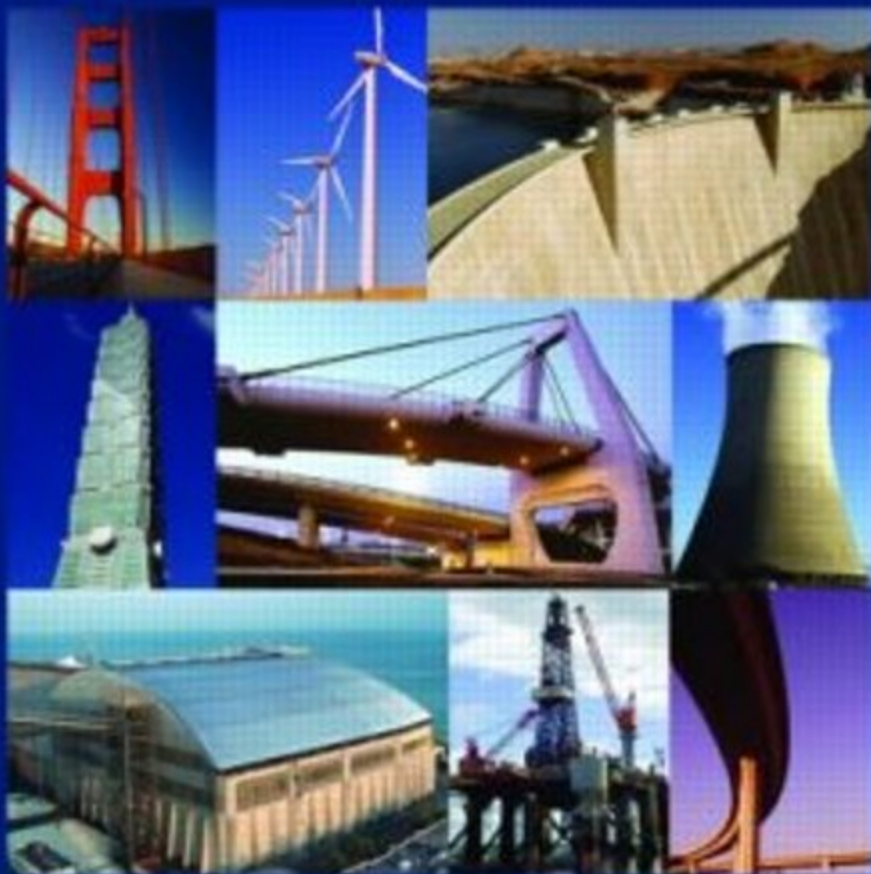


# Life-Cycle Civil Engineering

Editors

Fabio Biondini & Dan M. Frangopol



# LIFE-CYCLE CIVIL ENGINEERING



# Life-Cycle Civil Engineering

*Editors*

**Fabio Biondini**

*Department of Structural Engineering, Politecnico di Milano, Milan, Italy*

**Dan M. Frangopol**

*Department of Civil and Environmental Engineering, Center for Advanced Technology for  
Large Structural Systems, Lehigh University, Bethlehem, Pennsylvania, USA*



**CRC Press**

Taylor & Francis Group

Boca Raton London New York Leiden

---

CRC Press is an imprint of the  
Taylor & Francis Group, an **informa** business

A BALKEMA BOOK

*CRC Press/Balkema is an imprint of the Taylor & Francis Group, an informa business*

© 2008 Taylor & Francis Group, London, UK

Typeset by Vikatan Publishing Solutions (P) Ltd., Chennai, India

Printed and bound in Great Britain by Antony Rowe (A CPI-group Company), Chippenham, Wiltshire.

All rights reserved. No part of this publication or the information contained herein may be reproduced, stored in a retrieval system, or transmitted in any form or by any means, electronic, mechanical, by photocopying, recording or otherwise, without written prior permission from the publishers.

Although all care is taken to ensure integrity and the quality of this publication and the information herein, no responsibility is assumed by the publishers nor the author for any damage to the property or persons as a result of operation or use of this publication and/or the information contained herein.

Published by: CRC Press/Balkema

P.O. Box 447, 2300 AK Leiden, The Netherlands

e-mail: [Pub.NL@taylorandfrancis.com](mailto:Pub.NL@taylorandfrancis.com)

[www.crcpress.com](http://www.crcpress.com) – [www.taylorandfrancis.co.uk](http://www.taylorandfrancis.co.uk) – [www.balkema.nl](http://www.balkema.nl)

ISBN: 978-0-415-46857-2 (hbk)

# Table of Contents

Preface	XIII
Symposium Organization	XV
Acknowledgements	XIX
<i>Keynote lectures</i>	
Life-cycle considerations in risk-informed decisions for design of civil infrastructures <i>A.H-S. Ang</i>	3
Structural integrity monitoring for dependability <i>S. Arangio, F. Bontempi &amp; M. Ciampoli</i>	11
Practical approaches to the application of life-cycle civil engineering for infrastructures in Korea <i>H.-N. Cho</i>	21
Life cycle optimization in earthquake engineering <i>L. Esteva</i>	35
Life-cycle cost of civil infrastructure with emphasis on bridges <i>H. Furuta &amp; D.M. Frangopol</i>	47
The new life of the Theatre alla Scala <i>P.G. Malerba</i>	59
Life-cycle assessment of marine civil engineering structures <i>T. Moan</i>	73
Increasing a building's life-cycle in regions of high seismic risk <i>M.P. Sarkisian</i>	89
<i>Life-cycle damage processes</i>	
Mechanical behavior of clay bricks and restoration mortars subject to thermal actions <i>P. Antonaci &amp; P. Bocca</i>	101
Ageing and lifecycle of building envelopes and thin shells made of quasi-brittle conglomerates of glass and epoxy resin <i>F. Aymerich, G.P. Cossu &amp; L. Fenu</i>	107
Concrete composition and service life of reinforced concrete structures exposed to chloride bearing environments <i>L. Bertolini, F. Lollini &amp; E. Redaelli</i>	113
FEM-Models of cathodic protection systems for concrete structures <i>L. Bertolini, F. Lollini, E. Redaelli, R.B. Polder &amp; W.H.A. Peelen</i>	119
Structural behavior of cable-stayed bridges under damage <i>F. Biondini, P. Limonta, P.G. Malerba &amp; R. Stucchi</i>	125

Damage propagation and structural robustness <i>F. Biondini &amp; S. Restelli</i>	131
Increasing durability of recycled cement bound materials: laboratory investigation on the effects of bituminous emulsions <i>G. Da Rios, E. Toraldo &amp; E. Mariani</i>	137
Life cycle deterioration and cost comparison of bridge deck designs including rehabilitation strategies <i>L.R. Feldman, M. Boulfiza, J. Zaccaruk, P.N. Christensen &amp; G. Sparks</i>	143
In-situ chemical analysis for life cycle health management <i>M. Ghandehari</i>	149
Comparison of corrosion accelerated tests performed in reinforced concrete structures using voltage and current induction <i>A.G. Graeff, A.S. Torres &amp; L.C.P. Silva Filho</i>	153
Influence of localized corrosion of steel bars on structural performance of reinforced concrete beams <i>H. Hamada, E. Kato, M. Iwanami &amp; H. Yokota</i>	159
Development of a damage-recovery relationship based on variable re-curing of fire-damaged high-strength mortar <i>M. Henry, T.H. Ahn, Y. Kato &amp; T. Kishi</i>	165
New developed expansive ultra rapid hardening fiber reinforced concrete for bridge deck repair <i>I. Iwaki, S. Banchi &amp; Y. Koda</i>	171
Corrosion characterization of reinforcing bar in existing RC structure <i>E. Kato, M. Iwanami, H. Yokota &amp; H. Hamada</i>	177
Reasons for repair need in Finnish concrete facades in practice <i>J. Lahdensivu &amp; S. Varjonen</i>	183
The effects of mineral additions on chloride penetration into concrete under the frost action <i>B. Li &amp; L. Tang</i>	189
Stochastic modeling of corrosion propagation for service life prediction of chloride contaminated RC structures <i>Z.-H. Lu, Y.-G. Zhao &amp; K. Yu</i>	195
The critical role of marine bacterial processes in the development of models for pitting corrosion of structural steels <i>R.E. Melchers</i>	203
Feasibility analysis of the use of stainless steel reinforcement for concrete members subjected to aggressive exposure conditions <i>C. Molins, E. Real &amp; L. Medina</i>	209
Seismic loss estimation based on end-to-end simulation <i>M. Muto, S. Krishnan, J.L. Beck &amp; J. Mitrani-Reiser</i>	215
Fatigue damage measures with a statistical model for the Wöhler field <i>M.L. Ruiz-Ripoll, A. García, E. Castillo, A. Fernández-Canteli &amp; R. Koller</i>	221
Discussion concerning the multi-ranked deterioration forecasting model based on incomplete inspection data <i>Y. Shumuta</i>	227
The behavior of a building as a part of its conceiving <i>V. Spigai &amp; E. Dalla Vecchia</i>	233

Effect of spatially variable corrosion damage on strength and time-dependent reliability of RC beams	239
<i>M.G. Stewart &amp; Q. Suo</i>	
Service-life performance of reinforced concrete structures in corrosive environments	247
<i>D.V. Val &amp; L. Chernin</i>	
Effect of cracking on long-term performance of reinforced concrete slabs	253
<i>T. Yamamoto</i>	
Dilatometric tests combined with computer simulations and parameter identification for in-depth diagnostic analysis of concrete dams	259
<i>A. Zirpoli, G. Maier, G. Novati &amp; T. Garbowski</i>	
 <i>Life-cycle assessment and design</i>	
Life-cycle analysis of buildings with R/C frames	267
<i>D.O. Astafiev &amp; I.A. Fedotova</i>	
Direct Displacement Based Design and Force Based Design of precast concrete structures	273
<i>A. Belleri &amp; P. Riva</i>	
Lifetime seismic performance of precast reinforced concrete industrial buildings	279
<i>F. Biondini, A. Palermo &amp; G. Toniolo</i>	
Life-cycle multi-objective optimization of deteriorating structures	285
<i>F. Biondini &amp; G. Zani</i>	
Fatigue design of precast structural concrete plates for access floors	293
<i>M. Breccolotti, A.L. Materazzi &amp; I. Venanzi</i>	
Integration of degradation prognosis of concrete structures into life cycle management	299
<i>H. Budelmann, K. Hariri &amp; T. Starck</i>	
Increasing pavements durability through construction: a model for compaction design	305
<i>M. Crispino, E. Mariani &amp; R. Rampini</i>	
Service life predictions for new and rehabilitated concrete bridge structures	311
<i>B. Czarnecki &amp; R.L. Day</i>	
Combined reinforcement	317
<i>B. De Rivaz</i>	
New aspects on bridge design for durability	323
<i>M. Empelmann, V. Henke, G. Heumann &amp; M. Wichers</i>	
Fuzzy probabilistic analysis of prestressed concrete structures	329
<i>L. Giordano, G. Mancini &amp; F. Tondolo</i>	
Modeling maximum live load effects on highway bridges	335
<i>M. Ghosn, B. Sivakumar &amp; F. Moses</i>	
Analysis of the local ductility in reinforced concrete beams dimensioned according to Eurocode 8	343
<i>A. Kassoul, A. Bougara, M. Belkhatir &amp; K. Ezziane</i>	
Serviceability as a significant factor of the bridge life-cycle	349
<i>V. Kristek &amp; L. Vrablik</i>	
Inspection and evaluation of existing structures: a task for brave engineers	355
<i>J. León, H. Corres-Peirretti &amp; F. Prieto</i>	
Minimum life-cycle cost design and optimal earthquake intensity decision-making of aseismic structures based on finite element reliability analysis	361
<i>D.-G. Lu, X.-H. Yu, G. Li &amp; G.-Y. Wang</i>	

Evaluation of the response of concrete structures along their service life by nonlinear evolutive analysis methods	367
<i>A.R. Mari &amp; J.M. Bairán</i>	
Strengthening of aged RC structures using spreadsheet analyses with optimisation methods and linearised moment-curvature relations	373
<i>P. Mark</i>	
Uncertainty in structural capacity and influence on seismic demand and damage	379
<i>M. Mezzi</i>	
Cost-based design and renewal strategy for long-life structures	385
<i>J. Menčík</i>	
Probabilistic treatment of bridge monitoring data and associated errors for reliability assessment and prediction	391
<i>T.B. Messervey &amp; D.M. Frangopol</i>	
Life-cycle design of residential buildings: appearance and reality of ecological assessments	397
<i>M. Michlmair &amp; P. Maydl</i>	
The influence of design and detailing on the life and maintenance of a bridge	403
<i>A.G. Mordey</i>	
Life-cycle performance of structures: combining expert judgment and results of inspection	409
<i>L.C. Neves &amp; D.M. Frangopol</i>	
Bending performance of reinforced concrete member deteriorated by corrosion	415
<i>M. Oyado, T. Sato, T. Kanakubo &amp; Y. Yamamoto</i>	
Investigating the effects of corrosion on 45-year-old prestressed concrete bridge beams	421
<i>T.M. Papé &amp; R.E. Melchers</i>	
Analytical modelling of FRP strengthened steel beams	427
<i>C. Pellegrino, E. Maiorana &amp; C. Modena</i>	
Estimation of life-cycle fatigue damage for suspension bridge hangers	433
<i>F. Petrini &amp; F. Bontempi</i>	
Safety assessment of civil engineering structures throughout their life-cycle	439
<i>R. Pukl, D. Novák &amp; B. Teplý</i>	
Reliability-based fatigue assessment of welded connections	445
<i>S.G. Reid</i>	
Simple supported RC bridge design process considering durability	451
<i>X. Ruan, A.-R. Chen &amp; Z.-C. Pan</i>	
Probabilistic durability design of RC structures in Persian Gulf using DuraPGulf model	457
<i>M. Shekarchi, A. Rafiee, H. Layssi &amp; F.M. Marani</i>	
Strengthening with textile reinforced concrete—reliability based design with imprecise probability	463
<i>J.-U. Sickert, W. Graf &amp; S. Pannier</i>	
Fatigue life of precast decks of high speed railway bridges	469
<i>C.F. Sousa, R. Calçada &amp; A.S. Neves</i>	
Nonlinear dynamic analysis of frames with arbitrary plastic hinges	475
<i>Z.H. Yan &amp; F.T.K. Au</i>	
 <i>Life-cycle monitoring, maintenance, and rehabilitation</i>	
Life-cycle reliability analysis and selective maintenance of deteriorating structures	483
<i>F. Biondini, D.M. Frangopol &amp; E. Garavaglia</i>	

A comparison of tomographic reconstruction algorithms for acoustic non destructive testing of stone masonry	489
<i>B. Cannas, S. Carcangiu, M. Di Mauro, A. Fanni, A. Montisci, M.L. Mulas &amp; G. Concu</i>	
Features extraction techniques for sonic and ultrasonic NDT on building materials	495
<i>B. Cannas, F. Cau, M. Usai &amp; G. Concu</i>	
Measuring the displacements of a steel structure by GPS units	501
<i>F. Casciati &amp; C. Fuggini</i>	
Including structural monitoring activities in safety probabilistic formulations	507
<i>R. Ceravolo, A. De Stefano &amp; M. Pescatore</i>	
Maintenance strategies for large span suspension bridges against fatigue and corrosion	513
<i>A.-R. Chen, Y. Zeng &amp; R. Ma</i>	
Bridge management system techniques application to Italian highways network	519
<i>A. D'Andrea, D. Oggionni &amp; E. Spallarossa</i>	
Behavior of RC bridge girders strengthened with CFRP laminates	525
<i>A. El-Safty</i>	
Aspects of sustainability of repair-systems for concrete structures	531
<i>M. Empelmann, V. Henke, G. Heumann &amp; M. Wichers</i>	
Experimental identification of cable damping parameters towards robust design against aeroelastic instability	535
<i>L. Faravelli &amp; F. Ubertini</i>	
Seismic retrofitting of bridges	541
<i>G. Furlanetto, L. Ferretti Torricelli &amp; A. Marchiondelli</i>	
Widening and strengthening of bridge decks with composite materials	547
<i>G. Furlanetto &amp; R.L. Pefano</i>	
Maintenance and inspection of stay cables using prestressing steel at a German bridge	553
<i>C. Gläser &amp; H. Weiher</i>	
Assessment of bridge capacity through proof load testing	559
<i>J.D. Gómez &amp; J.R. Casas</i>	
Strengthening reinforced concrete T connections by steel straps	565
<i>M.N.S. Hadi</i>	
Development of a software-tool for the life-cycle management of bridges	571
<i>M. Kluth, A. Borrmann, E. Rank, T. Mayer &amp; P. Schiessl</i>	
Traffic load modeling based on structural health monitoring data	577
<i>C. Lan, H. Li &amp; J. Ou</i>	
Corrosion detection in reinforced concrete structures using static and dynamic response measurements	583
<i>F. Lanata &amp; A. Del Grosso</i>	
Prediction and quantification models of bridge condition in Korea	589
<i>K.-J. Lee, S.-H. Park, C.-H. Park, K.-H. Park &amp; J.S. Kong</i>	
Lifespan evaluation of 8 bridges of the Indiana Toll Road: A case study	595
<i>J. León, H. Corres-Peiretti, S. Pérez-Fadón, J.E. Herrero, F. Rodríguez &amp; F. Prieto</i>	
Birth certificate as an important tool for public-private-partnership projects	601
<i>T.F. Mayer, P. Schießl &amp; M. Zintel</i>	
Invention of crack inspection system using a light wave survey camera with a built-in crack scale	607
<i>K. Nakaniwa, M. Maeda, Y. Koyama &amp; T. Asakura</i>	
Structural health monitoring for life cycle management of bridges	613
<i>F.N. Catbas, M. Gul, R. Zaurin, H.B. Gokce, D. Maier &amp; T. Terrell</i>	



Peeling failure along the interface in FRP-strengthened beams subjected to transverse loads <i>E. Oller, A.R. Mari &amp; D. Cobo</i>	619
Optimal inspection and maintenance strategies for bridge network using supply and demand approach <i>A.D. Orcesi &amp; C.F. Cremona</i>	625
The life-cycle maintenance strategy for the bridge system <i>K.-H. Park, S.-Y. Lee, J.-H. Kim, J.-S. Kong &amp; H.-N. Cho</i>	631
Life time assessment of steel bridges via monitoring and testing <i>U. Peil, M. Frenz &amp; I. Schendel</i>	637
A risk ranking strategy for network level bridge management <i>S. Sathananthan, M.I. Rafiq &amp; T. Onoufriou</i>	643
Monitoring based structural performance assessment <i>A. Strauss, D.M. Frangopol &amp; S. Kim</i>	649
On the road of multi-performance profiles aided maintenance <i>A. Talon, D. Boissier &amp; J. Hans</i>	655
Development of a work carriage for tunnel maintenance <i>H. Terato, K. Yokozawa, N. Takemoto, Y. Miura &amp; Y. Inagawa</i>	661
Selection of repair method for concrete facades <i>S. Varjonen &amp; J. Lahdensivu</i>	667
Monitoring based performance prediction of steel bridges against traffic loading exemplified at the Europabrücke <i>R. Veit-Egerer &amp; H. Wenzel</i>	671
A maintenance concept for concrete tunnel linings in soft soil conditions <i>A.H.J.M. Vervuurt, G.A. Leegwater &amp; R.B. Polder</i>	677
Inspection of bridges in Austria—Practice and outlook <i>R. Wendner, S. Hoffmann, A. Strauss, K. Bergmeister &amp; R. Geier</i>	683
 <i>Life-cycle performance of special structures</i>	
Probability-based durability design and performance-based concrete quality control of a concrete harbor structure <i>V. Årskog &amp; O.E. Gjorv</i>	691
Structural safety evaluation of a r.c. arch bridge <i>A.M. Avossa, P. Famigliuolo &amp; P. Malangone</i>	697
Towards life-cycle assessment of foundations of guyed towers in electrical transmission lines <i>C.B.P. Azevedo &amp; S.M.C. Diniz</i>	703
Life-cycle performance of bridge decks in aggressive environments <i>F. Biondini, D.M. Frangopol &amp; P.G. Malerba</i>	709
Structural reliability of the "Palazzo della Civiltà Italiana" in Rome EUR <i>C. Ceccoli, T. Trombetti &amp; D. Biondi</i>	715
Maintenance and rehabilitation of the "Incoronata" viaduct along the Salerno Reggio Calabria highway <i>C. Ceccoli, T. Trombetti, A. Forlani &amp; F. Baroni</i>	721
Experiment based performance prediction of long span bridges subjected to non-uniform excitation <i>M.M.S. Cheung &amp; C.Y. Yang</i>	727
Functionality and strength of arch concrete dams cracked by shrinkage <i>M. Como &amp; S. Imperatore</i>	733

Effects of soil-structure interaction on the seismic damageability of coupled wall-frame structures on pile foundations	739
<i>F. Dezi, S. Carbonari &amp; G. Leoni</i>	
Rehabilitation and modernization of the Monte Bianco Tunnel	745
<i>G. Furlanetto &amp; L. Ferretti Torricelli</i>	
Design of durable bridges by using self-compacting concrete filled steel tubes	751
<i>G. Furlanetto, L. Ferretti Torricelli &amp; A. Marchiondelli</i>	
Structural reliability analysis and monitoring program applied to a roller-compacted concrete dam	757
<i>C.M. Krüger, A. Chaves Neto &amp; D.A.V. Krüger</i>	
Seismic vulnerability of historical buildings: the Royal Palace of Naples	763
<i>F.M. Mazzolani, B. Faggiano, A. Marzo, E. Guglielmo &amp; P. Mascilli Migliorini</i>	
Effect of unsteady aerodynamic admittances on life cycle of guyed masts	769
<i>U. Peil &amp; M. Clobes</i>	
Medium-term life-cycle monitoring of random behaviour components of in-service pile-supported wharves	775
<i>H. Yáñez-Godoy, J. Boéro &amp; F. Schoefs</i>	
 <i>Life-cycle cost of structures and infrastructures</i>	
Maintenance—LCC analysis based on real data	783
<i>C. Bahr &amp; K. Lennerts</i>	
A new efficient methodology for large scale outsourcing of maintenance	787
<i>J. Bakker, P. Boersma &amp; J. Vólwerk</i>	
Life cycle cost evaluation of the as-built cover layer in reinforced concrete bridge decks	793
<i>C.L. Barnes &amp; J.-F. Trottier</i>	
Recycling C&DW: a way for closing the concrete loop	799
<i>V. Corinaldesi, G. Moriconi &amp; L. Dezi</i>	
Life Cycle Cost Analysis in pavement type selection: state-of-the-practice	805
<i>Z. Guven, P.R. Rangaraju &amp; S.N. Amirkhanian</i>	
Financial viability of TPSM applied continuous composite bridges	811
<i>J.-H. Kim, J.-H. Ahn, C.-Y. Jung, &amp; S.-H. Kim</i>	
Effect of cumulative seismic damage on life-cycle cost of reinforced concrete bridges	819
<i>R. Kumar, P. Gardoni &amp; M. Sanchez-Silva</i>	
An information model for life-cycle cost management of cable-stayed bridge	825
<i>S.H. Lee, M.G. Huang, B.G. Kim &amp; Y.H. Park</i>	
Guidelines for LCC analysis and evaluation of public construction projects in Korea	829
<i>T.K. Kang &amp; Y.S. Lee</i>	
Design of green engineered cementitious composites for pavement overlay applications	837
<i>M.D. Lepech, G.A. Keoleian, S. Qian &amp; V.C. Li</i>	
Development of life-cycle cost based budget allocation system for bridge group	843
<i>A. Miyamoto &amp; H. Uchino</i>	
LCC case studies for bridges in different design phases	851
<i>S. Noponen &amp; A. Jutila</i>	
Life-cycle cost assessment and service life estimate of precast concrete culverts	857
<i>D.K. Panesar, C.J. Churchill, S.E. Chidiac &amp; E. Kling</i>	

A successive LCC model development of marine RC structures exposed to chloride attack using a Bayesian approach <i>H. Park, H. Jung, J. Kong &amp; G. Zi</i>	863
Optimal floor plan design of high-rise apartment buildings based on life-cycle cost consideration <i>K.J. Park &amp; A.H-S. Ang</i>	871
Life-cycle cost analysis for fire protection of buildings <i>L. Razdolsky</i>	877
FRP bridge deck life cycle cost analyzer <i>S. Sahirman, R.C. Creese &amp; H.V.S. GangaRao</i>	883
Life cycle cost and function analysis in value based design decision <i>C. Utomo &amp; A. Idrus</i>	889
Equipment replacement decisions based on life-cycle cost analysis <i>J. Weissmann &amp; A.J. Weissmann</i>	895
Life cycle analysis of waterfront structures (a qualitative process model) <i>J.L. Wilson &amp; C.B. Kubic</i>	901
An integrated life cycle assessment and life cycle analysis model for pavement overlay systems <i>H. Zhang, G.A. Keoleian &amp; M.D. Lepech</i>	907
 <i>Life-cycle oriented computational tools</i>	
Advanced fragility curves of Interdependent Lifelines Using Decision Making Process <i>M.N. Alexoudi, K.G. Kakderi &amp; K.D. Ptilakis</i>	915
Intelligent agents for life cycle management of structures and infrastructures in seismic areas <i>G.M. Atanasiu, F. Leon &amp; M.H. Zaharia</i>	921
Hierarchical ordering of extensometers readings from Itaipu dam <i>A.S. Dyminski, M.T.A. Steiner &amp; R. Villwock</i>	929
Algorithm for identification of damage on bridge piers <i>A.S. Kiremidjian, P. Sarabandi, A. Cheung, C. Cabrera, K.K. Nair &amp; G. Kiremidjian</i>	935
Analysis, heuristics, and uncertainty of hybrid life cycle assessment: agriculture and construction case studies <i>A.E. Landis &amp; M.M. Bilec</i>	941
Advanced performance evaluation system for existing concrete bridges with machine learning <i>A. Miyamoto &amp; J-I. Ishida</i>	947
Cost versus sustainability of reinforced concrete building frames by multiobjective optimization <i>I. Payá-Zaforteza, V. Yepes, F. González-Vidosa &amp; A. Hospitaler</i>	953
Model based reasoning for life-cycle structural engineering <i>I.F.C. Smith &amp; P. Kripakaran</i>	959
Value analysis for decision making on highway cross-sections <i>N. Villegas, B. De los Ríos, A. Aguado &amp; R. Núñez</i>	965

## Preface

In designing civil engineering systems, the system performance must be considered as time-dependent. Therefore, a consistent design approach should comply with the desired performance not only at the initial stage when the system is supposed to be in the intact state, but also during its expected life-cycle. This can be achieved by taking into account the effects induced by unavoidable sources of damage and by eventual maintenance interventions under uncertainty. At present design for durability with respect to chemical-physical damage phenomena is based on simplified criteria associated with prescribed environmental conditions. As an example, for concrete structures such criteria introduce threshold values for concrete cover, water-cement ratio, amount and type of cement, and others, to limit the effects of structural damage induced by carbonation of concrete and corrosion of reinforcement. However, a durable design cannot be based only on such indirect evaluations of the effects of damage, but also needs to take into account the global effects of the local damage phenomena on the overall system performance.

In recent years a considerable amount of research work has been done, and relevant advances have been accomplished in the fields of modeling, analysis, design, monitoring, maintenance and rehabilitation of deteriorating civil engineering systems. Nowadays these developments are perceived to be at the heart of civil engineering, which is currently undergoing a transition towards a life-cycle oriented design philosophy. For this reason, after a series of International Workshops on Life-Cycle Cost Analysis and Design of Civil Infrastructure Systems held in Honolulu, Hawaii, USA (LCC1, August 7–8, 2000), Ube, Yamaguchi, Japan (LCC2, September 27–29, 2001), Lausanne, Switzerland (LCC3, March 24–26, 2003), Cocoa Beach, Florida, USA (LCC4, May 8–11, 2005), and Seoul, Korea (LCC5, October 16–18, 2006), it was decided to create the International Association for Life-Cycle Civil Engineering (IALCCE, <http://www.ialcce.org>).

IALCCE was founded in October 2006 during the 5th International Workshop on Life-Cycle Cost Analysis and Design of Civil Infrastructure Systems (LCC5). This Association covers all aspects of life-cycle assessment, design, maintenance, rehabilitation and monitoring of civil engineering systems. The mission of the Association is to become the premier international organization for the advancement of the state-of-the-art in the field of life-cycle civil engineering. The objective of the Association is to promote international cooperation in the field of life-cycle civil engineering for the purpose of enhancing the welfare of society.

IALCCE has created fertile grounds for the stimulation and promotion of research in the field of life-cycle civil engineering. It was therefore decided to bring together the main advances in the field of life-cycle engineering and related topics at the First International Symposium on Life-Cycle Civil Engineering (IALCCE'08), held in Villa Monastero, Varenna, Lake Como, Italy, 10–14 June, 2008. This Symposium has been organized on behalf of IALCCE under the auspices of Politecnico di Milano. The interest of the international civil engineering community in the activities covered by IALCCE has been confirmed by the significant response to the IALCCE'08 call for papers. In fact, more than 200 abstracts were received by the Symposium Secretariat, and about 70% of them were selected for final publication as full papers and presentation at the Symposium.

IALCCE'08 covers all major aspects of life-cycle civil engineering and related topics. They include: life-cycle damage processes (aging of structures, deterioration modeling, durable materials, earthquake and accidental loadings, fatigue and damage, fire and high temperatures, marine and severe environments, structure-environment interaction); life-cycle assessment and design (design for durability, failure analysis and risk prevention, lifetime structural optimization, long-term performance analysis, performance based design, service life prediction, time-variant reliability, uncertainty modeling); life-cycle monitoring, maintenance and rehabilitation (damage identification, field testing, health monitoring, inspection and evaluation, maintenance strategies, rehabilitation techniques, strengthening and repair, structural integrity); life-cycle performance of special structures (bridges and viaducts, high-rise buildings, hydraulic structures, offshore structures, precast systems, roof systems and hangars, runway and highway pavements, tunnels and underground structures); life-cycle cost of structures and infrastructures (decision making processes, human factors in life-cycle engineering, life-cycle cost models, project management, risk-lifetime analysis and optimization, whole life costing); and life-cycle

oriented computational tools (artificial intelligence methods, evolutionary procedures, heuristic techniques, mathematical optimization, soft-computing methods, survival models and simulation).

*Life-Cycle Civil Engineering* collects papers on theories, methods, algorithms, and applications in the field of life-cycle civil engineering presented at IALCCE'08. It consists of a book and a CD-ROM containing 150 papers, including eight keynote papers and 142 technical contributions from 28 countries. These papers deal with the state of the art as well as emerging concepts and innovative applications related to all major aspects of life-cycle civil engineering and related topics. The Editors hope that these Proceedings will serve as a valuable reference to all concerned with life-cycle performance of civil engineering systems, including students, researchers, and engineers from all sections of civil engineering.

*Fabio Biondini and Dan M. Frangopol*  
Chairs, IALCCE'08  
Milan and Bethlehem, March 2008

# Symposium Organization

## Symposium Chairs

Fabio Biondini *Politecnico di Milano, Milan, Italy*  
Dan M. Frangopol *Lehigh University, Bethlehem, PA, USA*

## International Steering Committee

Dan M. Frangopol (Chair) *Lehigh University, Bethlehem, PA, USA*  
Alfredo H-S. Ang (Ex Officio) *University of California, Irvine, CA, USA*  
Fabio Biondini (Ex Officio) *Politecnico di Milano, Milan, Italy*  
Moe Cheung *Hong Kong University of Science and Technology, Hong Kong, P.R.C.*  
Hyo-Nam Cho *Hanyang University, Ansan, Korea*  
Luis Esteve *National University of Mexico, Mexico City, Mexico*  
Hitoshi Furuta *Kansai University, Osaka, Japan*  
Robert Melchers *University of Newcastle, Callaghan, NSW, Australia*  
Udo Peil *Technical University of Braunschweig, Braunschweig, Germany*  
Asko Sarja *Innokas Consulting Co, Espoo, Finland*

## International Scientific Committee

Alfredo H-S. Ang (Chair) *University of California, Irvine, CA, USA*  
Jaap Bakker *Ministry of Transport, Utrecht, The Netherlands*  
Larry Bergman *University of Illinois at Urbana-Champaign, IL, USA*  
Franco Bontempi *University of Rome "La Sapienza", Milan, Italy*  
Christian Bucher *Technical University of Vienna, Vienna, Austria*  
Harald Budelmann *Technical University of Braunschweig, Braunschweig, Germany*  
Joan R. Casas *Technical University of Catalonia, Barcelona, Spain*  
Marios K. Chryssanthopoulos *University of Surrey, Surrey, Guildford, UK*  
Ross Corotis *University of Colorado, Boulder, CO, USA*  
Paulo J.S. Cruz *University of Minho, Guimarães, Portugal*  
Sofia Diniz *Federal University of Minas Gerais, Belo Horizonte, Brazil*  
Bruce Ellingwood *Georgia Institute of Technology, Atlanta, GA, USA*  
Allen Estes *California Polytechnic State University, San Luis Obispo, CA, USA*  
Michel Ghosn *City College of New York, New York, NY, USA*  
Leo Klatter *Ministry of Transport, Utrecht, The Netherlands*  
Hyun-Moo Koh *Seoul National University, Seoul, Korea*  
Jung Sik Kong *Korea University, Seoul, Korea*  
Vladimir Kristek *Czech Technical University, Prague, Czech Republic*  
Xila L. Liu *Shanghai Jiaotong University, Shanghai, China*  
Pier Giorgio Malerba *Politecnico di Milano, Milan, Italy*  
Antonio Mari *Technical University of Catalonia, Barcelona, Spain*  
Ayaho Miyamoto *Yamaguchi University, Yamaguchi, Japan*  
Luis Neves *Univ. Nova de Lisboa, Monte de Caparica, Portugal*  
Andrzej Nowak *University of Nebraska, Lincoln, NE, USA*

Mark Stewart  
Man-Chung Tang  
Wilson Tang  
Palle Thoft-Christensen  
Eiichi Watanabe  
John L. Wilson

*University of Newcastle, Callaghan, NSW, Australia*  
*T.Y. Lin International, San Francisco, CA, USA*  
*Hong Kong University of Science and Technology, Hong Kong, P.R.C.*  
*Aalborg University, Aalborg, Denmark*  
*Kyoto University, Kyoto, Japan*  
*Lehigh University, Bethlehem, PA, USA*

### **Local Advisory Committee**

Pier Giorgio Malerba (Chair)	<i>Politecnico di Milano</i>
Franco Bontempi	<i>University of Rome "La Sapienza"</i>
Fabio Casciati	<i>University of Pavia</i>
Claudio Ceccoli	<i>University of Bologna</i>
Mario Como	<i>University of Rome "Tor Vergata"</i>
Edoardo Cosenza	<i>University of Naples "Federico II"</i>
Andrea Del Grosso	<i>University of Genoa</i>
Alessandro De Stefano	<i>Politecnico di Torino</i>
Luigino Dezi	<i>University of Ancona</i>
Pasquale Malangone	<i>Second University of Naples</i>
Giuseppe Mancini	<i>Politecnico di Torino</i>
Luigi Annibale Materazzi	<i>University of Perugia</i>
Claudio Modena	<i>University of Padua</i>
Alberto Parducci	<i>University of Perugia</i>
Emanuele F. Radogna	<i>University of Rome "La Sapienza"</i>
Paolo Spinelli	<i>University of Florence</i>
Giandomenico Toniolo	<i>Politecnico di Milano</i>

### **Local Organizing Committee**

Fabio Biondini (Chair)	<i>Politecnico di Milano</i>
Luca Bertolini	<i>Politecnico di Milano</i>
Marcello Ciampoli	<i>University of Rome "La Sapienza"</i>
Maurizio Crispino	<i>Politecnico di Milano</i>
Elsa Garavaglia	<i>Politecnico di Milano</i>
Massimiliano Gioffrè	<i>University of Perugia</i>
Stefano Malavasi	<i>Politecnico di Milano</i>
Alessandra Marchiondelli	<i>Spea Ingegneria Europea, Milan</i>
Livia Pardi	<i>Autostrade per l'Italia, Rome</i>
Zila Rinaldi	<i>University of Rome "Tor Vergata"</i>

### **Symposium Secretariat**

Ms. Paola Limonta and Ms. Roberta Stucchi  
*Department of Structural Engineering, Politecnico di Milano*  
*Piazza L. da Vinci, 32-20133 Milan, Italy*

### **Symposium Website**

<http://www.ialcce08.org>



## Organizing Association



IALCCE  
International Association for Life-Cycle Civil Engineering

## Organizing Institution



**POLITECNICO  
DI MILANO**

POLIMI  
Politecnico di Milano, Milan, Italy

## Sponsoring Institutions/Organizations



ACI  
American Concrete Institute



AICAP  
Italian Association for Reinforced and Prestressed Concrete  
*Associazione Italiana Calcestruzzo Armato e Precompresso*



AIOM  
Italian Association of Offshore and Marine Engineering  
*Associazione di Ingegneria Offshore e Marina*



ATLSS  
Center for Advanced Technology for Large Structural Systems,  
Lehigh University, Bethlehem, PA, USA



CTE  
Italian Society of Building Engineers  
*Collegio dei Tecnici dell'Edilizia*



IABMAS  
International Association for Bridge Maintenance and Safety



SEI-ASCE  
Structural Engineering Institute - American Society of Civil Engineers



Spea Ingegneria Europea, Milan, Italy



T.Y. Lin International, San Francisco, CA, USA



UPC  
Universitat Politècnica de Catalunya, Barcelona, Spain

## Supporting Local Authorities



**Regione Lombardia**  
*Casa e Opere Pubbliche*

Lombardy Regional Administration  
*Regione Lombardia*



Province of Como  
*Provincia di Como*



Provincia di Lecco

Province of Lecco  
*Provincia di Lecco*

## IALCCE Executive Board

Dan M. Frangopol (President)	<i>Lehigh University, Bethlehem, PA, USA</i>
Alfredo H-S. Ang (Honorary President)	<i>University of California, Irvine, CA, USA</i>
Harald Budelmann (Vice-President)	<i>Technical University of Braunschweig, Braunschweig, Germany</i>
Hyo-Nam Cho (Vice-President)	<i>Hanyang University, Kyungki, Korea</i>
Hitoshi Furuta (Vice-President)	<i>Kansai University, Osaka, Japan</i>
Fabio Biondini (General Secretary)	<i>Politecnico di Milano, Milan, Italy</i>
Jaap Bakker	<i>Ministry of Transport, Utrecht, The Netherlands</i>
Moe Cheung	<i>Hong Kong University of Science and Technology, Hong Kong, P.R.C.</i>
Luis Esteva	<i>National University of Mexico, Mexico City, Mexico</i>
Leo Klatter	<i>Ministry of Transport, Utrecht, The Netherlands</i>

## IALCCE Secretariat

Prof. Fabio Biondini  
*Department of Structural Engineering, Politecnico di Milano*  
*Piazza L. da Vinci, 32 - 20133 Milan, Italy*

## IALCCE Website

<http://www.ialcce.org>

## Acknowledgments

The Editors are extremely grateful to all people who contributed to the organization of the IALCCE'08 Symposium and to the production of this volume. Particularly, the Editors would like to express their sincere thanks to all the authors for their contributions, to the members of the International Scientific Committee and the Local Advisory Committee for their valuable support in the review process, and to the members of the Local Organizing Committee for the time and efforts dedicated to make IALCCE'08 a successful event.

Moreover, the Editors wish to thank all organizations, institutions, and authorities that offered their sponsorship. At the institutional level, a special acknowledgment has to be given to the Politecnico di Milano, for organizing and co-sponsoring this Symposium along with the International Association for Life-Cycle Civil Engineering (IALCCE), as well as to the Department of Structural Engineering and all people of its administrative staff, for important contributions to the Symposium organization.

IALCCE'08 has been conceived, planned, and developed in close consultation and cooperation with several individuals. Principally, the Editors wish to express their sincere gratitude to Pier Giorgio Malerba, Chair of the Local Advisory Committee, for his valuable and continuous support to both scientific and financial organization of this Symposium. His experience and advices have been of crucial importance. The Editors are also extremely thankful to Alfredo H-S. Ang for Chairing the International Scientific Committee.

Special thanks are due to Alessandra Marchiondelli, member of the Local Organizing Committee, who designed the Symposium website and closely followed all steps of the Symposium organization, providing many valuable insights and ideas which significantly contributed to the success of IALCCE'08.

Finally, the Editors wish to express their warmest appreciation to Paola Limonta and Roberta Stucchi, who professionally led the Symposium Secretariat, developed and maintained the Symposium website, and provided a tremendous amount of very dedicated teamwork. Their outstanding and continuous efforts have been of extreme importance for the organization of this Symposium.

*Keynote lectures*

# Life-cycle considerations in risk-informed decisions for design of civil infrastructures

A.H-S. Ang

*University of California, Irvine*

**ABSTRACT:** Civil structures and infrastructures, such as buildings, bridges, and other facilities, are constructed and built for long service lives; many for over 50 or 100 years. In this light, the performance of an engineered system over its useful life span is naturally of major concern. The concern must include the assurance of a minimum level of reliability of performance, which will necessarily require inspections, repair, and maybe even retrofitting or replacement. The whole-life cost associated with this life-cycle performance, therefore, is the pertinent cost that ought to be the basis for determining the cost during the design stage (in terms of present value); this must include the maintenance and potential damage costs, besides the initial cost, over the life of a system. In this regard, significant technical and economic uncertainties can be expected and are unavoidable; therefore, decisions required in the design of such systems must consider risk associated with the probability of non-performance and serious damage or failure, as well as of the financial risk. The importance of these factors in the decision process at the design stage is emphasized and a practical approach for life-cycle consideration in formulating risk-informed decisions in the planning and design of infrastructure systems is described. The approach is illustrated with specific applications in the optimal design of civil infrastructure systems.

## 1 INTRODUCTION

Civil infrastructures, such as bridges, buildings, power plants, dams, sewage treatment facilities are designed and built for long useful lives. Decisions made during the design stage of such a system are invariably fraught with significant uncertainties. This is especially true when considering the performance and cost of an infrastructure system over its useful life, which may be for over 50 or 100 years. In light of these uncertainties, there is risk of nonperformance (or even failure) of the system over its useful life—the loadings may vary significantly including forces from unforeseen or unexpected natural hazards, and the capacity of the system may deteriorate more than those assumed during the design stage; therefore, the performance of the system may be assured only in terms of probability or reliability, whereas the consequences to nonperformance (or failure) are also difficult to estimate with certainty. With respect to financial cost, there is similarly risk in under-estimating the whole life cost of the system, which must necessarily include the costs of operation, maintenance and repair, cost of failure, as well as the indirect costs of nonperformance or failure, each of which also contain significant uncertainties. These factors are clearly important in formulating the decisions required at the design stage.

## 2 DECISIONS UNDER UNCERTAINTY

### 2.1 *Basic concept*

Under conditions of uncertainty, any result obtained through analysis will also contain uncertainty; this uncertainty is often just as important as the relevant result of interest. For example, we mentioned above that in light of uncertainties in the loading on and capacity of a system, the performance of the system may be assured only in terms of probability or reliability, such as the probability of non-performance or failure. The uncertainty in the calculated probability of failure is clearly important, particularly on the decision in specifying what is a permissible or tolerable failure probability for the design of the system.

#### 2.1.1 *Modeling and significance of uncertainties*

Uncertainties may be classified broadly into two types (Ang and Tang, 2007)—the *aleatory* type and the *epistemic* type. The aleatory type is the variability inherent in nature, and can be observed in the variability of observed data; i.e., this type is data-based. Whereas, the epistemic type is uncertainty associated with our inability to accurately model or idealize reality; i.e., this type is knowledge-based.

The aleatory variability is not reducible as it is inherently part of the randomness of nature—additional observational data or improvement in the data collection process will increase the accuracy of the degree of variability, but may not reduce it; in fact it may even increase the degree of variability. On the other hand, the epistemic uncertainty can be reduced through the use of better or improved models of reality, or through more seasoned judgments of experts.

By separating uncertainties into two types—the aleatory and epistemic types, their respective significances in engineering applications can be delineated as follows:

*The probability of non-performance or failure of a system is associated with the aleatory variability, whereas the uncertainty in the calculated probability of failure is due to the epistemic type of uncertainty. This latter uncertainty (in the calculated failure probability) can be expressed in terms of its probability distribution (e.g., PDF).*

Observe that if the two types of uncertainties were combined into a total uncertainty, the calculated probability of failure would give its “best estimate” value (a single value). This best estimate value is, in fact, the mean value (or close to the mean) of the distribution of the failure probability indicated above.

### 2.1.2 Distribution of uncertainty

As mentioned above, the epistemic uncertainty can be represented by the distribution (PDF) of the relevant result of interest. This distribution clearly describes more complete information of the underlying result of interest, such as the failure probability. Similarly, the inverse of the failure probability distribution will yield the corresponding distribution of the safety index.

The probability distribution or the safety index is of special significance in the specification of the appropriate safety level for design. For risk averseness (Ang, 2006), a high percentile value may be specified, particularly for the design of an important system, in order to minimize the effect of the epistemic uncertainty. For example, by selecting the 90% value, there is implicitly a 10% probability that the selected value may be inadequate. Observe, on the other hand, that the “best estimate” value (or mean value) of the safety index could be inadequate by a probability of 50%.

Similarly, in estimating the life-cycle cost (at the design stage) of an engineering system under uncertainty, the distribution of its whole-life cost will permit the specification of a risk-averse cost (such as the 90% value) in order to minimize the chance of under-estimating the true cost of the system over its useful life.

## 3 ILLUSTRATIVE EXAMPLE

### 3.1 Optimal design of a cable-stayed bridge

In recent years, cable-stayed bridges have become one of the most popular type of long-span modern bridges in the world. The general concepts described above is applied to the optimal design of a cable-stayed bridge in Korea (Han and Ang, 2008). For this purpose, several designs of a bridge were considered in which the sections of the main members were increased or decreased relative to a standard design. Reliability analyses were then performed for each of the designs and the corresponding expected life-cycle costs were estimated.

#### 3.1.1 Profile and structural analysis of the cable-stayed bridge

Figure 1 shows the overall configuration of the cable-stayed bridge in Korea under consideration, which consisted of a steel box type girder that is 484 m in length and 11.3 m in width, 2 sets of steel box type towers that are 69 m in height, and 68 sets of lock coiled type cables. Also, Figure 1 shows the three dimensional model of the cable-stayed bridge (Han and Shin, 2005), indicating the locations of the critical members.

According to the design specification for a highway bridge in Korea (KICT, 1995), particularly for a long span bridge, the influence of the DB load is greater than that of the DL load. Therefore, when performing static analysis, the DL load was applied to two lanes simultaneously as live load, and the impact factor of  $i = 15/(40 + L) = 0.04$  was applied. The distributed

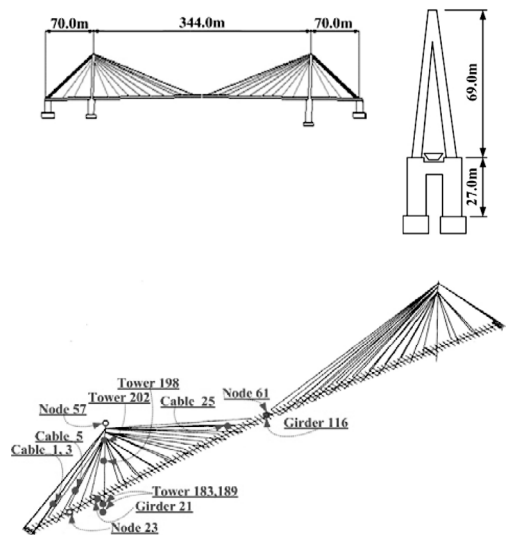


Figure 1. Profile and 3-D model of the cable-stayed bridge.

live load and concentrated live load under these conditions were 34.3 kN/m and 168.5 kN respectively, and these loads were applied so that the maximum positive bending moment occurred at the main span (distributed live load) and at the center point of the main span (concentrated live load), respectively.

Seismic response analysis (Nazmy and Abdel-Ghaffar, 1990) was performed by applying the acceleration time history to the elastic supporting points of all piers and abutments in the horizontal, lateral and vertical directions simultaneously. The applied force component of  $0.07(\text{coefficient of earthquake area}) \times 1.4(\text{importance factor}) = 0.098 \text{ g}$  in the horizontal direction is identical to those in the lateral direction, and the component in the vertical direction was assumed to be  $2/3$  of the component in the horizontal and lateral directions.

A reliability analysis was performed of the cable-stayed bridge under the lifetime maximum load; i.e., under the combined dead, live and earthquake loads. The reliability analysis was conducted with cable tensions, axial forces of girders and towers, and bending moments using first-order reliability method (FORM). The factors containing uncertainties include the ultimate stress, cable tensions, area, member forces and moment of inertia. Normal or lognormal distributions were assumed. In the case of the cables, the ultimate capacity was assumed to be 1,160.0 Mpa, whereas for the girders and towers, the material was SM400 steel with an ultimate stress of 240.0 Mpa. The coefficient of variation (c.o.v.) for the ultimate stress,  $\delta_C$ , was assumed to be 12%: whereas the c.o.v.'s of the area and moment of inertia,  $\delta_S$ ,  $\delta_I$ : were assumed to be 10%. The c.o.v. of the member forces by the dead load,  $\delta_D$ , was assumed to be 10%; and the c.o.v.'s of the member forces induced by the live load and acceleration time history,  $\delta_L$ ,  $\delta_E$ , were assumed to be 15%. These c.o.v.'s represent the respective aleatory uncertainties.

### 3.1.2 Results of reliability analysis

Reliability analysis was performed for the standard design of the bridge; similar analyses were also performed for the designs with increased and decreased sections of the members as shown in Figure 1. Figure 2 demonstrate the safety indices and failure probabilities of the critical members (Girder 21, Tower 189 and Cable 5) for the different designs. The values on the left axis in Figure 2 show the safety indices and those on the right axis represent the corresponding failure probabilities.

For the standard design, the failure probabilities of the critical members are as follows:

Girder:  $P_{F1} = 3.647\text{E-}03$ ,  
 Tower:  $P_{F2} = 6.664\text{E-}05$ ,  
 Cable:  $P_{F3} = 9.425\text{E-}05$

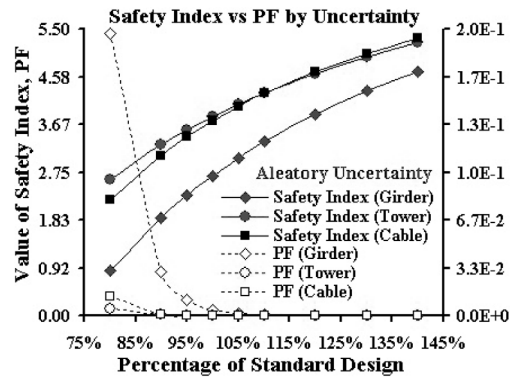


Figure 2. Failure probabilities and safety indices associated with aleatory uncertainties.

The failure probability of the bridge system is the union of the failure probabilities of the critical members, yielding therefore the system failure probability of  $P_{F,S} = 3.807\text{E-}03$ . The corresponding safety index would be  $\beta = 2.669$ .

The above results assume that there are no errors (or epistemic uncertainties) in the estimation of the properties, such as ultimate capacities of the critical members, and of the dead load, lifetime maximum live load and seismic load. Clearly, there will be inaccuracies in these estimations, and thus epistemic uncertainties in the estimated mean (or median) values. Assuming no biases in these estimations, the epistemic uncertainties may be expressed in terms of the respective c.o.v.'s as  $\Delta_C = 0.09$ ,  $\Delta_S = \Delta_I = \Delta_D = 0.10$ , and  $\Delta_L = \Delta_E = 0.20$ .

## 3.2 Determination of optimal design

In order to determine the optimal design based on minimum expected life-cycle cost, nine alternative designs were considered, including the standard one (based on current code), by increasing and decreasing the member sections relative to the standard design. On this basis, the initial costs corresponding to each of the alternative designs can be determined as summarized in Table 1.

### 3.2.1 Determination of initial cost

The initial cost for each of the alternative designs includes the design costs, construction costs and eventual load testing costs before use (Ang & De Leon, 2005). The initial cost for the standard design of the bridge is based on information from construction reports. All of the initial costs for the standard design and those of the different alternative designs are shown in Table 1 (in million US dollars).



### 3.2.2 Expected damage cost

The expected damage cost includes all the tangible and intangible losses resulting from a structural damage or failure of the cable-stayed bridge (including the cost associated with the closing of the bridge to traffic). Even though collapse of the bridge is highly unlikely under normal circumstances, the damage cost must include this as well as the insurance cost (Frangopol, & Lin, 1997). Therefore, the expected damage cost,  $C_D$ , may consist of several components  $C_i$  as follows:

$$C_D = C_{FR} + C_{FL} + C_{FH} + C_{FD} + C_{FEN};$$

where

$C_{FR}$  = bridge replacement cost;

$C_{FL}$  = loss of lives and equipment costs;

$C_{FH}$  = culture and historical costs;

$C_{FD}$  = functional disruption costs; and

$C_{FEN}$  = environmental and social costs.

Specifically, in estimating the life-cycle cost of the cable-stayed bridge, the initial cost items, plus the

Table 1. Initial costs of alternative designs (in million USD).

Design	Initial cost, $C_I$
80% of Standard Design	809.90 million USD
90% of Standard Design	845.50
95% of Standard Design	867.91
Standard Design	890.00
105% of Standard Design	934.50
110% of Standard Design	934.50
120% of Standard Design	1112.50
130% of Standard Design	1219.30
140% of Standard Design	1334.67

maintenance cost and damage cost items as percentage of the initial cost can be summarized as shown in Table 2. All the above future damage cost items must be expressed in present worth. For this purpose, each potential future damage cost item must be multiplied by the Present Value Factor,  $PVF$ , as follows (Ang, Pires, & Lee, 2004),

$$PVF = [1 - \exp(\alpha L)] / (\alpha L)$$

where

$$\alpha = \ln(1 + q);$$

$q$  = annual discount rate; and

$L$  = lifetime of structure

This study assumes that the lifetime of the cable-stayed bridge in question is  $L = 50$  years and the annual discount rate is  $q = 4.0\%$ .

### 3.2.3 The epistemic uncertainties

The estimate of the initial and maintenance costs,  $C_I$ ,  $C_M$ , for each of the alternative designs may contain some uncertainty (epistemic type). It may be reasonable to assume that the actual initial and maintenance costs could vary by  $\pm 20\%$ ; or expressed in terms of c.o.v.'s  $\Delta_{C_I} = \Delta_{C_M} = 0.20$ , representing the respective epistemic uncertainties in  $C_I$  and  $C_M$ . Moreover, for each of the damage cost components, the c.o.v.'s representing the respective epistemic uncertainties may be assumed to be those shown in Table 3.

Based on the information assumed in Table 2 and Table 3, the expected damage cost is

$$\begin{aligned} \bar{C}_D &= \bar{C}_{FR} + \bar{C}_{FL} + \bar{C}_{FH} + \bar{C}_{FD} + \bar{C}_{FEN} \\ &= 7.25\bar{C}_I \end{aligned}$$

Table 2. Total expected life-cycle cost items.

Cost items	Classification of cost items	% of Initial cost
Initial cost ( $C_I$ )	Design costs	7% $C_I$
	Construction costs	90% $C_I$
	Load testing costs	3% $C_I$
Maintenance cost ( $C_M$ )	Inspections costs (every 1 year)	
	Detailed inspections costs (every 5 year)	10% $C_I$
	Repair costs	
Damage cost ( $C_D$ )	Structural failure costs	–
	– Bridge replacement costs	150% $C_I$
	– Loss of lives and cost of injuries	500% $C_I$
	– Cultural and historical costs	10% $C_I$
	Functional disruption costs	50% $C_I$
	– Traffic delayed costs	
	– Traffic detour costs	–
	– Heavy traffic costs	
Environmental and social costs	15% $C_I$	

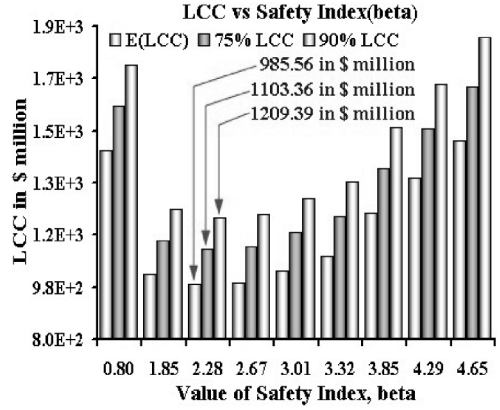
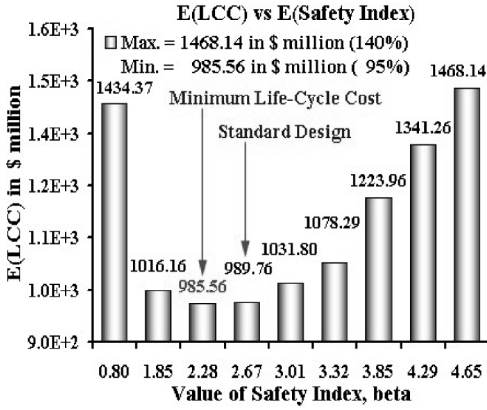


Figure 3. Mean or % LCC versus  $E(\beta)$  with epistemic uncertainties  $\Delta_{C_I} = \Delta_{C_M} = 0.20$  and  $\Delta_{C_D} = 0.28$ .

Table 3. Epistemic uncertainties in damage cost items.

Damage Cost Items	$C_{FR}$	$C_{FL}$	$C_{FH}$	$C_{FD}$	$C_{FEN}$
C.O.V. $\Delta_{C_i}$	0.20	0.40	0.40	0.40	0.80

and the variance of  $C_D$  will be,

$$\begin{aligned} Var(C_D) &= [0.2(1.5\bar{C}_I)]^2 + [0.4(5.0\bar{C}_I)]^2 \\ &\quad + [0.4(0.1\bar{C}_I)]^2 + [0.4(0.5\bar{C}_I)]^2 \\ &\quad + [0.8(0.15\bar{C}_I)]^2 = 4.16\bar{C}_I^2 \end{aligned}$$

Therefore,

$$\sigma_{C_D} = 2.04\bar{C}_I;$$

hence, the c.o.v. of  $C_D$  would be,

$$\Delta_{C_D} = 2.04\bar{C}_I / 7.25\bar{C}_I = 0.28,$$

from which the mean and variance of the expected life-cycle cost (LCC),  $C_T$ , becomes,

$$E(C_T) = \bar{C}_I + \bar{C}_M + \bar{C}_D \quad \text{and}$$

$$Var(C_T) = (0.20\bar{C}_I)^2 + (0.20\bar{C}_M)^2 + (0.28\bar{C}_D)^2$$

### 3.2.4 Minimum life-cycle cost designs

With the information summarized above, the LCC for all the nine alternative designs were evaluated; the results can then be plotted between the mean  $\beta$  and the expected LCC considering aleatory uncertainties only as shown in Figure 2. Similarly, the mean  $\beta$  may be plotted versus the 75% LCC and the 90% LCC. These results are summarized graphically in, Figure 3 which

shows that, irrespective of the percentile LCC used in the optimization process, the same optimal design is obtained at a mean safety index of  $E(\beta) = 2.284$ .

Finally, because of the epistemic uncertainties described earlier in Sect. 3.2.3 and in Table 3, the true failure probabilities and the corresponding safety indices will, respectively, be random variables. In particular, the histograms of the system failure probability and safety index generated through Monte Carlo simulation with a sample size of 10,000 are portrayed respectively in the two parts of Figure 4. From these two figures, the mean value, the 75% value, and the 90% values of  $P_F$  and corresponding  $\beta$ 's are determined as summarized in Table 4 for the optimal design of the cable-stayed bridge in Jindo, Korea.

The main results for the bridge can be summarized as follows:

Failure probabilities,

$$\begin{aligned} \text{Mean } P_F &= 1.112\text{E-}2, \\ 75\% P_F &= 1.394\text{E-}2, \\ 90\% P_F &= 1.627\text{E-}2. \end{aligned}$$

The corresponding safety indices are,

$$\begin{aligned} \text{Mean } \beta &= 2.281, \\ 75\% \beta &= 2.835, \\ 90\% \beta &= 3.324. \end{aligned}$$

It may also be of interest to observe the frequency diagram of the expected LCC for the optimal design as shown Figure 5. As expected, the LCC will increase with higher percentile level (the price for additional confidence). From Figure 5 the mean value, as well as the 75% and 90% values of the LCC for the optimal design are obtained as follows (in million USD):

$$\begin{aligned} \text{Mean LCC} &= 988.23, \\ 75\% \text{ LCC} &= 1,104.81, \\ 90\% \text{ LCC} &= 1,207.42. \end{aligned}$$

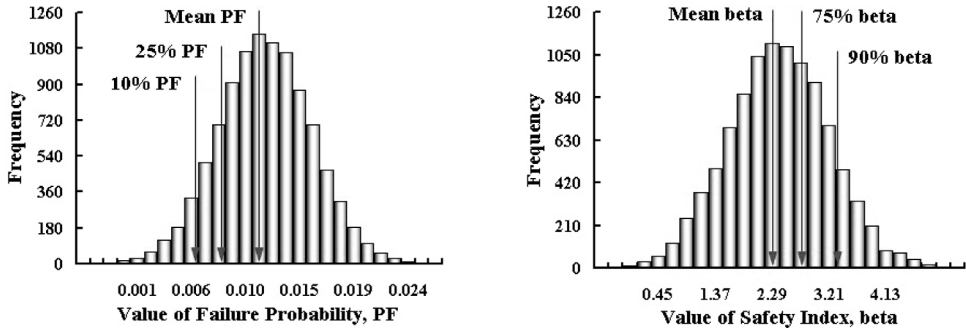


Figure 4. Frequency diagram of  $P_F$  and  $\beta$  for optimal design due to epistemic uncertainties.

Table 4. Failure probabilities and safety indices.

Percentile	Mean	25% $P_F$ ; 75% $\beta$	10% $P_F$ ; 90% $\beta$
$P_F$ ; $\beta$	1.112E-2; 2.281	8.600E-3; 2.835	6.149E-3; 3.324

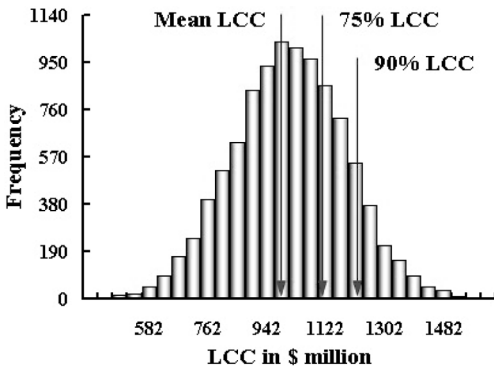


Figure 5. Frequency histogram of LCC of optimal design with  $\Delta_{C_I} = \Delta_{C_M} = 0.20$  and  $\Delta_{C_D} = 0.28$ .

### 3.2.5 Summary of results of example

This study performed the reliability analysis and determined the minimum life-cycle cost design of a cable-stayed bridge by considering separately the two types of uncertainties; namely the aleatory type and the epistemic type. The systematic procedures involved were illustrated for a cable-stayed bridge in Jindo, Korea under dead, live and earthquake loadings. Based on estimates of the aleatory uncertainties and reasonably realistic assumptions of epistemic uncertainties, complete information (i.e., distributions) of the failure probability and safety index, as well as of the LCC, were obtained for the optimal design of the bridge. This allows the specification of prescribed percentile values of the pertinent results. In this regard, for the

cable-stayed bridge in Jindo, Korea, the results indicated that the 90% value of the safety index for the optimal design is 3.324 and the corresponding 90% value of the LCC was estimated to be US\$1,207.42 million. The results of the study show that the current design of cable-stayed bridges in Korea is close to optimal from the standpoint of minimum life-cycle cost.

## 4 CONCLUSIONS

In risk-based engineering, it is important to distinguish the difference between two broad types of uncertainty; the aleatory type which is part of the randomness of natural phenomena whose significance can be expressed in terms of the probability of occurrence, and the epistemic type which is associated with imperfections in modeling and estimation of reality and leads to uncertainty (lack of complete confidence) in the calculated probability of occurrence.

For practical applications, epistemic uncertainty may be limited to the imperfections in the estimation or prediction of the mean (or median) value of a variable or parameter.

Because of these epistemic uncertainties the calculated results, such as failure probability, safety index, risk, and expected life-cycle cost, become random variables with respective distributions (or histograms). For decision-making purposes, the distributions of the respective calculated results allow the specifications of high percentile values of the essential design parameters (such as safety index) to ensure sufficient risk averseness. For example, the 90% value, or the 75%

value, of the safety index may be appropriate, leading to conservative designs (particularly important) for long span bridges or other major infrastructure systems.

## REFERENCES

- Ang, A.H-S. 2006. Practical Assessments of Risk and its Uncertainty. *Proc. IFIP Workshop, Kobe, Japan*.
- Ang, A.H-S. & Tang, W.H. 2007. *Probability Concepts in Engineering, 2nd Edition*. New York: John Wiley & Sons, Inc.
- Ang, A.H-S. & De Leon, D. 2005. Modeling and Analysis of Uncertainties for Risk-Informed Decisions in Infrastructures Engineering. *Journal of Structure & Infrastructure Engineering*, Taylor & Francis the Netherlands.
- Ang, A.H-S., Pires, Jose & Lee, J.C. 1996. Reliability-based optimal aseismic design of reinforced concrete building, Year 2. *Final Technical Report of Research Project* supported by CUREe/Kajima, Contract No. 19032.
- Frangopol, D.M. & Lin, K.Y. 1997. Life-Cycle Cost Design of Deteriorating Structures. *Journal of Structure Engineering, ASCE*. Vol. 123, No. 10, pp. 1390–1401.
- Han, S.H. & Shin, J.C. 2005. The Stochastic Finite Element Analysis and Reliability Analysis Subjected to Earthquake Load. *Journal of Computational Structural Engineering Institute of Korea*. Vol. 18. No. 1, pp. 29–42.
- Han, S.H., & Ang, A.H-S., 2008, Optimal Design of Cable-Stayed Bridges Based on Minimum Life-Cycle Cost, *Proceedings. IABMAS'08*, Seoul, Korea.
- Korea Institute of Construction Technology 1995. A Study on Design and Construction Method for Long Span Bridges. *Report ID KICT/95-SE-111-64*.
- Lee, K.M., Cho, H.N. & Choi, Y.M. 2004. Life-Cycle Cost Effective Optimum Design of Steel Bridges. *Journal of Constructional Research*, 60, Elsevier, pp. 1585–1613.
- Nazmy, A.S. & Abdel-Ghaffar, A.M. 1990. Nonlinear Earthquake Response Analysis of Long Span Cable- Stayed Bridges Theory. *Earthquake Engineering & Structure Dynamics*, Vol. 19, pp. 45–62.

# Structural integrity monitoring for dependability

S. Arangio, F. Bontempi & M. Ciampoli

*University of Rome "La Sapienza", Italy*

**ABSTRACT:** In recent years, structural integrity monitoring has become increasingly important in structural engineering and construction management. It represents an influential and effective tool for dependability assessment of existing structural systems, as integrates—in a unified perspective—systems engineering and performance based-design. Structural integrity monitoring includes issues like structural performances, from regular exercise to out-of-service and collapse, environmental conditions, sensor systems and their optimal placement, data transmission systems, signal processing techniques, state identification methods and model updating. The first part of this work deals with the concepts of dependability and structural integrity. The second part provides a reference framework for monitoring and damage identification of structures. In particular, techniques for monitoring using soft computing algorithms are illustrated and applied to an example case, a long-span suspension bridge.

## 1 INTRODUCTION

The realization of high-cost and safety-critical constructions has pointed out the necessity of advanced approaches that were able to consider the intrinsic complexity of the structures (Ciampoli 2005). The complexity can be related to the following aspects:

- a. nonlinear dynamic behavior;
- b. objective and cognitive uncertainties;
- c. strong interaction between the components.

Only considering these aspects, a consistent evaluation of the structural performance can be obtained. This requires evolving from a simplistic idealization of a structure to the idea of a structural system, intended as a set of interrelated components working together toward a common purpose (NASA System Engineering Handbook, 1995), and acting according to the techniques of system engineering, that is the robust approach to the creation, the design, the realization and the operation of an engineered system (Bontempi et al. 2007).

The structural design process needs to be reviewed in the framework of system engineering. Moreover, the advanced technologies for processing data collected on site on real structures shall be properly taken into account. In fact, these data are essential for evaluating the structural performance during the whole service life, validating the performance-based design (Smith 2001).

In this perspective, it is necessary to define the quality of a complex structural system in a comprehensive way by a global property, like its dependability that describes the overall quality performance

and the influencing factors: reliability, availability, maintainability and safety.

All these aspects are connected to the integrity of the structural systems, considered as the completeness and consistency of the structural configuration.

However, the integrity and consequently the overall dependability can be lowered by deterioration (considered as a continuous in time phenomenon) and damage (related to specific events during the service life). Structural integrity monitoring represents an essential tool to assess the evolution in time of the dependability of existing structural systems. It includes issues like structural performances, from regular exercise to out-of-service and collapse, environmental conditions, sensor systems and their optimal placement, data transmission systems, signal processing techniques, state identification methods and model updating.

In the first part of this work the concepts of dependability and structural integrity are discussed. In the second part, a framework for monitoring and identification of civil structural systems is presented. It is shown that different methods should properly be integrated for the dependability assessment.

In particular, a multi-step assessment strategy, applied to the analysis of the response of a long-span suspension bridge under wind action and traffic loads, and based on soft computing algorithms, is proposed.

## 2 DEPENDABILITY ASSESSMENT AND INTEGRITY MONITORING

For complex structural systems [that is also the case of large scale projects where there are significant dependencies between elements or subsystems], it is

important to have a solid knowledge of both how the system works as a whole, and how the elements behave singularly. In this contest, dependability is a global concept that describes the aspects assumed as relevant regard to the quality performance and its influencing factors (Bentley, 1993). System dependability can then be thought of as being composed of three elements (Fig. 1):

1. attributes: the aspects that describes the dependability;
2. threats: the elements that can affects the dependability;
3. means: the ways to increase the dependability.

The main attributes are reliability, availability, maintainability and safety. Basically, these properties are relevant to:

- the safety of the system under usual scenarios, generally defined in the structural engineering field by the ultimate limit states (ULS);
- the survivability of the system under accidental or exceptional scenarios, considering also security issues; in recent years this condition is defined by the integrity limit states (ILS);
- the functionality of the system under prescribed situations, generally defined in the structural engineering field by the serviceability limit states (SLS);
- the durability of the system.

The threats for system dependability can be subdivided into failure, errors and faults (Avizienis et al. 2004). The failure represents a permanent interruption of a system ability to perform a required function under specified operating conditions. In case of error, the system is in an incorrect state: it may or may not cause failure. On the other hand, a fault is a defect and represents a potential cause of error, active or dormant. In case of civil structures the possible faults are damage and deterioration. Within this framework, the problem of conceiving and realizing

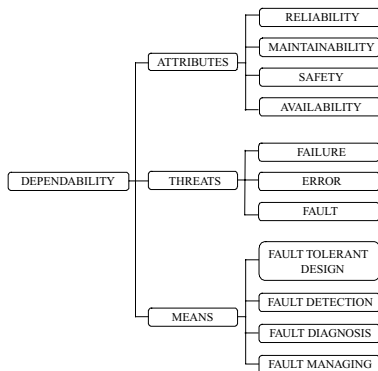


Figure 1. Dependability: attributes, threats and means.

a dependable structural system can be considered by four different points of view:

1. how to design a dependable system, that is a fault tolerant system;
2. how to detect faults of the systems, i.e. changes in its behavior;
3. how to locate a fault in the system, i.e. to find the place and the reason of the change in its behavior;
4. how to manage faults and failure.

This paper is focused on points 2 and 3: fault detection and fault diagnosis. These aspects are strictly related to the integrity monitoring of the structural system. An efficient integrity monitoring systems is expected to be able to proactively preserve the structural dependability, diagnosing deterioration and damage at their onset (Ou and Li 2005).

In particular, even if there is no general consensus on its definition, in analogy with biological systems, an intelligent monitoring system is expected to (Aktan et al. 1998, Isermann 2006):

- *sense* the loading environment as well as the structural response;
- *reason* by assessing the structural condition and health; even small faults should be detected and diagnosed;
- *communicate* through proper interface with other components and systems, including human managers;
- *learn* from experience as well as by interfacing with human for heuristic knowledge;
- *decide* and take action for alerting officials and control accidental or exceptional situations; it should be able to activate fault tolerant and reconfigurable systems.

In this sense, integrity monitoring allows to control the structural system in a proactive way. The circumstances that may eventually lead to deterioration, damage and unsafe operations can be diagnosed and mitigated in a timely manner, so that costly replacements can be avoided or delayed by effective preventive maintenance. Analyzing this aspects in terms of the expected payoff, it comes out that, in case of complex structures, the monitoring process should be planned since the design phase and should be carried out during the entire life in order to assess the structural health and performance under in-service conditions (Aktan et al. 2002).

A great research effort has been devoted in the past thirty years to establishing effective local and global methods for health monitoring in civil structures. An extensive survey of global methods is presented in Doebbling et al. (1996), and updated by Sohn et al. (2004). Usually, non destructive global methods are used for the task of fault detection, whereas local inspections and pattern recognition approaches for

fault diagnosis. Regarding the temporal extent of the measurements, in general, continuous measurements at low frequencies for long time (e.g. on a hourly basis) are needed to capture ambient effects such as those due to wind and temperature. On the other hand, programmed intermittent measurements are needed for shorter durations and at higher frequencies for capturing responses related to the operational conditions.

To take advantage from these methods, some of them can be jointly used for integrity monitoring.

### 3 FAULT-SYMPTOMS RELATIONSHIP

In order to detect and diagnose a system fault, it is necessary to evaluate the data coming from the monitoring, i.e. the system symptoms. However, this is a very complex task, that can be explained by Figures 2 and 3.

The relationship between fault and symptoms can be represented graphically by a pyramid (Fig. 2). The vertex of the pyramid represents the fault, the lower levels the possible events, and the base corresponds to the symptoms. The propagation of the fault to the observable symptoms follows in general a physical cause-effect relationships, and it is a top-down process: a fault in general determines events that, as intermediate steps, influence the measurable or observable symptoms (Isermann 2006).

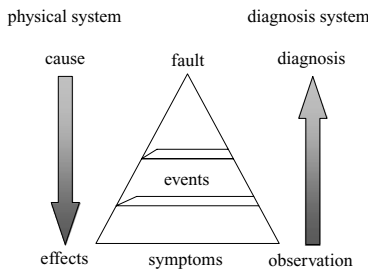


Figure 2. Fault-symptoms relationship in the physical and diagnosis systems.

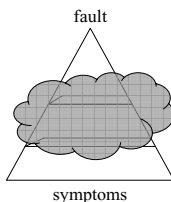


Figure 3. In the real situations the events are often not clear and the inverse process is difficult.

The fault diagnosis proceeds in the reverse way (Fig. 2, right side). It is a bottom-up process of inverse engineering that concludes from the observed symptoms to the faults. This implies the inversion of the causality principle.

However, the underlying physical laws are mostly not known in analytical form, or too complicated for numerical calculation.

One cannot expect to reconstruct the fault-symptom chains solely from measured data, because the causality is not reversible or the reversibility is ambiguous (Füssel 2002). Moreover, the intermediate events between faults and symptoms are not always visible from the symptoms behavior (Fig. 3). Therefore mostly structured knowledge has to be included, known from inspections, database and experience. In this case, the solving strategy requires to integrate different procedures, either forward or inverse procedures, in order to obtain what is needed in an efficient and accurate way. This mixed solving approach has been called the total approach by Liu & Han (2004), and different computational techniques have been developed.

For example, if no enough information is available on the fault-symptoms causalities, experimentally trained classification methods, such as methods based on pattern recognition and statistical classification, can be applied for fault diagnosis. If the fault symptoms causalities can be expressed in the form of if-then rules, inference methods, such as neural networks and fuzzy logic, can be applied.

### 4 KNOWLEDGE BASED FAULT DETECTION AND DIAGNOSIS

As shown in the previous section, fault diagnosis is a complex task that can be achieved only integrating forward and inverse procedures with the heuristic knowledge coming from experience or qualitative information.

A knowledge-base analysis procedure can be applied (Aktan et al. 1998) (Fig. 4). The results obtained by visual inspection or instrumented monitoring (the diagnosis system on the right side of Figure 2) are processed and combined with the results coming from the analytical model of the process (the physical system on the left side of Figure 2).

Information Technology provides the tool for such integration. The experimental data processing is an inverse process, where the output of the system (displacements, acceleration, natural frequencies) is known, but the parameters of the structure are to be determined; the analytical model is a forward process. The output of the information technology is then filtered by the heuristic knowledge.



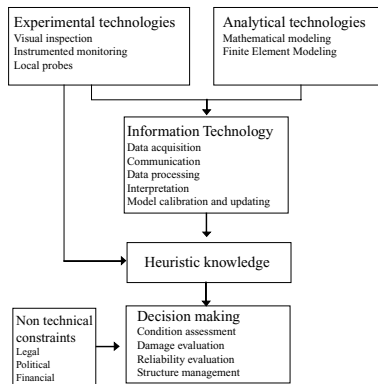


Figure 4. Knowledge-base analysis for structural integrity monitoring.

Different computational methods can be used. In several applications, soft computing algorithms, like the neural networks used in this work, have shown their effectiveness in processing information coming from monitoring (Barai & Pandai 1995, Chen & Kim 1994, Lam et al. 2006, Masri et al. 1996, Rytter & Kirkegaard 1997, Zhao et al. 1998).

The final part of the process in Figure 4 is referred to the management issue that is also related to non engineering aspects, like economics and politics.

## 5 NEURAL NETWORKS FOR FAULT DETECTION AND DIAGNOSIS

Neural networks are an effective technique to deal with the inverse diagnosis problem. The term neural network has its origins in attempts to find mathematical representations of information processing in biological systems. Actually, there is a definite probability model behind it; in fact a neural network is also a statistical model. Neural networks provide nonlinear regression functions that are estimated by optimizing a properly defined measure of fit to the training data. (Cheng and Titterington 1994). They consist of an extension of the general form of linear regression models:

$$y(\mathbf{x}, \mathbf{w}) = f \left( \sum_{j=1}^M w_j \phi_j(\mathbf{x}) \right) \quad (1)$$

where: the function  $f$  is an identity in case of linear regression;  $w_j$  are parameters; and  $\phi_j$  are the functions of the input variables  $x$  called basis functions. Neural networks assume that the basis functions  $\phi_j(x)$  are dependent on the parameters, and both basis functions and the parameters are updated during training.

The basic neural network model can be described by a series of functional transformations working at different correlated layers (Bishop 2006), given in case of two layers by:

$$y_k(\mathbf{x}, \mathbf{w}) = f \left( \sum_{j=1}^M w_{kj}^{(2)} g \left( \sum_{j=1}^D w_{ji}^{(1)} x_i + b_{j0}^{(1)} \right) \right) + b_{k0}^{(2)} \quad (2)$$

where the parameters  $w_{kj}$  and  $w_{ji}$  are the weights and the parameters  $b_{j0}$  and  $b_{k0}$  the biases of the first and second layer respectively. The quantities in the brackets are known as activations; each of them is transformed using a nonlinear activation function ( $f$  and  $g$ ). The nonlinear activation functions are generally chosen to be sigmoidal or tanh functions. Thus the neural network model is simply a nonlinear transformation from a set of input variables to a set of output variables controlled by a vector  $\mathbf{w}$  of adjustable parameters. The values of the network parameters  $\mathbf{w}$  are obtained during the training phase by minimizing an error function, that is, for example, the sum of squared errors.

It is important to note that the number of the adaptive parameters of the network model has to be fixed in advance. This choice, that defines the complexity of the model, has a fundamental importance. A too simple model gives a poor fit of the training data and consequently a poor representation of the underlying function; a too complex model gives an excellent fit of the training data but it has very poor generalization properties for new data. The problem of finding the optimal number of parameters provides an example of Ockham's razor, which is the principle that one should prefer simpler models to more complex models, and that this preference should be traded off against the extent to which the models fit the data. The best generalization performance is achieved by the model whose complexity is neither too small nor too large.

In this work the optimal architectures of the various models have been chosen by the Bayesian approach. It provides an objective and structured framework for dealing with the issue of model complexity, and allows an objective comparison between solutions using alternative network architectures (Beck and Yuen 2004). Bayes' Theorem is used to evaluate the posterior probability of the different models conditional on the set of data, as follows

$$p(M|D) \propto p(D|M)p(M) \quad (3)$$

where  $p(D|M)$  is the evidence and  $p(M)$  is the prior probability of the model. If there are no particular reasons to prefer one model, a non informative prior can be assigned to the models. They are thus compared by just evaluating the evidence for each

model: the optimal model is that with the higher evidence (MacKay 1994).

## 6 DEPENDABILITY ASSESSMENT OF A LONG SUSPENSION BRIDGE

A neural network approach has been used to formulate a multi-step strategy for dependability assessment.

A hierarchical approach (Fig. 5) has been followed because more effective to consider independently the tasks of damage detection and location (Ceravolo et al. 1995, Ko et al. 2002).

The considered structure is the long-span suspension bridge shown in Figure 5. It has a main span of 3.300 m and carries six road lanes and two railway tracks; detailed information on the bridge can be found in Bontempi (2006).

In the first step of the strategy the occurrence of damage or anomalies in the bridge is detected, and the damaged portion of the structure identified.

If some damage is detected, the second step of the procedure is set forth: using a pattern recognition approach, the specific damaged member within the whole portion is identified, and the extent of damage evaluated.

### 6.1 Damage detection

The response of the structure is monitored in various measurement points. In the considered example case, they are located every 30 m on the bridge deck (Fig. 6); correspondingly, different neural networks are trained, one for each point.

The neural network models are built and trained using the time-histories of the response of the structure subjected to wind actions and traffic loads (due to the passage of a train) in the undamaged situation. The time-histories are sampled at regular intervals, thus generating series of discrete values. A set of such values from the instant  $t - k$  to  $t$  is used as input for the feed-forward network models, and the value at the instant  $t + 1$  is used as the target output.

New input patterns, corresponding to both undamaged and damaged situations, are tested on the trained models. For each pattern, the value at  $t + 1$  is predicted and compared with the target output. If the error in the prediction is negligible, the structure is considered as undamaged; if the error is large, the presence of an anomaly is detected.

To distinguish the changes in the structural response due to variations in the excitation from those due to damage, the prediction errors are considered. In fact, if the error is large in all measurement points, the excitation has probably varied, and the network models cannot represent the considered time-history.

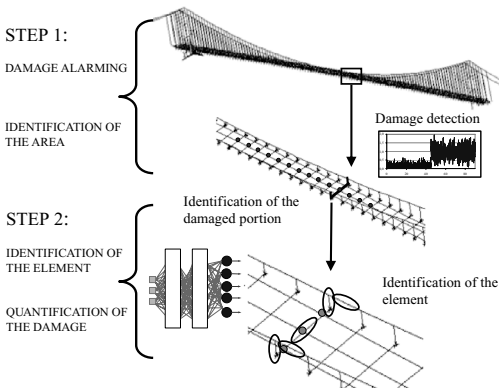


Figure 5. Steps of the damage identification strategy.

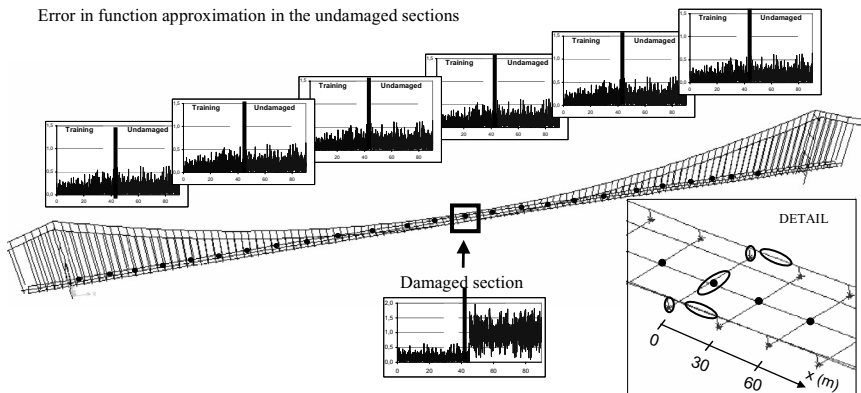


Figure 6. Location of the measurement points on the bridge deck and identification of the damaged portion by considering the errors in the approximation; also shown the potentially damaged elements of each portion.

The models are then updated according to the new excitation; for this reason, the proposed method can be considered as self-tuning.

On the other hand, if the error is large only in one or few points and generally decreases with the distance from those points, it can be concluded that that considered portion is damaged (Fig. 7).

In the example case, damage is intended as a reduction of the stiffness of a structural element. The following damage scenarios are considered:

- hanger: reduction of stiffness from 5% to 100%;
- cable: reduction of stiffness from 1% to 10%;
- transverse: reduction of stiffness from 5% to 30%.

The training data set for every network model includes 1000 samples of the time-history of the structural response. In case of excitation due to wind actions the monitored response is the rotation of the deck around the longitudinal axis; in case of traffic loads, the monitored response is the vertical displacement of the deck, that turned out to be the most sensitive quantity (Arangio and Petrini 2007).

### 6.2 Identification of damage location and intensity

Having recognized that a portion of the structure is damaged, the second step of the procedure is set up; it

is aimed at identifying the damaged element (a hanger, the cable or a transverse), and at evaluating the damage intensity. A pattern recognition approach is used.

To create the training data set, the errors in the approximation of the response time-histories in three different points of the damaged portion (denoted as A, B and C in Figure 8) are collected, considering different damage scenarios.

For each damage scenario, the training data set has as input the mean values of the errors, and, as output, the locations of damage (north hanger, north cable, transverse, south cable, south hanger) and its intensity, defined in a discrete scale (Fig. 8).

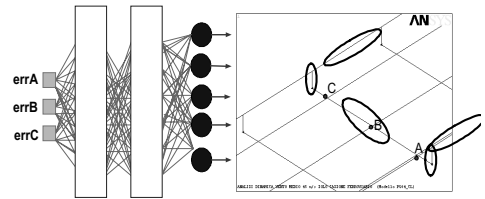


Figure 8. Neural network for the identification of damage location and intensity.

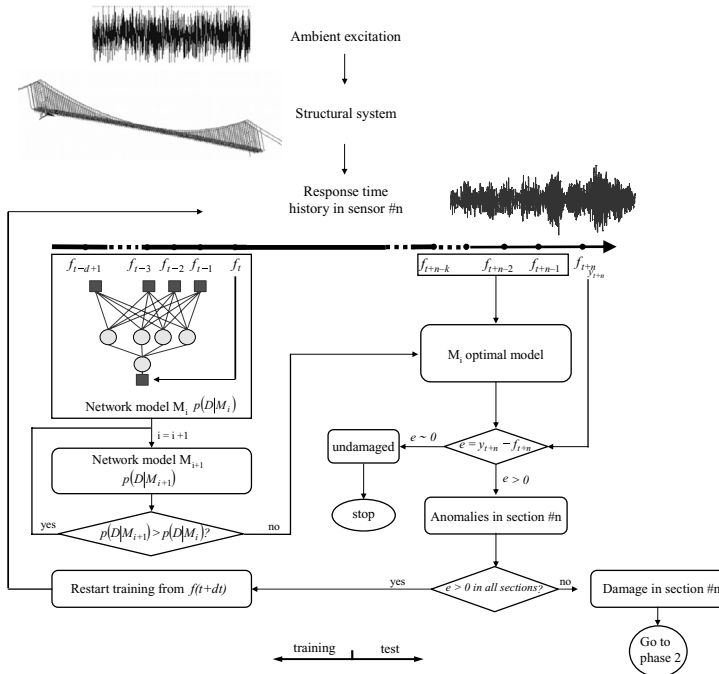


Figure 7. Flow chart of the procedure for damage detection.

## 7 RESULTS OF THE DEPENDABILITY ASSESSMENT PROCEDURE

### 7.1 Results of step 1: damage detection

Various network models have been trained using the time-histories of the response of the undamaged structure. The network architecture has been determined by the Bayesian approach discussed in section 5: the chosen network models consist of 2, 2 and 1 nodes in the input, hidden and output layers respectively.

In Figures 9 and 10, the difference between the predicted values and the target values for each instant of the training and test functions for the undamaged and damaged structure are reported.

In Figure 11 the mean values of the error in the approximation of the response of the undamaged structure, evaluated in three sections of each 30 m long portion, are shown. When new time-histories, corresponding to various damage scenarios, are proposed to the trained networks the errors in the approximation are greater.

In Figures 12 to 15 the increments of the mean value of the error with respect to the undamaged situation are shown for different levels of damage, in the hangers and the transverse. Both wind and traffic action have been considered. All signals have been normalized before training, so that normalized quantities are always compared.

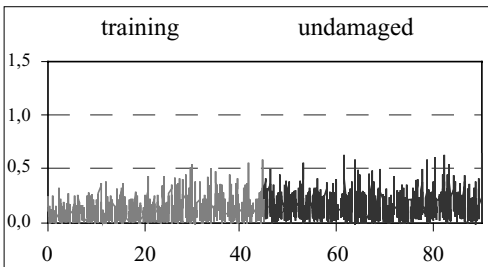


Figure 9. Differences between the network values and the correct value in case of undamaged structure.

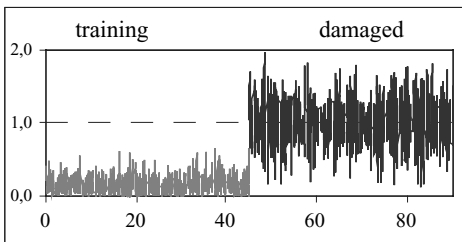


Figure 10. Differences between the network values and the correct value in case of damaged structure.

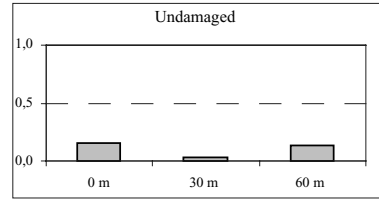


Figure 11. Mean error in the approximation of the time-history of the structural response in the undamaged situation in three different measurement points.

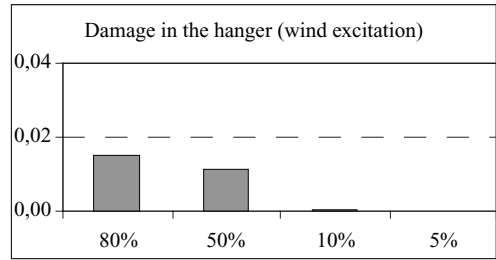


Figure 12. Increment of the error in the approximation of the time-history of the hanger response under wind action.

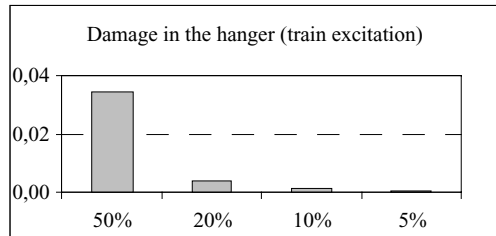


Figure 13. Increment of error in the approximation of the time-history of the hanger response under traffic action.

### 7.2 Results of step 2: location and quantification of damage

Once the damaged portion of the whole structure is identified, it was possible to recognize the specific damaged element and the intensity of damage using a pattern recognition approach.

As an example, only the structural response due to the passage of one train has been considered. In fact, by looking at the level of damage that is possible to detect using traffic or wind actions (Figures 11 to 15), it is possible to note that the proposed method is more effective when responses from high speed excitation (like traffic) are considered instead of responses due to slow speed excitation (like wind).

Various damage scenarios, corresponding to the reduction of the stiffness of the hangers, the two cables

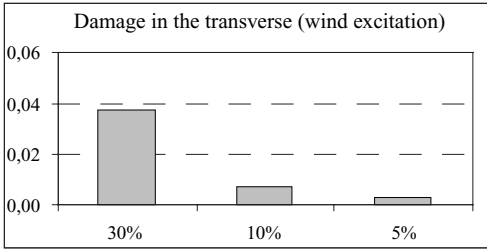


Figure 14. Increment of error in the approximation of the time-history of the transverse response under wind action.

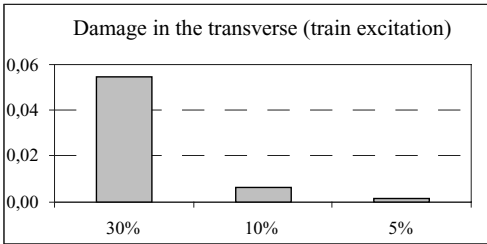


Figure 15. Increment of error in the approximation of the time-history of the transverse response under traffic action.

and the transverse in the damaged portion have been taken into account, and a training set consisting of 400 examples has been created. It. The network architecture has been always determined by the Bayesian approach discussed in section 5. The optimal network has 11 units in the hidden layer.

After the training phase, the network has been tested with 30 new input vectors, not included in the training set, and the related damage scenarios have been obtained. In order to give a global and intuitive representation of the results, two quantities have been defined as follows:

- position: it gives a measure of the error in the positioning of the damage

$$pos(i) = \frac{t \cdot y}{|t| \cdot |y|} \quad (3)$$

where  $t$  is the vector of the target values and  $y$  is the vector coming from the network model. If this quantity is equal to one the damage is well localized.

- intensity: it gives a measure of the error in quantifying the level of damage

$$int(i) = \frac{|t|}{|y|} \quad (4)$$

If it is equal to one, the level of damage is correctly estimated.

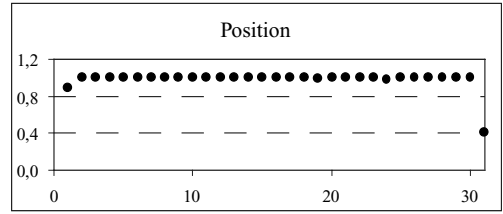


Figure 16. Identification of the damage position in the test examples.

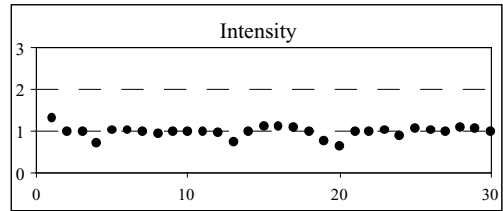


Figure 17. Identification of the intensity in the test examples.

The results of the test phase are given in Figures 16 and 17.

### 7.3 Analysis of the results

Analyzing the results of the first step, it is possible to note that the proposed method permits to detect the damaged portion when the reduction of stiffness is less than 50% in one hanger, or less than 10% in one cable, or less than 30% in the transverse.

The second step allows to identify the damaged element in 90% of the considered cases, and the intensity in 66% of the cases.

Therefore, the proposed method can be useful for damage identification of large structural systems instrumented with on-line monitoring systems because they furnish measurements of the structure in both damaged and undamaged situation; moreover, using the neural network approach, no other information on the structural model is needed.

## 8 CONCLUSIONS

In this work the concept of structural dependability has been discussed. It has been shown that this is a global term to describe the overall quality performance of a complex structural system and its influencing factors in a comprehensive way.

The different aspects related to dependability are strictly connected with the concept of structural integrity.

In order to assess the dependability of existing structural systems, integrity monitoring represents an essential tool.

Fundamental tasks of monitoring are fault detection and diagnosis. It has been shown that the diagnosis from experimental data is an inverse problem and the reconstruction of the fault-symptom chains cannot be done solely from measured data, because the causality is not reversible or the reversibility is ambiguous.

A solution can be achieved only applying a knowledge-based procedure that integrates forward and inverse solving procedures iteratively with the heuristic knowledge coming from experience or qualitative information.

For this task, different soft computing methods can be used. In particular the neural network model has been adopted to formulate a hierarchical dependability assessment strategy.

The strategy has been applied to the analysis of the time-history of the structural response a long-span suspension bridge subjected to ambient excitations.

## REFERENCES

Aktan, A.E., Helmicki, A.J. & Hunt V.J. 1998, Issues in health monitoring for intelligent infrastructure, *Smart Materials and Structures*, 7, 674–692.

Aktan, A.E., Catbas, F.N., Grimmelman, K.A. & Pervizpour, M. 2002, Development of a Model Health Monitoring Guide for Major Bridges, Report DTFH61-01-P-00347, submitted to Federal Highway administration Research and Development, Drexel Intelligent Infrastructure and Transportation Safety Institute.

Arangio, S. & Petrini, F. 2007, Application of neural networks for predicting the structural response of a long suspension bridge subjected to wind actions, Proceedings of SEMC 2007, Cape Town, South Africa.

Avizienis, I., Laprie, J.C. & Randell, B. 2004, Dependability and its threats: a taxonomy., 18th IFIP World Computer Congress, Toulouse (France), Building the Information Society. Kluwer Academic Publishers, 2004, ISBN 1-4020-8156-1, 12, 91–120.

Barai, S.V. & Pandey, P.C. 1995, Multilayer Perceptron in Damage Detection of Bridge structures, *Computer and Structures*, 54, 597–608.

Beck, J.L. & Yuen, K.V. 2004, Model selection using response measurements: Bayesian probabilistic approach, *Journal of Engineering Mechanics*, 130, 192–203.

Bentley, J.P. 1993, *An Introduction to Reliability and Quality Engineering*, Longman: Essex.

Bishop, C.M. 2006, *Pattern recognition and machine learning*, Springer.

Bontempi, F. 2006, Basis of Design and Expected Performances for the Messina Strait Bridge, Proceedings of the International Conference on Bridge Engineering—1–3 Nov. Hong Kong.

Bontempi, F., Gkoumas K. & Arangio S. 2007, Systemic approach to the maintenance for complex structural

systems, *Structure and Infrastructure Engineering*, DOI: 10.1080/15732470601155235.

Ceravolo, R., De Stefano, A. & Sabia, D. 1995, Hierarchical use of neural techniques in structural damage recognition, *Smart Material and Structures*, 4, 270–80.

Chen, S.S. & Kim, S. 1994, Neural network based signal monitoring in a smart structural system, *Smart Structures and Materials: Smart Sensing, Processing and Instrumentation*, 176–186.

Cheng, B. & Titterton, D.M. 1994, Neural Networks: A Review from a Statistical Perspective, *Statistical Science*, 9 (1), 2–54.

Ciampoli, M. 2005, Reliability assessment of complex structural systems, Proceedings of AIMETA 2005, Firenze University Press, ISBN 88-8453-248-5.

Doebbling, S.W., Farrar, C.R., Prime, M.B. & Shevitz, D.W. 1996, Damage Identification and Health Monitoring of Structural and Mechanical Systems from Changes in their Vibration Characteristics: A Literature Review, Los Alamos National Laboratory report LA-13070-MS.

Füssel, D. 2002, Fault diagnosis with tree-structured neuro-fuzzy systems, vol. Fortschr-Ber. VDI Reihe 8, 957. VDI Verlag, Düsseldorf.

Ko, J.M., Sun, Z.G. & Ni, Y.Q. 2002, Multi-stage identification scheme for detecting damage in cable-stayed Kap Shui Mun Bridge, *Eng. Struct.*, 24, 857–68.

Isermann, R. 2006, *Fault-Diagnosis Systems. An Introduction from Fault Detection to Fault Tolerance*, Springer.

Lam, H.F., Yuen, K.V. & Beck, J.L. 2006, Structural Health Monitoring via measured Ritz vectors utilizing Artificial Neural Networks, *Computer-Aided Civil and Infrastructure Engineering*, 21, 232–241.

Liu, G.R. & Han, X. 2004, *Computational inverse techniques in nondestructive evaluation*, CRC Press.

MacKay D.J.C. 1994, Bayesian methods for backpropagation networks, *Model of Neural Networks III*, chap. 6, 211–254, Springer.

Masri, S. F., Nakamura, M., Chassiakos, A.G. & Caughey, T.K., 1996, Neural network approach to detection of changes in structural parameters, *ASCE J. Eng. Mech.*, 122, 350–60.

National Aeronautics and Space Administration (NASA) 1995, *Systems Engineering Handbook*, Available online at: [www.nasa.gov](http://www.nasa.gov).

Ou, J. & Li, H. 2005, Smart Materials and Structures, Proceedings of the International Workshop on Durability and Reinforced Concrete under Combined Mechanical and Climatic Loads (CMCL), October 2005, Qingdao, China.

Rytter, A. & Kirkegaard P.H. 1997, Vibration based inspection using neural networks. Proc. DAMAS '97, University of Sheffield, UK, 97–108.

Smith, I. 2001, Increasing Knowledge of Structural Performance, *Structural Engineering International*, 12 (3), 191–195.

Sohn, H., Farrar, C.R., Hemez, F.M., Shunk, D.D., Stinemat, D.W., Nadler, B.R. & Czarnecki, J.J. 2004, A review of structural health monitoring literature: 1996–2001. Report LA-13976-MS, Los Alamos National Laboratory, New Mexico.

Zhao, J., Ivan, J.N. & DeWolf, J.T. 1998, Structural damage detection using artificial neural network, *ASCE Journal of Infrastructure System*, 4, 93–101.

# Practical approaches to the application of life-cycle civil engineering for infrastructures in Korea

Hyo-Nam Cho

*Department of Civil & Environmental Engineering, Hanyang University, Korea*

**ABSTRACT:** Recently in Korea, the demand is rapidly growing on the practical implementation of standard guides and softwares for life-cycle cost analysis, design and management of civil infrastructures, mainly because the Ministry of Construction & Transportation of Korea Government recognized the importance of the economic analysis of whole life investment for civil infrastructures, and thus now legally requires to apply VE/LCC analysis, and LCC-effective design and management to all the projects over 10 billion won (about 10 mil. \$). An overview is presented of recent progress of Life-Cycle Civil Engineering (LCCE) in Korea with a critical review of the state-of-the-practice, and the recent research & development of models and methodologies for LCC analysis, design, and management of civil infrastructures, with emphasis on bridge structures. Especially in the paper, practical approaches to the LCC methodologies are introduced with emphasis on uncertainty assessment of performance and cost data, either subjective or objective, using available statistical methods including Bayesian updating and Fuzzy uncertainty assessment based on historical records or experts opinion survey. Also, the LCC software systems developed in Korea for LCC analysis of highway and railroad bridge structures are reviewed with emphasis on integrated LCC system models that include the direct and indirect cost models, user friendly knowledge-based database incorporating statistical assessment and updating, reliability/risk assessment and optimization modules. Various application examples are briefly presented with those of LCC analysis for tenders at design stage, LCC-effective optimum design, LCC analysis for maintenance and management, and the optimal seismic risk-assessment for LCC-effective seismic maintenance and retrofit strategies, which demonstrate the applicability of the LCC models and methodologies suitable for the practice in Korea.

## 1 INTRODUCTION

Though the concept of Life-Cycle Cost (LCC) itself is not new and Life-Cycle Civil Engineering (LCCE) had started more than 20 years ago since early 1980's, its effectiveness is recognized only recently in practice for the optimal engineering decision problems such as the selection of optimal planning/design alternatives for bids together with Value Engineering (VE), optimal design of a project, optimal strategies for maintenance, rehabilitation and management of civil infrastructures over the whole life span.

For those decision problems as the LCC-effective maintenance of plant facilities, equipments, bridge decks, pavements, etc., Life-Cycle Cost Analysis (LCCA) is relatively simple, and thus its practical implementation is rather straightforward. However, when it comes to major infrastructures such as bridges, dams, tunnels, underground facilities, etc., LCCA problems become relatively, or sometimes extremely, complex simply because time-variant degrading/performance (resistance, serviceability, durability) and stochastic extreme environmental load

effects incur various deterioration and damage failures throughout the life span of a structure. Though, in the recent years in Korea, the application areas of LCCA have been largely limited only to these relatively complex problems of planning or design for the selection of LCC-effective optimal alternative design or rehabilitation mostly for bids at design stage, researchers in Korea realized the need to pursue more extensive studies on the LCC effectiveness mostly related to LCC models, methodologies, and S/W systems for the optimal design criteria and optimal maintenance/management of major civil infrastructures.

Moreover, recently in Korea the demand on the practical application of LCC-effective design and maintenance is rapidly growing unprecedentedly in civil engineering practice, with the need for the practical implementation of standard guides and softwares for life-cycle cost analysis, design and maintenance of civil infrastructures, mainly because the Ministry of Construction & Transportation of Korea Government recognized the importance of the economic analysis of whole life investment for civil infrastructures, and thus now legally requires to apply VE/LCC analysis,

and LCC-effective design and management to all the projects over 10 billion won (about 10 mil. \$).

In the paper an overview is presented of recent progress of LCCE in Korea with a critical review of the state-of-the-practice, and the recent research & development of models and methodologies for LCC analysis, design, and management of civil infrastructures, especially with emphasis on bridge structures. Especially in the paper practical approaches to the LCC methodologies are introduced with emphasis on uncertainty assessment of performance and cost data, either subjective or objective, using the available statistical methods including Bayesian updating and Fuzzy uncertainty assessment based on historical records or experts opinion survey. Also, the LCC softwares systems developed in Korea for LCC analysis of highway and railroad bridge structures, are reviewed with emphasis on integrated LCC system models that include direct and indirect cost models, user friendly knowledge-based database incorporating statistical assessment and updating, reliability/risk assessment and optimization modules.

## 2 RECENT PROGRESS OF LCCA IN KOREA

During the last two decades, in most of advanced countries, there has been impressive progress in the research on the LCC models and methodologies for LCCA for design, maintenance and rehabilitation of civil infrastructures, and in the application of Life-Cycle Civil Engineering in practice to various optimal decision problems involving engineering economics/value analysis from bids to design to maintenance/management to retrofit of optimal infrastructures (Ehlen, 1997; Frangopol et al. 1997). However in Korea, though the concept of LCC itself is not new and the research on LCC in Korea had been initiated only about a decade ago by the author as a part of U.S.-Korea cooperative research (Cho, et al. 1999). And the application of LCC in civil engineering practice had started when the Korea government had recognized the importance and potential benefits of Value Analysis/LCC, and thus required, by the legislation, that Value Engineering (VE) for design value analysis together with LCCA should be carried out for all the infrastructures projects over 50 billion won (about 50 million dollars), according to the enhanced law on the safety management of civil infrastructures right after the collapse of Sungsu Grand bridge (1994) and Sampung department store (1996), etc. Since then, the practical application areas of LCCA keep increasing for VE/LCC and LCCA for bids or design of major projects and for optimum LCC-effective design at design stage, LCCA for optimal maintenance strategies, risk-based LCCA analysis and design for the mitigation of natural hazards.

Though the demand on the LCCE for civil infrastructures is rapidly growing with the broad range of application areas including highway and railroad bridges, highway construction and pavement, dams, and water resource structures, harbor structures, underground structures, geotechnical structures, and sanitary structures, etc., yet the understanding of LCC and the application of LCCA software system by practitioners are not in mature state in civil engineering practice. Mainly because theoretically the LCCE problems, as stated above, become extremely complex simply because time-variant degrading resistance and stochastic nature of extreme load effects incur various damages/failures related with strength serviceability, durability, deterioration throughout the life span of a structure, which in turn, bring forth highly complicated cost and uncertainty assessment that often involves the lack of cost data associated with various direct and indirect losses, and the absence of uncertainty data available for the assessment.

As a result, recently in Korea, various LCCA softwares were developed for bids or optimal design or optimal maintenance strategies in Korea to assess the life cycle cost of various alternative construction materials, construction type, conceptual design, and maintenance of constructed facilities in practice. Especially similar to BridgeLCC 2.0 version (<http://www.bfrl.nist.gov/bridgelcc/>), developed by NIST, which makes up the weak points in BridgeLCC 1.0, a practical LCCA software system named PROLCC (PRObabilistic Life-Cycle Cost analysis program) has been developed for cost-effective design and maintenance of bridges. The essential feature of this program is such that it provides the benefits of utilizing statistical data available in Korea under the user-friendly system operating environment. Furthermore, in the last few years, the researchers on LCCE (Frangopol & Liu, 2004; Furuta et al. 2006) have pursued extensive studies on the LCC models and methodologies for LCCA for optimal decision, optimal design criteria and optimal maintenance/management of civil infrastructures. However in Korea, due to the lack of statistical data base available, the researches on LCCE have to be directed primarily to more practical approaches for LCCE applicable in practice in order to make up lack of available uncertainty data. Accordingly, recently in Korea in order to meet the demand on VE/LCC for major civil infrastructures at various levels and stages from bids to design to maintenance to retrofit of these infrastructures, a number of user-friendly LCC system have been developed or under development for highway and railroad bridges, tunnel, underground structures, harbor facilities, etc. Therefore, in the paper, the models and methodologies appropriate for the application under the construction environment of Korea are briefly summarized and reviewed with the recent trend of research &



development for upgraded implementation of LCCE in practice.

### 3 LCC MODELS FOR LIFE CYCLE CIVIL ENGINEERING

LCC may be simply defined as an economic evaluation of a civil infrastructure over a desired service life taking into consideration of all the expected costs incurred over the life span. These costs include a wide range of present and future expected costs such as initial cost, expected maintenance/repair cost and expected direct and/or indirect losses. Feasible improvements in each alternative decision on design or rehabilitation can then be evaluated or compared, using any of the equivalent values which are computed by converting a stream of all the time-related costs to a single equivalent value such as the present worth, annual worth, or future worth.

Expected lifetime investment cost could be evaluated relatively in an easy way, but it is extremely difficult to assess all the costs data based on prior prediction, especially expected direct/indirect costs associated with damage/failure consequences. Recently, with the availability of various models and data which are related to structural performance prediction, cost evaluation, reliability theory, optimization and various numerical analysis techniques, and with enhancement of computer technologies, the researches on the application of LCCE for civil infrastructures are pervasive and thus recently more elaborate models and methodologies are becoming available in practice. Based on the investigation of various kinds of LCC models available so far for the LCC-effective design and maintenance/management of civil infrastructures, the following three levels of LCC models may be defined depending upon the characteristics of applied problems for LCC assessment. In general, LCCA can be divided into Deterministic LCCA (DLCCA) and Probabilistic LCCA (PLCCA) and Reliability-based LCCA (RLCCA). All the approaches are applicable for the LCC design or management problems depending upon the uncertainty or desirable level of LCC assessment.

#### 3.1 LCC models for design-alternative analysis

A simple LCCA without reliability and uncertainty assessment may be effectively used in the conceptual design of a new civil structure, so that the economical efficiency of the structure over the life span can be achieved by the optimal selection of construction type, durable construction materials, and construction methods. Theoretically, these LCCA problems could be very complex or stochastic mainly due to time variant performance degradation loading history and operational environment. However, usually practical

approaches to LCCA are based on some simplified form of LCC model. In general, this simple LCCA can be divided into DLCCA and PLCCA. Both approaches are applicable for LCC analysis of infrastructures for bids and/or as an essential part of design VE works. However, these days, DLCCA is not any more used in practice simply because this model only uses a simple deterministic estimate for each cost item without considering uncertainties of input variables in a LCCA. In other words, only one deterministic result is evaluated by using only one likelihood expected or representative value for each of time and cost parameters of the model in conducting DLCCA, and thus often, stakeholders seize upon the uncertainties associated with LCCA inputs and vigorously debate the validity of the results or the decision on the alternatives.

Recently, PLCCA is predominantly used in the basic design for bids, as the method that utilizes MCS in the treatment of uncertain input variables (type of distribution, most likelihood expected value, and coefficient of variation, etc.) to generate probabilistic results. Therefore, it is recommended in FHWA (Walls III and Smith, 1998) that this PLCCA approach is more reasonable and scientific than DLCCA, which is usually analyzed by Monte Carlo simulation of the whole range of possible outcomes using occurrence probability of economic input factors. Similar to the inputs, the results of PLCCA are visually presented in the form of a probability distribution. Thus, more information such as distribution of LCC, and the chance (probability) for becoming optimal alternative, etc. can be acquired.

Therefore, a general form of LCC model, either deterministic or probabilistic may be formulated as follow:

$$E[C_T^{PV}(\vec{X})] = C_I^{PV}(\vec{X}) + E[C_M^{PV}(\vec{X})] + E[C_D^{PV}(\vec{X})] \quad (1a)$$

$$E[C_D^{PV}(\vec{X})] = \sum_{k=1}^K E[C_{DSP_k}^{PV}(\vec{X})] + E[C_{REC_k}^{PV}(\vec{X})] \quad (1b)$$

where  $E[C_T^{PV}(\vec{X})]$  = total expected LCC which are functions of the vector of design parameters  $\vec{X}$  in present worth;  $C_I^{PV}(\vec{X})$  = initial investment cost in present worth;  $E[C_M^{PV}(\vec{X})]$  = expected lifetime maintenance cost in present worth;  $E[C_D^{PV}(\vec{X})]$  = disposal costs that consist of the sum of demolition costs  $E[C_{DSP}(\vec{X})]$  and recycling costs  $E[C_{REC}(\vec{X})]$ , which depend upon design parameters  $\vec{X}$  associated with component  $k$  quantities of infrastructures.

### 3.1.1 Initial cost

The initial investment costs involved in design and construction of the structural and non-structural components of the structures such as planning and design, construction of foundation, superstructure, substructure and accessories in the case of bridges. Thus, in general, the initial cost may be expressed in the following form:

$$C_I^{PV}(\vec{X}) = (C_{Des}(\vec{X}) + C_{Con}(\vec{X}) + C_{Tes}(\vec{X})) \cdot i(t) \quad (2)$$

where  $C_{Des}(\vec{X})$  = planning and design cost;  $C_{Con}(\vec{X})$  = construction cost;  $C_{Tes}(\vec{X})$  = testing cost; and  $i(t)$  = discount rate function, which can be expressed as  $1/(1+q)^t$ ;  $q$  = discount rate; and  $t$  = time at which initial investment costs is implemented.

The construction cost should include all the costs of labor, materials, equipments, construction site management and quality control involved in the actual construction of civil infra-facilities. The construction costs can be expressed in terms of the initial cost, which may be approximately estimated at about 90% of the initial costs in the case of bridge, and the design cost and proof-load testing cost are also typically assumed as a percentage of construction cost.

### 3.1.2 Expected maintenance cost

Since the maintenance costs over a life span may be high, depending upon the quality, type, location, and environment of design and construction of facilities, the costs must be carefully regarded as one of the important costs in the evaluation of LCC.

In general, the maintenance costs can be classified in terms of the costs which are related to design parameters and maintenance strategy. Thus, the expected maintenance costs may be formulated as follows:

$$E[C_M^{PV}(\vec{X})] = E[C_{PM}^{PV}(\vec{X})] + E[C_{INS}^{PV}(\vec{X})] + E[C_{RM}^{PV}(\vec{X})] \quad (3a)$$

$$E[C_{RM}^{PV}(\vec{X})] = \int_0^L [C_{DRM}(\vec{X}) + C_{IDRM}(\vec{X})] \times P_{RM}(t) \cdot i(t) dt \quad (3b)$$

where  $E[C_{PM}^{PV}(\vec{X})]$  = expected ordinary repair maintenance cost;  $E[C_{INS}^{PV}(\vec{X})]$  = inspection/diagnosis costs which are function, expressed in terms of the facility types, scale, and construction year, etc.;  $E[C_{RM}^{PV}(\vec{X})]$  = expected repair cost;  $C_{DRM}(\vec{X})$ ,  $C_{IDRM}(\vec{X})$  = direct and indirect repair cost, respectively;  $P_{RM}(t)$  = repair probability of a facility at time  $t$ , which may be estimated based on performance degradation uncertainties; and  $L$  = life span.

### 3.1.3 Indirect cost

For an individual structure like a building structure, it can be argued that only the owner's cost may be relevant and thus it might have a minor influence on public user cost or socio-economic losses. However, when it comes to infrastructure such as bridge, tunnel, water delivery, and underground facilities, etc., the situation becomes completely different precisely because those infrastructures are primary public investments that provide vital service to entire urban areas. Thus, the indirect costs accruing to the public user of these infrastructural systems should also be accounted for. The models for highway and rail road bridges as for specific application examples are referred to the references (Cho, 2002; Cho et al. 2004).

## 3.2 LCC models for optimum design

### 3.2.1 LCC-effective optimum design model

Design of an infrastructure may be based on a comparison of risks (costs) with benefits. An optimal design solution, chosen from multiple alternative designs, can then be found by minimizing the LCC. Such a decision analysis can be formulated in a number of ways by considering various costs or benefits, which can also be referred to as a whole life costing or lifetime cost-benefit or cost-benefit-risk analysis. And thus LCC may be used to assess the cost-effectiveness of design decisions. If the benefits of each alternative are the same, then the total expected LCC up to the life span  $T_L$  of an infrastructure may be formulated as follows:

$$E[C_T^{PV}(\vec{X})] = C_I^{PV}(\vec{X}) + E[C_F^{PV}(\vec{X})] \quad (4)$$

where  $E[C_F^{PV}(\vec{X})]$  = expected (failure) rehabilitation cost for failure limit states considered in the model.

Because expected maintenance and disposal costs might usually have a minor or no influence on the optimum solution in LCC-effective design of infrastructures, they can be ignored in the LCC formulation.

The total expected LCC of an infrastructure, Eq (5) requires the assessment of the updated annual probability of failure for possible limit states considered in the cost model such as strength, fatigue, vibration, stability, serviceability, corrosion, etc. and of associated costs as well. Since costs may occur at different times, it is necessary for all costs to be discounted using a discount rate  $q$ . And then the general formulation for LCC-effective optimum design of an infrastructure may be represented as follows:

$$\text{Find} \quad \vec{X} \quad (5a)$$

$$\text{Minimize} \quad E[C_T^{PV}(\vec{X})] \quad (5b)$$

$$\text{Subject to } G_j(\cdot) \leq 0 \quad j = 1, 2, \dots, N_S \quad (5c)$$

$$P_{F_l}(\vec{X}) \leq P_{F_{allow}} \quad l = 1, 2, \dots, L \quad (5d)$$

$$\vec{X}^L \leq \vec{X} \leq \vec{X}^U \quad (5e)$$

where  $\vec{X}$  = the vector of design variables;  $G_j(\cdot)$  =  $j$ -th constraint (i.e., allowable stresses or resistance, combined stress/strength limits, geometric limits, etc.);  $N_S$  = the number of constraints;  $P_{F_l}(\vec{X})$  = probability of failure for limit state  $l$  considered in the design;  $P_{F_{allow}}$  = allowable probability of failure for the limit state  $l$ ; and  $\vec{X}^L, \vec{X}^U$  = the lower and upper bounds, respectively.

### 3.2.2 Expected rehabilitation cost

Expected rehabilitation costs may arise as a result of annual probability of failure or damage of various critical limit states that may occur any time during the life span of an infrastructure. Even though the rehabilitation costs do not have to be considered under normal circumstances, these costs should still be considered in an economic analysis as insurance costs (Cho, 2002). The expected rehabilitation costs can be obtained from direct/indirect rehabilitation costs and annual probability of failure for failure limit state  $l$  considered in the design as follows:

$$E[C_F^{PV}(\vec{X})] = \int_0^T \sum_{l=1}^L [(C_{DR}(\vec{X}) + C_{IR}(\vec{X})) \times P_{F_l}(\vec{X}, t | T)] \cdot i(t) dt \quad (6a)$$

$$C_{IR}(\vec{X}) = C_U \cdot t_l(\vec{X}) + C_H \cdot r_l(\vec{X}) + C_E \cdot t_l(\vec{X}) \quad (6b)$$

where  $l$  = index for a failure limit state;  $C_{DR}(\vec{X})$  = direct rehabilitation cost for failure limit state;  $P_{F_l}(\vec{X}, t | T)$  = updated annual probability of failure at any time  $t$  (i.e., probability that the failure will occur (annual) during time interval  $t$  conditional on updated loads or resistance);  $C_{IR}(\vec{X})$  = indirect rehabilitation cost for failure limit state in case of bridge;  $C_U, C_H, C_E$  = loss of user cost, contents or fatality and injury losses, and indirect socioeconomic losses, respectively;  $r_l(\vec{X})$  = increased accident rate during rehabilitation activities; and  $t_l(\vec{X})$  = period of rehabilitation activities.

The direct rehabilitation cost  $C_{DR}(\vec{X})$  and the loss of contents or fatality and injury loss cost  $C_H$  could

be evaluated in a relatively easy way. The direct rehabilitation costs could be estimated based on the various sources available, such as Construction Software Research's price information (CSR, [www.csr.co.kr](http://www.csr.co.kr)), opinions of the experts, and also obtained from various references (OCFM, 2002; KISTEC, 2000). And the loss of contents or fatality and injury losses cost  $C_H$  can be evaluated based on the research results of Korea Transport Institute, using the human capital approach of the traffic accident cost data (KOTI, <http://traffic.metro.seoul.kr>). Also, socioeconomic losses could be approximately evaluated as a percentage fraction ranging from 50% to 150% of road user costs.

Practical approaches to LCC models for optimum maintenance strategy and indirect cost models are not described herein due to the space limit but referred to the references (Park et al. 2006; Cho et al. 2004; Cho et al. 2006).

## 4 PRACTICAL APPROACHES TO METHODOLOGIES FOR LCCE

Civil infrastructures such as buildings, bridges, tunnels, dams, underground structures, etc. are invariably subject to appreciable diverse uncertainties in the evaluation of time variant performance degradations and loadings and environmental effects throughout the life span of the facilities. Moreover, in normal and abnormal service conditions and operational environments, most of civil infrastructures are subject to aging/deterioration/damages due to various man-made/natural hazard or physical process or chemical attacks. Also, the combined effect of environmental stressors, aggressive service conditions, and the absence of effective maintenance may accelerate the deterioration and/or damage failures of infrastructures. Accordingly, the evaluation of life cycle cost inevitably involves the assessment of time variant performance (condition states, carrying capacity, reliability, etc) of elements, component or system itself, associated with expected costs of maintenances, repairs, rehabilitation and retrofit, which, in turn involves the assessment of expected failure/damage probability, time variant reliability and risk of facilities. Accordingly, the LCCE itself theoretically becomes extremely complex stochastic problem, and moreover when the relevant databases are not available, the elaborate methodologies for LCCE become meaningless to come up with optimal decisions on engineering value and economics problems.

### 4.1 Assessment of performance degradation

In most conventional approaches developed so far, maintenance scenarios are based on time-controlled

maintenance (TCM) interventions for which the random application time is given as input data. Since the application time of maintenance interventions is decided only based on engineering experience or statistical data, these interventions depends on neither the condition state of the structure nor the target performance level. On the contrary, performance-controlled interventions represent maintenance actions applied when a specific condition is reached. The application times of these interventions depend on both the target performance level and previous maintenance interventions. That is, the performance-controlled maintenance (PCM) scenario can reflect previous maintenance intervention, thus, it seems that economical maintenance scenario which ensures a structure performance can be established (Kong & Frangopol, 2004).

In Korea, various FMSs (Facility Management Systems), such as Korea BMS (KRTA, 1998), KRIFIS (KORAIL, 2003) and FMS (KISTEC, 1995), have been used only for conventional maintenance & management of civil infra-facilities. Most of these FMS are only built upon discrete condition states based on subjective visual inspection and NDT data.

Accordingly in Korea, the assessment of performance degradation based on only raw database such as FMS, BMS is almost impossible because of the absence of relevant data and information on the structural performance. And, in PLCCA that includes the maintenance costs associated with performance-controlled interventions at design stage, the condition deterioration may be reasonable to use as performance degradation profile for the LCC evaluation of design-alternatives because the critical rehabilitation or retrofit due to structural failure or damage are not required under design loading environments. Therefore, for PLCCA incorporating performance degradation, condition indexes at both element and system levels may be used to construct condition deterioration profiles.

On the other hand, since for LCCA at maintenance stage, as indicated in the reference (Frangopol & Liu, 2004), the currently available FMSs have a number of limitations as mentioned above as the database for PCM decision information, the reliability deterioration profile should be preferably used to rationally quantify the structure performance indicator in term of reliability\_index.

However, in practice the time-variant reliability assessment of deteriorated facilities based on the BMS data of condition state is almost impossible due to the lack of actual local stiffness data with the associated uncertainties the extensive time-variant reliability analysis of each critical elements components/systems of civil infrastructure is extremely difficult if not impossible to apply in practice. Therefore, the methodology for the reliability deterioration profile from

direct reliability analysis has not yet arrived at matured stage to apply and use as performance degradation profile in practice.

Currently in an on-going research on the LCCA for bridge management, the author proposed an idea that the reliability deterioration profile can be drawn indirectly by fitting reliability index with carrying capacity based on BMS data from periodic inspection and assessment according to the categories of bridge types, traffic volume, environmental conditions, etc. And these performance-controlled intervention as a function of the life-cycle performance degradation could be estimated using knowledge-based DB and carrying capacity analysis. LCCA based on multi-performance indexes such as condition state index and approximate reliability or carrying-capacity may be used to estimate the optimal maintenance strategy. Detailed information about these LCCA models are not presented in the paper, but can be found in the reference (Park et al. 2006; Park, 2006).

#### 4.2 Uncertainty assessment

Uncertainties may easily lead to making the wrong decision, especially in selecting the best alternative from pairs of closely ranked competing strategies. For considering these uncertainties, generally, the uncertainty control and estimation independently considers three different cases corresponding to all of the three possible approaches in the following ways. 1) When historical data is sufficient and available, the probability of each variable can be evaluated by using a simple frequency analysis. 2) On the other hand, if the data is insufficient, engineering probability theories such as MCS or Bayesian approach could be used as uncertainty assessment methods. In other words, randomness and incompleteness of insufficient data is complemented by simulated or updated data. 3) Also, if the data is not available at all, the occurrence probability of each variable may have to be assessed by subjective judgments based on experienced experts' opinion and knowledge. In this case, fuzzy uncertainty concept has been proven as a valuable tool for handling uncertainties due to subjective estimates in decision making models (Cho et al. 2002).

However, it may be noted that all the three approaches aforementioned involve epistemic uncertainties, feature of incompleteness, fuzziness, and biases. Therefore, for evaluating subjective judgments based on experts' experiences and knowledge, it is to be noted that the biases in expert's opinion have to be considered rationally in the uncertainty control and estimation. In general, there are two major categories of the biases -namely, motivational bias and cognitive bias. Motivational biases arise when one or more experts provide intentionally biased opinions. A primary source of this type of bias is real or perceived

conflict of interest on the part of one or more experts. Cognitive biases are totally unintentional. Cognitive biases associates with epistemic uncertainties depend on the way the expert consolidates different pieces of information in formulating an opinion.

Both motivational and cognitive biases can be reduced from the aggregated results of the survey during the analysis and aggregation of the expert estimates. However, if only few experts' opinions are available, it is important to consider the uncertainty range that represents the degree of uncertainties involved in both probabilistic parameter estimates and subjective judgments. For example, since probabilistic parameter estimates are usually based on historical records, the uncertainties are considerably affected by the use of inadequate statistical analysis methods or the lack of data for accurate analysis. For uncertainties of subjective judgments, the major factors such as the complexity of working and health conditions for judgments and the level of education, assurance, and experience have influence on the epistemic uncertainties. Although there are a large number of factors that can be affected by the degree of uncertainties, these four major factors must be considered in the uncertainty assessment because of their major contributions to uncertainties. Moreover, it is especially more reasonable to use the uncertainty range in case when the experts' opinion may not be reliable or be in error (Cho et al. 2002).

Practical approaches to reliability assessment are not described herein but referred to the references (Cho et al. 2004; Cho et al. 2006).

### 4.3 Optimization algorithms and procedures

Various optimization techniques are applied to various optimum design and optimal decision-making problems for the selection of best alternatives with objectives of minimizing cost and/or maximizing performance. Recently, it is often used to make LCC-effective optimum design or optimal maintenance strategy of civil infrastructures.

Recently, general optimization algorithms for the reliability-based LCC-effective optimum design of bridges were developed by the author, which consists of a structural analysis module, reliability analysis module, optimization module, and LCC evaluation module.

In reality, since an infrastructure has a large number of design variables and shows complex structural behavior, it would be impractical to directly use the algorithm for its optimum design, especially for the LCC optimization problem. Thus, various approximation techniques, structural reanalysis techniques and multi-level optimization technique as well, can be applied for numerical efficiency. Also, the augmented Lagrange multiplier (ALM) method is applied,

with unconstrained minimization, and search techniques (Cho et. al, 1999). In particular, since bridge structures have a large number of design variables and shows complex structural behaviors, it would be impractical to directly use conventional optimization algorithm for its optimum design, especially for the LCC optimization problem. Thus, a multi-level (M/L) optimization design algorithm was introduced to improve the computational efficiency.

An automatic differentiation (AD) is incorporated into the M/L Optimization algorithm for the effective reanalysis of the main girders. However, recently, genetic algorithms (GA) one more often used to optimize discrete member design for civil infrastructure optimization. On the other hand, the optimization problem for generating LCC-effective maintenance scenario can be formulated in the form of a multi-objective combinatorial optimization problem. Managers of infrastructure will face the problem of selecting the optimal alternative scenario among many suggested scenarios. A fitness function (Park, 2006) can be applied to solve this problem for the optimum tradeoff solution, which is possible not only for the case of an optimal tradeoff solution among the conflicting objective functions but also for the case of a tradeoff solution satisfying manager's specific requirements and constraints. Multi-objective genetic algorithm (GA) may also be used for generating a set of the various maintenance scenarios.

Due to the space limit, detailed optimization procedures for these techniques are not presented in the paper, but referred to the references (Cho et al. 2001, Cho et al. 2004, Park et al. 2006; Cho et al. 2006; Lee et al. in press).

## 5 LCC SYSTEMS

### 5.1 LCC system model and knowledge-based data base

Though a number of LCC systems were developed so far, there are only few systems practically applicable to the real problems in practice. Moreover, nowadays practicing engineers are always concerned about the availability of integrated system applicable for LCC-effective decisions on design and rehabilitation of various kinds of infrastructures. For instance, in basic design phase for bids, engineers need some powerful LCC assessment tools for the selection of construction type, durable construction materials, and construction methods. For these problems, the DLCCA and PLCCA model may be applied effectively. In the case of the structural design of superstructure of a bridge, or in the case of repair/retrofit/strengthening design of a deteriorated and/or damaged bridge, design live loads will dominate the optimum LCC design in most cases, where

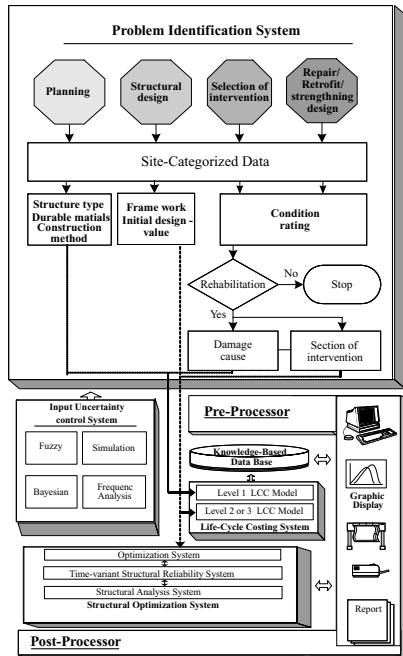


Figure 1. Schematic integrated LCC system model.

the time-invariant LCC model could be applied effectively. But, whenever the risk of earthquake or other natural hazards must be considered in the design of civil infrastructure like substructures of a bridge, it should be carried out by time-variant LCC model as shown in this paper.

From this point of view, a LCC system code practically applicable in practice was developed by the author with other research associates mainly based on PLCC and PLCCA models for superstructures and RLCCA seismic LCC models as well for substructures (Cho et al. 2006). The project was funded by the Ministry of Construction and Transportation (MOCT), which was carried out as one of the most strategic, important SOC research projects. Figure 1 shows the schematic diagram for integrated LCC system model mainly for bridge structures (KICT, 2006; Lee et al. 2004).

First of all, it may be noted that the construction of the knowledge-based DB is simply the most important part in the development of the LCC software system. Figure 2 shows the conceptual diagram for the knowledge-based DB. As shown in the figure, the main function of the knowledge-based DB is to store and assess all the cost and uncertainty data as well as all the information, such as essential information on rehabilitations (i.e., rehabilitation cost, time from first rehabilitation and period of subsequent rehabilitations corresponding to maintenance strategies, increase of performance or decrease

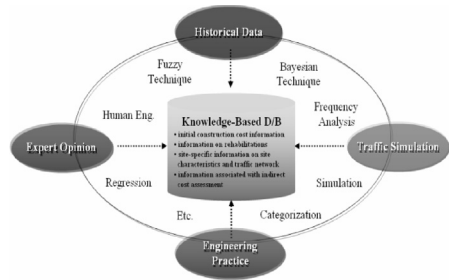


Figure 2. Conceptual diagram for knowledge-based base.

of deterioration rate after rehabilitation, duration of rehabilitation activity, work-zone condition, etc.), site-specific information on site characteristics and traffic network, etc., and various information associated with indirect cost assessment. The information can be acquired by historical data, expert's opinion, engineering practice and analytical damage prediction model which comprise of key components of the DB. Accordingly, these cost data and information are made to be stored and assessed in the knowledge-based DB of the LCCA systems. The input data related to the type of damages and the type of maintenance methods are incorporated into data base based on the sources available in Korea, such as "Method for Extension of Service life of Road.

Bridges" (KISTEC, 2000) and "Data for Design Guide to Maintenance and Repair of Infrastructure" (OCFM, 2002), etc. Also, the data related to the time from first rehabilitation and period of subsequent rehabilitations with respect to each alternative maintenance strategies associated with 'do nothing', 'essential maintenance', 'preventive maintenance' are based on the survey of expert's opinion and a reference such as "An Enhanced Strategy for Infra Facilities Safety Management System based on LCC Concept" (KICT & KISTEC, 2001). In addition, the information on evaluation of the indirect user cost and socio-economic losses (i.e., Input-Output table, the ratio of the number of workers, etc.) are also included in the database.

## 5.2 LCCA system for design stage

Recently in Korea, a number of LCCA systems have been developed and some of them are still under development by the author with other research associates. For example, the first standard LCCA system for highway steel bridges called LCCSTEB was developed using PLCCA model as a software package on personal computers with MS-windows platform and especially designed for individual steel bridges (KICT, 2006). It is used to make a decision for the selection of construction type, durable construction materials, and construction methods,

etc. Also, it will have additional ability to evaluate appropriate points in time of maintenance interventions of steel bridges associated with deterioration in the future. Basic theory of REHAB developed by Kong (2001) may be used for the additional development. It consists of the LCC computing and the DB management systems. Input data is automatically generated by the DB management system in LCCSTEB.

Figure 3 shows the simplified flow chart of LCCSTEB. Major sub-modules and their functional descriptions are presented in the flow chart. The followings are brief descriptions of development process for the DB management system.

It may be stated that DB has to be continuously complemented and updated for using LCCSTEB efficiently during lifetime of bridges. Therefore, a DB management system will be needed to provide user convenience and automatically updated data to LCCSTEB through DB processing and analyzing.

To build a DB for analyzing LCC of steel bridges, integration and networking of between DB systems in Korea were performed. As a result, a knowledge-based DB system has been developed for computing and estimating practical life-cycle cost at construction stages. Raw data is not particularly useful in LCCA. The DB management system has an important function of generating input data into LCCSTEB with the refined DB. The refined DB consists of maintenance time data and cost data obtained by statistical analyses using raw DBs. Those raw DBs were obtained from existing bridge management systems (BMS), surveys, and so on Figure 4. This refined DB is the core of the knowledge-based DB system. Main functions of DB management system are to manage data, to analyze data and to transfer data into LCCSTEB. The DB management module manages BMS data, survey data, field survey data, and reports data in the form of file. The DB analyzing module analyzes gathered DBs, and The DB transferring module transfers input data from the DB analyzing module into LCCSTEB.

Also, another LCCA system for railroad bridges, called RailBLCC has been almost developed by the author with other research associates, which also used PLCCA model and evaluates the expected maintenance costs based on performance-degradation regression model. Statistical and regression uncertainties are estimated and updated based on historical FMS/KRIFIS data and expert's opinion survey, which are used to define a maintenance intervention because maintenance characteristic and environment of railroad bridges are different from these of highway bridges (KRNA, 2007).

Practical approaches to LCC system for optimal maintenance strategy and optimal seismic retrofit for seismic LCC are not described herein due to the space limit but referred to the references (Park et al. 2006; Cho et al. 2006).

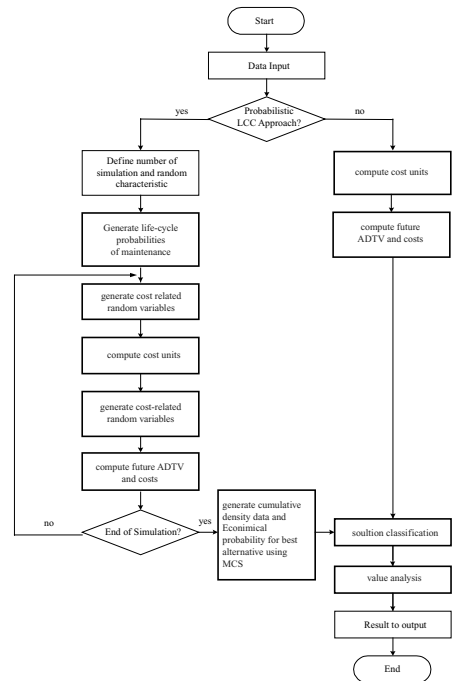


Figure 3. Life cycle cost analysis algorithm of LCCSTEB.

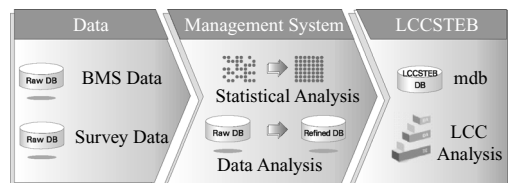


Figure 4. Data flow in LCCSTEB.

## 6 ILLUSTRATIVE EXAMPLES AND DISCUSSIONS

### 6.1 Example 1: life-cycle cost analysis for railroad bridges based on performance degradation uncertainty assessment

In Korea, almost all of LCCA systems and models rely on time-controlled maintenance (TCM) scenario to estimate maintenance cost of bridges. But a performance-controlled maintenance (PCM) scenario have advantage for preventive management that reflect previous maintenance intervention and the agency can make a rational decision on the desired safety level of civil infrastructures, etc. Thus, it seems that PCM can produce more rational and economical maintenance scenario which ensures a structure performance (Kong & Frangopol, 2004).

So, in an on-going research on the development of LCCA system for rail-road bridges (KRNA, 2007), by following the procedure shown in Figure 5, condition degradation models for components/systems of rail-road bridges have been developed based on uncertainty assessment and subsequently, performance-controlled intervention strategy that makes use of performance degradation model in terms of condition state index, which can be used to estimate lifetime maintenance probability and strategy.

The information required in the evaluation of the condition degradation can be obtained from the statistical analysis using existing data or expert's opinion survey data, because the assessment of these uncertainties based on only raw DBs such as FMS, KRIFISLCC is extremely difficult or even impossible in Korea.

Expert's opinion survey about maintenance parameters for LCC and deterioration rates are performed to make a prior distribution using classical statistical analysis and/or fuzzy uncertainty analysis and then the prior distributions are updated systematically based on Bayesian statistical analysis using a few historical data gained from available DB and field investigations.

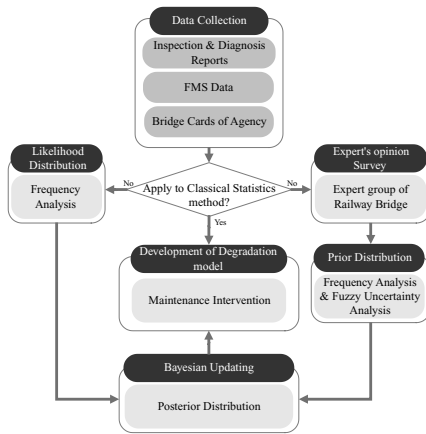


Figure 5. Procedure for development of degradation model.

Table 1. Weighting factor of experts.

WF		Content				
Certificate of qualification	0.2	Professional engineer	Certified engineer	engineer	technician	NO
		100%	80%	50%	50%	0%
Career	0.3	over 25	20–25	15–20	10–15	5–10
		100%	90%	80%	70%	60%
Experience	0.5	Yes			No	
		100%			0%	

Subjective data in a form of  $x, y$  ( $x$  = service life,  $y$  = performance index) are obtained from expert's opinion survey by the railway agency. And this data are considered as weighing factors which are function of qualification certificate, career, and experience of experts as shown in Table 1. Condition deterioration profiles of elements and systems can be estimated to using linear regression model because it was found that linear degradation model is most reasonable compared with exponential model, involution model and parabolic models.

In Korea, generally, the application times for repair is usually applied when a performance (deterioration) index is reached 67.5% (rank C), repair time of a PCS beam bridge is about 17 year as shown in Figure 6.

As for other type of bridges and members similar process is applied, the result is shown in Table 2.

As previously stated, the modified Event Tree Analysis (ETA) (Kong, 2001) is need for lifetime maintenance probability under the sequence of maintenance actions as shown in Figure 7.

When in near future the current BMS/FMS for various infrastructures are completely renovated or reconstructed so as to be compatible with database of LCCA systems, the database may be used to update uncertainties of condition deterioration profiles and thus to make updated performance-controlled interventions in practice.

## 6.2 Example 2: application of LCC models for design-alternative analysis & optimum design

The following is a typical example for the selection of LCC-effective optimal bridge type for bids at design stage, and the associated example for LCC-effective optimal design of the selected bridge (Cho, 2002). In this example, four bridge types—namely, Steel Box Girder bridge, Four Main Plate Girder bridge, PSC-Box Girder bridge by Free Cantilever Method (FCM), PSC-Box Girder bridge by Full Staging Method (FSM) are considered as the alternatives. The bridge will be constructed as a part of a rural highway which

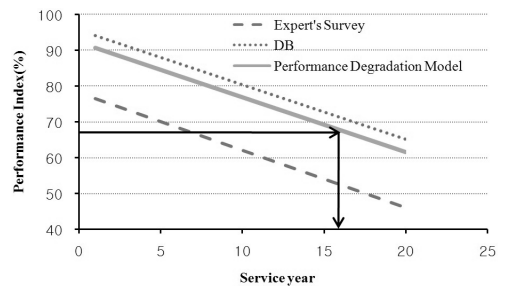


Figure 6. Performance degradation model of PSC beam bridge.



Table 2. Maintenance period of PSC girder bridges.

Element	Type of Damage	Expected Period of repair (year)	Standard deviation
Deck	Crack	18.58	4.497
	Deterioration, damage, rebar exposure	19.13	5.508
Expansion joint	Damage	19.38	5.882
		19.70	5.954
Bearing support	Steel bearing support damage	18.52	6.044
	Rubber bearing support damage	19.79	6.282
Girder over support	Surface condition, rebar exposure	17.30	4.863
	Crack	18.27	5.446
Girder at mid span	Surface condition, rebar exposure	18.98	5.089
	Crack	18.90	5.188
Girder on wire Anchorage	Damage		

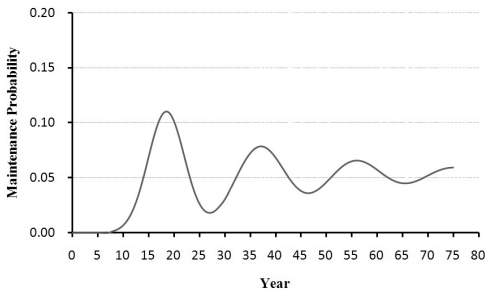


Figure 7. Lifetime maintenance probability.

has relatively moderate ADTV, expected to increase from 21,000 to 46,000 over 75-year design life. At the conceptual design stage, optimal bridge type should be selected by considering Value Engineering (VE) aspects incorporating economy (LCC), safety, aesthetic, workability, functionality, maintenance convenience and environmental effect, etc. Thus, for this bridge design problem, the LCCA is carried out as a part of VE evaluation of the alternative bridge types. In evaluating the LCC for each alternative, the maintenance is assumed to be conducted by preventive maintenance, which is based on the survey of expert's opinion (KIST and KISTEC, 2001). The more detailed data for each alternative applied in LCCA can be found in the reference (KECC—Korea Engineering Consultant Corp., 2002). The LCCA for this example is also performed by using PROLCC and LCCSTEB.

In Figure 8, the results of LCCA for the each alternative are comparatively shown. As shown in the figure, the expected LCC of the alternative-2—namely, Four Main Plate Girder bridge—shows the most economical result estimated as 20.89 billion won. Also, Figure 9 is cumulative distribution function for the each alternative, respectively.

Figure 8 shows that expected LCC of alternatives at 90% confidence level are 29, 26, 29 and 33 billion won, respectively; alternative 2 is most economical among others like a DLCCA. But PLCCA provides more information in terms of percentile probability

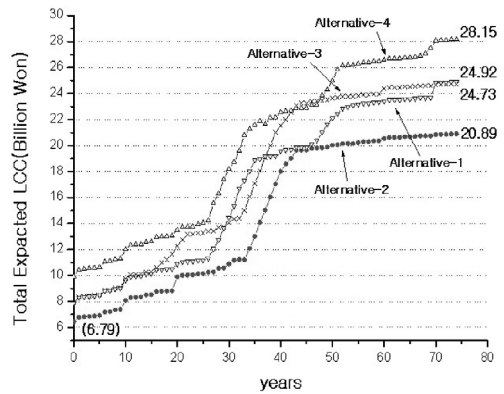


Figure 8. Total expected LCC for each alternative.

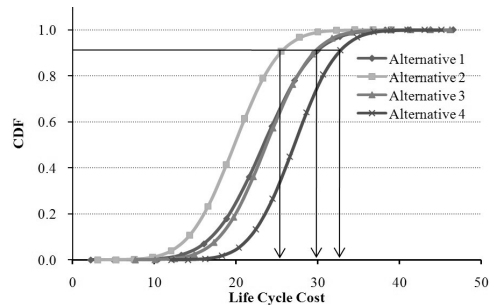


Figure 9. CDF of LCC for each alternative.

(occurrence possibility %) of one alternative relative to other alternatives. Thus, in view of decision-making, PLCCA is a lot more useful than DLCCA.

According to the results of VE evaluation incorporating those results of LCCA, the optimum alternative is chosen as the alternative-2, which is the same as that of the LCC assessment. As a result, the optimal bridge, Four Main Girder bridge, is shown in Figure 10, whose roadway is 280 m long and 20 m wide, and has two lanes for each way. In the LCC optimization for the alternative-2, the design variables are selected

as upper/lower flange and web thickness, and girder height. The design constraints are formulated based on Korean Bridge Design Specification.

The problem of optimum LCC design of the bridge is formulated as that of minimization of the expected total LCC that consists of initial cost, expected (failure) rehabilitation cost for strength and serviceability limit states. For instance, the cost associated with expected strength failure can be obtained from the probability of strength failure and the damage cost that consists of strengthening cost, human and property losses costs, road user costs due to traffic closure, and indirect regional economic losses.

The strength failure limit-state in terms of bending and shear of a main girder is defined as the ultimate limit state failure of flange and web of main girder system. As shown in Figure 8, the initial cost for initially assumed sections of the bridge is 6.79 billion won. The steel plate adhesion method is assumed to be used for the strengthening of main girder, the estimation criteria for unit repair cost is taken as 266.75 thousand won/m<sup>2</sup>, based on the reference (KISTEC, 2000).

Table 3. Major parameters used in design-alternative analysis and optimum design.

Parameter	Value	Unit	Reference
The traffic accident cost	0.12	bil. won	KOTI (http://traffic.
Traffic accident rate during repair work activity	2.2	mil. vehicle/km	metro. seoul. kr)
Traffic accident rate during normal condition	1.9	mil. vehicle/km	
The value of fatality	3.5	bil. won	Lee & Shim
The value of injury	21	mil. won	(1997)
The hourly driver cost	21,517	won/person	KOTI
Discount rate	4.51	%	KISTEC (2000)

Major parameters related to human and property losses costs and road user costs are given in Table 3. Though, detailed information on the assessment of indirect regional economic losses, uncertainty data related to reliability analysis and detailed procedure are not presented in this paper, due to space limitation which can be found in the references (Cho et al. 2001).

In this paper, only the economical aspects are focused and discussed. Since the LCC optimum design can be equivalently achieved by the initial cost optimization with a reasonable allowable stress ratio (Cho, 2001), the initial cost optimization is carried out by varying allowable stress ratio from 75% to 100% with increment of 5%.

As shown in Figure 11, the total expected LCC's for the 6 different levels of allowable stress ratio are estimated based on the Initial Cost Optimization (ICO).

It can be seen that the Initial Cost Optimization at the allowable stress ratio of 80% equivalently achieves the near optimum LCC design point. In Figure 12, for each of the three different optimizations—the conventional ICO, the ICO with allowable stress ratio of 80%, which is called ELCCO (Equivalent LCC optimization), and LCC Optimization (LCCO)—the results of initial cost, expected failure cost and total expected LCC are shown respectively. As shown in the figure, the results of the equivalent LCC (the ICO with optimal allowable stress ratio of 80%) and the LCCO are very similar.

However, in Figure 12, the results for the ICO are extremely different from other cases, mainly because more slender optimum sections of the ICO results in higher failure probably, which, in turn, yield higher expected failure costs. In the case of the ICO, the initial cost is little more economical by about 0.54 billion won compared with the case of LCCO. However, the LCCO can significantly reduce the total expected LCC by 10.47 billion won. Therefore it may be possibly stated that for the alternative-2, the more economical design may be induced in view of LCC if the initial cost optimization for allowable stress ratio of 80% or LCC

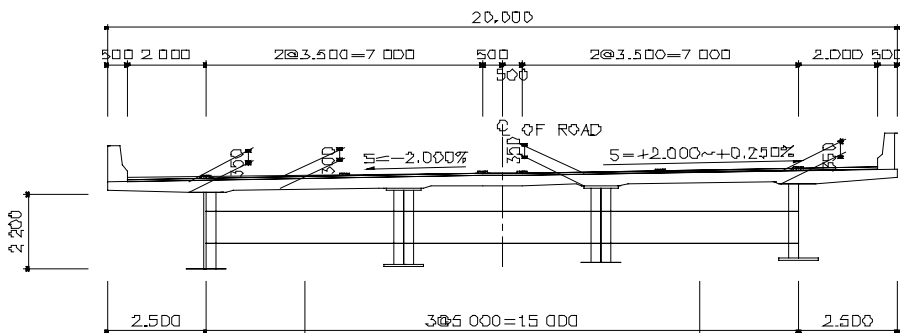


Figure 10. Typical section and profile of four main plate girder bridge.

optimization is applied. It has been invariably found that in a great number of other applications the equivalent LCC optimization, ELCCO, provides almost same results and thus may be effectively used instead of more rigorous and elaborate LCC optimization in practice, which means especially ELLC is very effective tool at basic design phase for LCC-effective optimum design of civil infrastructures.

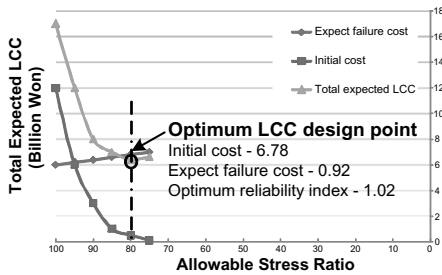


Figure 11. LCC of initial cost optimization to variation of allowable stress ratio.

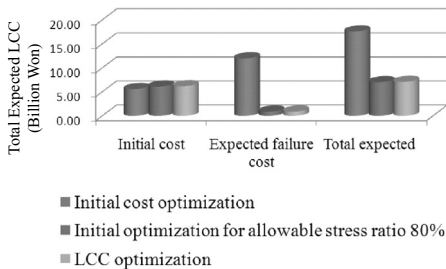


Figure 12. Comparison of costs of each optimization.

## 7 CONCLUDING REMARKS

In the paper, an overview is presented of recent progress of LCCE in Korea with a critical review of the state-of-the-practice, and the recent research & development of models and methodologies for LCC analysis, design, and management of civil infrastructures, with emphasis on practical approaches to LCC methodologies and uncertainty assessment using the available statistical method including Bayesian updating and Fuzzy uncertainty assessment based on historical records or expert's opinion survey. On the basis of the application experience with various LCCE problems in practice and the research experience with various research projects on the development of LCCA software system, the author spotted, in the paper, the current problems and critical issues, and then introduced practical approaches to the application of LCCE and LCC system model with an emphasis on uncertainty assessment and user-friendly knowledge-based database for its successful implementation.

The following concluding remarks can be made based on the critical review of the current situation and the limitations of LCCE applicable in Korea:

1. Practical approaches, rather than theoretical approaches, are inevitable and even more desirable since statistical database suitable and applicable for LCCA are not available so far in Korea.
2. The current BMS/FMS for various infrastructures have to be completely renovated or reconstructed so as to be compatible with database of LCCA system in order to implement LCCE system applicable in practice based on the available BMS or FMS.
3. Since the current PLCCA cannot incorporate the expected LCC including lifetime expected

Table 4. Maintenance interventions.

Element	Maintenance intervention	Unit cost (Thousand won)	Application Rate (%)	Improved condition index
Steel Girder	Painting (PG)	30.0/m <sup>2</sup>	100%	30%
	Welding (WE)	20.0/m	10%	40%
	Bolting (BO)	3.0/ea.	10%	30%
	Steel Attachment (SA)	750.0/m <sup>2</sup>	10%	70%
	Replacement (RG)	2,000.0/m <sup>2</sup>	100%	100%
Slab	Epoxy Injection (EI)	3.0/m	30%	24%
	Waterproofing (WP)	27.6/m <sup>2</sup>	80%	24%
	FRP Attaching (FA)	78.9/m <sup>2</sup>	50%	72%
	Replacement (RS)	150.0/m <sup>2</sup>	100%	100%
Pavement	Surface Treatment (ST)	10.0/m <sup>2</sup>	10%	30%
	Cutting-overlay (CO)	20.0/m <sup>2</sup>	30%	80%
	Patching (PA)	10.0/m <sup>2</sup>	5%	40%
	Re-pavement (RP)	25.0/m <sup>2</sup>	100%	100%

maintenance cost in terms of performance degradation profile and lifetime expected failure (rehabilitation) costs against various risk of hazards, reliability-based LCCA must be used in practice for most of major infrastructures, which are invariably subject to manmade and natural hazards such as explosion, flooding, wind and earthquake, etc.

4. So far, since the development of standard guides and software system for LCCE are limited mostly to building and bridge, the research and development of LCCE system should be extended to other major infra-facilities such as tunnels, dams, underground facilities, harbor facilities, offshore platforms among others.

Accordingly, in Korea the current researches are directed for the development of more realistic LCC models and methodologies practically applicable to each different type of infrastructures. However, the experts in LCCE in Korea realize that the R& D for LCCE systems may have to be more actively conducted in parallel with the development of compatible BMS/FMS and user-friendly knowledge-based database that incorporates more realistic deterioration/damage assessment modules and the associated cost assessment modules for each different kind of civil infrastructures.

## REFERENCES

- Cho, H.N., Ang, A.H-S. & Lim, J.K. 1999. Cost-effective optimal target reliability for seismic design and upgrading of long span PC bridges. *Proceedings of the 8th International Conference on Applications of Statistics and Probability*, 1999. Newcastle, Australia: Department of Civil, Surveying and Environmental Engineering, University of Newcastle.
- Cho, H.N., Min, D.H. & Lee, K.M. 2001. Optimum Life-Cycle Cost Design of Orthotropic Steel Deck Bridges. *Steel Structures*. 1 (2): 141–152.
- Cho, H.N. 2002. Life cycle cost effectiveness for design and rehabilitation of civil infrastructures. *Proceedings of SEWC02, October 2002*. Yokohama, Japan.
- Cho, H.N., Choi, H.H., & Kim, Y.B. 2002. A risk assessment methodology for incorporating uncertainties using fuzzy concepts. *Reliability Engineering and System Safety*. 78 (2):173–183.
- Cho, H.N., Kim, J.H., Choi, Y.M. & Lee, K.M. 2003. Practical Application of Life-Cycle Cost Effective Design and Rehabilitation of Civil Infrastructures. *3th International Workshop on Life-Cycle Cost Analysis and Design of Civil Infrastructure Systems*. 24–26 March 2003. Lausanne: Switzerland.
- Cho, H.N., and Lee, K.M. & Choi, Y.M. 2004. Life-Cycle Cost Effective Optimum Design of Steel Bridges. *Journal of Constructional Steel Research* 60: 1585–1613.
- Cho, H.N., Lee, K.M., Cha, C.J. & Kim, J.H. 2005. Life-Cycle Cost Effective Optimum Design of Orthotropic Steel Deck Bridges under Corrosion Environment. *4th International Workshop on Life-Cycle Cost Analysis and Design of Civil Infrastructure Systems*, 8–11 May 2005. Cocoa Beach, FL: USA.
- Cho, H.N., Lee, K.M., Choi, H.H. & Lim, J.K. 2006. Seismic reliability analysis of deteriorating bridges considering environmental stressors. *IABMAS. Proceedings of the 5th International Workshop on Life-Cycle Cost Analysis and Design of Civil Infrastructure Systems*, 16–18 October 2006. Seoul, Korea.
- Cho, H.N., Choi, H.H., Lee, K.M. & Park, K.H. 2006. Optimal seismic retrofit and maintenance strategy for steel bridges using Life-Cycle Cost analysis. *IABMAS. Proceedings of the 5th International Workshop on Life-Cycle Cost Analysis and Design of Civil Infrastructure Systems*, 16–18 October 2006. Seoul, Korea.
- Mark, A. Ehlen. 1997. Life-Cycle Costs of New Construction Materials. *Journal of Infrastructure systems*. 3 (4): 129–133
- Frangopol, D.M., Lin, K.Y. & Allen C. Estes. 1997. Life-Cycle Cost Design of Deteriorating Structures. *Journal of Structural Engineering*, 1230 (10) : 1390–1401.
- Frangopol, D.M. & Liu, M. 2004. Maintenance and management of civil infrastructure based on condition, safety, optimization, and life-cycle cost. *International Workshop on Integrated Life-Cycle Management of Infrastructures*, 9–11 December 2004. Hong Kong.
- Furuta, H., Kameda, T., Nakahara, K., Takahashi, Y. & Frangopol, D.M. 2006. Optimal bridge maintenance planning using improved multi-objective genetic algorithm. *Structure and Infrastructure Engineering*, 2 (1): 33–41.
- Kong, J.S. & Frangopol, D.M. 2004. Prediction of reliability and cost profiles of deteriorating structures under time- and performance-controlled maintenance. *Journal of Structural Engineering*, 130 (12): 1865–1874.
- Lee, K.M. Cho, H.M & Cha, C.J. 2006. Life-cycle cost-effective optimum design of steel bridges considering environmental stressors. *Engineering Structure* 28 (9):1252–1265.
- Lee, K.M. Choi, E.S. Cho, H.N. Choi, H.H. Lifetime Seismic Reliability Analysis of Deteriorating Bridges. *Probabilistic Engineering Mechanics* (in press).
- Park, K.H. 2006. *Comprehensive Framework of Optimum Management for Steel-Girder Bridges Based on Life-Cycle Performance and Cost*. Ph. D. Dissertation. Ansan, Korea: Hanyang University.
- Park, K-H., Hwang, Y.K., Lee, S.Y., Kong, J.S., Cho, H.N. & Lim, J.K. 2006. Multi performance based optimum maintenance system framework for existing bridge. *Proceeding of the Fifth International Workshop on Life-Cycle Cost Analysis and Design of Civil Infrastructure Systems*. October 16–18, 2006. Seoul, Korea: Taylor & Francis.
- Walls, J. & Smith, M.R. 1998. *Life-Cycle Cost Analysis In Pavement Design – Interim Technical Bulletin*. Fhwa-Sa-98-079. Research Report. Washington, DC: Federal Highway Administration.

# Life cycle optimization in earthquake engineering

Luis Esteve

*Institute of Engineering, National University of Mexico*

**ABSTRACT:** An overview is presented of life-cycle optimization in the establishment of reliability- and performance-based seismic design requirements for multistory systems. Alternative approaches are presented for the development of seismic vulnerability functions that do not require the determination of lateral deformation capacities. The influence of damage accumulation on the evolution of the seismic reliability functions is discussed, and some results are presented about the sensitivity of the seismic reliability and performance functions to the contribution of energy-dissipating devices to the lateral strength and stiffness of multistory frames. The process of structural damage accumulation resulting from the action of sequences of seismic excitations is taken into account in the assessment of life-cycle system reliability and performance, and in the formulation of reliability and optimization criteria and methods for the establishment of structural design requirements and for the adoption of repair and maintenance strategies. Problems related to the transformation of research results into practically applicable seismic design criteria are briefly discussed. Several illustrative examples are presented.

## 1 INTRODUCTION

For a long time, life-cycle optimization has been recognized as an implicit and essential objective of engineering design, construction and maintenance actions. For the establishment of recommended practical criteria and methods for the achievement of that objective, it is necessary to adopt a formal decision framework, based on the identification and evaluation of an adequate set of quantitative indicators to describe the performance of a given system. In general, this description will be strongly affected by significant uncertainties, associated with a) the random variability of the times and intensities of future excitations and of the mechanical properties of the system, b) our imperfect knowledge about these concepts, and c) the limitations of the mathematical models used to represent them. This leads to the adoption of a probabilistic framework to describe the expected performance of a system; it should be capable of dealing with two types of uncertainties: random or aleatory (group a, above) and epistemic (groups b and c). In earthquake engineering problems, the excitations include the gravitational loads (dead and live) and the seismic events. The expected performance of a system when subjected to any of those events depends on both the intensity of the latter and the mechanical properties of the former, which depend in turn on the level and distribution of damage that may have accumulated as a consequence of the system's response to previous seismic events or of the action of any other agent, such as differential settlements due to gravitational loads.

An important consequence of damage accumulation is the increase of the seismic vulnerability function of the system. In order to maintain the resulting vulnerability levels within acceptable limits, adequate maintenance and rehabilitation policies must be implemented, for which the scope, control variables and acceptance criteria should be based on a life-cycle optimization analysis, consistent with that adopted for the establishment of optimum seismic design criteria and quality control requirements.

An important problem in the formulation of optimum life-cycle decision criteria is related to the comparison of costs and benefits that may occur at different instants in time. The adoption of objective functions based on the present value of expected utilities, both positive (benefits) and negative (losses, costs) is ordinarily used to cope with this problem. As it is well known, very difficult questions arise in connection with the assignment of quantitative values to benefits and costs that cannot be directly expressed in monetary terms. They include the concepts known as intangible, such as losses of human lives, improvements or reductions in the quality of life, social and political problems. Although the formulations presented here avoid dealing explicitly with these concepts, it is expected that the general framework proposed can serve as a support for the formulation of decision criteria accounting for them.

This paper aims at presenting an overview of the general criteria and the available models and tools to formulate a framework for life-cycle optimization in earthquake engineering. Attention is focused

on multistory buildings with structural arrangements consisting of a rigid frame or a dual wall-frame system. Some problems associated with the determination of seismic vulnerability functions for those systems are discussed, and some ideas are presented about alternative approaches and desirable studies. Optimum maintenance programs that account for the influence of damage accumulation are examined. For systems with energy-dissipating devices, these programs include both repair of local damage in members of the structural system, and replacement of energy-dissipating devices that have failed or that are suspected to have developed high fatigue levels.

## 2 LIFE-CYCLE DECISION FRAMEWORK

### 2.1 Seismic hazard models

The seismic hazard at a site can be described by a stochastic process model of the occurrence of seismic events and of the conditional probability density function of the intensities; the latter may be described by a ground motion indicator showing significant correlation with the peak values of the structural response. Peak ground accelerations or velocities, or ordinates of response spectra for the fundamental period of the system of interest are often used for this purpose. Poisson and renewal stochastic process models with random selection of magnitudes are often used to represent the generation of seismic events at a source. These models have to be combined with adequate intensity attenuation functions in order to generate stochastic process models of the occurrence of earthquakes of different intensities at a site near one or more active sources.

A source-activity model considering the superposition of a renewal process of the occurrence of characteristic earthquakes and a Poisson process representing background activity was used by Singh *et al* (1983) for the development of a probabilistic seismic hazard model at sites near the subduction zone that runs along the southern coast of Mexico. Markov process models have been used by Lutz *et al* (1993) to represent seismic hazard in the vicinity of strike-slip faults near the Western coast of the United States.

For the Poisson model, the seismic hazard remains constant, regardless of the time elapsed since the last previous event; however, this is not true for the renewal and the Markov process models, which are characterized by the steady increase of the hazard level with the time without activity at a source.

### 2.2 Structural systems

Several multi-storey rigid frame and dual wall-frame systems were studied, assuming their non linear behaviour to be concentrated at the flexural member

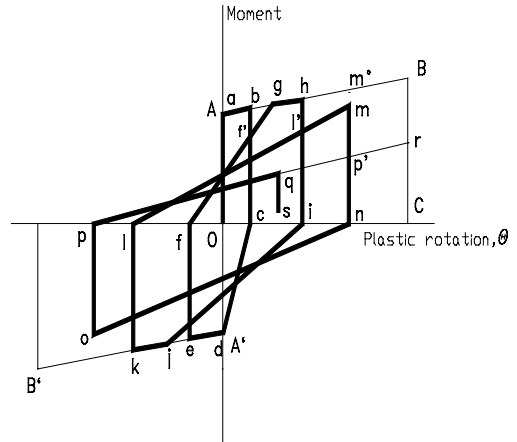


Figure 1. Constitutive function for moment vs plastic rotation at flexural member ends.

ends, characterized by a constitutive function similar to that shown in Figure 1, proposed by Wang & Shah (1987) and modified by Campos & Esteva (1997). Illustrative examples are also presented of the formulation of optimum repair and maintenance policies for systems with hysteretic energy-dissipating devices (Campos, 2004).

### 2.3 Optimization analysis

Let us consider first the simple case of a structural system built at instant  $t_0 = 0$ , and exposed to a sequence of seismic events with uncertainly known times of occurrence  $T_1, \dots, T_n$ , and intensities  $Y_1, \dots, Y_n$ , during the time interval  $0 < t < t_L$ , assumed here to correspond to the useful life-time of the system. Let  $C_0$  denote the initial construction cost (which is a function of the design parameters),  $D_i$  the cost of damage and maintenance actions occurring at the time of the  $i$ -th event, or immediately after it, and  $\gamma$  a discount rate used to transform values of benefits or losses that may be produced in the future into equivalent values assumed to be generated at instant  $t_0 = 0$ . The transformation would adopt the form  $U_0 = U_i \cdot \exp(-\gamma t)$ , where  $U_i$  and  $U_0$  are respectively the nominal value of the utility (a benefit, if positive; a loss if negative) generated at instant  $t$ , and its present value, at instant  $t_0 = 0$ . In the following only the special case when  $t_L \rightarrow \infty$  and the system is systematically rebuilt after failure will be considered, assuming that the vulnerability function of each new system will be equal to that of its predecessors. It is also assumed that the expected value of the benefits per unit time will remain constant while

the system remains in operation. Thus, the optimization analysis will consist in minimizing the absolute value of an objective function constituted by the addition of the initial cost (which is an increasing function of the strength and stiffness values determined by the structural design requirements) plus the present values of the expected losses,  $D_i$ . Under these assumptions, the objective function to be minimized is  $U$ , given by Equation 1, where  $E$  stands for the expected value function.

$$U = C_0 + E \left[ \sum_{i=1}^{\infty} D_i^{-\gamma T_i} \right] \quad (1)$$

The probability distribution of  $D_i$  depends on the intensity  $Y_i$  of the earthquake occurring at instant  $T_i$ . The joint probability distribution of the latter two variables is the subject of the seismic hazard model adopted. Rosenblueth (1976) and Rackwitz (2000) present analytical models based on the assumptions that earthquakes with intensities above a given threshold value occur in time as a Poisson process or as a renewal process, where the intensities are independent random variables with identical probability distribution. They also study more general cases than those considered in the preceding paragraph. For the particular case where earthquakes occur as a Poisson process, the last term in Equation 1 adopts the form  $\lambda \cdot E[D]/\gamma$ , where  $\lambda$  is the mean rate of occurrence per unit time of earthquakes with intensities above a specified threshold value (sufficiently low to include all intensities significant for engineering applications) and  $D$  is the expected value of damage and maintenance actions given the occurrence of any earthquake with intensity above the mentioned threshold value; its expected value is obtained by integration of the joint probability density function of the mechanical properties of the system under study and of the intensities given the occurrence of an earthquake.

Equation 1 does not explicitly take into account the epistemic uncertainties mentioned in the Introduction, and included in the analytical models presented by Rosenblueth (1976) and Rackwitz (2000); however, it can be easily modified as follows, to consider them:

$$U = C_0 + E_{\varepsilon} \left[ E \left[ \sum_{i=1}^{\infty} D_i^{-\gamma T_i} \mid \varepsilon \right] \right] \quad (2)$$

Here,  $\varepsilon$  is a vector used to represent the set of assumptions about the possible models used to estimate the last term in the second member in Equation 1, or about the values of the parameters adopted for those models, and  $E_{\varepsilon}$  is the expected value with respect to the probabilistic weights assigned to each of those assumptions.

## 2.4 Risk control considerations

Decisions made in accordance with the optimization analysis just presented may lead to excessively high, perhaps unacceptable, risk levels. This may occur as a consequence of adopting a structural system of arrangement that is not sufficiently efficient for the conditions considered. In those cases, two alternatives are available to the decision maker: look for a more efficient system or design for a pre-established risk level, even if that is not optimum on the basis of purely economic considerations.

It may also happen that an optimum design resulting from the minimization of the objective function presented in one of Equations 1 or 2, leading to acceptable risk levels at the moment of making the decision, may lead to unacceptable risk levels in the future, either because of an increase in the vulnerability that may arise as a consequence of damage accumulation on the system, or because of the steady increase in seismic hazard mentioned at the end of Section 2.1. The first source of risk enhancement can be controlled through the adoption of adequate repair and maintenance strategies and programs. This approach could also be applied to control the process associated with the increase in seismic hazard; however, this would be questionable because it would imply leaving to future generations risks that would not be acceptable to us. Therefore, the only option left would be to design a system capable of ensuring acceptable risk levels, provided adequate repair and maintenance policies are applied to prevent the vulnerability function of the system to raise higher than that corresponding to the initial, undamaged system.

## 3 SEISMIC VULNERABILITY AND RISK FUNCTIONS

### 3.1 Failure probabilities and expected damage under the action of a single excitation

In general, the seismic vulnerability function of a system can be represented as follows:

$$\bar{\delta}(y) = E[\delta \mid y] = p_F(y)\delta_F + (1 - p_F(y))\bar{\delta}(y \mid S) \quad (3)$$

Here,  $p_F(y)$  is the probability of ultimate failure (collapse) of the system when subjected to an earthquake of intensity  $y$ ,  $\delta_F$  is the expected cost of failure in case it occurs, normalized with respect to the initial cost,  $C_0$ , and  $\bar{\delta}(y \mid S)$  is the expected value of the normalized cost of damage for an earthquake with intensity  $y$ , conditional to survival of the system under the action of that event.

For a multistory building, the expected value of the damage produced by an earthquake with intensity  $y$  is often expressed as a function of the expected value

of the global distortion of the system,  $\Psi = \delta_N/H$ , where  $H$  is its height of the building above the ground surface and  $\delta_N$  is the peak value of the relative lateral displacement of its top with respect to its base. In many cases it results convenient to obtain the expected cost of damage as the sum of the contributions of several segments of the system, as given by Equation 4 (Esteva *et al*, 2002):

$$\bar{\delta}(y|S) = \lambda \sum_i r_{ci} \bar{g}(\Psi_i|y) \quad (4)$$

In this equation,  $r_{ci} = C_{0i}/C_0$ ,  $C_{0i}$  is the initial cost of the  $i$ -th segment of the system,  $g(\Psi_i)$  a function of the random value  $\Psi_i$  of the corresponding local distortion, and  $\bar{g}(\Psi_i|y)$  its expected value for intensity  $y$ . The initial costs  $C_0$  and  $C_{0i}$  are functions of the vector  $\alpha$  of structural parameters, and so is the joint probability density function of the local distortions  $\Psi_i$ . A factor  $\lambda$ , which is a function of the summation that follows it, is introduced to account for the fact that repair costs include the contribution of a fixed amount that reflects the costs of the logistic arrangements that have to be made before the actual repair work starts. As a consequence,  $\lambda$  will in general reach its maximum for infinitely small values of the summation mentioned above, and it will tend asymptotically to a smaller value as that summation grows. More details about the determination of the expected damage function given by Equation 4 have been presented by Esteva *et al* (2002).

Current approaches for the determination of the seismic reliability of a system subjected to an earthquake ground motion with a specified intensity propose to measure that reliability by the probability that  $\Psi$  is smaller than the deformation capacity,  $\Psi_C$ . Approximate estimates of second-moment probabilistic indicators of  $\Psi_C$  are often obtained with the aid of a simplified reference system, characterized by mechanical properties determined by means of a static pushover analysis of the detailed system. However, these estimates are tied to severe limitations, because according to this approach it is not possible to account for a) the influence of cumulative damage associated with the cyclic response, and b) the dependence of the lateral deformation capacity on the response configuration of the system when it approaches failure.

Trying to avoid the introduction of arbitrary assumptions about the determination of the deformation capacity of a complex system for the purpose of obtaining estimates of its seismic reliability, alternative criteria have been proposed, according to which system failure is assumed to take place when the displacements predicted by the dynamic response analysis become indefinitely large and non-reversible. The effective values of the elements of the resulting stiffness matrix are then infinitely small. This condition

is described as system collapse (Esteva, 1992; Shome and Cornell, 1999; Alamilla and Esteva, 2006). In order to determine the safety factor of a given system with respect to this type of failure for a given ground motion time history, it is necessary to obtain the scale factor that has to be applied to that time history in order to produce system collapse. The intensity leading to collapse is then denoted as "failure intensity". Because the determination of the needed scaling factor has to be attained by means of an iterative procedure, it may call for excessive demands of computer time.

The method of Incremental Dynamic Analysis (IDA, Vamvatsikos and Cornell, 2002) offers both possibilities for the estimation of probabilistic indicators of seismic reliability for given ground motion intensities: either on the basis of deformation capacities or using the concept of failure intensity. However, these advantages are often tied to excessive computer time demands (Dolsek and Fajfar, 2004). This has led Esteva and Ismael (2004) and Esteva and Díaz-López (2006) to explore an alternative approach, aiming at estimating reliability functions relating the reliability index  $\beta$  (Cornell, 1969) with the ground motion intensity, including the influence of cumulative damage and avoiding the need to obtain probabilistic definitions of lateral deformation capacities. This approach is based on the concept of "failure intensity", mentioned above. According to this approach, the collapse condition is expressed in terms of a secant-stiffness reduction index  $I_{SSR} = (K_0 - K)/K_0$ , where  $K_0$  is the initial tangent stiffness associated with the base-shear vs roof displacement curve resulting from pushover analysis and  $K$  is the secant stiffness (base shear divided by lateral roof displacement) when the lateral roof displacement reaches its maximum absolute value during the seismic response of the system. The failure condition is expressed as  $I_{SSR} = 1.0$ . For a given value of the intensity ( $y$ ), the probability density function of  $Q = \ln I_{SSR}$  is equal to  $f_Q(q)$ , which is continuous for  $q < 0$  and includes a discrete concentration at  $q = 0$ , which is equal to  $p_F(y) = P[Q = 0|y]$ , the failure probability for an intensity equal to  $y$ . In order to permit the joint analysis of information including cases with values of  $Q$  smaller than or equal to 0, an auxiliary variable  $U$  is introduced, such that  $Q = U$  for  $Q < 0$  and  $Q = 0$  for  $U \geq 0$  (that is, for the failure condition). The probability density function of  $U$  is designated by  $f_U(\cdot)$ , and the associated cumulative distribution function by  $F_U(\cdot)$ . These functions are characterized by a set of parameters  $\{\kappa\}$  that determine their basic properties, such as mean, standard deviation and skewness. (For instance, in the case of a Gaussian distribution,  $\{\kappa\}$  may be made by the mean and the standard deviation.) These parameters can in turn be expressed as functions of  $y$ ,  $G(y|\alpha)$ , with given form and unknown parameters. It is also assumed that we count with a set of  $m + n$  pairs of values of the



normalized intensity  $\mu_{0i}$ , and the corresponding logarithmic damage index  $Q = q_i$ , the latter obtained by means of a step-by-step time history dynamic response analysis. Under the assumption that these pairs of values are ordered so that  $Q$  is smaller than 0 (survival condition) for the first  $m$  cases, and equal to 0 for the remaining  $n$  cases, the likelihood function is expressed as follows in terms of  $\alpha$ :

$$L(\alpha) = \prod_{i=1}^m f_U(u_i | y_i, \alpha) \prod_{j=1}^n [1 - F_U(0 | y_j, \alpha)] \quad (5)$$

The vector of parameters  $\alpha$  is determined by means of a maximum likelihood approach applied to the sample of pairs of values of  $Y$  and  $Q$ .

According to the approach proposed by Esteva and Diaz-López (2006), a reliability function  $\beta(y)$  is obtained from a sample of pairs of values of  $I_{SSR}$  and  $y$ , where  $\beta$  is the safety index proposed by Cornell (1969) and  $y$  is the ground motion intensity. If the sample includes only cases with  $I_{SSR}$  smaller 1.0, the reliability function can be obtained by means of a regression analysis; if cases with  $I_{SSR} = 1.0$  are also included, a maximum likelihood analysis must be performed. Instead of formulating the problem as that of obtaining an indicator of the probability that  $I_{SSR} < 1.0$  (survival) for a given intensity, attention is focused on the determination of second moment indicators of the probability distribution of  $Z_F = \ln Y_F$ , where  $Y_F$  is the minimum value of the intensity leading to the condition  $I_{SSR} = 1.0$  (collapse). For an earthquake with intensity equal to  $y$ , a safety margin  $Z_M$  can be defined equal to the natural logarithm of the ratio of the system capacity to the amplitude of its response to the given intensity; it can also be defined as the natural logarithm of the ratio  $Y_F/y$ . The reliability function can then be expressed as follows:

$$\beta(y) = (E(Z_F) - \ln y) / \sigma(Z_F) \quad (6)$$

Here,  $E(\cdot)$  and  $\sigma(\cdot)$  stand for *expected value* and *standard deviation*, respectively.

For the structural system of interest, a sample of pairs of random values of  $Z$  and the stiffness reduction index,  $I_{SSR}$ , can be used to estimate means and standard deviations of  $Z(u)$ , the latter defined as the natural logarithm of the random intensity  $Y$  that corresponds to  $I_{SSR} = u$ . The values of  $Z$  in the sample that correspond to values of  $I_{SSR}$  equal to 1.0 are upper bounds of  $Z_F = \ln Y_F$ , where  $Y_F$  is the minimum value of  $Y$  required to produce system failure. Therefore, the points corresponding to these values of  $Z_F$  cannot be incorporated into the sample used to estimate  $E(Z(u))$  and  $\sigma(Z(u))$  by means of conventional minimum-squares regression analysis. However, they can be included in the estimation process, through a

maximum likelihood analysis slightly different from that proposed by Esteva and Ismael (2004).

Figure 2, taken from Rangel (2006), was presented by Esteva and Diaz (2006). It shows a plot of the values of earthquake intensities leading to different values of the stiffness reduction index,  $I_{SSR} = (K_0 - K)/K_0$ , for a twenty-story system with hysteretic energy dissipating devices, subjected to a set of synthetic ground motion records at a soft soil site in the Valley of Mexico. The records were simulated with the aid of the hybrid algorithm presented by Ismael and Esteva (2006). As shown in the figure, the results for values of  $I_{SSR}$  smaller than 1.0 were used to estimate the mean and the standard deviation of the natural logarithm of the failure intensity. The resulting reliability function is one of the three curves shown in Figure 3. The values of  $\beta(y)$  obtained following this approach were slightly higher than those obtained using the method of incremental dynamic analysis proposed by Vamvatsikos and Cornell (2002).

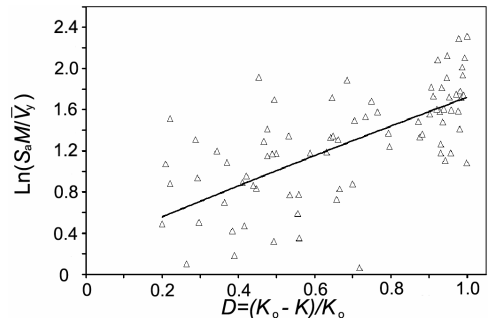


Figure 2. Normalized intensity vs  $I_{SSR}$  for 20-story system with EDD's.

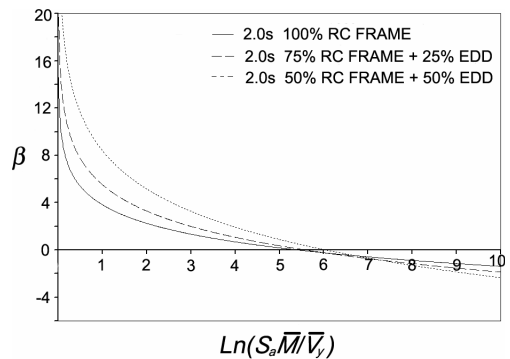


Figure 3. Reliability function in terms of normalized intensity for several twenty-story frame buildings with different contributions of EDD's to system lateral stiffness and strength.

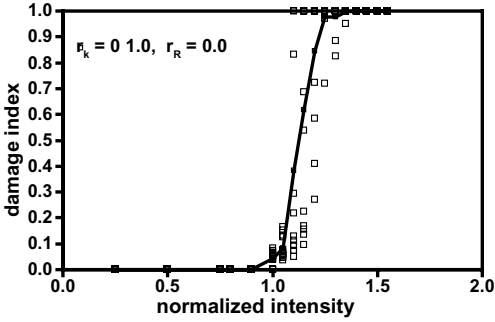


Figure 4. Expected damage function for conventional reinforced concrete frame.

### 3.2 Damage accumulation

It is well known that modern methods of earthquake-resistant design lead to structural systems that develop considerable nonlinear behavior when subjected to high-intensity earthquakes occurring at intervals of the order of a few tens of years. Thus, the possibility of significant damage is implicitly accepted, provided the probability of collapse under the action of future earthquakes is kept sufficiently low. Design intensities and safety factors are determined on the basis of an optimization analysis (either formal or informal) aiming at obtaining a balance between the expected values of repair costs, and other consequences of damage, and the construction cost increments needed to reduce them.

Some exploratory studies about the influence of initial damage on the seismic reliability of multistory rigid-frame buildings were made by Esteva and Díaz (1993), and Díaz and Esteva (1996, 1997). In the initial studies, the multistory frames were replaced by equivalent single-degree-of-freedom (sdf) systems, with constitutive functions for story shear *vs* lateral displacement similar to that shown in Figure 1; they were followed by studies on detailed models of the frames, assuming the nonlinear behavior to be concentrated at nonlinear hinges at the ends of bending members, with moment-rotation constitutive functions also similar to the mentioned figure. Some typical results for the sdf systems are shown in Figures 4 and 5, which correspond to a large-span reinforced concrete single-story frame, designed in accordance with Mexico City seismic design regulations of 1987. Its natural period is equal to 0.43s; its mechanical properties were taken deterministically equal to their expected values.

Figure 4 shows values of the damage index in the initially undamaged system subjected to an ensemble of simulated ground motion records of different intensities, which are represented in the figure in terms of

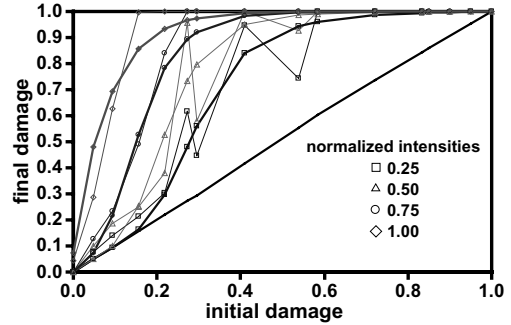


Figure 5. Influence of initial damage on the damaging potential of new earthquakes.

their normalized values, obtained in each case as the ratio of the ordinate of the linear pseudo-acceleration response spectrum for 0.05 damping, for the natural period of the system, divided by the lateral strength of the system, expressed in the same units as the intensity. Here, damage was measured by the ratio  $(K_0 - K)/K_0$ , where  $K_0$  is the initial value of the tangent story stiffness of the undamaged system, and  $K$  is the secant story stiffness computed as the ratio of the story deformation to the story drift at the instant when the latter reaches its peak absolute value. The figure shows a low damage level for a normalized intensity equal to unity, with fast growing values beyond it.

The influence of initial damage on the damaging potential of new earthquakes is illustrated in Figure 5, which shows the form of variation of the expected value of the final damage after an earthquake, in terms of the initial damage and the intensity of the earthquake. The horizontal axis represents initial damage, the vertical axis represents final damage, and the thin shaggy lines in the graph connect points that represent final damage levels corresponding to different values of the normalized intensity. The thicker, smooth curves are minimum square fittings to the original data, intended to represent the expected values of the final damage. The large uncertainties associated with the prediction of final damage indexes are evident, even for such a simple system.

According to Figure 5, the expected damage produced by a normalized intensity equal to 1.00 is smaller than 0.1; however, it grows very fast with the initial damage, reaching a final value of 0.7 for an initial value of 0.1. This calls the attention for the high reductions in the reliability indicators of the system that may be associated with initial damage levels. Optimum maintenance and rehabilitation policies and programs to control these reductions are studied in the following sections.

### 3.3 Mathematical models vs empirical information

Modern computational tools and systems allow professionals and researchers in earthquake engineering to generate simulated samples of the gravitational loads acting on large complex structural systems, as well as of the mechanical properties of their structural members, including models of the constitutive functions representing the relations between local internal forces and deformations at critical sections of members. This capability has been used to make estimates of the dynamic responses and hence the vulnerability functions of complex nonlinear systems, according to the concepts discussed in Sections 2.1 and 2.2. However, even though the uncertainties associated with the forms and parameters of those functions for individual members and critical sections have been recognized, very little attention has been paid to the evaluation of their impact on the uncertainties affecting the probabilistic estimates of responses and vulnerabilities of the full systems.

Two complementary approaches may be envisaged to account for the uncertainties mentioned above: one is to consider a set of assumptions related to the models of the constitutive functions and assign a probability value to each of them; another consists in comparing values of predicted and actual, measured responses of laboratory specimens or real systems. Bayesian probability methods might be applied to use available empirical results to update the prior probability distribution assigned to the mentioned set of assumptions and to determine probability distributions of actual versus computed responses for each of them. Uncertainties associated with the properties of the model should be handled as epistemic uncertainties, as described in the following section; those related to the ratios of observed versus computed responses for each model assumption should be handled as random.

### 3.4 Uncertainty analysis: random and epistemic

Rosenblueth (1976) obtains closed form solutions for the present values of expected costs of the possible failure events of a system subjected to seismic hazard conditions described by renewal process models of earthquake occurrence, with the intensities of the different events considered as stochastically independent, identically distributed random variables. He assumes that the system is immediately rebuilt after each failure event, with its loads and mechanical properties being random variables with the same probability distributions as for the original construction. For purposes of obtaining life-cycle indicators of system safety and vulnerability, he identifies three groups of uncertainly known variables, described below after introducing some slight changes:

- **Type 1:** Random fluctuations in the response of the system, resulting from the random characteristics of the earthquake ground motion. These fluctuations vary from one disturbance to another and are completely uncorrelated.
- **Type 2:** Random values of the gravitational loads and the mechanical properties of the system. They remain constant between reconstructions and are stochastically independent from one structure to the next
- **Type 3:** Epistemic uncertainties, associated with different concepts, such as our imperfect knowledge about the seismic hazard at the site or about the models used to represent the constitutive functions that describe the cyclic behavior of structural elements or critical sections.

Under the assumptions that earthquakes with intensities above a specified threshold value occur in accordance with a stochastic renewal process, and that the system is rebuilt immediately after each failure, the probability density functions of the times to the first and to the  $n$ -th failures are given by Equations 7 and 8, respectively:

$$g_1(t) = \sum_{i=1}^{\infty} f_i(t) P(1-P)^{i-1} \quad (7)$$

$$g_n(t) = \int_0^t g_{n-1}(t-\tau) g(\tau) d\tau \quad (8)$$

Here,  $f_i(t)$  is the probability density function to the first seismic event,  $P$  the failure probability given the occurrence of that event (for a system with deterministically known properties), and  $g(\tau)$  the probability density function of the time between successive failures. The present value of the expected loss for the rebuilding policy adopted is

$$D = D_F \sum_{n=1}^{\infty} \int_0^{\infty} g_n(t) e^{-\gamma t} dt \quad (9)$$

where  $D_F$  is the expected cost of failure in case it occurs. Replacing the values of  $g_n(t)$  in Equation 9 by those given by Equations 7 and 8, the following expression is obtained for  $D$ :

$$D = \frac{D_F P f_1^*(\gamma)}{1 - f^*(\gamma)} \quad (10)$$

Here,  $f^*(\gamma)$  and  $f_1^*(\gamma)$  stand for the Laplace transforms of  $f(t)$  and  $f_1(t)$ , respectively.

If uncertainties of type 2 are introduced, the value of  $P$  in Equation 7 is a function of the (random) vector

of system properties; the values of  $g_i(t)$  in Equations 8 and 9 have to be replaced by their expected values with respect to the joint probability density function of those properties, and  $D$  is given by Equation 11, where  $g^*(\gamma)$  and  $g_1(\gamma)$  are the Laplace transforms of  $g(t)$  and  $g_1(t)$ , respectively.

$$D = D_F \frac{E_2 [g_1^*(\gamma)]}{1 - E_2 [g^*(\gamma)]} \tag{11}$$

For the particular case where the occurrence of seismic events can be represented by a Poisson process with annual rate  $\lambda$ , Equations 10 and 11 lead to Equations 12 and 13, disregarding and including uncertainties of type 2, respectively:

$$D = \frac{D_F P \lambda}{\gamma} \tag{12}$$

$$D = D_F \frac{E_2 \left[ \frac{P \lambda}{P \lambda + \gamma} \right]}{1 - E_2 \left[ \frac{P \lambda}{P \lambda + \gamma} \right]} \tag{13}$$

In most cases of interest in engineering applications,  $E_2 [P \lambda] \ll \gamma$ . In this case, Equation 13 can be replaced by the following approximation:

$$D = \frac{D_F \lambda}{\gamma} E_2 [P] \tag{14}$$

For any of the cases considered in Equations 10–14, epistemic uncertainties can be taken into account by obtaining the expected values of  $D$  with respect to the probability density functions of the variables used to describe those uncertainties.

Equation 14 can be extended to cover structural and non-structural damage covering the possible conditions of failure and survival for each seismic event:

$$D = \frac{\lambda}{\gamma} E_2 [D_F P + D_S (1 - P)] \tag{15}$$

Here,  $D_S$  is the expected cost of damage given that the system survives when subjected to an earthquake with a randomly chosen intensity.

Cornell *et al* (2002) and Jalayer and Cornell (2003) have presented approximate expressions to estimate the expected failure rate  $\lambda \cdot E_2 [P]$ , as well as its expected value with respect to the probability density function of epistemic uncertainties (type 3), using simplified models to describe the probability density functions of earthquake intensities and dynamic responses given the intensity.

4.1 Evolution of risk functions with time

As a consequence of damage accumulation, seismic risk (expected cost of damage per unit time) grows with time after each rebuilding or maintenance action, even if seismic hazard remains constant, as assumed by Poisson process models. For those cases when seismic hazard is represented by renewal or Markov stochastic process models, the systematic increase in hazard associated with these models constitutes an additional source for risk increase. Extended forms of Equations 10–14 can be obtained to account for these effects. Alternatively, Monte Carlo simulation may be used to evaluate  $D$  as given by the last term in either Equation 1 or 2. For simplicity, this approach will be adopted in the following.

4.2 Repair and maintenance policies based on optimization analysis

For the purposes of illustration, consider the case of a simple (single-bay, single-story) system shown in Figure 6 (taken from Esteva and Diaz, 1993), constituted by a conventional frame (CF) and an energy-dissipating device (EDD); the nominal design values of its mechanical properties are summarized by the lateral strength ( $R_F, R_D$ ) and the initial stiffness ( $k_F, k_D$ ) of each of its components, where subscripts  $F$  and  $D$  denote the CF and EDD, respectively. Typical idealized load-deformation curves for these elements are shown in Figures 6b and 6c, which distinguish between the deterioration of stiffness and strength typical of reinforced concrete frames and the stability of the hysteretic cycles of the EDD. Every time that a moderate or high intensity earthquake occurs, damage increments take place on both elements. These increments are additive to those accumulated as a consequence of

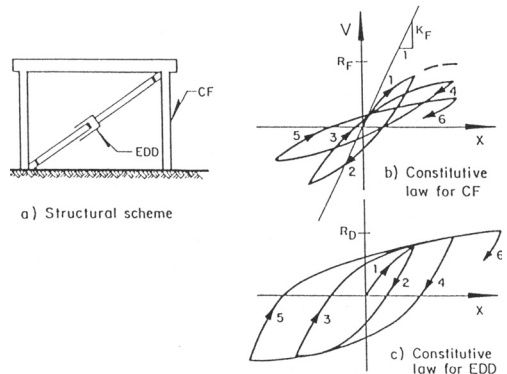


Figure 6. Single-story frame with energy-dissipating device.

previous events, provided the CF is not repaired and the EDE is not replaced. It is assumed that damage on the CF is visually identified, thus leading to repair actions when it reaches a pre-established level, and that the EED is replaced when it breaks or, according to a preventive strategy, when it has been subjected to a number of high intensity earthquakes such that the probability of failure in the event of the next potential earthquake is unacceptably high. An optimum strategy for the design, construction and maintenance of such a system implies selecting the structural design parameters and the threshold values for repair of the CF and for preventive replacement of the EDD, in such a way as to minimize the objective functions given by Equations 1 or 2.

The indicators of the damage accumulated in the CF and the EDD up to and including the  $j$ -th event are  $\delta_{Fj}$  and  $\delta_{Dj}$ , respectively. If a repair or replacement action takes place after the  $j$ -th earthquake,  $\delta_{Fj}$  and  $\delta_{Dj}$  are transformed into their updated values,  $\delta'_{Fj}$  and  $\delta'_{Dj}$ . The increments corresponding to the  $(j + 1)$ th earthquake are  $\Delta\delta_{F(j+1)}$  and  $\Delta\delta_{D(j+1)}$ , respectively. In the case of collapse of the structure during the  $i$ -th event, followed by immediate reconstruction, the value of  $D_i$  to be substituted into Equation 1 or 2 equals  $C_0 + C_F$ , where  $C_0$  is the initial construction cost and  $C_F$  includes all other related failure costs, including direct and indirect costs, as well as those associated with human losses or social impact. If collapse is not reached,  $D_i$  includes the repair costs of structural and infill elements, the replacement of those EDD that have failed or are estimated to have attained significant fatigue damage, and the losses inflicted by the eventual interruption of the normal operation of the system.

Every time that the damage accumulated on the CF exceeds a pre-established value  $\delta_{rF}$ , the repair must eliminate the accumulated damage; that is, it must restore the initial properties  $R_F$  and  $k_F$  of the structural frame. The replacement of the EDD follows a preventive strategy, based on an index of calculated damage,  $\delta_{cD}$ , to be defined later. Consequently,  $\delta'_{Fi} = \delta_{Fi}$  if  $\delta_{Fi} < \delta_{rF}$ ;  $\delta'_{Fi} = 0$ , otherwise. Also,  $\delta'_{Di} = \delta_{Di}$  if  $\delta_{Di} < 1.0$  and no preventive replacement takes place;  $\delta'_{Di} = 0$ , otherwise.

Because  $\Delta\delta_{F(j+1)}$  and  $\Delta\delta_{D(j+1)}$  depend on  $\delta_{Fj}$  and  $\delta_{Dj}$ , damage accumulation occurs as a Markov process, regardless of whether earthquakes are assumed to occur in accordance with a Poisson, a renewal or a Markov process. The transition probability matrices between the states of damage in consecutive events are obtained from the probability density functions of  $\Delta\delta_{F(j+1)}$  and  $\Delta\delta_{D(j+1)}$  conditional to  $\delta_{Fj}$  and  $\delta_{Dj}$ . The state of the system immediately after the  $j$ -th earthquake is expressed in terms of two sets of variables, describing respectively the state of damage on the system and the stage of the seismic process:  $\delta_{Fj}$

and  $\delta_{Dj}$  belong to the first set; the second is assumed to be described in terms of the vector  $S_j$  of seismological variables, if the characteristics of consecutive earthquakes are not stochastically independent. In the general case, in order to determine the conditional probability distribution functions of  $\delta_{F(j+1)}$ ,  $\delta_{D(j+1)}$  and  $S_{j+1}$  given their values just after the occurrence of the  $j$ -th event and the resulting maintenance actions, it is also required to determine the joint p. d. f. of  $Y_{j+1}$  and  $T_{i+1}$ , the intensity of the next earthquake and the waiting time for its occurrence, respectively. Following the Monte Carlo simulation process proposed above, the damage values after the  $j$ -th earthquake,  $\delta_{F(j+1)}$  and  $\delta_{D(j+1)}$ , would be obtained by step-by-step response analysis of the system, taking into account the information about accumulated damage (including local deformation history) at all critical members and sections. Alternatively, transition probability matrices for system damage may be previously generated for different values of the intensity of the new earthquake and used to determine joint probability density functions of  $\delta_{F(j+1)}$  and  $\delta_{D(j+1)}$ , conditional to  $\delta_{Fj}$ ,  $\delta_{Dj}$  and  $Y_{j+1}$ .

Closed-form expressions to determine  $f_{FD(j+1)}(u, v|\delta'_{Fj}, \delta'_{Dj})$ , the joint probability density function of  $\delta_{F(j+1)}$  and  $\delta_{D(j+1)}$  conditional to the values of the damage indicators  $\delta'_{Fj}$  and  $\delta'_{Dj}$  after the  $j$ -th earthquake and the maintenance actions following it, have been proposed by Esteva and Díaz (1993). They take into account the uncertainty about the intensity of the  $(j + 1)$ -th earthquake. However, use of those expressions may call for excessive computer time, which can be circumvented through the use of Monte Carlo simulation. This approach was followed in the life-cycle and optimization studies mentioned in sections 5.1 and 5.2.

## 5 ILLUSTRATIVE EXAMPLES

### 5.1 Life-cycle present values of expected costs

Campos (2004) made systematic studies about the values adopted by the utility function  $U$  defined in Equation 1. For this purpose, he considered several structural systems, as shown in Figure 7, with the properties summarized in Table 1 and examined the influence of the following variables, among others:  $\Psi_C$  = deformation capacity, measured as the lateral distortion corresponding to ultimate failure;  $r_1$  = ratio of indirect to direct repair costs;  $\alpha_C$  = expected cost of collapse divided by the initial construction cost;  $\delta_R$  = threshold damage ratio for repair of a member of the conventional system;  $\delta_D$  = threshold damage ratio for replacement of an energy-dissipating device (EDD).

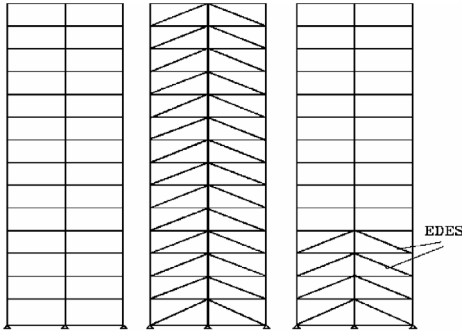


Figure 7. Systems considered in parametric study (Campos, 2004).

Table 1. Cases considered in parametric study.

Type	Stories with EDD's	Period (s)	$k_d/k$	$\delta_{yd}/\delta_{yc}$	$\mu$	Safety factor
<i>a</i>	None	1.46	–		4	1.0
<i>b</i>	All	1.48	0.25	0.50	4	1.0
<i>c</i>	All	1.49	0.25	0.50	5	1.0
<i>d</i>	All	1.48	0.50	0.50	4	1.0
<i>e</i>	All	1.55	0.50	0.50	5	1.0
<i>f</i>	All	1.44	0.50	1.00	5	1.0
<i>g</i>	1–4	1.41	0.50	1.00	5	1.0
<i>h</i>	1–4	1.41	0.50	1.00	5	1.1
<i>i</i>	1–4	1.41	0.50	1.00	5	1.2

Table 2. Present value of expected costs, normalized with respect to the initial cost of the system. Case 1:  $\delta_R = 0.2$ ,  $\psi_C = 0.04$ .

System	$\alpha_C = 20$			$\alpha_C = 100$		
	0.1	1.0	10.0	0.1	1.0	10.0
<i>a</i>	2.435	2.775	6.177	10.056	10.396	13.798
<i>d</i> : $\delta_D = 0, 5$	1.539	1.785	4.149	5.638	5.874	8.238
<i>d</i> : $\delta_D = 0, 5$	1.536	1.773	4.137	5.625	5.862	8.226
<i>d</i> : $\delta_D = 0, 5$	1.886	2.112	4.375	7.916	8.143	10.406
<i>d</i> : $\delta_D = 0, 5$	1.874	2.100	4.363	7.904	8.131	10.394
<i>d</i> : $\delta_D = 0, 5$	3.137	3.536	7.530	13.150	13.550	17.544
<i>d</i> : $\delta_D = 0, 5$	3.137	3.536	7.530	13.150	13.550	17.544

Some results are presented in Tables 2 and 3. All costs are normalized with respect to the initial construction cost of system *a* defined in Table 1. The lowest costs correspond to case *d*, followed by case *f*. The influence of the threshold values for the replacement of EDD's on the expected costs is negligible.

Table 3. Present value of expected costs, normalized with respect to the initial cost of the system. Case 2:  $\delta_R = 0.2$ ,  $\psi_C = 0.06$ .

System	$\alpha_C = 20$			$\alpha_C = 100$		
	0.1	1.0	10.0	0.1	1.0	10.0
<i>a</i>	0.928	1.311	5.135	2.274	2.656	6.480
<i>d</i> : $\delta_D = 0, 5$	0.569	0.827	3.404	1.102	1.359	3.936
<i>d</i> : $\delta_D = 0, 5$	0.557	0.815	3.392	1.089	1.347	3.924
<i>d</i> : $\delta_D = 0, 5$	0.596	0.847	3.353	1.316	1.566	4.073
<i>d</i> : $\delta_D = 0, 5$	0.584	0.835	3.341	1.304	1.554	4.061
<i>d</i> : $\delta_D = 0, 5$	1.167	1.618	6.125	2.999	3.450	7.957
<i>d</i> : $\delta_D = 0, 5$	1.167	1.618	6.125	2.999	3.450	7.957

## 5.2 Optimum repair and maintenance policies

The concepts introduced in Section 4 have been applied by Esteva et al [1999] to the study of the time-dependent process of damage accumulation and reliability evolution in building frames. They were also employed by the same authors for the study of optimum design criteria and maintenance strategies for structural frames with hysteretic energy-dissipating devices. Because of the complexity of the probability transition matrices involved, extensive use has been made of Monte Carlo simulation. One of the cases studied corresponds to a two-bay, fifteen-story frame system with hysteretic energy dissipating devices. The system was supposed to be built at a site in Mexico City where seismic hazard was represented by a Poisson process characterized by the function relating seismic intensity with annual exceedance rate. The state of damage at the end of each earthquake was measured by the maximum value attained at any story by the index  $I_{SSR}$  defined above.

Searching for a life-cycle optimum solution, several options were explored regarding the seismic design coefficient  $c$  and the threshold the values of  $I_{SSR}$  adopted as a condition for repair of the main frame and for replacement of the energy dissipating devices ( $D_{re}$  and  $D_{rd}$ , respectively). Values of a negative utility function  $U$ , calculated as the sum of initial construction cost,  $C_0$ , and expected present values of future expenditures, were obtained for each option. The resulting values of  $U$ , normalized with respect to the initial construction cost for the main frame designed for gravitational loads only, are depicted in Figure 8. The first section corresponds to the plain conventional frame, while the other three sections contain energy dissipating devices that contribute 75 percent of the lateral strength and stiffness of each story. It can be observed that the negative utility function is sensitive to both the seismic design coefficient and the repair and replacement strategies.

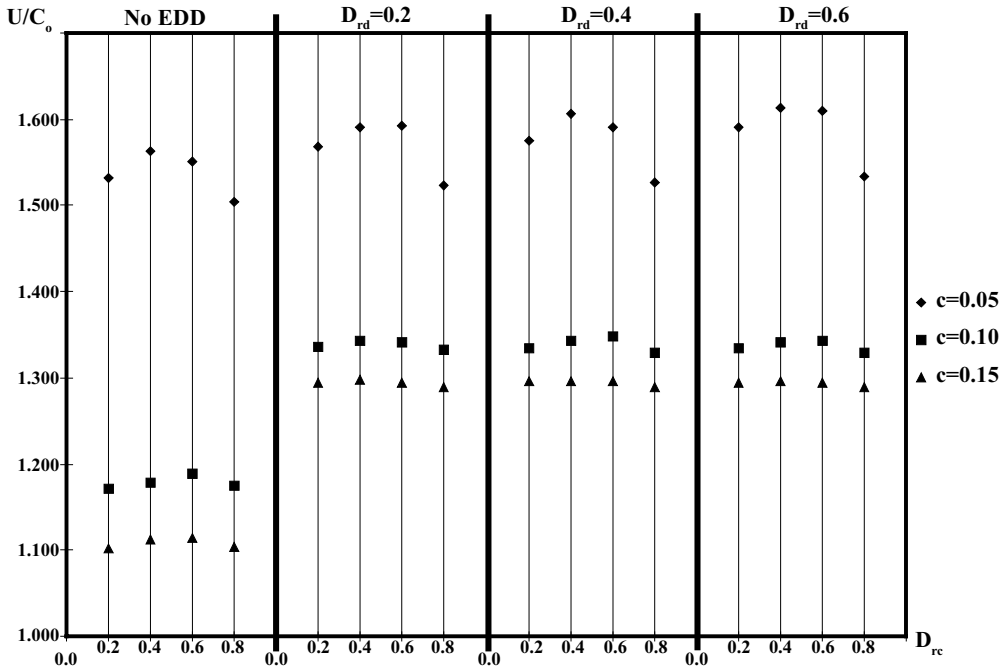


Figure 8. Life-cycle utility values for 15-story system: influence of design criteria and maintenance policies.

The large values that resulted for the initial and long term costs of the systems with EDD's are probably due to the excessively large values assumed for the contributions of those devices to the lateral strength and stiffness of the combined system. This fact may also be responsible for the high values shown by the optimum threshold value of the damage level for repair of the conventional frame. Because no analysis has been made of the sensitivity of these results to the constitutive functions, the damage-response models, the repair and replacement costs, and the consequences of ultimate failure, their value is limited to their role for the purpose of illustrating the application of the proposed life-cycle optimization criteria.

## 6 CONCLUDING REMARKS

Life-cycle optimization provides an adequate framework for the establishment of seismic design requirements and maintenance programs for systems built at sites with significant seismic hazard. Optimum design criteria formulated within that framework explicitly accept that under the action of each seismic excitation a system affected may experience one or more excursions into its range of nonlinear behavior; this

implies the occurrence of damage, as well as its accumulation during the life-cycle of that system. Hence the need to formulate damage control strategies and programs intended to keep failure probabilities and expected losses within tolerable limits. It is not sufficient to design and build a system capable of resisting a high intensity earthquake associated with a sufficiently long return interval: it is also necessary to prevent the consequences of damage accumulation on the increase of the system vulnerability for future earthquakes and to make repair actions easy, effective and inexpensive. Planning for this includes actions such as concentrating the expected nonlinear behavior and damage accumulation at easy-to-replace replace energy-dissipating devices or at easy-to-repair small segments at critical sections of structural members.

Modern computational tools permit the evaluation of expected performance of complex systems under sequences of earthquakes of different intensities. However, their results may be too sensitive to the models used to represent cyclic behavior and damage accumulation on the critical members and sections of those systems. Significant research efforts are desirable in the calibration of those models using experimental information from laboratory tests and from actual seismic events.

## REFERENCES

- Alamilla, J. & Esteve, L. 2006. Seismic reliability functions for multistory frame and wall-frame systems. *Earthquake Engineering and Structural Dynamics* 35 (15): 1899–1924.
- Campos, D. & Esteve, L. 1997. Modelo de comportamiento histerético y de daño para vigas de concreto reforzado (Hysteretic behavior and damage model for reinforced concrete beams). *Proceedings of XI National Conference on Earthquake Engineering*, Veracruz, Mexico (in Spanish).
- Campos, D. 2004. *Diseño sísmico de edificios con disipadores de energía (Optimum seismic design of buildings with energy dissipators)*. Ph D Thesis, School of Engineering, National University of Mexico, Mexico City (in Spanish).
- Cornell, C.A. 1969. A probability based structural code. *Journal of the American Concrete Institute* 66 (12).
- Cornell, C.A., Jalayer, F., Hamburger, R.O. & Foutch, D.A. 2002. Probabilistic Basis for 2000 SAC Federal Emergency Management Agency Steel Moment Frame Guidelines. *Journal of Structural Engineering*, 128 (4): 526–533.
- Díaz, O. & Esteve, L. 1996. Seismic damage indexes in decisions related to structural safety. *Proc. Seventh IFIP WG7.5 Working Conference*, Boulder, Co., USA.
- Díaz, O. & Esteve, L. 1997. Confiabilidad de estructuras y daño acumulado (Structural reliability and cumulative damage). *Proc. First Ibero-American Seminar on Earthquake Engineering*, La Serena, Chile (in Spanish).
- Dolsek, M. & Fajfar, P. 2004. IN2—A simple alternative for IDA. *Proc. 13th World Conference on Earthquake Engineering*, Vancouver, Canada: Paper 3353.
- Esteve, L. 1992. Nonlinear seismic response of soft-first-story buildings subjected to narrow-band accelerograms. *Earthquake Spectra* 8 (3): 373–389.
- Esteve, L. & Díaz, O. 1993. Influence of cumulative damage on the seismic reliability of multistory frames. *Proc. Fifth IFIP WG7.5 Working Conference*, Takamatsu, Japan.
- Esteve, L., Díaz-López, O., García-Pérez, J., Sierra, G. & Ismael, E. 2002. Life-cycle optimization in the establishment of performance-acceptance parameters for seismic design. *Structural Safety* 24: 187–204.
- Esteve, L. & Ismael, E. 2004. A maximum likelihood approach to system reliability with respect to seismic collapse. *Proc. International Federation for Information Processing, WG7.5 Working Conference*, Banff, Canada.
- Esteve, L. & Díaz-López, O. 2006. Seismic reliability functions for complex systems based on a secant-stiffness reduction index. *Proc. IFIP WG7.5 Working Conference*, Kobe, Japan.
- Ismael, E. & Esteve, L. 2006. A hybrid method for the generation of artificial strong ground motion records. *Proc. First European Conference on Earthquake Engineering and Seismology*, Geneva, Switzerland.
- Jalayer, F. & Cornell, C.A. 2003. A Technical Framework for Probability-Based Demand and Capacity Factor Design (DCFD) Seismic Formats. *Report PEER 2003/08, Pacific Earthquake Engineering Research Center, University of California, Berkeley, CA.*
- Lutz, K.A. & Kiremidjian, A.S. 1993. Generalized Semi-Markov Process for Modelling Spatially and Temporally Dependent Earthquakes. *Report 104, Blume Earthquake Engineering Center, Stanford University.*
- Rackwitz, R. 2000. Optimization—the basis of code-making and reliability verification. *Structural Safety* 22: 27–60.
- Rangel, J.G. 2006. Funciones de confiabilidad sísmica de sistemas con elementos disipadores de energía (Seismic reliability functions for systems with hysteretic energy dissipators). *M. Sc. Thesis, Graduate Program in Engineering, National University of Mexico.*
- Rosenblueth, E. 1976. Optimum design for infrequent disturbances. *ASCE Journal of the Structural Division* 102 (ST9): 1807–1825.
- Singh, S.K., Rodríguez, M. & Esteve, L. 1983. Statistics of small earthquakes and frequency of occurrence of large earthquakes along the Mexican subduction zone. *Bull. Seism. Soc. of Am.* 73 (6): 1779–1796.
- Shome, N. & Cornell, C.A. 1999. Probabilistic Seismic Demand Analysis of Nonlinear Structures. *Report No. RMS.35, Department of Civil Engineering, Stanford University, Stanford, California, USA.*
- Vamvatsikos, D. & Cornell, C.A. 2002. Incremental dynamic analysis. *Earthquake Engineering and Structural Dynamics*. 31 (3): 491–514.
- Wang, M.L. & Shah, S.P. 1987. Reinforced concrete hysteresis model based on the damage concept. *Earthquake Engineering and Structural Dynamics* 15: 993–1003.



# Life-cycle cost of civil infrastructure with emphasis on bridges

Hitoshi Furuta

*Kansai University, Takatsuki, Japan*

Dan M. Frangopol

*Lehigh University, Bethlehem, USA*

**ABSTRACT:** The Life-Cycle Cost (LCC) concepts and methods have remarkably advanced in the field of civil infrastructure. In this paper, LCC design concepts and methods are discussed with emphasis on bridges, in which the definition of structural performance, balance of structural performances, seismic risks and network effects are considered based on probabilistic approaches and genetic algorithms.

## 1 INTRODUCTION

The Life-Cycle Cost (LCC) concepts and methods have remarkably advanced in the field of civil infrastructure (Frangopol & Furuta 2001). Many international symposia and workshops have been held all over the world. The basic concept and methodology of LCC itself are not new and were already adopted several decades ago in the fields of electrical and mechanical engineering. In the field of civil engineering, seismic risk analysis was established on the basis of LCC. However, it is noted that the seismic risk analysis has not paid much attention to the structural maintenance activities.

LCC design is formulated as an optimization problem, which aims to implement an optimal inspection/repair strategy for the minimum expected total life-cycle cost that includes initial, preventive maintenance, inspection, repair and failure costs, while the civil structure maintains the target safety. As a representative civil structure, highway bridges follow the life-cycle that consists of design, construction, inspection, repair and replacement. At present, it is desirable to develop an optimal strategy for the bridge management through the lifetime in order to reduce the overall cost.

An efficient method that provides adequate inspection/repair strategies was proposed by Frangopol et al. (1997). This method can determine how many inspections are appropriate for lifetime, and at what time inspections and repairs should be done, while taking into account all bridge repair possibilities based on an event tree.

However, if the number of design variables increases, it is difficult to solve the problem. Therefore, an attempt was made to extend and improve

the work by Frangopol et al. (1997) using Genetic Algorithm (GA) (Furuta et al. 1998). Using GA, it is possible to easily decide the number of lifetime inspections, the time of each inspection, and which inspection has to be used. LCC is a useful measure for evaluating the structural performance of deteriorating structures. Then, the optimal strategy obtained by LCC optimization can be different according to the prescribed level of structural performance and required service life. The relationships among several performance measures are discussed and attempted to provide rational balances of these measures by using the Multi-Objective Genetic Algorithm (MOGA). So far the authors have discussed the relationships among the minimization of LCC, the optimal extension of structural service life, and the target safety level by using MOGA (Furuta et al. 2003). By introducing MOGA, it is possible to obtain several available solutions that have different structural life spans, safety levels, and LCC values.

Furthermore, LCC is evaluated focusing on the effects of earthquakes that are major natural disasters in Japan (Furuta & Koyama 2003). At first, LCC analysis is formulated to consider the social and economical effects due to the collapse of structures occurred by the earthquake as well as the minimization of maintenance cost. The loss by the collapse of structures due to the earthquake can be defined in terms of an expected cost and introduced into the calculation of LCC. A stochastic model of structural response is proposed, which accounts for the variation due to the uncertain characteristics of earthquake. Then, the probability of failure due to the earthquake excitation is calculated based on the reliability theory. In addition, LCC evaluations are performed not only for a single bridge but also for many bridges forming

road networks (Furuta et al. 2002, Liu & Frangopol 2004a, b).

## 2 APPLICATION OF GENETIC ALGORITHM TO LIFE-CYCLE COST OPTIMIZATION

LCC optimization is to minimize the expected total cost which includes the initial cost involving design and construction, routine or preventive maintenance cost, inspection, repair and failure cost. The details are provided in (Frangopol et al. 1997). Cost of repair is calculated by using the rate of the initial bridge condition and the deteriorated condition, taking into account the effects of aging and corrosion, and all possibilities of repair based on an event tree. Failure cost is calculated based on the changing rate of reliability. Moreover, expected total cost is calculated by introducing the net discount rate of money.

LCC optimization is a nonlinear problem that includes integer and discrete variables. Therefore, it is necessary to apply a combinatorial optimization method to solve it. The purpose of LCC optimization is to find the most economical plan for inspection/repair. It is evident that a non-uniform interval of inspection/repair strategy is more economical than a uniform one (Frangopol et al. 1997). It is easily understood that the combination of inspection techniques with different detection capabilities in a strategy is more economic. Discrete variables are useful in determining when and how inspections and repairs have to be performed and what methods have to be used. Genetic Algorithm (GA) is a representative algorithm of combinatorial optimization methods (Goldberg, 1989). Using GA, it is possible to decide the number of lifetime inspections, the time of each inspection, and which inspection has to be used. Then, the time of repair is decided based on an event tree analysis.

The LCC optimization is reduced to the following mathematical programming problem:

$$\begin{aligned} & \text{Minimize } C_{ET} \\ & \text{subject to } P_{f,life} \leq P_{f,life}^* \end{aligned} \quad (1)$$

where  $C_{ET}$  is the expected total cost,  $P_{f,life}$  is the lifetime probability of failure, and  $P_{f,life}^*$  is the maximum acceptable lifetime probability of failure.

## 3 MULTI-OBJECTIVE GENETIC ALGORITHM AND STRUCTURAL PERFORMANCE MEASURES

### 3.1 Structural performance

In order to establish a rational maintenance program for bridge structures, it is necessary to evaluate the structural performance of existing bridges

in a quantitative manner. So far, several structural performance indices have been developed, some of which are reliability, durability, and damage indices (Furuta et al. 2003, Neves et al. 2003). However, it is often necessary to discuss the structural performance from the economic or social points of view as well as the above structural performance indices.

LCC is one of the useful measures for evaluating the structural performance from another standpoint, which can reduce the overall cost and achieve an appropriate allocation of resources. In general, LCC optimization is to minimize the expected total cost which includes the initial cost involving design and construction, routine or preventive maintenance cost, inspection, repair and failure cost. Then, the optimal strategy obtained by LCC optimization can be different according to the prescribed level of structural performance and required service life. In this paper, an attempt is made to discuss the relationships among several performance measures and provide some good balances of them by using Multi-Objective Genetic Algorithm (MOGA).

### 3.2 Formulation using multi-objective genetic algorithm

Multi-objective optimization problem has several objectives, and Pareto solutions are obtained as a set of solutions. GA evaluates the optimal solution by random and multiple-point searches. The Multi-Objective Genetic Algorithm (MOGA) is performed according to the following five steps (Goldberg, 1989):

- Step 1: Generation of initial populations.
- Step 2: Crossover. Two-point crossover is used in this study.
- Step 3: Mutation.
- Step 4: Evaluation of fitness function.
- Step 5: Selection.

Although several performance measures have been so far developed, the following four measures are considered here (Furuta et al. 2003, Neves et al. 2003):

1. Safety Level; Safety level is defined in terms of structural capacity or durability.
2. Service Life; Service life means the prescribed expected period that the structure is used safely.
3. Life-Cycle Cost; Total cost including initial construction cost, maintenance cost, repairing cost, and replacement cost.
4. Condition Rate; Evaluation of damage state by inspection and defined in the range [0, 5]. 0, 1, 2, 3, 4, and 5 mean good, no damaged, slightly damaged, moderately damaged, severely damaged, collapse, respectively.

5. Reliability Index; Measure for structural safety obtained by reliability analysis.

The relationships among those performance measures are discussed by using MOGA. Paying attention to the two cases with three objective functions, the following two problems can be formulated:

*Problem 1:*

Objective function 1: Safety level should be maximized.

Objective function 2: Service life should be maximized.

Objective function 3: Life-cycle cost should be minimized.

*Problem 2:*

Objective function 1: Condition rate should be minimized.

Objective function 2: Safety index should be maximized.

Objective function 3: Life-cycle cost should be minimized.

By introducing MOGA, it is possible to obtain several available solutions that have different safety levels, service lives and LCC values, or condition rates, safety indices and LCC values.

3.3 Numerical examples

244 Pareto solutions are obtained by using MOGA, The 244 Pareto solutions can be classified into 13 patterns. Table 1 presents the maximum service life obtained for each of the 13 patterns. It is noted that the maximum service life is calculated assuming 0.6 for the allowable safety level. From Table 1, it is evident that the MOGA can provide many different solutions with various service lives and LCC values

Table 1. Maintenance plans.

LCC (yen)	Maximum service life (years)	Safety level
1,640,000	37	0.6
3,280,000	44	0.6
4,920,000	51	0.6
6,560,000	58	0.6
8,200,000	70	0.6
9,840,000	77	0.6
11,480,000	84	0.6
13,120,000	91	0.6
14,760,000	98	0.6
15,580,000	94	0.6
16,400,000	110	0.6
18,040,000	117	0.6
20,500,000	120	0.6

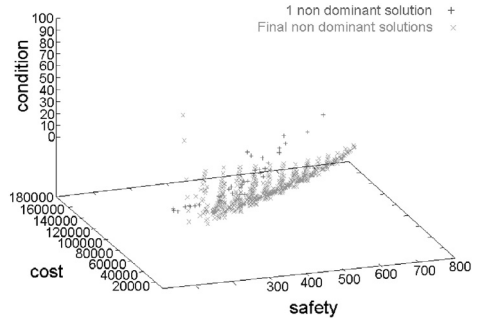


Figure 1. Pareto solutions for problem 2.

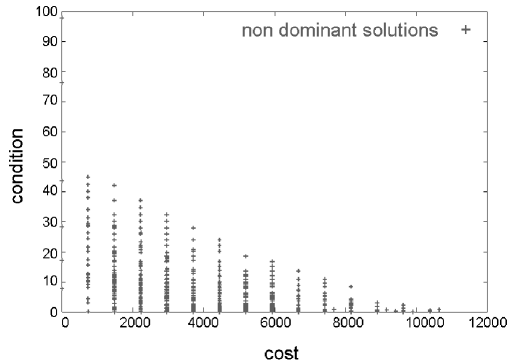


Figure 2. Relation between LCC and condition rate.

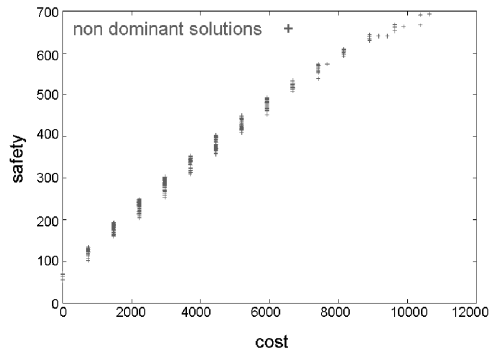


Figure 3. Relation between LCC and safety index.

under a constant safety level. Figure 1 presents the Pareto solutions obtained for problem 2. Figures 2, 3 and 4 show the relationships between LCC and condition rate, LCC and safety index, and safety index and condition rate, respectively. It is possible to choose an appropriate solution among the set of Pareto solutions by considering the corresponding condition.

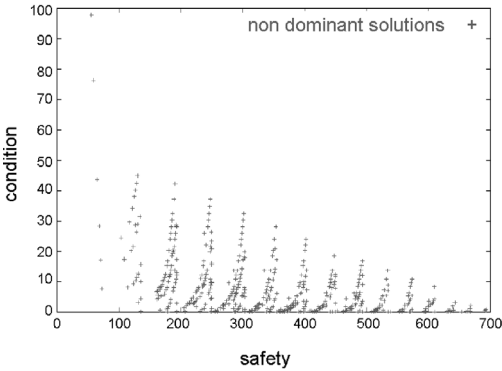


Figure 4. Relation between safety and condition rate.

#### 4 NEW MULTI-OBJECTIVE GENETIC ALGORITHM FOR LIFE-CYCLE COST OPTIMIZATION

Bridge maintenance planning has several constraints. In general, it is not easy to solve multi-objective optimization problems with constraints by applying a usual MOGA.

##### 4.1 A new MOGA

A new MOGA was developed by introducing the sorting technique into the selection process (Furuta et al. 2006). The selection is performed using so-called sorting rules which arrange the list of individuals in the order of higher evaluation values. Then, the fitness values are assigned to them by using the linear normalization technique. In general, if the fitness values are calculated directly according to the evaluation values, the differences among every individuals decrease so that the effective selection can not be done. In this study, the selection procedure is constructed coupling the linear normalization technique and the sorting technique. Using the evaluation values, the individuals are reordered and given the new fitness values. Figure 5 presents the process of the selection proposed here. The individuals of satisfying the constraints are arranged first according to the evaluation values and further the individuals of non-satisfying the constraints are arranged according to the degree of violating the constraints. Accordingly, all the individuals are given the fitness values using the linear normalization technique.

In order to apply the sorting rules to the multi-objective optimization problems, the non-dominated sorting method is used (Kitano 1995). In the non-dominated sorting method, the Pareto solutions are defined as *Front1*. Then, *Front2* is determined by

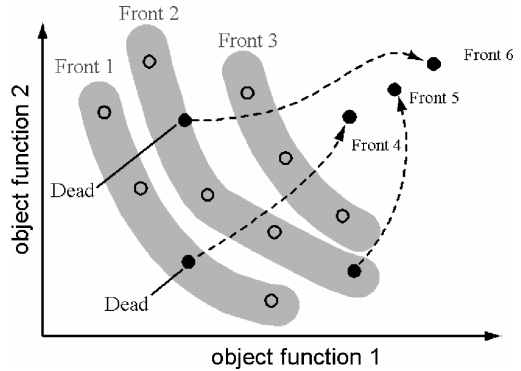


Figure 5. New sorting rules.

eliminating the *Front1* from the set of solution candidates. Repeating the process, the new *Front* is pursued until the solution candidates diminish. Further, the *Fronts* are stored in the pool of the next generation. If the pool is full, the individuals in the *Front* are divided into the solutions to survive or die based on the degree of congestion.

Then, the individuals are divided into the group of satisfying the constraints and the group without satisfying the constraints. The former is called as “alive individual”, and the latter “dead individual”. While the alive individuals are given the fitness values according to the evaluation values after the non-dominated sorting, the dead individuals are given the same fitness value. When implementing the non-dominated sorting, the Pareto *Front* may not exist at the initial generation, because a lot of dead individuals remain after the non-dominated sorting. Then, the dead individuals are arranged in the order of degree of violating the constraints and some of them are selected for the next generation. Thus, the multi-objective optimization problems with constraints are transformed into the minimization problem of violation of constraints. The elite preserve strategy is employed for the selection of survival individuals (Kitano 1995).

When the generation progresses, alive individuals appear and then both the alive individuals forming the Pareto front and the dead individuals arranged in the order of violation degree exist together. In this case, appropriate numbers of alive and dead individuals are selected for the next generation.

It is desirable to determine an appropriate life-cycle maintenance plan by comparing several solutions for various conditions. A new decision support system is developed here from the viewpoint of multi-objective optimization, in order to provide various solutions needed for decision-making.

#### 4.2 Formulation using new MOGA

In this study, LCC, safety level and service life are used as objective functions. LCC is minimized, safety level is maximized, and service life is maximized (Furuta et al., 2004). There are trade-off relations among the three objective functions. For example, LCC increases when service life is extended, and safety level and service life decrease due to the reduction of LCC. Then, multi-objective optimization can provide a set of Pareto solutions that can not improve an objective function without making other objective functions worse.

A group of ten concrete highway bridges are considered in this study. Maintenance management planning for ten consecutive piers and floor slabs (composite structure of steel girders and reinforced concrete (RC) slabs) is considered here (Furuta et al., 2006).

In this study, environmental corrosion due to neutralization of concrete, chloride attack, frost damage, chemical corrosion, or alkali-aggregate reaction are considered as major deteriorations. Deterioration of a bridge due to corrosion depends on the concrete cover of its components and environmental conditions, among other factors. For each component, the major degradation mechanism and its rate of deterioration are assumed corresponding to associated environmental conditions. In this study, four environmental conditions are considered; neutralization, mild, middle and severe environmental conditions.

#### 4.3 Numerical example

In the implementation of the proposed new MOGA, the GA parameters considered are as follows: number of individuals = 1000, crossover rate = 0.60, mutation rate = 0.05 and number of generations = 3000.

Figure 6 presents the results obtained by the new MOGA. This figure shows the evolution of the results from the 1st generation (iteration number) to the 100th generation. In Figure 6, the sum of penalty started to decrease from the 1st generation to around the 30th generation. The 20th generation was starting to increase the amount of alive solutions.

In Figure 7, the solutions at the 100th generation were not optimized. This means that the initial solutions can be generated uniformly. After the 120th generation, the solutions tend to converge to a surface, which finally forms the Pareto set as the envelope of all solutions. The number of solutions at the 3000th generation is larger than that at the 100th generation. This indicates that the proposed new MOGA could obtain various optimal solutions with different LCC values and safety levels. From Figure 8, it is seen that the new MOGA can find out good solutions, all of which evolve for all the objective functions, and the

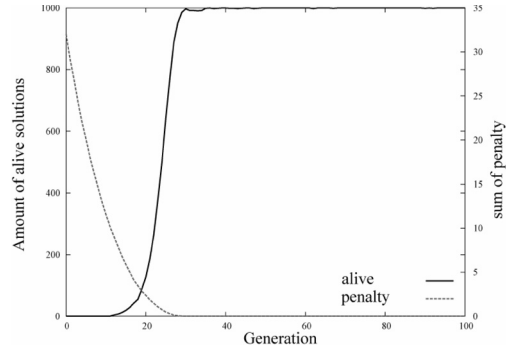


Figure 6. Evolution of new MOGA under neutralization environment (alive solutions and penalty).

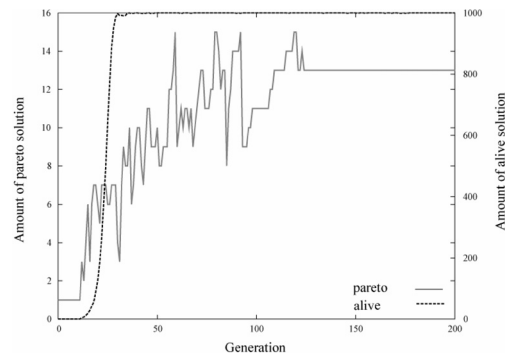


Figure 7. Evolution of new MOGA under neutralization environment (Pareto and alive solutions).

final solutions are sparse and have discontinuity. In other words, the surfaces associated with the trade-off relations are not smooth. This implies that an appropriate long term maintenance plan cannot be created by the repetition of the short term plans.

Figure 9 presents an optimal maintenance plan for the case of mild environment. It is noted that the simultaneous maintenance activities are considered to be preferable to reduce the LCC value.

Consequently, it is confirmed that the proposed method can provide many useful solutions with different characteristics for determining an appropriate maintenance plan available for practical use. It is clear that LCC can be reduced by adopting simultaneous repair works. Finally, it is confirmed that the proposed method using linear normalization technique and sorting technique can provide many near-optimal maintenance plans with various reasonable LCC values, safety levels, and service lives. Note that it is quite difficult to obtain such near-optimal solutions by the current MOGA.

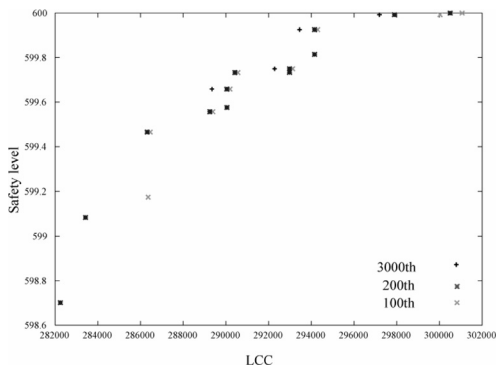


Figure 8. Evolution of new MOGA under neutralization environment (safety level and LCC).

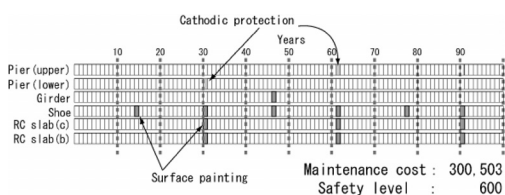


Figure 9. Maintenance scenarios for mild environment.

## 5 LIFE-CYCLE-COST OPTIOMIZATION CONSIDERING SEISMIC RISK

LCC of bridges consists of initial construction cost, maintenance cost, and failure cost (renewal cost, user cost, social and environmental costs and so on). In general, LCC analysis considers the damage and deterioration of materials and structures. However, in region that are exposed to frequent natural hazards such as typhoons and earthquakes, it is necessary to account for the effects of such natural hazards.

In this research, based on the seismic risk analysis, LCC is evaluated focusing on the effects of earthquakes that are major natural disasters in Japan. At first, LCC analysis is formulated to consider the social and economical effects due to the collapse of structures occurred by the earthquake as well as the minimization of maintenance cost. The loss by the collapse of structures due to the earthquake can be defined in terms of an expected cost and introduced into the calculation of LCC. A stochastic model of structural response is proposed, which accounts for the variation due to the uncertain characteristics of earthquake. Then, the probability of failure due to the earthquake excitation is calculated based on the reliability theory.

In general, LCC is defined in terms of initial construction cost, maintenance cost, and replacement cost. However, in this study, LCC is defined as the

sum of initial construction cost and seismic risk. As the initial construction cost, only piers are considered, because the sufficient data for the whole bridge is not available. Seismic risk includes both loss due to earthquake and user cost. Then, LCC considering seismic risk is calculated as

$$LCC = C_i + \sum P_d(a) \cdot C_d(a) \quad (2)$$

$$P_d(a) = P_h(a) \cdot P(DI, a) \quad (3)$$

where  $C_i$ : initial construction cost,  $P_d(a)$ : probability of seismic damage occurrence,  $C_d(a)$ : seismic loss,  $P_h(a)$ : earthquake occurrence probability,  $P(DI, a)$ : seismic damage probability,  $a$ : maximum acceleration,  $DI$ : damage index.

Eq. 3 provides the probability of damage occurrence due to the earthquake, which is the multiplication of earthquake occurrence probability with seismic damage probability. In this study, the earthquake occurrence probability is calculated by using the earthquake hazard curve shown in Figure 10, and the damage probability is calculated by using the damage curve.

### 5.1 Calculation of damage curve and definition of damage degree

Seismic damage probability is defined in terms of the probability that a bridge pier shows each damage degree among the prescribed damage ranges. The damage curve is calculated here by using the dynamic analysis of the bridge pier.

Reinforced Concrete (RC) bridge pier is used to obtain the damage curve. The RC pier is designed according to Design Specification of Highway

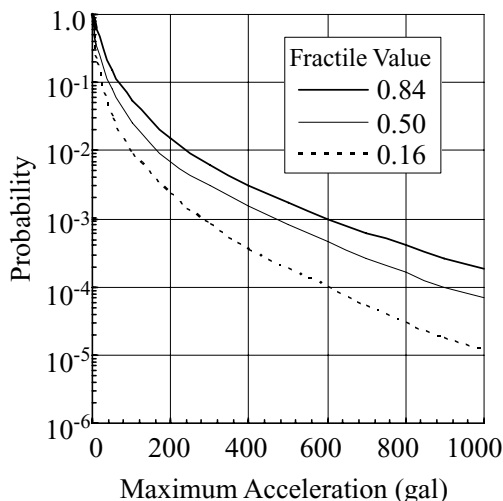


Figure 10. Earthquake hazard curve.

Bridges, Earthquake Version (MLIT 2002). Then, it is assumed that the ground condition is Type II and the importance of the bridge is B (MLIT 2002). Dynamic analysis is performed for bridges, in which a single mass and single degree of freedom model is used and Newmark  $\beta$  method is employed to do the dynamic analysis. It is assumed that the compression strength of concrete is  $f_c = 21$  (N/mm<sup>2</sup>) and the reinforcing bars are SD295. As input earthquake wave, the ground condition of Type II is used and Type I and II earthquakes are used. Table 2 presents six input earthquakes. Using these conditions, the dynamic analysis is performed for 600 times for a RC pier. Several damage indices have been proposed so far (Park & Ang 1985, Shoji et al. 1997). However, in this research, damage degree is defined in terms of the maximum response displacement, horizontal force, and horizontal displacement of pier. The damage degree is categorized into five ranks such as As, A, B, C, and D that mean collapse, severe damage, partial buckling and deformation, deformation, and no damage or minor damage, respectively. In order to calculate the damage probability, it is necessary to determine the distribution function of damage degree (damage index) corresponding to the maximum earthquake acceleration. In this study, the log-normal distribution is assumed. When the distribution of damage degree is determined, the damage probability can be calculated as

$$P(DI, a) = \int_a^b f_{DI}(x, a) dx \quad (4)$$

where [a, b] is the interval of each damage degree.

The damage probability is calculated for each damage degree and the results are plotted on a graph with the exceedance probability as the vertical axis and the maximum acceleration as the horizontal axis (JSCE 1996). Then, the damage curve can be obtained by combining them. Figure 11 shows the computed damage curve.

Table 2. Input data of six earthquake waves.

Earthquake type	Name	M	Direction
Type I	1968, Hyuga-Nada Earthquake	7.5	LG TR
	1994, Hokkaido-Toho Earthquake	8.1	TR
Type II	1995, Hyogo-Nanbu Earthquake	7.2	N-S E-W N27W

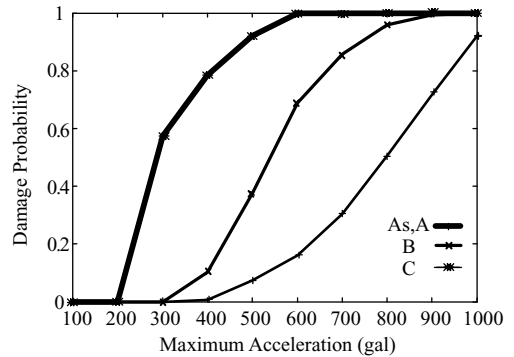


Figure 11. Earthquake hazard curve.

## 6 LCC OPTIMIZATION FOR ROAD NETWORK

Practically, it is necessary to consider the effects of network to calculate LCC of bridge systems. It can be expected that although the effects of seismic risk are not large in the case of a single bridge, they are large and important in the case of multiple bridges in a road network, because the user cost becomes quite large for the road network.

### 6.1 Road network model

For road networks, three network models (Model 1, Model 2, and Model 3) are employed, which are presented in Figure 12. In these models, it is assumed that each network model includes a road passing over a river, and that traffics reach the destination through detours when some bridges can not be passed. Moreover, it is assumed that the traffic volume and the velocity have a relation shown in Figure 13 (Kinki Branch, MLIT1999).

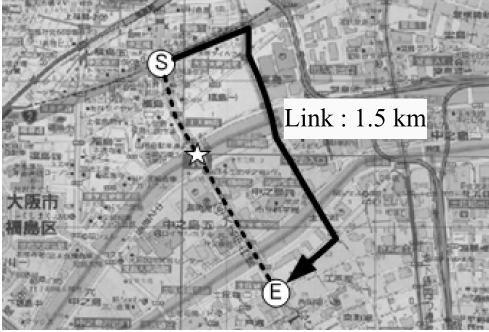
### 6.2 User cost

Here, user cost is defined in terms of the sum of the time cost and energy consumption cost due to the detour or closure of road. The cost associated with increasing driving time  $C_{UT}$  is calculated as the difference between (a) the cost associated with detour and road closure and (b) the usual cost (without detour and road closure).

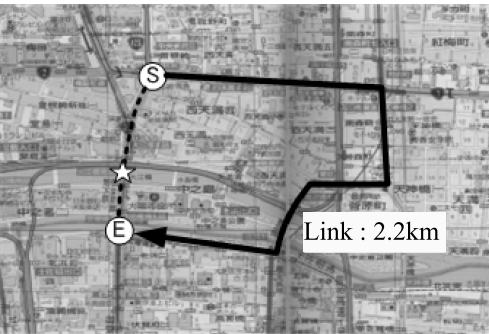
$$UC_T = \alpha \cdot \{(Q \cdot T) - (Q_0 \cdot T_0)\} \quad (5)$$

$$UC_C = \beta \cdot \{(Q \cdot L) - (Q_0 \cdot L_0)\} \quad (6)$$

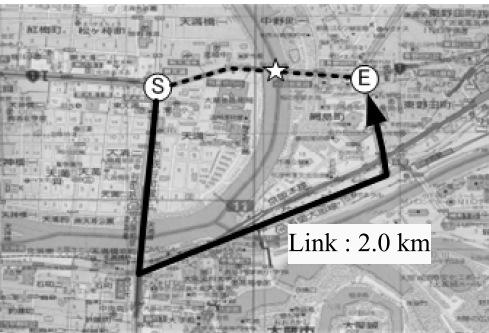
where  $\alpha$ : unit time cost,  $\beta$ : unit running cost,  $Q, T, L$ : detour traffic volume, running time, and link length



Model 1. Tamae-bashi  
Fukushima-ku, Osaka city



Model 2. Ohe-bashi  
Kita-ku, Osaka city



Model 3. Sakuranomiya-bashi  
Tyuo-ku, Osaka city

Figure 12. Three road network models.

at the time of road closure,  $Q_0, T_0, L_0$ : initial traffic volume, running time, and link length.

Using the data given in (Nihon Sogo Research Institute 1998) and assuming the ratio of small and medium trucks to be 10%, the unit time cost  $\alpha$  is estimated as 82 Yen/car/min., and  $\beta$  is assumed as 18 Yen/car/km to

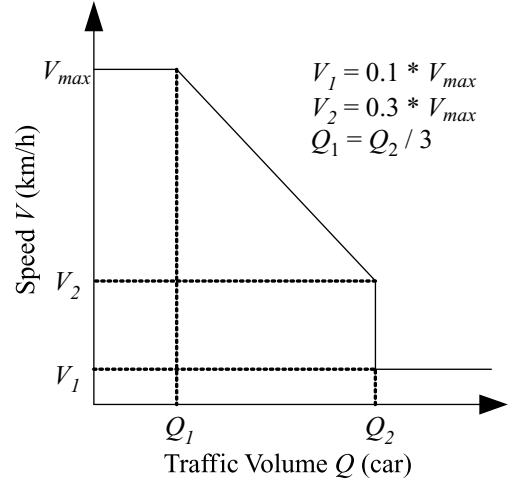


Figure 13. Relation between traffic volume and speed.

35 Yen/car/km. The restoring periods are assumed to be two months and two weeks for the damage (As, A) and B, respectively.

### 6.3 Calculation of LCC

#### 6.3.1 Calculation of LCC and repair cost

Taking into account the discount rate, LCC is calculated as

$$LCC = C_i + \sum P_f(a) \cdot P(DI, a) \times \left\{ \frac{C_m(DI, a) + UC(DI, a)}{(1+i)^T} \right\} \quad (7)$$

where  $C_m(DI, a)$ : repair cost for each damage degree,  $UC(DI, a)$ : UC for each damage degree,  $i$ : discount rate,  $T$ : service life.

For each damage degree, restoring method and cost are presented in Table 3.

#### 6.3.2 LCC results for three network models

For the three road networks, LCC is calculated by assuming that the fractile value in the hazard curve is 0.5, discount rate is 0, service life is 100 years. Figure 14 shows the calculated results, which indicate that there are important differences among the three networks, because of the differences in distances of detour and the initial traffic volumes. In the network with high traffics, seismic risk becomes 104,559,000 Yen that is 11 times the initial construction cost and 30 times the maintenance cost.

Comparing the case involving the user cost in the seismic risk and that without involving it, the seismic



Table 3. Restoring method and cost.

Damage index	Restoring method	Repair cost	Repair time
As, A	Rebuild	120% of initial construction cost	2 months
B	Repair	73,000 Yen/1 m <sup>2</sup>	1 month
C	Repair	35,000 Yen/1 m <sup>2</sup>	2 weeks
D	No Repair	–	–

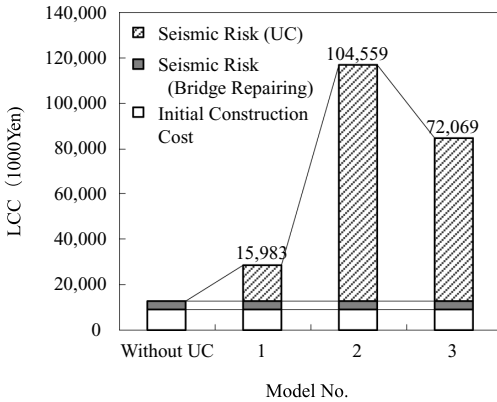


Figure 14. LCC of each model.

risk is only 1/3 of the initial cost when the user cost is not considered.

### 6.3.3 Relation between LCC and maximum acceleration

Paying attention to the damage probability curve in Figure 11, it is evident that there is some difference in the damage probabilities according to the earthquake intensity. Figure 15 shows the relation between the seismic risk and the maximum acceleration. This figure shows that it is obtained that the seismic risk decreases as the maximum acceleration increases. This is due to the facts that the bridge pier was designed to satisfy the requirement that the damage should be minor and the bridge function can be recovered in a short period. Therefore, the probabilities of damage B, C, and D become high.

### 6.3.4 Effects of damage degree on seismic risk

The effects of damage degree on the seismic risk are examined. Figure 16 presents the ratio of seismic risk corresponding to each damage degree, which implies that the damage degree C is 54% being the largest and the severe damages As and A have small portions of 28%. This is due to the fact that while the occurrence probabilities of As and A become larger as

the maximum acceleration increases, the earthquake occurrence probability decreases.

## 7 CONCLUSIONS

In this paper, an attempt was made to formulate LCC optimization based on GA and to discuss the relationships among several structural performance measures. In addition, seismic risk was introduced into the LCC optimization. The Multi-Objective Genetic Algorithm (MOGA) was adopted to successfully solve the large and complex combinatorial scheduling problems for the maintenance of damaged RC bridge structures.

By considering LCC, safety level, and service life as objective functions, it is possible to obtain the relationships among these three performance indicators and provide bridge maintenance management engineers with various maintenance plans and appropriate allocations of resources.

Based on the results presented in this paper, the following conclusions may be drawn:

1. Since the optimal maintenance problem is a very complex combinatorial problem, it is difficult to obtain reasonable solutions by the current optimization techniques.
2. Although Genetic Algorithm (GA) is applicable to solve multi-objective problems, it is difficult to apply it to large and very complex bridge network maintenance problems. By introducing the technique of Non-Dominated Sorting GA-2 (NSGA2), it is possible to obtain efficient near-optimal solutions for the maintenance planning of a group of bridge structures.
3. The Pareto solutions obtained by the proposed method show discontinuity. This means that the surfaces constructed by the trade-off relationships are not smooth so that an appropriate long term maintenance plan can not be created by the simple repetition of short term plans.
4. The optimal maintenance plans, especially repair methods, are quite different for the short term maintenance plan and the long term maintenance plan.

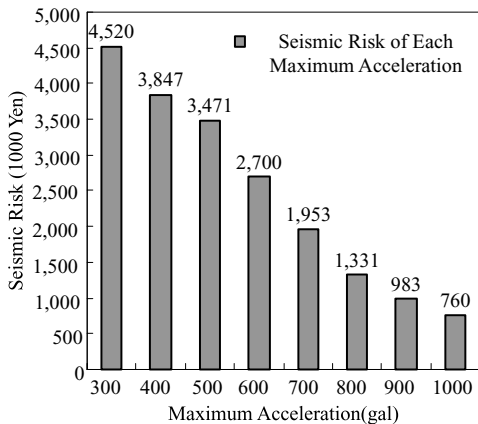


Figure 15. Seismic risk associated with each maximum acceleration.

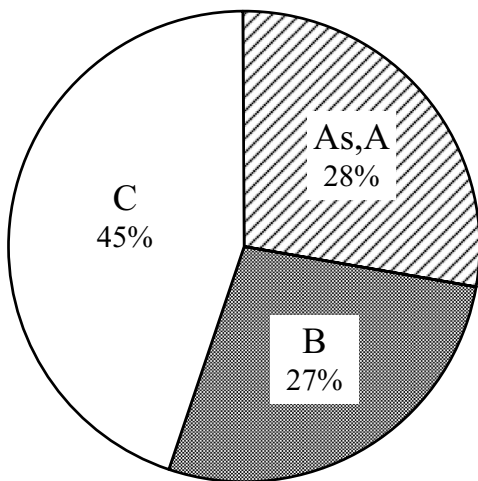


Figure 16. Relation between seismic risk and damage index.

- In the examples presented, the relation between safety level and LCC is non-linear. The increase of LCC hardly contributes to the improvement of safety level.
- LCC can be reduced by adopting simultaneous repair works. The proposed method using linear normalization technique and sorting technique can provide many near-optimal maintenance plans with various reasonable LCC values and safety levels.
- The damage degree is defined by using the maximum response displacement obtained by the dynamic analysis and the horizontal force and displacement of RC bridge pier.

- Through the LCC calculation of several representative road networks, it is concluded that the difference of road network greatly affects the seismic risk.
- Comparing the case with user cost and that without user cost, it is made clear that the effect of seismic risk is small unless user cost is considered.
- Paying attention to the change of LCC according to the change of the maximum acceleration of earthquake, the seismic risk decreases, as the maximum acceleration increases.

## REFERENCES

- Frangopol, D.M., & Furuta, H. (eds.) 2001, *Life-Cycle Cost Analysis and Design of Civil Infrastructure Systems*, ASCE, Reston Virginia.
- Frangopol, D.M., Lin, K.Y., & Estes, A.C. 1997, Life-cycle cost design of deteriorating structures, *Journal of Structural Engineering*, ASCE, Vol. 123(10), pp.1390–1401.
- Furuta, H., Frangopol, D.M., & Saito, M. 1998, Application of genetic algorithm to life-cycle cost maintenance of bridges, *Proc. of KKNN Symposium*, Seoul, Korea.
- Furuta, H., Nose, Y., Dogaki, M., & Frangopol, D.M. 2002, Bridge maintenance system of road network using life-cycle cost and benefit, *Proc. of IABMAS*, Barcelona, Spain, July.
- Furuta, H., Kameda, T., Fukuda, Y., & Frangopol, D.M. 2003, Life-cycle cost analysis for infrastructure systems: life-cycle cost vs. safety level vs. service life, *Proc. of 3rd Life-Cycle Cost Analysis and Design of Infrastructure Systems*, Lausanne, Switzerland.
- Furuta, H., & Koyama, K. 2003, Optimal maintenance planning of bridge structures considering earthquake effects, *Proc. of IFIP TC7 Conference*, Antipolis, France, 2003.
- Furuta, H., Kameda, T., & Frangopol, D.M. 2004, Balance of structural performance measures, *Proc. of Structures Congress, Nashville, Tennessee, ASCE, May*, CD-ROM.
- Furuta, H., Kameda, T., Nakahara, K., Takahashi, Y., & Frangopol, D.M. 2006, Optimal bridge maintenance planning using multi-objective genetic algorithm, *Structure and Infrastructure Engineering*, Vol. 2, No. 1, pp. 33–41.
- Goldberg, D.E. 1989, *Genetic Algorithms in Search, Optimization and Machine Learning*, Addison-Wesley Publishing Company, Inc.
- Japan Society of Civil Engineers 1996, *Report on Damage by Hanshin Awaji Earthquake* (in Japanese).
- Kinki Branch, Ministry of Land, Infrastructure and Transportation 1999, *Road Traffic Census* (in Japanese).
- Kitano, H. (eds.) 1995. *Genetic Algorithm 3*, Tokyo, Sangyotosho (in Japanese).
- Liu, M., & Frangopol, D.M. 2004a, Probabilistic maintenance prioritization for deteriorating bridges using a multi-objective genetic algorithm, *Proceedings of the Ninth ASCE Joint Specialty Conference on Probabilistic Mechanics and Structural Reliability, Hosted by Sandia National Laboratories, Omnipress, Albuquerque, New Mexico, July 26–28*, 6 pages on CD-ROM.
- Liu, M., & Frangopol, D.M. 2004b, Optimal bridge maintenance planning based on probabilistic performance

- prediction, *Engineering Structures*, Elsevier, Vol. 26, No. 7, pp. 991–1002.
- Ministry of Land, Infrastructure and Transportation 2002, *Design Specification of Highway Bridges*, Maruzen (in Japanese).
- Neves, L.C., Frangopol, D.M., & Hogg, V. 2003, Condition-reliability-cost interaction in bridge maintenance, *Proceedings of the Ninth International Conference on Applications of Statistics and Probability in Civil Engineering, ICASP9*, San Francisco, California, July 6–9, Millpress, Rotterdam, 2, 1117–1122.
- Nihon Sogo Research Institute 1998, *Draft of Guideline for Evaluation of Investment on Road* (in Japanese).
- Park, Y.J., & Ang, A.H.S. 1985, Mechanistic seismic damage model for reinforced concrete, *Journal of Structural Engineering*, ASCE, Vol. 111, No. 4, 722–739.
- Shoji, M., Fujino, Y., & Abe, M. 1997, Optimization of seismic damage allocation of viaduct systems, *Proc. of JSCE*, No. 563, 79–94 (in Japanese).
- ADDITIONAL REFERENCES**
- Biondini, F., Frangopol, D.M., & Malerba, P.G. 2006, Time-variant structural performance of the Certosa cable-stayed bridge, *Structural Engineering International*, Journal of IABSE, SEI, 16(2), 235–244.
- Biondini, F., Bontempi, F., Frangopol, D.M., & Malerba, P.G. 2006, Probabilistic service life assessment and maintenance planning of concrete structures,” *Journal of Structural Engineering*, ASCE, 132(4), 810–825.
- Biondini, F., & Frangopol, D.M. 2008, Collapse reliability and lifetime prediction of reinforced concrete framed structures, *Structure and Infrastructure Engineering*, Taylor & Francis (in press).
- Bucher, C., & Frangopol, D.M. 2006, Optimization of lifetime maintenance strategies for deteriorating structures considering probabilities of violating safety, condition, and cost thresholds, *Probabilistic Engineering Mechanics*, Elsevier, 21(1), 1–8.
- Cho, H.N., Frangopol, D.M., & Ang, A.H.S., eds. 2007, *Life-Cycle Cost and Performance of Civil Infrastructure* (ISBN 13: 978-0-415-41356-5 (hbk)), Taylor & Francis Group plc, London, 332 pages.
- Estes, A.C., & Frangopol, D.M. 2005, Life-cycle evaluation and condition assessment of structures, Chapter 36 in *Structural Engineering Handbook, 2nd Edition*, W-F. Chen and E.M. Lui, eds., CRC Press, 36–1 to 36–51.
- Frangopol, D.M., Estes, A.C., Augusti, G., & Ciampoli, M. 1997, Optimal bridge management based on lifetime reliability and life—cycle cost,” Chapter 8 in *Optimal Performance of Civil Infrastructure Systems*, D.M. Frangopol, ed., ASCE, New York, 98–115.
- Frangopol, D.M. 1997, Application of life cycle reliability—based criteria to bridge assessment and design, *Safety of Bridges*, P.C. Das, ed., Thomas Telford, London, 151–157.
- Frangopol, D.M. 1999, Life—cycle cost analysis for bridges, Chapter 9 in *Bridge Safety and Reliability*, D.M. Frangopol, ed., ASCE, Reston, Virginia, 210–236.
- Frangopol, D.M., Miyake, M., Kong, J.S., Gharaibeh, E.S., & Estes A.C. 2002, Reliability— and cost-oriented optimal bridge maintenance planning, Chapter 10 in *Recent Advances in Optimal Structural Design*, S. Burns, ed., ASCE, Reston, Virginia, 257–270.
- Frangopol, D.M., Brühwiler, E., Faber, M.H., & Adey, B., eds. 2004, *Life-Cycle Performance of Deteriorating Structures: Assessment, Design and Management*, ASCE (ISBN 0-7844-0707-X), Reston, Virginia, 456 pages.
- Frangopol, D.M., Kallen, M.J., & Van Noortwijk, J. 2004, Probabilistic models for life-cycle performance of deteriorating structures: review and future directions, *Progress in Structural Engineering and Mechanics*, John Wiley & Sons, 6(3), 197–212.
- Frangopol, D.M., & Liu, M. 2006, Life-cycle cost and performance of civil structures, *McGraw-Hill 2006 Yearbook of Science and Technology*, McGraw-Hill, New York, 183–185.
- Frangopol, D.M., Maute, K., & Liu, M. 2007, Design optimization with uncertainty, life-cycle performance and cost considerations, Chapter 11 in *Optimization of Structural and Mechanical Systems*, J.S. Arora, ed., World Scientific Publishing Co. Ptc. Ltd., 291–329.
- Frangopol, D.M., & Liu, M. 2007, Bridge network maintenance optimization using stochastic dynamic programming, *Journal of Structural Engineering*, ASCE, 133(12), 1772–1782.
- Frangopol, D.M., & Liu, M. 2007, Maintenance and management of civil infrastructure based on condition, safety, optimization, and life-cycle cost, *Structure and Infrastructure Engineering*, Taylor & Francis, 3(1), 29–41.
- Furuta, H., Dogaki, M., & Frangopol, D.M. 2003, Decision support system for optimal maintenance scheduling of highway RC bridge decks applying fuzzy reasoning and classifier system, *Proc. of 11th IFIP WG7.5 Working Conference, Banff, Canada*.
- Furuta, H., Kameda, T., Nakahara, K., & Takahashi, Y. 2003, Genetic algorithm for optimal maintenance planning of bridge structures”, *Proc. of GECCO, Chicago, US*.
- Furuta, H., & Frangopol, D.M. 2004, Life-cycle cost analysis for bridges: the basis of decision making in bridge management, *Proc. ICE Bridge Workshop*, Shanghai, China.
- Furuta, H., Kameda, T., & Frangopol, D.M. 2004, Balance of structural performance measures, *Proc. of Structures Congress, Nashville, Tennessee, ASCE, May*, CD-ROM.
- Furuta, H., Koyama, K., Dogaki, M., & Frangopol, D.M. 2004, Seismic risk evaluation and life-cycle cost analysis of bridge structures in Japan, *Proc. of 2nd ASRANeT Colloquium*, Barcelona, Spain.
- Furuta, H., Frangopol, D.M., & Kameda, T. 2004, Life-cycle cost analysis under uncertainty, *Proc. of Probabilistic Mechanics Conference*, Albuquerque, USA, CD-ROM.
- Furuta, H., Kameda, T., & Frangopol, D.M. 2004, Effects of environmental conditions on optimal bridge maintenance, *Proc. of International Workshop on Integrated Life-Cycle Management of Infrastructures*, Hong Kong.
- Furuta, H., & Frangopol, S.M. 2005, Optimal maintenance planning using multi-objective genetic algorithm, *Proc. of ICLODC*, Bochum, Germany.
- Furuta, H., Nakatsu, K., & Frangopol, D.M. 2005, Optimal restoration scheduling for earthquake disaster using life-cycle cost, *Proc. of 4th International Workshop on Life-Cycle Coast Analysis and Design of Civil Infrastructure Systems*, Coco Beach, USA.

- Furuta, H., & Kameda, K. 2005, Application of multi-objective genetic algorithm to bridge maintenance, *Proc. of IFIP TC7 Symposium*, Torino, Italy.
- Furuta, H., Koyama, K., Dogaki, M., & Frangopol, D.M. 2005, Seismic risk evaluation and life-cycle cost analysis of bridge structures, *Proc. of ICOSSAR '05*, Rome, Italy.
- Furuta, H., Kataoka, H., Dogaki, M., & Frangopol, D.M. 2005, Effects of seismic risk on life-cycle cost analysis for bridge maintenance, *Proc. of 4th International Conference on Current and Future Trends in Bridge, Construction and Maintenance*, Kuala Lumpur, Malaysia.
- Furuta, H., Koyama, O., M., 2005, Life-cycle analysis of bridge structures considering maintenance cost and seismic risk, *Proc. of IFIP WG7.5 Working Conference on Structural Reliability and Optimization*, Aalborg, Denmark.
- Furuta, H., Hirokane, M., Muraki, H., Tanaka, S., & Frangopol, D.M. 2005, Bridge maintenance system using digital photos, *Proc. of Structural Health Monitoring*, Winnipeg, Canada.
- Furuta, H., Dogaki, M., Fujii, H., & Frangopol, D.M. 2005, Bridge maintenance based on asset management, *Proc. of 2nd International Conference on Structural Health Monitoring of Intelligent Infrastructure*, Shenzhen, China.
- Furuta, H., Koyama, K., Oi, M., & Sugimoto, H. 2006, Life-cycle cost evaluation of multiple bridges in road network considering seismic risk, *Proc. of 6th International Bridge Engineering Conference*, Boston, USA.
- Furuta, H., Koyama, K., & Frangopol, D.M. 2006, Life-cycle performance and cost analysis of bridge network considering seismic risk, *Proc. of IFIP WG7.5 Conference on Structural Safety and Optimization*, Kobe, Japan.
- Furuta, H., Hattori, H., & Frangopol, D.M. 2007, Damage assessment of reinforced concrete bridge decks using Adaboost, *Proc. of 3rd International ASRANet Colloquium*, Glasgow, UK.
- Furuta, H., Kameda, T., & Erami, M. 2006, A practical bridge management system using new multi-objective genetic algorithm, *Proc. of the 4th IABMAS Conference*, Porto, Portugal.
- Furuta, H., Takenaka, Y., Kameda, T., & Tsukiyama, I. 2006, Development of bridge maintenance planning support system using multi-objective genetic algorithm, *Proc. of the 4th IABMAS Conference*, Porto, Portugal.
- Furuta, H., Enami, T., Kameda, T., & Frangopol, D.M. 2007, Bridge maintenance strategy considering user cost and connectivity, *Proc. of IABSE*, Budapest, Hungary.
- Furuta, H., & Kameda, T. 2007, Bridge management system based on life-cycle cost minimization, *Proc. the 5th Life-Cycle Cost Analysis and Design of Infrastructure Systems*, Seoul, Korea.
- Furuta, H., & Koyama, K. 2007, Life-cycle cost evaluation of bridge structures considering seismic risk, Chapter 10 in *Intelligent Computational Paradigms in Earthquake Engineering* (N. Lagaros & Y. Tsompanakis eds), John A. Martin & Associates, Inc., USA.
- Furuta, H., Kayano, M., & Watanabe, E. 2008, Current status and future issues on bridge management, *Proc. of SMSST'07*, Nanjing, China (in press).
- Ito H., Takahashi Y., Furuta, H., & Kameda, T. 2002. An optimal maintenance planning for many concrete bridges based on life-cycle costs. *Proc. of IABMAS*, Barcelona, Spain, CD-ROM.
- Liu, M., & Frangopol, D.M. 2006, Optimizing bridge network maintenance management under uncertainty with conflicting criteria: Life-cycle maintenance, failure, and user costs, *Journal of Structural Engineering*, ASCE, 132(11), 1835–1845.
- Liu, M., & Frangopol, D.M. 2005, Balancing connectivity of deteriorating bridge networks and long-term maintenance cost through optimization,” *Journal of Bridge Engineering*, ASCE, 10(4), 468–481.
- Liu, M., & Frangopol, D.M. 2005, Multi-objective maintenance planning optimization for deteriorating bridges considering condition, safety and life-cycle cost, *Journal of Structural Engineering*, ASCE, 131(5), 833–842.
- Liu, M., & Frangopol, D.M. 2006, Probability-based bridge network performance evaluation, *Journal of Bridge Engineering*, ASCE, 11(5), 633–641.
- Marsh, P.S., & Frangopol, D.M. 2007, Lifetime multi-objective optimization of cost and spacing of corrosion rate sensors embedded in a deteriorating reinforced concrete bridge deck,” *Journal of Structural Engineering*, ASCE, 133(6), 777–787.
- Miyamoto, A., & Frangopol, D.M., eds. 2002, *Maintaining the Safety of Deteriorating Civil Infrastructures*, University of Yamaguchi Press (ISBN 4-9901161-8-6 C3051), Ube, Japan, 374 pages.
- Neves, A.C., & Frangopol, D.M. 2005, Condition, safety and cost profiles for deteriorating structures with emphasis on bridges,” *Reliability Engineering & System Safety*, Elsevier, 89 (2), 185–198.
- Neves, L.A.C., Frangopol, D.M., & Petcherdchoo, A. 2006, Probabilistic lifetime-oriented multi-objective optimization of bridge maintenance: combination of maintenance types, *Journal of Structural Engineering*, ASCE, 132(11), 1821–1834.
- Neves, L.A.C., Frangopol, D.M., & Cruz, P.J. S. 2006, Probabilistic lifetime-oriented multi-objective optimization of bridge maintenance: single maintenance type, *Journal of Structural Engineering*, ASCE, 132(6), 991–1005.
- Kong, J.S., & Frangopol, D.M. 2003, Life-cycle reliability-based maintenance cost optimization of deteriorating structures with emphasis on bridges, *Journal of Structural Engineering*, ASCE, 129(6), 818–828.
- Kong, J.S., & Frangopol, D.M. 2003, Evaluation of expected life-cycle maintenance cost of deteriorating structures, *Journal of Structural Engineering*, ASCE, 129(5), 682–691.
- Kong, J.S., & Frangopol, D.M. 2004, Prediction of reliability and cost profiles of deteriorating structures under time- and performance-controlled maintenance, *Journal of Structural Engineering*, ASCE, 130(12), 1865–1874.
- Kong, J.S., & Frangopol, D.M. 2004, Cost-reliability interaction in life-cycle cost optimization of deteriorating structures,” *Journal of Structural Engineering*, ASCE, 130(11), 1704–1712.
- Petcherdchoo, A., Neves, L.A.C., & Frangopol, D.M. 2008, Optimizing lifetime condition and safety of deteriorating structures with emphasis on bridges, *Journal of Structural Engineering*, ASCE, 134(4) (in press).
- van Noortwijk, J.M., & Frangopol, D.M. 2004, Two probabilistic life-cycle maintenance models for deteriorating civil infrastructures,” *Probabilistic Engineering Mechanics*, Elsevier, 19(4), 345–359.

# The new life of the Theatre alla Scala

P.G. Malerba

*Department of Structural Engineering, Politecnico di Milano, Milan, Italy*

**ABSTRACT:** “The Scala is the first theatre in the world, because it is that which gives the maximum enjoyment” (Stendhal, 1816). Unfortunately, after two centuries of glorious service, the historical-monumental part and the hall of the Theatre clearly needed restoration interventions, while the backstage, subjected to the wear of time, having undergone haphazard additions and continual adaptations over the years, was no longer able to meet the request of a today’s theatre. The project of the New Teatro alla Scala was hence composed by two distinctive parts: the project of the refurbishment and of the restoration of the historical-monumental part and the project of the buildings for the new scenic plants. This paper present an overview of the design concepts and of the problems encountered during the design phases and during the restoring and construction works.

## 1 INTRODUCTION

There are artefacts for which the end of a life cycle coincides with the beginning of a new life. This was the common destiny of the major lyrical theatres during the two past centuries.

At the beginning of the ‘800, the first opera stages used oil lamps and bidimensional scenes, made of painted wings moving transversally along the stage. Between artists and spectators there was no clear separation. The following evolution of the scenic set involved tridimensional setups, with solid architectures, complex scenic machines and wide and rapid scenic movements of the ballet and of the singers. New hidden volumes were required under the stage and the wings became a set of layers moving vertically above the stage. All these transformations required a deepening of the scenic pit and a remarkable increase of the height of the scenic tower.

This continuous evolution was lived nearly at the same manner by all theatres: the stalls and the galleries of the boxes were maintained in their original form, while the changes regarded the scenic plant, which gradually became something completely separated behind the *boccascena* (the proscenium) front.

The invention of the *boccascena* and the parting between stage and spectators make the stage a magical place: this disjunction fostered the invention of perspective illusions, of special effects machines and, with the coming of electricity, of more and more complex light effects.

In the fight between Words and Music, the winner was the Spectacle (Malgrande, 2004).

## 2 SOME HISTORICAL NOTES

Dealing with monumental buildings, one of the major problems is represented by the necessity of manipulating (through modification, destruction, burial) material parts which belong to history.

In truth, the modification of the Theatre was continuous. Born as “New Royal Ducal Theatre”, it was designed by Giuseppe Piermarini, under the auspices of the Empress Maria Theresa of Austria and with the financial support of the Milanese aristocracy, who borne the costs in exchange for the ownership of the boxes. The new hall was inaugurated on 3 August 1778, and took the name of “Teatro alla Scala”, as it was built on the former location of the church of Santa Maria alla Scala. It was characterised by a plain neoclassic façade and by a sumptuous interior, with five orders of boxes, a luxurious central imperial box and eight proscenium boxes. The curtain was painted by Domenico Riccardo and represented the Muses in the Parnassus. The *platea* (main floor), destined to the lower classes, had no chairs and the same space was periodically used as dance hall. The lighting was originally provided by candles. In 1787 the lighting was improved by 84 oil lamps with a glass bulbs mounted in front of the stage, and by 996 lamps hanging from the roof. In 1807 the Theatre was closed, to allow important works on the decorations of the interiors. In 1814 the depth of the stage was increased by architect Pietro Canonica. In 1821, thanks to the director of stage design, Alessandro Sanquirico, the candle lighting was replaced by the famous great chandelier, with 84 oil lamps, replaced by gas lamps in 1860.

In 1838 all the decoration were unified in crimson colour. In 1875, the square in front of the Theatre was modified and acquired its present appearance. In 1883 electric power was installed.

Immediately after WW1, the Theatre closed, due to economic difficulties, and reopened in 1921 under the management of the Ente Autonomo Teatro alla Scala. In the same year, the height of the scenic tower was increased, so that the wings could be shifted vertically, instead of being rolled up on large wooden drums placed behind the roof.

In 1932, Luigi Lorenzo Secchi built the so called Scale degli Specchi (mirror stairs) which connect the stalls to foyer. The foyer had a new settlement and a new decoration in 1936. In 1937–38 a new stage hosted movable bridges and walls, moved by hydraulic devices. The central part of the stage became a wide platform of 330 sqm and a complex subdivision of the deck structures allowed a true tridimensional management of the stage volume.

In the night between August 15th and 16th 1943, a severe bombardment on Milan caused the collapse of the roof, of part of the galleries, of the boxes, of the stage and of all the service spaces.

In 1945 Andrea Greppi, the new Major of Milan, designated Antonio Ghiringhelli as temporary commissary and started the works to rebuild the Theatre. The inaugural concert, directed by Arturo Toscanini, was given on May 11th, 1946. Regular spectacles restarted on December 26th 1946.

Since the works which took place in 'thirties, it was clear that any further extension would be impossible, because of the intrinsic limits of the building box. Moreover, the obsolescence and wear of the electrical wiring, of the hydraulic plant, of the fire-extinguishing and of the heating system, clearly required new, wider and completely different spaces.

In January 2002 the Theatre was closed and all the activities was transferred to the Arcimboldi Theatre, in order to allow the radical works for the New Teatro alla Scala.

### 3 DESIGN CONCEPTS FOR A NEW THEATRE

When we imagine the “Teatro alla Scala”, the pictures that are brought to mind are those of its monumental front (Fig. 1), of its lounges and of its magnificent internal hall.

A lot less is known however about its interior, that is, what lies behind the *boccascena*, where the scenic machine, the auxiliary systems and the laboratories which form this complex theatrical mechanism, are to be found.

In 2001 the historical-monumental part and the hall of the Theatre clearly needed restoration interventions,

while the backstage, having gone continual adaptation over the years, was no longer able to meet the requests of a today's theatre.

The project of the New Teatro alla Scala was hence composed by two distinct parts: the project of the refurbishment and of the restoration of the historical-monumental part and the project of the buildings for the new scenic plants.

These two different views of the theatre have therefore been reflected in the two different objectives given to the project: its first aim was to safeguard the theatre's historical value and to maintain its right to remain an icon of Milan; the second was to create new structures and spaces in order to supply a solid platform to support a theatrical mechanism worthy of the Teatro alla Scala.

As shown in Figure 2, the historical and the new buildings are divided by the section line which, starting from Via Verdi, moves along the *boccascena*, the South East side of the Hall, and the rear part of the Scala Museum, up to Via Filodrammatici.

Such new buildings have been erected in the volume of the hold scenic tower, which has been demolished, and are composed by the new Scenic Tower, the Space for the Scenic supplies and the New Offices.

The main problems encountered during the design phases of the new structures were:

- the criteria for a selective demolition of the original structures;
- the design of the foundations and of the sheetpiling perimeter which envelopes the structures of the 56.5 m high scenic tower;
- the design of the Scenic Tower, which involves wide span deep beams, which cover the mouth of the stage and which support the five levels of the backstage in the rear;
- the design of the lateral sets, covered by wide span and heavily loaded floors and including the structure of the “ovoid”, which contributes to characterize the new image of the Theatre (Figs. 1 and 15);
- the hybrid interventions which involved both the historical and the new spaces;
- the special problems of the organization of a complex construction site, confined into the centre of Milan.

### 4 THE DEMOLITION PHASE

In order to build we first have to demolish, being careful not to destroy anything.

Our first step, therefore, was to decide how to demolish the scenic tower, which contained all its former theatrical equipment, and then how to clean out and gut all the basement volumes and re-model them to

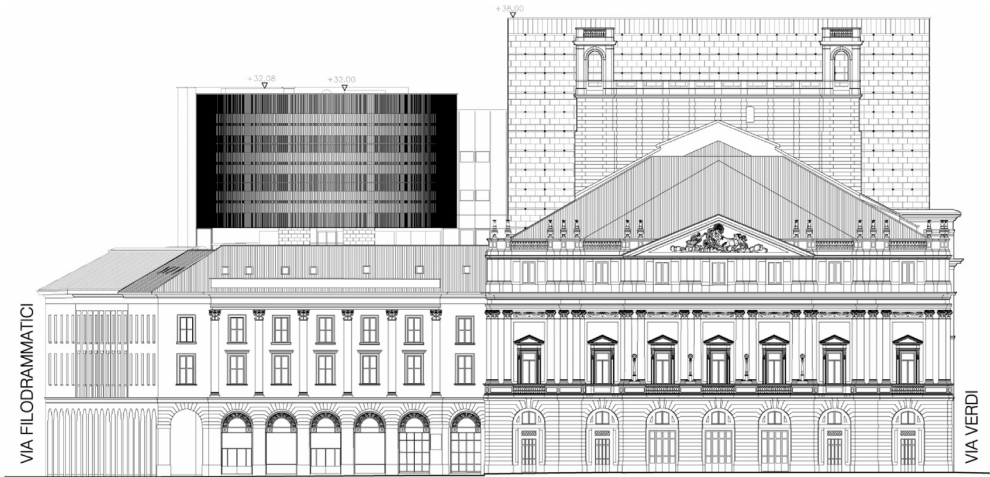


Figure 1. Frontal view of the historical front and of the new volumes of the Theatre alla Scala.

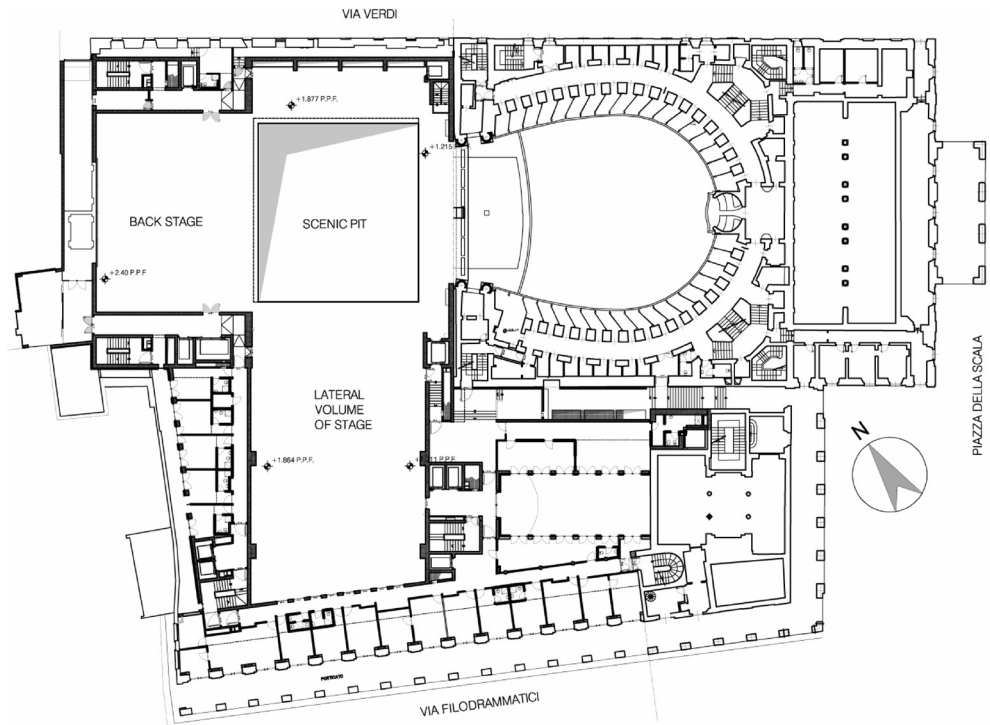


Figure 2. General plant of the Theatre at stage level.

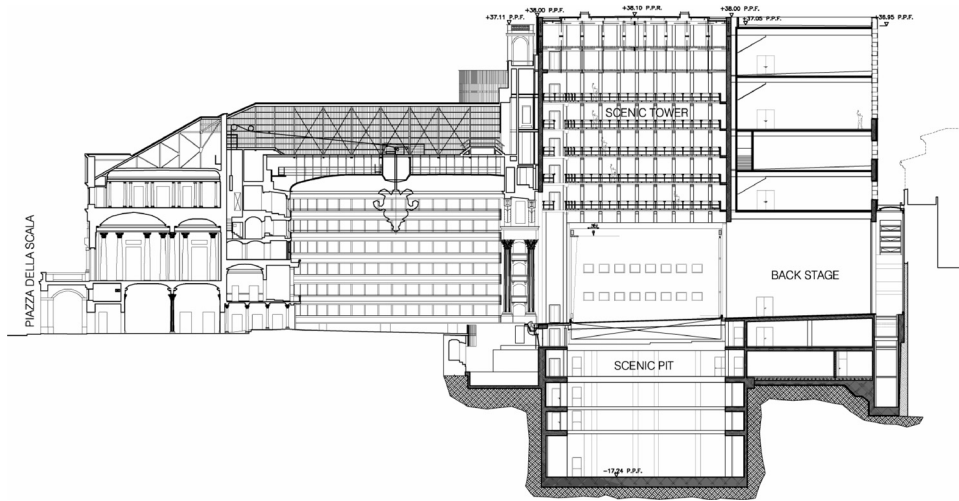


Figure 3. Longitudinal section.

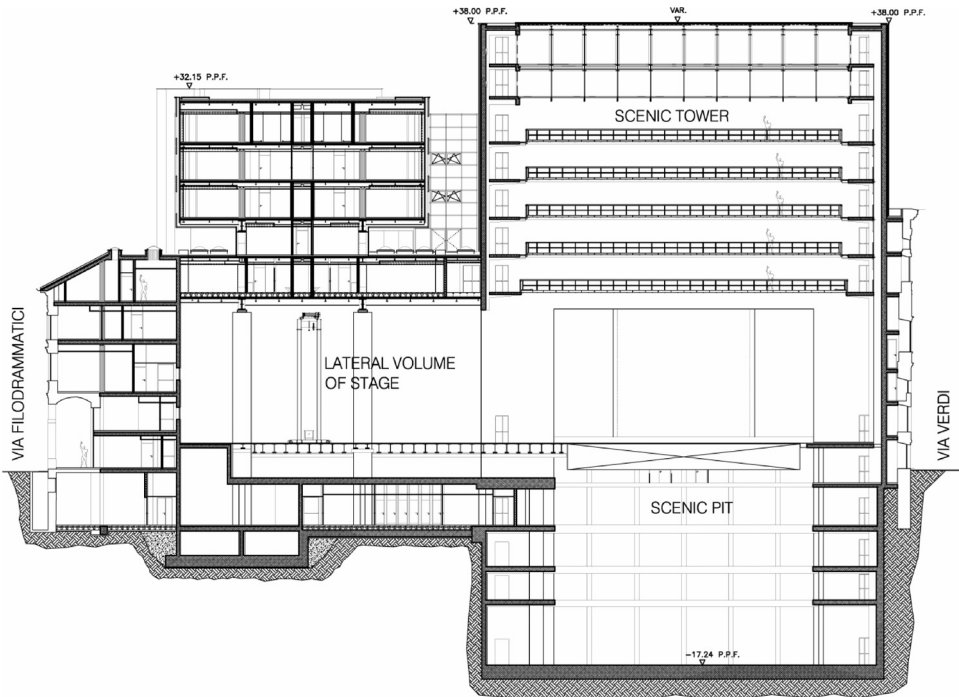


Figure 4. Transversal section in correspondence with the *boccascena*.

create one large area suitable to house new machinery and plants.

The greatest difficulties we faced in carrying this out were caused by having to maintain the two facades,

one on Via Verdi and the other on Via Filodrammatici, intact. These two facades have been re-adapted over the years but have now become part of the city's landscape.



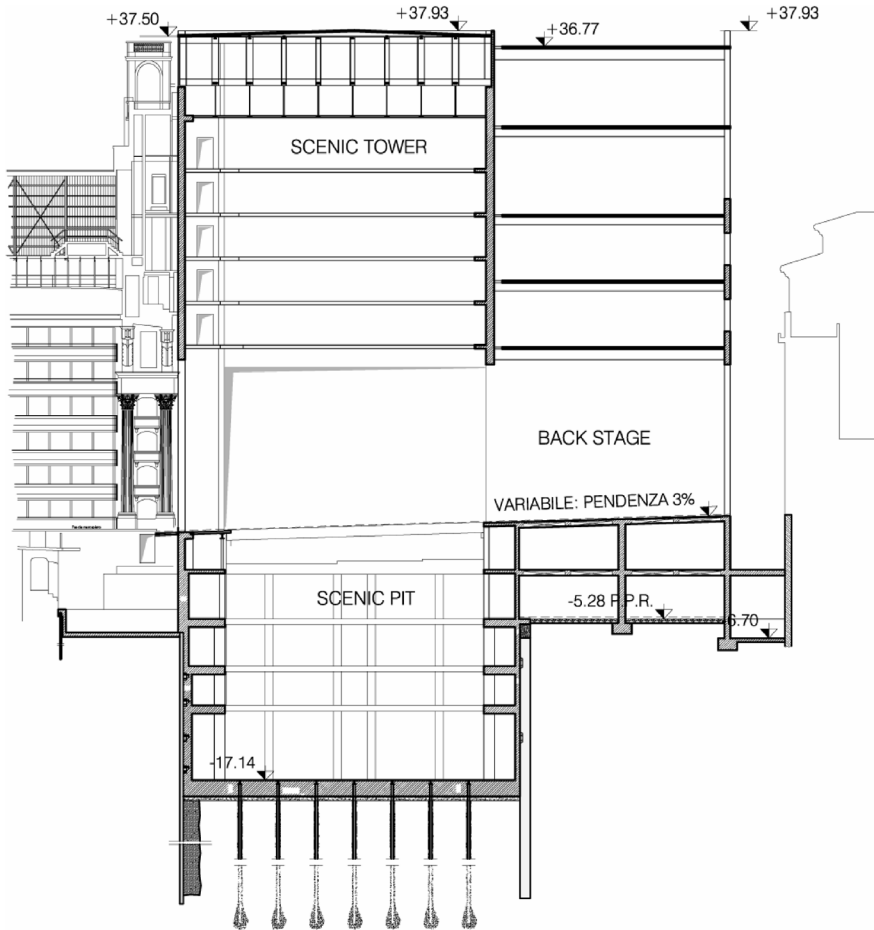


Figure 5. Longitudinal section of the backstage.

#### 4.1 The demolition project

The first step in the demolition project was to erect sturdy protection structures meant to support the façades in Via Verdi and Via Filodrammatici once the floors and the columns, which originally exerted the stabilising action, were removed.

The scenic pit, which is just behind of the façade along Via Verdi, had to be deepened to 18 metres below street level. This deepening left at the interior side an open front of about 42 m from the bottom of the excavation to the top of the façade and a front of 24 m at street side on the *boccascena* side. The free prospect was over 50 m.

We therefore had to erect support structures in open areas in Via Verdi. The idea was to fix the wall to metallic buttresses. These buttresses were shaped like

a portal with relatively restrict encumbrance. Thus, traffic could flow regularly along Via Verdi, even if only along one lane, supplying at the same time a basic structure for site facilities. Moreover, the area within the portal was suitable to house deposits and set up the cranes.

The portico and frontispiece support in Via Filodrammatici set several complex problems. On one hand, due to the fact that there were to be no excavations behind the pre-existing structure, there were minor static worries. On the other, the narrow width of the street wouldn't allow for any cumbersome structure.

At first it was planned to build a weighted scaffolding. However, on a second viewing, during work procedures it was decided to create a metallic truss which would occupy the same volume as the existing

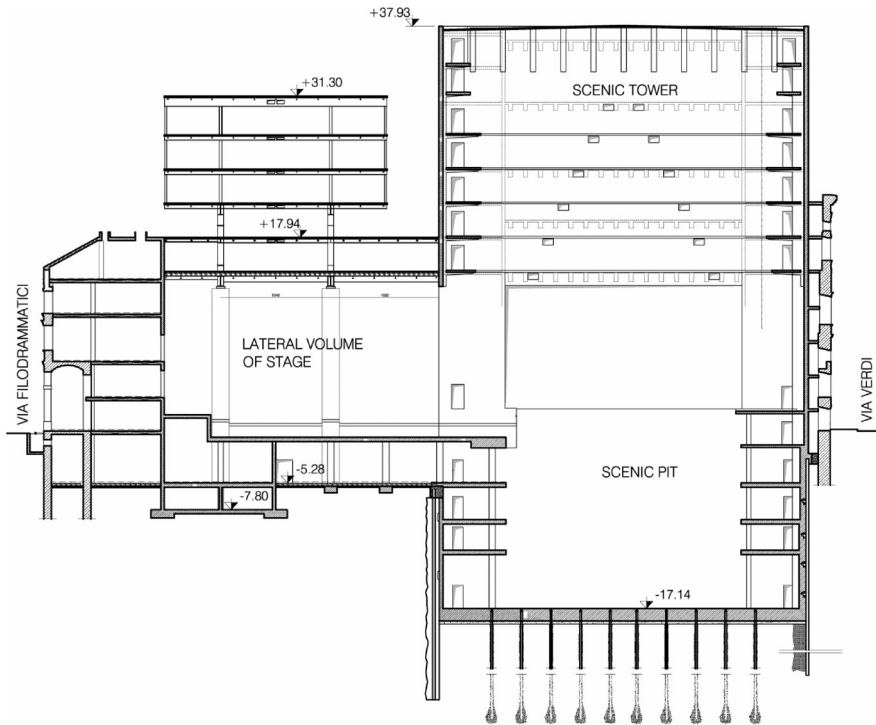


Figure 6. Transversal section of the backstage. The lateral volume can also be seen.

portico, reduce the encumbrance along the street and at the same time exploit the weight of the stonework structure to counterbalance accidental load forces.

All the support structures were built in such a way as to resist totally against any type of accidental force foreseen during work, especially forces caused by the wind. Particular attention was paid to deformation behaviour, making sure that the metallic structure support deformation was compatible with the static of the stonework to be garrisoned.

The attention was then focused on the demolition sequence. It was obviously impossible to demolish in an open area, by simply razing the building to the ground. Starting from the top and working down, each demolition phase was followed by a clearance phase. The problem was solved by first demolishing the roofing (Fig. 7) so as to reach the scenic pit area, where a sturdy crane was erected. The range of this crane was able to cover the whole work area, supplying the possibility to cut and lower the main structures, such as the reticular reinforced concrete beams of the tower roof, and move any medium to large sized elements.

Thus, high level demolition principally concerned secondary parts and linking elements. The larger structures were simply taken apart and then crushed or segmented on the ground. These complicated



Figure 7. The cutting of the roof truss beams.



Figure 8. Internal view after demolition.

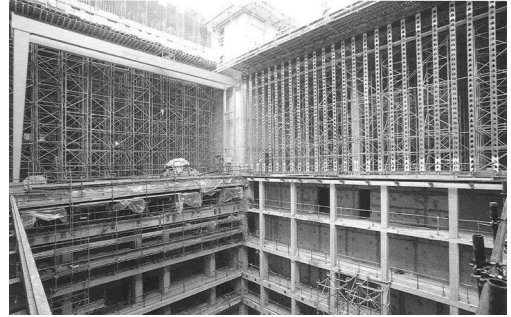


Figure 10. Scaffolding at the rear part of the tower.

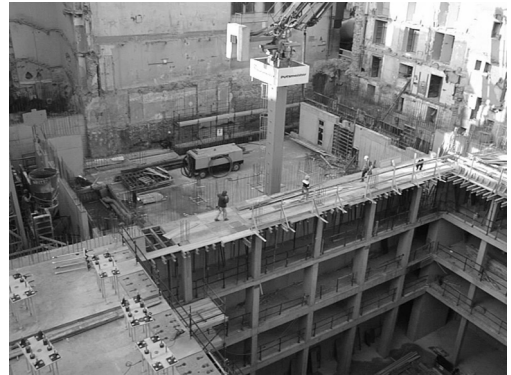


Figure 11. Building of the scenic tower.



Figure 9. Erection of a temporary platform.

manoeuvres were made possible and carried out in complete safety, thanks to advanced technologies and by using remote control machinery in dangerous areas. Great care was taken so as not to cause disruption to the surrounding buildings (Figs. 8–11).

#### 4.2 Monitoring scheme

During the works, an integrated system which was based on topographical surveys and instrumental surveys was set up. The topographic net was set in order to keep under control the façades of Via Verdi and Via Filodrammatici and other meaningful points on the adjacent buildings and all along the perimeter

of the new foundations. The electronic transducers were put in places where structural analyses seemed to detect the more relevant excavation settlements. The automatic monitoring allowed us to control the situation in real time, especially during the most critical stages. The topographic surveys permitted us to check the inclinometers results and therefore obtain a report on the period of the structure's first settling.

## 5 THE PROJECT OF THE NEW BUILDING

The directions as to the architectural plans for the scenic tower were clear and straightforward: deepen the pit from 12 metres to 18.60 m below street level in order to seat the new structures of the mobile stage, leaving vast unobstructed spaces around it.

From a structural point of view, this meant using special types of foundations and of frameworks able to cover long spans and support great weights, having to sustain overhead structures and scenic plants (Figs. 3–6).

## 5.1 The scenic tower

At the exterior, the Scenic Tower appears as a unique prismatic volume. Its interior is divided into two parts (Figs. 3–6): the volume containing the stage and, behind, the area which hosts the backstage, the laboratories and the training halls.

The main part of the Scenic Tower itself is a void prism with a basis of 26.0 m, in the direction of the axis of the theatre, per 36.00 m in the transversal direction. The ground level, at the bottom of the slab of the Scenic Pit, is  $-18.30$  m below the street level. The roof is at the quote  $38.00$  m. Total height is 57 m.

As shown in Figure 2, the whole volume of the Scenic Tower is separated into three parts:

- the part below stage level (the *Scenic Pit*), which hosts the lower scenic plant and which is edged, along its perimeter, by five different levels of service balconies ( $-11.64$ ,  $-8.56$ ,  $-5.16$ ,  $-1.56$ ,  $+1.08$  m “reference stage level”, Figs 5, 6). In this lower volume, a set of seven vertically movable platforms make up the main stage structures. These platforms can be moved independently from each other, or can be lowered simultaneously as whole, making the stage area completely free for a new stage. The deck for a new stage is cantilevered from the lateral volume of scene (Fig. 6), which will be described in the following:
- the volume of the stage itself, from level  $+1.08$  to level  $+14.57$  m;
- the part over the stage which hosts the set of the vertically movable scenes and, over this, the system of “*graticce*” (two wooden grillages), on which lies the system of suspension and of movement of the scenes.

### 5.1.1 The scenic pit

The Scenic Pit has plant  $24 \times 34$  m, plus a short prolongation along Via Verdi (Fig. 2). At the basis, the lower level of excavation was at  $-18.60$  m below street level (Via Verdi). This involved a deepening of 6 m of the previous basis level of the scenic pit at level 12 m.

The retaining of the lateral excavation fronts, was carried out by means of anchored sheet piles walls and of sheet walls made of jet-grouting columns.

The retaining wall at the foot of the historical front to be preserved along Via Verdi, is of *berlinese* type, made of 25 cm diameter micro-piles, internally reinforced by means of injections inside the steel tube and placed at a mutual distance of 35 cm. The piles were made transversally collaborating through six pairs of horizontal steel beams, anchored below Via Verdi through six levels of nearly horizontal pre-stressed tendons (Fig. 9). A similar solution was adopted along the section at the two sides of the *boccascena*. Due to the higher vertical loads acting in this zone, the retaining wall was made of two layers of piles at a distance

of 35 cm and with a relative shift of 17.5 cm. In the central part of the *boccascena*, corresponding to the stage width and carrying lower loads, the sheet wall is limited to a simple line of micro-piles and 5 levels of pre-stressed tendons.

On the other two sides of the perimeter, those parallel to Via Filodrammatici and along the ex San Paolo Bank, the increase of loads were lower and sheet walls made of jet grouting reinforced columns, having 120 cm diameter e spaced of 80 cm (hence partially compenetrated), were adopted.

In designing the scenic pit as a whole, the definition of a reference ground water level was carefully weighted. At present, the ground water level is 17.50 m. below street level and it is rising. To the design purposes the hypothesis of a possible future water level about 10.00 m. below street level, 8.0 m higher than the present one, was assumed. This means that the structures must be able to oppose the notable hydrostatic thrust of 8.00 m of water, equivalent to a maximum pressure of 80 kN/mq. The bottom floor of the pit and the boundary walls, placed behind the retaining walls, are all structures which behave like an “inverse tank”, loaded by an external hydraulic pressure and by a strong counter thrust from the bottom.

Generally, in underground construction, structure weight is distributed among the floors, which helps oppose the water’s upward thrust. On the contrary, the scenic pit, which is merely a container which houses the theatrical mechanism, notwithstanding the imposing mass formed by its walls, is actually a “light” structure when compared to its empty volume. As a consequence, the foundation flooring would have to be well anchored to the ground, in order to oppose the possible counter thrust due to the raising of the water level.

The contrast is carried out by means of 60 high strength thread bars, 21 m long and with a 36 mm diameter, earth anchored for 10 m through cement injections. Each bar, covered by a double protective sheath, was placed in such a way as to remain in contrast with the ground, even if the water level were to rise. Thanks to special inspection niches, which enable one to reach the anchor heads, each bar can be re-tensioned when required (Figs 5, 6 and 9).

### 5.1.2 The water proofing

The pit waterproofing adopted in the original design was made of a double impermeable membrane. During works, a special type of technology called “white basin” was used. According to this technology, concrete is assumed impermeable and waterproofing is entrusted only to the concrete walls.

This waterproofing technique makes use of low porosity concrete with a controlled shrinkage, cast

insegmented strips, separated by means of special ducts incorporated in the thickness of the walls. These little ducts create weak wall sections, which pay the effects of shrinkage and therefore give way to a pre-defined and regular crack patterns. These cracks are then sealed by injecting very low viscosity resin into the ducts, which, once hardened, makes the whole surface waterproof.

Such system would also be employed to achieve sealing in unexpected flaws or fissures caused as a consequence of casting.

The concrete characteristics were decided after a thorough study of mix and additives. When tracing the reinforcement, a great deal of attention was paid to every single local detail which could be sensible to the effects of the hardening phase.

By choosing the “white basin” technique, building time was notably cut. In fact, by avoiding the regularization of the surfaces of the sheet walls and by avoiding the laying of waterproofing membranes, it was possible, to carry out both horizontal and elevation casting at the same time, without other work interruptions.

### 5.1.3 The tower

The Scenic Tower is the case which houses the facilities, plants, systems, machinery and every other devices connected with scene manoeuvres.

Its internal volume has to allow for complete availability of space in order to hold and sustain all the mechanical scenic machines and plants.

Moreover, it should also consent a series of arrangements which are necessary for the performances.

In the case of the “Teatro alla Scala”, apart from difficulties deriving from the structure complexity, there was also the need to respect dimension and structure limitations, due to the fact that the scenic tower had to remain within the pre existing space limit, that is, between the historic façade in Via Verdi and the Piermarini hall *boccascena*, acting both as a connection and as a new support to the original structure.

The vertical mass of the tower is built in cast in place reinforced concrete. The roof is made of steel beams.

On planning the structures of the Tower, several requirements, connected to the running of the theatre, had to be borne in mind:

- the coordination of the scenic machine with the case made of the civil structures;
- the creation of service galleries, along with vertical connections, such as lifts and stair-ways;
- the building of vast openings onto the *boccascena*, on the sides and backstage, which would allow for quick and safe access to setting the scenes.

These requirements were met through wide edging floors, cantilevered from 40 ÷ 50 cm thick perimeter

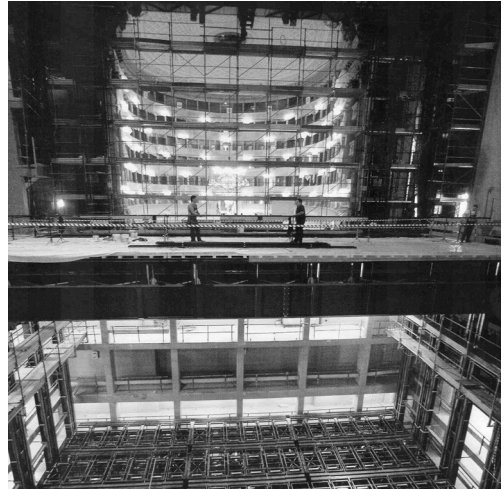


Figure 12. An internal view of the scenic tower.

walls, which form spacious galleries on different levels all along the perimeter of the pit (Figs 10–12). The voids opening onto the *boccascena*, the stage sides and backstage were covered by means of three deep beams spanning on 25 ÷ 30 m, which support the upper section of the tower, as far as the roof beams.

The roofing beams have two different purposes: supporting the actual roof and, at the same time, bracing the two wooden *graticce* from which, at two different levels, the scenes are hung.

Due to the fact that having easy access the work areas was of vital importance, in order to both manoeuvre machinery and to permit staff to move about their jobs, it was decided to opt for a “Vierendeel” beam type, that is a beam framework, having only horizontal and vertical elements, but no diagonal ones, as these would obstruct circulation (Fig. 13).

The lower flanges of these “Vierendeel” beams also sustain the first floor of work of the first *graticcia*. The second *graticcia* was hung from the main beams by means of steel braces and stabilised horizontally by connecting it to the surrounding concrete structures.

Apart from the problems deriving from having to coordinate the actual geometry of the roofing beams to every other need connected to the installation of theatrical equipment, other limits, such as methods and time of construction, were set.

One in particular was the need to transport enormous metallic elements through the centre of the city. A detailed study then had to be carried out as to the size and weight of each segmented beam, made of pre-fabricated elements, so as to travel and be manoeuvred unhindered on the site.





Figure 13. Steel Vierendeel beams of the roof.

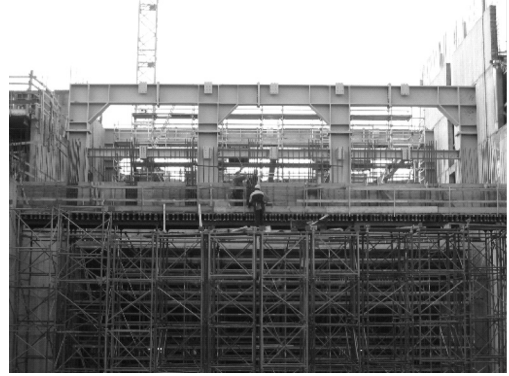


Figure 14. Inferior flange of the Ellipse supports.

In the end, the solution chosen allowed us to avoid welding in place and reduce bolted joints to a minimum.

#### 5.1.4 *The backstage*

Apart from the two basement floors, backstage had to have no intermediate structures whatsoever. For this reason the volume between +14.82 m and +36.77 m was set up on five different levels, made of wide span decks, which are borne by the boundary structure alone, without any other support (Figs. 2–5). In particular, in the area between the back-stage and the scenic pit, these decks weight on a 40 cm thick deep beam built in reinforced concrete columns 80 cm thick and 4.00 m wide.

At the other opposite sides, these same decks bear on the columns, erected on the vertical walls below. In order to build these decks, it was first decided to employ self carrying pre-cast elements. This choice was however discarded because of transportation and placing difficulties and a more traditional cast in place structure was chosen. The decks were thus built with beams of 17 m span having section 75 cm × 40 cm, and made collaborating through a 15 cm thick slab. For the deck at +14.82 m, directly above the stage area, the cross-section of the beams was increased to 95 cm × 40 cm, as this area undergoes major live loads.

#### 5.2 *The lateral volume of the stage*

For this part of the building, which is between the offices along Via Filodrammatici and the scenic tower (Fig. 3), the design process had to deal with two different types of restraints: functional and architectural ones.

On one side, in fact, there was the need to leave a large free space on the left side of the stage in order to mobilize the stage equipment by means of a bridge

crane; on the other, the need of covering this volume with six floors, intended as service spaces for the theatre.

In the original project, two reinforced concrete deep beam walls, having wide openings (Vierendeel type beams) were meant to reach the roofing, starting from +14.60 m of height, and were intended as central support for the floors.

The architectural update of the project has highlighted the need of having, above the stage, two large floors destined to technical services. The new elliptical body, designed by architect Botta and having four more floors, would have emerged, starting from 18.06 m of height, as an independent volume from the block below (Figs. 1, 14, 15 and 16).

The floors above the area at the side of the stage are supported by means of two steel beams, having 20 m long span and 7.50 m height, which allow to avoid the subdivision of the large spaces needed with pillars. These massive beams are supported by two walls, reinforced by strong pilaster strips, that, starting from the foundations, go through the two technical floors above the stage and sustain the four floors of the elliptical body.

The “Vierendeel” scheme, devoid of diagonal elements, was chosen in order to make fully available the two floors placed on the height of the beams. The main beams are the structures which support the steel skeleton of the elliptical body.

In order to avoid an excessive depth of the main beams of the floors, and to allow an easy ramification of the plans and systems, the cantilevered parts have been hung to the roofing beams, which therefore bear, together with their own weight, the loads of the floors below and the weight of the stony façades along the perimeter.

The bracing action is performed by staircases and elevator compartments, which are in cast-in-place reinforced concrete.

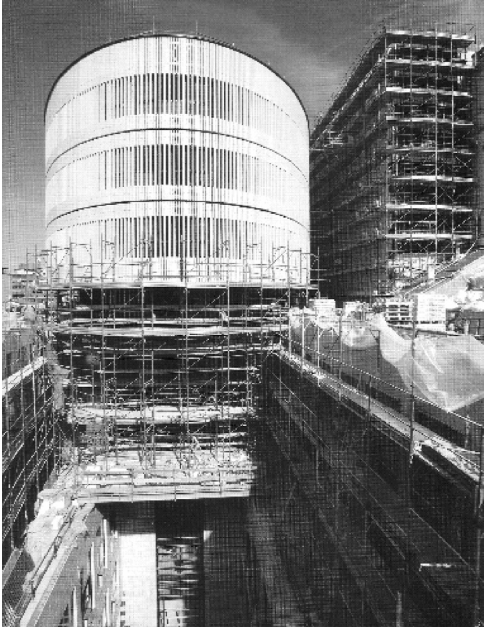


Figure 15. The Ovoid.



Figure 16. Front of the New Theatre alla Scala after completion.

### 5.3 *The body overlooking via Filodrammatici and the inner body*

The buildings overlooking via Filodrammatici and those of the inner body have smaller dimension with respect to other parts of the theatre, and were meant to become offices. Thus, they did not require any complex solution, and traditional elements, such as reinforced concrete beams, have been used. A part of these structural elements have been cast against the masonry and the via Filodrammatici portico, which has maintained its original configuration.

The foundations of the historical part have been reinforced by means of micro-piles connected by a

transversal beam. Particular care has been taken when connecting the new part of the building to existing structures, in order to increase the safety level of the latter.

### 5.4 *The structures of the monumental part*

The site investigations ordered by the Milan Municipality during the design stage, together with a new geometric survey of the building, allowed to ascertain with good precision where the bearing structures of the monumental body were located.

The bombardments in 1943 and the following reconstruction and modifications carried out in the 60 s and 70 s, have considerably modified the original layout designed by architect Piermarini, that is nowadays limited to the perimeter walls of the hall.

The project of the structural interventions on the monumental part has been preceded by an accurate analysis of the existing structural elements and of the materials they were made of, in order to evaluate their bearing capacity and whether they were fit to sustain the extra loads required by the use of the theatre.

As for the floors, sustained by vaults or by wooden or steel beams, the static tests have given, with few exceptions, good results, thus limited reinforcing works have been needed.

As for the wooden boxes that are placed along the perimeter of the hall, it has been ascertained that they had lack of stability in the horizontal direction and weak connections between wooden pillars and border beams.

To obviate these problems, low impact interventions have been studied: they had, as far as it was feasible, to involve technologies already used in the original state, which had to be modified as little as possible.

The global stability of the wooden structures is assured by steel bracings, having such a geometry that they are hidden by the roofing panels. The connections have been reinforced by light steel inserts and made integral by means of modern riveting.

## 6 THE CONSTRUCTION SITE

Before starting the demolition phases, provisional steel support structures have been erected in order to sustain the historical parts of the building which were intended to be maintained.

### 6.1 *Provisional support structures and demolitions*

The masonry along via Verdi has been fixed, by means of plates and rods, to new steel buttresses erected outside the construction site.

In order to proceed in a rational way, the interventions have been scheduled following a “geographical”

criterion which brought the division of the enormous complex into four areas:

- Area one: the scenic tower and the backstage;
- Area two: the area overlooking the backstage;
- Area three: the so called Piccola Scala and rooms nearby;
- Area four: all areas between area three and the monumental part of the building overlooking via Filodrammatici.

The demolition phase started from the above towards the lower parts, following a precise schedule and with the aid of a powerful crane that, after the preliminary demolition of the roofing, was placed in the middle of the scenic tower. Thanks to its placing, the crane served the entire building site, allowing the cutting and lowering of the most important structures, such as the tower roofing reinforced concrete trusses, and the mobilization of all elements of middle and big dimensions that can not be simply left free to fall to the ground. All demolitions have been performed with the most advanced technologies by highly qualified workers, who worked with elevated safety standards, operating machineries with remote controls and keeping everything under control with camcorders and from distant point of observations.

The intervention has produced more than 20,000 cubic meters of debris, the removal of which has been specifically planned. The congested traffic in the centre of Milan and the impossibility of certain activities to be performed daytime have made it necessary to remove the debris night time only.

In order to unload the debris to the recycle stations more than 1000 travel of 3 or 4-axles lorries have been necessary.

During the demolition phases 500 t of steel had already been separated from wooden materials, so that the latter did not mix up with concrete or masonry. The only space available for the storing or the building material outside the working area was that obtained fencing in one of the lanes in via Verdi. The other lane, with few exceptions, was always passable.

## 6.2 Excavation and foundations

The excavation phase has been monitored by means of instruments installed before the starting of the demolition stage, and by topographic surveys.

At each stage, during the installing of the provisional tension rods, data on the strain state of the bulkhead and of the structures supported by it have been collected. These data, summarized into tables and diagrams, allowed an instant and effective acknowledgment of possible anomalous strain processes or settlements.

The low values found have exceeded even the most optimistic previsions concerning the deformability of the earth sustaining structure.

The excavation works to  $-18.60$  m below ground level were carried out in complete safety and with no consequence whatsoever for the surrounding buildings.

An important feature is represented by the 1.20 m thick concrete bed at the bottom of the pit. The need of a good waterproofing has determined the casting to be made in a limited number of phases, in order to minimize the interfaces between concrete of different ages.

## 6.3 Cast in place and pre-cast structures

Given the placing of the theatre in the centre of a busy city, it has been necessary to deal with elements of limited dimensions that could be assembled on site. This has been the case of the bearing structures of the elliptic body and of the roofing structures of the pit. Cast in place and pre-cast structures.

Given the placing of the theatre in the centre of a busy city, it has been necessary to deal with elements of limited dimensions that could be assembled on site. This has been the case of the bearing structures of the elliptic body and of the roofing structures of the pit.

The big bearing beam of the elliptic body have been assembled in only 12 days between the beginning and the middle of January 2004.

In June 2004, with the same speed, the roofing of the scenic tower has been assembled.

Having 5 cranes (6, if we consider the one used for the demolitions, then removed) made it possible to minimize the downtimes. On the other hand, a good deal of attention has been required to the personnel which operated the cranes.

The big wall beams were erected with subsequent castings by means of metallic formworks. This construction method required, in the first place, the building of very high scaffoldings which would later support the formworks.

Having at disposal a fixed concrete pump has considerably increased the speed of casting of bigger casts.

For smaller volumes it has been chosen to transport the concrete by means of the cranes.

## 7 DURATION AND GENERAL DATA ON THE WORKS

Beginning: May 2002

Works on monumental part: May 2002–October 2004

Demolition works: June 2002–November 2002

Special foundations: December 2002–May 2003



Scenic tower: June 2003–June 2004 (16.000 cubic metres of concrete)  
 Roofing of scenic tower: June 2004 (1860 t of steel)  
 Elliptical body: January 2004–April 2004 (140 t of steel)  
 Lateral body along via Filodrammatici: March 2003–March 2004  
 Finishing works: September 2004–December 2004  
 Total labour: 98.700 hours  
 Technical Staff: 15 technician and administrators  
 Contractor Staff: 22 technician and administrators  
 Cost: 55 million euros  
 Opening: 7th December 2004 with the opera: “*Europa Ritrovata*” by Giovan Battista Salieri  
 Director: Riccardo Muti.

## 8 DESIGN STAFF

The design staff for the new structure was composed as follows:

- original architectural project: Giuliano Parmegiani;
- executive architectural project: Mario Botta;
- architecture and restoration of the monumental part: Elisabetta Fabbri;
- scenic plants: Franco Malgrande;
- original structural project project: Francesco Martinez y Cabrera<sup>†</sup>, Gabriele Salvatoni, Pier Giorgio Malerba;

- executive project of general structures: Aldo Bottini, Nicola Malatesta, Sergio Sgambati of BMS Progetti S.r.l., Milano, with Alberto Gentina, Alessandro Biondi, Gabriele Weisz;
- executive project of the monumental part: Emanuela Cristante, Carlo Kehrer, Roberto Uslenghi;
- special foundations problems: Paolo Marcellino.
- field engineering: Stefano Tugnoli, Mauro Turrini.

The Contractor was the temporary association of Consorzio Cooperative Costruzioni, Flli Panzeri S.p.A., DEC S.p.A.

## ACKNOWLEDGMENTS

Acknowledgements to Mr. Antonio Acerbo of the Milan Municipality, Project Manager and Works Director.

## REFERENCE

La Nuova Scala: Il Cantiere, il Restauro e l'Architettura, Marsilio Editore, Venezia, Dec. 2004, [www.marsilioeditori.it](http://www.marsilioeditori.it)

# Life-cycle assessment of marine civil engineering structures

T. Moan

*Centre for Ships and Ocean Structures and the Department of Marine Technology,  
Norwegian University of Science and Technology, Trondheim, Norway*

**ABSTRACT:** Based on operational experiences with offshore structures it is argued that adequate structural safety should be ensured by proper design, fabrication and operational criteria as well as by proper quality assurance and control through the life cycle. In this paper the focus is on design, inspection and repair procedures to ensure adequate safety with respect to degradation. While design and inspection criteria in modern codes have been calibrated on a generic basis, particular features of individual structures imply that it is necessary to update the initial inspection plan based on experiences obtained after fabrication and during operation. In this connection fatigue cracks are of special concern. Recent efforts to establish rational, reliability-based procedures for life cycle assessment of fixed offshore platforms are outlined. It is emphasized that the reliability methods should be calibrated to the semi-probabilistic approach that current codes are based on; as well as to operational experiences.

## 1 INTRODUCTION

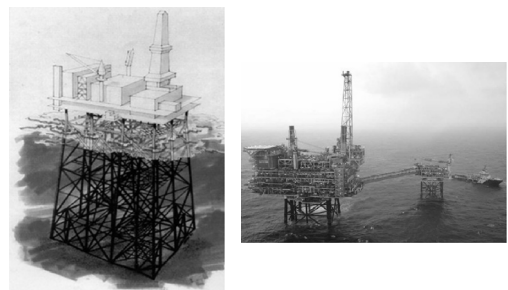
A variety of platform types are applied in the offshore oil and gas industry in the exploitation of hydrocarbons from beneath the seabed. Their primary function is to provide support of facilities for drilling for or production of the oil and gas. In this paper the focus is on the most common type of offshore platform, namely the jacket structure. Fig. 1 show typical jacket structures. Adequate performance of offshore structures is primarily ensured by designing them for a service life of 20 years or more. *Serviceability criteria* are introduced by the owner to ensure that the structure functions as required *Safety requirements* are imposed to avoid ultimate consequences such as fatalities, environmental damage or property damage.

Operational experiences (e.g. WOAD, 1996) show that accidental actions or abnormal resistance contribute significantly to failures of offshore structures. Such events can commonly be traced back to errors in design, fabrication or operation. To limit the risk of undesirable events it is therefore primarily important to avoid errors by those who do the work in the first place. Secondly, it is crucial to carry out quality assurance and control in all life cycle phases. An additional safety measure is to design the structural system to avoid global (system) failure due to the accidental damage. In principle, the structure can be designed to resist the accidental action locally (without damage) or by alternate paths.

Inspection and monitoring (IM), and, if necessary, maintenance and repair (MR) are also important measures for maintaining the adequate safety level,

especially with respect to fatigue, corrosion and other degradation phenomena. A particular issue for fixed platforms is the fact that the sea bed sometimes subsides when hydrocarbon reservoirs are emptied. This may increase the likelihood of direct wave loads on the deck structure, which normally is not supposed to be exposed, and hence the overall loading.

It is often found more economical to use existing structures than new buildings. Hence, there might be a need to reassess existing offshore structures during operation, for instance, because of planned change of function or occurrence of damage or need to extend the service life, see ISO 2394, ISO 19900, Dunlap and Ibbs (1994). A majority of the 5000 fixed offshore production platforms in the world have been operated more than the initially planned service life of 20 years.



a) Over-/underwater drawing of a jacket  
b) Above water photo of jackets and a supply vessel

Figure 1. Typical jacket platforms.

Since structural modifications to maintain acceptable safety level are much more expensive for existing structures than at the initial design stage—before fabrication—other strategies to achieve the necessary safety for existing structures are pursued. For instance, information about material and geometrical properties that is collected during fabrication and validation of structural response that can be made during operation, imply reduced uncertainties in predicted resistance and load effects and hence smaller safety margins (Moan, 2000).

The offshore industry early recognized that predicted structural loads and their effects as well as resistance are subjected to uncertainties. For this purpose risk and reliability methods were adopted to make more rational decisions, see e.g. the overview by Cornell (1995) and Moan (1995). In particular, reliability methods have especially been used to calibrate ultimate strength criteria (Fjeld, 1977; Moses, 1987; Lloyd & Karsan, 1988 and Jordaan & Maes, 1991; Moan, 1988). An evaluation of previous efforts on reliability-based calibration of offshore codes was provided by Moan (1995) in conjunction with the ISO effort to harmonize codes for offshore structures (ISO 1990, 1994). Assessment of degrading offshore structures involves significant uncertainties associated with the load effects and resistances, due to the large variability inherent in the degradation processes and the uncertainty associated with inspection approaches. Reliability methods are, hence, crucial to support decisions about safety and economy of degrading structures. Significant developments of structural reliability methodology, including Bayesian updating techniques, have taken place since the 1980's, as outlined e.g. by Madsen et al. (1987) and Melchers (1999). To achieve consistent design and inspection criteria, fatigue design criteria should be calibrated to reflect the consequences of failure and inspection plan (Moan et al., 1993).

While this calibration is done on the basis of the generic information available at the design stage, it is important that information obtained e.g. by inspections during operation, is used to update the inspection plan. This fact means that the IMMR efforts need to be dedicated to each individual structure, in contrast to ULS criteria which are based on a generic code calibration. However, service experiences from other structures with similar geometry, loading and site of operation could obviously also be utilized to update IMMR plans for a given structure.

To rely upon inspection and repair it is necessary that there is ample time to detect and remedy cracks during operation. This feature is ensured by a characteristic fatigue life of at least 20 years (i.e. a mean life of about 60 years). Similarly, adequate design on the corrosion protection or allowance would normally also ensure that corrosion would develop relatively slowly

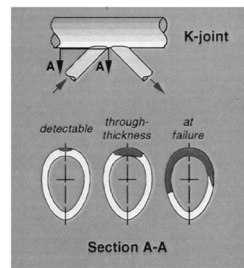
and become a safety problem only in case of lack of follow-up during operation.

The aim of this paper is to describe methods for management of an adequate safety level of fixed offshore steel structures in view of degradation processes during their life cycle. Particular focus is on how design for robustness, choice of inspection method and schedule inspection, maintenance and repair actions are combined to achieve the desired safety.

## 2 IN SERVICE EXPERIENCES

An assessment of the detailed causes of catastrophic accidents, such as that of the platforms Ranger I in 1979, Alexander Kielland in 1980, Ocean Ranger in 1982, Piper Alpha in 1988 and P-36 in 2001, as well as of accident statistics obtained from the World Offshore Data Bank (WOAD) is given by Moan (2004). It is emphasized that the causes of accidents should be assessed both from the technical and physical as well as from the human and organisational point of view. This is because the main causes of structural failures can be traced back to abnormal resistance or accidental actions due to human errors and omissions.

Ageing of offshore structures is a complex process of corrosion and crack growth (Figure 2), which is influenced by many factors. In-service experiences are therefore crucial to support laboratory data and theoretical considerations. An overview of experiences with fatigue cracks in offshore structures operating in the North Sea is given by Moan (2005). A brief account of experiences with cracks and corrosion in jackets is given below.



a) Crack growth in a tubular K-joint



b) Fracture of a tubular joint



c) Boat damage



d) Corrosion damage

Figure 2. Typical damages.

For jacket structures consisting of slender members, fatigue failures are confined to limited areas of the structure; namely the tubular joints where significant bending stresses occur. Proper fatigue design practice for jackets (in the North Sea) emerged around 1970–80. Due to lack of access inside the underwater jacket structure, inspections are carried out by divers or by remotely operated vehicles. This fact implies in general much higher inspection/repair costs per joint than for large volume structures. A significant amount of inspections has been devoted to North Sea fixed platforms since the last part of 1970, and especially after the fatigue failure of the Alexander Kielland platform in 1980. Vårdal and Moan (1997) compared cracks observed in about 4000 inspections of North Sea jackets with theoretical predictions. It was found that the number of predicted propagating cracks is typically 3 to 10 times larger than predicted. It was found that the theory is more conservative for new structures. On the other hand, it should be noted that 2–3% of the fatigue cracks detected, occur in joints which are not predicted to be susceptible to fatigue. This fact is attributed to the occurrence of gross fabrication defects, e.g. due to: abnormal initial defect size, e.g. due to wet electrodes; abnormal crack propagation caused by overprotection or loss of protection; abnormal eccentricity, or other bad design fabrication detailing; error in load (stress) analysis (environmental conditions, method, stress concentration factor . . .). Evidence from in-service inspections and laboratory investigations of fatigue clearly show that “abnormal” defects could occur. The possible occurrence of such defects could have implication on the design and inspection procedures. Hence, it may be considered whether such events should be taken as a damage condition for ALS criteria. The inspection strategy also needs to reflect the situation. Catastrophic accidents initiated by fatigue failures occurred for a jack-up and semi-submersible platform in 1979 and 80, respectively, due to inadequate fatigue design, inspection and reserve capacity.

The general corrosion rate for unprotected steel in seawater is about 0.1 mm/year. Corrosion rates fluctuate between 0.04 to 1.2 mm/yr and in some cases up to 3 mm/yr have been found in some ballast tanks (TSCF, 1997). Corrosion rates in ships exhibit a very large scatter depending upon location in the structure as well as the environmental conditions, e.g. North Sea as compared to Gulf of Mexico. Hence, follow-up of corrosion in service for individual ships becomes important. Normally offshore production platforms are protected with coating or by a cathodic protection. As soon as the corrosion protection system breaks down, free corrosion effects start to take place on the surface of the structural component, which implies a thickness reduction.

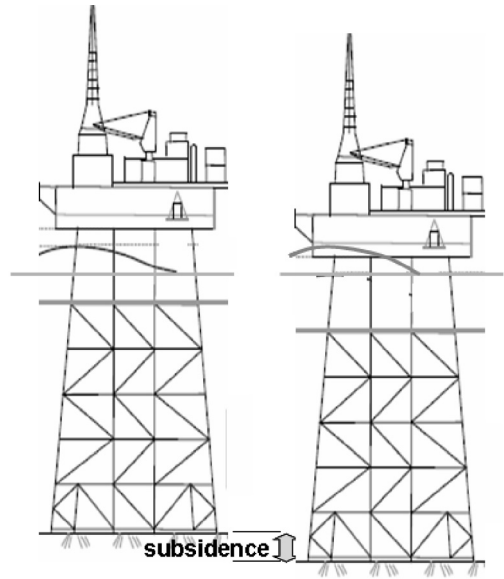


Figure 3. Platform subsidence.

A particular issue is concerned with the sinking of the seabed due to the emptying of the hydrocarbon reservoirs. This so-called subsidence implies that the air-gap between the sea level and the deck is reduced with an increased likelihood of waves hitting the deck and causing extreme loading, see Fig. 3.

### 3 LIFE CYCLE SAFETY MANAGEMENT

#### 3.1 General

Safety is a significant challenge for offshore structures due to the demanding ocean environment and the fire and explosion risk associated with hydrocarbons. While fatalities caused by structural failures would be related to global structural failure, smaller damages may result in pollution or property damage, which is expensive to repair, especially for underwater structure.

Various safety measures are required to control risks associated with different hazards. Primarily, gross errors should be avoided by adequate competence, skills, attitude and self-checking of those who do the design, fabrication or operation in the first place; and by exercising “self-checking” of their work. In addition, quality assurance and control (QA/QC) should be implemented in all stages of design, fabrication and operation. Moreover, as mentioned above, operational errors typically result in accidental actions such as fires or explosion. Such events may also be controlled by detecting the gas/oil leak and activating valve shut in; extinguishing of a fire by a deluge system

activated automatically etc.—often denoted “Event Control”.

Despite the efforts made to avoid error-induced accidental actions or resistance, they cannot be completely eliminated. For this reason Accidental Collapse Limit State (ALS) criteria are introduced to prevent progressive failure. The ALS is therefore also commonly denoted Progressive Failure Limit State.

To ensure adequate safety of degrading structures due to corrosion and crack growth, proper design and quality assurance of design as well as inspection during fabrication and operation are required. Relevant design criteria and inspection issues are briefly considered in the following.

### 3.2 Design

The determination of scantlings, material qualities, fabrication procedures and inspection plans during design need to be based on generic knowledge that reflect previous experiences with the relevant type of structure or related structures. The limit states for safety are indicated in Table 1. The FLS and ALS criteria are briefly commented upon in the following.

The fatigue limit state is defined by a crack size that represents an ultimate limit (ISO 19900, ISO 2394). However, partly because the critical crack size depends upon the load level, fatigue failure is commonly defined as the occurrence of a visible crack, or fracture (of test specimens with a small cross-sectional area). In particular the differences in the relationship between crack size and time for a plane plate as compared to a tubular joint, as shown in Fig 4, is noted. In a

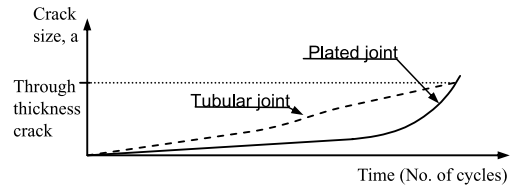


Figure 4. Crack size development in flat plate and tubular joint (adapted according to information in e.g. Almar Næss, 1985).

monocoque structure, like a ship hull, fatigue failure is normally taken to be a through-thickness crack. Final fracture in such structures will occur after significant propagation of the through-thickness crack (Bach-Gansmo et al, 1987). Fatigue design criteria for offshore structures are primarily based on consideration of wave induced loads, the Miner-Palmgren’s rule for fatigue damage accumulation and SN-curves that have been obtained by laboratory experiments.

The cumulative damage is commonly obtained by assuming that the SN-curve is defined by  $NS^m = K$  and the number,  $n(s)$  of stress ranges is given by the long term stress range probability distribution, often modelled by a Weibull distribution, with scale parameter  $A$  and shape parameter,  $h$ .  $A$  is  $A = s_0 / (\ln N_0)^{1/h}$  where  $s_0$  is given by  $P(s \geq s_0) = 1/N_0$ . The cumulative damage,  $D_d$  in a period,  $t$  with  $N_t$  cycles, is then given by

$$D_d = \sum_i \frac{n_i}{N_i} = \sum \frac{n(s_i)}{N(s_i)} = \frac{N_t}{K} \left[ \frac{s_0}{(\ln N_0)^{1/h}} \right]^m \Gamma(m/h + 1) \quad (1)$$

where  $\Gamma()$  is the Gamma function. Analogous expressions can be established when the SN-curve consists of two segments. Fracture mechanics methods have been adopted to assess the different stages of crack growth more accurately. Such detailed information about crack propagation is also required to plan inspections and repair, as briefly explained in Section 4.3.1.

At the design stage structural scantlings and local geometry to achieve a desired fatigue life and robustness in case of fatigue failure as well as inspection, maintenance and repair plan are decided. During fabrication it is ensured that the intended geometry is achieved and that the defects are below tolerances. Section 3.3 addresses the safety actions during operation.

Corrosion is not a separate limit state for offshore structures but reduces the thickness and hence, both the ultimate and fatigue strength. Moreover, the crack growth rate in a free corrosion is 3 times larger than for a protected structure. The design measure is to provide

Table 1. Safety criteria.

Limit states	Description	Remarks
Ultimate (ULS)	Overall “rigid body” stability Ultimate strength of structure and foundation	Different types of criteria apply Component design check
Fatigue (FLS)	Failure of (welded) joints	Component design check depending on residual system strength after fatigue failure
Accidental collapse (ALS)	Ultimate capacity <sup>1</sup> of damaged structure (due to fabrication defects or accidental loads) or operational error	System design check

<sup>1</sup>Capacity to resist “rigid body” instability or total structural failure.

a corrosion protection and a thickness allowance. Considerations at the design stage only ensure that there will be a reasonable time during operation before the thickness is reduced to the extent that actions to maintain safety level need to be carried out. This is essentially based on economic considerations. During fabrication it is ensured that the intended quality of possible coating for corrosion protection is achieved.

The main structural safety criterion is the so-called Accidental Collapse Limit State (ALS) which is motivated by the design philosophy that “small damages, which inevitably occur, should not cause disproportionate consequences”. The ALS check specified in NORSOK N-001 (1998) is an explicit and quantitative survival check of a damaged structural system. The damage is assumed to be due to accidental loads such as fires, explosions, ship impacts or fabrication defects corresponding to an annual exceedance probability of  $10^{-4}$  and should be identified by risk analysis (NORSOK N-003, 1999, Vinnem, 1999), considering relevant risk reduction actions such as e.g. use of sprinkler/inert gas system or fire walls for fires and fenders for collisions. To estimate damage, e.g. permanent deformation, rupture etc of parts of the structure, nonlinear material and geometrical structural behaviour need to be accounted for. See e.g. NORSOK N-001 (1998) and NORSOK N-004 (1998). The structure is required to survive the various damage conditions—without global failure, considering environmental loads with an annual exceedance probability of  $10^{-2}$ . Compliance with this requirement can in some cases be demonstrated by removing the damaged parts, and then accomplishing a conventional ULS component design check. It is found that a nonlinear finite element approach especially yields more realistic predictions of the ultimate strength of a damaged system than a conventional approach based on a linear global analysis and an ultimate strength assessment of the structural components (e.g. Skallerud and Amdahl, 2002; and Ultiguide, 1999). Nonlinear analysis methods are also applied to determine the ultimate global capacity after fatigue-induced fracture of members in connection with inspection planning (Moan et al., 2002b).

### 3.3 Inspection, maintenance and repair during fabrication and operation

Current design and inspection approaches for offshore structures are implemented in new codes issued by ISO 19900 (1994) and NORSOK N-001 (1998). The fatigue design criteria in such modern offshore codes depend upon the consequences of failure and access for inspection, see e.g. Table 2. The consequence measure in N-001 (1998) is based on the Accidental Collapse Limit State, as briefly described above. Slightly different criteria have been proposed by API (Karsan, 2005).

Table 2. Fatigue design factor,  $FDF = 1/\Delta_d$  to multiply the planned service life to obtain required design fatigue life (NORSOK N001, 2002).

Classification of structural components based on damage consequence <sup>1</sup>	Access for inspection and repair		
	No access or in the splash zone	Accessible (inspection according to generic scheme is carried out) Below splash zone	Above splash zone or internal
Substantial consequences	10	3	2
Without substantial consequences	3	2	1

<sup>1</sup>The consequences are substantial if the Accidental Collapse Limit State (ALS) criterion is not satisfied in case of a failure of the relevant welded joint considered in the fatigue check.

Moan et al. (1993) show the allowable cumulative damage ( $\Delta_d$ ) in design can be relaxed when an inspection and repair strategy is implemented. Hence, it was shown that the target level, corresponding to a design criterion with  $FDF = 10$  can be reached by a  $FDF = 4$  and  $FDF = 5$  for a tubular joint in a jacket and a tether butt weld, respectively, when inspections are carried out every 4th year using NDE methods with a mean detectable crack depth of 1.5 mm. This calculation is based upon predictions at the design stage, i.e. with a predicted outcome and not a known outcome of inspections. The reason for the larger relaxation of the fatigue design criterion for tubular joints is that cracks grow at a more constant rate over the plate thickness of a tubular joint than a plane plate. It is seen that these results indicate that the NORSOK code is non-conservative for these cases.

At the design stage only generic data about the variability and uncertainty that affect the reliability, is available. Hence, it is important to update the models on the basis of in-service experiences on an individual basis for each structure, depending on its life cycle history (Moan, 2005). By continuously updating the safety measure depending on actions initiated during use, decisions regarding inspection scheduling, maintenance and repair can be properly made, to ensure an acceptable safety level.

### 3.4 Cost-benefit optimization of design criteria and inspection plan for crack control

In addition to directly using the codified design and inspection criteria, cost-benefit optimization of the total expected costs over the service life may also be used to establish such criteria (e.g. Faber et al., 1992;

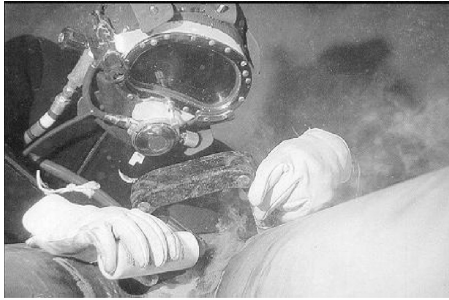


Figure 5. Underwater inspection by diver.

Moan, 2005; Straub and Faber, 2007). Then, fabrication costs as well as expected inspection, repair and failure costs should be considered.

The cost terms vary between the different types of platforms and between different areas of a given platform. The costs would also depend upon the geographical region. The costs of inspection, repair and failure is illustrated in the following by considering jackets in the North Sea.

Fixed platforms, e.g. jackets are inspected at the offshore site, partly below and partly above the water. Underwater inspections (Figure 5) are based on diver or ROV supported vessel under difficult conditions, due to the presence of marine growth, bad visibility, wave motions, etc. Moreover, underwater NDE are expensive because a time-consuming cleaning of the welded joints and diver support vessels, are needed (MTD 1992).

Eddy Current and Magnetic Particle inspection costs per joint might be US\$ 25–50 000. Flooded member detection may amount to US\$ 5–25 000. The cost of repairing a single tubular joint under water, may amount to US\$ 3–15 mill. However, repair of cracks which are less deep than 25% of the plate thickness, implies limited costs. This is because they are repaired by grinding which is carried out anyway to gauge the crack depth. Other failure costs can be neglected due to sufficient remaining fatigue life after through thickness crack or reserve capacity after failure of the relevant member.

Cost-benefit analyses that aim at balancing the total costs, need to be made based on generic data and hence, apply in principle for a fleet of platforms, as discussed by Straub and Faber (2007). The follow-up during operation generally needs to be on an individual platform basis. In this paper the focus is on individual platforms.

## 4 RELIABILITY AND RISK ANALYSIS

### 4.1 Overview

A rational safety management needs to be based on measures of the risk associated with relevant hazards

and failure modes. In general a quantitative risk analysis (QRA) (e.g. Vinnem, 1999), needs to be used to consider all uncertainties that affect the risk in the life cycle; including the effects of gross errors in design, fabrication or operation. However, if the risk assessment is limited to structural failures induced by natural and man-made hazards resulting from normal operations, structural reliability analysis (SRA) can be applied. This fact implies that the failure probability calculated by SRA will be much smaller than the total failure frequency.

In principle, design can be made by designing for a given target risk or reliability level. However, commonly risk or reliability methods have been applied to calibrate semi-probabilistic design codes for easy practical use.

### 4.2 Quantitative risk analysis

The application of Quantitative Risk Assessment (QRA) in the offshore industry has evolved since about 1980 (Moan and Holand, 1981, NPD, 1984). The Piper Alpha Disaster (PA, 1990), was the direct reason for introducing QRA in the UK (HSE, 1992). Risk analysis methodology is currently applied to validate offshore facilities at large, as outlined by e.g. Vinnem (1999). The focus herein is on the risk associated with total loss of offshore structures induced by accidental actions and abnormal resistance. Risk analyses to determine damage in terms of abnormal resistance due to fabrication defects, is generally not feasible. Some considerations of possible abnormal resistance associated with fatigue are made by Moan (2008) to shed some light on these issues.

### 4.3 Structural reliability analysis

#### 4.3.1 Component reliability

In a narrow sense *structural reliability* is the *probability* that a structure will not exceed any of a specified set of limit states (ultimate or serviceability) during a specified *reference period*. In general the failure probability for a *time-invariant* reliability problem, is

$$P_f = P [g(\mathbf{x}) \leq 0] \\ = \int \int_{g(\mathbf{x}) \leq 0} f_{\mathbf{x}}(\mathbf{x}) d\mathbf{x} = \int \int_{\mathbf{x}} I[g(\cdot)] f_{\mathbf{x}}(\mathbf{x}) d\mathbf{x} \quad (2)$$

where  $g(\mathbf{x})$  is the limit state function,  $\mathbf{X}$  is the set of  $n$  random variables used to formulate the problem,  $f_{\mathbf{x}}(\mathbf{x})$  in the joint probability density of the vector  $\mathbf{X}$ .  $I[g(\cdot)]$  is an indicator function, which is 0 and 1 for  $g(\mathbf{x}) > 0$  and  $g(\mathbf{x}) \leq 0$ , respectively. The expression  $g(\mathbf{x}) \leq 0$ , corresponds to failure. The integral of Eq. (2) may be calculated by direct integration, simulation or FORM/SORM methods (First Order/Second Order Reliability Method) as described in, e.g., the textbooks by Madsen et al. (1986); Ditlevsen and



Table 3. Relationship between  $\beta$  and  $P_f$ .

$\beta$	1.0	1.5	2.0	2.5
$P_f$	0.159	0.067	0.023	0.006
$\beta$	3.0	3.5	4.0	4.5
$P_f$	$0.14 \cdot 10^{-2}$	$0.23 \cdot 10^{-3}$	$0.32 \cdot 10^{-4}$	$0.34 \cdot 10^{-5}$

Madsen (1996) and Melchers (1999). Methods for reliability analysis of components, especially with time invariant properties, have become mature, as born out by the state-of-art regarding commercial software packages available (e.g. Schuëller, ed., 2006).

The reliability index,  $\beta$ , is defined as:

$$\beta \equiv -\Phi^{-1}(P_f) \quad (3)$$

where  $\Phi(\cdot)$  is the cumulative standard normal distribution. Hence, the *reliability index* is uniquely related to the *failure probability*,  $P_f$ , as shown in Table 3.

Determination of the failure probability when the resistance is degrading and the structure is subjected to a stochastic loading, require a truly time-variant approach, see e.g. Madsen *et al* (1986). Fortunately, accurate simplified methods are available (e.g. Ayala and Moan, 2006).

The probability of fatigue failure is a function of the time period,  $t$  which is considered. The distribution function of the time to failure is then  $F(t) = P_f(t)$ . Alternatively, the reliability may be expressed by the hazard function:

$$h(t) = P[T \leq (t + \Delta t) | T > t] \\ = \frac{P[t \leq T \leq t + \Delta t]}{\Delta t \cdot (1 - P[T \leq t])} = \frac{dP_f(t)/dt}{1 - P_f(t)} \quad (4)$$

The failure function  $g(t)$  for fatigue failure in the time  $t$ , may be obtained on the basis of the SN-approach

$$g(t) = \Delta - D_d \quad (5)$$

where  $D_d$  is given by Eq. (1) and where  $\Delta$  is the fatigue damage at failure, which is 1.0 according to Miner and Palmgren, but actually is a random variable with a mean value slightly less than 1.0. Several researchers have provided models for fatigue reliability assessment based on this framework Wirsching (1983) and Wirsching and Chen (1988) proposed a simple reliability model for fatigue reliability for offshore structures.

Alternatively, a fracture mechanics approach based upon Paris-Erdogan's crack propagation law (e.g. Almar-Næss, 1985) may be adopted:

$$\frac{da}{dN} = C(\Delta K)^m = C(\bar{S} \cdot Y(a)\sqrt{\pi a})^m \quad (6)$$

where  $a$  is crack depth,  $N$  is number of cycles,  $C$  is crack growth parameter,  $m$  is the inverse slope of the SN curve, and  $\Delta K$  is the stress intensity factor range

which is given as a function of  $a$  and depends on the geometry and loading, see e.g. BS 7910 (1999).  $\bar{S}$  is the equivalent constant stress range, given by

$$\bar{S}^m = [s_0/(\ell n N_0)^{1/h}]^m \Gamma(m/B + 1) \quad (7)$$

The limit state function may then in principle be written as:

$$g(\cdot) = a_f - a = a_f - \int_{a_0}^a da \quad (8)$$

where  $a_f$  is the crack size at failure. For special cases, Eq. (6) can be integrated to yield the crack size,  $a$  as a function of the number of cycles,  $N$ . Then Eq. (8) can be explicitly expressed in terms of the initial and critical crack sizes and the crack growth parameters. Eq. (8) can also be used in conjunction with Monte Carlo simulation, as illustrated in the comprehensive overview by Yang (1994). Efficient models suitable for application of FORM/SORM reliability analyses e.g. have been established by Madsen (1985) and Madsen *et al* (1987). Treatment of more general formulations of the crack propagation law (Eq. (6)) has been dealt with by e.g. Celant *et al.* (1983), Kam (1991) and Ayala and Moan (2007).

While in principle the fracture mechanics approach represents a refinement compared to the SN formulation the large uncertainties relating to the initial stages of crack growth suggest that the fracture mechanics formulation is calibrated by an SN-approach (Ayala-Uraga and Moan, 2007). Recently, reliability models that consider the second stage of crack propagation, namely of through the thickness cracks in stiffened plates, have been developed (Moan and Ayala-Uraga, 2007).

*Reliability updating.* The failure probability,  $P_f$ , of a specific structural component can be updated through additional information obtained by response measurement or observed damages. For instance when inspections are made with no detection of cracks in joint  $i$  after a time,  $t$  in-service, the failure probability of joint  $j$  may be updated as follows

$$P_{f_i,UPj} = P[(g_i(\cdot) \leq 0) | IE_j \leq 0] \\ = P[(g_i(\cdot) \leq 0) \cap (IE_j \leq 0)]/P[IE_j \leq 0] \quad (9)$$

where the inspection event for the  $j$ th joint is  $IE_j = a(t) - a_d$ ; where  $a_d$  is the detectable crack size; as described e.g. by Madsen (1987), Madsen *et al.* (1990) and Jiao and Moan (1990). The updated  $P_f$  of joint  $i$  based on the inspection of joint  $j$  depends on the correlation between the  $g_i(a)$  and  $IE_j$  events as illustrated by Moan and Song (1998).

As an alternative to using inspection events, the distribution of each random variable may be updated based upon the inspection information (e.g. Itagaki *et al.*, 1983, Shinozuka and Deodatis, 1989 and Yang, 1994). However, if several variables are updated based



on the same inspection event, the increased correlation between the updated variables due to the common information used, should be accounted for. The updating procedures mentioned so far provide updating e.g. of  $P_f$  or the random variables associated with individual joints. Rather than updating the  $P_f$  of individual joints Vårdal and Moan (1997) used observed crack occurrences identified in inspections of 30 North Sea jackets to establish an empirical correction of the prediction method by correlating the calculated and observed occurrence rate of cracks.

**Inspection quality.** The quality of NDE methods for detection of cracks in metal structures is expressed by a probability of detection (POD) curve, which corresponds to the distribution function of detectable crack size  $a_d$  (Visser, 2002; Dover & Rudlin, 1996; Rudlin & Austin, 1996). The mean detectable crack depth for methods such as MPI, Eddy current, alternate current methods and ultrasonic inspection is 1.5–2.0 mm. Moan et al. (1997, 2002a) inferred a POD curve with exponential distribution with a mean detectable depth of 1.95 mm, based on data from 3411 underwater NDE inspections of tubular joints in jackets. It is reasonable to consider the data from the latter reference as an “upper bound” of the mean detectable crack size, considering the difficult environment condition under which inspections are made.

The reliability of assessing corrosion damage relates to the accuracy of thickness change.

**Uncertainties.** The failure probability is crucially dependent upon the uncertainty measures of load and resistance parameters. It is important that authoritative values of the stochastic variables are used.

**Calculation of reliability.** It is noted that the FORM/SORM methodology is approximate and should be validated by using “converged” Monte Carlo simulation (e.g. Ayala-Uraga and Moan, 2002). This is particularly important for calculating the probability of intersections of events.

**Validation.** The various models that constitute the reliability analysis method may be validated by (Moan, 2002b): using model tests or full scale measurements to validate wave induced nominal stress; model tests to validate hot spot stress and fatigue strength and the reliability model at large by direct comparison of predicted and observed crack occurrences. The comparison by Vårdal and Moan (1997) showed that the number of predicted propagating cracks was typically 3 to 10 times larger than predicted. This discrepancy can be traced back to uncertainties in the prediction of the (nominal) stress.

**Example 1.** Fig. 6 shows the cumulative failure probability and the (maximum) hazard rate after 20 years, as a function of the fatigue design factor, FDF. For the base case of uncertainty measures it is seen that the difference between the implied probabilities for a FDF of 1 and 10 is nearly three orders of

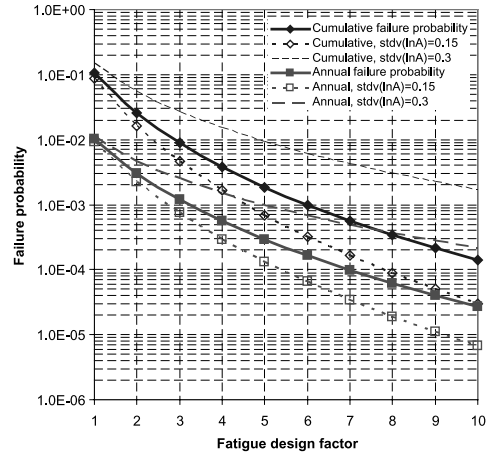


Figure 6. Fatigue failure probability and hazard rate for a welded joint in a structure in a harsh environment, as a function of the fatigue design factor FDF, which is multiplied with the service life to get the design fatigue life. The sensitivity to the uncertainty in the load effects is shown (Moan, 2004).

magnitude. The maximum hazard rate is about 1/10 to 1/4 of the cumulative probability, while the average hazard rate in 20 years is 1/20 of the cumulative probability.

The sensitivity of the implied hazard rate and cumulative failure probability to the uncertainty in the loading is also investigated. While in the base case the standard derivation of  $\ln A$  ( $A$ -scale parameter of the Weibull distribution of stress ranges) is 0.198, a lower bound of 0.15 and an upper bound of 0.30 are considered. The effect of the uncertainty measure is particularly significant for large FDFs.

Figure 6 also shows that the reliability level is critically dependent upon the design fatigue life. Good knowledge about calculated fatigue lives of all critical details and in-service experience on fatigue cracks is vital. Reduction of uncertainty in the loads, therefore, by using state-of-the-art methods in the analysis of old platforms may be worthwhile. In this way the effect of even gross errors made during initial design may be reduced.

**Example 2.** The initial crack size,  $a_0$  is very uncertain and may be abnormally large due to fabrication errors. Figure 7 shows the sensitivity of the reliability of a tubular and a plated joint with respect to the initial crack size for joints designed for a fatigue damage of either  $\Delta_d = 1/\text{FDF} = 1.0$  or  $\Delta_d = 1/\text{FDF} = 0.1$  for a 20-year service life. The uncertainty measures are based on Moan et al. (1994) while the weld magnification factor for the butt weld is calculated according to the recommendation of the BS-7910 (1999). The effect of the initial crack size,  $a_0$  is studied by assuming that it has an exponential distribution and a mean value

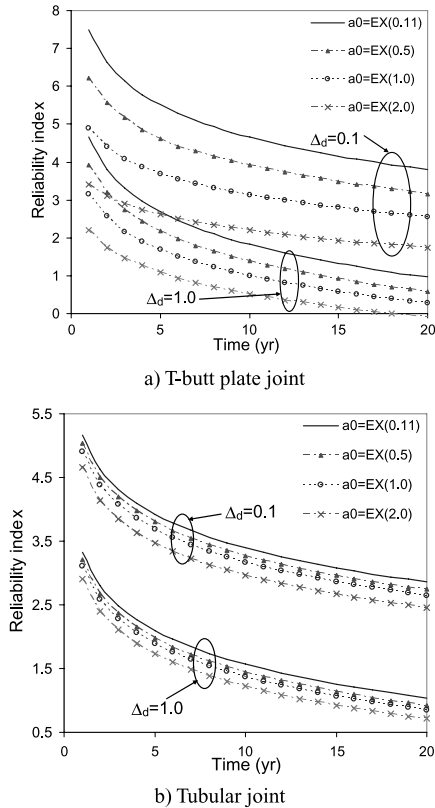


Figure 7. Sensitivity of the reliability to initial crack size ( $a_0$ ) for stress levels corresponding to both  $\Delta_d = 1/DFD = 1.0$  and  $\Delta_d = 1/DFD = 0.1$ .

between 0.11 and 2.0 mm. It is seen that the reliability of the flat plate is very sensitive to initial defect sizes that are smaller than the “detectable” crack size.

### 4.3.2 Systems reliability

Ultimate and fatigue design criteria in current codes are primarily based on component failure modes (limit states) and a linear global model of the structure to determine the load effects in the components.

Systems approaches are used in FLS and ALS design checks as indicated in Section 3.2. In reassessment of existing structures in the ULS, semi-probabilistic systems approaches are applied when simple conservative methods are insufficient (API, RP2A, 1993, 1997; Bea, 1993; Digré et al., 1995).

Systems approaches are attractive because the most significant failure consequences, and especially fatalities, are associated with system failure, and because a more realistic procedure would then pay in making decisions the very expensive possible strengthening of existing structures.

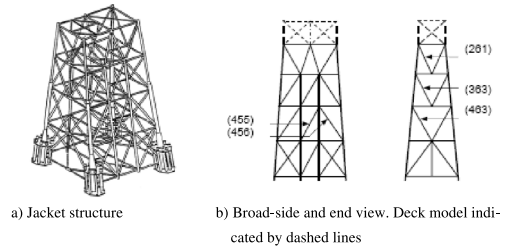


Figure 8. North Sea jacket.

System failure can be expressed mathematically by load—and resistance parameters relating to all failure modes for all structural components (members, joints, piles) and the probabilistic properties of these parameters (see e.g. Karamchandani, 1990; Moses and Liu, 1992; Shetty, 1992; Dalane, 1993 and Moan, 1994). Modeling of the uncertainties in loads and resistance variables of the components of the system is a crucial task, especially to estimate the correlation between variables in the different failure functions that represent the system. In general system reliability approaches become complex. Fortunately, for some systems, like jackets, accurate estimates of the systems failure probability under extreme sea loading can be achieved in many cases by considering a single system failure mode (e.g. De et al., 1989; and Wu & Moan, 1989). Then, the resistance ( $R_{sys}$ ) and load effect ( $S_{sys}$ ) are specified in terms of the base shear, or actually, the shear at the level of failure in a jacket. Assuming that both  $S_{sys}$  and  $R_{sys}$  are lognormally distributed, the annual reliability index  $\beta$  is

$$\beta = \frac{\ln [(B_R/B_S)REF]}{\sqrt{V_{R_{sys}}^2 + V_{S_{shear}}^2}} \quad (10)$$

where  $\mu$  and  $V$  denote mean and COV, respectively. The mean values for strength and load are related to their respective characteristic (nominal) values by

$$\mu_{R_{sys}} = B_R R_{c,sys} \quad \text{and} \quad \mu_{S_{sys}} = B_S S_{c,sys} \quad (11)$$

where  $B_R$  and  $B_S$  are bias factors. Subscript  $c$  indicates characteristic values. For  $S_{sys}$ , the characteristic value  $S_{c,sys}$  is defined as the most probable 100 years maximum load from the pushover analysis. For  $R_{sys}$ , the characteristic value  $R_{c,sys}$  is defined according to characteristic material properties. REF is defined as  $R_{c,sys}/S_{c,sys}$ . Typical values of  $R_{c,sys}$  and  $R_{c,d,sys}$  for the 8-legged North Sea jacket in a 109 m water depth shown in Fig. 8, are indicated in the Table 4. Damage in terms of removal of individual braces is considered as indicated in Fig. 8b.

The uncertainties for the load variable, are based on the API RP2A-LFRD calibration, (e.g. Moses and Larrabee, 1988) with some modifications which are relevant for the North Sea (Moan 1995).

Table 4. Residual strength of damaged North Sea jacket. Linear pile-soil behaviour (Moan, 2005).

Normalized strength	Loading and damage condition				
	Broad side loading			End-on loading	
	Brace 261	Brace 363	Brace 463	Brace 455	Brace 456
Ult. strength	2.73	2.73	2.73	2.89	2.89
$R_{c,sys}/S_{c,sys}$					
Res. strength	1.0	0.76	1.0	0.91	0.85
$R_{c,d,sys}/R_{c,sys}$					

Note:  $R_{c,sys}$ —ultimate strength,  
 $R_{c,d,sys}$ —ultimate strength of damaged platform.

The simple systems analysis method was extended to include fatigue failure modes, using the basic overload case as the reference case (Kirkemo, 1988; Moan, 2000). The system failure probability of an *inspected* structure, may be determined as follows:

$$P_{jSYS|up} = P[FSYS|I] \approx P[FSYS(U)] + \sum_{j=1}^n P[F_j|I] \cdot P[FSYS(U)|F_j] + \dots \quad (12)$$

where  $FSYS(U)$  is the overload system failure; and  $F_j$  the fatigue failure of component  $j$ . It is noted that the first term then covers all pure overload failure sequences, i.e. all kinds of failure modes like  $[FSYS|U_i, U_j, U_k, \dots]$ , and may be expressed by Eq. (10), as used in many requalification studies (API 1993/97). For a statically determinate system  $P[FSYS(U)|F_j]$  will be 1.0 since failure of each component implies system failure.

The formulation for updated failure probability in Eq. (12) is applicable when the inspection event  $I$  aims at *detecting cracks* before the failure of individual members, i.e. before they have caused rupture of the member. An alternative approach would be to apply visual inspection etc. to detect member failure, combined with a repair strategy (Moan, 2000).

A further simplification may be to update the failure probability of each joint based on the inspection of that joint (see e.g. Moan & Song, 1998).

#### 4.3.3 Limitation of structural reliability estimates

As mentioned above, the structural reliability analysis methodology accounts for failure and crack detection due to *normal uncertainties* in wave-induced loads (stresses) and fatigue resistance as well as normal variability of the inspection quality.

Cracks may also occur due e.g. to:

- abnormal initial defect size, e.g. due to wet electrodes.

- abnormal crack propagation e.g. due to corrosion fatigue caused by overprotection or loss of protection.
- abnormal local geometry (e.g. eccentricities) due to bad design or fabrication detailing.
- error in load (stress) analysis (environmental conditions, method, stress concentration factor . . .).

Due to the very nature (small size) of initial (fabrication) defects, an abnormal size of such defects often have been the cause of fatigue cracks. The experiences with e.g. jackets suggests that a small percentage (2–3%) of crack detections occurs in welds with a fatigue life which is many times the service life (Vårdal & Moan, 1997) and are, hence, caused by some “gross error”.

The effect of such an “abnormal” defect is significant, as described above in Section 4.3.1.

For a given inspection (with normal quality) with no crack detection in a joint with an abnormally large defect, the updating of  $P_f$  will be conservative.

However, the inspection itself can be subjected to gross errors. Thus, if abnormal defects are present in joints which are not inspected, the estimate of the failure probability will obviously be non-conservative. This fact should be accounted for in the estimate of the risk of system failure in view of the coverage of the inspection program.

#### 4.4 Target safety levels

Failure probabilities may be expressed as annual or service life values. The cumulative nature of fatigue suggests using the cumulative probability as an acceptance criterion. It is commonly accepted that the annual failure probability is most relevant when the consequences are fatalities, while the failure probability in the service life appears to be the most relevant when cost-benefit analyses are made.

As discussed e.g. by Moan (2002a), the target level should depend upon various factors such as the type of hazard and failure mode, the method to calculate the reliability, and the possible consequences in terms if risk to life, environment or economic loss. He also suggests to use a simplified approach in which target levels are defined separately for different hazards, failure modes, and phases. A certain portion of the total (target) failure probability may then be allocated to each case, assuming e.g. that the total failure probability is just equal to the sum of the individual probabilities. For instance, it may be convenient to apply a separate target level for each failure sequence implied by Eq. (12).

On the other hand, when considering fatigue reliability during the operation phase, the possible accumulation of fatigue damage during transport from the building site to the offshore site and during installation, should be included in a proper manner.

Regarding the effect of reliability methodology on selecting target values, a main issue is whether only normal uncertainties are considered or account of gross errors is to be made. Another aspect is whether normal uncertainties include both aleatory and epistemic or the aleatory uncertainty only. A final issue is the choice of distribution functions for the random variables in view of the tail sensitivity of reliability analysis.

In general it is recommended to calibrate the target level to that implicit in structures which are considered to have an acceptable safety, or modify it if this is not the case. Fatigue target levels may then be inferred from the cases e.g. in Table 2 preferably from cases which do not reflect the inspection effects but where fatigue failure implies “total loss”. The implicit failure probability should be estimated using the same reliability methodology as later will be used to demonstrate compliance with the target safety level. In this manner the structural reliability analysis will be a more robust tool for decision making. The implied failure probability for system failure due to fatigue would then be the following special case of Eq. (10); by omitting the inspection event,  $I$  and with  $P[FSYS|F_j] = 1.0$ ;  $P[F_j]$  is limited by the implied fatigue failure probability for an FDF equal to 10 (corresponding to substantial consequences). A simplified, practical approach is envisaged by separately considering each term of the sum in Eq. (12) and a corresponding target value. This approach has been applied in connection with inspection planning for jacket structures (Kirkemo, 1988; Moan et al., 1999).

## 5 INSPECTION, MONITORING, MAINTENANCE AND REPAIR PLANNING

### 5.1 Basic principles

The scope of the inspection, monitoring, maintenance and repair (IMMR) of concern herein is limited to strength degradation due to crack growth and corrosion, with an emphasis on the former phenomenon, and how IMMR should be managed by using reliability-based methods to ensure an acceptable safety level, yet, at a minimum of total expenditure.

The procedure for reliability-based assessment of the safety throughout the life cycle, including a possible service life extension, is based on the following principles:

- the degradation phenomena are accounted for by design for fatigue life and corrosion protection
- the degradation is monitored during operation by inspections or continuous surveillance and possible actions to maintain the acceptable safety level are implemented whenever necessary. Current practice

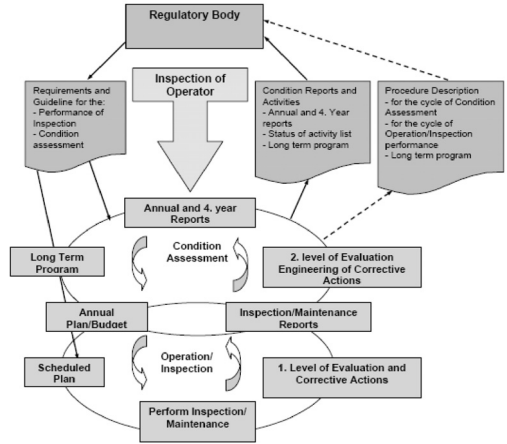


Figure 9. Inspection and maintenance process for offshore structures (Bruce et al., 2003).

for offshore structures is to rely on inspection, except for special components which are monitored.

- safety assessment which primarily refers to the component reliability, but which will increasingly refer to systems reliability, i.e. the risk of total loss.

At the initial design stage it is ensured that the various structural limit state criteria are fulfilled and an initial inspection plan is established based on generic data. The design should also ensure safe access for inspectors and the specification of equipment, e.g. X-ray equipment, ultrasonics and cameras. Hazardous areas require additional considerations.

Figure 9 shows the system for securing structural integrity within the offshore sector in the North Sea. The regulatory body defines the framework for safety. The operator (oil company or rig owner), is responsible for the safety during operation, defines inspection and maintenance needed, reports planned activity, finds and evaluates conditions annually and every fourth year. The procedure for condition assessment, inspection and maintenance is available to the regulatory body, which audits the Operator. Hence, the effect of the inspection history of a given structure is incorporated in planning future activities.

In this paper only structures for which there is experience is considered. Novel types of structures would need more monitoring and inspection as innovation often implies larger uncertainty in loads and resistance and may create new inspection problems, until adequate confidence is gained.

IMMR involve data which must be compatible with subsequent monitoring and evaluation processes and readily available. They must be cross-referenced to the as-built condition of the structure and the design analysis. The inspection and repair history will be important for a rational condition assessment procedure of

the relevant structure and other, especially “sister” structures.

### 5.2 IMMR planning and execution during service life

The objective of inspections is to detect cracks, buckling, corrosion (e.g. deterioration of coating and other protection systems as well as possible thickness reduction). Inspection and monitoring could also be used to validate design calculations etc, but such issues are not of concern herein.

The most refined fatigue design practice is to let the allowable damage depend upon consequences of member failure and access for inspection (e.g. Table 2). This relationship is generic, without account of the particular features of the structure and the relevant welded joints. Sometimes the relevant design criteria used have been less restrictive than the current code value. A more extensive or refined IMMR approach is then implemented.

It is important that a thorough condition assessment of the structure is made—preferably at the fabrication stage. There are often differences between “as-designed” and “as-is” conditions. Some discrepancies occur due to practical considerations during fabrications, such as the availability of space for welding. This can cause local changes of geometry that affect fatigue, which is sensitive to local details.

The safety level is maintained during operation by inspection or monitoring, maintenance and repair or intentional structural modification. The following factors are of influence

- fatigue design life (with respect to through thickness crack, beyond fatigue failure, failure).
- inspection of “as-is” structure after fabrication.
- leak control of through thickness cracks or inspections during operation.

Based on the specific information about the given structure and information collected through inspections, sometimes of strongly related structures, the inspection plan is continuously updated during service.

An inspection plan involves:

- prioritizing which locations are to be inspected.
- selecting inspection method (visual inspection, Magnet Particle Inspection, Eddy Current).
- scheduling inspections.
- repair strategy (size of damage to be repaired, repair method and repair schedule).

It is noted that the costs of the underwater inspections on jackets make it necessary to prioritize inspections. For instance, only 20% of tubular joints in jackets even in the North Sea which implies severe fatigue loading, might be inspected during the service life. Initially, North Sea inspections were executed more or less arbitrarily. Later, when fatigue analyses

became common, fatigue life estimates were used to prioritize NDE inspections to detect cracks. More recently, also failure consequences are considered, e.g. as related to the residual strength after fatigue failure of the relevant member.

The choice of inspection method depends upon its cost relative to its quality. Visual inspection and Penetrates have a low relative cost; Ultrasonic, Magnetic particle, Eddy Current and Leak testing imply medium costs while X-ray and deep ultrasonic involve high costs. Whether the inspection should be chosen to aim at detecting barely visible cracks, through-thickness cracks or member failures would depend on how much resources are spent to make the structure damage tolerant. Anyway, a certain minimum damage tolerance would be required because the damaged structure would need to carry the loads before the repair can be executed. This choice again would have implication on the inspection method; the main inspection methods being NDE methods, detection of through-thickness crack by e.g. member flooding, or failed members by visual inspection.

Typically major inspections of offshore structures (special surveys, renewal surveys) are carried every 4–5th year, while intermediate and annual inspections normally are less extensive.

Further refinement of the inspection planning has been made by introducing probabilistic methods as described below. Prioritization of inspection is, as mentioned above based upon fatigue life estimates, or more precisely, probability of fatigue failure and the consequence of damage. These two factors may be combined by requiring a target fatigue failure probability for joint  $i$  equal to  $P_{PFT(i)}$ . Inspections are then scheduled whenever the predicted reliability index is less than the target level, as shown in Fig. 10. In this example it is seen that the next inspection after a crack detection can take place 5 years after the detection; while the consecutive inspections become more frequent due to the relatively early (after 15 years) detection of a crack.

The target fatigue failure level  $P_{PFT(i)}$  is obtained by generalizing the approach implied by Table 2 as discussed above and by using a simplified systems approach based upon consideration of each failure mode ( $i$ ) of Eq. (12) separately, while omitting the inspection event,  $I$ . Hence, the target fatigue failure probability,  $P_{FJT(i)}$  is determined by:

$$P_{JSYS(i)} = P[FSYS|F_i] \cdot P_{FJT(i)} \leq P_{JSYS(T)} \quad (13)$$

where the system failure probability,  $P_{JSYS(i)}$  (associated with a fatigue failure of member ( $i$ )) complies with a system target level  $P_{JSYS(T)}$ .  $P[FSYS|F_i]$  is the conditional system failure probability of the structure, given fatigue failure of component ( $i$ ). The fatigue failure probability is determined by using a probabilistic fracture mechanics approach, while the latter probability

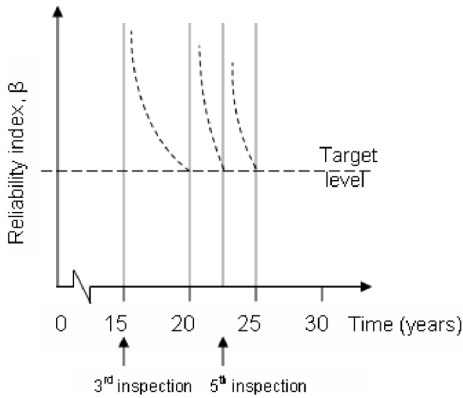


Figure 10. Schematic illustration of scheduling of inspections for a case where inspections after 5 and 10 years resulted in no crack detection and a crack was detected and repaired after 15 years.

is calculated based upon global ultimate strength of the damaged structure. This approach has for instance been implemented for template, space frame structures (Kirkemo, 1988, Moan et al., 1999). It is noted that this method might imply a system failure probability which is many times  $P_{SYS(T)}$  if many failure sequences with this failure probability are present. Even if this approach is not perfect, it represents an improvement of the “semi-probabilistic” approach given by Table 2.

Given the target level for a given joint, inspections and repairs by grinding or other modifications should be scheduled to maintain the reliability level at the target level. Fig. 10 indicates how inspections are scheduled when a thorough thickness crack is detected and repaired. Due to the repair conducted after the crack detection, it is not necessary to shorten the time for the first inspection after crack detection. But the subsequent inspections need to take place at intervals of about 2.5 years.

When inspections are prioritized, the potential of gross fabrication defects (e.g. because of difficult access), should also be a considered. If inspections during operation have a limited coverage it is important that all joints are carefully inspected before the structure is installed offshore and/or a continuous control such as leak-before-break detection in addition to the planned inspection, especially if they do not have adequate reserve strength.

A particular issue is concerned with welded joints which cannot be inspected in service, such as welds in piles. Adequate safety can then be ensured only by design margins and inspection of the fabricated pile. Since weld defects with a depth of less than 2 mm will be hard to detect, it is important that a sufficiently large

FDf or possibly design by assuming an ALS condition with abnormal defect size, is considered.

In service strengthening of structures can be made by increasing scantlings, grouting tubular joints to reduce bending. Increasing the fatigue strength by increasing plate thickness is very expensive. Local grinding of welds, or hammer peening etc. would be more relevant. Shallow cracks, especially in tubular joints, can be repaired by grinding or by use of other post-welding treatment. Cracks in tubular joints of North Sea jackets have often been repaired by successively grinding 0.5 mm in depth at the crack site, followed each time by an MPI/EC inspection to check whether the crack has been removed. This approach, hence, provides a measure of the crack depth (Vårdal and Moan, 1997). While the effect of toe grinding at the design stage corresponds approximately to a factor of 2 in terms of fatigue life, the effect on the remaining fatigue life is more significant if grinding is done at a later stage—when the cracks of larger magnitude are expected to have appeared. Moreover, it is noted that it is difficult to achieve high quality on the structural strength during modifications, especially undertaken at offshore sites.

Various methods for repairing corrosion damage are available (e.g. TSCF, 1997). They include: add/maintain anodes, spot blast and patch coat, reblast and recoat, as well as cut out other and replace plate and coat. Severe pitting corrosion could be dealt with by blasting, filling with weld and coating.

Inspection programs established in the 1970–80’ies turned out to be excessive, partly because the likelihood of fatigue cracks were overestimated, mainly due to conservative calculation of load effects. Frequently inspections were carried out with no crack detection. The result was an increased reliability (index) and less frequent inspections afterwards (Vårdal and Moan, 1997). (It is noted, however, that the inspection after an (early) detection and repair of a crack can be relatively long while subsequent inspection would have to be frequent). As a consequence, reliance on Leak Before Break principle has increased. However the high repair costs of large (through thickness) cracks suggest that use of non-destructive testing methods that can identify relatively shallow cracks, is cost beneficial.

The inspection strategy would normally be to inspect pre-selected potential crack sites. If the detected damage exceeds the acceptable level, the inspection would have to be extended to cover more possible crack sites, in the same or other sister platforms.

### 5.3 Service life extension

During operation structural reassessment may be necessary due to

- novel use or increase of payload.



- extension in service life.
- ageing or accidents.

Adequate safety in an extended service life may be ensured by a procedure involving the following steps:

- Collect information on previous and current operational and environmental conditions, records of inspection, maintenance and repair performed on the relevant structure and related structure.
- Screening by simple approach.
- Perform a detailed reliability based assessment, based on methods described in Section 3.
- Conclude and prepare a plan of necessary actions to ensure its safety during the extended service life.

An important consideration in connection with service life extension is the fulfillment of the fatigue design criterion. If the fatigue criterion is not fulfilled, mitigation may be achieved by implementing one or more of the following measures:

- Carrying out inspections to detect cracks and corrosion, and update reliability measure as shown in Section 3, according to inspection outcomes.
- If no crack is detected, increased fatigue life is implied, i.e. by updating the reliability level,
- Repair of possible cracks detected, by grinding, introducing additional brackets, or strengthening, or by reducing loads by removing unnecessary equipment, marine growth etc.
- Reducing potential failure consequences by reducing the personnel on-board.
- Increase the quality/frequency of inspections and repair.

If the ultimate strength criteria are not fulfilled due to general corrosion effects, replacement of plates or stiffeners, strengthening of stiffeners (e.g. by reducing the buckling length) need to be made. The follow-up of ultimate limit state component criteria can primarily be transformed into a check of

- corrosion protection by coating or cathodic protection.
- the average thickness reduction in view of the corrosion allowance.

## 6 CONCLUSIONS

Life cycle safety management of offshore structures should be based on a recognition of the effect of gross errors and normal variability in structural performance. The focus in this paper is on structural ageing, which should be controlled through adequate design as well as inspection, monitoring, maintenance and repair procedures.

Operational experiences with respect to degradation of jacket structures are summarized. The importance of Accidental Collapse Limit State design

criteria and use of the Leak Before Break principle, is emphasized. Utilisation of inspection outcomes such as: No crack detection as well as inspection, repair and failure costs vary significantly, provides a documentation of inherent reliability beyond that implied by design criteria and is beneficial.

It is proposed to prioritize and schedule inspections by using a reliability methodology which refers to a simplified system safety measure. Deterioration due to combined fatigue cracking and corrosion wastage of structural components is addressed. The reliability framework allows for explicit account of uncertainties as well as the effect of inspection.

The analyses show that the reliability may be maintained at the target level for a significant period of time beyond documented fatigue life, provided that adequate inspections are carried out at prescribed intervals and that any defects found are repaired to an acceptable standard.

Finally, the particular features of reliability-based structural reassessment for service life extension, is briefly outlined.

## ACKNOWLEDGEMENTS

I appreciate the cooperation with my many PhD students and other researchers, that resulted in many publications on which this work is based.

## REFERENCES

- Almar-Næss, A. (ed.) (1985). *Fatigue Handbook for Offshore Steel Structure*, Trondheim: Tapir Publisher.
- API (1993/1997). *Recommended Practice for Planning, Designing and Constructing Fixed Offshore Platforms*, API RP2A-WSD July 1993 with Supplement 1 with Sect., 17.0, *Assessment of Existing Platform*, February 1997, Dallas: American Petroleum Institute.
- Ayala-Uraga, E. and Moan, T. (2002). System reliability issues of offshore structures considering fatigue failure and updating based on inspection. *Proc. 1st Intnl. ASRANet Colloquium*, Glasgow, UK.
- Ayala-Uraga, E., and Moan, T. (2007). "Fatigue Reliability-based Assessment of Welded Joints Applying Consistent Fracture Mechanics Formulations," *Int J Fatigue*, 29, 3, 444–456.
- Bea, R.G. (1993). Reliability-based Requalification Criteria for Offshore Platforms. *Proc. 12th OMAE*, New York: ASME, II, 351–361.
- Bokalrud, T. and Karlsen, (1981). A Probabilistic Fracture Mechanics Evaluation of Fatigue Failure Form Weld Detects in Butt Welds Joints. *Proc. Conf. on Fitness for Purpose Validation of Welded Constructions*, London, UK: Paper 28.
- Bowness, D., Lee, M.M.K. (1999). Weld toe magnification factors for semi-elliptical cracks in T-butt joints. Offshore Technology Report—OTO 1999 014. Health Safety Executive.

- Bruce, G.J. et al. (2003). Report of Specialist Committee V.2. Inspection and Monitoring. *Int. Ship and Offshore Structure Congress*, A.E. Mansour and R.C. Ertekin (eds.), Amsterdam: Elsevier, 2, 37–70.
- BS 7910 (1999). *Guidance on Methods for Assessing the Acceptability of Flaws in Fusion Welded Structures*, BS 7910:1999, British Standards, London, UK.
- Celant, M.B. et al. (1983). Fatigue Characterization for Probabilistic Design of Submarine Pipelines. *Proc. The 1982 European Federation of Corrosion Meeting on Low Frequency Cyclic Loading Effects in Environment Sensitive Fracture*, Pergamon Press Ltd.
- Cornell, C.A. (1995). "Structural Reliability—Some contributions to Offshore Technology", Paper No. OTC 7753, *Proc. 27th Offshore Technology Conference*, Houston.
- Dalane, J.I. (1993). System Reliability in Design and Maintenance of Fixed Offshore Structures. PhD thesis, Dept. of Marine Structures, Norwegian Institute of Technology, Trondheim.
- De, R. et al. (1989). Study of Redundancy in near-Ideal Parallel Structural Systems. *Proc. 5th ICOSSAR*, San Francisco, New York: ASCE, 975–982.
- Det norske Veritas. (1996). PROBAN—General purpose probabilistic analysis program. Høvik, Norway, DnV.
- Digre, K.A. et al. (1995). Modification to and Applications of the Guidelines for Assessment of Existing Platforms Contained in Section 17.0 of API RP2A. *Proc. 27th Offshore Technology Conference*, Paper OTC 7779, Houston, 741–754.
- Dover, W.J. and Rudlin, J.R. (1996). Defect characterisation and classification for the ICON inspection reliability trials. *Proc. Conf. on Offshore Mechanics and Arctic Eng.*, ASME.
- Dunlap, W.A. and Ibbs, C.W. (eds) (1994). *Proc. Int. Workshop on Assessment and Requalification of Offshore Production Structures*, New Orleans, Offshore Technology Research Center, Texas A&M University and University of California, Berkeley, CA.
- Faber, M.H., Sorensen, J.D. and Kroon, I.B. (1992). Optimal Inspection Strategies for Offshore Structural Systems, *Proc. OMAE*, Calgary, Canada, 145–151.
- Fjeld, S. (1977). Reliability of Offshore Structures, *Proc. 9th Offshore Technology Conf.*, OTC 3027, Houston, 4, 459–472.
- ISO 19900 (1994), 'Petroleum and Natural Gas Industries—Offshore Structures—Part 1: General Requirements', Int. Standardization Organization, London.
- ISO 2394 (1998). General Principles on Reliability for Structures, Draft for approval.
- Itagaki, H., Akita, Y. and Nitta, A. (1983). Application of Subjective Reliability Analysis to the Evaluation of Inspection Procedures on Ship Structures, *Proc. Int. Symp. On the Role of Design, Inspection and Redundancy in Marine Structural Reliability*, National Academic Press, Nov.
- Jiao, G. and Moan, T. (1990). Methods of Reliability Model Updating through Additional Events. *Struct. Safety*, 9, 139–153.
- Jordaan, I.J. and Maes, M.A. (1991). Rational for Load Specifications and Load Factors in the New CSA Code for Fixed Offshore Structures. *C.J. Civil Engng.* 18, 3, 454–464.
- Kam, J.C.P. (1991). The Recent Development in Reliability Fatigue and Fracture Mechanics Analysis of Offshore Installations. *Proc. 10th OMAE*, Stavanger.
- Karamchandi, A. (1990). New Methods in Systems Reliability. Ph.D. Thesis. Stanford, CA: Department of Civil Engineering, Stanford University.
- Karsan, D.I. (2005). "Fixed Offshore Platform Design," Chap 6, *Handbook of Offshore Eng.*, S Chakrabarti, ed, Elsevier.
- Kirkemo, F. (1988). Applications of probabilistic fracture mechanics to offshore structures. *Applied Mechanics Revue*, 41, 2.
- Lloyd, J.R. and Karsan, D.I. (1988). Development of a Reliability-based Alternative to API RP2A, *Proc. 20th Offshore Technology Conf.*, OTC 5882, Houston, 4, 593–600.
- Madsen, H.O., Krenk, S. and Lind, N.C. (1986). *Methods for Structural Safety*, Prentice Hall, Englewood Cliffs, New Jersey.
- Madsen, H.O., Skjong, R.K., Tallin, A.G. and Kirkemo, A. (1987). Probabilistic Fatigue Crack Growth Analysis of Offshore Structures, with Reliability Updating Through Inspection, *Proc. Marine Structural Symposium*, Arlington, Virginia, USA, 45–55.
- Madsen, H.O. and S.D. Sørensen (1990). Probability-Based Optimization of Fatigue Design Inspection and Maintenance. Presented at *Int. Symp. on Offshore Structures*, University of Glasgow.
- Marshall, P.W. (1969). Risk Evaluations for Offshore Structures. *ASCE St. Div.* 95 (12).
- Marshall, P.W. and Luyties, W.H. (1982). Allowable Stresses for Fatigue Design, *Proc. BOSS '82*, New York: McGraw-Hill.
- Melchers, R.E. (1999). *Structural Reliability Analysis and Prediction*. 2nd ed. West Sussex, UK: John Wiley & Sons.
- Melchers, R.E. (2000). Probabilistic models of corrosion for reliability assessment and maintenance planning. *Proc 20th OMAE conf.*, Rio de Janeiro: ASME, Paper S&R-2108.
- Moan, T. (1988). The Inherent Safety of Structures Designed According to the NPD Regulations. Report No. F88043., Div. Structural Engineering, SINTEF, Trondheim.
- Moan, T. (1994). Reliability and Risk Analysis for Design and Operations Planning of Offshore Structures. *Proc. 6th ICOSSAR, Structural Safety and Reliability*, ed. Balkema, Rotterdam, Vol. I: 21–43.
- Moan, T. (1995). Safety Level Across Different Types of Structural Forms and Material—Implicit in Codes for Offshore Structures, SINTEF Report STF70 A95210, Trondheim, Prepared for ISO/TC250/SC7.
- Moan, T. et al. (1999). Probabilistic Inspection Planning of Jacket Structures. Paper No. 10848, *Proc. 31st Offshore Technology Conference*, Houston, TX.
- Moan, T. (2000). Recent Research and Development Relating to Platform Requalification, *J. OMAE*, New York: ASME, 122: 20–32.
- Moan, T. (2002a). Target levels for reliability-based assessment of offshore structures during design and operation, Offshore Technology report: OTO 060/1999. Health & Safety Executive, UK.
- Moan, T. (2002b). Review of Probabilistic Inspection Analysis Methods. Offshore Technology report: OTO 061/1999. Health & Safety Executive, UK.
- Moan, T. (2004). Safety of Offshore Structures, Keynote Lecture. *Proc 9th PRADS*, Lübeck-Travemünde, STG, Hamburg, 1, 10–38.



- Moan, T. (2005). "Reliability-based Management of Inspection, Maintenance and Repair of Offshore Structures," *J Struct and Infrastruct Eng*, 1, 1, 33–62.
- Moan, T. (2008). Development of Accidental Collapse Limit State Criteria for Offshore Structures, *J. Structural Safety*, to appear.
- Moan, T., Hovde, G.O. and Blanker, A.M. (1993). Reliability-Based Fatigue Design Criteria for Offshore Structures Considering the Effect of Inspection and Repair. OTC 7189. *Proc of 25th Offshore Technology Conference*, Houston, 2, 591–599.
- Moan, T., Vårdal, O.T., Hellevig, N.C. and Skjoldli, K. (1997). In-service observations of cracks in North Sea jackets—a study on initial crack depth and pod values. *Proc. of 16th OMAE Conf.*, Yokohama: ASME.
- Moan, T., Vårdal, O.T. and Johannesen, J.M. (1999). Probabilistic Inspection Planning of Fixed Offshore Structures, *Proc. ICASP 8, Applications of Statistics and Probability*, ed. A.A. Balkema, Rotterdam, 191–200.
- Moan, T. and Song, R. (2000). Implications of Inspection Updating on System Fatigue Reliability of Offshore Structures, *J. OMAE*, 122, 173–180.
- Moan, T., Wei, Z. and Vårdal, O.T. (2002a). Initial crack depth and POD data based on underwater inspection of fixed steel platforms. Corotis RB, Schuëller GI, Shinozuka M, editors. *Structural Safety and Reliability, Proc of 8th ICOSSAR '01*. ed. A.A. Balkema, Rotterdam.
- Moan, T., Amdahl, J. and Hellan, Ø. (2002b). Nonlinear Analysis for Ultimate and Accidental Limit State Design and Requalification of Offshore Platforms, *Fifth World Congress on Computational Mechanics*, July 7–12, Vienna, Austria.
- Moan, T. and Ayala-Uraga, E. (2007). Reliability-based assessment of FPSOs for service life extension. *J. Reliability Engineering and System Safety*, 93, 433–446.
- Moses, F. and Liu, Y.W. (1992). Methods of Redundancy Analysis for Offshore Platforms. *Proc. 11th OMAE Conf.*, New York: ASME, II, 411–416.
- Moses, F. (1987). Load and Resistance Factor Design-Recalibration LFRD Report API PRAC 87-22. API, Dallas, Texas.
- MTD (1992). Probability-based Fatigue Inspection Planning. Publication 92/100. Marine Technology Directorate Ltd., London.
- Newman, J.C. and Raju, J.S. (1981). An empirical stress-intensity factor equation for the surface crack. *Eng. Fracture Mech.*, 15 (1–2): 185–192.
- NORSOK N-001 (1998). Structural Design, Norwegian Technology Standards, Oslo.
- NORSOK N-004 (1998). Steel Structures, Norwegian Technology Standards, Oslo.
- NORSOK N-003 (1999). Actions and Action Effects, Norwegian Technology Standards, Oslo.
- NOU (1981:11). The Alexander L. Kielland Accident, The Report of the Royal Inquiry Commission, University Publishers, Oslo.
- NPD (1984). Regulations for load carrying structures, Norwegian Petroleum Directorate, Stavanger.
- Rudlin, J.R. and Austin, J. (1996). Topside inspection project: Phase I final report. Offshore Technology Report OTN 96 169. UK: Health & Safety Executive.
- Schuëller, G.I. (ed.) (2006). Structural Reliability Software. *Structural Safety*, 28, 1–2, 1–216.
- Shetty, N.K. (1992). System Reliability of Fixed Offshore Structures under Fatigue Deterioration. PhD thesis, Imperial College, London.
- Shinozuka, M. and Deodatis, O. (1989). Reliability of Marine Structures under Bayesian Inspection, Report of Princeton University, February.
- Sigurdsson, G. et al. (1993). Probabilistic Collapse Analysis of jackets. *Proc. 6th ICOSSAR Conf.*, ed. A.A. Balkema, Rotterdam.
- Sigurdsson, G., Lotsberg, I., Myhre, T. and Ørbeck-Nilssen, K. (2000). Fatigue Reliability of Old Semi-submersibles. OTC Paper no 11950, *Proc. Offshore Technology Conference*, Houston.
- Skallerud, B. and Amdahl, J. (2002). Nonlinear Analysis of Offshore Structures, Research Studies Press.
- Straub, D. and Faber, M.H. (2007). Risk based inspection planning for structural systems. *Marine Structures*, 27, 4, 335–355.
- Sucharski, D. (1997). Crude oil tanker hull structure fracturing: an operator's perspective. In: Ship Structure Committee. *Proc. Symposium and workshop on the prevention of fracture in ship structure*, Washington, D.C., 87–124.
- TSCF (1997). Guidance Manual for Tankers Structures. Tanker Structure Co-operative Forum & IACS, London, UK: Whitherby Publishers.
- Ultiguide (1999). Best Practice Guidelines for Use of Non-linear Analysis Methods in Documentation of Ultimate Limit States for Jacket Type Offshore Structures, DNV-SINTEF-BOMEL, Oslo, Trondheim, London.
- Vinnem, J.E. (1999). *Offshore Risk Assessment*, Kluwer Academic Publishers, Dordrecht.
- Visser, W. (2002). POD/POS curves for non-destructive examination. Offshore Technology Report OTO 2000/018, Health & Safety Executive, UK.
- Vårdal, O.T. and Moan, T. (1997). Predicted versus Observed Fatigue Crack Growth. Validation of Probabilistic Fracture Mechanics Analysis of Fatigue in North Sea Jackets. *Proc. 16th OMAE Conference*, Paper No. 1334, Yokohama, Japan.
- Vårdal, O.T., Moan, T. and Bjørheim, L.G. (2000). Applications of Probabilistic Fracture Mechanics Analysis for Reassessment of Fatigue Life of a Floating Production Unit-Philosophy and Target Levels, Paper No. 00-2078, *Proc. 19th OMAE Conference*, New Orleans.
- Wirsching, P.H. (1983). Probability based Fatigue Design Criteria for Offshore Structures. Report API PRAC Project No. 81 15, Dept. of Aerospace and Mechanical Engng. University of Arizona, Tucson.
- Wirsching, P.H. and Chen, Y.N. (1988). Considerations of Probability Based Fatigue Design for Marine Structures, *Marine Structures*, 1, 23–45.
- WOAD: Worldwide Offshore Accident Databank (1996), Det Norske Veritas, Oslo.
- Wu, Y.-L. and Moan, T. (1989). A Structural System Reliability Analysis of jacket using an Improved Truss Model. *Proc. 5th ICOSSAR*, San Francisco, ASCE, New York, 887–894.
- Yang Y.N. (1994). Application of reliability methods to fatigue, quality assurance and maintenance. In: Schuëller, Shinozuka & Yao, editors. *Structural Safety & Reliability, Proc. 6th ICOSSAR Conf.*, ed. Balkema, Rotterdam, The Freudenthal Lecture.

# Increasing a building's life-cycle in regions of high seismic risk

M.P. Sarkisian

*Skidmore, Owings & Merrill LLP, San Francisco, CA*

**ABSTRACT:** Beyond life safety considerations, increasing a building's service life is paramount in regions of high seismic risk. With the implementation of scientific structural devices and systems, building services, contents, and economic investments can be protected. Building codes specifying equivalent static analyses in many cases lead to conventional designs including members and joints that have limited ductility and have questionable economic value following a major seismic event.

What if structures were designed to behave dynamically moving freely at times, dissipating energy, protecting life safety, protecting investments, and allowing structures to remain elastic after a severe earthquake achieving the highest level of structural sustainability? What if these structures looked directly to nature for their mathematical derivations?

What if the solutions to superior performance use conventional building materials? These solutions could provide a scientific response without great expense and construction complexity while increase a building structure's life-cycle in regions of high seismic risk.

## 1 UNNATURAL BEHAVIOR

The 1995 Kobe Earthquake, or the Great Hanshin Earthquake as it has been formally named, was an important catalyst for considering building structures' long-term performance and life-cycle. Structures in Kobe exhibited unnatural behavior, many exhibited poor ductility and many collapsed during strong ground shaking. Mid-height and ground story collapses of structures (Figure 1) were common due large changes in stiffness and partial height use of structural steel within reinforced concrete columns. Reinforced concrete structures lacked confinement of vertical reinforcing steel. Because of this unnatural performance of buildings, 107,000 buildings were damaged, with 56,000 collapsed or heavily damaged. 300,000



Figure 1. Mid-height collapse, Kobe, Japan, 1995.

people were left initially homeless with 5000 people losing their lives. The total cost of the damage was well over US\$100 billion (1995 US dollars).

The solution is to increase behavior predictability in very unpredictable events. The nature, unpredictable event of an earthquake cannot be changed; however, forcing the structural system to behave in a predictable manner can be achieved. The solution is one that lies in elasticity of materials, which can be closely predicted, and in the passive dissipation of energy along with the inherent, internal damping of structural systems.

## 2 BEAM-TO-COLUMN TESTS

The mid 80's brought the conclusion of many steel beam-to-column moment connection tests. These pre-Northridge studies investigated frame connections that included fully welded top and bottom beam flanges and conventional shear tab web connections. The tests focused on these economical connections that incorporated typically available steel column and beam wide-flanged sections (Figure 2).

The tests compared the behavior of the connections without any column reinforcement, with flange continuity plates, and web doubler plates. Each connection was subjected to seven cycles of motion and was tested to at least two percent rotation to simulate expected rotation/drift in actual frame structures. Small rotations illustrated stress concentrations in beam and column flanges at complete penetration welded joints. Shear yielding in column webs could also be seen at

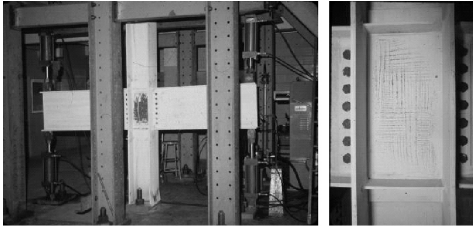


Figure 2. Beam-to-column joint testing, Lehigh University.

small rotations. As larger rotations were imposed and connections were subjected to further cyclic motion high material stress concentrations turned into fractures. Typically flange welds failed by either failure of the weld itself or laminar tearing of the beam flange. Continuity plates provided better results, typically protecting column—beam flange connections, however premature flange fractures were observed. Doubler plates protected the column webs but did little to reduce stress concentrations and eventual fracture of flange welds. These plates also severely limited rotation capabilities of the joint. In some tests flange welds were removed after fracture, re-welded, inspected and tested. These connections were further tested and in some cases met the required overall rotation and drift requirements. In all cases connections generally remained intact, beam and columns did maintain connectivity through the bolted web connections and the other full penetration welds that remained intact after the initial fracture.

The 1994 Northridge Earthquake in southern California proved what was found through the connection testing in the mid 80's. Steel moment frames experienced failure of welded flange connections but generally remained intact following the ground shaking. Life safety was protected, however, the economic loss was significant. Structural engineers were concerned about the effects of future events with questionable connections. Retrofits were made through a very difficult process of gaining access to connections through building finishes and while owners wished to keep buildings occupied. The reduced beam section or dog-bone connection was developed as an economical solution to the joint while protecting the column and ensuring ductility (Figure 3).

### 3 WOOD DOWELS AND STEEL PINS

Jesuit churches, built in the early 1900's, on the Island of Chiloe off the coast of Chile have performed well over their life when subjected to strong ground motion. The 1960 Chilean earthquake, perhaps the strongest earthquake ever recorded at 9.5 on the Richter Scale, did not cause major damage to these structures. Witnesses of this event describe wave forms in large open

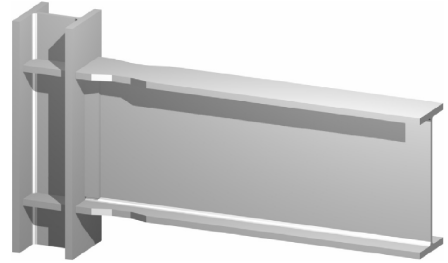


Figure 3. Post-Northridge dogbone connection.

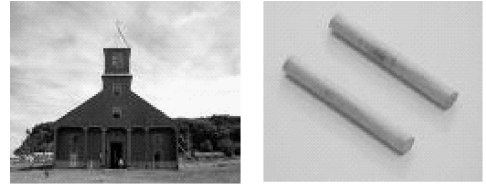


Figure 4. Wood dowel joints.

fields with amplitudes over 6 feet. Street light and poles used for telephone lines moved with large amplitudes and in some cases were observed to be almost parallel with the ground.

These churches have a common structural characteristic. Wood dowels from the indigenous Alerce Tree were typically used to connect structural wood members with no “fixed joint” mechanical fasteners. Wood dowels were driven through openings in the structural wood members so that the dowels were snug tight and “fixed” during typical service conditions with an ability to rotate during extreme loading conditions. When the joints rotated, energy was dissipated with the structures softening. With this softening the structures period lengthened, and as a result attracted less force from the ground motion.

Large diameter steel pins proved useful in the design of key structural elements of the Jin Mao Tower, Shanghai, The People's Republic of China. The structural system concept for the 421 meter-tall, 88 story Tower included lateral load resisting outrigger trusses that interconnected the central reinforced concrete core and eight (8) perimeter composite megacolumns. This interconnection occurred at three (3) two story segments between Levels 24 & 26, 51 & 53, and 85 & 87. Relative creep, shrinkage, and elastic shortening between core and the composite megacolumns was significant; if this behavior was not managed, the forces developed in the outrigger trusses would be large enough to overload the members causing significant over sizing, yielding, and potential failure. If fully connected at the time of erection, up to 45 mm of relative displacement was expected between the core and composite columns with only 16 mm

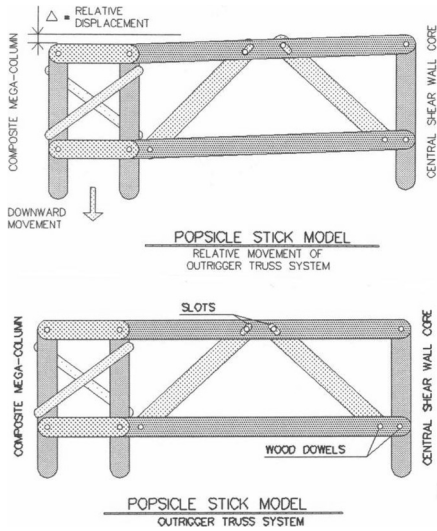


Figure 5. Popsicle stick model.

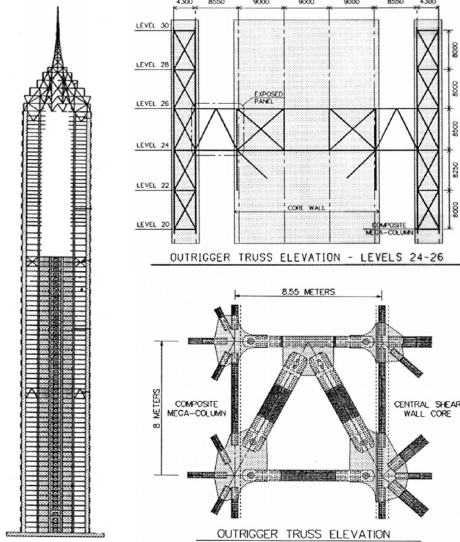


Figure 6. Structural system/outrigger elevation.

of relative displacement expected with 120 days of pinned connections only.

To manage these forces and reduce the amount of structural material required for the members and connections, large-diameter steel pins were incorporated into the truss system. Based on basic concepts of statics, these pins allow the trusses to behave as freely moving mechanisms prior to making final connections. This mechanism concept allowed the trusses to be constructed during normal steel erection procedures and allowed final bolted connections to

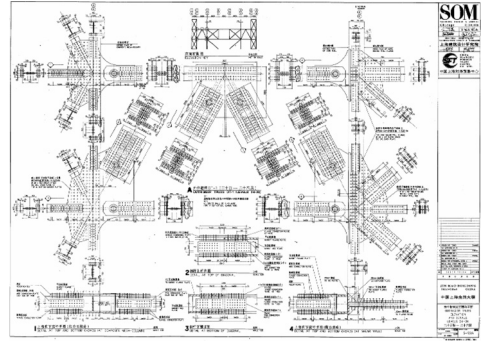


Figure 7. Outrigger truss working drawing.

be installed after a significant amount of relative movement had already taken place. Because diagonal members were used within the trusses, large slots were incorporated into end connections to allow movement to occur. These slots were the key component to all free movement of the system.

A simple model made up of popsicle sticks, wood dowels, and tongue depressors was used to study the behavior (Figure 5). This conceptual model was developed into a structural concept using building materials (Figure 6), analyzed, and developed full working drawings (Figure 7).

#### 4 PINNED JOINTS

The Jin Mao pinned-truss concept, based on the fundamentals of statics and behavior, led to the development of a series of structural systems that will behave predictably in an extreme seismic event. The systems are appropriate for building and other structures with varying heights and geometries allowing systems to remain elastic and dissipate energy while protecting economic investments.

Structural steel end connections of members contain pins or bolts and are installed to a well-calibrated torque by applying compression of joints through the pin or bolt tension. Faying surfaces are treated with an unsophisticated slip-type material such as brass, bronze, cast iron, aluminum or hard composite materials with a well-defined coefficient of friction, allowing for significant movement capabilities after the threshold of movement and without significant loss of bolt or pin tension. The material combination not only provides well-defined load-displacement characteristics, but also excellent cyclic behavioral attributes. Structural steel surfaces can be sandblasted or clean with mill scale present to minimize galling or binding. A force vs. displacement hysteresis curve of a combination of steel and brass illustrates the stable behavior (Figure 8).

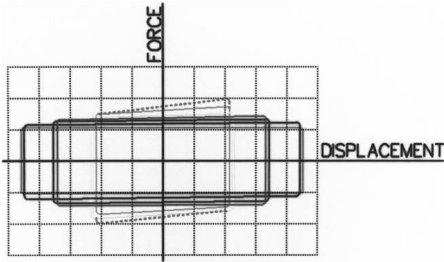


Figure 8. Representative hysteresis loop.

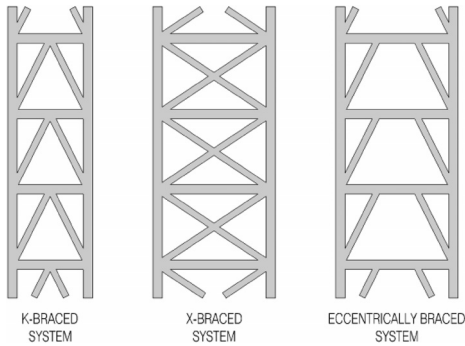


Figure 9. Truss system elevations.

Pins, installed into the end connections of trussed building frames (Figure 9), used in buildings subjected to extreme seismic events provide fixed joints for the typical service life of the structure and are allowed to slip during extreme events.

Circular holes are used in horizontal truss members for both connection plates and members. Circular holes are used in diagonal members with long-slotted holes used in connection plates. Slots are designed and installed in the direction of force (Figure 10). The length of the hole is dependent on the predicted drift and the dynamic characteristics of the structure when subjected to ground motion. A well-defined faying surface is used between connection plates and members. The material sandwiched between the steel surfaces is a shim or pad form (may be applied directly to the steel surfaces) and is stringently protected after application, during shipment, and during erection. The faying surface material is used in both slotted and circular connection joints. Pins are torqued in slip-defined joints at slotted connections of diagonal members. The size of the pin and the amount of torque are directly related to the coefficient of friction of the material being compressed between steel plates and the expected force that will initiate joint motion. Special Belleville Washers are used to help maintain bolt tension after slip has occurred in slotted joints. In addition, direct tension indicators (DTI's) are used

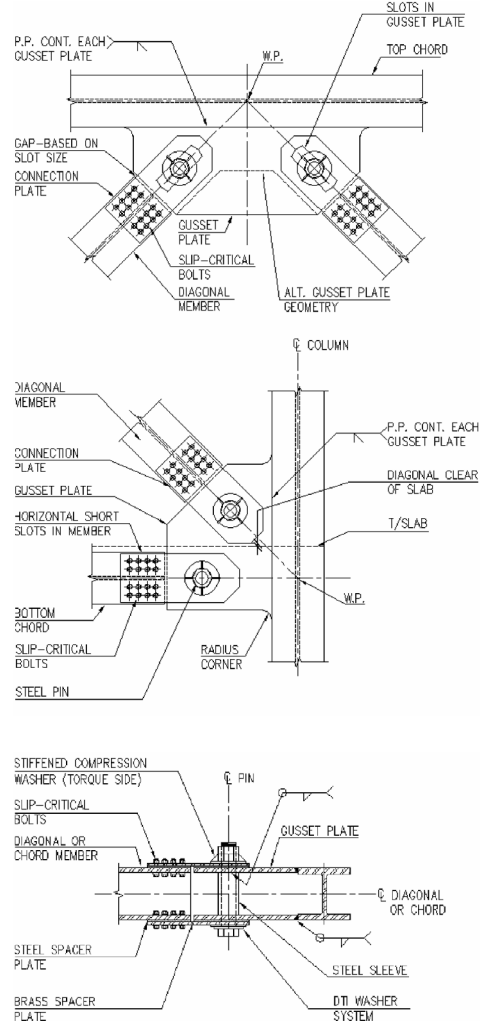


Figure 10. Pin-connection details.

under the head (non-torquing side) to ensure proper pin or bolt tension. Structural members are designed for forces required to initiate the onset of joint motion. Members are designed to remain elastic, not allowing yielding, local or global buckling.

Moment-resisting frames equally benefit when pins are introduced into end connections. Pins in long-slotted connections could be introduced into top and bottom beam flanges. The length of the beam flange slots can be predicted by evaluating the expected beam rotation and inter-story drift characteristics. A single pin in a circular hole is used in the web connection to provide the best rotational capabilities (Figure 11).

These fuses, whether placed in braced or moment frame systems, act to lengthen the structures period

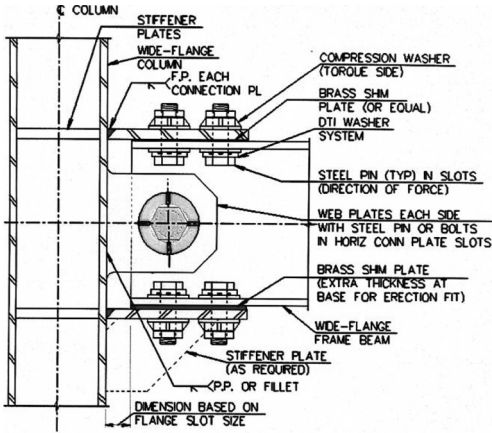


Figure 11. Moment frame beam-column joint detail.

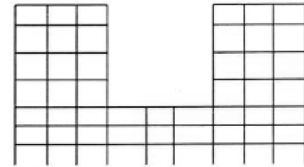
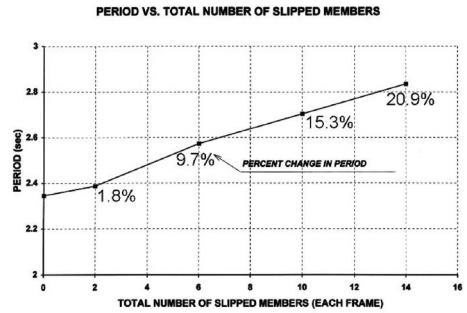


Figure 13. Period vs. total number of slipped members, frame example.

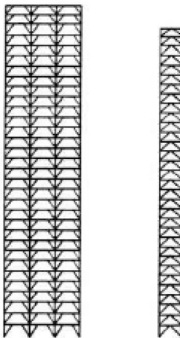
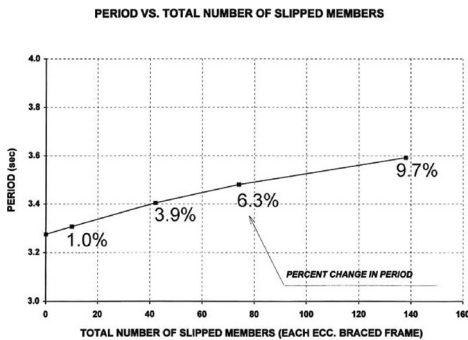


Figure 12. Period vs. total number of slipped members, truss example.

(Figures 12, 13). This lengthening of the period effectively softens the structure resulting in less force being attracted to the structure from the ground motion.

## 5 THE PIN-FUSE JOINT™

If structures were capable of altering their characteristics to resist potentially destructive forces during

extreme loading events without permanent deformation their expected life-cycle would significantly increase.

Structural frames previously utilizing beam-to-column moment connections that are welded with the frame beams perpendicular to the columns would become obsolete. Beams are typically connected to the face of columns rotate when subjected to racking of the building frame. These beams are designed to protect the column integrity and prevent potential collapse by plastically deforming during frame motion. This deformation, however, likely decreases post-earthquake integrity and economic viability in the process. Therefore, a new concept for this connection is warranted.

The *Pin-Fuse Joint*™ allows building movement caused by a seismic event while maintaining structural elasticity after strong ground motion. The joint introduces a circular-plated end connection for the steel beams framing into the steel or composite columns within a moment-resisting frame. Slip-critical friction-type bolts connect the curved steel end plates. A steel pin or hollow steel pipe in the center of the moment-frame beam to provides a well-defined rotation point. Under typical service conditions including wind and moderate seismic events, the joint remains fixed where applied forces do not overcome the friction resistance provided between the curved end plates. However, during an extreme event, the joint is designed to rotate around the pin joint, with the slip-critical bolts sliding in long-slotted holes in the curved end plates. With this slip, rotation is allowed, energy dissipated, and “fusing” occurs.

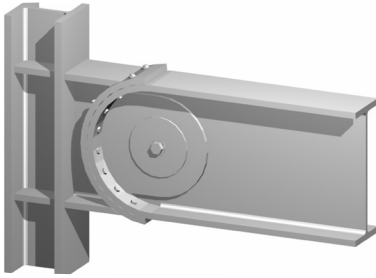


Figure 14. The Pin-Fuse Joint™, Patent No. US 6,681,538 B1.

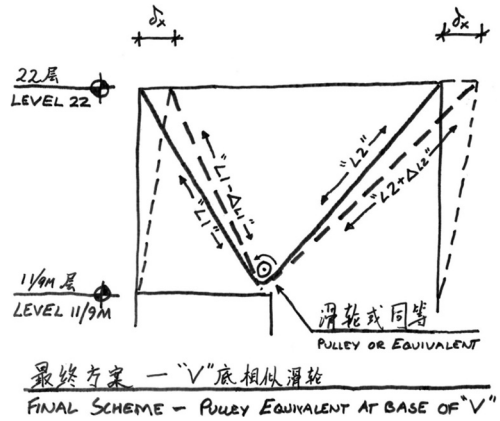


Figure 15. Pulley concept, China Poly Beijing.

The rotation of the *Pin-Fuse Joint™* during extreme seismic events occurs sequentially in designated locations within the frame. As the slip occurs, the building frame is softened. The dynamic characteristics of the frame are altered with a lengthening of the building period, less forces are attracted by the frame; however, no inelastic deformation is realized. After the seismic event, the elastic frame finds its pre-earthquake, natural-centered position. The brass shim located between the curved steel plates provides a predictable coefficient of friction required to determine the onset of slip and also enables the bolts to maintain their tension and consequently the clamping force after the earthquake has subsided (Figure 14).

## 6 MANAGING LARGE SEISMIC MOVEMENTS

The use of pinned mechanisms in structures are not limited to frame joints but may be used in large structural components that assist in natural building behavior during extreme seismic events and allow for increased building life-cycles.

A rocker mechanism, installed at the mid-height of the China Poly Beijing Project allowed the building to freely move during a significant earthquake while providing support for world's largest cable net and for a mid-height museum used to display some of China's most important antiquities (Figure 16). The cable net, 90 meters-tall and 60 meters-wide at its widest point, was conceived to provide support for the exterior wall system with minimal structure. Stainless steel cables were typically spaced at 1500 mm on-center with vertical cables 26 mm in diameter and horizontal cables 34 mm in diameter. A V-shaped cable stayed concept was used reduce the cable net span and reduce overall displacements when subjected to wind loads. 200 mm diameter cables not only provided lateral support for



Figure 16. China Poly Beijing, Beijing, China.

the cable net but were used to support the mid-height museum. It was found that these large cables acted as diagonal mega-braces when the building was subjected to strong ground motion. The displacement at the top of the building relative to the mid-height was approximately 900 mm. The forces developed in the cables and connections with this level of relative displacement resulted in designs that could not be reasonably achieved. If forces the primary cables could be relieve during lateral motion, then cables and connections could be designed for wind and gravity loads only. A pulley, located at the top of the museum, could achieve this behavior (Figure 15). However, because of a drum size nearly 6 meters in diameter was required to accommodate the primary cables and was aesthetically unacceptable; an alternate idea was required.

A rocker mechanism, capable of movements in two primary directions, was introduced into the top of the museum. Pins combined with steel castings provided the reverse pulley mechanism capable resisting the



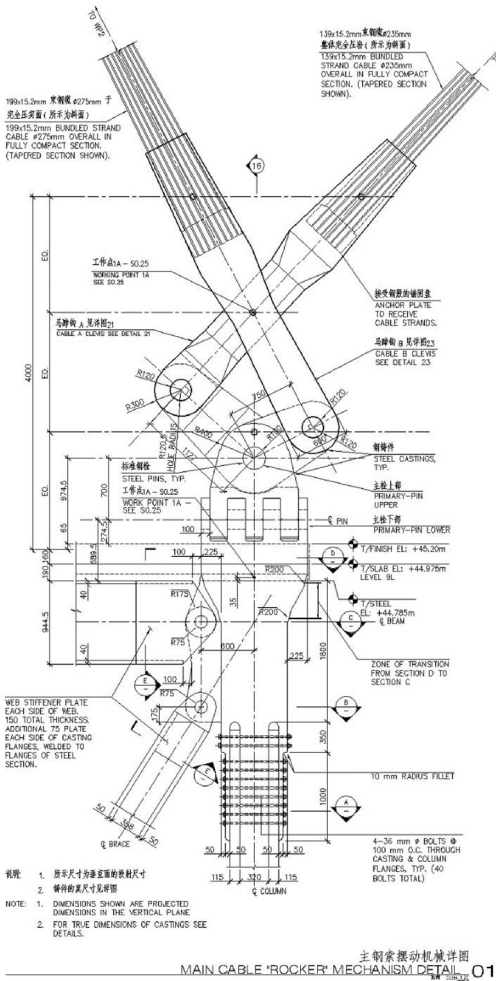


Figure 17. Rocker mechanism, China Poly Beijing.

imposed loads while remaining elastic during an extreme seismic event (Figure 17).

## 7 NATURAL STRUCTURAL RESPONSES

Perhaps natural forms commonly occurring in nature provide the clues to structures that will have the longest life-cycles (Figure 18). The shapes and structural systems are inspired by developing the optimal structural typology. The logarithmic spiral, repetitively occurring in nature through forms ranging from plant growth to nautilus shells to weather systems, provide the inspiration for the radiating lines of the exterior structure. Based on derivations such as the Fibonacci Sequence, the logarithmic spiral defines typological lines that directly relate to natural demands on a structure.

The spiral is a curve that winds around a fixed center and gradually recedes from the center. The hurricane exhibits greatest strength at the wall of its eye and least strength at the ends of its arms. Hurricane, typically observed in plan geometry, can be extrapolated vertically and applied to structures such as extremely tall buildings. Its shape, as well as the shape of other forms in nature such as the nautilus shell are not random, and can be mathematically described. Engineer Anthony Michell captured this behavior through his research in the early 1900's by describing the radiating lines of a pure cantilever where force flow lines of equivalent constant stress result in specific spacing and orientations from the base to the tip of the cantilever (Figure 19). The bracing system, mathematically described and overlaid on the building form as developed for the Transbay Tower in San Francisco (Figure 20), provides the optimal structural system considering the boundary conditions of height, width, and the desired base configuration (Figure 21).

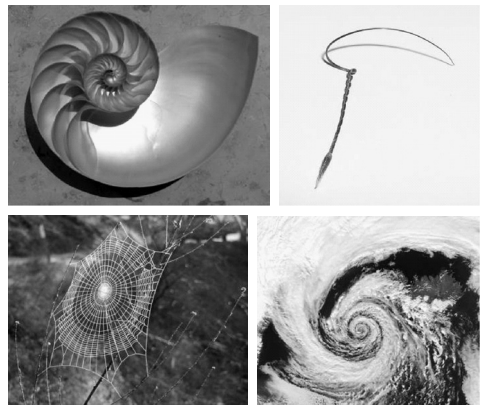


Figure 18. Natural forms (nautilus shell, storksbill seed, spider web, weather systems).



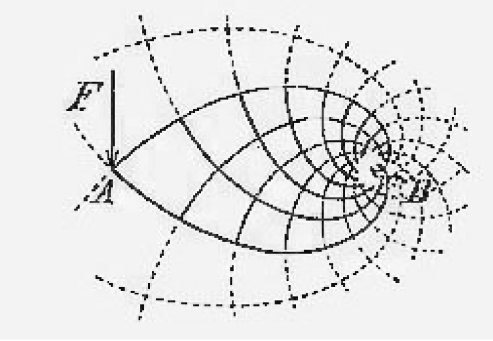


Figure 19. Original Mitchell truss diagram.

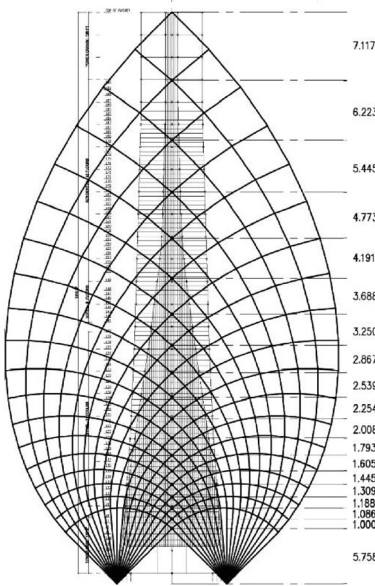


Figure 20. Mitchell truss applied to vertical elevation.

## 8 COMBINING NATURAL FORMS AND MECHANISMS

The combination of natural forms and mechanisms lead to the minimum use of material and the best life cycle. Therefore, a dual system could be incorporated into a structure; one system controlling lateral drift and one providing fused mechanisms used to protect the structure while maintaining permanent elasticity as illustrated in plan for the Transbay Tower (Figure 22).

The “Pin-Fuse Frame” (Figure 23), incorporated into braced frames (or between concrete shear walls) of structures allows braces to slip or “fuse” during extreme seismic events. High-strength bolts in long-slotted holes are used to clamp a sandwich of brass and steel plates (brass between the plates). Brass placed

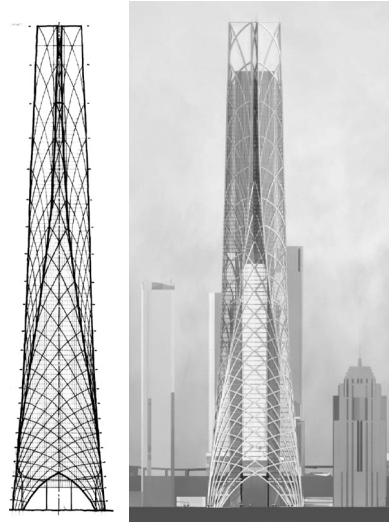


Figure 21. Resulting Tower elevation drawing and rendering.

between steel plates creates a well-defined threshold of slip when subjected to load. When the demand on the structure is extremely high, the moment-resisting frame with its circular bolt pattern provides additional resistance. If these joints are subjected to a high level of bending moment, they too will slip, rotating around a center steel pin. The combination in behavior of the braces and horizontal moment-resisting elements fuse the structure, dissipate energy, soften the building, lengthen the period, and reduce forces attracted from the ground motion. After the event, these joints return to their full structural capacity without permanent deformation. The tension in bolts used to clamp the plates together is not lost during the motion and, therefore, re-establishes the structural capacity by re-establishing the static friction within the joints. Although conventional steel braced frames have been proven to perform with some adequacy during extreme seismic events, their integrity is questionable in repetitive cyclic motions due to premature buckling. Damage in many cases may not be repairable.

The “Link-Fuse Joint” (Figure 24), incorporated into the reinforced concrete shear wall (or steel frames) of structures, allows links that typically occur over doorways and mechanical openings to fuse during extreme seismic events. The butterfly slot pattern in the steel connection plates is clamped together, developing static friction between plates. Brass shims located between the plates create a well-defined and consistent coefficient of friction. When the demand on the links is extreme, the joints slip in any necessary vertical or horizontal direction, dissipating energy, softening the building (period lengthens), and attracting less force from the ground. After the motion of

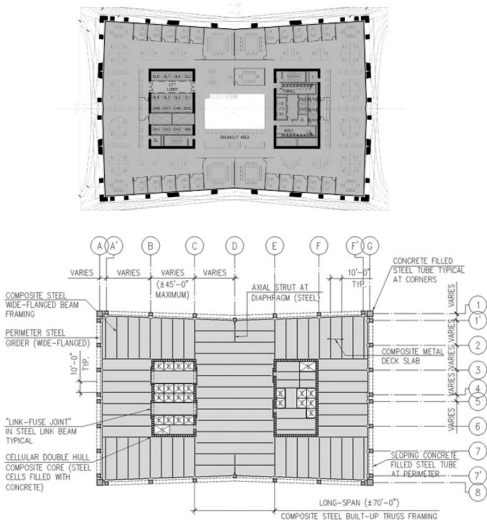
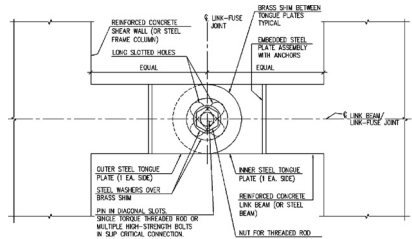
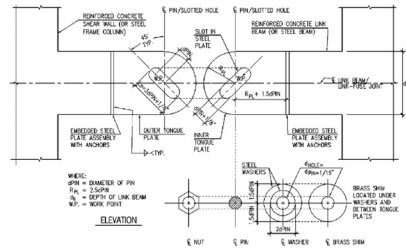


Figure 22. Structural system plan.



Completed Elevation



Exploded Elevation

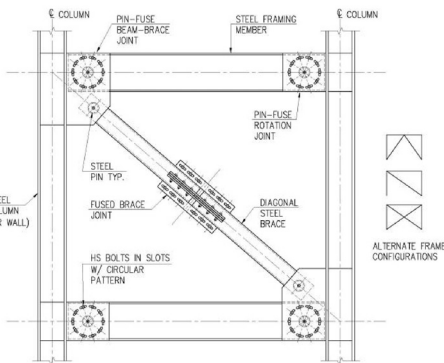


Figure 23. The pin-fuse frame, US Patent Pending.

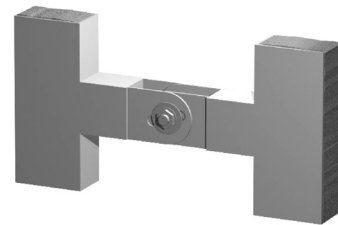


Figure 24. The link-fuse joint, US Patent Pending.

the building and the movement of the joints cease, the building and joints return to their natural at-rest position without permanent deformation. The tension in bolts used to clamp the plates together is not lost during the motion and, therefore, re-establishes the structural capacity by re-establishing the static friction within the joints. The structure is safe, its economic investment protected, and can remain in service. In contrast conventional reinforced concrete link beams are typically damaged and must be repaired or replaced, with the overall structure potentially deemed unfit for future service.

## REFERENCES

Sarkisian, M. 1985. Beam-to-Column Connections Subjected to Seismic Loads, *Master's Thesis*, Lehigh University.

Korista, S., Sarkisian, M., Abdelrazaq, A., Jin Mao Tower's Unique Structural System, 1995. *Shanghai International Seminar for Building Construction* ('95 SISBT).

Sarkisian, M. 2004. Structural Seismic Device, *United States Patent No. US 6,681,538 B1*.

*Life-cycle damage processes*

# Mechanical behavior of clay bricks and restoration mortars subject to thermal actions

P. Antonaci & P. Bocca

*Politecnico di Torino, Torino, Italy*

**ABSTRACT:** Environmental actions may have significant effects on masonry structures during their life-cycle. Therefore, in the effort to provide a contribution for a better understanding of masonry behavior when subjected to environmental actions, laboratory tests simulating freezing-thawing cycles have been conducted on clay bricks and restoration mortars. The clay brick samples have been taken from Venaria Reale Palace (Italy) and date back to the XVII–XVIII century. The mortar samples have been produced using commercially available mixes and are representative of common repair and maintenance works.

The effect of freezing-thawing cycles on the above materials has been evaluated through both standard laboratory tests and non-destructive tests, using a recently conceived technique named Impulse Method that is suitable for on-site investigations due to its non-destructiveness and ease of use.

The results obtained portray the response of the considered masonry components and show that the Impulse Method is potentially applicable with good effectiveness.

## 1 INTRODUCTION

In recent years, great attention has been devoted in Europe to the consolidation of architectural and infrastructural heritage, with special regard to the strengthening of historical structures requiring radical restoration works, whether because of their severe conditions of deterioration (caused by different types of environmental actions) or due to the damage suffered during seismic events. However, quite often damage phenomena are seen to affect previously repaired structures, thus raising doubts about the long-time effectiveness of the strengthening materials used. In particular, restoration materials having mechanical and elastic characteristics significantly dissimilar from the original ones are generally considered inadvisable (Morgan 1996, Emberson & Mays 1990a, b), in the absence of specific studies or standards concerning their durability.

In this paper, the results of an experimental investigation about the long-time behavior of historical clay bricks and different types of current restoration mortars subjected to repeated thermal actions are presented. In particular, the effect of freezing-thawing cycles has been simulated in the lab through accelerated techniques, with the aim to collect experimental data useful for a better comprehension of historical and modern materials' response to such environmental

actions. The information about the materials' behavior thus obtained can be subsequently used in order to select the most appropriate restoration material with regard to freezing-thawing solicitations, the selection criterion being the affinity of the mechanical and elastic characteristics of original and restoration materials in the medium and long term.

In addition to standard laboratory methods, also a recently conceived non-destructive technique, denoted as Impulse Method (Antonaci et al. 2007, Antonaci & Bocca 2004), has been used to detect the response of the materials under consideration to the action of the given freezing-thawing cycles. The aim was to evaluate the possible discrepancy between the results obtained by traditional laboratory methods and the Impulse Method, so as to check if the latter could be potentially applicable directly on-site in order to get information about the evolution of the masonry components' characteristics under the effect of environmental actions, during their life-time. In case of positive feedback, the Impulse Method (which is particularly interesting since it is a non-destructive, low-cost and easy-to-perform technique) could be furthermore developed in order to be used in the future in the framework of a specific experimental procedure aimed at the selection of the most appropriate repair material with the constraint to minimize the resort to extensive laboratory characterization tests.

## 2 EXPERIMENTAL PROGRAMME

Specimens made of historical clay bricks and common restoration mortars were produced according to the details reported in Section 2.1 and then characterized by means of standard laboratory tests, as described in Section 2.1. Subsequently, they were subjected to thermal solicitations represented by series of freezing-thawing cycles, performed in the lab (see Section 2.2). At the end of each series, the mechanical and elastic properties of the specimens in compression were evaluated through both standard compressive tests (see Section 2.3) and non-destructive tests using the Impulse Method (Antonaci et al. 2007, Antonaci & Bocca 2004) (see Section 2.4), in order to monitor the evolution of the materials' behavior due to the thermal actions applied. The results obtained are reported and discussed in Section 3.

### 2.1 Materials and specimens

Two classes of materials were examined in the present experimental investigation, i.e. historical clay bricks on the one hand and modern restoration products on the other. The first ones were taken from the royal restoration of Venaria Reale (Turin, Italy) during the restoration works of the building (Fig. 1), while the second ones are currently available on the market for building products and were chosen as representative of possible types of repair and maintenance work. Specifically, the following products were considered: a tixotropic mix for production of mortars and structural plasters, a cement-free binder for dehumidifying mortars, a cement-free grout to be used as



Figure 1. Facade of the Royal Residence of Venaria Reale (Turin, Italy) during its restoration works.

filler for voids and cavities in masonry structures, a one-component mortar for plaster repair. A description of their main characteristics, as certified by the producers, are reported in Tables 1–4. As far as bricks are concerned, instead, no information is available, except that they date back to the XVII–XVIII century.

Nine specimens sized  $40 \times 40 \times 160 \text{ mm}^3$  were cut from the historical bricks and subsequently tested. Similarly, nine test pieces sized  $40 \times 40 \times 160 \text{ mm}^3$  were produced per each type of mortar. They were cast in appropriate metallic frames and water-cured for 28 days. Their age before testing was approximately six months.

Preliminarily, the mechanical strength of the materials was determined through static compressive tests performed on three specimens per type of material with the aid of a 250 kN servo-controlled testing machine. The results are reported in Table 5.

Table 1. Nominal characteristics of mortar D.

DESCRIPTION	
Tixotropic mix for production of mortars and structural plasters.	
TECHNICAL DATA	
• Compressive strength (28 days):	15 ÷ 20 MPa
• Static modulus of elasticity (28 days):	16000 ± 500 MPa

Table 2. Nominal characteristics of mortar A.

DESCRIPTION	
Cement-free binder, for dehumidifying mortars for the restoration of damp stone, brick and tuff masonry.	
TECHNICAL DATA	
• Consistency:	powder
• Color:	light colored
• Composition:	with fine sand (0.5–2.5 mm) with large sand (0.5–5mm)
– binder	500 kg/m <sup>3</sup> 440 kg/m <sup>3</sup>
– sand	1000 kg/m <sup>3</sup> 1110 kg/m <sup>3</sup>
– water	225 kg/m <sup>3</sup> 200 kg/m <sup>3</sup>
• Density:	1600–1800 kg/m <sup>3</sup> 1700–1850 kg/m <sup>3</sup>
Flow table (UNI 7044):	70–100% 70–100%
Bleeding (UNI 7122):	none none
• Compressive strength:	
– 7 days	2–4 MPa 2–4 MPa
– 28 days	4–6 MPa 4–6 MPa
• Dynamic modulus of elasticity:	
– 7 days	3000–4000 MPa 3500–4500 MPa
– 28 days	4000–6000 MPa 4500–7000 MPa

Table 3. Nominal characteristics of mortar B.

DESCRIPTION	
Ready to use cement-free grout, filler for voids and cavities in masonry structures.	
TECHNICAL DATA	
• Color:	light grey
• Composition:	water/powder ratio: 0.3
• Density:	1900 kg/m <sup>3</sup>
• Bleeding:	none
• Compressive strength (28 days):	12 MPa
• Flexural strength (28 days):	2.5 MPa
• Static modulus of elasticity (28 days):	8000 MPa

Table 4. Nominal characteristics of mortar C.

DESCRIPTION	
One-component mortar for plaster repair.	
TECHNICAL DATA	
• Color:	grey
• Composition:	water/powder ratio: 0.12 ÷ 0.14 max. aggregate size: 2.5 mm
• Density:	1600 ÷ 1700 kg/m <sup>3</sup>
• Compressive strength (28 days):	>3.5 MPa
• Static modulus of elasticity (28 days):	950 MPa

Table 5. Mechanical characteristics of bricks and mortars.

Material	Failure stress (°) [MPa]
Mortar A (*)	8.95
Mortar B (*)	5.15
Mortar C (*)	4.20
Mortar D (*)	15.85
Historical brick	8.95

(\*) Tests on mortars were performed 28 days after casting.

(°) Average value of three tests.

Table 6. Elastic characteristics of bricks and mortars.

Material	Secant modulus of elasticity (°) [MPa]
Mortar A (*)	8650
Mortar B (*)	6900
Mortar C (*)	7950
Mortar D (*)	5700
Historical brick	4500

(\*) Tests on mortars were performed 6 months after casting.

(°) Average value of three tests.

Subsequently, the elastic modulus of each material was determined through compressive tests performed according to Italian Standard UNI 6556, with the aid of a 250 kN servo-controlled testing machine and electrical extensometers. The results are reported in Table 6.

## 2.2 Freezing-thawing tests

A potential damage similar to the one caused by natural thermal variations was induced in the specimens by means of freezing-thawing tests, performed in the lab with the aid of a freezing cell (Fig. 2). The test specimens in the steel chambers were water-saturated and thereafter cooled from  $20 \pm 5^\circ\text{C}$  to  $-10 \pm 2^\circ\text{C}$  with a cooling rate of  $4.6^\circ\text{C/h}$ . Warming rate was  $5^\circ\text{C/h}$  and temperature rose to  $20 \pm 5^\circ\text{C}$ . Cooling and warming procedure was repeated 25 times. Another series of 25 freezing-thawing cycles was successively executed with the same arrangement and test conditions.

The elastic characteristics of the specimens at the end of each series were evaluated as illustrated in Sections 2.3 and 2.4.

In this way, a realistic damage process due to thermal causes was simulated and monitored in the lab in an accelerated time period.

## 2.3 Mechanical characterization tests

At the end of each series of freezing-thawing cycles, the secant modulus of elasticity of brick and mortar specimens was determined. This was done because the evolution of the elastic modulus under the effect of the applied thermal solicitations was deemed representative of the integrity of the specimen, and hence related to the possible damage suffered (Kachanov 1986). Accordingly, it could be used as an indicator providing



Figure 2. Freezing cell.

information about the residual performances offered by the material during the structure life-cycle.

The elastic modulus tests were conducted in accordance with Italian Standard UNI 6556, using a 250 kN servo-controlled testing machine and two inductive bridge displacement transducers having a nominal stroke of  $\pm 10$  mm with precision class of 0.2%.

As prescribed, the elastic modulus tests were executed in the lab at ambient temperature and humidity, that were kept constant throughout the duration of the experiments.

At the beginning of each test, the displacement transducers were placed on two opposite faces of the specimen, at mid-height. They continuously recorded the specimen's deformation as a function of the applied compressive load. The specimen was then statically loaded in compression at a constant rate of 250 kPa/s up to 30% of the material's strength, as previously determined (see Tab. 5). The maximum load was maintained for 60 s, then the deformation readings were taken and subsequently the load was released at the same rate at which it was applied, up to a minimum level equal to 10% of the maximum load. Such a minimum load level was maintained in order to minimize possible vibrations of the specimen. The static loading-unloading process was repeated until proper stabilization of the deformation readings was achieved.

Finally, the elastic modulus value was computed as the ratio between stress and strain resulting from the test (see Section 3).

#### 2.4 Impulse method tests

The residual elastic modulus of the specimens at the end of each series of freezing-thawing cycles was determined also by means of a non-destructive technique referred to as Impulse Method.

The physical foundations of the method and the main experimental aspects concerning its practical implementation are extensively described in Antonaci et al. 2007, Antonaci & Bocca 2004; here it is sufficient to recall that it makes it possible to determine the elastic modulus of a material at a point based on the response of the material itself to the impact of a spherical mass having known geometric and elastic properties, under the hypotheses assumed in Hertz's theory of frictionless impact between elastic bodies. These concepts may be easily implemented into an experimental technique aimed at determining the elastic modulus of the material. It is just needed to:

- produce the impact of a known spherical mass against the surface of the specimen (or the structural member) to be examined;

- detect the force versus time curve describing the impact and consequently compute the parameters required for the local elastic modulus determination.

The testing equipment used in this study for elastic modulus determination according to the Impulse Method was composed as follows:

- a special impulse hammer, that is a completely self-contained instrument including an electrically activated mechanism that produces the impact of a hemispherical tip of bonded steel with controlled energy, a piezoelectric force sensor, a signal conditioner with an amplifier and a remote trigger hook-up;
- a portable data acquisition system which makes it possible to acquire and digitize the impulse hammer signals in a software-controlled manner;
- a post-processing system for subsequent data storage and elaboration, consisting of a common notebook.

Two points per specimen were tested via the Impulse Method using the above described technical apparatus. Series of multiple constant energy impacts were preliminarily applied to each point being tested, in order to achieve a stable local response of the system, as recommended in Antonaci et al. 2007, Antonaci & Bocca 2004. The values measured once stabilization was obtained were taken as representative of the material behavior at the point of investigation and the local value of the elastic modulus was computed accordingly.

### 3 RESULTS AND DISCUSSION

The response of the historical clay bricks and restoration mortars considered in this paper to the action of freezing-thawing cycles is reflected in the evolution of their secant modulus of elasticity. Reference elastic modulus values for each material were obtained by averaging the results of the tests on single specimens described in Section 2.3. They are reported in Figure 3 as a function of the number of freezing-thawing cycles.

With increasing number of freezing-thawing cycles, a progressive deterioration in the following form

$$-\frac{dE}{dN} = \lambda E \quad (1)$$

was expected, as illustrated in phenomenological studies such as Mutluturk et al. 2004.

In partial contrast with this theoretical expectation, the test results revealed that mortar A experienced a performance improvement, since its elastic modulus increased more than 16% after the first 25 cycles

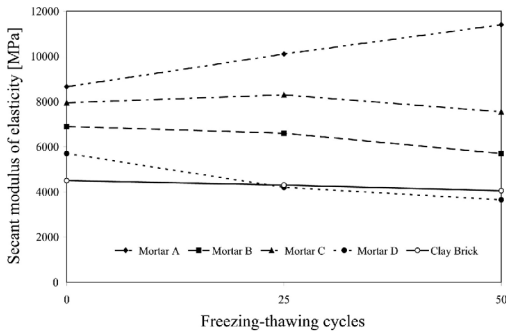


Figure 3. Evolution of secant moduli of elasticity with increasing freezing-thawing cycles.

and nearly 32% after 50 cycles. Similarly, the elastic modulus of mortar C increased in the first 25 cycles (although less markedly than in mortar A), but it regained a value substantially similar to the initial one at the end of the 50 cycles. This unusual behavior could be ascribed to the chemical composition of the mortars in question: according to the information provided by the producers, both contain pore agents and synthetic fibers. The positive influence of non-connected and uniformly distributed micro-pores on the freezing-thawing resistance of a cement or mortar matrix is well-known and is due their ability to dissipate the pressure gradients generated by ice formation. It is likely that also the presence of fibers positively contributes to the freezing-thawing resistance but it is still to be investigated how it can cause a performance enhancement.

The evolution of mortars B and brick samples did not deviate from the expected behavior, revealing a moderate elastic modulus decrease as a function of freezing-thawing cycles. Mortar D presented a more evident elastic modulus degradation.

The affinity with the historical clay brick behavior in terms of long-time thermal compatibility suggests that mortars B and C are particularly suitable to be used in combination with the original material. Therefore they represent the best choice among the four restoration products examined, with regard to the durability of the ensemble under the effect of environmental freezing-thawing actions. On the contrary, mortars A and D are deemed inadvisable because, due to opposite factors, their behavior is significantly dissimilar from the historical brick one and therefore could induce the onset of negative stress gradients in the ensemble, thus compromising its durability.

As far as Impulse Method tests are concerned, it must be remarked that the elastic modulus estimates provided by this technique are not adequately realistic: they significantly differ from point to point,

Table 7. Comparison of the results obtained by means of standard elastic modulus tests and Impulse Method tests.

Material	E [MPa] after $n$ thermal cycles				$\Delta E_{50-25}$ [MPa]	
	UNI 6556		Impulse method		UNI 6556	Impulse method
	$n = 25$	$n = 50$	$n = 25$	$n = 50$		
Mortar A	10100	11400	7500	8700	1300	1200
Mortar B	6600	5700	8150	7200	-900	-950
Mortar C	8300	7550	8200	7400	-750	-800
Mortar D	4200	3650	5700	5050	-550	-650
Brick	4300	4050	5700	5400	-250	-300

the material examined being the same, and in addition their average values are not representative of the actual elastic modulus values as resulting from standard mechanical characterization tests. This could be due to small material in-homogeneities, that may be present and alter the local elastic modulus measurements taken via the Impulse Method even though they have no influence on the behavior of the specimen as a whole. However, it should be noticed that the incremental measurements (i.e. the values of the difference between the elastic modulus estimates obtained through the Impulse Method at the end of two successive series of freezing-thawing cycles) are not affected by this kind of error and in fact the experimental evidence proved that on average they are reasonably representative of the difference between the actual elastic modulus values obtained through standard tests at the end of two consecutive series of thermal cycles. This result is illustrated in Table 7.

This experimental finding is fairly relevant if it is kept in mind that the incremental values of the elastic modulus, rather than the absolute values, are of interest within the process of material life-time assessment, as highlighted in Equation 1. For this reason, regardless of its limitations, the Impulse Method reveals to have interesting possibilities of application in the field of bricks and mortars characterization.

#### 4 CONCLUSIONS

The long-time mechanical behavior of historical clay bricks and modern restoration mortars subjected to series of freezing-thawing cycles has been analyzed by monitoring the evolution of the elastic modulus, whose value was taken as representative of the possible material degradation.

The use of accelerated laboratory techniques for thermal damage simulation in combination with standard methods for elastic modulus determination is proposed as an effective procedure for material



characterization and selection, that can support the design process of repair and restoration works, in view of their compatibility and durability.

In addition to standard laboratory methods for elastic modulus determination, also a recently conceived non-destructive technique, denoted as Impulse Method, has been used to monitor the response of the materials under consideration to the action of the given freezing-thawing cycles. The fairly good agreement between the results obtained by traditional laboratory methods and the Impulse Method (in terms of incremental values) revealed that the latter is potentially applicable directly on-site in order to get information about the evolution of the masonry components' characteristics due to repeated thermal solicitations. Consequently, the Impulse Method is seen to be an effective technique that could facilitate the process of selection of the most appropriate repair material reducing the resort to extensive laboratory characterization tests.

#### ACKNOWLEDGMENTS

The financial support to this study offered by Piedmont Region is gratefully acknowledged.

#### REFERENCES

- Antonaci, P., Bocca, P. & Sellone, F. 2007. Elastic modulus in large concrete structures by a sequential hypothesis testing procedure applied to impulse method data. *Structural engineering and mechanics* 26(5).
- Antonaci, P. & Bocca, P. 2004. On-site evaluation of concrete deformability characteristics: two non-destructive methods compared. *Scientific Israel – Technological advances* 6(3,4): 87–95.
- Emberson, N.K. & Mays, C.G. 1990a. Significance of property mismatch in the patch repair of structural concrete. Part 1: Properties of repair systems. *Magazine of concrete research* 42(152): 147–160.
- Emberson, N.K. & Mays, C.G. 1990b. Significance of property mismatch in the patch repair of structural concrete. Part 2: Axially loaded reinforced concrete members. *Magazine of concrete research* 42(152): 147–160.
- Kachanov, L.M. 1986. *Introduction to continuum damage mechanics*. Dordrecht: Kluwer.
- Morgan, D.R. 1996. Compatibility of concrete repair materials and systems. *Construction and building materials* 10(1): 57–67.
- Mutluturk, M., Altindag, R. & Turk, G. 2004. A decay function model for the integrity loss of rock when subjected to recurrent cycles of freezing-thawing and heating-cooling. *International journal of rock mechanics and mining sciences* 4(2): 237–244.

# Ageing and lifecycle of building envelopes and thin shells made of quasi-brittle conglomerates of glass and epoxy resin

F. Aymerich

*Department of Mechanical Engineering, University of Cagliari, Italy*

G.P. Cossu

*Building Engineer, Cagliari, Italy*

L. Fenu

*Department of Structural Engineering, University of Cagliari, Italy*

**ABSTRACT:** Ageing of conglomerates made of recycled glass and epoxy resin is studied. This material appears suitable for building envelopes, thin shells and design objects. It is quasi-brittle -with quite good mechanical characteristics and appearance- and translucent, taking color from its glass aggregates. Since envelopes are subjected to the action of the atmospheric agents, accelerated tests were conducted to investigate the ageing effects on the mechanical properties of the material and estimate the lifecycle of thin panels and shells.

## 1 INTRODUCTION

The ageing of a conglomerate made of glass aggregates and epoxy resin is studied. This material is quasi-brittle, and has high compressive strength. The tensile strength is much lower than the compressive strength, but rather high for a conglomerate. Due to the distributed granulometry, resin is saved, so reducing costs.

It is translucent, and both its colour and the amount of light that can pass through depend on the colours of the glass aggregates, that make it possible to obtain a number of colour gradations. This material appears to be suitable for building envelopes, small translucent plastic shells, design objects (even if big for urban furnish), as well as for a number of construction elements made of plastic materials that are increasingly available in the market.

Since envelopes, as well as shells, are subjected to the action of the atmospheric agents, accelerated ageing tests lasting more than eight months and simulating the action of the atmospheric agents have been performed on small sample panels of this material. The same tests made on unaged samples were conducted on aged samples to assess the effect of ageing on the material and to collect useful information for subsequent estimation of the lifecycle, especially of building envelopes and thin shells.

## 2 MATERIAL COMPOSITION AND SAMPLE PREPARATION

The conglomerate is made of aggregates of recycled glass and epoxy resin (Cossu, 2006). The aggregate colour affects the conglomerate one but, in order to obtain uniform and repeatable characteristics, recycled transparent float glass was crushed in a jaw mill and sieved to achieve the required granulometry. Table 1 shows the chosen granulometry.

Epoxy resin (14% in weight) was used as binding agent. Before mixing, the aggregates were wet with an adhesion promoter (amino-siloxane solution).

Conglomerate sheets  $400 \times 400 \text{ mm}^2$  with 10 mm thickness were prepared in a polyethylene formwork. Samples  $75 \times 140 \text{ mm}^2$  for subsequent accelerated ageing tests were obtained by cutting with a diamond-coated disc.

Table 1. Granulometry of glass aggregates.

Granulometric class [mm]	%
1.60 – 1.25	25.5
1.25 – 0.80	25.6
0.80 – 0.32	16.7
0.32 – 0.10	32.2

Finally, both aged and non aged samples (whose geometry is described in section 4) were cut for Three Point Bending tests on notched and unnotched specimens.

### 3 ACCELERATED AGEING

Since the material appears to be suitable for building envelopes and thin shells, a good ageing behaviour is necessary. Five 10 mm thick samples  $75 \times 140 \text{ mm}^2$  in size were subjected to accelerated ageing tests. A multi environmental stress test was performed, where the accelerated ageing is due to the combined action of UV rays, humidity and temperature changes.

The most widely used weathering and UV exposure test was performed, complying with numerous standard test methods and, among the other things, with the severe tests in the automotive field. Some general standards are defined (UNI EN ISO 11507, ASTM G-151, SAE J2020, JIS D 0205) as well as more specific ones (ASTM D-4329, DIN 53 384).

The conglomerate ageing was accelerated by means of a QUV Accelerated Weathering Tester, simply called QUV in the following. The test was conducted in accordance with the UNI EN ISO 11507–2002 standard, and the whole test lasted 6000 hours (250 days). The testing chamber was held under temperature control conditions. The samples were subjected to alternative cycles of 8 hours under UV exposure at  $50^\circ\text{C}$  and 4 hours under moisture conditions with condensing humidity at  $50^\circ\text{C}$  in the testing chamber, but cooling the other side surface of the sample till the dew-point was reached.

The test can be also run in an aggressive environment with chemical agents, like, for instance, solvents, salt and sulphurous anhydride. They have not been used in this case.

### 4 MECHANICAL CHARACTERISTICS BEFORE AND AFTER AGEING

Selected tests were performed in order to assess whether the structural performance of the material was deteriorated by the QUV test.

UV action, as well as humidity and temperature changes, can accelerate the ageing of a polymer. Moreover, since the material is a conglomerate, their action can be enhanced by cracking. Polymers are usually sensitive to the photochemical attack of UV rays, which are able to modify their molecular structure. Besides, when they absorb or release moisture, this causes a physical stress in the material, the greater the humidity and temperature variations in the environment, the greater the stress in the material. Whereas rain mainly affects the material surface, condensed

moisture is also absorbed inside the material, with a significant impact on the mechanical properties. In the range of the QUV test temperature, both Young's modulus and strength of epoxy resin decrease with temperature, even without reaching the glass temperature value, which is about  $120^\circ\text{C}$ . The combined effect of humidity cycles and temperature variations, together with cycles of UV exposure, causes irreversible changes in the polymer chain that are able to deteriorate the epoxy resin (Astawitz G. & Nicolais L., 1984). Therefore, also the conglomerate of glass and epoxy resin can be aged by the QUV tester, so that the ageing effects on the material properties can be detected.

Compressive and tensile strengths of the conglomerate were already known from a previous study (Cossu, 2006), during which compression tests on cubic samples with 30 mm side and Three Point Bending (TPB) tests on prismatic samples with size of  $30 \times 30 \times 160 \text{ mm}^3$  (span length = 150 mm) were carried out. Values of compressive strength of 114 MPa and of flexural tensile strength of 38 MPa were found. From TPB tests on  $30 \times 30 \times 160 \text{ mm}^3$  samples with a 10 mm notch (span length = 150 mm), a fracture energy of  $894 \text{ J/m}^2$  was obtained. TPB tests on notched samples showed a quasi-brittle behaviour with cohesive fracture (Carpinteri, 1986, Karihaloo, 1995).

For a first estimate of how much the ageing test is able to modify the mechanical characteristics of the conglomerate, TPB tests were run, and the results of aged and unaged samples compared.

Prismatic specimens were obtained by cutting them from both unaged and aged panels  $75 \times 140 \times 10 \text{ mm}^3$  in size. For in-plane bending (with respect to the original panel plane), specimens  $10 \times 20 \times 140 \text{ mm}^3$  were used with a span length equal to 110 mm. Some of these specimens were notched with a notch depth of 8 mm, that is  $\alpha = 8/20 = 0.4$ .

For out-of-plane bending (again with reference to the original panel plane), specimens  $20 \times 10 \times 70 \text{ mm}^3$  (span length = 55 mm) were used, with the notched samples having a notch depth of 4 mm ( $\alpha = 0.4$ ).

Typical load-displacement diagrams of the TPB tests on both  $10 \times 20 \times 140$  and  $20 \times 10 \times 70$  specimens (called A and B respectively) are shown in Figures 1–4.

Mechanical tests were conducted on a 5 kN servoelectrical testing machine operated under stroke control at velocity of 0.5 mm/min. At least five samples were tested for each specimen configuration.

Specimens A and B, as well the previously tested  $30 \times 30 \times 160$  ones, have different heights. Since the material is quasi-brittle, size-effect has to be expected (Bazant, 1976 and 1984).

Tests on unaged-unnotched A and B specimens (Figures 1a-2a and 6), show average peak loads of

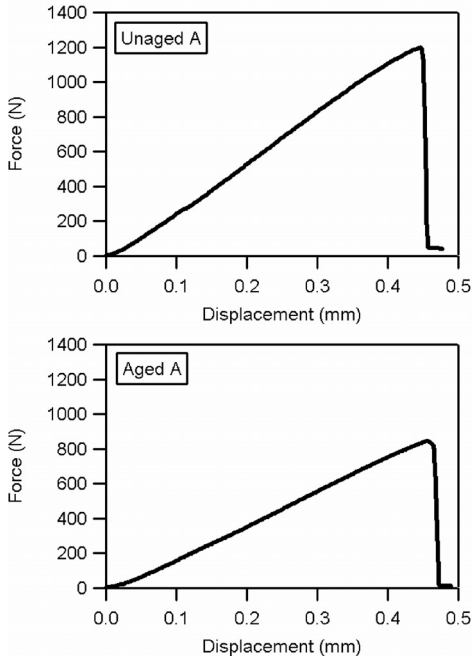


Figure 1. Typical load-displacement curves of flexural tests for unaged and aged A samples (in-plane bending).

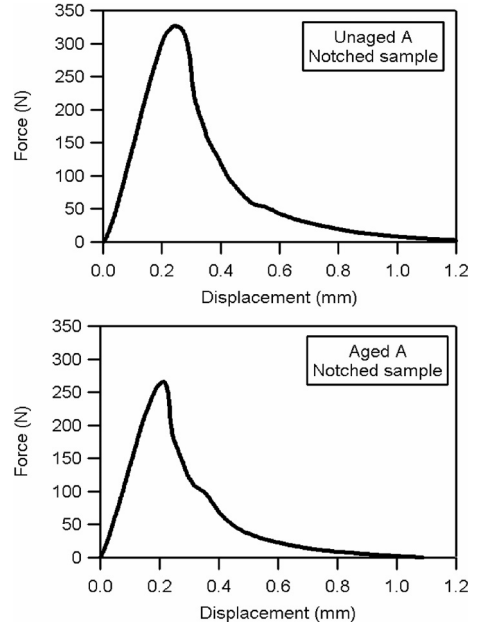


Figure 3. Typical load-displacement curves of flexural tests for notched unaged and aged A samples (in-plane bending).

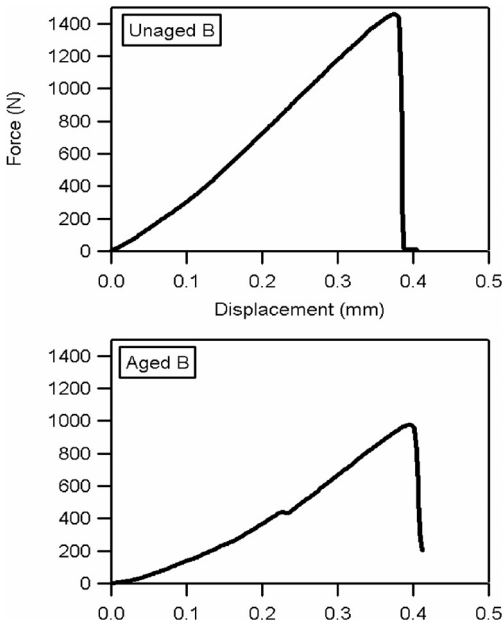


Figure 2. Typical load-displacement curves of flexural tests for unaged and aged B samples (out-of-plane bending).

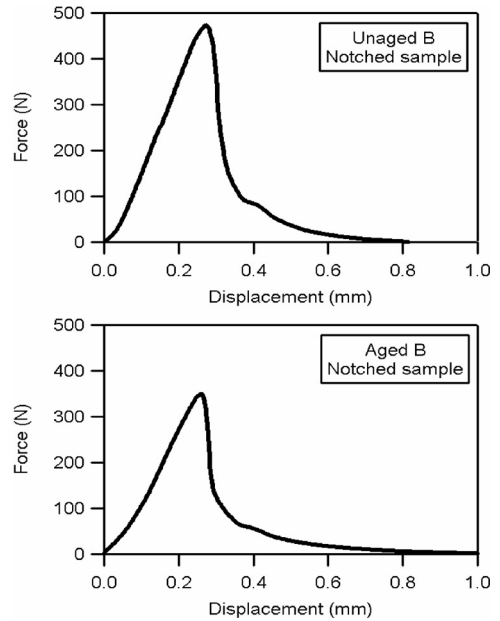


Figure 4. Typical load-displacement curves of flexural tests of notched unaged and aged B samples (out-of-plane bending).

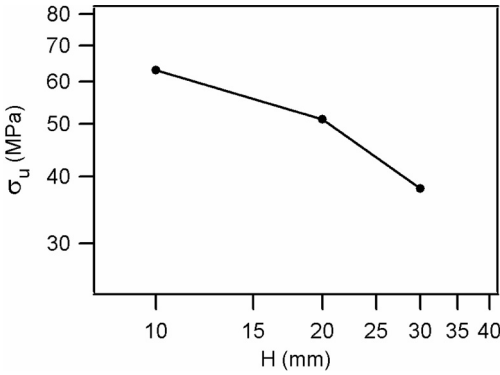


Figure 5. Size-effect for ultimate flexural tensile strength (log-scale axes).

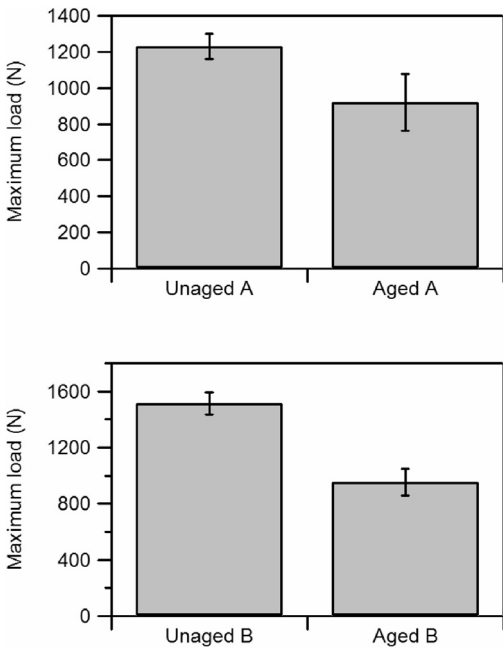


Figure 6. Maximum loads during flexural tests for unnotched unaged and aged samples.

1231 and 1524 N, respectively (which correspond to flexural tensile strengths of 51 and 63 MPa) with results in good accordance with the expected size-effect (Fig. 5).

This also means that their flexural strength does not change very much between in-plane and out-of-plane bending.

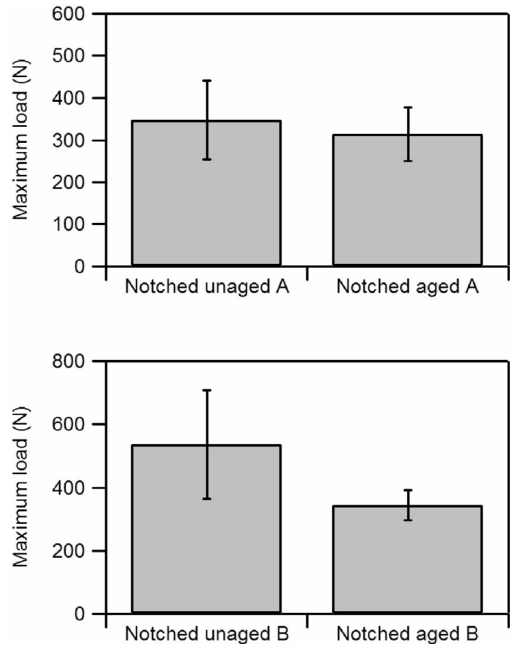


Figure 7. Maximum loads during flexural tests for notched unaged and aged samples.

It was also found that the accelerated ageing test reduced flexural tensile strengths of A and B samples, with average peak loads of 919 and 951 N, respectively, corresponding to nominal stresses of 38 and 39 MPa (Figs 1b-2b and 6). For both A and B types of aged samples, both fracture energies and peak loads of notched specimens were reduced (Figures 3-4 and 7-8).

The ageing effect is in fact confirmed by all the tests performed. The residual tensile strength is in any case higher than 35 MPa, that is a rather high value for a conglomerate where the amount of binder is quite low. Furthermore, toughness even though decreased by ageing- still maintains a good value for a conglomerated material.

## 5 ACCELERATED AGEING AND LIFE-CYCLE OF THE GLASS-EPOXY RESIN CONGLOMERATE IN THIN PANELS AND SHELLS

The accelerated ageing QUV test is a multi-environmental stress test that simulates extreme environmental conditions. It derives from the so called Florida test, that was restated to simulate the environmental conditions that can be found in some coastal

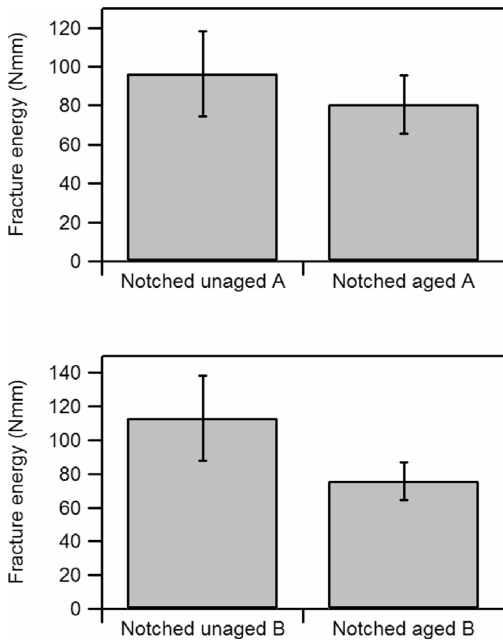


Figure 8. Fracture energies dissipated during flexural tests for notched unaged and aged samples.

regions of Florida, with intense UV irradiation and daily changes of temperature under high degree of relative humidity. It has been evaluated that a period of three weeks in the ageing tester should correspond to a one-year exposure in Florida (Schneider et al., 1993, Zhao & Allen Bernstore, 1998).

A test lasting six months corresponds thus to about eight years exposure in Florida, and to a more than twice longer exposure time for the environment of South-Europe regions. For an accelerated ageing test of 250 days, a correspondence of more than 11 years in Florida and more than 25 years in South-Europe may be therefore estimated. The actual relation between ageing tests and environment exposure in terms of material degradation and damage is however a very complex phenomenon, which cannot be expected to be described by a simple time-multiplier factor.

In any case, as a safe estimate, it can be assumed that thin panels and shells with the same thickness of the tested samples could be exposed for more than twenty-five years in South Europe -and even longer in northern european regions- while retaining good mechanical properties. In fact, flexural strengths and toughness values of aged samples appear to be sufficiently high to allow a structural use of the material, not only for the estimated durations of exposure, but even for longer times.

Furthermore, thicker panels and shells should be more durable, but allow less light to pass through, the thicker the less translucent.

With the peculiar good appearance given by the glass aggregates, perhaps also coloured, they suggest a structural use in both translucent building envelopes, like for instance it happens for structural glass facades, and thin translucent shells.

## 6 CONCLUSIONS

In contemporary architecture plastic materials are increasingly utilised, also with a structural use.

Costs are usually high, and durability under the environment agents not sufficiently known. Nevertheless they have some advantageous applications for both performance and appearance.

For realizing thin shells and panels, the proposed conglomerate of glass aggregates and epoxy resin allows us to save costly resin in comparison to the use of neat epoxy resin. For the good mechanical properties, together with translucency and good appearance, its use appears to be advantageous.

An estimate of the lifecycle of thin translucent structural elements made of this material is of course necessary. The epoxy resin, especially if conglomerated, and therefore unavoidably cracked, can be modified by the environment agents, so partially losing its favourable characteristics.

With reference to the above estimate, some samples of this material have been subjected to an accelerated ageing test, and flexural strengths and toughnesses of aged specimens have been compared with those of unaged samples.

The comparison has shown that ageing degrades the mechanical properties of the material. Nevertheless, the detected mechanical characteristics of the material have remained sufficiently good for a structural use in thin shells, panels, building envelopes and small thin plates.

Such structural elements made of this material, with the good appearance given from the glass aggregates (that can be also previously coloured) can then be realized. Among the other applications, their use appears to be suitable especially in contemporary architecture with a sufficiently long lifecycle. Also urban furnish and design objects appear to be a suitable field of application of this material.

## ACKNOWLEDGEMENTS

This study is fruit of a collaboration between the University of Cagliari, PhD course in Building Engineering, and the chemical company Sept Italia S.p.a., Cagliari; for his kind cooperation, special thanks go

from the authors to Dr. Gianluca Pettinau, whose valuable advices are acknowledged.

A particular thank goes to the student Filippa Pintus, for aiding in preparing the samples.

## REFERENCES

- Astawitz, G. & Nicolais, L., 1984. *Polymer processing and properties*, New York, Plenum.
- ASTM G-151, Standard practice for exposing nonmetallic materials in accelerated test devices that use laboratory light sources.
- ASTM D-4329, standard practice for light/water exposure of plastics.
- Bazant, Z.P. 1976. Instability, ductility and size effect in strain-softening concrete, *ASCE J Eng Mech*, 102, 331–344.
- Bazant, Z.P. 1984. Size effect in blunt fracture: concrete, rock, metal, *ASCE J Eng Mech*, 110, 518–535.
- Carpinteri, A., 1986. *Mechanical damage and crack growth in concrete*, Dordrecht, Martinus Nijhoff.
- Cossu, G.P. 2006. Nuovi materiali per l'architettura. Sperimentazione di un composito di vetro e resina epossidica, PhD Thesis in Building Engineering, Faculty of Engineering of the University of Cagliari.
- DIN 53 384, Testing of plastics, artificial weathering and exposure to artificial light.
- JIS D 0205, Test method of weatherability for automotive parts (Japan).
- Karihaloo, B.L. 1995. *Fracture mechanics and structural concrete*, Harlow, Longman Scientific & Technical.
- SAE J2020, Accelerated exp. of automotive exterior mats using a fluorescent uv/condensation apparatus.
- Schneider, H.M., Guidi, W.W., Burnham, J.T., Gorur R.S., Hall, J.F. 1993. Accelerated aging and flashover tests on 138 kV nonceramic line post insulators, *IEEE Transactions on Power Delivery*, Vol. 8, 1, 325–333.
- Zhao, T. & Allen Bernstore, R. 1998. Ageing tests of polymeric housing materials for non-ceramic insulators, *IEEE Electrical Insulation Magazine*, Vol.14, 2, 26–33.

# Concrete composition and service life of reinforced concrete structures exposed to chloride bearing environments

L. Bertolini, F. Lollini & E. Redaelli

*Dipartimento di Chimica, Materiali e Ingegneria Chimica "G. Natta", Politecnico di Milano, Milan, Italy*

**ABSTRACT:** Steel corrosion has become a critical issue in the management of reinforced concrete structures. The high costs related to maintenance and repair of corrosion-damaged structures have led to the awareness that steel corrosion has to be prevented since the design stage in order to reduce the life cycle cost of structures. Therefore, there is a need for tools aimed at the design of durable structures. Performance-based methods based on probabilistic or semiprobabilistic approaches have been recently proposed for this purpose, but there is lack of information about the parameters related to the long term behaviour of the materials. Preliminary results of a long-term experimental program aimed at the collection of parameters describing the behaviour of a wide range of concrete compositions and exposure conditions are presented in this paper. The role of concrete composition in relation to the service life of structures exposed to chlorides will be discussed.

## 1 INTRODUCTION

The service life of reinforced and prestressed structures exposed to chloride bearing environments, related to the exposure to seawater or de-icing salts, is limited by the corrosion of steel bars or strands (Bertolini et al. 2004). Corrosion may have several consequences on the serviceability and safety of reinforced concrete structures, such as cracking, spalling in localized areas, or delamination of concrete. Reduction of bond of the reinforcement to the concrete may also occur. The experience on these structures shows that the life cycle cost is usually strongly increased due to frequent repair works aimed at repairing the corrosion induced damages and restore the safety and serviceability of the structure. A proper design and execution of such structures could prevent or delay the damage of the structure and, thus, reduce the cost of the life-cycle. Nevertheless, for this purpose, reliable tools for the design of the service life are needed.

As far as corrosion of steel is concerned, the service life is the sum of the initiation time and the propagation time (Tuutti, 1982). The *initiation period* can be defined as the time required for the chloride to reach a critical threshold at the depth of the outermost steel bars. Once the chloride content has reached the threshold value at the steel surface, the *propagation period* begins and this terminates when a given limit state is reached beyond which consequences of corrosion cannot be further tolerated and a repair work is needed. This distinction between initiation and penetration periods is useful in the design of RC elements, since

different processes and variables should be considered in modelling the two phases (L. Bertolini, 2008).

Figure 1 summarizes the factors involved in the initiation of this type of attack. Chloride penetration through the concrete cover produces in time profiles of chloride content, as shown by the grey lines in Figure 1. Initiation of corrosion takes place at time  $t_i$  when the chloride profile is such that, as shown by the black line in Figure 1, a chloride threshold value ( $Cl_{th}$ ) is reached on the surface of the steel reinforcement, i.e. at a depth equal to the concrete cover thickness.

In order to model the initiation of corrosion, a reliable estimation of both chloride penetration and the chloride threshold is required. Nevertheless, both parameters are strongly influenced by many factors related to both the aggressive environment and the concrete.

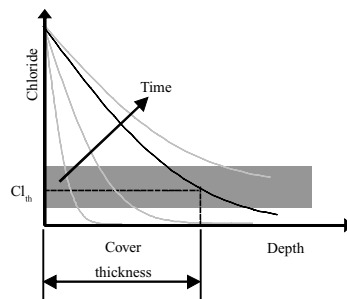


Figure 1. Parameters involved in the initiation of chloride induced corrosion.



As far as the penetration of chloride through the concrete cover is concerned, the complex nature of transport of chloride in concrete has led to the use of simplified procedures. Chloride profiles can be reasonably described by means of the relationship:

$$C(x, t) = C_s \left[ 1 - \operatorname{erf} \left( \frac{x}{2\sqrt{Dt}} \right) \right] \quad (1)$$

where:  $C(x, t)$  is the chloride concentration at depth  $x$  and time  $t$ ,  $C_s$  is the chloride content at the surface of concrete and  $D$  is the diffusion coefficient (Collepari et al., 1970). This relationship is a solution of Fick's second law of diffusion, but it is used by most of design models even for exposure conditions where the transport of chloride is also driven by other transport mechanisms, such as suction, and an apparent diffusion coefficient ( $D_{app}$ ) is introduced (Bertolini, 2008).

To prevent steel corrosion, EN 206-1 standard (2001) and Eurocode 2 (2002) define exposure classes and provide recommendations on the maximum water/cement ratio and the minimum cover thickness, aimed at assuring a service life of the order of 50 years. However, the requirements provided in European standards do not allow the use of a performance-based design procedure. Some models proposed to describe corrosion-related damage of concrete structures by the International Federation of Concrete (FIB) (1997, 2006) and in an European project, called DuraCrete (1997), are based on a probabilistic or semiprobabilistic approach similar to that used in the structural design: limit states that indicate the boundary between the desired and the adverse behaviour of the structure are defined. The resistance of the concrete to the penetration of chlorides is assessed by means of an accelerated test, usually the rapid chloride migration test for chloride induced corrosion (Nordtest, 1999). These models have a drawback in lacking reliable data for the parameters used in the evaluation of service life and also they require the knowledge of parameters characterizing the materials properties. Furthermore, the role of blended cements used in many Countries, obtained by replacing the clinker of portland cement with several types of pozzolanic, hydraulic or inert additions, should be assessed.

This paper shows the results of a long-term experimental program aimed at the collection of parameters describing the behaviour of different materials under different exposure conditions.

## 2 EXPERIMENTAL PROCEDURE

In order to investigate the influence of mineral additions, water/cement ratio and the dosage of cement on the performances of hardened concrete, 26 types of concrete were cast. Different types of binder were obtained by modifying, in a cement factory, a portland cement with the replacement of different percentages

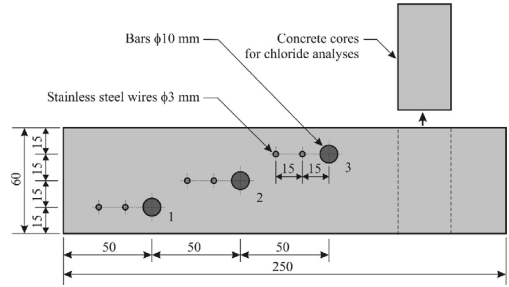


Figure 2. Reinforced specimen (dimensions in mm).

of cement with ground limestone (LI), coal fly ash (PFA), a natural pozzolan (P), and ground granulated blastfurnace slag (GGBS). Only results obtained on concretes made with ordinary portland cement (OPC), 15% and 30% ground limestone (15%LI, 30%LI) and 30% fly ash (30%FA) are presented in this paper. Water/binder ratios ranging from 0.42 to 0.61 and binder dosage ranging from 250 kg/m<sup>3</sup> to 400 kg/m<sup>3</sup> were considered. Major details on concrete compositions and their characterization with regard to mechanical properties, drying shrinkage, resistance to carbonation and chloride penetration properties are given elsewhere (Bertolini et al. 2007). Reinforced specimens were cast in order to simulate the behaviour of components exposed to the action of seawater, and collect data on the initiation and propagation of corrosion (Figure 2). Specimens had three rebars at different cover depth and stainless steel wires used as electrode for electrochemical measurements. A pond was mounted at the upper surface of the specimens and a 35 g/l chloride solution was poured inside, in order to simulate seawater. The corrosion behaviour of steel was monitored throughout the exposure period by means of electrochemical measurement of half-cell potential of steel versus saturated calomel electrode (SCE) and corrosion current density, measured from linear polarisation resistance measurements ( $R_p$ ) as:  $v_{corr} = B/(R_p)$ , where  $B$  was assumed equal to 26 mV. From the measured corrosion current density, an average corrosion rate was calculated and expressed in  $\mu\text{m}/\text{year}$ . Electrical resistivity of concrete was also monitored at different depths, by measuring the electrical conductance between the couples of stainless steel wires. When corrosion initiation was detected on any of the three rebars or after one year of exposure, a sample was cored and the chloride profile was measured, by analyzing the total chloride content (acid soluble) at intervals of 10 mm.

The resistance of the concretes to the penetration of chloride ions was also tested by means of the so-called rapid chloride migration (RCM) test (Nordtest 1999), which led to the calculation of a non-steady state chloride diffusion coefficient ( $D_{RCM}$ ).

### 3 RESULTS

Table 1 summarizes the main properties of the concretes, showing the average values at 28 days of curing of: compressive strength, density and electrical resistivity of water-saturated concrete. The non-steady state diffusion coefficient obtained from the rapid chloride migration test ( $D_{RCM}$ ) is also shown.

Figure 3 shows, as an example, the time evolution of the corrosion potential and the corrosion rate in the three bars of the reinforced specimen made with 15%LI,  $w/b$  0.61 and dosage of cement of 250 kg/m<sup>3</sup>. In time chloride penetration took place due to the ponding with the NaCl solution. When corrosion occurred on one of the three rebars, a sharp decrease in the corrosion potential and an increase in corrosion rate were observed. After only 10 days of ponding the potential of the upper bar dropped to about -400 mV vs SCE (Figure 3a) and corrosion ratio increased up to about 4 mA/m<sup>2</sup> (Figure 3d), indicating that corrosion had initiated on this bar. Later on, corrosion initiated also on the second and third bars.

As soon as corrosion initiation was detected on the bars (i.e. at times shown by × in Figure 3), chloride profiles were measured. By fitting these profiles with relationship (1), a surface content  $C_s$  and the apparent diffusion coefficient (named  $D_{pond}$ ) were calculated.

Table 1. Composition and properties of the tested concretes (average values of two replicate samples):  $w/b$  = water/binder ratio;  $b$  = binder content,  $\delta$  = density,  $C.S.$  = compressive strength,  $\rho$  = resistivity,  $D_{RCM}$  = chloride diffusion coefficient from RCM test (Bertolini et al. 2007).

	$w/b$	$b$	$\delta$	$C.S.$	$\rho$	$D_{RCM}$
	–	kg/m <sup>3</sup>	kg/m <sup>3</sup>	MPa	$\Omega \cdot m$	10 <sup>-12</sup> m <sup>2</sup> /s
Curing <sup>(*)</sup>	–	–	28	28	28	28
OPC	0.61	300	2489	59.2	38	12.5
	0.46	300	2544	87	53	7.7
		350	2461	70.7	44	7.7
	0.42	350	2525	86.6	52	5.4
15%LI	0.61	250	2474	54.5	27	18.9
		300	2431	45.2	29	19.8
	0.46	300	2571	47.8	40	15.1
		350	2461	67.3	38	13.6
	0.42	350	2511	83.3	40	11.3
	400	2470	63.7	39	11.4	
30%LI	0.61	300	2472	36.7	27	38.3
	0.46	300	2492	62	39	18.1
		350	2461	57.4	36	23.5
	0.42	350	2490	66.6	43	13.2
30%FA	0.61	300	2380	43.9	72	11.1
	0.46	300	2463	76.2	119	4.4
		350	2435	74.6	106	3.6
	0.42	350	2467	80.5	119	3.8

(\*) Days of wet curing at 23°C and 95% R.H.

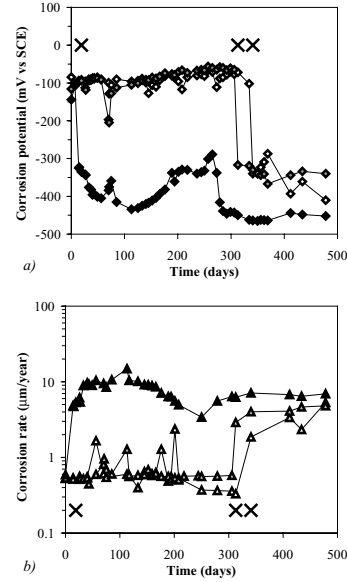


Figure 3. Corrosion potential (a) and corrosion rate (b) as a function of time in the specimen made of concrete with 15% limestone,  $w/b$  0.61 and binder content of 250 kg/m<sup>3</sup> (symbols: black = upper bar, grey intermediate bar, white = lower bar).

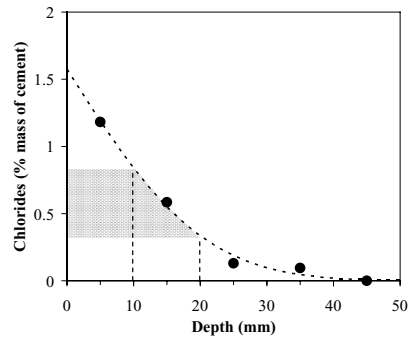


Figure 4. Chloride profile measured when corrosion occurred on the upper rebar (at depth of 10–20 mm) in the specimen made of concrete with 30% limestone,  $w/b$  0.46 and binder content of 300 kg/m<sup>3</sup>.

Figure 4 shows, as an example, the chloride profile measured after 10 days of exposure on the specimen made with 30%LI,  $w/b$  0.61 and dosage of cement of 300 kg/m<sup>3</sup>. Furthermore, the chloride content at the depth of the bar where corrosion had just initiated was assumed as a measure of the chloride threshold (Table 2), e.g. the upper bar, at depth of 10–20 mm, in Figure 4.

Table 2 summaries the results of all the tests, showing:  $C_s$ ,  $D_{pond}$  and the duration of exposure when these parameters were evaluated. Unfortunately, no data are

Table 2. Diffusion coefficient ( $D_{\text{pond}}$ ), surface chloride content ( $C_s$ ) and time of exposure at the time of testing ( $t$ ). Grey cells refer to cores taken when corrosion initiated on a rebar, while other cells refer to cores taken after about a year.

Binder	$w/b$	$b$ kg/m <sup>3</sup>	Curing (days)	$t$ (days)	$D_{\text{pond}}$ 10 <sup>-12</sup> m <sup>2</sup> /s	$C_s$ (% mass)	$C_{\text{th}}$ (% mass)	
OPC	0.61	300	7	150	16.7	2.82	1.66	
				366	6.1	5.09		
	0.46	300	7	349	8.2	1.98		
				366	7.4	1.94		
	0.46	350	7	323	8.6	1.29		
				362	2.3	1.96		
	0.42	350	7	28	362	13.2	0.12	
				7	368	13.1	0.99	
				7	357	35.2	0.66	
				28	357	7.00	1.05	
	15% LI	0.61	250	7	18	49.3	2.34	0.34
					298	35.5	2.28	1.08
0.61		300	7	318	12.5	3.77	0.13	
				13	20.9	2.47	0.19	
				106	12.9	5.14	0.34	
0.46		300	7	360	12.9	5.14		
				360	11.4	1.38		
				7	339	22.7	1.22	
0.46		300	28	367	6.9	2.08		
				10	166.1	1.01	0.38	
30% LI		0.61	300	7	145	28.3	3.8	0.96
					226	27.8	3.41	0.86
	0.46	300	7	204	11.4	2.11	1.19	
				7	18	82.9	1.57	0.55
	0.46	350	28	231	12.5	1.81	1.26	
				7	33	177.8	0.88	0.55
	0.46	350	7	83	35.0	1.88	1.06	
				28	244	13.5	1.29	0.73

available for concrete with fly ash, because, due to their high resistance to chloride penetration, corrosion has not occurred in any of the bars even after one year of exposure. In these specimens, the chloride profiles were measured after about one year of ponding.

#### 4 DISCUSSION

In order to discuss the effect of concrete composition on the service life of reinforced concrete structures exposed to chloride environment, its influence on different parameters related to the initiation and propagation will be analyzed.

**Concrete strength and microstructure.** The complex role of water/binder ratio ( $w/b$ ), wet curing, cement content and mineral addition in relation to the properties of the concrete has been described elsewhere (Bertolini et al. 2007). It is, however, useful to resume here the main findings. The replacement of portland cement with ground limestone (15%LI and 30%LI) led to a reduction in the compressive strength of concrete, due to the inert behaviour of such mineral addition. A

reduction in the 28-day compressive strength was also observed when 30% portland cement was replaced with fly ash (30%FA), although a longer curing, in this case, allowed concretes to reach strength values comparable to those reached by concretes with the same mix design made of portland cement. For a given  $w/b$ , a decrease in the strength was observed as the cement content increased; this could be explained by the increase in the amount of cement paste and, thus, in the increase in the total porosity of the concrete.

Electrical resistivity of concrete, which is an indirect measure of the porosity of the concrete (Bertolini et al. 2004), was also strongly influenced by the concrete composition. For any  $w/b$  ratio, the replacement of portland cement with 15% and 30% ground limestone decreased the electrical resistivity, whereas the replacement with 30% fly ash led to a remarkable increase in the resistivity. These results are a consequence of the inert behaviour of ground limestone, which thus has a negligible effect in decreasing the porosity of the hardened cement paste, and, conversely, of the pozzolanic behaviour of fly ash, which leads to the well known pore refinement of the microstructure of capillary pores.

**Chloride penetration.** The resistance of concrete to chloride penetration can be evaluated from results of the RCM test. The inverse of the non-steady state diffusion coefficient ( $D_{\text{RCM}}$ ) measured with the rapid chloride migration test on specimens cured for 28 days is often used to measure the resistance of concrete to the penetration of chloride ions.

Table 1 shows that, for any type of binder, this coefficient benefits of the reduction in porosity due to the reduction in the  $w/b$  ratio, while there is no significant role of the dosage of binder. A remarkable influence of the type of binder was also observed; in comparison to OPC,  $D_{\text{RCM}}$  was roughly halved by using 30%FA, while it was more than doubled with 15%LI. Very high values of  $D_{\text{RCM}}$  were obtained with 30%LI. Figure 4 shows that a relationship between  $D_{\text{RCM}}$  and the 28-day compressive strength could only be found for a given type of binder. This figure clearly shows the negative role of limestone cements and the beneficial role of fly ash cement on the chloride resistance, which is not reflected by changes in the compressive strength.

Chloride profiles measured on the reinforced concrete specimens subjected to ponding can also allow a comparison of the resistance of the tested concrete to the chloride penetration, by means of the coefficient  $D_{\text{pond}}$ . However, it was found that, as for the apparent diffusion coefficient measured in real structures, the  $D_{\text{pond}}$  is influenced by time of exposure (Table 2). High values were obtained after few days of exposure and they strongly decreased in time.

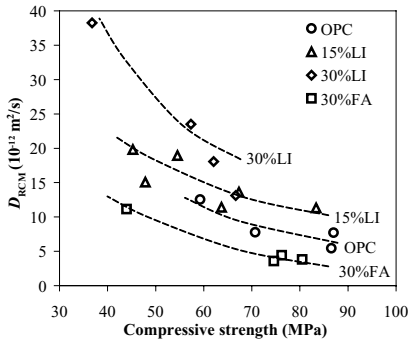


Figure 5. Relationship between  $D_{RCM}$  and 28-day compressive strength of concrete.

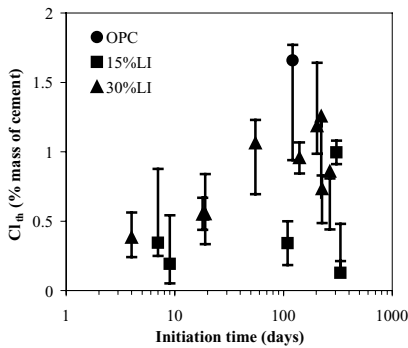


Figure 6. Chloride content measured at the depth of the bars just after corrosion initiation, as a function of initiation time.

As proposed in the literature (DuraCrete 2000, FIB 2007), the diffusion coefficient decreased in time following an exponential relationship; however, more data are necessary to assess the dependency of this correlation on the type of binder and the exposure. Further investigations are also necessary to correlate the diffusion coefficient found from accelerated tests and those obtained from ponding tests.

**Chloride threshold.** The initiation time does not only depend on the diffusion coefficient, but also on the critical chloride content, that is the chloride content required for the onset of corrosion. In order to investigate on this parameter, Figure 6 shows the chloride content measured at the depth of the bars were corrosion had just initiated (Table 2), as a function of the initiation time. The symbol shows the measured value, while the interval shows the range in the fitting profile at the same depth (shown, for instance, by the shadowed area in Figure 3).

No data are available for concretes with fly ash, because corrosion had not initiated after one year of exposure. The values shown in Figure 6 can be

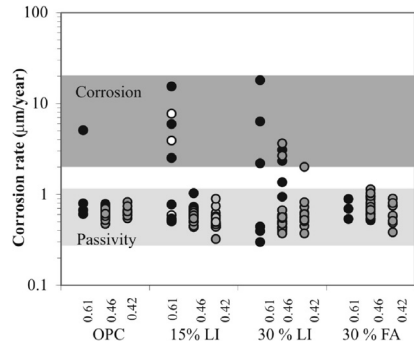


Figure 7. Average corrosion rate before (light grey) and after (dark grey) initiation time.

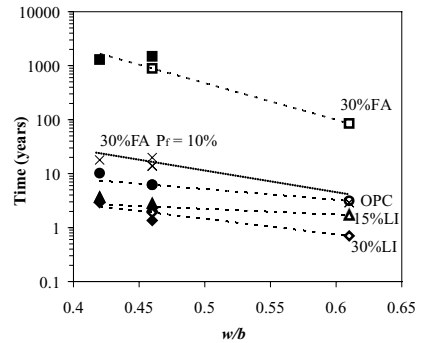


Figure 8. Initiation time evaluated by means of FIB model as a function of  $w/b$ , mineral addition and binder content assuming a probability of failure of 50%. A probability of failure of 10% is also given for concrete cast with fly ash.

assumed as an estimation of the critical chloride content. A wide scatter of results can be observed, which reflects the great variability of this parameter. Even though the experimental data normally fall in the range of 0.4–1% by mass of binder for *OPC* and 15%*LI* and 30%*LI*, which is the usual threshold reported in the literature for structures exposed to the atmosphere, several values below and above this range can be observed. The wide range of chloride contents where corrosion can initiate, makes the estimation of the time of initiation rather difficult, and requires further study on this subject in order to collect enough data for a reliable estimation of the chloride threshold as a function of the type of binder (Manera et al., 2008).

**Corrosion rate.** To estimate the propagation time, the corrosion rate of steel has to be estimated, as a function of the exposure conditions and the concrete composition. Figure 7 shows the corrosion rate measured in the steel embedded in the different types of concrete, both before and after the initiation of corrosion. Due to passivity, corrosion rate was lower than 1  $\mu\text{m}/\text{year}$

before initiation and no differences among specimens due to concrete composition were observed.

After the onset of corrosion, the corrosion rate increased reaching average values in the range of 2–20  $\mu\text{m}/\text{year}$ , and again no significant differences could be observed between bars embedded in *OPC*, 15%*LI* and 30%*LI*. In some specimens corrosion took place also in the deeper bars, and it was found that corrosion rate was always higher for the upper rebars than for the intermediate ones. This could be attributed to the higher chloride content and humidity. This suggests that chloride contamination and exposure conditions play a major role on the corrosion rate than the composition of concrete. Nevertheless, in order to clarify this point, further results are required, especially to collect data on the corrosion initiation on bars embedded in concretes with pozzolanic or hydraulic additions.

*Effect of concrete composition on the service life.* The results of tests showed a great variability of the parameters involved in the prediction of the service life of RC structures exposed to chloride environments. The model code published by FIB proposes a probabilistic approach aimed at taking into consideration such variability. Experimental data showed that corrosion rate could be quite high and the propagation period can be very short, so service life can be assumed equal to initiation period. According to the FIB model code the initiation time of a structure exposed to a marine environment can be evaluated when  $D_{\text{RCM}}$  is known. For instance, Figure 8 shows the initiation time that can be calculated from the values of  $D_{\text{RCM}}$  shown in Table 1, assuming a concrete cover of 40 mm, a reference temperature of 15° C and a probability of failure of 50%. The type of cement has a remarkable influence on the service life. For instance an initiation time of about 10 years can be calculated for concrete made of portland cement with  $w/b$  ratio between 0.42 and 0.61. The use of 15%*LI* and 30%*LI* leads to a further reduction of the initiation time. The beneficial role of fly ash in reducing the diffusion coefficient brings about initiation times of the order of 100 years with a  $w/b$  ratio of 0.61, and even longer initiation times with lower  $w/b$  ratios. Figure 8 shows that the use of 30%*FA* could provide a longer initiation time compared to the other concretes, even if a probability of failure of 10% is considered. Nevertheless, the reliability of the estimation of the service life provided by the FIB model code still needs to be validated.

## 5 CONCLUSIONS

The influence of several mix design parameters on the performance of RC structures exposed to chloride bearing environment was studied. The beneficial

effect related to the decrease in the water/binder ratio and the increase in curing time was estimated. Some influence of the dosage of binder was observed. The effect of mineral additions in blended cement was studied by replacing portland cement clinker with ground limestone and coal fly ash. Preliminary results of the research confirm the beneficial role of the latter in the resistance to chloride penetration, while show that the former leads to a remarkable decrease in the chloride diffusion coefficient. No significant influence of the concrete composition was observed on both the chloride threshold for corrosion initiation and the corrosion rate in the propagation stage.

## ACKNOWLEDGEMENTS

This research was financed by the Italian Ministry of University and Research (MIUR), Holcim Italia S.p.A. and Sismic. TNO is gratefully acknowledged for providing the software Prob2B<sup>TM</sup> used for the probabilistic calculations.

## REFERENCES

- Bertolini, L., Elsener, B., Pedferri, P. & Polder, R.B. 2004. *Corrosion of Steel in concrete: Prevention, Diagnosis, Repair*, Wiley-VCH, Weinheim, 392 pp.
- Bertolini, L., Lollini, F. & Redaelli E., Influence of concrete composition on parameters related to the durability of reinforced concrete structures, Proceeding of the International RILEM Workshop: Integral Service Life Modelling of Concrete Structures, Guimarães, 5–6 November 2007.
- Bertolini, L., 2008, Steel corrosion and Service Life of Reinforced Concrete Structures, *Structure & Infrastructure Engineering: Maintenance, Management, Life-Cycle Design and Performance*, 2.
- CEB 1997, *New approach to durability design*, Bulletin d'information N° 238.
- Collepari, M., Marcialis, A. and Turriziani, R., 1972, Penetration of chloride ions into cement pastes and concretes, *Journal of American ceramic society*, 55, 534.
- EN 1992-1-1 2002, *Eurocode 2: Design of concrete structures – Part 1: General rules and rules for buildings*.
- EN 206-1 2001, *Concrete—part 1. Specification, performance, production and conformity*.
- FIB 2006, *Model code for service life design*, Bulletin n° 34.
- The European Union-Brite Euram III 2000, *DuraCrete final technical report*, Delft.
- Manera, M., Vennesland, O. & Bertolini, L., Chloride threshold for rebar corrosion in concrete with addition of silica fume, *Corrosion Science*, in print.
- Nordtest, 1999, NT BUILD 492, “Concrete, mortar and cement-based repair materials: chloride migration coefficient from non-steady state migration experiment”.
- Tuutti, K. 1982, *Corrosion of steel in concrete*, Swedish foundation for concrete research, Stockholm.

# FEM-Models of cathodic protection systems for concrete structures

L. Bertolini, F. Lollini & E. Redaelli

*Dipartimento di Chimica, Materiali e Ingegneria Chimica "G. Natta", Politecnico di Milano, Milan, Italy*

R.B. Polder & W.H.A. Peelen

*TNO Built Environment and Geosciences, Delft, The Netherlands*

**ABSTRACT:** A significant number of reinforced concrete structures shows deterioration due to the reinforcement corrosion and requires interventions to guarantee their residual service life. A wide range of maintenance options is available, among which cathodic protection (CP) has been found to be a successful and reliable method even in heavily chloride contaminated structures. Presently, CP systems are designed without full consideration of electrochemical effects, but purely based on experience, which usually results in conservative design. Using numerical models for current and polarisation distributions, CP systems can be designed for critical aspects beforehand and made more effective and economical. In this paper numerical simulations for design of CP systems, in particular for protection of local damage in bridges (e.g. at leaking joints) are presented. From the solution of the models, potential and current distributions in the domain and on the boundary representing the steel/concrete interface are obtained.

## 1 INTRODUCTION

Nowadays a significant number of reinforced concrete structures, such as commercial buildings, marine structures, bridges, etc, begins to show sign of deterioration, particularly those over 30 years age. One of the most frequent degradation mechanism in concrete structures is chloride induced corrosion (Bertolini et al. 2004, EN 12969 2002, Pedferri 1996). A wide range of maintenance options is available to guarantee the residual service life of a concrete structure, among which cathodic protection (CP) has been found to be a successful and reliable method even in heavily chloride contaminated structures. CP is based on moving the potential of the steel to more negative values, reducing potential differences between the anodic and cathodic sites and so reducing the corrosion current to negligible value. This is realized by mounting an external electrode, the anode, on the concrete surface, connecting it with the positive terminal of a current source, while connecting the negative terminal to the reinforcement. On the short term, the polarisation resistance of the steel and the electrolytic resistance of the concrete govern the distribution of current and potential. Eventually the polarisation resistance will increase due to pH increase and chloride ion concentration decrease near the steel/concrete interface; consequently, potential and current distributions will change. Presently, CP systems are designed without taking these effects in

consideration, but purely based on experience, which results in conservative design. Their performance in the field is a matter of wait-and-see. However, using numerical models for current and polarisation distribution, CP systems can be designed for critical aspects beforehand and made more economical. Furthermore, the extent of protection outside the anode area or deeper into the cross section ("throwing power") can be predicted. These issues are illustrated by numerical analysis of part of a bridge deck that is modelled from an actual structure on which CP was applied (Polder 1998).

## 2 EXPERIMENTAL SETUP

### 2.1 Example structures

The structure for which the CP system was modelled consists of two parallel post-tensioned bridges over the river Dommel near 's-Hertogenbosch, The Netherlands. Corrosion was due to (de-icing salt) leakage of the joints between the abutments and the deck, see [Figure 1](#). Actual corrosion occurred of transverse bars within the first half meter from the joint edge. Deeper lying longitudinal bars and transverse bars further from the joint did not corrode. A conductive coating anode (AHEAD) was applied over one meter wide from the joint edge. Reference electrodes were placed near the reinforcing steel (for protection quality

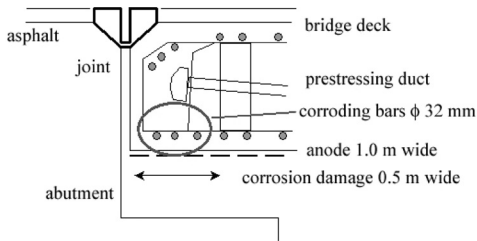


Figure 1. Schematic (longitudinal) cross section of bridge deck and abutment.

checking) and near the post-tensioning anchors (as a warning for reaching hydrogen evolution potentials).

Further details are given in (Polder 1998).

Numerical simulations were carried out using the finite element package COMSOL Multiphysics (formerly known as FEMLAB). The main objectives were to evaluate the CP system throwing power and to assess whether the prestressing steel was safe. The humidity and the number of corroding rebars were varied. It was assumed that the concrete slowly dried out to reach the equilibrium with the atmosphere, after replacing the joints and leakage stop. However, in the future the joint could start leaking again and the concrete would become wet again. As a result two extreme situations with respect to humidity were taken into account: equilibrium with air of 80% relative humidity (RH) and a temperature of 10°C or a RH higher than 90% and 10°C. In these conditions, the concrete was considered dry or wet, respectively, which is expressed by its electrical resistivity. The behaviour of steel in concrete under these specific conditions was described using data available in literature (Redaelli et al. 2006); no temporal variations in the steel conditions (active/passive) were considered.

## 2.2 Numerical model: Geometry

The geometry of the real case is quite complex, so in order to reduce the computation time a 2D model of a part of the deck longitudinal cross section was set up. Numerical simulations carried out on two different lengths of the modelled part (3 and 5 m) showed that the length influenced the results, but the effect was significant only for the rebar farthest from the anode, whereas for active bars (under the anode) it was negligible. Therefore it was assumed that a cross section with a height of 0.8 m and 5 m long was representative of the entire cross section of the bridge. The transverse bars have a concrete cover of 35 mm and are placed at 150 mm centre-to-centre distances, as shown in Figure 2. The three bars closest to the joint, which were actively corroding in the real case, have 32 mm diameter, the rest has 16 mm diameter. The

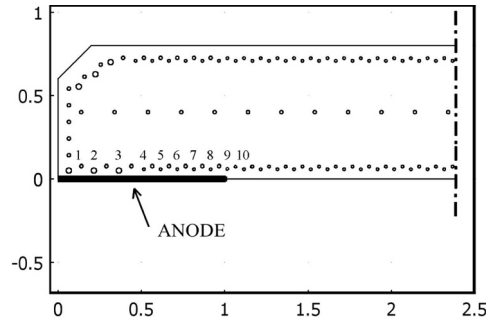


Figure 2. Part of the geometry of the domain (dimensions in m).

longitudinal bars have a diameter of 16 mm and have 100 mm centre-to-centre distances.

In the 2D model of the cross section, only transverse bars can be modelled in their real position. Infact longitudinal rebars cannot be modelled as such. However, their presence cannot be neglected because such bars close to the anode do influence the current flow and thus the power of cathodic protection. Therefore the longitudinal bars were implemented as a second layer of transverse rebars close to the first layer. Each of these rebars was placed in between two (outer) transverse bars taking care in avoiding overlapping with the transverse rebars. The real amount of steel was implemented, only the direction of the bars differs from reality. The diameter of these simulated bars was derived from the real steel surface area, about 0.5 m<sup>2</sup> of steel surface area per m<sup>2</sup> of concrete surface area. The longitudinal bars (simulated as transverse bars) had a concrete cover of 51 mm.

The bars in the upper side of the deck and the stirrups were modelled by mirroring the bars of the lower side. The presence of post-tensioning ducts and anchors, roughly in the middle of the deck thickness, was taken into account in the same way as the longitudinal bars. Taking into account ducts (or anchors) of 100 mm diameter placed at 1 m centre-to-centre distances, 5 bars per meter with a diameter of 20 mm were modelled. As in the real-life case, the anode had a width of one meter starting from the joint edge. The geometry of the model used is represented in Figure 2.

## 2.3 Numerical model: Boundary condition

Due to the high electrical conductivity of metals compared to that of concrete, the rebars and the anodes were assumed to be equipotential regions, and were not considered in the domain where Laplace's equation was solved. The electrochemical behaviour of active and passive steel was described through polarisation curves (that were used as boundary conditions



in the model). These curves were expressed as Butler-Volmer type of relations between current density and potential for active steel:

$$i_A = i_{corr,A} \cdot \left\{ \exp \left( 2.303 \frac{V - V_{corr,A}}{b_{a,A}} \right) + \exp \left( \frac{-2.303(V - V_{corr,A})}{b_{c,A}} \right) \right\} \quad (1)$$

and for passive steel

$$i_P = i_{corr,P} \cdot \left\{ \exp \left( 2.303 \frac{V - V_{corr,P}}{b_{a,P}} \right) + \exp \left( \frac{-2.303(V - V_{corr,P})}{b_{c,P}} \right) \right\} \quad (2)$$

Here  $i$  is the normal component of the current density at the steel surface,  $i_{corr}$  is the corrosion current density,  $V$  is the potential at the concrete side of the interface,  $V_{corr}$  is the free corrosion potential,  $b_a$  and  $b_c$  are the slopes of the anodic and cathodic polarisation curves. So, in order to describe thoroughly each polarisation curve, it is necessary to specify four parameters. In principle, each of these parameters may depend on environmental factors (wet, dry). The term  $V - V_{corr}$ , the polarisation from the corrosion potential due to current flow, is also termed overpotential.

Following previous work (Redaelli et al. 2006), for active bars it was assumed that the free corrosion potential was  $-300$  mV/SCE in dry conditions and  $-360$  mV/SCE in wet conditions and the corrosion current density in dry and wet conditions was  $5$  and  $10$  mA/m<sup>2</sup>, respectively.

The anodic and the cathodic slopes were equal to  $75$  mV/decade and to  $200$  mV/decade, respectively, identical for dry and wet conditions. For passive bars the parameters in expression (2) were considered independent of environmental factors. Free corrosion potential, corrosion current density, anodic and cathodic Tafel slopes were considered equal to  $+100$  mV/SCE,  $0.1$  mA/m<sup>2</sup>,  $10000$  mV/decade (i.e. virtually infinite) and  $200$  mV/decade, respectively. Table 1 summarises the parameters used in the polarization curves.

On the anode, a condition of constant current density was imposed:

$$i = i_{an} \quad (3)$$

Different values of  $i_{an}$  were considered (i.e.  $10$ ,  $20$ ,  $25$  and  $35$  mA/m<sup>2</sup>), in order to find the minimum value of anode current density that could guarantee a cathodic polarisation of  $100$  mV on the three actively corroding rebars.

Table 1. Values of parameters used in equation (1) and (2) (Redaelli et al. 2006).

Description	Symbol	Condition	
		Dry	Wet
Free corrosion potential of active steel	$V_{corr,A}$ (V/SCE)	$-0.30$	$-0.36$
Corrosion current density of active steel	$i_{corr,A}$ (mA/m <sup>2</sup> )	$5$	$10$
Anodic Tafel slope of active steel	$b_{a,A}$ (V/decade)	$0.075$	$0.075$
Cathodic Tafel slope of active steel	$b_{c,A}$ (V/decade)	$0.2$	$0.2$
Free corrosion potential of passive steel	$V_{corr,P}$ (V/SCE)	$+0.1$	$+0.1$
Corrosion current density of passive steel	$i_{corr,P}$ (mA/m <sup>2</sup> )	$0.1$	$0.1$
Anodic Tafel slope of passive steel	$b_{a,P}$ (V/decade)	$10$	$10$
Cathodic Tafel slope of passive steel	$b_{c,P}$ (V/decade)	$0.2$	$0.2$

All other boundaries were characterized by insulating conditions:

$$i = 0 \quad (4)$$

The model also required specifying the properties of the material in terms of electrical conductivity. Since the electrical resistivity of the repair mortar had roughly the same value as the parent concrete (made with OPC/CEM I), it was assumed that conductivity was constant in space. A value electrical resistivity of  $1000 \Omega \cdot m$  was chosen for dry concrete and of  $200 \Omega \cdot m$  for wet concrete (Redaelli et al. 2006).

The mesh was generated automatically by the program, and consisted of  $13115$  triangular elements in the simplified geometry and  $127443$  in the complete geometry with all the rebars. Using the 2D model described, computation times ranging from one to ten minutes were obtained.

### 3 RESULTS

Different series of numerical experiments were carried out, varying the number of the modelled bars and the number of corroding rebars.

The first series of numerical experiments was carried out for a simplified geometry, with rebars in the lower part of the deck only and without post-tensioning steel. Models were solved with different values of anodic current densities, i.e.  $10$ ,  $20$ ,  $25$  and  $35$  mA/m<sup>2</sup>. As it is shown in Figure 3, it was obtained that the lowest anodic current density that could polarize the three active rebars of  $100$  mV was  $35$  mA/m<sup>2</sup>. This value of



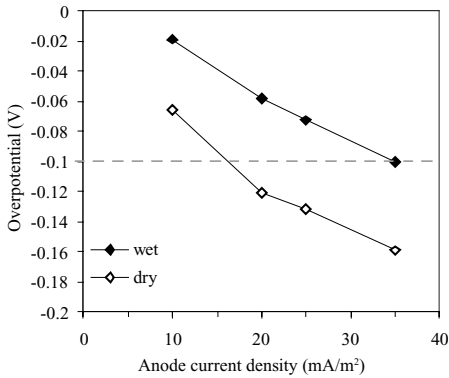


Figure 3. Average overpotential on the three active bars as a function of anode current density.

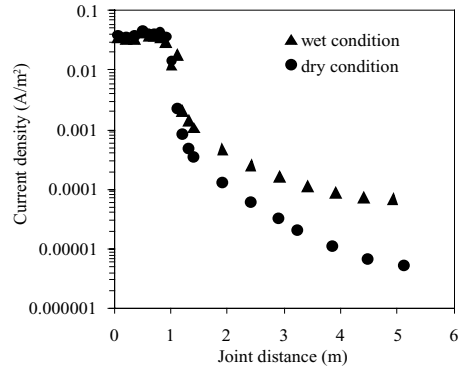


Figure 5. Current density on bars at different distance from the joint.

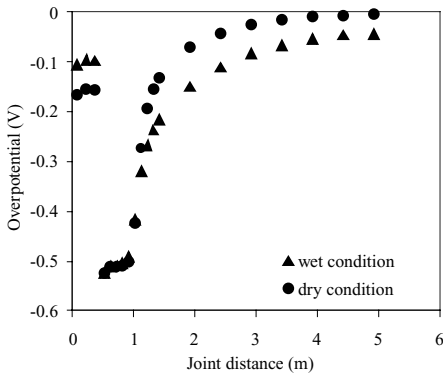


Figure 4. Overpotential on bars at different distance from the joint.

anodic current density was used also for the rest of the calculations. The average values of the overpotential on the steel surface and the steel current densities are shown in Figures 4 and 5, respectively, both for dry and wet conditions. It should be noted that the anode is only present on one meter on the left side. In dry concrete the polarization of the three active rebars was about 160 mV. The rest of the rebars below the anode, which were passive, had a polarization of 500 mV. The polarization of passive rebars decreased increasing the distance from the anode: for instance in dry concrete the steel polarization is 40 mV at about 1.5 m from the anode and becomes 0 mV at 4 m, whilst in wet concrete the steel polarization is 110 mV at 1.5 m and 44 mV at 5 m from the anode.

The cathodic current density was 36–39 mA/m<sup>2</sup> (dry) and 33–36 mA/m<sup>2</sup> (wet) for the three active bars (see Figure 1) and 41 mA/m<sup>2</sup> (dry) and 36 mA/m<sup>2</sup> (wet) for passive steel bars under the anode.

The potential close to the anode obtained from the calculation was 0.9 V in wet concrete and 2.7 V in dry concrete; these values can be considered as an estimation of the feeding voltage of the CP system.

In the second series of simulations, bars were added in the upper part or in the middle of the deck (results not shown).

It was found that overpotentials and current densities decreased slightly for bars in the lower part of the deck. Placing steel inside the deck (where the post-tensioning is located) did not have a significant influence on potentials and current density of the lower steel.

Further simulations were carried out with a complete set of rebars in the lower and upper deck and post-tensioning in the middle, as shown in Figure 2.

For the third series of simulations the number of active transverse rebars was varied. From the joint edge step-wise 3, 5, 8 (located at a distance of 0.916 m from the joint and so the last bar directly under the anode) or 10 (well outside the anode) bars were assumed to be actively corroding.

Figures 6 and 8 show the overpotential for active and passive steel for varying numbers of corroding bars in dry and wet concrete, respectively. Figures 7 and 9 illustrate the current densities on active and passive steel rebars for dry and wet conditions, respectively.

In general and in particular if high polarization is provided by a CP system, overprotection of the post-tensioning steel, ducts and anchors must be carefully regarded due to the possibility of hydrogen evolution (and subsequent embrittlement).

The absolute potentials of steel versus saturated calomel electrode at the position of the post-tensioning were calculated to check this possibility. Figures 10 and 11 show the potentials for a varying number of active rebars for dry and wet concrete.

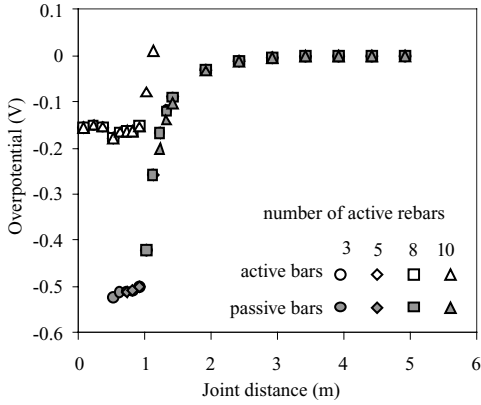


Figure 6. Overpotential on transverse bars in dry concrete at different distance from the joint.

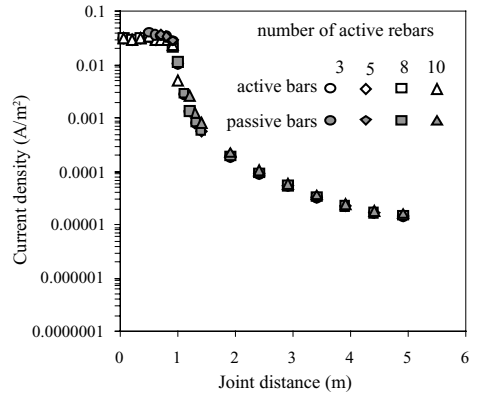


Figure 9. Current density on transverse bars in wet concrete, at different distance from the joint.

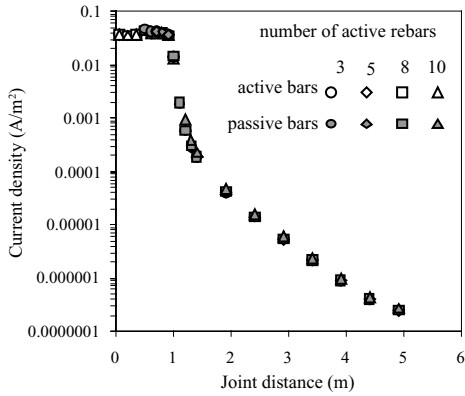


Figure 7. Current density on transverse bars in dry concrete at different distance from the joint.

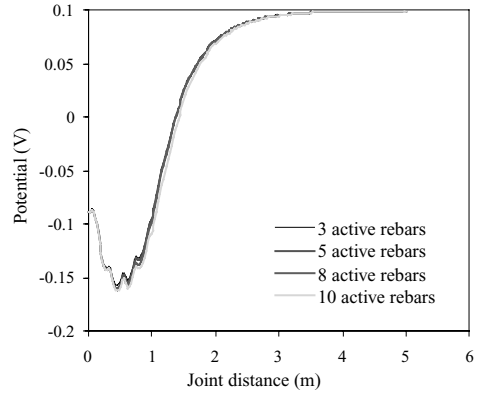


Figure 10. Potential vs SCE on post-tensioning steel in dry concrete.

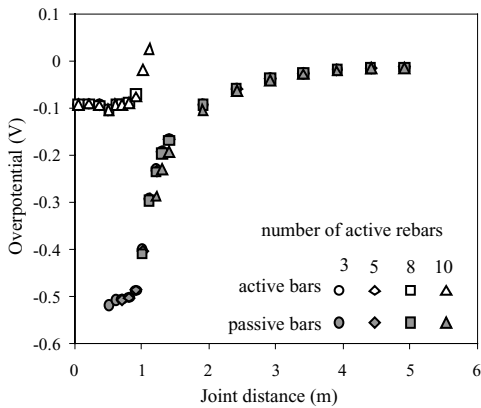


Figure 8. Overpotential on transverse bars in wet concrete, at different distance from the joint.

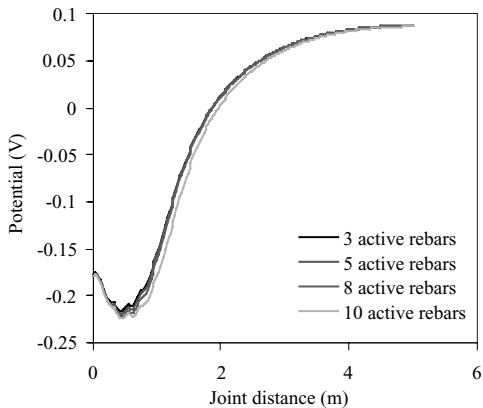


Figure 11. Potential vs SCE on post-tensioning steel in wet concrete.

## 4 DISCUSSION

As mentioned above, the potential calculated through the numerical simulations allows to calculate the overpotential which is the polarisation of the steel due to current flow. Assuming that this polarisation will relax to zero in the normal testing period of four to 24 hours after current switch-off, the “overpotential” could be interpreted as “depolarisation”. A value of 100 mV or more was taken as an indication of protection.

In the first (preliminary) set of numerical experiments, a cathodic polarisation of 100 mV for actively corroding bars in wet concrete was obtained with an anodic current density of 35 mA/m<sup>2</sup>; lower values of anodic current densities resulted in polarisation values lower than 100 mV, that was considered inadequate to protect active rebars. Much higher cathodic polarisation values were obtained on passive bars, about 500 mV for the rebars below the anode and 110 mV for rebars at 1.5 m from the anode. In dry concrete the steel polarization was about 160 mV for active rebars and 510 mV for passive rebars below the anode, and 40 mV at 1.5 m from the anode. The current density on the rebars (active and passive) below the anode was 37–40 mA/m<sup>2</sup>. Compared to measurements in the field, these calculated current densities seem rather high.

The second set of simulations showed that adding steel inside the modelled cross section or on the opposite side from the anode, did not have a big influence on the current to the steel immediately below the anode. Overpotentials reached at steel inside the cross section (e.g. post-tensioning steel) were negative but not so high.

In the third series, the number of corroding bars was varied in lateral direction with respect to the fixed anode surface. Numerical simulations showed that actively corroding bars are protected as long as they are below the anode; active rebars outside the anode (even a few centimeters) received less current and were less polarised; the protection falls off strongly from the edge of the anode. Passive bars were well polarised, more or less independent of the number of corroding bars, also outside the anode (as with the first series), in particular in wet concrete.

The steel current densities obtained with the simulations are higher than would be normally expected in a CP system (typically in the range of 10 to 20 mA/m<sup>2</sup>). This could be caused by several factors, such as assuming incorrect steel polarisation curves or boundary condition at the anode, incorrect values of concrete resistivities or making simplifications in the geometry.

Geometrical simplifications cannot be the main cause, as the real amount of steel and its approximate position were taken into account. Measurements on concrete resistivities in various climates suggest that more or less correct values were used. Other steel polarisation curves could be used, e.g. considering

the limiting current of oxygen or different values of corrosion potential and current density. However, it is hard to obtain polarisation curves from real cases and our estimate is the best guess we can make now. Further work is needed on this issue.

## 5 CONCLUSIONS

A finite element model was set up for cathodic protection of steel in concrete, taking into account the electrochemical properties of steel (active, passive) and concrete (dry, wet). The geometry of part of a bridge deck was simplified in 2 dimensions, including individual bars with realistic surface areas and positions; the anode covered only part of one side of the simulated bridge deck. Calculations for a section of the bridge deck of several meters long would take one to ten minutes. Local potentials and current densities were calculated using Butler-Volmer type steel polarisation behaviour. The amount of steel polarisation from the free corrosion potential (overpotential) is taken to represent the amount of depolarisation that is measured when the CP current is switched off, which is the usual way of checking the quality of protection.

Applying an anodic current density of 35 mA/m<sup>2</sup>, 100 mV polarisation (indicating protection) was obtained for corroding bars under the anode in a wet concrete; and for passive bars outside the immediate vicinity of the anode, both in lateral direction along the deck and deeper inside the cross section of the deck. Actively corroding bars would be protected only if they are under the anode. Steel inside the cross section would not reach very negative potentials that could allow hydrogen evolution (which should be avoided for prestressing steel).

## REFERENCES

- Bertolini, L., Elsener, B., Pedferri, P. & Polder, R.B. 2004. *Corrosion of Steel in Concrete: Prevention, Diagnosis, Repair*, Wiley-VCH Verlag GmbH & Co. KGaA, Weinheim, ISBN 3-527-30800-8, 392 pp.
- EN 12696, 2002, Cathodic protection of steel in concrete.
- Pedferri, P., 1996, Cathodic protection and Cathodic prevention, *Construction and Building Materials*, Vol. 10, (5), 391–402.
- Polder, R.B., 1998, Cathodic Protection of Reinforced Concrete Structures in The Netherlands—Experience and Developments, in: Corrosion of reinforcement in concrete – monitoring, prevention and rehabilitation, Papers from Eurocorr'97, Mietz, J., Elsener, B., Polder, R., Eds. The European Federation of Corrosion Publication number 25, The Institute of Materials, London, ISBN 1-86125-083-5, 172–184.
- Redaelli, E., Bertolini, L., Peelen, W. & Polder, R., 2006, FEM-models for the propagation of chloride induced reinforcement corrosion, *Materials and Corrosion*, Vol. 57, (8), 628–635.

# Structural behavior of cable-stayed bridges under damage

F. Biondini, P. Limonta, P.G. Malerba & R. Stucchi

*Department of Structural Engineering, Politecnico di Milano, Milan, Italy*

**ABSTRACT:** The paper is aimed to investigate the influence of localized or distributed structural weakening on the stability, post-critical and collapse behavior of cable-stayed bridges. The structural behavior of this kind of bridges is strongly influenced by non linear geometrical effects. These effects are studied through a numerical model, suitable to deal with large strains and large displacements. Comparative studies highlight the influence of the most typical damage causes (section reduction or break of one or more hangers or cables, lost of serviceability of a part of the deck, among others) for different cable layouts and/or for different geometrical, topological and stiffness characteristics.

## 1 INTRODUCTION

The collapse behavior of cable-stayed bridges is strongly influenced by non linear geometrical effects. According to their topological and geometrical characteristics, the equilibrium state of such structures may show stable paths or unstable paths with bifurcations, snap back or snap through (Biondini *et al.* 2006). Therefore, it is of noteworthy interest to study the effects of a structural weakening on the equilibrium paths of this kind of structures.

To afford this problem, a wide range of possible damage scenarios and deterioration effects associated with possible source of structural weakening are investigated. Damage is modeled by means of a reduction of cross-sectional properties. A numerical method suitable to deal with large strains and large displacements is used to trace the equilibrium paths of the damaged structures. An introductory example shows the effects of damage on the structural behavior of a truss beam. A set of comparative studies highlights the influence of damage on the stability, post-critical and collapse behavior of cable-stayed bridges.

## 2 LAGRANGIAN FORMULATION

In the hypothesis of large strain and large displacements, the Principle of Virtual Displacements (PVD) has to be formulated with reference to the actual deformed configuration  $C_t$ . According to an Updated Lagrangian formulation and with reference to an Hermitian beam element, the PVD assumes the following form:

$$\delta \mathbf{u}^T (\mathbf{K}_e + \mathbf{K}_g + \mathbf{S}_1 + \mathbf{S}_2 + \mathbf{S}_3) \mathbf{u} = \delta \mathbf{u}^T ({}^{t+\Delta t} \mathbf{f} - {}^t \mathbf{f}) \quad (1)$$

which, due to the arbitrary nature of virtual displacements, can be reduced to the following incremental equation of equilibrium at the configuration  $C_{t+\Delta t}$ , starting from the configuration  $C_t$  (Yang and Kuo 1994, Mc Guire *et al.* 2000):

$$(\mathbf{K}_e + \mathbf{K}_g + \mathbf{S}_1 + \mathbf{S}_2 + \mathbf{S}_3) \mathbf{u} = ({}^{t+\Delta t} \mathbf{f} - {}^t \mathbf{f}) \quad (2)$$

where  $\mathbf{K}_e$  and  $\mathbf{K}_g$  are, respectively, the elastic and geometric stiffness matrices,  $\mathbf{S}_1$ ,  $\mathbf{S}_2$ , and  $\mathbf{S}_3$  are the stiffness matrices associated to the higher order terms of strains and displacements,  $({}^{t+\Delta t} \mathbf{f} - {}^t \mathbf{f})$  is the load vector increment, and  $\mathbf{u}$  is the displacement vector.

The previous equations are based on the Updated Lagrangian formulation which allows us to write the equilibrium equation with reference to the deformed configuration and contains, in addition to the second order terms, also terms of higher order, which are function of the increments of the displacements.

The solution process of the incremental iterative non linear analysis includes two major phases: a prediction phase, which involves the solution in terms of displacements increments, and a correction phase, when the element forces, corresponding to the increments of the element displacements obtained in the first phase, are computed (Crisfield 1991).

An incremental equation with a lower degree of nonlinearity has been used for the prediction phase while another equation, with a higher degree of nonlinearity, has been adopted for the correction one. According to these strategies, the higher order stiffness matrices  $\mathbf{S}_1$ ,  $\mathbf{S}_2$ , and  $\mathbf{S}_3$  have been omitted in the prediction phase, while they are included in the correction one.

Numerical techniques for solving non linear problem in presence of singular points and unstable behaviors are also introduced. Since the classical Newton Raphson Method allows us to follow the equilibrium paths by load increments, but it is not able to follow the post critical behaviors, the arc length method is used (Riks 1979, Crisfield 1991). The method is improved by specific procedures able to detect bifurcation points and all paths departing from them (Bontempi and Malerba 1996, 1997).

### 3 DAMAGE MODELING

Damaging is introduced by means of a reduction of sectional properties (area and inertia). For each section, a suitable parameter  $\delta$  for describing damage is chosen and geometrical characteristics are computed as a function of this parameter.

Cross-sectional damage indices are defined as the ratio between the effective and the undamaged area or inertia, as follows:

$$\delta_A = \frac{A}{A_0} \quad \delta_I = \frac{I}{I_0} \quad (3)$$

Applications related to a truss system and a cable-stayed bridge are presented in the following. For all the elements of these structures, relationships between the cross-sectional damage indices  $\delta_A$  and  $\delta_I$  and the damage parameter  $\delta$  are represented in Figure 1, where different ratios of damage  $\delta$  in the range [0;1] are considered.

### 4 TRUSS SYSTEMS

Preliminary analyses are carried out on a series of simple structures, like an Euler beam, the Fujii-Perez-Choong structure, the Euler arch, and a truss beam, for which the exact solution is known. In this paper, only the results obtained for the truss beam are presented.

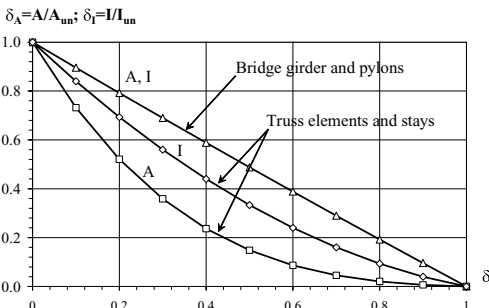


Figure 1. Cross-sectional damage indices.

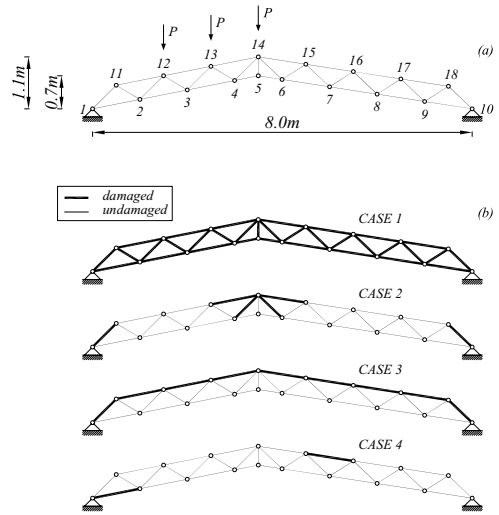


Figure 2. Truss System. (a) Geometry, static scheme, and loads. (b) Damage scenarios.

Table 1. Geometrical and mechanical characteristics of the truss system in Figure 1.

E[GPa]	A[mm <sup>2</sup> ]	I [mm <sup>4</sup> ]
206	1256.64	125663.71

Mechanical and geometrical parameters are summarized in Figure 2a and in Table 1. Sectional characteristics in Table 1 are referred to the undamaged condition.

The four damaging scenarios shown in Figure 2b are considered. In general, when the whole structure is uniformly damaged, the bearing capacity only is reduced, and the shape of equilibrium path remains unchanged. Figure 3a shows this behavior for Case 1. In this figure it is shown  $\mu$ , which is the amplification factor of the load  $P$ , versus the vertical displacement  $v_{14}$  of the node 14.

Figure 3b shows, for instance, a damaging scenario for which the bearing capacity decreases and the snap-back effects gradually disappear.

When damage involves only a part of the truss, like the whole upper flange, higher snap-back effects arise, accompanied by a stiffness recovering faster than in the undamaged case (Figure 3c).

Figure 3d shows the equilibrium paths with reference to the vertical displacement of the node 12,  $v_{12}$ , due to damage of two selected bars, one in tension and the other in compression. When damage on these elements exceed 20%, the snap-back disappears and the loss of carrying capacity becomes more gradual.

Since localized damage may influence favorably or unfavorably the structural behavior, various damage

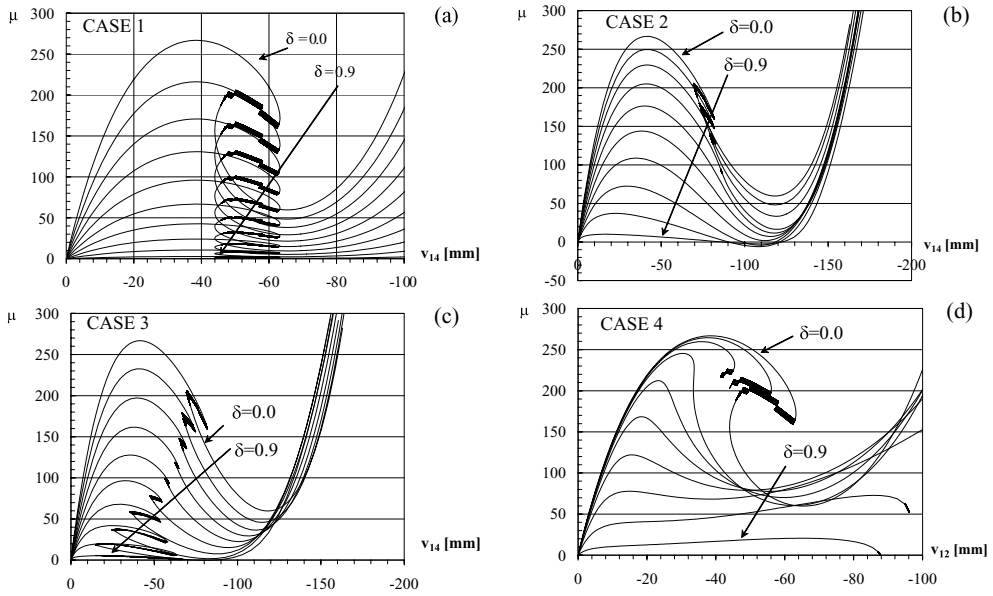


Figure 3. Equilibrium paths of the truss beam for the damaging scenarios in Figure 2b.

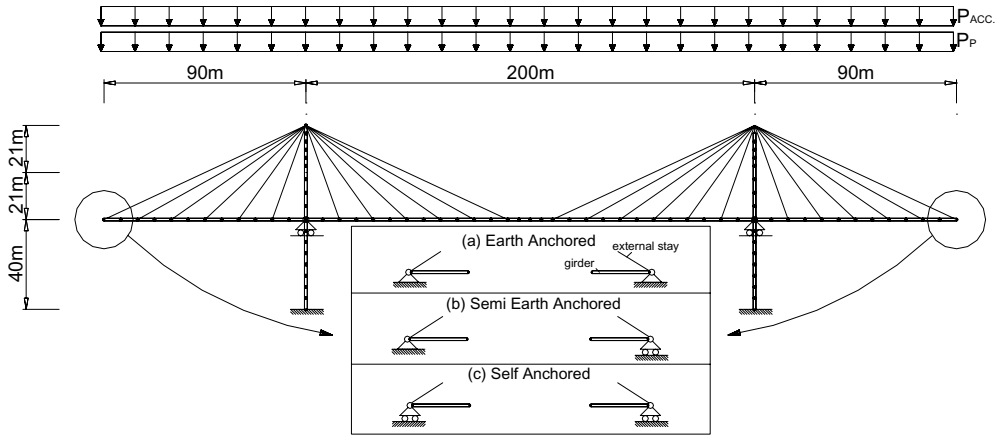


Figure 4. Cable-stayed bridge.

scenarios need to be investigated, especially when the structure is complex. However, these analyses demonstrated how, depending on which part of the structure is damaged, the structural behavior can significantly change.

## 5 CABLE-STAYED BRIDGES

The cable-stayed bridge shown in Figure 4 is considered. The geometrical and mechanical characteristics

are listed in Table 2. Sectional characteristics are referred to the undamaged condition (Di Domizio 2003, Biondini *et al.* 2004, Limonta and Stucchi 2005).

Three different restraint conditions have been taken into account: earth-anchored, semi-earth-anchored, and self-anchored. In all cases, each span of the bridge is uniformly loaded. Self-weight and stay pre-tensioning are also considered.

The equilibrium paths of the three bridge typologies are characterized by different kinds of stability, as shown in Figure 5 for the undamaged case.

Table 2. Geometrical and mechanical characteristics of the cable-stayed bridge in Figure 4.

Element	E[GPa]	$I_x[m^4]$	$I_y[m^4]$	A[m <sup>2</sup> ]	w[kN/m]
Girder	34	4.0896	236.09	8.0759	100
Tower (0–40)	34	1.3482	13.843	5.00	–
Tower (40–61)	34	0.7220	2.7750	2.70	–
Tower (61–62)	34	0.6219	2.6417	2.30	–
Stays	210	–	–	0.01	–
Ext. Stays	210	–	–	0.005	–

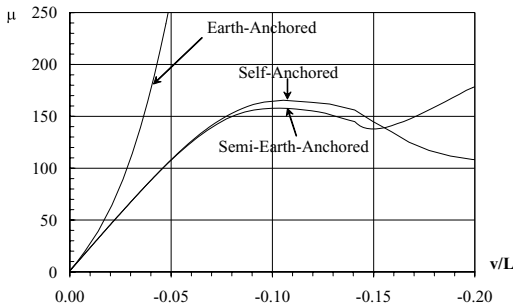


Figure 5. Equilibrium paths of the undamaged structures.

The damage scenarios in Figure 6 are investigated in the following.

The undamaged earth-anchored condition is characterized by a stable behavior. In the same way, when the stays, girder or towers are progressively damaged, the equilibrium path remains stable and does not show a remarkable loss of stiffness. Figure 7 shows the case of uniform damage of the girder.

For the semi-earth-anchored condition, the undamaged structure shows a limit point and a softening behavior. A qualitative different behavior can be observed as damage increases. Figure 8b shows the equilibrium paths when the girder is uniformly damaged. As damage increases, first the unstable behavior becomes more accentuated and then, when the damage is over 70%, the softening behavior is no longer followed by a stiffness recovering.

Figures 8a, 8c, and 8d, instead, refer to a uniform damage of the elements of the whole bridge, of the stays, and of the towers, respectively. In these cases, the unstable behavior tends to disappear, with larger displacements and reduced bearing capacity.

In fact, the reduction of the sectional properties of the towers gives a greater flexibility, so that a limit point is found for smaller loads. However, this does not affect the instability of the girder and, consequently, the behavior remains unchanged.

A different behavior can be found if a more localized damage is considered. Figures 8e and 8f describe

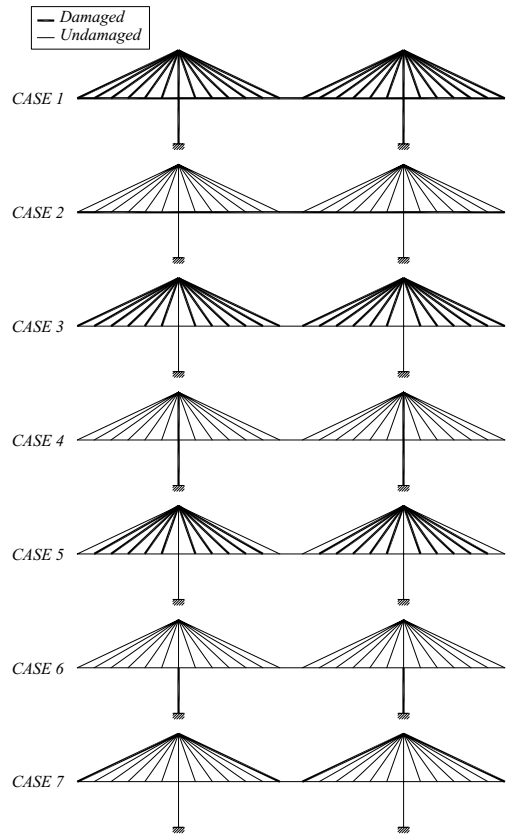


Figure 6. Cable-stayed bridge. Damage scenarios.

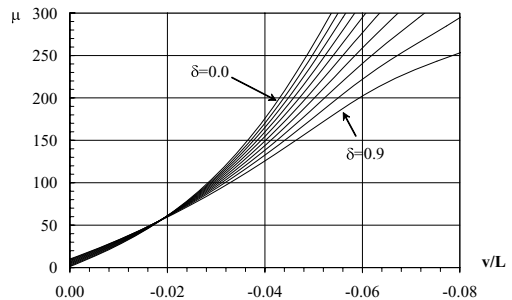


Figure 7. Equilibrium paths of the earth-anchored bridge (Case 2).

the equilibrium paths when damage affects all stays, with the exception of the external ones, or the part of the towers under the girder level, respectively.

In the first case, damage allows the equilibrium path to become stable, by means of a reduced bearing capacity in the first phase. Moreover, for larger displacements the bearing capacity of the damaged

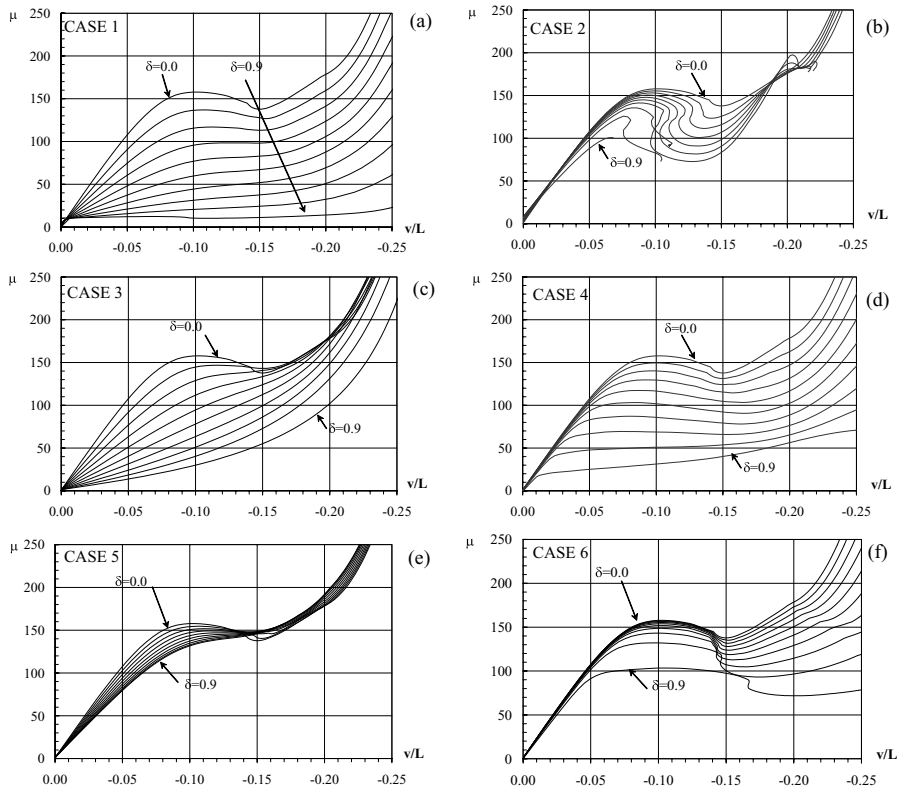


Figure 8. Equilibrium paths of the semi-anchored bridge for damaging scenarios in Figure 6.

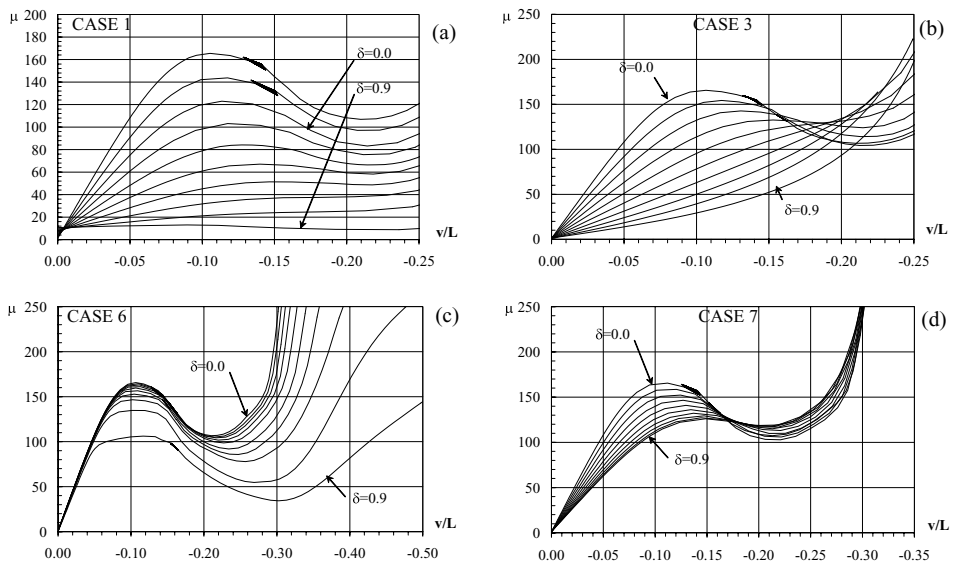


Figure 9. Equilibrium paths of the self-anchored bridge for damaging scenarios in Figure 6.



structure tends to become larger than in the undamaged case. In fact, as the stays are damaged, the horizontal force becomes smaller and the unstable behavior of the girder is progressively reduced.

Instead, when the lower part of the towers is damaged, the bearing capacity is always reduced and the behavior becomes unstable.

Consider now a self-anchored bridge with the same characteristics. The girder has a greater flexibility since it is not fixed at any of the two ends. As proved in the previous cases, the original stable behavior can become unstable under particular damage scenarios. For self-anchored bridges, a more stable behavior is observed when the stays are uniformly damaged. However, there is also a significant reduction of the bearing capacity, since the girder tends to be less supported by the stays (Figure 9c).

If damage is applied to all the elements of the bridge, again the bearing capacity is progressively reduced (Figure 9a).

In this condition, however, damage causes a structural behavior in which the stability recovering is significantly different with respect to the previous scenario.

A localized damage of the external stays causes a behavior similar to that of Figure 8e, as shown in Figure 9d. The structural behavior shows a recovery of stability. The bearing capacity is reduced for small displacements and for large rates of damage, while it tends to increase when displacements become large.

## 6 CONCLUSIONS

The influence of localized or distributed structural weakening, on stability, post critical and collapse behavior of cable supported bridges has been investigated.

The investigation has been based on the equilibrium paths traced through a numerical model. These analyses have been developed in the hypothesis of large displacements and large strains.

In the first part of the paper a simple truss structure affected by different kind of damage has been considered. Scenarios in which uniform damage is applied on the structure, and in which only a few element are damaged, have been taken into account. In the case of uniform damage the behavior remains always similar to the original one, even if the bearing capacity is reduced. Instead, in the case of localized damage, different structural response with different levels of stability can be obtained.

Similar considerations can be outlined for more complex systems, like cable-stayed bridges. Three different cable layouts and various geometrical,

topological and stiffness characteristics have been considered and the influence of the most typical damage causes (section reduction or break of one or more hangers or cables, lost of serviceability of a part of the deck, among others) have been studied.

The results of these analyses proved that, like for the truss beam, uniform damage on whole structure does not modify the stability behavior. On the contrary, different localized damage scenarios can affect structural behavior by increasing stability, or accentuating unstable behaviors, like snap-backs.

## ACKNOWLEDGEMENTS

This study is supported by research funds PRIN2005 (prot. 2005082490) from the Italian Ministry of University and Research—Department of Structural Engineering, Politecnico di Milano.

## REFERENCES

- Biondini, F., Di Domizio, M., Malerba, P.G., On the Structural Analysis of Cable-Stayed and Suspension Bridges, *2nd Int. Conf. on Bridge Maintenance and Safety (IABMAS'04)*, Kyoto, October, 19–22, 004.
- Biondini, F., Di Domizio, M., Malerba, P.G., 2006, Influence of Geometrical non Linearities on the Stability and Collapse Behaviour of Long Span Cable Supported Bridges, *International Conference on Bridge Engineering Challenges in the 21st Century*, 1–3 November, Hong Kong.
- Bontempi, F., Malerba, P.G., 1997. The Role of Softening in the Numerical Nonlinear Analysis of Reinforced Concrete Frames, *Structural Engineering and Mechanics*, 5 (6), 785–801.
- Bontempi, F., Malerba, P.G., 1996. The control of the tangent formulation in structural non linear problems, Studies and Researches, 17, *Graduate School for Concrete Structures*, Politecnico di Milano, Milan, Italy (in Italian).
- Crisfield, M.A., 1991. *Non-linear finite element analysis of solids and structures*. John Wiley & Sons.
- Di Domizio, M., 2003. *Geometrical non linear analysis of cable stayed and suspension structures*. Dissertation, Politecnico di Milano, Milan, Italy (In Italian).
- Limonta, P., Stucchi, R., 2005. *On the analysis of suspension bridges. Classical theories and numerical solutions*. Dissertation, Politecnico di Milano, Milan, Italy (In Italian).
- Mc Guire, W., Gallagher, R.H., Ziemian, R.D., 2000. *Matrix Structural Analysis*, John Wiley & Sons, Inc.
- Riks, E., 1979. An incremental approach to the solution of snapping and buckling problems, *International Journal of Solids Structures*. 15, 529–551.
- Yang, Y.-B., Kuo, S.-R., 1994. *Theory and Analysis of Nonlinear Framed Structures*, Prentice-Hall, Englewood Cliffs, N.J.

# Damage propagation and structural robustness

F. Biondini & S. Restelli

*Department of Structural Engineering, Politecnico di Milano, Milan, Italy*

**ABSTRACT:** The role of damage propagation on the structural robustness of deteriorating systems is investigated. The deterioration effects are evaluated with reference to suitable indicators of the structural response. The variation of these performance indicators with respect to the values associated with the undamaged system is used to formulate dimensionless measures of structural robustness. The damage paths associated with two alternative propagation mechanisms are identified by a fault-tree analysis and described at the system level by branched networks. The effectiveness of the proposed approach is shown through applications.

## 1 INTRODUCTION

In structural design the concept of robust structures, or damage-tolerant structures, is often an issue of controversy, since there are no well established and generally accepted criteria for a consistent definition and a quantitative measure of structural robustness. Moreover, robustness evaluations are usually related to damage suddenly provoked by accidental actions, like explosion or impacts. However, damage could also arise slowly in time from aging of structures, as induced for example by environmental aggressive agents. In this context, it is therefore of great interest to develop suitable life-cycle measures of structural robustness with respect to a progressive deterioration of the structural performance.

In this paper, a general approach to robustness assessment of structural systems undergoing damage is presented. The deterioration effects on the system performance are evaluated with reference to suitable performance indicators identified with parameters of the structural response. The variation of these indicators with respect to the values associated with the performance of the undamaged system is used to formulate dimensionless measures of structural robustness. Moreover, an index of structural integrity aimed to quantify the severity of the structural failure with regards to its consequences, is proposed.

In the proposed approach, damage is viewed as a progressive deterioration of the material properties and its amount is specified at the member level by means of a damage index associated with prescribed patterns of cross-sectional deterioration. Starting from this local definition of damage, a model of damage propagation at the system level is also developed by considering two alternative propagation mechanisms, and by using a damage-sensitive fault-tree analysis.

In such a way, all the feasible damage paths associated with the propagation mechanism and the actual topology of the system are described by branched networks where the level of activation of each nodal connection is properly tuned to account for the prescribed amount of local structural damage.

The effectiveness of the proposed approach is shown through the application to the robustness assessment of truss and frame systems.

## 2 STRUCTURAL PERFORMANCE INDICATORS

Strength and ductility, as well as other performance indicators of the ultimate conditions under nonlinear behavior, may result of great significance in robustness evaluations associated with damage induced by severe loadings, like explosions or impacts (Frangopol and Curley 1987, Biondini *et al.* 2008). However, performance indicators of the serviceability conditions under linear behavior, like elastic stiffness and first yielding, may become of major importance in life-cycle robustness evaluations associated with aging of structures. In the following, several performance indicators under linear elastic behavior are investigated (Restelli 2007).

### 2.1 Parameters of the structural behavior

The following performance indicators are considered:

$$d = \det(\mathbf{K}) \quad t = \sum_i \lambda_i(\mathbf{K}) \quad (1)$$

$$c = \frac{\max_i \lambda_i(\mathbf{K})}{\min_i \lambda_i(\mathbf{K})} \quad T = 2\pi \sqrt{\max_i \lambda_i(\mathbf{K}^{-1}\mathbf{M})} \quad (2)$$

where  $d$ ,  $t$ , and  $c$  are, respectively, the determinant, the trace, and the conditioning number of the stiffness matrix  $\mathbf{K}$ ,  $T$  is the first vibration period associated with the mass matrix  $\mathbf{M}$ , and  $\lambda_i(\mathbf{K})$  denotes the  $i$ th eigenvalue of the matrix  $\mathbf{K}$ . These indicators are quite general, since they are related to the properties of the structural system only. However, a structural system may have different performance under different loads. For this reason, the following indicators are also considered:

$$s = \|\mathbf{s}\| = \|\mathbf{K}^{-1}\mathbf{f}\| \quad \Phi = \frac{1}{2}\mathbf{s}^T\mathbf{K}\mathbf{s} = \frac{1}{2}\mathbf{s}^T\mathbf{f} \quad (3)$$

where  $\mathbf{s}$  is the displacement vector,  $\mathbf{f}$  is the applied load vector,  $\Phi$  is the stored energy, and  $\|\cdot\|$  denotes the euclidean scalar norm. These indicators depend on both the system properties and the loading condition, and they may refer either to the system in the original state, in which the structure is fully intact, or to the system in a perturbed state, in which a prescribed damage scenario is applied.

## 2.2 Pseudo-loads

For robustness evaluations it can also be of interest to define indicators able to simultaneously account for the structural performance of the intact system and of the damaged system. To this aim, it is useful to consider the following equilibrium equations:

$$\mathbf{K}_0\mathbf{s}_0 = \mathbf{f}_0 \quad \mathbf{K}_1\mathbf{s}_1 = \mathbf{f}_1 \quad (4)$$

where the subscripts “0” and “1” refer to the intact state and the damaged state of the structure, respectively (Figure 1.a). Based on these equations, the displacement vector of the intact system  $\mathbf{s}_0$  can be related to the displacement vector of the damaged system  $\mathbf{s}_1$  as follows:

$$\mathbf{s}_0 = \mathbf{s}_1 + \mathbf{K}_1^{-1}\hat{\mathbf{f}}_1 = \mathbf{K}_1^{-1}(\mathbf{f}_1 + \hat{\mathbf{f}}_1) \quad (5)$$

$$\hat{\mathbf{f}}_1 = (\mathbf{K}_1 - \mathbf{K}_0)\mathbf{s}_0 - (\mathbf{f}_1 - \mathbf{f}_0) = \Delta\mathbf{K}\mathbf{s}_0 - \Delta\mathbf{f} \quad (6)$$

where  $\hat{\mathbf{f}}_1$  is a vector of nodal forces equivalent to the effects of repair (Figure 1.b). This vector represents the additional nodal forces that must be applied to the damaged system to achieve the nodal displacements of the intact system, and it is called *backward pseudo-load vector*.

In a dual way, the displacement vector of the damaged system  $\mathbf{s}_1$  can be related to the displacement vector of the intact system  $\mathbf{s}_0$  as follows:

$$\mathbf{s}_1 = \mathbf{s}_0 + \mathbf{K}_0^{-1}\hat{\mathbf{f}}_0 = \mathbf{K}_0^{-1}(\mathbf{f}_0 + \hat{\mathbf{f}}_0) \quad (7)$$

$$\hat{\mathbf{f}}_0 = -(\mathbf{K}_1 - \mathbf{K}_0)\mathbf{s}_1 + (\mathbf{f}_1 - \mathbf{f}_0) = -\Delta\mathbf{K}\mathbf{s}_1 + \Delta\mathbf{f} \quad (8)$$

where  $\hat{\mathbf{f}}_0$  is a vector of nodal forces equivalent to the effects of damage (Figure 1.c). This vector represents the additional nodal forces that must be applied to the intact system to achieve the nodal displacements of the damaged system, and it is called *forward pseudo-load vector*. Backward and forward pseudo-loads can be related as follows:

$$\mathbf{K}_0^{-1}\hat{\mathbf{f}}_0 + \mathbf{K}_1^{-1}\hat{\mathbf{f}}_1 = 0 \quad (9)$$

The concept of pseudo-loads can be usefully exploited to define, in a dual way, two energy-based indicators related to the structural performance of both the intact system and the damaged system. The first one of these indicators is the difference of stored energy  $\Phi$  between the intact system ( $\Phi_0$ ) and the damaged system after the application of the backward pseudo-loads ( $\hat{\Phi}_1$ ):

$$\begin{aligned} \Delta\Phi_0 &= \Phi_0 - \hat{\Phi}_1 = \frac{1}{2}\mathbf{s}_0^T\mathbf{f}_0 - \frac{1}{2}\mathbf{s}_1^T(\mathbf{f}_1 + \hat{\mathbf{f}}_1) \\ &= -\frac{1}{2}\mathbf{s}_0^T(\hat{\mathbf{f}}_1 + \Delta\mathbf{f}) \end{aligned} \quad (10)$$

The area  $OP_0\hat{P}_1$  in Figure 1a represents the energy  $\Delta\Phi_0$  for the case  $\Delta\mathbf{f} = 0$ . The second indicator is the difference of stored energy  $\Phi$  between the intact system after the application of the forward pseudo-loads ( $\hat{\Phi}_0$ ) and the damaged system ( $\Phi_1$ ):

$$\begin{aligned} \Delta\Phi_1 &= \hat{\Phi}_0 - \Phi_1 = \frac{1}{2}\mathbf{s}_0^T(\mathbf{f}_0 + \hat{\mathbf{f}}_0) - \frac{1}{2}\mathbf{s}_1^T\mathbf{f}_1 \\ &= \frac{1}{2}\mathbf{s}_1^T(\hat{\mathbf{f}}_0 - \Delta\mathbf{f}) \end{aligned} \quad (11)$$

The area  $\hat{O}P_0P_1$  in Figure 1a represents the energy  $\Delta\Phi_1$  for the case  $\Delta\mathbf{f} = 0$ .

## 3 MEASURE OF STRUCTURAL ROBUSTNESS

### 3.1 Robustness indices

Structural robustness can be viewed as the ability of a system to suffer an amount of damage not disproportionate with respect to the causes of the damage itself. According to this general definition, a measure of structural robustness should arise by comparing the structural performance of the system in the original state, in which the structure is fully intact, and in a perturbed state, in which a prescribed damage scenario is applied (Frangopol and Curley 1987, Biondini *et al.* 2008). Based on this approach, the performance indicators are used as state variables, and a direct measure of structural robustness is obtained through robustness

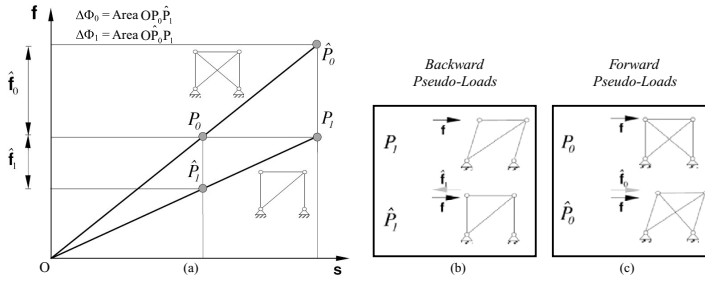


Figure 1. (a) Structural behavior of a truss system in the intact state and after elimination of one member. (b) Backward pseudo-loads (effects of repair). (c) Forward pseudo-loads (effects of damage).

indices, that are dimensionless functions of these variables varying in the range [0, 1]. In this study, the following robustness indices are considered:

$$\rho_d = \frac{d_1}{d_0} \quad \rho_t = \frac{t_1}{t_0} \quad (12)$$

$$\rho_c = \frac{c_0}{c_1} \quad \rho_T = \frac{T_0}{T_1} \quad (13)$$

$$\rho_s = \frac{s_0}{s_1} \quad \rho_\Phi = \frac{\Phi_0}{\Phi_1} \quad (14)$$

$$\rho_0 = 1 - \frac{\Delta\Phi_0}{\Phi_0} \quad \rho_1 = 1 - \frac{\Delta\Phi_1}{\hat{\Phi}_0} \quad (15)$$

The indices  $\rho_d$ ,  $\rho_t$ ,  $\rho_c$ , and  $\rho_T$ , are related to the properties of the structural system only, while the indices  $\rho_s$ ,  $\rho_\Phi$ ,  $\rho_0$ , and  $\rho_1$ , take also the loading condition into account.

To discuss the effectiveness of these indices, the structural robustness of the truss system shown in Figure 2 is evaluated under the progressive damage of each one of its members. The cross-section of all members is circular with radius  $r$ . For the damaged member an external layer of uniform thickness  $t$  is removed. Therefore, the amount of damage can be specified by means of the damage index  $\delta = t/r \in [0; 1]$ . The results are shown in Figure 3. It can be noted that, globally, the robustness indices allow to evaluate the role played by each member on the overall performance of the damaged system. However, the following critical aspects can also be outlined:

- The index  $\rho_c$  may show an increase of robustness under damage evolution ( $\rho_c > 1$ ).
- The index  $\rho_d$  is not able to catch the different role played by each element.
- The index  $\rho_t$  shows a very little sensitivity to damage.
- The indices  $\rho_t$  and  $\rho_0$  are not able to identify the failure condition  $\rho = 0$  for  $\delta = 1$ .

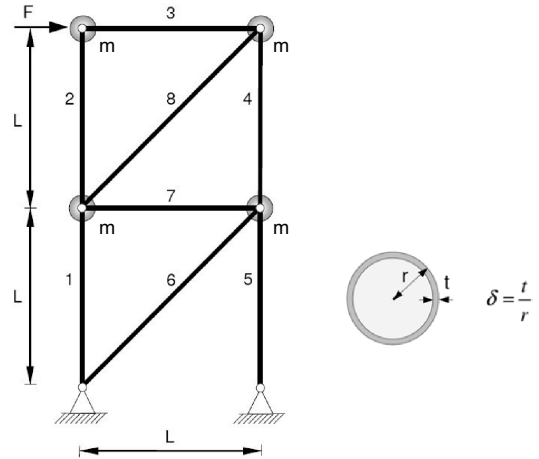


Figure 2. Truss system undergoing damage of one member.

Therefore, the indices  $\rho_c$ ,  $\rho_d$ ,  $\rho_t$ , and  $\rho_0$ , seem to be not suitable to fully describe the effects of damage on the structural performance. On the contrary, the indices  $\rho_t$ ,  $\rho_s$ ,  $\rho_\Phi$ , and  $\rho_1$ , can provide a very effective measure of structural robustness.

### 3.2 Structural integrity index

A robustness index should be able to identify the structural collapse by assuming at failure the value  $\rho = 0$ . However, in robustness evaluations may also be crucial to quantify the severity of a structural failure with regards to its consequences. For example, the collapse of the whole structural system should be considered much more important than the collapse of a single member. For this reason, a possible importance measure of a structural failure could be provided by the following structural integrity index:

$$\rho_V = \frac{V_1}{V_0} \quad (16)$$

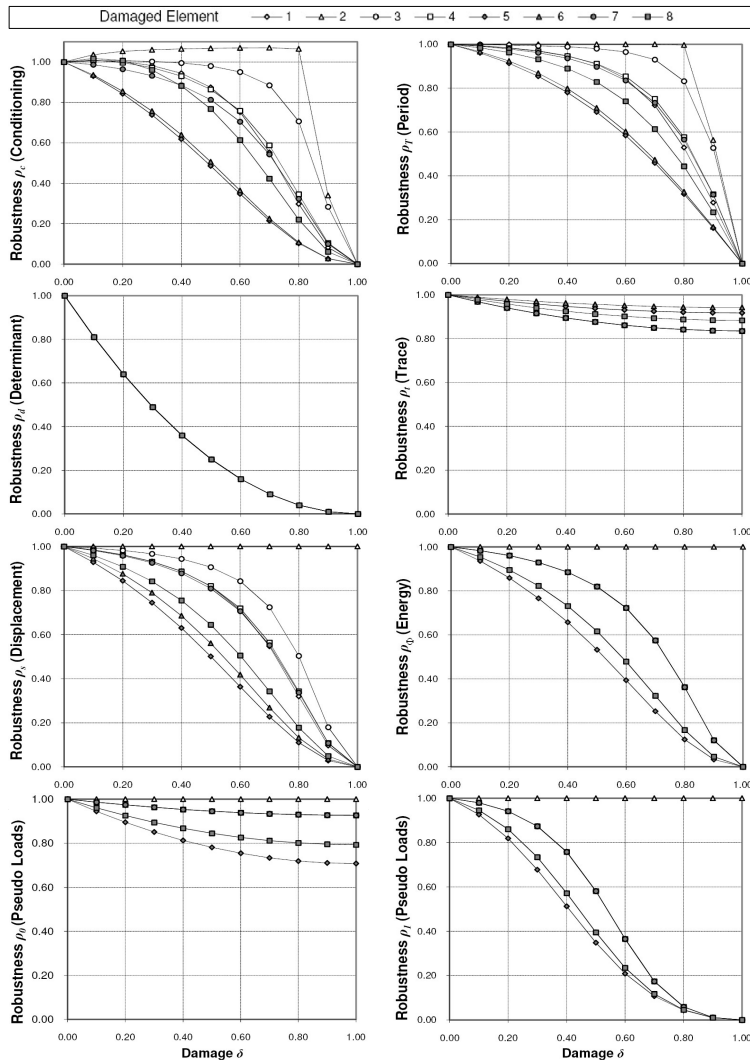


Figure 3. Truss system undergoing damage of one member. Robustness indices  $\rho$  versus damage  $\delta$ .

Table 1. Structural integrity index for the truss in Figure 2.

Damaged element	Structural integrity index $\rho_V$
1	0.25
2	0.75
3	0.75
4	0.50
5	0.00
6	0.00
7	0.25
8	0.50

where  $V_1$  is the portion of structural volume  $V_0$  which remains intact after damage. It is worth noting that also members not directly exposed to damage may fail. For example, a complete damage of member 8 of the truss shown in Figure 2 causes also the failure of members 2, 3, and 4 ( $\rho_V = 0.50$ ). Table 1 provides the structural integrity index associated to the failure of each single member. Failed members involved in a collapse mechanism can be identified based on the eigenvectors  $\mathbf{s}_i$  of the stiffness matrix  $\mathbf{K}$  associated with the eigenvalues  $\lambda_i(\mathbf{K}) = 0$ .

## 4 DAMAGE PROPAGATION

### 4.1 Propagation mechanisms

For redundant structures, local damage or failure of a member usually does not involve the collapse of the whole system. As a consequence, after failure of one member other members may fail, and the sequence of local failures propagates throughout the overall system until its collapse is reached. The mechanism of damage propagation is usually related to the causes of the damage itself. In Restelli (2007) two alternative propagation mechanisms, defined as directionality-based and adjacency-based, have been investigated.

In the directionality-based mechanism, damage propagates along the direction normal to the axis of the first failed member. For example, with reference to the frame system shown in Figure 4.a, the damage of member 1 is followed in sequence by the damage of elements 2, 3, and 4. The directionality-based mechanism is typical of damage induced by severe loadings, like explosions or impacts, which generally tends to propagate along the direction of loading.

In the adjacency-based mechanism, damage propagates towards the members directly connected with

other members already damaged. For example, with reference to the frame system shown in Figure 4.b, the damage of element 1 can be followed by the damage of the elements 5 and 13. The adjacency-based mechanism is typical of damage induced by aggressive agents, which generally tends to propagate through the structure based on diffusion processes.

### 4.2 Fault-tree analysis

Starting from the local definition of damage, and based on a prescribed propagation mechanism, a damage scenario at the system level can be developed by using a damage-sensitive fault-tree analysis. In such a way, all the feasible damage paths associated with the propagation mechanism and the actual topology of the system can be described by branched networks where the level of activation of each nodal connection is properly tuned to account for the prescribed amount of local structural damage (see Restelli 2007).

To describe the main features of this approach, the structural robustness of the frame system shown in Figure 5.a is evaluated under a distribution of lateral loads. The cross-sections of beams and columns, as well as the assumed cross-sectional damage patterns, are shown in Figures 5.b and 5.c. The fault-tree analysis is carried out by assuming an adjacency-based propagation mechanism and a damage level  $\delta = 1$  for each element. The results are represented in Figure 6 in terms of countoured branched network for the displacement-based robustness index  $\rho_s$ .

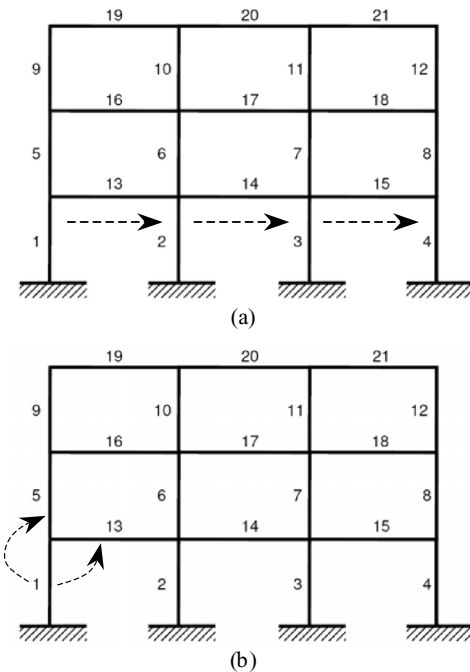


Figure 4. Mechanisms of damage propagation. (a) Directionality-based mechanism. (b) Adjacency-based mechanism.

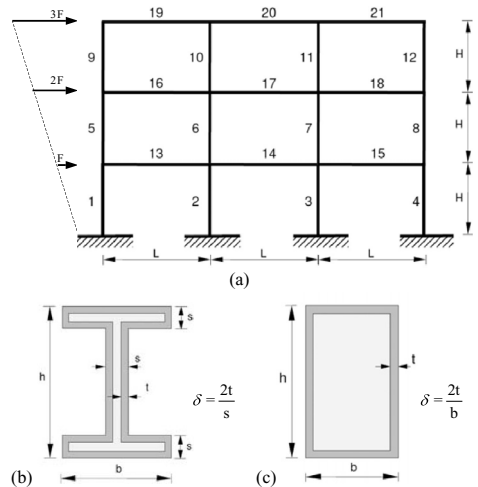


Figure 5. Frame system under damage. (a) Geometry ( $L/H = 2$ ), structural scheme, and loading. Cross-sections of (b) beams and (c) columns ( $h/b = 1.5$ ;  $h/s = 15$ ).

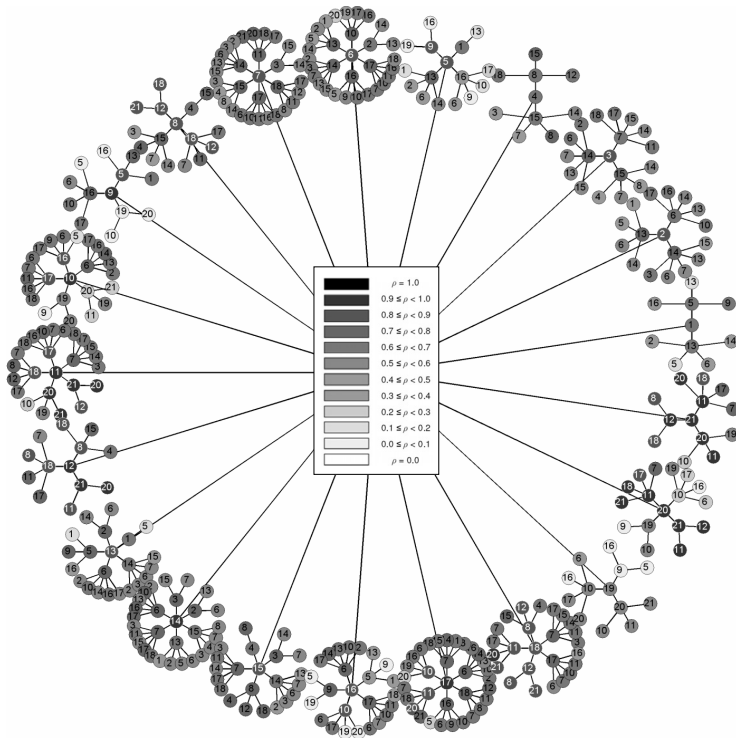


Figure 6. Fault-tree analysis of a frame system undergoing damage with adjacency-based propagation mechanism. Contoured branched network of structural robustness (displacement-based robustness index  $\rho_s$ ) for a damage level  $\delta = 1$ .

This mapping provides a comprehensive vision and a quantitative measure of the structural resources of the system with respect to all the considered damage propagation paths.

## 5 CONCLUSIONS

A general approach aimed to define a measure of structural robustness of deteriorating structural systems by means of a set of dimensionless indices has been presented. An index of structural integrity aimed to quantify the severity of a structural failure with regards to its consequences, has been also proposed. Moreover, a model of damage propagation at the system level has been developed by considering two alternative propagation mechanisms, defined as directionality-based mechanism and adjacency-based mechanism. In this way, all the feasible damage paths associated with the actual topology of the structural system have been identified by a damage-sensitive fault-tree analysis and described by branched networks. The presented applications demonstrated the effectiveness of the proposed measures of structural robustness, as well as of

the adopted damage propagation criteria, and highlighted the potentialities of the proposed approach in the context of a robust structural design.

## ACKNOWLEDGEMENT

This study is supported by research funds PRIN2005 (prot. 2005082490) from the Italian Ministry of University and Research—Department of Structural Engineering, Politecnico di Milano.

## REFERENCES

- Biondini, F., Frangopol, D.M. & Restelli, S., 2008. On Structural Robustness, Redundancy and Static Indeterminacy, *ASCE Structures Congress 2008*, Vancouver, Canada, April 24–26.
- Frangopol, D.M. & Curley, J.P., 1987. Effects of Damage and Redundancy on Structural Reliability, *Journal of Structural Engineering*, ASCE, **113**(7), 1533–1549.
- Restelli, S., 2007. *Measure of Structural Robustness of Deteriorating Systems*, Dissertation, Politecnico di Milano, Milan, Italy (In Italian).

# Increasing durability of recycled cement bound materials: laboratory investigation on the effects of bituminous emulsions

G. Da Rios, E. Toraldo & E. Mariani  
*DIAR, Politecnico di Milano, Milano, Italy*

**ABSTRACT:** Laboratory investigations of materials for road and/or airport construction deserve special attention from researchers since they have shown to be essential to create materials able to ensure in service high long-lasting performances. Moreover, the use of products deriving from recycling of waste materials is of extreme importance from an environmental and economical point of view. For these reasons and following previous research work in which the Authors developed a laboratory procedure for mix design of cement-bound mixtures, in this paper they present the results they obtained by focusing on the effects of different bituminous emulsions, used as additive, on volumetric mechanical and durability performances of such recycled cement-bound materials. In summary, the complete set of experimental data shows that, by means an appropriate use of bituminous emulsions in terms of type and dosage, it is possible to produce recycled materials characterized by mechanical properties suitable to different design requirements.

## 1 INTRODUCTION

In order to build civil infrastructures characterized by greater performance, high safety levels and by a durability proportioned to their value, both the use of innovative materials and the design of new pavement systems are becoming a need which has to be increasingly taken into account by Organizations and Administrations owners of the infrastructures, executing Contractors and Companies which develop and produce new materials. Moreover, the use of products deriving from the recycling of waste materials from industrial and civil activities is of extreme importance nowadays as a result of the advantages that can be obtained by an environmental and economical point of view.

In the last decades, a large number of research projects has been carried out thought the world in order to recycle and re-use demolition materials from civil and/or industrial activities, some of these are focused on the development of in-situ techniques (i.e. using foamed bitumen, bituminous emulsions, stabilization methods with lime and/or cement, etc), other are based on the re-generation in plant (Brandon et al. 2006, Crispino et al. 2007, Liddle et al. 2006, Little et al. 1998, Lund 2000, Moon 2007, Mountier 1982). Such last method allow to create new materials characterized by high levels of reliability in term of quality control of binders and aggregates, mix procedures and laying techniques. The in situ methods are normally used both for subbase layers and for structural layers (base) in pavements for secondary roads, whereas the

in-plant methods are favorite during construction of base layers for motorways or airports.

Taking these aspects into consideration and following a previous research in which the authors optimize the cement (4% by weight with respect the weight of the aggregates) and water (6% with respect the anhydrous aggregates) contents (Crispino et al. 2007), the investigation described in this paper is mainly focused on performance-based laboratory activities in which the aspect related to the main mechanical and volumetric characteristics of the studied materials were highlighted in order to help designer and practitioners during design of pavements characterized by high long-lasting performances.

The laboratory investigation was performed considering two different types and two dosage of bituminous emulsions, each mixture was subjected to traditional (Simple Compression and Indirect Tensile Stress at Failure) and performance tests (Indirect Tensile Elastic Modulus and Static Creep); a complete volumetric characterization was also performed. For comparative purposes and in order to investigate such volumetric characteristics as well in terms of workability and autocompaction, specimens were prepared with two different techniques: Proctor Hammer and Gyrotory Shear Compactor.

Obtained result shows that, by means an appropriate use of the bituminous emulsions in terms of dosage, it is possible to produce recycled materials for base and subbase layers characterized by mechanical properties suitable to different design requirements.



## 2 MATERIALS AND EXPERIMENTAL PROGRAM

Specimens were prepared by using Portland Cement (32.5 type), different bituminous emulsions and recycled aggregates.

Two cationic emulsions were considered: the first, following named BEA, derive from distilled bitumen (EN code: C 60 B 4 O); the second, named BEB, is obtained using SBS modified bitumen (EN code: C 60 BP 4 O). The main characteristics of both emulsions and bituminous binders are given in Table 1.

The recycled aggregates derived from a crushing and selecting process of old concrete slabs at the end of their life cycle. The crushing process was carried out in order to create recycled aggregates free from dust and impurities, in particular pieces of metal net used as reinforcement in old concrete slabs, while selection process was necessary in order to select aggregates in terms of particle size through a drum mill and a succession of sieves. Aggregates obtained from these operations presented a maximum size equal to 40 mm in diameter and a sieve particle size as reported in Table 2.

As far as the laboratory mix procedures, in order to obtain the right proportions of the binders (cement and bituminous emulsion) and recycled aggregates, each single specimen was mixed using a laboratory mixer complete with a measuring scale.

Table 1. Characteristics of emulsions and bitumen.

Emulsion characteristics		BEA	BEB
Content of water	EN 1428	41%	40%
Content of bitumen	EN 1431	59%	60%
pH	EN 12850	3	4
Bitumen characteristics		BEA	BEB
Penetration	EN 1426	74	54
Softening point	EN 1426	45°C	79°C
Fraass point	EN 12593	-12°C	-21°C

Table 2. Sieve size and Los Angeles index of the recycled lithic material.

Sieve size	Percent passing
2" (50.0 mm)	100.0
1" (25.0 mm)	70.0
3/8" (9.5 mm)	35.0
#4 (4.75 mm)	25.0
#10 (2.0 mm)	17.0
#40 (0.425 mm)	7.0
#200 (0.075 mm)	2.0
% L.A.	27.4

To this end, a preliminary investigation considering different mix procedures was necessary. In particular, it was observed that the preliminary combination of cement with aggregates and the subsequent adding of bituminous emulsion is the most proper technique.

Two different dosages (2% and 4% with respect to the weight of the aggregates) for each bituminous emulsion were combined obtaining four different mixtures; moreover for comparative purpose, an other mixture without emulsion was also studied.

Traditional mechanical tests were necessary in order to qualify the materials with respect the European Standard Specifications, while performance tests were focused to understand the mechanical and rheological effects of the bituminous emulsions and to define mechanical parameters able to help designer to achieve best long-lasting of a set of new pavement systems that include recycled materials.

## 3 EQUIPMENTS AND TEST PARAMETERS

As previously described, the laboratory investigation was carried out following two different ways: the first, using a traditional approach, was developed in order to evaluate the volumetric and mechanical characteristic of the analyzed materials in accordance with the European Specifications; the second was based on mechanical tests. In order to produce samples suitable for both testing approach, two different compaction apparatus were considered: Proctor Compactor, according with UNI EN 13286-2 and UNI EN 13286-50, and Gyratory Shear Compactor. For this last method, it was necessary a preliminary investigation devote to produce specimens compatible with the mechanical test equipments: as result of this preliminary investigation, it was found that the use of a cylindrical mould, 150 mm in diameter, and compacting in height control mode (70 mm), is the most suitable method.

For both the compaction methods, a special care was posed in order to create specimens characterized by the same volumetric characteristics, for this reason the Bulk Specific Gravity (AASHTO T166-93) and the Theoretical Maximum Density (AASHTO T209-93) were measured and compared; the average of the obtained results are given in Table 3, in which it is shown that the Bulk Specific Density is the same for each compaction technique used.

Specimens compacted by Proctor Hammer, after 7 days of curing in a climatic chamber at 20°C, were tested in Simple Compression mode (speed of load control) following the European Standard Specifications (UNI EN 13286-41).

The Indirect Tensile Stress at Failure was evaluated, on specimens compacted with the Gyratory Shear

Table 3. Volumetric characteristics of the studied mixtures.

	Proctor compactor			Gyratory compactor	
	T.M.D.	Bulk specific gravity	Content of voids	Bulk specific gravity	Content of voids
	[g/cm <sup>3</sup> ]	[g/cm <sup>3</sup> ]	[%]	[g/cm <sup>3</sup> ]	[%]
MC 00	2.600	2.120	18.5	2,120	18.5
MC BEA (2%)	2.597	2.120	18.4	2,120	18.4
MC BEB (2%)	2.611	2.130	18.4	2,120	18.8
MC BEA (4%)	2.567	2.120	17.4	2,120	17.4
MC BEB (4%)	2.530	2.110	16.6	2,110	16.6

Compactor, in speed of elongation control mode at different curing (7, 14 and 28 days).

Both Indirect Tensile Stiffness Modulus (ITSM) and Creep Tests were performed on specimens compacted with the Gyratory Shear Compactor.

ITSM tests were carried out in dynamic conditions, at 20°C, applying a vertical pulse of load that induce on the specimen a horizontal stress equal to 100 kPa. By such tests it was possible to evaluate both the effect of curing (repeating measurements after 7, 14 and 28 days of curing) and the effects of the bituminous emulsions on the rheological behavior of cement-bound material. For this goal different tests were performed varying the amplitude of load pulse from 60 ms (4.17 Hz) to 160 ms (1.56 Hz) and considering two additional frequency equal to 2.78 Hz and 2.02 Hz.

Creep compliance is a function of time-dependent strain over stress. The creep compliance curve represents the time-dependent behavior of visco-elastic mixture, thus it is commonly used to evaluate the rate of damage accumulation of bituminous mixtures (Paul et al. 2000, Van de Loo 1978). Taking this aspect into consideration and on the basis that the studied materials (cement-bound aggregates) are added with bituminous emulsions, it is considered important to use the same approach to study the rutting behavior of mixtures for base layers.

For this reason, Creep Tests were performed, cured at 20°C for 7 days, in order to investigate the effects of static load (100 kPa) at different temperatures (40°C and 60°C) in terms of permanent strain: both creep and recovery periods were equal to 3600 s.

## 4 RESULTS AND DISCUSSION

### 4.1 Traditional test investigation

As far as the traditional tests is concerning, Figure 1 shows that the simple compression resistance,

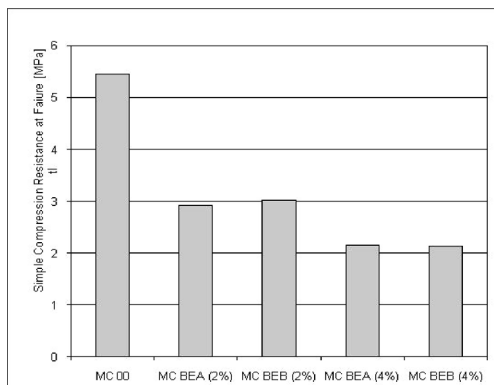


Figure 1. Results of the simple compression tests.

measured on specimens 7 days cured at 20°C in climatic chamber, decrease with the increase of the bituminous emulsion and it depend just from the content of emulsion and not from the bitumen used (there aren't significant contributions due to the SBS polymer contained in the BEB); such trend is also confirmed by the results plotted in Figure 2, where the indirect tensile failure results are given. These tests were performed in order to highlight the behavior of the mixture with respect the curing effects. For this reason, a set of specimens were prepared using Gyratory Compactor in accordance with the protocols above described and were tested after 7, 14 and 28 days of curing. Results in Figure 2, referred to the average of three nominally alike specimens, shows that the resistance at failure increase with the increase of the curing time for each mixture. Moreover, Figure 2 shows that the indirect tensile failure decrease with the increase of the bituminous emulsions dosage for each curing time investigated.

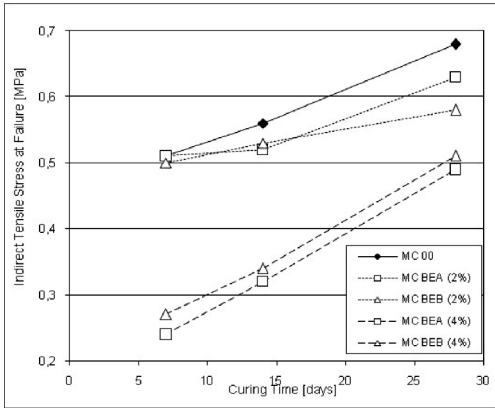


Figure 2. Results of the indirect tensile stress at failure tests.

#### 4.2 Investigation through performance tests

In order to highlight the effects of the bituminous emulsions on the cement-bound recycled materials, performance tests were oriented to obtain a set of mechanical parameters helpful during design and volumetric standards to achieve during construction.

As far as the volumetric characteristics of the mixtures is concerned, workability characteristics, for all the studied mixtures, were assessed from the data recorded during gyratory compaction: average compaction curves were derived by referring to the Equation 1 below:

$$\%C = C_1 + k \cdot \text{Log}(n) \quad (1)$$

in which  $C_1$  and  $k$  are respectively autocompaction and workability parameters, obtained by means of linear regression (Mountier 1982, Liddle et al. 2006). The dependence of these parameters from bituminous emulsion dosage and type is shown in Figure 3 and Figure 4.

It can be observed that for low values of bituminous emulsion dosage (e.g. 2%) no significant variations of workability and autocompaction are recorded. However, for greater values of the bituminous emulsion dosage (4%), a different common trend is identified for all the mixtures: it cause an increase of both workability and autocompaction. Such trend is probably due to the effects of the bituminous emulsion that cover the aggregates, reduce the mixture viscosity and play a significant role during compaction.

The performance-related mechanical characterization of the mixtures was performed measuring both the indirect tensile stiffness modulus and the creep resistance.

In Figure 5 and 6, the indirect tensile stiffness moduli, obtained as mean values three repetitions,

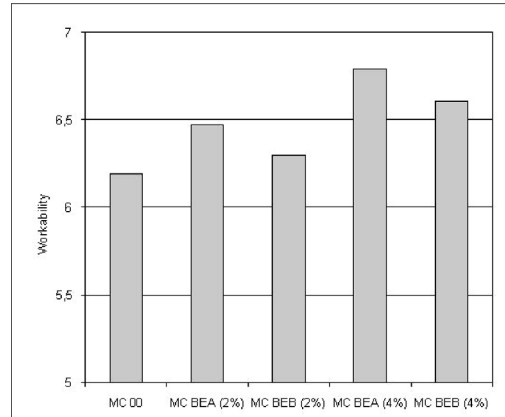


Figure 3. Workability derived from the gyratory compaction.

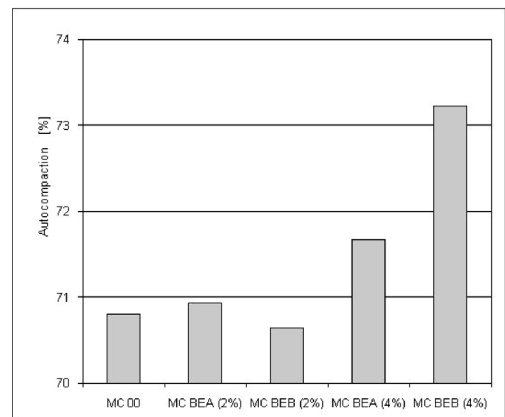


Figure 4. Autocompaction derived from the gyratory compaction.

are represented for all test configuration. In particular, Figure 5 shows the results obtained for each mixture at different frequency of load, while the results plotted in Figure 6 are referred to the curing effects on the analyzed mixtures at a single load frequency (2.04 Hz, 124 ms).

Analyzing the results in Figure 5, it is possible to note that there isn't a common trend of the mixture behavior with respect load frequency; moreover mechanical performances decrease with the increase of the bituminous emulsion dosage and there aren't significant variations in dependence of the emulsion type. Such results, clearly shows both in Figure 5 and Figure 6, are probably due to the effects of the bituminous emulsions that at the higher values of dosage (4%) cover a large part of the aggregates surface and

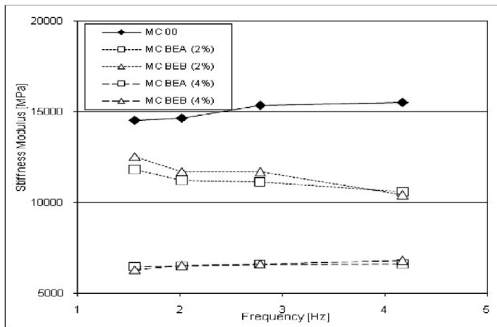


Figure 5. Stiffness moduli versus load frequency.

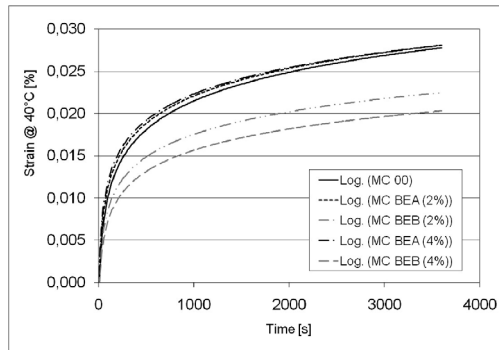


Figure 7. Creep curves at 40°C.

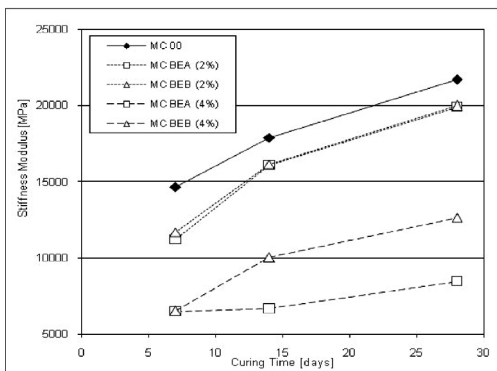


Figure 6. Curing effects on the stiffness moduli.

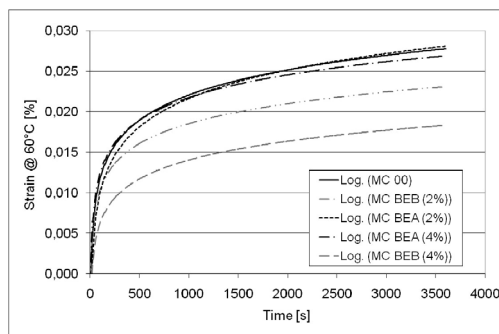


Figure 8. Creep curves at 60°C.

create discontinuity points on the internal structure of the mixtures, reducing the elastic stiffness.

Creep Tests were performed in order to define the rutting behavior of the mixtures both during the load application (creep curve and maximum strain) and for the period of recovery (reversible and permanent strains), the effects of the temperature were also studied.

Analyzing Figure 7 and Figure 8, in which the creep curves (strain versus time) are plotted, it is possible to note that the rutting of the mixtures containing unmodified bituminous emulsion (BEA) is similar with respect the MC 00 mixture (without bituminous emulsion), while both creep curves and value of the stain at the end of the load period (maximum strain) for the cement-bound materials added modified bituminous binder (BEB) shows a decrease if compared with the other tested mixtures. Moreover, a decrease of the maximum strain is notable with the increase of the BEB (modified bituminous emulsion), while no significant variations of the studied parameters derive from different test temperatures.

The benefits that derive from the use of bituminous emulsions as additive for recycled cement-bound

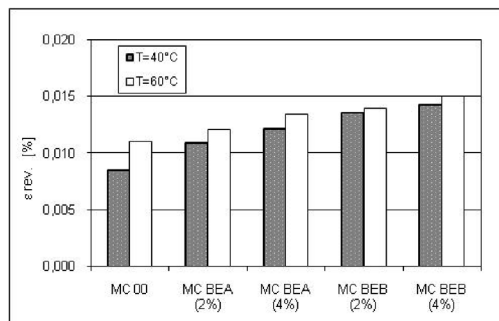


Figure 9. Reversible strains at 40°C and 60°C.

materials are clearly by analyzing the results reported in Figure 9 and Figure 10, in which the reversible and permanent strains at different test temperatures (40°C and 60°C) measured during the recovery period (3600 seconds) are given. As far as the effects of the temperature, no significant results it is possible to found, while interesting marks derive if compare different type and dosage of bituminous emulsions. Actually,

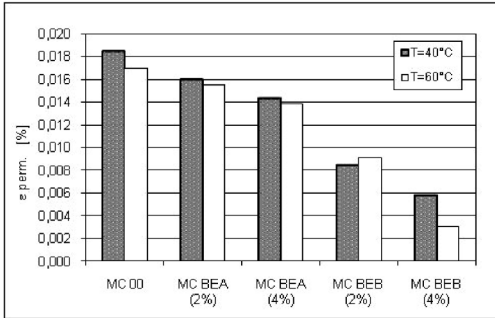


Figure 10. Permanent strains at 40°C and 60°C.

the reversible strain (strain recovered from the end of the load application up to 3600 s) increase (that mean decrease of permanent strain) with the increase of bituminous emulsion dosage. Furthermore, the mixture containing modified bituminous emulsion has the better performances and it increase with the increase of dosage.

## 5 CONCLUSIONS

The main conclusions that can be drawn from this study are represented as follows.

As far as traditional tests, Simple Compression e Indirect Tensile Failure Tests show that with the increase of the bituminous emulsion content decrease the mechanical performances of the mixtures, both referring to the seven days of curing results and if the curing process is considered (measures taken after 7, 4 and 28 days of curing).

Gyratory tests allowed to define both workability and autocompaction parameters of the studied mixtures, as result of the comparative analysis developed on these parameters, it is possible to declare that the increase of bituminous emulsion dosage improve the compaction ability of the recycled mixtures reducing the content of voids.

Data collected during stiffness tests clearly show that changing bituminous emulsion dosage it is possible to obtain different stiffness moduli of the cement-bound materials and consequently to combine such materials in order to design road and airport pavements with high long-lasting performances. In particular, if the studied material is combined with bituminous layers, the addition of bituminous emulsion allow to obtain a stiffness modulus comparable with the upper flexible layers, on the contrary if the recycled material is used for base for concrete slabs the addition of bituminous emulsion is not necessary.

Results obtained during Creep Tests show clearly the benefits that derive from the use of the modified bituminous emulsion in order to prevent rutting phenomena. These results are important for design purposes both in case of use the recycles materials combined with a bituminous multi-layer system (semi-rigid pavements), and in case of use for rural and secondary road whit an upper wearing course. For rigid pavements, concrete slabs prevents, by a particular stress-strain distribution, rutting distresses and not permit permanent deformations on the base layer.

## REFERENCES

- Brandon, J., Blankenagel, K. & Spencer Guthrie, W. 2006. Laboratory characterization of recycled concrete for use as pavement base material. *Transportation Research Board*. Washington D.C., USA.
- Crispino, M., Toraldo, E. & Pozzi, M. 2007. The use of crused concrete slabs in base layers of airport pavements. *5th MAIREPAV International Conference*, USA.
- Little, G., Oilver, J. & Alderson, A. 2006. Development of a workability index. *Pilot Study, Austroads Technical Report*.
- Little, D. et al. 1998. Cementitious stabilization. *Transportation Research Boar*: Washington D.C., USA.
- Lund, H.F. (2nd edition) 2000. *Recycling Handbook*. McGraw-Hill.
- Moon, C.W. 2007. Use of crushed concrete as aggregates in continuously reinforced concrete pavement. *5th MAIREPAV International Conference*, USA.
- Mountier, F. 1982. Prévision de la compactabilité des enrobés bitumineux à l'aide de la presse à cisaillement giratoire (PGC). *Bull. Liaison Labo. P. et Ch.* 121: 2472.
- Nardi, J.V. 2007. A methodology for selection treated bases and sub-base mixtures for pavement design and construction. *5th MAIREPAV International Conference*, USA.
- Paul, I., Braganca, A., Crespo, J., Diniz, B. & Sousa, J.B. 2000. Effect of binder type and air void content on the fatigue and permanent deformation performance of laboratory and field compacted mixes. *Eurasphalt & Eurobitume Congress*.
- Sherwood, P.T. 1995. *Alternative materials in road construction. A guide to the use of waste, recycles materials and byproduct*. Thomas Telford editor.
- Toraldo, E. & Mariani, E. 2007. Experimental investigation on the use of crushed concrete slabs for subbase layers in airport pavements. *VARIREI International Conference*, Italy.
- Van de Loo, P.J. 1978. The creep test: a key tool in asphalt mix design and in the prediction of pavement rutting. *Association of Asphalt Paving Technologists* vol. 47.

# Life cycle deterioration and cost comparison of bridge deck designs including rehabilitation strategies

L.R. Feldman, M. Boulfiza, J. Zacaruk, P.N. Christensen & G. Sparks

*University of Saskatchewan, Saskatoon, Saskatchewan, Canada*

**ABSTRACT:** Three reinforced concrete bridge deck designs combined with three rehabilitation strategies are compared in the context of their respective life-cycle costs. The bridge deck designs conform to the current edition of the Canadian Highway Bridge Design Code and differ only by the type of reinforcement used: black steel, stainless steel, and glass fibre reinforced polymer (GFRP). The rehabilitation strategies considered, from most to least proactive, are: chloride extraction, partial deck repair, and do nothing until deck replacement is required. The selected timing of rehabilitation work is forecasted using an integrated and systematic method of deterministic, sensitivity, and probabilistic analyses and is governed by the earliest onset of damage that interrupts and/or restricts the serviceability of the deck or reduces the structural safety to unacceptable levels. The results of this study show the sometimes surprising implications of total expected cost design when a relatively benign environment is considered.

## 1 INTRODUCTION

Approximately 40% of all bridges within Canada's transportation network are older than 30 years, and 30% of all bridges in the United States are functionally deficient or obsolete (Hassanain & Loov 2003). The current infrastructure deficit in Canada is estimated as \$125 billion and is a result of designing and building structures without regard for their continued satisfactory performance over their useful service lives (Mirza & Haider 2003). Other countries find themselves with similar deficit backlogs (e.g. Khan 2000, Kaneuji et al. 2007, Akgül 2007). Worldwide, municipalities are therefore facing similar quandaries: (1) how to effectively manage their aging infrastructures with the limited funds available, and (2) how to effectively design new structures with consideration to their performance and maintenance needs throughout their useful service lives. This paper addresses the latter topic.

The model presented herein uses a total expected cost method of design (Madsen et al. 1986) as a means of evaluating the sustainability and cost of a structure over its useful service life. Members are designed based on code requirements, deterioration models predict condition over time and provide the necessary triggers for rehabilitation intervention, and basic engineering economics determines the present-worth life-cycle cost over the design service life. Stochastic variation of all applicable parameters is incorporated into the analysis. The combination of these tools

provides a novel and effective means of establishing a total expected cost design process. A reinforced concrete bridge deck example is used to illustrate this method.

## 2 ANALYTICAL MODELS

Figure 1 shows the cross-section of the bridge deck. The bridge deck was designed in accordance with the Canadian Highway Bridge Design Code (CHBDC) (CSA 2006) empirical design method, and is representative of a typical midspan section of a highway overpass in Saskatoon, Canada. The bridge deck has an overall thickness of 245 mm, with clear concrete covers of 70 and 50 mm from the top surface and slab soffit, respectively, to the nearest layer of reinforcement. The clear cover to the top layer of reinforcement includes a 10 mm allowance for wear required for exposed concrete decks. Reinforcement consists of two layers of No. 15 bars at 250 mm on center in both the longitudinal and transverse directions, and the

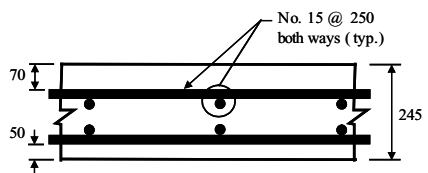


Figure 1. Bridge deck cross-section.

concrete compressive strength is equal to 40 MPa. The bridge deck designs differ only by the type of reinforcement used: black steel, type 316LN stainless steel, and glass fibre reinforced polymer (GFRP).

### 2.1 The corrosion deterioration process

Both the black steel and stainless steel reinforcing bars are subjected to localized pitting corrosion that initiates when the chloride content at the level of the reinforcing steel reaches its threshold value. Corrosion products have a larger volume than reinforcing steel, creating a radial expansion which eventually leads to cracking and spalling of the concrete. Pitting corrosion of stainless steel is delayed in comparison to black steel due to the thin protective chromium film layer that forms on the surface and increases the corrosion threshold level of these bars.

A Pitzer-based reactive transport model, based on first principles, is used to model the chloride ion ingress and the amount of various aqueous species available in the concrete within the clear cover depth (Boulfiza 2007). The model considers: flow and transport processes, chemical interactions between dissolved constituents in the pore solution and the solid phases (i.e. the concrete and the steel reinforcement), and the coupling between the transport and chemical

processes. The diffusion reaction equation that is central to the model can be expressed as (Boulfiza 2007):

$$\nabla \cdot \phi D \nabla c_j + \phi S_j = \frac{\partial \phi c_j}{\partial t} \quad (1)$$

where  $c_j$  is the concentration of the  $j$ th species,  $S_j$  is the source term representing the change in mass resulting from the chemical reactions of the  $j$ th species per unit volume of solution,  $D$  is the coefficient of modular diffusion, and  $\phi$  is the porosity. Earlier works present a detailed description of this mathematical model (Munshi & Boulfiza 2006, Boulfiza & Munshi 2006). Table 1 shows the statistical description of the parameters assuming that the bridge is located in Saskatoon, Canada.

### 2.2 In-situ alkalinity

The deterioration of GFRP bars subjected to in-situ alkalinity was established from the results of an experimental program (van der Wal & Boulfiza 2007). Results showed that only water, and not sodium hydroxide ions, penetrated the outside vinyl ester resin that serves as an outer boundary layer for these bars (van der Wal & Boulfiza 2007). Though water penetration leads to micro-blisters on the glass fibres, the resulting internal pressures are not large enough

Table 1. Statistical description of parameters.

Parameter*	Distribution	Units	Low	Nominal	High
Performance parameters:					
$C_0$	triangular	kg/m <sup>3</sup>	4	5	6
$D$	lognormal	m <sup>2</sup> /s	0.1	2.0	3.9
$\phi$	triangular	%	10	11	13
$S$	triangular	–	0.6	0.9	1
$\eta$	triangular	–	2.0	3.5	8.0
$X_{eff}$	triangular	%	50	66	75
Cost parameters:					
$C_i$ :					
black steel			700	867	1061
stnls. steel	triangular	\$/m <sup>2</sup>	939	1156	1450
GFRP			761	950	1167
$C_{r,x}$			437	583	729
$C_{r,p}$ :					
black steel			139	217	300
stnls. steel	triangular	\$/m <sup>2</sup>	228	333	444
$C_{r,r}$ :					
black steel			1082	1472	1875
stnls. steel	triangular	\$/m <sup>2</sup>	1321	1761	2264
GFRP			1143	1555	1981
$C_d$	triangular	\$/m <sup>2</sup>	57	105	139

\* where  $C_0$  is the near-surface chloride concentration,  $D$  is the diffusion coefficient,  $\phi$  is the concrete porosity,  $S$  is the degree of saturation,  $\eta$  is the expansion coefficient of the reinforcement to cause concrete spalling,  $X_{eff}$  is the effectiveness of the chloride extraction process,  $C_i$  is the initial construction cost,  $C_{r,x}$  is the chloride extraction cost,  $C_{r,p}$  is the partial deck rehabilitation cost,  $C_{r,r}$  is the deck replacement cost, and  $C_d$  is the decommissioning cost.

to propagate deterioration (van der Wal & Boulfiza 2007).

The experimental work performed to date was conducted exclusively on unstressed GFRP bars. Future research therefore needs to consider the influence of bar stress on the deterioration propagation rates of the reinforcement.

### 2.3 Triggers for rehabilitation

Figure 2 shows a schematic representation of the bridge deck performance over its design service life when subjected to different rehabilitation strategies. The bridge deck begins to deteriorate as soon as it is constructed due to the ingress of contaminants. Visual signs of deterioration eventually follow. Deterioration occurs gradually, and then more markedly, with increasing time in service. Figure 2 shows that a proactive or early corrective rehabilitation program requires intervention at relatively low levels of deterioration. Such a rehabilitation strategy, depending upon the method used, may or may not fully restore the original bridge deck condition. The scenario shown in Figure 2 suggests that only partial restoration of the bridge deck condition results. A proactive rehabilitation strategy allows the average bridge deck condition to remain at relatively high levels with comparatively low variation in condition over its entire design life. However, numerous interventions during the service life are therefore required.

A reactive rehabilitation strategy allows for intervention once physical deterioration has manifested. Figure 2 shows that a more invasive rehabilitation is then required to restore the bridge deck to its approximate original condition. The average bridge deck condition over its design service life is somewhat lower and more variable than that achieved using a proactive rehabilitation strategy.

Doing nothing until bridge deck replacement is required serves as a base-line for comparison with

more proactive rehabilitation strategies. This strategy allows deterioration to proceed until the resulting physical damage impairs the safety and rideability of the bridge deck. Figure 2 shows that a longer period of time prior to rehabilitation results. However, much more invasive and hence costly rehabilitation measures must be employed when finally required. The resulting average condition of the bridge deck over its design service life is low with a high degree of variability.

The selection of a rehabilitation strategy will affect the life-cycle cost of the bridge deck. The most suitable rehabilitation strategy may be dictated by the aggressiveness of the environment that the bridge deck is subject to and the design service life that is required.

The relevant rehabilitation strategies considered for this design example, from most to least proactive, are: chloride extraction, partial deck repair, and doing nothing until deck replacement is required. The bridge deck design that includes GFRP reinforcement is not subjected to chloride-induced deterioration. Therefore, only the do nothing strategy is applicable to decks containing GFRP reinforcement. Seven total deck design options including rehabilitation strategies result and are considered in the analysis that follows.

Chloride extraction requires a temporary power source and external anode system to be connected to the internal deck reinforcement. The concrete cover above the top layer of reinforcement acts as an electrolyte, and the impressed current drives the chloride ions away from the reinforcement (Emmons 1993). The passivity of the reinforcement is also reinstated (Emmons 1993). The chloride extraction method is nominally assumed to be 66% effective for the purposes of this analysis which is in line with industry standards (Velivasakis et al. 1998). Implementation of this rehabilitation strategy is triggered when the chloride concentration at the level of the top layer of reinforcement reaches the threshold value for pitting corrosion to initiate and internal pressure in the concrete due to the presence of corrosion products results.

The partial deck repair method consists of concrete removal to 20 mm below the top mat of reinforcement. The equivalent amount of new concrete is placed to restore the original elevation at the top surface of the bridge deck. This rehabilitation method physically removes the chloride ions surrounding the top layer of reinforcement, and the chloride diffusion process is initiated anew. This rehabilitation strategy is implemented when the internal pressure in the concrete as a result of corrosion product build-up is such that spalling of the bridge deck initiates.

The least proactive rehabilitation measure allows the bridge deck to remain in service and deteriorate until 50% of the cross-sectional area of the top layer of reinforcement results from pitting corrosion. It is assumed that at this stage chloride ions would have penetrated below the top mat of reinforcement and will

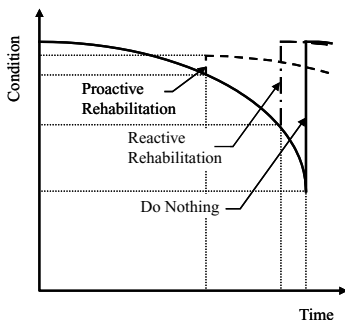


Figure 2. Schematic representation of bridge deck performance (after Kaneuji et al. 2007).



start to depassivate and corrode the bottom layer of reinforcement. Resulting spalling of the top surface of the bridge deck will affect deck rideability and has the potential to cause vehicle accidents.

#### 2.4 Life-cycle cost analysis

Table 2 shows the seven bridge deck designs that were evaluated using a comparison of their present worth equivalents. Local prices for construction materials and labour based on current Saskatoon, Canada market conditions were used.

Table 1 shows the statistical description of all initial, rehabilitation, and decommissioning costs in Canadian dollars. The initial construction costs of the bridge deck include costs for: formwork; concrete, including supply, placement, and finishing; and reinforcement. Complete deck replacement includes these material costs along with emergency concrete patching leading up to the replacement, and the cost of demolishing and disposing of the existing bridge deck. Partial deck repair costs include partial deck demolition; disposal of waste concrete; removal of corrosion products from the existing reinforcement; and the supply, placement, and finishing of new concrete. Chloride extraction costs include the cost of required utilities in addition to materials and labour. All construction and rehabilitation works also include costs for: mobilization, site access, traffic control, environmental protection, and line painting. It is assumed that the bridge is decommissioned at the end of its 100 year design life. At that time, the bridge deck, regardless of its actual condition, is demolished and a decommissioning cost is applied.

The present-worth life cycle cost,  $PWLCC$ , for each design option is then calculated as:

$$PWLCC = C_c + \sum_{j=1}^n C_{r_j}(P/F, i, t_{r_j}) + C_d(P/F, i, t_d) \quad (2)$$

where  $C_c$ ,  $C_r$ , and  $C_d$  are the initial construction, rehabilitation, and decommissioning costs for the bridge deck, respectively;  $i$  is the interest rate and is assumed

equal to 5%;  $t_r$  is the time at which a rehabilitation is performed; and  $t_d$  is the design service life of the bridge and is assumed equal to 100 years. The summation sign is required for the rehabilitation (i.e. second) term on the right-hand side of Eq. 2 since the selected rehabilitation method may need to be performed several times during the design service life of the bridge.

### 3 ANALYSIS AND RESULTS

A systematic and integrated application of deterministic, sensitivity, and probabilistic analysis methods was applied to the evaluation of the bridge deck designs. This section summarizes the findings of the three analysis methods and discusses the influence of all parameters on the expected present worth life-cycle cost of the seven bridge deck designs.

#### 3.1 Deterministic analysis

Table 2 summarizes the results of the initial deterministic analysis performed by setting all performance and cost parameters equal to their nominal values. The bridge deck reinforced with black steel rehabilitated by partial concrete removal (Option #2) is the most economical design based on the desired service life. The next most economical design consists of reinforcing the deck with black steel combine with doing nothing until bridge deck replacement is required (Option #1). The bridge deck reinforced with black steel and rehabilitated using chloride extraction (Option #3) is the least economical design.

Partial deck replacement is therefore the most economical rehabilitation method when considering bridge decks reinforced with black steel. However, the 2.8% cost savings that results when compared to doing nothing until bridge deck replacement is required is not particularly significant. A larger cost difference between these two rehabilitation measures would be apparent had a more aggressive chloride environment been considered in the analysis. In contrast, the do nothing rehabilitation option results in a 0.4% cost savings as compared to partial deck rehabilitation when considering only bridge decks reinforced with stainless steel. Again, the benign chloride environment coupled with the delay in pitting corrosion of the stainless steel reinforcement results in the change in the optimal rehabilitation measure when compared with bridge decks reinforced with black steel. Costs for chloride extraction for bridge decks reinforced with either black or stainless steel appear prohibitive. The relatively low concentration of chlorides at the top level of reinforcement that triggers this rehabilitation results in a large number of interventions over the design life and increases the  $PWLCC$  for these designs.

Table 2. Evaluated bridge design options.

#	Reinforcement	Rehab. method	Determ.	Prob.
			anal.	anal.
			$PWLCC$	$PLWCC$
			(\$CAD)	(\$CAD)
1	black steel	do nothing	937	963
2	black steel	partial removal	911	934
3	black steel	chloride ext.	1,380	1,635
4	stainless steel	do nothing	1,157	1,182
5	stainless steel	partial removal	1,160	1,188
6	stainless steel	chloride ext.	1,318	1,484
7	GFRP	do nothing	951	960

Analysis results show that nine and four interventions are required for bridge decks reinforced with black and stainless steel, respectively. However, user costs have not been considered and are expected to be comparatively low for this rehabilitation measure due to the short service interruptions required.

The results also suggest that the cost of advance metallic (i.e. stainless steel) reinforcement is too high to allow these design options to be competitive, while the cost of the option with non-metallic (i.e. GFRP) reinforcement is approximately 4.4% more expensive than the selected design option. However, these results need to be considered in the context of the current analysis. Saskatoon, Canada is a relatively benign environment when considering the corrosion of metallic reinforcements as described in Section 2.1 due to the low expected near-surface chloride concentration. The propagation of chloride ions through the concrete clear cover, and hence the initiation of pitting corrosion of the reinforcement, is a function of the near-surface chloride concentration. Pitting corrosion is therefore slow to occur when compared to other Canadian regions. The need for intervention is therefore delayed and allows the *PWLCC* for bridge decks with metallic reinforcement to remain comparatively low. The inclusion of user costs in the analysis would also drive up the *PWLCC*'s for the deck designs containing metallic reinforcements as rehabilitations requiring extensive traffic diversions are required within the selected design life. The widespread use of advanced reinforcing materials would also likely reduce the costs of these materials in the future.

### 3.2 Sensitivity analysis

A sensitivity analysis was performed using approximate 95% confidence bounds for all performance and cost parameters. The diffusion coefficient,  $D$ , which in part dictates the rate of chloride ion ingress in the concrete, is the only parameter that influences the determination of the most economical deck design. The diffusion coefficient is lognormally distributed with a nominal value of  $2.0 \times 10^{-12} \text{ m}^2/\text{s}$ . The deck reinforced with black steel rehabilitated by partial deck repair (Option #2) is the most economical design when  $D$  is close to its nominal value. However, the bridge deck reinforced with black steel under a do nothing and replace strategy (Option #1) is the most economical design option if  $D \leq 1.1 \times 10^{-12} \text{ m}^2/\text{s}$ . Although pitting corrosion and spalling occurs during the design life of the deck, the replacement trigger is not reached during the 100 year service life. Emergency repair costs are therefore incurred to provide satisfactory service, but replacement costs are avoided; ultimately leading to a relatively low life-cycle cost. In contrast, the GFRP reinforced bridge deck (Option #7) is the most economical design if  $D \geq 3.0 \times 10^{-12} \text{ m}^2/\text{s}$ .

Higher diffusion rates accelerate the propagation of chloride ions through the concrete cover, and pitting corrosion of metallic reinforcements initiate earlier. Bridge decks reinforced with metallic bars therefore require rehabilitation during the design life, thus inflating the *PWLCC* for these options (Options #1 to 6).

### 3.3 Probabilistic analysis

The statistical descriptions of all performance and cost parameters that significantly influenced the present worth life-cycle cost of the bridge deck designs and rehabilitation measures were included in a stochastic comparison of the seven options. Table 2 shows the expected results of this probabilistic analysis.

The rankings of the *PWLCC* for the seven bridge deck designs remain unchanged in comparison with the deterministic analysis with one notable exception. The results of the deterministic analysis show that the bridge deck reinforced with black steel combined with the do nothing rehabilitation strategy (Option #1) is the second most economical design while the GFRP reinforced bridge deck (Option #7) is the third most economical design. These results are reversed when the bridge deck designs are evaluated using a probabilistic analysis. Less uncertainty is associated with the GFRP reinforced bridge deck because it is highly unlikely that this reinforcement will deteriorate to the point that intervention is required during the 100 year design life. The uncertainty associated with the timing and cost of a rehabilitation is therefore effectively eliminated for this bridge deck design. This allows the GFRP reinforced bridge deck to have a more favourable *PWLCC* when compared to bridge deck designs that will have a higher likelihood of rehabilitation required during the selected design life (i.e. Options #1 to 6).

The inclusion of the statistical description of all relevant parameters increases the *PWLCC* for all evaluated bridge deck designs. The increase in the *PWLCC* in comparison with the results of the deterministic analysis is generally equal to approximately 2.5%. However, these values increase to 18.5% and 12.6% for the bridge decks reinforced with black and stainless steel, respectively, rehabilitated using chloride extraction (i.e. Options #3 and 6). The uncertainty in the effectiveness and cost of this rehabilitation method, in combination with the frequency of interventions required over the bridge design life, drive up the expected costs of these deck designs. The GFRP reinforced bridge deck (Option #7), with an increase in *PWLCC* of 0.9% over the results reported for the deterministic analysis, proves to be the least sensitive to uncertainty. Rehabilitation of this deck design over the intended bridge service life is not required due to the robustness of this reinforcement. The increase in the *PWLCC* for this option is therefore minimized.

## 4 CONCLUSIONS

A total expected cost design method is illustrated within the context of a design example that includes rehabilitation mitigation during the required design service life. The method, including analytical models for: the corrosion deterioration process, in-situ alkalinity, triggers for the implementation of the rehabilitation methods considered, and the life-cycle cost analysis, has been presented. An integrated and systematic method of deterministic, sensitivity, and probabilistic analyses was used to identify the most economical combination of selected reinforcement type and rehabilitation method for the example problem.

The design example consisted of a 245 mm thick reinforced concrete bridge deck designed in accordance with the Canadian Highway Bridge Design Code (CSA 2006) and located in Saskatoon, Canada. Three types of reinforcement and rehabilitation methods for the bridge deck were considered, however, not all rehabilitation measures applied to all reinforcing types considered. A total of seven bridge deck design options resulted and were evaluated using a comparison of their present worth equivalents.

The following significant conclusions are noted:

1. The bridge deck reinforced with black steel and rehabilitated by partial concrete removal was identified as the most economical option using both deterministic and probabilistic methods of analysis.
2. The use of advanced metallic and non-metallic reinforcement is not cost competitive for the relatively benign chloride environment considered in the design example.
3. User costs have not been incorporated in this analysis and would be expected to increase the competitiveness of chloride extraction as a rehabilitation measure.
4. Results of the sensitivity analysis show that the diffusion coefficient is the only parameter that influences the determination of the most economical bridge deck design.
5. With one exception, the rankings of the seven bridge deck designs do not change over point and expected value estimates.
6. Expected values of the present worth life-cycle costs are higher than those calculated using a deterministic analysis. The glass fibre reinforced bridge deck is the least sensitive to uncertainty of the performance and cost parameters because rehabilitation of this bridge deck is not required over the design service life.
7. Anticipated future work includes an evaluation of the selected reinforcement and rehabilitation options in different chloride environments to monitor the influence of near-surface chloride

concentration on the present worth life-cycle costs. The analysis model will also be expanded to consider freeze-thaw abrasion and alkali-aggregate reactivity as additional deterioration processes that may affect the long-term performance of the bridge deck.

## REFERENCES

- Akgül, F. 2007. Criteria for a bridge management system based on inspection, monitoring, and maintenance practices. In H.N. Cho, D.M. Frangopol & A.H.S. Ang (eds.), *Life-cycle cost and performance of civil infrastructure systems*, Seoul, 16–18 October 2006. London: Taylor & Francis.
- Boulfiza, M. & Munshi, S. 2006. A reactive transport model for carbonation and chloride ingress in concrete. *ISTC'06 Int. symp. of theoretical chemistry*, Algiers, 12–15 June 2006. Algiers: ISTC.
- Boulfiza, M. 2007. A reactive transport model for evaluating the long-term performance of stainless steels in concrete. In V.G. Degiorgi, C.A. Brebbia & R.A. Adey (eds.), *The simulation of electrochemical processes (ELECTROCOR07); Proc. 2nd int. conf.*, Myrtle Beach, 9–11 May 2007. Southampton: WIT Press.
- Canadian Standards Association 2006. *Canadian highway bridge design code CAN/CSA-S6-06*. Mississauga: Canadian Standards Association.
- Emmons, P.H. 1993. *Concrete Repair and Maintenance Illustrated*. Kingston, MA: R.S. Means.
- Hassanain, M. & Loov, R.E. 2003. Cost optimization of concrete bridge infrastructure. *Canadian journal of civil engineering* 30(5): 841–849.
- Kaneuji, M., Yamamoto, N., Watanabe, E., Furuta, H. & Kobayashi, K. 2007. Bridge management systems developed for the local governments in Japan. In H.N. Cho, D.M. Frangopol & A.H. S. Ang (eds.), *Life-cycle cost and performance of civil infrastructure systems*, Seoul, 16–18 October 2006. London: Taylor & Francis.
- Khan, M.S. 2000. Bridge management systems past, present, and future. *Concrete international* 22(8): 53–56.
- Madsen, H.O., Krenk, S. & Lind, N.C. 1986. *Methods of structural safety*. Englewood Cliffs: Prentice-Hall Inc.
- Mirza, M.S. & Haider, M. 2003. *The state of infrastructure in Canada: implications for infrastructure planning & policy*. Canada: Infrastructure Canada.
- Munshi, S., & Boulfiza, M. 2006. Effect of cations and carbonation on chlorides binding in concrete, *1st International structural specialty conference of the CSCE*, Calgary, 23–26 May 2006. 10 pp. paper in CD-ROM conf. proc.
- Van der Wal, J.S., & Boulfiza, M. 2007. A step forward in characterizing the performance of GFRP rods in concrete. *Durability and field applications of fibre reinforced polymer (FRP) composites for construction, 3rd int. conf.*, Quebec City, 22–24 May, 2007. 8 pp. paper in CD-ROM conf. proc.
- Velivasakis, E., Henriksen, S.K. & Whitmore, D. 1998. Chloride extraction and realkalization of reinforced concrete stop steel corrosion. *Journal of performance of constructed facilities* 12(2): 77–84.

# In-situ chemical analysis for life cycle health management

M. Ghandehari

*Civil Engineering Department, Brooklyn Polytechnic University, NY, USA*

**ABSTRACT:** Degradation processes in materials and structures are often catalyzed by, or accompanied by chemical reactions. Direct monitoring of such chemical processes, in advance of the emergence of the corresponding physical damage, is an effective means of enhancing infrastructure safety and serviceability. Complementing existing knowledge of materials performance, which is based on historical patterns and theoretical principles, real time in-situ chemical analysis is instrumental in improving practices of materials health management. This presentation describes the concept of real time in-situ Materials analysis in civil infrastructure using embedded optical fiber probes.

## 1 INTRODUCTION

Long term performance of materials and structures under variable and unpredictable conditions has always been of great interest to civil and materials engineers. A prime objective of the materials evaluation community is to increase safety while controlling costs by improving design and by optimizing maintenance and repair programs. Reliable tools for the prognosis of the material's health, durability and service life are therefore essential for the effective maintenance of the civil infrastructure including transportation, sanitation, waste containment and the utilities infrastructure.

Our work is focused on detection of a number of chemical species relevant to civil and environmental engineering. These include species that catalyze aging, such as moisture, chlorides, oxygen and extreme pH levels; those that are symptoms or byproducts of such aging, such as dissolved ions arising from metal dissolution; as well as the species that are a result of subsurface physical failures, such as leaks of hydrocarbons and waste products from pipelines and from sanitation and waste-storage facilities.

## 2 CHEMO OPTICAL SENSORS: TOOLS FOR MATERIALS HEALTH MANAGEMENT

Advances in photonics and developments in optical sensors and sensor components in the past decade have brought in-situ chemical analysis to the fields of biology, medicine, food processing, and environmental monitoring. Such technologies also present new opportunities for in-situ monitoring of transport processes and reaction chemistries in civil infrastructure materials.

In optical fibers, light is guided through the core of the fiber by total internal reflection at the interface of the core with the cladding. The total internal reflection generates an extended electromagnetic field, otherwise known as the evanescent field, which penetrates the cladding and travels along the fiber just outside of the core/cladding interface.

Optical fibers can be made to sample the environment in which they are embedded. They can be functionalized and tuned either at the fiber tip or along the fiber surface to detect a wide range of chemical species. In the latter case, it is accomplished through optical surface waves known as evanescent waves (Figure 1) [1, 2, 3, 4, 5, 6, 7].

The technology presented in this paper is configured for detection of liquid phase moisture using the near-infrared electromagnetic (EM) energy (figure 2). This choice of wave lengths is based on the availability of compact, robust and relatively low-cost optical components and fiber materials. The first and foremost focus of our research and development are selectivity and long term durability of the sensing probe.

### 2.1 Moisture detection

#### 2.1.1 Motivation

The service life of most porous construction materials depends to a great extent on their transport properties. Moisture detection is therefore relevant to durability of most engineering materials. The duration and distribution of moisture in concrete pores, for example, has a great deal of influence on shrinkage, creep, thermal conductivity, hydration rate and the long-term durability of cementitious materials. Water also carries with it chemical species, such as chlorides, that lead to accelerated corrosion of the steel in reinforced concrete.

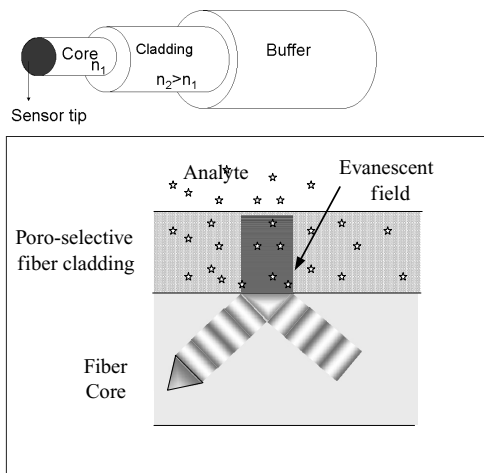


Figure 1. Anatomy of the optical fiber evanescent field chemical sensor. The evanescent wave travels along the fiber cladding at the interface with the fiber core. This surface wave interacts with the analyte in the cladding pore space, and signals the presence of target species by corresponding signal modulations.

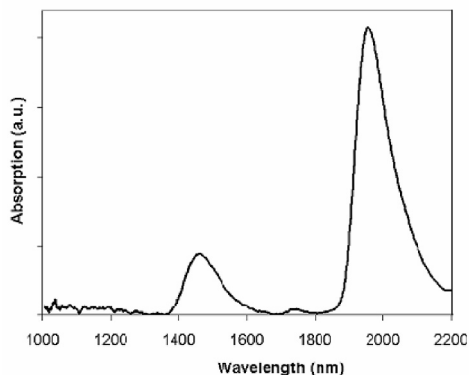


Figure 2. Near infrared absorption spectra of water.

Along with water also comes carbon dioxide, either in the liquid or in the complementary air phase, and this can lead to “carbonation” of the cement matrix. Meanwhile, ingress of acidic aqueous species, leads to calcium leaching and ingress of alkaline species—when in contact with siliceous aggregates present in concrete—may produce expansive products. Water contained in concrete pores can freeze and expand and lead to cracking and damage. Moisture is also a catalyst for deleterious reactions of internal sulfate and alkali deposits, as well as an agent for accelerated corrosion of reinforcing metals and protective coating.

In some cases, the objective is to keep the water out. In others, the aim is to keep it moving. Whichever the goal, long-term in-situ measurement of moisture content is of great benefit.

### 2.1.2 Molecular vibration spectroscopy for moisture detection

Vibration spectroscopy by infrared analysis is based on the principle that each material is a unique combination of atoms, and that no two compounds produce exactly the same infrared signature. Therefore, infrared spectroscopy can result in qualitative identification of numerous materials [8].

Water is a nonlinear polyatomic molecule—here, nonlinear refers to the non-collinear bonds of the hydrogen atoms to the oxygen atom (Figure 3).

In the graph shown above and in the remainder of this article, “Absorption”, shown in the vertical axis, is calculated according to the Beer-Lambert law as follows.

$$A = -\log(I/I_0) \quad (1)$$

where  $I_0$  and  $I$  are the intensity of light before and after interaction with an absorbing chemical species. An alternative expression for absorption, given by Beers Law is:

$$I = I_0 e^{-kx} \quad (2)$$

Where,  $k$  is an absorption coefficient and  $x$  is the interaction length. The sensitivity to the interaction length expressed in equation 2 plays a key role in evanescent field sensing. In other words, increasing the sensing length along the optical fiber enhances the signal and lowers the detection limit. Equation 1 and 2 hold for a single wave length. At other wave lengths, the absorption coefficient may be different and this leads to the “electromagnetic absorption spectra”, a fundamental material parameter.

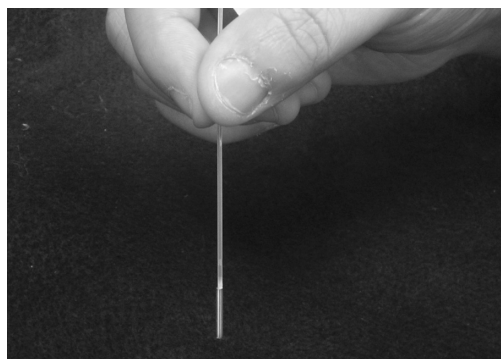


Figure 3. Fiber optic moisture sensor.

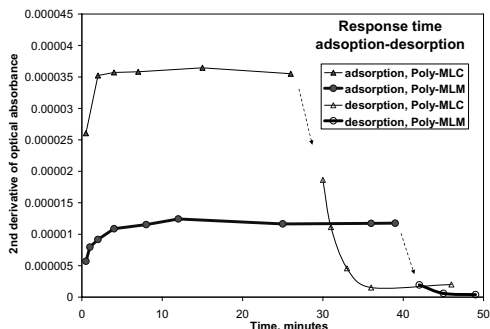


Figure 4. Response time of both sensor in adsorption and desorption.

### 2.1.3 Experiments

The objective of the experiments was to introduce typical models of fiber tip liquid phase moisture sensors.

The moisture sensor developed (Figure 4) is made from a low OH glass 0.6 mm diameter fiber with the polymeric tip and the stainless steel protective sleeve. The fiber is prepared by removing a portion of the original cladding from the tip and polishing it. The uncoated is then coated with sensor polymers poly-MLM<sup>®</sup> or poly-MLC<sup>®</sup> and then cured.

The experiment setup (Figure 4) includes an NIR spectrometer, NIR light source, NIR splitter, sensor (fiber with polymer coated tip) and computer (not shown). Before testing the sensor in water, reference intensities are recorded in dry ambient conditions. Using these references the optical absorption is checked and calibrated to zero. Once this setup is complete the sensor is dipped into water. The live signal coming from the sensor is observed on a computer and the absorbance spectrum is recorded at set intervals over a desired period of time. The second derivative of the absorbance is subsequently calculated.

The experimental procedure consisted of dipping the sensor into water until saturated, and then removing it.

## 3 CONCLUSIONS

Overall both sensor types using the two polymer types, show good results. In both cases full response time are approximately 5 minutes for ingress and approximately 15 minutes for egress. Yet in comparison the cellulose based sensor Chemsense-MLC showed greater signal level compared to the PMMA type sensor Chemsense-MLM.

## REFERENCES

- Engami C., Takeda K., Isai M. & Ogida E. Evanescent Wave Spectroscopic pH Sensor. *Optics Communications* 122, 122–124.
- Zhengfang, G. et al. “Fiber-Optic pH Sensor Based on Evanescent Wave Absorption Spectroscopy”, *Analytical Chemistry*, 65, 1993.
- Conzen J.P., Burck J. & Ache H.J. Characterization of a Fiber-Optic Evanescent Wave Absorbance Sensor for Nonpolar Organic Compounds. (1993), *Applied Spectroscopy*, 47(6), 753–763.
- Zataar Y., Zaouk D., Bechara J. et al. Fabrication and Characterization of an Evanescent Wave Fiber Optic Sensor for Air Pollution Control, (2000), *Materials Science and Engineering*, B74: 296–298.
- Ghandehari M. & Vimer C. “pH Monitoring in Civil Infrastructure by Fiber Optics Evanescent Field Spectroscopy,” *NDT & E International*, in Volume 37, Issue 8, December 2004, Pages 611–616.
- Ghandehari M. & Vimer C. “In-situ Monitoring of Moisture in Pavement Materials”, *TRB 2005 Annual Meeting Session 453—Pavement Monitoring*.
- Ghandehari M. & Khalil G. “Detection of gas leaks in the subsurface environment”, *SPIE, Smart Structures/NDE* [5769–22], San diego March 2005.
- Barton II, F.E. “Theory and Principles of Near-infrared Spectroscopy”, *Spectroscopy Europe*, Vol. 14/1, pp. 12–18, 2002.

# Comparison of corrosion accelerated tests performed in reinforced concrete structures using voltage and current induction

A.G. Graeff, A.S. Torres & L.C.P. Silva Filho

*Federal University of Rio Grande do Sul, Civil Engineering Post-Graduation Program, Porto Alegre, Brazil*

**ABSTRACT:** Rebar corrosion is one of the most important and widespread pathological manifestation in reinforced concrete structures. According to the prevailing bilinear deterioration model, the corrosion process is divided in two phases, initiation and propagation. Most studies in the area have been focused on the modeling of the initiation phase, because it defines the design service life. The propagation period, however, which starts after the depassivation of the rebar, is structurally more relevant, because the level of damage and the risk increase rapidly. Given the fact that the corrosion process in many structures has already entered the propagation phase, it is vital to increase the knowledge about how the propagation phase evolves. To ascertain the resistance or susceptibility to corrosion of different concrete mixes and protection measures, it is necessary to have adequate test procedures. There is a lack of standardization in this area, especially in Brazil, which leads to the use of several accelerated tests. The present work is focused on the study of a test procedure named CAIM (Accelerated Test by modified immersion), which evolved over the last 20 years in the Structural Test and Modeling Laboratory (LEME) of the Federal University of Rio Grande do Sul (UFRGS). The work compares data obtained using two different strategies for corrosion acceleration, based on the imposition of voltage or current differences. Results were successfully modelled using a Monte Carlo simulation.

## 1 INTRODUCTION

Throughout a great part of the XXth century, the notion that concrete was a naturally durable material, which almost avoided repairs during its life cycle, was widely accepted. Over time, however, several unexpected and premature deterioration processes that affected RC structures were recorded and studied, giving evidence to the contrary.

Near the end of the century, the idea that concrete durability was strongly related to the environmental conditions and material properties had already become established. To achieve a long service life it was therefore necessary to design the material with care, taking into account several deterioration agents and the effects of load and use patterns.

Several studies were conducted to identify the most frequent pathological manifestations, and the majority of them pointed out reinforcement corrosion as the most widespread and detrimental occurrence. In Brazil, Andrade (1997) found out that around 64% of the pathological manifestations in Pernambuco were due to reinforcement corrosion.

In the Amazon region, Aranha (1994) put the tally at nearly 43% of the cases analysed. According to Dal Molin (1988), reinforcement corrosion was also responsible for some 12% of the cracks found in structures of the state of Rio Grande do Sul.

Based on such data, it is easy to justify the undertaking of studies aimed at characterizing the phenomena and preventing corrosion onset and propagation. In order to accomplish this aim, it is necessary to develop adequate test procedures to determine the influential parameters and to analyse the impact of preventive and corrective measures. Unfortunately, there is a lack of accepted procedures to perform tests, which leads to the use of different experimental procedures. The diversity of techniques and the complexity of the area are hindering standardization and preventing useful result comparisons.

The research group of LEME/UFRGS has developed an accelerated corrosion test named CAIM—Modified Accelerated Corrosion by Immersion—to monitor corrosion propagation in reinforcement concrete specimens. The procedure involves the positioning of a rebar segment inside a concrete specimen, which is then partially submerged in a chloride-rich solution. In the earlier versions of the test, chloride ingress was stimulated by the application of an 80 V difference in electrical potential. The problem was that this voltage generated a lot of heat in the specimen, distorting the phenomena. The rate of corrosion would also vary over time, because of the increase in moisture content and cracking of the specimen, which reduces the electrical resistance.

Torres (2006) studied the effects of applying lower voltages and concluded that an electrical potential difference of 30 V would provide a better acceleration rate.

More recently, Graeff (2007), in order to study the effects of rebar corrosion on steel-concrete bonding, decided to change from voltage induction to corrosion induction, making the deterioration occur in a more homogeneous way along the test.

To enhance the knowledge about how test procedures affect results, this study was planned to compare how these two acceleration strategies worked, analysing if the use of voltage would distort the phenomena, as suggested in the literature. The general idea is to collect important data regarding the soundness, dynamic and reliability of this test procedure.

### 1.1 *Corrosion acceleration procedures*

The acceleration of corrosion in laboratory experiments is a fundamental measure to allow the collection of data in a reasonable amount of time, since the natural phenomenon occurs over a time-span of many years.

Corrosion acceleration is usually done by means of an electrochemical induction, which combines the exposition of specimens to an aggressive solution, often rich of chlorides, and the application of a potential difference or the impression of a corrosion current.

The choice of technique to accelerate corrosion varies among the authors and is often related with the focus of their studies. Amleh and Mirza (1999) and the ASTM 1202 C (1999) use corrosion acceleration procedures based on voltage application. Others authors, such as Rodriguez et al. (1997) and Gonzalez et al. (1995), accelerated the corrosion using the impression of a constant current in the specimens. They also added chlorides to the concrete mass, in order to reduce the length of the initiation phase, because they were focused on the study of the effects of corrosion in bonding strength.

There are as well variations in the cathodes used to make the electrical contact between the rebar and the source of voltage or current. They can be made of copper or steel, positioned internally or externally. The NaCl concentration in the aggressive solution is another factor that differs among researches, in general in a range from 3% to 5%. It was noticed, also, that some authors totally immerse the samples in the solution, while others do it partially.

### 1.2 *The CAIM test procedure*

The CAIM test was originally applied by Lima (1990), based on an initial conception proposed by Varela et al. (1988). Over time, Jadovski et al. (1991), Selistre et al. (1993/1994), Marchesan et al. (1997), Kirchheim

et al. (2005), Torres (2006) e Graeff (2007) have modified and improved the test procedure.

The basic idea of the test is to place a rebar segment inside a concrete block. The specimen is then placed in a container containing a salt solution with a NaCl concentration of 35 g/l. The specimen is submerged up to the level of bottom of the rebar, a set up that allows both moisture and oxygen to rapidly diffuse to the vicinity of the steel.

An electrical wire is positioned over the rebar, without direct contact, to act as cathode and attract chloride ions. Another wire is placed in the solution, to act as anode.

For the constant voltage test, chloride migration is stimulated by the application of a potential difference between the rebar and the solution. The output results are obtained in terms of corrosion currents over time and gravitational loss of weight. The latter is obtained by splitting the specimen after the test, allowing the recovery and weighing of the rebar. Before weighing, the corrosion products are removed by the immersion of the rebar in a cleaning solution containing chloridric acid and hexamethylenetetramine ( $C_6H_{12}N_4$ ), according to ASTM A380 (1996).

The initial length proposed for the test was a one-day continuous interval of 8 h, but results obtained by Kirchheim et al. (2005) demonstrated that, for low porosity concrete, with a w/c relationship lower than 0.5, up to 5 cycles of 8 h might be necessary to obtain significant corrosion in the rebars.

The power supply was specially designed to guarantee the maintenance of a constant voltage for the duration of the test.

In the case of the constant current test, chloride migration is stimulated by the impression of a constant corrosion current ( $500 \mu A/cm^2$ ) between the rebar and the solution. The length of the test is determined by the desired degree of corrosion, expressed as an average reduction in cross-section or weight of the rebar segment. The general idea is to use Faraday's Law to determine this time, but the estimates tend to be shorter than necessary because they do not consider the initiation period. For better results, a calibration curve obtained with results from similar concretes might be used. When the test is finished, the specimens are generally splitted and the bars removed and weighted, to check if the desired degree of corrosion was obtained.

## 2 EXPERIMENTAL PROGRAMME

### 2.1 *Materials and specimens size*

To perform the tests, concrete blocks with  $10 \times 20 \times 10$  cm were cast and a rebar was placed on their middle, positioned using plastic spacers.



Table 1. Materials used in the study.

Material	Specification
Cement	Portland cement high early strength, sulfate resistant type CP-V RS (conforming with NBR 5733)
Fine Aggregate	River sand quartz $\gamma = 2.62 \text{ g/cm}^3$ fineness module = 2.8
Coarse Aggregate	Crushed stone Basaltic $\gamma = 2.73 \text{ g/cm}^3$ Dmax = 19 mm
Rebar	CA 50-A (conforming with NBR 6118) diameter = 12.5 mm length = 14.5 cm

Table 2. Mix proportions used to cast specimens.

Mix proportion (cement: sand: coarse aggregate)	w/c ratio	Cement content (kg/m <sup>3</sup> )	Water content (kg/m <sup>3</sup> )
1 : 2.4 : 3.6	0.66	293	193.38

Three samples were produced for each test series (constant current and voltage tests). The materials used in the study are shown in Table 1.

### 2.2 Concrete mix

In this study, the w/c ratio used was 0.66, the same used by Graeff (2007) in her work. Mix proportions and cement content are presented in Table 2.

The mix resulted in a concrete with a compressive strength of 25 MPa at 28 days, value representative of that recorded in many existing structures in Brazil that may be subjected to corrosion.

During casting, specimens were compacted by external mechanical vibration. After 24 h at room temperature, covered by plastic sheets, the specimens were placed in a curing room, with a RH > 95% and a mean temperature of 23°C, for 20 days.

### 2.3 Test parameters

From the studies of Torres (2006) and Graeff (2007) it was possible to define the parameters to conduct the CAIM test with the two different strategies of corrosion induction: constant voltage and current, in order to produce a similar degree of corrosion. These test variables can be seen in Table 3.

The control variables (test output) are presented in Table 4.

Table 3. Description of defined characteristics.

	Variable	Id	Unit	Levels
CAIM voltage	Voltage	V	V (volts)	45
	Test period	T	h (hours)	24
	Immersion depth	P	cm	Bottom of rebar
CAIM current	Current	A	A (Amperes)	0,0283
	Test period	T	h (hours)	720
	Immersion depth	P	cm	Bottom of rebar

Table 4. Output variables.

Variable	Id	Unit
Gravimetric weight loss	Gwl	g
Electrochemical weight loss	Ewl	g

As explained before, the determination of the gravimetric weight loss is made by comparing the rebar weight before and after the test.

It is also possible to make an estimate of the electrochemical weight loss by monitoring the samples every 30 minutes in order to get the value of the passing current (this only makes sense in the CAIM procedure with constant voltage, since the current is always the same in the CAIM procedure with constant current). By multiplying the current (in Amperes) and the time (in seconds), the total charge (in Coulombs) is determined. It is then possible to estimate the weight loss by using Faraday's Law, described in equation 1.

$$\Delta m = \frac{M \times I \times t}{z \times F} \quad (1)$$

Where:

$\Delta m$  = weight of consumed steel (g);

M = atomic weight of metal (=55.85 g to Fe);

I = applied current (Amperes);

t = time spent to accelerate corrosion (s);

z = ionic charge (=2);

F = Faraday constant (=96.500 Amperes/second).

## 3 RESULTS

### 3.1 Weight loss

The results obtained in this study are summarized in Table 5 and Figure 1. It is easy to see the similarity between the values of the gravimetric weight loss

Table 5. Test results.

	CAIM Constant voltage		CAIM Constant current	
	Gwl	Ewl	Gwl	Ewl
	Specimen 1	18.80	27.88	16.6
Specimen 2	18.80	30.71	17.6	21
Specimen 3	15.10	26.91	16.6	21
Average	17.57	28.50	16.93	21.00
Standard deviation	2.14	1.97	0.58	0.00

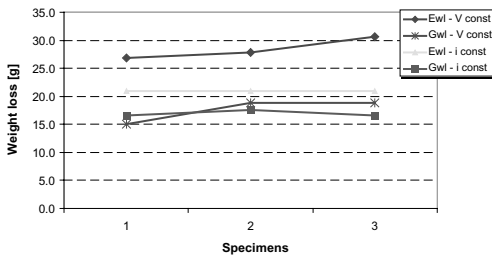


Figure 1. Graphic with results.

(Gwl) derived from both test procedures. This indicates that the choice of test parameters was adequate to produce similar results in both test series.

It is interesting to notice that the electrochemical weight loss estimates (Ewl) was superior to the real weight loss (Gwl) in both situations. However, the difference was smaller in the case of the constant current procedure.

The difference between Ewl and Gwl is attributed to the fact that there is an initiation period during which the impressed current or voltage does not produce an effective corrosion of the rebar. Further testing must be done to check if test conditions also play a role in this behavior.

It is also believed that the larger difference between Ewl and Gwl values (around 62%), verified in the results obtained with the constant voltage test procedure, is related to the more aggressive nature and shorter length of this kind of test, which distorts the corrosion phenomena. The initiation period might be more influential in shorter tests and the high voltage imposes temperature increases and quicker cracking, which reduces the resistance and allows the measured current to increase, without relationship with the actual corrosion current. To avoid this problem, the method will be adapted and current measurements will be taken on passive wires attached to the rebar, which are not connected to the main electrical circuit.

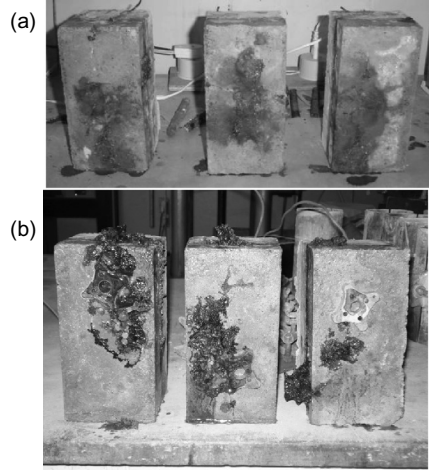


Figure 2. Specimens after CAIM test. (a) constant voltage (b) constant current.

On the other hand, the constant current test procedure, which required a longer acceleration time, seem to produce a more stable and reliable current profile.

In Figure 2, the condition of the specimens after the test can be visualized. The image shows the bottom face of the specimen after corrosion acceleration, induced by constant voltage (item “a”) and constant current (item “b”).

It is noticeable that the specimens are cracked and that a lot of corrosion products was deposited in these cracks. In fact, rust was visually noticed after some hours in the case of the constant voltage procedure and after 7 days of the constant current test. The deposition of corrosion products on cracks and voids around the bar may present an obstacle to oxygen and chloride access, leading to a lower gravitational weight loss (Gwl) than estimated by the current monitoring (Ewl).

### 3.2 Service life prediction using Monte Carlo simulation

In order to enhance this study, the deterioration of the concrete specimens was modeled using Monte Carlo simulation. The exercise was carried out considering the actual data and test conditions of both corrosion induction procedures. The idea was to check if the Monte Carlo Simulation and the corrosion propagation models proposed by Thoft-Chistensen (2001) for real structures could provide good results with data from accelerated tests. The failure condition adopted was a 20% average reduction in the cross section area.

Figures 3 and 4 show the service life histograms obtained. The service life estimates (50% of likelihood) were 0.036 years, or 13.24 days, for the data provided

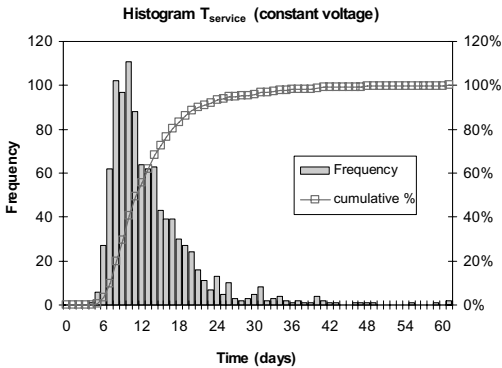


Figure 3. Histogram of service life prediction for the constant voltage test procedure.

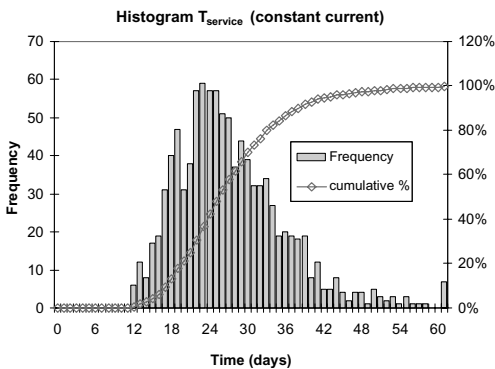


Figure 4. Histogram of service life prediction for the constant current test procedure.

by the CAIM test procedure using constant voltage, and 0.074 years, or 26.99 days, for the procedure with constant current.

The results confirm that, although test conditions were adjusted to produce similar results, the constant voltage procedure method seemed to be more aggressive, needing only 14 days to induce failure.

It is interesting to notice that the average value ( $P = 50\%$ ) found using the data from the constant current procedure was found to be in general accordance with the experimental results, given that the specimens presented 10 to 15% of gravimetric weight loss after 29 days of test. Most worrying, however, is the fact that, over the whole test period, the specimens showed only a few cracks and did not present any concrete spalling of the concrete cover, which would provide noticeable signs of impending failure.

The results of the constant voltage procedure also seem to be in accordance with the experimental ones. The differences in the service life estimates could be explained by the adoption, in the simulation, of an

initiation period longer than the one which occurs in reality.

The chloride diffusion conditions considered in the simulation included the average temperature of Porto Alegre throughout the year. However, in the case of the constant voltage specimens, the temperature of the solution is much higher, which would speed the deterioration. If the real temperature data was used, the initiation time and the corresponding service life prediction would be quite smaller, closer to the real ones.

#### 4 CONCLUSIONS

The tests performed indicate that the CAIM test was a good method to study the corrosion process in reinforced concrete specimens, specially when the procedure of acceleration by current impression is used.

Considering the results, in terms of comparison between test procedures for corrosion acceleration, it can be concluded that a careful choice of test parameters can lead to a good correlation of the results, in terms of rebar gravitational weight loss, for both test procedures. However, improvements in terms of current monitoring are necessary, because the lack of consideration of the initiation phase induces higher estimates of weight loss when the Faraday Law is applied to recorded current measurements.

As highlighted before, in Brazil there are few standards and a lack of knowledge about how test conditions affect the results of corrosion tests, which prevents correlation between test data. This study provides some useful information about the effects of using different acceleration strategies, which might be helpful to standardize other test methods. More tests should however be performed in order to improve the knowledge about how test conditions affect results. One example would be to analyze if the aggression level varies along the test, due to deposition of rust around the bar.

The use of the Monte Carlo Simulation technique in conjunction with the Thoft-Christensen model for corrosion propagation provide usable estimates of service life, for specimens subjected to accelerate condition. Further study in this area would be useful, specially if a correlation between simulations of accelerate condition and real-life structures could be obtained. This would allow us to have insights, from short term data, of the performance of reinforced concrete buildings subjected to chloride attack.

#### REFERENCES

- Standard test method for electrical indication of concrete's ability to resist chloride ion penetration. ASTM 1202 C. Philadelphia, 1999.

- American Society For Testing And Materials. Annual book of ASTM Standards. Standard practice for cleaning, descaling and passivation of stainless steel parts, equipment and systems. (Revision) ASTM A 380, Philadelphia, 1996.
- Amleh, L. Mirza, S. 1999. Corrosion influence on bond between steel and concrete. *ACI Structural Journal*. Vol. 96, no. 3, pp. 415–423.
- Andrade, J.J. 1997. Durabilidade das estruturas de concreto armado: análise das manifestações patológicas nas estruturas no estado de Pernambuco. Dissertação (Mestrado). Universidade Federal do Rio Grande do Sul, Porto Alegre-RS, 148 p. (*in Portuguese*)
- Aranha, P.M.S. 1994. Contribuição ao estudo das manifestações patológicas em estruturas de concreto armado na região amazônica. Dissertação (Mestrado). Universidade Federal do Rio Grande do Sul, Porto Alegre-RS, 120 p. (*in Portuguese*)
- Dal Molin, D.C.C. 1988. Fissuras em estruturas de concreto armado: análise das manifestações típicas e levantamento de casos ocorridos no estado do Rio Grande do Sul. Dissertação (Mestrado). Universidade Federal do Rio Grande do Sul, Porto Alegre-RS, 196 p. (*in portuguese*)
- González, J.A. Andrade, C. Alonso, C. Feliu, S. 1995. Comparison of rates of general corrosion and maximum pitting penetration on concrete embedded steel reinforcement. *Cement and Concrete Research*. Vol. 25, no. 2, pp. 257–264.
- Graeff, A.G. 2007. Avaliação experimental e modelagem dos efeitos estruturais da propagação da corrosão em elementos de concreto armado. Dissertação (Mestrado). Universidade Federal do Rio Grande do Sul. Porto Alegre-RS, (*in portuguese*)
- Jadovski, I. Lantelme, E.M.V. Kulakowski, M.P. Campagnolo, J.L. Dal Molin, D.C.C. 1992 A influencia da espessura do cobrimento no fenômeno da corrosão de armaduras. In: *Viii Congresso Regional De Iniciação Científica E Tecnológica Em Engenharia, Joinville*. Anais ... Joinville: FEJ/ UDESC. (*in portuguese*)
- Kirchheim, A.P. Pasa, V. Dal Molin, D.C.C. Silva Filho, L.C.P. 2005. Avaliação de revestimentos de proteção do aço no controle da corrosão das armaduras em concretos brancos. *VII Congresso Latinoamericano De Patologia De La Construccion, X Congreso De Control De Calidad En La Construccion*, Asunción, Paraguai. Anais ... CONPAT 2005. (*in portuguese*)
- Lima, M.G. 1990. Influencia dos componentes do concreto na corrosão de armaduras. Dissertação (Mestrado em Engenharia) – Universidade Federal do Rio Grande do Sul, Porto Alegre, 133 p. (*in portuguese*)
- Marchesan, P.R.C. Santarosa, D. Campagnolo, J.L. Filho, L.C.P.S. Pacheco, A.R. 1997. Estudo da influência da aplicação de revestimentos no controle da corrosão. In: *IV Congresso Iberoamericano De Patologia Das Construções E Vi Congresso De Controle De Qualidade*, Porto Alegre. Anais ... Porto Alegre: LEME/CPGEC/ UFRGS. (*in portuguese*)
- Rodriguez, J. Ortega, L.M. Casal, J. 1997. Load carrying capacity of concrete structures with corroded reinforcement. *Construction and Building Materials*. Vol. 11, no. 4, pp. 239–248.
- Selistre, F.P. Both, A.A. 1993. A influencia do fator A/C, do cobrimento e do tempo de cura na corrosão de armaduras. In: *V Salão De Iniciação Científica E II Feira De Iniciação Cinética*, Porto Alegre. Anais ... Porto Alegre: LEME/UFRGS. (*in portuguese*)
- Selistre, F.P. Gastal, S.L. Campagnolo, J.L. 1994. Estudo de técnicas para reversão do processo corrosivo em estruturas de concreto contaminadas com cloretos. In: *VI Salão De Iniciação Cinética E Iii Feira De Iniciação Cinética*, Porto Alegre. Anais ... Porto Alegre: LEME/ UFRGS. (*in portuguese*)
- Torres, A.S. Avaliação da Sensibilidade do Ensaio CAIM – Corrosão Acelerada por Imersão Modificada – frente ao processo de corrosão em armaduras de Concreto Armado. Dissertação (Mestrado). Universidade Federal do Rio Grande do Sul, Porto Alegre-RS, 2006. 159 p. (*in portuguese*)
- Varela, H. Espinoza, L.V. 1988. Penetrabilidade de Iones cloruors en Morteros con y sin Revestimiento. In: *VII Jornadas Chilenas Del Hormigón E I Jornada Lation-americana Del Cimento Y Hormigón*, Curso: Avances Tecnologicos en el Uso de Cementos y Hormigones, 1988, Santiago de Chile. Anais ... Santiago de Chile: Instituto Profesional de Santiago, p. 82–91.

# Influence of localized corrosion of steel bars on structural performance of reinforced concrete beams

H. Hamada

*TOA Corporation, Japan*

E. Kato, M. Iwanami & H. Yokota

*Port and Airport Research Institute, Japan*

**ABSTRACT:** This paper experimentally investigates an influence of localized corrosion of steel bars embedded in concrete on structural performance of reinforced concrete (RC) beams by flexural loading test. The localized corrosion was produced by controlling the area of direct current impression in which a wet sponge was attached to the limited part of the bottom surface of RC beam. As a result, it was possible to estimate the first yield load and deformability of RC beam by using the maximum loss in cross-sectional area of steel bars, even if steel bars showed localized corrosion. However, the maximum loads of RC beams were not adequately estimated by the maximum loss in cross-sectional area. After the first yield, influences of localized corrosion of steel bars on load carrying capacity and deformability were varied depending on the position of corrosion.

## 1 INTRODUCTION

Port and harbor structures are attacked by chloride ion in the sea water, which may cause serious deterioration of materials. Therefore, it is essential to carry out the rational and efficient maintenance to guarantee the required structural performance during service period. For this purpose, it is necessary to understand the degradation mechanism of structural performance and to predict the progress of degradation. Corrosion of steel bars embedded in concrete has a great influence on the structural performance. However, the relationship between the degree of corrosion of steel bar and structural performance has not been made clear adequately. In particular, the variation of corrosion including the localized corrosion has to be well understood for structural performance estimation.

In this study, through flexural loading test, an influence of localized corrosion of steel bars on load-carrying capacity and deformability of reinforced concrete (RC) beams has been experimentally investigated. The localized corrosion was produced by controlling the area of direct current impression in which a wet sponge was attached to the limited part of the bottom surface of RC beam.

## 2 EXPERIMENTAL PROGRAM

### 2.1 Test beam

Figure 1 shows the geometry and steel bar arrangements of tested RC beams. Five RC beams with identical dimensions were prepared. All the beams were designed in such a way that flexural failure precedes the occurrence of shear failure. The diameters of deformed steel bars were 16 mm for longitudinal bar and 6 mm for stirrup. Table 1 presents mixture proportion of concrete. Mechanical properties of concrete and steel bars are summarized in Table 2.

### 2.2 Impressed-current method

Corrosion of steel bar was artificially produced by an impressed-current method. Figure 2 shows the impressed-current method. The main bar was connected to anode, while the stainless plate was connected to cathode. To corrode the main bar locally, seawater was supplied by sucking up with a sponge of 50 mm wide. Table 3 lists the intended position of corrosion. For cases that main bars corroded only in the middle of span, the sponge was attached to the midspan of beam. For the case that the bar corroded in the outmost end of flexural span, the sponge was

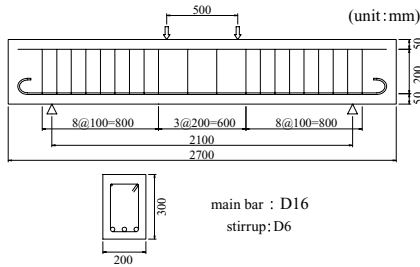


Figure 1. Layout of the RC beam.

Table 1. Mixture proportion of the concrete.

$G_{\max}$ (mm)	Slump (cm)	Air (%)	W/C (%)	$s/a$ (%)
20	18	4.5	57.2	47.3

Unit weight ( $\text{kg}/\text{m}^3$ )

W	C	S	G	Ad
179	313	839	964	3.3

$G_{\max}$ : maximum particle size of aggregate,  $s/a$ : sand-to-aggregate ratio, W: water, C: cement (OPC), S: sand, G: coarse aggregate, and Ad: air-entraining, water reducing agent.

Table 2. Mechanical properties of concrete and steel bar.

Concrete				
Compressive strength (MPa)		Young's modulus (GPa)		
43.0		30.0		
Steel bar				
Diameter	Yield strength (MPa)	Tensile strength (MPa)	Young's modulus (GPa)	
D16	366	528	180	
D6	361	524	190	

attached 250 mm apart from the midspan. For the case that corrosion only occurred in the shear span, the sponge was attached 500 mm apart from the midspan. The impressed-current was  $500 \text{ A} \cdot \text{day}/\text{m}^2$  against the initial surface area of the main bars.

### 2.3 Flexural loading test

Flexural loading test was performed for investigating structural performance of RC beams. RC beams were

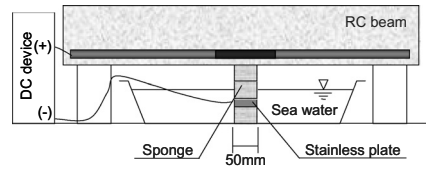


Figure 2. Impressed-current method.

Table 3. Position of corrosion.

Specimen No.	Corrosion position
-0	Healthy
-1	Middle of span
-2	Middle of span
-3	Outmost end of flexural span
-4	Shear span

simply supported with a span of 2100 mm. A monotonically increased load was applied symmetrically as shown in Figure 1. Steel plates of 100 mm wide were inserted in the loading points and the supports. Load, deflection, compressive strain of concrete, and crack width were measured and recorded. To measure crack widths, the array of LVDT was mounted on the side surface of beam. Since strain gauges were not glued on the steel bars, the first yield was assumed with a distinct bending point of a load-deflection curve.

### 2.4 Investigation of steel bar corrosion

After the loading test, the main bars were taken out from the concrete and cut into many pieces of 50 mm long. Their mass-losses were measured after the surface treatment with sandblasting followed by immersion into 10% diammonium hydrogen citrate solution.

## 3 RESULTS AND DISCUSSIONS

### 3.1 Distribution of steel bar corrosion

Figure 3 shows the distribution of mass-losses of steel bars due to corrosion. The mass-loss presented in this figure is an average of the data of three main bars at the corresponding positions. The maximum mass-losses were about 60% in D16-1 and D16-2, about 45% in D16-3, and about 20% in D16-4. The position having the most serious corrosion was the same as that intended, while the mass-loss was not uniform in the corrosion position. The area in which corrosion extended was limited within about 300 mm long. The maximum mass-loss appeared in the center span of

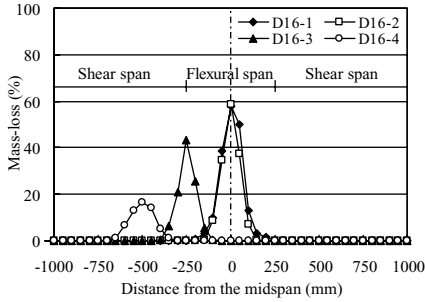


Figure 3. Distribution of steel bar corrosion.

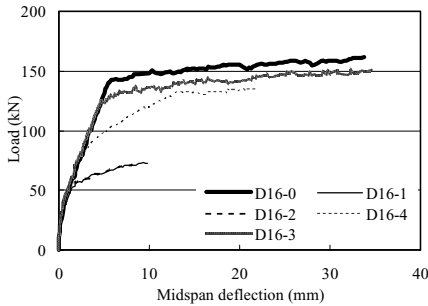


Figure 4. Load-deflection curves.

150 mm in the area and the remaining area showed the mass-loss of 10% or less. Every steel bar piece of 50 mm long seemed to have uniform corrosion; therefore, it was assumed that the mass-loss is exactly equivalent to the cross-sectional area loss of steel bar.

### 3.2 Load-deflection curve

Figure 4 shows the relationships between the midspan deflection and the load. The flexural stiffness up to the first yield was almost the same as that of the healthy beam (D16-0). In the past study by Kato, et al. 2005, the initial flexural stiffness became small in RC beam having uniformly corroded steel bars because of bond deterioration. In this study, however, the bond between concrete and steel bar was not heavily deteriorated in the locally corroded beam. Therefore, it can be considered that the flexural stiffness up to the first yield is not greatly influenced by localized corrosion of steel bars.

After the first yield, except for the healthy beam, the load-carrying capacity of the beam having only corrosion with the outmost end of flexural span (D16-3) was the largest. All the beams showed crushing of concrete at the ultimate. In addition, D16-1 and

D2 showed breakage of steel bars before crushing the concrete.

### 3.3 Load-carrying capacity

#### 3.3.1 Average cross-sectional area loss

Yokota, et al. 2003 concluded that load-carrying capacity of RC beam with uniform corrosion of steel bars can be evaluated by using the average loss in cross-sectional area of steel bars in the flexural span. The relationships between the average loss in cross-sectional area and load-carrying capacity of the beam having corrosion in its midspan are shown in Figures 5 and 6. In these figures, the load-carrying capacity is quantified in terms of the ratios of yield and maximum loads. They were the ratios of those loads of corroded beam to those of healthy beam. The average cross-sectional loss in these figures is an averaged data in the flexural span (500 mm long) that were measured with 50 mm long pieces. The straight line shows the relationship between cross-sectional area loss of steel bar and yield and maximum loads of beam based on the beam theory. Compared to uniformly corroded RC beams (Kato, et al., 2006), it was found that the degree of decrease in the load is remarkable in the locally corroded RC beams. Therefore,

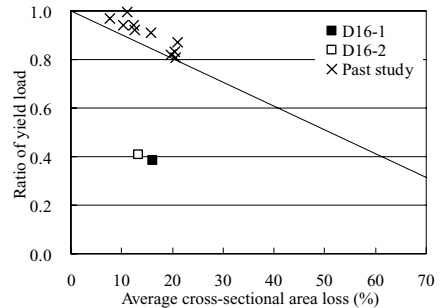


Figure 5. Relationship between average cross-sectional area loss and the ratio of yield load.

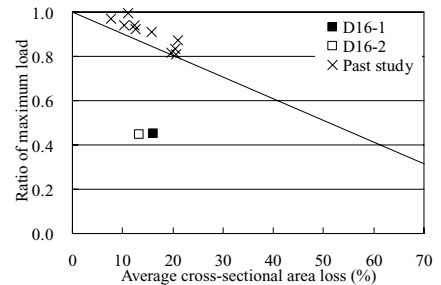


Figure 6. Relationship between average cross-sectional area loss and the ratio of maximum load.

in case of locally corroded RC beams, it is difficult to evaluate the load-carrying capacity by using the average loss in cross-sectional area of steel bar.

### 3.3.2 Maximum cross-sectional area loss

Instead of the average loss in cross-sectional area of steel bar, the applicability of the maximum loss in cross-sectional area of steel bar is examined for the evaluation of load-carrying capacity. The maximum loss in cross-sectional area in this paper is defined as the maximum loss in cross-sectional area measured in the piece of 50 mm long. Figure 7 shows the relationship between maximum cross-sectional area loss and the ratio of first yield load. The straight line shows the calculated value based on the beam theory using the maximum cross-sectional area loss. It was found that the first yield load can be evaluated by using the maximum cross-sectional area loss. In beam D16-4 (corrosion in the shear span only), it had been thought that the steel bars do not yield at the corroded position because its cross-sectional area loss was too small to make the steel bar become yield there. However, the crack width at the corroded position was extremely large at the first yield as shown in Figure 8. Therefore, bond deterioration there may have made the steel bar yielded due to tensile strain concentration.

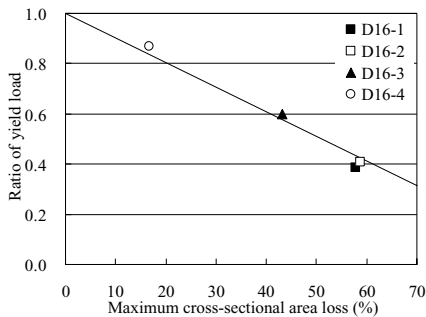


Figure 7. Relationship between maximum cross-sectional area loss and the ratio of yield load.

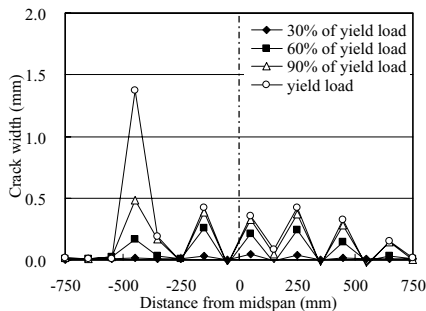


Figure 8. Increase in crack widths occurred in beam D16-4.

Figure 9 shows the relationship between maximum cross-sectional area loss and the ratio of maximum load. Compared to beams with corrosion in their midspans (D16-1 and 2), beams D16-3 and 4 showed small decrease in their maximum loads. Since those two beams had many numbers of cracks in their flexural spans as shown in Figure 10, in the beam having corrosion at either the outmost end of flexural span or the shear span corroded, tensile strain of the steel bar was considered not to concentrate because of no bond deterioration in the flexural span. Furthermore, an influence of corrosion of these beams on the maximum load seemed little compared to that of the beam with corrosion of its midspan.

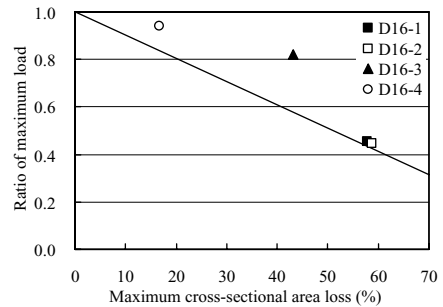


Figure 9. Relationship between maximum cross-sectional area loss and the ratio of maximum load.

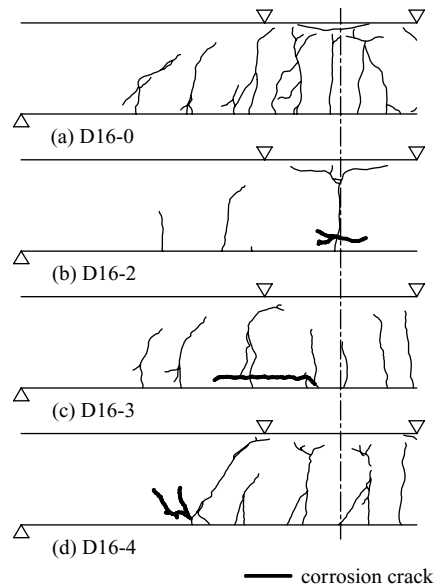


Figure 10. Crack formation at the maximum load.



### 3.4 Deformability

Figure 11 shows the deformation distribution of the beams at the first yield. The deformation distributions of corroded beams were almost the same as that of the healthy beam though the deflections varied. Figure 12 shows the deformation distribution of the beams at the ultimate. It was found that the deflection at the midspan was the largest, and the deformation distribution was almost linear in the beam having corrosion in its midspan (D16-2).

In the beam having corrosion at the outmost end of flexural span (D16-3), the deflection at the corroded position showed the maximum. Based on this result, it

was considered that the deformation of the beam concentrated because stresses are not distributed axially. On the other hand, in the beam with corrosion in its shear span (D16-4), the deformation distribution was almost the same as that of the healthy beam. Therefore, it was considered that the influence on the deformation distribution is small because the amount of corrosion was smaller than that of the other beams.

Figure 13 shows the relationship between maximum cross-sectional area loss and the ratio of deflection at the first yield of steel bar. The ratio of deflection is the ratio of the maximum deflection of the beam with corrosion to that of the healthy beam.

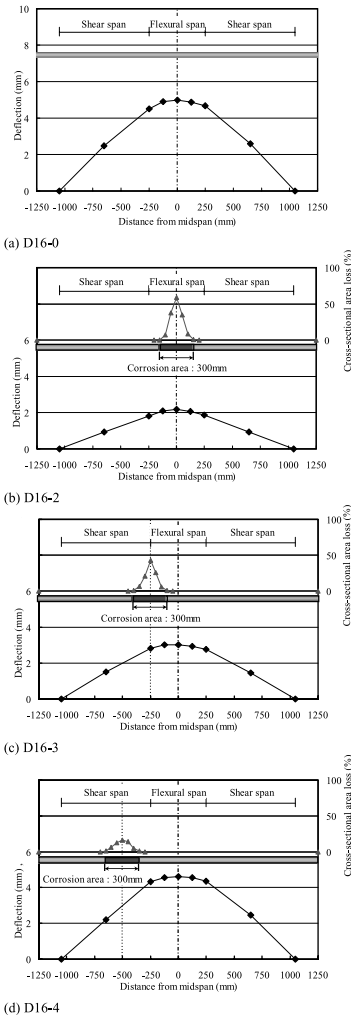


Figure 11. Distributions of deformation and steel bar corrosion at the first yield of steel bar.

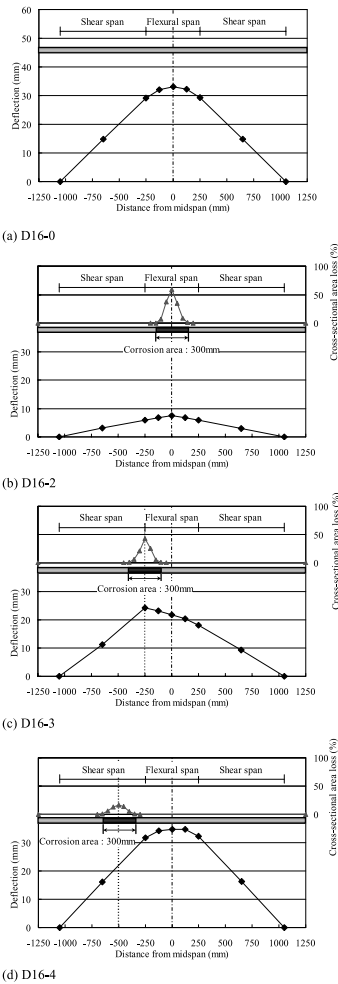


Figure 12. Distributions of deformation and steel bar corrosion at the ultimate state.

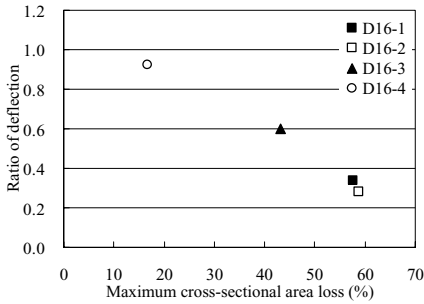


Figure 13. Relationship between maximum cross-sectional area loss and the ratio of deflection at the first yield.

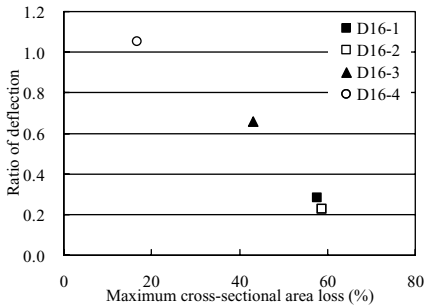


Figure 14. Relationship between maximum cross-sectional area loss and the ratio of deflection at the ultimate state.

It was found that the ratio of deflection tends to become small as the corrosion progresses. Furthermore, it was considered that an influence of corroded position on the decrement in the deformation is small. Figure 14 shows the relationship between the maximum cross-sectional area loss and the ratio of deflection at the ultimate state. It was found that the ratio of deflection tends to become small as the corrosion progresses though variations existed when the maximum loss in cross-sectional area was small.

#### 4 CONCLUSIONS

The following conclusions are drawn based on the flexural loading test of the RC beams with localized corrosion:

1. The flexural stiffness of the beam up to the first yield of steel bar is not largely influenced by localized corrosion because the bond deterioration due to corrosion seems small.
2. The first yield load can be accurately evaluated by using the maximum loss in cross-sectional area of

steel bars. However, it is not largely influenced by the position of corrosion.

3. After the first yield, the load-carrying capacity of beam is influenced by the mechanism of bond stress transfer between steel bar and concrete at the corroded position. Therefore, it was not possible to estimate the maximum load by the maximum loss in cross-sectional area of steel bar.
4. The deformation distribution of beam with corrosion is almost the same as that of the healthy beam regardless of corrosion position at the first yield. The deformation of beam concentrates at the corroded position in the beam with corrosion in its midspan or at its outmost end of flexural span because the stress is not distributed well. On the other hand, in the beam with corrosion in its shear span, the deformation distribution is almost the same as the healthy beam because the amount of corrosion was small compared to the other beam.
5. The deflection tends to be small as the corrosion progresses at the first yield. An influence of the corroded position on the decrement in deflection is small. At the ultimate state, as well as that at the first yield, deflection tends to be small as the corrosion progresses though variations existed when the maximum loss in cross-sectional area was small.

#### ACKNOWLEDGEMENTS

The authors would like to extend their appreciation to Ministry of Land, Infrastructure, and Transport for providing them chances to make full investigation of the existing wharf. The authors also thank Mr. Shingo Muramatsu, Graduate student in Nagaoka University of Technology, for his kind assistance in the experimental work.

#### REFERENCES

- Kato, E., Yokozawa, A., Akira, Y. & Yokota, H. 2005. Study on Durability of RC Deck of an Existing Pier. *Proc. of New Technologies for Urban Safety of Mega Cities in Asia*, Singapore, 69–78.
- Kato, E., Iwanami, M. & Yokota, H. 2006. Deterioration in Ductility of RC Beams with Corroded Reinforcement. *Proceedings of the 2nd fib International Congress*, Naples, Italy, 1–8.
- Yokota, H., Iwanami, M. & Sato, F. 2003. Quantitative Evaluation of Structural Performance of Reinforced Concrete Beams Damaged by Corrosion of Reinforcement. *Proceedings of the 6th CANMET/ACI International Conference on Durability of Concrete*, Thessaloniki, Greece, ACI-SP-212-35, 555–570.

# Development of a damage-recovery relationship based on variable re-curing of fire-damaged high-strength mortar

M. Henry & T.H. Ahn

*Department of Civil Engineering, University of Tokyo, Tokyo, Japan*

Y. Kato & T. Kishi

*Institute of Industrial Science, University of Tokyo, Tokyo, Japan*

**ABSTRACT:** Repair utilizing re-curing has the potential to restore strength and durability without removal and casting operations, thus reducing waste generation and material consumption. In this research, the effect of different post-fire cooling and re-curing conditions on the behavior of high-strength mortar was investigated. After removal from heating, specimens were placed in air or water conditions, and unstressed compressive strength and mercury intrusion porosimetry tests, as well as an epoxy injection process to observe the cracking pattern, were performed in order to understand the relationship between damage and recovery mechanisms. Results showed that air re-curing resulted in the formation of surface cracks due to differential thermal shrinkage, reducing strength. Immediate water submersion also resulted in large strength reductions, but was followed by strength, porosity, and crack recovery due to rehydration. Specimens which were cooled in the air before water submersion underwent less strength loss but also recovered less during re-curing.

## 1 INTRODUCTION

### 1.1 Background

Concrete undergoes a deterioration of properties when exposed to high temperatures such as those during a fire. This deterioration is caused by thermo-mechanical and thermo-hydral processes, and is typically qualified by cracking, loss of strength, and explosive spalling. In order to repair these damages, the damaged concrete is removed and a patching material is cast to restore strength, durability, and fire performance as necessary (Tovey, 1986).

However, for concrete which has not undergone explosive spalling, it may be possible to recover performance by re-curing the fire-damaged concrete under water supply. A repair process utilizing re-curing as a mechanism for strength or durability recovery would reduce waste generation and material consumption, as the area requiring removal and patching procedures would be reduced.

Crook & Murray (1970) first investigated this potential by studying concrete blocks re-cured in water after 620°C exposure. Strength recovery was observed, and it was found that extending the re-curing period resulted in higher strength. Recovery was attributed to the shrinkage of C-S-H gel in the capillary pore space, which allowed for the regrowth of smaller rehydration products by carbonation, resulting

in reduced porosity and increase strength. Expanding upon this, Sarshar & Khoury (1993) suggested that recovery was due to the regeneration of C-S-H during rehydration. Furthermore, they found that expansion due to rehydration in the outer layer of concrete may cause an initial strength reduction, and that re-curing in water for 7 days resulted in lower compressive strength than re-curing in 100% relative humidity (RH). This indicated that the re-curing process could have some effect on the damage and recovery mechanism.

A microstructure investigation was conducted by Lin et al. (1996), which found that water supply was the mechanism for rehydrating calcium hydroxide and unhydrated cement. Furthermore, the regrowth in void spaces due to rehydration led to the development of random pore structures, and they recommended that mercury intrusion porosimetry (MIP) be used to investigate.

In order to conduct a comprehensive quantitative analysis, MIP, as well as strength, durability, and scanning electron microscope, investigations were performed by Poon et al. (2001) to determine the effects of concrete type, exposure temperature, and re-curing condition on the strength and durability recovery of fire-damaged concrete. Constant water re-curing resulted in rapid rehydration during the first 7 days, whereas air re-curing was slow and gradual. High-strength concrete (HSC) recovered better than

normal-strength concrete (NSC). Finally, it was suggested that, if the exposure temperature is below 600°C, original properties can be recovered by re-curing alone, as C-S-H decomposition begins from 550°C.

These research works have established mechanical and chemical processes affecting the loss and recovery of strength. However, they have not established a connection between the loss and recovery mechanisms. For a given concrete and exposure condition, the damage and subsequent recovery should depend on the conditions to which the concrete is exposed after heating—that is, recovery behavior should depend on the damage suffered.

### 1.2 Objectives

This experimental program was conducted in order to determine the effect of different cooling and re-curing conditions on the damage and recovery mechanisms, and to investigate the relationship between these two mechanisms, for high-strength mortar exposed to fire. The cooling condition—defined in this research as the environmental condition immediately after removal from heating—and the re-curing condition—defined as the environmental condition after cooling until testing—are the variables in this program. The objective was to observe the effect of these variables on macro-(compressive strength, visible cracks) and micro-properties (pore structure, invisible cracks) after heating and re-curing, and to develop a relationship between the two behaviors.

## 2 EXPERIMENTAL PROGRAM

### 2.1 Materials

High-strength cement mortar was prepared from water, ordinary Portland cement (Type 1), Fujigawa river sand, and air-entraining (AE) and high-range water-reducing (HRWA) admixtures. A water-cement (W/C) ratio of 0.3 was used to achieve high strength conditions. Complete mix proportions are given in Table 1.

Table 1. Cement mortar mix proportions.

Water	(kg/m <sup>3</sup> )	230
Cement	(kg/m <sup>3</sup> )	767
Sand	(kg/m <sup>3</sup> )	1380
AE	(% cement mass)	0.4
HRWA	(% cement mass)	1.5
Water/cement	(by mass)	0.3
Sand/cement	(by mass)	1.8
28-day strength	(MPa)	100

### 2.2 Specimens

Cylinder specimens (5Ø × 10 cm) were cast using high-strength mortar. After casting, specimens were sealed and cured in the molds for 24 hours. They were then removed and placed in water curing (20°C) for 13 days, then transferred to air curing (20°C, 60% RH) until fire exposure at 28 days from casting.

### 2.3 Fire exposure

Fire exposure was emulated using an electric furnace. As this furnace does not have a control mechanism for the rate of heat increase, the furnace was preheated to the target temperature before beginning specimen exposure.

The exposure temperature was set at 550°C for this experimental program. This value was chosen by performing a trial series of tests in order to determine, for this specimen shape, size and mix proportions, the temperature at which the amount of fire damage was the highest yet the probability of spalling the lowest. A 2-hour exposure time was selected to achieve an even heating regime.

### 2.4 Re-curing conditions

After removal from heating, specimens were placed in one of three re-curing conditions, as shown in Table 2. The cooling period refers to the first hour after removal from heating, and the re-curing period is from cooling until testing. Air-cooled and re-cured specimens were removed from heating and placed in a controlled environment at 20°C and 60% RH. Water-cooled and re-cured specimens were placed into room-temperature (20°C) water immediately after removal from heating. In order to gauge the effect of the thermal shock caused by immediate submersion in water, air-water (AW) re-cured specimens were allowed to cool in the air for one hour before submersion in water.

### 2.5 Specimen testing

Testing consisted of three phases. The first phase measured strength and porosity recovery; the second

Table 2. Re-curing conditions.

	Cooling period Removal—1 hour	Re-curing period 1 hour—28 days
Air	Air	Air
Water	Water	Water
AW	Air	Water

phase observed cracking patterns using epoxy injection; the third phase observed crack self-healing behavior by microscope photography.

Compressive strength was measured under the unstressed residual condition. Three cylinders were tested at each data point and the average values are reported. MIP specimens, approximately 5 mm in size, were taken from compressive strength specimens after testing. These specimens were immediately submerged in acetone to stop the hydration reaction, then dried using a D-dry vacuum pump. Compressive strength and MIP specimens were tested before heating, 1 hour after heating (air and water cooling), and after 3 and 28 days (air, water, and air-water re-curing).

Compressive strength is reported as both absolute (in MPa) and in terms of the residual strength, calculated per Equation 1:

$$R = f/f_0 \times 100 (\%) \quad (1)$$

where  $R$  = residual strength (%);  $f$  = average strength (MPa); and  $f_0$  = average initial strength (MPa).

Strength loss and recovery are reported in terms of the change in residual strength relative to the initial strength.

In order to observe the cracking pattern and crack recovery under different re-curing conditions, an epoxy injection procedure was applied (Iwaki et al., 2004). After re-curing, epoxy was injected via vacuum pressure. This process can inject epoxy into cracks as small as 6 micrometers, and the hardening of the epoxy helps to prevent secondary defects from forming. After epoxy injection, specimens were cut in section 4 centimeters from the top of the specimen, and then placed under ultraviolet (black) light. The dispersion of epoxy was then recorded by photograph. Due to a limited number of specimens, only air re-cured (7 days) and water re-cured (1 hour and 7 days) specimens were observed.

Microscope observation was performed to investigate the progress and mechanism of crack self-healing. Specimens in this test series were allowed to cool in the air until surface cracking occurred, then placed in water to initiate self-healing. Observation was performed after 1, 3, 7, and 28 days.

### 3 RESULTS AND DISCUSSION

#### 3.1 Strength loss and recovery

Compressive strength test results are given in Table 3 and shown in Figure 1; strength loss and recovery is shown in Figure 2.

Air specimens underwent an initial strength loss of 29.5% after 1 hour, followed by a further 18.7% decrease by 3 days, for a total loss of 48.2%.

Table 3. Strength results by re-curing condition.

	Average strength (residual strength) MPa (% initial)		
	1 hour	3 days	28 days
Initial = 104.4 MPa			
Air	73.6 (70.5)	54.0 (51.8)	59.8 (57.3)
Water	40.2 (38.5)	65.3 (62.6)	75.6 (72.4)
AW	73.6 (70.5)	74.4 (71.3)	88.2 (84.5)

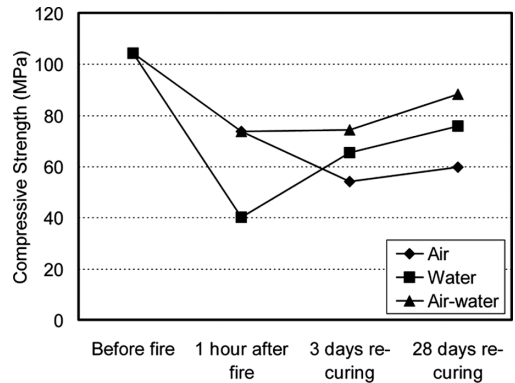


Figure 1. Strength behavior by re-curing condition.

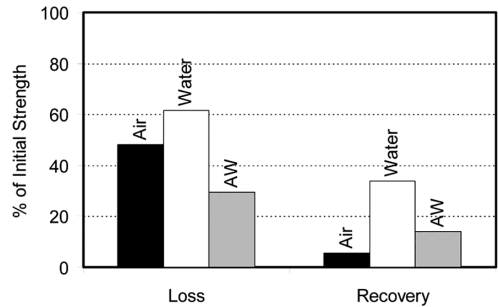


Figure 2. Strength loss and recovery.

Little strength recovery was observed between 3 and 28 days. The final residual strength for air specimens was 59.8% of the initial strength.

Water specimens lost 61.5% of the initial strength after 1 hour. However, from 1 hour to 28 days, constant strength recovery was observed, resulting in a 33.9% gain and a final residual strength of 75.6%.

Air-water specimens shared the same 1 hour strength loss of the air specimens at 29.5%. During the 1 hour to 3 day period, little change was observed, but between 3 and 28 days air-water specimens recovered 13.2%. The final residual strength was 88.2%.

The effect of thermal shock due to different cooling condition can be seen by comparing the air and water results after 1 hour. The residual strength was 33.4% lower for specimens immediately submerged in water after removal from the furnace.

Strength loss was highest for water specimens, followed by air and air-water specimens, respectively. However, water specimens had the greatest strength recovery. Air-water specimens lost the least amount of strength and regained a moderate amount, resulting in the highest final strength.

### 3.2 Pore structure loss and recovery

Porosity results are given in Table 4 and shown in Figure 3. Initial porosity was 0.139. Air specimens had an increase of 0.101 after 1 hour of cooling, and recovered 0.024 by 28 days; the final porosity was 0.217. The porosity of water specimens increased by 0.093 after 1 hour of water cooling, and recovered 0.091 by 28 days, for a final porosity of 0.141. Air-water specimens increased porosity by 0.101 and recovered 0.077, resulting in a final porosity of 0.164.

There is no apparent effect on the porosity due to thermal shock during the cooling period. However, immediate submersion in water, when compared to air

cooling before submersion, resulted in a decrease of 0.022 in final porosity.

### 3.3 Crack pattern and recovery

Epoxy injection was used to observe the crack pattern of air and water specimens. White areas show where epoxy penetrated through cracks; dark areas are uncracked, or where epoxy couldn't penetrate.

Figure 4 (left) shows the section of a specimen after 7 days air re-curing. In this image, the epoxy area is clearly defined. This indicates that discrete macro-cracking occurred. External inspection of air re-cured specimens showed that surface cracks were visible after 1 day re-curing (Fig. 4, right).

The effect of thermal shock and re-curing can be seen in Figure 5. In the left image, the epoxy can be seen in small, spidery radial lines with a less-defined area. This indicates the occurrence of micro-cracking; epoxy could only penetrate in the small cracks and radiate out from there, but these areas are relatively small, so the overall appearance is less-defined compared to the macro-cracking case. Furthermore, visual inspection of water specimens after 1 hour showed no cracks.

Figure 5 (right) shows the section of a specimen after 7 days water re-curing. There is almost no epoxy visible, indicating that there are no significant cracks to penetrate. From this image, the effectiveness of

Table 4. Porosity results by re-curing condition.

	Porosity ml/ml		
	1 hour	3 days	28 days
Initial = 0.139 ml/ml			
Air	0.240	0.237	0.217
Water	0.232	0.174	0.141
AW	0.240	0.190	0.164

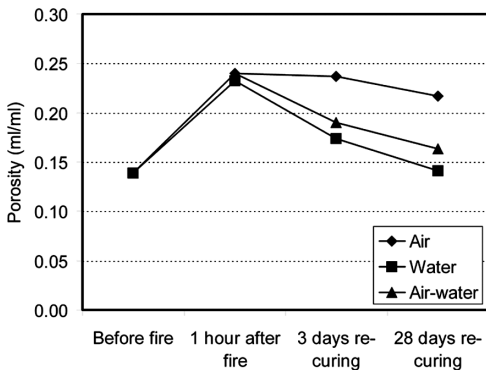


Figure 3. Porosity behavior by re-curing condition.

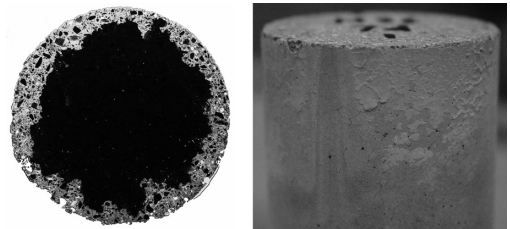


Figure 4. Crack pattern after 7 days air re-curing (left) and surface cracking (right).

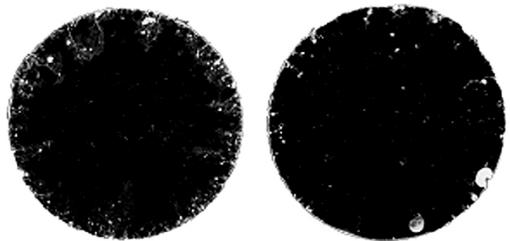


Figure 5. Crack pattern after 1 hour water cooling (left) and 7 days re-curing (right).

water re-curing to repair the cracks caused by thermal shock can be seen; within 7 days, self-healing under water supply closed most cracks.

### 3.4 Damage and recovery mechanisms

Porosity and strength share an inverse relationship; that is, an increase in porosity corresponds to a decrease in strength. Therefore, as porosity is a primary factor for strength, changes in the strength and porosity relationship should correspond. However, when comparing the strength and porosity behavior by re-curing condition, some differences arise: first, strength decreases for air re-cured specimens from 1 hour to 3 days without a corresponding decrease in porosity; second, thermal shock has little effect on porosity, yet there is a significant reduction in strength; and third, the strength of air-water specimens does not vary significantly between 1 hour and 3 days, but recovery of the pore structure occurs.

When cooling and re-curing in the air, heat is transferred by convection, which is a relatively slow process. Thermal gradients develop in the specimen as the outside cools more quickly than the inside, resulting in the formation of surface cracks, shown in Figure 4 (right), due to differential thermal shrinkage. Therefore, the strength loss between 1 hour and 3 days may be attributed to macro-cracking.

Water cooled specimens undergo thermal shock due to the large difference in temperature between the specimen (at 550°C) and the water (at 20°C). This causes a “quenching” effect, resulting in the formation of micro-cracks (Fig. 5, left). As the porosity of water and air cooled specimens after 1 hour is relatively similar, the strength reduction for water specimens is caused by micro-cracking.

When considering the recovery mechanism, water supply has been shown to be the most important factor for initiating rehydration. Therefore, the minor porosity and strength recovery of air specimens is understandable, as 60% RH provides only a small amount of water. Water and air-water specimens were both under water supply from 1 hour to 28 days; however, there is a 20.1% difference in the strength recovery. This difference is due to the initial cooling condition: for specimens immediately submerged, water is sucked into the pore structure as part of the cooling process. However, specimens initially cooled in the air have a much lower temperature when submerged, so less water is absorbed.

In order to show this difference, the mass loss due to heating and the mass gain one hour after water submersion were measured. While both water and air-water specimens lost the same mass under the same heating conditions, water specimens gained 44.7 grams of mass during the first hour of water submersion,

whereas air-water specimens gained 37.5 grams—a 16% difference. However, as the temperature of the air-water specimens is lower upon submersion, the effect of thermal shock is less as well. As a result, while less water is absorbed for rehydration, less damage occurs (Fig. 2).

### 3.5 Crack self-healing and secondary spalling

Crack recovery behavior was previously observed at the macro-scale. Micro-scale observation of crack self-healing ability under water supply can be seen in Figure 6. The initial crack width was 0.31 millimeters at its widest point (shown by black line in Fig. 6, top left); by 28 days, almost the entire cracked area had been filled with rehydration product.

Another damage-recovery mechanism is related to this self-healing rehydration at the specimen surface. In Figure 7, the concept of dehydration zones under heating is illustrated (Kalifa et al., 2000). In this figure, the dry/dehydrated zone is a brittle surface layer sintered due to complete dehydration and destruction of the cement paste—rehydration cannot occur in this zone. The layer below that, the drying/dehydrating zone, is where initial rehydration occurs during re-curing and is the source of the self-healing behavior in the crack. However, as rehydration occurs in this layer, expansion due to the formation of new hydration products also occurs. As the surface layer is brittle, this expansion causes secondary spalling, resulting in minor strength reduction. While not observed directly in this research, this effect has been studied before (Sarshar & Houry, 1993); however, it was not explicitly linked to sintering and dehydration zones.

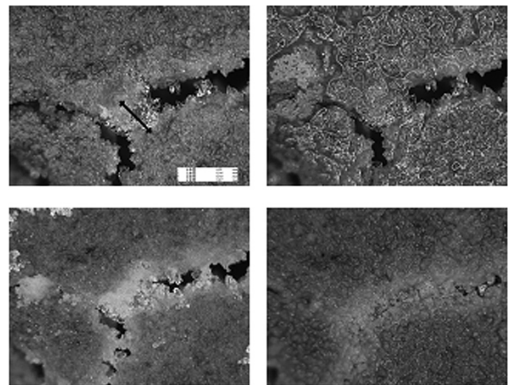


Figure 6. Crack self-healing under water supply. Top left: 1 day. Top right: 3 days. Bottom left: 7 days. Bottom right: 28 days.

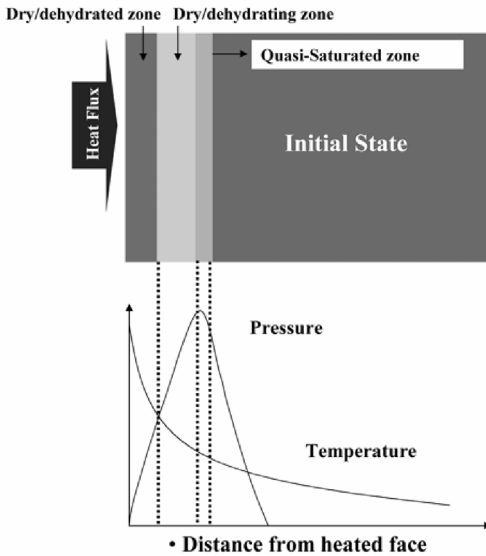


Figure 7. Concept of dehydration zones under heating.

#### 4 CONCLUSIONS

In this research, the relationship between damage and recovery mechanisms under re-curing was investigated for high-strength mortar exposed to fire.

Strength behavior was affected both by the changes in porosity and the formation of macro- and micro-cracks. The occurrence of cracking was used to bridge the difference in behavior between strength and porosity under the air, water, and air-water re-curing conditions. Re-curing by air led to the formation of macro-cracks due to differential thermal shrinkage, reducing the strength. Water submersion, while causing a large reduction in strength due to thermal shock, also increased the strength recovery behavior due to the absorption of water. As a result, the micro-cracks formed due to quenching were mostly healed within 7 days of water re-curing, and porosity was found to recover to pre-fire levels. Specimens allowed to cool in the air before water submersion, in order to reduce the effect of strength loss due to thermal shock, also absorbed less water due to the lower temperature of the specimen, thus reducing the recovery behavior.

Crack self-healing under water supply could recover within 28 days. However, this type of self-healing behavior may cause an initial reduction in strength, as the expansion due to rehydration causes secondary spalling of the brittle, sintered layer at the surface of the specimen. The time scale for testing in this research was not fine enough to detect this strength reduction; further experiments should be performed to clarify this mechanism.

While full recovery was observed for porosity and cracking in water re-cured specimens, the final residual strength did not recovery to 100%. One reason may be that, while micro-cracks visible in the crack pattern (Fig. 5) appeared to heal completely, there may be smaller cracks which could not be observed on the scale which the camera was taken. The smallest penetration size for the epoxy is 6 nanometers; therefore, it is difficult to see the nano-scale cracks without microscope observation. Subsequent investigations should attempt why complete strength recovery did not occur even when porosity and crack recovery was observed.

In order to reduce the effect of secondary spalling, future research should focus on the development of a chemical bonding agent to be used for the re-curing process. This agent would act to increase the bonding between the dehydration zones, thereby reducing the effect of the expansion caused during rehydration and increasing the effectiveness of the re-curing process. Development of such an agent would increase the attractiveness and practicality of repair utilizing re-curing.

#### ACKNOWLEDGMENT

The authors would like to thank Masamitsu Suzuki of the Shibaura Institute of Technology as well as the Tobishima Corporation for their support during the epoxy injection investigation.

#### REFERENCES

- Crook, D.N. & Murray, M.J. 1970. Regain of strength and firing of concrete. *Magazine of Concrete Research* 22(72): 149–154.
- Iwaki, K., Kato, J. Hirama, A. & Shiotani, T. 2004. Micro-structural evaluation of concrete damaged by acid attack using optical microscopy. *Proceedings of the Japan Concrete Institute* 26(1): 999–1004 (in Japanese).
- Kalifa, P., Menneteau, F.D. & Quenard, D. 2000. Spalling and pore pressure in HPC at high temperatures. *Cement and Concrete Research* 30: 1915–1927.
- Lin, W.M., Lin, T.D. Powers-Couche, L.J. 1996. Microstructures of fire-damaged concrete. *ACI Materials Journal* 93(3): 199–205.
- Poon, C.S., Azhar, S., Anson, M. & Wong, Y.L. 2001. Strength and durability recovery of fire-damaged concrete after post-fire-curing. *Cement and Concrete Research* 31: 1307–1318.
- Sarshar, R. & Khoury, G.A. 1993. Material and environmental factors influencing the compressive strength of unsealed cement paste and concrete at high temperatures. *Magazine of Concrete Research* 45(162): 51–61.
- Tovey, A.K. 1986. Assessment and repair of fire-damaged concrete structures—an update. *ACI Special Publication 92: Evaluation and Repair of Fire Damage to Concrete*: 47–62. Detroit: American Concrete Institute.



# New developed expansive ultra rapid hardening fiber reinforced concrete for bridge deck repair

I. Iwaki, S. Banchi & Y. Koda  
*Nihon University, Koriyama, Japan*

**ABSTRACT:** In Japan, many aging urban highway bridge decks have been severely deteriorated by fatigue due to heavy vehicle loadings. The purpose of this study is to develop expansive ultra rapid hardening fiber reinforced concrete as a new overlay concrete for achieving life-cycle maintenance of bridge decks in urban highway. In this study, the fresh and hardened properties of the concrete are investigated and the load-carrying capacities of RC members repaired by this are evaluated.

## 1 INTRODUCTION

Bridge maintenance in urban highway is becoming increasingly important due to increasing traffic volumes and heavier truck loads (Frangopol et al. 2007, Furuta et al. 2007). In Japan, many urban highway bridges have been constructed over the past 30 years and the reinforced concrete (RC) bridge decks have been severely damaged by fatigue. It is thought that overlaying the aging RC bridge decks with thin fiber reinforced concrete is one of the most effective repairing methods to increase the life-span of highway bridges (Detwiler et al. 1997). However, lots of problems exist to apply this method to urban highway RC bridge decks. For example, it is not allowed by nearby residents to compact overlay concrete with excessive vibration and noise at night. Additionally, it is known that shrinkage cracking which occurs in overlay concrete and debonding between overlay concrete and the existing concrete greatly influence to the durability of the repaired bridge deck. In this study, expansive ultra rapid hardening fiber reinforced concrete has been developed for solving these problems. Firstly, the fresh and hardened properties of this concrete are investigated. Next, the load-carrying capacities of RC members overlaid by this are evaluated. The required specifications and performances for this material are as follows; (1) Thickness of overlay is limited to 40 mm in comparison to the past, 60 mm, considering the composition of pavement and the anteroposterior level on the pavement. (2) Compressive strength of concrete at the age of 3 hours is satisfied with more than 24 MPa under sealed curing at 20C supposing to one overnight construction. (3) The consistency range in slump is within 5–15 cm, which is more workable than that of the existing one to enable to construct the concrete

overlay with low-noise. In order to compact this concrete, smaller and lighter concrete finisher equipped with high-frequency vibrator is being developed. The range of slump has been kept for at least 30 minutes after mixing. (4) Autogenous shrinkage can be remarkably compensated by the effect of expansive additive incorporated in concrete.

The experimental results reveals that the concrete has superior performances as a material for overlaying RC bridge deck, and the RC members overlaid by this shows good load-carrying capacities with bending and punching shear.

## 2 EXPERIMENTAL PROGRAM

### 2.1 Materials

The cement used was a regulated-set cement (density 3.01 g/cm<sup>3</sup>, Blaine 4690 cm<sup>2</sup>/g) developed in the United States and improved in Japan to meet the requirement that the compressive strength should be over 24 MPa at the age of 3 hours. The fine aggregate used was pit sand (density SSD 2.60 g/cm<sup>3</sup>, absorption 2.05%). The coarse aggregate used was crushed stone (density SSD 2.85 g/cm<sup>3</sup>, absorption 0.98%). The maximum size of coarse aggregate was limited to 13 mm because the thickness of overlay was specified as 40 mm. The fibers used were steel fiber (SF, density 7.69 g/cm<sup>3</sup>, length 30 mm, aspect ratio 50) and PVA fiber (VF, density 1.30 g/cm<sup>3</sup>, length 30 mm, aspect ratio 45). Superplasticizer and set-retarder for regulated-set cement were used as admixtures. Further, expansive additive (density 3.19 g/cm<sup>3</sup>, Blaine 4520 cm<sup>2</sup>/g) was used to compensate severe autogenous shrinkage by rapid hydration of regulated-set cement.

Table 1. Mixture proportions.

	Gmax (mm)	w/cm	s/a	Unit content (kg/m <sup>3</sup> )							
				W	C	Ex	S	G	Fiber	SP	JS
SF100	13	0.405	0.55	175	412	20	935	808	100	8.21	6.48
SF80							938	811	80		
VF15							937	810	15		
NF							954	825	0		

2.2 Mixture proportions

The water-cementitious materials ratio (w/cm) of concrete was kept constant at 0.405. The water content of all mixture proportions was 175 kg/m<sup>3</sup>.

The parameters were the type of fibers and the unit content. The concrete not incorporating any fiber (NF) was prepared for comparison. Table 1 shows these mixture proportions.

2.3 Test procedure

The slump test prescribed by ASTM C 143-90a was conducted after mixing and the change over time was measured. The compressive strength of concrete specimens was basically measured at the age of 3 hours, 7 days, and 28 days under sealed curing at 20C after placing concrete in 100 mm × 200 mm transverse-mounted cylindrical molds. In addition, the tensile bond strength between overlay concrete and the existing concrete at the age of 3 days was measured by adhesive strength test with reference to the previous report (FHWA, 1999). The behaviors of shrinkage and expansion after initial setting of concrete were measured using the method specified by the Japan Concrete Institute (Tazawa, 1998). Figure 1 shows the outline of this testing method.

Figure 2 shows the beam specimen for three point bending test. The specimen is 2000 mm long × 300 mm wide × 160 mm deep. The surface of this specimen is chipped to expose the coarse aggregates in concrete before overlaying. The concrete with the thickness of 40 mm, or 60 mm for comparison, was overlaid on the RC beam. All beams spanned 1800 mm and were simply supported. The load-displacement curve at the mid span was measured.

Figure 3 shows the slab specimen for punching shear test. The specimen is 1200 mm long × 1200 mm wide × 160 mm deep with the similar section size as the practical RC bridge deck slab. The concrete with the thickness of 40 mm or 60 mm was overlaid on the concrete slab. The deck slabs were supported on two steel girders spaced at 1000 mm center-to-center

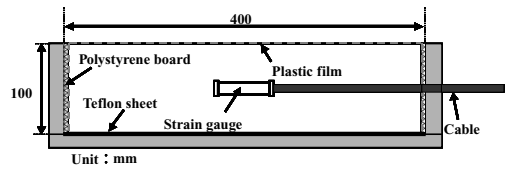


Figure 1. Testing method of shrinkage and expansion of concrete.

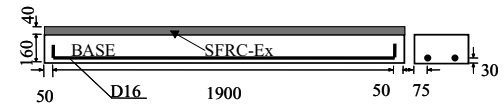


Figure 2. Beam specimens for bending test.

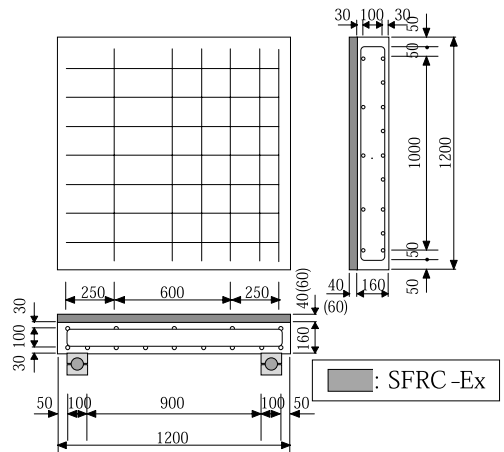


Figure 3. Slab specimens for punching shear test.

and were subjected to a monotonic single concentrated load over a contact area of 100 × 100 mm. The load-displacement curve at the center of slab was measured.

### 3 RESULTS AND DISCUSSION

#### 3.1 Fresh properties

Figure 4 shows the change of slump with time after mixing. As shown in this figure, the slump of concrete without fiber (NF) after mixing is over 20 cm. It is clarified as a semi-high fluidity concrete. On the other hand, the slump test results of concretes incorporating fibers (SF100, SF80, and VF15) within 30 minutes after mixing were 5–15 cm. The results reveal that this fiber reinforced concrete meets the requirement as fresh concrete and has superior workability. Thus, it is shown that this concrete could apply to a practical construction site and be compacted by a concrete finisher with high-frequency vibrator.

#### 3.2 Hardened properties

Figure 5 shows the results of compressive strength test. As shown in this figure, the compressive strength of concrete at the age of 3 hours reaches 24 MPa except in SF80. The reason why SF80 did not reach 24 MPa is that the setting time, that is, the start of hardening was delayed. If the setting time was appropriately controlled by the amount of set-retarder, it would have been satisfied with the requirement. The compressive strength at the age of 7 days and 28 days for all mixture proportions were over 60 MPa and 70 MPa, respectively. Consequently, these concretes are regarded as high strength concrete.

Figure 6 shows the strength development associated with SF100. As shown in this figure, the compressive strength rapidly increases until 6 hours and then slightly increases until 168 hours. The results show that this concrete has extremely high strength development at an early age.

Figure 7 shows the tensile bond strength for respective mixture proportion. As shown in this figure, the

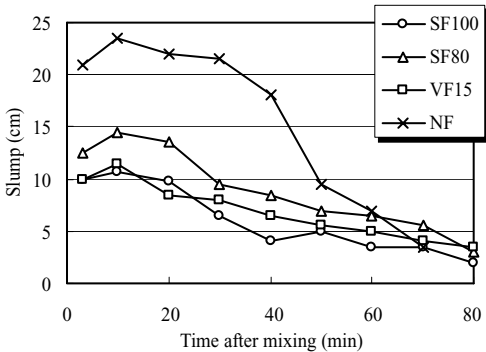


Figure 4. Change of slump with time after mixing.

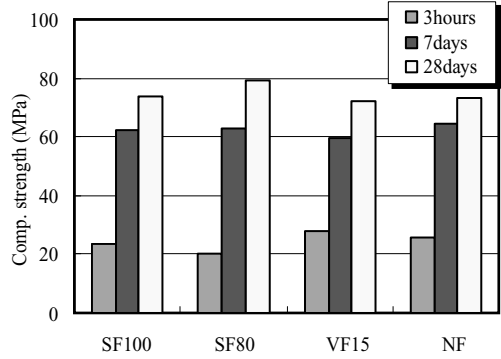


Figure 5. Compressive strength test results.

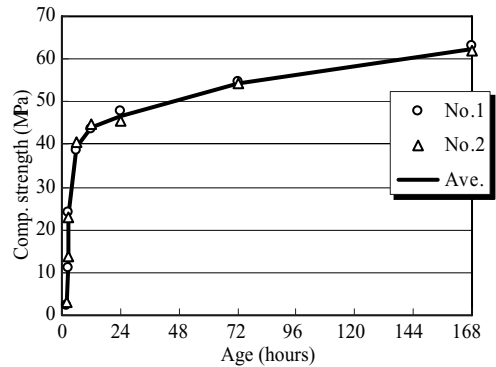


Figure 6. Strength development associated with SF100.

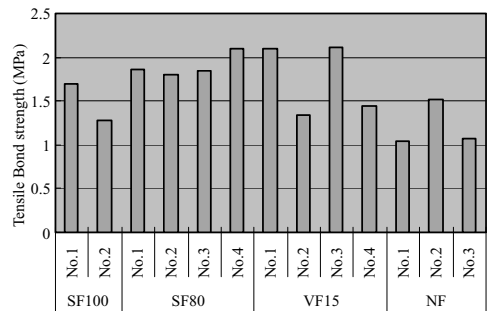


Figure 7. Tensile bond strength test results.

interfacial tensile bond strength between the existing concrete and overlay concrete is sufficiently high, more than 1 MPa at the age of 3 days.

Figure 8 shows the behaviors of shrinkage and expansion of concretes with or without expansive additive. The concrete without expansive additive (SFRC) shows rapid autogenous shrinkage soon after initial

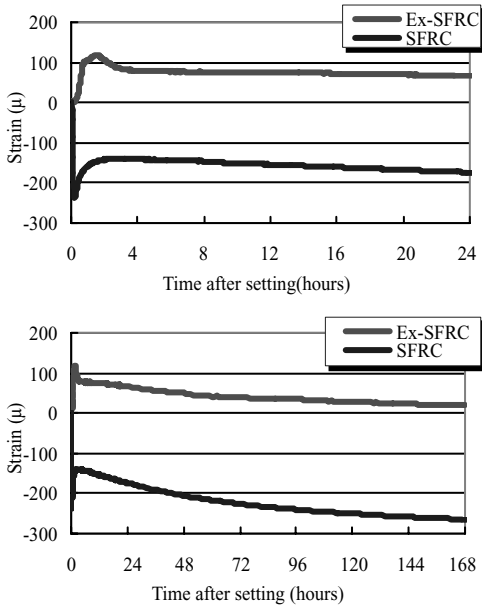


Figure 8. Shrinkage and expansion behaviors of concrete.

setting and the value reaches about 250  $\mu$ . On the other hand, the concrete with expansive additive (Ex-SFRC) does not show the remarkable shrinkage because the autogenous shrinkage is almost perfectly compensated by the action of expansive additive.

This result indicates that the usage of expansive additive is very effective in controlling the shrinkage cracking of overlay concrete.

### 3.3 Bending test

The mixture proportion was revised before bending test and punching shear test. Table 2 shows the mixture proportions, in which the water-cementitious materials ratio (w/cm) of concrete was reduced to 0.375 to improve the compressive strength at the age of 3 hours steadily. The fiber used was only steel fiber and the unit content was 100  $\text{kg}/\text{m}^3$ .

Figure 9 shows the change of slump with time for new mixture proportion. The test was conducted by two batches. As shown in this figure, the results of slump have been kept within the range of 5–15 cm for 40 minutes. The compressive strength at the age of 3 hours was over 30 MPa. Therefore, it is thought that fresh properties and hardened properties of this concrete were remarkably improved in comparison to the previous one. The compressive strength of the existing concrete and overlay concrete at the age of loading test was 45.1 MPa and 61.1 MPa, respectively while the

Table 2. Mixture proportions for bending test and punching shear test.

Gmax (mm)	Unit content ( $\text{kg}/\text{m}^3$ )									
	w/cm	s/a	W	C	Ex	S	G	Fiber	SP	JS
13	0.375	0.525	185	473	20	824	760	100	6.41	7.89

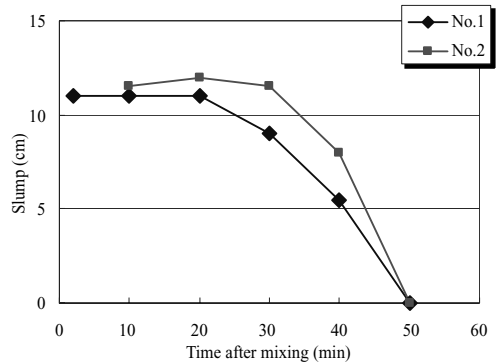


Figure 9. Change of slump with time for new mixture proportion.

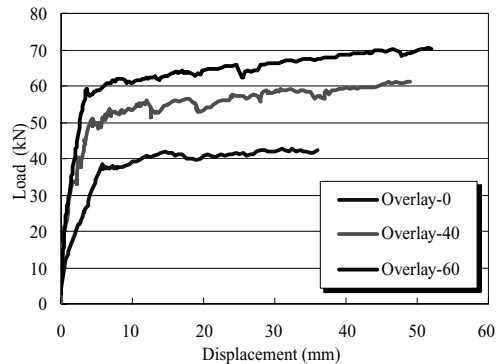


Figure 10. Load-displacement curves of bending test.

yield stress of reinforcement used in specimens was 321 MPa.

Figure 10 shows the load-displacement curves of bending test. As shown in this figure, the failure load associated with a 40 mm overlay (overlay-40) and a 60 mm overlay (overlay-60) are remarkably increased in comparison to that of concrete without overlay (overlay-0). The ratio of the failure load of overlay-40 to that of overlay-0 is 1.45 while the ratio corresponding to overlay-60 is 1.66. Thus, this concrete overlay has sufficient strengthening effect on load-carrying capacity for bending. The flexural cracks at failure

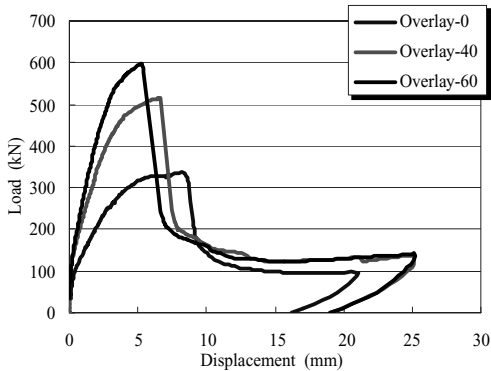


Figure 11. Load-displacement curves of punching shear test.

load penetrated from the concrete base to the concrete overlay. Additionally, any delamination between concrete base and concrete overlay was not observed. This fact indicates that the bond strength between both concretes is sufficient. Additionally, the displacement at failure load is increased as the thickness of overlay is increased. The results reveal that the performance in terms of deflection is improved by overlaying, too.

### 3.4 Punching shear test

Figure 11 shows the load-displacement curves of punching shear test. As shown in this figure, the failure loads associated with overlay-40 and overlay-60 are remarkably increased in comparison to that of overlay-0. The ratio of the failure load of overlay-40 to that of overlay-0 is 1.53 while the ratio corresponding to overlay-60 is 1.77. Thus, this concrete overlay has sufficient strengthening effect on load-carrying capacity for punching shear as well as bending. The stiffness is also increased as the thickness of overlay is increased. However, the deflection at failure is slightly decreased as the thickness of overlay is increased.

## 4 CONCLUSIONS

In this study, an expansive ultra rapid hardening fiber reinforced concrete has been developed to enable life cycle maintenance of urban highway bridge decks and increase their life-span remarkably.

From the experimental results, it is recognized that this concrete has superior workability in comparison

to the past overlay concrete. The compressive strength at the age of 3 hours is satisfied with 24 MPa. Further, this concrete can perfectly compensate the autogenous shrinkage inducing shrinkage cracking due to the action of expansive additive.

From the results of bending test and punching shear test, the RC members overlaid by this concrete shows superior load-carrying capacities in terms of the failure loads.

At present, the fatigue capacity of RC deck overlaid by this concrete is being evaluated by wheel loading fatigue test. In future, on-site test should be conducted using a concrete finisher with high-frequency vibrator being developed for this concrete.

## ACKNOWLEDGEMENTS

This study has been conducted by a collaboration of TAIHEIYO CEMENT CORPORATION, ONODA CHEMICO CO., LTD, NIPPO CORPORATION, METROPOLITAN EXPRESSWAY CO., LTD, and NIHON UNIVERSITY. The authors would like to express their appreciation to all researchers and engineers concerned.

## REFERENCES

- Banchi, S., Kajio, S., Koda, Y. & Iwaki, I. 2007. Study on properties of expansive ultra rapid hardening overlay concrete, *Proceedings of the Japan Concrete Institute*, 29 (2): 805–810: JCI (in Japanese).
- Banchi, S., Kajio, S., Koda, Y. & Iwaki, I. 2007. on load-carrying capacity of RC members overlaid by expansive ultra rapid hardening fiber reinforced concrete, *Proceedings of the Concrete Structure Scenarios*, 7: 141–146: JSMS (in Japanese).
- Detwiler, R.J., Kojundic, T. & Fidjestol, P. 1997. Evaluation of bridge deck overlays, *Concrete International*, 19 (8): 43–45: the American Concrete Institute.
- FHWA, 2000. Tensile Bond Strength of a High Performance Concrete Bridge Deck Overlay, Field test report.
- Frangopol, D.M. & Liu, M. 2007. Maintenance and management of civil infrastructure based on condition, safety, optimization, and life-cycle cost. *Structure and Infrastructure Engineering*, 3 (1): 29–41. Rotterdam: Balkema.
- Furuta, H., Kayano, M. & Watanabe, E. 2007. Current status and future issues on bridge maintenance and bridge management system. *JSCE journal*, 63 (3): 287–294 (in Japanese).
- Tazawa, E. 1998. *Autogenous shrinkage of concrete*. In E. Tazawa (ed.), E & FN SPON.

# Corrosion characterization of reinforcing bar in existing RC structure

E. Kato, M. Iwanami & H. Yokota  
Port and Airport Research Institute, Yokosuka, Japan

H. Hamada  
TOA Corporation, Japan

**ABSTRACT:** To develop an evaluation method for accurately assessing the structural performance of existing reinforced concrete structure, it is necessary to discuss the corrosion characterization of reinforcing bar, which has a large effect on the structural performance. In this paper, the variations in corrosion characteristics and mechanical properties of corroded reinforcing bars in reinforced concrete slabs and beams of open-type wharves were discussed. From the tests and analyses, unevenness of cross-sectional loss had a great influence on the mechanical properties of corroded steel bar because of the lopsided action of tensile stress.

## 1 INTRODUCTION

### 1.1 Background

When reinforced concrete structures are located in coastal and offshore areas, the most important deterioration phenomenon to which attention should be paid in design and maintenance is corrosion of reinforcing bar embedded into concrete. Corrosion of reinforcing bar can initiate a crack of concrete due to the volume expansion of corrosion products. Such a crack may accelerate further progress of corrosion, and subsequently structural performance such as load carrying capacity and ductility will be deteriorated (Kato, et al. 2006). To keep structural performance of these structures over the required levels during the service life, it is necessary to implement a well organized maintenance strategy and to conduct suitable maintenance work according to the grade of deterioration.

### 1.2 Life-cycle management system

The authors have tried to establish the life-cycle management system for a reinforced concrete superstructure of open-type wharf that is one of the most vulnerable structural types in ports and harbors, as shown in Figure 1 (Port and Airport Research Institute, 2007). The life-cycle management is a series of actions to evaluate the grade of deterioration by periodic inspection, to assess the structural performance and to predict the future progress of performance degradation, and to propose alternatives of appropriate remedial action based on life-cycle cost minimization or performance maximization under budget capping.

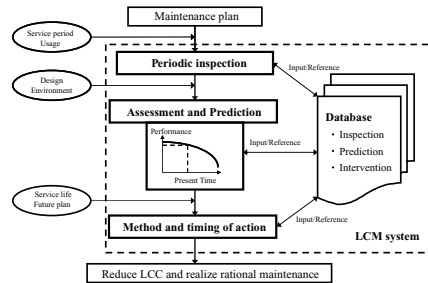


Figure 1. Procedure of life-cycle management.

### 1.3 Simplified assessment of structural performance

During inspection on the present conditions of structural members and assessment of performance of structure, in general, appearances of reinforced concrete members are visually observed and are more or less subjectively evaluated based on the grading system specified in the manual (Port and Airport Research Institute, 2007). However, the relationship between the grade of deterioration and performance of reinforced concrete members has not yet been quantitatively evaluated.

Aiming at the achievement of life-cycle management, the authors have tried to establish the simplified assessment of performance of reinforced concrete member by focusing on the relationship between the degree of deterioration and structural performance of reinforced concrete deck (Yokota et al. 2007). The simplified assessment of structural performance was

Table 1. Criterion for grading RC slab of open-type wharf from the viewpoint of corrosion of reinforcing bar.

Degree of deterioration	Criteria
<i>a</i>	Map cracking (over 50%) Spalling off of concrete cover Heavy rust stain
<i>b</i>	Map cracking (less than 50%) Much rust stain
<i>c</i>	One directional crack or gel extraction Partial rust stain
<i>d</i>	None

considered based on the results of loading test of real floor slabs taken out from decks in existing open-type wharves that have been used for 30–40 years. These slabs had wide variations in their grade of deterioration. Before the load application, the slabs were visually inspected on their surfaces, of which degrees of deterioration were judged by the grading system using degrees *a*, *b*, *c*, and *d*. The criterion is summarized in Table 1 (Port and Airport Research Institute, 2007). Visual inspection was carried out by focusing on cracks and their directions, spalling off of cover concrete, rust stain, and corrosion appearances.

When the performance of deck of open-type wharf is determined only by Table 1, degrees of deterioration *a*, *b*, *c*, and *d* can be translated in the following grades for the judgment of maintenance:

- Grade A: Seriously deteriorated; urgent remedial actions are necessary
- Grade B: Deteriorated; remedial actions may be considered in the near future
- Grade C: Slightly deteriorated; continuous inspection is necessary
- Grade D: Not deteriorated

After the visual inspection and judgment, the slab was experimentally load tested as an one-way slab. Figure 2 shows the relationships between the degree of deterioration and ultimate loads of tested slabs. The structural details and degrees of deterioration of all the slabs are given in Table 2. The loads were normalized by corresponding calculated results based on the beam theory by using designed values of strengths, dimensions, and the initial areas of reinforcing bar. The design values of compressive strength of concrete and yield strength of reinforcing bars are assumed to be 24 N/mm<sup>2</sup> and 345 N/mm<sup>2</sup> respectively. Their Young's moduli are also assumed as 25 kN/mm<sup>2</sup> and 200 kN/mm<sup>2</sup>.

In slabs judged as degrees of deterioration *c* and *b*, there were large variations in the load-carrying capacity. There existed the cases of which ultimate load ratios are smaller than 1.0 in degrees of

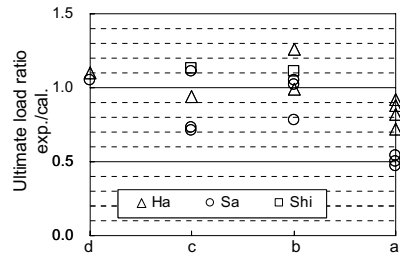


Figure 2. Structural capacity vs. degree of deterioration.

Table 2. Configuration and degree of deterioration of tested slabs.

No.	Year	Degree	Width (mm)	Thickness (mm)	Tensile reinforcing bar		Shear span (mm)
					Upper	Lower	
Ha-1	40	<i>c</i>	1520	270	4-D13	8-D13	400
Ha-2	40	<i>b</i>	1490	370	4-D13	8-D13	400
Ha-3	40	<i>a</i>	1500	310	4-D13	8-D13	400
Ha-4*	40	<i>b</i>	532	255	3-D13	3-D13	450
Ha-5*	40	<i>c</i>	389	255	2-D13	2-D13	450
Ha-6*	40	<i>d</i>	575	261	3-D13	3-D13	450
Ha-7*	40	<i>a</i>	492	178	3-D13	3-D13	450
Ha-8*	40	<i>a</i>	408	170	2-D13	2-D13	450
Ha-9*	40	<i>a</i>	585	172	3-D13	3-D13	450
Sa-1	40	<i>d</i>	699	300	3-R13	5-R13	700
Sa-2	40	<i>b</i>	535	300	4-R13	4-R13	700
Sa-3	40	<i>c</i>	798	300	3-R13	6-R13	700
Sa-4	40	<i>c</i>	732	310	3-R13	5-R13	700
Sa-5	40	<i>b</i>	569	310	3-R13	5-R13	700
Sa-6	40	<i>c</i>	812	310	3-R13	6-R13	700
Sa-7*	40	<i>b</i>	1940	253	13-D16	5-D16	750
Sa-8*	40	<i>a</i>	1987	226	13-D16	5-D16	750
Sa-9*	40	<i>a</i>	1984	275	13-D16	5-D16	750
Sa-10*	40	<i>a</i>	1964	262	13-D16	5-D16	750
Shi-1	30	<i>c</i>	1010	350	2-D16	5-D13	1450
Shi-2	30	<i>b</i>	1010	350	2-D16	5-D13	1450

\*Kato et al. 2007.

deterioration *c*, *b*, and *a*. This means that, when symptom of deterioration appeared on the surface of concrete members, the load-carrying capacity may become smaller than the design expectations. In case of the degree of deterioration *a*, in particular, the load-carrying capacity dropped to around 70 percent of the design expectations. Some of the load-carrying capacities of slabs of which degrees of deterioration was *c* were reduced to the same level as that of degrees of deterioration *a*. Delamination of cover concrete was detected by hammering test at the midspan area of these slabs. However, the delamination was not directly related to the judgment on the degree of deterioration as listed in Table 2. Furthermore, many small cracks and honeycomb existing on the surface layer

of concrete disturbed the change in appearance due to corrosion, which may mislead the healthier degree of deterioration. The degree of corrosion of reinforcing bar considered to not always contribute to the surface appearance of slab; that is, judgment of the degree of deterioration. As a result, it was made clear that the load-carrying capacities of tested slabs are affected by localized corrosion of reinforcing bar.

To accurately estimate the load-carrying capacity of deteriorated reinforced concrete members, it is necessary to obtain the degree and cross-sectional (weight) loss of corroded reinforcing bar. Moreover, to develop a structural performance evaluation method having reasonable accuracy, it is necessary to discuss the corrosion characteristics of reinforcing bar, which has a large effect on the structural performance of reinforced concrete members.

### 1.4 Research objectives

Many researchers and engineers are now actively studying the remaining structural capacities and producing a lot of useful results on them with testing artificially deteriorated reinforced concrete members. However, in a real structural member, a reinforcing bar is not uniformly corroded compared with an artificially corroded one in laboratories. Moreover, the mechanical properties of corroded reinforcing bar may be affected by the non-uniformity of corrosion. In this paper, corrosion profiles of reinforcing bars were investigated for several real reinforced concrete slabs and beams of open-type wharves that have been in service under marine environment for 30–40 years. Through the tests and analyses, the variation of corrosion characteristics and mechanical properties of corroded reinforcing bars are discussed.

## 2 METHODS OF INVESTIGATION AND TEST

### 2.1 Outline of tested reinforcing bars

Three Slabs Sa-A, Sa-B, Ha-1 and Ha-2, and Beam Ha-A were extracted from two open-type wharves. The symbols, Sa and Ha, have the same meaning as those listed in Table 2. The details of the materials used, such as the mix proportion of concrete and the strength of reinforcing bars, are not available because of lack of design and execution records. Tested reinforcing bars were sampled from 4 slabs and 1 beam. Table 3 lists the service years, degree of deterioration judged according to Table 1, positions and total numbers of sampled reinforcing bar pieces were randomly chosen from each concrete member. The length of each piece was 60–200 mm depending on the diameter of steel bar described in the following section.

Table 3. Sampled reinforcing bars.

Member	Year	Degree	Sampled piece		
			Type	Diameter	Total
Slab Sa-A	40	<i>b</i>	Round	16 mm	12
Slab Sa-B	40	<i>b</i>	Round	16	14
Slab Ha-1	30	<i>c</i>	Deformed	13	36
Slab Ha-2	30	<i>b</i>	Deformed	13	
Slab Ha-3	30	<i>a</i>	Deformed	13	
Beam Ha-A	30	<i>b</i>	Deformed	22	8

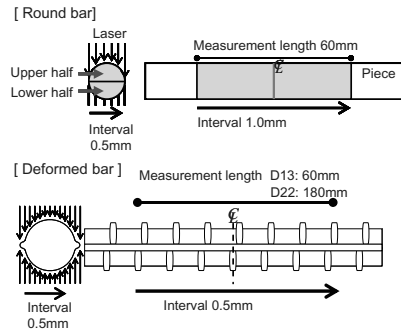


Figure 3. Outlines of surface geometries measurement.

### 2.2 Removal of corrosion products

Weight losses of sampled pieces were measured with the following procedures: at first, sample pieces were sand blasted to remove corrosion products and concrete sticking on its surface. Then, the piece was immersed in 10% diammonium hydrogen citrate solution to completely remove corrosion products.

### 2.3 Distribution of cross-sectional area of steel bar

Surface geometries of sampled pieces were measured by laser-scanning techniques. Outline of the measurement is shown in Figure 3.

For the round bar pieces taken from Slabs Sa-A and Sa-B, the surface geometry measurement was conducted separately for the lower and upper halves of piece. The measurement length was 60 mm and measurement pitches were set at 0.5 mm in the cross-sectional direction and 1.0 mm in the axial direction. Distribution of cross-sectional area of each piece was obtained by integrating the laser irradiation distances in the cross-sectional direction of lower and upper halves. Figure 4 shows three examples of the distribution of cross-sectional area. Its nominal cross-sectional area is 132.7 mm<sup>2</sup> if not corroded.

For the deformed bar pieces taken from Slabs Ha-1 and Ha-2 and Beam Ha-A, the surface geometry measurement was conducted separately as shown in



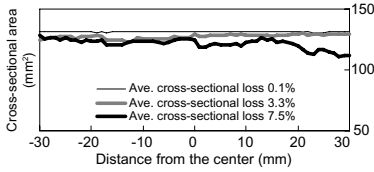


Figure 4. Distribution of cross-sectional area of round bars.

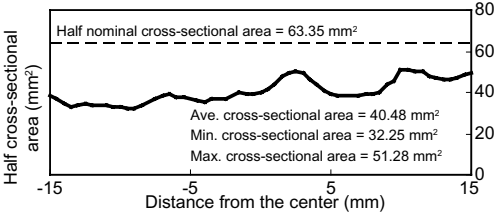


Figure 5. Distribution of cross-sectional area of deformed bar.

Figure 3. The measurement length was 60 mm for pieces of 13 mm in diameter, and 180 mm for pieces of 22 mm in diameter. Measurement pitches were set at 0.5 mm in the cross-sectional direction and 0.5 mm in the axial direction. Distribution of cross-sectional area of each piece was obtained by integrating the laser irradiation distances in the cross-sectional direction of measurement halves. Figure 5 shows the examples of the distribution of the half of cross-sectional area. Nominal cross-sectional area of D13 is 126.7 mm<sup>2</sup> and that of D22 is 387.1 mm<sup>2</sup> if they are not corroded.

All the measured cross-sectional areas were not exactly the same as the real cross-sectional area because of the interference of the pit-hole corrosion.

#### 2.4 Measurements of mechanical properties of steel bar

The tension test was conducted to obtain yield and tensile strengths and elongation of bar piece. Tension test of all pieces was carried out after measurement of surface geometries described in Section 2.3.

Figure 6 shows the test setup of round bars. Two deformed bars (SD295-D16) of 150 mm long were welded at the both ends of the piece with 20 mm lap. The total length of the piece for the tension test was about 60 mm. Targets for the elongation measurement were mounted near the end of the welding device as shown in Figure 6. Three pieces which were failed by slipping out from the welding device were excluded from the following discussion.

In the case of deformed bar pieces, a tensile load was directly applied from the both ends of pieces. Distances between targets for the elongation measurement were set at 4 times of nominal diameters of

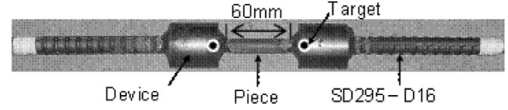


Figure 6. Testing specimen for tension test of round bar piece.

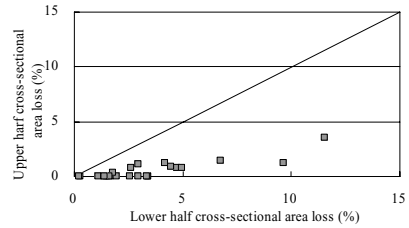


Figure 7. Cross-sectional loss in lower and upper halves of round bar pieces.

deformed bar. Two pieces of D22 which were failed by slipping were excluded from the following discussion.

### 3 CORROSION CHARACTERIZATION OF REINFORCING BAR

#### 3.1 Variation of cross-sectional loss

##### 3.1.1 Corrosion at lower and upper halves of piece

Figure 6 shows the relationship between average cross-sectional area losses of piece in lower and upper halves of the round bar pieces. The average cross-sectional area losses of the lower half were larger than those of the upper half. This was considerably caused by smaller cover depth and the existence of the interfacial transition zone formed on the lower half surface due to bleeding.

##### 3.1.2 Variation of cross-sectional loss

The average and maximum cross-sectional area losses of round bar piece were calculated by Equations 1 and 2:

$$\Delta A_{s,ave} = (A_{s,ave} - A_{s,nom})/A_{s,nom} \quad (1)$$

$$\Delta A_{s,max} = (A_{s,min} - A_{s,nom})/A_{s,nom} \quad (2)$$

where  $\Delta A_{s,ave}$ : average cross-sectional area loss,  $\Delta A_{s,max}$ : maximum cross-sectional area loss,  $A_{s,ave}$ : measured average cross-sectional area,  $A_{s,min}$ : measured minimum cross-sectional area, and  $A_{s,nom}$ : nominal cross-sectional area.

Those of deformed bar piece were calculated as follows:

$$\Delta A_{s,ave} = (A_{s,ave} - A_{s,0,ave})/A_{s,0,ave} \quad (3)$$

$$\Delta A_{s,max} = (A_{s,min} - A_{s,0,min})/A_{s,0,min} \quad (4)$$

Table 4. Cross-sectional area of deformed bars.

Diameter (mm)	Nominal (mm <sup>2</sup> )	Meas. ave. $A_{s,ave}$ (mm <sup>2</sup> )	Meas. min. $A_{s,min}$ (mm <sup>2</sup> )
13	126.7	132.5	120.1
22	387.1	378.2	354.0

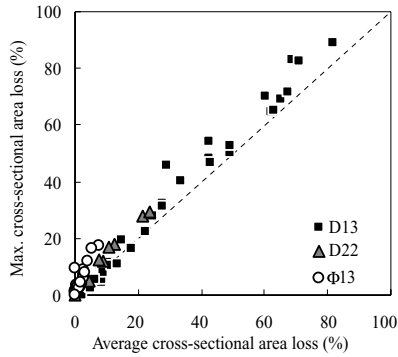


Figure 8. Average and Maximum cross-sectional losses.

Table 5. inclination based on liner approximation.

Type	Diameter (mm)	Inclination	Correlation coef. $R^2$
Deformed	13	1.11	0.98
Deformed	22	1.33	0.97
Round	16	2.56	0.74

where  $A_{s,0,ave}$ : measured average cross-sectional area of sound piece, and  $A_{s,0,min}$ : measured minimum cross-sectional area of sound piece. Measured average and minimum cross-sectional areas of deformed bars are summarized in Table 4.

Figure 8 shows the relationship between average and maximum cross-sectional area losses of all the pieces. Table 5 lists inclinations of those relationships based on the linear approximation. In the case of round bar, the maximum cross-sectional area loss was 2.56 times of the average one. This value was larger than that of deformed bar pieces. The difference is considered to be caused by the differences in the corrosion condition, such as quality of cover concrete, cover depth and oxygen-supplying, in addition to the surface geometries of reinforcing bar.

### 3.2 Influence of corrosion on mechanical properties

Mechanical properties of corroded reinforcing bars were usually evaluated by weight loss because of its easiness for measurement. However, the weight loss was considered to be insufficient as a corrosion index

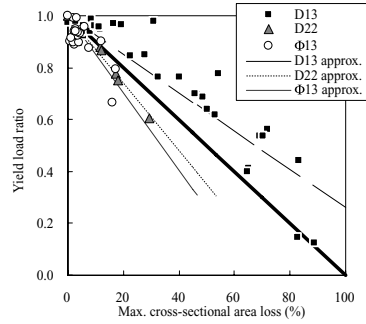


Figure 9. Maximum cross-sectional loss vs. yield load ratio.

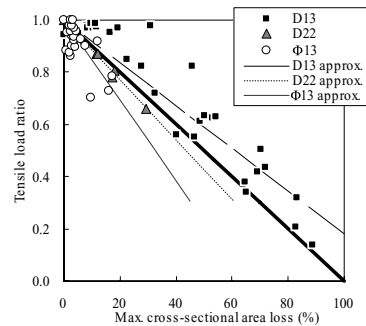


Figure 10. Maximum cross-sectional loss vs. tensile load ratio.

because the surface geometry of corroded reinforcing bar was varied as shown in Figures 4 and 5. In this study, mechanical properties of corroded reinforcing bar were examined with consideration of the variation in the cross-sectional loss.

Figures 9 and 10 show the relationships between maximum cross-sectional area losses and yield and tensile load ratios, respectively. Yield and tensile load ratios were calculated by dividing applied yield and tensile loads by those obtained with the non-corroded pieces. The yield and tensile load ratios became small as the maximum cross-sectional area loss increases. The straight lines show an approximation obtained by the least square method. Because the theoretical yield and tensile load ratios of reinforcing bar depend on its cross-sectional area, the inclinations of approximate lines are considered to be 1.0, which is drawn as a thick straight line in the same figures. However, inclinations of approximation line were not 1.0. It was considered to be caused by the localization of corrosion and those degrees. The inclinations of approximate lines became large as the inclinations of relationship between the average and the maximum cross-sectional area losses listed in Table 5 increases.

Figure 11 shows the relationships between maximum cross-sectional area loss and elongation ratio.

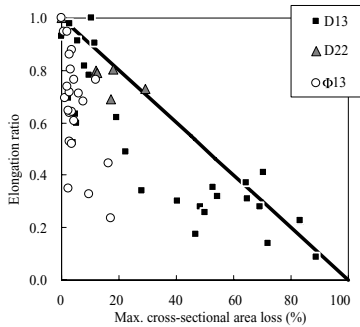


Figure 11. Maximum cross-sectional loss vs. elongation ratio.

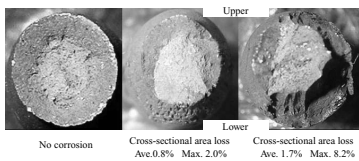


Figure 12. Cross-section of round bar at breaking location.

The elongation ratio became small as the cross-sectional area loss increases, and the effect of corrosion on the elongation was larger than that on the strengths. Kobayashi (2006) also drew the same conclusion. However, the relationship between maximum cross-sectional area loss and elongation ratio was more widely distributed compared with that between maximum cross-sectional area loss and yield and tensile load ratio.

Figure 12 shows the cross-sections of round bar pieces at the location of breakage. In the case of sound piece, because the cross-section was not lopsided, the tensile stress was considered to distribute uniformly on the cross-section. On the other hand, the cross-sectional shape of corroded piece was asymmetry even though the cross-sectional area loss was small. According to the previous research on fatigue property of corroded reinforcing bar by Moriwake, et al. (1996), uneven cross-section due to corrosion caused a crack under fatigue stress, and consequently, the progress of that crack greatly influenced on the fatigue property. Though the way of current loading test was different from fatigue test, the lopsided stress seems to have effects on the yield and tensile strengths and elongation. Therefore, the mechanical properties of corroded reinforcing bar are significantly affected by the unevenness of cross-sectional area. In this study, the cross-sectional area loss of the lower half of round bar piece was larger than that of the upper half as mentioned in Section 3.1.1. This fact was particularly

considered to affect the yield and tensile strengths of round bar. Moreover, because this effect considerably became large after yielding, the variation of the elongation was relatively large as shown in Figure 11.

## 4 CONCLUSIONS

To develop a structural performance evaluation method, it is necessary to discuss the corrosion characterization of reinforcing bar, which has a large effect on the structural performance of reinforced concrete members. In this paper, the variation of corrosion characteristics and mechanical properties of corroded reinforcing bars in real reinforced concrete slabs and beams of open-type wharves were discussed. From the tests and analyses, the following conclusions were drawn:

1. The load-carrying capacities of tested slabs extracted from exiting open-type wharves were affected by localized corrosion of reinforcing bar.
2. The cross-sectional loss of the lower half of round steel bar was larger than that of the upper half because of the small cover depth and existence of the interfacial transition zone formed due to bleeding.
3. Unevenness of cross-sectional loss had an influence on the mechanical properties of corroded steel bar because of the lopsided action of tensile stress.

## REFERENCES

- Kato, E., Iwanami, M. and Yokota, H., 2006. Deterioration in ductility of RC beams with corroded reinforcement, *Proceedings of the 2nd Fédération Internationale du Béton Congress*, Naples, Italy.
- Kato, E., Iwanami, M. and Yokota, H., 2007. Deterioration and structural performance of reinforced concrete deck of existing piers, *Proceedings of the 62nd JSCE Annual Meeting*. (in Japanese)
- Kobayashi, K., 2006. The seismic behavior of RC member suffering from chloride-induced corrosion, *Proceedings of the 2nd Fédération Internationale du Béton Congress*, Naples, Italy.
- Port and Airport Research Institute, 2007. Manual on maintenance and rehabilitation of port and harbour facilities, Coastal Development Institute of Technology. (in Japanese)
- Moriwake, A., et al., 1996. Estimation of fatigue life of reinforced concrete members deteriorated by chloride attack, *Proceedings of the Japan Concrete Institute*, 18(2), 1529–1534. (in Japanese)
- Yokota, H., Iwanami, M. and Kato, E., 2007. Structural capacity of deteriorated reinforced concrete deck in marine environment, *Proceedings of the 4th International Conference on Concrete under Severe Conditions: Environment & Loading*, Tours, France.

# Reasons for repair need in Finnish concrete facades in practice

J. Lahdensivu & S. Varjonen

*Department of Structural Engineering, Tampere University of Technology, Tampere, Finland*

**ABSTRACT:** Concrete structures exposed to outdoor climate are deteriorated by several different degradation mechanisms, whose existence and progress depend on many structural, exposure and material factors. Under Finnish outdoor climate the frost damage of concrete together with corrosion of reinforcing steel is the major degradation mechanism that causes the need to repair of concrete facades. During ongoing project *Repair strategies of concrete facades and balconies*, it has been gathered the condition investigation data from 946 buildings to a database. 89% of protective pore ratios in Finnish concrete balconies are less than 0.20 and 78% are less than 0.15. Despite this 56–70% of buildings, depending on buildings location has any visible frost damage. This means, it is possible to have good results with thorough patch repair and protective coatings with balcony glazing in most of the cases. Protective measures slows corrosion rate 30–80% and frost damage stops completely.

## 1 INTRODUCTION

### 1.1 Background

Since the 1960s a total of about 44 million square metres of concrete-panel facades have been built in Finland as well as almost a million concrete balconies (Vainio et al. 2005). In fact, more than 60% of Finnish building stock has been built in the 1960s or later. Compared with the rest of Europe the Finnish building stock is quite young.

Despite of quite young age of Finnish building stock, several problems have been encountered in their maintenance and repair. The structures have deteriorated due to several different degradation mechanisms whose progress depends on many structural, exposure and material factors. Thus, the service lives of structures vary widely. In some cases the structures have required, often unexpected, technically significant and costly remarkable repairs less than 10 years after their completion. For that reason, Finland has during the last 20 years developed many new methods for maintaining and repairing these structures. The methods include a condition investigation practice and its extensive utilization, rational repair methods and their selection as well as first-rate repair products and appropriate instructions for managing repair projects.

The value of Finnish buildings and infrastructure is about 300 billion euros (Vainio et al. 2002). The construction and real estate business accounts for more than 30% of Finnish gross domestic product. Concrete structures have been repaired extensively in Finland since early 1990s. During that almost 20 years period about 10 percent of the stock built in 1960–1980

has been repaired once. It is estimated that the total annual value of building repair work in Finland is about 5500 million of euros, of which about 30% involves external structures (walls, balconies, roofs, windows, etc.). The total annual volume of facade renovation is about 15 million m<sup>2</sup>. In addition, 40,000 balconies are repaired annually and 4500 new balconies are added to old buildings. It is estimated that the volume of facade renovation will grow 2% annually (Vainio et al. 2005 and Vainio et al. 2002).

Because of great amount of those existing concrete structures, it is very important to solve their incident repair need economically and technically durable. This means, we have to use the most suitable repair methods for each case and it is also important to be able to determine the optimal time of those repairs.

### 1.2 Structures in concrete buildings

Prefabricated concrete facades have been the most common facade of residential buildings in Finland since late 1960s, at least in blocks of flats. A typical concrete element consists of an outer layer, thermal insulation (typically mineral wool) and an inner layer. The outer and inner layers are connected by trusses. The outer layer is typically 40–85 mm thick, and the strength of concrete is typically near C20. The thermal insulation is usually mineral wool with a design thickness of 70–140 mm. Due to the compaction of thermal insulation, the actual thickness is usually between 40–100 mm. The thickness of the inner layer is normally 150–160 mm (load bearing element) or 70–100 mm (non-load bearing elements).

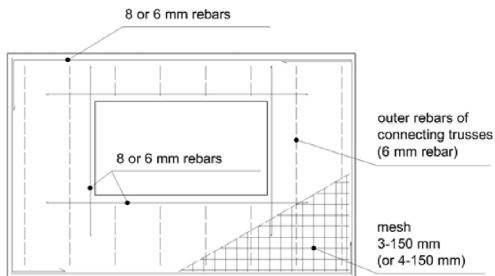


Figure 1. Typical outer layer of a Finnish concrete facade element.

The most common type of balcony from late 1960s in Finland consist on frame, slab and parapet elements which are prefabricated from concrete. Those balcony elements consist so called balcony-tower, which has own foundations and the whole tower has been connected to buildings frame only for horizontal loads. Typical thickness of frame element is normally 150–160 mm and in parapets 70–85 mm. Parapets usually have quite heavy reinforcement near both surfaces.

### 1.3 Objectives

This paper is based on the authors' experiences from about 150 condition investigations of concrete structures, long-continued development of condition investigation systematic, and a ongoing project called *Repair strategies of concrete facades and balconies*. The general objective of this research is to study the factors that have actually had an impact on the service life, existence and progress of deterioration in concrete facades and balconies. The three subgoals of the research are:

1. To find out the factors that has actually had an impact on the existence and progress of different deterioration mechanisms in concrete facades.
2. To find out the relative importance of said factors.
3. To provide new reliable data on the service-lives of concrete facades and balconies for use in calculational durability design and LCC-analyses of concrete structures.

The research project has started in March 2006 and it will continue until the end of March 2009.

## 2 CONDITION INVESTIGATION

Damage to structures, its degree and extent, due to various degradation phenomena can be determined by a comprehensive systematic condition investigation. A condition investigation involves systematic

determination of the condition and performance of a structural element or an aggregate of structural elements (e.g. a facade or balcony) and their repair need with respect to different degradation mechanisms by various research methods such as examining design documents, various field measurements and investigations and sampling and laboratory tests.

The wide variation in the states of degradation of buildings, and the fact that the most significant deterioration is not visible until it has progressed very far, necessitate thorough condition investigation at most concrete-structure repair sites. Evaluation of reinforcement corrosion and the degree of frost damage suffered by concrete are examples of such investigations.

### 2.1 Instructions for thorough condition investigation

Information about the condition of concrete structures needed for the planning and design of repair work can only be acquired by a systematically conducted condition investigation. The main reason for this is that the general degradation mechanisms related to concrete structures normally proceed for relatively long before becoming visible.

The following instructions should be followed in a condition investigation in order to ensure its reliability (Anon 2002 and Pentti 1999):

1. The investigator must have sufficient knowledge about the performance and properties of the examined structures. He must also thoroughly understand the degradation mechanisms, defects, deficiencies, and repair methods at issue. Then, he can focus on studying the appropriate problems and collecting information and observations that are relevant to the client's needs.
2. The examined subject must be divided up into structure groups according to performance, type, material and exposure conditions, so that the systematic variation in the state of degradation and properties of structures between the groups can be detected.
3. The investigation must be able to determine the state of all potential degradation mechanisms that endanger the performance and durability of the structure as well as the structural and exposure factors that affect their progress.
4. An effort must be made to examine each issue under scrutiny using several parallel information collection and measurement methods.
5. Observations and measurements describing the state of different degradation mechanisms must be produced in sufficiently representative and large samples, so that the conclusions drawn on the basis of samples are reliable.

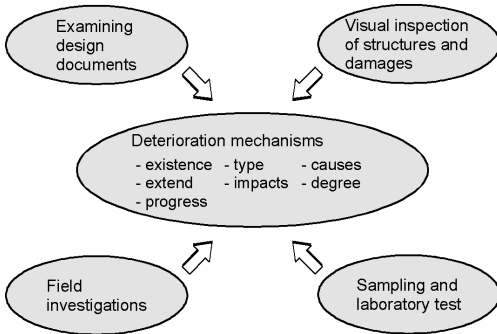


Figure 2. Different research methods in systematic condition investigation (Anon 2002).

6. Sufficiently valid and reliable methods must be used for observations and measurements.
7. The collected information must be analysed carefully, so that the condition and repair need of structure groups can be determined. Conclusions must be clearly based on collected factual information. The existence, extent, degree and reasons for different types of degradation are examined as factors governing the condition of each structure group. Then, the impact of degradation on the structure's performance (e.g. safety), the propagation of degradation, suitable repair methods, and recommended timing of repairs can be assessed.

### 3 CREATING A DATABASE

Condition investigation systematics for concrete facades and balconies have been developed in Finland since the mid-1980s. A large body of data on implemented repair projects has been accumulated in the form of documents prepared in connection with condition investigations. About a thousand precast concrete apartment blocks have been subjected to a condition investigation, and painstakingly documented material on each one exists, including the buildings' structures and accurate reports on observed damage and need for repairs based on accurate field surveys and laboratory analyses.

During ongoing project *Repair strategies of concrete facades and balconies*, it has been gathered the condition investigation data from 946 buildings for now to a database. Those condition investigation reports have been collected from companies which have conducted such investigations as well as from property companies owned by cities.

#### 3.1 Distributions of buildings and structures

Most of the blocks of flats stock in Finland is situated southern part of Finland. In the database those

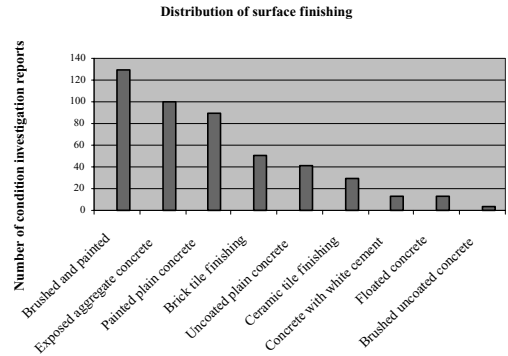


Figure 3. Distribution of surface finishing in the database (n = 946 single buildings).

buildings has been divided in three different group based on their geographical position: coastal area, inland and North Finland. About thirds of those buildings are situated on coastal area and two-thirds on inland. Only few of buildings in the database is situated North Finland.

Basically all prefabricated concrete panels has been made in the same way, but there is a lot of differences in their surface finishing and manufacturing. Those have a strong effect, for instance, on the situation of rebars and the quality of concrete. In the database the most common surface finishing are brushed and painted concrete, exposed aggregate concrete and painted plain concrete. The distribution of surface finishing on the database is shown in Fig. 3.

### 4 DEGRADATION

#### 4.1 General

The most common degradation mechanisms causing the need to repair concrete facades and balconies in Finland, and concrete structures in general, are corrosion of reinforcement due to carbonation or chlorides as well as insufficient frost resistance of concrete which leads to, for instance, frost damage (Pentti et al. 1998).

In following text there are the first results concerning mostly concrete balconies and small parts also concrete facades. These results bases on analyzing our database.

#### 4.2 Corrosion of steel

Reinforcing bars in concrete are normally well protected from corrosion due to the high alkalinity of the concrete pore water. Corrosion may start when the passivity is destroyed, either by chloride penetration

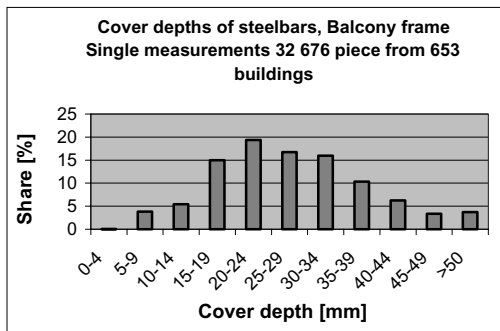


Figure 4. Distribution of cover depths of steel bars in balcony frames in the database.

or due to the lowering of the pH in the carbonated concrete. Steel corrosion in carbonated concrete or in chloride migrated concrete has been widely studied (Tuutti 1982, Parrott 1987, Schiessl 1994, Richardson 1988, Broomfield 1997, Mattila 2003 etc.).

In condition investigation reports there is a lot of measured data concerning corrosion of steel in concrete. When we are studying carbonation induced corrosion we have to find out the distribution of cover depths of steel bars and carbonation of concrete. Average carbonation factor  $k$  [mm/va] in balcony frames is 2.60 in outer surface and 2.91 in inner surface to same extent in parapets are 2.10 and 2.15. The standard deviation in carbonation factor is relatively high, it is between 1.31–1.51 as mentioned cases. Carbonation factors are in general remarkable smaller in buildings made 1990 and after. This is mostly consequence on raising the concrete strength up to C30–C45.

The distribution of cover depths of steel bars in balcony frame elements is shown in figure 3. If we think to use so called light repair methods, like patch repairs, we have to look the amount cover depths which are = 10 mm. Carbonation of concrete is in many cases advanced more than mentioned 10 mm, steel bars deeper than that causes very seldom visible corrosion damage, because the diameter in ordinary concrete elements varies usually between 6–10 mm and is mostly 12 mm.

Chlorides are not general problem causing corrosion in Finnish concrete buildings, because only in four buildings out of 946 there is chlorides = 0.05 weight-% of concrete weight in concrete. Concrete bridges and their edge beams is another story.

#### 4.3 Active corrosion

Once the passivity is destroyed either by carbonation or by chloride contamination, active corrosion may start in the presence of moisture and oxygen (Parrott

1987). Corrosion may run for a long time before it can be noticed on the surface of the structure. Because corrosion products are not water soluble, they accumulate on the surface of steel nearby the anodic area (Mattila 1995). This generates an internal pressure, because the volume of the corrosion products induced by carbonation is four to six times bigger than original steel bars (Tuutti 1982).

Internal pressure caused by corrosion products leads to cracking or spalling of the concrete cover. Visible damage appears first on the spots where the concrete cover is smallest.

The amount and state of visible damage depends firstly on the age of building when condition investigation was completed. In every case there is either smaller local damage or far advanced and wide spread damage, when the balcony was completed before 1990s. In 1990 and after that built balconies there was local visible damage in 27% of buildings. Visible damage has no correlation on situation of buildings, visible damage appears as well in coastal area as in inland.

#### 4.4 Disintegration of concrete

Concrete is a very brittle material. It can stand only extremely limited tensile strains without cracking. Internal tensile stresses due to expansion processes inside concrete may result in internal cracking and, therefore, disintegration of concrete. Disintegration of concrete accelerates carbonation and this way also steel corrosion. Concrete may disintegrate as a result several phenomenons causing internal expansion, such as frost weathering, formation of late ettringite or alkali-aggregate reaction. In Finland frost weathering of concrete is the most important disintegration mechanism, the others are very rare.

#### 4.5 Frost resistance of corrosion

Concrete is a porous material whose pore system may, depending on the conditions, hold varying amounts of water. As the water in the pore system freezes, it expands about 9% by volume which creates hydraulic pressure in the system (Pigeon & Pleau 1995). If the level of water saturation of the system is high, the overpressure cannot escape into air-filled pores and thus damage the internal structure of the concrete resulting in its degradation. Far advanced frost damage leads to total loss of concrete strength.

The frost resistance of concrete can be ensured by air-entraining which creates a sufficient amount of permanently air-filled so-called protective pores where the pressure from the freezing dilation of water can escape. Finnish guidelines for the air-entraining of facade concrete mixes were issued in 1976 (Anon. 2002).

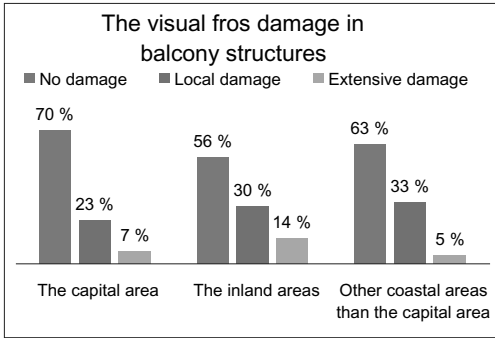


Figure 5. Distribution of visible frost damage in Finnish balconies in the database.

In those guidelines mentioned above, protective pore ratio [ $p_r$ ] should be = 0.20 in normal Finnish outdoor climate. According to condition investigations in Finnish balconies  $p_r$  is <0.10 in 59% of sample, between 0.10–0.14 in 19% of samples and between 0.15–0.19 in 11% of samples. Total number of samples is 1907. Distribution of protective pore ratio is slowly getting better year after year since 1976 because of air-entraining in concrete mixes.

Moisture behaviour and environmental stress conditions have an impact on frost stress. For instance, the stress on balcony structures depends on the existence of proper waterproofing. Despite of non frost resistant concrete in Finnish balconies, the share of visible frost damage is quite small (see fig. 5).

Protective pore ratio test and thin-section analysis gives congruent information on frost resistance of concrete. Of course thin-section analysis gives more accurate information about pore size distribution and degree of frost damage e.g. beginning frost damage.

## 5 REPAIR POSSIBILITIES

In Finland concrete facade renovation methods are divided into three categories (repair principles):

- protective repair methods
- cladding
- demolition of outer layer or balcony and rebuilding.

Protective repair methods are suitable mainly for structures where deterioration has just begun and the damage is not widespread. Possible protective repair methods suitable for concrete facades are divided into:

- resealing of element joints with elastic sealants
- painting over the old paint
- protective painting after removal of old paint
- thorough patch repair and protective painting.

If the existing structures are more severely damaged, protective repair methods are no longer effective. In Finland different cladding methods are widely used with concrete facades. Generally, the old structure is covered with additional thermal insulation and new outer layer. Cladding usually consists of:

- external thermal insulation with rendering
- different facade panel products (e.g. metal cassettes, fibre cement panels, polymer composite panels, etc.)
- a brick wall
- new concrete facade elements.

If the facade is severely damaged, the outer layer and thermal insulation can usually be demolished quite easily. The new thermal insulation and new cladding system can be selected from the above-mentioned alternatives. In balconies whole balcony structure is usually demolished and replaced with new concrete balconies.

## 6 CONCLUSIONS

The most common degradation mechanisms causing the need to repair concrete facades and balconies in Finland, and concrete structures in general, are corrosion of reinforcement due to carbonation or chlorides as well as insufficient frost resistance of concrete which leads to, for instance, frost damage (Pentti et al. 1998).

Concrete used in Finnish facades and balconies is not frost resistant, 89% of protective pore ratios in concrete balconies are lower than 0.20 and 78% are lower than 0.15. Despite this 56–70% of buildings depending on buildings location has not any visible frost damage. This means, it is possible to have good results with thorough patch repair and protective coatings with balcony glazing in most of the cases. According previous research project *Performance of protective measures in Finnish concrete facades and balconies* (Mattila & Pentti 2004), protective measures decrease effectively moisture content in concrete and this slows corrosion rate 30–80% and frost damage stops completely. Again, it has been estimated it is possible to get 20–25 years more service life for concrete facades and balconies with protective measures mentioned before compared with doing any measures.

This is remarkable result for property owners and in perspective of global climate change. It has been estimated, that heavy rains and freeze-thaw actions will increase during following decades remarkably. If we use early enough those protective measures in our concrete structures, perhaps we do not have to demolish and rebuild all Finnish concrete facades and balconies at all. Unfortunately those protective coatings are not suitable repair alternative in case exposed aggregate



concrete facades and brick or ceramic tile finishing. It is impossible to get consistent surface from protective coatings on exposed aggregate concrete and ceramic tiles.

## REFERENCES

- Anon. 2002: Condition investigation manual for concrete facade panels. Helsinki. Concrete Association of Finland BY 42 178 p. (In Finnish)
- Broomfield J. 1997: Corrosion of steel in concrete—understanding, investigation and repair. London. E & FN Spon. 240 p.
- Mattila J. 1995: Realkalisation of concrete by cement-based coatings. Tampere, Tampere University of Technology, Structural Engineering. Licentiate's Thesis. 161 p. (In Finnish).
- Mattila J. 2003: On the durability of cement-based patch repairs on Finnish concrete facades and balconies. Tampere, Tampere University of Technology, Structural Engineering. Publication 123. 69 p. (In Finnish).
- Mattila J., Pentti M. 2004: Performance of protective measures in Finnish concrete facades and balconies. Tampere, Tampere University of Technology, Publication 450. 111 p.
- Parrott L.J. 1987: Review of carbonation in reinforced concrete. Cement and Concrete Association. Wexham Springs. 42 p.
- Pigeon M., Pleau R. 1995: Durability of Concrete in Cold Climates. Suffolk. E & FN Spon. 244 p.
- Pentti Matti, Mattila Jussi, Wahlman Jyrki 1998: Repair of concrete facades and balconies, part I: structures, degradation and condition investigation. Tampere, Tampere University of Technology, Structural Engineering. Publication 87. 157 p. (In Finnish).
- Pentti, M. 1999. The Accuracy of the Extent-of-Corrosion Estimate Based on the Sampling of Carbonation and Cover Depths of Reinforced Concrete Façade Panels. Tampere, Tampere University of Technology, Publication 274. 105 p.
- Richardson M. 1988: Carbonation of reinforced concrete. Dublin, CITIS. 203 p.
- Schiessl P, Breit W, Raupach M. 1994: Durability of local repair measures on concrete structures damaged by reinforcement corrosion. Mathora, V. M- (editor). Durability of concrete. Detroit. American Concrete Institute. pp. 1195–1215.
- Tuutti K. 1982: *Corrosion of Steel in Concrete*. Stockholm. Swedish Cement and Concrete Research Institute. CBI Research 4:82. 304 p.
- Vainio et al. 2002: Korjausrakentaminen 2000–2010 (Repair, maintenance and improvement work in Finland). Espoo 2002. VTT Research Notes 2154. 60 p. + app. 25 p. (In Finnish).
- Vainio et al. 2005: Julkisivujen uudis- ja korjausrakentaminen. (Building and renovation of facades) Tampere, 2005. VTT 26 p. + app. 13 (In Finnish).

# The effects of mineral additions on chloride penetration into concrete under the frost action

B. Li & L. Tang

*Chalmers University of Technology, Gothenburg, Sweden*

**ABSTRACT:** This paper presents the results from a study of the effects of mineral additions on chloride penetration into concrete under the frost action. Mineral additions namely fly-ash (FA), silica fume (SF), GGBF slag (SL) were used to replace some part of cement in concrete. Seven types of concrete were investigated. All specimens were immersed in tap water or NaCl solutions under the freeze-thaw (F-T) and the climate room conditions. The results showed that the frost action significantly increase liquid uptake in both plain Portland cement concrete and concrete with mineral additions whatever specimens were exposed to tap water or salt solutions. Incorporation of mineral additions in concrete can in general reduce the amount of uptaken liquid. As a conclusion, incorporation of mineral additions and proper entraining air pores in concrete can improve resistance of concrete to chloride penetration even under the frost action.

## 1 INTRODUCTION

The manufacture of Portland cement is a highly energy-intensive process. In an energy-hungry world, considerable efforts are therefore being made to find substitutes—the so-called supplementary cementing materials—to replace part of the cement in concrete. The less energy-intensive materials being sought are industrial by-products such as fly ash; slag and silica fume as potential resources rather than as waste materials that are easily available, require little or no pyro-processing, and have inherent or latent cementitious properties (Malhotra 1993). Permeability is an important property of concrete, which mainly depending on cement composition, pozzolanic additions, water/binder ratio, curing conditions and period. Low permeability delays ionic and moisture transfer within concrete and prevents chemical erosion or attack in chemically severe environments. The advantages of supplementary cementing materials lie in a high resistance to severe environmental ingress especially sea water, freezing-thawing cycles, deicing salt agents etc. Concrete incorporating pozzolanic and cementitious materials placed in aggressive environment exhibits a substantial decreasing in permeability due to the transformation of larger pores into finer pores as a result of pozzolanic reaction of the mineral additions (Meira et al 2007, Wang et al 2007, Gjorv 1983, Manmohan et al 1981, Song et al 2005, Tahir et al 2007).

This paper presents a study of the effects of a few kinds and replacement ratios of mineral additions on

chloride penetration into concrete under the freeze-thaw condition were reported.

## 2 EXPERIMENTAL

### 2.1 *Materials and mix proportions of concrete*

Swedish SRPC of type CEM I, 42.5 N BV/SR/LA, SF—silica fume (Elkem, Norway), FA—Fly ash (Aalborg, Denmark) and Swedish GGBF Slag (Merit 5000) were used as binder. The coarse aggregate was crushed rock of size 8–16 mm and the fine aggregate was natural sand of size 0–8 mm. Five types of concrete with air-entraining agent (AEA), w/b 0.40, and two types of concrete without AEA, w/b 0.4 and 0.30, were used in the investigation. The proportions of concrete and some physical properties are listed in [Table 1](#), where the superplasticizer (SP) was Glenium 51 and AEA was SikaAer-5.

### 2.2 *Preparation of specimens*

The concrete cubes of size 150 × 150 × 150 mm and 100 × 100 × 100 mm and cylinders of size Ø100 × 200 mm were cast and stored in the moulds at the air temperature of 20°C, covered with plastic sheet to prevent from drying. After 24 h they were demoulded and placed in a water bath at 20°C for 90 days.

Table 1. Mix proportion of specimens.

Concrete mix	SF040	SF040NA	SF040FA	FA040	FA030	SL040	PC040
Binder type	SF	SF	SF + FA	FA	FA	SL	PC
Water/binder ratio	0.40	0.40	0.40	0.40	0.30	0.40	0.40
Cement, %	95	95	78	80	80	70	100
Mineral add., %	5	5	5 + 17	20	20	30	–
SP (% of binder)	0.31	0.37	0.40	0.55	0.57	0.41	0.22
AEA (% of binder)	0.72	0	0.55	0.61	0.19	0.37	0.10
Slump (mm)	88	60	120	70	70	60	70
Measured air content (vol %)	7.25	3.8	6.6	6	6.2	3	6
Compressive strength at 28 days (MPa)	65	84.5	73.2	76.4	109.9	68.6	66.6

Table 2. Exposure conditions.

Specimens	Exposure condition				
	Freeze-thaw, 3% NaCl	Freeze-thaw, 10% NaCl	Freeze-thaw, tap water	Climate room, tap water	Climate room, 3% NaCl
150 × 150 × 50mm	Two parallel slabs	–	Two parallel slabs	Two parallel slabs	–
Φ100 × 50 mm	One disc at different freeze-thaw cycles	One disc at different freeze-thaw cycles	–	–	One disc at certain exposure period

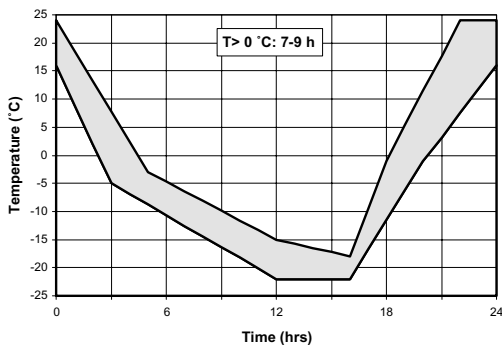


Figure 1. Temperature regime for freeze-thaw cycles according to EN 12390-9, the slab test.

The cubes of size 100 × 100 × 100 mm were used for compressive strength test at the age of 28 days.

At the age of about 91 days, slab specimens of size 150 × 150 × 50 mm were cut from the 150 mm cubes according to the instruction given in EN 12390-9, the slab test. These specimens were used for water absorption and standard frost test. In parallel, disc specimens of size Ø100 × 50 mm were cut from the central portion of cylinders. These specimens were used for chloride migration test according to NT BUILD 492 and for chloride penetration tests under different exposure conditions as will be described later.

Other procedures of specimen preparation, such as sealing with rubber cloth, conditioning and pre-wetting, were in accordance with EN 12390-9, the slab test.

### 2.3 Exposure conditions

In this investigation, 3% or 10% sodium chloride solution and tap water were used as immersion liquid. The specimens exposed to different conditions are shown in Table 2. The air temperature in the climate room was 20 ± 2°C and the temperature regime for freeze-thaw cycles was in accordance with EN 12390-9, the slab test, as shown in Figure 1, where the time-temperature cycle in the freezing medium is to fall within the shaded area in the graph. From Figure 1 it can be seen that the unfreezing period (assuming the temperature > -5°C) is less than a half of cycle.

### 2.4 Measurements

Prior to the freeze-thaw test the mass of each slab specimen (including the sealing materials) under the surface dry condition was measured.

After 7, 14, 28, 56, 84 and 112 cycles of freeze-thaw, the following measurements were carried out:

- Scaling on each slab specimen,
- Liquid uptake in each slab specimen,
- Chloride penetration profile in one of the disc specimens of each type of concrete.

### 2.4.1 Scaling

The scaling measurement was carried out in accordance with the procedures described in EN 12390-9, the slab test.

### 2.4.2 Liquid uptake

The liquid uptake was calculated based on the mass changes using the following equation.

$$\Delta W_i = \left\{ \left[ m_i + (1 + W_c^s) * \sum M_i - m_0 \right] * 10^{-3} \right\} / A \quad (1)$$

Where  $\Delta W_i$  = the liquid uptake after  $i$  cycles of freeze-thaw,  $\text{kg/m}^2$ ;  $m_i$  = the mass measured after  $i$  cycles of freeze-thaw, g;  $W_c^s$  = the evaporable water content of concrete, which was approximately estimated from the mixture proportion and concrete age;  $\sum M_i$  = the dry mass of accumulated scaled materials after  $i$  cycles of freeze-thaw, g;  $m_0$  = the initial mass, i.e. measured after pre-wetting, g; and  $A$  = the area of the test surface,  $\text{m}^2$ .

### 2.4.3 Chloride penetration profile

After the specified cycles of freeze-thaw, pulverized samples were taken from the cylinders by dry-grinding on a lathe with a diamond tool, successively from the exposed surface to a certain depth and dried at  $105^\circ\text{C}$  to a constant weight, then stored in a desiccator.

The total chloride content (acid soluble) in each sample was determined by potentiometric titration with a chloride ion selective electrode and silver nitrate solution of 0.01 N. After titration of chloride ions, calcium content was analysed by potentiometric titration with a calcium ion selective electrode and EDTA solution of 0.1 N. This calcium content was used to estimate the content of binder in each sample so as to be able to express chloride content as mass % of binder (TANG Luping, 1996).

## 3 RESULTS AND DISCUSSION

### 3.1 Surface scaling

The accumulative scaled material of each type of concrete after 7, 14, 28, 56, 84 and 112 cycles of freeze-thaw with 3% and 10% sodium chloride solution are shown in Figure 2.

The results showed that the non-air-entrained SF concrete exhibited increasing of scaling after 7–14 freeze-thaw cycles with both 3% and 10% sodium chloride solutions. The maximum scaling after 112 cycles of freeze-thaw is, however, less than  $1 \text{ kg/m}^2$ , the criterion for acceptable frost resistance in Sweden. From Table 1 it can be seen that the measured air content in Mix SF040NA is 3.8%, higher than natural entrapped air volume (normally 1%~2%).

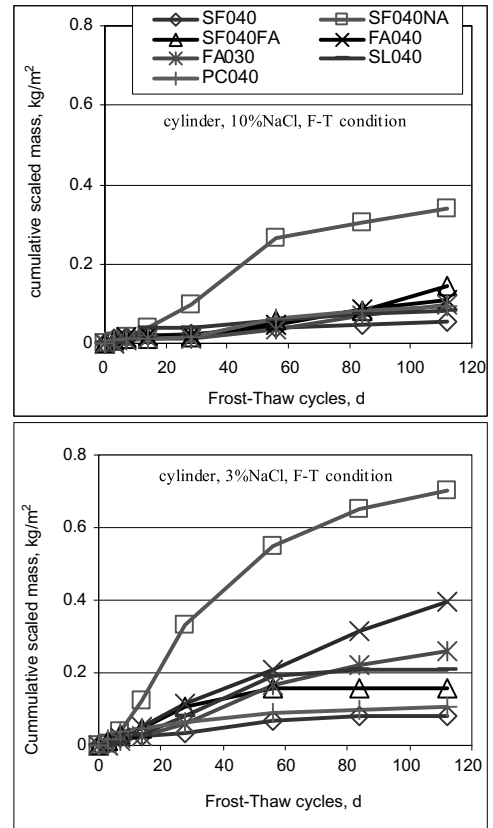


Figure 2. Results of scaling.

This is probably due to the use of superplasticizer Glenium 51, which might have introduced a certain air pores in the concrete, partly improved the resistance to scaling. Salt scaling was higher with 3% sodium chloride solution (moderate amount of solute) than with 10% one, which is in agreement with previous other researchers' findings. The concretes containing 20% fly ash with w/b ratio 0.40 and 0.30 (FA040 and FA030) got a little higher amount of scaling among all the air-entrained concretes. It was normally attributed to its relatively slower hydration development by the pozzolanic reaction. In this study, however, the compressive strength of fly ash concrete at 28 days is higher than that of PC concrete (see Table 1). Further study is needed in order to find convincing explanations.

### 3.2 Liquid uptake

Figure 3 shows the results of liquid uptake under different exposure conditions. It is obvious that the freeze-thaw action greatly increased the liquid uptake when compared with the natural water absorption in

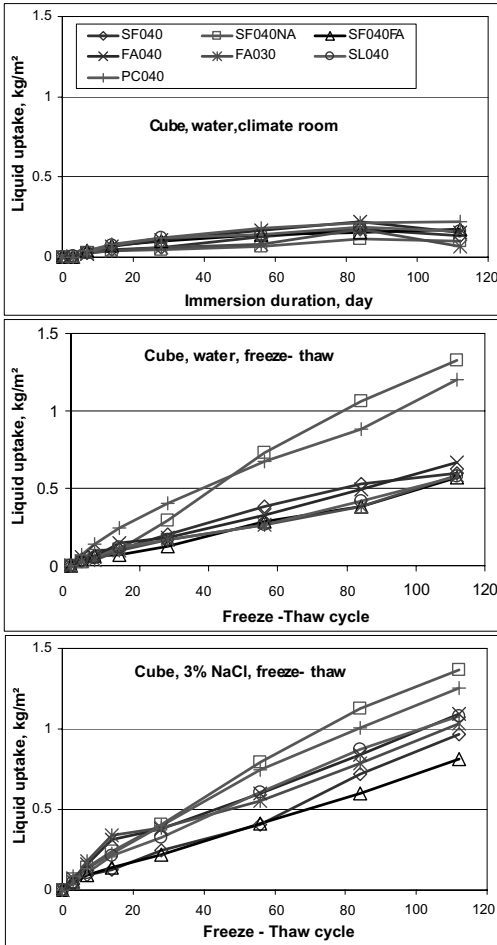


Figure 3. Liquid uptake in cube specimens.

the climate room at 20°C with both sodium chloride solution and tap water immersion liquid among all kinds of concretes. Figure 3 clearly shows the pumping effect due to frost action, which significantly increases liquid uptake, as reported by Jacobsen 1995, Tang & Petersson 2002, Palecki & Setzer 2002, and so on.

Using 3% NaCl solution as immersion medium slightly increased the liquid uptake in the concrete with mineral additions under the freeze-thaw cycles condition. This probably could be explained by the decreased freezing temperature of ionic solution in combination with the finer pore structures in the concrete with mineral additions, resulting in a longer non-frozen period for liquid uptake.

Figure 4 shows the water absorption in the climate room including the pre-wetting period. As can

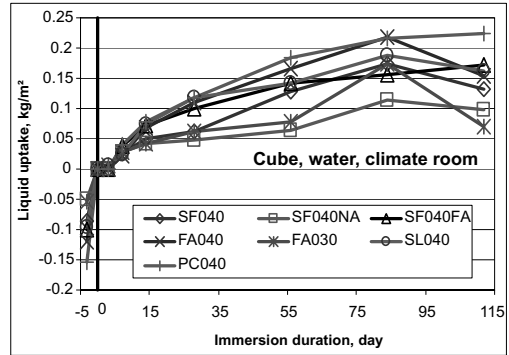


Figure 4. Water uptake in concrete in the climate room.

be expected, the concrete with lower air content or low w/b (SF040NA and FA030) revealed lower water uptake while the plain cement concrete (PC040) revealed the highest water uptake due to its relatively coarser pore structures.

### 3.3 Chloride penetration profiles

It is well known that supplementary cementing materials namely fly ash, silica fume and slag, are normally finer than cement particles and can fill voids between adjacent cement grains and aggregates, resulting in finer pore structures after pozzolanic reactions. Microstructure and porosity decide permeability of concrete, which further affect the penetration of moisture, gas and ions etc. Figure 5 showed the results of chloride ion penetration after 56 immersion days in the climate room of 20°C and 112 cycles of freeze-thaw, which may correspond to diffusion for about 56 days under the non-frozen period. It can be seen that, under the frost action, chloride penetration in the plain cement concrete (PC040) remarkably increased and in the concrete without AEA (SF040NA) significantly increased. This is in agreement with the results of liquid uptake as shown in Fig. 3. The uptaken liquid brought chloride ions into the concrete through the coarse pores in the plain cement concrete (PC040) and possible micro-cracks in the silica fume non-air-entrained concrete (SF040NA) due to the frost action.

It seems that the frost action did not remarkably increase chloride penetration in the air-entrained concrete with mineral additions, even though there was significant increase in liquid uptake as shown in Fig. 3. One of possible explanations could be the filter effect of very fine pores which only allow water flows in but exclude chloride ions outside. Temperature effect may be another reason. At the averagely low temperature under the freeze-thaw cycles the movement of chloride ions is slow and chloride binding capacity is relatively high (Tang 1996), retarding chloride ingress.

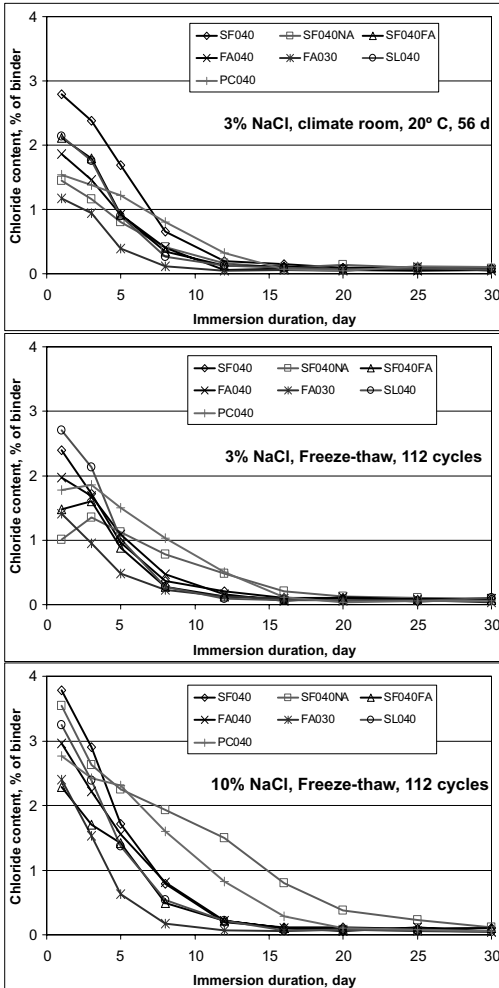


Figure 5. Chloride penetration profiles.

The 30% fly ash concrete with w/b 0.3 (FA030) revealed lowest chloride penetration under all the exposure conditions used in this study.

As expected, chloride penetration was higher in 10% than in 3% NaCl solution, especially in the non-air-entrained concrete (SF040NA), due to possible internal damage (micro-cracks) under the frost action.

#### 4 CONCLUDING REMARKS

From this study it has been demonstrated again that frost action significantly increase the liquid uptake in both plain Portland cement concrete and concrete with mineral additions whatever specimens were exposed

to tap water or salt solution. Incorporation of mineral additions in concrete can in general reduce the amount of uptaken liquid.

Without air entraining agent, even the concrete with mineral additions (5% silica fume in this study) may be damaged by the frost action, resulting in a higher liquid uptake and significant increase in chloride penetration.

The frost action influences chloride transport in concrete in two ways: 1) accelerating chloride penetration by increasing liquid uptake, and 2) retarding chloride penetration by short non-frozen period and low temperature, both of which retard diffusion process. For the plain cement concrete and the concrete without air entraining agent, the accelerating effect seems superior to the retarding effect, which for the concrete with mineral additions and sufficiently entrained air pores, the accelerating effect may be compensated or eliminated by the retarding effect, resulting in no remarkable changes in chloride penetration when compared with that at the constant temperature of 20°C.

As a conclusion, incorporation of mineral additions and proper entraining air pores in concrete can improve resistance of concrete to chloride penetration even under the frost action.

#### ACKNOWLEDGEMENTS

Financial supports granted by The Swedish Research Council FORMAS (project No. 243-2004-1197) are greatly appreciated.

#### REFERENCES

- Gjorv, O.E., 1983. Durability of concrete containing condensed silica fume. In First International Conference on Fly Ash, Silica Fume, Slag and Other Mineral By-Products in Concrete, *ACI publication SP-79*, vol. 2, 695–708.
- Jacobsen, S., 1995. Frost testing of high strength concrete: internal cracking vs. scaling of OPC silica fume concretes, *Doctoral thesis 1995:101, NTH, Trondheim, Norway*.
- John, J. et al, 2007. A review of salt scaling: 1. Phenomenology. *Cement and Concrete Research*, 37, 1007–1021.
- Malhotra, V.M. 1993. Fly ash, slag, silica fume, and rice-husk ash in concrete: a review. *Concrete International*, 23–28.
- Manmohan, D. et al, 1981. Influence of pozzolanic slag, and chemical admixtures on pore size distribution and permeability of hardened cement pastes. *Cement Concrete & Aggregates* 3 (1).
- Meira, G.R. et al, 2007. Chloride penetration into concrete structures in the marine atmosphere zone—Relationship between deposition of chlorides on the wet candle and chlorides accumulated into concrete. *Cement & Concrete Composites* 29, 667–676.

- Palecki, S. & Setzer, M.J., 2002. Investigations of high-performance concrete under frost attack—internal damage and water uptake. In M.J. Setzer, R. Auberg & H.-J. Keck (eds), *Frost Resistance of Concrete—From Nano-Structure and Pore Solution to Macroscopic Behaviour and Testing*; RILEM Publications PRO 24, 317–326.
- Song, H.-W. et al, 2005. An estimation of the diffusivity of silica fume concrete, *Building and Environment* 42, 1358–1367.
- Tahir, G. et al, 2007. The influence of mineral admixtures on the short and long-term performance of concrete. *Building and Environment* 42, 3080–3085.
- Tang, L. & Petersson, P.-E., 2002. Water uptake, dilation and internal deterioration of concrete due to freezing-and-thawing. In M.J. Setzer, R. Auberg & H.-J. Keck (eds), *Frost Resistance of Concrete—From Nano-Structure and Pore Solution to Macroscopic Behaviour and Testing*; RILEM Publications PRO 24, 287–294.
- Tang, L., 1996. Chloride Transport in Concrete—Measurement and prediction, *Doctoral thesis, Publication P-96:6, Dept. of Building Materials, Chalmers Universities of Technology, Gothenburg, Sweden.*
- Wang, S.Z. et al, 2007, Durability of biomass fly ash concrete: Freezing and thawing and rapid chloride permeability tests, *FUEL* 87, 359–364.

# Stochastic modeling of corrosion propagation for service life prediction of chloride contaminated RC structures

Zhao-Hui Lu, Yan-Gang Zhao & Ke Yu

*Department of Architecture, Nagoya Institute of Technology, Japan*

**ABSTRACT:** The intention of this paper is to present a reliability-based methodology for service life prediction of chloride contaminated RC structures. An improved time-variant probabilistic model of corrosion current density for representing the corrosion propagation in chloride contaminated RC structures is proposed. A corrosion model with the consideration of both uniform corrosion and pitting corrosion is also proposed. In the present study, for a corrosion-affected RC beam, it is assumed that the deterioration of structural strength is mainly due to the reduction in cross-sectional area of reinforcing bar. The fourth-moment method is applied to conduct time-dependent system reliability analysis. With the present strength deterioration model, the service life of chloride contaminated RC structures can be predicted using the present time-dependent system reliability assessment method.

## 1 INTRODUCTION

Corrosion of reinforcing bars due to chloride contamination is the primary cause of deterioration of RC structures. Reinforcing bars are normally passive in concrete due to high alkalinity of the concrete pore solution; however, penetration into the concrete of chlorides destroys this inhibitive property of the concrete and leads to corrosion. The deterioration process associated with corrosion can be divided into two stages: an initiation stage related to chloride diffusion that ends with the initiation of corrosion; and a propagation stage during which structural deterioration develops (Tuutti 1982).

The initiation stage has been the focus of research in the area of reinforcement corrosion for decades (e.g., Takewaka & Matsumoto 1988, Bamforth 1999, Roberts et al. 2000). Recent research has provided a wealth of evidence that for RC structures with load-induced cracks and subjected to constant chloride invasion, as represented by a marine environment, the initiation of reinforcement corrosion at the root of cracks occurs within a short period of time in service and the initiation time period is negligibly short if service life is considered (e.g., Leeming 1998, Otsuki et al. 2000, Francois & Castel 2001, Li 2003a) and therefore will not be discussed in details in the present paper.

On the contrary, little research has been done on the corrosion propagation in concrete as measured by the corrosion rate or corrosion current density. In general, because the corrosion rate or corrosion current density varies in different structures, it should be obtained from site-specific measurement of the structure to be

assessed over as long a period of time as practical. Obviously, the above method for determining the corrosion rate or corrosion current density is unrealistic. Therefore, the corrosion rate or corrosion current density is often simply modeled by using a constant value (e.g., Ting 1989, Val & Melchers 1997, Val 2007) or a time-invariant random variable (e.g., Mori and Ellingwood 1994, Frangopol et al. 1997). However, there is a clear experimental evidence, from a variety of sources (e.g., Tuutti 1982, Yalcyn & Ergun 1996, Liu & Weyers 1998), that the corrosion rate or corrosion current density is actually not a constant value but that it accentually changes (usually reduces) with increased exposure time (Melchers & Li 2006). It is in this regard that the present paper attempts to develop a time-dependent probabilistic model of the corrosion current density and focuses on the structural strength deterioration as reinforcement corrosion propagates.

In the following sections, an improved time-dependent probabilistic model of the corrosion current density, which is an extension and simplification of those proposed by Liu & Weyers (1998) and Vu & Stewart (2000), is proposed and a corrosion model with the consideration of both uniform corrosion and pitting corrosion is also proposed. Next, the time-dependent reliability analysis of a chloride contaminated RC beam using the fourth-moment method (e.g., Zhao & Ono 2001, Zhao & Lu 2007) is illustrated in detail. Finally, the service life of the chloride contaminated RC beam is predicted using the present time-dependent system reliability assessment method.



## 2 AN IMPROVED TIME-DEPENDENT PROBABILISTIC MODEL OF CORROSION CURRENT DENSITY

### 2.1 Model of the corrosion current density at the start of corrosion propagation

After corrosion initiation, the corrosion propagation in reinforcing rebars is controlled by a well-known electrochemical process. A quantitative description of corrosion propagation is usually given in terms of the corrosion rate,  $v_{corr}$  ( $\mu\text{m}/\text{year}$ ), which is defined as the loss of metal per unit of surface area per unit of time. The most reliable data on the corrosion rate can be obtained by measuring weight differences in the reinforcing steel with reference to its surface area exposed corrosion. However, this requires the removal of reinforcing bars from concrete and thus cannot be used for RC structures in service. Most non-destructive techniques currently used for monitoring of corrosion are based on electrochemical measurements, with the corrosion rate estimated in terms of a corrosion current density,  $i_{corr}$  (normally expressed in  $\mu\text{A}/\text{cm}^2$ ). Major factors affecting the corrosion current density are the ambient environmental condition (e.g., relative humidity and temperature), the concrete quality (mainly depend on water/cement ratio) and cover. For an ambient relative humidity of 75% and temperature of  $20^\circ\text{C}$ , the corrosion current density at the start of corrosion propagation is empirically estimated as proposed by Vu & Stewart (2000)

$$i_{corr}(T_i) = \frac{37.8(1 - w/c)^{-1.64}}{d_c} \quad (1)$$

in which,  $w/c$  is estimated from Bolomey's formula (1935); namely,

$$w/c = \frac{27}{f_{cyl} + 13.5} \quad (2)$$

where  $T_i$  is the time to initiation;  $i_{corr}(T_i)$  ( $\mu\text{A}/\text{cm}^2$ ) is the corrosion current density at the start of corrosion propagation;  $w/c$  is a water/cement ratio;  $f_{cyl}$  (MPa) is the concrete compressive strength of a standard test cylinder; and  $d_c$  (mm) is the depth of the concrete cover.

Because the ambient environmental conditions are greatly different from each other for many locations in Asia, Europe, American and Australia, and Eq. (1) can only be used for a particular environmental condition, it is necessary to develop a more general expression. In this paper, for arbitrary ambient environmental conditions, concrete quality and cover, an empirical formula for estimating the corrosion current density at the start of corrosion propagation is proposed as

$$i_{corr}(T_i) = \frac{T_K H_r (w/c)}{d_c} \quad (3)$$

where  $T_K$  is the average temperature in degree Kelvin and  $H_r$  is the average relative humidity.

For the ambient environmental condition mentioned above, Eq. (3) can be simplified as

$$i_{corr}(T_i) = \frac{220(w/c)}{d_c} \quad (4)$$

Comparisons between  $i_{corr}(T_i)$  changed with  $d_c$  for  $w/c = 0.3, 0.35, 0.4, 0.45$ , and  $0.5$  obtained by Eq. (4) and those given by Eq. (1), respectively, are shown in Figure 1. From Figure 1, one can see that although the present formula is simply, it gives almost the same results with those obtained by Eq. (1). Also, there are visible differences between the results provided by the present formula and Eq. (1) when the quality of concrete is poor (i.e., high water/cement ratio and small depth of the concrete cover).

### 2.2 Model of the corrosion current density during corrosion propagation

Many reliability analyses have assumed that the corrosion rates are constant or a time-invariant random variable during the propagation period. However, it is expected that the formulation of rust products on the steel surface will reduce the diffusion of the iron ions away from the steel surface. Also, the area ratio between the anode and cathode is reduced. This suggests that the corrosion rate will reduce with time; namely, rapidly during the first few years after initiation but then more slowly as it approaches a nearly uniform level (Tuutti 1982, Yalcyn & Ergun 1996, Liu & Weyers 1998). Using the data reported by Liu & Weyers (1998), a relationship between time since initiation and the corrosion rate was developed by Vu & Stewart (2000), which is expressed empirically as

$$i_{corr}(t) = i_{corr}(T_i) \cdot 0.85t_p^{-0.29} \quad (5)$$

where  $t$  (years) is time since corrosion initiation and  $i_{corr}(T_i)$  is the corrosion current density at the start of corrosion propagation, which is given by Eq. (1).

According to Eq. (5), when  $t < 0.5$ , one obtains,  $i_{corr}(t) > i_{corr}(T_i)$ , which is inconsistent with the

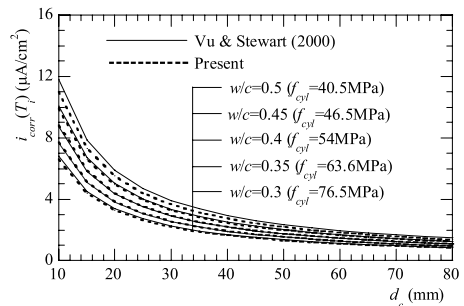


Figure 1. Comparisons between Eq. (1) and Eq. (4).

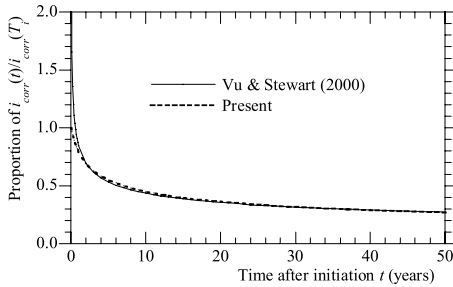


Figure 2. Comparisons between Eq. (5) and Eq. (6).

experimental evidence that the corrosion current density reduces rapidly during the first few years, as described earlier. For this reason, an improved relationship is proposed as the follows.

$$i_{corr}(t) = \frac{i_{corr}(T_i)}{\sqrt[3]{1 + t_p}} \quad (6)$$

where  $i_{corr}(T_i)$  is given by Eq. (4).

The effects of time on corrosion current density determined by Eq. (5) and Eq. (6) are depicted in Figure 2. As can be seen from the Figure, the results given by the present equation are in very close agreement with those of Eq. (5) when  $t > 1$ . In the mean time, the present equation eliminates the shortcomings of Eq. (5) when  $t$  is small (e.g.,  $t < 0.5$ ).

### 2.3 Model error

The corrosion current densities at the start of corrosion propagation  $i_{corr}(T_i)$  predicted by Eq. (4) for typical  $w/c$  ratios (less than 0.5) appear to be not unreasonable and within the range of typical corrosion current densities found in the literature (see the above reference) and so that it is expected that the model error ( $M_i$ ) is not high. In the absence of any data to conduct a statistical analysis, it is assumed herein that the distribution for  $M_i$  is a normal distribution and the corresponding mean and coefficients of variation are 1.0 and 0.2, respective.

## 3 MODEL OF CORROSION PROPAGATION

It should be noted that the corrosion current densities  $i_{corr}(t)$  above mentioned are average values for the overall concrete surface. As corrosion in reinforcement propagates, two types of corrosion—general and localized—are possible (Vassie 1984). So-called general or “uniform” corrosion (see Figure 3) consists of approximately uniform loss of metal over the whole exposed surface of a reinforcing bar. In this case, Faraday’s law indicates that a corrosion current density of  $i_{corr} = 1 \mu\text{A}/\text{cm}^2$  corresponds to a uniform corrosion penetration of  $11.6 \mu\text{m}/\text{year}$  (Jones 1992). Thus,

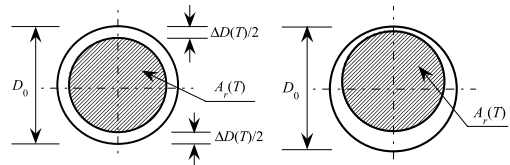


Figure 3. Uniform corrosion. Figure 4. Hybrid corrosion.

the reduction of the diameter of a corroding bar,  $\Delta D$  (mm), at time  $T > T_i$ , can be estimated directly as

$$\Delta D(T) = 0.0232 \cdot M_i \cdot \int_{T_i}^T i_{corr}(t) dt \quad (7)$$

Then the net cross-sectional area of a reinforcing bar  $A_r$  (the shaded area in Figure 3), at time  $T$ , is then equal to

$$A_r(T) = \begin{cases} \frac{\pi D_0^2}{4} & T \leq T_i \\ \frac{\pi [D_0 - \Delta D(T)]^2}{4} & T > T_i \end{cases} \quad (8)$$

where  $D_0$  is the initial diameter of the reinforcing bar (in mm).

Pitting or localized corrosion, in contrast to uniform corrosion, concentrates over small areas of reinforcement. As a result, a corroding area of a reinforcing bar may be much smaller than the area associated with the measurement of  $i_{corr}$ . Thus,  $i_{corr}$  cannot be converted directly into loss of cross-sectional area of a reinforcing bar. Although pitting or localized corrosion of the reinforcing steel is observed usually in chloride-contaminated RC structures (e.g., Gonzales et al. 1995, Rodriguez et al. 1997, Torres-Acosta & Martinez-Madrid 2003), robust and validated pitting models, particularly for larger diameter reinforcing bar have not been developed to compute the reduction of the diameter of a corroding bar and the deterioration of structural strength. Field and laboratory studies have shown that pitting corrosion is generally distributed all over the bar (Birbilis et al. 2002), so that it may be reasonable to introduce a factor ( $P$ ) that includes the effect of highly localized pitting associated with chloride contamination into the general corrosion model (see Figure 4). In this paper, it is called as hybrid corrosion. The reduction of the diameter of a corroding bar,  $\Delta D$  (mm), at time  $T > T_i$ , may be approximated by

$$\Delta D(T) = 0.0232 \cdot P \cdot M_i \cdot \int_{T_i}^T i_{corr}(t) dt \quad (9)$$

in which  $P$  is assumed as a lognormal random variable with mean and coefficient of variation of 2.0 and 0.3, respectively.

Therefore, the net cross-sectional area of a reinforcing bar  $A_r$  (the shaded area in Figure 4), at time  $T$ ,

is similar with Eq. (8), in which  $\Delta D(T)$  is given by Eq. (9).

#### 4 DETERIATION OF STRUCTURAL STRENGTH

General corrosion also affects the bond between the concrete and reinforcement. Since the general corrosion product, common rust, occupies a much larger volume than that of the original reinforcing steel, it causes cracking and ultimately spalling and delamination of the concrete cover, with subsequent reduction of bond strength. According to available experimental data (e.g., Al-Sulaimani et al. 1990, Cabrera 1996), after the initiation of corrosion the bond strength initially increases slightly (before cracking), but then decreases as the corrosion propagates. However, the effect of reduction of bond on structural strength will not be considered in the following sections as it appears that the complete loss of bond has a relatively insignificant influence on bridge reliability in flexure (Val et al. 1998). Therefore, the flexural strength of corrosion-affected RC structures depends mainly on the total available cross-sectional area of longitudinal rebars in the tension zone. From Figure 4, the total bending reinforcement area  $A_L$ , at time  $T$ , can be expressed as

$$A_L(T) = \begin{cases} \frac{n\pi D_0^2}{4} & T \leq T_i \\ \frac{n\pi [D_0 - \Delta D(T)]^2}{4} & T > T_i \end{cases} \quad (10)$$

where  $n$  = number of bars and  $\Delta D(T)$  is given by Eq. (9).

The flexural strength of a RC beam at time  $T$ ,  $M_R(T)$ , may be approximately computed as (ACI 2005)

$$M_R(T) = A_L(T)F_{yL} \left[ h_0 - \frac{A_L(T)F_{yL}}{1.7F_c b} \right] \quad (11)$$

where  $F_{yL}$  = yield strength of a longitudinal reinforcing bar;  $F_c$  = compressive strength of concrete;  $b$  = cross-sectional width; and  $h_0$  = effective depth of cross section.

According to ACI (2005), the time-dependent shear strength of a RC beam may be given by

$$V(T) = V_C + V_S(T) \quad (12)$$

In Eq. 12, it is assumed that the shear strength of concrete  $V_C$  is time-independent, which can be computed by using the following equation.

$$V_C = \frac{\sqrt{F_c}}{6} bh_0 \quad (13)$$

When only shear reinforce perpendicular to the axis of the member is used, the shear strength due to stirrups

is given as

$$V_S(T) = \frac{A_S(T)F_{yS}h_0}{s} \quad (14)$$

where  $F_{yS}$  = the yield strength of a stirrups and  $s$  = spacing between stirrups. Under hybrid corrosion (also see Figure 4), the cross-sectional area of a stirrup as a function of time,  $A_S(T)$  is given by

$$A_S(T) = \begin{cases} \frac{2\pi D_0^2}{4} & T \leq T_i \\ \frac{2\pi [D_0 - \Delta D(T)]^2}{4} & T > T_i \end{cases} \quad (15)$$

where  $\Delta D(T)$  is given by Eq. (9).

#### 5 TIME-DEPENDENT RELIABILITY ANALYSIS OF A CHLORIDE CONTAMINATED RC BEAM

Consider a simply supported RC beam located in a marine environment as shown in Figure 5. The performance function corresponding to the flexural strength failure mode can be expressed as

$$G_1(\mathbf{X}) = A_L(T)F_{yL} \left[ h_0 - \frac{A_L(T)F_{yL}}{1.7F_c b} \right] - \frac{(D+L)}{8} l^2 \quad (16)$$

For the shear strength failure mode, the performance function is given as

$$G_2(\mathbf{X}) = \frac{\sqrt{F_c}}{6} bh_0 + \frac{A_S(t)F_{yS}h_0}{s} - \frac{(D+L)}{2} l \quad (17)$$

where  $A_L(t)$  and  $A_S(t)$  are given by Eq. (10) and Eq. (15), respectively;  $D$  = the dead load;  $L$  = the live load. The probability characteristics of the basic random variables are listed in Table 1.

According to Eq. (16) and Eq. (17), the performance functions corresponding to flexural failure and shear failure can be rewritten as the following forms, respectively

$$G_1(\mathbf{X}) = 8A_L(T)F_{yL} \left[ h_0 - \frac{A_L(T)F_{yL}}{1.7F_c b} \right] / l^2 - (D+L) \quad (18)$$

$$G_2(\mathbf{X}) = 2 \left[ \frac{\sqrt{F_c}}{6} bh_0 + \frac{A_S(t)F_{yS}h_0}{s} \right] / l - (D+L) \quad (19)$$

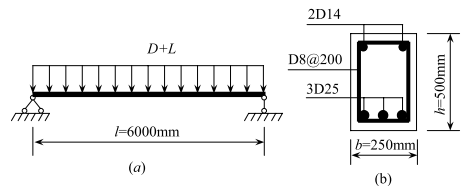


Figure 5. A simply supported RC beam.

Table 1. Statistical parameters for basic variables.

Basic variables	Mean	Coefficient of variation	Distributions
Model error			
$of i_{corr}(M_i)$	1.0	0.2	Normal
$P$	2	0.3	Lognormal
$F_{yL}$	350 MPa	0.1	Lognormal
$F_{yS}$	250 MPa	0.1	Lognormal
$F_c$	40 MPa	0.2	Lognormal
$D$	20 kN/m	0.1	Normal
$L$	10 kN/m	0.5	Gumbel

The performance function of the system can be defined as the minimum of the above; i.e.,

$$G(\mathbf{X}) = \min\{G_1(\mathbf{X}), G_2(\mathbf{X})\} \quad (20)$$

Assume that the structure is under the typical ambient environmental condition as described earlier. The depth of concrete cover  $d_c = 30$  mm and  $f_{cyl} = F_c + 7.5 = 47.5$  MPa (Vu & Stewart 2000). According to Eq. (4), the corrosion current density at the start of corrosion propagation  $i_{corr}(T_i)$  is obtained as  $3.25 \mu\text{A}/\text{cm}^2$ .

As has been described, the initiation time period is negligibly short if the service life is considered and it has been shown that the different values of  $T_i$  has only a slight effect on the structural failure,  $T_i$  is suggested to be equal to 1.0 year (Lu & Zhao 2007).

The first four moments of  $G(\mathbf{X})$  in Eq. (20), i.e., the mean ( $\mu_G$ ), standard deviation ( $\sigma_G$ ), skewness ( $\alpha_{3G}$ ), and the kurtosis ( $\alpha_{4G}$ ), at service time of  $T = 0, 1, 10, 20, 30, 40, 50, 60, 70$ , and 80 years obtained by using the point estimate method (Zhao & Ono 2000) are listed in Table 2. The corresponding time-dependent reliability indexes are also listed in Table 2, which are obtained by using the fourth-moment method (Zhao & Lu 2007)

$$\beta_{4M} = \frac{\sqrt[3]{2}p}{\sqrt[3]{-q + \Delta}} - \frac{\sqrt[3]{-q + \Delta}}{\sqrt[3]{2}} - \frac{\tilde{h}_3}{3\tilde{h}_4} \quad (21)$$

$$P_f = \Phi(-\beta_{4M}) \quad (22)$$

where

$$\Delta = \sqrt{q^2 + 4p^3} \quad (23)$$

$$p = \frac{3\tilde{h}_4(1 - 3\tilde{h}_4) - \tilde{h}_3^2}{9\tilde{h}_4^2}, \quad q = \frac{2\tilde{h}_3^3 - 9\tilde{h}_3\tilde{h}_4}{27\tilde{h}_4^3} \quad (24)$$

in which  $\beta_{4M}$  is the fourth-moment reliability index;  $P_f$  is the probability of failure;  $\Phi$  is the cumulative distribution function (CDF) of a standard normal random variable; and  $\tilde{h}_3$  and  $\tilde{h}_4$  are the parameters in the

Table 2. Results corresponding to system failure.

$T$	$\mu_G$	$\sigma_G$	$\alpha_{3G}$	$\alpha_{4G}$	$\beta_{4M}$	$P_f$
0	18.70	6.98	-0.40	3.58	2.34	$9.63 \times 10^{-3}$
1	18.70	6.98	-0.40	3.58	2.34	$9.63 \times 10^{-3}$
10	15.77	6.90	-0.42	3.61	2.06	$1.98 \times 10^{-2}$
20	13.63	6.94	-0.42	3.61	1.82	$3.44 \times 10^{-2}$
30	11.87	7.04	-0.42	3.59	1.61	$5.37 \times 10^{-2}$
40	10.33	7.16	-0.41	3.56	1.41	$7.93 \times 10^{-2}$
50	8.95	7.31	-0.39	3.54	1.22	$1.11 \times 10^{-1}$
60	7.68	7.46	-0.38	3.51	1.05	$1.47 \times 10^{-1}$
70	6.50	7.61	-0.37	3.48	0.89	$1.87 \times 10^{-1}$
80	5.38	7.76	-0.36	3.46	0.74	$2.30 \times 10^{-1}$

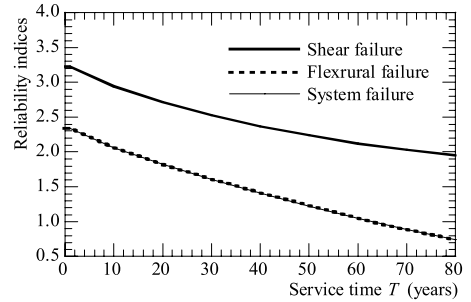


Figure 6. Time-dependent reliability indices.

Winterstein formula (1988), which are given by

$$\tilde{h}_3 = \frac{\alpha_{3G}}{4 + 2\sqrt{1 + 1.5(\alpha_{4G} - 3)}} \quad (25a)$$

$$\tilde{h}_4 = \frac{\sqrt{1 + 1.5(\alpha_{4G} - 3)} - 1}{18} \quad (25b)$$

The time-dependent reliability indices corresponding to flexural failure, shear failure and system failure (both flexural and shear failure are considered in the same time) obtained by using the fourth-moment method with respect to the service time are depicted in Figure 6. From Figure 6, one can clearly see that: (1) the reliability indices decrease as the reinforcement corrosion in the RC structure propagates; (2) the reliability indices corresponding to system failure are almost the same with those corresponding to flexural failure, which means the shear failure has negligibly effect on the reliability of this chloride contaminated RC beam.

## 6 PREDICTION OF SERVICE LIFE OF THE CHLORIDE CONTAMINATED RC BEAM

With the proposed models of structural strength deterioration, it is not difficult to predict the time for corrosion-affected RC structures to be unsafe once the acceptance criteria is determined. However, it is

quite difficult to decide an acceptable limit for the strength deterioration since the determination of it involves social-economical considerations, in addition to risk analysis for the structure. Clearly, different acceptance criteria will result in different times for the structure to be unsafe. This is the risk involved in decision-making. Gonzales et al. (1996) observe that a damage level of 25% in terms of the reduction in cross-sectional area of reinforcement bars seems to be prominent in corrosion-affected RC structures. This observation is based on data from the Eurointernational Committee of Concrete which classifies structural deterioration according to external signs, such as rust spots, concrete cracks, and cover delamination, as well as reduction of the cross-sectional area of reinforcement bars. Amey et al. (1998) predict the service life of corrosion-affected concrete structures using a more simplistic 30% rebar reduction as the failure criterion. Li (2003b) takes the acceptable limit for strength deterioration as 0.6 and predicts the time at which the structure becomes unsafe using a confidence level of 90%. Because the collapse of the frame beam will result in a serious loss of property and life, the minimum acceptable risk in terms of the reliability index,  $\beta_a$ , is taken as 1.5, and the time for the structure to become unsafe (failure)  $T_f$ , can be predicted from Eq. (26), i.e.,

$$\beta(T_f) \leq \beta_a = 1.5 \quad (26)$$

which gives  $T_f \approx 35$  years.

## 7 CONCLUSIONS

1. A time-dependent probabilistic model of corrosion current density is proposed.
2. A factor that includes the effect of highly localized pitting associated with chloride contamination is introduced into the general corrosion model.
3. The fourth-moment method is applied to time-dependent reliability analysis. The method, being very simple, is expected to apply in practical engineering.
4. The methodology presented in the paper can be used as a tool for structural engineers and asset managers to assess a corrosion-affected concrete infrastructure and make decisions with regard to its maintenance and rehabilitation.

## ACKNOWLEDGMENTS

This study is partially supported by a "Grant-in-Aid for Scientific Research (*Tokubetsu Kenkyuin Shorei-hi*)" from Japan Society for the Promotion of Science (JSPS) (No: 19-07399). The support is gratefully acknowledged.

## REFERENCES

- Al-Sulaimani, G.J., Kaleemullah, M., Basunbul, I.A., & Rasheeduzzafar, I.A. 1990. Influence of corrosion and cracking on bond behavior and strength of concrete members. *ACI Structural Journal* 87(2):220–231.
- American Concrete Institute (ACI). 2005. *Building code requirements for structural concrete*. Detroit: ACI 318–05, ACI.
- Amey, S.L., Johnson, D.A., Miltenberger, M.A., & Farzam, H. 1998. Predicting the service life of concrete marine structures: An environment methodology. *ACI Materials Journal* 95(2): 205–214.
- Bamforth, P.B. 1999. The derivation of input data for modeling chloride ingress from eight-year UK coastal exposure trials. *Magazine of Concrete Research* 51(2):89–96.
- Bolomey, J. 1935. Granulation et prevision de la resistance probable de betons. *Traavaux* 19(30): 228–230.
- Biribilis, Y.Y.N., Sanjayan, J.G., & Taplin, G. 2002. Corrosion behavior of loaded reinforced concrete beams housed in an environment chamber. *Corrosion and Prevention* 02, 10–13 November, Adelaide, Australia (CD-ROM).
- Cabrera, J.G. 1996. Deterioration of concrete due to reinforcement steel corrosion. *Cement and Concrete Composites* 18(1):47–59.
- Francois, R., & Castel, A. 2001. Discussion on influences of bending crack and water-cement ratio on chloride-induced corrosion of main reinforcing bars and stirrups. *ACI Materials Journal* 98(3):276–278.
- Frangopol, D.M., Lin, K.Y., & Estes, A. 1997. Reliability of reinforced concrete girders under corrosion attack. *Journal of Structural Engineering* 123(3):286–297.
- Gonzales, J.A., Andrade, C., Alonso, C., & Feliu, S. 1995. Comparison of rates of general corrosion and maximum pitting penetration on concrete embedded steel reinforcement. *Cement and Concrete Research* 25(2): 257–264.
- Gonzales, J.A., Feliu, S., Rodriguez, P., Lopez, W., Alonso, C., & Andrade, C. 1996. Some questions on the corrosion of steel in concrete. II: Corrosion mechanism and monitoring, service life prediction and protection methods. *Materials Structure* 29:97–104.
- Jones, D.A. 1992. *Principles and prevention of corrosion*. New York: Macmillan Publishing Corporation.
- Leeming, M.B. 1998. *Durability of concrete in and near sea*. *Concrete in coastal structures*, R.T.L. Allen, ed., Thomas Telford, London, 73–98.
- Li, C.Q. 2003a. Life-cycle modeling of corrosion-affected concrete structures—Initiation. *Journal of Materials in Civil Engineering* 15(6):594–601.
- Li, C.Q. 2003b. Life-cycle modeling of corrosion-affected concrete structures—Propagation. *Journal of Structural Engineering* 129(6):753–761.
- Liu T, & Weyers, R.E. 1998. Modeling the dynamic corrosion process in chloride contaminated concrete structures. *Cement and Concrete Research* 28(3):365–379.
- Lu, Z.H. & Zhao, Y.G. 2007. Performance assessment of corroded reinforced concrete Structures. *ACI Structural Journal* (in review).
- Melchers, R.E., & Li, C.Q. 2006. Phenomenological modeling of corrosion loss of steel reinforcement in marine environments. *ACI Material Journal* 103(1):25–32.

- Mori, Y., & Ellingwood, B.R. 1994. Maintaining reliability of concrete structures II: optimum of inspection/repair, *Journal of Structural Engineering* 120(3):846–862.
- Otsuki, N., Miyazato, S., Diola, N.B., & Suzuki, H. 2000. Influences of bending crack and water-cement ratio on chloride-induced corrosion of main reinforcing bars and stirrups. *ACI Material Journal* 97(4):454–465.
- Roberts, M.B., Atkins, C., Hogg, V., & Middleton, C. 2000. A proposed empirical corrosion model for reinforced concrete. *Struct. Bldg. I.C.E.* 140(1):1–11.
- Rodriguez, J. Ortega, L.M., & Casal, J. 1997. Load carrying capacity of concrete structures with corroded reinforcement. *Constructional Building Materials* 11(4):239–248.
- Stewart, M.G., & Rosowsky, D.V. 1998. Time-dependent reliability of deteriorating reinforced concrete bridge decks. *Structural Safety* 20(1):91–109.
- Takewaka, K. & Matsumoto, S. 1988. Quality and cover thickness of concrete based on estimation of chloride penetration in marine environments. *Concrete in Marine Environment*. Detroit, V.M. Malhprtra, ed., SP-109, American Concrete Institute (ACI): 381–400.
- Ting, S.-C. 1989. The effects of corrosion on the reliability of concrete bridge girders. PhD thesis, Department of Civil Engineering, University of Michigan, Ann Arbor, Michigan.
- Torres-Acosta, A.A. & Martinez-Madrid, M. 2003. Residual life of corroding reinforced concrete structures in Marine environment. *Journal of Materials in Civil Engineering* 15(4), 344–353.
- Tuutti, K. 1982. *Corrosion of steel in concrete*, Swedish Cement and Concrete Research Institute, Stockholm, Sweden.
- Val, D.V. 2007. Deterioration of strength of RC beams due corrosion and its influence on beam reliability. *Journal of Structural Engineering* 133(9):1297–1306.
- Val, D.V. & Melchers, R.E. 1997. Reliability of deteriorating RC slab bridges. *Journal of Structural Engineering* 123(12):1638–1644.
- Val, D.V., Stewart, M.G., & Melchers, R.E. 1998. Effect of reinforcement corrosion on reliability of highway bridge. *Engineering Structures* 20(11):1010–1019.
- Vassie, P. 1984. Reinforcement corrosion and the durability of concrete bridges. Proc. Institution of Civil Engineers, Part I, 76, 713–723.
- Vu, K. & Stewart, M.G. 2000. Structural reliability of concrete bridges including improved chloride-induced corrosion models. *Structural Safety* 22(4):313–333.
- Winterstein, S.R. 1988. Nonlinear vibration models for extremes and fatigue. *Journal of Engineering Mechanics* 114(10):1772–1790.
- Yalcyn, J.R. & Ergun, M. 1996. the prediction of corrosion rates of reinforcing steels in concrete. *Cement and Concrete Research* 26(10):1593–1599.
- Zhao, Y.G. & Lu, Z.H. 2007. Applicable range of the fourth-moment method for structural reliability. *Journal of Asia Architecture and Building Engineering* 6(1): 151–158.
- Zhao, Y.G. & Ono, T. 2000. New point estimates for probability moments *Journal of Engineering Mechanics* 126(4):433–436.
- Zhao, Y.G. & Ono, T. 2001. Moment methods for structural reliability *Structural Safety* 23(1): 47–75.

# The critical role of marine bacterial processes in the development of models for pitting corrosion of structural steels

R.E. Melchers

*Centre for Infrastructure Performance and Reliability, The University of Newcastle, Australia*

**ABSTRACT:** The modelling of both short- and long-term corrosion loss and maximum pit depth is increasingly of interest to engineers and others interested in prediction the remaining life of coastal and ocean infrastructure. This paper reviews a recent advanced modelling approach and simplifies this to development of a model for predicting maximum pit depth for mild steel subject to long-term marine environment exposure. A crucial aspect is that the model development considers, for the first time and explicitly, the influence of microbially induced corrosion (MIC). It is shown that uncertainty in longer-term pitting depth is likely to be time-invariant and is best represented by a Frechet distribution.

## 1 INTRODUCTION

Models for the marine corrosion of structural steels are important for interpreting observations of the degree of corrosion of existing structures, for predicting the likely future rate of corrosion of existing structures and for setting realistic and economically rational allowances for possible corrosion in the design of new structures. This applies both to general (or uniform) corrosion in which there is a more or less uniform thinning of plates and fittings, and pitting corrosion in which there is highly localized penetration, typically causing plate or wall perforation.

The present paper is concerned with pitting corrosion. It is important where structural integrity, and in particular containment, is an issue, such as for tanks, pipelines, pressure vessels and containments for nuclear wastes (Marsh et al. 1989).

For infrastructure evaluation, probabilistic assessment tools, including probabilistic models for resistances and for loads are desirable to deal with the uncertainties (statistical and other) inevitable in models of the natural and man-made environment. Typically, there are many factors that influence corrosion, including (a) physical factors (such as temperature, wave action, water velocity, metal surface finish, (b) chemical factors (e.g. salinity, pollutants, metal composition) and (c) biological factors (e.g. bacteria, marine growth). These may be collected together in a vector  $\mathbf{E}$ . They would be expected to influence also the modelling of pitting corrosion.

In the simplest terms, the pit depth  $d(t)$  as a function of time  $t$  and of environmental conditions and

material properties  $\mathbf{E}$  can be represented as (Melchers 2003b)

$$d(t, \mathbf{E}) = b(t, \mathbf{E}) \cdot \bar{f}n(t, \mathbf{E}) + \varepsilon(t, \mathbf{E}) \quad (1)$$

where  $\bar{f}n(t, \mathbf{E})$  is a mean-valued function,  $\varepsilon(t, \mathbf{E})$  is a zero mean error function picking-up the uncertainties not accounted for in  $\bar{f}n(t, \mathbf{E})$  (and therefore sometimes called a called probability bucket), and  $b(t, \mathbf{E})$  is a bias factor, expected to be unity for good-quality models. Evidently there is a balance between  $\bar{f}n(t, \mathbf{E})$  and  $\varepsilon(t, \mathbf{E})$  with poor modelling of the former likely to increase the latter, often substantially. Of course, a model with high quality  $\bar{f}n(t, \mathbf{E})$  and low  $\varepsilon(t, \mathbf{E})$  is likely to be complex and will require much more detailed data for its calibration. Examples of poor quality models for  $\bar{f}n(t, \mathbf{E})$  and the resulting high levels of uncertainty have been discussed elsewhere (e.g. Melchers 2007a).

The next section outlines the recent development of an appropriate model for  $\bar{f}n(t, \mathbf{E})$  based on actual and very detailed observations of steels exposed to natural seawater. The model has been shown to be applicable to immersion, tidal and coastal atmospheric corrosion environments (Melchers 2003a, 2007b). Next is described how the model may be slightly simplified for practical application under longer-term exposure conditions. Field data is then used to estimate the variability in maximum pit depth at a given exposure location, derived from the application of extreme value statistics. Some comments are made also about the application of the simplified model.

## 2 BACKGROUND

Pitting corrosion is known to commence almost immediately upon first exposure of bare steel to seawater, the pits soon developing, typically, to a diameter of around 50–100 microns and similar depths (Butler et al. 1972). Only moderate increases in depth and diameter occur for some considerable time thereafter. Typically the pits are spaced some distance apart and this is consistent with the notion that a pit represents a localized and concentrated anodic region that loses metal ions to the surrounding cathodic region (Wranglen 1974). During this time new pits may develop and others may stop growing. Such pitting is known in the corrosion literature as meta-stable pitting (Burstein et al. 1993). In contrast, stable pitting is associated with pits that do not stop growing (at some positive semi-definite rate) once they commence. Also, there is a degree of randomness in the initiation and in the development of pitting (Szklańska-Smiałowska 1986). This has led to pit depth being considered as an ideal example for the application of extreme value theory (Galambos 1987). However, it should be clear also that the two categories of pitting (stable and meta-stable) represent two different statistical populations. Surprisingly, the implication of this appears only recently to have been considered in extreme value analysis (Melchers 2005, 2006b). In brief, by their very definition, meta-stable pits are, except perhaps for very short exposure periods, never able to be pits deeper than any of the stable pits, assuming that there are no fundamental differences in the mechanisms of pit depth propagation. It follows that the population of meta-stable pits should not be considered in an extreme value analysis.

Close observation of the development of pit depth and pit diameter and of the overall surface topology reveals that each of these changes with longer exposures. Typically, a relatively sharp increase in pit depth is observed after some period and the previously individual isolated pits commence to coalesce, forming more or less uniform depressions. Later, new pits can be seen to initiate and develop on the surface of the depressions (Jeffrey & Melchers 2007). This has been associated with the development of anaerobic conditions within the pits and on the corroding surface underneath the surface rusts (Melchers 2003a). Such conditions do not support metal oxidation by oxygen but are known to be suitable for the development of microbial influenced corrosion (Cragolino and Tuovinen 1984). For this the sulphate-reducing bacteria (SRB) in particular have been implicated. However, it is important to note that in natural conditions bacteria seldom occur in isolation (as is the usual case in laboratory studies) and almost always occur in microbial communities. The bacteria in such communities lend support and essential energy and food to each other and help bacterial survival under (perhaps

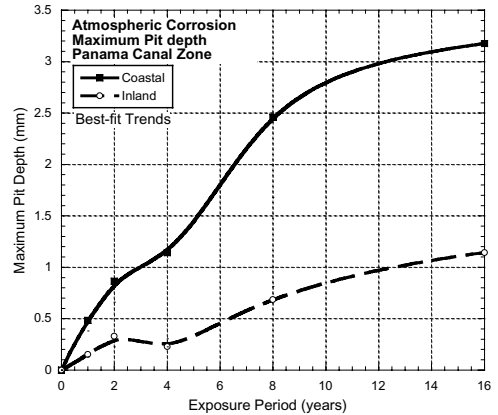


Figure 1. Typical trends in maximum pit depth development with increased exposure time.

temporary or cyclic) adverse conditions (Hamilton 1986).

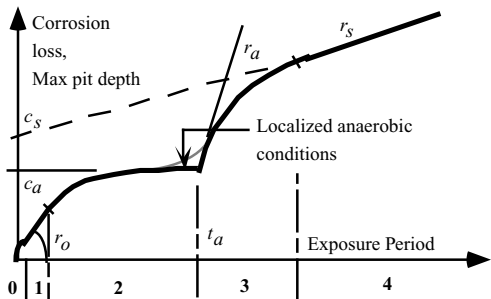
There has been much dispute and some controversy associated with the long history of understanding the mechanisms of corrosion associated with SRB (Cragolino and Tuovinen 1984). However, it is now largely agreed that the main driver of SRB-influenced corrosion are the metabolites (waste products) resulting from the metabolism of the SRB on and close to the corroding metal surface (Crolet 1992). The main metabolic product is  $H_2S$ . It reacts with iron but also with many other metals and materials.

Corrosion associated with SRB can be particularly aggressive under marine exposure conditions. Figure 1 shows a typical plot of maximum pit depth for exposure of steel to the marine coastal atmosphere in the Panama Canal Zone (Southwell et al. 1979). Similar results are available for marine immersion and for atmospheric corrosion losses (Melchers 2004a, b, 2007b).

## 3 MODEL FOR MAXIMUM DEPTH OF PITTING CORROSION

The important observation from Figure 1 is that there is a change in pitting behaviour after some period of exposure. This has been proposed as being the result of the mechanism controlling the corrosion process changing from oxidation by oxygen to that caused by  $H_2S$  attack (Melchers 2003a). The idealized model proposed to represent this behaviour is shown in Figure 2 together with a summary description of each of the model phases. The model and its parameters have been extensive calibrated to field data obtained from a wide range of coastal exposure sites worldwide (Melchers 2003a). Moreover, the effects of water





**Phase 0** - Surface colonized by bacteria etc.

**Phase 1** - Oxidation controlled by rate of arrival of oxygen from the seawater

**Phase 2** - Corrosion products progressively inhibit rate of oxygen diffusion

**Phase 3** - SRB flourish under ample nutrient supply

**Phase 4** - Metabolism of SRB and loss of rust through erosion and wear

Figure 2. Corrosion model with summary descriptions of each phase. The model parameters are shown also.

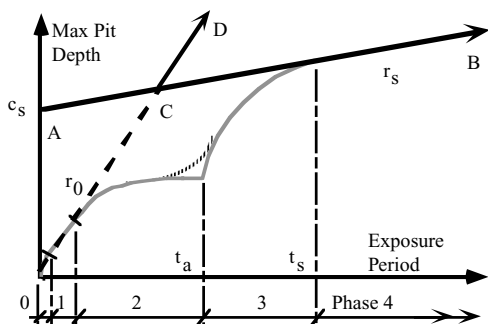


Figure 3. Simplified pit depth model 0AB (bold) showing also over-estimation by 0CD.

temperature, water pollution and metal composition have been described (Melchers 2006b).

The parameter  $t_a$  in Figure 2 describes the change-over from oxidation by oxygen diffusion through the rust layers. For practical purposes the model of Figure 2 may be simplified to that of Figure 3. It has only the long-term corrosion rate given by  $r_s$  located at  $c_s$  on the pit depth axis. This means that after an initial transition period, only Phase 4 is relevant for the description of long-term corrosion.

A similar simplified model has been proposed for general corrosion (Melchers 2006c). Since even for very cold immersion conditions  $t_a$  is not much more

than 4–5 years from first exposure (although it is rather longer for atmospheric conditions), the parameter  $t_s$  is likely to be less than 10 years even in the harshest exposure conditions. This means that the simplified model is a reasonable approximation for long-term exposures and an upper bound for intermediate exposure periods.

In any case, the model of Figure 3 (and also that of Figure 2) is a much better approximation than assuming a constant corrosion rate through the origin (for example 0CD in Figure 3).

#### 4 VARIABILITY OF MAXIMUM PIT DEPTH

Since Phase 4 of the model of Figures 2 and 3 is governed by the rate of metabolism of anaerobic bacteria, the critical parameter for determining the variability of maximum pit depth becomes the rate of supply of nutrients (cf. Melchers and Wells 2006). A simple model may be used to represent this situation. Let  $e(t, T)$  represent the rate of supply of nutrients to the region of the corroding surface. Here  $t$  is time since the commencement of phase 3 and  $T$  is mean water temperature. The metabolic material produced may be assumed distributed between the pits on the surface. Let pitting be assumed to cover a proportion  $\rho(t, T)$  of the total surface. Then the rate of nutrient supply per pit is  $e(t, T)/\rho(t, T)$ .

Assuming now that the rate of increase in pit depth, given by  $\dot{x}(t, T)$  is proportional to the rate of supply of nutrients per pit and that this occurs at a roughly constant rate during Phase 4, it follows that the pit depth at any time  $t$  is given by  $x(t, T) = Ae(t, T)/\rho(t, T)$ , where  $A$  is a constant of proportionality between instantaneous corrosion rate and rate of nutrient supply.

In general neither  $e(t, T)$  nor  $\rho(t, T)$  will be known precisely. Both may be modelled as random variables. Both also are positive semi-definite. Consistent with First Order reliability concepts the uncertainty associated with each may be postulated as being modelled as Lognormal distributed. As a result, the pit depth of an individual pit  $x(t, T)$  is proportional the quotient of two independent lognormal random variables. This quotient also will be Lognormal, limited on the left at zero.

For the maximum pit depth the domain of attraction of the Lognormal is, theoretically, the Type 1 (or Gumbel) extreme value (EV) distribution (Galambos 1987). However, it is undefined on the left, and in practice the Type 2 (Frechet) distribution is often used since, for the maximum, it is limited on the left (in this case at zero). This more closely corresponds to physical reality. Probably for this reason there is a long history of using the Frechet distribution as the extreme value distribution for left-limited (usually zero) physical phenomena

such as wind and wave loads (Benjamin & Cornell 1970).

The Frechet distribution is given by the cumulative distribution function (CDF)  $F_Y(y)$

$$F_Y(y) = \exp[-(u/y)^k] \quad y \geq 0 \quad (2)$$

with parameters  $u$  and  $k$  related to the mean and variance of the random variable  $Y$  by

$$m_Y = u\Gamma(1 - 1/k) \quad k > 1 \quad (3)$$

$$\sigma_Y^2 = u^2 [\Gamma(1 - 2/k) - \Gamma^2(1 - 1/k)] \quad k > 2 \quad (4)$$

The Frechet distribution is related to the Gumbel through a simple logarithmic mapping of  $Y$ . Thus  $Z = \ln Y$  is Gumbel distributed and a Frechet plot is obtained when pit depths  $Y$  are plotted to a log scale on the horizontal axis of a Gumbel plot (Galambos 1987). For both distributions the vertical axis usually is given by the standardized variable  $w = (y - \hat{u})\alpha$  where  $\hat{u}$  and  $\alpha$  respectively are the mode and slope of the Gumbel distribution. Also  $k = \alpha$ .

Data ideally Frechet distributed plots as a linear trend on a Frechet plot. Figure 4 shows an example for data obtained at Taylors Beach, Australia using pit depth observations over 9 coupons (18 faces) (Melchers 2004a). This data source is unique in that almost no multiple coupon pit depth data have been reported in the literature. Almost all previous statistical analyses have relied on combining pit depth data from different periods of exposures. Generally this is invalid (Melchers 2005).

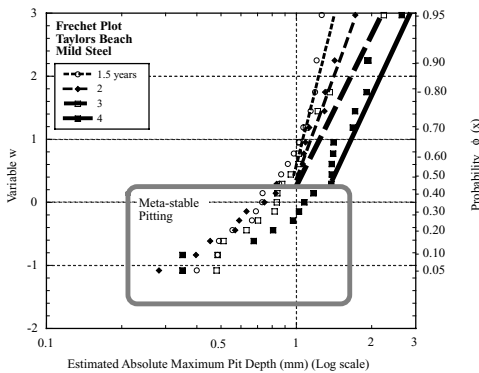


Figure 4. Frechet plot of maximum pit depth data recorded for 9 multiple coupons exposed at Taylors Beach, Australia. The straight lines represent fits to the Frechet distribution for different exposure periods. The data corresponding to meta-stable pitting have been isolated as shown. They have not been considered in fitting the Frechet lines.

## 5 MAXIMUM PIT DEPTH UNCERTAINTY

For the simplified model of Figure 3 only the variability corresponding to Phase 4 of the model in Figure 2 is of interest. This may be estimated from the data shown in Figure 4 for  $t = 3, 4$  years using Eqn (4). Evidently estimates of parameters  $u$  and  $k$  are required. First the data points corresponding to meta-stable pitting, as evident from the change in the trend of the data (Figure 4), are discarded. The remaining ones are used to estimate the Frechet distribution and hence the parameters  $u$  and  $k$ . An example is shown in Figure 5 for  $t = 4$  years. Similar analyses for other exposure periods result in the parameter values shown in Table 1. It is seen that all parameters vary systematically with greater exposure time  $t$ .

The standard deviation is plotted in Figure 6 as a function of exposure period. Evidently, the standard deviation steadies during the period corresponding to Phase 4. This might be expected also from inspection of the trend shown in Figure 4. It also would be expected from fundamental considerations, noting that Phase 4, which represents the dominant long-term corrosion process, is essentially dependent on the rate of

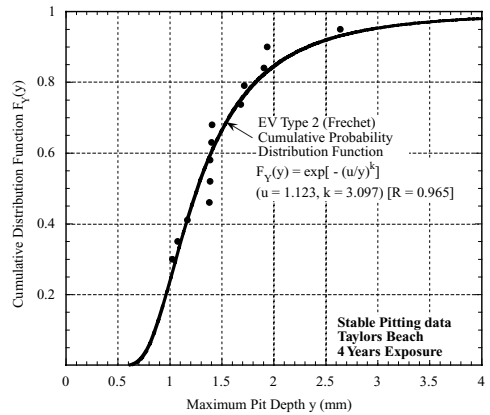


Figure 5. Cumulative distribution function of Frechet distribution fitted to maximum stable pit data at 4 years exposure.

Table 1. Parameters for fitted Frechet distributions.

$t$ (years)	Parameter $u$	Parameter $k$	Mean $m_Y$	Standard Devn. $\sigma_Y$
4	1.123	3.097	1.51	0.95
3	0.835	3.75	1.04	0.97
2	0.907	4.72	1.07	0.36
1.5	0.898	4.74	0.958	0.32
1	0.427	8.53	0.462	0.08

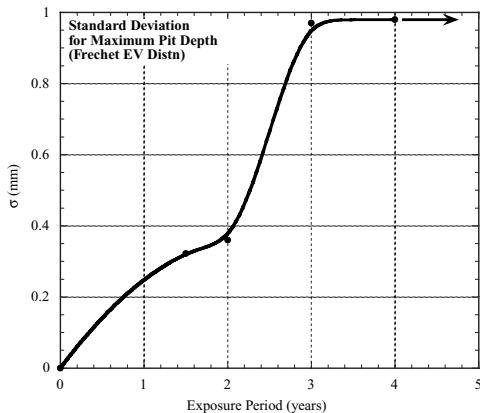


Figure 6. Variation of standard deviation for Frechet distribution with increased exposure period. The standard deviation appears to level-out after 3 years exposure.

supply of nutrients, the slow loss of external rust layers and the conversion of pits through coalescence into general corrosion loss.

## 6 DISCUSSION

Although estimates of the statistical uncertainty associated with pit depth, and in particular maximum pit depth is important for estimating the life of containment vessels and piping, there is remarkably little information in the corrosion or engineering literature that can be used for this purpose (Melchers 2004a). Efforts to obtain such estimates have in the past invariably resorted to combining data for pit depths obtained at different periods of exposure, and correcting the data to a common time point using the assumption that pit depth  $d(t)$  follows the power law function  $d(t) = At^B$  where  $A$  and  $B$  are constants obtained by fitting this function to the data. This function is based entirely on the assumption that the rate of supply of oxygen to the anodic regions (e.g. pits) governs the rate of corrosion progression. However, as Figure 2 shows, the simple power law function does not represent the progression of pitting corrosion in the longer term since eventually, after about  $t_a$ , the corrosion process becomes controlled by the rate of metabolism of anaerobic bacteria, principally the SRB. In very cold seawaters the power law function ceases to be valid after about 4–5 years and it is valid for much shorter periods in warmer waters (Melchers 2004a). The times are somewhat longer for marine atmospheric corrosion.

As a result of the changing corrosion behaviour seen in Figures 1 and 2 and in other cases reported in the literature, combination of data from different

time periods is not valid. Evidently, estimates of pit depth uncertainty so obtained are erroneous. The only way to progress is to ensure that future test programs are designed specifically using multiple coupons to allow statistical analysis of the data at each time point, without combination with other data.

The theory outlined herein is based on the important observation that longer-term pit depth is governed by the rate of metabolism of the SRB and the assumption that this is influenced only by the rate of arrival of essential nutrients. For structures that are exposed to natural seawater immersion or to seawater spray, such nutrients are immediately available and this means that the conditions for corrosion, and hence the uncertainty in the long-term corrosion rate are likely to remain essentially constant. This is the underlying assumption indicated by the arrow in Figure 6. It is supported to some degree by the steadying of the standard deviation estimated at years 3 and 4.

It is known that bacterial activity in seawater depends on a variety of nutrients. Sulphates are abundant in seawater and organic carbon usually also is available. The corrosion process provides iron. Invariably the limiting nutrient for metabolic activity under steel corrosion conditions in seawater is nitrogen. One consequence is that seawaters polluted by nitrogenous material are likely to display higher rates of long-term steel corrosion and also some increased early corrosion. This can arise from pollution of coastal seawaters by fertilizers and at sea at offshore oil platform operational areas (Melchers 2007c). The relationships between nutrient pollution and corrosion loss and pit depth are currently being explored in controlled field experiments.

Another consequence of the involvement of bacteria in long-term corrosion and pitting of steels is that testing for corrosion behaviour in artificial media such as 3.5% saltwater solutions or in abiotic artificial seawaters is highly likely to give misleading results. Key components in both the very short term and in the long term corrosion of steels in seawater are biotic content and nutrient availability.

In practice infrastructure often is protected by protective coatings and, in appropriate circumstances, by cathodic protection. However, there are situations where these measures cannot be applied, or where they become ineffective after some years. Unless maintenance is of a high order, corrosion can be expected. Even casual observation in industrial and coastal zones shows that advanced stages of corrosion are in evidence.

## 7 CONCLUSION

The recently developed corrosion model applicable to immersion, tidal and coastal marine environments

may be simplified for predicting maximum pit depth for mild steel subject to long-term marine environment exposure. A crucial aspect is that the model, for the first time and explicitly, builds on the observation that long-term corrosion and pitting is largely a function of bacterial activity (microbially-induced corrosion). Using data available in the literature it is shown that the uncertainty in pitting depth under longer-term exposures is likely to be time-invariant and is best represented by a Frechet distribution.

## ACKNOWLEDGEMENT

The work reported here is part of a project on the effect of deterioration and corrosion on the structural reliability of infrastructure in aggressive environments. The financial support of the Australian Research Council is gratefully acknowledged.

## REFERENCES

- Benjamin JR & Cornell CA (1970) Probability, Statistics and Decision for Civil Engineers, McGraw-Hill Book Co., New York.
- Burstein GT, Pistorius PC & Mattin SP (1993) The nucleation and growth of corrosion pits on stainless steel, *Corrosion Science*, 35 (1–4) 57–62.
- Butler G, Stretton P & Beynon JG (1972) Initiation and growth of pits on high-purity iron and its alloys with chromium and copper in neutral chloride solutions, *British Corrosion Journal*, 7 (7) 168–173.
- Cragolino G & Tuovinen OH (1984) The role of sulphate-reducing and sulphur-oxidizing bacteria on the localized corrosion of iron-base alloys—A review, *International Biodeterioration*, 20 (1) 9–26.
- Crolet J-L (1992) From biology and corrosion to biocorrosion, (In) *Microbial Corrosion*, (Ed) Sequeira CAC and Tiller AK, (Proceedings of the 2nd EFC Workshop, Portugal 1991) European Federation of Corrosion Publication No. 8, The Institute of Metals, London, 50–60.
- Galambos J (1987) *The asymptotic theory of extreme order statistics*, Second Edition, Krieger, Malabar, FL.
- Hamilton AW (1986) The sulphate reducing bacteria and anaerobic corrosion, *Annual Review of Microbiology*, 39: 195–217.
- Jeffrey R & Melchers RE (2007) The changing topography of corroding mild steel surfaces in seawater, *Corrosion Science* 49: 2270–2288.
- Marsh GP, Harker AH & Taylor KJ (1989) Corrosion of carbon steel nuclear waste containers in marine sediment, *Corrosion (NACE)* 45 (7) 579–589.
- Melchers RE (2003a) Modeling of marine immersion corrosion for mild and low alloy steels—Part 1: Phenomenological model, *Corrosion (NACE)* 59 (3) 319–334.
- Melchers RE (2003b) Modeling of marine immersion corrosion for mild and low alloy steels—Part 2: Uncertainty estimation, *Corrosion (NACE)* 59 (3) 335–344.
- Melchers RE (2004a) Pitting corrosion of mild steel in marine immersion environment—1: maximum pit depth, *Corrosion (NACE)* 60 (9) 824–836.
- Melchers RE (2004b) Pitting corrosion of mild steel in marine immersion environment—2: variability of maximum pit depth, *Corrosion (NACE)* 60 (10) 937–944.
- Melchers RE (2005) Statistical characterization of pitting corrosion—2: Probabilistic modelling for maximum pit depth, *Corrosion (NACE)* 61 (8) 766–777.
- Melchers RE (2006a) Pitting corrosion of mild steel under marine anaerobic conditions—Part 2: Statistical representation of maximum pit depth, *Corrosion (NACE)* 62 (12) 1074–1081.
- Melchers RE (2006b) The marine corrosion of structural steels in brackish and fresh waters, *Journal of Structure & Infrastructure Engineering* 2 (1) 53–61.
- Melchers RE (2006c) The corrosion in seawater of structural steels in infrastructure applications, *Australian Journal of Structural Engineering*, 6 (1) 159–168.
- Melchers RE (2007a) Development of new applied models for steel corrosion in marine applications including shipping, Proceedings, PRADS, Practical Design of Ships and Offshore Structures, Houston, American Bureau of Shipping, Houston, USA, 919–927.
- Melchers RE (2007b) The transition from marine immersion to coastal atmospheric corrosion for structural steels, *Corrosion (NACE)* 63 (6) 500–514.
- Melchers RE (2007c) The influence of seawater nutrient content on the early immersion corrosion of mild steel—1 Empirical observations, *Corrosion (NACE)* 64 (1) 318–329.
- Melchers RE & Wells PA (2006) Models for the anaerobic phases of marine immersion corrosion, *Corrosion Science* 48 (7) 1791–1811.
- Southwell CR, Bultman JD & Hummer CW (1979) Estimating service life of steel in seawater (in) Schumacher, M (Ed) *Seawater Corrosion Handbook*, Park Ridge, NJ: Noyes Data Corporation, 374–387.
- Szklarska-Smialowska Z (1986) *Pitting corrosion of metals*, Houston: NACE.
- Wranglen G (1974) Pitting and sulphide inclusions in steel, *Corrosion Science*, 14: 331–349.

# Feasibility analysis of the use of stainless steel reinforcement for concrete members subjected to aggressive exposure conditions

C. Molins, E. Real & L. Medina

*Universitat Politècnica de Catalunya, Barcelona, Spain*

**ABSTRACT:** This paper analyses the economical and environmental viability of the use of stainless steel reinforcement in structural members subjected to aggressive environments like wastewater. Analyses are based on the comparison of a reinforced concrete wastewater tank using conventional carbon steel or stainless steel, regarding environmental and economical aspects. The use of corrosion resistant reinforcement allows: smaller coverings, greater crack width limits and smaller cement quantities, which reduces the global cost. Although water tightness does not allowed relaxing the crack width, stainless steel reinforced tank global cost is reduced to twice the cost of the carbon steel one. Two favourable aspects of the use of stainless steel were disregarded: maintenance costs during service life and a possible relaxation of the crack width limit when using stainless steel.

## 1 INTRODUCTION

### 1.1 *Environmental impact of building industry*

Environmental sustainability of building products is a very common subject at present time but poorly studied, even though environmental burdens of this kind of products are very significant.

Building industry causes significant environmental impacts: it uses 15% of the world-wide water consumption. With regard to weight, volume and money, construction industry is the greatest materials consumer in our society. Around 40% of the materials used in industrial production are related to construction industry. Many construction materials cause a great environmental impact. This is the case of cement, one of the most used construction materials: 2.1 billion tonnes were produced in 2004 (Cembureau 2005). In addition to a huge consumption of raw materials, cement production implies a very polluting industrial process that consumes a great amount of energy. The production of each tone of Portland cement releases to the atmosphere, at least, one tone of CO<sub>2</sub> in addition to other pollutants. It is responsible of a 5% of total CO<sub>2</sub> emission (Gjorv 2003).

### 1.2 *Possibilities of stainless steel*

Durability and service life are critical aspects of carbon steel reinforced concrete structures. That has made actual design rules and standards require very restricting covers and crack width limits when the exposure conditions are aggressive, like structures exposed to seawater or wastewater. In some structural members,

those restrictions can lead to the use of concrete and steel amounts larger than those strictly required for strength. In spite of its higher cost of about three times, the use of a corrosion resistant reinforcement material may produce not so large effect on the overall cost because it allows reducing covers and also permits a greater crack width. This means less concrete and reinforcement amounts.

This work sets out to study the economical and environmental viability of the use of stainless steel reinforcement in structures subjected to aggressive environments like wastewater.

### 1.3 *LCA methodology*

LCA is a scientific way of studying environmental impacts whose methodology is described by the international standards ISO 14040 to 14043. In particular, LCA is a process for evaluating the environmental burdens associated with a product or system. This assessment includes identifying and describing quantitatively or qualitatively the wastes released into the environment, the energy and material consumption, and the impact of these items on the environment along the entire lifecycle of the product or activity. Environmental impact categories considered are: greenhouse effect, acidification, eutrophication, summer smog and heavy metals. Global impact is weighed by the Eco-Indicator 95 which scores each different impact category depending on their particular effects on present environmental situation.

To include the costs of CO<sub>2</sub> emissions in the economical analysis, an average prize of the emission rights has been used.

## 2 STAINLESS STEEL REINFORCEMENT

### 2.1 *Stainless steel and concrete*

Stainless steel is an alloy of iron and carbon with a minimum content of 10.5% chromium. Besides chromium, typical alloying elements are molybdenum, nickel and nitrogen. Alloying these elements brings out different crystal structures for different properties in machining, forming, welding, etc. The corrosion resistance of stainless steels is due to the formation of stable passive film on the surface. The environment inside concrete is characterized by highly alkaline conditions ( $\text{pH} > 12$ ). Under such conditions, both steels are passive. However, when exposed to chlorides, the passivity of carbon steels is lost and corrosion can initiate.

### 2.2 *Previous experience in stainless steel reinforcement*

The earliest known significant example was a 2.1 Km loading jetty on the Yucatan Peninsula in Mexico erected between 1937 and 1941. In fact, most structural members were built in plain concrete however the arches between columns were reinforced with austenitic stainless steel. In 1998, a survey of the structure concluded that it was in a quite well condition, despite the actual cover was lesser than modern standard specifications for marine environment.

After that example, there are almost no significant structures of stainless steel reinforcement till the early 1970's, when the Building Research Establishment (BRE) in UK carried out a series of studies to investigate the use of corrosion resistant materials for reinforcement, particularly the long term performance of stainless steel reinforcement even in worst conditions than those considered in modern design codes. It was not until 1998 that the Concrete Society published a technical report about specific uses of stainless reinforcement. But it did not give a definitive guidance in key questions like when and what grade to use. The UK Highways Agency began its own investigation program about the use of stainless steel for road structures with the aim of establishing a framework and a definitive guide for the use of stainless steel. The result was the publication in 2002 of a departmental advice note (Highways Agency 2002) for the use of stainless steel reinforcement in road structures.

### 2.3 *Selection of steel grade*

Only austenitic and duplex stainless steels are recommended for concrete due to their corrosion resistance. Austenitic steel is the most used because of its widely known corrosion resistance in concrete with significant chloride content. Its tolerance towards chloride content is 5 to 10 times larger than that of the carbon

steel (Whiteway 1998). Austenitic steel 1.4301 (AISI 304) would be the adequate for low chloride ion concentration or no marine atmospheric exposure (Highways Agency 2002). Under severer conditions, AISI 316 is recommended.

### 2.4 *Design implications of using stainless steel reinforcement*

Stainless steel reinforcement do not change design and building criteria, except with respect to durability oriented measures because it offers the possibility of relaxing some of the design requirements for durability, originally thought for carbon steel (Highways Agency 2002, Gedge 2003). That relaxation can be introduced in four design conditions: concrete mix, covers, allowable crack width and hydrophobic impregnation materials. This relaxation produces some saving that minimizes the inevitable additional cost associated to the use of stainless steel reinforcement. In relation to concrete quality, it is no recommended to design relaxed concrete mixes although there is no need to adopt more onerous mix designs (Gedge 2003). With respect to the cover, in absolute terms a 30 mm covering or less would be enough irrespective of the concrete quality and exposure condition (Highways Agency 2002). Crack width limit can achieve the 0.30 mm (Highways Agency 2002) or 0.35 mm (Gedge 2000). However, the effects of this measure would only be perceivable where this factor determines the design. On the other hand, waterproofing coatings can be eliminated where they only protect reinforcement from chloride ion ingress.

Table 1. Steel environmental profile (per tone).

Energy (GJ/t)	19
<i>Raw materials</i>	
Iron ore (kg/t)	1500
Limestone (kg/t)	225
Coal (kg/t)	750
<i>Emissions (*)</i>	
Slag (kg/t)	145
Granulated slag (kg/t)	230
Residual water (l/t)	150,000
Gaseous emissions (t/t)	2
Carbon dioxide (CO <sub>2</sub> ) (kg/t)	1,950.000
Nitrogen oxides (NO <sub>x</sub> ) (kg/t)	3.000
Sulfuric oxide (SO <sub>2</sub> ) (kg/t)	4.000
Methane (CH <sub>4</sub> ) (kg/t)	0.626
Volatile organic compounds (VOC)	0.234
Dust (kg/t)	15.000
Heavy metals (kg/t)	0.037
(Pb, Cd, Hg, As, Cr, Cu, Ni, Se, Zn, V)	

(\*)Values of gaseous emissions from table 1 have been obtained from the statistics of emissions of the British iron and steel industry (1997).

### 3 MATERIAL FLOW

Table 1 shows the amount of raw materials and energy consumed and the byproducts and emissions generated for each tone of steel (Lawson 1996).

There are few references available that scientifically quantify concrete emissions. Comparative life cycle assessments are often not feasible due to the lack of homogeneity of data, due to the uncertainties of system boundaries or due to the insufficient information about the analytical methods used or the geographical scope (Josa et al. 2004). Such panorama requires an effort to gather and adapt the most reliable data available.

Cement is concrete main polluting agent, representing more than the 70% of emissions and energy consumption in concrete manufacturing due to the high temperatures needed for its production and for the lime-carbonate decomposition. Therefore, concrete manufacturing environmental effects depend mainly on its cement content, which is about 10% to 15% on weight. Minimum cement content is fixed by the exposure conditions of the structure: 250 Kg/m<sup>3</sup> for a non aggressive atmospheric exposure and 325 Kg/m<sup>3</sup> for a non marine chloride exposition (Ministerio de Fomento 1998).

CO<sub>2</sub> emission per concrete volume varies depending on the source, ranging between 1 and 1.25 CO<sub>2</sub> tones per cement tone (Gjorv 2003, Wilson 1993). In this work, CO<sub>2</sub> emissions per concrete tone due to cement production is obtained considering one tone of CO<sub>2</sub> emissions per cement tone and a concrete density of 2350 kg/m<sup>3</sup>. Cement represents the 83% of CO<sub>2</sub> emissions from concrete manufacturing (Häkkinen & Vares, 1998). Therefore, total CO<sub>2</sub> emissions would be between 128 and 166 g CO<sub>2</sub>/kg concrete, depending on the exposure condition. Table 2 show selected values for the environmental profile of concrete.

Table 2. Concrete environmental profile (per kg).

Energy	
Fuel	0.93 MJ
Electricity	0.20 MJ
<i>Raw materials</i>	
Limestone	170 g
Other mineral products	850 g
Water	80 g
<i>Emissions</i>	
Carbon dioxide (CO <sub>2</sub> )	120 g
Nitrogen oxides (NO <sub>x</sub> )	0.55 g
Sulphuric oxide (SO <sub>2</sub> )	0.14 g
Methane (CH <sub>4</sub> )	0.13 g
Volatile organic compounds (VOC <sub>tot</sub> )	0.18 g
Dust	0.023 g
Heavy metals (Cr, As, Cd, Hg, Tl, Pb)	20 µg

Table 3. Main characteristics of the tank.

Water height	5.00 m
Liquid density	9.81 kN/m <sup>3</sup>
Effective depth of the wall	400 mm
Effective depth of the ground slab	200 mm
Steel strength (f <sub>y,k</sub> )	500 N/mm <sup>2</sup>
Exposure conditions inside:	chloride of non marine origin
Exposure conditions outside:	external non aggressive
Crack width limit:	0.20 mm

## 4 COMPARISON BETWEEN THE USE OF STAINLESS OR CARBON STEEL AS REINFORCEMENT IN CONCRETE TANKS

### 4.1 LCA process: objectives

LCA can be done for different reasons or with different goals. A typical goal can be the environmental comparison between two products, services or processes, however other modalities are possible. In this case, the comparison between the use of stainless steel or carbon steel as reinforcement in concrete tanks is selected.

The functional unit chosen is a tank of undefined plan sizes on the ground surface containing highly aggressive wastewater, which main characteristics are summarized in Table 3. The tank is supposed to have a ground slab and a straight wall, which resists water pressure acting as a cantilever. In order to generalize the case, tanks are supposed to be enough long and wide to consider corner effects negligible. Then, the functional unit is divided in two parts: wall and slab.

The selected water height is very common in such tanks. The limitation of crack width to 0.20 mm owes to watertightness requirement. Minimum cement content allowed by stainless steel is 250 Kg/m<sup>3</sup>, with a concrete strength around 25 N/mm<sup>2</sup>. Carbon steel reinforcement under aggressive exposure conditions requires a minimum cement content of 325 Kg/m<sup>3</sup>, such content normally produces a 30 N/mm<sup>2</sup> concrete. Stainless steel rebar allows reducing cover as far as the minimum value for normal exposure conditions (20 mm), whereas carbon steel requires 35 mm. By using the same level of execution control, nominal covers are 30 mm and 50 mm, respectively. Adding the different covers to the fixed effective depth results a total wall depth of 500 mm for carbon steel and 450 mm for stainless steel (it would be 460 but it is rounded off for execution precision reasons). Similarly, for the ground slab results a total depth of 300 mm and 250 mm respectively.

### 4.2 LCA process: Life cycle inventory analysis

Inventory assessment begins defining the system to study, next divides the system in different stages in order to organize the study and finally establish the material and energetic flows involved in each stage. Most representative stages are (Fig. 1): (1) concrete and steel production, (2) concrete and steel transport,

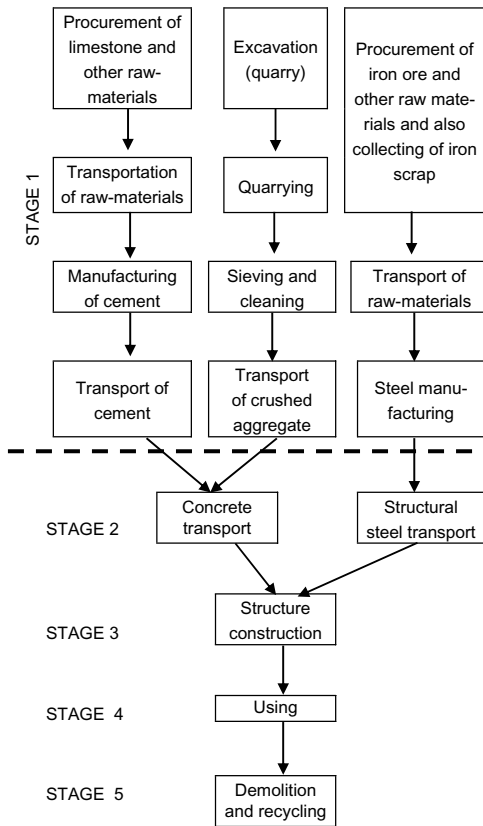


Figure 1. Reinforced concrete tank life cycle tree.

Table 4. Transport energy consumption and emissions.

Energy	13.2 MJ/veh/km
CO	8.0 g/veh/km
NO <sub>x</sub>	17.5 g/veh/km
VOC	2.8 g/veh/km
CO <sub>2</sub>	1158.0 g/veh/km
SO <sub>2</sub>	1.58 g/veh/km

(3) structure construction, (4) use of the structure and (5) demolition and recycling.

Stage 1: Concrete and steel production. After estimating the material amounts required for each tank, total emissions generated during concrete and steel production can be evaluated using the data of unitary emissions from Tables 1 and 2.

Stage 2: Concrete and steel transport. Average range of materials transport is 40 km and of fuel consumption 0.33 l/km. If one liter of diesel fuel is equivalent to 40 MJ, energetic consumption will be 13.20 MJ/km. Table 4 shows the energy consumptions and the emissions per vehicle and km.

Stage 3: Structure construction and Stage 4: Use of the structure, present similar environmental costs in both tanks.

Table 5. Global warming potential in CO<sub>2</sub>-eq per m<sup>2</sup> of ground slab or per m wall.

Stage	Carbon steel tank		Stainless steel tank	
	Wall	Ground slab	Wall	Ground slab
Manufacturing (concrete + steel)	2817.16	279.73	2283.36	200.35
Transport	10.13	1.18	9.14	0.98
Demolition	7.09	0.83	6.40	0.69
TOTAL	2834.38	281.74	2298.90	202.02

Stage 5: Demolition and recycling. Once the structure life is ended, it will be demolished and possibly recycled. Demolition waste weight quantities result:

Carbon steel tank wall = 6.12 t/m

Stainless steel tank wall = 5.53 t/m

Carbon steel ground slab = 0.71 t/m<sup>2</sup>

Stainless steel ground slab = 0.59 t/m<sup>2</sup>

For the waste transport at this stage, the hypotheses about material transport are those of stage 2.

With regard to waste recycling, it is necessary to say that waste recycling in Spain is practically nonexistent (10%) although its great potential. In this stage only emissions generated during waste transportation to deposition place are considered.

#### 4.3 Life cycle impact evaluation (ISO 14042)

Each environmental inventory category must have a coefficient in order to do a weighed sum and obtain a single index for each product or component that it is being analyzed. At present time, theoretical bases for impact evaluation and even more, for interpreting and comparing the wide range of sources and environmental impacts, are not fully stated. In next paragraphs the impact categories selected are described.

Global warming: The contribution to global warming is calculated in CO<sub>2</sub>-equivalents or Global Warming Potentials (GWPs). GWPs are based on the radiative efficiency of each gas relative to that of CO<sub>2</sub>, as well as the relative decay rate of each gas, according to the Intergovernmental Panel on Climate Change (IPCC). Gas emissions generated during the structure life cycle which contribute to global warming are CO<sub>2</sub>, CH<sub>4</sub> and NO<sub>x</sub> (Table 5). Results yield that the use of stainless steel allows a reduction of a 20% of CO<sub>2</sub> emissions.

Acidification: is the process whereby air pollution is converted into acid substances causing damage to forests and lakes. The potential contribution to acidification from SO<sub>2</sub> and NO<sub>x</sub> is calculated in SO<sub>2</sub>-eq (Tab. 6). The results indicate that the use of stainless steel allows a 13% reduction of acidification per m of wall and a 20% per m<sup>2</sup> of ground slab.

Eutrophication is a process whereby water bodies receive excess of nutrients that stimulate an excessive plant growth which reduces dissolved oxygen in the water and can cause other organisms to die. Gas emissions generated during lifecycle which contribute



Table 6. Equivalence factors Eco-indicator 95 (SimaPro 4.0).

Substances	g SO <sub>2</sub> -eq/g substance
SO <sub>x</sub>	1.00
NH <sub>3</sub>	1.88
NO <sub>x</sub>	0.70

Table 7. Eutrophication potential in g PO<sub>4</sub>-eq per m<sup>2</sup> of ground slab or per wall m.

Stage	Carbon steel tank		Stainless steel tank	
	Wall	Ground slab	Wall	Ground slab
Manufacturing (concrete + steel)	586.10	62.40	492.10	47.40
Transportation	19.90	2.32	17.96	1.94
Demolition	13.93	1.62	12.57	1.35
TOTAL	619.93	66.34	522.63	50.69

Table 8. Equivalence factors Eco-indicator 95 (SimaPro 4.0).

Substance	g C <sub>2</sub> H <sub>4</sub> -eq/g substance
C <sub>2</sub> H <sub>4</sub>	1.000
CH <sub>4</sub>	0.007
VOC	0.398

Table 9. Contribution of each stage to photochemical smog in g C<sub>2</sub>H<sub>4</sub>-eq per m<sup>2</sup> of ground slab and per m of wall.

Stage	Carbon steel tank		Stainless steel tank	
	Wall	Ground slab	Wall	Ground slab
Manufacturing (concrete + steel)	450.60	52.10	407.00	43.40
Transport	9.75	1.14	8.80	0.95
Demolition	6.83	0.80	6.16	0.66
TOTAL	467.18	54.04	421.96	45.01

to eutrophication are PO<sub>4</sub>-eq. Table 7 reflects the contribution of each stage to eutrophication. Stainless steel allows a reduction of the 16% of eutrophication per wall m and 24% per ground slab m<sup>2</sup>.

Photochemical smog is the chemical reaction of sunlight, nitrogen oxides (NO<sub>x</sub>) and volatile organic compounds (VOC's) in the atmosphere, which leaves airborne particles and ground-level ozone. The potential contribution from various substances is calculated in CH<sub>4</sub>-eq (Tab. 8). Gas emissions which contribute to photochemical smog are CH<sub>4</sub> and VOC (volatile organic compounds). The use of stainless steel allows a reduction of a 10% of smog per wall m and a 17% per ground slab m<sup>2</sup> (Tab. 9).

Embodied energy is the energy consumed by all the processes associated with the whole lifecycle of the tank. The use of stainless steel allows a reduction of a 16% of energy consumption per wall m and 27% per ground slab m<sup>2</sup> (Tab. 10).

Table 10. Embodied energy in MJ per m<sup>2</sup> of ground slab and per m of wall.

Stage	Carbon steel tank		Stainless steel tank	
	Wall	Ground slab	Wall	Ground slab
Manufacturing (concrete + steel)	12728.56	1138.92	10682.97	831.60
Transport	115.49	13.47	104.23	11.23
Demolition	80.84	9.43	72.96	7.86
TOTAL	12924.89	1161.82	10859.19	850.69

Table 11. Waste generation during the wall lifecycle in kg per m for the solid waste and l for the liquid.

Stage	Carbon steel tank		Stainless steel tank	
	Solid	Liquid	Solid	Liquid
Manufacturing (concrete + steel)	93.52	37409.65	89.79	35916.91
Demolition	6120.00		5530.00	
TOTAL	6213.52	37409.65	5619.79	35916.91

Table 12. Waste generation during the ground slab lifecycle in kg per m<sup>2</sup> for the solid waste and l for the liquid.

Stage	Carbon steel tank		Stainless steel tank	
	Solid	Liquid	Solid	Liquid
Manufacturing (concrete + steel)	3.55	1422.00	2.97	1185.00
Demolition	714.00		595.00	
TOTAL	717.55	1422.00	597.97	1185.00

Table 13. Heavy metal emitted (g) during lifecycle, per m of wall and m<sup>2</sup> of ground slab.

Stage	Carbon steel tank		Stainless steel tank	
	Wall	Ground slab	wall	Ground slab
Concrete	0.15	0.02	0.11	0.01
Steel	9227.71	350.76	8859.50	292.30
TOTAL	9227.86	350.78	8859.61	292.31

In order to obtain the solid and liquid waste generation for each tank typology, the values of every stage are added up. Stainless steel allows a 16% reduction of solid waste per wall m and a 27% per m<sup>2</sup> of ground slab, whereas the liquid waste reduction is of a 4% and a 17%, respectively (Tabs. 11 and 12).

Table 13 shows the results obtained of the heavy metal emission, which indicate that the use of stainless steel allows a 4% reduction of their emission per wall m and a 17% per m<sup>2</sup> of ground slab.

In order to compare the environmental impact of each kind of tank, a global value which considers each impact category is necessary. Table 14 shows

Table 14. Impact potential contribution by Eco-Indicator 95.

Impact category	Value per functional unit	Functional unit
Global warming	2.5	Kg CO <sub>2</sub> -eq
Acidification	10.0	Kg SO <sub>2</sub> -eq
Eutrophication	5.0	Kg PO <sub>4</sub> -eq
Summer smog	2.5	Kg C <sub>2</sub> H <sub>4</sub> -eq
Heavy metal emission	5.0	Kg

Table 15. Environmental impact potential per wall meter.

Environmental impact category	Carbon steel	Stainless steel
Global warming (kg CO <sub>2</sub> -eq)	7085.95	5747.25
Acidification (kg SO <sub>2</sub> -eq)	51.82	45.34
Eutrophication (kg PO <sub>4</sub> -eq)	3.10	2.61
Summer smog (kg C <sub>2</sub> H <sub>4</sub> -eq)	1.17	1.06
Heavy metal emission (kg)	46.15	44.30
Eco-Indicator 95	7188.19	5840.56

Table 16. Environmental impact potential per square m of slab.

Environmental impact category	Carbon steel	Stainless steel
Global warming (kg CO <sub>2</sub> -eq)	704.35	505.05
Acidification (kg SO <sub>2</sub> -eq)	4.96	3.89
Eutrophication (kg PO <sub>4</sub> -eq)	0.33	0.26
Summer smog (kg C <sub>2</sub> H <sub>4</sub> -eq)	0.13	0.11
Heavy metal emission (kg)	1.75	1.45
Eco-Indicator 95	711.52	510.76

the impact category contribution potential to global environmental impact according to Eco-Indicator 95 methodology. The use of stainless steel reinforcement reduces a 19% environmental impact per wall m and a 28% per ground slab m<sup>2</sup> (Tables 15 and 16).

Global warming is the most significant impact category during the tank lifecycle (98%), independently of the kind of steel used. In particular, concrete and steel production is the main contributors to global warming, acidification, water eutrophication, photochemical smog creation, embodied energy and liquid waste emission. Steel production is the stage that most contributes to heavy metal emission.

#### 4.4 Economical analysis

The economical costs of the tank during its lifecycle can be divided in two: direct costs and the costs derived from the CO<sub>2</sub> emissions. The stage that introduces the greatest differences between both tanks is the acquisition of materials, steel and concrete. Costs of construction and use would be similar in both types of tanks whereas transport cost differences would be almost negligible. The same comment is valid for demolition and recycling costs. 26 €/t is the prize considered for CO<sub>2</sub> emission rights. Costs shown in Table 17 include materials direct costs and those from CO<sub>2</sub> emission rights. Results obtained indicate that, although stainless steel bars are 3.5 times more expensive than carbon

Table 17. Costs during the lifecycle of the two tanks in €.

	Carbon steel tank		Stainless steel tank	
	Wall	Ground slab	Wall	Ground slab
Materials	674.38	33.26	1217.83	45.40
CO <sub>2</sub> emissions	73.69	7.32	59.77	5.25
TOTAL	748.07	40.58	1277.61	50.65

steel ones, the cost of a stainless steel reinforced concrete wall is only 1.7 times the price of a carbon steel one. This factor for the ground slab is merely 1.25.

## 5 CONCLUSIONS

LCA methodology was applied to study the feasibility of building wastewater concrete tanks with stainless steel reinforcement. Nowadays there is guidance and experience for the use of stainless steel as an alternative for the reinforcement of concrete structures. The use of stainless steel reinforcement allows relaxing some restrictive prescriptions of current structural concrete codes, in aggressive exposure conditions.

Under these conditions, the cost of erecting a tank with stainless steel reinforcement is a 70% larger than the cost of the carbon steel one. This result was achieved disregarding the maintenance costs that would reduce the economical difference. Besides, life cycle assessment concludes that building a tank with stainless steel reinforcement allows reducing a 20% its environmental impact.

## REFERENCES

- Cembureau 2005. *Activity Report 2004*.
- Concrete Society. Guidance on the use of stainless steel reinforcement. Article published by the *Concrete Society direction committee*.
- Gedge, G. 2000. Structural Properties of Stainless Steel Rebar *Symposium Structural Applications of Stainless Steel in Building and Architecture*, organized by Euro Inox. Brussels.
- Gedge, G. 2003. Rationale for using stainless steel reinforcement in the UK construction industry. *International Stainless Steel Forum-7*, Berlin, December 2003.
- Gjorv, O.E. 2003. Durability Design and Construction Quality. *International Conference in Concrete and Structures Advances 2003*, Xuzhou, Jiangsu, China.
- Häkkinen, T. & Vares, S. 1998. *Environmental Burdens of concrete and concrete products*, Technical Research Centre of Finland.
- Highways Agency 2002. BA 84/02 Use of stainless Steel reinforcement in highway structures. *Part 15 Design manual for roads and bridges*. UK.
- Josa, A., Aguado, A., Heino, A. & Cardim, A. 2004. Comparative analysis of available life cycle inventories of cement in the EU *Cement and Concrete Research* 34: 1313–1320.
- Lawson, B. 1996. *Building materials, energy and the environment: Towards ecologically sustainable development*. Red Hill, A.C. T.: Royal Australian Institute of Architects.
- Ministerio de Fomento 1999. *Instrucción de hormigón estructural (EHE)*.
- Whiteway, P. 1998. Building Better Bridges. *Nickel Magazine*, 14(1).
- Wilson, A. 1993. Cement and Concrete: Environmental Considerations; *Environmental Building News*, 2 (2); <http://www.buildinggreen.com/features/cem/cementconcl>.

# Seismic loss estimation based on end-to-end simulation

M. Muto, S. Krishnan & J.L. Beck

*California Institute of Technology, Pasadena, California*

J. Mitrani-Reiser

*Johns Hopkins University, Baltimore, Maryland*

**ABSTRACT:** Recently, there has been increasing interest in simulating all aspects of the seismic risk problem, from the source mechanism to the propagation of seismic waves to nonlinear time-history analysis of structural response and finally to building damage and repair costs. This study presents a framework for performing truly “end-to-end” simulation. A recent region-wide study of tall steel-frame building response to a  $M_w$  7.9 scenario earthquake on the southern portion of the San Andreas Fault is extended to consider economic losses. In that study a source mechanism model and a velocity model, in conjunction with a finite-element model of Southern California, were used to calculate ground motions at 636 sites throughout the San Fernando and Los Angeles basins. At each site, time history analyses of a nonlinear deteriorating structural model of an 18-story steel moment-resisting frame building were performed, using both a pre-Northridge earthquake design (with welds at the moment-resisting connections that are susceptible to fracture) and a modern code (UBC 1997) design. This work uses the simulation results to estimate losses by applying the MDLA (Matlab Damage and Loss Analysis) toolbox, developed to implement the PEER loss-estimation methodology. The toolbox includes damage prediction and repair cost estimation for structural and non-structural components and allows for the computation of the mean and variance of building repair costs conditional on engineering demand parameters (i. e. inter-story drift ratios and peak floor accelerations). Here, it is modified to treat steel-frame high-rises, including aspects such as mechanical, electrical and plumbing systems, traction elevators, and the possibility of irreparable structural damage. Contour plots of conditional mean losses are generated for the San Fernando and the Los Angeles basins for the pre-Northridge and modern code designed buildings, allowing for comparison of the economic effects of the updated code for the scenario event. In principle, by simulating multiple seismic events, consistent with the probabilistic seismic hazard for a building site, the same basic approach could be used to quantify the uncertain losses from future earthquakes.

## 1 INTRODUCTION

Advances in computational seismology and earthquake engineering allow for increasingly sophisticated predictions of seismic response of buildings, including end-to-end simulation (Krishnan et al. 2006a, 2006b). However, for these methods to be of value to decision-makers, they need to be translated into financial terms.

Seismologists have created 3-D Earth models, and with advances in parallel computing can simulate global and regional seismic wave propagation using Finite Element and Finite Difference methods. Similarly, advances in the finite-element modeling of structures now make it possible to produce three-dimensional models of tall buildings which capture many of the material and geometric nonlinearities associated with strong seismic loading, and to facilitate the modeling of structural stability and damage.

As these computational tools in seismology and structural engineering become more accurate, and the increasing availability of computational power makes the application of these tools on a large scale feasible, there exists an opportunity to use these tools to perform so called “end-to-end” earthquake simulations, modeling the process from the rupture physics to structural performance and economic loss. This approach in particular has the potential to be a very powerful tool for performance-based earthquake engineering (PBEE).

The Pacific Earthquake Engineering Center (PEER) has developed a modular approach for PBEE (Porter 2003; Moehle and Deierlein 2004; Goulet et al. 2007). The first step is a seismic hazard analysis for a site, to establish an intensity measure (IM) for potential ground motions. The second step is a structural analysis, in which the IM and structural design are used to determine the resulting values for structural response measures such as peak transient

inter-story drift ratio (IDR) or peak floor acceleration, which are referred to as engineering demand parameters (EDP). In the damage analysis phase, the EDP is used with experimentally or empirically determined fragility functions to compute damage measures (DM) for the building components. Finally, the DM values are used in a loss analysis, where the losses are calculated using measures such as repair cost, repair duration, and loss of life. The modules are designed to implement a probabilistic approach to hazard analysis, so that the final result is essentially an integral involving a set of conditional probability density functions, which are used to “integrate out” the uncertainties associated with each module.

In the PEER methodology, the first two steps are usually carried out using probabilistic seismic hazard and building vulnerability curves. Here, a full seismic risk analysis is not attempted; instead, only the damage and loss steps are implemented by applying an extended version of the MDLA toolbox developed at Caltech (Mitrani-Reiser 2007) to the results of a Southern California-wide study of the response of two steel-frame buildings to a  $M_w$  7.9 scenario earthquake (Krishnan et al. 2006a, 2006b). This effectively extends the PBEE methodology to include simulation of the source rupture mechanism and wave propagation to the building site. Only one scenario event is considered here but work is underway to combine the results presented here with a probabilistic seismic hazard analysis to quantify uncertain losses from future earthquakes and hence, ultimately, to life-cycle costs for a building at one of the sites in the Southern California region.

## 2 SCENARIO EARTHQUAKE AND BUILDING RESPONSE

The regions of interest for this study are the Los Angeles basin and the San Fernando valley, areas with large inventories of high-rise buildings and high levels of seismic risk. The chosen scenario event is a  $M_w$  7.9 earthquake along a 290-km segment of the southern San Andreas fault (similar to the 1857 Fort Tejon earthquake), with the slip model derived from a finite-source inversion of the November 3, 2002 Denali earthquake in Alaska (Ji et al. 2003). The rupture was initiated at Parkfield in central California, propagated in a south-easterly direction, and terminated just north of the San Gabriel valley, as shown in Figure 1 (inset). Krishnan et al. (2006a, 2006b) computed ground motion time histories for the 636 analysis sites (spaced uniformly at approximately 3.5 km, as shown in Figure 1) using the spectral element method (e. g. Komatitsch and Tromp 1999), with peak velocities of up to 2 m/s and peak displacements of about 2 m.

At each analysis site, they performed three-dimensional nonlinear dynamic analyses of two

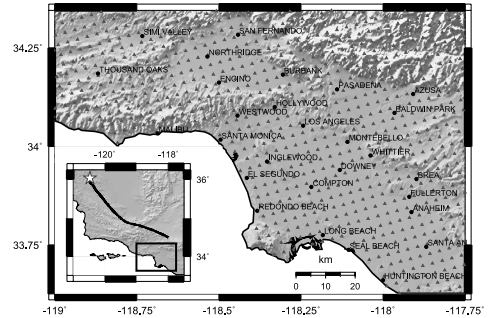


Figure 1. Scope of study area. Small triangles indicate locations where ground motion time histories are computed. Major cities are shown for reference. The inset shows the rupture trace in relation to the study area and the star represents the rupture initiation point (Parkfield).

building models using the program FRAME3D (Krishnan 2003; Krishnan and Hall 2006a, 2006b). Building response time histories were calculated, in addition to the induced structural damage, for two building designs.

Building 1 is based on an existing 18-story steel moment frame building, designed according to the 1982 Uniform Building Code (UBC) and constructed in 1986–87, that experienced significant damage (moment-frame connection fractures) during the 1994 Northridge earthquake. The existing building has 17 office stories above ground and a mechanical penthouse on top. The height above ground is 75.7 m. The typical floor plan is shown in Figure 2. The lateral force-resisting system consists of two-bay welded steel moment frames, two in each direction. The location of the north frame at one bay inside the perimeter results in some torsional eccentricity. Many of the moment-frame connections in the building fractured during the 1994 Northridge earthquake, leading to extensive studies of the building (SAC 1995; Carlson 1999). The finite-element model was developed from the building plans, and the material properties were based on samples of the structural steel from the building. The brittle failure of moment connections is also modeled in a probabilistic manner.

Building 2 uses the same architecture as Building 1, but the lateral force-resisting system has been re-designed according to the 1997 UBC. It has greater redundancy and strength than Building 1, with eight moment-frame bays in each direction (Figure 3). Additionally, moment connections designed after the 1994 Northridge earthquake are expected to behave in a ductile fashion, so connection fractures are not included in the analysis of Building 2.

Detailed floor plans, beam and column sizes, and gravity, wind, and seismic loading criteria for both buildings are given in Krishnan et al. (2005).

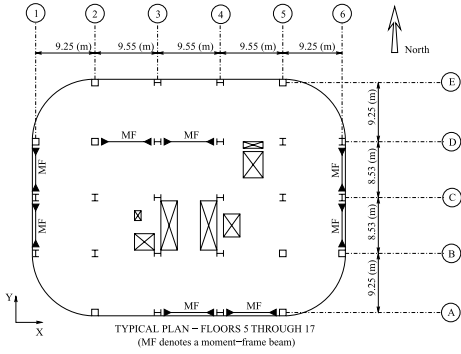


Figure 2. Typical plan for Building 1. Lines marked with 'MF' indicate moment-frame bays.

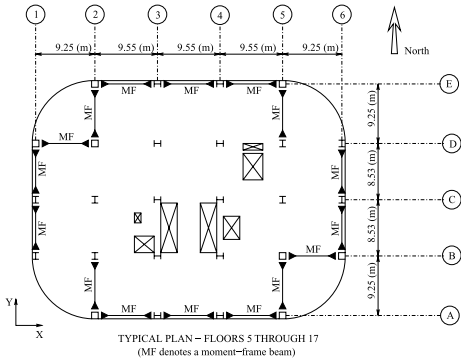


Figure 3. Typical plan for Building 2. Lines marked with 'MF' indicate moment-frame bays.

Values of peak IDR from the nonlinear analyses of the Buildings 1 and 2, subjected to the simulated ground motion time histories, are summarized in Figures 4 and 5, respectively. Shading is used to indicate building performance levels defined by FEMA 356 (2000) for Immediate Occupancy (IO), Life Safety (LS), and Collapse Prevention (CP). In addition to these performance categories, we classify buildings with greater damage as being Red-Tagged (RT) or Collapsed (CO). The peak IDR for Building 1 exceeds 0.05, the maximum value for performance level CP, throughout the San Fernando valley and in a major portion of the Los Angeles basin. For Building 2, values of peak IDR are reduced in the Los Angeles basin (but still exceed the maximum value for performance level LS of 0.025), and exceed 0.05 for most of the San Fernando valley.

### 3 BASIS FOR LOSS ESTIMATION

While it has been demonstrated that for smaller events, damage to non-structural components can contribute significantly to life-cycle costs (e. g. Goulet et al.

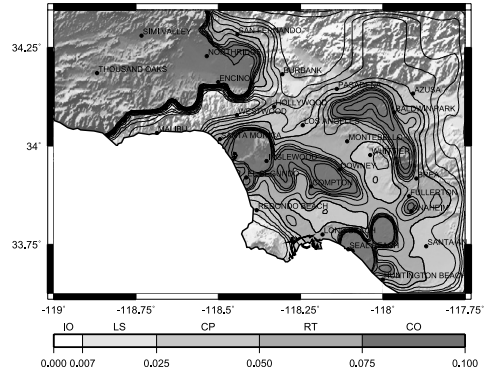


Figure 4. Peak IDR for Building 1 in the scenario earthquake, with regions classified according to FEMA limits for Immediate Occupancy (IO), Life Safety (LS), and Collapse Prevention (CP), and two additional damage states, Red-Tagged (RT) and Collapsed (CO).

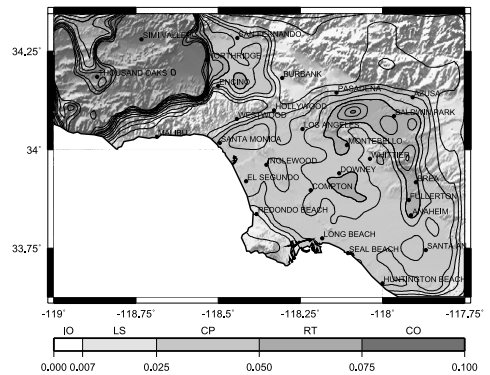


Figure 5. Peak IDR for Building 2 in the scenario earthquake, with regions classified according to FEMA limits for Immediate Occupancy (IO), Life Safety (LS), and Collapse Prevention (CP), and two additional damage states, Red-Tagged (RT) and Collapsed (CO).

2007), in large seismic events such as the one considered in this study, there is a significant probability for a building to suffer irreparable damage or even complete collapse.

Iwata et al. (2006) present a study of twelve steel structures damaged in the 1995 Kobe earthquake. Using the measured residual peak IDR and reported repair costs, they estimate a reparability limit of 0.015 for the peak residual IDR. However, there are two cases presented by Iwata et al. (2006) where buildings with peak residual IDR greater than 0.02 were successfully repaired. Based on this description, we chose to describe the probability of irreparable damage as a lognormal cumulative distribution function (CDF) parameterized with logarithmic median  $\mu = 0.02$ , and logarithmic standard deviation  $\beta = 0.5$ . The

Table 1. Repair/Replacement costs and fragility functions for building components.

Assembly	Unit	Quantity	EDP	Fragility parameters		Action	Cost (\$ U.S.)
				$\mu$	$\beta$		
<i>Structure in irreparable state</i>							
Structure and cladding	ft <sup>2</sup>	280,988	Perm. IDR	0.02	0.5	Replace	180
Plumbing systems	ft <sup>2</sup>	280,988	Perm. IDR	0.02	0.5	Replace	9
Electrical systems	ft <sup>2</sup>	280,988	Perm. IDR	0.02	0.5	Replace	25
HVAC	ft <sup>2</sup>	280,988	Perm. IDR	0.02	0.5	Replace	30
Elevators	ea	3	Perm. IDR	0.02	0.5	Replace	1,300,000
Non-structural elements	ft <sup>2</sup>	280,988	Perm. IDR	0.02	0.5	Replace	82
Construction costs	ft <sup>2</sup>	280,988	Perm. IDR	0.02	0.5	Replace	60
Total cost							112,400,000
<i>Structure in a reparable damage state</i>							
Moment conn. (Bldg. 1; fracture mode)	ea	284	Damage calculated in FEA			Repair	20,000
Moment conn. (Bldg. 2; flange buckling)	ea	550	IDR	0.05	0.5	Repair	20,000
Drywall partitions (visible damage)	64 ft <sup>2</sup>	6,098	IDR	0.0039	0.17	Repair	88
Drywall partitions (significant damage)	64 ft <sup>2</sup>	6,098	IDR	0.0085	0.23	Repair	525
Drywall finish (visible damage)	64 ft <sup>2</sup>	6,098	IDR	0.0039	0.17	Repair	88
Drywall finish (significant damage)	64 ft <sup>2</sup>	6,098	IDR	0.0085	0.23	Repair	253
Exterior glazing	panel	3,423	IDR	0.040	0.36	Repair	439
Elevators	ea	3	Perm. IDR	0.01	0.25	Replace	1,300,000
Automatic sprinklers	12 ft	2,757	Accel.	32	1.4	Repair	900
Acoustical ceiling	ft <sup>2</sup>	280,988	Accel.	92/(1 + w)		Repair	2.21
Interior paint	ft <sup>2</sup>	280,988	Based on ratio of dmg. to undmg. area			Repair	1.52

cost of replacing Building 1 or 2 with a current state-of-the-art structure is estimated to be approximately \$112 M (U.S.), including the cost of structural and non-structural components, and plumbing, electrical, and heating, ventilation and air-conditioning (HVAC) systems; the latter costs are based on estimates for current construction, as shown in the first part of Table 1.

The MDLA toolbox estimates repair costs using an assembly-based vulnerability approach (Porter 2000). The second part of Table 1 summarizes the damageable components in the buildings. In Building 1, damage to moment connections takes the form of connection fractures, which are calculated directly during the finite-element analysis. In Building 2, the moment connections are assumed to remain ductile. However, for large inter-story drifts, connections are expected to fail in a local flange-buckling mode. Since this mode of failure is not incorporated in the structural analysis, damage to connections for Building 2 is modeled using a probabilistic approach. The connections are grouped by story (e. g. connections at the second floor are associated with the first story) and direction of the moment-frame bay, and damage to each group is estimated using a fragility function based on the peak transient IDR at each story in the same direction as the connection group. This function is defined by a lognormal CDF with  $\mu = 0.05$  and  $\beta = 0.5$ . Probabilistic descriptions of damage to the interior partitions, exterior glazing, acoustical ceiling, and sprinkler system

are calculated using fragility functions developed by Porter (2000) that have the form of lognormal CDFs. The governing EDP and fragility function parameters are summarized in the second part of Table 1.

Fragility functions for hydraulic elevators are given by Porter (2007). However, there is little published information on the repair and replacement of the traction elevators used in high-rise buildings. Following the Northridge earthquake, the elevators in Building 1 were unable to properly function due to approximately six inches of permanent roof displacement. Based on the observed damage pattern, a major portion of this displacement was most likely accommodated over four stories, resulting in a peak permanent IDR of 0.01. Therefore, the fragility function for the elevators is taken as a lognormal CDF on residual peak IDR with  $\mu = 0.01$  and  $\beta = 0.25$ . The plumbing, electrical, and HVAC systems are assumed to be robust, since we felt that serious damage to these components would likely be associated with irreparable structural damage, in which case the entire building must be replaced anyway.

Repair and replacement costs for components are also shown in Table 1. Average repair costs for the fractured moment connections in Building 1 are based on a collection of reported values for repairs to fractured connections in steel moment-frame buildings following the 1994 Northridge earthquake (Bonowitz and Maison 2003). Since a major portion of the cost is

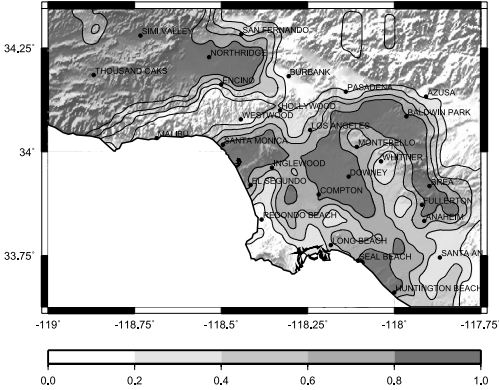


Figure 6. Mean loss for Building 1, normalized by building replacement cost. Near-total losses are calculated for the San Fernando valley and much of the Los Angeles basin.

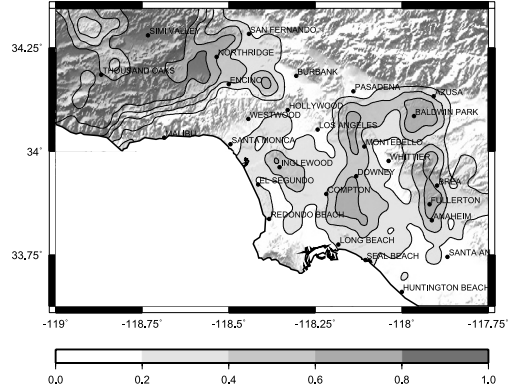


Figure 7. Mean loss for Building 2, normalized by building replacement cost. Compared to Building 1, losses in the Los Angeles basin are significantly lower, but losses in the San Fernando valley remain high.

related to accessing the connection, which will be necessary for both fracture and local flange buckling, the cost for repair for both modes of failure is taken to be the same. Repair and replacement costs for the interior partitions, interior paint, exterior glazing, acoustical ceiling tiles, and sprinklers are given by Porter (2000).

#### 4 ESTIMATION OF REPAIR/REPLACEMENT COSTS FOR BUILDINGS UNDER THE SCENARIO EARTHQUAKE

To estimate the losses in Buildings 1 and 2 from the scenario earthquake, the EDPs (peak transient IDR, peak residual IDR, peak floor acceleration) obtained from Krishnan et al. (2006a, 2006b), are used with the fragility and repair/replacement cost functions summarized in Section 3. The geographical distribution of mean (expected) losses for Building 1 is shown in Figure 6. The building performs poorly, with complete losses for locations throughout the San Fernando valley and much of the Los Angeles basin. The performance of Building 2, shown in Figure 7, is much better; the predicted impact of the scenario earthquake in the Los Angeles basin is considerably lower than for Building 1, though significant losses are predicted in some areas of the San Fernando valley.

Figure 8 shows the losses plotted against the residual peak IDR for all 636 analysis sites. It is clear that at higher excitation levels, losses are dominated by the probability of irreparable damage. For Building 1, 309 of the 636 analysis sites have a greater than 50% chance of irreparable damage, while 176 sites for Building 2 fall into that category. Shown in Figure 9 are the losses plotted against the transient peak IDR. We see that for a peak transient of IDR of 0.05, the FEMA acceptance criterion for the collapse prevention (CP) performance level, building losses exceed 50% for much of the

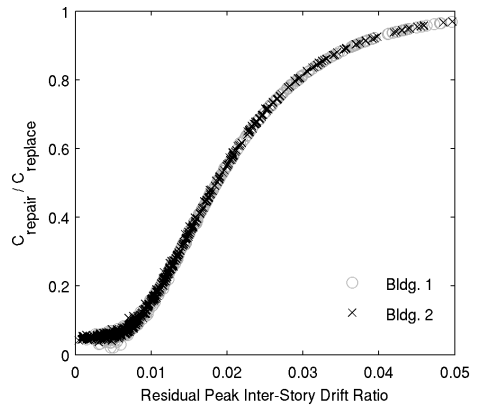


Figure 8. Normalized mean losses for Buildings 1 and 2 plotted against the peak residual inter-story drift ratio (IDR). For values greater than about 0.05, cost is dominated by the probability of irreparable damage, as discussed in Section 3.

region, with near-total losses occurring when the peak IDR exceeds 0.075.

#### 5 CONCLUSIONS

In this prototype study, we have laid the framework for performing a quantitative seismic hazard analysis by detailed simulations at all stages: source rupture, seismic wave propagation, structural response, and induced economic loss. The framework allows for effects such as source rupture directivity and slip distribution, both of which play a critical role in determining the intensity of ground motion at a particular site, to be considered. By simulating a large number of



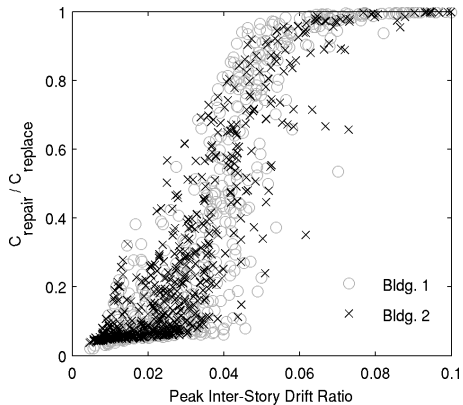


Figure 9. Normalized mean losses for Buildings 1 and 2 plotted against the peak transient IDR. Note that the mean loss for both buildings reaches the replacement cost for peak IDR greater than about 0.075.

plausible earthquakes of varying magnitude from the relevant regional faults and weighing them by their probability of occurrence over a specified time period, it will be possible to develop a more accurate picture of the economic seismic risk faced by a given building. Additionally, by developing a realistic inventory of buildings and other engineered structures, this method can be applied to combine advanced earthquake simulations with structural modeling and PBEE loss methodologies to estimate region-wide losses for major scenario events, which would be very useful in recovery planning.

## REFERENCES

- Bonowitz, & Maison, B. 2003. Northridge welded steel moment-frame damage data and its use for rapid loss estimation. *Earthquake Spectra* 19(3): 335–364.
- Carlson, A. 1999. Three-dimensional nonlinear inelastic analysis of steel moment frame buildings damaged by earthquake excitations. Report EERL 99-02, Earthquake Engineering Laboratory, California Institute of Technology, Pasadena, California, USA.
- FEMA (2000). Prestandard and commentary for the seismic rehabilitation of buildings. Report FEMA 356. Federal Emergency Management Agency, USA.
- Goulet, C., Haselton, C., Mitrani-Reiser, J., Beck, J., Deierlein, G., Porter, K. & Stewart, J., 2007. Evaluation of the seismic performance of a code-conforming reinforced-concrete frame building—from seismic hazard to collapse safety to economic loss. *Earthquake Engineering and Structural Dynamics* 36: 1973–1997.
- Iwata, Y., Sugimoto, H., & Kuwamura, H. 2006. Reparability limit of steel structural buildings based on the actual data of Hyogoken-Nanbu earthquake. *Technical Memorandum of Public Works Research Institute* 4022: 86–95.
- Ji, C., Tan, Y., Helmberger, D., & Tromp, J. 2003. Modeling teleseismic P and SH static offsets for great strike-slip earthquakes. In *Proceedings of the American Geophysical Union Fall Meeting*, USA.
- Komatitsch, D. & Tromp, J. 1999. Introduction to the spectral element method for three-dimensional seismic wave propagation. *Geophys. J. Int.* 139: 806–822.
- Krishnan, S. 2003. FRAME3D—a program for three-dimensional nonlinear time-history analysis of steel buildings: User guide. Report EERL 2003-03, Earthquake Engineering Research Laboratory, California Institute of Technology, Pasadena, California, USA.
- Krishnan, S. & Hall, J. 2006a. Modeling steel frame buildings in three dimensions—Part I: Panel zone and plastic hinge beam elements. *Journal of Engineering Mechanics* 132(4): 345–358.
- Krishnan, S. & Hall, J. 2006b. Modeling steel frame buildings in three dimensions—Part II: Elastofiber beam elements and examples. *Journal of Engineering Mechanics* 132(4): 359–374.
- Krishnan, S., Ji, C., Komatitsch, D., & Tromp, J. 2005. Performance of 18-story steel moment frame buildings during a large San Andreas earthquake—a Southern California-wide end-to-end simulation. Report EERL 2005-01, Earthquake Engineering Research Laboratory, California Institute of Technology, Pasadena, California, USA.
- Krishnan, S., Ji, C., Komatitsch, D., & Tromp, J. 2006a. Case studies of damage to tall steel moment frame buildings in southern California during large San Andreas earthquakes. *Bulletin of the Seismological Society of America* 96(4): 1523–1537.
- Krishnan, S., Ji, C., Komatitsch, D., & Tromp, J. 2006b. Performance of two 18-story steel moment frame buildings in southern California during two large simulated San Andreas earthquakes. *Earthquake Spectra* 22(4): 1035–1061.
- Mitrani-Reiser, J. 2007. *An Ounce of Prevention: Probabilistic Loss Estimation for Performance-Based Earthquake Engineering*. Ph. D. thesis, California Institute of Technology, Pasadena, California, USA.
- Moehle, J. & Deierlein, G. 2004. A framework methodology for performance-based earthquake engineering. In *International Workshop on Performance-Based Engineering*, Bled, Slovenia.
- Porter, K. 2000. *Assembly-Based Vulnerability of Buildings and its Uses in Seismic Performance Evaluation and Risk-Management Decision-Making*. Ph. D. thesis, Stanford University, Stanford, California, USA.
- Porter, K. 2003. An overview of PEER's performance-based earthquake engineering methodology. In *Proceedings of the Ninth International Conference on Applications of Statistics and Probability in Civil Engineering*, San Francisco, California, USA.
- Porter, K. 2007. Fragility of hydraulic elevators for use in performance-based earthquake engineering. *Earthquake Spectra* 23(2): 459–469.
- SAC. 1995. Analytical and field investigations of buildings affected by the Northridge earthquake of January 17, 1994 – Part 2. Report SAC 95-04, Structural Engineers Association of California, Applied Technology Council, and California Universities for Research in Earthquake Engineering, USA.



# Fatigue damage measures with a statistical model for the Wöhler field

M.L. Ruiz-Ripoll, A. García & E. Castillo

*Department of Applied Mathematics and Computational Sciences, University of Cantabria, Spain*

A. Fernández-Canteli

*Department of Construction and Manufacturing Engineering, University of Oviedo, Spain*

R. Koller

*Empa, Dübendorf, Switzerland*

**ABSTRACT:** This paper deals with the problem of accumulating damage due to any fatigue load history. First, some desirable properties for a damage model are discussed and different possible alternatives fulfilling these properties are analyzed. Generally, current damage measures, such as the Palmgren-Miner's rule, do not satisfy these properties. Next, a statistical fatigue regression model, able to predict the Wöhler field for any combination of  $\sigma_{\min}$ ,  $\sigma_{\max}$  or  $R = \sigma_{\min}/\sigma_{\max}$  is presented. This model is based on physical, statistical and compatibility conditions rather than on arbitrary functions. The probability of failure is assumed to be the most suitable option to assess damage measure. According to this, the procedure for obtaining the basic information for constant load, i.e. the probabilistic Wöhler field, is discussed, and formulas for calculating the associated damage are given. Finally, the proposed damage accumulation approach is applied to failure prediction of pieces under a Gaussian and FALSTAFF load spectra.

## 1 INTRODUCTION AND MOTIVATION

The evaluation of fatigue damage is basic and very important in design of structures, because fatigue is becoming determinant and the cause of a high number of failures of mechanical components and structural elements in real practice.

Laboratory tests are usually carried out under constant stress ranges and levels (S-N curves) or under a particular accelerated load history (ASTM E606), but real structures are subjected to fatigue load histories involving much more complex varying stress ranges and stress levels.

There is a long list of models dealing with the parametric definition of the S-N curves for a constant reference stress level, however, for these models to be applicable to real situations, they must be complemented with a damage accumulation model to allow engineers the evaluation of fatigue damage. The complex load history furthermore needs a counting method (ASTM E1049) and other transformations of the real load history to get an equivalent simplified load spectrum. The mean stress must be considered as a secondary parameter besides the stress range, as the main parameter. Models based on empirical assumptions have been already proposed (Collins, 1993).

An important question was risen in Castillo et al. (Castillo et al., 2007c): *what is damage? Or, equivalently how is damage related to failure?* A physical concept of failure, such as crack size, seems to be adequate to define a service limit state, but fatigue failure, as an ultimate limit state, requires a probabilistic framework allowing relating damage levels to probabilities of occurrence. The solution to these question is one of the principal objectives of this paper. Furthermore, several methods to measure damage will be analyzed and discuss to identify which is the best one and which of them are inadequate for measuring damage.

## 2 THE GUMBEL-WÖHLER FIELD

Consider a fatigue test with an alternating constant load, from minimum,  $\sigma_m$ , to maximum,  $\sigma_M$ , stresses, respectively. Castillo et al. (Castillo et al., 2007a) determine the cumulative distribution function of the random lifetime  $N$  (number of cycles to failure) associated with the test, a Gumbel family of models able to reproduce not only the whole Wöhler field for  $\sigma_M$  constant and varying  $\sigma_m$ , but the whole Wöhler field for  $\sigma_m$  constant and varying  $\sigma_M$ .

The proposed Gumbel model is:

$$p = 1 - \exp \left\{ - \exp \left[ \frac{(\log N^* - B)(\log \Delta \sigma^* - C) - E}{D} \right] \right\} \quad (1)$$

where  $0 \leq p \leq 1$  refers to the percentile,  $\Delta \sigma^* = \sigma_M^* - \sigma_m^*$ ,  $\sigma_M^* = \sigma_M / \sigma_0$ ,  $\sigma_m^* = \sigma_m / \sigma_0$ ,  $N^* = N / N_0$  and  $\sigma_0$  and  $N_0$  are some reference stress and number of cycles, respectively, to make the formulas dimensionless.

The physical meanings of the parameters are:  $A$  is the Weibull shape parameter of the cumulative distribution function (cdf) in the S-N field,  $B$  is the threshold value of log-lifetime,  $C$  is the endurance limit ( $\Delta \sigma^*$ ),  $E$  is the parameter defining the position of the corresponding zero-percentile hyperbola and  $D$  is the Weibull scale factor.

Since the model must be valid for any fixed values of  $\sigma_m$  and  $\sigma_M$ , and because for different constant values of  $\sigma_M$  one must have different models of the form (1), the parameters  $A; B; C; D$  and  $E$  must be functions of  $\sigma_M$ . Similarly, if the constant load fatigue tests are run for constant values of  $\sigma_m$ , one has another family of models, where now the parameters  $A; B; C; D$  and  $E$  are functions of  $\sigma_m$ . In order all these functions to be compatible, the final model must be of the form (Castillo et al., 2006), (Castillo et al., 2008), (Castillo et al., 2007b), (Koller et al., 2007b) and (Koller et al., 2007a):

$$F(N) = 1 - \exp \left\{ - \exp \left[ C_0 + C_1 \sigma_m^* + C_2 \sigma_M^* + C_3 \sigma_m^* \sigma_M^* + (C_4 + C_5 \sigma_m^* + C_6 \sigma_M^* + C_7 \sigma_m^* \sigma_M^*) \log N^* \right] \right\} \quad (2)$$

where  $F$  is de CDF function of  $N^*$ , subject to:

$$C_4 \geq 0 \quad (3)$$

$$C_5 - C_4 \leq 0 \quad (4)$$

$$-C_5 - C_4 \leq 0 \quad (5)$$

$$-C_4 + C_5 - C_6 + C_7 \leq 0 \quad (6)$$

$$-C_4 - C_5 - C_6 - C_7 \leq 0 \quad (7)$$

$$C_3 C_6 - C_2 C_7 \geq 0 \quad (8)$$

$$C_3 C_5 - C_1 C_7 \geq 0 \quad (9)$$

$$C_6 (C_6 (C_0 + \gamma) - C_2 C_4) \leq 0 \quad (10)$$

$$C_5 (C_5 (C_0 + \gamma) - C_1 C_4) \leq 0 \quad (11)$$

where  $\gamma = 0.57772$  is the Euler-Mascheroni number. Constraints (3)–(11) come from the following physical conditions:

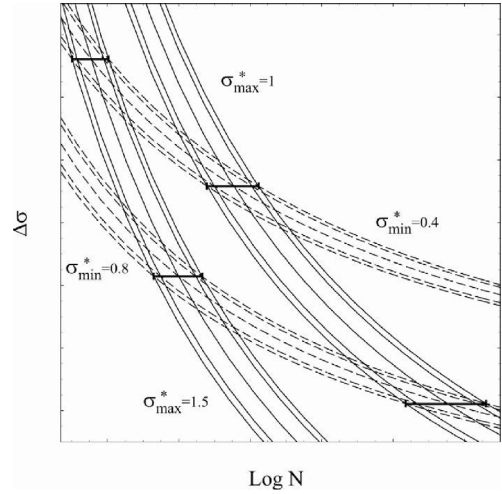


Figure 1. Schematic Wöhler curves for percentiles  $\{0.01, 0.05, 0.5, 0.95, 0.99\}$  for  $\sigma_{\max} = 1$  and  $\sigma_{\max} = 1.5$ , and  $\sigma_{\min} = 0.4$  and  $\sigma_{\min} = 0.8$ , illustrating the compatibility condition. Dashed lines refer to Wöhler curves for constant  $\sigma_{\min}$ , and continuous lines refer to Wöhler curves for constant  $\sigma_{\max}$ .

- The asymptotic value  $\Delta \sigma_{m0}$  or  $\Delta \sigma_{M0}$  must be non-negative, and, due to physical reasons, must be non-increasing in  $\sigma_m$  or  $\sigma_M$  respectively.
- The cdf in (2) must be non-decreasing in  $\log N$ , non-increasing in  $\sigma_m$  and non-decreasing in  $\sigma_M$ .
- The curvature of the zero-percentile of  $(\log N, \Delta \sigma)$  for constant  $\sigma_{\min}$  must be nonnegative, and, in the case of constant  $\sigma_{\max}$  must be non-negative.

We remind the reader that the cumulative distribution function of the two parameter Gumbel family is given by:

$$F(x; \lambda; \delta) = 1 - \exp \left\{ - \exp \left[ \frac{x - \lambda}{\delta} \right] \right\}; \quad x \geq \lambda \quad (12)$$

Where  $\lambda$  and  $\delta$  are the location and the scale parameters, respectively. When  $X$  follows a Gumbel distribution  $G(x; \lambda, \delta)$ , we write  $X \sim G(x; \lambda, \delta)$ , Its mean  $\mu = \lambda - 0.57772\delta$  and variance  $\sigma^2 = \pi^2 \delta^2 / 6$ .

One important property of the Gumbel family is that it is stable with respect to location and scale transformations, and also with respect to minimum operations (Castillo, 1988) and (Castillo et al., 2004). More precisely:

$$X \sim G(\lambda, \delta) \Leftrightarrow \frac{X - a}{b} \sim G \left( \frac{\lambda - a}{b}, \frac{\delta}{b} \right) \quad (13)$$

and

$$X_i \sim G(\lambda, \delta) \Leftrightarrow \text{Min}(X_1, X_2, \dots, X_n) \sim G(\lambda - \delta n, \delta) \quad (14)$$

### 2.1 Parameter estimation

The parameter estimation of the model can be done by several methods. The most well known method for estimating the parameters of a statistical model is the maximum likelihood method, which shows good statistical properties (Castillo et al., 2008).

Other estimation methods, can be seen in (Castillo & Hadi, 1995) and (Castillo et al., 1999).

### 2.2 Normalization of the Gumbel model

Normalization will be applied with the aim of establishing a relation among the fatigue data pertaining to different load levels, thus enabling us not only a pooled parameter estimation, but the statistical interpretation of the damage measure to be done.

According to Eq. (13), it is generally accepted in the case of fatigue lives,  $U = (x - \mu_x)/\sigma_x$  (corresponding normalized value) also follows a Gumbel distribution with parameters  $\lambda^*$  and  $\delta^*$ , given by:

$$\lambda^* = \frac{\lambda - \mu}{\sigma} = \frac{0.57772\sqrt{6}}{\pi}; \quad \delta^* = \frac{\delta}{\sigma} = \frac{\sqrt{6}}{\pi} \quad (15)$$

Thus, it follows, that all distributions sharing common parameters, and  $\pm$  transform, after normalization, to the same distribution.

An alternative normalization consists of using the random variable

$$Z = \frac{(\log N^* - B)(\log \Delta\sigma^* - C) - E}{D} \quad (16)$$

## 3 DAMAGE MEASURES

The problem of defining and selecting damage measures must be done with care if one desires they to be useful in practice. This problem is discussed in this section, with the main ideas taken from Castillo et al. (Castillo et al., 2007c).

### 3.1 Some requirements for damage measures

Some properties to get a valid damage measure are:

- Property 1. Increasing with damage: The larger the damage, the larger must be the value of the damage measure.
- Property 2. Interpretability: The damage measures must provide a clear information of the associated damage level.
- Property 3. Dimensionless measures: The use of dimensions causes problems in the estimation of

lifetime and requires indication of the measure units used in the analysis. So, dimensionless measures are much more convenient.

- Property 4. Known and fixed range: The range of variation of the damage measure must be fixed and known, independently of the type of load and, if possible, of the material.
- Property 5. Of known distribution: To know the probability of failure of a piece chosen at random, its damage must have a known distribution.

### 3.2 Some damage measures

Measures based on the number of cycles: As fatigue damage increases with the number of cycles  $N$ , the number of cycles to failure or any increasing function of it are possible candidates for damage measures.

1. *The number of cycles*: The damage measure is the number of cycles  $N$ . This measure does not satisfy Property 3 above (is not dimensionless), because if we use thousands or dozens of cycles, instead of cycles, we have  $N/1000$  or  $N/12$ , respectively.

The range depends on the stress range  $\Delta\sigma_i^*$ , so it satisfies Property 5 but not Property 4.

2. *The logarithm of the number of cycles*: Other alternative is the logarithm of the number of cycles  $N$ . Unfortunately, this index satisfies neither Property 3 nor Property 4.

If  $\log N$  is a Gumbel distribution, and the range depends on the stress level, this alternative has the same problems and limitations as the previous one.

3. *The normalized logarithm of the number of cycles*: A third alternative is the normalized logarithm of the number of cycles to failure.

$$D_i = \frac{\log N_i^*}{\mu_i} \quad (17)$$

where  $\mu_i$  is the mean of  $\log N_i^*$  when the stress range is  $\Delta\sigma_i^*$ . This measure it is not easily interpretable, so it does not satisfy Property 2. Furthermore  $D_i$  does not satisfy Property 4.

4. *The standardized logarithm of the number of cycles*: The last option analyzed, is the standardized logarithm of the number of cycles:

$$N_i^* = \frac{\log N_i^* - \mu_i}{\sigma_i} \quad (18)$$

This alternative does not depend on the stress range and material, so we can conclude that  $N_i^* \Leftrightarrow N^*$  and does not satisfy all the properties.

*Based on the Palmgren-Miner number:*

5. *The Palmgren-Miner number*:

$$M_i = N_i/\mu_i' \quad (19)$$

where  $\mu_i'$  is the mean value of the number of cycles to failure  $N_i$  for a stress level  $\Delta\sigma_i^*$ .

The Palmgren-Miner number is dimensionless (because the random variable is divided by its mean) so it satisfies Property 3. Taking logarithms one gets:

$$\log M_i = \log N_i - \log \mu'_i \quad (20)$$

Again, the range of  $M_i$  depend of the material, so it does not satisfy Property 4.

6. *The logarithm the Palmgren-Miner number:* Similarly to the previous measure, the range does not satisfy Property 4.

*Based on the Gumbel variable:* In Section 2.2 (eq. (16)), a very convenient candidate for a damage measure, the normalized variable  $Z$  was presented. It satisfies all the Properties: increasing with damage, interpretable, non-dimensional, with fixed range, and  $Z \sim G(0, 1)$ . Thus, we propose  $Z$  as a convenient measure for the cumulative fatigue damage associated with a given stress level or load history.

*Based on the failure probability:* Above the zero-percentile curve, we can define our damage measure as the failure probability (Castillo et al., 2007c):

$$P_F = F_{G(B-\lambda_i, \delta_i)}(\log N_i) = F_D(D) \quad (21)$$

where  $P_F$  is non-dimensional and has a uniform distribution ( $P_F \sim U(0, 1)$ ). This measure satisfies all desired Properties 1-5.

To define a damage measure below the zero percentile, in the non-failure zone, a proportionality criterion is used. This criteria was defined in (Castillo et al., 2007c), damage in this zone is proportional to the number of cycles if the stress level is held constant.

*Critical comparison:* A comparison between all the cases studied is made. Table 1 summarizes the main

characteristics and properties of several proposals of damage measures.

The main conclusion derived from this table is only measures  $Z$  and  $P_F$  satisfy all the properties, so these measures are the best, followed by  $N^*$ .

### 3.3 Damage accumulation

Model (2) provides probabilistic bases for calculating the damage accumulation for any type of loading being considered. In fact, due to the possible identification of the probability of failure  $P$ , represented by the percentile curves in the Wöhler field for any  $\sigma_{\min}$  and  $\sigma_{\max}$  with the damage state (Castillo et al., 2007c), the model can be used in cumulative damage calculations for fatigue life prediction of components subject to complex loading histories. To evaluate the accumulated damage, we proceed as shown in (Koller et al., 2007b).

## 4 EXAMPLE OF APPLICATION

As indicated, this model provides probabilistic bases for calculating the damage accumulation for any type of loading being considered. In fact, due to the possible identification of the probability of failure ( $p$ ), represented by the percentile curves in the Wöhler field, with any damage state (Castillo et al., 2007c), the model can be used in cumulative damage calculations for fatigue life prediction of components subject to complex loading histories.

### 4.1 Parameter estimation

To characterize the material, different load fatigue tests were conducted with steel 42CrMo4. The static characteristics of the material were  $R_m = 1067$  MPa and  $R_{p0.2} = 967.3$  MPa.

Table 1. Properties and characteristics of different damage measures for the case of constant stress levels (Legend: \*\*\*\*Very Good, \*\*\*Good, \*\*Medium and \*Bad).

Damage measure	Property				
	Increasing	Interpretability	Dimensionless	Range	Distribution
$N_i$	Yes	**	No	$(e^{\lambda_i}, \infty)$	$\log G(B - \lambda_i, \delta_i)$
$\log N_i$	Yes	*	No	$(\lambda_i, \infty)$	$G(B - \lambda_i, \delta_i)$
$D_i = \log N_i^* / \mu_i$	Yes	*	Yes	$(\lambda_i / \mu_i, \infty)$	$G(\lambda_i / \mu_i, \delta_i / \mu_i)$
$N^* = (\log N_i^* - \mu_i) / \sigma_i$	Yes	***	Yes	$(\lambda_i^*, \infty)$	$G(\lambda_i^*, \delta_i^*)$
$M_i = N_i / \mu'_i$	Yes	**	Yes	$(e^{\lambda_i / \mu_i}, \infty)$	$\log G(\lambda_i - \log \mu'_i, \delta_i)$
$\log M_i = \log N_i - \log \mu'_i$	Yes	*	Yes	$(\lambda_i - \log \mu'_i, \infty)$	$G(\lambda_i - \log \mu'_i, \delta_i)$
$Z = (\log N^* - B - \lambda_i) / \delta_i$	Yes	***	Yes	$(-\infty, \infty)$	$G(0, 1)$
$P = F(\log N_i)$	Yes	****	Yes	$(0, 1)$	$U(0, 1)$

$$\lambda^* = 0.57772\sqrt{6}/\pi; \delta^* = \sqrt{6}/\pi$$

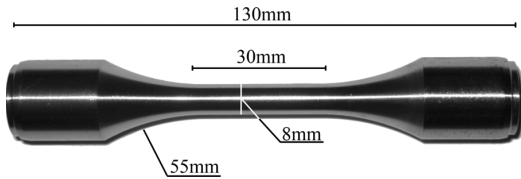


Figure 2. Geometry of the testing specimen.

The test specimens (Figure 2) were cylindrical of 8 mm diameter. The total and free lengths were 130 mm and 30 mm, respectively, and the transition radius to the test section of the specimen was 55 mm.

All the tests were conducted as shown in (Koller et al., 2007a) and (Koller et al., 2007b). The test data are shown in these references.

With all these data, the model parameters were estimated using by the maximum likelihood method. The resulting model is:

$$F(N) = 1 - \exp \left\{ - \exp \left[ -53.21712 - 33.5721\sigma_m^* + 47.3862\sigma_M^* + 24.9346\sigma_m^*\sigma_M^* + (0.5102(1 - \sigma_m^*) + 0.0439\sigma_M^* + 0.0231\sigma_m^*\sigma_M^*) \log N^* \right] \right\} \quad (22)$$

The damage probabilities calculated from (2) were obtained, using these parameters. To test the good ness of the model, the Kolmogorov-Smirnov and chi-square uniformity tests were applied (Koller et al., 2007a).

#### 4.2 Damage evaluation

To check the validity of the proposed model for the calculation of the accumulated damage for failure prediction, different load histories have been used:

- Constant load history: Described by  $\Delta\sigma_i^* = 1130$  MPa.
- Lineal variable load history: Two different cases are studied,  $\Delta\sigma_i^* = 300 - 5 \cdot 10^{-3} N$  MPa and  $\Delta\sigma_i^* = 1000 + 10^{-3} N$  MPa where  $N$  is the number of cycles.
- Variable load history: Two different spectra: FALSTAFF, which represents a contrasting spectrum of pseudo-random form and blocked form for fighter aircraft (Fillis et al., 2004), and a Gaussian 0.99 spectrum with  $\sigma_{mean} = 0$  MPa) have been used to check the model. Both spectra were applied by defining the maximum peak stress value. In this example, this value was fixed to 956 MPa = 0.98 ·  $R_y$ .

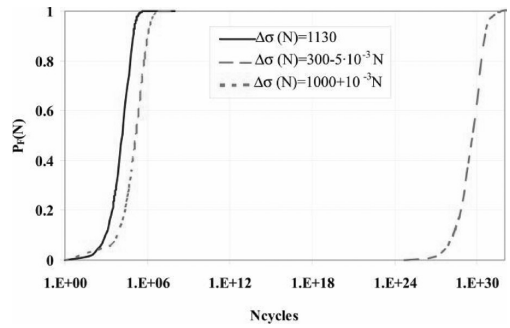


Figure 3. Accumulated damage  $P_F$  as a function of the number of cycles for the three different loads: (a) Constant:  $\Delta\sigma_i^* = 1130$  MPa (continuous line), (b) linearly increasing  $\Delta\sigma_i^* = 300 - 5 \cdot 10^{-3} N$  MPa (dashed line) and (c) linearly decreasing:  $\Delta\sigma_i^* = 1000 + 10^{-3} N$  MPa (dotted line).

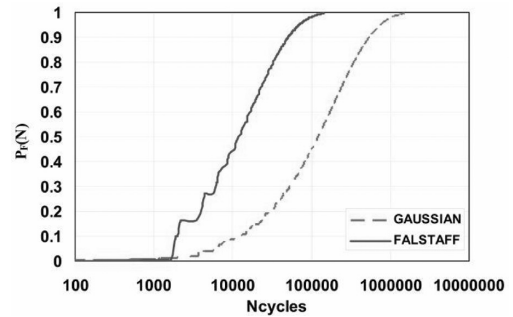


Figure 4. PF accumulated damage as a function of the number of cycles for the FALSTAFF and Gaussian spectra.

Figure 3 shows the resulting accumulated values of damage obtained from the model with the parameters for the three loading types cited before. It can be appreciated how the model is capable of evaluating the cumulative damage of different types of loads. This Figure illustrates how the damage  $P(N)$  increases with the number of cycles, and with this model it would be easy to fix a probability of failure, say  $10^{-4}$ , and then calculate the associated design number of cycles.

Figure 4 shows the  $P_F$  damage curves resulting from the model for both spectra. In this Figure, it can be observed how from this model the damage or failure probability of the sample is null or very low during the first cycles. Later, the damage increases until it approaches one. One of the main advantages of this model is that it permits to know the probability range in which a sample will break, so that an engineer could know with precision the number of cycles below which the failure probability of the sample is sufficiently low.

## 5 CONCLUSIONS

The main conclusions from this paper are the following:

1. The normalized random variable in Eq. (16) described in Section 2 appears to be a useful tool to facilitate the comparison of the cumulative fatigue damage produced by different load histories involving constant or changing stress levels.
2. A wide range of possible alternatives for selecting damage indices, including the logarithm of the number of cycles, the number of cycles to failure, the Palmgren- Miner number, its logarithm, its normalized or standardized form, the reference Weibull variable and the failure probability, are possible, and have been described in this paper. However, some of them are more convenient than others in the sense that they satisfy some desirable properties, such as adimensionality, fixed range, interpretability, known distribution, invariance with respect to load histories, etc.
3. The probability of failure is a very reasonable criterion for defining cumulative damage associated with different load histories. In fact, the Wöhler percentile curves allow us an easy interpretation of damage.
4. The new model (2) is a good method for evaluating the damage in all ranges and load histories.
5. Finally, it can be concluded that the model can be used for any type of load, constant, Gaussian or other. In our study we could observe that the model is very sensitive to the parameters used so, the data used for estimating these parameters have to be carefully chosen. Anyway, more research is needed about this subject.

## REFERENCES

- Annual Book of ASTM Standards, Vol. 03.01.2005. ASTM E606-92.
- ASTM Standard E1049-85 (1985). Standard Practices for Cycle Counting in Fatigue Analysis, Philadelphia, PA.
- Castillo E. (1988), *Extreme Value Theory in Engineering*, New York: Academic Press.
- Castillo E. and Hadi, A.S. (1995). Modelling Lifetime Data with Application to Fatigue Models, *Journal of the American Statistical Association*, 90, 1041.1054.
- Castillo, E. and Fernández-Canteli, A. and Hadi A.S. (1999). On Fitting a Fatigue Model to Data, *International Journal of Fatigue*, 21:97.106.
- Castillo, E., Hadi, A.S., Balakrishnan, N., and Sarabia, J.M. (2004). *Extreme Value and Related Models with Applications in Engineering and Science*, New York: John Wiley & Sons.
- Castillo, E. and Fernández -Canteli, A. A parametric life-time model for the prediction of high cycle fatigue based on stress level and amplitude. *Fatigue and Fracture of Engineering Materials and Structures*, 29, 1031–1038, 2006.
- Castillo, E. and Fernández -Canteli, A., Hadi, A.S. and López-Aenlle, M. (2007a). A fatigue model with local sensitivity analysis, *Fatigue and Fracture of Engineering Materials and Structures*, 30, 149.168.
- Castillo, E., Fernández -Canteli, A., Koller, R., Ruiz-Ripoll, M.L. and García, A. (2007b). A statistical fatigue model covering the tension and compression Wöhler fields. *Submitted to Probabilistic Engineering Mechanics*.
- Castillo, E., Fernández -Canteli, A., López-Aenlle M., and Ruiz-Ripoll, M.L. (2007c). Some fatigue damage measures for longitudinal elements based on the Wöhler field. *Fatigue Fract. Engng. Mater. Struct.*, 30, 1063–1075.
- Castillo, E., Fernández -Canteli, A. and Ruiz-Ripoll, M.L. A General Model for Fatigue Damage due to any Stress History, *International Journal of Fatigue*, 30:1, 150.164, 2008.
- Collins J.A. (1993). *Failure of Materials in Mechanical Design*, JohnWiley, New York.
- Filis P.A., Farrow I.R. and Bond I.P. Classical fatigue analysis and load cycle mix-event damage accumulation in fiber reinforced laminates. *International Journal of Fatigue* 2004; 25; 565–573.
- Koller R., Ruiz-Ripoll M.L., García A., Fernández—Canteli A. and Castillo E. (2007a). Experimental Validation of a Statistical model for the Wöhler Field Characterization for Different Reference Stress Levels and Damage Accumulation. *Submitted*.
- Koller R., García A., Ruiz-Ripoll M.L., Castillo E. and Fernández-Canteli A. (2007b). Damage accumulation with a Statistical Model for the Wöhler Field Characterization. *Submitted*.

# Discussion concerning the multi-ranked deterioration forecasting model based on incomplete inspection data

Y. Shumuta

*Central Research Institute of Electric Power Industry, Chiba, Japan*

**ABSTRACT:** This paper presents a multi-ranked deterioration model for a civil engineering structure. The Markov chain model is widely used for engineering structures. Though the model has the advantage of easy handling, it needs a strong assumption that the transition rate for a unit time is always constant. On the other hand, the current time-dependent multi-ranked deterioration model has some difficulties when practically applied to actual incomplete inspection data. This paper tries to forecast a multi-ranked deterioration state based on incomplete inspection data without assuming a specific probability distribution. The proposed model is applied to inspection data for an actual tunnel structure and discusses the effectiveness of the proposed model.

## 1 INTRODUCTION

The Markov chain model is widely used as a multi-ranked deterioration forecasting model for engineering structures. Though the model has the advantage of easy handling, it needs a strong assumption that the transition rate for a unit time is always constant (Ang & Tang 1984). However, the deterioration of a civil engineering structure invariably changes with respect to the elapsed time. The transition rate may generally depend on the prior state.

On the other hand, Aoki et al. (2005) proposed a time-dependent forecasting model in which the transition rate is dynamically changed according to the duration for use. The model was formulated using a weibull hazard model based on the Chapman Kolmogorov equation. The multi-ranked deterioration state for a target structure is evaluated by the multiple integration of a simultaneous occurrence probability defined by the weibull hazard functions. However, this model has difficulties such as (1) a lot of sample data is needed for estimating the parameters of an assumed probability function, (2) a complex multiple integration is needed for the evaluation, and (3) it is difficult to determine an appropriate probability function based on incomplete sampling data.

The tunnel structure targeted by this study is deteriorated by various external factors such as a water leak, harmful water, frost damage, salt damage, and smoke pollution. Therefore, the physical deterioration mechanism is not well understood, and the possibility that the speed of the deterioration changes depending on the elapsed time, is not controvertible. Moreover, the inspection history data of the tunnel structure are often incomplete and includes many censored data, which are well known as data with unknown state transition

time in the survival time analysis (Nakamura, 2003), because it has so far been treated as a maintenance free structure. The detail discussion for the censored data for a civil engineering structure is referred to Shumuta et al. (2007). From the life cycle cost minimization point of view, even with incomplete sampling data, it is important to quantitatively discuss the possibility of the deterioration progress in consideration of the uncertainty.

The author has proposed a deterioration forecasting model for the two ranked deterioration states using the incomplete inspection data (Shumuta et al., 2007). On the basis of this research, this paper proposes a multi-ranked deterioration forecasting model without assuming a specific probability distribution. Chapter 2 describes the outline and the problem of the existing model. Chapter 3 formulates the proposed model. Chapter 4 applies the proposed model to the actual tunnel structure, and discusses the effectiveness of the proposed model. Chapter 5 contains the closing remarks.

## 2 EXISTING MODEL

### 2.1 *Transition rate evaluation model*

This paper focuses on the civil engineering structures whose deterioration degrees are shown by two or more ratings. When the deterioration states are expressed by  $i$  and  $j$  ( $i \leq j$ ,  $i = 1, \dots, K$ ,  $j = 1, \dots, K$ ) and the elapsed time, in which the deterioration state changes from  $i$  to  $j$ , is shown by the random variable  $T$ , the transition probability distribution, density functions and non-transition probability distribution function are given by

$$F_{ij}(t) = \Pr_{ij}\{T \leq t\}, \quad F_{ij}(0) = 0 \quad (1)$$

$$F_{ij}(t) = \int_0^t f_{ij}(t) dt \quad (2)$$

$$R_{ij}(t) = \Pr_{ij}\{T > t\} = 1 - F_{ij}(t), \quad i \neq j \quad (3)$$

$$\text{if } i = j \quad R_{ii}(t) = F_{ii}(t) \quad (4)$$

Note that though the existing model applies equation (3), in a multi-ranked situation, if all the transition states from state  $i$  are considered simultaneously, equation (3) changes into

$$R_{ij}(t) = \Pr_{ij}\{T > t\} = 1 - \sum_{j=1}^K F_{ij}(t), \quad i \neq j \quad (5)$$

where  $K$  = the total number of deterioration states.

The transition rate in a unit time that will change from state  $i$  at elapsed time  $t$  to  $j$  at  $t + \Delta t$  is usually called a hazard. In this paper, the hazard is defined as the transition rate and is given by

$$\lambda_{ij}(t) = \lim_{\Delta t \rightarrow 0} \frac{1}{R_{ij}(t)} \cdot \frac{F_{ij}(t + \Delta t) - F_{ij}(t)}{\Delta t} = \frac{f_{ij}(t)}{R_{ij}(t)} \quad (6)$$

Thus, the non-transition probability distribution function is defined by

$$R_{ij}(t) = \exp \left\{ - \int_0^t \lambda_{ij}(t) dt \right\} = \exp \{ -\Lambda_{ij}(t) \} \quad (7)$$

$$R_{ij}(0) = 1$$

where  $\Lambda$  = the cumulative hazard function.

When the target samples in which the deterioration state changed from  $i$  to  $j$  were collected at a constant interval, the transition rate function is given by

$$\lambda_{ij}(t) = \bar{\lambda}_{ij} = \frac{\sum_n (h(t+1) = j/h(t) = i)}{\sum_n (h(t) = i)} \quad (8)$$

where  $(h(t) = i)$  = the deterioration state  $i$  at discrete time  $t$ .  $(h(t+1) = j/h(t) = i)$  = deterioration state  $j$  at  $t+1$  on the condition that its state is  $i$  at  $t$ .  $n$  = the total number of components which is state  $(h(t) = i)$ .  $m$  = the total number of components which is state  $(h(t+1) = j/h(t) = i)$ .

## 2.2 Transition rate evaluation model with censored data

The inspection data, which can be used for the forecasting, is often incomplete because the observed period is limited. Therefore, the collected samples cannot often be clarified when the state transition occurred. Shumuta et al. (2007) treated such incomplete sample data, which were collected from a civil engineering structure, as the censored data and proposed its transition rate evaluation model which focuses on the two ranked deterioration state (damage or non-damage) samples. In order to expand the above model for the multi-ranked samples with the

censored data, the likelihood method (point estimation) is often applied. This method enables us to evaluate the parameters for the target theoretical probability distribution from the observed sample data.

When a discrete time is expressed as  $(t_l, r_l; t_0 = 0, r_0 = 0)$  during an observed period, the observed times of the transition samples are expressed as  $t_1, t_2, \dots, t_n$ , and the observed periods of the non-transition samples are expressed as  $r_1, r_2, \dots, r_m$ . The probability distribution and density functions, which transit the deterioration state from  $i$  to  $j$ , are defined as  $F_{ij}(r)$  and  $f_{ij}(t; \theta)$ , and the simultaneous transition probability is given by

$$f_{ij}(t_1; \theta) dt_1 f_{ij}(t_2; \theta) dt_2 \dots f_{ij}(t_n; \theta) \times \{1 - F_{ij}(r_1)\} \cdot \{1 - F_{ij}(r_2)\} \dots \{1 - F_{ij}(r_m)\} \quad (9)$$

where  $n$  = the total number of observed samples, whose deterioration state changes from  $i$  to  $j$ .  $m$  = the total number of censored data.  $t_n$  = the observed time of the transition.  $\theta$  = the parameters of the probability density function such as the mean and standard deviation.

According to the likelihood method, the parameter  $\theta$  is determined so that the simultaneous transition rate of equation (9) may be maximized. The likelihood function is given by

$$L(\vec{t}, \vec{r}; \theta) = \prod_{t=1}^n f_{ij}(t_r; \theta) \prod_{r=1}^m \{1 - F(t_r)\} \Rightarrow \max \quad (10)$$

Next, if the logarithm of both sides of equation (10) is taken,  $\theta$  determined for the partial differential value becomes 0 as follows:

$$\frac{\partial \ln(L(\vec{t}, \vec{r}; \theta))}{\partial \theta} = 0 \quad (11)$$

Note that it is usually difficult to determine the parameter  $\theta$  using equation (11) on the condition that 1) the number of samples is few, 2) the observed period is short, and 3) much censored data exist.

## 2.3 Multi-ranked deterioration model

IF the transition rate depends only on the current state, the process of change may be modeled by the Markov process. If the state space is a countable finite state, and the change can occur only at discrete points, the process is modeled by a transition matrix as shown in

$$\vec{\pi} = \begin{pmatrix} \pi_{11} & \dots & \pi_{1K} \\ \vdots & \ddots & \vdots \\ \pi_{K1} & \dots & \pi_{KK} \end{pmatrix} \quad (12)$$

$$\pi_{ij} \geq 0, \quad \pi_{ij} = 0 (i > j), \quad \sum_{j=1}^K \pi_{ij} = 1 \quad (13)$$



On the basis of equation (8), each component of the Markov transition matrix is given by

$$\pi_{ij} = \overline{\lambda}_{ij} \quad (14)$$

Tsuda et al. (2004) also proposed a model to evaluate  $\pi_{ij}$  based on equation (6) assuming that  $f_{ij}(t)$  is an exponential function.

If the Markov transition matrix, which describes the deterioration state between the fixed discrete intervals, is evaluated, the multi-ranked deterioration share vector of the time step  $t_i(\overrightarrow{S}(t_i))$  is given by

$$\overrightarrow{S}(t_i) = \overrightarrow{S}(t_0) \cdot [\overrightarrow{\pi}]^i \quad (15)$$

On the other hand, if the deterioration transition rate change depends on the prior state and time, it is difficult to apply the Markov model. Aoki et al. (2005) proposed a time-dependent deterioration forecasting model whereby the deterioration process is evaluated by the multi-ranked weibull hazard function based on the Chapman-Kolmogorov equation. The definition is given by

$$\pi_{ij}(t) = \int_0^t \int_0^{t-t_1} \dots \int_0^{t-\sum_{m=1}^{i-2} t_m} g_{ij}(t_1, t_2, \dots, t_{i-1}) dt_{i-1} dt_{i-2} \dots dt_1 \quad (16)$$

$$g_{ij}(t_1, \dots, t_{n-1}) = \prod_{m=1}^{i-1} f_{mj}(t_m) \cdot R_{ij} \left( t - \sum_{m=1}^{i-1} t_m \right) \quad (17)$$

$0 \leq t_1 + t_2 + \dots + t_{i-1} < t, \quad i > j$

where  $\pi_{ij}(t)$  = the transition rate whose deterioration state changes from  $i$  to  $j$  at time  $t$ .

Note that it is usually difficult to evaluate equation (16) if the assumed probability function is complicated or sampling data includes much censored data.

When the last deterioration state  $J$  is assumed as an absorbing state, the transition rate of the target structure is given by

$$\pi_{iJ}(t) = 1 - \sum_{m=1}^{J-1} \pi_{im}(t) \quad (18)$$

Finally, the time-dependent multi-ranked deterioration share vector of the time step  $t$ ,  $\overrightarrow{S}(t)$  is given by

$$\overrightarrow{S}(t) = \overrightarrow{S}(t_0) \cdot \overrightarrow{\pi}(t) \quad (19)$$

### 3 PROPOSED MODEL

#### 3.1 Multi-ranked deterioration model

The proposed model tries to estimate the multi-ranked transition rate at a discrete time without assuming the theoretical probability distribution. The basic idea is based on the Kaplan-Maier (KM) method. Refer to Andersen et al. (1993) for the theoretical details of the KM method.

It is assumed that the deterioration transition time is  $t_1 < t_2 < \dots < t_r < \dots$  and the transition rate is constant during the time interval  $t_{r-1} < t \leq t_r$ . The transition rate at time  $t_r$  is given by

$$\lambda_{ij}(t_r) = \frac{d_{ij}(t_r)}{n_i(t_{r-1})} \quad (20)$$

where  $d_{ij}(t_r)$  = the total number of components which changes the deterioration state from  $i$  to  $j$  at the observed time  $t_r$ .  $n_i(t_{r-1})$  = the total number of components which are the deterioration state  $i$  at the observed time  $t_{r-1}$ .

The transition share, which changes the deterioration state from  $i$  to  $j$  at time  $t_r$ , is given by

$$S_i(t_r) = S_i(t_{r-1}) \cdot \lambda_{ij}(t_r) \quad (21)$$

When the initial vector of the rating share for each deterioration state is defined as

$$\overrightarrow{S}(t_0) = [s_1(t_0) \quad s_2(t_0) \quad \dots \quad s_K(t_0)] \quad (22)$$

and the transition rate matrix at time  $t_r$  is defined as

$$\overrightarrow{\lambda}(t_r) = \begin{pmatrix} \lambda_{11}(t_r) & \dots & \lambda_{1K}(t_r) \\ \vdots & \ddots & \vdots \\ 0 & \dots & \lambda_{KK}(t_r) \end{pmatrix} \quad (23)$$

As a result, the deterioration rating share vector at the discrete time  $t_r$  is given by

$$\overrightarrow{S}(t_r) = \overrightarrow{S}(t_0) \cdot \prod_{j=1}^r \overrightarrow{\lambda}(t_j) \quad (24)$$

Equation (24) indicates that the transition shares of the  $K$  ranks are composed of the  $K \times K$  transition rate matrix for every discrete time  $t_j$ .

Next, the transition rate decomposition process is explained in detail as follows:

It is assumed that a civil engineering structure consists of 95 components which are independently deteriorating and their deteriorations are evaluated by three ranks (ranks 1, 2, and 3). Table 1 shows the element of the transition rate matrix of  $3 \times 3$ , of which the deterioration rates at each discrete time has been decomposed. As the initial condition, which is indicated at time 0, in Table 1, the 95 components are divided into 60 of rank1, 20 of rank2 and 15 of rank3. At time 1, their numbers change to 55 of rank1, 23 of rank2 and 17 of rank3. As a result, the rank share vector  $\overrightarrow{S}(t_r) = [s_1(t_r) \quad s_2(t_r) \quad s_3(t_r)]$  becomes

$$\overrightarrow{S}(0) = [0.63 \quad 0.21 \quad 0.16],$$

$$\overrightarrow{S}(1) = [0.58 \quad 0.24 \quad 0.18].$$

The matrix elements in equation (23) is given by

$$\overrightarrow{\lambda}(t_r) = \begin{pmatrix} rmd_{11}(t_r) & rmd_{12}(t_r) & rmd_{13}(t_r) \\ rmd_{21}(t_r) & rmd_{22}(t_r) & rmd_{23}(t_r) \\ rmd_{31}(t_r) & rmd_{32}(t_r) & rmd_{33}(t_r) \end{pmatrix} \quad (25)$$

Table 1. Example of the transition rates at discrete time.

time (tr)	T number(tr)				Atrisk1 (tr)	Trate(tr)			S1(tr)
	rs11	rs12	rs13			rmd11	rmd12	rmd13	
0	60	0	0	60	1.00	0.00	0.00	0.63	
1	55	3	2	60	0.92	0.05	0.03	0.58	
:	:	:	:	:	:	:	:	:	
time (tr)	T number (tr)				Atrisk2 (tr)	Trate(tr)		S2(tr)	
	rs12	rs22	rs23			rmd22	rmd23		
0	0	0	20	0	20	1.00	0.00	0.21	
1	3	3	20	0	20	1.00	0.00	0.24	
:	:	:	:	:	:	:	:	:	
time (tr)	T number(tr)				Atrisk3 (tr)	Trate(tr)		S3(tr)	
	rs13	rs23	trs23	rs33		rmd33			
0	0	0	0	0	15	15	1.00	0.16	
1	2	0	2	0	15	15	1.00	0.18	
:	:	:	:	:	:	:	:	:	

Number(tr): Number of transition at time tr.  
 Trate(tr): Transition rate at time tr.

where  $rmd_{ij}(t_r)$  = the transition rate at the discrete time  $t_r$  for  $ij$  element. In Table 1,  $rmd_{ij}(t_r)$  is evaluated by

$$rmd_{ij}(t_r) = \frac{rs_{ij}(t_r)}{Atrisk_i(t_r)} \tag{26}$$

where  $rs_{ij}$  = the total number of components whose deterioration states changes from  $i$  to  $j$ .  $Atrisk_i(t_r)$  = the total number of components whose deterioration state keeps  $i$  until the discrete time  $t_r$ . For example,  $Atrisk_2(t_r)$  of rank2 shown in Table 1 is given by

$$Atrisk_2(t_r) = -rs_{12}(t_r) + trs_{12}(t_r) + rs_{22}(t_r) + rs_{23}(t_r) \tag{27}$$

where  $trs_{12}(t_r)$  = the cumulative number of components whose deterioration rank changes from 1 to 2 at the discrete time  $t_r$ . Note that the decomposition process in this paper improved that of the KM method by Nakamura (2003).

Finally, on the basis of equation (24), each rank share at the discrete time 1 in Table 1 is given by

$$\begin{aligned} \vec{S}(1) &= \vec{S}(0) \times \vec{\lambda}(0) \times \vec{\lambda}(1) = [0.63 \quad 0.21 \quad 0.16] \\ &= \begin{pmatrix} 1.00 & 0 & 0 \\ 0 & 1.00 & 0 \\ 0 & 0 & 1.00 \end{pmatrix} \times \begin{pmatrix} 0.92 & 0.05 & 0.03 \\ 0 & 1.00 & 0.00 \\ 0 & 0 & 1.0 \end{pmatrix} \\ &= [0.58 \quad 0.24 \quad 0.18] \end{aligned} \tag{28}$$

Each share evaluated by equation (28) corresponds to the share which is directly counted, such as  $[0.58 = 55/950.24 = 23/95018 = 17/95]$ .

### 3.2 Multi-ranked extrapolating model

In order to evaluate the transition rate matrix  $(\vec{\lambda}(t_r))$  for the time range of the extrapolation, the least square fitting method is applied. Specifically, in the time range of the extrapolation, the transition rate function is evaluated based on the least-square fitting method using linear, non-linear and polynomial functions.

IF the observed and estimated transition rates are expressed by  $\lambda_{ij}^o(t_1), \lambda_{ij}^o(t_2), \dots, \lambda_{ij}^o(t_r)$ , and  $\lambda_{ij}^e(t_1), \lambda_{ij}^e(t_2), \dots, \lambda_{ij}^e(t_r)$ , respectively, the evaluation function is given by

$$F = \sum_{t=1}^r (\lambda_{ij}^o(t_r) - \lambda_{ij}^e(t_r; \theta))^2 \Rightarrow \min \tag{29}$$

Finally, parameter  $\theta$  determined for the partial differential value becomes 0 as follows:

$$\frac{\partial(F(\vec{t}; \theta))}{\partial \theta} = 0 \tag{30}$$

The proposed model enables us to easily and flexibly determine the parameters for the evaluation function even if the observed data include much censored data. However, the proposed model does not satisfy a time corresponding condition between  $\vec{\lambda}(t_r)$  and  $\prod \vec{\lambda}(t_j)$ , which was mentioned by Tsuda et al. (2005). Thus, this paper assumes that the discrete time interval basically corresponds to the observed one. However, if the time intervals of the observed samples are not unique, their average time interval is used for the extrapolation in the proposed model.

## 4 NUMERICAL EXAMPLES

### 4.1 Inspection data for the target tunnel structure

In numerical examples, the proposed model was applied to an actual tunnel structure. The target tunnel structure is divided into two parts, the arch and the sidewall, which are made of brick and stone, respectively. The total length of the tunnel is 670 m, which is separated into 67 parts with the same intervals of 10 m, and the deterioration degree of each part was inspected, which focused on some deterioration phenomenon including cracks, water leaks, and separations. Finally, on the basis of this inspection, the deterioration ranking was determined.

Table 2 shows the definition of the deterioration ranking, which consists of four ranks (S, A, B, C). The target inspection data were recorded in 1997, 1998, 2000, 2002, 2003, and 2004.

Note that it is assumed that if an observed deterioration ranking recovers (becomes a lower rank) without maintenance after the observed time, its ranking record

Table 2. Definition of deterioration ranking.

Rank	Safety in operation (Deterioration degree)
A	necessary to care, functional loss in near future
B	if progress, necessary to care
C	no problem at present, negligible
S	no problem for the time being

Table 3. The transition number and the transition rate of the observed samples for every inspection time.

ET (Tr)	Tnumber(Tr)				AtriskS	Trate(Tr)			
	rsSS	rsSC	rsSB	rsSA		rmdSS	rmdSC	rmdSB	rmdSA
0	29				29	1.00	0.00	0.00	0.00
1	29				29	1.00	0.00	0.00	0.00
3	28		1		29	0.97	0.00	0.03	0.00
5	16	2	8	2	28	0.57	0.07	0.29	0.07
6	13	3			16	0.81	0.19	0.00	0.00
7	13				13	1.00	0.00	0.00	0.00
ET	trsSC	rsCB	rsCA	AtriskC	rmdCC	rmdCB	rmdCA		
0	0	11		11	1.00	0.00	0.00		
1	0	11		11	1.00	0.00	0.00		
3	0	11		11	1.00	0.00	0.00		
5	2	3	5	3	11	0.27	0.45	0.27	
6	5	-2	4	1	5	0.00	0.80	0.20	
7	5	-2	0	0	3	1.00	0.00	0.00	
ET	trsSB	rsBB	rsBA	AtriskB	rmdBB	rmdAA			
0	0	0	22	22		1.00	0.00		
1	0	0	22	22		1.00	0.00		
3	1	0	22	22		1.00	0.00		
5	9	5	20	2	23	0.91	0.09		
6	9	9	18	2	34		0.94	0.06	
7	9	9	18	0	36		1.00	0.00	

ET(Tr):elapsed time, rmd: hazard

is neglected due to a measurement error as well as the assumption of the Markov model shown in equation (13). In this paper, Rank A is also assumed as an absorbing state.

Table 3 shows the change in the transition number and the transition rate associated with rank *S*, rank *C*, and rank *B* for every discrete time. Year 1997 is assumed as reference time 0. The ET column shows the elapsed time from 1997. The data finally used to evaluate the transition rate associated with rank *S*, rank *C*, rank *B* and rank *A* is 355 among 402 observed samples.

#### 4.2 Discussion

Fig. 1 shows a comparison of the change in the transition rates from *S* to other states during the observed time period. The transition rate of Proposed in Fig. 1 corresponds to [1-rmdSS] in Table 3. Fig. 2 also shows the comparison of the change in the share of rank *S* during the observed period. The transition rates and the share of rank *S* were estimated by the Markov, the weibull, the lognormal and the proposed models. Because the proposed model is based on the KM method, the transition rate and the share rate become step functions as shown in both figures. The transition rate and the share rate by the proposed model correspond to the observed one at time 0, 1, 3, 5, 6 and 7. On the other hand, the transition rate of the markov in Fig. 1 is always constant. Furthermore, the weibull and the lognormal, who are the time dependence models in Fig. 2, evaluate a decrease of the share of rank *S* with increase of the elapsed time more excessively than the observed share. These results suggest that it is difficult for the existing models to simulate the characteristics of the observed samples in the given condition.

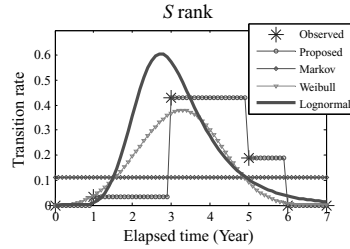


Figure 1. Comparison of the change in the transition rates which change from state *S* to other states.

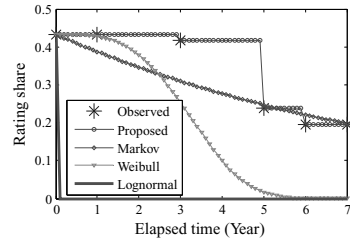


Figure 2. Comparison of the change in the share of rank *S*.

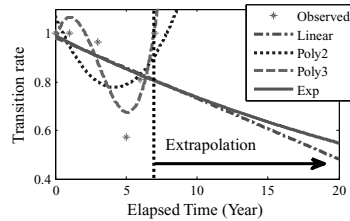


Figure 3. Results of the extrapolation estimated by the four regression models.

Table 4. The four regression models and their sum of squares due to errors.

Name	Function $f(x)$	SSE
Linear	$-0.0251x + 0.9835$	0.1248
Poly3	$0.0118x^3 - 0.1093x^2 + 0.1914x + 0.9718$	0.0282
Poly2	$0.0167x^2 - 0.1406x + 1.0730$	0.0905
Exp	$0.9908 \exp(-0.0296x)$	0.1233

SSE: Sum of squares due to errors.

Fig. 3 shows the extrapolation results of the rmdSS element in Table 3 using four regression models based on the proposed method. Table 4 shows evaluation functions for the regression models and the sum of squares due to errors (SSE) with the observed samples. Table 4 suggests that the Poly3 who is the cubic polynomial model is the best fit model in the four models. However, Fig. 3 suggests that the Poly3 is not appropriate as the forecasting model because its

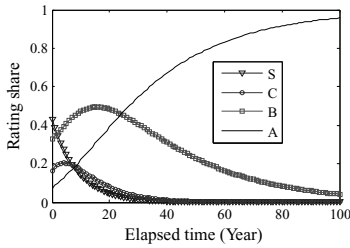


Figure 4. Change of the rating shares estimated by the Markov model (time independent model).

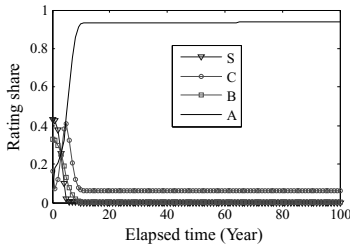


Figure 5. Change of the rating shares estimated by the weibull model (time dependent model).

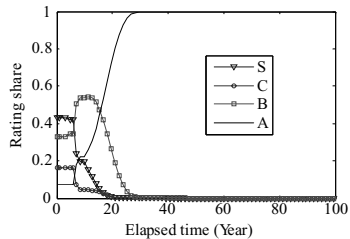


Figure 6. Change of the rating shares estimated by the proposed model (time dependent model).

transition rate is diverging in the time range of the extrapolation. These results suggest that the proposed method enables us to easily make some alternatives in order to quantitatively discuss the adequacy of them.

Figs. 4–6 show the forecasting results of the rate shares for 100 years from 1997 through 2097, by the markov, the weibull, and the proposed models with some exponential extrapolation functions such as Exp in Table 4, respectively. Figs. 4–6 also show that even if the same sample data is used, the forecasting results are different due to the assumed models. These results suggest that in the given incomplete sample condition, it is difficult to determine a unique model for the forecasting. In this situation, the proposed model enables us to easily produce some alternatives for the comparison.

## 5 CONCLUSIONS

This paper proposed a method to forecast the multi-ranked deterioration rate share for a civil engineering structure based on incomplete inspection data. The proposed method was applied to the inspection data monitoring from an actual tunnel structure. The main results of this research are as follows:

1. On the basis of the Kaplan-Mayer method, a method was proposed to decompose the multi-ranked deterioration transition share to the transition rate matrix for every observed discrete time. As a result, it was shown that the multi-ranked deterioration share could be reproduced using the transition rate matrix.
2. It was clarified that the estimated results based on the existing models did not correspond well with the observed one.
3. It was clarified that the proposed method enables us to forecast the transition rate share even if the sample data are few and incomplete. The proposed method could easily produce some alternatives in order to quantitatively discuss the effect of uncertainty.

## ACKNOWLEDGEMENTS

This research was supported by the Hokkaido Electric Power Company. I would like to thank them for all their help with this study.

## REFERENCES

- Ang, A.H-S., & Tang, W.H. 1984. *Probability Concepts in Engineering Planning and Design, Volume II—Decision, Risk, and Reliability*: John Wiley & Sons.
- Aoki, K., Yamamoto, K., Tsuda, Y., & Kobayashi, K. 2005. A deterioration forecasting model with multi-stage weibull hazard functions, *Journal of the Japan Society of Civil Engineers, No.798/VI-68*:125–136 (in Japanese).
- Andersen, P.K., Borgan, O., Gill, R.D. & Keiding, N. 1993. *Statistical Models Based on Counting Processes*, New York: Springer.
- Nakamura, T. 2003. *Cox proportional hazard model*: Asakura Publishing Co. Ltd. (in Japanese).
- Shumuta, Y., Saito, K., Kamimura, H., Yasui, M., & Shibata, M. 2007. Defect probability evaluation for hoist equipment of dam spillway gates, Proceedings of the Sixth Japan Conference on Structural Safety and Reliability, (A):181–186 (in Japanese).
- Tsuda, Y., Kaito, K., Aoki, K., & Kobayashi, K. 2005. Estimating markovian transition probabilities for bridge deterioration forecasting, *Journal of the Japan Society of Civil Engineers, No.801/I-73*:69–82 (in Japanese).

# The behavior of a building as a part of its conceiving

V. Spigai & E. Dalla Vecchia

*Università IUAV di Venezia, Venice, Italy*

**ABSTRACT:** The research group held by Prof. Spigai “Architecture of steel, glass and high technologies” at Università IUAV—Venice dealt a remarkable number of technological and compositive themes, with the collaboration and help of a large numbers of colleagues from IUAV’s Construction and Design Departments. Above these themes, the durability of a building and its behavior during the time has been thoroughly investigated.

## 1 THE RELATION BETWEEN DESIGN AND A BUILDING’S DURABILITY

### 1.1 *Introduction*

At the basis of the work held by Prof. Spigai’s group there is the understanding of the professional designing as an activity that can’t ignore, nowadays, the maintenance and management through time of a new building. This is both due to the laws in force and to the need for a higher awareness while interacting with natural resources and territory. The aim is to have the knowledges about engineering, mechanics and CAD-CAM productive techniques melted and integrated with those more creative, cultural and emotional aspects of design. In order to obtain this, a conscious and contemporary design methodology, having also the long-run behavior of a building as part of the design phase itself, is being taught in the Architecture faculty of IUAV.

One of the goals is also to make architecture more deeply linked to the territory from a technological and environmental point of view, by considering technical and local factors, in addition to the more classical ones about language, materials. . .while studying the settling strategy.

During these years, it has been possible to deal with a remarkable number of shared themes, both technical and technological, constituting a branch on which theoretical and experimental tendencies have been formed during last years through many interconnected design verifications. Themes as: steel and mixed structures, with a particular remark on their fireproof performances; use of advanced technologies in architecture; use in complex contexts of advanced technologies and techniques for the sustainability of architecture and for the innovative use of traditional materials. . .have been occasion and object of a theoretical and practical confrontation among students and

professors, creating a deeper design awareness about the themes themselves and making the graduation theses short scientific research experiences, enriched and completed by their thematic interconnection.

We will show and comment the most meaningful works among more than thirty design experimental projects, presenting the technological research path at the basis of the research group’s integrated design philosophy.

## 2 FIRE AND HIGH TEMPERATURES

In this section we will present two experimentations regarding mixed structures in steel and concrete; these have been held aiming to verify the interaction possibilities of these two materials, to optimize their performances both from the technical-technological and from the designing-aesthetic points of view. In particular, regarding the theme of steel’s fire proof performances, the possibility to integrate reinforced concrete in steel structures has been investigated, so to make the two materials structurally collaborating, in order to integrate their mechanical features as it already happens in normal reinforced concrete structures. From the fire proof performances point of view, we can say that the reinforced concrete, if properly calculated, will—for a limited span of time—perform the structural work made by steel if the latter is no more efficient because melted by fire; a more economical thinking will also find some advantages in such a structure, since it is less expensive than a totally steel one; and from the constructive point of view it’s easier and quicker to build than a totally reinforced concrete one; finally, such a material’s combination allows the designer to imagine a greater variety of possible sections’ shapes, and this not only for the sake of aesthetic and originality, but also in order to better integrate structure and technological and electrical systems.

The works have been articulated in following phases of deepening on the investigated materials' properties and features, and on applicative solutions already utilized by other designers, in order to draw a critic general picture of the state of art and organize search results about technical and technological possibilities and main running researches in the field. Subsequently, designing hypotheses have been formulated, with the aim of proposing a some kind of innovation regarding the utilization of materials themselves; following, we will illustrate two works thoroughly studying the possibilities of combining reinforced concrete with cold-plied steel plates.

2.1 *"Steel and fire, new languages: project for a mediatheque nearby Saracinesca gate, in Padova"* by Lisa Bortolotto

The research field for this work has been searching for new interaction possibilities for steel and reinforced concrete in structures. Beyond the fire proof performances, which was the main interest, the research also aimed to study the possibilities of pre-construction and modularization of such a structure, even while working on a functionally complex and volumetrically composed design hypothesis, also using a variety of materials.

A first phase has been dedicated to deepen the knowledge of the research group about various kinds of steel and concrete, in relation to their mechanical features and stress performances.

The project plans a glass volume working as entrance, main hall and internal fluxes distribution and vector; for this wing in particular, a number of junctions has been studied: not only the obvious beam-beam and pillar-beam joints, but also some composite structure-concrete structure (constituting the remaining part of the building), composite structure-glass skin joints . . . in order to systematically investigate the features and/or problems of such a structure.

In particular, beams and pillars are composed—as it will be in the next work presented—by a pre-fabricated metallic shaping frame, made of a cold-formed, 5 mm thick steel plate and to be left on the final beam, plus a section of self-compacting concrete done on site. The concrete section silhouette is defined and completed by a second metallic shaping-frame, which will be re-used on many beams, again constituted by a cold-formed steel plate.

The possibility of efficiently pre-build and assemble on site the main part of this structure is proved by the relatively small abacus of joints and sticks resulting by the thorough study and design of the project.

In this hypothesis, concrete sections are calculated as sufficient by themselves to bear the loads (as they have to be counted by law); this feature may look like a loss for the project's meaning itself, but it has

been done following some considerations about the functional aspects of the glass volume itself.

To this work, the merit of having been the first in the group proposing such a kind of structure assembling method for steel and concrete to be investigated.

2.2 *"Steel and glass: composite structures in cold-formed steel plate and reinforced concrete: project for a library in Cervia, Ravenna"* by Fabiomassimo Focaccia e Nicola Brunelli

In this work, which continues the study on cold-formed steel plate in junction with reinforced concrete, the focus has been posed on the possibility of application in an historical building's restoration, adding the challenge of a function as heavily defined by laws as a library is.

The first, learning phase has been based not only on collecting a number of technical and mathematical data about materials' performances, but also—and mainly—on the various working techniques and machinery applicable in this field, and their consequences on the materials' mechanical and aesthetic results and performances.

As a first design application of this just described deepening phase has been the production of a number of prototypes (both by drawing and modeling) of pillar-beam systems, in order to explore as thoroughly as possible the various morphological, mechanical and designing possibilities and consequences of such composite elements. Since the structural elements have been designed as half-prebuilt, also the possibility to integrate, in the metallic sections, part of the technological systems has been studied again, with a particular remark to the electrical and electronic systems.

The pillar-beam prototype finally chosen for the complete design experimental proposal has been also verified in relation to the actual fire-safety laws; it consists, as in the hypothesis of the previously presented work, of a cold-formed steel plate, for which folding the exact machinery to be used has been individuated, and a part of self-compacting reinforced concrete.

The calculation of structural elements is based on actual Italian laws, and it is obviously connected to the forecasts of a fire's effects on such a structure. In particular, the external steel plate, which has a structural role in normal conditions, is considered to be inefficient because of melting by the fire warm. Therefore, the whole structure (concrete plus metal) is calculated for the normal load conditions, while the concrete section reinforcement is verified on a reduced load, corresponding to the hypnotized load after the fire (all the fixed load plus the 30% of the special load), so to have a total section as thin as possible.

### 3 INTERACTION AMONG STRUCTURE AND ENVIRONMENT

Reinforcing and deepening the control of interactions between a building and the natural environment surrounding is another goal to improve the long-term behavior of a building, and we will present tree researches on this theme, each of them considering the aspect from a personal and original point of view. The connecting theme is the will of considering the sustainable design not as the adaptation of a building to its natural environment, but as the use of natural and climatic features really as morphogenetic factors characterizing the designer's work: therefore, in relation to the natural context, to have not an "adapted design", but a "consequent design" philosophy.

Therefore, after considering and studying a number of environment factors—not only sun angles and exposition, but also winds strength and path, average temperature and humidity . . . and materials, typologies and structural features deriving from the local natural environment, different settling strategies on the territory have been proposed, aiming not to a nearly utopian "zero impact" on the territory itself, but to maximize the effect of natural factors on the design and on the building itself, to make it more efficient from the energetic needs point of view, and also more inserted, and therefore durable, in relation to the natural context hosting it.

#### 3.1 *"Environment and sustainable architecture—Ecotec software as a design tool: a diving centre in Sistiana Bay, Trieste"* by Paola Iaschi e Martina Meloni

This project was born from the need to create a sustainable architecture, using technology as an instrument and able to work in harmony with the natural environment in which it is inserted, instead of overcoming it.

The use of Ecotec software as a design and conceptual development tool for the project allows us to implement the overall architectural quality of the design, while constantly controlling energetic, environmental and usage comfort consequences and impacts, so to fund the design choices on real performances' verifications.

During the various phases of conceiving and designing we stick to a small group of concepts and principles: first of all, regarding the interaction among formal choices and performative-constructive needs, it was fundamental to optimize the efficiency of those factors which could be controlled through the design, as: sun exposition; materials' choice (for obvious reasons, we addressed to materials having a strong thermic inertia); the study of weather, for a correct placement of the natural ventilation's openings; and finally the solar irradiation control, to optimize the

shadowing systems. Moreover, a rational utilization of both conventional and renewable energy sources has been planned, by inserting in the building highly performing technical systems and a solar system to produce warm water, necessary to the building's function and usage. In third place, in order to limit water losses, it has been planned the re-use and re-cycle of gray waters, and the restitution to soil of rain waters.

Finally, we tried in general to use recycled and/or recyclable materials.

The analysis run through Ecotec software along all the design phases allowed us to pursue and obtain a meaningful, general reduction of heating energy needs; in particular, for what concerns the cooling of internal spaces during summer, only the most critical temperatures will require the use of cooling systems.

#### 3.2 *"Air, water, architecture: project for a bioclimatical building on quarry lakes in Istrana, Treviso"* by Emanuele Guerra e Mauro Berto

The first cue of this research has been the will of studying the possibility of a constructive recovery of environmentally damaged areas as an abandoned quarry can be. In Veneto's zones interested by gravel quarries there are artificial lakes as the result of the quarries' themselves excavations, once they reach the natural underground water level; so formed lakes have quite notable dimensions (some hundreds of meters as side length, and about eighty—hundred meters deep) and, because of their very same nature, are totally alien to the surrounding landscape—may it be natural or anthropic—and are somehow kept out from it (in fact they're often hidden by on-purpose grown trees, or earthworks); however, even if only for their dimensions, they have a huge impact on the landscape quality and on the surrounding territory organization.

Once the hypothesis of filling up the lakes with ground is obviously discarded, such a notable water mass can be considered as interesting to verify the possibility to design a building which, based on Venturi effect and working in collaboration with the surrounding natural landscape elements, can convey and use those air fluxes blowing over the water itself to create a natural and efficient cooling and ventilation system of itself. The Venturi effect describes the pressure variations of a fluid flux in relation with its speed, and it can be assumed as the mathematical basis to design a building which should reproduce, through its volumetric composition, those condition to make the Venturi effect happen: meaning, the aim is to control the air fluxes and pressure via the building's volumetric composition itself.

The initial research and deepening phase has been facing more aspects: obviously the site has been thoroughly studied from the climatic and meteorological

points of view, to evaluate the real possibilities to use Veneto's territory in this way. At the same time, a series of case-studies, focused on natural ventilation building and the relationship between a building and surrounding water, have been investigated and deeply understood. Finally, some studies about gravel quarries have been run, in order to understand some geological and technical implications of constructing in such a special site.

The artificial lake's shores and the surrounding tree lines have been designed so to amplify as much as possible the wind's currents effects, which are not so strong in the area.

After a number of hypotheses and crossed checking, the efficiency and convenience of such an intervention philosophy, which use the natural landscape as a living part of itself, has been proved: the building inserted in this way in the landscape is really a part of the environment itself, not from an aesthetic or mimetic point of view, but really concerning its intrinsic functioning and its interactions with the territory itself. The so-designed building is also efficient from the Venturi effect point of view.

The building is composed by two main volumes, shaped and placed so to create between them the spatial conformation allowing the Venturi effect verification; this space, three stores high, is protected by a roof which is both contributing to the natural ventilation and supporting solar panels, to produce electricity (in this way, the building is nearly auto-sufficient, as for concerns its electrical energy needs). Internal spaces and functions distribution is also partially determined by the ventilation and technological needs: the various halls and rooms characterizing the functional program of the building (research center) always point out to the central main covered hall, which is crossed by some thin bridges—working both as link for users' movements and as structural stiffeners.

The main facades are constituted by a double-skin glass system, which creates a very wide buffer zone and contributes to the internal temperature and humidity control.

### 3.3 *"Solar architecture. A lido in Borgo Valsugana, Trento" by Katia Stenghel*

The project studies the possibility to create a quite big building, in this case the functional use is a water sports and wellness center, nearby a water course in a small town at the feet of Alps mountain. The whole project aims at using sun and water as a source and vector to heat and give energy to the building.

The site has an highly precious natural landscape surrounding it, and it is directly nearby the historical center of Borgo Valsugana town: therefore, both these factors have to carefully considered, and a total interpenetration and an efficient interaction

between building and environment are even more necessary.

The building itself is composed by a series of volumes, variedly orientated and with differently inclined green roofs; they are linked by a central passage, working as main servant distributional space from the functional point of view, and also as a connection to the decreasing ground from the volumes composition point of view. From an exquisitely architectural point of view, the whole building group is based on the revaluation and recovery of disappeared traces and directions, coming from the history and the evolution of the town and territory themselves, therefore re-proposing spatial suggestions of the historical center and declaring its appurtenance to the site.

Used materials are: CorTen steel structures, local stone cut in panels studied for the north facade skin, and glass and wood, characterizing internal spaces.

The technological systems, both active and passive, characterizing the sustainability of this building are based, as already said, on sun and water. It is possible to briefly list them, distinguishing the two categories—active and passive systems.

Passive systems:

- glass surfaces on south facade, and two conservatories to gain energy—directly and indirectly;
- heat storage in water-walls systems, and in thick roofing systems studied on purpose (in particular, the water-wall system is made of a series of plastic cans, designed on purpose for this project, which can be filled up with water; placed in strategical points in the internal spaces of the building, they provide a big mass of water, which allows the heat storage and slow release);
- good thermic insulation (earthwork on the north side, green roofs);
- good exposition of the building and volumes' composition optimized so to maximize the orientation advantages.

Active systems:

- tubular solar system to produce warm water, maintain the pools' temperature and help the internal space cooling during summer. This system, usually very evident and aesthetically invasive, has been integrated in the green roof, without compromising its efficiency;
- photovoltaic shading system.

## 4 CONCLUSIONS

Through the work hold in the universities, it is fundamental to give to future designers the knowledge of, in the history of a building, technological and material



choices taken during the designing phases have a deep impact not only on structural and aesthetic aspects, but also on the long-term behavior of a building and on its durability; moreover, this approach has to be considered as usual, and not an exception for rare and special buildings.

For this reason, especially during the graduation theses works, which are an important summarizing moment in a student's academic career and a possible starting point for future professionals, it is very important to face the evaluations on long-term consequences of designing choices and to learn to consider a number of aspects and criteria range, wider than the singular specialization of the various aspects of the design discipline.

## REFERENCES

- Bortolotto, Lisa. 2003. *Acciaio e fuoco—Nuovi linguaggi. Progetto per una mediateca a Porta saracinesca (PD)*. Venezia. Tesi di laurea presso l'Università IUAV di Venezia. Co-tutor Prof. P. Foraboschi.
- Focaccia, F. & Brunelli, N. 2006. *Acciaio e fuoco—Strutture composte in lamiera sagomata e cemento armato. Progetto per una biblioteca a Cervia, Ravenna*. Venezia. Tesi di laurea presso l'Università IUAV di Venezia. Co-tutor Prof. P. Foraboschi.
- Iaschi, P. & Meloni, M. 2004. *Ambiente ed architettura sostenibile. Il software Ecotec come strumento progettuale: un diving center nella baia di Sistiana (TS)*. Venezia. Tesi di laurea presso l'Università IUAV di Venezia. Co-tutor Prof. L. Schibuola.
- Guerra, E. & Berto, M. 2007. *Acqua, aria, architettura: progetto per un edificio bioclimatico sui laghi di cava ad Istrana (TV)*. Venezia. Tesi di Laurea presso l'Università IUAV di Venezia. Co-tutor Prof. F. Peron, Arch. E. Dalla Vecchia.
- Stenghel, Katia. 2006. *Architettura solare. Un lido per Borgo Vasugana*. Venezia. Tesi di Laurea presso l'Università IUAV di Venezia. Co-tutor Prof. F. Peron.
- Brown, G.Z. & Al. 2001. *Sun, wind and light: architectural design strategy*. New York. Wiley ed.
- Lione, R & Al. 2002. *Il legno: caratteristiche tecniche e progettazione*. Roma. Carocci Faber.
- Mazria, E. 1990. *Sistemi solari passivi*. Padova. Nuova edizioni.
- Cirillo, Antonio. 2006. *Acciaio. Calcoli strutturali, progettazione e prassi del costruire*. Napoli. Esselibri editrice.
- Florida, Sebastiano. 2003. *Acciaio: collegamenti nelle strutture*. Palermo. D. Flaccovio.
- Buccino, Giampaolo. 2001. *Acciaio. Elementi strutturali e particolari costruttivi*. Roma. Librerie Dedalo.
- Spigai, V. & Dalla Vecchia, E. 2007. Architettura e sistemi impiantistici innovativi. In: *Architettura\_Energia—Un'indagine sul complesso rapporto tra la professione dell'architetto e la questione energetica*. (A cura di Barucco, M. & Trabucco, D. , Edicom Edizioni). Pagine da 125 a 132.

# Effect of spatially variable corrosion damage on strength and time-dependent reliability of RC beams

M.G. Stewart & Q. Suo

*Centre for Infrastructure Performance and Reliability, School of Engineering, The University of Newcastle, New South Wales, Australia*

**ABSTRACT:** A spatial time-dependent reliability model is developed for a RC beam subject to corrosion-induced pitting corrosion. The analysis considers the spatial and time-dependent variability of pitting corrosion and its effect on cover cracking and shear and flexural resistance. The model uses extreme value theory to predict maximum pit depth as a function of bar diameter and reinforcing bar length. The effect of corrosion on the mechanical behaviour of reinforcement and associated loss of ductility is also considered. A 1D spatial model is included where concrete properties, concrete cover and the surface chloride concentration are treated as random fields. The spatial time-dependent reliability model allows the loss of structural capacity and reliability to be calculated conditional on the observed extent of corrosion damage. This allows the interaction between corrosion damage and loss of structural safety to be inferred for a deteriorating RC beam.

## 1 INTRODUCTION

There is overwhelming evidence from laboratory and field observations of deteriorated structures that the deterioration process is spatially and time-dependent in nature. In other words, corrosion damage is not homogenous along a structure, but is highly spatially variable (heterogeneous) due to the spatial variability of concrete and steel material properties, environment, moisture, concrete cover, surface cracking, pitting corrosion, etc. While much work has progressed on the structural reliability of deteriorating structures, there is relatively little work on spatial modelling of deterioration processes.

The main objective of the present paper is to consider the spatial variability of cover cracking and pitting corrosion and their effect on serviceability, strength and conditional limit states. While some work has investigated the interaction of multiple limit states (Stewart and Val 2003), this work assumed homogeneous material, dimensional and deterioration properties and a simplified crack width prediction model. The present paper considers spatial variability for pit depth, concrete cover, concrete properties, concrete cover, surface chloride concentration, time to corrosion initiation, corrosion rate and crack propagation. A spatial time-dependent reliability model is thus developed for a reinforced concrete (RC) beam subject to corrosion-induced pitting corrosion. The analysis considers the spatial and time-dependent variability of pitting corrosion and its effect on cover cracking

(damage) and shear and flexural resistance. The model uses extreme value theory to predict maximum pit depth. A 1D spatial model is included where material, dimension and deterioration variables are treated as random fields. The term ‘damage’ refers to concrete with corrosion-induced surface crack widths exceeding 0.3 mm. The effect of corrosion on the mechanical behaviour of reinforcement and associated loss of ductility is also considered as for most realistic structural and deterioration scenarios some reinforcement will fail by ductile yielding, and others by brittle fracture. The progression from ductile to brittle behaviour is spatially and time-dependent. To estimate how such phenomena affects structural reliability the structural resistance of reinforcement is modelled as either (i) perfectly ductile parallel system or (ii) perfectly brittle parallel system.

The spatial time-dependent reliability model allows the loss of structural capacity and reliability to be calculated conditional on the observed extent of corrosion damage. This allows the interaction between corrosion damage and loss of structural safety to be inferred. Results are presented for a simply supported RC beam comprising Y27 main reinforcement and Y10 stirrups.

## 2 DETERIORATION PROCESS

Predictive models for corrosion initiation and propagation are described in detail by Vu and Stewart (2000, 2005).

## 2.1 Time to severe cracking

The time (after corrosion initiation) for cracking of the concrete surface to reach a limit crack width ( $w_{lim}$ ) is (Vu et al. 2005):

$$t_{sp} = t_{1st} + t_{ser} = t_{1st} + k_R \frac{0.0114}{i_{corr}} \left[ A \left( \frac{C}{w/c} \right)^B \right] \quad (1)$$

where  $t_{1st}$  is the time to crack initiation,  $t_{ser}$  is the time since crack initiation to reach a limit crack width (years),  $i_{corr}$  is the corrosion current density ( $\mu A/cm^2$ ) assumed constant with time, A and B are empirical constants,  $k_R$  is a rate of loading correction factor, C is concrete cover (mm) and w/c is the water-cement ratio. The water-cement ratio is correlated to concrete compressive strength ( $f'_c$ ). The model is valid for 16 mm diameter bars.

The Liu and Weyers (1998) model is a popular method for predicting time to crack initiation ( $t_{1st}$ ). However, Chernin and Val (2008) prove that the derivation of a key parameter ( $k_p$ ) in the Liu and Weyers (1998) model is incorrect and not solvable. The Liu and Weyers (1998) model now seems invalid and should not be used as a predictive tool. Hence, the El Maaddawy and Souki (2007) model for crack initiation is used herein.

An accurate predictive model of the effect of bar diameter on crack propagation ( $t_{ser}$ ) is not available. In the present case, the effect on  $t_{ser}$  when using 27 mm (main reinforcement) and 10 mm (stirrups) diameter bars is of interest. Accelerated corrosion tests at The University of Newcastle show that increasing the bar diameter from 16 mm to 27 mm reduces  $t_{ser}$  by 12% to 32% (Al-Harthy et al. 2007). A model by Vidal et al. (2004) predicts a 30% to 40% decrease (for various corrosion rates and covers) in  $t_{ser}$  if bar diameter increases from 16 mm to 27 mm. If bar diameter reduces from 16 mm to 10 mm, then Vidal et al. (2004) predicts a 40% to 60% increase in  $t_{ser}$ . In the absence of other data or models, it is assumed herein that:

- 10 mm diameter bar:  $t_{ser}$  given by Eqn. (1) is increased by 50%.
- 27 mm diameter bar:  $t_{ser}$  given by Eqn. (1) is reduced by 25%.

See Vu et al. (2005) for details on time to reach the limit crack width for a time-variant corrosion rate.

## 2.2 Pitting corrosion and ultimate strength of a RC section

A pitting factor  $R = p/P_{av}$  is used to define the extent of corrosion pitting, where p is the maximum pit depth and  $P_{av}$  is the penetration calculated based on general corrosion. A Gumbel (EV-Type I) distribution is selected herein for modelling maximum pit depths for reinforcing bars. Experimental results from The University of Newcastle show that R was found to be

statistically independent for 100 mm lengths. To predict the distribution of maximum pitting factor for a reinforcing bar of length ( $L_U$ ), the Gumbel statistical parameters are:

$$\mu = \mu_o + \frac{1}{\alpha_o} \ln \left( \frac{L_U}{L_o} \right) \quad \alpha = \alpha_o \quad (2)$$

where the Gumbel parameters  $\mu_o$  and  $\alpha_o$  are derived from statistical analysis of pitting data for reinforcement of length  $L_o$ , see Table 1.

The maximum pit depth along a reinforcing bar is

$$p(t) = 0.0116R \int_{T_i}^t i_{corr}(t) dt \quad t > T_i \quad (3)$$

where p(t) is in mm and  $T_i$  is the time to corrosion initiation. The cross-sectional area of the pit ( $A_{pit}$ ) is calculated from p(t).

Reinforcement yield strength ( $f_y$ ) reduces linearly with corrosion loss (Du et al. 2005).

$$f_y(t) = (1 - \alpha_y Q_{corr}) f_{y0} \quad (4)$$

where  $f_{y0}$  is the yield stress of an uncorroded reinforcing bar,  $\alpha_y$  is an empirical coefficient (=0.005), and percentage corrosion loss ( $Q_{corr}$ ) is measured as  $A_{pit}(t)/A_{stnom} \times 100\%$  where  $A_{stnom}$  is the cross-sectional area of an uncorroded reinforcing bar. For more details see Stewart (2004) and Stewart and Al-Harthy (2008).

While there is a gradual transition from ductile to brittle behaviour as corrosion loss increases (e.g., Cairns et al. 2005), for the present paper it is conveniently assumed that complete loss of ductility in corroded reinforcing bars occurs after corrosion loss ( $Q_{corr}$ ) exceeds a threshold value of  $Q_{limit}$ . This leads to two types of mechanical behaviour:

1. Ductile behaviour:  $Q_{corr} \leq Q_{limit}$
2. Brittle behaviour:  $Q_{corr} > Q_{limit}$

The literature shows that it is reasonable to quantify  $Q_{limit} = 20\%$ , although more research is needed.

The reinforcement layout for a typical singly reinforced RC beam is shown in Figure 1. The time-dependent ultimate flexural capacity (M) is

$$M(t) = ME_M \times A_{st}(t) f_y(t) \left( d - \frac{A_{st}(t) f_y(t)}{1.7 f'_c(t) b} \right) \quad (5)$$

which is a function of model error ( $ME_M$ ), concrete compressive strength ( $f'_c$ ), effective depth (d), beam

Table 1. Statistics of Pitting Corrosion ( $L_o = 100$  mm).

Rebar	$\mu_o$	$\alpha_o$	Reference
Y10	5.08	1.02	Stewart (2004)
Y16	5.56	1.16	Stewart & Al-Harthy (2008)
Y27	6.55	1.07	Stewart & Al-Harthy (2008)

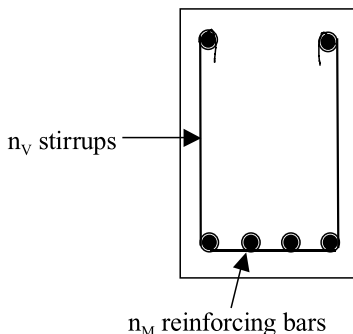


Figure 1. Cross-section of RC beam.

width ( $b$ ), yield stress ( $f_y$ ) and cross-sectional area of reinforcement ( $A_{st}$ ) (ACI318-2005).

The ultimate shear capacity is

$$V(t) = ME_V \left[ 0.17 \sqrt{f'_c} b d + A_v(t) f_y(t) \right] \quad (6)$$

where  $A_v(t)$  is the cross sectional area of all shear reinforcement (stirrups) in a section of beam of length  $d$  and  $ME_V$  is the model error.

Strength capacity of a RC section is based on a layout comprising of  $n$  reinforcing bars that comprise a parallel system. For ductile behaviour there is equal load sharing between all reinforcement. However, brittle fracture will completely exhaust a reinforcing bars load-carrying capacity, resulting in load redistribution to the remaining bars, possibly leading to progressive failure of adjacent reinforcing bars. The strength of a RC section is thus dependent on the mechanical behaviour and strength of reinforcement and the cross-sectional area of each reinforcing bar, such that:

1. Perfectly ductile parallel system:

$$f_y(t) A_{st}(t) = \sum_{i=1}^n f_{yi}(t) A_{iM}(t)$$

$$f_y(t) A_V(t) = \sum_{i=1}^n f_{yi}(t) A_{iV}(t) \quad (7)$$

2. Perfectly brittle parallel system:

$$f_y(t) A_{st}(t) = \max(n f_{y1}(t) A_{1M}(t), (n-1) f_{y2}(t) A_{2M}(t), \dots, f_{yn}(t) A_{nM}(t))$$

where  $f_{y1}(t) A_{1M}(t) < f_{y2}(t) A_{2M}(t) < \dots < f_{yn}(t) A_{nM}(t)$

$$f_y(t) A_V(t) = \max(n f_{y1}(t) A_{1V}(t), (n-1) f_{y2}(t) A_{2V}(t), \dots, f_{yn}(t) A_{nV}(t)) \quad (8)$$

where  $f_{y1} A_{1V}(t) < f_{y2}(t) A_{2V}(t) < \dots < f_{yn}(t) A_{nV}(t)$  and where  $A_{iM}(t)$  and  $A_{iV}(t)$  are the cross-sectional

areas of the  $i^{\text{th}}$  main reinforcing bar and stirrup at time  $t$ , respectively, and  $f_{yi}(t)$  is the yield strength for each reinforcing bar. The effects of corrosion on reduction of bond and delamination or spalling of concrete cover are not considered.

### 3 RANDOM FIELD MODELLING

The spatial variables for the RC beam are:

1. concrete compressive strength
2. concrete cover
  - a. main reinforcement
  - b. stirrups
3. chloride surface concentration
4. reinforcement corrosion pitting factor
  - a. main reinforcement
  - b. stirrups

The spatial variability may be modelled by random fields. The midpoint method is preferred herein due to its ease of computation, numerically stable results and is applicable to Gaussian and non-Gaussian random fields. In this method the random field needs to be discretised into  $N$  elements of identical size and shape ( $\Delta$ ). For more details see Vanmarcke (1983).

#### 3.1 Discretisation of RC beam

For a spatial analysis of pitting corrosion a reinforcing bar is subdivided into equal lengths  $L_U$ , referred to herein as 'uniform capacity length', see Figure 2. This length refers to the distance along a structural member in which localised corrosion will have a detrimental effect on structural capacity. The uniform capacity length is likely to be dependent on (i) the ability of corroded reinforcement to redistribute stresses to adjacent (less corroded) reinforcement via the concrete matrix, (ii) mechanical behaviour of the reinforcement (yield, brittle), (iii) development length of reinforcement (function of diameter of reinforcement and concrete cover) and (iv) geometry and spacing of reinforcement. The understanding of this phenomena is incomplete, with recent reliability studies assuming values of  $L_U$  varying from 100 mm to

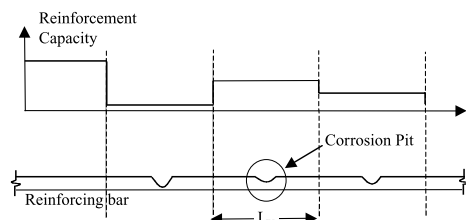


Figure 2. Spatial capacity of corroded reinforcing bar.

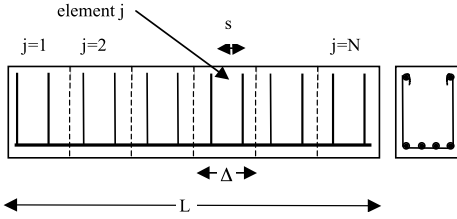


Figure 3. Discretisation of RC beam.

over 1000 mm (Stewart 2004, Stewart and Al-Harthy 2008, Val 2007).

A 1D random field is applied to a RC beam discretised into  $N$  elements of length  $\Delta$ , see Figure 3. The failure mode for shear is diagonal cracking inclined at approximately  $45^\circ$  at locations of large shear force and small bending moment. Hence, shear and flexural capacity is calculated for an element length of  $\Delta = d$  (effective depth of beam). It follows that uniform capacity length  $L_U$  for main reinforcement is the element length ( $\Delta$ ). Shear diagonal cracking can occur anywhere along a stirrup within an element, so in this case the maximum pit along a stirrup is obtained using  $L_U = \text{length of stirrup}$ .

Concrete cover, concrete compressive strength and surface chloride concentration are modelled as a 1D random field. The chloride diffusion coefficient, w/c ratio and corrosion rate are dependant variables on the concrete compressive strength and/or cover and are thus also spatially variable. The maximum pit depth  $R$  for an element is modelled from the Gumbel distribution. Since experimental data shows it is reasonable to model pit depths for adjacent elements and between each reinforcing bar within an element as statistically independent, then this is equivalent to a random field with zero correlation between elements.

### 3.2 Probabilistic measures of performance

The following performance indicators are obtained from the spatial time-dependent reliability analysis for deteriorating RC structures.

#### 3.2.1 Serviceability limit states

Corrosion-induced cracking can occur as a result of corrosion to main reinforcement and/or stirrups. Hence, corrosion-induced cracking can affect the soffit and sides of a RC beam. In the present case, the proportion of a concrete surface with crack widths exceeding the limit crack width at time  $t$  for the soffit and sides of a RC beam are referred to as  $d_M(w, t)$  and  $d_V(w, t)$ , respectively. Monte-Carlo simulation analysis can then be used to infer the distribution of  $d_M(w, t)$  and  $d_V(w, t)$ . As shown by Stewart and Mullard (2007) the probability distribution of corrosion damage is

highly non-Gaussian and so percentile values of probability distribution of corrosion damage can only be predicted from simulation methods.

The probability that at least  $x\%$  of a concrete surface has cracked at time  $t$  is referred to herein as  $\Pr(d_M(w, t) \geq x\%)$  and  $\Pr(d_V(w, t) \geq x\%)$  for main reinforcement and stirrups, respectively.

#### 3.2.2 Strength limit states

The critical limit state occurs when actual load effects exceed resistance at any element. In general, if it is assumed that  $K$  load events occur within the time interval  $(0, t)$  at times  $t_i (i = 1, 2, \dots, K)$ , then for this series system the critical strength limit state for a beam comprising  $N$  elements is

$$G_{M,t_i}(X) = \min_{j=1,N} (M_j(t_i) - S_{M_j}(t_i))$$

$$G_{V,t_i}(X) = \min_{j=1,N} (V_j(t_i) - S_{V_j}(t_i)) \quad (9)$$

where  $M_j(t_1), M_j(t_2), \dots, M_j(t_K)$  and  $V_j(t_1), V_j(t_2), \dots, V_j(t_K)$  represent the flexural and shear resistance at the mid-point of each element  $j$ , respectively; and  $S_{M_j}(t_i)$  and  $S_{V_j}(t_i)$  represents the bending moment and shear force at the mid-point of each element due to the  $i^{\text{th}}$  load. The flexural resistance at any element  $j$  at time  $t$  is obtained from Eqn. (5) where  $f_y(t)A_{st}(t)$  is obtained from Eqn. (7) or (8) for  $n_M$  reinforcing bars. The shear resistance at any element  $j$  at time  $t$  is obtained from Eqn. (6) where  $f_y(t)A_V(t)$  is obtained from Eqn. (7) or (8) for  $n_V$  stirrups.

The cumulative probabilities of failure for flexure ( $p_{fM}$ ) and shear ( $p_{fV}$ ) limit states anytime during this time interval are, respectively

$$P_{fM}(0, t) = 1 - PR [G_{M,t_1}(X) > 0 \cap \dots \cap G_{m,t_k}(X) > 0]$$

$$P_{fV}(0, t) = 1 - PR [G_{V,t_1}(X) > 0 \cap \dots \cap G_{V,t_k}(X) > 0] \quad (10)$$

where  $t_1 < t_2 < \dots < t_k \leq t$

For any corroding RC structural component that comprises of many reinforcing bars and elements there is a strong likelihood of non-ductile behaviour irrespective of structural configuration. Hence, some reinforcement which is more heavily corroded than other reinforcement will exhibit brittle behaviour, and other (less corroded) reinforcement ductile behaviour. Clearly, this phenomena is very difficult to model either numerically or by stochastic FEA. In light of such difficulties, it is reasonable to assume two bounds on structural reliability, namely, all reinforcement in a RC structural component exhibits: (i) ductile behaviour ( $p_{f-ductile}$ ) or (ii) brittle behaviour ( $p_{f-brittle}$ ). As the capacity of a perfectly brittle parallel system

is less than that of a perfectly ductile parallel system, it follows that the actual structural reliability ( $p_f$ ) of the RC structural component will thus lie somewhere between these structural reliabilities such that  $P_{f-ductile} < P_f < P_{f-brittle}$ .

### 3.2.3 Conditional limit states

It is of interest to assess the relative loss of strength and reliability conditional on the observation of extent of corrosion damage. Hence, conditional limit states of interest may include:

Probability of flexural or shear collapse conditional on  $w$  mm crack widths being  $x_1$  to  $x_2\%$  of the surface area:

$$\begin{aligned} p_{fM}(w, t) | d_M(w, t) &= (x_1\% - x_2\%) \\ p_{fV}(w, t) | d_V(w, t) &= (x_1\% - x_2\%) \end{aligned} \quad (11)$$

where  $x_1 - x_2$  is 0%, 10–20%, 30–40%, etc.

The proportion of cracking at the time when flexure failure occurs (at time  $t_M$ ) or when shear failure occurs (at time  $t_V$ ):

$$\begin{aligned} d_M(w, t_M) | G_{M,t_M}(X) &< 0 \\ d_V(w, t_V) | G_{V,t_V}(X) &< 0 \end{aligned} \quad (12)$$

The corrosion loss ( $Q_{corr}$ ) at the time when flexure failure occurs (at time  $t_M$ ) or when shear failure occurs (at time  $t_V$ ):

$$\begin{aligned} Q_{corr-M}(w, t_M) | G_{M,t_M}(X) &< 0 \\ Q_{corr-V}(w, t_V) | G_{V,t_V}(X) &< 0 \end{aligned} \quad (13)$$

### 3.3 Computational analysis

Due to the complicated nature of the spatial time-dependant reliability analysis used herein it is not possible to derive closed-form solutions. The analysis includes a large number of random variables, spatial random fields and dependant variables as well as non-linear and conditional limit state functions for corrosion damage, capacity reduction and time-dependant material properties and corrosion processes. Hence, Monte Carlo simulation methods are used herein.

## 4 RESULTS

### 4.1 RC beam

The structural configuration is a simply supported RC beam supporting a uniformly distributed load. The specified nominal concrete strength is  $F'_c = 34.5$  MPa and reinforcement yield strength is 413.5 MPa. A 400 mm  $\times$  800 mm RC section with 4Y27 main reinforcement ( $n_M = 4$ ) is designed as a typical RC section for  $L = 7.5$  m, 50 mm cover and live-to-dead

Table 2. Statistical Parameters For Corrosion Parameters, Material Properties and Dimensions (normally distributed).

Parameter	Mean	COV
$C_o$ (surface Cl concentration)	3.05 kg/m <sup>3</sup>	0.74
$C_r$ (threshold Cl concentration)	2.4 kg/m <sup>3</sup>	0.2
Model errors for D and $i_{corr}$	1.0	0.2
Model error: $t_{sp}(w_{lim} = 0.3 \text{ mm})$	1.09	0.19
$t_{sp}(w_{lim} = 1.0 \text{ mm})$	1.05	0.20
Model error: Flexural capacity	1.02	0.06
Shear capacity	1.075	0.10
Cover	+1.6 mm	$\sigma =$ 11.1 mm
Reinforcement yield strength $f_{y0}$	467.5 MPa	0.03
Concrete cylinder strength $f'_{cyl}$	$F'_c + 7.4 \text{ MPa}$	$\sigma =$ 6 MPa
$k_w(f'_c(28) = k_w f'_{cyl})$	0.87	0.06
Concrete tensile strength $f'_{ct}(t)$	$0.53 (f'_c(t))^{0.5}$	0.13
Concrete elastic modulus $E'_c(t)$	$4600 (f'_c(t))^{0.5}$	0.12

load ratio of one (ACI318-2005). Shear capacity is provided by Y10 stirrups spaced at  $s/d = 0.5$ .

The RC beam is discretised into  $N = 10$  elements of length  $\Delta = d = 750$  mm. Each element contains  $n_V = 2$  stirrups. Hence,  $L_U = 750$  mm for main reinforcement and  $L_U = 700$  mm for stirrups.

A 1D random field is applied to the RC beam considering the spatial variability of concrete cover, concrete compressive strength and surface chloride concentration. The random field is assumed stationary with respect to space. The corrosion rate is assumed as time-variant. The statistical parameters for the spatial time-dependent reliability analysis are given in Table 2. Statistical parameters for a stochastic office floor load are summarised by Stewart (2004). The time period is taken as 100 years.

Data to date suggests that a scale of fluctuation for concrete compressive strength, cover and surface chloride concentration is approximately 3.5 m (Stewart and Mullard, 2007). The Gaussian correlation function is used herein.

### 4.2 Results

Figure 4 shows the effect of mechanical behaviour on the cumulative probabilities of failure calculated from Eqn. (10), for flexure and shear limit states. The probabilities of failure considering all reinforcement to exhibit brittle behaviour are up to 123% higher than probabilities of failure assuming all reinforcement exhibits ductile behaviour. Clearly, the mechanical behaviour of reinforcement has a significant effect on structural reliability, and the bounds on the actual probability of failure  $P_{f-ductile} < P_f < P_{f-brittle}$  can be considerable.

The probability of flexural collapse conditional on 1 mm crack widths being  $x_1 - x_2\%$  of the surface area

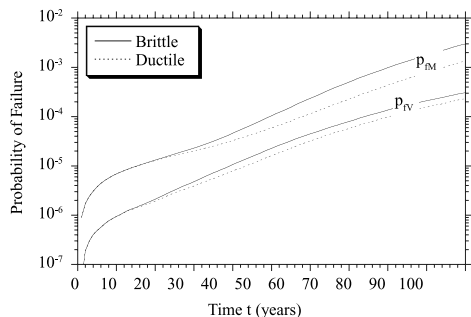


Figure 4. Probabilities of failure,  $p_{FM}(0, t)$  and  $p_{FV}(0, t)$ .

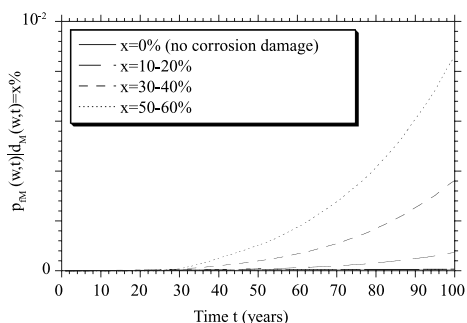


Figure 5. Probabilities of flexural failure conditional on extent of 1 mm cover cracking, for ductile behaviour.

obtained from Eqn. (12) are shown in Figure 5, for ductile behaviour. It is observed, for example, that the probability of flexural failure when extent of cracking is between 50–60% [ $p_{FM}(t) | d_M(t) = (50-60\%)$ ] is 142 times higher than  $p_{FM}$  when no cracking is evident [ $p_{FM}(t) | d_M(t) = 0\%$ ]. Even if only 10–20% of cracking damage is observed the probability of flexural failure is 12.1 times higher than if no damage is observed. If the shear limit state is considered then  $p_{FV}(t) | d_V(t) = (50-60\%)$  is 113 times higher than  $p_{FM}$  when no cracking is evident [ $p_{FV}(t) | d_V(t) = 0\%$ ]. If the limit crack width ( $w_{lim}$ ) is reduced to 0.3 mm (i.e., stricter definition of ‘damage’) the differentials are smaller but the general trends remain unchanged.

Figure 6 shows that the mean proportion of cracking at the time when flexure or shear failure occurs [obtained from Eqn. (12)] increases to 40% when  $t_M$  or  $t_V$  is 100 years. In all cases, the COV is very high (typically 0.3 to 0.5).

The mean corrosion loss ( $Q_{corr-M}$ ) for all reinforcement in a section at the time when flexure failure occurs [obtained from Eqn. (13)] varies from 30% at  $t_M = 50$  years to 40% after  $t_M = 100$  years. The mean corrosion loss ( $Q_{corr-V}$ ) at the time when shear failure occurs is significantly higher, with a maximum value of nearly 80% at  $t_V = 100$  years.

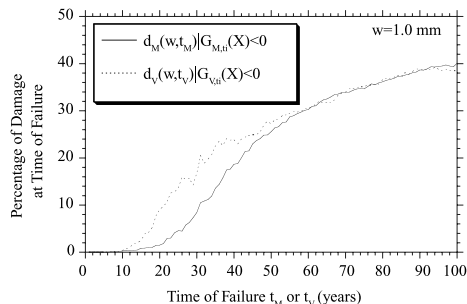


Figure 6. Mean percentage of damage at the time of flexural or shear failure, for ductile behaviour and  $w = 1.0$  mm.

The results clearly show that the observed extent of cover cracking is an important indicator of structural reliability. Such information can be measured from an existing structure and thus can be used to update the reliability of existing structures.

## 5 CONCLUSIONS

A spatial time-dependent reliability analysis considering collapse and damage (cover cracking) limit states allowed the interaction between corrosion damage and loss of structural safety to be inferred for a deteriorating RC beam. It was shown that extent of cover cracking is an important indicator of structural reliability.

## ACKNOWLEDGEMENTS

The support of the Cooperative Research Centre for Integrated Engineering Asset Management under grant ID207 is gratefully acknowledged.

## REFERENCES

- Al-Harthy, A.S., Mullard, J. and Stewart, M.G. (2007), Cracking in Concrete Due to Corrosion of Steel Reinforcement, *Fifth Int. Conf. on Concrete Under Severe Conditions, Environment and Loading*, F. Toutlemonde (ed.), 383–390.
- Cairns, J., Plizzari, G.A., Du, Y., Law, D.W. and Franzoni, C. (2005), Mechanical Properties of Corrosion-Damaged Reinforcement, *ACI Materials Journal*, 102(4):256–264.
- Chernin, L. and Val, D.V. (2008), Prediction of Cover Cracking in Reinforced Concrete Structures due to Corrosion, *MEDACHS 08: 1st Int. Conf. on Construction Heritage in Coastal and Marine Environments*, 28–30 January, Lisbon.
- Du, Y.G., Clark, L.A. and Chan, A.H.C. (2005), Residual Capacity of Corroded Reinforcing Bars, *Magazine of Concrete Research*, 57(3):135–147.

- El Maaddawy, T. and Soudki, K. (2007), A Model for Prediction of Time from Corrosion Initiation to Corrosion Cracking, *Cement & Concrete Composites*, 29(3):168–175.
- Liu Y, Weyers RE, (1998), Modelling The Time-to-Corrosion Cracking in Chloride Contaminated Reinforced Concrete Structures, *ACI Materials Journal*, 95(6):675–681.
- Stewart, M.G. and Val, D.V. (2003), Multiple Limit States and Expected Failure Costs for Deteriorating RC Bridges, ASCE, *Journal of Bridge Engineering*, 8(6):405–415.
- Stewart, M.G. (2004), Spatial Variability of Pitting Corrosion and its Influence on Structural Fragility and Reliability of RC Beams In Flexure, *Structural Safety*, 26(4):453–470.
- Stewart, M.G. and Mullard, J.A. (2007), Spatial Time-Dependent Reliability Analysis of Corrosion Damage and the Timing of First Repair for RC Structures, *Engineering Structures*, 29(4):1457–1464.
- Stewart, M.G. and Al-Harthy, A. (2008), Pitting Corrosion and Structural Reliability of Corroding RC Structures: Experimental Data and Probabilistic Analysis, *Reliability Engineering and System Safety*, 93(3):273–382.
- Vanmarcke, E.H. (1983), *Random Field: Analysis and Synthesis*, Cambridge, Massachusetts, London, The LIT Press.
- Val, D.V. (2007), Deterioration of Strength of RC Beams Due to Corrosion and its Influence on Beam Reliability, *Journal of Structural Engineering*, ASCE, 133(9):1297–1306.
- Vidal, T., Castel, A. and Francois, R. (2004), Analyzing Crack Width to Predict Corrosion of Reinforced Concrete, *Cement and Concrete Research*, 34:165–174.
- Vu, K. and Stewart, M.G. (2000), Structural Reliability of Concrete Bridges Including Improved Chloride-Induced Corrosion Models, *Structural Safety*, 22(4):313–333.
- Vu, K. and Stewart, M.G. (2005), Predicting the Likelihood and Extent of RC Corrosion-Induced Cracking, *Journal of Structural Engineering*, ASCE, 131(11):1681–1689.
- Vu, K.A.T., Stewart, M.G. and Mullard, J.A. (2005), Corrosion-Induced Cracking: Experimental Data And Predictive Models, *ACI Structural Journal*, 102(5): 719–726.



# Service-life performance of reinforced concrete structures in corrosive environments

D.V. Val

*Heriot-Watt University, Edinburgh, UK*

L. Chernin

*Technion, Israel Institute of Technology, Haifa, Israel*

**ABSTRACT:** Reinforced concrete (RC) structures in marine environments are susceptible to deterioration caused by corrosion of reinforcing steel. Various measures can be employed to protect RC structures against corrosion and prevent deterioration. The measures increase the initial cost of a RC structure but reduce costs associated with its future service life. Thus, a cost-effective solution can only be determined on a life-cycle cost basis. Obviously, results of a life-cycle cost analysis depend on the predictive models used to describe corrosion initiation, propagation, and corresponding deterioration. The paper examines the influence of various predictive models on results of life-cycle cost analysis. Serviceability failure due to excessive corrosion-induced cracking is considered.

## 1 INTRODUCTION

Chloride-induced corrosion of reinforcing steel is the main course of deterioration of reinforced concrete (RC) structures in marine environments. Various measures can be employed to protect RC structures against corrosion and prevent/delay deterioration. The measures usually increase the initial cost of a RC structure but reduce costs associated with its future service life. Thus, in order to make a decision about a cost-effective solution life-cycle cost (LCC) of a structure needs to be considered, i.e. all costs associated with design, construction, maintenance and possible failure modes of the structure (e.g. Val & Stewart 2003, Frangopol & Liu 2007).

Usually, excessive cracking and spalling of the concrete cover due to corrosion appear before corrosion has any significant influence on strength of a RC structure (e.g. Val 2005). Thus, times of corrective actions (e.g. repair, replacement) are normally controlled by serviceability failure associated with these phenomena. In the present study, only failure costs due to serviceability failure caused by corrosion-induced cracking/spalling are taken into account.

To estimate failure costs due to corrosion at the stage of design, when decisions about the use of corrosion protection measures are usually made, models to predict corrosion initiation, propagation, and corresponding deterioration are necessary. There is significant uncertainty associated with the models, including statistical data required for their calibration.

The influence of different sources of uncertainty on the prediction of corrosion initiation, propagation, and corresponding structural damage on results of LCC analysis was investigated in Val (2007). However, not only available statistical data but the predictive models themselves are being updated and improved with time. In particular, major projects such as DuraCrete (2000) and LIFECON (2003), which were completed recently, contributed significantly to understanding of deterioration mechanisms in RC structures and development of new improved models for their prediction, especially it concerns corrosion-induced deterioration. Another important document published lately, which provides models for prediction of corrosion initiation, is *fib* Model Code for Service Life Design (*fib* 2006).

The objective of this paper is to examine the influence of models employed for prediction of corrosion initiation, propagation, and corresponding structural damage on results of LCC analysis and based on them design recommendations. For this purpose, design specifications (i.e. concrete grade and thickness of the concrete cover) will be selected based on the minimum expected LCC for RC structures in marine environments (splash zone and atmospheric zone adjacent to the cost). In order to estimate the expected LCC time-dependent probabilities of spalling (i.e. failure) will be calculated using predictive models from DuraCrete (2000), LIFECON (2003), *fib* (2006), and Chernin & Val (2008). Results will be compared with those from the previous study (Val & Stewart 2003), in which more simple predictive models were employed.

## 2 MODELLING CORROSION-INDUCED DETERIORATION

### 2.1 Corrosion initiation

Corrosion in RC structures in marine environments is caused by chloride contamination and starts when the concentration of chloride ions near reinforcing steel reaches a threshold value. In reality, the penetration of chloride ions into concrete is a complex process involving such transport mechanisms as ionic diffusion and convection. However, in practical applications it is usually modelled as a pure diffusion process, which can be described by Fick's 2nd law of diffusion. In Val & Stewart (2003) the simplest solution with constant values of the surface chloride concentration,  $C_s$ , and the chloride diffusion coefficient,  $D_C$

$$C(x, t) = C_s \left[ 1 - \operatorname{erf} \left( \frac{x}{2\sqrt{D_C t}} \right) \right] \quad (1)$$

was used, where  $C(x, t)$  = chloride concentration at a distance  $x$  from the concrete surface at time  $t$ .  $D_C$  was estimated by the formula proposed by Papadakis et al. (1996).

According to recent studies (e.g., DuraCrete 2000, LIFECON 2003) there is strong evidence that the chloride diffusion coefficient decreases with time, which may have significant influence on the prediction of chloride ingress. Thus, in the present paper a more advanced model recommended by fib (2006) is adopted. The model leads to the solution given by Eq. (1), in which  $D_C$  is replaced by the apparent chloride diffusion coefficient

$$D_{app,C} = k_e D_{RCM,0} \left( \frac{t_0}{t} \right)^a \quad (2)$$

where  $k_e = \exp[1/T_{ref} - 1/T_{real}]$  = environmental transfer variable;  $b_e$  = regression variable;  $T_{ref}$  = standard test temperature (K);  $T_{real}$  = temperature of the ambient air;  $D_{RCM,0}$  = chloride migration coefficient from the rapid chloride migration test;  $t_0$  = reference time; and  $a$  = ageing exponent. The time to corrosion initiation,  $t_i$ , is determined as the time when the chloride concentration near reinforcing steel (i.e. at  $x$  equal to the thickness of the concrete cover,  $c$ ) reaches the threshold chloride concentration,  $C_{cr}$ .

In the analysis  $b_e$ ,  $c$ ,  $C_{cr}$ ,  $D_{RCM,0}$ , and  $a$  are treated as random variables, whose statistical properties are assigned in accordance to recommendations of fib (2006).  $C_s$  is also considered as a random variable. However, in order to ensure consistency of comparison with results from Val & Stewart (2003) statistical parameters of  $C_s$ , which represents environmental load, are adopted from the above paper. For details see Table 1.

Table 1. Statistical parameters of random variables.

Variable	Mean	COV*	Distribution
$c$	nominal	10 mm**	Lognormal
$C_s$			
in splash zone	7.35 kg/m <sup>3</sup>	0.70	Lognormal
on coast	2.95 kg/m <sup>3</sup>	0.70	Lognormal
$C_{cr}$	0.6 wt.-%cement	0.25	Beta on [0.2;2.0]
$b_e$	4800 K	0.146	Normal
$D_{RCM,0}$			
$f'_c = 30$ MPa	$15.8 \times 10^{-12}$ m <sup>2</sup> /s	0.20	Normal
$f'_c = 40$ MPa	$10.0 \times 10^{-12}$ m <sup>2</sup> /s	0.20	Normal
$f'_c = 50$ MPa	$8.9 \times 10^{-12}$ m <sup>2</sup> /s	0.20	Normal
$a$	0.30	0.40	Beta on [0;1]
$k$	2.63	1.335	Shift. lognormal min. 1.09
$\rho_0$			
$f'_c = 30$ MPa	116 $\Omega$ m	0.16	Normal
$f'_c = 40$ MPa	134 $\Omega$ m	0.16	Normal
$f'_c = 50$ MPa	155 $\Omega$ m	0.16	Normal
$b_{R,T}$	3815 K	0.15	Lognormal
$k_{R,RH}$			
in splash zone	1.0	–	Deterministic
on coast	1.07	0.13	Lognormal
$a_{Cl}(C < 2\%)$	0.72	0.153	Normal
$k_{R,Cl}(C \geq 2\%)$	0.72	0.153	Normal
$n$	0.23	0.174	Normal
$\delta_0$	30 $\mu$ m	0.90	Lognormal
$b$	0.0104 mm/ $\mu$ m	0.125	Normal
$f_{ct}$	$0.3(f'_c)^{2/3}$ MPa	0.18	Lognormal
$E_c$	$22(f'_c/10)^{0.3}$ GPa	0.10	Lognormal

\* Coefficient of variation.

\*\* Standard deviation.

### 2.2 Corrosion propagation

In Val & Stewart (2003) the corrosion rate was expressed in terms of a corrosion current density,  $i_{corr}$ , which was estimated as proposed by Vu & Stewart (2000)

$$i_{corr} = \frac{0.378 (1 - w/c)}{c} (\mu\text{A}/\text{mm}^2) \quad (3)$$

where  $w/c$  = water/cement ratio. The corrosion current density was then transformed into the loss of steel by the use of Faraday's law of electrochemical equivalence.

In the present paper a more advanced model from DuraCrete (2000) and LIFECON (2003) is employed. According to the model, the actual corrosion penetration,  $V_{corr}$ , is estimated as

$$V_{corr} = V w_i (\mu\text{m}/\text{year}) \quad (4)$$

where  $V$  = corrosion rate; and  $w_i$  = relative time of wetness. The corrosion rate is expressed via the concrete resistivity,  $\rho(t)$

$$V = \frac{m_0}{\rho(t)} F_{Cl} \quad (5)$$

where  $m_0 = 882 \mu\text{m} \cdot \Omega\text{m}/\text{year}$ ; and  $F_{Cl} = 1 + k(C - C_{cr}) = \text{chloride corrosion rate factor}$  ( $F_{Cl} \geq 1$ ). The concrete resistivity is time-variant and depends on a number of factors

$$\rho(t) = \rho_0 k_{R,T} k_{R,RH} k_{R,Cl} \left( \frac{t}{t_0} \right)^n \quad (6)$$

where  $\rho_0 = \text{specific electrical resistivity of concrete at time } t_0$ ;  $k_{R,T} = \exp[b_{R,T}(1/T_{real} - 1/T_0)] = \text{temperature factor}$ ;  $b_{R,T} = \text{regression variable}$ ;  $T_0 = 293 \text{ K}$ ;  $k_{R,RH} = \text{relative humidity factor}$ ;  $k_{R,Cl} = 1 - (1 - a_{Cl})/2 = \text{chloride factor}$ ;  $t_0 = 28 \text{ days}$ ;  $t = \text{age of concrete (in analysis } t \leq 1 \text{ year)}$ ; and  $n = \text{age factor for resistivity}$ . In analysis  $k$ ,  $\rho_0$ ,  $b_{R,T}$ ,  $k_{R,RH}$ ,  $k_{R,Cl}$  (or  $a_{Cl}$ ), and  $n$  are treated as random variables, whose statistical properties are assigned in accordance to DuraCrete (2000) and LIFECON (2003) (see Table 1).

### 2.3 Cracking and spalling

In Val & Stewart (2003) the time between corrosion initiation and first cover cracking,  $t_{cr1}$ , was estimated using the Liu & Weyers (1998) model, while the time from corrosion initiation to spalling,  $t_{cr}$ , was assumed to be equal to  $10 t_{cr1}$ . However, as has been demonstrated recently (see Chernin & Val 2008) the Liu & Weyers model is incorrect. In the present study,  $t_{cr1}$  is calculated based on an analytical model proposed by Chernin & Val (2008).

Like the previously proposed analytical models, the Chernin & Val model is based on a thick-walled cylinder approach when concrete surrounding a corroding reinforcing bar is considered as a thick-walled hollow cylinder with the wall thickness equal to that of the concrete cover. The corrosion-induced pressure leads to formation of radial cracks near the inner surface of the cylinder after which it is divided into two cylinders—a partially cracked inner cylinder and an uncracked outer one. Concrete in the outer cylinder is treated as an isotropic linearly elastic material. Cracks in the inner cylinder are considered as smeared and their influence is taken into account by gradually reducing the stiffness of concrete in the tangential direction of the cylinder, which is described by a power function of the radial coordinate; the stiffness in the radial direction remains unchanged. Thus, concrete in the inner cylinder is treated as an inhomogeneous orthotropic linearly elastic material. The model ensures a consistent stress-strain description within both inner and outer cylinders and complete compatibility of stresses and strains on the boundary between the cylinders. The model was calibrated using available experimental data. With the help of the

model the expansion around a corroding reinforcing bar corresponding to formation of a throughout crack in the concrete cover (i.e. crack initiation),  $\delta_{cr1,a}$ , is evaluated. Parameters of the model treated as random variables are the tensile strength of concrete,  $f_{ct}$ , and the modulus of elasticity of concrete,  $E_c$  (see Table 1).

In order to take into account penetration of part of forming corrosion products into concrete pores it is assumed that there is a porous zone of thickness  $\delta_0$  around a reinforcing bar and the corrosion products do not exert any pressure on the surrounding concrete until they fully fill this zone. Values of  $\delta_0$  have been estimated by fitting the model predictions to results of a number of accelerated corrosion tests (see Chernin & Val 2008). According to the results,  $\delta_0$  can be treated as a random variable with mean of  $30 \mu\text{m}$  and standard deviation of  $27 \mu\text{m}$ . Thus, the corrosion penetration corresponding to crack initiation,  $p_{cr1}$ , can be found as

$$p_{cr1} = \frac{\delta_{cr1,a} + \delta_0}{\alpha_v - 1} \quad (7)$$

where  $\alpha_v = \text{volumetric expansion ratio of the corrosion products}$ , and  $t_{cr1} = p_{cr1}/V_{corr}$ .

After crack initiation, the crack width,  $w_{cr}$ , is evaluated as (DuraCrete 2000)

$$w_{cr} = w_0 + b(p - p_{cr1}) \quad (8)$$

where  $w_0 = 0.05 \text{ mm} = \text{width of the initial visible crack}$ ;  $b = \text{constant depending on the position of the reinforcing bar}$ ; and  $p = \text{corrosion penetration}$ . According to DuraCrete (2000) the critical crack width inducing spalling is  $w_{cr,sp} = 1 \text{ mm}$ . The corrosion penetration corresponding to spalling is then  $p_{cr} = (w_{cr,sp} - w_0)/b + p_{cr1}$  and the time from corrosion initiation to spalling  $t_{cr} = p_{cr}/V_{corr}$ . The constant  $b$  is treated as a random variable, whose statistical properties are adopted from DuraCrete (2000).

## 3 LIFE-CYCLE COST ANALYSIS

In order to compare different alternatives with the same benefits the LCC of a structure over its design life  $t_d$  may be expressed as (e.g. Val & Stewart 2003)

$$LCC(t_d) = C_C + C_{QA} + C_{IN}(t_d) + C_M(t_d) + C_F(t_d) \quad (9)$$

where  $C_C = \text{cost design and construction}$ ;  $C_{QA} = \text{cost of quality assurance (i.e. additional protection against corrosion)}$ ;  $C_{IN}(t_d) = \text{cost of inspections}$ ;  $C_M(t_d) = \text{cost of maintenance}$ ; and  $C_F(t_d) = \text{cost of failure}$ . Like in Val & Stewart (2003), it is assumed that  $C_{IN}(t_d)$  and  $C_M(t_d)$  are similar for different alternatives and so are omitted from the analysis. Since failures of different alternatives may occur at different times in order

to obtain consistent results costs of failure are usually discounted to their present values

$$C_F(t_d) = \frac{c_F}{(1+r)^{t_f}} \quad (10)$$

where  $c_F$  = cost of failure at the time of decision making;  $t_f$  = time of failure; and  $r$  = discount rate.

As noted previously, many parameters controlling the time of failure (i.e. spalling) are random variables, subsequently,  $t_f$  is a random variable as well. Since values of  $C_F(t_d)$  depend on  $t_f$  it is also a random variable and so is  $LCC(t_d)$ . In such situations decisions are usually made using the expected LCC,  $E[LCC(t_d)]$ , which obviously depends on the expected cost of failure,  $E[C_F(t_d)]$ . If to assume that failure (i.e. spalling) is discovered during a visual inspection of the structure and that the inspections are carried out over regular time intervals,  $\Delta t$ ,  $E[C_F(t_d)]$  can be found as (Val & Stewart 2003)

$$E[C_F(t_d)] = \sum_{i=1}^{t_d/\Delta t} \Delta P_{sp,i} \frac{c_F}{(1+r)^{i\Delta t}} \quad (11)$$

where  $\Delta P_{sp,i}$  = probability of a spalling incident between the  $(i-1)$ -th and  $i$ th inspections. Values of  $\Delta P_{sp,i}$  are calculated via the cumulative distribution function of the time to spalling  $P_f(t) = \Pr[t_i + t_{cr} \leq t]$  and their calculation depends on a selected repair strategy (see Val & Stewart (2003) for details).

Two repair strategies are considered (Val & Stewart 2003). In both strategies repair/replacement is carried out immediately after spalling has been discovered during an inspection. It is also assumed that a repair/replacement restores the repaired structure to “as new” condition. However, in Repair Strategy I repairs do not provide any improvement in durability performance of the repaired structures, i.e. spalling may re-occur during the remaining life of the structure and multiple repairs may be needed. In Repair Strategy II repair improves durability performance of the structure so that the probability of spalling re-occurrence is neglected.

#### 4 RESULTS OF LCC ANALYSIS

A common approach to protect reinforcing steel against corrosion is to use higher grade concrete and thicker concrete cover. In this study, similar to Val & Stewart (2000), combinations of 30, 40, and 50-MPa concrete grades (ordinary Portland cement concretes) with 30, 50, and 70-mm covers are considered for two locations: (1) splash zone; (2) atmospheric zone adjacent to the coast. Spalling of exposed surfaces of a RC structure subject to chloride contamination is treated as failure.

Table 2. Costs of durability design specifications ( $C_{QA}$ ).

Cover	$f'_c = 30$ MPa	$f'_c = 40$ MPa	$f'_c = 50$ MPa
30 mm	$-0.072C_C$	$-0.048C_C$	$-0.027C_C$
50 mm	$-0.025C_C$	0.0	$0.022C_C$
70 mm	$0.026C_C$	$0.052C_C$	$0.075C_C$

The baseline case for costs is 40-MPa concrete with 50-mm cover, for which is assumed that  $C_C = 1.0$ . Costs of durability specifications (i.e. quality assurance  $C_{QA}$ ) are given in terms of the construction cost for the baseline case in Table 2 (Val & Stewart 2003). Negative values of  $C_{QA}$  reflect cost reduction compared with the baseline case.

It is assumed that the cost of repair/replacement (excluding user associated costs) without improving durability performance is equal to the double construction cost and the cost of quality assurance, i.e.  $c_F = 2C_C + C_{QA}$  (Val & Stewart 2003). Repair/replacement with improved durability performance implies the maximum concrete grade and cover (i.e. 50-MPa concrete and 70-mm cover). The probabilities of spalling calculated for this design specification in Val & Stewart (2003) were small for both considered locations that justified its use in Repair Strategy II since the probability of spalling re-occurrence in a RC structure after it had been repaired could be neglected.

Life-cycle costs are evaluated using a 4% discount rate (i.e.  $r = 0.04$ ) for a design life of 100 years. It is assumed that inspections are conducted every two years (i.e.  $\Delta t = 2$  years). For the splash zone the relative time of wetness is unity (i.e.  $w_t = 1.0$ ), while for the atmospheric zone adjacent to the coast  $w_t = 0.75$  is assumed (DuraCrete 2000). The temperature of the ambient air is  $T_{real} = 293$  K. In order to convert values of the chloride threshold concentration from % by weight of cement into  $\text{kg/m}^3$  the following cement contents are adopted for different concrete grades:  $320 \text{ kg/m}^3$  for 30-MPa concrete,  $350 \text{ kg/m}^3$  for 40-MPa, and  $370 \text{ kg/m}^3$  for 50-MPa, respectively. Probabilistic analysis is carried out using Monte Carlo simulation. Results of the present analyses as well as from Val & Stewart (2003) (for comparison)—cumulative probabilities of spalling  $P_f(t)$  and expected LCCs (normalised to  $C_C$ ), are presented in Figures 1–8.

Comparing the new results with the old ones, a noticeable increase in the probabilities of spalling in the splash zone, especially for 50-MPa concrete, can be observed (Figs. 1–2). The rather significant probabilities of spalling for 50-MPa concrete with 70-mm cover cast doubts on validity of the assumption adopted in Repair Strategy II that if this design specification used in repair/replacement then the possibility

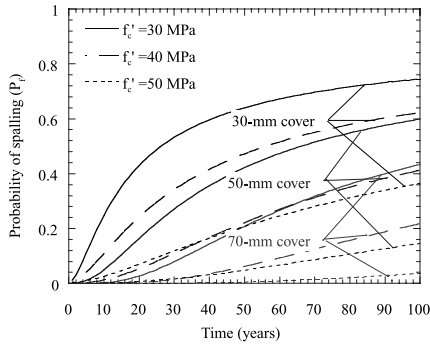


Figure 1. Probabilities of spalling in splash zone (Val & Stewart 2003).

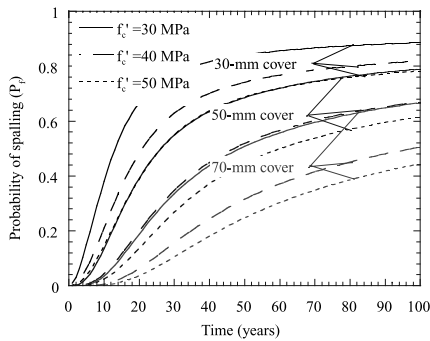


Figure 2. Probabilities of spalling in splash zone (new models).

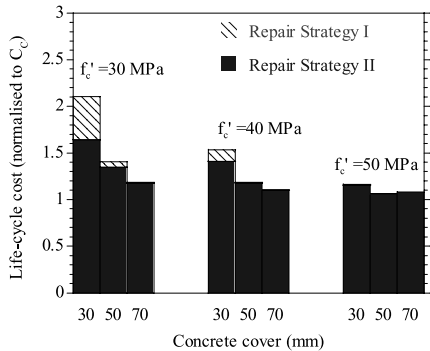


Figure 3. Expected life-cycle costs in splash zone (Val & Stewart 2003).

of re-occurrence of spalling can be neglected. However, very small difference between the two repair strategies in the expected LCCs obtained for this design specification in the splash zone (Fig. 4) indicates that the error associated with the use of this assumption still remains sufficiently small. For the atmospheric zone on the coast differences between the

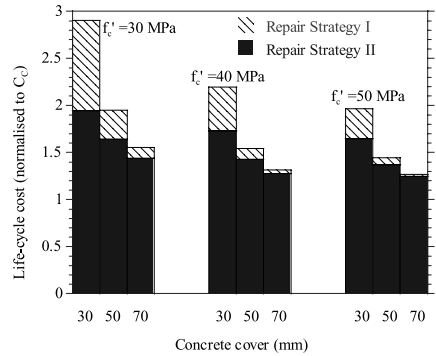


Figure 4. Expected life-cycle costs in splash zone (new models).

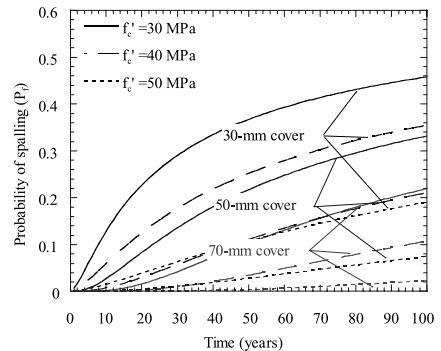


Figure 5. Probabilities of spalling on coast (Val & Stewart 2003).

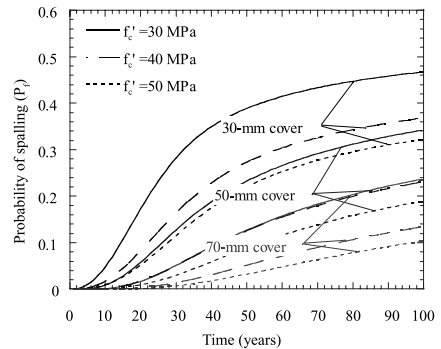


Figure 6. Probabilities of spalling on coast (new models).

probabilities of spalling obtained in this study and in Val & Stewart (2003) are insignificant, apart from the results for 50-MPa concrete (Figs. 5–6).

Taking into account that the predictive models employed in this study distinct in many respects from those used in Val & Stewart (2003) it is difficult to

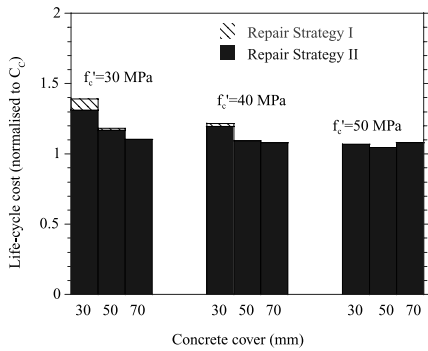


Figure 7. Expected life-cycle costs on coast (Val & Stewart 2003).

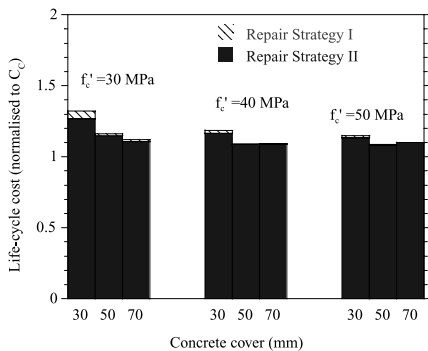


Figure 8. Expected life-cycle costs on coast (new models).

identify the main causes of these differences. The only cause, which is worth to mention, is different description of the chloride threshold concentration. In Val & Stewart (2003) it was presented by a normal random variable with a mean of 0.95% by weight of cement and coefficient of variation (COV) of 0.375; in the new study it was modelled by a Beta random variable defined on [0.2; 2] with a mean of 0.6% by weight of cement and COV of 0.25. In this respect it should be noted that in Val (2007) the threshold chloride concentration was identified as the second most important parameter (after the surface chloride concentration) in terms of its effect on the time of spalling.

The differences in the probabilities of spalling found its reflection in the expected LCCs (Figs. 3–4, 7–8). However, in terms of recommended design specifications difference between the two studies is not significant. For the atmospheric zone on the coast the design specification corresponding to the lowest expected LCC in both studies is 50-MPa concrete with 50-mm cover; for the splash zone it is also 50-MPa concrete with 50-mm cover in Val & Stewart (2003), while in the present study it is 50-MPa concrete with 70-mm cover.

## 5 CONCLUSIONS

The paper examined the influence of various predictive models for corrosion initiation, propagation, and corresponding structural damage on results of LCC analysis of RC structures in marine environments. According to obtained results, despite very significant changes in the predictive models the recommended design specifications remained almost the same. This result demonstrates the maturity of the LCC approach in terms of its use for decision making concerning RC structures in corrosive environments.

## REFERENCES

- Chernin, L. & Val, D.V. 2008. Prediction of cover cracking in RC structures due to corrosion. In *Proc. 1st International Conference on Heritage and Construction in Coastal and Marine Environment (MEDACHS'08) Lisbon, 28–30 January 2008*.
- DuraCrete. 2000. General Guidelines for Durability Design and Redesign. *Rep. No. BE95-1347/R17 Prepared for DuraCrete: Probabilistic Performance-Based Durability Design of Concrete Structures*, The European Union—Brite EuRam III.
- fib. 2006. *Bulletin N°. 34: Model Code for Service Life Design*, Lausanne: International Federation for Structural Concrete.
- Frangopol, D.M. & Liu, M. 2007. Maintenance and management of civil infrastructure based on condition, safety, optimization, and life-cycle cost. *Structure and Infrastructure Engineering* 3(1): 29–41.
- LIFECON. 2003. LIFECON Deliverable D 3.2 Service Life Models, *RDT Project: Life Cycle Management of Concrete Infrastructures for Improved Sustainability*, European Community, Fifth Framework Program: GROWTH.
- Liu, Y. & Weyers, R.E. 1998. Modeling the time-to-corrosion cracking in chloride contaminated reinforced concrete structures. *ACI Materials Journal* 95(6): 675–681.
- Papadakis, V.G., Roumeliotis, A.P., Fardis, M.N. & Vagenas, C.G. 1996. Mathematical modelling of chloride effect on concrete durability and protection measures. In R.K. Dhir & M.R. Jones (eds), *Concrete Repair, Rehabilitation and Protection*: 165–174. London: E & FN Spon.
- Val, D.V. 2005. Effect of different limit states on life-cycle cost of RC structures in corrosive environments. *Journal of Infrastructure Systems, ASCE* 11(4): 231–240.
- Val, D.V. 2007. Factors affecting life-cycle cost analysis of RC structures in chloride contaminated environments. *Journal of Infrastructure Systems, ASCE* 13(2): 135–143.
- Val, D.V. & Stewart, M.G. 2003. Life-cycle cost analysis of reinforced concrete structures in marine environments. *Structural Safety* 25(4): 343–362.
- Vu, K. & Stewart, M.G. 2000. Structural reliability of concrete bridges including improved chloride-induced corrosion models. *Structural Safety* 22(4): 313–333.

# Effect of cracking on long-term performance of reinforced concrete slabs

T. Yamamoto

*Daido Institute of Technology, Nagoya, Japan*

**ABSTRACT:** This paper presents the long-term loading test of reinforced concrete slabs to examine the effect of cracking on the long-term deflections and changes in natural frequencies. The shrinkage of the slabs was restricted and the restriction ratio of the shrinkage was supposed to be in the case of low or moderate-rise beam-column system buildings. The test results showed that the long-term deflections of the slabs after six years loading increased up to 21 times as much as the calculated elastic deflections. Although the effect of the shrinkage rate was small, the final slab deflections were quite different due to the slab thickness. The dynamic rigidity of the slabs decreased to about a half of the initial values.

## 1 INTRODUCTION

The long-term performance of reinforced concrete members is affected by creep and shrinkage of concrete and structural codes deal with the estimation method for these effects (ACI 2005, CEB-FIP 1978). However, concrete slabs are relatively thin compared with beams and columns and tend to crack by drying shrinkage of concrete when the shrinkage is restricted. The occurrence of cracking decreases the rigidity of reinforced concrete slabs and affects their life time serviceability. It is difficult to predict accurately the effect of cracking, hence, a long-term loading test of reinforced concrete slabs was conducted.

## 2 DESCRIPTION OF TEST

### 2.1 Specimens

The specimens are shown in Figure 1 and Table 1. In the test various thicknesses (from 120 mm to 240 mm) with 400 mm width one-way slabs fixed at both ends were used to examine the effect of the rate and ultimate value of concrete shrinkage. The length of the fixed end is 450 mm with the prominence upward and downward part of 100 mm. The test slab is partially restricted by the thicker (360 mm) concrete member connected to it through the taper part of 45 degrees from the straight line part of 100 mm in one unit. The restriction ratio was supposed to be in the case of low or moderate-rise beam-column system buildings. The span-depth ratio is constant 30 and the flexural reinforcing ratios are from 0.29% to 0.38%. The longitudinal reinforcing ratio of the restriction member is 0.83%.

### 2.2 Elastic properties of the test slabs

The elastic properties of the test slabs are shown in Table 2. The flexural stress due to the load is about

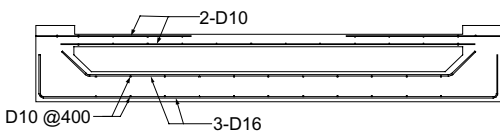


Figure 1. Specimen D.

Table 1. Specimens.

Specimen	Reinforcement		Span (mm)	Slab cross section			Load		
	Bar	$pt(\%)$		Thickness (mm)	Width (mm)	Restriction member thickness (mm)	Dead (kN/m)	Applied (kN/m)	Effective depth (mm)
A	4-D10	0.33	7200	240	400	360	2.26	0.00	215
B	3-D10	0.35	5400	180	400	360	1.70	0.56	155
C	2-D10	0.29	4500	150	400	360	1.41	0.76	125
D	2-D10	0.38	3600	120	400	360	1.13	1.09	95

2.5 MPa and assumed to be equal to the concrete flexural strength. The span-elastic deflection ratio is constant 4340. The natural frequencies of the slabs are from 14.1 Hz to 19.9 Hz.

### 2.3 Properties of concrete and reinforcing steel

Tables 3 and 4 show the mix proportions of the concrete and the properties of hardened concrete, respectively. The concrete strength at 28 days was 27.0 MPa. The type of reinforcing steels is SD295 (nominal yield point 295 N/mm<sup>2</sup>).

### 2.4 Loading test procedures and condition

The specimens were stored in wet conditions until the loading test started. The load applied evenly by the

10 kg concrete blocks at 28 days just after the slab shores were removed. The temperature and humidity were not controlled and the Specimens are subjected to the ambient conditions. The average temperature and humidity were about 16°C and 65% RH.

### 2.5 Measurement

The slab deflections and longitudinal shrinkage were measured by dial gauges. The steel and concrete strains in the slabs were measured by wire strain gauges and embedded type strain gauges, respectively. The creep and shrinkage of plain concrete were also measured at the same ambient condition. The natural frequencies of the slabs were measured at various ages by dropping 0.5 kg sandbag onto the slabs from a height of 25 cm.

Table 2. Calculated elastic properties of the slabs.

Specimen	Total load (kN/m)	Flexural stress (MPa)	Deflection (mm)	Natural frequency (Hz)	Steel stress (MPa)
A	2.26	2.54	1.66	14.1	181
B	2.24	2.52	1.25	16.3	187
C	2.28	2.57	1.04	17.8	246
D	2.22	2.49	0.832	19.9	201

Table 3. Mix proportions of concrete.

Cement (kg/m <sup>3</sup> )	Water (kg/m <sup>3</sup> )	W/C (%)	Sand (kg/m <sup>3</sup> )	Gravel (kg/m <sup>3</sup> )	S/A (%)
302	172	57.0	818	1002	44.9

Table 4. Properties of concrete.

Part	Age (days)	Density	Compressive strength (MPa)	Young's modulus (GPa)
Test slab	28	2.30	27.0	23.6
Restriction member	28	2.33	29.1	27.3

Table 5. Short-term properties of the slabs.

Specimen	Deflection			Natural frequency		
	Measured: $\delta_m$ (mm)	Calculated: $\delta_c$ (mm)	Ratio ( $\delta_m/\delta_c$ )	Measured (Hz)	Calculated (Hz)	Ratio (fm/fcal)
A	1.27	1.44	0.88	15.1	14.1	1.07
B	0.91	1.09	0.84	17.6	16.3	1.08
C	0.87	0.90	0.96	19.4	17.8	1.09
D	0.65	0.72	0.90	21.6	19.9	1.08

## 3 RESULTS OF TEST

### 3.1 Short-term properties

The short-term properties of the slabs are shown in Table 5. In the calculations the measured concrete Young's Modulus 23.6 GPa is used. The ratios between measured and calculated short-term deflections of the slabs were from 0.88 to 0.96. The natural frequencies of the slabs were from 14.1 Hz to 19.9 Hz. The rigidities of the slabs were slightly high compared with the calculated ones. The properties among the short-term deflections and natural frequencies were in good agreement. No cracking was observed in all the specimens at the initial loading.

### 3.2 Long-term deflections

The long-term deflections of the slabs are shown in Table 6 and Figure 2. The deflections of the slabs increased rapidly in the early stage. After the age of 373 days, the increasing rate of the deflections gradually decreased with the seasonal changes. The deflections recovered in the wet seasons due to the ambient high humidity. The ratios of the long-term deflections of the slabs to the calculated short-term deflections are shown in Figure 3. The deflections of



Specimen A reached 19.3 mm at 2254 days and the ratio to the calculated short-term deflection was 13.4. The ratio of the spans to the deflection of Specimen A at 2254 days is 374. The ratios of the deflections of the other Specimens B, C, and D to the calculated short-term deflections are from 15.0 to 21.3. The thicker slabs showed the smaller long-term deflection ratios. The ratios of the spans to the long-term deflections of Specimens B, C, and D are from 235 to 331. They were relatively high compared with the proposed estimation methods (Branson 1977, MC90 1990, AIJ

1999). Figure 4 shows the rates of long-term deflections which are the ratios of the long-term deflections to the deflections at 2254 days. Except for the early stage before 373 days the rates of the long-term deflections of the slabs were almost the same among the specimens which had different slab thicknesses. The long-term deflections of the specimens reached about 79% and 87% of the final long-term deflections at one year and two years, respectively. After three years the long-term deflections of the slabs were stable.

Table 6. Long-term deflections.

Specimen	Deflection (mm)						Ratio ( $\delta_{\text{days}}/\delta_c$ )			Ratio ( $\delta_{\text{days}}/\delta_{2254}$ )			Ratio span/ $\delta_{2254}$
	$\delta_c$	373	518	731	1301	2254	373	731	2254	373	731	2254	
A	1.44	15.0	15.6	16.8	18.7	19.3	10.4	11.7	13.4	0.78	0.87	1.00	374
B	1.09	12.9	13.4	14.2	15.7	16.3	11.9	13.0	15.0	0.79	0.87	1.00	331
C	0.90	13.8	14.3	15.1	16.6	17.6	15.4	16.7	19.5	0.79	0.86	1.00	256
D	0.72	12.2	12.6	13.2	14.5	15.3	16.9	18.4	21.3	0.80	0.86	1.00	235

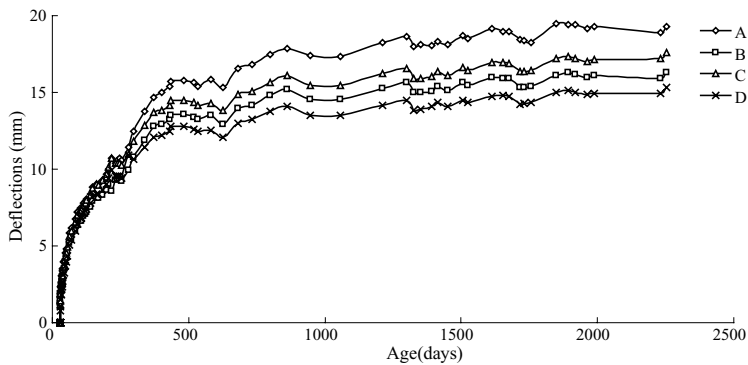


Figure 2. Long-term deflections of the slabs.

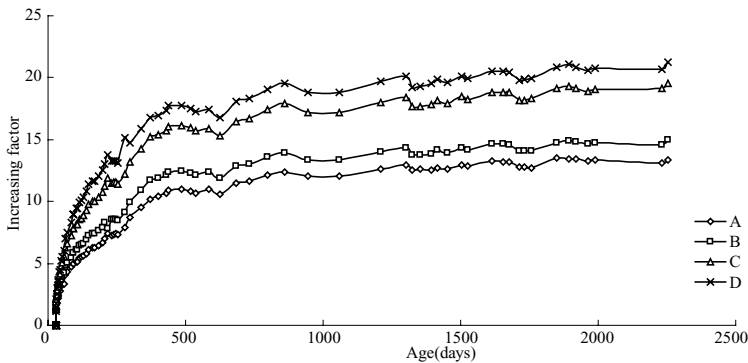


Figure 3. Deflection increasing factor.

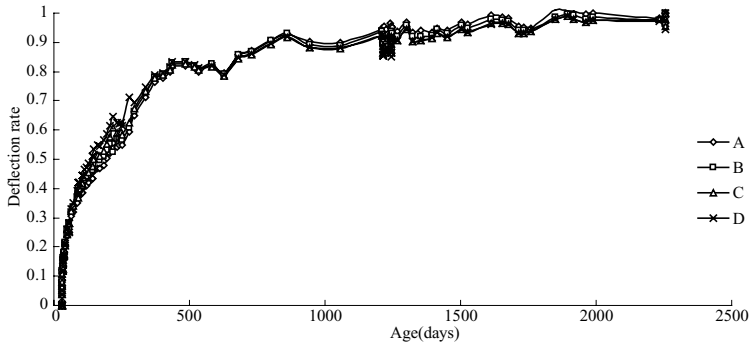


Figure 4. Deflection rate.

Table 7. Longitudinal slab shrinkage.

Specimen	Slab shrinkage ( $\mu$ )					Slab model shrinkage ( $\mu$ )				Ratio (ss/sm)			
	ss373	ss518	ss731	ss1301	ss2254	sm373	sm731	sm1301	sm2254	373	731	1301	2254
A	400	390	440	528	507	700	730	820	780	0.57	0.60	0.64	0.65
B	424	406	433	515	498	750	770	840	810	0.57	0.56	0.61	0.61
C	449	438	462	542	504	740	770	830	820	0.61	0.60	0.65	0.62
D	450	436	464	547	514	830	830	905	830	0.54	0.56	0.60	0.62

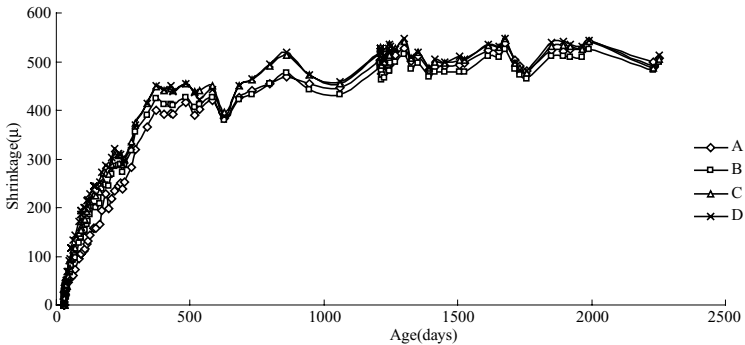


Figure 5. Longitudinal shrinkage of the slabs.

### 3.3 Shrinkage of slab concrete

The longitudinal shrinkage of the slabs is shown in Table 7 and Figure 5. The longitudinal shrinkage of the slabs showed almost the same behavior as the long-term deflections. In the wet seasons the shrinkage decreased so much. Although in the early stages of the loading test the longitudinal shrinkage of the slabs somewhat differed among the Specimens, the shrinkage reached about the same 500  $\mu$  at 2254 days. The shrinkage of the model slabs which were 400 mm length and stored in the same ambient are also shown in Table 7. The shrinkage of model slabs was about

800  $\mu$  at 2254 days. The restriction ratios of the shrinkage strain were about 0.4. The restricted longitudinal shrinkage strain is supposed to be about 300  $\mu$ . Even if stress relaxation is made by creep, this restricted strain was large enough to cause the formation of cracking.

### 3.4 Cracking of the slabs

Figure 6 shows the crack patterns of the Specimens A, B, C and D. After the loading test many cracks were observed along the whole slab spans. At the initial loading cracking did not occur. The first cracking

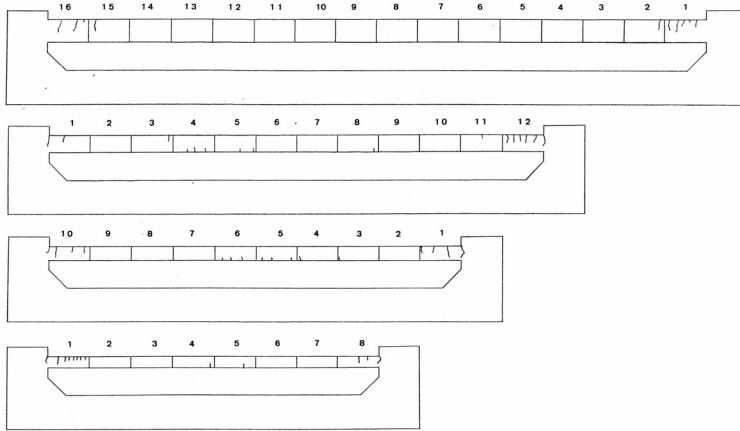


Figure 6. Crack patterns of the specimens: shown crack width 0.1 mm or more.

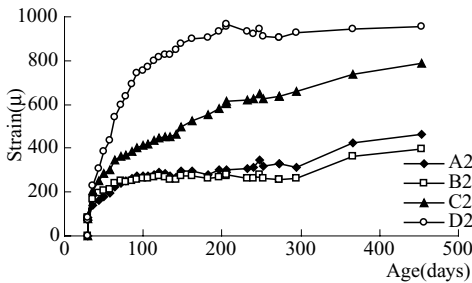


Figure 7. Change in steel strain at fixed end.

occurred at the fixed end of the slabs due to shrinkage of concrete, then at the mid-spans. Most of the crack widths were equal or less than 0.3 mm.

### 3.5 Change in steel strain

The steel strains of the slabs were measured by wire strain gauges. Changes in the steel strains at fixed end of the slabs and anchorage part located in 200 mm in the stubs are shown in Figures 7 and 8, respectively. The calculated tensile steel strain at fixed end of Specimen D is  $980 \mu$ . The measured steel strain of Specimen D was  $970 \mu$  at about 200 days. After that it showed an almost constant value except small movement by the change of the humidity. The tensile strains of the other Specimens showed from  $400 \mu$  to  $800 \mu$  and were smaller compared with the calculated strains. The steel strains at the anchorage part located in 200 mm in the stubs were compressive  $-280 \sim -430 \mu$ . They showed enough fixations at the position of 200 mm in the stubs and the influence of the shrinkage of the concrete was big.

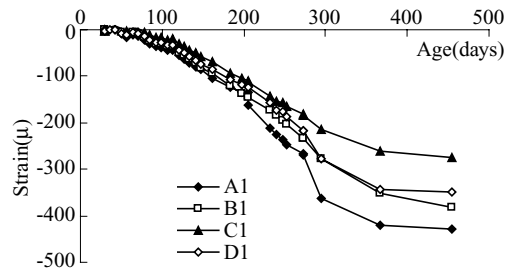


Figure 8. Change in steel strain at anchorage.

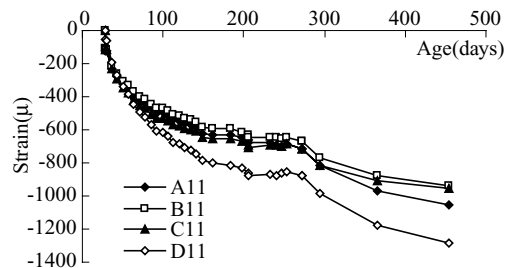


Figure 9. Change in concrete strain.

### 3.6 Change in concrete strain

Changes in the concrete strain at fixed end are shown in Figure 9. The compressive concrete strains were  $-900 \mu \sim -1300 \mu$ . There was still the shrinkage of the concrete in a tendency to increase at that stage.

Table 8. Natural frequencies of the slabs.

Specimen	Natural frequency (Hz)						Ratio (fdays/f29)				
	f <sub>cal</sub>	f <sub>29</sub>	f <sub>56</sub>	f <sub>373</sub>	f <sub>1301</sub>	f <sub>2254</sub>	f <sub>29</sub>	f <sub>56</sub>	f <sub>373</sub>	f <sub>1301</sub>	f <sub>2254</sub>
A	14.1	15.1	14.4	12.9	12.2	12.1	1.00	0.95	0.86	0.81	0.80
B	16.3	17.6	16.4	14.5	13.6	13.7	1.00	0.93	0.82	0.77	0.78
C	17.8	19.4	17.6	14.5	14.0	14.1	1.00	0.91	0.75	0.72	0.73
D	19.9	21.6	19.5	16.0	15.8	15.7	1.00	0.90	0.74	0.73	0.72

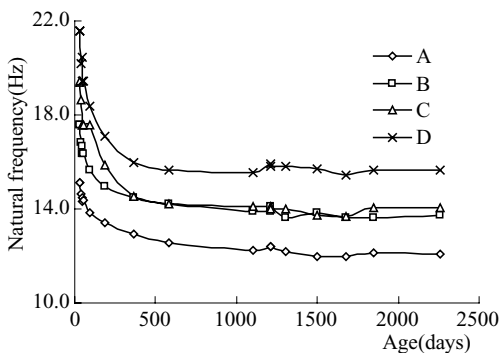


Figure 10. Change in natural frequency.

### 3.7 Natural frequencies of the slabs

Changes in the natural frequencies of the slabs are shown in Table 8 and Figure 10. The natural frequencies decreased rapidly in the early stage of the loading test and showed an approximately stable value after 373 days. The ratios of measured frequencies at 2254 days to those at 29 days are from 0.72 to 0.80. Thinner slabs showed smaller ratios. These ratios becomes from 0.52 to 0.64 when converted into static rigidity.

## 4 CONCLUSIONS

Based on the long-term loading test conducted in this study, the following conclusions are derived.

1. The occurrence of cracking affects the short and long-term performance of reinforced concrete slabs. The restriction ratio of the slabs was about 0.4 of the free shrinkage of the concrete.
2. The long-term slab deflections increased up to 21 times as much as the calculated elastic deflections for six years loading. The thicker slabs showed the smaller long-term deflection ratios.
3. After the age of 373 days, the increasing rate of the deflections gradually decreased with the seasonal changes. The long-term deflections of the specimens reached about 79% and 87% of the final long-term deflections at one year and two years, respectively.
4. The natural frequencies decreased rapidly in the early stage of the loading test and showed an approximately stable value after 373 days.
5. Thinner slabs showed smaller ratios. These ratios becomes from 0.52 to 0.64 when converted into static rigidity.

## REFERENCES

ACI 318-05. 2005. *Building Code Requirements for Structural Concrete and Commentary*. American Concrete Institute.

AIJ. 1999. *Standard for Structural Calculation of Reinforced Concrete Structures*. Architectural Institute of Japan: pp. 350–364.

Branson, D.E. 1977. *Deformation of Concrete Structures*. New York. McGraw-Hill.

CEB-FIP. 1978. *Model Code for Concrete Structures*, 3rd edition. Paris.

CEB-FIP. 1990. *Model Code 1990*. London. Thomas Telford.

# Dilatometric tests combined with computer simulations and parameter identification for in-depth diagnostic analysis of concrete dams

A. Zirpoli, G. Maier, G. Novati & T. Garbowski

*Dept. of Structural Engineering, Politecnico di Milano, Milan, Italy*

**ABSTRACT:** Diagnostic analysis of dams means here assessment of possible structural damages (due to, e.g., alkali-silica reaction in concrete). Such damages may be primarily self-equilibrated stresses due to material expansion, elastic stiffness degradation, decrease of compressive and tensile strength, and of fracture energy. The procedure presented in this paper is intended to perform such diagnosis deep inside the concrete dam and is based on “ad hoc” devised substantially novel mechanical experiments, on their finite element modelling and on deterministic parameter identification through the minimization of the discrepancy norm between measured quantities and their counterparts computed as functions of the sought parameters.

## 1 PRELIMINARY REMARKS

In present dam engineering the assessment of possibly deteriorated material properties and of the stress state, both in dam concrete and in foundation rocks, is necessary in order to compute the present safety factors with respect to various kinds of possible failures. Typical structural problems in concrete dam engineering are dealt with e.g. in Pedro (1999) and Bourdarot et al. (1994).

As for diagnostic analysis of possible damages in concrete dams (due to alkali-silica reactions and/or extreme loads like exceptional floods and earthquakes), the following methodological classification can provide a concise overview, see e.g. Maier et al. (2004), Fedele et al. (2006):

(a) overall dynamic excitation and accelerometric measurements; (b) hydrostatical loading due to seasonal variations of reservoir level and measurement of consequent displacements by pendula, collimators, and, recently, radar; (c) same as at (b), but with “fast” hydrostatical loading performed by “ad hoc” changes of the reservoir level; (d) local, traditional flat-jack tests on dam surface and extensimetric or, in the future, “digital image correlation” measurements; (e) traditional “overcoring” for damage and stress assessment in-depth.

Overall diagnosis procedures are clearly limited to the assessment of elastic stiffness distribution; the static approaches provide more data if radar is employed and are especially inexpensive if seasonal. Local tests are needed in order to assess fairly accurately stress states and inelastic material properties.

In this paper a new methodology is proposed in order to perform diagnostic analyses locally, in-depth and in a relatively inexpensive and non-destructive fashion. The diagnostic method here presented, inspired by the traditional overcoring technique but substantially different from it, is centered on inverse analyses and is articulated in the operative phases specified in the subsequent Section. The in-depth material characterization has been, since several decades, a research subject, particularly in rock mechanics, and a widely employed practice in geotechnical engineering. Wittke (1990) and Sjöberg & Klasson (2003) can be regarded as representative references to the relevant vast literature.

## 2 OUTLINE OF THE EXPERIMENTAL PROCEDURE AND RELATED PARAMETER IDENTIFICATION

The operative phases of the proposed diagnostic method are listed below and schematically illustrated in Figure 1.

- a. A hole is drilled in the dam (Figure 1a).
- b. A device called “dilatometer” is inserted in it. The dilatometer basically consists of two sleeves equipped with radial displacement gouges and, between them, of two movable steel “arches” (Figure 1b).
- c. The drilling goes ahead, making the hole longer, while the gouges measure the displacements due

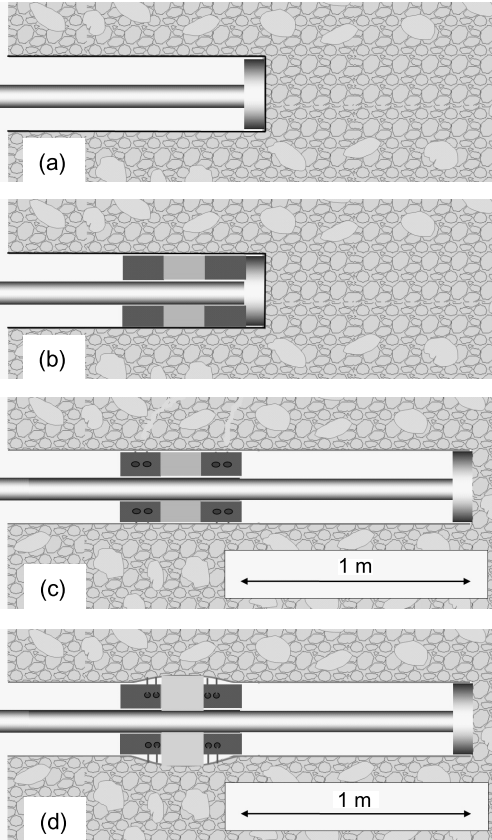


Figure 1. Operative phases of the proposed procedure.

- to the stress state modification caused by the excavation advancement (Figure 1c).
- d. The two steel “arches”, governed by two small hydraulic jacks (fed by a volumetric external pump), apply two growing radial forces (equal magnitude, opposite directions) on the hole’s wall. The gauges measure the displacements, first generated in the linear elastic range (Figure 1d).
  - e. The same operations of phase (d) are performed, but this time the elastic limit is overcome by increasing the jack pressure. The pump feeds the jacks through small pipes placed into the tube which supports the dilatometer and contains the drill shaft.
  - f. A laptop containing an artificial neural network, trained through computer simulations of the mechanical tests, collects the signals from the gauges, digitalizes them and performs inverse analyses which provide the sought parameters, in the following sequence: (i) Young modulus and Poisson coefficient (under the hypothesis of isotropic material), on the basis of the experimental data collected during phase (d); (ii) the stresses, two normal

and one tangential, in the plane orthogonal to the hole axis, on the basis of the data coming from phase (c); (iii) the parameters governing a plastic constitutive model and/or a quasi-brittle fracture model (e.g.: the three parameters of Drucker-Prager model and/or the two of the simplest cohesive crack model).

- g. The drilling goes ahead and the sequence of the above outlined phases is repeated at a new position and direction in the dam.

For the repeated inexpensive “in situ” use of the equipment, accurate nonlinear finite element modeling is needed, but once-for-all only, in order to generate by the “forward operators” a suitable number of “patterns” for the “training” and the “testing” of the neural networks to be employed on site.

The above outline of the proposed diagnostic procedure for concrete dams can be clarified and motivated by the following remarks.

- α. No specimen is extracted from the borehole to be tested in laboratory, at a basic difference from traditional core drilling procedures. Since dam concrete is inhomogeneous with aggregate sizes larger in average than in the usual concrete employed with steel reinforcement for buildings and bridges, carots should be rather large and, hence, damaging (say, with a diameter an order of magnitude larger than expected maximal aggregates) in order to avoid misleading inaccurate experimental data.
- β. Displacements, not strains, are measured. In fact, strain gauges usually adopted for overcoring techniques would be unsuitable for concrete, since, clearly, strains are sensitive to local material properties (quite different from mortar to aggregate), whereas displacements reflect, in a sense, average properties, namely the large-scale material properties of structural engineering interest.
- γ. Inelastic properties are the main targets of the proposed procedure, since so far such properties are not assessed “in situ” and in-depth according to the present practice of concrete dam engineering.
- δ. The instrumented equipment envisaged herein is not available at present on the market, but it is clearly possible (and relatively inexpensive) to produce it by the present technology, even if with major changes with respect to the current practice. Therefore, the preliminary validation of the method presented in what follows rests on a pseudo-experimental approach, namely measurable data are computed by means of simulations of foreseen experiments through a finite element model, starting from reasonably assumed values of the sought parameters; then these values are compared to those arrived at by the inverse analyses, and a suitable discrepancy function is

minimized, taking those parameters as mathematical optimization variables. Clearly, recourse to pseudo-experimental data for methodological validation implies that the systematic (not random) modeling errors are not considered.

- e. The proposed diagnostic technique is dealt with at a preliminary design stage. To its further improvement “sensitivity analyses” are useful, namely numerical tests apt to make sure that the quantities (here displacements) to be measured as “effects” are sufficiently influenced by the sought parameters acting as “causes”, see e.g. Kleiber et al. (1997). Some analyses of this kind are presented within the computational exercises summarized in Section 3.

### 3 COMPUTATIONAL VALIDATION OF THE DIAGNOSTIC TECHNIQUE

The finite element model built up for the computer simulation of tests is visualized in Figure 2 and its main features are specified below.

- a. In order to mitigate the computing efforts, the following simplifying assumptions are adopted for the subsequent comparative numerical tests: (i) material isotropy (which is not always acceptable for dam concrete, particularly for rolled compacted concrete (RCC)), in view of the frequently consequent non-negligible orthotropy with horizontal isotropy only; (ii) symmetries with respect to the vertical and horizontal planes through the hole axis; (iii) the three-dimensional domain of the problem exhibits typical lengths which are 10 times longer than the hole radius, so that the boundary can be regarded as unaffected by the mechanical events produced by the tests; (iv) rigid constraints are imposed on the remote boundary (statical condensation or infinite elements will be employed in future investigations); (v) the longitudinal direction represents a principal direction for the stress state with vanishing normal stress; (vi) the original stress field before testing is uniform and generated at Gauss points; (vii) the drilling of the hole is simulated by removing radial restraints placed along the hole boundary (such restraints being active when the initial “in situ” stresses are enforced at the Gauss points).
- b. The traditional finite element model qualitatively described above, can quantitatively be specified as follows: 57781 tetrahedral elements with linear interpolations for displacements; 36111 degrees of freedom; commercial code Abaqus (version 6.6).
- c. The constitutive models adopted herein for a first validation are the following classical ones, see Figure 3 and, e.g., Jirasek & Bažant (2001) or

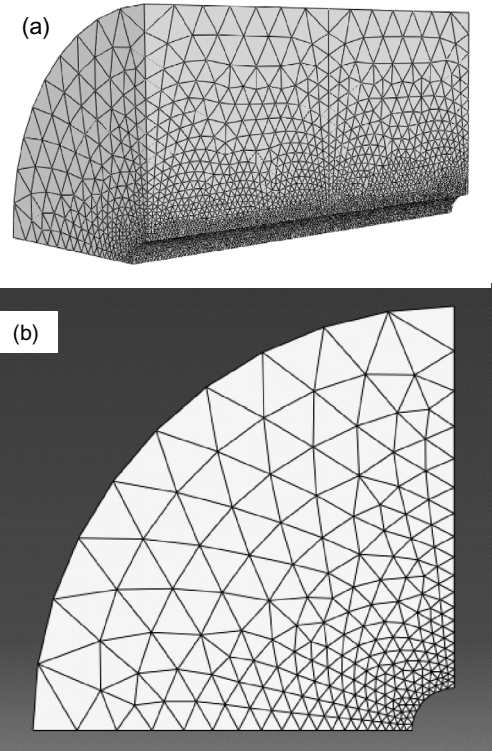


Figure 2. Finite element mesh adopted for the computational validation of the method; (a) 3D view, (b) mesh in the transversal plane.

Kaliszky (1989): linear elasticity with 2 parameters, of which only the Young modulus  $E$  is to identify, while Poisson ratio is assumed as  $\nu = 0.2$ ; Drucker-Prager perfect plasticity (3 parameters: cohesion  $d$ , hydrostatic compressive strength  $p_b$  and internal friction angle  $\beta$ ), improved by a “cap” (1 parameter: cap eccentricity  $R$ ) in view of expected stress states with dominant compression.

Reference values reasonably expected in dam concrete are attributed to the material parameters and stresses to identify, namely:  $E = 28000$  MPa, hydrostatic compressive strength  $P_b = 35$  MPa, cohesion  $d = 3.5$  MPa, friction angle  $\beta = 51^\circ$ , and cap eccentricity  $R = 0.65$ ; pre-existing horizontal and vertical principal stresses:  $\sigma_H = 5$  MPa and  $\sigma_V = 10$  MPa, respectively, both compressions. The other two parameters required by the model, i.e. the transition surface radius ( $\alpha$ ) and the initial plastic volumetric deformation, were considered respectively equal to 0.6 and to 0.

Figure 4 shows some plots of imposed force vs measured displacement of the “arches” with different values attributed to the parameter  $p_b$  which, together

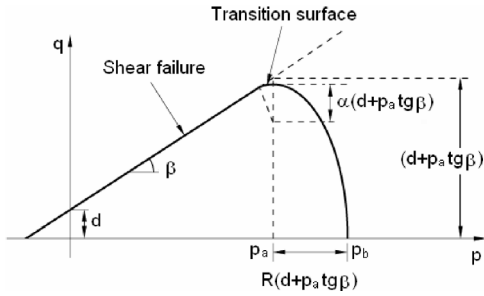


Figure 3. Drucker-Prager model with “cap” and relevant parameters  $d$ ,  $p_b$ ,  $\beta$  and  $R$  are to identify.

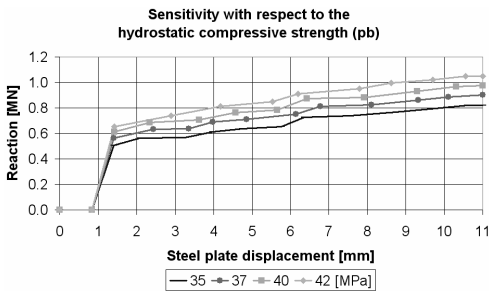


Figure 4. Force vs displacement concerning the “arches” for various values for parameter  $p_b$ .

with  $R$ , governs the “cap” on Drucker-Prager model. Plots like these visualize the sensitivity of measurable quantities with respect to sought parameters, as a simplified alternative to the sensitivity analysis in terms of derivatives (Kleiber et al. 1997).

Using such values and the finite element model shown in Figure 2, the radial displacement of the arch is computed (up to 10 mm) as a function of the force generated on it by the small jack. Such computations are repeated and their results plotted in Figure 4 after having each time assigned a value indicated in the figure to one of the material parameters to identify. The above sensitivity analyses show that the measurements planned by means of the envisaged instruments are likely to be adequate for the identification of the sought parameters.

Present parameter identification by a deterministic batch (non sequential) approach to inverse analysis, means solution of a generally non-convex mathematical programming problem. Such problems are tackled here first, to methodological validation purposes, by the “Trust Region” iterative algorithm. This algorithm is a special case of sequential quadratic programming method: it implies at each step finite difference evaluation of the gradient only (“first order algorithm”) and solution of a quadratic program in two variables, see

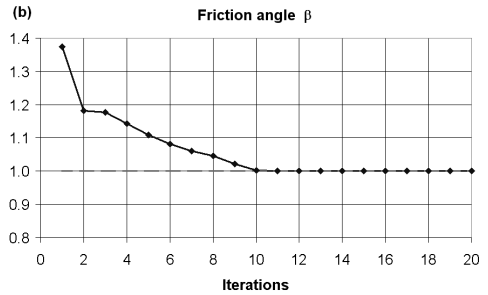
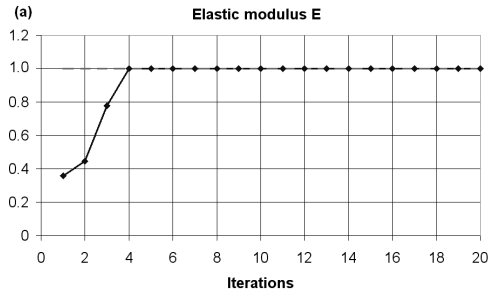


Figure 5. Convergence of the identification process: (a) normalized elastic modulus  $E$ ; (b) normalized internal friction angle  $\beta$ .

e.g. Coleman & Li (1996). The discrepancy function to minimize is here defined as the Eulerian quadratic norm of the differences between pseudo-experimental data and their computed counterparts. In fact, the inverse of the covariance matrix of measurement random errors can be reasonably assumed as equal to the identity matrix, since the instruments are all equal and correlation is negligible.

The convergence processes resulting from some of the exercises performed so far in this study, are visualized in the following figures: elastic modulus and friction angle (see Figure 5a and 5b), hydrostatic compressive strength, cohesion and cap eccentricity (see Figure 6a, 6b and 6c), horizontal and vertical normal stresses (see Figure 7a and 7b).

All parameters are “normalized” with respect to their (above specified) values assumed in order to generate by “direct analyses” the pseudo-experimental data employed as input of the inverse analyses. The chosen initializations are rather distant from the values attributed to the parameters. This circumstance helps to conjecture the absence of local minima of the discrepancy function, a conjecture also supported by visual maps of the discrepancy functions here omitted for brevity.

The average computing time required by the above outlined inverse analyses amounts to 35 hours with a computer characterized by a 2GB RAM and a 2.4 GHz velocity. Clearly, this circumstance represents a significant burden in terms of cost and time, a burden



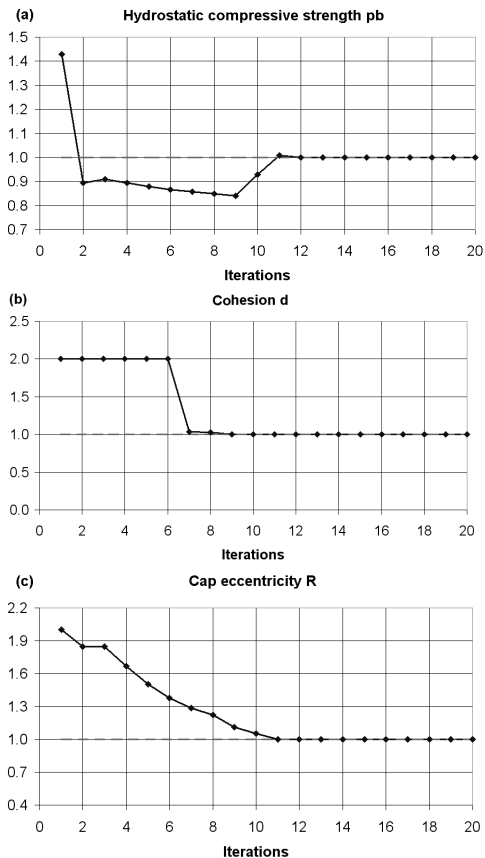


Figure 6. Convergence of the identification processes: (a) hydrostatic compressive strength  $p_b$ , (b) cohesion  $d$ , (c) cap eccentricity  $R$ .

which can at present be avoided by recourse to soft computing, specifically here to artificial neural networks (ANNs), see Haykin (1999). Such practically important feature of the diagnostic method proposed herein can be outlined as follows (details and numerical results will be presented in the full paper in preparation).

The outline holds for each one of the three parameter identifications described in what precedes.

$\alpha$ . The set of experimental data which should represent the input of the inverse analysis is approximated in order to achieve a balance between input and output of the ANN (the output consisting of one or two parameters in the present context, of three or four at most in future applications). Such approximation is achieved by polynomials here

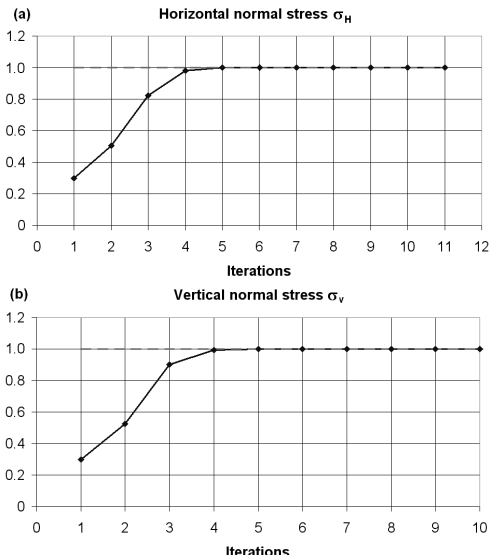


Figure 7. Convergence of the identification processes: (a) horizontal normal stress  $\sigma_H$ , (b) vertical normal stress  $\sigma_v$ .

(cf. e.g. Waszczyszyn (1999)), by proper orthogonal decomposition (probably better) in future developments (see e.g. Ostrowski et al. (2005)).

- $\beta$ . The ANN “architecture” is designed according to the criteria expounded in the literature (see e.g. Waszczyszyn (1999) ) primarily in order to avoid “overfitting” (here specifically two “hidden layers”, each one with 5 active neurons).
- $\gamma$ . A grid of points is selected on a reasonably bounded domain in the space of the sought parameters and for each point the corresponding vector of measurable quantities is computed by direct analysis (through the finite element model) and approximated as hinted at phase ( $\alpha$ ).
- $\delta$ . A subset (here 500) of the patterns generated in the preceding phase, after perturbation by a suitable random “noise” (here with uniform probability density over  $\pm 5\%$ ), is employed for the ANN “training”, namely for the identification of “weights” and “biases” of active neurons by means of a traditional “back propagation” algorithm. The remaining patterns (here 200) are used for the ANN “testing”.

#### 4 CLOSING REMARKS

The diagnostic technique briefly described in what precedes exhibits several substantial novelties, potentially advantageous in engineering practice. The most promising features arise from accurate once-for-all

computer simulations of the tests and on-site use of artificial neural networks for inverse analyses in situ. Investigations now in progress are intended to further improve the efficiency of the method and to increase the number of identifiable parameters, particularly by means of the following prospects: sharp indenters, employed after the arches, in order to provoke fracture in an easier and more intensive fashion apt to accurate assessment of fracture properties (fracture energy “in primis”); optimized geometries of the dilatometer positions and of the whole equipment; repeated tests after 90 degree rotation of the instrument in order to increase the available experimental data.

## REFERENCES

- Bourdarot, E., Mazars, J. & Saouma V. (eds) 1994. *Dam Fracture and Damage*. Rotterdam, Balkema.
- Coleman, T.F. & Li, Y. 1996. An interior trust region approach for nonlinear minimization subject to bound. *SIAM Journal on Optimization* 6: 418–445.
- Fedele, R., Maier, G. & Miller, B. 2006. Health assessment of concrete dams by overall inverse analyses and neural networks. *Int. J. of Fracture* 137: 151–172.
- Fedele, R. & Maier, G. 2007. Flat-jack tests and inverse analysis for the identification of stress states and elastic properties in concrete dams. *Meccanica* 42: 387–402.
- Haykin, S. 1998. *Neural Networks: A Comprehensive Foundation (2nd edition)*. Upper Saddle River, NJ (USA), Prentice Hall.
- Jirasek, M. & Bažant, Z.P. 2001. *Inelastic Analysis of Structures*. New York, Wiley.
- Kaliszky, S. 1989. *Plasticity, Theory and Engineering Applications*. Elsevier.
- Kleiber, M. et al. 1997. *Parameter Sensitivity in Nonlinear Mechanics. Theory and Finite Element Computations*. New York, Wiley.
- Maier, G., Ardito, R. & Fedele, R. 2004. Inverse analysis problems in structural engineering of concrete dams. In Z.H. Yao et al. (eds), *Computational Mechanics: Proc. WCCM VI in conjunction with APCOM'04, Beijing, Sept.5–10, 2004*. Tsinghua Univ. Press & Springer-Verlag.
- Ostrowski, Z., Bialecki, R.A., & Kassab, A.J. 2005. Advances application of proper orthogonal decomposition on inverse problems. In D. Lesnic (ed.), *5th International Conference on Inverse Problems in Engineering, Cambridge, 2005*. Leeds University Press.
- Pedro, O. (ed.) 2000. *Arch Dams: Designing and Monitoring for Safety*. CISM Courses and Lectures, Wien, Springer.
- Sjöberg, J. & Klasson, H. 2003. Stress measurements in deep boreholes using the Borre (SSPB) probe. *Int. J. Rock Mech. and Min. Sci.* 40: 1205–1223.
- Waszczyszyn, Z. (ed.) (1999). *Neural Networks in the Analysis and Design of Structures*. CISM Courses and Lectures, Wien, Springer
- Wittke, W. 1990. *Rock Mechanics*. Berlin: Springer-Verlag.

*Life-cycle assessment and design*

# Life-cycle analysis of buildings with R/C frames

D.O. Astafiev & I.A. Fedotova

*Investment Construction Company «Mayak», Saint Petersburg, Russia*

**ABSTRACT:** The R/C load-carrying frameworks of multistorey buildings as arbitrary spatial rod systems, consisting of columns and crossbars, are considered in the paper. The floor slabs and wall panels can be also involved in joint work with the framework. These frameworks are a classical example of statically indeterminate composite structures. A proper analysis of a stress-strain state and setting the criteria of these systems stability require the accounting of both their physical and geometrical nonlinearity. It allows one to describe the R/C structure life-cycle more exactly and to give a real prediction of its durability.

## 1 INTRODUCTION

The rapid development of St. Petersburg building industry and the formation of a quickly growing market of real estate against the general growth of the Russian economy have caused the necessity of searching cheaper raw materials and working out the optimum structure arrangements of designed residential buildings. It is the speed of construction and the relative cheapness of dwelling houses that will permit to solve the urgent problem of providing the population with accessible inexpensive habitation.

For this reason the application of the frame constructive system consisting of R/C members is the most appropriate, as it possesses a number of advantages in comparison with constructive schemes of buildings where the bearing elements are the walls made of reinforced concrete or of brick. Using the frame construction arrangement leads to decreasing the load-carrying structure weight by 40 per cent, which is really important for St. Petersburg weak soils, as well as to decreasing expenses on building materials. Besides, the possibility of both the free planning of flats and of a large variety of the buildings architectural facade decisions results in a greater demand for such flats, which strengthens the position of a civil engineering firm as a whole and its competitiveness on the real estate market.

For a climatic zone of the northwest of Russia where the period of frosts sometimes lasts from November till March, the usage of precast concrete is much more preferable, than of the cast one, as it increases the speed of multistorey housing construction. Consequently, perfecting the models and methods of calculating frame buildings made of precast concrete and optimization of their constructive decisions is a very urgent engineering problem now.

## 2 STATEMENT OF THE PROBLEM AND ITS SOLUTION

### 2.1 *Statement of the problem*

The paper deals with the problem of creating the optimum frame structure which, on the one hand, could correspond to the architectural peculiarities of the building and the layout of its apartments, and on the other hand, would have the necessary rigidity. It would permit to use as few of diaphragms as possible and to make the construction light enough and to have an economical use of reinforced concrete. For this purpose a comprehensive investigation of a multistorey frame building, which is being designed was carried out. It consisted in estimating the strength and stability of the framework structure as a whole and its separate elements components.

In their analysis the authors took into account the joint work of the building and the soil basis, the non-linear behavior of the structure materials and its design model deformations, and also the real rigidity of joints, connecting the precast components of the R/C framework. The multilevel approach consisting of modeling the construction as a whole, and modeling its separate members was used.

### 2.2 *Features of the building constructive arrangement*

As an example the behavior of a block of the designed frame building made of precast concrete is considered. The scheme of arranging the columns, crossbars and diaphragms of the block under consideration is presented in [Figure 1](#). It consists of 22 floors. The sizes of the column cross-sections change depending on the building height and are equal to  $60 \times 60$  cm from the

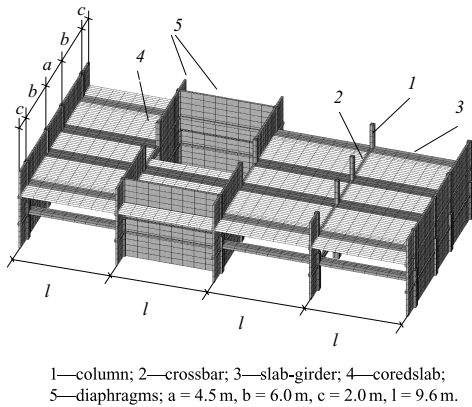


Figure 1. Features of the building constructive arrangement.

ground to the eleventh floor and  $40 \times 40$  cm up. These types of columns have different strength qualities of concrete: B50 and B40 respectively. The diaphragm thickness changes depending on the block height from 200 mm down to 140 mm. The precast concrete floor slab is composed of slab-girders involved in the joint work with the framework and of cored slabs, which are not the load-carrying components of the building frame. The building is set on the foundation slab supported by piles.

### 2.3 Description of the framework design model

Two design models of the structure are studied: finite-element model of the building block with the foundation slab on the rigid basis and the same model on the elastic basis, which allows the authors to take into account the soil-structure interaction. The rigidities of the “piled field-soil” system are defined by numerical calculating and the system is modeled by elastic supports. The values of the rigidity characteristics of nonlinear springs, simulating the performance of piles in the ground, changed from 700 to 5000 tones per meter (from 7 to 50 MN/M).

The framework load-bearing elements of the building block—columns, crossbars, diaphragms, slab-girders and the foundation slab are modeled by rod and shell finite elements. Besides, it is also necessary to take into account the non-bearing elements of the block frame—the cored slabs, which influence significantly on the stability of the construction as a whole and its displacements from the building facade plane.

In the places, where the precast components of the R/C frame are connected with each other, the model of the elastic nonlinear hinge is used. The rigidities of this hinge are determined by solving three-dimensional

problems modeling the immediate junction of these elements.

The calculation of the structure under consideration presupposes the following kinds of loading: the static one caused by the framework own weight and the quasistatic, corresponding to the combination of the weight and wind loads, the active component of which affects the building facade. The value of the pulsation component of the wind load was obtained on the basis of the structure frequency analysis with the account of the change of its stiffness depending on the building height. In this loading case the total wind load changed from 132.9 to 927.86 Pa depending on the building floor.

The parameters of finite-element model of the building precast frame are the following: the number of degrees of freedom is 328 505, the number of nodes is 64 266 and the number of the elements is 29 349.

### 2.4 The account of the framework non-linear behavior

The correct analysis of a stress-strain state and setting the criteria of the framework stability require the account of not only geometrical non-linearity of the problem, connected with the change of the deformed design model of the structure in the course of time, but also physical non-linearity of its material behaviour. It means that the material of the structure elements is considered to be anisotropic, the concrete and reinforcement have non-linear stress-strain diagrams and possess the property of plasticity.

From the point of view of the authors for the analytical approximation of the stress-strain diagram of concrete it is the most preferable to use the following polynomial of the fifth degree:

$$\sigma = A\varepsilon + B\varepsilon^2 + C\varepsilon^3 + D\varepsilon^4 + F\varepsilon^5 \quad (1)$$

where  $\sigma$  = stress;  $\varepsilon$  = strain;  $A, B, C, D$  and  $F$  = coefficients, the values of which depend on the strength quality of concrete and are defined by using the characteristic points of the above mentioned diagram from the solution of the system of algebraic equations of the fifth order. For example, for the strength quality of concrete 50 the values of these coefficients in describing this material behavior in the compression field are the following:  $A = 3.9 \cdot 10^4$  MPa,  $B = -1.737 \cdot 10^7$  MPa,  $C = 4.6 \cdot 10^9$  MPa,  $D = -7.504 \cdot 10^{11}$  MPa,  $F = 4.768 \cdot 10^{13}$  MPa.

### 2.5 The account of the real stiffness of the frame connection joints

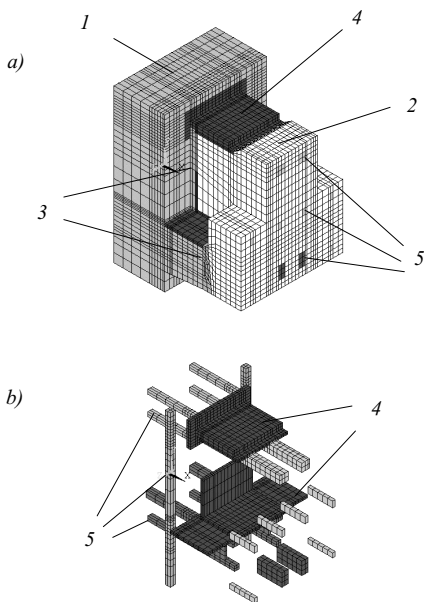
Typical decisions of the connection joints of precast members, which are applied at a number of concrete plants in our country, are considered in the paper.

The real stiffness characteristics of the frame elements connection joints are taken into account in the behavior analysis of the multistorey building block model. That is really significant for a proper estimation of the framework deformability, strength and stability.

Therefore in the proposed structure finite-elements models the joints of the framework precast members are simulated by means of elastic fixing connection, longitudinal and rotational rigidities of which are defined by calculating the separate joints. In modeling of any connection joints both the real scheme of reinforcing of the precast members, the behavior of embedded items and of solution seams are taken into consideration.

For example, a three-dimensional finite-element model of the joint of a vertical column and a horizontal crossbar, which represents a complex composite construction with unilateral connections, is shown in Figure 2a). To show it more clearly, the arrangement of the structure metal elements (embedded items and reinforcement) is presented separately in Figure 2b). The parameters of this joint finite-element model are the following: the number of degrees of freedom is 80 021, the number of nodes is 27 323 and the number of elements is 23 418.

As a result of the numerical experiments the longitudinal and rotational rigidities of a column and a



1 – column; 2 – crossbar; 3 – solution seam; 4 – embedded items; 5 – reinforcement bars

Figure 2. Finite-element model of the connection joint of a vertical column and a horizontal crossbar.

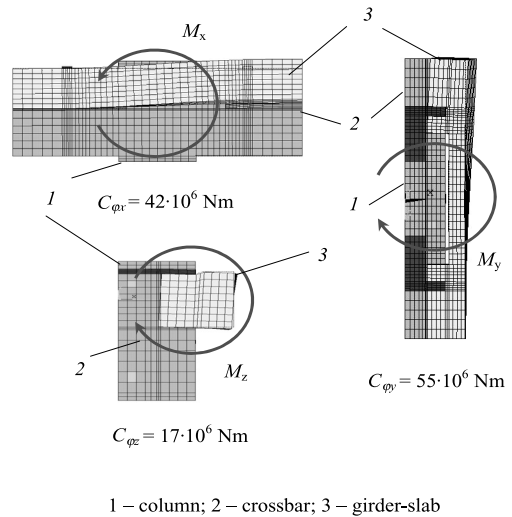


Figure 3. Defining the rotational rigidities of the connection joint of a crossbar and a girder-slab.

crossbar connection joint have been calculated. The problems were solved in linear-elastic statement taking into account the contact zones. In defining the joint rotational rigidities, connected with rotary degrees of freedom, the values of moment loads producing by the crossbar section were set, and the corresponding angles of rotation caused by these moment loads were defined. For example, rotational rigidities of the joint under consideration round the horizontal and vertical axes of the facade plane are accordingly:  $C_{\phi x} = 61 \cdot 10^6 \text{ Nm}$  and  $C_{\phi y} = 75 \cdot 10^6 \text{ Nm}$ . The rotational rigidity of this connection joint round the axis perpendicular to the facade plane appears to be 2–2.5 times higher:  $C_{\phi z} = 151 \cdot 10^6 \text{ Nm}$ .

Stages of defining the rotational rigidities of a crossbar and a girder-slab connection and the corresponding rigidity values are given in Fig. 3. It is obvious, that this joint rotational rigidity round the axis perpendicular to the facade plane, appears to be 2.5–3.2 times lower, than two other connection joint rigidities. That indicates the necessity of strengthening the metal plate connecting the crossbar with the girder-slab.

To estimate the degree of influence of the connection joints flexibility on the investigation results, calculations of the building design model with absolutely rigid joints have been also carried out.

### 3 METHOD OF THE INVESTIGATION

Nowadays the world tendency of developing methods of engineering structures computation is to build up

an actual model of structure behavior, simultaneously taking into account both physical and geometrical non-linearity of the structures and all regimes and kinds of loadings. But this kind of analysis based on traditionally used computer programs is likely to cause essential difficulties and may not always be adequate. So, in order to reveal the true character of the structure behavior under the external loads, the authors have used not only standard computer programs, but also their own software.

It is founded on the method the main propositions of which are thoroughly described by the authors in (Astafiev & Fedotova 2004), (Astafiev & Fedotova 2005), (Astafiev & Fedotova 2006). To describe the behavior of the whole constructive rod element, the obtained systems of non-linear geometrical and equilibrium equations have to be added by the equations, used for the design sections computation and both of them have to be differentiated with respect to time. This procedure makes the problem linear relatively to the time derivatives from the parameters of the structure stress-strain state and their generalized coordinates and essentially simplifies the problem solving.

The joint solution of the systems of differential equations obtained for each constructive rod element allows us to describe the whole structure behavior caused either by changing the external load or by the material creep.

It should be noted, that in case of the static and quasi-static setting of the problem the equations contain the first and the second time derivatives of the parameters of the structure stress-strain state. In case of dynamic loading the equations contain the third derivatives with respect to time.

To solve the systems of linear differential equations, incremental-iterative procedure is carried out, and both the durability of the design sections and the stability of the whole structure and of its separate members are analyzed at each step.

#### 4 RESULTS OF THE INVESTIGATION

As a result of the computation we have managed to reveal the real behavior of the building block under the normative loads recommended by Building Codes accepted in Russia. The calculation results in accordance with different design models of the structure are shown in Figures 4–6.

Figure 4 illustrates the horizontal displacements distribution of the building three-dimensional finite-element model. The graphs of horizontal displacements of the frame perpendicular to the building facade plane depending on the floor height are presented in Figure 5. Each graph corresponds to a definite design model of the “building-soil” system.

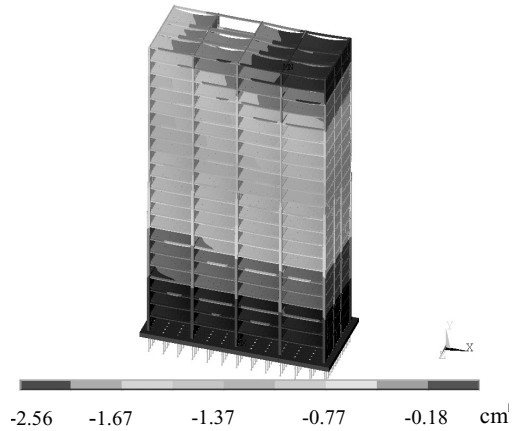
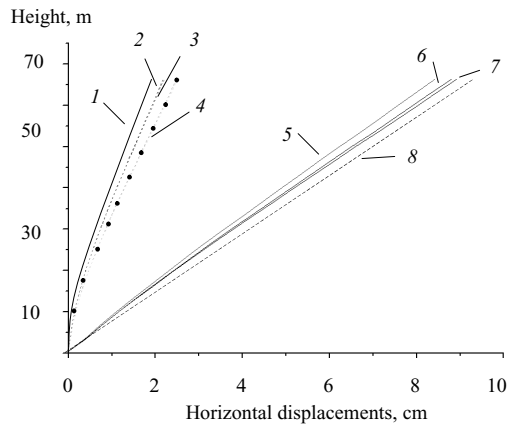


Figure 4. Horizontal displacements of the building three-dimensional finite-element model from the facade plane.



Solid basis: 1 – linear computation; 2 – accounting of geometrical nonlinearity; 3 – accounting of physical nonlinearity; 4 – accounting of both nonlinearities.

Elastic basis: 5 – linear computation; 6 – accounting of geometrical nonlinearity; 7 – accounting of physical nonlinearity; 8 – accounting of both nonlinearities.

Figure 5. Horizontal displacements of the frame depending on the building height.

The diagram of the maximal horizontal displacements of the frame top is given in Figure 6.

It is obvious, that the account of the nonlinear behavior of the superstructure on the rigid basis results in increasing the displacements by 1.4 times in comparison with the results obtained for the linear model. At the account of the soil elasticity these displacements appear to be 4.7 times higher. The contribution of the

Horizontal displacements  
of the building top

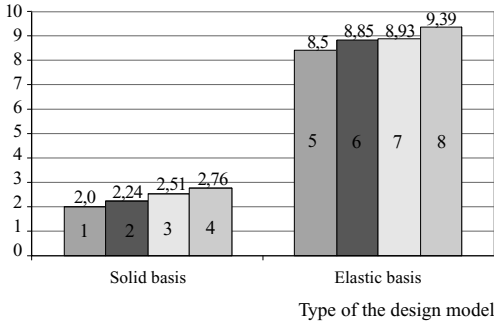


Figure 6. Maximum values of horizontal displacements depending on the type of the structure design model.

basis performance into the values of the building horizontal displacements is more considerable, than the framework, because the basis is composed of weak soils.

It should be noted, that taking into account the real rigidities of the structure connection joints leads to increasing the horizontal displacements by approximately 10 per cent.

According to the Russian Building Codes, for the building calculated by using linear model on the elastic

basis, the displacements of the structure top should not exceed 1/1000 of its height. In nonlinear calculations these displacements are not limited. The results of the investigation shows, that in accordance with linear approach, the building framework is not rigid enough and demands strengthening by 20 per cent by means of either introducing any new pre-cast components or increasing the cross-sections of the existing members. The displacements obtained in nonlinear computation are in a good agreement with the requirements to high-rise buildings. Consequently, the frame constructive arrangement proposed meets the demands of both the economic efficiency and the structure serviceability.

## REFERENCES

- Astafiev, D.O. & Fedotova, I.A. 2003. Stability of physically and geometrically non-linear spatial composite rod systems. *The conceptual approach to structural design; Proc. intern. conf., Milan*, 1–2 June: 233–240.
- Astafiev, D.O., & Fedotova, I.A. 2005. Comprehensive non-linear mathematical model of the work of spatial rod R/C structures. *Keep concrete attractive; Proc. intern. symp., Budapest*, 23–25 May: 507–512.
- Astafiev, D.O., & Fedotova, I.A. 2006. Analysis of rod R/C structures design life considering their non-linear work. *Service life and serviceability of concrete structures; Proc. intern. symp., Espoo*, 12–14 June: 139–144.



# Direct Displacement Based Design and Force Based Design of precast concrete structures

A. Belleri & P. Riva

Department of Design and Technology, University of Bergamo, Bergamo, Italy

**ABSTRACT:** In the following paper we deal with the application of Direct Displacement Based Design (DDBD) to precast concrete buildings with a structural layout typical of Italian warehouses and commercial malls: one story cantilever columns connected by simply supported precast and prestressed beams, supporting prestressed concrete roof elements. To outline the advantages and the limitations of the DDBD procedure compared to the Force Based Design (FBD), we need to find a way to compare the two procedures. Beyond that we make general considerations on how to deal with the equivalent viscous damping equations available in literature to include into the design different types of column-to-foundation connections typical of precast concrete elements.

## 1 INTRODUCTION

### 1.1 Precast concrete structures

The structural layout of precast concrete structures sensibly reduces the construction time and is extremely cost effective. This is the main reason for which the precast technique applied to reinforced concrete building is widely diffused in Italy, especially in the industrial sector. The typical structural layout of Italian warehouses and commercial malls consists of cantilever columns, connected by simply supported precast and prestressed beams, supporting prestressed concrete roof elements. The columns are inserted and grouted in-situ in isolated precast cup-footings.

This kind of structures are usually designed for the seismic event neglecting the moment capacity between the top column and supporting beam connection and adopting the FBD procedure. The new performance criteria which are taking place in the current codes are moving the attention from the ultimate resisting force to the displacement and deformation under the seismic event.

Compared to other reinforced concrete structures, we note how story height of the typical precast concrete structures is usually 2–3 times bigger; this leads to a lower amount of ductility demand as it could be easily determined from a comparison:

$$\frac{\mu_{\Delta}^{precast}}{\mu_{\Delta}^{usual}} = \frac{H_{usual}}{H_{precast}} \quad (1)$$

Thus, if  $H_{precast}$  is three times bigger than the usual reinforced concrete story height, the ductility

associated to the precast system is three times less: the target ductility could be very small compared to usual reinforced concrete structures. We note that the low amount of ductility required leads to a limit state related to the interstory drift control rather than a material strain limit requirement.

### 1.2 Case study

The case study under consideration can be schematized as a set of cantilever column connected at the top by pinned elements as part of a rigid diaphragm. Therefore we can analyze a single column ( $h = 7.9$  m) with the mass ( $m = 82946$  kg) corresponding to the tributary area concentrated at the column end; the target drift chosen is 2.5% (0.1975 m). The material adopted are concrete C40/50 and steel B430H and the design has been done according to EC8–1:2004, for type 1 spectrum, soil type C and a peak ground acceleration of 0.5 g.

Table 1. Ground motions definition.

Earthquake	Duration (s)	Scale factor
Duzce	25.89	1.2
Kalamata	29.995	3.1
Kocaeli–1	70.38	2.1
Northridge–Baldwin	60.00	4.5
Hella	60.00	2.0
SIMQKE 1	19.99	artificial record
SIMQKE 2	19.99	artificial record

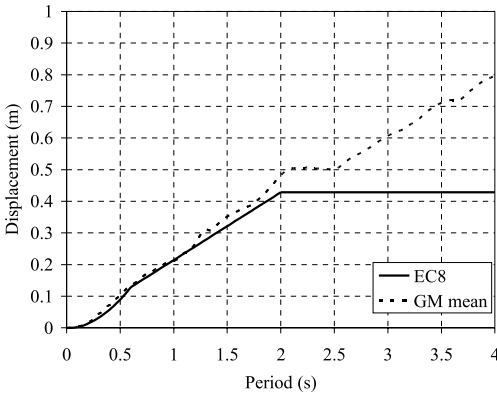


Figure 1. Displacement spectra comparison.

The ground motion used to validate the results in the non linear time history analyses are the one proposed by the line 4 of the RELUIS national project (Table 1), which leads to a mean pseudo acceleration spectrum in good accordance with the EC8 one but a mean displacement spectrum (Figure 1) which doesn't reflect the EC8 constant displacement beyond the corner period (2 s).

## 2 FORCE BASED DESIGN

### 2.1 FBD procedure

The FBD procedure starts with the definition of a force reduction factor ( $q$ -factor) for the structure which depends on the structural type under examination. After the definition of an effective module of inertia  $I_{eff}$  as a percentage of the gross module  $I_g$  we obtain the system stiffness and the system period:

$$T = \frac{2\pi}{\omega} = 2\pi \sqrt{\frac{mH^3}{3EI_{eff}}} \quad (2)$$

We determine the spectral acceleration corresponding to the structural period from the design spectrum,  $S_a(T, q)$  and we get the base shear and the base moment:

$$M_u = V_b \cdot H = S_a \cdot m \cdot g \cdot H \quad (3)$$

The corresponding top displacement is computed, according to EC8, as:

$$\Delta_{inelastic} = q \cdot \Delta_{el} = q \cdot \left( V_b \cdot \frac{H^3}{3EI_{eff}} \right) \quad (4)$$

After that we evaluate the second order effects computing the Theta value, defined as the ratio between the second order moment and the moment from analysis, which should be less than 0.3.

### 2.2 FBD limitations

We individuated three sources of approximation in the FBD procedure which can affect the results: the force reduction factor, the equal displacement approximation and the effective module of inertia definition.

The first limitation is the choice of the force reduction factor. According to EC8, if we consider that the columns are connected in one direction directly by means of L-beams or inverted T-beams, and in the other direction indirectly by TT or Omega beams, we can consider the precast system as a one story frame system, whose  $q$ -factor is 3.3 for a medium ductility class (DCM). This ductility class is justified by the low amount of ductility associated to precast concrete structures as mentioned before. In the particular case of precast concrete structures we get that the previous  $q$ -factor value should be reduced by half if the connections are not designed on the basis of the capacity design rules, which is not the case under examination.

We note that in this definition we deal with the system resisting capacity in terms of force with no specific consideration on the inelastic displacement. If we assume correct the equal displacement approximation we should reduce the  $q$ -factor according to the target inelastic displacement to obtain a better design procedure.

The second limitation is the equal displacement approximation which states that the displacement ductility is equal to the force reduction factor. This approximation could be bypassed by the adoption of inelastic displacement spectra which relate the inelastic displacement directly to the structural period.

The last limitation identified is the choice of the gross modulus of inertia reduction, which is adopted to estimate the secant stiffness at yield. For columns with low axial load, as it is in our cases, the recommended value (Paulay & Priestley 1992) is  $0.4 I_{gross}$ : this leads to a wrong period evaluation and so to a wrong system design, because the FBD procedure considers the stiffness as a property of the section, while the system property that does not change is the yield displacement (Priestley 2005). As it is clear in the Table 2 the system period depends on the actual longitudinal steel ratio.

It is so clear how the steel ratio affects the period and therefore the demand predicted by the FBD procedure. In our specific case we note how the period evaluated with a reduced modulus of inertia ( $0.4 I_{gross}$ ) is close to the period corresponding to 2% steel ratio, which is the ratio commonly adopted.

Table 2. Steel ratio period dependence.

Section size (cm)	Steel ratio				$0.4I_{gross}$ (s)
	1% (s)	2% (s)	3% (s)	4% (s)	
60	2.85	2.16	1.90	1.73	2.11
70	2.00	1.71	1.41	1.30	1.55
80	1.56	1.27	1.08	0.97	1.19
90	1.25	0.99	0.87	0.78	0.94
100	1.05	0.83	0.71	0.62	0.76
110	0.88	0.69	0.58	0.51	0.63

### 3 DIRECT DISPLACEMENT BASED DESIGN

#### 3.1 DDBD procedure

The DDBD procedure (Sullivan et al. 2005) adopts a substitute structure approach. We start with the definition of the structural deformed shape ( $\Delta_i$ ), linear in this case, and with the choice of the target displacement ( $\Delta_d$ ), which for the considerations previously stated is related in this case to the interstorey drift value rather than to material strain limit states. With these two definitions we can define the single degree of freedom substitute structure, which is characterized by the effective height ( $h_{eff}$ ), mass ( $m_{eff}$ ):

$$h_e = \frac{\sum_{i=1}^n m_i \Delta_i h_i}{\sum_{i=1}^n m_i \Delta_i} \tag{5}$$

$$m_e = \frac{\sum_{i=1}^n m_i \Delta_i}{\Delta_d} \tag{6}$$

The next step is the determination of the equivalent viscous damping, adopted by DDBD to represent the elastic and the hysteretic damping  $\xi_d = 5 + \xi_{hyst}\%$ ; the first term, the elastic viscous damping, takes into account material viscous damping, radiation damping due to the foundation system and damping due to the non linear behavior of the connections, while the second term, the hysteretic damping, depends on the hysteretic relationship of the structural elements and takes into account in somehow the capacity of the system to dissipate energy.

The equivalent viscous damping value is used to determine the design displacement spectrum reduction for damping values different from 5%. According to EC8, this reduction should be:

$$\frac{SD(\xi)}{SD(5\%)} = \sqrt{\frac{10}{5 + \xi_{eq}}} \tag{7}$$

Because we are concerned about the comparison between the FBD and the DDBD procedures, we will

use the mean displacement spectrum deriving from the ground motion under considerations and we will consider their effective dependence from damping. With a least square procedure, we find out that the spectrum reduction factor for the ground motions adopted can be well described (in the period range 0–2s) by:

$$\frac{SD(\xi)}{SD(5\%)} = \sqrt{\frac{7.8}{2.8 + \xi_{eq}}} \tag{8}$$

With the displacement spectrum so reduced we can evaluate the substitute structure effective period associated to the target displacement, and from that the effective stiffness associated to the substitute structure maximum response. The design base shear is so:

$$V_b = k_{eff} \Delta_d = 4\pi^2 \frac{m_{eff}}{T_{eff}^2} \Delta_d \tag{10}$$

#### 3.2 Equivalent viscous damping

The equivalent viscous damping formulation adopted in this study is the one proposed by Blandon et al. (2005) and subsequently modified by Grant et al. (2005), which relates the equivalent viscous damping to the target system ductility ( $\mu_\Delta = \Delta_d/\Delta_y$ ) and to the substitute structure effective period:

$$\xi_{eq} = 0.05 + a \left(1 - \frac{1}{\mu^b}\right) \left(1 + \frac{1}{(T_e + c)^d}\right) \tag{11}$$

The previous parameters have been calibrated for different hysteretic models: the one adopted for this research is the Takeda model (Figure 2), with  $\alpha = 0.3, \beta = 0.6, r = 0.05$ , the corresponding parameters for design purposes are  $a = 0.249, b = 0.527, c = 0.761$  and  $d = 3.250$  (Takeda “fat” model).

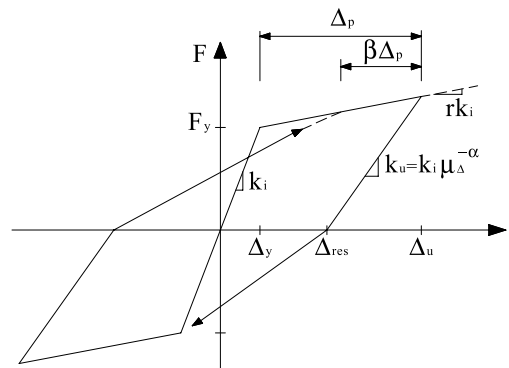


Figure 2. Force-displacement Takeda model.

The procedure adopted by the authors to calibrate the damping equation parameters is based on the force-displacement response of SDOF systems subjected to a ductility range from 2 to 6 and to an effective period range from 0.5 s to 4 s. Therefore we need to check if the damping equation is still conservative for low ductility values, typical of precast concrete structures, and to define the correlation between force-displacement and moment-curvature Takeda parameters; the latter will be used in the finite element non linear analyses with the software Ruaumoko (Carr 2006).

The equation behavior for low ductility values has been checked by means of non linear time history analyses for section size ranging from 60 cm to 110 cm. The results are presented in Figure 3, where the ratio between the target ductility and the ductility obtained is shown as a function of the target ductility. As we can see the equation is still conservative for low ductility values.

In this research the Takeda model has been adopted to describe the column moment-curvature relationship. Thus we need to define the relationship between the parameters for the force-displacement (Figure 3) and moment-curvature Takeda model (Figure 4).

The relationship between curvature and displacement ductility, considering a plastic hinge region of length  $L_p$  with constant plastic curvature  $\phi_p$  located at the element ends, is:

$$\mu_\phi = 1 + \frac{\mu_\Delta - 1}{r' + 3 \frac{L_p}{H} (1 - r')} \quad (12)$$

The relationship between  $r$  and  $r'$  is:

$$r = r' \frac{H}{3L_p} \quad (13)$$

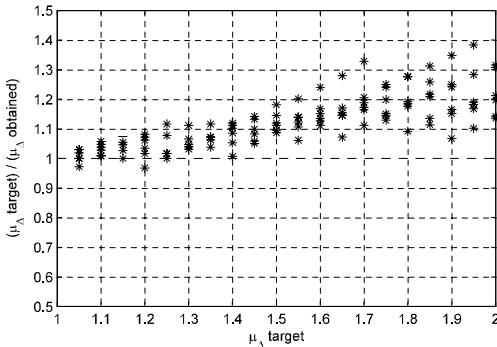


Figure 3. Ductility values ratio comparison.

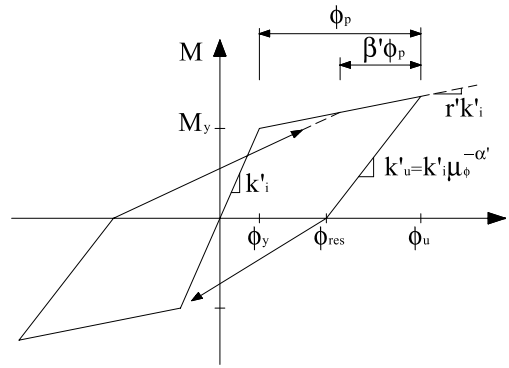


Figure 4. Moment-curvature Takeda model.

The relationship between  $\alpha$  and  $\alpha'$  is:

$$\alpha' = \left\{ \ln \left[ -\frac{H}{3L_p} + 1 + \frac{H}{3L_p} \mu_\Delta^\alpha [1 + r'(\mu_\phi - 1)] \right] + -\ln[1 + r'(\mu_\phi - 1)] \right\} \frac{1}{\ln(\mu_\phi)} \quad (14)$$

The relationship between  $\beta$  and  $\beta'$  is  $\beta = \beta'$ .

### 3.3 DDBD limitations

At the state of the art we individuated two limitations in the DDBD procedure: the evaluation of the response for structures with an effective period greater than the displacement spectrum corner period and for structures whose behavior is described by a Takeda hysteretic model with parameters different from the ones in the literature.

A substitute structure effective period greater than the corner period, according to EC8 displacement spectrum, means that the DDBD procedure has an inelastic response at a ductility level less than the one corresponding to the target displacement chosen. Therefore we should reduce the target displacement until we reach the corner period. We observe that anytime the displacement obtained from the DDBD procedure is less than the target displacement, this procedure assigns automatically to the structure an effective period corresponding to the corner period, in this case 2 s. We note that this procedure is not applicable in this research because the mean displacement spectrum obtained from the ground motions does not present a clear corner period and a constant displacement region (Figure 1).

Regarding the choice of the Takeda parameters to match the actual structure behavior, we carried out an experimental test for a pocket foundation precast concrete column with 40 cm cross section size, 3.2 m

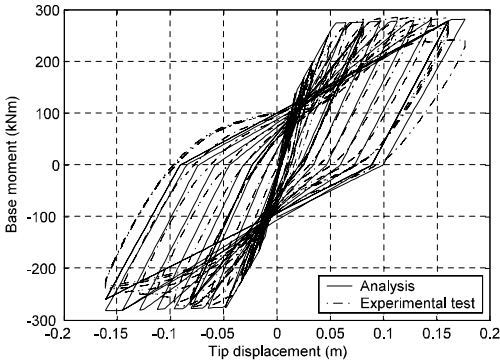


Figure 5. Takeda model calibration.

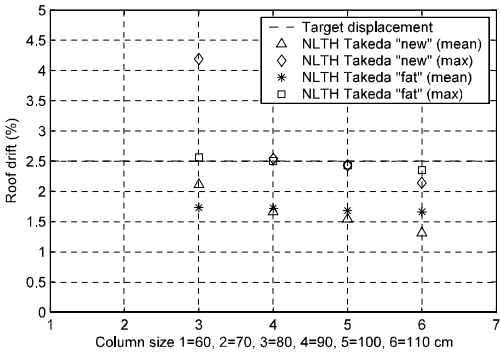


Figure 6. THNL analysis for different Takeda models.

height and the same magnitude axial load ratio of the case under considerations. As it is clear in Figure 5, the experimental behavior is well described by a moment-curvature Takeda model with  $\alpha' = 0.35$ ,  $\beta' = 0.2$  and  $r' = 0.00063$ , which, for the previous considerations, leads to parameters corresponding to force-displacement relationship of  $\alpha = 0.26$ ,  $\beta = 0.2$  and  $r = 0.0022$ .

If we plot the results obtained from time history non linear (THNL) analyses with the moment-curvature Takeda model parameters just presented and the ones corresponding to the Takeda “fat” model (Figure 6), we see how the former results, even if we can control the mean values, are not as stable as the latter. This means that a new calibration of Equation 11 is necessary for different sets of Takeda parameters.

#### 4 FBD AND DDBD COMPARISON

In this paragraph we outline two possible ways to compare the FBD and DDBD procedure. We used a hysteretic model for the NLTH analyses which reflects the assumptions made: Takeda “fat” model for both

procedures and  $I_{eff} = 0.4 I_{gross}$  for the FBD one. In both cases we do not take into account second order effects, we consider the mean displacement spectrum obtained from the ground motions and we use Equation 8 to get the spectrum reduction for damping values different from 5%.

The first way of comparison starts from FBD: after designing the column cross section, we calculate the inelastic displacement (Equation 5) and we use this value as the target displacement for the DDBD procedure. The results are shown in Figure 7.

The good agreement observed for the FBD procedure is due to the hysteretic model used which reflects the assumptions made in the design.

If we give priority to displacement control and we adopt the DDBD procedure to match a target displacement set at 2.5% of the roof drift, as a damage limitation requirement limit used in this research, we can use that value to get the q-factor to use in the FBD procedure from the equivalent displacement approximation ( $q = \mu_{\Delta}$ ), as stated in the actual Codes. The results are shown in Figure 8.

Looking at the computed displacement it is clear that, even if we have set the q-factor according to

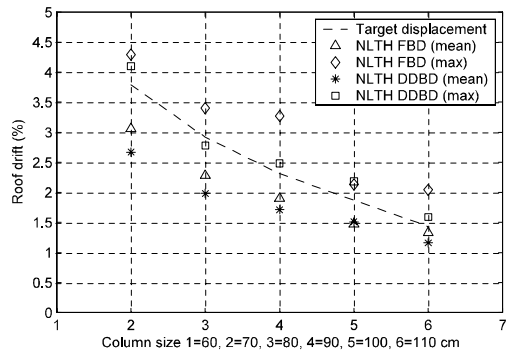


Figure 7. THNL analysis FBD-DDBD comparison.

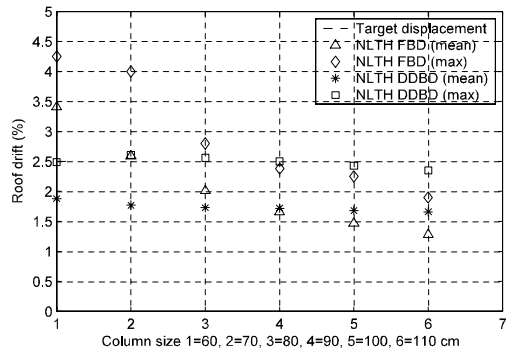


Figure 8. THNL analysis DDBD-FBD comparison.

the target displacement in the DDBD (2.5% drift), the displacement computed for the FBD procedure is different from the target displacement. This is due to the equal displacements approximation ( $q = \mu_{\Delta}$ ). It is clear how the DDBD procedure succeeds in predicting and controlling the displacements with a stable trend for both maximum and mean values. We note that the main drawback of the FBD procedure is the incapacity of the procedure to determine the target displacement at the beginning of the analysis.

## 5 CONCLUSIONS

Trying to compare the FBD and the DDBD procedure, we note that at the state of the art the comparison is hard because of a series of drawbacks in the FBD procedure: the main one is the failure to predict the inelastic displacements, which is due to the way the latter are related to the q-factor and to the arbitrary choice of the effective stiffness. If we overpass these limitations the two procedures give comparable results.

Regarding the FBD procedure, the q-factor takes into account the system ductility by reducing the system seismic force; it depends on the structural system type and once the system type is chosen the q-factor is fixed. In the current codes the inelastic displacements are related directly to the elastic ones by the equivalent displacement approximation. Even if we could better predict the inelastic displacements, the FBD procedure does not provide convergence to the target displacements which could be associated to a q-factor different from the chosen one; thus the section designed following the FBD is not optimized to limit the target displacement.

This problem is overcome in the DDBD procedure that, starting from the target displacement, controls the non-linearity of the problem with the hysteretic damping formulation. In the DDBD design procedure, once we have obtained the effective period of the substitute structure  $T_{eff}$ , the reinforcement needed is the one which leads a period  $T$  associated to the secant stiffness at yield greater than

$$T_{eff} \sqrt{\frac{1 + r(\mu_{\Delta} - 1)}{\mu_{\Delta}}} \quad (15)$$

A possible drawback of the DDBD is the displacement evaluation of structures with an effective period greater than the corner period (2 s in this case). Anytime this happens we assign automatically to the structure an effective period corresponding to the corner period. This behavior is not observed in this research because the mean displacement spectrum of the ground motions adopted does not clearly present the constant displacement region after the corner period.

At the state of the art the DDBD hysteretic damping equations have been calibrated (Grant et al. 2004) for two sets of Takeda parameters. The NLTH analyses for structures governed by these hysteretic models, with the considerations made in paragraph 3.2, give very good results, but for different hysteretic models (Figure 6) the parameters of Equation 11 need to be recalibrated.

## ACKNOWLEDGMENTS

This research is being supported by the DPC-Reluis national research. The experimental test is part of a research program on precast column-to-foundation connections financed by Moretti SpA, Erbusco (BS), Italy.

## REFERENCES

- Blandon, C.A. & Priestley, M.J.N. 2005. Equivalent Viscous Damping Equations for Direct Displacement Based Design, *Journal of Earthquake Engineering*, Vol. 9, Special Issue 2 pp 257–278.
- Carr, A.J. 2006. Ruaumoko—Users manuals, University of Canterbury, Christchurch, New Zealand.
- Eurocode 8–2004. Design of Structures for Earthquake Resistance, Part 1: General rules, seismic actions and rules for buildings.
- Grant, D.N. Blandon, C.A. & Priestley, M.J.N. 2004. *Modelling Inelastic Response in Direct Displacement-Based Design*, IUSS Press Pavia, Italy.
- Jacobsen, L.S. 1960. Damping in composite structures, *Proceedings of the Second World Conference on Earthquake Engineering*, pp 1029–1044.
- Paulay, T. & Priestley, M.J.N. 1992. *Seismic Design of Reinforced Concrete and Masonry Buildings*, John Wiley and Sons, Inc.
- Paulay, T. 2002. A Displacement-Focused Seismic Design of Mixed Building Systems, *Earthquake Spectra*, Vol. 18, No. 4, pp. 689–718.
- Paulay, T. 2003. Seismic Displacement Capacity Of Ductile Reinforced Concrete Building Systems, *Bulletin of the New Zealand society for Earthquake Engineering*, Vol 36, No. 1.
- Pettinga, J.D. & Priestley, M.J.N. 2005. *Dynamic Behaviour of Reinforced Concrete Frames Designed with Direct Displacement-Based Design*, IUSS Press, Pavia, Italy.
- Priestley, M.J.N. 2003. *Myths and Fallacies in Earthquake Engineering, Revisited*, The Ninth Mallet Milne Lecture, IUSS Press, Pavia, Italy.
- Priestley, M.J.N. & Grant, D.N. 2005. Viscous Damping, in Seismic Design and Analysis, *Journal of Earthquake Engineering*, Vol. 9, Special Issue 2 pp 229–255.
- Priestley, M.J.N. Calvi, G.M. & Kowalsky, M.J. 2007. *Displacement-Based Seismic Design of Structures*, IUSS Press, Pavia, Italy.
- Sullivan, T.J. Priestley, M.J.N. & Calvi, G.M. 2005. Development of an Innovative Seismic Design Procedure for Frame-Wall Structures, *Journal of Earthquake Engineering*, Vol. 9, Special Issue 2 pp 279–307.

# Lifetime seismic performance of precast reinforced concrete industrial buildings

F. Biondini, A. Palermo & G. Toniolo

*Department of Structural Engineering, Politecnico di Milano, Milan, Italy*

**ABSTRACT:** In the Southern part of Europe the 80% of the industrial buildings and low-rise multi-storey commercial buildings have been constructed with precast concrete members. Especially in the 70's–80's the structural frames, i.e. columns and beams, were directly exposed to environmental conditions without any protection. The aim of the paper is to assess the seismic behaviour of industrial precast concrete buildings considering the material degradation within the lifetime of the structure. A typical one-storey industrial building prototype has been investigated. After life-cycle structural analyses on the columns sections, where plastic hinges occur during an earthquake event, push-over and push-pull cyclic analyses have been carried out on the whole structure with the intent to assess both the global (total base shear, displacement ductility) and local structural behaviour (moment-curvature) within the lifetime. At this stage, the preliminary results state a relevant reduction of both the total strength and the displacement ductility within 50 years lifetime.

## 1 INTRODUCTION

Precast reinforced concrete buildings are quite spread in Italy and South Europe, both for commercial and industrial use. These buildings are generally limited to two-three storeys and, especially for industrial purposes, most of them are typically characterised by one-storey hinged frames. All the structural members generally are prefabricated, and dry connections with mechanical devices between the members are adopted. Since the beam-to-column connections are designed for transferring shear only (hinge) the only dissipative zones of the structural system are located at the bottom of the columns, where a plastic hinge is expected to develop when an earthquake occurs.

If interior concrete panels or masonry/concrete bricks are considered as external façade elements, the structural members of the building are directly exposed to the environmental aggressive agents, which can be quite severe for specific conditions. This phenomenon within the lifetime of the structure can drastically reduce local strength and ductility, modifying, for some particular structural configurations, also the failure mechanism (Biondini and Frangopol 2008). Recent research investigations (Biondini and Toniolo 2006, 2008) have been focused on a proper calibration of the behaviour factor  $q$  for precast systems, i.e. the parameter estimating the global ductility of the structure, since in the first editions of Eurocode 8, precast concrete buildings were particularly penalised with an

unjustified low value of the  $q$ -factor compared to the traditional cast-in-situ monolithic buildings. The purpose of the present work is to evaluate the seismic performance, i.e. total strength and global ductility, considering the mechanical damage due to aggressive agents of the structural members during the structural lifetime.

After a life-cycle analysis on the column sections in correspondence of the possible formation of plastic hinges, push-over and push-pull cyclic analysis are carried out on a typical one-storey industrial building prototype to investigate the time evolution of its seismic performance.

The structural prototype is shown in [Figure 1](#). The prototype (35.0 × 28.7 m) is composed of 10 columns (70 × 70 cm) 11 m high, and 5 I-beams with variable longitudinal profile. Five frames with internal hinge restraints at the top between the beams and the columns are located in the Y direction, while in X direction, ribbed roof elements, 7 meters long, guarantee the structural connection between the columns. Also in the X direction the connection roof-element-to-beam can be assumed as a hinge restraint. Due the similar structural schemes in both directions, in the following the numerical investigations will be limited to the Y direction only.

The numerical results have been obtained through refined lumped plasticity finite element modelling, which has been already adopted for the validation of experimental full-scale tests on similar industrial building prototypes (Palermo *et. al* 2007).

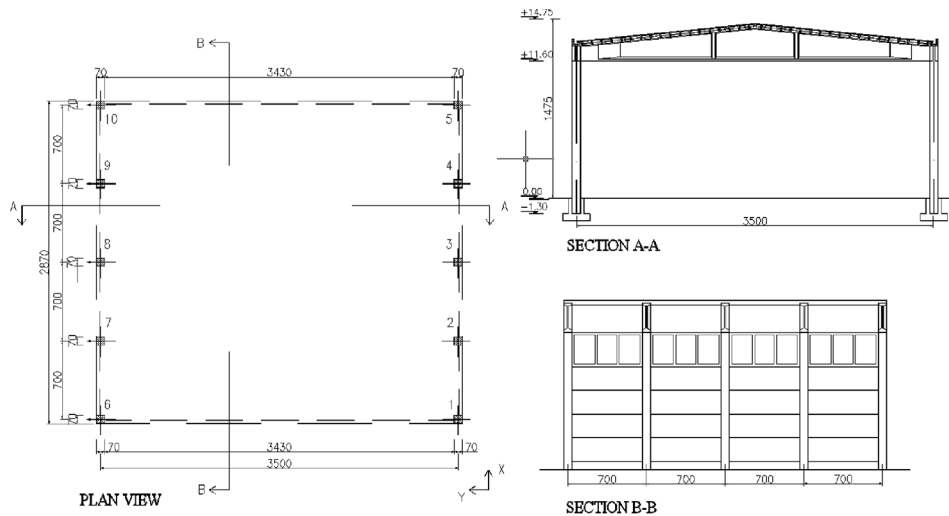


Figure 1. Transversal section and plan view of the precast industrial building.

## 2 DAMAGE MODELING AND PERFORMANCE ANALYSIS UNDER AGGRESSIVE AGENTS

### 2.1 Life-cycle performance of concrete structures

The life-cycle structural analyses are carried out by using a general procedure for concrete structures in aggressive environments proposed in (Biondini *et al.* 2004, 2006a, 2006b). In the proposed approach, the diffusion process is described by the Fick's laws and reproduced by using a special class of evolutionary algorithms called cellular automata. Based on this modeling, the concentration of the aggressive agent  $C = C(\mathbf{x}, t)$  at point  $\mathbf{x}$  and time  $t$  is obtained. Structural damage induced by diffusion is modeled by introducing a degradation law of the effective resistant areas for the concrete matrix and steel bars. The amount of degradation is described by means of dimensionless damage indices for concrete and steel which provide a direct measure of the damage level of the materials. The damage indices are correlated to the diffusion process by assuming, for each material, a linear relationship between the rate of damage and the mass concentration  $C = C(\mathbf{x}, t)$  of the aggressive agent.

### 2.2 Constitutive laws of the materials

The constitutive laws of the materials are required to define the bending behavior of the cross-section. For concrete, the stress-strain diagram is described by the Saenz's law in compression and by an elastic perfectly plastic model in tension, with: compression strength  $f_c = -35$  MPa; tension strength  $f_{ct} = 0.25|f_c|^{2/3}$ ; initial modulus  $E_{c0} = 9500|f_c|^{1/3}$ ; peak strain in compression  $\varepsilon_{c0} = -0.20\%$ ; unconfined strain limit in compression  $\varepsilon_{cu} = -0.35\%$ ; strain limit in tension

$\varepsilon_{cu} = 2 f_{ct}/E_{c0}$ . The effects of confinement are also taken into account by assuming the concrete ultimate strain as a function of the stirrup mechanical ratio  $\omega_w$  as follows:

$$\varepsilon_{cu}^* \cong \varepsilon_{cu} + 0.05\omega_w \quad (1)$$

where  $\omega_w$  is computed for stirrups  $\varnothing 8/75$  mm. For steel, the stress-strain diagram is described by an elastic perfectly plastic model in both tension and compression, with: yielding strength  $f_{sy} = 430$  MPa; elastic modulus  $E_s = 206$  GPa; strain limit  $\varepsilon_{su} = 6.00\%$ . Regarding the geometric characteristics, the section is square  $70 \times 70$  cm, within  $8\phi 22$  (diameter 22 mm) bars, as shown in Figure 2a.

### 2.3 Life-cycle structural analysis

The life-cycle analysis is carried out by assuming that the columns of the building are exposed on the external surface only with prescribed concentration  $C_0$  of the aggressive agent. As a consequence, the cross-sections of the external columns are exposed along two sides, and the cross-sections of the internal columns along one side. Figures 2b, 2c, 2d show the structural model and the grid of the cellular automaton. Figures 2c and 2d also show the location of the aggressive agent for the external and internal columns.

With reference to a diffusivity coefficient  $D = 10^{-11}$  m<sup>2</sup>/sec, the cellular automaton is defined by a grid dimension equal 25 mm and a time step equal 0.25 years. The diffusion process is described by the maps of concentration  $C(\mathbf{x}, t)/C_0$  shown in Figure 3 for the case of external columns only.

The mechanical damage induced by diffusion is evaluated by assuming a damage rate equal  $0.04C_0$  for concrete, and  $0.02C_0$  for steel. Figures 4a, 4b respectively shows the time evolution of the resistant



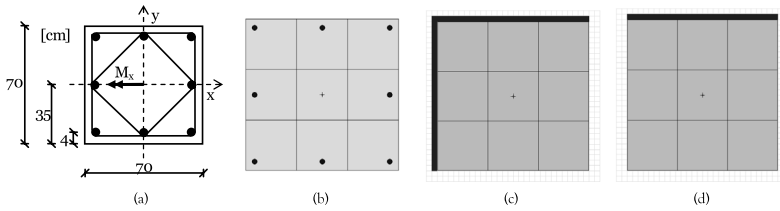


Figure 2. Cross-section at the base of the columns. (a) Geometrical dimensions and reinforcement. (b) Structural model for life-cycle analysis. Grid of the cellular automaton with location of the aggressive agent for (c) the external and (d) the internal columns.

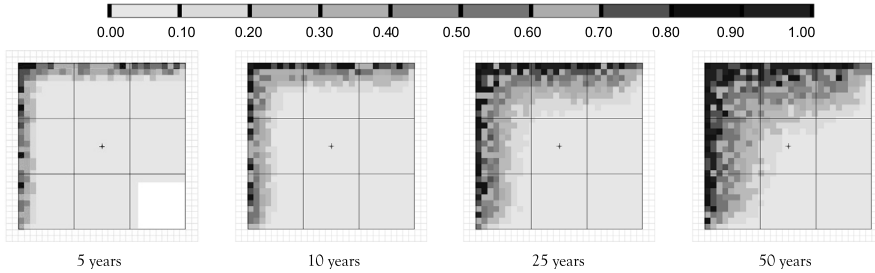


Figure 3. Maps of concentration  $C(x, t)/C_0$  of the aggressive agent after 5, 10, 25, and 50 years from the initial time of diffusion penetration in the cross-section at the base of the external columns.

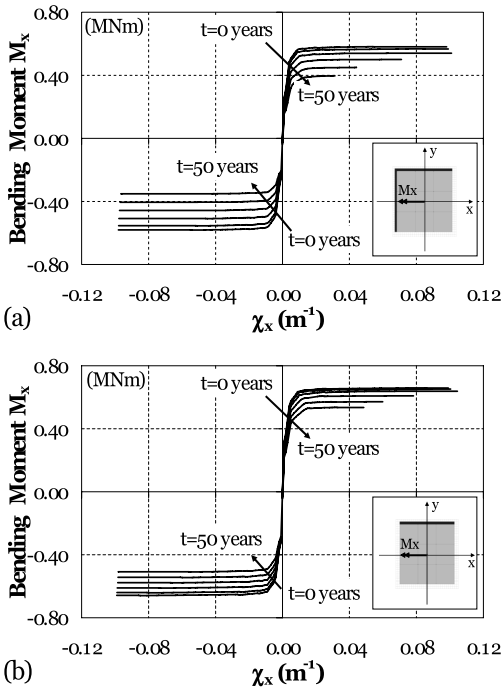


Figure 4. Lifetime evolution of the bending moment-curvature diagrams for the (a) external columns and (b) internal columns.

bending moments  $M_x$ , during the first 50 years of lifetime with time step of 10 years (0, 10, 20, 30, 40, 50 years) for external and internal columns.

Since the exposure of the columns to the aggressive agent is not symmetric, the positive and negative bending moment-curvature curves assume a different behaviour varying within the lifetime. In particular, since the bars are in tension in the damaged exposed part, a higher reduction of the ultimate moment capacity strength is evident for the negative curves. An opposite trend is vice-versa observed for the positive ultimate curvatures, which are drastically reduced within the 50 years lifetime. The reduction of the ultimate curvature of the section is mainly due to the fact that failure is governed by the concrete crushing of the compressive zone which also correspond to the most damaged-exposed part, if the positive bending moments are considered.

Figure 5 clearly shows the trend of the dimensionless ultimate moment varying the lifetime. Being the external columns the most exposed, a higher reduction of the ultimate moment capacity has been expected compared to the internal columns. (30–35% against 20–25%).

In terms of curvature ductility  $\mu_\chi$ , as shown in Figure 6, negligible differences are noticeable between external and internal columns for negative curvatures; while, after 50 years lifetime, a reduction of the curvature ductility (positive curvatures) of 75% for external columns and 55% for internal columns can be observed. The threshold lifetime, where the reduction of curvature becomes significant, approximately corresponds to 30 years.

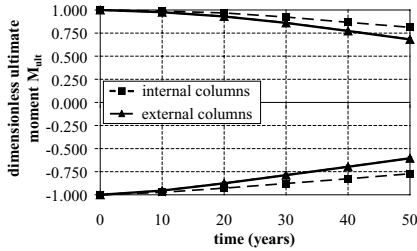


Figure 5. Dimensionless ultimate/nominal yielding moment versus structural lifetime.

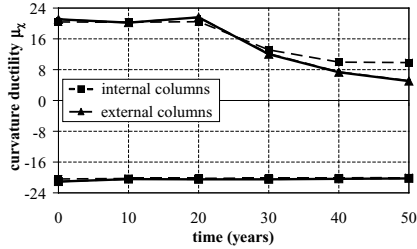


Figure 6. Curvature ductility versus structural lifetime.

### 3 STRUCTURAL MODELING

The industrial building prototype shown in Figure 1 was modelled with elastic beam-type elements and with lumped inelastic rotational springs to simulate the cyclic behaviour of the plastic hinges. The beams were modelled with linear-elastic beam-type elements (uncracked second moment of areas), while for the roof elements, due to their high stiffness, a rigid diaphragm constraint has been assumed between the structural frames. For the columns, where formation of plastic hinges is expected to occur near the base foundations, a linear elastic element (cracked second moment of areas,  $I_x = I_y = 0.4I_g$ ) with inelastic rotational spring at its edges has been adopted.

The cyclic behaviour of the plastic hinge, i.e. rotational inelastic springs is defined by the relationship between moment and rotation, achieved by means of integration of a proper adopted moment-curvature hysteresis rule, assuming a parabolic distribution of the curvature along a fixed length region of the plastic hinge  $L_p$  calculated as proposed in (Paulay and Priestley 1992).

Beam-column connections were modelled as hinged restraints both in the x-z and y-z plane as shown in Figure 7, while the socket-column foundation restraint (section A-A, Figure 1) has been assumed as a fully fixed joint.

For sake of brevity, the seismic performance of the building prototype has been evaluated in one direction only (x direction), parallel to the main beams (section A-A, Figure 1). Similar results, not herein presented, have been obtained also in the Y direction.

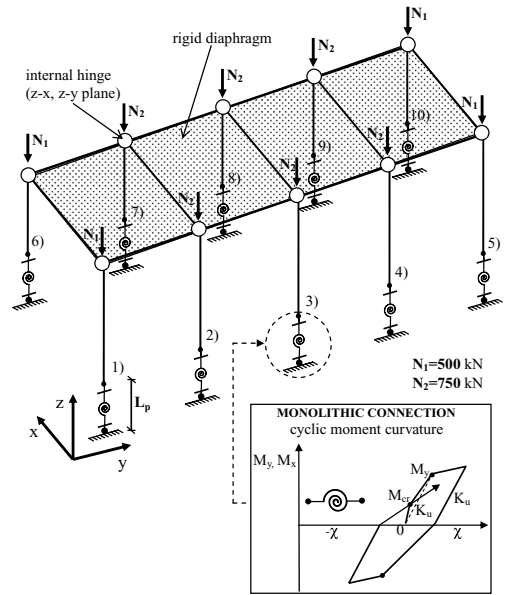


Figure 7. Lumped plasticity model of the structural prototype.

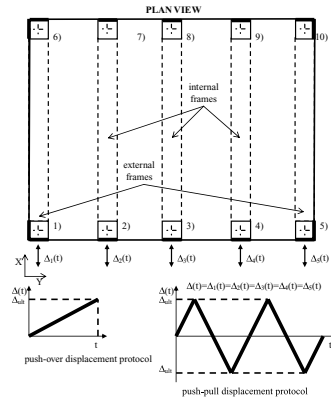


Figure 8. Displacement loading protocol.

Push-over and quasi-static cyclic analyses, carried out on the prototype, through the program Ruaumoko 3D (Carr, 2006), were referred to the loading displacement protocol and the scheme shown in Figure 8. For both the analyses the second order effects ( $P - \Delta$ effect) have been included. The values of the axial loads applied to the columns are shown in Figure 7.

The most important part in the model preparation is related to the linearization of the moment-curvature relationships of the internal and external columns shown in Figure 9. For each time step considered, the linearization has been carried out for both the negative and the positive moment-curvature relationship, as shown in Figures 4.a and 4.b.

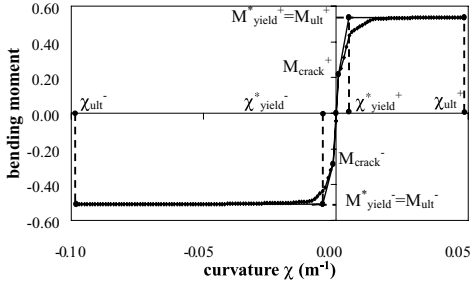


Figure 9. Linearization of the moment-curvature diagram.

Once the main parameters, as the cracking ( $M_{crack}$ ) and the nominal yielding moment ( $M_{yield}^*$ ), the initial stiffness, the nominal yielding ( $\chi_{yield}^*$ ) and ultimate curvature ( $\chi_{ult}^*$ ), have been calibrated, the cyclic behaviour of the column plastic hinges is defined through the Fukada hysteresis rule (Fukada, 1969). Due to lack of information, the unloading stiffness factor  $\beta$  has been empirically assumed 0.2, constant for all the time steps considered (typical value for beams and columns with low axial loading).

## 4 NUMERICAL NON LINEAR ANALYSES

### 4.1 Push-over analysis

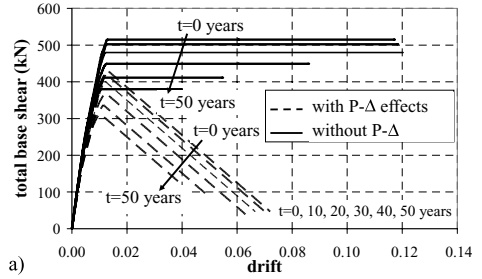
A monotonic increasing displacement up to the failure condition has been imposed to the five frames in the X direction (Figure 8). Referring to the above mentioned lifetime steps (0, 10, 20, 30, 40, 50 years), Figure 10.a shows the total base shear vs. drift (top column displacement divided by column height) with and without P- $\Delta$  effects.

For both the cases, with the increment of lifetime a marked reduction of the total strength and of the ultimate drift is evident. The collapse of the structure is governed by the instability failure of the internal columns 7, 8, and 9 up to 40 years of lifetime, while for higher lifetimes a material failure of the external columns 6 and 10 occurs.

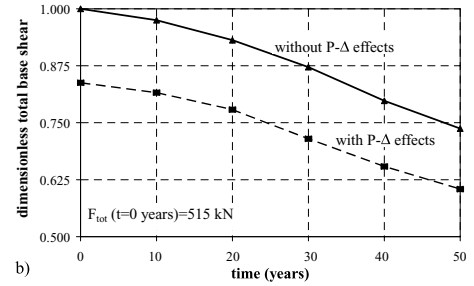
The effect of P- $\Delta$  effects, as shown in Figure 10.b, drastically reduces the global strength of about 20% in proximity of the yielding drift remaining almost constant within the lifetime. The material degradation and the P- $\Delta$  effects bring to a global strength reduction of 40% after 50 years of lifetime.

Figure 11 shows the displacement ductility  $\mu_{\Delta}$ , or the behaviour factor  $q$ , versus the lifetime. The material degradation strongly affects the ductility of the structure after 20–25 years of lifetime, while P- $\Delta$  effects are more relevant in the first 25 years.

Including both the P- $\Delta$  effects and the material degradation, after 50 years lifetime a reduction of 30% of the displacement ductility or behaviour factor  $q$  can be observed. The interaction of P- $\Delta$  effects and material degradation can affect the distribution of the



a)



b)

Figure 10. (a) Lifetime total base shear versus column drift. (b) Dimensionless base shear versus lifetime.

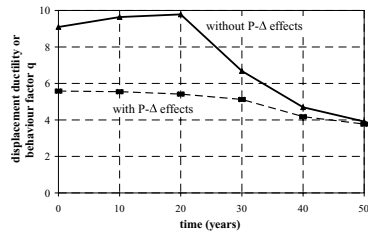


Figure 11. Displacement ductility, or behaviour factor  $q$ , versus lifetime.

shear strength provided by the above-mentioned five frames, which can be distinguished in two external and three internal frames. As shown in Figure 12, the P- $\Delta$  effects, which are more marked for the internal frames due to the higher axial load ( $N_2 = 750$  kN) affect the redistribution of the total base shear, leading to an increment of the percentage of total base shear capacity given by the external frames. Vice-versa, the material degradation is more evident in the external columns, being the exposed to the environmental conditions with two faces. Hence, as shown in Figure 12 for 50 years of lifetime, a higher percentage of total base shear capacity is provided by the internal frames.

### 4.2 Quasi-static cyclic analysis

A cyclic displacement loading history (two cycles with amplitude corresponding to the ultimate displacement  $\Delta_{ult}$ ) has been imposed to the five frames in the X direction (Figure 8). For sake of brevity only the two lifetime steps (0, 50 years) have been considered for

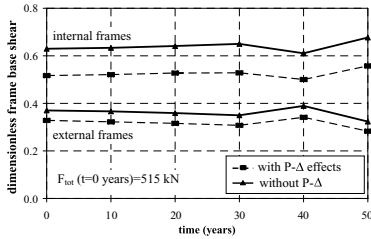


Figure 12. Distribution of frame base shears versus lifetime.

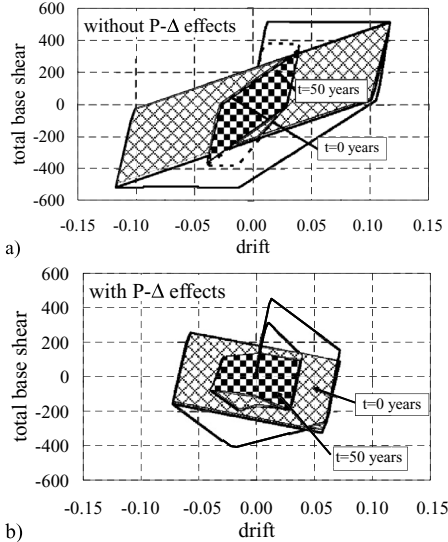


Figure 13. Base shear versus column drift: (a)  $t = 0$ ; (b)  $t = 50$  years.

the analyses. The global cyclic behaviour in terms of base shear versus drift, with and without P- $\Delta$  effects, is shown respectively in Figure 13a and Figure 13b. The typical cyclic behaviour of concrete structures is well represented by the above-mentioned Fukada hysteresis rule. It is evident a drastic reduction of the total energy dissipated, respectively at section failure and collapse limit, after 50 years lifetime as emphasized by the shaded areas reported in the Figures 13a and 13b. In fact, as a confirmation of this result, the equivalent viscous damping  $\xi_{\text{equiv}}$  moves from 30.8% to 27.6% within a reduction of 11% during 50 years lifetime (Figure 13a). The inclusion of P- $\Delta$  effects (Figure 13b) affects not only the shape of the cyclic loops, but bring to a reduction of the total dissipation capacity of the structure ( $\xi_{\text{equiv}} = 29\%$  at initial condition,  $\xi_{\text{equiv}} = 23.6\%$  after 50 years lifetime).

## 5 CONCLUSIONS

The preliminary numerical investigations carried out on the precast concrete building prototype confirmed that the seismic performance both in terms of

strength (total base shear) and ductility displacement (behaviour factor  $q$ ) is drastically reduced during the structural lifetime. The collapse of the structure, which is typically governed by the instability failure of the internal columns, moves towards a material failure of the external columns for a lifetime higher than 45 years. The distribution of the strength and stiffness with the internal and external structural frames is also affected during the structural lifetime.

All these aspects need to be further investigated considering different precast building typologies, including multi-storey buildings. Moreover, further investigations will be oriented to both new designed buildings for a proper lifetime evaluation of the behaviour factor  $q$ , and existing buildings for a correct seismic vulnerability assessment of the structure.

## ACKNOWLEDGEMENTS

This study is supported by Research funds PRIN2005 (prot. 2005082490) from the Italian Ministry of University and Research—Dept. of Structural Engineering, Politecnico di Milano, and by the National Research Project RELUIS “Seismic Assessment and Reduction of the Vulnerability of Reinforced Concrete Buildings” funded by the Department of Civil Protection.

## REFERENCES

- Biondini, F., Bontempi, F., Frangopol, D.M., and Malerba, P.G., (2004). Cellular Automata Approach to Durability Analysis of Concrete Structures in Aggressive Environments. *Journal of Structural Engineering*, ASCE, **130**(11), 1724–1737.
- Biondini, F., Bontempi, F., Frangopol, D.M., and Malerba, P.G., (2006a). Probabilistic Service Life Assessment and Maintenance Planning of Concrete Structures. *Journal of Structural Engineering*, ASCE, **132**(5), 810–825.
- Biondini, F., Frangopol, D.M., and Malerba, P.G., (2006b). Time-variant Performance of the Certosa Cable-stayed Bridge. *Structural Engineering International*, **16**(3), 235–244.
- Biondini, F., and Frangopol, D.M., (2008). Probabilistic Limit Analysis and Lifetime Prediction of Concrete Structures. *Structure and Infrastructure Engineering*. Published online as forthcoming article on January 2007—In print.
- Biondini, F., and Toniolo, G., (2006). Probabilistic Calibration of Behaviour Factor for Concrete Frames, *2nd fib Congress*, Paper 8–28, Naples, June 5–8, 2006.
- Biondini, F., and Toniolo, G., (2008). Probabilistic Calibration and Experimental Verification of the Seismic Design Criteria for Concrete Frames. Submitted for possible publication on *Journal of Earthquake Engineering*.
- Carr, A.J., (2006). RUAUMOKO Program for Inelastic Dynamic Analysis. Department of Civil Engineering, University of Canterbury, Christchurch, New Zealand.
- Fukada, Y., (1969). Study on the Restoring Force Characteristics and Design of Reinforced Concrete Buildings. *Kanto District Symposium*, Architectural Institute of Japan, Tokyo, Japan, No. 40 (In Japanese).
- Paulay, T., and Priestley, M.J.N., (1992). *Seismic Design of Reinforced Concrete and Masonry Buildings*. John Wiley & Sons.
- Palermo, A., Carabellese, A., and Toniolo, G., (2007). Numerical Validation of Pseudo-Dynamic and Quasi-Static Cyclic Tests on Full-Scale Precast Industrial Building Prototypes. *8th Pacific Conference on Earthquake Engineering*, December 5th–7th, 2007, Singapore, pp 8, CD-ROM.

# Life-cycle multi-objective optimization of deteriorating structures

F. Biondini & G. Zani

*Department of Structural Engineering, Politecnico di Milano, Milan, Italy*

**ABSTRACT:** This paper presents a new approach to life-cycle multi-objective optimization of deteriorating structures. The time-variant performance is evaluated with reference to a proper modeling of structural damage. The effects of maintenance interventions are taken into account by relating the cost of maintenance to the actual damage level. A genetic algorithm is used to solve the multi-objective optimization problem. The effectiveness of the proposed approach is demonstrated with a simple benchmark and a final application to the life-cycle optimization of a prestressed box-girder bridge. The results highlight the fundamental role of the time-variant performance and of the maintenance planning in the selection of the Pareto set of optimum design solutions.

## 1 INTRODUCTION

In the classical approach to multi-objective optimum structural design, the objective functions and the design constraints are defined by considering the structural performance at the initial time of construction, when the system is undamaged. However, for structures exposed to damaging environments the structural performance must be considered as time-dependent, mainly because of the progressive deterioration of the materials. For this reason, a consistent approach to optimum design of durable structures should be able to comply with the desired performance not only at the initial time of construction, but also during the overall structural lifetime, by taking into account the effects of the unavoidable sources of mechanical damage and of eventual maintenance and rehabilitation interventions.

To overcome the inconsistencies associated with a damage-free formulation of the optimum design problem, a new approach to the minimum cost design of structural systems with time-variant performance has been proposed in previous works (Azzarello *et al.* 2006, 2007). In the proposed approach, the structural damage is modeled by a proper material degradation law and the structural analysis is carried out at different time instants in order to assess the time evolution of the system performance. The design constraints are related to both the time-variant stress and displacement state, as well as to the amount of structural damage. The objective cost function is formulated by accounting for both the initial cost of the structure and the costs of possible maintenance interventions, that are properly discounted over time and assumed to be proportional to the actual level of structural damage. This procedure has been developed for truss

and framed systems made by homogeneous members (Azzarello *et al.* 2006), as well as for reinforced concrete structures (Azzarello *et al.* 2007).

In this paper, the proposed approach is extended to consider multiple design targets related not only to the life-cycle cost, but also to other life-cycle performance indicators. To this aim, the design problem is formulated in the context of the multi-objective structural optimization and solved by using a genetic algorithm. A simple benchmark related to the life-cycle optimization of a tensioned bar undergoing damage is presented to demonstrate the effectiveness of the proposed approach. The multi-objective optimization procedure is finally applied to the life-cycle design of a prestressed box-girder bridge. The results highlight the important role played by both the time-variant performance and the maintenance plan in the selection of the Pareto set of optimum design solutions.

## 2 MODELING OF STRUCTURAL DAMAGE

With reference to truss and framed systems, damage is considered to affect the cross-sectional area  $A = A(t)$ , the elastic modulus  $E = E(t)$ , and the material strength  $\bar{\sigma} = \bar{\sigma}(t)$  of each structural member:

$$A(t) = [1 - \delta_A(t)]A_0 \quad (1)$$

$$E(t) = [1 - \delta_E(t)]E_0 \quad (2)$$

$$\bar{\sigma}(t) = [1 - \delta_{\bar{\sigma}}(t)]\bar{\sigma}_0 \quad (3)$$

where  $\delta_A, \delta_E, \delta_{\bar{\sigma}}$ , are dimensionless damage indices which provide a direct measure of the damage level within the range [0; 1]. Proper correlation laws can

be introduced to define the corresponding variation of other geometrical properties of the member cross-section, like the inertia moment.

The time evolution of the damage indices  $\delta_A$ ,  $\delta_E$ ,  $\delta_{\bar{\sigma}}$ , depends on the physics of the deterioration process, and it is usually related to the acting stress  $\sigma = \sigma(t)$  (Figure 1a). Therefore, a reliable assessment of the time-variant structural performance requires deterioration models suitable to describe the damage evolution and its interaction with the structural behavior (Biondini *et al.* 2004). However, despite the inherent complexity of the damage laws, very simple degradation models could be successfully adopted to define an effective hierarchical classification of the design alternatives (Biondini and Marchiondelli 2006).

Without any loss of generality, in this study it is assumed that all material properties undergo the same damage process, or  $\delta_A = \delta_E = \delta_{\bar{\sigma}} \equiv \delta$ . Moreover, the damage index  $\delta = \delta(t)$  is correlated to the stress  $\sigma = \sigma(t)$  by assuming the following relationship (Figure 1b):

$$\frac{d\delta(t)}{dt} = \frac{1}{T_{\delta}} \left[ \frac{\sigma(t)}{\bar{\sigma}_0} \right]^{\alpha} \quad \bar{\sigma}_0 = \begin{cases} \bar{\sigma}_0^+ & \text{if } \sigma \geq 0 \\ \bar{\sigma}_0^- & \text{if } \sigma < 0 \end{cases} \quad (4)$$

where  $\alpha \geq 0$  is a suitable constant,  $\bar{\sigma}_0^-$  and  $\bar{\sigma}_0^+$  are the minimum and maximum allowable stress at the initial time  $t = t_0$ , respectively, and  $T_{\delta}$  represents the time period required for a complete damage under a constant stress level  $\sigma(t) = \bar{\sigma}_0$  (Figure 1c). The initial condition  $\delta(t_{cr}) = 0$  with  $t_{cr} = \max\{t | \sigma(t) \leq \sigma_{cr}\}$  is assumed, where  $\sigma_{cr} \leq \bar{\sigma}_0$  is a critical stress threshold.

The index  $\delta = \delta(t)$  fully describes the damage evolution in each point of the structure. However, due to its *local* nature, it does not seem handy for design purposes. A more synthetic *global* measure of damage may be computed as the weighted average of  $\delta$  over the volume  $V$  of the structure (Biondini 2004). For a structural system composed by  $p$  members, a global damage index can be defined as follows:

$$\hat{\delta}(t) = \sum_{i=1}^p \hat{\delta}_i(t) = \sum_{i=1}^p \int_{V_i} w_i \delta_i(t) dV \quad (5)$$

where  $w_i$  are weight functions with  $\sum_{i=1}^p \int_{V_i} w_i dV = 1$ .

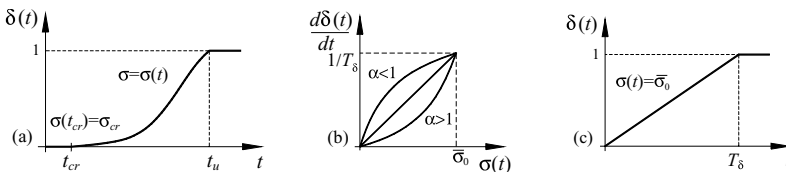


Figure 1. Modeling of structural damage. (a) Time evolution of the damage index  $\delta = \delta(t)$ . (b) Linear relationship between the rate of damage and the stress level  $\sigma = \sigma(t)$ . (c) Meaning of the damage parameter  $T_{\delta}$ .

### 3 LIFE-CYCLE COST OPTIMALITY

#### 3.1 Life-cycle structural cost

The total cost  $C$  of the structure over its life-cycle is given by the sum of the initial cost  $C_0$  and the maintenance cost  $C_m$ :

$$C = C_0 + C_m \quad (6)$$

The initial cost  $C_0$  is computed as follows:

$$C_0 = cV_0 \quad (7)$$

where  $V_0$  is the total volume of the material and  $c$  is the corresponding unit cost. For reinforced or prestressed concrete structures the cost of both materials, concrete and steel, are considered:

$$C_0 = c_c V_{c,0} + c_s V_{s,0} = c_c (V_{c,0} + c V_{s,0}) = c_c V_{c,0}^* \quad (8)$$

where  $V_{0,c}$ ,  $V_{0,s}$ , are the total volumes of concrete and steel, respectively,  $c_c$ ,  $c_s$ , are the corresponding unit costs,  $c = c_s/c_c$  is the unit cost ratio, and  $V_{c,0}^*$  is the equivalent volume of concrete.

The maintenance cost  $C_m$  can be evaluated by summing the costs of the individual interventions:

$$C_m = \sum_{k=1}^r \frac{C_m^k}{(1+v)^{(t_k-t_0)}} \quad (9)$$

where the cost  $C_m^k$  of each intervention  $k = 1, \dots, r$  is referred to the initial time  $t_0$  by taking a discount rate  $v$  into account (Kong and Frangopol 2003).

#### 3.2 Maintenance scenario

The previous general formulation is now specialized to a prescribed maintenance scenario. In this scenario an essential maintenance aimed to totally restore the initial structural performance is performed after each design period  $T_D$ , or at each time instant  $t_k = (t_0 + kT_D)$ . In this way, all the interventions have the same cost  $C_m^k = C_m^1$ , and the number of interventions applied during a prescribed service lifetime  $T_S$  is  $r = \text{int}(T_S/T_D)$  if  $\text{mod}(T_S/T_D) > 0$ , or  $r = [\text{int}(T_S/T_D) - 1]$  if  $\text{mod}(T_S/T_D) = 0$ . Therefore,

the cost of maintenance is:

$$C_m = C_m^1 \sum_{k=1}^r \frac{1}{(1+v)^{kT_D}} = C_m^1 q \quad (10)$$

where the factor  $q = q(T_S, T_D, v) \leq r$  depends on the prescribed parameters  $T_S$ ,  $T_D$ , and  $v$  only.

The cost  $C_m^1$  of the single intervention is related to the level of damage developed during each design period  $T_D$ . Since damage is not recovered over time, a measure of this damage is given by the global damage index evaluated at the end of each period  $T_D$ , or:

$$\tilde{\delta} = \hat{\delta}(t_k) = \hat{\delta}(t_{k-1} + T_D), \quad k = 1, \dots, r \quad (11)$$

Based on the life-cycle global damage index  $\tilde{\delta}$ , the following linear relationship is assumed:

$$C_m^1 = C_0(\beta + \tilde{\delta}) \quad (12)$$

where  $\beta$  is a coefficient which takes the fixed cost of each intervention into account. In this way, the total life-cycle cost  $C$  is finally formulated as follows:

$$C = C_0[1 + (\beta + \tilde{\delta})q] \quad (13)$$

### 3.3 The role of maintenance cost

To highlight the actual role played by a prescribed maintenance program, the design of the tensioned bar shown at the top of Figure 2 is investigated. By denoting with  $d_0$  the diameter of the undamaged cross-section and by assuming  $\beta = 0$ , the total cost of the bar over the prescribed service lifetime  $T_S$  is:

$$C = C_0(1 + \tilde{\delta}q) = cA_0L(1 + \tilde{\delta}q) = c \frac{\pi d_0^2 L}{4} (1 + \tilde{\delta}q) \quad (14)$$

with  $\tilde{\delta} = \tilde{\delta}(d_0)$ . The diameter  $d_0$  must be chosen in such a way that the acting stress  $\sigma = \sigma(t)$  is no larger than the allowable stress  $\bar{\sigma} = \bar{\sigma}(t)$  over the prescribed design period  $T_D$ :

$$\sigma(t) = \frac{F}{A(t)} = \frac{4F}{\pi d_0^2 [1 - \delta(t)]} \leq \bar{\sigma}(t) = \bar{\sigma}_0 [1 - \delta(t)] \quad (15)$$

with  $\delta(t) = \delta(d_0, t)$ . Without damage ( $\delta = \tilde{\delta} = 0$ ), the minimum cost solution  $d_0^*$  is given by the minimum diameter  $d_0$  which satisfies the stress constraint:

$$d_0^* = d_{0,\min} = \sqrt{\frac{4F}{\pi \bar{\sigma}_0}} \quad (16)$$

On the contrary, when damage is included, the minimum cost solution  $d_0^*$  is, in general, no longer associated with the diameter  $d_{0,\min}$ . In fact, higher

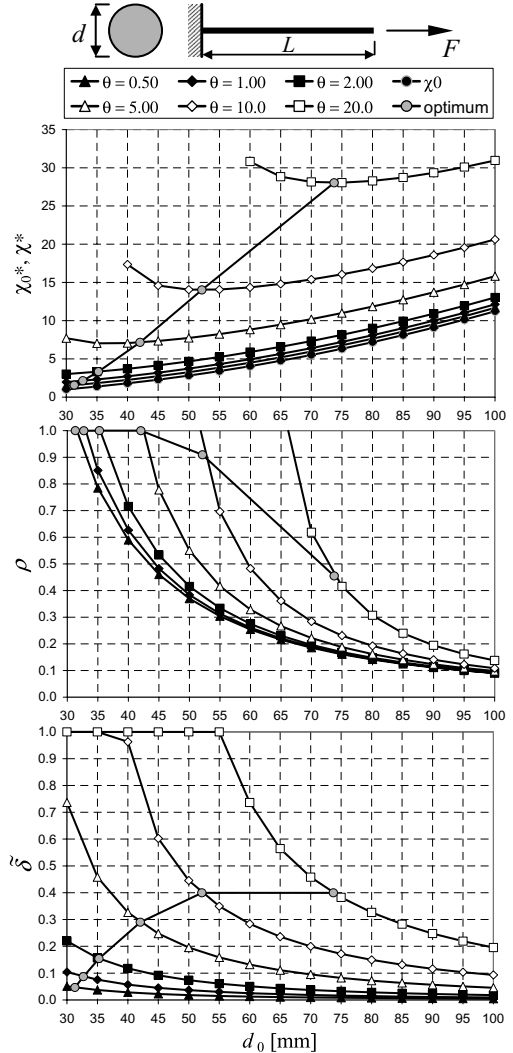


Figure 2. Initial cost  $\chi_0^*$ , life-cycle cost  $\chi^*$ , stress ratio  $\rho$ , and global damage  $\tilde{\delta}$  for a tensioned bar undergoing damage.

$d_0^*$ -values may be required to achieve a balance between the maintenance cost and the amount of damage.

These aspects are highlighted in Figure 2, where both the cost and structural efficiency of the bar versus its diameter  $d_0$  are shown for different damage rates  $\theta = T_S/T_\delta$ , with  $t_0 = 0$ ,  $\sigma_{cr} = 0$ ,  $\alpha = 1$ , and with reference to the following case study:  $F = 70$  kN,  $\bar{\sigma}_0 = 100$  MPa,  $T_S = 100$  years,  $T_D = 10$  years, and  $v = 0$  ( $q = r$ ). The diagrams in Figure 2 refer to the following quantities:

$$\chi^* = \chi_0^* + \chi_m^* \quad \chi_0^* = C_0/C^* \quad \chi_m^* = C_m/C^* \quad (17)$$

$$\rho = \sigma(T_D)/\bar{\sigma}(T_D) \quad \bar{\delta} = \hat{\delta}(T_D) \quad (18)$$

where  $C^* = C(d_{0,\min}) = cFL/\bar{\sigma}_0$  denotes the optimal cost for  $\theta = 0$ . The following remarks can be made:

- The minimum feasible diameter without damage is  $d_{0,\min} = 29.9$  mm. Its value increases with  $\theta$ .
- The initial cost  $\chi_0^*$  increases and the maintenance cost  $\chi_m^*$  decreases when  $d_0$  increases. For a given  $d_0$ , the maintenance cost  $\chi_m^*$  increases with  $\theta$ .
- The total cost  $\chi^*$  has a minimum for  $d_0^* \geq d_{0,\min}$ , and the optimal diameter  $d_0^*$  increases with  $\theta$ .
- The stress ratio  $\rho$  decreases with  $d_0$  and increases with  $\theta$ . The optimal solution  $d_0^*$  at the end of the design period  $T_D$  may be not fully stressed ( $\rho^* \leq 1$ ).
- The damage index  $\bar{\delta}$  decreases with  $d_0$  and increases with  $\theta$ . For the optimal solution, such quantity tends to saturate for the higher  $\theta$ -values.

Similar results are obtained by varying  $T_D$ .

## 4 LIFE-CYCLE STRUCTURAL OPTIMIZATION

### 4.1 Multi-objective optimization problem

The purpose of a life-cycle multi-objective design process is to find a vector of design variables  $\mathbf{x} = [x_1 \ x_2 \ \dots]^T$  which optimizes the value of a set of objective functions  $\mathbf{f}(\mathbf{x}) = [f_1(\mathbf{x}) \ f_2(\mathbf{x}) \ \dots]^T$ , according to both side constraints with bounds  $\mathbf{x}^-$  and  $\mathbf{x}^+$ , and inequality time-variant behavioral constraints  $\mathbf{g}(\mathbf{x}, t) \leq 0$ :

$$\min_{\mathbf{x} \in D} \mathbf{f}(\mathbf{x}) \quad D = \{ \mathbf{x} | \mathbf{x}^- \leq \mathbf{x} \leq \mathbf{x}^+, \mathbf{g}(\mathbf{x}, t) \leq 0 \} \quad (19)$$

The time-variant behavioral constraints are related to the structural response in terms of stress  $\sigma_{i,\ell} = \sigma_{i,\ell}(t)$  and displacement  $u_{j,\ell} = u_{j,\ell}(t)$  in each element  $i$  is nodal point  $j$ , and loading condition  $\ell$ , as follows:

$$\begin{cases} \bar{\sigma}_{i,\ell}^-(\mathbf{x}, t) \leq \sigma_{i,\ell}(\mathbf{x}, t) \leq \bar{\sigma}_{i,\ell}^+(\mathbf{x}, t) \\ \bar{u}_{j,\ell}^- \leq u_{j,\ell}(\mathbf{x}, t) \leq \bar{u}_{j,\ell}^+ \end{cases} \quad (20)$$

where  $\bar{\sigma}_{i,\ell}^- = \bar{\sigma}_{i,\ell}^-(t)$  and  $\bar{\sigma}_{i,\ell}^+ = \bar{\sigma}_{i,\ell}^+(t)$  are allowable stress values,  $\bar{u}_{j,\ell}^-$  and  $\bar{u}_{j,\ell}^+$  are prescribed displacement bounds. Constraints on structural stability, as well as on both local and global damage, can also be considered (Azzarello *et al.* 2006). In this study, the Pareto set of optimum design solutions is found by using a genetic algorithm properly formulated to effectively solve multi-objective optimization problems (Deb 2001, Biondini and Riboldi 2006).

### 4.2 Life-cycle optimization of a tensioned bar

The life-cycle design of the tensioned bar shown in Figure 2 is carried out by considering two objective functions to be minimized: the life-cycle cost

$C$  and the maximum displacement  $u_{\max} = \max u(t)$ . The displacement  $u(t) = FL/[EA(t)]$  is computed by assuming  $F = 70$  kN,  $E = 210$  GPa, and  $L = 5$  m. The design variables are the diameter  $d_0$  of the undamaged cross-section and the design period  $T_D \leq T_S$ , with  $T_S = 100$  years. A time-variant stress constraint with material strength  $\bar{\sigma}_0 = 100$  MPa is considered. The life-cycle optimization problem is solved by assuming  $\theta = 20$ ,  $\beta = 0.01$ , and  $\nu = 0$ . Figure 3 makes a comparison between the target solution of the optimization problem and the numerical results obtained by using a genetic algorithm. The following remarks can be made:

- A good agreement between the target solution and the numerical results is obtained for the Pareto set, the optimal diameter  $d_0$ , and the stress ratio  $\rho$ . For the optimal design period  $T_D$  and the global damage  $\bar{\delta}$  a deviation from the target solution is observed. This is due to the discretization adopted for  $d_0$ .
- The optimal values of the design variables  $d_0$  and  $T_D$  increase as the life-cycle cost  $C$  increases.
- The optimal values of the design period  $T_D$  are properly selected in such a way that the ratio  $T_S/T_D$  assumes only integer values, or  $\text{mod}(T_S/T_D) = 0$ .
- The minimum cost solution is fully stressed and it is characterized by an optimal design period  $T_D = 1$  year. However, the other Pareto optimum solutions are not fully stressed and the stress ratio  $\rho$  significantly decreases as the life-cycle cost  $C$  increases.
- The global damage  $\bar{\delta}$  tends to decrease as the life-cycle cost  $C$  increases, with abrupt variations when the optimal design period  $T_D$  changes.

Finally, Figure 4 shows the Pareto curves obtained for different values of the damage rate  $\theta$ , fixed maintenance cost  $\beta$ , and discount rate  $\nu$ . It is noted that the life-cycle cost  $C$  increases when the damage rate  $\theta$  and the fixed maintenance cost  $\beta$  increase. This tendency is reduced by the discount rate  $\nu$ .

### 4.3 Life-cycle optimization of a prestressed bridge

The proposed formulation is applied to the life-cycle optimization of the prestressed box girder bridge shown in Figure 5. The following data are assumed:  $L = 40$  m,  $b = 13$  m,  $b_0 = 7$  m,  $b_{\text{web}} = 0.75(h_{\text{bot}} + h_{\text{top}})$ . The bridge is subjected to a set of applied loads: a dead load  $g = \gamma A_c + 25$  kN/m, where  $\gamma = 25$  kN/m<sup>3</sup> is the weight density and  $A_c$  is the area of the box cross-section; the live loads  $q_1 = q_2 = 75$  kN/m; the prestressing loads  $P = \sigma_{p0} A_s$  and  $p = P\kappa$ , where  $P$  is the prestressing force,  $\sigma_{p0} = 1000$  MPa is the initial prestressing,  $A_s$  is the area of prestressing steel, and  $\kappa$  is the geometric curvature of the prestressing cable. The cable eccentricity



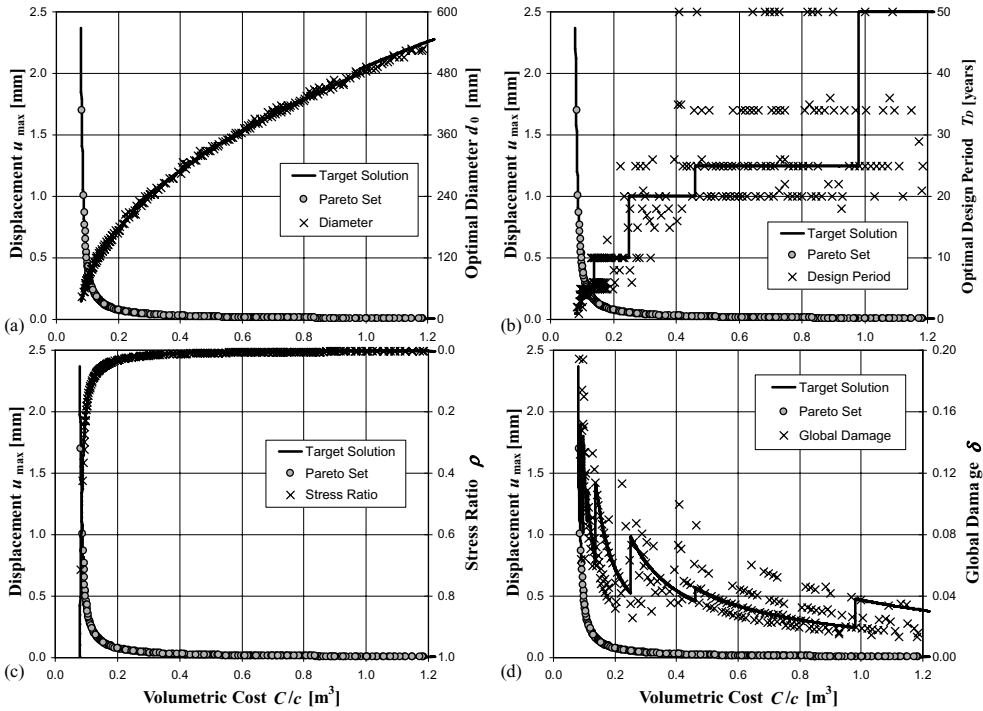


Figure 3. Tensioned bar undergoing damage. Pareto set of the optimum design solutions (life-cycle cost  $C$  versus maximum displacement  $u_{\max}$ ) compared with (a) optimal diameter  $d_0$ , (b) optimal design period  $T_D$ , (c) stress ratio  $\rho$ , and (d) life-cycle global damage  $\delta$  (damage rate  $\theta = 20$ , fixed cost of maintenance interventions  $\beta = 0.01$ , discount rate  $\nu = 0$ ).

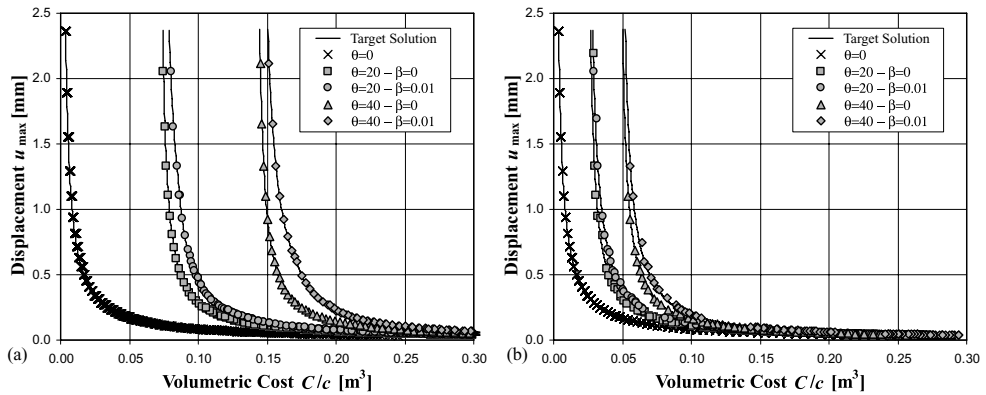


Figure 4. Tensioned bar undergoing damage. Pareto sets of the optimum design solutions (life-cycle cost  $C$  versus maximum displacement  $u_{\max}$ ) for different values of the damage rate  $\theta$  and of the fixed cost of maintenance interventions  $\beta$ : (a)  $\nu = 0$ , and (b)  $\nu = 0.03$ .

$e$  is parabolic, with  $e = 0$  at the ends,  $e = e_1$  at the middle of each span, and  $e = e_2 = 0.95 h - h_G$  at the middle support. Three load conditions are considered for the live loads: (1)  $q_1 = q_2 = 0$ ; (2)  $q_1 = q_2 = 75 \text{ kN/m}$ ; (3)  $q_1 = 0$  and  $q_2 = 75 \text{ kN/m}$ .

The damage and maintenance scenarios are defined by assuming  $\theta = 0.5$ ,  $\sigma_{cr} = 0$ ,  $\alpha = 1$ ,  $T_S = 100$  years,  $T_D = 5$  years,  $\beta = 0.05$ , and  $\nu = 0$  ( $q = r$ ). The bridge is subdivided in 16 elements and the time evolution of the damage index  $\delta$  is computed with reference

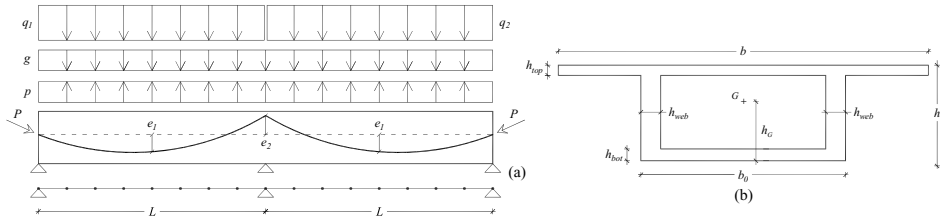


Figure 5. Box girder bridge undergoing damage. (a) Structural scheme and loading conditions. (b) Geometry of the box cross-section.

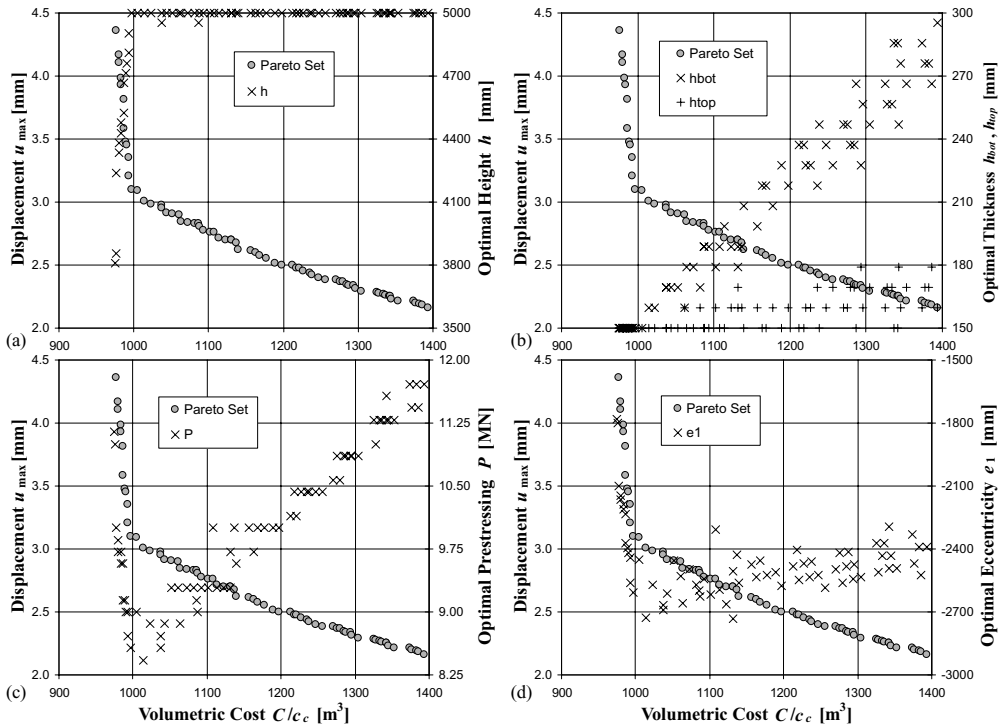


Figure 6. Box girder bridge undergoing damage. Pareto set of the optimum design solutions (life-cycle cost  $C$  versus maximum deflection  $u_{\max}$ ) compared with the optimal values of the design variables: (a) deck height  $h$ , (b) slab thickness  $h_{\text{bot}}$  and  $h_{\text{top}}$ , (c) prestressing force  $P$ , and (d) cable eccentricity  $e_1$  at middle span (damage rate  $\theta=0.5$ , fixed cost of maintenance interventions  $\beta=0.05$ , discount rate  $\nu=0$ ).

to the maximum stress in each segment. Based on a prescribed damage pattern, the inertia moment of the damaged cross-section is computed with a damage index  $\delta' = \delta(2 - \delta)$ .

The objective functions to be minimized are the life-cycle cost  $C$  and the maximum deflection  $u_{\max}$  at middle span over the service life  $T_S$ . The life-cycle cost  $C$  is computed by assuming a unit cost ratio of concrete

and steel  $c = c_s/c_c = 100$ . The displacements are evaluated with  $E = 34$  GPa.

The following design variables and side constraints are assumed: height of the box section  $2 \text{ m} \leq h \leq 5 \text{ m}$ ; thickness of top and bottom slabs  $0.15 \text{ m} \leq h_{\text{top}} \leq 0.45 \text{ m}$  and  $0.15 \text{ m} \leq h_{\text{bot}} \leq 0.45 \text{ m}$ , respectively; prestressing force  $7 \text{ MN} \leq P \leq 16 \text{ MN}$ ; eccentricity  $0 \leq h_G + e_1 \leq h$ .

The time-variant stress constraints are applied, for each loading condition, in each segment of the box girder with reference to the initial allowable stresses  $\bar{\sigma}_0^- = -10$  MPa and  $\bar{\sigma}_0^+ = 0$ . Moreover, the displacement constraint  $u_{1max} \geq 0$  on the maximum deflection at middle span under the load condition (1) is applied. Finally, the constraints  $0.5 \leq h_{top}/h_{bot} \leq 2$ ,  $A_s/A_c \leq 0.05$ , and  $50 \text{ mm} \leq (h_G + e) \leq (h - 50 \text{ mm})$  are considered.

Figure 6 shows the results of the optimization process. It can be noted that the upper side constraint on the height  $h$  subdivides the Pareto set into two parts. This transition strongly influences the relationship between the life-cycle cost  $C$  and the variables  $P$  and  $e_1$ .

## 5 CONCLUSIONS

A new approach to the life-cycle multi-objective optimization of deteriorating structures under multiple loading conditions has been presented. This approach allowed to overcome the inconsistencies associated with a damage-free formulation of the optimum design problem. In fact, in the proposed formulation, the structural damage is accounted for by means of a material degradation law of the mechanical properties, and the design constraints of the optimization problem are related to the corresponding time-variant performance over the expected structural lifetime. Moreover, the life-cycle cost is evaluated by considering both the initial cost of the structure and the costs of possible maintenance interventions, that are properly discounted over time and assumed to be proportional to the actual level of structural damage.

The proposed approach has been applied to a simple benchmark related to a tensioned bar undergoing damage, and to the life-cycle optimization of a prestressed box-girder bridge under multiple loading conditions. The results proved the effectiveness of the proposed approach by highlighting that the Pareto set of optimum design solutions strongly depends on both the time-variant structural performance and the maintenance planning.

## ACKNOWLEDGEMENTS

This study is supported by research funds PRIN2005 (prot. 2005082490) from the Italian Ministry of University and Research, Department of Structural Engineering, Politecnico di Milano.

## REFERENCES

- Azzarello, L., Biondini, F., Marchiondelli, A., 2006. Optimal Design of Deteriorating Structural Systems. *3rd International Conference on Bridge Maintenance, Safety and Management (IABMAS'06)*, Porto, July, 16–19.
- Azzarello, L., Biondini, F., Marchiondelli, A., 2007. Lifetime Optimization of Reinforced Concrete Structures in Aggressive Environments, *Life-Cycle Cost and Performance of Civil Infrastructure Systems*, H.N. Cho, D.M. Frangopol, A.H.-S. Ang (Eds), Taylor & Francis, pp. 93–102.
- Biondini, F., 2004. A Three-Dimensional Finite Beam Element for Multiscale Damage Measure and Seismic Analysis of Concrete Structures. *13th World Conf. on Earthquake Engineering*, Vancouver, B.C., Canada, August 1–6, Paper 2963.
- Biondini, F., Bontempi, F., Frangopol, D.M., and Malerba, P.G., 2004. Cellular Automata Approach to Durability Analysis of Concrete Structures in Aggressive Environments. *Journal of Structural Engineering*, ASCE, **130**(11), 1724–1737.
- Biondini, F., Marchiondelli, A., 2006. Evolutionary Design of Structural Systems with Time-variant Performance. *Structure and Infrastructure Engineering*, **4**(2), 163–176, Special Issue, F. Biondini (Ed.), Taylor & Francis Publisher.
- Biondini F., Riboldi E., 2006. Multi-Objective Structural Optimization using Genetic Algorithms, *16th CTE Congress*, Parma, November 9–11 (In Italian).
- Deb, K., 2001. *Multi-Objective Optimization using Evolutionary Algorithms*, John Wiley & Sons.
- Kong, J.S., Frangopol, D.M., 2003. Evaluation of Expected Life-Cycle Maintenance Cost of Deteriorating Structures. *Journal of Structural Engineering*, ASCE, **129**(5), 682–691.

# Fatigue design of precast structural concrete plates for access floors

Marco Breccolotti, Annibale L. Materazzi & I. Venanzi

*Department of Civil and Environmental Engineering, University of Perugia, Italy*

**ABSTRACT:** In the present paper are presented the investigations carried out to evaluate the fatigue resistance of RC panels used as access floors for office, commercial and warehouse spaces. The comparison between the results of numerical models and experimental tests allowed to tune a numerical model to predict the fatigue life of the precast structural concrete panels for different values of the external loads.

## 1 INTRODUCTION

The access floors represent a fast, economic and flexible way to cover great surfaces for offices, commercial activity and warehouses. They are built with modular square plates of reduced size (usually  $50 \times 50$  and  $60 \times 60$  cm in plan), made with structural concrete. Their weight and thickness are carefully calibrated through stringent in-factory quality controls to reduce the cost of transport and setting in place. Nevertheless the attempt of reducing the self-weight makes these elements more sensitive to static and dynamic loads. Moreover during their service lives the plates are exposed to moving loads that induce the risk of fatigue failure. In fact, the duration of fatigue life represents one of the major concerns in the design of the plates. Some standards, such as the *Recommended test procedures for access floors* issued in the U.S. by C.I.S.C.A. (Ceiling & Interior System Construction Association) (CISCA 2004), point out the minimum acceptable resistance to moving loads of these products and specify the way to verify this resistance. While the static load bearing capacity can be easily predicted, assessed and even improved, the fatigue resistance evaluation needs more accurate and complicate considerations requiring a design phase that may include both numerical simulations and experimental verifications.

The work presented in this paper is the continuation of a previous study by the Authors (Breccolotti et al. 2006) and regards the investigation on a different type of concrete panel for access floors. After the review of the current knowledge about fatigue resistance of RC elements, the experimental tests carried out to evaluate the performance of the panels are described, paying particular attention to the testing machine used for the rolling load tests. Numerical simulations have been performed to estimate the fatigue endurance of the concrete access floors.

## 2 FATIGUE STRENGTH OF REINFORCED CONCRETE

Fatigue resistance of plain and reinforced concrete has been studied for many years in the past (Nordby 1958; Hsu 1981; Cannon et al. 1992; RILEM 1984), establishing a well defined level of knowledge, especially for structures like buildings and bridges.

As it regards low carbon steel rebars for reinforced concrete, the S-N lines that describe the relation between the stress cycle amplitude and the corresponding number of cycles to the failure are composed by a decreasing branch, with an horizontal asymptote at a constant  $\Delta\sigma$  value, that represents the stress level that can be sustained by the material for a boundless duration (fatigue limit). If fatigue damage builds up in an aggressive environment, the corrosion induced damage interacts with the fatigue damage (corrosion fatigue) reducing the material resistance and the fatigue limit disappears.

The existence of a fatigue limit in the case of plain concrete elements is still a matter of scientific debate. The more recent experimental tests have not allowed to detect such limit yet, at least below 20 million cycles, even if theoretical considerations, based on the methods of Fracture Mechanics, lead to believe that it should exist maybe at 30–40% of the static strength.

From the point of view of the structural safety it appears prudent to use for the concrete S-N curves without fatigue limits, as done, for instance, by international standards such as the Model Code 1990 issued by CEB and FIP (CEB-FIP 1990). More recent standards, such as the Eurocode 2 (CEN 2004), do not provide satisfactory information to allow a comprehensive understanding of experimental tests.

More recently, the attention has been focused also on the fatigue performance of fiber reinforced concrete (Li and Matsumoto 1998; Naaman and Hamoud 1998; Zhang et al. 2001; Cachim et al. 2002;

Lee and Barr 2004) and on the fatigue behaviour to 2D and 3D stresses (Subramaniam and Shah 2003; Alliche 2004). While steel fibers reinforced concrete elements exhibit flexural or tensile strength higher than normal reinforced concrete, contradictory opinions exist about the use of fibers to increase the fatigue strength. Two opposite effects can in fact be introduced using fibers in reinforced concrete from the fatigue resistance point of view. By one side their addition can limit the microcracks' amplitude and can retard their growth, while on the other side it increases the pore and the initial microcrack density, causing a decrease in concrete strength. Finally the buckling of the thin steel fibers can occur.

### 3 REINFORCED CONCRETE PANELS FOR ACCESS FLOORS

The reinforced concrete panels for access floors analyzed in the present paper are depicted in the Figure 1. They are produced casting concrete into plastic moulds and mechanically smoothing the elements after concrete hardening to respect the required tolerances. The dimensions of the panels are 500 by 500 mm with a maximum thickness of 36 mm. The reinforcing bars are placed in the lower part of the panels. The external rebars are 8 mm in diameter while the central ones have 6 mm diameter. In the upper part of the panel is placed a fine 2 mm diameter steel mesh with 25 mm spacing. The concrete used for the panels has a cylindrical characteristic strength ( $f_{ck}$ ) at 28 days of 50 MPa. It is made up following the mix design listed in Table 1. As can

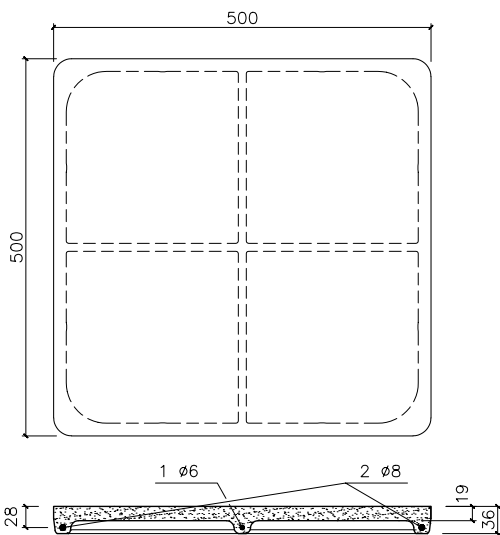


Figure 1. Plan view and section of the RC panels.

Table 1. RC panels admixtures.

Material	Quantity
Cement CEM I 52.5 R	450 kg/m <sup>3</sup>
Water (W/C = 0.44)	198 kg/m <sup>3</sup>
Fine Sand (0–4 mm)	706 kg/m <sup>3</sup>
Sand (0–6 mm)	1061 kg/m <sup>3</sup>
Hyperplasticiser	5.35 kg/m <sup>3</sup>

be seen, this type of concrete is different from the conventional one for the absence of coarse aggregates.

### 4 NUMERICAL SIMULATIONS OF THE ROLLING LOAD TESTS

#### 4.1 Modelling of the structural response

To correctly organize the experimental tests, a finite element model has been set up to estimate the stress in the rebars and in the concrete of the access floor panels. The use of a numerical models is mandatory in consequence of the difficulty of quantify the stress levels coming from experimental tests. In fact, due to the small dimensions of the concrete samples and to the large dimensions of the strain gauges suitable for concrete, the direct measurement of the strain will most likely possess poor accuracy.

Once the numerical model has been constructed and the experiment tests executed, the tuning of the FE model, through the comparison of its results with those observed from the tests, could allow to predict the behaviour of concrete panels for different design parameters such as concrete compressive strength and position and amount of steel rebars.

The finite element model is composed of 256 shells that represent the flat part of the panel and 96 beam elements to model the ribs along the edges and the mid sections of the panel, for a total number of nodes equal to 289 (see Figures 2 and 3). The presence of the reinforcing rebars has been neglected in the FE model while the concrete has been considered uncracked, as it is usually done for RC elements. The external load has been modelled in the time domain defining triangular time history functions applied to all the nodes between node no. 137 and node no. 153 with different arrival times.

#### 4.2 Analytical evaluation of the fatigue life

The fatigue resistance of the RC panels has been estimated using the provision of the Model Code 90. Nevertheless it has to be emphasized that this standard has been prepared for RC elements with dimensions several times bigger than those of the access floor panels, thus producing inaccuracy in the evaluation

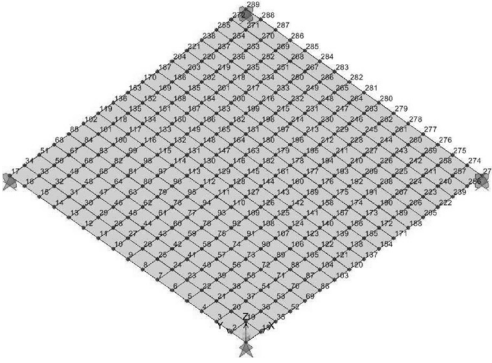


Figure 2. Finite element model—joints numbering.

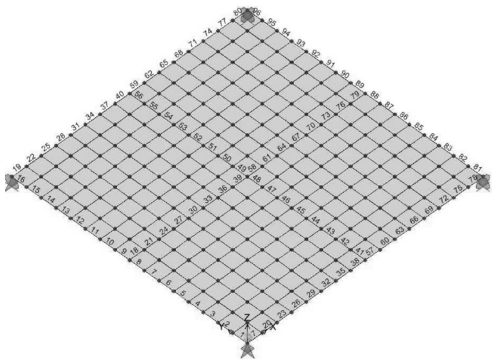


Figure 3. Finite element model—frames numbering.

of fatigue resistance of small RC components. Fatigue endurance has been evaluated for the beam element no. 38 that is the most stressed one according to the numerical analyses. It will be later seen that it is in fact located at the place where the collapse occurred during the experimental tests.

Several types of fatigue failure can happen in RC elements. As indicated by the numerical analysis and confirmed by the experimental tests, the steel rebars are not responsible for the fatigue collapse of the slabs, resulting almost undamaged at the end of the tests. The collapse has thus to be ascribed to the deterioration of the concrete properties.

The Model Code 90 gives three different S-N laws:

- i. for concrete in pure compression;
- ii. for compression-tension concrete;
- iii. for concrete in pure tension or tension-compression.

Again the numerical analysis suggested that the failure of the panel should be ascribed to the fatigue crushing of the concrete placed in the upper part of

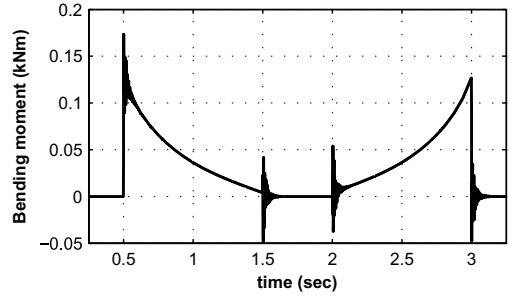


Figure 4. Example of time histories of bending moments.

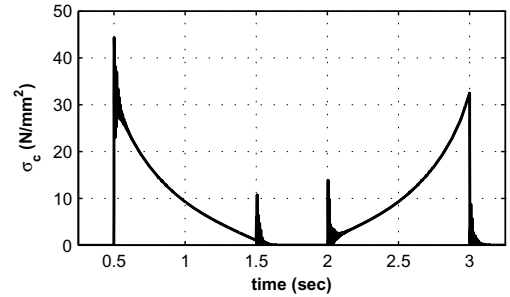


Figure 5. Example of time histories of concrete stresses.

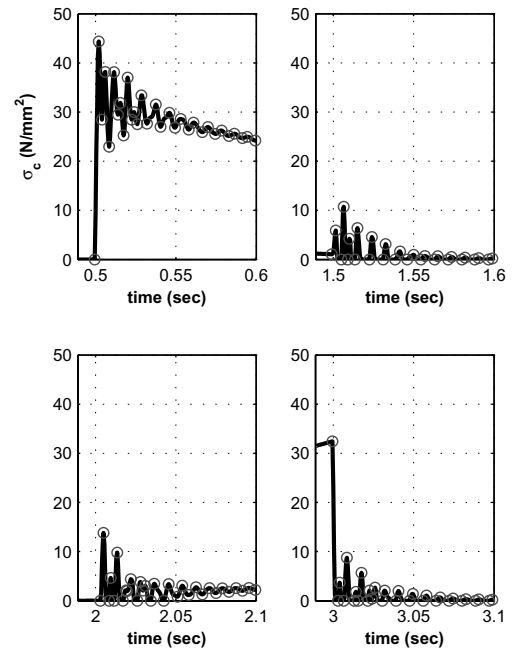


Figure 6. Examples of turning points extraction.

the panel. Assuming that the concrete in tension is cracked, the time history of the compressive stress has been calculated using the hypotheses of linearity between strains and stresses and linear strain variation across the sections. The homogenization technique was applied considering the actual ratio between the elastic modulus of concrete and steel. The computed time histories of the bending moment and of the concrete compressive stress are reported in the Figures 4 and 5, respectively. Then, the turning points have been extracted from the stresses time history, as depicted in the Figure 6, where the most important time intervals have been emphasized. Applying the rain-flow method (Matsuishi and Endo 1968) to this sequence of turning points, the stress cycles characterized by different amplitudes have been obtained and counted. The Palmgren-Miner rule was used to compute the accumulated fatigue damage. The S-N laws given by the Model Code 90 for the case of concrete in pure compression, reported in the Equations from 1 to 8, were used:

$$\log N_1 = (12 + 16S_{c,\min} + 8S_{c,\min}^2)(1 - S_{c,\max}) \quad (1)$$

$$\log N_2 = 0.2 \log N_1 (\log N_1 - 1) \quad (2)$$

$$\log N_3 = \log N_2 (0.3 - 0.375S_{c,\min}) / (\Delta S_c) \quad (3)$$

$$S_{c,\max} = |\sigma_{c,\max}| / f_{ck,fat} \quad (4)$$

$$S_{c,\min} = |\sigma_{c,\min}| / f_{ck,fat} \quad (5)$$

$$\Delta S_c = |\sigma_{c,\max}| - |\sigma_{c,\min}| \quad (6)$$

$$f_{ck,fat} = \beta_{cc}(t) \cdot \beta_{c,sus}(t, t_0) \cdot f_{ck} \times \left( 1 - \frac{f_{ck}}{25f_{ck0}} \right) \quad (7)$$

$$\beta_{cc}(t) = \exp \left\{ s \left[ 1 - \sqrt{\frac{28}{t/t_1}} \right] \right\} \quad (8)$$

where  $N$  is the number of cycles,  $\sigma_{c,\max}$  and  $\sigma_{c,\min}$  are the maximum and minimum stress in the concrete,  $\beta_{c,sus}$  is equal to 0.85,  $f_{ck}$  and  $f_{ck0}$  are equal to 50 and 10 MPa and  $t$  and  $t_1$  are equal to 28 and 1 days, respectively. In the Equation 1 if  $\log N_1 \leq 6$  than  $N = N_1$ ; if  $\log N_1 > 6$  and  $\Delta S_c > 0.3 - 0.375S_{c,\min}$ , than  $N = N_2$ ; if  $\log N_1 > 6$  and  $\Delta S_c < 0.3 - 0.375S_{c,\min}$ , than  $N = N_3$ . The results of the numerical simulations are summed up in the Table 2.

Table 2. Results of the numerical simulations.

Passages	2500 N	2750 N	3000 N
Theoretical value	13980	11162	10531

## 5 ROLLING LOAD TESTS

### 5.1 Programme of the experimental tests

As regards the experimental part, a dedicated testing machine complying with the requirements of the previously mentioned standard was designed and built. Then a statistically significant number of plates has been tested to failure.

According to the tests procedure described in the CISCA standard, the fatigue tests have been carried out applying a rolling load over three panels until failure. Three different values of the rolling load, 2500 N, 2750 N and 3000 N, have been used to estimate the relationship between the intensity of the load and the number of cycles to failure. For a satisfactory test the panel should sustain at least 10,000 passages of the moving load.

### 5.2 The experimental set-up

The machine used for the experimental tests is shown in the Figure 7. It is composed of a rigid steel frame, 3 m long and 1 m wide, that can accommodate up to five concrete panels mounted on suitable steel legs. A basket containing several removable steel plates (see Figure 8), that makes possible to change the value of the applied load, is supported by a hard rubber wheel with 12" diameter and 2" width. A low-friction driving system moves the basket along the major dimension of the frame. Two linear guides connected to an electric engine commanded by a control panel drive the basket along the support structure. The control panel,

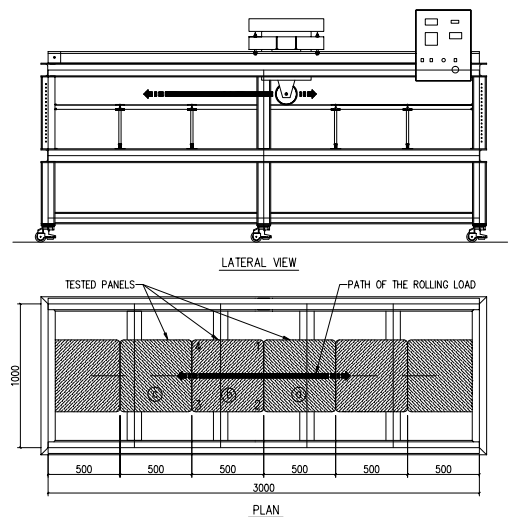


Figure 7. Plan view and lateral view of the experimental set-up.

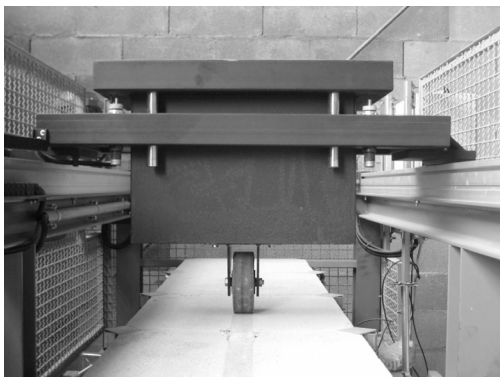


Figure 8. Experimental set-up.

Table 3. Summary of experimental results.

Test	2500 N	2750 N	3000 N
1st	11874	7110	1826
2nd	17275	10395	594
3rd	13122	8210	749
mean	14090	8572	1056
st.dev.	2827	1672	671

composed by a programmable inverter, a LVDT and a counter allows a complete control of the path of the moveable mass and the interruption of the test when the panel starts to fail. A load cell connected to the control panel can be used to measure the weight of the moveable mass. In the tests described in this paper the path of the wheel that applies the load passes through the mid axis of the panel, as depicted in the Figure 7.

### 5.3 Results of the experimental tests

The results of the experimental tests are summed up in the Table 3. As usual in the case of fatigue tests the results show a considerable scatter, probably caused by the many variables involved (global and local concrete properties, bond between concrete and steel, position of the reinforcing rebars, presence and location of defects, etc.), but provide in any case a reference for the evaluation of the fatigue life of the RC panels.

## 6 COMMENTS ON THE OBTAINED RESULTS

The hypothesis of the fatigue concrete crushing and the absence on fatigue collapse of the reinforcing bars found justification in the type of failure occurred during the experimental tests (see Figure 9). The comparison between the numerical simulations and the



Figure 9. Example of panel collapse.

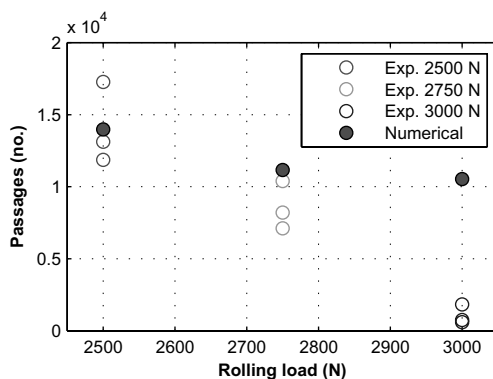


Figure 10. Comparison between numerical and experimental results.

experimental tests showed a good agreement especially for the lower levels of the external loads. On the contrary, for the higher values of the rolling load, the failure during the experimental tests occurred well before the predicted values (see Figure 10).

## 7 CONCLUSIONS

In the present paper the analytical and experimental work carried out to evaluate the fatigue behaviour of reinforced concrete panels used for access floors is reported. The experimental tests, executed following the indications of the CISCA recommendations, highlighted a fast decrease of the fatigue resistance for rolling loads above 2.5 kN. Numerical simulations, carried out along with the experimental tests, allowed a better understanding of the fatigue collapse mechanism, thus indicating the way for improving the elements endurance.



## ACKNOWLEDGMENTS

The financial support of the firm EDIL BETON, based in Perugia (Italy) is gratefully acknowledged.

## REFERENCES

- Alliche, A. (2004). Damage model for fatigue loading of concrete. *International Journal of Fatigue* 26, 915–921.
- Breccolotti, M. et al. (2006). Crack control and fatigue behaviour improvement of precast reinforced concrete access floors. In *Fatigue 2006*.
- Cachim, P. et al. (2002). Fatigue behavior of fiber-reinforced concrete in compression. *Cement and Concrete Composite* 24, 211–217.
- Cannon, R. et al. (1992). Considerations for design of concrete structures subjected to fatigue loading. Technical report, American Concrete Institute.
- CEB-FIP (1990). Model code 1990 final draft, bulletin information no. 203, 204, 205. Technical report, CEB-FIP.
- CEN (2004). En 1992-1-1:2004 eurocode 2: Design of concrete structures—part 1-1: General rules and rules for building. Technical report, CEN.
- CISCA (2004). *Recommended test procedures for access floors*. Ceilings Interior Systems Construction Association.
- Hsu, T. (1981). Fatigue of plain concrete. *ACL Journal* 78, 292–305.
- Lee, M. and B. Barr (2004). An overview of the fatigue behaviour of plain and fibre reinforced concrete. *Cement & Concrete Composite* 26, 299–305.
- Li, V. and T. Matsumoto (1998). Fatigue crack growth analysis of fiber reinforced concrete with effect of interfacial bond degradation. *Cement and Concrete Composite* 20, 339–351.
- Matsuishi, M. and T. Endo (1968). Fatigue of metals subjected to varying stress. In J. S. M. Engng. (Ed.), *Kyushu District Meeting*.
- Naaman, A. and H. Hammoud (1998). Fatigue characteristics of high performance fiber-reinforced concrete. *Cement and Concrete Composite* 20, 353–363.
- Nordby, G. (1958). Fatigue of concrete—a review of research. *ACL Journal* 55(2), 191–219.
- RILEM (1984). Long term random dynamic loading of concrete structures. *Mater Struct* 17(97), 1–28. 36-RDL RILEM Committee.
- Subramaniam, K. and S. Shah (2003). Biaxial tension fatigue response of concrete. *Cement and Concrete Composite* 25, 617–623.
- Zhang, J. et al. (2001). Crack bridging model for fibre reinforced concrete under fatigue tension. *International Journal of Fatigue* 23, 655–670.

# Integration of degradation prognosis of concrete structures into life cycle management

H. Budelmann, K. Hariri & T. Starck

*Institute for Building Materials, Concrete Construction and Fire Protection (iBMB),  
Technical University of Braunschweig, Germany*

**ABSTRACT:** Every structure holds an initial resistance inventory against degradation. During its service life a structure degrades due to deterioration and wearing down. These processes should be estimated in advance for the purpose of a provident life cycle management.

With respect to the deterioration processes of reinforced concrete structures several mechanisms of concrete attack and reinforcing steel corrosion, repairing measures such as coatings included, have to be regarded.

In the contribution the state and potentials of different forecasting models are presented with respect to the application in life cycle management systems. Such models can either be based on process oriented transport/reaction formulations or on constitutive engineering models, both being able to take reliability into account if the scatterings of the variables are known. As a deterioration model Markov chains can be used to predict the change of a structure or component. In any case the prognosis can be updated considerably by monitoring data.

## 1 INTRODUCTION

For reasons of durability and concluding economy life cycle management systems (LMS) have been developed, being up to evaluate today's structures. A first step in conducting a reliability-based analysis for LMS is to model the problem. One important component of a LMS is basically the integration of degradation prognosis which is based upon a large-scale of structure assessments and the thus following integration of prognosis models to predict the lifetime and the durability.

In this paper the basics of a LMS and of degradation prediction in combination with the importance of monitoring a structure will be discussed. Proposals for evaluating monitoring data in the safety concept are made and illustrated through a few scientific approved material models gathering the load-independent deteriorations. There are also some probabilistic programs available, which are outlined within this context. With the aid of Markov-chains the durability with respect to the lifetime prognosis can be evaluated. The concluding example should demonstrate the possibilities of lifetime prediction by application of Markov-chains.

## 2 LIFE CYCLE MANAGEMENT

### 2.1 *Purposes and components*

The development of LMS is a systematic approach for the organisation and execution of all activities, which belong to the stages of planning, assessment, construction, maintenance and monitoring. The purpose of a LMS is to identify potential impairments at an early state and to forecast the development of the structure's condition in order to enable an economically optimised and sustainable structure maintenance. Elemental components of a LMS are:

- Probabilistic lifetime assessment procedures for the decisive mechanisms of deterioration
- Periodic condition data gathering beginning with a so-called "Birth-Certificate"
- Application of monitoring-systems for a continuous condition assessment
- Improvement of the lifetime prognosis on the basis of surveyed data
- Probabilistic models for assessing the durability of maintenance measures

Because of large and unavoidable scatters on side of both the exposures and the resistances equally probabilistic assessments must be adapted.

Essential component of a LMS is the planning of monitoring and maintenance. During the structure's service life the most important resistance parameters must be continuously acquired by sensors or within inspections, so scatters will be reduced. Probabilistic methods are adequate for the planning of a cost-optimised inquiry. For new buildings it is possible to apply probabilistic lifetime assessment models already within the design stage and to execute an update of the structural elements resistances. Buildings of different ages and complexity or different usage must be maintained also. In these cases an individual adaptation of the methods and results with previous information must take place.

## 2.2 Online monitoring of the structure

The continuous condition assessment of a structure with non-destructive test methods assigns a special importance in LMS. As sensors become smaller, more affordable, less power consuming and wireless, the use of LMS in civil infrastructures is increasing. The monitoring results of the actions resp. exposures and resistances are essential for the improvement of the lifetime prognosis. The identification and selection of suitable methods for decision define separate processes within a LMS. Hence flexible strategies based upon the following aspects are required which have to be adjusted to the building's specific requirements:

- Formulation of a classification of the monitoring values separated by structural elements and symptoms
- Compilation of methods and sensors
- Compilation of monitoring parameters

Local areas, which are not gathered by the exposition classes of the DIN 1045-2 have to be evaluated separately.

## 3 SAFETY CONCEPT

Generally in a safety concept the probability of the occurrence of a certain limit state has to be defined. The aim is to ensure that this limit state will not be reached within the designed life time with reasonable certainty. (Gehlen 2000). The purpose of the safety concept is to achieve a sufficient safety during the designed lifetime. In general two variables are compared. The action resp. exposure S is on the one hand and the structural element's resistance R is on the other hand. These parameters follow strong variances, therefore probabilistic failure likelihoods have to be determined. A common method for calculating these

failure probabilities is based upon the following limit state equation

$$p\{Failure\} = p_f = p\{R - S < 0\} \quad (1)$$

Where  $p\{Failure\} = p_f$  = failure probability; R = structure's resistance; S = exposure.

With the following equations it is possible to calculate the reliability index  $\beta$ .

$$\beta = \frac{\mu_Z}{\sigma_Z} = \frac{\mu_R - \mu_S}{\sqrt{\sigma_R^2 + \sigma_S^2}} \quad (2)$$

Where  $\mu$  = mean value;  $\sigma$  = standard deviation.

The following table shows the coherence of the reliability index  $\beta$  and the failure probability  $p_f$

Table 1. Correlation between reliability index and failure probability (Gehlen 2000).

Reliability index $\beta$	Failure probability $p_f$ in %
0,00	50,000
1,28	10,000
1,50	6,681
1,64	5,000
1,80	3,593
2,00	2,275
3,00	0,135
3,60	0,016
3,80	0,007

Civil engineering applications define two limit states:

SLS: serviceability limit state

ULS: ultimate limit state

Both limit states may be relevant for LMS as shown in the following.

## 4 DETERIORATION PROCESS MODELS FOR REINFORCED CONCRETE STRUCTURES

### 4.1 Carbonation

Carbonation is the diffusion controlled transformation process of  $\text{Ca(OH)}_2$  into  $\text{CaCO}_3$  resulting in the reduction of the pH-value and the corresponding decomposition of the reinforcement's passivation.

A reliable model is the following constitutive equation that was designed by Gehlen (Gehlen 2000).

$$x_c(t) = \sqrt{2 \cdot k_e \cdot k_c \cdot (k_t \cdot R_{ACC,0}^{-1} + \varepsilon_t) \cdot \Delta C_s} \times \sqrt{t} \cdot \left(\frac{t_0}{t}\right)^w \quad (3)$$

The output parameter  $x_c(t)$  describes the time dependent carbonation depth considering the following parameters:

- Different conduction parameters  $k$
- Material resistance  $R$
- Diffusion coefficient  $C$
- $\text{CO}_2$ -concentration
- Aging of the structure

Equation (3) is validated and based upon practical values. Through comparing the existing concrete cover with the expected depth of carbonation it is possible to design a limit state formula. The SLS is reached if the difference between the two values is zero.

#### 4.2 Chloride ingress

The currently most reliable constitutive model for chloride ingress is based upon the following transport mechanisms:

- Diffusion due to concentration differences
- Capillary suction and Permeation

Gehlen (Gehlen 2000) designed the following limit state equation.

$$C_{crit} = C_{S,\Delta x} \times \left( 1 - \text{erf} \cdot \frac{d_c - \Delta x}{2 \cdot \sqrt{k_e \cdot k_t \cdot D_{RCM,0} \cdot t \cdot \left(\frac{t_0}{t}\right)^a}} \right) \quad (4)$$

The parameters to be quantified are:

- Basic material resistance  $D_{RCM,0}$
- Basic impacts  $C_{S,\Delta x}$
- Different conduction parameters  $k$
- Geometric variable  $\Delta x$

The limit state will be reached when the present chloride concentration is higher than the critical chloride concentration at the level of the reinforcement.

#### 4.3 Other complex exposures

To consider the complex coherences within prediction calculations for different affecting agents the transport-reaction-model Transreac was developed (Budelman et al. 2004). By means of this numerical model for the calculation of chemical attacks on concrete it is possible to calculate time-variant destruction processes. This basically deterministic model consists of a calculation tool for mass and for heat transport processes in combination with a simulation tool of the chemical reactions and the resulting corrosive effects.

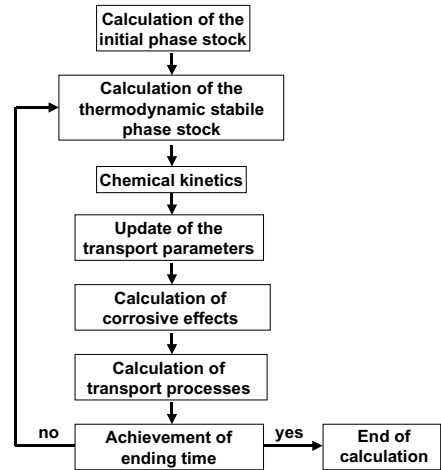


Figure 1. Function chart of Transreac (Bruder 2006).

Using Transreac the surveyed structure is divided into discrete volume elements (VE), which are assigned to a thermodynamic and kinetic stable state as a start value for further calculation steps. Between two neighbored VE heat transport, humidity transport and other mass transports are calculated until stable thermo-dynamic and kinetic states are evaluated. Then the next time step is calculated implicating the evaluated parameters. The algorithms implicated in Transreac enable the calculation of heat conduction, capillary transports and heat and moisture transmission in several mineral building materials.

In addition to algorithms an extensive physical and chemical data base of the mineral building material and of the aggressive media regarded is essential for calculation. The required thermodynamic data are available within the database of Transreac.

## 5 PREDICTION OF THE LIFETIME

### 5.1 Basic agreements

A reasonable definition of the service lifetime of a structure is the time of arriving the SLS. In case of reinforced concrete (rc) structures this state is achieved if the reinforcement depassivates and the rebar begins to corrode. The lifetime until  $t = t_{SLS}$  is called initiation period. Thus following is the deterioration period that ends by reaching the ULS. According to Holst (Holst 2007) in terms of monitoring criteria the time span until SLS is defined as monitoring-level I (can be controlled by help of sensors) and the following time span until ULS as monitoring-level II (can not yet be controlled by help of sensors; some non-destructive test methods available). The described safety concept

has to be applied in every limit state consideration in order to assess the reliability. Any prediction method of lifetime should take into account both the probabilistic nature of actions and resistances and the need of improvement and updating of prediction by actual condition data.

### 5.2 Extension of transreac to a probabilistic model

To issue a statement about the durability of a structure Transreac (see chapter 4.3) was expanded to a probabilistic model while keeping all of its flexibility (Budelmann & Rigo 2005). Therefore the main algorithm of Transreac was incorporated into a Monte Carlo-method. The results were verified by laboratory experiments. Besides of computing the failure of probability it is possible to conduct a sensitivity analysis. The results are so-called factors of weighting to identify the material property that significantly influences the system. Actual work aims at the implementation of the model into the design concept for the assessment of the lifetime based on equations of limit states  $G = R - S$ .

This model is also prepared to compare calculated data of the structure's behaviour with characteristics observed by monitoring sensors and to adapt the calculation's transport-parameters when necessary. So we achieve an adaptation of predicted properties to the real behaviour of the structure, even if started from initial values of minor quality.

### 5.3 PROBILAS

The main focus of the computer code PROBILAS is to optimize structural health monitoring measures by identifying the weak points of probabilistically modelled structures and to perform lifespan predictions using reliability analysis (Hosser 2005).

Its methodology is a reliability-based system assessment as a combination of methods of system and reliability theory. In Figure 2 the application flow of PROBILAS is illustrated. The required information is:

- Material models
- Structure properties
- Imposed loads
- Resulting failure mechanisms

Based on this information a fault tree can be constructed, which describes how dependencies and relations of components can lead to an overall system failure. The interaction between components is described via logical knots. Components can interact in serial systems, where the failure of one component leads directly to the failure of the system. The parameters of the limit state equation  $G = R - S$  are statistically

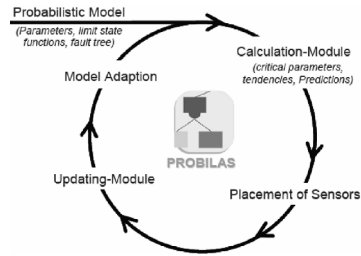


Figure 2. Structural evaluation process of PROBILAS (Hosser 2006).

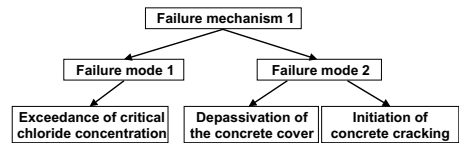


Figure 3. Example for failure mechanisms and failure modes (Hosser 2006).

evolved. Important values are the probability of failure  $p_f$ , the safety index  $\beta$  and sensitivity factors  $\alpha_i$ .

The creation of the probabilistic system model with the fault tree and the limit state equations is the most sensitive part in this reliability analysis. Each local damage is defined as a specific failure mode. Such modes can be described by simple mechanical models or have to be modeled considering quite complex relations. A combination of failure modes, which leads to an overall system failure, can be called failure mechanism as it is shown in Figure 3.

PROBILAS makes suggestions, which may be included in the future monitoring process. The monitoring data are analysed by the updating-module. The structure's performance is assessed by evaluating the time development of the failure probability.

### 5.4 STRUREL

The program system STRUREL is a complete software tool for structural, statistical and reliability analysis and has been developed to perform random processes of reliability based on the most recent theoretical findings (RCP GmbH 2007). It is originated from applications in structural reliability. The set of stochastic models includes 44 models and can be used either in parameter form or in terms of the first two moments and additional parameters if necessary.

STRUREL consists of several independent but highly interrelated programs. One module for time-invariant and time variant compartmental reliability analysis of components is COMREL. This module

can deal with arbitrary dependence structures in the stochastic model. System reliability evaluations with multiple failure criteria are covered by the module SYSREL. STATREL is the module for the reliability-oriented statistical analysis of data. It performs parameter estimation, confidence interval and quantile estimation as well as hypothesis testing including tests for sample validity, distribution functions and parameters. Import of data and stochastic models from spreadsheet programs like Excel is possible.

### 5.5 Markov-chains

Markov-Chains are a mathematical model to describe degradation processes for which analytical or empiric models do not exist (Biondini 2005). The probability of a discrete state  $X_n = i$  turning within a time increment into the state  $X_{n+1} = j$  is calculated. Markov-Chains are based on the assumption that the condition of a structural element at the point of time  $n+1$ ,  $X_{n+1}$  depends only on the structural element's condition until the point of time  $n$ , but not on the previous conditions.

$$P(X_{n+1} = j | X_1 = i_1, \dots, X_n = i_n) = P(X_{n+1} = j | X_n = i_n) \tag{6}$$

If there are  $k$  discrete structural conditions  $P$  is a  $(k \times k)$ -matrix whose entries  $p_{ij}$  describe the probability, that the structural element will change its condition within the next time-step. The current structural condition will be described by a condition vector  $w(k \times 1)$ . To reach the structural condition of a later point of time  $n+m$  the condition vector  $w$  has to be multiplied  $m$ -times with the transfer matrix  $P$ .

$$w_{n+m} = w_n \cdot P^m = \begin{pmatrix} w_0 \\ w_1 \\ \dots \\ w_k \end{pmatrix} \cdot \begin{bmatrix} p_{00} & p_{01} & \dots & p_{0k} \\ p_{10} & p_{11} & \dots & p_{1k} \\ \dots & \dots & \dots & \dots \\ p_{k0} & p_{k1} & \dots & p_{kk} \end{bmatrix} \tag{7}$$

Following boundary conditions for the degradation of concrete structures are existent:

- While modelling the degradation the user can assume that the structures cannot change into a better condition without maintenance measures, so the transfer matrix is changed into  $p_{ij} = 0, i > j$  (upper triangular matrix) and  $p_{kk} = 1$
- The sum of the transfer probabilities within one row is equal to 1 (stochastic matrix)

Thus the transfer matrix  $P$  can be simplified into the following upper triangular matrix:

$$P = \begin{bmatrix} 1 - p_{01} & p_{01} & \dots & 0 \\ 0 & 1 - p_{12} & p_{12} & 0 \\ 0 & \dots & 1 - p_{k-1,k} & p_{k-1,k} \\ 0 & 0 & \dots & 1 \end{bmatrix} \tag{8}$$

In order to avoid a high calculation effort, systems with five to seven conditions at most should be used. A very special advantage of Markov-Chains is the simple implementation of the calculation.

The information about the processes of degradation is held within the entries of the transfer matrix. Hence the definition of the transfer probabilities is a constitutive task. Following approaches are used to determine the probabilities:

- Application of the systematic interactive forecasting Delphi-method from a panel of independent experts. It is believed that during this process the range of the answers will decrease and the group will converge towards the "correct" answer.
- If test results for structures are available, it is possible to determine transfer probabilities from two consecutive results.
- If probabilistic models for degradation processes are available, Markov-Chains could be modified.

### 5.6 Application of markov chains

The application is shown exemplarily for the case of steel corrosion of a rc-member. First of all, the transformation function and a stochastic matrix with single probabilities have to be generated. Figure 4 defines the six lifetime states which are most relevant for this example. The definitions of these single states explain the state of the art, the specific transition probabilities are estimated and not verified. The basics of this calculation are included in the mentioned research report F 31006/05 (Schießl 2007).

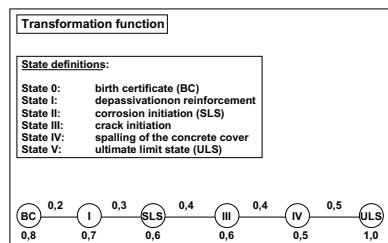


Figure 4. Transformation function of Markov-chains.

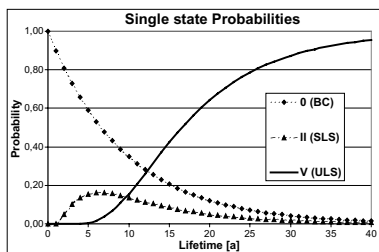


Figure 5. Single state probabilities of Markov-chains.

Depending on the transformation function the transformation matrix is generated in equation (9):

$$P = \begin{bmatrix} 0,8 & 0,2 & 0 & 0 & 0 & 0 \\ 0 & 0,7 & 0,3 & 0 & 0 & 0 \\ 0 & 0 & 0,6 & 0,4 & 0 & 0 \\ 0 & 0 & 0 & 0,6 & 0,4 & 0 \\ 0 & 0 & 0 & 0 & 0,5 & 0,5 \\ 0 & 0 & 0 & 0 & 0 & 1 \end{bmatrix} \quad (9)$$

Each of the contiguous states only has access to the next one. So the left side of the matrix is 0. The corresponding probabilities for the single states are defined in Figure 5. For better recognisability only three of the six states are presented in Figure 5.

The evaluation of the complete set of functions gives the following occurrence probabilities.

Table 2. Year of occurrence of single Markov-states.

State		Year of occurrence
0	BC	0
I	Depass	6
II	SLS	9,5
III	Crack ini	14
IV	Spalling	21
V	ULS	–

Although these results are only an engineering appraisal it shows that Markov-chains are an easy to apply tool to determine failure probabilities of defined states with a relatively small effort.

## 6 CONCLUSIONS

In this paper the basics of integration of degradation prognoses into life cycle management are discussed. This comprises the components and the purposes including the requirements of online monitoring as well as several load-independent deterioration formulations. Moreover some probabilistic lifetime prognosis software tools (Transreac, PROBILAS, STRUREL

and Markov-chains) based on different assumptions, allowing the user to perform durability prognoses, are introduced. Markov-chains enable the user to estimate the next system state by knowing the boundary conditions. Finally an application of the method of Markov-chains as an engineering appraisal should demonstrate exemplarily the usefulness of this method.

These several methods and tools are available to evaluate different structure's states and to predict the structure's lifetime with an adequate reliability. Since usually we neither do not know nor cannot correctly evaluate the present and future boundary conditions an appropriate prognosis quality can only be achieved by help of probabilistic methods.

## ACKNOWLEDGEMENT

The support of this research work within the project "Nachhaltig Bauen mit Beton, Teilprojekt D: Lebensdauermanagement", organized by the German Committee for Structural Concrete (DAFStb) and funded by the Federal Ministry of Education and Research is appreciated.

## REFERENCES

- Biondini, F. & Garavaglia, E. (2005). Markovian Modelling for Lifetime Prediction and Maintenance Planning of Deterioration Structures, 9th Int. Conf. On Structural Safety and Reliability, Rome
- Bruder, S. (2006). Adaptive Modellierung der Dauerhaftigkeit im Zuge der Überwachung von Betonbauwerken, Doctoral Thesis, Braunschweig
- Budelmann, H. & Bruder, S. (2004). Adaptives Modell zur Dauerhaftigkeitsprognose im Zuge der Überwachung von Betonbauwerken, Braunschweig
- Budelmann, H. & Rigo, E. (2005). Simulationsverfahren TRANSREAC—Erweiterung zum probabilistischen Modell, Braunschweig
- DIN 1045-2 (2001). Tragwerke aus Beton, Stahlbeton und Spannbeton; Festlegung, Eigenschaften, Herstellung und Konformität, Beuth, Berlin
- Gehlen, C. (2000). Probabilistische Lebensdauerbemessung von Stahlbetonbauwerken—Zuverlässigkeitsbetrachtungen zur wirksamen Vermeidung von Bewehrungskorrosion, Doctoral Thesis, Aachen
- Holst, A. (2007). Korrosionsmonitoring und Bruchortung vorgespannter Zugglieder in Bauwerken, Doctoral Thesis, Braunschweig
- Hosser, D. & Schnetgöke, R. (2005). PROBILAS—Zuverlässigkeitsorientierte Bauwerksüberwachung, Braunschweig
- Hosser, D. & Klinzmann, C. (2006). Probabilistic Building Inspection and Life Assessment—a computer program for reliability based system assessment, Braunschweig
- RCP GmbH (2007). Reliability Consulting Programs, [www.strurel.de](http://www.strurel.de), München
- Schießl, P. & Mayer, T. (2007). Forschungsbericht F 31006/05, DAFStb-Verbundvorhaben "Nachhaltig Bauen mit Beton" Teilprojekt A3, München

# Increasing pavements durability through construction: a model for compaction design

M. Crispino, E. Mariani & R. Rampini

*Polytechnic of Milan, Milan, Italy*

**ABSTRACT:** The overall quality and durability of asphalt pavements mainly depends on its “design”, which generally includes materials selection, mix design, structural (and functional) design. In the “design” phase, less attention is generally given to the definition of the construction procedures, which somehow seem to assume a secondary importance. The selection of the most suitable rollers and their use (number of passes, vibration settings) is rarely defined before the job, and the definitive choice often depends on the contractor’s available equipments and on the experience of the staff. This paper presents the result of a full-scale experimental study carried out to test the effects of different compaction procedures on the final degree of compaction of different asphalt mixes. After introducing a new variable able to represent the compaction action carried out by the roller, a relation was identified which allows to preliminary evaluate the degree of compaction of a layer when a compaction procedure is defined.

## 1 BACKGROUND ON COMPACTION

### 1.1 *Phenomenon*

As it is well known, the main goal of asphalt concrete compaction is to rearrange the distribution of the aggregates of the mix, allowing them to assume the configuration that generates the desired density (Aste & Weaire 2000; Ludwig et. al. 2006; Murali Krishnan & Lakshmana Rao 1999; Murali Krishnan & Rengaraju 1998; Philippe & Bideau 2001). Compaction plays a major role in the performance of flexible pavements conferring to the pavement the indispensable characteristics of bearing capacity, stability, impermeability and durability.

The energy needed to perform compaction is transmitted to the asphalt layer by means of the temporary application of either a static or a dynamic load (Floss 2001; Forssblad 1981; Jaselskis 2001).

Static compaction uses the pressure of a dead-weight applied on the surface to compress the material. The effect of static compaction decreases with increasing layer depth, and its efficacy can only be enhanced by increasing the weight. Example of static compactors are steel-wheeled static rollers and pneumatic rollers.

Vibratory (or dynamic) compaction consists in a rapid succession of impacts on the surface, which generates a vibration through the material; the pressure waves thus created reduce the internal friction of the aggregate, allowing the grains to rearrange and, consequently, be pressed into a denser position. Example

of vibratory compactors are single-drum vibratory rollers, tandem vibratory rollers, vibratory plates and tampers.

### 1.2 *Influencing factors*

Several machine-related parameters can be recognized as directly influencing the compaction results; above all, particular attention must be focused on the type of roller, its operating mass, vibration amplitude and frequency, rolling speed and number of passes (Floss 2001; Forssblad 1981; Khan et. al. 1998; Ter Huerne 2004).

A more significant parameter called Static Linear Load (SLL) can be recognized as being suitable in characterizing the compaction effectiveness of steel drum rollers (Crispino et. al. 2007; Crispino & Rampini 2008; Rampini 2007).

The Static Linear Load (SLL) represents the ratio between the load of a single drum module and its width:

$$SLL_i = \frac{W_i}{w_i} \quad (1)$$

where  $SLL_i$  = Static Linear Load of a single drum [Force/Length];  $W_i$  = weight of the single drum module [Force];  $w_i$  = width of the single drum [Length].

Since the actual pressure transferred to the ground directly depends on drum width, this parameter, calculated for each drum, is considered to be more significant than the mere roller operating mass.



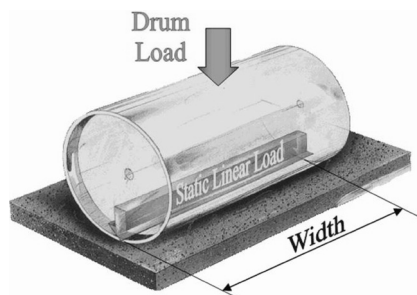


Figure 1. Static linear load.

Typical values of SLL vary from about 5 daN/cm for light equipments to more than 60 daN/cm for heavy duty soil works.

## 2 FULL-SCALE EXPERIMENTATION

This study is based on full-scale tests carried out by the Road Research Laboratory of Polytechnic of Milan (Italy) and by the International High Comp Center (Karlskrona, Sweden).

These tests were aimed at comparing the effectiveness of the three most diffused types of vibration (circular vibration, directed vibration and oscillation) on the degree of compaction of different asphalt mixes, with different layer thicknesses.

### 2.1 Rollers

The tests were performed using four different tandem rollers (hereafter indicated as R1, R2, R3, R4).

Rollers R1 and R2 were equipped with circular vibration on both drums, R3 with directed vibration on the front drum and circular vibration on the rear one, while R4 with circular vibration on the front drum and oscillation on the rear one.

In particular, R3 was tested in the automatic mode; therefore, the most suitable direction was automatically decided by the on-board computer system. The rollers were chosen so that their operating characteristics could be as similar as possible. R1 and R2 have the same vibrating system but different static weights (roller R1 is actually a heavier than roller R2). The main characteristics of the rollers are reported in [Table 1](#).

### 2.2 Asphalt mixes

Two different asphalt mixes were tested: an Asphalt Base mix (layer thicknesses 45 mm and 70 mm) and a Stone Mastic Asphalt mix (layer thickness 40 mm). Their main characteristics comply with Swedish requirements.

The required minimum degree of compaction was 97% for both mixes.

### 2.3 Testing conditions

The tests were performed under strictly controlled conditions, which can be summarized as follows:

- all asphalt mixes were laid and compacted under controlled and uniform conditions;
- only one paver with determinate settings was used;
- all four rollers operated at the constant speed of 5 km/h;
- the same roller was tested on each asphalt mix experimenting different vibration settings, amplitudes and frequencies, and number of vibrating drums;
- each compaction procedure, on each asphalt mix, was tested executing 4, 6 and 8 passes;
- for Asphalt Base compaction, between roller R1 and R2, both with circular vibration, the first one was preferred to the latter, whereas for Stone Mastic Asphalt all rollers were used.

The data collected contains a total of 108 values of compaction degree each one calculated as the average of the 9 core samples. The dataset is distributed as follows:

- Asphalt Base, 45 mm: 24 values.
- Asphalt Base, 70 mm: 30 values.
- Stone Mastic Asphalt, 40 mm: 54 values.

## 3 DATA ANALYSIS

### 3.1 Preliminary analysis

A first analysis of the results shows that most of the rolling techniques chosen allowed to successfully achieve the compaction requirements ([Fig. 2](#)), even if different performances are showed by the rollers, mostly in relation to the layer thickness.

Whereas such an “easy” analysis cannot show/highlight any evident correlation, more detailed data analyses, that take into account the effective compaction load transmitted to the layer, provide a more exhaustive understanding of the compaction phenomenon. The way the load is taken into account is able to strongly affect the interpretation of the phenomenon, therefore different analysis were carried out:

- “Static Load” Analysis;
- “Dynamic Load” Analysis;
- “Advanced Dynamic Load” Analysis.

### 3.2 “Static load” analysis

The results of compaction tests are generally compared to the number of passes executed by the roller.

Table 1. Main operating characteristics of the rollers used in the experimentation.

		Roller abbreviation			
		R1	R2	R3	R4
Operating weight kg		10,400	8400	9560	9700
Static linear	Front	30.7	28.7	30.2	29.8
Load daN/cm	Rear	31.2	28.7	26.7	28.0
Amplitude	Front	0.7/0.3	0.5/0.2	Variable	0.6/0.4
low/high mm	Rear	0.7/0.3	0.5/0.2	5.31	**
Frequency	Front	50/62	54/71	46*	42/50
low/hi Hz	Rear	50/62	54/71	46	33/39**
Drum diameter mm		1300	1120	1220	1200
Drum width mm		1680	1450	1680	1680
Type of vibration	Front	circular	circular	directed	circular
	Rear	circular	circular	circular	oscillation

\* Directed vibration \*\* Oscillation.

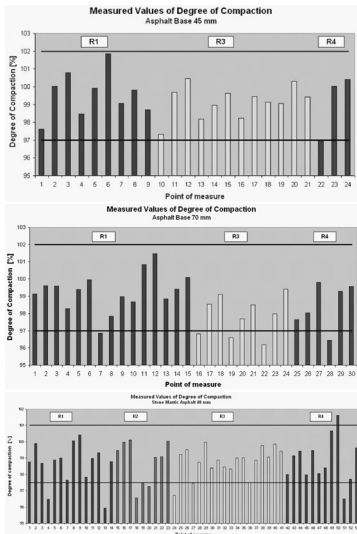


Figure 2. Degree of compaction achieved by each roller for each layer and comparison with the compaction requirement.

The number of passes itself, in spite of its easiness of application, often cannot be considered a reliable parameter, since it doesn't consider the actual compaction load transmitted to the ground by the roller. Same considerations can also be made about the roller operating mass, whose value is not directly related to the actual pressure transmitted to the material by each drum.

In this analysis a new parameter named "Total Static Load" (TSL) was therefore used.

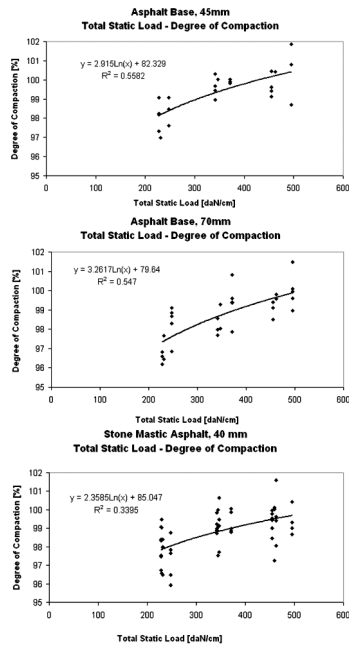


Figure 3. Static analysis: general trends between TSL and DoC without considering vibratory effects.

The Total Static Load represents the sum of all Static Linear Loads (of both front and rear drums) run over a fixed section:

$$TSL = \sum_{i=1}^n (SLL_i^f + SLL_i^r) \quad (2)$$

where:  $TSL$  = Total Static Load;  $n$  = number of passes;  $SLL^f$  = Static Linear Load (front drum);  $SLL^r$  = Static Linear Load (rear drum).

In case of uniform passes, the formula can be easily simplified, obtaining:

$$TSL = n \cdot (SLL^f + SLL^r) \quad (3)$$

The use of the TSL allows to incorporate in just one parameter all the information about roller loads and number of passes.

The first analysis was made considering the data obtained for each asphalt mix, without making any distinction between the rollers used.

Reporting the degree of compaction to the TSL, without considering any contribution given to the load by the vibration, a general logarithmic trend can be observed for all materials.

The TSL can be considered a first attempt to represent the compaction load transmitted to the pavement, but still no satisfying results can be obtained through it.

### 3.3 "Dynamic load" analysis

As compaction due to vibratory passes is different from compaction due to static passes, a coefficient  $k$ , representative of the dynamic contribution given by vibration, was introduced.

The coefficient  $k$  can therefore be considered as the static equivalent compaction factor for a dynamic pass. The TSL assumes now a different meaning, representing the Total Equivalent Static Load. This new parameter can be written in the following form:

$$TeSL = \sum_{i=1}^n (k_i^f \cdot SLL_i^f + k_i^r \cdot SLL_i^r) \quad (4)$$

where:  $k_i$  = equivalent vibratory coefficient for the  $i$ -th pass ( $k=1$  in case of a static pass);  $f$  = front drum while  $r$  = rear drum.

Considering all single mixes separately, once again without making any distinction among the rollers, a first evaluation of the general effect of vibration were drawn. The coefficient  $k$  for each asphalt mix were calculated by means of the Least Square Matching (LSM) method (Table 2).

Table 2. Dynamic analysis: dynamic coefficients and relative correlations.

Asphalt mix	$R_{k=1}^2$	$k$	$R_k^2$
Asphalt base, 45 mm	0.56	1.26	0.58
Asphalt base, 70 mm	0.55	1.43	0.59
Stone mastic asphalt, 40 mm	0.34	1.41	0.36

The results show that the dynamic effect increases the compaction load, and its positive contribution ranges from 25% to about 40% of a static pass.

### 3.4 "Advanced dynamic load" analysis

Since each asphalt mix was compacted experimenting different types of rollers and vibrations, a thorough examination of the different dynamic effects was made.

Considering all the data, and making a distinction between the types of roller used (hence the types of vibration involved) and the different amplitudes, it was possible to assign different values of  $k$  to the compaction techniques and asphalt mixes experimented in the tests.

The dynamic contributions, compared to the compaction results, also allowed to evaluate the suitability of the different rollers and techniques for the tested asphalt mixes.

All  $k_k$  coefficients were simultaneously calculated aiming at the maximization of the values of  $R^2$ . They are summarized in Table 3.

The coefficients  $k$  reported in Table 3 show remarkable differences depending on the roller and the material type. It means that the compaction effect due to vibration is not a proper characteristic of the roller, but it is highly dependent on the vibrating system of the roller and, above all (as for all dynamic systems), on the dynamic interaction between the roller (with that vibrating system) and the layer to be compacted. Actually, the vibrating effect varies from null or very low values (increase of very few points per cent) up to high values (increase of 40–60%).

The introduction of the different coefficients  $k$  produced an adjustment of the correlations between the Total Equivalent Static Load and the Degree of Compaction (Fig. 4). The obtained values of  $R^2$  became more consistent, especially for the Asphalt Base mixes.

Table 3. Dynamic contribution given by the different vibration systems to each asphalt mix.

Roller	Amplitude	Asphalt base, 45 mm	Asphalt base, 70 mm	Stone Mastic asphalt, 40 mm
		$k$	$k$	$k$
R1	High	–	1.62	–
	Low	1.22	–	1.03
R2	High	–	–	–
	Low	–	–	1.29
R3	High	1.27	1.24	1.13
	Medium	1.06	1.00	1.41
R4	Low	1.04	–	1.16
	High	–	1.17	–
	Low	1.09	–	1.29

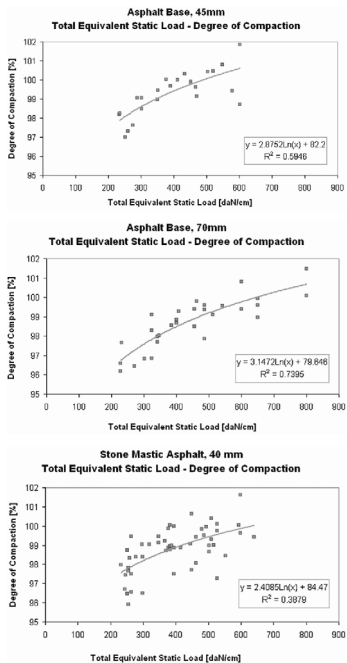


Figure 4. Dynamic analysis: correlations between TSL and DoC considering all vibratory coefficients.

These results reveal some significant correspondences and represent the background to come to the final relations.

### 3.5 The DoC-TeSL relation

Examining the single logarithmic relations, obtained for the different materials, between the Degree of Compaction (DoC) and the Total Equivalent Static Load (TeSL), some interesting analogies can be identified.

All three logarithmic trends are very similar, even if they were obtained after a significant number of tests carried out on different materials and with various compaction techniques.

The logarithmic curves that describe the compaction phenomenon have the generic expression:

$$DoC = a \cdot \ln(1 + TeSL) + b \quad (5)$$

the relations obtained from the data analysis of the three asphalt mixes, then, assume the following forms:

— Stone Mastic Asphalt, 40 mm

$$DoC = 2.41 \cdot \ln(1 + TeSL) + 85 (R^2 = 0.39) \quad (6)$$

— Asphalt Base, 45 mm

$$DoC = 2.87 \cdot \ln(1 + TeSL) + 82 (R^2 = 0.60) \quad (7)$$

— Asphalt Base, 70 mm

$$DoC = 3.14 \cdot \ln(1 + TeSL) + 80 (R^2 = 0.74) \quad (8)$$

It can be noticed that, for the different formulas, the coefficient  $a$  assumes values approximately in the range  $2.4 \div 3.1$ , while the term  $b$  varies from 80 to 85.

A further look at the equations shows that the coefficients  $a$  and  $b$  have specific trends respect to the thickness of the layer.

Moreover, it is clear that the term  $b$  can be seen as the degree of compaction of the layer at zero passes ( $TeSL = 0$ ), that is to say the degree of compaction produced by the paving process only.

In addition, the coefficient  $a$ , indicating the growth rapidity of the curve, can be considered representative of the compaction susceptibility of the material, which results higher during the first passes as far as relatively thick layers are concerned.

## 4 VALIDATION OF THE RESULTS

The results obtained have been verified using the data collected in a further survey campaign carried out during the recent runway paving operations in one of the main Italian international airports.

In this case, the analysed mix was a high-module wearing course asphalt concrete, containing polymer modified bitumen, with a layer thickness of 60 mm.

Five different rollers were used, all of them equipped with circular vibration. Their main characteristics are summarized in Table 4.

A thorough “on-site” monitoring of the paving operations was carried out during each phase of the job, including constant temperature check, number of passes of each roller, vibration settings and rolling speed.

Due to the kind of job, only eight couples of sample cores could be taken, each one exactly in correspondence of the monitored check-spots; the data were then elaborated and the Total Equivalent Static Load calculated.

Table 4. Operating characteristics of the rollers employed in the airport paving jobs.

Roller abbreviation	Operating weight	Static linear load (for each drum)
	kg	daN/cm
R1	1300	7.9
R2	1450	9.0
R3	7200	25.7
R4	9400	28.0
R5	8400	29.0

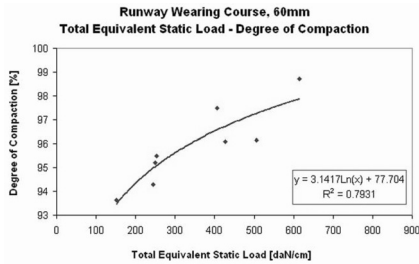


Figure 5. Airport paving data analysis: validation of the TSL-DoC correlation.

The coefficient  $k$  thus calculated was supposed to be unique for all rollers and equal to 1.3. That value was used to calculate the TeSL for each point. Finally, the LSM method allowed to find the best curve able to interpolate the experimental points. Once again, the results showed a very good logarithmic trend (Fig. 5).

Even though both the material laid and the rollers used were different from those of the real-scale test, the equation obtained still confirms the relation between the degree of compaction and the Total Equivalent Static Load:

$$DoC = 3.14 \cdot \ln(1 + TeSL) + 78 (R^2 = 0.79) \quad (9)$$

It can be noticed that the coefficient  $a$  of the equation is identical to the one obtained for the Asphalt Base—70 mm (the wear course thickness is 60 mm).

The coefficient  $b$ , instead, results little lower, indicating a lower compaction performance of the paver.

In conclusion, the Equation 5 can be considered as the general description of the evolution of Degree of Compaction in relation to the Total Equivalent Static Load:

$$DoC = a \cdot \ln(1 + TeSL) + b \quad (10)$$

with:  $a \approx 3$ ;  $b \approx 80$ .

## 5 CONCLUSIONS

A full scale experimentation was carried out using two different asphalt mixes (Asphalt Base and Stone Mastic Asphalt) and four asphalt rollers with different vibration settings, carrying out different numbers of passes.

The results showed that different compaction procedures applied to a defined asphalt layer can lead to considerably different results in terms of degree of compaction. A thorough analysis of the data and the introduction of a new reference variable, the Total Equivalent Static Load (TeSL), allowed to

observe good relations between the compaction procedure (well represented by TeSL) and the degree of compaction obtained using different rollers.

Further analysis, including the use of dynamic factors to take into account vibrating effects, allowed to obtain relations valid for different types of roller and compaction procedure, providing a good prediction of the degree of compaction obtainable with different number of passes. Such relations were successfully validated using the data collected during a further survey campaign carried out in one of the main Italian international airports.

The relations found show a steady logarithmic trend between the Total Equivalent Static Load and the Degree of Compaction. The equations obtained, even if referred to different mixes, compaction procedures and rollers, denote very interesting analogies; their coefficients vary coherently to the expectations and the value of the constant term assumes a correct physical meaning.

The results obtained allow to extend the relations found to any compaction machine and technique, representing a useful prevision tool for researchers and technicians.

## REFERENCES

- Aste, T. & Weaire, D. 2000. *The pursuit of perfect packing*. Bristol, United Kingdom: Institute of Physics Publishing (IoP).
- Crispino, M., Rampini, R. & Pozzi, M. 2007. An experimental analysis of the effects of compaction on asphalt pavement macrotexture. *Advanced Characterisation of Pavement and Soil Engineering Materials Conference, Athens, Greece*.
- Crispino, M. & Rampini, R. 2008. Constitutive laws of hot asphalt mix during compaction: a numerical experimental evaluation. *Submitted for publication*.
- Floss, R. 2001. *Compaction technology in Earthwork, highway and transportation engineering*. Vol. 1. Bomag GmbH & Co. OHG.
- Forsssblad, L. 1981. *Vibratory soil and rock fill compaction*. Sweden: Svedala Dynapac Publication.
- Khan, Z.A. et al. 1998. Comparative study of asphalt concrete laboratory compaction methods to simulate field compaction. *Construction and building materials* 12(1998): 373–384.
- Jaselskis, E.J. 2001. Status of roller mountable microwave asphalt pavement density sensor. *Journal of construction engineering and management*.
- Ludwig, F. et al. 2006. *Compaction of granular mixtures*. *Granular Matter* 8(2006): 87–91. Springer-Verlag.
- Murali Krishnan, J. & Lakshmana Rao, C. 1999. Mechanics of air voids reduction of asphalt concrete using mixture theory. *International Journal of Engineering Science* 38(2000): 1331–1354.
- Murali Krishnan, J. & Rengaraju, V.R. 1998. Air voids reduction phenomena of asphalt concrete—A continuum approach. *International Journal of Fracture* 97(1999): 337–354. Holland: Kluwer Academic Publishers.
- Philippe, P. & Bideau, D. 2001. Numerical model for granular compaction under vertical tapping. *Physical Review E, Volume 63, 051304*. USA: The American Physical Society.
- Rampini, R. 2007. *Development of an empirical-rational methodology for the optimization of compaction techniques of hot asphalt concrete*. Ph. D. Thesis, Politecnico di Milano, Milan, Italy.
- Ter Huerne, H.L. 2004. *Compaction of Asphalt Road Pavements*. Ph. D. Thesis. CT & M Department, University of Twente, Holland.

# Service life predictions for new and rehabilitated concrete bridge structures

Bozena Czarnecki

*EBA Engineering Consultants Ltd. Calgary, Alberta, Canada*

Robert L. Day

*Schulich School of Engineering, University of Calgary, Alberta, Canada*

**ABSTRACT:** Concrete bridge structures in Canada experience exposure to extreme environmental conditions such as extended durations at low temperatures, frequent freezing and thawing cycles, and, in urban maintenance conditions, extensive use of deicing salts. Chloride-induced corrosion is one of the major causes of deterioration in reinforced concrete structures. The focus of this study is (a) to examine the impact of this severe environment on High Performance Concrete (HPC) structures, and especially on corrosion of the steel reinforcement, and (b) to develop methods for estimating the remaining service life of existing rehabilitated bridge structures. Several methods of measuring chloride ion diffusion are compared as a contribution to the development of a universal performance-test that satisfies the demands of the fast-paced construction environment. The model for service life predictions is discussed and the impact of chloride binding in cold climates is assessed. Based on the results of the study the model used for service life predictions of new structures showed the highest sensitivity to the production controls exercised by ready-mix producers. An old-bridge rehabilitation strategy that has proved to be most effective is also described.

## 1 INTRODUCTION

Chloride-induced corrosion of steel reinforcement is one of the major causes of deterioration in reinforced concrete structures. The rate of deterioration has accelerated since the use of deicing salts began in the 1960s. Many of Canada's structures are in urgent need of substantial rehabilitation as our infrastructure is aging. In recent years the need to consider resistance of concrete to corrosion related damage has been recognized. However, chloride induced concrete deterioration should not be taken out of the context of complex durability issues. An analysis of concrete durability failure can often identify only the most obvious failure mechanism. The recognition of other contributing factors such as inadequate protection against freezing and thawing, damage due to chemical attack on concrete or non compliant concrete production is necessary. The lessons from such investigations extend to recommendations for the rehabilitation strategy of existing structures and new designs. The ultimate goal of testing and condition surveys is to determine the remaining service life of existing structures, or the life cycle of new structures in the context of resistance to corrosion related damage. Service life of a structure consists of two stages; the initiation stage extends up to the onset of active corrosion (i.e. time to reach a critical concentration of chloride ions at the reinforcing steel,

for example), and the propagation stage when the corrosion related damage to the structure exceeds acceptable limits. A number of methods and procedures, both long-term and short-term, have been developed in recent years to describe and predict chloride movement in concrete. However, while some of the methods are standardized and more are under development, much controversy surrounds the applicability of the results obtained to the actual structure performance.

## 2 REVIEW OF CHLORIDE TRANSPORT TESTS

The ability of the concrete to resist chloride ion penetration is one of the most essential properties in determining the service life of concrete structures. A number of long-term and accelerated methods to test concrete for chloride penetrability have been developed. The long-term methods are based on prolonged exposure of concrete samples to chlorides followed by profiling of chloride content after a specified time of exposure. These methods are very accurate in research projects but they are time consuming and in construction quality control demands the results may be too late for remedial measures. Transport of chlorides in the 90-day ponding test (AASHTO T259-80) is due to a combination of absorption, diffusion and wicking. Pure diffusion of chloride ions is assumed

in the Nordtest NT Build 443-95 and in the ASTM C1556-03 and the diffusion coefficient is determined by fitting the solution equation of Fick's Second Law to the measured chloride ion contents in non-linear regression analysis.

Any accelerated test should meet several criteria. Testing time should be short, commencing after 28 days of curing. The test should be easy to perform and evaluate and the theory behind the procedure should be sound. In addition, the test should be used for diffusion coefficient determination and possibly for service life predictions. As the rate of chloride ion penetration due to diffusion alone is slow, techniques are used to accelerate this process for evaluating concrete. A commonly used method is the application of electrical potential. In migration tests an electrical field accelerates the transport of chlorides through the concrete in a two-compartment cell, and then the amount of chloride arriving in the downstream compartment is measured. The migration due to the electrical field is dominant and the diffusion is minimal. In the AASHTO test method T277, commonly called the rapid chloride permeability test (RCPT), the classification of permeability is based on the charge passed, similarly to ASTM C1202. Several modifications to these methods were proposed to improve correlation between the ponding test and accelerated test (McGrath et al. 1999, Castellote et al. 2001, Yang et al. 2002). The studies to develop the criteria in AASHTO T277 adopted in 1983 and in ASTM C1202 adopted in 1991 did not investigate any concretes containing SCM. However, these two tests are still used to evaluate the resistance to chloride ion penetration in concretes with fly ash, silica fume and granulated blast furnace slag. It has been recognized that SCMs change the composition of the pore solution of concrete, thus affecting the electrical conductivity of concrete (Shi et al. 1998, Wee et al. 2000). The rapid migration test (RMT) was developed by Tang et al. 1991 and standardized as the Nordtest method NT Build 492. The non-steady state migration coefficient is calculated based on the applied voltage, temperature of the anolyte solution, specimen thickness and the chloride penetration depth determined by the colour change after treatment with silver nitrate solution. The RMT was modified based on the study conducted by Stanish et al. 2000 and is standardized in AASHTO TP 64-03. The modified procedure is similar to NT Build 492 but the coefficient of diffusion is replaced by the rate of chloride penetration and classified for different grades of high performance concrete (HPC) based on research by Hooton et al. 2001.

### 3 EXPERIMENTAL PROGRAMME

A total of six commercial HPC mixes were studied. The mixes were produced by two ready-mix suppliers

in Calgary, Alberta. The concrete utilized Type GU cement (General Use Hydraulic Cement, similar to Type I, ASTM) with an alkali content of 0.5% ( $\text{Na}_2\text{O}_{eq.}$ ). Good quality local aggregate composed of sound quartzite and limestone was incorporated in the mixes. The concrete was produced at the batch plants and used for 2004 and 2005 infrastructure projects in Calgary. The design compressive strength was specified for each mix and the chloride ion penetrability requirement as per ASTM C 1202 was 1000 coulombs at 28 days. Plastic concrete samples were obtained from batch plants and concrete was cast to determine the ability to resist chloride penetration using different methods. The summary of the mix properties is presented in Table 1.

The summary of the chloride ion penetration test results measured by different methods is in Table 2.

The results indicate two distinct groups of penetration rates in the concretes produced by the ready mix producers and are not consistent with the mix properties. It is expected that lower w/cm ratio would result in a lower migration coefficient. However, mixes 1 and 2 with a w/cm ratio of 0.35 had a lower migration coefficient than mix 3 with w/cm ratio of 0.31. Similarly, mixes 2 and 6 that had the same w/cm ratio and cement content had a migration coefficient of 2.29 and  $3.63 \times 10^{-12} \text{m}^2/\text{s}$ . A comparison of results by ready-mix suppliers confirmed significantly higher results for mixes 4 and 5 than for mixes 1, 2, 3, and 6, regardless of the mix design. Mixes 1, 2, 3, and 6 had the penetration rates classified as HPC grade 3. The corresponding RCPT results were also below 800 coulombs. Mixes 4 and 5 had the penetration rates classified as HPC grade 2 and the corresponding RCPT values were above 800 coulombs. The discrepancies in the results cannot be simply explained by the differences in the mix designs, but rather by the different level of production controls executed by each concrete producer. Other durability requirements such as freeze/thaw durability and scaling resistance met specification requirements (Czarnecki 2006).

Table 1. Commercial HPC mix properties.

Mix number	1	2	3	4	5	6
Design strength at 28 days (MPa)	50	50	50	35	50	45
Cement ( $\text{kg}/\text{m}^3$ )	380	370	380	380	430	370
Fly ash (% by total cementitious mat.)	11.0	11.0	13.5	0	10.5	11.0
Silica fume (% by total cementitious mat.)	7.5	7.5	6.3	7.3	8.0	7.6
w/cm	0.35	0.35	0.31	0.36	0.31	0.35
28-day compressive strength results (MPa)	64.4	63.8	65.2	38.2	54.2	64.0

Table 2. Chloride ion penetration of HPC mixes.

Mix number	1	2	3	4	5	6
Chloride ion penetrability at 28 days (coulombs)	800	678	557	972	972	509
ASTM C1202 migration coefficient at 28 days ( $\times 10^{-12} \text{m}^2/\text{s}$ )	2.28	2.29	3.41	6.29	6.02	3.63
NT build 492 rate of penetration at 28 days ( $\text{mm}/\text{V} - \text{h}^* 10^{-3}$ )	64	73	87	163	125	73
AASHTO64-03	64	73	87	163	125	73

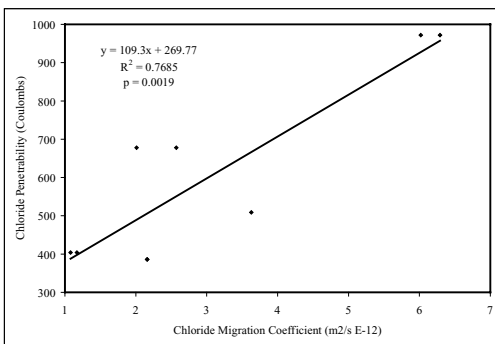


Figure 1. Correlation between chloride migration coefficient and RCTP.

Correlations between the test methods were established for the commercial HPC mixes. Good correlation between the depth of chloride penetration and the migration coefficient was established. The correlation is statistically significant with p value of 0.0019. Similarly, reasonable correlations were obtained for the RCTP and migration coefficient (Figure 1) and between the migration coefficient and migration rates (Figure 2). However, the correlation between migration rate and RCTP was poor with p value of 0.058.

The difference in the performance of the commercially produced HPC mixes that otherwise have similar mix proportions should raise some concerns. While they all meet the HPC compliance specifications, using the varying test results to predict service life may lead to a significant range of estimated time to initiation of corrosion (presented in Chapter 6). The dependence of the mix characteristics on the ready-mix supplier is not taken into consideration at the design stage of the structure, but if accounted for, it results in either worst case scenario assumptions or the demand for the over-designed concrete mix to meet

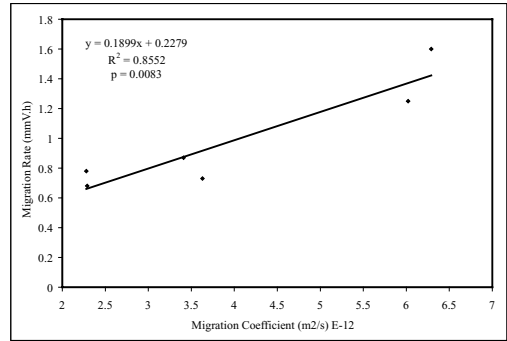


Figure 2. Correlation between chloride migration coefficient and migration rates.

the mid-range criteria for the properties. Since the aggregate, cement and SCM sources are comparable for these mixes the difference in the results can only be explained by the different standards of the production controls.

#### 4 BRIDGE DECK ANALYSIS

Concrete bridge decks in Calgary are exposed to deicing salts leading to deterioration due to chloride induced corrosion of steel reinforcement. Service life predictions of older concrete bridge decks are essential in developing cost-effective repair and rehabilitation strategies. The current methodology to determine the condition of the bridge deck consists of two parts; (1) determination of potential for corrosion by the half-cell potential test and (2) determination of the chloride ion content profile on concrete cores obtained from the deck, combined with petrographic examination of the concrete. Chloride profiles from the bridge decks were used for the determination of traffic patterns and the diffusion coefficients. Service life predictions were aided by the results of half-cell potentials. Since all bridge decks in Calgary receive asphalt or PMA overlay at the time of construction the seasonal variations in the surface chloride concentrations and their impact on the chloride profiles were assumed negligible. Based on the data from the bridge deck surveys the apparent diffusion coefficient was estimated analytically using the error function equation from the solution to Fick's Second Law of diffusion for each measured point. The apparent chloride diffusion constant coefficient was also determined from the chloride profile by fitting the solution of Fick's Second Law to the measured chloride ion profile in non-linear regression analysis. The bridges selected for the analysis were chosen to illustrate the effect of different design and rehabilitation techniques on the overall performance of the



Table 3. Constant diffusion coefficient  $D_a$  from cores.

Bridge number	Bridge design	$D_a$ ( $m^2/s * 10^{-12}$ )
1	Rubber membrane and asphalt overlay on concrete deck	0.4
2	25 mm concrete cover over reinforcing steel, high density concrete	0.51
3	40 mm concrete cover and 50 mm asphalt wearing surface. Pyrament concrete overlain with PMA	1.3
4	Concrete and 40 mm asphalt wearing surface	3.8

structure. Since in the service life predictions a constant diffusion coefficient is considered, the constant diffusion coefficient was calculated from the composite chloride profile and non-linear regression analysis using the Solver feature of Excel. Constant diffusion coefficients from non-linear regression analysis are summarized in Table 3.

The bridges selected for the analysis represent a variety of initial design, protection of steel reinforcement against corrosion and rehabilitation procedures. Bridge 1 had a membrane and asphalt placed on the concrete deck. The membrane and asphalt wearing surface was later removed and replaced with PMA (polymer modified asphalt). Bridge 2 had the original asphalt on the concrete deck that later was removed and replaced with the concrete wearing surface. Bridge 3 had the original asphalt wearing surface placed on the concrete deck without a membrane. During subsequent rehabilitation the asphalt and concrete were removed, Pyrament concrete was used to repair the deck and PMA was placed on the surface. Bridge 4 had the original asphalt placed on timber. Rehabilitation programs resulted in concrete with asphalt as a wearing surface and subsequently asphalt was removed and replaced with concrete. The diffusion coefficient values are consistent with the design and rehabilitation strategy. The lowest diffusion rate was noted for the rubber and asphalt cover design. Higher results were noted for the Pyrament concrete and the old concrete with asphalt wearing surface (Table 3).

Both acid and water soluble chlorides were measured in the cores extracted from the bridge decks. The amount of bound chlorides measured as a difference between acid and water soluble chlorides is very small and on average is 2.7%. The correlation between the total and free chlorides is very good (Figure 3).

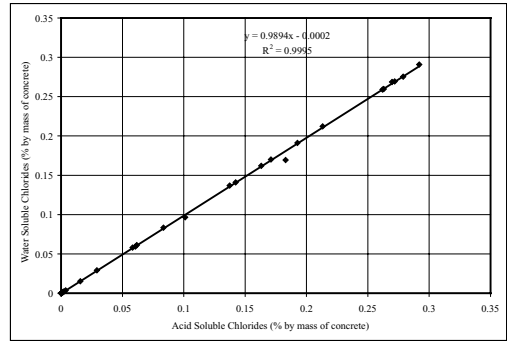


Figure 3. Correlation between total and free chlorides in bridge decks.

## 5 SERVICE LIFE PREDICTIONS

There have been several models developed in recent years that purport to predict the service life of concrete structures and estimate the life-cycle cost of different corrosion protection strategies. However, as the assumptions and approach of different models vary significantly, the solutions produced by these models also produce highly variable service life predictions and life cycle cost analyses.

The prediction of service life consists of two parts; predictions from the early age tests conducted in this programme and service life predictions of the existing bridge structures based on the bridge deck core analysis.

### 5.1 Prediction of service life from early age tests

The analysis presented in this study is intended to show the sensitivity of long term predictions that rely on the early-age measured properties. Only a simple model is used to focus on readily measured design parameters and materials' properties instead of numerically developed parameters not supported by experimental data.

The following model is based on the diffusion being the predominant mechanism of the chloride transport in concrete. The model uses a time-dependent and a temperature-dependent diffusion coefficient. The model is used for the service life predictions of the bridge structures constructed in accordance with the current practices specified by the City of Calgary. The ultimate goal of the analysis is to estimate from the model the time needed for the chloride concentration to reach the critical concentration at the reinforcing steel. The sorptivity, wicking, partial saturation, cracking and seasonal chloride variations due to winter salt application and summer rains were not considered in this model since concrete decks are covered with a

polymer modified asphalt wearing course. Chloride binding, impact of curing, and the type of steel were also not considered based on historical research.

The service life prediction is for a typical bridge deck in Calgary. HPC for bridge deck applications is designed to have chloride ion penetrability below 1000 coulombs at 28 days as determined by the ASTM C1202 test method. The design concrete cover over the reinforcing steel is 70 mm (+5 mm; -10 mm tolerance) and 50 mm of PMA (polymer modified asphalt) overlay. The deck will not be exposed to chlorides until 6 months after placement and it is assumed that the low permeability PMA will effectively block the chloride ingress into concrete for 3 to 5 years. The reduction in the cover due to sorption and seasonal changes in concrete saturation and surface chloride concentrations are not considered since the deck is overlaid with PMA. The average annual temperature for Calgary reported by Environment Canada is 4.1°C. The HPC commercial mixes will be considered for this case. The early diffusion coefficients were determined from the non-steady-state migration experiments (NT Build 492). The chloride diffusion coefficients obtained from non-steady migration experiments were adjusted for the time-dependency using the relationship developed by Maage et al. 1995. Chloride diffusivity in concrete decreases with a decrease in temperature and was adjusted for the Calgary annual average temperature using Arrhenius Law. The adjusted diffusion coefficients are presented in Table 4.

The time to reach the critical chloride content to initiate corrosion at the top of the steel reinforcement (service life) was calculated using Crank's solution of Fick's second law of diffusion and the service life summary for HPC mixes is presented in Table 5.

Service life was also computed for different time to exposure to chlorides (5.5 years), as well as for different threshold limits and concrete cover over steel. The sensitivity analysis based on these parameters is presented in Table 6.

Table 4. Adjusted diffusion coefficients for HPC mixes.

Mix number	1	2	3	4	5	6
Migration coefficient at 28 days ( $\times 10^{-12} \text{m}^2/\text{s}$ )	2.28	2.29	3.41	6.29	6.02	3.63
NT build 492 time adjustment at 3.5 years ( $\times 10^{-12} \text{m}^2/\text{s}$ )	0.82	0.82	1.77	2.05	3.13	1.30
Temperature adjustment to 4.1°C $\times 10^{-12} \text{m}^2/\text{s}$	0.35	0.35	0.77	0.89	1.36	0.57

Table 5. Time to reach threshold limit of 0.2% at 60 mm depth based on diffusion coefficient at 3.5 years.

Mix number	1	2	3	4	5	6
Service life (years)	129	129	59	51	33	79

Table 6. Service life sensitivity analysis.

Parameter	Service life increase (%)
Change in diffusion coefficient prior to exposure to chlorides (from 3.5 years to 5.5 years)	12
Change in cover depth within specified range (from 60 mm to 75 mm)	55
Change in threshold limit from codes (from 0.2% to 0.6%)	40
Change in diffusion coefficient due to concrete mix variations (from Mix 5 to Mix 1)	300

Initial assumptions of the chloride diffusion have the smallest impact on the corrosion initiation. Cover depth variations and the threshold limits result in average 50% change in the predicted time to corrosion. The impact of production controls of the concrete mixes is the most significant and from a practical standpoint raises a significant concern about the service life predictions analyzed in this study.

## 5.2 Prediction of service life for old bridge structure

The analysis was conducted on Bridge 2. After the rehabilitation work in 1985 the bridge was surveyed in 2003. For the service life predictions several assumptions were made; threshold chloride content was 0.2%, surface chloride concentration was assumed at 2%, cover depth including high density concrete was 75 mm and the depth of sorption influence on the cover was 5 mm. Measured chloride ion concentrations versus depth were plotted and the chloride diffusion coefficient was determined from the non-linear regression analysis using Excel Solver. The diffusion coefficient based on chloride profile is  $0.51 \times 10^{-12} \text{m}^2/\text{s}$ . Since the chloride profiles were obtained from the bridge deck exposed to the elements over time, the temperature adjustment of the diffusion coefficient for the climatic conditions in Calgary is not calculated. The time to corrosion initiation is estimated to be 109 years. Similar to the two models predicting the service life from early age properties of concrete, this simplified model does not take into consideration any other influence on the time to corrosion

initiation. However, the results show how the bridge rehabilitation is expected to extend the service life by approximately 109 years from the time of the deck rehabilitation to the time to reach chloride threshold limit at the reinforcement depth.

## 6 CONCLUSIONS

A good correlation was established between the RCPT procedure and RMT procedure for HPC mixes. The RMT procedure is more practical for service life predictions based on early age properties. The amount of bound chlorides confirmed in the cores obtained from the bridges in Calgary was small. Since Friedel's salt is metastable and present in small amounts, the impact of bound chlorides on the transport of chloride ions in the concrete and on the service life predictions is considered negligible in Alberta due to cold climate and historically low  $C_3A$  content in local cements. The analysis of the data from the bridge deck surveys shows that the membranes, asphalt and PMA wearing surfaces offer good protection against chloride ion ingress into concrete cover. The quality of concrete, as produced at the ready-mix batch plants in Calgary and placed in the structure, is the most sensitive parameter affecting service life predictions. The predictive value of complex empirical or theoretical solutions that include almost unlimited physical and chemical variables will remain limited until tighter controls on the materials production parameters and workmanship are exercised. This conclusion should be limited to the two ready-mix plants analyzed in this study and can only be generalized upon more extensive research of concrete produced in other concrete plants.

## REFERENCES

- Castellote, M., Alonso, C., Andrade, C., Chadbourn, G.A. & Page, C.L. 2001(a). Oxygen and chloride diffusion coefficients obtained by steady-state migration tests. *Cement and Concrete Research* 31: 621–625.
- Czarnecki, B. Chloride mass transfer and concrete durability. 2006. *PhD Thesis*. The University of Calgary.
- Hooton, R.D., Thomas, M.D.A. & Stanish, K. 2001. Prediction of chloride penetration in concrete. *Publication No. FWHA-RD-00142, Department of Transportation, Federal Highway Administration*. McLean, VA.
- Maage, M., Poulsen, E., Vennesland, O. & Carlsen, J.E. 1995. Service life model for concrete structures exposed to marine environment—Initial period. *SINTEF Report No. STF 70 A94082*. Trondheim.
- Shi, C., Stegemann, J. & Caldwell R.J. 1998. Effect of supplementary cementing materials on the specific conductivity of pore solution and its implications on the rapid chloride permeability test (AASHTO T277 and ASTM C1202) results. *ACI Materials Journal* 95 (4): 389–394.
- Stanish, K., Hooton, R.D. & Thomas, M.D.A. 2000. Evaluation of four short-term methods for determining chloride penetrability in concrete. *Water-Cement Ratio and Other Durability Parameters, Techniques for Determination ACI International*. SP-191-7: 81–97.
- Tang, L. & Nilsson, L-O. 1991. Chloride diffusivity in high strength concrete. *Nordic Concrete Research* 11: 162–170.
- Wee, A., Suryavanshi, A.K. & Tin, S.S. 2000. Evaluation of rapid chloride permeability test results for concrete containing mineral admixtures. *ACI Materials Journal* 97 (2): 221–232.
- Yang, C.C., & Huang, S.W. Chor. 2002. The relationship between charge passed and the chloride-ion concentration in concrete using steady-state chloride migration test. *Cement and Concrete Research* 32: 217–222.

# Combined reinforcement

Benoit De Rivaz

*NV Bekaert, Zwevegem, Belgium*

**ABSTRACT:** Cracks in concrete are a matter of fact due to the nature of this material. Furthermore, they are necessary as in the design of concrete structures always a cracked section is assumed. Otherwise the reinforcing effect of rebar or mesh would not be given. If these cracks do not exceed a specific size, they are neither harmful to a structure nor to its serviceability. In order to prepare the concrete to meet the requirements of small crack widths, a minimum reinforcement ratio is introduced. When following additional rules, concrete structures with limited crack width can also be used as a second barrier against water-endangering fluids. Steel fibre reinforced concrete can significantly contribute to reduce crack width in concrete structures. However, in most cases this is only possible in interaction with a traditional reinforcement. Only in very few cases additional reinforcement is not necessary.

## 1 INTRODUCTION

Cracks in concrete are a matter of fact due to the nature of this material. Furthermore, they are necessary as in the design of concrete structures always a cracked section is assumed. Otherwise the reinforcing effect of rebar or mesh would not be given.

If these cracks do not exceed a specific size, they are neither harmful to a structure nor to its serviceability. In order to prepare the concrete to meet the requirements of small crack widths, a minimum reinforcement ratio is introduced. When following additional rules, concrete structures with limited crack width can also be used as a second barrier against water-endangering fluids.

Steel fibre reinforced concrete can significantly contribute to reduce crack width in concrete structures. However, in most cases this is only possible in interaction with a traditional reinforcement. Only in very few cases additional reinforcement is not necessary. On the following pages a short introduction to the design of combined reinforcement will be given.

## 2 CRACKS IN REINFORCED CONCRETE

When concrete is exposed to load and/or restraint deformation, cracks are a consequence. The width of these cracks mainly depends on these parameters:

- concrete tensile strength  $f_{ct,t}$
- type of loading            tensile, flexural, bending—load or restraint
- concrete cover             $c$

- rebar diameter             $d_s$
- thickness of structure     $h$
- steel section               $A_s$

The most important parameter is the tensile strength of the concrete. It is a time dependent material property which can be calculated according to the following equation.

$$\beta_{cc,t} = e^{s \cdot (1 - \sqrt{28/t})} \quad (1)$$

(where  $0, 20 \leq s \leq 0, 38$ , function of cement-type)

Therefore it is important to know at what time cracking will occur. In many cases, such as where the dominant imposed deformation arises from dissipation of the heat of hydration, it is sufficient to consider 2–5 days old concrete (e.g. many ground supported slabs). This leads to an effective tensile strength of ca. 50% of the values at 28 days. When the time of cracking cannot be established with confidence as being less than 28 days, the tensile strength of hardened concrete has to be taken into account (e.g. inner walls of underground parking lots).

The other factors are mainly given by design rules, workability and loading and are much easier to determine.

The concrete cover is depending of the exposure class and has an influence on the effective area.

The crack limiting effect of the reinforcement can only be observed within this area. It is equal to the area of concrete surrounding the tension reinforcement of a depth equal to 2,5 times the distance from

the tension face to the section to the centroid of the reinforcement (see figure 1).

Therefore an increase of slab thickness will not automatically lead to an increase of reinforcement for crack control (regarding the statically required minimum reinforcement there will be an influence, of course).

In case of thick members this might lead to the formation of wide, collecting cracks in the concrete outside the effective area (see figure 2).

Furthermore, the thickness of the structure influences the size of non-uniform self-equilibrating stresses within the concrete. The thicker a structure is the higher these stresses will be and the lower the released energy is when the concrete cracks. Subsequently it is important to know what the nature of stress distribution is within the section immediately prior to cracking: A section under pure tension will release more energy than a section subject to pure bending (see figure 3).

Keeping these principles in mind, crack formation can be divided into two different phases:

Assuming a member subject to restraint deformation, in the initial phase of cracking the first crack will form at that place where the concrete tensile strength is lowest (see figure 4).

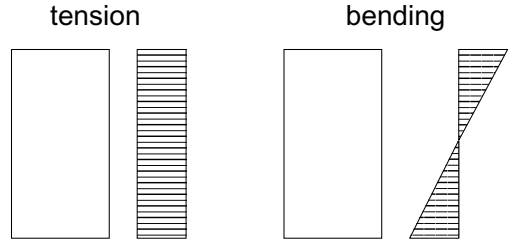


Figure 3. Stress distribution.

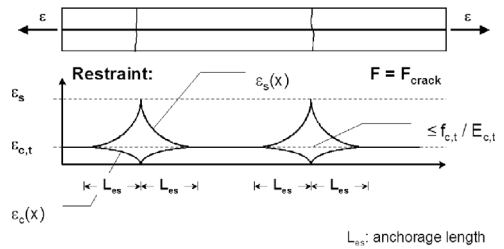


Figure 4. Initial phase of cracking.

Directly in the crack only the reinforcement can take up stresses. The concrete does not contribute at all. Therefore steel strain reaches its maximum while concrete strain is zero. Over the anchorage length of the reinforcement, stresses are now retransferred in the concrete. Steel strain is reduced, but concrete strain increases at the same time. At the point of full anchorage of the reinforcement steel and concrete strain have the same value.

The section is uncracked and there is no slip between reinforcement and concrete any more.

If now restraint deformation ( $=\Delta l$  of the member) is increased, more cracks will form based on the same principle (see figure 5).

It is obvious that another crack just can form, if enough load has been transferred from steel back to concrete to exceed concrete tensile strength again. The more cracks form, the shorter the remaining anchorage length between two cracks will be. When there is not enough anchorage length available, no additional cracks can form and concrete tensile strength can not be exceeded any more. Even at very high imposed deformations it is not possible to make the concrete crack again. At this state the existing cracks just will become wider and the final state of cracking is reached. Therefore the minimum crack distance is  $1 \times$  anchorage length, the maximum crack distance is  $2 \times$  anchorage length (see figure 5).

In practice, concrete structures usually are in-between these two phases and the final state of cracking is not reached.

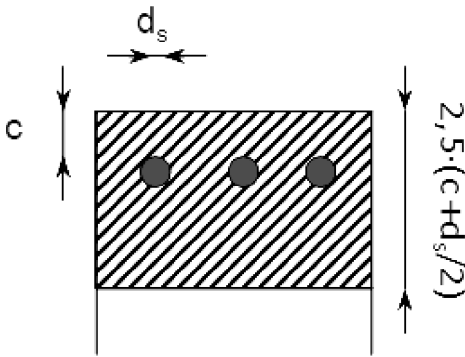


Figure 1. Effective area.

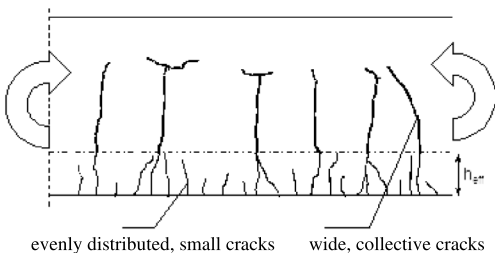


Figure 2. Collective cracks outside effective area.

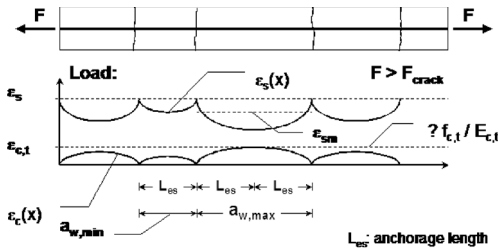


Figure 5. Final state of cracking.

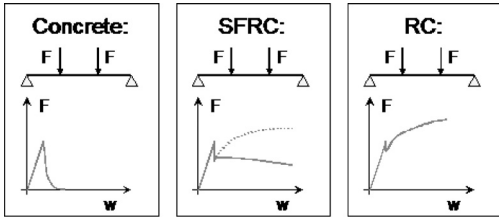


Figure 6. Bending test with plain concrete, steel fibre reinforced and reinforced.

For serviceability design, yielding of the steel is not taken into account. The design is usually based on a steel stress between  $150 \text{ N/mm}^2$  and  $350 \text{ N/mm}^2$ ,  $200 \text{ N/mm}^2$  seems to be quite common. However, it is always necessary to provide an over-critical reinforcement which can take up the stresses that are released at cracking without yielding. Otherwise the cracked section would always be the weakest part of the structure (see figure 6). With undercritical reinforcement, only one crack would form which's width would permanently increase (restraint deformation according figures 4 and 5). Here the yield point of the reinforcement situated in the crack would be exceeded and subsequently multiple cracking would not be possible.

### 3 EFFECT OF STEEL FIBRES ON COMBINED REINFORCEMENT

Keeping these basic mechanisms of cracking and crack formation in mind, there remains only one possibility to reduce crack width: reduce the required anchorage length in order to get more and therefore smaller cracks.

This goal can be achieved by several means:

- increase bond by reducing steel bar diameter
- increase the amount of steel
- reduce the load which is released when cracking

In practice, the possibilities to reduce steel diameter or increase the amount of steel is limited. Sometimes an amount of reinforcement is foreseen which makes it impossible to cast and compact the concrete properly. But the quality of casting and compaction is evident to the quality (cracking) of the structure. . .

#### 3.1 Properties of steel fibre reinforced concrete

The use of steel fibre reinforced concrete (SFRC) is another option. But before the mechanism can be explained some principles about steel fibre reinforced concrete need to be described:

It is well known that steel fibres provide a post crack strength to the concrete. After cracking, the fibres bridge the cracks and transfer loads from one side to the other. For normal fibre dosages the post crack strength is always lower than the first crack strength (see straight line in figure 6, SFRC). Therefore steel fibre reinforced concrete can be considered as an undercritical reinforcement. Only with high performing fibres at high dosages (e.g.  $50 \text{ kg/m}^3$  Dramix® RC-80/60-BN) the ultimate load derived from a bending test is higher for the cracked than for the uncracked section (see dotted line in figure 6, SFRC).

Due to this undercritical behaviour, steel fibre reinforced concrete without additional reinforcement can not be used to calculate a crack width—except in those cases where a compressive zone is permanently present (pre-stressed structures or those with compressive loads, statically indeterminate structures without axial restraint, . . .).

However, when using steel fibre reinforced concrete without additional reinforcement cracks will always be smaller in practice than those in plain concrete. Even if one cannot calculate the crack width in some cases it is reasonable to use steel fibre reinforced concrete instead of plain concrete. Apart from the effect of steel fibres on crack width, the geometry of the crack itself is influenced in a positive way, too:

Usually steel fibres bridge a crack at a non-perpendicular angle. Therefore the fibre will be bent already at small crack widths. Due to the locally increased friction, compressive stresses parallel to the crack surface are induced. As a consequence, the associated tensile stresses perpendicular to the crack can lead to a secondary crack (see figure 7). They can be compared with those cracks in reinforced concrete which can be found in the zone directly around the rebars. With steel fibre concrete they can be observed over the whole cracked section.

Subsequently cracks become more curved. Fragmentation, offset and ramification can be identified (see figure 8). Resistance to intruding substances, especially liquids, is substantially increased, even outside the effective area (see figure 1) of a combined or traditional reinforcement.

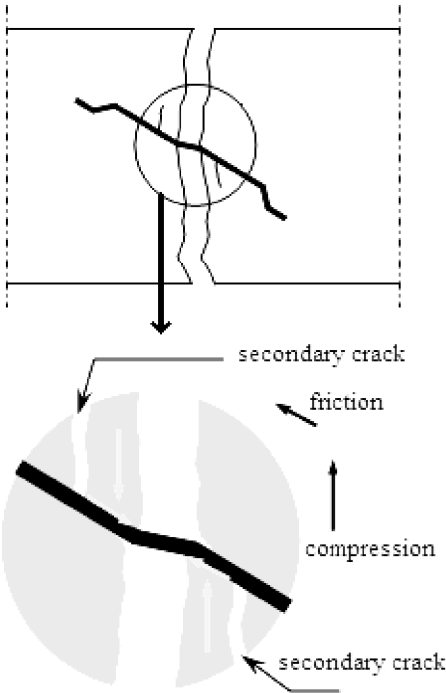


Figure 7. Secondary cracks due to steel fibres.

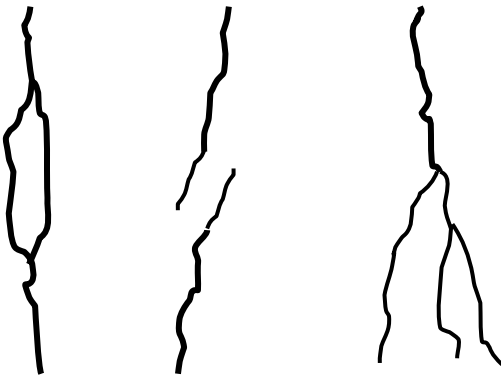


Figure 8. Fragmentation, offset ramification.

### 3.2 Design of combined reinforcement

Despite that, many applications have to be designed for crack width. For instance, an estimation of the expected crack width has to be given to prevent corrosion of rebars or esthetical damage, ensure water tightness or protect the environment from dangerous substances. In these cases steel fibres can contribute significantly to reduce crack width and/or to reduce the amount of required minimum reinforcement.

As some part of the load still can be taken by the “concrete” after cracking, not the full amount of energy is released compared to concrete without steel fibres. Assuming a concrete tensile strength of e.g.  $3.0 \text{ N/mm}^2$  while providing an equivalent tensile strength (post crack strength) of  $1.0 \text{ N/mm}^2$  when using steel fibres, only  $2/3$  of the full crack load has to be considered for the design. This has a strong effect on the required reinforcement.

As crack width is a function of concrete tensile strength, know formula or other standards can be adopted easily by subtracting equivalent tensile strength  $f_{ct,eq}$  from effective concrete tensile strength  $f_{ct,ef}$ .

$$w_{cal} = f (f_{ct,ef} - f_{ct,eq,t}) \quad (2)$$

In order to eliminate the influence of time, a neutral factor (here:  $\alpha_f$ ) shall be introduced. By doing so, the material properties of tensile strength and equivalent tensile strength are based on the same concrete age—which is evident. A time correction factor according (1) can be used to achieve the resulting value  $f'_{ct,ef}$ .

$$f'_{ct,ef} = f_{ct,t} \cdot (1 - \alpha_f) \cdot \beta_{cc,t} \quad (3)$$

$$\text{with: } \alpha_f = f_{ct,eq,t=28} / f_{ct,t=28} \quad (4)$$

The reduced tensile strength  $f'_{ct,eff}$  can be applied in calculations according chapter 4.4.2, EC2-1, to determine the crack width for a combined reinforcement.

In some design rules are given for control of cracking without direct calculation. This method is very practical and easy to use but more economic (and realistic) results can be achieved with direct calculation of crack width.

$$d_s^f = d_s \cdot \sqrt{1 + \frac{f_{ct,eq}}{f_{ct}}} \quad (5)$$

$$s_{max}^f = s_{max} \cdot \frac{f_{ct}}{f_{ct} - f_{ct,eq}} \quad (6)$$

(concrete age 28 days) with:

$d_s$  adjusted maximum bar diameter without the effect of fibres

$d_s^f$  adjusted maximum bar diameter including the effect of fibres

$s_{max}$  maximum bar spacing without the effect of fibres

$s_{max}^f$  maximum bar spacing including the effect of fibres

## 4 APPLICATION PROJECTS

A variety of projects has been built with combined reinforcement in countries all over the world. Some examples shall highlight and support the use of combined reinforcement.

The surface of an existing floor was damaged after some years in use (industrial park in Ismaning, Germany 2003). A layer of 8 cm was milled and replaced by 8 cm new floor with combined reinforcement. The new layer was separated from the old slab by a double layer of plastic sheet. The joint distance was 27 m × 30 m, the total size 3,400 m<sup>2</sup>. A mesh Q295 (steel section 2.95 cm<sup>2</sup>/m in both directions) was combined with 35 kg/m<sup>3</sup> Dramix<sup>®</sup> RC-65/60-BN (end-hooked, length 60 mm, diameter 0.9 mm). The calculated crack width of 0.2 mm was not exceeded. Construction was simplified and sped up due to the use of a light mesh. A concrete pump was not needed as the truck mixers could drive directly to the pouring point. Laying the light mesh could be done simultaneously with the pouring when needed.

An industrial floor should act as a secondary barrier against hazardous substances eventually leaking from their containments (production facility, Waldenburg, Germany 2003). Crack width needed to be limited to 0.1 mm in this case. The 20 cm thick slab was poured on a double layer of plastic sheets to reduce the stresses due to restraint deformation. Joint distances were about 30 m × 30 m. A top mesh Q513 (steel section 5.13 cm<sup>2</sup>/m in both directions) was combined with 30 kg/m<sup>3</sup> Dramix<sup>®</sup> RC-80/60-BN (end-hooked, length 60 mm, diameter 0.75 mm). The total size of the project was 15,000 m<sup>2</sup>. Instead of a heavy reinforcement consisting of a large number of single rebars, a strong mesh could be combined with high performing steel fibres. The time for installing the reinforcement was significantly reduced so that laser screed and topping spreader could be used. This reduced construction time and improved the total quality of the floor.

The foundation slab of a production facility had to resist any possible vibrations which could affect the production of very precise optical equipment (Carl Zeiss, Oberkochen, Germany 2001). A slab thickness of 150 cm was needed to meet the requirements. The traditional, very heavy reinforcement for crack control due to dissipation of hydration heat was replaced by a four layer combined reinforcement: 1st layer (bottom) was 40 cm with 40 kg Dramix<sup>®</sup> RC-65/60-BN (see above) and a double mesh Q513 (see above), 2nd and 3rd layer were 40 cm with 15 kg Dramix<sup>®</sup> RC-65/60-BN while the 4th layer was 30 cm with 40 kg Dramix<sup>®</sup> RC-65/60-BN and rebar Ø16–10 cm. The layers were poured “fresh in fresh” with a maximum field size of 7,430 m<sup>3</sup> and a total project size of 12,000 m<sup>2</sup>. The installation time for the reinforcement was considerably reduced. Still

acceptable rebar diameters at sufficient distance and mesh could be used. Pouring and compacting the concrete was not interfered by a narrow reinforcement. The top of the final slab is indicated by the wooden beam.

In 2004, a combined reinforcement was applied to the concrete face rock-filled dam in the Longshou 2nd phase project, China. The highest height of the dam is 146.5 m. The dam is located in an area with frequent seismic activity, dry and cold weather with large temperature differences between day and night. For some panels only traditionally reinforced concrete was used, for the other panels the same amount of reinforcing steel plus steel fibres were used. The main steel mesh ratio was 0.4%, the transverse steel mesh ratio was 0.35%, the dosage of Dramix<sup>®</sup> RC-80/60-BN (see above) was 35 kg/m<sup>3</sup>. The longest steel fibre panel has a length of 75 m, thickness varies from 70 cm at the dam base to 30 cm at the crest. 1,440 m<sup>3</sup> concrete were installed. Panels without steel fibres showed non tolerable cracking already after a short time. Quite some repair efforts had to be done. The combined reinforced panels could even resist an earthquake without visible cracks.

In Valencia, a combined reinforcement was used for a thin shell structure in the oceanographic park. 50 kg/m<sup>3</sup> Dramix<sup>®</sup> RC-80/35-BN (end-hooked, length 35 mm, diameter 0.45 mm) and a single mesh Ø8–15 cm were applied. Due to the curvature and the limited shell thickness of 6 cm to 12 cm it would have been very difficult to install a complicated traditional reinforcement in an accurate and safe way. With the chosen combination, both serviceability and ultimate limit state could be designed.

## 5 STEEL FIBRES IN CONCRETE

The EN 14 889-1 specifies requirements for steel fibres for use in mortar and concrete. It covers fibres intended for use in mortar and concrete, including sprayed concrete, flooring, precast and repair.

Steel fibres are available in different sizes, shapes and qualities. All of them will have their own effect on the concrete behaviour and quality. Therefore the required steel fibre dosage to meet design and structural requirements has to be related to the steel fibre performance.

### 5.1 Length/diameter ratio

The longer the fibre, the better the bond of the steel fibres in the matrix, the more difficult to pull the fibre out of the matrix. It is generally recommended to use a fibre length of at least three times the size of the maximum aggregate. The smaller the diameter the higher the number of fibres per unit weight and therefore



Table 1. Tolerances on fibre length and diameter.

Symbol	Deviation of the individual value relative to the declared value	Deviation of the average value relative to the declared value	
$l, l_d^*$	$\pm 10\%$	$\pm 5\%$	$\pm 1.5$ mm
$D$	$\pm 10\%$	$\pm 5\%$	$\pm 0.015$ mm
$\lambda$	$\pm 15\%$	$\pm 7.5\%$	

\*(if applicable).

the more efficient the reinforcement becomes. Steel fibres with a high length/diameter ratio have a better performance.

### 5.2 Tolerances

#### 5.3 Hooked ends

Tensile stresses induced in the concrete are transferred to the steel fibres thanks to the durable bond characteristics between both basic materials. The adherence can be improved by enhancing the mechanical anchorage and choosing a suitable shape of the steel fibres. Hooked ends, enlarged ends, crimped wire, . . . are different shapes which are available on the market.

#### 5.4 Tensile strength

An efficient load transfer will result in a high tensile stress in a small diameter steel fibre. Efficient steel fibres need to have a high tensile strength to avoid fibre fracture. The use of high strength concrete and shotcrete have enhanced the need to develop high tensile steel fibres.

#### 5.5 Glued fibres

Good fibres should have a high length/diameter ratio. This can however cause problems when mixing. Loose fibres, particularly those with a high length/diameter ratio, are difficult to spread evenly in the concrete mixture. Bekaert has overcome this problem of “fibre balling” by glueing the Dramix fibres.

## 6 CONCLUSION AND OUTLOOK

Steel fibre reinforced concrete in combination with traditional reinforcement can significantly reduce crack width and/or the required amount of reinforcement. The quality of the structure is increased due to better material properties and workability.

Existing design rules can “easily” be modified for the use of combined reinforcement. However, specific and more detailed design rules are also available and verified by testing.

The use of combined reinforcement will certainly increase in fields of application which are now dominated by conventionally reinforced concrete like huge jointless structures, water and liquid tight structures etc. The excellent experiences from the past with those structures where combined reinforcement was used will give a strong support.

## REFERENCES

- Brite-Euram, BRPR-CT98-0813. *Test and design methods for steel fibre reinforced concrete.*
- Deutscher Ausschluß für Stahlbeton 1996. *Richtlinie für Betonbau beim Umgang mit wassergefährdenden Stoffen.* Berlin: Beuth-Verlag GmbH.
- Deutscher Beton- und Bautechnik-Verein e. V. Fassung Oktober 2001. *DBV-Merkblatt Stahlfaserbeton.* Berlin: Eigenverlag.
- European Committee for Standardization: EC2-1. *Design of Concrete Structures—Part 1: General rules and rules for buildings.*
- Schnütgen, B. Schriftenreihe des Instituts für Baustoffe, Massivbau und Brandschutz der TU Braunschweig (iBMB). *Stahlfaserbeton für den Umweltschutz, Fachbeitrag zum Heft 100 der Schriftenreihe des Ibm.* Braunschweig: Eigenverlag.
- Winterberg, R. Deutscher Ausschluß für Stahlbeton, *Einfluß von Stahlfasern auf die Durchlässigkeit von Beton, Heft 483.* Berlin: Beuth-Verlag GmbH.

# New aspects on bridge design for durability

M. Empelmann, V. Henke, G. Heumann & M. Wichers

*Institute for Building Materials, Concrete Construction and Fire Protection (iBMB),  
Technical University of Braunschweig, Germany*

**ABSTRACT:** The present paper deals with design aspects of the life-cycle optimization of reinforced and prestressed concrete bridges. The main aspects such as “structural system”, “concrete technology” and “structural detailing” will be dealt with more closely. Based on a typical example the possibilities and the effectiveness of optimization measures will be quantified.

## 1 INTRODUCTION

Bridges are important, linking structures in the traffic infrastructure of each country. Within the Federal road system of Germany approximately 36,000 bridges existed until the end of 2001, with an assumed value of almost 40 billion euros. As shown in Figure 1, most of these bridges were constructed with reinforced or prestressed concrete. The turbulences within the commodity markets and the price development for construction steel will make sure that this trend continues in the future, which means that bridges will be predominantly erected using concrete as the main construction material.

With regard to the aimed life-expectancy of 100 years for bridge constructions, maintenance and repair strategies have to be developed for the existing bridges, but as well for new bridge constructions. The durability has to be used as the fundamental basis, in order to ensure a sufficient serviceability during the life-cycle of the structure. This aim can be achieved by the erection of “durable bridge constructions”. These have a far higher life expectancy and require

a lower maintenance expenditure, i.e. lower costs for supervision, maintenance and repair.

## 2 OPTIMIZATION APPROACHES FOR BRIDGE CONSTRUCTIONS AND ITS CONCRETE COMPONENTS

### 2.1 Fundamentals

Within the scope of the own reflections, regarding an improved life-cycle for concrete and prestressed concrete bridges, four main categories were chosen: “construction”, “structural system”, “concrete technology” and “structural detailing”. As the improvement of the actual construction was already dealt with in numerous papers, and is a fundamental erection problem, this aspect will not be regarded in this paper more closely. In the following the main aspects will be the “structural system”, “concrete technology” and “structural detailing”.

### 2.2 Structural system

An old design rule specifies that the number of bearings and joints in bridges should be kept low in order to reduce their high construction and maintenance costs (design aim: integral bridges). Contrary to this design aim it is often tried to reduce restrained forces in bridges by the arrangement of bearings and joints, in order to neglect this forces in the structural design.

Compact cross sections show a much more favourable behaviour with regard to damaging environmental influences. This means that compact cross sections, such as slabs, wide T-beams or sections with a continuous bottom surface are superior to filigree load carrying systems with regard to their durability.

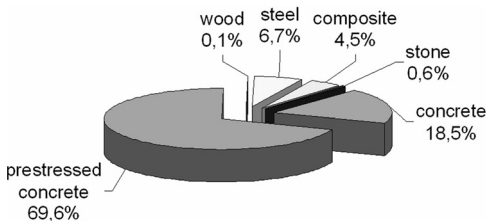


Figure 1. Percentage of different bridge constructions for Federal roads according to the bridge surface, state 2004 (Bundesministerium für Verkehr, Bau und Stadtentwicklung (2006)).

### 2.3 Concrete technology

The use of high performance concrete (HPC) is very often only taken in consideration for bridge construction, due to its higher compression strength. Considerations taking durability aspects for bridge superstructures into account have so far very seldom carried out, though HPC has many advantages in this respect.

Contrary to normal strength concretes, HPC provides a very high density, especially if silicate flour is used as an aggregate. The density has a very positive influence on the durability, especially on the resistance against chemical and corrosive influences on the reinforcement. Additionally an improved resistance against mechanical abrasion and frost and/or frost chloride (due to de-icing salts) effects can be obtained. In other countries HPC has been used for years and favourable experiences were obtained in Scandinavia, America and Australia.

### 2.4 Structural detailing

The minimum and additional safety concrete cover according to DIN 1045-1 is based on the exposure classes. The concrete cover has to fulfil different tasks: bond securing, protection of the reinforcement against damaging chemical influences and protection of the reinforcement against fire. An upper limit of the concrete cover is not given in DIN 1045-1 nor in the special report for bridge design "DIN Fachbericht 102". With an increased concrete cover the protection of the reinforcement against carbonization and chemical influences will be improved.

Damages, which occur in spite of the fulfilment of conventional serviceability limit state design requirements, normally are due to a lack of robustness. The robustness is normally secured by constructive measures, such as the arrangement of a nominal reinforcement. Sufficient robustness means that damages will be noticeable in time (i.e. by large deformations) but their influence will not lead to the complete failure of the structure (i.e. by the formation of plastic hinges).

## 3 EFFECTIVENESS QUANTIFICATION OF SINGLE OPTIMIZATION APPROACHES BY PROBABILISTIC LIFE-CYCLE PROGNOSIS

### 3.1 Basics of life-cycle prognosis or design

The design of durable bridge structures is, with regard to the economical aspects of the owner or operating company, an optimization task. This means that it should be tried, by a well considered construction and material choice, to minimize the erection costs, later

maintenance, inspection and repair expenditure and possible closure costs for the whole structure.

The aim is to derive from the accumulation of single building element states the overall state of the complete structure. So far, this has been, due to the lack of appropriate numerical methods and basic data, only been possible with a great deal of effort and for simple applications. A method, which has been developed in the meantime, is the probabilistic life-cycle prognosis and its application potential will be shown in the following simple example.

### 3.2 Differentiation between descriptive design concept and life-cycle design

For time being, the durability of concrete constructions is assured according to DIN EN 206 and/or DIN 1045 by a descriptive design concept. The design is based on the choice of decisive exposure classes. To these exposure classes minimum requirements with regard to the concrete used and the minimum concrete cover are assigned. Contrary to the load carrying design of construction elements, a safety concept is not recognizable for this procedure, which is supposed to secure the durability of a structural element with regard to the serviceability limit state design. For the structural engineer involved in such a design procedure the meaning and / or relevancy of these limit state elements (concrete cover, cement content) remain unclear.

These basic deficiencies can be resolved by a probabilistic life-cycle design. The basics of such a life-cycle design and the design fundamentals for the main concrete damaging factors were mainly, e.g. formulated in Gehlen (2000).

With regard to the durability of bridge structures, the effectiveness of single materials against damaging environmental effects, in connection with structural details, can be assessed by a life-cycle design. The results of such a design are verifiable and offer the possibility to compare different materials and constructive influences (e.g. concrete cover) with regard to their influence on the durability in a transparent way.

### 3.3 Example for the use of a life-cycle prognosis and design

Based on a typical prestressed concrete superstructure and by the use of the design model described in Gehlen (2000), the anticipated life-cycle of this building member and the effect of the main basic variables on the life-cycle, will be assessed with regard to the influence of carbonization and chloride effects. The reliability calculation for the determination of the safety index  $\beta$  and the parameter sensitivities will be carried out using the programme system COMREL.

The system used for this design and the decisive locations for the life-cycle design in the span (U1)

and support (U2) region are given in Figure 2. The most important damaging effect on a concrete bridge superstructure is the spread of corrosion on the reinforcement. Normally this is induced by carbonization of the concrete or chloride penetration.

These damaging mechanism will be investigated in two different time-step life-cycle prognoses for the relevant locations. The building member will be regarded as damaged, as soon as the carbonization front or the critical chloride concentration has reached the steel reinforcement. If this state is reached and no maintenance measures will be undertaken, it is unavoidable that reinforcement corrosion occurs and on the long run cracks and surface spillings will occur on the concrete superstructure. With regard to carbonization the bottom of the superstructure, which is protection from the rain, is decisive. Contrary, for the design with regard to chloride penetration the upper side of the building member will be investigated. The chloride penetration results from de-icing salts used during the winter on the bridge surface. In the region of untight expansion joints or sealings these chlorides can reach the concrete surface.

According to the German "DIN Fachbericht 102" for the environmental influences the exposure classes XC 4 and XD 1 have to be used. The nominal value of the concrete cover is 45 mm for both cases, as the minimum values for the concrete cover according to "DIN Fachbericht 102" are independent from the decisive exposure class. The minimum requirements (see parameter configuration PM1) are given in table 1. The necessary additional requirements (e.g. for the local

Table 1. Compilation of the basic design parameter.

Parameter configuration	Concrete	Concrete cover $c_{nom}$	Remarks
PM1	C35/45	45 mm	Minimum requirement according to "DIN Fachbericht 102"
PM2	C60/75	45 mm	Use of a higher strength concrete
PM3	C35/45	55 mm	Use of an increased concrete cover
PM4	C35/45	35 mm	Use of an reduced concrete cover
PM5	C60/75	35 mm	Use of an reduced concrete cover and a higher strength concrete

climate in the region of the structure and the magnitude of the environmental effects) are assumed according to the normal bridge design in Germany. It should be considered, that these basic conditions normally have to be specified individually for each bridge.

A quantification of the construction parameters influences can be achieved by a sensitivity analysis, which can be carried out with the programme system COMREL. This analysis was carried out for a time-span of  $t = 100$  years, this is equivalent to the expected life-cycle, with the given design parameters PM1 and additional influence factors given in Figure 3. It can be seen from the results, that the basis variables

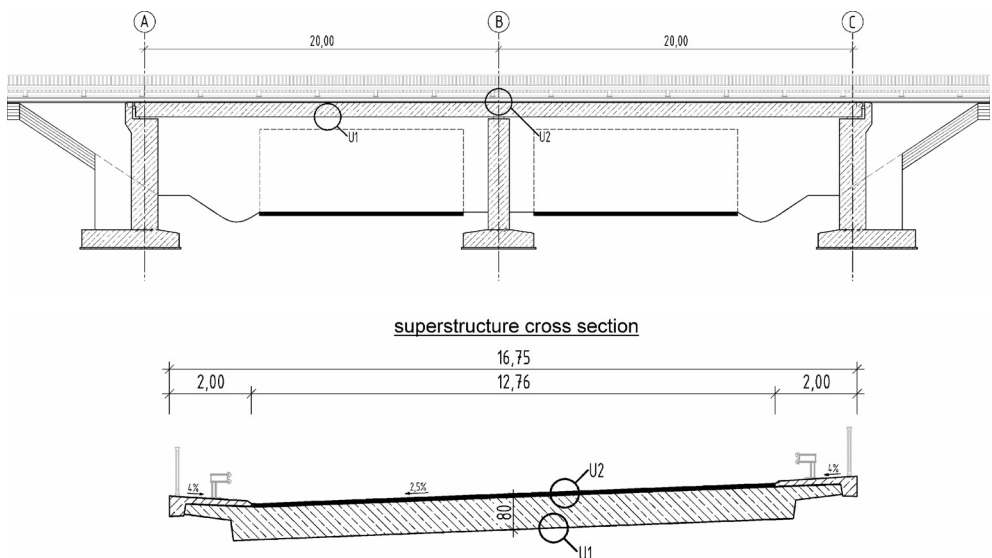


Figure 2. Example for a prestressed concrete bridge and design regions U1 and U2.

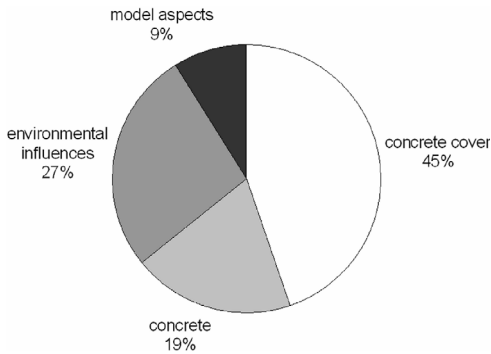


Figure 3. Sensitivity of the basic variables of a life-cycle design for a time-span of 100 years and parameters PM1.

“concrete” and “concrete cover”, which can be influenced, result in approximately 65 % of the relative influence.

The reliability index with regard to carbonization, depending on the life-span of the construction and the parameter constellation according to the minimum requirements (PM1) is given in Figure 4. After the definition of a socially accepted safety level, in analogy to a load carrying design, the derived safety index can be compared with the necessary safety level. This verification will be carried out for the serviceability limit state. If the reliability of the building member has to be increased, the practical question which measures or alternatives have the maximum effects has to be answered.

The options, available for the present example are:

- Use of a higher strength concrete with a higher density.
- Increase of the concrete cover.

In order to clarify these influences, life-cycle design for the variants PM2 and PM3 was additionally carried out. As can be expected and is shown for the design region U1, the use of a higher strength concrete (PM2) or an increased concrete cover by 1 cm (PM3) can increase the life-cycle of the structure, for the same target reliability, considerably, see Figure 4. But the results show too, that the descriptive procedure according to “DIN Fachbericht 102” (PM1) results in a sufficient reliability (reliability index between 1.3 and 2.3 according to Joint Committee on Structural Safety).

The additional investigations (PM4 and PM5) show the high influence of a reduced concrete cover on the time-dependent development of the reliability index, which can occur due to inadequate construction. It can be shown, that by the use of a higher strength concrete the target reliability according to “DIN Fachbericht 102”, despite of the reduced concrete cover,

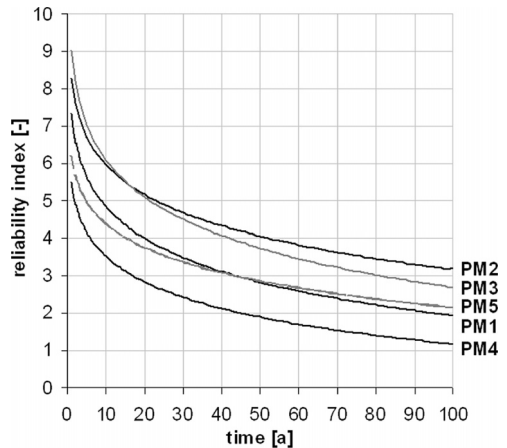


Figure 4. Time-dependent limit state building member reliability for corrosion induced by carbonisation.

can be reached. As far as corrosion induced by carbonisation is concerned, the use of a higher strength concrete can provide an additional safety reserve.

Figure 5 shows the reliability index with regard to chloride induced reinforcement corrosion for the design region U2, according to the minimum requirements (PM1). Basically for the design model and the model parameters the statements given above are valid.

It was assumed, that a sealing failure can be assumed after its mean life-expectancy of approximately 20 years and the concrete is exposed to the chloride effects as an unprotected building member.

As the effect of constructive measures to avoid a chloride exposure is very often limited, as a numerous damages on bridges have shown in the recent years, the resistance against chloride penetration into a bridge superstructure should be improved. This can be achieved by an increased concrete cover and / or an optimization of the concrete resistance against chloride penetration. As an example the effect of the use of a higher strength concrete, with a higher density (PM2), is given in Figure 5.

These design examples show, that by the use of a probabilistic life-cycle prognosis as a design instrument for securing the durability of a structural element, it is possible to obtain a very differentiated information about the building element under investigation. Additionally, the reliability of the construction can be increased by selective optimization measures, and thus can be secured for the relatively long bridge life-cycle. Specific aspects, such as the environmental exposure, as well as the economical interest of the owner and/or operating company can be incorporated in such a “performance-based-design”.

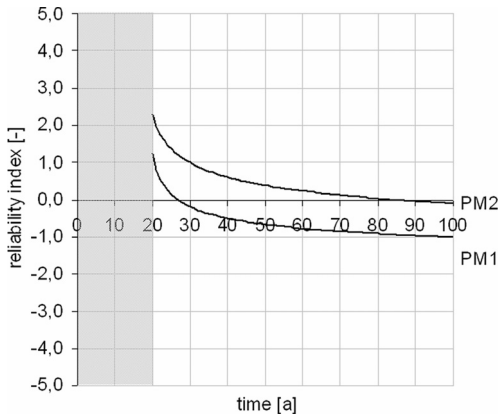


Figure 5. Time-dependent limit state building member reliability for corrosion induced by chloride penetration, assumed sealing failure after 20 years.

#### 4 SUMMARY

In the future the already existing bridges will require an enormous maintenance and repair measures. Therefore, for new constructions the design should be focussed on durable and low-maintenance bridge constructions. In the scope of this paper considerations concerning the life-cycle of single building elements and the relative future maintenance and repair efforts as well as a weak-point analysis was given. On this basis conclusions on the improvement of concrete bridges can be drawn.

By the use of new building materials, e. g. high performance concrete, it is possible to optimize the main influence parameters with regard to the durability, i.e. concrete density and concrete cover. The choice of an appropriate cross-section offers the possibility to reduce the surfaces exposed to the environment. Constructive measures, such as an increased concrete cover, further increase the durability and are an approach for a “performance-based-design” defined by the operating company.

All measures aimed at increasing the durability reflect more or less in the construction costs. Nevertheless it is profitable to incorporate measures for increasing the durability with regard to “low-maintenance bridges” already in the design, as the initial investments have to be compared with the higher life-time of the structure. Additionally, the very often neglected economical aspects, which result from construction sites and increased pollution due to traffic hindrance, have to be evaluated financially.

The influences of the proposed optimization measures can be quantified by a life-cycle prognosis and design. This was shown with a simple example. For the time being there is a lack of systematic considerations and engineering design models for the proposed optimization possibilities. With regard of an overall durability optimization for bridge constructions, further research efforts are necessary.

#### REFERENCES

- NORM DIN 1045-1: 2001-07: *Tragwerke aus Beton, Stahlbeton und Spannbeton—Teil 1: Bemessung und Konstruktion.*
- Deutsches Institut für Normung 2003. *DIN-Fachbericht 102. Betonbrücken.* Berlin: Beuth Verlag.
- Joint Committee on Structural Safety (JCSS) 2002. *Probabilistic Model Code.* 12th draft.
- Bundesministerium für Verkehr, Bau und Stadtentwicklung 2006. *Bericht über die Qualität, Dauerhaftigkeit und Sicherheit von Spannbetonbrücken.* Berlin.
- Gehlen, C. 2000. Deutscher Ausschuss für Stahlbeton. *Probabilistische Lebensdauerbemessung von Stahlbetonbauwerken. Zuverlässigkeitsbetrachtungen zur wirksamen Vermeidung von Bewehrungskorrosion.* *DAfStb, Heft 510,* Berlin: Beuth Verlag.
- Haardt, P. 2002. Bundesanstalt für Straßenwesen. *Entwicklung eines Bauwerks-Management-Systems für das deutsche Fernstraßennetz—Stufe 1 und 2.* Schlussbericht zum AP-Projekt 99245. Bergisch Gladbach.
- Reliability Consulting Programs (RCP) 2004. STRUREL, a Structural Reliability Analysis Program-System, COMREL & SYSREL: *Users Manual.* München.

# Fuzzy probabilistic analysis of prestressed concrete structures

L. Giordano, G. Mancini & F. Tondolo

*Politecnico di Torino, Torino, Italy*

**ABSTRACT:** the evaluation of the safety level in concrete structures should be carried out considering the stochastic behaviour of the main parameters involved, not only under ultimate conditions, but also under serviceability and durability conditions. Particularly in concrete structures, the large variability of mechanical and rheological parameters may give rise to important deviations from the expected behaviour if a deterministic approach is used.

On the other hand, it is well known as some parameters required to define the mean values of the probability density functions are themselves subjected to some uncertainties, but it is not always possible to define the corresponding statistical distributions. The problem can be solved assuming those parameters as fuzzy variables, and converting the probabilistic analysis in a fuzzy-probabilistic one.

In this paper, a probabilistic analysis and a fuzzy probabilistic analysis of a prestressed roof beam is performed in order to evaluate its behaviour under serviceability conditions, with particular attention to the crack formation limit state. Loads, shrinkage, creep and tensile strength are considered to be stochastic variables, whilst for the other variables involved (e.g. geometric dimensions, relaxation of prestressing steel, etc.) are considered to be deterministic values. The comparison between the two approaches demonstrates the peculiarity of the fuzzy probabilistic procedure that reproduces a more comprehensive safety estimate method.

## 1 INTRODUCTION

The evaluation of the stochastic character of variables involved in structural analysis has been a subject of interest over recent years (JCSS, 2002). Such an approach allows for a more effective consideration of the design influencing parameters and for the establishment of sensitivity analysis criteria. Consequently, methods of level 3 and level 2 (within the structural safety framework) are then used for the calibration of partial safety factors, thus characterising the limit states semi-probabilistic approach (Leporati, 1979). However, it should be pointed out that the nature of the variables involved cannot be described by means of their statistical characterization only (Möller et al., 2002). A theory that handles other kinds of uncertainty, like the theory of fuzzy sets, also needs to be considered. For this purpose, in the past, convex sets and interval analysis have also been used (Moore, 1966 and Ben-Haim & Elishakoff, 1990). The theory of fuzzy sets enables the mathematical consideration of uncertainties that otherwise could not be taken into account within a conventional structural analysis. The uncertainties are essentially the lack of statistically representative samples for the evaluation of design parameters, the lack of conformity

of conventional tests on materials, the uncertainty in the correlation between the different variables, the difficulties in the evaluation of effective limit state attainment, and the human error influence. Finally, the merging between probabilistic and fuzzy sets theories produces the fuzzy probabilistic analysis.

In this paper, the evaluation of the variability effect of rheological parameters such as creep and shrinkage and their influence in concrete structures is considered. The stochastic behaviour of tensile strength, permanent loads and variable loads is also considered in the same way. The randomness of such parameters may imply a result deviation of 20% to 30% [EN1992-1-1 2003] in serviceability conditions, in particular in the evaluation of stress and deformation conditions. This randomness appears to be particularly relevant for prestressed concrete structures, in which the rheological parameters play a relevant role, particularly if variations of static schemes during the construction are to be expected. In the following, the probability of crack formation is considered as the parameter controlling the verification of the corresponding serviceability limit state. An analysis of the effects of the random variables will be performed on a pretensioned beam of a concrete roofing, first by means of a fully probabilistic procedure, and then by a fuzzy probabilistic approach,

introducing as fuzzy variables the relative humidity of the environment, the age of concrete at the introduction of permanent loads and some coefficients which depend on the type of cement and affect the shrinkage value.

It will be shown that the fuzzy probabilistic approach can be considered as a generalization of the fully probabilistic procedure; in fact, the fuzzy probabilistic method is a more detailed and comprehensive safety tool.

## 2 CRACK FORMATION IN PRESTRESSED STRUCTURES

In a prestressed structure, the crack formation may be attributed to a reduction of compressive stresses in the extreme fibres of the element. An important role in this reduction is played by prestress losses, due to shrinkage, creep and steel relaxation, whose effects are mutually dependent.

Several simplified methods have been proposed in order to calculate the prestress losses, such as the Effective Modulus method, the Mean Stress method and the Age Adjusted Effective Modulus method. On the other hand, the exactly evaluation of losses for any load history, need the use of a step-by-step numerical procedure able to describe the interaction between the concrete stress and the residual prestress force (M. Tadros et al. 1977, CEB 1984). In fact as the prestressing strand tension is decreased, concrete creeps less, resulting in some recovery. To account for the continuous interactions in time between creep and shrinkage of concrete and the relaxation of strands, time will be divided into intervals; the duration of each time interval can be made progressively larger as the concrete age increases. The stress in the strands at the end of each interval equals the initial conditions at the beginning of that time interval minus the calculated prestress losses during the interval.

The stresses and deformations at the beginning of an interval are the same as those at the end of the preceding interval. With this time-step method, the prestress level can be estimated at any critical time of the life of the structure.

Then the stress at time  $t$  in a simply supported beam in the midspan section at the edge with lower compression may be expressed as:

$$\sigma_c(t) = \sigma_c(t_0) + \frac{\Delta N_p(t)}{A} + \frac{\Delta M_p(t)}{W} + \frac{M_{G2} + M_Q}{W} \quad (1)$$

The crack formation is reached when the following inequality is violated

$$\sigma_{int}(t) \leq f_{ct} \quad (2)$$

Table 1. Symbols for equations (1) and (2).

Parameters	Definitions
$\Delta N_p(t) = \sum \Delta \sigma_{p,i}(t) \cdot A_{p,i}$	Variation of prestressing axial force due to creep, shrinkage and relaxation
$\Delta M_p(t) = \sum \Delta N_{p,i}(t) \cdot e_{p,i}$	Variation of prestressing bending moment due to creep, shrinkage and relaxation
$\Delta \sigma_{p,i}(t)$	Variation of stress in the any strand levels due to creep, shrinkage and relaxation
$A_{p,i}, e_{p,i}$	Area and eccentricity of any strand levels
$A, W$	Area and resistance modulus for tensed edge of concrete section
$\sigma_c(t_0)$	Stress in tensed edge of the beam due to the self weight and initial prestressing
$\sigma_c(t)$	Stress in tensed edge of the beam at time $t$
$M_{G2}, M_Q$	Bending moment due to permanent and live load
$f_{ct}$	Tensile strength of concrete

All symbols in equations (1) and (2) are declared in Table 1.

## 3 PROBABILITY OF CRACK FORMATION IN PRESTRESSED STRUCTURES

If variables in equations (1) are deterministic the internal actions level corresponding to crack formation can be directly evaluated transforming the inequality (2) in the corresponding equality. Instead the variables present a stochastic nature described by corresponding probability distributions. However, as usual in engineering field, only the variables characterised by significant variation are considered as stochastic parameters, assuming the remaining ones as deterministic; in such a way the problem maintains a dimension that can be easily handled.

In particular in this work the variable assumed with stochastic behaviour and the corresponding probability density functions (PDF) are listed below:

- shrinkage: gaussian distribution with coefficient of variation (COV)  $r_\epsilon = 0.30$  (EN 1992-1-1, 2003);
- creep: gaussian distribution with COV  $r_\phi = 0.20$  (EN 1992-1-1, 2003);
- tensile strength: gaussian distribution with COV  $r_{f_{ct}} = 0.185$  (corresponding to the 0.05 and 0.95 fractiles equal to  $0.7f_{ctm}$  and  $1.3f_{ctm}$  respectively, EN 1992-1-1, 2003);
- self-weight load: gaussian distribution with COV  $r_{G1} = 0.04$  (JCSS, 2002);



- permanent load: gaussian distribution with COV  $r_{G2} = 0.04$  (JCSS, 2002);
- live (snow) load: Gumbel distribution with COV  $r_{SN} = 0.40$  (Del Corso, 2004).

All the other variable are described as deterministic one, supposing that their variation can be neglected either due to the strict tolerances in the production process (i.e. steel relaxation of prestressing steel, steel elastic modulus) or to the small contribution in the considered topic (i.e. modulus of elasticity of concrete, concrete compressive strength, geometrical dimensions).

Let  $f_r(x)$  be the PDF of the tensile strength of concrete and  $f_s(x)$  be the PDF of the tensile stress at the tensed edge and accepting that resistance and stress are independent variables, the probability of crack formation can be expressed by the following integral

$$P_r = P_r(s > r) = \int_{D'} f_r(r) f_s(s) dr ds \quad (3)$$

where  $D'$  is the uncertainty domain.

At last it is necessary to point out how some parameters required for the definition of the stochastic variables presented above, can be described neither as stochastic variables nor as deterministic ones, but can have a satisfactory formalization using the fuzzy theory described in the following.

## 4 FUZZY THEORY

### 4.1 Theory of fuzzy set

The theory of fuzzy sets has been established by Lofti A. Zadeh (1965); its basic concept is that of "undefined extreme sets" (Dubois & Prade, 1980) or "fuzzy extreme sets". If the variables under consideration are numerically expressed, the definition of their characterizing values, rather than be binary or following an interval logic, is evaluated in agreement to a degree of membership, defined membership function  $\mu(x_i)$ . A typical representation of a one-dimensional fuzzy variable  $x$  is pictured in Figure 1, where the membership function  $\mu(x)$  is represented according with the corresponding values of  $x$  variable. Values "a" and "c" are defined extremes and "b" represents the central value; the deterministic variable is clearly identified because the event may be represent by a fuzzy variable with  $a_{i,j} \equiv b_{i,j} \equiv c_{i,j}$ .

Every event may be considered as characterized by some uncertainties and then all the variable involved can be evaluated in agreement to fuzzy approach. In general the representation of an  $X$  set is:

$$X = \{(x, \mu_A(x)), x \in X, \mu_A(x) \in [0, 1]\} \quad (4)$$

where  $A$  is the fuzzy set of  $X$ .

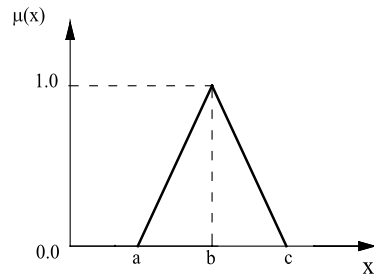


Figure 1. Representation of a one-dimensional fuzzy variable.

The fuzzy sets application can be very interesting in civil engineering application (Biondini et al., 2004), particularly in static and dynamic simulations where variability of both actions and resistance should be accounted for (Möller & Beer, 1997) in the evaluation of structural behaviour. For instance, on the resistance side, the uncertainties deriving by the construction process and by the exposition conditions during the structure service life may substantially affect the structural behaviour. In particular in re-design process of existing structures one should take into account some variables, the uncertainties of which are expressed with some difficulties or can be defined only qualitatively.

Finally the fuzzy approach, in general terms, can be considered as complementary to the probabilistic one: the two approaches are in fact used for the evaluation of substantially different kinds of information and may coexist in the structural safety field.

### 4.2 Theory of fuzzy random variables

The theoretical formulation of a fuzzy random variable may be derived from the conventional real random variable. A random variable corresponds to an event  $\omega$  within the field of  $\Omega$  events, with  $\omega \in \Omega$ ; if the events are real a real random variable may be evaluated. But if the events are affected by uncertainties is not possible to assign univocal values to the  $\omega$  events, so fuzzy values, on the opposite, should be assigned. A fuzzy random variable can then be defined by a membership function  $\mu(x_i)$ . A very clear representation of a fuzzy random variable has been given by Möller B. et al. (2003), and is pictured in Figure 2.

Similarly to the case of real random variables, fuzzy probability density functions  $\tilde{f}(x)$  and fuzzy probability distribution functions (Figure 3) can be defined; fuzzy probability function  $\tilde{P}(A_i)$  can be defined too, where  $A_i$  stands for the generic event.

The evaluation of such functions can be performed by means of  $\alpha$  level discretization method by which the determination of  $\tilde{P}(A_i)$  corresponds to that of  $P_\alpha(A_i)$  in

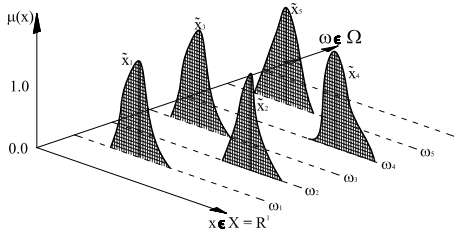


Figure 2. Realization of a one-dimensional fuzzy-random variable.

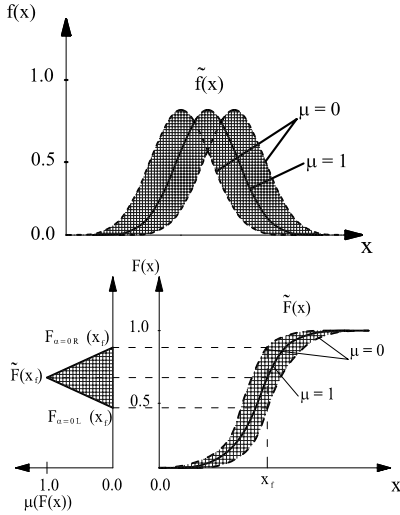


Figure 3.  $\tilde{f}(x)$  and  $\tilde{F}(x)$  of a one-dimensional continuous fuzzy-random variable.

the real probability field where kolmogorovian axioms are applicable, so avoiding the use of a fuzzy  $\sigma$ -algebra (Möller et al. 2002); in such a way a very onerous optimization problem for the definition of the extremes for every  $\alpha$  can be avoided.

Generally, the structural analysis is performed using a set of fuzzy random variables for actions and for the model; in such a way the structure behaviour is represented by a vector that includes fuzzy random variables. An optimization method for different  $\alpha$  levels is performed (Möller et al., 2000) in agreement to the extension principle of Zadeh, 1965: membership of output variables  $z_i$  is evaluated by an optimization algorithm able to give the maximum and minimum value of  $z_i$  variable for every  $\alpha$  level. At the end of the process, a fuzzy safety level may be evaluated, that is a safety level having the same character of input data. Using the procedure described by Möller et al., 2000, fuzzy random variables, fuzzy variables and real variables can be considered simultaneously and the uncertainties in

input data and in mathematical model may be appreciated in the output, transforming the safety index into the fuzzy safety index. Then a fuzziness characterizes the new format for the safety evaluation, in comparison to that of purely probabilistic methods.

#### 4.3 Fuzzy probability of crack formation in prestressed structures

The fuzzy probability of crack formation  $\tilde{P}_r$  can be evaluated by equation (5), similar to equation (4), where  $\tilde{f}_r$  and  $\tilde{f}_s$  are fuzzy probability densities of resistance and internal actions and  $\tilde{D}$  is the domain of fuzzy uncertainties:

$$\tilde{P}_r = \tilde{P}(r > s) = \int_{\tilde{D}} \tilde{f}_r(r) \tilde{f}_s(s) dr ds \quad (5)$$

In order to evaluate the fuzzy probability density of internal actions  $\tilde{f}_s$ , equations (1) and (2) can be used considering creep and shrinkage as fuzzy-random variables. The fuzzyness is introduced through the following parameters:

- relative humidity of the environment (triangular membership function with central values  $b = 70\%$  and extreme value  $a = 60\%$ ,  $c = 80\%$ ).
- age of concrete at the introduction of permanent loads (triangular membership function with central value  $b = 28$  days and extreme values  $a = 14$  days,  $c = 60$  days).
- $\alpha_{ds1}$  coefficient (triangular membership function with central value  $b = 4$  and extreme values  $a = 3.5$ ,  $c = 5$ ).
- $\alpha_{ds2}$  coefficient (triangular membership function with central value  $b = 0.12$  and extreme values  $a = 0.115$ ,  $c = 0.125$ ).

## 5 NUMERICAL APPLICATION

The effects of the stochastic variables described above are evaluated on a typical simply supported

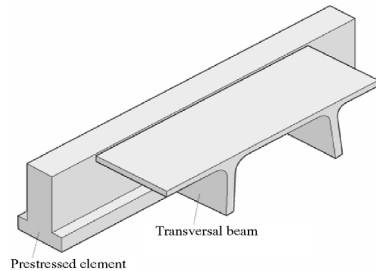


Figure 4. Schematic view of the roof system.

roof element prestressed by pretensioning (Figure 4). The element carries the transversal beams as well as the permanent and variable (snow) load applied on the roof. The main geometrical and mechanical properties of the prestressed element are summarized in Table 2. The load values are given in the same table. The structural design is performed so that the stress at the intrados in midspan equals the mean tensile strength in the serviceability limit state combination of actions (mean values for permanent loads and characteristic values for variable load). In this situation the prestress losses are evaluated adopting the mean value of shrinkage and creep.

A purely probabilistic analysis using level 2 method is performed. In particular the first order reliability method (FORM) has been used. A  $\beta$  value of 1.79 and a corresponding probability of crack opening  $Pr = 3.65\%$  is obtained. Although this probability value is aligned with the expected value for a serviceability limit state verification, it is quite low due to the magnitude of the permanent actions (characterized by a very low COV) with respect to the total actions. In order to validate the FORM approach for the analyzed problem, a Monte Carlo simulation (MCS) is performed too. The samples number is increased up to 500'000 for each stochastic variable, obtaining the

same failure probability evaluated with the level 2 method.

A sensitivity analysis may be performed to take into account the uncertainties related to the coefficients of variation of creep and shrinkage. They are the variables that have the biggest uncertainties and, at the same time, the main influence on prestress losses. Figure 5 shows as  $r_\epsilon$  and  $r_\phi$  coefficients played a secondary role in the failure probability definition. In fact a high variation of the two values can change the failure probability only from 3.4% to 3.9%, with a higher effect of shrinkage.

In this context it is possible to consider the fuzzy-probabilistic approach. Firstly the role of the value of some parameters needed to define the PDF of the stochastic variables is put in evidence. For instance Figure 6 shows the shrinkage PDF corresponding to three environmental relative humidity values, plotted assuming the same coefficient of variation  $r_\epsilon = 0.30$ .

The optimization procedure described by Möller et al.(2000) is performed in order to evaluate the extreme failure probability values. The  $\beta$  values and  $P_r$  values pictured in Figure 7 are obtained using six  $\alpha$ -levels ( $\alpha = 0.0/0.2/0.4/0.6/0.8/1.0$ ). The central values of the membership functions ( $\alpha = 1$ ) correspond to a purely probabilistic approach. The figures put in evidence that the fuzziness of the involved parameters imply an important variation of the safety

Table 2. Prestressed beam definition.

Parameter	Value	
Beam span L (m)	15.0	
Area A (m <sup>2</sup> )	0.535	
Resistant modulus for tensed edge W (m <sup>3</sup> )	0.029	
Perimeter u (m)	3.40	
Characteristic concrete compressive strength $f_{ck}$ (MPa)	45.0	
Average tensile strength $f_{ctm}$ (MPa)	3.80	
Cement type	N	
Coefficient for shrinkage calculation*	$\alpha_{ds1}$	4
	$\alpha_{ds2}$	0.12
Prestressing steel strength $f_{pk}$ (MPa)	1860.0	
Initial strand stress (MPa)	1419.0	
Strand area (mm <sup>2</sup> )	139	
Strands number:	1st level	15
	2nd level	7
Strands eccentricity (m):	1st level	0.293
	2nd level	0.243
Self-weight $g_1$ (kN/m)	12.80	
Permanent load $g_2$ (kN/m)	35.20	
Snow load (kN/m)	$q_{sk}$	5.9**
	$q_{sm}$	7.79
Age of concrete at prestressing $t_0$ (days)	4	
Permanent load introduction $t_1$ (days)	28	
Relative humidity of the environment RH (%)	70	

\* Depending on type of cement.

\*\* 98% quantile in the distribution function for the annual maximum load (50 years' return period).

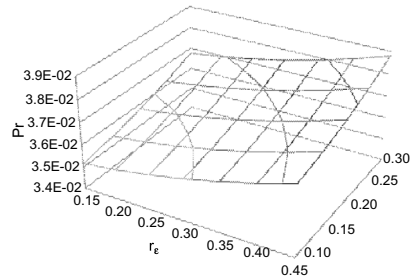


Figure 5. Probability of crack formation as a function of  $r_\phi$  and  $r_\epsilon$ .

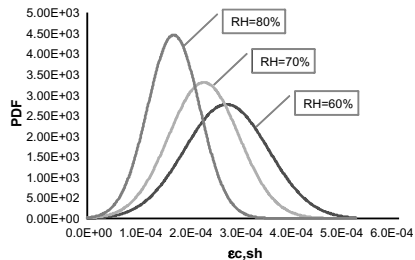


Figure 6. Shrinkage probability density function for different RH value.

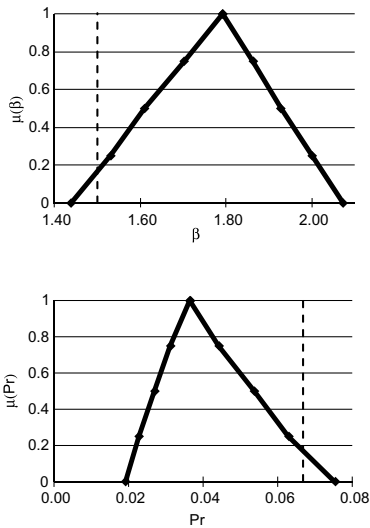


Figure 7. Membership function of  $\beta$  and  $Pr$ .

level. The maximum failure probability value obtained is greater than the maximum one computed with the sensitivity analysis. In any case, the safety level falls under the values usually accepted for the serviceability limit state ( $\beta = 1.5$  or  $Pr = 6.67\%$ ) only for the  $\alpha$ -level zero, in the specific case study considered.

Finally, using the centroid defuzzification method (Möller and Beer 2003) a single value of  $\beta$  (1.76) and  $Pr$  (4.13%) have been found.

## 6 CONCLUSION

In this paper, a pure probabilistic and a fuzzy probabilistic method for the evaluation of the probability of crack formation in prestressed concrete structures by a level 2 method have been presented. In the first case shrinkage, creep, tensile strength, permanent and variable load have been considered as stochastic variable. The second approach was based on the theory of fuzzy random variables that extends the classical concept of random variables. In particular, relative environmental humidity, time of application of permanent loads and two parameters required for shrinkage evaluation were assumed with a given degree of fuzziness; in this way the mean value and standard deviation of creep and shrinkage became fuzzy variables. Both these methods have been used for a simply supported prestressed concrete roof element in order to evaluate the probability of crack formation.

The probabilistic approach was performed both by the FORM and by a MCS; a sensitivity analysis was carry out, putting in evidence the small variation of the

probability failure from the coefficient of variation on creep and shrinkage.

With the extension to the fuzzy probabilistic approach, the single values of the probability failure were substituted by function that showed the extreme probability conditions for different  $\alpha$ -levels. Finally, using a defuzzification procedure, it was possible to determine a new value of the probability of the crack opening that took into account the overall uncertainty.

## REFERENCES

- Ben-Haim, Y. and Elishakoff, I., *Convex Models of Uncertainty in Applied Mechanics*, 1990 (Elsevier: Amsterdam).
- Biondini, F., Bontempi, F. and Malerba, P.G., Fuzzy reliability analysis of concrete structures. *Comput. Struct.*, 2004, 82, 1033–1052.
- CEB, *CEB design manual on structural effects of time-dependent behavior of concrete*, Bulletin D'Information No. 142/142 Bis, Paris, 1984.
- Del Corso, R. and Formichi, P., A proposal for a new normative snow load map for the Italian territory, *Snow Engineering. Proceedings of the Fifth International Conference on Snow Engineering*, 5–8 July 2004, Davos, Switzerland, pp. 85–94
- Dubois, D. and Prade, H., *Fuzzy Sets and Systems*, 1980 (Academic Press: London).
- EN1992-1-1, *Design of Concrete Structures, General Rules and Rules for Buildings*, 2003 (CEN: Brussels).
- JCSS, *Probabilistic Model Code*, Joint Committee on Structural Safety, 2002.
- Leporati, E., *The Assessment of Structural Safety*, 1979, Forest Grove, Research Studies Press.
- Möller, B. and Beer, M., Uncertainty analysis in civil engineering using fuzzy modelling, in *ICCCBE-VII, Proceedings of the 7th International Conference on Computing in Civil and Building Engineering*, 1997, pp. 1425–1430.
- Möller, B. and Beer, M., *Fuzzy Randomness*, 2003 (Springer: Berlin).
- Möller, B., Graf, W. and Beer, M., Fuzzy structural analysis using a-level optimization. *Comput. Mech.*, 2000, 26 (6), 547–565.
- Möller, B., Graf, W. and Beer, M., Safety assessment of structures in view of fuzzy randomness. *Comput. Struct.*, 2003, 81, 1567–1582.
- Möller, B., Graf, W., Beer, M. and Sikert, J.U., Fuzzy randomness towards a new modelling of uncertainty. In *Proceedings of the Fifth World Congress on Computational Mechanics, WCCM V*, edited by A.H.
- Mang, F.G., Rammerstorfer and J. Eberhardsteiner, pp. 1–10, 2002.
- Moore, R.E., *Interval Analysis*, 1966 (Prentice-Hall: New York).
- Papoulis, A., *Probability, Random Variables, and Stochastic Process*, 1965 (McGraw-Hill: New York).
- Tadros, M.K., Ghali, A. and Dilger, W.H., Time-dependent analysis of composite frames, *ASCE Journal of Structural Division*, April 1977, pp. 871–884.
- Zadeh, L.A., Fuzzy sets. *Inform. Control*, 1965, 8, 338–353.

# Modeling maximum live load effects on highway bridges

Michel Ghosn

Department of Civil Engineering, The City College of New York/CUNY, New York, NY, USA

Bala Sivakumar

Transystems/Licthenstein, Paramus, NJ, USA

Fred Moses

Department of Civil Engineering, University of Pittsburgh, Pittsburgh, PA, USA

**ABSTRACT:** This paper presents a procedure that describes how site-specific truck weight and traffic data collected using Weigh-In-Motion (WIM) systems can be used to obtain estimates of the maximum live load for the 75-year design life of new bridges or the two-year return period to be used for the load capacity evaluation of an existing bridge. The application of the results for the reliability-based calibration of live load factors is also presented.

## 1 INTRODUCTION

The HL-93 live load model of the *AASHTO LRFD* was developed using a 1975 truck data set collected at a single site in Ontario Canada (Nowak; 1999). Because truck traffic volume and weights have increased and truck configurations have become more complex and because of site-to-site variations, the Ontario data may no longer be representative of current U.S. vehicular bridge loads. Therefore, U.S. Federal and State highway authorities are reviewing methods for updating the HL-93 load model and live load factors so that the design of new bridges and the safety assessment of existing bridges would be more consistent with current loading conditions.

Weigh-In-Motion (WIM) systems have been developed to capture truck characteristics in an undetected manner and obtain true unbiased representations of current highway loads. The object of this paper is to outline a methodology that utilizes WIM traffic data for developing load models for bridge design and evaluation. The paper is based on the research being conducted under NCHRP Project 12-76 (Sivakumar, Ghosn & Moses; 2006).

## 2 WIM DATA FOR BRIDGE LOAD MODELING

Characterizing the design live load effect requires the quantification of the mean of the maximum value expected over the appropriate return period, the standard deviation, and the probability distribution

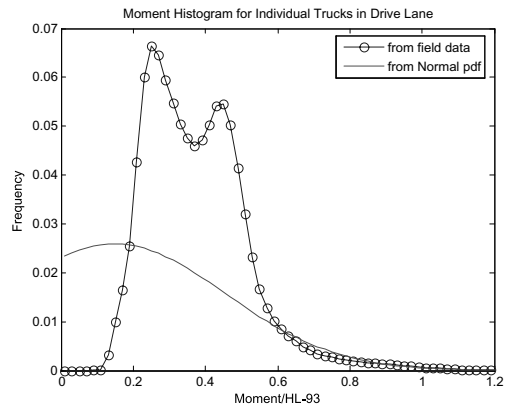


Figure 1. Normalized moment histogram for trucks in drive lane of I-81 NB.

function. The maximum bridge loading depends on the weight and axle configuration of all the trucks on a bridge span and their headway. This information can be assembled from existing WIM systems. The WIM data collected over a one-year period at Site 9121 on I-81 are used for illustration. The ratio of each truck's maximum moment and shear to those of the HL-93 maximum effect are assembled in histograms similar to that found in Figure 1. Additional normalized histograms are assembled for single truck or multiple lane loading events for simple and continuous spans.

Because of statistical variability, the estimation of the maximum live load effect for a 75-year design life

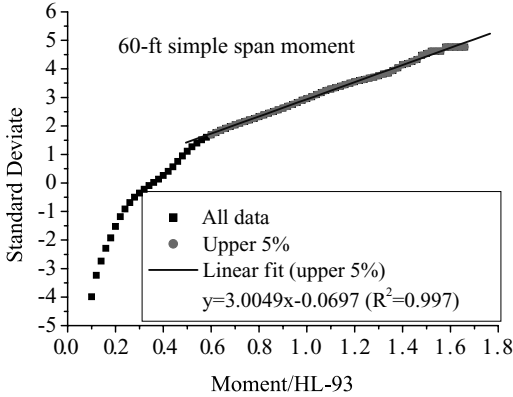


Figure 2. Normal plot for trucks in drive lane of I-81 NB.

or a two-year return period for the safety assessment of existing bridges would require several cycles of WIM data for each return period. Since this is not possible to achieve, some form of statistical projection of the tail end of the available WIM data is necessary. Careful observations of the tail ends of the WIM data histograms assembled from several sites indicate that the tail ends match the tail ends of Normal probability distributions. Figure 2 illustrates how a linear fit on the Normal probability plot of the upper 5% of the data collected at the I-81 site will produce a slope,  $m$ , and an intercept,  $n$ , which will give the mean of the Normal distribution that best fits the tail end as  $\mu_{event} = -n/m$ . The standard deviation of the best-fit Normal is  $\sigma_{event} = (1 - n)/m - \mu_{event}$ . For the I-81 data, single truck events give  $\mu_{event} = 0.0333$  and  $\sigma_{event} = 0.333$ . The red curve in Figure 1 shows how the Normal distribution matches the tail end of the actual WIM histogram. Additionally, the number of events for the I-81 site are obtained as  $n_{day} = 3200$  single truck events and  $n_{day} = 72$  multiple lane events.

To find the cumulative distribution for the maximum loading event in a return period,  $T$ , we have to start by determining the number of loading events,  $N$ . The magnitudes of these events are designated as  $S_1, S_2, \dots, S_N$ , the maximum of which is  $S_{max,N}$ . The cumulative probability distribution,  $F_{s_{max,N}}(S)$ , gives the probability that  $S_{max,N}$  is less than or equal to a value  $S$ . If  $S_{max,N}$  is less than  $S$ , this implies that all  $S_i$  are less than  $S$ . Hence, assuming that the loading events are independent and they are all drawn from the same parent distribution, the probability that  $S_{max,N} \leq S$  can be calculated from:

$$F_{s_{max,N}}(S) = [F_S(S)]^N \quad (1)$$

where  $F_S()$  is the cumulative distribution function of an event  $S_i$ .

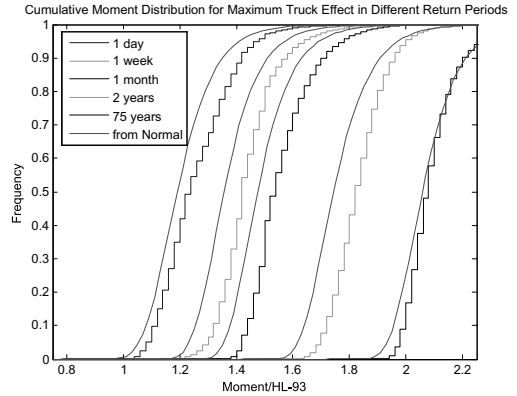


Figure 3. Cumulative distribution of maximum load effect of side-by-side of events for different return periods.

Figure 3 shows the cumulative probability function for the maximum load effect for periods ranging from one day to 75 years for the data collected on the I-81 site for side-by-side events  $F_S(S)$ . The figure shows good agreement between the projections obtained from the Normal fit of the tail (in red) and simulated data. The mean value and the standard deviation of the maximum effect for each return period can be obtained from the cumulative distribution functions  $F_{s_{max,N}}()$ .

### 3 EXTREME VALUE DISTRIBUTION OF MAXIMUM LOAD EFFECTS

Although the application of Eq. 1 can be executed numerically for any parent probability distribution, the fact that the tail end of the WIM data matches that of a Normal distribution allows for the application of extreme value theory to obtain the statistics of the maximum load effect in closed form. The approach is based on the following known concept as provided in Ang and Tang (2007): “if the parent distribution of the initial variable  $S$  has a general Normal distribution with mean  $\mu_{event}$  and standard deviation  $\sigma_{event}$ , then the maximum value after  $N$  repetitions approaches asymptotically an Extreme Value Type I (Gumbel) distribution” with a dispersion  $\alpha_N$  given by:

$$\alpha_N = \frac{\sqrt{2 \ln(K)}}{\sigma_{event}} \quad (2)$$

and a most probable value  $u_N$  given by:

$$u_N = \mu_{event} + \sigma_{event} \left( \sqrt{2 \ln(N)} - \frac{\log(\log(N)) + \log(4\pi)}{2\sqrt{2 \ln(N)}} \right) \quad (3)$$

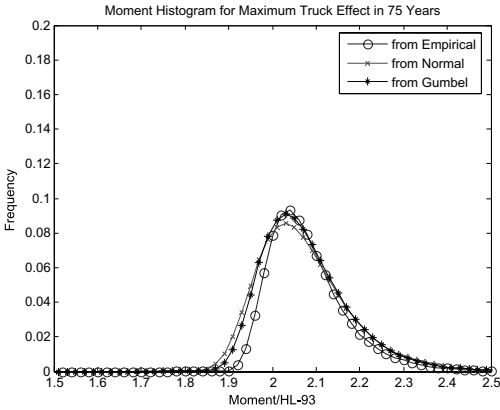


Figure 4. Comparison of Gumbel fit on Normal distribution tail for 75-year maximum side-by-side trucks.

$\alpha_N$  and  $u_N$  can be used to find the means,  $L_{max}$ , and standard deviations,  $\sigma_{max}$ , for the maximum load effect for any return period having  $N$  repetitions as:

$$\bar{L}_{max} = \mu_{max} = u_N + \frac{0.577216}{\alpha_N} \quad (4)$$

and

$$\sigma_{max} = \frac{\pi}{\sqrt{6}\alpha_N} \quad (5)$$

For 75 years, the I-81 data lead to a dispersion coefficient  $\alpha_N = 18.17$  for the normalized moment effect on a 60-ft simple span. The most probable value is  $u_N = 1.896$ . The mean of the maximum value for a 75-year bridge design life is  $\bar{L}_{max} = \mu_{max} = 1.86$  and the standard deviation is  $\sigma_{max} = 0.0706$ . Figure 4 shows in black the results obtained when the Gumbel distribution function is plotted using as parameters the values of  $\alpha_N$  and  $u_N$  obtained from Eq. 2 and 3.

The results of the Gumbel fit are compared in Figure 4 to the results obtained when Eq (1) is used with  $F_S(S)$  being the cumulative Normal distribution (plotted in red) and the results when  $F_S(S)$  is the simulated function for side-by-side events obtained from the raw WIM data (plotted in blue). These three curves essentially coincide with only small differences due to the numerical execution of the equations.

#### 4 L<sub>MAX</sub> RESULTS FOR REPRESENTATIVE U.S. SITES

WIM data sets from 59 representative sites in six U.S. states were analyzed and the maximum live load effects for single lanes and for multiple lanes were calculated as explained in Section 3.

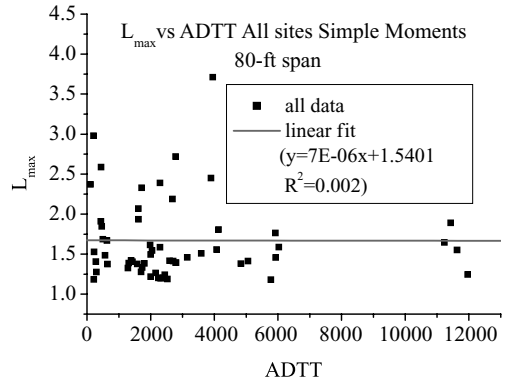


Figure 5. Plot of  $L_{max}$  versus ADTT.

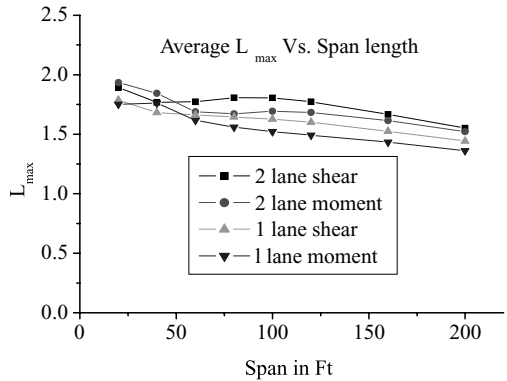


Figure 6. Plot of average  $L_{max}$  versus span length.

The results are analyzed to study the relationship between  $L_{max}$  and the HL-93 design live load as a function of span length, Average Daily Truck Traffic (ADTT) and other factors. For example, Figure 5 gives a plot of the individual Normalized  $L_{max}/HL-93$  values obtained for the moments of a simple 80-ft span from multiple lanes versus ADTT. Figure 6 shows how the average  $L_{max}/HL-93$  values from all the sites for single and multiple lanes, for both moment and shear vary with span length. Overall the analysis of the WIM data and  $L_{max}$  results shows the following trends:

1. There seems to be no correlation between multiple lane  $L_{max}$  and ADTT.
2. The average  $L_{max}/HL-93$  decreases with span length indicating that the HL-93 design load is not consistent with current truck loading data.
3. The ratio of multiple lane  $L_{max}$  divided by one lane  $L_{max}$  is reasonably constant for shear and moments within a range of 1.05 to 1.13 which indicates that the multiple presence factor  $MP = 1.2$  specified in the AASHTO LRFD is not consistent with current loading conditions.

4. The spread in  $L_{max}$  from different U.S. sites is very high producing site-to-site variability with a COV 0.36 to 0.24 with a tendency to go lower with span length.
5. The one lane COV is generally lower and decreases faster with span length than the multiple lanes COV.
6. The  $L_{max}$  values for the multiple lanes seem to be lower than those implied by the AASHTO LRFD while the  $L_{max}$  for the single lanes appear to be higher than those implied in the AASHTO LRFD.
7. The WIM data show that the actual percentage of side-by-side multiple truck event cases is significantly lower than assumed by the AASHTO LRFD.
8. There is some negative correlation between the weights of side-by-side trucks.

## 5 APPLICATION OF $L_{MAX}$ RESULTS FOR LIVE LOAD MODELING

The work performed as part of NCHRP 12-76 consisted of collecting WIM truck traffic data on various sites within the U.S. and using these data to project for the maximum expected live load effects,  $L_{max}$ . For example, Tables 1 and 2 provide a set of normalized 75-year  $L_{max}$  values obtained for the maximum bending moments of simple span bridges from 8 sites in California (CA). The  $L_{max}$  values were calculated for one lane of traffic and for two lanes of traffic and they are normalized with respect to the effect of one lane of HL-93 loading. The results show higher COV values for the two-lane effects that may be due to the lower

Table 1.  $L_{max}$  values for one lane for the moment effect of simple span beams.

1-Lane event $L_{max}$ for simple span moment				Span length (ft)								Max Value
State	Site ID	Direction	ADTT	20	40	60	80	100	120	160	200	
CA	0001	E/N	5058	1.370	1.278	1.239	1.206	1.173	1.164	1.137	1.086	1.370
CA	0001	W/S	4839	1.400	1.354	1.305	1.237	1.174	1.161	1.124	1.069	1.400
CA	0003	E	2790	1.190	1.216	1.293	1.268	1.219	1.191	1.149	1.106	1.293
CA	0004	W	3149	1.365	1.354	1.382	1.337	1.253	1.189	1.114	1.051	1.382
CA	0059	S	11627	1.340	1.291	1.368	1.358	1.338	1.293	1.212	1.127	1.368
CA	0060	N	11432	1.989	1.635	1.413	1.392	1.351	1.311	1.227	1.168	1.989
CA	0072	E/N	2318	1.138	1.228	1.297	1.255	1.221	1.140	1.052	1.003	1.297
CA	0072	W/S	2159	1.217	1.227	1.272	1.213	1.149	1.094	1.046	0.976	1.272
			Min value	1.138	1.216	1.239	1.206	1.149	1.094	1.046	0.976	
			Avg value	1.376	1.323	1.321	1.283	1.235	1.193	1.132	1.073	
			Max value	1.989	1.635	1.413	1.392	1.351	1.311	1.227	1.168	
			Stand.dev.	0.266	0.137	0.060	0.070	0.076	0.074	0.065	0.063	0.101
			COV	0.193	0.104	0.045	0.054	0.061	0.062	0.058	0.059	0.057

Table 2.  $L_{max}$  values for two lanes for the moment effect of simple span beams.

2-Lane event $L_{max}$ for simple span moment				Span length (ft)								Max Value
State	Site ID	Direction	ADTT	20	40	60	80	100	120	160	200	
CA	0001	E/N	5058	1.663	1.706	1.515	1.412	1.456	1.450	1.386	1.299	1.706
CA	0001	W/S	4839	1.592	1.475	1.324	1.382	1.445	1.460	1.410	1.341	1.592
CA	0003	E	2790	1.447	1.421	1.429	1.392	1.374	1.332	1.281	1.213	1.447
CA	0004	W	3149	1.575	1.441	1.440	1.460	1.515	1.529	1.479	1.388	1.575
CA	0059	S	11627	1.678	1.665	1.490	1.553	1.562	1.578	1.506	1.419	1.678
CA	0060	N	11432	1.955	1.823	1.844	1.891	1.859	1.783	1.676	1.544	1.955
CA	0072	E/N	2318	1.368	1.235	1.172	1.199	1.224	1.233	1.177	1.122	1.368
CA	0072	W/S	2159	1.499	1.428	1.335	1.265	1.286	1.247	1.198	1.125	1.499
			Min value	1.368	1.235	1.172	1.199	1.224	1.233	1.177	1.122	
			Avg value	1.597	1.524	1.444	1.444	1.465	1.452	1.389	1.306	
			Max value	1.955	1.823	1.844	1.891	1.859	1.783	1.676	1.544	
			Stand.dev.	0.179	0.191	0.196	0.211	0.195	0.183	0.168	0.148	
			COV	0.112	0.125	0.136	0.146	0.133	0.126	0.121	0.113	0.127



number of multiple lane events and the differences in the frequency of heavy legal and overloaded vehicles (illegal, exclusion, or permit) in each site's truck traffic stream, and the probability of having two lanes loaded by such vehicles.

In addition to the site-to-site variability, the uncertainties associated with the estimated values for  $L_{max}$  include the uncertainties within a site due to the random nature of  $L_{max}$  and the fact that the WIM data histograms do not necessarily include all the extreme load events that may occur within the 75-year design period of the bridge. An analysis of the results of the projections as obtained from Eq. (5) show that the uncertainties within a site are associated with a COV on  $L_{max}$  on the order of  $V_{projection} = 3.5\%$  for the one-lane maximum effect and a COV of  $V_{projection} = 5\%$  for the multiple lanes. Additional uncertainties associated with  $L_{max}$  are due to the limited number of data points used in the projections and the confidence levels associated with the size of the data sample collected over a one-year period for each site. Using the  $\pm 95\%$  confidence limits, it is estimated that the COV is on the order of  $V_{data} = 2\%$  for the one-lane case and about  $V_{data} = 3\%$  for the two-lane case.

The  $L_{max}$  values as assembled using the methods of Section 3 give the total static load effect on a bridge. The motion of the vehicles over the flexible bridge structure will introduce a dynamic amplification, which according to Nowak (1999) will augment the  $L_{max}$  load effect by an average of 13% for one lane of traffic and by 9% for side-by-side trucks. The dynamic amplification also results in a COV of  $V_{IM} = 9\%$  on the one-lane load effect and  $V_{IM} = 5.5\%$  on the two-lane effect.

Finally, for multi-girder bridges the most loaded girder will carry a fraction of the total load effect, which according to the AASHTO LRFD is obtained from the load distribution factor D.F. provided in the code. In previous studies on live load modeling, Ghosn & Moses (1986) included the uncertainties in estimating the lane distribution factor which was associated with a COV equal to  $V_{DF} = 8\%$  based on field measurements on typical steel and prestressed concrete bridges.

Observing that the  $L_{max}$  values are for the total static load effect on a bridge and observing that the D.F. provided by the AASHTO LRFD for a single lane already includes a multiple presence factor  $MP = 1.2$ , the final mean value for maximum load effect on a single girder of a multi-girder bridge can be calculated for one lane and two lanes as:

For one lane:

$$\overline{LL} = L_{max\ beam} = L_{max} \times IM \times D.F. / 1.2$$

For two lanes:

$$\overline{LL} = L_{max\ beam} = L_{max} \times IM \times D.F. / 2$$

(6)

Dividing D.F. of one lane by 1.2 is done to remove the multiple presence factor, while dividing the D.F. of two lanes by 2 is done to account for the fact that the  $L_{max}$  for two lanes are normalized in this study by dividing the calculated total effect by the effect of one lane of HL-93 loading.

The mean value of the live load effect on the most critical girder can then be obtained from Eq. (6). The COV's of the maximum girder live load effect can be obtained from:

$$V_{LL} = \sqrt{V_{site-to-site}^2 + V_{projection}^2 + V_{data}^2 + V_{IM}^2 + V_{DF}^2} \quad (7)$$

Table 3 provides values for the means and standard deviations of the girder moment live load, LL, for 60-ft, 120-ft and 200-ft simple span bridges. Note that in the calculations performed in this study and following the procedure of Nowak (1999), it is assumed that the load distribution factor, D.F., values provided by AASHTO LRFD are mean values. It should also be mentioned that the statistics for the dynamic impact and for the load distribution factors as used by Nowak (1999) are based on very limited data and much more research is needed on these topics to study how these factors change from site to site and how they relate to the truck weights and traffic data. However, these issues are beyond the scope of this study and in this case, this study uses the same data applied during the AASHTO LRFD calibration.

## 6 CALCULATION OF RELIABILITY INDEX AND CALIBRATION OF LIVE LOAD FACTORS

In addition to the live loads, the random variables that control the safety of a bridge member include the actual resistance and the applied dead loads. Nowak (1999) provided models to represent the mean values and the COV's of these random variables, which are used to obtain the values provided in Table 3 for the bridge cases considered.

A measure of the safety of bridge members is the reliability index,  $\beta$ , which is related to the probability of failure,  $P_f$ , by:

$$\beta = \Phi^{-1}(P_f) \quad (8)$$

where  $\Phi^{-1}()$  is the inverse of the Gaussian cumulative distribution function. Assuming that all the random variables representing the resistance, dead load and live load effects follow Gaussian (Normal) probability distributions, the reliability index,  $\beta$ , can be calculated as:

$$\beta = \frac{\bar{R} - \overline{DL} - \overline{LL}}{\sqrt{\sigma_R^2 + \sigma_{DL}^2 + \sigma_{LL}^2}} \quad (9)$$

Table 3. Reliability index calculation for bending moment of simple span composite steel bridges based on California WIM data.

Span	Spacing	Ave. Res. 1	Av. Res. 2	$\sigma$ Res. 1	$\sigma$ Res. 2	Mean DL	$\sigma$ DL	Mean LL 1	Mean LL 2	$\sigma$ LL 1	$\sigma$ LL 2	beta 1-lane	beta 2-lane
60	4	1356	1602	136	160	346	28	447	362	60	64	3.73	5.11
60	6	1770	2134	177	213	474	38	567	476	76	84	3.71	5.09
60	8	2163	2646	216	265	604	48	675	583	91	103	3.69	5.07
60	10	2572	3171	257	317	756	61	776	684	105	121	3.66	5.02
60	12	2989	3704	299	370	923	74	870	782	117	138	3.63	4.97
Span	Spacing	Ave. Res. 1	Av. Res. 2	$\sigma$ Res. 1	$\sigma$ Res. 2	Mean DL	$\sigma$ DL	Mean LL 1	Mean LL 2	$\sigma$ LL 1	$\sigma$ LL 2	beta 1-lane	beta 2-lane
120	4	4396	5099	440	510	1741	117	949	904	134	153	3.60	4.50
120	6	5726	6742	573	674	2325	160	1193	1181	169	200	3.57	4.49
120	8	6853	8179	685	818	2797	199	1414	1440	200	244	3.57	4.50
120	10	8087	9718	809	972	3375	247	1618	1686	229	286	3.53	4.47
120	12	9446	11378	945	1138	4063	301	1811	1923	256	326	3.49	4.42
Span	Spacing	Ave. Res. 1	Av. Res. 2	$\sigma$ Res. 1	$\sigma$ Res. 2	Mean DL	$\sigma$ DL	Mean LL 1	Mean LL 2	$\sigma$ LL 1	$\sigma$ LL 2	beta 1-lane	beta 2-lane
200	4	12306	13796	1231	1380	6265	377	1630	1611	228	258	3.38	4.07
200	6	15810	17938	1581	1794	8123	500	2035	2095	285	335	3.36	4.08
200	8	18999	21753	1900	2175	9814	614	2401	2547	336	408	3.35	4.09
200	10	22444	25812	2244	2581	11743	749	2740	2977	384	476	3.32	4.06
200	12	26416	30389	2642	3039	14096	906	3059	3390	428	542	3.28	4.01

If a representative set of composite steel bridges are designed to exactly meet the requirements of the AASHTO LRFD Strength criteria, and if these bridges are subjected to the average live loads observed on the California sites,  $\beta$  is obtained as shown in the last two columns of Table 3.

Generally speaking, the results of Table 3 and other similar calculations show that for the California truck traffic conditions, the reliability index for one lane is on the average equal to  $\beta = 3.55$  which is close to the target  $\beta = 3.50$  set during the calibration of the AASHTO LRFD based on the Ontario live load data. For two lanes of truck traffic, the average reliability index is  $\beta = 4.63$ . This indicates that for the two-lane loading of California bridges, the current AASHTO LRFD is conservative producing higher reliability index values than the target  $\beta = 3.50$ . The range of the  $\beta$ 's however is large varying between a  $\beta = 5.32$  for short span prestressed concrete bridges with closely spaced beams to  $\beta = 4.0$  for long span prestressed concrete bridges with closely spaced beams. The fact that the loading of the short span bridges is dominated by the live loads while the long span bridges' loading is dominated by the dead load indicates that for

California bridges, the HL-93 nominal design live load is conservative.

To reduce the reliability index for the two lane cases and achieve an average reliability index for the equal to the target  $\beta = 3.5$ , a live load factor  $\gamma_L = 1.20$  should be used rather than the specified  $\gamma_L = 1.75$ . This means that the HL-93 loading should have a multiple lane reduction factor = 1.46 (1.75/1.20) when checking the design for two lanes of traffic.

The results of Table 3 for the California WIM data may not be consistent with the data from other states. The differences are mainly due to the legal truck weight limits or exemptions and the permit overload frequencies and weight regulations that vary from state to state. For example, if the  $L_{max}$  values Florida WIM data sites are used, the reliability index values for one lane of loading drops to an average of  $\beta = 2.58$ . The two-lane  $L_{max}$  leads to an average reliability index  $\beta = 3.96$ . The latter value is still higher than the target  $\beta = 3.5$  while the one lane reliability is lower than the target. It is noted that the Florida data shows high site-to-site variations leading to a high COV for  $L_{max}$  and subsequently lower reliability index values than those observed for California. If the live load factor is raised

to  $\gamma_L = 2.37$  from the specified  $\gamma_L = 1.75$ , then the reliability indexes for the Florida sites would increase to  $\beta = 3.50$  for the one-lane cases, and  $\beta = 4.95$  for the two-lane cases, bringing the reliability indexes more in line with the California results.

Using the  $L_{\max}$  values generated from the Indiana WIM data sites, the reliability index values for one lane of loading is on the average equal to  $\beta = 3.16$ . The two-lane  $L_{\max}$  would lead to an average reliability index  $\beta = 4.71$ . The latter value is higher than the target  $\beta = 3.5$  while the one lane reliability is slightly lower than the target. The Indiana data show a site-to-site variability in COV's on the order of 11% to 15% for both one-lane and two-lanes loadings. These are compared to the CA data that show low site-to-site variability in the one-lane loading cases (typically less than 10% for spans greater than 40ft) and the Florida data that shows high COV's for both the one-lane and two-lane cases (typically greater than 20%).

## 7 CONCLUSIONS

This paper presented a procedure to develop live load models based on actual truck weight measurements using WIM technology. A reliability-based procedure

to adjust the live load factors in the AASHTO LRFD code to account for the variation in the loadings observed in different states is also presented. The results show that the average reliability index values vary considerably from state to state. Also, the results show that in most cases, one-lane loadings are dominating the safety of bridge members due to the lower number of side-by-side events and the lower load effects produced by these events when compared to the data used during the calibration of the AASHTO LRFD.

## REFERENCES

- AASHTO, LRFD Bridge Design Specifications, (2007), 4th edition, Washington DC.
- Ang, A. H-S, & Tang, W.H., (2007), *Probability Concepts in Engineering*, 2nd Edition, Wiley.
- Ghosn, M. & Moses, F., (1986), "Reliability Calibration of a Bridge Design Code", ASCE Journal of Structural Engineering, April.
- Nowak, A.S., (1999), Calibration of LRFD Bridge Design Code, NCHRP Report 368. Washington, DC.
- Sivakumar, B., Ghosn, M. & Moses, F. (2006), "Protocols for Collecting and Using Traffic Data in Bridge Design", Interim Report, NCHRP Project 12-76, TRB, Washington, DC.

# Analysis of the local ductility in reinforced concrete beams dimensioned according to Eurocode 8

A. Kassoul, A. Bougara, M. Belkhatir & K. Ezziane

*Faculty of Sciences and Sciences of Engineer, University of H.H.B., Chlef, Algeria*

**ABSTRACT:** The present work deals with the principle of the evaluation method of the curvature ductility factor. The parameters affecting the available curvature ductility are examined. In order to better understand the local ductility in the reinforced concrete beams dimensioned according to Eurocode 8, an Eurocode 8 vision concerning the local ductility is presented. Furthermore, the maximum tension reinforcement ratio  $\rho_{\max}$  of the Eurocode 8 for a given ductility is estimated. Then, the available curvature ductility factor in beams corresponding at  $\rho_{\max}$  is evaluated. As a consequence, a new maximum tension reinforcement ratio  $\rho$  for the local ductility condition similar to  $\rho_{\max}$  of Eurocode 8, is suggested.

## 1 INTRODUCTION

Currently, the modern codes of design of constructions in the seismic zones give a particular importance to the local ductility during the dimensioning. The Eurocode 8 (Eurocode 8 2003) is one of the codes which has benefited from advanced scientific research in the field of analysis of the inelastic behavior of the reinforced concrete structures; by considering the local ductility during the dimensioning.

The objective of this work is to present an analysis of the local ductility in cross-sections of the beams dimensioned according to the recommendations of Eurocode 2 (Eurocode 2 2004) and Eurocode 8 (Eurocode 8 2003). After then, we examine the condition of the local ductility presented in Eurocode 8. Finally, we have tried to propose a new relation of tension reinforcement ratio  $\rho$  for the local ductility condition for the cross-sections of the reinforced concrete beams.

In the beginning, this work presents the principle of the evaluation method of curvature ductility factor in the reinforced concrete beams, taking into account the characteristics of Eurocode 2 (Eurocode 2 2004). This method is articulated on the use of the static equilibrium equations of the internal and external efforts and the relations of compatibility of the deformations for the limiting states of service and ultimate. Then, a parametric analysis of the factors influencing the local ductility is presented. The requirements of Eurocode 8 (Eurocode 8 2003) concerning the local ductility are included, in order to evaluate the ratios of local ductility in the cross-sections of reinforced concrete beams. Finally, an analysis of these last ratios are examined, which contributes to propose a new relation

of the tension reinforcement ratio  $\rho$  for the local ductility condition, similar to the one used by Eurocode 8 (Eurocode 8 2003) and generalized for high strength concretes.

## 2 PARAMETERS AFFECTING THE AVAILABLE CURVATURE DUCTILITY

### 2.1 Principle of the evaluation procedure of the available curvature ductility factor

The inelastic behaviour of a reinforced concrete beam with unconfined concrete will be treated by using the procedure developed by (Park & Ruitong 1988). It is based on the equations of static equilibrium of forces acting on the cross section and the relation of strain compatibility at the limit of the elastic and ultimate state.

The curvature at first yield  $\varphi_y$  is defined when the longitudinal tension reinforcement first reaches the yield strain  $f_{yd}/E_s$ . From figure 1-a, we can write:

$$\varphi_y = \frac{f_{yd}/E_s}{d(1-k)} \quad (1)$$

where  $E_s$  = Design value of modulus of elasticity of reinforcing steel;  $d$  = Effective depth of a cross-section;  $f_{cd}$  = Design value of concrete compressive strength;  $f_{yd}$  = Design yield strength of reinforcement;  $k$  = Neutral axis depth factor  $\varepsilon_{sy,d}$  = Design value of steel strain at yield.

The curvature at ultimate state  $\varphi_u$  is defined when the concrete strain, at the extreme compressive fiber, reaches the limiting value  $\varepsilon_{cu1}$ , recommended by the code (Eurocode 2 2004) for unconfined sections.

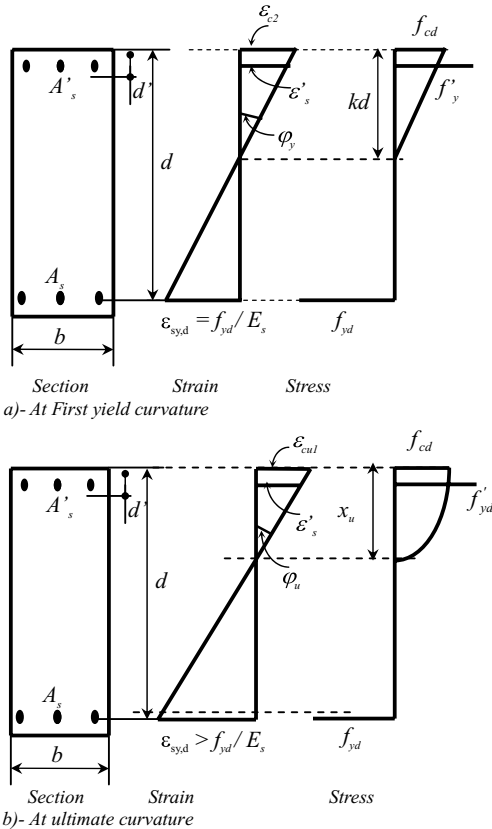


Figure 1. Doubly reinforced concrete beam section with flexure.

According to figure 1-b, the curvature can be written as:

$$\varphi_u = \frac{\varepsilon_{cu1}}{x_u} \quad (2)$$

where  $x_u$  = Neutral axis depth;  $\varepsilon_{cu1}$  = Ultimate strain of unconfined concrete.

The curvature ductility factor  $\mu_\varphi$  defined as the ratio of the post-ultimate strength curvature at 85% of the moment of resistance, to the curvature at yield, provided that the limiting strains of concrete and steel  $\varepsilon_{cu1}$  and  $\varepsilon_{su,k}$  are not exceeded. The ratio  $\mu_\varphi = \varphi_u / \varphi_y$ , in which  $\varphi_u$  and  $\varphi_y$ , are respectively the curvatures computed from eqs. (1) and (2), represents the analytical expression of the available curvature ductility factor in the unconfined beam sections and it is merely expressed by:

$$\mu_\varphi = \frac{\varepsilon_{cu1}}{\varepsilon_{sy,d}} \frac{d(1-k)}{x_u} \quad (3)$$

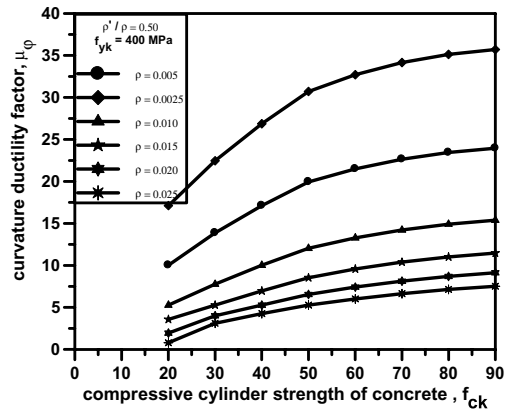


Figure 2. Variation of the curvature ductility factor with the cylindrical compressive strength of the concrete  $f_{ck}$ .

## 2.2 Effect of the cylindrical compressive strength of the concrete $f_{ck}$

In this study, we varied the values of the Characteristic compressive cylinder strength of concrete at 28 days  $f_{ck}$  of 20 MPa (for ordinary concrete) at 90 MPa (for a high strength concrete). The Characteristic yield strength of reinforcement  $f_{yk}$  remains constant and equal to 400 MPa. Figure 3 presents six curves each one corresponds to a value of the tension reinforcement ratio  $\rho$ . We note that each curve increases with  $f_{ck}$ . This increase has a considerable effect on the cross sections beams having a small tension reinforcement ratio  $\rho$  ( $\rho < 0.005$ ), however this effect decrease for the sections where  $\rho$  is greater than 0.01.

In general, although the concrete is a brittle material and its ultimate strain of unconfined concrete  $\varepsilon_{cu1}$  decreases with increasing in  $f_{ck}$ , the increase in  $f_{ck}$  improves considerably local ductility in the reinforced concrete beams.

## 2.3 Effect of the characteristic yield strength of reinforcement $f_{yk}$

To specify the influence of the characteristic yield strength of reinforcement  $f_{yk}$  of the longitudinal reinforcements, various curves of the curvature ductility factor illustrated according to  $f_{yk}$ . Figure 5, shows that the shape of the various curves of curvature ductility factor corresponding to the various values of  $\rho$  decrease with the increase in  $f_{yk}$ . Indeed, the increase in the yield strength of reinforcement has a negative purpose on the local ductility in the reinforced concrete beams.

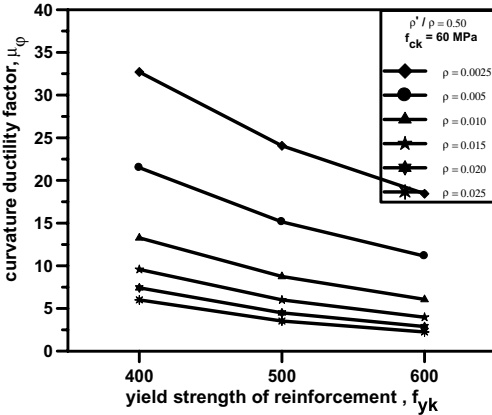


Figure 3. Variation of the curvature ductility factor with the yield strength of reinforcement  $f_{yk}$ .

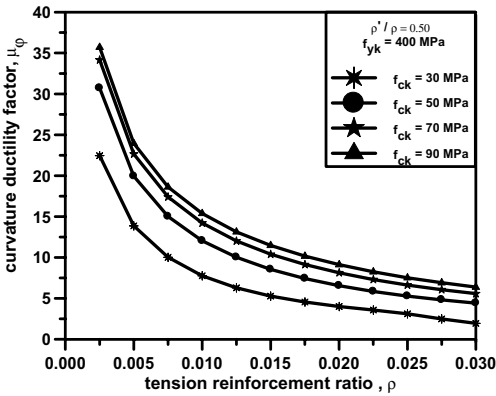


Figure 4. Variation of the curvature ductility factor with the tension reinforcement ratio,  $\rho$ .

#### 2.4 Effect of the tension reinforcement ratio $\rho$

Contrary, to the effect of  $f_{ck}$  and  $f_{yk}$  which influence the entire length of the reinforced concrete beam, the ratio  $\rho$  and  $\rho'$  influence each cross section of the beam according to the variation of the neutral axis. Figure 4 illustrates the evolution of the curves of ductility according to the tension reinforcement ratio  $\rho$  for a constant value of  $\rho'/\rho = 0.5$  and  $f_{yk} = 400$  MPa, we note that the shape of the curves of  $\mu_\phi$  is inversely proportional with the increase of  $\rho$ . This report is observed for all curves carried out with  $f_{ck} = 30, 50, 70$  and  $90$  MPa. Consequently, the increase of  $\rho$  in the sections of reinforced concrete beams has an unfavourable purpose on local ductility.

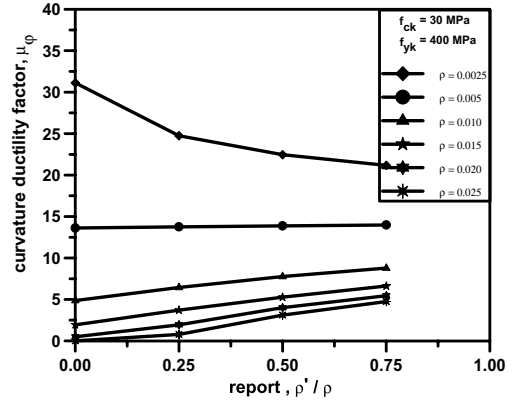


Figure 5. Variation of the curvature ductility factor with the report  $\rho'/\rho$ .

#### 2.5 Effect of compression steel ratio in beam $\rho'$

The effect of tension reinforcement ratio  $\rho$  was represented in §2.4 without holding account of the compression steel ratio in beams  $\rho'$ . In figure 5, we illustrate this effect for constant values of  $\rho$ . It is seen that the increase in  $\rho'/\rho$  from 0.0 to 0.75, the shape of  $\mu_\phi$  for low values of  $\rho$  ( $\rho < 0.005$ )  $\mu_\phi$  decreases, however for high values of  $\rho$  ( $\rho \geq 0.01$ )  $\mu_\phi$  increases. Generally, the designers of the reinforced concrete structures avoid dimensioning with small ratios of reinforcements  $\rho$  that represents the case of the section weakly reinforced; the increase of the report  $\rho'/\rho$  influence favorably the ductility of the cross sections reinforced concrete beams.

### 3 EUROCODE 8 VISION CONCERNING LOCAL DUCTILITY

It is very interesting to illustrate the Eurocode 8 (Eurocode 8 2003) vision with respect the local ductility during dimensioning of the cross sections of the reinforced concrete beams. In that way, the recommendations of this code require in the critical region of beam a minimal value of the curvature ductility factor  $\mu_\phi$  in order to satisfy the local ductility condition. Indeed, it requires that to satisfy this local ductility requirement, the value of the available curvature ductility factor  $\mu_\phi$  shall be at least equal to the value obtained by the following expressions:

$$\mu_\phi = 2q_0 - 1 \quad \text{if } T_1 \geq T_C$$

$$\mu_\phi = 1 + 2(q_0 - 1) \frac{T_C}{T_1} \quad \text{if } T_1 < T_C$$

where  $T_1$  = Fundamental period of the building in the horizontal direction of interest;  $T_C$  = Corner period at the upper limit of the constant acceleration region of the elastic spectrum.

And the basic value of the behaviour factor  $q_0$  for the frame system is given by  $q_0 3 (\alpha_u/\alpha_1)$  for medium class ductility (DCM) and  $q_0 4.5 (\alpha_u/\alpha_1)$  for high class of ductility (DCH). The report  $\alpha_u/\alpha_1 = 1.1$  for frames system at one-storey and  $\alpha_u/\alpha_1 = 1.3$  for system multistory, multi-bay frames. In general, the basic value of the behaviour factor  $q_0$  varies between 3 and 6 and the correspondent minimal curvature ductility factor  $\mu_\phi$  varies between 6 and 12.

In addition, Eurocode 8 (Eurocode 8 2003), requires a detailing for the provision of the reinforcements, in order to satisfy local ductility in the cross sections beams. The reinforcement ratio of the tension zone  $\rho$  does not exceed  $\rho_{max}$  value equal to:

$$\rho_{max} = \rho' + \frac{0.0018 f_{cd}}{\mu_\phi \varepsilon_{sy,d} f_{yd}} \quad (4)$$

And the compression steel ratio  $\rho'$  in beam equals at least less than half of the reinforcement ratio  $\rho$  provided at the tension zone, or:

$$\rho' \geq 0.5\rho$$

In order to avoid a brittle fracture of the entire length of beam and to ensure an adequate local ductility, it recommends that the tensile reinforcement ratio shall be not less than the following minimum value  $\rho_{min}$ :

$$\rho_{min} = 0.5 \frac{f_{ctm}}{f_{yk}} \quad (5)$$

Other works have proposed expressions for  $\rho$  as follows:

a- ACI 318 (2005)

$$\rho - \rho' \leq 0.75 \left( \frac{0.85 \beta_1 f'_c}{f_y} \left( \frac{600}{600 + f_y} \right) \right) \quad (6)$$

With

$$\rho_{max} \leq 0.025$$

b- Park & Ruitong (1988)

$$\rho \leq k_1 \left( \frac{f'_c + 1000}{1000} \right) \quad (7)$$

for  $\mu_\phi \geq 8$  and  $\rho'/\rho \geq 0.5$

c- Kassoul et al. (2004)

$$\rho = 0.11 k \varepsilon_{cu1} f_{ck} \quad (8)$$

for  $\mu_\phi \geq 8$  and  $\rho'/\rho \geq 0.5$

## 4 EVALUATION OF THE AVAILABLE CURVATURE DUCTILITY FACTOR

### 4.1 Ratio $\rho_{max}$ of tensile reinforcement for a given ductility

Table 1 shows the variation of the values of the ratio  $\rho_{max}$  adopted according to Eurocode 8 (Eurocode 8 2003) of the equation (4), determined for minimal curvature ductility factor  $\mu_\phi$  given, equal to 10, 8 and 6 with the various values of  $f'_{ck}$ , and  $f_{yk} = 400$  and 600 MPa with a report  $\rho'/\rho = 0.5$ . According to this table, we note that the values of  $\rho_{max}$  obtained for strength  $f'_{ck} > 50$  MPa, are very high, causing inappropriate practical provision.

Furthermore, high values of  $\rho$  substantially disadvantage the local ductility according to §2.4. These ratios will decrease when  $f_{yk}$  increases to 600 MPa, but it has always negative effects on the ductility when  $f_{yk}$  increases according to §2.3.

### 4.2 Available curvature ductility factor in beams dimensioned according to Eurocode 8

Table 2 illustrates the available curvature ductility factor which can be obtained by the method presented in § 2.1 for selected values of  $\rho_{max}$  expressed in Table 1, and the  $\rho_{min}$  (equation 6) (Eurocode 8 2003). According to this table, we note that for the minimal values of  $\mu_\phi$  of 10 and 8, the corresponding  $\rho_{max}$  offer real available curvature ductility factor ranging from 7 to 5 for  $\mu_{\phi, minimal} = 10$  and from 6 to 4 for  $\mu_{\phi, minimal} = 8$ . These results really show that the values of the available curvature ductility factor obtained by the analytical method represents in general only half value of the minimal curvature ductility factor. In the

Table 1. Variation of the tension reinforcement ratio  $\rho_{max}$  adopted by (Eurocode 8 2003), ( $\rho'/\rho = 0.5$ ).

$f_{yk}$ MPa	$f'_{ck}$ MPa	$\mu_\phi = 10$	$\mu_\phi = 8$	$\mu_\phi = 6$
400	30	0.011	0.014	0.019
	50	0.019	0.023	0.031
	70	0.026	0.033	0.044
	90	0.034	0.042	0.056
600	30	0.005	0.006	0.008
	50	0.008	0.010	0.014
	70	0.012	0.015	0.019
	90	0.015	0.019	0.025

Table 2. Variation of the factor of ductility in the sections dimensioned by  $\rho_{\min}$  and  $\rho_{\max}$  for Eurocode 8, ( $\rho'/\rho = 0.5$ ).

$\mu_{\varphi, \text{minimal}}$		10		8			
$f_{yk}$ MPa	$f_{ck}$ MPa	$\rho_{\max}$	$\mu_{\varphi}$	$\rho_{\max}$	$\mu_{\varphi}$	$\rho_{\min}$	$\mu_{\varphi}$
400	30	0.0113	6.9	0.0141	5.6	0.0036	17.6
	50	0.0190	6.9	0.0234	5.6	0.0051	19.7
	70	0.0260	6.4	0.0330	5.1	0.0058	20.6
600	90	0.0340	5.7	0.0420	4.6	0.0063	20.8
	30	0.0050	6.4	0.0063	5.1	0.0024	23.0
	50	0.0083	6.4	0.0104	5.1	0.0034	25.5
	70	0.0117	5.7	0.0146	4.5	0.0038	26.8
	90	0.0150	5.0	0.0188	4.0	0.0042	26.6

same table, we notice that the available curvature ductility factor obtained for the minimal ratio  $\rho_{\min}$  exceeds 3 to 5 times the values corresponding to  $\rho_{\max}$ . Based on these previous results, we observe that the variation of the available curvature ductility factor in the cross sections of the reinforced concrete beams varies from 5 for the sections highly reinforced to 27 for the sections weakly reinforced.

#### 4.3 New ratio $\rho_{\max}$ for the local ductility condition

Table 3 presents a comparison between  $\rho$  determined by the equation (4) adopted by EC8 and the values of  $\rho$  obtained by the inverse procedure of the method used previously in §2.1. According to this result, it is to be noted that the values obtained by the equation (4) exceed the values obtained by the analytical method. Also, with the respect to the result given in Table 2, we observed that the values of the factors of ductility determined for the  $\rho_{\max}$  of EC8 do not correspond to the minimal curvature ductility factor required.

Indeed, Although Eurocode 8 (Eurocode 8 2003) recommends in equation (4) a very advanced relation for the ratio  $\rho_{\max}$  to take into account the local ductility condition during dimensioning for the DCM and DCH ductility classes. Nevertheless, this relation gives very high values of  $\rho_{\max}$  which do not correspond to the values of the minimal curvature ductility factor required. From this result, we need to modify the equation (4).

Thus, In order to have the available curvature ductility factor near to the minimal curvature ductility factor and to take an explicit consideration of the ultimate deformation of the concrete of high strength ( $f_{ck} > 50$  MPa), it is necessary to decrease the quantity of the tension reinforcement ratio  $\rho_{\max}$  obtained by the equation (4) recommended by Eurocode 8 (Eurocode 8 2003). Taking into account the study realized in this investigation presented in table 3, we suggest to modify the equation (4) of the EC8 by introducing the

Table 3. Comparison between  $\rho$  determined by the equation (4) of Eurocode 8 and those obtained by the analytical procedure.

$\mu_{\varphi, \text{minimal}}$		10		8		6	
$f_{yk}$ MPa	$f_{ck}$ MPa	$\rho_{\max}^*$	$\rho^{**}$	$\rho_{\max}^*$	$\rho^{**}$	$\rho_{\max}^*$	$\rho^{**}$
400	30	0.011	0.007	0.014	0.009	0.019	0.012
	50	0.019	0.012	0.023	0.015	0.031	0.021
	70	0.026	0.015	0.033	0.020	0.044	0.026
600	90	0.034	0.017	0.042	0.022	0.056	0.030
	30	0.005	0.003	0.006	0.004	0.008	0.005
	50	0.008	0.005	0.010	0.006	0.014	0.008
	70	0.012	0.006	0.015	0.008	0.019	0.011
	90	0.015	0.007	0.019	0.009	0.025	0.012

$\rho_{\max}^*$ .  $\rho$  obtained by the equation (4) (Eurocode 8 2003).

$\rho^{**}$ .  $\rho$  obtained by the inverse procedure of the method used previously in §2.1.

ultimate deformation of unconfined concrete  $\varepsilon_{cu1}$  multiplied by coefficient of correction equal to 0.4 instead of 0.0018, as expressed in the following equation:

$$\rho_{\max} = \rho' + \frac{0.4 \varepsilon_{cu1} f_{cd}}{\mu_{\varphi} \varepsilon_{sy,d} f_{yd}} \quad (9)$$

where  $f_{cd}$  = Design value of concrete compressive strength;  $f_{yd}$  = Design yield strength of reinforcement;  $\mu_{\varphi}$  = Minimal curvature ductility factor;  $\varepsilon_{cu1}$  = Ultimate strain of unconfined concrete;  $\varepsilon_{sy,d}$  = Design value of steel strain at yield.

The values of the ratio  $\rho_{\max}$  obtained by the equation (9) should not be exceeded in all cases an ultimate value of the tension reinforcement ratio  $\rho$  equal to 0.025 ( $\rho_{\max} \leq 0.025$ ).

This last condition has already adopted by the PS92 (PS92. 1998) and the ACI (ACI 318 2005).

Table 4 illustrates a comparison between the values obtained for the tension reinforcement ratio  $\rho_{\max}$  given by Eurocode 8 (Eurocode 8 2003) and those determined by the equation suggested in equation (9), for  $\rho'/\rho = 0.5$  and  $f_{yk} = 400$  MPa. We observe a clear reduction of the value of  $\rho_{\max}$  from 22 to 38%. This is attributed to the ultimate deformation of the concrete  $\varepsilon_{cu1}$  for strength  $f_{ck} > 50$  MPa, since this deformation decreases for high strength. This justifies the modification of the equation proposed earlier in (9).

Table 5 presents a comparison between the various ratio  $\rho$  obtained first by (Park & Ruitong 1988), (Kasoul et al. 2004) then analytical method, Eurocode 8 (Eurocode 8 2003) and the proposed equation (9) in this investigation, with  $f_{yk} = 400$  MPa,  $\rho'/\rho = 0.5$  and  $\mu_{\varphi} = 8$ . From this table, we can say that the various values obtained are approximately the same in



Table 4. Comparison of  $\rho_{\max}$  proposed by Eurocode 8 and those proposed in this investigation ( $f_{yk} = 400$  MPa,  $\rho'/\rho = 0.5$ ).

$\mu_{\varphi, \text{minimal}}$		10			8		
$f_{yk}$ MPa	$f_{ck}$ MPa	$\rho^*$	$\rho^{**}$	%	$\rho^*$	$\rho^{**}$	%
400	30	0.011	0.009	22	0.014	0.011	23
	50	0.019	0.015	22	0.023	0.018	22
	70	0.026	0.016	38	0.033	0.020	38
	90	0.034	0.021	38	0.042	0.026	38
600	30	0.005	0.004	22	0.006	0.005	22
	50	0.008	0.007	22	0.010	0.008	22
	70	0.012	0.007	38	0.015	0.009	38
	90	0.015	0.009	38	0.019	0.012	38

$\rho_{\max}^* \cdot \rho$  obtained by the equation (4) (Eurocode 8 2003).

$\rho^{**} \cdot \rho$  obtained by this investigation in the equation (9).

Table 5. Comparison between various ratio  $\rho$  obtained from various investigations, for  $f_{yk} = 400$  MPa,  $\rho'/\rho = 0.5$  et  $\mu_{\varphi} = 8$ .

$f_{ck}$ MPa	$\rho^{(1)}$	$\rho^{(2)}$	$\rho^{(3)}$	$\rho^{(4)}$	$\rho^{(5)}$
20	0.0091	0.0077	0.0060	0.0094	0.0073
30	0.0124	0.0116	0.0090	0.0141	0.0109
40	0.0158	0.0154	0.0120	0.0188	0.0146
50	0.0192	0.0193	0.0150	0.0234	0.0182
60			0.0180	0.0281	0.0188
70			0.0200	0.0328	0.0204
80			0.0210	0.0375	0.0233
90			0.0220	0.0422	0.0263

$\rho^{(1)}\rho$  by (Park & Ruitong 1988).

$\rho^{(2)}\rho$  obtained by (Kassoul et al. 2004).

$\rho^{(3)}\rho$  obtained by the inverse procedure of the method used previously in §2.1.

$\rho^{(4)}\rho$  obtained by the equation (4) (Eurocode 8 2003).

$\rho^{(5)}\rho$  obtained by this investigation in the equation (9).

general. However, the two first proposition are limited for only for  $\mu_{\varphi} = 8$ , and  $f_{ck}$  less than 50 MPa. Also, the proposed equation in (9) and that of Eurocode 8 (Eurocode 8 2003) take into account explicitly the

local ductility, which may be generalized for very high strength up to  $f_{ck} = 90$  MPa. Although the advantages of the two later approaches, our approach gives the best accurate results.

## 5 CONCLUSION

The tension reinforcement ratio  $\rho_{\max}$  recommended by EC8 has been examined to determine the variation of the curvature ductility factor in the cross sections in the reinforced concrete beams. According to the analysis, we suggest a modification of the equation proposed earlier in (9) in order to take into account the effect of the ultimate deformation of the concrete, which decreases for very high strength. In addition, the proposed relation does not exceed the value of 0.025 in all cases.

## REFERENCES

- ACI 318M. 2005. Building code requirements for structural concrete and commentary, ACI Committee 318—Structural Building Code, p438.
- Eurocode 2. 2004. Design of concrete structures—Part 1-1: General rules and rules for buildings, EN 1992-1-1:2004 (E), p225.
- Eurocode 8. 2003. Design of structures for earthquake resistance—Part 1: General rules, seismic actions and rules for buildings, prEN 1998-1:2003 (E), p229.
- Kassoul, A., Ezziiane, K. & Kadri, A. 2004. Nouveau pourcentage d'armature pour la condition de ductilité dans les poutres. Revue française de génie civil, 8 (7): 769–791.
- Park, R. & Ruitong, D. 1988. Ductility of doubly reinforced concrete beam sections. ACI-Structural Journal 85 (S24): 217–225.
- PS92. 1998. Règles de construction parasismique—Règles PS aux bâtiments—PS92. Édition Eyrolles, Paris, 283 pages.

# Serviceability as a significant factor of the bridge life-cycle

V. Kristek & L. Vrablik

*CTU Prague, Faculty of Civil Engineering, Czech Republic*

**ABSTRACT:** Prestressed concrete bridges are very sensitive to long-term increase of deflections. The cost of reduced service life of such bridges is tremendous for society, the owners and users. Reliable prediction of bridge deflections during their construction as well as during their service life is of crucial importance for achieving good durability and long-term serviceability. The excessive and with time increasing deflections of long-span prestressed bridges are caused by a combination of several simultaneously acting factors. Two of them are discussed in detail. Special attention is directed to effects of the differential shrinkage and to arrangement of prestressing—a procedure to find the optimal arrangement of tendons layout is presented, allowing to avoid the tendons contributing to deflection increases. Developed computer programs are freely available; repair examples, as well as recommendations for the design practice are also presented. Results of the presented solutions and the developed analytical and design methods can help creating suitable theoretical tools for reliable and economic structural design of prestressed concrete box girder bridges without deflection impairments.

## 1 INTRODUCTION

The design of structures is more and more directed towards the entire lifetime design with multiple concurrent objectives. Apart from durability, the most important factor in the whole life design of reinforced and, in particular, prestressed concrete bridges, is the Service Limit State. From this point of view, prestressed concrete bridges are very sensitive to long-term increase of deflections. A survey of many bridges monitored in various countries showed that all of them have experienced similar deflection histories.

The long-term deflection behavior of long-span prestressed concrete box girder bridges has often deceived engineers monitoring the deflections. This phenomenon has paramount importance for serviceability, durability and long-time reliability of such bridges.

Due to excessive deflections, several bridges had to be either closed or repaired well before the end of their initially projected lifespan. The cost of reduced service life of structures is tremendous for society, the owners and users. In fact, it greatly exceeds, in strictly economic terms, the cost of catastrophic failure due to mispredicted safety margin.

As an example of remediation due to excessive deflections, bridge over river Elbe in Decin in North Bohemia can be presented. Structural system of this bridge is a three span continuous box girder beam (62.5 + 104 + 62.5 m—[Fig. 1](#)) with tapered shape, erected applying the cantilever technology.

The bridge structure was monitored since 1993, annual increment of midspan deflection was about 8 mm. Total differences between the theoretical road level and the result of measurement immediately before start of remediation were about 140 mm. Some probable reasons of this phenomenon can be summarized below:

- lower value of Young's modulus of concrete
- the shear effects (incl. the shear lag) on deflection in the design stage were ignored
- wrong function for time prediction of creep
- unexpected higher influence of relaxation of prestressing steel

During remediation, the stiffness of the structure was increased and an additional upward directed relieving loading were provided by additional external prestressing tendons—[Fig. 2](#).

The Koror-Babeldaob Bridge in the Republic of Palau, an island nation in the Pacific Ocean, is an example of the significance of the problem of serviceability. The bridge was designed in 1975 and when completed in 1977 it was the longest spanning, prestressed concrete box girder bridge in the world. However, the severe long-term serviceability problems appeared (deflection at mid-span of this bridge was much greater than anticipated; by the early 1990s the centre of the bridge had sagged 1.2 m). Structural remediation of the bridge was completed by June 1996, but on 26 September 1996, the bridge abruptly and catastrophically collapsed.

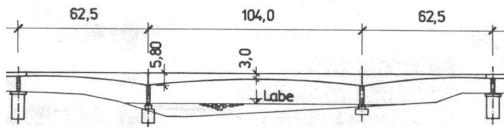


Figure 1. Bridge over river Elbe in Decin Czech Republic.



Figure 2. External tendons for structure relieving.

Reliable prediction of bridge deflections during their construction as well as during their service life is of crucial importance for achieving good durability and long-term serviceability. This is why the development of means to avoid excessive and in time increasing deflections already in the design stage is so significant.

Obviously, difficulty of predicting deflections is closely related to the properties of concrete (strength, elastic modulus, nonlinearity, creep, shrinkage, etc.), both initially and with time.

The total calculated deflection of a prestressed box girder bridge represents a small difference between a downward deflection due to dead and live loads, and an upward deflection due to prestress. This small difference between two large, variable quantities is very sensitive to small errors in these deflections. A small change in one may cause a large percentage change in the total deflection.

The excessive and with time increasing deflections of long-span prestressed bridges are caused by a combination of several simultaneously acting factors. Two of them are discussed in more detail.

## 2 DIFFERENTIAL CREEP AND SHRINKAGE

In large-span prestressed concrete box girder bridges, the thickness of the top slab is typically uniform or nearly uniform (equal to about 0.2 m) while the thickness of the bottom plate varies greatly, increasing from the midspan to the supports (from about 0.2 m to even as high as 1 m or much more). The web thickness is also variable. The thickness differences greatly affect the rate of drying (which is roughly inversely proportional to thickness square), and this in turn greatly affects concrete shrinkage and also influences creep. Further discrepancies in the rate of drying, and thus in shrinkage and creep, are caused by differences in the temperature and humidity conditions at the surface.

Drying shrinkage of the thinner top slab initially offsets downward deflections. However, once the thinner top slab has dried out and stopped shrinking, the slower shrinkage of the thicker bottom slab increases, causing large downward deflections.

The deflections of the cantilevers due to the differential shrinkage evolve freely only until their free ends are joined to create the final structural system of the bridge. Because, in the case of moment-resisting joints, further relative rotations between the joined ends are prevented after the girder is made continuous, a bending moment gradually develops in the joint. Significant additional redundant bending moments may develop due to the differential shrinkage after installing a moment-resisting joint. Their evolution can be quite complex, possibly changing from negative to positive values. The magnitude of these moments is roughly proportional to the girder stiffness. Thus stiff cross sections near the support may engender bending moments that are quite high for the light cross sections near the midspan, resulting in significant additional stresses in the midspan region.

The creep and shrinkage effects on prestressed concrete box girder bridges are usually analyzed assuming the shrinkage and the creep compliance (or creep coefficient) to be uniform over the entire cross section of the box girder. One of the objectives of this paper is to show that the result may be an incorrect prediction of long-term deflections, stress redistributions, and incorrect extrapolation of the trend of deflections observed during the initial years.

Measuring small deflections over the first few years, the engineer is tempted to extrapolate and optimistically expect the deflections to remain small, only to be unpleasantly surprised when, after several years, the deflections suddenly accelerate. Without realistic calculations, one may even misinterpret the

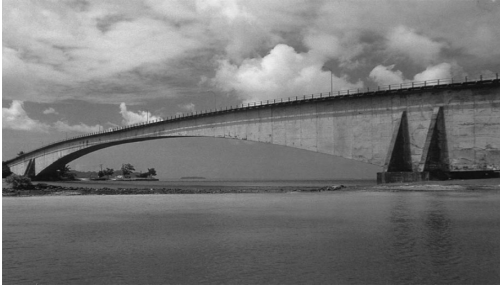


Figure 3. The Koror-Babeldaob Bridge in the Republic of Palau (Macdonald at all).

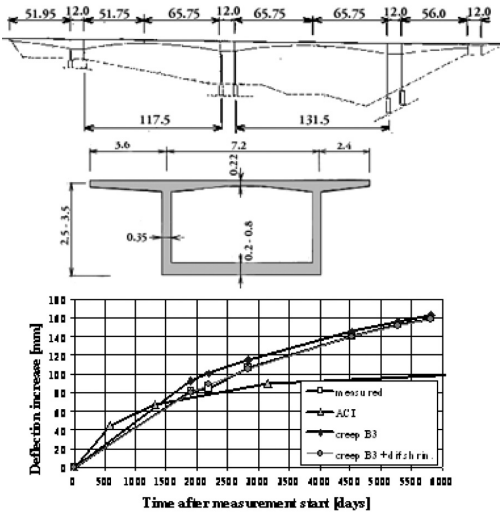


Figure 4. La Lutrive bridge: results of analysis and comparisons with observation. a) elevation, b) cross-section, c) deflections—measured and predicted by various models.

reasons for such a sudden acceleration of deflection and undertake inappropriate corrective actions that may induce excessive bending moments, overstressing the bridge, and possibly causing serious damage (e.g. as seen in Fig. 3).

An analysis was performed for the Lutrive Bridge, built in 1973 in Switzerland, which had midspan hinges (Fig. 4(a) and (b)). The midspan deflections gradually increased to over 150 mm (5.9 in.) after 15 years, as depicted in Fig. 4(c). The maximum upward deflection due to the differential shrinkage was about 22 mm (0.87 in.) after 1300 days. A comparison of the calculated and measured deflections is shown in Fig. 4(c), and it confirms that:

1. The measured deflections agree well with the calculations, taking into account differential shrinkage according to Model B3 (see Fig. 4(c));

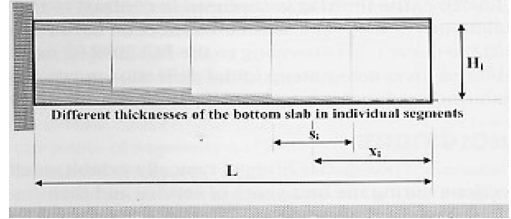


Figure 5. Simple illustrative example of a cantilever with a varying bottom flange thickness.

2. The time lag is captured in contrast to the calculations based on the mean cross-section behavior;
3. The curve corresponding to the ACI 209R-92 model exhibits an excessively steep initial deflection curve and grossly underestimates long-term deflections.

For the cantilever stage, it's instructive to give a simplified tool amenable to short formulae that anyone can evaluate by hand calculation. Consider a cantilever of length  $L$ , drying in a constant environment, and consisting of an ideal box beam (with massless webs) and two flanges of different thicknesses  $d_1$  and  $d_2$ , uniform over the individual segment lengths (Fig. 5) but small enough for the moment of inertia of each flange cross section to be negligible.

The deflection line curvature of a segment due to differential shrinkage may be approximated as

$$\psi_i = (\varepsilon_{sh,t} - \varepsilon_{sh,b,i})/H_i \quad (1)$$

in which  $\varepsilon_{sh,t}$  and  $\varepsilon_{sh,b,i}$  are the shrinkage strains in the top and bottom flanges and  $H_i$  is the box depth (Fig. 3).

The contribution of a single ( $i$ -th) segment to deflection of the cantilever end due to differential shrinkage is

$$\Delta y_i = \psi_i s_i x_i \quad (2)$$

in which  $s_i$  is the length of the  $i$ -th segment, and  $x_i$  is the distance of its center from the cantilever free end ( $i = 1, 2, \dots, N$ ). Thus, the deflection of the cantilever end due to differential shrinkage can be obtained as a sum of the contributions of individual segments

$$y = \sum \psi_i s_i x_i \quad (3)$$

Considering the special case of uniform thicknesses of flanges over the span length  $L$ , the deflection at the end of cantilever due to the differential shrinkage can be approximated as

$$y = \psi L^2/2 \quad (4)$$

### 3 ARRANGEMENT OF TENDON LAYOUT

Prestressed slender bridges are extremely sensitive to deflections in general. Deflection is a result of two opposite actions: the first one is caused by the external (vertical) loadings like dead load and live load, the other one, which has the opposite direction, is the effect of prestressing. Both mentioned actions, when acting separately, would produce individually significant deflections of opposite directions. The resulting deformation due to simultaneous action of the both loadings—due to external (vertical) loads and due to prestressing—is the difference of the mentioned deflections—this difference of large numbers is very sensitive: a small change in one of these numbers may result in a very significant change of their difference, i.e. in a significant change of the final deflection value.

In reality, all the parameters are of a random nature. The dead and live loads are usually known rather reliably. On the other hand, the prestressing can show much larger deviations from the assumed values. Due to the above-mentioned sensitivity of deflections on the contributing components, the randomness of prestressing plays very significant role when predicting deflections.

The tendon profile is often determined by construction staging and the geometry of the cross-section. But it is necessary to optimize the layout arrangement of tendons to achieve the highest efficiency of prestressing to reduce deflections.

It can be shown that low deflections of the bridge during the cantilever construction stages do not automatically result also in acceptable deflections during the bridge service life. The cantilever tendons, applied in erection stages, are usually very efficient during construction. However, after changes of the structural system making the structure continuous in the final structural system (e.g. closing of the midspan joints), their efficiency on the long term growth of deflections may be significantly limited, since the additional forces are developed due to the redundancy in the new structural system.

This can easily be demonstrated by an elementary example: two cantilevers are prestressed by tendons anchored at their end cross-sections as shown by arrows in Fig. 6. This arrangement of prestressing layout is very efficient to reduce deflections in the cantilever stage, but it can be easily proven that this arrangement of prestressing is absolutely inefficient to reduce *deflection increments* after the cantilevers are made continuous to form a final structural system. Such a final system (a clamped beam) deforms as being without any prestressing.

Importance of sensitivity of the tendon location can be shown on the following example: the final structural system of a bridge has a form of a three-span continuous beam as in Fig. 7. The effects of two locations

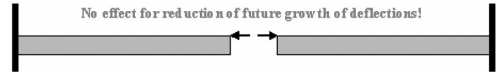


Figure 6. Prestressing in the cantilever stage.

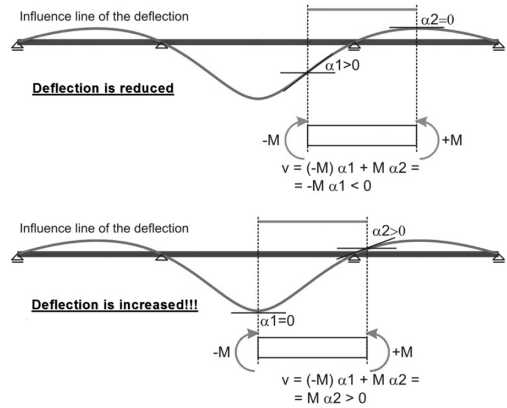


Figure 7. Different arrangement of a prestressing tendon location resulting in opposite midspan deflections: a) midspan deflection is reduced; b) midspan deflection is increased.

of a prestressing tendon on the midspan deflection are compared. Using the influence line of the midspan deflection, it can easily be shown that a relatively small shift of the tendon location results in quite opposite effects on the midspan deflection (Fig. 7).

An example elucidating significance of the tendon arrangement layout and assessment of efficiency of prestressing tendon layout for reduction of deflections of a real existing bridge is presented below.

The bridge over the River Labe in Melnik built in 1992 in Central Bohemia—a three span continuous box girder bridge (72.05 + 146.2 + 72.05 m—Fig. 8) with tapered shape, erected using the cantilever technology—is considered and analyzed. The task is to identify a possible unsuitable arrangement of the tendon layout that can result in harmful effects—as such tendons cause long-time increase (instead of reduction) of the midspan cross-section deflections.

Several categories of tendons, corresponding to individual stages of the construction process, were used during construction (see Fig. 9):

- A. Tendons located at the top surface, applied during cantilever erection stage
- B. Tendons located at the bottom surface of the middle (main) span
- C. Tendons located at the bottom surface of the first and third spans

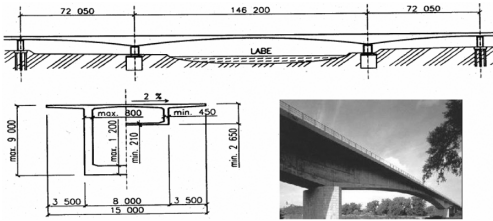


Figure 8. Bridge over the River Labe in Melnik.

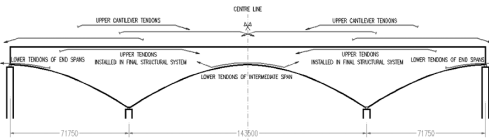


Figure 9. Scheme of layout of prestressing tendons.

Table 1.

Tendon category	Total number of tendons	Tendons increasing midspan deflection	
		Number	[%]
A	80	14	18
B	12	1	8
C	8	8	100
D	4	0	0
<b>Total</b>	<b>104</b>	<b>23</b>	<b>22</b>

D. Tendons located at the top surface over internal supports, applied at the time when box girder cantilevers are joined continuously at their ends to form the final structural system.

Effects of individual tendons were evaluated applying a developed program OPTI 1.1; the results, indicating how individual tendons affect the midspan deflection, are summarized in Tab. 1.

It is seen that 22% of the total prestressing tendons affect the investigated bridge unfavorably, contributing to an increase of deflections. The tendons of category C, located at the bottom surface of the first and third spans (see Fig. 9), proved to be extremely harmful, since all of them produce deflection increase in the central region of the main span of the bridge.

Among the tendons located at the top surface, applied during cantilever erection, the straight tendons, which are passively anchored in the vicinity of internal supports and follow the top surface, are harmful. In the discussed bridge, the unfavorable tendons in

the first (and in the third) span are anchored typically at distance of approximately 15 m from the ends of the bridge, the unfavorable tendons in the main span are anchored typically at distances of approximately 30 m from the midspan (see Fig. 9).

Significance of the tendon arrangement layout is elucidated in this way and a method to assess its efficiency on bridge deflections has been developed. The advantage of the proposed method is its ease of application, which allows the optimal tendon layout to be determined from the developed procedure. The method was programmed and is freely available on a web site and proposed as a design aid without recourse to expensive solutions. Practicing engineers can benefit in the design of sensitive bridges from a computer program OPTI 1.1., which has been developed at the Czech Technical University in Prague, making the assessment of the tendon layout immediately accessible to any engineer. This program is free to download from the internet address:

[http://concrete.fsv.cvut.cz/veda/science\\_en.php](http://concrete.fsv.cvut.cz/veda/science_en.php)

Program OPTI 1.1, which on filling the boxes for the data of the bridge and the tendon layouts gives values of deflection contributions due to individual tendons instantly.

A simple versatile method is also proposed to determine the most efficient location of a tendon (parallel with the girder neutral axis) for reduction of deflections. The method, which is intended for use as a design aid, allows the determination of the most efficient tendon location from a very simple graphical procedure.

The task is to determine the location of a tendon of length  $s$  with eccentricity  $e$  to produce maximum upward deflection of a bridge at cross-section  $P$  (see Fig. 10).

Provided that concrete creep represents a dominant effect, the time increment of deflections of a bridge of common arrangement in the final structural system caused by creep may be approximated as

$$\Delta y(t) = [\varphi(t, t_0) - \varphi(t_r, t_0)] y_e$$

in which  $\varphi$  is the creep coefficient,  $t_0$  is the age of concrete at loading,  $t_r$  is age of concrete at the instant of change of structural system,  $t$  is the age of concrete at the investigated time,  $y_e$  is the instantaneous deflection in the final structural system due to the applied loads.

It is evident that this relationship is quite simple—the time increment of deflections may be approximated simply as a product of the instantaneous deflection and the difference of the creep coefficients. The proposed graphical procedure for determination of location of a tendon to produce maximum upward deflection is based on this relation.

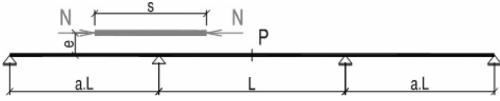


Figure 10. Location of the tendon.

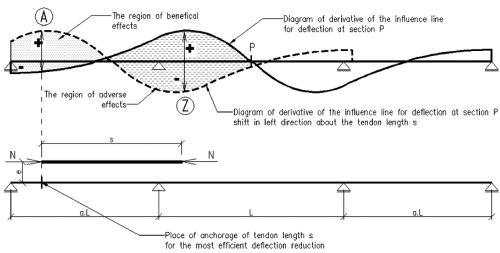


Figure 11. Simple graphical tool to determine the most efficient location of a tendon for deflection reduction.

The procedure consists of the following consequent steps:

1. Construct the diagram of the derivative of the influence line of bridge deflection at section  $P$  (the full line in Fig. 11)
2. Move this diagram to the left direction along the bridge axis about the tendon length  $s$  (the dashed line in Fig. 11)
3. The cross-sections with extreme differences of the both lines indicate the most efficient cross section  $A$  in Fig. 11 (or the most harmful cross section  $Z$  in Fig. 11) for location of the left tendon anchor
4. Intersections of the both lines indicate the anchorage locations without any effect on deflection of cross-section  $P$
5. Intersections of the both lines demark the regions of beneficial effects (the dotted area in Fig. 11) and adverse effects (the dashed area in Fig. 11)

There is no longer any need for blindly trying to find an optimal tendon layout that is really efficient from the point of view of reduction of deflections. Such a simple tool allows the tricky tendons (that—on the one hand—are beneficial to eliminate tensile stresses but whose layout—on the other hand—significantly contribute to deflection increases) to be eliminated.

#### 4 CONCLUSIONS

The prestressed box girder bridges typically exhibit only a portion of deflections during the first period and then continue to deflect. Extensive monitoring on many bridges confirms these observations.

The research on this problem is important, not only to avoid excessive deflections resulting in long-term serviceability impairments. It also should be noted that a wrong prediction of the development of deflections means that also prediction of the distribution of internal forces, particularly in bridges changing the structural systems, can be far from reality.

Lessons from assessment of existing bridges can be learnt: bridge design should be performed on two different levels, including two equivalent parts—not only common stress analysis, but also optimization of prestressing tendon layout should be compulsorily performed to reach acceptable deflection variations.

Presented results can enable increase of economy of materials, energy and costs and their better utilisation and offer objective and effective tools increasing the level of serviceability, durability and efficiency of prestressed concrete box girder bridges. The achieved results will enable not only to avoid excessive deflections resulting in long-time serviceability problems, but also possibly other impairments.

#### ACKNOWLEDGMENTS

This outcome has been achieved with the financial support of the Ministry of Education, Youth and Sports, project No.1M680470001, within activities of the CIDEAS research center. The support of the Grant Agency of the Czech Republic Grant Projects No. 103/06/0674 and 103/08/1677 is also gratefully acknowledged.

#### REFERENCES

- Kristek, V. & Kohoutkova, A. 2002 Service Limit State of Prestressed Concrete Bridges, *fib Congress, Osaka, 2002*
- Kristek, V. & Vitek, J.L. 1999 Deformations of Prestressed Concrete Structures—Measurement and Analysis, *Proceedings of the fib symposium 1999, Prague, pp. 463–469*
- Vitek, J.L. & Kristek, V. & Kohoutkova, A. 2004 Time development of deflections of large prestressed bridges, *New Delhi, November 2004*
- Kristek V. & Bazant, Z.P. & Zich, M. & Kohoutkova, A. 2006 Box Girder Bridge Deflections—Why is the initial trend deceptive?, *Concrete international/January 2006, pp. 1–9*
- Kristek V. & Vrablik, L. 2005 To deflection control of prestressed concrete bridges (in Czech), *BETON No. 4, July 2005*
- Macdonald, B & Saraf, V. & Ross, B. A Spectacular Collapse: The Koror-Babeldaob (Palau) Balanced Cantilever Prestressed, Post-Tensioned Bridge, *Failure Analysis Associates, USA*

# Inspection and evaluation of existing structures: a task for brave engineers

J. León

*Maintenance Engineering Department of FHECOR & Civil Engineering School of Madrid, Spain*

H. Corres-Peiretti

*FHECOR Ingenieros Consultores & Civil Engineering School of Madrid, Spain*

F. Prieto

*Maintenance Engineering Department of FHECOR, Madrid, Spain*

**ABSTRACT:** Assessing an existing structure implies its in-depth understanding. In the world of Medicine, full understanding of the patient is based on a well studied clinical history, a visual check, analytical tests and, consequently, a comprehensive diagnosis of the causes of the diseases. There is no reason not to apply a similar *modus operandi* to existing structures. This paper claims for a better education of young engineers, to enable them to understand an existing structure as a part of a fascinating whole and not merely as a mathematical model.

## 1 INTRODUCTION

Le Corbusier conceived Architecture as ‘a wise, concrete and magnificent combination of volumes grouped under light’, implicitly supposing eternal or, at least, sufficient life for them. Fernández-Casado (1975) qualified such an assertion in the sense that ‘it is not a matter of volumes, but masses that weigh and resist; the architecture of engineers is rooted in a cosmic vision, forcing them to an ascetic attitude in relation to Nature, to stoical withstand the attraction of superfluosity; a non-timeless attitude, independent of momentary tendencies’.

During the last fifteen years, a new concept is present in the basis of design of engineers, together with safety against failure and an adequate serviceability: durability. Modern standards, as the Spanish Concrete Code EHE (1998), state: ‘A structure must be designed and erected in such a way that it can resist all corresponding actions both during construction and along the lifetime foreseen in design, with acceptable safety, as well as environmental aggressiveness’. To ensure durability, a fourth aspect is gaining importance in engineering practice: maintenance. The oncoming edition of the Spanish Concrete Code EHE (2008) already includes this idea: ‘Maintenance can be defined as the set of actions necessary to ensure that the features of a structure, as a basis of design, do not fall below a certain threshold value along its lifespan. This threshold value is related to the strength, durability, functionality and even aesthetics’.

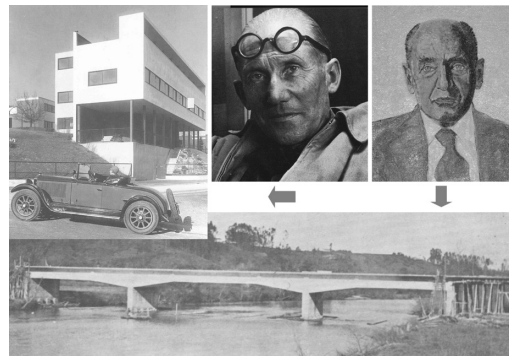


Figure 1. Le Corbusier and Fernández-Casado. Two different but complementary visions of the structures of 20th century.

Certain established attitudes defended the idea that structures should not be in service beyond a nominal lifetime, independently of the condition of the structure, and then replaced. However, the increasingly present sustainable principles are pushing towards new strategies of decision, including the possibility of enlarging the service life of existing structures. Indeed, little attention has been paid to the structural maintenance, from the technical, economical and educational points of view, which is also a symptom that society has not considered structural maintenance as important as the maintenance of aircrafts or high speed trains.



## 2 THE 'LIFE-CYCLE' CONCEPT



Figure 2. Collapse of the bridge over the Mississippi River in Minneapolis (August 1st, 2007).



Figure 3. Degradation processes affect a great variety of structures and condition, always increasing with age.

Unfortunately, due to some accidents, it seems that this tendency is changing (figure 2).

The opinion of the authors is that this new attitude opens new possibilities and challenges for engineers, but also new requirements regarding their skills and education. This paper tries to shed light on this topic.

The need of maintenance involves structures of all ages, materials and typologies (figure 3), requiring, as Poul Beckman (2004) says, 'a couple of open eyes and an open mind', which means an overall knowledge and expertise in structural engineering. It is also worthwhile mentioning that, once again, the experience gained in the field of structural concrete has settled the basis for a general and comprehensive treatment of this problem.

Figure 4 shows the evolution of the life expectancy in Spain over the last 108 years. It is evident how the application of preventive measures and an adequate sanitary policy ('maintenance') has practically doubled this expectancy. There is no reason to think that an adequate maintenance policy, applied to the existing structures, can not lead to an enlarged, engineer based, life of the structures. Figure 5 shows a summarized but clarifying chart of the life process of a structure, paralleling to the one of a human being, and the related attitude of engineers.

Although in this figure the first step, the decision for construction, is usually outside of the scope of a technician, it is also very useful for him to know about the historical circumstances of such a decision. A skilled technical inspector can extract a lot of information from the history of construction: regulatory guidelines on actions, quality of materials used (strength and durability properties), methods of construction, etc.

In any case, both design and construction take few months, a relatively reduced time compared to the long and usually forgotten period of service. However, the inexorable degradation of materials, some design mistakes or construction defaults, condition the lifetime of the structures. The knowledge of all these causes could help to improve the processes of design and construction and, as a consequence, it seems clear that the inspector engineers can give important feedback information. Nevertheless, the truth is that the biggest part of the effort of universities and other training institutions, e.g. engineering companies, has been devoted to project. In this regard, designing engineers are assisted by standards or procedures, which make

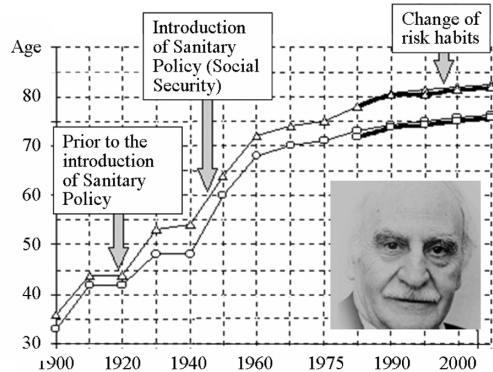


Figure 4. Evolution of life-expectancy in Spain and an example of increasingly more frequent exceptions: the writer Francisco Ayala, 102 years old and still active.

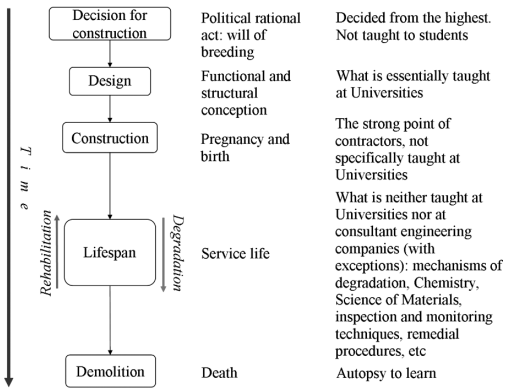


Figure 5. The life cycle and the frame of tasks of inspection and maintenance.

easy their task and reduce the responsibility of the technicians. Although it seems rather unfair and probably excessive, it does not matter if the engineer understands what he is doing; the important thing is that he is under the comfortable umbrella of a standard.

### 3 INTERPRETING DAMAGES

There are several classification catalogues (León et al. 2003) of damages available for technicians. The problem is that excessive task specialization unfortunately has led to a situation of only partial understanding and even misuse of such documents. Thus, on one hand, specialists on structures feel happy when dealing with structural diseases (i.e. cracking due to shear or bending, etc.), but, on the other hand, they become uncomfortable when they have to understand the electrochemical process of steel corrosion or the sulphate attack on concrete. On the contrary, when chemists are called to inspect a construction showing structural problems, they tend to discover corrosion processes, although the cause is quite simple (e.g. cracking due to overloading, not foreseen for modern live loads, or originally produced during construction). Therefore, it may be concluded that interpreting damages requires 'complete' technicians, that is, engineers who are well trained and educated, in cooperation, of course, with many other specialists. The following are just few examples of these ideas.

It is well known that structural movements (figure 6) induce, it is well known, reduced consequences in statically determined structures and, in theory, more important ones in statically undetermined structures. The structural engineer must be aware that even the latter may be less important than derived after a classical, conventional, but untrue, elastic analysis, provided



Figure 6. Settlement: a relatively easy symptom to qualify.

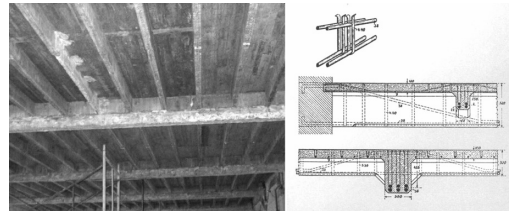


Figure 7. Apparent sound old structures: a potential trap.

that they were designed with sufficient ductility (this amount of ductility has not been quantified yet as a function of the imposed displacement).

At the other extreme, the engineer may find structures, with no cracking patterns, although with big delayed deformations. Designed in the early times of structural concrete, when the concepts or arranging steel bars on the compression zones were not clear yet, this type of structures may be rather brittle and admit no repair techniques by means of the always promising techniques of carbon fiber strips. In spite of their good appearance, these structures hide their poor condition and might be a real trap to an unaware inspector (figure 7).

In front of a diagonal crack (figure 8), the inspector who had to study structural concrete (or, even better, teaches it nowadays), feels the ineffable sensation of identifying real strut-and-tie models, which seemed rather arbitrary simplifications of textbooks. From the point of view of durability, it is not yet clear why, even under aggressive environmental conditions and with crack widths beyond the conventional limits, there is no higher level of corrosion in these zones than in other, even uncracked ones.

Figure 9 shows a specific case of confusion between the consequence of differential settlement of fresh concrete mass of the webs with respect to the flanges and the effects of longitudinal shear between flanges and webs. It is not uncommon to find reports recommending strengthening webs and flanges with transverse reinforcement.

Some inspectors feel frightened when they discover large but single cracks on masonry or plain concrete vaults, in crown and springing zones (figure 10). In fact, such cracks are a mere consequence of the normal



Figure 8. Diagonal cracks announcing a compressed strut.

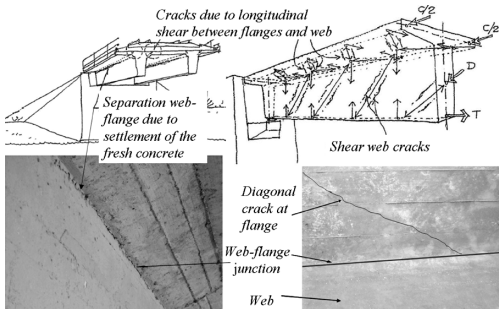


Figure 9. Misunderstanding of web top part separation in relation to the flange, and cracks due to longitudinal shear.

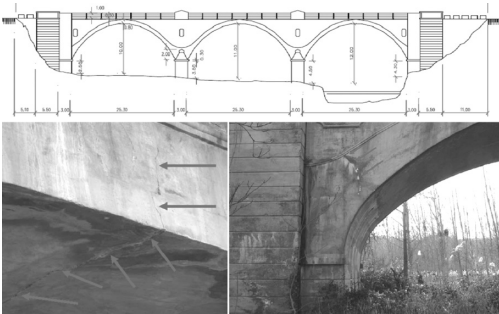


Figure 10. Normal, harmless cracks, showing normal behaviour, although alarming to an inexperienced technician.

functioning of the structure. However, the fear of the inspectors is justified because they do not understand the working mechanism of such structures, which are not taught at the University because this old typology is no longer used in modern design and construction. Another reason to underline the vast formation required to inspectors, much broader than supplied today at universities.



Figure 11. Collapsed column of a building with durability problems as well as poor design of details and construction.

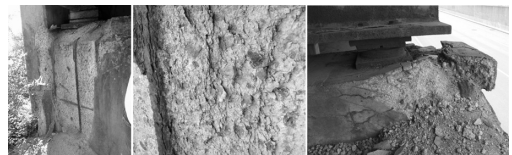


Figure 12. Effects of deicing salts. It is normally believed that salt=chlorides=corrosion of reinforcement, but it is even worse, in extreme weather conditions, the effect of the local freezing-thaw, producing scaling of concrete.

Hidden design or construction defaults may lead to situations of collapse as shown in figure 11. Surprisingly, in this case the architect decided to repair the structure. Indeed, there are modern techniques to rehabilitate columns by means of new confined concrete covers, but a sensible engineer must establish a logical limit to the reparability, closely related to the importance of the damages, the costs of repair and the remaining lifespan.

Deicing salts, in zones of continuous low temperatures, may produce important damages to concrete, threatening even the stability of bearing devices, as shown in figure 12. The problem is especially important in zones of water leakage, i.e. in joints, and could be avoided by means of simple devices to keep the water off. The authors wish to express at this stage the rewarding experience gained when inspecting structures abroad, in zones with climates and engineering traditions different from own's.

Chemical attacks are not easily identified, since similar symptoms may have radically different origins (figure 13). Thus, plastic shrinkage shortly after casting concrete, thermal effects also during the hardening process of the cement paste, or chemical attacks due to water with sulphates produce cracking with the same appearance. The capability of the inspector on the site is essential to properly identify the most



Figure 13. The coincidence of symptoms with different origins calls the attention specifically of well trained inspectors.

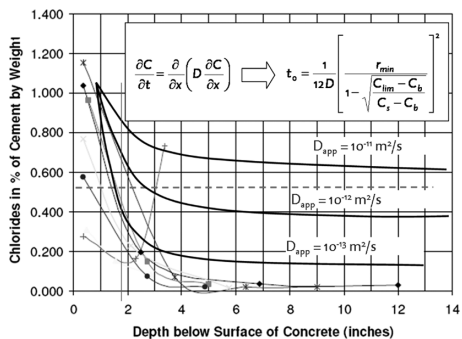


Figure 14. Available model, based on Fick's second law, to predict the initiation period of the corrosion process of re-bars.

probable cause (or causes) of the problems he comes across and to prescribe the complementary analyses and remedies.

In recent years corrosion processes have been studied in depth, providing models that supply a reasonable good estimation of structural lifespan (figure 14). By means of these models, the engineer is able to evaluate the residual lifespan and to design the eventual repair procedure. This last activity is still considered a minor task, but implies a great responsibility, since a badly conceived or executed repair may disguise other real diseases and, therefore, shorten the life of the repaired structure.

#### 4 MAINTENANCE ENGINEERING

Once accepted that structures suffer inexorable degradation processes, the task of engineers is to define the most suitable strategy to maintain their safety, functionality and durability. Figure 15 shows a diagram of Prof. Mola (1997), summarizing the elements of the eternal fight against failure. Every repair operation leads, if well directed, to an increasing of the lifespan.

Figure 16 shows the same ideas on a variation of the classical diagram of Tuutti (1982). Lifespan  $t_1$  of the structure is the sum of both the initiation and propagation periods. The time  $t_2$  could be understood as an 'extended' lifespan forced by the circumstances. 'Reactive' interventions (unfortunately,

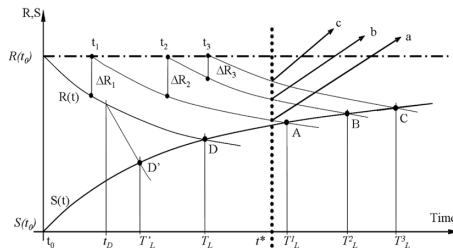


Figure 15. Evolution of actions  $S_d(t)$  and capacities of the structure  $R_d(t)$ . Possible interventions to increase the lifetime.

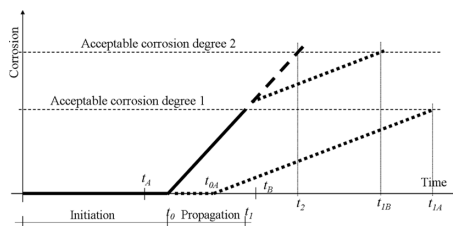


Figure 16. Variations on the classical diagram of Tuutti, expressing the predictable lifespan and how to enlarge it by means of timely intelligent interventions.

the most common which take place just after surpassing an acceptable or limit situation) at age  $t_{1B}$ , lead to an increased lifespan equal to  $t_{1A} - t_{1B}$ . Frequently, when the time of intervention is higher than  $t_{1B}$ , the repair or strengthening operations are more expensive or even unaffordable and the structure must be replaced.

Figure 16 also shows how the success of an intervention may be much more profitable if a 'proactive' intervention is adequately programmed. The closer, but not later, to the end of the initiation period and the more effective intervention (with the smallest slope of the damage evolution), the most durable (and probably cheaper) solution shall be obtained. When intervening at time  $t_A$ , it is possible to delay  $t_0$  until  $t_{0,A}$  and the propagation period, till  $t_{1,A}$  is also enlarged, even for a more strict accepted level of corrosion. The quantification of the end of both the initiation period and the propagation periods requires a correct diagnosis of the degradation mechanisms and a correct evaluation of the relevant parameters of the available models: again a task requiring expert engineers.

It is very interesting to detect that some societies have assumed the need of a maintenance policy, as in the case of the Mosque of Djanné, in Mali (figure 17). Whenever necessary, the citizens are requested to make a personal effort to repair the old mudwalls.

This is an admirable example of 'proactive' intervention. The example goes beyond that, since horizontal protruding logs, permanently attached to the



Figure 17. The Mosque of Djanné (Mali).



Figure 18. Railings: a topic that relates user's safety and structural aspects.

walls, serve as auxiliary elements to allow people to climb up and carry out the operations of inspection and maintenance. Auxiliary devices for this purpose are required by new Standards, i.e. the new Spanish Code for Structural Concrete.

In recent times, a complementary concept of safety is growing and affecting engineers: the user's safety. It is not only a matter of torsional cracks or chloride contents, that is, the security of the structure itself, but something more concrete to the citizen and to the politicians: it results unacceptable (political and economically expensive) that structures or their equipment might become dangerous to users in case of foreseeable accidents (figure 18). The question is located in a not well defined frontier: it belongs neither to the structural engineer nor to the expert in bridge railings. It is worth to mention that the problem is of tremendous complexity and that the common way of solving it is empirical, by means of tests, leading to empirical proposals that are valid for a given set of circumstances.

## 5 EDUCATION

The need for housing and infrastructures has conditioned the professional profile of the current engineers, directed only towards new structures. Besides, young engineers seem to be rather 'blinded' by the new and huge bridges, buildings or facilities, symbols of prestige and social success. But once such constructions start showing defaults, it becomes essential to inspect them to value their condition and intervene in the most intelligent possible way. This task requires truly interested, well trained and brave engineers, capable to accept the challenge of this fascinating field of the professional activity.

Universities must complete their educational offer including a sufficient formation of such disciplines

related to Structural Analysis, involving all kind of structural materials, typologies, ages or functions, but also Chemistry, Science of Materials, Non Destructive Techniques of inspection and monitoring and even Linguistics and Terminology (Bauder, 2007). It is the right time now to mention such a need, at least in Europe, where a new 'space of common education' tries, theoretically, to offer to the society the required professionals. To teach students it becomes necessary to stimulate the participation of professional engineers in the teaching process, as medical doctors teach at faculties and hospitals, at the open air of reality, bringing also the freshness of the relation that such activity has with history, politics, economics, art, etc. This approach will also contribute to cure the 'blind calculism', an illness affecting young engineers that believe that their professional activity consist in conceiving the world through powerful, coloured but even vain finite element models.

## REFERENCES

- Bauder, E. Las edades del puente de fábrica. Terminología y metáfora. Doctoral Thesis, directed by Aguado, G. and León, J. March 2007.
- Beckman, P.; Bowles, R. Aspects of Building Conservation. Elsevier-Butterworth-Heinemann, Oxford 2004.
- EHE. Spanish Code for Structural Concrete. December 1998.
- Fernández-Casado, C. La Arquitectura del Ingeniero. Colegio de Ingenieros de Caminos, Canales y Puertos. Madrid 2005 (first edition, 1975).
- León, J.; Espeche, A.; Corres, H. et al. Daños en puentes ferroviarios de hormigón. Grupo de Hormigón Estructural. Universidad Politécnica de Madrid. December, 2003.
- Mola, F.; Vitaliani, R. Analysis, diagnosis and preservation of ancient monuments: the St. Mark's Basilica in Venice. CIMNE. Barcelona 1997.
- Tuutti. Corrosión of steel in concrete. Swedish Cement and Concrete Research Institute. CBI Research 4:81, 1982.

# Minimum life-cycle cost design and optimal earthquake intensity decision-making of aseismic structures based on finite element reliability analysis

Da-Gang Lu, Xiao-Hui Yu, Gang Li & Guang-Yuan Wang

*School of Civil Engineering, Harbin Institute of Technology, P.R. China*

**ABSTRACT:** A new model of life-cycle cost optimization for the optimal earthquake intensity decision-making is put forward in the present paper, in which the un-optimized initial material/construction cost dependent on the traditional trial-and-error design whose arbitrariness in nature is unavoidable now is replaced by the minimum initial cost. The functional relationship between the minimum initial cost and the earthquake intensity is derived through a series of minimum initial cost seismic design subjected to the provisions of the Chinese codes by successively adjusting the design earthquake intensity. A two-stage optimal design methodology is presented, in which the decision of the optimal earthquake intensity is made during the first stage, while the minimum-cost design under the optimal earthquake intensity is conducted in the second stage. To account for the uncertainties more efficiently and accurately, the finite element reliability analysis based on first order reliability method (FORM) is used in this paper to calculate the probability of exceedance of structural responses in four damage states given the occurrence of seismic events. The discrete seismic fragilities, i.e. damage probability matrix of the slight, moderate, severe and collapse performance levels are computed by using the nonlinear finite element reliability module in OpenSees. The limit state probabilities are then calculated by the summation of the product of discrete damage fragilities and hazard probabilities. The proposed procedure is applied in seismic design optimization of steel frame buildings subjected to Chinese seismic design codes. A numerical example demonstrates the feasibilities and the merits of the proposed methodology.

## 1 INTRODUCTION

Significant progress has been made in the preceding decades in the area of minimum life-cycle cost design optimization for aseismic structures. The life-cycle cost model in the existing literature is the total summation of initial material/construction cost and the lifetime seismic damage cost. Liu & Neghabat (1972) are among the first researchers who incorporated lifetime seismic damage cost into the initial design stage. Recent studies by Ang & De Leon (1997), Rackwitz (2000), Wen (2001), Wen & Kang (2001a, 2001b), Ang & Lee (2001), Esteva et al. (2002), Frangopol & Maute (2003), Wang & Lu (2001), Wang et al. (2003), Liu et al. (2003, 2004), Lu et al. (2002, 2006), Alimoradi et al. (2007), Foley et al. (2007), among others, have developed the minimum expected life cycle cost criteria and methodologies for performance-based seismic design of structures.

In minimum life-cycle cost design of structures, the optimal reliability generally is taken as the acceptable risk level (Ang & De Leon 1997, Rackwitz 2000, Ang & Lee 2001). In the present paper, however, the optimal earthquake intensity is chosen as

a risk-informed decision-making parameter, instead of the target reliability. A new model of life-cycle cost optimization for the optimal earthquake intensity decision-making is put forward, in which the un-optimized initial material/construction cost dependent on the traditional trial-and-error design whose arbitrariness in nature is unavoidable now is replaced by the minimum initial cost. A two-stage optimization methodology for aseismic structures is then presented to realize the minimum life-cycle cost design.

To compute the expected lifetime seismic damage cost in the minimum life-cycle cost model, the limit state probabilities are usually evaluated by some practical methods in order to lessen the computational burden during the optimization process, such as, the procedure proposed by Wen and his group based on the uniform hazard ground motion and the equivalent SDOF system (Wen & Kang 2001a,b, Liu et al. 2003), the SAC/FEMA method based on the assumptions of lognormal distributions for randomness in seismic demands and capacity (Liu et al. 2004, Foley et al. 2007, Alimoradi et al. 2007), and the simplified fragility analysis method formerly proposed by the authors based on the three levels of seismic design



criteria in Chinese code (Wang & Lu 2001, Wang et al. 2003, Lu et al. 2002, 2006). However, all the above mentioned methods are approximate in nature. To account for the uncertainties more accurately and efficiently, the finite element reliability method is used in this paper to calculate the probability of exceedance of structural responses given the occurrence of seismic events.

## 2 REVIEWS OF LIMIT STATE PROBABILITY CALCULATION METHODS

### 2.1 Wen's method

To evaluate the probability of exceedance of a given response level of the system, Wen (2001), Wen & Kang (2001b), Liu et al. (2003). proposed a practical method. In this method, the response of a MDOF nonlinear system was approximated by that of an equivalent nonlinear SDOF system, based on the results of a static pushover analysis. The maximum interstory drift ratio of the MDOF system was then calculated based on the uniform hazard response spectra for a given soil condition and a given level of probability of exceedance for both linear and nonlinear systems. The 50-year probability of exceedance of structural response in both the linear and nonlinear range was evaluated using the uniform hazard response spectra and the equivalent SDOF system. The errors introduced by the SDOF system were corrected by bias factors.

### 2.2 Cornell's method

The SAC/FEMA guidelines developed by Cornell et al. (2002) calculate the mean limit state probability as the following, assuming lognormal distributions for randomness/uncertainty in seismic demands and capacity, respectively:

$$P_{LS} = H(S_a^{\hat{C}}) \exp \left[ \frac{1}{2} \frac{k^2}{b^2} \beta_T^2 \right] \quad (1)$$

where  $H(S_a^{\hat{C}})$  is the point estimate of spectra acceleration hazard associated with median drift capacity  $S_a^{\hat{C}}$ ;  $k$  is the slope of the seismic hazard curve, in log-log coordinates, at the hazard level of interest;  $b$  is a coefficient relating incremental change in demand to incremental change in ground shaking intensity;  $\beta_T$  is the coefficient of variation of the total randomness and uncertainty in demand and capacity.

### 2.3 Finite element reliability method

The methods proposed by Wen and Cornell are approximate in nature. To account for the uncertainties more accurately and efficiently, the finite element reliability method (Haukaas & Der Kiureghian 2007) is used

herein to calculate the limit state probabilities of the structure in different damage states.

For a given limit state function  $g(\mathbf{x})$ , where  $\mathbf{x}$  is the basic random variables vector, the first order approximation of the failure probability is

$$P_{LS} = P[g(\mathbf{x}) \leq 0] \approx \Phi(-\beta_{HL}) = \Phi(-\alpha^{*T} \mathbf{u}^*) \quad (2)$$

where  $\Phi(\bullet)$  is the cumulative distribution function (CDF) of standard normal variate;  $\beta_{HL}$  is the Hasofer-Lind reliability index;  $\mathbf{u}^*$  is the design point in standard normal space  $\mathbf{u}$ ;  $\alpha^*$  is the normalized negative gradient at  $\mathbf{u}^*$ .

The design point  $\mathbf{u}^*$  generally is iteratively searched by the well-known HLRF algorithm:

$$\mathbf{u}_{i+1} = \left( \frac{G(\mathbf{u}_i)}{\|\nabla G(\mathbf{u}_i)\|} + \alpha_i^T \mathbf{u}_i \right) \alpha_i \quad (3)$$

where  $\mathbf{u}_i$  and  $\alpha_i$  are the design point and its normalized negative gradient in the  $i$ th iteration respectively;  $G(\mathbf{u}) = g[T^{-1}(\mathbf{x})]$  is limit state function in  $\mathbf{u}$  space, in which  $\mathbf{u} = T^{-1}(\mathbf{x})$  is the inverse transformation of  $\mathbf{x}$ ;  $\nabla G(\mathbf{u})$  is the gradient of  $G(\mathbf{u})$ , which relates the gradients of limit state function and structural responses function in the original  $\mathbf{x}$  space as

$$\nabla G(\mathbf{u}) = (\mathbf{J}_{\mathbf{u},\mathbf{x}}^{-1})^T \mathbf{J}_{\mathbf{s},\mathbf{x}} [\nabla g(\mathbf{s}) \cdot \mathbf{J}_{\mathbf{s},\mathbf{x}} + \nabla g(\mathbf{x})] \quad (4)$$

where  $\nabla g(\mathbf{x})$  and  $\nabla g(\mathbf{s})$  are gradients of  $g(\mathbf{x})$  and  $g(\mathbf{s})$ , respectively;  $\mathbf{J}_{\mathbf{u},\mathbf{x}}$  and  $\mathbf{J}_{\mathbf{s},\mathbf{x}}$  are Jacobian matrix of probability transformation  $\mathbf{u} = T^{-1}(\mathbf{x})$  and mechanical transformation  $\mathbf{s} = \mathbf{s}(\mathbf{x})$ , respectively.

The Jacobian  $\mathbf{J}_{\mathbf{s},\mathbf{x}}$ , i.e., the gradient of structural responses  $\mathbf{s}$  with respect to basic variables  $\mathbf{x}$ , can be obtained by finite element response sensitivity analysis with the direct differential methods. For example, the gradient of displacement responses can be directly computed as

$$\mathbf{K}_T \frac{\partial \delta}{\partial \mathbf{x}} = \frac{\partial \mathbf{F}}{\partial \delta} - \frac{\partial \mathbf{R}}{\partial \mathbf{x}} \Big|_{\delta} \quad (5)$$

where  $\delta$  is the nodal displacement vector in the global coordinates,  $\mathbf{F}$  and  $\mathbf{R}$  are external and internal forces vectors, respectively;  $\mathbf{K}_T$  is the global tangent stiffness matrix;  $(\partial \mathbf{R} / \partial \mathbf{x})|_{\delta}$  is the conditional gradient of internal forces vectors.

The response sensitivities by direct differentiation as well as finite element reliability analysis have been developed by Haukaas & Der Kiureghian (2007) in object-oriented finite element computation platform OpenSees.

### 3 MINIMUM LIFE-CYCLE COST DESIGN OF ASEISMIC STRUCTURES

#### 3.1 A new model of optimal earthquake intensity decision-making for aseismic structures

The design earthquake intensity  $I_d$ , instead of the target reliability, is taken as the acceptable risk level of a structure. We herein propose a more rational optimization objective function for performance-based seismic design considering expected life cycle cost as follows:

$$E[C(T, I_d)] = C_{\min}[\mathbf{d}(I_d)] + \frac{\nu}{\lambda}(1 - e^{-\lambda T})L[\mathbf{d}(I_d)] \quad (6)$$

where  $\mathbf{d}(I_d)$  is the structural scheme designed according to the design earthquake intensity  $I_d$ .  $C_{\min}[\mathbf{d}(I_d)]$  is its initial minimum cost;  $L[\mathbf{d}(I_d)]$  is its corresponding loss expectation;  $\nu$  is the mean occurrence rate of earthquake;  $e^{-\lambda T}$  is the discounted factor of over time  $t$ ;  $\lambda$  is the constant discount rate/year;  $T$  is the design life of a new structure.

#### 3.2 Two-stage minimum expected life-cycle cost optimization methodology

The minimum expected life cycle cost optimization for performance-based seismic design is divided into the following two design stages:

Stage 1: Decision-making for the optimal earthquake intensity of aseismic structures considering expected life cycle cost.

In this stage, the optimal earthquake intensity of aseismic structures is determined according to the following optimization model:

$$E[C(T, I_d)] = C_{\min}(I_d) + \frac{\nu}{\lambda}(1 - e^{-\lambda T})L(I_d) \rightarrow \min \quad (7)$$

where the minimum-cost function  $C_{\min}(I_d)$  can be obtained from the regression analysis of a series of minimum initial cost seismic design by adjusting the design earthquake intensity  $I_d$ , which is an increasing function of  $I_d$ ; the total loss expectation function  $L(I_d)$  can be obtained from the regression analysis of a series of seismic risk and loss assessment processes by adjusting  $I_d$ , which is a decreasing function of  $I_d$ .

The total expected life cycle cost curve  $E[C(T, I_d)]$  by composing the above two curves generally have the lowest point. The design earthquake intensity  $I_d$  corresponding to this point is called the optimal earthquake intensity  $I_d^*$ , which represents the minimum acceptable seismic risk level of a structure.

Stage 2: Minimum initial cost seismic design under the optimal earthquake intensity.

Once the optimal earthquake intensity  $I_d^*$  has been obtained, the minimum initial cost seismic design can be made under this  $I_d^*$ . Therefore, the optimization model in this stage should be:

Find the design scheme  $\mathbf{d}(I_d^*)$ , to make the structural cost

$$C[\mathbf{d}(I_d^*)] \rightarrow \min \quad (8)$$

subjected to all constraints and requirements of design codes of structures.

The final solution is the optimal design scheme in consideration of the total loss expectation  $L(\mathbf{d})$ . Since the loss expectation has been taken into consideration when deciding  $I_d^*$  during the first design stage, it is only necessary to counteract the optimal resistance  $I_d^*$  by the minimum initial cost design scheme during the second design stage.

#### 3.3 Minimum initial cost design of aseismic structures

Under the given earthquake intensity  $I_d$ , the minimum initial cost design problem of a structure can be conceptually stated as:

To find the design scheme  $\mathbf{d}(I_d)$ , so as to make the initial cost of the structure

$$C[\mathbf{d}(I_d)] \rightarrow \min \quad (9)$$

subjected to provisions of Chinese Seismic Design Code of Buildings and other specific design codes of structures.

Since gradient information can greatly improve the optimization efficiency, the Polak-Ribiere conjugate gradient direction algorithm is made use of, which performs the optimization loop according to the search direction as follows:

$$\mathbf{r}^{(j)} = -\nabla Q(\mathbf{d}^{(j)}) + \theta_{j-1} \mathbf{r}^{(j-1)} \quad (10)$$

where  $\mathbf{r}^{(j)}$  = search direction vector in the  $j$ th iteration;  $\mathbf{d}^{(j)}$  = design variable vector in the  $j$ th iteration;  $Q(\bullet)$  = the dimensionless, unconstrained objective function via penalty function method;  $\nabla Q(\bullet)$  = the gradient vector of the function  $Q$  with respect to design variable vector;  $\theta_{j-1}$  = the conjugate direction coefficient in the  $(j-1)$ th iteration, whose formula is

$$\theta_{j-1} = \frac{[\nabla Q(\mathbf{d}^{(j)}) - \nabla Q(\mathbf{d}^{(j-1)})]^T \nabla Q(\mathbf{d}^{(j)})}{\|\nabla Q(\mathbf{d}^{(j-1)})\|^2} \quad (11)$$

where  $\|\bullet\|$  represents  $l_2$  norm.

#### 3.4 Earthquake loss evaluation of structures

In China, five seismic damage states of engineering structures in general are specified: (1) nonstructural damage, (2) slight damage, (3) moderate damage, (4) severe damage, and (5) collapse.

Let  $B_j$  represent the  $j$ th damage state. Then the earthquake loss of a structure in damage state  $B_j$  can be evaluated as follows:

$$D_j = D_j^{(1)} + D_j^{(2)} + D_j^{(3)} \quad (j = 1, \dots, 5) \quad (12)$$



where  $D_j^{(1)}$  = the direct loss of from both structural and non-structural damage as well as the cost of maintenance and demolition;  $D_j^{(2)}$  = the indoor loss induced by the structural damage;  $D_j^{(3)}$  = the indirect loss induced by the structural damage.

To simplify the earthquake loss evaluation approach, the three kinds of economic losses for five seismic damage states can be assessed according to the loss coefficients method which depends on the earthquake filed investigations and experts' judgment.

For direct economic loss, the cost is evaluated by

$$D_j^{(1)} = \xi(B_j)C_I(I_d) \quad (13)$$

where  $\xi(B_j)$  = the direct loss coefficient for damage state  $B_j$ ;  $C_I(I_d)$  = the initial cost designed according to the design earthquake intensity  $I_d$ .

For indoor economic loss, the cost is evaluated by

$$D_j^{(2)} = \eta(B_j)C_{eq} \quad (14)$$

where  $\eta(B_j)$  = the indoor loss coefficient for damage state  $B_j$ ;  $C_{eq}$  = the equivalent merit of the indoor asset.

For indirect economic loss, the cost is evaluated by

$$D_j^{(3)} = \gamma(B_j)D_j^{(1)} \quad (15)$$

where  $\gamma(B_j)$  = the indirect loss coefficient for damage state  $B_j$ .

### 3.5 Expected failure cost analysis of aseismic structures

The values of loss coefficients in Eqs. (13) to (15) depend on the types and importance of the buildings. The loss  $D_j$  should be evaluated according to the specific situation of a structure and the seismic damage states. The total loss expectation value with five seismic damage levels can be obtained by the following formula:

$$L[\mathbf{d}(I_d)] = \sum_{j=1}^5 P_f[B_j, \mathbf{d}(I_d)] \cdot D_j \quad (16)$$

## 4 PROBABILISTIC SEISMIC RISK ASSESSMENT OF STRUCTURES BASED ON FINITE ELEMENT RELIABILITY ANALYSIS

### 4.1 Probabilistic seismic hazard analysis in mainland of China

The seismic hazard at a building site is displayed through a cumulative distribution function (CDF) or its complementary one (CCDF) of earthquake ground motion parameters, e.g., seismic intensity, peak ground acceleration, spectral acceleration, etc. Gao & Bao (1985) analyzed 45 cities in the northern, northwestern and southwestern mainland of China by probabilistic seismic hazard analysis (PSHA) method, derived a conclusion that the cumulative distribution function of the seismic intensity during the design

lifetime in mainland of China is type-three extreme value distribution, which takes the form of

$$F_I(i) = \exp \left[ - \left( \frac{\omega - i}{\omega - \varepsilon} \right)^\zeta \right] \quad (17)$$

where  $\exp(\bullet)$  = exponent distribution function;  $\omega$  = the upper limit value of the random variable  $I$ , it takes 12 for seismic intensity;  $\varepsilon$  = characteristic value of  $I$ , which equals to the basic intensity  $I_0$  minus 1.55, i.e.,  $\varepsilon = I_0 - 1.55$ ;  $\zeta$  = shape parameter of the distribution function, whose value depends on the basic intensity  $I_0$  of the site.

### 4.2 Probabilistic seismic fragility analysis of structures based on finite element reliability method

The seismic fragility of a structural system is defined as the conditional probability of failure of the system for a given intensity of the ground motion. In a performance-based seismic design approach, the failure event is said to have occurred when the structure fails to satisfy the requirements of a prescribed performance level. The conditional probability of failure as a function of the ground motion intensity (e.g., seismic intensity, peak ground acceleration or spectra acceleration) can be described by continuous seismic fragility curves or discrete damage probability matrix.

Let the symbol  $B_j^*$  represents the seismic damage state larger than the state  $B_j$ . Then  $P_f [B_j^*, \mathbf{d}(I_d)|I]$  can represent the seismic fragility for the damage state  $B_j^*$  ( $j = 1, \dots, 4$ ) of design scheme  $\mathbf{d}(I_d)$  under the design earthquake intensity  $I_d$  when the seismic intensity  $I$  is given.

$P_f [B_j^*, \mathbf{d}(I_d)|I]$  can be obtained using the global deformation limit states in terms of the maximum inter-storey drift ratio for building structures:

$$P_f [B_j^*, \mathbf{d}(I_d)|I_k] = P[\Delta(I_d, I_k) > \Delta_j] \quad (18)$$

where  $\Delta(I_d, I_k)$  is the maximum inter-storey drift ratio of structures with design earthquake intensity  $I_d$  given occurrence of earthquake  $I_k$ ;  $\Delta_j$  is the corresponding drift ratio limit value, according to the Chinese Seismic Code of Buildings,  $\Delta_j$  is listed in Table 1.

Eq. (18) can be computed by combining finite element reliability method based on FORM described

Table 1. Performance and damage level in terms of drift ratio.

Performance level	Damage state	Drift ratio (%)
I	B <sub>1</sub> : None	$\Delta < 0.2$
II	B <sub>2</sub> : Slight	$0.2 < \Delta < 0.4$
III	B <sub>3</sub> : Moderate	$0.4 < \Delta < 0.8$
IV	B <sub>4</sub> : Severe	$0.8 < \Delta < 2.0$
V	B <sub>5</sub> : Collapse	$\Delta > 2.0$

in section 2.3 with nonlinear static procedure based on nonlinear fiber-section beam-column elements in OpenSees platform.

### 4.3 Probabilistic seismic risk assessment of structures

The failure probability for larger than damage state  $j$  can be obtained with the summation of product of the discrete seismic fragility and hazard:

$$P_f[B_j^*, \mathbf{d}(I_d)] = \sum_{I_k} P_f[B_j^*, \mathbf{d}(I_d)|I_k] \cdot P(I_k) \quad (19)$$

where  $P(I_k)$  is the occurrence probability of the earthquake when earthquake intensity  $I$  takes discrete value  $I_k$ .  $I_k$  usually takes from 6 degree to 9 degree with 0.5 spacing in Chinese seismic design practice. To compute  $P(I_k)$ , the following formula are taken:

$$\begin{aligned} P(I_k = 6.0) &= F_I(6.25), \\ P(I_k = 6.5) &= F_I(6.75) - F_I(6.25), \\ P(I_k = 7.0) &= F_I(7.25) - F_I(6.75), \\ P(I_k = 7.5) &= F_I(7.75) - F_I(7.25), \\ P(I_k = 8.0) &= F_I(8.25) - F_I(7.75), \\ P(I_k = 8.5) &= F_I(8.75) - F_I(8.25), \\ P(I_k = 9.0) &= 1 - F_I(8.75). \end{aligned} \quad (20)$$

The limit state probability for seismic risk in five damage states can be evaluated as:

$$P_f[B_1, \mathbf{d}(I_d)] = 1 - P_f[B_1^*, \mathbf{d}(I_d)] \quad (21a)$$

$$P_f[B_j, \mathbf{d}(I_d)] = P_f[B_{j-1}^*, \mathbf{d}(I_d)] - P_f[B_j^*, \mathbf{d}(I_d)] \quad (j = 2, 3, 4) \quad (21b)$$

$$P_f[B_5, \mathbf{d}(I_d)] = P_f[B_4^*, \mathbf{d}(I_d)] \quad (21c)$$

## 5 CASE STUDY: AN APPLICATION IN STEEL FRAME BUILDINGS

A three-bay and four-storey plane steel frame structure, as shown in Figure 1, is demonstrated by the method proposed in this paper. All beams of the frame are made of Q235B steel, while all columns are made of Q345B steel. The soil type of the building site is type III, and the basic seismic intensity is 7 degree. The equivalent static horizontal seismic forces are calculated using base shear method according to the Chinese seismic design code.

At the stage of initial optimum design, the finite element model for this structure is built in ANSYS. All beams and columns are modeled using Beam3 element during the elastic design stage under minor earthquake, while they are modeled using Beam24 element during the elastoplastic design stage under major earthquake. The minimum initial cost seismic design is performed using ANSYS design optimization tool. The global optimization strategy is used to treat with both elastic and elastoplastic inter-storey drift angle

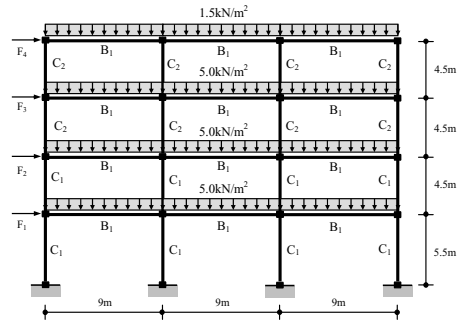


Figure 1. Three-bay and four-storey plane steel frame.

Table 2. Loss coefficients.

Damage State	$\xi$	$\eta$	$\gamma$
B1: None	0.00	0.00	0.00
B2: Slight	0.10	0.05	0.00
B3: Moderate	0.30	0.15	0.50
B4: Severe	0.90	0.50	2.00
B5: Collapse	1.00	0.95	6.00

Table 3. Seismic risk probabilities for five damage states.

Intensity $I_d$	$P_f[B_1]$	$P_f[B_2]$	$P_f[B_3]$	$P_f[B_4]$	$P_f[B_5]$
6.0	0.1754	0.3776	0.0001	0.4443	0.0026
6.5	0.2381	0.3203	0.2798	0.1615	0.0003
7.0	0.1250	0.6624	0.1758	0.0364	0.0004
7.5	0.6000	0.3014	0.0710	0.0260	0.0016
8.0	0.7229	0.2417	0.0249	0.0105	0.0000
8.5	0.7254	0.2417	0.0287	0.0042	0.0000
9.0	0.7287	0.2680	0.0033	0.0000	0.0000

constraints simultaneously. The first-order optimization method is adopted, in which the gradients are calculated by the forward finite difference method.

The shape parameter  $\zeta = 8.3339$ . The design life-time  $T = 50$  years. The mean occurrence rate of earthquake  $\nu = 0.03/\text{year}$ . Assume that  $\lambda = 5\%$ ,  $C_{eq} = 1.5C_I$ . The loss coefficients for five damage states are listed in Table 2.

The seismic risk probabilities for five damage states are calculated using Eqs. (18) to (21), whose results are listed in Table 3.

The original initial cost, the minimum initial cost, the expected damage cost as well as the total expected life cycle cost are summarized in Table 4 and Figure 2. From Figure 2, it can be readily seen that the optimal earthquake intensity corresponding to the minimum total expected life cycle cost point is  $I_d^* = 6.5$ . The optimum solution corresponding to this optimal earthquake intensity is the final seismic design scheme considering the expected life cycle cost. The result of this paper is consistent to that by using simplified fragility method (Lu et al. 2006).

Table 4. Total expected life cycle cost ( $\times 10^5$ RMB).

Intensity $I_d$	$C_0$	$C_{\min}$	$L$	$E[C_T]$
6.0	27.812	21.032	34.0905	39.8073
6.5	35.213	23.875	19.2103	34.4551
7.0	45.897	30.846	11.2136	37.0219
7.5	73.911	36.336	7.4071	40.4155
8.0	87.296	40.374	3.8489	42.4938
8.5	97.553	55.867	4.2548	58.2103
9.0	115.27	61.254	3.0009	62.9113

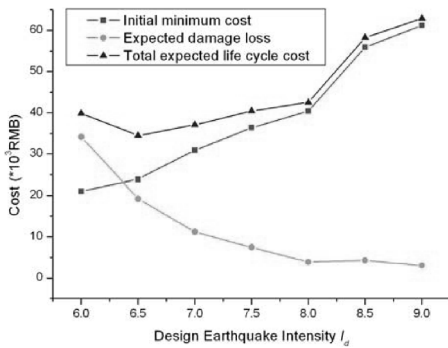


Figure 2. Decision-making of optimal earthquake intensity.

## 6 CONCLUSIONS

As is well known, the design schemes are changing during the process of searching optimum solutions, hence, it needs computing the limit state probability of all design schemes. Actually, the efficiency and accuracy of the limit state probability computation takes an important part in life-cycle cost design optimization of aseismic structures. It is shown in this paper that it usually takes about ten times of iterations to find the design point and the corresponding failure probability by using finite element reliability method (FERM). Therefore, FERM is a good alternative of traditional Monte Carlo simulation or other approximate methods in this aspect.

## ACKNOWLEDGEMENTS

The support of National Science Foundation of China through projects (Grant No. 90715021, 50678057, 50108005) is greatly appreciated.

## REFERENCES

Alimoradi, A., Pezeshk, S. & Foley, C.M. 2007. Probabilistic performance-based optimal design of steel moment-resisting frames. II: Applications. *ASCE Journal of Structural Engineering* 133(6): 757–766.

Ang, A.H.-S. & De Leon, D. 1997. Development of target reliability for design and upgrading of structures. *Structural Safety* 14(1): 91–103.

Ang, A.H.-S. & Lee, J.-C. 2001. Cost optimal design of R/C buildings. *Reliability Engineering and System Safety* 73: 233–238.

Cornell, C.A. et al. 2002. Probabilistic basis for 2000 SAC Federal Emergency Management Agency steel moment frame guidelines. *ASCE Journal of Structural Engineering* 128(4): 526–533.

Esteva, L. et al. 2002. Life-cycle optimization in the establishment of performance-acceptance parameters for seismic design. *Structural Safety* 24(2&4): 187–204.

Foley, C.M., Pezeshk, S. & Alimoradi, A. 2007. Probabilistic performance-based optimal design of steel moment-resisting frames. I: Formulation. *ASCE Journal of Structural Engineering* 133(6): 757–766.

Frangopol, D.M. & Maute, K. 2003. Life-cycle reliability-based optimization of civil and aerospace structures. *Computers & Structures* 81: 397–410.

Gao, X.W. & Bao, A.B. 1986. Determination of Seismic design standards using probability methods. *China Building Structures Journal* 7(2): 55–63.

Haukass, T. & Der Kiureghian, A. 2007. Methods and object-oriented software for reliability and sensitivity analysis with application to a bridge structure. *ASCE Journal of Computing in Civil Engineering* 21(3): 151–163.

Liu, M. et al. 2003. Optimal seismic design of steel frame buildings based on life cycle cost considerations. *Earthquake Engineering and Structural Dynamics* 32: 1313–1332.

Liu, M. et al. 2004. Life cycle cost oriented seismic risk optimization of steel moment frame structures with risk-taking preference. *Engineering Structures* 26: 1407–1421.

Liu, S.C. & Neghabat, F. 1972. A cost optimization model for seismic design of structures. *The Bell System Technical Journal* 51(10): 2209–2225.

Lu, D.G. et al. 2002. Minimum total life cycle cost design of aseismic structures: Principle and method. *Proc. the Second China-Japan-Korea Joint Symposium on Optimization of Structural and Mechanical Systems (CJK-OSM2), Busan, Korea, Nov. 4–8, 2002*: 129–134.

Lu, D.G. et al. 2006. Optimal fortification load decision-making and life-cycle cost design for aseismic structures according to Chinese codes. In Cho, H.-N. et al. (eds), *Life-Cycle Cost and Performance of Civil Infrastructure Systems*: 239–248, *Proc. 5th intern. workshop on life-cycle cost analysis and design of civil infrastructure systems, Seoul, Korea, Oct. 16–18, 2006*. London: Talyor & Francis.

National Standard of China P.R. 2001. *Seismic Design Code of Buildings (GB50011–2001)*. Beijing: Building Industry Press of China.

Rackwitz, R. 2000. Optimization—the basis of code-making and reliability verification. *Structural Safety* 22(1): 27–60.

Wang, G.Y. et al. 2003. An optimal design for total lifetime cost of aseismic structures. *China Civil Engineering Journal* 36(6): 1–6 (in Chinese).

Wang, G.Y. & Lu, D.G. 2001. Optimal fortification load and reliability of aseismic structures. *Earthquake Engineering Frontiers in the New Millennium*: 371–376. In Spencer & Hu (eds), Lisse: Swets and Zeitlinger.

Wen, Y.K. 2001. Reliability and performance-based design. *Structural Safety* 23(4): 407–428.

Wen, Y.K. & Kang, Y.J. 2001a. Minimum building life-cycle cost design criteria. I: Methodology. *ASCE Journal of Structural Engineering* 127(3): 330–337.

Wen, Y.K. & Kang, Y.J. 2001b. Minimum building life-cycle cost design criteria. I: Applications. *ASCE Journal of Structural Engineering* 127(3): 338–346.

# Evaluation of the response of concrete structures along their service life by nonlinear evolutive analysis methods

Antonio R. Mari & Jesús M. Bairán

*Dept. Construction Engineering, School of Civil Engineering  
Universitat Politècnica de Catalunya (UPC), Barcelona, Spain*

**ABSTRACT:** During the construction process and along their service life, structures may suffer changes in their geometry, static configuration and changes in the material properties due to time-dependent effects and environmental effects. Special analytical methods to capture the actual structural response at each stage are needed to accurately evaluate the functionality and safety of structures along their service life. In this paper, a step by step time-dependent nonlinear analytical model is presented, capable to reproduce the actual construction sequence, the load history and the evolution of materials, support conditions and geometry of 3D frames along their service life. A RC pedestrian bridge subjected to a deterioration process and a subsequent retrofit is analysed and conclusions are drawn about the capabilities of the model for structural assessment.

## 1 INTRODUCTION

Along their service life, reinforced, pre-stressed and composite concrete and steel structures may suffer changes in their geometry, structural configuration and material properties. These changes may be due to the construction process adopted, to deterioration of the materials due to environmental actions or to modifications of the structural geometry, supports and reinforcement due to repair and retrofit systems.

In addition, time-dependent effects due to creep, shrinkage and evolution of concrete properties, relaxation of pre-stressing steel, combined with the non-linear material's behaviour produce a non-linear structural response. Such aspects must be considered when trying to accurately evaluate the serviceability and safety of structures along their service life.

Among the large number of analytical models developed to predict the nonlinear and time dependent structural response of concrete frame structures, only few of them include the effects of segmental construction configuration and changes along the service life. The most relevant models were developed by Ghali & Elbadry (1985), Kang (1990), Abbas & Scordelis (1993), Cruz et al. (1998), and Mari (2000). A general review of the mathematical modeling and structural effects of creep, shrinkage and segmental construction was presented by Bazant (1988).

In this paper a numerical model for the nonlinear and time dependent analysis of three dimensional reinforced, pre-stressed and composite concrete frames, which takes into account the effects of changes on the

structural scheme during the construction process and along the structural service life, is presented.

An illustrative example shows the capabilities of the model to simulate the effects of the materials deterioration, the repair and the retrofit of a 3-span continuous footbridge, on its structural response. The efficiency of the selected retrofit system is evaluated by studying the service load response and ultimate capacity of the bridge before and after such operation.

## 2 DESCRIPTION OF THE ANALYTICAL MODEL

### 2.1 *Material properties*

In order to incorporate the varied material properties within a frame in evaluating element properties, the element is divided into a discrete number of concrete and reinforcing steel filaments, as shown in figure 1, each of which is assumed to be in a uniaxial stress state.

It is assumed that plane sections remain plane and the deformations due to shearing strains are neglected. The total strain at a given time and point in the structure  $\varepsilon(t)$ , is taken as the direct sum of mechanical strain  $\varepsilon^m(t)$ , and non-mechanical strain  $\varepsilon^{nm}(t)$ , consisting of creep strain  $\varepsilon^c(t)$ , shrinkage strain  $\varepsilon^s(t)$ , ageing strain  $\varepsilon^a(t)$ , and thermal strain  $\varepsilon^T(t)$ .

$$\varepsilon(t) = \varepsilon^m(t) + \varepsilon^{nm}(t) \quad (1)$$

$$\varepsilon^{nm}(t) = \varepsilon^c(t) + \varepsilon^s(t) + \varepsilon^a(t) + \varepsilon^T(t) \quad (2)$$

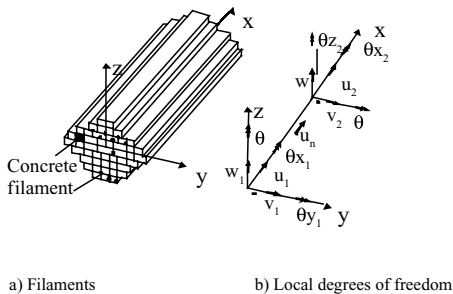


Figure 1. Fibre beam element.

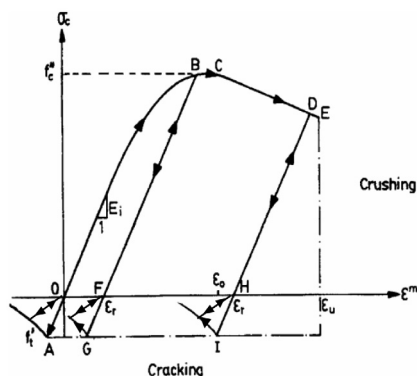


Figure 2. Uniaxial stress-strain curve in concrete.

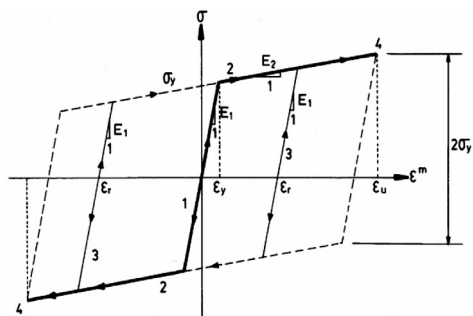


Figure 3. Stress-strain curve of reinforcing steel.

The short-time uniaxial stress-strain relationship governing the response of the individual concrete filaments is based on a parabolic-linear curve, including cracking, tension stiffness and load reversals, as shown in figure 2. For the reinforcing steel, a bilinear stress-strain relationship is assumed with load reversals (fig. 3). A multilinear stress-strain curve is used for prestressing steel (fig. 4).

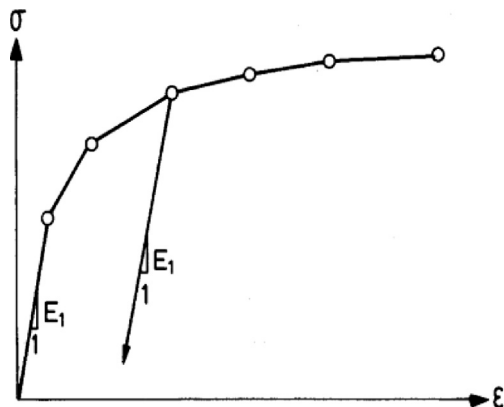


Figure 4. Stress-strain curve of prestressing steel.

## 2.2 Age dependent integral formulation for creep

Creep strain  $\epsilon^c(t)$  of concrete is evaluated by an age dependent integral formulation based on the principle of superposition. Thus,

$$\epsilon^c(t) = \int_0^t c(\tau, t - \tau) \cdot \frac{\partial \sigma(\tau)}{\partial \tau} d\tau \quad (3)$$

where  $c(\tau, t - \tau)$  is the specific creep function, dependent on the age at loading  $\tau$ , and  $\sigma(\tau)$  is the stress applied at instant  $\tau$ . Numerical creep analysis may be performed by subdividing the total time interval of interest into time intervals  $\Delta t$ , separated by time steps. A detailed explanation of the can be found in Mari (2000).

## 2.3 Three-dimensional beam element

A typical three dimensional frame structure consists of one dimensional beam elements interconnected by joints. Each element has a prismatic cross section of arbitrary shape which is assumed to be composed by filaments, which can be made from a different concrete or steel. For each finite element, the reinforcing steel is considered constant along its length and parallel to the longitudinal axis. There is a discrete number of pre-stressing steel tendons in the frame, each of which has a given profile and constant sectional area along its length.

The Hermitian 13 degrees of freedom finite element beam is used. (fig. 1). An axial displacement, that is eliminated by static condensation, is associated to an internal node placed at the element mid length. Such DOF is necessary to correctly capture the material non-linear response in RC elements.

The elastic stiffness of a beam element is obtained by the following known expression:

$$K_e = \iiint_V B^T \cdot E \cdot B \cdot dV \quad (4)$$

where E represents the material tangent modulus associated either with flexural or torsional DOF, and B is the matrix relating nodal displacements and strains at the Gauss points. The model allows also considering the second order effects, by adding the geometric stiffness matrix, to the elastic one, and by updating the nodal coordinates after deformation.

The element internal resisting load vector due to stresses in the concrete and steel fibres can be evaluated by:

$$R^i = \iiint_V B^T \sigma dV \quad (5)$$

The equivalent load vector due to non-mechanical strains  $\epsilon^{nm}$ , is calculated by the equation:

$$R^{nm} = \iiint_V B^T \cdot E \cdot \epsilon^{nm} dV \quad (6)$$

The material properties of the concrete and steel at any time and load level, depend on the age of concrete and the state of the material, and can be obtained from the respective material nonlinear stress-strain relationship. A tri-linear torque-twist relationship is used to represent the torsional response.

The active effect of pre-stressing is introduced in the structure as an equivalent load vector. After grouting, bond between concrete and steel is assumed. Therefore, its contribution to the stiffness and strength will be considered and increment of strains and stresses at each point of the pre-stressing tendons will take place according to the deformation of the structure.

#### 2.4 Solution strategy for the time dependent nonlinear problem

A number of construction steps are defined along the time domain. A construction step is a situation of the structure in which any variation on its geometry, loading or boundary conditions takes place. For each construction step, pre-stressing, external loads, temperature distributions, instantaneous stress-strain curves, materials properties and structure scheme are given.

The time elapsed from one construction step to the next is subdivided into time intervals, separated by time steps. At each time step the material properties, the stiffness matrix and the load vector are updated. Increments of non-mechanical strains  $\Delta\epsilon^{nm}$  occurred

during the time interval from  $t_{n-1}$  to  $t_n$  are evaluated. The equivalent joint load increments  $\Delta R^{nm}$  at time  $t_n$ , summed for the concrete, reinforcing steel and prestressing steel, are then calculated from their respective non-mechanical strain increments  $\Delta\epsilon^{nm}$ . Thus, at a time  $t_n$ , the load increment  $\Delta R_n$  to be applied to the structure is obtained by adding the external joint load increment  $\Delta R_n^i$  and the unbalanced load  $R_{n-1}^u$  left over from time  $t_{n-1}$  to the equivalent joint load increments  $\Delta R_n^{nm}$

$$\Delta R_n = \Delta R_n^i + \Delta R_n^{nm} + R_{n-1}^u \quad (7)$$

The total load obtained at each time step is divided into load increments, so that the load-displacement curve can be traced along the elastic, cracking, inelastic and ultimate ranges.

### 3 SIMULATION OF DETERIORATION, REPAIR AND RETROFIT PROCESSES

The present model has been designed to simulate most of the structural changes that take place during the construction process and along the entire service life of structures. Deterioration effects such as loss of concrete or steel sections, repair or retrofit operations and demolition of parts of the structure are considered also as construction steps.

At each construction step, changes in the longitudinal or transverse geometry of the structure can be accounted for by adding or removing elements or filaments of the cross section. Pre-stressing tendons, and stays can be stressed, unstressed or removed at any time. External supports and connections between elements can be modified at any time. Variations in the external boundary conditions are also recognised in the model so that new supports can be added or releasing of a constraint can be considered by introducing a force equal and opposite to the reaction of the removed support.

The cross section of each element can be made of different concrete and steel types. For each material, the instant of placement and removal are specified at the beginning of the process. When a concrete or steel filament is placed in the element, its stiffness is included in the element stiffness; when it is removed, its stiffness and its contribution to the internal force vector is not taken into account any more in the step by step analysis. In this case, an unbalanced load vector will appear in the next time step, which is automatically introduced in the iterative procedure until equilibrium is obtained.

According to these principles, the following situations related to deterioration, repair and retrofit of concrete structures can be simulated:

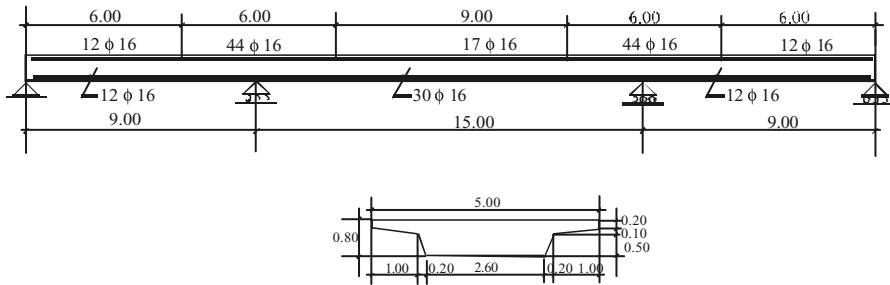


Figure 5. Elevation and cross section of the studied structure.

- *Loss of concrete and reinforcement section*, due to carbonation, steel corrosion and spalling of concrete cover or by eliminating a damaged concrete before substituting it by a new one. It can be made by specifying the time in which concrete and steel filament are placed and removed.
- *Sealing of Cracks*. If a cracked concrete is repaired and cracks are sealed, it can be specified that at a certain time the concrete is again capable of resisting tensile stresses, by modifying the constitutive equation.
- *Enlargement of concrete cross section, adding of reinforcement or fastening a steel plate*. It can be simulated by specifying that a part of the concrete section or a number of steel filaments are placed on the structure at a specific age. The steel plate is considered as reinforcement, with a specific constitutive equation.
- *External prestressing*. This type of reinforcement is treated as an unbonded prestressing. The loads introduced by the prestressing are automatically obtained by equilibrium from the tendons layout.
- *Temporary shores and imposed movements*. They can be simulated thanks to the possibility of modification of the boundary conditions (adding or removal of supports) along the entire service life.

#### 4 APPLICATION EXAMPLE: SIMULATION OF THE DEGRADATION AND RETROFIT OF A CONTINUOUS R/C PEDESTRIAN BRIDGE

##### 4.1 Description and modelling

A 3-span continuous reinforced concrete pedestrian bridge affected by corrosion of the upper reinforcement and concrete cover of the top face is analyzed.

The structure dimensions and reinforcement layout considered are shown in figure 5. The bridge is subjected to its self weight (7 kN/ml), dead load (DL = 0,2 kN/m<sup>2</sup>), and live load (LL = 0,5 kN/m<sup>2</sup>). The concrete and steel strength are  $f_{ck} = 30$  N/mm<sup>2</sup> and  $f_{yk} = 500$  N/mm<sup>2</sup>, respectively.

The assumed evolution of the deterioration effects is shown in figure 6 for both loss of effective area of reinforcement and concrete cover.

It has been considered that due to use of de-icing products, a strict concrete cover of the top reinforcement (30 mm) and a lack of water proofing, the top reinforcement of the bridge is subjected to corrosion. Loss of reinforcement steel area and concrete cover takes place progressively as shown in figure 6. It is considered that elapsed time until the penetration of chlorides affect the reinforcement is 3 years. This is a theoretical example; therefore, the rate of deterioration has been exaggerated.

The structure is idealized by means of 66 beam elements, each of 0,5 m length. The cross section is subdivided into concrete trapezoids and steel filaments, each with different age of vanishing. At the age of 28 days, the structure is subjected to the total nominal load and then unloaded to reach the level of quasi-permanent loads (SW + DL + 0,4LL = 9 kN/ml). This load is maintained constant along the time, while the time dependent effects (creep, shrinkage, corrosion, etc) take place.

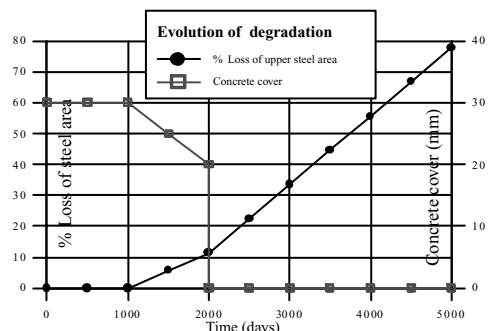


Figure 6. Evolution of deterioration effects on reinforcement and concrete cover.

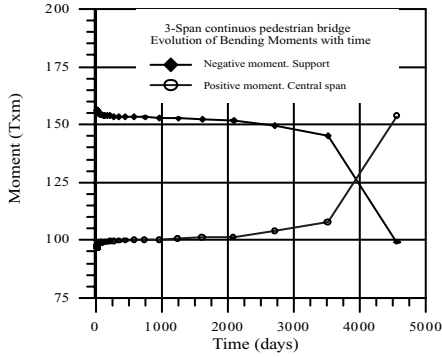


Figure 7. Bending moments at support and midspan sections.

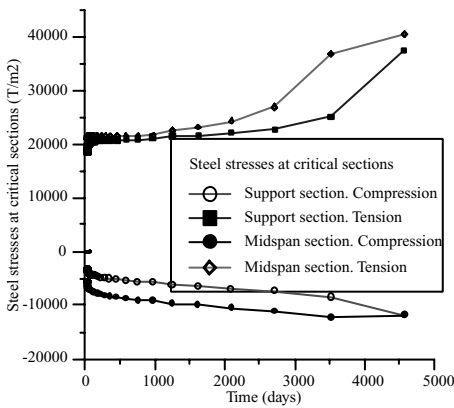


Figure 8. Steel stresses at support and mid-span sections.

#### 4.2 Effects of deterioration

Figure 7 shows the evolution with time of the bending moments at the support and at the bridge midspan. It can be observed that a redistribution of bending moments due to the materials deterioration takes place, decreasing the negative bending moment from 157 kN m to 99 kN m, and increasing the positive moment from 97 kN · m to 154 kN · m just before failure.

Figure 8 shows the steel stresses at the support and mid-span sections. It is observed that the tensile steel stresses at the support section increase with time, due to the loss of steel section, while the tensile stresses at the centre span also increase due to forces redistribution.

Compressive stresses increase in both cases due to creep of concrete and reduction of effective inertia of the cross section. At the mid-span section the increase of bending moment due to forces redistribution also affects the level of stress in the reinforcements.

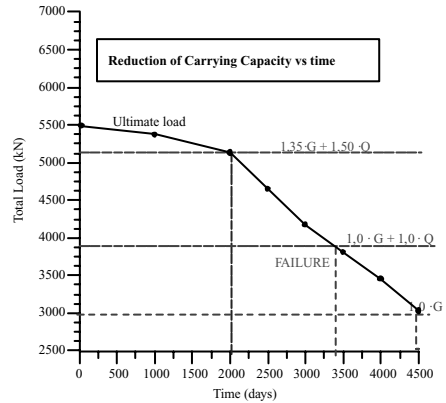


Figure 9. Evolution of load carrying capacity.

In order to study the evolution of the structural carrying capacity with time, an incremental non-linear analysis up to failure has been made. In these analyses it is assumed, for simplicity purposes, that the live load is extended to the whole bridge length.

Figure 9 shows the reduction of carrying capacity of the bridge with time. Different remarkable times can be observed in this figure: Until 2000 days the structure resists the external load with the safety coefficients required by current codes. Between 2000 and 3400 days the structure resists the nominal loads but with a safety level below the required one. After 3400 days the structure can not carry the self weight and permanent loads, and after 4500 days the structure is unable to carry its self weight.

#### 4.3 Effects of retrofitting

It is assumed now that the structure is retrofitted at the age of 3000 days, when the structure is able to carry the total loads with a safety coefficient near 1,0. The retrofit consists on substituting the degraded top 50 mm of concrete by a new concrete layer of the same thickness and the upper reinforcement by another with the same amount of steel, increasing the cover to 40 mm, to avoid future corrosion. Active shores will be utilized to compensate the self weight of the bridge and resist the weight of the new concrete. The shores are removed at the end of the retrofit operation.

Figure 10 shows the deflection at the central section of the bridge in three cases: with degradation, without degradation and having been retrofitted at 3000 days. It is observed that near 4000 days, with degradation, the deflection increases quickly until failure takes place. The retrofit avoids the collapse and keeps the deflection parallel to the curve without degradation.



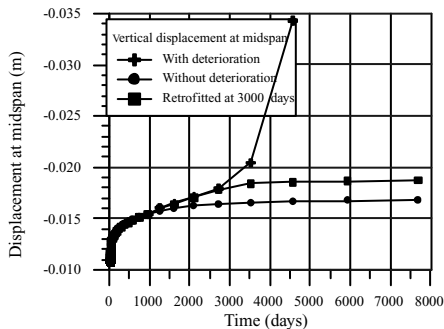


Figure 10. Evolution of displacement at midspan.

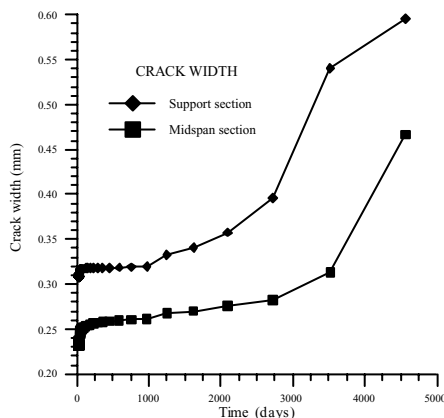


Figure 11. Evolution of crack widths.

Figure 11 shows the evolution of the crack width with time, under the quasi-permanent load combination, obtained from the results of non-linear analysis. These results take into account the tension-stiffening, the spacing and diameter of the reinforcement and concrete cover. It can be observed that deterioration produces an increase of crack width, making the structure unacceptable under the serviceability and durability points of view. Appearance of new cracks can be also captured by the model.

## 5 CONCLUSIONS

An analytical model capable to trace the structural response of reinforced and prestressed concrete frame structures during construction and along their entire service life has been presented. The model uses a filament beam finite element and takes into account the material and geometric non-linearities, the time dependent effects of creep, shrinkage and relaxation of

prestressing steel and any changes in geometry, loads, reinforcement or support conditions that could take place along the structure service life.

An application example has been studied to show the capabilities of the model to reproduce the structural effects of materials degradation and the efficiency of a retrofit system. Bending moments, stresses, deflections and crack widths have been obtained for different ages and degradation levels of the structure.

Redistributions of internal forces between the support and centre span sections and redistributions of stresses between concrete and steel have been observed due to the loss of concrete and steel areas, increasing cracking and rotations at the support section, and creep effects. The evolution of deflections as well as the ultimate carrying capacity of the structure, before and after being retrofitted has been obtained for a given load case.

The proposed model has shown to be a proper tool for the serviceability and durability assessment of structures along their lifetime. The model is capable of evaluating the structural effects of different degradation processes; therefore, it can be also useful to calibrate models of degradation mechanisms.

## ACKNOWLEDGEMENTS

The present investigation has been developed under the Research Projects SEDUREC (Safety and Durability of Construction Structures, CSD2006-00060) and BIA2006-05614 funded by the Spanish Ministry of Education.

## REFERENCES

- Ghali & Elbadry (1985) "User's Manual and Computer Program CPF: Cracked Plane Frames in Prestressed Concrete" Department of Civil Engineering, The University of Calgary, Research Report CE 85-2, Calgary, Alberta, Canada.
- Kang & Scordelis (1990) "Non-linear Segmental Analysis of Reinforced and Prestressed Concrete Bridges", 3rd International Conference on Short and Medium Span Bridges. Toronto, Ontario, Canada, pp. 229-240.
- Abbas & Scordelis (1993) "Nonlinear Geometric, Material and Time-Dependent Analysis of Segmentally Erected Three-Dimensional Cable Stayed Bridges", Report UCB/SEMM-93/09, University of California at Berkeley.
- Cruz, Mari & Roca (1998) "Nonlinear Time-Dependent Analysis of Segmentally Constructed Structures", *J. Structural Engineering ASCE*, Vol. 124, No. 3, pp. 278-287.
- Mari (2000) "Numerical Simulation of the Segmental Construction of Three Dimensional Concrete Frames", *Engineering Structures*, Vol. 22, 585-596.
- Bazant, Z.P. (1988), Ed., "Mathematical Modeling of Creep and Shrinkage of Concrete". John Wiley and Sons.

# Strengthening of aged RC structures using spreadsheet analyses with optimisation methods and linearised moment-curvature relations

P. Mark

Grassl Consultant Engineers, Düsseldorf, Germany

**ABSTRACT:** A nonlinear numerical calculation method is presented that allows for a specific strengthening of the bending resistances of aged reinforced concrete (RC) beam or slab structures. Cross sections may consist of different aged or new materials (concrete, reinforcement or others with linear or nonlinear material properties) and may have arbitrary shapes. The method starts from estimating required strengthenings and elaborates the moment-curvature relations of the different composite sections using spreadsheet tools and optimisation methods. A nonlinear structural analysis is carried out and sectional forces in serviceability and ultimate limit states are derived and input into the design routine back in the spreadsheets. A typical example shows the practical application.

## 1 INTRODUCTION

Rehabilitation, strengthening and repair of aged constructions more and more grow in structural engineering. Their major difficulties are the constraints given by the existing structural elements, as those constraints complicate the execution of construction work as well as the design. Individual and elaborated solutions become necessary (Petryna & Krätzig 2005, Krätzig & Petryna 2006, Hankers 2000).

With respect to the design, the major focus lies on the existing structural elements, as they provide reduced bearing capacities and can not be changed any more. Consequently, strengthenings must be designed and arranged in such a way that they activate redistribution effects relieving weakened building components. This requires a realistic modelling of the nonlinear properties of the complex composite elements with initial and complementing partitions and thus elaborated strategies: Effects from cracking, yielding, stiffness reductions and redistributions are already introduced during the evaluation of sectional forces by nonlinear moment-curvature relations. Moreover, those relations arise from composite sections with complex shapes and versatile nonlinear constitutive laws. Even biaxial bending—with or without axial forces—may occur.

The contribution presents a method based on spreadsheet analyses, optimisation methods and nonlinear evaluations of sectional forces as well as a corresponding design to specifically strengthen the bending resistances of aged RC beam or slab structures. The fundamental steps are:

- Calculations of arbitrarily shaped composite sections with aged and new RC partitions exposed to biaxial bending and axial forces.
- Linearised moment-curvature relations of the composite sections.
- Nonlinear calculations of sectional forces and corresponding design strategies.

## 2 STRENGTHENED CROSS SECTIONS

The cross sections considered may have arbitrary shapes and consist of four kinds of materials, namely the concrete of the initial, aged section (concrete 1), the concrete of the strengthened partition (concrete 2) as well as corresponding reinforcements 1 and 2 (Fig. 1).

The limitation to four materials is made due to practical reasons. From the mathematical point of view the method is open for extensions to  $n$  material types, where  $n \geq 1$  (Mark 2005).

### 2.1 Fundamentals

The governing equations and assumptions are:

- The familiar equilibrium conditions of spatial, slender bars (Krätzig & Basar 1997)

$$N = \iint_{(A)} \sigma \, dA$$

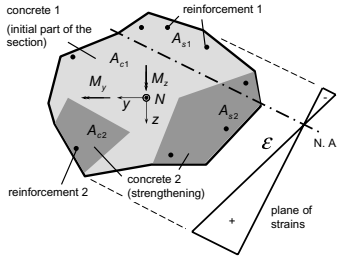


Figure 1. Strengthened RC section with two kinds of concretes and reinforcements.

$$M_y = \iint_{(A)} \sigma z \, dA$$

$$M_z = \iint_{(A)} \sigma (-y) \, dA \quad (1)$$

that combine the sectional forces of actions  $N$ ,  $M_y$ ,  $M_z$  with corresponding resistances  $N_R$ ,  $M_{yR}$ ,  $M_{zR}$ —arising from normal stress integrals—on the right hand sides of equation (1). Thus, uniaxial as well as biaxial bending with or without axial forces may occur.

- The Bernoulli hypothesis, so plane sections remain plane and strain values  $\varepsilon$  are linearly distributed over the cross sectional area  $A_c$  with  $A_c = A_{c1} + A_{c2}$  (gross areas including reinforcements).

$$\varepsilon = b_1 + b_2 y + b_3 z, \quad \mathbf{b}^T = (b_1 \quad b_2 \quad b_3) \quad (2)$$

The three variable parameters, being the axial strain  $b_1$  and the curvatures  $b_2, b_3$  with respect to the principle axis, are summarised to a vector  $\mathbf{b}$ . An ideal, slip free bond is assumed between the partitions.

- Linear or nonlinear relations—separately formulated for each material type—combine stresses and strains.

$$\begin{aligned} \sigma_{c1} &= \sigma_{c1}(\varepsilon), & \sigma_{c2} &= \sigma_{c2}(\varepsilon) \\ \sigma_{s1} &= \sigma_{s1}(\varepsilon), & \sigma_{s2} &= \sigma_{s2}(\varepsilon) \end{aligned} \quad (3)$$

For the practical solution of the equilibrium conditions (1) it is convenient to separate between the materials and lump the reinforcement areas to points. Integrating over the gross areas  $A_{c1}$  and  $A_{c2}$  equation (1) is transferred into

$$N = \iint_{(A_{c1})} \sigma_{c1} \, dA_{c1} + \iint_{(A_{c2})} \sigma_{c2} \, dA_{c2}$$

$$+ \sum_i (\sigma_{s1i} - \sigma_{c1i}) A_{s1i} + \sum_j (\sigma_{s2j} - \sigma_{c2j}) A_{s2j}$$

$$M_y = \iint_{(A_{c1})} \sigma_{c1} z \, dA_{c1} + \iint_{(A_{c2})} \sigma_{c2} z \, dA_{c2}$$

$$+ \sum_i (\sigma_{s1i} - \sigma_{c1i}) z_i A_{s1i} + \sum_j (\sigma_{s2j} - \sigma_{c2j}) z_j A_{s2j}$$

$$M_z = \iint_{(A_{c1})} \sigma_{c1} (-y) \, dA_{c1} + \iint_{(A_{c2})} \sigma_{c2} (-y) \, dA_{c2}$$

$$+ \sum_i (\sigma_{s1i} - \sigma_{c1i}) (-y_i) A_{s1i}$$

$$+ \sum_j (\sigma_{s2j} - \sigma_{c2j}) (-y_j) A_{s2j} \quad (4)$$

where the concrete stresses  $\sigma_{c1}$ ,  $\sigma_{c2}$  are subtracted from the steel stresses  $\sigma_{s1}$ ,  $\sigma_{s2}$  in the terms of the reinforcement points to ensure a correct integration over the four net sectional areas.

## 2.2 Materials

Generally, any kinds of scalar material relations may be introduced, if they make sense from the physical point of view. This variety is especially important for rehabilitation or strengthening procedures to realistically model the material properties of the aged materials derived from on side tests. For the sake of simplicity, the following formulations are taken from European Standards (EN 1992-1-1 2004, NA EN 1992-1-1 2007) and restricted to normal strength concretes as well as usual reinforcement types with high or normal ductility. For the calculation of sectional forces medium strength values are assumed ( $f_c$ ,  $f_y$ ,  $f_t$ , see Fig. 2). During the design procedure they are reduced to design values  $f_{cd}$ ,  $f_{yd}$  by partial factors

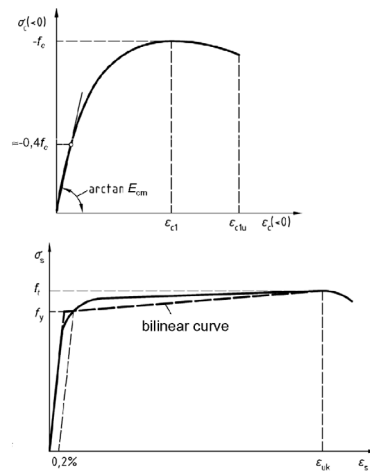


Figure 2. Stress-strain relations for concrete and reinforcing steel (evaluation of sectional forces).

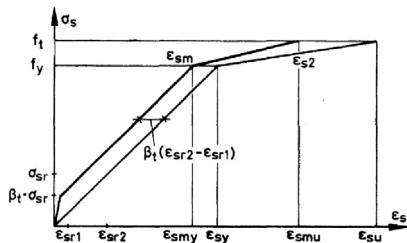


Figure 3. Simplified stress-strain relation for the reinforcing steel accounting for tension-stiffening effects, acc. (DAfStb 2003).

$\gamma_R$  of safety.

$$\sigma_c = f_c \frac{E_{cm}(\varepsilon_{c1}/f_c)(\varepsilon/\varepsilon_{c1}) + (\varepsilon/\varepsilon_{c1})^2}{1 - (E_{cm}(\varepsilon_{c1}/f_c) + 2)(\varepsilon/\varepsilon_{c1})} \quad (5)$$

$$f_y = 1, 1f_{yk} \quad f_t = \begin{cases} 1,08f_y \\ 1,05f_y \end{cases} \quad (6)$$

A modification of the stress-strain relation for the reinforcements accounts for tension-stiffening effects (Fig. 3) in a simplified way. The trilinear approach is taken from (DAfStb 2003). It activates stresses for smaller strain values smearing the alteration of cracked and uncracked sections to a medium stiffness property of a stepwise continuous cross section. It is assumed for a realistic calculation of sectional forces and of course omitted in design.

### 2.3 Spreadsheet analysis with optimisation methods

Modern spreadsheet analysis programs and included optimisation tools (Fylstra et al. 1998) offer very suitable methods to solve the coupled equilibrium problem of equation (4) with (3), (5) and (6) (Powell & Baker 2004, Mark 2005). The cross section with its aged or new material properties as well as actions is given. The corresponding plane of strains, characterised by  $b_1 = \varepsilon_1$ ,  $b_2 = \kappa_z$  and  $b_3 = \kappa_y$  must be iteratively found.

The solution has two major aspects: First, the problem itself must be iteratively solved. For this purpose, the coupled equation problem of the equilibrium is transferred into an optimisation problem (Mark 2005, Bhatti 2000). Doing so, the three equations in (4) are combined to a positive sum of errors between actions  $N$ ,  $M_y$ ,  $M_z$  and corresponding resistances ( $N_R$ ,  $M_{yR}$ ,  $M_{zR}$  abbreviating the stress integrals).

$$f(\mathbf{b}) = a_1(N - N_R(\mathbf{b}))^2 + a_2(M_y - M_{yR}(\mathbf{b}))^2 + a_3(M_z - M_{zR}(\mathbf{b}))^2 \rightarrow \min \quad (7)$$

Finding the minimum of the sum—namely zero—means finding the equilibrium state. The task of the weighing parameters  $a_1$  to  $a_3$  is to adapt the extents of

the three error terms. Usually, they are set to unity. The numerical solution of the optimisation problem itself is accomplished with the Generalised Reduced Gradient (GRG) algorithm (Lasdon et al. 1978, Smith & Lasdon 1992).

Second, in each step of the iterative solution the stress integrals of the resistances have to be solved. This is also done numerically using a simple integration scheme of the form

$$\iint_{(A_c)} \sigma_c dA_c \cong \sum_{i=1}^k \sigma_{ci} \Delta A_{ci}$$

$$\iint_{(A_c)} \sigma_c z dA_c \cong \sum_{i=1}^k \sigma_{ci} z_i \Delta A_{1i} \quad (8)$$

and the principle of the fibre models (Hsu 1985, Furlong 2004).  $k$  should be a large integer value, typically several hundreds or thousands, to achieve a sufficient accuracy. The fibre principle complies well with the cell structure of columns and rows in the spreadsheet (Fig. 4). Using “drag and drop” as well as

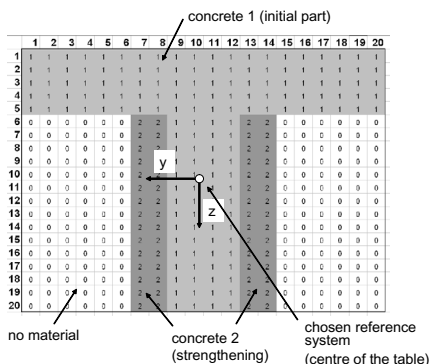


Figure 4. Example for material assignments in the spreadsheet (T-girder strengthened at its web).

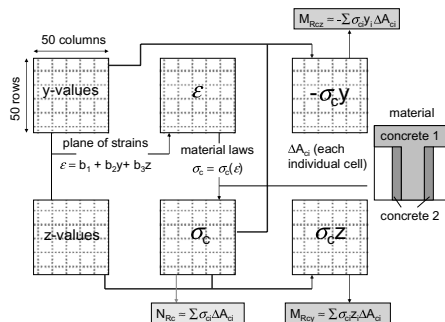


Figure 5. Schematic way of stress integration to the resistances of the concrete partitions.

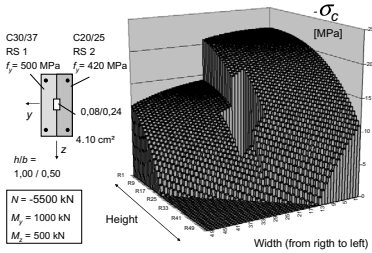


Figure 6. Stress distribution of a section with different concrete strengths exposed to biaxial bending and axial force.

“copy and paste” techniques any cross sectional shape is easily implemented and visually checked.

Cell ranges of  $y$ - and  $z$ -coordinates of the fibre centroids, strains, stresses as well as moment increment are defined and summed up to yield resistances (Fig. 5).

Figure 6 shows a typical application. A rectangular section with two different concrete materials, two different steel materials and a rectangular blockout is exposed to biaxial bending and longitudinal compression. As expected, a curved stress surface arises with a pronounced stress jump at the material joint. Note that the usual time effort for computations remains negligible.

### 3 LINEARISED MOMENT-CURVATURE RELATIONS

The derived method is now applied to develop moment-curvature relations of composite cross sections. As the relations are simplified to trilinear shapes (Fig. 7), only the three kinking points (1) to (3) have to be computed from equilibrium iterations. Note that just the bending moment varies. Axial forces  $N$ —if any—remain constant. For uniaxial bending  $M_y = M$  the curvature  $(1/r) = \kappa$  is obtained from  $b_2 = \kappa_z = (1/r)$ . Points (1) to (3) are determined in the following ways:

Point (1): linear-elastic calculation, boundary condition: tensile concrete stress is reached ( $\sigma_{c,max} = f_{ctm}$ ).

Point (2): spreadsheet analysis, boundary condition: first yielding of the reinforcement ( $\epsilon_{s,max} = \epsilon_{smy}$ , incl. tension-stiffening).

Point (3): spreadsheet analysis, boundary condition: ultimate bearing capacity  $\epsilon_s = \epsilon_{smu}$  (steel failure) or  $\epsilon_c = \epsilon_{c,min}$  (concrete crushing).

The three inclinations of the branches characterise the variable stiffness  $B$ . It is obtained from relations of moment and curvature differences by  $B = \Delta M / \Delta (1/r)$ .

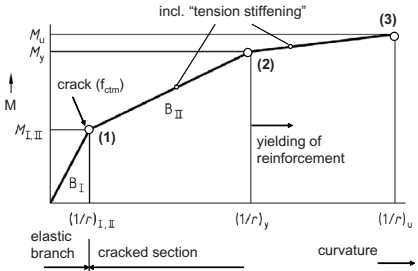


Figure 7. Linearised moment-curvature relation.

## 4 STRUCTURAL ANALYSIS AND DESIGN

For the structural analysis the structural system is discretised into a fine pattern of Finite Elements like beam or slab elements and moment-curvature relations are assigned to each element corresponding to its individual cross section. All reinforcement amounts—including required strengthenings—must be estimated in advance. They are not determined during the design process but only verified in their predesigned amounts. Iterative solution techniques are needed to solve the governing equations, because of the nonlinearity of the constitutive laws (Bathe 1996). However, due to the linear branches even purely linear solutions operate, if stepwise computations are carried out. So, standard software tools may be applied.

For the design, sectional forces derived for the ultimate limit state (ULS) and the serviceability limit state (SLS) are input into the spreadsheet solution routine. The equilibrium search produces steel and concrete stresses and strains. Compared to admissible values bending designs in ULS ( $\epsilon_{c,min} \leq \epsilon_{c1u}$  or  $\epsilon_{s,max} \geq \epsilon_{su}$ ) as well as verifications of concrete or steel stresses or calculative crack width in SLS are obtained in the common way.

## 5 EXAMPLE: SLAB WITH INCREASED LIVE LOADS

An aged slab—fixed at its both ends—should be improved in its bending resistance against distributed live loads (Fig. 8). Live loads grow from initially  $LL_0 = 2 \text{ kN/m}^2$  to now  $LL_0 + LL_1 = 2 + 4 = 6 \text{ kN/m}^2$ .

Material parameters of the existing concrete (concrete 1) derived from non-destructive tests, the supplementary concrete 2 (C30/37), the initial reinforcement 1 (normal ductility,  $E_s = 210.000 \text{ MPa}$ ) as well as the supplementary reinforcement 2 (high ductility,  $E_s = 200.000 \text{ MPa}$ ) are given in Figure 8 or assumed according to standard values of (EN 1992-1-1 2004).

The general idea is to enhance the bending resistance of the slab by locally providing an additional reinforced concrete layer either on top or at the bottom of the slab.

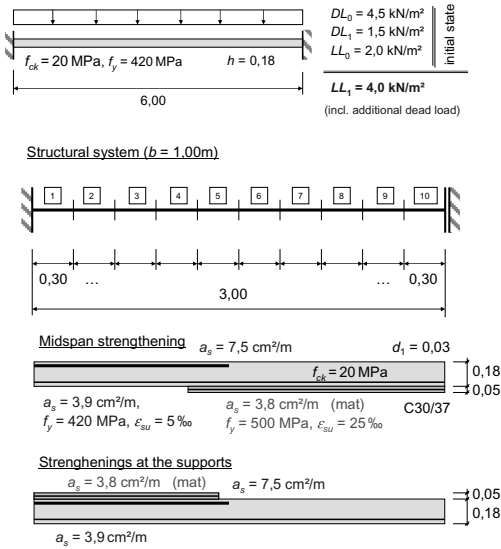


Figure 8. Strengthening of a slab: geometry, loads and structural systems.

- Span strengthening: shotcrete only at midspan (bottom layer).
- Strengthening at the supports: cast in place RC layer only at the supports (top layer).

Consequently, nonlinear calculations of sectional forces are needed, as—otherwise—strengthening at both sides of the slab would be compulsory, because positive as well as negative moments pronouncedly rise and existing reinforcement amounts do not include sufficient reserves.

The required amount of the reinforcement 2 is estimated in advance from the total increase of the design value of the bending moment to about 3 to 4 cm<sup>2</sup>/m. Thus, a reinforcement mat of 3,77 cm<sup>2</sup>/m is provided in both cases (bottom or top).

### 5.1 Moment-curvature relations

The parameters of the initial and strengthened cross sections are determined using spreadsheet analyses to yield four different moment-curvature relations, namely the ones at

- midspan, initial section
- midspan, strengthened section
- support, initial section
- support, strengthened section

which are illustrated in Figure 9. Even the linear calculations are made with the software tool to easily consider the correct influence of the reinforcement on section properties. Because of the uniaxial bending conditions and the rectangular shape of the

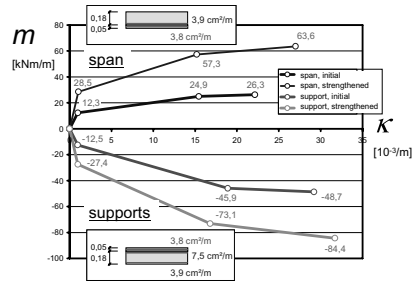


Figure 9. Moment-curvature relations for initial and strengthened sections.

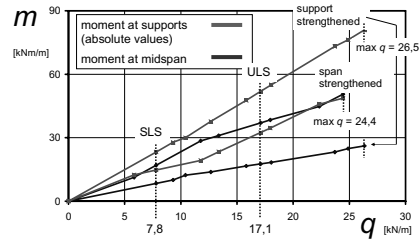


Figure 10. Developments of bending moments for the different strengthening types.

sections, the modelling within the spreadsheet is rather straightforward. One loading parameter (moment  $m_y = m$ ) and one curvature ( $\kappa_z = \kappa$ ) remain.

The strengthening almost doubles the resistances, as inner lever arms grow and yield strengths are increased. This accounts for the span as well as for the supports.

### 5.2 Sectional forces and development of the stiffness parameters

Figure 10 shows the nonlinear rise of the sectional moment  $m$  over the total load  $q = q$  ( $DL_0$ ,  $DL_1$ ,  $LL_0$ ,  $LL_1$ ) The strengthening at midspan adjusts span and support moments to almost the same (absolute) extents.

On the contrary, span moments decrease to about 1/3 of the support moments, if the strength enhancement is supplied at the fixed ends. Pronounced redistributions take place induced by the stiffness variations provided initially or by the progressive cracking during loading. Figure 11 shows this development from the uncracked sections ( $B_I$ ), over the serviceability limit state (SLS) with a first damage at the supports, the ultimate limit state (ULS) with pronounced cracking and the final calculative failure at the supports. As expected, failure occurs where no strengthening is provided.

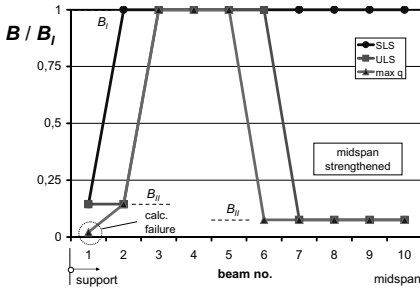


Figure 11. Distributions of stiffness parameters.

Table 1. Design for strengthening in midspan.

	ULS	SLS
Midspan	$M_{Rd} = 49,6 \text{ kNm/m}$ $\geq M_{Ed} = 37 \text{ kNm/m}$ $(\epsilon_c/\epsilon_{s1}/\epsilon_{s2} = -1,64/5,00/7,22[\text{‰}])$	$\sigma_{c,min} = -4,5 \text{ MN/m}^2 \geq 0,45f_{ck}$ (permanent) $\sigma_{s1} = 113 \text{ MN/m}^2 \leq 0,8 f_{yk}$ $\sigma_{s2} = 158 \text{ MN/m}^2 \leq 0,8 f_{yk}$ Crack width ( $w_{p,cal} = 0,4 \text{ mm}$ )
Support	$M_{Rd} = -38 \text{ kNm/m}$ $\approx M_{Ed} = -39 \text{ kNm/m}$ $(\epsilon_c/\epsilon_{s1o}/\epsilon_{s1u} = -1,46/5,00/-0,17[\text{‰}])$	similar calc. for midspan

### 5.3 Design

The design verifies the *á priori* choice of the reinforcement amounts and their suitable longitudinal distributions over the structural elements. Doing so, a bending design in SLS, stress limitations and crack limitations in ULS's are carried out with the help of the spreadsheets. Input parameters are the sectional moments of the design states, material functions and material parameters (design values) corresponding to the nonlinear evaluation of the sectional forces (EN 1992-1-1 2004, NA EN 1992-1-1 2007). Outputs are extreme strain and stress values and bending resistances. Table 1 summarises the key results for a strengthening in midspan. Note that the limitation of the ultimate steel strain to 5 ‰ (reinforcement I with normal ductility) limits the bearing capacities. Concrete and steel stresses as well as crack widths remains far above admissible values.

## 6 CONCLUSIONS

The proposed method solves the complex design problem of strengthening aged RC structures with just practical solution techniques. Redistributions induced by stiffness reductions (cracking, yielding) are realistically modelled. Even if sections have arbitrary shapes and consist of several materials—this often occurs due to the constraints introduced by the initial geometries and material properties—the method only requires a usual spreadsheet analysis program and a linear solver for the structural analysis. All nonlinear

calculations, being the evaluation of moment-curvature relations and the final verification process, are performed within the spreadsheets. The common idea of the fibre models is used to discretise the section in the grid of columns and rows and a gradient method to solve the equilibrium problem. The nonlinear calculations for sectional forces are reduced to stepwise linear ones, as moment-curvature relations have linear branches. Usually, the governing sectional forces of SLS and ULS are found after a few steps and efforts remain acceptable.

## REFERENCES

- Bathe, K.-J. 1996. *Finite Element Procedures*, Upper Saddle River: Prentice Hall.
- Bhatti, A.M. 2000. *Practical Optimization Methods*. New York: Springer.
- DAfStb. 2003. *Erläuterungen zu DIN 1045-1, DAfStb H. 525*, Berlin: Beuth Verlag (In German).
- EN 1992-1-1. 2004. *Eurocode 2: Design of concrete structures—Part 1-1: General rules and rules for buildings*. European Committee for Standardization.
- Furlong, R.W., Hsu, T.T.C. & Mirza, S.A. 2004. Analysis and design of concrete columns for biaxial bending-overview. *ACI Structural Journal* 101 (3): 413–423.
- Fylstra, D., Lasdon, L., Watson, J. & Waren, A. 1998. Design and use of the Microsoft Excel Solver. *Interfaces* 28 (5): 29–55.
- Hankers, C. 2000. Möglichkeiten zur Verstärkung von Stahlbetonbauteilen, *Beton- und Stahlbetonbau* 95 (9): 531–536 (in German).
- Hsu, T.T.C. 1985. Biaxially loaded L-shaped reinforced concrete columns. *Journal of Structural Engineering* 111 (12): 2576–2595.
- Krätzig, W.B. & Basar, Y. 1997. *Tragwerke 3, Theorie und Anwendung der Methode der finiten Elemente*. Berlin: Springer Verlag (In German).
- Krätzig, W.B. & Petryna, Y.S. 2006. Iterative Berechnung inelastischer Stahlbetonstabwerke mit linearer FE-Software. *Bauingenieur* 81 (4): 181–188 (In German).
- Lasdon, L.S., Waren, A., Jain, A. & Ratner, M. 1978. Design and testing of a Generalized Reduced Gradient code for nonlinear programming. *ACM Transactions on Mathematical Software* 4: 34–50.
- Mark, P. Design and optimisation of cross sections using spreadsheet analyses. In B.H.V. Topping (ed.). *Proceedings of the Tenth International Conference on Civil, Structural and Environmental Computing*. Rom. Sept. 2005, Stirling: Civil-Comp Press.
- National Appendix (Germany) to EN 1992-1-1: 2004. Draft 02/2007. *Eurocode 2: Design of concrete structures—Part 1-1: General rules and rules for buildings*.
- Petryna, Y.S. & Krätzig, W.B. 2005. Computational framework for long-term reliability of RC structures. *Computer Methods in Applied Mechanics and Engineering* 194 (12–16): 1619–1639.
- Powell, S.G. & Baker, K.R. 2004. *The Art of Modeling with Spreadsheets*. Hoboken: Wiley.
- Smith, S. & Lasdon, L. 1992. Solving large sparse nonlinear programs using GRG. *ORSA Journal on Computing* 4: 2–15.

# Uncertainty in structural capacity and influence on seismic demand and damage

M. Mezzi

*Dip. Ingegneria Civile ed Ambientale, Università degli Studi di Perugia, Perugia, Italia*

**ABSTRACT:** The variation in member capacities is an important source of response uncertainty and PBSD methods based on a probabilistic definition of the correlation among the parameters controlling the consequences of the seismic events shall account for it. The parameters defining the plastic hinges' properties, particularly the yielding moments, can be assumed as reference random variables. Once generated a set of configurations, corresponding to a random distribution of the capacities of all the members, accounting for the uncertainty in their capacity, the simulations of the seismic response allow to define the statistics of the demand parameters and to point out the PDF's of their distributions. The most interesting result, finalized to the application of a probabilistic PBSD procedure, consists of fragility curves of the demand parameters, both global and local, to which the damage status can be, in its turn, correlated. Contrarily to some current assumptions, results show the relevant influence of the capacity uncertainty in damage characterization and the strong influence of the accelerograms used for the analyses, even if chosen with spectrum-fitting criteria.

## 1 INTRODUCTION

A correct and comprehensive procedure for the seismic assessment of buildings according to the Performance-Based Seismic Design method should provide for a probabilistic definition of the correlations among the parameters controlling each step of the procedure. The probabilistic characterization of the hazard, usually expressed through intensity levels, with assigned return period, associated to response spectrum shapes, is well known and accepted. Moreover, a set of spectrum-fitting accelerograms, both recorded or even artificially generated, provides for a large scattering of the Engineered Demand Parameters (EDP) characterizing the response, and requires a probabilistic interpretation.

Within the path leading to a complete probabilistic formulation of the *consequences* provoked by an earthquake on a construction, it is important to investigate the influence of the random variation in member capacities on the response uncertainty. Attention should be paid to the random variation of the member capacity associated to the random variations of the strength and ductility of its component. Once defined the reference damage state, different procedures can be applied: (1) data from numerical simulations or tests or field survey can be used, if available; (2) experimental campaigns can be carried out; (3) numerical simulation analyses can be carried out. The first two methods do not give enough information due to

the lack of large experimentations and field observations and the analytical method can be very onerous. Therefore a simplifying procedure has been outlined and is presented in the present paper. It makes reference to higher level parameters and it is allowed by the engineered knowledge of the structural problem. The flexural response of a r/c member depends on the random variation of the material mechanical characteristics, on their distribution on the sections, on the member geometry, but the non linear behaviour of such member is usually modelled with plastic hinges located at the member ends and characterised by elastic-plastic diagrams. The parameters defining the hinges' behaviour (yielding moment and curvature, ultimate moment and curvature, residual moment) can be assumed as reference random variables, in place of the detail material and geometry characteristics.

A research has been carried out providing for the generation of a set of variants of a structural model, resulting from a random distribution of the capacities of all the members, accounting for the uncertainty in member capacity. Simulations of the seismic response of the variants allow to obtain a sample of the response parameters, from which the probability density functions (PDF) of their distribution can be identified and the corresponding fragility curves can be finally drawn. The fragility curves will enter in a performance-based procedure leading to the probabilistic evaluation of the earthquake consequences.



## 2 STRUCTURAL RANDOMNESS

### 2.1 *Randomness of structural parameters*

The parameters on which the mechanical behaviour of the structures depends, are characterized by uncertainty that can be represented by their PDF's. In r. c. elements both the concrete and steel parameters should be accounted for. For the concrete: compressive strength, elastic modulus, ultimate deformation, confinement effect. For the steel: yield strength, elastic modulus. The PDF's of these parameters can be derived from the test results and values can be found in literature (Mirza et al. 1979a, b). Also the member geometry, alignment and dimensions, can be assumed to be characterised by random distributions (Mirza et al. 1979c).

The randomness of the geometry and mechanical parameters influence the characterization of both the structural response and the damage status, but these aspects should be examined separately.

### 2.2 *Influence on structural response*

The randomness of the geometry definition and that of the mechanical parameters of the materials result in a scattering of the mechanical characterization of the element: stiffness, resistant moment and shear, flexural ductility. It is evident that different distributions of member stiffness and strength in the same structural scheme determine different responses to the same external input.

These aspects are currently ignored in the design practice, or better they are implicitly accounted for, through the assumptions of characteristics values (with predefined percentiles) of the mechanical parameters of the materials, leading to a conventional representation of the structure.

In procedures where the actual structural response has to be considered, instead of a conventional one, as in the case of the evaluation of EDP's for a performance assessment, the scattering of the mechanical parameters of the structure should be explicitly considered. Because it does not seem to be negligible, numerical investigations have been carried out for evaluating its influence and the results are reported and commented in the present paper.

### 2.3 *Influence on damage status*

The randomness of the detail mechanical parameters should not be considered at the only macro-scale of the global structural response, but it also influences the local member behaviour in terms of consequences to the structural response.

The levels of the damage states related to the structural demand depend on the randomness of the structural parameters. Fragility curves of the local

curvature related to the story drift ratio are reported in literature (Yong et al. 2005) and studies are being currently carried out by the authors within the same research line illustrated in this paper. The damage conditions at the member ends are assumed in a severity order: initial concrete cracking, concrete cover spalling, wide and deep concrete cracking, steel yielding, core concrete crushing, steel buckling, stirrups' rupture. Fragility curves of the listed damage states are derived, related to the story drift ratio, accounting for the randomness of the material and geometry parameters. This aspect lies outside the aims of this paper and the related results are not reported.

## 3 SAMPLE STRUCTURES

### 3.1 *Fixed-base frame*

The sample structure used for the evaluations is a 2-bays 4-story r/c frame. It is designed according to the Italian guidelines (OPCM3431 2005) under the following assumptions: seismic Zone I (PGA equal 0.35 g), soil profile B (medium stiff soil), ductility class high (DCH). The dimensions of the members' sections are:  $300 \times 500$  mm for the beams,  $400 \times 400$  mm for the columns, kept constant for all the members. The following assumptions have been adopted for the load and the consequent mass data. Dead loads of the structural members, corresponding to a concrete dead load of  $25 \text{ kN/m}^3$ . Floor dead and permanent loads:  $g_{k,s} = 6.0 \text{ kN/m}^2$ . Floor live loads:  $q_{k,s} = 1,5 \text{ kN/m}^2$  at roof level,  $q_{k,s} = 2,0 \text{ kN/m}^2$  at the intermediate floors. The frames are hypothesized at a distance of 5 m.

### 3.2 *Modelling of non linearity*

The non linear behaviour of the model frames is modelled, in the adopted computer code, by means of the automatic insertion of a plastic hinge at the member end when the force equals the elastic strength. The flexural plastic hinges are characterized by the typical moment-curvature behaviour shown in Figure 1: Point B is defined by the yielding moment and by zero rotation (a yielding curvature is defined anyhow), point C is defined by the ultimate moment and rotation, point D and E are defined by the residual moment and by the ultimate rotation. The initial member behaviour is elastic, when the bending moment reaches the yielding value, the hinge starts to work with the plastic rotations required by the deformations undergone by the structure.

The model used in the study provides for some simplified hypotheses of the non linear behaviour:

1. the interaction between bending moment and axial force is ignored, the moment-rotation diagram refers the average axial force;

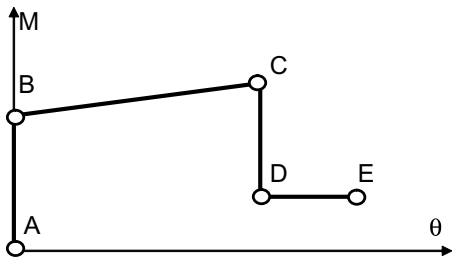


Figure 1. Moment-curvature relationship of the plastic hinges.

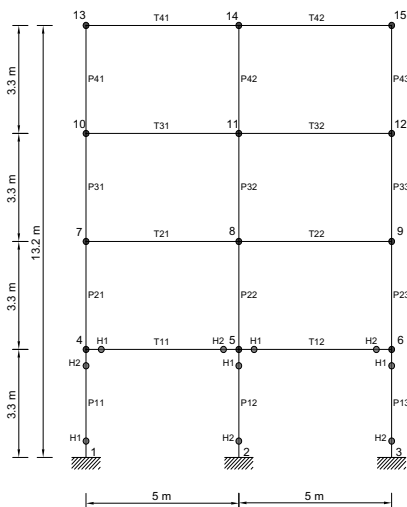


Figure 2. Sample model with columns, beams and hinges identification codes.

2. the moment-rotation diagram is assumed to be elastic-perfectly-plastic, the strength is characterized only by the yielding moment.

Figure 2 reports the general scheme of the sample model used in the analyses.

#### 4 SIMPLIFIED RANDOMNESS MODEL

As previously stated, a detailed randomness model should account for a probabilistic characterization of the material characteristics and section geometry. The PDF of these parameters should be defined according to their scattering parameters. A combination of values of the parameters, randomly assumed, defines a different curve characterizing the plastic hinge. The influence of the scattering on the response should be simulated repeating the dynamic analyses for a large number of hinges' characterizations, corresponding to the assumed combinations.

The outlined methodology is very hard to follow because of the large number of combinations to be used for obtaining a statistically stable population of the input hinges and response parameters.

A simplified model of the randomness of the structural characteristics can be used considering directly the randomness of the hinges' characteristics: yielding moment and curvature, ultimate moment and curvature, residual moment. Figure 3 reports a graphical representation of this assumption: the dashed areas identify the domains of the probable values of the characterizing parameters.

Actually, because in the present study the moment-rotation diagram is assumed to be elastic-perfectly-plastic, an even simpler model has been actually used providing for the probabilistic definition of the only yielding moment, as shown in Figure 4.

As a consequence of the scattering of the parameters affecting the r/c section strength, a coefficient of variation of 0.25 is assumed for characterizing the scattering of the yielding moment of the sections. According to the usual assumptions (ATC58 2005) of the probabilistic laws of the main structural parameters, a lognormal PDF is assumed for representing the yielding moment statistics.

For each plastic hinge a lognormal PDF is defined. Assuming the nominal value of the resistant moment,  $m_Y$ , as mean value of the moment statistics and the chosen coefficient of variation CV, the corresponding parameters of the lognormal distribution result

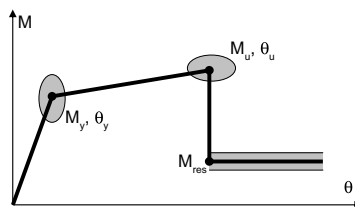


Figure 3. Random parameters of the plastic hinge diagrams.

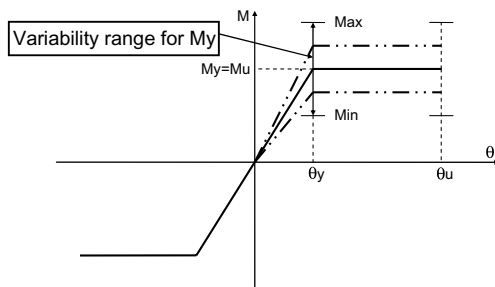


Figure 4. Actual random characterization of the plastic hinges.

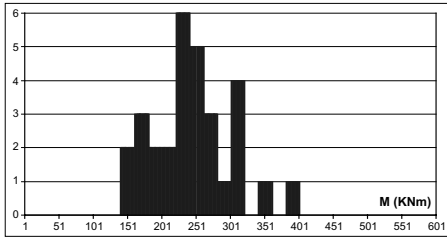


Figure 5. Frequency histogram of the resistant moments of the hinge P1 1b (bottom section of the left column at 1st story).

$$\sigma_{\ln y} = \sqrt{\ln(CV^2 + 1)} \quad (1)$$

$$m_{\ln y} = \ln \left[ m_Y \cdot \exp(-0.5 \cdot \sigma_{\ln y}^2) \right] \quad (2)$$

the median of the distribution is

$$\mu_Y = m_Y \exp(-0.5 \cdot \sigma_{\ln y}^2) \quad (3)$$

and the PDF expression results

$$f_Y(y) = \frac{1}{y \sqrt{2\pi} \sigma_{\ln y}} \exp \left\{ -\frac{1}{2} \left[ \frac{\ln(y/\mu_Y)}{\sigma_{\ln y}} \right]^2 \right\}. \quad (4)$$

Once defined the PDF of the resistant moment of each potential plastic hinge, that is at each end of columns and beams, a large number of possible configurations of the model frame can be pointed out. Each configuration is characterized by a random distribution of the hinge characteristics. Actually, thirty configurations have been created. Each configuration corresponds to a combination of randomly defined values of the resistant moment of each plastic hinge, extracted considering the PDF of the resistant moment of that hinge. Figure 5 reports the frequency histogram of the resistant moments attributed to the bottom hinge of the first-story left column having a nominal value of 240 kNm.

## 5 DYNAMIC ANALYSES

The seismic intensity is modelled by the 5% damped elastic acceleration response spectrum. The reference spectrum provided by the Italian guidelines (OPCM3431 2005) for medium stiff soils (Class B) and for a PGA equal 0.35 g (high seismicity area), is assumed.

Seven recorded ground motions are selected matching the specified intensity spectrum (the accelerograms are reported in [www.reluis.it](http://www.reluis.it)). More detailed information concerning the strong motion data base, the characteristics of the accelerograms, the selection

criteria, the matching rules, are reported in (Iervolino et al. 2006).

Non linear time histories analyses are carried out on the variants of the designed model. The main response parameters are considered as Engineered Demand Parameters (EDP) characterizing the structural behaviour: the top displacement, the story drift ratios, the plastic hinges' rotations, the floor accelerations. A probabilistic characterization of these parameters is carried out assuming a log-normal Probability Density Function (PDF) according to the assumptions reported in the literature (D'Ambrisi & Mezzi 2005, ATC58 2005).

## 6 RESPONSE PARAMETERS

### 6.1 Story drift ratios

The first examined parameter for checking the influence of the scattering of the structural characteristics is the story drift ratio. It is the most representative EDP characterizing the performances requested to the structural elements. The member status can be related to it, many damage indicators are based on it, many guidelines provide for controlling the structural performance by limiting its value.

The statistics of the responses of the model variants allow to identify the PDF's of their distribution. Figure 6 shows the lognormal PDF's of the 1st-story drift ratio for the seven accelerograms used in the analyses. The validity of the lognormal assumption has been checked by carrying out, for each assumed distribution, a Kolmogorov-Smirnov test. Figure 7 gives

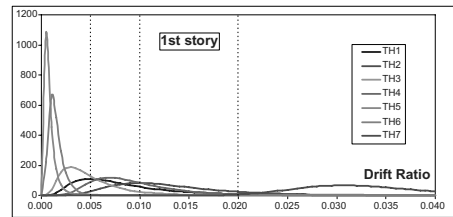


Figure 6. PDF's of the 1st-story drift ratio for the seven accelerogram.

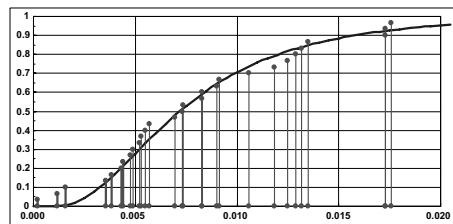


Figure 7. Kolmogorov-Smirnov test on the 1st-story drift ratio distribution.

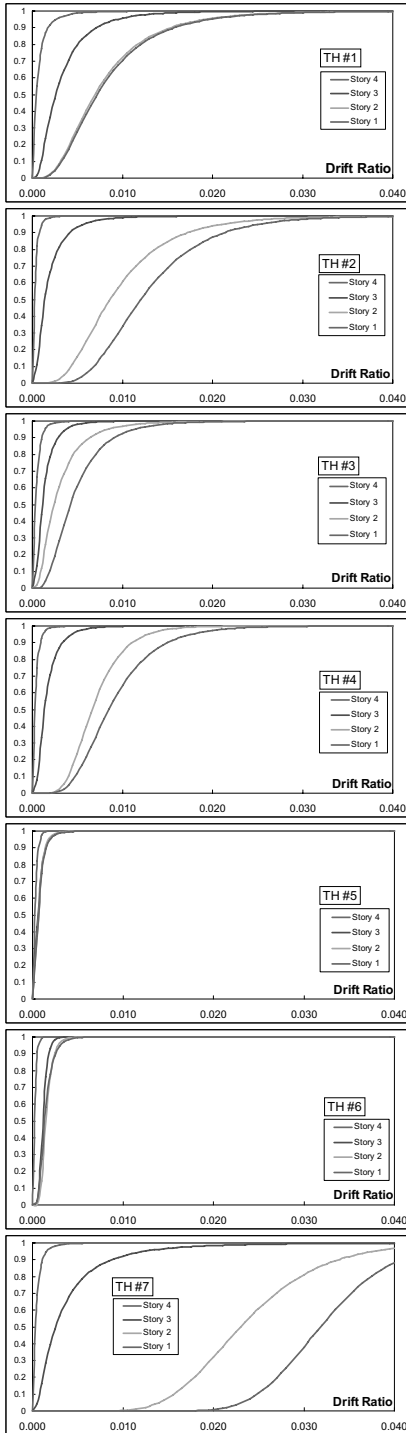


Figure 8. Fragility curves of the story drift ratio at the four stories for the seven accelerograms.

a graphical wisdom of the goodness of fit of the cumulated frequency values (vertical red lines) with the lognormal CDF (blue diagram).

The seven graphs of Figure 8 report the fragility curves of the drift ratios of the four stories, evaluated correspondently to the seven accelerograms used. The relevance of the influence of the scattering of the mechanical characterization of the member detail is evident. It is especially evident the strong influence of the input characteristics, because the graphs vary from one accelerogram to another one. This fact is better evident if the diagrams are collected by story, as shown in the graphs of Figure 9.

It can be observed that at the first story the probability to overcome a story drift ratio of 0.01 varies from 100% for the accelerogram #7 to 0% for the accelerograms #5 and #6, with intermediate values of 70%, 35%, 30% and 8%, given by the other accelerograms. The results evidence that:

- the influence of the scattering of the mechanical characterization is not negligible, except at the higher stories, where the plasticization are not present or strongly limited;
- the choice of the design accelerograms is a critical issue and the spectrum fitting criterion is not adequate for the non linear analyses;

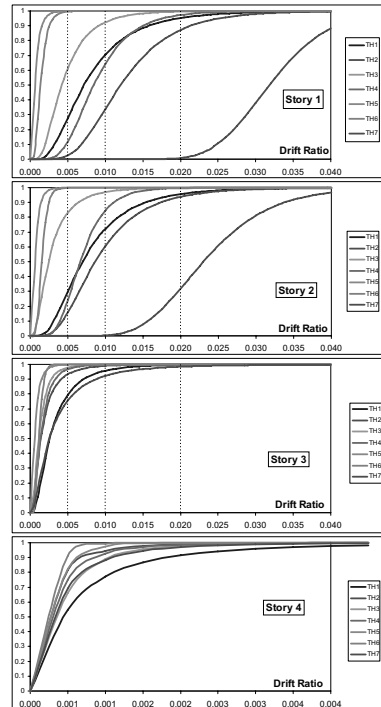


Figure 9. Fragility curves of the story drift ratios collected for each story level.

- a criterion for defining a reference fragility curve for the performance evaluations is required.

## 6.2 Plastic rotations

The local demand of the structural members is evaluated in terms of rotations of the plastic hinges rising up at the ends of beams and columns when the forces reach the values of the elastic strengths. When the elastic limits are not overcome, the continuity of the rotation values is preserved adopting a pseudo-rotation, evaluated multiplying the elastic curvature by the length assumed for defining the plastic hinge. The elastic curvature is computed as the portion of the yielding curvature proportional to the ratio of the actual moment to the yielding moment.

Figure 10 shows the fragility curves of the rotations of the top and bottom hinges of the lateral and central columns at the first story.

Also the local response in the post-elastic range is strongly influenced by the scattering of the strength parameters and exalted by the characteristics of the accelerograms used in the analyses.

For the base hinge of the lateral column, the couple of rotations having the non exceedance probability of 10% and 90% are 0.007–0.049, 0.018–0.051,

0.014–0.022, 0.013–0.024, 0.006–0.009, 0.009–0.013, 0.038–0.055 radian, respectively for the seven time histories analyzed.

## 7 CONCLUSIONS

Results show the relevant influence of the randomness of the flexural capacity, controlling the hinges' behaviour, in the global and local demand. The characteristics of the input accelerograms, even if chosen according to standard spectrum-fitting criteria, strongly influence the correlation. The fragility curves of the demand parameters can be finalized for deriving a damage evaluation within a probabilistic PBSB procedure.

## ACKNOWLEDGEMENTS

The research is carried out within the project DPC-ReLUI5 2005–2008, Research line 7 “Technologies for isolation and control of structure and infrastructure”.

## REFERENCES

- ATC58. 2005. Guidelines for Seismic Performance Assessment of Buildings. 25% Draft. *Applied Technology Council*.
- D'Ambrisi, A. & Mezzi, M. 2005. A Probabilistic Approach for Estimating the Seismic Response of EP SDOF Systems. *Earthquake Eng. & Struct. Dynamics*, 34(14), 1737–1753.
- FEMA445. 2006. Next-Generation Performance-Based Seismic Design Guidelines. *Federal Emergency Management Agency*, Washington, D.C., USA.
- Iervolino, I., Maddaloni, G. & Cosenza, E. 2006. Accelerogrammi Naturali Compatibili con le Specifiche dell'OPCM 3274 per l'Analisi Non Lineare delle Strutture. 6° *Congresso CTE*. Parma, Italy (*in Italian*).
- OPCM3431. 2005. Ulteriori modifiche ed integrazioni alla Ordinanza PCM 2374 «Primi elementi in materia di criteri generali per la classificazione sismica del territorio nazionale e di normative tecniche per le costruzioni in zona sismica». Roma, Italia (*in Italian*).
- Mirza, S.A., Hatzinkolas, M. & MacGregor, J.G. 1979a. Statistical descriptions of strength of concrete. *J. Struct. Div. ASCE* 105(6), 1021–1037.
- Mirza, S.A. & MacGregor, J.G. 1979b. Variability of the mechanical properties of reinforcing bars. *J. Struct. Div. ASCE* 105(5), 921–937.
- Mirza, S.A. & MacGregor, J.G. 1979c. Variations in dimensions of reinforced concrete. *J. Struct. Div. ASCE* 105(4), 751–766.
- Yong L., Xiaoming G. & Jiong G. 2005. Probabilistic Drift Limits and Performance Evaluation of Reinforced Concrete Columns. *J. Struct. Div. ASCE*, 131(6), 966–978.

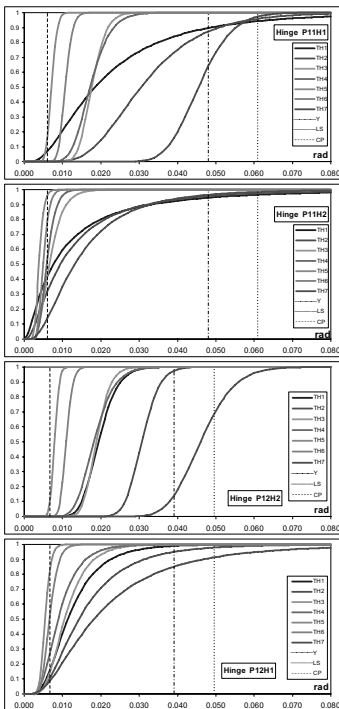


Figure 10. Fragility curves of the plastic rotations of the columns' hinges.

# Cost-based design and renewal strategy for long-life structures

J. Menčík

University of Pardubice, Pardubice, Czech Republic

**ABSTRACT:** Long-life structures suffer by gradual deterioration due to corrosion, fatigue or carbonation, and after some time they must be repaired or replaced by a new object. In addition to safety, a criterion for design and maintenance is cost effectiveness, characterised by the total money expended per unit time of service. A new construction should be dimensioned so as to ensure the minimum unit costs. The paper brings formulae relating the dimensions, lifetime and costs for basic forms of deterioration function, and analyses the problem of optimum life for typical stress distributions and deterioration rates. Only in some cases can the absolute minimum be achieved within a suitable interval of sizes and service times. Decisions about repairs are facilitated by proposing several variants and comparing the costs per unit of service, calculated from those for operation, inspections, maintenance and repair, with respect to the time value of money.

## 1 INTRODUCTION

Long-life structures, such as bridges, should be designed, dimensioned and maintained so as to guarantee safe operation during a demanded time, but for reasonable price. These structures are usually very expensive, so that great effort is devoted to the improvement of their design and maintenance management with respect to costs. A typical example is bridges, also due to great numbers of objects in road and railway networks. Numerous papers have been published and also several extensive research projects have dealt with this topic. For all, the projects Bridge Management in Europe (BRIME 2001) or Sustainable bridges (2003–2007) can be named.

The general aim is to minimise the total life-cycle costs, consisting of the costs associated with design, building, maintenance and removal at the end of life, and also the costs caused by failures; for bridges see, e.g. the classic papers by Branco & Brito 1995, Frangopol & Estes 1997, Frangopol et al. 1997, or Nowak et al (1990). As it is impossible to predict accurately the conditions of operation in distant future (loading, climatic influences, etc.), it is reasonable to divide the total life into two stages: design and operation. In the design stage, the structure is dimensioned for the demanded service time. In the operation stage, we try to maintain it so that the total costs from the putting into operation till the demolition or replacement are minimal. In this paper, approaches for both stages are discussed.

## 2 BASIC FORMULAE FOR DETERIORATING STRUCTURES

The costs, which can be influenced by dimensioning,  $C$ , consist of the price  $C_0$  of the new structure or component and of the rotable costs  $C_f$  caused by a premature failure (see further):

$$C = C_0 + C_f \quad (1)$$

Long-life structures deteriorate gradually due to load effects (e.g. in fatigue) and/or due to the action of environment (corrosion, carbonation of concrete, etc.). In all these cases, failure occurs after some time of operation. The costs must, therefore, be related to the lifetime  $T$  of the component or structure, and the cost-effectiveness must be evaluated according to the costs per unit-time of operation,

$$C_1 = C/T \quad (2)$$

The time  $T$  to replacement depends on the load effect  $S$ , which can be the stress magnitude or amplitude in cyclic loading, but also the intensity of corrosive environment. In the simplest case,  $T$  decreases with increasing  $S$  according to the formula

$$T = BS^{-m} \quad (3)$$

$B$  and  $m$  are constants. Equation (3) is known as Woehler curve for fatigue, with  $S$  denoting the stress amplitude. Also the time to failure of a body with a

crack, based on the Paris-Erdogan equation for crack velocity, can be expressed by Eq. (3), and even the time necessary for carbonation of a concrete wall or beam into some depth can be expressed in similar way. The thickness of a carbonated layer, no more able to protect steel reinforcement against corrosion, grows approximately with the square root of time,  $h = \varphi T^{1/2}$ , so that the time until the layer of thickness  $h$  gets carbonated, is

$$T = (h/\varphi)^2 \quad (4)$$

This corresponds to Eq. (3) with  $m = 2$ ; the layer thickness  $h$  characterises the protective ability of the structure against corrosion of the rebars ( $h^2$  corresponds to  $B$  in Eq. 3), and  $\varphi$  characterises the intensity of chemical attack. The rate of deterioration in actual structure can vary due to varying temperature, air humidity and other factors, and a more general value of exponent  $m$  instead of 2 may sometimes be more appropriate, similarly to Eq. (3).

The total time to failure of a reinforced-concrete component consists of two stages: carbonation of concrete and corrosion of steel rebars. Often, the time of the steel corrosion is short compared to the carbonation process, and can be neglected. Nevertheless, it is possible to determine the time to failure, or lifetime, using a two-stages model. The choice of a particular model also depends on what is considered as the limit state in the particular case.

The load effect  $S$  depends on the load  $L$  and the resistance  $Z$  of the loaded cross-section; in the simplest case

$$S = L/Z \quad (5)$$

$Z$  is, for example, the cross-section area or section modulus. The characteristic load  $L$  can be expressed as a sum of a load-independent value  $L_0$  and a term depending on the own weight of the component, and thus on the cross-section area  $A$ :

$$L = L_0 + k_{AL}A \quad (6)$$

$k_{AL}$  is a proportionality constant.

The demanded lifetime  $T$  can be ensured by proper dimensioning. Larger cross section means higher manufacturing costs, but usually also lower stresses, and thus longer life with lower unit costs. This allows one to seek the dimensions guaranteeing the minimum life-cycle costs. The price of the component can approximately be expressed as a sum of a fix value  $C_{00}$  and a value proportional to the cross-section area,

$$C_0 = C_{00} + k_{AC}A \quad (7)$$

where  $k_{AC}$  is a constant. The actual relationship can be more complex. Equation (7), however, is correct

for small deviations from the optimum dimensions. Sometimes, the cross-section cannot be changed continuously, but in steps (for standardised parts, e.g.). In such cases one must calculate and compare the costs for individual variants.

### 3 DIMENSIONING FOR THE DEMANDED SERVICE TIME

In dimensioning for the prescribed service time  $T$ , the allowable characteristic load effect  $S$  is calculated from Eq. (3) first, and then the necessary cross-section characteristics ( $Z$ ,  $A$ ) for the given load  $L$  using Eqs. (5) and (6). Then, the characteristic dimension  $D$  (e.g. beam thickness) is determined. If necessary, the cross-section dependent component of the load must be considered in Eq. (6). Then, the costs  $C_0$  and  $C$  are determined from Eqs. (7) and (1), and the unit costs  $C_1$  from Eq. (2).

However, one must be aware that many uncertainties enter the design computations. Some quantities either vary randomly or are not known accurately in advance. The examples of random variables are loads, deterioration rate and the time to failure, which vary in specimens used for the determination of fatigue characteristics as well as in the real construction. Also the strength or characteristic dimensions of structural parts exhibit some scatter.

Another kind of uncertainties originates from our limited knowledge. For example, costs for materials or prefabricated parts are often known only roughly in the design phase—the suppliers of material and work are chosen later. Some values must be only estimated. In these cases, various methods for working with uncertainties can be advised, such as calculations for the optimistic, probable and pesimistic data, the “worst-case” method or “what-if” method, fuzzy techniques, and others. The following text is limited on cases where data on probability distributions are available.

The constants  $B$ ,  $m$  or  $\varphi$  are determined from tests. As the times to failure vary from test to test, also these “constants” vary. In semi-probabilistic design, the mean value of exponent  $m$  is used and the quantile of  $B$  (e.g. 5%), corresponding to the allowable probability  $P_f$  of failing before  $T$ . (In fully probabilistic approach, both  $B$  and  $m$  can be considered as random variables, in addition to random variability of load and other quantities, and simulation methods such as Monte Carlo must be used.)

When calculating the total costs  $C$  from Eq. (1), it is necessary to respect the possible costs  $C_f$  caused by a premature failure. However, as we assume such failure happening only with probability  $P_f$ , only the probable costs are usually considered:

$$C_f = P_f \times C_{ff} \quad (8)$$

where  $C_{ff}$  are the direct and indirect costs associated with the collapse. The direct costs are those for the repair (they can be as high as the price of a new object), while the indirect costs cover all additional damages including the compensation for casualties. Nevertheless, there is one problem in this simple approach (8): the probable failure costs  $C_f$  can be significant for  $P_f > 10^{-1}$ , but they become negligible for very low failure probabilities ( $P_f < 10^{-4}$ ), regardless the value of actual damage. However, while a collapse of a structure with very costly consequences can be bearable for an owner who has a large portfolio of many objects, it can be fatal for an owner without sufficient funds. Therefore, insurance is used in some cases, and then also the insurance costs must be included into the cost balance. Also, if the damages could be very extensive (more fatalities, heavy environmental damages), it is impossible to use purely economic approach, and a socially acceptable or a law-prescribed value of failure probability is worked with (cf. Eq. 11 in Section 4).

For deteriorating processes, the probability of failure  $P_f$  can be expressed as a function of service time. The computations are based on models for crack propagation, reduction of load carrying cross-section due to corrosion, carbonatation etc., combined with probabilistic techniques.

#### 4 COST-BASED OPTIMISATION OF CROSS-SECTION DIMENSIONS

In optimum case, the component has such dimensions and lifetime, that the unit costs for this time are minimum. In principle, equations (1)–(7) should be combined so as to express  $C_1$  as a function of characteristic dimension  $D$ . Then, the optimum size  $D_{opt}$  could be found from the condition  $dC_1/dD = 0$ .

However, analytical solution is practically impossible, especially for complex shapes of cross-section, and also if the weight of the component (with yet unknown cross-section size) contributes to the total load. Much easier procedure consists of calculating the quantities  $T$ ,  $C$  and  $C_1$  for various values of  $D$ ,  $A$  and  $Z$ , and then expressing  $D$ ,  $A$ ,  $Z$ ,  $C$  and  $C_1$  as functions of  $T$ . Very useful is plotting of these curves (also for various values of  $P_f$ ). These graphs show if an optimum exists, how the costs vary around it, and what will be the consequences of using a different cross-section.

The graphs can also be constructed as non-dimensional, as well, by dividing the costs and dimensions by a suitable reference value. Then, they show the relative cost changes as functions of relative change of cross-section.

A simple computer program has been created for studying the influence of the main parameters (Menčík 2006a,b). Figures 1 and 2 show the development of unit costs and time to failure as the functions of the

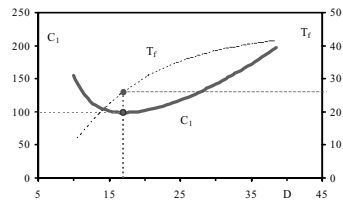


Figure 1. Unit costs  $C_1$  and time to failure  $T_f$  as functions of bar diameter  $D$ . Tensile cyclic loading, fatigue exponent  $m = 3.0$ . After Menčík 2006a,b.

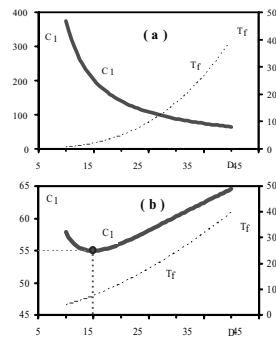


Figure 2. Unit costs  $C_1$  and time to failure  $T_f$  as functions of beam thickness  $D$ . Cyclic loading in bending, fatigue exponent  $m = 3.0$  (fig. a) and  $m = 1.7$  (fig. b). After Menčík 2006a,b.

thickness of a component loaded in tension (Fig. 1) and bending (Fig. 2a, b).

Several important conclusions can be drawn from this analysis. First, only in some cases an optimum (with minimum unit costs) exists (Figs. 1 and 2b). Sometimes it lies outside the suitable interval of sizes or service times. An important role is played by the kind of loading and fatigue exponent  $m$ . For tensile loading of steels with common values of fatigue exponent ( $2 < m < 6$ ), an optimum with minimum unit costs often exists (Fig. 1). In cyclic bending, the increase of the characteristic cross-section dimension  $D$  causes the increase of the section modulus  $Z$ , and much faster growth of useful life ( $T \sim Z^m$ ). As a consequence, any enlargement of cross-section usually leads to the reduction of unit costs  $C_1$  (Fig. 2a). Other criteria for design are then decisive. However, for low values of  $m$  (for example  $m = 1.7$ ), a minimum of unit costs also exists (Fig. 2b).

The model (4) for carbonatation of concrete has indicated that for  $m = 2$  the unit costs decrease monotonously with growing thickness of the protective layer. However, the situation in other cases of deterioration, with other values of  $m$ , can be different.

Because of many factors involved, it is impossible to formulate simple universal rules for finding the optimum size. A more practical way is to model the



situation for reasonable ranges of the input quantities and for several design variants. Graphical representation can reveal that the unit costs vary monotonously or insignificantly in the possible range of input variables, which makes the choice of dimensions easier. To probabilistic cost-based dimensioning, the reader is also referred to Menčík 2004.

## 5 COST-BASED MAINTENANCE OPTIMISATION

Two cases can be distinguished here: maintenance optimisation of a single object, and maintenance of a group of similar objects, such as bridges in a railway network.

### 5.1 Single object—cost components

The optimisation tries to minimise the total costs spent from the putting the structure into operation till its replacement or reconstruction. In addition to direct costs for maintenance and repair, also other cost components must be considered. The total costs  $C$  in the period  $T$  are (Frangopol et al. 1997):

$$C = C_i + C_m + C_r + C_f + C_u + C_a - V_s \quad (9)$$

$C_i$  = inspection costs,  $C_m$  = maintenance costs,  $C_r$  = repair costs,  $C_f$  = failure costs,  $C_u$  = user costs,  $C_a$  = additional costs, and  $V_s$  = salvage value of the object at the end of the considered period. Remarks to some cost components follow.

If more inspections are performed during the considered period, the costs for each inspection must be included into  $C_i$ . Maintenance costs  $C_m$  cover only minor repairs, but not the costs of large repairs or reconstructions, which are included into  $C_r$ . The costs of a repair depend on the actual condition of the structure, for example a bridge, and thus also on the time when it will be done. If an old bridge is to be replaced by a new one, also the demolition costs must be considered here.

Failure costs  $C_f$  include the costs resulting from a collapse of the bridge or from its closure when a collapse is imminent and the bridge must be closed to traffic. The costs of a collapse can be divided into the direct costs (e.g. for bridge replacement), and the indirect costs (the damages caused by the collapse). Also the expenses of bridge users,  $C_u$ , must be included (delays and the necessity to use longer alternative routes). The traffic limitation causes losses to the whole society, and should be considered from this point of view. On the other hand, we do everything to prevent such collapse, so that we expect that it can happen only with some probability  $P_f$ . Therefore, only the probable costs (8) are considered for  $C_f$  when comparing various maintenance strategies, similarly to the approach used in design.

Additional costs  $C_a$  characterise the economic influence of repair works on nearby localities, the necessity of more expensive night work, installation of signalling appliances etc.

### 5.2 Time value of money

In long-term planning, one must be aware that there can be a difference between spending money today or in the future. Due to interests, the value of (suitably deposited) money gradually increases, so that the today's value  $V$  will—in  $n$  years—correspond to  $V(1+r)^n$ , where  $r$  is the interest rate. Thus, when the total costs during a long period are calculated as a sum of expenses arising in various times, the values of individual components should be converted to the same time base, usually to the time  $T_0$  when the study is made. The common formula for the conversion of the  $j$ -th component  $C_{j,T_i}$  paid at time  $T_i$  is

$$C_{j,T_0} = C_{j,T_i} \frac{1}{(1+r)^{T_i-T_0}} \quad (10)$$

Due to inflation, however, also the prices for material, components and work gradually grow, and the gain from postponing an investment is smaller. If the inflation rate is close to the interest rate, the profit can be negligible, and the standardisation (1) is not necessary.

### 5.3 Single object—maintenance optimisation

Various strategies can be used for managing the maintenance and repairs, for example no repair until the replacement, or regular maintenance plus small repairs, which would enable longer time of operation till replacement. The optimisation consists of comparing the costs  $C$  for several variants and choosing the best one with lowest possible costs. For each variant, the total costs  $C$ , Eq. (9), are calculated for the time interval considered (e.g. 5 or 20 years), and the costs for individual variants are rank-ordered and compared (Fig. 3 and Menčík & Rudolf 2005).

As some of the input data were only estimated, it is recommended to make several estimates for each maintenance strategy: with optimistic, probable, and pessimistic input values. Also, the sensitivity of total costs to individual components should be evaluated, and the accuracy of input data should be adjusted to the relative influence of individual factors.

Often, some constraints must be respected. An important condition is that the safety cannot drop below certain level. Usually, this condition is expressed as

$$P_f \leq P_f^* \quad (11)$$

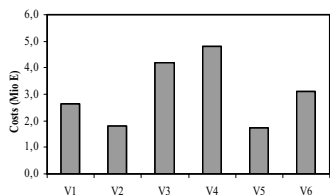


Figure 3. Comparison of total costs for 6 variants.

where  $P_f$  is probability of failure and  $P_f^*$  is the allowable, or target, probability of failure. (As an alternative measure, index of safety  $\beta$  is used in some cases, with the condition  $\beta \geq \beta^*$ .) Another very important constraint can be the availability of money or working capacities for a big reconstruction; the situation can differ from year to year.

Sometimes it is easier to compare relative differences between individual variants. For this purpose, so-called repair index  $RI$  may be used,

$$RI = \frac{(C_i + C_m + C_r + C_f + C_u + C_a - V_s)_{var}}{(C_i + C_m + C_r + C_f + C_u + C_a - V_s)_{ref}} \quad (12)$$

which compares the total costs for some maintenance variant (*var*) with the total costs for a reference case (*ref*). The smaller the repair index, the better is the maintenance variant.

#### 5.4 Maintenance optimisation in a group of objects

In an ideal case without any limitations and priorities, the optimum variant for maintenance and repairs for each object in the network (e.g. a bridge) could be found by the manner described above. Then, the objects (=bridges) would be repaired according to the time schedule corresponding to the optima for individual bridges. In real life, however, this is usually impossible because of various constraints, which must be respected. The most important constraints and factors will be briefly discussed in the following section, as well as the strategy for the optimum choice of bridges for repair.

A very important constraint is the amount of money available for maintenance and repairs in individual years. If every bridge should be repaired or reconstructed in its optimum time, it could happen that more bridges should be reconstructed simultaneously than the possible budget would permit, while in other years, the working capacities for repairs would be used only partly. Generally, the money spent for the renewal of the bridge stock should not vary too much from year to year. Thus, it is not sufficient to calculate and compare only the total costs  $C$ , defined by Eq. (9). Instead, it is necessary to calculate the cost components for every bridge and maintenance variant for every year

	2008	2009	...	2024	2025	SUM
Br.1, V2						
Br.2, V1						
Br.3, V2						
Br.4, V1						
Br.5, V3						
Br.6, V2						
Br.7, V1						
SUM						

Figure 4. Example of cost matrix for seven bridges during the period 2005–2025. Br—bridge, Vi—maintenance variant.

in the considered time interval  $T$ , in which the bridge maintenance and renewal should be optimised (e.g. 20 years). If these yearly costs are written into a table with the columns corresponding to years and the rows to individual bridges and maintenance variants (Fig. 4), one can see from the sum in each column, whether the demands for money in individual years are distributed uniformly or not. In the latter case, the times for repairs of some bridges must be changed so that the total money needed in individual years is close to the assumed sources. A consequence of any deviation from the repair schedule “optimal for each bridge” is that the total sum of money for all bridges in the interval  $T$  would be higher. Thus, the changes in the time schedule for the maintenance of chosen bridges should be such that the increase of total costs in the interval  $T$  is as low as possible. When proposing these changes, one should consider the sensitivity of the total costs (in individual variants) to the deviations of repair time from the absolute optimum. The best strategy can be found by comparing several variants.

In addition to the demand of relatively uniform flow of money for maintenance and repairs, several other factors must be considered when prioritising the bridges for repairs:

- the condition of individual bridges and of the bridge stock as a whole (the bridges that are in the worst condition or have a reduced load carrying capacity are of special interest),
- the rate of deterioration; some bridges can be in a better condition, but deteriorate faster; their repair thus becomes urgent sooner,
- the importance of the bridge in the whole network or in some region (also the importance of the route on which the bridge is located),
- unpredictable events, such as floodings, earthquakes, or traffic accidents with heavy damages to some bridges.

For these reasons, the maintenance optimisation process is sometimes divided into three steps (BRIME 2001, Menčík & Rudolf 2005), described in the following section.

#### Step 1. Condition rating prioritisation.

All bridges are ranked according to their condition revealed by inspections and described by safety

index or another criterion, characterising the general condition (corrosion, condition of the pillars, superstructure, the carriageway etc.). Also some tools of the Failure Mode and Effect Analysis (FMEA) can be used, such as the classification of failure consequences and of the possibility of detecting the imminent collapse before it happens. Only the bridges whose condition is worse than some limit value, will be considered for the maintenance in the near future. This pre-selection significantly reduces the number of candidates for further steps.

The bridges can also be ranked according to the remaining life till the reconstruction—a criterion which combines the current condition and the rate of deterioration. Deterioration rates can be assessed by plotting condition against age; the slope of this curve gives the rate, and the residual life can be obtained by extrapolation. This estimate is more reliable if the data from more inspections are available.

#### Step 2. Bridge importance prioritisation.

The second step considers the role of individual bridges in the road or railway network. One bridge can be in a worse condition than another bridge. However, if it lies on an unimportant road in a rural area, while the latter bridge is on a main road with dense traffic, where the consequences of bridge failure or closure for long time would be much worse, the latter will be repaired preferably. The importance of a bridge was also considered in the “single bridge” maintenance optimisation described above, by means of “user costs”  $C_u$  in Eq. (9). The pre-selection from the whole bridge stock can consider more aspects (e.g. importance of the route and the traffic volume, the importance of the particular bridge due to its width, or even its historical value), and can further reduce the number of candidates and make the following cost-based optimisation easier.

Especially those bridges should be chosen preferably, which are ranked high according to both the condition and importance criteria. In such selection, weights can be assigned to some criteria, which cannot be measured easily.

#### Step 3. Optimisation of money allocation

In this step, the individual possible maintenance strategies are compared, taking into account the total amount of money and the work capacities necessary for each strategy in individual years. Then, the strategy is chosen, which is economically most favourable for the bridge stock within the longer period under consideration. Various techniques of multi-criteria optimisation are used for this purpose, including linear programming or neural networks. Sometimes, however, the choice can be influenced also by other criteria—for example, the repair of bridges on one route or in some area. Generally, the maintenance strategy for the bridge stock should be so that the condition

of the stock as a whole should gradually not get worse, but improve.

## 6 SUMMARY AND CONCLUSION

Cost-based design and maintenance optimisation of long-life structures aims at minimising the costs per unit time of operation. In design, this can be achieved by suitable dimensioning. However, the absolute unit-costs minimum can be achieved only in some cases. In maintenance management, the unit costs are calculated from those for operation, inspections, maintenance and repair. The optimum strategy is found by comparing several variants.

## ACKNOWLEDGMENT

The work has been supported by the Czech Science Foundation project GAČR 103/05/2066, and its presentation by the project GAČR 103/08/1340. This support is gratefully appreciated.

## REFERENCES

- Branco, F.A. & Brito, J. 1995. Decision criteria for concrete bridge repair. *Structural Engineering International*, Vol. 5, No. 2: 92–95.
- BRIME 2001. *Bridge Management in Europe*. Final Report and Deliverables of the 4th EU Framework Programme BRIME (1998–1999); [www.trl.co.uk/brime](http://www.trl.co.uk/brime).
- Frangopol, D.M. & Estes, A.C. 1997. Lifetime bridge maintenance strategies based on system reliability. *Structural Engineering International*, No. 3, October 1997: 193–198.
- Frangopol, D.M., Lin, K.Y. & Estes, A.C. 1997. Life-cycle cost design of deteriorating structures. *Journal of Structural Engineering*. No. 10, October 1997: 1390–1401.
- Menčík, J. 2004. Effective use of probabilistic methods for ensuring the reliability of structures. (In Czech). Conf. *Probability of structural failure, PPK 2004*, 6–7 October 2004. VUT & ÚAM, Brno: 85–90.
- Menčík, J. 2006a. Economic questions of dimensioning of constructions with limited lifetime. (In Czech). Conf. *Probability of structural failure, PPK 2006*, 3–4 October 2006. VUT Brno & ÚAM, Brno: 65–70.
- Menčík, J. 2006b. Optimum-reliability dimensioning: Cost-based approach. *3rd Int. Colloquium ASRANet*. Glasgow, 10–12th July 2006. Universities of Glasgow & Strathclyde. Paper No. 63. Book of abstracts, p. 29, full text: CD-ROM.
- Menčík, J. & Rudolf, P. 2005. Optimisation of maintenance strategy in a bridge network. *2nd Int. Conf. “Reliability, Safety and Diagnostics of Transport Structures and Means”*. Pardubice, 7–8 July 2005. University of Pardubice: 224–23. ISBN 80–7194–769–5.
- Nowak, A. (editor) 1990. *Bridge Evaluation, Repair and Rehabilitation*. Dordrecht: Kluwer Academic Publishers.
- Sustainable bridges 2003. Reports of the 6th EU Framework Programme, 2003–2007; [www.sustainablebridges.net](http://www.sustainablebridges.net).

# Probabilistic treatment of bridge monitoring data and associated errors for reliability assessment and prediction

Thomas B. Messervey

*University of Pavia, Pavia, Italy*

Dan M. Frangopol

*Lehigh University, Bethlehem, PA, USA*

**ABSTRACT:** Using and expanding upon past studies of a bridge monitored during construction, for controlled tests, and for 90 days while in service, this paper uses monitoring data to conduct a reliability-based structural assessment using the appropriate code specified return period for live loads. Extreme value statistics are utilized to characterize the live-load distribution and a method for assessing and incorporating the error associated with the characterization of monitoring-based distributions is proposed and developed.

## 1 INTRODUCTION

This paper continues work on the development of a method to incorporate monitoring information into reliability-based life-cycle bridge management programs. Specifically, the use of extreme value distributions to model live-load demands is investigated and applied to a reliability analysis of the Lehigh River Bridge located in Bethlehem, Pennsylvania, USA. Messervey & Frangopol (2007a, b) proposed and developed the idea of peak picking maximum daily strain recordings from monitoring data to model the live-load demand of highway trucks. In these papers, the idea was generally that once designed, a highway bridge could be assessed using a site-specific monitoring-based replacement for the HS-20 design truck by characterizing the distribution of the extreme values. Due to the asymptotic behavior of extreme value distributions, once such a distribution is characterized in a specific timeframe, or if the average daily truck volume is provided, the distribution can be projected to a 75-year return period consistent with code requirements for live loads (Ghosn et al. 2003). Such a transformation considers the time effects that must be accounted for when working with monitoring data in order to rationally predict bridge reliability with respect to future performance.

Although conceptually correct, developing monitoring-based distribution specifically for a design truck may be difficult to achieve and of limited use. Perhaps for a single-lane structure with a constant

number of truck crossings each day, the method would be well-suited. However, for a more realistic structure, the live-load demand is a much more uncertain phenomenon. For a typical highway bridge the number of truck crossings fluctuates daily, multiple lanes result in side-by-side truck occurrences, and vehicle speeds and surface roughness impact recorded measurements. In addition, recorded load effects are not only due to truck crossings but also to other loads as well such as wind and temperature.

As such, a more appropriate approach is to model the extreme value distribution of the total live-load demand instead of isolating the truck load. Such an approach is developed in Messervey & Frangopol (2008) and serves as the theoretical basis for this paper. Of particular importance and focus in this work was researching how much data (number of observations) is necessary to adequately define the extreme value live load distribution and in which timeframe (daily, weekly, monthly) peak picking should occur to observe the phenomenon. To begin investigating these questions, a simulation was constructed to approximately model traffic, wind, and temperature loads on a bridge structure. From this simulation, convergence to an extreme value distribution was confirmed by peak picking maximum recordings and a discussion of the amount of error associated with short observation timeframes was initiated. However, application of the method to a real structure was lacking. This is the purpose of the study presented herein.



Figure 1. Photograph of the main span of the SR33 Lehigh River Bridge (photo taken by Sunyong Kim on 8 January 2008).

## 2 MONITORING DATA COLLECTION

### 2.1 *Bridge and monitoring project description*

The Lehigh River Bridge SR-33 (Fig. 1) was constructed in 2001 and is situated in Bethlehem, PA, USA. The bridge is a four-span continuous weathering steel deck truss with a main span over the Lehigh River of 181.05 m. The depth of the truss varies from 10.97 m (at midspans) to 21.95 m (over the supports). The structure is subjected to light to medium truck traffic.

The Lehigh River Bridge is unique because the reinforced concrete deck is not only composite with the longitudinal steel stringers and transverse floor beams, but also with the upper chord members of the truss through the use of shear studs connecting the upper chords directly to the bridge deck. This structure is the only composite truss in the State of Pennsylvania and possibly the United States (Connor & McCarthy 2006). The main truss members (i.e., upper chords, lower chords and diagonals) are fabricated from structural steel plates into box or "H" shapes. The steel stringers, sway bracing, and cross bracing members are all rolled "W" shapes.

Monitoring of the Lehigh River Bridge was conducted during construction, for controlled load tests using test trucks, over time for temperature measurements, and for several short periods of in-service usage (Connor & Santosuosso 2002, Connor & McCarthy 2006). The objective of the testing was to measure mechanical strains and thermal strains during construction and while in-service to better understand the performance of the structure. Data is available from representative periods that include all seasons. Instrumentation and testing were conducted by personnel from Lehigh University's Center for Advanced Technology for Large Structural Systems (ATLSS). Complete descriptions of the bridge layout as well as the field and instrumentation program are available in ATLSS reports prepared by Connor & Santosuosso (2002) and by Connor & McCarthy (2006).

Frangopol et al. (2008) used data collected from this instrumentation program to assess the reliability of the truss upper chord, truss lower chord, and deck stringers at each construction or testing milestone. Sensors were located and measurements taken on member's cross sections and from positions on the bridge that maximized strain responses. The end result of this work with respect to the reliability assessment of these members is reported in Frangopol et al. (2008) and determines that the structure had a high reliability during construction, for the controlled crawl load test, and for the one day of in-service live load monitoring. The next step is an extrapolation of the future reliability of the bridge based upon monitored live-loads over time. Such an analysis requires the consideration of the appropriate return period for the monitored live-load and the consideration of the error associated with ability of the monitoring data to adequately characterize the live-load demand distribution. This analysis is the purpose of this work.

### 2.2 *Data selection from monitoring records*

Periodic in-service data is available from 24 sensors on various members during dates that range from June 2004 to February 2005 (Connor & McCarthy 2006). For each sensor, approximately 90 days of data are available. Measurements are trigger-based meaning that sensors were only activated when prescribed strain thresholds were exceeded. Two control units (one for each direction of traffic) were utilized to coordinate and log sensor data. Noise spikes often associated with vibrating wire strain gauges are present in the data, can be identified because they are instantaneous in nature, and for this analysis were manually removed from each record.

Because this work is focused on developing a method for the use of extreme values and because of the time associated with managing the data after-the-fact from a program not specifically designed for the purpose of peak picking, it was undesirable to consider all 24 sensors. Instead, it was desirable to identify and consider the most critical members and sensors from the structure. Such a process is in fact applicable and practical as bridge managers currently operate in a resource-constrained environment, funding for SHM is very limited, and monitoring technologies will likely be gradually implemented for critical concerns instead of complete monitoring systems as techniques and methods are improved (Frangopol & Messervey 2008).

Selection of the critical members and sensors for the Lehigh River Bridge was aided significantly by dynamic tests conducted and reported by Connor & McCarthy (2006) and by the reliability analysis conducted by Frangopol et al. (2008). The response of a lower chord, upper chord, and two stringers to a series of vehicles traveling eastbound is shown in Figure 2

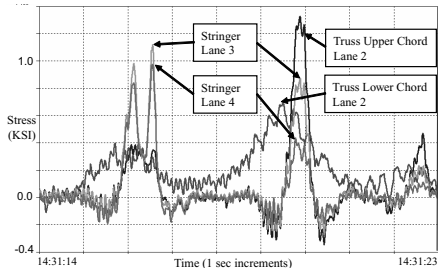


Figure 2. Strain response of two stringers, truss upper chord, and truss lower chord to four separate vehicles traveling eastbound (adapted from Connor & McCarthy (2006)).

(adapted from Connor & McCarthy 2006). The global response of the lower chord can be seen from its early response to the load. It gradually increases its response as the load traverses the main river span and peaks when the truck is above the sensor. The local responses of the upper chord and stringers are seen by their more abrupt response when the load is directly above these members. The upper chord and stringers primarily exhibit local bending. Lane position can also be inferred from this figure. Stringers 3 and 4 have a significant response to the first two stress cycles indicating that the vehicles are traveling in Lane 3 (these two stringers are directly beneath this lane of traffic). The next stress cycle indicates that the vehicle is positioned in Lane 2. Here, the upper chord and lower chord, which are both beneath this lane of traffic, have more significant responses whereas the stringers do not (Connor & McCarthy 2006). These and similar dynamic tests consistently identify the upper truss chords and four (of nine) stringers as having the most significant responses to traffic loading.

The upper truss chords at two locations (above a support and at bridge midspan) are selected as the critical members for this structure. Although the stringers have the lowest reliability index (Frangopol et al. 2008) the failure of one stringer does not typically lead to global failure or even local failure due to load redistribution within the deck. In contrast, the failure of a truss component may result in global failure and

as such these members are deemed more important. Figure 3 shows the selected locations on the structure and member for analysis in this paper. Two locations are selected due to the composite nature of this particular truss. Although one may expect the upper truss chord to be in compression at midspan, local bending (with the deck) dominates the response. This local bending of the upper chord members is also of interest at midspan because the deck is thinner and the upper chord truss members also have smaller cross sections resulting in potentially larger stress demands.

### 3 IN-SERVICE LIVE-LOAD RELIABILITY ANALYSIS

#### 3.1 Definition of the extreme value distributions

A daily timeframe is selected to observe maximum stress recordings. The observation period of one day is consistent with work done in Messervey & Frangopol (2008) and the implications of this decision are discussed further in section 3.2. Daily maximum stresses are taken from four sensors. Each sensor is located on the bottom flange of an upper chord member at member midspan. Two sensors are located above the main support (one in each direction of traffic) and two sensors are located at the center of the main span of the bridge (again one in each direction of traffic). Each sensor records approximately 90 days of data. The number of days observed are not equal due to the data being trigger based, controller malfunction, and/or sensor malfunction on particular days. Based on the results reported by Connor & McCarthy (2006), Table 1 shows the statistical descriptors of the daily maximum stresses for each of the four sensors.

From this data, it appears the eastbound lane experiences slightly greater stress demands and that the upper chord at bridge midspan is subjected to greater live-load stresses. Additionally, it is clear that the bridge experiences very small live-load stresses compared to its yield strength descriptors of 380 MPa (mean) and

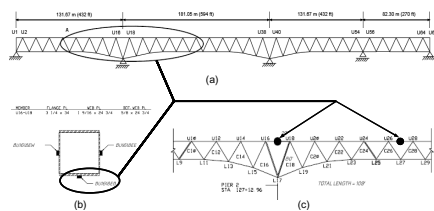


Figure 3. General schematic of (a) section of bridge (b) section of member and (c) location of members selected for extreme value distribution reliability analysis.

Table 1. Daily maximum live-load stress descriptors for the upper truss chord at midspan and above main support in both directions of traffic.

	Span 1618 over support (East- bound)	Span 1618 over support (West- bound)	Span 2628 Midspan (East- bound)	Span 2628 Midspan (West- bound)
# of Obs.	92	88	93	88
$\mu_y$ (MPa)	8.33	7.99	12.75	12.01
$\sigma_y$ (MPa)	1.13	1.12	2.16	1.56
Max (MPa)	10.75	1.12	2.16	1.56
Min (MPa)	3.63	3.20	5.61	5.56

28 MPa (standard deviation) for the M270 Grade 50 W steel (Frangopol et al. 2008). To continue, a reliability analysis of the eastbound lane at both midspan and above the support will be conducted. Both members will be analyzed due to the differences member sizes and recorded stresses.

Using the descriptors in Table 1, the two parameters of a Type I (Gumbel) extreme value distribution (EVD) are calculated as (Ang & Tang, 1984)

$$\alpha_n = \frac{\pi}{\sqrt{6}\sigma_{Yn}} \quad \text{and} \quad \mu_n = \mu_{Yn} - \frac{\gamma}{\alpha_n} \quad (1)$$

where  $\alpha$  is a shape parameter,  $n$  the number of samples (if known) or timeframe from which maximum values are selected,  $\mu_{Yn}$  and  $\sigma_{Yn}$  the mean and standard deviation of the observed extreme data respectively,  $\gamma = 0.5772$  is the Euler's number, and  $\mu_n$  the characteristic value of the EVD. Once characterized, the Type I distribution can be transformed from a daily observation timeframe to a 75-year return period using

$$\mu_{Yn} = \mu_X + \frac{\ln(n)}{\alpha} \quad (2)$$

where  $\mu_{Yn}$  is the mean in the desired timeframe (e.g. 75 years),  $\mu_{Xg}$  the mean in the observed timeframe (e.g. daily), and  $n$  is the number of observation timeframes involved in the transformation (e.g. 75 years = 27394 days =  $n$ ).

Using the formulas provided in Equations 1–2 and the monitoring-based results from Table 1, Table 2 shows the Type I Gumbel EVD descriptors of the 75-year live load consistent with code requirements and appropriate for use in the reliability analysis for both eastbound upper chord sensors of interest.

### 3.2 Consideration of error in characterizing monitoring-based EVDs

Before using the 75-year EVD descriptors provided in Table 2 to conduct a reliability analysis, it is both appropriate and necessary to consider the

Table 2. Characterization of live-load EVD parameters for truss upper chord and transformation from a daily observation timeframe to a 75-year return period.

	Daily EVD				75 year EVD			
	$\mu_{Y1}$ (MPa)	$\sigma_{Y1}$ (Mpa)	$\mu_1$ (MPa)	$\alpha_1$	$\mu_{Y75}$ (MPa)	$\sigma_{Y75}$ (MPa)	$\mu_{75}$ (MPa)	$\alpha_{75}$
Over support (East-bound)	8.33	1.13	7.82	1.14	17.33	1.13	16.82	1.14
Midspan (East-bound)	12.75	2.16	11.78	0.59	29.93	2.16	28.96	0.59

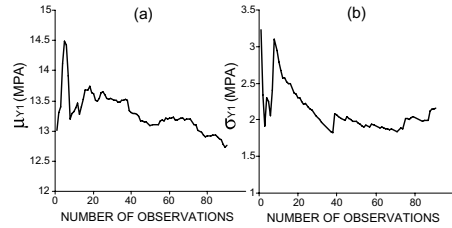


Figure 4. Beginning with two observations, (a) the mean and (b) the standard deviation of the daily maximum recorded stress (MPa) vs. the number of observations considered.

error associated with characterizing the distributions. Unlike a park test or controlled experiment where the end result is a single measured structural response, any use of in-service monitoring seeks to define the distribution of structural responses over time. As such, the amount of data collected and how that data is processed is of significance. Although being termed here as error, this is perhaps more appropriately regarded as a manner to statistically treat the incomplete information associated with any monitoring record.

With respect to extreme value distributions, two types of error are identified for consideration. The first type of error is concerned with the number of observations or amount of data collected and is denoted  $\epsilon_{obs}$ . For example, in determining the average daily maximum demand on a structural member, the result and degree of variability of that result will vary with respect to the number of days observed. Figure 4 illustrates this using the data from the eastbound upper chord sensor at bridge midspan. Beginning with the second day, the mean and standard deviation of the daily maximums are calculated each day using all previous information. The results show that both parameters change as more observations are considered. For this data, after 90 observations (days) neither parameter has reached a stable result indicating a longer monitoring period may be desirable if possible and/or some consideration of this variability is necessary in the reliability analysis.

The second type of error is specific to the timeframe selected to observe maximum values and is denoted  $\epsilon_{timeframe}$ . With respect to bridge monitoring, although live-load demand is dominated by daily truck crossings, other highly random phenomena such as wind, severe temperatures, accidents, or other unforeseen events are more sporadic. Daily traffic fluctuations are also important as picking the largest occurrence from 500 vs. 1000 samples (trucks) yields significantly different results. Although a longer observation timeframe minimizes this type of error, it also requires a longer monitoring period or results in a greater amount of the error associated with the number of observations (first type of error discussed).

Figure 5 illustrates this second type of error and the effects of uncertainty on the characterization of



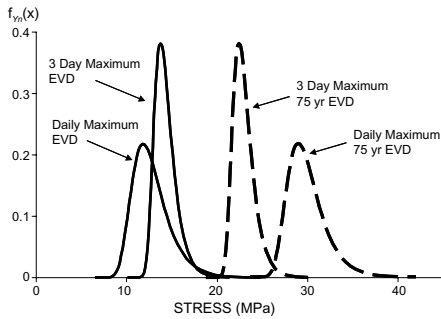


Figure 5. Type I Gumbel EVDs using identical data but selected maximum values from a daily selected timeframe vs. a 3 day timeframe, and both corresponding 75-year EVDs.

the EVDs. The data is again taken from the eastbound upper chord at bridge midspan. Instead of selecting daily maximum responses, the maximum response is selected every three days. As a result, from approximately 90 days of data, 30 extreme values are available to characterize the EVD again using the formulas provided in Equations 1–2. As one would expect, the resulting EVD has a greater mean as maximums are selected from a larger number of samples. The fact that the distribution also has a smaller standard deviation (change in shape) indicates that the daily timeframe window does not completely capture the random process. This results in a greater degree of measurement/modeling uncertainty (epistemic) in addition to the uncertainty inherent to the live load (aleatory). With respect to the transformations to the 75-year EVD, it is noted that although the 3-day timeframe begins with a higher mean, its 75-year EVD has a lower mean and smaller associated shift. This results from the decrease in standard deviation and associated increase in the shape parameter for the 3-day EVD with respect to the daily EVD. For this example, a comparison of these two timeframes yields meaningfully different results for the 75 year live load. However, not considered or shown in Figure 5 is that the 3-day timeframe has only 30 observations available to define the distribution (instead of 90 for the daily). Selecting the optimal timeframe requires the consideration of both types of error.

Although more data and longer monitoring periods are desirable with respect to reducing error, it must also be balanced against the cost of obtaining the data. Furthermore, an important objective of permanent monitoring systems is to characterize a distribution and then to repeat the process to investigate changes in the distribution indicating damage or deterioration. As such, an appropriate cutoff needs to be identified for distribution characterization and the associated error for that cutoff period appropriately incorporated into a reliability analysis.

### 3.3 Reliability analysis using the monitoring-based EVD with the incorporation of error

Two methods can be utilized to account for the incomplete information associated with monitoring data, to statistically treat this uncertainty as error, and to incorporate this error into a reliability analysis. Either the random variable distribution parameters can themselves be treated as random variables or separate error terms can be added to the performance function. Here the latter is chosen resulting in the generalized performance function

$$g(1) = R - L_D - (L_L + \varepsilon_{obs} + \varepsilon_{timeframe}) \quad (3)$$

where  $R$  is the member resistance,  $L_D$  the dead load,  $L_L$  the monitoring-based EVD,  $\varepsilon_{obs}$  the error associated with the amount of data available, and  $\varepsilon_{timeframe}$  the error associated with the selected observation timeframe. Both error terms are modeled as normally distributed random variables. Each has a mean of zero indicating an equal likelihood of underestimating or overestimating the live load. The standard deviation of both types of error is calculated as the product of a coefficient and the mean value of the EVD. As such, the magnitude of the error is a function of the magnitude of the monitored observations. Tables 3–4 provide a starting point for the estimation of two separate error coefficients,  $a$  and  $b$ , associated  $\varepsilon_{obs}$  and  $\varepsilon_{timeframe}$  respectively. Coefficient values are estimated from previous simulation work (Messervey & Frangopol 2008) and are preliminary estimates only. Their refinement is a future area of research.

As an example illustrating the use of these tables, the eastbound upper chord at bridge midspan is considered. This member has a mean 75 year EVD live load demand of 29.93 MPa (Table 2) and a daily observation timeframe is selected. Using this information,  $\varepsilon_{obs}$  is normally distributed with parameters  $\sim N(0, 1.5)$  where  $29.93 \times 0.05 = 1.5$  MPa for 90 days of

Table 3. Coefficient to determine the standard deviation of  $\varepsilon_{obs}$  as a function of the mean of the monitored extreme value distribution and amount of data considered.

	Number of observation					
	7	14	30	90	180	365
a	0.25	0.15	0.1	0.05	0.03	0.01

Table 4. Coefficient to determine the standard deviation of  $\varepsilon_{timeframe}$  as a function of the mean of the monitored extreme value distribution and timeframe selected.

	Selected timeframe		
	Daily	Weekly	Monthly
b	0.06	0.03	0.01



Table 5. Reliability analysis distributions, parameters, and sources.

Member	Random variable	Distribution and parameters (MPa)	Source
Upper chord support Eastbound	$R$	Normal (380, 28)	Frangopol et al. (2008)
	$L_D$	Normal (109, 5.7)	Frangopol et al. (2008)
	$L_L$	Gumbel (17.33, 1.13)	Table 2
	$\varepsilon_{obs}$	Normal (0, 0.867)	Table 3
Upper chord support Eastbound	$\varepsilon_{timeframe}$	Normal (0, 1.03)	Table 4
	$R$	Normal (380, 28)	Frangopol et al. (2008)
	$L_D$	Normal (92.7, 4.9)	Frangopol et al. (2008)
	$L_L$	Gumbel (29.93, 2.16)	Table 2
	$\varepsilon_{obs}$	Normal (0, 1.5)	Table 3
	$\varepsilon_{timeframe}$	Normal (0, 1.8)	Table 4

data. Likewise,  $\varepsilon_{timeframe}$  is normally distributed with parameters  $\sim N(0, 1.8)$  where  $29.93 \times 0.06 = 1.8$  MPa for the daily observation timeframe.

Table 5 provides the random variable distributions, parameters, and sources utilized to conduct a FORM analysis for the performance function identified in Equation 3. All parameters are reported as stresses in MPa (linear elastic behavior has been assumed in this work). Each distribution is reported in terms of its mean and standard deviation.

Conducting the analysis, the reliability index for the upper truss chord above the support is  $\beta = 8.87$  and for the upper chord at bridge midspan is  $\beta = 9.0$ . These results are consistent with the park and crawl tests conducted after construction and the bridge maintains a high level of in-service safety. This particular structure has an extremely low live to dead load ratio. For the analysis developed in this work, the error terms discussed Section 3 have little impact on the final result. This will likely not be the case for other types of structures. Also of interest, because the live-load demand is small relative to the resistance and dead load, changes in the distribution over time may be easier to detect and be more accurately correlated to member deterioration.

#### 4 CONCLUSIONS

This work accomplished three main objectives with respect to the treatment and use of monitoring data for an in-service bridge. First, a methodology to select the most critical sensors, locations, and members was implemented. Fortunately, this analysis had access to previous reports and work to facilitate the process. Second, the statistics of extreme values were applied to in-service monitoring data to characterize an extreme value distribution and through a transformation the appropriate code required live

load demand (in this case a 75-year return period) was obtained. Third, a method for the consideration and treatment of the error associated with the characterization of monitoring-based distributions was developed and applied. This area in particular is an area in need of future research.

#### ACKNOWLEDGEMENTS

The support by grants (PITA X, PITA XI) from the Commonwealth of Pennsylvania, Department of Community and Economic Development, through the Pennsylvania Infrastructure Technology Alliance (PITA) is gratefully acknowledged. The support of the National Science Foundation through grants CMS-0638728 and CMS-0639428 to Lehigh University is also gratefully acknowledged. The opinions and conclusions presented in this paper are those of the authors and do not necessarily reflect the views of the sponsoring organizations.

#### REFERENCES

- Ang, A.H.S. & Tang, W.H. 1984. Probability Concepts in Engineering Planning and Design, John Wiley & Sons, II, New York.
- Connor, R.J. & McCarthy, J.R. 2006. Report on Field Measurements and Uncontrolled Load Testing of the Lehigh River Bridge (SR-33). Lehigh University's Center for Advanced Technology for Large Structural Systems (ATLSS), ATLSS Phase II Final Report No. 06-12.
- Connor, R.J. & Santosuosso, B.J. 2002. Field Measurements and Controlled Load Testing on the Lehigh River Bridge (SR-33). Lehigh University's Center for Advanced Technology for Large Structural Systems (ATLSS), ATLSS Report 02-07.
- Ghosn, M., Moses, F. & Wang, J. 2003. Design of Highway Bridges for Extreme Events. NCHRP TRB Report 489, Washington, D.C.
- Frangopol, D.M. & Messervey, T.B. 2008. Integrated Maintenance-Monitoring-Management for Optimal Decision Making in Bridge Life-Cycle Performance. Proceedings of the NSF Civil, Mechanical and Manufacturing Innovation (CMMI) Engineering Research and Innovation Conference, Knoxville, Tennessee, January 7-10, 2008.
- Frangopol, D.M., Strauss, A. & Kim, S. 2008. Bridge Reliability Assessment Based on Monitoring. Journal of Bridge Engineering, ASCE, Vol. 13, No. 5 (in press).
- Messervey, T. & Frangopol, D.M. 2007a. Bridge live load effects based on statistics of extremes using on-site load monitoring. *Reliability and Optimization of Structural Systems: Assessment, design, and life-cycle performance*, Frangopol, D.M., Kawatani, M., and C-W. Kim, eds., Taylor & Francis Group plc, London, 2007, 173-180.
- Messervey, T. & Frangopol, D.M. 2007b. Updating the time-dependent reliability using load monitoring data and the statistics of extremes. *Life-Cycle Performance and Cost of Civil Infrastructure*, Cho, H-N., Frangopol, D.M., and Ang, A-H.S., eds., Taylor & Francis Group plc, London, 2007, 269-276.
- Messervey, T.B. & Frangopol, D.M. 2008. Innovative Treatment of Monitoring Data for Reliability-Based Assessment, *Proceedings of the Fourth International Conference on Bridge Maintenance and Safety*, Seoul, Korea, July 13-17, 2008, IABMAS'08 (submitted).

# Life-cycle design of residential buildings: appearance and reality of ecological assessments

M. Michlmair

*Institute of Thermal Engineering, Graz University of Technology, Graz, Austria*

P. Maydl

*Institute of Technology and Testing of Building Materials, Graz University of Technology, Graz, Austria*

**ABSTRACT:** Residential buildings require, more than other construction works, the simultaneous consideration of all three dimensions of sustainability: environmental impacts, cost effectiveness and social aspects such as the affordability of flats. On the other hand, many European countries spend considerable public funds on the residential sector and try to use these subsidies to realise environmentally buildings.

In the past, environmental assessments focused mainly on the construction stage and ignored operation and dismantling. Future international standards to be developed by ISO and CEN require life-cycle analyses for all construction works. Against the background of the current discussion about climate change and global warming, the Federal and Laender authorities in Austria are considering to tighten the guidelines for public funding of residential buildings: low-energy and passive-house technologies, low-emission construction materials etc.

The paper reports about life-cycle analyses of four residential buildings planned and partly constructed in Styria. Comparisons of the different stages of the building's life cycle show that the influence of the selected materials and the construction stage is overestimated compared to the use stage with heating, cooling and maintenance. Another aspect is the relevance of the estimated life time and the transfer rates of components. These analyses should sharpen the eye for the essential parameters in environmental assessments and demonstrate what can be neglected as the integrated performance of buildings requested by future standards according to CEN/TC 350 is complex enough, so that a limitation to a few essential parameters will be imperative to ensure acceptance on a broad basis.

## 1 INTRODUCTION

### 1.1 *Motivation and background*

The ecology-based assessment of building products as well as of entire buildings has increasingly gained in importance in recent years. Not only has the general public become more and more aware of environmental issues, but political decision-makers world-wide have begun to change the framework conditions as well. Sustainable development has been an immaterial component of the European Union for several years. Considering the importance of the building sector and the development of densely populated areas, the European Commission published its "Thematic Strategy for the Urban Environment" (European Commission 2006) as well as mandate M 350 (European Commission 2004). At the same time, national activities can be observed in almost all EU member countries, accelerated by the world-wide discussion about climate change. In Austria, the Federal government published

a strategy on sustainable development in 2002, which was followed by a national climate protection programme (Austrian Federal Ministry 2002) as well as numerous activities at the level of the Laender. Building law and subsidies for social housing fall within the competence of the Laender in Austria, and in recent years especially these housing subsidies have increasingly been used as an instrument by the Austrian Laender to promote aspects of climate and environmental protection in residential building construction subsidised by the public.

As the biggest contributor to waste and, when considering the use stage, also the largest consumer of energy, the building sector plays a particular role in climate and environmental protection. Against this background, strategy programmes were adopted by the Laender. The aims of these programmes are to translate the requirements for ecological, economic and social sustainability in subsidised residential building and communal building into practice.

## 1.2 Aims of the study

The assessment of buildings from an ecological perspective, which is to judge these buildings for their environmental impact, is a complex matter, complicated additionally by the need for a holistic approach which includes all three dimensions of sustainability. Thus, very few assessment models which are suitable for practical application and may claim comprehensiveness have existed so far. Normally, these models suggest themselves only for retrospective assessment. This is usually too late for optimisation measures at the draft, design or building product level. What would be desirable for the future are assessment concepts which are applicable all along the way from the project development phase to the phase of detailed planning.

This study should demonstrate in which areas substantial impacts on the environment are likely to occur due to building measures and which stages of life and segments of performance are chiefly affected, so that the right priorities can be set in the future given the inevitable need for simplification of ecological assessments during the planning stage.

## 2 DEVELOPMENTS IN INTERNATIONAL REGULATIONS

### 2.1 At ISO level

For many years, extensive work has been going on in the international standardisation organisation ISO in the effort to develop internationally harmonised regulations on environmental issues. The best-known results so far include the ISO 14040 series. Since

2003, the ISO committee ISO/TC 59/SC 17 “Building Construction / Sustainability in Building Construction” has been discussing how to implement aspects of sustainability in the building sector.

The following table gives an overview of the most important currently available draft standards.

### 2.2 At CEN level

In parallel to the ISO activities, attempts are being made at the level of the European standardisation institute CEN to develop a regulatory scheme for sustainable building. The basis is mandate M 350 of the European Commission “Development of horizontal standardised methods for the assessment of integrated environmental performance of buildings” (European Commission 2004) issued in 2004. The outcome of these activities will be a number of European standards as well as of technical reports on the following selected topics:

- Framework for assessment of integrated building performance (umbrella document and resub documents for the three dimensions of sustainability)
- Building life cycle
- Environmental performance of buildings
- Environmental product declaration
- Communication formats b2b and b2c
- Generic data

The cornerstone of all these assessments is the focus on the entire life cycle of buildings as well as comprehensive, i.e. holistic, analyses in all three dimensions of sustainability: the ecological one, the social one and the economic one.

Since European standards are national standards as well, these regulations are expected to have a considerable influence on the building sector. In general, they are an integral part of all building contracts, not just in Austria. Even if, for the time being, these standards are voluntary in their nature, they will change competition among the individual building products quite considerably.

## 3 FUNDAMENTALS FOR THE ASSESSMENT OF BUILDINGS

To compare the environmental impacts of buildings in their phases of life—construction, use and end of life—,life-cycle analyses were performed on four residential building blocks. In order to be able to provide a judgement on the relevance of different approaches to reduce their environmental effects, the different causes for the environmental impacts of these buildings were to be investigated in as great a detail as possible. The methodology used to collect the data underlying this study is described in the following chapter.

Table 1. ISO drafts.

Environmental labels and declarations	
ISO 14020	General principles
ISO 14025	Type III environmental declarations— Principles and procedures
Environmental management	
ISO 14040	Life cycle assessment— Principles and framework
ISO 14044	Life cycle assessment— Requirements and guidelines
ISO 14050	Vocabulary
Sustainability in building construction	
ISO 15392	General principles
ISO 21929	Sustainability indicators
ISO 21930	Environmental declaration— of building products
ISO 21931	Framework for methods of assessment for environmental performance of construction works
ISO 21932	Terminology

### 3.1 Assessment concept

Following the rules of CEN/TC 350, an assessment concept was chosen in which nine categories of impacts were studied (prCEN/TS 15643-1 unpubl.). A further aggregation towards highly aggregating parameters was not performed as this would have not allowed the desired comprehensive description of the environmental impacts. Instead, the investigation was based on the following quantitative impact indicators in accordance with the quantitative classification as proposed by CML (Heijungs 1992) in low-aggregating, multi-criterial form. These nine indicators have been investigated: global warming potential (GWP), ozone depletion potential (ODP), photochemical ozone creation potential (POCP), acidification potential (AP), eutrophication potential (EP), human toxicity potential (HTP), terrestrial eco-toxicity potential (TETP), abiotic resource depletion potential (MR), cumulative energy demand (ER).

The life-cycle analysis was prepared on the basis of an execution-oriented breakdown (according to the Austrian standard ÖNORM B 1801-1 / ÖNORM B 1801-1 1995). The individual performance items were collected on the basis of the tender documents of all trades and crafts. Thus, the common practice in establishing life-cycle analyses of entire buildings by combining performances into subassemblies was abandoned, resulting in a higher data collection accuracy compared to similar studies.

### 3.2 Investigated product system

The product system analysed in this study for its life-cycle performance consisted of four residential housing blocks, constructed as subsidised multi-storied residential buildings in the Land of Styria. One block of flats was already in use at the time the study was conducted, the three others were under construction.

The selection of the concrete projects was made by two non-profitable builders who were approached with the request to make available the respective data and documents for two blocks of flats each.

The four chosen residential blocks consist of ten to 17 dwellings each, two blocks were solid constructions

Table 2. Characteristic values of the investigated residential building blocks (GFA... gross floor area; HED... heating energy demand; FED<sub>heat</sub>... final energy demand for heating).

Residential buildings	Support structure	GFA	HED	FED <sub>heat</sub>
		m <sup>2</sup>	kWh/m <sup>2</sup> a	kWh/m <sup>2</sup> a
project 1	brick	744	49.0	67.9
project 2	brick	1054	41.1	51.8
project 3	timber	1381	36.4	68.7
project 4	timber	1609	62.7	114.8

and two were timber constructions. Table 2 shows the characteristic values of the residential building blocks which were investigated.

### 3.3 Structure and scope of the study

As far as the temporal system boundaries are concerned, the study covered the entire life cycle of the residential buildings analysed for their life cycle performance. Following the breakdown of the life cycle as suggested by CEN/TC 350, the breakdown as shown in Figure 1 was chosen (prCEN/TS 15643-1 unpubl.).

The scope of the individual life-cycle stages is described in the following:

- The construction stage starts with the extraction of the necessary resources and raw materials and ends as the facility is handed over to its users.
- During the use stage, the intended usage of the residential building has to be safeguarded by continuous operation and maintenance. The length of the use stage was defined to be 70 years. The service life of the individual building components was ascertained individually.
- The end-of-life stage comprises the demolition of the residential buildings and their final removal—which means disposal of the rubble in landfills or incineration. Recycling measures were not considered in this study as this would not have allowed us to consider the life of the buildings in terms of a completed cycle.

Analogue to the division of the use stage, the spatial system boundaries were divided into two levels: construction work and operation. The further breakdown into the constructional segments carcassing, building services, interior work, outdoor facilities and transport and the operational segments freshwater supply, waste-water disposal, supply with electricity and supply with heat for space heating and the preparation of hot water enabled us to perform a detailed analysis of these environmental impacts also within the life-cycle phases.

### 3.4 Data origin and data quality

When determining the material and energy flows of the residential buildings during their life cycle, data of different origin and of differing quality were included. In the description of this aspect of the study, a differentiation is made between the construction work level and the level of operation.

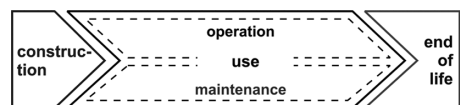


Figure 1. Breakdown of the life cycle.

a) *Construction work*: The material flows in this segment ascertained in the inventory analysis of the life-cycle analysis were determined on the one hand on the basis of manufacturers' specifications on the building products and by using non-building-product-specific information on the density and geometry of the building products on the other.

Depending on the constructional segment investigated, the information available varied in quality. While, for example, data of good quality existed for the constructional segments carcassing and outdoor facilities, across-the-board and rough estimates had to be resorted to for building services and transport.

b) *Operation*: For the assessment of the operation of the building, statistical data were used as well as simplified calculation methods to determine need values.

The investigation of the operational segments fresh-water supply, waste-water disposal and electricity supply was made on the basis of statistical data using mean consumption values provided by utility companies.

The need for heat for space heating and warm-water preparation was assessed by using the calculation algorithms which are applied in Austria for the calculation of the energy performance of buildings. Using this method, the individual heat requirement values could be determined at the level of useful energy as well as at the level of delivered energy. The assessment was made at level of delivered energy.

The impact-indicator results were then assigned to the identified material and energy flows with the help of the database "ecoinvent", version v1.3 (Frischknecht & Jungbluth 2004). For individual products which could not be assigned to any ecoinvent data set, product life-cycle analyses—validated by sensitivity analyses—were used to assess the environmental impacts caused by these products.

## 4 RESULTS

The results are presented at two levels. At level 1, the entire environmental impact throughout the life cycle and to which extent the individual life phases are affected are shown. At the second level it is shown in detail how the impacts are composed at the building work level and at the level of operation.

### 4.1 Influence of the life-cycle stages

Figure 2 illustrates how the entire environmental impacts throughout the life cycle are distributed to the stages construction, usage-maintenance, usage-operation, and removal. Depending on which indicator was investigated, the shares contributed by the individual stages vary considerably.

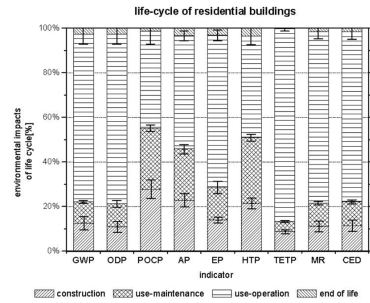


Figure 2. Distribution of environmental impacts throughout the entire life cycle of the residential buildings.

The predominant part of environmental impacts throughout the life cycle is caused in the 70-year period of use, which accounts for 70 to 90%. However, it has to be noted that this includes both operation and the necessary maintenance work. A more detailed analysis of the two levels of consideration in the use stage—operation and maintenance—shows that operation accounts for about 45 to 85% and maintenance for about 5 to 30% of all environmental impacts throughout the life cycle.

Depending on the indicator investigated, about 10 to 30% of the environmental impacts are caused in the construction stage. The share of the end-of-use or removal stage does not exceed 4%.

The deviation of the individual values for the four residential buildings, which are due to averaging, is 6% at a maximum. For the majority of the investigated values the deviation ranges from 0 to 3%.

If the environmental impacts which are caused by the operation of the building are disregarded, the distribution of the environmental impacts arising from building work to the individual life cycle stages is as shown in Figure 3. From this figure it can be inferred that the share of the construction stage in the construction work is only slightly higher than the share of

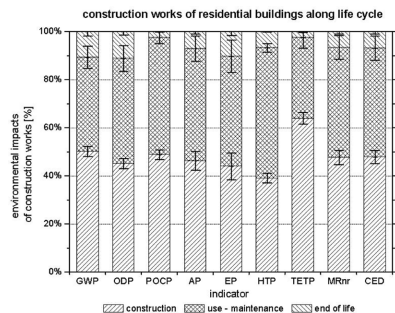


Figure 3. Distribution of the environmental impacts of building work to the entire life cycle of the residential buildings.

the necessary maintenance work during the use stage. Depending on which indicator was investigated, the aggregate share of these two stages is between 30 and 50%. The share of removal in the impacts of building work reaches a maximum value of 12%.

#### 4.2 Influence of the constructional segments

The results of the investigated constructional segments make obvious that the chief environmental impacts arise in the areas carcassing, interior work and—with some limitations—building services. The environmental impacts caused by transport are responsible for 1 to 3% of all environmental impacts throughout the life cycle, depending on which impact indicator is being investigated. Outdoor facilities account for 1 to 6%, again depending on the investigated indicator.

The constructional segment carcass is the most crucial factor among the building measures which are necessary in the course of the life cycle of a building. It is in particular during the construction stage that the share of environmental impacts caused by carcassing is comparatively high. Depending on which indicator is

investigated, the values may scatter quite considerably in some cases, so that the share of the carcass in the environmental impacts in the construction stage may vary between 30 and 75%.

Due to the long service life of the carcass components, their share in maintenance is low. In the end-of-use stage, on the other hand, which has only minor environmental impacts in general, the share of the structural works rises and accounts for 40 to 60% of the environmental impacts in this stage.

The environmental impacts caused by the constructional segment interior work contribute, after the carcass, the second largest share in the construction stage. Due to the relatively short service life of the components used for interior work—compared to the carcass—the share caused by the interior work is slightly higher in the use-maintenance stage than in the construction stage. Compared to the carcass, the share of interior work in the end-of-life stage is fairly insignificant.

#### 4.3 Influence of the operational segments

Figure 6 shows how the environmental impacts of operation are divided up among the individual segments. The overwhelming part of the environmental impacts in this stage is caused by the delivery of electric power and heat for space heating and the preparation of hot water. In eight of the nine investigated indicator categories, these two segments together are responsible for more than 90% of the environmental impacts arising from operation. The share for which electricity and heat respectively are responsible varies depending on the indicator.

An exception in the distribution of the impacts is the indicator EP, which reflects the danger of over-fertilising soils and water bodies. Since phosphorus, which is the limiting factor for the growth of plants, is present in waste water in a concentrated form, the eutrophication potential is particularly high for the operational segment waste water.

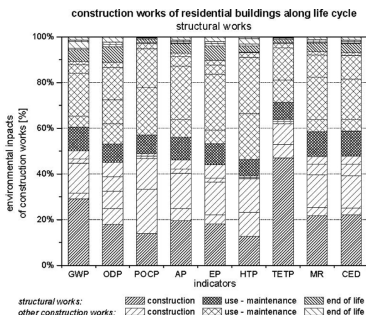


Figure 4. Influence of the carcass / structural works on the environmental impacts of building measures throughout the life cycle of the residential buildings.

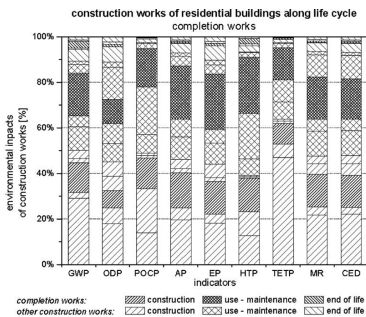


Figure 5. Influence of the interior work on the environmental impacts of the building measures throughout the life cycle of the residential buildings.

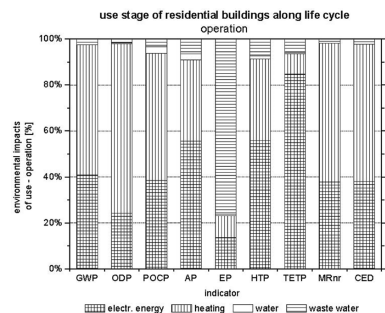


Figure 6. Environmental impacts of the operational segments in the life-cycle stage use-operation.

#### 4.4 Summary

The environmental impacts caused during the use stage account for the overwhelming part of all environmental impacts throughout the life cycle. During the 70-year service life, major impacts arise in particular from providing the necessary electric power and from satisfying the requirements for heat for space heating and the preparation of hot water.

When considering the building works in the life cycle of the building, it is striking that the environmental impacts which arise from maintenance during the use of the buildings are almost as high as those which are caused in the construction stage, with the biggest share in environmental impacts of building work being contributed by the construction and maintenance of the carcass, followed by interior work. Outdoor facilities and transport play an inferior role while building service installations feature relatively high impacts for some indicators.

## 5 CONCLUSIONS

Preparing an exhaustive life-cycle analysis for residential building covering their entire life cycle is a comprehensive and complex task. In particular, determining the material and energy flows as part of the inventory analysis (LCI) is in most cases very time-consuming. Using the life-cycle analysis as a practical tool for the assessment and optimisation of environmental impacts of buildings in an approach as chosen for this study is rather inconceivable. This would require numerous changes in methodology.

As regards the assessment of the environmental impacts, it may be stated based on this study that there are pros and cons associated with the assessment using nine different impact indicators.

On the one hand major differences were noted in the distribution of the environmental impacts for the categories investigated. It is therefore impossible in many cases to provide information on the environmental impacts of individual stages or segments and, subsequently, on individual building materials. In order to do so, better-correlating parameters would be required. Presenting the results in the form of nine different impact indicator results does not appear to be a sufficiently transparent way of informing decision makers involved in the building and planning process.

On the other hand it can be clearly inferred from figure 6 that aggregating the individual impact categories to one single figure is fraught with difficulties. The wide scatter in the distribution of the environmental impacts arising from the supply with electric power and heat does neither permit the aggregation to one single figure nor does it permit the non-consideration

of individual impact categories. At the moment it is not possible to provide an explicit answer as to which impact categories are of particular relevance for the assessment of ecological sustainability. Given the wide scatter of the various indicator results for the respective segments of operation, such a simplification would be penalised by a loss in quality and in informative value of the results. In addition, numerous output flows—such as CO<sub>2</sub> emissions—come to bear on several impact categories. An aggregation to one single figure based on impact indicator results would mean these output flows would be considered several times.

Thus, the question suggests itself in which way the method of preparing a life-cycle analysis can be applied to translate ecological sustainability throughout the life cycle of buildings into building practice. Presenting the results in a form which is clear and easy to interpret is an important prerequisite to encourage the use of a life-cycle analysis to optimise impacts throughout the life cycle of buildings. Thus, it is presumably communication which is the biggest hurdle for this method. One way to circumvent this could be the focus on some few impact categories which, would have to reflect most environmental impacts without any double tracking.

It will be a task incumbent upon CEN/TC 350 to find a trade-off between the demand for completeness and sufficient suitability for practical application. However, this will require ongoing studies.

## REFERENCES

- Austrian Federal Ministry of Agriculture, Forestry, Environment and Water Management (ed.) (2002): *Die österreichische Strategie zur Nachhaltigen Entwicklung. Eine Initiative der Bundesregierung*. Vienna.
- European Commission (2004): M/350 EN. Standardisation Mandate of CEN. *Development of Horizontal Methods for the Assessment of the Integrated Environmental Performance of Buildings of 29 March 2004*.
- European Commission (2006): *Communication from the Commission to the Council and the European Parliament on Thematic Strategy on the Urban Environment of 11 January 2006*.
- Frischknecht, R. & Jungbluth, N. (eds.) 2004. *Overview and Methodology. Data v1.1 (2004). ecoinvent report No. 1/* Swiss Centre for Life Cycle Inventories. Dübendorf, 2004.
- Heijungs et al. 1992. *Environmental Life Cycle Assessment of Products. Guide.* / Centre of Environmental Science (CML). Leiden.
- Standard prCEN/TS 15643—1 (unpubl.): *Sustainability of construction works—Framework for assessment of integrated building performance—Part 1: Environmental, health and comfort and life cycle cost performances*.
- Standard ÖNORM B 1801—1 (1995): *Kosten im Hoch- und Tiefbau—Teil 1: Kostengliederung*.

# The influence of design and detailing on the life and maintenance of a bridge

A.G. Mordey

*Atkins Highways and Transportation, Birmingham, England*

**ABSTRACT:** Each new structure is designed in accordance with the standards and details which are codified at the time of its design and conception, and with the requirements of the owner of the bridge who will be responsible for its maintenance in the long term. The codes and standards are guidelines, but are not generally definitive, which gives the design engineer scope to use best practice and his own experience when designing an individual structure. The main enemy of a bridge, in the UK at least, is uncontrolled water, but careful attention to the use of materials and the shaping of the vulnerable areas to shed water and take it away in a controlled manner can ensure that the maintenance requirements of a structure can be minimized.

## 1 INTRODUCTION

Many ancient structures standing today are assumed to have been well built, and remain standing because they were well built, but this is not necessarily the case.

To extend the idea to nature, even the most durable rocks are attacked by the elements and gradually deteriorate, so it is unreasonable to assume that a structure made from the same materials will last without any maintenance. In fact, we tend to use the weaker, more workable material in our structures, which makes the problem worse.

Any structures which are out in the open in all weathers will be affected by wind and rain, and alternating heat and cold, in the same way as cliffs or crags.

The normal process leading to damage of a structure built of stone is that wind-driven rain penetrates the stone or the joints which are in any way porous, then freezes and breaks up the stone. An example of this can be found in Durham Cathedral, built from 1092 AD onwards; this has had scaffolding somewhere about it to allow the repair of stonework for as long as I have known it, which is over 50 years, and this is probably the case with most large and ancient structures. Those which have not been constantly maintained have fallen into disrepair and in some cases are now ruins.

The performance of the foundations of a structure must also be considered as one of the defining factors in the life of a structure.

Foundation failure is normally avoided by the robustness of the design, be it spread footing or piled foundation, but the ground conditions themselves can lead to material failure.



Figure 1. Durham Viaduct.

Before the application of soil mechanics theory to foundations, whether a structure stood up or not was a matter of trial and error. There was an understanding of soft ground, and rock, and where there was a need for piles, but much of this was based on local knowledge, not theory. Where piles were used, which was usually in a marshy situation, timber was the preferred material, because that was all that was available. Its properties were such that being kept wet preserved it. The most vulnerable part of a pile was the short length near the surface which was subject to wetting and drying, so as long as this was protected, the life of the pile could be limitless.

Other natural materials used in the past were “withy mats and sheep’s wool”. During the railway building era in Britain there was a need for large numbers of viaducts, which were usually built in stone or brick, or



even a mixture of both. In marshy ground it was not uncommon to found the arch structures on mats made from willow staves woven together, with sheep's wool layered into it, which acted as a spreader. Durham Viaduct (Fig. 1), on the main line from London to Edinburgh, is reputed to be built on such a foundation, and has been there from 1856. At the time the local pundits said that it would not last, but it is still there, still taking mainline trains, after more than 150 years.

## 2 BRIDGES

If we consider bridges, the oldest structures from modern times are railway bridges. These are usually either arch structures in brick or stone, beam bridges in wrought or cast iron, or trusses in the same material.

### 2.1 *The life of arch bridge*

The life of arch bridges has been shown to be variable, and they fail in different ways.

The essence of an arch bridge is that the foundations are sound, and that the arch barrel itself is supported by a firm backing. It also is of benefit if the span of the arch is square and the backing to the arch is drained.

It is unfortunate that not all of these conditions were met in the railway boom in Britain, nor in other parts of the world.

The railways were built largely between the 1840s and the start of the 20th century to link industrial centres, over routes where the founding material could be variable, so problems arose through settlement of the foundations leading to arch distortion, which reduced the arch's capacity and led to failure.

But arches were constructed by artisans and were largely undesigned in modern engineering terms. Their sizing was estimated by the masons who worked to drawings prepared by draughtsmen with little theoretical basis.

By and large, however, masonry arches, and modern concrete developments, have been found to be durable and reliable in terms of performance.

### 2.2 *Metal bridges*

With the advent of cast and wrought iron, and later of steel, which were capable of withstanding tensile forces, structures spanning as beams became possible.

These took various forms according to the spans involved, but it can be presumed that none of these were designed with a finite life in mind. They were designed to perform a function, and not fall down, and that was as far as it went.

### 2.3 *The failure of metal bridges*

As rail loading changed, various bridges which had never been designed to modern levels of sophistication were assessed to modern codes, and were found in many cases to be below standard. Part of the assessment was to inspect the bridges for condition, and these inspections found that bridges were often corroded at similar details.

It was found that the detailing of beams and trusses almost invariably resulted in corners where water and leaves or other detritus could be retained. Typically this would be at the junction of vertical stiffeners and bottom flanges, or at a point where truss members came together. The most serious corrosion of this kind would be at the bearing seating, where the shear stress would be at its highest, or else at mid-span at the point of maximum flange tension, which was equally undesirable. The message from this is that if these places had been regularly and frequently cleaned the life of the members could have been prolonged.

That having been said, some of these bridges are still in service after a hundred years, so good detailing is not necessarily the most important factor; making members bigger than strictly necessary for strength reasons can be beneficial in terms of sacrificial material being available. The better the detailing however, the smaller the sacrificial steel thickness required and this is especially true of unprotected weathering steel bridges today.

### 2.4 *Definition of the end of the life of a bridge.*

As long as the repair or maintenance of a bridge is economically viable, and its design or assessed capacity is adequate for the duty it is being asked to perform, then it can be considered to be within its design life.

Once the cost of replacement is less than the cost of repair over a defined period then a structure can be considered to have reached the end of its life.

An alternative to replacement is to downgrade the duty of the bridge and re-route whatever it is carrying. In this way a highway bridge can become a footbridge, while the road it used to carry is diverted onto a new structure. Thus the old bridge lives on.

In the case of metal bridges, if the deck is in good condition, but the details are not in accordance with current practice, then the choice is between strengthening or replacement, which comes down to a matter of cost. This is not a simple choice based on the extent of strengthening; the cost of disruption to rail timetables or road closures must be added into the works cost, which can make replacement almost as economical as adding on strengthening material.

The decision on the end of life of a metal bridge is easiest when corrosion is considered. The loss of section in critical areas is usually difficult to repair

because by definition they are highly stressed, and relieving the stress is not generally easy. In economic terms, the cost of relieving stress by jacking or other means can exceed the cost of the repair, making deck replacement a more attractive option, since all of the deck will be renewed, giving a more predictable future to the bridge.

### 3 MODERN BRIDGES

The foregoing has been related to historic bridges, so now attention will be turned to modern structures. In the same way that rapid expansion of the railways led to a boom in construction of bridges to carry them, the spread of the motor car and expansion of road transport led to construction of motorways and other major trunk roads. In Britain this was largely from the 1960s onwards, suggesting a period of some 40 years during which the defects arising in modern bridges have been able to develop.

However, the design and detailing of structures in modern materials was carried out in the early years of the motorway expansion, the 1960s and 1970s, with limited knowledge of their long-term properties, and with no clear idea of how they would deteriorate, other than knowing that steel rusted and would need painting.

Concrete, once believed to be permanent, has been subject to alkali-silica reaction, carbonation, chloride attack, sulphate attack, and thaumasite attack, to name the common ones.

Structural steelwork fails in a number of ways, which are not always immediately detected by visual methods. Fatigue and buckling failures are both sudden, but can not normally be seen in advance of the event. Fatigue failure is avoided by careful detailing, and buckling, including lateral torsional buckling, is avoided by design, but standards can change with increasing traffic loading and with continuing research into structural behaviour. "Steady-state" assessment can lead to the conclusion that the bridge could fail, but there is no visual evidence, so in such cases the bridge must be monitored using instruments. Strain gauges can detect the stress regime, dye penetration can detect cracks in welds, and the advance of fatigue cracks can be sensed by the use of Acoustic Emission Monitoring, or AEM, where each reversal of stress producing an advance in the crack can be "heard" by continuous monitors.

The condition of closed structures where access is difficult can be ascertained by use of air sampling, which can indicate an atmosphere conducive to corrosion, or by viewing through an aperture using remote optical or video recording instruments.

Most modern bridges incorporate concrete within their structure as supports, with decks being of rein-

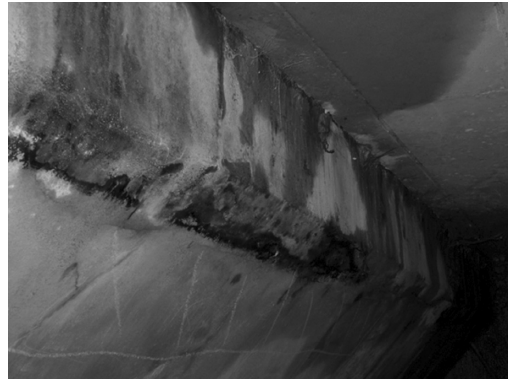


Figure 2. Result of leaking deck joint.

forced or prestressed concrete, or steel and composite concrete. Larger bridges may be of suspension form or, more recently, cable stayed.

In the early days of the design and detailing of concrete bridges, it was in the hands of named individuals such as Messrs Freysinnet or Hennebique, who personally supervised the construction of their designs, but then when there was a huge expansion of the roads programme design moved into the hands of ordinary engineers, working to the then current codes and standards, and their own experience. At the time it was believed that deck joints could be sealed adequately, so no attempt was made to protect the concrete of the beam seatings or the bearing shelves. At around the same time, because of the increase in motor traffic, and the fact that more modern, faster, cars were becoming available, the practice of salting roads to prevent icing in winter became more widespread, obviously to prevent accidents.

The bearing shelves were almost always detailed as being flat, so water was able to pond and soak into the concrete. The chloride ions in the salt migrated to the reinforcement and changed the chemical environment, causing the steel to corrode and break off the concrete cover.

An example is a cross-head of an elevated road in the Midlands. As a trial, an existing flat-topped cross-head was modified by the addition of a screed on the top surface which fell in such a way as to shed water.

The costing showed this to be very expensive in terms of access and man-hours, but the result was that the condition of this cross-head remained good, while others which were left with a flat top suffered all of the effects of chloride penetration. Had the top been shaped to shed water from the beginning then the expenditure could have been avoided.

#### 4 THE IMPORTANCE OF SEALING DECK JOINTS

Before the boom in motorway construction little attention had been paid to the sealing of deck joints. Long span railway bridges were generally of arch form, which did not have joints, and long metal railway bridges had open deck joints, because the running rails spanned them and they were not detected by the rail vehicles. Any water going through the joints was picked up in gutters, or launders as the railwaymen call them, and taken away to a drainage system. Other than possible frost damage, this was never a problem, since the water from the permanent way did not contain salts, and the engineering brickwork commonly used for the abutment was not particularly susceptible to chemical attack. However, open joints are not desirable in road bridges because of the noise of tyres when they cross them and the potential for joints to be prevented from closing by any debris that may fall down them. Deck seals were intended to reduce the noise and prevent the ingress of debris, but were also intended to prevent surface water from reaching the structure beneath. (Fig. 2).

The pursuit of a joint which does not leak has led to many designs. The design depends on the expected movement of the deck. In Britain this is covered by a Departmental Standard BD 33/94 (1994), which recommends buried joints for less than 20 mm, asphaltic plug joints for the range 5 mm to 40 mm, nosings with a poured sealant 5 mm to 12 mm, which is less than a buried joint, nosing with a preformed compression seal 5 mm to 40 mm, and proprietary joints above that, according to their design. Over the years, however, there have been varying degrees of success.

Various methods have been devised by design engineers using the materials available at the time. In the early days of motorway bridges, steel angles to retain the surfacing were bolted to the deck and a sealant put into the gap; epoxy concrete was tried as a nosing to retain the surfacing, again with a sealant in the gap, as was fibre reinforced concrete but these were largely unsuccessful.

A successful development in the late 1970s was the “asphaltic plug joint”, or APJ, which by the addition of a polymer to bitumen binder was rendered stable in summer but flexible in winter, so is ideal for use as a deck joint.

There are drawbacks to APJs, so there have been further developments.

“Elastomeric in metal runner” deck joints were developed for larger deck joint movements but the weak point of these is that the bolts which hold the frame to the deck eventually work loose.

Combining the idea of “Elastomeric in metal runner” with polymer concrete nosings has largely been



Figure 3. Failure of metal runner fixing in nosing.

successful, but performance does depend on the workmanship of the nosing installation. (Fig. 3).

However, the maintenance of a deck joint, particularly the removal of grit which accumulates with time, is crucial to its life, since any trapped grit compacts and prevents the joint from acting properly when it closes with the seasonal increase in ambient temperature, and in many cases causes damage to it.

Joints for very large movements of decks are a subject of their own.

Their purpose is to provide a smooth surface for the passage of traffic, while controlling any water passing through it such that it is channelled away. Various different designs are available from a number of manufacturers, and involve various principles including beams which span the gap supporting plates, or lazy tong arrangements which again support plates, or a number of transverse plates which are guided in rails to beneath the deck as the bridge moves.

#### 5 THE LIFE OF BRIDGE BEARINGS

In the early days of motorway bridge design short span structures were given a free and a fixed end to cater for temperature expansion and contraction in the longitudinal direction, but often the fact that the bridge was wider than its span was overlooked, and failure or displacement of elastomeric bearings occurred because the design movement was exceeded, so either the bearing split, or it moved bodily from its original position. Thirty or forty years on, the restoration of the bearings to their original position is a major exercise frequently involving lifting of the entire bridge deck.

Sliding bearings usually consist of a layer of PTFE bonded to a steel substrate, which slides against a polished stainless steel plate that is also bonded to a steel substrate. Such bearings have a measurably limited life, which can be derived from the number of cycles

they undergo, and the distance they travel. The life can be extended by greasing the bearings, but wear is inevitable, and the bearings must be replaced, which involves lifting the bridge. The cost of lifting the bridge can far outweigh the cost of the bearing itself, therefore the easier it is made at the design stage, the less it will cost in the future.

## 6 AVOIDANCE OF DIFFICULT DETAILS WHICH CAN BE BADLY CONSTRUCTED

There is often a conflict between the needs of the long-term design and the method of construction, and it is not uncommon for a contractor to ask for design details to be altered or simplified to suit his methods, therefore if the designer uses his experience to detail his structure to be easily constructed he will reduce the need to change it under the pressure of having to do a redesign within a construction programme.

The precasting of parts of a bridge should be considered; unless it is a very complicated structure which cannot be simplified, a significant proportion of a bridge deck can be precast. It is normal to precast beams, but, if properly detailed, diaphragms can also be precast, the main problem then being to connect them to the main structure in such a way that they become an integral part of the bridge. The advantage of this is reduced dependency on workmanship and reduced time on site. Eurocode EN4 (2005) allows shear connectors to be clustered, which opens the door to precasting composite concrete decks over their whole width.

## 7 THE COMPARISON OF INITIAL COST VERSUS LONG-TERM MAINTENANCE

It must be assumed that no structure can be left for its design life without any maintenance being required. Steelwork must be painted, deck joints fail, bearings wear out and despite the designer's best efforts, concrete may deteriorate. Comparative maintenance costs for steel and concrete structures are evaluated in the British Departmental Standard BD36/92 (1992).

Where access to a bridge is easy, and jacking up the deck is comparatively simple, bearing replacement is not a problem, particularly since it has long been the case in Britain that provision should be made in the original design for the future replacement of bearings. However, costs escalate when access is difficult.

As an example, a major viaduct over a river estuary in the south of England was built in the 1970 s with PTPE on stainless steel sliding bearings.

Because the bridge as constructed did not have provision for bearing replacement, the estimated cost of

the exercise of replacing the bearings is over £2 m, of which just £20,000 is the cost of the bearings.

In designing a bridge to last 120 years, which is the case for structures in Britain, it is necessary to acknowledge that at some time in its life either the bridge must be lifted to allow replacement, or the bearings must be designed to last that length of time.

An approach to be considered is to change the philosophy of bearing design. Normally bearings are designed to the stresses allowed by the codes or standards, but this sets the stress level at the maximum for the material chosen; an alternative approach would be to overdesign the bearings, by making the contact areas bigger to reduce the stress. The effect of this would be to increase the cost of the bearings when first purchased, but this could be set against the savings in cost of replacement.

## 8 PRESERVING THE LIFE OF BRIDGES

With the experience built up over the last few decades, there is much that has been done in terms of specification to prolong the life of a bridge, but there is also much that can also be done in terms of detail.

With regards to concrete bridges, the current specification for concrete attempts to eliminate corrosion of the steel due to carbonation by increasing the cover, the aggregates and cement are specified such as to avoid alkali-silica reaction, additives such as calcium chloride which are deleterious to the concrete are forbidden.

In addition to this, exposed areas of concrete which can be subject to chloride or other external attack are normally coated with a layer that prevents the ingress of chlorides or other unwanted material. These layers can either be barriers which are applied to the surface, or liquids which can be applied to the surface and penetrate the concrete to form a barrier beneath the surface.

Cladding the concrete in brickwork or other ceramic material which prevents penetration by rain or surface water has been shown in the past to preserve the structural concrete, although it can become a maintenance liability in its own right.

The deck edge beams can be clad with an environmental barrier, such as GRP panels, which protects them from chloride ingress, but the cladding should be easily replaceable or again it becomes a maintenance liability in its own right.

Decks should be made continuous over piers to avoid the need for deck joints, and abutments should be integral or semi-integral where appropriate, depending on span or skew.

Flat surfaces should be profiled to prevent water from ponding.

With regard structural steelwork bridges, the concrete deck usually associated with composite bridges can be treated in all of the ways described in the section above, but the steelwork itself should be detailed to avoid the retention of water or debris, including nesting birds.

Corrosion protection is necessary, unless weathering steel is used, but certain areas are more vulnerable than others, and should receive special attention, such as additional coats of paint.

In hostile environments, or where access is difficult, which might be the same location, cladding the entire deck in GRP or similar material should be considered to provide both an environmental barrier and a permanent inspection access which, again, will require maintenance over its own design life.

### 8.1 *The importance of detailing*

There are certain rules in addition to those found in codes and standards which, if used for guidance, can go some way towards ensuring the long and trouble-free life of a bridge. These are:

- assume that water will get in, and let it out
- do not depend on one agent; assume that the first could fail, and have a back-up
- assume sealants will fail, for instance, and provide a channel to pick up the water leaking through them
- detail bearings which have sliding surfaces such that the surface more susceptible to damage from grit is uppermost
- detail bearings for easy replacement
- spend money on larger bearings at a lower stress to increase life between replacements
- eliminate bearings altogether through integral construction where possible

### 8.2 *The importance of simple maintenance*

Repeated simple minor maintenance can avoid major maintenance, or defer it for a long time. Such minor maintenance can be:

- regular washing of bearing seatings
- yearly cleaning of drains after the gritting season
- yearly inspection of movement joints and removal of grit
- providing drains in closed boxes to let the water out
- washing down external stiffeners

- local touching-up of paintwork
- preventing birds from nesting, or removing their nests once finished with

### 8.3 *Plan for major maintenance*

Major maintenance which can be expected is the replacement of bearings and deck joints, which must be planned for and funds set aside. The contribution which the designer can make to make this as infrequent as possible, and as easy as possible, is to:

- design jacking points into the supports to allow the deck to be lifted to replace bearings
- design the deck to be lifted from those points; this can induce reverse moments, which will be important in the case of prestressed beams
- overdesign the bearings to reduce the stress and thus wear on the bearing material
- use prefabricated deck joints where possible to reduce dependency on site workmanship, which is frequently subject to the extremes of weather
- detail the deck ends for specific joints to ensure optimum performance

## 9 CONCLUSION

It is unrealistic to assume that once a structure has been completed it can be left unmaintained for the whole of its design life. However, the need for maintenance or repair can be reduced by careful detailing by the original designer and, where components have an identifiable design life, detailing the bridge to make their replacement as simple and convenient as possible.

## REFERENCES

- The Chief Highway Engineer 1992. BD36/92—Evaluation of Maintenance Costs in Comparing Alternative Designs for Highway Structures. London: The Department of Transport, 123, Buckingham Palace Road, SW1 W 9SR
- The Chief Highway Engineer 1994. BD33/94—Expansion Joints for Use in Highway Bridge Decks. London: The Department of Transport, 123, Buckingham Palace Road, SW1 W 9SR
- Eurocode EN4 2005—Design of composite steel and concrete structures—Part 2: General rules and rules for bridges. London: BSI Publications, 389, Chiswick High Road, W4 4AL.

# Life-cycle performance of structures: combining expert judgment and results of inspection

L.C. Neves

*New University of Lisbon, Caparica, Portugal*

D.M. Frangopol

*Lehigh University, Bethlehem, Pennsylvania, USA*

**ABSTRACT:** Current bridge management systems base decisions on the results of visual inspections. These systems consider visual inspection results as accurate and disregard any further information available. In the present study, the result of each inspection is considered as a random variable, dependent of a wide range of factors, that can be integrated with other sources of information, including expert judgment and results of other inspections. The combination of different sources of information results in reliable posterior information and allows more accurate predictions of future deterioration. In the present paper, performance of an existing structure is obtained in terms of the condition index, which describes the effects of deterioration as can be seen by an inspector, and the safety index, which measures the safety margin of the structure. The reduction in uncertainty associated with periodical inspections is considered through updating of performance profiles. The updating of the condition index is direct, as new information on this parameter is collected by the inspector. In terms of safety, however, only indirect information is collected and the uncertainty reduction associated with an inspection is significantly lower. Several realistic examples show the impact of inspections on the predicted life-cycle performance of structures.

## 1 INTRODUCTION

Inspections of existing structures are a fundamental aspect of every structural management system. In fact, structural deterioration depends on such a wide range of factors, that direct observation must be considered the prime source of accurate and reliable information on the structure.

Inspections are not, however, free of errors and uncertainty (Phares *et al.* 2004). In fact, the result of an inspection depends on several factors such as the experience of the inspector, the deterioration mechanisms present, location of the bridge, and means available for the inspection. Moreover, the results of inspections alone do not allow a medium or long term planning, and any decisions based on the results of inspections alone will result in application of maintenance to very deteriorated structures, resulting in a very high life-cycle maintenance costs (Neves, Frangopol and Cruz 2006; Neves, Frangopol and Petcherdchoo 2006).

For these reasons, it is fundamental to integrate the results of inspection with a prediction model for the deterioration of existing civil infrastructure. In this manner, more accurate predictions of future deterioration will be possible, and more efficient decisions can be made.

In this paper, the deterioration of existing structures is analyzed considering the model developed by the authors (Neves and Frangopol 2005). In this model, the performance of structures is defined in terms of lifetime probabilistic condition, safety, and cost profiles. The main advantages of this model are the ability to consider the entire performance history of the structure, including deterioration and effects of maintenance actions as well as the ability to combine common performance indicators, namely the condition index, with more consistent indicators, such as the safety index.

The model proposed by the authors (Neves and Frangopol 2005) does not include any information resulting from inspections or tests in the analysis, as it bases the evolution over time of performance on expert judgment alone.

In this paper, a model for combining expert judgment in the form of the model proposed by Neves and Frangopol (2005) with information from inspections is proposed. This new approach is based on the use of Bayesian updating combined with simulation for improving expert judgment. The results obtained in the examples analyzed show the significant impact on performance prediction of the inclusion of information obtained from inspections.

## 2 CONDITION, SAFETY AND COST

In the model proposed by Neves and Frangopol (2005) life-cycle performance of an existing structure is characterized by three different time-dependent probabilistic indicators: condition index, safety index, and the cumulative maintenance cost. The condition index is an indicator of deterioration as recorded by a bridge inspector. It might be associated with the severity of cracking in reinforced concrete structures, deterioration of painting and rusting in steel structures, or any other visually observable deterioration effect. The safety index is a measure of the reliability or the safety margin of a structure, and can only result from a structural safety evaluation.

These two indicators are related, in the sense that both refer to the effects of deterioration on a certain structure. However, full knowledge on one of these factors is not enough to determine the value of the other. In fact, the condition index is only influenced by the observable defects, and only indirectly includes the effects of corrosion, fatigue or cracking. The safety index includes all these aspects directly. In short, the safety index would be a much more interesting measure of performance. However, it is extremely expensive to determine the safety margin of a structure, and the network system reliability analysis of all structures in a large network is close to impossible.

In the model proposed by Frangopol (1998) and Neves and Frangopol (2005), the condition and safety indices under no maintenance are defined as bi-linear functions, in terms of 6 random parameters: initial condition,  $C_0$ , initial safety index,  $S_0$ , time of initiation of deterioration of condition and safety,  $t_{ic}$  and  $t_i$ , respectively, and deterioration rate of condition and safety,  $\alpha_c$  and  $\alpha$ , respectively. The effect of maintenance actions is defined in terms of 8 random parameters, as follows: (a) improvement in condition index and safety index immediately after application,  $\gamma_c$  and  $\gamma$ , respectively; (b) time during which the deterioration processes of condition index and safety index are suppressed,  $t_{dc}$  and  $t_d$ , respectively; (c) time during which the deterioration rate in condition index and safety index are suppressed or reduced,  $t_{pdc}$  and  $t_{pd}$ , respectively; and (d) deterioration rate reduction of condition index and safety index,  $\delta_c$  and  $\delta$ , respectively. The meaning of each of these random variables is shown in Figure 1.

The mean, standard deviation, histograms and percentiles of the life-cycle condition index, safety index, and cumulative cost are computed using Monte-Carlo simulation. A detailed description of the computational platform employed can be found Neves and Frangopol (2005).

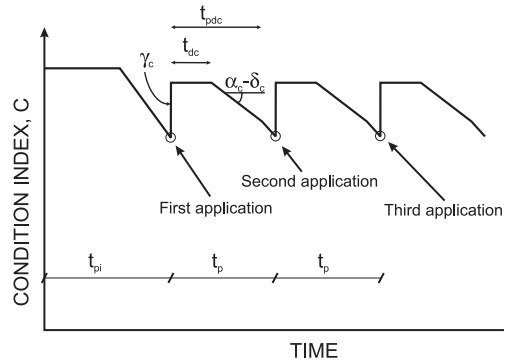


Figure 1. Condition index profile.

## 3 CONDITION AND SAFETY UPDATING

When an inspection is executed, new information on the condition index of the structure at a certain point in time becomes available. If the inspection was perfect, it would be possible to know, exactly, the condition index at that point in time. Since the inspection is affected by errors and uncertainty, this new information must be regarded as probabilistic, and must be used as such.

At the time of an inspection, the condition index can be characterized as a probabilistic variable, with a probability density function dependent on the results obtained by the inspector, but also on the quality of the inspection. Common practice defines the results of an inspection in terms of a set of possible outcomes  $(0, 1, \dots, n)$ . However, deterioration has, for most cases, a continuous or almost continuous evolution, and these results are a simplification of reality. We can consider that for a given condition index at time  $T$ ,  $C_T$ , the result of an inspection,  $C_{ins}$ , is given as a likelihood function  $P(C_{ins}|C_T) = L(C_T)$ . This function can be approximated by a normal distribution with mean  $\mu$  and standard deviation  $\sigma$ . The mean will be equal to the result of inspection  $C_{ins}$ , if the results of inspections are unbiased, and lower or higher than  $C_{ins}$ , if inspectors are consistently optimistic or pessimistic, respectively. In this paper, it is assumed that inspections are unbiased and that a lower condition index is associated with a lower deterioration. The uncertainty in the results is measured by the standard deviation  $\sigma$ , which is related to the quality of inspection, dependent on the experience of the inspector and the conditions for inspection.

Based on Bayes theorem, the probability density function of the condition index, considering the

result of inspection and the information from expert judgment can be defined as (Ang and Tang 2007):

$$f''(C_T) = K \cdot L(C_T) \cdot f'(C_T) \quad (1)$$

where  $f''(C_T)$  is the probability density function of the condition index at time  $T$  considering both expert judgment and results of inspections, also designated posterior distribution,  $f'(C_T)$  is the probability density function of the condition index at time  $T$  considering only expert judgment, also designated prior distribution  $L(C_T)$  is the likelihood function, and  $K$  is a normalizing constant defined by:

$$K = \frac{1}{\int_{-\infty}^{\infty} L(C_T) \cdot f'(C_T) dC_T} \quad (2)$$

Considering Monte-Carlo simulation was used to computed the probabilistic indicators of performance, the mean and standard deviation of the condition index at time  $\tau$ , can be computed as (Chen and Ibrahim 2000, Frangopol and Neves 2008):

$$\mu_C^\tau = \frac{\sum_{i=1}^n C_\tau^i \cdot L(C_T^i)}{\sum_{i=1}^n L(C_T^i)} \quad (3)$$

$$\sigma_C^\tau = \sqrt{\frac{\sum_{i=1}^n (C_\tau^i)^2 \cdot L(C_T^i)}{\sum_{i=1}^n L(C_T^i)} - \left( \frac{\sum_{i=1}^n C_\tau^i \cdot L(C_T^i)}{\sum_{i=1}^n L(C_T^i)} \right)^2} \quad (4)$$

where  $\mu_C^\tau$  and  $\sigma_C^\tau$  are the mean and standard deviation of the condition index at time  $\tau$  considering both expert judgment and results of inspections,  $C_\tau^i$  is the condition index at time  $\tau$  associated with sample  $i$ ,  $C_T^i$  is the condition index at time of inspection  $T$  associated with sample  $i$ , and  $n$  is the number of samples.

In terms of the safety index, a similar approach can be employed, resulting in a mean and standard deviation given, respectively, as:

$$\mu_S^\tau = \frac{\sum_{i=1}^n S_\tau^i \cdot L(C_T^i)}{\sum_{i=1}^n L(C_T^i)} \quad (5)$$

$$\sigma_S^\tau = \sqrt{\frac{\sum_{i=1}^n (S_\tau^i)^2 \cdot L(C_T^i)}{\sum_{i=1}^n L(C_T^i)} - \left( \frac{\sum_{i=1}^n S_\tau^i \cdot L(C_T^i)}{\sum_{i=1}^n L(C_T^i)} \right)^2} \quad (6)$$

where  $\mu_S^\tau$  and  $\sigma_S^\tau$  are the mean and standard deviation of the safety index at time  $\tau$  considering both expert judgment and results of inspections and  $S_\tau^i$  is the safety index at time  $\tau$  associated with sample  $i$ .

In this manner, it is possible to obtain new updated condition and safety profiles. It must be noted that the inspection only provides direct information on the condition index. If the safety index is considered independent of the condition index, then the prior and posterior safety profiles will coincide. Nevertheless, since both the condition index and safety index depend on the deterioration, some correlation is to be expected, and some information on the safety of the structure can be extracted from an inspection.

#### 4 EXAMPLES

As an example, the life-cycle condition and safety profiles of existing reinforced concrete bridge elements are analyzed considering data provided in Denton (2002). This data is thoroughly analyzed in Neves and Frangopol (2005), considering the life-cycle performance under no maintenance and under different maintenance strategies. The condition and safety profiles under no maintenance obtained are presented in Figure 2.

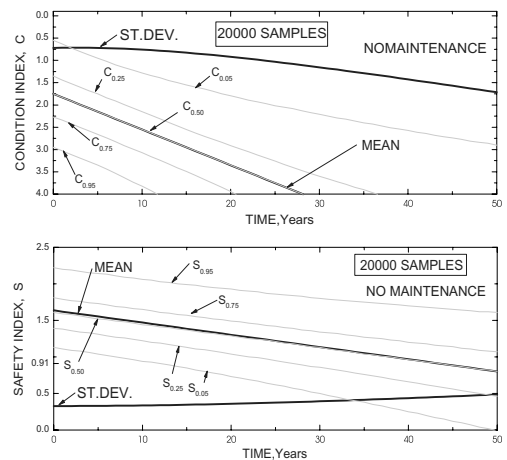


Figure 2. Condition and safety index under no maintenance.



As can be observed from these results, under no maintenance the performance presents very significant dispersion, as denoted by the difference between the values of the 5 and 95 percentiles ( $C_{0.05}$  and  $C_{0.95}$ , respectively).

Let's now consider that an inspection is carried out at year 20. It is considered that the inspector classifies the bridge element as having a condition index equal to 2, 3, or 4. Considering the experience of the inspector, different levels of quality are defined, each associated with a probability of misclassification. Assuming a normal distribution for the likelihood function, the probability of misclassification is associated with the different standard deviations, as follows (Frangopol and Neves 2008).

Quality	Probability of misclassification	Standard deviation
High	5%	0.255
Medium	10%	0.304
Low	20%	0.390
Very Low	40%	0.595

Considering no correlation between the condition index and the safety index, this inspection does not affect the safety index. However, in terms of condition, the updated condition index is significantly different from the profile predicted based on expert judgment as shown in Figure 3, considering a high quality inspection.

These results show that an inspection has a significant impact of the predicted condition index. In fact, for different results of inspection, a significant reduction in the standard deviation of the condition index occurs. Moreover, an important change in the predicted mean condition is also observable. The latter is more dramatic if the observed condition is 2.0, as this is significantly different from the mean predicted value.

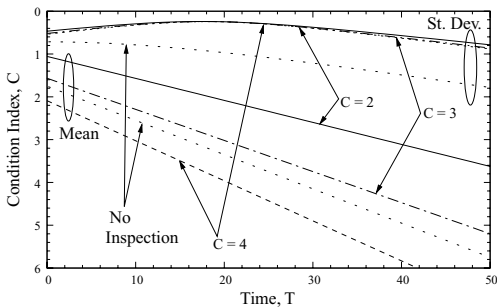


Figure 3. Comparison of the mean and standard deviation of condition index considering only prior knowledge and prior knowledge and inspection.

In Figures 4 and 5 the PDFs of the condition index considering an inspection with an observed condition index equal to 2 and equal to 3, respectively, are shown.

These PDFs show the effect of maintenance on the degree of knowledge on the condition of a structure. In fact, for both inspection results, the updated condition PDFs show a reduction in dispersion but also a large shift in the mode. In all cases, there is an important change in the distribution of the initial parameters, namely the initial condition index and the deterioration rate.

#### 4.1 Effect of quality of inspection

An inspection should yield a condition index very close to the real condition of the bridge. This is not the case for two major reasons. Firstly, it is very difficult to the inspector to give a precise indication of the condition, and usual systems use only a limited number of condition classes (e.g., five different classes). As a consequence, even for a perfect inspection a result of 3 means the condition is close to 3.0 (i.e., between 2.5 and 3.5). Moreover, limited experience, difficult

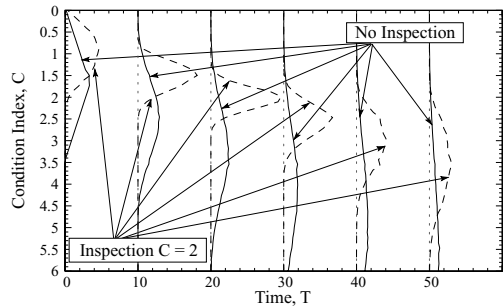


Figure 4. Comparison of the PDFs of the condition index at 10 years time intervals considering only prior knowledge and prior knowledge and inspection,  $C = 2$ .

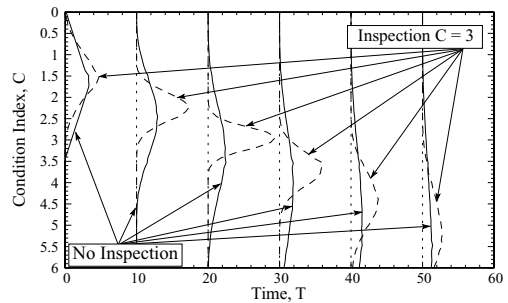


Figure 5. Comparison of the PDFs of the condition index at 10 years time intervals considering only prior knowledge and prior knowledge and inspection,  $C = 3$ .

accessibility to the structure, or human error also result in errors in the classification of the condition of structures. In the present work, as previously stated, four different types of inspections were considered. A high quality inspection will provide a good indication on the condition of a structure and can be extremely informative. However, the amount of information provided is reduced when the quality of the inspection decreases. Let's consider an example similar to the previous one, but assuming different inspection qualities. The results obtained, assuming that all inspections resulted in a classification of condition index  $C = 2$  are shown in Figure 6.

Figure 6 shows that, even very low quality inspections have a large impact on the condition index profiles, resulting in a reduction in the standard deviation and an increase in mean condition. This is mostly a consequence of the initial data available. In fact, the data presented in Denton (2002) refers to a large set of bridges with very different ages, and not to a single bridge, the information gathered reduces significantly the uncertainty over present, past and future condition.

#### 4.2 Effect of inspection on the safety index

Although an inspection yields no direct information on the safety index of a structure, this information can be obtained in an indirect manner. In fact, changes in the condition index and the safety index are both the result of deterioration, and, as a consequence, worst condition index is often associated with lower safety.

The probabilistic relation between the condition index and the safety index can be measured by the correlation between these two indicators at any point in time. If no maintenance is considered and the parameters defining the profiles under no maintenance (*i.e.*, the initial condition, initial safety, deterioration rate of condition index and deterioration rate of

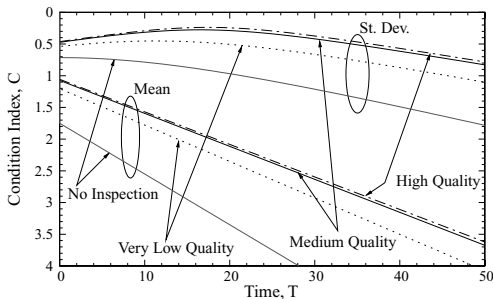


Figure 6. Comparison of the mean and standard deviation of the condition index considering only prior knowledge and prior knowledge and inspection with different quality levels.

Table 1. Correlation coefficient between parameters defining the condition index and the safety index under no maintenance.

	$\alpha_c$	$\alpha$	$C_0$	$S_0$
$\alpha_c$	1	$\rho$	0	0
$\alpha$	$\rho$	1	0	0
$C_0$	0	0	1	$\rho$
$S_0$	0	0	$\rho$	1

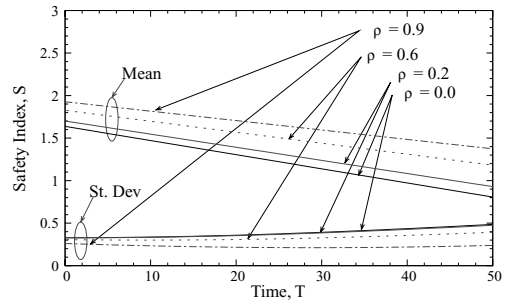


Figure 7. Comparison of the mean and standard deviation of the safety index considering prior knowledge and inspection with different correlations.

safety index) are assumed independent, the resulting condition index and safety index will be independent.

If, on the other hand, the parameters defining the condition index and the safety index are correlated, the resulting profiles will also be correlated, and an inspection will improve the knowledge on the condition index, but also on the safety index.

In general, no information on the correlation between parameters defining the condition index and the safety index exists. Let's assume the correlations between these parameters as denoted in Table 1.

In this table, the correlation coefficient between parameters,  $\rho$ , is taken as 0, 0.2, 0.6, and 0.9.

In Figure 7 the safety index profiles are obtained considering that an inspection is performed at year 20 and a condition index equal to 2.0 is observed. These results show that, even for relatively low correlation coefficients, there is a significant improvement in mean safety, as a consequence of the observed condition index being better than the initial prediction. Moreover, a reduction in the dispersion of the safety index over the entire lifetime is also observed.

## 5 UPDATE OF INITIAL PARAMETERS

The condition index and safety index profiles are defined in terms of a set of random parameters. When

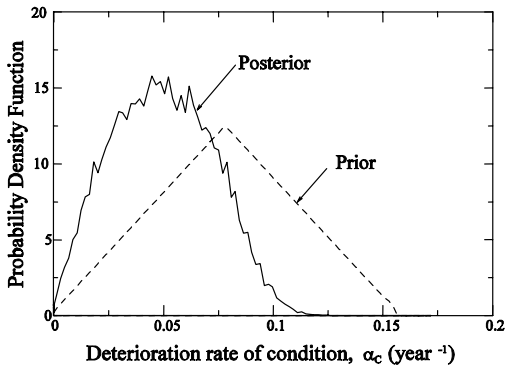


Figure 8. Comparison of the deterioration rate of condition considering only prior knowledge and prior knowledge and inspection.

updating is carried out, new information on these parameters becomes available. This information can be used to make more accurate predictions for other structures.

As an example, in Figure 8, the distribution of the deterioration rate of condition considering only expert judgment is compared to the updated distribution. Inspection causes a reduction in uncertainty, but also a reduction in the deterioration rate, as the observed condition is better (i.e., less deteriorated) than initially predicted.

## 6 CONCLUSIONS

In the present study, a methodology to combine expert judgment and results of inspection on the life-cycle prediction of deteriorating structures is proposed. The methodology uses the probabilistic deterioration model proposed by the authors. The effects on this prediction of inspections are defined in a Bayesian framework. The obtained results show that an inspection, even of low quality, results in a significant reduction in uncertainty.

The results obtained show the importance of incorporating the outcome of inspections in the deterioration models in a consistent manner. As a result, more accurate predictions of performance can be obtained, and more sound decisions can be made.

## ACKNOWLEDGMENTS

The support to Lehigh University from (a) the National Science Foundation through grants CMS-0638728 and CMS-0639428, (b) the Commonwealth of Pennsylvania, Department of Community and Economic Development, through the Pennsylvania Infrastructure Technology Alliance (PITA), and (c) the U.S. Federal Highway Administration Cooperative Agreement Award DTFH61-07-H-00040, are gratefully acknowledged. Also, the support of the Science and Technology Foundation to UNIC Research Center in the New University of Lisbon is gratefully acknowledged. The opinions and conclusions presented in this paper are those of the authors and do not necessarily reflect the views of the sponsoring organizations.

## REFERENCES

- Ang, A. and W. Tang (2007). *Probability Concepts in Engineering: Emphasis on Applications in Civil & Environmental Engineering*. Wiley.
- Chen, M. and J. Ibrahim (2000). *Monte Carlo Methods in Bayesian Computation*. Springer Series in Statistics. Springer.
- Denton, S. (2002). Data estimates for different maintenance options for reinforced concrete cross-heads. Draft Report for Highways Agency, U.K., Brinckerhoff Ltd.
- Frangopol, D. (1998). A probabilistic model based on eight random variables for preventive maintenance of bridges. Technical report, Highways Agency, London, U.K. *Optimum Maintenance Strategies for Different Bridge Types*.
- Frangopol, D. and L. Neves (2008). Structural performance updating and optimization with conflicting objectives under uncertainty. In *2008 Structures Congress - Crossing Borders*. Vancouver, Canada, April (in press).
- Neves, L. and D. Frangopol (2005). Condition, safety, and cost profiles for deteriorating structures with emphasis on bridges. *Reliability Engineering & System Safety* 89, 185–198.
- Neves, L., D. Frangopol, and P. Cruz (2006). Probabilistic lifetime-oriented multiobjective optimization of bridge maintenance: Single maintenance type. *ASCE Journal of Structural Engineering*: 132 (6), 991–1005.
- Neves, L., D. Frangopol, and A. Petcherdchoo (2006). Probabilistic lifetime-oriented Multiobjective optimization of bridge maintenance: combination of maintenance types. *ASCE Journal of Structural Engineering* 132 (11), 1821–1834.
- Phares, B., G. Washer, D. Rolander, B. Graybeal, and M. Moore (2004). Routine Highway Bridge Inspection Condition Documentation Accuracy and Reliability. *Journal of Bridge Engineering* 9 (4), 403–413.

# Bending performance of reinforced concrete member deteriorated by corrosion

M. Oyado & T. Sato

*Railway Technical Research Institute, Tokyo, Japan*

T. Kanakubo & Y. Yamamoto

*University of Tsukuba, Ibaraki, Japan*

**ABSTRACT:** This paper presents the study results about the influence of corrosion of reinforcing bars on the bending performance of reinforced concrete (RC) members in order to serve for maintenance of RC structures. In this study, static bending tests were carried out for 13 corroded RC members and a three dimensional shape scanning method of the corroded reinforcing bar was developed and applied to measurement of the corrosion amount. From the test result, it was proved that the tensile strength of reinforcing bars and the ultimate strength of RC members were decreased not only by the averaged reduction of cross section of reinforcing bars but also by the localized corrosion.

## 1 INTRODUCTIONS

It is important to confirm the safety performance of existing reinforced concrete (RC) structures, especially when they are damaged by the corrosion. It is considered that the bending performance of RC beams or columns decreases due to the corrosion of reinforcing bars.

According to the some previous studies, the ratio of weight reduction of reinforcing bars caused by the corrosion to the original weight before corrosion was adopted as the corrosion amount index to evaluate the relationship between the strength and the corrosion. The ratio of weight reduction can be calculated by the following equation (1).

$$C = \Delta w/w \quad (1)$$

where  $C$  = ratio of weight reduction;  $\Delta w$  = weight reduction caused by the corrosion; and  $w$  = original weight before corrosion.

The ratio of weight reduction shows the ratio of cross sectional reduction averaged for the measured region. Using this index, the ultimate bending strength of the RC member can be evaluated in the equation (2), in an example.

$$P_{uc}/P_{un} = 1 - kC \quad (2)$$

where  $P_{uc}$  = ultimate bending strength of the RC member after corrosion;  $P_{un}$  = ultimate bending strength of the RC member before corrosion; and  $k$  = reduction coefficient.

These equations (1) and (2) have often been adopted in some of previous studies and even been considered as standard procedures. In this method, the coefficient  $k$  has an important meaning in evaluating corroded RC members or reinforcing bars. However, the test results of the coefficient  $k$  in the equation (2) have so much variance depending on each study because of various reasons including unexpected uncertainties of the experimental data; therefore no appropriate assessment procedure for the corroded RC member has ever been proposed so far.

This paper presents the study results about the influence of corrosion of reinforcing bars on the bending performance of RC members in order to serve for maintenance of RC structures.

## 2 STATIC BENDING TEST

### 2.1 Details of test specimen

In this study, bending tests were carried out for 13 corroded RC members, among which eight beam specimens were exposed to the open air (EX), and the remained five beam specimens were subjected to the electric accelerated corrosion process (EL). Table 1 gives the relevant properties of the specimens and Fig. 1 shows the details of the specimens. All of the specimens were designed to have the same dimensions overall. Series S and M were corroded by EX, and Series C were corroded by EL.

Fig. 2 shows the method of EX, which was conducted near the urban (not coastal) area. The

Table 1. Relevant properties of the specimens.

Corrosion method	specimen			
	No corr. (0)	small (0.35)	medium (0.84)	large (1.33)
EL	C1	C2	C3	C4, C5
Corrosion method	No corr.	Exposed for 20 months		Exposed for 12 years
EX	S-0N	SD-1N, SD-2N, SD-3N, SD-4S		M1, M2, M3

Figure inside the bracket() means the accumulated electric current density(A · h/cm<sup>2</sup>)

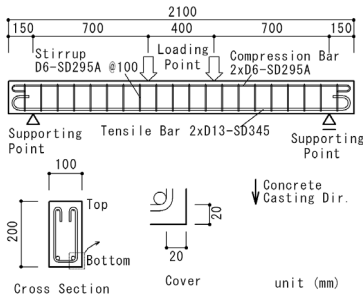


Figure 1. Details of the specimens.

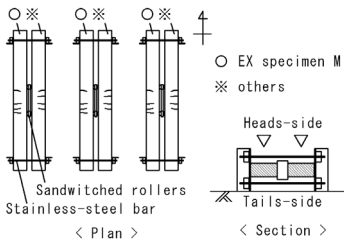


Figure 2. EX corrosion method.

specimens were combined together with the specimens tested in another study (by Nishiwaki and Authors) by using sandwiched rollers and stainless-steel bars, while holding flexural cracks pre-induced by the static loading open. Sodium chloride solution was sprayed periodically three times in every day for 17 months after starting exposure, in an attempt to soak NaCl into the concrete and to accelerate corrosion. Amount of chloride ion at the 50 mm depth from heads-side surface reached to 5kg/m<sup>3</sup>. Approximate exposing period of Series S is 20 months, and that of Series M is 12 years.

EL specimens were planned to have variations of the weight reduction of the reinforcing bars so as to make weight reduction a testing parameter, and prepared together with the other specimen. Fig. 3 shows the experimental setup of the EL accelerated corrosion test, which was intended for all of reinforcing bars including longitudinal reinforcing bars and stirrups to corrode, in order to compare with the EX specimens. The maximum corrosion amount was targeted for the weight reduction of 50% by controlling corrosion duration and accumulation of the electric current.

### 2.2 Loading test and material inspection

Fig. 1 also shows the loading and supporting points of the loading test. After the loading test, tensile reinforcing bars were retrieved from each specimen to determine their weight reduction and mechanical properties. The former was measured by weighing rust-removed bars after soaking in the solution of the diammonium hydrogen citrate (in accordance with the Japanese test code of JCI-SCI), and the latter was achieved by the direct tension test.

### 2.3 Test result—crack pattern

Fig. 4 shows the examples of the crack pattern observed after loading test. In EL specimen C2, fewer loading cracks were observed in comparison with no corroded control specimen C1, because many corrosion cracks along the longitudinal bars and stirrupshad

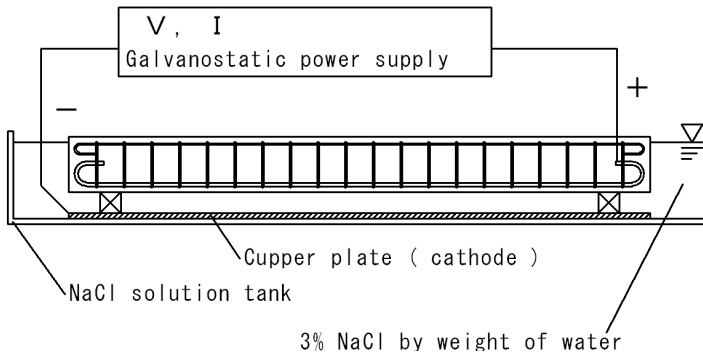


Figure 3. EL accelerated corrosion process.

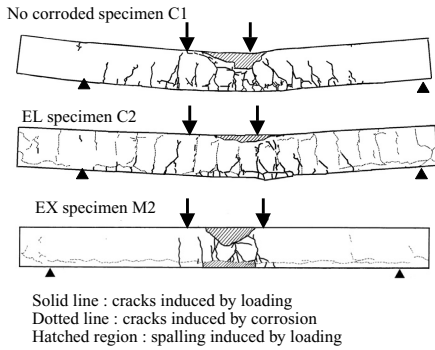


Figure 4. Examples of crack pattern.

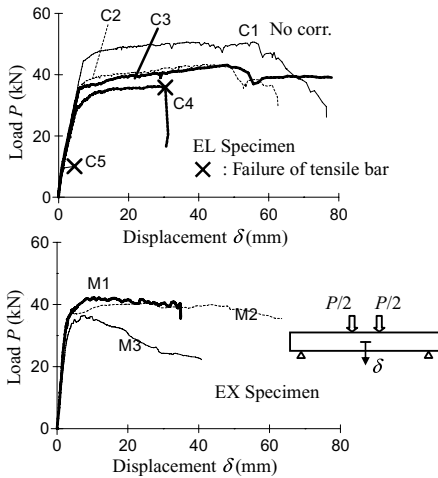


Figure 5. Load-displacement relationships.

already appeared before the loading test. Cracks induced at the bottom side reached to the longitudinal corrosion crack, with its direction being changed or even with its progression being disturbed.

On the other hand, in EX specimen M2, very few loading cracks were observed, especially in the shear span region, almost no cracks were induced. On top of that, in the bottom surface under the longitudinal bars, few cracks were observed and the cover concrete in the pure bending region almost fell off. It is apparent that the bond failure is one reason of those phenomena.

#### 2.4 Test result—load-displacement relationship

Fig. 5 shows the relationship between the load  $P$  and the displacement  $\delta$ . All specimens except the EL specimen C4 and C5 failed due to the concrete compression failure after yielding of the tensile reinforcing bar. In these cases, every specimen except M3 showed sufficient ductility, however in case of M3, immediate load dropping was observed due to the concrete spalling on the top surface. On the other hand, EL specimen C4 and C5 showed sudden brittle failure of the tensile reinforcing bar. These sudden failures of the specimen M3, C4 and C5 should be predicted in order to keep safety against the deterioration. However, no appropriate prediction method has been proposed until now.

Table 2 shows the ratio of weight reduction  $C$  and ultimate strength of the RC member  $P_u$ . Fig. 6 shows the relationship between the ratio of the weight reduction  $C$  and the ratio of the ultimate strength  $P_{uc}/P_{un}$ , which is the quotient of the ultimate strength of the corroded RC member  $P_{uc}$  divided by that of the non-corroded RC member  $P_{un}$ . The failure mode of each specimen is also shown in Table 2. In calculation of  $P_{uc}/P_{un}$ , specimen S-0N was assumed to have no corrosion for EX specimens, and specimen C1 was also

Table 2. Test result  $P_u$  and  $C$ .

Name	$P_u^*$	$(P_{uc}/P_{un})$	C of each test piece				< ave. >	mode**
C1	50.6	(1.00)	-				< 0.00 >	1
C2	43.0	(0.85)	0.20,	0.22			< 0.21 >	1
C3	42.7	(0.84)	0.10,	0.11			< 0.10 >	1
C4	36.2	(0.72)	0.22,	0.26			< 0.24 >	3
C5	8.7	(0.17)	0.37,	0.50			< 0.44 >	4
M1	36.4	(0.72)	0.13,	0.14,	0.16		< 0.14 >	2
M2	40.5	(0.80)	0.13,	0.13,	0.12,	0.15	< 0.13 >	1
M3	42.2	(0.83)	0.10,	0.11,	0.12,	0.12	< 0.11 >	2
S-0N	52.5	(1.00)	-				< 0.00 >	1
SD-1N	47.1	(0.90)	0.00,	0.03			< 0.02 >	1
SD-2N	45.6	(0.87)	0.03,	0.04			< 0.04 >	1
SD-3N	48.1	(0.92)	0.00,	0.03			< 0.01 >	1
SD-4N	49.5	(0.94)	0.02,	0.02			< 0.02 >	1

\*unit: kN; \*\* mode: Failure mode.

1: Concrete compression failure after yielding.

2: l(Max. strength = yielding strength).

3: Failure of tensile reinforcing bar.

4: 3(Max strength = cracking strength).

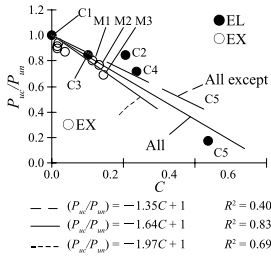


Figure 6.  $C$  vs  $P_{uc}/P_{un}$ .

assumed to have no corrosion for EL specimens. The equations in Fig. 6 were given by a linear regression analysis of the experimental data. The value  $k$  of the coefficient in the equation for all specimens is 1.64, and that for the specimens excluding C5 is 1.35. (The specimen C5 was excluded because it showed too much degradation of the ultimate strength.) Both of these coefficients exceed the original value 1.0, which means that the ratio of the ultimate strength reduction of the RC member is larger than that of the weight reduction of the reinforcing bar.

To evaluate the degradation in ultimate strength of the RC member caused by the corrosion, it is important to understand physical behavior of their internal corroded bar. Fig. 7 shows the relationship between the ratio of the weight reduction  $C$  and the ratio of  $f_{suc}/f_{sun}$ , in which  $f_{suc}$  means the ultimate tensile strength of the corroded bar, and  $f_{sun}$  means that of no corroded bar.

In this examination, the equation (2) is converted to the equation (3), in which  $P_{uc}/P_{un}$  in the equation (2) is substituted by  $f_{suc}/f_{sun}$ . The coefficient  $k$  in the regression line corresponding to all the points is 1.35. That is larger than 1.0, in the same way as in the Fig. 6.

$$f_{suc}/f_{sun} = 1 - kC \quad (3)$$

Table 3 shows the summarized result of the coefficient  $k$  derived from the experiments and the other previous test concerning the yield point. The coefficient  $k$  varies from about 1 to about 2, and shows neither specific tendency nor special relationship with each condition. When the value  $k$  is nearly equal to 1.0, it means that the reduction rate of the strength is as much as the ratio of weight reduction. On the other hand, when the  $k$  is larger than 1.0, it is obvious that the reduction ratio of the strength is larger than the ratio of the weight reduction.

It is apparent that the main reason why the value  $k$  is different depending on each study is the difference of their measurement method. In this study, the corrosion product of the reinforcing bar was cleaned and scrubbed with a stiff metal brush and picking out needle after soaking of the reinforcing bar in the citric acid solution for a long period, and the ratio of weight reduction was calculated as the value for the entire region of the test piece. On the other hand in a

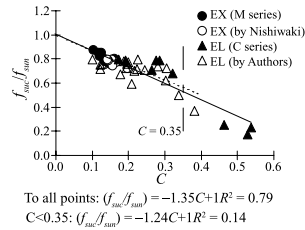


Figure 7.  $C$  vs  $f_{suc}/f_{sun}$ .

Table 3. Coefficient  $k$ .

	This paper			Previous test
	EX	EL	All	
Bar	1.41	1.34	1.35	1.17
RC member	1.97	1.59	1.64	--

\* : value for yield strength

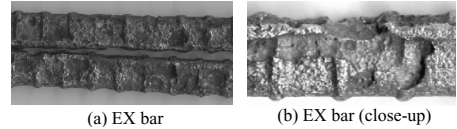


Figure 8. Outward appearance of corroded bar.

previous study sand-blasting is adopted as the cleaning method in order for the test piece to be free from any adhering corrosion products, and the ratio of the weight reduction was calculated as the value for the only 128mm length span near the failure section.

In addition, another reason that causes the difference of the coefficient  $k$  can be pointed out. Fig. 8 shows the outward appearance of the corroded bar of an EX specimen. In this figure, the severe localized corrosion caused by the chloride ion attack can be observed. Such severe localized corrosion should have a significant influence on the mechanical properties of the corroded bar and RC member.

As stated above, corrosion doesn't progress uniformly. Therefore the investigation method of the corrosion amount should be defined clearly and standardized for the accurate evaluation of the coefficient  $k$ .

### 3 EVALUATION OF CORROSION

#### 3.1 Inspection method

To evaluate the mechanical performance of the corroded bar and RC member, it is essential to clarify the uniformity of the localized shape in the every corroded bar through the whole evaluating region. However, there had been no effective method to investigate the extent of the localized corrosion of the corroded bar.

Table 4. General features of 3D laser scanner.

Scan method	Laser beam spot tracking method by triangulation
Laser	Wavelength: 600~700nm Max. output power:1.0mW
Scan pitch	Circumferential: 0.2~60° Vertical: 0.2~406.4 mm
Max. scan region	Diameter: 254 mm, Height: 406.4 mm

Therefore in order to clarify the accurate shape and cross section of the corroded bar, a three dimensional (3D) shape scanning method using the laser beam device without contact was newly developed in this study.

Fig. 9 shows the 3D laser scanner adopted in this experiment, and Table 4 shows its general features. It can digitize the shape of the objective set on the internal turntable through the following steps;

At the first step, the laser beam horizontally emitted at the particular height  $z$  projects a beamspot whose position  $(x,y)$  on the cross sectional plane surface can be specified by means of triangulation method. At the second step, the measuring objective on the turntable is revolved with tracing the position-specified beamspot equiangularly. At the third step, after a 360-degree roll of the turntable, the laser unit (beam device & sensor) is moved upward in the vertical direction within the short interval. These three steps are continuously repeated till the laser unit reaches to the upper limit of the evaluating region, which leads to obtain the whole shape of the objective. In these ways, this 3D scanner can measure the shape not only from a particular point of view but also from all the directions around so that it has very few dead angles.

This 3D scanner can measure the shape of the corroded bar effectively, however, it isn't the perfect method because of its inherent signal noise. Therefore to reduce this noise, white paint is sprayed to the surface of the objective bar. It can be considered that the usage of white paint for noise reduction and the software for calculation of the laser beam intensity adjusted for general measuring objective will generate difference between measured data and the actual shape. In this way, it isn't necessarily proper to use the original output for direct evaluation. However as shown in Fig. 10, measured shape of the cross section (Fig. 10 (b)) is

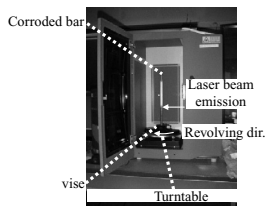


Figure 9. 3D laser scanner.

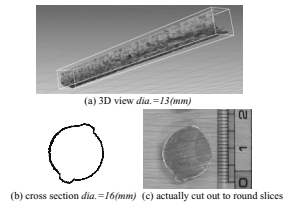




Figure 10. An example of measured data.

Table 5. Objective test pieces.

No.	Reinf. bar	Dia.	C , L	Note
1	No corr.	13	0 , 70	
2	EX	13	0.15 , 150	Specimen M2
3	EL	13	0.12 , 360	Specimen by Authors
4		13	0.40 , 360	Specimen C5
5	ST	16	0.39 , 250	Slab*
6		10	- , 270	Column (Hoop)

L: Measured length (mm) – : No data

\* Wave shaped lateral rib  Others 

almost equal to the actual shape cut out to round slices (Fig. 10 (c)). So it can be judged that this 3D scanner with moderate calibration can digitize the shape of corroded bar effectively with sufficient accuracy.

### 3.2 Inspection result

Distribution of cross section of the tensile reinforcing bar was inspected using this 3D scanner. Table 5 shows the properties of the inspected reinforcing bar, taken out of the EL and EX specimens and the actual structures (ST). The interval of the measurement is 1 degree in the angular direction and 1 mm in the longitudinal direction.

Fig. 11 shows the distribution of the net cross section. The lateral rib and plain body can be regularly observed in the no corroded bar No.1. The lateral rib of the EX bar No.2 can also be observed. On the other hand, the lateral rib of the EL bar No.3 cannot be clearly observed. It is obvious that the electric corrosion firstly makes the lateral rib smaller, and secondly makes the body slenderer.

From the viewpoint of the ST bar, the lateral rib of the ST bar No.6 can be observed clearly, that is similar to the EX bar rather than the EL bar. On the other hand, the ST bar No.5 (Studied by Kashiwabara, see Fig. 12) has rather averaged corrosion in a plain shape. The corrosion of the ST bar No.6 was supposed to be due to the salt injury, and that of No.5 contains the effect of the carbonation. Obviously, the corrosion property depends on their particular corrosion circumstances.

Here suppose the averaged ratio of the cross sectional reduction  $C_2$  as the equivalent index of the ratio of weight reduction  $C$ .



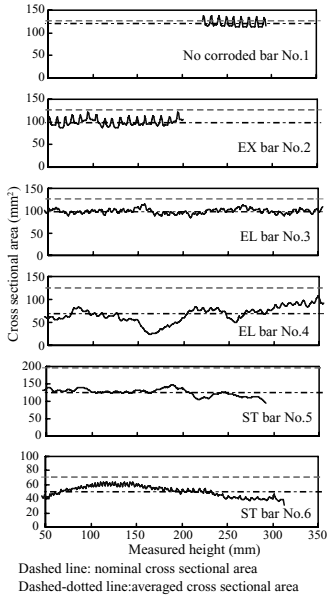


Figure 11. Distribution of net cross section.



Figure 12. ST bar No.5.

$$C_2 = (A_n - A_c) / A_n \quad (4)$$

where  $A_n$  = averaged cross sectional area of no corroded bar,  $A_c$  = averaged cross sectional area of corroded bar. The ratio of reduction of the minimum cross sectional area can be expressed by  $A_{mc}/A_{mn}$ , where  $A_{mc}$  = the minimum cross sectional area of corroded bar,  $A_{mn}$  = that of no corroded bar. Fig. 13 shows the relationship between  $C_2$  and  $A_{mc}/A_{mn}$ . In this consideration, the equation (2) is converted to the equation (5), in which the value  $P_{uc}/P_{un}$  is substituted by  $A_{mc}/A_{mn}$ , the index  $C$  is substituted by  $C_2$  and the index  $k$  is substituted by  $k_2$ .

$$A_{mc}/A_{mn} = 1 - k_2 C_2 \quad (5)$$

The index  $k_2$  of the equation (5) is 1.76 as shown in Fig. 13. According to this value, the reduction rate of the minimum cross sectional area shows about 1.8 times as much as that of the averaged cross sectional area. According to Table 3, the coefficient  $k$  varies from about 1 to 2. The value of the coefficient  $k_2$  is within the range of the coefficient  $k$ .

It is obvious that the index  $k_2$  has a significant influence on the mechanical performance of the corroded bar and the RC member.

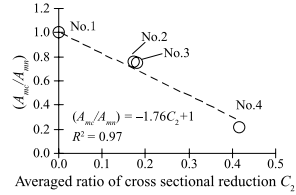


Figure 13.  $C_2$  vs  $A_{mc}/A_{mn}$ .

According to Fig. 11, the EL bar No.3 was in smoothed shape. Despite that, Fig. 13 shows that there is the same tendency and the less difference between the EX bar No.2 and the EL bar No.3. There is a possibility that there is no difference between the EX bar and the EL bar from the viewpoint of the reduction of the minimum cross sectional area. Consequently, it can also be supposed that the mechanical performance of the corroded EX bar is similar to that of the EL bar.

#### 4 CONCLUSION

In this paper, it was proved that the mechanical performance of the corroded bars and RC members could be evaluated not only by the averaged reduction of cross section but also by the localized reduction. Therefore to solve the problem about evaluation for corroded bars and RC members, accurate inspection of the shape of the corroded bar should be carried out. From this point of view, a 3D shape scanning method was proposed in this paper, and proved its sufficient efficiency for inspection in the shape of the corroded bar. These evaluation methods can be expected to be in widespread use.

#### ACKNOWLEDGMENT

This work is financially supported in part by the Japanese Ministry of Land, Infrastructure and Transport.

#### REFERENCES

- Iwanami, M., et al. 2002. Influence of Rebar Corrosion on Load Carrying Capacity of RC Beams, *Proceedings of the Japan Concrete Institute*, Vol. 24, No. 2: 1501–1506. (in Japanese)
- Kashiwabara, S., et al. 2000. A Study on Evaluation Method of the Tensile Yield Strength of Corroded Reinforcing Bar Cut Out from Structure, *the proceeding of the 55th JSCE Annual Meeting*, V-358: 718–719. (in Japanese)
- Nishiwaki, K., et al. 2002. "Fatigue Property of Reinforced Concrete Beam with Corroded Reinforcement," *Proceedings of the Japan Concrete Institute*, Vol. 24, No. 1: 783–788. (in Japanese)
- Oyado, M., et al. 2002. "Characteristics of Fatigue of Reinforced Concrete Beam Damaged by Accelerated Corrosion," *Proceedings of the Japan Concrete Institute*, Vol. 24, No. 2, pp. 961–966. (in Japanese)

# Investigating the effects of corrosion on 45-year-old prestressed concrete bridge beams

Torill M. Papé & Robert E. Melchers

*Centre for Infrastructure Performance & Reliability, University of Newcastle*

**ABSTRACT:** The Sorell Causeway Bridge spanned the Pittwater Estuary in Tasmania, Australia until 2002 when it was replaced after 45 years of service. Demolition occurred due to the formation of longitudinal web cracks along some beams, appearing to follow the trajectory of the post-tensioning tendons, which were suspected to be caused by corrosion. Three beams of varying condition and location were salvaged and load tested to destruction. The beam in the worst condition achieved only 51% of its good-condition counterpart and failed catastrophically. It was confirmed that the longitudinal web cracking followed the tendon trajectory. Generally, corrosion was most severe in areas where concrete cracking was significant, however the majority of rust staining stemmed from the conventional reinforcement. The most severely corroded post-tensioning strands had lost between 75–100% of their cross-section. Corrosion varied from general corrosion to elongated, irregular and deep pitting. Evidence of green rusts, chloride weeping and silvery-gold zones on steel surfaces were also observed.

## 1 INTRODUCTION

The Sorell Causeway Bridge was the first prestressed concrete bridge of its kind in Australia when completed in 1956 (Coombs 1957). It is located over the Pittwater Estuary in Tasmania, Australia and links Hobart to Port Arthur and the popular East Coast. In 1993, longitudinal cracks began appearing along the webs of some beams apparently following the trajectory of the post-tensioning tendons. The bridge was demolished in 2002. Subsequently, a Linkage Grant was obtained from the Australian Research Council to consider the correlation between investigative test results prior to demolition with observations and detailed analysis of beams after demolition. The state road authority, DIER, set aside a number of beams after demolition and three beams were selected, representing the worst, average and best condition beams from the bridge. These were transported to the University's structural engineering laboratory.

## 2 BACKGROUND

The bridge was 457m in length, with 34 spans each approximately 13m long. Each span comprised 14 precast, post-tensioned "T" beams, transversely post-tensioned through a set of five diaphragms per beam to form a stiffened deck. The beam sections between the diaphragms will be referred to herein as bays. The beams, prefabricated using steel moulds, had minimal conventional reinforcement and two longitudinal,

parabolically-draped post-tensioning tendons formed using inflatable rubber tubes (Anon. 1959; Gibbens and Selby-Smith 2004). Each tendon comprised  $18 \times 5$ mm diameter high-tensile wires stressed using the Freyssinet method. Minimum cover to the steel was specified at 25mm. A typical beam cross-section is shown in Figure 1.

The beams were supported on cast-in-situ crossheads and precast, prestressed piles. A nominal 35mm asphalt seal was placed over the beams. The post-tensioning process is shown in Figure 2.

In 1976, the state road authority was informed that calcium chloride had been used as an additive to the concrete during construction to aid early setting of the concrete. This was common practice for the day but has since been banned (Cook 1976). A detailed inspection of the bridge in 1978 revealed corrosion-related defects on the piles and crossheads but no significant defects were identified on the beams (Hurd 1979). In 1993, an underbridge inspection revealed a crack had instigated along the web of beam #12 within the seventeenth span from the western abutment (Giana 1993; van Grieken 1994). Consequently, the frequency of underbridge inspections were increased and by 2000, some 51 beams showed similar cracking. In some instances the cracks were in excess of 20mm width and some prestressing strands were directly exposed to the elements. Figure 3 shows one of the worst cases of longitudinal web cracking.

In 2000 a risk assessment carried out by the University of Newcastle concluded that the adequacy of the

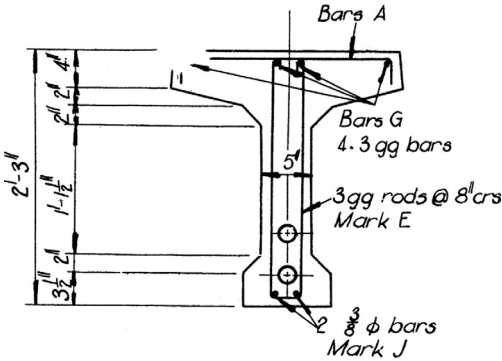


Figure 1. Beam cross-section showing post-tensioning details (courtesy of DIER).



Figure 2. Finalising the post-tensioning procedure on a beam (Coombs 1957).



Figure 3. Typical longitudinal web crack along a beam.

post-tensioning tendons in both longitudinal and transverse directions could not be guaranteed in the light of corrosion damage and that catastrophic failure could not be ruled out. Later that year the decision was made

Table 1. Selected beam description and location.

Beam No.	Beam Location	Cast No.	Casting Date
17/4	Span17, No.3	256	18 Aug 1956
17/3	Span17, No.12	254	17 Aug 1956
118	Unknown	118	18 Jun 1956

to completely replace the bridge and in 2002 the new Sorell Causeway Bridge, entitled McGee's Bridge, was completed.

Out of the interactions between the University and DIER, a research project was initiated with the assistance of the Australian Research Council to investigate the effects and extent of corrosion on the beams. In November 2005 three beams were retrieved from the demolished bridge and relocated to the structural engineering laboratory at The University of Newcastle. A brief description of each beam is shown in Table 1.

The following sections will detail the investigation findings to date, including performance of the beams under load and the extent and severity of corrosion.

### 3 LOAD TESTING

#### 3.1 Equipment requirements and setup

According to DIER records, the bridge was designed to sustain AASHO H20-S16-44-P60 loading (AASHO 1957) or the more realistic scenario of a Foden Semi-Trailer and H10 loading (Anon. 1954). These were the standard minimum loadings at the time of design.

In the laboratory tests the beams were supported on specially fabricated steel bearings to replicate the in-situ beam supports. Two 250kN hydraulic jacks with displacement control, operated remotely from a computer console, were suspended from steel frames to apply the load at the third points along the beam (Figure 4). The load points were aligned as close as possible with the beam vertical centreline to attempt to eliminate eccentric loading and to avoid twisting action.

Twelve 10mm potentiometers were placed evenly across both faces of each beam at centre span to measure concrete strains throughout the load tests. Also, two 100mm travel displacement potentiometers, placed at the same location, were used to measure overall beam deflection. The load was applied incrementally with displacement control throughout.

#### 3.2 Results

Loading increments were set at 5kN steps initially in the elastic range and then at 10kN steps. At higher

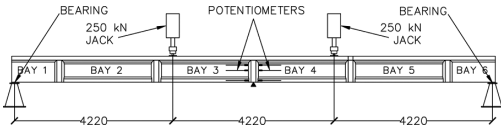


Figure 4. Diagram showing load test setup.

Table 2. Summary of load test results.

Beam No.	Beam Condition	Failure Load (kN)	% of B17/4	Failure Loc <sup>n</sup>
7/4	Good, minor rusting	112	100	Centre
7/3	Poor, web cracks	57	51	Under load
18	Medium, web cracks	78	70	Under load

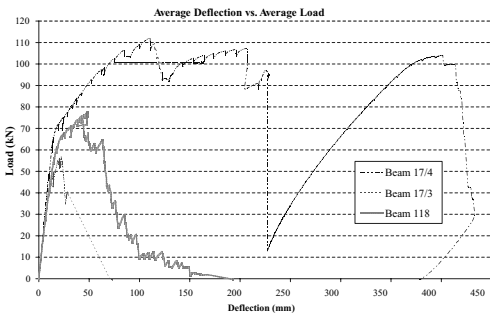


Figure 5. Deflection vs. applied load plot.

load levels, it became increasingly difficult to sustain the loading at a constant level, due to what was eventually identified as the progressive failure of prestressing strands. This was noted by a series of “popping” sounds, starting at approximately a 50kN jack load. “Popping” continued even during pauses in load application for beams 17/3 and 118. Table 2 summarises the load test results, while Figure 5 shows the load-deflection plots for each beam tested.

Beam 17/4 failed in bending at about mid-span close to the central diaphragm at an average point load of 112kN. Figure 5 shows the load deflection plot in blue. Approximately 10 strands failed. Regularly spaced vertical cracks were observed across the face of the beam, becoming finer further away from the centre of the beam. The largest cracks observed at the failure point were approximately 20mm in width.

Beam 17/3 failed in shear at the fourth diaphragm stemming from the longitudinal web cracking evident in bay 5. It reached a maximum average load of 57kN, which is approximately half the load capacity achieved

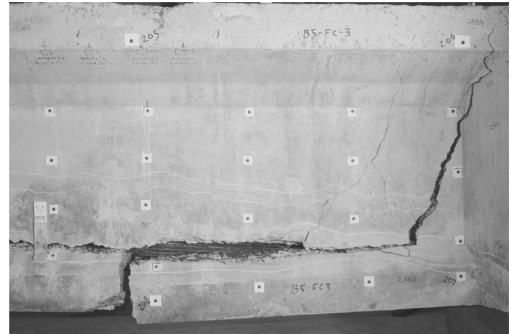


Figure 6. Failure mechanism of Beam 17/3.

by beam 17/4. The deflection plot is shown in red in Figure 5. Some 17 strands failed during the loading process. Several large diagonal cracks running from the diaphragm in towards the prestressing crack formed during the test (Figure 6).

Beam 118 failed in shear, in a manner similar to beam 17/3 at a maximum load of 83kN. It achieved 70% of the capacity observed for beam 17/4. The deflection plot is shown in green in Figure 5. Approximately 33 strands failed. The cracking patterns were similar to those occurring on beam 17/3. Evidently, the reduction in the capacity of the beams tested is roughly proportional to the severity of corrosion identified in the prestressing steel.

After the load tests had been completed, the reinforcing details were examined in some detail. There was evidence that the splicing of the longitudinal reinforcement which should have had splices approximately 1ft (350mm) long over each diaphragm did not comply with the design requirements. Exposure of some of the joints overlaps revealed splices of only approximately 75mm length. This may have contributed to the observed behaviour of the beams under load (especially beam 17/4).

## 4 CORROSION OBSERVATIONS

### 4.1 External visual observations

Of the beams tested, beams 17/3 and 118 exhibited longitudinal web cracking on both webs in bay 5. External cracking appeared to follow the trajectory of the post-tensioning tendons which was confirmed after load testing. Crack widths varied from 0.5mm to 15mm. Similar but much smaller cracks were observed in bay 4 of both beams. Rust staining was visible on the exterior concrete surfaces of all beams tested, in particular adjacent to spalls, cracks and zones of low cover. Closer inspection showed that this was mainly at shear ligatures and lower longitudinal bars, but little

or no corrosion products were observed adjacent to the longitudinal web cracking.

#### 4.2 Strands from post-tensioning tendons

As anticipated, beams exhibiting longitudinal cracking had severe strand corrosion, especially those from bay 5 of beam 17/3. Where cracking was most severe, more than 75% of the cross-section had been lost to corrosion (by inspection). It was observed that a small number of strands had lost its entire section due to corrosion whilst in service. Corrosion patterns were indicative of both general and pitting corrosion, however qualification is continuing. Strands subjected to severe corrosion are shown in Figure 7.

Minimal rust staining was noted adjacent to the corroded strands, despite substantial section loss. Areas that did have a buildup of corrosion products were photographed and analysed. Colours varied between yellow, orange, and shades of green to dark red, brown, and black. Green and black corrosion products oxidised quickly once exposed to air, suggesting anaerobic products. XRD results indicate the presence of magnetite, lepidocrocite and goethite. Lesser traces of ferric oxychloride and akaganeite were also noted. Portlandite and other cement-related products were identified.

During the dissection of a heavily corroded section from beam 17/3, an intact segment from the lower tendon was retrieved, revealing the profile of the strand group (Figure 8). Strands have preferentially corroded along the top and sides of the tendon, showing irregular, semi-circular, concave corrosion profiles.

#### 4.3 Conventional reinforcement

Most conventional reinforcement retrieved from the beams tested was found to be in good condition. However some areas exhibited spalling and cracking. As



Figure 7. Profile of corroded strands.

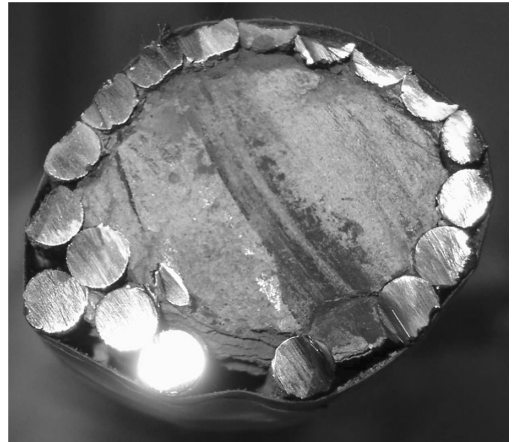


Figure 8. Profile of strand group.



Figure 9. Extent of rust staining.

previously noted, corrosion of the conventional reinforcement was observed as the predominant source of rust staining. Corrosion products had migrated considerable distances, as shown in Figure 9.

Detailed analysis of corrosion products is continuing, however initial results from XRD analysis have indicated typical corrosion products such as magnetite, haematite, lepidocrocite, goethite, and wustite. Traces of quartz and calcite were also detected in samples, which originate from the surrounding concrete.

Reinforcement from bay 5 of beam 17/3 showed the most severe corrosion, with section losses greater than 75% by geometric inspection. Corrosion patterns for both longitudinal and shear reinforcement were general and localised. Deep and irregular pitting was observed particularly on shear ligatures where longitudinal cracking was most severe (Figure 10).

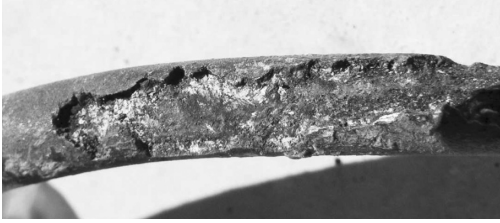


Figure 10. Deep and irregular pitting of shear ligature.

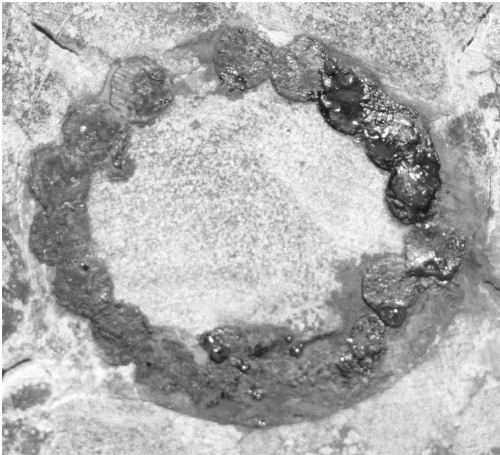


Figure 11. Evidence of ferric chloride.

#### 4.4 Evidence of ferric chloride

Upon exposing freshly cut concrete surfaces to air, it was noted that small beads of iridescent fluid were weeping from steel/concrete interfaces (Figure 11). Occurrences of this phenomenon were more frequent on sections where the beam condition was poor. Upon drying, the fluid formed an orange-brown crystalline crust. A sample was analysed using XRD and SEM, which identified the presence of ferric chloride.

Ferric chloride has been recorded in previous archaeological studies for iron artefacts and is often referred to as “sweating” or “chloride weeping”. The phenomenon occurs when steel with high chloride ion concentrations dries out rapidly or there are changes in relative humidity (Gilberg and Seeley 1981; Sel-wyn et al. 1999). Typically due to the instability of ferric chloride in the presence of water, it will oxidise and only small quantities are found in archaeological practice. Due to the presence of moisture and the soluble nature of chloride ions, the ferric chloride is often considered to have been washed away or incorporated into other corrosion products (Copson 1945).

#### 4.5 Other observations

Where corroded steel was exposed, areas of bright blue-green rust were noted on or adjacent to both prestressing and reinforcing steel surfaces (Figure 12). The rust oxidised quickly to a black powder, most likely magnetite. This behaviour suggests the presence of green rusts which results from the oxidation of iron (II) hydroxides (Cornell and Schwertmann 2003). Green rusts are normally associated with chloride, sulphate or carbonate ions and also with marine environments (Gilberg and Seeley 1981).

Some of the corrosion products indicate corrosion may have been influenced by bacterial action. For example, there was black spotting on the surface of various prestressing strands retrieved from beams 118 and 17/3 (Figure 13). The product oxidised quickly to brown rust once exposed to air. This suggests that it is an anaerobic corrosion product and in turn this suggests the presence of bacteria (Chaves 2005; Genin 2002). This is currently under investigation.

Moist, black rust was found in pits on several strands in bay 5 of beam 118 (Figure 14). Due to the rapid oxidation of the rust, the exact composition is

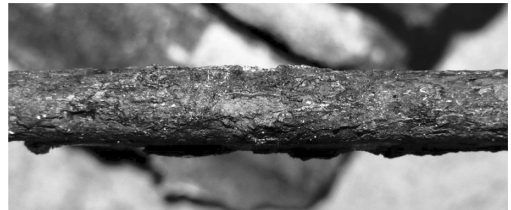


Figure 12. Green rust on strand.



Figure 13. Black spotting across strands.

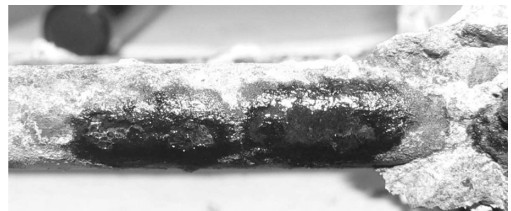


Figure 14. Moist, black rust on strand.





Figure 15. Silvery gold surface on ligature.

unknown. However SEM analysis revealed high levels of chloride.

Zones of silvery-gold coloured steel were noted on some shear ligatures and also strands (Figure 15). This is indicative of the presence of sulphur and perhaps bacterial activity. Tests are continuing.

## 5 CONCLUSIONS

Several beams were taken from the Sorell Causeway Bridge to investigate the extent and severity of corrosion that had been identified whilst the bridge was in service. Load testing revealed that beam capacity was significantly impaired due to corrosion of the prestressing strands and conventional reinforcement, with the reduction in capacity roughly proportional to the severity of corrosion. It was confirmed that the longitudinal web cracking followed the tendon trajectory, however the majority of rust staining was from the conventional reinforcement. Corrosion products were typical for steel embedded in concrete. Pitting corrosion was observed on strands located at the top of tendons in the worst affected areas, with black and green corrosion products observed. Evidence of ferric chloride was also noted weeping out of prestressing strand and tendon interfaces. The observations presented in this paper suggest that bacteria may have influenced the corrosion process of both prestressing strands and conventional reinforcement.

## ACKNOWLEDGEMENTS

The work reported herein forms part of project 2096 supported financially by the Australian Research Council. In addition, the Department of Infrastructure, Energy & Resources provides financial and in-kind support. Both sources are gratefully acknowledged.

## REFERENCES

- AASHO (1957). *Standard Specifications for Highway Bridges*. Washington, DC: American Association of State Highway Officials. 7th Edition.
- Anon. (1954). Sorell causeway no. 1—design of pre-stressed concrete superstructure. Technical report, Department of Public Works. Design Calculations.
- Anon. (1959). Forming cores in concrete with inflated rubber tubes. *Concrete Construction Magazine*.
- Chaves, L.H. (2005). The role of green rust in the environment: A review. *Revista Brasileira de Engenharia Agrícola e Ambiental* 9(2), 284-288. 2005.
- Cook, G. (1976). Use of calcium chloride in bridge girders. Letter.
- Coombs, W. (1957). The sorell causeway bridge: Longest pre-stressed concrete bridge in australia. *Tasmanian Architect June*, 24-25.
- Copson, H. (1945). A theory of the mechanism of rusting of low alloy steels in the atmosphere. *ASTM Bulletin* 45, 554-590.
- Cornell, R. and U. Schwertmann (2003). Chapter 1: Introduction. In *The Iron Oxides: Structure, Properties, Reactions, Occurrences and Uses*, pp. 1-7. Weinheim: Wiley-VCH Verlag GmbH & Co.
- Genin, J.-M. (2002). Green rusts and their relationship to iron corrosion; a key role in microbially induced corrosion. *Hyperfine Interactions* 139/140, 119-131. 2002.
- Giana, F. (1993). Bridge inspection record: Sorell causeway—tasman highway. Technical report, Department of Transport. Bridge Inspection Report.
- Gibbins, B. and P. Selby-Smith (2004). Design—construction of sorell causeway channel bridge, hobart, tasmania. *PCI Journal May-June*, 56-66.
- Gilberg, M.R. and N.J. Seeley (1981). The identity of compounds containing chloride ions in marine iron corrosion products: A critical review. *Studies in Conservation* 26(2), 50-56.
- Hurd, R. (1979). Sorell causeway—inspection of underside of deck and piles to waterline. Technical report, Department of Public Works, Hobart. Condition Report.
- Selwyn, L.S., P.J. Sirois, and V. Argyropoulos (1999). The corrosion of excavated archaeological iron with details on weeping and akaganite. *Studies in Conservation* 44(4), 217-232.
- van Grieken, A.N. (1994). Sorell causeway no. 1 bridge hobart tasmania—preliminary report. Technical report, Remedial Engineering. Condition Report.

# Analytical modelling of FRP strengthened steel beams

C. Pellegrino, E. Maiorana & C. Modena

*Department of Structural and Transportation Engineering, University of Padova, Italy*

**ABSTRACT:** In this paper an analytical procedure to predict flexural behaviour of FRP strengthened steel and steel-composed elements, based on the cross-section behaviour, taking into account non-linear behaviour of the materials with any configuration of FRP reinforcement is shown. Analytical provisions are compared to some experimental results available in literature about flexural behaviour of FRP strengthened steel and steel composed elements showing a good agreement of the results also in the non-linear-phase until failure.

## 1 INTRODUCTION

The degradation of aging steel bridges over the years have led to the need for structural strengthening. At the same time, traffic volumes and allowable truck loads have steadily increased. As a result, most of the old bridges are now underdesigned according to current design codes. In the ambit of life-cycle infrastructure engineering, the strengthening of existing bridges has become a new engineering challenge and cost-effective rehabilitation methods are in high demand.

FRP materials have a high strength-weight ratio, do not involve problems due to corrosion, are extremely manageable and are commonly used for strengthening of structural reinforced concrete members (Pellegrino and Modena 2002, Pellegrino and Modena 2006, Pellegrino et al. 2008) but limitedly studied and used for strengthening of steel elements and, above all, steel-composed elements. A number of studies about FRP strengthening of concrete structures have resulted in the first design guidelines for concrete structures strengthened with externally applied FRP. American ACI 440-02 (ACI Committee 440 2002), European fib bulletin 14 (fib T.G. 9.3, 2001) and Italian Recommendations (CNR-DT 200 2004) are examples of such guidelines.

Main approaches proposed in literature to study the phenomenon of the delamination (Buyukozturk et al. 2004), are those based on linear elastic analysis of internal stresses (Täljsten 1997) and those based on the linear elastic fracture mechanics (Lenwari et al. 2005, Lenwari et al. 2006, Colombi 2006). These theories have not been validated with a sufficient number of experimental results due to the few experimental data available in literature.

In this paper the general method based on cross-sectional equilibrium, which takes into account material non-linearities, is proposed for the study of the global behaviour of generic steel and steel-composite elements strengthened in flexure with FRP. This method is general and allows to take into account material non-linearities and any geometry of the structural steel or steel-composite element and FRP reinforcement.

## 2 SHEAR AND AXIAL STRESS IN THE FRP

One of the first works in which a rigorous procedure to determine shear and axial stress in the FRP is shown in (Täljsten 1997). This approach is based on the following hypotheses:

- plane sections remain plane;
- shear deformation of the metallic beam and reinforcement are neglected;
- perfect bond between materials;
- linear elastic constitutive laws for the materials;
- normal and shear stress does not change with the thickness of the adhesive layer and the reinforcement;
- bending stiffness of the beam that is to be strengthened is much greater than the stiffness of the strengthening plate.

Axial stress in the FRP is calculated on the basis of the shear stress  $\tau(x)$  in the adhesive layer (Fig. 1):

$$\tau(x) = \frac{G_a P}{2sE_s W_s} \frac{(2l + a - b)}{(l + a)} \frac{(a\lambda e^{-\lambda x} + 1)}{\lambda^2} \quad (1)$$



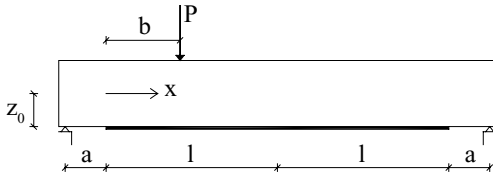


Figure 1. FRP strengthened beam.

where the meaning of the symbols is indicated in appendix and  $\lambda$  is expressed as follows (Täljsten 1997):

$$\lambda^2 = \frac{G_a b_f}{s} \left( \frac{1}{E_s A_s} + \frac{1}{E_f A_f} + \frac{z_0}{E_s W_s} \right) \quad (2)$$

For concentrated and symmetrical loads Eq. (1) can be simplified in Eq. (3):

$$\tau(x) = \frac{G_a P}{2s E_s W_s} \frac{(a\lambda e^{-\lambda x} + 1)}{\lambda^2} \quad (3)$$

Axial stresses can be obtained integrating shear stresses along beam axis:

$$\sigma(x) = \int_0^l \tau(x) dx \quad (4)$$

and therefore:

$$\sigma(x) = \int_0^l \frac{G_a P}{2s E_s W_s} \frac{(a\lambda e^{-\lambda x} + 1)}{\lambda^2} dx \quad (5)$$

Solving the integral the following equation is obtained:

$$\sigma(x) = \frac{b_f G_a P}{2s A_f E_s W_s} \frac{x + a(1 - e^{-\lambda x})}{\lambda^2} \quad (6)$$

An important parameter influencing shear stress in the adhesive, and therefore delamination phenomenon, is the distance between the support and the end of the anchorage  $a$ . From Eq. (3) it is possible to obtain an expression for the maximum distance between the support and the end of the reinforcement:

$$a_{\max} = \frac{2s E_s W_s \lambda}{G_a P} \tau_k - \frac{1}{\lambda} \quad (7)$$

End delamination occurs before steel yielding for  $a > a_{\max}$  and therefore potentialities of the reinforcement cannot be fully developed.

Italian Recommendations CNR-DT 202/2005 (Italian Research Council, 2005) give a simplified formulation only for the maximum value of shear and normal

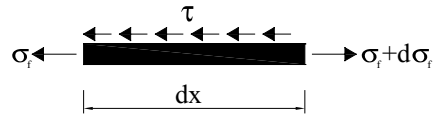


Figure 2. Equilibrium of a segment of FRP plate.

stresses in the adhesive. The formulation of the shear stress is the following:

$$\tau_{\max} = \frac{G_a y_s}{\lambda s E_s I_s} \Delta M(0) \quad (8)$$

$\Delta M(0)$  it is the bending moment in the point in which  $x = 0$  (the beginning of the FRP plate).

The following analytical procedure (Pellegrino and Modena 2008) can be implemented for the calculation of the shear stress in the adhesive on the basis of the deformations in the FRP. Bond behaviour is governed by the following equation:

$$\frac{d^2 s}{dx^2} - \frac{1}{n \cdot t \cdot E_f} \cdot \tau(s(x)) = 0 \quad (9)$$

The values of bond/shear stress  $\tau$  are calculated by a simple equilibrium equation of a segment of FRP sheet (see Fig. 2) subjected to normal stresses  $\sigma_f$  and  $\sigma_f + d\sigma_f$  and to shear stresses  $\tau(x)$  along length  $dx$  of the segment.

The equilibrium equation may be written as follows:

$$n_f t_f d\sigma_f = \tau(x) dx \quad (10)$$

Assuming linear elastic behavior until failure:

$$d\sigma_f = E_f d\varepsilon_f \quad (11)$$

Therefore, substituting Eq. (14) into Eq. (13), one obtains:

$$\tau(x) = n \cdot t \cdot E_f \frac{d\varepsilon_f}{dx} \quad (12)$$

The calculation of shear stress and slip can be obtained by means of Finite Differences method through discrete values of the strains along the FRP:

$$\tau(x_i) = \frac{1}{2} n \cdot t \cdot E_f \left( \frac{\varepsilon_{i-1} - \varepsilon_i}{x_i - x_{i-1}} + \frac{\varepsilon_i - \varepsilon_{i+1}}{x_{i+1} - x_i} \right) \quad (13)$$

where index  $\varepsilon_i$  indicates deformation at generic position  $i$ , and  $x_i$  the position  $i$ .

### 3 PROPOSED METHOD

The proposed method is based on the equilibrium of the cross-section and consists in an iterative procedure which takes into account non-linear behaviour of the materials. The iterative method consists in the following steps:

- the value of the stress in the extreme fiber of the section is assumed and the corresponding deformation is obtained on the basis of the assumed constitutive law;
- a tentative value of the depth of the neutral axis and therefore the strain diagram is obtained on the basis of the hypothesis of plane sections;
- stresses in the section are computed with the different constitutive laws;
- translational equilibrium is imposed (see Fig. 3).

$$F_1 + F_2 + F_3 = F_4 + F_5 + F_6 + F_7 \quad (14)$$

The method is general and also applicable for steel composite sections (see Fig. 4):

$$F_1 = F_2 + F_3 + F_4 + F_5 \quad (15)$$

- if Eq. 14 (or Eq. 15) is not satisfied one returns to points *b*), *c*), *d*) with a different position of the neutral axis, up to the satisfaction of Eq. 14 (or Eq. 15);
- when exact position of the neutral axis is determined, the ultimate moment of the strengthened section can be obtained with the following expression (see Fig. 3 or Fig. 4):

$$M = \sum F_i \cdot d_i \quad (16)$$

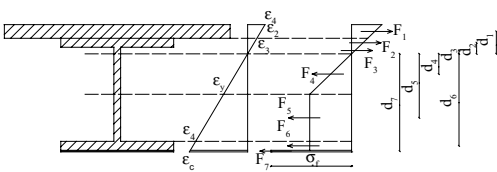


Figure 3. Strain and stress diagram and internal forces distribution for the steel section.

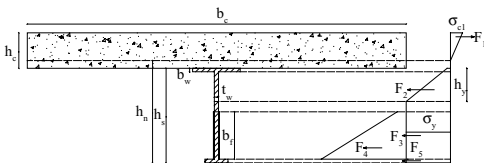


Figure 4. Stress diagram and internal forces distribution for the steel composite section.

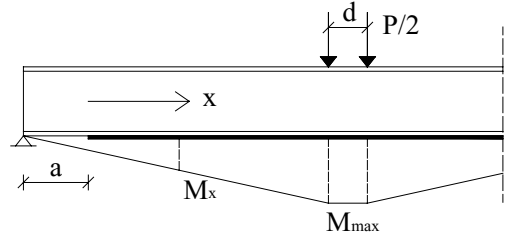


Figure 5. Example of load scheme for the calculation of the stress in the FRP along the beam.

The iterative procedure continues for each increase of the stress in the FRP, correlating the stress in the FRP to the bending moment.

For each value of the load *P*, the value of the maximum moment *M*<sub>max</sub> and the corresponding coordinate can be found on the basis of the load scheme (see Fig. 5):

$$x_{\text{equiv}} = \frac{M_x \cdot \frac{l-d}{2}}{M_{\text{max}}} - a \quad (17)$$

The coordinate *x* is therefore correlated to the value of the moment, the load and finally the corresponding stress in the FRP  $\sigma(x)$ . The curve  $\sigma = \sigma(x)$  is not obtained with the assumption of linear elastic behaviour of the materials but for each material the correspondent non-linear constitutive law is used until failure. The procedure can also be applied to steel-composed beams with collaborating concrete slab and any configuration of the external FRP reinforcement (both at the inferior edge and along web of the beam) assuming the rigid connection (no sliding is allowed) between steel and concrete.

It is also possible to obtain, at discrete points, through the previous analytical procedure (Eq. 13), the diagram of the shear stresses  $\tau = \tau(x)$  between steel and FRP on the basis of the deformation  $\varepsilon = \varepsilon(x)$  also in presence of plastic deformations of the steel and non-linear behaviour of the concrete for steel-composed sections.

### 4 VALIDATION WITH EXPERIMENTAL TESTS

Few experimental tests are currently available in literature on steel flexural elements strengthened with FRP. Three experimental investigations about flexural steel and steel-composed beams strengthened with FRP are considered to validate the proposed analytical procedure.

#### 4.1 Commercially available profile strengthened with FRP at the tensile edge

The experimental investigation of Colombi and Poggi (2006) has been developed on four beams: the first beam was not strengthened, two beams were strengthened with one CFRP (Carbon FRP) layer, one was strengthened with two layers (Fig. 6).

The aim of the experimental investigation has been the study of the behaviour of the steel beams strengthened with CFRP under normal service conditions (steel yielding did not occurred).

Results are reported in terms of stress  $\sigma(x)$  of the CFRP at strain-gauges' position. Corresponding strains  $\varepsilon(x)$  are calculated on the basis of the hypothesis of linear elastic behaviour of the CFRP until rupture to obtain the corresponding shear stresses  $\tau(x)$  between steel and CFRP.

In Fig. 7 theoretical curves and experimental results (Colombi and Poggi 2006) in terms of maximum longitudinal stress in the reinforcement  $\sigma_{CFRP}$  versus distance from plate end are shown for one FRP layer (Fig. 7a) and two FRP layers (Fig. 7b). The proposed method based on the equilibrium of the cross-section and Täljsten (1997) theory follow enough well the experimental data.

#### 4.2 Welded beam with steel plate in compressed zone strengthened with FRP at the tensile edge

The experimental investigation has been developed by Lenwari et al. (2005, 2006) on five beams with steel plates welded in compressed zone to prevent rupture due to instability (Fig. 8). FRP reinforcement had different lengths.

Results were expressed in terms of strain  $\varepsilon(x)$  of the FRP reinforcement at strain-gauges' position.

In Fig. 9 FRP stress  $\sigma_f$  at midspan vs. applied load obtained with Täljsten theory and proposed method based on the equilibrium of the section are compared with experimental results (Lenwari et al. 2005, 2006).

Values of  $\sigma_f$  in the FRP at midspan are well approximated by both Täljsten theory and proposed method until yielding of the steel. After yielding of the steel Täljsten theory fails to follow experimental results because it is based on the hypothesis of linearity of the

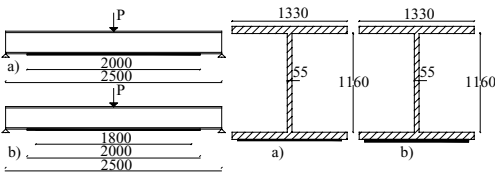


Figure 6. Specimens of Colombi and Poggi (2006). (a) strengthened with 1 FRP layer; (b) strengthened with 2 FRP layers (lengths in mm).

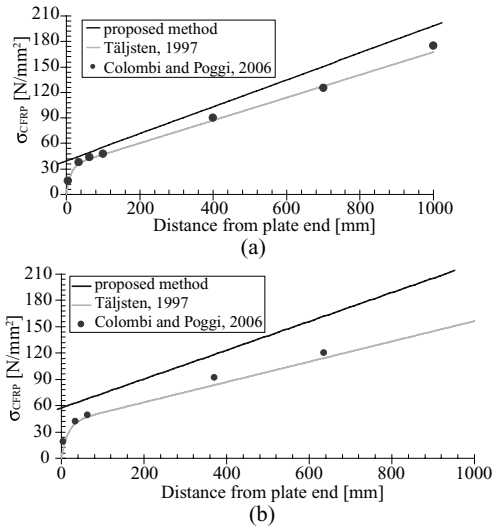


Figure 7. Theoretical curves and experimental results (Colombi and Poggi 2006) in terms of maximum longitudinal stress in the reinforcement  $\sigma_{CFRP}$  versus distance from plate end for one FRP layer (a) and two FRP layers (b).

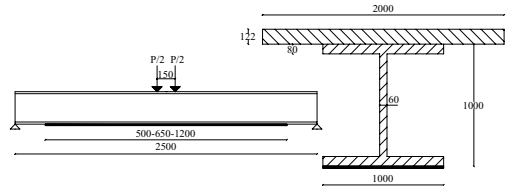


Figure 8. Load scheme and geometry of the cross-section of Lenwari's (2005, 2006) experimental investigation (lengths in mm).

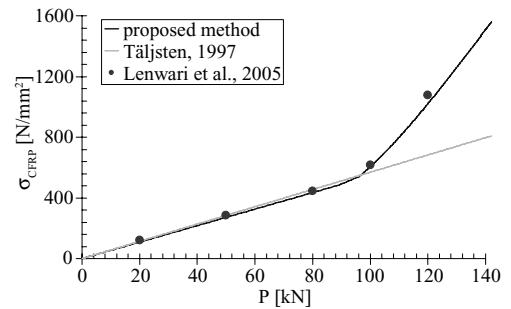


Figure 9. Stress in the FRP at midspan vs. applied load obtained with Täljsten theory and proposed method compared with experimental results (Lenwari et al. 2005, 2006).

materials while the proposed analytical method based on the equilibrium of the section gives a good approximation of the experimental values also in the plastic phase.

The diagram in Fig. 10 shows the variation of the shear stresses between FRP and steel along the longitudinal axis of the beam obtained with Täljsten and present method.

The first sudden increase of the shear stress shown by the curve obtained with the proposed method points out the beginning of the yielding in the inferior flange while the following sudden increase is due to the complete yielding of the flange with the beginning of the yielding of the web.

The violent increase of the shear stress is due to the strong reduction of the resisting contribution of the steel substrate and the consequent relevant transfer of forces from steel to FRP.

The non-linear behaviour of the shear stresses near midspan is due to the progressive yielding of the web when neutral axis moves rapidly towards the flange.

The proposed method based on equilibrium equations allows to deeply study the global behaviour of the FRP strengthened beam also in the plastic phase, both in terms of axial and shear stresses.

#### 4.3 Steel-composed beam with FRP reinforcement at the tensile edge and on the web

The experimental investigation about steel-composed beams has been developed by Al-Saidy et al. (2004) (see Fig. 11).

The aim of the experimental investigation has been the study of the behaviour of damaged steel-composed beams, strengthened with different types and geometries of CFRP reinforcement.

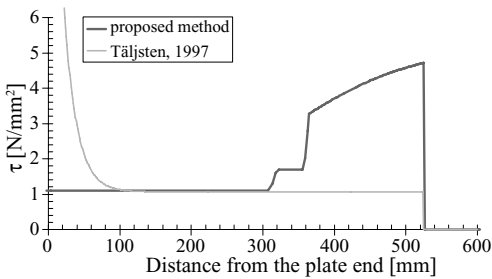


Figure 10. Variation of the shear stresses along the longitudinal axis of the beam of Lenwari et al. (2005, 2006) obtained with Täljsten and proposed method.

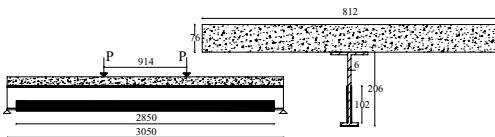


Figure 11. Longitudinal section and load geometry during the experimental tests (lengths in mm).

previously damaged removing a portion (50% or 75%) of the inferior flange of the steel beam. Externally bonded FRP reinforcement has been applied on web and inferior flange of the steel beam.

In this case, not only the presence of the concrete slab in the superior part of the composed section (that introduces a further non-linearity of material), but also the application of the FRP on a vertical portion of the web (see Fig. 11) (which does not allow to assume a constant distribution of the stress in the FRP) are taken into account. The parabolic equation of Hognestad (1951) is assumed as concrete constitutive law. The hypothesis of rigid connection is also assumed.

In Figs. 12 and 13 theoretical load—displacement diagram, obtained with the proposed method, at midspan for specimens D50R2 and D75R1 and the experimental one (Al-Saidy et al. 2004) are respectively shown.

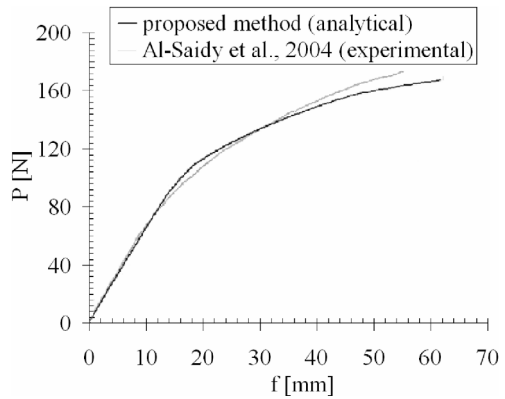


Figure 12. Analytical-experimental comparison for specimen D50R2 (Al-Saidy et al. 2004).

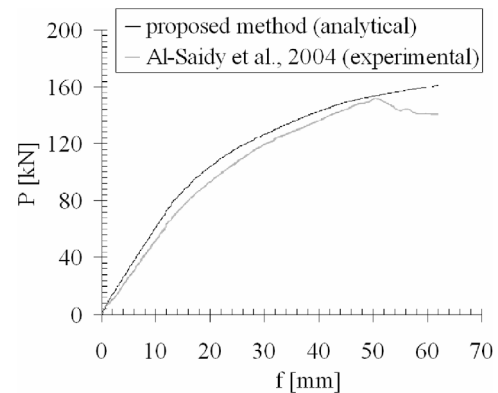


Figure 13. Analytical-experimental comparison for specimen D75R1 (Al-Saidy et al. 2004).

Three FRP plates have been applied for specimen D50R2: two at both sides of the web and one below the tensile flange. The proposed method well approximate the experimental behaviour of the steel-composed beam including a good estimation of the ultimate load (Fig. 12).

A portion of the inferior flange (75%) has been removed for the specimen D75R1 (Fig. 13). It has been strengthened with two FRP plates in the inferior part of the web at both sides.

Also in this case the proposed method well approximate the experimental behaviour of the steel-composed beam except for a small difference of the failure load due to sliding between concrete and steel. The application of the FRP plates almost until the supports has avoided the delamination.

Finally the proposed analytical method, based on equilibrium of the section, provides with good degree of accuracy the behaviour of steel-composed beams, damaged or not, strengthened with FRP plates both on the flange and on the web when delamination of the FRP and sliding between steel and concrete are avoided.

## 5 CONCLUSION

In the ambit of life-cycle infrastructure engineering, the strengthening of existing steel bridges has become a new engineering challenge and cost-effective rehabilitation methods are in high demand.

In this paper, a method based on the equilibrium of the cross-section of the flexural element is proposed for the study of the global behaviour of steel and steel-composed beams with any FRP reinforcement configurations, taking into account material non-linearities. The method was implemented to describe the structural behaviour (for example load-displacement diagram, axial and shear stress diagram along the longitudinal axis of the beam) of steel and steel-composed elements until failure. The theoretical behaviour obtained with the proposed method was compared with the experimental results described in some of the few experimental investigations available in literature about steel flexural elements (Colombi and Poggi 2006, Lenwari et al. 2005, 2006), and steel-composed (Al-Saidy et al. 2004) obtaining a good agreement of results.

The proposed method is completely general and can be used to describe the global structural behaviour of steel and steel-composed beams (assuming rigid steel-concrete connection) strengthened with FRP materials, taking into account material non-linearities and with any reinforcement geometry, well approximating experimental behaviour.

## REFERENCES

- ACI Committee 440 (2002). "Guide for the design and construction of externally bonded FRP systems for strengthening concrete structures (ACI 440.2R-02)", American Concrete Institute, Farmington Hills, Michigan, USA.
- Al-Saidy A.H., Klaber F.W., Wipf T.J. (2004). "Repair of steel composite beams with carbon fiber-reinforced polymer plates", *Journal of Composites for Construction*, 8(2), pp. 163–172.
- Buyukozturk O., Gunes O., Karaca E. (2004). "Progress on understanding debonding problems in reinforced concrete and steel members strengthened using FRP composites", *Construction and Building Materials*, 18, pp. 9–19.
- CNR Italian Advisory Committee on Technical Recommendations for Construction (2004). "Guide for the Design and Construction of Externally Bonded FRP Systems for Strengthening Existing Structures. Materials, RC and PC structures, masonry structures (CNR-DT 200/2004)", Italian Research Council, Rome, Italy.
- CNR Italian Research Council, Italian Advisory Committee on Technical Recommendations for Construction (2005). "Guidelines for the Design and Construction of Externally Bonded FRP Systems for Strengthening Existing Structures. Preliminary study. Metallic structures" (CNR-DT 202/2005). Italian Research Council, Rome, Italy.
- Colombi P. (2006). "Reinforcement delamination of metallic beams strengthened by FRP strips: Fracture mechanics based approach", *Engineering Fracture Mechanism*, 73, pp. 1980–1996.
- Colombi P., Poggi C. (2006). "An experimental, analytical and numerical study of the static behaviour of steel beams reinforced by pultruded CFRP strips", *Composites: Part B*, 37, pp. 64–73.
- fib Task Group 9.3. (2001). "Externally bonded FRP reinforcement for RC structures", fib bulletin 14, Lausanne, Switzerland.
- Hognestad E. (1951). "A study of combined bending and axial load in reinforced concrete members", *Bulletin No. 399*, Univ. of Illinois, Engineering Experimental Station, Urbana, USA.
- Lenwari A., Thepchatri T, Albrecht P. (2005). "Flexural response of steel beams strengthened with partial-length CFRP plates", *Journal of Composites for Construction*, 9(4), pp. 296–303.
- Lenwari A., Thepchatri T, Albrecht P. (2006). "Debonding strength of steel beams strengthened with CFRP strips", *Journal of Composites for Construction*, 10(1), pp. 69–78.
- Pellegrino C., Modena C. (2002). "FRP shear strengthening of RC beams with transverse steel reinforcement", *Journal of Composites for Construction*, 6(2), pp. 104–111.
- Pellegrino C., Modena C. (2006). "FRP shear strengthening of RC beams: experimental study and analytical modelling", *ACI Structural Journal*, 103(5), pp. 720–728.
- Pellegrino C., Modena C. (2008). "An experimental study on bond behaviour between concrete and FRP reinforcement", *Journal of Composites for Construction*, in print.
- Täljsten B. (1997). "Strengthening of beams by plate bonding", *Journal of Materials in Civil Engineering*, 9(4), pp. 206–212.

# Estimation of life-cycle fatigue damage for suspension bridge hangers

F. Petrini & F. Bontempi

*University of Rome "La Sapienza", Rome, Italy*

**ABSTRACT:** Steel structures are subjected to several vibrations due to wind action. Therefore, in order to ensure an adequate safety level for the users, the life-cycle design of this kind of structures must consider the high cycle fatigue effects. In the case of suspension bridges serving railway traffic, an analysis to prevent the failure due to fatigue effects should take into account the vibrations due to both train transit and wind action. In the present paper this problem is investigated with respect of the case study of long span suspension bridge, where the life duration of different structural members is assessed.

## 1 INTRODUCTION

Wind and traffic induced vibrations are the main causes of fatigue damage in the cables and hangers of suspension bridges. Cause of the high flexibility and reduced weight (in relation of the whole dimension of the structure), suspension cable system of these type of bridges can experiment a great number of tension-cycles with significant amplitude during their life-cycle. In this paper the fatigue problem regarding hangers of the bridge is treated. These members are subjected to axial fatigue effect that can be faced with simplified damage laws and fatigue curves referring to axial experimental data.

Concerning wind fatigue damage, several authors have done studies to assess fatigue behavior of structures (Repetto & Solari 2001 and 2007, Aprile & Benedetti 2000) and cables (e. g. Cluni et al. 2007) under wind action. Because of wind stochastic nature, the problem has to be treated in a probabilistic way. The fatigue damage is correlated with the mean wind velocity magnitude (Ubertini & Bontempi 2008), and the last one can be viewed like a stochastic variable having an annual Weibull probability density function. Consequently, each parameter which can describe adequately the response of the structure will be a stochastic variable too.

The fatigue damage induced by traffic is different in the different members of suspension bridges, depending on the stress rate induced by the transit of the vehicles: in the members which experience low excursions of the stress rate in respect the permanent load, such as the main cables, the expected fatigue damage is low, especially in the case of long span bridges, for which the permanent load is very high. Vice versa,

hangers, deck and secondary components have high change in the stress during the transit of vehicles, and so they are prone to be damaged and substituted several times during the service life of the bridge.

The third aspect of discussion, concerning the subject of the paper, is the interaction mechanism between train and wind. First, there is an aerodynamic interaction caused from the local changes in aerodynamic forces due to the train presence on the bridge deck (Petrini et al. 2005). This effect increase in importance when the geometrical dimension ratios between train and structure (length of the train vs length of the span, height and width of the train vs height and width of the deck section) increase. The second interaction mechanism concerns the structural dynamic behavior, it can be significant in the case of large deflection of the bridge. Third interaction mechanism concerns the fatigue damage interaction: the sum of damages due to wind and train is not equal to the damage caused from train transit when the structure is subjected to the wind action. In the present paper, interaction mechanisms are not considered.

## 2 WIND FATIGUE ANALYSIS

### 2.1 *Wind mathematical and numerical models*

A Cartesian three-dimensional coordinate system  $x, y, z$ , having its origin on the ground is adopted. For each spatial point  $j$  of the domain, the wind velocity field can be decomposed in the three corresponding components ( $V_x(j), V_y(j), V_z(j)$ ). Decomposing  $V_x(j), V_y(j), V_z(j)$  in its medium (time invariant) and its turbulent (fluctuating in time) components, orienting the coordinate system in such a way that the

wind velocity mean component has nonzero magnitude along only one axis ( $y$  axis in the present paper), one can write:

$$V_x^{(j)} = u_j(t); \quad \mathbf{V}_y^{(j)} = V_{mj} + v_j(t); \quad \mathbf{V}_z^{(j)} = w_j(t) \quad (1)$$

in which  $u_j(t)$ ,  $v_j(t)$ ,  $w_j(t)$ , represent the three turbulent components, and  $V_{mj}$  represents the mean velocity magnitude at location  $j$ .

Concerning the mean velocity component, it is a function which varies with  $z$  following the logarithmic law:

$$V_m(z) = u_{fri} \cdot \frac{1}{k} \cdot \ln\left(\frac{z}{z_0}\right) \quad (2)$$

where  $k$  is the Von Karman constant, set to 0,4 by experimental way,  $z_0$  is the rugosity length,  $u_{fri}$  is the friction velocity (Simiu & Scanlan 1996).

Concerning wind turbulent velocity components, they are modeled like a Gaussian stationary and ergodic stochastic processes with zero mean value. The single turbulent spatial component of wind velocity ( $u$ ,  $v$  or  $w$  component) is considered independent from each other. By means of a discretization of the spatial domain in  $n$  points representing the locations where the wind acts on the structure. Adopting an Eulerian point of view,  $u$ ,  $v$  and  $w$  on the whole domain can be represented by three  $n$ -order stochastic vectors in which elements are Gaussian zero-mean stochastic processes. Each of these vectors is completely characterized by the Power Density Spectral (PDS) matrix which assumes the form (e. g. for  $u$  component)

$$\begin{bmatrix} S_{u1u1}(\omega) & \dots & \dots & S_{u1un}(\omega) \\ \vdots & S_{u2u2}(\omega) & \dots & \vdots \\ \vdots & \vdots & \dots & \vdots \\ S_{umu1}(\omega) & \dots & \dots & S_{unun}(\omega) \end{bmatrix} \quad (3)$$

in which  $\omega$  represents the circular frequency of the generic time history signal,  $n$  represents the number of spatial points in which one wants to generate wind velocity time histories. Diagonal terms are called the auto spectra functions, and represent (in some manner) the frequency content of a hypothetic, isolated, punctual time history. The out of diagonal terms, represents the correlation between two different spatial points and are called crossed spectra.

The numerical wind time history simulation is possible by various techniques (Carassale & Solari 2006); in this paper the Weighted Amplitude Wave Superposition method (W.A. W.S.) by using of Proper Orthogonal Decomposition (P.O.D.) of PSD matrix (Ubertini & Giuliano 2008) is adopted. Starting from the wind velocity time histories, the computing of the

acting forces by use of aeroelastic theories is possible (Petrini et al. 2007, Salvatori & Borri 2007).

## 2.2 Probabilistic point of view: Stochastic system analysis

In wind engineering problems, there are many uncertainties parameters, which can be divided into three groups (see Fig. 1):

1. wind uncertainties: divided into mean wind velocity and turbulence intensity caused by the terrain rugosity before the structure
2. structure uncertainties: stiffness, damping, material characteristics, etc.

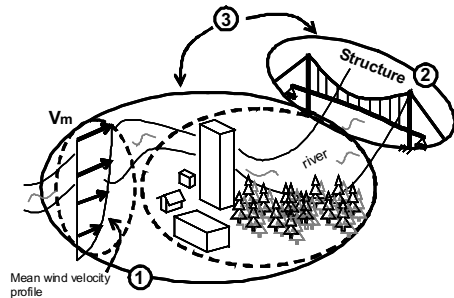


Figure 1. Uncertainties parameters in wind engineering problems.

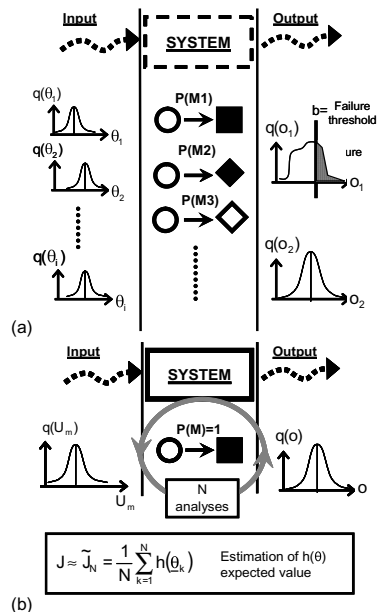


Figure 2. Stochastic system analysis: general (a), by using of Monte Carlo approach in present paper (b).

3. interaction mechanism uncertainties: typically aerodynamic and aeroelastic interactions.

To handling correctly these uncertainties, a stochastic system analysis is required in facing this problem (Augusti & Ciampoli). A general synthesis of stochastic system analysis is shown in Figure 2(a): there are a certain number of stochastic input parameters  $\theta_i$   $i = 1, \dots, n$  having corresponding joint Probability Density Functions (PDFs)  $q(\theta_i)$ , the system can be represented by various deterministic models  $M_i$  (Input/output relations), each of them has a probability of occurrence  $P(M_i)$  (with  $\sum P(M_i) = 1$ ) and, consequently, both output parameters and failure relations are probabilistic too.

In the stochastic system analysis, the expected value  $J$  of a certain function (model)  $h(\theta)$ , can be computed by the probability integral:

$$J = E[h(\underline{\theta})] = \int h(\underline{\theta})q(\underline{\theta})d\underline{\theta} \quad (4)$$

where  $\underline{\theta} \in R^d$  = vector of uncertainties parameters;  $q(\underline{\theta})$  = PDF of uncertainties parameters, and the underline indicates a vector.

A particular case of the stochastic system analysis is the reliability analysis, in which the main objective is to determine the probability of overcoming a certain failure threshold value by an output value. In this case, the probability integral becomes the reliability integral:

$$J = P(F) = \int_{g(\underline{\theta}) \leq 0} q(\underline{\theta})d\underline{\theta} = \int_{R^d} I_F(\underline{\theta})q(\underline{\theta})d\underline{\theta} \quad (5)$$

where, with reference to (4):

$$h(\underline{\theta}) = I_F(\underline{\theta}) = \begin{cases} 0 & \text{if } \theta \notin g(\underline{\theta}) \\ 1 & \text{if } \theta \in g(\underline{\theta}) \end{cases}$$

= indicator function;

$g(\underline{\theta}) \leq 0$  = failure domain.

There are several methods to compute the integral (5); in this paper Monte Carlo method is adopted. By this way, a single deterministic model  $M$  (input/output relations) is assumed. Concerning input parameters, in the case study the mean wind velocity magnitude is assumed as stochastic, having a Weibull annual PDF. Following these positions, the stochastic problem of structural response under wind is faced by the approach synthesized in fig. 2(b). In the case of stochastic fatigue analysis, referring to expression (4), the output is the fatigue damage, and a function  $h(\theta)$  is represented by a damage accumulation law (in the present case the Palmgreen-Miner law). The

expected value of  $h(\theta)$  is the mean damage caused by the wind velocity magnitude probability distribution. Using Monte Carlo method doing  $N$  analyses, the total damage is the sum of the damages caused from each one of the  $N$  analyses, and it becomes a deterministic parameter (associated with the number  $N$ ), instead of that a distribution of probability.

### 3 TRAIN FATIGUE ANALYSIS

In the case of ordinary bridges, and especially the railway ones, the fatigue effects have great impact in the verification and in the design procedures.

In the present paper the fatigue effects are evaluated by means of deterministic analyses, assuming two kinds of trains: the LM71 Eurocode train, whose weight is 8,8 ton/m and 750 meters long, representing a goods train, and a passenger light train, whose weight is 2,44 ton/m and 390 meters long (see Tab 2). The analyses use deterministic crossing timetables, so the fatigue life of the components can be evaluated if the traffic volume is known. The analysis in the domain of time can assess the stress rate in the structural components. The real load scenarios are generally complicated because more train can cross the bridge, at different speed and so with different dynamic impact, and crossing each other at different location. Consequently a reliable evaluation of the fatigue effect can use the results of deterministic simulations coupling them with probabilistic treatment of the data: one can work on the spectral density functions of the crossing, in terms of weight, length, speed and number of train per day, and that of the crossing at certain location of two train running in opposite sense. The same damage accumulation law of the wind simulations is considered, at first keeping separated the contemporary occurrence of wind and traffic loading and neglecting the contemporary presence of two trains on the deck.

The analyses show that different hangers of the structural system have greater vulnerability to traffic induced fatigue than the wind induced one, while other components such as main cables and towers are more sensitive to wind fluctuation and damage accumulation.

### 4 APPLICATION ON A LONG SPAN SUSPENSION BRIDGE

A case study of long span suspension bridge (Petrini et al. 2005) is presented to apply the fatigue damage calculation under wind action and train traffic. The main span of the bridge is 3300 m long, while the total length of the deck, 60 m wide, is 3666 m (including the side spans). The deck is formed by three box sections, the outer ones for the roadways and the central one for the railway.



#### 4.1 Preliminary investigations

Following the indication of Eurocode 3, preliminary static and dynamic analyses have been conducted to assess the sensitivity of various hangers (in various positions along the span) to the fatigue damage.

The wind field in only  $y$  (transversal to the bridge main span), and  $z$  (vertical directions) has been generated numerically, the wind in  $x$  direction (parallel to the span) has been neglected. The mean velocity component has  $y$  direction.

The damage of the same hangers has been investigated under the action of the train type 2 (see Tab. 2) transit.

The analyses have been developed in time domain both for wind action and train transit effects investigation. In the case of wind, it has been applied both along the deck and along the main cables (as shown in Fig. 5(a)), a total of 27 points of action application has been considered (so 27 time histories for each component of wind velocity are needed every analysis). The damage of the hangers represented in Figure 3 and in Table 1 has been investigated under the action of specific wind time histories having  $V_m = 15$  m/s.

The train has been modeled as a system of mobile forces. In Figure 4, time histories of axial force acting in the hanger 352 are shown. In the analyses, the rainflow method is assumed as the fatigue counting method, the Palmgreen-Miner law is assumed as the damage accumulation criterion, the fatigue curve from the Eurocode 3 is assumed for the structural elements damage calculation. In Figure 5(d), the adopted fatigue curve is shown, the detail category has been chosen as 160 (N/mm<sup>2</sup>) and, in this preliminary phase, no fatigue limit has been considered.

#### 4.2 Fatigue damage during life-cycle

In this case, the adopted fatigue curve considers a limit of fatigue (Fig. 7).

To estimate the fatigue damage during life-cycle under wind action, a Monte Carlo simulation has been

done. A set of 450 ( $N = 450$  in Fig. 2(b)) of the analyses described in section (4.1) has been done, each one corresponding to a sample of  $V_m$  which (as previously stated), is assumed as a stochastic variable having annual Weibull distribution of probability. The sampling histogram is shown in Figure 6(a). Focusing on the damage in the critic hanger number 352 (the most damaged by the wind action in the previous section par 4.1), only 30 of the 450 runs produce a damage, in Figure 6(b) the damages are represented versus the mean wind velocity magnitude. One can see that there is a tendency in increase the damage (more than linear), corresponding to an increment of wind mean velocity. However it is also clear that the tendency is not properly monotone, this is probably due to the fact that each analysis has a casual distribution of turbulent velocity peaks along the bridge deck and it is different from each other.

Concerning the fatigue damage caused by the train transit, two typologies of train have been considered (see Tab. 2). In the estimation of the life cycle fatigue, the trains velocities have been considered the same for each transit. To estimate the fatigue damage during life-cycle under train transit, a hypothesis on the traffic intensity has been done: the transit of three type 2 trains (passengers) and the transit of one type 1 train every hour have been hypnotized, for a total of 18 hour every day, six days every week, fifty weeks every year. We have a total of 16200 transits per year of the type 2 train and 8100 transits per year of the type 1 train. The life cycle of the structure has been established to be 200 years long.

Table 1. Damages in investigated hangers (preliminary analysis).

	Hanger number	Wind damage (Um = 15 m/s)	Train damage (LM71 V = 135 Km/h)
Near tower	351	2,44E-07	1,93E-07
	352	3,08E-07	1,68E-07
	353	7,59E-09	8,54E-09
	354	5,44E-09	7,38E-09
	359	4,24E-09	8,96E-09
	360	1,60E-08	7,76E-09
	361	8,00E-09	9,66E-09
	362	6,97E-09	2,12E-08
Quarter span	409	7,80E-08	2,04E-07
	410	8,17E-08	1,80E-07
Midspan	513	2,22E-07	4,04E-07
	514	1,72E-07	3,56E-07
	515	1,71E-07	4,08E-07
	516	1,72E-07	3,60E-07
	517	1,56E-07	4,08E-07
	518	1,63E-07	3,60E-07

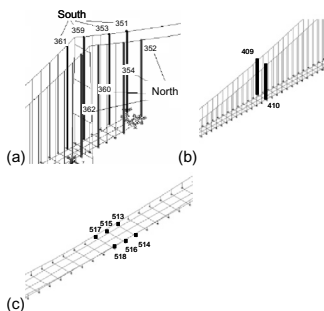


Figure 3. Hangers under investigation: near tower (a), quarter span (b), midspan (c).

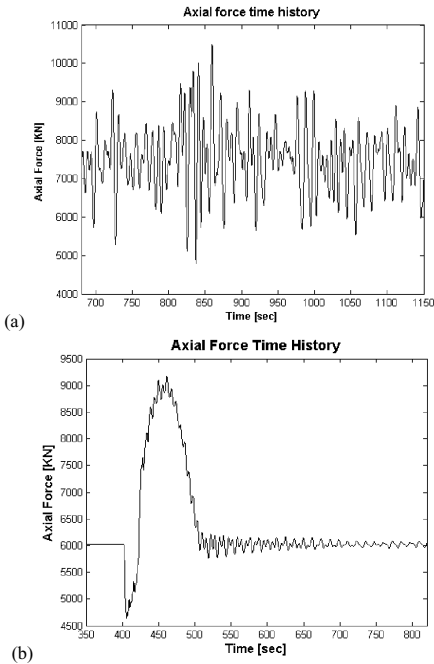


Figure 4. Axial force in the hanger 352: under wind action (a), under train traffic (b).

For the hanger number 352 (critic for wind action), the total damage computed by Monte Carlo analysis is the sum of the damages represented in Figure 6(b), it results equal to 9,67312 exp (-5) and it can be consider

Table 2. Considered train type and train traffic intensity and relative damage in critic hangers.

	Train type	
	1(LM 71)	(2 EC3)
Length [m]	750	390
Weight [ton/m]	8,80	2,44
Velocity [Km/h]	135	250
One transit damage on hanger 517 (critic hanger)	3,072E-07	8,200E-08
One transit damage on hanger 352 (critic hanger for wind action)	1,67E-07	3,90E-08
Total annual transits	16200	8100

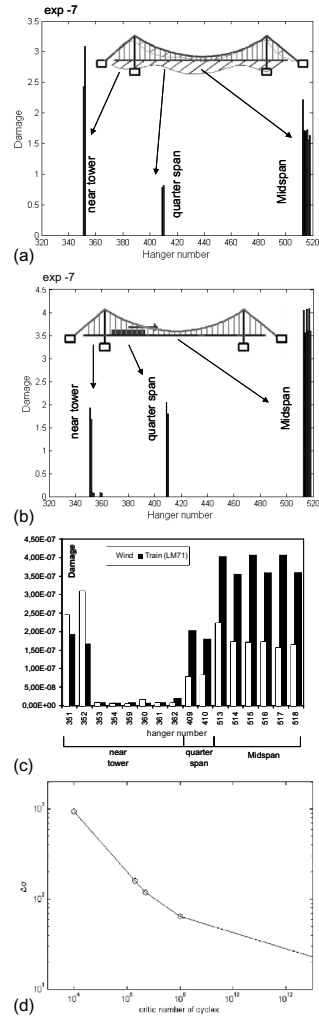


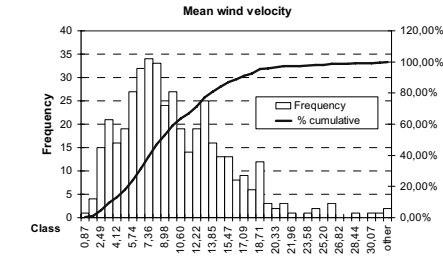
Figure 5. Damages in investigated hangers (preliminary analysis): under wind action (a), under train traffic (b), comparison between wind and train damages (c), adopted fatigue curve (d).

representing an annual damage due to wind action. Consequently the fatigue life of the hanger number 352 under wind action results of 10337,93 years (computed as the inverse of the annual damage).

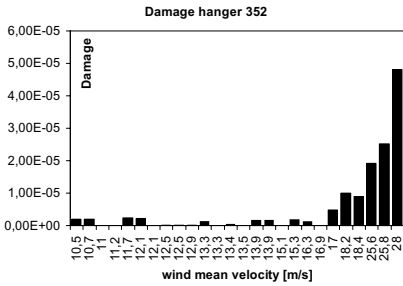
Concerning damages due to train transit in the critic hangers (number 517), they are resumed in Table 4.

## 5 CONCLUSIONS

In the present paper, the estimation of the life-cycle fatigue damage in long span suspension bridge hangers due to both wind action and train transit has



(a)



(b)

Figure 6. Mean wind velocity magnitude sampling (a), damages versus stochastic variable (b).

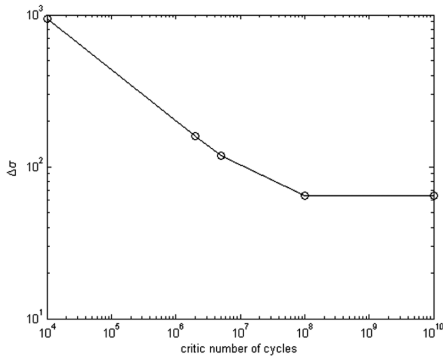


Figure 7. Adopted fatigue curve (evaluation of fatigue damage during life cycle).

Table 3. Life Cycle damage in critic hangers due to train transit and evaluated fatigue life.

Hanger number	Critic for	Total annual damage for train transit	Fatigue Life [years]
517	Train	0,005641	177,2786
352	Wind	0,003021	330,9834

been assessed. Analyses have been conducted in time domain and, concerning the wind-induced fatigue

damage, Monte Carlo technique has been adopted to consider the stochastic nature of the action. Analyses results show that the train transit influences the fatigue life more than wind action; it is also shown that the critic hanger (more damaged from fatigue point of view) is in different location along the deck for the two actions. Further analyses have to be developed to implement wind-train interaction effects.

## ACKNOWLEDGEMENTS

The observations on the theme of this paper with Prof. G. Augusti and Prof M. Ciampoli are gratefully recognized.

## REFERENCES

Aprile, A. & Benedetti, A. 2000. Damage evaluation and control for fatigue under stochastic excitation, Proceedings of 8th ASCE Probabilistic Mechanics and Structural Reliability Conference (PCM2000), Notre Dame, USA (2000).

Augusti, G. & Ciampoli, M. Performance-Based Design as a decision strategy for risk reduction, Probabilistic Engineering Mechanics, (submitted for publication).

Carassale, L. & Solari, G. 2006. Monte Carlo simulation of wind velocity field on complex structures, Journal of Wind Engineering and Industrial Aerodynamic 94 (2006) 323–339.

Cluni, F., Gusella, V. & Ubertini, F. 2007. A parametric investigation of wind-induced cable fatigue, Engineering Structures 29 (11): 3094–3105.

Petrini, F., Giuliano, F. & Bontempi, F. 2005. Modeling and simulations of aerodynamic in a long span suspension bridge, Proceedings of the ninth International Conference on Structural Safety And Reliability, ICOSSAR '05, Rome, Italy (2005) 83.

Petrini, F., Giuliano, F. & Bontempi, F. 2007. Comparison of time domain techniques for the evaluation of the response and the stability in long span suspension bridges, Computer & Structures 85: 1032–1048.

Salvatori, L. & Borri, C. 2007. Frequency and time-domain methods for the numerical modeling of full-bridge aerolasticity. Computer & Structures 85: 675–687.

Simiu, E. & Scanlan, R.H. 1996. Wind effects on structures, John Wiley e sons Inc., third edition 1996.

Ubertini, F. & Bontempi, F. 2008. Wind-induced fatigue assessment in main cables and hangers of suspension bridges. Proceedings of the fourth International Conference on Bridge Maintenance, Safety and Management (IABMAS'08).

Ubertini, F. & Giuliano, F. A comparative study on efficiency and accuracy of Gaussian wind simulation, Journal of Wind Engineering and Industrial Aerodynamic (submitted for publication).

# Safety assessment of civil engineering structures throughout their life-cycle

R. Pukl

Červenka Consulting, Prague, Czech Republic

D. Novák & B. Teplý

Brno University of Technology, Brno, Czech Republic

**ABSTRACT:** The decision-making tools for life-cycle analysis should capture the degradation and retrofitting processes in order to support maintenance of structures. Most of the current approaches to the life-cycle analysis are based on more or less simplified mechanical models or formulas. A more realistic reliability analysis can be achieved using non-linear FEM modeling. The particular methodologies are available and have been verified in practice. In the presented work they are integrated into an innovative tool for safety assessment of engineering structures throughout whole their service life. The life-cycle analysis combines modeling of nonlinearities in material and structure and degradation effects including uncertainties involved in all these phenomena. As the nonlinear structural analysis used for realistic prediction of structural response is computationally very demanding, a suitable technique of statistical sampling is employed in order to allow relatively small number of simulations. The proposed methodology allows evaluating structural safety using reliability index during and after the degradation and retrofitting processes in order to calculate the safety level for the service life conditions.

## 1 INTRODUCTION

Safety and economy have to be ensured for the structure during its service life. From this emerges the necessity for:

- i. reliability assessment technique of newly designed as well of existing structures (i.e. an assessment of *design* or *residual reliability* level);
- ii. design or assessment of structures for durability;
- iii. instruments for balancing service life vs. initial costs, maintenance and repair costs.

In this context, or in the concept of performance-based approaches, sustainability and whole life costing, time is the decisive variable and the durability issues are pronounced. This approach deals with *durability* and *reliability* issues, which both rank amongst the most decisive structural performance characteristics. This is clearly demonstrated at numerous international conferences, by international joint projects, in the work of several technical committees, and it is reflected also in current standardization activities: the ISO/WD 13823 (in prep.) and *fib* Model Code 2008 (see *fib Bulletin* No. 34, 2006). Both these documents are based on probabilistic approaches and will introduce (or enhance) the *design of structures for durability*—i.e. a time-dependent

limit state approach with service life consideration. Also, Japanese *Recommendations* (Noguchi et al. 2006) specifically deal with durability design and apart from other approaches also encompass probabilistic method for assessment of durability of structures.

The utilization of design for durability may bring positive economical and sustainability impacts. The level of reliability in the context of durability should be left to the client's decision as well as the choice of appropriate serviceability criteria; unfortunately there is a lack of recognition from investors in this respect, in spite of the fact that the mutual impact of these values on the cost of the project may be crucial. Thus, the durability implications in the context of reliability should be addressed during the design process and discussed with the client. Broad application is, unfortunately, still prevented by the insufficient dissemination of basic ideas, relevant knowledge or by the lack of experimental evidence and lack of efficient and user-friendly design instruments (software and other).

The service life of a building or structure is determined by its design, construction, ageing and maintenance during use. While assessing the service life, the combined effect of both the structural performance and ageing should be considered.

## 2 MODELING OF DEGRADATION

### 2.1 General

Modeling of degradation processes may be based on different levels of sophistication:

- a. macro-level;
- b. simplified models, probabilistic approach;
- c. micro-level.

The *a-level* is the most simple, often called the “deemed-to-satisfy” set of rules (mostly according to current codes) and does not allow for the design/assessment of a specified service life with a specified reliability level. The *b-level* comprises simple models (often semi-empirical), verified by comparison with the results of testing under experimental and real conditions. The variables are treated as random quantities; therefore the outputs are also capable of expressing statistical and probabilistic quality with respect to time evolution (service life assessment). In the present work this level is dealt with. The *c-level* is the most refined; the models are complex and are developed making use of basic physical laws and often constitutive laws of mechanics, thus leading to the problem of needing to solve partial differential equations. This level of sophistication is not suitable for everyday design practice. Note that levels *b* and *c* may be viewed as performance-based design.

### 2.2 Tools for durability design of concrete structures

Within the framework of the new probabilistic and performance-based approach to durability design, some software tools for concrete structures have recently been developed by authors and coworkers. These SW comply with ideas of the future codes (ISO/WD 13823, *fib* Model Code 2008) and are briefly introduced below:

- i. *RC-LifeTime* utilizes the model of the carbonation process for concretes made from Portland or blended cements, considers the input data as random variables and performs a stochastic simulation technique. An assessment of service life is provided which considers the concrete cover quality and exposition type, and this together with reliability index assessment. It enables the user to make some assessment of CO<sub>2</sub> emissions and cost consequences among variants of concrete mix (see [Rovnanik et al. 2007](#)). *RC-LifeTime* is a rather simple and user friendly tool, freely accessible on <http://rc-lifetime.stm.fce.vutbr.cz/>;
- ii. *FReET-D*: A complex software tool for degradation assessment. Presently, it is available in a configuration encompassing several models for carbonation, for chloride ingress and reinforcement

corrosion. The tool is based on the probabilistic multipurpose software package FReET (Novák et al. 2003, 2007). It will enable the incorporation of any degradation closed-form numerical model in the form of a limit state/response function. For more details see below, and [Teplý et al. \(2006, 2007, in press\)](#);

- iii. *SARA* is a complex software system, which combines efficient techniques for nonlinear numerical analysis of engineering structures and probabilistic methods to offer an advanced tool for assessment of realistic behavior of civil engineering structures from reliability point of view (Pukl et al. 2007). Structural safety can be calculated at any stage of the life-cycle. FReET-D is used within the framework of this complex system to model degradation phenomena. The principal parts of the *SARA* system are described below in more detail.

### 2.3 FReET-D

FReET-D provides:

- i. modeling of degradation phenomena in concrete structures, statistical and sensitivity analyses;
- ii. assessment of service life;
- iii. assessment of reliability measures.

For the purposes of options (ii) and (iii) different simple limit conditions can be created.

The FReET-D module has been developed by implementing a number of degradation models for reinforced concrete structures. Degradation models are time dependent mathematical functions that show the average increase of cumulative degradation with time. These models are parameterized with several material, structural and environmental parameters that are considered to be random variables.

The main criteria in selecting the degradation model for each specific use are e.g.:

- type of relevant degradation mechanism, definition of appropriate limit state and given exposure conditions;
- availability of statistical data or the testing method for the input variables of each model;
- accuracy of the model when using the available data in relation to the required accuracy/strategy level.

The list of models currently implemented in FReET-D is summarized in [Table 1](#). Implementation of additional models is still in process.

The single models listed in [Table 1](#) can be used to construct different limit states (LS). Some types of durability limit states (DLS) have to be described by more than one model: a series of two or more models must be used—such composition may be called a “chained” model. For example a limit state based on reinforcement corrosion necessitates the existence of

Table 1. Degradation models implemented in FReET-D.

Degradation mechanism	Model notation	Output	Note
Carbonation	Carb1a Carb1b	Carbonation depth at time $t$ ; time to depassivation	Concretes from Portland cement; model b differs by RH function
	Carb2a Carb2b Carb3		Ditto; simplified model Concretes from Portland cement; influence of temperature
	Carb4a Carb4b		Concretes from blended cements; model b differs by RH function
	Carb5a Carb5b		Concretes from blended cements; model b is for HVFA concretes
	Carb6		Concretes from blended cements; type of cement considered
	Carb7 Carb8		Concretes from blended cements; <i>fib</i> Model Code 2008 model
	Carb9		Concrete from Portland cement with lime-cement mortar coating
	Chlor1a Chlor1b	Depth of chlorination at time $t$ ; time to depassivation	Model b provides calculation of saturation concentration of $Cl^-$ by analytical formula
	Chlor2a Chlor2b	Concentration of chlorides at depth $x$ and time $t$	Model b provides calculation of diffusion coefficient by experimentally derived formula
	Chlor3a Chlor3b		<i>fib</i> Model Code 2008 model; model b provides calculation of surface $Cl^-$ conc. for specific conditions by analytical formula
Reinforcement corrosion	Corr1	Net rebar diameter at time $t$	Uniform type of corrosion
	Corr2	Pit depth at time $t$	Pitting type of corrosion
	Corr3	Net cross sectional area of rebar at time $t$	Pitting type of corrosion
	Corr4	Time to cracking due to corrosion	Crack initiation on the steel-concrete interface; uniform corrosion

(Continued)

Table 1. (Continued)

Degradation mechanism	Model notation	Output	Note
	Corr5	Crack width due to corrosion at time $t$	Crack width on concrete surface; uniform corrosion
	Scc1a Scc1b	Stress intensity factor at the pit tip at time $t$	Prestressed reinforcement, pitting corrosion; fracture mechanics approach

depassivation. In such cases one output of the preceding model is time, which serves subsequently as an input (random variable) for the following model.

### 2.3.1 Inputs

Input parameters for the computational model are defined as random variables. Random variables can be divided into categories in order to make the handling of a large number of random variables easier and more transparent. Variables are described by their probability density functions (PDF) and statistical definition, which includes statistical characteristics, statistical parameters or their combination. The user can select an appropriate PDF from the set of 29 theoretical models in a user-friendly manner. The shape of the probability distribution of a particular random variable is displayed in graphic form. Random variables can also be described by user-defined raw data.

A mutual statistical dependence (correlation) between input variables can be prescribed and is arranged by a simulated annealing method.

Some models may be highly input demanding; in order to simplify the handling of inputs their statistical sensitivity is provided by means of Spearman rank-order correlation coefficients, i.e. the user may easily gain measures of the relative effect of each basic variable. The sensitivity analysis used in FReET-D is based on the assumption that the randomly generated input variables which significantly influence the output (both positively and negatively) have a high absolute value of correlation coefficient. In the opposite way, a low correlation coefficient will signalize a low influence. The sensitivity coefficients (their value being within the range from  $-1$  to  $+1$ ) thus provide information on the relative influence of the change in input random variables on the change in output values.

There are two main benefits from understanding the sensitivity of individual input parameters for a model:

- i. The "dominancy" of an individual input parameter is assessed by the value of the sensitivity

coefficient: for less sensitive parameters less effort can be devoted to investigating the input values. Consequently such input variables may also be considered to be deterministic ones within a similar computation

- ii. The most sensitive input quantities should be determined and verified more carefully in technological or constructional processes.

The user can also automatically perform a simple parametric study of the dependence of an output parameter on a selected input variable. For a definition of a limit state function, the user may create an appropriate value for barrier, called the comparative value within FReET. It is possible (and in many cases even desirable) to regard the comparative value as a random variable.

### 2.3.2 Outputs

According to the user-defined type of analysis FReET-D provides the following type of outputs:

- after performing the statistical analysis (by the Monte Carlo method or Latin Hypercube sampling method), the statistical moments of output variables are shown in a numerical and graphical way; also the values of the sensitivity coefficients for individual inputs are provided;
- reliability analysis provides the probability of failure value or reliability index relevant to a user-designed limit condition. For this purpose the FORM technique may also optionally be utilized;
- for the output quantity the best-fitted PDF may be automatically found.

## 3 PROBABILISTIC APPROACH

The stochastic engine of the SARA system is the probabilistic program FReET - Feasible Reliability Engineering Tool. This module for statistical, sensitivity and reliability analysis of engineering problems was designed with focus especially on the computationally intensive problems, which do not allow performing thousands of samples (Novák et al. 2003, 2007).

### 3.1 Small-sample simulation

For time-intensive calculations like nonlinear mechanics of concrete, the small-sample simulation techniques based on stratified sampling represent a rational compromise between feasibility and accuracy. Therefore Latin hypercube sampling (LHS) was selected as a key fundamental technique. It is a special type of the Monte Carlo simulation, which uses the stratification of the theoretical probability distribution function of input random variables. It requires a relatively small number of simulations to estimate statistics of response—repetitive calculations of the structural response (tens or hundreds).

The basic feature of LHS is that the probability distribution functions for all random variables are divided into  $N_{Sim}$  equivalent intervals ( $N_{Sim}$  is a number of simulations); the values from the intervals are then used in the simulation process. This means that the range of the probability distribution function of each random variable is divided into intervals of equal probability. The samples are chosen directly from the distribution function based on an inverse transformation of distribution function. The representative parameters of variables are selected randomly, being based on random permutations of integers  $1, 2, \dots, j, N_{Sim}$ . Every interval of each variable must be used only once during the simulation. Being based on this precondition, a table of random permutations can be used conveniently, each row of such a table belongs to a specific simulation and the column corresponds to one of the input random variables.

### 3.2 Statistical correlation

Once samples are generated, the correlation structure according to the target correlation matrix must be taken into account. There are generally two problems related to the statistical correlation: First, during sampling an undesired correlation can occur between the random variables. It can happen especially in the case of a very small number of simulations (tens), where the number of interval combination is rather limited. The second task is to introduce the prescribed statistical correlation between the random variables defined by the correlation matrix. The columns in LHS simulation plan should be rearranged in such a way that they may fulfill the following two requirements: to diminish the undesired random correlation and to introduce the prescribed correlation.

A robust technique to impose statistical correlation based on the stochastic method of optimization called simulated annealing is used in FReET. The imposition of the prescribed correlation matrix into the sampling scheme can be understood as an optimization problem: The difference between the prescribed  $K$  and the generated  $S$  correlation matrices should be as small as possible. A suitable measure of quality of the overall statistical properties can be introduced, e.g. a norm which utilizes the deviations of all correlation coefficients:

$$E_{overall} = \sqrt{\sum_{i=1}^{N_V-1} \sum_{j=i+1}^{N_V} (S_{i,j} - K_{i,j})^2} \quad (1)$$

The norm  $E$  has to be minimized from the point of view of the definition of the optimization problem using simulated annealing optimization approach.

### 3.3 Random fields

Spatial variability of structural properties, in particular of material properties, is an important phenomenon, which can have substantial influence on the structural damage and failure—e.g. crack initiation and localization in homogeneous stress state region as it occurs in four point bending tests. Therefore, it should be properly accounted in the computer simulation of structures if realistic results are desired.

The representation of spatial variability of structural properties by random fields is a high level of their modeling with a scientific background (Vořechovský & Novák 2005). Random fields describe the spatial distribution of a structural (material) property over the region representing the structure. The spatial correlation of the generated random fields, defined by correlation length (and the autocorrelation function), is of crucial importance. Randomly selected examples of realizations of 2D random fields over a rectangular support for different correlation lengths are shown in Fig. 1 for illustration.

This methodology is implemented in FReET as a level of random fields, which can represent the spatial variability of material properties for the structural analysis in SARA system.

### 3.4 Sensitivity analysis

An important task in the structural reliability analysis is to determine the significance of random variables. The sensitivity analysis is obtained as an additional result of LHS, and no additional computational effort is necessary.

The relative effect of each basic variable on the structural response can be measured using the partial correlation coefficient between each basic input variable and the response variable. The method is based on the assumption that the random variable which influences the response variable most considerably (either in a positive or negative sense) will have a higher correlation coefficient than the other variables. Because the model for the structural response is generally nonlinear, a non-parametric rank-order correlation is used by means of the Spearman correlation coefficient or Kendall tau.

### 3.5 Reliability assessment

In cases when we are constrained by small number of simulations (tens, hundreds) it can be difficult to

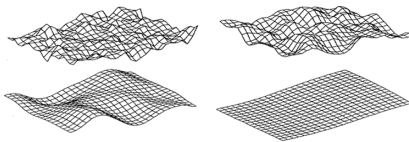


Figure 1. Realizations of 2D random fields with increasing spatial correlation.

estimate the failure probability. The following approaches are therefore utilized here; they are approximately ordered from elementary (extremely small number of simulations, inaccurate) to more advanced techniques.

- Cornell's reliability index—the calculation of reliability index from the estimation of the statistical characteristics of the safety margin.
- Curve fitting approach—based on the selection of the most suitable probability distribution of the safety margin.
- FORM approximation (Hasofer-Lind's index).
- Importance sampling techniques.
- Response surface methods.

These approaches are well known in reliability literature. In spite of the fact that the calculation of the failure probability (or/and reliability index) using some of these techniques does not always belong to the category of very accurate reliability techniques (first three in the list), they represent a feasible alternative in many practical cases.

## 4 NONLINEAR ANALYSIS

The structural resistance is modeled in the SARA system by nonlinear finite element computer program ATENA. Software ATENA is well established for realistic assessment of structural load-carrying capacity and simulation of damage and failure of concrete and reinforced concrete structures (Červenka 2000, <http://www.cervenka.cz>). It can analyze the structure in intact or deteriorated conditions.

An algorithm for nonlinear analysis is based on three basic parts (Fig. 2): Finite element technique, constitutive model, and non-linear solution methods, which should compose a balanced approximation.

Nevertheless, the constitutive models decide about the material behavior, and therefore they are treated here more extensively. Since concrete is a complex material with strongly nonlinear response, special constitutive models for the finite element analysis of concrete structures are employed.

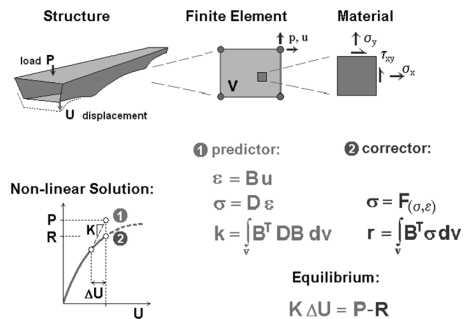


Figure 2. Scheme of the nonlinear finite element method.



## 4.1 Constitutive models

For computer simulation of concrete and reinforced concrete structures including its interaction with neighborhood ATENA offers variety of nonlinear material models for concrete, quasi-brittle materials, soils and metals, namely:

- Damage-based material model.
- Fracture-plastic cementitious material.
- Microplane material model.
- Drucker-Prager plasticity model.
- Von Mises plasticity model.
- Plasticity with hardening for reinforcement etc.

Tensile behavior of concrete is modeled by nonlinear fracture mechanics combined with the crack band method and smeared crack concept. Main material parameters are tensile strength, fracture energy and shape of the stress-crack opening curve. A real discrete crack is simulated by a band of localized strains. The crack strain is related to the element size. Consequently, the softening law in terms of strains for the smeared model is calculated for each element individually, while the crack-opening law is preserved. This model is objective due to the energy formulation and its dependency on the finite element mesh size is neglectable.

The compressive behavior of concrete is covered by theory of plasticity with a non-associated flow rule. This model describes well specific phenomena in concrete in compression, namely volume change after crushing or influence of the lateral stresses to the compressive strength, so called confinement effect.

## 4.2 Input parameters

The input parameters for ATENA calculation are usually assumed to be deterministic values. However, in reality they have random nature; they are uncertain and often even unknown, and the deterministic value can be only estimated. In order to account the randomness and uncertainty of input parameters, probabilistic approach methods should be employed. Therefore in the SARA system the input parameters are generated randomly by FReET from prescribed statistical parameters. Reduced material parameters (or their statistic) for deteriorated structure can be obtained from FReET-D. All variables and results in degradation analysis are time-dependent.

## 4.3 Safety issues

Application of appropriate stochastic methods allows statistical evaluation of the structural response (resistance) and direct assessment of structural safety in SARA system. In case of deterministic calculation, which works optimal in terms of mean values, safety issues should be addressed by means of global safety factors.

## 5 CONCLUSIONS

Described software packages are applicable for the assessment of service life (for newly designed concrete structures) or residual service life (for existing concrete structures) and relevant safety and reliability levels. The consideration of input parameters as random variables is essential for more realistic results enabling a reasonable decision-making.

## ACKNOWLEDGEMENTS

The presented work is related to the research funded by the project No. MSM0021630519 from the Ministry of Education of the Czech Republic and by the grant No.103/08/1527 "Safety formats" from the Grant Agency of the Czech Republic. Authors gratefully acknowledge this support.

## REFERENCES

- Červenka, V. 2000. Simulating a Response. *Concrete Engineering International* 4(4): 45–49.
- fib* Bulletin No. 34, 2006. Service Life Design—Part of the future *fib* Model Code 2008.
- ISO/WD 13823 (in prep.). General Principles on the Design of Structures for Durability (currently under development). ISO TC 98/SC2/WG10.
- Noguchi, T., Kanematsu, M. and Masuda, Y. 2006. Outline of Recommendations for Durability Design and Construction Practice of Reinforced Concrete Buildings in Japan. In Malhotra VM, editor. *7th CANMET/ACI International Conference*. Montreal, Canada, p. 347–373.
- Novák, D., Vořechovský, M. and Rusina, R. 2003. Small-sample probabilistic assessment—software FReET. In *9th Int. Conf. on Applications of Statistics and Probability in Civil Engineering—ICASP 9*, San Francisco, USA, Rotterdam Millpress: 91–96.
- Novák, D., Vořechovský, M. and Rusina, R. 2007. FReET - Feasible Reliability Engineering Efficient Tool, User's and Theory guides. Brno/Cervenka Consulting, Czech Republic, <http://www.freet.cz>.
- Pukl, R., Červenka, V. and Novák, D. 2007. Virtual reliability assessment of structures with damage, SARA— Part II. In *Proc. of 3rd International Conference on Structural Health Monitoring of Intelligent Infrastructure* (SHMII-3), Vancouver, Canada.
- Rovnaník, P., Teplý, B. and Rovnaníková, P. 2007. Concrete mix and environmental load in the context of durability and reliability. In *Proc. Vol.2, CEBS 07 Prague Conference*, p.772–778.
- Teplý, B., Chromá, M., Matesová, D., Rovnaník, P. and Veselý, V. 2006. FReET-D—Deterioration Module Program Documentation and User's Manual. Brno, Czech Republic.
- Teplý, B., Chromá, M. and Rovnaník, P. (in press). Durability assessment of concrete structures: Reinforcement depassivation due to carbonation. *Structure and Infrastructure*
- Teplý, B., Matesová, D., Chromá, M. and Rovnaník, P. 2007. Stochastic degradation models for durability limit state evaluation: SARA— Part VI. In *Proc. of 3rd International Conference on Structural Health Monitoring of Intelligent Infrastructure* (SHMII-3), Vancouver, Canada.
- Vořechovský, M. and Novák, D. 2005. Simulation of random fields for stochastic finite element analysis. *Proceedings of 9th Int. conf. on Structural Safety and Reliability Icosar 2005*, Rome, Italy.

# Reliability-based fatigue assessment of welded connections

S.G. Reid

*School of Civil Engineering, University of Sydney, NSW, Australia*

**ABSTRACT:** The paper describes a probabilistic method of fatigue assessment for welded connections. The fatigue assessment is based on probabilistic models of fatigue loading (represented by rainflow data) and fatigue resistance (represented by S-N curves). The fatigue reliability of a welded connection cannot be expressed simply in terms of a separable “load” and “resistance” because the failure criterion (fatigue limit state) is related to a cumulative fatigue damage indicator (the Palmgren-Miner summation) that is a function of both a load spectrum and a corresponding resistance spectrum (for variable stress ranges). Furthermore, the resistance spectra are based on S-N curves that have discontinuities associated with “constant stress range fatigue limits” and “cut-off limits”, at low stresses. Accordingly, fatigue damage is a highly non-linear function of the levels of fatigue loading and fatigue strengths. To accommodate the response non-linearity and discontinuities, the analysis presented in the paper is based on an estimated distribution of the individual S-N curves that are represented by the ensemble test statistics on which the characteristic design curves are based (noting that individual S-N curves cannot be determined by testing). Accordingly, the reliability assessment is based on the summation of conditional probabilities of failure for various levels of fatigue strengths represented by individual S-N curves. The paper outlines the probabilistic method of fatigue assessment and presents illustrative results concerning time-dependent fatigue reliability. The probabilistic method of fatigue assessment is illustrated in an assessment of the reliability of a welded connection with a design life determined in accordance with the deterministic design criteria for fatigue specified in the Australian Standard AS4100.

## 1 INTRODUCTION

In engineering practice, the fatigue strengths and design lives of welded connections are normally assessed using S-N curves (relating the stress-range  $S$  to the number of cycles to failure  $N$ ) specified in design standards. The S-N curves specified for design purposes in accordance with the Australian Standard AS 4100 (and similar standards such as BS 7608) correspond to results that are 2 standard deviations below the expected values (based on test results). A capacity factor  $\Phi$  is also applied to the strength, and this factor takes a value of 1.0 for “reference design conditions” and a value less than or equal to 0.70 for other (more critical or more severe) conditions. Accordingly, the specified design criteria give estimates of fatigue design strengths and design lives that are generally “safe”.

However, deterministic fatigue life assessments in accordance with standards such as AS4100 do not give any indication of the level of safety or reliability of a welded connection, nor do they give any indication of the expected fatigue life. Moreover, in some circumstances, the potential consequences of a fatigue failure can be very significant, and estimates of the structural reliability and the uncertain distribution of the fatigue

life are necessary to provide a rational basis for the assessment and management of the associated risks. This paper describes a method to estimate the structural reliability and the uncertain distribution of the fatigue life for welded connections.

The fatigue assessment is based on probabilistic models of fatigue loading and fatigue resistance (related to S-N curves). However, the fatigue reliability of a welded connection cannot be expressed simply in terms of a separable “load” and “resistance” because the failure criterion (limit state) is related to a cumulative fatigue damage indicator (normally based on the Palmgren-Miner summation) that is a function of both a load spectrum and a corresponding resistance spectrum (for variable stress ranges). Furthermore, the resistance spectra are based on S-N curves that have discontinuities associated with “constant stress range fatigue limits” and “cut-off limits”, at low stresses. Hence, fatigue damage is a highly non-linear function of the levels of fatigue loading and fatigue strengths. Accordingly, the proposed method of reliability assessment is based on the summation of conditional probabilities of failure for various levels of fatigue strengths.

The paper outlines the reliability-based method of fatigue assessment and presents illustrative results

concerning time-dependent fatigue reliability (which can be readily related to the probability distribution of the fatigue life or time to failure). The probabilistic method of fatigue assessment is illustrated in an assessment of the reliability of a welded connection with a design life determined in accordance with the deterministic design criteria for fatigue specified in the Australian Standard AS4100.

## 2 DETERMINISTIC FATIGUE ASSESSMENT

In accordance with AS4100, the resistance to fatigue is expressed in terms of S-N curves, based on a constant stress range fatigue limit ( $f_3$ ) applicable at  $5 \times 10^6$  stress cycles, and a cut-off stress limit ( $f_5$ ) applicable at  $10^8$  stress cycles, as shown in Figure 1.

The uncorrected fatigue strength ( $f_f$ ) for a particular detail category ( $f_{rn}$ ) with a constant stress range limit  $f_3$  and a number of stress cycles  $n_{sc}$  (of constant stress range) may be calculated as:

$$f_f^3 = \frac{f_3^3 \times 5 \times 10^6}{n_{sc}} \quad (1)$$

for stresses above the constant stress range fatigue limit  $f_3$ , and

$$f_f^5 = \frac{f_3^5 \times 5 \times 10^6}{n_{sc}} \quad (2)$$

for stresses between  $f_3$  and the cut-off stress limit  $f_5$ .

For a transverse fillet or butt welded connection involving a plate thickness  $t_p$  greater than 25 mm, the uncorrected fatigue strength is corrected in accordance with a thickness correction factor  $\beta_{tf}$ :

$$\beta_{tf} = (25/t_p)^{0.25} \quad (3)$$

For connections subjected to variable stress ranges  $f$  and corresponding numbers of stress cycles  $n(f)$ , the strength is required to satisfy Miner's cumulative damage rule, based on the corrected stress limits  $f_{3c}$  and  $f_{5c}$ :

$$\frac{\sum_i n_i (f_i)^3}{5 \times 10^6 (\phi f_{3c})^3} + \frac{\sum_j n_j (f_j)^5}{5 \times 10^6 (\phi f_{5c})^5} \leq 1.0 \quad (4)$$

where  $f_i \geq \phi f_{3c}$  and  $\phi f_{5c} < f_j < \phi f_{3c}$ .

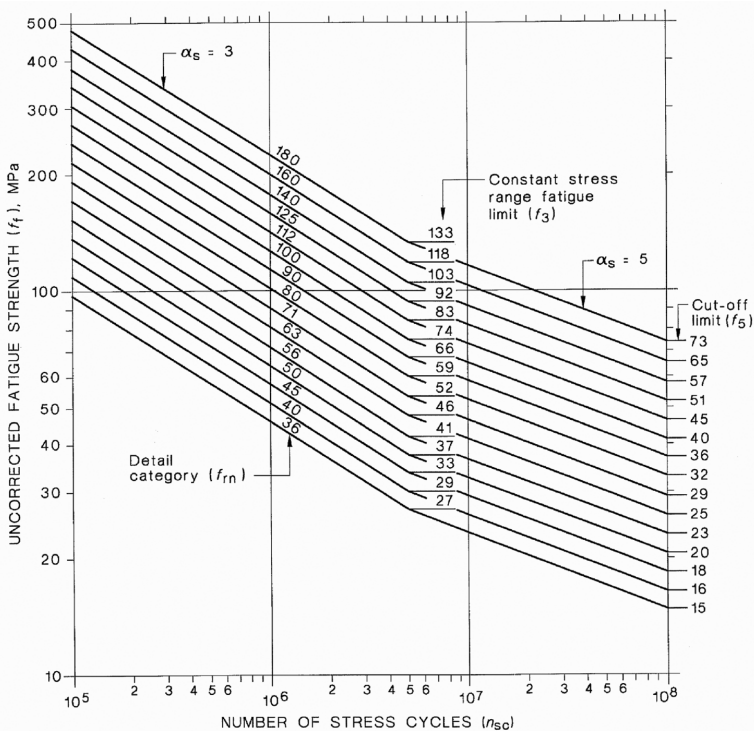


Figure 1. S-N curves for design in accordance with AS4100.

AS4100 defines specific detail categories that take into consideration the local stress concentration at a detail, the size and shape of the maximum acceptable discontinuity, the loading condition, metallurgical effects, residual stresses, the welding process and any post-weld improvement. Each detail category is given a number ( $f_m$ ) that defines the fatigue strength (in MPa) at  $2 \times 10^6$  cycles on the relevant S-N curve.

### 3 PROBABILISTIC FATIGUE ASSESSMENT

Probabilistic fatigue assessments can be based on cumulative damage models characterized by S-N curves or fracture mechanics models of stochastic crack growth calibrated to fit the S-N curves (e.g., Wirsching, 1995).

The conventional approach to probabilistic fatigue analysis based on S-N curves (e.g., Wirsching, 1995) considers 'linear' segments of the curves (such as the AS4100 curves above the constant stress range limit) for which the relationship between  $N$  and  $S$  may be described simply as:

$$NS^m = A \quad (5)$$

where  $m$  is the inverse of the slope of the relevant S-N curve, and for any particular value of the stress range, the parameters  $S$ ,  $N$  and  $A$  may be treated as random variables.

If the stress ranges are also treated as random variables, after  $n$  cycles of loading the damage  $D$  due to the expected loading is (in accordance with Miner's rule):

$$D = nE[S^m]/A \quad (6)$$

where  $E[S^m]$  is the expected value of  $S^m$ . Expressions for  $E[S^m]$  have been reported for several distributions of  $S$ , including results for a Rayleigh distribution of stress ranges (for which the stress-time history is a stationary Gaussian narrow-band process) (Wirsching, 1995), and for a Weibull distribution including a result for a bilinear S-N curve with a discontinuity at a fixed value of  $S$  (Ayala-Uraga & Moan, 2007).

For the purposes of probabilistic analysis, the damage due to a random distribution of stress ranges can also be related to the damage due to an 'equivalent constant-amplitude stress range'  $S_e$ , giving:

$$D = \frac{n}{A} B^m S_e^m \quad (7)$$

where  $B$  is a random variable that accounts for uncertainties associated with the fatigue 'loading'. The

probability of failure may then be simply evaluated as the probability that the uncertain damage  $D$  exceeds a critical value  $\Delta$  (a random variable representing the resistance to the cumulative damage assessed in accordance with Miner's rule).

On the other hand, probabilistic fracture mechanics approaches model the initiation and propagation of fatigue cracks leading to failure (e.g., Ayala-Uraga & Moan, 2007). The fracture mechanics models are usually based on the Paris crack propagation law, and these models can be used to estimate the time to failure (associated with a critical crack size). An advantage of the fracture mechanics models based on fatigue crack growth is that they can be used in conjunction with crack inspection programs to facilitate reliability-based updating of the remaining fatigue life of an existing structure.

In this paper, a new probabilistic approach is developed on the basis of a cumulative damage model characterized by probability distributions of S-N curves. A new feature of this model is the inclusion of discontinuities associated with uncertain values of the constant stress range limit and the cut-off stress limit. The probabilistic model is based on reported statistics of the test data that were used to obtain the S-N curves given in AS4100, and some reported statistics of the uncertainty associated with the failure condition defined by Miner's Rule. The time-dependent probability of failure is assessed with regard to conditional probabilities of failure for a range of strength fractiles, as described below.

#### 3.1 Statistical expressions for fatigue resistance

The S-N curves in AS4100 are based on test data for which detailed statistics have been reported by Gurney (1979). The S-N curves are based on test results for pulsating tension loading and it is generally assumed that such results are not affected by mean-stress levels or residual stresses or related thickness effects (but a thickness correction factor is nevertheless included in AS4100, as noted above).

The particular design categories specified in AS4100 correspond to particular classes of welds for which the mean  $\log S - \log N$  relationship (least squares fit) and the standard deviation of  $\log N$  (for a given stress range) have been reported. The S-N curves given in AS4100 are based on characteristic results lying 2 standard deviations below the mean.

Whereas the variability of the S-N test results has been previously reported with regard to the standard deviation of  $\log N$  (Gurney, 1979), for the purposes of probabilistic analysis as described in this paper, the variability has been reassessed in terms of the corresponding variability of  $\log S$  (for a given value of  $N$ ). Thus the variability of strength within a particular design category is modeled as an uncertain shift of the

S-N curve along the S axis (rather than the N axis), similar to the variability of strength between design categories. This distinction is important with regard to the variable values of the constant stress range fatigue limit  $f_3$  and the cut-off limit  $f_5$ .

Some statistics of critical values of the cumulative damage parameter  $\sum_i (n_i/N_i)$  have also been reported and these statistics have been used to estimate the uncertain bias inherent in Miner's Rule and to estimate the distribution of the critical values ( $\Sigma_{crit}$ ). Based on 401 test results, Jacoby (1968) reported that the critical value (at failure) of  $\sum_i (n_i/N_i)$  was greater than 1 for 62.6% of the results and it exceeded 5.3 for 6% of the results. Based on these results, the distribution of  $\Sigma_{crit}$  has been approximated by a LogNormal distribution with a median value of 1.331 and a coefficient of variation of 0.864 (after subtracting the variability due to  $N_i$  associated with the S-N curves for constant stress range test results).

### 3.2 Probabilistic expressions for fatigue damage

The results reported in this paper were derived from probabilistic expressions for fatigue damage, based on the statistical distributions of the standard S-N curves.

Two types of S-N curves were considered, including bilinear curves of the type given in AS4100 and linear curves for which the relationship for constant amplitude loading was assumed to apply also for variable amplitude loading down to a cut-off stress at  $2 \times 10^7$  cycles of loading, giving:

$$f_f^3 = \frac{f_3^3 \times 5 \times 10^6}{n_{sc}} \text{ for } n_{sc} \text{ up to } 2 \times 10^7 \quad (8)$$

Gurney (1979) reported that curves of this type have been shown to provide reasonable results for several types of variable amplitude loading (and curves of this type are referred to as Gurney-type curves in the following).

For the purposes of probabilistic modeling, S-N curves corresponding to a range of selected fractiles of the fatigue strength distribution were obtained (by shifting curves up and down the stress axis).

For each selected strength fractile, the cumulative damage parameter  $\sum_i (n_i/N_i)$  was evaluated based on the values of  $S_i$  and  $n_i$  (from the rainflow data) and the values of  $N_i$  obtained from the relevant S-N curve.

### 3.3 Probability of failure due to fatigue

For each selected strength fractile, the conditional probability of fatigue failure (dependent on the service

life) was evaluated with regard to the time-dependent limit state function:

$$\sum_i (n_i/N_i) = \Sigma_{crit} \quad (9)$$

For a given service life, the cumulative damage parameter  $\sum_i (n_i/N_i)$  was taken to be LogNormally distributed with a coefficient of variation of 0.1 (to account for loading uncertainty) and  $\Sigma_{crit}$  was taken to be LogNormally distributed with a median value of 1.331 and a coefficient of variation of 0.864 (as explained above).

For each selected strength fractile, the time-dependent failure probability density was then evaluated as the product of the conditional probability of failure and the relevant probability density of the strength distribution (dependent on the strength fractile).

Finally, the total probability of failure at a critical section was obtained by integrating the relevant failure probability density function (for a specified service life).

## 4 EXAMPLE

To illustrate the probabilistic method of fatigue assessment discussed in this paper, an analysis is presented for a welded connection that has been assessed in a bridge structure in Sydney, Australia.

The welded connection is a transverse butt weld in a support bar ( $t_p = 100\text{mm}$ ). The relevant constructional detail is AS4100 Constructional Detail (19) and the applicable Detail Category is 90 (noting that NDT inspection has not been carried out on the welded connection).

### 4.1 Fatigue loading—rainflow data

Fatigue loading of the welded connection has been assessed based on strain measurements, and the results have been expressed in terms of rainflow cycle counts (per fortnight) for stress range intervals of 5 MPa, as shown in Figure 1.

The rainflow data for this welded connection (and other critical connections in the structure) are reasonably approximated by functions of the form

$$n = k \cdot \exp(-ms) \quad (10)$$

where  $n$  denotes the cycle count (for a stress range interval of 5 MPa),  $s$  denotes the stress range (upper value for a stress range interval of 5 MPa) and  $k$  and  $m$  are fitted distribution parameters. For this welded connection the value of  $k$  was 2.63E6 and the value of  $m$  was 0.1664. The fitted function is shown in Figure 2 (for  $s \geq 10 \text{ MPa}$ ). The fitted functions have

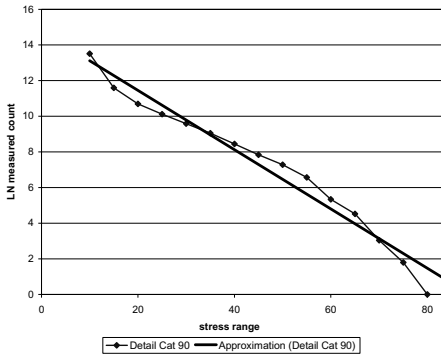


Figure 2. Rainflow (stress-range) data for welded connection.

Table 1. AS4100 design life.

$\beta_{if}$	Design Life (years)	
	$\phi = 1.0$	$\phi = 0.7$
1.0	259	29.0
0.71	31	5.5

been used to provide a generalized form of the sample results (smoothed with regard to sampling variations) and to allow extrapolation to stress ranges greater than those included in the sample. (However, the relatively infrequent high stress cycles do not significantly affect the estimated fatigue life.)

#### 4.2 AS4100 design life estimate

The AS4100 design life estimate for the welded connection has been obtained in accordance with Miner's cumulative damage rule (Equation 4), and the results are shown in Table 1. Results are given for alternative values of the capacity factor ( $\phi = 1.0$  or  $0.7$ ), ignoring or including the thickness correction factor ( $\beta_{if} = 0.71$ )

Clearly, the reduced design strengths associated with the reduced capacity factor ( $\phi = 0.7$ ) and the application of the thickness correction factor result in significant reductions of the estimated design lives. This is due not only to the reduced design life for any particular stress range, but also the additional damage due to the additional number of low-stress cycles which contribute to the damage when the lower stress limits  $f_3$  and  $f_5$  are reduced.

The relative contributions to the cumulative fatigue damage due to stress cycles at different stress ranges are shown in Figure 3 which gives the results as a function of  $(\beta_{if}, \phi)$ . Clearly, the cumulative fatigue

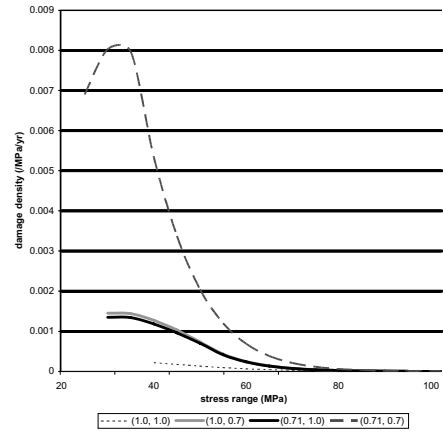


Figure 3. Cumulative damage density ( $\beta_{if}, \phi$ ) based on Palmgren-Miner summation (MPa/yr).

damage is very sensitive to the value of the cut-off stress limit because of the very large number of low-stress cycles in the region of the limit.

#### 4.3 Probabilistic fatigue life

Probabilistic fatigue life estimates have been obtained based on the rainflow data (Figure 1 and Equation 8), and taking account of the reported value of  $\sigma_{\ln N} = 0.4824$  (Gurney, 1979) based on constant stress range test results for the relevant weld detail category (implying  $\sigma_{\ln S} = 0.1608$ ).

For a range of strength fractiles, the conditional probabilities of fatigue failure (dependent on the service life) have been evaluated with regard to the time-dependent limit state function given by Equation 7, as described above.

The corresponding failure probability density functions (given by the product of the conditional probability of failure and the relevant probability density of the strength distribution) are shown in Figures 4–5 for service lives corresponding to the AS4100 design lives noted in Table 1 (taking  $\beta_{if} = 1$ ). The failure probability densities are plotted with respect to a normalized strength which indicates the number of standard deviations by which the strength deviates from the median value.

The failure probability densities calculated using Gurney-type S-N curves are generally larger than those calculated using Code-type curves. Also, the figures show that the failure probability densities for Code design lives based on  $\phi = 1$  (Figure 4) are generally concentrated in the region of strengths about 2 standard deviations below the median values, whilst for the reduced design strengths based on  $\phi = 0.7$

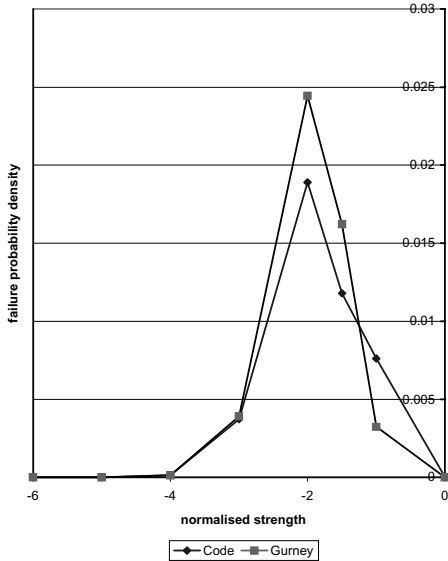


Figure 4. Failure probability density function for service life of 259 years. (Total probability of failure: 0.0297, Code-type; 0.0329, Gurney-type).

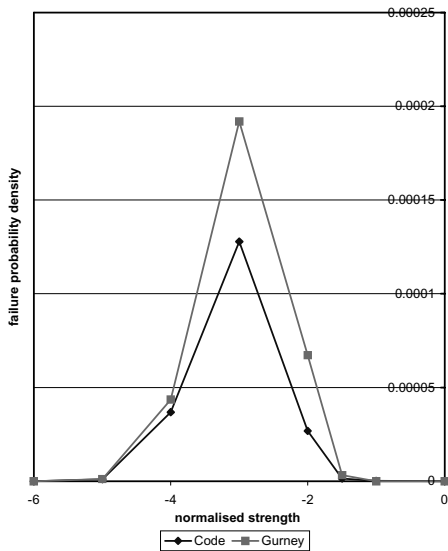


Figure 5. Failure probability density function for service life of 29 years. (Total probability of failure: 0.000187, Code-type; 0.000289, Gurney-type).

(Figure 5) the failure probability densities are generally concentrated in the region of strengths about 3 standard deviations below the median values.

The total probability of failure is obtained by integrating the relevant failure probability density function (for a specified service life). The total probabilities of failure corresponding to the failure probability density functions shown in Figures 4–5 are noted in the figure captions.

For a service life corresponding to the AS4100 design life based on a capacity factor  $\phi$  of 1.0, the estimated probability of fatigue failure was about 3%. For a service life corresponding to the AS4100 design life based on a capacity factor  $\phi$  of 0.7, the estimated probability of failure was reduced by about 2 orders of magnitude (due to the more conservative value of  $\phi$ ).

In this example, the probability of fatigue failure has been evaluated for specified values of the ‘design life’ (corresponding to deterministic values of the design life in accordance with AS4100). Similarly, the probabilistic assessment of fatigue could also be used to assess the probability of failure as a function of the service-life (or time in service) and the associated probability distribution of the time to failure.

## 5 CONCLUSION

A new method of reliability-based fatigue assessment for welded connections has been described and illustrated by assessing the reliability of a critical welded connection with a design life determined in accordance with the deterministic design criteria for fatigue specified in the Australian Standard AS4100. The probabilistic method accounts for uncertainties in S-N curves, including the uncertain values of stress limits associated with discontinuities in the curves. Also it has been shown that fatigue damage can be very sensitive to fatigue loading in the region of these discontinuities.

## REFERENCES

- AS 4100. 1998. *Australian Standard: Steel structures*. Sydney, Australia: Standards Australia.
- Ayala-Uraga E & Moan T. 2007. Fatigue reliability-based assessment of welded joints applying consistent fracture mechanics formulations. *International Journal of Fatigue* 29(3): 444–456
- BS 7608. 1993. *Code of practice for fatigue design and assessment of steel structures*. London (UK); British Standards.
- Gurney TR. 1979. *Fatigue of welded structures*. Cambridge University Press.
- Jacoby G. 1968. Comparison of fatigue life estimation processes for irregularly varying loads, *Proc. 3rd Conf. on Dimensioning*, Budapest.
- Wirsching, PH. 1995. Probabilistic fatigue analysis. In C. Sundararajan (ed.), *Probabilistic Structural Mechanics Handbook*: 146–165. New York: Chapman & Hall.

# Simple supported RC bridge design process considering durability

Xin Ruan, Ai-Rong Chen & Zi-Chao Pan  
*Dept. of Bridge Eng., Tongji Univ., Shanghai, China*

**ABSTRACT:** Durable problems about existing bridges are widely concerned in recent years. Researches related to materials, structures, maintenances are rapidly carried out. And at the same, with influence of life-cycle method, the relationship about the durable problems and life-cycle methods are also discussed. Based on basic consideration of life-cycle methods, durable problems are related to the whole life process of bridges, the countermeasures to this problems should be considered in the whole processes of bridge life, which include materials selection, structures detail design, mechanics design, maintenance and repair plan design, and also reinforce design. And all those problems should be well considered in the design period, so that the design practice will become an integrated process. An primary framework of bridge design processes considering durability is given in this paper, which are composed of setting durable index, safety and serving ability design, durability assessment, structure detail design optimize, maintenance and repair plan design, and finally reinforce design. A design process for a simple supported RC bridge is given as an example. Based on the practice, it is reasonable to believe that the process controlled design method will become an effective method to solve those complex decision problems in currently practices, including durable problems.

## 1 INTRODUCTION

Along with the rapid development of bridge construction, it had been gradually found that the deterioration process of many bridges were so rapid that much beyond anticipation. The causes of those phenomena consist of many aspects. For the objective reasons, the influence of environment and increasing of traffic volume have imposed great burden on the maintenance work of bridge. For the subjective reasons, the traditional design method can't ensure the durability of bridge during the whole life cycle efficiently. But the life cycle design method of bridge which is widely discussed all over the world considers the process of design, construction, operation and demolishment as a whole. In this way, the bridge designers can predict the deterioration process of bridge performance clearly, and establish the maintenance scheme accordingly. This innovation in design method will greatly improve the durability of bridge.

Simple supported RC bridge has been widely used due to its advantage in structure, cost and many aspects. This paper will mainly discuss the durability design process of simple supported RC bridge on the basis of existing research achievements.

## 2 DURABILITY DESIGN PROCESS

The durability should be taking into consideration at the very beginning of the whole design stage, and integrated into the whole processes. In the whole design process, not only the internal force and deformation of the structure should be calculated in detail, but also the deterioration processes and their countermeasures should be designed. A new design frame is suggested below, which composed of four sub steps.

### 2.1 *Design life-span determination*

Design life-span is a basic index which is related to anticipate durability of structure. The index will help designers to realize the basic time range to consider the durable problem. Basic required design life-span of bridge is already established in many countries' design code. For example, the design life-span for highway bridges in AASHTO is 75 years, while the Euro standard requires the design life-span for some infrastructures including bridge should be 100 years.

But according to the life cycle design theory, to reach the lowest cost of the whole life span, repaired



and even replace can also be considered in the design process. So the design life-span can be considered as an index, which is determined in the design process based on the life cycle theory, design experiences and also the environment, but not only by the design code at the beginning. Suggested basic flow to determine the design life-span is given in Figure 1.

### 2.2 Performance design

To find the optimal design life-span, a feedback relationship between design life-span and design requirements should be established (Fig.2). So we can adjust design project according to different requests of performance through this feedback relationship.

As discussed above, the traditional design process has only considered the safety and performance of bridge as perfect or in an undeterioration condition. So it is difficult to make a judgment whether the design result can ensure the durability performance of structure during the whole life cycle at the initial design stage. To solve this problem, a suggested adopting the design process is given in Figure 3.

### 2.3 Improvement of initial design project

After durability estimation, if the initial design scheme cannot ensure the durability performance of the requirements, some improvements should be considered. Changing design parameters and designing maintenance scheme are two main countermeasures to make improvement.

### 2.3.1 Changing design parameters

The parameters which control the design scheme should be varied according with different structure types and materials. Taking the simple supported RC bridge for example, the basic parameters include the shape of section, the thickness of concrete protective cover, and the prosperities of concrete and steel. If the initial design project cannot meet the requirements of life-span durability, it can be considered to increase the thickness of concrete protective cover, or to use special material with higher performance to enhance the durability performance of structure.

After changing design parameters, designers should estimate the durability of design project again.

### 2.3.2 Designing maintenance schemes

Another way to improve the initial design scheme is to design maintenance scheme according to the result of durability estimation. Based on the material deterioration model, the durability of the structure on a certain time can be calculated, which can help the designer to making the maintenance scheme at the design stage. Of course, considering the inaccuracy of the calculation model, the practical experience also plays an important role in the process of decision.

The maintenance scheme considering in the design process will also help the designers to make some special detail design which will make the maintenance work in operation stage more convenient.

When the maintenance scheme has been designed, designers should estimate the durability of design project again.

### 2.4 Life-cycle cost analysis

Life-Cycle Cost Analysis (LCCA) is also integrated into the process to ensure the whole cost performance the design, which considering not only the design and construction cost, but also the operation and maintenance cost as it designed.

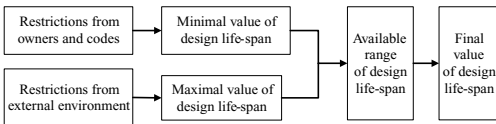


Figure 1. Process of design life-span determination.

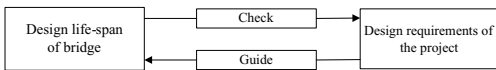


Figure 2. Feedback relationships between design life-span and design requirements of the project.

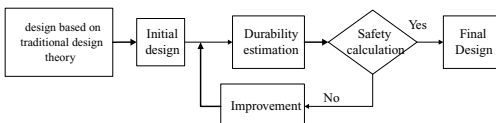


Figure 3. Process of performance design.

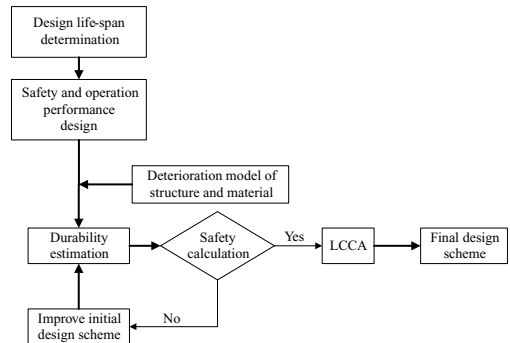


Figure 4. Durability design process.

To sum up the whole design process that discussed above, the whole durability design process is given in Figure 4.

### 3 EXAMPLE

In order to demonstrate the durability design process more clearly, an example of simple supported RC bridge will be given below.

#### 3.1 Profile of design

Basic environmental parameters, including average temperature, relative humidity and the consistency of CO<sub>2</sub> are given in Table 1. The bridge will be built far from the sea. It is not necessary to consider chloride induced deterioration.

#### 3.2 Design life-span determination

Considering the requirements of bridge owners and the conditions of local environment, the design life-span of bridge is estimated as 60 years. Meanwhile, the design life-span of components of bridge can also be determined according to the data provided by the manufacturers (Table 2).

#### 3.3 Performance design

##### 3.3.1 Safety and operation performance design

First of all, in order to ensure the safety and operation performance in the undeterioration condition, designers should select the girder which is under the most disadvantageous appearance to decide the geometric dimension of section and configuration of steel according to present design standards. After that, the initial design project can be created. In this example, the section of girder and the positions of steel of the

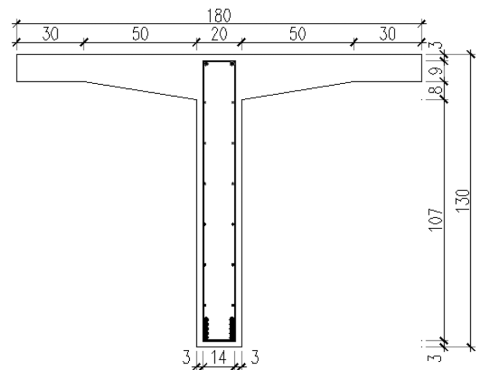


Figure 5. The girder's section of initial design scheme (cm).

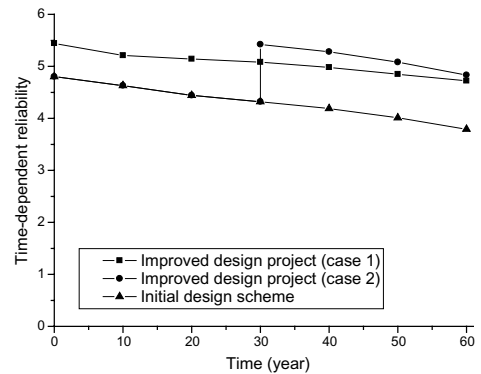


Figure 6. Time-dependent reliability of design scheme.

initial design project can be expressed in Figure 5. The grade of concrete is C35, while the grade of steel is HRB335.

##### 3.3.2 Durability estimation

According to the existing research achievements, the main reason of the deterioration of this bridge will be carbonization. It can predict that the steel of this bridge will be corroded from the 26th year according to the calculation model recommended in references (Hai-jun Wu 2006, Wen-ya Ye et al. 2006). Furthermore, we can get the time-dependent reliability of this bridge according to references (Wang Yi & Cai Min 2006, Moriy & Ellengwood R.1993, Suo Qing-hui & Qian Yong-jiu 2006, Jin Da-de 2006, Melchers Re.2001). (Fig. 6).

According to the result of durability estimation, the initial design scheme cannot ensure the durability requirements of the bridge in the whole life cycle since the time-dependent reliability will be lower than the restriction. So the initial design scheme has to be improved.

Table 1. Basic environmental parameters.

Item	Average temperature	Average relative humidity	Consistency of CO <sub>2</sub>
Value	16°C	75%	3.8%

Table 2. Design life-span of components of bridge.

Item	Girder	Bearing	Expansion	Joint	Pave-ment
Design life-span (Year)	60	40	20	60	15

Table 3. Improvement of girder design.

	Basic method	Improvements
Case 1	Changing design parameters	<ol style="list-style-type: none"> <li>1. Increasing the thickness of concrete protective cover to 35 mm.</li> <li>2. Using stainless steel instead of ordinary steel.</li> </ol>
Case 2	Designing maintenance schemes	<ol style="list-style-type: none"> <li>1. Reinforce the structure by planting 2Φ 25 HRB335 steel into the girder in the 30th year.</li> </ol>

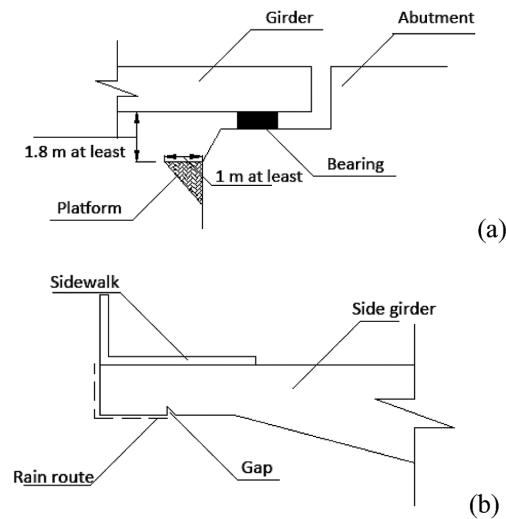


Figure 7. Improvement of detail design.

### 3.3.3 Improvement of initial design scheme

The improvement of initial design scheme should include the improvement of girder design and also some details. To improve the girder design, two kinds of improvement are considered which are listed in Table 3.

Once the initial design scheme has been improved, the durability estimation should be calculated again (Fig 6). Obviously, these two kinds of improvement can both ensure the durability of bridge structure during the whole life cycle.

In addition, some of the bridge's components such as bearings, expansion joints and pavements should be replaced periodically according to their design life-span listed in Table 2.

It is necessary to do some detail design for the maintenance work. Taking the bearing for example, in order to make the replacement more convenient, a platform should be designed as showed in Figure 7a.

Furthermore, designers should pay enough attention to the detail of the structure. For example, when it rains, the raindrop will easily run along the surface of the flange plate of the side girder to the web plate. In order to protect the web plate from corroding by the raindrop, it is suggested to set a small gap on the surface of the flange plate to change the route of raindrop (see Fig. 7b).

### 3.4 Analysis of life-cycle cost

Considering the complexity of the process of LCCA, the detail calculation process of LCCA will not be given in detail. But from the above discussion, it is obviously that some detail design are improved beforehand to make the maintenance work more convenient. So the new design method has much advantage in reducing the cost of maintenance.

## 4 CONCLUSIONS

The traditional design method has mainly considered the safety and undeterioration condition performance of bridge, but not the durability performance in design stage. It is necessary to establish an integrated durability design method to solve this problem. Therefore, with the basic idea of life-cycle design method, a basic design process that considering the durability problem is given in this paper, which is composed of design life-span determination, performance design, improvement if initial design scheme and analysis of life-cycle cost. Although the example is give in a simple supported RC bridge, the suggested method can also be applied in other kinds of bridge design.

The proposed design method is also an example of process controlled design method. Compared with traditionally index controlled design method, the former one is more effective to excite the creativity of the designed, also more effective to solve those complex decision problems in currently practices, including durable problems.

## ACKNOWLEDGEMENT

The research is financially supported by National High-tech R&D Program (863 Program) (2007AA11 Z104) from Ministry of Science and Technology of the People's Republic of China.

## REFERENCES

- Hai-jun WU. 2006. Research on durability design methods of bridge structures[D]. Degree thesis for Tongji University, Shanghai, China.

- YE Wen-ya, LI Guo-Ping, Fan LI-Chu. 2006. Preliminary analysis of life cycle cost for bridge. Highway, 2006 VOL.6, 101–104.
- Wang Yi, Cai Min.2006. Analysis on the reliability and forecast of service life of existing reinforced concrete structures. Engineering and Construction, 2006, 20(2):100–103.
- MORIY, ELLINGWOOD R.1993. Reliability Based Service-Life Assessment of Aging Concrete Structures. Journal of Structural Engineering 1993, 119(5):1600–1621.
- SUO Qing-hui, QIAN Yong-jiu.2006. Time-Dependent reliability index calculation of existed highway bridge. Journal of Traffic and Transportation Engineering. 2006, 6(1):69–71.
- JIN Da-de.2006. Durability analysis of existing reinforced concrete bridges based on reliability[D] Degree thesis for Chang'an University, Xi'an, China.
- Melchers RE.2001. Assessment of existing structures-some approaches and research needs. J Struct Eng ASCE 2001;127(4):406–11.

# Probabilistic durability design of RC structures in Persian Gulf using DuraPGulf model

M. Shekarchi, A. Rafiee, H. Layssi & F.M. Marani

*Construction Materials Institute (CMI), School of Civil Engineering, University of Tehran*

**ABSTRACT:** A probabilistic approach in durability design of reinforced concrete structures has been studied using DuraPGulf model. DuraPGulf is a service life design model, the first version of which provides a realistic prediction of corrosion initiation for RC structures in Persian Gulf region. Output parameters are interpolated using a complete database of conducted experiments in this region.

Although relevant data is still lacking, this approach has been successfully applied to a concrete structure in Persian Gulf environment. In order to facilitate the probability-based durability analysis, simple analysis has been developed, where the probabilistic approach is based on a Monte Carlo simulation. A comparative study of deterministic and probabilistic approach has been carried out using the data available from durability assessment of a jetty in Persian Gulf. In particular, probability based design seems to provide more realistic results than deterministic durability design analysis.

## 1 INTRODUCTION

Reinforced concrete has proved to be a reliable structural material with good durability performance when used properly. It has been one of the most used building materials in the last decades. However, there are many structures which show early, premature deterioration, and sometimes failure, namely those exposed to aggressive environments (Vaysburd & Emmons 2004).

The Persian Gulf environment has a long record of stigma for its harsh climate, desert features and saline waters, that increases the chloride penetration and consequently chloride induced reinforcement corrosion rates (Haque et al. 2007).

In many cases in the Persian Gulf, even structures which have been designed and constructed in compliance with Iranian code for durability of concrete structures in Persian Gulf region (BHRC-PNS428 2005), express corrosion problems in early age of their service life. In order to solve this problem, besides changing the code requirements in respect of durability, one should represent methods of durability design so that to find the most economical solution according to the desired service life for reinforced concrete structures (Ghalibafian et al. 2003). Since all parameters both for concrete durability and environmental exposure typically show a high scatter, a probability-based approach provides a very powerful basis for durability analysis (Gehlen & Schiessl 1999, Bentz 2003). This approach is primarily applied in order to obtain

more controlled durability and long-term performance of new concrete structures.

During the past decades, many physical and mathematical models have been introduced to calculate the chloride diffusion parameters into concrete and to estimate the time to corrosion initiation. DuraPGulf (Chini et al. 2004, Ghods et al. 2007), like many other programs, was deterministic in its operation, meaning that it will produce only one predicted time to initiation of corrosion for one set of input parameters. This single output contrasts with the well-known fact that concrete structures are quite variable in properties both throughout the structure and in terms of quality of construction and materials from one project to another. It would be useful if programs like DuraPGulf were able to predict a range of expected times to initiate corrosion rather than a single value to allow owners in a better risk management (Bentz 2003).

This paper describes the DuraPGulf model structure. The demonstration of this practical application is also explained through an example in this paper. Results obtained from the model have been verified with the data available from durability assessment of a jetty in Persian Gulf region.

## 2 EXPERIMENTAL PROGRAM

Concerning the fact that there was few data available for concrete durability studies specially regarding the

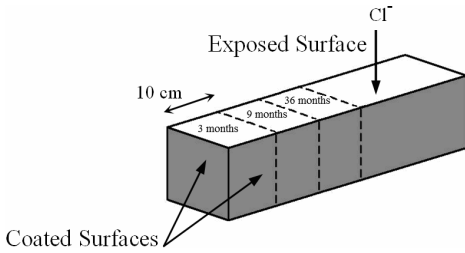


Figure 1. Concrete prism specimens (150 × 150 × 600 mm) exposed to marine environment for long-term durability studies.

chloride diffusion in Persian Gulf region, a complete set of field experiments were conducted in order to investigate the effect of different parameters on chloride diffusion such as water to cement ratio, silica fume content, curing condition, exposure condition, environment temperature and surface coating. A detailed review regarding this experiment can be found elsewhere (Chini et al. 2004, Ghods et al. 2007). In this project, 120 prism specimens measuring 150 × 150 × 600 mm were exposed to marine environment of Bandar-Abbas city. Sampling of the specimens for chloride diffusion has been carried out at the ages of 3, 9 and 36 months. Figure 1 shows the concrete prism specimens for the long-term durability studies. By curve fitting of chloride profiles of each specimen to Fick's second law (Crank 1975), data for diffusion coefficient and surface chloride content were calculated. Data have been used in order to develop the DuraPGulf database.

### 3 NUMERICAL MODELING

DuraPGulf uses advanced mathematical concepts for analyzing input data in order to predict Diffusion Coefficient ( $D_c$ ) and Surface Chloride Content ( $C_s$ ) values for new cases. Moving Least Squares method (MLS) is used for data regression. Accordingly, for each set of new input data in the  $n$ -dimensional space of primary data, a regression is conducted so that the nearby primary data have the highest effect on the final output (i.e. diffusion coefficient and surface chloride content). According to the Figure 2, in the Moving Least Squares approach the weighting function  $F$  is defined in shape and size, and is translated over the domain so that it takes the maximum value over the point  $k$  identified by the coordinate  $X_k$  where the unknown function  $\hat{u}$  is to be evaluated. The weight factor in this regard, which influences the effect width, can be calibrated after trial and error for new set of experiments (Lancaster & Salkauskas 1981).

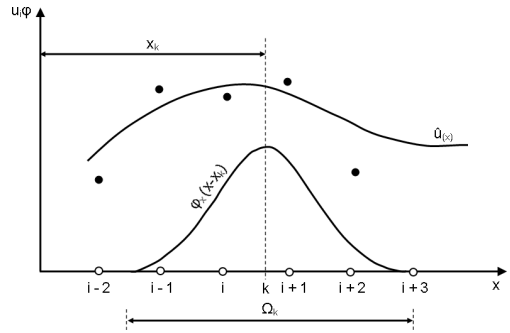


Figure 2. Schematic illustration of Moving Least Squares (MLS) method.

Finite Difference Method (FDM) is used to solve differential equation of the Fick's second law of diffusion over time:

$$\frac{\delta C}{\delta t} = D_c \frac{\delta^2 C}{\delta X^2} \quad (1)$$

Considering the following boundary conditions:

$$C(X > 0, t = 0) = 0$$

$$C(X = 0, t > 0) = C_s$$

$$C(X = \infty, t > 0) = 0$$

The solution for this differential equation is:

$$C(X, t) = C_s \cdot \left[ 1 - \operatorname{erf} \left( \frac{X}{2\sqrt{D_c t}} \right) \right] \quad (2)$$

Where  $D_c$  is the chloride diffusion coefficient,  $C_s$  is the equilibrium chloride concentration on concrete surface and  $C$  is the chloride content at the depth of  $X$  from the surface at the time  $t$ . The time, at which chloride content on the reinforcement surface reaches the chloride threshold value, is considered as the corrosion initiation time. In the DuraPGulf software, the percentage of chloride threshold is depended on mixture proportion and thickness of concrete cover.

The time dependence of the diffusion coefficient is normally expressed as (Thomas & Bentz 2001):

$$D(t) = D_0 \cdot \left( \frac{t}{t_0} \right)^\alpha \quad (3)$$

Where  $D_0$  is the diffusion coefficient at a given time  $t_0$  and the exponent  $\alpha$  represents the time dependence of the diffusion coefficient or the increased ability of the concrete to resist chloride penetration over time.

Table 1. Input data for initial probability analysis.

Parameter	Average	Coefficient of variation	Standard deviation	Distribution
Chloride diffusivity (m <sup>2</sup> /s.10 <sup>-12</sup> )	0.56	0.25	0.140	Normal
Surface chloride content (% weight of concrete)	0.80	0.30	0.24	Normal
Critical chloride content (% weight of concrete)	0.13	0.20	0.027	Normal
Concrete cover (mm)	75	0.10	7.5	Normal
Aging factor	0.31	0.25	0.078	Normal

Employing Ahrenius equation, the effect of temperature is considered on the diffusion coefficient for different months during the year (Page et al. 1981):

$$\frac{D_T}{D_0} = \exp \left[ \frac{U}{R} \times \left( \frac{1}{T_0} - \frac{1}{T} \right) \right] \tag{4}$$

Where **T** and **T<sub>0</sub>** are temperature in Kelvin degree, **R** is the gas general constant value and **U** is the activation energy of the diffusion process. A special value of 2948 for **U/R** was suggested in this study for DuraPGulf based on the experiments at the Construction Materials Institute (Chini et al. 2004). Similar to the temperature, the effect of humidity on the diffusion coefficient is considered through the model proposed (Bazant & Najjar 1972):

$$\frac{D_H}{D_0} = \left[ 1 + 256 \left( 1 - \frac{h}{100} \right)^4 \right]^{-1} \tag{5}$$

Where **h** is the humidity of environment (%).

#### 4 PROBABILISTIC APPROACH

The probabilistic approach is based on the Monte Carlo Method, which can be briefly described as a statistical simulation method, where sequences of random numbers are applied to perform the simulation (Gehlen & Schiessl 1999, Bentz 2003). In the present application of the simulation, the physical process is simulated directly by use of the modified Fick's Second Law of Diffusion for describing the transport process. The only requirement is that all the input parameters to the equation be described by a probability density function. Once the probability density functions of the various durability parameters of the system are known, the probability of failure is based on the evaluation of the limit state function for a large number of trials. Figure 3 shows a normal curve divided into eight sections, each with a probability of 0.125 (Bentz 2003). At about the centroid of each region is a discrete point that represents the characteristic value for that

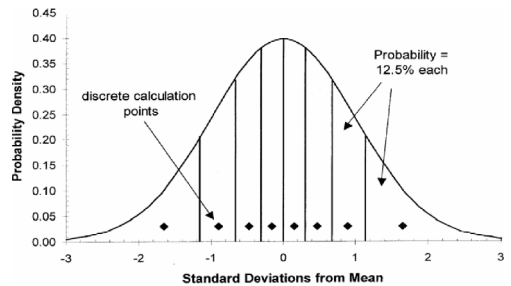


Figure 3. Division of normal curve into discrete regions (Bentz 2003).

region. The locations of these points are positive and negative 1.65, 0.89, 0.47 and 0.155 standard deviations from mean. By varying each set of the input parameters through all eight of these calculation points, it becomes possible to know exactly the number of iterations necessary to fully cover the input domain and produce a reasonable estimate of the solution. The accuracy of the Monte Carlo Method depends mainly on the number of trials undertaken and the method is easy to implement, a simulation based on this method appears to be both simple and intuitive.

#### 5 PROGRAMMING

DuraPGulf software has been developed based on data regression and analyses according to the mathematical methods mentioned earlier. The program uses a FDM kernel and graphic user interface (GUI) provided by VISUAL BASIC programming.

#### 6 EXAMPLE

A typical reinforced concrete pier of a jetty in Bandar-Emam port is subjected to the tidal zone exposure of the Gulf. The thickness of the concrete cover

is assumed to be 75 mm. Temperature diagram of Bandar-Emam is also shown in Figure 4.

Concrete has been cured for 3 days after demolding in July. The concrete mixes were developed at the water to cementitious ratios of 0.38, cementitious materials content of approximately 450 kg/m<sup>3</sup> and 6.5% silica fume. These parameters were used as input to the program. Running DuraPGulf, the calculated profile of chloride concentration versus depths for a given time of 27 months and the result of the sampling are shown in Figure 5.

The corrosion initiation time is calculated with the deterministic approach to be 128 years, which is very high.

In order to analyze the probability levels of the above combinations of concrete quality and concrete cover, initial probability analysis with input parameters as shown in table 1 were carried out. In this table, the surface chloride content of 0.8% by weight of concrete, which reflects the exposure conditions in tidal zone, was adopted. Based on a complete database of experiments, a threshold chloride content of 0.13% (Frederiksen, J.M., 2000) by weight of concrete and aging factor of 0.31 was assigned. Using Monte Carlo simulation, the probability of steel corrosion and development of further chloride penetration

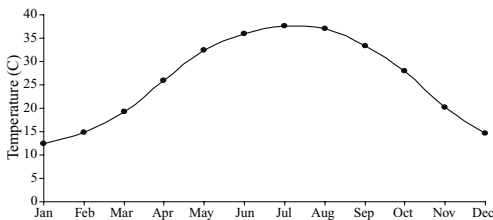


Figure 4. Annual temperature diagram of Bandar-Emam.

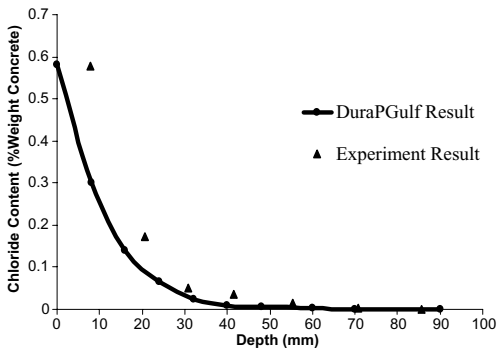


Figure 5. Comparison of the results of experiment with the results predicted by DuraPGulf model.

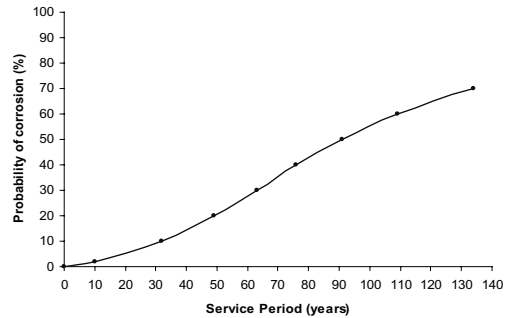


Figure 6. Development of risk for steel corrosion.

is illustrated in Figure 6. In most codes for reliability of structures, an upper level of 10% for probability of failure is normally accepted (NS 3490, 2004). As can be seen from Figure 6, a 10% level for the risk of steel corrosion will result in a service period of 32 years and for a service period of 128 years, the level of risk would be 65%.

## 7 CONCLUSIONS

Regarding results and experiments following conclusions can be drawn:

1. Durability design of RC structures has received a great concern in the recent decades;
2. In Iran, the need for a model for service life design of concrete structures in Persian Gulf region is highly necessary;
3. The predicted chloride profile by DuraPGulf model is generally in agreement with the experimental results.
4. Probabilistic durability model provides more realistic solutions than deterministic durability design.

## ACKNOWLEDGEMENTS

Authors are deeply indebted to Late Professor M. Ghalibafian for his continuous support and discussions. The financial support of Management and Planning Organization of Iran is greatly acknowledged.

## REFERENCES

- Bazant, Z.P. & Najjar, L.J. 1972. Nonlinear water diffusion of nonsaturated concrete. *Materials and Structural Journal*, 5 (1): 3–20.



- Bentz, E.C. 2003. Probabilistic modeling of service life for structures subjected to chlorides. *ACI Materials Journal*, 100 (5): 391–397.
- BHRC-PNS428. 2005. *National code of practice for concrete durability in the Persian Gulf and Oman Sea (proposed)*. Building and Housing Research Center, Ministry of Housing and Urban Development, Tehran: Iran.
- Chini, M. Ghods, P. Alizadeh, R. Hoseini, M. Montazer, Sh. Shekarchi & M. Ghalibafian, M. 2004. *Developing the first version of the model for service life prediction of reinforced concrete structures in Persian Gulf and Oman Sea*. 2nd report, NO. CMI8309144, Construction Materials Institute at the University of Tehran: Tehran, Iran.
- Crank, J. 1975. *The mathematics of diffusion (2nd Ed.)*. Oxford Press: London.
- Frederiksen, J.M., 2000 (approved 2002–03). Method for determination of chloride threshold values for steel in concrete. Nordtest report TR 500.
- Gehlen, C. & Schiessl, P. 1999. Probability-based Durability design for the Western Scheldt Tunnel. *Structural Concrete*, No 2: 1–7.
- Ghalibafian, M. Shekatchi, M. Zare, A. & Tadayon M. 2003. Chloride penetration testing of silica fume concretes under Persian Gulf conditions. *Proc. 6th CANMET/ACI intern. Conf. On durability of concrete, SP—212–46, Thessaloniki, Greece: 737–754*.
- Ghods, P. Alizadeh, R. Chini, M. Hoseini, M. Ghalibafian, M. & Shekarchi, M. 2007. Durability-based design in the Persian Gulf, *Concrete International*, 29(12): 50–55.
- Haque A.M. Al-khaiat, H. & John B. 2007. Climatic zones-A prelude to designing durable concrete structures in the Arabian Gulf. *Building and Environment*, 42(6): 2410–2416.
- Lancaster, P. & Salkauskas, K. 1981. Surface generated by moving least square methods. *Mathematics and Computer*, No. 37: 141–158.
- NS 3490. 2004. Design of structures. Requirements to reliability, Standards Norway, Oslo.
- Page, C.L. Short, N.R. & Tarras, A. El. 1981. Diffusion of chloride ion in hardened cement pastes. *Cement and Concrete Research*, 11(30): 395–406.
- Thomas, M.D. A & Bentz E.C. 2001. *Life 365: Computer program for predicting the service life and life cycle costs of reinforced concrete exposed to chlorides*. American Concrete Institute, Committee 365, Service life prediction, Detroit, Michigan.
- Vaysburd, A.M. & Emmons, P.H. 2004. Corrosion inhibitors and other protective systems in concrete repair. *Cement and Concrete Composites*, 26(3): 255–263.

# Strengthening with textile reinforced concrete—reliability based design with imprecise probability

J.-U. Sickert, W. Graf & S. Pannier

*Institute for Structural Analysis, TU Dresden, Germany*

**ABSTRACT:** The purpose of this contribution is to introduce on the one hand a new technology for strengthening damaged and deteriorated RC structures and on the other hand a basically new solution technique to perform a reliability based design. For the latter, an inverse solution of the design problem regarding reliability constraints is suggested. This solution enables the computation of design parameters in dependency of design constraints directly avoiding an iterative search or a solution of an optimization problem.

## 1 INTRODUCTION

The load-bearing capacity of steel reinforced concrete (RC) structures is time-dependent. In most cases mechanical and environmental stresses lead to damage and deterioration, e.g. in the form of concrete cracking, steel corrosion, and spalling. In addition, structures were planned to resist smaller loads in comparison to today's requirements. Therefore, the reliability of the structures varies and may fall down below permissible levels.

In order to increase the reliability up to required levels structural engineers are confronted with the challenge of strengthening and repair of those structures. They have to evaluate and quantify the damaged state of the structure as well as design the strengthening. The design comprises the selection of adequate strengthening technology as well as materials and the the respective dimensioning. Furthermore, the time-dependent reliability and the associated lifetime have to be determined.

In this paper, the focus is set on the new strengthening technology which bases on the new material textile reinforced concrete (TRC) (Brameshuber 2006). Thereby, TRC layers are applied on the surface of RC structures. A short introduction regarding TRC is given in Section 2.

Design is usually understood as the determination of design parameters in an iterative search process. Partly, it is also formulated as an optimization problem, see e.g. (Frangopol and Maute 2003). The inverse solution of the design problem suggested in Section 3 allows the computation of design parameters in dependency of design constraints directly and avoids so the iterative search or the solution of an optimization problem. The presented algorithm may also be applied for

the solution of the lifetime-oriented design problem in (Möller et al. 2007) and for the design of robust structures in (Beer and Liebscher 2007).

## 2 STRENGTHENING OF RC STRUCTURES WITH TEXTILE REINFORCED CONCRETE

Textile reinforced concrete (TRC) is a new composite material made of fine grained concrete and mul-tiaxial warp knitted fabrics, so called textiles. These textiles consist of filament yarns (rovings) which are connected with the aid of stitching yarn. Each roving is composed by a lot of single filaments. The filaments can consist of different material, e.g. alcali-resistant glass (AR glass) or carbon. TRC may be used for new structures and for new structural members as well as for strengthening of existing steel reinforced concrete (RC) structures. In this paper, the focus is set on the application of TRC for strengthening of existing RC structures. Thereby, TRC layers are applied on the surface of the existing structures.

The load-bearing behavior of RC structures with textile strengthening may appropriately described with the multi-reference-plane model (MRM). The MRM enables to model multi-layered composite materials with a discontinuous multi-BERNOULLI-kinematics (Möller et al. 2005). The FE discretization of the MRM is based on a hybrid energy functional. A MRM element comprises  $k + 1$  layered sub-elements and  $k$  interfaces. The sub-element  $i$  with its corresponding reference plane  $RP_i$  ( $i = 0, \dots, k$ ) is subdivided into  $s_i$  sub-layers (concrete and steel sub-layers or fine grained concrete and textile sub-layers). The reference plane  $RP_i$  is located in the middle of the sub-layer 0 or so-called reference layer, which may

be selected arbitrarily. The same stress shape functions, boundary displacement shape functions and element displacement shape functions are chosen for all sub-elements.

In order to describe the composite structure comprised of reinforced concrete and textile strengthening, different nonlinear material laws are applied to the individual sub-layers of concrete, steel and textile. Endochronic material laws for concrete and steel are utilized for general loading, unloading, and cyclic loading processes, and taking into account the accumulated material damage during the load history. In the case of cyclic loading, the textile reinforced fine grained concrete layers are split into sublayers of fine grained concrete and of textile reinforcement. The endochronic material law for concrete is adapted to the fine grained concrete. A nonlinear elastic brittle material law is used for the textile reinforcement. Under cyclic loading, damage occurs in the strengthening layer in the fine grained concrete matrix and the textile structure as well as disruption of the bond between the old concrete and the textile strengthening. These forms of damage and the additional plastic deformations may be described theoretically by means of plasticity and continuum damage theory (Möller et al. 2005). The subsequent strengthening of a RC structure is linked with a system modification, i.e. a changing of a preloaded and possibly damaged construction. The process of system modification is simulated numerically by an incremental iterative execution on the basis of the MRM.

The introduction of these new materials and technologies is accompanied by data uncertainty, (Möller et al. 2006). Aware of the governing uncertainty in the development of textile reinforced concrete structures, e.g. regarding the bond between filaments in textile yarns or the determination of sensitive material parameters, enhanced uncertainty dependent numerical concepts are required to simulate the load-bearing behavior realistically. In the case of plane textile reinforced concrete structures, spatially distributed uncertainty depending on the position vector also arises. This uncertainty may be accounted for using uncertain functions (Möller et al. 2006). Furthermore, the uncertain time-dependent material behavior of the textiles and the fine grained concrete requires the formulation of uncertain processes.

Textile reinforced concrete structures show data uncertainty of different characteristic. If an event (regarding its occurrence), as a random result of a test, may be observed as a crisp value on an almost unlimited number of occasions under constant boundary conditions, this represents a stochastic uncertainty.

The uncertainty characteristic randomness is assigned to this stochastic uncertainty. If the boundary conditions are (apparently) subject to arbitrary fluctuations, a comprehensive system overview is lacking, the

number of observations are only available to a limited extend, or the sample elements are of doubtful accuracy (non-precise), an information deficit exists. The outcome of this is a gap between the mathematical quality requirements of data if using stochastic methods and the real available non-precise data. The data do not fully satisfy real valued probability laws. In fact, the data may be quantified by imprecise probability, see e.g. (Viertl 1996).

The impreciseness results from informal uncertainty in terms of non-precise recognition of data or statistical inference (determining stochastic input parameters, such as expected values, variances and probability distribution functions). Here, this informal uncertainty is described by the uncertainty characteristic fuzziness and is mathematically quantified on the basis of the fuzzy set theory. The uncertainty consisting of randomness and fuzziness is summarized in the characteristic fuzzy randomness. The fuzzy random data are assessed with the aid of the uncertain measure fuzzy probability (Möller et al. 2006). The uncertainty characteristic fuzzy randomness includes both randomness and fuzziness as special cases. If data only show random properties, fuzziness is in-existent, i.e. a real-valued random variable is used. Non-precise data without random properties are quantified by fuzzy values.

### 3 RELIABILITY BASED DESIGN WITH IMPRECISE PROBABILITY

The reliability based design method presented herein has been developed for solving the inverse problem in combination with a nonlinear structural analysis using the MRM under uncertainty with emphasis on numerical efficiency and bases on (Beer and Liebscher 2007). The general scheme of the reliability-based design procedure introduced here may be summarized with the flowchart in Figure 1.

The procedure starts with specification and quantification of all design and structural parameters. Design parameters are usually the total thickness of the strengthening layer and the amount and form of the textiles. Potential values of the design parameters may be merged in intervals, reasonably in engineering sense. The intervals form the space of design parameters and each point of this space specifies a potential design. The intervals may be interpreted as uncertain information about the design parameters. If they are modeled as fuzzy sets the inverse solution of the design problem succeeds. Structural parameters are all non-controllable deterministic and non-deterministic input parameters.

The reliability based design task may be solved with the aid of the fuzzy stochastic structural analysis which is contained in the time-dependent safety assessment

selection of the design variables $\tilde{x}_{k,d}$ , $k = 1, \dots, n_d$
selection of the non-controllable uncertain structural parameters $\tilde{x}_{k,str}$ , $k = 1, \dots, n_{str}$
selection of numerical models assessing damage and deterioration
determination of reliability based design
uncertain time-dependent reliability analysis
selection of points from design space $\mathbb{X}_d$
computation of $\tilde{P}_i(\tau_i)   i = 1, \dots, n_i$
determination of time $\tilde{\tau}_i   \tilde{P}_i < \text{perm}_P$
marking of time $\tau_i \in \tilde{\tau}_i$ as lifetime
cluster analysis in design space - determination of fuzzy design vectors
evaluation of the $\tilde{x}^{[k]}$ - selection of optimal design

Figure 1. Flowchart of the design procedure.

of textile strengthened RC structures (Möller et al. 2006). Within the fuzzy stochastic structural analysis a set of input points  $x_i \in \mathbb{X}_d$  are mapped onto a set  $\mathbb{Z}$  of result points  $z_i$ . The result points  $z_i$  are assigned to the input points  $x_i$  by means of the mapping model on a point-to-point basis with

$$z_i = f(x_i). \quad (1)$$

This provides also an inverse assignment according to Figure 2. The fact that these dependencies are only known in a discrete form, excludes a closed solution of the design problem; continuous sets of feasible design parameter vectors cannot be determined by simply applying

$$x_i = f^{-1}(z_i). \quad (2)$$

The point-wise information, however, permits designing structures virtually directly with the aid of cluster analysis methods.

In the case of reliability based design the failure probability  $P_f$  or the reliability index  $\beta$  for different limit states are selected as coordinates  $z_j$ . Then, prescribed design conditions  $DC_h$ , available e.g. in codes, subdivide the point set  $M_z$  into two disjoint subsets  $M_{z^+}$  and  $M_{z^-}$ , comprising exclusively feasible points  $z^+$  or non-feasible points  $z_i$ , respectively. As a consequence, the points  $x_i$  may be assigned to the point sets  $M_{x^+}$  and  $M_{x^-}$  due to the point-to-point dependency. The set  $M_{x^+}$  comprises the design points  $x_{i^+}$  which fulfill all prescribed reliability requirements. These points  $x_{i^+}$

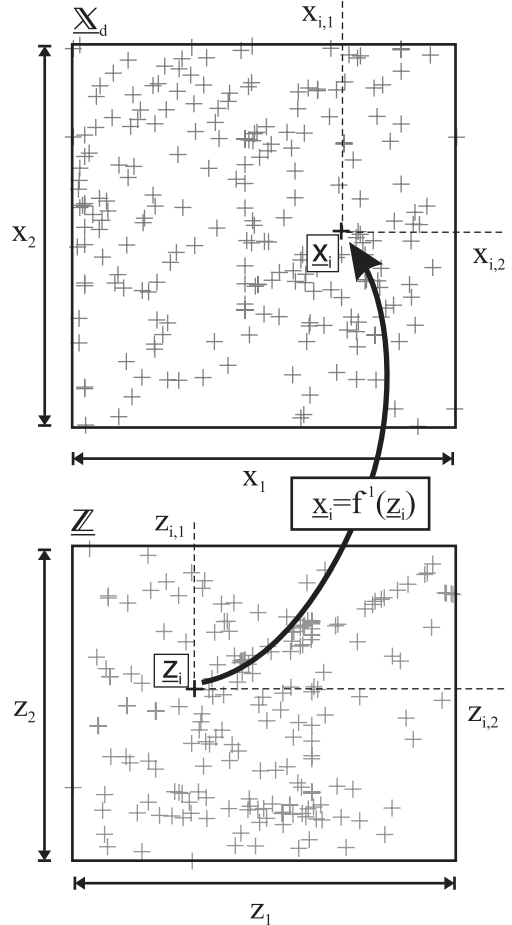


Figure 2. Point sets  $M_x$  and  $M_z$  in the design space and in the space of structural responses.

represent the basis for the numerical determination of  $n_c$  alternative point sets

$$C_k \subseteq M_{x^+}, k = 1, \dots, n_c \quad (3)$$

of feasible design variants. The point sets  $C_k$  are referred to as *clusters* which describe a partitioning of the points  $x_{i^+}$ .

The obtained clusters  $C_k$  form the basis for constructing alternative design variants. In a first step, a connected domain  $\underline{D}_k$  of points  $\underline{d}_1$  is deduced from each cluster  $C_k$ ,

$$C_k \rightarrow \underline{D}_k, k = 1, \dots, n_c. \quad (4)$$

These cluster domains  $\underline{D}_k$  possess the form of hyper-cubes in the design space  $\mathbb{X}_d$  with maximum extent in

each direction  $x_j$  and containing feasible points  $x_i \in M_{x^+}$  exclusively. Selected clusters domain  $D_k \in \mathcal{D}$  are taken as a basis to construct an associated fuzzy design vector  $\tilde{x}^{[k]}$ ,

$$D_k \rightarrow \tilde{x}^{[k]}, k = 1, \dots, n_D, \quad (5)$$

see Figure 3. Basically, this construction of design vectors can be extended to formulate a variety of appropriate design vectors from each cluster domain.

This can be reasonable, e.g., if some additional restrictions or preferences are applicable directly to the value ranges defined by the cluster domains  $D_k$ . The obtained fuzzy vectors  $\tilde{x}^{[k]}$  are needed to finally verify the feasibility of the design variant with respect to the design constraints  $DC_h$ ,  $h = 1, \dots, q$  and to evaluate their robustness. The formulation of the fuzzy design vector  $\tilde{x}^{[k]}$  is primarily determined by the information contained in the cluster domains  $D_k$ . Their geometry defines the support sets of the fuzzy design vectors  $\tilde{x}^{[k]}$ . The specification of the membership function  $\mu(\tilde{x}^{[k]})$ , however, provides some flexibility in incorporating objective and subjective preferences as well as problem specific characteristics. A reasonable strategy may be to first select an element  $\underline{x}^{[k]} = \underline{d}_1^* \in D_k$  of elevated preference for the final design and assign the membership value  $\mu(\underline{x}^{[k]}) = (\underline{d}_1^*) = 1$ , and then define the remaining membership function in correspondence with the requirement for convexity of  $\tilde{x}^{[k]}$ . For example, a simple, linear membership function may be assigned if no particular requirements are specified. This yields the membership values  $0 \leq \mu(\tilde{x}^{[k]}) < 1$  for all remaining points  $\tilde{x}^{[k]} = \underline{d}_1 \in D_k \setminus \underline{d}_1^*$ , see Figure 3.

The permissible design variants characterized by the fuzzy design vectors  $\tilde{x}^{[k]}$  represent  $n_D$  alternatives for selecting the optimum structural design variant  $\tilde{x}_{opt}$ . This selection is solved as a discrete multi-criteria optimization problem. The particular criteria of this problem are determined on the basis of the results

from  $n_D$  fuzzy structural analysis for the  $\tilde{x}^{[k]}$ . In (Beer and Liebscher 2007) three optimization criteria are formulated. Criterion I aims at an optimum structural design “in the mean” and corresponds with traditional optimization objectives, e.g., minimum cost, minimum mass, or maximum esthetics of the structure. In correspondence with probabilistic approaches, the criterion II assesses the robustness of the design variants [k]. This criterion may further be extended by introducing additional components which corresponds with the understanding of *robustness with respect to violation of a constraint*. This additional robustness component aims at evaluating the  $\tilde{x}^{[k]}$  by means of the distance of  $\tilde{x}^{[k]}$  from the design constraints  $DC_h$ . The desire for providing preferably large decision margins to the construction engineer motivates the formulation of criterion III. The decision margin of design variant [k] is determined by the  $\tilde{x}^{[k]}$ . This covers the whole range of possible choices for the final design  $\underline{x}^{[k]}$  weighted by the associated membership values  $\mu(\underline{x}^{[k]})$ . The overall optimization problem is formulated by combining the criteria I–III. To obtain a problem specific solution the criteria may be weighted and summarized.

#### 4 EXAMPLE

The new reliability based design method is applied to a T-beam floor construction in order to design strengthening layers made of textile reinforced concrete. A section of the T-beam floor construction with two beams is shown in Figure 4. The time-dependent reliability in relation to serviceability limit state is computed with the aid of fuzzy Monte-Carlo simulation (FMCS) with response surface approximation using an artificial neuronal network (Lagaros et al. 2005), (Liebscher et al. 2007). The serviceability limit state is achieved, if the deflection in the middle of the beam  $v_3$  exceeds 3.0 cm.

The structure is discretized by means of 156 finite elements. The beams are modeled with 12 concrete

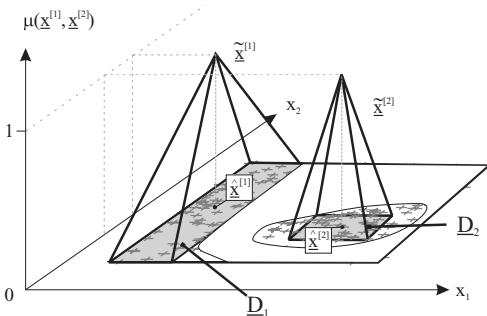


Figure 3. Fuzzy design vectors.

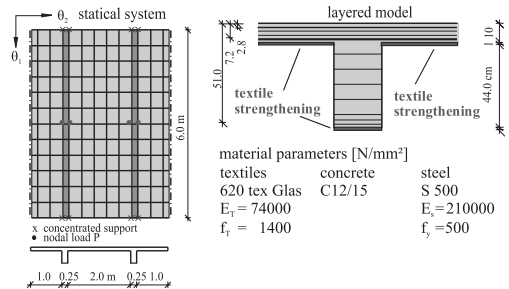


Figure 4. Geometry, material, and FE model.

layers and the plate portion with five concrete layers. The steel reinforcement is specified as a uniaxial smeared layer. The physically nonlinear analysis is carried out using endochronic material laws for concrete and steel. Crack formation, tension stiffening, and steel yielding are taken into consideration. The T-beam floor was primarily designed for a dead weight  $g$  of the floor construction, an additional load  $g_1$ , and a live load  $p_1$ . A change of use presupposes an updated dimensioning of the floor for an additional life load  $p_2$  and point loads  $P$ . For this reason textile strengthening is applied to the underside of the structure.

The aim of the investigation is to determine design parameters, which ensure a lifetime of 30 years. The lifetime  $L$  is attained, if the fuzzy failure probability  $\tilde{P}_f(\tau)$  exceeds the value of 0.005. Design parameters are the mean value  $x_{1,d}$  of the randomly distributed tensile strength of the fine grained concrete  $f_{c,d}$  and the amount of reinforcement  $x_{2,d}$ . The uncertainty of both parameters is considered by means of the intervals  $X_{1,d} = [5.5; 6.3]$  N/mm<sup>2</sup> and  $X_{2,d} = [0.5; 3.0]$  cm<sup>2</sup>/m. The interval forms the support of accompanying fuzzy values.

The remaining geometrical, material, and load parameters are a-priori parameters. The loads  $g_1$ ,  $p_1$ , and  $p_2$  are modeled as uniformly distributed superficial loads. The point loads  $P$  are modeled as nodal loads of magnitude  $P = 30$  kN. The live load  $p_1$  is modeled as a real random variable (GUMBEL distribution with  $a = 2.565$  and  $u = 5.699$ ) and the live load  $p_2$  as a fuzzy random variable (GUMBEL distribution with the bunch parameters  $\tilde{E}p_2 = \langle 5.7, 6.0, 6.3 \rangle$  kN/m and  $\sigma_{p_2} = 0.5$  kN/m). The concrete compressive strength  $f_c$  is specified as a GAUSSian distributed fuzzy random variable ( $E[f_c]$  N/mm,  $\tilde{\sigma}_{f_c} = (2.0, 2.5, 3.0)$  N/mm). Furthermore, deteriorating effects have to be considered. The deterioration is influenced by several factors, which are not precisely known. This information deficit leads to uncertainty and at the end to an uncertain service life. In the framework of this example, the deterioration is simplified by a fuzzy process

$$\tilde{d}_k(\tau) = e^{-\int_0^\tau \lambda(\tau, \tilde{s})} \quad \text{with}$$

$$\lambda(\tau, \tilde{s}) = \begin{cases} 10^{-4} & \text{if } \tau \leq \tau_0 \\ 10^{-4} + \frac{1}{3000} \left( e^{\frac{\tau \cdot \tilde{s}}{20}} - e^{\frac{\tau_0 \tilde{s}}{20}} \right) & \text{else} \end{cases} \quad (6)$$

with  $\tau_0 = 20$  years and the bunch parameter  $\tilde{s} = \langle 0.9, 1.0, 1.1 \rangle$ , which acts on the global tangential stiffness matrix.

As an intermediate result, Figure 5 shows the time-dependent fuzzy reliability and the fuzzy lifetime

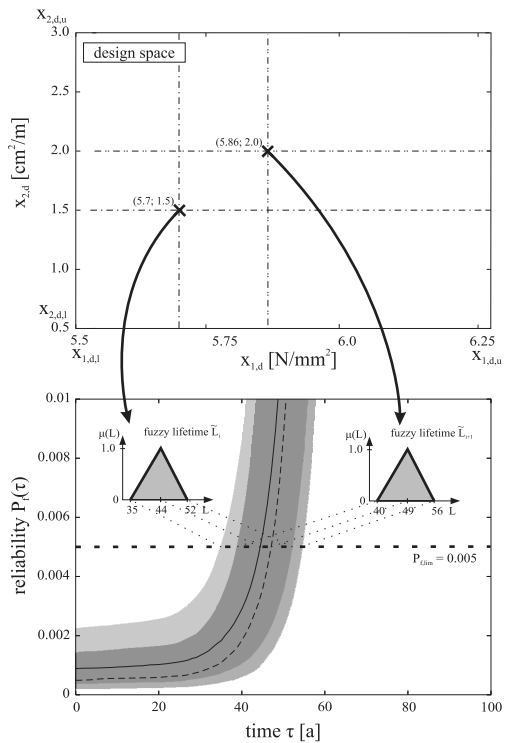


Figure 5. Time-dependent fuzzy reliability and fuzzy lifetime.

$\tilde{L}_i$  for two specific points  $x_i$  out of the design space. The repetition of the time-dependent reliability analysis yields the point set  $M_x = \{\min_{L_i \in \tilde{L}_i} [L_i = z_i]\}$  and allocates the point-to-point dependency. In the next step, the design space is subdivided into feasible and non-feasible points under consideration of two design constraints (Figure 6). The first design constraint DC1 is predefined with a minimal lifetime  $L_{min}$  of 30 years. Designs, exhibiting a lower lifetime, are assessed as non-feasible. Additionally, economical design constraints have to be met by the design parameters. Therefore, a specific design represented by design parameters is evaluated with the aid of a cost function  $f_c$  given by

$$f_c(X_{k,d}) = \left( 0.53 \left( \frac{x_{1,d} - x_{1,d,1}}{x_{1,d,u} - x_{1,d,1}} \right) + 0.2 \right) + \left( 0.9 \left( \frac{x_{2,d} - x_{2,d,1}}{x_{2,d,u} - x_{2,d,1}} \right) - 0.328 \right). \quad (7)$$

The second design constraint  $DC_2$  limits the costs of the design. The maximal cost of  $f_{c,max} = 1$  must not be exceeded.

The cluster procedure is initiated with 1,000 points which are lumped together to form the point set  $M_x$ .

This is subdivided by means of the design constraints  $DC_1$  and  $DC_2$  into the point set  $M_{x^+}$  with  $|M_{x^+}| = 434$  feasible points. The feasible points are introduced into a cluster analysis with the fuzzy c-means algorithm, see (Höllerrpner et al. 1999), (Bezdek et al. 1984). The obtained cluster configuration consists of three clusters  $C_k, k = 1, 2, 3$ . The associated cluster domains  $D_k, k = 1, 2, 3$  are determined with the membership-based approach according to (Beer and Liebscher 2007), see Figure 6.

The optimum design variant  $\tilde{x}_{opt}$  is then selected assessing the clusters received. Thereby, criterion I

$$K_I^{[k]^+}(\tilde{x}^{[k]^+}) = \frac{1}{A} \cdot \int_{x \in \tilde{x}^{[k]^+}} \left(1 - \frac{f_e(x)}{2}\right) dx, \quad (8)$$

is an optimum structural design “in the mean” in view of economical aspects. It is formulated by evaluating the cluster domains with the aid of the cost function  $f_e(x)$  according to Equation 7. Furthermore, criterion II assesses the size of the decision margins, covering the range of possible choices, computed according to

$$K_{II}^{[k]}(\tilde{x}^{[k]^+}) = A = \int_{x \in \tilde{x}^{[k]^+}} 1 dx. \quad (9)$$

For each of the measures the preferred variant is highlighted in Table 1. As  $\tilde{x}^{[2]^+}$  provides reasonable decision margins with respect to the other variants and an optimum structural design “in the mean” in

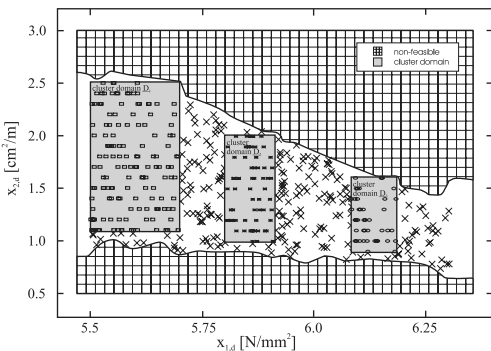


Figure 6. Clustering.

Table 1. Selection of optimum structural design.

	criterion I $K_I^{[k]}$	criterion II $K_{II}^{[k]}$
$\tilde{x}^{[1]^+}$	0.728	0.107
$\tilde{x}^{[2]^+}$	0.740	0.272
$\tilde{x}^{[3]^+}$	0.698	0.069

view of economical aspects, it is finally selected as the optimum design variant  $\tilde{x}_{opt} = \tilde{x}^{[2]^+}$ . The associated intervals of the design parameters are  $X_1, d = [5.5; 5.7]$  N/mm<sup>2</sup> and  $X_{2,d} = [1.1; 2.5]$  cm<sup>2</sup>/m. Considering the uncertainty of the a-priori parameters and design parameters the fuzzy lifetime  $\tilde{L}$  of at least  $L = (33, 43, 51)$  years is ensured.

## ACKNOWLEDGMENT

The authors gratefully acknowledge the support of the German Research Foundation (DFG).

## REFERENCES

- Beer, M. and Liebscher, M. (2007). Designing robust structures— a nonlinear simulation based approach. *Special Issue of Computers & Structures*. doi:10.1016/j.compstruc.2007.05.037 (in press).
- Bezdek, J. C., Ehrlich, R., and Full, W. E. (1984). FCM: The fuzzy c-means clustering algorithm. *Computers & Geosciences* 10, 191–203.
- Brameshuber, W. (Ed.) (2006). *Textile Reinforced Concrete*. State-of-the-Art Report of RILEM Technical Committee 201-TRC: Textile Reinforced Concrete.
- Frangopol, D. and Maute, K. (2003). Life-cycle reliability-based optimization of civil and aerospace structures. *Computers & Structures* 81, 397–410.
- Höllerrpner, F., Klawonn, F., Kruse, R., and Runkler, T. (1999). *Fuzzy Cluster Analysis: Methods for Classification, Data Analysis and Image Recognition*. Chichester New York Weinheim: Wiley.
- Lagaros, N. D., Charmpis, D. C., and Papadrakakis, M. (2005). An adaptive neural network strategy for improving the computational performance of evolutionary structural optimization. *Computer Methods in Applied Mechanics and Engineering* 194(30-33), 3374–3393.
- Liebscher, M., Beer, M., Pannier, S., Thiele, M., and Graf, W. (2007). Sampling schemes for crashworthiness investigations in view of robustness and reliability. In *COMPADYN 2007—Computational Methods in Structural Dynamics and Earthquake Engineering*. CD-ROM.
- Möller, B., Beer, M., Graf, W., and Sickert, J.-U. (2006). Time-dependent reliability of textile strengthened rc structures under consideration of fuzzy randomness. *Computers & Structures* 84(8–9), 585–603.
- Möller, B., Graf, W., Hoffmann, A., and Steinigen, F. (2005). Numerical simulation of rc structures with textile reinforcement. *Computers & Structures* 83(19-20), 1659–1688.
- Möller, B., Graf, W., Liebscher, M., Pannier, S., and Sickert, J.-U. (2007). An inverse solution of the lifetime-oriented design problem. In F. Stangenberg, O. Bruhns, D. Hartmann, and G. Meschke (Eds.), *3rd International Conference Lifetime Oriented Design Concepts*, Bochum, pp. 21–40.
- Viertl, R. (1996). *Statistical Methods for Non-Precise Data*. Boca Raton New York London Tokyo: CRC Press.

# Fatigue life of precast decks of high speed railway bridges

C.F. Sousa, R. Calçada & A.S. Neves

*Faculty of Engineering of the University of Porto, Porto, Portugal*

**ABSTRACT:** Fatigue verification doesn't govern the design of the majority of civil engineering structures, but, in the case of railway bridges (namely those constructed with prefabricated beams) fatigue needs to be taken into account because of the high value and the cyclic nature of the traffic actions. The main objective of the present paper is the identification of the critical points where fatigue verification is more severe than ultimate limit state verification, in the case of railway bridge decks constructed with precast "U" beams carrying heavy freight traffic.

## 1 INTRODUCTION

Prefabrication has been one of the most employed techniques in the construction of modern railway bridges. Precast decks are commonly composed by prefabricated "U" beams connected by a thin slab cast in situ (eventually using prefabricated planks). The cross section is usually constructed with 2 precast beams when the bridge carries two railway tracks (Fig. 1) and a single beam if there is only one track.

A common structural scheme in the longitudinal direction comprehends continuous spans, monolithically connected without prestressing steel (Fig. 2). This solution has been employed in railway bridges with a maximum span approximately equal to 35 m.

The main objective of the present paper is to identify the critical points, in this kind of structures, where fatigue verification is determinant, that is, the points where fatigue verification is more severe than ultimate limit state verification.

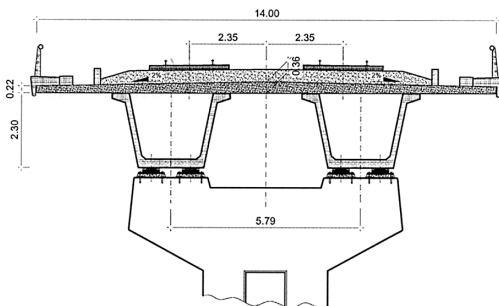


Figure 1. Railway bridge deck constructed with two precast "U" beams.

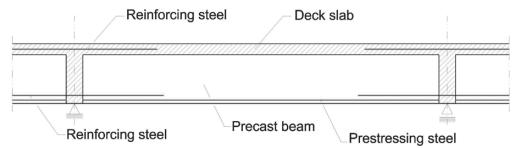


Figure 2. Schematic representation of the structural scheme in the longitudinal direction.

The following procedure is adopted:

- a bridge deck with typical geometrical configuration is adopted as a case study;
- for all the critical sections, both in the longitudinal and in the transverse direction, the area of reinforcement required for ultimate limit state verification (under the effect of permanent loads and traffic loads) is quantified;
- fatigue verification is carried out for the critical sections, considering the quantity of reinforcement previously evaluated.

This paper presents the case of a structure inserted in a high speed railway line, composed by two separate decks: one carries high speed traffic, whereas the other carries heavy freight traffic. This paper refers to the fatigue verification of the precast deck carrying heavy freight traffic.

Fatigue verification is carried out for reinforcement and also for concrete subjected to compression. During the fatigue verification, the effect of bending moments and shear forces is taken into account.

At last, the results of the analysis are discussed and the main consequences of fatigue in this kind of structures are pointed out.



## 2 FATIGUE VERIFICATION ACCORDING TO THE EUROCODES

European design codes include rules for fatigue verification. In the case of reinforced and prestressed concrete structures, fatigue verification must be carried out according to one of the following methodologies:

- damage accumulation method;
- damage equivalent stress method;
- simplified analysis (only suitable for a few simple cases).

The general procedure for fatigue verification is based on the damage accumulation method. This method involves the calculation of the stress history caused by the passage of each train (belonging to the traffic scenario, for the line under analysis). Then, the stress history must be converted into a stress histogram and the total damage must be calculated using the Palmgren-Miner Rule.

EN 1992-2 (CEN, 2005) presents a simplified procedure for calculating the damage equivalent stress. The damage equivalent stress is the stress which causes (with a reference number of repetitions, usually  $10^6$ ) a fatigue damage equal to the one produced by the real trains along the service life of the structure. In the case of reinforcing and prestressing steel, the damage equivalent stress range shall be calculated according to the equation 1:

$$\Delta\sigma_{S, equ} = \lambda_{S,1} \cdot \lambda_{S,2} \cdot \lambda_{S,3} \cdot \lambda_{S,4} \cdot \phi \cdot \Delta\sigma_{S,71} \quad (1)$$

where  $\Delta\sigma_{S,71}$  = steel stress range due to the static traffic loads;  $\phi$  = dynamic factor; and  $\lambda_{S,i}$  = parameters which take into account the span length, annual traffic volume, design life and the existence of multiple tracks.

The determination of the parameters included in the equation 1 is exposed in EN 1992-2. Concerning concrete, the upper and lower stresses of the damage equivalent stress spectrum are determined by a similar procedure. Adequate fatigue resistance exists if the damage equivalent stress range is lower than the corresponding maximum stress range indicated in EN1992-1-1 (CEN, 2004).

The methodology employed in the present paper is the damage equivalent stress method, because the structure under analysis carries freight traffic, with maximum speed lower than 200 km/h.

If the structure under analysis was a bridge with maximum line speed at the site greater than 200 km/h, the employment of the damage accumulation method would be compulsory. In that case, the stress history caused by the passage of the trains should be calculated through dynamic analyses, so that resonance phenomenon could be taken into account.

## 3 CASE STUDY

The cross section of the bridge deck under analysis is composed by a precast “U” beam (2,± m high) and a slab, carrying a railway line with a single track (Fig. 3). The slab has a thickness equal to 0.30 m and is 8.96 m wide. The bridge deck has four continuous spans: two end spans with a length equal to 26.5 m plus two centre spans with a length equal to 33.5 m. The sequence of construction of the deck is presented in Table 1.

### 3.1 Geometry

Table 2 presents the geometrical properties of the precast beam. The effective width of the slab (flange of the composite beam) was determined according to EN1992-1-1, in order to take into account the shear lag effect. The following values were considered in the structural analysis: 8.96 m in the span region; 6 m in the support region.

### 3.2 Materials

The characteristic strength in cylinders,  $f_{ck}$ , of the concrete employed in precast beams is 50 MPa (strength class C50 according to EN1992-1-1). The characteristic strength of the remaining concrete elements is

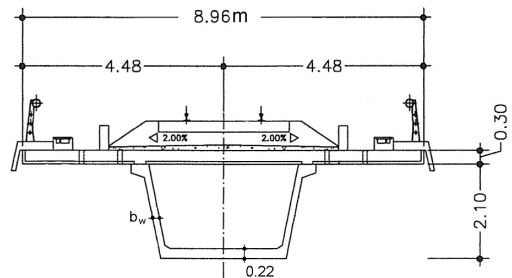


Figure 3. Cross section of the bridge deck under analysis.

Table 1. Sequence of construction.

Time days	Action
-3.5	Casting of the girders
0	Transfer of the prestress
60	Erection of the precast planks and casting of the central strip of the deck, in the region above the continuity supports
67	Casting of the central strip of the deck, in the middle span region
74	Casting of the remaining part of the deck
104	Placing of the additional permanent loads (ballast and others)

Table 2. Geometrical properties of the precast beam.

	Along 7.5 m near the end of the beam	Central part of the beam
$A(\text{m}^2)$	1.557	1.332
$I(\text{m}^4)$	0.8194	0.7190
$h(\text{m})$	2.10	2.10
$v_i(\text{m})$	0.8012	0.7405
$b_w(\text{m})$	0.21	0.15

$A$  = area;  $I$  = second moment of area;  $h$  = total height;  $v_i$  = distance between the centre of gravity and the bottom fibre; and  $b_w$  = thickness of the web.

30 MPa. Creep and shrinkage behaviour was modelled according to Model Code 1990 (CEB, 1993). The yield strength of the reinforcing steel,  $f_{yk}$ , is 500 MPa. The tensile strength of the prestressing steel,  $f_{pk}$ , is 1860 MPa. The maximum stress applied to the tendon during tensioning is equal to  $0.75 f_{pk}$ .

### 3.3 Loads

The self weight of the structure is 106.14 kN/m at the support region and 100.5 kN/m at the middle span region. The weight of the ballast is 41.9 kN/m, (characteristic value). The weight of other permanent loads is 38.51 kN/m. Table 1 describes the sequence of application of the permanent loads.

The static effect of the traffic load is represented by Load Models 71 and SW/0, according to EN1991-2.

It must be realized that the methodology based on damage equivalent stress is not valid when classified loads with  $\alpha > 1$  are required to represent the effect of freight trains. In those cases, fatigue verification must be carried out according to the damage accumulation methodology, considering the specific traffic scenario of the railway line.

The dynamic magnification of stresses is represented by the dynamic factor  $\phi$  as defined in EN1991-2.

### 3.4 Numerical analysis

#### 3.4.1 Phased analysis considering creep and shrinkage

A linear viscoelastic model, considering the sequence of construction (Table 1) and the effects of creep and shrinkage, was employed for the evaluation of the effects of the permanent loads. This kind of analysis evaluates the temporal evolution of the stresses and strains that occur in this kind of structures as a result of the modification of the static system during the construction phase and the delayed deformation of the concrete.

DIANA Finite Element Analysis software (TNO DIANA, 2007) was employed. Structural discretization was carried out using Mindlin beam finite elements, numerically integrated along the beam axis and in its cross section. Concrete behaviour was modelled using a strain decomposition model, which allows for creep, shrinkage and cracking effects to be handled simultaneously.

Figure 4 illustrates the evolution of the normal stress at the upper fibre of the support section and the evolution of the bending moment at the same section, respectively.

By observing Figure 4 we can conclude that the value of the tensile stress (at the upper fibre of the section above the support) after the delayed deformation of the concrete is greater than the value immediately after the end of the construction. However, this doesn't happen in the case of the bending moment at the same section.

An important conclusion of this analysis is the fact that the value of the tensile stress is greater than the tensile strength of the concrete ( $f_{ctm} = 2.9$  MPa), even without the effect of the traffic loads. The consequences of this event (such as modification of the natural frequencies and change of the structural response under the effect of the passage of trains) will be analysed in future developments of this work.

#### 3.4.2 Effect of traffic actions

The determination of the effects of traffic actions was performed using Bernoulli beam finite elements, considering the linear-elastic behaviour of the concrete, that is, cracking of the slab (above the supports) wasn't considered during the calculation of the forces caused by traffic loads.

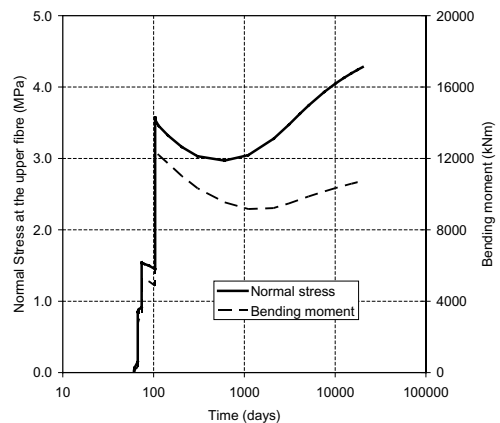


Figure 4. Evolution of the normal stress at the upper fibre of the support section, and bending moment at the same section.

Separate models were employed for the calculation of the forces in the longitudinal direction and in the transverse direction.

In the longitudinal direction, the numerical model consists of a single beam.

In the transverse direction, the numerical model consists of a 1 m wide strip, whose axis is represented in Figure 5. This figure represents also the transverse distribution of the point forces of Load Model 71, due to the effect of the sleeper and the ballast (according to EN1991-2). The longitudinal distribution of the point forces (wheel loads)

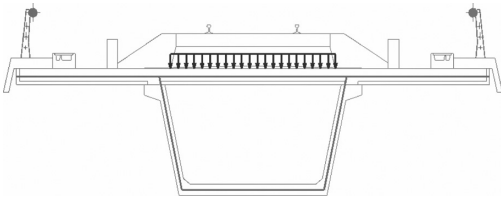


Figure 5. Numerical model for the determination of forces in the transverse direction.

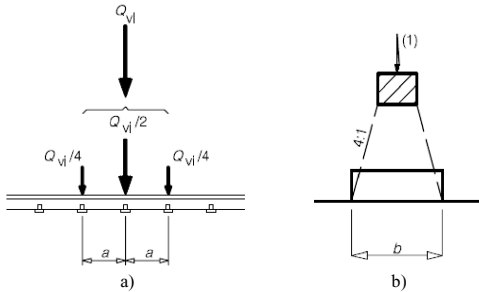


Figure 6. Longitudinal distribution of a point force or wheel load; a) by the rail; b) by the sleeper and the ballast.

by the rail, the sleepers and the ballast was carried out according to EN1991-2 (Figure 6), resulting in a uniform distribution of forces in the longitudinal direction.

### 3.5 Results

Tables 3 and 4 present a synthesis of the results regarding the longitudinal behaviour. Tables 5 and 6 present the results regarding the transversal behaviour.

The main results comprehend the quantification of the amount of reinforcement required for ultimate limit state and the fatigue verifications (considering that amount of reinforcement) in order to identify the situations where fatigue phenomenon governs the design.

The results of the fatigue verification are exposed in the following way:

- In the case of the steel,  $\Delta\sigma_{S, equ}$  represents the damage equivalent stress range. Adequate fatigue resistance exists if  $\Delta\sigma_{S, equ}$  is lower than the maximum stress range at  $N^*$  cycles,  $\Delta\sigma_{RSk}(N^*)$ .
- In the case of the concrete under compression,  $N_{i, max}$  represents the maximum number of cycles (having the upper and the lower stress of the damage equivalent stress spectrum) which are resisted by the structure. Adequate fatigue resistance exists if  $N_{i, max}$  is greater than  $N^*$ .

The situations where fatigue verification governs the design are pointed out with the symbol <sup>(F)</sup> in tables 3 to 6.

In the case of shear force, steel stresses are quantified under the effect of shear at a distance  $d$  from the support ( $d$  = effective depth of the cross section), whereas concrete stresses are quantified considering the shear force at the support section. During the fatigue verification of the webs compressed by the effect of shear, the fatigue strength of the concrete  $f_{cd, fat}$  was affected by the reduction factor  $\nu$ ,

Table 3. Synthesis of the results regarding the longitudinal bending moment.

Ultimate limit state			Fatigue verification				
$M_G$	$M_{\phi-LM71}$	$A_{s, required}$	Steel		Concrete under compression		
kN · m	kN · m	cm <sup>2</sup>	$\Delta\sigma_{s, equ}$	$\Delta\sigma_{RSk}(N^*)$	$N_{i, max}$	$N^*$	
Support section	-12370	-11322	368.7	117.6	162.5	$2.4 \cdot 10^{5(F)}$	$1 \cdot 10^6$
Middle span section	+13264	+9925	0*	**	**	$2.2 \cdot 10^{13}$	$1 \cdot 10^6$

\*No reinforcing steel is required in addition to prestressing steel.

\*\*Cracking does not occur under the characteristic combination of actions.

<sup>(F)</sup> Fatigue verification governs the design.

Table 4. Synthesis of the results regarding the longitudinal shear force.

	Ultimate limit state				Fatigue verification			
					Steel		Concrete under compression	
	$V_G$	$V_{\phi-LM71}$	$\theta$	$A_{sw}/s_{required}$	$\Delta\sigma_{s,equ}$	$\Delta\sigma_{RSk}(N^*)$	$N_{i,max}$	$N^*$
	kN	kN	°	cm <sup>2</sup> /m	MPa	MPa		
Support section	3069	2116	28*	**	**		$1.7 \cdot 10^{3(F)}$	$1 \cdot 10^6$
At a distance $d$ from the support	2659	1892	***	19.9	137.4	162.5	***	

\*Considering  $\nu = 0, 6$  and  $f_{wd} = 400$  MPa.

\*\*Shear reinforcement is determined by shear force at a distance  $d$  from the support section.

\*\*\*Inclination of the compression struts is determined by shear force in the support section.

<sup>(F)</sup>Fatigue verification governs the design.

Table 5. Synthesis of the results regarding the transverse bending moment.

	Ultimate limit state			Fatigue verification			
				Steel		Concrete under compression	
	$M_G$	$M_{\phi-LM71}$	$A_{s,required}$	$\Delta\sigma_{s,equ}$	$\Delta\sigma_{RSk}(N^*)$	$N_{i,max}$	$N^*$
	kN · m/m	kN · m/m	cm <sup>2</sup> /m	MPa	MPa		
Support section of the deck slab	-39.0	-38.4	10.23*	119.0	162.5	$2.5 \cdot 10^8$	$1 \cdot 10^6$
Middle span section of the deck slab	-8.88	+77.4	25.84	198.9 <sup>(F)</sup>	162.5	$9.9 \cdot 10^7$	$1 \cdot 10^6$

\*Without consideration of the effect of shear between web and flange of the box section.

<sup>(F)</sup>Fatigue verification governs the design.

Table 6. Synthesis of the results regarding the transverse shear force.

	Ultimate limit state				Fatigue verification			
					Steel		Concrete under compression	
	$V_G$	$V_{\phi-LM71}$	$\theta$	$A_{sw}/s_{required}$	$\Delta\sigma_{s,equ}$	$\Delta\sigma_{RSk}(N^*)$	$N_{i,max}$	$N^*$
	kN/m	kN/m	°	cm <sup>2</sup> /m/m	MPa	MPa		
Support section of the deck slab	34.8	113	21.8	*	*		$6.0 \cdot 10^{13}$	$1 \cdot 10^6$
At a distance $d$ from the support	29.4	113	**	8.8	263.1 <sup>(F)</sup>	162.5	**	

\*Shear reinforcement is determined by shear force at a distance  $d$  from the support section.

\*\*Inclination of the compression struts is determined by shear force in the support section.

<sup>(F)</sup>Fatigue verification governs the design.

as imposed by EN1992-1-1, in order to take into account the strength reduction caused by transverse cracking. It should be realized that strength reduction must be applied because the combination of shear and bending moment is sufficient to cause cracking,

although the beams are prestressed in the longitudinal direction.

By observing tables 3 to 6, we can conclude that there are several situations where fatigue verification governs the design. The situations where fatigue

determines the amount of reinforcement can be easily taken into consideration in the design of new structures.

The situations where insufficient fatigue resistance of the concrete was detected are more complex (namely in the case of the webs of the precast beams) because they imply the modification of the standard geometry of precast beams. However, several authors mention that when the fatigue verification of the concrete governs the design, this does not necessarily mean that there is insufficient fatigue resistance, because it could mean that there is insufficient knowledge about the fatigue phenomenon, which leads to conservative design codes (ERRI D 216, 1999). For example, in the cases where a stress gradient occurs in the compression zone of a concrete section, a redistribution of stresses takes place. This effect is not mentioned in EN1992-1-1. If it is taken into account according to the procedure indicated in Model Code 1990, the fatigue verification included in Table 3 does not govern the design any more.

This redistribution may not be applied in the cases where the compression results from the shear force. By observing Table 4 we can conclude that, according to EN1992-1-1, the fatigue resistance of the compression struts of the webs ( $N_{i,max} = 1.7 \cdot 10^3$ ) is, in this case, 600 times less than the required value ( $N^* = 1 \cdot 10^6$ ). However, it must be realized that the relation between compressive stress and fatigue life is not linear. In this case, an increase of the web thickness equal to 17% would be sufficient to obtain adequate fatigue resistance.

Finally, it must be pointed out that two aspects are not dealt with in this paper:

- fatigue verification of the webs considering the interaction between shear and transverse bending;
- fatigue verification of the connection between concrete cast at different times.

These complex aspects, which are not explicitly treated in the Eurocodes, are beyond the scope of the present paper. These aspects will be the object of future developments of this work.

#### 4 CONCLUSIONS

The main objective of the present paper was the identification of the critical points where fatigue verification is more severe than ultimate limit state verification, in the case of railway bridge decks constructed with precast “U” beams carrying heavy freight traffic.

The synthesis of the results identified several critical sections where fatigue governs the design, both in the longitudinal and in the transverse direction of the bridge. In the case under analysis, fatigue verification is critical in the case of both bending and shear.

The situations where fatigue determines the amount of reinforcement can be easily taken into consideration in the design of new structures. However, the situations where insufficient fatigue resistance of the concrete was detected are more complex (namely in the case of the webs of the precast beams) because they imply the modification of the standard geometry of precast beams.

This paper presents the results of a single case, which can not be immediately generalized, but the work in this domain is in progress, within the scope of the research project mentioned in §5.

#### ACKNOWLEDGMENTS

This paper refers to a research performed with financial support from the Portuguese Foundation for Science and Technology (FCT), through the research project PTDC/ECM/68430/2006.

Financial support from FCT, through the PhD grant SFRH/BD/29125/2006, is also acknowledged by the first author.

#### REFERENCES

- CEB, Comité Euro-International du Béton. 1993. *CEB-FIP Model Code 1990*. Thomas Telford.
- CEN, Comité Européen de Normalisation. 2004. *EN1992-1-1-Eurocode 2: Design of concrete structures - Part 1-1: General rules and rules for buildings*. Brussels.
- CEN, Comité Européen de Normalisation. 2005. *EN1992-2-Eurocode 2: Design of concrete structures—Concrete bridges—Design and detailing rules*. Brussels.
- ERRI D 216, European Rail Research Institute. 1999. *Fatigue of railway bridges. State of the art report*. Study undertaken for the International Union of Railways.
- TNO DIANA BV. 2007. *DIANA User's Manual—Release 9.2*. Delft, The Netherlands.

# Nonlinear dynamic analysis of frames with arbitrary plastic hinges

Z.H. Yan & F.T.K. Au

*Department of Civil Engineering, The University of Hong Kong, Hong Kong, China*

**ABSTRACT:** This paper presents a method for nonlinear dynamic analysis of frames subjected to distributed loads, which is based on the semi-rigid technique and moving node strategy. The plastic hinge that accounts for the material nonlinearity is modelled as a pseudo-semi-rigid connection at the element end. The stiffness matrix of a frame member with material and geometric nonlinearities is expressed as the sum of products of the standard stiffness matrix and the geometric stiffness matrix of the member with their corresponding correction matrices. Each beam member is modelled by two elements. The moving node strategy is applied to the intermediate node to track the exact location of any intermediate plastic hinge that may be formed. The method presented is efficient in computation and it needs no additional connection elements. A portal frame and a five-storey frame are used to verify and illustrate the applicability of the method.

## 1 INTRODUCTION

The influence of material and geometric nonlinearities on the behaviour of frames is particularly significant during extreme events such as earthquakes and typhoons. The dynamic response of a frame is very much complicated by the phenomena of yielding, unloading, reloading, etc. especially around the plastic hinges. Furthermore in practical cases, members of frames are subjected to distributed loads such as the self-weight, the live load, the wind load, etc. Under the action of distributed loading, plastic hinges may be formed at intermediate positions besides the ends of member. In addition, modern structures also suffer from more significant “ $P$ - $\Delta$  effects” since they are often taller and more slender because of the use of stronger materials and more advanced construction techniques. To better understand their behaviour and to improve the design of modern buildings, it is necessary to develop methods for dynamic analysis taking into account such factors.

The semi-rigid technique is a method to analyze frames with semi-rigid connections (Monforton & Wu 1963). Recently the geometric nonlinearity (Xu 1992) and the plastification concept (Hasan et al. 2002) were also included in the technique, and a series of advanced analyses of steel frame structures were developed (Xu et al. 2005, Gong et al. 2005, Gong 2006, Gong et al. 2006, Grierson et al. 2006). So far, the semi-rigid technique is mainly applied to static and pushover analyses. Although various researchers are trying to develop the pushover analysis as a means of practical design, nonlinear dynamic analysis is still essential especially to

those structures that are irregular and those of which the higher mode effects cannot be ignored. Besides, the strong-motion peculiarity is also a problem that the pushover analysis needs to overcome (Elnashai 2002). Therefore dynamic analysis is still important to frames with nonlinearities.

The moving node strategy was presented for the elasto-plastic analysis of frames subjected to loads including linearly varying distributed load (Wong 1996). In addition, certain practical applications of the moving node strategy were carried out in the second-order inelastic analysis of two-dimensional and three-dimensional steel frames (Kim et al. 2004, Kim & Choi 2005). However, the research work above on the intermediate plastic hinge was only for the static analysis of frames. In actual practice, the plastic hinges are formed when the frame is subjected to strong dynamic excitations such as earthquakes. Therefore the local behaviour of the intermediate plastic hinges and the global responses of frames under distributed loads need to be studied in detail.

The dynamic analysis of frames with semi-rigid joints has been studied for over ten years. Although various methods for dynamic analysis of frames with different nonlinear semi-rigid connections taking into account geometric nonlinearity were developed (Lui & Lopes 1997, Awkar & Lui 1999), the nonlinear connections could only be located in the beams but not the columns, since the stability functions used for geometric nonlinearity were not compatible with the nonlinear connections. It is not easy to extend the method to inelastic analysis because the bending moments in the columns of the lower floors are usually so large that

they yield at the base. Recently, Au & Yan (2008) presented a method for nonlinear dynamic analysis of frames with material and geometric nonlinearities based on the semi-rigid technique.

This paper presents a method for nonlinear dynamic analysis of frames subjected to distributed loads, which is based on the semi-rigid technique and moving node strategy. The plastic hinge that accounts for the material nonlinearity is modelled as a pseudo-semi-rigid connection at the element end. Each beam member is modelled by two elements and the moving node strategy is applied to the intermediate node to trace the exact location of any intermediate plastic hinge that may be formed. A portal frame and a five-storey frame are used to verify and illustrate the applicability of the method.

## 2 DEVELOPMENT OF SEMI-RIGID TECHNIQUE

Semi-rigid behaviour often exists in the frame connections since there is no perfectly rigid or pinned connection in reality. Monforton and Wu (1963) modelled the semi-rigid connection as a zero-length linear spring at each end of a member as shown in Figure 1 and presented the fixity factor as

$$\lambda_i = \frac{\alpha_i^e}{\alpha_i^e + \alpha_i^s} = \frac{\alpha_i^e}{\alpha_i^{total}} = \frac{1}{1 + (3EI/r_iL)} \quad (i = 1, 2) \quad (1)$$

where  $\alpha_i^e$  is the elastic end-rotation at end  $i$  of the member,  $\alpha_i^s$  is the spring rotation at end  $i$  of the member,  $\alpha_i^{total}$  is the total end-rotation at end  $i$  of the member,  $r_i$  is the rotational stiffness of the semi-rigid connection at end  $i$ ,  $E$  is elastic modulus of the member,  $I$  is moment of inertia of the member, and  $L$  is the length of the member. The fixity factor is defined as the ratio of the rotational stiffness of the semi-rigid connection to the total stiffness comprising the connection and the member. It can also be interpreted as the ratio of the elastic end-rotation of the member to the total end-rotation of the member. The fixity factor  $\lambda_i$  lies between 1 and 0, which correspond to the rotational stiffness of the semi-rigid connection  $r_i$  of infinity

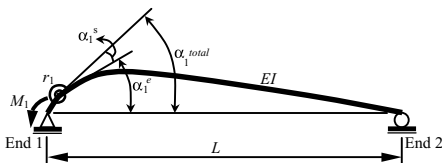


Figure 1. Concept of fixity factor.

and zero respectively, namely the rigid connection and pinned connection.

Monforton & Wu (1963) also presented a correction matrix  $S_e$  as a function of the fixity-factors to develop a first-order elastic analysis approach for semi-rigid frames. The stiffness matrix of a member with semi-rigid connections is taken as the product of the standard elastic stiffness matrix  $K_e$  and the correction matrix  $S_e$ , i.e.

$$K_{semi-rigid} = K_e S_e \quad (2)$$

Much later Xu (1992) presented another correction matrix  $S_g$  as a function of the fixity-factors to develop a second-order elastic analysis for semi-rigid frames. To account for both first-order and second-order effects, the stiffness matrix of a member with semi-rigid connection is written as the sum of product of the standard elastic stiffness matrix  $K_e$  with the correction matrix  $S_e$  and the product of the geometric stiffness matrix  $K_g$  with the correction matrix  $S_g$ , i.e.

$$K_{semi-rigid} = K_e S_e + K_g S_g \quad (3)$$

Hasan et al. (2002) later discovered that the model for post-elastic behaviour of a plastic hinge section is similar to that for the elastic behaviour of a semi-rigid connection. Therefore regarding the spring rotation  $\alpha_i^s$  at end  $i$  of the member as the plastic rotation  $\alpha_i^p$  of the plastic hinge at the corresponding end of the member, and assuming that the rotational stiffness of the semi-rigid connection  $r_i$  can vary under the external bending moment according to certain nonlinear moment-curvature relation, then a potential plastic-hinge section can be regarded as a pseudo-semi-rigid connection. A plasticity factor can then be introduced based on the fixity factor to describe the behaviour of a plastic hinge from the initial elastic state to the plastic state under monotonic loading (Hasan et al. 2002). Let the zero-length connection rotational stiffness  $r_i$  be the section flexural stiffness  $dM_i/d\alpha_i^p$ , namely

$$r_i = \frac{dM_i}{d\alpha_i^p} \quad (4)$$

where  $\alpha_i^p$  is the plastic end-rotation of the member at end  $i$  under the external bending moment. The plasticity factor (Hasan et al. 2002) can be defined as

$$p_i = \frac{1}{1 + 3EI/(L dM_i/d\alpha_i^p)} \quad (5)$$

The stiffness matrix with material and geometric nonlinearities can be expressed in the form of plasticity

factors by replacing the fixity factor  $\lambda_i (i = 1, 2)$  with  $p_i (i = 1, 2)$  in Equation 3 as follows:

$$\mathbf{K} = \mathbf{K}_e \mathbf{S}_e^p + \mathbf{K}_g \mathbf{S}_g^p \quad (6)$$

where  $\mathbf{S}_e^p$  and  $\mathbf{S}_g^p$  are the corresponding matrix functions of plasticity factors.

### 3 MOVING NODE STRATEGY IN DYNAMIC ANALYSIS

When a member is subjected to a distributed load, the location of intermediate plastic hinge varies according to the member forces and loads acting on it. In order to capture the location and behaviour of the intermediate plastic hinge, Wong (1996) first presented a moving node strategy for the elasto-plastic analysis of frames subjected to loads including linearly varying distributed load. In the moving node strategy, the location of intermediate plastic hinge is described by a moving node that tracks the location of maximum bending moment calculated on the basis of member forces and loads. Once the maximum bending moment reaches the yielding moment of the member, an intermediate plastic hinge is formed there.

The moving node strategy is introduced to the dynamic analysis of frames in the present work to capture the real behaviour of frames under distributed loads. In order to apply the moving node strategy to dynamic analysis, the following assumptions are normally made:

- Once a plastic hinge is formed, its location will not change any more; and
- The intermediate plastic hinge cannot be too close to the ends of the member.

In the application of the strategy, each beam member is modelled by two elements and three nodes. Consider the portal frame under a uniformly distributed load and an earthquake in Figure 2 as an example. At first the intermediate moving node 3 is set at an arbitrary location, e.g. at the mid-span, of the beam member. In each time step, the location of the maximum total bending moment where the total shear

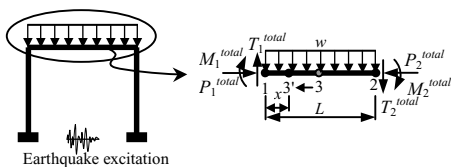


Figure 2. Illustration of the moving node strategy.

force equal to 0 is obtained as

$$x = \frac{T_1^{total}}{w} \quad (7)$$

where  $x$  is the distance of the maximum total bending moment from the left end of the member,  $w$  is the uniformly distributed load, and  $T_1^{total}$  is the total shear force at the left end of the member.

Then the maximum total bending moment of the member can be calculated using

$$M_{max}^{total} = \frac{wx^2}{2} - T_1^{total}x - M_1^{total} \quad (8)$$

where  $M_{max}^{total}$  is the maximum total bending moment including the effects from the inertial force, the damping force, the stiffness force, the earthquake excitation, and the uniformly distributed load applied on the beam member, and  $M_1^{total}$  is the total bending moment at the left end of the member. Then if the maximum total bending moment is larger than the yielding moment of the beam member, the moving node 3 is shifted to node 3' where the total bending moment is the maximum and the plastic hinge is formed. Afterwards the dynamic analysis of the whole structure can proceed assuming this new configuration.

### 4 NUMERICAL EXAMPLES

A MATLAB programme for nonlinear time history analysis of frames with arbitrary plastic hinge is developed based on the above method. A comparison is carried out for verification between the results obtained using the arbitrary plastic hinge method in which the location of the plastic hinge is determined during the process of dynamic analysis based on the moving node strategy and the fixed plastic hinge method in which the potential location of plastic hinge is assumed before the dynamic analysis. Finally a practical example is analyzed to illustrate the applicability and performance of the proposed method.

#### 4.1 Seismic response of a portal frame

A portal frame made up of steel W-type I-beams as shown in Fig. 3 is used for verification. Through trial calculations, the accurate location of the plastic hinge is determined beforehand. Then the results from the arbitrary plastic hinge method and the fixed plastic hinge method are compared. As the bending capacity of the beam is lower than that of the column, the top of column is less likely to yield. The internal forces will be redistributed after the beam yields. The Young's modulus is  $2 \times 10^{11} \text{ N/m}^2$  while the yield stress is  $2.48 \times 10^8 \text{ N/m}^2$ . The other properties of the steel W-type I-beams are given in Table 1.



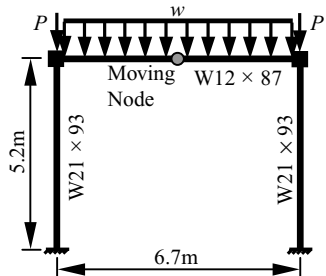


Figure 3. A portal frame for verification.

Table 1. Properties of steel W-type I-beams.

Member	Area (m <sup>2</sup> )	Moment of inertia (m <sup>4</sup> )	Yield moment (Nm)
Column (W21 x 93)	$1.7613 \times 10^{-2}$	$8.6160 \times 10^{-4}$	$8.9814 \times 10^5$
Beam (W12 x 87)	$1.6516 \times 10^{-2}$	$3.0801 \times 10^{-4}$	$5.3645 \times 10^5$

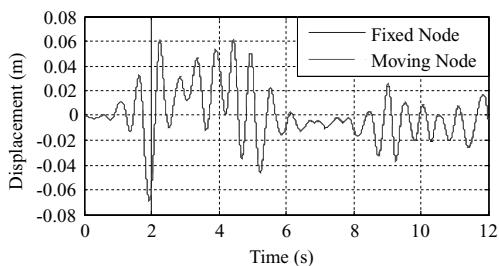


Figure 4. Horizontal beam displacement of portal frame under magnified E1 Centro earthquake ( $t = 0.0022s$ ).

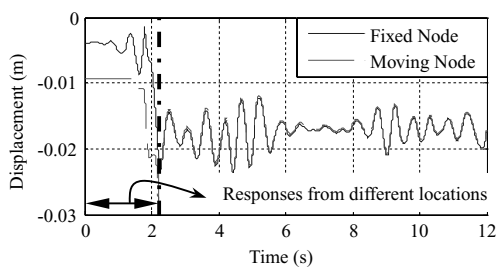


Figure 5. Vertical displacement of the moving node of the roof in portal frame under magnified E1 Centro earthquake ( $t = 0.002s$ ).

For simplicity, the rotational inertial effect of the beam and slab is ignored and the lumped mass matrix is adopted. Two 50,000 kg mass points are placed on the beam-column joints of the frame to simulate the mass of the floor. There is a vertically downward load of

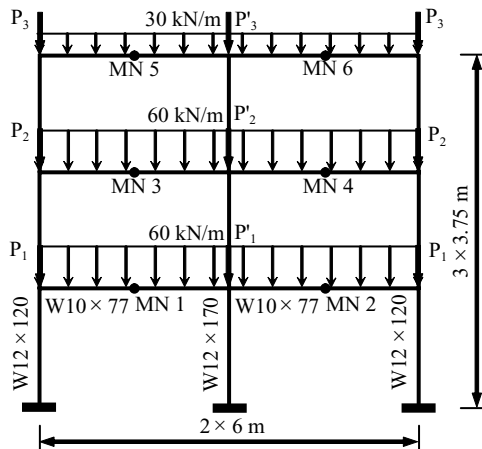


Figure 6. A three-storey steel frame (MN: Moving Node).

500 kN on each beam-column joint to account for the gravity effect. Mass-proportional damping is assumed, and the critical damping ratio is taken to be 5%. As the aim of the example is only to verify the correctness of the programme, the yield criterion (Au & Yan 2008) adopted accounts for the bending moment only while the effect of axial load is ignored. At first the moving node is set at the middle of the beam. The uniformly distributed load on the roof is 70 kN/m. The assumed excitation is that of E1 Centro earthquake with magnified peak ground acceleration of 0.5 g, where g is the acceleration due to gravity. The time step has been chosen as 0.002 s. As the available E1 Centro earthquake excitation has been sampled at 50Hz with time steps of 0.02 s, piecewise cubic Hermite interpolation is used to provide excitation data of time steps of 0.002 s. Through the trial calculation the accurate location of the plastic hinge at the roof is 1.18 m from the left column of the frame. Therefore in the fixed plastic hinge method the roof member is meshed into two beam elements with lengths of 1.18 m and 5.52 m. The horizontal beam displacement of the portal frame is shown in Figure 4, while the vertical displacement of the plastic hinge is presented in Figure 5.

Figures 4 and 5 show that the moving node strategy can be used in dynamic analysis effectively. In Figure 5, the reason for the apparent difference within the first few seconds is that the chosen nodes in the two methods are different before the formation of intermediate plastic hinge. After the plastic hinge is formed at the roof 2.22 s after the start of analysis, the responses from the two methods are nearly the same.

#### 4.2 Seismic response of a multi-storey frame

A more realistic three-storey frame made up of steel W-type I-beams as shown in Figure 6 is then studied

Table 2. Properties of members for five—storey steel frame.

Member	Area (m <sup>2</sup> )	Moment of inertia (m <sup>4</sup> )	Yield moment (Nm)
Ext.Column* (W12 × 120)	$2.2774 \times 10^{-2}$	$4.4537 \times 10^{-4}$	$7.5590 \times 10^5$
Int.Column† (W12 × 170)	$3.2258 \times 10^{-2}$	$6.8678 \times 10^{-4}$	$1.1176 \times 10^6$
Beam (W10 × 77)	$1.4581 \times 10^{-2}$	$1.8939 \times 10^{-4}$	$3.9665 \times 10^5$

\* Ext. Column is Exterior Column.

† Int. Column is Interior Column.

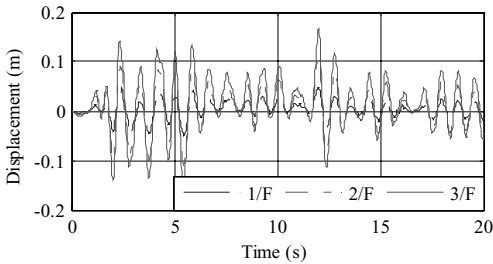


Figure 7. Horizontal floor displacements under magnified E1 Centro earthquake with multi-parameter yield criterion.

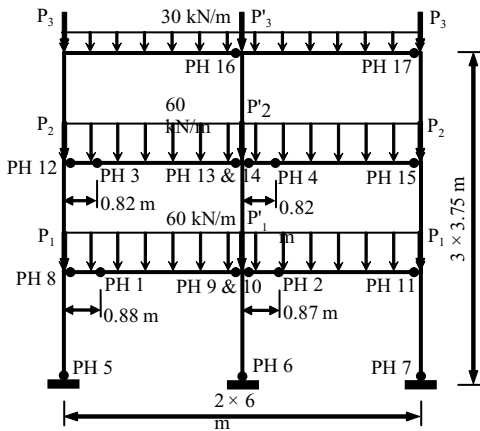


Figure 8. Final locations of plastic hinges (PH: Plastic Hinge).

to illustrate the capability of the proposed method. The exterior and interior columns are of W12 × 120 and W12 × 170 sections respectively, while all the beams are made of W10 × 77 sections. The member properties are shown in Table 2. The Young's modulus is  $2 \times 10^{11}$  N/m<sup>2</sup> while the yield stress is  $2.48 \times 10^8$  N/m<sup>2</sup>.

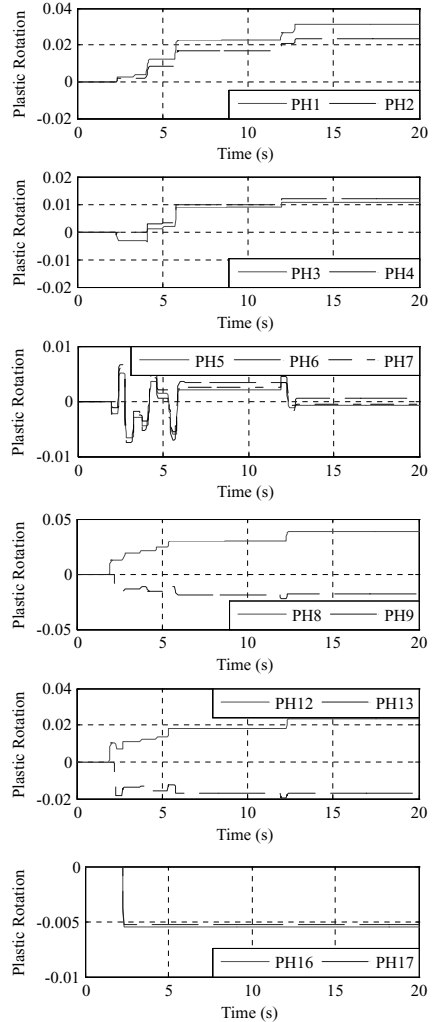


Figure 9. Plastic rotations at selected plastic hinges of frame.

The lumped mass matrix is adopted. On each floor below the roof, the mass on each exterior column is 20,000 kg, and that on each interior column is 40,000 kg. At the roof level, the mass on each exterior column is 10,000 kg, while that on each interior column is 20,000 kg. The axial forces in the columns are as follows:  $P_1 = 500$  kN,  $P'_1 = 1000$  kN,  $P_2 = 300$  kN,  $P'_2 = 600$  kN,  $P_3 = 100$  kN and  $P'_3 = 200$  kN. The assumed excitation is that of the E1 Centro earthquake with magnified peak ground acceleration of 0.7g. Mass-proportional damping is assumed, and the critical damping ratio is taken to be 5%. The selective time discretization scheme with further subdivision of the time step within which plastic hinges are

formed and the multi-parameter yield criterion taking into account both axial force and bending moment as adopted by Au & Yan (2008) are used in this example. The dynamic analysis of the frame is carried out with standard time steps of 0.02 s and refined time steps of 0.002 s. The horizontal displacements at various floors of the frame are shown in Figure 7, and the final locations of the plastic hinges are shown in Figure 8.

Figure 8 shows that besides the ends of beam members and the ends of columns at ground level, plastic hinges can also be formed at intermediate locations within beam members. To evaluate the dynamic response of frames accurately, it is important that such phenomena be taken into account.

Furthermore, the time histories of plastic rotations at selected plastic hinges shown in Figure 9 demonstrate that in general both the plastic rotations at the beam ends and the intermediate locations are larger than those at the bottom of columns. One may therefore conclude in this case that the damage of the columns is less than that of the beams, and that the goal of having “strong columns and weak beams” has been achieved. The proposed method is also capable of analyzing complicated multi-storey frames commonly encountered in practice.

## 5 CONCLUSIONS

The paper describes a method for nonlinear dynamic analysis of frames subjected to distributed loads, which is based on the semi-rigid technique and moving node strategy. The method uses pseudo-semi-rigid connections to simulate the plastic hinges that may form in a frame. The stiffness matrix is constructed by the standard elastic stiffness matrix and geometric stiffness matrix with their respective correction matrices. The moving node strategy is applied in the dynamic analysis of frames with distributed loads so that the plastic hinges can be accurately located in the process of dynamic analysis. Compared with the traditional methods for nonlinear dynamic analysis of frames, the proposed method has the following merits:

- The plastic hinges can be accurately located by the moving node strategy in the process of dynamic analysis. Therefore the dynamic behaviour of frames with distributed load can be predicted with better accuracy.
- Since the proposed method does not require additional connection elements, it reduces the necessary computational effort and enables the use of existing linear dynamic analysis programmes with minimal modification.
- Each semi-rigid frame member comprises a finite-length frame member with a zero-length rotational

spring attached to each end, with clear physical meaning associated with each component.

- The effects of plastic hinges on the geometric nonlinearity are considered through the correction matrix of the geometric stiffness matrix. It has practical applications since plastic hinges and geometric nonlinearity may occur in most frame structures when they are subject to extreme events.

The numerical examples provided demonstrate the feasibility and applicability of the method.

## REFERENCES

- Au, F.T.K. & Yan, Z.H. 2008. Dynamic analysis of frames with material and geometric nonlinearities based on semi-rigid technique. *International Journal of Structural Stability and Dynamics* (to appear).
- Awkar, J.C. & Lui, E.M. 1999. Seismic analysis and response of multistory semirigid frames. *Engineering Structures* 21: 425–441.
- Elnashai, A.S. 2002. Do we really need inelastic dynamic analysis? *Journal of Earthquake Engineering* 6 Special Issue 1: 123–130.
- Gong, Y. et al. 2005. Performance-based design sensitivity analysis of steel moment frames under earthquake loading. *International Journal for Numerical Method in Engineering* 63: 1229–1249.
- Gong, Y. 2006. Adaptive gradual plastic hinge model for nonlinear analysis of steel frameworks. *Canadian Journal of Civil Engineering* 33(9): 1125–1139.
- Gong, Y. et al. 2006. Sensitivity analysis of steel moment frames accounting for geometric and material nonlinearity. *Computers and Structures* 84: 462–475.
- Grierson, D.E. et al. 2006. Optimal performance-based seismic design using modal pushover analysis. *Journal of Earthquake Engineering* 10(1): 73–96.
- Hasan, R. et al. 2002. Push-over analysis for performance-based seismic design. *Computers and Structures* 80: 2483–2493.
- Kim, S.E. et al. 2004. Practical second-order inelastic analysis for steel frames subjected to distributed load. *Engineering Structures* 26: 51–61.
- Kim, S.E. & Choi, S.H. 2005. Practical second-order inelastic analysis for three-dimensional steel frames subjected to distributed load. *Thin-Wall Structures* 43: 125–160.
- Lui, E.M. & Lopes, A. 1997. Dynamic analysis and response of semirigid frames. *Engineering Structures* 19(8): 644–654.
- Monforton, G.R. & Wu, T.S. 1963. Matrix analysis of semi-rigidly connected frames. *Journal of the Structural Division ASCE* 89(6): 13–42.
- Wong, M.B. 1996. Effects of linearly varying distributed load on the collapse behaviour of frames. *Computers and Structures* 61(5): 909–914.
- Xu, L. 1992. Geometrical stiffness and sensitivity matrices for optimization of semi-rigid steel frameworks. *Structural Optimization* 5: 95–99.
- Xu, L. et al. 2005. Nonlinear analysis of steel frameworks through direct modification of member stiffness properties. *Advances in Engineering Software* 36: 312–324.

*Life-cycle monitoring, maintenance, and rehabilitation*

# Life-cycle reliability analysis and selective maintenance of deteriorating structures

F. Biondini

*Department of Engineering, Politecnico di Milano, Milan, Italy*

D.M. Frangopol

*Department of Civil and Environmental Engineering, ATLSS Center, Lehigh University, Bethlehem, PA, USA*

E. Garavaglia

*Department of Structural Engineering, Politecnico di Milano, Milan, Italy*

**ABSTRACT:** The life-cycle reliability and maintenance planning of deteriorating structural systems is investigated. The probabilistic analysis is developed within a semi-Markov modeling of the deterioration process. Selective maintenance scenarios are considered by applying the repair interventions only to elements heavily deteriorated and/or characterized by a low safety margin. The life-cycle reliability of statically determinate and indeterminate truss systems is compared by considering the effects of selective maintenance.

## 1 INTRODUCTION

The assessment of the life-cycle performance of deteriorating structures can be formulated as a reliability problem where a loss of performance greater than prescribed threshold values is considered as a *failure*. Therefore, when a failure is reached, the system passes from the current state to another state characterized by a lower level of performance. On the other hand, structural performance can also be improved by maintenance and/or rehabilitation interventions. In this case the system may move from the current state to another state characterized by a higher level of performance. However, in both cases the *failure process* may be defined as a *transition process* through different service states due to environmental attacks and/or maintenance actions. Clearly, since the problem is affected by several sources of uncertainty, the assessment of the life-cycle performance must be based on a suitable damage modeling and on a probabilistic analysis able to model the main features of the time-variant deterioration process (Biondini *et al.* 2004, 2006a, Biondini and Frangopol 2008).

In this paper, a procedure for life-cycle reliability assessment and maintenance planning of deteriorating structural systems is proposed. Material damage is described in probabilistic terms within a semi-Markov modeling of the deterioration process aimed to evaluate the reliability of the system. Selective maintenance scenarios are considered by applying the repair interventions only to elements heavily deteriorated and/or

characterized by a low safety margin. To this aim, a suitable condition index is introduced. The proposed procedure is applied to compare the life-cycle reliability of statically determinate and indeterminate truss systems by considering the effects of selective maintenance.

## 2 LIFE-CYCLE RELIABILITY ANALYSIS

### 2.1 Case study

The life-cycle reliability of the truss structure shown in Figure 1 is investigated. The following four cases are considered: (1) statically determinate truss with members area  $A = 2000 \text{ mm}^2$  and total volume  $V = 0.055 \text{ m}^3$ ; (2) statically indeterminate truss with members area  $0.83 A$  and total volume  $1.09 V$ ; (3) statically indeterminate truss with area  $A$  for members 10–11, area  $0.83 A$  for all other members, and total volume  $1.1 V$ ; (4) statically indeterminate truss with area  $A$  for members 8–13, area  $0.83 A$  for all other members, and total volume  $1.13 V$ . The allowable material strength is  $\bar{\sigma} = 150 \text{ MPa}$ .

### 2.2 Damage modeling

The structures in Figure 1 are considered to undergo a deterioration process due to aging that involves reduction in the cross-sectional area  $A$  and material strength

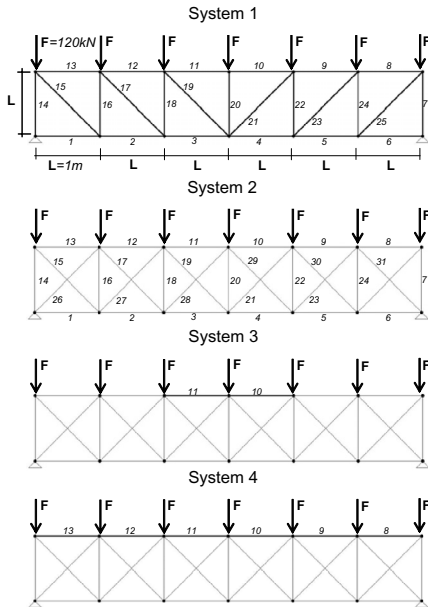


Figure 1. Truss structure undergoing damage. Cases studied: (1) statically determinate truss with members area  $A$  and total structural volume  $V$ ; (2) statically indeterminate truss with members area  $0.83 A$  and total structural volume  $1.09 V$ ; (3) statically indeterminate truss with area  $A$  for members 10–11, area  $0.83 A$  for all other members, and total structural volume  $1.1 V$ ; (4) statically indeterminate truss with area  $A$  for members 8–13, area  $0.83 A$  for all other members, and total structural volume  $1.13 V$ .

$\bar{\sigma}$  of each member as follows:

$$A(t) = A_0[1 - \delta(t)] \quad (1)$$

$$\bar{\sigma}(t) = \bar{\sigma}_0[1 - \delta(t)] \quad (2)$$

where “0” denotes the initial undamaged state, and the deterioration over time  $t$  is measured by the time-variant damage index  $\delta = \delta(t) \in [0; 1]$ . In this study, the following general damage model is used:

$$\delta(t) = \begin{cases} \omega^{1-\rho} \tau^\rho, & \tau \leq \omega \\ 1 - (1 - \omega)^{1-\rho} (1 - \tau)^\rho, & \omega < \tau < 1 \\ 1, & \tau \geq 1 \end{cases} \quad (3)$$

where  $\tau = t/T_1$ ,  $T_1$  is the time instant of reaching the failure threshold  $\delta = 1$ ,  $\omega$  and  $\rho$  are damage parameters defining the shape of the damage curve, as shown in Figure 2.

The damage parameters  $\rho$  and  $\omega$  must be chosen according to the actual evolution of the damage process. Damage rates may be associated with the aggressiveness of the environment, as well as with the level of acting stress  $\sigma$  with respect to the material

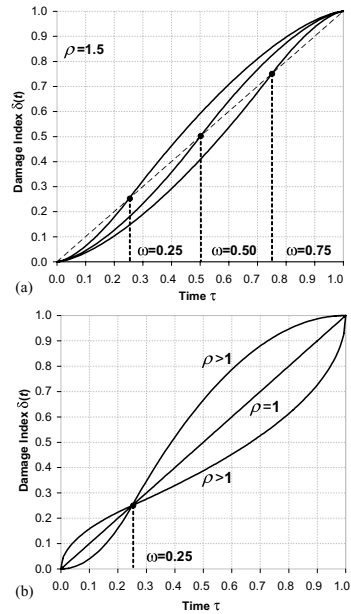


Figure 2. Material damage index  $\delta$  vs time  $\tau = t/T_c$ . (a) Damage laws for  $\rho = 1.5$  and varying  $\omega$ . (b) Damage laws for  $\omega = 0.25$  and varying  $\rho$ .

strength  $\bar{\sigma}$ , or  $\xi = \sigma/\bar{\sigma}$ . In this study, the following linear relationship is assumed:

$$\rho = \rho_a + (\rho_b - \rho_a) \xi \quad (4)$$

$$\omega = \omega_a + (\omega_b - \omega_a) \xi \quad (5)$$

where the subscript “a” refers to damage associated with environmental aggression, and the subscript “b” refers to damage associated with loading effects. In this way, the proposed damage law is able to represent damage mechanisms induced by environmental deterioration, like carbonation of concrete and corrosion of steel, or material fatigue.

Generally, both these mechanisms are present and interacting, and a proper calibration of the damage parameters is required based on experimental observations and/or laboratory accelerated test data.

### 2.3 Probabilistic analysis

The evolution of the system performance can be considered as a transition process described by a random variable representing the waiting time  $t_i$  spent by the system into a service state  $i$  before a transition to another service state. This type of transition process can be modeled as a semi-Markov Process (s-MP). This modeling requires the following information to

be known (Howard, 1971):

- The state  $i$  of the system at the initial time  $t = 0$ , and the time  $t_i = t_0$  spent in the initial state (i.e. the initial conditions).
- The probability density function  $f_{ik}(t)$  of the waiting time  $t_{ik}$  spent by the system into the service state  $i$  provided that the next state after transition is  $k$ , or  $f_{ik}(t) = P\{t < t_{ik} < t + dt\}$ .
- The transition probability  $p_{ik} = P\{\text{present state } i; \text{ next state } k\}$ .

In this way, the probability density function  $f_i(t)$  of the waiting time  $t_i$  between two subsequent transitions (i.e. the lifetime in the state  $i$ ), whatever is the next destination, can be obtained:

$$f_i(t) = \sum_k f_{ik}(t) p_{ik} \quad (6)$$

Based on this distribution function, the probability  $\Pi_{ij}(t, t_0)$  that the system will occupy the state  $j$  at the time  $t$  after it was in the state  $i$  at the time  $t = 0$ , can be computed as follows:

$$\begin{aligned} \Pi_{ij}(t, t_0) &= \delta_{ij} \mathfrak{S}_i(t, t_0) \\ &+ \sum_k p_{ik}(t_0) \int_0^t f_{ik}(u, t_0) \Pi_{kj}(t-u) du \end{aligned} \quad (7)$$

where  $\delta_{ij}$  is the Kronecker operator,  $\mathfrak{S}_i(t)$  is the survival function related to the first waiting time  $t_0$  in the initial state  $t = 0$ , and where:

$$\begin{aligned} \Pi_{kj}(t) &= \delta_{kj} \mathfrak{S}_i(t) \\ &+ \sum_r p_{kr} \int_0^t f_{kr}(u) \Pi_{rj}(t-u) du \end{aligned} \quad (8)$$

The previous two integral equations are convolution-integrals and they can be effectively computed by using Laplace transforms.

The choice of an adequate waiting time probability density function  $f_{ik}(t)$  should be based on the knowledge of the physics of the deterioration phenomenon under investigation and on the shape of the hazard rate function that describes the behavior of a given distribution in its tails where the prediction of an immediate occurrence risk is made (Grandori, Guagenti and Molina 1981, Guagenti and Molina 1990). After a suitable density function is selected, its parameters needs to be estimated based on data samples built with data obtained by laboratory tests or monitoring. The choice of a suitable size of these

samples is usually a critical point, since samples are often too small to be representative for a probabilistic approach. However, effective procedures based on limited data samples have been developed (Biondini and Garavaglia 2005, Biondini *et al.*, 2006b).

In this study, the waiting time probability density distribution  $f_{ik}(t)$  is modeled by using a Gamma function, and its parameters are estimated by using the maximum likelihood and Rosenbrock's optimization methods. The data samples for parameter estimation are obtained by means of a Monte Carlo simulation of the life-cycle structural performance based on the damage modeling previously introduced. In this simulation process the damage parameters  $\rho_a, \rho_b, \omega_a, \omega_b$ , and  $T_1$ , are modeled as random variables with prescribed probability distribution and, for each simulation cycle, the time-variant structural analysis is carried out by updating step-by-step the stiffness matrix of the deteriorated structural members. In this way the transition among states is detected for each member, as well as for the structural system, and the probability of failure  $P_F$ , or the corresponding reliability index  $\beta$ , can be estimated.

Based on this procedure, the time evolution of the reliability index  $\beta$  has been computed for each one of the four systems in Figure 1. The results are shown in Figure 3. The following comments can be made:

- For a reliability threshold  $\beta = 3$ , the computed values of structural lifetime are:  $t_1 = 16$  years;  $t_2 = 17$  years;  $t_3 = 22$  years;  $t_4 = 21$  years.
- Systems (1) and (2), having the same size for all members, are less reliable than systems (3) and (4), for which the size of selected members is bigger.
- System (3), with only two members having bigger size, is more reliable than system (4), for which six members have bigger size.

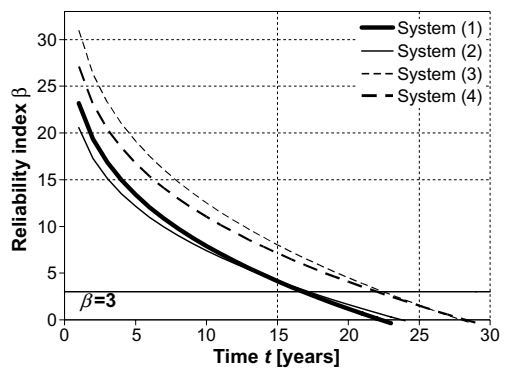


Figure 3. Comparison between the reliability indexes  $\beta$  related to the four different static schemas presented in Figure 1.

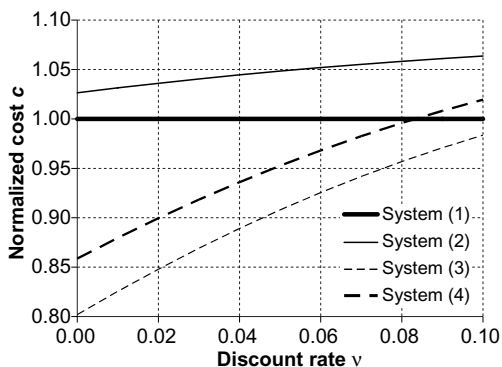


Figure 4. Annual cost  $C_i$  of the system ( $i$ ) normalized to the cost  $C_1$  of the system (1), or  $c_i = C_i/C_1$ , versus the discount rate  $\nu$ .

- In general, for statically indeterminate structures the over-design of some members does not necessarily lead to an increase of reliability. In fact, damage produces a stress redistribution over time towards the bigger members which, in this way, may become critical with respect to failure.

### 2.4 Cost analysis

From the economic point of view, if the structural cost is associated only with the initial cost of the materials, the optimal solution is represented by the structure of minimum volume. Therefore, among the cases in Figure 1, the minimum cost solution is the statically determinate truss system (1). However, when the expected structural lifetime  $t_i$  is also taken into account, the annual structural cost  $C_i$  of the system ( $i$ ) can be computed as follows:

$$C_i = C_{0,i} \frac{\nu(1 + \nu)^{t_i}}{(1 + \nu)^{t_i} - 1} \quad (9)$$

where  $C_{0,i}$  is the initial structural cost and  $\nu$  is the discount rate. Figure 4 shows the annual cost  $C_i$  of the system ( $i$ ) normalized to the cost  $C_1$  of the system (1), or  $c_i = C_i/C_1$ , versus the discount rate  $\nu$ . It can be noted that the best solution is represented by the system (3), the worst by the system (2).

## 3 MAINTENANCE PLANNING

### 3.1 Condition index and selective maintenance

Based on the results of the life-cycle reliability analysis, a maintenance plan can also be decided and, by comparing different maintenance scenarios,

optimal maintenance interventions can be selected. Two main approaches can be generally applied for maintenance:

1. *Replacing* damaged members: the initial reliability of the system is fully restored and future maintenance can be applied at constant time intervals.
2. *Repairing* damaged members: the initial reliability of the system is only partially restored.

For complex structural systems it is crucial to decide which elements require maintenance and to investigate scenarios where repairing involves the deteriorated members only, or *selective maintenance scenarios*. Clearly, a selective maintenance requires suitable life-cycle performance indicators to effectively select the elements that actually need repair. To this aim, the following condition index  $\mu$  has been defined:

$$\mu = (1 - \delta) \cdot \frac{R - S}{R} \quad (10)$$

where  $\delta$  is the damage index,  $R$  is the strength of the considered element, and  $S$  is the corresponding loading demand. Based on this definition, the index  $\mu$  can be evaluated for each element and at each time instant during the structural lifetime, and high values of this index may identify elements heavily deteriorated and/or characterized by a low safety margin.

As an example, a selective maintenance is applied to the truss systems (1) and (3) in Figure 1, by repairing deteriorated elements with condition index  $\mu < 0.35$  when a reliability threshold  $\beta_g = 3$  is reached. If more than 75% of the members need to be repaired, maintenance is applied to the whole system.

Figure 5 shows the time evolution of the reliability index  $\beta$  for both the systems (1) and (3). Figure 6 shows the corresponding time evolution of

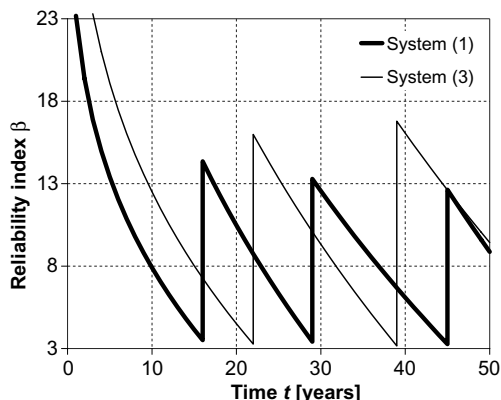


Figure 5. Time evolution of the reliability index  $\beta$  for systems (1) and (3) under selective maintenance.



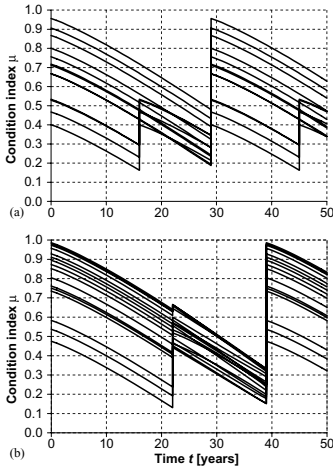


Figure 6. Time evolution of the condition index  $\mu$  associated with each truss member of (a) system (1), and (b) system (3).

the condition index  $\mu$  for each member of the systems (1) and (3). The time of application of the selective maintenance and the repaired members are also listed in Table 1. These results highlight the effectiveness of the condition index  $\mu$  in selecting the members to be repaired.

### 3.2 Cost of maintenance

For a prescribed maintenance scenario, the total cost of maintenance  $C_m$  can be evaluated by summing the costs  $C_q$  of the individual interventions (Frangopol *et al.* 1997, Kong and Frangopol 2003):

$$C_m = \sum_{q=1}^n \frac{C_q}{(1 + \nu)^{t_q}} = \sum_{q=1}^n C_{0q} \quad (11)$$

where the cost  $C_q$  of the  $q$ th rehabilitation has been referred to the initial time of construction by taking a proper discount rate of money  $\nu$  into account (Kong and Frangopol 2003).

In this study, the cost  $C_q$  of the individual intervention is assumed as follows:

$$C_q = C_f + \sum_{k=1}^m \delta_k \cdot V_k \cdot c_{qk} \quad (12)$$

where  $C_f = \alpha C_0$  is a fixed cost computed as a percentage  $\alpha$  of the initial cost  $C_0$ ,  $\delta_k$  is the damage index of element  $k$  of the structural system,  $V_k$  is the volume of element  $k$ , and  $c_{qk}$  is the volume unit cost for restoring the element  $k$ . Based on this

Table 1. Time of application of selective maintenance for the members of systems (1) and (3). System (1): 16, 29, 45 years. System (3): 22, 39 years.

Years	System (1)			System (3)	
	16	29	45	22	39
<b>Elements</b>					
1		X			X
2		X			X
3		X			X
4		X			X
5		X			X
6		X			X
7	X	X	X		X
8		X			X
9	X	X	X	X	X
10	X	X	X	X	X
11	X	X	X	X	X
12	X	X	X	X	X
13		X			X
14	X	X	X		X
15	X	X	X		X
16		X			X
17		X			X
18		X			X
19		X			X
20		X			X
21		X			X
22		X			X
23		X			X
24		X			X
25	X	X	X		X
26				X	X
27					X
28					X
29					X
30					X
31				X	X

cost model, different maintenance scenarios can be compared and an optimal maintenance strategy can be selected (Biondini *et al.*, 2006a, 2006b).

Figure 7 shows the total cost  $C_i$ , computed as the sum of initial cost  $C_0$  and maintenance cost  $C_m$ , of the system ( $i$ ) normalized to the cost  $C_1$  of the system (1), or  $c_i = C_i/C_1$ , versus the discount rate  $\nu$ , for different values  $\alpha$  of the fixed cost of maintenance  $C_f = \alpha C_0$ . It can be noted that the advantage in economic terms of the statically indeterminate system (3) over the statically determinate system (1), that was pointed out in Figure 4, it does no longer hold if a selective maintenance is applied. In fact, as shown in Figure 7, if the statically determinate system (1) is properly maintained, its total cost is lower than the cost required for the statically indeterminate system (3). Clearly, the economic primacy of system (1) over system (3) becomes less emphasized as the fixed

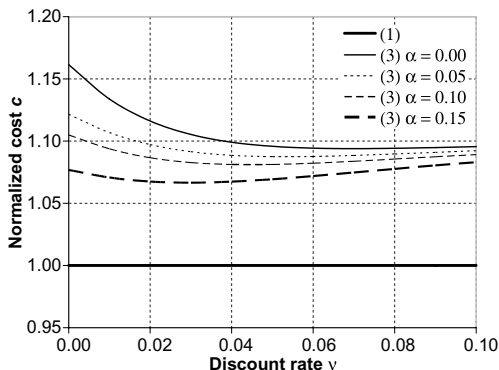


Figure 7. Total cost  $C_i$ , computed as the sum of initial cost  $C_0$  and maintenance cost  $C_m$ , of the system ( $i$ ) normalized to the cost  $C_1$  of the system (1), or  $c_i = C_i/C_1$ , versus the discount rate  $v$ , for different values  $\alpha$  of the fixed cost of maintenance  $C_f = \alpha C_0$ .

cost of maintenance increases, since in this way the importance of the role played by a proper selective maintenance is reduced.

#### 4 CONCLUSIONS

The main features of a procedure for life-cycle reliability assessment and maintenance planning of deteriorating structural systems have been presented. This procedure is based on an effective modeling of structural damage and takes advantage from the generality of a semi-Markov modeling of the deterioration process where every loss of performance greater than prescribed threshold values is considered as a failure. Special attention has been paid to the definition of a condition index aimed to identify selective maintenance scenarios, where repair interventions are applied only to elements heavily deteriorated and/or characterized by a low safety margin. The proposed procedure is applied to compare the life-cycle reliability of statically determinate and indeterminate truss systems by considering the effects of selective maintenance. The results proved that for statically indeterminate structures the over-design of some members does not necessarily lead to an increase of reliability. In fact, damage tends to produce a stress redistribution over time and, in this way, the overloaded members may become critical with respect to failure. However, when properly dimensioned, the cost of statically indeterminate systems can be lower than the cost of statically determinate systems. On the contrary, the primacy of statically indeterminate over statically determinate systems can be reversed

if a selective maintenance is applied. However, the positive effect of the selective maintenance can be reduced when the fixed costs of maintenance become important.

#### ACKNOWLEDGEMENT

This study is supported by research funds PRIN2005 (prot. 2005082490) from the Italian Ministry of University and Research—Department of Structural Engineering, Politecnico di Milano.

#### REFERENCES

- Biondini, F., Bontempi, F., Frangopol, D.M., and Malerba, P.G., 2004. Cellular Automata Approach to Durability Analysis of Concrete Structures in Aggressive Environments. *Journal of Structural Engineering*, ASCE, **130**(11), 1724–1737.
- Biondini, F., Bontempi, F., Frangopol, D.M., and Malerba, P.G., 2006a. Probabilistic service life assessment and maintenance planning of concrete structures, *Journal of Structural Engineering*, ASCE **132**(5), 810–825.
- Biondini, F., Frangopol, D.M., and Garavaglia, E., 2006b. Probabilistic Lifetime Assessment based on Limited Monitoring, *3rd Int. Conf. on Bridge Maintenance, Safety and Management (IABMAS'06)*, Porto, Portugal, July 16–19, 2006, Ed. Paulo J.S. Cruz, Dan M. Frangopol & Luis C. Neves, Taylor & Francis Groups. Leiden, The Netherlands, CD-ROM, Paper\_030.
- Biondini, F., and Frangopol, D.M., 2008. Long-term Performance of Structural Systems, *Structure and Infrastructure Engineering*, **4**(2), 72, Special Issue, Fabio Biondini (ed.), Taylor & Francis Publisher.
- Biondini, F., and Garavaglia, E., 2005. Probabilistic Service Life Prediction and Maintenance Planning of Deteriorating Structures, *Int. Conf. on Structural Safety and Reliability (ICOSSAR'05)*, Rome, Italy, June 19–22, 2005, G. Augusti, G.I. Schuëller, M. Ciampoli Eds. Millpress, Rotterdam, The Netherlands, CD-ROM, pp. 495–501.
- Ciccardi, R., and Consoli, S., 2006. *Reliability Analysis of Deteriorating Structural Systems*, Degree Thesis, Politecnico di Milano, pp. 225 (In Italian).
- Frangopol, D.M., Lin, K.-Y., and Estes, A.C. 1997. Life-Cycle Cost Design of Deteriorating Structures, *Journal of Structural Engineering*, ASCE, **123**(10), pp.1390–1401.
- Grandori Guagenti, E., and Molina, C., 1981. A dynamic system approach to structural rehabilitation planning, *Mechanics research communications*, **8**(3), pp 137–142.
- Guagenti, E., and Molina, C., 1990. Structural rehabilitation—a semi-Markov decision approach. *Structural Safety*, Elsevier, **8**, pp.255–262.
- Howard, R.A., 1971, *Dynamic Probabilistic Systems*, John Wiley and Sons, New York, NJ, USA.
- Kong, J.S., and Frangopol, D.M., 2003. Life-Cycle Reliability-Based Maintenance Cost Optimization of Deteriorating Structures with Emphasis on Bridges. *Journal of Structural Engineering*, ASCE **129**(6), 818–824.

# A comparison of tomographic reconstruction algorithms for acoustic non destructive testing of stone masonry

B. Cannas, S. Carcangiu, M. Di Mauro, A. Fanni, A. Montisci & M.L. Mulas

*Electric and Electronic Dept., Univ. of Cagliari, Cagliari, Italy*

G. Concu

*Dept. of Structural Engineering, Univ. of Cagliari, Cagliari, Italy*

**ABSTRACT:** An experimental program has been started with the purpose of evaluating the reliability of acoustic tomography in the characterisation and non destructive testing of concrete and stone masonry. The research has been carried out analysing the acoustic wave propagation crossing selected sections of stone masonry elements. Different reconstruction algorithms, chosen between the most commonly used, were implemented for determining the distribution of waves velocity in these sections. In particular, the following iterative algorithms, *Singular Value Decomposition*, *Regularized Singular Value Decomposition*, *Algebraic Reconstruction Technique*, *Simultaneous Iterative Reconstruction Technique*, and were adapted and tested in order to evaluate their performance for practical use.

## 1 INTRODUCTION

The goal of extending the useful service life of structures and infrastructures has become of crucial importance over the last decades, due to cultural, social, and economic factors. There is a general interest in achieving this goal, and special care is reserved to the management of the increasing cost of building estate maintenance. That cost increases especially because many structures, exposed to age and to aggressive environmental conditions, are not as durable as wished.

The response to this demand has included the development and implementation of management and maintenance systems for assets and structures, in order to handle the information flow and store relevant data, to plan and organize the maintenance activities, and to prepare and manage maintenance budgets. Particular attention has been devoted to the development of non destructive techniques (NDT) for buildings diagnosis and evaluation. NDTs are particularly suitable when dealing with structures and infrastructures because they allow one to not interfere with the state of the asset (Fib 2002).

Among the non destructive techniques, sonic and ultrasonic methods, based on measurements of the velocity  $v$  of acoustic waves propagating through the material, seem to be very suitable for evaluating a building condition because they give information

with immediacy, rapidity and relatively low cost (Krautkramer & Krautkramer 1990).

Those methods are preferentially carried out applying the Through Transmission Technique, in which the wave is transmitted by a transducer (Emitter) through the test object and received by a second transducer (Receiver) on the opposite side. This allows to measure the time  $t$  that the wave needs to travel through the object's thickness, from the emitter to the receiver, along a path of length  $l$ ; the average velocity of the wave is then obtained from the ratio  $l/t$  (Cianfrone 1993).

The major limit of the Through Transmission Technique consists of describing the velocity field in each section of the object using only one value of velocity for each path, i.e., hypothesizing that the mean is homogeneous along each wave path. The Tomographic Technique overcomes this limit using numerical analysis as a real measurement instrument, combining the results of several Through Transmission Technique applications for a sharper and reliable investigation of the object.

The present work aims to point out the reliability of acoustic tomography in the diagnosis and characterisation of stone masonry buildings, deepening the analysis of the issues which affect the algebraic problem conditioning and highlighting the most suitable techniques for the algebraic problem solution.

## 2 THE TOMOGRAPHIC PROBLEM

As previously cited, an acoustic wave propagating through any object spends a definite time to travel from a point to another of the object. The wave covers the path between the two points spending the time  $t$  and propagating with a mean velocity  $v$ . When the distance between the two points reduces to zero a local velocity  $v_p$ , and a local slowness  $s = 1/v_p$  can be defined for the point  $p$ .

The acoustic behaviour of a selected section of the object is then defined when the slowness  $s$  is known continuously in every point of the investigated section. This function can be approximated dividing the section into a grid of  $N$  rectangular cells (pixels) in which  $v$  is supposed to be constant (Fig. 1).

The Tomographic Problem consists of obtaining the slowness of the  $N$  pixels starting from the knowledge of  $M$  travel times measured along a series of paths joining couples of transducers located on opposite or adjacent sides of the section. The ray-paths of waves depend on the velocity distribution, and their sharp definition is a not easy problem to solve, especially when dealing with structures made of different elements such as stone masonry.

In this study, the Linear Tomography has been applied, which considers the ray-paths to be rectilinear.

In order to obtain the values of the slowness in the grid, the following equations system has to be solved:

$$\mathbf{L}\mathbf{s} = \mathbf{t} \quad (1)$$

where

$\mathbf{t} = [t_1, t_2, \dots, t_M]$  is the vector of measured travel times;

$\mathbf{s} = [s_1, s_2, \dots, s_N]$  is the vector of slowness;

$\mathbf{L} = [l_{11}, l_{12}, \dots, l_{NM}]$  is the coefficients matrix, whose generic element  $l_{ij}$  is the length of the  $i$ th ray in the  $j$ th cell.

Thus, the Tomographic solution consists of determining the vector  $\mathbf{s}$  as:

$$\mathbf{s} = \mathbf{L}^{-1}\mathbf{t} \quad (2)$$

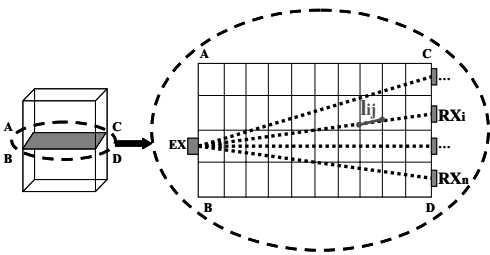


Figure 1. Schema of linear tomographic problem.

To avoid instability in matrix inversion, the number of cells must be smaller than the number of measured travel times. If the inverse of  $\mathbf{L}$  exists it can be directly evaluated.

However, the inverse of  $\mathbf{L}$  generally doesn't exist since  $\mathbf{L}$  is not a square matrix, it is ill-conditioned, and it has not full rank. Thus, other methods have to be used to solve the problem.

In this paper three conventional inversion algorithms have been implemented.

To compare their performance, the residual:

$$R = \frac{\|\mathbf{t} - \mathbf{L}\hat{\mathbf{s}}\|}{\|\mathbf{t}\|} \quad (3)$$

has been evaluated, where  $\hat{\mathbf{s}}$  is the obtained slowness distribution.

### 2.1 Singular value decomposition

A common method to obtain the solution of equations system (1) in the least square sense is the Singular Value Decomposition (SVD) (Berriman 1991, Herman 1980, Ivansson 1986). The singular value decomposition can be used for computing the pseudo-inverse of the  $\mathbf{L}$  matrix. Indeed, this method produces a diagonal matrix  $\mathbf{D}$ , of the same dimension of  $\mathbf{L}$  and with non-negative diagonal elements in decreasing order, and two unitary matrices  $\mathbf{U}$  and  $\mathbf{V}$  so that  $\mathbf{L} = \mathbf{U}\mathbf{D}\mathbf{V}^T$ . Then, the pseudo-inverse of the matrix  $\mathbf{L}$  with singular value decomposition is  $\mathbf{L}^+ = \mathbf{V}\mathbf{D}^{-1}\mathbf{U}^T$  and the solution of equations system (1) can be written as  $\mathbf{s} = \mathbf{L}^+\mathbf{t}$ .

This solution is the minimum norm solution and it is only mathematically suitable. The inverse problem is ill posed and ill conditioned, making the solution sensitive to measurement errors and noise. Regularization methods are needed to treat this ill-posedness. It can be shown that the small singular values mainly represents the noise and can be discarded. Truncated SVD may be considered as having a filter, and hence it is less sensitive to high frequency noise in the measurements.

Because of the nonlinear relationship between the velocity and the travel time, it is almost impossible to find the solution by a single step algorithm using a linear approximation. Thus, iterative methods can be used, such as ART (Algebraic Reconstruction Technique) and SIRT (Simultaneous Iteration Reconstruction Technique). Both methods need a starting value of velocity, and then they modify iteratively this value by minimizing the difference between the measured travel times and the travel times calculated in the previous iteration. While ART goes on ray-path after ray-path, SIRT takes into account the effect of all ray-paths crossing each cell.

## 2.2 Iterative methods

In the  $N$ -dimensional space each equation in (1) represents a hyperplane. When a unique solution exists, the intersection of all the hyperplanes is a single point. A computational procedure to locate the solution consists of starting with an initial solution, denoted by

$$\mathbf{s}^{(0)} = (s_1^{(0)}, s_2^{(0)}, \dots, s_N^{(0)})$$

This initial solution is projected on the hyperplane represented by the first equation in (1) giving  $\mathbf{s}^{(1)}$ .  $\mathbf{s}^{(1)}$  is then projected on the hyperplane represented by the second equation in (1) to yield  $\mathbf{s}^{(2)}$  and so on. When  $\mathbf{s}^{(i-1)}$  is projected on the hyperplane represented by the  $i$ th equation to yield  $\mathbf{s}^{(i)}$ , the process can be mathematically described by

$$\mathbf{s}^{(i)} = \mathbf{s}^{(i-1)} + \frac{t_i - \mathbf{l}_i^T \cdot \mathbf{s}^{(i-1)}}{\mathbf{l}_i^T \mathbf{l}_i} \mathbf{l}_i \quad (4)$$

where  $\mathbf{l}_i$  is the  $i$ th row of the matrix  $\mathbf{L}$ .

For an over determined problem,  $M > N$ , ART does not give a unique solution, but this depends on the starting point. The tomographic system is often over determined and measurement noise is present. In this case an unique solution does not exist and the solution found by ART will oscillate in the neighbourhood of the intersections of the hyperplanes.

The Simultaneous Iterative Reconstruction Technique (SIRT) algorithm (Berriman 1991, Herman 1980, Ivansson 1986) uses the same equations as in the ART algorithm; the difference is that SIRT modifies the slowness model taking into account at each iteration the effect of all ray-paths crossing each cell. The new value of each cell is the average value of all the computed values for each hyperplane. Then, using the SIRT algorithm, better solutions are usually obtained at the expense of slower convergence.

## 3 CASE STUDY

The experimental program has been carried out on a full scale stone masonry model.

The wall is 90 cm wide, 62 cm high and 38 cm thick, and it is made of Trachite blocks sized  $20 \times 38 \times 12 \text{ cm}^3$ , settled as shown in Figures 2–4 and joined with cement lime mortar. The block assigned to the central position of the wall was not settled, thus realizing a macro-cavity with the same size of the missing block (Fig. 3), and assumed as a known anomaly. Mortar joints have been assumed to be 1 cm thick, but since the wall was manually built by a builder, actual dimensions are not so precise. Trachite specimens have been prepared and then tested for

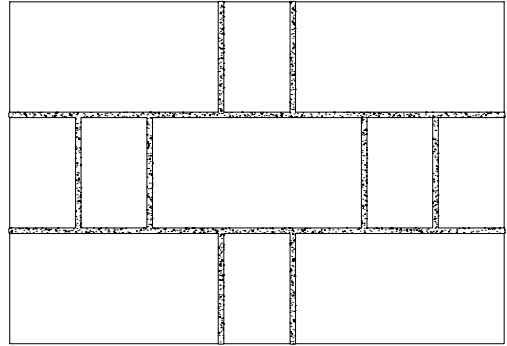


Figure 2. Front view of the wall.

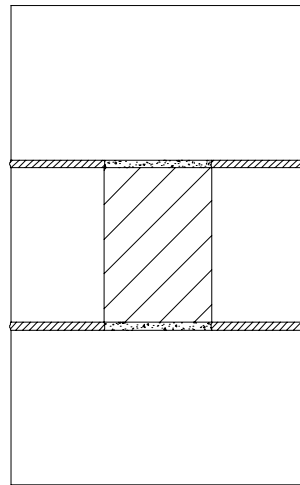


Figure 3. Vertical plane section: position of the cavity.

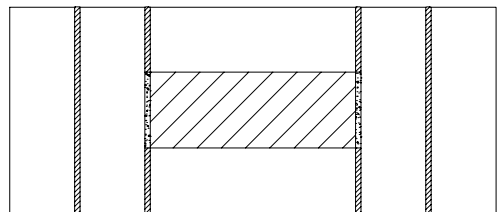


Figure 4. Horizontal plane tomographic section intercepting the cavity.

the determination of compressive strength and elastic modulus, following the Italian standards UNI EN 1926 and UNI EN 14580. Results are shown in Table 1.

The Tomographic Technique has been applied to a horizontal plane section crossing the wall in order to intercept the central void (Fig. 4).

Table 1. Trachite properties.

Properties	Value (MPa)
Compressive strength	40,5
Static elastic modulus	6100

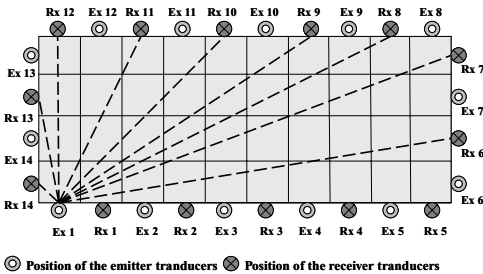


Figure 5. Measures scheme.

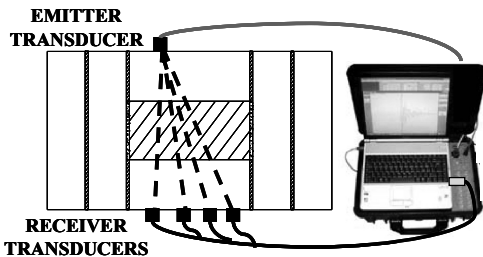


Figure 6. Measurement set-up.

The investigated section was 90 cm wide and 38 cm thick, and it has been divided in 40 cells 5 cm × 5 cm.

Emitters and receivers have been alternatively positioned along the side of the section, in the centres of the cells. Each acquisition has been run activating the receivers positioned in the sides of the wall parallel and adjacent to the side where the emitter was positioned (Fig. 5).

Using this measurements configuration, the section is crossed by 138 paths, whose relative travel times have been measured. Thus, system (1) consists of 138 equations and 40 unknowns.

The testing equipment, developed by Boviar s. r. l., includes:

- a piezoelectric transducer for emitting signals;
- 4 piezoelectric transducers for receiving signals;
- a multi-channel acquisition system for signals generation and preliminary analysis;
- a PC for data storage and signal processing.

The measurement set-up and the operative procedure are shown in Figure 6.

The software for tomographic data analysis was developed in Matlab® and Python®.

#### 4 RESULTS

The technique described in Section 2 has been applied to the case study of Section 3.

Due to the different density of the cells, the velocity should be spread within the range between  $10^3$  and  $3 \cdot 10^3$  m/s, which correspond to the velocity of the wave respectively in the air and in the Trachite.

The map of velocities is represented by a 256 levels gray scale diagram, where the lowest level (white) corresponds to the minimum velocity, and the highest level (black) corresponds to the maximum velocity. The 256 levels are normalized with respect to the range of velocities measured in the represented tomography.

The  $10 \times 4$  cells are represented by using the Kriging method (Isaaks & Srivastava 1989, Watson 1992, Deutsch & Journel 1992).

The ideal velocity map of the selected section has been elaborated assuming a velocity of  $10^3$  m/s for the cavity and a velocity of  $3 \cdot 10^3$  m/s for the stones, without taking into account the mortar (Fig. 7).

In Figure 8 the map obtained with the SVD method is shown. The calculation time has been of 5 ms, and the final residual was  $R = 9.97 \cdot 10^{-2}$ .

As it can be seen, the Kriging method identifies a central region, corresponding to the position of the cavity, where the velocity of the wave is lower.

Figure 9 shows the map obtained with the regularized SVD method. For elaborating this solution 5 ms have been spent and the final residual was equal to  $10.0 \cdot 10^{-2}$ . As it can be noted, the regularization attenuates the noising components, so that the region associated to the central cavity is here wider, and the peripheral regions with low velocity are no longer present.

In Figure 10 the result obtained with the ART method is shown. The time calculation for this solution has been of 1.5 s and the residual was  $R = 13.04 \cdot 10^{-2}$ . The average slowness of the ray-paths crossing each cell has been assumed as starting point of the iterative procedure, and 9 iterations has been performed. In this case, the residual is bigger than those of the other algorithms, but this is mainly due to the high value of velocity in some cells placed in the left side of the structure. On the other hand, the central region is here more clearly distinguishable than before.

Figure 11 shows the results obtained with the SIRT method. The calculation time has been of 2 s and the residual was  $R = 9.97 \cdot 10^{-2}$ . The same starting point of ART has been assumed as starting solution, and the procedure did converge in 8 iterations. This map is similar to the one obtained with the regularized SVD

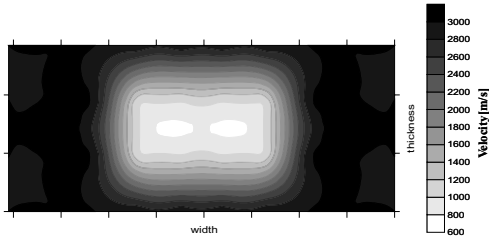


Figure 7. Ideal tomographic map of the structure.

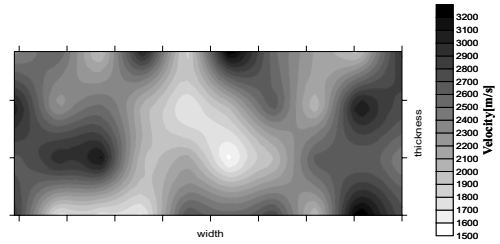


Figure 11. Tomographic map obtained with SIRT method.

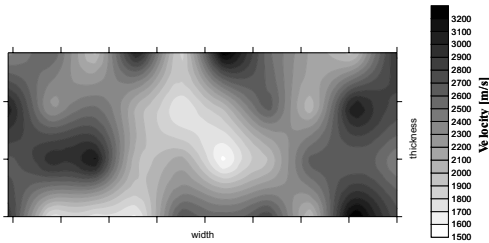


Figure 8. Tomographic map obtained with SVD method.

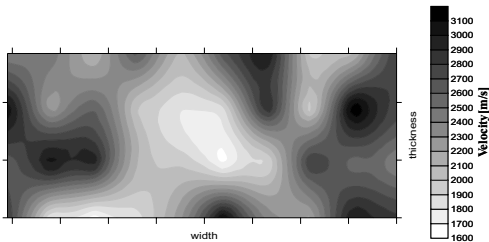


Figure 9. Tomographic map obtained with regularized SVD method.

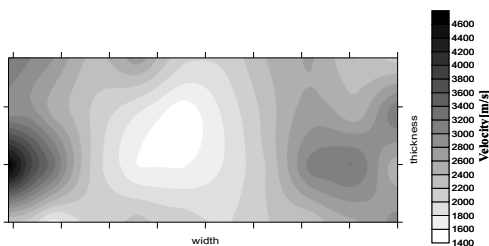


Figure 10. Tomographic map obtained with ART method.

method (Fig. 9), so the same considerations can be done in this case.

## 5 CONCLUSIONS

In this paper a procedure for the tomography of stone masonry is described. The aim of the procedure is

to detect defects inside masonries, by exploiting the dependence of the acoustic velocity on the density of the material mean. Due to the uncertainties of measurements, a set of redundant measures has to be acquired, so that an over determined equations system has to be solved. Four different algorithms have been used to solve such equations system and the results have been compared.

The procedure has been tested on a real case, and the suitability of the approach for such case has been shown.

The obtained results show that all the algorithms are able to identify the presence of an anomaly in the stone masonry. In spite of a bigger value of the residual, the ART algorithm seems to be the most suitable one for the reconstruction of the tomography, because it shows more clearly than the other considered algorithms the presence of the defect inside the wall.

## REFERENCES

- Berryman, J.G. 1991. Non linear inversion and tomography, Lecture notes, Earth Resource Laboratory, MIT, 1991.
- Cianfrone, F. 1993. Indagini microsismiche e ultrasoniche, Atti del Seminario. "Sperimentazione su strutture" Venezia 12–13 Febbraio 1993.
- Deutsch, C.V. & Journal, A.G. 1992. GSLIB Geostatistical Software Library and User's Guide Oxford University Press, New York, USA.
- Fib bulletin 17. Management, maintenance and strengthening of concrete structures, April 2002.
- Herman, G.T. 1980. Image Reconstruction from Projection: the Fundamentals of Computerized Tomography, Academic New York, 1980.
- Isaaks, E.H. & Srivastava, R.M. 1989. An Introduction to Applied Geostatistics, Oxford University Press, Oxford.
- Ivansson, S. 1986. Seismic Borehole Tomography—Theory and Computational Methods. Proc. IEEE 74, 328–338.
- Krautkramer, J. & Krautkramer, H. (ed.) 1990. Ultrasonic testing of materials, Berlin: Springer-Verlag.
- Watson, D.F. 1992. Contouring: A Guide To The Analysis And Display Of Spatial Data, Pergamon Press, New York, USA.

# Features extraction techniques for sonic and ultrasonic NDT on building materials

B. Cannas, F. Cau & M. Usai

*Dept. of Electric and Electronic Engineering, Univ. of Cagliari, Cagliari, Italy*

G. Concu

*Dept. of Structural Engineering, Univ. of Cagliari, Cagliari, Italy*

**ABSTRACT:** An experimental program has been started, with the purpose of evaluating the reliability in buildings diagnosis and characterization of integrated analysis of features related to several acoustic parameters, associated with acoustic waves propagating through the material. The Through Transmission Technique has been applied, processing the wave incident on a grid of detecting probes after it has been transmitted through a stone masonry model with known anomalies. As a first step, the process has been simulated implementing a finite element 3-D model with the LS DYNA ANSYS modulus. Various wave's features e.g., propagation velocity, signal power, signals spectrum, have been extracted. Then a distribution map of each feature has been derived interpolating the data acquired in the grid's nodes. It has been evaluated how each feature correlates with materials properties, and a novel approach based on the clustering of the high dimensional features space has been proposed for data interpretation.

## 1 INTRODUCTION

Inspection and monitoring of structural condition is an essential part of civil engineering systems' life-cycle management: in fact, outputs from inspections and assessments of a structure become inputs into maintenance, rehabilitation and replacement strategies, with the objectives to ensure public safety, to monitor the performance of structural components and materials, to identify deficiencies and thus to facilitate immediate intervention.

In the field of assessment methodologies, particular importance is given to developments in Non-Destructive Techniques (NDTs), including automated procedures and information technology to support decision making and evaluation of data. NDTs for buildings diagnosis and evaluation allow one to not interfere with the state of the asset.

Among NDTs, sonic and ultrasonic techniques give information with immediacy, rapidity and relatively low cost, thus they are often used to evaluate building materials conditions.

Sonic and ultrasonic material analysis is based on a simple principle of physics: the propagation of any wave will be affected by the medium through which it travels. Thus, changes in measurable parameters associated with the passage of a wave through a material can be correlated with changes in physical

properties of the material (Krautkammer & Krautkammer 1990).

Traditional application of sonic and ultrasonic techniques is based on measurements of the velocity  $v$  of acoustic waves propagating through the material. The velocity is obtained from the ratio  $l/t$ , where  $t$  (travel time) is the time wave needs to travel along the path of length  $l$ . It is a function of material elastic modulus  $E$ , Poisson's number  $\nu$  and density  $\rho$ .

Nevertheless, other wave's characteristics such as attenuation, scattering and frequency content, primarily related to the elastic wave power, allow one to get more and relevant information about the material. In fact, wave power is absorbed or attenuated at different rates in different materials, determined in a complex manner by interactive effects of density, hardness, viscosity, and structure. Moreover, waves reflect from boundaries between dissimilar materials, thus changes in material structure, e.g. presence of discontinuities or defects, can affect the amplitude, direction, and frequency content of scattered signals. Finally, all materials tend to act to some degree as a low pass filter, attenuating or scattering the higher frequency components of a broadband wave more than the lower frequency components. Thus, analysis of changes in the remaining frequency content of a selected broadband pulse that has passed through the test material can keep track of the combined effects of attenuation and



scattering as previously described (Cianfrone 1993, Nelligan 2007).

In the light of this, an experimental program has been started, with the purpose of evaluating the reliability in buildings diagnosis and characterisation, of integrated analysis of features related to several waves parameters.

## 2 CASE STUDY

The experimental program has been carried out simulating the propagation of acoustic signals through a stone masonry wall. Finite Elements numerical techniques have been used to model a wall 0,90 m wide, 0,62 m high and 0,38 m thick, made of Trachite blocks sized  $0,20 \times 0,38 \times 0,12$  m, jointed with cement lime mortar joints 0,01 m sized. The wall is affected by a defect consisting of a macro-cavity set in central position. A picture of the wall is shown in Figure 1.

The material properties assumed for the trachite and the mortar are reported in Table 1.

The test method is the Through Transmission Technique. In this method, the ultrasonic wave is transmitted through the test object and received by a second transducer on the opposite side of the structure. Changes in received signal provide indications of variations in material continuity. 220 emitters and 220 receivers have been positioned on a grid of  $11 \times 20$  nodes in the opposite surfaces of the wall (see Fig. 2).

In order to simulate the wave propagation through the wall, a finite element 3-D model has been developed using the commercial code ANSYS (ANSYS 2007).

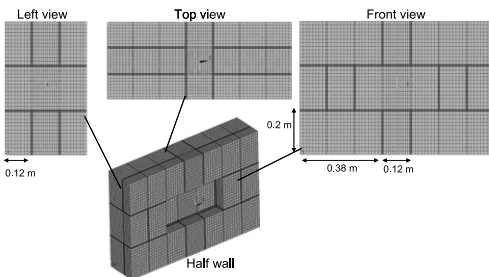


Figure 1. Views of the test wall.

Table 1. Geometrical dimensions and material properties of the wall.

	Young's modulus [GN/m <sup>2</sup> ]	Poisson's coefficient	Density [kg/m <sup>3</sup> ]
Trachite	6	0.2	1750
Mortar	15	0.1	1800

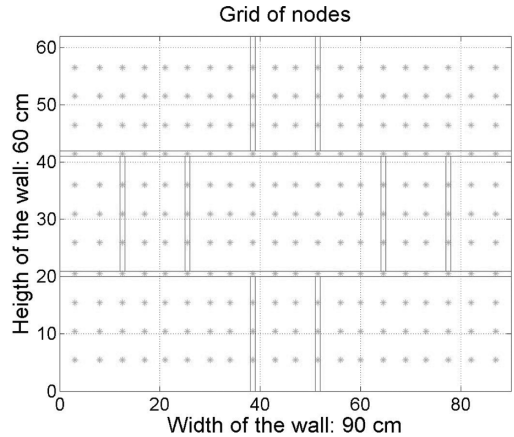


Figure 2. Grid of test points.

In particular, the LS DYNA modulus, which solves structural and mechanical problems in a transient domain, has been used.

Numerical models are mainly useful to reproduce the signals obtained with real measurements and to collect a large amount of data in a relatively short time.

The model implemented to simulate the wave propagation through the test wall is shown in Figure 1, in which both trachite areas and mortar layers are presented. In the centre of the wall the cavity has been modelled by removing the corresponding elements.

The numerical analyses have been carried out simulating the use of piezoelectric transducers for emitting and receiving the signal. Simulations have been performed on a Hewlett-Packard Workstation xw9300 with Opteron tm Processor 250, 2.39 Ghz, 3.50 GB of RAM Physical Address Extension. Each simulation (one ray path) lasted 35 minutes.

Due to symmetry of the structure, it has been sufficient to analyse only one quarter of the wall. The excitation  $y(t)$  is an acceleration signal applied in the grid's nodes on one side of the wall. It is a seven and half-cycle tone burst enclosed in a Hanning window as described by (1) and reported in Figure 3 (Jackson 1995):

$$y(t) = \frac{1}{2} \sin(2\pi ft) \cdot \left[ 1 - \cos\left(\frac{2}{15} 2\pi ft\right) \right] \quad (1)$$

The parameter  $f$  is the excitation frequency equal to 60 kHz, which corresponds to the characteristic frequency of the transducer previously described. The Hanning windowing is largely used to reduce the leakage in NDT. In fact, when the signals are measured for a short time the Fourier Transform works as if the data

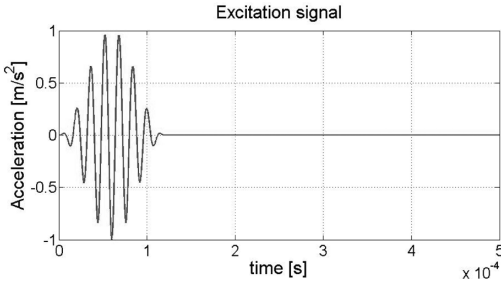


Figure 3. Excitation signal.

were periodic for all time introducing spurious spectral lines in the signal spectrum.

The aliasing has been avoided by suitably sampling the data (the sampling frequency is around 1 MHz).

### 3 FEATURES EXTRACTION FOR CLASSIFICATION OF ANOMALIES AND MATERIAL

At the end of the simulation sessions, 220 signals have been obtained, one for each point of the grid of receivers. From each node of the grid, 21 parameters both in time domain and in frequency domain have been extracted in order to investigate the presence of anomalies and obtain some information on the material. Each parameter is associated with a matrix  $A_i(11 \times 20)$ ,  $i = 1, \dots, 21$ , containing the parameter values in each node of the grid.

The time domain features are extracted from the waveform and from its envelope. The envelope of signals has been determined by applying a smoothing function to the positive amplitude peaks of the signal. The waveforms and their envelopes have been normalized between 0 and 1. The frequency domain features are measured from the power spectrum of the normalized waveform. The selected 21 features (Cohen 1995, Vergara et al. 2004, Salzar et al. 2006, Liu et al. 1988, Hinton 1999, Miralles et al. 2005) are listed in Table 2, where the number in the second column is referred to the elaboration sequence.

Time-reversibility (Miralles et al. 2005, Schreiber & Schmitz 1999) and Third order autocovariance (Gautama et al. 2004) are two traditional metrics that give information on non-linearity of the signal. Time-reversibility is the skewness of the slopes normalized by standard deviation of the slopes taken to the third power. Third order autocovariance is the higher order extension of the traditional autocovariance (a slide of the third order moment estimation).

Input signal attenuation (Liu et al. 1998) has been estimated from spectral centroid down-shift using a statistically based method.

Table 2. Selected features.

Time domain	
Propagation velocity	21
Maximum peak-peak amplitude	18
Maximum absolute amplitude	17
Minimum absolute amplitude	1
Mean value of normalized amplitude	11
Variance of normalized amplitude	12
Time-reversibility	9
Third order auto-covariance	10
Mean value of normalized signal envelope	16
Variance of normalized signal envelope	20
Local rise time from 25% level to peak of normalized signal envelope	15
Local rise time from 50% level to peak of normalized signal envelope	13
Signal power	14
Travel time	19
Frequency domain	
Spectrum principal frequency	7
Spectrum normalized maximum amplitude	5
Input signal attenuation	2
Spectrum central frequency	4
Spectrum Bandwidth	3
Spectrum normalized mean value	6
Spectrum normalized variance	8

A map of the distribution of each feature has been derived interpolating the data recorded in the grid's nodes. Each map emphasizes areas where anomalies are located, according to feature's specific diagnostic skill.

### 4 PROCESSING OF FEATURES MAPS

In order to evaluate how each feature correlates with materials properties, a matrix  $M(20 \times 11)$  has been built. The element  $m_{ij}$  identifies the type of path the wave, emitted in the  $i, j$  position of the grid, propagates through. In particular, the wave can propagate through four types of paths: trachite, mortar-trachite, mortar, air-trachite. Figure 4 shows the map associated to the  $M$  matrix.

The absolute values of the correlation coefficients between the material properties ( $M$ ) and the single features ( $A_i, i = 1, \dots, 21$ ) are reported in Figure 5 where numbers are referred to those reported in table 2. As it can be noticed, the signal power and the amplitude variance show the higher correlation coefficients.

As an example, Figure 6 shows the distribution map of the signal power. It can be noticed that this feature, as for the amplitude variance, is able to well-define the contour of the defect, but not the mortar joints.

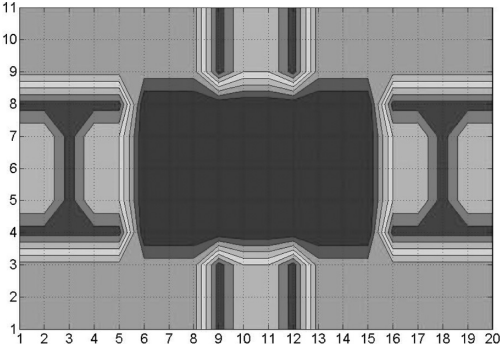


Figure 4. Map associated to the M matrix.

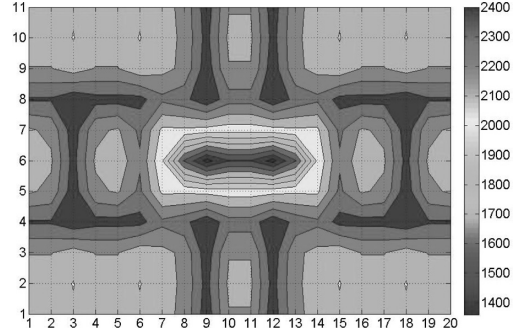


Figure 7. Propagation velocity: distribution map.

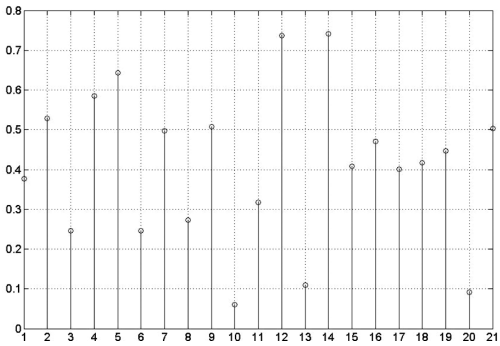


Figure 5. Materials and features: correlation coefficients.

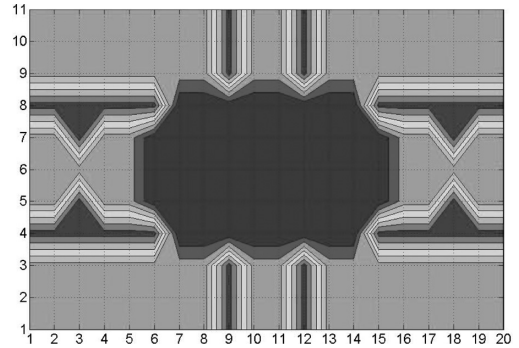


Figure 8. Map derived from clustering of selected features.

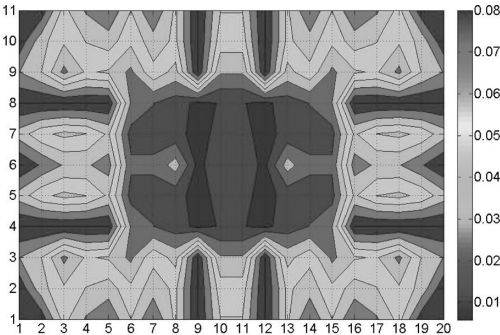


Figure 6. Signal power: distribution map.

The propagation velocity, frequently used in NDTs, shows a correlation coefficient of 0.5.

Despite its correlation coefficient is lower than those relative to signal power and amplitude variance, the map of the velocity, shown in Figure 7, is able to discriminate three main types of ray-paths.

Only the paths through trachite and those through mortar-trachite are undistinguishable. In the center of

the map the presence of the cavity region can be clearly seen, although it is smaller than expected.

In order to exploit the complementary contribution of the information contained in the various features, the high-dimensional distribution obtained by the union of the most significant features has been considered.

In particular, features with a correlation coefficient less than 0.2 have been discarded, thus obtaining a 18-dimensional features space.

The resulting distribution has been mapped in the material distribution in order to identify the four principal ray-paths. For this task, discretization techniques have been used, partitioning the 18-dimensional features space into four clusters corresponding to the four types of ray paths. K-means algorithm has been used to identify the clusters (MacQueen 1967). K-means performs the grouping by minimizing some metric relative to the centroids of the clusters. In this case, the metric is the euclidean distance between data and the corresponding cluster centroid. Figure 8 reports the obtained map.

In this map, the paths crossing the trachite and those crossing mortar-trachite cannot be still clearly distinguished. Nevertheless, the cavity inside the structure is accurately defined, as well as the mortar joints.

## 5 CONCLUSIONS

In the present paper a novel approach for acoustic non-destructive testing of structures, based on the extraction of several features from waves propagating through the structures' thickness, is proposed.

The propagation of ultrasonic signals through a stone masonry wall has been simulated using a finite element method, and various wave's features, both in time and frequency domains, have been extracted from the received signal.

The method consists in three fundamental steps: derivation of a distribution map for every feature extracted; analysis of how features correlate with structures' characteristics; clustering of the high dimensional features space for exploiting the complementary contribution of the information contained in most significant features, and for compressing data.

Results show that it is possible to extract several waves features, each one strongly related to one or more information on structures' properties.

The use of clustering procedures permits to compress all these information in a single map, which represents a signature of the examined structure allowing one to clearly detect materials properties and structures' discontinuities.

Future research will investigate the method reliability processing such kind of maps for different cases of anomalies and defects, applying PCA (Principal Component Analysis) method, FFT2 (Bidimensional Fast Fourier Transform), and using these maps for training a neural network in order to predict the presence and the position of anomalies and defects not detectable by visual inspection. Moreover, test on a full scale real stone masonry wall will be performed to confirm the effectiveness of the method.

## REFERENCES

- Ansys, Release 10, Documentation for ANSYS, Release 10.0.
- Cianfrone, F. 1993. *Indagini microsismiche e ultrasoniche, Sperimentazione su strutture; attualità ed affidabilità delle metodologie d'indagine, Proc. of symp.*, Venice, 1993.
- Cohen, L. 1995. Time-frequency analysis. Englewood Cliffs, Prentice Hall.
- Gautama, T. Van Hulle, M.M. & Mandic, D.P. 2004. On the characterization of the deterministic/stochastic and linear/nonlinear nature of time series. Technical report DPM-04-5, London: Imperial College.
- Hinton, Y.L. 1999. Problems associated with statistical pattern recognition of acoustic emission signals in a compact tension fatigue specimen, NASA/TP-1999-209351 ARL-TR-1691.
- Jackson, L.B. 1995. Digital Filters and Signal Processing, Kluwer Academic Publishers.
- Krautkramer, J. & Krautkramer H. 1990. Ultrasonic testing of materials, Springer Verlag.
- Liu, L. Lane, J.W. & Quan, Y. 1988. Radar attenuation tomography using the centroid frequency downshift method. *Journal of Applied Geophysics* (40): 105–116.
- MacQueen, J.B. 1967. Some Methods for classification and Analysis of Multivariate Observations. Proceedings of 5-th Berkeley Symposium on Mathematical Statistics and Probability, Berkeley: University of California Press.
- Miralles, R. Gosalbes, J. & Salzar, A. 2005. Detection of non linearities caused by bubbles in ultrasonic signals. Proc. of EUSIPCO, Antalya, Turkey, 2005.
- Nelligan, T. 2007. An introduction to ultrasonic material analysis. Olympus NDT. www.olympusndt.com, 2007.
- Salzar, A. Miralles, R. Parra, A. Vergara, L. & Carrascosa, B. 2006. Ultrasonic non-destructive testing of archaeological ceramics. Proc. of ECTNDT, 2006.
- Schreiber, T. & Schmitz, T. 1999. Testing for non linearity in unevenly sampled time series. *Phys. Rev.* (59): 4044–4047.
- Vergara, L. Gosalbez, J. Miralles, R. & Bosch, I. 2004. On estimating the center frequency of ultrasonic pulses. *Ultrasonic*, Elsevier, (42): 813–818.

# Measuring the displacements of a steel structure by GPS units

F. Casciati & C. Fuggini

*Department of Structural Mechanics, University of Pavia*

**ABSTRACT:** Global Navigation Satellites Systems (GPS, GLONASS and the future GALILEO) have been proved to be suitable for displacement monitoring in structural engineering. The American Global Positioning System (GPS) provides sampling rates sufficient to track the displacement of dynamically objects with the accuracy of sub-centimetres. In the past few years the GPS has appeared as an alternative to common accelerometers in measuring the vibration of flexible structures. It was applied to monitor the structural response of many different structures, like bridges, dams and tall buildings.

This paper investigates the reliability and the accuracy in real time measurement of dual frequency GPS receivers located on the roof of a steel building. The goal is to estimate the precision of such GPS receivers to acquire the movements of the monitored points due to wind action, temperature change and to the dynamic vibration induced by the internal bridge-crane.

## 1 INTRODUCTION

The American Global Positioning System (GPS) provides sampling rates sufficient to track the displacement of dynamically excited objects with an accuracy of the order of millimetres. Thus it is becoming an alternative to common accelerometers to measure the dynamic response of long-period structures (Celebi 2000) (Nikitopoulou et al. 2006) (Kijewsji-Correa et al. 2006). The high-precision GPS technology has been applied to monitor wind-induced deformation of tall flexible buildings (Kijewsji-Correa et al. 2003), (Campbell et al. 2006) (Seco et al. 2007), to assess the vibrations of suspension and cable-stayed bridges (Xu et al. 2001) (Lekidis et al. 2004), the displacements of high chimneys (Breuer et al. 2002) and dams (Barnes et al. 2006), (Cazzaniga et al. 2006). Many applications were developed by installing GPS receivers at key locations to capture their static and dynamic displacements of the structures in real time and in all weather conditions (Tamura et al. 2002). In other cases, the GPS was incorporated in the monitoring of a major suspension bridge (Wong 2004).

## 2 GOVERNING RELATIONS

GPS positions are calculated using the concept of triangulation; the known position of satellites overhead allows one to determine the position of a GPS receiver/antenna pair on the Earth (Figure 1). Each satellite continuously transmits the current time kept by atomic clocks, as well as information about its

current position  $x^j, y^j, z^j$  in its orbital path. The distance  $r_i^j$  of the  $j$ th satellite to the unknown position on the Earth  $x_i, y_i, z_i$  is determined from the travel time of the transmitted electromagnetic signals (with  $c = 290,000$  km/s).

For a constellation of  $N_{sat}$  ( $j = 1, 2, \dots, N_{sat}$ ) satellites, the distance satellite-receiver can be defined as:

$$r_i^j = c \cdot \Delta t = c \cdot (T^A - T^B) \tag{1}$$

where  $T^A$  represent the epoch of arrival of the signal and  $T^B$  the epoch of start. Equation (1) can be written as the geometrical distance between satellite and receiver:

$$r_i^j = \sqrt{(x^j - x_i)^2 + (y^j - y_i)^2 + (z^j - z_i)^2} \tag{2}$$

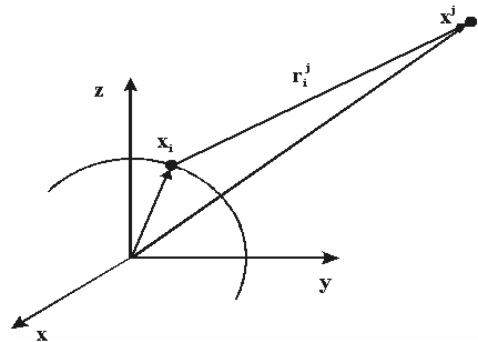


Figure 1. Satellite—receiver distance.

To account for clock inaccuracies, due to the lower power accuracy of the receivers clocks than those of satellites, the pseudo-range distance can be calculated as:

$$\rho_i^j = r_i^j + c^*(\delta t^j - \delta t_i) + \Delta T_i^j + \Delta I_i^j + \varepsilon_r + \varepsilon_m \quad (3)$$

where  $\delta t^j - \delta t_i$  = time delay of the signal;  $\Delta T_i^j$  = ionospheric delay (proportional to the frequency of the signals; it can be removed by tracking the two L1 and L2 frequencies carried by the GPS signal);  $\Delta I_i^j$  = tropospheric delay (can be deleted by the Hopfield model);  $\varepsilon_r$  = errors due to the receiver and electromagnetic interference;  $\varepsilon_m$  = multi-path effect.

In synthesis the error due to multi-path effect is the result of a signal arriving at the receiver with a slight delay having been reflected off by one or more objects. In urban zones this is one of the challenges that the GPS monitoring has to solve. Many efforts were focused on estimating this error and different solutions were proposed (Lovse et al.) (Kijewski-Correa et al. 2007).

Two main methods were developed for obtaining the coordinates  $x, y, z$ , of a static or moving receiver. In the static mode a GPS antenna is fixed in a certain position and receives information sent by a number of tracked satellites. In the kinematic mode the signal recorded by the moving receiver (rover) is corrected, in real time or in post processing, by a stationary receiver (reference) fixed in a nearby position. The kinematic GPS mode guarantees the identification of frequencies in the range 0.1–20 Hz. In order to achieve high levels of accuracy a pair of dual frequency GPS receivers are needed and a real time communication between the moving and the fixed receivers is necessary to avoid GPS positioning errors. Indeed, the quality of GPS position solutions depends on the number and the geometric distribution of available satellites. At least five satellites available in the sky (with at least 10 degree of elevation angle) are necessary and the line-of-sight to each of them has not to be obstructed.

In the kinematic mode the information (3D point coordinates) collected at the reference are used to make corrections for atmospheric delays and other error sources to enhance the stand alone accuracy of the rover unit. The position of the two GPS antennas has to be chosen to satisfy some requirements: both the antennas must have a clear view of the sky above in order to track the orbiting satellites, the reference and the rover could be in close proximity to minimize baseline errors, both antennas need to be installed on a rigid surface. Moreover the verification of GPS receiver positions data allows to quantify the dilution of precision (DOP) in the signal due to a deviation from the idealized geometric distribution of satellites. This source of error is inherent in the technology and

can only be practically removed by adding more satellites. Others sources of errors in the GPS receiver position are due to electromagnetic interference and to the multi-paths effect as in Equation (3).

### 3 EXPERIMENTAL MOCK-UP

Two GPS antennas have been placed on the roof of an industrial steel building in Pavia, at the height of 15 m, in order to guarantee an open field location sufficiently free from potential sources of multi-paths errors and from buildings that may obstruct the view of the lower elevation satellites (around 15–30°). In these conditions a sufficient number of satellites is visible all over the day, with a maximum of twelve satellites in the early morning.

The antennas were anchored on a small stiff concrete surface, placed on the flat roof at a distance of around 13 m one from the other. They are linked to the receivers by wire connections, and others wires connect the receivers to a computer for the acquisition of the GPS signal.

In order to guarantee the accuracy of millimetres in the positioning, two dual frequency L1/L2 GPS receiver are used. The rover and the reference, communicate each to the other to guarantee the correction of position errors. For this purpose the GPS technique of *differential point positioning (DGPS)* is used (Dana, 1997). The correct position of the fix reference receiver is sent towards a wire connection to an acquisition software, that in real time acquires the coordinates and the information from the reference position, computes new coordinates and transmits the correction of position to the rover receiver. This kind of differential positioning allows, through the data of a reference receiver, to delete the rover errors of position and to obtain, with sub-centimetres resolution, the correct position of the rover.

The components used in *DGPS* are: a) a dual frequency high precision Leica GMX902 GPS receiver, working as rover, with a maximum sampling rate of 20 Hz; b) a dual frequency high precision Leica GRX1200 Pro GPS receiver, working as reference,

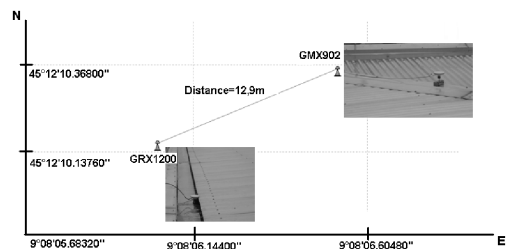


Figure 2. GPS ground configuration.

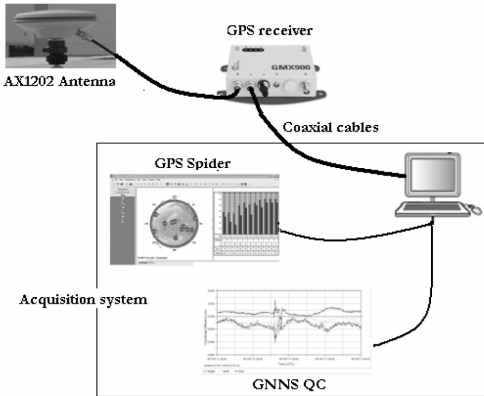


Figure 3. System architecture.

with a maximum sampling rate of 20 Hz (Leica 2005). The antennas are a pair of dual frequencies Leica AXI202 recording signal with a sampling rate up to 20 Hz.

The GPS signals are recorded by Leica GPS Spider software, that furnishes information on the satellites configuration and allows corrections of data for a single-base real time positioning product. GPS spider is combined with the Leica GNNS QC data analysis and quality control software, used for elaboration of data recorded as ambiguity fixed positions (Brown et al. 2006).

As figure 3 shows, the system architecture is made of an outdoor part, the antennas (6.2 cm height, 17.0 cm of diameter, 0.4 Kg weight) mounted on the roof, and of an indoor part assembling the receivers and a computer running the two Leica software products. They display the displacements in terms of their North-East-Vertical components or in terms of longitudinal directions. The recorded signals are then analyzed using a system identification toolbox.

#### 4 DYNAMIC TESTS

The system architecture of Figure 3 was used to monitor movements due to natural actions (wind, temperature changes) and man-made excitation obtained by driving a bridge-crane along rails supported at the height of 8 m.

Some preliminary calibration tests had shown the performance of a dual frequency GPS receiver in a early architecture configuration (Casciati et al. 2007). In these tests the amplitudes of the oscillations were varied in the range from  $\pm 0.5$  cm up to  $\pm 5$  cm with frequencies of 0.1; 0.2; 0.5; 1; 2, 4 Hz.

#### 4.1 Wind action

On November 11, 2007 a wind event occurred in Pavia. During this event the wind approached from the West-North direction and produced predominant along wind response in the N-E reference axes of the rover.

Near the industrial steel building where the GPS receivers are placed, a wind station (Cascina Pelizza) recorded the velocity and the direction of the wind all over the day. The data recorded by the station could be considered the same produced at the top of the steel building, as the two buildings are really near and their heights are quite similar.

In particular from 14.00. to 16.30 the wind speed was in the range from 10 to 17.5 m/s, with around ten minutes of significant peaks up to 20.7 m/s; this maximum intensity was reached at 14.22. For the two hours of registration shown in this paper, i.e., from 2 to 4 p.m., the wind approached from North.

The GPS rover sensor mounted on the roof of the industrial building recorded the oscillations of the building due to this wind action. The main amplitude of the GPS movements was in the North direction, corresponding to the along wind line, while in the East direction the amplitude was quite smaller.

Others authors (Kijewsji-Correa et al. 2006) analyze the wind-induced response of tall buildings by decomposing the wind action in three components: mean, background (quasi-static), resonant. They further applied to this three components a filtering scheme to obtain a clearer and more consistent with physically parameters response. In this paper one only adopts a filtering scheme to show the global wind response of the building.

Figures 4 and 5 show the intensity and the direction of the wind event, respectively, as it was recorded by the permanent station at Cascina Pelizza on November 9, 2007. The displacements of the building measured by the GPS unit during the wind event are plotted in the next Figures 6 and 7 in term of N-E component time histories:

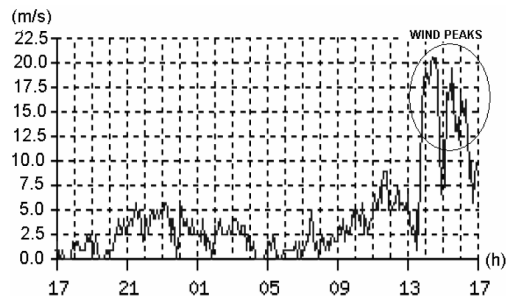


Figure 4. Wind speed from 5 pm of November 8, 2007 to 5 pm of November 9, 2007.



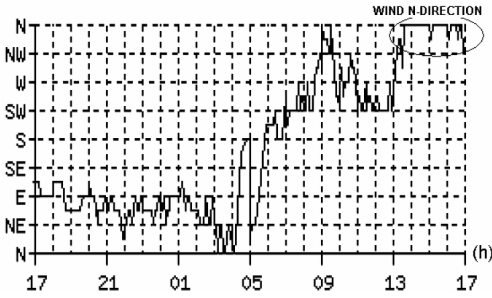


Figure 5. Wind direction from 5 pm of November 8, 2007 to 5 of 09 pm of November 9, 2007.

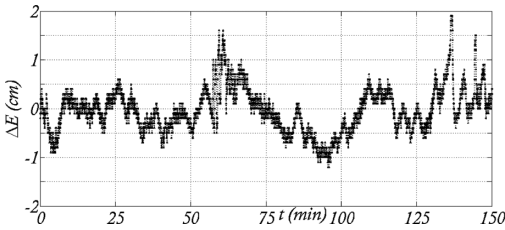


Figure 6. Time histories of the displacements during wind event: East component ( $\Delta E$ ).

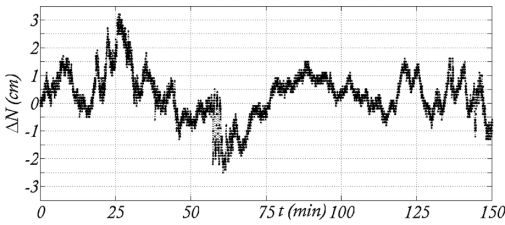


Figure 7. Time histories of the displacements during wind event: North component ( $\Delta N$ ).

Figure 8 shows the North and East components of the displacement of the rover sensor for the wind event approaching from the North. Figure 9 gives for the East component, 50 sec of the time histories recorded on November 9, 2007 and November 10, 2007 when no significant wind events had occurred.

The signal recorded is then filtered using a low frequencies bandstop technique. Figures 10 and 11 show the filtered East and North component of the signal.

According to a finite elements model of the steel building, the peaks displacement in the structure response have a maximum value of around 3.5 cm, in the main wind direction.

Figure 12 shows the deformed shape of the building in the finite element model reporting the localization of the rover and of the reference GPS receiver.

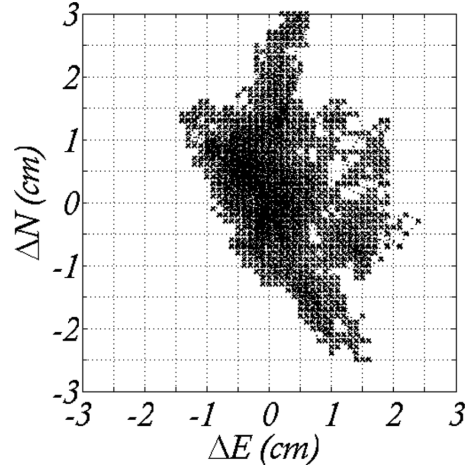


Figure 8. North-East component response during wind event.

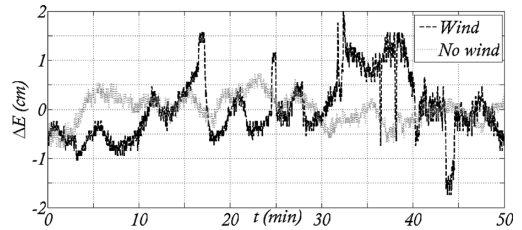


Figure 9. East component ( $\Delta E$ ) correlation between wind action and no wind event.

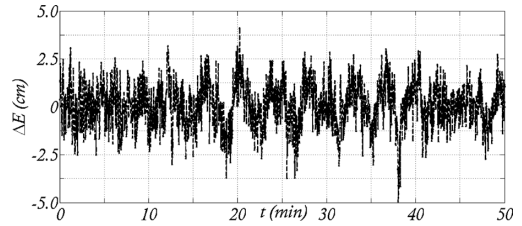


Figure 10. Time histories of the displacements during wind event: filtered East component ( $\Delta E$ ).

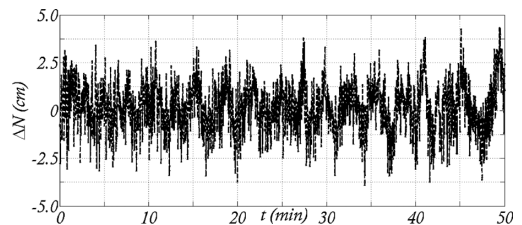


Figure 11. Time histories of the displacements during wind event: filtered North component ( $\Delta N$ ).



The X axis direction coincide with the North direction of the wind event.

#### 4.2 Bridge-crane movements

A bridge-crane is mounted on rails running inside the industrial steel building at the height of 8 m and covering a span of around 20 m. It allows three types of movements: vertical movements of the load, longitudinal horizontal movements along its way beam, transversal displacements for horizontal movements of the load. The longitudinal bridge-crane movements induce significant vibrations of the steel structure. The amplitude can also be estimated by the finite element model in Figure 12. While the bridge-crane is moving along the longitudinal direction, the GPS placed on the roof records these oscillations. Note that when the bridge-crane stops, at the end of his ride a peak force of 10,93 KN is introduced.

The bridge-crane can be moved at two different speed: low and fast. The low mode has the speed of 0,33 m/s, the fast mode of 0,67 m/s. In this paper the fast mode is adopted.

Figure 13 shows some results in term of longitudinal ( $\Delta L$ ) time histories. The observed peak is relative to the force applied to the structure when the bridge-crane is pulled up. The two parts in which Figure 13 is divided by the peak, show the bridge crane movements at the high speed.

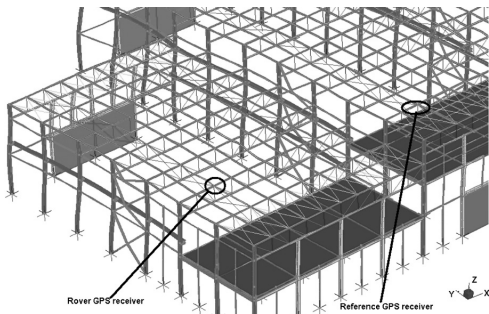


Figure 12. Wind displacements, of the wind recorded time histories applied to the finite element model.

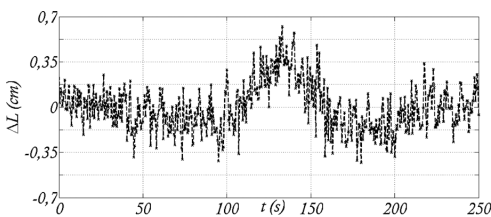


Figure 13. Longitudinal ( $\Delta L$ ) bridge-crane movements recorded by GPS.

The signal recorded by GPS rover receiver is also filtered applying a low frequencies stopband filter scheme and plotted in Figure 14.

Others tests have been made when the bridge-crane moves backward and forward along its rails, inducing symmetric oscillations to the steel building. The speed was always chosen as the faster one. These tests are quite valuable because the movements chosen were enough fast to induce strong motion to the structure.

Figure 15 reports the results in term of longitudinal displacement time histories.

The values of the displacements, in the two bridge-crane cases are similar to those obtained by a finite element model of the steel building, when a linear transient dynamic analysis is developed.

Figure 16 shows the structure response due to longitudinal movements of the bridge-crane along the Y axis direction, when the bridge-crane is pulled up.

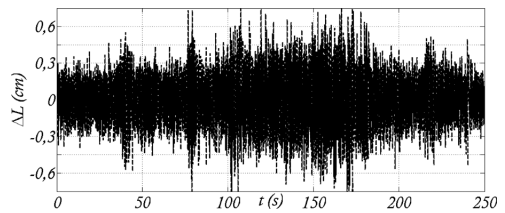


Figure 14. Filtered longitudinal ( $\Delta L$ ) bridge-crane movements recorded by GPS.

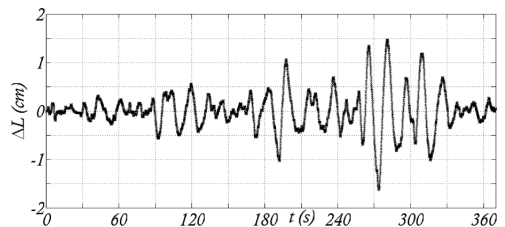


Figure 15. Longitudinal ( $\Delta L$ ) oscillations of bridge-crane movements recorded by GPS.

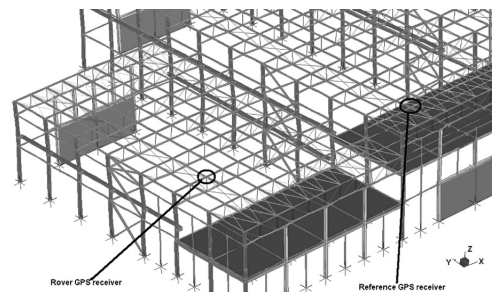


Figure 16. Bridge-crane induced displacements.

## 5 CONCLUSIONS

This paper considers the use of a high-precision global position system for monitoring the displacements of flexible structures due to wind and man made actions.

The performance of a pair of dual frequency GPS receivers have been already verified in static tests.

The level of accuracy achieved by the GPS receivers was also investigated for dynamic movements. The dynamic tests of calibration compare the receivers records with known time histories oscillations.

The present full-scale test assesses the ability of the GPS receivers to measure the displacements induced in a steel structure by the wind action and by movements of an internal bridge-crane. The data recorded by the GPS unit are compared with the response of a finite element model of the structure.

For each test, a filtering technique is applied, in order to remove the noise in the signal low frequencies.

The study confirms the expectation in the GPS accuracy for monitoring dynamic displacements induced by wind or man made actions.

Further validation is required for long acquisition periods in static tests and for imposed vibrations of very low amplitudes (less than 1 cm) and high frequencies (more than 2 Hz).

The full-scale tests could also be carried out by a parallel installation of accelerometers. A comparison of the recorded responses would show the range of feasibility of the GPS monitoring.

## ACKNOWLEDGEMENT

The authors acknowledge the GPS installation and the technical support obtained by the company Leica Geosystems Italia.

## REFERENCES

- Barnes, J. & Cranenbroeck, J. Van. 2006. The potential of a ground based transceivers network for water dam deformation monitoring, *International Conference Hydropower, Kunming, 23–25 October 2006*, 765–795.
- Breuer, P., Chmielewski, T., Gorski, P. & Konopka, E. 2002. Application of GPS technology to measurements of displacements of high-rise structures due to weak winds, *Journal of Wind Engineering and Industrial Aerodynamics* 90, 223–230.
- Brown, N., Troyer L., Zelzer O. & Cranenbroeck J. Van. 2006. Advances in RTK and post processed monitoring with Single Frequency GPS, *Journal of Global Positioning Systems* 9, 145–151.
- Campbell, S. Kwok, K.C.S., Keung, Y.L. & Hitchcock, P.A. 2006. Full-scale monitoring of a high-residential building using GPS under typhoon conditions, *4th World Conference on Structural Control and Monitoring, San Diego, 11–13 July 2006*.
- Casciati, F., Fuggini, C. & Bonanno, C. 2007. Dual frequency GPS receivers: reliability of precision of the measures, *Proceedings of 4th C2I, Nancy, 15–17 October 2007*, 604–612.
- Cazzaniga, N.E. & Pinto, L. 2006. Structural monitoring with GPS and accelerometers: the chimney of the power plant in Piacenza, Italy, *3rd IAG Symposium on Geodesy for Geotechnical and Structural Engineering and 12th FIG Symposium on Deformation Measurements, Baden, 22–24 May 2006*.
- Celebi, M. 2000. GPS in dynamic monitoring of long-period structures, *Soil Dynamics and Earthquake Engineering* 20, 477–483.
- Dana, P.H. 1997. Global Positioning System (GPS) Time Dissemination for Real-Time Applications, Real-Time Systems: The International Journal of Time Critical Computing Systems, 12, 9–40.
- Kijewski-Correa, T.L. & Kareem, A. 2003. The Chicago monitoring project: a fusion of information technologies and advanced sensing for civil infrastructures, *Proceedings of 1st International Conference on Structural Health Monitoring and Intelligent Infrastructure, Tokyo, 13–15 November 2003*, 1003–1010.
- Kijewski-Correa, T., Kareem, A. & Kochly, M. 2006. Experimental Verification and Full-Scale Deployment of Global Positioning Systems to Monitor the Dynamic Response of Tall Buildings, *Journal of Structural Engineering* 132(8), 1242–1253.
- Kijewski-Correa, T.L. & Kochly, M. 2007. Monitoring the wind-induced response of tall buildings: GPS performance and the issue of multipath effect, *Journal of Wind Engineering and Industrial Aerodynamics* 95, 1176–1198.
- Leica 2005. GMX 902 user manual, *Leica Geosystems AG, Heerbrugg, Switzerland*.
- Lekidis, V., Tsakiria, M., Makrab, K., Karakostasb, C., Klimisb, N. & Sous, I. 2005. Evaluation of dynamic response and local soil effects of the Evripos cable-stayed bridge using multi-sensor monitoring systems, *Engineering Geology* 79, 43–59.
- Lovse, J.W., Teskey, W.F., Lachapelle, G. & Cannon, M.E. 1995. Dynamic deformation monitoring of tall structure using GPS technology, *Journal of Surveying Engineering*, 121(1), 35–40.
- Nickitopoulou, A., Protopsalti, K. & Stiros, S. 2006. Monitoring dynamic and quasi-static deformations of large flexible engineering structures with GPS: accuracy, limitations and promises, *Engineering Structures* 28, 1471–1482.
- Seco, A., Tirapu, F., Ramirez, F., Garcia, B. & Cabrejas, J. 2007. Assessing building displacement with GPS, *Building and Environment* 42, 393–399.
- Tamura, Y., Matsui, M., Pagnini, L.C., Ishibashi, R. & Yoshida, A. 2002. Measurement of wind induced response of building using RTK-GPS, *Journal of wind engineering and industrial aerodynamics* 90, 1783–1793.
- Wong, K.Y. 2004. Instrumentation and health monitoring of cable-supported bridges, *Structural Control and Health Monitoring* 11, 91–124.
- Xu, L., Guo, J.J. & Jiang, J.J. 2002. Time-frequency analysis of a suspension bridge based on GPS, *Journal of Sound and Vibration* 254(1), 105–116.

# Including structural monitoring activities in safety probabilistic formulations

R. Ceravolo, A. De Stefano & M. Pescatore

Politecnico di Torino, Torino, Italy

**ABSTRACT:** Safety assessment of existing structures should take into account the additional knowledge obtained from monitoring activities. In fact, information about safety degradation over time is needed when estimating the residual lifetime of a structure, which must be a factor in the assessment of the overall economic utility of a strengthening intervention. In this paper, two symptoms, namely the reduction in stiffness and the increase in energy dissipation, were assumed to be directly associated with structural damage and safety degradation. In the last part of the paper, in order to show possible strategies for relating dynamic measurements to reliability with respect to collapse, a numerical application to a bridge pier subjected to periodic monitoring is reported.

## 1 INTRODUCTION

When the degradation of reliability over time is taken into account, the lifetime of a structure is a random variable (Lawless 1982) and reliability can be characterised in relation to the so-called “hazard function” (the damage rate in the infinitesimal time interval), which assumes various forms depending on the distribution model adopted (Weibull, Gamma, etc.). In this connection, a monitoring-oriented approach (Natke & Cempel 1997, Ceravolo et al. 2007) is of great interest, as the monitoring process is able to supply useful data both to plot the reliability curves, defined as a function of the symptom, and to interpret the diagrams obtained.

In the second part of the paper, in order to show possible strategies for relating dynamic measurements to reliability with respect to collapse, a numerical application to a bridge pier subjected to periodic monitoring is reported. In this example, two symptoms, namely reduction in stiffness and increase in energy dissipation, were assumed to be associated with degradation in structural safety performances.

## 2 SYMPTOM-BASED APPROACH TO SAFETY ASSESSMENT

According to a symptom based approach, structural safety will depend on measurable quantities. The reliability of a structure,  $R(t)$ , is defined as the probability that the time it takes a system to reach a damage limit state associated to the structure’s lifetime,  $t_b$ , is greater than a generic time  $t$ :

$$R(t) = P(t \leq t_b). \tag{1}$$

Eq. (1) may be reformulated in the terms of a symptom variable,  $S$ ; in this case, reliability is defined as the probability that a system, which is still able to meet the requirements for which it has been designed ( $S < S_l$ ), is active and displays a value of the  $S$  smaller than  $S_b$ , where  $S_l$  is the maximum value that a symptom can reach in a system according to statistical decision theory, and  $S_b$  is the value of the symptom corresponding to the reference limit state. Accordingly,  $R(S)$  can be expressed by the integral of the symptom’s distribution probability density  $f_S$ :

$$R(S) = P(S \leq S_b | S < S_l) = \int_S^{\infty} f_S dS \tag{2}$$

With the symptomatic approach it is also possible to work out, for the  $R(S)$  function, expressions similar to those used by the time-based approach, that is to say for  $R(t)$ ; the hazard function,  $h(t)$ , specifies the instantaneous rate of reliability deterioration during the infinitesimal time interval,  $\Delta t$ , assuming that integrity is guaranteed up to time  $t$  (Lawless 1982):

$$h(t) = \lim_{\Delta t \rightarrow 0} \frac{P(t \leq t_b < t + \Delta t | t_b \geq t)}{\Delta t}; \tag{3}$$

$h(t)$  is correlated to the reliability function,  $R(t)$ , by the following relationship:

$$R(t) = \exp \left( - \int_0^t h(x) dx \right). \tag{4}$$

In a similar manner, the so-called symptom hazard function,  $h(S)$ , is defined as the reliability deterioration rate per unit of increment of the symptom (Cempel 2000):

$$R(S) = \exp \left( - \int_0^S h(x) dx \right). \quad (5)$$

For example, if the time law of the evolution of the symptom can be approximated with Pareto's model (Natke & Cempel 1997), we get:

$$S(t) = S_{(t=0)}(1 - t/t_b)^{-1/\gamma} \quad (6)$$

where  $S_{(t=0)}$  is the value of the symptom at time  $t = 0$ , and  $t_b$  is the time of attainment of a damage limit state or the total lifetime. Hence:

$$R(S) = 1 - t/t_b = (S_{(t=0)}/S)^\gamma \quad \gamma > 0 \quad (7)$$

where the  $\gamma$  coefficient determines the law of evolution of the symptom over time.

Reliability as a function of the symptom gives the residual damage capacity,  $\Delta D$ , of the structure:

$$R(S) = (S_{(t=0)}/S)^\gamma = 1 - D \equiv \Delta D(S), \quad (8)$$

where  $D = t/t_b$  represents the system's aging as well as the measure of the damage.

Eq. (8) lends itself to a diagnostic use: assuming that one knows the evolution of reliability through the observation of a set of systems, the value of the symptom as observed in a given unit makes it possible to determine the residual lifetime of the unit itself.

Under this approach monitoring plays a key role, in that reliability is no longer expressed as a function of time, but rather as a function of a symptom, which is a measurable quantity.

### 3 EXTENSION TO STRUCTURAL CLASSES

Reliability can be described starting from a primary reliability,  $R_0(S)$ , that applies to a given type of systems and can be characterised for a particular system by the introduction of a logistic vector  $L_i$ , with  $i = 1, \dots, N$ , where  $N$  is the total number of systems to be monitored (Cempel 2000).

$L_i$  denotes the individual element of the sample, it may contain a series of specific parameters depending on which aspect of the system we want to monitor.

The  $L_i$  vector appears in the formulations of system reliability starting from  $h(S)$ , which depends on  $L$ :

$$h(S(L)) = h(S, L); \quad (9)$$

whence, by integration, by analogy with eq. (5), we can express the value of reliability,  $R(S, L)$ , as a function of the symptom considered and the  $L$  vector:

$$R(S, L) = \exp \left\{ - \int_0^S h(x, L) dx \right\}. \quad (10)$$

For the hazard function, we can use a multiplicative form:

$$h(S, L) = h_0(S)g(L) \quad (11)$$

in order to explore how the logistic vector,  $L$ , affects the survival function  $R(S, L)$ . In the assumption of small changes of  $L$ , system reliability can be determined as (Cempel 2000):

$$R(S, L)|_{L_0+\Delta L} = R_0(S, L_0) \left\{ 1 + \Delta L^T \frac{\delta g}{\delta L} \ln(R_0(S)) \right\} \quad (12)$$

being:

$$R_0(S, L_0) = \exp \left\{ - \int_0^S h_0(x) g(L_0) dx \right\} \quad (13)$$

where  $g(L)$  is an unknown function to be defined, and  $\Delta L$  is a vector containing the variations made to the parameters of the  $L$  vector.

As an alternative, considering that reliability characterised as a function the symptom,  $R(S)$ , gives the residual life time of a system based on the value of the current symptom, by extending the dependence of  $R(S)$  to  $L$  it becomes possible to obtain an expression of this type (Li 2007):

$$R(S, L) = R_0(S)^{\exp(BL)}, \quad (14)$$

which can be used to determine the residual lifetime of a system with greater accuracy, compared to the determination obtained from  $R_0(S)$ , in view of the dependence of reliability in eq. (14) on logistic vector  $L$ .

$B$  is a weight coefficients vector to be determined.

### 4 DYNAMIC MONITORING OF A BRIDGE PIER

The safety assessment strategy is illustrated by referring to a structure that is ideally subjected to periodic dynamic testing.

The application example described below is about a reinforced concrete bridge pier ( $H = 5$  m, section diameter  $\phi = 1.1$  m,  $f_{ck} = 40$  N/mm<sup>2</sup>, concentrated mass at the top of the pier = 410.000 kg, geometric reinforcement ratio  $\rho_l = 2.41\%$  and horizontal design load  $H_d = 868$  KN, initial cracking moment for the section  $M_{cr} = 1.13$  MN m).

The symptoms that we assume to monitor over time, through customary experimental modal testing procedures, are the fundamental period of the pier, whose variation is associated with the decrease in stiffness, and an equivalent viscous damping. Due

to the purely methodological value of this example, the symptom's evolution is not measured but calculated according to an analytical damage model. The first cracking moment of the pier section,  $M_{cr}$ , is 1.13 MNm, as determined according to the following formula (Eurocode 2):

$$M_{cr} = f_{ctm} \cdot W_i \quad (15)$$

where  $f_{ctm} = 3.5 \text{ N/mm}^2$  is the average tensile strength of concrete and  $W_i$  is the section modulus of the uncracked section at the lower chord.

Having defined a normal statistical distribution of horizontal load  $H$  applied to the top of the pier (mean value 575 KN, and variation coefficient of the distribution 0.2) over a one year period, the analysis is performed for each time step and each load level envisaged.

The damage model considered is based on the elastic theory of damage (Ju 1989), so that the deterioration process in the bridge, triggered when the damage threshold envisaged was exceeded, translates into a reduction in bending stiffness,  $EI$ , according to the following expression (DiPasquale 1990):

$$EI = EI_0(1 - d), \quad (16)$$

where  $EI_0$  is the stiffness of the uncracked section, and  $d$  is the damage parameter. The deformation energy, corresponding to the first cracking moment,  $M_{cr}$ , is assumed as the threshold value,  $\xi_0$ , beyond which the damage mechanism is triggered in the beam.

For a given time step, each statistical value of the load  $H$  corresponds to an accumulated deformation energy,  $\xi$ , and a certain size of the crack zone in the pier. The damage to the structure, reflected by parameter  $d$ , affects only the cracked zone and propagates over time according to the elastic model: at the  $n+1$  interaction, the elastic deformation energy,  $\xi_{n+1}(\varepsilon_{n+1})$ , a function of the state of strain,  $\varepsilon_{n+1}$ , is determined; we get the damage parameter,  $d_{n+1}$ , and the damage threshold,  $r_{n+1}$ , as given below (Ju 1989):

$$d_{n+1} = \begin{cases} d_n & \text{if } \xi_{n+1} < r_n \\ 1 - (1 - A) \cdot \xi_0 / \xi_{n+1} - A \\ \quad \times \exp[B(\xi_0 - \xi_{n+1})] & \end{cases} \quad (17)$$

$$r_{n+1} = \max(r_n, \xi_{n+1})$$

In eq. (26), the deformation energy,  $\xi_{n+1}$ , is compared with the limit,  $r_n$ , and the damage parameter,  $d_{n+1}$ , is maintained the same as in the previous step if the accumulated energy,  $\xi_{n+1}$ , does not exceed the limit  $r_n$ ; conversely,  $d_{n+1}$  is defined with eq. (17) if  $\xi_{n+1}$  exceeds  $r_n$ . In eq. (17),  $A$  and  $B$  stand for the growth coefficients of the damage law, which are 0.68 and 1.41, respectively, for high resistance concrete (Ju 1989).

#### 4.1 Reliability assessment, symptom monitored: Fundamental period

The fundamental period is calculated by taking the mean value, as resulting from the statistical distribution assumed for loads.

The residual damage capacity of the system, or its reliability as a function of the symptom observed,  $R(S)$ , is given by (Natke & Cempel 1997):

$$R(S) = \Delta D(S) = 1 - \frac{t(S)}{t_b}, \quad (18)$$

In this application it was assumed for the bridge's lifetime  $t_b = 100$  years, which is associated with a complete degradation of the reliability with respect to a Damage Limit State (DLS).

In evaluating the reliability of existing structures one cannot rely on monitoring data covering the entire life of a structure, on the other hand it has been ascertained that a few initial data regarding the symptom observed over time are sufficient to identify the underlying trend evidenced by it. The symptom-based approach makes it possible to choose, from among different variation curves of the symptom over time, the one that best reflects the trend observed so as to obtain a tool for the evaluation of the current and future conditions of the system.

Knowing the current value of  $S$ , eq. (18) supplies an evaluation of the current and future conditions of the structure in terms of residual lifetime.

Given the reliability function,  $R_0(S)$ , valid for a family of structures of the same type, by monitoring the structure examined it is possible to calibrate with greater accuracy the estimate of its residual damage capacity,  $R(S)$ .

If monitoring results reveal an evolution of the symptom faster, or slower, than the standard rate assumed for the structural family, the estimate for the specific structure in question can be modified through eq. (12), where  $R_0(S, L_0)$  is the survival function for the standard structure, and  $R(S, L)_{L_0+\Delta L}$  is the survival function for a specific structure characterised by increment  $\Delta L$  of the basic logistic vector,  $L_0$ .

If  $R_0(S, L_0)$  is made to coincide with  $R_0(S)$  and the measured fundamental period  $T_m$  is the only monitored quantity to be inserted in the logistic vector, the following form may be assumed for eq. (11):

$$\begin{aligned} h(S, L) &= h_0(S) \cdot g(L) = h_0(S) \cdot L \\ &= h_0(S) \cdot \frac{T_m}{T_m(t=0)}, \end{aligned} \quad (19)$$

In other words, hazard function  $h(S, L)$  is assumed to be modified proportionally to the measured symptom  $T_m$  referred to its initial value,  $T_m(t=0)$ .

Correspondingly eq. (12) becomes:

$$R(S, L)|_{L_0+\Delta L} = R_0(S) \left\{ 1 + \frac{\Delta T}{T_m(t=0)} \ln(R_0(S)) \right\} \quad (20)$$

where a positive deviation in the symptom,  $\Delta T = T_0 - T_m$ , indicates a reduction in reliability. The evolution of the fundamental period of the structure in time is represented in Fig. 1, while the graphs of  $R_{DLS}(t)$ , corresponding to different evolutions of natural period, are showed in Fig. 2.

#### 4.2 Reliability assessment, symptoms monitored: Fundamental period and damping

In addition to the fundamental period,  $T$ , a viscous equivalent damping,  $\xi_{eq}$ , as obtained from monitoring, is herein included. The results obtained on reinforced concrete structures, in fact, have shown that, in this material, stress intensity, i. e., cracking state, has a decisive influence on equivalent damping. The value of this parameter is seen to increase with increasing stress level until the structural element is fully cracked; after cracking, damping begins to decrease (Fig. 3) (Chowdhury 1999). In the application described below, the evolution of damping

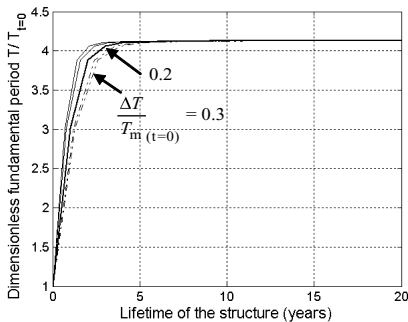


Figure 1. Interaction between monitoring and reliability: Dimensionless fundamental period  $T/T(t=0)$ .

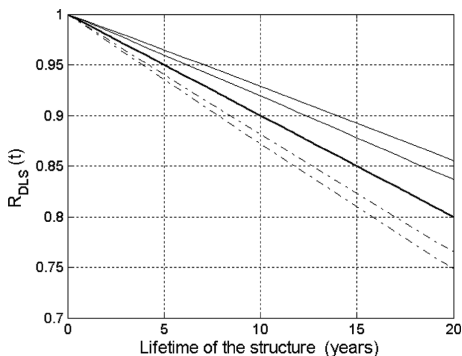


Figure 2. Interaction between monitoring and reliability: Damage limit state reliability  $R_{DLS}$ .

for purposes of reliability assessment is determined with reference to the conditions that precede the fully cracked state. To this end, a hysteretic mechanical model has been adopted, such as the one proposed by Ramberg-Osgood (Otani 1981)(Fig. 4):

$$D = \frac{F}{K} \left( 1 + \left| \frac{F}{F_y} \right|^{\gamma-1} \right) \quad (21)$$

where  $D$  is the generic displacement, which is a function of the dynamic load applied,  $F$ ;  $\gamma$  is the exponent of Ramberg's model, to be calibrated;  $F_y$  is the force applied at yielding. The evolution over time of equivalent stiffness,  $K$ , is worked out from the fundamental period (e. g. via the damage model reported above (Ju 1989)), and therefore the Ramberg-Osgood model is updated on a yearly basis in its  $K$  and  $F_y$  parameters. By exciting the structure by means of a vibrodyne, for each step of the analysis it is possible to quantify the corresponding equivalent damping,  $\xi_{eq}$ , according to the following formula (Otani 1981):

$$\xi_{eq}(t) = \frac{2}{\pi} \left( 1 - \frac{2}{(\gamma+1)} \right) \cdot \left( 1 - \frac{F_{vib}/D_{vib}(t)}{K(t)} \right), \quad (22)$$

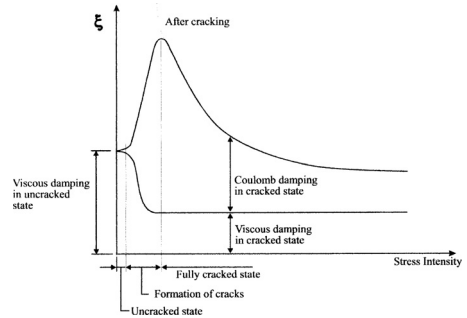


Figure 3. Equivalent damping values in a reinforced concrete element in different cracking states (Chowdhury 1999).

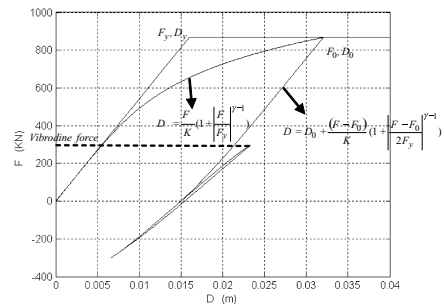


Figure 4. Ramberg-Osgood model for the evaluation of equivalent damping.

where  $F_{vib}$  is the dynamic load ideally generated by the vibrodyne, and  $D_{vib}$  is the ensuing displacement observed in the structure.

The reliability of the system monitored, as a function of small variations of the logistic vector,  $L$ , is worked out from eq. (12), i. e.:

$$R(S, L)|_{L_0+\Delta L} = R_0(S, L_0) \left\{ 1 + \Delta L^T \frac{\delta g}{\delta L} \ln(R_0(S)) \right\} \quad (23)$$

In this case, the logistic vector,  $L$ , reflects both parameters monitored, i. e., fundamental period,  $T$ , and equivalent damping,  $\xi_{eq}$ ;  $\Delta L^T$  contains the deviations of these parameters over time,  $T_m$  and  $\xi_{eq,m}$ , from their standard values,  $T_0$  and  $\xi_{eq,0}$ :

$$\Delta L^T = \left\{ \frac{\Delta T}{T_m(t=0)}, \frac{\Delta \xi_{eq}}{\xi_{eq}(t=0)} \right\} \quad (24)$$

$$\Delta T = T_0 - T_m; \quad \Delta \xi_{eq} = \xi_{eq,0} - \xi_{eq,m}$$

In the case of the two symptoms monitored, eq. (23) becomes:

$$R(S, L)|_{L_0+\Delta L} = R_0(S, L_0) \times \left\{ 1 + \left\{ \frac{\Delta T}{T_m(t=0)}, \frac{\Delta \xi_{eq}}{\xi_{eq}(t=0)} \right\} \times \left( \begin{matrix} p_1 \\ p_2 \end{matrix} \right) \ln(R_0(S)) \right\} \quad (25)$$

where  $\delta g/\delta L$  reduces to a weight vector  $(p_1, p_2)^T$  to be associated with the two symptoms.

## 5 DYNAMIC MONITORING OF A BRIDGE PIER: RESULTS

The application example described below is about a reinforced concrete bridge pier. Thus we get the evolution over time of the fundamental period,  $T$ , and equivalent stiffness,  $K$ , according to elastic damage theory. Assuming that the pier was excited yearly with a vibrodyne calibrated at a constant value ( $F_{vib} = 300$  KN), the initial displacement value produced by the vibrodyne at the top of the pier,  $D_{vib,0}$ , is determined from the following formula:

$$D_{vib,0} = \frac{F_{vib}}{K_0} \left( 1 + \left| \frac{F_{vib}}{F_y} \right|^{\gamma-1} \right); \quad (26)$$

where  $K_0$  is the initial equivalent stiffness of the pier.

In the absence of experimental data, the temporal evolution of the displacement of the pier, caused by the vibrodyne,  $D_{vib}$ , is assigned the following asymptotic law:

$$D_{vib}(t) = D_{vib,0} \cdot [1 + 7.63 \cdot \arctan(t)]. \quad (27)$$

The evolution over time of equivalent damping is determined as follows:

$$\xi_{eq}(t) = \frac{2}{\pi} \left( 1 - \frac{2}{(\gamma + 1)} \right) \cdot \left( 1 - \frac{F_{vib}/D_{vib}(t)}{K(t)} \right). \quad (28)$$

The analysis was conducted for a predetermined dynamic load  $F_{vib}$  and various values of  $\gamma$  (Fig. 5) in order to attest the strong influence of parameter  $\gamma$  on the variation of damping over time, which means that this parameter should be determined on a preliminary basis with sufficient accuracy. It should also be noted that equivalent damping increases over time in accordance with the experimental data of damping recorded for r. c. structures in partial cracking conditions (Chowdhury 1999). Fig. 6 exemplifies the correlation between monitoring results and reliability: the correct reliability profile (6b) is worked out as a function of the deviation of equivalent damping as recorded during the monitoring period from the standard evolution of this symptom (6a).

Finally, let us consider the evolution over time of reliability at the limit state of damage  $R_{DLS}$  in the case of both symptoms, i. e.,  $T$  and  $\xi_{eq}$  (eq. (15)), and in the case of  $T$  alone (Fig. 7). For this application, the weights that appear in the vector  $(p_1, p_2)^T$  were both taken to be 1.

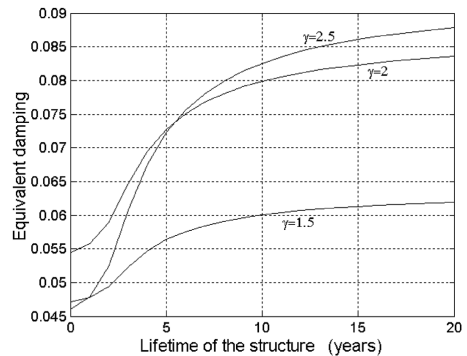


Figure 5. Evolution of equivalent damping  $\xi_{eq}$  over time for various values of the Ramberg-Osgood  $\gamma$  coefficient and vibrodyne excitation  $F_{vib} = 300$  KN.

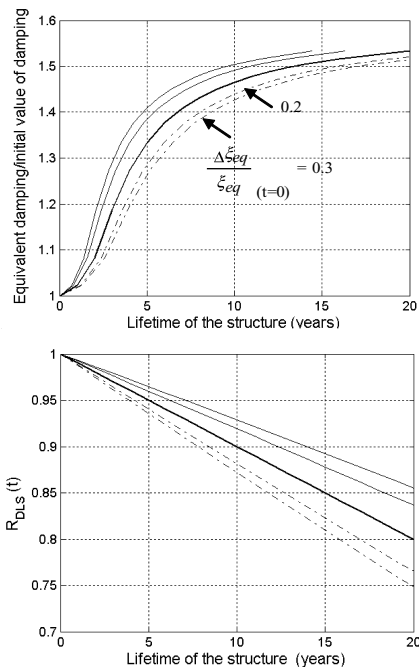


Figure 6. Correlation between monitoring results and initial reliability: a) ratio between equivalent damping and initial damping; b) reliability at the damage limit state  $R_{DLS}$ .

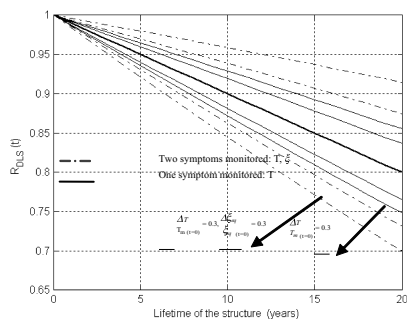


Figure 7. Correlation between monitoring results and initial reliability: reliability at damage limit state  $R_{DLS}$  in the case of monitoring of both symptoms,  $T$  and  $\xi_{eq}$ , or a single symptom,  $T$ .

## 6 CONCLUSIONS

This paper addressed the probabilistic assessment of structural reliability through a symptomatic approach. The final aim of this research is to create an appropriate theoretical framework for taking into account, in safety checks, periodic or continuous monitoring activities. In particular, such an approach lends itself to the use

of dynamic parameters (e. g. modal frequencies and damping), identified either through non-destructive tests performed on existing civil structures set up to this end, for the estimate of the residual lifetime of a construction.

A numerical application to a bridge pier, subjected to periodic monitoring, has been illustrated, in which two symptoms were considered: the reduction in stiffness and the increase in an equivalent viscous damping. Damping is known to be sensitive to the presence of cracks, though its estimation is often rather inaccurate. Moreover, differently from modal frequencies, damping typically shows a gradual evolution in time.

The results obtained for the pier show that, while a detectable change in the fundamental period is restricted to first five years of service, the damping parameter continues to increase slowly and consistently with the bridge effective age. We conclude that the practical feasibility of dynamic monitoring systems might be conditioned by the availability of accurate damping measurements, possibly identified from ambient excitation signals.

## REFERENCES

Cempel, C., Natke, H.G. & Yao, J.T.P. 2000. Symptom reliability and hazard for systems condition monitoring. *Mechanical Systems and Signal Processing* 14(3), 495–505.

Ceravolo, R., De Stefano, A. & Pescatore, M. 2007. Symptom based reliability and generalized repairing cost in monitored bridges. *Proc. of EVACES'97*, Porto, 24–26 October 2007. 935–944.

Chowdhury, S.H., 1999. *Damping Characteristics of reinforced and partially prestressed concrete beams*, PhD thesis, Faculty Engineering Griffith University.

DiPasquale, E., Ju, J.W., Askar A. & Cakmak A.S. 1990. Relation between global damage indices and local stiffness degradation. *Journal of Structural Engineering* 116(5), 1440–1456.

Eurocode 2—UNI ENV 1992-2:2000 Part 2: Concrete bridges.

Ju, J.W., Monteiro P.J. M. & Rashed A.I. 1989. Continuum damage of cement paste and mortar as affected by porosity and sand concentration. *Journal of Engineering Mechanics* 115(1), 105–130.

Lawless, J.F., 1982. *Statistical models and methods for lifetime data*. J. Wiley & Sons, New York.

Li, Z., Zhou, S., Choubey, S. & Sievenpiper C. 2007. Failure event prediction using the Cox proportional hazard model driven by frequent failure signatures. *IIE Transactions on Quality and Reliability Engineering* 39, 303–315.

Natke, H.G. & Cempel, C. 1997. *Model—Aided Diagnosis of Mechanical Systems*. Springer, Germany.

Otani, S. 1981. Hysteresis models of reinforced concrete for earthquake response analysis. *Journal of Faculty of Engineering, University of Tokio*, Vol. XXXVI(2), 407–441.



# Maintenance strategies for large span suspension bridges against fatigue and corrosion

Ai-rong Chen, Yong Zeng & Rujin Ma

*Department of Bridge Engineering, Tongji University, Shanghai, China*

**ABSTRACT:** Jiangyin bridge, a suspension bridge built in 1999, has been the second longest bridge in China. The span arrangements are 336 m + 1385 m + 309 m. Like all other civil engineering structures, Jiang Yin Bridge is subjected to long-term formidable environment, such as fatigue and corrosion. After its open to traffic, degradation and damage of its components appear in Jiangyin bridge, which causes the reduction of bearing capacity and reliability of Jiangyin bridge. Therefore, the service safety of Jiangyin bridge is a topic of importance, particularly for its managers. This paper provides maintenance strategies for managing and maintaining the structural safety of suspension bridge in a life cycle framework in order to rationalize maintenance actions economically. Firstly, investigation and analysis of in-situ operation are performed, which are diseases and damage of components, characters of vehicle flux and so on. Maintenance strategies of the hangers are proposed. In the end, probabilistic multi-scale time-dependent model are put forward considering corrosion for the main cable and closed box steel girder. Based on the model, maintenance strategies for main cables and close box steel girder are proposed.

## 1 INTRODUCTION

Jiangyin Bridge is a suspension bridge with the main span of 1385 m, which has been the second longest bridge in China (Figure.1). The span arrangement is 336 m+1385 m+309 m (Zhou Shizhou 2005). Like all other civil engineering structures, Jiangyin Bridge is subjected to long-term formidable environment, such as fatigue and corrosion. After open traffic, degradation and damage of its components appear in Jiangyin Bridge, which causes the reduction of bearing capacity and reliability of Jiangyin Bridge.

Hangers, main cables and main girders are the most important structural components of suspension bridges, therefore, ensuring their safety under different load conditions is of great importance to engineers and managers. Occurrence of fatigue cracks and corrosion in suspension bridge is always an important concern for bridge managers, and efforts should be devoted in order to ensure safety of the bridges during the service life (Wang Chunsheng 2003, Wang Chun sheng, Chen Wei zhen, & Ai-rong Chen 2002). In this paper, traffic investigation, corrosion maintenance strategies for the hangers and main cable, and fatigue maintenance strategies for steel box girder will be presented respectively.



Figure 1. General view of Jiangyin suspension bridge.

## 2 TRUCK MODELS FOR LARGE-SPAN SUSPENSION BRIDGES

Fatigue loads for steel bridges are generally developed from passing vehicles. As the foundation of the life-cycle analysis, the truck load models of bridge for reliability evaluation should be investigated firstly.

After put into service, traffic volume of Jiangyin Bridge grows rapidly. Annual rate of increase is more than 20 percent. Traffic volume data were collected from 2000 to 2006 (Ai-rong Chen 2007), seen in Figure.2. With the increasing of traffic volume, it is very dangerous the components of Jiangyin Bridge, which may induce cracks and reduce the service life.

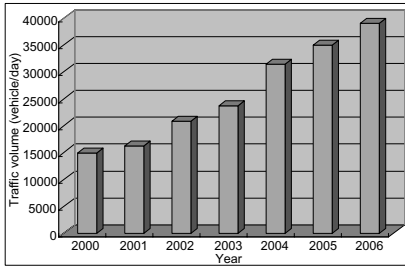


Figure 2. Traffic flow of Jiangyin bridge from 2000 to 2006.

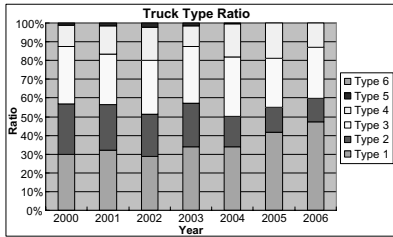


Figure 3. Constituent ratio of each vehicle (%).

Table 1. Classification and criterion of trucks.

Classification	Criterion
1	Less than 6 seats of bus.
2	Bus with 7~20 seats, less than 2 tons' truck.
3	Bus with 20~50 seats, 2~5 tons' truck.
4	More than 50 seats bus, 5~10 tons' truck.
5	10~20 tons' heavy truck'
6	More than 20 tons' heavy truck

According to the traffic investigation, the trucks with same axles are classified to same classification and fatigue truck model is established for each classification. Traffic flow is divided into below- mentioned classification for simplicity.

It is obvious that trucks of Group 1 have the largest amount, followed by Group 2, Group 4, Group 5 and Group 6 respectively. We also found that, trucks of Group 1~3 often occupy main lane and overtake lane, while trucks of Group 4~6 occupy main lane and slow lane. Main lane is the busiest lane, which carries the majority of traffic flow.

### 3 MAINTENANCE APPROACH

Maintenance actions are series of activities which can not only keep the bearing capacity of a bridge and but fulfill its design requirements with sufficient

reliability of its performance in its lifetime. It also refers to operations performed to keep the structure in an acceptable performance level from the point of both serviceability and safety.

As shown in Figure.4, the maintenance actions may be classified into two types (Kevin Kin-lam Cheung, Moe M.S ZHANG& Eric Xue-qing 2007, TaeHoon Hong, Makarand Hastak 2007, Zhu Jinson, Xiao Rucheng 2006). One type is corrective maintenance, which means that no inspection is necessary and repairing is performed to restore the structure into required level only after failure of components (or when required serviceability level or safety level is exceeded). The other type is preventive maintenance, which can keep the structure in a serviceability level by delaying and mitigating some aging effects, such as fatigue and related phenomena.

Jiangyin Bridge has a significant amount of steel-works, therefore, the major concerns of the structures are corrosion and fatigue. Generally, two types of corrosion are mostly considered, which are general corrosion or pitting corrosion. For the same site, there is a high variability because the varying conditions of the very local environment. Among the corrosion forms, the general corrosion is the most common form. Fatigue is caused by dynamic loads, such as heavy truck passing through bridges. Figure. 4 summarizes the repair methods for damaged steel bridges (Z.X. Li, T.H.T 2006 , Raimondo Betti,Bojidar Yanev 1999, Leendertz JS, Weijde H, Kolstein H 1997, Piya Chotickai, Mark D. Bowman 2006).

Jiangyin Bridge has a significant amount of steel structures, therefore, the major concerns of the structures are corrosion and fatigue. Generally, two types of corrosion are mostly considered, which are general corrosion or pitting corrosion. For the same site, corrosion has a high variability because the varying conditions of the very local environment. Among the corrosion forms, the general corrosion is the most common form. Fatigue is caused by heavy trucks passing through bridges.

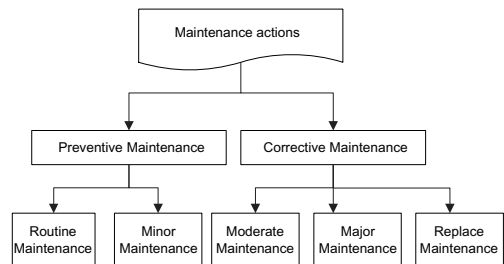


Figure 4. Classification of different maintenance actions of bridge.

#### 4 MAINTENANCE STRATEGY FOR HANGERS

Two types of hangers are used in Jiangyin Bridge. One is the hanger with helical wires, the other is the hanger with straight wires (ZHOU Shizhou, 2005). If the length of hangers is more than 10 meters, hangers with straight wires are adopted. If the length of hangers is less than 10 meters, hangers with helical wires are adopted, which are located in the mid-span of the bridge. The hanger spacing is 16.0 m.

Assessment of the safety of hangers was based on many structural reliability analyses with a detailed modeling of the physical behavior of parallel wires. In life cycle cost analysis, shorter replacement interval of hangers is accompanied with higher annual replacement cost, but lower annual failure cost. On the contrary, longer replacement interval of hangers is followed by lower annual replacement cost, but higher annual failure cost. Inspections and replacements are performed to control and reduce the failure risk of hangers. However, inspections and replacements are cost-dependent. A rational maintenance strategy should balance the cost and the failure risk. According to the computation, optimum replacement interval of 13~17 years for the hangers of Jiangyin Bridge is obtained. For the longest hanger, the optimum replacement interval will be 15 years as shown in Figure.5. Table 2 below lists the maintenance interval, method and items for hangers.

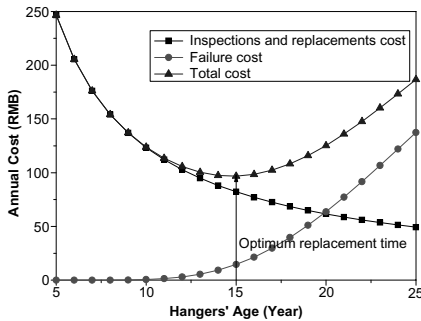


Figure 5. Optimum replacement interval of the longest hanger.



Figure 6. Surface cleaning by trained personnel.

Table 2. Maintenance interval, method and items for hangers.

Maintenance items	Interval	Inspection methods and instruments
Surface cleaning	1 year	Trained personnel*
PE Pipe	1 year	Inspection on deck, visual inspection
Anchorage	1 year	Inspection on deck, ultrasonic testing
Corrosion of wires	3 years	Magnetic flux leakage
Crack of wires	3 years	Magnetic flux leakage or radiography
Broken wires in hangers	3 years	Magnetic flux leakage or radiography
Cable force	Each year	Inspection on deck, accelerometer
Replacement of hangers	1317 years	Between deck and main cable, special replacement

\*Surface cleaning of hangers are shown in Figure. 6.

#### 5 SAFETY ASSESSMENT AND MAINTENANCE STRATEGY FOR MAIN CABLES

Deterioration and damage of main cables have more types than hangers, which have general corrosion, pitting, stress corrosion cracking, corrosion fatigue and hydrogen embrittlement. Deterioration will reduce the strength and ductility of wires, and consequently will lead to a reduced service life of main cables. However, the main cables are significant important components for a suspension bridge. Cable system of Jiangyin Bridge is comprised of many parallel wires. Each main cable in central span is composed of 169 strands and the outer diameter is 876 mm. In side span, the main cable is composed of 177 strands, and the outer diameter is 897 mm. The diameter of galvanized wire is 5.35 mm. Figure.7 shows the section and protection system of main cables in Jiangyin Bridge.

Because the length of cable, the section of cable and the damage of wire, such as fatigue cracks and corrosion pits, have different geometric scales, the response and local damage of main cables are analyzed according to different scales. Thus safety assessment of main cables is performed from three geometric scales, which are the scale in main cables, the scale in strands and the scale in wires. Figure.8 shows the three geometric scales for Jiangyin Bridge.

##### 5.1 Fracture analysis of wires of main cable

Main cables are composed of many wires, therefore, the behavior of each wire will contribute to the performance of the whole cable. Assessment of their ultimate capacity is essential for the evaluation of

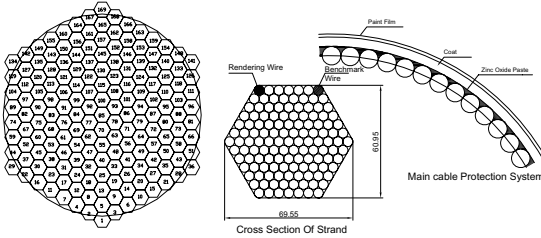


Figure 7. The constitute and protection system of main cable.

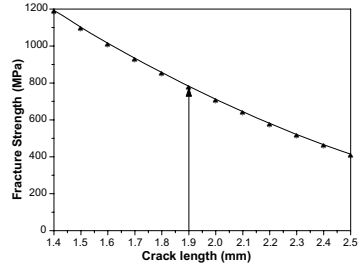


Figure 10. Fracture strength vs. crack length.

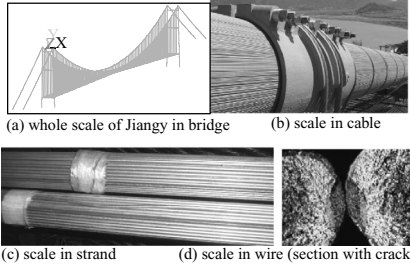


Figure 8. Three scales of Jiangyin bridge.

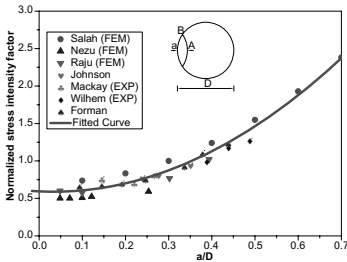


Figure 9. Normalized SIF for semicircular crack in tension.

the load carrying capacity of main cables. Figure.9 demonstrates the various normalized stress intensity factor (SIF) results for a semicircular surface crack front under tension.

A polynomial equation is fitted through the results to express SIF, as follows:

$$Y\left(\frac{a}{D}\right) = 0.5964 - 0.2686\left(\frac{a}{D}\right) + 4.0122\left(\frac{a}{D}\right)^2 \quad (1)$$

After fracture strength analysis, fracture strength varying with crack length can be obtained, shown in Figure.10. For the wires of main cables in Jiangyin Bridge, fracture of wire will happen when crack length is 1.9 mm.

## 5.2 Time-dependent reliability of main cable

Corrosion of wires is a spatial and time-dependent random process. Corrosion will evolve from the surface towards the core. Because of the presence and evolution of deterioration, the safety of main cables is also time dependent. If the load is considered to be constant, the probability can be expressed by:

$$P_f = \Phi\left(\frac{\bar{R}_c(t) - S}{\bar{R}_c(t)}\right) = \Phi(-\beta_{rel}) \quad (2)$$

$\beta_{rel}$  is the Cornell reliability index,  $\Phi(\cdot)$  is the cumulative distribution function of the standard normal distribution and  $S$  the service load.

The safety index  $\theta$  is defined as:

$$\theta = \frac{T_u}{T_c} \quad (3)$$

$T_u$  is the ultimate tension force and  $T_c$  is the tension force in service.

For simplicity,

$$T_c = \frac{l(w+p)\sqrt{l^2+f^2}}{16f}, \quad T_u = A_c\sigma_c \quad (4)$$

The limit state equation is:

$$G = \sigma_c - \frac{\gamma l(w+p)\sqrt{l^2+f^2}}{16fA_c} \quad (5)$$

The safety index is:

$$\theta = \frac{16fA_c\sigma_c}{l(w+p)\sqrt{l^2+f^2}} \quad (6)$$

$w, p, A_c, \sigma_c$  are all stochastic variables. Their statistical values can be obtained from reference (Ai-rong CHEN 2007).

The tension force induced by live load is 29180 KN, while the tension force induced by dead load is

Table 3. Maintenance intervals, methods and items of main cable.

Maintenance items	Interval	Methods and instruments
Surface cleaning	1 year	Trained personnel
Paint inspection	1 year	By special inspection car or inspection on deck
Coat inspection	1 year	By special inspection car or inspection on deck
Corrosion of wires	3 years	Magnetic flux leakage or radiography
Crack of wires	3 years	Magnetic flux leakage or radiography
Temperature and humidity of anchorage	1 month	Thermometer, hygrometer
Slippage	1 year	By special inspection vehicle
Water penetration	2 years	By special inspection vehicle
Saddle cleaning	1 year	By special inspection vehicle
Slippage between cable and saddle	1 year	Square caliper or visual inspection
Geometric change of cable	1 year	Inspection on deck
Crack of strands	3 years	By special inspection car, NDE
Special inspection	Specific condition	Typhoon, earthquake, overweight truck, ship impact and etc.

350160 KN. The ratio of the tension force between live load and dead load is 8.3%. It is obvious that the dead load effect is dominant.

The initial reliability index of main cables is 5.04, which will decrease with time. When the service time is 68 years, the reliability index will be 3.72, while the fail probability will be 0.01 percent. At that time, upgrading maintenance will be necessary.

### 5.3 Maintenance strategy for main cables

Main cables are important components for a suspension bridge and can't be replaced during the service period. Keeping cables in a better working condition is very important. Table 3 gives maintenance intervals, methods and items of main cables for Jiangyin Bridge.

## 6 MAINTENANCE STRATEGY FOR STEEL BOX GIRDER

The steel box girder of Jiangyin Bridge has a significant amount of steelworks, such as orthotropic decks with closed stiffeners, which are vulnerable and sensitive to fatigue loads induced by heavy trucks, particularly in the vicinity of welds area where cracks and voids may possibly appear. Therefore, fatigue

inspection planning has long been important issues in the scheduled inspection of welded steel structures. For welded structures subjected to cyclic repetitive loading, the allowable stresses in the vicinity of welded joints are relatively low due to the vulnerability of the joints under fatigue loads. Corrosion has been the most contributing factor to the deterioration of steel bridges. Fatigue is the primary cause of damage to steel box girders induced by heavy trucks.

Heavy trucks do harms to girder nearly 10 times than ordinary trucks. It is necessary to monitor the stress and deformation of the girder when heavy trucks pass through. Existing defects will promote small cracks to appear. They are often localized at weld toes and can grow under loading. The factors governing the growth of cracks are structural deformation, initiation site, material characteristics, loadings, and so on. Small cracks will propagate under cyclic repetitive loading, therefore inspection and repair should be carried out in time.

The steel box girder has been put into use for about 9 years. The girder is enough safe for anti-fatigue now. Figure.11. and Figure.12 shows field welding inspection and rust cleaning of steel box girder, respectively. Figure.13. below shows the flow chart of fatigue and corrosion inspection of steel box girder.

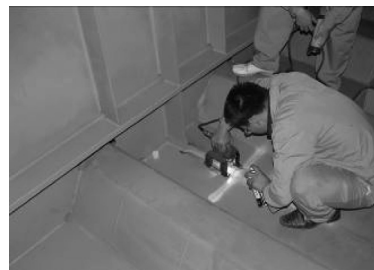


Figure 11. Welding repair.



Figure 12. Rust cleaning of girder.

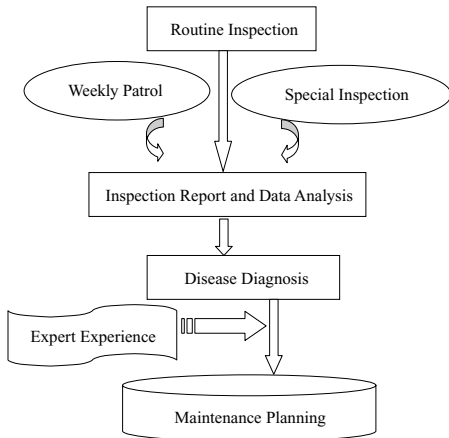


Figure 13. Flow chart of inspection of steel box girder.

## 7 CONCLUSIONS

Bridges are deteriorating faster than they are being maintained, and rehabilitated. The maintenance of bridges becomes an vital concern for bridge managers. Among all the factors of deterioration, fatigue and corrosion are the most destructive to suspension bridges. The design service life of Jiangyin Bidge is 100 years, during which the bridge will inevitably suffer from environmental corrosion, long-term loads or fatigue effects. Maintenances against fatigue and corrosion are increasingly important.

Because inspections and replacements of hangers are cost-dependent, rational maintenance strategy of hangers must balance the cost and failure risk. According to the computation, optimum replacement intervals for hangers of Jiangyin Bridge is about 13~17 years.

The main cables are cardinal important components for a suspension bridge. General corrosion, pitting, stress corrosion cracking, corrosion fatigue and hydrogen embrittlement are main diseases in main cables. After safety assessment for the main cables, it can be concluded that upgrading maintenance is necessary when the life of the bridge is 68 years

Heavy trucks have most harmful effect to girder. Micro cracks will propagate under cyclic repetitive loading and should be inspected and mended as soon as possible. The steel box girder of Jiangyin Bridge is enough safe for fatigue now.

## ACKNOWLEDGMENTS

The partial financial support of the China the Science and Technology Project by Ministry of

Transportation and Communication through grants No.200431882225 and No.200631882302-1. This paper is supported by the Traffic Scientific and Technological Project by Jiangsu Province Highways Agency (No.05Y50) and by National Key Project of Scientific and Technical Supporting Programs Funded by Ministry of Science & Technology of China (No. 2006BAG04B0).

## REFERENCES

- Zhou Shizhou. Technology Summary of Jiangyin Yangtze Bridge[M]. Beijing: China Science and Technology Press, 2005. (in Chinese)
- Wang Chunsheng. Assessment of remaining fatigue life and service safety for riveted steel bridges[D]. Shanghai: Tongji University, 2003. (in Chinese)
- Wang Chun sheng, Chen Wei zhen & Chen Ai rong. Damage safety assessment and maintenance management strategy of bridges. Journal of Traffic and Transportation Engineering. 2002, 4(2) 21-28. (in Chinese)
- Airong Chen. Life-circle based monitor, maintenance and management research of Jiangyin Yangtse River Bridge[R]. Shanghai: Tongji University, 2007 (in Chinese)
- Ying Li. Effect of Spatial Variability on Maintenance and Repair Decisions for Concrete Structures[D]. Neerland: Technische Universiteit Delft, 2004.
- Kevin Kin-lam Cheung, Moe M.S Zhang & Eric Xue-qing. Maintenance repair methods and cost optimization in highway structures. Shanghai: ILDMI 2007[C].
- TaeHoon Hong & Makarand Hastak. Evaluation and determination of optimal MR& R strategies in concrete bridge decks. Automation in Construction [J], Vol.16, Iss.2, March 2007, P.165-175.
- Zhu Jinson & Xiao Rucheng. A study on the safety assessment method for stay cables of long-span cable-stayed bridges. China Civil Engineering Journal.2006, 39(9), 75-80. (in Chinese)
- Z.X. Li & T.H.T. Chan. Fatigue criteria for integrity assessment of long-span steel bridge with health monitoring. Theoretical and Applied Fracture Mechanics[J]. Volume 46, Issue 2, October 2006, Pages 114-127.
- Raimondo Betti & Bojidar Yanev. Conditions of Suspension Bridge Cables New York City Case Study. Transportation Research Record 1654. 105-111.
- Leendertz JS, Weijde H & Kolstein H. Inspection of bridges with orthotropic decks with particular attention to fatigue. In: Proc. IABSE workshop: Evaluation of existing steel and composite bridges. 1997.
- Piya Chotickai & Mark Bowman D. Truck Models for Improved Fatigue Life Predictions of Steel Bridges. Journal of Bridge Engineering[J] 2006(1): 71-80.
- British Standards BS5400 (1980): Steel, concrete and composite bridges, Part 10, code of practice for fatigue. British Standards Institution.

# Bridge management system techniques application to Italian highways network

A. D'Andrea & D. Oggionni

*Sineco S.p.A., Milano, Italy*

E. Spallarossa

*Archimede s.r.l., Genova, Italy*

**ABSTRACT:** This paper describes the main bridge management techniques applied by Sineco to manage the highway bridge network. Using two integrated approaches Sineco can verify the actual maintenance needs and grow maintenance program reliability. The paper describes two integrated Bridge Management System. Integrating the two systems allows Sineco to manage inspection data and process them focusing on maintenance actions programming and prioritizing and on budgeted allocation, on the basis of both deterioration probabilistic models definition and different maintenance program simulations. The two tools are used to calculate maintenance needs, and provide 5–10 years time frame maintenance programs and annual projects details. Programs identify the maintenance policy that minimizes the annual expenditure by the agency, while integrating the objectives of public safety and risk reduction, user convenience and preservation of program policies.

## 1 INTRODUCTION

This paper describes the main bridge management techniques and tools Sineco adopts to assess more than 1000 km of Italian highways infrastructures network, on which the company yearly performs inspections, evaluates needs, programs maintenance activities and develops single-bridge rehabilitation projects. The Bridge Management Systems tools Sineco adopts are:

- SIOS (Sistema Ispezione Opere Sineco), an inspection system, directly developed by Sineco since 1994, actually applied to 1300 highway assets (including bridges and viaducts).
- PONTIS, a computer-based bridge management system licensed through the American Association of State Highway and Transportation Officials (AASHTO) to over 45 state transportation departments and other agencies nationally and internationally.

## 2 BRIDGE MANAGEMENT SYSTEM AIMS

A BMS allows bridge owners to manage a large number of data and to assess items such as:

- Economic analysis and programming: defining an adequate programming, on one hand, helps owners to reduce economical efforts and, on the other hand, planning maintenance and improvement

activities ensures structure safety and functionality and increases structures life cycle;

- Maintenance costs optimization: a BMS recommends a preservation strategy that minimizes the long term maintenance funding requirements while keeping the structures out of risk of failure and evaluates the economic impact of delaying any recommended action or taking extra actions;
- Serviceability targeting: defining a performance measure limit for posting the bridge or closing it, allows maintenance planning on the basis of logistic opportunities directed to minimize and reduce work impact on traffic.

In the present paper BMS is intended both as a technique, both as a tool able to assist highway agencies to choose the optimal bridge network maintenance or improvement policies, consistent with agency's usual policies, long term targets and budget constraints. Using BMS techniques and tools allows Sineco in addressing the bridge life cycle, and in developing policies and programs that help ensure the safety and functionality of agencies' structures.

On these basis Sineco has been developing an integrated system based both on SIOS both on Pontis.

## 3 INSPECTING STRUCTURES

It is widely recognized that performing periodical inspections aimed at the condition state evaluation is

one of the most effective way to assess structures. Periodical inspections should be performed following well-defined procedures, with the purpose of acquiring information about deterioration evolution, on the basis of which it is possible to understand, explain and asses the actual state.

The experience acquired performing inspections simultaneously on a great number of structures and the need of attaining to synthetic evaluations have induced Sineco to refine inspection procedures adopting the following operating methodologies:

- associate a number or an index representing the inspector observations to the corresponding qualitative condition state evaluation;
- computerize inspections;
- employing adequate staffing, provided with special training on the structures to inspect;
- employ and maintain the same staff inspecting structures belonging to the same highway network;
- grant the presence of supervisors whose objective is to control the different inspectors evaluation uniformity.

All structures in the network are classified on the basis of structural types and grouped in homogeneous groups, on the basis of deck design, materials and structural elements morphology. Each structure is successively divided into its own elementary structural elements.

The detailed inspection collects data on the element level basis that are stored in the database:

- inventory data;
- structural and morphology data;
- environment data;
- maintenance data;
- condition state of the structure, in terms of damage description and extension.

For every different kind of structures or of structural components a list of defects that may be found has been created. To each defect a class coefficient, depending on the structural element considered, has been assigned. This coefficient is one of the parameters in the index value calculation.

Performing the inspection each defect is divided into three gravity classes, (low, medium, high). To each gravity class and to each defect a numeric coefficient is assigned to be entered in the index value calculation.

Defects inspected and registered in the sketches are accurately computerized and recorded on the corresponding graphical file.

A software tool is provided to:

- separate defects on the basis of classes (defect type) and gravity (inspectors judgement);
- calculate defects areas;

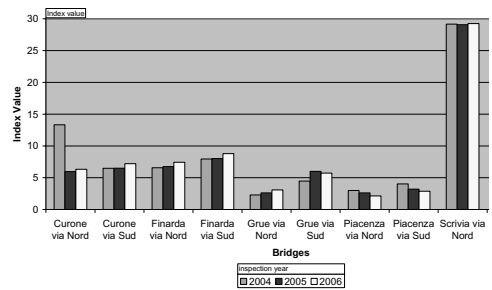


Figure 1. Summary index value graph of ten bridges during three inspection years.

- calculate index values, based on an algorithm considering classes and gravity coefficients, and deterioration extension (in terms of effectively deteriorated area).

All the index values calculated are loaded into a database that allows for sorting, averaging, statistical incidence calculation, maximum and minimum values calculation, etc. To define the structure condition state, the index value is contextualized and related to the structure environment aggressivity.

This method predicts how the condition of the infrastructure would be adopting statistical criteria capable of evaluating the future damage evolution, on the basis of historical observations. Priorities are determined on the basis of the statistical analysis, both of the structure, both of each component performance levels changes.

The provisional method is efficient in the short—medium period thanks to the great amount of data collected during annual inspections, since 1998 and recorded in the Sineco database, in order to evaluate the short term needs and actions.

#### 4 ADVANCED BMS METHODS

The SIOS methodology provides a detailed database intended to:

- collect historical deterioration data, in order to measure deterioration evolution;
- associate and collect as detailed as possible deterioration data, even graphically, for each element in each span;
- allow specific evaluations, damaged areas calculations, single defect evaluation;
- provide data for estimated bill of quantities.

The integrated SIOS-PONTIS system achievement is based on using detailed database information provided by the first to perform life cycle cost analysis and long term programming with Pontis BMS tool.



This software supports a bridge management comprehending: data analysis, optimal preservation policy identification and recommendation, bridge needs and performance measure forecasts and development of projects to include in agencies' economical planning.

In order to apply Pontis BMS methodology to SIOS inspection data, the databases were "normalized" to adapt the two different structural models and the two different damage evaluation.

#### 4.1 *Commonly recognized elements*

In Pontis each structure is divided into one or more smaller units, called structure units. A structure unit is any logical grouping of structure components usually having the same structural design and material. Structure units can be used to represent groups of spans having the same structural design and material, or portions of the structure that might be rehabilitated separately. Each structure unit is made of elements, the "Commonly Recognized" (CoRe) structural elements developed by Federal Highway Administration. Sineco, on the basis of the AASHTO Guide for CoRe structural elements, has customized commonly recognized elements for Italian roads needs.

#### 4.2 *Deterioration models conversion*

In Pontis the condition state categorizes the nature and extent of damage or deterioration on a bridge element. Each CoRe element can have up to five condition states. Condition states for each element have been precisely defined in terms of the specific types of distresses that the elements can develop.

As the deterioration of a structure is partially determined by its environment and operating practices (e.g. weather conditions or use of road salt), each element on a structure can belong to one or more of four environment classifications (benign, low, moderate, severe). Association between CoRe elements and environments defines condition units.

In order to normalize the SIOS database, a conversion criteria was used to "translate" the ratings described through the "Index value" into the Pontis condition-unit language. The conversion has been completed considering different items, relatively to environmental aggressiveness class and to different material tests and specialistic surveys performed on some structures. Each CoRe element area has been divided into the five or less condition states required by Pontis.

## 5 PRESERVATION POLICY

The preservation policy is the set of recommended preservation actions for each state of each condition

unit, it is defined on the basis of deterioration and cost models. This policy consists of actions applied to bridge elements, that minimizes life cycle costs while keeping elements out of risk of failure. The preservation policy for a condition unit (CoRe element in one of the four environments) is determined by formulating a Markov decision model with an infinite time horizon, discounted future costs, and the objective of minimizing long-term agency costs.

Important assumptions in solving the preservation policy include the following:

- Preservation actions are based on a policy that specifies the action that must be taken, given the current state of a particular element/environment combination (condition unit);
- The optimal policy may be determined independently for each condition unit;
- Cost and deterioration transition probabilities may be specified for each condition state for a given condition unit. The costs and probabilities depend only upon the condition unit most recent state.

#### 5.1 *Forecasting models*

Pontis forecasting models are developed for each type of element of a bridge (e.g., timber deck, painted steel column). These models are probabilistic, rather than deterministic, and are structured to predict the behaviour of a population of elements within the network of bridges. Models consist of a set of transition probabilities, which predict the chances that the element, with a particular action applied during the following year, improve to a higher condition state (taking an action), or, not applying any action (Do Nothing), stay in the same condition state or pass to a worse condition state.

Deterioration models can be developed from different source of information. Sineco first step in defining forecasting models has been compiling expert elicitation data. Elicitation data is assembled into transition probability matrices, defined from most of the USA Department of Transportations. This elicitation process is used to create deterioration models based solely on expert judgment. This allows reasonable models to be developed in advance of having actual data, which takes several years to assemble.

Expert transition probabilities are updated using historical inspection data collected by Sineco for several years accumulating all possible pairs of successive condition observations of element conditions, subject to certain constraints (e.g., there should not have been a spontaneous improvement in element condition between inspections).

The updating procedure, based on linear multiple regression, provides a transition probability matrix for each structural element as showed in [figure 2](#).

Transition Probabilities				
	1	2	3	4
<b>State: 1 No deterioration</b>				
>> 0 Do Nothing	96.20	3.80	0.00	0.00
<b>State: 2 Minor cracks/spalls</b>				
>> 0 Do Nothing	0.00	97.90	2.10	0.00
1 Seal cracks	86.00	14.00	0.00	0.00
<b>State: 3 Delams/spalls</b>				
>> 0 Do Nothing	0.00	0.00	96.17	3.83
1 Clean steel and patch	53.00	47.00	0.00	0.00
<b>State: 4 Analysis warranted</b>				
0 Do Nothing	0.00	0.00	0.00	87.06
1 Rehab unit	16.00	8.00	16.00	60.00
>> 2 Replace unit	100.00	0.00	0.00	0.00

Figure 2. Prestressed concrete girders—transition probability matrix for the structural element.

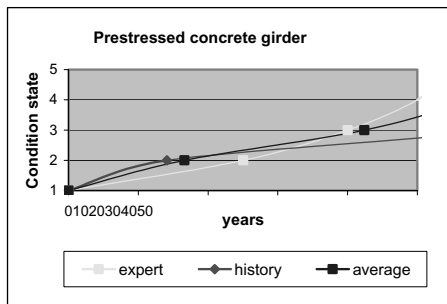


Figure 3. Prestressed concrete girders—forecasting models on historical inspection data and expert elicitation.

For the do nothing action, probabilities matrices have been transformed into graphs showing deterioration flow during the time, applying three different models: the only expert-based, the historical updated model or their combined averaged values.

Figure 3 shows deterioration graph for prestressed concrete girders.

For what concerns Italian highways network Sineco inspects and assesses, the most reliable models have been proven to be the averaged ones as these models follow historical data for condition states providing many observations (state 1 and 2) and follow expert evaluation for those other states characterizing a low number of structures (state 4 and 5). Transition probabilities are stored in the database for every combination of element, environment, condition state, and action.

Rules - Agency Policy Rule 10 of 18				
1 Scoping   2 Look Ahead   3 Major Rehab   4 Agency Policy				
Existing Rules				
Agency Policy Set: <input type="text" value="sineco"/> <input type="button" value="Edit"/> <input type="button" value="Delete"/> <input type="button" value="Help"/> <input type="button" value="Back"/> <input type="button" value="Forward"/> <input type="button" value="Add"/>				
Rule in English				
If R/Conc Floor Beam has >= 1% in State 3 or worse, then for R/Conc Floor Beam do actions [S1] Do Nothing, [S2] Element Repair, [S3] Element Repair, [S4] Element Rehabilitati, and [S5] Replace Element 6.0				
If R/Conc Abutment has >= 34% in State 3 or worse, then for R/Conc Abutment do actions [S1] Do Nothing, [S2] Element Repair, [S3] Element Repair, [S4] Element Rehabilitati, and [S5] Replace Element 7.0				
If R/Conc Cap has >= 39% in State 3 or worse, then for R/Conc Cap do actions [S1] Do Nothing, [S2] Element Repair, [S3] Element Repair, [S4] Element Rehabilitati, and [S5] Replace Element 8.0				
If Pot Bearing has >= 60% in State 3 or worse, then for Pot Bearing do actions [S1] Do Nothing, [S2] Element Repair, [S3] Replace Element, [S4] Element Rehabilitati, and [S5] Replace 9.0				
If this object		Then for this object		Take Th
1 Element Number	<input type="text" value="1"/>	1 Element Number	<input type="text" value="1"/>	S1: 1 Action Type
Elements	<input type="text" value="Moveable Bearing"/>	Elements	<input type="text" value="Elastomeric Bearing"/>	S2: 1 Action Type
has >= than <input type="text" value="7"/> %		in this state (or worse)		S3: 1 Action Type
State 2		Rule Priority: <input type="text" value="1"/>		S4: 1 Action Type
				S5: 1 Action Type

Figure 4. Maintenance practices applied by the Agency and translated into simulation rules.

## 5.2 Cost models

The optimal policy and the benefit/cost ratio evaluation are defined on the basis of unit costs associated to each of the defined maintenance feasible actions associated to each element (cost matrix).

For each maintenance action associated to each element a unit cost has been defined, on the basis of reference prices used by Sineco for the rehabilitation projects.

A typical 30 years old structure maintenance project includes:

- curbs and joints rehabilitation;
- concrete columns and caps seal cracks and minor patching and concrete repair;
- concrete girders and deck rehabilitation.

Assembling different group of these kind of works, maintenance action are defined, and associated to a unit cost, that varies depending on the importance of the action (minimum repair, rehabilitation or replace element).

## 6 BENEFIT-COST ANALYSIS

### 6.1 Scenarios parameters

On the basis of actual inspection data and of the previously described models, maintenance actions to maintain the actual network condition state are provided (work candidates). To obtain this, simulations are performed defining different scenarios governed by a set of parameters such as annual budget, simulation period, bridges considered, elements considered, simulation rules and benefits calculation method.

Simulation outputs are:

- bridge needs (amount of money needed annually to maintain the actual network condition state);
- set of the generated work candidates (maintenance actions needed to maintain the actual network condition state).

Work candidates are prioritized on the basis of incremental benefit/cost ratios in order to maximize the benefits obtained from a fixed maximum budget.

## 6.2 Benefits calculation

The benefits calculation method is strategic for work candidates selection and prioritization.

Benefits can be calculated according to two different main methods: "shadow cost analysis" and "condition state analysis".

In the first one benefits are obtained by multiplying the unit benefit of the recommended action by the quantity of the element. Unit benefit is defined as the difference between the shadow cost of doing nothing and the shadow cost of the recommended action.

In the second one benefits are function of:

- the difference between health index assuming that an action is taken and health index assuming that nothing is done;
- the asset value of the bridge: Sineco assumes it equal to the sum of failure costs of all the bridge elements.

According to Pontis standards, the health index adopted is a percentage indicator (from 0%, which corresponds to the worst possible condition, to 100% in the best condition) calculated as a function of the fractional distribution of the bridge elements' quantities across the range of their applicable condition states.

## 7 MAINTENANCE PROGRAM

### 7.1 Priority list and projects

The result obtained running the simulation with the selected scenario is the single elements maintenance works (work candidates) priority list. Work candidates are grouped for each structure according to the year during which the simulation program performs single work candidates.

This way a structure priority list is obtained, ordered by the ratio between benefits deriving from the action application and costs of the single work candidates selected. A preliminary maintenance project is developed on each structure, modifying and optimizing selected work candidates, in order to satisfy logistical needs and match previous maintenance plans.

To update maintenance program on the basis of work quantities and programmed year changes, simulation will be repeated refining results. Maintenance program effects are reviewed and refined analyzing each bridge single structural elements graphs. These graphs show projected condition distribution for each element of the bridge, according to maintenance actions applied during the program period considered (Figures 5 and 6).

### 7.2 Maintenance minimum cost

Once achieved maintenance objectives necessary to maintain the network at the current condition state, and, consequently, necessary to maintain the actual performance measures (Health Index) maximizing benefits and minimizing costs, it is possible to evaluate the additional annual costs necessary to target a particular performance measure value, eventually increasing the actual one. Similarly, the minimum annual cost necessary for preserving network elements at a specified minimum performance measure value can be evaluated. These two items, strictly connected, are shown on the graph in Figure 7 obtained for decks elements in a network section (115 Km, 220 bridges).

The Health Index minimizing annual long term cost is 55%. Minimum annual costs to maintain the actual network health index (70%) is about 4.000.000,00€.

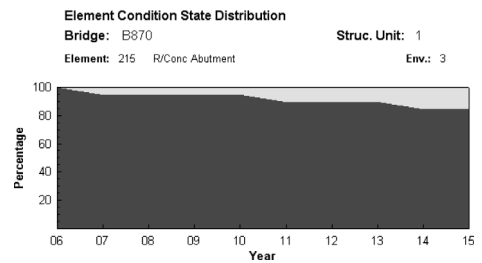


Figure 5. Reinforced concrete abutment element, belonging to a single structure, condition distribution projected from 2006 to 2015, with no actions selected.

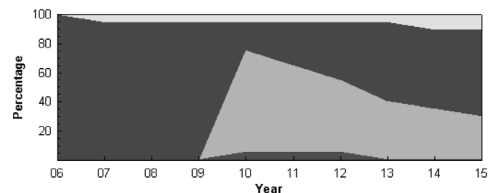


Figure 6. Reinforced concrete abutment element, belonging to a single structure, condition distribution projected from 2006 to 2015 with maintenance actions performed in 2010.

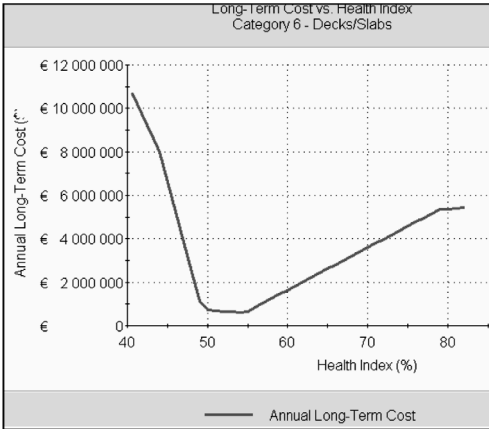


Figure 7. Annual long term Cost/Health Index.

## 8 CONCLUSIONS

The two BMS integration has provided medium to long term (five or ten years) scenarios forecasts detailing annually maintenance programs. Operative annual maintenance programs are drawn up focusing on minimizing users discomfort also considering other Assets maintenance needs. Development and continuous update of the following items have to be considered:

- deterioration and forecasting refining on the basis of annual inspections and maintenance programs updated on the network operations activities;
- managing bridges contextually to other assets applying asset management techniques to the entire network.

Sineco is actually implementing an Asset Management system able to support agencies in allocating economical resources among all the network linear Asset.

## REFERENCES

- AA.VV. 2005. "Manuale di riconoscimento e valutazione delle anomalie". Sineco S.p.A.
- AA.VV. 2005. "Manuale per la gestione dei dati ispettivi". Sineco S.p.A.
- AA.VV. 2005. "Manuale per le ispezioni alle opere d'arte". Sineco S.p.A.
- Cambridge Systematics, Inc. 2005. Pontis Technical Manual. American Association of State Highway and Transportation Officials.
- Cambridge Systematics, Inc. 2005. Pontis User's Manual Release 4. American Association of State Highway and Transportation Officials.
- CEB Comité Euro-International du Béton. 1998. Bulletin 243 "Strategies for Testing and Assessment of Concrete Structures". Guidance Report from the Task Group 5.4 on Assessment, maintenance and Repair.
- Federal Highway Administration. 2002. "Bridge Inspector's Reference Manual" Publication No. FHWA NHI 03-001, National Highway Institute. U.S. Department of Transportation.
- Hearn, G. & Cavallin, J. & Frangopol, Dan M. January, 1997. "Generation of NBI Condition from Condition Reports for Commonly Recognized (CoRe) Elements". University of Colorado at Boulder.
- National Cooperative Highway Research Program. 2003. "Bridge Life-Cycle Cost Analysis" NCHRP Report 483, Transportation Research Board, Washington, D.C.
- Robert, W., Marshall, A., Shepard, R. & Aldayuz, J. 2003. Pontis Bridge Management System: State of the Practice in Implementation and Development. 9th International Bridge Management Conference, Transportation Research Circular E-C049.
- Subcommittee on Bridges and Structures of the Standing Committee of Highways. 2005. Guide for Commonly Recognized (CoRe) Structural Elements. American Association of State Highway and Transportation Officials.

# Behavior of RC bridge girders strengthened with CFRP laminates

A. El-Safty

*University of North Florida, Jacksonville, Florida, USA*

**ABSTRACT:** Carbon Fiber Reinforced Polymer (CFRP) laminates have been used for strengthening reinforced concrete bridge girders. This research investigates the effectiveness of using CFRP laminates in strengthening girders in flexure. Experimental work was conducted on two groups of 11 beams. Instrumentations of LVDT's mounted for deflection measurements were connected to a data acquisition system to automatically record the load and displacements data. A 100 kips capacity displacement-controlled hydraulic actuator ram was used to apply static loading at mid-span. The results were analyzed for the flexural behavior of the strengthened beams including load-deflection, mode of failure, and debonding of CFRP. The results indicated a significant gain of 41.9% to 89% in the capacity of the strengthened girders than that of control ones, and that beams failed before reaching the rupture strength of the laminates. The study covered key parameters such as the number of CFRP layers and using U-Shaped laminates.

## 1 INTRODUCTION

Composite materials made of fibers in a polymeric resin, known as fiber-reinforced-polymers (FRP) have emerged as an alternative to traditional materials. There are a number of available externally bonded FRP systems, such as Wet Layup FRP system, Prepreg FRP system, and Procured FRP system (ACI 440 2002). The main advantages of the externally bonded FRP system include lightweight, noncorrosive and high-tensile strength of the FRP. Substantial experimental and theoretical research has been conducted over the last decade into the effectiveness of using FRP sheets/strips to strengthen or retrofit RC members and the behavior of the strengthened structural elements (Grace et. al. 1999, Grace 2002, ACI 440 2002, Tavakkolizdeh & Saadatmanesh 2003, and El-Hacha & Rizkalla 2004). Most of these investigation used non-prestressed method by gluing or bolting the FRPs to the members' surfaces. However, the method of gluing or bolting FRPs to the members' surface has a common problem of debonding and hence could not fully utilize the full tensile strength of the FRP (Lopez & Naaman 2003).

Extensive research has shown that externally bonded CFRP laminates improve both short term (Nanni 1997, Okeil et al. 2001) as well as long term behavior of concrete girders. The technique of externally bonding carbon fiber reinforced polymer (CFRP) laminates to reinforced concrete girders is becoming more established as an alternative to traditional structural rehabilitation methods. CFRP laminates has proven effective for both strengthening and stiffening

reinforced concrete (RC) bridge girders. CFRP provide extra tensile resistance and are attached to the bottom surface or wrapped around the stem of RC beams using epoxy adhesives.

Bonding FRP to the tension face of a concrete flexural member with fibers oriented along the length of the member provides an increase in flexural strength. Increases in flexural strength from 10 to 160% have been documented (Sharif et al. 1994). Possible failure mechanisms are crushing of the concrete in compression before yielding of the reinforcing steel; yielding of the steel in tension followed by rupture of the FRP laminate; yielding of the steel in tension followed by concrete crushing; shear/tension delamination of the concrete cover; and debonding of the FRP from the concrete substrate. There is a concern regarding the effectiveness and safety of this method of FRP beam strengthening that is the potential of brittle debonding failures. Such failures, unless adequately considered in the design process, may significantly decrease the effectiveness of the strengthening or repair application. FRP Strengthening may increase beam flexural or shear load capacities and increase stiffness for reduced deflections under service and design loads.

## 2 RESEARCH DESCRIPTION

### 2.1 *Research outlines*

The flexural strength and behavior of steel reinforced concrete beams strengthened with carbon fiber-reinforced polymer (CFRP) laminates were

investigated. The beams were tested in three-point bending. Instrumentations of strain gages bonded to the internal steel reinforcement and to external concrete side surface, and LVDTs mounted to measure deflections were connected to a data acquisition system to automatically record the data of load, displacements, and strains in steel and concrete. However, the attempt of strain gage monitoring failed. A 100 kip capacity displacement-controlled hydraulic actuator ram controlled with an electric pump was used to apply static loading at mid-span. Both control beams and the repaired beams with CFRP laminates were loaded in a three-point flexural configuration. Continuous visual inspection was performed to determine any possible debonding between the CFRP membranes and the concrete. The test variables were the spacing of stirrups and the number of CFRP laminates in flexure. This paper provides investigative efforts to study the effectiveness of flexure strengthening of girders with CFRP laminates.

## 2.2 Beam description

Two sets of beams were tested. The beams had a concrete ultimate compressive strength of around 8000 psi. The beams' dimensions were 6 inches wide, 9.5 inches deep, and 8 feet long for the first set and 6 feet long for the second set. The span lengths were 7.5 feet and 5.5 feet, for groups 1 and 2, respectively. The longitudinal reinforcement was 2 # 4 bars at the bottom for flexure and # 3 stirrups for shear at variable spacings. Three control beams in the first group and two control beams in the second group having no FRP lamintae were tested.

For the first set, stirrups of beams (B1 & B2) were spaced at 6" on center throughout its entire length from one support to the other. For beams (B3 & B6), stirrups were spaced at 11.25" throughout its entire length between supports. Stirrups in beams (B4 and B5) were spaced at 22.5". For the second set, control beam (B1) had one stirrup at each support and six stirrups spaced at 6" and centered at midspan. Control beam (B2) had stirrups spaced at 6" on center throughout its entire length. The standard reinforcing configuration indicated that beams (B3) and (B4) were similar to control beam (B2), and beam (B5) was similar to control beam (B1).

Carbon Fiber reinforced polymers (CFRP) laminates were uniaxial mesh. This was a substrate element stitched carbon uni-axial fabric tape. The characteristics of light weight, high strength, and corrosion resistance of FRP made them ideally suited for quick and effective structural repairs. This material has adhesion strength to concrete of 500 psi per ASTM D 4541, and the following mechanical properties: Dry fabric weight = 13 ounces per square yard, tensile strength = 123,000 psi, tensile modulus

= 11,400,000 psi, compressive strength = 20,000 psi, and interlaminar shear strength = 2,800 psi.

Table 1 shows three control beams without FRP and three CFRP strengthened beams (B2), (B6), and (B5). Comparisons were made between beams in each of the following pairs (B1 & B2), (B3 & B6), and (B4 & B5). Table 2 shows the CFRP application used on beams (B3, B4, and B5) as follows: beam B3 had three flexure layers on the bottom and three U-Shaped shear layers on the sides at three locations, beam (B4) had four flexure layers on the bottom and four U-shaped shear layers at three locations, and beam (B5) had three straight layers for flexure on the tension side of the beam.

## 2.3 FRP application

Debonding failures pose a critical problem in using FRP composites in structural strengthening and repair applications. The preparation and application of FRP to concrete surface were performed according to the following steps. (1) Remove all loose materials, depressions, and dust from the surface and deep clean with 2000 psi water pressure; (2) Allow the surface

Table 1. Beams details—1st set.

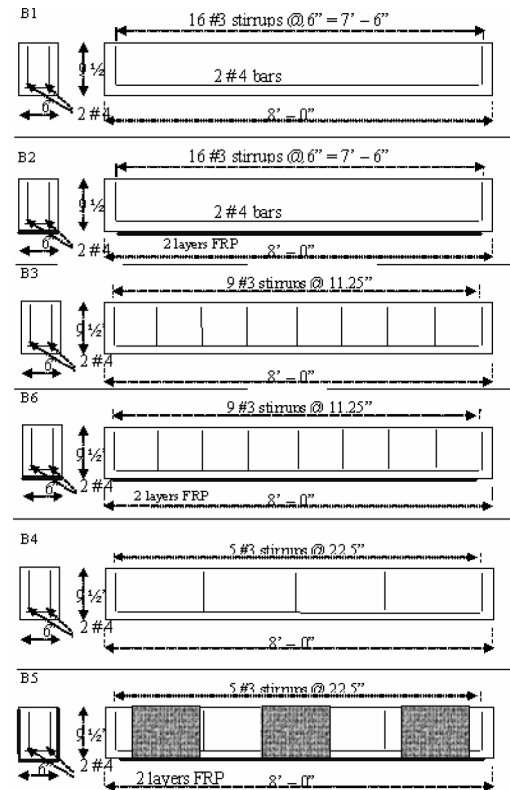
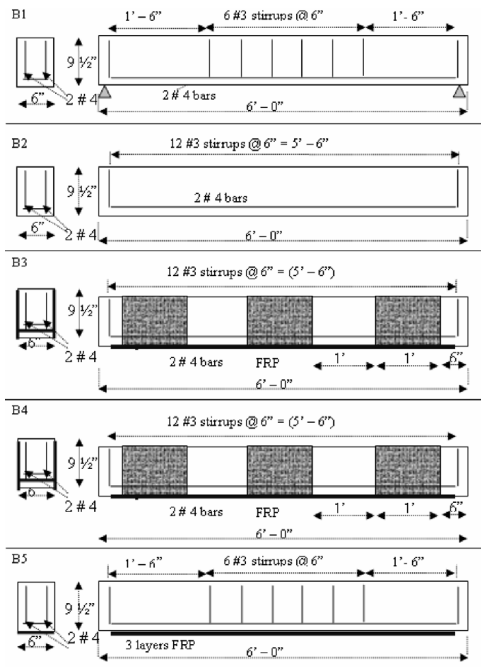


Table 2. Beams details—2nd set.



to dry; (3) Measure and mark placement of the FRP overlays; (4) Mix the Base primer with the adhesive; (5) Apply it to the marked surface using a 1/4" – 3/8" paint roller. Use only enough to wet the surface without causing excessive foaming. Only apply to small areas at a time, as this mixture will dry within a half hour; (6) Allow the previously applied mixture to become "tacky" (which should take about 15 minutes) before attaching the 1st layer of laminate; (7) The first layer of FRP laminate is the most critical for optimal adhesion between the surfaces, and must be applied with no air bubbles. This requires that pressure must be repeatedly applied to the laminate while it is on the concrete surface to remove all trapped air; (8) Using a garden hose, or something similar, spray low water pressure to cover the entire 1st layer thoroughly; (9) Apply the remaining layers similarly on top of the 1st, up to a maximum of four layers total.

Shear strength can be improved by wrapping the FRP system around three sides of the member (U-wrap). In all wrapping schemes, the CFRP system can be installed continuously along the span length of a member or placed as discrete strips.

#### 2.4 Instrumentation of beams

Instrumentations of strain gages bonded to internal steel reinforcement and to external concrete side surface and LVDTs mounted under the concrete

beams were connected to a data acquisition system to automatically record the data of load, displacements, and strains in steel and concrete. However, the attempt of strain gage monitoring failed. A 100 kip capacity displacement-controlled hydraulic actuator ram controlled with an electric pump was used to apply static loading at mid-span. Beams were loaded in a three-point flexural configuration. The performance of beams was evaluated by conducting bending static loading. Visual inspection was used to determine the possible failure by debonding of the FRP laminate from the concrete surface.

### 3 BEAMS TESTING AND RESULTS

The beams were tested using the Shorewestern load cell actuator in three-point bending over simply supported clear spans of 90 inches (7.5 feet) and 66 inches (5.5 feet), for beams of groups 1 and 2, respectively. The displacement controlled load application was applied. The load and displacement data were correlated with the LVDT's deflection readings, as well as with physical readings made during loading sequences. The applied load and displacements readings were electronically recorded during the test using a data acquisition system monitored by a computer. Figures 1–4 show the tested beams of the first set.

Table 3 and Figure 5 show the flexural test results of the beams, including the cracking and ultimate loads. There was a 51.1% increase in the load carrying capacity for beam (B2) compared to control beam (B1). The cracking load of beam (B2) also increased by 13.6% than that of control beam (B1). There were also increases of 8.1% and 41.9% for beam (B6) than that



Figure 1. Beam (B1) after testing—1st set.



Figure 2. Beam (B2) testing—1st set.



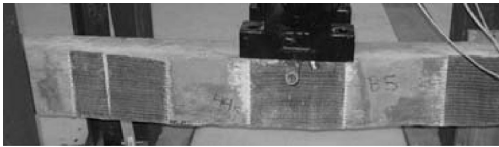


Figure 3. Beam (B5) during testing (1st set).



Figure 4. Debonding of CFRP in Beam (B6).

Table 3. Summary of test results for the first beams group.

Beam	Cracking load		Failure load	
	lb	N	lb	N
B1	3417	15,200	7,410	32,960
B2	3867	17,200	11,195	49,800
B3	3597	16,000	7,407	32,950
B4	3545	15,770	6,385	28,400
B5	4316	19,200	10,813	48,100
B6	3889	17,300	10,510	46,750

for control beam (B3), in the cracking load and failure load, respectively. Also, there were increases of 21.8% and 69.4% for beam (B5) than that for control beam (B4), in the cracking load and failure load, respectively. Such a higher increased cracking and failure load for beam (B5) indicated the effectiveness of using U-wrapped CFRP laminate combined with the straight laminates, as it extended the desired behavior of the strengthened beams and delayed debonding of the longitudinal laminate at the bottom.

The failure mode of control beams (B1), (B3), and (B4) was due to steel yielding in flexure. However, the failure mode for strengthened beam (B5) was steel yielding followed by crushing of concrete in compression at mid span and debonding of U-shaped and straight CFRP laminates. The strengthened beams (B2) and (B6) experienced steel yielding followed by CFRP debonding from the concrete substrate.

The 6-feet long beams of the second group were also tested in three-point bending. Figures 6–10 show the tested beams.

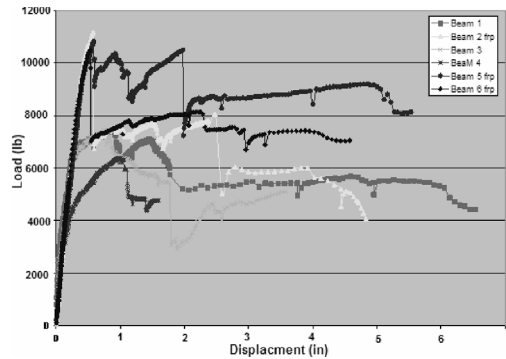


Figure 5. Load-deflection curves for beams of 1st set.



Figure 6. Beam (B1) testing—2nd set.



Figure 7. Testing of beam (B2).



Figure 8. Testing of beam (B3).



Figure 9. Beam (B4) after testing.





Figure 10. Beam (B5) after testing.

Table 4. Summary of test results for the second beams group.

Beam	Cracking load		Failure load	
	lb	N	lb	N
B1	6,070	27,000	10,116	45,000
B2	5,620	25,000	9,554	42,500
B3	—	—	—	—
B4	10,116	45,000	21,357	95,000
B5	14,613	65,000	19,109	85,000

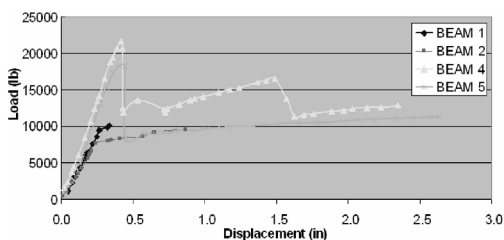


Figure 11. Load-deflection curves for second beams set.

Table 4 and Figure 11 show the results of the tested beams of the second group. The results included the cracking loads and ultimate loads. The loadings results were as expected, with the exception of beam (B3), which had erratic load capacity due to a malfunctioning chord in the load frame. The expected beam flexural capacity for control beams was about 15 k-ft. Figure 11 showed the load versus midspan deflection relationships for tested beams of the second set. There was a 78.8% increase in the load carrying capacity for beam (B4) compared to control beam (B2). The cracking load of beam (B4) also increased by 80% than that of control beam (B2). There were also increases of 141% and 89% for beam (B5) than that for control beam (B1), in the cracking and failure loads, respectively. Figure 11 showed increase in the stiffness of the strengthened beams than that of the control beams. A possible inaccuracy was noticed in recording the first cracking load for beam (B5), as it is believed that recording an earlier first cracking was missed. The load-deflection curve showed enhanced performance of beam (B4) than that of beam (B5).

The failure mode of control beams (B1) & (B2) was due to steel yielding in flexure. The failure of strengthened beam (B4) was steel yielding followed by debonding of U-shaped CFRP laminates at mid-span and at the support, debonding of CFRP laminates, and crushing of concrete in compression at mid span. The failure mode of strengthened beam (B5) was steel yielding followed by CFRP debonding from the concrete substrate.

## 4 CONCLUSIONS

1. Strengthening beams in flexure using CFRP laminates bonded to the tension side proved to be an effective alternative.
2. Significant increases in the load carrying capacity ranged from 41.9% to 89% were achieved using CFRP laminates in flexure strengthening.
3. The use of U-wrapped CFRP laminate combined with straight laminates proved to be effective in increasing the load capacity. It extended the desired behavior of strengthened beams and delayed debonding of the longitudinal laminate at the tension side.
4. Proper preparation of the beam, resin, and CFRP laminate should be focused on the right application of the CRRP to ensure proper repair and to avoid CFRP debonding.

## REFERENCES

- ACI 440 American Concrete Institute committee 440, 2002 Guide for the design and construction of externally bonded FRP systems for strengthening concrete structures. American Concrete Institute committee 440, Farmington Hills, Michigan, 45 pages.
- El-Hacha, R. & Rizkalla, S.H. 2004. Near-surface mounted fibre-reinforced polymer reinforcements for flexural strengthening of concrete structures, *ACI structural journal* 101(5): 717–721.
- Grace, N.F., Abdel-Sayed, G. & Rajheb, W.F. 2002. Strengthening of Concrete Beams Using Innovative Ductile Fiber-Reinforced Polymer Fabric. *ACI Structural Journal* Vol. 99, No. 5, pp. 692–700.
- Grace, N.F., Sayed, G.A., Soliman, A.K. & Saleh, K.R. 1999. Strengthening Reinforced Concrete Beams Using Fiber Reinforced Polymer (FRP) Laminates. *ACI Structural Journal* Vol. 96, No. 5, pp. 865–874.
- Lopez, M.M. & Naaman, A.E. 2003. Concrete cover failure or tooth type failure in RC beams strengthened with FRP laminates, Fibre-Reinforced polymer reinforcement for concrete structures (Proceeding of the sixth international symposium on FRP reinforcement for concrete structures (FRPRCS-6), (Tan K.H. editor), Vol 1: 317–726
- Nanni, A., Bakis, C.E., Boothby, T.E., Lee, Y.J., & Frigo, E.L. 1997. Tensile Reinforcement by FRP Sheets

- Applied to RC. 9C/1–8, *ICE 97 International Composites Exposition*, Jan., Nashville, Tenn., pp. 9C/1 to 8.
- Okeil, A.M., El-Tawil, S. & Shahawy, M. 2001. Short-Term Tensile Strength of CFRP Laminates for Flexural Strengthening of Concrete Girders. *ACI Structural Journal*, July–August 2001, Vol. 98 No. 4, pp. 470–478.
- Sharif, A., Al-Sulaimani, G., Basunbul, I., Baluch, M. & Ghaleb, B. 1994. “Strengthening of Initially Loaded Reinforced Concrete Beams Using FRP Plates,” *ACI Structural Journal*, Vol. 91, No. 2, Mar.–Apr. pp. 160–168.
- Shouping Shang, et al. 2005. Avoiding De-Bonding in FRP Strengthened Reinforced Concrete Beams Using Prestressing Techniques. *Proceedings of the International Symposium on Bond Behaviour of FRP in Structures (BBFS 2005)*.
- Tavakkolizadeh & Saadatmanesh 2003. Repair of damaged steel-concrete composite girders using carbon fibre reinforced polymer sheets, *ASCE Journal of Composite* 7(4): 302–322.

# Aspects of sustainability of repair-systems for concrete structures

M. Empelmann, V. Henke, G. Heumann & M. Wichers

*Institute for Building Materials, Concrete Construction and Fire Protection (iBMB),  
Technical University of Braunschweig, Germany*

**ABSTRACT:** The present paper deals at first with the “traditional” method for the planning of rehabilitation measures for concrete structures. In a further step the principle effect of different rehabilitation measures on the reliability of concrete structures will be shown. Finally, based on a typical failure example, it will be presented how the selection process for rehabilitation measures can be optimized by using a life-cycle prognosis.

## 1 INTRODUCTION AND PROBLEM DEFINITION

Numerous different repair measures are available for the rehabilitation of concrete structures. The requirements for these measures are mainly orientated with regard to an increase of the remaining service life, the economical aspects and the conditions for the use and practicability of the respective repair measure. Depending on specific structural aspects further criteria may become decisive.

The decision between competing rehabilitation measures will normally be taken on the basis of already existing experiences with the respective method, the material, as well as economical considerations.

Alternatively, for new constructions there is the increasing possibility to use a probabilistic life-cycle prognosis, which offers the option to implement repair measures within a life-cycle orientated building management. This means a transparent planning and objective choice of an optimal method. Specific structural aspects, such as environmental exposure, as well as the economical interests of the owner and/or the operating company can therefore be taken into account.

## 2 OPTIMIZATION OF THE REHABILITATION PLANNING

### 2.1 *Potentials of life-cycle prognosis*

With the choice of a rehabilitation strategy, technical as well as economical aspects are closely connected. Therefore, the decision for a special strategy depends on specific particularities of the structure and the interests and requirements of the owner and/or user.

The use of the increasingly applied method of a probabilistic life-cycle prognosis for newly

erected structures (e.g. see [Gehlen \(2000\)](#)) offers the possibility to consider the state or failure development of a structural member during its total life-span. If it can be achieved to incorporate rehabilitation measures into these prognosis models, it is possible to obtain a connection between technical aspects and economical interests.

The basics for a life-cycle prognosis, even under the consideration of rehabilitation measures and by the use of Markov-chains are given by [Vesikari \(2003\)](#). These methods are based on the principle, to describe the stochastic process of a damaging mechanism by a time-dependent state prognosis. The characteristic of Markov-chains is that it is not necessary to regard the time-dependent development of a building member, but to describe the probability that a building member changes from the actual state into next damage state within a specific time-step. For these assessments it is necessary to multiply a state vector with a transition matrix. Similar methods can be used to introduce a rehabilitation transition matrix into the prognosis.

### 2.2 *Implementation of rehabilitation measures in a life-cycle prognosis*

Basically, rehabilitation measures are carried out to achieve two aims (see [Hillemeier et al. \(1999\)](#)). For a restoring or strengthening measure the state of the building member is increased by leaps at the time of their execution. In contrary, with a protective or delaying measure the damage advancement will be stopped at the long run or at least delayed. The effect of a rehabilitation measure, i.e. the interaction with the building member to be restored, can be described at two levels.

- Serviceability Limit State (SLS) and
- Ultimate Limit State (ULS).

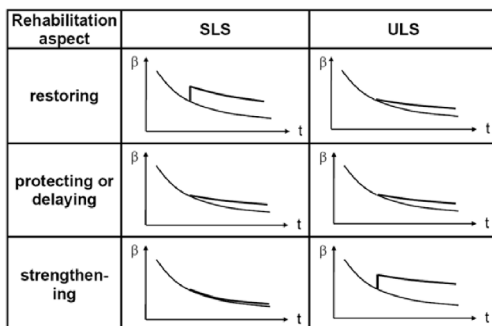
In table 1 and 2 rehabilitation measures, their mode of action and the quantitative course of effectiveness, after the rehabilitation has been carried out, are given with regard to these limit states.

For the time being there is still a lack of models, which are able to quantify this mode of action depending on the special border conditions. But it can be assumed, that this gap of knowledge will be closed within the next couple of years, e.g. Kluth et al. (2007). These models have to be able to describe the time-dependent material properties and their actions, with regard to the life-span and the load-carrying capacity of a building member. In order to carry out this task,

Table 1. Rehabilitation measures for concrete structures.

Rehabilitation measure	Rehabilitation aspect		
	Restoring	Protecting or delaying	Strengthening
Concrete replacement or local concrete replacement	X		
Increase of concrete cover		X	
Surface protection systems		X	
Cathodic corrosion protection, electro-chemical re-alkalisation, chloride extraction		X	
Sealing crack injection	X		
Strengthening with carbon fibre strips or steel plates, additional reinforcement, external prestress			X

Table 2. Qualitative course of the building member reliability for SLS and ULS, after a rehabilitation measure has been carried out.



it is necessary to formulate the theoretical principles for the description of the specific building member interactions.

### 2.3 Life-cycle cost consideration

During the life-span of a building, the owner has to carry the respective costs arising from the building use. These costs can originate from the carrying-out of a rehabilitation measure, but as well may originate from its omission and the resulting poor state of the building. The total costs, depending on the actual measure originate mainly from:

- Costs for carrying-out the measure: Construction costs (erection, demolition), administration costs, costs due to loss of use (here: loss of revenue), costs arising from noise, environmental and climate protection.
- Supervision costs: Costs for the determination of the building state or recognition of unexpected damages by inspection and / or monitoring.
- Costs due to use restrictions or possible failure: Costs, which arise from a reduced user acceptance due to the building state (i.e. multi-storey parking) and costs arising from the risk of a building member failure and its consequences.

These three cost aspects do not represent the total costs of a building, but represent all economical influences, which are essential for the choice of a rehabilitation strategy or a rehabilitation method.

### 2.4 Optimization process—interaction between life-cycle prognosis and life-cycle costs

The aim of the model described in the following, is to compare different rehabilitation measures and strategies with each other. The optimal rehabilitation measure for an actual failure will not be determined, but a long-term concept dealing with a kind of damage will be developed. For each of the regarded rehabilitation measures the optimal time of action, with regard to the economical aspects, will be determined. The rehabilitation intensity results from the total life-span of the building. Subsequently, the optimal measure for a certain kind of damage will be determined. This optimization process will be shown for the following example.

The regarded system is given in Fig. 1 and consists of a reinforced concrete slab in a multi-storey car park with chloride penetration.

The task is to establish an appropriate rehabilitation strategy for this building member already at the planning stage and to choose a suitable state-of-the-art rehabilitation measure. The computations were carried out for a life-span of 50 years and are based on the basics given in table 3. The costs described above for carrying out the rehabilitation measure, the

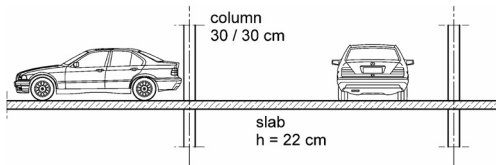


Figure 1. Regarded reinforced concrete slab in a multi-storey car park.

Table 3. Basic data.

Life-span	50 years
Interest rate	3%
Rehabilitated area	100 m <sup>2</sup>
Construction costs	300 Euro/m <sup>2</sup>

supervision costs and the costs due to use restrictions or possible failure will be assessed for this example in a practical way. For an actual application the data of a more exact cost assessment have to be considered.

At the beginning, the time-dependent course of the damage or the state development of the building member has to be investigated and described. This can be carried out exemplarily by the use of probabilistic design approaches (e.g. see Gehlen (2000)). As the optimization process will be carried out by the use of Markov-chains, the transition of the prognosis results into a transition matrix is necessary. The evaluation of the computed transition matrix, for an average condition state between 0 and 4, is given in Fig. 2. An average condition state of 0 describes the state of an undamaged building member and the state 3 a building member which has already failed with regard to the serviceability limit state. The criteria for the serviceability limit state will be exceeded after approximately 11 years. At this time a rehabilitation measure has to start at the latest.

The rehabilitation will be carried out by removing the concrete in the damaged area and replacing the concrete and if necessary the corroded reinforcement. Alternatively the case will be regarded that the reinforced concrete slab is protected by a sealing layer right from the beginning. This protecting sealing layer delays the chloride penetration into the concrete. In tendency, a building member damage will arise at a later stage. On the other hand side, such a sealing layer degrades as well, which means that this sealing layer has to be replaced after a couple of years.

In order to describe the effectiveness of both rehabilitation measures, the necessary data and their consideration will be assessed in a practical way from their average life-span.

Figure 2 & 3 show the results of this optimization process. It can be seen that a rehabilitation by concrete replacement, without additional sealing, has been

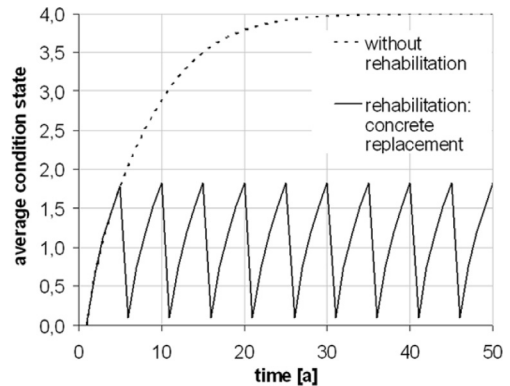


Figure 2. Time-dependent development of the average condition state of the building member without rehabilitation and with rehabilitation measures: concrete replacement.

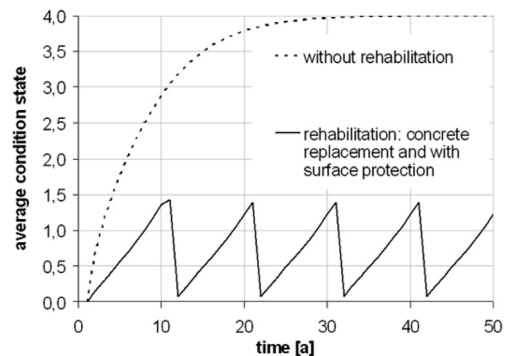


Figure 3. Time-dependent development of the average condition state of the building member without rehabilitation and with rehabilitation measures: concrete replacement with surface protection.

carried out fairly often, here every 6 years. If with each rehabilitation by concrete replacement a surface protection system is applied at the same time, the interval between the necessary rehabilitations can be increased. From the additional surface protection measures additional costs arise, which have to be considered as well.

The development of the capitalized costs depending on the state of the building at the beginning of the rehabilitation measures is given for both variants in Figure 4 & 5. By comparing both variants, it can be seen that the rehabilitation measure with additional sealing is the more economical measure, under the assumptions given above. The minimal total costs occur, if a rehabilitation is carried out approximately every 11 years. Due to the sealing effect of the protection layer the occurring damages are not severe, which means that the necessary measures which have to be carried out are relatively small.

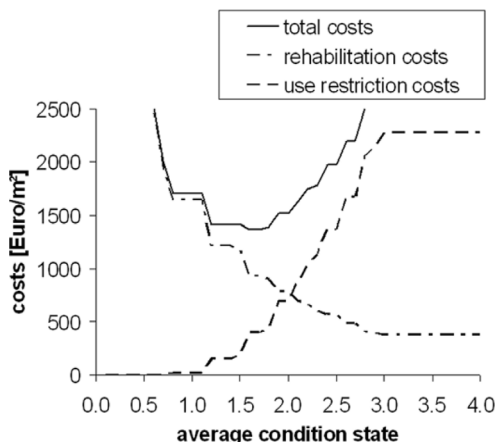


Figure 4. Capitalized total costs of the building with regard to the building state at the start of a rehabilitation measure for the variant “concrete replacement”.

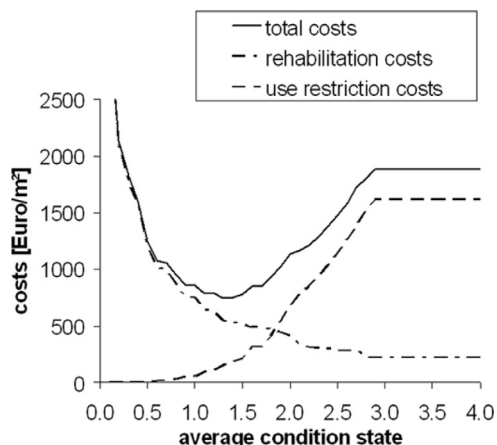


Figure 5. Capitalized total costs of the building with regard to the building state at the start of a rehabilitation measure for the variant “concrete replacement with sealing”.

For this case, the capitalized costs arising for the user during the regarded life-span are 2.5-times the original costs of the regarded area of 100 m<sup>2</sup>. The user, at the time of the building construction, has to put aside 75,000€ in order to assure an optimal maintenance. With these maintenance costs all expenditures for inspection, rehabilitation and loss of use are covered.

If, divergent from this recommendation, a rehabilitation is carried out in shorter time intervals, the capitalized total costs are considerably higher, as the number of measures during the life-span of the building and the connected costs increase. If a rehabilitation

is alternatively carried out in longer time intervals the total costs rise as well, as the costs due to failure and loss of use increase, caused by the restricted use.

The rehabilitation strategy, shown here as an example, and the choice of an optimal rehabilitation measure from the two regarded alternatives reflects the at the time being useable knowledge about the state-of-the-art. The main advantage of the method shown here can be seen in the fact that the choice of a suitable rehabilitation strategy can be carried out with scientific methods and therefore is verifiable. This means that an essential part of objectivity can be incorporated into the planning process for rehabilitation measures.

### 3 SUMMARY

For the planning of rehabilitation measures for concrete structures numerous different rehabilitation methods are available. In order to carry out a decision between competing rehabilitation measures with much more objectivity, the methods of a probabilistic life-cycle prognosis and building management have to be joined.

For the optimization of rehabilitation measures the life-cycle prognosis and the use of Markov-chains was introduced. This means, that it is possible to reflect the whole life-span of a building member with regard to the state development or course of the damage and the incorporation of possible rehabilitation methods.

In order to come to an optimal decision towards a rehabilitation strategy in connection with a rehabilitation method, the costs arising during the life-span of the building for the user are analysed. Subsequently, the optimization process is shown with an example and the results are given.

### REFERENCES

- Kluth, M., Bormann, A., Rank, E. & Mayer, T. 2007. Development of a software-tool for the life-cycle management of bridges. *Proceedings of the 1st International Symposium on Life-Cycle Civil Engineering (IALCCE'08)*, Varenna 2008.
- Gehlen, C. 2000. Deutscher Ausschuss für Stahlbeton. Probabilistische Lebensdauerbemessung von Stahlbetonbauwerken. Zuverlässigkeitsbetrachtungen zur wirksamen Vermeidung von Bewehrungskorrosion. *DAfStb, Heft 510*, Berlin: Beuth Verlag.
- Vesikari, E.; LIVECON 2003. Deliverable D 2.2. *Statistical Condition Management and Financial Optimisation in Lifetime Management of Structures*.
- Hillemeier, B., Stenner, R., Flohrer, C., Polster, H. & Buchenau, G. 1999. Instandsetzung und Erhaltung von Betonbauwerken. *Beton-Kalender*: Teil II, 88. Jahrgang, Karlsruhe: Ernst & Sohn Verlag.

# Experimental identification of cable damping parameters towards robust design against aeroelastic instability

L. Faravelli & F. Ubertini

*Department of Structural Mechanics, University of Pavia*

**ABSTRACT:** Steel cables are lightly damped structural elements for which ambient loads may produce large amplitude oscillations, which may eventually determine fatigue ruptures. The dynamics of cables have been extensively explored in the literature and evidence was given of the fundamental role played by structural damping in determining the quality of the vibration. Particularly, it was either numerically or experimentally observed that bifurcated solutions exist when modal damping ratios are sufficiently small. Provided this scenario, an accurate identification of the cable damping parameters is essential for robust design against ambient vibrations and for life cycle assessments. To this end, wavelet analysis is here applied in order to identify the damping parameters of a suspended cable model. The aim is to explore the robustness and the repeatability of the results with respect to different test conditions. Afterwards, the nonlinear forced harmonic vibrations of the system are numerically explored, devoting particular care to the role of damping uncertainties on the cable response. Finally, the use of a secondary tuned mass damper system is discussed as a way to increase the robustness against cable aeroelastic instability.

## 1 INTRODUCTION

The life cycle assessment and the fatigue analysis (Cluni et al. 2007) of steel cables require an accurate identification of the damping parameters of the system. A very convenient way to do so is represented by wavelet analysis (Staszewski 1997). After briefly reviewing the theoretical background of this approach, the damping parameters of an experimental suspended cable model are here identified. The repeatability of the results is explored, at first, with respect to different test conditions.

Some relevant references on nonlinear cable dynamics are given in (Rega 2004a, b). In this paper, some attention is devoted to the role of damping uncertainties on the prediction of the nonlinear response of the system to forced harmonic vibrations. Galloping aeroelastic instability is considered as an example of catastrophic event. The problem has been studied by Luongo & Piccardo (2005). After reviewing the principal aspects of the problem, in both resonant and non-resonant cases, a discussion is added on the role of added damping towards the robust design against such a dynamic instability. The use of a small tuned mass damper is considered to this purpose, since it revealed to be particularly effective for cable vibration mitigation (Casciati & Ubertini, in press; Gattulli et al. 2003).

## 2 IDENTIFICATION OF MODAL DAMPING PARAMETERS VIA WAVELET ANALYSIS

Let a structural dynamic signal  $x(t)$  be expressed by the following general form:

$$x(t) = \sum_{n=1}^N x_n(t) = \sum_{n=1}^N k_n(t) \cos(\phi_n(t)) \quad (1)$$

which is obtained from the superposition of  $N$  uncoupled vibration modes of amplitude  $k_n(t)$ . In force of Hilbert's transform, the  $n$ -th real-valued signal  $x_n(t)$  is usually expressed as the real part of its associated analytical signal  $Z_{xn}(t)$ , namely:

$$\begin{aligned} Z_{xn}(t) &= k_n(t) e^{i\phi_n(t)} \\ x_n(t) &= \text{Re}[Z_{xn}(t)] \end{aligned} \quad (2)$$

where  $i$  is the imaginary unit. In force of Equation (2), no hypothesis on the analyticity of  $x(t)$  is required. Modulus and angle of  $Z_{xn}(t)$  can be expressed according to the following equations:

$$\begin{aligned} k_n(t) &= |Z_{xn}(t)| \\ \phi_n(t) &= \angle[Z_{xn}(t)] \end{aligned} \quad (3)$$

Given those definitions, we introduce the continuous wavelet transform  $W_x(a, b)$  of  $x(t)$  as:

$$W_x(a, b) = \frac{1}{a} \int_{-\infty}^{\infty} x(t) h^* \left( \frac{t-b}{a} \right) dt \quad (4)$$

being  $h^*$  the complex conjugate of the  $L^2$  piecewise continuous function  $h$ , called “mother function”. We consider herein the Morlet-type mother function, which is defined as:

$$h(t) = e^{i\omega_0|t|} e^{-|t|^2/2} \quad (5)$$

The pair  $(a, b)$  in Equation (4) is the time-scale variable of the analysis. When the signal  $x(t)$  is sufficiently “oscillatory”, which means that the amplitude functions  $k_n(t)$  are slowly varying (with respect to the harmonic oscillations), the wavelet transform  $W_x(a, b)$  is locally maximum along fixed values of the parameter  $a$ , say for  $a = a_n$ , called “ridges”. The restriction of the wavelet transform along a ridge is called the skeleton of the wavelet transform. Since the square of the modulus of  $W_x(a, b)$  represents the energy of the signal, one can observe that in the neighborhood of the ridge  $a = a_n$  corresponding to the frequency  $\omega_n$  of the  $n$ -th mode, the wavelet transform  $W_x(a_n, b)$  approximately corresponds to the wavelet transform of the single vibration mode  $W_{xn}(a_n, b)$ . This last condition obviously requires well-separated modes. Looking at the previous definitions, the following relation can also be given:

$$\begin{aligned} |W_{xn}(a_n, b)| &\cong |Z_{xn}(b)| |\hat{h}(\dot{\phi}_n(b)a_n)| \\ &= k_n(b) |\hat{h}(\dot{\phi}_n(b)a_n)| \end{aligned} \quad (6)$$

For the  $n$ -th vibration mode, the amplitude and the phase of the signal can be expressed in the form:

$$\begin{aligned} k_n(t) &= A_0 e^{-\xi_n \omega_n t} \\ \phi_n(t) &= \omega_n \sqrt{1 - \xi_n^2} t + \phi_0 \end{aligned} \quad (7)$$

where  $\xi_n$  assumes the meaning of modal damping ratio of the  $n$ -th mode and  $\phi_0$  is a phase shift. By substituting Equations (7) into Equation (6) and by passing to the natural logarithms one thus obtains:

$$\log(|W_{xn}(a_n, b)|) = -\xi_n \omega_n b + C \quad (8)$$

where  $C$  is a scalar constant. From equation (8) one can conclude that the damping ratio of the  $n$ -th vibration mode can be identified as the slope of the straight line of the wavelet modulus skeleton in a semi-logarithmic plane. Conversely, when  $|W_{xn}(a_n, b)|$  is almost straight in a semi-logarithmic plane, evidence is given of the physical meaning of a viscous damping.

### 3 EXPERIMENTAL DAMPING IDENTIFICATION

An experimental suspended cable model is here considered (Figure 1) with span length  $L = 2.30$  m, diameter  $d = 0.002$  m and sag  $f = 0.032$  m. A triaxial crossbow accelerometer is placed along the cable at a quarter of its span.

Several in-plane and out-of-plane free vibration tests have been considered in order to identify the system natural frequencies. As an example, the time history of the in-plane acceleration, at the location of the accelerometer, is represented in Figure 2, for a sample case. The power spectral density functions of the in-plane and out-of-plane accelerations, measured by the accelerometer, are also reported in Figure 2. The identification of the model was reported elsewhere (Ubertini & Fuggini 2007) and led to the modal frequencies summarized in table 1. The presented values

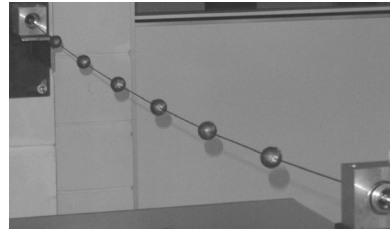


Figure 1. Experimental cable model.

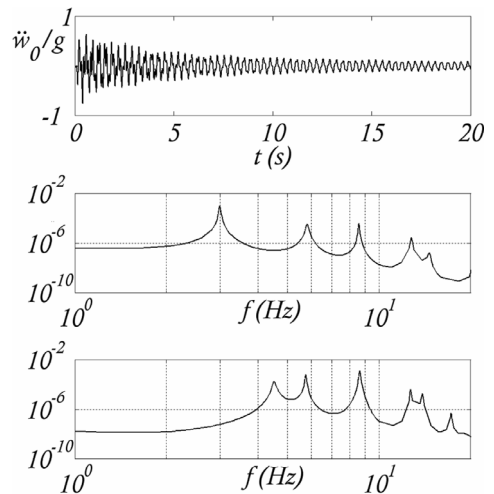


Figure 2. From the top: in-plane free acceleration (normalized to the gravity acceleration  $g$ ) at the position of the accelerometer; PSD function of out-of-plane acceleration; PSD function of in-plane acceleration.



correspond to a non-dimensional Irvine parameter  $\lambda^2 = 1.81\pi^2$ .

Figure 3 represents the logarithm of the modulus of the wavelet transform of the in-plane and out-of-plane experimental accelerations. After performing several experimental tests, under free spatial vibrations, the damping ratios  $\xi_n$  of the first three in-plane and out-of-plane modes have been identified using Equation (8). Particularly, for each test, one identified three values of the modal damping ratios, corresponding to three distinct intervals in which the wavelet skeletons were subdivided. The damping ratio  $\xi_n$  of the  $n$ -th mode was calculated, in the most significant test (i.e. in the one in which the skeleton showed the most linear behavior), as the maximum of those three values. The mean damping ratio  $\xi_{n,mean}$  of the  $n$ -th mode, was also calculated by considering different intervals in several experimental tests. The obtained results are summarized in Table 2, where the

Table 1. Identified modal frequencies (IP: in-plane; OP: out-of-plane).

IP mode no.	Frequency Hz	OP mode no.	Frequency Hz
1	4.467	1	2.991
2	5.737	2	5.767
3	8.667	3	8.606

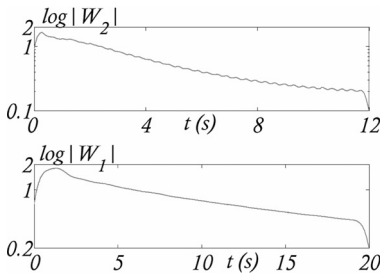


Figure 3. From the top: time-variation of wavelet modulus along the ridges corresponding to the first in-plane and out-of-plane modes, respectively.

Table 2. Identified damping ratios.

IP mode no.	$\xi_n$ %	$\xi_{n,mean}$ %	$\Delta$ %
1	2.60	1.98	24
2	2.14	1.52	29
3	1.50	1.10	27
$\Delta_{mean} = 27\%$			
OP mode no.			
1	1.90	1.56	18
2	2.20	1.96	11
3	1.65	0.98	41
$\Delta_{mean} = 23\%$			

percentage difference  $\Delta$  between  $\xi_n$  and  $\xi_{n,mean}$  is also reported. As evidenced by the obtained results, the damping ratios of the six considered modes have been clearly identified and the difference between  $\xi_n$  and  $\xi_{n,mean}$  is around 25%.

#### 4 DAMPING EFFECTS ON CABLE RESPONSE AND ITS STABILITY

##### 4.1 Nonlinear cable response under harmonic excitation

In order to analyze how damping uncertainties reflect on the cable nonlinear response, the frequency response curves of the first in-plane and out-of-plane cable modes, have been calculated by means of a continuation technique implemented in a dedicated software (AUTO2000) (see Figures 4–5). A nonlinear Galerkin model, with two degrees of freedom, has been adopted for this purpose assuming that the response of the considered modes is weakly influenced by the neglected higher order modes.

The results presented in Figure 4 refer to a harmonic in-plane excitation of normalized amplitude  $p$  and frequency ratio  $\Omega$  with respect to the first in-plane cable frequency. The amplitude  $q_2$  of the harmonic response is normalized to the cable span and it is represented as a function of  $\Omega$ . Three different values of the damping ratios are assumed, by reducing the experimentally measured value  $\xi_2 = 0.026$  by 25% and 50%. As it can be observed from such a figure, a softening-hardening behavior of the system is observed around the primary resonance ( $\Omega = 1$ ). Subharmonic resonant peaks are also observed at  $\Omega = 1/2$ ,  $\Omega = 1/4$ , etc. Those observations indicate that the cable behavior is essentially nonlinear, even at low vibration amplitudes. The figure also shows that reducing the damping ratio reflects on a drastic cut-off of the cable hardening harmonic branch around the main resonance. Consequently, the frequency range in which the cable may undergo the largest displacements is also cut-off. Analogous

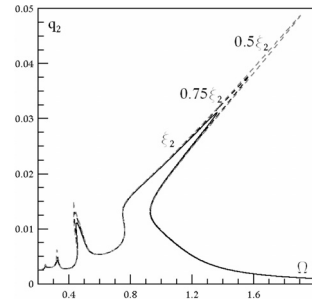


Figure 4. Frequency response curves of the first in-plane mode assuming different modal damping ratios ( $p = 0.003$ ,  $\xi_2 = 0.026$ ).

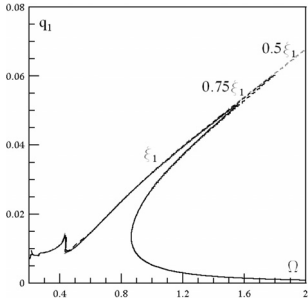


Figure 5. Frequency response curves of the first out-of-plane mode assuming different modal damping ratios ( $p = 0.003$ ,  $\xi_1 = 0.019$ ).

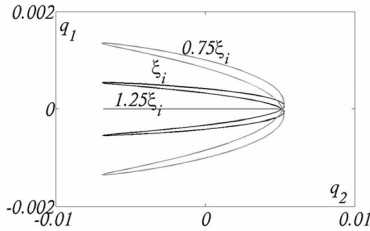


Figure 6. Phase plane projections of relevant harmonic limit cycles for different damping ratios ( $\Omega = 1.1$ ,  $p = 0.002$ ).

results are presented in Figure 5, with reference to the out-of-plane harmonic vibrations.

A Galerkin model with 4 in-plane and 4 out-of-plane degrees of freedom has also been considered. Figure 6 represents the phase plane projections of the steady harmonic limit cycles obtained, under in-plane harmonic excitation, for  $\Omega = 1.1$ . As one can observe from such a figure, depending on the initial conditions, the system, at the considered amplitude of excitation, may undergo a bifurcated spatial motion involving the out-of-plane mode  $q_1$ . Nevertheless, if one slightly increases the damping, the limit cycle is destroyed and the out-of-plane bifurcation does not appear. In contrast, a reduction of the damping of the system reflects on a larger participation of the out-of-plane mode.

#### 4.2 Linear instability mechanism under wind action

The results presented in Section 4.1 have shown that underestimating the cable damping ratios may result in dramatically unconservative results, due to the inherent nonlinear cable behavior. Linear instability mechanisms are also strongly influenced by damping variations, as it can be observed in flutter instabilities of long-span bridges, crowd-induced instabilities of footbridges, etc.

In order to discuss damping effects on linear cable instabilities, the 2-degrees-of-freedom (dofs) cable galloping is considered herein. As it is wellknown,

the critic condition is represented by a Hopf bifurcation, which is the case in which two complex conjugate eigenvalues cross the imaginary axis. In the case of cables, this may happen when icing conditions modify the aerodynamics of the system, originating lift forces. A simple linear two-dofs cable sectional model, subjected to an incoming wind flow of velocity  $U$ , can be written as (Luongo & Piccardo 2005):

$$\ddot{q}_1 + (2\omega\xi_s + 2\mu C_D)\dot{q}_1 + \mu(C'_D - C_L)\dot{q}_2 + \omega^2 q_1 = 0 \quad (9)$$

$$\ddot{q}_2 + 2\mu C_L\dot{q}_1 + (2\xi_s + \mu(C_D + C'_L))\dot{q}_2 + q_2 = 0$$

In which  $q_1$  represents the out-of-plane displacement and  $q_2$  denotes the in-plane one. In Equation (9)  $C_D$  and  $C_L$  represent the cable drag and lift coefficients, while  $C'_D$  and  $C'_L$  denote their derivatives with respect to the effective wind angle of attack. A same structural damping  $\xi_s$  is assumed in the two directions, while  $\omega = \omega_1/\omega_2$  is the ratio between the first out-of-plane and in-plane circular frequencies. In this work it is assumed  $\xi_s = 0.026$  and  $\omega = 0.67$ , since these values characterize the identified cable. The case in which  $\omega = 1$  will also be considered (resonant case). The non-dimensional wind velocity  $\mu$  has been defined as  $\mu = 0.5\rho BU/(m\omega^2)$ , where  $\rho$  is the air density,  $b$  is a reference dimension of the cylinder cross-section and  $m$  is the cylinder mass per unit length. The following eigenvalue problem can be written from Equations (9), to analyze the incipient instability of the trivial solution ( $q_1 = 0, q_2 = 0$ ):

$$\det[\lambda^2 \mathbf{M} + \lambda \mathbf{D} + \mathbf{K}] = 0 \quad (10)$$

where  $\mathbf{M}$  is the mass matrix,  $\mathbf{D}$  is the aerodynamic damping matrix and  $\mathbf{K}$  is the stiffness matrix which can be immediately derived from Equations (9). In the non-resonant case ( $|\omega - 1| > \varepsilon$ ,  $\varepsilon$  being a small perturbation parameter), a first order approximation of the system eigenvalues can be achieved by means of the multiple scale method (Luongo & Piccardo 2005), leading to the approximate critic wind velocity  $\mu_{crit}^0 = -2\xi_s/(C_D + C'_L)$ , which is positive for  $C_D + C'_L < 0$ . When the system is under internal resonance conditions ( $|\omega - 1| = 0$ ), the linear stability diagram can be drawn in the  $\det \mathbf{D} - \text{tr} \mathbf{D}$  plane, where  $\det$  and  $\text{tr}$  denote the determinant and the trace operators, respectively, and an approximate expression of the critic velocity can still be derived (Luongo & Piccardo 2005).

## 5 ROBUST DESIGN AGAINST CABLE AEROELASTIC INSTABILITY VIA ADDED DAMPING

When the TMD is not introduced in the system, the critic wind velocity grows linearly with the structural damping, in both the resonant and nonresonant cases. A way to increase the structural robustness against aeroelastic instabilities is therefore to increase the

damping of the system by adopting a small TMD. The relevant mass, damping and stiffness structural matrices then become:

$$\mathbf{M} = \begin{bmatrix} 1 & 0 & 0 \\ 0 & 1 & 0 \\ 0 & 0 & 1 \end{bmatrix}$$

$$\mathbf{D} = \begin{bmatrix} 2\omega\xi_s + 2\mu C_D & & \\ & 2\mu C_L & \\ & & 0 \end{bmatrix}$$

$$\mathbf{K} = \begin{bmatrix} \omega^2 & 0 & 0 \\ 0 & 1 + \psi\omega_t^2 & -\psi\omega_t^2 \\ 0 & -\omega_t^2 & \omega_t^2 \end{bmatrix} \quad (11)$$

where  $\psi$  is the ratio between the mass of the TMD and the mass of the cable, while  $\omega_t$  is the ratio between the circular frequency of the TMD and the in-plane cable circular frequency. In the following developments it is assumed  $\psi = 0.01$ , as usual in technical applications. The third rows of the matrices reported in Equation (11), are referred to the degree of freedom  $q_t$  of the TMD.

A linear eigenvalue problem, analogous to Equation (10), can be written also to evaluate the incipient instability of the controlled system. Figure 7 represents the root locus (obtained by solving numerically the eigenvalue problem) of the perfectly tuned controlled system ( $\omega_t = 1$ ) with optimal damping parameter  $\xi_{t,opt} = [3/8\psi/(1 + \psi)]^{0.5}$ , by varying the control variable  $\mu$  from 0 to  $\mu_{crit}^0$  (critic value for the uncontrolled system). It must be noted that, even by assuming  $\omega_t = 1$ , the perfect tuning of the system is never achieved as a consequence of *veering* interactions between closed eigenvalues. From the presented results one can also note that, at the value  $\mu_{crit}^0$ , the cable-TMD system is still in the stability region. The root locus of the eigenvalues for higher values of  $\mu$  is also reported in Figure 7. The resonant case is analyzed in Figure 8.

Figure 9 investigates the effect of the tuning of the TMD and of the damping uncertainties on the increment of the critic wind velocities. As it was expected, the increment of the critic velocity is very sensitive to variations of the frequency tuning  $\omega_t$  and attains a maximum at the perfectly tuned condition ( $\omega_t = 1$ ). A way to increase the robustness of the system against detuning effects is to adopt multiple tuned mass damper systems. The investigation of such a control strategy goes beyond the aims of the present work and will be its major future development. Figure 9 also shows that reducing the structural

damping increases the relative performance of the TMD. In particular, the ratio  $\mu_{crit}/\mu_{crit}^0$  grows as the structural damping is decreased. This suggests that the decrement of  $\mu_{crit}^0$  is faster than the increment of  $\mu_{crit}$ . This was however expected since  $\mu_{crit}$  mainly depends on the damping of the TMD  $\xi_t \gg \xi_s$ . Similar

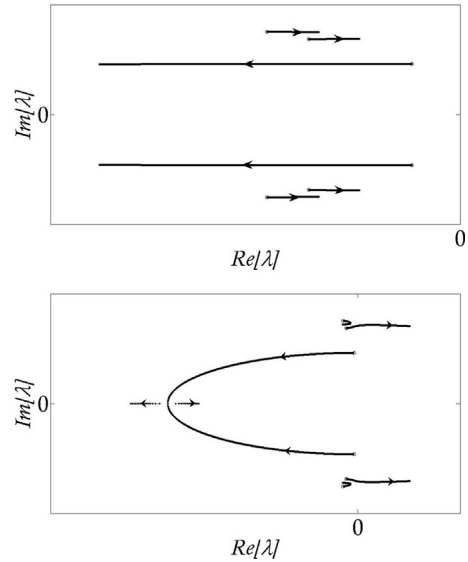


Figure 7. From the top: root locus of controlled system eigenvalues by increasing the control variable  $\mu$  below and above the critic condition (nonresonant solution).

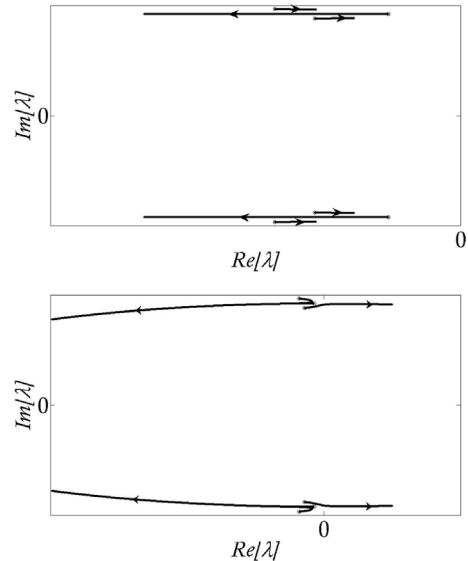


Figure 8. From the top: root locus of controlled system eigenvalues by increasing the control variable  $\mu$  below and above the critic condition (resonant solution).

conclusions can be made in the resonant case, reported in Figure 10.

The effect of the damping ratio of the TMD on the critic wind velocity is analyzed in Figure 11. The results show that the optimal damping value of the TMD, against structural galloping, is smaller than the classic optimum  $\xi_{t,opt}$ . Moreover, this optimum value seems to be substantially independent on the cable structural damping. It must also be noted that the critic wind velocity grows in a faster way, below the optimum value, than above the said value. This circumstance is also evident in the resonant case (see Figure 12). Particularly the ratio  $\mu_{crit}/\mu_{crit}^0$  grows almost linearly below the optimum damping value, while it decreases nonlinearly elsewhere.

## 6 CONCLUSIONS

The identification of six modal damping parameters of a physical cable, has been pursued via wavelet analysis evidencing an experimental uncertainty of less than 25%. Afterwards, it has been numerically shown that overestimating the cable modal damping reflects on a drastic cut off of the hardening harmonic branch of the main resonance. As a final result, the role of added damping (via the use of a small TMD) is investigated as a way to enhance the robustness against linear aeroelastic instability. Both resonant and non-resonant cases are considered in this analysis. A high sensitivity of the considered passive control strategy

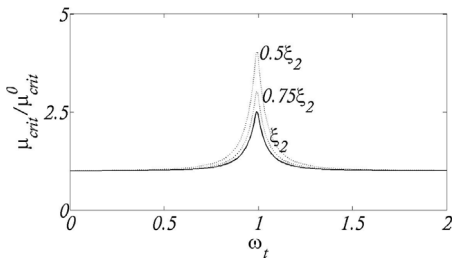


Figure 9. Increment of critic velocity (robustness against aeroelastic instability) as a function of the frequency ratio of the TMD (nonresonant solution).

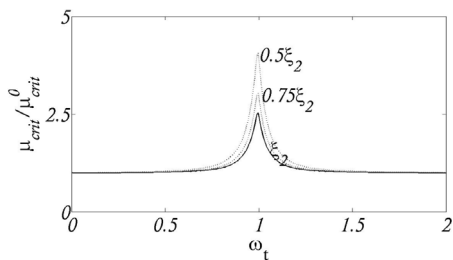


Figure 10. Increment of critic velocity as a function of the frequency ratio of the TMD (resonant solution).

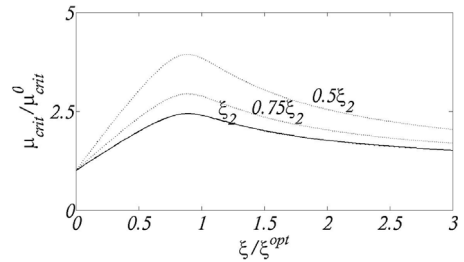


Figure 11. Increment of critic velocity as a function of the TMD damping ratio (nonresonant solution).

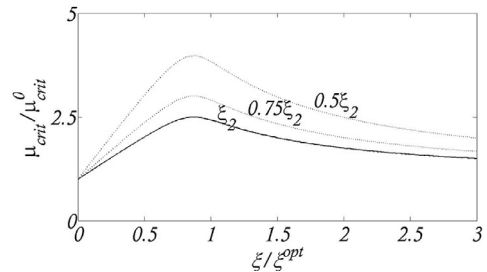


Figure 12. Increment of critic velocity as a function of the TMD damping ratio (resonant solution).

with respect to detuning effects is observed from the presented results.

## REFERENCES

- Casciati, F. & Ubertini, F. in press. Nonlinear vibration of shallow cables with semiactive tuned mass camper. *Nonlinear Dynamics*, in press (DOI 10.1007/s11071-007-9298-y).
- Cluni, F., Gusella, V. & Ubertini, F. 2007. A parametric investigation of wind-induced cable fatigue. *Engineering Structures* 29(11): 3094–3105.
- Doedel, E.J., Paffenroth, R.C., Champneys, A.R., Fairgrieve, T.F., Kuznetsov, Y.A., Oldeman, B.E., Sandstede, B. & Wang, X.: AUTO2000: continuation and bifurcation software for ordinary differential equations. Available online from <http://indy.cs.concordia.ca/auto/>
- Gattulli, V., Lepidi, M. & Luongo, A. 2003. Controllo con una massa accordata dell'instabilità aeroelastica di un cavo sospeso (In Italian). *Proceedings of the 16th Italian Conference on Theoretic and Applied Mechanics (AIMETA)*.
- Luongo, A. & Piccardo, G. 2005. Linear instability mechanism for coupled translational galloping. *Journal of Sound and Vibration* 288, 1027–1047.
- Rega, G. 2004a. Nonlinear vibrations of suspended cables, part I: modelling and analysis. *Applied Mechanics Reviews* 57, 443–478.
- Rega, G. 2004b. Nonlinear vibrations of suspended cables, part II: deterministic phenomena. *Applied Mechanics Reviews* 57, 479–514.
- Staszewski, W.J. 1997. Identification of damping in mdof systems using time-scale decomposition. *Journal of Sound and Vibration* 203(2), 283–305.
- Ubertini, F. & Fuggini, C. 2007. Confronto di due tecniche per l'identificazione e il monitoraggio di cavi strutturali mediante prove sperimentali (in Italian). *Proceedings of the Italian Conference on Non-Destructive Tests (AIPND)*, Milan, Italy.

# Seismic retrofitting of bridges

G. Furlanetto, L. Ferretti Torricelli & A. Marchiondelli

*Bridge Design Department, SPEA Ingegneria Europea s. p. a., Milan, Italy*

**ABSTRACT:** In Italy, in the last years the problem of retrofitting existing bridges received a progressively growing attention, mainly for the new safety requirements during seismic events imposed by the recently issued Italian codes. In this context, Autostrade per l'Italia, the main national transportation agency, and SPEA Ingegneria Europea, its design company, spent a great effort in developing basic guidelines for the upgrading of existing bridges aimed to support all the designers involved in the rehabilitation design activities. In particular, two alternative approaches for seismic retrofitting are adopted: the first approach is focused on the upgrading of the structural performance during seismic events, while the second one is aimed at the reduction of the seismic induced forces. In the former case, the structural capacity upgrading is achieved by intervening on specific structural members, while, in the latter case, base isolation or seismic protective systems are used. This paper presents some representative cases of retrofitted bridge structures, by using both the above described retrofitting techniques.

## 1 INTRODUCTION

The former bridge structures belonging to the Italian highway system were built in the 60's, and nowadays many of them result inadequate to comply with the actual functional and safety standards anymore. This is also due to a recent upgrading of the national seismic code (OPCM 3274/2003). In fact, the former national code imposed prescriptive requirements based on a conventional design approach, while the new one introduced concepts proper of the capacity design, based on the actual structural performance under seismic events, in accordance with the Eurocode 8. Moreover, national seismic hazard maps, based on the most recent studies, are issued by dividing the whole national territory into seismic zones including the regions previously considered as non-seismic or "zero hazard regions".

The main feature of the new seismic design philosophy consists of ensuring the stability of the structural response in the post-elastic range. To this aim, great attention is spent on the concept of ductility by providing specific construction details in new designs.

The new code also stated as mandatory the check of the seismic performance of all the existing structures to be considered strategic. Due to the more stringent safety requirements and the increased seismic forces to be accounted for, many existing structures usually reveal deficiencies related to inadequate ductility caused by poor attention dedicated to construction details such as efficient anchorages for both longitudinal and transversal reinforcements, adequate amount of stirrups in order to improve the confinement of

the structural members in correspondence of critical nodes, proper staggered position of longitudinal reinforcement in order to avoid weak sections, and so on. In order to adequate the structural response to the new required safety level, proper strengthening interventions are often requested.

In this context, Autostrade per l'Italia, the main Italian transportation agency, and SPEA Ingegneria Europea, its design company, have been involved in a wide design activity for seismic retrofitting of a large number of different bridge structures, and in handling peculiar problems and critical situations, which often required the setting up of a tailor-made rehabilitation procedure.

In particular, two alternative approaches for seismic retrofitting can be adopted. The first approach acts on the seismic demand by reducing the induced forces by means of base isolation or seismic protective systems. The second approach, instead, influences the structural capacity by intervening on specific structural members. In this latter case, a typical retrofit strategy consists of increasing the strength and/or the stiffness, or upgrading the mechanical properties of the structure. Another efficient, even if counterintuitive, retrofit strategy consists of a rational weakening of selected structural members. In fact, by using this strategy, the seismic demand can be reduced and the inelastic mechanism can be changed according to capacity design principles in order to avoid non-ductile failure modes.

In the following, representative cases of retrofitted bridge structures by using the above mentioned retrofitting techniques, acting at both the seismic demand and capacity level, are presented.

## 2 WIDENING AND RETROFITTING OF TWO HIGHWAY BRIDGES

The design of widening and retrofitting of the two highway bridges shown in Figure 1 is presented.

Both the as-built bridges are composed by simply supported prestressed concrete decks sustained by framed bents. Basically, the widening intervention consisted of an enlargement of both superstructure and piers in continuity with the existing parts (Furlanetto

et al., 2007). The proportion of the new structural elements are chosen to comply with the geometric characteristics and mechanical properties of the old ones. After the new structural elements are designed, a performance evaluation of the widen bridges is carried out by means of pushover analysis aimed to verify the seismic suitability of the old part of the structure. In both cases, the existing columns resulted to be inadequate for ductility and confinement during longitudinal seismic events. In addition, bearing deficiencies associated with insufficient seat width and inability to accommodate seismic displacements are found.

Retrofitting interventions leading to uniform distribution of seismic forces are designed to improve the whole seismic performance. The existing bearings are replaced by elastomeric pads (Figure 2.a). To prevent jumping of the superstructure, longitudinal and transversal seismic restrainers are realized by means of reinforced concrete elements doweled to the existing cap beams (Figures 2.b-c). New expansion joints are also provided.

Since a sufficient level of deformation ductility in plastic hinge regions needed to be achieved, the chosen seismic retrofitting of the existing columns consisted of an external FRP jacket (FIB Task Group 9.3, 2001). To improve the seismic structural performance in longitudinal direction, the FRP jacket is only needed at the end of the columns.

For the Cesano bridge, having circular columns, the FRP jacket is made by unidirectional fiber epoxy-impregnated sheets wrapped around columns, with the main fibers oriented in the hoop direction (Figure 1.a). Instead, for the columns of the Morignano bridge, having rectangular cross-section of dimensions 0.70 m × 2.30 m, the intervention was more complex. Since the

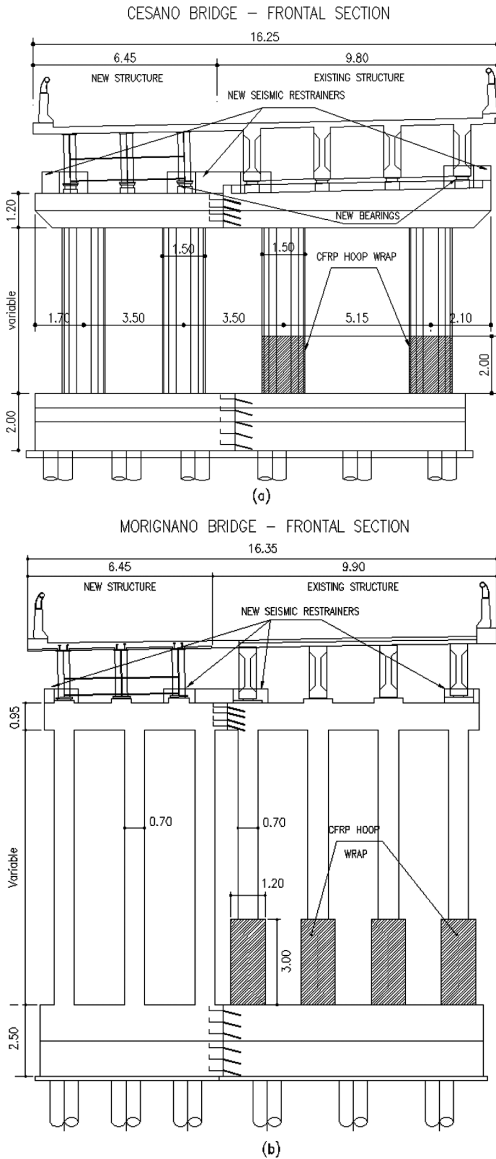


Figure 1. Widening and retrofitting of two bridges.

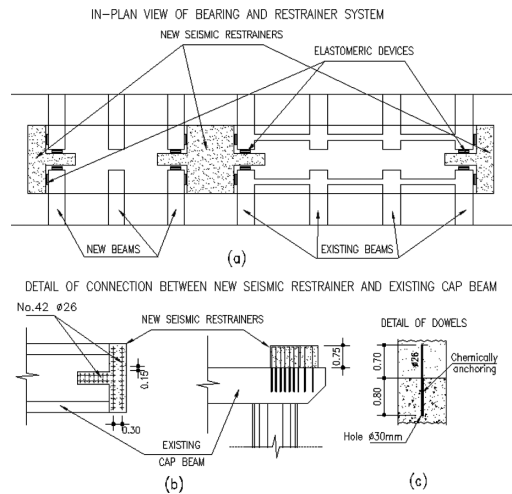


Figure 2. Retrofitting of bearing and restrainer system.

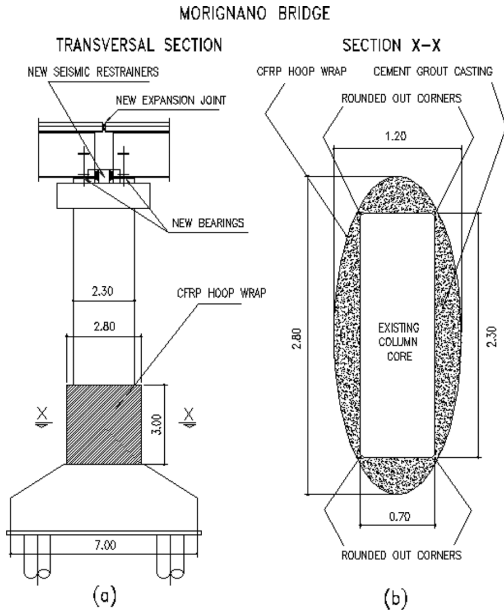


Figure 3. FRP jacketing of rectangular columns.

confinement effectiveness of the externally bonded FRP jackets depends, among other parameters, on the shape of cross-sections and radius of the corners, a modification of the cross-sectional shape is needed. To reduce any detrimental effect of the sharp corners on the tensile strength of the FRP, in the chosen solution the corners are rounded and an elliptical-shaped external cover surrounding the old rectangular cross-section is realized by using cement grout (FIB Task Group 7.1, 2003). Finally a multilayer FRP jacket is wrapped around the elliptical-shaped region (Figure 3).

### 3 STRENGTHENING OF BRIDGE PIERS

The bridge in Figure 4 is composed by simply supported prestressed concrete spans, 33.0m long. The bents consist of framed structures formed by two elevations, distant about 13.0 m (Figure 4.a). They are connected at the top by means of a cap beam. The height of the piers is varying about from 12.0 m to 32.0 m. Each elevation, having in-plant dimensions of 3.70 m × 4.50 m, is composed by two T-shaped columns, distant 1.5 m each other, linked by thin transversal beams every 7.50 m (Figure 4.b). The foundation system consists of an isolated footing, 2.5 m thick, for each elevation. Due to the good characteristics of the ground, a direct foundation is chosen. The bearing system is composed by elastomeric pads, and seismic restrainers aimed to avoid the deck unseating are provided for both transversal and longitudinal directions.

The carried out pushover analysis aimed to verify the seismic suitability of the whole structure highlighted the inadequacy of the elevations in terms of strength resistance. In fact, the pier columns are

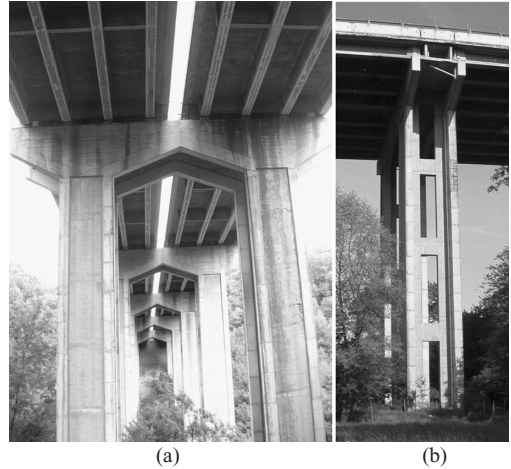


Figure 4. As-built Mulinaccia Viaduct.

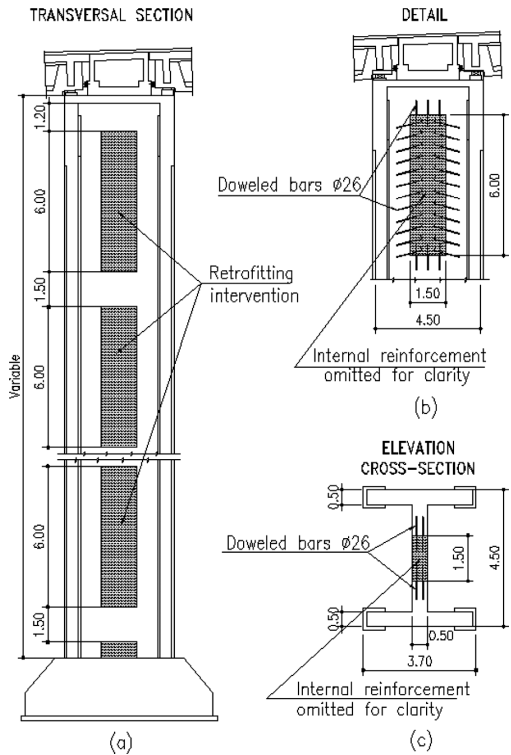


Figure 5. Strengthening of pier elevation.

not able to sustain the high tensile forces caused by earthquake loadings acting in longitudinal direction.

In order to reduce the flexibility of the high piers and to improve the tensile strength resistance, the two T-shaped columns forming each elevation are connected along the whole height by filling the openings among the transversal beams by reinforced concrete casting (Figure 5.a). As result, the elevation cross-section, presenting a I-shape in the final configuration, results to be much more efficient than the previous one (Figure 5.c).

By adopting this solution, great care is paid to the details aimed to assure the cooperation between the old and new parts. Before intervention, the roughening of existing surface by removing the concrete cover, the arrest of any reinforcement corrosion phenomena, and the injection of open cracks by low-viscosity epoxy resin are provided (Priestley et al. 1995). Finally, the shear transfer among existing columns and adding portions is ensured by the use of doweled bars (Figure 5.b). The casting of the new parts is made by using a special concrete aimed to reduce shrinkage phenomena.

#### 4 A SELECTIVE WEAKENING STRATEGY FOR RETROFITTING A PIER-FOUNDATION SYSTEMS

The widening and seismic retrofitting design of a highway bridge is presented.

The bridge in Figure 6.a is composed by an existing simply supported prestressed concrete deck, monolithically connected with a new steel-concrete composite deck. Each bent consist of a wall 2.20 m thick and 33.90 m wide, having height of about 10 m. The existing portion of the pier presents a three-cellular box cross-section, having walls 0.50 m thick (Figure 6.c). The foundation is formed by a footing, 4.0 m wide and 1.20 m thick, sustained by a system of micropiles. The widening pier portion consists of an enlargement of both the wall and footing in continuity with the existing parts (Figures 6.c–d).

The existing structure does not comply with the seismic requirements of the Italian code for several aspects. In particular, the pier elevations result to be over-designed, while the foundations are not able to sustain the resistant bending moment of the cross-section at the wall base. For this reason the capacity design criteria aimed to favor the flexural collapse of the wall and to avoid the early collapse of the footing, are not satisfied.

Among different design solutions, the chosen retrofitting strategy is aimed to strengthen the footing as well as to reduce the bending capacity of the pier wall. In particular, the strengthening of the footing is realized by means of the widening intervention shown in Figure 6.d, aimed to improve the bending capacity of the foundation system. Instead, the reduction of the

bending capacity of the pier wall is obtained by means of a local weakening of the base cross-section (Ireland et al., 2006). To this aim, a circular opening, with diameter of 1.20 m, is made in the wall of each box of the existing pier, as shown in Figure 6.a and Figure 6.e. In this way, it was possible for a worker to access the internal part of each box, and to demolish the concrete cover at the bottom part of the pier along the whole internal perimeter of the cross-section. Therefore, the required weakening is obtained by cutting a selected number of reinforcing steel bars. Finally, the concrete cover is completely restored. The sequence of these steps is shown in Figure 6.f. It is worth noting that, as shown in Figure 6.e, at the end of the retrofitting intervention, the effectiveness of the reinforcing bars in correspondence of the circular openings is also restored, and the provisional openings are then closed with a casting made by using special concrete able to reduce shrinkage phenomena.

#### 5 BRIDGE SEISMIC PROTECTION BY USING SHOCK TRANSMITTER DEVICES

The bridge in Figure 7.a is subdivided into three parts. The central one consist of a framed structure composed by a continuous concrete box girder, having variable height, monolithically connected to the central pier. The two lateral structures are formed, instead, by simply supported decks having constant height. The static scheme presents a fixed point in correspondence with the central pier, while longitudinal unidirectional bearings are provided at the remaining supports.

The bridge, built in the 60s, is designed without considering seismic loadings because the previous national seismic hazard map classified the area as “zero hazard region”. In accordance with the most recent classification, the area results to be seismic zone of 3rd category, with a correspondent Peak Ground Acceleration (PGA) of 0.15 g.

The structural performance evaluation, carried out according to the new Italian seismic code, highlighted the inadequacy of the bridge. In particular the abutments, consisting of a thin wall, 0.80 m thick and 7.0 m high, originally designed to sustain static loads only, are not able to comply with the horizontal seismic forces due to earth pressure as well as to deck inertial effects.

In order to allow the insertion of an additional traffic lane, a widening intervention is also considered by providing an enlargement of both superstructure and supports in continuity with the existing parts (Figure 7.c). In particular, the widening deck solution, consisting of a composite structure, is chosen so to minimize the increase of mass of the superstructure as well as to comply with the flexibility of the concrete deck. The widening configuration of the



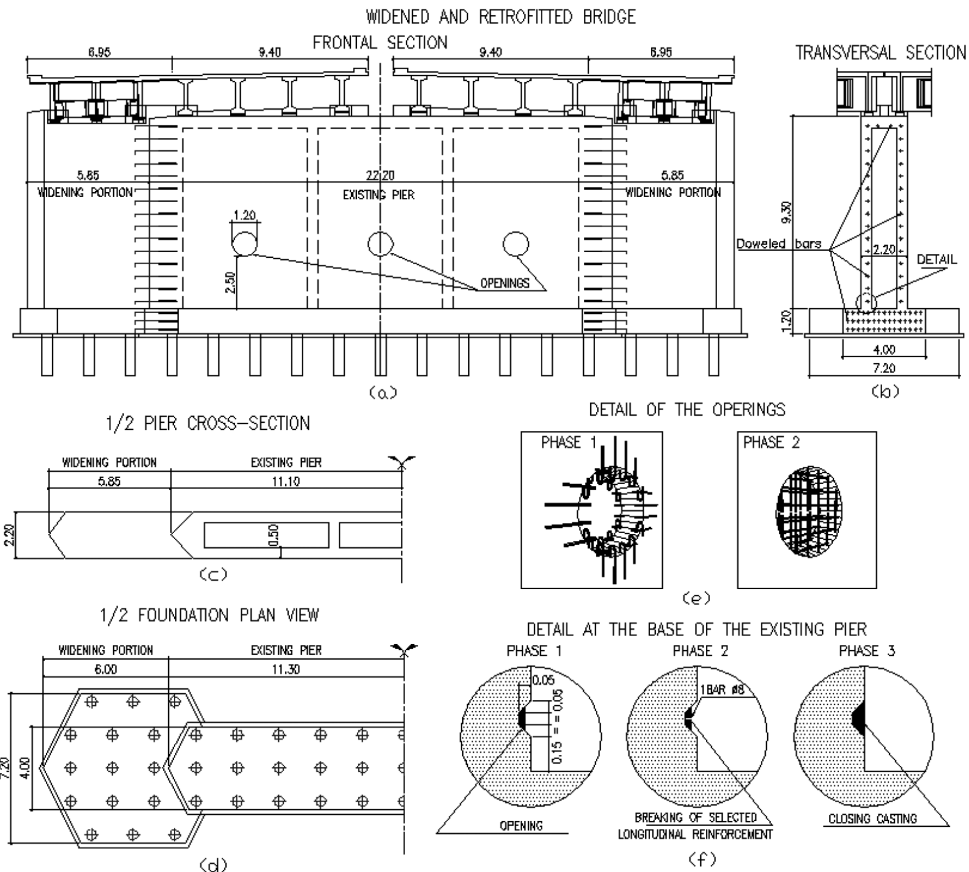


Figure 6. Retrofitting of pier foundation system.

bents is designed according to both aesthetic and structural requirements by reproducing the geometric and mechanical characteristics of the existing parts.

The retrofitting intervention (Figure 7.b) is designed with the aim of safeguarding the bridge, and consisted of inserting a seismic protective system composed by shock transmitter devices in correspondence of the abutments and the lateral piers (Pinto et al., 2001). Special diaphragms are also provided at the ends of the deck so to strengthen the box-girders against the concentrate loads due to the seismic devices (Figures 7.d–e). More in detail, the shock transmitters are hydraulic devices able to allow slow displacements, like those due to thermal variations, but to block those of sudden onset, due to earthquake, that may produce damage to joints, bearings and other structural members. In case of violent acceleration due to seismic event, the shock transmitter devices behave as fixed restrainers by blocking any relative displacements between the connected parts, and by transferring the seismic forces to the properly designed

new structures. To this aim, in the retrofitting planning, a modification of the abutment configuration is proposed (Figure 8). In particular, the vertical loads are still sustained by the abutment, but, after the demolition of the top part of the abutment wall, an additional structure, formed by a reinforced concrete plate sustained by a system of piles, is built in order to sustain the horizontal forces due to shock transmitter devices.

## 6 CONCLUSIONS

In Italy, in the last years the problem of retrofitting existing bridges received a progressively growing attention, mainly for the new safety requirements during seismic events imposed by the recently issued Italian codes. In this context, Autostrade per l'Italia, the main national transportation agency, and SPEA Ingegneria Europea, its design company, are widely involved in the upgrading of existing bridges. Two alternative approaches for seismic retrofitting are mainly adopted.

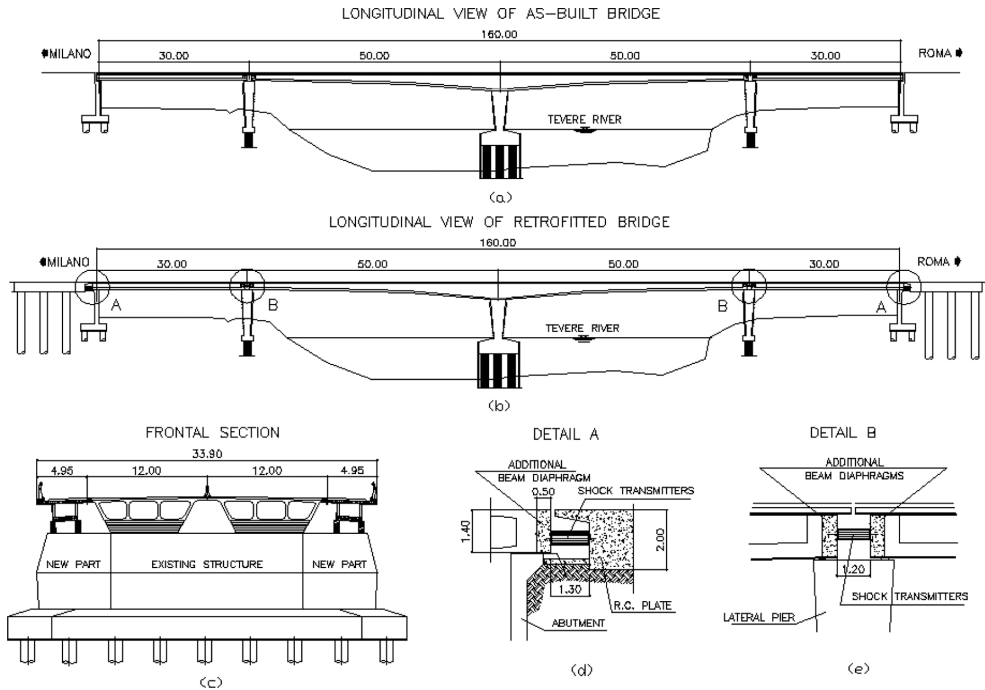


Figure 7. Bridge retrofitting by using shock transmitter devices.

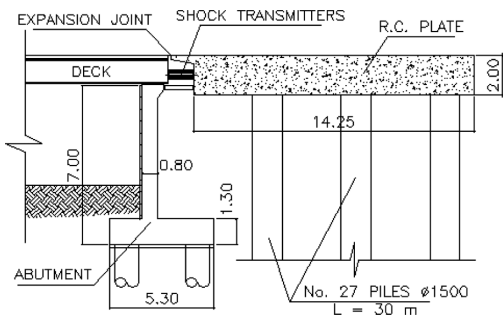


Figure 8. Abutment retrofitting intervention.

The first one is aimed at reducing the induced forces by means of base isolation or seismic protective systems. The second one is aimed at improving the structural capacity by intervening on specific elements. In this latter case, two alternative retrofit strategies are possible: the most common consists of increasing the strength of inadequate structural members, the less intuitive, even if equally efficient, consists of a rational weakening of selected structural members so to change the inelastic mechanism according to capacity design principles in order to avoid non-ductile failure modes. In the paper, representative cases of retrofitted bridge structures by using all the recalled retrofitting techniques are discussed.

## REFERENCES

- fib Task Group 9.3, 2001. *Externally bonded FRP reinforcement for RC structures*. fib Bulletin 14. Lausanne: Fédération International du Béton.
- fib Task Group 7.1, 2003. *Seismic assessment and retrofit of reinforced concrete buildings*, fib Bulletin 24. Lausanne: Fédération International du Béton.
- Furlanetto, G., Ferretti Torricelli, L. & Marchiondelli, A. 2007. Structural Assessment and Rehabilitation of Concrete Bridges, *Proceedings of the IABSE Symposium*, Weimar, Germany, September 19–21, 2007.
- Ireland, M.G., Pampanin, S. & Bull, D.K. Concept and Implementation of a Selective Weakening. Approach for the Seismic Retrofit of R.C. Buildings., *Proceedings of the Annual NZSEE Conference*, Napier, March 2006.
- OPCM 3274/2003: "General criteria for the seismic classification of Italian territory and technical specification for structures", and following modifications.
- Pinto, P.E., Calvi, G.M. & Priestley, M.J.N. 2001. Seismic Protection Of Bridges And Viaducts; Achievements And Future Developments, *Proceedings of 7th Int. Seminar on Seismic Isolation, Passive Energy Dissipation and Active Control of Vibrations of Structures*, Invited Paper, Assisi, October 2–5, 2001.
- Priestley, M.J.N., Seible, F. & Calvi, M. 1995. *Seismic Design and Retrofit of Bridges*, John Wiley & Sons, Inc., New York, NY, Sep. 1995, 672 pp.

# Widening and strengthening of bridge decks with composite materials

G. Furlanetto & R.L. Pefano

*Bridge Design Department, SPEA Ingegneria Europea, Milan, Italy*

**ABSTRACT:** For the widening of the motorway A1 between Orte and Fiano Romano and the upgrading of the Bologna motorway ring-road, widening of bridge decks and strengthening of existing structures were carried out using innovative materials such as carbon fiber-reinforced polymers (CFRP), having considered the highly desirable features of these materials for bridge applications in terms of high strength, high fatigue resistance, lightweight and corrosion resistance. The use of CFRP materials made also possible the observance of a very tight construction programme, with the further benefits of minimal disruption to traffic and ability of working under restricted conditions.

## 1 INTRODUCTION

In the last few years, the Italian motorway network has seen a strong growth of traffic level. The need of providing additional capacity along the most critical areas became evident and a program of widening existing motorways was set up. This included the widening of the motorway A1 between Orte and Fiano Romano for a total length of 38 Km and the upgrading of the 18 km long section of the motorway ring-road around Bologna.

A large number of existing bridges were affected by the widening project. The above mentioned motorways were built in the Sixties and the majority of the bridges had not deteriorated appreciably. In this case, the option of widening the existing structures is generally more cost-effective than their complete replacement; so it was decided to widen the bridges, retaining the existing structures.

In the case of widening of decks, the standard option is connecting the old and the new structures, avoiding longitudinal joints between them, which entail a number of inconveniences such as the creation of differential deflections and offsets in the riding surface, which may result in hazardous driving conditions, or the possible leakage of corrosion inducing materials, as de-icing salts, through the joints into the girders and substructures.

The decision of providing a structural connection between the decks led, in the majority of the cases, to the necessity of strengthening the existing bridges that had to be checked and, if necessary, upgraded to new standards, as the resulting structure, in its final configuration, has to comply with current design codes. The existing bridges were in fact designed in accordance with old Italian codes, which prescribed lower traffic loads; other kinds of loads, such as thermal, braking or earthquake forces, were differently or not

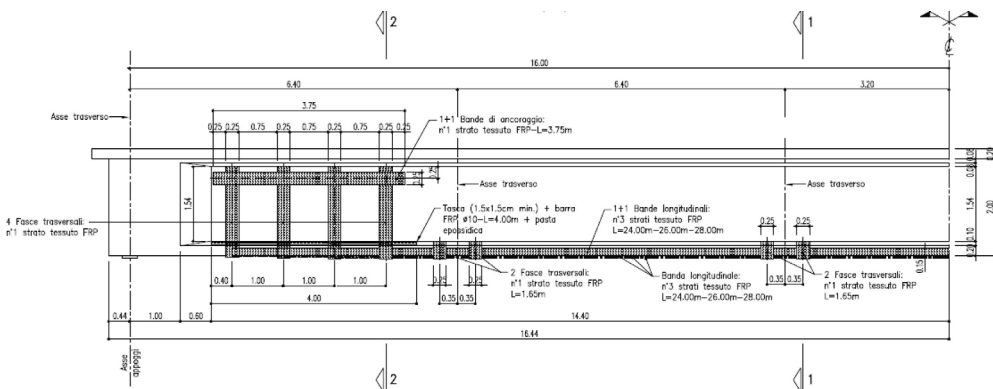


Figure 1. Flexural and shear strengthening of the girder with CFRP sheets.

at all taken into account; the materials used were in general of lower strength and poorer quality than the materials used today.

In the Orte—Fiano Romano project, the use of carbon fiber-reinforced polymers (CFRP) composite materials was proposed for both the extension of the deck cantilever slab, for which carbon fiber bars were used, and the strengthening of the deck beams, where CFRP fabric sheets were adopted. In the Bologna ring-road project the strengthening of the beams of the existing decks was carried out using pre-stressed CFRP strips.

Load tests were conducted before and after the CFRP materials were installed in order to evaluate their effectiveness.

## 2 WIDENING OF THE A1 BRIDGES

### 2.1 Design considerations

The original motorway section is composed by dual-two lane carriageways, carried by two separate decks. The prevailing existing deck type is formed by reinforced concrete post-tensioned beams with cast-in-situ slab and cross-beams; plain reinforced concrete deck beams and concrete arch structures are also present. A multiple, simply supported beam is the static scheme most often met. The substructure consists of reinforced concrete piers and cantilever wall abutments, founded mostly on bored piles.

The need of minimizing the interference of the widening works with the traffic and the necessity to observe a tight construction programme led to the final proposal of widening the deck overhang only, without the aid of a supplementary beam (the required additional width was around 1 meter). From a static point of view, this solution is more demanding for some structural elements, namely the outer deck beam and the overhang slab itself, considering also the obligation set by the Italian codes to verify the structure, in its new design configuration, in compliance with current bridge standards.

For these reasons, it was decided to use high quality components, such as CFRP materials, choosing an emerging technology, which is becoming a more and more employed alternative to steel for concrete structure strengthening.

CFRP materials consist in a weave of small carbon fibers, which are the principal stress bearing constituents, bundled in a resinous matrix, which assures transfer of stress among the fibers and protection against environment and mechanical damages. They offer both remarkable mechanical properties in terms of tensile strength and elastic modulus, and a number of advantages such as immunity from corrosion, good fatigue strength, drastic weight reduction compared to

steel, which allows quick and safe operations, even in impervious positions.

Static calculations have been based on analytical and empirical models as provided by some international codes; the design, which is similar to that adopted for ordinary reinforced concrete members, has been carried out in accordance with the Limit State Design principles. In this respect, the following assumptions have been made: a parabolic-rectangular stress-strain relationship has been adopted for concrete, a bilinear stress-strain relationship has been adopted for steel and a linear elastic stress-strain relationship has been adopted for CFRP materials. Perfect bond among all the section components (concrete, steel and composite material) and planarity of loaded sections have been also assumed.

### 2.2 Description of the works

The use of CFRP composite materials has been proposed for both the extension of the cantilever slab, in the form of carbon fiber bars, and the strengthening of the beams, for which CFRP fabric sheets have been adopted.

The features of simplicity and rapidity connected with the application of CFRP materials should not overlook the importance of the application process on the site, which is very important for the good result of the work. This is why CFRP application techniques are often designated as 'systems', made up of materials (not only the composite reinforcement, but also the complementary materials as primers, resins, mortars, etc. used in the whole process) and site operations, for which skilled and highly trained operators should always be appointed. In the following, a brief description of the various steps related to the execution of the works is given.



Figure 2. Rust-proofing of uncovered steel reinforcement during preliminary operations.

### 2.2.1 Strengthening of the beams

Strengthening of the beams proved necessary due to the rise of live loads of the current Italian bridge design code and the increment of their eccentricity in the new design configuration.

The preliminary operations were related to the preparation of surfaces, that have to present a regular and smooth finish before the CFRP sheets are applied: all loose and deteriorated parts of concrete must be removed; sharp edges around the beam are rounded off and sandblasting is carried out to remove small particles and roughen the surfaces for the following operations; uncovered steel reinforcement, if present, has to be cleaned and passivated. Water jet blasting is used for further cleaning and wetting of the surface. A layer of a modified-polymer mortar is then applied to the surface in order to ensure planarity and regularity of the support.

In order to guarantee an effective adhesion between the substrate and the CFRP sheet, a primer, which penetrates and saturates the concrete pores, is laid on the support and, after that, the first layer of an epoxy adhesive is spread evenly on the prepared surface. With the particular technique adopted, the so-called ‘wet lay up system’, the adhesive has the double task to ensure the development of bond between the fabric sheet and the support and to impregnate the sheets made of dry fabric, that must be clean, integral and dust-free. The CFRP sheets are then applied on the supporting surfaces and pressed by rollers to eliminate air entrapment and to guarantee the complete penetration of the adhesive into the fiber sheets. The sequence adhesive-fabric must be repeated as many times as the numbers of layers prescribed in the design (the final number of adhesive layers is equal to the number of fabric layers plus one). The process is completed by the application of a protective polyurethane layer against ultra-violet light.



Figure 3. Application of CFRP sheets on the beam.

For shear strengthening and in order to provide additional anchorage for the main composite reinforcement, U-jackets made of CFRP fabric sheets were also applied near the supports of the beam, with similar procedures. Careful detailing was also developed to contrast diverting forces that may arise at concave angles and to avoid possible formation of high stress concentration at singular points.

### 2.2.2 Extension and strengthening of the slab

Also in this case the preparation of surfaces (bush-hammering, cleaning, saturation with water, etc.) was carried out with particular care as this is fundamental to obtain a good adherence between the support and the reinforcing materials.

After the demolition of part of the existing cantilever slab and the removal of the superficial upper concrete layer of the slab over the outer beam, the CFRP bars are laid on suitable spacers and fixed to prevent movements during concrete casting. As composite carbon materials are good electrical conductors, the CFRP bars are insulated from ordinary steel reinforcement in order to avoid the possibility, although unlikely in road bridges, of galvanic corrosion of steel. Complete collaboration between the support and subsequent castings is ensured by the provision of steel hooks drilled and grouted into the existing slab.

The additional casting incorporates the supplementary reinforcement together with the old reinforcement left in place during the hydro-demolition of the old cantilever and produces an over-thickness in the existing slab of 6–8 cm. The material used for the integrating casting over the existing deck (concrete or mortar according to the thickness required) presents high quality features in terms of fluidity, workability, shrinkage-free properties and mechanical strength.

Operations had to be fast and were carried out during the night at lower air temperature, due to the limited workability of mortar; they were able to cast up to six

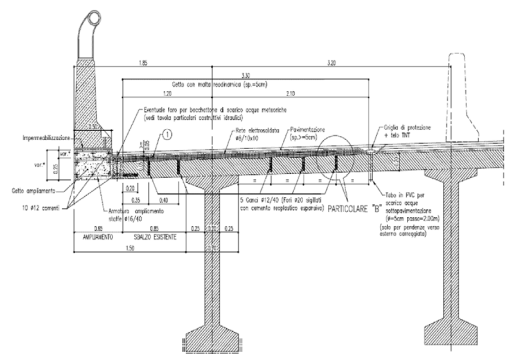


Figure 4. Extension and strengthening of the cantilever slab with CFRP bars.

spans in one night (190 m). In two months, a total length of 2500 m of widened slab was carried out by the Contractor.

### 2.3 Testing plan

Despite CFRP materials have now being used for some years for civil structural applications, a lack of experience and clear rules for design in bridge applications of CFRP composites was acknowledged at the time of design work. This is the reason why a testing campaign has been set up in order to provide direct information and a higher degree of confidence on the use of these relatively new techniques.

- a. With the cooperation of the University of Padova and Bologna, several tests were performed in laboratory and on the site; among them the following can be mentioned.
- b. Direct pull-out test on mortar-concrete for the integrative slab casting, carried out on site. The failure always took place into the existing concrete and not at the interface between support and new castings.
- c. Expansion plate test on mortar-concrete carried out on site, in order to assess the shrinkage-free property of the materials used for integrative castings.
- d. Tensile test for the assessment of the tensile strength, elastic modulus and ultimate strain of CFRP sheets and bars.
- e. Flexural test on beams reinforced with CFRP bars in order to monitor bonding both between bars and concrete and between different layers of concrete.
- f. Failure load-test on a full-scale model reproducing the deck cantilever slab, the results of which proved to be in accordance with the theoretical model, represented by a finite element model, where non-linear properties of steel and concrete have been taken into account.
- g. Traditional load tests with full-load lorries.

## 3 POST-STRENGTHENING OF A BRIDGE WITH PRESTRESSED CFRP STRIPS

### 3.1 General framework

For the upgrading of the motorway ring-road around the city of Bologna, a bridge rehabilitation project using pre-stressed CFRP strip was carried out on a large scale for the first time in Italy. A structural analysis to current standards of the deck of the Battiferro-Navile Viaduct showed that the bending resistance of the existing post-tensioned beams was not satisfactory. Considering various factors, among which the necessity to work under restricted condition, maintaining the bridge open to traffic throughout the whole construction period, the difficulties connected with

the adoption of a traditional external post-tensioning system and the very short time available for the work, it was decided to strengthen the deck beams with pre-stressed CFRP strips.

The adoption of a carbon-fiber pre-stressing system allows the use of high performance materials together with lightweight and handy equipment, that in turn increase security in operations and shorten construction time schedules.

### 3.2 Description of the work

The existing bridge was built in the early 60's and consists of a three span, simply-supported structure. The deck carries a double four-lane carriageways and is composed by post-tensioned concrete girders,



Figure 5. Battiferro-Navile Viaduct. General view during widening and strengthening operations.



Figure 6. Application of the CFRP strip to be pre-stressed at the beam intrados.

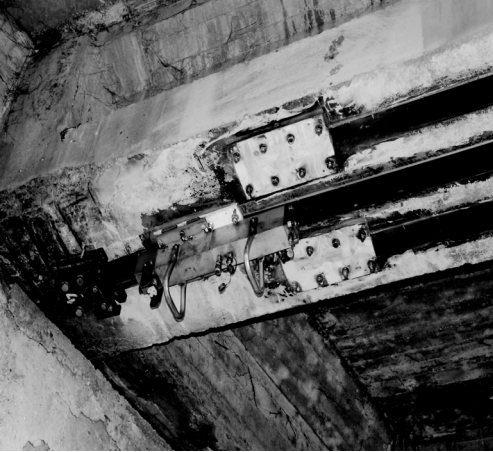


Figure 7. Tensoning jack placed at the mobile end anchorage plate of the CFRP strip.



Figure 8. Fixed end anchorage plate of the CFRP strip with lock wedge.

24 meter long, with slab and cross-beams. The widening project included the strengthening of 48 existing beams.

The cross beams were strengthened with the application of plain CFRP laminates at the intrados, as flexure reinforcement, and a wrapping made by CFRP fabric in the support area, as shear reinforcement, using a solution similar to that already described for the A1 bridges.

The strengthening of the girders was achieved with the use of tensioned CFRP strips applied on the beam intrados, in order to give the beam a pre-stress with a maximum eccentricity. This allows to reduce the stress on the beams at the service level and to lower vertical deflections, increasing at the same time the ultimate flexural strength of the girders.

Three 23 meter long CFRP strips are applied on each beam. Every strip is pre-stressed at 120 kN for a total tensile force of 360 kN, applied at the beam intrados. The checking of the applied tension is carried out through the measurement of the lengthening of the carbon strip during the tensioning phase, considering the linear relationship between stress and strain of composite materials; the strip was tensioned up to an extension of around 13 cm, corresponding to 0.6% of the ultimate strain, which is a value commonly recommended by reference documentation.

The installation of the CFRP pre-stressed laminate system can be described briefly by the following steps.

- a. Repair and smoothing of the concrete surface, treatment (rust-proofing) of possible uncovered steel reinforcement and rectification of the beam intrados (with a tolerance of 5 mm/2 m).

- b. Drilling of holes at the beam intrados for the housing of the end anchorage plates, taking care that no structural reinforcement bars were cut.
- c. Placement and bonding of the anchorage plates.
- d. Preparation of the support surfaces with the application of a primer to enhance adhesion between the surface and the laminates.
- e. Fastening of the CFRP strip to the fixed plate, placing of wedge plates at the fixed end that act as a contrast during the tensioning phase.
- f. Application of an epoxy resin to the surface, followed by the placement of the CFRP strip.
- g. Fastening of the strip to the mobile plate and preparation of the tensoning jack.
- h. Application of the design stress to the CFRP strip followed by locking of the jack.
- i. Rolling of the strip to ensure adherence to the resin layer and the substrate.
- j. Heating of the strip heads to guarantee a suitable polymerization of the resin.
- k. Removal of the jack and the wedge plates (24 hours after the pre-stressing of the strip).

### 3.3 Load tests

Load tests were conducted to evaluate the effectiveness of the proposed strengthening system. With the support of the Material Testing Laboratory of the University of Padova, some beams with different reinforcement and anchorage have loaded for traditional flexural tests (see Figure 9). The comparison was carried out among the following test beams: ordinary reinforced concrete beam (RC-C), reinforced concrete beam strengthened with CFRP laminates

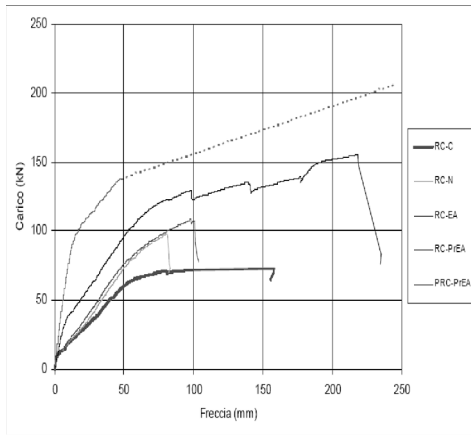


Figure 9. Load—deflection graphs for the 5 tested beams.

applied on undercoat resin (RC-N), reinforced concrete beam strengthened with CFRP laminates applied with resin and anchored with end plates (RC-EA), reinforced concrete beam strengthened with pre-stressed CFRP laminates (RC-PrEA), pre-tensioned reinforced concrete beam strengthened with pre-stressed CFRP laminates (PRC-PrEA).

In short, the beams strengthened with pre-stressed CFRP strips showed a better response in terms of a notable increase of the ultimate flexural strength and the first cracking moment, together with a better exploitation of CFRP material, which was capable to work at higher strain levels.

## 4 CONCLUSIONS

CFRP materials offers interesting opportunities for bridge strengthening and widening design. Thanks to their high quality characteristics, such as high strength, corrosion resistance and lightweight, and the simplicity and rapidity of their application, carbon-based composite materials are taking over traditional materials in bridge rehabilitation projects. The initial high cost of the materials may be offset by increased long-term durability, faster and safer installation and the consequent reduction of economic losses due to disruption of traffic during site operations, which is particularly important for works affecting toll-roads.

## REFERENCES

- ACI Committee 440, 2001. Guide for the design and construction of concrete reinforced with FRP bars. Farmington Hill (USA): American Concrete Institute.
- ACI Committee 440, 2002. Guide for the design and construction of externally bonded FRP systems for strengthening concrete structures. Farmington Hill (USA): American Concrete Institute.
- FIB Task Group 9.3, 2001. Externally bonded FRP reinforcement for RC structures. FIB Bulletin 14. Lausanne: Fédération International du Béton.
- CNR-DT 200/2004. Istruzioni per la progettazione, l'esecuzione e il controllo di interventi di consolidamento statico mediante l'utilizzo di compositi fibrorinforzati. Materiali, strutture in c. a. e c. a. p., strutture murarie. Roma: Consiglio Nazionale delle Ricerche.



# Maintenance and inspection of stay cables using prestressing steel at a German bridge

Christian Gläser & Hermann Weiher

*Department of concrete structures, Technische Universität München, Munich, Germany*

**ABSTRACT:** In the past all large stay cable bridges in Germany were built with locked wire ropes. For a new project, Ziegelgraben-Bridge crossing the “Strelasound”, the contract award also had allowed offers with stay cables using prestressing strands for tendoring. Before executing the bridges with stay cables using prestressing strands special requirements for the life time of the bridge were defined to ensure the durability and sustainability of the structure. The exchangeability of a stay cable as well as of a single strand has to be possible. The possibility for load measurements has to be given. Ducts and corrosion protection systems shall be visitable. Exchangeability had to be verified with special tests. For load measuring direct (lock-off-test) and indirect methods (vibration analysis) were applied. For vibration analysis reference measurements were performed after completion of the bridges. As most of the ducts of stay cables using prestressing steel have an outer helix to reduce vibrations common methods for visual inspection with cameras had to be modified. After the test methods had been planned a maintenance manual was created which defines the inspection periods as well as type and number of tests for the inspection period. By this an effective maintenance of the stay cables with adequate durability and safety shall be guaranteed.

## 1 PROJECT

### 1.1 Preface

First, it was planned, that locked wire ropes shall get installed as stay cables for the bridge crossing the “Ziegelgraben”, an anabranch of the Strelasound (Kleinhanß, et al 2007). Referring to the tender, the contractor submitted a design proposal, to use prestressing strands instead of strand stay cables.

In history locked wire ropes were almost exclusively used for all stay cable bridges in Germany. This type of cable consists in the core of round non alloyed steel wires and outside of shaped non alloyed steel wires. The biggest cable that has been manufactured in Germany until now has a diameter of 167 mm and a load capacity of 30 MN. The buildup of the cables, that have a big inner surface, requires a durable inner corrosion protection. This corrosion protection has to offer also a lubricating effect to decrease the internal friction of the single wires. The corrosion protection is done by galvanizing. Additional coating by polyurethane increases the protection on the outer surface of the cable. This coating has to be renewed several times in the life-time of a stay cable bridge.

In the tender for the construction of the bridge crossing the Strelasound it was first time in Germany that beside the locked wire ropes also cables using prestressing strands were enquired. The tender included

an extensive and detailed description that also contains the conditions for a specific project approval.

### 1.2 Bridge crossing the Strelasound (Baltic Sea)

The stay cable bridge crossing the Strelasound was constructed with a total length of 583 m and a main span of 198 m (see Figure 1). The steel superstructure with width of 16 m is connected to the pylon by cables arranged in harp-shape in two plains. The pylon is 128 m in height.



Figure 1. Cables of the bridge crossing the Strelasound.

### 1.3 Approval procedure

The German approval body (Deutsches Institut für Bautechnik, DIBt, Berlin) was charged to establish an experts' report, based on that the specific project approval could be given (Schellenberg 2006). On basis of the requirements of the tender and the regulations of the *fib*-recommendations (*fib* 2005) the DIBt together with an expert team defined requirements for the specific project approval:

- static and fatigue tests on the single strands
- full scale tests (fatigue tests with subsequent static loading) on a stay cable specimen (full scale test)
- water-tightness-test on the anchors
- exchangeability of single strands under service load of the cable
- identity tests
- proof of transversal and longitudinal stresses in the anchor area
- details for construction
- assembly of the stay cables and recording of the prestressing
- quality control
- evidence or prevention of cable vibrations
- measurements
- Monitoring measures.

## 2 STAY CABLE SYSTEM

32 stay cables DYWIDAG DYNA Grip® type DG-P 37 with 34 strands each support the superstructure in the area of the large spans of the bridge crossing the Strelasound. All strands have a steel cross section of 150 mm<sup>2</sup> and a characteristic tensile strength  $f_{pk} = 1770 \text{ N/mm}^2$ . In the anchors, there is free space for three extra strands to offer the possibility of strengthening later. Altogether 150 t of strands were installed at the bridge crossing the Strelasound.

The stay cables have a stressing anchor (consisting of an anchor-block with an adjustable ring nut) at the side of the superstructure and a dead anchor at the pylon-side. All anchors include sealing elements to avoid infiltration of water in the wedge area (see Figure 2).

As tensile elements 7-wire cold-drawn strands  $\varnothing 15.7 \text{ mm}$ , hot-dip galvanised and waxed, PE-coated are used. They are anchored with three part wedges. To reduce transversal bending effects in the anchorage zones, because of traffic, wind and temperature, an elastomeric bearing element is inserted which also has a damping effect and bundling function of the single strands (see Figure 2).

The whole strand bundle is surrounded by an alloy-coloured HDPE duct with an external helix, which has to prevent the occurrence of rain-wind induced vibrations (Caetano 2007).

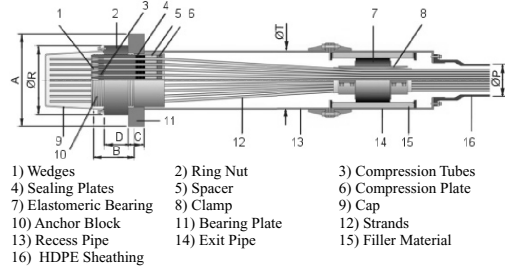


Figure 2. Detail of the anchorage zone of a stay cable type DYNA-Grip® using prestressing strands.

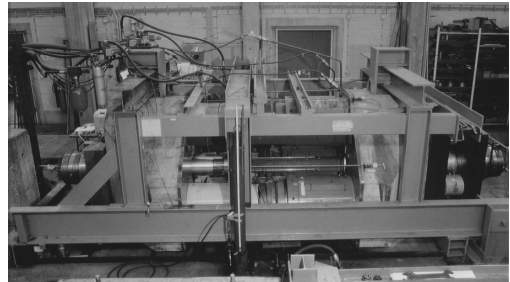


Figure 3. Machine for testing fatigue and static properties of stay cables at Technische Universität München, Munich.

## 3 CONSIDERATIONS FOR DESIGN AND ERECTION OF THE BRIDGE

### 3.1 Static tensile tests and fatigue test required for the approval

After a lot of fatigue tests and static tensile tests on single strands had been performed according to the test-program coordinated with the DIBt three full scale tests (fatigue tests with subsequent static tensile loading) on a DYWIDAG stay cable DYNA-Grip® DG-P 37 with 37 strands were carried out. The tests took place between November 2004 and March 2005 at the laboratory for structural engineering of Technische Universität München (TUM, Munich) according to the *fib*-recommendations (*fib* 2005).

TUM was selected because it is the only institution in Germany that has an appropriate testing machine (see Figure 3) and has long-range experience (Zilch & Gläser 2001) in testing of stay cables (testing for 68 stay cable bridges all over the world).

On basis of these tests the S-N-curve for the cables could be verified. By these assumptions the fatigue verification was done considering a design life of 100 years.



Figure 4. Exchange of a single strand in a test.

### 3.2 Exchangeability test

One advantage of stay cables using prestressing strands compared to locked wire ropes is the possibility to exchange single strands of the bundle. Because of the corrosion protection of the strands consisting of two barriers, which is furthermore produced in a factory, and a complex quality assurance concept on the production of strands, a fracture of the single strand seems nearly impossible. Nevertheless, the possibility of exchange was checked within the approval tests. In a test it was shown that a single strand of a cable DYNA Grip® type DG-P 37 could be exchanged under load.

After stressing again to service load, the tightness of the anchors was demonstrated by vacuum test. An inner strand was chosen for exchange. It could be removed without any problems. After removing the wedge, the strand could be pulled out and simultaneously the new strand could be inserted.

### 3.3 Monitoring during construction of the bridge

With regard to the special exposures, a large monitoring- and measuring-program was installed at this stay cable bridge. In the period up to the start of service it was the aim to assure the assumptions of the planning, as well as to establish a database for the future inspections and the maintenance.

Throughout the design the connection devices to the superstructure for the retrofitting with cable dampers were already provided. By permanent measuring of the cable vibrations of the longest cables seawards it was detected, that additional methods for damping must be considered. Therefore both horizontal and vertical vibrations in the lower part of the cables were recorded (Kleinhanß 2007).

Figure 1 shows some recordings of horizontal vibrations on a cable with an amplitude in the middle of the cable of about 90 mm, which was induced by wind with

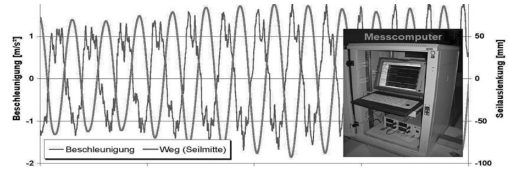


Figure 5. Cable vibrations, measuring unit (Kleinhanß 2007).

wind force 4 in longitudinal direction of the bridge. After first analysis, vertical vibrations also occur on moderate wind force but transversal to the bridge. A correlation of windstorms with the cable-vibrations has not been detected until now.

By these first results it was decided to do vibration analysis also in future. The measurements can also be used to calculate the cable force.

## 4 ACCEPTANCE OF THE QUALITY OF THE STRUCTURE

The owner of the bridge has considered that within the acceptance procedure a first main inspection has to be made by a competent inspector. During the first main inspection the relevant data of the structure and the stay cables have to be detected for inspectors in the future.

Additionally to the required inspections according to the national inspection code DIN 1076, the following tasks have to be done:

- Inspection of the arrangement of the anchorages at the superstructure and at the pylon.
- Recording of the actual stay cable-forces and comparison with the calculated forces.
- Recording of the temperature (surrounding, bearing structure and stay cable during the inspection).

## 5 SUITABILITY OF INSPECTION METHODS

A lot of testing methods are available for stay cables consisting of full locked wire ropes. Some of them have to be modified for stay cables using prestressing steel.

### 5.1 Inspection of ducts by camera

On the surface of the ducts a special helix is arranged to avoid rain- and wind-induced vibrations. Caused by this helix the surface of the ducts is not smooth and it is not easy to use common devices to travel on the stay cables. For the travelling on stay cables, a device produced by the company Alpin Technik and

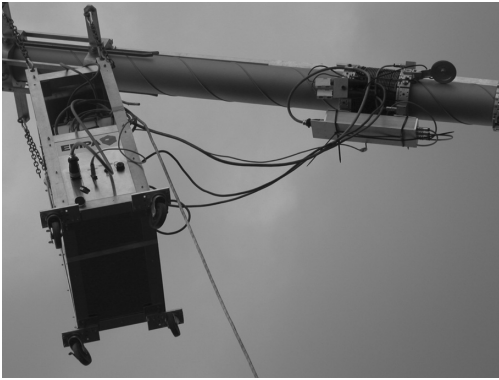


Figure 6. Cable testing using magnetic induction.

Ingenieurservice GmbH, which can be moved over the free length of the cable, was tested. The device is controlled from the ground. Cameras were installed on this device to check the status of the ducts and their couplers.

### 5.2 Cable testing using magnetic induction

Regular tests on full-locked wire ropes can show early the deterioration progress. Magnetic-inductive tests of the free cable lengths respectively supersonic tests on the anchorages were performed. Depending on the diameter of the cable, the EMPA respectively the DMT has developed different types of devices for the magnetic-inductive cable tests. This system was developed especially for cables with large diameters due to small filling ratios, like stay cables using prestressing steel. This system is especially developed for cable constructions which have a large cable-diameter caused by their small filling factor. For diameters of cables up to 250 mm reliable test results can be achieved.

The stay cables were tested by the measuring device travelling along it (see Figure 6). Initially the voltages developed by the hall probes are measured and recorded in defined steps along the cable. The image of the scatter field is made along the axis of the cable. Besides of wire fractures also initial corrosion can be detected.

It could be shown that the method can also be used for stay cables using prestressing steel.

### 5.3 Lift-off test on a single strand

To determine the load of a single strand of a cable, first of all the anchor cap has to be removed.



Figure 7. Preparation for lift-off test.



Figure 8. Lift-off test.

To reach the anchor a bridge soffit inspection device was used. After the cap was lifted (see Figure 7) the wax used for corrosion protection was removed.

A steel ring was pushed over one end of a strand so that the wedge was surrounded. A monostrand jack was seated on this steel ring. Then the load of the jack was increased until movement of the wedge was observed (see Figure 8). This procedure was repeated for all strands of the cable. Then the anchor cap was mounted again and was re-filled with wax. The measured load agreed very well with the calculated load.

## 6 INSPECTION AND MAINTENANCE

### 6.1 Preface

During the life cycle of the bearing structure, the stay cables have to be inspected and observed regularly according to DIN 1076 to guarantee their bearing capacity and durability or to prevent them from damages. If unexpected results during random inspections are made, the amount of testing has to be increased.

If damages are detected, special tests defined by the owner of the bridge will be required.

In the inspection manual, the main features of inspection and maintenance of the stay cables after the completion of the bridge have to be described. For this manual the results of the suitability testing of the different methods (camera inspection, magnetic induction, lift-off-tests) had been considered. This manual includes:

- General instructions about the building and the stay cable-system that was used.
- Schedule of the inspection and the structural monitoring.
- Type and number of tests and monitoring measures (at basic inspection, detailed inspection or extraordinary inspection).
- Maintenance work on the stay cables and their components.
- Documentation.

The documentation about the life-cycle of the stay cable, that has to be archived during the life-time of the building, must include at least the following information:

- Date of the inspection and name of the inspector.
- Description of the inspection and the nomenclature of the stay cables.
- Data, detected damages and photos of the damage that were collected during the inspection.
- Used tools and methods.

## 6.2 Basic inspection

During the basic inspections the whole bearing structure is examined in particular with regard to the stay cables as well as the anchorage area at the pylon and the superstructure. The basic inspection which is performed visually and without any tools has the following steps:

- Inspection of the correct state and position of the ducts, welding, deviation elements clamps, damping devices,
- Inspection for spots, leakages or deformations on the anchorage,
- Inspection of the integrated monitoring system.

## 6.3 Detailed inspection

Detailed inspections will be performed according to DIN 1076 in intervals of six years. Type and number of the inspection activities are defined in the maintenance manual. In addition to the basic inspection,

the detailed inspection should include the following inquiries:

- Visual check of the surface of the ducts (e.g. by cameras).
- After the random dismantling of the anchor-caps, the anchor-heads have to be examined, whether signs of water, modification or leaking of the filling material, can be observed. If unexpected results during random inspections are made, the amount of testing has to be increased. Opened anchor-caps have to be closed professionally.
- Tightness of the couplers of the duct.
- State of the deviation elements, damping devices and clamps.
- Corrosion protection of the anchorage and transmission areas.
- State of the installed drainages in the anchorage and transmission areas.
- State of the bearing elements.
- Random, non-destructive inspection of the stay cables, can be made via magnetic or other appropriate non-destructive testing methods.
- Random lift-off-tests of the anchorage or at single strands with an appropriate jack at opened anchorages.
- Random check of the Eigen frequencies.

## 6.4 Extraordinary inspection

The program of the extraordinary inspection has to be adapted to the special task.

# 7 CONCLUSIONS

The good experience of Strelasound Bridge initiates to execute an additional pilot project with stay cables using prestressing steel. This second bridge is executed at the moment near Wesel. It crosses the river Rhine. The durability and long-term-behaviour of the cables using prestressing steel will be observed in the following years. Thereby it will be shown, if the requirements defined in the maintenance manual contain the main features that have to be considered for inspection and maintenance.

## REFERENCES

- Gläser, Ch., Zilch, K. 2005. First German Application with stay cables using prestressing strands according to fib-recommendations. *Proceedings of the 6th Japanese German Bridge Symposium*, Munich.
- Gläser, Ch., Scheibe, M., Zilch, K. 2007. Die 2. Strelasundquerung—Erste deutsche Anwendung von Parallel-litzenseilen. *Bauingenieur* 98, Heft 4, pp. 8–16, Berlin: Springer.

- Fédération internationale du béton (*fib*). 2005. Recommendations for the acceptance of Stay Cable Systems, using Prestressing Steels. *fib-Bulletin* 30.
- de Sá Caetano, E. 2007. *Cable Vibrations in Cable-Stayed Bridges*. SED 9. Zurich: IABSE.
- Kleinhanß, K., Romberg, M., Saul, R. Schmidt-Hurtienne, B. 2007. Die 2. Strelasundquerung mit der Schrägseilbrücke über den Ziegelgraben. *Bauingenieur* 98, Heft 4, pp. 17–29, Berlin: Springer.
- Schellenberg, T. 2006. Innovation im deutschen Großbrückenbau durch Zustimmung im Einzelfall—Erstmalige Anwendung von großen Schrägkabeln aus Litzenbündeln. *DIBt-Mitteilungen* 66, Heft 3, pp. 100–110, Berlin: Ernst & Sohn.
- Zilch, K., Gläser, Ch. 2001. Developments in Testing Stay Cables. *Proceedings of IABSE Conference on Cable-Supported Bridges—Challenging Technical Limits*. Seoul.
- Gläser, Ch., Zilch, K. 2007. Tests for German applications with stay cables using prestressing strands according to fib-recommendations: Bridges crossing the Strelasund and the river Rhine near Wesel. *Proceedings of SEMC'07—The Third International Conference on Structural Engineering, mechanics and computation*. Capetown.
- Deutsches Institut für Normung (DIN). 1999. DIN 1076 - Engineering structures in combination with roads; inspection and test. German standard, Berlin.
- DMT-Prüflaboratorium für Zerstörungsfreie und Zerstörende Prüfung - Seilprüfstelle. *Hochfeste Zugglieder in abgespannten Bauwerken*. Information sheet of DMT. 2007, Essen.

# Assessment of bridge capacity through proof load testing

J.D. Gómez & J.R. Casas

*Universitat Politècnica de Catalunya, Barcelona, Spain*

**ABSTRACT:** Aging is a matter of increasing concern for most bridges that are part of the road and railway systems of the European Union. Many of these bridges are very old bridges without documentation. A possible way to assess their capacity is by means of a proof load test.

Two main questions should be solved when facing the execution of such a test: a) Which is the load level that the bridge should resist during the proof test to guarantee a predetermined service load with a required and appropriate safety level? and b) When the increase of loading should stop in order to not damage the structure?

The answer to these questions is part of the task of the EC 6th Framework Programme European Project ARCHES (Assessment and Rehabilitation of Central European Highway Structures). In the project a methodology of proof load testing for existing bridges in new member states will be proposed. The paper shows the basis of the method as well as the application to an existing bridge located in Barcza (Poland). The bridge should be removed in the next future and therefore the proposed methodology can be fully checked.

## 1 INTRODUCTION

Existing bridges in several parts of the world, including Europe, are aging. This is because of the great expansion in road construction occurred during the postwar period, the fifties and sixties. For this reason the evaluation of the existing structures is every day more and more important.

The increase of traffic and specifically the increase of the vehicles load capacity cause a greater effect on bridges. This increase along with a deficient maintenance has caused in some countries the deterioration of these structures. The consequences are serious in main road bridges. The consequences can be enhanced due to fatigue, corrosion and other forms of material degradation.

For the reasons exposed above, it is common to find that old bridges carrying normal traffic satisfactorily fail to pass the assessment calculation. In other cases, bridges that were designed with old codes or standards fail to pass the assessment when new codes prescribe higher levels of live load. These bridges are ranked as deficient, so, theoretically, they need to be posted, strengthened or in the worst case closed and replaced. These situations make to the highway administration invest a big part of its budget, in solving these problems.

The capacity assessment of a bridge tries generally: a) to confirm the maximum load that the structure can support under acceptable safety conditions or

b) increasing the service load limit. Nevertheless, usually the methods used in structural evaluation give very conservative results and the real resistance is much greater. This is because many of the used methods do not exactly reflect the structural behavior. The normal methods for calculating the bridge resistance tend to be conservative and often do not take into account some reserve capacity that comes from additional and/or hidden sources of strength (composite action between slab and girders in bridges that were designed as non-composite, rigid or semi-rigid connections that were designed as flexible, ...). Thus, the objective of load testing is to optimize bridge assessment by finding reserves in its behavior and load carrying capacity. Savings in such optimized assessment and, consequently, in less severe rehabilitation measures on deteriorated structures, can be significant.

Another problem when evaluating old structures is the difficulty to identify the actual properties, as well as the selection of a suitable safety level, especially considering the regulations of load of new trucks.

A good approach in the verification of the safety can be obtained by means of a proof load test where existing bridges are proven before keep them opened to traffic (Moses et al 1994). During the proof load test performed, often, the structure reveals resistance reserves, due to the nonstructural elements contribution, supports contribution, better materials properties, etc. In many cases, the cost derived from the replacement or reinforcement of posted bridges can

be avoided proving the structure safe through a proof load test. In other cases, as bridges with lack of documentation a complete theoretical assessment can not be carried out. (Minervino et al 2004)

The difficulty of the realization of a proof load test is in the estimation of the value of the proof load to apply during the test, so that this is sufficiently representative to evaluate the resistant capacity of the bridge with a relevant safety, without causing irreversible damages or the collapse of the structure.

Additionally the used deterministic methods in the evaluation of structures do not consider the uncertainty associated with the applied loads and the resistance of the structure, reason why we set out to study the determination of the structural reliability through proof load tests.

## 2 EVALUATION THROUGH PROOF LOAD TEST

### 2.1 Reliability model

As mentioned before, the deterministic assessment does not account for the uncertainties associated to resistance and load. For this reason, the assessment via proof load test is analyzed here in a reliability-based perspective. If  $R$  and  $S$  are the resistance and action variables respectively, the limit state function is defined as:

$$G(x) = R - S = 0 \quad (1)$$

And the safety margin,  $Z$ , can be defined as:

$$Z = R - S \quad (2)$$

The safety margin can be expressed as: (Fu et al 1995)

$$Z = R - G - \alpha Q = R' - \alpha Q \quad (3)$$

And the failure probability

$$P_f = \text{Prob}(R - S \leq 0) = \text{Prob}(Z \leq 0) \quad (4)$$

Where  $R$ ,  $G$  and  $Q$  are the real resistance values, effects of the permanent and variable actions respectively.  $R' = R - G$  is the margin of resistance for additional variable actions.  $\alpha$  is the traffic action adjustment coefficient. In agreement with Eurocode 1—Part 3 (EN 1991-3), a coefficient  $\alpha$  can be used. This coefficient is function of the highway type and expected or existing traffic, that must be defined by the National authority.

If  $R$  and  $Q$  are independent variables with normal distributions, the reliability index  $\beta$ , can be defined in

function of the inverse normal probability distribution,  $\Phi^{-1}$ , as:

$$\beta = \Phi^{-1}(-P_f) = \frac{\mu_R - \mu_s}{\sqrt{\sigma_R^2 + \sigma_S^2}} \quad (5)$$

### 2.2 Bridge description

The methodology described is applied here to a bridge that is fully documented and that should be removed in the next future. In this case, the proposed methodology could be compared to the standard assessment procedure and the posterior execution of the proof load will allow to go beyond the usual limits to not damage the structure.

The bridge is a three span concrete bridge, made of pre-stressed pre-cast beams (figure 1). The bridge has a 46°41' skew and is located in the Warsaw—Krakow highway, near to Barcza's town in Poland.

The bridge was designed and erected in the middle sixties of the previous century. It was designed according to the ancient Polish Code, to fulfill the requirements of Class I+T80. That means that unlimited traffic of 30 tons vehicles was permitted. This is equivalent to the class C of appropriate Polish Code PN-85/S-10030, which is being used nowadays.

The objective of the assessment is to know if the bridge in the actual conditions will be able to carry the traffic live load as prescribed in the Eurocode for actions on highway bridges (EN 1991-3). The question regarding the proof load test is: how much load should we put in the bridge to guarantee that the total traffic action (or a certain percentage of it) defined in the Eurocode can be carried out by the bridge with a predefined safety level?

The bridge structure is supported in four sections, with four columns (40 × 60 cm reinforced concrete) in each section. The exterior supports are founded in the ground with a 2,20 × 1,80 m slab (under each column), while the interior ones are founded on wells made of



Figure 1. Bridge lateral view.



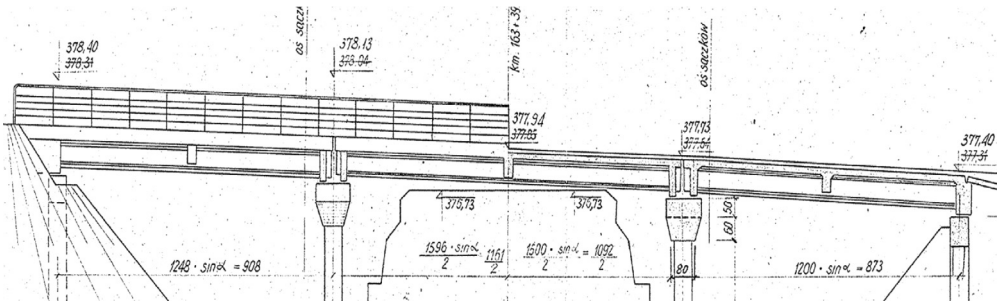


Figure 2. Bridge longitudinal section showing the foundation conditions.

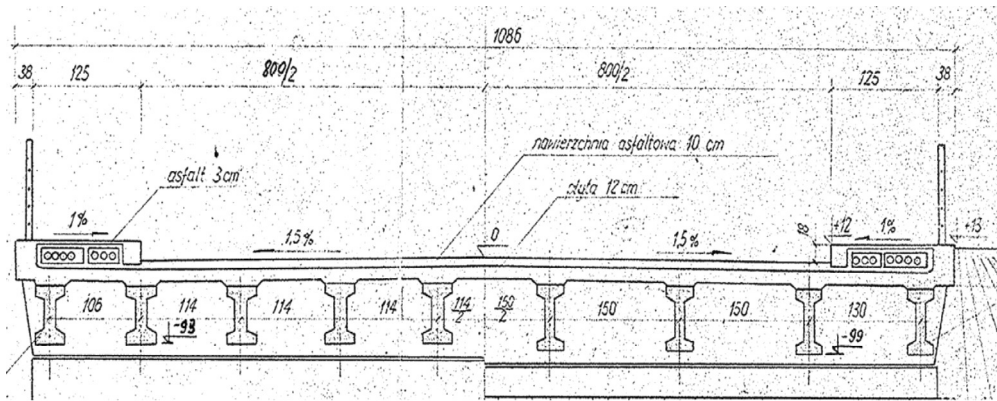


Figure 3. Beams and deck bridge section. Left: center span. Right: lateral spans.



Figure 4. Bridge bottom view.

of pre-cast. There are 10 girders in the main span with a separation of 1.14 m and 8 in the side spans with a separation of 1.5 m. (figure 4). The precast girders are made of C 40/50 class concrete, with a characteristic resistance,  $f_{ck} = 40 \text{ N/mm}^2$ .

In the center span, eight inner beams are stressed with 4 cables (18  $\sigma$  5), while the two outer ones with 5 cables. In the lateral spans, the six inner beams are stressed with 4 cables (16  $\sigma$  5), while the two outer ones with 4 (but 18  $\sigma$  5) cables. The design pre-stressing force in the cables is 330 kN.

The girders in all three spans are covered with 12 cm thick concrete slab made in situ. This is made of C16/20 concrete, with a characteristic resistance  $f_{ck} = 16 \text{ N/mm}^2$ . According to the original design there should be a 10 cm thick of asphalt pavement.

concrete rings (filled with concrete), which are dug 4,50 m under the ground (figure 2).

There are cross beams over the supports and a cross beam in the middle of the longest span (see figure 3). The span-length of the central span is 15,96 m. The lateral spans have a span-length equal to 12,48 m. The spans are simply-supported. The cross section is made

### 2.3 Deterministic model

In order to perform the main-span bridge structural analysis a 3-D finite elements model has been elaborated. The software used was the SAP2000. The precast girders have been modeled as beam elements,

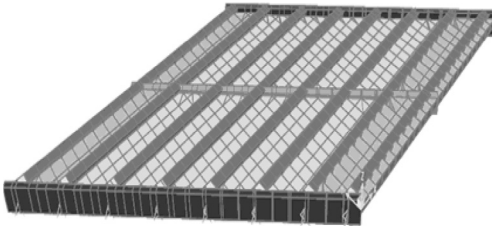


Figure 5. Finite Element Model of girders and deck.

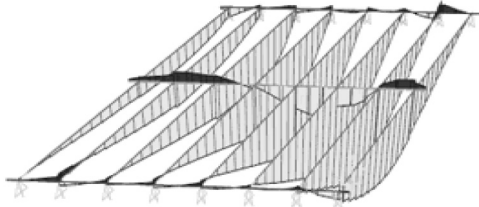


Figure 6. Longitudinal bending moments in girders and cross-beams for eccentric actuation of the traffic live load as defined in the Eurocode.

and deck and walkways as shell elements (figure 5). The variation of the cross-sectional section of the main beams is considering modeling them as nonprismatic sections.

The structural analysis allows to determine the effects of the Eurocode characteristic variable action,  $Q_{0,95}$ , in the different beams (figure 6). The most loaded beam is submitted to a bending moment in the center span equal to  $523 \text{ kN} \cdot \text{m}$  when the live-load action  $Q_{0,95}$  is applied. In the Ultimate State Limit, the total design bending moment  $S$ , due to the Eurocode characteristic variable action is:

$$S = \gamma_G G + \gamma_Q Q = 1.083 \text{ kN} \cdot \text{m} \quad (6)$$

Where  $\gamma_G (=1.35)$  and  $\gamma_Q (=1.5)$  are the load factors and  $G$  and  $Q$  are the of the dead and live load effect respectively.

From the drawings and the additional information provided, the ultimate bending moment of the girder+deck cross-section at mid-span with the partial safety factors for concrete ( $=1.5$ ) and steel ( $=1.15$ ) is evaluated as:

$$R = 1.216 \text{ kN} \cdot \text{m} \quad (7)$$

As  $R > S$ , then the bridge can safely support the Eurocode action in the ULS. Also it is verified that no cracking occurs for the frequent combination of actions. Therefore, the bridge can be rated as able to support the traffic action as presented in the Eurocode

for actions on bridges. In this case, this is possible because the bridge has a complete documentation. If there were not documentation or the analytical method would result on a negative assessment, then the proof load test is a good alternative as presented next.

## 2.4 Proof load determination

The objective is to obtain the proof load to be introduced in the main span that will guarantee the passage of a defined percentage of the Eurocode traffic action with a predefined reliability level. Once the target reliability index is defined, through equations (3) and (4) it is possible to obtain the required resistance for a predefined level of traffic load. Of course, first, the type of distribution as well as the main parameters (mean and standard deviation) of the variables involved should be defined. For example, in the case that both resistance and actions are all defined as Normal variables, the target value of the reliability index,  $\beta = 2.3$ , can be calculated from equation (5) as follows (Lichtenstein 1993):

$$\beta = \frac{\text{BIAS}(\gamma_{PL} \times Q_{d(0.95)} + \mu_D) - (\mu_Q + \mu_D)}{\sqrt{\sigma_R^2 + \sigma_Q^2 + \sigma_D^2}} \quad (8)$$

$R$  is the resistance,  $Q$  = variable actions effect;  $D$  = Effect of the permanent actions and self weight;  $\mu_Q$  = variable mean value;  $\sigma$  = standard deviation of the variable;  $Q_{d(0.95)}$  = characteristic variable action effect and  $\gamma_{PL}$  = variable actions safety partial factor. The mean value of the resistance can be defined by use of a BIAS factor applied to the nominal value of the resistance. The nominal value of the resistance is equal to the proof load applied during the test plus the permanent loads.

Because the evaluation of the structure will be made by means of the application of a proof load, the resistance of the bridge could accurately be well-known and its value can be handled like deterministic. Similarly we can accept that the value of the effects due to the actions of the self weight and permanent loads do not have uncertainty and therefore they are deterministic and therefore  $\sigma_R = \sigma_D = 0$ . This is because they are present on the bridge during the proof load test: Therefore in the equation (8) it is left to determine the partial factor of safety for the variable actions,  $\gamma_{PL}$  to reach a reliability index  $\beta = 2.3$ .  $\gamma_{PL}$  represents the number of times that the characteristic value of the traffic action should be applied in the test.

In this study, the influence of the type of distribution and the variability of the traffic action is investigated. The required proof load is obtained for 3 different

Table 1. Statistical definition of the variables used in reliability analysis.

Variable	Type	$\mu$ (kN · m)	COV	$Q_{(0,95)}$ (kN · m)
Q	Gumbel	360.2	0.25	529.0
		445.8	0.10	
	Normal	374.9	0.25	
		454.3	0.10	
	Lognormal	363.5	0.25	
		451.1	0.10	
G	Deterministic	158.2	—	—

distributions for the traffic action (Normal, Lognormal, Gumbel) as well as for 2 different coefficients of variation, 10 and 25%.

A sensitivity analysis will be also performed to find out the variation of the proof load factor for  $\alpha$  (as defined in 2.1) between 0.5 and 1.0. This will show the load to be applied during the test in order to guarantee the safely crossing in the bridge of a certain percentage of the live load in the Eurocode.

Next, the results of the sensitivity analysis for each variable distribution, and values of  $\alpha$  and  $COV$  are presented.

In the case that an explicit expression as presented in (8) is not available for the calculation of the reliability index, the FORM method is applied. This is the case when the traffic action is assumed as Gumbel.

Assuming that  $Q_{(0,95)}$  as defined in the Eurocode is the characteristic traffic action corresponding to a 5% probability of exceeding in 50 years (in other words, a return period of 1.000 years (Bruls et al 1996)) and for the corresponding values of the  $COV = \sigma\mu$  and depending on the distribution type, the mean values of the traffic action  $Q$  as presented in table 1 were calculated.

Additionally, the BIAS for material strength has been taken as 1.12. The effect value of the self weight and permanent loads were calculated from bridge drawings and specifications.

### 2.5 Results

In figure 7 is shown the influence of the type of distribution, variability and percentage of characteristic live load as defined in the Eurocode, in the proof load effect (bending moment) to be introduced in the most loaded beam of the bridge. Alternatively, in figure 8 it is shown the value of the partial safety factor  $\gamma_{PL}$  to be applied to the live load model for highway traffic actions in the Eurocode.

As can be seen in figures 7 and 8, the type of distribution is almost negligible for low values of the coefficient of variation of the traffic load. However,

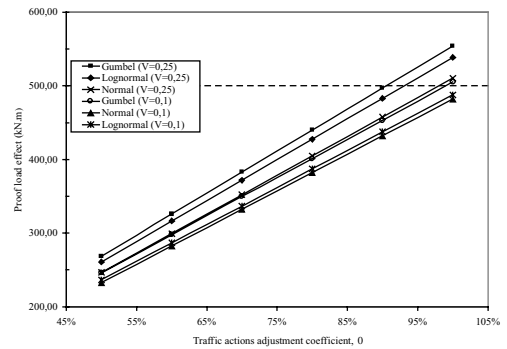


Figure 7. Proof load effect (bending moment in the most loaded beam) for  $\beta = 2, 3$ .

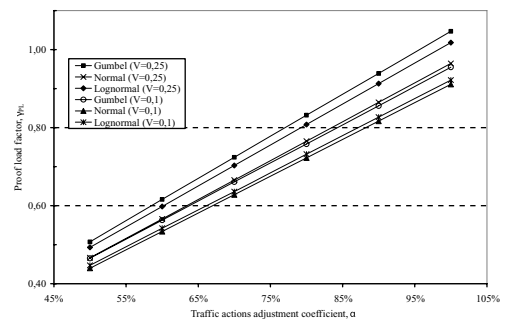


Figure 8. Proof load factor effect  $\gamma_{PL}$  for  $\beta = 2, 3$ .

the coefficient of variation seems to have a higher influence. The influence of the percentage of total traffic in the proof load effect is almost linear independently of the type of distribution and coefficient of variation.

### 3 CONCLUSIONS

The paper presents the application of a proof load test to assess the possibility of an existing bridge to carry higher loads than in the design. In particular, the objective is to see if the bridge can carry the traffic load as presented in the Eurocode for actions in highway bridges. In fact, due to the uncertainty in the variables involved (mainly the traffic), a reliability-based approach has been applied. Because the final results can be highly sensitive to the type of distribution and variability assumed for such random variables, the influence of the type of distribution and coefficient of variation of the traffic action on the final target proof load has been investigated. The Gumbel distribution produces the highest values of the target proof load,

whereas the lowest are due to the Normal distribution. Nevertheless, it is found that the type of distribution has a lower significance in the final results than the coefficient of variation. The example has been worked out with a target value of the reliability index of 2.3. Having the present results in mind, further analysis will be performed in the future for other values of the target reliability index. In this case, the reliability index gives the indication of the safety behind the load level attained in the test.

Because in the present case the bridge under study has a complete documentation, the results have been compared with those coming from a standard assessment based on a theoretical analysis using the dimensions and material qualities as presented in the design and the safety factors as taken in the Eurocode. In fact, this analysis shows that the bridge can safely carry the traffic load corresponding to the live-load model of the Eurocode. This result is also obtained with the reliability-based approach. In fact, the cracking moment of the most loaded beam in 750 kN m. The results of the analysis show how loading the bridge with a load producing in this beam a bending moment less than 600 kN m, the crossing of a 100% of the Eurocode traffic load will be also guaranteed. The level of 600 kN m, is completely feasible to be achieved as no cracking will be present in the bridge because of the load testing.

#### ACKNOWLEDGEMENTS

The authors want to thank the financial supports provided by the European Union 6th Framework Program through the European Project ARCHES (Assessment and Rehabilitation of Central European

Highway Structures) and the Spanish Government through projects BIA2005-24136-E and HP-2005-0101 (Acción Integrada España-Portugal). The authors also thank IBDIM (Dr. Piotr Olaszek) from Poland, for providing the documentation and data on the Barcza bridge.

#### REFERENCES

- Bruls A., Calgaro J., Mathieu H., Prat M. 1996. ENV 1991 Part 3: The main models of traffic load on road bridges Background studies. Proceedings of IABSE Colloquium, Delft, The Netherlands, IABSE-AIPC-IVBH, 215–228.
- EN 1991-3. 1998. Eurocode 1. Part 3. Basis of design and actions on structures. Traffic loads on bridges. European Committee for Standardization.
- Fu G., Tang J. 1995. Risk-based proof load requirements for bridge evaluation. *Journal of Structural Engineering* Vol. 121(3):542–556.
- Lichtenstein A.G. 1993. Bridge rating through nondestructive load testing. Technical report on NCHRP 12-38(13) A. Transport Research Board.
- Minervino C., Sivakumar B., Moses F., Mertz D., Edberg W. 2004. New AASHTO Guide Manual for Load and Resistance Factor Rating of Highway Bridges. *Journal of Bridge Engineering*. Vol. 9, (1):43–54
- Moses F., Lebelt J.P., Bez R. 1994. Applications of Field Testing to Bridge Evaluation. *Journal of Structural Engineering* Vol. 120, No. 6.

# Strengthening reinforced concrete T connections by steel straps

M.N.S. Hadi

*University of Wollongong, Wollongong, Australia*

**ABSTRACT:** The aim of this paper is to present results of testing a full scale reinforced concrete T connection by static loading. The connection is a T connection representing a beam-column connection. The beam and column had a square cross section with a 300 mm dimension. The height of the column was 2.9 m and the clear beam length was 1.4 m. The connection was initially tested to failure. Galvanised steel straps were used to strengthen the connection. Epoxy resin was used to fix the steel straps to the concrete surface. The connection was tested after the rehabilitation. Results of testing the rehabilitated connection show that the yield and ultimate loads were 65 kN and 95 kN, respectively, compared with the original test results of 75 kN and 84 kN, respectively.

## 1 INTRODUCTION

Connections are defined as a common point of intersection of the columns and beams and provide resistance to applied external loads due to the bending moment encountered at the joint. Therefore, connections play an important part in structures. The loading on structures pass through the beam-column connections. Load paths are developed in the concrete members and this allows the transfer of the externally applied loads to the support structures. Connections are critical and have to be designed so that failure due to shear, torsion and moment are minimised or eliminated. Research studies have indicated that some of the factors that have an important influence on the beam-column RC connections are: concrete confinement, confinement of reinforcement, axial compression on columns and the panel geometry of connection. Past events have shown that the collapses of structures are due mainly to the failure of the beam-column connections. Therefore, it is vital that beam-column connections are designed to the optimum possible ability. Research has been done to highlight the different factors that attribute to the failure of concrete connections and the methods used to counteract these failures.

This paper presents an investigation of testing a T connection. This T connection was originally cast and tested to failure in 2006. In 2007, the same connection was rehabilitated and tested to failure with the aim to test the viability of the strengthening technique. The rehabilitation technique composed of using galvanised steel straps with epoxy. Results of the test showed that the rehabilitation technique is an effective technique.

## 2 REVIEW OF LITERATURE

The Portland Cement Association conducted the first experimental tests on beam-column connections in the early 1960s (Hanson and Conner 1967). Since then other research studies have been done to provide applicable data for beam-column connection design problems. Some of these research studies are discussed below.

One such study was done to investigate the shear strength of reinforced concrete beam column connections by Meinheit and Jirsa (1981). The objective of this investigation was to examine the methods to improve the shear strength and measure the basic shear strength characteristics of a beam-column connection. Several reinforced concrete beam-column connections were developed and tested under cyclic loads. Meinheit and Jirsa (1981) found that the strength of the connection differed according to the axial load on the column, the presence of transverse beams and the amount of closed hoop reinforcement within the connection. Meinheit and Jirsa (1981) concluded that shear capacity improved due to transverse reinforcement in the connection, unloaded transverse beams improved the shear capacity, column axial load did not influence ultimate shear capacity of the connection, the connection geometry had no influence on the shear strength of the joint if the shear area of the connection remained constant and the increase in column longitudinal reinforcement did not result in the increase in shear strength.

Scott (1992) investigated the behaviour of reinforced concrete beam-column connections due to the different detailing methods of reinforcement.

This research made detailed measurements occurring inside the connection specimen by using internally strain-gauged reinforcement. This was done to obtain detailed distributions of strain along the column and beam reinforcement bars. As such, the intrinsic mechanisms of the connection behaviour could be comprehended.

Scott (1992) used three detailing arrangements for the reinforcement and three beam tension steel percentages in this research. They were: bending beam tension bars down into the column, bending beam tension bars up into the column and 'U' bars, in which the lower legs formed the bottom beam reinforcement. The beam tension steel percentage depended on the size of the steel bar used. This comprised of 1.0% and 1.9% respectively in a 12 mm or 16 mm diameter steel bar for shallow beam specimens and 1.3% in a 16 mm diameter steel bar for deep beam specimens. Several specimens were developed and tested in a purpose built testing rig. A full column load of 50 kN or 275 kN was used in increments of 25 kN. The load was held as the beam was loaded downwards in 1 kN increments till failure. Strain measurements of the steel reinforcement bars were measured together with the concrete surface strains.

Scott (1992) found that specimens with 1.0% beam tension reinforcement bent down into the column or bent into the 'U' bar failed due to development of a plastic hinge on the beam at the face of the column when a column load of 275 kN was used. Gross yield of the reinforcement beam bars resulted in high reinforcement strains. However, when a column load of 50 kN was used on similar specimens, failure due to extensive joint cracking and strains was recorded. Other specimens failed due to extensive joint cracking and the strains were lower occasionally in the elastic range. The load transfer in the three beam details was mainly due to the development of bond stresses at the bend up to the point of cracking. Upon cracking, the loss of bond in bars bent down and the 'U' bars was provided for by bond development stresses over their length. This enabled a large load increment between joint cracking and failure. In contrast, the bars bent up detail failed to account for the loss of bond and resulted in a brittle failure. Scott (1992) concluded that the bars bent down and the 'U' bar details performed better than the bars bent up detail and recommended the use of the bars bent down detail if ductility was of main importance.

### 3 TESTING THE INITIAL CONNECTION

In 2006, a helically reinforced T connection was tested to failure. The dimensions for the beam-column connection and the testing geometry are shown in Table 1 and Figure 1, respectively.

Table 1. Dimensions of the structural elements.

Structural element	Dimension (mm)
Column length	2900
Beam length	1400
Column cross-section	300 × 300
Beam cross section	300 × 300

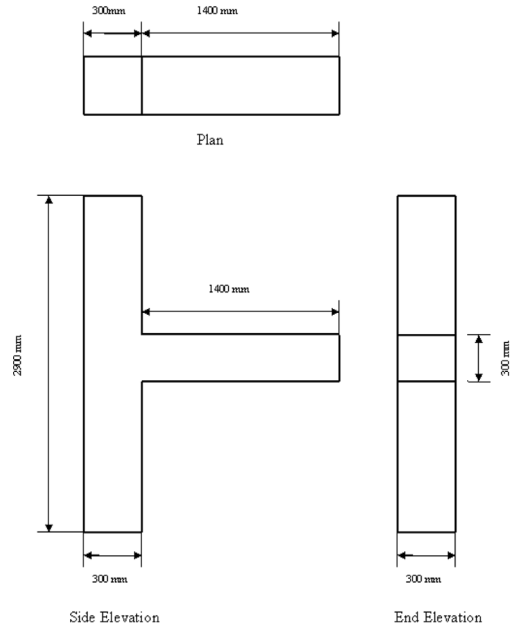


Figure 1. Dimensions of the beam-column connection.

#### 3.1 Materials used

A grade 32 NSC with a compressive strength of 32 MPa was used to build the beam-column connection. The average concrete strength after 29 days was found to be 46.78 MPa.

D500 N deformed steel bars were used in building the beam-column connection. The steel bar had a specified yield stress of 500 MPa and had normal ductility. R10 plain steel bars were used for the stirrups, having a specified yield stress of 250 MPa and normal ductility. Three samples 300 mm long were tested in the Instron testing machine. The steel bars were found to have an average tensile strength of 538.6 MPa. This was above the specified value of 500 MPa.

#### 3.2 Reinforcement

The specimen was reinforced with N20 and N16 bars as shown in Table 2 and Figure 2.

Table 2. Specimen reinforcement.

Member	Reinforcement location	Steel used
Beam	Tensile reinforcement	2N20
	Compressive reinforcement	2N16
	Stirrups—normal spacing	150 mm
	Stirrups—joint spacing	50 mm
Column	Tensile reinforcement	2N20
	Compressive reinforcement	2N16
	Stirrups—normal spacing	150 mm
	Stirrups—joint spacing	50 mm

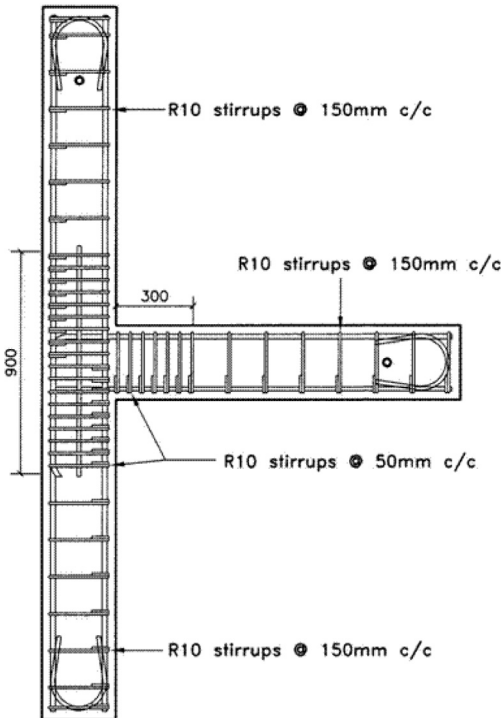


Figure 2. Reinforcement details.

### 3.3 Testing the specimen

The testing frame shown in Figure 3 was used to test the specimen both the initial specimen in 2006 and the rehabilitated specimen in 2007.

The loading regime was chosen in line with the capabilities of the frame and the loading jack. An increasing single load was adopted.

The hydraulic jack applied a downward vertical load onto the beam to create a large turning moment within the concrete connection. The load was applied at a distance of 1100 mm from the column beam interface while the column was held securely in place.



Figure 3. Testing frame.

The hydraulic jack applied a constantly increasing point load at the end of the beam until the beam reached ultimate failure. The loading rate was determined by the increase or decrease in pressure applied to the hydraulic jack by the hydraulic pump. The hydraulic pressure supplied to the jack was adjusted by using the turning the knob on the hydraulic pump and was constantly increased to keep the deflection rate of around 2.5 to 5 mm per minute until the beam yields, at which the applied pressure was kept constant as the beam continued to deflect at approximately 3 to 5 mm per minute. The pressure began to decrease as the beam reached ultimate failure and the internal tensile steel ruptures.

The beam was loaded with a 550 kN universal hydraulic jack from 0 kN to the ultimate load point whilst deflections, strain readings and rotation measurements were taken throughout the test. All measurements were attached via a data logger into the computer for a constant readout of the performance of the beam logged at around 5 Hz, five readings per second.

An 111.5 kN load cell that was connected above the hydraulic jack during testing measured the applied load. The 111.5 kN load cell was calibrated on the INSTRON by technical staff. An LVDT measured the deflection directly above the loading point of the beam in millimetres.

Steel reinforcement strains within the beam were read by the change in resistance of the strain gauges that were logged onto the computer. The concrete tensile strains were measured using a concrete embedment gauge developed at the University of Wollongong. The embedment gauge consists of a normal steel strain gauge that is embedded within an epoxy resin shape that can bend and stretch to measure the strain of the concrete. Several strain gauges during testing stopped reading after yield of the beam occurred as concrete movement can destroy the small strain gauge wires or scratch the gauge surface.

The rotation of the beam during the test indicates exactly the rotational capacity of the connection. Two inclinometers were used to measure the degree of rotation of the beam and column during testing. The inclinometers logged the rotation in degrees during the entire test. The overall rotation of the joint will be equal to the rotation of the inclinometer on the beam minus the inclinometer on the column. Table 3 shows results of testing the original specimen.

## 4 REHABILITATION OF THE SPECIMEN

### 4.1 Preliminary testing

Four main materials were used in rehabilitating the specimen, viz. epoxy (EP40 and EP10), galvanised steel and steel straps. Two specimens (cylinder with a nominal diameter of 50 mm and nominal height of 90 mm) of EP40 were tested for compressive strength which yielded an average compressive strength of 99.6 MPa. Two specimens of EP10 epoxy specimens were tested for tensile strength. The shape of the specimens was dog bone 360 mm long and 20 mm by 6.5 mm nominal cross sectional area in the test region. The average tensile strength of the EP10 epoxy specimens was 46.2 MPa. Three specimens of galvanised steel were tested. The specimens were dog bone in shape and had an overall length of 360 and cross sectional nominal dimensions of 20 mm by 0.5 mm. The average tensile strength of the galvanised steel specimens was 358.4 MPa. Two steel strapping samples were tested in the Instron machine for their tensile strength. The samples were cut off from the bulk roll of steel straps and were 270 mm long. The nominal cross sectional dimensions of the steel strap specimens was 0.5 mm by 19 mm. The average tensile strength of the steel straps was calculated to be 711.5 MPa.

### 4.2 Preparing the specimen

During the initial test, three major tensile cracks were formed and there was a major crushing of the concrete in the compression zone of the connection. Two of the major tensile cracks propagated right through the

beam cross section while the other tensile crack did not. Some minor cracks formed on the surface of the beam and column.

The following procedures were undertaken to repair and retrofit the damaged T connection. Each procedure is explained below.

The contact surfaces had to be cleaned before the application of epoxy into the cracks. Loose concrete, oil, grease, free standing water and dust were to be removed. The contact surfaces were free of oil, grease and free standing water. Loose concrete and dust were removed by hand and air blasted. Air blasting was done through the operation of an air compressor.

A problem was encountered while trying to lift the beam. The whole structure moved while an upward force was applied through a hydraulic jack to lift the beam. Apparently, there was not enough restraint on the top end of the column. The self weight of the column could not resist the load applied. As a result the force from the hydraulic jack caused the whole structure to move. Therefore, a restraint had to be applied on the top end of the column before the beam could be lifted.

A chain block was used to restraint the column on the top end to counter the problem. A hole had been drilled on the top of the column to aid its transportation previously. A steel rod was placed through the hole and the chain block was anchored.

The beam was lifted through the application of an upward force by the hydraulic jack after the column was restrained. There was no movement of the structure and the beam was lifted to its horizontal position. After the beam was put to its horizontal position it was supported by a wooden prop to prevent the beam from falling against its own weight.

A designed to fit formwork was constructed to prevent the leakage of epoxy on the underside and the sides of the gap. The formwork was made of plywood and screwed using threaded rods and bolts to hold it together. The formwork was installed after the beam was aligned to its horizontal position. The formwork was sealed along its edges using Bostik Silicone. This was done to prevent any leaking of the epoxy.

There was a large removal of concrete in the underside of the beam. For this particular region, injection of epoxy was not practical. Hence, a different grade of epoxy was used to patch it up. The Conbextra EP40 was used to fill the gap. The epoxy based resin and hardener were mixed in the ratio 1 to 4, respectively. Three samples were made to test for the compressive strength. The samples were cast on the same day as the epoxy was applied. Care was taken while handling the epoxy because of its corrosive nature. Safety goggles, mouth mask and rubber gloves were worn at all times when handling the epoxy.

Epoxy was then applied into the underside of the beam. A hole had been drilled into the formwork prior



to installation to create an opening for the pouring of epoxy. The epoxy was poured through a funnel that was connected to a hose fitted into the opening in the formwork.

Epoxy was injected into the tensile cracks after the removal of loose concrete and dust. The Conbextra EP10 was used to fill the tensile cracks that ranged from 0.2 mm to 0.01 mm. Holes were meant to be driven to inject the epoxy if needed. However, it was not needed in this case as the epoxy was very viscous. In fact the epoxy flowed just like water. Hence, the epoxy flowed very well into the cracks. The epoxy was injected using the Nitofill LV injection system. The cartridge containing the epoxy was inserted into the injection gun and a static mixer hose was fitted onto the cartridge. The epoxy was then left to cure for 7 days to gain its specified strengths.

A galvanised steel jacket was fabricated from galvanised steel. The steel jacket was measured, cut and bent to the required shape. The dimensions of the fabricated steel jacket are shown in Figure 4.

The dimensions of the steel jacket were marked onto the steel sheet, the sheet was then clamped with G-clamps onto a large working table and finally the steel sheet was cut using an electric cutter. Subsequently it was bent along the dotted lines to achieve its final form and was then fitted into the connection. The galvanised steel sheet was bent to the required shape using the bending machine. The steel jacket was then placed into the connection. Steel straps were used to hold the steel jacket in place and apply a confining pressure. The straps were spaced at 20 mm intervals. 22 steel straps and 19 steel straps were clamped onto the column and beam, respectively. A special band-it tool was used to apply a confining pressure to the steel straps and clamp them in place. The tool consists of a cutting handle, a grip lock and a turning handle.

The steel straps were provided in a bulk roll. The steel straps were first cut into lengths of 1800 mm to ease the application of the straps onto the connection

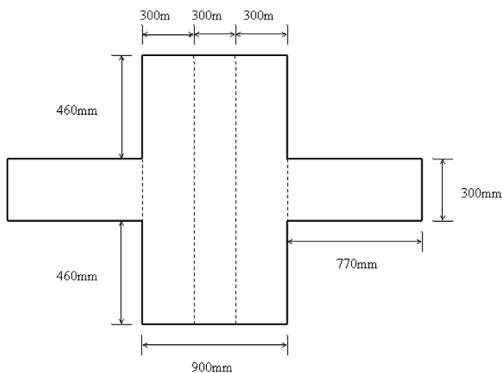


Figure 4. Dimensions of steel jacket.



Figure 5. T-connection completed with steel straps.

using the band-it tool. The above mentioned procedure was necessary as the accessibility was restricted due to the testing frame. A buckle was used to lock the steel straps in place.

Figure 5 shows the completed strapping of the galvanised steel sheet onto the connection with the steel straps.

## 5 TESTING PROCEDURE

An increasing single load was applied to simulate progressive collapse loading as done during testing the initial specimen. A hydraulic jack applied a downward vertical load onto the beam to create a turning moment within the connection. The load was applied at a distance of 1100 mm from the column-beam interface. The hydraulic jack applied an increasing point load until ultimate failure of the beam was reached. The loading rate was set to keep the deflection rate between 2.5 mm and 5 mm per minute and was determined by increasing or decreasing the pressure applied by the hydraulic pump to the hydraulic jack. An increasing single load was applied onto the beam with a 550 kN universal hydraulic jack from 0 kN to ultimate failure load. The deflections of the beam and the rotation measurements were taken throughout the testing period. The measurements were attached to a computer data logger to obtain a constant readout of the performance throughout the test. The applied load was measured via a 111.5 kN load cell which was connected on top of the hydraulic jack. The load cell was calibrated by technical staff before it was fixed on top of the hydraulic jack. A LVDT was placed to measure the beam deflection and was placed on the edge of the beam at a distance of 1100 mm from the column-beam interface. Two inclinometers were used to measure the rotation of the column and beam. The inclinometers logged the rotation in degrees for the whole test. One inclinometer was placed on the column and the other on the beam.

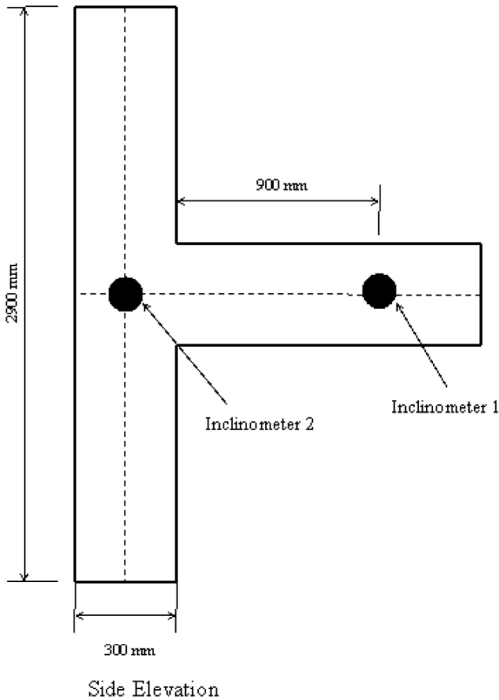


Figure 6. Position of inclinometers.

Table 3. Comparison of results.

	Original	Rehabilitated
Yield load (kN)	75.83	65.37
Yield deflection (mm)	20.15	28.2
Yield rotation (degrees)	0.665	0.8
Ultimate load (kN)	84.69	95.48
Ultimate deflection (mm)	167.89	170.8
Ultimate rotation (degrees)	10.94	7.3

The overall rotation of the joint is equal to the rotation of the beam minus the rotation of the column. The position of the inclinometers is shown in Figure 6.

The performance of the rehabilitated specimen was determined by comparing its results with the results obtained in 2006. The overall comparison of the results is summarised in Table 3.

From Table 3 several conclusions can be made:

- The yield load for the rehabilitated specimen was lower than the original specimen.
- The ultimate load for the rehabilitated specimen was higher than the original specimen.
- The rehabilitated specimen did not increase the joint rotation.
- The rehabilitated specimen reached ultimate failure.

## 6 CONCLUSIONS

The performance level of the rehabilitated specimen was determined by comparing the results obtained with the results of the original specimen. It was found that the rehabilitated specimen had no increase in the rotational capacity of the joint. The rehabilitated specimen had a yield load of 65.37 kN. This value was lower than that of the original standard specimen which had a yield load of 75.83 kN. However, the rehabilitated specimen achieved a higher ultimate load of 95.48 kN compared to an ultimate load of 84 kN achieved by the original standard specimen. This was an approximate increase of 13.67% in the ultimate load.

It was found that the rehabilitated specimen had a brittle failure as opposed to a ductile failure of the original specimen. In addition, a single major tensile crack developed in the rehabilitated specimen. This crack was ripped off the column. This failure pattern was totally different from the original specimen in which case multiple tensile cracks had occurred in the beam. Therefore, it shows that the stresses were not evenly spread along the beam for the rehabilitated specimen resulting in a brittle failure.

It was also observed that the region repaired with epoxy did not reopen. The epoxy, Conbextra EP10, managed to withstand the tensile load applied. There was no epoxy crushing in the compression zone of the beam as opposed to a large crushing of concrete in the original specimen. This shows that the epoxy, Conbextra EP40, managed to withstand the applied compressive load. The two primary tensile reinforcement bars were totally ruptured upon ultimate failure.

The epoxy performed satisfactorily. However, the contribution of the external steel reinforcement on the performance of the structure was difficult to gauge.

Finally, although the reinforcing steel did yield during the initial test, the rehabilitated specimen proved to be capable of carrying considerable loads before failure.

## REFERENCES

- Hanson, N.W. & Conner, H.W. 1967. *Seismic resistance of reinforced concrete beam-column joints*—Portland Cement Association, Research and Development.
- Meinheit, F.D. & Jirsa, O.J. 1981. Shear strength of RC beam-column connections. *ASCE 107 (ST11)*: pp. 43–45.
- Scott, R.H. 1992. The effects of detailing on RC beam/column connection behaviour. *The Structural Engineer* 70 (18): 318–324.

# Development of a software-tool for the life-cycle management of bridges

M. Kluth, A. Borrmann & E. Rank

*Chair for Computation in Engineering, Technische Universität München, Munich, Germany*

T. Mayer & P. Schiessl

*Centre for Building Materials, Technische Universität München, Munich, Germany*

**ABSTRACT:** This paper introduces a software tool for the predictive life-cycle management of reinforced concrete bridges. The novel aspect of this particular tool is the integration of non-destructive inspection techniques in combination with fully-probabilistic deterioration models. The use of these models requires that the building under examination be subdivided into multiple levels of detail. We employ a 3D model of the building for creating and visualizing the different system levels. At the same time the 3D model forms the basis of any data acquisition, analysis and evaluation. The system is implemented by coupling a Java 3D front-end with a relational database, in which the construction geometry and all related information is stored. Due to the long life span of bridge structures, the software is required to satisfy special requirements in terms of its flexibility. It is shown how new materials, inspection techniques, deterioration models, repair procedures etc. can easily be integrated into the software tool.

## 1 INTRODUCTION

### 1.1 Motivation

According to statistics published by the German Federal Ministry for Transport, Building and Urban Development (Bundesministerium für Verkehr, Bau und Stadtentwicklung 2006) there is a stock of about 120,000 bridges in Germany. The institutions that own these bridges are faced with the problem of maintaining these aging structures with just limited funds at their disposal (Schiessl & Mayer 2006). During the past 20 years or so, numerous so-called computer-aided bridge management systems (BMS) were developed to support engineers involved in the inspection or repair planning of bridge structures (see [Section 1.2](#)): information from inspections is stored in a BMS and can be consulted at any time. This data is also used to compute the condition of the structure, described as part of a marking system. One disadvantage of many existing BMS systems is that the lack of adequate deterioration models only allows for the detection of damage through visual inspection (e.g. cracking, staining, spalling). In most cases, the best time for (preventive) repair work on concrete component parts has already passed once erosion becomes visible on the concrete surface. Predictive life-cycle management systems (LMS) are a novel approach to overcome this major drawback of conventional BMS. To detect

decay earlier on, additional non-destructive and visual inspection techniques are used in combination with fully-probabilistic deterioration models to predict the endurance and longevity of component parts. The prognosis will be constantly updated, thus being more precise concerning rate of deterioration. Such a LMS can thus be used to optimize the operation of bridges over their entire service life (Schiessl & Mayer 2006, see also [Budelmann & Starck 2008](#)). Furthermore, the system supports the institutions responsible for bridge maintenance in the long-term planning of inspections and repair measures at both bridge level and network level. Another advantage is that the required budget for funding the reconditioning measures can be planned more precisely.

In an ongoing research project we develop a software tool for the predictive life-cycle management of reinforced concrete bridges. A 3D building information model (BIM) is at the heart of this system. All relevant data like measurement results, photos or condition prognoses are stored in this BIM. In this way, the owner of a stock of bridges can easily obtain an overview of the condition of individual structures or the complete bridge stock. The hierarchic subdivision of structures into component parts, sub-elements and hotspots chosen for the BIM allows for a more precise allocation of information.

## 1.2 Related work

Several life-cycle management systems for bridges are already in operation. In Germany “SIB-Bauwerke” was developed by the Federal Highway Research Institute (Bundesanstalt für Strassenwesen). This software is used on a national and federal state level (Haardt 2002). The city of Düsseldorf developed another system for the maintenance planning of all bridges and tunnels within the city (Landeshauptstadt Düsseldorf 2007). The following list shows some systems from other countries (the list does not claim to be complete):

- Bridgelifa in Finland (Vesikari 2006),
- Danbro in Denmark (Henriksen 1999),
- Eirspan in Ireland (Duffy 2004),
- Kuba-MS in Switzerland (Haller & Basurco 2006),
- Pontis (Robert et al. 2003) and Bridgit (Hawk 1999) in the USA
- Ontario Bridge Management System in Canada (Thompson et al. 1999).
- “Mobile model-based bridge lifecycle management systems” are currently being developed in Canada (Hammad et al. 2006).

The aforementioned systems are characterized by the following properties:

- Except for the “mobile model-based bridge lifecycle management systems” (Hammad et al. 2006) no explicit geometry is used. Photos or measurement results can only be allocated to component parts as text information.

- Adding a bridge to a system of this kind, the bridge is structured horizontally into “parts” and vertically into levels. The number of levels differs from system to system. The smallest “unit” in all these systems is a component part. No further subdivision is used in any of these systems.
- For predicting the progressive condition of component parts or the whole bridge, respectively, deterministic models (such as Haardt (2002), Landeshauptstadt Düsseldorf (2007), Henriksen (1999)) or Markovian Chain systems (Vesikari (2006) etc.) are used. Fully-probabilistic deterioration models are not used in any of these systems.
- The condition of a building is assessed manually, solely on the basis of visual inspections. Hardly any other non-destructive inspection methods are ever used.

## 2 PREDICTIVE LIFE-CYCLE MANAGEMENT

### 2.1 Architecture

The architecture of the life-cycle management system we are developing is shown in Figure 1. This system is primarily developed for bridges but it can also be used for other reinforced concrete structures subject to severe environmental loading (such as tunnels, multi-storey car parks and offshore structures). The features of the system are described for bridges without loss of generality. The system consists of five modules: acquisition module, condition acquisition module, assessment module, repair module, prognosis module.

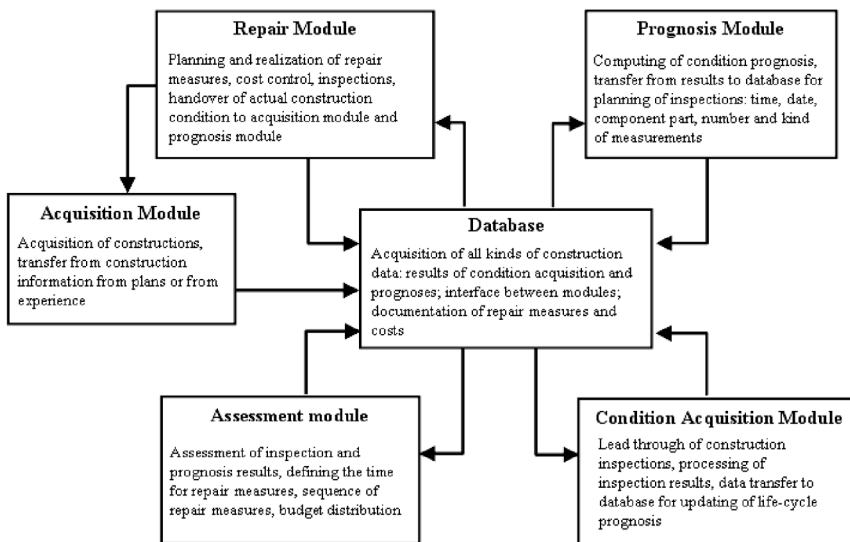


Figure 1. Assembly of the predictive life-cycle management system (according to Schiessl & Mayer 2006).

module, prognosis module, assessment module and repair module.

The database represents the centre of this system, in which the following information of every construction is stored:

- general information,
- geometric data,
- characteristic material properties for every component part,
- environmental loads,
- inspection results,
- located deteriorations,
- inspection and repair planning,
- type of structure.

The database is the interface between all modules in this system. With the help of the acquisition module it is possible to store new constructions in the database. Once all construction information has been stored, all the other modules can make use of it.

The prognosis module can be used to calculate and predict changes in the condition of every component part over the course of time. Non-destructive inspection methods are used for updating the original prognosis results for each component part. It is accordingly necessary to define and store deterioration models in the database.

At the moment, sufficiently quantified deterioration models only exist for the depassivation of reinforcement due to carbonation or chloride ingress (see Gehlen 2000, for instance). For most reinforced concrete elements, reinforcement corrosion forms the main cause of decay. However, to allow for a deterioration prognosis for phenomena that cannot be properly modelled today (such as freeze-thaw-attack, ASR), simpler models like Markovian Chain-systems are used. These models can be replaced by suitable fully-probabilistic deterioration models at any time. Predicting the progressive decline (in a structure's condition) will be probabilistically calculated using the software package STRUREL (RCP 2007). We intend to establish a corresponding interface between STRUREL and the LMS to enable the required data exchange. If the system is used for a new bridge still under construction, an initial prognosis can be carried out during the planning stage and updated with the results of the acceptance inspection ("birth certificate", Mayer, Schiessl & Zintel 2008).

The condition acquisition module is used to plan and carry out inspections. This module will be used to assign measurement results, which were collected during inspections, to component parts. These results are mainly generated by means of non-destructive inspection techniques. In this way, it is possible to detect damage (like depassivation of reinforcement) at a very early stage. The correct interpretation of the inspection results still relies on engineering experience and

cannot be left to the software. Using the measurement results and deterioration models, the condition prognosis for every part is updated by means of the prognosis module. In the next step, the acquisition module develops an inspection programme based on the computed condition changes. This programme not only contains all the inspection methods available but also the number of inspections (per component part, for example).

The assessment module determines the optimum time for any kind of repair measures on the basis of the predicted condition changes at any one time. One purpose of repair measures is to eliminate possible damage at an early stage, thus enabling the construction to last longer while saving money because such "preventive" repair work is usually cheaper than mending a damaged component part. Further information about planning of repair measures is given in Empelmann et al. (2008). The repair measures are approved using the repair module. The structural condition following these repair measures is stored on the database. The prognosis module uses this information to compute a so-called Bayesian update for all condition prognoses.

## 2.2 3D Building model

In conventional life-cycle management systems the allocation of information is done textually. In the system we propose, a 3D building information model forms the core of the data acquisition and data retention system. This is because we regard 3D building models as the most suitable form of data representation in the LMS context. This model stores the components' geometry as well as all the information on material properties, environmental loads, deterioration, inspections, repair measures and condition changes related to the geometry. In addition, all the results of non-destructive inspection techniques or photos taken during inspections can be attached to the geometric representation of the corresponding component. This way, information is easily allocated and a very good overview is guaranteed.

To adapt a construction to the building information model, it is subdivided vertically into levels and horizontally into "parts" to achieve the best allocation of measurements, deteriorations, repair measures, etc. So up to five levels of detail (LoD) are used. These are shown in Figure 2 (Schiessl & Mayer 2007).

The first step is to subdivide the construction (level 1) under consideration into modules (level 2). This subdivision is done from an organizational or functional point of view (Schiessl & Mayer 2007). For instance, the modules of a construction of type *bridge* are: foundation, bridgehead, pylon and superstructure. Although the system is mainly developed for bridges, it is also possible to organize other constructions with

this tool. For this reason, a fifth type of module is defined: a *general module*. Whereas the four aforementioned modules may appear only once in every construction, the general module can appear several times. Every general module is defined by a different name.

A module consists of component parts (level 3) of comparable material resistance, which are subdivided into sub-elements (level 4) of comparable environmental stresses. Furthermore every sub-element can be subdivided into hotspots (level 5). Hotspots are used for sections which have a low material resistance and/or extraordinarily high environmental loads which are critical for the condition of the construction. These hotspots can be set by the engineer or bridge-owner during planning. New hotspots can be defined at the implementation stage if local changes in environmental stress are observed during the course of inspections (Schiesl & Mayer 2007). Material resistance, environmental loads and geometric details are allocated only to elements at levels 3 to 5.

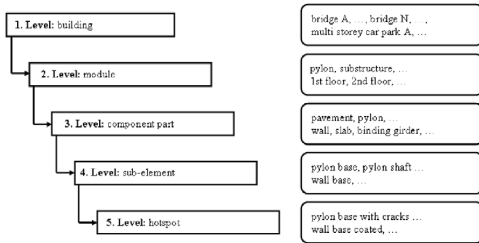


Figure 2. Structure for a bridge (according to Schiesl & Mayer, 2007).

This subdivision of component parts into sub-elements and hotspots is tedious, but it is absolutely necessary in order to make optimum use of the fully-probabilistic deterioration models mentioned above. This makes it possible to achieve a much better allocation of deterioration to different areas, and the prognosis for the whole structure will be more precise.

All constructions that are stored in the database collectively form the network level. Inspections and repair measures can be planned at network level or building level.

Determining the condition of a structure is done by aggregation of the condition of all building levels. With the described levels of detail approach, the owner of a bridge can easily acquire detailed information or assess a construction's condition from the hotspot level to the whole construction at network level.

### 3 SOFTWARE TOOL

#### 3.1 General information

The software tool presented in this paper is implemented by coupling a Java application (Sun Microsystems 2006a) with a relational database. All construction information, including geometric data, is stored in this database. A relational MySQL database (MySQL 2007) was chosen as the database management system (DBMS). The advantages of this DBMS are fast access to data, the possibility of storing large amounts of data, and no licence fees. The three-dimensional representation of the construction's geometry is achieved with the Java 3D library (Sun Microsystems 2006b). A screenshot of the acquisition module is shown in Figure 3.

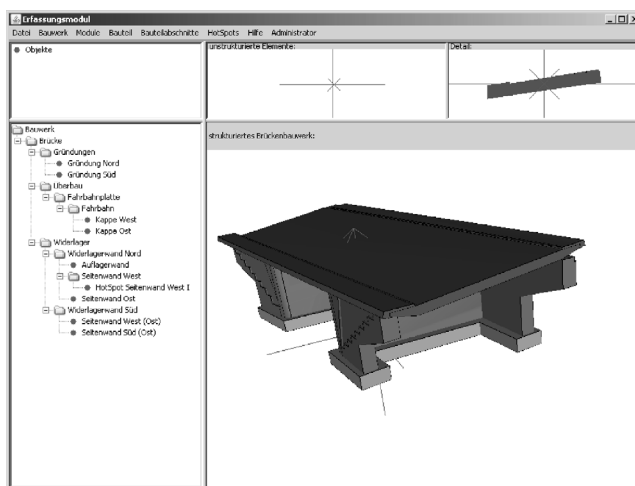


Figure 3. Graphical user interface of the software tool (under development).

All geometric data is stored in the database in the form of a boundary representation model (B-Rep). For this purpose, a data structure similar to the geometric kernel ACIS is used (Spatial 2006).

The advantage of the programming language Java is that applications written in this language can easily be used on different operating systems like MS Windows or Linux. This aspect is very important because potential users of this application (such as administrations, construction firms with PPP-projects) may use different operating systems.

Although the first steps are done to develop a product data model for bridges (IFC-Bridge, Yabuki et al. 2006), no such product data model is available for practical services yet. As soon as it becomes available, we intend to use it as the basis of our lifecycle management system.

All construction information stored in the database can be visualized and edited by the graphical user interface (GUI). One special aspect of this GUI is that an intuitive and user-friendly interaction is possible everywhere—at an office desk or during a bridge inspection on the construction site. This is achieved in two ways:

- All dialogue boxes are clearly structured. The system provides assistance with every input. This is done using tooltip texts and a support system. In addition, the user is informed if incorrect information has been entered or information is missing when closing a dialogue box.
- The user can rotate, translate and scale the 3D model. This is done with the mouse device. Furthermore the user can select any single element (component part, sub-element, hotspot) in the graphic window or the tree view. The selected geometry is shown in a separate graphic window and can also be translated, rotated and scaled.

### 3.2 Data input

All data input is done at the graphical user interface (GUI). For easier and even faster input, extendable lists have been integrated for recurring inputs. There are lists for

- materials,
- defined material parameters,
- environmental loads,
- measurement methods,
- repair measures,
- deterioration models,
- types of component parts, and
- construction types.

Using these lists in conjunction with the software tool achieves highly effective standards of work. The lists are stored in the database and can be updated by the user or the administrator, respectively. For example,

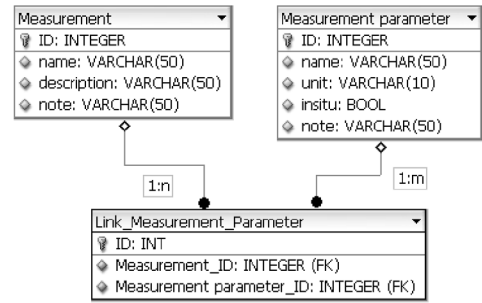


Figure 4. Generic database structure for measurement methods and measurement parameters.

it is possible to define an arbitrary number of measurement methods, each of which is defined by a number of measurement parameters. This functionality for (re) defining measurement methods renders the systems extremely flexible, which is necessary to ensure its usability over the long life-span of a concrete building.

Measurement methods and parameters are stored in different tables on the database. A third table links measurement parameters and measurement methods. One parameter can be assigned to more than one measurement method. The generic database structure, which can hold any kind of measurement method, is shown in Figure 4. Materials and material-specific values are defined in the same way.

It is also possible to store new fully-probabilistic deterioration models on the database. To this end, the model's equation has to be defined by the user in a form readable by STRUREL.

All other lists are permanently stored in a single table.

Using dynamic programme structures inside the software-tool, not only the measurement methods and measurement parameters but also the materials and material parameters are employed to compute degrees of deterioration and prognosis.

## 4 SUMMARY

In an ongoing research project, we develop a software tool for the predictive life-cycle management of reinforced concrete bridges. A key feature of our LMS is a 3D building information model which forms the basis of all data acquisition and evaluation functionality. This model serves to store all the information on component parts together with their relation to the geometry. What first distinguishes this software tool from other existing building management systems is the fact that a construction is subdivided into up to five levels (levels of detail). In an initial step,

structures are first subdivided into modules and then into component parts. Component parts are subdivided into sub-elements and hotspots. The advantage of this approach is that results of inspections or photos can be directly allotted to the according geometries. This subdivision is necessary in order to use the fully probabilistic deterioration models in a goal-oriented manner.

For predicting future changes in the condition of a structure, these fully probabilistic deterioration models are used in conjunction with non-destructive inspection methods. The construction's condition is computed by aggregating the conditions on all five levels. It is accordingly possible to detect damage at a very early stage and plan repair measures to eliminate such damage. This consequently means a reduction in the financial outlay for the maintenance of the structure.

The predictive life-cycle management system is implemented by coupling a Java application with a relational MySQL database. The graphical user interface is a simple, innovative way to store new constructions in the database. All information can be entered and modified using this interface.

The software tool includes lists for recurrent inputs. These lists can be updated by the user or the administrator, respectively. Defined programme structures are used to compute the degree of deterioration or the prognosis for a component part with the information from these lists.

## REFERENCES

Budelmann, H. & Starck, T. 2008. Integration of Degradation Prognosis of Concrete Structures into Life Cycle Management. Proceedings of the 1st International Symposium on Life-Cycle Civil Engineering (IALCCE'08), Varenna 2008.

Bundesministerium für Verkehr, Bau und Stadtentwicklung. 2006. *Bericht über die Qualität, Dauerhaftigkeit und Sicherheit von Spannbetonbrücken*. Berlin: Bundesministerium für Verkehr, Bau und Stadtentwicklung.

Duffy, L. 2004. Development of Eirspan: Ireland's bridge management system. *Proceedings of the Institution of Civil Engineering* 157: 139–146.

Empelmann, M., Henke, V., Heumann, G. & Wichers, M. 2008. *Aspects of Sustainability of Repair-Systems for Concrete Structures*. Proceedings of the 1st International Symposium on Life-Cycle Civil Engineering (IALCCE'08), Varenna 2008.

Gehlen, C. 2000. *Probabilistische Lebensdauerbemessung von Stahlbetonbauwerken—Zuverlässigkeitsbetrachtungen zur wirksamen Vermeidung von Bewehrungskorrosion*. Berlin: Deutscher Ausschuss für Stahlbetonbau (DAfStb), Heft 510.

Haardt, P. 2002. *Entwicklung eines Bauwerks-Management-Systems für das deutsche Fernstraßennetz, Stufe 1 und 2, Schlussbericht zum AP-Projekt 99 245*. Bergisch-Gladbach: Bundesanstalt für das Straßenwesen.

Haller, H. & Basurco, G. 2006. *KUBA-DB Benutzerhandbuch*. Bern: Eidg. Drucksachen- und Materialzentrale.

Hammad, A. Zhang, C. & Hu, Y. 2006. Mobile Model-Based Bridge Lifecycle Management System. *Computer-Aided Civil and Infrastructure Engineering* (21): 530–547.

Hawk, H. 1999. BRIDGIT: User-Friendly Approach to Bridge Management. *Proceedings of the 8th International Bridge Management Conference*: E-7/1–15.

Henriksen, A. 1999. Bridge Management—Routine Maintenance: Recent Experience with the Routine Management Module in the DANBRo Bridge Management System. *Proceedings of the 8th International Bridge Management Conference*: 1-5/1–13.

Landeshauptstadt Düsseldorf 2007: *Lebensdauermanagement für Ingenieurbauwerke der Landeshauptstadt Düsseldorf*. Düsseldorf Homepage ([http://www.duesseldorf.de/verkehrsmanagement/bruecken\\_und\\_tunnel/index.shtml](http://www.duesseldorf.de/verkehrsmanagement/bruecken_und_tunnel/index.shtml))

Mayer, T., Schiessl, P. & Zintel, M. 2008. *Birth Certificate as an Important Tool for Public-Private-Partnership Projects*. Proceedings of the 1st International Symposium on Life-Cycle Civil Engineering (IALCCE'08), Varenna 2008.

MySQL, 2007. *Documentation of MySQL Ed. 1.5*. Uppsala: MySQL AB.

RCP, 2007. *Documentation of STRUREL Ed. 8*. Munich: RCP.

Robert, W., Marshall, A., Shepard, R., Aldayuz, J. 2003. Pontis Bridge Management System—State of Practice in Implementation and Development. *Proceedings of the 9th International Bridge Management Conference*: 49–60.

Schiessl, P. & Mayer T. 2006. Lebensdauermanagement von Stahlbetonbauwerken. *Statusseminar zum Verbundforschungsvorhaben "Nachhaltig Bauen mit Beton"*: 65–74.

Schiessl, P. & Mayer, T. 2007. *Forschungsbericht 31006/05, DAfStB-Verbundforschungsvorhaben "Nachhaltig Bauen mit Beton", Teilprojekt A3 "Wesentliche Bausteine eines Bauwerksmanagementsystems"*. Berlin: Deutscher Ausschuss für Stahlbetonbau (DAfStb), Heft 572..

Spatial 2006. *Documentation of 3D ACIS Modeler*. Westminster: Spatial.

Sun Microsystems 2006a. *Documentation of Java™ Platform Standard Ed. 6*. Santa Clara: Sun Microsystems.

Sun Microsystems 2006b. *Documentation of Java3D Ed. 1.5.0*. Santa Clara: Sun Microsystems.

Thompson, P., Merlo, T., Kerr, B., Cheetham, A. & Ellis, R. 1999: The New Ontario Bridge Management System. *Proceedings of the 8th International Bridge Management Conference*: F-6/1–15.

Vesikari, E. 2006. *BRIDGELIFE, User Manual*. VTT, Finland.

Yabuki, N., Lebegue, E., Gual, J., Shitani, T. & Zhan- tao, L. 2006. International Collaboration for Developing the Bridge Product Model "IFC-Bridge". *Proceedings of the Joint International Conference on Computing and Decision Making In Civil and Building Engineering*. 1: 1927–1936.



# Traffic load modeling based on structural health monitoring data

Chengming Lan & Hui Li

*School of Civil Engineering, Harbin Institute of Technology, Harbin, China*

Jinping Ou

*School of Civil Engineering, Harbin Institute of Technology, Harbin, China; School of Civil and Hydraulic Engineering, Dalian University of Technology, Dalian, China*

**ABSTRACT:** Live load models are foundation for life-cycle design of highway bridges. Many highway bridges are now equipped with structural health monitoring systems, which provide valuable data to establish load models. In this paper, traffic load models of the Binzhou Yellow River Highway Bridge are developed based on the field measurement of vehicles by an already installed structural health monitoring system. The probabilistic distribution model and extreme value distribution of gross vehicle weight are statistically analyzed using the monitoring data and the results indicate that they follow the Bimodal-Lognormal Distribution and Gumbel Distribution, respectively.

## 1 INTRODUCTION

Traffic load is one of the most critical factors that influence a bridge design, analysis and maintenance. Important traffic load information includes the most possible maximum gross vehicle weight during the design return period. The extrapolation and statistical analysis are frequently employed to obtain the most possible maximum gross vehicle weight within the design return period. The extrapolation approach was proposed by Nowak (1994). This approach provides an easy and effective way to obtain the maximum value of related parameters. It can avoid complicated simulation. Nowak (1994) used this approach to obtain the traffic load model of the Ontario Highway Bridge Design Code. However, the approach is subjective and the accuracy depends on the experience of the researchers. The statistical analysis approach is an effective method to obtain the cumulative distribution function (CDF) of gross vehicle weight and axle weight. Miao and Chan (2002) used this approach to obtain the traffic load model for Hong Kong. The disadvantage of the statistical analysis approach is its complexity.

In this paper, traffic load models are established based on the measurement of vehicles by a structural health monitoring system installed on the Binzhou Yellow River Highway Bridge (BYRHB). The probabilistic distribution model and extreme value distribution of gross vehicle weight are statistically analyzed using the monitoring data.

## 2 DESCRIPTION OF THE BRIDGE

The Shandong Binzhou Yellow River Highway Bridge is a three-tower cable-stayed bridge carrying a dual three-lane carriageway over the Yellow River, as shown in Figure 1. This bridge is located in Shandong Province, China, providing an important connection between Eastern and Northern China. The construction of the bridge began in August, 2001, and was completed in November, 2003, and opened to traffic in July, 2004. The entire length of the bridge is 1698.4 m with a 13.102 km highway approach and connection line. The main bridge has a total length of 768 m, consisting of two 300 m spans and two 84 m side-spans.

A sophisticated structural health monitoring system was installed on this bridge and became operational since 2004 (Ou, 2003; Li *et al.*, 2006). The measurement of vehicles passing through this bridge provides the valuable raw data to model the traffic loads.

## 3 EXTREME VALUE DISTRIBUTION OF VEHICLE LOAD

### 3.1 Probability distribution of vehicle load

The data of gross vehicle weight have been collected by the SHM system since 2004. One-day data is taken to be an observation unit for analyzing the probability distribution and extreme value distribution of vehicle

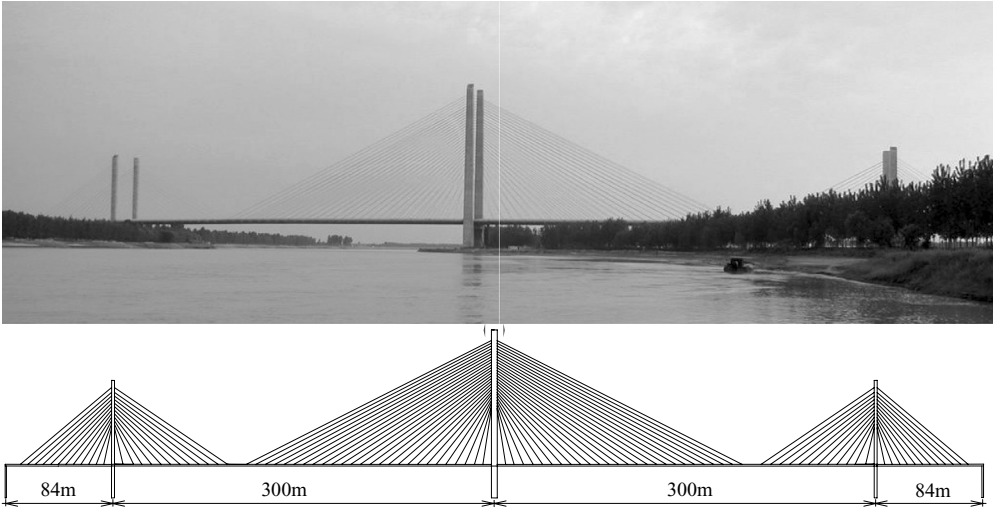


Figure 1. General view of the Shandong Binzhou Yellow River Highway Bridge.

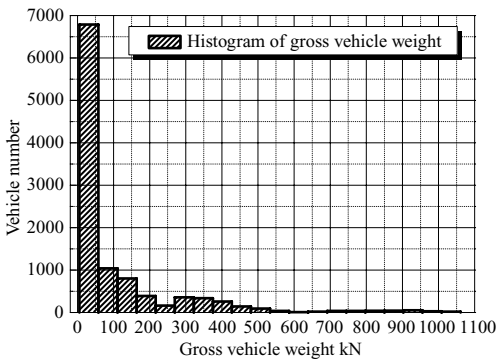


Figure 2. The histogram of gross vehicle weight.

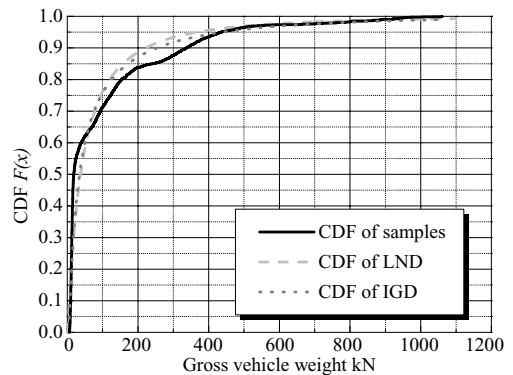


Figure 3. Cumulative distribution functions of LND and IGD of the gross vehicle weight.

gross weight for this bridge. Statistic operation is repeatedly conducted on every day data and the results indicate that the statistic characteristics of gross weight for all days are almost the same. Therefore, a sample drawn randomly from the data in 2005 is employed to modeling the traffic load. The histogram of gross vehicle weight is shown in Figure 2. It can be seen from Figure 2 that vehicle with weights less than 100 kN (light vehicles) are dominant, however, heavy trucks with weight of more than 700 kN are also observed. The mean, standard deviation and coefficient of variation of the sample are 104.94 kN, 172.83 kN and 1.647, respectively.

Generally, the Lognormal Normal Distribution (LND) and Inverse Gaussian Distribution (IGD) which are the unimodal distribution are frequently used to

fit the cumulative distribution function (CDF) of the samples and the results are shown in Figure 3. The Kolmogorov-Smirnov test (KS-test) (Hahn, 1994) is adopted herein to determine if a sample comes from a population with a specific distribution, which can offer a critical value following a given reliable parameter. The advantage of this approach is that all deviations can be obtained between every observed distribution point and theoretical distribution point. The LND and IGD cannot be accepted by the KS-test at the 5% significance level. Therefore, the LND and IGD cannot be used to model the probability distribution of the gross vehicle weight. Since the regularity of the logarithm of gross load is clearly observed from Figure 4,

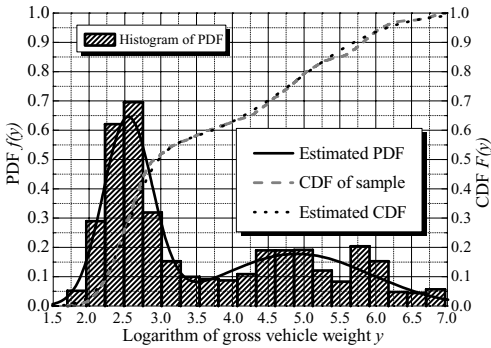


Figure 4. Probability density function and cumulative distribution function of variable  $Y$ .

the logarithmic distribution of gross vehicle weight can be obtained by univariate finite mixtures of Normal Distribution.  $X$  denotes the gross vehicle weight with a unit of kN and  $Y$  is the natural logarithm of  $X$ , i.e.  $Y = \ln(X)$ .  $\hat{F}(y)$  is the CDF of  $Y$  and expressed by

$$\hat{F}(y) = p_1 \Phi\left(\frac{y - \mu_{Y1}}{\sigma_{Y1}}\right) + p_2 \Phi\left(\frac{y - \mu_{Y2}}{\sigma_{Y2}}\right) \quad (1)$$

where  $p_1$  and  $p_2$  respectively represent the weight or mixing coefficients for the first and second term, and  $p_1 + p_2 = 1$ ;  $\Phi(\cdot)$  is the CDF of standard normal distribution;  $\mu_{Y1}$ ,  $\sigma_{Y1}$ ,  $\mu_{Y2}$  and  $\sigma_{Y2}$  are the statistical parameters of the distribution in Eq. (1). The Maximum Likelihood Estimation (MLE) method is used to obtain the statistical parameters from the samples in this paper. Let  $f_X(x; \theta)$  be the density function of variable  $X$ , where, for simplicity,  $\theta$  is the only parameter to be estimated from a set of sample values  $x_1, x_2, \dots, x_n$ . The likelihood function of  $\theta$  is defined as,

$$L(\theta) = \prod_{i=1}^n f_X(x_i; \theta) \quad (2)$$

When the sample values are given, the likelihood function  $L$  becomes a function of a single variable  $\theta$ . The estimation procedure for  $\theta$  based on the method of maximum likelihood consists of choosing, as an estimate of  $\theta$ , the particular value of  $\theta$  that maximizes  $L$ . The maximum of  $L(\theta)$  occurs in most cases at the value of  $\theta$ , where  $dL/d\theta$  is zero. Hence, the maximum likelihood estimate  $\hat{\theta}$  of  $\theta$  based on sample values  $x_1, x_2, \dots, x_n$  can be determined from,

$$\frac{dL(x_1, x_2, \dots, x_n; \hat{\theta})}{d\hat{\theta}} = 0 \quad (3)$$

$L$  is always nonnegative and attains its maximum for the same value of  $\hat{\theta}$  as  $\ln L$ . Since  $\ln L$  is in the form of a sum rather than a product, it is generally easier to obtain  $\hat{\theta}$  by solving

$$\frac{d \ln L(x_1, x_2, \dots, x_n; \hat{\theta})}{d\hat{\theta}} \quad (4)$$

The single parameter estimation procedure can be directly extended to multi-parameter estimation. In the case of  $m$  parameters, the likelihood function becomes

$$L(\theta) = \prod_{i=1}^n f_X(x_i; \theta_1, \theta_2, \dots, \theta_m) \quad (5)$$

and the MLEs of  $\theta_j$ ,  $j = 1, 2, \dots, m$ , are obtained by simultaneously solving the system of likelihood equations

$$\frac{\partial \ln L}{\partial \hat{\theta}_j} = 0, \quad j = 1, 2, \dots, m \quad (6)$$

In this way the greatest probability is given to the observed set of events, provided that the true form of probability density distribution is known.

A 180-day vehicle weight data are used as samples to estimate the statistical parameters in Eq. (1). The estimated values of the statistical parameters in Eq. (1) are 0.543, 0.457, 2.542, 0.342, 4.901 and 1.024 for  $p_1, p_2, \mu_{Y1}, \sigma_{Y1}, \mu_{Y2}$  and  $\sigma_{Y2}$ . The PDF and CDF of  $Y$  are shown in Figure 4. Based on the estimated results, the CDF of  $X$  can be written as,

$$\begin{aligned} F_X(x) &= P(X \leq x) = P(Y \leq \ln x) = F_Y(\ln x) \\ &= p_1 \Phi\left(\frac{\ln x - \mu_{Y1}}{\sigma_{Y1}}\right) + p_2 \Phi\left(\frac{\ln x - \mu_{Y2}}{\sigma_{Y2}}\right) \end{aligned} \quad (7)$$

It is clear that the CDF of  $X$  are the mixtures of two LND (called Bimodal-Lognormal Distribution, BLD) with different parameters. For the gross weight of light cars, it follows the LND (LN (13.472, 4.746<sup>2</sup>)) with a probability of occurrence  $p_1 = 0.543$ , whereas, for the gross weight of heavy trucks, it follows LND (LN (227.125, 309.396<sup>2</sup>)) with a probability of occurrence  $p_2 = 0.457$ . The CDF of  $X$  obtained from Eq. (7) are shown in Figure 5. It is observed that the curve of CDF of  $X$  shown in Figure 5 can better trace the measured one than that shown in Figure 3. The CDF of BLD with the estimated parameters is accepted by KS-test at the significance level of 1%. Therefore, the Bimodal-Lognormal Distribution can be used to model the CDF of the gross vehicle weight.

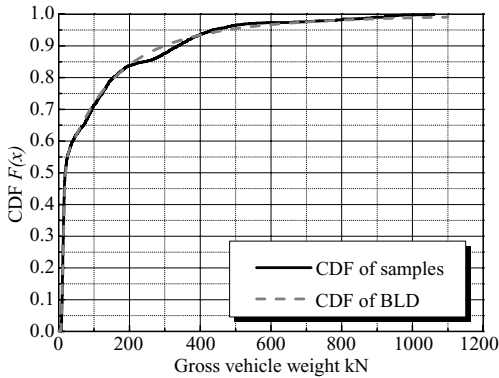


Figure 5. Cumulative distribution function of BLD of the gross vehicle weight.

### 3.2 Extreme value distribution of traffic load

Since the load duration of a vehicle on a bridge is very short, the gross vehicle load stochastic process on a bridge can be described approximately by a filtered Poisson process (Lin, 1990). Hence, a filtered Poisson process is employed to simulate the gross vehicle load stochastic process  $\{s(t), t \in [0, T]\}$  in this paper. The diagrammatic sketch of filtered Poisson process is shown in Figure 6.

The filtered Poisson process which is used to simulate gross vehicle load stochastic process is

$$s(t) = \sum_{n=0}^{N(t)} \xi_n \cdot I(t, \tau_n) \quad (8)$$

where  $\{N(t), t \in [0, T]\}$  is a Poisson process with parameter  $\lambda$ , and  $\xi_n (n = 1, 2, \dots)$  are variables following  $F(x)$ , independent of each other and  $\xi_0 = 0$ . The responding function is expressed by

$$I(t, \tau_n) = \begin{cases} 1, & t \in \tau_n; \\ 0, & t \notin \tau_n, \end{cases} \quad (9)$$

where  $\tau_n$  is the load duration of the  $n$ th vehicle and  $\tau_0 = 0$ .

The extreme value probability distribution of a filtered Poisson process is expressed by

$$F_M(x) = \begin{cases} \exp[-\lambda T(1 - F(x))], & x \geq 0; \\ 0, & x < 0, \end{cases} \quad (10)$$

where  $F(x)$  is the CDF of gross vehicle weight mentioned above;  $\lambda$  is the parameter of Poisson process and can be calculated by the MLE approach based on the survey data; and  $T$  is the period of requirement.

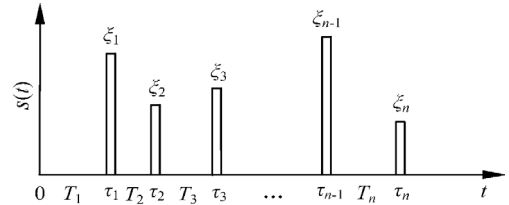


Figure 6. Diagrammatic sketch of filtered Poisson process.

For the purpose of obtaining the extreme value probability distribution of gross vehicle weight, the first peak associated with light vehicles is not of interest. For this reason, the splitting of Poisson process is discussed next. Let  $\{N(t), t \geq 0\}$  be a Poisson process with rate  $\lambda'$ . Suppose that each arrival of the process is classified as being either type 1 arrivals or type 2 arrivals with respectively independent probabilities  $p'_1$  and  $p'_2$  of all other arrivals. Let  $N_i(t)$  be the number of type  $i$  ( $i = 1, 2$ ) arrivals up to time  $t$ . Then  $\{N_1(t)\}$  and  $\{N_2(t)\}$  are two independent Poisson processes with respective rates  $\lambda p'_1$  and  $\lambda p'_2$  (Tijms, 2003). Therefore, stochastic process of the gross vehicle weight can be split into two independent Poisson processes with rate  $\lambda p_1$  and  $\lambda p_2$ , the former for modeling light vehicles, while the latter for heavy trucks. The extreme value distribution of heavy truck in one day is expressed as,

$$F_M(x) = \exp\{-\lambda p_2 T_1 [1 - F_Z(x)]\}, \quad x \geq 0 \quad (11)$$

where  $F_M(x)$  is the CDF of extreme value in one day, the time intervals can be approximately described as the Exponential Distribution,  $F_Z(x)$  is the CDF of heavy trucks followed LND (LN(227.125, 309.396<sup>2</sup>)), obviously,  $T_1 = 86400$  s. For the Shandong Binzhou Yellow River Highway Bridge, the estimation value of  $\lambda$  obtained using measurement data is 0.02385. Based on the Unified Standard for Reliability Design of Highway Engineering Structures (China, GB/T 50283-1999), the extreme value distribution of gross vehicle weight in one day is used to represent their extreme value distribution in one year, and then the extreme value distribution of vehicles in service-life can be written as

$$F_T(x) = \exp\{-\lambda p_2 T_2 [1 - F_M(x)]\}, \quad x \geq 0 \quad (12)$$

where  $F_T(x)$  is extreme value distribution of gross vehicle weight in service-life;  $T_2$  is service-life or remaining service life with units of year.

Solving Eq. (12) directly is more difficult due to the complicated function  $F_M(x)$  in this equation. Therefore, the Monte Carlo simulation method (Kottegoda, 1998), which is one of the most commonly effective approaches to simulate complicated random variables

and stochastic processes, is adopted to solve Eq. (12). It has been proven that the CDF is always uniformly distributed on  $[0, 1]$  (Eckhardt *et al.* 1987). Since the random variable  $x$  and the CDF  $F(x)$  are 1-to-1, one can sample  $x$  by first sampling  $y = F(x)$  and then solving for  $x$  by inverting  $F(x)$ , or  $x = F^{-1}(y)$ . Therefore, a random numbers sample  $\xi$  from  $U[0, 1]$  are generated and the value of  $x$  is determined by inversion,  $x = F^{-1}(\xi)$ . This method sometimes called the “Golden Rule for Sampling”. According to this method, many counterfeit functions could be produced by means of the Monte Carlo approach. Supposed that the service-life is 100 years, 100 counterfeit random numbers of extreme value distribution are obtained by Monte Carlo approach and checked by KS-test whether the Normal, the Lognormal, the Weibull, the Gamma, the Inverse Gauss, and the Gumbel Distribution (Extreme-Value Type-I Distribution) can describe the extreme value distribution of the gross vehicle weight or not. Based on the simulated results, only the Gumbel distribution can be accepted by KS-test at the significance level of 1%. Therefore, the extreme value distribution of the gross vehicle weight is as follows

$$F_T(x) = \exp(-\exp(-(x - b)/a)), \quad x \geq 0 \quad (13)$$

where  $a = 38.79$  and  $b = 1676.51$  which are obtained by MLE and the units of gross vehicle weight is kN.

#### 4 CONCLUSION

Traffic load models of the Shandong Binzhou Yellow River Highway Bridge are established in this case study based on the field measurement by a structural health monitoring system installed on this bridge. The following conclusions are obtained from this case study:

- i. The probability distribution of the gross vehicle weight follows the Bimodal-Lognormal Distribution, one peak for light cars and another for heavy trucks. In this case study, for the gross weight of light cars, it follows the LND (LN (13.472, 4.746<sup>2</sup>)) with a probability of occurrence  $p_1 = 0.543$ ; whereas, for the gross weight of heavy trucks, it follows LND (LN (227.125, 309.396<sup>2</sup>)) with a probability of occurrence  $p_2 = 0.457$ .
- ii. The gross vehicle load stochastic process on a bridge can be described approximately by a filtered Poisson process. Further study indicates that the extreme value distribution of the gross vehicle weight follows the Gumbel Distribution.

#### ACKNOWLEDGEMENT

This study is financially supported by the National Natural Science Foundation of China under the following grants: 50525823, 50538020 and 50278029.

#### REFERENCES

- Eckhardt R., Ulam J. and Neumann J.V. (1987). “*The Monte Carlo Method*”. Los Alamos Science.
- Hahn G.J. and Shapiro S.S. (1994) “*Statistical Models in Engineering*”. John Wiley & Sons Ltd, New York.
- Kottegoda N.T. and Rosso R. (1998). “*Statistics Probability and Reliability for Civil and Environmental Engineers*”. The McGraw Hills Companies Inc, Singapore.
- Li H., Ou J.P., Zhao X.F., Zhou W.S., Li H.W., Zhou Z. and Yang Y.S. (2006). “Structural health monitoring system for the Shandong Binzhou Yellow River Highway Bridge.” *Computer-Aided Civil and Infrastructure Engineering*, 21, 306–317.
- Lin Z.M. (1990). “*The Reliability Design and Estimation of Structure Engineering*”. China Communications Press (in Chinese)
- Miao T.J. and Chan T.H.T. (2002). “Bridge live load models from WIM data.” *Engineering Structures*, 24, 1071–1084.
- Nowak A.S. (1994). “Load model for bridge design code.” *Canadian Journal of Civil Engineering*, 21, 36–49.
- Ou J.P. (2003). “Some recent advances of structural health monitoring systems for civil infrastructure in mainland China.” *Proceedings of the First International Conference on Structural Health Monitoring and Intelligent Infrastructure*, Tokyo, Japan, 131–144.
- Shandong Transportation Bureau (1998). “*The Feasibility Research Report of the Shandong Binzhou Yellow River Highway Bridge on 205 National Highway*,” Technique report. (In Chinese)
- Tijms H.C. (2003). “*A First Course in Stochastic Models*”. John Wiley & Sons Ltd, Chichester.

# Corrosion detection in reinforced concrete structures using static and dynamic response measurements

F. Lanata & A. Del Grosso

*Department of Civil, Environmental and Architectural Engineering, University of Genoa, Italy*

**ABSTRACT:** Corrosion of steel bars in reinforced concrete structures is the main cause of structural degradation; the detection of the early propagation stage of reinforcement corrosion is therefore a crucial aspect in structural health monitoring applications. The paper reports about the assessment of corrosion of the reinforcements through the observation of the dynamic and static structural responses. A reinforced concrete beam modelled by plane stress finite elements will be used as a benchmark. The capacity of simulating corrosion damages and structural behaviours will be discussed in function of the detection of the early propagation of reinforcement corrosion. For damage identification, different techniques will be used. For the dynamic measurements, Single Value Decomposition and Wavelet Packet Decomposition will be applied and compared. The static measurements will be analysed with the Proper Orthogonal Decomposition. The results from the benchmark will be compared with experimental studies in the laboratory on damaged concrete beams.

## 1 INTRODUCTION

In the last years the development of integrated monitoring systems for new and existing reinforced concrete structures has been recognized as an important tool to reduce maintenance costs allowing a rational approach to the assessment of repair options, scheduling of inspection and maintenance programs. Continuous monitoring of reinforced concrete can allow a better knowledge of present and future performances of the structure in order to prevent premature deterioration. This issue is particularly significant for reinforced concrete bridges, because corrosion phenomena in reinforcing bars are the main cause of the reduction of the load bearing capacity and of the design security levels (Yoshihiro et al. 1990, Cairns 1998, Perno et al. 2005). The evaluation of service life for reinforced concrete structures with corroded reinforcements is a very significant topic in the literature (Rodriguez et al. 1997, Capozucca & Cerri 2003, Razak & Choi 2001, Ahmed et al. 2006).

Sensor positioning is the most important component of an integrated system. A variety of sensors and associated monitoring systems have been proposed in the last fifteen years (Baessler et al. 2000, McCarter & Vennesland 2004, AICAP 2005), usually representing a direct method for the assessment of the corrosion level, for example in terms of corrosion rate, concrete resistivity, critical chloride content and carbonation depth but they are essentially utilized for new structures and for particular applications. It is very difficult to generalize about positioning of sensor systems for

direct measurements, as the number, type and location of sensors within the structure are related to the knowledge of the most critical points from the design details. In addition, sensors are only able to give local information on the corrosion level.

An indirect method based on the dynamic and static monitoring of concrete structures is proposed in this paper. The aim of the study is to evaluate the influence of the local corrosion conditions on the global responses of the structure, comparing the static and dynamic approaches. Experimental laboratory studies as well as computer simulations have been used to test the capability of the above health monitoring approaches in identifying the insurgence of corrosion in reinforcing bars. A reinforced concrete beam modelled by plane stress finite elements will be used as a benchmark in order to get some information on the structural response of the healthy and damaged structures. For laboratory studies, a set of sample reinforced concrete beams artificially damaged and corroded to known limits has been used. The objective of the tests was the damage detection in concrete structures with two different monitoring systems: classic accelerometric sensors and static/dynamic fiber optic extensometers. In this paper, special emphasis will be given to the signal processing techniques that have been used for damage identification. In particular, for the dynamic measurements, the use of Single Value Decomposition (SVD) and Wavelet Packet Decomposition will be discussed and compared. Static deformation measurements have been processed with the Proper Orthogonal Decomposition

technique. The experiences have shown that in simple beams the effect of corrosion at an initial stage on the bars can be accompanied by secondary phenomena that may hide stiffness degradation.

## 2 EXPERIMENTAL PROGRAM

### 2.1 Beams description

Three reinforced concrete beams were cast with the aim to simulate the behavior of the beams composing highway viaducts. All beams were 2.60 m in length and had identical cross sections measuring  $180 \times 270$  mm (Fig. 1). The longitudinal reinforcement consisted of 2Ø16 bars in the tension zone, and 2Ø12 bars in the compression zone. Shear reinforcement consisted of 8 mm diameter stirrups spaced at 150 mm. The tests have been carried out to validate the application in detecting corrosion damage and to check the effects of corrosion products on the bond strength.

The first specimen was cast without defects and was used as the reference in the undamaged state. The second beam had mechanical damages: three cracks were artificially located around the central section of the beam (Fig. 2). The third beam was mechanically damaged like Beam 2 and it was also subjected to accelerated corrosion with chloride in the central part of the beam.

### 2.2 Experimental tests

Dynamic measurements have been performed using output-only tests. Loads have been applied by a hammer in different positions of the beam. The same load conditions have been repeated for the three beams in order to compare the results. From this impulsive excitation the natural frequencies of vibration for the three beams have been retrieved. A set of deformation sensors temporarily attached to the lower surface of the beams have been used for the measurements (Fig. 1). For the measurements, the SOFO (Surveillance d'Ouvrages par Fibre Optique) System, one of the most diffused fiber optic sensory systems for the

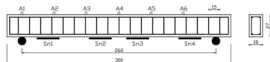


Figure 1. Sensors location for the two experimental tests (A: accelerometer; Sn: fibre optic extensometer).

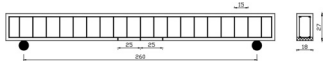


Figure 2. Geometry and crack locations for beams 2 and 3.

monitoring of civil structures (Inaudi & Del Grosso 2007) has been used. Four fiber optic extensometers with a base length of 300 mm have been fixed with clamps on the beams (Fig. 3). A frequency of acquisition of 100 Hz has been chosen even if the instrumentation can reach a frequency of acquisition of 1000 Hz. Dynamic measurements with the same excitations have been also repeated with 6 conventional accelerometers fixed at the upper surface of the beams in order to compare the results (Figs. 1 and 4). In this case a frequency of acquisition of 500 Hz has been used and a cut-off frequency of 200 Hz has been decided.

Static measurements have not been performed on the beams. The preparation of new sets of laboratory beams for the static experiments is presently under way.

## 3 NUMERICAL SIMULATIONS

### 3.1 The finite element model

A numerical model of the experimental beams has been developed in order to investigate and compare the efficiency of dynamic and static approaches in detecting small levels of damage. The results of the model will be compared with the experimental results. The concrete properties in the model reproduce the experimental values as follows:

Young's elastic modulus:  $E_c = 29.0 \text{ kN/mm}^2$

Poisson's ratio:  $\nu = 0.15$ ;

Density:  $\rho_c = 23 \times 10^{-9} \text{ kN/mm}^3$



Figure 3. Detail of a fibre optic extensometer mounted to include the crack.



Figure 4. Accelerometric sensors location on the cracked and corroded beam.

The beam is discretized into 840 'four node' quadrilateral elements, i.e. 120 elements in the x-direction (beam length) and 7 elements in the y-direction. Each element of the mesh is 0.025 metres length and 0.038 metres height. A MATLAB® based programming language is used and the output of the mesh is shown in Fig. 5.

The simulation considers the concrete and the steel components separately. The longitudinal reinforcing bars have been superimposed on the defined mesh using axial elements having no flexural stiffness. In order to reproduce the experimental results correctly, accurate values of steel properties have been specified in the analysis:

Young's elastic modulus:  $E_s = 207.0 \text{ kN/mm}^2$

Density:  $\rho_s = 78.5 \times 10^{-9} \text{ kN/mm}^3$

For the undamaged beam a perfect bond behavior without slip has been supposed at the interface.

The constraints of the beam have been considered partially fixed and updated using the dynamic model in order to converge to the measured experimental frequencies of the undamaged beam. The same values for the constraint conditions have been also used for the damaged and the static models to better reproduce experimental beams.

### 3.2 Simulation of damages

After the study of the structural model in the healthy state, damages corresponding to the experimentally damaged beams have been simulated. The procedure has been implemented in MATLAB® environment by modifying the previous finite element analysis.

The mechanical damages are supposed to affect six different elements of the mesh around the central section of the beam (Fig. 2). The damage is assumed to be represented by a finite element of the mesh with a reduced flexural rigidity. In other words, it is assumed that the damage affects the stiffness matrix of the defected element but not the mass matrix. As a consequence, the stiffness matrix of the damaged element is represented as a certain fraction of the healthy element stiffness matrix, i.e. with a localised reduction in the Young's elasticity modulus. The severity of damage can range between 0 (no damage) and 100% ('complete' damage, i.e. no rigidity at all).

For the cracked beam a perfect bond behavior without slip has been supposed at the interface. The secondary phenomena observed from the experimental results at the initial corrosion stage (see paragraph 4.1)



Figure 5. Numerical discretization of the experimental beams.

require a deeper investigation of the bond strength between concrete and corroded bars. For this reason, a modified model taking into account the adherence and the bond strength will be used for the cracked and corroded beam; in this case the bond behavior will be described by means of a couple of axial springs at the edges of each bar element.

The finite element model has been solved for both the dynamic and the static models, in order to have the frequencies of vibration and the nodal displacements corresponding to the damaged beams.

### 3.3 The dynamic model

For the dynamic approach the equation of motion has been developed in the finite element procedure as follows:

1. discretize the structure into nodes and elements, and choose the type of shape functions; thereby create the nodal displacement vector;
2. calculate the elemental stiffness matrix and the elemental mass matrix;
3. assemble the global system stiffness matrix and the global mass matrix to solve the second order differential equation;
4. solve the eigenvalue problem to obtain the natural frequencies and the modal shapes of the beam.

### 3.4 The static model

The finite element solution procedure for the static approach can be summarized as follows:

1. create the global nodal displacement vector as in the dynamic approach;
2. calculate the elemental stiffness matrix and load vector for all the elements;
3. assemble the global unconstrained system stiffness matrix and the global force vector;
4. impose constraints of nodal displacements and the applied loads to get the constrained system equations;
5. solve for the global nodal displacement vector using the constrained system equations.

For the study of the structural response under static ambient excitations, a thermal load has been applied to the simulated beam. In this case the structure is supposed to be equipped with a set of SOFO displacement sensors located on the lower surface of the beam as in the experimental tests.

The structural responses have been generated in time in terms of shortening/elongation of the installed sensors.



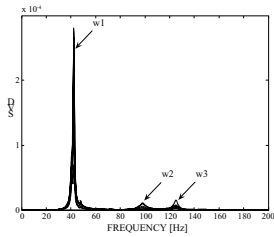


Figure 6. Singular values for the undamaged beam from which the first three frequencies are identified.

Table 2. Comparison of the first three frequencies for the undamaged beam.

	1° frequency	2° frequency	3° frequency
	Hz	Hz	Hz
Experimental	42	98	125
Simulated	49.98	93.52	126.41

#### 4 DYNAMIC RESPONSE PROCESSING

##### 4.1 Natural frequencies comparison

The analysis of the measured responses from accelerometers has been performed in terms of spectral energy using the output-only algorithm. The analysis in the frequency domain has been used to retrieve the natural frequencies of the specimens from the measured responses under dynamic impulses. In particular, the technique known as Enhanced Frequency Domain Decomposition has been used (Brincker et al. 2003). The first step has been the computation of the Power Spectral Density matrix which has been decomposed into its singular values, each corresponding to one vibrational mode.

From the analysis on the undamaged beam the first three experimental frequencies have been retrieved. The singular values deriving from the EFDD for each load position are reported in Figure 6 for the reference beam. The comparison of the results for the experimental and the simulated beams in the undamaged state is reported in Table 2. The frequencies are in good agreement.

The first three experimental frequencies have been extracted also for the cracked and for the cracked and corroded beams. While the first frequency is substantially independent from the damage, the second and the third frequencies present more significant variations (Fig. 7). The computed frequencies from the model are coherent with the reduction observed in the measured frequencies, but variations are smaller than measured ones. The simulations confirm the fact that small

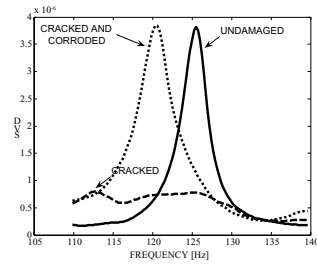


Figure 7. Variation of the third frequency in function of damage level from accelerometric measurements.

damages in particular are only a local phenomenon and their influence on the dynamic behavior may be of the same order of magnitude than the variation due to environmental conditions (Wenzel & Pichler 2005).

For the cracked and corroded beam, the corrosion has been first introduced in the model as a diameter reduction of the reinforcement bars. In this way the computed frequencies for the cracked and corroded model show a little decrease in comparison with the cracked beam, in contradiction with experimental results. In fact, the analysis of experimental measurements suggests that the second and third frequencies decrease when both cracking and corrosion damages are present (Fig. 7). However, the stiffness decrease is greater when only cracks are present in the beam. When corrosion is also induced in the beam, a small difference of the frequencies in comparison with the cracked beam can be observed. All compared frequencies show this behavior, that could be related to the increasing of the bond strength due to corrosion, as observed in literature (Mangat & Elgarf 1999, Razak & Choi 2001). Different authors confirm the fact that the bond strength between the corroded reinforcement and concrete cover increases and reaches its peak value because the radial expansion of corroded reinforcement increases the normal pressure on its surface. However, when the corrosion level increases, the development of concrete cracks caused by radial expansion reduces gradually the rate of increase of bond strength (Du et al. 2006). It can be observed that the theoretically computed rate of corrosion in tested beams is in good agreement with the low corrosion level associated with the increase of bond strength.

A more accurate modeling of the bond behavior between concrete and bars needs to be introduced in the corroded sections of the model in order to simulate the measured increase of bond strength and correctly retrieve the experimental frequencies. The development of the corroded model is actually under study.

While the first three frequencies could be extracted from acceleration responses, with SOFO sensors only

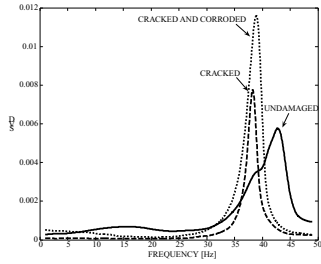


Figure 8. Variation of the first frequency in function of damage level from SOFO sensors measurements.

the first frequency could be obtained due to the low frequency of acquisition. As a consequence, the comparison of the results between the two acquisition techniques has been only possible for the first frequency. Figure 8 shows the comparison between the singular values from the analysis of the SOFO sensor responses for the three beams. Also with the SOFO measurements the cracked and corroded beam has shown higher frequencies of vibration in comparison with the cracked beam, confirming the results of the accelerometers.

#### 4.2 Wavelet packet decomposition on dynamic experimental results

Interpretation of the measurements can also be conducted in terms of time-history responses. As the modal properties such as natural frequencies and mode shapes are not good sensitive indicators of structural damage, a damage detection index called Wavelet Packet Energy Rate Index can be proposed for damage detection of beam structures (Han et al. 2005). This index has been shown to be less sensitive to environmental conditions that could negatively affect damage detection when natural frequencies are used. The procedure can be applied on both strain time-histories and acceleration measurements. Dynamic signals measured from the beams have been first decomposed into the wavelet packet components. The energy stored in each decomposed component of the initial signal at a generic level of decomposition has to be computed. Physically, the total signal energy is decomposed into a summation of wavelet packet component energies that correspond to different frequency bands. The component energies are more sensitive than the total energy to shift due to damages; the rate of signal wavelet packet energy at  $j$  level is defined as

$$\Delta(E_{f_j}) = \sum_{i=1}^{2^j} \frac{|(E_{f_j^i}) - (E_{f_j^i})_{REF}|}{(E_{f_j^i})_{REF}} \quad (1)$$

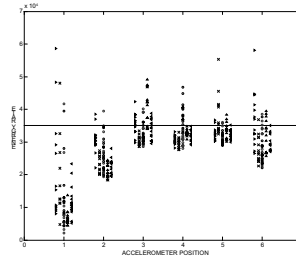


Figure 9. Wavelet energy rate for each measurement section (accelerometers) with the confidence limit at 98%. Each point represents a different load position.

where  $(E_{f_j^i})$  is the energy stored in the component signal  $f_j^i(t)$  at the time  $t$  and at the  $j$  level of decomposition. The *REF* pedex indicates the energy content in the reference configuration (undamaged beam).

In order to set adequate threshold values for damage alarms, a reliable undamaged situation has to be available. The thresholds have to be established using the statistical properties and the one-side confidence limit of the damage indicators from successive measurements. The algorithm shows that also small changes in frequency can be detected by the wavelet packet decomposition.

Figure 9 shows the results of wavelet packet decomposition for the cracked laboratory beam, it is clear that something happened in the central sections of the beam but the damage location strongly depends on the choice of the reference signal.

Deeper investigation and simulations are under study to improve the algorithm and to establish if the results obtained are badly conditioned by tests performed on different beams.

## 5 STATIC RESPONSE PROCESSING

The POD (Kreuzer & Kust 1996; Solari et al. 2005) has been used to extract a spatial and temporal correlation between the installed sensors, related in a certain way to the normal modes contained in the structural response. A Level 3 damage detection procedure can be possible with the definition of three indices: a damage function DF, indicating the insurgence of damage, a damage localization index DLI, indicating the location of damage and a threshold value, allowing the determination of the damage intensity (Lanata & Del Grosso 2006).

As static tests have not been performed, a numerical benchmark have been modeled in order to simulate a long-term database of structural static responses. The algorithm has been tested and validated using the simulated time series. In the simulation, the POD has

demonstrated to be reliable to detect also small damages. The procedure has to be validated on real data from laboratory experiments that will be carried out in the next future.

## 6 CONCLUSIONS

The two monitoring systems installed on the laboratory beams have shown to be equally reliable and able to detect changes in frequencies due to damages. The results are in good agreement even if the comparison has been possible only for the first frequency. The experimental results have shown that cracks and corrosion are detected in different ways; while mechanical damage causes a stiffness reduction in the beam, corrosion damage shows a stiffness reduction in comparison with the undamaged beam, but a greater stiffness in comparison with the beam having the same mechanical damage. This effect has been related to the increase in bond strength for small levels of corrosion.

Observing that different analysis methods allow to have a better reliability in the damage identification, a signal analysis algorithm has been also applied to the dynamic measurements. A damage detection index called Wavelet Packet Energy Index has been computed for both strain time-histories and acceleration measurements. The identification of damage is clear but the difference between mechanical and corrosion damages is very hard to detect also because usually both types of damage are present and simultaneous in the structure.

The modeling of the damaged beams has shown to be very complex and few works on the subject have already been presented in the literature. The corrosion damage in the simulated model is very difficult to introduce. The dynamic simulation in particular has shown that small damages may cause very small changes in natural frequencies. In this sense the static approach has showed to be much more sensitive than the dynamic one to identification of small levels of damage.

Future developments of the research are focused on the improvement of the finite element model and on the realization of a static campaign of measurements on physical beam models and laboratory test to characterize the phenomenon of the bond strength increase.

## REFERENCES

Ahmed, S.F.U., Maalej, M., Paramasivam, P. & Mihashi, H. 2006. Assessment of corrosion-induced damage and its effect on the structural behavior of RC beams containing supplementary cementitious materials. *Prog. Struct. Engng. Mater.* 8:69–77.

AICAP Associazione Italiana Calcestruzzo Armato e Precompresso 2005. *La corrosione nel calcestruzzo: fenomenologia, prevenzione, diagnosi, rimedi*. Pubblicità.

Baessler, R., Mietz, J., Raupach, M. & Klinghoffer, O. 2000. Corrosion monitoring sensors for durability assessment of concrete structures. *Smart Structures and Materials 2000: Smart Systems for Bridges, Structures, and Highways* 3988: 32–39.

Brincker, R., Ventura, C. & Andersen, P. 2003. Why output-only modal analysis is a desirable tool for a wide range of practical applications. *21st Int. Modal Analysis Conf.*, Kissimmee, FL, SEM, Inc.

Cairns, J. 1998. Assessment of effects of reinforcement corrosion on residual strength of deteriorating concrete structures, 1st *International Conference on Behaviour of Damaged Structures*, Rio de Janeiro.

Capozucca, R. & Cerri, M.N. 2003. Influence of reinforcement corrosion-in the compressive zone-on the behaviour of RC beams. *Engng. Struct.* 25 (13):1575–1583.

Du, Y.G., Chan, A.H.C. & Clark, L.A. 2006. Finite element analysis of the effects of radial expansion of corroded reinforcement. *Computers and Structures* 84: 917–929.

Han, J.-G., Ren, W.-X. & Sun, Z.-S. 2005. Wavelet packet based damage identification of beam structures. *International Journal of Solids and Structures* 42: 6610–6627.

Inaudi, D. & Del Grosso, A. 2007. Fiber Optic Sensing Technologies for Smart Materials and Structures. *SMSST'07*, Chongqing & Nanjing, China, May 22–27 (on CD-ROM).

Kreuzer, E. & Kust, O. 1996. Analysis of long torsional strings by proper orthogonal decomposition. *Arch. Appl. Mech.* 67:68–80.

Lanata, F. & Del Grosso, A. 2006. Damage detection and localization for continuous static monitoring of structures using a Proper Orthogonal Decomposition (POD) of signals. *Smart Materials and Structures* 15 (6):1811–1829.

Mangat, P.S. & Elgarf, M.S. 1999. Bond characteristics of corroding reinforcement in concrete beams. *Materials and Structures* 32:89–97.

McCarter, W.J. & Vennesland, Ø. 2004. Sensor systems for use in reinforced concrete structures. *Construction and Building Materials* 18:351–358.

Perno, S., Rinaldi, Z., Valente, C. & Pardi, L. 2005. Experimental evaluation of the load bearing capacity of corroded beams, *5th Int. Conf. on Bridge Management* 508–516.

Razak, H.A. & Choi, F.C. 2001. The effect of corrosion on the natural frequency and modal damping of reinforced concrete beams. *Engineering Structures* 23: 1126–1133.

Rodriguez, J., Ortega, L.M. & Casal, J. 1997. Load carrying capacity of concrete structures with corroded reinforcement. *Construction and Building Materials* 11 (4): 239–248.

Solari, G., Carassale, L. & Tubino, F. 2005. POD methods and applications in wind engineering. *6th Asia-Pacific Symp. on Wind Engng.*, Seoul.

Wenzel, H. & Pichler, D. 2005. *Ambient vibration monitoring*. England: Wiley.

Yoshihiro, T., Ken-Ichi, M., Yasuo, K. & Mitsunori, K. 1990. Mechanical behaviour of RC beams damaged by corrosion of reinforcement. Page CL, Treadaway KWJ, Bamforth PB, editors, *Corrosion of reinforcement in concrete*, Elsevier Applied Science, 178–187.

# Prediction and quantification models of bridge condition in Korea

Kwang-Joo Lee & Seong-Hyun Park

*Department of Civil, Environmental and Architectural Engineering, Korea University, Korea*

Chang-Ho Park

*Korea Expressway & Transportation Technology Institute, Technical Support Center, Korea*

Kyung-Hoon Park

*Hybrid Structure Research Division, Korea Institute of Construction Technology, Korea*

Jung Sik Kong

*Department of Civil, Environmental and Architectural Engineering, Korea University, Korea*

**ABSTRACT:** In Bridge Management Systems (BMS), the role of condition profiles is important to predict the condition in the future subject to diverse circumstances. The accuracy of the profiles is directly related to the accuracy of BMS and the reliability of the profiles is important to produce the optimal solution to distribute a maintenance budget reasonably. To predict the future condition of bridges, condition rating models based on experts' opinions have been used widely because of the lack of quantitative inspection and maintenance records. A weakness of these conventional systems is that experts' opinions are very subjective, moreover, the quality of condition profile is not good enough to be used for more advanced BMS. To overcome this limitation, an advanced regression technique is suggested to make reasonable condition profiles. To apply the suggested technique, the database of the Highway Bridge Management System (HBMS) in Korea is used and condition profiles are produced.

## 1 INSTRUCTION

The condition or the performance profiles are the most important perspectives among many factors and parameters consisting BMSs. Reasonable results and the confidence of the results depends on the quality of the condition and/or performance profiles. As a matter of fact, the decision making process and solutions provided by the modern management systems such as the optimal maintenance scenario (Frangopol & Liu 2007) are meaningless if the quality of condition or performance profiles as fundamental data cannot be assured to some extent. Therefore, providing higher quality condition/performance profile models are very important.

It's been commonly accepted that condition/performance profiles can be constructed based on existing inspection data. Based on this, significant investments have been made for last a couple of decades to establish databases storing inspection results. However, the result is not so satisfactory. In Korea, only 20–25% of inspection data for highway bridges have been collected for last 7 years and about

25% data is not continuously gathered and 50% of data are not even available. Besides, experts' opinions on condition and/or performance profiles of bridges are so subjective that it is doubt to be used with some quantitative accuracy. To overcome this inefficient data problem, we may use some additional information such as numerical or experimental analysis results (Kong *et al.* 2007).

Modern BMSs has to provide decision supporting solutions such as optimal lifetime scenarios for target structures. Complicated civil infrastructures such as bridges are associated with various inspections and maintenance interventions. Therefore, finding the optimum solution of bridges requires a very complicated process and serious computation time.

As we consider these aspects involved with a BMS, it is evident that a condition and/or performance profile model of BMS should be not only elaborate to insure the accuracy including uncertainties but also simple enough to guarantee the efficiency in computation.

The purpose of this study is provide a method to produce bridge condition profiles even though we do not have enough data at this moment. As a result,

quantitative condition profile models for different types of bridges were developed. Comprehensive, yet insufficient database HBMS which the Korea Expressway Corporation currently maintains has been used for this purpose.

## 2 EXISTING BRIDGE CONDITIONS AND CURRENT PRACTICES

Figure 1 shows the accumulated number of bridges built in Korea during 1973 and 2004. As we can see, almost a half of bridges have been built since the beginning of 1990.

The current structure management system in Korea was designed to be supplemented by regular inspection programs enforced by the law. By a special ordinance for management of infrastructures (MOCT 2003) announced by the Ministry of Construction and Transportation in Korea (Act 2003-170), the regular inspection (level 1), mainly based on visual inspection, has to be performed more than once every six months and the regular precise-inspection (level 2) has to be conducted more than once within two years. For important structures, the regular precise examination of level 3 has to be performed more than once every 5 years if the structure is more than 10-years-old.

Although the Act 2003-170 does not indicate the exact type of inspection or examination for different types of structures, it is necessary to have different examination strategies for different infrastructures. More detailed examination strategies for different infrastructures have been prepared and maintained by the Korea Infrastructures Safety and Technology Corporation (KICT 2006).

For bridges, regular inspection includes visual inspection of concrete and steel members and sub-structures. For concrete members, inspectors have to check the existence of crack, spalling, exposure of reinforcements, surface and drainage condition, deformation of members. Corrosion, bolt connection,

welding, deformation, painting, crack, support conditions have to be all investigated for steel members.

The regular inspection programs are essential for current bridge management systems and its importance cannot be underestimated. A significant budget is required to maintain the program. Figure 2 shows the maintenance cost for infrastructures in Korea in 2001. The increase becomes more significant if the indirect user cost which occurred by restriction of usage of structures is considered. Therefore, it is very important to develop a cost effective structure management system.

Five levels of condition states have been used for member condition assessment and decision making. Table 1 shows the typical five discrete condition status used for the regular inspection program in Korea. More detailed descriptions for condition states are prepared according to the type of members.

Most of current structural management systems support decisions based on the maintenance records of the past. These systems analyze maintenance frequencies, durations, and costs from the past records of similar structures with an assumption that a similar maintenance scenario can be applied to target

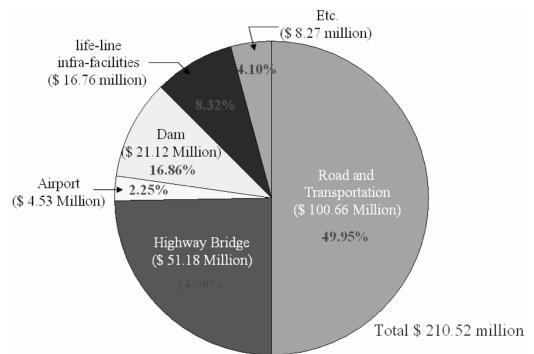


Figure 2. Direct maintenance cost of civil infrastructures in Korea (KISTEC, 2001) (million USD dollars, 1 USD  $\approx$  1,000 won).

Table 1. Typical discrete condition states used for the regular inspection program in Korea.

Status	Condition
A	Best condition without defects
B	Good condition with minor defects
C	Normal condition with some defects
D	Condition needs assessment for opening to the public because of deterioration or damage of important members
E	Structure cannot be opened to the public and needs immediate maintenance because of severe damage of important members

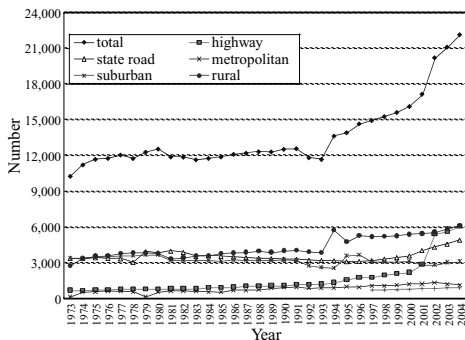


Figure 1. Accumulated number of bridges built in Korea.

Table 2. Available condition data of rigid-frame bridge members.

Materials	Number of data						Total number of good data	Ratio of good data
	A	B	C	D	E	N.A.		
Girder	146	20	11	0	0	14,130	177	1.24%
Slab	5,224	1,363	213	0	0	7,480	6,800	47.62%
Bearing	211	176	32	0	0	13,861	419	2.93%
Substructure	5,153	1,467	193	0	0	7,467	6,813	47.71%
Foundation	6,147	501	78	0	0	7,554	6,726	47.10%
Expan. joint	129	27	11	0	0	14,113	167	1.17%
Pavement	5,280	1,172	259	0	0	7,641	6,639	46.49%
Handrail	4,627	780	96	2	0	8,775	5,505	38.55%
Drain	4,724	682	128	0	0	8,746	5,534	38.75%

structures in the future. This type of approach can be found in many Life-cycle cost (LCC) analysis programs (Cho *et al.* 2003, 2007).

Highway bridges in Korea have been inspected regularly from 2000. Inspection data is not sufficient enough to produce highly reliable condition profiles because data have been accumulated for only 7 years. In this study, the present status of bridges in Korea has been investigated and bridge condition profiles have been evaluated. Regression analysis has been performed for different types of bridges but only summarized results for RA (rigid-frame) bridges are presented in this paper.

The first problem of the HBMS database is the completeness and reliability. The completeness of data input is less than 25%. Besides, the condition of bridges seldom reaches to status C apart from status D or E. Table 2 shows the available inspection data of rigid-frame bridges. From the table it can be investigated that the members closely related to the safety of bridges such as girders and bearings have very low ratio of completeness because it is not easy to access to inspect. Therefore, the performance of bridges instead of the condition cannot be assessed appropriately.

Nevertheless, regression analyses has been carried out in this study. The reasons are 1) to provide a prototype of condition profile so it can be undated continuously in the future and 2) to check the feasibility of database and to suggest improvements to be used with more advanced management systems in the future.

### 3 REGRESSION ANALYSIS MODEL

#### 3.1 Nonlinear regression analysis

Condition and/or performance profiles are one of the important data for Life-cycle analysis for bridges. Because of the importance many institutes suggested some condition and/or performance profiles. In general these profiles obtained based on expert's opinion or the regression analysis by using database

for bridge inventories. Most of current BMSs use condition and/or performance profiles to help decision making process for better management.

The final decision can be changed significantly depending on the reliability of the profiles. Until a recent date, however, the importance of the profiles has not been recognized well, so only some simple regression models have been suggested. For instance, New York DOT suggested linear condition profiles. University of Alabama and ALDOT suggested bi-linear functions for slab, superstructures, and substructures after investigating 15,500 bridges.

Because of its natural variance caused by environmental effects and of the statistical characteristics to represent a group of similar bridges these profiles contains big uncertainties. To obtain reliable results from BMS it is important to reduce these uncertainties and increase the reliability of profiles. To increase the reliability, condition profiles can be classified by characteristics of bridges and environmental conditions. For instance, span length or ADTT could be major parameters for classification. Of course the level of reliability can be improved only when we have enough number of data for analysis.

Nonlinear regression analysis can be performed with different type of functions such as polynomial, irrational, exponential, and inverse functions. Among them polynomial functions are used widely. In this study, polynomial functions with different orders are compared. However, we will not produce any final conclusions at this moment because this study is an on-going research project which will suggest representative condition profiles for important types of bridges. Equation 1 is the shape of general regression function based on polynomial functions.

$$y = \sum_{i=0} a_i x^i + u \tag{1}$$

where  $a_i$  = regression coefficient,  $x$ : time factor,  $u$  = error term.

Table 3. Nonlinear regression coefficient of rigid-frame bridge slab and substructure.

Time factor	3th order		4th order		5th order	
	Slab	Substructure	Slab	Substructure	Slab	Substructure
$a^5$					$4.794 \times 10^{-7}$	$3.742 \times 10^{-7}$
$a^4$			$-1.001 \times 10^{-5}$	$-7.808 \times 10^{-6}$	$-4.948 \times 10^{-5}$	$-3.862 \times 10^{-5}$
$a^3$	$1.286 \times 10^{-5}$	$6.746 \times 10^{-6}$	$6.361 \times 10^{-4}$	$4.926 \times 10^{-4}$	$1.747 \times 10^{-3}$	$1.361 \times 10^{-3}$
$a^2$	$-7.202 \times 10^{-4}$	$-6.567 \times 10^{-4}$	$-1.229 \times 10^{-2}$	$-9.686 \times 10^{-3}$	$-2.479 \times 10^{-2}$	$-1.945 \times 10^{-2}$
$a^1$	$-3.785 \times 10^{-2}$	$-3.328 \times 10^{-2}$	$3.078 \times 10^{-2}$	$2.036 \times 10^{-2}$	$8.796 \times 10^{-2}$	$5.994 \times 10^{-2}$
$a^0$	5.016	4.984	4.927	4.915	4.880	4.878
$R^2$	0.320	0.315	0.331	0.355	0.334	0.381

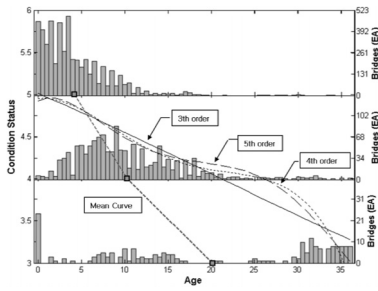


Figure 3. Nonlinear regression curves of RA slab.

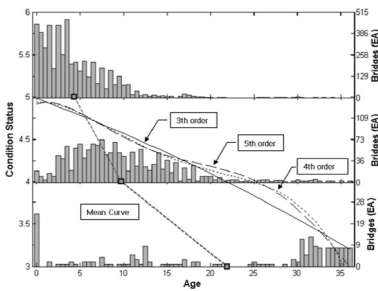


Figure 4. Nonlinear regression curves of RA substructure.

First, a simple nonlinear regression analysis has been performed by using whole data base. About 1900 rigid-framed bridges were investigated. Regression functions of linear, second, third, fourth, and fifth order were investigated for slab and substructures, respectively. Table 3 shows coefficients of regression function as the order of function are third, fourth, and fifth power, respectively. Figures 3 and 4 show the regression results of condition profiles. First and second order regression functions show similar trends even though those are not on the figures.

Histograms show the distribution of bridges belonging to condition status 3, 4, and 5 depending on their service life. Also mean points were connected to be compared with the regression analysis. As we can see

big differences are observed between the regression curves and the mean curve. It's because the number of bridges belonging to condition status 3 is greater than others. Also it has to be noted that bridge condition data cannot represent the pure degree of deterioration because the data include the variation by maintenance interventions.

Unfortunately, the maintenance activities cannot be separated because of the inappropriate design of data field of HBMS. To improve the reliability and efficiency of database for BMS, the application time of maintenance and quantitative measure of the improvement on condition by maintenance must be investigated and recorded. From the figures it can be observe that high order regression functions do not give a good approximation always.

### 3.2 Multiple linear regression analysis

To obtain more meaningful condition profiles, multiple regression analyses have been performed. The most important thing in multiple regression analysis is not only to decide the shape of regression function but also to identify important design variables (dependent variables).

The simplest multiple linear regression function can be expressed as follows.

$$y = a_0 + a_1x_1 + \dots + a_nx_n + u \tag{2}$$

where  $\beta_0, \beta_1, \dots, \beta_p$  are regression coefficients and  $u$  is the error term. In this study, four fundamental design variables were selected and linear and nonlinear multiple regression analyses have been performed. Those dependent variables are bridge span length, effective width of bridge, AADT (Annual Average Daily Traffic), and age of bridges, respectively. Equation (2) shows multiple linear regression function consists of four dependent variables ignoring error term.

$$y = a_0 + a_1x_1 + a_2x_2 + a_3x_3 + a_4x_4 \tag{3}$$

Table 4 shows the multiple linear regression analysis results for RA slab and substructure. Figure 5 shows the multiple linear regression surfaces of RA bridge slab. Because of the limitation of visualization, only age and AADT have been used to construct the surfaces. In this case, the length of bridge and the effective width are assumed as 11.4 m and 12 m, respectively. Bridges with relatively short span length have been

used because the span length of rigid-frame bridges is short in general. It is interesting that AADT do not have a significant effect on condition status.

### 3.3 Multiple nonlinear regression analysis

If there is significant dependency between dependent variables, linear regression analysis is not appropriate to represent this relationship. To investigate the dependency between variables multiple nonlinear regression analysis has been performed. The concept of multiple nonlinear regression analysis is similar to that of the multiple linear regression analysis. However, regression equation has to be modified depending on the way that the dependency between variables is assumed.

In this study only the first order dependency considered between design variables. Quadratic or cubic function of major design variables is assumed. Four variables such as bridge span length, bridge effective width, AADT, and age are used like multiple linear regression analysis. For the cubic function only a dependent variable of *age* is considered up to the third order.

Equation 4 shows a typical multiple nonlinear regression function associated with first order dependency between dependent variables.

$$y = a_0 + \sum_{i=1}^m \sum_{j=1}^n a_{ij} x_i^j + \sum_{i=1}^m \sum_{j=1}^{i-1} b_{ij} x_i x_j \quad (4)$$

where *m* is the number of dependent variables, *n* is the order of polynomial function, and *a<sub>ij</sub>*, *b<sub>ij</sub>* are regression coefficients for dependent variables. Especially, *b<sub>ij</sub>* represent the mutual relationship between dependent variables.

Table 5 shows the multiple nonlinear regression analysis results for RA slab. Subscript 1, 2, 3, and 4 represent span length, AADT, effective bridge width,

Table 4. Regression coefficients of RA slab and substructure obtained from multiple linear regression analysis.

Regress. coeffi.	Variable	Slab	Substructure
<i>a</i> <sub>0</sub>	Nondimensional coeffi.	5.022	5.067
<i>a</i> <sub>1</sub>	Span length	$2.578 \times 10^{-3}$	$-3.209 \times 10^{-3}$
<i>a</i> <sub>2</sub>	AADT	$1.975 \times 10^{-3}$	$1.058 \times 10^{-3}$
<i>a</i> <sub>3</sub>	Effective bridge width	$-1.751 \times 10^{-6}$	$-4.985 \times 10^{-7}$
<i>a</i> <sub>4</sub>	Age (years)	$-4.579 \times 10^{-2}$	$-4.643 \times 10^{-2}$
<i>R</i> <sup>2</sup>	Coefficient of determination	0.329	0.312

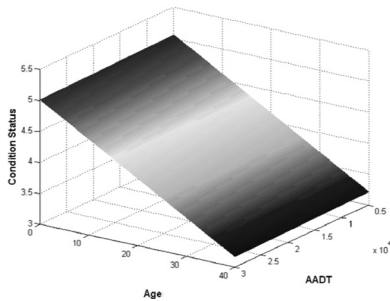


Figure 5. Multiple linear regression surface of slab.

Table 5. Regression coefficient of RA slab obtained from multiple nonlinear regression analysis.

Quadratic regression function				Cubic regression function			
Coeffi.	Value	Coeffi.	Value	Coeffi.	Value	Term	Coefficient
<i>a</i> <sub>0</sub>	5.518	<i>a</i> <sub>4</sub> <sup>2</sup>	$-6.716 \times 10^{-4}$	<i>a</i> <sub>0</sub>	5.512	<i>a</i> <sub>4</sub> <sup>2</sup>	$-1.244 \times 10^{-3}$
<i>a</i> <sub>1</sub>	$-3.567 \times 10^{-2}$	<i>b</i> <sub>12</sub>	$6.771 \times 10^{-4}$	<i>a</i> <sub>1</sub>	$-3.567 \times 10^{-2}$	<i>a</i> <sub>4</sub> <sup>3</sup>	$1.384 \times 10^{-5}$
<i>a</i> <sub>1</sub> <sup>2</sup>	$4.945 \times 10^{-4}$	<i>b</i> <sub>13</sub>	$-1.021 \times 10^{-8}$	<i>a</i> <sub>1</sub> <sup>2</sup>	$4.945 \times 10^{-4}$	<i>b</i> <sub>12</sub>	$6.677 \times 10^{-4}$
<i>a</i> <sub>2</sub>	$-1.606 \times 10^{-2}$	<i>b</i> <sub>23</sub>	$1.654 \times 10^{-3}$	<i>a</i> <sub>2</sub>	$-1.606 \times 10^{-2}$	<i>b</i> <sub>13</sub>	$-1.648 \times 10^{-8}$
<i>a</i> <sub>2</sub> <sup>2</sup>	$2.138 \times 10^{-4}$	<i>b</i> <sub>14</sub>	$-1.868 \times 10^{-8}$	<i>a</i> <sub>2</sub> <sup>2</sup>	$2.138 \times 10^{-4}$	<i>b</i> <sub>23</sub>	$1.741 \times 10^{-3}$
<i>a</i> <sub>3</sub>	$-5.211 \times 10^{-6}$	<i>b</i> <sub>24</sub>	$-3.666 \times 10^{-4}$	<i>a</i> <sub>3</sub>	$-5.211 \times 10^{-6}$	<i>b</i> <sub>14</sub>	$-2.048 \times 10^{-8}$
<i>a</i> <sub>3</sub> <sup>2</sup>	$3.803 \times 10^{-11}$	<i>b</i> <sub>34</sub>	$-2.736 \times 10^{-7}$	<i>a</i> <sub>3</sub> <sup>2</sup>	$3.803 \times 10^{-11}$	<i>b</i> <sub>24</sub>	$-3.436 \times 10^{-4}$
<i>a</i> <sub>4</sub>	$-3.915 \times 10^{-2}$	<i>R</i> <sup>2</sup>	$3.631 \times 10^{-1}$	<i>a</i> <sub>4</sub>	$-3.915 \times 10^{-2}$	<i>b</i> <sub>34</sub>	$-2.665 \times 10^{-7}$
						<i>R</i> <sup>2</sup>	$3.633 \times 10^{-1}$



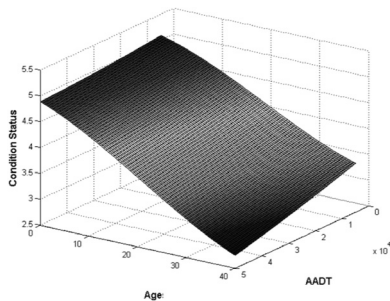


Figure 6. Third order regression surface of RA slab.

and age (years), respectively. It can be observed that values of regression coefficients are similar for those quadratic or cubic function cases. It is also shown that the effect of width of bridge is relatively small for the variation of condition over time. The contribution of the third order term related to the variable *age* is not significant compared to the second order term.

Figure 6 show the multiple nonlinear regression surfaces of slab when the third order polynomial function is used. Because of the limitation of visualization, only age and AADT have been used to construct the surfaces. In this case, the length of bridge and the effective width are 11.4 m and 12 m, respectively.

Unlike the multiple linear regression analysis results it can be shown that AADT have an effect on condition status. This can be predicted by investigating regression coefficients  $a_2$ ,  $b_{24}$  also.

#### 4 CONCLUSIONS

In this study, the present status of bridges in Korea has been investigated and bridge condition profiles have been evaluated. Database in HBMS has been used for this analysis even though the data has been accumulating for only 7 years. It cannot be said the reliability of obtained regression functions is high because of the quality of data, however, it can be improved as the period of data collection increases. The purpose of this study is to provide a method to produce bridge condition profiles even though we do not have enough data at this moment. Simple regression analysis and more complicated linear and nonlinear multiple

regression analyses have been performed to obtain condition profiles of rigid-frame bridges at Korean Highway. Especially, multiple nonlinear regression analysis gives considerable results and we can see that it could be an important technique for bridge assessment. Similar analyses have been performing for other major types of bridges such as pre-stressed concrete I-style bridge (PSCI), steel box bridge (STB), reinforced concrete slab bridge (RCS), preflex bridge (PF), and pre-stressed concrete box bridge (PSCB). The final report will be provided by the end of 2008.

#### ACKNOWLEDGEMENT

This study was partially sponsored by the Korea Expressway & Transportation Technology Institute and by the Korea Research Foundation Grant funded by the Korean Government (MOEHRD)" (KRF-2006-331-D00564). The supports received are gratefully acknowledged.

#### REFERENCES

- Cho, H-N., Frangopol, D.M. & Ang, A.H-S. (eds) 2007. *Life-Cycle Cost and Performance of Civil Infrastructure Systems*, Taylor and Francis.
- Cho, H-N, Kim, J-H., Choi, Y-M. & Lee, K-M., 2003, "Practical Application of Life-Cycle Cost Effective Design and Rehabilitation of Civil Infrastructures", *Proc. of JSSC03*
- Frangopol, D.M. & Liu, M. 2007. Maintenance and management of civil infrastructure based on condition, safety, optimization, and life-cycle cost, *Structure and Infrastructure Engineering*, 3(1): 29–41.
- Korea Institute of Construction Technology (KICT) 2006. *Development of life-cycle cost analysis method and system for the life-cycle cost optimum design and the life-time management of steel bridges*, Research Report, MOCT and KICTTEP, Korea (in Korean).
- Kong, J.S., Park, K.H., Lim, J.K. & Cho, H.N. 2007. Performance regression model for the optimal maintenance evaluation of steel box bridges, IABMAS, *Proceedings of the 5th International Workshop on Life-Cycle Cost Analysis and Design of Civil Infrastructure Systems*, 16–18 October 2006. Seoul, Korea.
- Ministry of Construction and Transportation (MOCT) & Korea Infrastructure Safety and Technology Corporation (KISTEC). 2003. *Detailed Guidelines of Safety Inspection and Precise Safety Diagnosis*. Korea (in Korean).

# Lifespan evaluation of 8 bridges of the Indiana Toll Road: A case study

J. León & H. Corres-Peiretti

*FHECOR Ingenieros Consultores & Polytechnical University of Madrid, Spain*

Santiago Pérez-Fadón & J.E. Herrero

*Technical Direction of FERROVIAL, Madrid, Spain*

F. Rodríguez

*Polytechnical University of Madrid, Spain*

F. Prieto

*FHECOR Ingenieros Consultores, Madrid, Spain*

**ABSTRACT:** This paper shows the practical experience achieved by evaluating the lifespan of some existing structures under extreme weather conditions, in order to decide on either demolition or repair. The applied methodology shows the feasibility of the approach based on “durability engineering” according to mainframe of current models of degradation. Thus, by using both relatively conventional testing methods and the mentioned available models, it was possible to estimate the remaining lifetime of these structures. Nevertheless, some difficulties appear when applying theory to practice, as pointed out in this paper.

## 1 DESCRIPTION OF STRUCTURES

The Indiana Toll Road is a part of the New York—Chicago Toll Road system running east-west across the upper north side of Indiana. The eight analysed structures share similar typologies and are exposed to the same extreme weather and aggressive environment conditions. All eight structures were built in 1956 and underwent repair and widening operations during the 1980s. Table 1 contains the main geometrical dimensions of these structures.

Their general typological properties may be summarized as follows:

Most of these structures are made up of twin decks of almost equal dimensions. Each structure consists of statically determined decks of a reinforced concrete slab on several longitudinal steel stringers, simply supported on abutments and bents. Every deck shows transversal joints on abutments and bents.

Bents are made up of square reinforced concrete piers and rectangular lintels, with the exception of the Broadway St structure, containing a combination of R.C. elements and steel struts. Bents are founded on reinforced concrete pile-caps.

Abutments are closed, with a breast wall founded on piles, transversal wing walls and a back slipper on piles supporting an approach slab.

Although the Indiana Toll Road suffered several repair works in the past, the effectiveness of the maintenance was rather poor.

Table 1. Summary of the structures analyzed.

Structure	Number of spans	Length (ft)	Width (ft)	Area (sf)	%Length over total	
I-12, R.R. traks and Gary W.T.P.	WB	40 3,013.70	35	105,480	18.21	36.4
	EB	3,013.70	35	105,480	18.21	
Grand calumet	WB	216.43	35	7,575	1.31	
River West Bridge	EB	3 216.43	35	7,575	1.31	2.62
	WB	7 340.85	35	11,930	2.06	
Street	EB	11 546	35	19,110	3.3	5.36
Grand calumet	WB	165.59	42	6,955	1	
River East	EB	5 167.47	43.3	7,251	1.01	2.01
	WB	218.74	42	9,187	1.32	
Buchanan street	EB	3 218.74	53.3	11,659	1.32	2.64
BroadWay St., Virginia St., E.J. & E.R.R.	WB	3,941.29	41.2	162,381	23.82	
Tennessee Street	EB	75 3,941.29	41.2	162,381	23.82	47.6
	WB	128.13	41.7	5,343	0.77	
Old Hobart Road	EB	3 128.13	41.7	5,343	0.77	1.55
	WB	146.49	35	5,127	0.89	
	EB	3 146.49	35	5,127	0.89	1.77
		16,549.47		637,904	100	100

## 2 GENERAL CONDITION OF BRIDGES

The structural steel has undergone different levels of degradation.

Concrete shows evidences of damages not induced by steel corrosion. The local freezing-thaw effects of de-icing salts produced successive scaling of concrete (figure 1, left). Water leakage with de-icing agents also favours the circulation of liquid water, even under low temperatures, with an important amount of chlorides, which ineluctably led to corrosion of reinforcement (figure 1, right).

It is worthwhile mentioning that damages on the original structures (1950s) and on the broadened ones (1980s) were very similar. This analogous condition is probably due to a similar time of exposure to de-icing agents, extensively applied after the second part of the 1960s.

It is also interesting to observe that past concrete repairs usually show map cracking, probably due to either exothermic reactions (the thickness of the repaired zones is relatively high, about 10–15 cm) or to drying shrinkage due to poor curing. In any case, it is necessary to point out that the technical basis for durability knowledge and strategies of intervention are relatively new (about twenty years), which left former repair interventions without a proper diagnosis. In addition, although undoubtedly the main reason for corrosion on structural steel girders and concrete bents and piers lies on the poor ability of joints to keep water away, another reason to explain the apparent lack of efficiency of the repaired concrete cover is to be found on the formation of macro-cells between apparently healthy zones, formerly cathodic zones, and the repaired zones, formerly anodic and transformed into well protected cathodics.

No significant structural damages (differential settlements, shear cracks, etc.) were detected, highlighting the fact, once again, that the vast majority of structures arrive on the end of their lifetime after durability problems. In some cases, vertical cracking due to horizontal restrained shrinkage was found at abutment walls. Although the crack width is about 0.3 mm, no special evidence of corrosion of reinforcement is associated to such cracking.



Figure 1. Left: concrete scaling, threatening the stability of a bearing device. Right: chloride induced corrosion attack.

Transverse cracking at top slabs (perpendicular to main girders) is due to the lack of sufficient longitudinal reinforcement to control crack width. Anyhow, cracks are small and do not necessarily coincide with corroded areas.

Another interesting case is the special structure over Broadway St. Petrographic analysis detected the existence of chert, sensitive to Alkali-Silica-Reaction (ASR). In fact, it seems that gel is already appearing and filling up the neighbouring voids of these fine aggregates, but the potential effects on these structures' future service life are negligible in practice.

Obviously, the intensity and extent of the damages are closely related to the state of joints and the drainage system.

## 3 AUSCULTATION PLAN AND RESULTS

### 3.1 Auscultation plan and taking of cores

Several techniques were used in order to measure the significant properties related to structural and durable behaviour:

- Tests to quantify both structural parameters and the extension of damages (acoustic sounding, impact echo and spectral analysis of surface wave and ground penetrating radar).
- Tests to characterize mechanical properties of materials (compressive strength, Ultrasonic Pulse Velocity, Rebound Index and density for concrete and the tensile strength, resilience and weldability for structural steel).
- Tests to identify properties related to the durability of materials (chloride contents profiles, carbonation depth, chemical water analysis of the Grand Calumet River in order to quantify its potential aggressivity, electrical half-cell potential of reinforcing steel, corrosion rate ( $I_{corr}$ ) by Galvanostatic Pulse Method and estimation of concrete cover of reinforcement from the ground penetration radar readings).

Table 2. Summary of cores taken and related ratios.

Structure	Cores	Deck surface (m <sup>2</sup> )	Ratio (cores / deck area m <sup>2</sup> )
Gary	25	34,483	1/1,380
Grand Calumet West	10	2,476	1/250
Bridge Street	14	5,073	1/360
Buchanan Street	19	2,910	1/150
Grand Calumet East	14	1,376	1/100
Broadway	30	41,797	1/1,400
Tennessee Street	15	1,359	1/90
Old Hobart Road	11	1,819	1/170
<i>Total identified cores</i>	<i>138</i>	<i>91,320</i>	<i>1/660</i>

138 cores were taken: 57% from slabs and 43% from substructures (abutments and bents), as summarized in table 2.

### 3.2 General criteria for auscultation results

Since all eight structures possess similar typologies, were built during the same period of time and, apparently, with the same materials, as well as their exposure to analogous environmental factors, a global layout for all structures may be considered valid for all of them. Thus, general strategies are valid for all cases and to be applied to each type of damage in any of these structures. Unfortunately, obtained results do not confirm this hypothesis, as will be explained in the following paragraphs. Therefore, it was necessary to define a specific strategy for each and every structure.

Firstly, an analysis of the mechanical properties of concrete was carried out in order to identify the types of concrete used for each structure. From the 'as built' project could be deduced that class D concrete was done using 1.50 barrels of cement per cubic yard, while 1.25 and 1.75 barrels were used for concrete classes E and F, respectively (a barrel equals to 375 lb of cement).

Afterwards, an analysis of densities was made. According to design two types of concrete can be clearly distinguished: class F used for decks and class D for substructures. The specified concrete strength was 4,000 psi (27, 6 MPa) for decks and 3,500 psi (24, 1 MPa) for substructures. Figure 2 summarizes results.

Despite the scatter, a great heterogeneity of values was also detected, with some apparent inconsistencies,

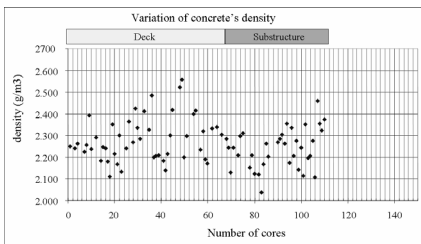


Figure 2. Variation of concrete densities. Abscissas: sequence of cores. Ordinates: obtained density of each core.

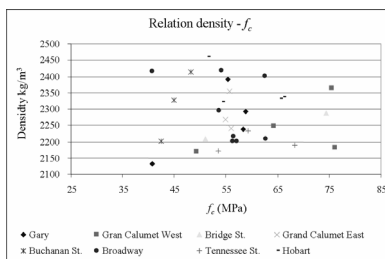


Figure 3. Scatter of concrete densities and strength.

particularly after analysing the relationship concrete strength vs density, as shown in figure 3.

In relation to the evolution of concrete strengths of decks and substructures, the following expression relates design vs obtained mean, real and characteristics values.

$$\begin{aligned} \frac{f_{ck,deck,real}}{f_{ck,substructure,real}} &= \frac{59.08 - 1.645 \times 8.88}{49.01 - 1.645 \times 6.03} = 1.138 \\ &\approx \frac{f_{c,deck,project}}{f_{c,substructure,project}} \\ &= \frac{4000 \text{ psi}}{3500 \text{ psi}} = 1.143 \\ \frac{\bar{f}_{c,deck,real}}{f_{c,substructure,real}} &= \frac{59.08}{49.01} = 1.21 \\ &> \frac{f_{c,deck,project}}{f_{c,substructure,project}} = \frac{4000 \text{ psi}}{3500 \text{ psi}} = 1.143 \end{aligned}$$

It seemed that both types of concrete equally developed their characteristic strengths. In order to explain the obtained scatter, it was assumed that one part of the concrete might have been produced by using different air-entraining admixtures. To confirm it, the decrease of strength was analysed as a function of the decrease of density by accepting the hypothesis of different percentages of air-entraining admixtures (figure 4). After literature, 1% of air-entrained represents a decreasing strength up to 4% and 5%.

As a consequence, the hypothesis of a deck made up by air-entrained admixtures and a substructure free of them seems uncertain. In addition, it seems that any degradation process acting along the life of the structure may have affected both decks and substructures in a homogeneous way (appearance of freezing-thaw processes, etc.). Summarizing, the obtained results denote great heterogeneities, much greater than expected from similar structures with analogous concrete specifications in project and built during the same period. As a consequence, the initial methodology of adopting standard solutions and the hypothesis of similar behaviour among the different structures could not be maintained. Thus, a specific study for each structure had to be carried out.

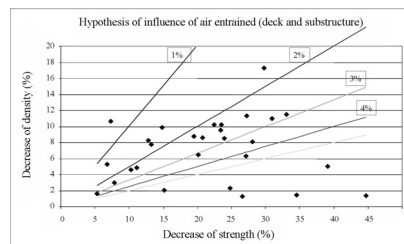


Figure 4. Potential influence of the air-entraining percentage on decreased strength.

## 4 GENERAL CRITERIA ADOPTED

### 4.1 Exposure conditions

All analyzed structures are located in the same geographical area, which is exposed to a rather extreme climate, with extremely low temperatures during several months in late autumn and winter. According to its annual temperatures and rainfalls the massive use of de-icing agents to maintain traffic is evident, which may be responsible for the development of chloride induced corrosion mechanisms on reinforcing bars and specific concrete degradation.

### 4.2 General criteria for lifespan estimation

In this document, the adopted criteria to estimate the lifespan of these structures are based on the fact that the conditioning phenomenon for their degradation process is chloride induced corrosion of reinforcing bars, since this type of attack is predominant and is, therefore, strongly conditioning their life expectancy.

Accordingly, the methodology to estimate the lifespan of the structures follows these steps:

- Analysis of experimental results, in order to identify possible uncertainties or mistakes.
- Modelling of the main cause for degradation (corrosion induced by de-icing agents) and estimation of the relevant parameters for material behaviour (chloride diffusion coefficient).
- Estimation of limit conditions of durability of the structures under real exposure conditions (chloride threshold or limit value of chloride contents leading to corrosion under real moisture and temperature conditions).
- Estimation of the time-dependent model of behaviour to describe relevant mechanisms of durability (estimation of chlorides distribution in time and depth).
- Estimation of the remaining lifespan, that is, the age at which the durability conditions can no longer be fulfilled: elapsing time when chloride contents at reinforcement level reach the aforementioned threshold value for real environmental conditions).

Therefore, in order to minimize possible uncertainties of this layout, it is essential to count maximum warrants of the carried out experimental determinations for the true identification of chloride contents, cover values and half-cell potentials. In the particular case of diffusion coefficient estimation of the, accuracy depends on sufficient number of valid data from tests, that is, sufficient measures of chloride contents per core.

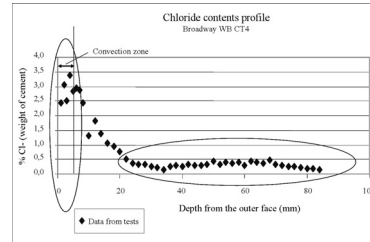


Figure 5. Corrections imposed by convection zone and components effect.

### 4.3 Modelling of the chloride induced degradation process

The accepted model for the diffusion of chlorides across the concrete mass, under non-stationary conditions, is governed by Fick's second law:

$$\frac{\partial C}{\partial t} = \frac{\partial}{\partial x} \left( D \frac{\partial C}{\partial x} \right) \quad (1)$$

This equation expresses the flux of concentration  $C$  of the diffusing species (chlorides) at a depth  $x$  from the outer surface along time  $t$ .  $D$  is the diffusion coefficient, expressed in  $\text{m}^2/\text{s}$ , which depends on concrete characteristics and on environmental conditions.

An approximate solution is given by

$$C_x - C_b = (C_s - C_b) \left[ 1 - \text{erf} \left( \frac{x}{2\sqrt{Dt}} \right) \right] \quad (2)$$

with the following meanings:

- $C_s$  contents of chlorides  $\text{Cl}^-$  at convection zone;
- $C_x$  contents of chlorides  $\text{Cl}^-$  at a distance  $x$  from the outer concrete surface; and
- $C_b$  contents of chlorides  $\text{Cl}^-$  already present in concrete mass and provided by its components;

In order to apply this model, it is necessary to obtain the diffusion coefficient  $D$  (which may typically vary from  $10^{-11}$  and  $10^{-13}$   $\text{m}^2/\text{s}$  as a function of concrete characteristics). As stated above, the precision of such sensitive value depends on available information. Therefore, when the number of chloride contents per concrete core at a given position is limited to 3 or 4, the precision may be reduced, especially considering that a convection zone is to be expected due to variable environmental conditions. In addition, it is essential to correct the chloride contents in order to consider their already present amount at construction, as illustrated in figure 5.

Therefore, for any determination on the different test cores, it is necessary to identify the region that really provides the diffusion of chlorides, disregarding the results outside This procedure implies the movement of both axes in figure 5. The distances are  $C_b$  for y-axis and  $x_{conv}$  for x-axis, being  $x_{conv}$  the depth affected by the above described convection

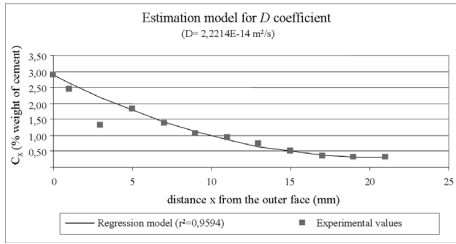


Figure 6. Example of regression in one of the cores.

mechanism. The obtained chloride profile is analysed by optimising the fit of the approximate equation given above by using the least square method after a linearization of the equation throughout a variable transformation (figure 6).

Indeed, the diffusion coefficient is not constant and may change in function of position and time, following variations in the pore structure or due to external humidity and temperature. This variation in  $D$  may be modelled by means of an ageing function given by:

$$D(t) = D(t_0) A(t) \quad \therefore A(t) = \left(\frac{t_0}{t}\right)^m \quad (3)$$

In the case of the structures analysed in this document,  $t_0 = 50$  years (current age after construction); and  $t = 100$  years (50 years of remaining desired life). Exponent  $m$  depends on type of cement. According to indications of *fib*, an  $m$  value of 0.50 has been adopted.

The chloride threshold for initiation of pitting corrosion for a given structure depends on numerous factors, i. e. pH of concrete, electrochemical potential of steel and presence of voids at steel/concrete interface. Traditionally, the threshold chloride content that may produce electrochemical reactions of corrosion corresponds to the weight of cement and is related to the binding capacity of the cement paste, among others. Therefore, according to *fib* recommendations, an average value of 0.6% (respect to mass of cement) for such a threshold is adopted. However, it is frequent to find some discrepancies or anomalous results provided by the labs, as happened in this case. This problem could be eluded since some measures, such as the corrosion potential, were also available. This means that if cement content values could not be determined, chloride contents should be related to concrete weight instead of cement weight.

As an important number of half-cell potential, basic parameter for the quantification of electrochemical phenomenon, were measured, an alternative procedure was adopted to quantify the chloride threshold throughout the relationship between half-cell potentials, chloride contents and the existence of damages at the positions where such measurements were taken. It therefore seems that the presence of damages could be related to threshold values corresponding to half-cell

potential of  $-300$  mV and 0.085% of chloride content of the mass of concrete. It is worth mentioning that this percentage perfectly fits the theoretical value of 0.6% recommended by *fib*, although expressed in terms of chlorides mass with respect to mass of cement in the case of a cement contents of about  $333 \text{ kg/m}^3$ , which is the value defined in the project of substructure elements, where the presence of damages is greater.

#### 4.4 Estimation of time-dependent evolution of chloride penetration

The model of Tuutti (1982) is accepted as a basis of this strategy. Usually, propagation time is negligible in relation to the initiation period, so  $t_1 = 0$  has been adopted.

The initiation period  $t_0$  is conditioned by the chloride diffusion processes from the outer surface to the reinforcing steel bars. From equation (2) derives:

$$t_0 = \frac{1}{12D} \left[ \frac{r_{\min}}{1 - \sqrt{\frac{C_{\text{lim}} - C_b}{C_s - C_b}}} \right]^2 \quad (4)$$

Thus, for each structure it is necessary to give diffusion coefficient  $D$ , concrete cover  $2''$  (corrected in order to consider the convection zone (0,5'') due to the fact that the maximum chloride content does not correspond to the surface but to a depth of 0,5'' that is,  $r_{\min} = 2 - 0,5 = 1,5''$ , a chloride threshold value  $C_{\text{lim}} = 0.085\%$  (referred to the mass of concrete, equivalent to 0.6% in mass of cement), and a chloride concentration  $C_s$  measured at the surface (maximum value, for a already elapsed time of 50 years, equal to the desired remaining lifespan) equivalent to 0.31% referred to the mass of concrete. Chloride concentrations  $C_b$  provided at construction stage by the cement and aggregates correspond to the horizontal line measured at reasonable depth, in order to ensure their independence from chloride diffusion mechanisms.

To assess the lifespan with a given failure probability, it is possible to develop a 'semi probabilistic' method, similar to the usual limit states method for structural assessment. For the purpose of this study, a probability failure  $p_f = 0.50$  has been considered. A partial safety factor for lifespan  $\gamma_L = 1.1$  was adopted, according to the new Spanish Code.

#### 5 GENERAL CRITERIA TO DECIDE ON REPAIR STRATEGIES

The election of an adequate repair strategy had to be based on the data collected during the auscultation phase, and was based on the following methodology. Figure 7 shows the chart of decisions and explains the significance of all related proposals of intervention. The process starts with the intensity  $I_{\text{corr}}$  measurement of the electrical current on bars.

If  $I_{corr} = 0$ , no corrosion process is taking place at the moment. Thus, it is necessary to compare chloride contents at level of reinforcement  $Cl_0$  with the chloride threshold  $Cl_{th}$ . If  $Cl_0 > Cl_{th}$ , showing no evidence of generalized damages, delamination of concrete and acceleration of corrosion will be taking place shortly after. In that case, the only possible intervention is to eliminate the contaminated concrete cover even behind reinforcement (according to the distribution of chlorides), although there are also different strategies available, as i.e. cathodic protection. If  $Cl_0 > Cl_{th}$ , the concrete member exhibits generalized damages and its reinforcement shows generalized corrosion too, with a significant loss of section, demolition would be the best option. If  $Cl_0 < Cl_{th}$  and the concrete member shows generalized damages and its reinforcement shows a fine layer of rust, but without relevant loss of section, the elimination of the deteriorated concrete even behind the reinforcement shall be necessary.

If  $Cl_{50}$  is the foreseen chloride contents at the level of reinforcement (according to available models, as explained above) at time  $t=50$  years. If  $Cl_0 < Cl_{th}$ ,  $Cl_{50} > Cl_{th}$  or  $Cl_0 < Cl_{th}$ ,  $Cl_{50} < Cl_{th}$  and the concrete member exhibits generalized damages (i.e. due to freeze-thawing effects), the removal of the concrete cover and its repair with new concrete is proposed. If  $Cl_0 < Cl_{th}$ ,  $Cl_{50} > Cl_{th}$  and the concrete member does not show generalized damages, patching repair may be carried out.

If  $Cl_0 < Cl_{th}$ ,  $Cl_{50} > Cl_{th}$  and the concrete member does not exhibit generalized damages painting with corrosion inhibitors or watertight layer may be applied to the existing surface.

If  $I_{corr} > 0$ , a corrosion process is taking place. If, in addition, the concrete member shows generalized damages, demolition might be inevitable. On the contrary, if no generalized damages are present, the above mentioned technique of removal the old cover and its replacement by a new one is proposed.

## 6 CONCLUSIONS

The current knowledge of the durability models for degradation processes allowed the development of effective strategies for the assessment of the remaining lifespan in existent structures. The applied methodology for the Indiana Toll Road bridges shows the feasibility of this approach based on “durability engineering”. By using relative conventional testing methods, it was possible to assess the remaining lifetime for the different structures located in very aggressive environment conditions. Nonetheless, some practical difficulties appeared when auscultation methods were carried out and theoretical models were applied. The main identified problems were the following:

- The number of cores must be limited, although representative in order to minimize the scattering of results, claiming to coordinate both auscultation and engineering activities.
- On some occasions, the obtained results did not fit expected theoretical behaviour. In these cases, the application of several simultaneous techniques for significant parameters may be highly effective.
- In practice, the application of Fick’s second law is associated to the assumption of values for some parameters which are very sensitive. Chloride threshold for corrosion and surface chloride contents may be good examples of that.
- The decision making process from obtained lifespan values may be defined according to an adequate repair strategy.

## REFERENCES

- Bertolini, L., Elsener, B., Pedferri, P. & Poldere, R. Corrosion of steel in concrete. Wiley-VCH. 2003.
- CEB. Strategies for testing and assessment of concrete structures. Guidance report. Bulletin 243. May 1998.
- Federation Internationale du Beton. Model Code for service life design. Bulletin FIB 34. February 2006.
- León, J., Espeche, A., Corres, H. et al. Daños en puentes ferroviarios de hormigón. Universidad Politécnica de Madrid. December, 2003.
- León, J. Durability of eight existing structures. Diagnosis report from Fhecór to Ferrovial. June 2007. Unpublished.
- Tuutti. Corrosión of steel in concrete. Swedish Cement and Concrete Research Institute. CBI Research 4:81, 1982.

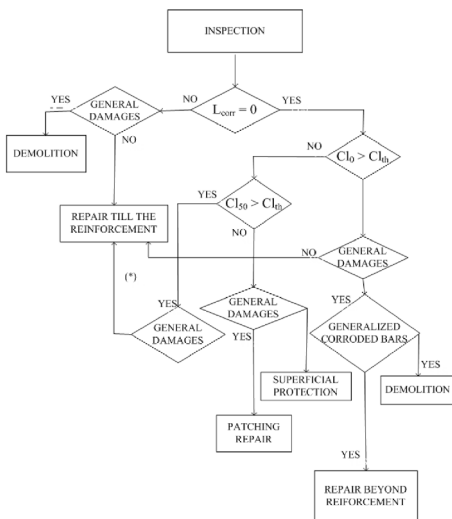


Figure 7. Flow-chart to decide the repair strategy.

# Birth certificate as an important tool for public-private-partnership projects

T.F. Mayer, P. Schießl & M. Zintel

*Centre for Building Materials, Technische Universität München, Munich, Germany*

**ABSTRACT:** In recent years, public-private-partnerships projects have gained increasing importance in various fields of the building sector. The need for the contractor not only to plan and construct, but also to maintain a structure over a period of normally about 30 years has caused a considerable interest in tools for an economically optimised planning and maintenance of structures exposed to environmental loads. A “birth certificate” can help with this task as it combines novel probabilistic deterioration models with non-destructive inspections carried out during and directly after completion of the structure. This paper presents an approach for the development of birth certificates by discussing characteristic parameters to be assessed, possible inspection techniques and the use of inspection results for the update of the original prognosis by means of a case study.

## 1 INTRODUCTION

On the background of scarce public budget resources, public-private-partnership-projects (PPP) have gained increasing importance in the public building sector. As a consequence, since 2004 the number of PPP-projects in Germany has increased by more than 100% on a yearly base. The majority of PPP-projects is in the field of building construction (hospitals, schools, administration buildings), but infrastructure projects (bridges, tunnels) with a quota of 20% form a vital part as well (BMVBS (2007)). There are different types of PPP-models ranging from so-called ‘Build-Operate-Transfer’—to ‘Build-Operate-Own’—models, but all of them have in common that the construction company is not only responsible for the planning and construction phase but also for the maintenance of the structure over a period of twenty to thirty years, depending on the model chosen.

A first evaluation of 46 PPP-projects conducted in 2007 has shown an increase in efficiency of 16% on average with respect to conventional project financing. This increase in efficiency is mainly due to an improved cost and planning reliability and an increased interest of the contractor in the quality of the structure. For the construction companies on the other hand, the need to maintain the structure over a period longer than the warranty offers an opportunity to turn away from the aggressive dumping prices of the last decade towards a quality-oriented construction philosophy. Especially in the field of infrastructure systems the durability of the constructed assets therefore gains importance due to considerable environmental stresses.

## 2 BIRTH CERTIFICATE

### 2.1 General

The Birth Certificate can form a valuable tool in the improvement of durability and quality control. Although the term itself is learnt from the field of medicine, “Birth Certificate” in this context is not limited to the mere documentation of the state of the structure directly after its completion (“birth”), but it also includes both the optimisation of the structure during design and planning and the quality control during construction and after completion. The approach followed in this paper is schematically illustrated in figure 1.

The development of a birth certificate can thus be subdivided into the following stages:

### 2.2 Design stage

During design stage, most of the crucial decisions concerning the durability of a structure have to be made. In the past, durability design of concrete structures mainly involved the observation of solely empirical ‘deemed to satisfy’ rules. However, recent achievements in the field of deterioration modelling (Gehlen (2000) nowadays allow for a durability design comparable to load design. For instance, for the depassivation of the reinforcement due to carbonation or chloride ingress, probabilistic models have been developed and applied successfully over the last decade for various structures.

Analogous to the load design, the first step in durability design is the assessment of environmental



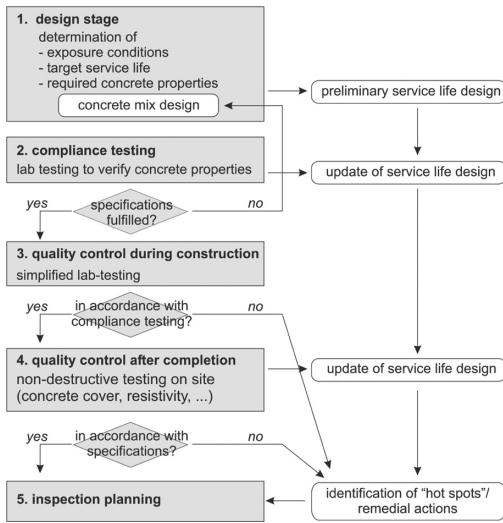


Figure 1. Stages in the development of a birth certificate.

stresses. Guidelines for their quantification can be found in literature. Furthermore, the target service life, limit states to be considered and corresponding safety indices required at the end of service life have to be quantified. For ultimate limit states, safety indices are subject to national standards, but for elements of minor structural relevance, lower safety indices can be agreed upon. Probabilistic prognosis using deterioration modelling as mentioned above renders requirements for specific concrete characteristics as for instance the chloride migration resistance  $D_{RCM,0}$  or the carbonation resistance  $R_{ACC,0}$ . These requirements can be compared to specific resistances of concrete mixes tested earlier or stated in literature. For illustration purposes, the influence of cement type and water-cement-ratio on the chloride migration coefficient is shown in figure 2.

If the deterioration modelling yields that due to very severe environmental stresses the durability requirements cannot be met with concrete alone, further protective measures (coating, cladding) have to be considered. As an alternative, the installation of monitoring devices in heavily exposed areas ('hot spots') does not lead to an increase of the structural resistance, but allows for a steady control of the structure's condition state while the structure is in use (Sodeikat et al. 2006).

### 2.3 Compliance testing

The design stage yields a concrete mix design that is supposed to fulfil the concrete properties as specified

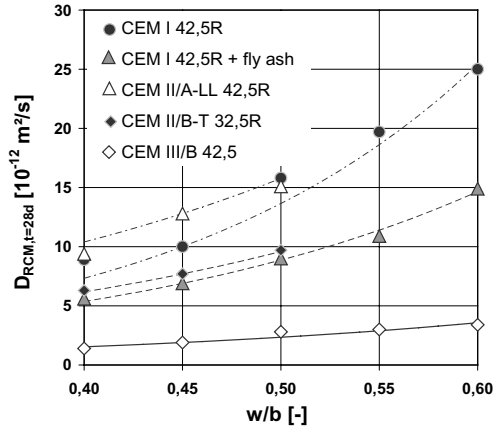


Figure 2. Rapid chloride migration coefficient  $D_{RCM,0,28d}$  versus w/b ratio for different binder types (Schiessl & Lay 2004).

before. However, due to considerable scatter in the properties of concretes produced for instance with cements from different cement plants, the compliance of the concrete mix with the target values specified earlier has to be checked. Test methods used for compliance testing are intended to give a direct and reliable quantification of the concrete characteristics. Therefore, indirect test methods such as electrolytic resistivity measurements in order to quantify the chloride diffusion properties of concrete are considered to be inadequate. However, the slow progress of deterioration mechanisms as for instance carbonation calls for accelerated test methods in order to gain reliable results within a comparably short time period. Therefore, rapid chloride migration testing and accelerated carbonation testing have been established as standard procedures for quantification of chloride migration and carbonation properties respectively (Gehlen 2000, Tang 1996). For freeze- and freeze-thaw-exposure CDF—('capillary suction of deicing solution and freeze thaw test') and CIF-test ('capillary suction, internal damage and freeze thaw test') appear to be adequate test methods. Due to the lack of deterioration models for these mechanisms, durability design with respect to freeze- and freeze-thaw-impact is still limited to 'deemed-to-satisfy' approaches (Schiessl & Mayer 2007).

The results of compliance testing can be used for a first update of the original deterioration prognosis. If the concrete characteristics determined in the tests are not sufficient to satisfy the requirements specified during design stage, an adjustment of the original concrete mix design has to be made or changes in the structural design itself (increase of concrete cover, application of coating) have to be considered.

## 2.4 *Quality control during construction*

Compliance testing is used to verify that the concrete meets the requirements when produced and tested under lab conditions. Unfortunately, the properties of the concrete produced in the concrete plant or on site can differ significantly from concrete produced in the lab. To become a valuable tool for the quality control during construction, the birth certificate also has to provide test methods in order to control the regularity of the concrete used on site.

It is obvious that for quality control purposes simple, easy-to-use test methods have to be chosen that can be included in the regular control procedures which have already been established for compressive strength testing. Electrolytic resistivity measurement appears to be an adequate test method as it can be conducted on the same concrete cubes already produced for compressive strength testing. Even though the electrolytic resistivity was classified as inappropriate for compliance testing, it is sufficient to assess the regularity of the concrete production. Test series conducted earlier indicated that once the characteristic properties of the concrete with respect to the prevailing exposure classes have been identified, the electrolytic resistivity can be used as a conformity indicator for concretes exposed to chloride ingress, carbonation, freeze- and freeze-thaw-attack. Different test methods can be used for the determination of the electrolytic resistivity. Among them, the Wenner-probe-Method and the two-electrode-method are the most common ones (Büteführ et al. 2006, Polder, 2001).

Threshold values for the minimum allowable electrolytic resistivity have to be formulated during the compliance testing stage already. If quality control shows that fractions of the concrete do not meet these requirements, possible consequences have to be evaluated and in some cases remedial actions have to be taken (coating, cladding, reduction of inspection interval length).

## 2.5 *Quality control after completion*

The inspections carried out after the completion of the structure resemble the classical acceptance inspection. The major difference is that the deterioration modelling carried out during the design stage allows for a more durability-oriented inspection planning. In contrast to inspections performed while the structure is already in use, quality control directly after completion yields no information about the environmental stresses that the structure is subject to or structure-environment interactions, so that only the structural resistance can be assessed. Therefore, a number of inspection techniques as for instance potential mapping, determination of chloride profile etc. cannot be used at this early stage in the life cycle of the structure. Depending on the exposure of the structural

elements, non-destructive techniques to be used for quality control are for instance concrete cover mapping, electrolytic resistivity measurements or crack mapping. As concrete cover is one of the key parameters for the time until depassivation both due to chloride ingress and carbonation, large parts of the concrete surfaces should be inspected. If for some reason this is not possible, at least small fractions of every element should be checked to make sure that systematic errors can be excluded.

In contrast to the resistivity measurements carried out in the lab on water-stored specimens during the construction phase, the structure's surfaces have been subject to a differing curing regime. Furthermore, as the concrete of the structure is not water-saturated even if extensively wetted directly before the measurement, a direct comparison with the threshold values defined for lab testing is inappropriate. For this purpose, additional specimens should be produced on site, demoulded and cured in accordance with the structural concrete and—if possible—stored on site. Methods for the determination of the electrolytic resistivity on site are the Wenner-probe-method or a two-electrode-measurement between the outer reinforcement and a stainless steel electrode placed on the concrete surface as described in Polder, 2001.

The use of the torrent permeability test to assess the surface quality is confined to very dry surfaces. Besides, even very small surface-near cracks can strongly influence the test results. Despite these drawbacks permeability measurements are used extensively for instance in Switzerland for the evaluation of the cover concrete quality of bridge structures etc. (Roelfstra et al. 2004).

Visual inspections yield no quantitative results for the update of the deterioration prognosis. Still, they form an important part of the acceptance inspection as they help to identify potential 'hot spots' due to cracking, risk of ponding or other irregularities. The results of the acceptance inspections can be used to update the original prognosis. If the update leads to a significant decrease of the expected life time for single elements or the visual examination yielded damages as described above, remedial measures have to be taken or an intensified inspection plan to monitor the future development has to be agreed upon.

## 2.6 *Inspection planning*

Inspection planning forms the last part of the birth certificate. Based on the updated service life prognosis, optimal inspection intervals for individual structural members can be identified. If very short inspection intervals are chosen, subsequent inspections are very likely to lead to no significant gain in information. On the other hand, very long inspection intervals bear the risk that the condition state of the structure might

already have passed a limit state considered optimal for maintenance actions.

The optimal point of time for inspections strongly depends on the individual maintenance strategy of the owner. If for instance a condition state  $n_m$  is considered adequate to carry out maintenance works, an inspection should only be scheduled when the probability that the structure has reached condition state  $n_m$  is larger than a target probability  $p_{f,target}$  (for example 20%):

$$t_{insp,a}: Pf[(n_m - 1) - n(t_{insp,a}) \leq 0] \geq p_{f,target}.$$

On the other hand, inspections should not be carried out too late to avoid that the structure is already in a worse state  $n_m + 1$ :

$$t_{insp,b}: Pf[(n_m) - n(t_{insp,b}) \leq 0] \leq p_{f,target}.$$

This approach renders a timeframe between  $t_{insp,a}$  and  $t_{insp,b}$  during which inspections should be carried out. As inspections are usually not conducted for single elements, but for the whole structure, the analysis of the timeframes for individual elements yields an optimal point of time for an inspection of the whole structure. Independent of the maintenance strategy, an inspection has to be scheduled when the failure probability exceeds the acceptable failure probabilities defined in the relevant standards or requirements formulated by the owner.

### 3 CASE STUDY

#### 3.1 General

The following case study is intended to illustrate the theoretical concept developed above.

The new Munich football stadium 'Allianz Arena' was completed in 2005. To provide sufficient parking space for almost 70.000 visitors, Europe's largest parking garage was integrated into the architectural concept. It comprises 9.800 parking places on four levels of 125 m length and 152 m width each, figure 3. The target service life of the parking garage is fifty years. To make sure that this service life can be accomplished with a minimum of maintenance costs, a lifecycle management system was agreed upon with a birth certificate as the first step.

#### 3.2 Design stage

For the parking decks a construction of prestressed concrete slabs supported on concrete columns was chosen, yielding a very slender slab structure of only 20 cm height without any additional down-stand beams. According to German standard DIN EN 1045-1:2001, the concrete slabs had to be classified as



Figure 3. View of the Allianz Arena and the adjacent parking garage during construction.

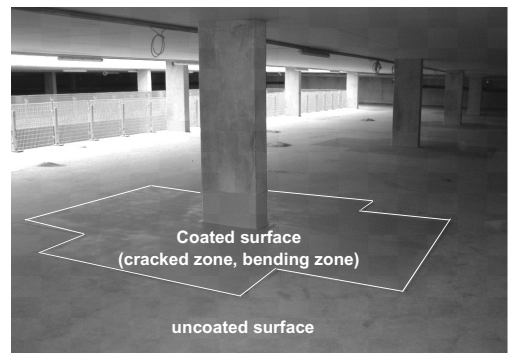


Figure 4. Coating of concrete surfaces in the bending zone only. Surfaces under compression are left uncoated and visually checked for cracking.

XD3—surface subject to chloride attack, alternatingly wet and dry.

For concrete surfaces which are directly driven upon, the German standard demands the application of a crack-bridging coating or alternative concepts to avoid depassivation of the reinforcement. Taking the considerable costs for the coating of 270,000 m<sup>2</sup> parking deck area and the comparably short life time of coating systems into account, an alternative corrosion protection concept was agreed upon. As the parking decks were constructed as continuous slabs, cracking due to bending was only to be expected close to the columns. Therefore, coating was limited to the tension zone, figure 4, whereas no coating was applied to surface areas under compression due to bending. To make sure that no cracking occurred in these uncoated areas, a regular visual inspection routine of both uncoated and coated areas was defined. A CEM I concrete with 50 kg/m<sup>3</sup> fly ash addition and an effective water-cement ratio of 0.45 was chosen. Due to the

slenderness of the slab construction the nominal concrete cover was limited to 45 mm. To compensate for this, additional quality control activities were planned to achieve a significant reduction of the concrete cover variability ( $\sigma = 3$  mm instead of  $\sigma = 8$  mm).

A preliminary durability design was carried out during design stage with values for material resistance for the planned concrete composition and environmental stresses taken from literature. The calculation yielded a probability of depassivation of 14.5% at the end of the target service life of 50 years, figure 5. As this failure probability was considered to be inadequate for parking deck slabs, the installation of a corrosion monitoring system of 30 anode ladders was agreed upon. The anode ladders allow for a non-destructive determination of the time-dependent chloride ingress into the concrete and can thus be used to update the original durability prognosis and identify possible corrosion risks before depassivation.

### 3.3 Compliance testing

As chloride-induced reinforcement corrosion is the core deterioration mechanism for parking decks, the chloride diffusion properties of the concrete were further investigated during compliance testing. The chloride migration coefficient  $D_{RCM,0}$  at an age of 28 days was determined by means of rapid chloride migration testing. The tests yielded an average chloride migration coefficient of  $D_{RCM,0} = 11.1 \cdot 10^{-12} \text{ m}^2/\text{s}$  ( $350 \text{ mm}^2/\text{a}$ ) which is in good agreement with the migration coefficient estimated during the design stage ( $D_{RCM,0,des.} = 10.6 \cdot 10^{-12} \text{ m}^2/\text{s} = 334.3 \text{ mm}^2/\text{a}$ ). Consequently, an update of the preliminary durability prognosis led to no significant change in failure probability.

### 3.4 Quality control during construction

As mentioned before, special attention was paid to a strict observance of the concrete cover on site. For

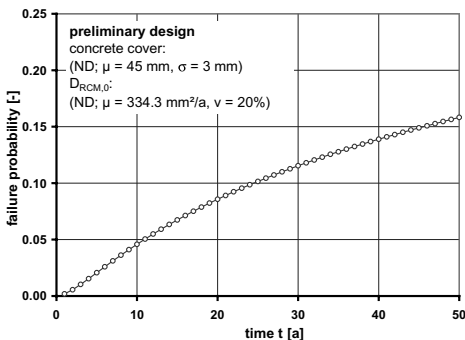


Figure 5. Failure probability vs. time (preliminary design).

this purpose, the staff was specifically trained and test surfaces not subject to chloride exposure were cast first and then investigated thoroughly.

The uniformity of concrete quality was controlled by means of resistivity measurements and Torrent permeability testing. The tests were carried out both on the structure itself and on specimens with different curing regimes ranging from two days under water and then under lab atmosphere up to 28 days under water (Kubens et al., 2005).

### 3.5 Quality control after completion

The alternative corrosion concept for the parking decks is based on the assumption that no cracking on the upper surface occurs outside of the coated areas. Therefore, the complete parking deck surfaces had to be visually checked for cracking after completion. The inspection yielded the formation of cracks close to fire retaining walls, as these walls apparently induced unexpected restraints. Deck surfaces adjacent to fire retaining walls were thus coated as well. Besides, only minor cracking was observed. Cracked surface areas discovered during visual inspection were locally coated to avoid accelerated chloride ingress into the deck slabs.

Concrete cover measurements were carried out on the complete parking deck surfaces. The average concrete cover was determined to be 50.3 mm and thus fulfilled the specifications formulated during the design stage. However, the quality control during construction did not meet the expectations, as the scatter of the concrete cover was significantly higher than planned ( $\sigma = 9.0$  mm).

The results of the compliance testing and the concrete cover mapping were used for a first update of the durability design, figure 6. As illustrated, the update after completion of the structure led to a slight decrease of failure probability with time.

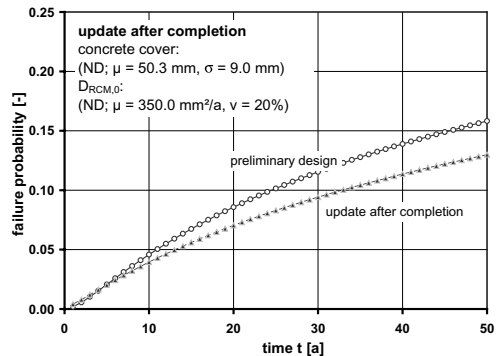


Figure 6. Updated failure probability vs. time after completion of the structure.

### 3.6 Inspection planning

In the case of the Allianz Arena parking garage, the installation of a corrosion monitoring system comprising thirty anode ladders in both coated and uncoated surface areas allows for a constant control of the degradation process. Therefore, the primary goal of the inspections is to control whether additional cracking occurred in both coated and uncoated areas. Visual inspections of the concrete surfaces are executed annually.

The results of the monitoring devices can directly be used to update the initial durability prognosis. Further information on the implementation of sensor data for update purposes can be found in Sodeikat (2006). A first evaluation of the monitoring data in 2007 led to a further increase of the prognosis reliability and as a consequence to a decrease of failure probability.

## 4 BIRTH CERTIFICATE IN THE CONTEXT OF LIFE CYCLE MANAGEMENT SYSTEMS

The “birth certificate” concept presented in this paper is intended as an element of a full probabilistic life cycle management system (LMS) which is currently being developed by a German research group from the Technical University of Stuttgart, the Technical University of Braunschweig and the Technische Universität München.

This computer-based LMS employs full probabilistic deterioration models on a structural element level. The subdivision of the structure into elements of comparable environmental stresses and material resistance allows for a detailed and exact prognosis of the condition development. The preliminary deterioration prognosis can then be constantly updated by means of non-destructive testing as presented in this paper. This way, possible future damages can be detected in time and preventive remedial actions can be taken before extensive repair actions are inevitable. The improved knowledge of the current and the future condition of the structure allows for a proper scheduling of remedial actions and budget allocation over a longer period of time.

Further information on the LMS software prototype under development and the deterioration modeling approaches used can be found in Kluth et al. (2008) and Budelmann & Starck (2008).

## REFERENCES

- BMVBS 2007. Erfahrungsbericht Öffentlich-Private-Partnerschaften in Deutschland, Berlin, Bundesministerium für Verkehr, Bau und Stadtentwicklung.
- Budelmann, H. & Starck, T. 2008. *Integration of degradation prognosis of concrete structures into life cycle management*. Proceedings of the 1st International Symposium on Life Cycle Management, Varenna, Italy.
- Büteführ, M., Fischer, C., Gehlen, C., Menzel, K. & Nürnberger, U. 2006. On-site investigation on Concrete Resistivity—a parameter of durability calculation of reinforced concrete structures. *Materials and Corrosion*, Vol. 57, Issue 12, pp. 932–939.
- Gehlen, Ch. 2000. *Probabilistische Lebensdauerbemessung von Stahlbetonbauwerken*. Deutscher Ausschuss für Stahlbeton, Issue 510, Berlin, Beuth-Verlag.
- Kluth, M. Borrmann, A., Rank, E., Mayer, T. & Schießl, P. *Development of a software-tool for the life-cycle management of bridges*. Proceedings of the 1st International Symposium on Life Cycle Management, Varenna, Italy.
- Kubens, S., Zellhuber, E., Rabald, K & Heidel, R. 2005. Einfluss der Nachbehandlung auf die Dichtigkeit und Druckfestigkeit von Beton. *Beton*, issue 2, pp. 20–22.
- Polder, R. 2001. Test methods for on site measurement of resistivity of concrete—a RILEM TC-154 technical recommendation. *Construction and Building Materials*, Vol. 15, pp. 125–131.
- Roelfstra, G., Hajdin, R., Adey, B. & Brühwiler, E. 2004. Condition evolution in bridge management systems and corrosion-induced deterioration. *Journal of Bridge Engineering*, Vol. 9, Issue 3, pp. 268–277.
- Schiessl, P. & Lay, S. 2004. Influence of concrete composition on reinforcement corrosion. In: Böhni, H. (ed.): *Corrosion in reinforced concrete structures*. Cambridge, Woodhead Publishing Ltd.
- Schiessl, P. & Mayer, T.F. 2007. *Lebensdauermanagementsystem*. Deutscher Ausschuss für Stahlbeton, Issue 572, Berlin, Beuth-Verlag.
- Sodeikat, Ch., Dauberschmidt, Ch., Schießl, P., Gehlen, Ch. & Kapteina, G. 2006. Korrosionsmonitoring von Stahlbetonbauwerken für Public Private Partnership Projekte. *Beton-und Stahlbetonbau*, Vol. 101, Issue 12, pp. 932–942.
- Tang, L. 1996. *Chloride Transport in Concrete—Measurement and Prediction*. Dissertation, Chalmers University of Technology, Gothenburg.

# Invention of crack inspection system using a light wave survey camera with a built-in crack scale

K. Nakaniwa

*Kansai Kouji Sokuryo Co., Ltd., Osaka, Japan*

M. Maeda

*NTT Infrastructure Network Corp., Tokyo, Japan*

Y. Koyama

*Geo-Research Institute, Tokyo, Japan*

T. Asakura

*Kyoto University, Kyoto, Japan*

**ABSTRACT:** In this paper, the newly developed crack inspection system using a light-wave with a built-in crack scale is proposed. This inspection system is more precise and higher speed than a conventional crack inspection method. The demonstration tests for proving the preciseness of this system in the case of perpendicular and nonperpendicular measurement are described. Moreover, the minimum measurable crack width and the maximum measurable distance are determined and tested. By using this newly developed crack inspection system, it is not necessary to construct temporary footholds for observing cracks at high place. Thus the injury risk of inspectors and inspection work duration can be reduced significantly. This inspection system can automatically transform the observed crack data into three dimensional digital data and link with CAD software, to create the unique 3D database crack management system.

## 1 INTRODUCTION

Normally crack and deformation inspections are necessary before planning repair and maintenance works for bridges, tunnel linings and other construction structures. In Japan, a conventional method, close visual inspection, is normally used for inspecting cracks of concrete infrastructures. The conventional method, temporary footholds must be constructed or a man-lift truck must be used for inspecting cracks of high rise bridges or tunnel crowns. This causes injury risks of inspectors, more working duration and more overall inspection cost. Moreover, the close visual inspection cannot be performed at some parts of structures at high place.

From these reasons, it is necessary to develop the long distance inspection method that can add the inspection data such as crack shape, length, width on CAD drawings simply and automatically. The newly developed method should be possible to use for inspecting the deterioration of structures precisely, and tracking the changes of structures in long term.

In this paper, the development and three demonstration tests for proving the preciseness, accuracy

and reliability of the newly development system are described.

## 2 CONVENTIONAL CRACK INSPECTION METHOD

In Japan, the close visual inspection method is widely used as described in RTRI (2007). In this conventional method, an inspector observes cracks on concrete surface visually. Normally, an inspector uses a chalk to mark crack positions and uses a crack scale to compare and evaluate a crack width. After taking photos of cracks, crack details such as crack position, shape, length, width, and inspection date are recorded in a sketch book on site. Finally, the inspection data is written down on CAD drawings manually. The problems of using this conventional method are as follows.

1. The accuracy of inspection results greatly depends on the experiences of each inspector.
2. Human errors occur easily in inspecting, sketching processes.
3. Difficult to observe and evaluate small cracks.

4. Necessary to construct temporary footholds or to use a man-lift truck for inspecting cracks at high places.
5. Requiring a great deal of time for drawing the crack information on CAD drawings.
6. Difficult to investigate crack progressing.
7. Requiring a great deal of time for updating the inspection data in the long term.

### 3 DEVELOPED CRACK INSPECTION SYSTEM

#### 3.1 Development background

The new crack inspection system was developed by combining a non-prism type light wave distance-measuring system with a crack scale. The non-prism type light wave is used for measuring a distance up to long-distance range. The built-in crack scale is used for evaluating a crack width.

The normal focal scope of a light-wave survey camera is shown in Figure 1. The newly developed focal scope with a built-in crack scale is shown in Figure 2. The crack scale was created as a spider's web shape that is easy to compare and match a crack direction by rotating the crack scale.

#### 3.2 Features of the developed crack inspection system

Figure 3 shows the newly developed survey camera, light-wave survey camera with a built-in crack scale. This new survey camera has the features as follows.

##### 1) A built-in crack scale

The spider's web shape crack scale is attached on a focal scope as shown in Figure 2. The light wave



Figure 1. Normal focal scope.

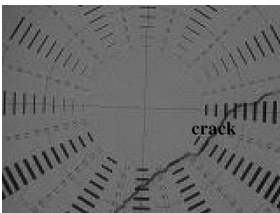


Figure 2. Newly developed focal scope.



Figure 3. The developed light-wave survey camera with a built-in crack scale.

distance survey camera with a built-in crack scale can be used to observe the crack in a long-distance. An inspector can choose the most suitable number on a crack gauge by rotating the focal scope and comparing the crack gauge with a crack observed through the camera. Then the crack width can be calculated from a crack gauge number, a distance and an angle between a camera and a crack.

##### 2) A 40-time zoom telescope lens

Normally, a light wave survey camera uses a 30-time zoom lens. As for the developed camera, in order to improve the observation efficiency of a built-in crack scale for observing cracks in the long-distance, the 40-time zoom lens is used. By using a high magnification lens with a built-in crack scale, this new camera can be used to inspect the crack width and three dimensional coordinates of cracks in the long-distance effectively and accuracy.

Based on the test results, this new camera has the capacity to detect 0.3 mm width cracks in the range of 39 m, and 0.1 mm width cracks in the range of 12 m. Hence, it is not necessary to use footholds or a man-lift truck to inspect the cracks at high places.

##### 3) A non-prism type light wave measuring function

The invented camera has a high efficiency to measure the distance in a long distance by using the light wave measuring system with a non-prism type without using a reflection prism and seal. In good environmental conditions, the non-prism type light wave measuring function can measure the distance up to 350 m.

##### 4) A collimation angle correction measuring

The measured size and width of an object depend on measured distance and angle. The actual crack width can be measured perpendicular to a crack and a structure surface. In the case of measuring angularly, the measured crack width changes depend on the measure angle. Three dimensional coordinates of cracks are calculated from the distance and the angle between the survey camera and observed cracks. By combining the crack width obtained from a built-in crack scale, and the three dimensional coordinates of the crack, the collimation angle correction is performed automatically to calculate the actual crack width.

## 5) Camera application software

Four application programs were also developed for processing and transforming the measured data to be digital data and CAD drawings. An inspector can use these developed programs on a personal computer link with CAD software, to create a three dimensional view, plan view, elevation view and unfolded view automatically and easily. The time required for post processing and drawing works can be reduced remarkably by using these developed programs.

### (a) Automatic connecting line program

The automatic connecting line program is used for connecting the start, end, broken points of crack lines. An angle correction is also performed at the same time of connecting line. A crack shape can be recorded exactly and precisely by using this program.

### (b) Specific planer projection and unfolded curve surface program

The specific planer projection program is applied for processing crack data at a slope or a wall surface. In the case of a bridge pier and a tunnel lining, the unfolded curve surface program is applied for processing the measured data.

### (c) High speed drawing program

The measured data can link with any CAD software on the market. By using the high speed drawing program together with CAD software, a deformation view, a plan view, an elevation view and an unfolded view with crack shape of the observed surface can be drawn easily and in the short time.

### (d) Data exchange program

The data exchange program is used to exchange digital measured data with other types such as 3D laser scanner data, GIS data, National Spatial Data Infrastructure (NSDI). Hence, it is possible to combine measured data with other types of data for performing the three dimensional analysis of observed structures.

## 4 DEMONSTRATION TESTS

In this session the results of three demonstration tests carried out for investigating the scattering of measured results caused by human factor, the minimum measurable crack width and the maximum measurable distance and the preciseness of angular measurement, are shown and described.

### 4.1 Tests of scattering caused by human factor

#### 1) Test objectives

In the crack inspection operation, an inspector observes a crack through a camera and selects the most suitable crack gauge number from a built-in crack scale. After that, the crack width is calculated automatically from the selected gauge number

and the measured distance. Hence, the selection of a gauge number by an inspector has the most effect on measured results. Thus the demonstration tests for investigating the scattering of measured results caused by human factor or an inspector were carried out.

#### 2) Test method

As shown in Figure 4, a wall with an imitation crack was made and placed outdoor then the developed camera was set at the same height and perpendicular to an imitation crack. The operation of selecting the gauge number is shown in Figure 5. By rotating the built-in crack scale and comparing an observed crack with a crack gauge, the gauge number of the crack gauge that has the same size as the observed crack is selected and recorded. After this manual operation, the crack width is calculated automatically.

#### 3) Test conditions

The test conditions are shown in Table 1. This test was carried out by 100 surveyors who have experiences in surveying varying from few years to expert and licensed surveyor. The real crack width of the imitation crack is measured by a microscope.

#### 4) Test results

The test results of the measure distance of 20 m, the measured crack width and its number of results are shown in Figure 6 ~ 10. Figure 6 shows that there are some measured data that have errors more than 0.05 mm in the case of 0.1 mm crack width. While for the wider crack, all measured data has an error less

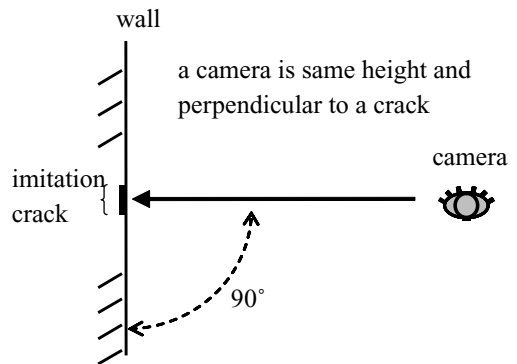


Figure 4. Outline of the scattering test.

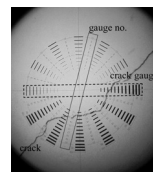


Figure 5. Comparing an imitation crack with a crack gauge.



Table 1. Conditions of the scattering test.

Subject	Condition
Distance (m)	10, 20, 30, 40, 50
Crack width (mm)	0.1, 0.2, 0.3, 0.4, 0.5
Place	Outdoor
Object	Imitation crack which has a uniform crack width
Date at time	9:00~17:30, 3 days in the first week of June (summer)
Acceptable error	All errors are not more than 0.05 mm

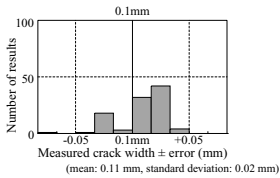


Figure 6. Test results of crack width 0.1 mm, distance 20 m.

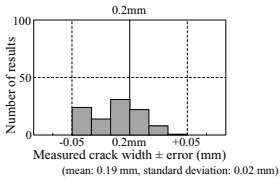


Figure 7. Test results of crack width 0.2 mm, distance 20 m.

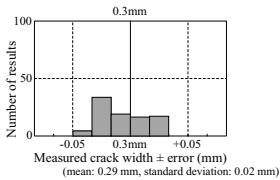


Figure 8. Test result of crack width 0.3 mm, distance 20 m.

than 0.05 mm. Based on the test criteria, the minimum measurable crack width for measure distance 20 m is 0.2 mm.

Moreover, the minimum measurable crack widths for each measure distance are summarized in Table 2. These results show obviously that the minimum measurable crack width depends on the measure distance. The measurable crack is wider when the measure distance is shorter.

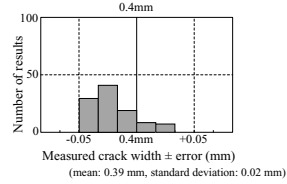


Figure 9. Test result of crack width 0.4 mm, distance 20 m.

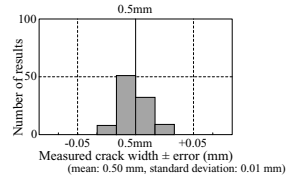


Figure 10. Test results of crack width 0.5 mm, distance 20 m.

Table 2. Minimum measurable crack width.

Distance (m)	Min. crack width (mm)	Maximum error (mm)
10	0.1	0.05
20	0.2	0.05
30	0.3	0.05
40	0.4	0.05
50	0.4	0.05

#### 4.2 Tests of minimum measurable crack width and maximum measurable distance

In order to determine the minimum measurable and the maximum measurable distance, the same test procedures as described in the previous session were carried out. The tests were carried out at the distance of 5, 10, 15, 20, 25, 30, 35, 40, 45 and 50 m. The measurable crack width is defined as the measured result that has an error within 0.05 mm.

The relation between the minimum measurable crack width and the measurement distance is shown in Figure 11.

In Japan, normal requirement of crack inspection for road tunnels is 0.2 mm, for telecommunication tunnels is 0.3 mm, and for bridges is 0.3 mm (ref. RTRI 2000 etc.). These results show that the maximum measurable distance for 0.2 m cracks is 27 m, and for a 0.3 mm cracks is 39 m. Hence it is possible to set the camera on a pavement or a tunnel invert for inspecting the crack at tunnel crown without using any foothold

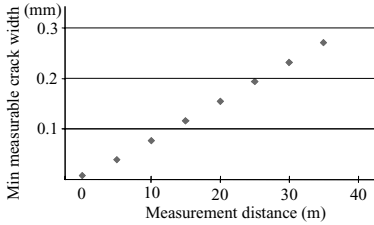


Figure 11. Relation between the minimum measurable crack width and the measure distance.

Table 3. Maximum measurable distance.

Crack width (m)	Max. measurable distance (m)
0.1	12
0.2	27
0.3	39

or a lift-man truck. It is also possible to inspect in the long distance up to 27~39 m.

### 4.3 Tests of angular measurement

#### 1) Test objectives

The precision of perpendicular measurement is demonstrated and proved in the previous two sessions. In usual inspection works, the measurement cannot be performed perpendicular to a target wall due to nearby obstacles. Theoretically, the measured crack width from an angular measurement is smaller than a perpendicular measurement. Thus, the collimation correction of an angular measurement should be performed for obtaining an actual width.

The automatic collimation function is included in this developed camera. In this session the tests for demonstrating the precision of this function is described. From past experiences of many surveyors, an angular measurement less than 30° causes too large error and unreliable results. Thus in this test, the range of a camera angle was set as 30°~80°.

#### 2) Test method

Figure 12 shows an outline of the tests of angular measurement. The camera was set at the same height and at the angular range of 30°~80° to an imitation crack. Firstly, both ends of crack were measured and then a reference point on the wall was measured. The coordinates of three points are used to define a surface and correct the crack width automatically by the collimation correction program. Finally the measured results were compared with the real crack width that measured by a microscope.

#### 3) Test conditions

The test conditions are shown in Table 4. This test was carried out by 100 surveyors. The imitation crack

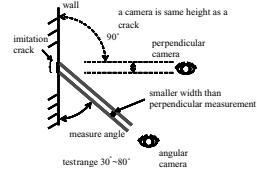


Figure 12. Outline of the angular measurement test.

Table 4. Conditions of the angular measurement test.

Subject	Condition
Distance (m)	10, 20
Crack width (mm)	0.1, 0.2
Object	Imitation crack which has a uniform crack width
Measure angle	30°, 40°, 50°, 60°, 70°, 80°
Date at time	9:00~17:30, 3 days in the first week of June (summer)
Acceptable error	All errors are not more than 0.05 mm

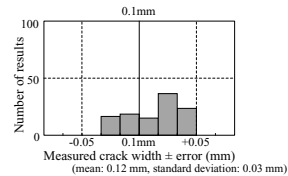


Figure 13. Test result of crack width 0.1 mm, angle 30°.

widths are 0.1 and 0.2 mm, and the measure angle are 30°, 40°, 50°, 60°, 70° and 80°.

#### 4) Test results

Test results of the measure distance of 20 m, camera angle of 30°, 60°, and 80° of both 0.1 and 0.2 mm crack are shown in Figure 13~18. The range of errors and the maximum absolute error of the measured results are summarized in Table 5~6. This results show that all measured results from the angular camera has an error less than 0.05 mm. Thus it can be concluded that the crack width can also be measured precisely in the case of angular measurement in the range of 30°~80° by using the included collimation correction function.

## 5 SUMMARY

In this paper, the development and the features of the new crack inspection systems using a light wave survey camera with a built-in crack scale is described. Then the demonstration tests results for investigating the scattering due to human factor in the case of perpendicular and angular measurement are shown. The

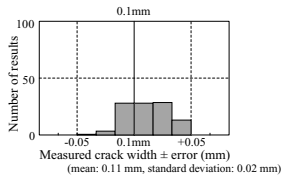


Figure 14. Test result of crack width 0.1 mm, angle 60°.

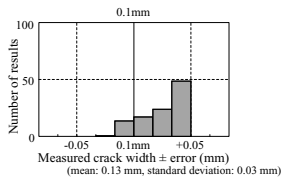


Figure 15. Test result of crack width 0.1 mm, angle 80°.

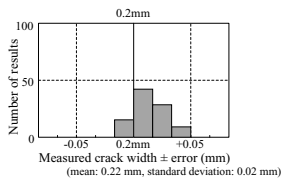


Figure 16. Test result of crack width 0.2 mm, angle 30°.

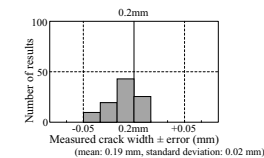


Figure 17. Test result of crack width 0.2 mm, angle 60°.

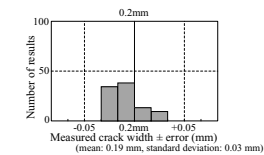


Figure 18. Test result of crack width 0.1 mm, angle 80°.

results proved that the crack width obtained from both cases using this inspection system is precise and accurate enough in practical. Moreover, the tests of the maximum measurable distance show that, this developed camera can be used for measuring the crack in the long distance effectively.

Table 5. Test results of the 0.1 mm wide crack.

Distance (m)	Range of error (mm)	Max absolute error (mm)
10	-0.02~+0.02	0.02
20	-0.02~+0.03	0.03

Table 6. Test results of the 0.2 mm wide crack.

Distance (m)	Range of error (mm)	Max absolute error (mm)
10	-0.04~+0.01	0.04
20	-0.04~+0.01	0.04

This crack inspection system was applied for inspecting the cracks at the 582 m-long, 4-lane pier bridge in Aomori prefecture, Japan. The inspection works completed safely and economically in 4 days. In this application, the three dimensional cracks information were drawn together with structure drawings by CAD software and saved digitally.

From the applications on site the following features of this newly developed inspection systems have been proved.

1. Capable to inspect at the long distance and the high place.
2. Easy to create the digital CAD drawings.
3. Capable to investigate the progressive of cracks.
4. Capable to inspect only the newly occurring cracks.

Now, the developed inspection systems are used in many sites, and many environments in Japan. New features such as automatic image processing and automatic tracking systems are under developing. The effective utilization of the observed crack information for maintenance concrete structures in the long term is also under investigating.

## REFERENCES

- Railway Technical Research Institute (RTRI) 2000. *Manual of Tunnel Repairing and Reinforcement*: 115. Tokyo: Maruzen (in Japanese).
- Railway Technical Research Institute (RTRI) 2007. *Maintenance Standards for Railway Structures and Commentary*: 102–104. Tokyo: Maruzen (in Japanese).

# Structural health monitoring for life cycle management of bridges

F.N. Catbas, M. Gul, R. Zaurin, H.B. Gokce, D. Maier & T. Terrell

*University of Central Florida, Orlando, FL, USA*

**ABSTRACT:** The infrastructure, more specifically bridges, in the US is aging. Visual bridge inspections with limited non-destructive evaluation and simplified load rating are the main data generation program for decision making. The shortcomings of this program for providing objective data are well established. As a result, application of new technologies and approaches has become a major need. Bridge health monitoring (BHM) offers promise in better understanding the actual condition of the structures for life cycle management of bridges. BHM can be defined as continuously or intermittently monitoring of the structural systems/components/elements to track the condition and to determine damage. With this, it is expected to develop condition-based maintenance strategies, prioritize maintenance applications for better use of funds and mitigate unexpected structural problems. However, there are major research needs in BHM before it becomes a standard practice by infrastructure owners. The purpose of this paper is to discuss the effective use of information technologies to facilitate the use of data by infrastructure users. This effort is expected to serve integration of bridge management and bridge health monitoring system applications. Together, these two systems will help infrastructure owners to make better decisions for the management of an entire fleet of bridges. In this paper, the writers are presenting an overview of their recent studies on the movable bridges within the state of Florida.

## 1 INTRODUCTION

Structural Health monitoring (SHM) can be defined as measurement of operating and loading environment and critical responses of a system to track and evaluate incidents, anomalies, damage and deterioration. Transportation infrastructure, especially long-span bridges, is one of the main subjects of application for SHM. Implementation of SHM can reveal global and local structural parameters, generate data for structural identification, lead to effective maintenance and operation, improve future designs and help diagnosing pre- & post- hazard conditions and emergency management. All SHM applications involve the basic phases of planning, instrumentation, data collection, processing and decision making. Type, scope and scale of the application determine types of sensor and data acquisition devices and evaluation methods. Advancing technology is making it simple and inexpensive to deploy large numbers of sensors and collect real-time or archived data. Therefore, data management technologies and data processing algorithms need to be developed in order to be able to make use of the data in the most effective way to supplement bridge management systems.

## 2 BRIDGE MANAGEMENT SYSTEMS

### 2.1 *General*

Bridge management system (BMS) is a system of decision making, budget allocation, and maintenance scheduling operations for an inventory of bridges. Project-level BMS is the applications of the maintenance engineer and the district offices, which have the immediate control of the bridge and carry out inspection and maintenance operations. Network-level BMS establishes policies and decides budget allocation for the project level. Efficient BMS should designate evaluation and decision making to the network level, which requires comprehensive information from the project-level, regarding bridge characteristics, structural condition, usage level and maintenance information. With sufficient data, inventory of bridges can be managed as transportation assets to minimize their life-cycle cost, therefore, utilizing the available budget efficiently while keeping the bridges at satisfactory conditions.

### 2.2 *Current Practice in the US*

Currently, common practice is that ordinary bridges are inspected with a fixed frequency to check for

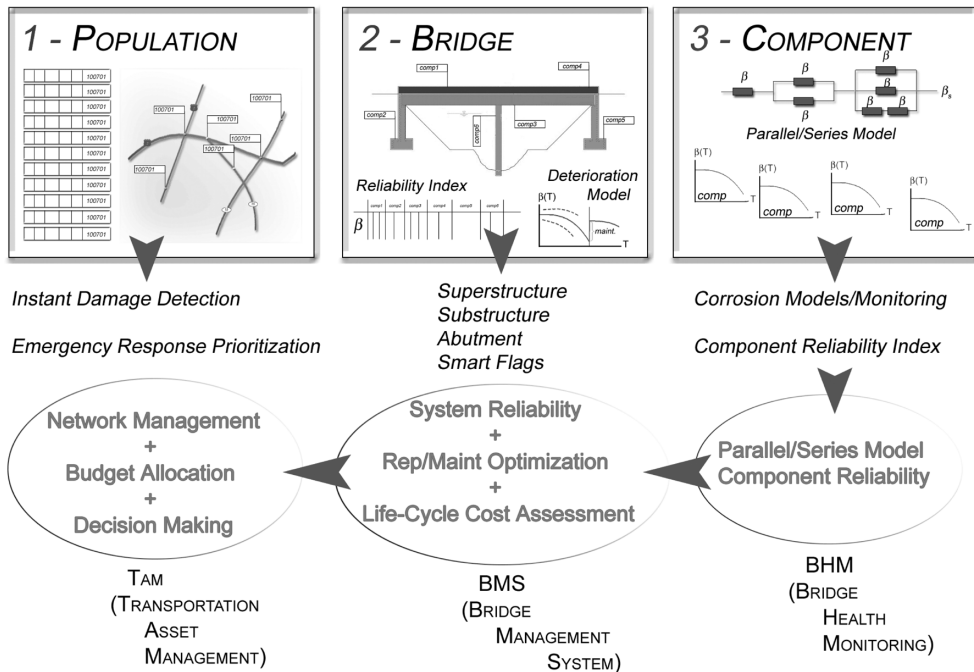


Figure 1. Health monitoring for life cycle management of bridge populations.

deterioration and assign repair tasks for deficient parts according to the urgency of intervention and available budget. Inspection frequency in the United States is once in every two years. Routine inspections are done only visually, allowing only the problems reaching the surface to be detected. A lot of common and critical problems like corrosion of reinforcing steel in reinforced concrete members, hairline cracks in steel members, loss of tension in prestressing strands, fatigue effects cannot be determined with visual inspections. Also, results of these inspections depend on the expertise and thoroughness of the inspection crew, and studies indicate that they also include considerable subjectivity.

Established by the Federal Highway Administration (FHWA), detailed characteristic information for all bridges is stored in a common database called National Bridge Inventory (NBI), which is updated every two years with routine inspection reports, also including a basic condition state appraisal. NBI involves dimensions, location, type, design criteria, traffic, structural and functional condition, and lots of other information. Also, bridge management software were developed and implemented in many states. Two examples are PONTIS and BRIDGIT. These software incorporate NBI data, store inspection records, keep track of maintenance work, and even have capability of budget optimization using Markovian decision processes.

However, their application is limited to visual inspections only and thus incorporates the uncertainties associated with the visual inspection process. Data for bridge condition and management activities are usually kept by the respective transportation district office, without any information sharing mechanism within the agency. Also, data is often found to be incompatible for comparison between different time periods or different districts. Therefore, although extensive bridge management programs exist, the data used is unreliable and insufficient, and information sharing within departments is inadequate.

### 2.3 Emerging role of SHM for integrated bridge management

SHM can be an indispensable tool by providing accurate, abundant and up-to-date data for BMS. As well as revealing global structural properties such as natural frequencies; component monitoring, shown in Figure 1 (3), yields condition state based on monitored parameters, such as strain, corrosion, etc. Component-based monitoring data should be assessed to produce reliability of each monitored structural component, and deterioration with time. Components to be instrumented should be carefully selected, as well as the parameters to monitor. Reliability analysis is based on statistical calculation of the safety buffer, or,

distance from the limit state. Method of reliability index, calculated from the load effects and capacity, is selected according to the considered parameter.

Structural condition state and reliability is then to be determined from component data. Reliability of the structural system depends on reliability of its components, so if there is no redundancy, weakest link will determine the overall reliability. Presence of redundant members makes it necessary to perform a system reliability analysis, modeling the structure as parallel and/or series combinations of the components.

Bridge management systems can be easily developed to function with condition rating and system reliability of a bridge obtained from SHM data. The ideal case is operating with real-time monitoring, but intermittent data collection is also fine. Then, deterioration of the bridge can be fit to models to predict the future condition of the bridge without maintenance interventions. Bridge management system will use this data to evaluate the life-cycle cost (LCC) of the bridge with alternative maintenance types and plans, in order to minimize the LCC.

In Figure 1 (1), inventory of bridges were combined as a bridge network. This is the network-level management stage, where budget allocation and optimization is done at the network level. Another crucial application of bridge population monitoring is prioritization of incident management activities during extreme events such as hurricanes and earthquakes.

These three stages of monitoring should be involved in the integrated bridge management, forming a network-level bridge management database. In addition, the common database should be based on the conventional internet backbone, allowing access with

web browsers, in order to make the system easily accessible from any worldwide location and for any user, including the general public, to the extent of their allowed level of authorization.

### 3 BRIDGE HEALTH MONITORING AND LIFE CYCLE MANAGEMENT

#### 3.1 Integration issues

Integration of all bridge management aspects requires implementation of information technologies. All data flow; sensor data, inspection reports, traffic information, security, should be organized under an integrated framework, accessible through a secure internet connection. In the following schema (Fig. 2), integration of BHM and BMS is illustrated. Sensors on the structure transmit signals to the data acquisition stations through wired or wireless connections, according to the SHM design. Raw data delivered by data acquisition stations are processed and converted into meaningful data, which is then logged into the database. Inspection reports from visual inspection of the structure are also added to the database in electronic format. Then, the integrated database containing bridge information, legacy data and condition state serves as a hub for all related agencies and individuals for reaching, updating and sharing this information.

Advantages of utilizing internet for bridge management and database applications are numerous. A system working on internet will be much more convenient for the users, who will have access with any kind

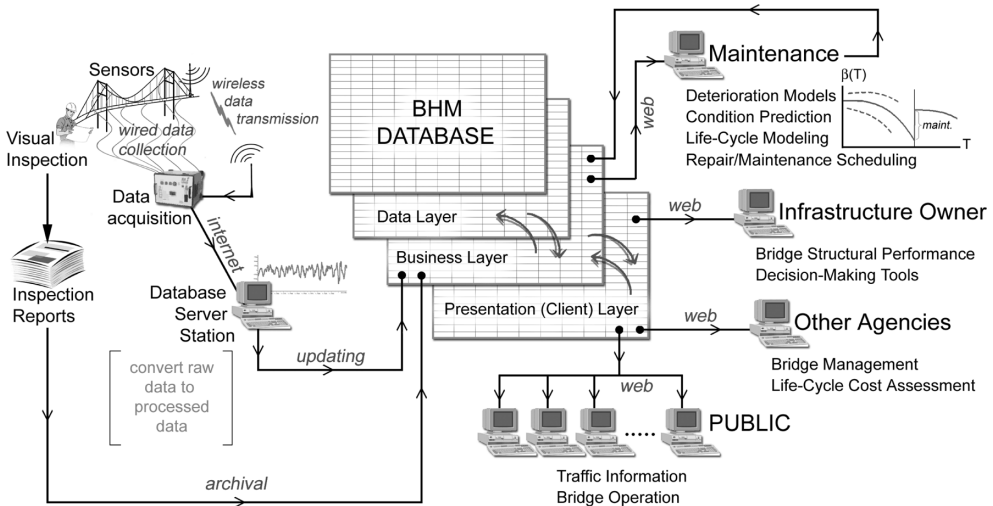


Figure 2. Database implementation issues for health monitoring system.

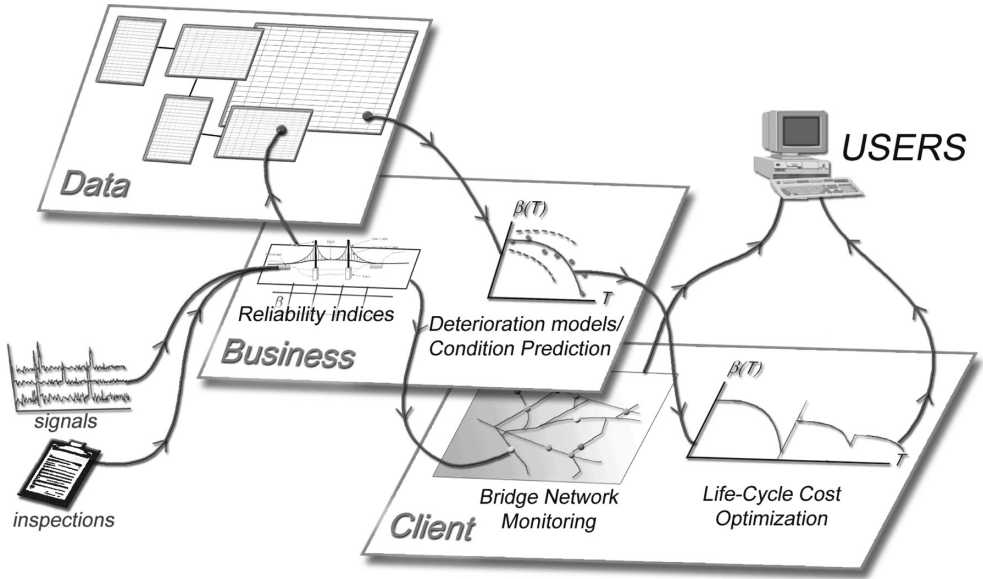


Figure 3. Database functional layers.

of internet connection. There will be no compatibility issues or installation and maintenance of software for each user, since regular internet browsers will be enough for all tasks. Intra-agency information sharing and collaboration can be maximized.

### 3.2 Database structure

Database consists of three conceptual layers, each of which is associated with certain functions of its mechanism. These are;

1. Data Layer
2. Business Layer
3. Presentation (Client) Layer

An example of database working schema is given in Figure 3. The data layer is a static layer, representing stored physical data. Data layer is the foundation of the database, containing all data and tables. This layer is at the background and accesses only through the business layer. The business layer contains the rules, policies and algorithms for manipulating the data layer. Algorithms that determine the reliability indices from SHM data and store into appropriate fields/tables in the database are parts of the business layer. Client layer is the interface that the user interacts and sends/receives information. When the user requests bridge network monitoring or life-cycle cost optimization display from the client layer, business layer retrieves the necessary information from the data

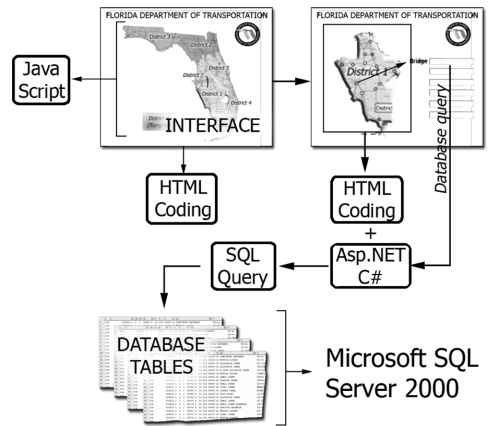


Figure 4. Internet-based database framework.

layer, converts into required format, and sends to the client layer for display (Fig. 3).

An example web-based database structure is shown below (Fig. 4). The database was created using Microsoft SQL Server 2000 database management software. This software was found to be convenient, robust and inexpensive, and its performance satisfactory for the application involving the highway bridge inventory of Florida. However, for bigger applications, database management software having higher performance, for example Oracle, can be considered.

Database management software communicates with the HTML (hypertext markup language—most common and basic form of webpage coding) interface via SQL (Structured Query Language) queries. SQL queries are specific codes for searching, filtering, editing or manipulating database fields. C# code on the interface connects to the database and translates user input into SQL queries. Web page was created with HTML code, with Java code incorporated for interactive selections.

### 3.3 Some issues for internet-based database implementation

First type of issues for BMS database application is the problems of dealing with large-scale databases. Database design criteria are scalability, interoperability, extensibility, fault tolerance and, ultimately, good performance. From a technical point of view for the web application design, important considerations are bandwidth, latency, load and security. Bandwidth determines the speed of the network, latency is the delay in response from the server and load is the maximum number of simultaneous clients the server can support. Security of the system is a very critical issue since the bridges as well as the management system are important assets. Security of the system should therefore be top priority. Access to the database should be limited by defining users with passwords and their position, task and privileges. So, only certain sections of the database should be allowed to each user.

## 4 CONCLUSIONS

Integrating bridge management systems as a combined system including health monitoring and decision making components can improve management of highway bridges by providing reliable data and realizing effective sharing of available data. Highest functionality is provided by designing a world-wide-web interface for accessing and using the system. Also, decision making processes can be improved by employing structural reliability analyses, for cost-benefit and tradeoff assessments using budget optimization techniques. Integrated bridge management system will also be extremely helpful for hazard management and provide reference data for future structural designs, maintenance and traffic operations.

## ACKNOWLEDGEMENTS

The authors would like to acknowledge the support from the Florida Department of Transportation (FDOT) and the U.S. Federal Highway Administration (FHWA). This material was mainly based

on FDOT Research Project BD548-RPWO#1. The authors greatly appreciate the feedback and guidance of Mr Marcus Ansley of FDOT. Also, Dr Hamid Ghasemi of FHWA provided valuable feedback on the requirements of the long term bridge performance. The authors would like to acknowledge Prof. Dan Frangopol of Lehigh University for their collaboration and joint studies. Finally, contribution of past graduate students Melih Susoy and Pavel Babenko is appreciated. Any opinions, findings and conclusions or recommendations expressed in this publication are those of the authors and do not reflect the view of the Florida Department of Transportation or Federal Highway Administration.

## REFERENCES

- Ang, A.H-S. & De Leon, D. 2005. Modeling and analysis of uncertainties for risk-informed decision in infrastructures engineering. *Structure and Infrastructure Engineering, Taylor & Francis* 1 (1): 19–31.
- Akgul, F. & Frangopol, D.M. 2003. Rating and Reliability of Existing Bridges in a Network. *Journal of Bridge Engineering, ASCE* 8 (6): 383–393.
- Aktan, A.E., F.N. Catbas, et al. 2000. Issues in Infrastructure Health Monitoring for Management. *Journal of Engineering Mechanics, ASCE* 126 (7): 711–724.
- Aktan, A.E., D.N. Farhey, et al. 1996. Condition Assessment for Bridge Management. *Journal of Infrastructure Systems, ASCE* 2 (3): 108–117.
- Aktan, A.E., A.J. Helmicki, et al. 1998. Issues in Health Monitoring for Intelligent Infrastructure. *Smart Materials and Structures* 7: 674–692.
- Bolukbasi, M., J. Mohammadi, et al. 2004. Estimating the Future Condition of Highway Bridge Components Using National Bridge Inventory Data. *Practice Periodical on Structural Design and Construction* (91): 16–25.
- Catbas, F.N. & A.E. Aktan 2002. Condition and Damage Assessment: Issues and Some Promising Indices. *Journal of Structural Engineering, ASCE* 128 (8): 1026–1036.
- Catbas, F.N., Susoy, M., & Frangopol, D.M. 2008. Structural health monitoring and reliability estimation: Long span truss bridge application with environmental monitoring data. *Engineering Structures, Elsevier* (in press).
- Chen, C.J. & D.W. Johnston 1987. Bridge Management under a Level of Service Concept Providing Optimum Improvement Action, Time and Budget Prediction. Raleigh, NC, FHWA.
- Ellingwood, B.R. 2005. Risk-Informed Condition Assessment of Civil Infrastructure: State of Practice and Research Issues. *Structure and Infrastructure Engineering* 1 (1): 7–18.
- Enright, M.P. & D.M. Frangopol 1999. Condition Prediction of Deteriorating Concrete Bridges Using Bayesian Updating. *Journal of Structural Engineering, ASCE* 125 (10): 1118–1125.
- Estes, A.C. & D.M. Frangopol 2001. Bridge Lifetime System Reliability under Multiple Limit States. *Journal of Bridge Engineering, ASCE* 6 (6): 523–528.



- Federal Highway Administration (FHWA) 1995. Recording and Coding Guide for the Structural Inventory and Appraisal of the Nation's Bridges. FHWA.
- Hudson, W.R., R.C.G. Haas, et al. 1997. *Infrastructure management: integrating design, construction, maintenance, rehabilitation, and renovation*. New York, McGraw-Hill.
- Pagano, A.M. & E. Ogard 2005. Linking Asset Management to Strategic Planning Processes: Best Practices from State DOT's. *TRB 84th Annual Meeting*, Washington D.C.
- Thompson, P.D., J.O. Sobanjo, et al. 2003. Florida DOT Project-Level Bridge Management Models. *Journal of Bridge Engineering, ASCE* 8 (6).
- Wang, X., S. Kangas, et al. 2005. Overview of a Modal-Based Condition Assessment Procedure. *Journal of Bridge Engineering* 10 (4): 460–467.
- Weyers, R.E., P.D. Cady, et al. 1988. Cost Effective Bridge Maintenance and Rehabilitation Procedures. Washington, D.C., *Transportation Research Board*.

# Peeling failure along the interface in FRP-strengthened beams subjected to transverse loads

E. Oller & A.R. Mari

*Construction Engineering Department, Technical University of Catalonia, Barcelona, Spain*

D. Cobo

*Tec-cuatro, S.A., Barcelona, Spain*

**ABSTRACT:** Existing experimental research has shown that the application of externally bonded laminates to strengthen reinforced concrete structures can lead to brittle failures involving the laminate debonding before the design load is reached and a classical failure mode occurs. In an externally bonded RC beam, this peeling failure can initiate either near midspan due to the effects of flexural or shear cracks, or at the laminate end due to stress concentration at the laminate cut-off point. The design procedure to obtain the laminate area to strengthen a reinforced concrete element should avoid these premature peeling failures. Therefore, there is a need to understand the mechanics of the laminate debonding process in order to prevent it. This paper studies the evolution of the debonding process using Non-Linear Fracture Mechanics assuming a bilinear constitutive law for the interface between the concrete and the externally bonded laminate. The crack's propagation process is described through the evolution of different stages, in which the interfacial shear stresses can be obtained. The integration of the shear stress distribution gives the force transferred between the laminate and the support. Since the transfer of stresses from laminate to concrete through the interface is a critical parameter in the correct performance of externally bonded structures, the transferred force should be limited to a maximum value in order to prevent peeling failure.

## 1 INTRODUCTION

Existing RC structures may be damaged or in need of repair due to a loss of carrying capacity, or may need to upgrade their resistance or stiffness in order to withstand an increase in load demand or to eliminate structural deficiencies. FRP laminates have successfully been used as external reinforcement since the early nineties. However, the existing experimental programs have shown the appearance of brittle failure modes involving the laminate peeling-off that limit the gains under ultimate and service conditions provided by the externally bonded reinforcement. Many investigators have attempted to predict these peeling failure modes and most of the existing theoretical work has been focused on the stress behavior at the laminate end. However, experimental studies have shown that the premature laminate debonding may also start at the opening of a flexural or shear crack. Therefore, there is a need to improve the knowledge of the peeling process in both locations to be able to predict premature failures.

To solve the weaknesses of the existing theoretical models, Non-Linear Fracture Mechanics theory has been applied to model the behavior of the interface and its failure modes.

## 2 INTERFACE BEHAVIOR IN A PURE SHEAR SPECIMEN

### 2.1 *Application of non-linear fracture mechanics theory to bonded laminates*

The debonding process of a laminate can be analyzed as the formation and propagation of an interfacial crack assuming the bond line as a pure shear medium. The shear stresses which are locally transferred between the concrete and the external reinforcement are related to the relative displacement between both materials through the constitutive behavior of the interface using a bond-slip function.

Figure 1 shows a typical bond-slip relationship for a bonded joint. In this bond-slip curve, two zones are distinguished:

1. While the slip is lower than the value  $s_{LM}$ , the shear stress is a growing function representing the adhesive deformation. The joint is in Zone I. The maximum shear stress at a slip value of  $s_{LM}$  is  $\tau_{LM}$ .
2. For slip values higher than  $s_{LM}$ , the shear stress is a decreasing function that reproduces the post-peak behavior. The joint is in Zone II. While in Zone I, the material is assumed to be undamaged,

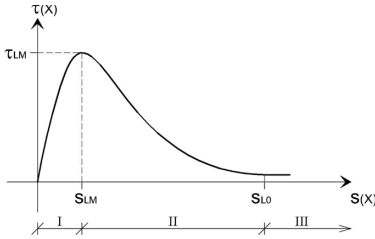


Figure 1. Bond-slip relationship.

in Zone II, microcracks develop in the joint. Shear stress transfer is still possible by aggregate interlock. The function is valid up to a slip value of  $s_{L0}$ . At this point, the joint is assumed to be locally broken with the opening of an interfacial macrocrack.

The area enclosed by the bond-slip relationship is the strain energy stored in a joint (per unit bonded area). When a crack opens, the store energy is released. At this point, the energy release, is called fracture energy  $G_F$  (per unit bonded area).

The external work done by a particular force value  $P$  will be stored as strain energy in the laminate, in the support and in the joint. Fracture growth is caused by a critical value of the applied force  $P_{max}$  that generates a strain energy release (fracture energy) compatible with an equal energy increase in the laminate. This critical value of the applied force is given by Equation 1.

$$P_{max} = b_L \sqrt{2G_F E_L t_L} \quad (1)$$

where  $b_L$  and  $t_L$  are the width and thickness of the bonded laminate respectively, and  $E_L$  is the laminate modulus of elasticity.

This analysis has been based mainly on the work of Täljsten (1994) and has the advantage of being very simple, intuitive, and theoretically more accurate in describing the physics of the FRP debonding than other theoretical models. However, it does not give a clear idea of which is the process involved in the formation and propagation of a crack. Therefore, in order to describe the crack propagation process, a strength approach (rather than an energy approach) is presented in this section.

### 2.2 Bilinear bond-slip relationship

In the following analysis, the bond-slip relationship given by Figure 1 will be simplified to a bilinear function, whose enclosed area is the fracture energy,  $G_F$ , as shown in Figure 2.

As observed, the bilinear bond-slip relationship may be divided into three areas depending on the value of the relative displacement between the support and the reinforcement: Zone I (upward branch), Zone II (downward branch), Zone III (horizontal branch).

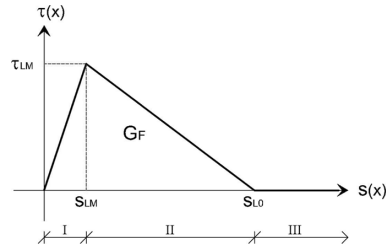


Figure 2. Bilinear bond-slip relationship.

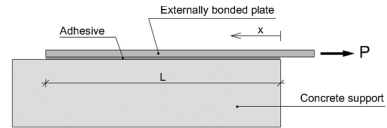


Figure 3. Pure shear specimen.

### 2.3 Behavior of a bonded joint during the debonding process

In order to describe the stress and strain distribution on the interface between the support and the laminate in a beam under transverse loads, it is necessary to deal with a simplified case at first. Therefore, a pure shear specimen (see Fig. 3) has been studied and its formulation will be useful to understand the behavior of a general beam case.

The laminate debonding process has been analyzed assuming the bond line as a pure shear medium. The shear stresses which are locally transferred between the concrete and the external reinforcement are related to the relative displacement between both materials through the bilinear bond-slip function described in section 2.2.

By applying equilibrium to a differential element, the laminate tensile stress,  $\sigma_L$ , can be obtained through the interfacial shear stresses  $\tau(x)$  as shown in Equation 2, where  $t_L$  is the laminate thickness.

$$\tau(x) = t_L \frac{d\sigma_L(x)}{dx} \quad (2)$$

Since the concrete axial strain is neglected, the first derivative of the slip (or relative displacement between support and external reinforcement represented by  $s$ ) becomes equal to the laminate strain, which can be expressed as a function of the tensile stress  $\sigma_L$  and the laminate modulus of elasticity  $E_L$ . By incorporating Equation 2 into the second derivative of the slip, the governing equation (Eq. 3) can be written.

$$\frac{d^2 s(x)}{dx^2} - \frac{1}{E_L t_L} \tau(x) = 0 \quad (3)$$

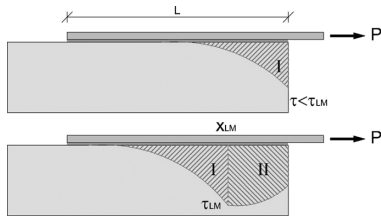


Figure 4. Shear stresses in a pure shear specimen during Stages 1 and 2 respectively.

As observed this equation is expressed in terms of relative displacement (or slip) between support and external reinforcement and the shear stress which is a function of the slip,  $\tau = f(s)$ . The second order differential equation (Eq. 3) describing the behavior of a bonded joint was first derived by Volkersen in 1938 (referenced by Brosens 2001). Equation 3 can be solved by assuming a constitutive relationship between the shear stress and the slip,  $\tau = f(s)$ , such as the bilinear bond-slip relationship, and applying the appropriate boundary conditions.

The evolution of the debonding process has been studied as the applied load increases through the solution of the governing equation for both Zones I and II of the bilinear bond-slip relationship. Some different stages have been observed by increasing the prescribed displacement at the loaded laminate end. Expressions for the laminate tensile stresses and the interfacial shear stresses can be found in Oller (2005).

Initially during Stage 1, the complete interface is under a linear elastic state, which corresponds to Zone I of the  $\tau$ - $s$  curve. The shear stress at the loaded end increases to its maximum value, while the transferred force increases as well (see Fig. 4).

Stage 1 finishes when the maximum shear stress is reached at the load application point. During Stage 2, two regions can be distinguished in the bonded connection: Zone I and Zone II. The concrete remains uncracked in Zone I, whereas some microcracks appear in the interface of Zone II, which is still able to transfer forces. As long as the sliding at the load application point increases, Zone II will increase in length, the maximum shear stress  $\tau_{LM}$  will move towards the free laminate end and, the transferred force will increase (see Fig. 4).

If the laminate is long enough, that is longer than a limit value ( $L \geq L_{lim}$ ), the shear stress at the load application point will decrease to a zero value during the evolution of Stage 2 (see Fig. 5). At this instant, the transferred force, which is the area enclosed by the shear stress distribution, will reach its maximum value, given by Equation 4 which has the same expression as Equation 1. From this point on, a macrocrack will open and propagate towards the free laminate end. As observed, the shear stress distribution has been completely developed.

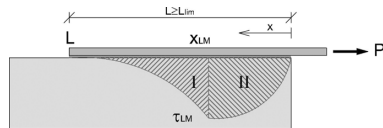


Figure 5. Maximum transferred force in a pure shear specimen with a long bonded laminate.

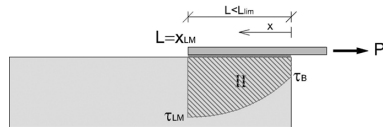


Figure 6. Maximum transferred force in a pure shear specimen with a short bonded laminate.

If the laminate is short ( $L \leq L_{lim}$ ), the maximum shear stress  $\tau_{LM}$  will eventually reach the free laminate end during the evolution of Stage 2. At this point, the transferred force will reach its maximum value given by Equation 4.

$$P_{max} = b_L \sqrt{2G_F E_L t_L} \begin{cases} \sin(\Omega_2 L) & L \leq L_{lim} \\ 1 & L > L_{lim} \end{cases} \quad (4)$$

As observed in Figure 6, in the short laminate case, the transferred force will be reached before the shear stress distribution has completely been developed.

For both long and short bonded lengths, once the maximum transferred force is reached, any attempt to increase the applied load will lead into laminate debonding.

The limit length between a short and a long laminate can be obtained as a function of the fracture energy  $G_F$  and the maximum shear stress of the  $\tau$ - $s$  curve,  $\tau_{LM}$ .

$$L_{lim} = \frac{\pi}{2} \frac{\sqrt{2G_F E_L t_L}}{\tau_{LM}} \quad (5)$$

### 3 BEAM SUBJECTED TO TRANSVERSE LOADS

Existing experimental studies on beams subjected to transverse loads confirmed that the laminate commonly peels-off in the concrete near the surface. This premature debonding can initiate at the laminate end or along the span, between flexural or shear cracks. These peeling failure modes can be predicted by knowing the maximum value of the force transferred between the laminate and the support. This is the main concern of this section.

To obtain this maximum transferred force, the formulae of a pure shear specimen have been extended to a general case of a beam under transverse loads. The evolution of the debonding process as well as the

strain and stress distributions have been studied for two specific cases as shown below.

For both cases, the governing equations of interfacial shear stresses and laminate tensile stresses can be derived by assuming a bilinear bond-slip relationship between the support and the external reinforcement. The main difference with the pure shear specimen equations is a term related to the slip reduction resulting from the strain in the concrete support.

### 3.1 Element at the laminate end

The debonding process in an element between the laminate end and the nearest crack (crack  $J$ ) of a beam subjected to transverse loads is similar to that of a pure shear specimen. Therefore, the same stages described in section 2.3 can be assumed for this specific element. Depending on the bonded length, two possible situations may arise during Stage 2. In a long bonded length, the maximum sliding is reached in crack  $J$  before the maximum shear stress reaches the free laminate end. In a short bonded length, the maximum shear stress reaches the free laminate end before the shear stress has decreased to a zero value in crack  $J$ . Under both situations, the transferred force reaches its maximum value which has the same expression of a pure shear specimen when the concrete contribution in tension is not considered (Eq. 4).

### 3.2 Element between cracks

Focusing on an element between two adjacent cracks (Fig. 8), it is observed that the existence of shear forces causes an increase of the laminate tensile stresses between cracks which requires shear stresses to achieve equilibrium in the laminate. In addition, the concrete between the two cracks contributes to the transfer of tensile stresses between the external reinforcement and the concrete itself. This concrete stress contribution, known as tension stiffening, is only possible if shear stresses are induced between concrete and laminate. In short, the shear stresses that appear between two cracks are, on one hand, required for equilibrium and are, on the other hand, induced by a tension stiffening effect. When no shear force is acting between both cracks, the shear stresses only appear due to the tension stiffening effect.

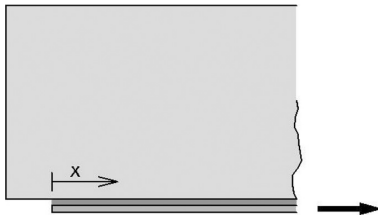


Figure 7. Element at the laminate end.

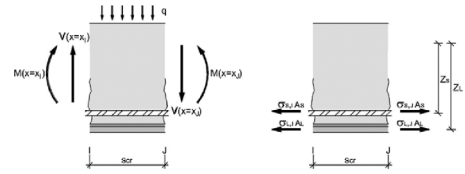


Figure 8. Element between two subsequent cracks  $I$  and  $J$ .

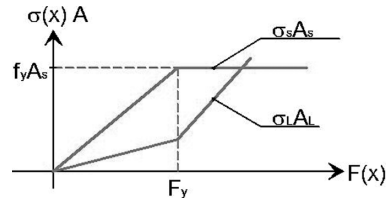


Figure 9. Applied force vs. tensile stress in the laminate and internal steel reinforcement.

In a beam under transverse loads, yielding of the internal steel constitutes an important factor of the debonding process. As observed in Figure 9, both the laminate and the internal steel increase their tensile stress before steel yielding. Once the steel yields, the internal reinforcement is not able to increase its tensile stress and the external reinforcement alone assumes the subsequent load increments. As a consequence, the laminate tensile force increases more rapidly, and the debonding process accelerates.

In a similar manner than in a pure shear specimen, some different stages can be observed during the debonding process as the applied load increases. The main difference between the pure shear specimen case and the element between cracks is on the contour conditions. As shown in Figure 8, in an element between two cracks, the laminate is under the effect of a tensile force acting on each crack tip. However, in a pure shear specimen, the tensile force is applied at one laminate end and the other one remains free. Except for the pure flexure case, the tensile force acting in each crack tip is different. The interfacial shear stress distribution in an element between two cracks is like a combination of two shear stress distributions along an equivalent pure shear specimen whose bonded length is equal to the crack spacing. Each shear stress distribution corresponds to a case where the laminate tensile force acting at one end is equal to the tensile force in each crack tip.

The long and short bonded lengths described in the pure shear specimen case can be extrapolated for this case.

A conceptual description of the different stages observed during the debonding process is given below through the analysis of a long and a short element between two cracks  $I$  and  $J$ . In the following discussion, the bending moment in crack  $J$  will be higher

than in crack  $I$ , that is, crack  $J$  will be the section under the highest tensile stresses. Expressions for the laminate tensile stresses and the interfacial shear stresses can be found in Oller (2005).

### 3.2.1 Long crack spacing

For a long crack spacing case, the following stages are observed as long as the applied load on the beam or the laminate tensile force increases.

During Stage 1, the complete interface is in Zone I of the bond-slip curve. As observed in Figure 10, the shear stresses follow a hyperbolic distribution, with a maximum value under each crack (lower than  $\tau_{LM}$ ) and a zero value between them,  $x_K$ . As Stage 1 evolves, the transferred force increases and the zero shear stress location moves towards crack  $I$ .

Stage 2.1 initiates when the shear stress reaches the maximum value,  $\tau_{LM}$ , in crack  $J$ . Then, as observed in Figure 11, the bonded connection between crack  $J$  and the maximum shear stress ( $x_{LM}$ ) location is in Zone II of the  $\tau$ - $s$  curve. Although microcracks can appear in Zone II, the interface is still able to transfer forces by aggregate interlock. As Stage 2.1 evolves, the maximum shear stress location approaches the zero shear stress location which is simultaneously moving towards the less loaded crack (crack  $I$ ). Similar to Stage 1, the transferred force continues to increase during Stage 2.1.

Stage 2.2 starts once the maximum shear stress is reached not only in crack  $J$  but in crack  $I$  as well. As observed in Figure 12, the regions between each crack tip and the points where the maximum shear stress is reached are located in the descending branch of the bond-slip relationship (Zone II). Between the maximum shear stress locations, the interface behaves like a linear elastic material, in the ascending branch of the bond-slip relationship (Zone I). At increasing deformations, the length of both Zones II increases to the detriment of the length of Zone I. At the same time, the zero shear stress point  $x_K$  moves towards the less-loaded crack ( $I$ ).

During the evolution of Stage 2.2, the slip in crack  $J$  can eventually reach the maximum value  $s_{L0}$ . At this

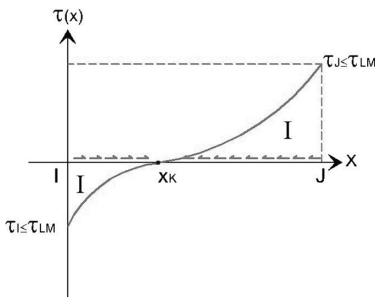


Figure 10. Shear stress distribution between cracks  $I$  and  $J$  during Stage 1.

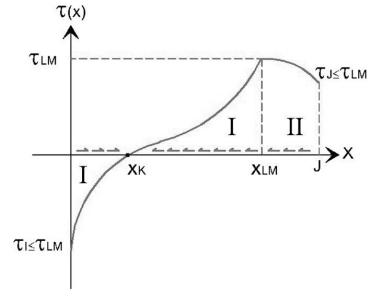


Figure 11. Shear stress distribution between cracks  $I$  and  $J$  during Stage 2.1.

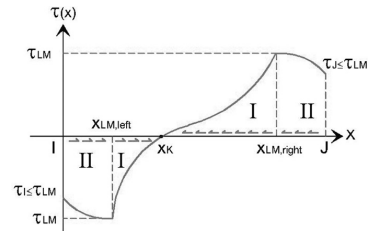


Figure 12. Shear stress distribution between cracks  $I$  and  $J$  during Stage 2.2.

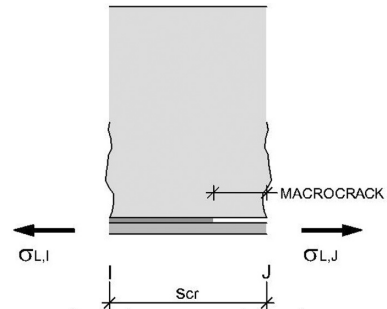


Figure 13. Macrocrack opening during Stage 3.

point, Stage 3 initiates. A real macrocrack opens between laminate and support, and propagates towards crack  $I$  (Fig. 13).

During the development of Stage 3, the maximum shear stress can eventually reach crack  $I$  (see Fig. 14). At this point, the transferred force, which is the area enclosed by the shear stress profile, reaches its maximum value. From this point on, if the applied load increases, the laminate will debond.

### 3.2.2 Short crack spacing

In a short crack spacing, the conceptual description of the debonding process is similar to a long crack spacing case. The main difference occurs during Stages

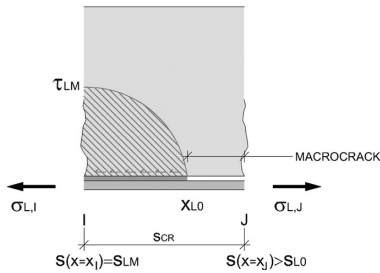


Figure 14. Maximum transferred force.

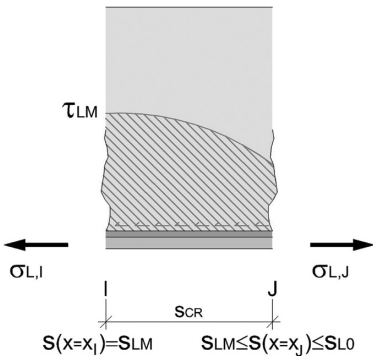


Figure 15. Maximum transferred force.

2.1 or 2.2, when the maximum shear stress reaches crack *I* before the shear stress decrease to a zero value in crack *J* (see Fig. 15). At this point the transferred force reaches its maximum value, and the laminate will completely debond with any attempt to increase the transferred force.

Since the laminate debonds once the maximum transferred force is reached, the laminate tensile force increment between two subsequent cracks should be controlled and maintained below this theoretical maximum value to avoid peeling failure. Equations for the maximum transferred force can be found in Oller (2005).

The limit between a short and a long crack spacing can be obtained as a function of the ratio between the laminate tensile stress in both cracks ( $\sigma_{L,I}$ ,  $\sigma_{L,J}$ ) as shown in Equation 6.

$$s_{cr,lim} = \frac{2}{\pi} L_{lim} \arccos \left( \frac{\sigma_{L,I}}{\sigma_{L,J}} \right) \quad (6)$$

### 3.2.3 Pure flexure case

In a pure flexure case, the shear stresses are only required due to a tension stiffening effect. The shear stress distribution is skew-symmetric in relation to

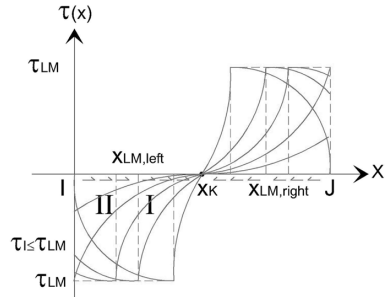


Figure 16. Shear stress distribution in a pure flexure case.

the middle of the crack spacing (see Fig. 16). The transferred force along the crack spacing is zero since the tensile force in both cracks tips is equal. Debonding will occur when the shear stress decreases to a zero value at the crack tip.

## 4 CONCLUSIONS

Since the laminate peeling-off is the most common failure in beams externally strengthened by plate bonding, Non-Linear Fracture Mechanics has been applied to a general case of a beam in order to understand the mechanics of the debonding process.

A pure shear specimen has been studied at first and its formulation has been extended to a general case of a beam subjected to transverse loads. In both cases, several load stages have been observed during the evolution of the debonding process. By assuming a bilinear bond-slip relationship, the shear stress distribution can be obtained for each stage. The area enclosed by the shear stress distribution is the transferred force along the bonded length.

By limiting the transferred force along the bonded length to a maximum value, laminate debonding can be avoided.

## REFERENCES

- Brosens, K. 2001. *Anchorage of externally bonded steel plates and CFRP laminates for the strengthening of concrete elements*, PhD thesis. Katholieke Universiteit Leuven, Belgium.
- Oller, E. 2005. *Peeling failure in beams strengthened by plate bonding. A design proposal*. PhD thesis. Technical University of Catalonia, Barcelona, Spain.
- Täljsten, B. 1994. *Plate Bonding. Strengthening of Existing Concrete Structures with Epoxy Bonded Plates of Steel or Fibre Reinforced Plastics*. PhD thesis. Lulea University of Technology, Sweden.

# Optimal inspection and maintenance strategies for bridge network using supply and demand approach

A.D. Orcesi & C.F. Cremona

*Laboratoire Central des Ponts et Chaussées, Paris, France*

**ABSTRACT:** This paper presents a mathematical model to determine a network-level bridge management system. A supply and demand approach is combined with a probability-based formulation of the inspection and maintenance activities to determine the optimal maintenance planning for each bridge within the network. Reliability and serviceability aspects are taken into account to determine such optimal strategies. This methodology is illustrated with the example of a part of the French national network in which the optimal maintenance planning is found for the different bridges located on this network.

## 1 INTRODUCTION

The objective of this study is to provide a methodology to be used to determine optimal maintenance planning for several bridges within a network. A supply and demand approach (Adey *et al.* 2003) is combined with a probability-based formulation of the inspection and maintenance activities (Thoft-Christensen and Sorensen 1987, Madsen *et al.* 1989, Sorensen 1993). The model that evaluates user costs is described firstly. This model takes into account traffic jams and assigns the traffic on the network by supposing that vehicles always try to minimize their travel cost. Then, the model that determines the time-performance of the bridges is introduced. This model uses a probabilistic approach to assess the performance of degraded structures. The optimization problem and the methodology to find optimal maintenance planning are detailed afterwards. This optimization helps to find a good compromise between bridge reliability and users/agency costs. Finally, to illustrate theoretical aspects, an application example is introduced. The studied network is a part of the French national road network managed by the Road Directorate of the Ministry of Ecology, Sustainable Development and Spatial Planning.

## 2 TRAFFIC FLOW MODEL

The road users are always supposed to take the fastest way. This search of the best route combined with traffic jams leads to an equilibrium where the traffic volume is distributed among the different routes of the network. The objective of this study is then being able

to assess the traffic distribution when there is one or several links that are failed and then to evaluate the incurred users costs. This methodology needs first to evaluate the effect of congestion on users' behaviour. As vehicle speed is limited by traffic volume, the greater the number of vehicles being simultaneously on a link, the more the speed being reduced. Speed, and consequently travel time depend both on the traffic congestion according to the Highway Capacity Manual (Martin and McGuskin 1998) formulae given in equation

$$V = \frac{V_0}{1 + 0.15 \left( \frac{\xi}{C} \right)^\eta} \quad (1)$$

with  $V_0$  the free-flow speed,  $\xi$  the occupancy on the road,  $C$  the capacity of the road and  $\eta$  a parameter generally fixed at 4. It is then obvious that the sum of users' costs increases when the traffic is congested and that users will always try to avoid this congestion. The methodology is to find the equilibrium, named Wardrop equilibrium, when no user can change his way to improve his travel cost. To approach this equilibrium in a satisfactory way, the traffic assessment is found using Frank-Wolfe algorithm (Lotito *et al.* 2002). In this model, impact of inadequate service on road users is taken into account directly and is given in a monetary value. Indeed, costs of travelling in case of loss of connectivity are assessed for each new Wardrop equilibrium in case of failure of the bridge network. The cost database QUADRO (*Queues And Delays at Roadworks*) developed by the British Department for Transport provides a method for assessing road user costs. This model is used in this paper to determine



vehicle operating costs (VOC), which are estimated using equations below:

$$C_1 = a + bV + cV^2 + dV^3, \quad C_2 = a' + \frac{b'}{V} \quad (2)$$

where  $C_1$  is the fuel cost and  $C_2$  is the non-fuel cost in euros per kilometre per vehicle,  $V$  the average link speed in kilometres per hour, and  $a, b, c, a'$  and  $b'$  the VOC formulae parameter values in 2002 prices by type of vehicle are those used in QUADRO. The other users costs are travel time costs (12€/h/veh) and accident costs. Finally, the traffic cost is defined as the sum of the vehicle operating costs, the travel time costs and the accident costs.

### 3 BRIDGE MODEL

#### 3.1 Bridge performance

##### 3.1.1 Bridge reliability

The limit state is willingly expressed in a global way to be adapted to a large number of failure modes. The general form of the safety margin is given in equation

$$M = R g(t) - S \quad (3)$$

where  $R$  is the initial strength of the bridge,  $g(t)$  represents the deterioration of the element ( $g$  decreases with time),  $S$  models the load effects. The notation is very general and can handle structural safety performance as well as serviceability performance and then be linked to any failure modes. Finally, as  $R, S$  and  $g$  are random variables, the failure probability is expressed in a first order approach (Melchers 1999).

##### 3.1.2 Bridge serviceability

The IQOA principle is to give a score to the bridges according to their condition. There are five possible scores, which are described in table 1. The difference of the defects between the IQOA condition states 2 and 2E and the IQOA states 3 and 3U is substantial. The two first ones represent serviceability defects whereas the two others represent structural deficiencies of the bridge. The present condition is sufficient enough to

Table 1. Definition of IQOA scores.

Score	Definition
1	Good overall state.
2	Equipment failures or minor structure damage. Non urgent maintenance needed.
2E	Equipment failures or minor structure damage. Urgent maintenance needed.
3	Structure deterioration. Non urgent maintenance needed.
3U	Serious structure deterioration. Urgent maintenance needed.

determine the future condition of bridge because of the independence between different scores of the IQOA categorization (Orcesi and Cremona 2007). Homogeneity is also assumed, leading to consider a constant transition matrix over time. The access to the scoring data of approximately 10,000 bridges between 1996 and 2005 makes it possible to determine the probability for 1 m<sup>2</sup> of bridge deck to move from one condition rating to another one within one year.

Hence, the probability to move from quotation  $i$  to  $j$ , is the total surface of bridges that were scored  $i$  at year  $p$  and  $j$  at year  $p + 1$  divided by the total surface of bridges that were in  $i$  at year  $p$ , for  $p$  between 1996 and 2004. The obtained pure ageing transition matrices are shown in equation (4) for different types of structures such as reinforced concrete bridges (matrix  $P_1$ ) and prestressed concrete box girder (matrix  $P_2$ ). It should be pointed out that values under the diagonal line are summed up to the diagonal term to obtain pure ageing matrices  $P_1$  and  $P_2$  without any maintenance action.

$$P_1 = \begin{pmatrix} 0.53 & 0.47 & 0 & 0 & 0 \\ 0 & 0.87 & 0.07 & 0 & 0.06 \\ 0 & 0 & 0.99 & 0.01 & 0 \\ 0 & 0 & 0 & 0.95 & 0.05 \\ 0 & 0 & 0 & 0 & 1 \end{pmatrix}$$

$$P_2 = \begin{pmatrix} 0.83 & 0.15 & 0.02 & 0 & 0 \\ 0 & 0.83 & 0.15 & 0.02 & 0 \\ 0 & 0 & 0.97 & 0.03 & 0 \\ 0 & 0 & 0 & 0.99 & 0.01 \\ 0 & 0 & 0 & 0 & 1 \end{pmatrix} \quad (4)$$

Hence, if a bridge  $i$ , with transition matrix  $P_i$  is characterized by its probability vector  $q_{0,i}$  at time 0, i.e.  $q_{0,i}(j)$  is the probability to be quoted in  $j$ , then at year  $k$ ,  $q_{k,i} = q_{0,i} P_i^k$ . Finally, the probability for a bridge having equipment maintenance at year  $k$  is the scalar product of  $q_{k,i}$  and  $\hat{p}_{r,eq}$  the probability vector to have equipment maintenance according to IQOA score.

#### 3.2 Event tree decisions

There is often an offset of several years between the inspection result and the beginning of maintenance works, which is due to budget-restrained financing. In practice, inspections are performed regularly to update bridge information given to the bridge owner who finally decides when repair works have to be performed. This offset is taken into account in the following since two embedded calendars are introduced in the maintenance decision process. The structural and equipment decisions are respectively illustrated in figures 1 and 2. It is supposed that the investigation process allows assessing structural performance of bridge members and then the global loss of performance. The structural decision is then directly linked to the outcome of the bridge inspection and can be divided in three possible actions (figure 1) whereas

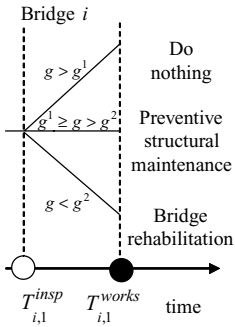


Figure 1. Reliability event tree decision.

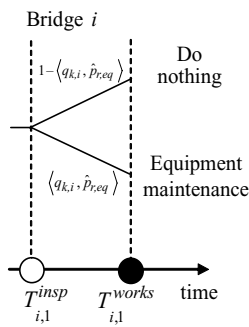


Figure 2. Serviceability event tree decision.

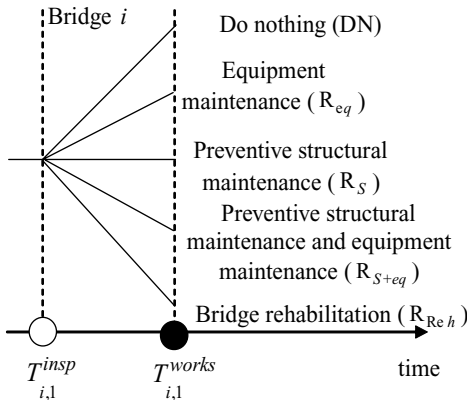


Figure 3. Mixed reliability and serviceability event tree decision.

the equipment decision is expressed in a statistical way (figure 2).

The figure 3 is a mixed event tree events built on both previous ones, which allows to split the two first branches of structural event tree.

Indeed the first branch that was doing nothing becomes either doing nothing or doing only equipment maintenance. In the same way, the second branch “preventive structural maintenance” can now be performed without or with equipment maintenance. Finally, the last branch that is bridge rehabilitation remains the same because it deals with great maintenance works on the bridge that takes into account possible equipment repairs. The construction of an event tree enables then to assess failure maintenance probabilities at each inspection time. The effect of maintenance actions on bridge reliability is expressed in a very general way. It is supposed that preventive maintenance actions allow to temporary stop the degradation process. This effect is modeled in this paper by supposing that the bridge failure probability remains constants during an average time period characteristic for each bridge and for each deterioration profile. It is also supposed

that the rehabilitation maintenance also permits to stop the deterioration process during a longer period and that once the deterioration process restarts, its rate is lower than before the maintenance. The impact of maintenance works on the IQOA score is assessed by introducing maintenance transition matrices. Two examples of maintenance transition matrices are given in equation (5). The position of the 1 in those matrices indicates a pro-active maintenance decision. For instance, an action is decided to move 1 m<sup>2</sup> of bridges in score 2E to score 2. Of course, only a percentage of the total bridge deck surface will be affected by this maintenance action.

$$M_1 = \begin{pmatrix} 1 & 0 & 0 & 0 & 0 \\ 0 & 1 & 0 & 0 & 0 \\ 0 & 1 & 0 & 0 & 0 \\ 0 & 0 & 0 & 1 & 0 \\ 0 & 0 & 0 & 0 & 1 \end{pmatrix},$$

$$M_2 = \begin{pmatrix} 1 & 0 & 0 & 0 & 0 \\ 0 & 1 & 0 & 0 & 0 \\ 0 & 1 & 0 & 0 & 0 \\ 0 & 0 & 0 & 1 & 0 \\ 0 & 0 & 0 & 1 & 0 \end{pmatrix} \quad (5)$$

### 3.3 Cost study

The different costs involved in the optimization problem are detailed below. The repair costs are given by equation

$$C_{REP,k}^p = c_{rep,k}^p + (c_{cars,rep,k}^p + c_{HGV,rep,k}^p) d_{rep,k}^p \quad (6)$$

with  $c_{rep,k}^p$ : costs for maintenance  $k$  on bridge  $p$ ;  $c_{cars,rep,k}^p$  and  $c_{HGV,rep,k}^p$ : cars and Heavy Gross Vehicles (HGV) daily costs induced by works  $k$  on bridge  $p$ ;  $d_{rep,k}^p$ : time interval for works (in days)  $k$  on bridge  $p$ . This repair cost takes into account the fact that users are diverted and increase the cost of their travel. The failure costs are detailed below:

$$\forall \theta \in \Theta, \quad C_f^\theta = c_{reh}^\theta + (c_{cars,reh,k}^\theta + c_{HGV,reh,k}^\theta) d_{reh,k}^\theta \quad (7)$$

with  $\Theta$ : the set of possible failed bridges combinations;  $c_{reh}^\theta$ : rehabilitation costs on the failed set of bridges  $\theta$ ;  $c_{cars,reh,k}^\theta$  and  $c_{HGV,reh,k}^\theta$ : cars and HGV daily costs induced by rehabilitation works on the failed set bridges  $\theta$ ;  $d_{reh,k}^\theta$ : time interval for rehabilitation works (in days) on the failed set bridges  $\theta$ . An analysis was led on around 180 bridge maintenance works cases in Ile-de-France, planned between 2005 and 2009 by the French Highway Agency (table 2).

Table 2. Works characteristics.

	Average cost (10 <sup>3</sup> €)	length (in days)	Traffic capacity reduction
Equipment maintenance :	100	7	–
Preventive structural Maintenance :	200	21	10%
Rehabilitation :	400	31 × 5	50%

It is supposed here that the first type of maintenance has no significant impact on the traffic condition because it can be generally performed during night when the traffic demand is low and can lead to very small risks of traffic jams. However, preventive structural maintenance and rehabilitation are supposed to disrupt the traffic even during daytime because of scaffolding presence for example. In case of traffic disruption, vehicle operating costs incurred by maintenance works and bridges failures are obtained by assessing the new Wardrop equilibrium as it was described in paragraph 2.

$$\left\{ \begin{array}{l} \min_{T_1^1, \dots, T_{n_1}^1, \dots, T_1^p, \dots, T_{n_p}^p} C_{INSP}, \text{ with :} \\ C_{INSP} = \sum_{p=1}^{n_b} \left( \sum_{i=1}^{n_{insp}^p} (C_{insp}^p (1 - P_f^p(T_i))) \frac{1}{(1 + \alpha)^{T_i}} + \sum_{i=1}^{n_{int}^p} \left( \sum_{k=1}^{n_r} C_{REP,k}^p P_{REP,k}^p(T_i) \right) \frac{1}{(1 + \alpha)^{T_i}} \right. \\ \left. + \dots + \sum_{i=1}^{n_{insp}^p + n_{int}^p} \left( \sum_{\theta \in \Theta} C_f^\theta P_f^\theta(T_i) \right) \frac{1}{(1 + \alpha)^{T_i}} \right), \text{ such that :} \\ \forall p = 1 \dots n_b, \quad \forall i = 1 \dots n_{insp}^p, \quad \beta^p(T_i) \approx \Phi^{-1}(P_f^p(T_i)) > \beta_0^p, \quad CI_{2E}^p(T_i) < CI_{2E,0}^p \quad \text{and} \quad CI_{3U}^p(T_i) < CI_{3U,0}^p \end{array} \right. \quad (8)$$

$$\left\{ \begin{array}{l} \min_{T_1^1, \dots, T_{n_1}^1, \dots, T_1^p, \dots, T_{n_p}^p} C_{REP}, \text{ with :} \\ C_{REP} = \sum_{p=1}^{n_b} \left( \sum_{i=1}^{n_{insp}^p} (C_{REP,i}^p (1 - P_f^p(T_i))) \frac{1}{(1 + \alpha)^{T_i}} + \sum_{i=1}^{n_{int}^p} \left( \sum_{\theta \in \Theta} C_f^\theta P_f^\theta(T_i) \right) \frac{1}{(1 + \alpha)^{T_i}} \right), \text{ such that :} \\ \forall p = 1 \dots n_b, \quad \forall i = 1 \dots n_{insp}^p, \quad \beta^p(T_i) \approx \Phi^{-1}(P_f^p(T_i)) > \beta_0^p, \quad CI_{2E}^p(T_i) < CI_{2E,0}^p \quad \text{and} \quad CI_{3U}^p(T_i) < CI_{3U,0}^p \end{array} \right. \quad (9)$$

#### 4 FORMULATION OF THE OPTIMIZATION PROBLEM

##### 4.1 Optimization of the intervention times

Based on the IQOA scoring system introduced in paragraph 4.1.2, the condition index called  $CI_\xi$  is defined as the probability for a bridge to be quoted in  $\xi$ , which is the  $\xi$ th value of the condition vector  $\mathbf{q}$ . Indeed, if this score is the one in which the bridge can no longer assure its initial level of service, it has to be reevaluated. The minimization problem

of the network costs is given in equation (8) with  $n_b$ : number of bridges;  $n_{insp}^p$ ,  $n_{int}^p$  and  $n_{insp}$ : number of inspection times, intervention times for bridge  $p$ , total number of inspections for the bridge network;  $n_r$ : number of possible maintenance decisions;  $\Theta$ : set of possible failed bridges combinations;  $P_f^\theta(T_i)$ : failure probability of the bridges combination at intervention time  $T_i$ ;  $P_{REP,k}^p(T_i)$ : probability for maintenance  $k$  at intervention time  $T_i$ ;  $C_{insp}^p$  and  $C_{REP,k}^p$ : cost for intervention and for maintenance  $k$  for bridge  $p$ ;  $C_f^\theta$ : failure cost for the combination of bridges  $\theta$ ;  $\alpha$ : discount rate;  $\beta_0^p$ : the inverse cumulative probability function of a standard distribution;  $CI_\xi^p(T_i)$ : condition index of bridge  $p$  at intervention time  $T_i$  (i.e. probability for bridge  $p$  being quoted in IQOA score  $\xi$ );  $\beta_0^p$  and  $CI_{\xi,0}^p$ : minimal reliability index and minimal condition index for bridge  $p$  in IQOA score  $\xi$ . A Genetic Algorithm based procedure is used here with an initial GA population of 51 solutions, a crossover and mutation operations used with probabilities of 85% and 10%. The fitter individual is the one with the lower expected intervention cost. Since the maintenance planning is a

constraint optimization problem, the penalty method is used to ensure that the solutions respect the constraints.

##### 4.2 Optimization of the maintenance actions

Once the optimal intervention times are found, the optimal actions are searched. These actions have to be applied at the intervention times to ensure that constraints on reliability and serviceability are respected until the end of the planning. The minimization problem is given in equation (9) with using the same notations as in the equation (8). The same Genetic

Algorithm procedure as in paragraph 4.1. is used to find optimal actions.

## 5 EXAMPLE

The studied road network is a part of the French national network located at the east of Paris (figure 4). This network has a strategic role in the overall traffic distribution of the East road network of the Ile-de-France county and is directly concerned by possible traffic disruption that can have quickly tremendous consequences. Hourly traffic flow is shown in figure 5 by applying traffic model described in paragraph 2. However, because network users do not know the overall network paths and stay on the main roads in general even where there is congestion, the network is simplified by only keeping primary networks. The corresponding origin / destination matrix is then determined by counting all the vehicles that move from one point to another one of the primary network (figure 6). Impact on traffic distribution can then be found for

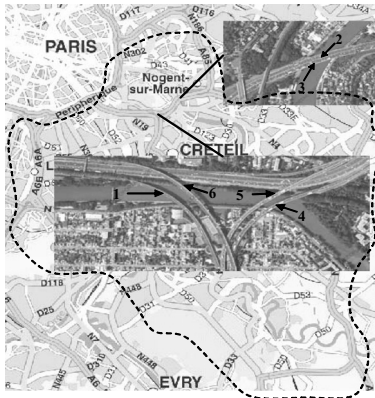


Figure 4. Network bridges.

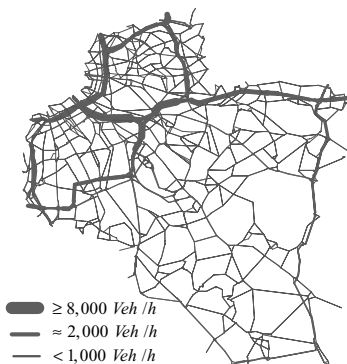


Figure 5. Hourly traffic flow at peak hour on the overall network.



Figure 6. Hourly traffic flow at peak hour on the primary network.



Figure 7. Hourly traffic flow at peak hour on the primary network if bridge 2 capacity is reduced by 90%.

any situation. One case is shown in figure 7 when bridge 2 capacity (figure 4) is reduced by 90% because of rehabilitation works or of bridge failure for example. Besides, users costs for each of the six bridges of figure 4 are given in figure 8 according to each level of capacity loss. These different costs can now be used in the optimization problem described in paragraph 4 to determine intervention schedules of the six bridges of figure 8. It is supposed here that these prestressed bridges have a deterioration profile that slows down with time, representing durability profile. Besides, the initial probability of being in one of the five IQOA scores is  $q_{0,1} = q_{0,4} = q_{0,5} = q_{0,6} = (0 \ 0.02 \ 0.96 \ 0.02 \ 0)$  and  $q_{0,2} = q_{0,3} = (0 \ 0 \ 0.05 \ 0.90 \ 0.05)$ , which allows to consider the uncertainty of the IQOA scoring process. The equipment maintenance introduced in paragraph 3.1.2 is  $\hat{p}_{r,eq} = (0 \ 0 \ 0.6 \ 0.5 \ 0.5)$ . The optimal maintenance planning is determined for a minimal reliability index of 3.0, a minimal probability of being quoted in 2E and 3U at the end of the planning respectively fixed at 70% and 50% and a rate of discount  $\alpha = 4\%$ . Figures 9 and 10 show the development of reliability index linked to cumulative failure probability for two different situations (notations are those of figure 3). In figure 9, the optimal schedule is determined for each bridge in an individual way by supposing each time that other bridges are always reliable. The optimal intervention time is in around 15 years for all bridges

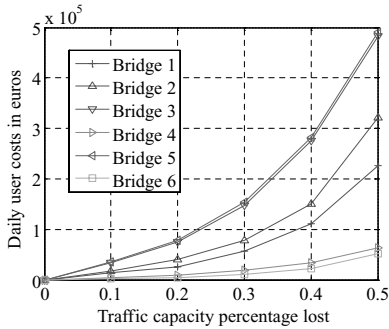


Figure 8. Traffic disruption impact on daily user's costs.

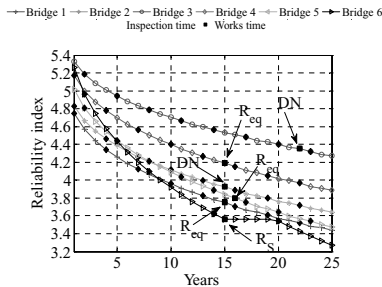


Figure 9. Intervention planning for bridges if considered individually.

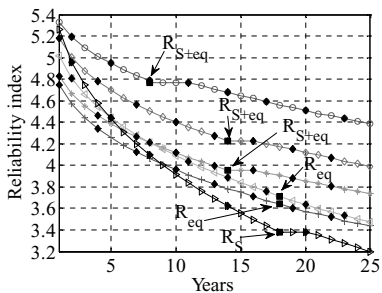


Figure 10. Intervention planning for bridges if considered globally.

except for bridge 3 which is in 22 years (figure 9) but at which nothing is done. In figure 10, the optimal schedule is determined by considering all the bridges together during the optimization process.

It is interesting to highlight the change in the optimal instant times. Indeed, works are spread out in a more important way than in figure 9. Moreover, works are performed for all bridges and are more consequent than in figure 9. This difference can be explained by the tremendous financial impacts for the network users when there are simultaneous bridges failure, this

phenomenon being not taken into account when bridges are managed in an individual way.

## 6 CONCLUSIONS

In this study, the methodology to be used to determine optimal maintenance planning for several bridges within a network has been presented. The combination of the supply and demand approach with the formulation of a probability based intervention and maintenance planning allows determining optimal strategies for the different bridges. Moreover, the combination of reliability aspects with condition scoring enables to take into account not only structural performance of the bridge but its overall condition. The originality of this method is to keep a very general expression for the development of the performance of the bridges, which allows adapting the methodology to a large number of failure modes. The objective is finally to provide to decision makers a good basis in the field of decision processes where multiple criteria are considered on a bridge network.

## REFERENCES

Adey, B., Hajdin, R. & Brühwiler, E. (2003). Risk-based approach to the determination of optimal interventions for bridges affected by multiple hazards, *Engineering Structures*, 25, 903–912.

Lotito, P., Mancinelli, E. & Quadrat, J.P. (2002). Traffic assignment algorithms: a Scilab tool-box, numerical comparisons, 9th Meeting of the EURO Working Group on Transportation Intermodality, Sustainability and Intelligent Transportation Systems, Polytechnic University of Bari, Faculty of Engineering, Bari, Italy, June 10–13, 2002.

Madsen, H.O., Sorensen, J.D. & Olesen, R. (1989). Optimal intervention planning for fatigue damage of offshore structures, *Proceedings ICOSSAR 89*, San Francisco, 2099–2106.

Martin, W.A. & Mc Guskin N.A. (1998). “Travel estimation techniques for urban planning”, National Cooperative Research Program Report 365, Transportation Research Board, National Research Council, Washington, D.C.

Melchers, R.E. *Structural reliability analysis and prediction*, Wiley, 1999.

Orcesi, A. & Cremona, C. (2007). Optimization of management strategies applied to the national reinforced concrete bridge stock in France, *Structure and Infrastructure Engineering*, 16 June 2007.

Sorensen, J.D. (1993). Reliability-based intervention planning for structural systems, *Reliability and Optimisation of Structural Systems*, V (B-12), 31–46.

Thoft-Christensen, P. & Sorensen, J.D. (1987). Optimal strategies for intervention and repair of structural systems, *Civil Engineering Systems*, 4, 94–100.

Thompson, P.D., Small, E.P., Johnson, M. & Marshall, A.R. (1998). The Pontis bridge management system, *Structural Engineering International*, IABSE, 8 (4), 303–308.

# The life-cycle maintenance strategy for the bridge system

Kyung-Hoon Park

*Hybrid Structure Research Division, Korea Institute of Construction Technology, Korea*

Sang-Yoon Lee

*Hybrid Structure Research Division, Korea Institute of Construction Technology  
and Department of Civil, Environmental and Architectural Engineering, Korea University, Korea*

Jung-Ho Kim

*Hybrid Structure Research Division, Korea Institute of Construction Technology, Korea*

Jung-Sik Kong

*Department of Civil, Environmental and Architectural Engineering, Korea University, Korea*

Hyo-Nam Cho

*Department of Civil and Environmental Engineering, Hanyang University, Korea*

**ABSTRACT:** This paper presents the proposed bridge maintenance method and the developed program establishing a lifetime optimum maintenance strategy of a deteriorating bridge considering the lifetime performance and the life-cycle cost. The optimum maintenance scenario can be generated not only at the individual member level but also at the system level of the bridge by taking account of the subordinate relation due to the replacement of member. This paper discusses the generation of system level maintenance strategy considering the members which consist of the bridge as well as the optimum maintenance strategy in the member level, and studies more practical and rational method through the comparison of analytical examples between different levels. The optimum maintenance scenario is selected on the basis of the performance and cost of the bridge system by considering the subordinate relation.

## 1 INSTRUCTIONS

The establishment and development of bridge maintenance system have been on the process not only in Korea but also in most advanced countries due to the collapse of bridges which were built in the development-oriented time. However, the existing method of bridge maintenance has a certain limit and it is necessary to apply more advanced maintenance techniques in order to bring in the real preventive maintenance system (Casas 2006). Recently, a method has been suggested for establishing the strategy of the optimum maintenance in the deteriorating bridge by considering the life-cycle performance (LCP) as well as the life-cycle cost (LCC) (Frangopol and Liu 2007, Furuta et al. 2006, Patidar et al. 2007). In the stage of bridge maintenance, it is required to have a method which can make the developed theory into the reality and the reliable data which support such a method

so as to consider LCP and LCC. There have recently been various researches and developments undergoing in the world for overcoming the limit of current bridge maintenance and applying the actual preventive maintenance system (Cho et al. 2007, TRB 2003).

The members of bridge have a mutual correlation in which one replacement can trigger another replacement. And thus, a system level maintenance scenario would be a realistic proposal as it simultaneously considers maintenance interventions in each member which consists of bridge system not a simple combination of optimum maintenance scenario in each member. Therefore, this paper discussed the generation of optimum maintenance strategy in the system level considering the members which consist of the bridge as well as in the member level, and studied more practical and rational method through the comparison of analytical examples between different levels. It also dealt with the feasibility of the optimum maintenance

strategy considering its limit in the real situation by applying the proposed method.

## 2 METHOD FOR GENERATING AN OPTIMUM MAINTENANCE STRATEGY

### 2.1 Life-Cycle Performance and Cost Evaluation

To evaluate the bridge performance, it needs a selection of performance index and the appropriate models for evaluating the LCP as well as for quantifying the performance changes. This study introduces reliability index and condition index. In here, response surface method (RSM) which is one of probabilistic safety evaluation methods is applied to the time-variant reliability analysis and the quantification of maintenance effects (Kong et al. 2007). The condition index used in this study sequentializes and generalizes the discontinuous condition states based on the sight inspection applied to the current bridge maintenance in Korea (MOCT & KISTEC 2003). The information required in the condition index evaluation is obtained from the statistical analysis using the existing data or the professional research data (KICT 2006).

Cost in LCC analysis for bridge maintenance is composed of direct cost which directly relates to the bridge maintenance intervention during life-cycle and user cost which is caused by the traffic control from the bridge maintenance actions, and failure cost from deterioration of the bridge or failure probability caused by environmental and social factor can be taken into account. The establishment of maintenance cost classification, formulation of each cost and estimation of user cost and failure cost are conducted (KICT 2006). As for the life-cycle analysis like this study considering LCC and LCP, it considers the time-variant cost corresponding to the maintenance interventions.

### 2.2 Optimum maintenance scenario

This paper uses Genetic Algorithm (GA) to solve multi-objective optimization problem considering condition index, reliability index and cost during the lifetime, and selects optimum tradeoff solution automatically in the normalized Pareto optimum solution space by using fitness function (Park et al. 2006). It also tries to solve a problem from the inappropriate definition of initial boundary in the fixed fitness function by renewing the fitness function with the change of solution space in each generation. That is, with the renewal of fitness function in each generation, it induces more specific direction of the optimum solution for each generation so as to enhance the convergence of Pareto optimum solution as shown in Figure 1. The following Equation 1 expresses the adaptive normalize contour fitness function in each generation.

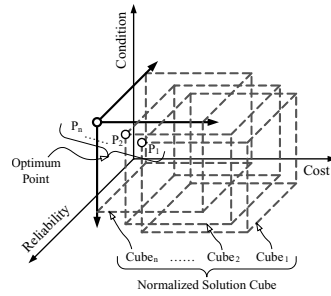


Figure 1. Change of solution space and optimal point.

$$f_k(\cdot) = \prod_{l=1}^p \left[ 1 - \left\{ \frac{P^l - \min_{i=1}^k (\min_{j=1}^m P_{ij}^k)}{\max_{i=1}^k (\max_{j=1}^m P_{ij}^k) - \min_{i=1}^k (\min_{j=1}^m P_{ij}^k)} \right\}^2 \right] \quad (1)$$

where  $f_k(\cdot)$  = fitness function at  $k$ -th generation;  $P_{ij}^l$  = value of the  $l$ -th normalized performance (i.e. cost, condition, reliability) at  $k$ -th generation and  $j$ -th individual;  $P^l$  =  $l$ -th normalized performance as a variable.

The solution space in each generation maintains itself as it is just up to the previous generation, and the solution space expands in case that a new developed solution is out of the existing solution space. Eventually, the solution area of the final generation becomes a domain including all solutions produced in all generations.

The individuals in each generation are generated through the cross over and the mutation, and at this moment, the elite group of the previous generation is utilized as parents for cross over. The elite group of each generation is selected according to the designated rate in advance based on the value of fitness function among Pareto Front. The elite group continuously succeeds into the parents of next generation and repeats the renewal process as passing by the generation. Therefore, it can be defined that the Pareto front of the final generation considers all solutions which have been produced over all generations.

### 2.3 The optimum maintenance scenario in the system level

The maintenance of the bridge should be focused on the applying time and type of maintenance actions and the efficient management of the budget for the bridge system with various members rather than the individual members. As the bridge is a systematic structure connecting with various members, it will be

realistic to generate a scenario considering the mutual influence of members from the maintenance intervention for each member. To generate the system level analysis, this study establishes a method to integrate the condition index and the reliability index of each member.

The basic concept of condition index is founded on bridge safety guidelines (MOCT & KISTEC, 2003) of Korea so that this paper evaluates the system condition index through the weight factor for each member indicated in the guideline. The system reliability method can be used for estimating the reliability index of the system level from the one of the member level. The composition of bridge system with various members can be considered as a series, parallel and a combined system connected with these two systems. The time history of maintenance cost in the system level is calculated by the summation of time history of maintenance cost in each member.

### 3 SELECTION OF BRIDGE AND ANALYTIC CONDITION

#### 3.1 Bridge information and general matters

In order to study the feasibility and rationality of the proposed model and method to generate the optimum maintenance scenario, a steel box-girder bridge which is a simple and typical case in national road is selected for the life-cycle analysis. The plane figure and longitudinal section of the bridge are shown in Figure 2 and Figure 3 respectively. The bridge was built in 2001 with 45 m length, 19.5 m width and 3-steel boxes in a simple span. It has been used in public service without special maintenance intervention.

This paper performs the life-cycle analyses of the bridge members limited in slab and pavement because the purposes of this study are to suggest a model for establishing the optimum maintenance strategy of the bridge system and to compare the analysis of member level with the analysis of system level.

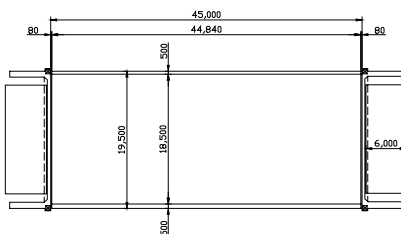


Figure 2. Plane figure of the example bridge.

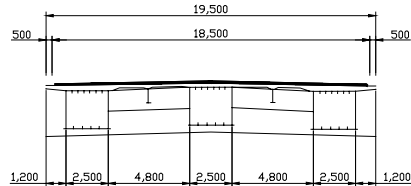


Figure 3. Longitudinal section of the example bridge.

Table 1. Effects of maintenance interventions.

Member	Maintenance Intervention	Improved Condition Index	Unit Cost (Thousand Won*)	Application Ratio (%)
Slab	Epoxy Injection (EI)	40%	3.0/m <sup>2</sup>	30%
	Waterproofing (WP)	60%	27.6/m <sup>2</sup>	80%
	FRP Attaching (FA)	75%	78.9/m <sup>2</sup>	50%
	Replacement (RS)	100%	150.0/m <sup>2</sup>	100%
Pavement	Surface Treatment (ST)	30%	10.0/m <sup>2</sup>	10%
	Cutting-overlay (CO)	80%	20.0/m <sup>2</sup>	30%
	Patching (PA)	40%	10.0/m <sup>2</sup>	5%
	Re-pavement (RP)	100%	26.4/m <sup>2</sup>	100%

\*Note: Thousand won is about one dollar.

#### 3.2 Performance evaluation

In this paper, the condition index is only considered as the performance. In case of non-intervention, the condition index profile, determined by the survey from the experts and references, is decided by using the period of maintaining the initial condition and the deterioration rate of the condition dropped into the lowest value.

The maintenance interventions of the selected member are considered as Table 1. The improvement of condition index with the retrofit or replacement is evaluated by superposing the initial condition index profile over the improved condition index value at the time applying the maintenance intervention. It is assumed that the deterioration curve after the retrofit is applied with the initial deterioration curve.

#### 3.3 Cost estimation

The cost for each maintenance intervention selected in the life-cycle analysis considers the direct maintenance cost which can be estimated from the results of construction expenses, quotation, survey, etc. The unit



cost and the application ratio for each maintenance intervention are estimated from the expert survey.

#### 4 MAINTENANCE STRATEGY OF MEMBER AND SYSTEM LEVEL

##### 4.1 Maintenance strategy of member level

This study executes the life-cycle analyses to generate the optimum maintenance scenario during the service life for individual member such as slab and pavement. The period of analysis is considered to be 50 years after the completion of construction and 45 years from the analytical point of time (i.e. 2006). The number of population and generation applied to the GA execution is 1,000 individuals and 1,000 generations and the probability of crossover and mutation is 50% and 5%, respectively.

The left side of Table 2 shows the annual maintenance scenario, the minimum condition index value and the cumulative LCC for each member during the analytic period in the member level. In here, these present output results of the optimum tradeoff solution among tradeoff solution sets in each member. In the member level, the system condition index is a value simply calculated by applying the weight factor to the condition index for each member.

The generation and combination of maintenance scenario in each member has the serious problem with the asynchronous replacement of pavement when replacing the slab. Such problem will block the rational generation of the maintenance strategy and the budget establishment.

##### 4.2 Generation of maintenance strategy for the bridge system

For suggesting the maintenance scenario of the bridge system, the optimum maintenance scenario analysis in the system level is executed by considering the subordinate relation between slab and pavement. The maintenance intervention of a member can influence on other members, but it is defined to have subordinate relation when only replacing each member. For instance, the replacement of slab accompanies with the replacement of pavement. The number of population and generation applies in the analysis is 1,000 and 5,000 respectively, and the probability of cross over and mutation is applied as same as the analysis of member level.

Among the solutions obtained from the result of basic analysis, the elite group stored in each generation distributes as shown in Figure 4. Each point of Figure 4 means a solution which has annual information of maintenance intervention, performance and cost. Figure 5 and Figure 6 show the condition index profile and the maintenance cost profile of optimum

Table 2. Comparison of the member level and system level maintenance scenarios.

No.	Year	Member Level		System Level	
		Slab	Pavement	Slab	Pavement
1	2006		ST		
2	2007	EI			PA
3	2008				
4	2009		PA	EI	
5	2010		ST		PA
6	2011				ST
7	2012		PA		
8	2013		CO		RP
9	2014		ST	WP	
10	2015		RP		PA
11	2016				
12	2017				CO
13	2018				ST
14	2019		ST		
15	2020	EI	PA	EI	PA
16	2021		CO		CO
17	2022		ST		RP
18	2023	WP	PA		
19	2024		RP	FA	ST
20	2025				PA
21	2026		PA	WP	
22	2027	FA	ST		
23	2028				RP
24	2029		PA		PA
25	2030				
26	2031	EI	CO	EI	
27	2032		RP		PA
28	2033	RS	ST		CO
29	2034			RS	RP
30	2035		PA		
31	2036		ST		
32	2037				CO
33	2038		CO		ST
34	2039		PA		
35	2040		ST		
36	2041		RP	WP	RP
37	2042		PA		ST
38	2043				
39	2044			EI	CO
40	2045				
41	2046		PA		ST
42	2047	EI	CO		
43	2048		RP		RP
44	2049				CO
45	2050				
Min. Condition Index of Member		93.3	82.6	91.6	77.8
Maintenance Cost of Member (Thousand Won)		54,886	48,407	69,836	55,457
Min. Condition Index of System		90.7		92.6	
Maintenance Cost of System (Thousand Won)		103,294		125,292	

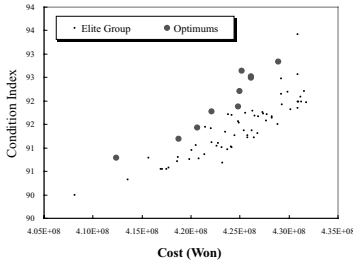


Figure 4. Elite group and Pareto solutions at the system level.

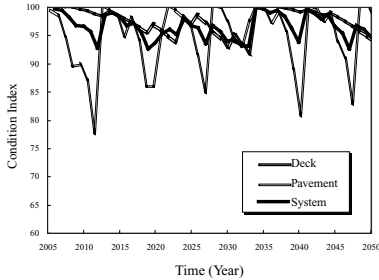


Figure 5. Condition index profile at the system level.

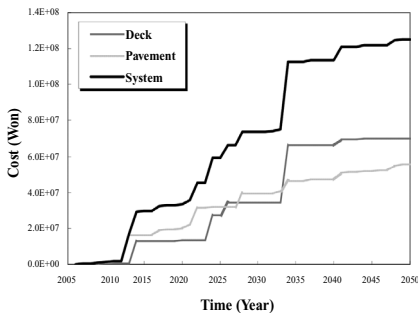


Figure 6. Maintenance cost profile at the system level.

tradeoff solution at the system level. The right part of Table 2 shows the annual maintenance scenario, performance and cost of the slab and pavement for the optimum tradeoff solution among the derived elite solution sets.

#### 4.3 Comparison the system level with the member level

The maintenance scenarios in Table 2 are located on the uppermost part among the sets of optimum trade-off scenarios occurring in the member and system level analysis. The optimum maintenance scenario in the system level is decided in order to improve the performance of the entire bridge system by considering the mutual subordinate relation between members.

Therefore it gives different result from the optimum maintenance scenario produced in the member level.

The optimum maintenance scenario in the system level shows a little bit large amount of maintenance cost compared to the cost result of member level which is combined with the optimum maintenance scenario in each member. To compare the minimum condition index of the system, the condition index of each member which is estimated in the system level is lower than the result in the member level as shown Table 2, but the minimum condition index of the system level is a bit higher than the member level. That is, member level maintenance scenario will be likely to manage the performance of each member during the lifetime, however, there is a limit in the performance management of the combined system with each member. This limit can be overcome by estimating the optimum maintenance scenario in the system level.

In Table 2, it is verified that the pavement is not replaced in the point of time when occurring the replacement of slab with the comparison of the optimum maintenance scenario between slab and pavement. Therefore, the optimum maintenance scenario in the member level has a meaning if there is no replacement of upper level member, and however, it does not give any significance as the optimum solution in case of the inevitability of replacement. Furthermore, if the unexpected replacement of the upper level member occurs in the member level analysis, the additional cost will be generated from the replacement of lower level member, which causes the increase of maintenance cost in the entire bridge system.

This paper also reanalyzes the optimum maintenance scenario produced from each of slab and pavement in member level by reorganizing the imaginary system level scenario, which the pavement is compulsorily replaced with the replacement of slab by considering the subordinate relation between members. From the result of reanalysis, the cost of imaginary system level scenario has additional cost from the compulsory replacement of pavement which increases to 108,677 thousand won. However, the minimum condition index is not changed with the value of 90.7 despite the increase of maintenance cost (Figure 7 and Figure 8). This tendency means that the optimum maintenance scenario estimated by the combination of the member level analysis causes the unnecessary maintenance intervention which does not contribute to the improvement of system performance and the unexpected increase of budget. After all, this scenario does not have the significant meaning as an actual optimal solution. Therefore, the actual optimal solution of the maintenance scenario of the system should be obtained from the system level analysis considering the subordinate relation among members not from the combination of optimal solution in the member level analysis.

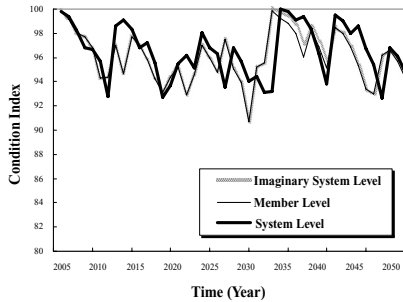


Figure 7. Comparison of condition indexes of system.

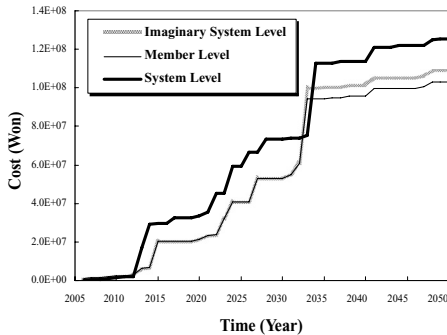


Figure 8. Comparison of maintenance cost of system.

## 5 SUMMARY AND CONCLUSIONS

In order to reasonable maintenance of the bridge, this paper proposes a method to set up the optimum maintenance strategy through the connection of bridge performance change and cost during the lifetime. It performs the life-cycle analysis not only at the member level but also at the system level according to the proposed method, and compares and studies the maintenance strategy generated from each analysis.

This paper quantitatively suggested the result of life-cycle analysis of the member and system level for the bridge in service by applying the developed method to generate the maintenance scenario. It would give more rational result, which the optimum maintenance scenario is selected on the basis of the performance and cost of the bridge system by considering the subordinate relation.

In order to utilize the next generation maintenance technique for making safe and rational bridge maintenance, the proposed life-cycle analysis is required to make more actual estimation corresponding to the quantification of performance evaluation for each member and performance change by the maintenance intervention. In addition, it is considered that the more research and development for the network level

analysis should be continued on the basis of the bridge system level analysis in order to make the optimum management for the group of bridges.

## ACKNOWLEDGEMENT

This study was supported by the Technical Innovation Project (No. 10) of Ministry of Construction and Transportation (MOCT) and Korea Institute of Construction and Transportation Technology Evaluation and Planning (KICTTEP) and KTAM-40 Project of Korea Institute of Construction Technology (KICT).

## REFERENCES

- Casas, J.R. 2006. Bridge management: actual and future trends, CD ROM of *Bridge Maintenance, Safety, Management, Life-Cycle Performance and Cost*, IABMAS, Porto, Portugal.
- Cho, H-N., Frangopol, D.M. & Ang, A.H-S. (eds) 2007. *Life-Cycle Cost and Performance of Civil Infrastructure Systems*, Taylor and Francis.
- Furuta, H., Kameda, T., Nakahara, K., Takahashi, Y. & Frangopol, D.M. 2006. Optimal bridge maintenance planning using improved multi-objective genetic algorithm, *Structure and Infrastructure Engineering*, 2 (1): 33- 41.
- Frangopol, D.M. & Liu, M. 2007. Maintenance and management of civil infrastructure based on condition, safety, optimization, and life-cycle cost, *Structure and Infrastructure Engineering*, 3 (1): 29- 41.
- Korea Institute of Construction Technology (KICT) 2006. *Development of life-cycle cost analysis method and system for the life-cycle cost optimum design and the life-time management of steel bridges*, Research Report, MOCT and KICTTEP, Korea (in Korean).
- Kong, J.S., Park, K.H., Lim, J.K. & Cho, H.N. 2007. Performance regression model for the optimal maintenance evaluation of steel box bridges, IABMAS, *Proceedings of the 5th International Workshop on Life-Cycle Cost Analysis and Design of Civil Infrastructure Systems*, 16–18 October 2006. Seoul, Korea.
- Ministry of Construction and Transportation (MOCT) & Korea Infrastructure Safety and Technology Corporation (KISTEC). 2003. *Detailed Guidelines of Safety Inspection and Precise Safety Diagnosis*. Korea (in Korean).
- Park, K-H., Lee, S-Y., Kim, J-H., Cho, H-N. & Kong, J-S. 2006. The Model to Generate Optimum Maintenance Scenario for Steel Bridges considering Life-Cycle Cost and Performance, *Journal of Korean Society of Steel Construction* 18 (6): 677–686 (in Korean).
- Patidar V., Labi, S., Sinha, K.C. & Thompson, P. 2007. *Multi-Objective Optimization for Bridge Management Systems*, NCHRP report 590, TRB.
- Transportation Research Board (TRB). 2003. *Proceedings of 9th International Bridge Management Conference, Transportation Research Circular No. E-C049*. Orlando: Florida.

# Life time assessment of steel bridges via monitoring and testing

U. Peil, M. Frenz & I. Schendel

*Institute of Steel Structures, Technical University Braunschweig, Germany*

**ABSTRACT:** The prediction of a realistic lifetime and the prolongation of the service life of a structure are important factors to reduce costs. The commonly used theoretical predictions of fatigue in steel-structures have often not proven to be accurate. The commonly used prediction model consists of a load model, a system-transfer model and a damage model. The results of these sequentially coupled models are usually unreliable, especially as the influence of the uncertain load and damage models controls the reliability of the result. A method based on monitoring strategies which avoids these problems is presented in this paper. To avoid the damage model, an artificial generated time history is used as an input for the digitally controlled test rig, in which a specimen of the actual constructional detail, or even a part of it, is tested. Following this concept, the knowledge of the critical details in the structure is of particular importance. In old structures the choice of the few details at which the monitoring is necessary can be done in a deterministic way. In contrast, new structures normally cover a broad range of critical details with an equally distributed failure level. Monitoring of all these points is far too expensive. Software is presented here to determine the critical details in a probabilistic way.

## 1 INTRODUCTION

The prediction of a realistic lifetime and the prolongation of the service life of a structure are important factors to reduce cost. It will therefore be necessary to determine the real lifetime of structures which is often much longer than estimated by usual theoretical models. As a result most structures could be used much longer than their calculated life cycle. This would reduce the overall costs of the structure. However, a lot of structures show unexpected damages, due to increased and unpredictable usage, higher strengthening of the structure, corrosion by environmental conditions, carelessness during construction and maintenance.

The theoretical models usually consist of a load model, a system-transfer model and a damage model. Because the results of one model serve as an input for the next model, the systematic and random errors of all models flow together which then are multiplied. Thus the results of this chain of models are usually unreliable. Especially the influence of the uncertain load and damage models controls the reliability of the result.

The uncertainties of the above mentioned three models can be minimized when using monitored data of the random strains at the critical points and additional tests in the laboratory. The Method can be used for new and existing structures as well. The reliability of the results is high.

## 2 GENERAL CONCEPT

In a first step, the random strains at critical details are monitored. The reliable determination of the critical details in the structure is therefore a substantial need. Due to the monitored strains, a load model and a system model is not required any more, thus the uncertainties of both models can be avoided, [Figure 1](#).

Using the monitored data, the load histories can be classified by means of the Rainflow-Method. The resulting stress collectives can then be used for common cumulative linear or non-linear damage rules (Fujiwara et al. 1993). The result of such life cycle assessment will always be un-certain (Schütz 1994). To achieve a more reliable prediction, it is essential to avoid the damage model as well (Andkjær, Agerskov & Vejrum 1995).

To avoid the damage model within the concept presented here, an artificial i.e. generated time history is used as an input for a digitally controlled test rig, in which a sample of the actual constructional detail (or a part of it) is tested. The monitored time history is reduced, eliminating small i.e. non-damaging stress cycles and breaks of action.

The artificial time history contains the overall statistics of the load process, taking into account the past and the estimated future of the loading situation including e.g. clustering of trucks and traffic jam (Peil, Frenz & Weilert 2007). The generation is based on a Markov-Process. In the following, the generation

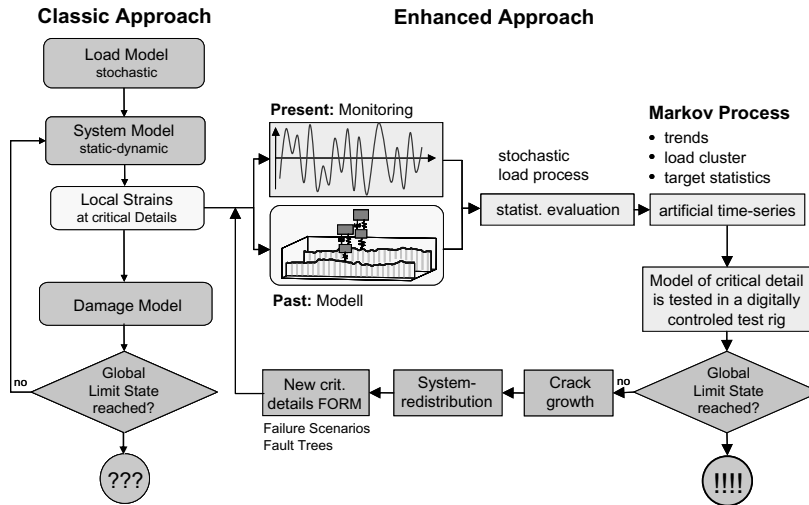


Figure 1. General concept.

of artificial time histories which are used as an input for the digitally controlled test rig will be shortly discussed. The main point is, that not only the last load class induced by a vehicle is used as a starting class but previously generated load classes as well.

Different methods were investigated. As a first method a transitions matrix method is used. This method doesn't guarantee however that all target classes occur with their theoretical probabilities if finite time histories are used. A correspondence between the input and the output transition matrix generated from the synthetic time history becomes much better, if very long time histories are used as an input. Thus a large number of realizations are computed and the resulting time histories are evaluated by an automatic selection using a criterion of best cluster matrix or best collective shape.

The next method uses a 3-dimensional transition matrix. Not only is the transition probability of the last load class used, but also the previously generated ones. For every previous load class taken into account a special transition matrix is needed. In Figure 2 the transition probability from class 6 to the new unknown class depends on the transition probabilities of the previous transition probabilities of class 10, class 0 and class 9, which could be determined using the transition matrices of the last 3 load classes.

The third method used is a so called snake algorithm. This method determines the load classes step by step by means of a random generator. To take the load sequences into consideration, a pattern recognition of the load classes at the actual end of the synthetic time history is used for the decision of the new target class.

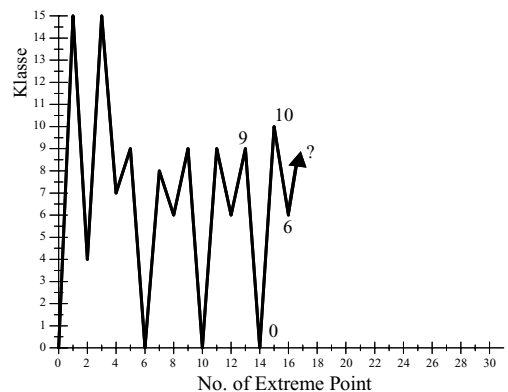


Figure 2. Part of a generated time history.

If the pattern of the last  $n$  classes is used as a feature of the new class to be generated, the  $n$ -dimensional feature vector can be written as follows:

$$M_{new\ class} = \begin{pmatrix} \text{Class No. Sequence start} \\ \dots \\ \dots \\ \dots \\ \text{Class No. Sequence end} \end{pmatrix} \quad (1)$$

Snake is the name of an elastic curve, which is defined by different points defining the classes. It is used to find again a typical pattern at any point of the measured time history and to set up a statistic. The

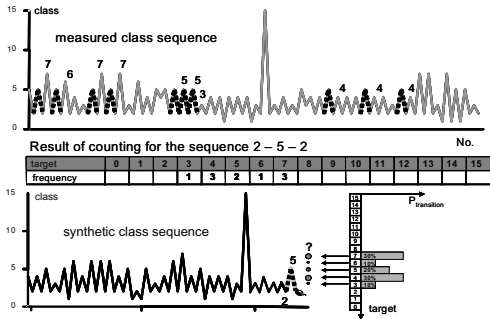


Figure 3. Principle of generation with the snake-algorithm.

principle is shown in Figure 3. In this example  $n$  is assumed to be 3 defined by the sequence 2-5-2. The accompanying distribution of possible target classes is shown in the lower part of Figure 3. The probable target classes are symbolized by points of different diameter in front of the snake. The investigations showed that short snakes with a sequence of 3 to 5 can be used.

The trend of the process is included, using a step by step procedure, testing only a chosen time interval (e.g. 5 years) of the future load process. If the specimen survives this time interval, the detail will survive as well. After having reached the end of the time interval, the same specimen will be tested further with the next artificial strain history, including the latest information about the new trend. If there is a difference between the fatigue states of the specimen and the real constructional detail, the fatigue state must be adjusted before starting the next testing interval. This can simply be done by adding the difference of load cycles monitored for the real detail minus the actual load cycles of the specimen, provided the real structure has a higher fatigue state after the chosen time interval than the specimen. The Markov matrices of both processes have to be subtracted. Because the damage state of the specimen which is loaded by a certain number of cycles is compared with the same number of cycles for the real structure, there is no need to determine the real damage state. We can therefore just compare the cycles. If the fatigue state of the real structure is less than the fatigue state of the specimen, one has to wait for the point in time until the structure has the same damage state as the specimen. The specimen will not be destroyed. After testing and in order to guarantee the same environmental impacts, the specimen will be stored close to the structure.

If a structure is monitored from the beginning, the procedure is straight forward. To predict the remaining fatigue life of an existing structure, load histories from the past would be required. Since they cannot be monitored by nature, they must be generated.

The generating method consists of two procedures: a load generating procedure and a strain generating procedure. Those procedures are explained in (Peil, Frenz & Weilert 2007), (Peil, Mehdiانpour, Scharff & Frenz 2002).

However, a validation of the described method is usually impossible because the remaining life cycle of real buildings is fairly high. To avoid this problem, so called building substitutes (BS) with different weak points and matching specimen are tested under different load histories in the laboratory, (Peil, Mehdiانpour, Scharff & Frenz 2002).

Up to now three different types of load-collectives have been tested. For the first investigations single-step tests on four different load-levels have been used. In a next step a measured time history, monitored at a critical detail of a highway bridge, was used. In order to validate the procedure for a greater range of applications, a load time history presented by Fischer et al. (Fischer, Hück, Köbler & Schütz 1970) was tested in the lab. This time history is similar to a Gaussian Process and was especially designed as a general time history for service-strength investigations of materials and critical details. It is based on a given rainflow-matrix and a specific generation procedure which is always reproducible.

Up to now 56 building substitutes and 180 specimens have been tested. Figure 4 shows a comparison of the time the first crack arises in the BS and in the specimen. If the point hit the 45° line the life time prediction by means of the specimen is exact. The precise agreement is clearly visible, as the results lies always near the 45° line.

### 3 DETERMINATION OF CRITICAL DETAILS

Independent of the type of the structure to be monitored, the assessment of critical weak points is one of the most important tasks. Weak points or weak spots are areas of the structure which are prone to damages or where possible damages cause non-tolerable consequences. Weak points of older structures, usually designed with very different safety levels (from our today's point of view), are normally well known and can be determined by existing structural calculations or by experience.

Newer structures however show an equally distributed safety level over a high number of critical details. Because of the increasing costs for every new detail to be monitored, the critical details can be detected using probabilistic methods, leading to a lower number of measuring points.

The procedure for reliability-oriented determination of weak points classifies critical weak points as those which contribute the largest part to the overall failure probability of the structure. These points must

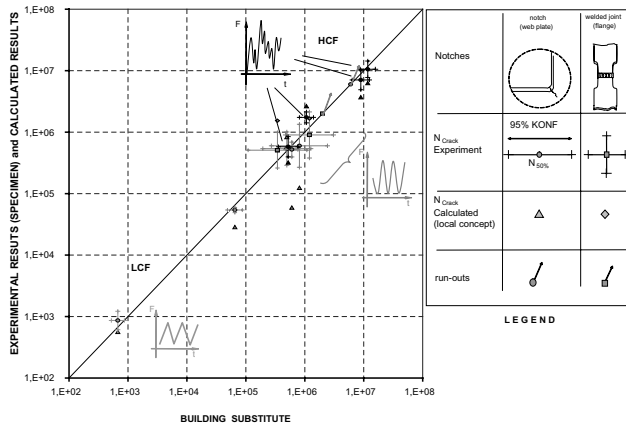


Figure 4. Comparison of results.

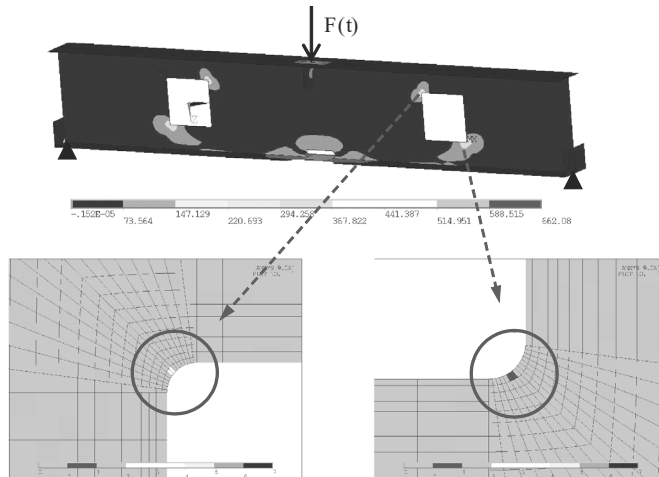


Figure 5. Display of calculated critical points at the building substitute.

be monitored. To determine the failure probability the description of

- limit state functions, limit values
- stochastic model
- mechanical model
- analysis of sequences of events, fault trees

are prerequisites. The probabilistic calculations have to be done by software, which matches the need within this project for cyclically loaded steel-structures.

For this reason, and in close co-operation with the subproject A1 (Klinzmann, Schnetgöke & Hosser 2006) of the Collaborative Research Center 477 (SFB 477) “Life Cycle Assessment of Structures via innovative Monitoring”, an automatic procedure was developed. On the basis of an exact FE-analysis, weak points

are identified, depending on its contribution to the overall failure probability of the structure. The optimal location for placing sensors on the structure can be determined. Software at present available in the market are insufficient to fulfill the requirements, see also (Pellissetti & Schueller 2006) with an overview of the existing Structural Reliability software.

As a first step an anamnesis of the concerning structure has to be accomplished, in order to know the current condition of the building as well as the used materials as exactly as possible. In this step e.g. deviations of the building from planning, changed design details and possible pre-existing damage are determined.

In order to execute a probabilistic calculation, the structure is then modeled in a FE-Program under

consideration of the anamnesis-results. Geometric parameters and e.g. steel grades are part of the stochastic model. The limit state function is described by the theoretical calculated occurrence of the first crack via the concept of local strain. This calculation can be done for every Gaussian point in the FE-model.

To reduce calculating time, the used commercial FEA-program was extended by integrating different subroutines into the menu structure. Thereby on the one hand local disturbances in the structure e.g. sharp notches and also welding seams can be represented by the definition of flaw-factors for the appropriate FE elements. As a result, complex local refinements of the net can be avoided. On the other hand a selection of the points to be examined (i.e. assumed critical details) in the FE model can be made by the user, so that it is not necessary to examine all existing points. The amount of computing time is thereby reduced substantially.

For the now selected group of possible critical details—or also optionally for the entire structure—a damage computation is accomplished using the local strain concept. The results of the stochastic model of the structure are passed via a data interface to the program named PROBILAS (Klinzmann, Schnetgöke & Hosser 2006). This software calculates the failure probability for each of the preselected points by means of the First and Second Order Reliability Method (FORM/SORM).

The FORM calculations are based on the general definition of the limit state equation:

$$G = R - S \quad (2)$$

with  $R$  as resistance quantity and  $S$  as action quantity of the system.  $R$  and  $S$  are both stochastic variables (basic variables).

Safety is guaranteed, when the resistance is greater than the action, while failure occurs when  $G < 0$ . The failure probability can be interpreted by equation (1).

$$p_f = \int_{-\infty}^{+\infty} f_s(x) \cdot F_R(x) dx \quad (3)$$

with:  $f_R(x)$  distribution density of  $S$  at  $x$  and  $F_R(x)$  distribution function of  $R$  at  $x$ .

One method for the determination of failure probabilities is the First Order Reliability Method (FORM). This method has been performed for normally distributed variables (Hasofer & Lind 1974) and later extended to arbitrarily distributed parameters (Rackwitz & Fiessler 1978). For the explanation of this method, it is supposed that  $R$  and  $S$  in Equation 3 are uncorrelated and normally distributed. When the failure probability is calculated according to FORM,

the basic variables and thus the limit state equation are transformed into standard normal distributions. This is done by the transformation equation. The procedure then follows the classical First-Order-Reliability-Method (FORM).

The calculation of our example results in a probability of occurrence, described by the safety index  $\beta$ . The lower the  $\beta$ -value, the greater is the failure probability of the particular critical detail. The calculated  $\beta$ -values are returned to the FE-program, which was extended in order to show the critical points in an order of rising  $\beta$ -values, see Figure 5. The stresses of the former described building-substitute are shown, followed by the calculated critical points. The first critical point is located at the lower outside corner of the girder, third at the opposite upper out-side corner. Due to the information given by this display the user can now decide whether parts of the concerning structure have to be monitored or not. The procedure is now upgraded to automatically perform the overall analysis of a fatigue endangered structure under consideration of fatigue crack growth.

#### 4 LIFE TIME ASSESSMENT OF EXISTING STRUCTURES

For existing structures different aspects have to be taken into account. In addition of the challenge of the knowledge and simulation of the former loading (Peil, Mehdiانpour, Scharff & Frenz 2002), the original steel will often not be available for the making of the specimen. In contrast to new structures, steel from different charges must therefore be used and the influence of the different material behavior in fatigue must be taken into account.

In order to assess the influence of different steel charges on the result of the lifetime until the occurrence of the first crack, additional comparative tests with specimen from three different steel charges were compared with the results of the building substitutes. For each steel charge two different one-step tests series were carried out (named “W IIa”, “W IIb”), followed by a tests series using the measured random time series (“R II”). For each test series 10 specimens per charge were tested.

In order to assess the influence of different steel charges on the result of the lifetime until the occurrence of the first crack, additional comparative tests with specimen from three different steel charges were compared with the results of the building substitutes. For each steel charge two different one-step tests series were carried out (named “W IIa”, “W IIb”), followed by a tests series using the measured random time series (“R II”). For each test series 10 specimens per charge were tested.



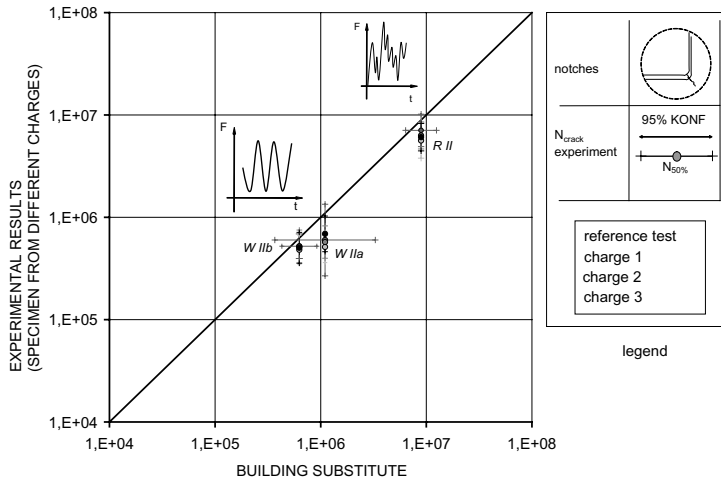


Figure 6. Comparison of results between different charges.

In order to take the different cyclic and fatigue behavior between the charges into account, the adjusted strains of the specimen in the test-rig were corrected. Based on the measured strains at the building substitute, the required strains for the same number of cycles until the occurrence of the first crack with the different charge were calculated. The calculations were performed by means of the concept of local strains (Bäumel & Seeger 1990).

The results are shown in Figure 6. It is clearly visible from the graph, that the results of the different steel charges lay within the 95% confidence level of the original measurements.

## ACKNOWLEDGEMENT

The research work reported here was supported by the Deutsche Forschungsgemeinschaft (German Research Foundation) within the framework of the Collaborative Research Center SFB 477. The authors wish to express their appreciation for the financial support.

## REFERENCES

Andkjær Nielsen, Agerskov H. & Vejrum, T. 1995. Fatigue damage accumulation in steel bridges under highway random loading Proc. 1st European Conf. On Steel Struct. Eurosteel 95. Athens 1995.

- Bäumel Jr., A. & Seeger, T. 1990. Materials Data for Cyclic Loading, Supplement 1. Materials Science Monographs 61, Elsevier Science Publishers B.V., 1990.
- Fischer, R., Hück, M., Köbler, H.-G. & Schütz, W. 1970. Eine dem stationären Gaussprozess verwandte Beanspruchungs-Zeit-Funktion VDI-Fortschrittsberichte, VDI-Z 5, Nr. 30, 1970, 2–29.
- Fujiwara, M. et. al. 1993. Stress Histograms and Fatigue Life Evaluation of Highway Bridges. Bericht IVBH-Colloq. Copenhagen, 301–308.
- Hasofer, A.M. & Lind, N.C. 1974. An Exact and Invariant First-Order Reliability Format. In: Journ. Of. Eng. Mech., ASCE, 199, EM1, pp. 111–121.
- Klinzmann, C., Schnetgöke, R. & Hossler, D. Framework for the Optimization of Structural Health Monitoring on a Probabilistic Basis. In Guemes (ed.) Structural Health Monitoring 2006, SHM 2006, Granada, pp. 57–64.
- Peil, U., Frenz, M. & Weilert, K. Life Time Assessment of Bridges. ICLODC 2007, Bochum.
- Peil, U., Mehdiانpour, M., Scharff, R. & Frenz, M. 2002. Life Time Assessment of Existing Bridges. Proceedings of the First European Workshop: Structural Health Monitoring. Paris 2002, S. 999–1006.
- Pellisetti, M.F. & Schueller, G.I. On general purpose software in structural reliability—An overview. Structural Safety 28 (2006), pp. 3–16.
- Rackwitz, R. & Fiessler, B., 1978. Structural Reliability under Combined Random Load Sequences. In: Computers & Structures, 9, pp. 484–494.
- Schütz, W. 1994. “Fatigue life prediction by calculation: Facts and fantasies.” Structural Safety & Reliability (Ed. Schueller & Yao). Rotterdam, Baalkema, 1125–1131.

# A risk ranking strategy for network level bridge management

S. Sathananthan & M.I. Rafiq

*Faculty of Engineering and Physical Sciences, University of Surrey, Guildford, UK*

T. Onoufriou

*Department of Civil Engineering, Cyprus University of Technology, Cyprus*

**ABSTRACT:** At present almost all bridge owners and managers, i.e. Network Rail, Highways Agency and local authorities in the UK, carry out bridge inspections at regular intervals to collect information on condition and performance of bridges. Introduction of risk based approaches in the selection of inspection regimes can provide consistent safety levels within the network in a cost effective manner. This paper presents the development of a qualitative risk ranking strategy to characterize a network of bridges into groups with similar risk levels, which can form the basis for developing a risk based inspection regime over the network. There are a multitude of factors that affect risk. These factors are identified and rationally combined to present various attributes of bridges. A qualitative scoring system is then introduced which utilizes the attributes to rank bridges in terms of their relative risk. Sensitivity analysis is performed to quantify the effect of relative weights of the attributes on the risk scores. The methodology is demonstrated through its application on UK's Network Rail bridge stock comprising of about 40,000 bridges. The criteria to classify the severity of the attributes are established for the network. A random sample of bridges is ranked to illustrate the proposed methodology.

## 1 INTRODUCTION

Bridges deteriorate with time and need intermittent inspections to ensure that they are capable of carrying traffic. However, inspecting a network of bridges at regular intervals without considering issues related with bridge characteristics, functionality and significance may not provide optimum level of safety. A risk based inspection methodology can be useful in this context as it has the potential of rationalising the inspection planning with significant safety and cost benefits.

The early use of risk based inspections can be found in various industries such as air craft (e.g. Yang and Tang, 1974), and offshore (e.g. Faber *et al*, 1996, Onoufriou, 1999). These techniques have recently been utilised in transport infrastructure, in particular for maintenance management of bridges. [e.g. Sommer *et al* (1993), Frangopol *et al*, 1997, Liu & Frangopol (2005)].

The previous studies have concentrated at an element/structure level or a small group of structures with similar characteristics, which are not readily applicable to a large stock of bridges. In this case, bridge specific analyses may not be feasible. Even if all the bridges are analysed individually and inspections are scheduled accordingly that will result in large variations in inspection intervals over the network causing

practical difficulties and additional expenses. Instead of having the same inspection regime throughout the entire network or bridge specific inspection intervals, scheduling inspections for groups of bridges according to their relative risk would optimize the inspection resources in a cost effective manner. Therefore, it is necessary to categorise the bridges with similar characteristics into groups before developing a risk based inspection (RBI) methodology.

This paper presents a systematic risk ranking approach to a network of bridges considering the factors which influence their relative risk. This approach is beneficial to bridge owners to identify the safety critical bridges in their network and to plan interventions/inspections according to their risk levels to maintain the same risk level throughout the network.

## 2 FACTORS AFFECTING RISK AND BRIDGE ATTRIBUTES

Based on a study of available literature, and discussions with bridge owners, sixteen key factors have been identified as having a significant impact in determining the relative risk levels of bridges in a network. Many of the attributes affect the same attribute of a bridge and hence can be grouped together. Five bridge attributes have been identified that are affected

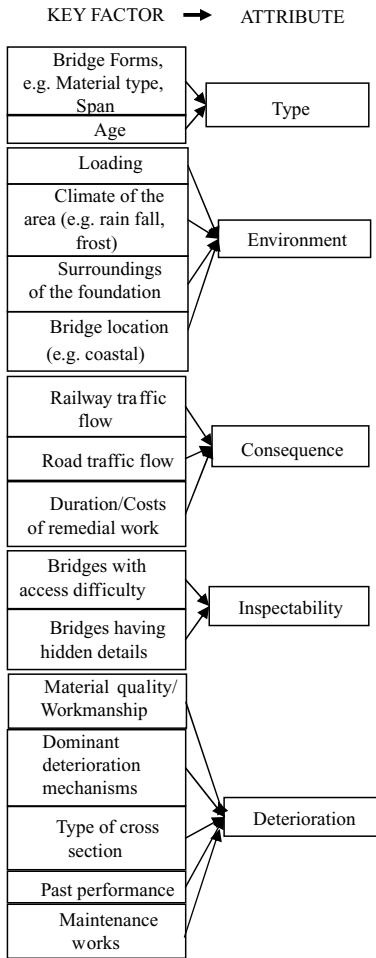


Figure 1. Relationship between key factors and bridge attributes.

by these factors. A list of the key factors and their relationship with the bridge attributes is outlined in Figure 1. The attributes are elaborated in more detail in the following sub sections.

### 2.1 *Type*

In a network, there may be different forms of bridges with variations in the material type, span, etc. Since different materials have different mechanisms and rates of deterioration, material variation is one of the most significant factors affecting risk. Bridge age is another decisive factor. The rate of deterioration and hence the risk increases with age. Normally, a correlation between the bridge age and bridge form within a network can be observed. This may be due to the fact that the construction methods are similar

over a certain period of time until another method is introduced. For instance, all the arch bridges owned by Network Rail were built more than 100 years ago (Bell, 2004). Therefore, these factors are grouped under a bridge attribute called 'Type'. This attribute will be used to divide a network into groups of bridges having similar characteristics in relation to risk.

### 2.2 *Environment*

The environment attribute is represented by the factors that are external to the structure but play an important role in determining the risk associated. These include loading, climate, location of a bridge and surroundings of the foundation. The effects of these factors will be different for different material types. For example, a reinforced concrete or a steel bridge located in a coastal area may have severe corrosion attack, whereas a masonry bridge in a similar location might be least affected. Therefore, the environment attribute must be classified independently for each group of bridges defined through type attribute.

### 2.3 *Consequence*

The consequence attribute covers a wide range of factors from direct consequences of failure such as human loss, repair/replacement cost and the loss of income to indirect consequences such as traffic delay costs, environmental impacts, political impact, etc. Evaluating and interpreting all these consequences in numerical terms is difficult. Therefore, by considering parameters such as traffic flow and duration/cost of remedial works reasonable judgement can be made regarding the consequence. Higher traffic flow can be used as an indicator for high traffic delay cost, if flow is interrupted or high human loss in case of an accident. Similarly, length of a bridge (multiple spans or long span) may be related to high maintenance costs and/or long duration of remedial works, etc.

### 2.4 *Inspectability*

If all main elements of a bridge are not inspectable then some defects may remain undetected, and result in higher risk of failure. The two scenarios leading to this include bridges having hidden details and bridges having difficulty in accessing main elements for inspection. For example, tenanted arches may have unidentified defects and if some parts of a bridge are under water then it may be difficult to inspect them during the visual inspection. These factors are grouped separately under the inspectability attribute.

### 2.5 *Deterioration*

The deterioration attribute incorporates all the factors that contribute to degradation of the structure with time. These include factors such as dominant deterioration mechanisms, workmanship and material

quality, past performance and maintenance and the cross sectional make up of the structure. The dominant deterioration mechanisms will be different for each bridge type (as defined in section 2.1). Information on the other factors will also help in the classification, e.g. good workmanship and material quality and good past performance can be used as an indicator for a lower deterioration rate.

The bridge attributes in Sections 2.1 to 2.4 are all time independent and are utilised to provide an initial screening of the bridges in terms of their relative risk. The deterioration attribute provides the variation of the risk with time. This can be used, along with the initial relative risk, to develop a framework for risk based inspection planning of bridge stock.

### 3 QUALITATIVE RISK SCORING SYSTEM

A simple and practical approach for ranking the bridges is introduced by defining groups and sub groups of bridges in a network. ‘Type’ attribute is used as the basis to define the main groups. Three other attributes environment, consequence and inspectability are classified into two categories, in terms of the severity and subgroups are derived according to these classifications. Therefore, the subgroups serve as a risk ranking tool within a main group of bridges. A flow chart highlighting the grouping procedure is shown in Figure 2. A scoring system is then introduced to express the relative risk numerically.

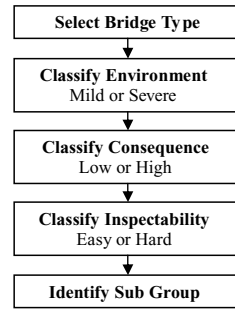


Figure 2. Selection procedure for grouping.

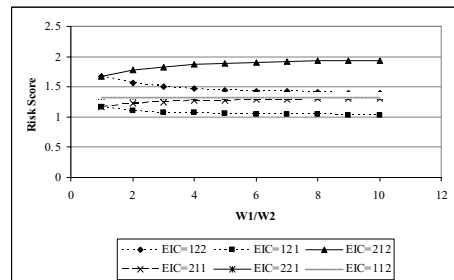


Figure 3. Variation of risk score with relative weight of environment/inspectability.

#### 3.1 Relative risk score

Initially, a score of 1 for the best cases and 2 for the worse cases are assigned to the attributes. For example, a score of 1 is allocated for the mild environment whereas 2 is assigned to the severe environment. Risk is defined as the multiplication of the probability of failure and consequence of failure. The environment and inspectability attributes are related to the probability of failure ( $P_f$ ) and the consequence attribute represents the consequence of failure ( $C_f$ ). Therefore, a score representing the relative risk of a subgroup,  $R$ , can be expressed through Equation 1.

$$R = (W_1 S_E + W_2 S_I) \times S_C \quad (1)$$

where  $S_C$  = consequence score;  $S_E$  = environment score;  $S_I$  = inspectability score;  $W_1, W_2$  = Weight factors representing relative importance of  $S_E$  and  $S_I$  within the overall risk score  $R$ .

#### 3.2 Weight factors for environment and inspectability scores

The weighting of consequence attribute will not have any impact on the final risk score since it will be multiplied to the scores and  $R$  only represents the

relative risk among the sub groups. Hence the relative weighting between environment and inspectability scores is considered in Equation 1. In some structures environment may be a critical factor in defining the relative risk whereas inspectability may be more critical in others. Sensitivity analysis is carried out to find the effect of weight factors  $W_1$  and  $W_2$  on the final risk score,  $R$ . The results are presented in Figure 3. Final risk scores can be arranged to vary between 1 and 2 by linear interpolation in order to compare the relative scores for different combinations of weight factors.

Initially, the risk score ( $R$ ) of each sub-group for different combinations of environment ( $E$ ), inspectability ( $I$ ) and consequence ( $C$ ) factors (e.g. mild environment, hard inspectability and high consequence), while changing the relative weight of  $W_1/W_2$  are calculated. These are plotted in Figure 3.

The notation  $EIC = 122$  represent the group of bridges which belongs to Mild Environment ( $E = 1$ ), Hard Inspectability ( $I = 2$ ) and High Consequence ( $C = 2$ ). Altogether 8 groups can be obtained by changing this combination. However, the group with mild environment, easy inspectability and low consequence ( $EIC = 111$ ) and the group with severe environment, hard inspectability and high consequence ( $EIC = 222$ ) are not plotted in the graph as their scores always remain as 1 and 2 respectively. From, this graph

Table 1. Differences in scores with and without weight factors.

Condition	Score		Percentage difference (%)
	Without weight factor	With weight factor	
EIC = 111	1.00	1.00	0
EIC = 112	1.33	1.33	0
EIC = 121	1.17	1.25	6.8
EIC = 122	1.67	1.83	9.6
EIC = 211	1.17	1.25	6.8
EIC = 212	1.67	1.83	9.6
EIC = 221	1.33	1.33	0
EIC = 222	2.00	2.00	0

it can be seen that the variation in the risk scores with the relative weights is small, particularly with weight factors higher than 3. Therefore, a maximum relative weight of 3 between the environment and inspectability factor can be used.

A new method for incorporating the weight factor is proposed and the sensitivity tested again. In this method the worse case is assigned a weight of 3. That is, if the environment is severe, then use a relative weight 3 for the environment and if the inspectability is hard, assign inspectability a weight of 3. In the cases where both environment and inspectability are in worse or better conditions, the weight factors have no effect. The scores obtained using this approach and the scores obtained without using weight factors are given in Table 1.

It can be seen from Table 1, that the difference between the two methods is small with a maximum percentage difference of 9.6%. Based on the results of the sensitivity studies and bearing in mind that the scoring system is only a qualitative measure of the relative risk among the sub groups of bridges it was decided to ignore the weighting factors from the scoring system. Therefore the relative risk score 'R' is calculated using Equation 2.

$$R = (S_E + S_I) \times S_C \quad (2)$$

These values are normalized to vary between 1 and 2 by linear interpolation. This adjustment was considered desirable so that 1 and 2 always represent the best and worse cases respectively. The risk ranking system is provided in Table 2.

#### 4 APPLICATION OF RISK RANKING STRATEGY TO NETWORK RAIL BRIDGE STOCK

The proposed risk ranking strategy is demonstrated through its application on the UK Network Rail

Table 2. Risk ranking system.

Environment	Consequence	Inspectability	Risk Score
Mild	Low	Easy	1.00
Mild	Low	Hard	1.17
Mild	High	Easy	1.33
Mild	High	Hard	1.67
Severe	Low	Easy	1.17
Severe	Low	Hard	1.33
Severe	High	Easy	1.67
Severe	High	Hard	2.00

bridge stock that comprises over 40,000 bridges. This includes bridges carrying railway traffic (under line bridges) and bridges carrying roads which pass over the railway lines (over line bridges). Initially the main groups are identified based on the 'type' attribute and then the criteria to rank the bridges within those main groups are developed.

##### 4.1 Identification of main group

Analyzing Network Rail bridge stock it was observed that about half of the network bridges are masonry arch bridges, either brick or stone, and almost all of them are over 100 years old. Metallic bridges are about 40% of the stock and spread over three age ranges <50, 50–100 & >100 years. Concrete has been used in the remaining bridges and were constructed mostly within the last 50 years (Bell, 2004). It was also observed that metallic bridges can be classified in to three types, namely cast iron riveted steel and welded steel. Therefore, based on the forms and age of the bridges in the network following six main groups are proposed; stone arch bridges, masonry arch bridges, cast iron bridges, riveted steel bridges, welded steel bridges and concrete bridges.

##### 4.2 Classification criteria for environment

The environment of a bridge will be considered as severe if two or more of the following factors are severe/heavy.

###### 4.2.1 Loading

Loading is one of the external factors that affect deterioration due to fatigue and/or ring separation. A qualitative classification of loads has been used that is based on the type of traffic. Railway routes are classified by the Network Rail into the following categories; primary, LSE (London South Eastern), main secondary, secondary, rural and freight. Among them, primary, LSE and freight routes are considered to carry heavy traffic and the bridges in these routes are considered as heavily loaded bridges. Over line

bridges serving motorways and trunk roads can also be considered as heavily loaded bridges.

#### 4.2.2 *Climate of the area*

Frost and rain are the two most common causes for the deterioration of mortar and brick. Therefore, the bridges can be classified into two groups in terms of frost and rainfall. Based on the annual average rain fall and frost level records from the Met office website (<http://www.metoffice.gov.uk/climate/uk/averages/index.html>) the climate of the UK can be classified into two regions; severe and mild. In this procedure, regions having annual rainfall under 1125 mm or regions with air frost less than 55 days are considered as mild since these are the national average values.

#### 4.2.3 *Location of bridge*

Susceptibility of masonry bridges due to its location is relatively low when compared to concrete or metallic bridges. Concrete or metallic bridges are prone to corrosion attack if they are exposed to salty environment. However, masonry bridges in highly polluted industrial areas also can be taken as severe in terms of the location since the mortar in bridges is vulnerable to chemical attacks.

### 4.3 *Classification criteria for consequence*

Factors identified as having influence on the consequence (see [Figure. 1](#)) are categorized into two groups, namely 'high' and 'low'. If two or more of the factors are classified as high, then the consequence factor is considered as 'high'.

#### 4.3.1 *Railway traffic flow*

Railway traffic flow can be considered as an indirect indicator of the possible consequences of an underline bridge failure such as human life loss/or injuries, loss of income, etc. It is assumed that the underline bridges in primary and LSE lines have high traffic flow rate.

#### 4.3.2 *Road traffic flow*

Over line bridges carry road traffic. Therefore, their failure consequence can be estimated in a similar manner to the underline bridges. Motorways and trunk roads can be assumed to have higher traffic flow rate. In addition, bridges on traffic sensitive roads (as designated by the Street works act <http://www.opsi.gov.uk/si/si2007/20071951.htm>) can be considered as of high consequence.

#### 4.3.3 *Cost and/or duration of remedial actions*

Cost and duration of remedial actions are difficult to estimate as they will be more bridge specific and will depend on the type of damage. However, it is assumed that the bridges with multi or long spans may encounter high cost and/or duration. This includes

an implicit assumption that all spans of a multi span bridge perform in a similar manner.

### 4.4 *Classification criteria for inspectability*

The inspectability can be affected in two ways. Firstly, inspections will not be able to reveal condition of hidden details of the bridge and the other factor is the difficulties in access to the bridge due to its location. This information is obtained from the past inspection reports. Normally, the examiners make a note in the examination report whether or not they were able to examine all major parts of the bridge.

### 4.5 *Case studies on selected bridges*

In this section a random selection of masonry bridges from Network Rail are ranked according to the above guidelines to demonstrate the procedure. The railway traffic type and SCMI details are obtained electronically from the Network Rail database. The locations of bridges are obtained from past inspection records and they are compared with the rain fall and frost maps to identify the relevant climatic condition. The roads adjacent to the bridges are identified using [www.streetmap.co.uk](http://www.streetmap.co.uk) and used to establish the consequence attribute. The required information about the inspectability is obtained from the past inspection reports.

As an example, asset Reference ANG030 is a masonry underline bridge in a primary line near to Harlesden area. From the met office records the rain fall and frost are identified as low. There are no noticeable heavily pollutant industries near the bridge. Therefore, the environment is taken as 'mild'. Its land ranger is TQ210839. From [streetmap.com](http://streetmap.com) the road adjacent to this is A407 which is not a critical road. However, since this bridge is a multi span bridge and it is on a primary line its consequence is 'high'. Past inspection record for this bridge indicates no inspection difficulties or hidden details of the structure hence inspectability is assigned as 'easy'. Therefore, this bridge has mild environment, high consequence and easy inspectability, hence according to [Table 2](#), a risk score of 1.33 is assigned to this bridge. [Table 3](#) presents a list of sample structures ranked according to their relative risk.

These risk scores can be used to establish the inspection strategy within a main group of bridges. Since they are indications of the relative risk levels of the bridges, selecting inspection intervals proportional to these scores would ensure same risk level is maintained. For instance, if the bridges with the score of 1.00 are inspected at 6 year intervals, then the bridges with score of 1.33 must be inspected every 4<sup>1</sup>/<sub>2</sub> years to maintain the consistent risk levels within bridges. A method to identify the inspection intervals for

Table 3. Bridge groups and SCMI scores.

Asset Ref	E	C	I	Risk Score
ANG034	Mild	Low	Easy	1.00
ANG006	Mild	Low	Easy	1.00
NW006	Mild	Low	Easy	1.00
GW006	Mild	Low	Easy	1.00
ANG031	Mild	Low	Easy	1.00
LNW-MID002	Mild	Low	Easy	1.00
STH030	Mild	Low	Easy	1.00
ANG033	Mild	Low	Hard	1.17
LNE030	Mild	Low	Hard	1.17
ANG007	Mild	Low	Hard	1.17
SCO104	Severe	Low	Hard	1.17
LNE-MID001	Mild	High	Hard	1.33
LNE008	Mild	High	Hard	1.33
ANG030	Mild	High	Easy	1.33
LNE-MID106	Mild	High	Hard	1.33
SCO103	Severe	Low	Hard	1.33
LNW-MID025	Severe	Low	Easy	1.33
GW101	Severe	High	Easy	1.67

bridges with score 1.00 is currently being developed by the authors.

## 5 CONCLUSION

The development of a risk ranking strategy is presented in this paper, which can serve as a screening process to rank the bridges in a network according to their relative risk levels. Main factors that may affect risk in relation to safety and serviceability of bridges are identified and linked to various bridge attributes. These attributes can be used to divide a network of bridges into groups according to their relative risks. A scoring system is developed to rank the groups in terms of their relative risk. Sensitivity analysis yielded the effects of different weights of the attributes on the relative risk scores.

The proposed method is demonstrated through its application on the UK railway network bridge stock. Six main groups are proposed based on the type attribute. Eight subgroups within each main group are proposed using the environment, consequence and inspectability attributes. Each of the attributes is classified into two categories based on the severity and relative risk score for each group is established. The classification system and the use of attributes in deriving relative risk is demonstrated on a sample of bridges from the network.

The risk ranking methodology will help the bridge owners to identify critical bridges in their network in a systematic and rational manner. The risk scores along with the deterioration profiles for each bridge type can be used to establish inspection/intervention intervals

for each group. This will ensure that a consistent risk level is maintained over the network. A process for the risk based inspection planning is being developed and will be published in the near future.

## ACKNOWLEDGEMENTS

The authors express their sincere gratitude to Network Rail for sponsoring this project and Mouchel for providing data. We also thank the steering committee members from various bridge related organizations who attended regular meetings for their valuable comments. We extend our sincere thanks to Brian Bell from Network Rail for all his contributions to this project.

## REFERENCES

- Bell, B. 2004. *European railway bridge demography, Deliverable D 1.2, Technical report*, UK: Sustainable bridges, Sixth framework programme, Sustainable development global change & ecosystems.
- Daly, A.F. 1999. Modelling of deterioration in bridges, Deliverable D11, European Commission DG VII-4th Framework Programme. *Bridge Management in Europe*. Available from: <http://www.trl.co.uk/brime/d11.pdf>.
- Faber, M.H. Kroon, I.B. & Sorensen, J.D. 1996. Sensitivities in structural maintenance planning. *Reliability engineering and system safety* 51: 317–329.
- Frangopol, D.M. Lin, K.Y. & Estes, A.C. 1997. Life cycle cost design of deteriorating structures. *Journal of structural engineering* 123 (10): 1390–1401.
- Liu, M. & Frangopol, D.M. 2005. Multi-objective maintenance planning optimization for deteriorating bridges considering condition, safety, and life-cycle cost. *Journal of structural engineering* 131 (5): 833–842.
- Mckibbins, L.D. Melbourne, C. Sawar, N. & Gaillard, C.S. 2006. *Masonry arch bridges: Condition appraisal and remedial treatment-CIRIA C656*. London: CIRIA.
- Melbourne, C. & Gilbert, M. 1995. The behaviour of multi-ring brickwork arch bridges. *Structural Engineer* 73 (3): 39–47.
- Onoufriou, T. 1999. Reliability based inspection planning for offshore structures, *Journal of Marine Structures* 12 (7–8): 521–539.
- Page, J. 1993. *Masonry arch bridges*, London: TRL. HMSO.
- SACP, pers. comm. 2005. *SACP Feasibilities*, London: Mouchel Parkman.
- Sommer, A.M. Nowak, A.S. & Thoft-Christenson, P. 1993. Probability based bridge inspection strategy, *Journal of structural engineering* 119 (12): 3521–3535.
- Stupart, A.W. 1989. A survey of literature relating to frost damage in bricks. *Masonry international* 3 (2): 42–50.
- Yang, J.N. & Trapp, W.J. 1974. Reliability analysis of aircraft structures under random loading and periodic inspection, *AIAA Journal* 12 (12): 1623–1630.
- [www.metoffice.gov.uk](http://www.metoffice.gov.uk)
- <http://www.opsi.gov.uk/si/si2007/20071951.htm>
- [www.streetmap.co.uk](http://www.streetmap.co.uk)

# Monitoring based structural performance assessment

Alfred Strauss, Dan M. Frangopol & Sunyong Kim

*Lehigh University, Bethlehem, PA, USA*

**ABSTRACT:** Engineering structures are subjected during lifetime to numerous stressors associated with environmental (chemical and physical) and mechanical loading. All these stressors and their associated uncertainties have to be considered during the structural design and assessment processes. Unfortunately, uncertainties in the prediction of stressors, their occurrence time and magnitude increase with prediction horizon. Cost optimization considerations associated with the maintenance and strengthening of structures are significantly influenced by such uncertainties. Therefore, for effective cost optimization approaches, for instance based on time dependent probabilistic methods, there is the need for the reduction of epistemic uncertainties associated with stressors by monitoring systems. The objective of this paper is to present statistical based tools for cost effective monitoring for structural performance assessment and prediction under environmental and mechanical stressors.

## 1 INTRODUCTION

An important part for the economic growth and social development of a modern society is the safety and reliability performance of its civil infrastructure (Frangopol and Liu, 2007). Valuable assets for most countries are their existing structures which are deteriorating at an alarming rate due to overuse, overloading, aging or damage (Frangopol and Messervey, 2007). For instance, bridges, which are vulnerable beyond doubt, are subjected to aggressive environment such as chemical attack from deicing salts, environmental stressors, as well as continuously increasing traffic volumes (Frangopol and Liu, 2007). In addition, many existing structures are close or above their planned lifetime.

Due to the urgent need of maintenance, repair, or replacement of many structures, there is a great demand for methods and technologies that allow an accurate assessment of these structures by prioritizing repairs and the efficient allocation of funds (ASCE, 2005). Nowadays site-specific response data, providing decision support for an efficient maintenance and rehabilitation of civil infrastructure, can be obtained by advanced monitoring systems. The main objectives using such systems are (a) the detection of threshold violations associated with defined reliability levels during the lifetime of a structure, (b) the determination of optimum intervention periods, and (c) the determination of optimum monitoring periods.

Nevertheless, despite high developed monitoring systems (MS) a comprehensive assessment and inspection of all elements composing an engineering structure is not feasible due to monetary constraints.

Hence, MS have to focus on the components and failure modes that are important to the reliability of structural systems during their lifetime.

The selection of structural components to be monitored must be based on statistical and reliability considerations. Statistical methods also enable the utilization of historical monitoring information for the formulation of structural degradation predictions. The aim of this paper is to present (a) statistical sampling based concepts for the determination of the necessary number of locations to be monitored, and (b) extreme data concepts for the prediction of physical quantities or the detection of degradation processes of structures.

## 2 MONITORING BASED STRUCTURAL PERFORMANCE ASSESSMENT

### 2.1 *Number of sensors based on sampling by attributes and variables*

The effectiveness of long term monitoring systems applied to engineering structures depends on their capability to capture the aging of the engineering structure. Sensors of MS in most cases are allocated according to (a) the mechanical, physical or chemical loading, (b) the geometrical characteristics, and (c) the reliability importance of the components of the structural system.

#### 2.1.1 *Monitoring by attributes*

In general, the number of components to be monitored is large. Statistical methods, until now hardly used for the layout of monitoring systems, can assist



in such cases. Such methods are known as acceptance criteria and provide the required number of sensors  $n$  on selected structural components out of all components, necessary for reliable statements with respect to the condition of physical quantities. This kind of monitoring allows the assessment of the entire lot of selected structural members  $N$  by indicating a bad performance for defined  $r$  violations out of  $n$  sensors. The definition of the acceptable  $r$  violations (Ang and Tang (2007), Frangopol et al. (2007)) for a given number of sensors  $n$  installed on selected structural members  $N$  and an accepted probability of  $f$  threshold violations can be based on the hyper-geometric distribution as follows (Ang and Tang (2007)):

$$P(f) = \sum_{x=0}^r \frac{\binom{N \cdot f}{x} \binom{N \cdot h}{n-x}}{\binom{N}{n}} \quad (1)$$

where  $h = 1 - f$ . This formulation is valid by assuming that the performance of each monitored component is recorded by only one sensor. The lot will be accepted, if there are  $r$  or less sensors indicating a threshold violation. The hyper-geometric distribution, as indicated in Eq. (1), serves for (a) finding the probability  $P(f)$  of accepting a lot of size  $N$  with an actual fraction of threshold violations  $f$  monitored by  $n$  sensors from which  $r$  indicate threshold violations, and (b) finding the necessary number of sensors  $n$  by limiting the probability of accepting an actual fraction  $f$  of threshold violations. The no threshold violation requirement,  $r = 0$  out of  $n$  sensor measurements, yields the probability of accepting a lot  $N$  with an actual fraction  $f$  of threshold violations as follows (Hald, 1952)

$$P(f) \approx \sum_{x=0}^{r=0} \frac{n!}{x!(n-x)!} \cdot f^x \cdot h^{n-x} \quad (2)$$

Therefore, for a given confidence level  $C = 1 - h^n$ , with  $h = 1 - f$ , the necessary number of sensors  $n$  can be computed as

$$n = \frac{\ln(1 - C)}{\ln(h)} \quad (3)$$

Figure 1 presents the necessary number of sensors  $n$ , monitoring a physical quantity from  $N$  structural components, for a defined fraction of accepted threshold violations with respect to a desired confidence level  $C$ .

Equation 3 and Fig. 1 provide the required number of sensors  $n$  associated with a desired confidence level  $C$  on the assumption that the considered monitored components, under comparable mechanical,

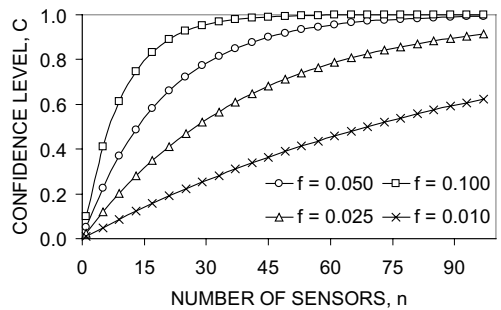


Figure 1. Confidence level vs. necessary number of sensors  $n$  for several fractions of accepted threshold-violations.

physical and chemical stressors, belong to the same population  $N$ .

This formulation (monitoring by attributes) does not take into account (a) the range of the considered population  $N$  nor (b) the quality of the single sensor measurements. The components or sensor measurements are classified simply as good or bad. Hence, a poor measurement obtained from one out of  $n$  sensors is associated with the violation of defined requirements according to an acceptable fraction  $f$  of bad elements and the desired confidence level  $C$ . A simply bad or good classification does not fully utilize the information that can be achieved from monitoring systems.

### 2.1.2 Monitoring by variables

An alternative method for the determination of the necessary number of sensors  $n$  and for the treatment of good and bad sensor readings provides the so called monitoring by variables approach (Ang and Tang 2007). It allows the assessment of monitored physical processes by mean monitored data  $\bar{X}$  with respect to a threshold  $\gamma$ . The threshold  $\gamma$  can be determined from defined good and bad processes (e.g.,  $N(\mu_G, \sigma_G)$  and  $N(\mu_B, \sigma_B)$ , respectively) and from acceptable probabilities  $\kappa$  and  $\lambda$ , where  $N$  indicates normal probability density function and  $\kappa$  indicates the probability that a good monitored physical quantity will be rejected and  $\lambda$  that a poor (bad) monitored physical quantity will be accepted, see Fig. 2, where PDF denotes probability density function. Equations 4 and 5 provide the analytical format for the computation of the threshold location  $\gamma$  and the associated necessary number of sensors  $n$ .

Equation 4 indicates the probability  $\kappa$  that a sensor measurement will indicate a bad condition for no violation of the threshold  $\gamma$  by the mean  $\bar{X}$  as follows:

$$P(\bar{X} > \gamma \mid \mu_G) = 1 - \Phi\left(\frac{\gamma - \mu_G}{\sigma/\sqrt{n}}\right) = \kappa \quad (4)$$

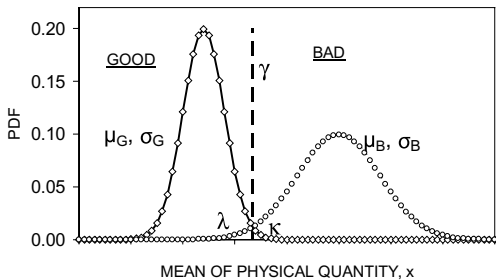


Figure 2. Threshold  $\gamma$  separating good (G) and bad processes (B) and associated acceptable probabilities  $\kappa$  and  $\lambda$ .

The probability  $\lambda$  that a sensor measurement will indicate a good condition for violation of the threshold  $\gamma$  by the mean  $\bar{X}$ , can be written as

$$P(\bar{X} < \gamma \mid \mu_B) = \Phi\left(\frac{\gamma - \mu_B}{\sigma/\sqrt{n}}\right) = \lambda \quad (5)$$

Hence, the determination of necessary number of sensors  $n$  for monitoring of mechanical, physical similar loaded elements of an engineering structure can be based, as shown in Fig. 2, on defined acceptable (“good”) PDF and not acceptable (“bad”) PDF. These PDFs can be generated from acceptable monitored extreme data processes obtained at sensor locations during structural loading and from destructive or non destructive testing of monitored details or materials. The previously discussed probabilities  $\kappa$  and  $\lambda$  serve for the definition of the required distance between the PDFs in Fig. 2.

In addition, the computed threshold  $\gamma$  allows a simplified assessment of the dispersion of the monitored data (e.g., obtained from a set of sensors). Fig. 2 shows for  $\bar{X} \leq \gamma$  a good and for  $\bar{X} \geq \gamma$  a bad situation, respectively. This approach assumes that the acceptable (“good”) and not acceptable (“bad”) PDFs, constant or variable in time, are known from experience or can be derived from prediction models.

## 2.2 Utilization

For example, consider similar mechanical notched tension cases of a steel structure with an associated normal distributed ultimate strength of  $N(145 \text{ MPa}, 21.8 \text{ MPa})$ . This strength is only allowed to be reached by existing normal stress processes by an acceptable probability (e.g., defined by  $\kappa$  and  $\lambda$ ). Figure 3 shows for an initial (i.e., time = 0) normal stress process, specified as a normal distribution  $N(79 \text{ MPa}, 7.9 \text{ MPa})$ , and acceptance probabilities  $\kappa$  and  $\lambda = 0.025$  according to Eqs. 4 and 5 a threshold  $\gamma = 96.6 \text{ MPa}$  and a necessary number of sensors  $n = 1$  (see Table 1). On the assumption that the dispersion of the normal

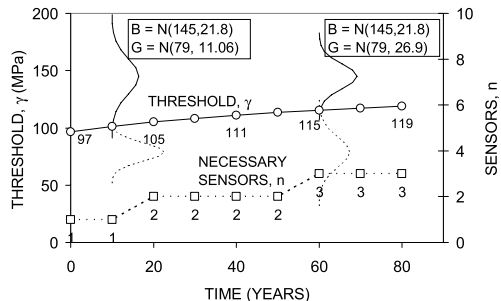


Figure 3. Threshold  $\gamma$  and necessary number of sensors  $n$  for a linear increase in the coefficient of variation with time (indicated by  $\Delta\text{COV}_{\text{good}} = 0.004/\text{year}$ , see Table 1).

Table 1. Threshold  $\gamma$  and necessary, number of sensors  $n$  and the reliability index  $\beta$  as function of the linear increasing uncertainties, indicated by  $\Delta\text{COV}_{\text{good}} = 0.004/\text{year}$ .

YEARS	$\gamma$	$n$	$\beta$	$\mu_G$	$\text{COV}_{\text{good}}$
0	96.6	1	2.85	79	0.10
10	101.3	1	2.70	79	0.14
20	105.1	2	2.54	79	0.18
30	108.3	2	2.37	79	0.22
40	111.1	2	2.21	79	0.26
50	113.4	2	2.05	79	0.30
60	115.5	3	1.91	79	0.34
70	117.3	3	1.78	79	0.38
80	118.9	3	1.66	79	0.42

stress processes will increase linearly, due to uncertainties, over the years (e.g., indicated by  $\Delta\text{COV}_{\text{good}} = 0.004/\text{year}$ , see Table 1) equations 4 and 5 are associated with a threshold  $\gamma = 119 \text{ MPa}$  and a necessary number of sensors  $n = 3$  at 80 years. The defined acceptable process characteristics are warranted in the case where the mean values of the monitored sensor data do not violate the threshold  $\gamma$ . Figure 3 also shows with increasing  $\text{COV}_{\text{good}}$  a reduction of the distance between the PDFs, which is also associated with an increase in the number of sensors  $n$  to guarantee the acceptable probabilities  $\kappa$  and  $\lambda = 0.025$ .

The reliability index (as a measure of the probability of satisfactory performance) is decreasing with an increase in  $\text{COV}_{\text{good}}$ . Fig. 4 shows a direct relation between the reliability index  $\beta$  (as a measure of the probability of no violation of the threshold  $\gamma$ ) and the required number of sensors  $n$ .

Therefore the determination of necessary number of sensors  $n$ , must be based on the minimum acceptable reliability index  $\beta$ . For the considered example of mechanical notched tension cases the reliability index  $\beta = 1.66$  is associated with  $n = 3$  sensors at 80 years. This monitoring by variables approach

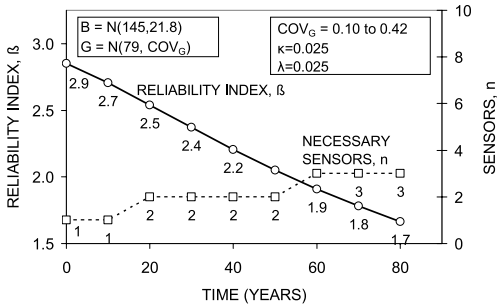


Figure 4. Reliability index  $\beta$  associated with the necessary number of sensors  $n$  vs. monitoring duration.

allows the incorporation of the randomness of monitored data and a reduction in the required number of sensors  $n$  by assuring the same assessment quality compared to monitoring by attributes. It has to be emphasized that these computations are based on the assumption that the standard deviation  $\sigma$  of the measurements is known in advance (e.g., from experience) and the measurements are Gaussian distributed. Equations (4) and (5) provide also the basis for the extension to non-Gaussian considerations.

### 3 PREDICTIONS BASED ON MONITORED EXTREME VALUES

In general, there are two types of monitoring: (a) short term monitoring activities focusing on detecting damaged zones of a structure, and (b) long-term monitoring providing the basis for predicting the performance of the structural degradation. The performance prediction of engineering structures associated with monitoring programs needs a suitable treatment of monitored data (e.g., extreme data).

#### 3.1 Extreme value distributions for monitoring-based predictions

Extreme values are associated with the largest and smallest values from a monitored sample of size  $n$  within a known population. Therefore, the largest and the smallest value are associated with a probability distribution. A monitored physical quantity recorded at defined locations of a structure can be considered as a random variable  $X$  (or population). The monitored sample of size  $n$  from this population will have a largest and a smallest value which are related to the probability density distribution (PDF)  $f_X(x)$  or cumulative probability distribution (CDF)  $F_X(x)$ . These extreme values will also have their respective distributions which are related to the distribution of the initial variable  $X$ , (Ang and Tang, 1984).

The monitored sample of size  $n$  can be considered as a set of observations  $(x_1, x_2, \dots, x_n)$  representing the first, second,  $\dots$ ,  $n$ th observed values. Nevertheless, the monitored values are unpredictable, they are a specific realization, whichever underlies a set of random variables  $(X_1, X_2, \dots, X_n)$ . Therefore, the interest is in the maximum and minimum of  $(X_1, X_2, \dots, X_n)$ , which can be expressed as follows (Ang and Tang, 1984)

$$Y^{\max} = \max(X_1, X_2, \dots, X_n) \quad (6)$$

and

$$Y^{\min} = \min(X_1, X_2, \dots, X_n) \quad (7)$$

Based on certain assumptions (Ang and Tang, 1984) it is possible to develop the exact probability distributions of  $Y^{\min}$  and  $Y^{\max}$ . These assumptions can be derived as follows (Ang and Tang, 1984). Consider a specified value  $y$ , in case of  $Y^{\max}$  lesser than  $y$ , all the sample associated random variables  $X_1, X_2, \dots, X_n$  must also be less, see Eq. (6). Assuming that  $X_1, X_2, \dots, X_n$  are statistically independent and identically distributed yields the CDF (Ang and Tang, 1984):

$$F_{Y^{\max}}(y) = [F_X(y)]^n \quad (8)$$

and the PDF

$$f_{Y^{\max}}(y) = n \cdot [F_X(y)]^{n-1} \cdot f_X(y) \quad (9)$$

where  $F_X(y)$  and  $f_X(y)$  are, respectively, the CDF and PDF of the initial variable  $X$ . The same consideration can be performed for the minimum  $Y^{\min}$  with the survival function, resulting in the CDF (Ang and Tang, 1984):

$$F_{Y^{\min}}(y) = 1 - [1 - F_X(y)]^n \quad (10)$$

and the corresponding PDF

$$f_{Y^{\min}}(y) = n \cdot [1 - F_X(y)]^{n-1} \cdot f_X(y) \quad (11)$$

Therefore, the exact distribution of the largest and smallest values from samples of size  $n$  is a function of the distribution of the initial variable. There is the possibility to capture the exact solutions with asymptotic distributions. The following statements are valid according to Ang and Tang (1984): (a) the extreme value from an initial distribution with an exponential decaying tail (in the direction of the extreme) will converge asymptotically to a *Type I*, (b) the distribution of an extreme value of an initial variate with a PDF that decays with the polynomial tail will converge to a *Type II* (Eq. 12), (c) if the extreme value is limited,

the corresponding extremal distribution will converge asymptotically to a *Type III* (Eq. 13),

$$\text{Type II: } F_{Y^{\max}}(y) = \exp \left[ - (v_n/y)^k \right]^n \quad (12)$$

$$\text{Type III: } F_{Y^{\min}}(y) = 1 - \exp \left[ - \left( \frac{y - \varepsilon}{w_1 - \varepsilon} \right)^k \right] \quad (13)$$

with  $y \geq \varepsilon$

where  $v_n$  = most probable value of  $Y^{\max}$ ,  $k$  = shape parameter, which is an inverse measure of the dispersion of values  $Y^{\max}$ ,  $w_1$  = most probable smallest value, and  $\varepsilon$  = lower bound value of  $y$  (Ang and Tang, 1984).

### 3.2 Application to the Wisconsin Bridge

The I-39 Northbound Bridge over the Wisconsin River in Wausau, Wisconsin was built in 1961. The total length of the bridge is 196.04 m. It is a five span continuous steel plate girder bridge. The monitoring of this bridge included the strain/stress behavior of specified structural components (Mahmoud et al, 2005). The solid line of Figure 5 shows the recorded extreme monitored data per day provided by one sensor, and the dashed line presents an artificial monitored degradation process.

The artificial process relies on the monitored data and is modified by  $\sigma_{\text{modified}} = \sigma_{\text{existing}} + a_1 \times t + a_2 \times t^2$ , where  $a_1 = 1/500$  and  $a_2 = 1/20$ , and  $t$  is time in days. The continuously, according to Eq. (12), computed  $F_Y^{\max}$  of the existing and modified monitored extreme data served as input for the reliability assessment. Parameters of Eq.12 are:  $n = t =$  time in days,  $v_n$  = mean value of the  $n$  monitored  $y$  extreme values, and  $k = [2 \times \ln(n)]^{1/2} / \zeta_X$ , where  $\zeta_X$  is the parameter of the lognormal distribution related to the dispersion of  $\ln X$ . Figure 6 presents the reliability

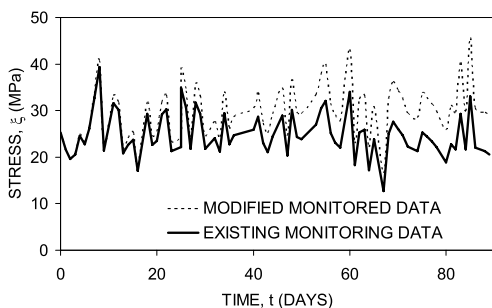


Figure 5. Recorded extreme monitored data per day provided by the sensor CH15.

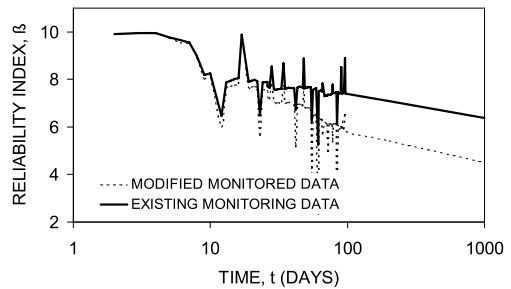


Figure 6. Computed reliability profiles based on the monitored and modified monitored data associated with the extreme value distributions of Eq. (12).

index  $\beta$  with respect to the yield strength  $f_y = \text{LN}$  (377 MPa, 30.16 MPa) of the used structural steel for both the existing (solid line) and the modified monitored extreme data (dashed line). As indicated in Fig. 6, the computed future trend of the extreme value based reliability index distribution can be used (a) to detect performance degradation detecting deviations during monitoring (e.g., 0 to 90 days), and (b) to predict the future values of the reliability index (e.g., from 90 days to the end of the lifetime).

## 4 CONCLUSIONS

The paper presents approaches for the incorporation of monitoring data in the performance assessment of existing structures. An effective incorporation needs (a) the optimum number of sensors, (b) the optimum location of sensors, and (c) the rational use of monitored data for the assessment, the detection and prediction of degradation processes. Extreme value considerations as proposed and applied to the I-39 Northbound Bridge over the Wisconsin River demonstrate their capabilities. Additional information can be found in Frangopol et al. (2007, 2008).

## ACKNOWLEDGMENTS

The support by grants from the Commonwealth of Pennsylvania, Department of Community and Economic Development, through the Pennsylvania Infrastructure Technology Alliance (PITA) is gratefully acknowledged. The support of the National Science Foundation through grants CMS-0638728 and CMS-0639428 to Lehigh University is also gratefully acknowledged. The opinions and conclusions presented in this paper are those of the authors and do not necessarily reflect the views of the sponsoring organization. The authors want to express their profound thanks to Professor Ben T. Yen and Mr. Ian Hodgson,

Lehigh University, for their constructive comments and suggestions and access to the data obtained during the long term monitoring of the Lehigh River Bridge SR-33.

## REFERENCES

- Ang, A.H.-S. and Tang, W.H. 1984. *Probabilistic Concepts in Engineering Planning and Design—Volume II: Decision, risk and reliability*. New York, NY: John Wiley & Sons.
- Ang, A.H.-S. and Tang, W.H. 2007. *Probability Concepts in Engineering Planning, 2nd Edition*. New York, NY: John Wiley & Sons.
- ASCE 2005. *Report card for America's Infrastructure, American Society of Civil Engineers*. Reston, VA.
- Frangopol, D.M. and Liu, M. 2007. Maintenance and Management of Civil Infrastructure based on Condition, Safety, Optimization, and Life-Cycle Cost. *Structure and Infrastructure Engineering* 3 (1): 29–41.
- Frangopol, D.M. and Messervey, T.B. 2007. Integrated life-cycle health monitoring, maintenance, management and cost of civil infrastructure. *International Symposium on Integrated Life-Cycle Design and Management of Infrastructures, Shanghai, China*.
- Frangopol, D.M., Strauss, A. and Kim, S. 2007. Sensor-based monitoring systems for performance assessment of engineering structures. Submitted for publication.
- Frangopol, D.M., Strauss, A. and Kim, S. 2008. Use of monitoring extreme data for the performance prediction of structures. Submitted for publication.
- Hald, A. 1952. *Statistical Theory with Engineering Applications*. New York, NY: John Wiley & Sons.
- Mahmoud, H.N, Connor, R.J. and Bowman, C.A. 2005. Results of the fatigue evaluation and field monitoring of the I-39 Northbound Bridge over the Wisconsin River. Bethlehem: Lehigh University.

# On the road of multi-performance profiles aided maintenance

A. Talon & D. Boissier

*Civil Engineering Laboratory, Polytech 'Clermont-Ferrand, Aubière, France*

J. Hans

*CSTB, Sustainable Development Department, Sustainable Buildings and Products Division, Saint Martin d'Hères, France*

**ABSTRACT:** The performance maintain of a building component in service (double glass unit, brick wall, concrete floor, etc.) is led by the knowledge and so the assessment of this performance at different moments of its life-cycle. We firstly propose a methodology that allows providing a multi-performance profile associated to a considered building component in service. Our second proposition is to aid the maintenance of building components on the basis of these multi-performance profiles. This paper presents: (1) the methodology to obtain the multi-performance profiles, (2) the application of this methodology to aid the maintenance of building components and, (3) an illustration of this methodology on the case study of a brick wall.

## 1 INTRODUCTION

The construction domain is increasingly involved in attaining objectives for ensuring sustainable development that allows for satisfying the needs of present and, in particular, future generations. The principles espoused by those focused on sustainable development necessarily influence on building design and on the need to maintain the functional performance of building over time (Lee & Barrett, 2004).

The maintenance optimization associated with diagnosis of experts is a common practice in some civil engineering domains such as roads, dams and railways. However, this approach is not so advanced in the building domain because, for few explanations, different structures, building components and materials exist, many persons are in charge of building maintenance and because, in almost of the cases, the economic impact of building degradations is badly known. This problem, at the building level, is quite the same at the building component one.

The performance of a building component is not only related to its mechanical stability but also to its thermal insulation, to its acoustic insulation, to its integrity as regards the contact of climatic and usage conditions (rain, micro-organisms, wind, ...), ... In consequence, one must judge essential to take into account the whole set of functions that ensure the performance of building components. This approach is on the opposite of the classical approach of the durability assessment of building components (Jernberg *et al.* 2004) and on the opposite of the Performance Limits

Method developed by Iacono (2005). Our approach that takes into account all the functions for the construction domain is quite similar to the approach proposed by Serre (2005) for the performance assessment of dykes.

In order to maintain building components as efficiency as possible, the knowledge of the degraded elements and their degradation modes (phenomena) is essential; indeed these phenomena lead to the decreasing of the performance of these building components. It is also of major interest to know the date and the occurrence probability of these phenomena. In consequence, we propose a methodology to qualitatively identify degradation phenomena, as well as chains of phenomena (i.e. degradation scenarios), and then to quantify the duration and the occurrence probability of these scenarios.

The data of duration and occurrence probability is multi-source (sightings, experimentations, instrumentations, simulations, statistics, expert opinions, probabilities) and multi-scale (geometrical scale, functional scale, phenomenological scale and temporal scale), so our approach is based on: (1) the assessment of the quality of this data, (2) the transformation of this data within a possibility format and, (3) the combination of this data by unification using data fusion and by aggregation in order to obtain an consensual data (that contains the maximum of consensus) and a indicator of the quality of this consensual data.

From an operational point of view, we develop this methodology to be applied to all building components in all in-service conditions.

## 2 METHODOLOGY OF ASSESSMENT OF MULTI-PERFORMANCE PROFILES

### 2.1 Overview of the methodology

In order to respond to the objectives defined in the introduction (multi-function approach, qualitative identification of degradation scenarios, quantification in terms of duration and occurrence probability of these scenarios with taking into account the entire set of multi-scale and multi-source information, applicability to all building components) a methodology is proposed that associates qualitative and quantitative methods, databases and representation tools. The methodology is compound of two main stages: (1) one qualitative phase for the identification of the scenario and (2) four quantitative phases for the assessment of the duration of these scenarios, for the assessment of the occurrence probability of these scenarios and for the assessment of the relation between degradation scenarios and functional performances. The relations between the phases of the methodology, the methods, the databases and the representation tools are schematized in the Figure 1 and are detailed in the following sections.

### 2.2 Phase of qualitative analysis

The phase of qualitative analysis consists in: (1) a functional analysis of the studied building component and, (2) a failure mode and effects analysis (FMEA).

The functional analysis aims to model the functioning of the building component in-service by: (1) decomposing the building components into elements, (2) identifying the functions ensured by each element and, (3) determining the behavior of each triplet {element, function, item of the climatic and usage conditions}.

On the basis of functional analysis results, the FMEA provides the entire set of possible degradation phenomena of the building component. Moreover causes of each phenomenon, consequences of the

phenomenon and {element, function} pairs associated to a phenomenon are determined. Based on the iterative principle that consequences of a phenomenon may generate causes of a subsequent phenomenon, chains of phenomena (i.e. degradation scenarios) are identified.

An application of this qualitative analysis on the case study of a solar panel is presented in Talon *et al.* (2004). Other researches and applications of FMEA are detailed in Talon *et al.* (2006a).

### 2.3 Phases of quantitative analysis

The quantitative analyses are threefold: (1) temporal analysis, (2) analysis of criticality and, (3) analysis of performance.

The first phase of the methodology provides a qualitative description of a set of degradation scenarios; the aim of the temporal quantitative analysis is to provide the duration and the occurrence probability of this set of degradation scenarios. The process of this analysis depends on the available data. When duration and probability of occurrence data are available for each scenario but are obtained from several origins, quality analysis of data, transformation of data and unification of data are led. On the contrary, when duration and probability of occurrence data are available only for each phenomenon and are obtained from several origins, quality analysis of data, transformation of data, unification of data for each phenomenon and aggregation of data from phenomenon level to scenario level are led. This temporal quantitative analysis is further detailed in Talon *et al.* (2006b).

The goal of the quantitative analysis of criticality is to select the scenarios that have a high impact on the performance of the building component and so, to reduce the number of scenarios to consider for the continuation of the methodology process. This methodology phase is based on the classification into three classes (major, significant and minor) of scenarios using three criteria: (1) scenario duration, (2) occurrence probability of scenario and (3) gravity of the scenario consequence on functioning of the building component. The major scenarios only are selected for the continuation of the methodology process.

The objective of the quantitative analysis of performance is to provide a multi-performance profile at different dates of the service life of the building component. A multi-performance profile is a model of the performance levels of the primary functions and combinations of functions that the building component has to ensure. These multi-performance profiles are obtained by determining the relations between degradation states of the major scenarios and the function levels. These relations are established for each {phenomenon  $Ph_i$  of major scenario; function  $F_j$  of building component} pair and the result is a function

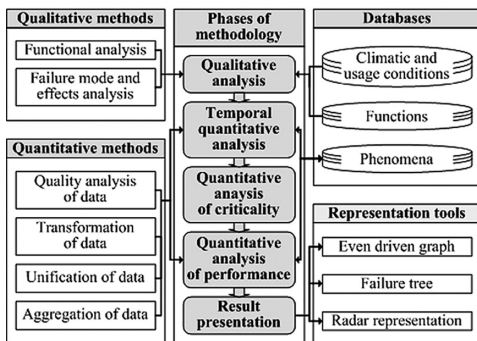


Figure 1. Relations between methodology, methods, databases and representation tools.

level  $\mu (Ph_i, F_j)$ . The relation “degradation state  $DS_i$  of a phenomenon  $Ph_i$ —date  $t$ ” is deduced from the temporal quantitative analysis. Consequently, at a date  $t$ , a function level  $\mu (F_j)$  of a function  $F_j$  is provided by:

$$\mu (F_j) = \min(\mu(Ph_i, F_j)) \quad (1)$$

where the considered set of  $\{Ph_i\}$  is the phenomena of major scenarios that are started and not finished at the date  $t$ .

## 2.4 Methods of quantification

Four methods of quantification are developed: (1) method of quality analysis of data, (2) method of transformation in a possibility format of data, (3) method of unification of data by data fusion and, (4) method of data aggregation.

For the assessment of duration, occurrence probability or performance of building components, several sources of information are available: (1) sightings, (2) experimentations, (3) instrumentations, (4) simulations, (5) statistics, (6) expert opinions and, (7) probabilities. These sources of information don't have the same reliability but our approach consists in taking into account all the available set of information; consequently, a method is proposed to assess the confidence one can attribute to each type of source. The result of this assessment is a belief mass associated to each collected data for a given problem. To make homogeneous the assessment, a quality grid, based on the work of Funtowicz & Ravetz (1990), is provided. This grid is compound of eight criteria (data modeling, hypothesis of modeling, obtaining mode, source, censorship, coherence of the modeling of data, correspondence between data and given objective, Shannon's entropy) assessed on a scale with four levels (1, 2/3, 1/3 and 0). The belief mass associated to a collected data is so equal to the average of the note attributed to each criterion. This method of data quality analysis is further detailed in Talon *et al.* (2007a, c).

The treatment models of data requires to use a common format of data and as the main available format of data (probabilities, expert opinions, statistics, . . . ) can be transformed in a possibility format, as proposed in Boissier & Talon (2007), we propose to transform all available data in a possibility format; this possibility format is detailed in Bouchon-Menier (1995).

The method of data unification is applied when several data relevant to a same problem but providing from different sources is available. As a example, when the duration of a phenomenon is given by an experimentation, a sighting and an expert opinion, the data unification will provide a consensual data of the duration of this phenomenon with using these three sources of information. The method of unification of data is based on the fusion of data developed by Shafer (1976) and detailed in Talon *et al.* (2007b).

The data aggregation is applied when several data relevant to different sub-problems of a given problem is available. As an example, let  $Sc_k$  be a scenario compound of 5 phenomena  $Ph_i$ , and  $t_k, t_i$  the durations of respectively the scenario and the phenomena, the method of data aggregation provides:

$$t_k = \sum_{i=1}^5 t_i \quad (2)$$

In spite of the fact that the principle of aggregation is the same for all type of data (duration, occurrence probability and performance), each assessment presents specificity as detailed in Talon (2006).

## 2.5 Databases

Three databases have been developed for aiding the methodology process: (1) a climatic and usage conditions database that regroups the environmental items that can damage building components in-service, (2) a function database that contains the generic function ensured by all the building components, (3) a phenomena database that compounds qualitative (cause, consequence, . . . ) and quantitative (duration, occurrence probability, performance, . . . ) information on phenomena of materials, elements and building components.

At the moment, the two first databases are completed (93 items for the first one and 97 items for the second one) and the third one is implemented with case studies. Five case studies (solar panel, reinforced concrete wall, brick wall, double glass unit, concrete facade) have been used to complete the phenomena database (120 generic phenomena are completed with qualitative information and duration data).

## 2.6 Representation tools

Three representation tools have been developed or adapted for this construction domain application: (1) the even driven graph that allows representing phenomena of major scenarios on a temporal axis as well as the causes, the elements and the functions damaged by these phenomena, (2) the failure tree that allows schematizing the combination between phenomena and (3) the radar representation that allows presenting the levels of the functions and combination of functions of the considered building component, i.e. its multi-performance profile.

The complete methodology and applications on case studies are developed in Talon (2006).

## 3 APPLICATION TO THE MAINTENANCE OF BUILDING COMPONENTS

The proposed methodology offers qualitative and quantitative information in order to aid the maintenance of building components; it is detailed in the following



sections 3.1 and 3.2. However, researches have to be proceeded, as presented in section 3.3, in order to improve the efficiency of this methodology to aid the planning of conditional and corrective maintenance.

### 3.1 Qualitative information for maintenance

The result of the proposed methodology is the obtaining of the multi-performance profiles of a building component at different dates of its service-life in relation with the even-driven graph (i.e. major scenarios represented on a temporal axis). Consequently, each functional decreasing can be associated to one or several scenarios and elements of the building components. This relation is illustrated on the Figure 2.

The even-driven graph on Figure 2 represents three scenarios compound of ten phenomena that affect five functions and three elements. The dates  $t_1$  to  $t_{12}$  (except  $t_4$  and  $t_9$ ) represent the moment when the successive phenomenon can start, for example the phenomenon  $Ph_2$  starts at the date  $t_1$ . At the date  $t_4$ , the multi-performance profile is the result of: (1)  $F_1$  is affected by  $Ph_1$  and  $Ph_2$ , (2)  $F_2$  is affected by  $Ph_8$  and  $Ph_9$ , (3)  $F_3$  is affected by  $Ph_7$ , (4)  $F_4$  is affected by  $Ph_6$  and, (5)  $F_5$  is not affected so its functional level is equal to 1 (if considering that no degradation occurs before the starting of time). At the date  $t_9$ , the changing of the previous multi-performance is due to: (1) the evolution of previously starting phenomena for functions  $F_1$  to  $F_4$ , (2) the start of  $Ph_3$  for  $F_2$ , (3) the start of  $Ph_4$  for  $F_3$  and, (4) the start of  $Ph_{10}$  for  $F_5$ .

As an example, if considering that the performance level of function  $F_5$  must never be decreasing, then the remedy may be to modify the element 2 or to protect this element from the occurrence of the causes of phenomenon  $Ph_{10}$ .

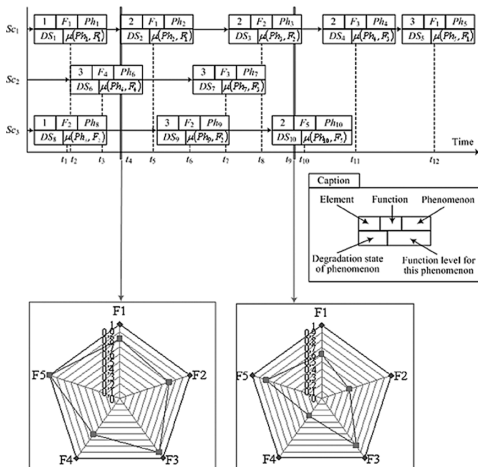


Figure 2. Illustration of the relation between even-driven graph and multi-performance profile.

Considering this qualitative information, one can efficiently choose the element to be repaired or to be added in order to protect the building component against the climatic and usage conditions that generated the considered scenario. However, knowing how to repair is essential but knowing when to repair is the most important.

### 3.2 Quantitative information for maintenance

The quantitative information, as result of the methodology, for helping the maintenance is (1) the multi-performance profile at different dates of the building components service life and, (2) an indicator of the kinetics of these multi-performance profiles over their service life.

The approach is to calculate, using the proposed methodology, the multi-performance profiles at different dates (for example, 0 year, 5 years, 10 years, ...). By considering these profiles and the thresholds (defined by the user) that functions must not overrun, the maintenance dates are highlighted. The principle of this approach is illustrated in Figure 3, red lines represent the thresholds and blue lines represent the performance levels of functions.

The proposed indicator  $Ic\mu^j$  of the kinetics of the multi-performance profiles is provided by:

$$Ic\mu^j = \frac{|\mu^j(t_i + \Delta t) - \mu^j(t_i)|}{|\Delta t|} \quad (3)$$

where  $\mu^j(t_i)$  corresponds to the performance level of a function  $F_j$  at a date  $t_i$  and  $\Delta t$  is a step of time.

$Ic\mu^j$  allows defining if, for different successive and identical steps of time, the evolution of a performance level of one function is accelerating or not. The same analysis can be made for several functions and a same step of time.

### 3.3 Perspectives

The two primary perspectives of this research as regards maintenance aspect are: (1) to determine the evolution curve of degradation phenomena after maintenance actions and, (2) to associate this prevision tool to a multi-criteria decision tool of the best strategy of maintenance actions.

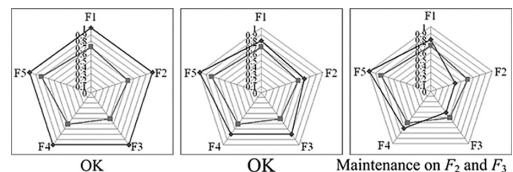


Figure 3. Illustration of the determination of maintenance dates using multi-performance profiles.

Currently, the proposed methodology provides an assessment of the performance levels of the functions of building component when no maintenance actions occurs. Consequently, only preventive maintenance can be done with this approach. An interesting issue for this research will be to know the evolution of multi-performance profiles when maintenance action are made; that could be possible if evolution curve of degradation phenomena are built and injected in the temporal quantitative analysis of our methodology.

The multi-criteria decision tool will help: (1) to assess the consequences of each solution of maintenance actions, in terms of maintenance efficiency, maintenance reliability, maintenance cost, etc. and, (2) to aggregate these results to obtain the best solution of maintenance action.

#### 4 ILLUSTRATION ON THE CASE STUDY OF A BRICK WALL

This paragraph aims to apply the proposed methodology to the maintenance of building components on the case study of a brick wall. The elements that compound this wall are described in Figure 4.

This brick wall ensures five functions: (1)  $F_1$ —to stop the flow of climatic and usage conditions, (2)  $F_2$ —to absorb the infrared radiation, the temperatures and the noises, (3)  $F_3$ —to mechanically resist, (4)  $F_4$ —non to be damaged by the contact of climatic and usage conditions, (5)  $F_5$ —to be in accordance with the standards and requirements.

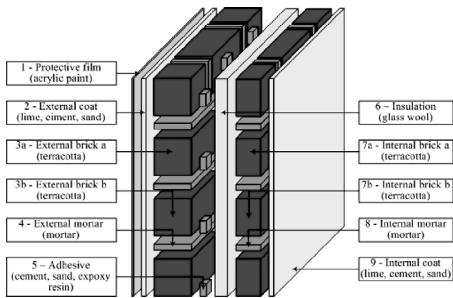


Figure 4. Description of the elements of the brick wall.

Table 1. Description of the major scenarios of the brick wall and their characteristics.

Scenario	Cause	Duration (years)	Function	Element
$Sc_1$ —Uniform leaching	Rain	[4; 14]	$F_3, F_4, F_5$	1
$Sc_2$ —Erosion and chalking	Wind, dust	[4; 14]	$F_3, F_4, F_5$	1
$Sc_3$ —Settling of insulation	Water infiltration	[21; 59]	$F_2, F_3, F_4, F_5$	1, 2, 3, 5, 6
$Sc_4$ —Immediate breakdown of wall	Setting to work error	[0; 10]	$F_1$ to $F_5$	3, 4, 7, 8
$Sc_5$ —Breakdown of wall	Water infiltration + shock	[43; 99]	$F_1$ to $F_5$	1, 2, 3, 4, 7, 8

The main result of the qualitative analysis and of the temporal quantitative analysis are summarized in Table 1. Authors notify that Table 1 results are only illustrative.

The multi-performance profiles obtained for the brick wall at the dates 0, 10, 20, 30, 40, 50 and 60 years with or without considering the scenario  $Sc_4$  (as this scenario is generated by really pessimistic causes that have low probabilities) are respectively presented in Figure 5 and in Figure 6. The indicators of the kinetics of the brick wall performance, for 10, 20, 30, 40, 50 and 60 years without considering the scenario  $Sc_4$ , are regrouped in Table 2.

On the basis of these results, the qualitative and quantitative information for the maintenance of the brick wall are the followings:

- Decreasing of the respect of requirement function ( $F_5$ ) from 0 to 10 years is due to the scenario of uniform leaching ( $Sc_1$ ) and the scenario of erosion and chalking ( $Sc_2$ ). These scenarios have influence on the esthetical aspect of the wall that can be remedied by a renovating when the facade aspect is no more acceptable;
- Decreasing of the mechanical resistance function ( $F_3$ ) is due to the water infiltration through the

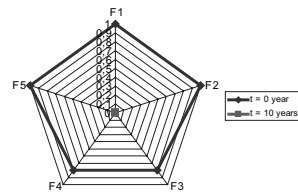


Figure 5. Multi-performance profiles of the brick wall with considering the scenario  $Sc_4$ .

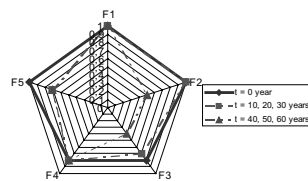


Figure 6. Multi-performance profiles of the brick wall without considering the scenario  $Sc_4$ .

Table 2. Indicators of kinetics of the brick wall performance without considering  $Sc_4$ .

Function	$Ic\mu^j$ (10)	$Ic\mu^j$ (20, 30)	$Ic\mu^j$ (40)	$Ic\mu^j$ (50, 60)
$F_1$	0	0	0	0
$F_2$	0	0	0.05	0
$F_3$	0.01	0	0.03	0
$F_4$	0	0	0	0
$F_5$	0.03	0	0	0

protective film (beginning of the scenario  $Sc_3$ ); consequently one should control regularly the porosity of the protective film in order to stop or to slow down this scenario;

- Decreasing of the absorb function ( $F_2$ ) and of the mechanical resistance function ( $F_3$ ) from 30 to 40 years is due to the settling of insulation ( $Sc_3$ ) that pushes the down of the wall. A preventive remedy for this degradation scenario is to control the porosity of the protective film before 10 years and to ensure a good gluing of the insulation on the external bricks during the construction. A corrective remedy to this scenario is to reinforce the button of the wall and to fix an other insulation on the internal bricks (i.e. build an other insulation on the internal side of the wall);
- Breakdown of the wall ( $Sc_5$ ) from 43 to 99 years should be avoid by applying the previously cited remedies and as far as possible protecting the wall against hard shocks.

## 5 CONCLUSIONS

A methodology to assess the multi-performance profiles of a building component at different instant of its service life is proposed. The main advantage of this methodology is: (1) to take into account all the functions ensured by the considered building component, (2) to provide a functional performance assessment related to the degradation scenarios and, (3) to use and assess the quality of all available source of data for the assessment of duration of scenarios, occurrence probability of scenarios and performance of building components.

This methodology provides precious qualitative and quantitative information for helping the maintenance of building components: (1) the qualitative information is used to identify the elements, the scenarios, the phenomena and their causes, that cause the decrease of the performance of building component and (2) the quantitative information allows to know the dates of the multi-performance profiles and the evolution tendencies of multi-performance profiles in time.

Finally, further researches have to be proceeded in order to improve the helping for conditional and corrective maintenance.

## REFERENCES

- Boissier, D. & Talon, A. 2007. Etat de l'art des méthodes de prise en compte de l'incertain pour l'analyse de risque. *Projet National ISI (Ingénierie Sécurité Incendie)*.
- Bouchon-Meunier, B. 1995. *La logique floue et ses applications*. Amsterdam: Addison-Wesley.
- Funtowicz, S.O. & Ravetz, J.R. 1990. *Uncertainty and Quality in Science for Policy*. Dordrecht: Kluwer Academic Publishers.
- Iacono P. 2005. Propositione di un percorso metodologico applicabile alla valutazione della durabilità di elementi tecnici edilizi e degli elementi funzionali costituenti. *Thesis (PhD) of Polytechnic of Milan*.
- Jernberg, P., Lacasse, M.A., Haagenrud, S.E. & Sjöström, C. 2004. Guide and Bibliography to Service Life and Durability Research for Building Materials and Components. *CIB Report*, Publication no. 295.
- Lee, A. & Barrett, P. 2003. Performance based building: First International State-of-the Art Report [online]. Available from: <http://www.pebbu.nl> [cited 21 February 2005].
- Serre D. 2005. Evaluation de la performance des digues de protection contre les inondations—Modélisation de critères de décision dans un Système d'Information Géographique. *Thesis (PhD) of Marne-La-Vallée University*.
- Shafer, G. 1976. *A mathematical Theory of evidence*. Chichester: Princeton University Press.
- Talon, A., Boissier, D. & Hans, J. 2007a. Durée de vie des produits de construction—Evaluation de la qualité des données. *Annales du Bâtiment et des Travaux Publics* (5): 66–70.
- Talon, A., Boissier, D. & Lair, J. 2007b. Service life assessment of building components: Application of evidence theory. *Canadian Journal of Civil Engineering*. Accepted for publication.
- Talon, A. & Boissier, D. 2007c. Risk faced decision: optimization of decision shedule. In M. Stewart (ed.), *Third International Forum on Engineering Decision Making; Proc. intern. symp., Port Stephens, 12–15 December 2007*.
- Talon, A. 2006. Evaluation des scénarii de dégradation des produits de construction. *Thesis (PhD) of Clermont-Ferrand University*. CSTB and LGC.
- Talon, A., Chevalier, J-L. & Hans, J. 2006a. Failure Modes Effects and Criticality Analysis Research for and Application to the Building Domain. *CIB Report*, Publication no. 310.
- Talon, A., Boissier, D., Hans, J., & Capra, B. 2006b. A Multi-Scale Approach for Service Life Evaluation. In A. Sarja (ed.), *European Symposium on Service Life and Serviceability of Concrete Structures; Proc. intern. symp., Helsinki, 12–14 June 2006*.
- Talon, A., Boissier, D., Chevalier, J-L. & Hans, J. 2004. A methodological and graphical decision tool for evaluating building component failure. In H. Elmahdy (ed.), *CIB World Building Congress 2004; Proc. intern. symp., Toronto, 2–7 May 2004*. Ottawa: National Research Council of Canada.

# Development of a work carriage for tunnel maintenance

H. Terato, K. Yokozawa & N. Takemoto

*Japan Construction Method and Machinery Research Institute, Shizuoka, Japan*

Y. Miura

*Sanshin Corporation, Tokyo, Japan*

Y. Inagawa

*Gifu Kogyo Company, Limited, Gifu, Japan*

**ABSTRACT:** This paper describes the concept of a carriage intended for use in inspection and repairs of road tunnels. In the present situation, inspection and repairs of the two-lane tunnels in service are often conducted in such a way that traffic along one lane is banned while the other remains in use. In that case, the work on the crown sections that stretch over between the two lanes must be restricted, resulting in time-consuming undertaking as a whole. The carriage aims at facilitating such tasks for the crown sections of two-lane road tunnels where the jobs have met with difficulty.

## 1 INTRODUCTION

In recent years, the concept of social assets has changed to the point where we should make an effective use of them instead of building them. An increasing importance is now placed on maintenance of such assets since their “effective use” is seriously called for. This holds also true to tunnels that reportedly extend to 20,000 km altogether in Japan (Japan Society of Civil Engineering 2005). Therefore, it seems urgent to come up with plans for rational way of tunnel maintenance.

Application fields where what we call tunnels are used are multifarious—roads, railway, aqueducts, gas and electricity supply, communications, etc. Therefore, careful attention should be paid to a difference in them. An upgraded approach to their maintenance is based on the two factors: software and hardware. Applicable combination of these factors is considered to be essential.

Against the background stated above, the authors are working on the development of a work carriage for highway tunnel maintenance (hereinafter referred to as the work carriage) as one of the models of hardware-related approach. This paper delineates main specifications of the work carriage and such in addition to the estimates on effects gained from the carriage to be operational in tunnel repairs.

## 2 TECHNOLOGICAL PROBLEMS

The authors take up tunnels containing a highway with more than two traffic lanes. When maintenance is to

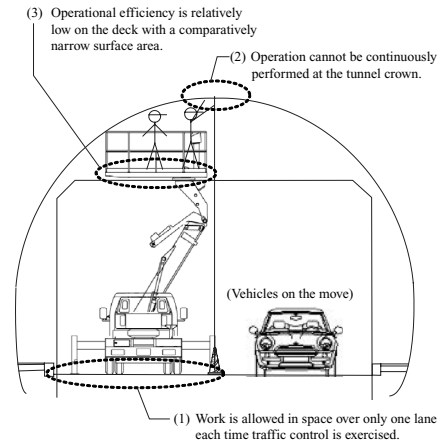


Figure 1. Problems with the current maintenance (in the case of two-lane highway tunnel in service).

be carried out in such tunnels where traffic is partially restricted, the following problems are believed to be posed:

1. Since there must be limited use of traffic lanes, the work space is allowable only over either lane. (Refer to (1) in Fig. 1).
2. At the tunnel crown over the boundary between the lane where the work is done and the lane where traffic is allowed, any work overreaching the latter lane must be restricted. Therefore, fiber sheeting and other materials must be discontinuously applied there. (Refer to (2) in Fig. 1).

3. The deck where the operator does his job usually has a surface area of 2 to 3 square meters. In such a relatively narrow space, operational efficiency is relatively low. (Refer to (3) in Fig. 1).

The authors have tried to find solutions to the foregoing problems in the course of the development of the work carriage.

### 3 CHARACTERISTICS OF THE WORK CARRIAGE

#### 3.1 Main components

Fig. 2 outlines the construction of the work carriage and its main components. The carriage consists mainly of the following components:

1. Carriage body frame that can move over one of the two lanes in the tunnel. (Refer to (1) in Fig. 2).
2. Scaffold that is mounted on the carriage body frame by means of a lifting mechanism. (Refer to (2) in Fig. 2).
3. Extender that lets the scaffold mentioned in 2) above hang over the other lane. (Refer to (3) in Fig. 2).
4. Foot that prevents the scaffold from falling over during maintenance. (Refer to (4) in Fig. 2).

#### 3.2 Status of execution

The status of execution with the work carriage is shown in Fig. 3. As is clear in the front view (2) in the figure, the scaffold can be stretched over the other lane of a two-lane highway in the tunnel with the work carriage staying in one lane. In this state, job can be done at the tunnel crown without interference by running vehicles.

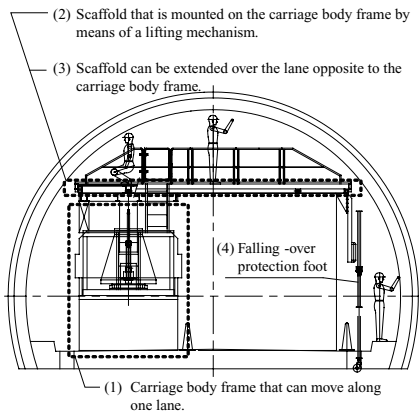


Figure 2. Construction and main components of the work carriage.

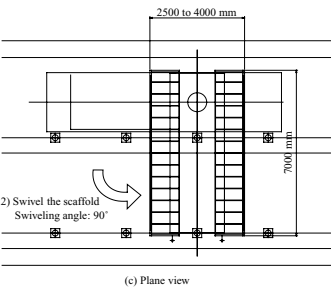
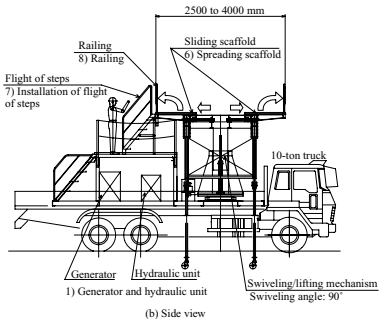
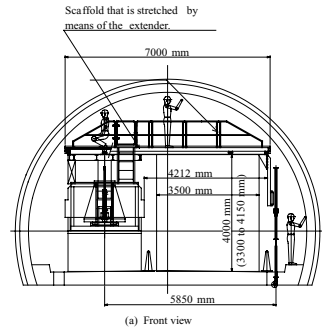


Figure 3. Status of execution (numbers in the figure correspond to the steps of setup. See Fig. 4 for other steps).

Moreover, scope of the job includes the space over both lanes at one time. The carriage can travel during job with its scaffold stretched.

As is shown at (b) in Fig. 3, the scaffold edge can be extended up to 2.5 to 4 m in a longitudinal direction of the tunnel by means of a scaffold extension mechanism shown at (a) in Fig. 3. Operable space can thus be expanded.

It is only the scaffold lifting mechanism in the carriage body frame that supports the load of the working personnel on the scaffold. In the interest of safety, the foot against scaffold falling over is installed at the far end of the frame shown in Fig. 2. The foot is positioned at the shoulder of the right-hand lane in Fig. 2.

As illustrated at (a) in Fig. 3, job may also be done on the sidewalk concurrently with that on the scaffold.

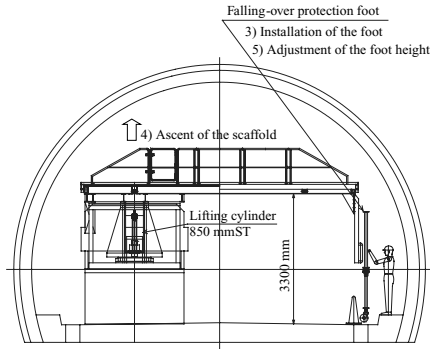


Figure 4. Installation of the falling-over protection foot (Numbers in the figure correspond to the steps of setup. See Fig. 3 for other numbers).

### 3.3 Scaffold swiveling during operational setup and upon its completion

The scaffold swivels when it is extended during operational setup or when it is withdrawn upon completion of execution. The scaffold extension procedure is described below using Figs. 3 and 4. The scaffold is withdrawn at the end of job in the reverse order of its extension.

1. Start up the generator and the hydraulic unit (see (b) in Fig. 3).
2. Swivel the scaffold installed on the carriage body frame 90 degrees so that it overhangs the lane opposite that where the carriage stays as shown at (c) in Fig. 3.
3. Attach the falling-over protection foot to the overhanging scaffold as shown in Fig. 4.
4. Raise the scaffold.
5. Adjust the height of the foot.
6. Slide the scaffold to increase its surface area in a longitudinal direction of the tunnel. (See Fig. 3(b)).
7. Install a flight of steps to the scaffold shown at (b) in Fig. 3.
8. Install a railing to the scaffold shown at (b) in Fig. 3. Since this railing is collapsible, it is stowed away on the scaffold when job is finished.

All the procedural steps described above can be followed inside or outside the tunnel depending on the specific conditions. When the operation must be performed over all the traffic lanes in the tunnel, operational setup or component withdrawal may be made outside the tunnel or in the area where traffic is unaffected. When partial repairs are to be made in a comparatively long tunnel, the carriage may approach the job site with the scaffold withdrawn and, upon reaching it, start preparatory and stowing operations.

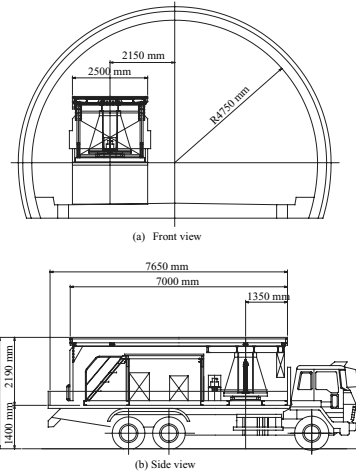


Figure 5. Status of traveling carriage.

Operational setup and component withdrawal are assumed to require about 3 minutes and about 2 minutes, respectively, depending on the carriage specifications given later in this paper.

### 3.4 Status of traveling carriage

The scaffold shown in Fig. 3 should be withdrawn before the carriage travels toward the job site or upon completion of the job. Fig. 5 illustrates the carriage in such a status. The scaffold itself can be accommodated on the load platform of a commercially available 10-ton truck.

## 4 WORK CARRIAGE SPECIFICATIONS

### 4.1 Main specifications

Table 1 lists the main specifications for the work carriage. The scaffold is light in weight since its material is aluminum. There are several different types of the feet available for protection of the scaffold against falling over (see Fig. 4a). The contractor is allowed to single out the foot that best suits the inner breadth of the tunnel where the work is to be done.

### 4.2 Safety measures

The work carriage is supplied with several safety devices since it is put to operation along the highway in service. Such devices are detailed below.

#### (1) Revolving light with a horn

The location where the revolving light with a horn is installed is indicated by (1) in Fig. 6. Traveling vehicles are warned off the job site when the lights are

Table 1. Work carriage specifications.

Parameter	Description	
Carrying vehicle	10-ton truck	
Carriage dimensions	Height	2190 mm
	Length	7000 mm
	Width	2500 mm
Scaffold dimensions	Height	7000 mm
	Length	2500 to 4000 mm
Carriage weight	9800 kg	
Maximum loading capacity	400 kg (150 kg/m <sup>2</sup> )	
Swiveling unit	Drive source	Hydraulic cylinder
	Stroke	90°
	Maximum operating speed	1.5 rpm (10 sec/90°)
Lifting unit	Drive source	Hydraulic cylinder
	Stroke	850 mm ST
	Maximum operating speed	Ascent: 18 sec/850 mm ST Descent: 9 sec/850 mm ST
Sliding scaffold	Drive source	Hydraulic cylinder (4 in total)
	Stroke	750 mm ST
	Maximum operating speed	Extension: 10 sec/750 mm ST Withdrawal: 7 sec/750 mm ST
Hydraulic unit	200 VAC, 60 Hz, 7.5 kW	
	Pump discharge	23.1 l/min
	Pump discharge pressure	14 MPa
Generator	25 kVA	
Safety device	Obstruction sensor	
	Laser marker for center line check	
	Revolving light with a horn	
	Warning siren	

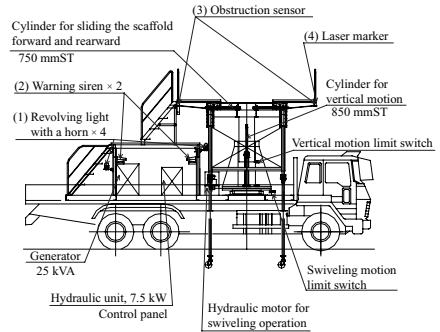


Figure 6. Locations of safety devices.

or any other object. As a means against such a contact, the obstruction sensor is furnished on the scaffold. An alarm buzzer sounds when the sensor has found any obstruction ahead so as to alert the operator to the possibility of collision.

(4) *Laser marker*

The location where the laser marker is installed is shown by (4) in Fig. 6. This marker is designed to make sure that the truck that is running with its scaffold overhanging is taking its right course. An erratic travel of the carriage can thus be avoided.

The idea is that the laser marker at the front of the scaffold projects a light to the center line of the highway so that the driver in the cabin may easily recognize an irradiated position on the highway. The driver is thus capable of keeping the truck right on the track.

(5) *Manual scaffold swiveling clutch and lowering lever*

In the event that the scaffold cannot be swiveled or lowered hydraulically, the hand-operated clutch and lever serves the purpose intended.

5 ADVANTAGES AND DISADVANTAGES OF THE WORK CARRIAGE

The work carriage is reasonably expected to excel the existing system of its kind as described below.

1. Continuous job can be done beyond one lane at the tunnel crown.
2. Job required can be done for two lanes at a time with traffic along either lane prohibited, meaning that the traffic-regulated lane need not be changed during execution.

The proposed work carriage, however, is disadvantageous as follows:

3. The main scope of work is limited to the area around the tunnel crown.
4. Since the scaffold needs to be situated with sufficient clearance from traveling vehicles as shown in Fig. 3(a), work space may not be secured sufficiently in some tunnels.

flashing. A total of 4 lights are installed, two at the rear of the carriage and two near its center.

The revolving light has chimes that ring each time its drive components (the hydraulic cylinder and the motor) start operation so as to attract the operator's attention.

(2) *Warning siren*

Fig. 6(2) indicates the locations where the warning sirens are installed. The personnel are urged to evacuate when they sound in an emergency. Pressing the button on the control panel triggers them.

(3) *Obstruction sensor*

The location where the obstruction sensor is installed is shown by (3) in Fig. 6. When the work carriage is moving in the tunnel, its overhanging scaffold must not come into contact with the tunnel wall

Table 2. Estimated requirements for the work with continuous fiber reinforced sheets (case 1).

		Existing system	Work carriage	Remarks
Conditions		– Area covered by continuous fiber reinforced sheets: 2,000 m <sup>2</sup> – Night shift (Workhours: 20:00 to 5:00)		
Working group		Two groups	One group	– A special driver as the owner of a driver's license for large vehicles, including the work carriage for tunnel maintenance, must be employed.
		– Manager: 1	– Manager: 1	
		– Special workers: 4	– Special workers: 4	
		– Ordinary workers: 2	– Common workers: 2 – Special driver: 1	
Work efficiency	Surface preparation for undercoat: 22 m <sup>2</sup> /day	23 days	19 days	– Operational efficiency is assumed to be 1.2 times higher than that of the existing system since the work carriage's deck has a comparatively large surface area.
	Primer coating: 50 m <sup>2</sup> /day	10 days	9 days	
	Touch-up of uncoated area: 22 m <sup>2</sup> /day	23 days	19 days	
	Sheeting application: 18 m <sup>2</sup> /day	28 days	24 days	
	Total	84 days	71 days	
Cost-effectiveness (with effect from the previous system = 1)		1	1.05	– Comparison is made in terms of direct work cost.

Table 3. Estimated requirements for the work with continuous fiber reinforced sheets (Case 2).

		Existing system	Work carriage	Remarks
Conditions		– Area covered by continuous fiber reinforced sheets: 2,000 m <sup>2</sup> – Night shift (Workhours: 20:00 to 5:00)		
Working group		Two groups	One group	– A special driver as the owner of a driver's license for large vehicles, including the work carriage for tunnel maintenance, must be employed.
		– Manager: 1	– Manager: 1	
		– Special workers: 4	– Special workers: 4	
		– Ordinary workers: 2	– Common workers: 2 – Special driver: 1	
Work efficiency	Surface preparation for undercoat: 22 m <sup>2</sup> /day	91 days	76 days	– Operational efficiency is assumed to be 1.2 times higher than that of the existing system since the work carriage's deck has a comparatively large surface area.
	Primer coating: 50 m <sup>2</sup> /day	40 days	34 days	
	Touch-up of uncoated area: 22 m <sup>2</sup> /day	91 days	76 days	
	Sheeting application: 18 m <sup>2</sup> /day	112 days	93 days	
	Total	334 days	279 days	
Cost-effectiveness (with effect from the previous system = 1)		1	0.96	– Comparison is made in terms of direct work cost.

Since manufacture of the carriage under discussion has not yet started, the detail of its operational capability remains unavailable. Its possibly obtainable advantages are discussed below, however, in consideration of such desirability that the traffic line need not be changed as mentioned in subsection 2) above.

In the discussion, the following two cases where continuous fiber reinforced sheets are applied are taken up and compared with each other in terms of cost-effectiveness and workdays.

Case 1: An area of 500 m<sup>2</sup> is covered.

Case 2: An area of 2,000 m<sup>2</sup> is covered.



Workers who are engaged in application of the sheets are supposed to do their job on night shift (workhours: 20:00 to 5:00). Since the new work carriage has a wider deck, an increase in operational efficiency is reasonably expected. To be more specific, the increased efficiency is considered to result from the following:

- Since the area that is worked at a time is relatively large, the frequency of the carriage's movement is lessened.
- During application, the number of times the sheeting strips must be joined together can be decreased.
- Teamwork among the workers could be improved.

At present, the fact that the carriage is not yet manufactured makes it rather difficult to quantitatively determine the operational efficiency. The authors, therefore, directly contacted the workers, who apply fiber reinforced sheets, for surveying purposes. As a result, it could be surmised that the efficiency could probably increase 1.2 times that gained from the existing system by reason of a more spacious deck of the carriage.

Tables 2 and 3 list the estimates made for Cases 1 and 2, respectively. Informational material (SRS Research Group, Civil Engineering Division 2003) was consulted for estimation.

As is clear in Table 2 for Case 1, the proposed carriage is inferior to the existing system in terms of cost-effectiveness although the former excels the latter in operational efficiency. In Case 2, on the other hand, the carriage has the advantage over its predecessor in both working efficiency and cost-effectiveness as indicated in Table 3.

Indeed, one more worker is required for the carriage and, in addition, the basic cost of the carriage is more expensive than that for the existing system. It follows that an increased personnel cost as well as its hire would offset the benefits derived from the use of the carriage, meaning that it is economically disadvantageous. If prime consideration should be given to economic benefits, then the carriage will most probably have an economic advantage only when it is used at the site where the scope of work extends beyond a certain limit.

On the other hand, when the point concerns solely the operational efficiency, the carriage under discussion presumably outperforms the conventional system in either case. However, note should be taken of the fact that the foregoing estimates are based on the assumption that an increase rate of the operational efficiency is 1.2. In order to further increase the rate, discussion should be had over the field test results and other data obtained from a commercial model. The details are yet to be furnished.

## 6 CONCLUSION

This paper describes the background of introducing a maintenance carriage that handles the highway tunnel in service. Its detailed design has already come off the drawing board. According to the plans, manufacture of the commercial model is in the offing.

Conceivable operational problems with the carriage will come to light through a series of activities, including manufacture of a prototype as well as field tests. After that, necessary improvements will be made on it.

Tunnel maintenance job by use of the carriage under discussion is considered to be preferable as compared with that done by the existing system in that:

1. Continuous repairs are allowed at the tunnel crown beyond the traffic lane;
2. During the work, changing of the lane along which traffic must be prohibited is unnecessary;
3. Operational efficiency is expected to increase; and
4. Execution can become highly economical depending on the size of the area worked on.

It should be noted that the foregoing assumptions are not based on accurate verification since no testing has not yet been conducted with a commercial model. However, the fact still remains that the contemplated model is probably a meaningful attempt at bringing a preferable tunnel maintenance method to reality.

Aside from the forthcoming manufacture of a prototype as well as field tests for the purpose of accurate verification, the authors have plans of identifying potential advantages and disadvantages of the carriage under discussion.

The authors wish to add that the patent on the said proprietary carriage was disclosed on May 25, 2006 (Patent disclosure No. 2006-132119).

## ACKNOWLEDGMENTS

The carriage discussed in this paper represents an outcome from the research jointly conducted by Sanshin Corporation, Gifu Kogyo Co., Ltd., and Japan Construction Method and Machinery Research Institute. The authors are indebted to all the people affiliated with them for providing them with generous and valuable assistance.

## REFERENCES

- Japan Society of Civil Engineering 2005. *Tunnel Maintenance in Japan*. 1.
- SRS Research Group, Civil Engineering Division 2003. *CRS Method (Repairs and reinforcement of structures using carbon fibers)*, *Collected Data on Estimation (2nd ed.)*.

# Selection of repair method for concrete facades

S. Varjonen & J. Lahdensivu

*Department of Structural Engineering, Tampere University of Technology, Finland*

**ABSTRACT:** Concrete facades have been repaired extensively during the last 20 years in Finland. The common structural solutions and materials used in concrete facades have not been able to ensure a long service life. The concrete structures exposed to outdoor climate are deteriorated by several different mechanisms, whose propagation depends on many structural, climatic exposure and material factors. This paper presents an ongoing project studying the decision making process related to repairing of concrete facades. Selection of suitable repair method for each case has several demands: technical feasibility, cost-effectiveness, service life requirements, requirements concerning the reliability of the repair, aesthetics, architectural or conservation demands and juridical demands. The choice of an economically and technically suitable and ideally scheduled repair method is always based on the technical condition of the structure. Reliable data on the condition can be established only when employing a systematic condition investigation procedure.

## 1 INTRODUCTION

### 1.1 Background

Reinforced concrete is a common building material in facades all over the world. For example in Finland, around 44 million square metres of facades made of concrete have been built since the 1960s as well as more than half a million concrete balconies (Vainio et al. 2005).

However, the common structural solutions and materials used in these precast concrete facades have not been able to ensure a long service life. Often due to unexpectedly rapid deterioration, facades only 20–30 years old have had to be repaired by severe methods. Concrete structures exposed to an outdoor climate deteriorate by several different mechanisms, whose propagation depends on many structural, climatic exposure and material factors. Consequently, their service lives vary significantly in practice.

Concrete structures have been repaired extensively in Finland since the early 1990s. Many new repair methods, products and materials for maintaining and repairing these structures have been developed in Finland since that as well as guidelines for determining repair needs and for managing repair projects. Renovation of concrete facades is however, a quite complex procedure. The selection of suitable repair method for each case has several demands: technical feasibility, cost-effectiveness, service life requirements, requirements concerning the reliability of the repair, aesthetics, architectural or conservation demands and juridical demands. Besides the correct repair method,

it is also important to be able to determine the technically and economically optimal time to execute repair measures. Even if the repairing of concrete facades is nowadays quite common, there is still a need for better understanding on how the management of these projects can be improved.

### 1.2 Degradation of concrete structures

The degradation of concrete structures with age is due primarily to weathering action, which deteriorates material properties of concrete. Degradation may be unexpectedly quick if used materials or the work performance have been of poor quality or the structural solutions erroneous or non-performing. Weathering action may launch several parallel deterioration phenomena whereby a facade is degraded by the combined impact of several adverse mechanisms. Degradation phenomena proceed slowly initially, but as the damage propagates, the rate of degradation generally increases.

The most common degradation mechanisms causing the need to repair concrete facades and other concrete structures in Finland, are corrosion of reinforcement due to carbonation or chlorides (Fig. 1) as well as insufficient frost resistance of concrete which leads to, for instance, frost damage (Pentti et al. 1998).

These degradation mechanisms may result in, for instance, reduced bearing capacity or bonding reliability of structures. Defective performance of structural joints and connection details generally causes localized damage thereby accelerating local propagation of deterioration.

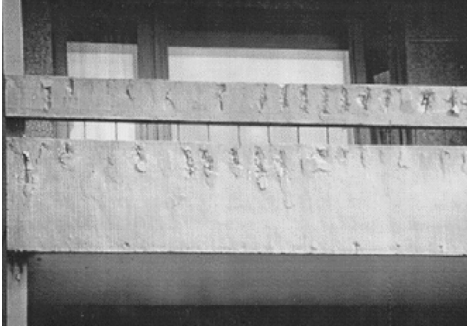


Figure 1. Corrosion of reinforcement is a common degradation mechanism in concrete facades and balconies.

### 1.3 Repair methods

The alternative repair methods for concrete facades are typically divided into three categories: patching in combination with protective repair methods, covering or claddings and demolition of the outer concrete layer and rebuilding.

Protective repair methods are suitable mainly for structures, in which the deterioration has only just begun and the damage is not wide spread.

If there is more severe damage in the existing structures, protective repair methods are no longer sufficient. In Finland different kind of covering repair methods are widely used with concrete facades. The old structure is covered with an additional thermal insulation and a new cladding.

If the facade is severe damaged, the outer layer and the thermal insulation can usually quite easily be demolished and a new thermal insulation and cladding system can be applied.

### 1.4 Objective

This paper presents a part of a larger ongoing project called Service life of concrete facades—Existence and progress of deterioration. The general objective of the research is to study the factors that have actually had an impact on the service life, existence and progress of deterioration in concrete facades and balconies. The subject is studied based on a unique extensive database, which has been gathered during the project. The database contains concrete facade condition investigation data from about 950 buildings giving reliable information on the deterioration of concrete facades and balconies in practise.

As a part of this project, the factors that have had an effect on the success of a facade renovation project are studied. The aim is to find out what kind of issues actually affects on the success and is there a need for further developing of condition investigation systematic or managing renovation process.

## 2 DEMANDS FOR REPAIR METHOD

### 2.1 General

The principles of selection of repair method are shown in Figure 2.

### 2.2 Technical condition

Suitable repair method cannot be chosen without knowing the actual condition of the target structure. The basis to ensure a long service life for renovated facade is that the selected repair method is suitable for the damage situation. It is not enough that one has durable materials or structures if the whole renovation system is not suitable for the damage situation. The basic rule is that with severe damage, heavy repair methods have to be used. So-called protective methods (painting, patch repair) are usually suitable only if there is quite limited damage.

Condition investigation is a systematic procedure to find out the actual condition of a concrete facade, the possible propagation of deterioration and the remaining service-life. A condition investigation involves systematic determination of the condition and performance of a structural element or an aggregate of structural elements (e.g. a facade or balcony) and their repair need with respect to different degradation mechanisms by various research methods such as examining design documents, various field measurements and investigations and sampling and laboratory tests. Evaluation of reinforcement corrosion and the degree of frost damage in concrete are examples of such investigations.

The wide variation in the states of degradation of buildings, and the fact that the most significant deterioration is not visible until it has progressed very

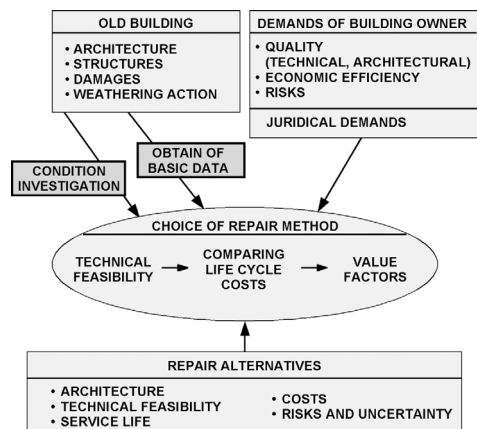


Figure 2. Different factors, which have influence on decision of repair method.

far, necessitate thorough condition investigation at most concrete structure repair sites.

### 2.3 Strategy of building management

Building management consists of such repair and maintenance measures that maintain the function of the building. There are at least four different types of building management:

1. Proactive building management, where the original properties of the facade are restored during the whole lifetime.
2. Programmed building management, where structures are maintained according to guidelines or standard maintenance periods.
3. Monitored building management, which is based on condition surveys and investigations.
4. No management, when the degradation of structure may proceed until it cannot be repaired anymore. After this the structure is renewed.

Selection of the repair method depends on which building management type is controlling. For example in historically significant buildings, the proactive maintenance is usually applied even if the costs of proactive building management are more than in other alternatives.

### 2.4 Requirements of real estate owner

For a successful repair project it is important that the real estate owner sets well-defined objectives for the project. The most important objective is that the repaired structure is safe to use and to maintain. This means for example that the structure does not contain any substances harmful to health and all the fastenings are safe.

The real estate owner should specify also other objectives, such as requirements concerning

- the architecture and appearance,
- the service life and
- the possibilities to maintenance.

### 2.5 Aesthetic requirements

The propagation of degradation causes finally visible damage. The corrosion of reinforcing steel and frost damage leads to cracking or spalling of the concrete cover. Malfunction of moisture behaviour may cause contamination or pigmentation of concrete surface. The optimal timing for the repair measures depends strongly on aesthetic requirements. Often the technical condition of concrete facade may still be sufficient, but the aesthetics of the facade are at non-acceptable level.

In case of historically significant buildings or important areas, the requirements for the appearance of the building may have a crucial role when deciding on repairs.



Figure 3. Degradation of concrete facade may cause aesthetic problems before the technical service life of the facade comes to end.

### 2.6 Service life requirements

The question of service life of facade structures is quite complex. To ensure a long service life for a facade repair, there are at least four conditions that has to be fulfilled: the repair method has to be suitable to the damage situation, the progress of deterioration of the old structure has to stop or at least slow down, the repaired structure has to be durable and the maintenance of repaired structure has to be adequate.

There are various repair methods available. The service life of renovated structure can be from 10 to 100 years depending on the selected repair method and work performance.

With structures that are severe damaged, a light repair methods are no longer useful and a more thorough repair method should be selected. If nonetheless a light, protective type repair method is in this case selected, the service life of the repair will be essentially shorten. Usually light protective repair methods contain more or less severe risks of future damage. If the real estate owner requires a secure repair, it is advisable to choose heavier repair methods. Heavier repair method means distinctively higher investment cost, but on the other hand, maintenance and energy costs are lower in the future.

### 2.7 Architectural demands

The degradation of reinforced concrete facades cannot be retarded efficiently enough by appearance-saving light methods if the structures are of poor quality, or if repairs are postponed too much. Therefore, in most cases, the repair measures applied as part of standard maintenance will, sooner or later, change the original nature of the buildings and townscapes remarkably.

The stock of buildings with concrete panel facades is mainly concentrated in suburban areas, which were built in the 1960's and 1970's. Nowadays, this modern

urban architecture has begun to regard as part of European cultural heritage (Varjonen et al. 2006). Seen from the point of view of cultural sustainability, suburban landscapes are primarily endangered by long-term repair activity. The possible aim to restore the appearance of the building during its lifetime limits the number of alternative repair measures and effects on the optimal time for maintenance or repair measures. When the general aim is to preserve the original appearance of a concrete facade for as long as possible, it is important to apply well in advance measures that can protect the facade from deterioration processes, or at least retard them as much as possible.

### 3 EXECUTION OF THE RESEARCH

#### 3.1 *Analyzing repair plans*

The study will be executed as a case study. About 20 different renovation cases will be selected from different areas of Finland. Running or just finished concrete facade renovation cases will be selected for the research.

The construction plans of these repairs and the condition investigation reports of the target buildings will be gathered and compared with each other. The resources available for condition investigations are usually limited, which is why the investigations are made with the sampling method with so small amount of samples as possible. For the comparison, the condition investigations will be classified into three classes according to their extent or sufficiency. A database of condition investigations and a Finnish guideline for condition investigations (Anon. 2002) will be used as a criteria for the classification.

#### 3.2 *Interviews*

The analyse of the construction plans of the repair and the condition investigation reports of the target buildings will be completed with the interviews of the decision-makers of selected concrete facade renovation projects.

#### 3.3 *Expected results*

The research will produce at least the following benefits:

- Information on which actions in practice effects on the success of a facade renovation project.
- Information on the reliability and impacts of condition investigations. Is the repair method, which is recommended by condition investigation selected? Is there after condition investigation need for further tests or investigations before the repair method can be selected?
- Information on the criteria when selecting repair methods. Is the repair method selected based on technical, architectural or economical demands?
- Information on the effects of light or extensive condition investigations. If a light condition investigation is conducted, does it lead to heavy repair measures?

As a final conclusion, the research will give information on the further development needs of renovation process or condition investigation systematic.

The results of the research can be used to develop the concrete facade renovation project so that the repair is successful. The results may also be used in the development of condition investigations by giving information of what kind of impacts condition investigations have had.

### 4 CONCLUSIONS

All the requirements of selection of repair method have not the same value. The choice of an economically and technically suitable and ideally scheduled repair method is always based on the technical condition of the structure. Therefore, the repair methods are selected primarily on the basis of the technical condition of the structure.

The technical condition of facade and the service life which facade has left can be determined by systematic condition investigation. Ensuring a long service life for repaired facade structures requires that the repair method have to be suited to the existing damage, deterioration of the old structure has to end or at least decelerate, the repaired structure has to be durable, maintenance of the repaired structure has to be adequate and the repair should also be cost effective. The one repair method that best meets the property owner's requirements and architectural and financial criteria of the project is selected from among those that meet the technical requirements.

### REFERENCES

- Anon 2002. *Condition investigation manual for concrete facade panels*. Helsinki: Concrete Association of Finland BY 42 (In Finnish).
- Pentti Matti, Mattila Jussi, Wahlman Jyrki 1998. *Repair of concrete facades and balconies, part I: structures, degradation and condition investigation*. Tampere: Tampere University of Technology, Structural Engineering. Publication 87 (In Finnish).
- Vainio et al. 2005. *Julkisivujen uudis- ja korjausrakentaminen*. Tampere: VTT (In Finnish).
- Varjonen S. et al. 2006. *Conservation and Maintenance of Concrete Facades—Technical Possibilities and Restrictions*. Tampere: Tampere University of Technology, Structural Engineering, Publication 136.

# Monitoring based performance prediction of steel bridges against traffic loading exemplified at the Europabrücke

R. Veit-Egerer & H. Wenzel

VCE—Vienna Consulting Engineers, Vienna, Austria

**ABSTRACT:** Bridges are ageing and traffic is growing, which creates a demand for accurate fatigue life assessment. The Europabrücke—a well known Austrian steel bridge near Innsbruck, opened in 1963—is one of the main alpine north-south routes for urban and freight traffic. It represents a bridge generation, where bridge designers acted on a maxim of building material economisation. A long-term preoccupation of VCE with BRIMOS® (BRIDGE MONITORING SYSTEM) on the Europabrücke (since 1997) with regard to fatigue problems and possible damage led to the installation of a permanent monitoring system in 2003. Since that time a lot of investigations and additional special measurements were devoted to innovative, mainly monitoring-based fatigue assessment. As life-time predictions in modern standards depend on lots of assumptions, the emphasis is to replace those premises—referring to loading—by measurements.

## 1 INTRODUCTION

In the abstract's context the present work is focused on three levels:

- Level I: Global behaviour—primary load bearing members (traffic loading observation mainly based on laser-supported global deflection measurement)
- Level II: Cross-sectional behaviour (dynamic traffic-weight registration system, which utilises laser-calibrated accelerometers reproducing vertical cantilever deformations based on pattern recognition.
- Level III: Local systems—e.g. the bottom and top joints of the bridge's torsional bracings (verification with additional strain gauge measurements)

In each of these levels of analysis the consumption of the structure's overall-capacity per year is to be determined. A continuative methodology was prepared, which uses the isolated hot spot areas for detailed fatigue analysis to determine, how grave the present situation is with regard to the remaining service lifetime of the analysed structural members. As the present lifetime calculations are performed in terms of stresses by means of damage-accumulation, comprehensive Finite Element Analysis is necessary to quantify the real fatigue-threat. The calculation's loading-input is going to be strictly measurement based. This methodology of course implies additional strain gauge measurements for verification purposes.

## 2 METHODOLOGY

An extensive explanation of the present research work as well as an insight into its methodology in detail is given in Wenzel et. al 2008 and is visualised in Fig 1.

Even if the present methodology represents a tailor-made approach, it can be modified and transferred to other bridge structures. For reasons of a limited extension of the present contribution it is mainly going to be focused on showing the development of a tailor-made loading model for performance prediction.

## 3 TAILOR-MADE LOADING MODEL FOR PERFORMANCE PREDICTION

Based on the hot spot areas isolated in [Veit-Egerer & Wenzel 2007], detailed fatigue analysis is demanded to determine, how grave the present situation of the relevant structural members is with regard to the remaining service lifetime—using the monitoring based impact. In the following an insight is given into the idea, how the results for a one week lasting measurement campaign are extracted and implemented into the developed methodology for performance prediction.

Firstly accompanying video recordings were undertaken to eliminate possible uncertainties and to provide complementary information. Extensive data mining lead to frequency distributions including all different kinds of occurring loading scenarios (Fig. 2). One of these loading configurations—two trucks simultaneously stressing the bridge's side span by driving in

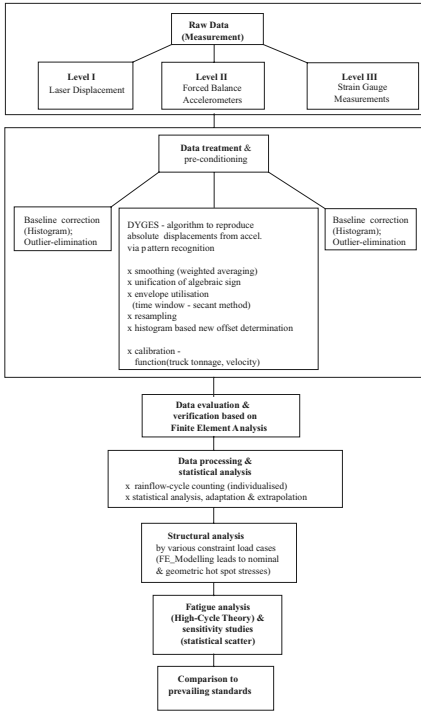


Figure 1. Detailed flowchart of the methodology.



Figure 3. Video based observation of relevant loading scenarios.



Figure 2. Typical, exemplary loading scenario—two trucks causing unsymmetrical traffic impact—highlighted in Fig. 4.

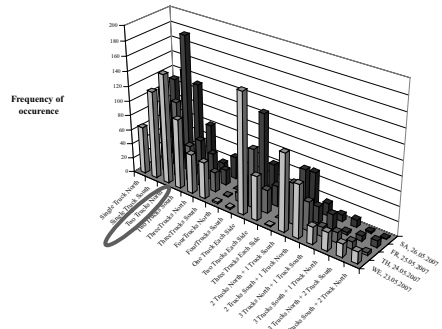


Figure 4. Video supported classification of loading scenarios and resulting frequency distribution.

the downhill direction—was chosen to show its consequence for the three levels of performance analysis (Fig. 5), which have been introduced.

Global response in terms of vertical deflection due to the chosen scenario was recorded using a transmitter unit at the bridge abutment and a receiver unit

located at the southern side span (laser supported global deflection measurement)

In the course of [Wenzel & Veit-Egerer 2007] the main feature of the permanent monitoring system—the DYGES algorithm (Dynamic Freight Traffic Classification)—was introduced. This feature



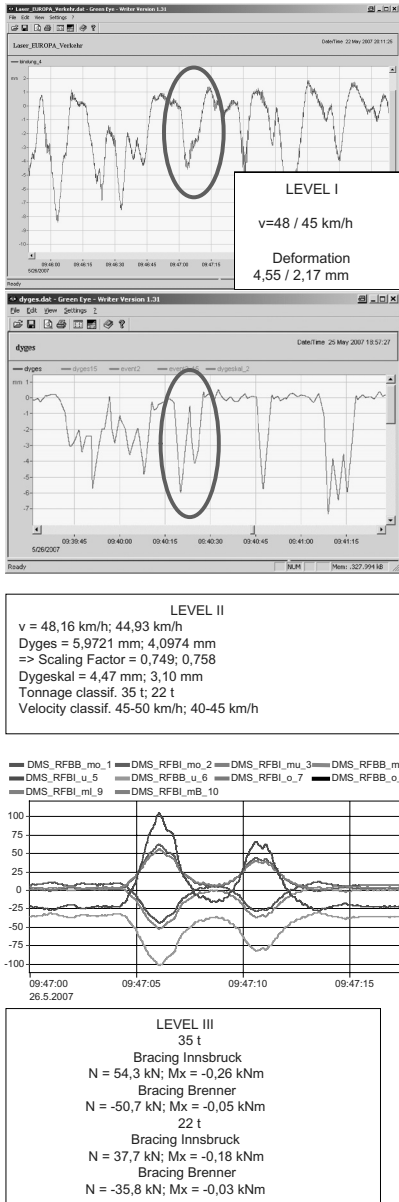


Figure 5. Randomly selected loading scenario and the corresponding structural response—expressed by means of the Three Level Approach.

explicitly provides the truck loads corresponding with the observed global bridge span deflection.

Finally the effective axial forces and bending moments acting on the bracings as well as the occurring stress cycles can be extracted from the monitored strain data recorded at the directly stressed

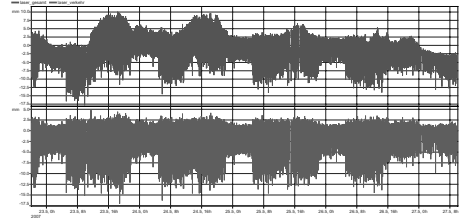


Figure 6. Traffic induced response in terms of vertical displacement (red)—isolated from the overall impact (blue) for the bridge's side-span V; 22.05.2007 19:00–27.05.2007 10:00.

bracings. In the following it is explained, how the established, tailor-made loading model (Fig. 2) is utilised for performance analysis of Level I (Global Impact):

Monitoring based global impact data for a certain, representative time period (one day, one week—e.g. Fig. 6) are assessed using Rainflow Analysis. To express the Damage Rate for this loading function each of the observed, typically occurring loading scenarios (Fig. 4) is implemented one by one into a Structural Finite Element Model using certain truck loads (DYGES). This leads to a corresponding structural stress cycle  $\Delta\sigma$ . As it has to be dealt with truck traffic causing High Cycle Fatigue, linear elastic material behaviour can be assumed. Stresses and strains are assumed to remain elastic. This facilitates the calculations, as a single load case due to the chosen scenario is to be calculated in terms of stresses, while all other occurring truck loads are automatically included within the Rainflow Matrix. The latter, the calculated stress cycle value and the stress life curve corresponding with the analysed relevant structural detail lead to a Damage Matrix. This assumes only the chosen loading scenario to be occurring. Based on the frequency distribution of the observed loading scenarios (Fig. 2) the chosen entry gets its weighting within all other relevant loading cases to quantify the consumed loading capacity related to a certain observation period. The same procedure is repeated for all other entries of the observed loading scenario distribution leading to an accumulated damage per determined observation period.

In the course of the performed Finite Element calculations—following the consequence for the fatigue resistance of structural details relevant for Level I, a parallel determination for those structural details relevant for Level III can be done. Additionally there is always the possibility to make a crosscheck for those stresses from analytical calculations by comparing them to the ones given by explicit strain measurements at representative positions, which shows the capability of this integral methodology (Fig. 7).



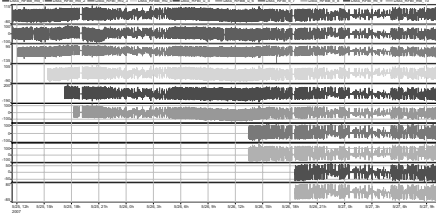


Figure 7. Successively added strain gauges—installed along an assembly of two corresponding torsional bracings; 25.05.2007 11:00–27.05.2007 11:00.

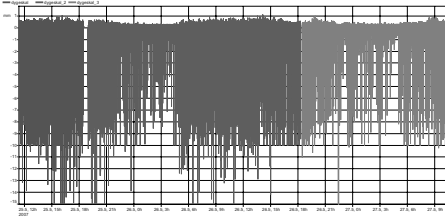


Figure 8. Corresponding pattern of the Dynamic weight registration based on cantilever acceleration measurements (reproduced cantilever deformations via pattern recognition)—a feature implemented into permanent monitoring; 25.05.2007 11:00–27.05.2007 11:00.

Performance analysis for Level II (Cantilever impact) seems to be less complex, as the consequence on fatigue relevant structural details in terms of principal structural stresses occurs perpendicular to the stress cycles—previously analysed for Level I. The DYGES based truck loading impact (Fig. 8) is again implemented into structural models by means of a deformation constraint load case affecting the cantilever's outer edges.

#### 4 REMAINING SERVICE LIFETIME BY MEANS OF EXISTING TRAFFIC DATA

The demonstrated damage calculations refer to a sufficient amount of workdays and weekend-days, that enable a representative extraction of a damage rate per week, which consequently enables its extrapolation to enlarged time periods. Thus the assessment of an analysed detail via Damage Matrix calculated for the measuring time of a whole year (=> 'Damage-per-year effect') is possible to determine the consumption of the overall loading-capacity per year for the corresponding detail. The detailed knowledge about the progression of the prevailing traffic from the very beginning up to these days and the implementation of published future trend studies with regard to the

next ten years (until 2015) are used for fatigue analysis (variation of traffic volume & variation of the notional truck-weight). Fig. 9 shows the increase of the freight traffic volume at the Europabrücke. According to [Verkehrsentwicklung in Tirol 2006], traffic volume in 2006 increased to an amount of 472% in relation to 1964 and is expected to grow 2.9% per year until 2015 [Verkehrsprognose 2015]. To derive every considered year's Damage Matrix affected by the variation of traffic volume, fatigue analysis approximately demands a uniform adaptation of the number of occurrences for all elements of the derived Rain-flow Matrix before extrapolation techniques of the measured impact for the whole lifetime—discussed in [Wenzel et al. 2008]—are applied.

Fig. 8 shows the increase of the effective amount of transported goods compared to a calculated cargo per notional truck. The calculations showed that this truck weight in 2006 increased to an amount of 503% in relation to 1964 and is assumed to have already reached a maximum. This means, that a further increase of transported goods is likely to be a consequence of the

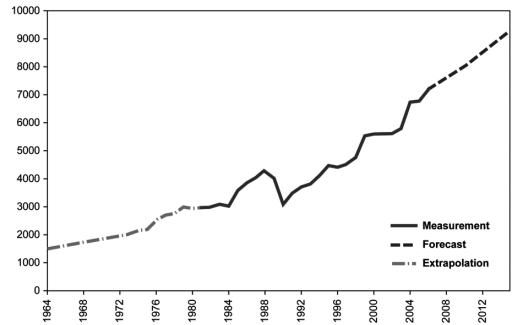


Figure 9. Progression of freight traffic volume at the Europabrücke from 1964 until 2015 [trucks/day].

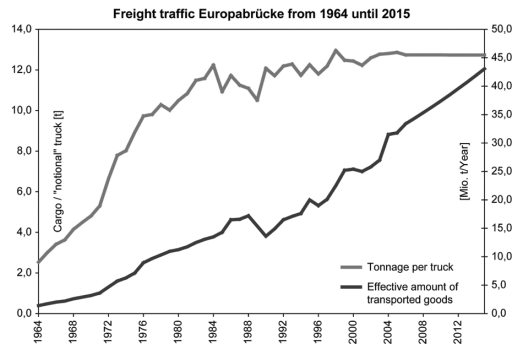


Figure 10. Effective amount of transported goods on the Brenner route compared to a calculated cargo per notional truck.

still growing traffic volume. An adaptation for fatigue analysis due to the variation of the notional truck-weight is realised by re-scaling the Rainflow Matrice's subdivision. The information included in both of these functions can be broadened crucially, as the DYGES based freight traffic classification delivers exact truck weight data for the analysed bridge object—starting with the summer of 2004.

## 5 CONCLUSIONS AND FUTURE WORK

The present contribution explicitly deals with measurement data and the procedures, how they were provided and conditioned for continuative performance analysis. The methodology provides strictly in-situ based loading input parameters for continuative fatigue analysis leading to a “tailor-made” performance prediction. In addition strain gauge measurements in each of the considered levels of analysis (*Level I—Level III*) are done for verification purposes of the Finite Element based stress-life approach. Thus the main goal, the substitution of the standard's premises—referring to loading—has been reached in a quite innovative manner with regard to determine the consumption of the structure's overall-capacity per year by means of a three level approach. One of the main innovations within the present methodology is the introduced *DYGES Algorithm*, which is necessarily based on a pattern recognition algorithm by Wenzel & Veit-Egerer [Wenzel & Veit-Egerer 2007] in order to reproduce vertical cantilever deformations from accelerometers (major feature of the permanent monitoring system). The development of the *DYGES Algorithm* was nominated for the Austrian Award for Telematics, by the Federal Ministry of Transport, Innovation and Technology.

Besides the traffic induced impact, additional monitoring campaigns revealed, that there is a strong influence due to sun-radiation (Fig. 11 & Fig. 12). In addition to the described laser supported global deflection measurements the progression of the offset of the bridge's reference accelerometer in the lateral direction was transformed into an angle of inclination. The resulting temperature gradient function induces additional axial forces and deformations explicitly into the outer bridge spans. Approximate analysis indicates that this constraint's intensity level can occur up to the range of the traffic-impact itself. The affection due to temperature and radiation impact needs to be analysed seperately, before it is necessarily going to be superimposed with the strictly traffic induced fatigue impact.

Contrary to the general doctrine in conjunction with structural performance analysis of welded components the authors assume, that the influence of temperature

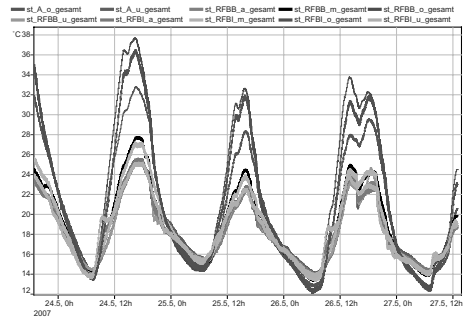


Figure 11. Integral Assessment of environmental conditions: Steel-temperature and Air-temperature along on a certain cross section (pier V): 23.05.2007 19:00–27.05.2007 13:00.

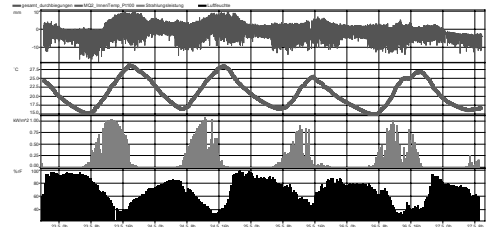


Figure 12. Integral Assessment of Traffic impact and comparison with environmental conditions: Global vertical deformations vs Air-temperature vs. Radiation efficiency vs. Humidity: 23.05.2007 20:00–26.05.2007 12:00.

leading to varying mean stresses will have to be considered. The authors are convinced that shrinkage effects that lead to residual stresses in the welds are minimized or already vanished in this almost 45 year old and constantly stressed structure. In that case varying mean stresses become relevant even for welded structural members and demand the application of appropriate correction rules.

Starting with May 2007 the in-situ distribution of temperature impact as well as the sun-radiation itself is assessed via permanent monitoring using a profile of temperature sensors over a certain box-girder's cross section (9). An explicit temperature load case is going to be created and again implemented into the Finite Element calculations.

The implementation of strictly measurement based loading impact into Finite Element calculations strongly supports quantitative estimation of the service-lifetime via separation of fatigue relevant loading cycles from the randomly occurring overall traffic. The Palmgren-Miner based accumulation of all calculated Damage Matrices from the very beginning of

the bridge's existence up to now leads to the remaining capacity of loading cycles for the analyzed detail. As a superior conclusion in addition to a quantitative estimation of the service-lifetime another key figure FR (Fatigue Relevance) is also derived (eq. (1)). It separates remaining, fatigue relevant loading cycles  $n_i$  (registered by sensors and taken from the Damage Matrix) from the randomly occurring traffic (ADTV = average daily traffic volume). It is obvious that the investigation's results are going to be improved by progressive stages; the longer the observation period lasts.

$$FR = \frac{\sum n_i}{ADTV} \quad (1)$$

This whole conception assures the determination and observation of slowly progressing processes in the structure, which might lead to local damage or to deterioration of the structure's operational integrity. The results of these hot spot analysis calculations with regard to the fatigue resistance itself are going to be undertaken and discussed in the course of further publications.

## REFERENCES

- Veit-Egerer, R. & Wenzel H. 2007. Monitoring based weak point determination of a steel bridges's torsional bracings with regard to fatigue threat in "Proceedings of the 2nd International Conference—Experimental Vibration Analysis for Civil Engineering Structures (EVACES'07)". Portugal: ISBN 978-972-752-095-4
- Verkehrsprognose 2015—vorläufige Ergebnisse hochrangiges Straßennetz Österreich. BMVIT-Abteilung II/A/1. Wien. 2000.
- Verkehrsentwicklung in Tirol—Berichte 1984–2006. Amt der Tiroler Landesregierung-Abteilung Gesamtverkehrsplanung. Innsbruck.
- Wenzel H. et al. 2008. Structural Health Monitoring of Bridges. England: J. Wiley and Sons Ltd. (under examination).
- Wenzel H., Veit-Egerer R.: Measurent based traffic loading assessment of steel bridges—a basis for performance prediction. International Journal of Structure and Infrastructure Engineering. Taylor & Francis Group. New York. 2007 (submitted and already scientifically reviewed).

# A maintenance concept for concrete tunnel linings in soft soil conditions

A.H.J.M. Vervuurt, G.A. Leegwater & R.B. Polder

*Netherlands Organization for Applied Scientific Research (TNO), The Netherlands*

**ABSTRACT:** In the European project TUNCONSTRUCT a life cycle cost method for management and maintenance of underground structures is developed. Within the project TNO is concerned with the durability of the concrete lining. In this paper the concept is explained by means of a case of a bored road tunnel (in soft soil) with exposure to de-icing salts (internal) and seawater (external). The example concerns a real structure, with input chosen such that at some point in time during the service life corrosion and spalling will occur and repairs will be needed. Moreover, for elucidating the optimization possibilities of the method two types of intervention are concerned: (1) conventional repair with a relatively short life of the repairs, such that new repairs will be needed during the remaining life of the tunnel and (2) cathodic protection with a relatively long life, so that only minor interventions are needed during the remaining life of the tunnel.

## 1 INTRODUCTION

In 2005 the European Integrated Project TUNCONSTRUCT was started. The project promotes the development and implementation of European technological innovation in underground construction. The project is co-financed by the European Commission, under its 6th framework program. Coordination of the project rests on the Graz University of Technology, Austria.

The TUNCONSTRUCT project is divided in four subprojects, namely:

- SP 1. Design.* Focusing on advanced modeling and expert based design tools.
- SP 2. Technologies.* Within SP 2, among others, new technologies aiming at innovative Tunnel Boring Machines for different soil types are developed.
- SP 3. Processes.* For improving the building process new technologies for data transfer are developed.
- SP 4. Services.* In SP 4 new measuring techniques and monitoring devices are developed for a more efficient management of underground structures.

This paper focuses on SP 4 and the development of a management and maintenance framework for tunnels. SP 4 is coordinated by Dragados from Spain and next to TNO the management and maintenance method is developed by, among others, STUVA, AMBERG, Mott MacDonald, CETU and ACCIONA.

In the sub project, TNO is concerned with the development of the life cycle cost model related to the durability of the concrete lining. In this paper the methodology of the concept is explained. Moreover, for elucidating the optimization possibilities of the method two types of intervention are considered: (1) conventional repair with a relatively short life of the repairs, such that new repairs will be needed during the remaining life of the tunnel and (2) cathodic protection with a relatively long life, so that only minor interventions are needed during the remaining life of the tunnel.

## 2 PERFORMANCE BASED DESIGN

In the future more management and maintenance contracts for civil infrastructures are expected; therefore the need increases for decision tools with respect to the most optimal choices regarding maintenance. Within these decisions on the one hand functionality (performance) of a structure during its service life plays an important role, whereas on the other hand the costs are to be considered. Generally the structural performance is to be maintained within accepted reliability ranges and with a minimum of costs.

During the service life of the structure different damage mechanisms may be distinguished that cause deterioration of the structure and a decrease of the performance. Most damage mechanisms show typical patterns in time and different strategies varying from repair to replacement may be adopted for maintaining

the required level of performance. Asphalt for example has a relatively short service life compared to other components such as the structural components. Generally, asphalt is repaired during a certain period and periodically (every 5–15 years) replaced for maintaining the required comfort performance. On the other hand the structural components are designed in such a way that a minimum of repair is expected during the service life of the structure (80–120 years, depending on the design requirements).

Because a lot of aspects are not certain when predicting the service life of the different components, there is a possibility that the actual performance level is less than required. In such a case the maintenance strategy has to be adjusted. For monitoring the actual performance level, generally measurements are performed. Such measurements may vary from periodical visual inspection to drilling cores, laboratory tests and in situ tests. Monitoring leads to an increase of the reliability of the expected performance in time.

### 3 PERFORMANCE BASED MAINTENANCE STRATEGY

With respect to the durability of the concrete lining in (bored) tunnels, the performance is dominated by possible corrosion of the reinforcement. For ensuring reliably that corrosion during the design service life is not likely, the chloride content of the concrete at the reinforcement is to be sufficiently low, e.g. lower than the critical chloride content at which corrosion may occur ( $Cl_{crit}^-$ ), see Figure 1.

For corrosion attack of the reinforcement the time dependent chloride content may be considered as the loading component (solicitation  $S(t)$ ), whereas the critical chloride content  $Cl_{crit}^-$  is defined as the resistance  $R$ . The limit state related to chloride attack is exceeded when  $R - S(t) < 0$ .

The values for  $R$  and  $S(t)$  may be determined on the forehand, based on known aspects such as applied materials and environmental conditions. However, especially for time depending parameters such as  $S(t)$  lots of uncertainties exist, that must be accounted for. For larger time spans these uncertainties increase and lead to a larger variation in the predictions with respect to  $R$  and  $S$ . Monitoring and measurements decrease the uncertainty resulting in more reliable predictions with respect to the actual performance level.

Generally the requirements with respect to chloride attack are related to the probability ( $P_f$ ) that the chloride content exceeds the critical chloride content, i.e.:

$$P_f(Cl^- < Cl_{crit}^- | t < t_{life;d}) = P_f(R - S < 0 | t < t_{life;d}) < P_{f,target}$$

When the performance is defined as the degree to which the different requirements are met, Figure 2 may be constructed. In the figure both the resistance and the solicitation are divided by  $S$ . In that case the required performance is 100% by definition and deterministic by nature. The actual performance level in that case equals  $P(t) = R/S(t)$  and is probabilistic by nature. A performance level of 100% indicates that the requirements are just met. On the horizontal axis the expected service life is given.

Traditionally structures are designed in such a way that the required performance level is met reliably during the service life. The reliability is denoted by the reliability index  $\beta$ , indicating the probability that the requirements (the limit states) are NOT met. For larger  $\beta$ , the reliability increases and the probability for exceeding the predefined limit state decreases. An optimal design aims at  $P_f = P_{f,target}$ . For structural concrete elements the above mentioned design method was developed in the project DuraCrete (2000).

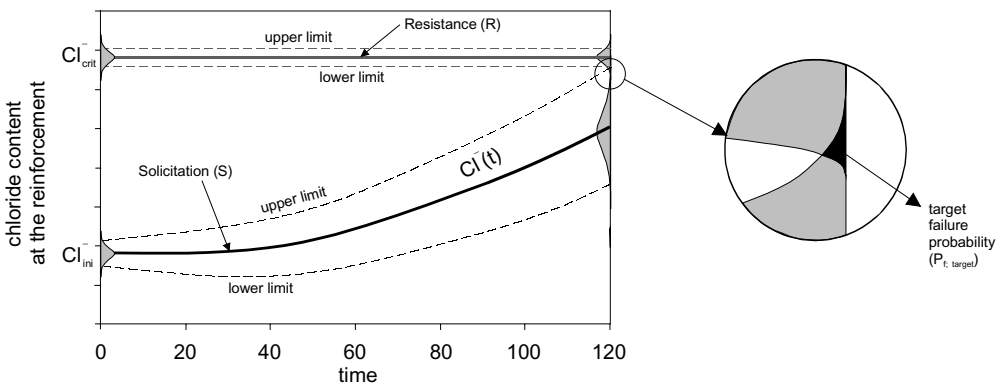


Figure 1. Performance based design with respect to the durability of the concrete: Chloride attack.

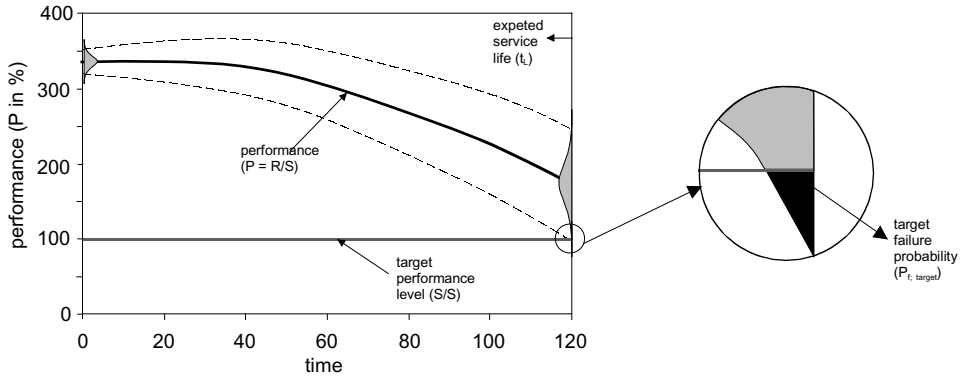


Figure 2. Performance based design on the basis of a normalized performance criterion.

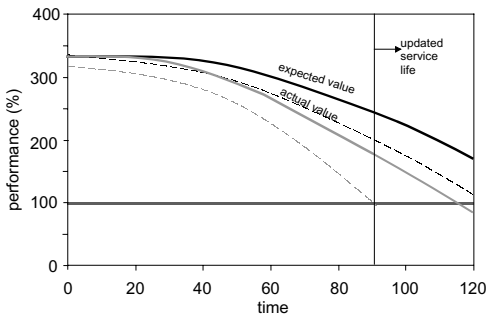


Figure 3. Effect of monitoring on the expected design life.

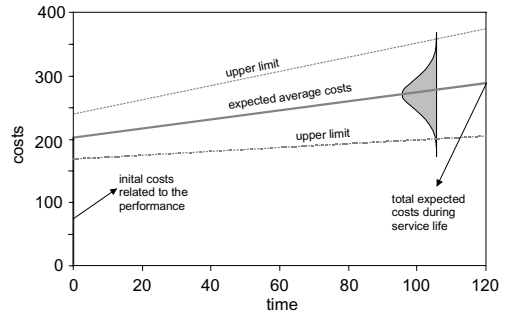


Figure 4. Expected cost developments during service life.

Moreover, the method is suggested for using in the new *fib* Model Code, *fib* (2006).

In practice the actual performance will differ from the calculated performance, due to differences in the loading ( $S$ ) and resistance ( $R$ ). These differences are generally noticed by observing the structure and/or monitoring. In Figure 3 the possible effect of monitoring on the expected design life is illustrated. In the example the updated design life is shorter than the original design life. Of course it's also possible that measurements indicate a longer updated life. It may be obvious that these observations may be important for decisions in the maintenance strategy that is followed.

Generally monitoring may have the following consequences:

1. The updated service life differs from the calculated design life
2. More certainties are obtained affecting the representative value (lower/upper limit) of the updated design life

As mentioned above, it may appear that the actual performance level is lagging behind the requirements.

Usually this necessitates additional measures. The effects of the type of measures on the costs and the expected performance level are discussed below.

For the example of Figure 2, in Figure 4 the cost developments are graphically shown. In the figure on the horizontal axes the time is given, whereas on the vertical axis the cost investments and total costs related to the concrete lining are given. In the example it is assumed that the total costs during the service life of the structure are determined by, on the one hand the initial costs and on the other hand by costs linearly depending on time. In the example of Figure 4 no incidental repair costs are considered and the time dependent costs are restricted to regular maintenance (surveillance).

It is noted that the total costs depend on the different performance criteria that may be related to different functions (asphalt, concrete, electrical installations, etc.). In the given example only one performance criterion is considered. The costs considered, therefore, only should reflect that part of the costs that is related to the durability of the concrete lining. In reality the costs related to the different performance criteria are

highly correlated and can not be separated. For this example, however, this effect is neglected.

In the design phase of the tunnel certain measures can be taken to influence the total costs during maintenance of the structure. These measures may affect the performance level on the one hand or the limit state on the other hand. Two obvious examples in the respect are given below:

#### *Example 1*

By applying stainless reinforcing steel the chloride content is of less importance when the performance is considered. Stainless steel increases the resistance  $R$  and allows for a higher limit state, Bertolini et al. (2004).

With respect to the costs, stainless steel will increase the initial costs, but will decrease the maintenance costs. Moreover a more slender structure may be designed because the requirements to the concrete cover are less.

#### *Example 2*

Protecting the reinforcing steel from corroding, for example by using cathodic protection (CP) as elucidated by Bertolini et. al. (2004), increases the performance (Figure 2) and as a result the expected service life. CP implies additional initial and time depending costs that must be accounted for.

In order to make a rational decision about the measures to be taken (or not taken) and the scenario to be followed, both options must be considered and worked out in detail. Generally in the design of concrete structures such special measures are not considered and it is assumed that no measures are necessary. This in contradiction to for example the asphalt construction and the electrical installations for which it is assumed on the forehand that replacement is required after a certain number of years.

Nevertheless, during the service life it may appear that measures have to be taken for maintaining the required performance level of the concrete structure. Mostly rust spots appearing on the surface indicate local corrosion and globally an insufficient performance level. In the following section the possible maintenance strategies for such cases will be considered.

## 4 PERFORMANCE BASED MANAGEMENT

As mentioned previously, generally a design aims that the design life requirements with respect to durability are met with sufficient reliability. However, due to uncertainties in the design, the actual performance differs from the calculated performance and measures have to be taken for maintaining the required service life. Measures related to the durability of the concrete structure are mostly related to repair

of the structure and are generally quite expensive. Consequently the costs of such measures cannot be neglected compared to the total (maintenance) costs. When the costs appear to be too high it even may lead to a decision for replacing the structure. Generally such decisions are also affected by changing functionalities to which the structure should comply. It may be obvious that for tunnels, and especially for bored tunnels, replacement is less easy than for, for example, bridges.

In the project TUNCONSTRUCT it is assumed that the maintenance strategy may be optimized on the basis of different possible scenarios. In such a case it is important to predict the benefits and the costs of the different scenarios, taking into account the uncertainties that play a role. As mentioned different scenarios may be adopted. The most important strategies that may be distinguished in this respect are rebuilding, corrective repair and preventive repair.

In the case of corrective repair, only damaged spots are repaired, whereas in the case of preventive repair measures are taken that prevent actual damage to occur. Advantage of corrective repair is that the costs are postponed and only limited to the necessary spots. Disadvantage is that the time spans between repair moments become smaller in time because generally, the durability of repairs is less than the durability of sound concrete. As a result it may be expected that the periods between repairs decrease in time. Finally, the costs for repairing are quite expensive, also because of secondary costs such as closure and consequently unavailability of the infrastructure.

In the case of preventive repair, measures are taken that prevent damage rather than repairing damaged spots. Corrosion of the steel reinforcement is suppressed. Consequently the costs are made earlier in time, but large-scale maintenance costs are avoided. Examples of preventive maintenance are the use of coatings or applying cathodic protection.

Two examples are addressed qualitatively. The results are illustrated in Figure 5. Within the remainder of the project TUNCONSTRUCT the applied method will be quantified and made applicable for comparable structures.

In both examples it is assumed that the actual design service life is not likely to be reached without taking any measures. Moreover, actual damage has not developed yet and replacement is not aimed at.

The red lines in Figure 5 indicate the design values for the expected performance in time. For both examples the first period (until  $t = 60$  years) no specific (repair) measures are taken and no differences are observed.

After 60 years it appears that the required service life (120 years) is not reached with the required reliability and a decision is made for upgrading the structure. In the example two different scenarios are considered: (1) periodic (corrective) repair after

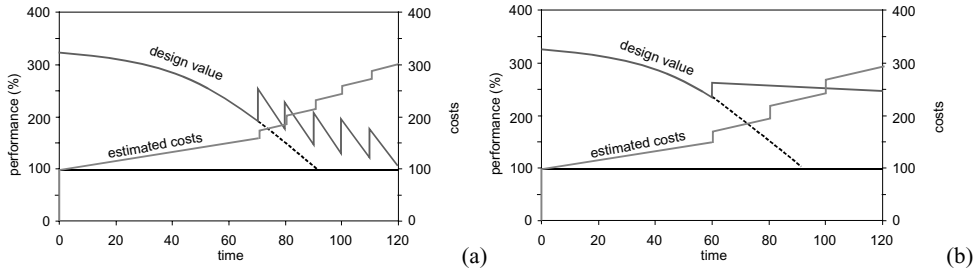


Figure 5. Expected cost developments during service life.

expectedly 70 years and (2) cathodic protection after 60 years.

From Figure 5a it can be seen that scenario 1 is characterized by no additional costs until 70 years. Thereafter periodically a leap in the costs is observed indicating the repair costs. Each time repairs are carried out the performance level is increased. In the period thereafter the performance level decreases again in time. Because the durability of repaired concrete is less than for sound concrete, the decreasing slope is assumed steeper than before repairing the concrete. In the example, moreover it is assumed that repairing the structure shows a repeating pattern.

The most important variables that play a role of importance in this respect, and have a stochastic distribution are:

- The repair costs and the periodic maintenance costs in between the repairs.
- The decreasing slope of the performance level, as well as the increase in the performance level after repair.
- The intervals between repairs.

It may be obvious that there is a correlation between the different variables. The costs will be related strongly to the amount of repairs and the incidental increase in the performance level. Moreover it may be expected that the costs for repair will increase in time due to increasing amounts of damage in time.

For scenario 2 (Figure 5b) it is decided that the moment for damage is not waited for but, instead, preventive measures are taken at  $t = 60$  years. It is assumed that at that time a cathodic protection (CP) system is applied. As a result quite an investment is made at  $t = 60$  years. Moreover it is assumed that the regular maintenance costs after applying the CP system are larger compared to scenario 1. Finally it must be accounted for that after some time parts of the CP system need to be replaced. In the current example it is assumed that this is every 20 years.

With respect to the performance level it is expected that, after applying the CP system, there is hardly any decrease in the performance. This is attributed

mainly to the change in the limit state requirements (the critical chloride content is of less interest). The decrease of the performance level is only expected when the CP system does not function.

As well as for scenario 1, also scenario 2 contains different uncertain parameters that need to be quantified. In this respect, first of all the costs of the CP system are important: the initial costs as well as the costs for maintenance of the system (including periodic replacement of parts of the system). Decisions will be taken on the basis of the total costs.

With respect to the scenarios elucidated in Figure 5 it is noticed that the performance level at  $t = 120$  years is higher for scenario 2 than for scenario 1. In a rational decision making method it seems obvious that the residual value (residual performance) of the structure is also accounted for.

Moreover it is noted that for the costs only the costs are taken into account that can be attributed to the performance indicator considered. On the other hand, the total costs cannot be assessed without taking into account the remaining performance indicators. Moreover, a strong interaction and correlation between the different costs may be expected. Nevertheless, at this moment for simplicity, a method is adopted in which the different performance indicators are treated separately. Afterwards the different performance indicators will be combined.

## REFERENCES

- DuraCrete R17, 2000, *DuraCrete Final Technical Report, Document BE95-1347/R17*, May 2000, The European Union—Brite EuRam III, DuraCrete—Probabilistic Performance based Durability Design of Concrete Structures, CUR, Gouda.
- fib, 2006, *Model Code for Service Life Design*, Task Group 5.6, fib Bulletin 34.
- Bertolini, L., Elsener, B., Pedferri, P., Polder, R.B., 2004, *Corrosion of Steel in Concrete: Prevention, Diagnosis, Repair*, Wiley-VCH Verlag GmbH & Co. KGaA, Weinheim, ISBN 3-527-30800-8, 392 pp.



# Inspection of bridges in Austria—Practice and outlook

R. Wendner, S. Hoffmann, A. Strauss & K. Bergmeister  
*University of Applied Life Sciences and Natural Resources, Vienna, Austria*

R. Geier  
*Schimetta Consulting, Vienna, Austria*

**ABSTRACT:** During the last decades many structures—buildings and bridges—have been erected, many of which have already reached their initial design life demanding high efforts in inspection and maintenance. Due its geographical characteristics the Austrian railroad and street network consists of a high number of bridges, further complicating the task at hand. In course of a research project called AIFIT demands by operators and engineers were listed and future possibilities for more efficient inspection in accordance with current codes were derived.

## 1 INTRODUCTION

Every operator is obliged by law and codes to ensure safe usage of all structures. This encompasses especially guaranteeing a sufficiently high reliability level, with respect to the ultimate limit state (ULS), the serviceability limit state (SLS) and the durability limit state (DLS). Furthermore in case of bridges traffic safety has to be considered.

Technically a structure thus has to be inspected regularly with adequate documentation and assessment of its condition and possible damages. Additionally all necessary steps to maintain its condition and durability have to be taken and damage has to be repaired in case of some incident. Unfortunately limited monetary assets complicate matters. So a balance between inspection, maintenance, repair and obstruction of traffic resulting in economic losses has to be found.

In course of project AIFIT, which is aimed at developing user orientated approaches for damage identification and assessment, demands and experience coming from Austria’s largest operators of bridges were collected, evaluated and can be summarized as follows.

The main causes for interruption in usage and demand for repair are (a) changes in loadpaths in hyperstatic systems due to creep, shrinkage, relaxation, settling in the underground, changes in cable forces and from idealization deviating boundary conditions; (b) not detected damage and problems; (c) dynamic excitation by means of wind, wind/rain and traffic over time leading to fatigue, abrasion and other types of deterioration over time. (d) Finally extreme

or not foreseeable incidents like earthquakes, flood, and storm or vehicle impact on important structural members.

A sudden interruption or limitation of usage caused by damages as mentioned above causes high costs for necessary immediate action accompanied with problems with investors, insurance companies and authorities. Apart from national economic losses due to traffic obstructions, the damage itself and costs for repair an important aspect for operators is a possible loss of image and reputation especially in case of human casualties, which hardly can be quantified in monetary terms.

Not all kinds of damage require immediate action. In many cases of smaller problems a risk analysis is performed to determine the necessity of rehabilitation. In Figure 1 a possible schema for the evaluation of the operator’s risk is given.

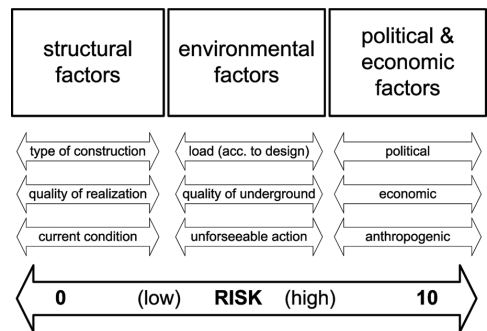


Figure 1. Assessment of operator’s risk.

## 2 CODES RELEVANT TO INSPECTION AND ASSESSMENT

As already stated, inspection and assessment are essential for maintenance planning to ensure sufficient reliability and cost efficiency. In Austria the following codes are currently to be applied by operators and engineers respectively.

### 2.1 *RVS 13.71 (1995) Überwachung, Kontrolle und Prüfung von Kunstbauten/Straßenbrücken*

RVS 13.71 is a directive issued by the Austrian government giving guidelines regarding the inspection of road bridges and familiar structures with respect to ULS, SLS, DLS and traffic safety. Basically early detection should be ensured in order to allow the operator to rehabilitate the structure in time before traffic safety is endangered or economic loss is caused.

This guideline differentiates between regular supervision (every 4 months), control (every 2 years) and full inspection (every 6 years).

Supervision is done visually by an employee of the operator and all changes in deflection, cracking as well as in the condition of the paving and the bridge equipment are noted.

Control is scheduled every 2 years and has to be performed by an engineer or a specially educated employee. Again only visual changes are noted and compared to earlier findings. If the condition of the structure is poor or due to extraordinary circumstances the time between controls is reduced.

A full inspection ordinarily is done every 6 years by an experienced engineer or if results from the control demand for it. During a full inspection all damages are registered, all statically relevant elements are evaluated and the structure's safety level is assessed with respect to ULS, SLS and DLS. Based on the results a finding is authored including the current assessment, possible limitations in usage, necessary maintenance steps or additional instructions for the next inspection.

However RVS 13.71 does not specify how results from monitoring systems, global identification or other sophisticated tools can be included or utilized. So basically the engineer doing the inspection takes the full responsibility for applied new technology, which could save time, money and even improve the quality of inspection.

### 2.2 *DIN 1076 (1999)—Ingenieurbauwerke im Zuge von Straßen und Wegen: Überwachung und Prüfung*

DIN 1076 describes inspection and supervision of engineering structures part of the road network with regard to ULS, SLS, DLS and traffic safety. Similar to the RVS 13.71 there are different levels of inspection

with varying repetition times and extensiveness. As demanded by the RVS 13.71 demands for documentation and detail increase with level inspection according to DIN 1076 as well. Apart from the final inspection report there are several types of documents which have to be kept listing structures, describing their elements and characteristics, observed damages and actions taken.

### 2.3 *ISO 13822 (2003)—Bases for design of structures. Assessment of existing structures*

This international code describes requirements and necessary steps during assessment of existing structures and the evaluations of effects of damage. This approach is based on an analysis of the entire structure considering some initial parameters and their adaptation to the current or a possible future situation. Again different levels of analysis can be considered. Instructions for including inspection results are provided but no statements are made regarding monitoring or inspection.

### 2.4 *ÖNORM B 4706 (2003)—Betonbau: Instandsetzung, Umbau & Verstärkung*

ÖNORM B4706 is the Austrian code detailing rehabilitation, repair, backfitting and strengthening of concrete structures to ensure, restore or improve durability and serviceability related properties. This code refers to inspection in general and solely gives instructions during which actions supervision and documentation is necessary and to what extent to ensure continuous safety and the achievement of the desired results.

## 3 MONITORING AND DATA ACQUISITION

The most important step in inspection and consequently maintenance planning is data acquisition. Codes relevant in Austria currently focus only on visual inspection. Thus depending on the level of detail changes to the structure are registered superficially or in great detail but all information is limited to what can be determined on the surface. In course of a full inspection cracking, wetting of the concrete surface, changed inclination of structural member, the condition of the bearings and joints and effects of corrosion to the reinforcement like visible rust or spalling can be registered. However there is no way to determine the condition of elements of the structure not accessible for instance due to pavement above it and results highly depend on the experience of the engineer performing the inspection. Although expert knowledge is an important and not dismissible factor more objective approaches should be considered as well.

During the last years many tools have been developed which allow a better insight into the structure and an improved assessment of existing damage, ranging from local tools like ultrasound, thermal imagery, radar surveillance and chemical analysis up to checking global characteristics like modal properties. More and more sophisticated tools are applied in practice by engineers but without proper support by codes and lacking any guidelines how to include the data acquired during assessment.

Apart from the ‘traditional’ inspection strategies based on a visual survey and maybe even sophisticated local tests there is the huge topic of digital data acquisition mostly referred to as monitoring. Generally monitoring includes the placement of certain types of sensors onto the structure, getting a digital signal, storing it and analysing it. This way changes of certain structural properties over time can be observed. Thus degradation processes and damage can be discovered at an early stage and necessary steps can be taken to ensure safety and save funds.

Depending on the length a monitoring system is applied to a structure permanent, periodic monitoring as well as monitoring on demand can be differentiated. During the last years monitoring has become an important factor in maintaining structures and many new as well as existing bridges have been equipped. However considering monetary aspects both in terms of installation costs and operation costs the implementation of a certain type of monitoring system has to be pondered carefully.

Given several thousands of structures which have to be maintained a full permanent monitoring system can only be applied to very few complex or endangered structures for which the direct and indirect consequences of failure clearly outweigh the costs of the monitoring system. Especially considering the huge amount of data collected by such a system and the human manpower needed to actually work with and analyse the data.

For the larger number of smaller structures only periodic monitoring or monitoring on demand is a feasible option. A typical example of monitoring on demand would be some structure the condition of which is not clear after for instance an explosion or a vehicle impact. In this case only few carefully chosen sensors such as a laser to measure deflection would be enough to monitor the structure in real time and alert authorities in case of a critical development. Costs of installation and especially data analysis are comparably low since there is no need for data storage and data evaluation can be automated simply by defining a trigger value denoting danger. In Figure 2 this is shown schematically.

In case there has been no obvious damage still periodic monitoring for instance accompanying every full inspection can be useful and worth

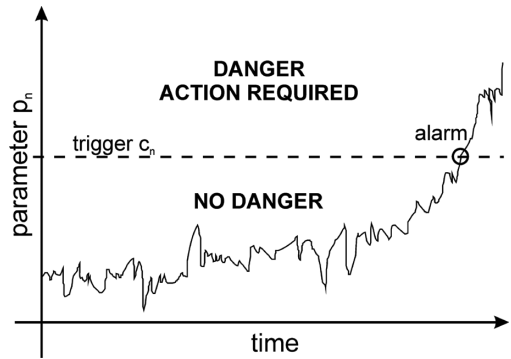


Figure 2. Monitoring of key sensors considering a trigger value.

the expenses. Basically there are two approaches possible.

Firstly a comparison between the currently measured properties and some kind of baseline, regardless whether this is a reference measurement done after completion of construction or the measurement during the last inspection. This approach allows identification of changes in structural characteristics and consequently possible damage. However the influence of changing boundary conditions and environmental influences like temperature can hardly be determined and included in the assessment which might lead to wrong conclusions.

Alternatively data from periodic monitoring can be used to determine certain structural properties which can be used to identify damage without the need for a baseline measurement. Hoffmann et. al (2007a, b) could show that directly measured influence lines for bearing reactions of hyperstatic systems can be used to determine the relative stiffness distribution within a structure. Through comparison with the ideal distribution based on known material properties and the cross section along the structure areas with possible damage can be localized and even the severity estimated. In a similar way mode shape data can be used to identify the stiffness distribution on an idealized structure without the need to consider material properties and cross section area at this point (Wendner et al. 2007). Again identification of damage is possible simply by evaluating the course of stiffness distribution without the need of considering external factors.

Both tools mentioned use global properties of the structure—static and dynamic respectively—to identify, localize and even quantify damage. The main advantage of those approaches lies in the ability to find damage even in areas which are not easily accessible. During a field test within project AIFIT damage in a 3 span plate-bridge above the middle supports could be

identified although the pavement did not permit access to the concrete itself.

Regardless of the type of monitoring system used or inspection performed important data about a structure is captured which allows a better understanding of the structural properties, the design itself and the influence of environmental impact. Based on this data bridge network's operator can optimize maintenance and construction of new structures with respect to safety requirements and cost efficiency.

#### 4 DAMAGE INVESTIGATION FROM OPERATOR'S PERSPECTIVE

Damage investigation from operators' point of view starts with the determination of the existence of damage followed by damage localization to identify areas which might lead to problems. After having identified damage the most important question is to determine whether immediate action to ensure safety is necessary or not. Only afterwards the extrapolation of the remaining life time and the optimization of maintenance can be started. From a practical point of view learning from damages and mistakes made is highly important since the analysis of existing damages, their causes and consequences allows to identify damage at an early stage and to classify damages to individual structural members according to their severity. In Vienna 3000 cases of damage affecting 900 bridges during the last 20 years have been analysed, see [Leitl \(2004\)](#).

Based on this report seven damage classes could be defined, as shown in Figure 3.

Apart from getting a statistical analysis of existing types of bridges, also types of damage were evaluated. Only 9% of overall costs due to damage were

<p><b>class 1: superficial damage</b> no consequence to usage and life time</p>
<p><b>class 2: slight local damage</b> only 1 element, slight influence on life time</p>
<p><b>class 3: slight structural damage</b> several elements, influence on life time</p>
<p><b>class 4: medium damage</b> failure of single element, limitation of usage possible</p>
<p><b>class 5: severe damage</b> immediate stop to usage, permanent limitation of usage possible</p>
<p><b>class 6: very severe damage</b> no rehabilitation possible, limited life time and usage</p>
<p><b>class 7: total failure</b> immediate and permanent failure of entire structure</p>

Figure 3. Possible classification of damage.

related with problems of the bearing structure, 10% were caused by the pavement and a total of 67% by damages to the bridge equipment mainly in connection with water tightness.

Further analysis of the data available resulted in a statistical evaluation of causes. According to this study 50% of all damages originate during construction. Consequently quality control during planning and construction are as essential as regular inspection of existing structures. Maintenance already starts during design, a fact that is well covered by various books on durability and robustness.

Given a big network of structures it's not easy to detect all damages in time, to assess the structures future condition correctly and to allocate funds in an optimal way to satisfy safety issues and budget restrictions. This is only possible using an intelligent management system with the following requirements ([Gitzelmann, 2003](#)): quick data acquisition, reduction in effort, objectivity, determination of characteristics and support for planning and decision making including documentation.

##### 4.1 Experts' experience

In general inspections are carried out according to the codes and guidelines already mentioned ordinarily by contracted engineers. Currently most data is acquired by performing a visual survey of the structure accompanied by tapping the concrete surface especially in highly reinforced areas and where some kind of rehabilitation has been done. Additionally the bridge equipment is controlled with special attention to joints and bearings. All damages are numbered increasingly and put into the report specifying the type of damage, its localisation and the structural element which is affected. In course of an ordinary inspection no geodetic survey of the structure is done as well as no recalculation of the bearing capacity or any planning of maintenance or rehabilitation actions.

After the inspection is finished a report is filed which has to contain information about the structure, its owner, and the inspector apart from the description of the inspection and the results. Additionally necessary actions regarding safety or durability are pointed out, instructions for future inspections are issued and possible necessary special tests are demanded.

##### 4.2 Typical damages in RC

Depending on the type of structural member different types of damage have to be considered. Generally damage to the superstructure, substructure and the bridge equipment can be differentiated which have varying effects on the reliability level with respect to ULS, SLS, DLS and traffic safety.

Since the damage to bridge equipment amounts to a large part of total maintenance costs special care has to be taken during inspection of those elements. In case of bearings the condition as well as the current position—angles and displacement—with respect to the temperature are registered. During inspection of joints the most important information apart from the visual condition is its width at the current temperature.

During investigation of the bearing structure the concrete surface is searched for signs of damage in the concrete itself as well as of corrosion of the reinforcement. Obvious damages like not covered reinforcement bars, pre-stressing cables and missing parts of the concrete body are documented. Spalling can be detected visually, which can be caused simply by frost or by corrosion due to chloride ingress or carbonisation. Naturally a rusty colour of the concrete surface can also denote corrosion of the reinforcement and is registered. Areas which are wetted due to bad sealing or bad drainage are noted too since they can lead to corrosion. By tapping the concrete surface hollow areas can be detected which is especially important during the first inspection. Hollow areas can have a big influence on durability and on bearing capacity if bonding is impaired.

A very interesting aspect is cracking since on one hand this is to be expected in a reinforced concrete structure but on the other hand can denote a serious loss of bearing capacity and endanger durability. In general cracks smaller than 0.3 mm or 0.1 mm for pre-stressed concrete are considered to be harmless. Everything above is documented in detail. In case the cause of cracking is obvious or cracking is accompanied by wetting, rusty colour or sintering this is noted as well. Laboratory tests in course of project AIFIT have shown that almost invisible cracking already lead to a significant loss of bending stiffness (Hoffmann, 2007b). Consequently the investigation of cracking has to be ascribed high importance to.

## 5 STRUCTURAL ASSESSMENT

After conclusion of the inspection itself the condition is assessed. This can be done according to different guidelines and approaches for the entire structure or for each member individually on basis of the classified damages resulting in a condition rating for instance ranging from 1 to 6—denoting excellent condition to immediate danger. In case of single assessment of structural members the assessment of the entire structure can be derived using weighting factors considering the importance of each member with respect to the safety level, see Bergmeister (1997). Based on this rating necessary steps in maintenance are

scheduled. Currently all data acquired during inspection—visual, ultrasound, thermal imagery, chemical analysis, etc.—are considered during damage investigation only.

In order to allocate funds more efficiently also the future condition of all structures has to be taken into account. Consequently the need for prediction arises for instance based on degradation models. Furthermore using all available physical data during assessment and considering changes of several physical parameters over time can significantly decrease uncertainty in prediction and thus allow for better management of funds. In Figure 4 the condition index over time is shown depending on start condition  $C_I$  and target condition  $C_H$  at lifetime  $t_H$  (Strauss et. al, 2007). Of course the more data available the better results can be expected. However due to the high costs for monitoring and especially data analysis only periodic monitoring with a limited number of sensors is feasible from a practical point of view.

Since codes specify required safety levels both with respect to ULS and SLS in terms of failure probability the determination of reliability at least for critical structures will gain in importance. Thus the identification of relevant parameters for instance material properties using one time or periodic measurement is essential to be able to accurately describe structural behaviour. Based on this data for example a non-linear finite element analysis can be performed to determine the structure's reliability level. In general identification tools should be robust, impartial, highly automated and work without the need for engineering judgement to be applicable in practice. Alternatively stiffness distributions can be identified directly using global parameters and used for the assessment of failure probability apart from getting information about possibly damaged areas of the structure (Wendner et. al, 2007).

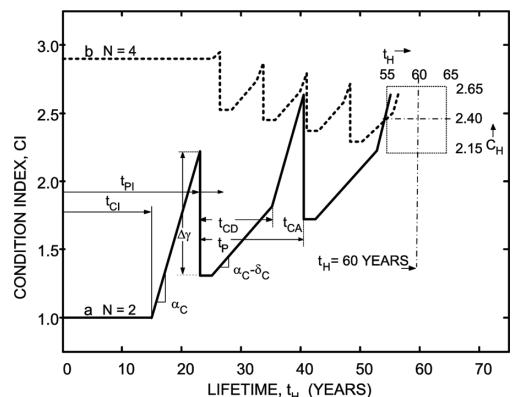


Figure 4. Condition profile over time.

## 6 CONCLUSIONS

In Austria there is an established and working system for bridge inspection based on visual survey of structures and experts' experience. Since there is an increasing number of structures which have to be inspected regularly and are reaching their initial lifetime demands for more efficient and automated inspection, assessment and maintenance arise. Although there are already many tools especially for local testing available which can improve inspection codes do not support them. Additionally suitable robust, unbiased and highly automated global identification tools, which allow a direct determination of the structures condition based on limited global measurements, are still in development and are not accounted for in guidelines either. Finally instructions regarding life time prediction and assessment of existing structures need to be issued in order to allow for more efficient allocation of funds and management of structures belonging to Austria's road and railroad network.

## ACKNOWLEDGEMENT

The authors wish to express their gratitude to the Austrian research foundation FFG for financial support of project AIFIT and to our partners Schimetta Consult, ÖBB (Austrian railway) and Maurer Söhne. Finally we express our thanks to Konrad Bergmeister, who made this project possible.

## REFERENCES

Bergmeister, K. (1997). *Assessment Procedures and Safety—Evaluation on Concrete Bridges*. CEB, Bulletin 239.  
DIN 1076 (1999). *Ingenieurbauwerke im Zuge von Straßen und Wege: Überwachung und Prüfung*.  
Gitzelmann, H. (2003). *Intelligente Inspektionssysteme für Eisenbahnen*. in german. BPI-Consult GmbH, Wiesbaden.

Hoffmann, S., Bergmeister, K., Strauss, A., Preslmayr, M. (2007a). *Identifying Stiffness Distributions by Direct Influence Line Measurements*. proceedings of 10th International Conference on Application of Statistics and Probability in Civil Engineering, July 31—August 3 2007, Tokio, Japan.  
Hoffmann, S., Wendner, R., Strauss, A., Bergmeister, K. (2007b). *Comparison of stiffness identification methods for reinforced concrete structures*. Proceedings of the 6th International Workshop on Structural Health Monitoring, Sept 11–13 2007, Stanford, CA, USA.  
ISO 13822 (2003). *Bases for design of structures. Assessment of existing structures*.  
Leitl, D. (2004). *Dauerhaftigkeit und Robustheit von Straßenbrücken. diploma thesis (in german)*, Institute of Structural Engineering, Univ. BOKU, Vienna, Austria.  
Kong, J.S., Frangopol, D.M. (2004). *Cost-Reliability Interaction in Life-Cycle Cost Optimization of Deteriorating Structures*. Journal of Structural Engineering, ASCE, 130 (11), 1704–1712.  
ÖN B4702 (2000). *Straßenbrücken aus Beton—und Stahlbeton—Berechnung und konstruktive Durchbildung*.  
ÖN B4706 (2003). *Betonbau—Instandsetzung, Umbau, Verstärkung*.  
Preslmayr, M. (2006). *Analyse von Steifigkeitsänderungen bei Ingenieurtragwerken- Modellierung mittels nichtlinearer Finite Elementen Methoden*. diploma thesis (in german), Institute of Structural Engineering, Univ. BOKU, Vienna, Austria.  
RVS 13.71 (1995). *Überwachung, Kontrolle und Prüfung von Kunstbauten—Straßenbrücken*.  
Strauss, A, Frangopol, D.M., Bergmeister, K. (2007). *Condition—reliability aspects for the probabilistic lifetime optimization of structures*. proceedings of 10th International Conference on Application of Statistics and Probability in Civil Engineering, July 31—August 3 2007, Tokio, Japan.  
Wendner, R., Strauss, A., Hoffmann, S., Bergmeister, K. (2007). *Novel Identification Methods for the Assessment of Engineering Structures*. proceedings of 5th International Probabilistic Symposium, Nov 28–29 2007, Ghent, Belgium.

*Life-cycle performance of special structures*

# Probability-based durability design and performance-based concrete quality control of a concrete harbor structure

V. Årskog

*Ålesund University College, Ålesund, Norway*

O.E. GjØrv

*Norwegian University of Science and Technology, NTNU, Trondheim, Norway*

**ABSTRACT:** In the present paper, experience with probability-based durability design and performance-based concrete quality control of a new container harbor in Oslo City is briefly outlined and discussed. As an overall durability requirement, a service period of at least 100 years was required before a probability of 10% for steel corrosion would be reached. Based on a durability analysis of the given structure in the given environment, requirements to both chloride diffusivity and concrete cover for the given structure were established, and this provided the basis for the performance-based concrete quality control during concrete construction. Based on the relationship between chloride diffusivity and electrical resistivity of the given concrete, a regular quality control of the chloride diffusivity based on electrical resistivity measurements on all concrete specimens used for the testing of compressive strength was carried out. In combination with a regular control of achieved concrete cover, this provided the basis for control of the specified durability. Upon completion of the concrete construction, compliance with the specified durability with a good margin was obtained. Additional documentation on achieved durability on the construction site and achieved potential durability of the structure also showed very good results.

## 1 INTRODUCTION

During the period from January 2005 to June 2007, the first part of a new container harbor for Oslo City was constructed. The 650 m water front consists of an open concrete deck on top of solid columns consisting of driven steel tubes filled with concrete. The major part of the 22,900 m<sup>2</sup> concrete deck is a slab type of deck with deep girders. For this part, a large number of slab elements were prefabricated and placed between the in situ cast concrete girders as formwork for the following concreting of the deck. Another part of the deck is a flat slab deck constructed on top of the deck of an old existing concrete harbor structure, which was used as formwork for the production of the new concrete deck.

According to the current Norwegian concrete codes (NS-EN 206-1 2003, NS 3473 2003), the durability requirements to the new concrete harbor structure primarily included a maximum water-binder ratio of 0.40, a minimum binder content of 330 kg/m<sup>3</sup> and a minimum concrete cover of 60 mm. For ensuring proper frost resistance, a total air content of 4–6% was also required. In order to obtain an increased and

more controlled safety against steel corrosion, however, the local harbor authorities decided to apply the new recommendations and guidelines for durability design published by The Norwegian Association for Harbor Engineers (2004a, b). Although such a durability design does not guarantee a given service life of a structure, this design is based on engineering judgment of all those factors which are considered relevant for the durability, including the scatter and variability of all factors involved. As a result, durability requirements are specified which can be verified and controlled during the construction period. Thus, during concrete construction, a regular monitoring of the most important durability parameters is carried out, and upon completion of the construction period, a documentation of achieved construction quality and durability is provided before the structure is handed over to the owner. As part of the durability design, the owner is also provided with a service manual on how to carry out a regular monitoring of the real chloride penetration during the service period and how to apply protective measures in order to control this chloride penetration. After some time of observed chloride penetration, probability-based extrapolations of the



further chloride penetration and evaluation of corrosion probability provide the basis for how frequent the further control of chloride penetration shall be carried out. Also, if the probability of steel corrosion eventually becomes too high, protective measures are recommended in order to retard or stop the further chloride penetration and thus obtain a more controlled service life.

In the following, the experience from this durability design and the following quality control for ensuring that the specified durability would be achieved during concrete construction is briefly outlined and discussed.

## 2 SPECIFIED DURABILITY

As an overall durability requirement to the new concrete harbor structure, the owner required a service period of at least 100 years before a probability of steel corrosion of 10% would be reached. In order to calculate such a probability for steel corrosion, a simple calculation of chloride penetration rates based on Fick's Second Law of diffusion with a time-dependent chloride diffusion coefficient (Luping & Gulikers 2007) in combination with a Monte Carlo Simulation was carried out (Gjørøv 2002 & 2004, Ferreira & al. 2004).

The conventional expression for the error function solution to Fick's 2nd law can be written as:

$$C(x, t) = C_S \left[ 1 - \operatorname{erf} \left( \frac{x}{2\sqrt{D_a \cdot t}} \right) \right] \quad (1)$$

where  $C(x, t)$  is chloride content at depth  $x$ ;  $C_S$  is chloride content at the exposed surface;  $D_a$  is apparent chloride diffusion coefficient; and  $t$  is time of exposure. The time dependency of the chloride diffusion coefficient can be expressed as:

$$D_a = \frac{D_0}{1 - \alpha} \cdot \left[ \left( 1 + \frac{t'_{ex}}{t} \right)^{1-\alpha} - \left( \frac{t'_{ex}}{t} \right)^{1-\alpha} \right] \cdot \left( \frac{t'_0}{t} \right)^\alpha \quad (2)$$

where  $\alpha$  is aging factor;  $D_0$  is chloride diffusion coefficient at time  $t'_0$ ;  $t'_{ex}$  is age of concrete at the start of exposure; and  $t$  is time of exposure. The model also includes the annual average temperature (Polder & deRoos 2005).

An unacceptable rate of corrosion will start when the chloride content at the depth of reinforcement exceeds a certain critical value,  $C_{CR}$ .

Based on the above requirement to probability of corrosion, an initial durability analysis was carried out in order to establish the necessary requirements to concrete quality and concrete cover. The individual input parameters for this analysis are shown in

Table 1. Input data for initial durability analysis.

Environmental load, $C_S$ (% by wt. of binder)	N (3.8;0.9)*
Annual average temperature ( $^{\circ}\text{C}$ )	10
Age of concrete at start of exposure, $t'_{ex}$ (days)	28
Chloride diffusivity, $D_{28}$ ( $\times 10^{-12}$ m <sup>2</sup> /s)	N (5.0;1.0)
Testing age for chloride diffusivity, $t'_0$ (days)	28
Aging factor, $\alpha$	N (0.6;0.12)
Critical chloride content, $C_{CR}$ (% by wt. of binder)	N (0.4;0.08)
Concrete cover, $X$ (mm)	N (90;0.11)
Service period, (years)	100

\*Normal distribution (Average value; standard deviation).

Table 1. In this table,  $D_{28}$  is the chloride diffusion coefficient ( $D_0$ ) measured according to the NT Build 492 Method (1999) at an age of concrete  $t'_0 = 28$  days. The environmental load ( $C_S$ ) was based on long-term experience from existing concrete structures in Oslo Harbor after service periods of up to 80 years. For the critical chloride content ( $C_{CR}$ ), an empirical value of 0.40 by weight of binder was adopted. An average value of 0.60 for the aging factor was also used as input parameter for the analysis.

Based on this durability analysis, it was shown that a chloride diffusivity of  $D_{28} \leq 5.0 \times 10^{-12}$  m<sup>2</sup>/s in combination with a concrete cover of  $90 \pm 15$  mm would satisfy the required durability with a proper margin. These results, therefore, were used as a basis for the specified requirements to chloride diffusivity and concrete cover.

In order to establish a concrete mixture which would meet the required chloride diffusivity, some preliminary tests were carried out by the contractor. Based on a pure portland cement of type CEM I 52,5 LA and 4% silica fume by weight of cement, three different concrete mixtures with 20, 40 and 60% replacements of the cement by fly ash were produced. Based on these tests, the mixture based on 60% replacement was selected by the contractor. Although this type of concrete showed a somewhat higher value of  $D_{28}$  than that specified, the further development of the chloride diffusivity showed very good results. Therefore, this type of concrete was accepted for the further concrete production (Table 2).

Extensive experience has shown that much of the durability problems which develop after some time can be related to lack of proper quality control and special problems during concrete construction. For the concrete structure in question, therefore, it was very important to carry out a performance-based concrete quality control which would ensure that the specified durability would be achieved during concrete construction (Gjørøv 2003).

Table 2. Composition of the concrete mixture.

Constituents	kg/m <sup>3</sup>
Portland cement (CEM I 52,5 LA)	270
Silica fume(4%)	10.8
Fly ash	162
Superplastiziser	6
Air entraining admixture	3
Fine aggregate (0–8 mm)	850
Coarse aggregate (8–16 mm)	200
Coarse aggregate (16–24 mm)	665
Water	139
Air content (%)	>4
w/b-ratio	0.31

### 3 ACHIEVED DURABILITY

#### 3.1 General

Shortly after start of the concrete construction work, a solid concrete test slab with dimensions of 2.0 × 2.0 × 0.5 m without any reinforcement was produced on the construction site. From this test slab which was produced and cured as representative as possible for the real concrete structure, a number of Ø 100 mm concrete cores were later on removed at various ages in order to observe the development of chloride diffusivity on the construction site. During the production of the test slab, a number of 100 mm concrete cubes and Ø 100 × 200 mm concrete cylinders were also produced. Already the next day, these test specimens were sent to the laboratory for establishing the necessary calibration curve to be used for the later control of chloride diffusivity based on electrical resistivity measurements. All electrical resistivity measurements were based on the Wenner Method (Sengul & Gjorv 2007), and in the laboratory all specimens were kept in water until time of testing. After the calibration curve was established, it was required that some of the concrete cylinders should be kept in water for further testing of the chloride diffusivity at various intervals of up to at least half a year.

#### 3.2 Compliance with specified durability

Based on combined testing of chloride diffusivity (cylinders) and electrical resistivity (cubes) after curing periods of 14, 28, 56 and 89 days (Table 3), a calibration curve as shown in Figure 1 was established, where the electrical conductivity is the inverse value of the electrical resistivity. This calibration curve was later on used as the basis for an indirect control of the chloride diffusivity ( $D_{28}$ ) based on electrical resistivity measurements. This testing was carried out on all concrete cubes which were used for the testing of the 28 day compressive strength.

Table 3. Development of chloride diffusivity and electrical resistivity under laboratory conditions.

Testing age days	Chloride diffusivity ( $\times 10^{-12}$ m <sup>2</sup> /s)*	Electrical resistivity (ohm m)
14	14.0;1.9	146;9
28	6.9;0.1	307;21
56	4.6;0.6	508;41
89	2.4;0.5	699;55
186	1.2;0.3	1201;131
365	0.7;0.02	1836;232

\* Average value; standard deviation.

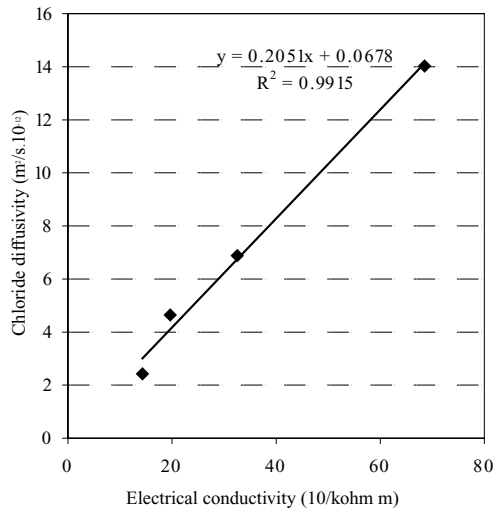


Figure 1. Calibration curve for control of chloride diffusivity based on measurements of electrical resistivity.

Table 4. Achieved chloride diffusivity ( $D_{28}$ ) based on electrical resistivity measurements during concrete construction.

Testing age (days)	Electrical resistivity (ohm m)*	Chloride diffusivity ( $\times 10^{-12}$ m <sup>2</sup> /s)
28	260;102	7.9;3.2

\* Average value; standard deviation.

During the whole period of concrete construction, a total of 344 individual measurements of electrical resistivity were carried out, and this was the basis for the regular control of the chloride diffusivity. This quality control showed an acceptable level of chloride diffusivity throughout the concrete construction without large deviations. As a result, an average value of chloride diffusivity of  $7.9 \times 10^{-12}$  m<sup>2</sup>/s with a standard deviation of 3.2 was achieved (Table 4).

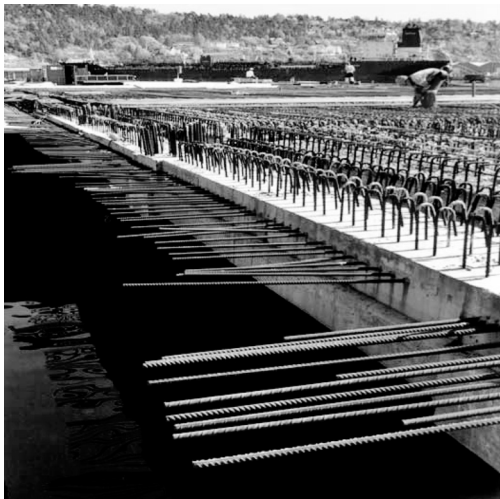


Figure 2. Protruding bars in the concrete deck.



Figure 3. The concrete deck had very congested reinforcement.

Throughout the construction period, a number of control measurements of achieved concrete cover were also carried out. Due to the very thick concrete cover and very congested reinforcement as shown in Figures 2 and 3, however, it was not possible to obtain reliable measurements based on conventional cover meters. Therefore, all control measurements were based on observed concrete covers on protruding bars in concrete joints. Based on altogether 68 individual measurements, an average concrete cover of 99 mm with a standard deviation 11 mm was obtained.

Upon completion of the concrete construction work, a new durability analysis based on the input parameters shown in Table 5 was carried out. A probability of 4.9% of corrosion over a 100 years service

Table 5. Input data for analysis of the compliance with specified durability.

Environmental load, $C_S$ (% by wt. of binder)	N (3.8;0.9)*
Annual average temperature ( $^{\circ}$ C)	10
Age of concrete at start of exposure, $t'_{ex}$ (days)	28
Chloride diffusivity, $D_{28}$ ( $\times 10^{-12}$ m <sup>2</sup> /s)	N (7.9;3.2)
Testing age for chloride diffusivity (days)	28
Aging factor, $\alpha$	N (0.6;0.12)
Chritical chloride content, $C_{CR}$ (% by wt. of binder)	N (0.4;0.08)
Concrete cover, $X$ (mm)	N (99;11)
Service period (years)	100

\*Normal distribution (Average value; standard deviation).

Table 6. Development of chloride diffusivity on the construction site.

Testing age (days)	Chloride diffusivity ( $\times 10^{-12}$ m <sup>2</sup> /s)*	
	Test slab	Structure
28	6.9;1.7	
56	4.3;0.4	
62		6.2;0.3
89	4.7;0.4	
168		1.7;0.2
186		3.4;0.1
250		2.5;0.1
365	1.7;0.1	1.4;0.2

\*Average value; standard deviation.

period showed that the specified durability had been achieved with a good margin during the construction period.

### 3.3 Achieved in situ durability

In order to provide some additional information on achieved durability on the construction site, a number of  $\varnothing$  100 mm concrete cores were removed from the test slab which had been produced on the construction site at an early stage of the concrete construction. These cores were removed at various ages of up to one year, and immediately upon removal, the cores were sent to the laboratory for testing of achieved chloride diffusivity. In addition, achieved chloride diffusivity was also tested on a number of concrete cores which were removed from the real concrete structure where possible. All these results are shown in Table 6 and graphically demonstrated in Figure 4. In this figure, the development of chloride diffusivity based on water cured specimens in the laboratory is also shown.

Based on achieved chloride diffusivity on the construction site after periods of 180 and 365 days in combination with achieved concrete cover, new durability

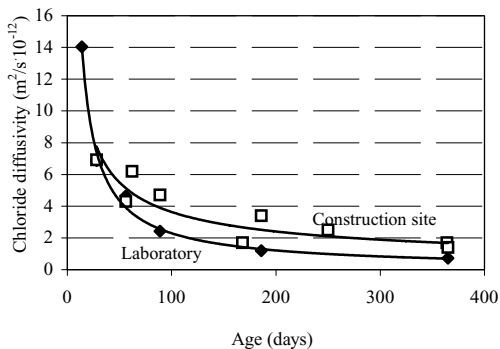


Figure 4. Development of chloride diffusivity on the construction site and in the laboratory.

analyses were carried out. For a chloride diffusivity after 180 days of  $2.86 \times 10^{-12} \text{ m}^2/\text{s}$  with standard deviation of 0.76 and  $1.47 \times 10^{-12} \text{ m}^2/\text{s}$  with standard deviation of 0.76 after 365 days, the durability analyses showed probabilities of 2.0 and 0.6 % of corrosion after a service period of up to 100 years, respectively. These results indicate that achieved durability on the construction site was very good.

### 3.4 Achieved potential durability

Based on achieved chloride diffusivities after 180 and 365 days of water curing in the laboratory in combination with achieved concrete cover, further durability analyses were carried out. For a chloride diffusivity after 180 days of  $1.2 \times 10^{-12} \text{ m}^2/\text{s}$  with standard deviation of 0.3 and  $0.7 \times 10^{-12} \text{ m}^2/\text{s}$  with standard deviation of 0.02 after 365 days, these durability analyses showed probabilities of 0.02 and 0.01% of corrosion after a service period of up to 100 years, respectively. These results indicate that achieved potential durability of the structure was also very good.

## 4 CONCLUDING REMARKS

As an overall durability requirement to the given concrete structure, it was specified that the structure should have a service period of at least 100 years before a probability of 10% for corrosion would be reached. On the basis of the durability analysis carried out, requirements to both chloride diffusivity and concrete cover could be established, and this provided the basis for the performance-based concrete quality control during concrete construction.

Based on the data on chloride diffusivity and concrete cover obtained from the concrete quality control during concrete construction, a new durability analysis showed a probability of 5.9% of corrosion, which

demonstrates a very good compliance with the specified durability. The quality control also revealed a very good achieved durability on the construction site and a very good achieved potential durability of the structure, with probability levels of 2.0 and 0.6% after a period of one year, respectively.

It should be noted that the above “service period” should not be considered as a real service period for the given concrete structure. As a basis for the durability design, a very simple diffusion model for the calculation of chloride penetration was applied. The durability analyses were also based on accelerated migration testing of the chloride diffusivity and an aging factor for the chloride diffusivity for which there is a lack of reliable data. However, the probabilities obtained are the result of an engineering judgement of the most important factors relevant for the durability including the scatter and variability of all factors involved. From the performance-based concrete quality control carried out, it appears that a very good durability had been achieved. For the concrete structure in question, it is only a regular monitoring of the real chloride penetration during operation and evaluation of the future corrosion probability in combination with proper protective measures which provide the ultimate basis for achieving a more controlled service life.

## ACKNOWLEDGEMENTS

The opportunity to carry out the durability design and the following concrete quality control for Oslo Harbor KF and to publish current test results and experience is greatly appreciated.

## REFERENCES

- Ferreira M., Jalali S. and Gjrv O.E., 2004. Software for Probability-Based Durability Analysis of Concrete Structures. *Proc. 4th Int. Conf. on Concrete under Severe Conditions-Environment and Loading*, Vol. 1, ed. by B.H. Oh, K. Sakai, O.E. Gjrv and N. Banthia, Seoul National University and Korea Concrete Institute, Seoul, ISBN 89-894-02-X 93530, 1015–1024.
- Gjrv O.E. 2002. Durability and Service Life of Concrete Structures, *Proc. First fib Congress 2002*, Session 8, Vol. 6, Japan Prestressed Concrete Engineering Association, Tokyo, 1–16.
- Gjrv O.E. 2003. Durability of Concrete Structures and Performance-Based Quality Control. *Proc. Int. Conf. on Performance of Construction Materials in the New Millennium*, ed. by A.S. El-Dieb, M.M. R. Taha and S.L. Lissel, Shams University, Cairo, ISBN 977-237-191, 10 p.
- Gjrv O.E. 2004. Durability Design and Construction Quality of Concrete Structures, *Proc. 4th Int. Conf. on Concrete under Severe Conditions-Environment and Loading*, Vol. 1, ed. by B.H. Oh, K. Sakai, O.E. Gjrv and N. Banthia, Seoul National University and Korea Concrete Institute., Seoul, ISBN 89-894-02-X 93530, 44–55.

- Luping T. and Gulikers J. 2007. On the Mathematics of Time-Dependent Apparent Chloride Diffusion Coefficient in Concrete. *Cement and Concrete Research* 37(4), 589–595.
- Norwegian Association for Harbor Engineers, 2004a. *Recommended Specifications for Increased Durability of New Concrete Harbor Structures*, TEKNA, Oslo, 2. edition, 18 p (In Norwegian).
- Norwegian Association for Harbor Engineers, 2004b. *Practical Guidelines for Durability Design of New Concrete Harbor Structures*, TEKNA, Oslo, 2. edition, 48 p (In Norwegian).
- NS-EN 206-1, 2003. Concrete—Part 1: Specifications, properties, execution and conformity, Standards Norway, Oslo.
- NS 3473, 2003. Design of concrete structures. Design- and detailing rules, Standards Norway, Oslo.
- NT Build 492, 1999. Concrete, Mortar and Cement Based Repair Materials: Chloride Migration Coefficient from Non-Steady State Migration Experiments, NORDTEST, Espoo, ISSN 0283-7153, 8 p.
- Polder R.B. and deRoos M.R. 2005. Durability of Marine Concrete Structures – Field Investigations and Modelling, *HERON* 50(3), 133–153.
- Sengul, O. and Gjorv, O.E. 2007. Electrical Resistivity Measurements for Quality Control of Concrete Durability. *Proc. 5th Int. Conf. on Concrete Under Severe Conditions— Environment and Loading*, Vol. 1, ed. by F. Toutlemonde, K. Sakai, O.E. Gjorv and N. Banthia, Laboratoire Central des Ponts et Chaussées, Paris, ISSN 1626-4704, 871–880.

# Structural safety evaluation of a r.c. arch bridge

A.M. Avossa, P. Famigliuolo & P. Malangone

*Department of Civil Engineering, Second University of Naples, Aversa (CE), Italy*

**ABSTRACT:** The paper presents the analytical and experimental modal analysis of an existing reinforced concrete arch bridge, built in the fifties across the Volturno river on “Domitiana” state road. First the modal properties of different 3D finite element models of the bridge were determined with/without reference to some structural strengthening carried out in the seventies. Then ambient vibration tests under traffic excitation are designed and developed in order to identify the bridge modal properties and calibrate its theoretical model. Finally starting from results obtained by that model, the structural response under different load conditions (traffic and seismic loads) was carried out in order to evaluate the real bridge behaviour and the structural safety assessment according to current seismic code provisions.

## 1 INTRODUCTION

Structural safety assessment of existing bridges is a topic in the field of structural engineering, especially for structures nearly to their lifetime. In particular, bridge strengthening capacity evaluation requires an analysis criteria based on hypotheses different as regard to design criteria used for new structures. In fact some of these old bridges are subjected to service loads (traffic loads) very different than design ones.

On the other hand the need to assess the real characteristics of stiffness and strength as a result of inevitable phenomena of damage and degradation over time is very important too. In detail, the degradation of the mechanical properties of the constituent materials comes from the deterioration induced by environmental like chemical or physical causes as well as any design flaws or constructive errors. Other causes of damage are related to specific phenomena such as the type of impulsive actions, the fatigue of materials under repeated loads, the seismic actions and the possibly high temperatures caused by fire.

The assessment of the state of health and conservation for the scheduled maintenance of bridge structures is usually obtained through visual checks, not always based on objective criteria for damage classification. This approach, although improved by use computerized protocols that allow the definition of specific “damage indices”, however, does not permit to obtain a full bridge life cycle assessment. In fact there is no specific assessments, such as those relating to the mechanical parameters of materials, the depth of a possible chemical attack, etc.

In particular, the structural materials characterization in terms of quality and strength can be obtained

through destructive and non-destructive tests, that increase the information provided by visual inspection but do not allow alone to fully assess the functioning of the structure alone.

Alternatively it is possible to perform static test operations, or to use techniques of limited impact on bridge functionality, such as the dynamic tests. Through the monitoring of dynamic parameters (frequencies, modal shapes, damping ratios) and more generally by comparison with numerical models, it is possible to evaluate the local or global stiffness degradation related to structural problems. Therefore it is necessary to support the theoretical results with specific experimental activities, in order to validate the model parameters and to provide analytical results representative of the real structural response. Therefore these experimental activities play a key role for structural capacity assessment and for estimate of their level of accuracy.

In this context the paper concerns the dynamic identification and the structural safety assessment of a r. c. arch bridge built in the fifties across the Volturno river.

The study, which is of interest also of a social issue on the need to determine the bridge structural safety under the seismic actions, aims also to identify any improving interventions according to the current code provisions.

## 2 THE VOLTURNO RIVER ARCH BRIDGE

The bridge on Volturno river, built on “Domitiana” state road in the municipality of Castelvolturno (Caserta), is a typical open spandrel deck arch bridge according to Maillart’s type. In particular the entire

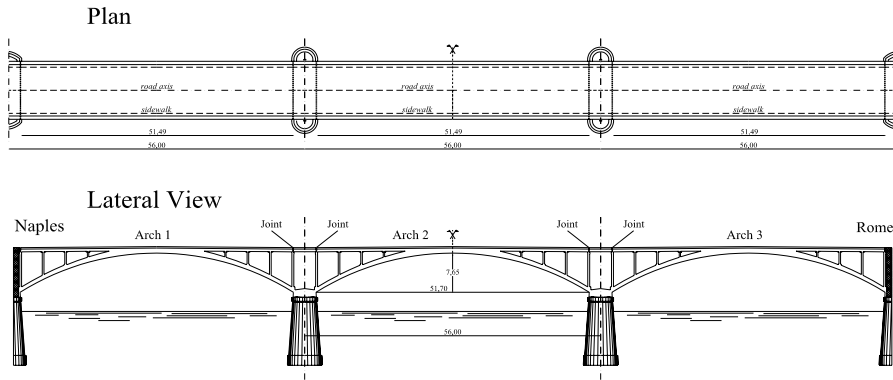


Figure 1. The Volturno river arch bridge geometry (plan and upriver lateral view).

structural scheme consists of three independent twin reinforced concrete arches, tapered from crown to springing, with a span length of 51.70 m and with a rise to span ratio of 1:7 (Fig. 1). The slab deck sustained by main girders and floor girders transmits dead and moving loads to arches through columns of variable heights. Piles and abutments are founded respectively on caissons and foundation piles.

In the late seventies the bridge shown some local situations of significant structural deterioration. In fact the bridge exhibited cracks both in the parts exposed to flood water both in elements in immediate contact with the vehicular traffic, such as slab deck, girders and joints systems. The last damages were caused likely by high levels of traffic conditions because of frequency, intensity and speed of moving loads. The efficiency of foundation structures over time and the substantial structural integrity of arches were crucial to target the decision-making process to the bridge retrofit. Therefore the static verifications pointed out the possibility of the bridge retrofit according to existing requirements for the 1st category roads (*Circolare No.384, 14/2/1962*), whereas the bridge had been design in order to support the traffic loads required by *Normale No.6081, 9/6/1945*.

Bridge retrofit was achieved by repair, replacement and strengthening interventions of some existing members. In particular, the twin arches were strengthened into the interior parts with a steel lattice covered with a new concrete jet. The arch ribs near the springing were also stiffened by an integrative new concrete thin slab placed to the extrados. The upgrade of columns and of floor beams was also carried out with a partial jacketing technique. Moreover slab deck was strengthened by two main girder in addition to the four already existing, and by a new thin slab of about 6 cm dowelled to the extrados. Finally the bridge joints were remodeled in order to obtain the roadway continuity and a suitable structural gap under the road pavement. Overall, the bridge was fully inspected and repaired

by replacement interventions of corroded reinforcing bars and by the sealing of cracks.

The current structure shows obvious signs of deterioration, mainly due to physical and chemical aggression produced by weathering and by river waters. In particular some parts of abutment walls and some parts of arches are interested by reinforcing bars corrosion with related spalling phenomena.

### 3 THE BRIDGE STRUCTURAL MODELLING

Before the implementation of dynamical tests some bridge structural FEM models have been developed both in order to identify an appropriate positioning of the acceleration measuring instruments both to conduct a preliminary assessment of structural modal parameters. In particular the 3D finite element models of the bridge, defined in linear field, were determined also with reference to structural retrofit interventions carried out in the seventies. Given the particular twin arches geometry with a variable arch ribs (twin arches are joined at springing while there are hole ribs at crown), solid “brick” elements with 8 nodes and 3 degrees of freedom per node has been chosen in order to define the theoretical model. The three arches can be considered structurally independent because of the deck joints existence. That has allowed to examine a single arch bridge, characterized appropriately by a specific FEM model.

At first step the FEM1 arch modeling was carried out with reference to current geometry, estimating the structural contribution of integrative elements as perfectly joined to the original structures (Fig. 2). With reference to FEM1 model, modal shapes and corresponding modal participating mass ratios values of more significant six modes are represented in Figure 3. In particular, can be pointed out that the modal shapes more involved in bridge response are mainly bending in XZ plane, with exception of the mode 2 bending in

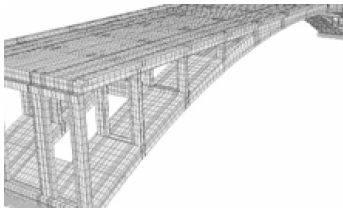


Figure 2. Retrofitted Arch model (FEM1).

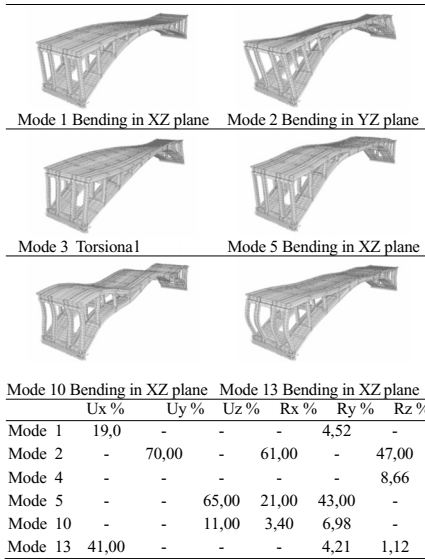


Figure 3. Bridge FEM1 model: modal shapes and corresponding participating mass ratio.

the XY plane and of the mode 3 which is torsional. Modal shapes shown in figure are related to a levrotatory axes of coordinates with origin at external corner of the springing and axis of X parallel to bridge longitudinal direction.

Then the contribution provided to global bridge response by repair structural interventions carried out in the seventies was partially neglected. In particular a situation of structural separation between the existing concrete surface and the concrete jet added to the arch extrados has been considered. Therefore a new FEM2 model which takes into account of the original arch rib has been defined. In this model the structural role of these new reinforced concrete elements has been reduced to lumped mass only. In Figure 4 are shown the modal dynamic characteristics of FEM2 model that show minor differences as compared to the corresponding ones of previous FEM1 model.

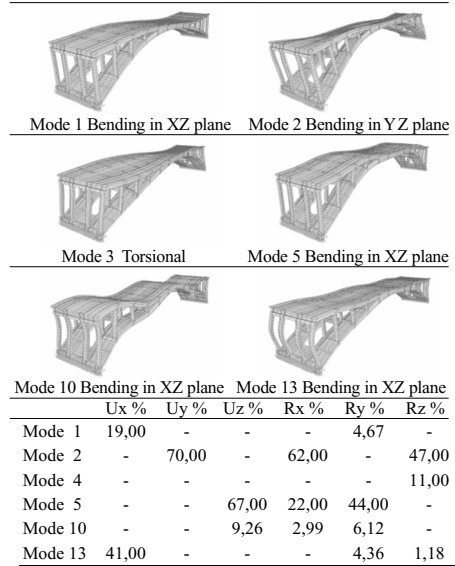


Figure 4. Bridge FEM2 model: modal shapes and corresponding participating mass ratio.

#### 4 DYNAMIC TESTS AND SIGNAL PROCESSING OF EXPERIMENTAL DATA

##### 4.1 Dynamic tests

In the recent years the use of dynamical tests in order to carry out the structural parameters identification has met an increasing development especially in the case of bridges and viaducts. In fact the methodology effectiveness, the increasing accuracy of measurement instruments and the data acquisitions systems capacity provide an accurate and reliable prediction of structural global modal parameters of these structures. In particular the experimental dynamic analysis allows: a) to check the correspondence between the real dynamic response and the theoretical model one; b) the validation of structural material parameters; c) the identification and position of structural defects or anomalies through the comparison between experimental modal shapes and theoretical ones. In order to avoid or to limit the bridge out of service, in this case first have been carried out ambient vibration tests through the recording of accelerations due to the ordinary vehicular traffic. Then the bridge has been dynamically excited both by passages of lorry and tractor at different velocity (40, 60, 80 Km/h) both by passages of a lorry over a prominence placed at 1/4 of span length. Accelerations in various positions over the bridge have been measured by using 8 piezoelectric accelerometers PCB/393A03 with sensitivity of 5 Volt/g. The equipment used for the tests also includes signal cables, a 16-channel data acquisition



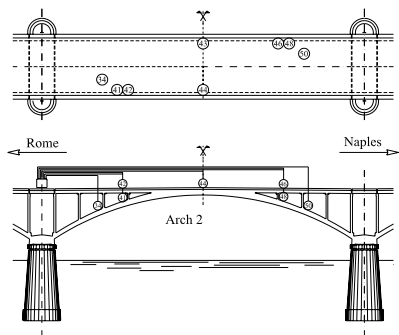


Figure 5. Measurement stations arrangement for ambient vibration test.

systems with signal amplifier and conditioner directly connected with a notebook for the storage and the analysis of data. The above-mentioned instrumentation is available at the Department of Civil Engineering—Second University of Naples and all dynamic tests were organized and carried out by the authors of this work. Bridge dynamic response was investigated through the 8 measurement stations placed in anti-symmetric way according to the information obtained from the mode shapes of the preliminary finite element models (Fig. 5). In particular 4 accelerometers was placed on the slab deck at mid span length and at 1/4 span length. The other 4 accelerometers had been placed on the arch extrados respectively at 1/4 and at 1/8 of span length. All accelerometers had been mounted in the vertical direction according to the preliminary theoretical analysis indications that allowed to neglected the accelerations in transverse direction. In all cases the sampling acceleration frequency on site was 50 Hz.

#### 4.2 Modal parameter identification

Dynamic parameter identifications was carried out by peak picking method (PP) that is initially based on the fact that the frequency response function goes through an extreme value around the natural frequency. In the context of ambient vibrations measurements, the frequency response function is replaced by the auto spectra and cross spectra of the output-only data (Bendat & Piersol 1993).

The PP approach leads to reliable estimates in the cases of low damping and sufficiently spaced modal frequencies. In this case the frequency response function  $H(\omega)$  can be evaluate with good approximation starting from autospectrum  $S_{xx}$  of the response signal  $x$  recording by the accelerometer as follow:

$$H(\omega) = S_{xx}/S_{ff} \quad (1)$$

where  $f$  indicates the unknown random bandwidth excitation signal (similar to white noise) due to

vehicular traffic which corresponding a  $S_{ff}$  autospectrum constant ( $1/c$ ) for each frequency value. The recording signals have been filtered by Hanning window and corresponding spectra have been calculated using the Welch's method. The results of the PP approach in terms of natural frequencies (for vertical modes) can be represented through spectral diagrams reported in Figure 6 where are represented the autospectra of accelerations recorded at different deck and arch points of measure with reference to the passage of ordinary vehicular traffic. The spectral diagrams show distinctly a well-defined series of peaks corresponding to the following six frequency values: 2.93 Hz, 5.86 Hz, 8.79 Hz, 10.93 Hz, 12.89 Hz, 16.01 Hz. For the same conditions of excitation are set, in Table 1, the values of frequencies identified by reference to autospectra obtained starting from each registration. It may be pointed out that the processing of recorded data due to ordinary vehicular traffic has allowed the identification of a great number of modal frequencies with a well-defined spectrum obtained by a signal not affected by noise. These results also were confirmed by processing of recorded signals starting by the other types of bridge excitation carried out. In fact there are good correlations among the natural frequency values identified starting by recorded data with different types of excitation. In particular, can be observed that the asymmetrical load condition excites the higher frequency vibration modes, as can be remarked by autospectra peaks values corresponding to 5.86 Hz and 8.79 Hz frequency values (Fig. 7).

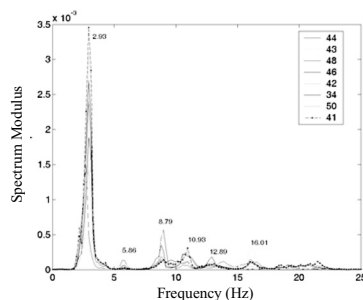


Figure 6. Acceleration autospectra due to the ordinary vehicular traffic.

Table 1. Frequency identified values.

Sensor	F1[Hz]	F2 [Hz]	F3 [Hz]	F4 [Hz]	F5 [Hz]	F6 [Hz]
34	2.93	5.86	8.79	10.94	12.89	16.60
41	2.93	5.86	8.98	10.94	13.08	16.01
42	2.93	5.86	9.57	10.94	12.70	16.01
43	2.93	5.86	8.98	10.55	12.89	16.01
44	2.73	5.86	8.98	10.55	12.30	16.01
46	2.93	5.86	8.79	10.74	12.50	16.01
48	2.93	5.86	8.79	10.74	12.50	16.01

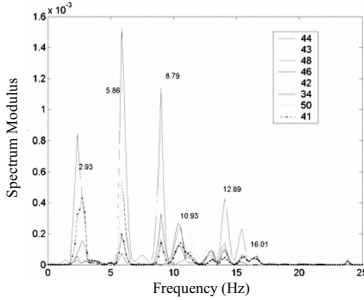


Figure 7. Acceleration autospectra due to lorry passages over a prominence placed at 1/4 of span length.

## 5 THEORETICAL MODEL VALIDATION

The identification of bridge natural frequencies obtained by recorded acceleration data processing has allowed then the characterization and validation of the bridge theoretical model. In this case the model parameters to calibrate are the values of the concrete elastic modulus  $E_C$  and the structural joining level between original members and the strengthening parts or elements added in the seventies. This last aspect has been taken into account developed the two different theoretical model FEM1 and FEM2. Regarding to these models, the concrete elastic modulus values were determined in order to make equal the fundamental period of theoretical bridge model with the experimental one. This has allowed to complete the dynamic characterization of FEM1 and FEM2 models through the evaluation of bridge natural frequencies of the six mode shapes (bending in the XZ plane and torsional) identified with dynamic tests. A first comparison between experimental and theoretical results can be carried out with reference to first two columns of Tables 2–3 that shows respectively the experimental and theoretical natural frequency values for the two considered FEM models. Then a measure of correlation between theoretical and experimental results was obtained by evaluating the percentage error  $\varepsilon_f$  through the following relationship:

$$\varepsilon_{f,i} = \frac{|f_{Exp,i} - f_{Theo,i}|}{f_{Exp}} \quad (2)$$

where for the  $i^{\text{th}}$  modal shape  $f_{Exp}$  and  $f_{Theo}$  represent respectively the natural frequency experimental values and theoretical ones. The identification of mechanical model whose results provide better approximation of the experimental data was carried out, for both theoretical models examined, by assessing the values of following  $J$  error function:

$$J = \sum_{i=1}^N w_i \cdot \varepsilon_{f,i}^2 \quad (3)$$

Table 2. Comparison between theoretical and experimental natural frequencies (FEM1 model).

	$f_{EXP}$ [Hz]	$f_{THEO}$ [Hz]	$\varepsilon_{f,i}$	$w_i$
Modo 1	2.930	2.930	0.0001	0.2401
Modo 3	5.860	5.793	0.0114	0.0871
Modo 5	8.790	7.675	0.1269	1.2900
Modo 7	10.930	9.770	0.1062	0.0437
Modo 10	12.890	13.895	0.0780	0.2139
Modo 13	16.010	15.985	0.0016	0.4633
$E_{FEM1} = 26076.0$ [MPa]			$J = 0.02258$	

Table 3. Comparison between theoretical and experimental natural frequencies (FEM2 model).

	$f_{EXP}$ [Hz]	$f_{THEO}$ [Hz]	$\varepsilon_{f,i}$	$w_i$
Mode 1	2.930	2.930	0.0001	0.2413
Mode 4	5.860	5.864	0.0007	0.1089
Mode 5	8.790	8.050	0.0842	1.3263
Mode 7	10.930	9.701	0.1124	0.0405
Mode 10	12.890	13.832	0.0731	0.0617
Mode 13	16.010	16.836	0.0516	0.4893
$E_{FEM2} = 30198.8$ [MPa]			$J = 0.01155$	

Table 4. Error function  $J$  evaluation to varying of flexural restraint level.

Restraint Level	$k_\varphi$ [kN*m]	$J_{FEM1}$	$J_{FEM2}$
0	0	0.06336	0.04052
1/2	1.95E + 07	0.02676	0.01208
2/3	3.90E + 07	0.02673	0.01207
3/4	5.85E + 07	0.02673	0.01207
1	$\infty$	0.02258	0.01155

where the square percentage error value (standard deviation) for  $i^{\text{th}}$  modal shape is weighted by a  $w_i$  coefficient equal to the sum of the six modal participating mass ratios taken into account. The identified values of concrete elastic modulus with the corresponding values given by error function (3), for each structural model analyzed, are reported in Tables 2–3. The comparison between the FEM1 and FEM2 theoretical models shows that the experimental structural response is better approximate by the FEM2 model which presents the lower value of error function.

Finally the possibility of a different restraint condition at the springing of arches was considered, including in both FEM models a rotational springs with flexural stiffness value  $k_\varphi$ . In Table 4 are shown the values that the error function  $J$  takes for varying of the rotational stiffness parameter  $k_\varphi$ , characterized on equivalent beam scheme, for different values of restraint level (RL) at the ends.

Table 5. Loads combination factors for ULS safety check.

	$g_1$	$g_2$	$q_1$	$q_2$	$q_3$	$q_5$
$U_I$	1.4	1.4	0	0	0	1.5
$U_{II}$	1.4	1.4	1.5	1.5	0	0.9
$U_{III}$	1.4	1.4	1.5	1.5	1.5	0.3

## 6 STRUCTURAL SAFETY EVALUATION

Starting from the dynamic identification and theoretical model calibration results, structural response of FEM2 model under different load conditions (traffic and seismic loads) was fulfilled according to current Italian Code provisions (Norme Tecniche, 2005 and OPCM 3431, 2005). In particular the safety checks of cross sections at the ends of columns and in correspondence of four significant arch cross sections such as the arch rib at springing, the two mirror arch ribs of haunch (spaced of 6.90 m from springing) and the crown arch rib were carried out. The structural safety assessment was fulfilled considering the following different load cases: dead load of structural and non structural elements ( $g_1$ ,  $g_2$ ), moving load and its dynamic amplification effects ( $q_1$ ,  $q_2$ ), longitudinal braking/acceleration load ( $q_3$ ), snow or wind load ( $q_5$ ). The maximum and minimum stress diagrams due to moving loads were carried out starting from the influence lines calculation. Load combinations used in order to evaluate the structural safety checks for ultimate limit state (ULS) conditions are shown in Table 5. For all load combinations taken into account, the ultimate limit state stress values are not exceeded. In particular the arch ribs at springing and the cross sections at the ends of shorter columns presented stress values closed to the failure ones relating to  $U_{II}$  and  $U_{III}$  combinations while the safety checks for the other structural members and for all combinations are satisfied with a large margin of safety.

The bridge structural safety assessment under seismic loads was also carried out through a response spectrum analysis based on the smoothed elastic spectra for type C soil with  $PGA = 0.15$  g (corresponding to third category seismic hazard level) provided by current Italian Code. The corresponding structural members safety checks under all gravity and seismic loads combinations are satisfied with a large margin of safety if compared to the ultimate conditions force values.

## 7 CONCLUSIONS

The paper presents the analytical and experimental modal analysis of an existing reinforced concrete three arch bridge built in the fifties across the Volturno river. First the description of bridge typology and geometry

was presented also with reference to some structural strengthening carried out in the seventies. Then the modal properties of different 3D finite element models of the bridge were determined with/without reference to aforementioned structural strengthening. The identification of bridge dynamic parameters has allowed then the calibration and validation of the bridge theoretical model whose results are more closed with real experimental behaviour. In particular for FEM2 model were estimated the concrete elastic modulus value and the restraint level at springing. Finally starting from these results the structural response of FEM2 model under different load conditions (traffic and seismic loads) was carried out in order to evaluate the real bridge behaviour and the structural safety assessment according to current seismic code provisions.

## REFERENCES

- Bendat, J.S. & Piersol, A.G. 1993. *Engineering applications of correlation and spectral analysis*. Wiley Interscience, 2nd Ed.
- Douglas, B.M. & Reid, W.H. 1982. Dynamic test and system identification of bridge, *Journal of Structural Division*, ASCE, 108: 2295–2312.
- Ewins, D.J. 1986. *Modal Testing: theory and practice*. Research Study Press, UK.
- Ferraioli, M., Malangone, P. & Zambrano, A. 2003. Some iron railway bridges of the 19th century built in Italy: recent experimental investigations and analytical modelling, *8th International Conference on Inspection Appraisal & Maintenance of Structures*, Singapore.
- Friiba, L. 1972. *Vibration of solids and structures under moving loads*, Academia, Publishing House of the Czechoslovak Academy of Sciences, Prague.
- Gentile, C. 2000. *Comportamento dinamico e identificazione strutturale di ponti e viadotti*, Pitagora Editrice, Bologna.
- Italian Code, 2005. *Consiglio Superiore dei LL.PP. Norme Tecniche per le Costruzioni*, and OPCM 3431, *Allegato 3 —Ponti*.
- Maya, N.M.M. & Silva, J.M.M., 1997. *Theoretical and experimental modal analysis*, Research Studies Press Ltd.
- Miyamoto, A., Kawamura, K. & Nakamura, H. 2001. Development of a bridge management system for existing bridges. *Advances in Engineering Software*, Elsevier, 32: 821–833.
- Ren, W.X. & Zong, Z.H., 2004. Output only modal parameter identification of civil engineering structures. *Struct Engng Mech*; 17(3–4): 429–444.
- Thoft Christensen, P. 1995. Advanced bridge management systems. *Engineering Structures*, Elsevier, 3: 151–163.
- Welch, P.D. 1967. The use of Fast Fourier Transform for the estimation of Power Spectra: a method based on time averaging over short modified periodograms. *IEEE Trans. Audio Electroacoustic*, 15: 70–73.

# Towards life-cycle assessment of foundations of guyed towers in electrical transmission lines

C.B.P. Azevedo & S.M.C. Diniz

*Federal University of Minas Gerais, Belo Horizonte, Brazil*

**ABSTRACT:** Nowadays there has been a great interest in the use of probabilistic methods in problems related to electrical transmission lines. While different types of towers may be used along a transmission line, preference is usually given to guyed towers for its smaller weights and resulting smaller foundation costs. Due to the complex interaction soil-guy-tower, information on this subject is mostly obtained by experimental methods. In this work, experimental results are coupled to systems reliability techniques in the evaluation of failure probabilities of guyed towers foundations. These probabilities represent main ingredients in the estimation of risks associated with potential foundation failures. This is an important step towards the implementation of life cycle methods in the design, operation, and maintenance of electrical transmission lines.

## 1 INTRODUCTION

The demands for a sustainable development have put a strong emphasis on the use of renewable energy sources. In this regard, Brazil is in a privileged position with its large hydropower potential for electricity generation. On the other hand, there has been an increase in the distance between generation and consumption locations. As a result, the transmission of energy,—its technological aspects, dependability, and attendant costs—,is of great importance in the decision among different competing energy sources.

A transmission line is made of different mechanical components,—cables, towers, foundations—, and its reliability can be estimated by the methods of system reliability (Ang & Tang 1990). Due to uncertainties in the parameters involved, the reliability of the transmission line system can be established in probabilistic terms only. While different types of towers may be used, preference is usually given to guyed towers for its smaller weights and resulting smaller foundation costs. Typically, these structures are comprised by two main towers (with foundations under compression) and four guys (with foundations under tensile forces).

Nowadays there has been a great interest in the use of probabilistic methods in problems related to electrical transmission lines. However, most of the studies performed so far are related to the reliability of towers (e.g. Kempner et al. 2002) or foundations under compression loads (e.g. Phoon et al. 2000). Due to the complex interaction soil-guy-tower, information on this subject is mostly obtained by experimental methods. As such, the availability of a large number of test

results for guyed-tower foundation behavior obtained during the construction of the North-Northeastern line in Brazil offers a unique opportunity for a realistic analysis. In this work, experimental results are coupled to systems reliability techniques in the evaluation of failure probabilities of guyed towers foundations. These probabilities represent main ingredients in the estimation of risks associated with potential foundation failures. This is an important step towards the implementation of life cycle methods in the design, operation, and maintenance of transmission lines.

## 2 FOUNDATIONS IN THE NORTH-NORTHEASTERN SYSTEM

The North-Northeastern system has been designed and built to attend the increased electricity demand in the North-Northeastern region of the Brazilian territory. This 500 kV system comprises the following branches: (i) Tucuruí—Vila do Conde, (ii) Tucuruí—Marabá, (iii) Marabá—Açailândia, (iv) Açailândia—Imperatriz, and (v) Açailândia—Presidente Dutra (see Fig. 1). These transmission lines were built in 2001 and 2002 in the Pará and Maranhão states, and started operations in March 2003.

Standard Penetration Tests (SPT) have been performed along the transmission lines for the estimation of the soil geotechnical parameters. As a design criterion, these tests have been performed on average at each 5 km. Initially, two main groups have been defined: sand and a combination of sand-clay soils. Based on the number of strokes ( $N_{SPT}$ ) in the SPT

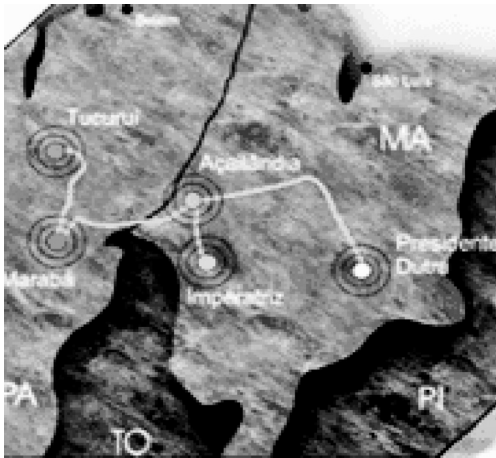


Figure 1. Transmission line branches of the North-Northeastern system in the Pará and Maranhão states, Brazil.



Figure 2. General view of the pull-out test (Azevedo 2006).

tests, each soil group has been further subdivided as Type I ( $N_{SPT} \geq 12$ ), Type II ( $8 \leq N_{SPT} < 12$ ), Type III and Type IV ( $4 \leq N_{SPT} < 8$ ). The distinction between types III and IV is that the latter corresponds to a submerged terrain (water level above the foundation level). Most of the foundations corresponding to soils Type I, II, and III have been designed as cylindrical blocks with 80 cm-diameter and located at depths 320, 350, and 400 cm, for soils I, II, and III, respectively.

Out of 7,780 stay foundations in the N-NE transmission line, 471 had pull-out tests performed (see Table 1 and Figure 2). A detailed description of these tests is found in Azevedo (2006). These tests have been planned and executed in order to check the following performance criteria: (i) maximum displacement under axial loads (50 mm allowable limit), and (ii) maximum residual displacement (unloaded condition, 25 mm allowable limit).

Table 1. Extension, number of foundations, and number of tests performed in each branch of the transmission line.

Transmission Line	Extension (km)	Number of foundations	Number of tests
Tucuruí – Vila do Conde	324.1	1976	351
Tucuruí – Marabá	217.5	1152	36
Marabá – Açailândia	237.6	1736	20
Açailândia – Imperatriz	56.8	356	14
Açailândia – Pres. Dutra	414.9	2560	50

### 3 STATISTICAL MODELING OF MAXIMUM AND RESIDUAL DISPLACEMENTS

The results obtained in each of the 471 foundation pull-out tests have been documented in spreadsheets as reported in Azevedo (2006). The data has been separated according to each of the standard soil type: 97 tests for soil Type I, 211 tests for soil Type II, and 163 tests for soil Type III. Each test comprises data for maximum,  $D_{MAX}$ , and residual,  $D_{RES}$ , displacements. The largest values corresponding to each data set have been extracted, the corresponding histograms have been plotted, and a probability distribution has been fitted to each data set ( $D_{MAX}$  and  $D_{RES}$  for each soil type). The adequacy of fitted probability distributions was checked by the chi square goodness of fit test (Haldar & Mahadevan 2000). The histograms, and superimposed selected probability distributions, for maximum and residual stresses are shown in Figures 3–8.

The performance criteria: (i) maximum displacement under axial loads (50 mm allowable limit), and (ii) maximum residual displacement (unloaded condition, 25 mm allowable limit) may be represented in terms of the following performance functions:

$$g_1(D_{MAX}) = 50 - D_{MAX} \quad (1)$$

$$g_2(D_{RES}) = 25 - D_{RES} \quad (2)$$

where  $g_1(\cdot)$  represents the limit state associated to foundation maximum displacement under load conditions and  $g_2(\cdot)$  represents the limit state associated to foundation residual displacement in unload conditions. The events  $[g_1(\cdot) < 0]$  and/or  $[g_2(\cdot) < 0]$

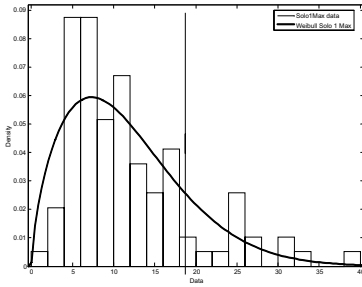


Figure 3. Histogram and superimposed Weibull distribution for maximum displacements in soil Type I.

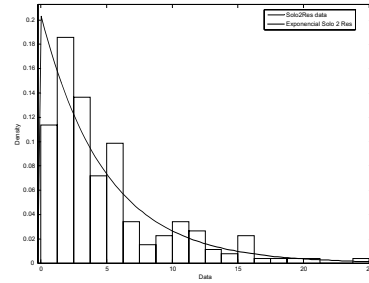


Figure 6. Histogram and superimposed exponential distribution for residual displacements in soil Type II.

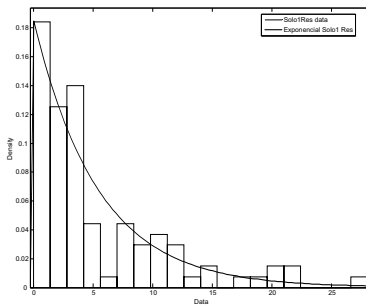


Figure 4. Histogram and superimposed exponential distribution for residual displacements in soil Type I.

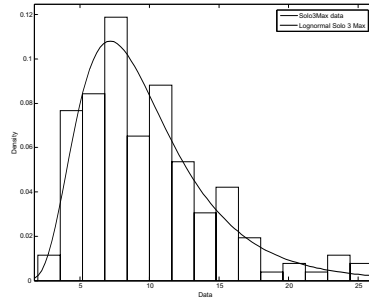


Figure 7. Histogram and superimposed Lognormal distribution for maximum displacements in soil Type III.

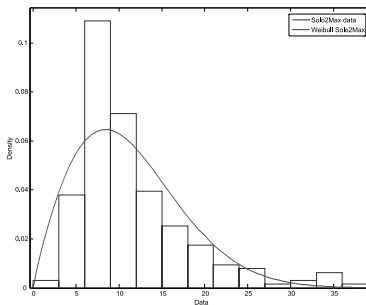


Figure 5. Histogram and superimposed Weibull distribution for maximum displacements in soil Type II.

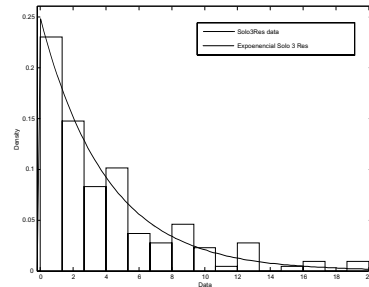


Figure 8. Histogram and superimposed exponential distribution for residual displacements in soil Type II.

represent failure (or nonperformance) of each stay foundation.

Table 2 displays the computed mean, standard deviation for performance functions  $g_1(\cdot)$  and  $g_2(\cdot)$  and corresponding correlation coefficient  $\rho(g_1, g_2)$  for each of the three standard soil types. The correlation coefficients between failure modes show similar values for each soil type. Additionally, these values are positive, as expected, and close to unity, i.e. perfect

correlation ( $\rho = 1.0$ ). This can also be seen in Figure 9 which shows a plot of maximum displacements versus residual displacements for soil Type II.

#### 4 ESTIMATION OF PROBABILITIES OF FAILURES

A schematic representation of an electrical transmission line system is shown in Figure 10. This is a highly complex system comprised by mechanical and

Table 2. Mean, standard deviation for performance functions  $g_1(X)$  and  $g_2(X)$  and corresponding correlation coefficient.

Soil type	Sample size	$g_1$		$g_2$		$\rho(g_1, g_2)$
		Mean	St.Dev.	Mean	St.Dev.	
I	97	38,52	7,62	19,66	5,81	0,83
II	211	38,80	6,52	20,08	4,40	0,84
III	163	40,12	4,67	20,97	3,97	0,82

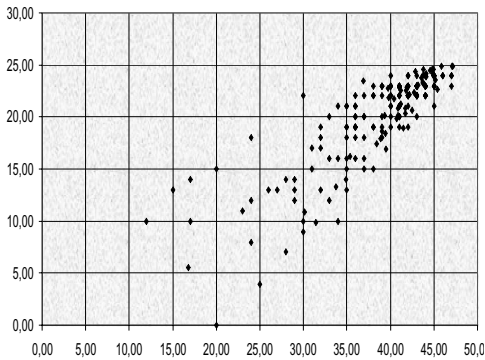


Figure 9. Maximum displacements versus residual displacements for soil Type II.

electrical components where each component is a system of its own (or a subsystem in a larger system). In the present study, the focus is on failure (or nonperformance) of the foundations of stays in guyed towers. The fault tree representation of the foundation system is shown in Figure 11.

Failure or nonperformance of the system may be estimated based on concepts and methods of systems reliability (Ang & Tang 1990, Melchers 1999). For positive correlation between failure modes, the uni-modal bounds for the probability of failure are given by:

$$\max_i p_{F_i} \leq p_F \leq 1 - \prod_{i=1}^k (1 - p_{F_i}) \quad (4)$$

where  $p_{F_i}$  is the probability of failure corresponding to the  $i$ -th failure mode. For small values of  $p_{F_i}$ , the right-hand side in Equation 4 may be approximated as:

$$1 - \prod_{i=1}^k (1 - p_{F_i}) \cong \sum_{i=1}^k p_{F_i} \quad (5)$$

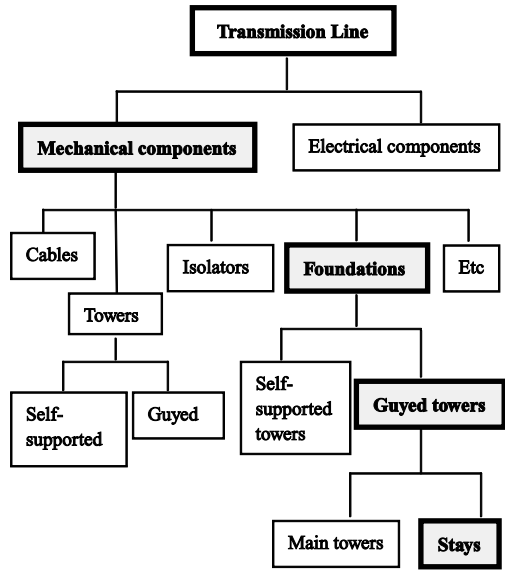


Figure 10. Schematic representation of the transmission line system.

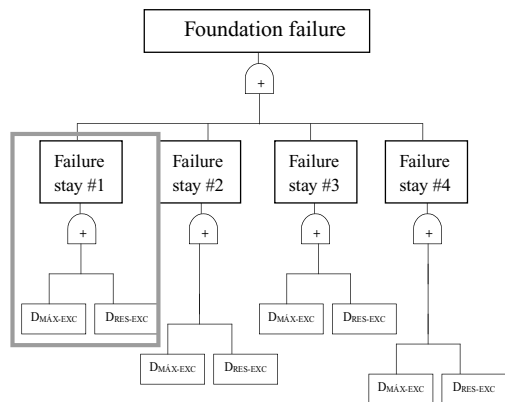


Figure 11. Fault tree representation of failure in the foundation system. Failure of the subsystem “stay”, i.e. secondary event is highlighted.

#### 4.1 Failure in the subsystem “stay”

Each guyed tower is supported by 4 stays. As presented in section 3, in this work it is considered that the foundation of each stay may fail either by excessive displacements under loads or excessive residual displacements. These failure modes for each stay are represented by the performance functions in Equations 1 and 2. These two performance functions comprise deterministic limits (50 mm for



maximum displacements under loads and 25 mm for residual displacements) proposed by experts in the field. Rather than physical failure, these limits are associated to nonperformance of the system. The first is related to requirements for proper performance of the electrical equipment, and the second is a practical limit implying that retensioning of the stays is required in the case of excessive residual displacements.

The primary events  $E_1 = [g_1(.) < 0]$  and/or  $E_2 = [g_2(.) < 0]$  represent failure of each stay foundation. This can be mathematically represented as  $P(E_1 E_2)$ , i.e. the probability of the intersection of events  $E_1$  and  $E_2$ . The event failure in the subsystem “stay” is highlighted in Figure 11.

The computed probabilities of failure,  $P(E_1)$  and  $P(E_2)$ , for soil types I, II, and III are shown in Table 3. Also shown in this table are the lower and upper bounds of the probability of failure for the  $i$ -th stay foundation,  $P(E_1 E_2)$ . These limits have been obtained through Equation 4. The lower and upper bounds correspond to perfectly correlated and statistically independent failure modes, respectively.

As it can be seen in Table 3, for soil Type I, the probability of failure due to excessive maximum displacements under load conditions,  $P(E_1)$ , is about 10 times smaller than the probability of failure due to excessive residual displacements,  $P(E_2)$ . Regarding soils Type II and III, the probability of failure due to excessive maximum displacements,  $P(E_1)$ , is about 1000 times smaller than the probability of failure due to excessive residual displacements,  $P(E_2)$ . These results indicate that the primary failure mode “excessive residual displacements” is dominant in all the three soil types. This implies in narrow limits for the probability of failure of the subsystem “stay” as it can be observed in the fourth and fifth column of Table 3.

Additionally, based solely on the number of strokes,  $N_{SPT}$ , in the SPT tests ( $N_{SPT} \geq 12$  for soil Type I,  $8 \leq N_{SPT} < 12$  for soil Type II, and  $4 \leq N_{SPT} < 8$  for soil Type III), it could be expected that the probability of failure for the subsystem “stay” in soil Type II would be smaller than that corresponding to soil Type III. However, as it can be observed in Table 3, this is not true. While a number of reasons may be responsible for these results, it should be reminded

that different depths have been used for the cylindrical blocks, i.e. 320, 350, and 400 cm, for soils I, II, and III, respectively. It can be concluded that both soil type and foundation depth do play a role in the stay foundation reliability.

#### 4.2 Failure in the system “foundation”

As already mentioned, each guyed tower is supported by 4 stays. It is assumed herein that all 4 stay foundations are built in the same soil type. Based on the fault tree in Figure 11, it is further assumed that failure of a single stay will result in the failure of the system “foundation”, i.e. it is assumed that the foundation system behaves as a series system. In the previous section, the probability of failure of the  $i$ -th stay foundation, i.e. the probability of the secondary event, has been obtained. Based on these probabilities associated to the secondary events, the uni-modal bounds for the foundation system can be obtained.

Table 4 presents results for the lower and upper bounds for the probability of failure of the foundation system for secondary events assumed as: (a) perfectly correlated (columns 2 and 3), and (b) statistically independent (columns 4 and 5). For the perfect correlation assumption for the secondary failure modes, column 2 corresponds to perfectly correlated primary modes, and column 3 to statistically independent primary modes. For the statistical independence assumption for the secondary failure modes, column 4 corresponds to perfectly correlated primary modes, and column 5 to statistically independent primary modes.

An analysis of Table 4 indicates that overall bounds correspond to the results listed in column 2 for the lower bounds (perfectly correlated primary events and perfectly correlated secondary events) and column 5 for the upper bounds (statistically independent primary events and statistically independent secondary events). A comparison of the upper and lower bound for each soil type indicates that the latter are 4.4, 3.96, and 4.0 times larger than the former for soil type I, II, and III, respectively. If needed, further refinements could be made by using bi-modal bounds (Ang & Tang 1990). In this case, information on the correlation between pairs of secondary events, i.e. failure of the subsystem

Table 3. Probabilities of failure  $P(E_1)$  and  $P(E_2)$  for the primary events and lower and upper bounds for the subsystem failure.

Soil	$P(E_1)$	$P(E_2)$	$P_f$ (lower bound)	$P_f$ (upper bound)
I	1.10 E-04	1.05 E-03	1.05 E-03	1.16 E-03
II	1.00 E-06	6.22 E-03	6.22 E-03	6.22 E-03
III	9.00 E-06	2.02 E-03	2.02 E-03	2.03 E-03

Table 4. Lower and upper bounds for the probability of failure of the foundation system for secondary events: perfectly correlated and statistically independent.

Soil	Perfectly correlated		Statistically independent	
	Lower bound	Upper bound	Lower bound	Upper bound
I	1.05 E-03	1.16 E-03	4.193 E-03	4.631 E-03
II	6.22 E-03	6.22 E-03	2.465 E-02	2.465 E-02
III	2.02 E-03	2.03 E-03	8.056 E-03	8.091 E-03



“stay  $i$ ” and failure of the subsystem “stay  $j$ ”,  $i, j = 1, \dots, 4$ , are required. It can be submitted, however, that, similarly to primary events, this correlation should be high and corresponding probabilities of failure close to the lower bound. Additionally, it is interesting to observe that probabilities of failure of  $10^{-3}$ , as obtained in the present study, are common for structural components in other civil engineering systems (see Galambos et al. 1982). This also shows the adequacy of simple rules used in practice for describing much more complex phenomena.

## 5 SUMMARY, CONCLUSIONS, AND SUGGESTIONS

Nowadays, the transmission of energy,—its technological aspects, dependability, and attendant costs—, is of great importance in the decision among different competing energy sources. An electrical transmission line is a highly complex system comprised by mechanical and electrical components where each component is a system of its own. While different types of towers may be used, preference is usually given to guyed towers for its smaller weights and resulting smaller foundation costs and overall initial costs. Typically, these structures are comprised by two main towers (with foundations under compression) and four guys (with foundations under tensile forces). The survival of such towers is highly dependent on the performance of the guy foundations. Due to the complex interaction soil-guy-tower, information on this subject is mostly obtained by experimental methods.

In the present study, the focus has been on failure (or nonperformance) of the foundations of stays in guyed towers. The availability of a large number of test results for in-situ guyed-tower foundation behavior obtained during the construction of the North-Northeastern line in Brazil has offered a unique opportunity for a realistic analysis. In this work, these experimental results have been coupled to systems reliability techniques in the evaluation of failure probabilities of guyed towers foundations.

The estimation of the probability of failure of the foundation system involves the computation of the probability of failure for each primary event (“excessive displacements under loads” and “excessive residual displacements”) and then the probability of failure for the subsystem “stay” (secondary event). Experimental results for 471 pull-out tests were used in the statistical modeling of the maximum and residual displacements. Two performance functions, comprising deterministic limits proposed by experts in the field, have been used. A high positive correlation between the primary failure modes has been observed ( $\rho = 0.83, 0.84$ , and  $0.82$ , for soils Type I, II, and III, respectively).

The results obtained for the probability of failure for the subsystem “stay” indicate that the primary failure mode “excessive residual displacements” is dominant in all the three soil types. This implies in narrow limits for the probability of failure associated to the secondary events. In the sequence, the probability of failure of the foundation system has been estimated. Lower and upper bounds for the probability of failure of the foundation system for the assumptions of: (i) perfect correlation, and (ii) statistical independence of the secondary failure modes, have been obtained. A comparison of the upper and lower bounds for each soil type indicates that the latter are roughly four times larger than the former for all soil types. If needed, further refinements could be made by using bi-modal bounds. It can be submitted, however, that, similarly to primary events, correlation between pairs of secondary events should be high, leading to corresponding probabilities of failure close to the lower bound.

The probabilities of failure computed in this study represent main ingredients in the estimation of risks associated with potential foundation failures. Their use will depend on the particular monetary information available for describing different failure events (primary, secondary or any other combination thereof). The information obtained in this study can be linked to the reliability of other transmission line components, e.g. towers (Kempner et al. 2002) and foundations under compression (Phoon et al. 2000) for a life-cycle analysis of the electrical transmission line system.

## REFERENCES

- Ang, A.H-S. & Tang, W.H 1990. *Probability Concepts in Engineering Planning and Design – Decision, Risk and Reliability*, Vol. II, New York.
- Azevedo, C.P.B. 2006. *Avaliação da Confiabilidade de Fundações de Torres Estaiadas de Linhas de Transmissão* (in Portuguese). Master’s Dissertation, Federal University of Minas Gerais (UFMG). Belo Horizonte, 131 p.
- Galambos, T.V., Ellingwood, B., MacGregor, J.G. & CORNELL, C.A. 1982. Probability based load criteria: assesment of current design practice, *Journal of the Structural Division*, ASCE, Vol. 108: 959–977.
- Haldar, A. & Mahadevan, S. 2000. *Probability, Reliability and Statistical Methods in Engineering Design*, John Wiley & Sons, New York.
- Kempner, Jr., L., Mueller III, W.H., Kitipornchai, S., Albermani, F., de Menezes, R.C. & da Silva, J.B.G.F. 2002. Lattice transmission tower analysis: beyond simple truss model, *Electrical Transmission in a New Age*: 175–187.
- Melchers, R.E. 1999. *Structural Reliability Analysis and Prediction*, John Wiley & Sons.
- Phoon, K-K., Kulhawy, F.K. & Grigoriu, M.D. 2000. Reliability-based design for transmission line structure foundations, *Computers and Geotechnics*. (26): 169–185.

# Life-cycle performance of bridge decks in aggressive environments

F. Biondini

*Department of Structural Engineering, Politecnico di Milano, Milan, Italy*

D.M. Frangopol

*Department of Civil and Environmental Engineering, ATLSS Center, Lehigh University, Bethlehem, PA, USA*

P.G. Malerba

*Department of Structural Engineering, Politecnico di Milano, Milan, Italy*

**ABSTRACT:** The life-cycle performance of multi-cellular bridge decks is investigated in both deterministic and probabilistic terms. The study is developed by using a general methodology for time-variant reliability analysis of concrete structures subjected to diffusive attacks from external aggressive agents. The beneficial effects of repair interventions are also taken into account. The results show that the repair interventions allow to decrease the rate of deterioration, as well as the dispersion of the associated uncertainty.

## 1 INTRODUCTION

Concrete bridge decks have a noteworthy sensitivity to the damaging effects due to diffusive attacks from environmental aggressive agents. These effects usually involve a deterioration of concrete and corrosion of reinforcement, and may lead to a significant variation of structural performance over time (Biondini and Frangopol 2008). As a consequence, maintenance and rehabilitation interventions are often required to restore, partially or totally, the original performance of the undamaged structure (CEB 1992).

These aspects are here investigated in both deterministic and probabilistic terms with reference to the case of a multi-cellular bridge deck. The life-cycle structural performance is investigated at cross-sectional level by using a general method for time-variant probabilistic analysis of concrete structures in aggressive environments (Biondini *et al.* 2004, 2006a). In this approach the diffusion process is modeled by using a special class of evolutionary algorithms, called cellular automata (Wolfram 1994), and the mechanical damage coupled to diffusion is evaluated by introducing proper material degradation laws. The probabilistic analysis is carried out by Monte Carlo simulation and the corresponding time evolution of the structural performance is investigated with reference to a suitable indicator of the nonlinear behavior. The beneficial effects of prescribed rehabilitation interventions on this indicator are also taken into account (Biondini *et al.* 2008). The direct comparison of the results shows that the adopted rehabilitation

intervention leads to a relevant decrease of the rate of deterioration and, consequently, to a significant reduction of the costs related to future inspections and maintenance actions. In addition, a decrease in the dispersion of the associated uncertainty is also achieved. From the probabilistic point of view this reduction in uncertainty clearly allows a more reliable maintenance planning of the rehabilitated structure.

## 2 CASE STUDY

The five cells box girder bridge deck shown in [Figure 1](#) is considered (Martinez Y Cabrera 2002). The cross-section of the bridge deck has main nominal dimensions  $b = 11.75$  m and  $h = 1.35$  m. The upper and lower slabs are 0.25 m and 0.20 m thick, respectively. Figures 1a and 1b show the detailing of the steel reinforcement and the location of the prestressing cables, respectively. The deck is prestressed with cables made up respectively of 19 strands of 0.6 inches. The nominal values of the material strengths for concrete, reinforcing steel, and prestressing steel are  $f_c = -45$  MPa,  $f_{sy} = 500$  MPa, and  $f_{py} = 1800$  MPa, respectively. The nominal value of the prestressing is  $\sigma_{p0} = 1300$  MPa.

The time-variant structural performance of the bridge deck is evaluated to provide a basis for informed decision-making concerning inspection activities and eventual maintenance actions (Biondini *et al.* 2006b, 2008). In particular, the effects of a maintenance intervention aimed to protect the skin surfaces and to

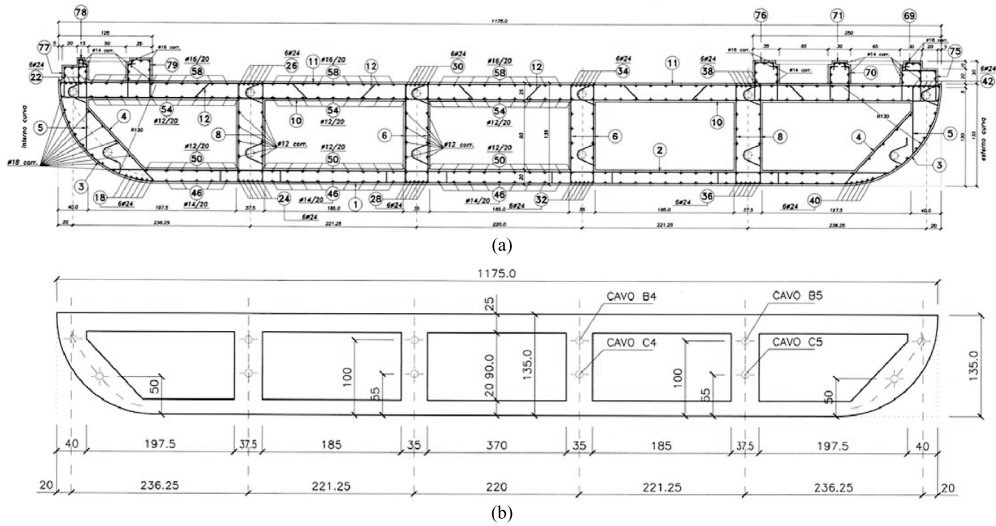


Figure 1. Multi-cellular bridge deck. (a) Reinforcement layout. (b) Prestressing cables.

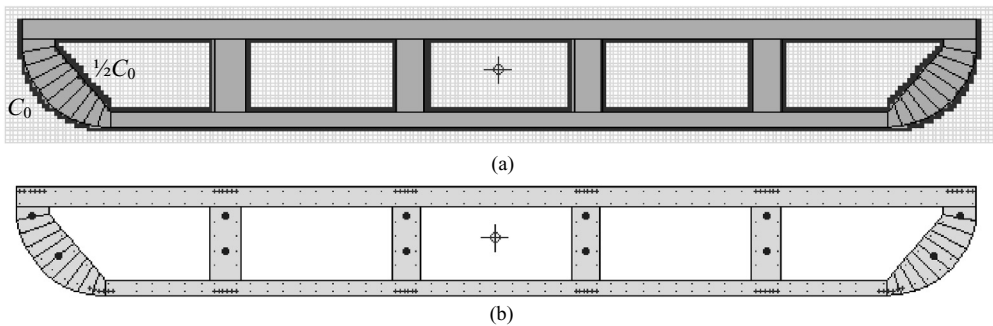


Figure 2. Multi-cellular bridge deck. (a) Grid of the cellular automaton and location of the aggressive agent. (b) Structural model.

prevent future diffusive attacks from external aggressive agents are investigated.

To this aim, two cases are studied. In the first one the structure is left free to undergo damage without any intervention. In the second one the effects of a maintenance intervention are taken into account after ten years of service, by placing a diffusive barrier along the external boundary of the cross-section. This barrier allows to stop the diffusion of aggressive agents from outside, and the future damage can be induced only by the agent already existing inside the structure.

### 3 DAMAGE SCENARIO AND SIMULATION OF THE DIFFUSION PROCESS

Since the attention is focused on the effectiveness of the repair intervention rather than on the actual

evolution of the structural performance, the role of the deterioration process on the life-cycle performance is emphasized by assuming the hypothesis of a very severe damage scenario. In this scenario, the deck cross-section is assumed to be subjected to a diffusive attack from an environmental aggressive agent located along the whole bottom external perimeter with constant concentration  $C_1 = C_0$ , as well as along the whole internal perimeter of each one of the five cells with constant concentration  $C_2 = 1/2C_0$  (Figure 2a). In fact, differences in oxygen levels and moisture contents, among other factors, may contribute to generate an aggressive environment also inside the cells of the box girder.

The diffusion process of the aggressive agent inside the structure is described according to the Fick's laws (Glicksman 2000) and is effectively simulated by using a special class of evolutionary algorithms

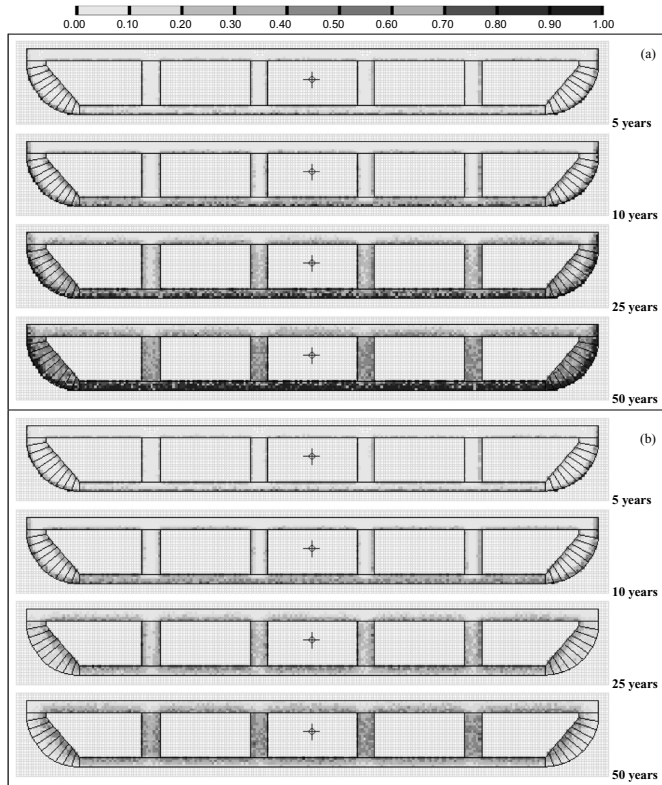


Figure 3. Maps of concentration  $C(t)/C_0$  of the aggressive agent after 5, 10, 25, and 50 years from the initial time of diffusion penetration. (a) Damaged structure. (b) Rehabilitated structure (repair intervention applied after 10 years of lifetime).

called cellular automata (Biondini *et al.* 2004, 2006a). Figure 2a shows the grid of the cellular automaton, with highlighted the location of the aggressive agent. With reference to a nominal diffusivity coefficient  $D = 10^{-11} \text{ m}^2/\text{sec}$  for concrete, the diffusion process associated with the two investigated scenarios, without and with maintenance intervention, is described by the maps of concentration shown in Figure 3. The direct comparison of the concentration maps in Figures 3a and 3b highlights the high effectiveness of the rehabilitation intervention with regards to the limitation of the diffusive attack of the aggressive agent.

#### 4 DAMAGE MODELING AND PREDICTION OF THE LIFE-CYCLE PERFORMANCE

Structural damage induced by diffusion is modeled by introducing a degradation law of the effective resistant area for concrete matrix, steel bars, and prestressing cables. In this study, damage is coupled to the

diffusion process by assuming, for both materials, a linear relationship between the rate of damage and the mass concentration of the aggressive agent. The proportionality coefficients which define such linear relationships are denoted by  $q_c = (C_c \Delta t_c)^{-1}$ ,  $q_s = (C_s \Delta t_s)^{-1}$ , and  $q_p = (C_p \Delta t_p)^{-1}$ , where  $C_c$ ,  $C_s$ , and  $C_p$  represent the values of constant concentration which lead to a complete damage of the materials, concrete, reinforcing steel, and prestressing steel after the time periods  $\Delta t_c$ ,  $\Delta t_s$ , and  $\Delta t_p$ , respectively (Biondini *et al.* 2004, 2008). For the cases under investigation the nominal values  $C_c = C_s = C_p = C_0$  and  $\Delta t_c = \Delta t_s = \Delta t_p = 50$  years, are adopted.

The time-variant bending behavior of the bridge deck is investigated with reference to the structural model in Figure 2b and by adopting the following constitutive laws. For concrete, the stress-strain diagram is described by the Saenz's law in compression and by an elastic perfectly plastic model in tension, with: tension strength  $f_{ct} = 0.25|f_c|^{2/3}$ ; initial modulus  $E_{c0} = 9500|f_c|^{1/3}$ ; peak strain in compression

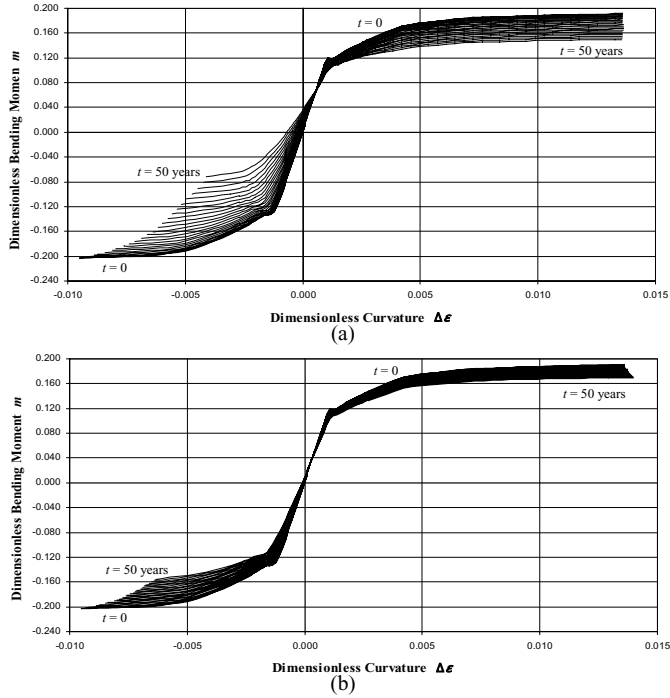


Figure 4. Evolution of bending moment  $m = M/(|f_c|A_{c0}h)$  – curvature  $\Delta\varepsilon = 100\chi h$  diagrams during the first 50 years of the lifetime ( $\Delta t = 2$  years). (a) Damaged structure. (b) Rehabilitated structure (repair intervention applied after 10 years of lifetime).

$\varepsilon_{c0} = -0.20\%$ ; strain limit in compression  $\varepsilon_{cu} = -0.35\%$ ; strain limit in tension  $\varepsilon_{ctu} = 2f_{ct}/E_{c0}$ . For reinforcing steel, the stress-strain diagram is described by an elastic perfectly plastic model in both tension and compression with elastic modulus  $E_s = 206$  GPa, and strain limit  $\varepsilon_{su} = 1.00\%$ . For prestressing steel, the stress-strain diagram is described by an elastic perfectly plastic model in both tension and compression with elastic modulus  $E_p = 200$  GPa, and strain limit  $\varepsilon_{pu} = \varepsilon_{p0} + 1.00\%$ .

Figure 4 shows for the two investigated scenarios the time evolution of the dimensionless bending moment  $m = M/(|f_c|A_{c0}h)$  versus curvature  $\Delta\varepsilon = 100\chi h$  diagrams under the axial force  $N = -(P + 20$  MN), where  $P = \sum_n \sigma_{p0n} A_{pn}$  is the total prestressing force. The direct comparison of the diagrams in Figures 4a and 4b highlights the high effectiveness of the repair intervention with regards to the deterioration of the structural performance over time.

## 5 EVOLUTION OF THE COUPLING EFFECTS OF THE AXIAL-BENDING BEHAVIOR

With reference to the diagrams in Figure 4, among the several parameters which could be adopted as suitable

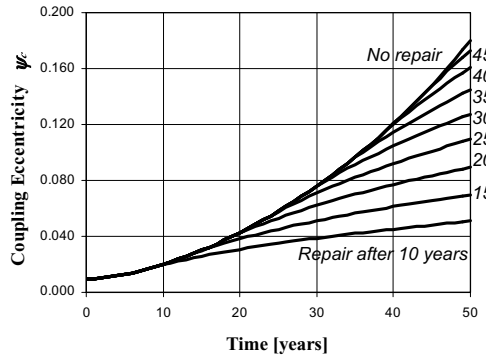


Figure 5. Time evolution of the coupling eccentricity of the deck cross-section. Effects of the repair intervention applied at different time instants during the structural lifetime.

measures of structural performance, particularly interesting is the bending moment associated with zero curvature, or the coupling moment  $M_c = M(\chi = 0)$ . This moment is associated with the coupling effects between axial and bending behavior arising from the eccentricity  $e_c = M_c/N$  of the centre of gravity of the

Table 1. Probability distributions and their parameters.

Random Variable ( $t = t_0$ )	Distribution Type	$\mu$	$\sigma$
Concrete strength, $f_c$	Lognormal	$f_{c,nom}$	5 MPa
Reinforcing steel strength, $f_{sy}$	Lognormal	$f_{sy,nom}$	30 MPa
Prestressing steel strength, $f_{py}$	Lognormal	$f_{py,nom}$	100 MPa
Coordinates of the nodal points, $(y_r, z_r)$	Normal	$(y_r, z_r)_{nom}$	5 mm
Coordinates of the reinforcing bars, $(y_m, z_m)$	Normal	$(y_m, z_m)_{nom}$	5 mm
Coordinates of the prestressing cables, $(y_n, z_n)$	Normal	$(y_n, z_n)_{nom}$	5 mm
Diameter of the reinforcing bars, $\emptyset_m$	Normal(*)	$\emptyset_{m,nom}$	$0.10\emptyset_{m,nom}$
Diameter of the prestressing cables, $\emptyset_n$	Normal(*)	$\emptyset_{n,nom}$	$0.10\emptyset_{n,nom}$
Cables prestressing, $\sigma_{p0n}$	Normal(*)	$\sigma_{p0n,nom}$	$0.10\sigma_{p0n,nom}$
Diffusivity coefficient, $D$	Normal(*)	$D_{nom}$	$0.10 D_{nom}$
Concrete damage rate, $q_c$	Normal(*)	$q_{c,nom}$	$0.30 q_{c,nom}$
Reinforcing steel damage rate, $q_s$	Normal(*)	$q_{s,nom}$	$0.30 q_{s,nom}$
Prestressing steel damage rate, $q_p$	Normal(*)	$q_{p,nom}$	$0.30 q_{p,nom}$
Concentration of the aggressive agent inside the cells, $C_2$	Normal(*)	$\frac{1}{2} C_0$	$0.15 C_0$

(\*)Truncated distributions with non negative outcomes are adopted in the simulation process.

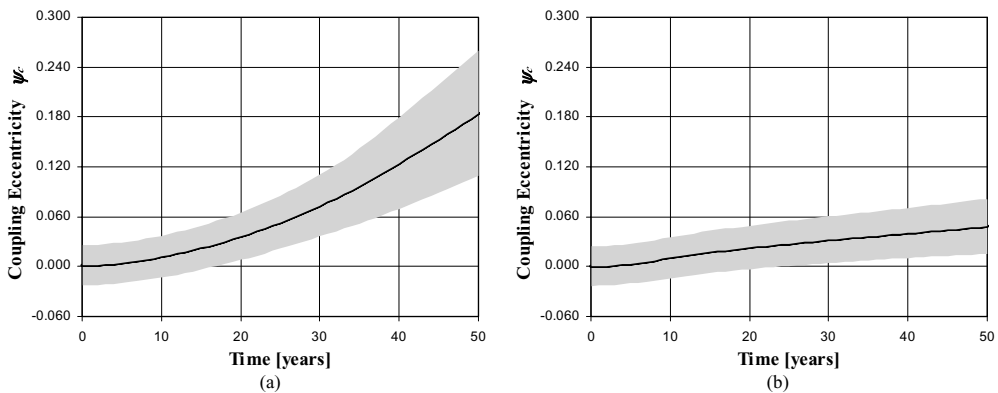


Figure 6. Time evolution of the statistical parameters of the coupling eccentricity. The shaded region is bounded by the mean plus one standard deviation (upper bound) and the mean minus one standard deviation (lower bound). (a) Damaged structure. (b) Rehabilitated structure (repair intervention applied after 10 years of lifetime).

composite cross-section with respect to the deck axis (Malerba 2003). The eccentricity  $e_c$  is a measure of the structural resources over the cross-section and its variation over time can be assumed as suitable indicator of the deteriorating effects induced by damage. The time evolution of the dimensionless eccentricity  $\psi_c = e_c/h$  is given in the diagram of Figure 5. Beside the two basic cases without repair and with repair applied after ten years of lifetime, this diagram shows a series of intermediate cases where repair is assumed to be delayed in time with intervals of 5 years. The results highlight three relevant aspects: (1) the noteworthy sensitivity of the dimensionless eccentricity to the damaging process; (2) a significant reduction of the

rate of variation of the eccentricity over time if the repair intervention is promptly applied; (3) a decrease of the effectiveness of the repair as the delay of the intervention increases.

## 6 PROBABILISTIC ANALYSIS AND ROLE OF UNCERTAINTY

The previous deterministic comparison is now extended to account for the uncertainty associated with the problem. The probabilistic model assumes as random variables the material strengths  $f_c$ ,  $f_{sy}$ , and  $f_{py}$ , the coordinates  $(y_r, z_r)$  of the nodal points

$r = 1, 2, \dots$  which define the two-dimensional model of the concrete cross-section, the coordinates  $(y_m, z_m)$  and the diameter  $\varnothing_m$  of the reinforcing bars  $m = 1, 2, \dots$ , the coordinates  $(y_n, z_n)$  and the diameter  $\varnothing_n$  of the prestressing cables  $n = 1, 2, \dots$ , the initial prestressing  $\sigma_{p0n}$ , the diffusion coefficient  $D$ , the damage rates  $q_c = (C_c \Delta t_c)^{-1}$ ,  $q_s = (C_s \Delta t_s)^{-1}$ , and  $q_p = (C_p \Delta t_p)^{-1}$ , and the concentration of the aggressive agent inside the cells. These variables are assumed to be uncorrelated and having the probabilistic distribution with the mean  $\mu$  and standard deviation  $\sigma$  values listed in Table 1 (Biondini *et al.* 2008).

The probabilistic analysis is carried out by Monte Carlo simulation. With reference to a sample of 2000 simulations for each one of the two basic investigated scenarios, Figure 6 shows the time evolution of the statistical parameters of the coupling eccentricity during the first 50 years of service life.

The direct comparison of Figure 6.a and Figure 6.b demonstrates the high effectiveness of the adopted maintenance intervention, which leads to a relevant decrease of the rate of deterioration and, consequently, to a significant reduction of the costs related to future inspections and maintenance actions. In addition, a decrease in the dispersion of the associated uncertainty is also achieved. From the probabilistic point of view this reduction in uncertainty clearly allows a more reliable maintenance planning of the rehabilitated structure.

## 7 CONCLUSIONS

This paper investigated the life-cycle performance of multi-cellular bridge decks. In order to outline the importance of an early diagnosis and to investigate the effectiveness of eventual repair interventions, a life-cycle nonlinear analysis under diffusive attacks from external agents has been developed by taking the beneficial effects of prescribed repair interventions into account. In this analysis, the time evolution of the structural performance of these bridges has been analyzed under the hypothesis of a very severe damage scenario in order to emphasize the role of the deterioration process and of the associated uncertainty effects.

The life-cycle performance has been evaluated with reference to the bending moment associated with the coupling effects between axial and bending behavior arising from the eccentricity of the centre of gravity of the composite cross-section with respect to the deck axis. The coupling eccentricity is a very effective measure of performance in concrete elements. In fact, this parameter represents a measure of the distribution of the structural resources over the cross-section and its

variation over time due to damage can be assumed as suitable indicator of the deteriorating effects induced by damage.

The results demonstrated that the assumed repair intervention led to a relevant decrease of the rate of deterioration and, consequently, to a significant reduction of the costs related to future inspections and maintenance actions. In addition, a decrease in the dispersion of the associated uncertainty has been also achieved. From the probabilistic point of view this reduction in uncertainty clearly allows a more reliable maintenance planning of the rehabilitated structure.

## ACKNOWLEDGEMENTS

This study is supported by research funds PRIN2005 (prot. 2005082490) from the Italian Ministry of University and Research – Department of Structural Engineering, Politecnico di Milano.

## REFERENCES

- Biondini, F., Bontempi, F., Frangopol, D.M. & Malerba, P.G. 2004. Cellular Automata Approach to Durability Analysis of Concrete Structures in Aggressive Environments. *ASCE Journal of Structural Engineering*, **130**(11), 1724–1737.
- Biondini, F., Bontempi, F., Frangopol, D.M. & Malerba, 2006a. Probabilistic Service Life Assessment and Maintenance Planning of Concrete Structures. *ASCE Journal of Structural Engineering*, **132**(5), 810–825.
- Biondini, F., Frangopol, D.M. & Malerba, 2006b. Time-variant Performance of the Certosa Cable-stayed Bridge. *Structural Engineering International*, **16**(3), 235–244.
- Biondini, F., Frangopol, D.M. & Malerba, 2008. Uncertainty Effects on Lifetime Structural Performance. *Probabilistic Engineering Mechanics* (in press).
- Biondini, F. & Frangopol, D.M., 2008. Long-term Performance of Structural Systems, *Structure and Infrastructure Engineering*, **4**(2), 72, Special Issue, Fabio Biondini (ed.), Taylor & Francis Publisher.
- CEB, 1992. *Durable Concrete Structures—Design Guide*, Thomas Telford.
- Glicksman, M.E., 2000. *Diffusion in Solids*, John Wiley and Sons.
- Malerba, P.G. (Ed.), 2003. *Limit and Nonlinear Analysis of Reinforced Concrete Structures*. International Centre for Mechanical Sciences (CISM), Udine, Italy (in Italian).
- Martinez, Y. Cabrera, F., 2002. *Collected Papers—In memory of Francesco Martinez Y Cabrera*, Politecnico di Milano, 511–542 (reprinted from *L'Industria Italiana del Cemento*, **757**, 2000).
- Wolfram, S., 1994. *Cellular Automata and Complexity—Collected Papers*, Addison-Wesley.



# Structural reliability of the “Palazzo della Civiltà Italiana” in Rome EUR

C. Ceccoli & T. Trombetti

*DISTART, Università degli studi di Bologna, Italy*

D. Biondi

*Ceccoli e Associati, Bologna, Italy*

**ABSTRACT:** The “*Palazzo della Civiltà Italiana*” is a monumental building characterized by structural system made of reinforced concrete frames (cast in situ) and composite floors (reinforced concrete and hollow bricks), following a construction technology quite common in Italy. The floors are characterised by relatively large spans of about 10.0 meters. The construction took place between 1939 and 1943, presumably according to the construction code of the time published in 1939. The authors have coordinated a comprehensive experimental campaign aimed at the identification of the characteristics of the construction materials and members, as well as the identification of possible damages. Based upon the experimental results a number of analytical and numerical investigations have been developed in order to identify the structural actions and deformations. Fortunate circumstances have allowed the authors to have at hand the original technical drawings of the structural designer. This has proved crucial in order to develop grounded reliability analysis for the building structure in its present state, which still sees the building in its “original” configuration (no substantial intervention of structural retrofit or rehabilitation have indeed been implemented so far). In order to assess the seismic risk of the building structure a specific hazard analysis (PSHA) was developed to obtain a more precise probabilistic characterization of the expected seismic action (than that suggested for new building construction). The two major reliability issues identified though the analysis are relate to: (a) the load bearing capacities of the floors (the live load of the original design are inferior to those required nowadays to guarantee a sufficiently “flexible” use of the spaces), and (b) the seismic vulnerability of the building original structure. The authors have developed simple (non invasive) structural solutions in order to bring the “*Palazzo*” to the level of structural safety required by current standards. The strengthening and retrofit design encompasses the use of seismic dampers to be inserted in a central “light well” (already present in the building) and of “preloaded” steel beams to be placed underneath the floors.

## 1 INTRODUCTION

The “*Palazzo della civiltà italiana*” in Rome is a monumental symbol of the project for the “*Esposizione Universale di Roma*” programmed for 1941. The project for this exhibition was only partially built and the exhibition itself was never held due world war II. The construction works for this building started in 1938 and were completed (in almost all areas) by 1943. From a structural point of view the building is carried by a series of concrete frames with floors made of mixed (reinforced concrete-masonry) slabs. The span of the slab is quite large. Due to lucky circumstances (it is not always the case in Italy) an ample and thorough documentation of the construction of the building which encompasses the original technical drawings together with structural details. The present work summarizes the evaluations that the authors have carried out regarding the safety and conservation state

of this construction designed and built according to the knowledge and technology of about 65 years ago.

In order to carry out the above mentioned evaluations it has been necessary to develop, on the basis of the available technical documentation, a series of experimental investigations regarding the materials used for the construction. Also a number of numerical analysis and simulations were developed with special attention devoted to the correct modelling of the non structural components of the building. Finally specific seismic hazard analysis was developed for the site in order to estimate the seismic risk of the building.

## 2 THE STRUCTURE

The building is characterized by a squared plan with sides measuring about 51,50 meters. The overall building height is about 65 meters. Externally the





Figure 1. The external view of the “Palazzo della civiltà italiana”.

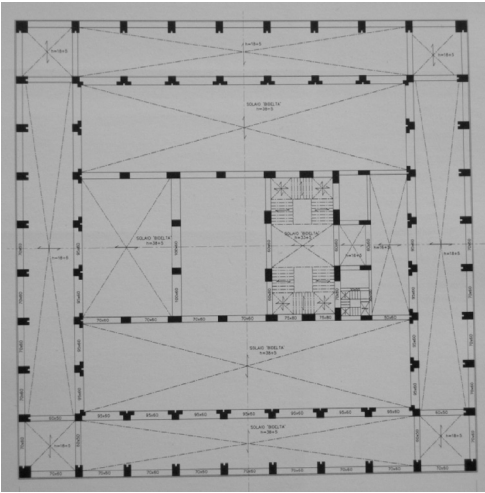


Figure 2. The plan of the building.

construction is characterized by 6 orders of arcades (porches). Each one composed of nine vaults on each side. An internal “cloister” (which starts at the second floor) provides light the central area of the building.

Figure 2 shows the typical building plan with the position of the pillars, beams and direction of the floors. The floors (mixed in reinforced concrete + masonry elements – hollow bricks called “pignatte”) over the porches span about 5,6 meters with a thickness of about 18 + 5 cm. The floors of the central part of the building spans about 10 m with a thickness of about 38 + 5 cm (see Fig. 3). The beams are characterized by a depth which varies (depending on the type) between 95 and 70 cm with a constant width of about 60 cm. All floor were originally designed to carry a live load of about  $4 \text{ kN/m}^2$ . At the base the pillars are characterised by generous dimensions with a cross section of about 1,50 m by 0,80 m, while at the top show a square cross section with a side length of about 70 cm.

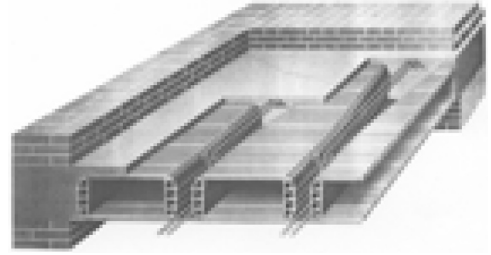


Figure 3. The concrete hollow bricks floor system, as described in an original brochure of the time of construction. It is worth to notice the widening of the concrete beams (“travetti”) in correspondence of the bearing edges.



Figure 4. The brick vaults during the construction phase.

Overall the structure in elevation is massive with “poor” reinforcing details, mainly in the pillars where, in spite of the large number of longitudinal bars it is inserted only one hoop to confine them and prevent lateral instability. Also the beams show little transversal (shear) reinforcement as well as short reinforcement overlaps and length of anchorage. Most likely the relatively sparse use of reinforcement is a consequence of the economic condition of the time, Casciato & Poretti (2002). Reasonably the design was carried out according to the construction code (for reinforced concrete structures) published 1939, design code that replaced the preceding one published in 1907.

The whole structure rests upon a soil of average bearing capacity. Due to the large self weight of the massive structure and of the marble cladding of the exterior, the foundations rests upon piles.

It is to be pointed out the building is characterized by the presence of:

- extensive and thick marble cladding;
- internal brick partitions, and

- brick vaults (cross) inserted in all porches which structurally work in parallel with the columns and beams (as depicted in Fig. 4).

### 3 CHARACTERISTICS OF THE MATERIALS, THEIR CONSERVATION AND THE WORKING CONDITION OF THE STRUCTURE

In order to obtain the characteristics of strength for the concrete of the pillars use was made of a combined approach ultrasound/sclerometer at one storey. This was used to calibrate the results obtainable from the use of the sclerometer only. After this “calibration” effort and extensive campaign was carried out using the sclerometer upon all pillars at all floors. Using Brinnell hardness tests upon the reinforcing steel of the columns and beams (exposed by removal of the cover), it was possible to estimate the strength of the re-bars. The concrete of the structure was also extensively investigated in order to evaluate its possible carbonation. Also a number of tests were performed in order to check the correspondence between the reinforcement prescribed in the original technical drawings and the what was actually placed in the construction. Similar verifications were developed to check the reliability of the geometry described in the original design.

Finally a number of dynamic tests were performed in order to evaluate the properties of the floors characterized by the large spans.

In summary the average strength of the concrete of the pillars was found to be:

Ground level (first floor)	41 MPa
Second floor	42 ”
Third floor	32 ”
Fourth floor	38 ”
Fifth floor	26 ”
Sixth floor	30 ”
Seventh floor	26 ”

On the other hand, the strength of the steel reinforcement varies between a maximum of 429 and a minimum of 400 MPa.

As far as the materials are concerned the good quality of the concrete has been verified (with respect to their working load) and, tracing back to the original technical literature it was possible to estimate the yield strength of the steel to be equal to 350 N/mm<sup>2</sup>.

The practical absence of carbonation in the concrete is probably to be ascribed to the “generous” marble cladding and mortar.

The dynamic tests indicate that all floors are characterized by a homogeneous behavior with a fundamental frequency of vibration of about 12 Hz.

Comparison with the analytical/numerical counterparts clearly indicates that the masonry inserted in

the floors mainly as non load bearing elements (they are characterized by the presence of voids to reduce weight) do actually contribute to the structural functioning of the reinforced concrete system. Also the thin layer of concrete (about 5 cm) positioned above the floor for construction reasons (non load bearing element) together with the thick marble flooring seems to collaborate to the structural functioning of the floor system.

Overall, after more than 65 years of service work and in the absence of significant maintenance and retrofitting works, the structure in elevation seems to be in good condition.

There is no evidence of differential foundation settlements. The structural design of the time was carried out using conventional methods, nonetheless the structures, as verified by the authors, show level of stress (under working condition) which are fully compatible with reduced deformations and limited cracking. The over strength of the floors, beams and columns, has allowed the building to accommodate easily the unavoidable deformations due to creep which occurred in the reinforced concrete members.

### 4 THE ANALYSIS OF SEISMIC HAZARD

A Probabilistic Seismic Hazard Analysis (PSHA) has been carried out with reference to the site of Roma EUR. The PSHA procedure, based upon the consolidated approach suggested by Cornell (1968), is here carried out through the identification of the Probability Density Function (PDF) and the Cumulative Distribution Function (CDF) of the Peak Ground Acceleration (PGA), as computed over a given observation time *t*. It consists of the following basic steps:

1. choice of an appropriate earthquake catalogue and identification of the areas of homogeneous seismic activity;
2. definition of an appropriate recurrence law, which gives, for example, an analytical relationship between a quantity describing the seismic event (e.g., the magnitude) and the return period of the seismic event for each seismic source zone;
3. definition of an appropriate occurrence law (e.g., Poisson process or other different laws), which statistically describes the number of events in any time period for each seismic source zone;
4. development, from the above assumptions (steps 1 to 3) and from basic probability theory, of the PDF and the CDF of the parameter describing the seismic event (e.g., the magnitude) for each seismic source zone;
5. identification of the appropriate ground motion prediction model (attenuation law) for the territory and the site under investigation;

6. development, from the above assumptions and results (steps 1 to 5) and from basic probability theory, of the PDF and the CDF of the prediction of the peak ground acceleration  $PGA'$  due to the seismic action of each seismic source zone;
7. development, from the above results (step 6) and from basic probability theory, of the PDF and the CDF of the prediction of the peak ground acceleration  $PGA'$  due to the seismic action of all seismic source zones considered;
8. derivation, introducing the epistemic uncertainty, of the PDF and the CDF of the peak ground acceleration  $PGA$  due to the seismic action of all seismic source zones considered.

Following these steps, a PSHA is developed which makes use of the following assumptions:

- the surface-wave magnitude ( $M$ ) as magnitude measure;
- the CPTI2 earthquake catalogue of the Italian territory, INGV (2003). This catalogue accounts, independently of the intensity ( $I_0$ ) and the surface-wave magnitude ( $M$ ), only for the largest event within time-space frames of  $\pm 90$  days and radius of 30 km of each seismic event;
- the ZS9 seismic subdivision for the Italian territory, INGV (2003), which refers to 40 area source zones;
- the “completeness analysis” proposed by Mulargia *et al.* (1987), to filter the historical data;
- the PGA attenuation law by Sabetta & Pugliese (1996) specifically developed for the Italian territory, which provides the values of the  $PGA'$ , together with the values of the standard error  $SE_{\log_{10} PGA}$ .

As illustrative example, Fig. 5 plots the CDF curve of the PGA, as obtained over an observation time of  $t = 50$  years, Bertero & Bertero (2002). With the

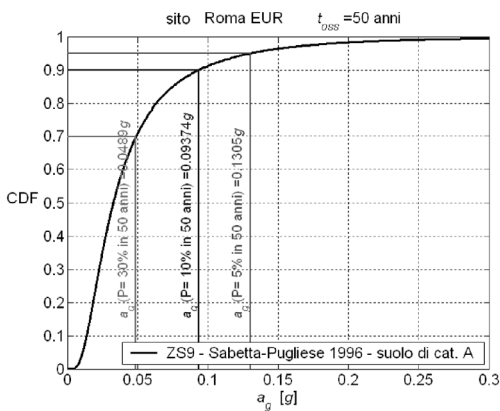


Figure 5. The CDF of the Peak Ground Acceleration (PGA) as evaluated for the site under investigation.

aim of identifying groups of earthquake inputs characterised by seismic hazard level corresponding to a rare event (probability of exceedance  $\bar{P}$  equal to 10% in 50 years), this curve allows to identify the numerical value of PGA corresponding to  $\bar{P} = 10\%$  in 50 years:  $a_g \cong 0.10$  g.

## 5 THE SEISMIC BEHAVIOR OF THE STRUCTURE AND ITS RETROFIT

Analysis of the seismic behaviour of the structure were developed with the support of numerical models. The first 3 periods of vibration of the system are estimated to be about 1,7 second, with the first two mode of vibration being characterised by a lateral deformation and the third mode of vibration by a torsional one. The relatively large value of the first period being due mainly to the large masses of both load bearing and non load bearing elements. The numerical model developed takes appropriately into account the effects (both in terms of mass and stiffness) of all non structural elements such as partitioning walls, the external walls and the external vaults.

The seismic response of the system under the input corresponding to the PGA of 0,1 g (which corresponds, according to the probabilistic seismic hazard analysis summarised above, to the design ultimate limit state – ULS) lead to structural action which are approximately the double of the structural system capacity. In particular the beams showed an insufficient reinforcement at their intrados in correspondence of their connection to the columns. On the other hand, the columns, thanks to their massive size shoed larger capabilities to carry the seismic loads. The capacity of the beams was estimated considering a ductility of the system of about 3.5, this estimation being made taking into account the fact that:

1. the poor reinforcing details leads to a reduced ductility of the elements,
2. the limited amount of reinforced used in the system, lead to an increased ductile behaviour of the elements.

Overall, with respect to the seismic hazard the building shows a level of vulnerability which is not capable to meet the current (high) standard of structural reliability required for the new construction. Considering the historical value and nature of *Palazzo*, the level of seismic protection (for specific use of the building) can be considered acceptable. However, in light of a possible (but not programmed) retrofit of the building in order to bring it to the same level of safety of newly built construction, the retrofit solution described below was developed.

Considering the monumental characteristics of the *Palazzo* a direct intervention upon the structure itself

(beams) was considered infeasible. For this reason a retrofit strategy aimed at reducing the actions imposed by the seismic input upon the structure was followed. Seismic isolation was not taken in consideration due to the specific problems connected to the insertion of the bearing under such (massive) building. On the other hand, the presence of a cloister (light well) in the centre of the building plan has suggested the insertion in this position of an additional steel structure (that, from an architectural point of view, could be realized as a totally distinct and removable way) to which seismic viscous dampers could be inserted. This solution allows to increase (in a totally reversible way) seismic damping to the structural system, thus reducing the actions imposed by the ULS earthquake input.

The use of an additional steel structure (connected to the historical building through horizontal members pinned at both ends) to insert the dampers allows exert only beneficial horizontal action on the original construction (which in this was somehow “restrained” in its horizontal motion) without introducing other undesired actions (see Figure 6).

Also, the use of viscous dampers is selected for their capability of providing non degrading actions as well as a calibration of their maximum effect. The effect of such a solution was firstly estimated using the results of theoretical work recently published in literature, and then checked through numerical dynamical analysis performed using time step integration. Two solutions were envisaged for the introduction of the dampers in the new system, Trombetti & Silvestri, (2007):

- MPD implementation (which sees the dampers placed horizontally between the historical building and the steel frame, as represented in Fig. 7).

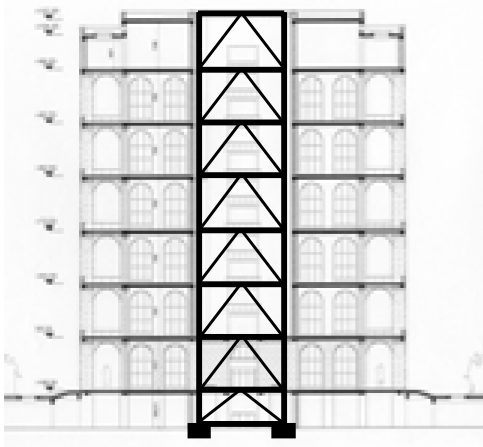


Figure 6. Transversal section of the building, with the additional steel structure placed inside the light well.

- SPD implementation (which sees the dampers placed between adjacent stories in the additional frame structure and this latter connected to the historical building through pinned beams, as represented in Fig. 8).

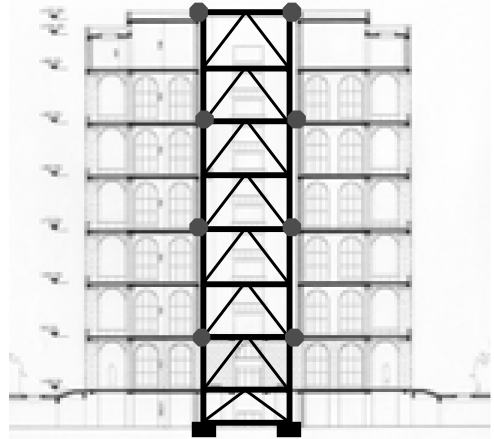


Figure 7. The MPD placement: dampers connect the new steel structure to the historical building. The dampers (here schematically represented with red dots) “work” in function of the differential velocity developed between the historical building and the added steel structure.

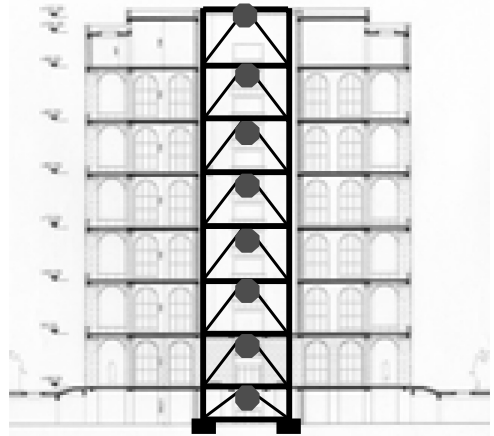


Figure 8. The SPD placement: dampers are placed between adjacent stories of the new steel structure which is linked through axially inextensible beams (pinned at the ends) to the historical building. The dampers (here schematically represented with red dots) “work” in function of the differential velocity developed between adjacent storey of the added steel structure.

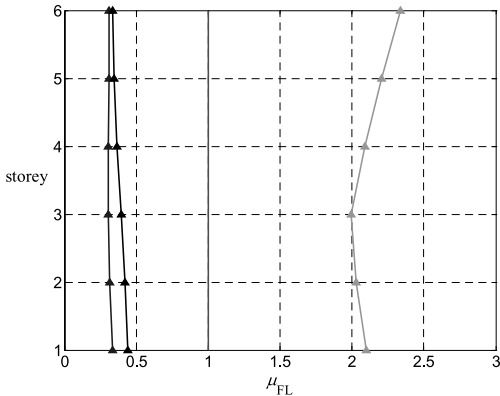


Figure 9. The storey shear profiles (relative values) for the different structural systems considered (green line = undamped system, red line = SPD system, Blue and black lines = MPD systems).

All analysis developed indicate that the insertion of two viscous dampers per floor for each direction (each one characterized by a damping coefficient  $c = 40 \text{ t s/cm}$ ) lead to a reduction of the seismic response of the historical building (with respect to the undamped solution) of about 1/2 for the SPD solution. On the other hand the more efficient MPD solution leads to a reduction of the seismic response of the historical building to 1/4 of that of the building without the insertion of any devices.

This result is summarized in Fig. 9 where the red line represent the profiles of the storey shear for the historical building in the case of the SPD solution, the blue and black lines represent the profiles of the storey shear in the historical building (in the case of MPD solution, with two slightly different solution of damper sizing), and the green line represent the profiles of the storey shear of the historical building in absence of seismic retrofit.

It is clear how in the light of the preceding considerations, in order to bring the *Palazzo della Civiltà Italiana* to the same levels of structural seismic safety of new building constructions, the SPD solution is sufficient.

## 6 CONCLUSIONS

The extensive experimental and analytical campaign developed for the *Palazzo della Civiltà Italiana* in Rome indicates that the building in its present condition shows sufficient levels of safety as far as the static

and dynamic (not seismic) actions. Only with regard to the seismic effects its level of safety (acceptable for an historical building structure) does not matches that required for new building construction. A seismic retrofit solution which encompasses the addition of viscous dampers to the structural system (placed in an additional steel structure to be realized in the light well positioned in the centre of the building) allows to raise the level of seismic safety of the historical building to values comparable to those required for new constructions.

At the time of writing, the retrofit proposal, though fully developed, is not programmed for actual implementation.

## ACKNOWLEDGEMENTS

The authors thanks eng. Filippo Russo and arch. Solange Signorini for the kind support offered during the development of the investigations here described. Also the authors are grateful to CME S.R.L. for the accurate experimental tests carried out.

## REFERENCES

- Bertero R.D. & Bertero V.V. (2002), Performance-based seismic engineering: the need for a reliable conceptual comprehensive approach. *Earthquake Engineering and Structural Dynamics* 2002; **31**(3): 627–652.
- Casciati M. & Poretti S. (2002), *Il palazzo della civiltà italiana*, Federico Motta Editore, Milano, 2002.
- Cornell C.A.. (1968), Engineering seismic risk analysis. *Bulletin of the Seismological Society of America* 1968; **58**: 1583–1605.
- INGV (2003), *Redazione della Mappa di Pericolosità Sismica prevista dalla Ordinanza PCM del 20 marzo 2003, n. 3274, all. 1. Rapporto Conclusivo*. Coordinator: Stucchi, M., Istituto Nazionale di Geofisica e Vulcanologia, Roma, April 2004.
- Mulargia F., Gasperini P., & Tinti S. Contour mapping of Italian seismicity. *Tectonophysics* 1987; **142**: 203–216.
- Sabetta F. & Pugliese A. (1987), Attenuation of Peak Horizontal Acceleration and Velocity from Italian Strong-motion Records. *Bulletin of the Seismological Society of America* 1987; **77**: 1491–1513.
- Sabetta F. & Pugliese A. (1996), Estimation of Response Spectra and Simulation of Nonstationary Earthquake Ground Motions. *Bulletin of the Seismological Society of America* 1996; **86**: 337–352.
- Trombetti T. & Silvestri S. (2007), “Novel schemes for inserting seismic dampers in shear-type systems based upon the mass proportional component of the Rayleigh damping matrix”, *Journal of Sound and Vibration* 302 (2007) 486–526.

# Maintenance and rehabilitation of the “Incoronata” viaduct along the Salerno Reggio Calabria highway

C. Ceccoli & T. Trombetti

*Distart – Università degli studi di Bologna, Italy*

A. Forlani

*SGAI Srl, Rimini, Italy*

F. Baroni

*Ceccoli ed Associati, Bologna, Italy*

**ABSTRACT:** This paper describes the inspections and field testing, as well as the analytical development for the retrofitting of the “*Incoronata*” viaduct (originally built at the beginning of the ‘60s) along the Salerno Reggio Calabria highway in southern Italy. The “*Incoronata*” viaduct is a cantilever type bridge, with cast in situ segments. The analysis developed indicates that the sound structural design of the original structure (designed at a time when the segmental bridge construction technology was still experimental and the numerical analysis tools not common) has allowed the bridge to maintain sufficient degrees of reliability over a time span of about 50 years.

## 1 INTRODUCTION

This paper relates the about the exhaustive campaign of analysis and tests carried out in order to retrofit the structure of the “*Incoronata*” viaduct along the Salerno-Reggio Calabria highway in southern Italy. The work carried out has allowed to effectively estimate the reliability and performances the bridge as well as to identify an effective solution for the upgrade of the structure. This upgrade being necessary in order to obtain an increase in bearing capacity in terms of both live and seismic load, and to modify the geometry of the bridge. In particular, the extensive analyses carried to obtain a complete knowledge of the bridge in its present condition may represent a significant example of structural reliability and performance assessment.

## 2 THE BRIDGE

### 2.1 Characteristics and history of the viaduct

The “*Incoronata*” viaduct was completed in the beginning of the ‘60 and is characterized by a total length of 527 meters.

Its central portion is made with two consecutive cantilever box girder of 55.0 m in length. Thus creating a system of 55 m + 110 m + 55.0 meters. This central system is joined at both north (Salerno) and south (Reggio Calabria) sides by 4 simple spans of 38 meters in length each. The northbound and southbound ways

(composed of two lanes each) are completely separate from each other, thus creating two independent bridges (see Fig. 4). The structure of the bridge consists of a hollow concrete box girder of variable depth: 2.2 meters at the centre of the 110 meter span and 5.5 meters at the junction with the pier. The hollow deck was built following a segmental construction with the hollow decks cast in situ (Fig. 2).

The central piers show a rectangular hollow section and have height of about 45 meters.

The post tensioning at the extrados was introduced using cables, following a common technique of



Figure 1. Longitudinal view of the central span of the viaduct (110 meter in length). At midspan the thickness of the box girder is 2200 mm while in correspondence of the piers is about 5500 mm. Overall this dimensions provide the bridge with a pleasant slenderness.

Note the portion of steel deck of the new viaduct which is being built alongside the existing structure.

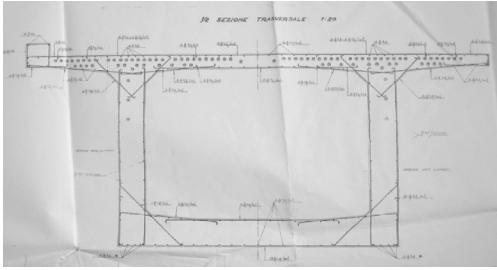


Figure 2. Transversal section of the girder in correspondence of the pier, as per the *original* technical drawings. Note the “historical” reinforcement: the transversal one is made with stirrup 10 mm in diameters spaced at 200 mm, also the anchoring of the bars has a short length but shows a partial hook.

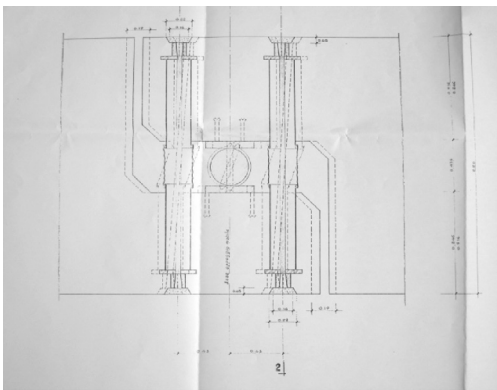


Figure 3. The particular solution devised to obtain the central pendulum: the horizontal steel cylinder acts to transmit the compressive shear while the two tendon transmit the traction shear. Note that the system was slightly pre-tensioned. Note also how the device does not present any specific solution to ensure its durability with time.

beginning of the 60 (instead of the solid bars which became widely in Italy used after 1970). The viaduct is characterized by a remarkable slenderness of both the piers and the deck. This slenderness, however, did not compromise the sound structural behavior of the system. At the time of construction, the deck was restrained both vertically and horizontally in correspondence of the external piers (fixed hinges). While the link in the deck at the mid-span was a pendulum (Fig. 3). The authors, for the development of the retrofit project could access only to the original drawings, as all other technical documents (including the technical report) could not be traced. Anyway, the authors have developed a numerical analysis of the structure in the condition it was originally designed and built. It was quite surprising to find that the stress levels are in good accordance with

the values commonly adopted nowadays for this type of structures. On the other hand, the deformations thus evaluated cannot not satisfy the standards current required. A first check upon the viaduct conditions was carried out in 1985, by the firm CND (Controlli Non Distruttivi) s.r.l. This work was performed following the recognition of: (1) a vertical deformation in excess of 250 mm observed at the center of the bridge, and (2) a malfunctioning of the bearing and connecting devices respectively placed at the extremities and at center span.

In 1992 the bridge underwent a first substantial rehabilitation which encompassed the seismic retrofitting. Overall, this intervention has modified the static scheme of the viaduct according to the following (see Fig. 7).

At midspan the pendulum was removed and a deck continuity was created. The concrete slab at the bridge intrados was strengthened through an increase in its thickness and the addition of a post tension imposed through the placement of additional bounded pre-stressing cables. Also, the original fixed hinges at the external extremities of the viaduct were replaced with unidirectional sliding bearings (along the longitudinal direction) equipped with appropriate shock absorbers (for seismic reasons).

Finally (most likely at the same time of this retrofit) all concrete surfaces were protected with epoxy paint.

## 2.2 The new requirements

In order to increase the highway capacity the bridge is currently subjected to a complete renovation which encompasses the connection of the two (north and south) lanes in order to obtain a single road composed of three lanes for regular traffic + a service lane, this will serve the north bound traffic (Figure 4). The new way heading south is obtained building a completely

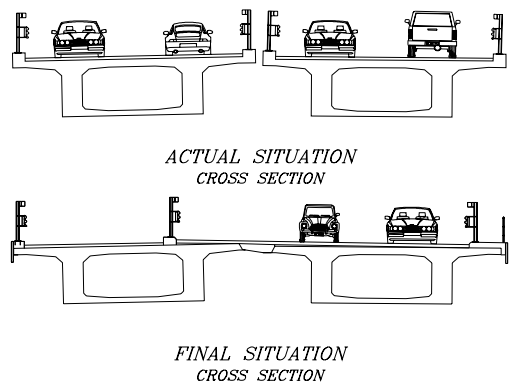


Figure 4. Transversal section of the bridge: the original and final configuration.



new (and independent) bridge geometrically similar to the existing one but characterized by a steel structure (Fig. 1).

### 3 THE INVESTIGATION CAMPAIGN FOR THE IDENTIFICATION OF THE PROPERTIES OF THE VIADUCT

A consistent amount of resources were devoted to obtain a knowledge as complete as possible of the bridge conditions. In particular, in addition to the knowledge of the geometry of the viaduct (the original design drawings were available) which was checked through a control campaign, both non destructive and destructive tests were performed in order to identify:

1. the mechanical characteristics of the materials used (strength & Young's Modulus);
2. the geometry of rebar and foundations;
3. the level of pre-stressing in the cables acting at present time;
4. the level of stress in the concrete;
5. the dynamic characteristics of the structure;
6. eventual damages present in both concrete and steel.

#### 3.1 Concrete strength and level of stress

Pull out" tests (extraction of portion of concrete), as well as "SonReb" tests (ultrasonic sclerometer) and compressive (destructive) tests performed upon of concrete sections removed from the viaduct were performed. All results were congruent and in accordance with the design prescription reported on the original drawings. The concrete of the deck has shown an average compressive strength of about 47 Mpa, while that of the piers about 35 MPa.

#### 3.2 Carbonation depth in the concrete

The concrete of the deck has shown a carbonation depth of about 20 mm, while that of the piers about 40 mm. The carbonation of the outer layers of concrete leads to an increase in the superficial compressive strength. This phenomenon was well captured also by the investigation performed using the sclerometers.

#### 3.3 Tests performed upon the post-tensioned cables

A number of analysis were performed using different methodologies and with different purposes. Direct inspection of the prestressing (post tensioned) tendons were performed through the use of endoscope.

RIMT investigations were performed for about 30% of the cables and have indicated that:

1. almost all cables show a lack of injected grout within the duct (corrugated steel sheeting) for about 30 to 35% of the cross section. In addition the grout is cracked and exposed to aggressive agents over about 20% of the length of the ducts;
2. water is present within most of the ducts;
3. the post tensioning cables show corrosion which has reduced their effective cross section of about 12 to 15%. This corrosion extends cumulatively over about the 25–30% of the length of the cables.

Release of some of the pre-stressing cables which are located in the deck have shown that the current level of pre-stress varies between a minimum of 590 MPa and 830 MPa. These values are approximately 10–15% inferior to the original design prescriptions.

#### 3.4 Chemical tests

The chloride content was estimated both for the concrete of the deck (at 11 different positions) and for the grout injected in the corrugated sheets. The results have shown that maximum title of chloride is between 0.038% (for the grout) and 0.025% (for the concrete of the deck). Both these values are inferior to the limits and considered acceptable.

A chemical analysis of the paint which cover the bridge was performed. The results indicate that is still water repellent and thus deemed sufficient to protect the artifact.

#### 3.5 Tests for the identification of the dynamic properties of the viaduct

Dynamic field investigations were performed in collaboration with the DISTART Department of the University of Bologna. In particular the first frequencies of vibration (as well as the corresponding modes) of the bridge were identified through interpretation of recorded bridge accelerations (due to traffic excitation). The fundamental frequency—Anil Chopra (1996)—is about 0,97 Hz and the corresponding modal damping is identified at about 2%. The experimental data were compared to their numerical counterparts (as obtained through a FEM model) and shoed a good agreement modeling the structure as clamped at the base.

### 4 THE DIFFERENT MODELS DEVELOPED FOR THE ESTIMATION OF THE VIADUCT CONDITIONS

Five different numerical (FEM) models were developed:

1. Iso-static scheme (represented in Fig. 5). This bi-dimensional scheme is representative of the viaduct



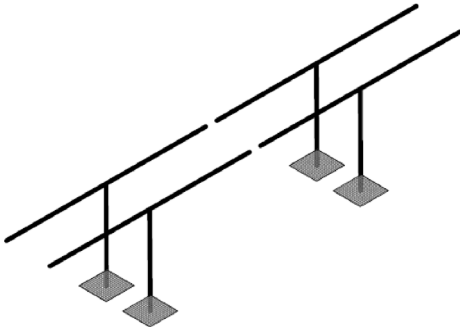


Figure 5. The isostatic scheme.

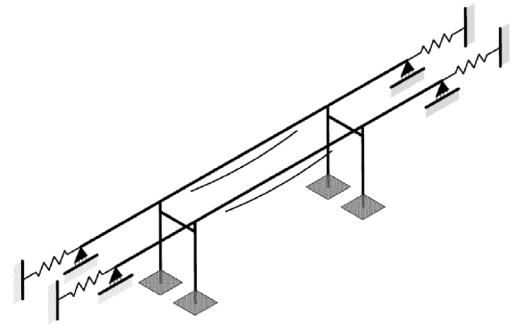


Figure 7. The frame model. Note the two “springs” representing the connection of the central system to the lateral simple span structure (connection which is functioning only in dynamic conditions thanks to the shock transmitters). Also the schematic representation in the center of the midspan indicates the addition of prestress at the intrados due to post-tensioning cables. Also, the two beams connecting the piers of the adjacent viaducts represent the physical connection inserted with this retrofit.

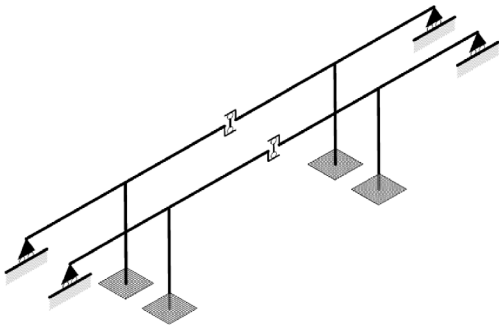


Figure 6. The iperstatic “gerber” scheme. Note the schematic representation at the two longitudinal edges indicate hinges fixed at the lateral simple span structures.

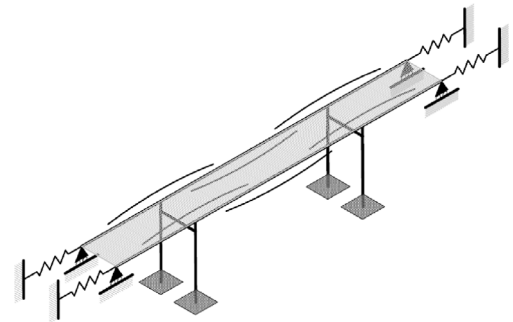


Figure 8. The three-dimensional model. Note, in addition to the schemes of Fig. 7, the schematic representation in correspondence of the piers which indicates the addition of prestress the extrados of the box girder due to post-tensioning cables. Also the grey surface between the two frames symbolically indicates the structural connection between the two adjacent viaducts.

- conditions during the construction phase (before the solidarization of the two decks).
2. Iper-static scheme following a so called “Gerber” deck (represented in Fig. 6). This bi-dimensional scheme is representative of the viaduct conditions at the end of the original construction.
  3. Iper-static “portal” frame (represented in Fig. 7). This bi-dimensional scheme is representative of the viaduct conditions after the 1992 “seismic” retrofit.
  4. Iper-static “thermal” frame (bi-dimensional). This model is structurally the same described above, but “tuned” to effectively evaluate the effects of thermal expansion.
  5. Three-dimensional iperstatic frame represented in Fig. 8. This three-dimensional model is representative of the viaduct conditions after the proposed interventions.

The first model was mainly use to evaluate the actions in deck during the (staged) construction phase.

The second model was used to evaluate the loss in the post-tensioning and the creep effects in the bridge after its first completion.

The third model was used to evaluate the change in internal actions due to the seismic retrofit of 1992. This retrofit encompassed:

1. the increase of the thickness of the deck,
2. the removal of the hinge at the connection between adjacent decks,
3. the introduction of additional post tension in the intrados of the deck,
4. the transversal connection of the two deck realize in correspondence of the piers,
5. the modification of the longitudinal retain systems at the abutments.

The fourth model was used only to evaluate the effects of thermal variation upon the bridge in the present configuration.

The fifth model was used to evaluate the effectiveness of the proposed new retrofit solution.

## 5 THE NEW RETROFIT SOLUTION

The new retrofit was introduced in order to:

- Bring the viaduct to levels of safety with respect to the seismic action, which is comparable to that of new bridges, as required by current Italian design codes – Ministero dei lavori pubblici, (2005);
- Bring the viaduct to levels of safety with respect to the static and live action, comparable to that of new bridges, as required by current Italian design codes (in the years that have passed between the original construction, the 1992 first retrofit, and now, the live load for class A Bridges have substantially increased);
- Satisfy the new geometric requirements (changes in the ways) already described.

### 5.1 General description of the interventions proposed

The new retrofit solution encompasses the following:

1. Structural connection of the original north and south way (which will become the new north way, for the south way a new viaduct will be built).
2. Insertion of an additional longitudinal post tensioning of the deck, through external cables placed inside the hollow deck (unbounded post-tensioning).
3. Insertion of four steel diaphragms connecting the two box girders. These diaphragms were inserted in order to better ensure a uniform behavior of the two decks (now structurally linked) under the effect of asymmetric longitudinal loads.
4. Increase of the section of the base of the piers.

### 5.2 The deck

In order to bring the viaduct to satisfactory levels of safety it was deemed necessary to provide additional post tensioning in the deck (to compensate for the loss due to creep) and to connect structurally the two original box girders of the viaduct with the introduction of diaphragms. In order to optimally calibrate the new post tension it was chosen to insert an “external” action thought the insertion of “unbounded” cables (Fig. 9).

Overall 10 post tensioning tendons are added to the deck. Each tendon is composed of 19 strands of 0,

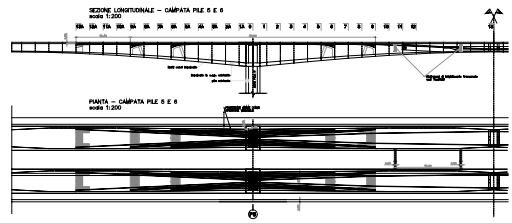


Figure 9. Longitudinal section and plan of the viaduct, as per the proposed new retrofit solution.

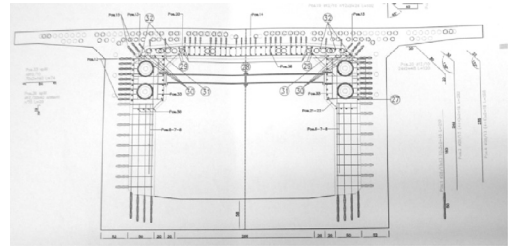


Figure 10. The system devised to anchor the new tendons for post tensioning to the original girder: details.

6 inches in diameter, and is capable of carrying up to 3.600 kN at tensioning. The increase in the longitudinal action due to this additional post tensioning is about 25% of the existing prestress. All tendons are positioned at the exterior of the deck in correspondence of the piers and are symmetrically anchored at special head placed laterally on the sides of the decks.

This solutions allows to adapt the actions in the cables to the structural response during placement. For this reasons the cable heads were chosen to be adjustable so that the actions could be varied up to  $\pm 15\%$  with respect to the design additional prestress (about 25% of the original pre-stress). This possible variation has, on the other hand, required a specific design of the reinforced concrete structure in the area around the anchoring (Fig. 10).

### 5.3 The piers

The central piers (which are rigidly connected to the deck) are those who carry the largest actions. These had to be upgraded both due to carbonation of the concrete and due to high level of stress to which they were subjected in their life cycle with respect to the actual concrete bearing capacity (as evaluated through in the experimental campaign developed for the project). The solution which was considered the most reliable, in terms of correct execution and of durability, is jacketing. For this reason a 300 mm thick jacket will be added to the piers up to a height of

15 m (in correspondence of the section in which the maximum bending moment is reduced to about 40% of its maximum value).

#### 5.4 *The execution phases*

A careful planning of the retrofit intervention sequence was developed, according to the subsequent series of operations summarized below:

##### *Intervention on the deck (right side)*

1. Construction of the anchoring heads,
2. Placement and tensioning of the cables.

##### *Intervention on the deck (left side)*

3. Construction of the anchoring heads,
4. Placement and tensioning of the cables.

##### *Intervention upon both decks*

5. Construction and placement of the transversal steel beams (transverses),
6. Demolition of the two adjacent (and facing) edges of the deck,
7. Structural linkage of the two decks (in reinforced concrete),
8. Realization of the road pavement,
9. Final treatment of the existing structure for weather protection using resins.

Great importance and attention has been devoted to the placement and tensioning of the cables for which a specific procedure was identified (it was prescribed to tension one cable at a time, while the deformation of the deck was being monitored).

It is to be noted that all intervention works had to be planned to take place while the viaduct was under regular (even though, restricted) use.

## 6 CONCLUSIONS

A project for the upgrade and retrofit of the “*Incoronata*” viaduct along the Salerno Reggio Calabria

highway in southern Italy has been developed by the authors and it is here briefly described. On the basis of the results of an exhaustive experimental campaign and of inspection of the original technical report of the '60 a comprehensive analysis has been developed in order to identify the repair, strengthening, retrofitting strategies to be adopted for the bridge. Of particular interest (and complexity) has been the development of a series of analysis (through numerical and analytical models) capable to account for the different (and successive) bridge configurations. From the analysis developed it emerged the need to increase the pre-stressing of the original structure. This was obtained through the introduction of additional (“unbounded”) pretension cable positioned inside the hollow box section of the deck. The analysis developed indicates that the sound structural design of the original structure (designed at a time when the segmental bridge construction technology was still experimental and the numerical analysis tools not common) has allowed the viaduct to maintain sufficient degrees of reliability over a life span of about 50 years.

## ACKNOWLEDGEMENTS

The authors want to thank the *Impresa C.M.C. Cooperativa Muratori e Cementisti Ravenna* and engs. Paolo Casalini and Gaetano Cassano for their contributions during the instigation campaign as well as during the design process. Also, *Società Modo s.a.*, *CND s.r.l.*, and the laboratory of *Tecnica delle costruzioni* of the Department *DISTART* of the *Università di Bologna*, are thankfully acknowledged for their contributions. Finally, a special thank to *A.N.A.S. s.p.a.* for providing the original technical documents and as well as historical information.

## REFERENCES

- Chopra A. (1996) *Dynamics of structures, Theory and Applications to earthquake engineering*, Prentice Hall.  
Ministero dei lavori pubblici (2005), *Norme Tecniche per le Costruzioni*, G.U. 23 Settembre 2005.

# Experiment based performance prediction of long span bridges subjected to non-uniform excitation

Moe M.S. Cheung

*Department of Civil Engineering, the Hong Kong University of Science and Technology, Hong Kong*

C.Y. Yang

*Department of Bridge Engineering, Tongji University, Shanghai, China*

**ABSTRACT:** Spatial variation of seismic waves has significant effects on the life-cycle performance prediction of long span bridges under earthquake loading. Since long span bridges have multi-supports and extreme lengths, due to the spatial variation effects, the ground motions at different supports may have noticeable discrepancies in terms of vibration amplitudes, frequency characteristics and arrival times; therefore, the seismic performance of long span bridges are greatly influenced. Though, lots of efforts have been put into the numerical analysis of long span bridges subjected to non-uniform earthquake excitation, the severe similitude requirements for seismic testing and the lack of multiple shake-table testing systems result in that few experimental studies have been carried out in this area. Shake table testing of a long span bridge subjected to non-uniform earthquake excitation is introduced in this paper. A specially designed dual shake table testing system is constructed for performing non-uniform excitation testing. A 1:120 model of a 750 m long cable-stayed bridge is designed by using the artificial mass simulation (AMS) modeling approach. Structurally uncoupled masses are attached to the physical model in order to satisfy the similitude requirements of seismic testing. Earthquake records from dense digital arrays of strong motion seismographs are adopted as inputs in this study. The testing results shed some light on the performance prediction of long span bridges subjected to non-uniform excitation.

## 1 INSTRUCTION

The routine analysis method for seismic performance prediction of long span bridges is based on a uniform excitation assumption, which postulates that earthquake excitations at all the points along the base are identical. However, four factors may cause the spatial variation of seismic waves, which are a) Incoherence effect. Due to the impurities consisting in ground material, the reflection and refraction of waves in the strata cause loss of coherency of seismic waves. b) Attenuation effect. The energy of the wave may decrease along with propagation, which results in a reduction in excitation amplitude. c) Site effect. Different soils have different wave characteristics. When a certain wave travels through various strata, some strata may amplify the response, yet some may do just the opposite. and d) Propagation effect. The velocity of seismic wave propagation isn't infinite. The uniform excitation assumption only works when the seismic wave velocity is rather large compared to the dimension of structures. Since long span bridges have multi-supports and extreme lengths, due

to the spatial variation effects, the ground motions at different supports may contain noticeable discrepancies in terms of vibration amplitudes, frequency characteristics and arrival times; therefore, the seismic performance of long span bridges are greatly influenced.

Experiment plays an important role in civil engineering research. Model testing can be applied to study the behavior of the prototype under different loading or to verify the analysis results from different numerical methods. However, it's very difficult and complex to perform the experiment based performance prediction of long span bridges subjected to earthquake loading. The space and payload limitation of the shake table and the severe similitude requirements for seismic experiments significantly increase the research difficulty. One of the first shake-table testing of a reduced scale model of long span bridge was carried out by Godden and Aslam (1978). The Ruck-A-Chucky cable-stayed bridge was structurally scaled to 1:200 and tested on the shake table of the Earthquake Simulation Laboratory of the University of California Berkeley. Garevski et al. (1991) conducted a shake table test of the Jindo

Bridge, a cable-stayed bridge with a main span of 344 m, at the University of Bristol. In order to fit the size of the shake table, the geometrical scale was set to 1:150. A 1:60 suspension bridge model was constructed and tested on shake table by Wang et al. (2006). However, the aforementioned tests were all performed on single shake table, none of them could take into account the non-uniform excitation cases.

Shake table testing of a long span bridge subjected to non-uniform earthquake excitation is introduced in this paper. A specially designed dual shake table testing system is constructed for performing non-uniform excitation testing. A 1:120 model of a 750 m long cable-stayed bridge is designed by using the artificial mass simulation (AMS) modeling approach. Earthquake records from dense digital arrays of strong motion seismographs are adopted as inputs in this study. The testing results shed some light on the performance prediction of long span bridges subjected to non-uniform excitation.

## 2 DUAL SHAKE TABLE TESTING SYSTEM

One prerequisite for dynamic model testing of non-uniform excitation is the multiple shake table system. Although there are many shake tables in universities and research institutes all over the world, very few have a multiple shake table system which can provide non-uniform excitations to different parts of the structural model. Based on the results of requirements estimation (Yang, 2007), an innovative dual shake table testing system is designed and constructed for the purpose of this study. The specifications of the proposed dual shake table are summarized in Table 1.

The table-board is made of machined honeycomb structure, covered the top and bottom surfaces with plates. The construction material is steel. In order to achieve a good working performance and avoid vibration interference, the table design prefers to high natural frequencies and high table-mass to specimen-mass ratio. However, an extremely stiff and massive design

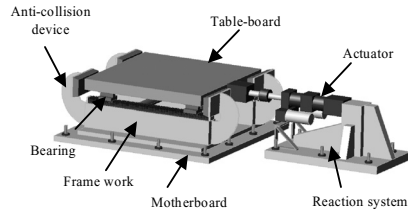


Figure 1. Design outline of one shake table.

is unpractical, considering the high construction costs and the excessive consumption of hydraulic power to drive the table. Therefore, the proposed design of honeycomb structure with plate skins provides an optimum trade-off between performance and cost. The FEM analysis results show that the natural frequencies of the first 3 modes of the table-board are 362 Hz, 500 Hz and 537 Hz, which are much higher than the highest operating frequency of the shake table (50 Hz).

Each table is supported by 4 linear ball bearings rested on 2 guide rails. The linear ball bearing design is provided to allow very low frictional and smooth motion of table-board along the length of guide rails, and restrict the motion along the perpendicular direction. The guide rails are installed on the frame work, and the frame work are fixed on the motherboard, as shown in Fig. 1. Each table is driven by a MTS 244.22 hydraulic actuator, with a forcing rate of 10 ton and maximum stroke of  $\pm 75$  mm. Each actuator is supported by a steel-made reaction system with high rigidity. Since each table and reaction system are anchored to the strong floor at grid holes, it can be easily relocated and rotated. Therefore, not only the center-to-center distance can be changed, but also the dual shake table system can provide three different working modes to satisfy different testing purposes, i.e., in-line excitation, parallel excitation and perpendicular excitation.

## 3 PROTOTYPE AND MODEL DESIGN

The bridge example adopted in this study is a double-deck cable-stayed bridge with a main span of 430 m and side spans of 160 m on either side, as shown in Fig. 2. Most of the main span, 387 m, is made of steel/concrete composite construction, consisting of steel frames, steel webs and concrete slabs. The rest of the main span and both side spans are constructed by using prestressed concrete box girders. The two H-shape concrete towers are founded on bedrock, with a height of 150 m above the water level. Each tower consists of 2 shafts and 3 cross beams. The bridge consists of 176 stay cables, arranged in two vertical planes. The bridge girder is vertically supported by 4 piers and 2 towers. Along the longitudinal direction, the deck is

Table 1. Specifications of the dual shake table system.

Table size	1.5 × 1.5 m
Maximum payload	2 ton
Actuator	MTS 244.22 (force rating 10 ton)
Shaking direction	1-D (X direction)
Maximum travel	+75 mm
Maximum acceleration	1 g
Operating frequency	0–50 Hz
Distance between two tables	4.8 m (center to center)
Working mode	In-line excitation Parallel excitation Perpendicular excitation

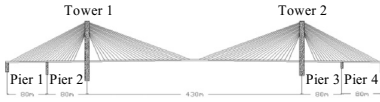


Figure 2. Elevation of the cable-stayed bridge.

Table 2. Summary of main scale factors used in the model.

Quantity	Scale factor
Length	1:120
Acceleration	1:1
Time	1:10.954
Frequency	1:0.0913
Modulus	1:11.182
Strain	1:1
Model weight	1:161022

only fixed at the cross beam of the Tower 2, and is movable at the other supports. Along the transverse direction, the deck is fixed at all six supports.

A reduced scale model of the cable-stayed bridge is designed based on the similitude requirement for seismic experiments. In model testing, it is the similitude requirements that relate the reduced scale model to the prototype structure. The similitude requirements are based on the theory of modeling, and can be derived from dimensional analysis (Harris, 1979; Liam Finn and Gohl, 1987; Blaney and Mallow, 1987). The artificial mass simulation (AMS) modeling approach (Harris and Sabnis, 1999) is adopted in this study.

The geometric scale  $S_L$  is 120, determined by the length of the prototype and the dimensions of the dual shake table. Although the prototype tower is made of concrete, acrylic is selected to fabricate the model tower in this study. The main purpose is to reduce the total weight of the model. Besides, acrylic also provides a good fabricating performance in machining and bonding. In view of the fact that Young's Modulus of concrete and acrylic are 35 GPa and 3.13 GPa, respectively, the scale factor for Young's Modulus  $S_E$  in the proposed physical model is 11.182. After  $S_L$  and  $S_E$  are determined, all the scale factors for different quantities can be derived accordingly. A summary of main scale factors adopted in the proposed model can be found in Table 2.

Aluminum plate with rectangular cross-section is selected to model the girder. Scaling requirement of vertical and transversal bending stiffness is satisfied. Since axial stiffness and torsional stiffness have little influence on the overall structure performance subjected to earthquake loading (Godden and Aslam, 1978; Garevski et al., 1991; Wang et al., 2006), their scaling requirement is neglected. High-strength stainless steel wire is used for modeling cables, with the scaling requirement of axial stiffness being

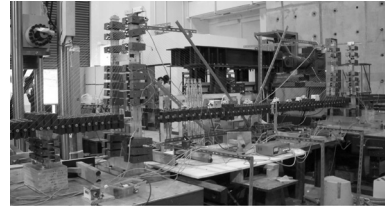


Figure 3. Finished model of the cable-stayed bridge.

satisfied. In order to satisfy the similitude requirements of seismic testing, machined iron blocks are attached to the model as artificial mass. The blocks are evenly distributed along the tower and girder, without inducing significant stiffness variation in the model. The photograph of finished model is shown in Fig. 3.

#### 4 INPUT GROUND MOTION AND TEST PROTOCOL

Earthquake records from SMART-1 seismograph array are used in this test. SMART-1 (Strong Motion Array in Taiwan, phase I) is a dense digital array of strong-motion seismographs, which was built up by the Institute of Earth Sciences (Taiwan) and the University of California at Berkeley, in 1980. The array consists of 36 stations which are configured in three concentric circles, with radii of 200 m (inner ring), 1000 m (middle ring) and 2000 m (outer ring). In view of the fact that each pair of stations (along the diametrical direction) in the inner ring are spaced at a distance of 400 m, which is quite close to the span length of the example bridge (430 m); two pairs of selected records from the inner ring stations are used in this study as the non-uniform seismic records. Since the displacement time-histories are required for shake table testing, the numerical processing scheme suggested by the USGS (United States Geological Survey) is adopted in this study to transform the collected acceleration records to the displacement records. The acceleration time-histories and the corresponding displacement time-histories used in this study are shown in Fig. 4.

Table 3 lists the test protocol for the shake table testing. In test stage I, a modal test is performed by using 0.1 g white noise input excitation. In test stage II, two groups of earthquake records from SMART-1 are used for performing the uniform and non-uniform excitation test. In the "identical input" case, both tables have the same input wave; while in the "varying input" case, different input waves are applied to different tables. The wave propagation effect is studied by changing the wave passage velocity, including five cases, i.e. 400 m/s, 600 m/s, 1000 m/s, 2000 m/s and infinite. The distance between the two main towers (430 m) is

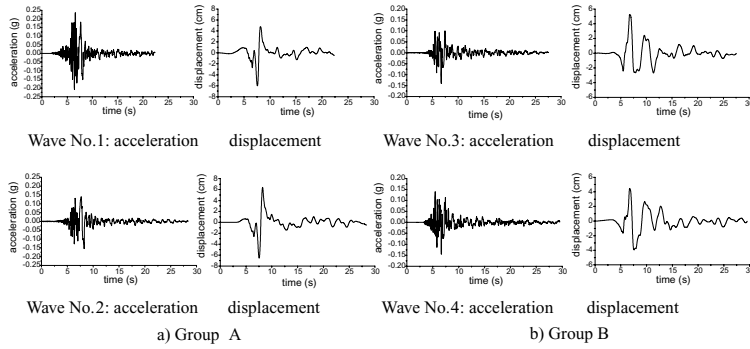


Figure 4. Acceleration and corresponding displacement inputs used in this study.

Table 3. Summary of main scale factors used in the model.

Cases		Input at Tower 1, Pier 1 and Pier 2	Input at Tower 2, Pier 3 and Pier 4	Arrival time delay (sec)	Wave length (m/s)
Stage I-Model Test		0.1 g white noise		N/A	N/A
Stage II- Group A	Identical Input	Wave No.1	Wave No.1	0	Infinite
		Wave No.1	Wave No.1	0.215	2000
		Wave No.1	Wave No.1	0.43	1000
		Wave No.1	Wave No.1	0.717	600
		Wave No.1	Wave No.1	1.075	400
	Varying Input	Wave No.1	Wave No.2	0	Infinite
		Wave No.1	Wave No.2	0.215	2000
		Wave No.1	Wave No.2	0.43	1000
		Wave No.1	Wave No.2	0.717	600
		Wave No.1	Wave No.2	1.075	400
Stage II- Group B	Identical Input	Wave No.3	Wave No.3	0	Infinite
		Wave No.3	Wave No.3	0.215	2000
		Wave No.3	Wave No.3	0.43	1000
		Wave No.3	Wave No.3	0.717	600
		Wave No.3	Wave No.3	1.075	400
	Varying Input	Wave No.3	Wave No.4	0	Infinite
		Wave No.3	Wave No.4	0.215	2000
		Wave No.3	Wave No.4	0.43	1000
		Wave No.3	Wave No.4	0.717	600
		Wave No.3	Wave No.4	1.075	400

used to calculate the difference of the arrival time for the two tables.

An instrumentation scheme including 39 channels of accelerometers, displacement transducers and strain gauges is designed for the shake table testing. The data are recorded at a rate of 256 Hz.

## 5 TEST RESULTS AND DISCUSSION

Modal test is carried out before the earthquake ground motion excitation tests. A refine 3-D finite element model of the example bridge is developed using SAP2000. In comparing the results from modal test

with the results from numerical analysis, it shows that the designed reduced scale model represents the dynamic nature of the prototype quite well (Yang, 2007).

Typical results of test stage II-Group A (Input wave No.1 and No. 2) are presented in Fig. 5–Fig. 7. From these figures, one finds that non-uniform excitation strongly influences the dynamic response of the bridge model. Comparing the results at the same wave velocity, in most cases the “varying input” excitation results in a much larger response than the “identical input”. The wave propagation effect also has a significant influence on the results. As shown in Fig. 5, in most cases, the wave propagation effect

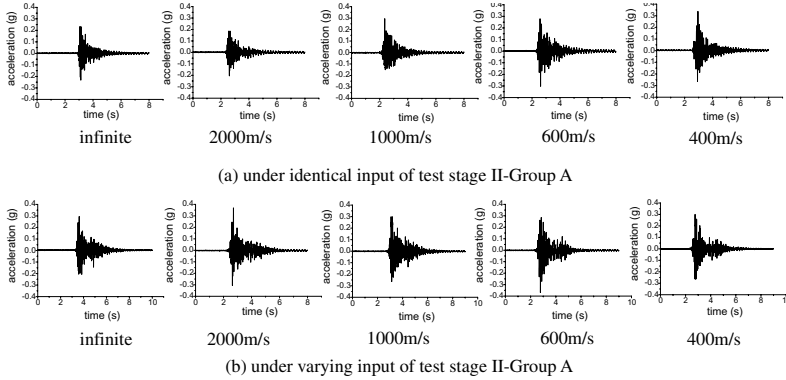


Figure 5. Vertical acceleration time-histories at quarter location of the girder.

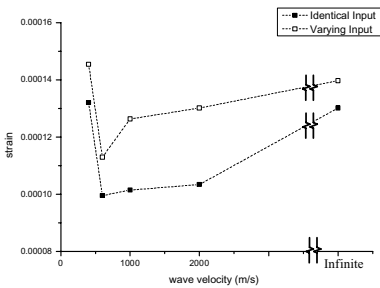


Figure 6. Strain gauge records near the top of Tower 2 under test stage II-Group A.

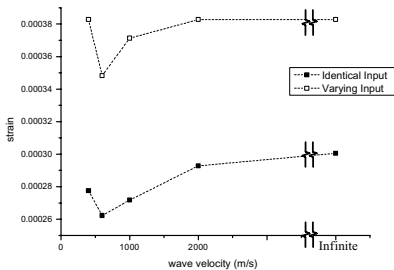


Figure 7. Strain gauge records near the bottom of Tower 2 under test stage II-Group A.

observably increases the vertical acceleration at the quarter location of the girder. While from Fig. 6 and 7, it can be seen that except for the case of a wave velocity equal to 400 m/s, the wave propagation effect slightly reduces the strain at the top and the bottom of the tower. The above results imply that, in general, the wave propagation effect may increase the vertical response while slightly reduce the longitudinal response of the cable-stayed bridge.

Typical results of test stage II-Group B (Input wave No. 3 and No. 4) are presented in Figs. 8 and 9. Studying the longitudinal accelerations in Fig. 8, and the strain records shown in Fig. 9, when comparing the result from non-uniform excitation with the one from uniform excitation, an amplification of more than 50% can easily be observed. When studying the effect of wave propagation, it can be found that, in general, the wave passage effect may decrease the longitudinal response of the tower (Figs. 8 and 9), which agrees with the previous findings.

## 6 CONCLUSIONS

The experiment based performance prediction of long span bridges subjected to non-uniform excitation is studied in this paper. The following conclusions can be drawn.

1. The designed dual shake table testing system and the reduced scale cable-stayed bridge model perform quite well in this study. The favorable match of the modal test results with the numerical analysis results in terms of dynamic characteristics of the prototype implies that the AMS (Artificial Mass Simulation) model, which can adequately simulate the dynamic behavior of the prototype, provides a practical modeling method for shake table testing.
2. The results of shake table testing show that non-uniform excitation strongly influences the seismic response of the bridge model. In most cases, the “varying input” excitation results in a much larger response than the “identical input”.
3. The results show that in general, the wave passage effect may significantly increase the vertical responses while decreasing the longitudinal responses of long span bridges under non-uniform



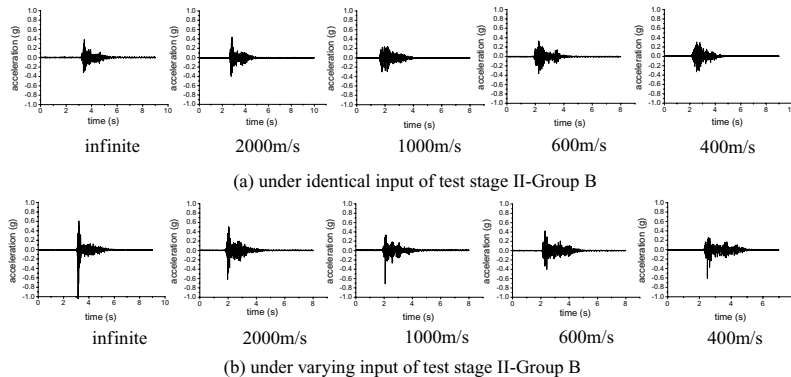


Figure 8. Longitudinal acceleration time-histories at the top of Tower 2.

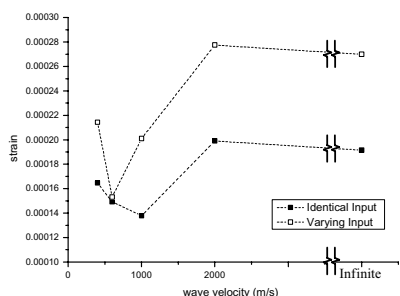


Figure 9. Strain gauge records near the bottom of Tower 2 under test stage II-Group B.

excitation. Further, the value of wave propagation velocity also plays an important role in this study.

#### ACKNOWLEDGEMENTS

Financial support from the Research Grants Council of Hong Kong under Competitive Earmarked Research Grant # 612106 is highly appreciated.

#### REFERENCES

Blaney, G.W. & Mallow, W.A. 1987. Synthetic clay soil for dynamic model pile tests. Dynamic response of pile foundations—experiment, analysis, and observation: proceedings of the Geotechnical Engineering Division, ASCE Convention in Atlantic City, New Jersey, 27 April 1987: 127–148.

Garevski, M.A. et al. 1991. Resonance-search tests on a small-scale model of a cable-stayed bridge. *Engineering Structures*, 13:59–66.

Godden, W.G. & Aslam, M. 1978. Dynamic model studies of Ruck-A-Chucky Bridge. *Journal of the Structural Division, ASCE*, 104 (ST12): 1827–1844.

Harris, H.G. 1979. Use of structural models as an alternative to full-scale testing. Full-scale load testing of structures: a symposium/jointly sponsored by ASTM Committee E06 on Performance of Building Constructions and the ASCE Committee on the Professional Practice for Full-Scale Structural Testing, ASTM, Philadelphia, Pa. 2 April 1979: 25–44.

Harris, H.G. & Sabnis, G.M. 1999. *Structural Modeling and Experimental Techniques*, 2nd edition, CRC Press.

Liam Finn, W.D. & Gohl, W.B. 1987. Centrifuge model studies of piles under simulated earthquake lateral loading. Dynamic response of pile foundations—experiment, analysis, and observation: proceedings of the Geotechnical Engineering Division, ASCE Convention in Atlantic City, New Jersey, 27 April 1987: 21–37.

Wang, J.J. et al. 2006. A brief introduction to the shaking-table test of Liede Bridge. Proceedings of the 4th PRC-US Workshop on Seismic Analysis and Design of Special Bridges, Chongqing, China, June 2006.

Yang, C.Y. 2007. *Seismic Analysis of Long Span Bridges Including the Effects of Spatial Variation of Seismic Waves on Bridges*. PhD Thesis, Department of Civil Engineering, The Hong Kong University of Science and Technology.

# Functionality and strength of arch concrete dams cracked by shrinkage

M. Como & S. Imperatore

University of Rome "Tor Vergata", Italy

**ABSTRACT:** Aim of the paper is to present a step by step approach able to obtain information on the strength capacity, particularly under hydrostatic loads, of cracked concrete dams. The functionality control of a cracked dam requires to set up a computational procedure able to reproduce the gradual dam crack formation during the loading history. The proposed approach makes use of the program Atena 3D, based on a Fracture Mechanics context. Dams with different front shape are considered. To verify the validity of the obtained result, a comparison with the behavior of a real dam is carried out.

## 1 INTRODUCTION

A large number of Italian arch dams date back to the early twentieth century. Generally, these structures were erected without vertical contraction joints, required to control tensile stresses due to concrete shrinkage and temperature effects. Due to this lack, long sub-vertical cracks are frequently detected in these dams, since the used massive plain concrete has almost zero tensile strength.

Resistant capacity of undamaged arch concrete dams to hydrostatic loads is generally high: unknown, on the contrary, is the reduction of this capacity in presence of cracks.

An arch/gravity dam can be considered as a complex structural system obtained by assembling vertical cantilevers and horizontal arches, interacting each others. Hydrostatic loads are mostly sustained by the horizontal arches in an efficient working of the dam with dominating compression stresses. In the damaged dam, on the contrary, the long sub-vertical cracks cut the arches and can produce a dominating cantilever behavior and a consequent strong reduction of the dam strength.

Aim of the paper is to present a step by step approach able to obtain information on the strength capacity, particularly under hydrostatic loads, of cracked concrete dams.

The functionality control of a cracked dam requires to set up a computational procedure able to reproduce the gradual dam cracking during the loading history. The proposed approach makes use of the program Atena 3D, based on a Fracture Mechanics context.

A large number of parameters is involved in this analysis, as the definition of a suitable energy fracture, the mesh geometry, the boundary conditions, the creep effects of the concrete, the geometry of the dam and

so on. A important case study, the old Corfino dam, with its detected crack pattern, is taken as reference.

The main steps of the proposed approach are:

- analysis of the dam under gravity loads;
- overlap of the concrete shrinkage effects;
- crack pattern evaluation and comparison with the real detected damage;
- analysis of the dam to the overlapping water effects.

Different typologies of concrete dams are considered: arch dams with rectangular or like triangular front. To the latter typology belongs the case studio of the Corfino dam.

## 2 THE NONLINEAR MODEL OF THE DAM

To evaluate the crack pattern and the crack widths, a stress analysis of the dam was carried up with Atena 3D, a program based on the principles of Fracture Mechanics. The numerical model reproduces the geometry and the boundary conditions of the dam.

A nonlinear stress-strain relationships is associated to the concrete macro-elements constituting the dam, (Fig. 1).

The tensile stress-strain branch is particularly relevant to crack development.

When the concrete tensile strength  $\sigma_{cr}$  is reached in a section, a crack localizes and then gradually grows up. The softening branch thus does not represents an effective increasing of strains, but only the strain localization across the crack. The area subtended by the diagram stress-crack opening ( $\sigma - w$ ), that is constant for each material, is defined as energy of fracture  $G_f$ :

$$G_f = \int_0^{w_c} \sigma(w) dw \quad (1)$$

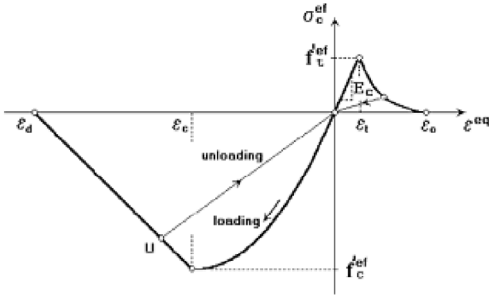


Figure 1. Uniaxial stress-strain law for concrete.

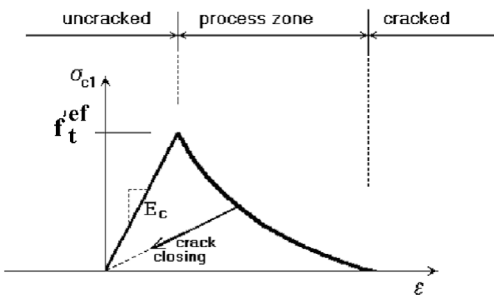


Figure 2. Stages of crack opening.

where  $w_c$  = is the crack opening at  $\sigma = 0$ . Various equations of the law  $\sigma(w)$  have been proposed; very effective is the Foote law (1986):

$$\frac{\sigma}{\sigma_{crt}} = \left(1 - \frac{w}{w_c}\right)^n \quad (2)$$

Different softening curves can be obtained according to the chosen value of the exponent  $n$ .

The process of crack formation is divided into three stages (Fig. 2). The un-cracked stage last when the peak tensile strength is reached. The crack formation takes place in the process zone of a potential crack with decreasing tensile stress on a crack face due to a bridging effect. Finally, after a complete release of the stress, the crack opening continues without the stress. It is also possible, that the second stress, parallel to the crack direction, exceeds the tensile strength. Then the second crack, in the direction orthogonal to the first one, is formed using the same softening model as the first crack.

Moreover, in the model, between dam and fixed supports, is introduced an interfacial zone, in order to consider the interaction between the dam and the surrounding rock. Obviously, the dam behavior changes with the elastic modulus associated to the interfacial zone. So a parametric study is carried out, in order to

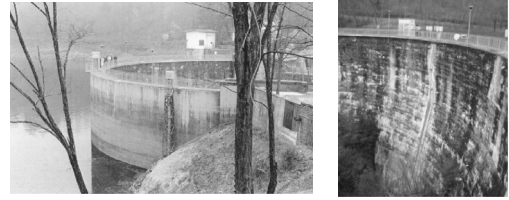


Figure 3. The Corfino dam.

evaluate a range of elastic moduli that provides a dam behavior, in terms of crack pattern, comparable with the actual one. The same logic is adopted to establish the size of the interfacial zone.

### 3 THE CASE OF THE CORFINO DAM

#### 3.1 The Corfino dam

To evaluate the effectiveness of the model, a first analysis is carried out in order to simulate the behavior of the Corfino dam. For this structure, the constructive features and the damage states are quite well known. Built at the early '900, the dam has a simple curvature vault, with a radius of 23,5 m at the extrados and a width linearly variable with the height at the intrados.

The cross section of the dam has a trapezium shape from the basement up to the level of 494,72 m; beyond this height the section has constant thickness. The section width varies between 7,00 m and 1,50 m. The dam height is 38,50 m and has circular arc sections in plan, with a radius of curvature at the extrados of 25,00 m and a taffrail length of 65,00 m.

The dam was assembled in horizontal layers of concrete 3,00 m thick. Each layer was cast with different cement contents. There aren't vertical contraction joints. Monolithic rocks are present at the foundation while fractured rocks have been found at the side boundaries.

Few years after the dam was completed, vertical cracks were detected, probably due to the concrete shrinkage.

Damage monitoring of the dam started later: from the 1997, the crack pattern is practically unvaried and is characterized by four main cracks crossing the dam, with a sub-vertical orientation.

#### 3.2 Effects of the gravity loads

A qualitative description of the dam deformation under self-weight is reported in Fig. 4.

The structural behavior is influenced by the interaction of horizontal arches and vertical cantilevers. Due to the eccentricity of the vertical load, the vertical layers, weakly restrained by the upper horizontal

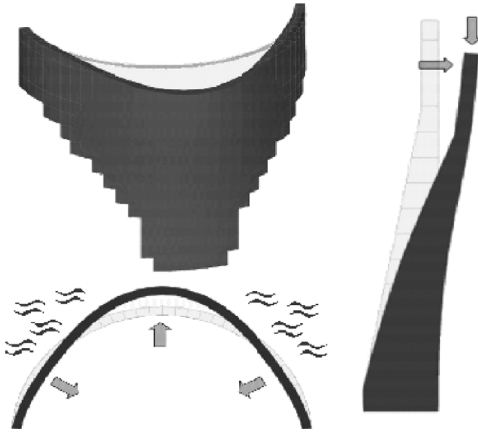


Figure 4. Deformations due to the gravity loads.

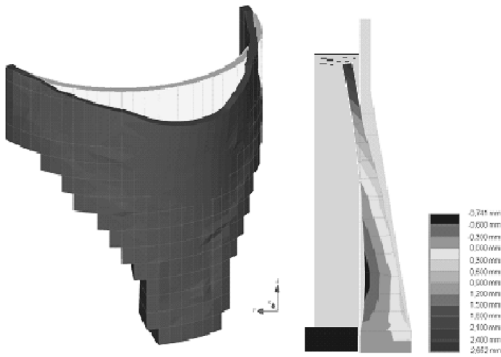


Figure 5. Dam's displacements due to gravity loads and shrinkage.

arches, inflects toward down stream. Consequently, the bending of the vertical cantilevers distort the upper arches.

### 3.3 Shrinkage cracking

To verify the actual functionality of an old dam, it is reasonable to assume that all the concrete shrinkage is run out. A constant temperature reduction occurring across the dam simulates the shrinkage of the concrete. In the present study, the reduction of temperature is assumed  $-15^{\circ}\text{C}$ . Fig. 5 gives a synthetic description of the dam bending.

Transversal sections look distorted like in the case of the simple self-weight, but the magnitude of the displacements in this case is higher. This result is caused by the cracks that, cutting the structure, increase the cantilever effect.

The crack pattern evaluated by means of the numerical model is consistent and coherent with the detected

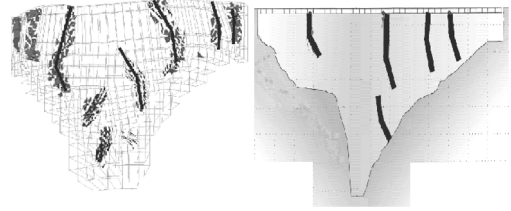


Figure 6. Crack pattern in the numerical model and in the real dam.

cracks in the existing dam. The larger cracks, with a width ranging between 0,5–5,4 mm, occur on the upper zone.

## 4 PARAMETRIC STUDY ON THE NUMERICAL RESPONSE OF THE DAM

In the following, a parametric study on the factors that influence the numerical response of the dam is carried out. In addition, a range of variation for this parameters, is fixed. To reduce the computational cost, the model represent half of the dam (Fig. 7).

The examined parameters are:

- The elastic modulus of the interfacial zone;
- The size of the interfacial zone;
- The mesh shape;
- The fracture energy.

The elastic modulus adopted for the interfacial zone is taken in order to have a ratio  $E_{\text{rock}}/E_{\text{concrete}}$  varying between 0,050 and 1,5. The results, in terms of crack pattern, are reported in (Fig. 8). When the ratio is grater than 0,50 the results are realistic.

To establish the influence of the size of the interfacial zone is considered a layer of 2,7 m and 14 m respectively. The thickness of the dam at the foundation is 7 m. The result, in terms of crack pattern, are reported in (Fig. 9). May be observed how the result are compatible with the size of the interfacial zone is the same of the thickness of the dam.

To obtain reasonable results, it is necessary select appropriate meshing parameters. The program Atena 3D permit to choose element of different shape (tetrahedron, brick, pyramid), further than different dimension. The better solution is achieved for structured mesh composed only with brick elements. However, such method is useful only for very regular structures. Indeed, the time of analysis become almost elevated. Tetrahedron and mixed meshes are more flexible and suitable for most geometries. The mixed meshes consist of an uniform brick mesh in the interior or the model and tetrahedral elements in the remaining regions. This method works satisfactory only if the selected mesh size is sufficiently small.

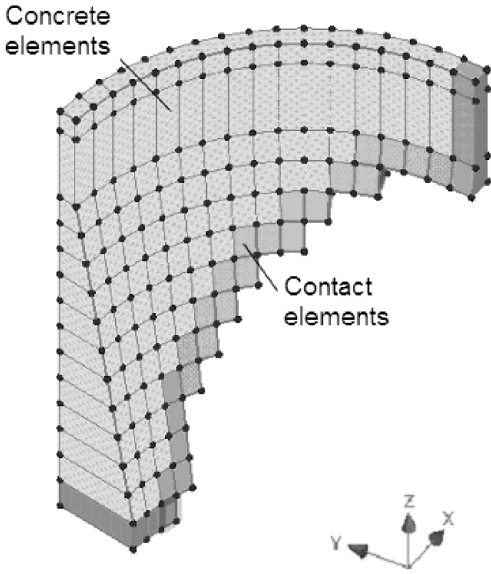


Figure 7. The model of the dam.

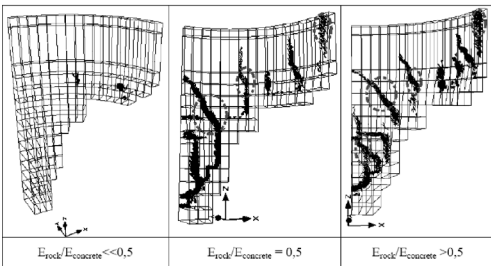


Figure 8. Crack pattern for various  $E_{\text{rock}}/E_{\text{concrete}}$  ratio.

So, also in this case, the time of analysis is high. To reduce the computational cost, in the examined cases are used only tetrahedron meshes. The ratio of refined size to global size is chosen 0,5-1-2, respectively (the tetrahedron sides have length 30–60–175 cm, while the width of foundation is of 700 cm). The result, in terms of crack pattern, are reported in (Fig. 10). The best compromise between the time of analysis and the accuracy of results there is when the ratio of is 1.

Due to shrinkage, tensile stresses occur. This causes cracks that gradually grow up in the specimen extension. The energy of fracture  $G_f$  represents the area subtended by the diagram  $\sigma - w$  and physically represents the more or less brittle behaviour of the concrete. Then, changing this parameter the structural response of the dam varies. In particular may be observed (Fig. 11) how the crack pattern enlarge when the exponent  $n$  increase from 5 to 15.

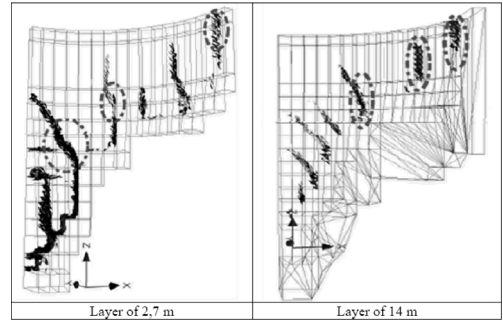


Figure 9. Crack pattern for various size of the interfacial zone.

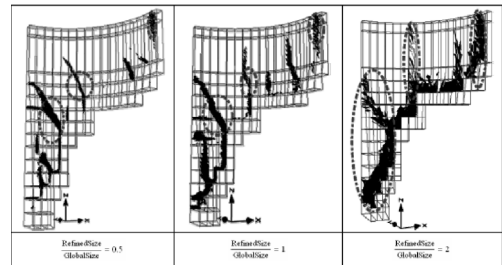


Figure 10. Crack pattern for various size of the tetrahedron meshes.

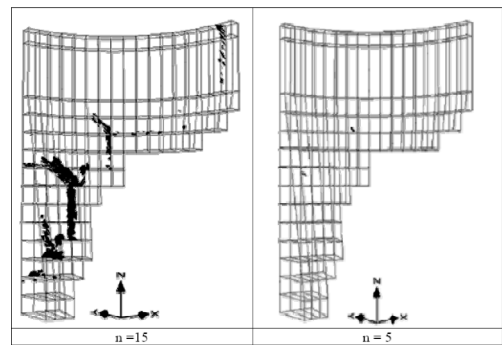


Figure 11. Crack pattern for  $n = 15$  and  $n = 5$ .

## 5 INFLUENCE OF CREEP AND SHRINKAGE

Under sustained loads, the process of cracking continues and the concrete strains increase. This phenomenon is taken into account by means of a fictitious elastic modulus, so to have a strain greater than that employed for short-term loads.

To evaluate the influence of the creep on the structural behavior of the dam, various elastic modulus for the concrete are launched. The result, in terms of crack pattern, are reported in (Fig. 12).

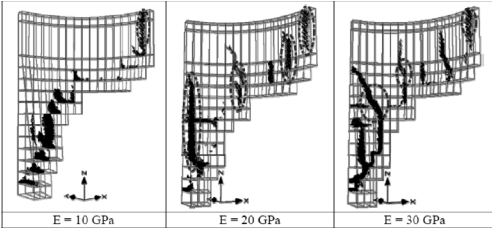


Figure 12. Crack pattern for various values of creep at parity of shrinkage.

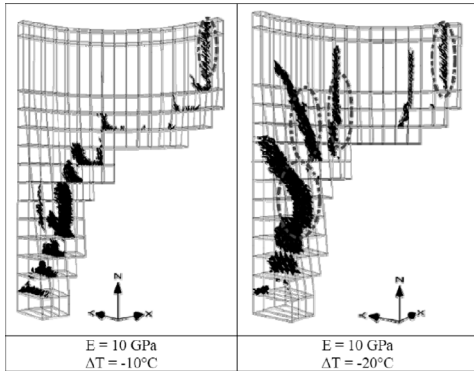


Figure 13. Crack pattern enlarging with the shrinkage strains.

May be observed that as the elastic modulus of concrete decrease, the cracking decrease. Then, the shrinkage strains may become more consistent (Fig. 13).

## 6 THE SERVICE BEHAVIOR

In the following, the life-cycle behavior is presented with and without the cracking effects due to shrinkage.

Strains of the undamaged dam are presented in Fig. 14. The deformation of the vertical cantilevers has a typical “S” shape, due to the load distribution and to the upper arches deformation. The dam behaves like an arch.

This behavior is modified by shrinkage damage. Vertical cracks cut the restraint supplied by the horizontal cantilevers. So, for each cantilever, a bending deformation occurs. Besides, displacement due to shrinkage opposes that due to the hydrostatic pressure (Fig. 15). Then the water pressure has a benefic effect, sealing shrinkage cracks.

The analysis shows that the hydrostatic pressure does not cause any new crack at the upstream side of the dam. Then it is headed off the uplift hazard.

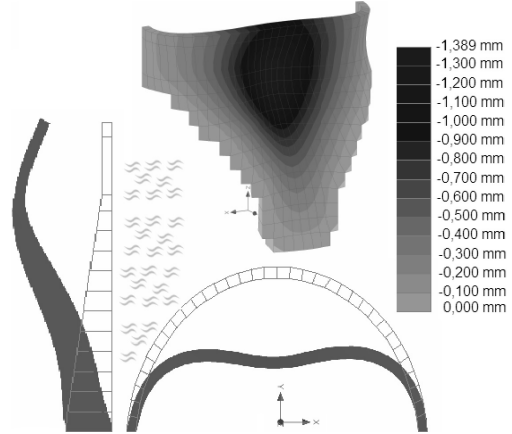


Figure 14. Dam's displacements due to gravity loads and hydrostatic pressure, without damage.

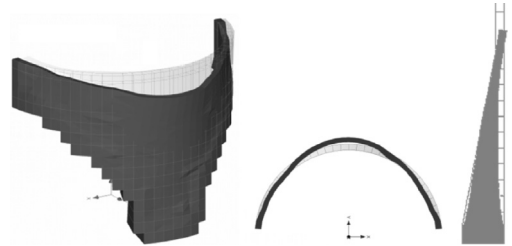


Figure 15. Dam's displacements due to gravity loads and hydrostatic pressure, with damage.

## 7 THE CASE OF ARCH/GRAVITY DAMS WITH RECTANGULAR FRONT

Three different geometries of dams have been considered. The horizontal section of the dam a circular sectors with an angular width of 60°, 75° and 90°, respectively (Fig. 16). It has been assumed, for the concrete, a delayed modulus, to take in account the creep effects,  $E_c = 10$  GPa and an uniform temperature reduction  $\Delta t = -15^\circ\text{C}$ .

Due to the particular geometry, under gravity loads and shrinkage effects long vertical cracks grow. Those cracks are extended on the height of the dam and the distance between two following cracks is quite constant (Fig. 17).

In this typology of dam, the hydrostatic pressure induces strong cracking on the base (on the upstream side), due to the dominating vertical cantilever behavior (Fig. 18–19). So the crack damage in this typology yield an unsafe service behavior.

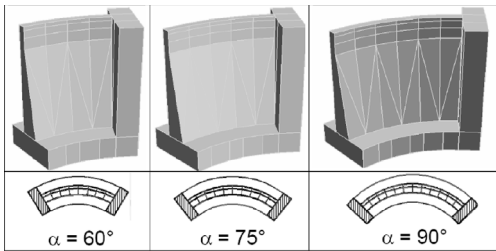


Figure 16. The mesh geometry and the considered angular widths.

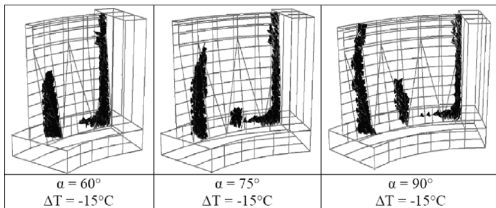


Figure 17. Crack pattern occurring in the dam under gravity loads and shrinkage.

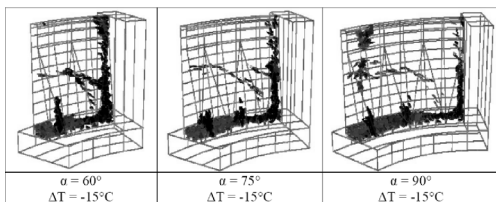


Figure 18. Crack pattern occurring in the dam under gravity loads, shrinkage and hydrostatic pressure.

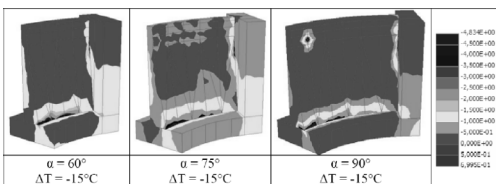


Figure 19. Stress distribution occurring in the dam under gravity loads, shrinkage and hydrostatic pressure.

## 8 CONCLUSIONS

In the paper is presented a procedure able to verify the functionality of old arch/gravity dams has been set up. In fact, the presence of long cracks due to concrete shrinkage may reduce the load capacity of the dam and render unsafe the structure.

The functionality control requires to reproduce the gradual dam cracking during the loading history.

A step by step procedure has been followed to take in account the non linear effects due to the concrete cracking into the sequence of the working phases of the dam. The shrinkage effects have been considered acting on the dam stressed only by dead loads. The creep effects are considered by introducing a delayed elastic modulus. The influence on the numerical response of parameters like the fracture energy, the mesh geometry and the boundary conditions have been investigated. Different typologies of concrete dams are studied: arch dams with rectangular or like triangular front. To the latter belongs the case studio of the Corfino dam, useful to compare the crack pattern obtained in the numerical model with the detected one.

The shrinkage vertical cracks are sealed by the water pressure. Thus, the shrinkage damage does not produce relevant reduction of functionality capacity in the dams with a like triangular front.

Like rectangular front dams, on the contrary, behave differently. The action of the hydrostatic pressure on these damaged dams, in fact, produces new cracks on the upstream side, due to the dominating cantilever behaviour.

## ACKNOWLEDGEMENT

The authors acknowledge ingg. Matteo Agliocchi, Fabio Fattori and Antonio Rossetti for the numerical analyses developed during their graduation thesis.

## REFERENCES

- Batti, M.A., Teng, S. & Ashton, W.D. 1994. Simplified finite element analysis of a cracked concrete arch dam, *Engineering Structures* 26(2004): 27–37. ACI.
- Lan, S. & Yang J. 1997. Nonlinear finite elements analysis of arch dam—I. Constitutive relationship, *Advances in engineering software* 28(1997): 403–408. Elsevier.
- Lan, S. & Yang J. 1997. Nonlinear finite elements analysis of arch dam—II. Nonlinear analysis, *Advances in engineering software* 28(1997): 409–415. Elsevier.
- Ahmadi, M.T., Izadinia, M. & Bachmann H. 2001. A discrete crack joint model for nonlinear dynamic analysis of concrete arch dam, *Computers and Structures* 79(2001): 403–420. Elsevier.
- Azmi, M. & Paultre, P. 2002. Three-dimensional analysis of concrete dams including contraction joint non-linearity, *Engineering Structures* 24(2002): 757–771. Elsevier.
- Lofli, V. & Espandar, R. 2004. Seismic analysis of concrete arch dams by combined discrete crack and non-orthogonal smeared crack technique, *Engineering Structures* 26(2004): 27–37. Elsevier.
- Cervenka, V, Jendele, L.. & Cervenka, J. 2007. ATENA Program Documentation, Part 1—Theory, Cervenka Consulting, Prague, Czech Republic.



# Effects of soil-structure interaction on the seismic damageability of coupled wall-frame structures on pile foundations

F. Dezi

*Department of Materials and Environment Engineering and Physics, Università Politecnica delle Marche, Ancona, Italy*

S. Carbonari

*Department of Architecture, Constructions, Structures, Università Politecnica delle Marche, Ancona, Italy*

G. Leoni

*Department ProCAm, Università di Camerino, Ascoli Piceno, Italy*

**ABSTRACT:** The paper presents a study on the seismic damageability of coupled wall-frame structures founded on piles. A complete soil-structure interaction analysis is carried out with reference to a case study. Three different soils and seven real accelerograms are considered. Local site response analyses are performed in order to evaluate the incoming free-field motion at different depths and the ground motion amplifications. A numerical model, accounting for the pile-soil-pile interaction and for material and radiation damping, is used to evaluate the impedance matrix and the foundation input motion. Dynamic analyses are then performed in the time domain by considering fixed and deformable base models. In the second case, the effects of the soil-foundation system deformability are taken into account with Lumped Parameter Models calibrated on the impedance functions previously evaluated. Rocking phenomena affect the behaviour of the structure by increasing the interstorey drifts. Evaluation of the return period of damaging events shows how for soft soils the usual design procedure may be not effective in protecting the building against seismic damages.

## 1 INTRODUCTION

In the conventional building design, structures are generally assumed to be fixed at their bases and the input motion is defined at the outcropping soil according to suitable design spectra. In reality, the deformability of the soil-foundation system makes the problem more complex. Firstly, the input motion of the structure is filtered by the embedded pile foundation subjected to ground motions variable with depth; secondly, the foundation deformability reduces the overall stiffness of the structure and increases the damping due to energy radiated into the soil.

For wall and coupled wall-frame structures it is important to guarantee a suitable degree of restraint at the base. Commonly, pile foundations are considered to be enough rigid against rocking motions and a fixed base model is supposed to be conservative because it overestimates the actual seismic action. In reality the wall rocking may affect the behaviour of the structure by changing the local displacement demand. Structural displacements can be directly related to damage potential though material strains (structural damage)

and drift (non structural damage). Consequently, by considering the real foundation deformability, the events that lead to damage may be characterised by a lower return period.

A reliable analysis should account for the main features previously described by carrying out a complete soil-structure interaction study.

The first step consists in performing a local site response analysis of the soil profile (for usual purposes a one-dimensional analysis is sufficient) by deconvoluting the accelerograms defined at the bedrock outcropping and studying the polarized shear wave propagation (Bardet J.P. et al. 2000). This permits to evaluate the effects of the free-field motion variable with depth. The second step consists in the structural analysis including the soil-foundation system. The problem is governed, in the frequency domain, by a system of complex linear equations

$$\begin{bmatrix} \mathbf{K}_{SS} & \mathbf{K}_{SF} & \mathbf{0} \\ \mathbf{K}_{FS} & \mathbf{K}_{FF}^{[S]} + \mathbf{K}_{FF}^{[F]} & \mathbf{K}_{FE} \\ \mathbf{0} & \mathbf{K}_{EF} & \mathbf{K}_{EE} \end{bmatrix} \begin{bmatrix} \mathbf{d}_S \\ \mathbf{d}_F \\ \mathbf{d}_E \end{bmatrix} = \begin{bmatrix} \mathbf{0} \\ \mathbf{f}_F \\ \mathbf{f}_E \end{bmatrix} \quad (1)$$



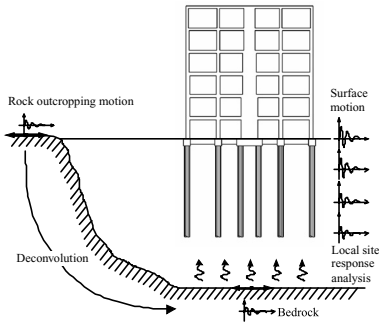


Figure 1. Soil-structure interaction problem.

where the partition descends from the separation of the displacements in the structure ( $d_S$ ), foundation ( $d_F$ ) and embedded piles ( $d_E$ ) components (Dezi et al, 2007). Foundation impedances have to account for pile-soil-pile interaction and radiation damping and should be able to describe also the foundation rocking response. The known term collects the forces descending from the local site response analysis previously carried out.

In the sequel the influence on the seismic damageability of coupled wall-frame structures is investigated according to the methodology previously introduced. The soil-pile-structure interaction analysis is performed by means of the substructure method which consists in studying separately the soil-foundation system (kinematic interaction analysis) and the superstructure on deformable restraints (inertial interaction analysis) (Wolf 1988).

## 2 SEISMIC DAMAGEABILITY ANALYSIS OF A COUPLED WALL-FRAME SYSTEM

The problem of the seismic damageability of coupled wall-frame systems is investigated with reference to the 6-storey 4-bays building shown in the figures 2 and 3. The building is supposed to have a square plan with a side length of 18.00 m. Four coupled wall-frame systems, placed at the boundaries in order to achieve a torsionally restrained system, constitute the seismic-resistant structure. The total height  $h_t$  is 19.20 m and the storey height  $h_i$  is 3.20 m. The structure was designed by considering fixed base restraints and by assuring interstorey drifts less than 5‰ (Damageability Limit State).

Thanks to the plan symmetry, the structural analysis is carried out by considering only one seismic-resistant wall-frame system. The masses associated to each floor of the system, shown in Fig. 3a, refer to half storey and are not comprehensive of the structural self weight that is automatically accounted for in the model.

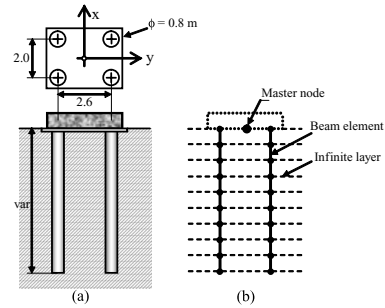


Figure 2. (a) Foundation of the wall; (b) Finite element model.

The wall-frame system is founded on piles: a single pile foundation is considered for each column of the frame, while a  $2 \times 2$  pile group foundation is assumed for the wall. The piles are floating and characterized by the same diameter ( $\phi = 0.8$  m). Fig. 2a shows the geometry of the wall foundation used in the numerical application.

The soil profile consists of a deformable homogeneous soil layer of 30 m thickness overlying a rigid bedrock which is supposed to be elastic. Three kinds of soils, characterized by different shear wave velocities and densities, are considered for the deformable layer. A constant hysteretic material damping ratio  $\xi = 10\%$  and a constant Poisson's ratio  $\nu = 0.4$  are assumed for all the soils. Table 1 shows the soil properties chosen for each soil profile.

The pile lengths, varying with the soil properties of table 1, are 14 m for soil profile A, 16 m for soil profile B and 22 m for soil profile C.

### 2.1 Structural modelling

Structural models are separately developed for the foundation and the superstructure according to the substructure method.

The foundation is modelled by considering the piles as beam elements embedded in a Winkler-type layered soil (Makris & Gazetas 1992). The numerical procedure proposed by the authors (Leoni et al. 2007, Dezi et al. 2007) for the kinematic analysis of pile groups is used to effectively study the soil-foundation and the pile-to-pile interaction. The procedure is used to compute the foundation input motion and the frequency-dependent impedances of the soil-foundation systems. Each pile is modelled by 1 m long finite elements to provide a suitable level of accuracy. Concerning the wall foundation, a rigid cap is considered and a master node is introduced at the centroid of the pile group at the level of pile heads (Fig. 2b).

Two structural models were considered for the superstructure: one is fully restrained at the base (FB model) while the other is supported by deformable restraints (SSI model).

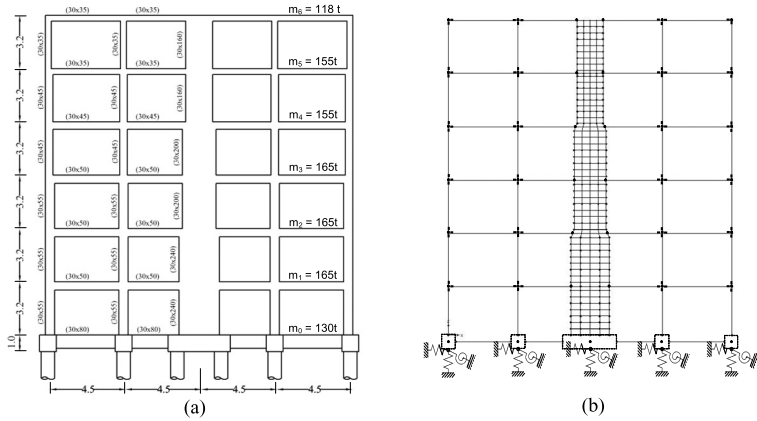


Figure 3. (a) Coupled wall-frame system; (b) SAP2000® model.

Table 1. Soil properties.

Profile	$V_s$ m/s	$\rho$ t/m <sup>3</sup>	$\nu$	$\xi$ %	NSPT	$C_u$ kN/m <sup>2</sup>
Bedrock	1200	2.0	0.4	—	—	—
A	400	1.8	0.4	10	40	220
B	250	1.6	0.4	10	22	150
C	100	1.6	0.4	10	8	70

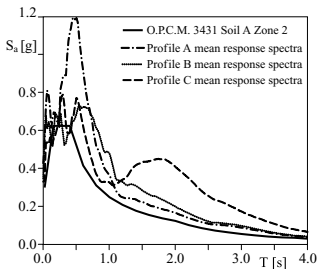


Figure 4. Mean response spectra at the outcropping soil for the three profiles.

The finite element models were developed in SAP2000® (CSI—Computers and Structures inc., 2005). Frame members are modelled by beam elements while shell elements are used to simulate the concrete wall (Fig. 3b). Rigid links, automatically introduced by the program, are used to simulate the beam-to-column joints; in particular, the actual length of the rigid link is assumed to be 50% of the joint region to take into account the strain penetration effect. To incorporate the in-plane rigidity of the floor, a stiff diaphragm constraint is introduced at each storey. Mass of the foundations and tie-beams at the pile cap level were also incorporated in the flexible base model.

The concrete (C30/37) is considered to be linearly elastic, with a Young's modulus  $E_c = 3.5 \times$

$10^7$  kN/m<sup>2</sup>. The effects of members cracking is taken into account by considering 75% of the concrete Young's modulus for the wall and the columns and 50% for beams. A structural damping is introduced in term of Rayleigh damping: stiffness and mass proportional terms were evaluated to provide a 5% effective damping for the first and second mode.

## 2.2 Kinematic interaction analysis

The incoming seismic action at the outcropping bedrock is represented through seven real accelerograms matching the elastic response spectrum of the Italian Code (OPCM 3431, 2005) for soil type A and hazard level 2, obtained from the European Strong Motion Database (<http://www.isesd.cv.ic.ac.uk>). The accelerograms are divided by a factor 2.5 to reduce the action to the damage limitation level hazard corresponding to a 50% probability of exceedence in 50 years.

A one-dimensional ground response analysis was performed by using EERA (Bardet et al. 2000). The three soil profiles and the seven accelerograms were considered. The time histories of the free-field motion at the ground surface and at different depths corresponding to the finite element nodes of the foundation model were calculated. The time histories obtained from the site response analyses were used as input, at different depths, for the kinematic interaction analysis, whereas the motions obtained at the ground surface were used for FB model. Fig. 4 shows the mean response spectra of the motion at the ground surface where amplifications due to the different site responses are evident.

The frequency-dependent impedance functions shown in Fig. 5 are also obtained. In particular columns (a) and (c) show the impedances of the single pile and the  $2 \times 2$  pile group foundation, respectively.

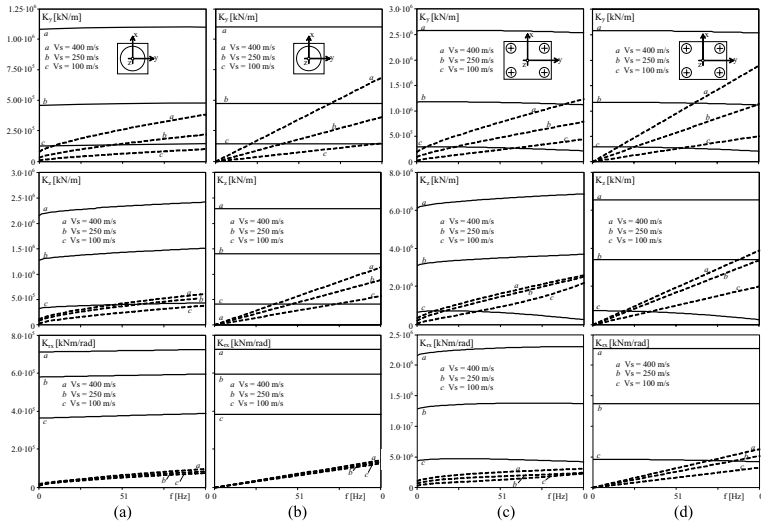


Figure 5. Dynamic foundation impedances: (a) dynamic impedances of single pile foundations for each soil profile and (b) approximated behaviours; (c) dynamic impedances of pile group foundation for each soil profile and (d) approximated behaviour.

### 2.3 Inertial interaction analysis

Suitable Lumped Parameter Models (LPMs) are used to catch the frequency dependent behaviour of foundations in the time domain analysis. The simplest of these models consists of one spring, one damper and one mass for each degree of freedom of the rigid cap. The relevant constants are calibrated so that both the real part and the imaginary part of the foundation impedances are well approximated in the frequency range of interest.

The dynamic stiffness relevant to the  $j$ -th dof of the foundation is thus approximated by

$$Z_j(\omega) = [(K_j - \omega^2 M_j) + i\omega C_j] \quad (1)$$

where the real part varies with frequency as a second order parabola while the imaginary part varies linearly with frequency.

The frequency-independent coefficients of springs, viscous dampers and masses are calibrated to better reproduce, in the low and medium frequency range (0–10 Hz), the trend of the frequency dependent impedances obtained from the soil-pile-foundation interaction analysis previously described.

In SAP2000® the lumped parameter models were introduced as visco-elastic grounded springs and additional masses applied to the master node of each foundation.

In Fig. 5 columns (b) and (d) show the approximated dynamic impedance functions of the single pile and the  $2 \times 2$  pile group foundation, respectively. Notice that some curves relevant to LPMs look quite different from the theoretical ones, especially for

imaginary parts. This is due to the model adopted but the approximation can be improved by choosing more sophisticated LPMs (Wolf 1988). However, the loss of precision is compensated by the advantage of using commercial structural analysis software.

## 3 MAIN RESULTS

The main parameter monitored in the application was the interstorey drift that is considered to be a good measure of the seismic damage level of non-structural elements.

Fig. 6 shows the time histories of the interstorey displacements relevant to floor 6 for the three different soil profiles obtained from one of the real accelerograms considered. The dashed straight lines represent the limit values of 5‰ of the storey height as prescribed by many seismic codes. Obviously, the soil-structure interaction effects on the structural response revealed to be more important in the soil profile with a lower value of  $V_s$ .

In Fig. 7 the interstorey drifts obtained from the 14 analyses performed for each soil profile are presented (dots) together with the relevant mean values (curves). It can be observed that for the fixed base analyses the mean curves (dashed) are all below the limiting line for every soil profile.

For the soil profile A ( $V_s = 400$  m/s) no differences are observed between the fixed base model and that including the soil-structure-interaction. For the soil profile B, mean interstorey drifts obtained with the SSI model are slightly higher than those obtained

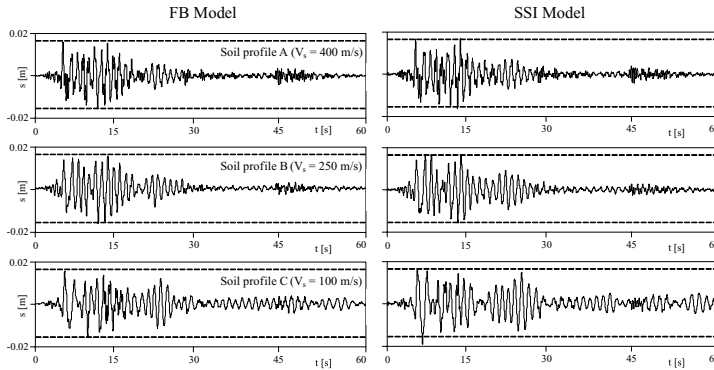


Figure 6. Time histories of the interstorey displacements relative to the 6th storey (accelerogram 190xa).

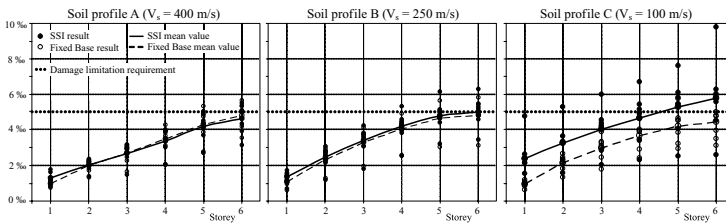


Figure 7. Interstorey drifts obtained from all the accelerograms used in the analyses for both the fixed and the flexible base models.

with FB model even if the results are more scattered. The mean values are still lower than the limit of 5‰. In the case of soil profile C, the mean interstorey drifts obtained with the two models are very different. The mean value obtained at the sixth storey with the SSI model is more than 30% higher than that relevant to the FB model and reaches more than 100% at the first storey. Differences are due to the foundation rocking that adds more than 1‰ storey drift corresponding to the maximum rocking angle of about 1 mrad. Additionally, it should be noted that results referred to flexible base models are very scattered. The verifications are not satisfied at the last two levels. To clearly appreciate differences between the two models results of the interstorey drifts, obtained under all the seismic excitations, are presented in Table 2 for the sixth storey. Mean values are presented together with variance to give a measure of the statistical dispersion.

### 3.1 Evaluation of return periods of damaging events

In an attempt to evaluate the frequency of occurrence of the limit damage level, the Peak Ground Accelerations (PGA) producing a maximum interstorey drift equal to 5‰ for both FB and SSI models were evaluated.

Table 2. Interstorey drift of the sixth floor [‰].

Earthquake	Profile A		Profile B		Profile C	
	Fixed	SSI	Fixed	SSI	Fixed	SSI
Record						
55xa	4.98	5.01	5.93	4.71	3.52	4.55
182ya	5.56	4.24	5.73	6.23	4.84	9.84
198xa	4.58	4.89	4.77	5.38	5.94	6.32
198ya	5.23	5.41	4.74	5.11	4.81	5.80
200xa	3.45	3.06	3.05	3.37	3.14	2.60
190xa	4.96	5.26	5.40	5.21	5.04	3.09
1231ya	4.10	3.84	4.74	4.51	4.01	5.61
Mean	<b>4.69</b>	<b>4.53</b>	<b>4.76</b>	<b>4.93</b>	<b>4.47</b>	<b>5.83</b>
$\sigma^2$	<b>0.44</b>	<b>0.63</b>	<b>0.62</b>	<b>0.67</b>	<b>0.80</b>	<b>4.07</b>

By supposing that the structure behaves linearly till 5‰ interstorey drift, and that the spectrum shapes do not change with the probability of occurrence, the PGAs were calculated by a linear interpolation. Fig. 8 shows the seismic hazard curve associated to the site considered for the case study (Italian seismic hazard maps provided by the INGV-DPC). The design PGA of 0.10 g, as already stated, is associated to a probability of exceedence of 50% in 50 years.

The probabilities of exceedence  $P_E^{FB}$  and  $P_E^{SSI}$  related to the PGA values, calculated for the FB and

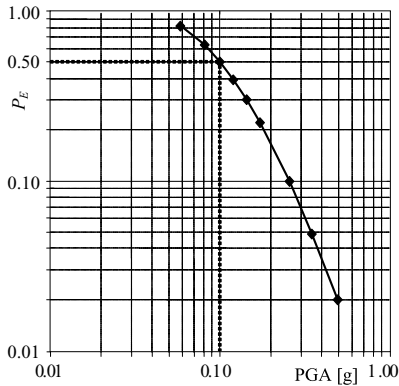


Figure 8. PGA values for different probability of exceedence in 50 years.

Table 3. Probabilities of exceedence and return periods referred to the sixth floor.

Soil profile	FB		SSI	
	$P_E$ %	$P_R$ years	$P_E$ %	$P_R$ years
A	44	85	42	91
B	45	83	47	78
C	42	93	57	59

SSI models, can be derived from the hazard curve and are reported in Table 3. The mean return periods  $P_R$ , relevant to such exceedence probabilities, have been calculated from equation

$$P_R = \frac{-50}{\ln(1 - P_E)} \quad (2)$$

Except for the case of soil profile A, for which the return period increases by considering the SSI, a reduction of the mean return period is registered for soils B and C. In particular, for soil profile C the mean return period  $P_R^{SSI}$  is 59 years that is not acceptable in terms of damageability limit state.

#### 4 CONCLUSIONS

In this paper the seismic damageability of wall-frame systems founded on piles was investigated. In order to understand the importance of the foundation deformability, a complete SSI analysis was performed.

The domain decomposition technique was adopted to perform time-domain seismic analyses introducing LPMs to take into account the frequency dependent impedance of the soil-structure system.

Local response analyses were performed to compute the free-field input motion by considering seven

real accelerograms at the outcropping bedrock. The foundation kinematic interaction analysis was performed by means of a numerical model proposed by the authors accounting for pile-soil-pile interaction.

The following conclusions may be drawn:

- the local site response analysis is necessary to catch the free-field motion variable with depth and the spectral amplification of the input signals;
- even if the deformability of the soil-foundation system reduce the seismic base shear, this does not result in the reduction of the interstorey drift responsible of the building damage;
- the foundation rocking induces an additional drift that is almost constant for all the storeys;
- soil-structure interaction effects increase the probability of occurrence of the seismic action that produce a maximum interstorey drift equal to the 5% of the storey height and consequently increase the probability of damage during the life-cycle of the structure.

Although the previous remarks are derived from a case study they support evidence on the significance of considering SSI effects on seismic damageability of wall-frame structures.

#### REFERENCES

- Bardet J.P., Ichii K. & Lin C.H. (2000). EERA: Equivalent-linear Earthquake site Response Analyses of Layered Soil Deposit. University of Southern California.
- Dezi F., Carbonari S., Dall'Asta A. & Leoni G. (2007). Dynamic spatial response of structures considering soil-foundation-structure interaction: analytical model, *A.N.I.D.I.S. 2007—12° Convegno Nazionale—L'ingegneria sismica in Italia, Pisa*, paper n. 310.
- Dezi F., Dall'Asta A., Leoni G. & Scarpelli G. (2007). Influence of the soil-structure interaction in the seismic response of a railway bridge, *ICEGE 2007—4th International Conference on Earthquake Geotechnical Engineering—Thessaloniki—Greece*, paper n. 1711
- European Strong Motion Database—[www.isesd.cv.ic.ac.uk](http://www.isesd.cv.ic.ac.uk).
- INGV-DPC S1 Project (2006), Italian seismic hazard maps adopted by the OPCM 3274 (<http://esse1.mi.ingv.it>).
- Leoni G., Dezi F. & Carbonari S. (2007). A model for 3D kinematic interaction analysis of pile groups in layered soils—*Submitted to Earthquake Engineering and Structural Dynamics*.
- Makris, N. & Gazetas, G. (1992). Dynamic Pile-Soil-Pile Interaction—Part II: Lateral and Seismic Response. *Earthquake Engineering Structural Dynamics*, 21 (2), pp.145–162.
- OPCM n. 3431, Italian seismic code, 2005.
- SAP2000 (October 2005). “CSI analysis reference manual”. *Computer and Structures, Inc.*, Berkeley, California, U.S.A.
- Wolf J.P. (1988). *Soil-structure Interaction Analysis in Time Domain*, Prentice-Hall, Englewood Cliffs, N.

# Rehabilitation and modernization of the Monte Bianco Tunnel

G. Furlanetto & L. Ferretti Torricelli

*Bridge Design Department SPEA Ingegneria Europea S.p.A., Milan, Italy*

**ABSTRACT:** After the tragic event of the march 1999, in which the fire broken out from a truck destroyed a wide portion of the internal structures of the Monte Bianco Tunnel, an extensive plan of rehabilitation and modernization of this important link between Italy and France was started, in order both to repair the damages caused by the fire and to improve the safety of the tunnel. The tunnel carriageway runs onto a box prestressed concrete structure, laying on the bottom of the tunnel, that went irreparably destroyed in three distinct points of the upper slab, together with a wide portion of the vault. The paper, after an overview of the main features of the structure and of the modernization plan, which have strongly improved the safety standards of this important link, will show in detail the peculiarities of the structural interventions on the internal structure.

## 1 INTRODUCTION

The Monte Bianco tunnel was opened to traffic in 1965; with its 11.6 km, excavated under a medium cover of more than 2000.0 m in very hard geological conditions represented, more than the realization of a strategic link with Europe, a challenge that remained unequalled for many years.

Due to the complexity of the excavation conditions, compared with the equipment available at that time, the tunnel was designed in order to strictly allow a single two-lane carriageway 8.60 m wide, composed by two 3.50 m wide lanes and two sidewalks of approximately 0.8 m.

The carriageway runs on the top slab of a box concrete structure, whose internal cells are used as canalization of the ventilation system.

For the realization of this internal structure, two typologies have been adopted: for the segment under the competence of the Italian authority, from chainage 0.00 to 5800.00 a precast box section was used, whilst the portion under the competence of French authorities was realized for the greater part by a multiple arch cast-in place structure.

In correspondence of the border between the two portions the continuity of the ducts was successively interrupted closing the internal cell with a massive concrete diaphragm.

Along the "Italian" portion, the number of the cells varies from a maximum of five, near the entrance, to a minimum of three in the middle of the tunnel; one of the side cells is dedicated to the suction of foul air through intake points located every 300 m; the other cells are reserved to the injection of fresh air through inlets located every 10 m. For the "French" portion,

the subdivision and use of the internal ducts is similar. The concrete structure is composed by precast box segments 10 m long; they rest on the bottom slab of the tunnel with the interposition of linear reinforced elastomeric bearings located under the web axes.

The lateral haunches were installed in a second stage, rigidly fixed to the box with a cast-in-place junction, and simply supported on a longitudinal saddle provided on the lining of the tunnel. The air tightness is here ensured by means of continuous packing, which allows longitudinal movement to take place. Water-stops sealing were also provided in correspondence of the cast in place junction between lateral haunches and box structure.

Seen in cross section the structure appears as a box girder, completely independent from the lining, floating on the bottom slab of the tunnel. In the longitudinal direction, the "deck" is a continuous structure fixed at the ground in correspondence of three abutments provided at chainage 0.00, 2.900 and 5.800; the abutments were realized by means of vertical cables, subdividing the Italian portion into two segments having approximately equal length.

In transversal direction, in addition to traffic loads, the design required to account for the air pressure loads in the internal ducts, ranging from 7 to 12 kN/m<sup>2</sup> and the loads arising from the air temperature gradient between air in the tunnel and that in the ventilation ducts, giving rise to stresses of the same order as the traffic loads. The client organization decided to achieve the air tightness of the internal ducts without making use of either coating or painting, resorting to the prestressing of the structure. The prestress was obtained giving a permanent constraint compressive

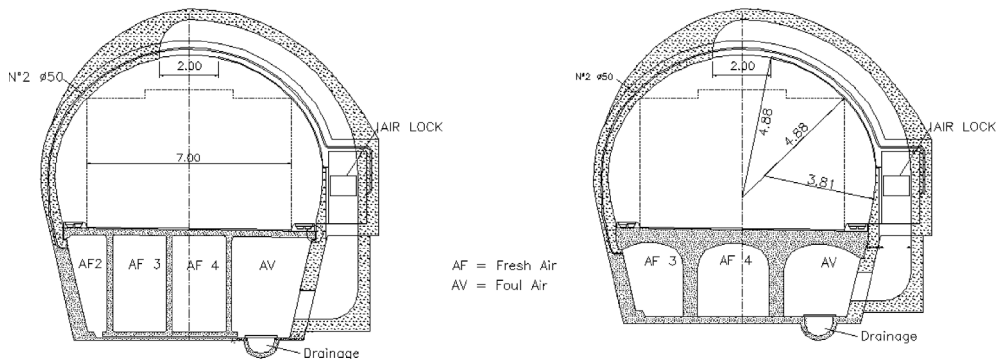


Figure 1. The two typologies of internal structure in correspondence of intake points.

state through special “stressing sections” located every 180 m, using flat jacks uniformly distributed along the transversal section of the deck. The amount of prestress was determined in order to guarantee, accounting for the long term losses, a minimum compression stress of at least  $-1.5$  MPa in presence of the lowest ambient temperature, during winter time; each abutment was designed to withstand a maximum design thrust of 77000.0 kN, determined on the basis of the initial prestress (without long term losses) and the maximum temperature rise. The prestressing was given following a long and complex cycle of stressing adjustment, set up in order to minimize the effect of long term losses, at the end of which the stressing sections were definitively sealed. In the service state, under the design seasonal temperature difference of  $35^{\circ}\text{C}$ , the longitudinal stress acting in the transversal deck sections could range from  $-1.5$  to  $-8.5$  MPa.

### 1.1 The damages

On march 1999 the fire burst out from a truck broken down approximately in the middle of the tunnel. In this tragic event 39 people lost their lives, mainly due to the exceptionally dense smoke curtain that immediately invaded the tunnel, preventing the fire brigades from reaching the centre of the fire that was extinguished after more than 50 hours from its rise.

The most serious structural damages of the internal deck structure interested a portion about 800 m long; in this segment the concrete vault went almost completely destroyed, together with the top slab of the internal structure.

The deck structure suffered both for the presence of the vehicles burning on the top slab and for the extremely high temperatures of the air flowing into the ventilation tunnel, that caused the spalling of the concrete cover of the slab and webs in many points and the melting of the longitudinal rubber bearings supporting the lateral haunches.



Figure 2. Archive photo: positioning of precast box segments and lateral haunches.



Figure 3. Archive photo: the internal structure finished.

### 1.2 The modernization and rehabilitation plan

These heavy damages, in conjunction with minor damages due to the old age of the structure and, above all, the need to improve the safety standard of the infrastructure, induced the Italian and French managing firms (SITMB and ATMB) to start an intensive plan of rehabilitation and modernization.

On February 2000, the international call for tenders was won by the joint-venture SPEA Ingegneria Europea (Italy)—Scetaroute (France), whose designs were



Figure 4. Vault and top slab damages.



Figure 5. Concrete spalling of the carriageway slab intrados.

approved by an intergovernmental supervising commission and, for Italy, by the National Authority for roads and highways A.N. A.S.

Here below are summarized the main works involved by the rehabilitation and modernization plan. The first provides:

- The integral demolition and replacement of the box segments in three distinct zones, for a total length of 100 m (10 segments);
- The demolition and replacement of the concrete vault directly interested by the fire;
- The replacement of the bearings of the lateral haunches for the whole length of the tunnel;
- The repairing of the parts characterized by minor damages, with demolition and restoration of the concrete cover.

The most important structural works on the internal structure involved by the modernization plan, were related to the realization of a safety escape paths along the fresh air ducts, with:

- demolition of the diaphragm obstructing the abutment n. 3, located in correspondence of French-Italy border, which required the realization of a completely new abutment;
- realization of gaps through the prestressed box webs, fitted with air tight doors;

- improvement of the air tightness of the internal ducts, providing a special seal in correspondence of the continuous longitudinal bearing of the lateral haunches.

The other main works involved by the modernization plan, which interested the whole length of the structure, includes the realization of:

- laybys, located every 600 m, ensuring the easy U-turn of commercial vehicles;
- 37 pressurized shelters (one every 300 m), linked with the internal duct;
- fire places every 150 m, equipped with emergency telephone and fire extinguishers;
- additional smoke intakes;
- three water tanks located along the tunnel and dedicated to the fire extinguishing system
- a fire-brigade station, located in the middle of the tunnel.

In addition, the control system has been radically renewed, together with the alert-intervention procedures.

## 2 REHABILITATION OF THE INTERNAL STRUCTURE

The interventions provided for the rehabilitation of the internal structure consist in the repairing of the less damaged zone, where the deterioration affects generally only the concrete cover, and in the integral replacement of the precast segments characterized by damages whose repairing could have compromised the prestressing state originally provided.

### 2.1 Replacement of damaged segments

As previously mentioned, the damages suffered by the top slab and by the webs obliged to the integral replacement of the box segments in three distinct zones (“A”, “B” and “C”) located between the abutment “2” and abutment “3” in a range of about 800 m. In correspondence of these points the slab appeared buckled, and crossed by wide cracks through the thickness.

The sections were also tested by measuring the natural frequencies of the frame, which, compared with measures made on non-damaged sections confirmed an hard decay of the original properties. For this reason the complete replacement of the segments damaged was planned.

Due to its peculiarity, all the interventions provided along the internal box structure had to be planned in order to minimally disturb the design prestressing state imposed during the construction; in fact, the demolition of the segments, would have caused of the loss of prestress on a portion of length hardly to establish.



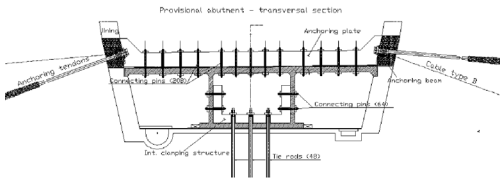


Figure 6. Provisional abutment at chainage 4900.00.



Figure 7. Provisional abutment—anchorage of the box.

For this reason it was decided to “isolate” the portion under intervention, providing a provisional fixed point at chainage 4900.00, in order to preserve the restraint state due to the prestressing in the non-damaged portion. The restoring of the prestress should have been carried out acting through new “active” joints located along the replaced segments

The provisional abutment was conceived not only to guarantee the transferring of the resultant prestressing force to the rock without any slip, but also with the aim of making its realization and demolition as easy as possible. For this purpose was designed a sort of “clamping” structure, formed by an upper concrete plate, restraining the top slab, anchored to the rock with steel side cables, completed by an U-shaped concrete plate, which restrains the lower part of the deck, located into the central box and anchored to the rock with steel rods; the top and the internal concrete plates are anchored to the deck structure with steel prestressed pins. The interface between the existing structure and the “clamping” device were protected with steel plates provided in order to facilitate the removal of the elements at the end of the works.

The abutment was dimensioned on the basis of a maximum force of 30000 kN, evaluated accounting for the total maximum resultant force due to design prestressing force and temperature heating, plus the overstresses due to the friction losses occurring during the restressing stage of the isolated portion. The total length of the clamping structure was 24 m, needed to install the anchorages to the rock, for a total of 32 subhorizontal cables formed by 7 strands  $\phi$  0.6”

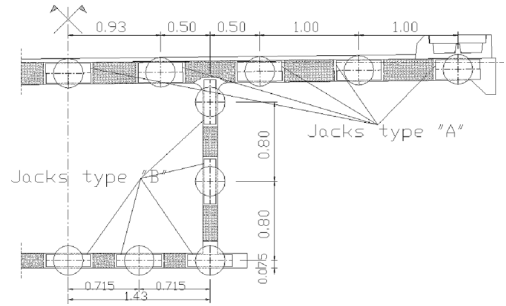


Figure 8. Stressing section.

and 48 vertical tie rods, and the anchorage of the clamping structure to the deck, for a total of 276 steel pins. The figure below shows the internal “U” shaped clamping structure before the casting. In the picture it can be appreciated the restriction characterizing the intervention conditions.

The demolition of the damaged segments was carried out using the hydro-demolition technology and interested a total of ten “original” segments (two segments respectively for zone “A” and “C”, and six segments for zone “B”) that were cut from the structure exactly in correspondence of the original joint sections. After this operation the “new” segments were cast in place in continuity with the existing, providing the accurate preparation of the joint between old and new structure, that was fitted with PVC water-stops. The demolition and casting was carried out for one segment per time.

One “active” joint was provided along each of the three interventions zones “A”, “B” and “C”, realized by a gap of 0.5 m, needed for the installation of the prestressing jacks. Preventive testing of the stress state of the structure carried out along the undamaged portion, gave evidence of the presence of a mean stress of  $-3.5/ -4.0$  MPa, value fairly agreeing with the original design provisions. The segment to prestress, which had a total length of 900.0 m, was instrumented providing four monitoring sections equipped with four strain gauges and seven thermometric sounds each one, in order to evaluate the actual stress during restressing for each of the four segments located between adjacent active joints and between the active joints and the abutments. Each stressing section was equipped with a total of 20 flat jacks having a maximum stroke of 100.0 mm and providing a maximum force of 1500.0 kN each.

The mean target stress, depending from the mean temperature during the works, was about  $-4.0$  MPa. The total resultant force to provided at the stressing section, reached 22000.0 kN.

The stressing operations were carried out under strain control, providing in every section a resultant

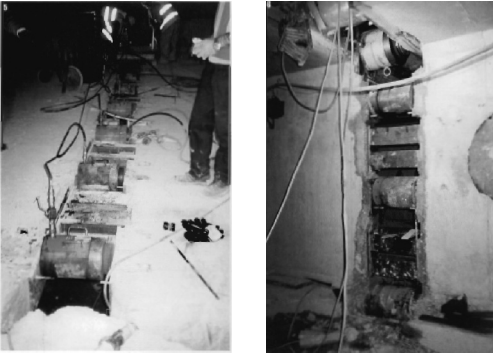


Figure 9. Stressing jacks along slab and webs.



Figure 10. Replacement of abutment 3 – transition between box structure and arch structure at chainage 5.800.00.

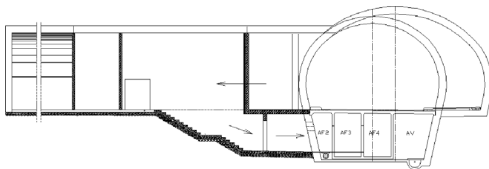


Figure 11. Evacuation path from a fire shelter.

force almost centered, acting cyclically on the three stressing sections. The stress was continuously adjusted until the end of the works in order to minimize the effect of long term loss affecting the new segments. At the end of restressing cycle, the jacks were replaced by steel striker devices, followed by the positioning of the reinforcement and the casting of the gap, made with low shrinkage concrete.

After the completion of the restressing operations that obviously followed the replacement of the abutment n. 3 (see the following chapter), the provisional abutment was removed by cutting the concrete plates with a diamond disk. The steel rods used for the anchoring of the bottom slab were completely removed in order to allow the restore the correct stress-strain flow between the adjacent sections.

## 2.2 Repairing of the less damaged zones

The zones characterized by minor damages, were preventively scarified with “selective” hydrodemolition; during this operation, the water pressure was accurately tuned in order to act only on the incoherent portion of concrete; after the passivation and, at the occurrence, substitution of the damaged reinforcing bars, the concrete was reconstituted operating for layers having thickness not more than 50 mm with a special low-shrinkage bi-component mortar reinforced with steel fibers.

## 3 REPLACEMENT OF THE ABUTMENT AT THE FRENCH-ITALY BORDER

For the restoration of the continuity of the internal ventilation ducts in correspondence of the French-Italy border, the demolition of the abutment n. 3, located at chainage 5800.00 was needed. This replacement was carried out contextually with the replacement of the damaged segments, taking advantage from the presence of the provisional abutment. The 37 m long abutment was replaced with a cast in place box segment. For the anchoring of the segment to the rock 36 sub-vertical cables made by 7 strand  $\phi$  0.6” were provided, located along the box webs. The design horizontal bearing capacity provided with prestressing was about 32000.0 kN, slightly greater than the maximum expected horizontal force transferred by the internal deck under the maximum temperature raising. Due to the presence of the fixed anchorage to the rock, this segment was prestressed independently, with longitudinal post-tensioned tendons providing an almost centroidal resultant. The longitudinal prestressing was realized with a total of six tendons formed by four strands each one (respectively 4 tendons and two tendons in the top and bottom slab), ensuring a residual compressive stress of about  $-1.0$  MPa under the worst temperature condition. The stressing of these cables was carried out before the stressing of the anchorages in order to allow the free longitudinal strain of the element.

## 4 REALIZATION OF OPENINGS ALONG THE DECK WEBS

The accident dramatically highlighted the need to provide alternative escape paths located safe from fire and smoke. For this purpose, the pressurized shelters were linked with the fresh air ventilation ducts through appropriate escape paths.

The realization of the openings along the webs of the prestressed structure required the design of special steel frames capable to resist and to properly spread

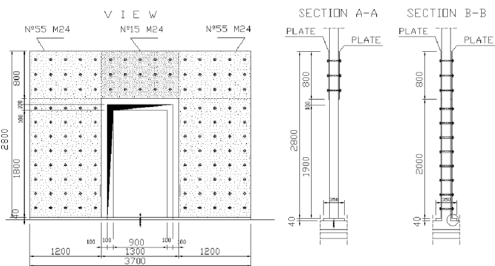


Figure 12. Steel frames for realization of web openings.



Figure 13. Emergency escape path from shelter – doors through the ventilation ducts.

the longitudinal compression stress flow of prestress acting in the webs after the realization of the opening.

The openings are of various typology, dependently from the deck cross section into which are located; they have constant height of 2.0 m and length form 0.9 to 1.80 m.

As shown in the following figure, the frames are realized with large steel plates 15 mm thick forming an inverted “U”, positioned outside and inside the web and connected at the base by a steel beam. The frames are connected together by 125 pretensioned pins crossing the web, dimensioned in order to ensure the transmission of the compressive force from the concrete web to the steel frame by friction.

The adequacy of the frame has been verified with a non linear finite element model, modeling also the interface between web and steel plate.

The sequence of realization of the opening provides was rather complicate because the frame had to be positioned and completely fixed to the web before the cutting of the opening, to avoid the formation of shear cracks due to the heavy perturbation caused by the opening and the loss of prestress the adjacent zones of the web.

The work sequence was as follows:

- preparation of the concrete surfaces;
- positioning of the inward steel plates;
- realization of the hole across webs;
- positioning of the outward steel plates;
- injection of resin through steel concrete interface;
- positioning and tensioning of the bolts.
- realization of the opening with concrete cutting using a diamond disk.

Afterwards, the frame was fitted with special airtight doors.

## 5 CONCLUSIONS

This paper describes the main interventions carried out for the rehabilitation of the internal structures of the Monte Bianco Tunnel after the tragic fire of march 1999. The originally adopted design solution provides an internal prestressed structure similar to a box girder, whose internal cells are used for canalization of fresh and foul air.

The replacement of the damaged portions of this structure, and the realization of the escape facilities, required the set up of a special intervention strategy aimed at the preservation of the original imposed prestressing state needed to ensure the air tightness of the ventilation system.

These interventions belong to the extensive modernization plan that started after the accident and whose works were completed in an extremely short period of time, which allowed the reopening of the infrastructure on February 2001.

## REFERENCES

- Portier, M., 1966. *La ventilation du tunnel routier sous le Mont Blanc*. Revue Generale des Routes et des Aerodromes n. 408, P61/79.
- Portier, M., 1967. *La construction des conduits de ventilation et de la dalle sous chaussée*. Revue Generale des Routes et des Aerodromes n. 427, P95/106.
- ACI 360R-92, 1997: *Design of Slabs on Grade*, ACI Manual of Concrete Practice part 5.
- Ferro, V., 2000. *Temperature e pressioni all'interno della condotta di ventilazione*. Studio Associato Ferro—Cerioni, Torino.
- DTU, 1987: *Méthode de prévision par le calcul du comportement au feu des structures en béton*. Secretariat de groupe DTU, Paris 1987.
- Società Italiana Traforo del Monte Bianco, 1964. *Soletta e condotte di ventilazione*. Project Documentation SITMB, Rome.
- Furlanetto, G., Ferretti Torricelli, L., 2000. *Reparazione des caissons—Mémoire Thécnique*. Project de Réhabilitation et modernization du tunnel du Mont Blanc, SPEA, Milano.

# Design of durable bridges by using self-compacting concrete filled steel tubes

G. Furlanetto, L. Ferretti Torricelli & A. Marchiondelli

*Bridge Design Department, SPEA Ingegneria Europea s.p.a., Milan, Italy*

**ABSTRACT:** In recent years, a wider vision of the quality and durability of constructions allowed a rapid increase of the applications of innovative materials and technologies in civil engineering. The design of Concrete Filled Steel Tubular (CFST) structures become familiar and the structural performance of several existing constructions demonstrated the advantages of this system. In addition, the development of affordable Self-Compacting Concrete (SCC) mixture showed the greater benefits provided by this relatively new material in comparison with conventional vibrated concrete in many critical situations. This paper is aimed to highlight the advantages offered by the synergy arising from the use of these two innovative technologies in designing high quality bridge structures. In fact, the use of systems composed by self-compacting concrete filled steel tubes (SCC-FST) gives important benefits in terms of costs and durability, like time construction reduction, major quality of workmanship, high safety of workers, elimination of noise and vibrations resulting from compaction, lower environmental impact, etc. However, it is worth noting that these goals can only be achieved by fulfilling special requirements and accurate quality control procedures during the construction phase.

## 1 INTRODUCTION

In recent years, a growing attention has been devoted to the quality and durability of constructions. This new sensibility has been pushed by the designers in developing advanced technologies and using innovative materials. In the field of civil engineering, the design of Concrete Filled Steel Tubular (CFST) structures has been rapidly increased, as well as the development of affordable Self-Compacting Concrete (SCC) mixture has been reached greater advantages in comparison with conventional vibrated concrete for solving many critical situations.

The CFST structures show many advantages with respect to both reinforced concrete structures and steel structures because they utilise the advantages of both steel and concrete. In fact, the CFST members are comprised of a steel hollow section, usually having circular or rectangular shape, filled with plain or reinforced concrete. By using self-compacting concrete instead of conventional concrete for the inner core, additional benefits may be obtained. In fact, SCC is a highly fluid concrete which, unlike its normal counterpart, does not require extra compacting power to flow into formwork and is able to fully surround the reinforcement. The peculiar characteristics of this innovative technology that we have called Self-Compacting Concrete Filled Steel Tube (SCC-FST) system allow to save considerable amount of

time during the construction stage by improving, at the same time, the quality of workmanship and the environmental impact.

Nowadays this kind of system has achieved great importance and in the last decade many constructions, some of them with complex structural schemes, have been successfully built. In particular, in this paper two peculiar bridges will be presented in order to highlight the advantages offered by the synergy of SCC and CFST in forming Self-Compacting Concrete Filled Steel Tube (SCC-FST) system. However, it is worth highlighting that these benefits can only be achieved by fulfilling special requirements and accurate quality control procedures.

## 2 ADVANTAGES AND DISADVANTAGES IN USING SCC-FST

The enhancement provided by CFST to structural properties is due to the composite action between the constituent elements. Steel members have the advantages of high tensile strength and ductility, while concrete members may be advantageous in compressive strength and stiffness (CNR 10016/1999).

More in detail, the major benefits of the steel shell derives from its action as integral formwork during concrete pumping and permanent shield for the inner core against external attacks. In service conditions,

the steel shell works as longitudinal and transverse reinforcement able to carry stresses due to axial, shear and bending loadings, as well as to internal passive pressure caused by concrete deformation. In addition, it provides confining pressure on concrete, putting it under a beneficial triaxial state of stress. Finally, the steel supports several levels of construction prior to concrete being pumped, by assuring a lower stress state in the concrete core.

On the other hand, the major benefits of the concrete core consists of stiffening the external shell, preventing the local buckling of the thin steel tube, and finally increasing the strength and stability of the whole system. In addition, in the restrained state, the concrete core is able to sustain higher stresses and strains (Knowles et al., 1996).

By adopting self-compacting concrete instead of conventional vibrated concrete, additional benefits could be reached, and in particular a considerable amount of time can be saved during the construction stage due to the no need of vibration. Moreover SCC is highly advantageous in terms of its handling, which dispenses with physically stressful, noisy and time-consuming compaction in structures. In addition, SCC improves the corrosion resistance of reinforcement by fully surrounding them and perfectly bonding steel to concrete core; for this reason, it is convenient moreover in elements characterized by restricted sections or in areas particularly congested by reinforcements. Finally, SCC can improve the quality and durability of the structure by providing the resistance against environmental effects.

On the basis of the above mentioned reasons, the CFST system results to be convenient since it has much better constructability than ordinary concrete structures, and provides higher strength and stiffness compared with reinforced concrete systems with the same materials properties. Also compared to steel structures, the cost is minor due to the reduced usage of steel and the increased stiffness. In particular, the CFST system is useful in seismic regions because of excellent earthquake-resistant properties such as high strength, high ductility, and large energy absorption capacity. Finally it also provides high fire resistance (ENV 1994-1-2).

On the contrary, this kind of system also presents some disadvantages. In particular, for CFST framed structures the connections are quite complicated (Couchman et al., 1998). Critical zones are also the ends of the steel tube: here local plastic buckling may occur followed by the crushing of internal concrete. The worst aspect is that this type of failure is very difficult, or even impossible, to be repaired. Moreover, since the steel tube is used as longitudinal reinforcement to resist axial force or bending moment, when the steel tube yields under excessive longitudinal stresses, its transverse confinement to the internal

concrete is drastically reduced and its beneficial effect is lost.

Additional disadvantages can derive from using SCC for filling the tube. In contrast to normal concrete, the quality of SCC strongly depends on viscosity and flowing properties of fresh concrete. Even slight changes in consistency of fresh concrete can consequently worsen the serviceability or even the load-bearing capacity of the structure. The suitability of SCC, in fact, can only be ascertained after a processing test of the mixture under conditions corresponding to those at the construction site because the concreting crew can no longer influence the strength or density of SCC through compaction inside the component. Due to the lack of specific standards for SCC as well as prescriptions oriented to establish an in situ acceptance quality control for testing the rheological prerequisites of fresh concrete, it is fundamental that the crew is highly familiar with fresh SCC peculiarities. Relatively close cooperation and coordination between the construction company and concrete manufacturer is also necessary. Another critical aspect in using SCC is the economic factor. In Italy the cost of SCC is slightly higher with respect to normal concrete of the same strength class, so it is very important to draw cost/benefit comparisons to confirm the real advantages in using SCC. In addition, the extra costs related to the quality control are not negligible and this aspect, added to the intrinsic higher cost of the material, represents a significant limitation for a wide use of this special material.

In conclusion, the use of steel tube structures filled by self-compacting concrete can improve the quality and durability requirements and make construction techniques more economical. However, special technologies are needed to manufacture and process this system. In particular, the CFST system is more convenient for special structures for which great attention is devoted to the expected high quality of workmanship, low environmental impact, high safety level for workers, speed and easy constructability, time reduction, among other aspects.

### 3 SCC-FST DESIGN SOLUTIONS FOR BRIDGE STRUCTURES

In the following, two bridge design solutions are presented in order to highlight the benefits derived from using steel tubular elements filled by self-compacting concrete in terms of both quality and durability.

#### 3.1 *Special piers for the Reno bridge*

Along the new Italian motorway called "Variante di Valico" connecting Bologna to Florence, a new bridge over the Reno river has been recently realized by

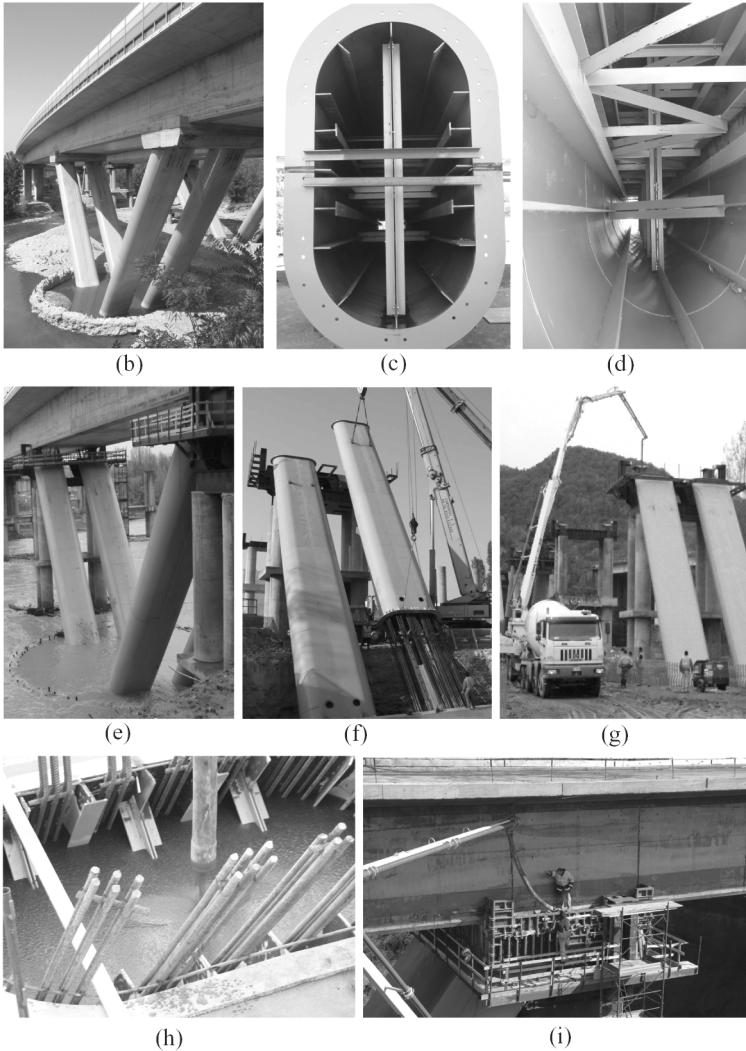
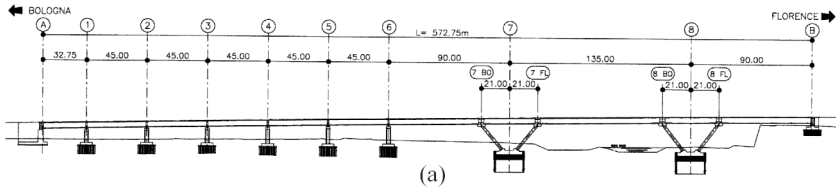


Figure 1. The Reno bridge.

adopting a particular design solution mainly motivated by the need of complying with several constraints of different nature.

The Reno bridge consists of a curved continuous prestressed concrete box girder, organized in nine

spans for a total length of 572.75 m (Figure 1a). The first six spans are simply supported by typical reinforced concrete piers, while a framed system is realized for the last three longer spans by clamping the deck to two special piers formed

by inclined steel shells filled by self-compacting concrete.

The structural characteristics of the Reno bridge have been presented in detail in previous papers (Furlanetto et al., 2006). This work is mainly focused on the special design solution chosen for the long span zone.

The framed system designed for over-crossing the Reno river is organized into two special piers presenting a V-shaped configuration formed by a pair of arms, about 32 m long and 42° inclined with respect to the vertical axis (Figure 1b). The arms are doubled into two CFST elements. They are realized by an outer steel shell with elliptical cross-sectional shape, having principal axes of 3.5 m and 1.8 m and thickness of 12 mm (Figure 1c). Proper ribbed trusses are internally provided both to stabilize the thin shell acting as formwork during the concrete core casting, and to strengthen the composite cross-section by working as internal reinforcement in service conditions (Figure 1d). Another important role played by the outer shell consists of realizing a protective barrier for the inner concrete core against water erosive effects due to the river flow (Figure 1e).

In the construction phase, the steel shells are moved in the final inclined position by using cranes. After lifting, the shell is slipped down to fit two steel drive-tubes fixed in the pier foundation as well as longitudinal reinforcement emerging from the footing in order to block the shell at the bottom (Figure 1f). In addition, a provisional pier sustains the shell at the top to achieve a greater safety level during the filling operations (Figure 1g).

The inner shell core is made by C35/45 self-compacting concrete. Before casting, it was fundamental to define accurately the sequence of concreting operations taking into account the peculiarities of SCC. Before beginning the pumping process, the fluidity of SCC has been properly checked through measurements of rheological properties. To this aim conventional tests have been used (Slump-flow, V-Funnel and J-ring) according to Italian Standards (UNI 11040-11041-11042-11045).

The casting phase has been subdivided into four stages, each one about 6 m high, for a total amount of about 30 m<sup>3</sup>/cast. Pumping has been carried out with 100–125 mm diameter pipes, not more than 100 m long, directly positioned at the top of the pier (Figures 1g–h). Since SCC has higher velocity of flowing in the pipe with respect to normal concrete, a greater loss of pressure has been expected during pumping operations. This effect may cause an increasing of the lateral pressure on formwork. For this reason the steel shell has been provided by internal ribs and trusses in order to improve its carrying capacity. Another crucial point is the control of the ambient conditions in which concreting occurs: in particular,

during and immediately after concreting, the ambient temperature should not drop below 5°C.

Since the connections in CFST framed structures usually present very complex aspects, a great attention has been focussed on the joints of the special piers. In particular, before casting the last upper portion of steel shell, longitudinal reinforcement have been provided for the monolithic connection with the deck realized by means of a traditional reinforced concrete pulvino. Due to the complexity of working in a high reinforcement density area, the realization of the pier-deck joint has been subdivided into two steps. The first step was particularly complex since it consisted in casting the top part of the steel shell together with the pulvino, which was a zone characterized by strong inaccessibility (Figure 1i). Instead, the second step has been focussed on accurately sealing the interface between pulvino and deck. In particular, the perfect closure of the interface has been needed a preliminary preparation of the surfaces by washing and brushing; subsequently, an injection of a very fluid cement mortar in the interface section has been made in order to assure a perfect contact.

After the completion of all these operations, the steel shells have been coated by two layers of painting and a final layer of anti-abrasive protection in order to achieve a proper durability level.

The choice of this particular design solution consisting in a framed structure realized by adopting traditional reinforced concrete elements as well as composite elements, both with self-compacting concrete, is motivated by the need of complying with very peculiar technical problems. More in detail, the main advantages in using CFST for the special piers of the Reno bridge are related to the beneficial actions developed by the cooperation of both steel and concrete. In particular, the steel shell acts as formwork during the concrete core casting, as structural reinforcement in service condition, and finally as protective barrier against water erosive effects. On the other hand, concrete assures strength and stability to the whole system. In addition, the use of SCC allowed to speed up the construction, to fit the complex geometric shape, to avoid the need of concrete vibration in very dense reinforcement zones with limited accessibility by guaranteeing at the same time the elimination of internal voids.

### 3.2 *The arch bridge over Tevere river*

Within the project of a new highway connecting Rome to Latina a new bridge with total length of 777 m has been designed. Two different solutions have been adopted: the first portion, having length of 225 m, is realized by a composite superstructure, and the second one, having length of 552 m, consists of a post-tensioned concrete box girder. In particular, for

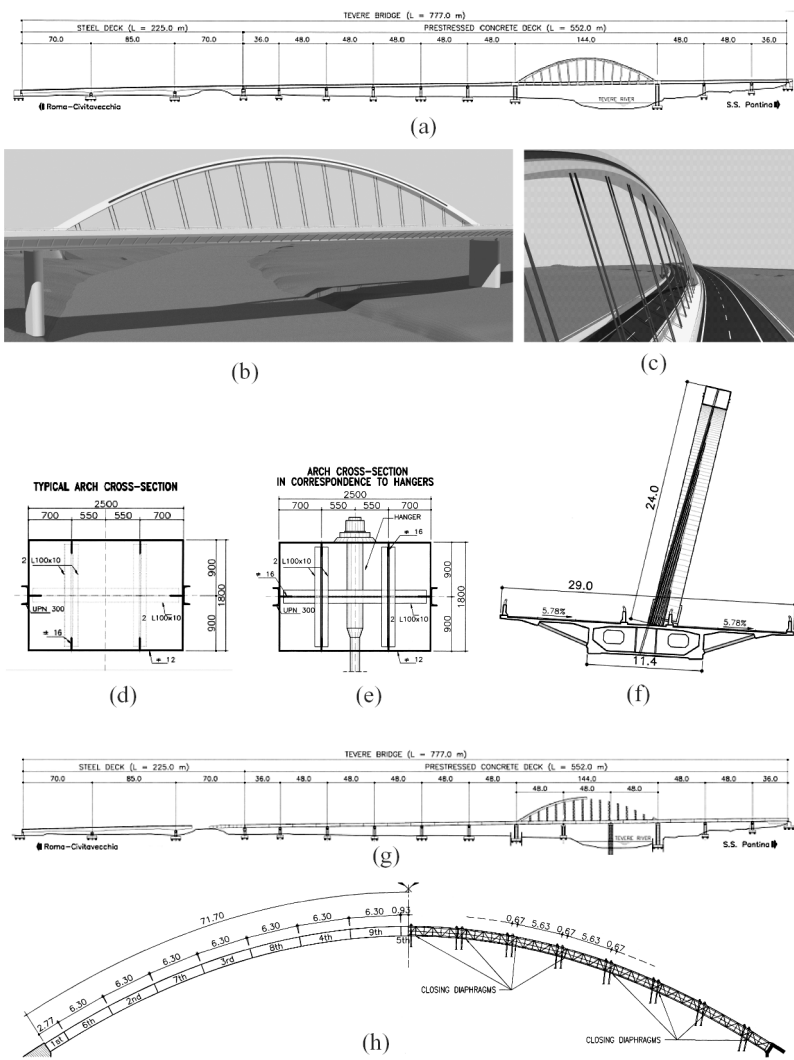


Figure 2. The Tevere arch bridge.

over-crossing the Tevere river an arch solution with span of 144 m is chosen (Figure 2a).

The structural characteristics of the Tevere bridge have been presented in a previous work (Furlanetto et al., 2007). In this paper the attention will be focussed only on the design solution chosen for the arch structure, which is the main peculiarity of the whole bridge. This structure is composed by a tied-arch designed by adopting a post-tensioned concrete box girder sustained by the arch structure by means of a system of hangers (Figure 2b). The curve planimetric profile enforces the arch to be 13.2° inclined respect to the vertical axis (Figure 2c).

The arch presents a parabolic shape with 24.0 m rise and is realized by adopting a concrete filled steel tubular (CFST) cross-section. More in detail, the arch is composed by an outer rectangular steel shell having dimensions 2.50 × 1.80 m and thickness 12 mm (Figures 2d–e), which is filled by self-compacting concrete. The outer shell, properly ribbed, is even more stiffened by internal steel elements such as transversal L-profiles and two longitudinal continuous trusses. The stiffness of the ribbing system is accurately designed on the basis of the hydraulic pressure of concrete core during pouring phases and the need of improving the confinement



effect exerted by the shell to the inner core in service conditions.

Self-compacting concrete is used for both the arch core and the deck, by choosing respectively C50/60 and C40/50 strength classes.

The deck consists of a continuous post-tensioned concrete girder subdivided into 48 m long precast segments and realized by adopting incremental launching method (Figure 2f).

The monolithic connection between deck and arch is realized by casting two special diaphragms, 8 m long, characterized by high density of reinforcement. In addition, a system of hangers, having a fan configuration, is provided to sustain the 144 m long span.

Great attention is paid to study the construction process in order to save time and costs, as well as to achieve a successful structural quality and high safety level for workers (Figure 2g). To this aim, the key-choices consist of using incremental launching method for the deck and steel tubular structure filled by self-compacting concrete for realizing the arch.

In order to push the deck by incremental launching method, two provisional piers are provided in the long span zone to limit the maximum pushing span to 48 m. After the deck launching, the assembly of the steel structures of the two half-arch is made directly on the deck slab. Each half-arch is then lifted by cranes and fixed in the final position by means of provisional steel trusses. After the rigid connection of the arch structure at the bottom ends as well as at the crown, the casting phase of the inner core is started.

The SCC casting process has to respect a strict working schedule. Due to the slenderness of the arch, special attention is focussed on the control of deflections. In particular, in order to avoid undesired strains, the SCC casting schedule is articulated into nine stages aimed to maintain the anti-funicular loading of the arch (Figure 2h). Moreover, a special SCC mixture, composed by calcareous filler and acrylic additives, is designed to reduce the hydration heating, due to the large dimensions of the arch cross-section.

After SCC hardening, the hangers are positioned and their stressing process is realized in three consequential steps by gradually removing, at the same time, the provisional steel trusses sustaining the arch.

The final structure, beside to demonstrate an efficient performance under service conditions, also shows excellent performance against seismic events. In fact, due to the high strength-to-weight ratio and the confinement effect exerted by the steel shell to the inner concrete core, the CFST arch solution shows improved damping behaviour as well as enhanced ductility and toughness compared to the traditional steel arches.

Another important factor which played a crucial role in choosing CFST arch solution consists

of the great resistance in fire condition. In fact, many researchers demonstrated that a CFST element presents a better behaviour than a steel one, as well as a reinforced concrete one during fire (Edwards, M., 2000). In order to improve the fire resistance of the Tevere arch bridge an external protection is provided by using isolating materials. In particular, after the completion of the arch, two layers of painting and a final intumescent coating have been applied in order to achieve proper durability and fire resistance levels.

#### 4 CONCLUSIONS

The present paper has been highlighted the advantages offered by the synergy of CFST innovative technology and SCC new material in designing high quality bridge structures. The two presented bridge structures demonstrated the achieved important benefits in terms of costs and durability, like time construction reduction, high safety of workmanship, elimination of noise and vibrations resulting from compaction, lower environmental impact, etc. At the same time, great attention has been focussed on fulfilling special requirements and accurate quality control procedures during construction phase in order to achieve high durable and quality levels.

#### REFERENCES

- Couchman, G.H. & Way, A., 1998. *Joints in steel construction: Composite connections*. The Steel Construction Institute/The British Constructional Steelwork Association, P213/98.
- CNR 10016: *Struttura composta di acciaio e calcestruzzo. Istruzioni per l'impiego nelle costruzioni*, CNR Bollettino Ufficiale n. 192—Norme Tecniche, 1999.
- Edwards, M., 2000. The performance in fire of fully utilised concrete filled SHS columns with external fire protection, *Proc. 9th International Symposium on Tubular Structures*, Balkema, Rotterdam, Netherlands.
- ENV 1994-1-2: Eurocode 4: Design of composite steel and concrete structures. Part 1.2: General rules. Structural fire design.
- Furlanetto, G., Ferretti Torricelli, L. & Marchiondelli, A., 2006. The new Reno bridge on the A1 Milan-Naples Motorway, *Proc. 2nd International fib Congress*, June 5–8, 2006, Naples, Italy.
- Furlanetto, G., Ferretti Torricelli, L. & Marchiondelli, A., 2006. Durability design criteria for the Reno bridge, *Proc. 3rd International Conference on Bridge Maintenance, Safety and Management (IABMAS06)*, July 16–19, 2006, Porto, Portugal.
- Furlanetto, G. & Ferretti Torricelli L., 2007. New Structural Frontiers for Self-Compacting Concrete. The Tevere River Bridge, *Proc. IABSE Symposium*, September 19–21, 2007, Weimar, Germany.
- Knowles, R.B. & Park, R., 1996. Axial load for concrete filled steel tubes, *Journal of the Structural Division*, ASCE, Vol. 96, No. 10, pp. 2125–2155.

# Structural reliability analysis and monitoring program applied to a roller-compacted concrete dam

C.M. Krüger

*Graduate Program in Numerical Methods, Universidade Federal do Paraná, Curitiba, Brazil  
Universidade Positivo – UnicenP – Curitiba, Brazil*

A. Chaves Neto

*Graduate Program in Numerical Methods, Universidade Federal do Paraná, Curitiba, Brazil*

D.A.V. Krüger

*Energy Company of the State of Paraná, COPEL, Curitiba, Brazil*

**ABSTRACT:** Dam construction is a complex civil engineering activity that involves multiple areas of knowledge. The determination of risk and uncertainty is essential to the design of these structures offering adequate levels of safety and performance for their entire lifetime. This paper demonstrates the application of methodologies for structural reliability analysis of concrete dams that could be readily employed in the design of such structures. First order reliability procedures such as FORM and Hasofer-Lind's AFOSM, as well as Monte Carlo simulations, are applied to estimate the reliability of a typical section of a roller-compacted concrete (RCC) dam located in the Iguazu river basin in southern Brazil. The dam safety monitoring system, present at the dam since its construction, provided the data for the analysis. The results obtained with the reliability methods allowed important information for the maintenance program of the Salto Caxias dam.

## 1 INTRODUCTION

Concerned with the responsibility of building safe structures, engineers normally design in a conservative manner, through the use of safety coefficients or overload factors. In many cases, these safety factors are defined by standards and official rules that represent the skill and experience of past designers. Nonetheless, failures still happen, some of them catastrophic. At the same time, it is common to find structures that are excessively conservative and over-dimensioned.

The main requisites of an engineering project, beyond its functionality, are the cost adequacy, safety, and minimization of environmental impacts. Among these objectives, safety is the most important, because an eventual loss of lives in a catastrophic event cannot be compensated. The cost is also very important, because a structure inappropriately designed can cause maintenance expenses which can be of the same order or greater than the cost of the structure components. The principal goal of a project is to ensure a satisfactory performance, i.e., to provide a capacity or resistance greater than the loads during the system lifetime. Having in mind the uncertainties of the problem, the satisfactory performance cannot be provided

with absolute confidence. In this case, the probability of failure has to satisfy some performance criteria. In engineering terms, reliability would be "the probability of occurrence of the satisfactory performance" (Haldar & Mahadevan 2000).

The design and feasibility analysis of concrete structures must focus on their performance, safety and durability during their lifetime. Concrete dam design involves structural analysis, material and construction process specifications, and the implementation of a monitoring program to verify the structure's behavior during and after the construction. The evaluation of safety of structures is a complex problem because of uncertainties related to the prediction of spatial and temporal variations of material properties and applied loadings such as temperature and external loads. The prediction of stress levels due to time- and space-variable loads is essential to the correct design of structures, and it involves aspects such as the limitation of maximum stresses and the structure durability. Dam structures are constructed for long service, usually for over 50 years, and the assurance of a minimum level of reliability is necessary. This requires the establishment of a monitoring system, including visual inspections and provisions for the repair of eventual damages.

Structural reliability methods can be a useful framework to guide decisions required during the design phase and during the lifetime of structures. The approach contemplates the risk associated with the probability of inadequate performance or serious damage or failure.

## 2 STRUCTURAL RELIABILITY METHODS

Hurtado & Alvarez (2003), among others, present a taxonomy of methods available for reliability analysis. The most common and widely accepted methods can be classified as those based on the probability theory (and Taylor series expansions), and methods based on the synthetic generation of series (Monte Carlo simulations). Figure 1 illustrates this classification. In the first category, one can find methods that estimate reliability by computing low order moments (usually means and covariances) of the structural responses. The reliability estimation must refer to some basic hypothesis, such as the normality of the analyzed variables. Beyond these methods, there are procedures that seek to estimate the probability density functions of the relevant variables. According to many researchers, by following these methods the estimation of reliability can be done without great difficulty. Methods in the second category, based on Monte Carlo simulations, can be considered indirect methods, because they normally use computational procedures, such as finite elements, to compute the structural response variables. Figure 1 illustrates this classification.

### 2.1 First Order Reliability Method (FORM)

The FORM approach has been historically derived from second order methods, which use the first and second moments of the random variables. These methods can be further separated into first order, second moment (FOSM) and advanced first order, second moment methods (AFOSM). In the FOSM methods, the information about the random variables distribution is ignored, while in the AFOSM approach this information is appropriately used.

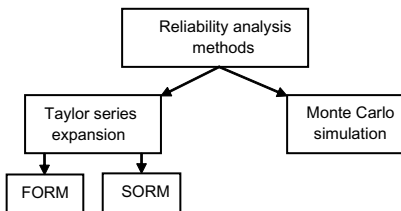


Figure 1. Classification of most common reliability analysis methods.

### 2.1.1 First Order, Second Moment Method (FOSM) or MVFOSM method

The FOSM method is also known in the literature as the mean value, first order, second moment method (MVFOSM). MVFOSM received this denomination due to the fact that they are based on first order Taylor series, where a performance function is linearized at the mean values of the random variables, and also because the method uses only statistics of up to second order (mean and covariances).

### 2.1.2 FORM for normal variables

Considering a limit state function  $Z = g(\mathbf{X})$  for a vector  $\mathbf{X}$  of  $n$  relevant variables  $X_1, X_2, \dots, X_n$ , representing the structural behavior of the system under analysis, the FORM procedure can be summarized as shown in Figure 2.

By using the reliability index  $\beta$ , it is possible to compute the exact failure probabilities only for a few cases. For example, if all the  $X_i$  are normal and independent,  $Z$  is normal, and the failure probability can be calculated by the equation  $p_f = 1 - \Phi(\beta)$ , where  $\Phi(\beta)$  is the cumulative normal distribution probability associated with  $\beta$ . Similarly, if all  $X_i$  are independent lognormal variables and  $g(\mathbf{X})$  is a multiplicative function of  $X_i$ ,  $Z = \ln g(\mathbf{X})$  is normal, and the probability of failure can also be computed by  $p_f = 1 - \Phi(\beta)$ .

However, in the majority of cases, not all the variables are independent and with normal or lognormal distribution. In addition, the performance function will

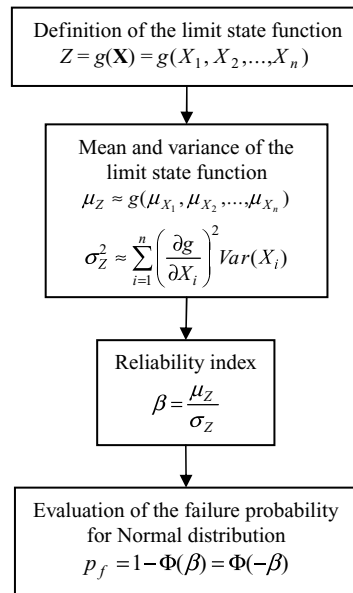


Figure 2. FORM procedure.

not necessarily be an additive or multiplicative function of the variables. In these cases, the reliability index  $\beta$  cannot be related directly to the failure probability, but it is still worth considering that the FORM procedure can provide a first approximation of the true risk level or of the project reliability (Rackwitz 2001).

### 2.1.3 AFOSM or Hasofer-Lind method for normal variables

The Hasofer-Lind (H-L) method is applied to normal random variables. The method uses reduced normal variables (Melchers 1987):

$$Z_i = \frac{X_i - \mu_{X_i}}{\sigma_{X_i}} \quad (i = 1, 2, \dots, n) \quad (1)$$

where  $Z_i$  is a zero mean and unit standard deviation random variable and  $\mu$  and  $\sigma$  are the mean and standard deviation of the variable  $X_i$ . The above equation is used to transform the original limit state  $g(\mathbf{X}) = 0$  to the reduced limit state  $g(\mathbf{Z}) = 0$ . The coordinate system  $\mathbf{X}$  is called the original coordinate system and the new system  $\mathbf{Z}$  is the reduced or transformed coordinate system. It is important to note that if  $X_i$  is normal,  $Z_i$  is standard normal.

In the Hasofer-Lind procedure, the reliability index  $\beta_{H-L}$  is defined as the minimum distance from the origin of a coordinate system defined by the reduced variables to the limit state surface (or failure surface). This distance can be evaluated by:

$$\beta_{H-L} = \sqrt{(\mathbf{z}^*)^T (\mathbf{z}^*)} \quad (2)$$

The point of minimum distance in the limit state surface is known as the design point (Figure 3). This point is represented by the vector  $\mathbf{x}^*$  in the original variables space and the vector  $\mathbf{z}^*$  in the reduced variables space. These vectors represent the values of all the relevant variables, i.e.,  $X_1, X_2, \dots, X_n$  in the design point in the coordinate system used.

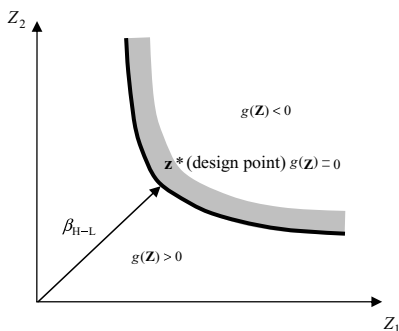


Figure 3. Hasofer-Lind method. Nonlinear limit state.

For nonlinear limit states, the calculation of the minimum distance is an optimization problem:

$$\text{minimize } D = \sqrt{\mathbf{z}^T \mathbf{z}} \quad (3)$$

$$\text{subject to } g(\mathbf{X}) = g(\mathbf{Z}) = 0 \quad (4)$$

where the vector  $\mathbf{z}$ , to be estimated, represents the coordinates of the point of calculation in the limit state equation in reduced coordinates. Figure 4 shows the steps of this optimization procedure.

### 2.2 Monte Carlo Simulation

Obtaining an estimate of the probability of failure using the Monte Carlo simulation technique involves the following steps: (1) defining the problem and the random variables; (2) defining the probabilistic characteristics of the random variables; (3) generating values for these random variables; (4) evaluating the problem deterministically for each set of realizations of random variables; (5) estimating probabilistic information from  $N$  realizations; and (6) determining the efficiency and accuracy of the simulation. Figure 5 illustrates the Monte Carlo procedure used in this study, for uncorrelated normal variables.

## 3 DEFINITION OF THE STRUCTURAL PROBLEM

A concrete gravity dam must be relatively impermeable to water and designed to support the loads acting on it with a large safety margin.

Gravity dams may fail by sliding over the foundation or along a horizontal plane, by rotation about the toe (bottom end of downstream face), or by material disruption. Material failure can happen at the terrain level or in any plane in the dam. Sliding (or shear failure) can occur if the horizontal resultant of the loads in any elevation exceeds the shear strength at the same level. In the preliminary phase of design of a gravity dam, it is customary to consider an isolated typical cross section of unit width. It is assumed that this section works independently of the adjacent sections. The adequacy of the terrain must also be analyzed. It is usually assumed that the normal stresses in the concrete at the base of the dam are transferred to the soil. Maximum compressive strengths for each terrain type must be respected.

Although the procedure is very simplified and considers that the concrete behaves as an elastic material, structural analyses as described above are still valid and adopted in preliminary studies worldwide (US Department of the Interior 1993), and are accepted by Brazil's official code for dam design (Eletrobrás 2003). For large dams, this procedure is normally followed by a structural analysis using finite elements.

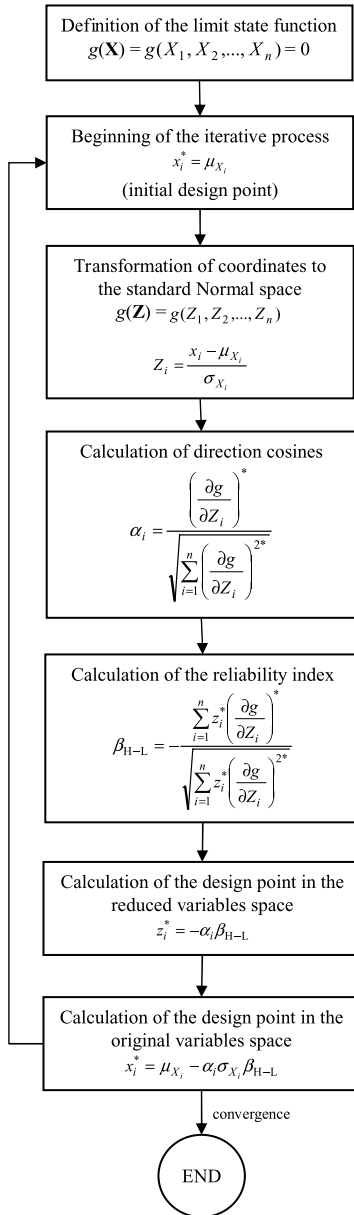


Figure 4. AFOSM procedure.

#### 4 DEFINITION OF THE PROBABILISTIC PROBLEM

##### 4.1 Normal stresses

In the analysis of normal stresses, in the foundation or concrete, for any horizontal plane of the cross

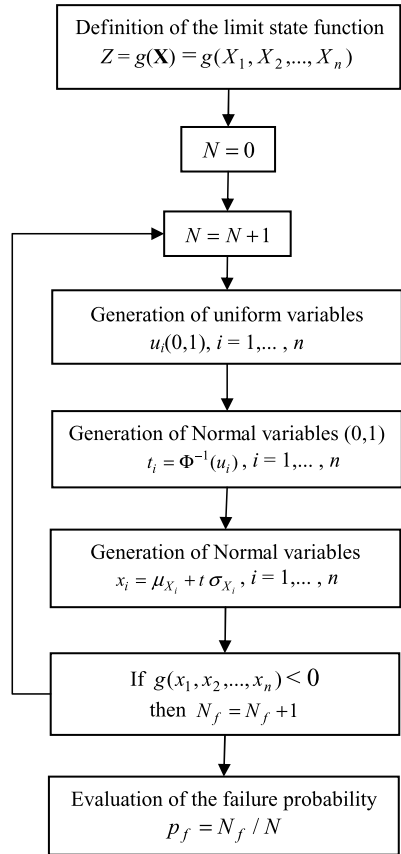


Figure 5. Monte Carlo simulation procedure.

section, the intervenient random variables are the allowed traction and compressive strengths, and the concrete specific weight.

Stress on the base of the blocks results from the action of vertical forces and the bending due to the moment produced by load eccentricity. Supposing initially that there are no moments transversal to the dam section:

$$s = \frac{V}{A} \pm \frac{M\eta}{I} \quad (5)$$

where:  $s$  is the maximum and minimum stresses at the section borders;  $V$  is the resultant of vertical forces;  $A$  is the section base area;  $I$  is the moment of inertia of the section base;  $M = Ve$ , where  $e$  is the eccentricity of the resultant force, and  $\eta = h/2$ , where  $h$  is the base height. The base width is unitary.

In order to avoid traction stresses in the section, the resultant load must be applied within the central core of inertia, which has the shape of a lozenge in the case

of a rectangular section. Then,  $e = \eta - d$ . The distance  $d$  can be calculated, in the case of a full reservoir:

$$d = \frac{\sum Moments}{V} \quad (6)$$

where  $\Sigma Moments$  means that the total turning moment must be subtracted from the stabilizing moment. In the case of an empty reservoir, the only vertical force will be the weight of the section, and the eccentricity  $e$  is the distance from the center of the base to the point of application of the weight load. The limit state equations for the compression and traction verification can be written as:

$$Z_c = \frac{V}{A} + \frac{M\eta}{I} - s_{c,adm} \quad \text{and} \quad (7)$$

$$Z_t = \frac{V}{A} - \frac{M\eta}{I} - s_{t,adm} \quad (8)$$

where  $s_{c,adm}$  and  $s_{t,adm}$  are the admissible compression and traction stresses. The probability of failure for compression and traction can be calculated separately, as:

$$p_{fc} = P[Z_c < 0] \quad \text{and} \quad (9)$$

$$p_{ft} = P[Z_t < 0]. \quad (10)$$

## 5 SALTO CAXIAS DAM

Salto Caxias hydroelectric power plant was built between 1995 and 1998 in the Iguazu river, state of Paraná, in Brazil. With an installed capacity of 1240 MW, at the time of completion, Salto Caxias dam was the largest RCC dam in volume in the world, with the total concrete volume of  $1.01 \times 10^6 \text{ m}^3$ . Owned by Energy Company of the State of Paraná—COPEL, the project was awarded the International Milestone RCC Project, received in Guiyang, China, in November, 2007. The catchment area at the dam site is 57,000 km<sup>2</sup> and the mean flow is 1240 m<sup>3</sup>/s, although during the construction it was 2380 m<sup>3</sup>/s, almost double the expected flow. Reservoir area is 141 km<sup>2</sup> with 3573.0  $10^6 \text{ m}^3$  storage capacity.

The dam is a gravity roller-compacted concrete—RCC dam with a maximum height of 67 m and length of 1100 m, including the spillway (Figure 6). The dam is built with RCC up to Elevation (El.) 327.00 m, and the crest was finished with conventional concrete (CVC) to El. 329.30 m. The upstream face is vertical and built with CVC. The downstream face, also built with CVC, in steps, has a 0.75 H:1.0 V slope below El. 315.00 m and, it is vertical above this elevation. Two galleries were designed for drainage and for an injection curtain. The dam stability analysis was performed



Figure 6. Aerial view of Salto Caxias dam.

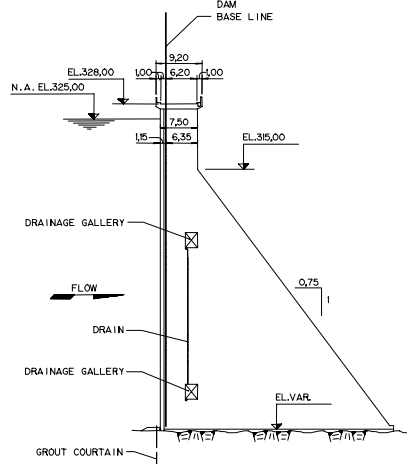


Figure 7. Salto Caxias—typical section.

taking into account its geometry, the physical characteristics of the materials used, and standard safety factors. Figure 6 presents the general layout of Salto Caxias; Figure 7 shows the main section of the dam.

The permanent controlling and monitoring system involves 9 different types of instruments, totaling 192 devices distributed into 8 blocks, 2 at the spillway, 4 at the dam, 1 at the water intake and 1 at the river bed. The instruments embedded in the concrete and foundation masses are of the vibrating wire type. Data acquisition from 167 instruments is automated and remotely operated (62 thermometers, 28 joint extensometers, 23 embankment piezometers, 41 foundation piezometers, 8 flow gauges and 3 pendulums). Non-automated instruments amount to 24 (6 multiple extensometers, 5 tri-orthogonal gauges and 13 topographical marks). The behavior analysis also includes a visual inspection program, and a geodesic survey of the dam and surroundings. Since its construction, no unusual deformations, temperatures, deflections, or water pressures have been recorded.

The reliability analysis presented here uses data gathered at the construction site. It includes concrete mix properties and results of concrete strength from samples of RCC taken at the dam.

Table 1. Structural analysis results—deterministic and reliability analysis.

RCC	Specific weight
Mean	24.5 kN/m <sup>3</sup>
Standard dev.	578.9 kN/m <sup>3</sup>
Compression	
$s_c$ (max)	0.93 MPa
$s_c$ (adm)	6.0 MPa
Mean ( $s_c$ )	13.7 MPa
Standard dev ( $s_c$ )	3.4 MPa
$\beta_{FORM}$	3.756
$\beta_{AFOSM}$	3.756
$P_{fFORM}$	0.0086%
$P_{fAFOSM}$	0.0086%
$P_{fMC}$	0.0086%
Traction	
$s_t$ (max)	-0.027 MPa
$s_t$ (adm)	-0.48 MPa
Mean ( $s_t$ )	-0.60 MPa
Standard dev ( $s_t$ )	0.20 MPa
$\beta_{FORM}$	2.820
$\beta_{AFOSM}$	2.820
$P_{fFORM}$	0.24%
$P_{fAFOSM}$	0.24%
$P_{fMC}$	0.25%

## 6 RESULTS

The methods described above, namely FORM, Hasofer-Lind's AFOSM, and Monte Carlo simulation, were applied in the verification of normal stresses for a section of unit width of the Salto Caxias dam. The deterministic results of the rigid body structural analysis are compared to the probabilistic results. Table 1 shows the RCC characteristics, and means and standard deviations of concrete strength obtained from concrete samples. The reliability indexes  $\beta$  and probabilities of failure are compared.

As is confirmed by the literature (Haldar & Mahadevan 2000), with the performance function being linear, and considering normal variables in the models, the results of the FORM and AFOSM are the same, except for minor differences due to numerical approximations. Monte Carlo simulations confirmed the same results.

It is important to highlight the importance of the quality of the RCC data sample and its influence on safety analysis. Special care must be taken in the data collection and during laboratory tests, in order to reduce the variance of the concrete data due to sample handling. In the present study, the coefficient of variation (CV) of the tensile strength is high (CV = 33%). For example, with a standard deviation of  $s_t = 0.15$  MPa (CV = 25%), the traction failure probability is reduced to 0.0094%, obtained by Monte

Carlo simulation. The high values of probabilities of failure for traction loads are not confirmed by the deterministic structural analysis, where the maximum traction stresses are within the allowable limits.

The methods above were applied to an exceptional situation, with the water level upstream of the dam at the maximum possible, and with no operation of drains under the dam foundation. The AFOSM procedure converged in only 3 iterations, and the Monte Carlo procedure used  $10^6$  simulations. All methods were coded in Visual Fortran™ with IMSL™ mathematical library (Compaq 2000).

## 7 CONCLUSION

The modeling technique presented here can be used to support the structural and safety analysis of concrete structures. The procedure is also useful in the definition of a construction design that minimizes the occurrence of cracks, while determining the most cost effective arrangement for the structure.

Dam safety evaluations require a realistic definition of all loads and material properties that influence the structural behavior. The designer should be concerned with the definition of material characteristics, weather conditions, and model restraints. Significant and unforeseeable changes in the materials or in the construction process could increase the risk of damages. Modeling can be useful in determining the influence of each of these factors. The advantage of this technique is that it allows a technical and economical support to maintenance activities during the structure's lifetime, which takes into account different factors to reduce costs while maintaining the quality and safety of the structures.

## REFERENCES

- Compaq Computer Corporation 2000. *Compaq Visual Fortran Professional Edition*.
- Eletrobrás—Centrais Elétricas Brasileiras S.A. *Critérios de projeto civil de usinas hidrelétricas*. Brazil.
- Haldar, A., Mahadevan, S. 2003. *Reliability assessment using stochastic finite element analysis*. John Wiley & Sons. 2000.
- Melchers, R.E. 1987. *Structural Reliability. Analysis and Prediction*. Ellis Horwood Limited. John Wiley & Sons.
- Rackwitz, R. 2001. Structural reliability—a preview and some perspectives. *Structural Safety* (23). Elsevier.
- United States Department of the Interior 1993. *Design criteria for concrete arch and gravity dams*. Engineering Monograph No. 19.
- Weber, M.A. 1995. Risk assessment through probabilistic structural analysis. *International Journal on Pressure Vessels & Piping* 61.

# Seismic vulnerability of historical buildings: the Royal Palace of Naples

F.M. Mazzolani, B. Faggiano & A. Marzo

*DIST, University of Naples "Federico II", Naples, Italy*

E. Guglielmo & P. Mascilli Migliorini

*Soprintendenza per i Beni Architettonici del Paesaggio, del Patrimonio Storico Artistico e Demoantropologico di Napoli e Provincia, Naples, Italy*

**ABSTRACT:** The paper deals with an extensive study concerning the application of an integrated multilevel methodology for the evaluation of the seismic vulnerability of the Royal Palace of Naples. In particular the paper focuses on the north-west wing of the Royal Palace of Naples. The first phase of the vulnerability evaluation, which consists in the application of the GNDT Level II method for the vulnerability index estimate and in the use of the vulnerability function for the damage index calculation, is presented. The applied methodology is suitable for a global vulnerability estimation of those structural typologies, such as historical monumental masonry building, characterized by complex structural configurations and proportions. Complementary in depth mechanical both localized and global investigations will be performed in succeeding phases.

## 1 INTRODUCTION

The seismic vulnerability of buildings can be defined as the susceptibility to be damaged, that is the resources that can be lost, in case of earthquake. Several methodologies of analysis exist for its evaluation, at both national and international level, among all the following three are the most common ones: 1) the two Level (I and II) method by the National Group for Earthquake Defense (GNDT, 1994), for the Build-up Areas, which is mainly referred to masonry constructions; 2) the HAZUS method by the U.S. Federal Emergency Management Agency (FEMA, 1999), which focuses on the exceptional events; 3) the RISK-UE method, which is the output of the European project "An advanced approach to earthquake risk scenarios with applications to different European towns", coordinated by Bureau de Recherches Geologiques et Minieres (BRGM, France, 2001–2003).

The GNDT method is based on the identification of the main parameters controlling the damage in buildings caused by a seismic event, such as nature and distribution of structural elements, both horizontal and vertical regularity of buildings, etc. (Benedetti et al., 1984). In particular, the Level I method, which is referred to Build-up Areas, defines three vulnerability classes (A, B, C), each one characterized by a relationship between seismic intensity and damage, based on damage probability matrixes (DPM). The probabilistic damage distribution derives by the collection of a great amount of survey data, related to relevant seismic

events occurred in Italy (Braga et al., 1982). Therefore, a direct correlation between building typologies and vulnerability classes is established. The Level II method, which is referred to a single building, is based on the analysis of all constructional and typological indicators, having some influence on the building seismic behavior, which is weighted by means of a specific factor. The indicators are quantified by applying four different scores, corresponding to four classes, and then combined for defining the vulnerability index  $I_v$ , which characterizes the attitude of the analyzed building to damage.

HAZUS and RISK-UE mechanical methods evaluate the seismic performance of buildings in terms of damage limit states. They consist in assigning to each building the Capacity Curve in an acceleration-displacement format and the earthquake Inelastic Demand Curve; the intersection of the two curves provides the performance point which corresponds to a damage limit state (Lagomarsino et al., 2004). In particular, focusing the study on masonry buildings, constant-ductility inelastic spectra can be adopted for the demand spectrum. Besides, capacity curves are used to characterize in a risk analysis classes of buildings ascribed to each typology (Cattari et al., 2004). They can be defined in a simplified approach as bilinear elastic perfectly plastic curves, based on some hypotheses on structural post-elastic behavior and a limited number of easily traceable parameters such as: true fundamental period of vibration; strength and ultimate displacement capacity.



The selection of the appropriate methodology, for the seismic vulnerability evaluation, is dictated by the building type. This is a very complex matter when the historical and architectural heritage is concerned, due to the peculiarities of the structural elements, the geometric proportions and not least the need for conservation of the building and the high artistic value assets housed inside (frescoes, canvases, altars, etc.).

In this framework, the research activity, which this paper deals with, is an extensive study concerning the application of an integrated multilevel methodology for the evaluation of the seismic vulnerability to the Royal Palace of Naples, which has already been selected as a study case within the international research project PROHITECH (scientific coordinator Prof. F. M. Mazzolani, 2005–2008) concerning the earthquake PROtection of HIstorical buildings by reversible mixed TECHnologies (Marzo et al., 2006). The proposed methodology is composed of three phases: 1) the application of the GNDT Level II method to parts of the whole extremely complex building; 2) the application of damage limit state based performance analysis methods to the same building parts; 3) the application of the same analysis methods to the whole building.

In this context the paper presents the first phase of the proposed methodology focusing on the north-west wing of the Royal Palace of Naples, the geometrical and mechanical survey of this part being up to today already comprehensive and exhaustive.

## 2 THE STUDY CASE

### 2.1 *The Royal Palace of Naples*

The Royal Palace of Naples is located in the historical centre of the town (Fig. 1a). It has been Royal Palace from 1600 to 1946; now it houses the Museum of the Royal Apartment, the National Library and the Superintendence to architectural heritage offices. The square body which encircles the honour court was built between 1600 and 1613; it corresponds to the original design by the architect Domenico Fontana (1543–1607). The extension works were carried out between 1700 and 1800. The actual layout of the Palace is shown in Figure 1b.

The Palace is distributed on three levels: the ground floor, which in the past was used for the services related to the royal activities and at present it houses the offices of the Superintendence; the first floor, where the Royal Apartment at the northern-west part and the National Library at the northern-east part are located; the second floor, which in the past was used as servants' accommodations and now it houses the National Library.

The main vertical structures are made of tuff masonry walls, whereas the horizontal structures are

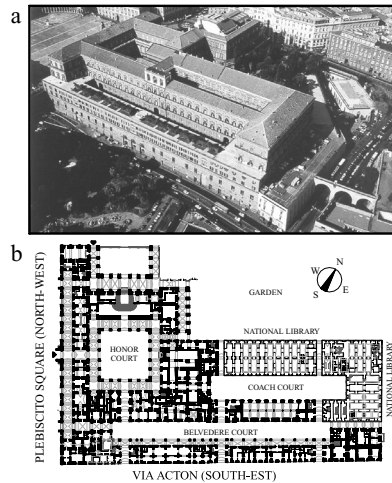


Figure 1. The Royal Palace of Naples: a) Bird's eye view; b) General layout at ground floor.

made of either wood (beam floors and vaults) and tuff masonry (vaults).

In some part of the buildings the type of foundations has been identified thanks to some excavation works carried out during the time for archeological purposes, in a small area located in the Plebiscito square front side of the ground floor, as well as to the presence of an accessible underground level at the seafront side of the palace. According to the constructional practice of the age relating to the tuff masonry buildings, vertical walls basements were simply obtained by tuff rock blocks, rising at the basement with very large width. Where caves were situated, arch and vaults masonry structures were realized for horizontally connecting and stiffening the vertical walls each other.

The roofing structures are generally made of trusses and tiles. All the trusses were originally made of wood, but some of them, due to the weather degradation and some accidents occurred during time, have been recently substituted by trusses made of either reinforced concrete, steel or glued timber.

### 2.2 *The north-west wing of the palace*

The main façade of the N-W wing of the Royal Palace, which faces on Plebiscito Square, together with both the horizontal and vertical sections are plotted in Figures 2 and 3.

As it appears from the geometrical survey, the construction is characterized by both in plan and in elevation irregularities, mainly due to the presence of arcades at both the façade and the honour court. In particular, at the ground floor the arcades are extended along 121.50 m at the façade and 71.00 m at the internal court, such as about the 80% and 45% of the whole length of the building, respectively (Fig. 2b);

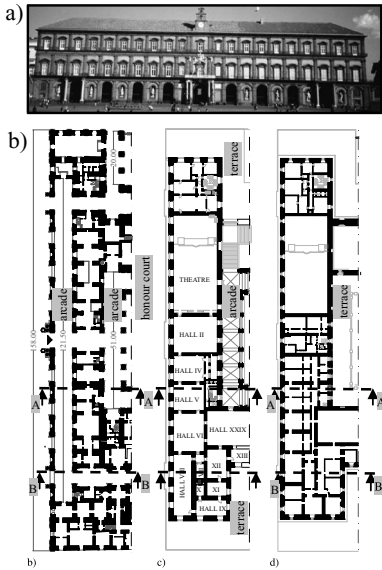


Figure 2. The north-west part: a) Main façade facing on Plebiscito square; b) Ground floor; c) First floor; d) Second floor.

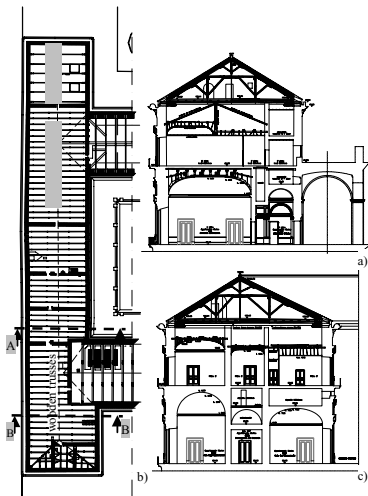


Figure 3. The north-west wing: a) Roofing floor; b) Section A-A; c) Section B-B.

at the 1st floor arcades only continues at the internal side of the building, where the ambulacro of the Royal Apartment is located (Fig. 2c).

Here arcades are extended along 51 m, such as about the 40% of the whole length. Further to this the N-W wing of the palace at the 1st floor houses the Court



Figure 4. Horizontal structures: a) Wooden self-bearing vaults; b) Complex wooden structure; c) Wooden beam floor. Roofing structures: d) Wooden truss; e) R. c. trusses.

Theatre, the Diplomatic Hall (II) of the Royal apartment, they being very large rooms, and the monumental stairs reaching the 1st floor (Fig. 2c).

The horizontal floors are made of three different structural types (Fig. 4): at the 1st floor they are masonry vaults; at the 2nd floor they are masonry vaults, as the roofing structures of the Halls from VII to XIII and the arcade, while both self bearing timber vaults and complex timber structures composed by beam floors and vaults connected each other, as for the remaining Halls (Fig. 4a, b); at the 3rd floor they are timber beam floors (Fig. 4c).

The roofing structures are made of timber truss (Fig. 4d), with the exception of trusses located at the Northern part adjacent to the Royal Theatre, which are made of reinforced concrete (Fig. 4e).

With reference to the non structural elements, the main peculiarity is that at the Royal apartment halls the false ceilings are made of timber structures shaped as vaults, realized by grids of curved ribs and splines, as support for the layer of canes and stucco, which are the base of the frescos. The partition walls are made of wooden panels or bricks. The façades are generally decorated with parapets and cornices; in addition, the main one on Plebiscito square is enriched with some balconies (Fig. 5).

The survey of the damage state has evidenced some degradations of both timber and masonry structures. Timber beams are affected by typical defects like cracks, splits, ring shakes, moreover some of them show damage due to overstress (Fig. 6a) and to insect or fungi attacks as a consequence of rain seepage (Fig. 6b). Cracks are detected in some masonry vaults and walls at the beam supports at the 2nd floor (Fig. 6c, d, e), further to damage due to rain seepage of the roofing r.c. structures.

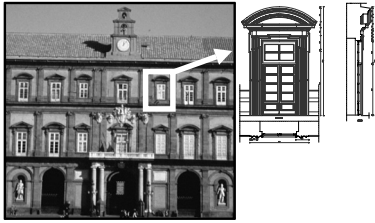


Figure 5. Details of the main façades.

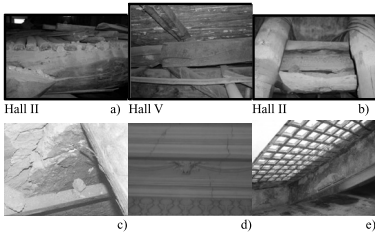


Figure 6. Damage in timber beams: a) overstressed beams; b) rain seepage effects. Crack distribution in masonries: c) walls; d) vaults; e) rain seepage effects.

### 3 EVALUATION OF THE SEISMIC RISK

#### 3.1 The applied methodology

The Level II GNDT method is based on the classification of the building according to ten indicators, such as ten items which are assumed to strongly influence the seismic behaviour of the construction. These are qualified through four different scores ( $c_i$ ), ranging from 0 to 45, identifying four classes, from A to D, A corresponding to optimal features up to D corresponding to unfavourable features. Moreover, their contribution is appraised by means of appropriate weight factors ( $w_i$ ), ranging from 0.25 to 1.5. The items, the qualification classes and the weight factors are listed in Table 1 (Benedetti et al., 1984).

Each items is briefly introduced hereafter:

1. *Organization of vertical structures.* It deals with the connection among vertical structures. Accordingly the classes from A to D characterize buildings with connection at each floor by means of stringcourses or chains up to buildings with unconnected vertical walls. A penalty of one class must be assigned in case of walls with span more than 15 times the thickness.
2. *Typology of vertical structures.* It deals with the material nature, the shape and the constructive type of walls. Accordingly the classes from A to D characterize buildings made of tuff or brick

Table 1. Indicators for the vulnerability classification of masonry buildings.

Item		Class				Weight factor $w_i$
		A $c_i$	B	C	D	
1	Organization of vertical structures	0	5	20	45	1
2	Typology of vertical structures	0	5	25	45	0.25
3	Building site and foundation type	0	5	25	45	0.75
4	Distribution of the resisting elements	0	5	25	45	1.5
5	Horizontal regularity	0	5	25	45	0.5
6	Vertical regularity	0	5	25	45	1
7	Type of horizontal structures	0	5	15	45	variable
8	Roofing structures	0	15	25	45	variable
9	Details	0	5	25	45	0.25
10	State of preservation	0	5	25	45	1

homogeneous and regular masonry up to buildings made of bad quality and irregular masonry.

3. *Building site and foundation type.* It deals with the type and slope of soil and the foundation stringcourses. Accordingly the classes from A to D are characterized by stable soils, slopes smaller than 5 degree, foundation stringcourse up to no stringcourses and either clay soil, slopes smaller than 15 degrees, or rock soil, slopes smaller than 25 degrees. The weight factor of the item is equal to 0.75, all possible cases being not considered.
4. *Distribution of resisting elements.* It deals with the ultimate strength of vertical structures. The attribution of the appropriate class is based on the coefficient  $\alpha$ , which is related to the ratio between the ultimate base shear and the weight of the building. Such coefficient is calculated as a function of the following parameters: the area of the structural walls as respect to the whole building areas, the masonry shear strength; the weight of one floor of the building per unit surface; the number of stories. Therefore classes from A to D are associated to ranges of  $\alpha$  values not smaller than 1 up to smaller than 0.4.
5. *Horizontal regularity.* It deals with the shape of the building. In case of rectangular shaped buildings it is evaluated by the ratio ( $\beta_1$ ) between width and length, which should be coupled to another coefficient accounting for shape irregularities if the case. Therefore the classes from A to D are associated to ranges of  $\beta_1$  values smaller than 0.1 up to larger than 0.3. Although this item is commonly very significant, in case of masonry

buildings resisting structures are generally uniformly distributed, therefore the weight factor is assumed as equal to 0.5.

6. *Vertical regularity.* It deals with the distribution of both strength and stiffness in elevation. The classes are mainly defined in relation with either the reduction of the floor area from one story to another, depending on the presence and extent of arcades and terraces, or the presence and height of towers. Therefore the classes from A to D are associated to ranges of area reductions smaller than 10% up to larger than 20%, buildings with arcades and terrace for an extent smaller than 10% of the whole floor area up to larger than 20%, and towers. Moreover, a penalty of one class (two from class A) must be assigned in case different materials are used at different stories.
7. *Type of horizontal structures.* It deals with both the efficiency of slabs to guarantee the suitable distribution of horizontal forces to vertical structural elements, thanks to the in plane stiffness and the degree of connection to the vertical walls, which also reduces the risk of the slab collapse. In particular class A buildings are characterized by horizontal structures affected by small in plane deformations, effective connection of slabs to the vertical walls, regular vertical distribution; the lack of one of these features penalizes the building class. The weight factor is determined as a function of the number of floors in class B as respect to the total one.
8. *Roofing structures.* It deals with the type of roofing structures, they being thrusting or plane roofs, with or without perimeter stringcourses. The classes from A to D are defined accordingly. The weight factor depends on the self-load and on the ratio between the roof perimeter and the support length.
9. *Details.* It deals with the completion elements or decorations, whose damage could provoke any injury to both people and things. The classes from A to D are defined accordingly.
10. *State of preservation.* It deals with the actual conditions of the structural elements, such as the presence, the diffusion and the amplitude of cracks, or any other decay form. The classes from A to D are defined accordingly.

Also the collaboration of the building with adjacent ones is another qualification items, but this aspect can not be generalized, due to the extreme variability of the actual situations. Then, it must be evaluated in each specific case.

The combination of the class coefficients and weight factors defines the vulnerability index ( $I_v$ , Eq. 1) that varies on a scale ranging from 0, which corresponds to all class A items, to 385.5,

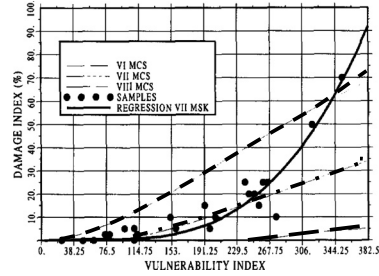


Figure 7. Vulnerability functions (Barbat et al., 1996).

which corresponds to all class D items (Benedetti et al., 1984):

$$I_v = \sum_{i=1}^{10} c_i W_i \quad (1)$$

Based on the vulnerability index, the global damage index  $D$  characterizes the structural state of a building after an earthquake. It is expressed in percentage of damage through the so called vulnerability function, which is achieved by statistical analyses of data referred to many study buildings and to assigned seismic intensities. In Figure 7 the ( $I_v$ ,  $D$ ) relationships referred to a VII MSK intensity (Barbat et al., 1996) and to the VI, VII and VIII MCS intensities (Angeletti et al., 1988) are drawn.

### 3.2 Application to the study case

With reference to the study case the evaluation of the seismic vulnerability based on the GNDT Level II method, has provided the following results.

1. *Organization of vertical structures:* generally, the orthogonal vertical walls are efficiently connected, they being sewed each other, but spans are larger than 15 times the thickness; then the building belongs to class D.
2. *Typology of vertical structures:* the lack of broad in situ investigations suggests an assumption in the safe side, then the building belongs to class C.
3. *Building site and foundation type:* due to the large extension of the building, the localized investigations on foundations cannot be reliably generalized, therefore the building is precautionary assigned to class C.
4. *Distribution of resisting elements:* the building belongs to class A, being  $\alpha = 1.8$ , according to the following estimated values of the peculiar parameters: the area of the structural walls is the 42% and 58% of the whole building area, in the main X (transversal) and Y (longitudinal) directions, respectively; the masonry shear strength is equal to 6 t/mq; the weight of one floor of the building is equal to 6.8 t/mq; the number of stories is 3.

5. *Horizontal regularity*: the building has a rectangular shape ( $BXL = 28 \text{ m} \times 157 \text{ m}$ ); the corresponding ratio  $\beta_1$  is equal to 0.18, therefore the building belongs to class B.
6. *Vertical regularity*: the building is characterized by arcades at both ground and first floors, for an extent of more than 20% of the floor area; therefore the building belongs to class D.
7. *Type of horizontal structures*: wooden beam floors are characterized by in plane deformability and a small degree of connection between parallel masonry walls, the building belongs to class D. The weight factor is equal to 1.
8. *Roofing structures*: they are realized by means of trusses provided with chains and without string-courses. This corresponds to a class B building. The weight factor is equal to 0.50.
9. *Details*: the main façades of the building is decorated by parapets and cornices, which could slump in case of a seismic events; therefore the building belongs to class D.
10. *State of preservation*: the visual survey has evidenced some structural and non structural damages; therefore the building belong to class C.

The connection of the analyzed part of the building to the other ones is ignored; its stiffening action will be evaluated in the next phase of analysis.

In conclusion, the calculated vulnerability index  $I_v$  is equal to 206.25, such as the 53% of the maximum value 385.5. The damage index  $D$  is equal to about 6%, with reference to VII MSK intensity, while with reference to the VII and VIII MCS intensities, it results equal to about 12% and 32%, respectively. Therefore, the level of damage, as a global estimation, is quite limited; however, in case of monumental buildings, it should be necessary to know where and in which extent damage is located.

#### 4 CONCLUSIONS

The evaluation of the seismic vulnerability is a very important task when the historical and architectural heritage is concerned; due to the peculiarities of the structural elements, the geometric proportions among parts and the need for conservation of constructions and assets of high artistic value. In this context, after a brief state of the art on the topic, the paper deals with the application of the first phase of a multilevel methodology for the evaluation of the seismic vulnerability of the Royal Palace of Naples, which has been selected as a study case within the international research project PROHITECH. In particular, the paper focuses on the north-west wing of the Palace.

The vulnerability index  $I_v$  has been calculated through the GNDT Level II method, according to the Benedetti-Petrini procedure, hence the damage index

$D$  has been calculated by means of the regression functions proposed by Angeletti et al. with reference to the VII and VIII MCS intensities. The results of the applied method provide low seismic vulnerability and damage index values, as a global estimation; however, dealing with a monumental construction, more careful levels of analyses should be performed, in order to preserve the historical and architectural heritage represented also by non structural elements, such as decorations, frescos and furniture. As a consequence, the completion of the study on the north-west wing of the Palace will consist on the seismic vulnerability evaluation by means of simplified mechanical models. Further the analysis will be extended to other parts of the Palace and then to the whole construction.

#### ACKNOWLEDGMENT

The research activity is developed within the PROHITECH European project "Earthquake Protection of Historical Buildings by Reversible Mixed Technologies" (2005–2008) coordinated by F.M. Mazzolani.

#### REFERENCES

- Angeletti, P., Bellina, A., Guagenti, E., Moretti, A. & Petrini, V. 1988. Comparison between vulnerability assessment and damage index, some results. *Proc. of the 9th World Conference on Earthquake Engineering*, Tokyo-Kyoto, Vol. 8: 181–186.
- Barbat A.H., EERI M., Yépez Moya F. & Canas J.A. 1996. Damage scenario simulation for seismic risk assessment in Urban zones. *Earthquake Spectra*, Vol. 12, N. 3.
- Benedetti D., Petrini V., 1984. On seismic vulnerability of masonry buildings: proposal of an evaluation procedure, *L'industria delle costruzioni*; 18, 66–78.
- Braga, F., Dolce, M. & Liberatore, D. 1982. A statistical study on damaged buildings and ensuring review of MSK-76 Scale (in Italian). *Terremoto dell'Irpinia 23 Novembre 1980, Cap. 5, Progetto Nazionale Geodinamica (CNR)*, Roma: Ed Scientifiche Associate.
- Cattari, S., Curti, E. Giovinazzi, S., Lagomarsino, S., Parodi, S. & Penna, A. 2004. A mechanical model for the vulnerability analysis of the masonry build-up on the urban scale (in Italian). *Proc. of the 11th National Congress ANIDIS: L'ingegneria sismica in Italia*, Genoa, 2004.
- FEMA 1999 (Federal Emergency Management Agency), HAZUS 1999. HAZUS Earthquake Loss Estimation Methodology, *Technical Manual, U.S.A.*
- GNDT 1994. Scheda di esposizione e vulnerabilità e di rilevamento danni di primo livello e di secondo livello (muratura e cemento armato), *Gruppo Nazionale per la Difesa dai terremoti*, Roma.
- Lagomarsino S., Podestà S. & Risemini S., 2004. Observational and mechanical models for the vulnerability assessment of monumental buildings. *13th World Conference on Earthquake Engineering Vancouver*, B.C., Canada.

# Effect of unsteady aerodynamic admittances on life cycle of guyed masts

U. Peil & M. Clobes

*Institute of Steel Structures, Technische Universität Carolo-Wilhelmina zu Braunschweig, Germany*

**ABSTRACT:** For predicting the life cycle of guyed structures under turbulent wind, a model-chain has to be applied including models for: the wind-loading, the structures mechanical behaviour and the fatigue analysis. Each model affects the predicted life-time. Unsteady wind load models in the frequency domain require a linearisation of the structure's nonlinearities due to the sagging cables. Quasi-steady wind loading models for the time domain lead to forces that correspond to measurements only in high winds. In this paper, identified complex aerodynamic admittances in combination with nonlinear numerical simulations of guyed masts in the time-domain under turbulent wind are used for a life cycle analysis. The results indicate a reduction of the predicted damage compared with common quasi-steady simulations of the buffeting wind loads.

## 1 INTRODUCTION

Dynamically excited steel structures are vulnerable to fatigue damages because cyclic loading can lead to inherent damages, although the resulting stresses are significantly below the material strength.

For high and slender structures like guyed masts wind is the only relevant dynamic load. If these loads are buffeting wind loads due to the natural turbulence, there are two possibilities for their mathematical modelling. Either quasi-steady wind load models in the time domain or unsteady wind load models in the frequency domain are available. However, unsteady models in the frequency domain—modelled by aerodynamic admittance functions—require a linearisation of the structure's nonlinearities. Quasi-steady models lead to forces that correspond to measurements only in high winds. However, these wind events with high wind speeds are rare and hence they do not contribute for fatigue.

In this paper complex aerodynamic admittances from full-scale measurements in combination with numerical simulations of guyed masts in turbulent wind fields are used for a life cycle analysis to account for frequency-dependent aerodynamic admittance in the time domain.

Aim of the presented enhanced calculation of the life cycle of guyed masts is to use the advantages of modelling the wind forces in the frequency domain in combination with a dynamic structural analysis in the time domain. The latter allows for taking nonlinearities due to sagging cables into account.

## 2 MODEL OF UNSTEADY AERODYNAMIC ADMITTANCE

Figure 1 and figure 2 show the instrumentation of the data acquisition tower Gartow II. The installation of claddings fixed on load cells and wind sensors on cantilevers at each side allows for measuring wind velocities and directions as well as total lift and drag forces. The cladding is installed at 66 m an 102 m above the ground. Since 2007 turbulence measurements are done with ultrasonic anemometers



Figure 1. Covered part of the guyed mast Gartow II at 66 m.

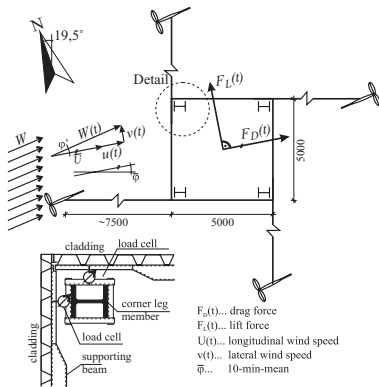


Figure 2. Instrumentation for the measurement of the aerodynamic admittance at the mast.

(USA). For further details of the whole data acquisition tower Gartow II see (Behrens 2004; Clobes 2008).

For the transmission of the longitudinal and lateral turbulence to buffeting wind loads a MiSo-LTI-model is used to describe the time-dependent loads due to the external turbulent wind velocity fluctuations. The model is based on the two inputs  $u(t)$  and  $v(t)$  of the windward sensor, the transfer functions  $H(f)$  or  $h(t)$  and the output fluctuating drag  $F'_D(t)$  or lift  $F'_L(t)$ , see figure 2.

The complex admittance  $H(f)$  between the input and the output can be calculated from the corresponding cross spectral densities e.g.  $S_{u, D}(f)$  and the auto spectral density of the input (Bendat and Piersol 2000). See eq. (1) for the drag force transfer functions due to longitudinal turbulence.

$$H_{D,u}(f) = \frac{S_{u, F_D}(f)}{S_{uu}(f)} \quad (1)$$

The transfer functions for the lift force and those due to the lateral turbulence  $v(t)$  can be calculated likewise. Equation (1) provides an noise minimising description of the mathematic relations of input an output if there is any correlation between the model uncertainty, e.g. vortex excitation, and the system's input.

### 2.1 Unsteady aerodynamic transfer in the time domain

If the admittance in the frequency domain is known with its real and imaginary part it can be transformed into the time domain via *Fourier* transform without any loss of information. Hence, the time domain representation of the admittance  $H(f)$  that is the impulse response  $h(t)$  can be obtained. With these

impulse response functions an equivalent description of unsteady wind loads in the time domain is available. The buffeting wind forces can thus be calculated via

$$F'_{b,u}(t) = \int_{-\infty}^{\infty} h_{b,u}(t - \tau)u(\tau)d\tau \quad (2)$$

If the continuous time signal  $u(\tau)$  is divided into impulses of the width  $d\tau$ , the system's output can be calculated based on the conditions that the impulse response of the transfer system is known and that a linear system transfer can be accepted. Thus, the continuous system output results from a superposition of the system's responses to the single impuls  $u(t)$ .

### 2.2 Causal system transfer

A system is called causal if its response is only due to present and past but not to the future input signals. For real physical systems it can be stated (Rupprecht 2003):

$$h(t) \begin{cases} = 0 & \text{if } t < 0 \\ \neq 0 & \text{if } t \geq 0 \end{cases} \quad (3)$$

In the frequency domain causality of the complex admittance can be verified by the *Hilbert* transform. Aerodynamic impulse response functions directly calculated from the measured auto and cross spectral densities violate these conditions (Clobes 2008).

That is a result of the necessary digital filtering of the measured data. Then the region of the *Gibbs* phenomenon is broadened and leads to a not satisfying at and around the point of discontinuity (Papoulis 1962).

Additionally, the transfer functions from eq. (1) ensure a minimalisation of the noise only if the convolution is also done with the non causal parts, see eq. (2). Convolution in the time domain and multiplication in the frequency domain thus leads to identical results only if non-causal parts were also taken into account. But the transfer system has a finite memory size that should be connected with the integral time scale  $T_{ux}$ . Inputs beyond  $T_h$  must not be taken into account.

As a result it can be stated that transfer systems that only depend on measured spectral values violate the causality conditions and result in physically meaningless relationships.

Hence, it is feasible to fit continuous functions on the measured admittances that fulfil the *Hilbert* transform in order to smooth the measured data and to get causal impulse responses in the time domain via the *Fourier* transform. This is done with rational functions.



### 2.3 Rational function approximation of complex admittances

An approximation of the step response  $\phi(t)$

$$\phi(t) = \begin{cases} 0 & \text{for } t < 0 \\ a_0 - \sum_{n=1}^N a_n \cdot e^{-b_n \cdot t} & \text{for } t \geq 0 \end{cases} \quad (4)$$

that is the integral of the impulse response leads via *Laplace* transform to an approximation of the complex admittance with equation (5), see (Chen and Kareem 2001; Clobes 2008) for details.

$$H(\omega) = a_0 - \sum_{n=1}^N \frac{a_n \cdot i\omega}{b_n + i\omega} \quad (5)$$

From the idea that high frequency gusts have a small scale, no wind forces will be induced on the structure in the case of  $\omega \rightarrow \infty$ . Hence, the upper limit of the admittance function tends to zero, and it follows for the impulse response

$$h(t) = \sum_{n=1}^N a_n \cdot b_n \cdot e^{-b_n \cdot t} \quad (6)$$

If  $N = 1$ , the complex admittance can solely be calculated from the amplitude response only because there are no zeros in the right complex half-plane (Papoulis 1962). Hence, the phase response is explicit given by an approximation of the amplitude response with rational functions. For  $N > 1$ , the measured phase has to be taken into account because zeros in the right complex half-plane are possible. The calculation of the phase response that is only due to aerodynamic effects and not due to the geometry of the measuring arrangement is not possible. The distance between the anemometer and the mast is always included in the phase. A phase correction from *Taylor's* hypothesis has to be rejected because of the deformation of the gusts when approaching the mast (Hunt et al. 1990). The amplitudes are thus stronger weighted in the approximation and only the low-frequency phases are used. In addition the assumption of starting from zero is made for the phase spectrum for low frequencies.

The highly nonlinear fitting of equation (5) to the measured data is done with a genetic algorithm.

### 3 AERODYNAMIC TRANSFER-FUNCTIONS FROM FULL-SCALE MEASUREMENTS

The full-scale data obtained at the mast Gartow II is used to identify the unsteady transfer system with respect to the considerations mentioned in the preceding paragraphs. In the following, only those transfer

paths with an ordinary coherence larger than 0.3 are considered (Bendat and Piersol 2000).

In figure 3 and figure 4 the aerodynamic transfer functions for five different data sets with similar flow characteristic perpendicular to the cladding are compared. The differences between each transfer function are negligibly small. Only the transfer function identified in the data set that was recorded by an ultrasonic anemometer stronger decreases in the frequency domain due to the missing of any inertia effects. This causes a lower increase of the step response function.

However, this phenomenon cannot be analyzed with respect to statistical certainty due to the small amount of ultrasonic data. Especially in the low frequency range the scatter of the transfer functions shown in figure 5 and figure 6 is strong. Nevertheless, the approximated transfer functions are basically similar

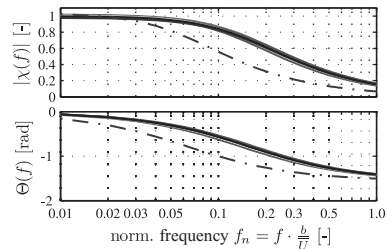


Figure 3. Aerodynamic admittance  $\chi_{W,u}(f)$  for  $F'_W(t)$  from  $u(t)$  with  $\bar{\varphi} = 0^\circ$  from different full-scale measurements.

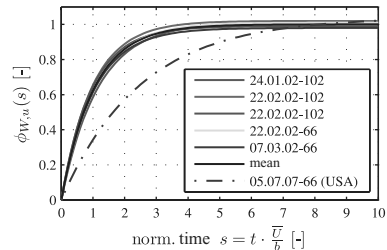


Figure 4. Step response  $\phi_{W,u}(s)$  for  $F'_W(t)$  from  $u(t)$  with  $\bar{\varphi} = 0^\circ$  from different full-scale measurements.

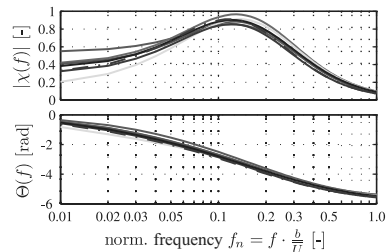


Figure 5. Aerodynamic admittance  $\chi_{Q,v}(f)$  for  $F'_Q(t)$  from  $v(t)$  with  $\bar{\varphi} = 0^\circ$  from different full-scale measurements.



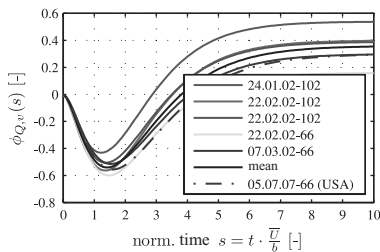


Figure 6. Step response  $\phi_{Q,v}(s)$  for  $F'_Q(t)$  from  $v(t)$  with  $\bar{\varphi} = 0^\circ$  from different full-scale measurements.

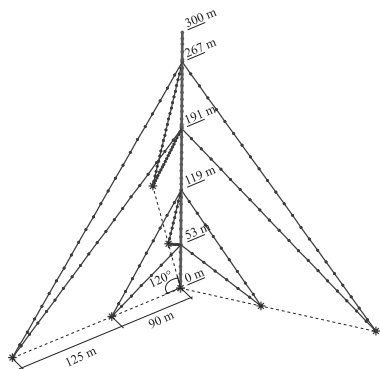


Figure 7. Dimensions and elementation of the 300-m-Mast.

for each data set, although their flow parameters like turbulence intensities or integral length scales  $L_{ux}$  differ significantly for each set, see (Clobes 2008) for details. Thus, the functions can at least be described well by their mean value.

#### 4 STRUCTURAL DYNAMICS OF GUYED MASTS UNDER BUFFETING WINDLOAD

The numerical simulations were done for different types of guyed masts. In figure 7 the mechanical model and its elementation of a 300 m high mast is shown.

##### 4.1 Unsteady wind loads in the time domain

The application of the identified aerodynamic transfer from a covered square cylinder on lattice structures like masts is associated with simplifications whose influences cannot be verified within the presented investigations. Nevertheless, an application is done in such a manner that the identified aerodynamic impulse response functions are scaled with quasi-steady force coefficients  $C_D$  and  $C_L$  for lattice structures coming from the methodology given in (ESDU 1991).

A direct use of the identified impulse response functions in the numerical simulation would only describe

linearly-involved parts of the wind forces. It is thus assumed that the quasi-steady transfer model can properly describe the fluctuating part of the wind loads for the steady state  $f \rightarrow 0$ . Therefore, step responses that converge to 1 are used in order to simulate the influence of a frequency-dependent transfer only. Although no correlation between the velocity fluctuations and the corresponding orthogonal forces could be identified, this transfer is also modelled using the same aerodynamic impulse response for the unsteady wind loading model as well. Hence, for the unsteady model the equivalent total energy of the wind process for the steady state is the same compared to the quasi-steady model.

With respect to orthogonal incoming flow, the lateral forces and the corresponding admittances  $\chi_{Q,v}(f)$  the identified transfer system are strongly influenced by the body-induced turbulence (Hölscher 1999). Regarding lattice structures, lateral forces due to vortex excitation having the same magnitude cannot be expected. Only the memory size  $T_h$  is therefore taken from the identified impulse responses for the description of the lift forces. The parameters of the assumed unsteady transfer model and the wind directions simulated in the numerical investigations are listed in table 1.

The non-normalized, real-time aerodynamic impulse response  $I_{F,k}(t)$  is defined by equation (7) (Papoulis 1962).

$$I_{F,k}(t) = \frac{\bar{U}}{b} \cdot \sum_{n=1}^N a_n \cdot b_n \cdot e^{-b_n t \cdot \frac{\bar{U}}{b}} \quad (7)$$

The unsteady wind forces are described by an extended description of the quasi-steady wind forces. Thus, the quadratic term of the fluctuating wind velocities and the nonlinear characteristics of the aerodynamic coefficients are retained.

$$F_D(t) = \frac{\rho}{2} A \int_0^t I_{D,u}(t-\tau) W^2(t) C_D(t) \cos(\varphi'(t)) dt - \frac{\rho}{2} A \int_0^t I_{D,v}(t-\tau) W^2(t) C_L(t) \sin(\varphi'(t)) dt \quad (8)$$

Table 1. Estimated coefficients of aerodynamic transfer functions for the numerical simulations.

Wind-direction	Admittance-function	Coefficients				
		$a_0$	$a_1$	$b_1$	$a_2$	$b_2$
$\bar{\varphi} = 0^\circ, 90^\circ, 180^\circ$	$\chi_{D,u}, \chi_{D,v}$	1	1	1	-	-
	$\chi_{L,u}, \chi_{L,v}$	1	1	0.5	-	-
$\bar{\varphi} = 45^\circ, 135^\circ$	$\chi_{D,u}, \chi_{D,v}$	1	1.2	0.5	-0.2	1.4
	$\chi_{L,u}, \chi_{L,v}$	1	1.2	0.85	-0.2	3.9

#### 4.2 Simulation of the guyed masts' life time

Normally, different locations have a distinctive wind-direction-dependent frequency distribution of the occurring wind speeds. In the presented investigations it is assumed that the wind directions are uniformly distributed and that the results obtained from the wind directions  $\bar{\varphi} = 0^\circ, 45^\circ, 90^\circ, 135^\circ$  and  $180^\circ$  are characteristic for their respective sectors.

In general, the probability density of the current wind velocities is defined by the *Weibull* curve.

This *Weibull* distribution is only feasible for probabilities  $P(\bar{U}) > 0,01$  and therefore an improper description of extreme wind statistics (Peil and Nölle 1995). The probability of occurrence of wind situations with  $\bar{U} > 10$  m/s is normally about or below this limit in Germany and the terrain categorie II (CEN 2005). Hence, instead of the *Weibull* curve with parameters from (Troen and Petersen 1990) long-term data from the Gartow II mast was used. The 14.000 mean values of the wind velocities from the years 1993-1994 cover 40% of the two years period and can be generally accepted as representative.

A conversion of these measurements at a level of 30 m above the ground from a rougher terrain between terrain categorie III and IV into the smoother terrain of categorie II and the reference height of 10 mis done by the assumption of equal wind speeds in the gradient height. For the full-scale measurements a gradient height of  $z_G = 400$  m and for the terrain of categorie II a gradient height of  $z_G = 300$  m is used (Ruscheweyh 1982).

The long-term measurements show that a mean exponent of  $\alpha = 0,25$  for the wind profile can be used at the site of the mast Gartow II (Clobes 2008). The conversion of the mean wind speed can thus be done with

$$\bar{U}(10)_{II} = \bar{U}(30)_{Gtw} \cdot \frac{(400/30)^{0,25}}{(300/10)^{0,16}} \quad (9)$$

This leads to the empirical distribution function shown in figure 8. The number of wind fields with a specified mean wind velocity within 50-years from this distribution function is given in table 2.

For an estimation of the influence of unsteady buffeting admittance the fatigue of guyed masts under turbulent wind load is calculated. Three-dimensional numerical wind fields with a reference wind speed according to table 2 were generated with *Shino-zoukas* method. Here a computational efficient algorithm based on the FFT is used. The wind fields were generated for the wind directions given in table 1. The time length of each wind field is 10 minutes. The statistical properties were taken from *Eurocode 1* as well as from our full-scale measurements or other literature if available. Under these wind fields, a nonlinear dynamic calculation of several guyed masts is done

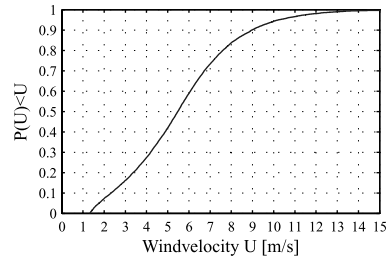


Figure 8. Empirical distribution function of wind velocities in a height of 10 m for Gartow.

Table 2. Probability of occurrence and 50-years frequency of mean wind velocities

Interval $\bar{U}_{Int}$ [m/s]	$\bar{U}_{ref}$ [m/s]	Probability $p(\bar{U}_{Int})$	Frequency $N_{50a}(\bar{U}_{Int})$
7,5–12,5	10	$1,97 \cdot 10^{-1}$	518000
12,5–17,5	15	$1,35 \cdot 10^{-2}$	36000
17,5–22,5	20	$4,86 \cdot 10^{-4}$	1300
>22,5	25	$(3,81 \cdot 10^{-7})^\circ$	1

$^\circ$ theoretic probability for a 50-years event with  $P_a = 0.02$ .

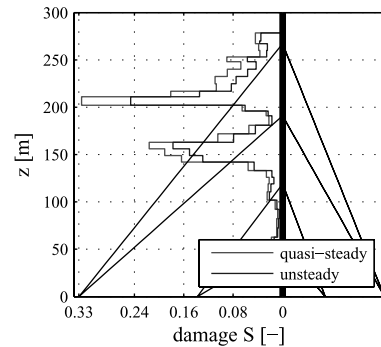


Figure 9. 300-m-mast: maximum of the damage in the four corner leg members for fatigue detail category 71.

in the time domain using the unsteady wind loading model according to equation (8) as well as an ordinary quasi-steady wind loading model.

The resulting stress-time-series under quasisteady and unsteady wind load for different wind directions were counted with the *Rainflow*-algorithm from (Clormann and Seeger 1986). The stress collectives are multiplied with the occurrence frequencies given in table 2 and the probability of the wind direction. A calculation of the inherent damage is done with the well-known linear *Palmgreen-Miner* hypothesis.

In figure 9 and figure 10 the maximum damage  $S$  of the corner leg members of a 300 m mast for two different detail categories are shown. The reduction of

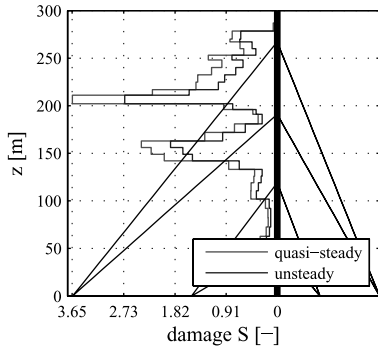


Figure 10. 300-m-mast: maximum of the damage in the four corner leg members for fatigue detail category 36.

damage when modelling the wind loads with impulse response functions accounts 30%. The mast having a detail category of 36 N/mm<sup>2</sup> will not reach a life time of 50 years.

## 5 CONCLUSIONS

The life cycle analysis of guyed structures was done in the time domain regarding the influence of geometric nonlinearities due to the sagging cables. Because of the need of a simulation of frequency dependent aerodynamic admittance for low wind speeds, the complex admittance-functions were identified in full-scale measurements und transformed into the time domain.

The identified step responses are well comparable for similar wind flows. But the influence of inertia free measurements with ultrasonic anemometers is remarkable.

Former investigations have shown that the ordinary coherence functions indicate that 90% of the low-frequency drag is linearly related to  $u(t)$  and that the correlation between  $F'_L(t)$  and longitudinal turbulence as well as the correlation of  $v(t)$  and  $F'_D(t)$  is negligible. About 50% of the lift in the region of the *Strouhal* frequency is linearly related to the lateral turbulence. Hence, the high frequency drag and most of the lift cannot be modelled by the MiSo-Lti-system. So the aerodynamic admittance functions used here are not suitable for practical considerations. Further data from full-scale measurements and wind tunnel experiments has to be analysed and the model for the aerodynamic transfer has to be enhanced.

The assumption made in section 4.1 that the force fluctuations due to the corresponding orthogonal wind velocities can be modelled with the same impulse response functions although there is no correlation between the velocity fluctuations and the corresponding orthogonal forces, leads to an overestimation of the real stresses.

Nevertheless the unsteady admittance shows a remarkable influence on the masts life cycle. The total damage under 50 years of wind loading is reduced to about 70%.

The abandonment of fatigue calculations for masts with detail categories greater than 71 N/mm<sup>2</sup> as it is given in the EN 1993-3-1 can be accepted.

## ACKNOWLEDGEMENTS

We gratefully acknowledge the support given by the German Research Foundation (DFG). Thanks also to the Deutsche Telekom AG for the allowance of carrying out measurements on their guyed mast Gartow II.

## REFERENCES

- Behrens, M. (2004). *Aerodynamische Admittanzansätze zur Böenwirkung auf hohe, schlanke Bauwerke*. Ph. D. thesis, Technische Universität Carolo-Wilhelmina zu Braunschweig.
- Bendat, J.S. & A.G. Piersol (2000). *Random data: Analysis and Measurement Procedures* (3. ed.). John Wiley & Sons, Chichester, New York.
- CEN (2005). Eurocode 1: Actions on structures—part 1-4: General actions, wind actions. Technical report, CEN.
- Chen, X. & A. Kareem (2001). Nonlinear response analysis of long-span bridges under turbulent winds. *Journal of Wind Engineering* 89, 1335–1350.
- Clobes, M. (2008). *Identifikation und Simulation instationärer Übertragung der Windturbulenz im Zeitbereich*. Ph. D. thesis, Technische Universität Carolo-Wilhelmina zu Braunschweig.
- Clormann, U. & T. Seeger (1986). Rainflow-hcm, ein zählverfahren für betriebsfestigkeitsnachweise auf werkstofflicher grundlage. *Stahlbau* 55, 65–71.
- ESDU (1991). Esdu 81028, lattice structures. part ii: mean fluid forces on tower like space frames. Technical report, ESDU International plc.
- Hunt, J.C.R., H. Kawai, S.R. Ramsey, G. Pedrizzetti & R.J. Perkins (1990). A review of velocity and pressure fluctuations in turbulent flows around bluff bodies. *Journal of Wind Engineering and Industrial Aerodynamics* 35, 49–85.
- Hölscher, N. (1999). *Ein multivariater Ansatz für die aerodynamische Übertragungsfunktion der Winddrücke in atmosphärischer Grenzschichtströmung*. Ph. D. thesis, Ruhr Universität Bochum.
- Papoulis, A. (1962). *The fourier integral and its applications*. McGraw Hill Book Company, New York, London.
- Peil, U. and H. Nölle (1995). Ermittlung der lebensdauer hoher windbeanspruchter bauwerke. *Bauingenieur* 70, 21–33.
- Rupprecht, W. (2003). *Signale und Übertragungssysteme: Modelle und Verfahren für die Informationstechnik*. Springer-Verlag, Berlin, Heidelberg, New York.
- Ruscheweyh, H. (1982). *Dynamische Windwirkung an Bauwerken, Band 1 & 2*. Bauverlag GmbH, Wiesbaden und Berlin.
- Troen, I. and E.L. Petersen (1990). *Europäischer Windatlas*.

# Medium-term life-cycle monitoring of random behaviour components of in-service pile-supported wharves

H. Yáñez-Godoy & J. Boéro

*Oxand S.A., Avon and Lyon, France*

F. Schoefs

*Institute for Research in Civil and Mechanical Engineering (GeM) Nantes Atlantique University, Nantes, France*

**ABSTRACT:** In the Nantes Harbour, France, two recently built pile-supported wharves have been instrumented in 30% of the cross sections where tie-rods have been installed. Tie-rods are identified by a risk analysis as fundamental components for two main reasons: the first being that their behaviour is very sensitive to building conditions and secondly they support a significantly great portion of horizontal loading due to ship mooring or wind loading on container cranes. This paper aims to assess the structural health from the information acquired by monitoring and its probabilistic analysis during post-building step but before complete service loading (no ship mooring). A decomposition of measured loads in tie-rods on polynomial chaos is selected. Response distribution leads to assess both the probability of failure (considering a limit state design criterion) and the medium-term evolution of steel corrosion (considering an acceptable corrosion level).

## 1 INTRODUCTION

Harbour structures are subjected to great hazards during their building due to the long period of construction (at least one year) and the wide set of available techniques to install their various components. Respecting the mechanical design hypotheses during their construction is a key-point for ensuring safety, availability and durability. However due to weather or non-foreseen situations, it is necessary to carry out a review of incidents. This and the knowledge of observed or predicted events during construction and exploitation of a structure allow updating the model and for an optimization of its survey, leading to an improvement of the inspection, maintenance and repair programs. The monitoring is then the only way to improve models and update assumptions. It has been shown that the real state of the structure after building can be far from the design one (Yáñez-Godoy et al., 2008a).

In this paper we present two recently built pile-supported wharves in the Nantes Harbour, in France. They have been instrumented in 30% of the cross sections where tie-rods have been installed. Data collected from 2003 to 2006 are available. An original instrumentation strategy has been achieved: it aims to follow the global behaviour of every wharf during at least the first 5 years after building with a view to setup prediction models. These validated models will allow basing the maintenance policy on a better understanding of the in-service behaviour. Indeed, the large

dimensions of these structures, the building hazards and the soil behaviour induce the choice of conservative and too theoretical hypotheses at the design stage that make the design easier but the re-analysis more difficult.

A risk analysis is performed on the design phase. It highlights tie-rods as key components of the structure. We monitor these components which are hardly accessible after the building period and the sensitivity of which can be measured with the present accuracy of available sensors (Verdure et al., 2005).

In this paper, we focus mainly on the tie-rods during service loading but without ship loading in order to identify first the behaviour of the structures with basic loading. The polynomial chaos decomposition of measured loads in the tie-rods is selected. Response distribution leads to assess both the probability of failure (considering a limit state design criterion) and the medium-term evolution of steel corrosion (considering an acceptable corrosion level).

## 2 CONTEXT

The two in-service monitored pile-supported wharves presented here are located in the estuary of the river Loire, in the west of France. They are managed by the Port Authority of Nantes Saint-Nazaire (PANSN). These studies deal with the extension of the timber terminal of Cheviré, the station 4 (so called Cheviré-4

wharf) and the extension of the containers terminal of Montoir (so called TMDC-4 wharf). Their detailed description is available in (Yáñez-Godoy et al., 2008a). A sketch of a typical cross section is represented on Figure 2. Collaboration with the PANSN permitted the survey of the structures.

### 3 RISK ANALYSIS

Risk analysis can be used in design stage but also during operation of infrastructures (Billard et al., 2007). The aims are to provide the owners with formal and objective maintenance decision-making indicators based on technical and financial aspects. In this study, FMECA (Failure Mode Effects and Criticality Analysis) is applied on two pile-supported wharves during design stage. The expert approach is shown in Figure 1. This is a very common method that has been shown to be very efficient when studying coastal structures (Billard et al., 2006, Billard et al., 2007, Crouigneau et al., 2008).

#### 3.1 Functional analysis

The first step of the study consists in system decomposition according to environment, loadings, geometry or material. In case of pile-supported structures, six main components are identified (see Fig. 2).

Main functions filled by wharves are: (1) ship support for berthing and mooring; (2) connection between ship and open area; support for operational charges and discharges from ships; (3) ground support. Each

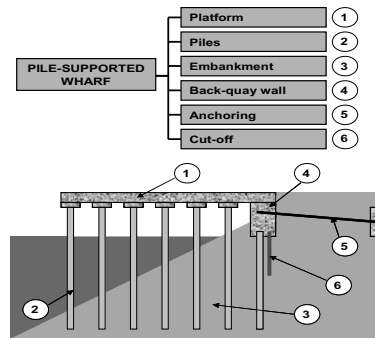


Figure 2. Decomposition of “pile-supported wharf” system.

component plays a specific role in the functioning of the pile-supported wharf in a functional context.

#### 3.2 Failure modes identification and assessment

The exhaustive list of potential failure modes is obtained thanks to a crossing between the components and the expected functions of the pile-supported wharves. For each component, an analysis of the different causes which could lead to a failure of the associated function is carried out.

For example, the components “platform”, “piles” must resist mechanically to vertical loading due to both overcharges (container cranes, goods traffic, etc.) and dead loads. The component “anchoring” must support a significantly great portion of horizontal loading due to ship mooring or wind loading on container cranes. If they couldn’t resist to loadings, because of a resistance decrease due to both building conditions and infrastructure ageing or of an increasing stress with traffic evolution, failures could lead to consequences like loss of human life, interruption of traffic, and damage to environment. The component “cut-off (sheet-pile wall)” must prevent leakage of particles from the back-fill to the river. Failure can be caused by holes in the sheet-pile wall due to corrosion and could damage the open area.

Criticality (C) is affected for each failure mode. The criticality assessment allows ranking identified failure modes. In the present methodology, criticality is calculated with three parameters:

- the frequency of failure mode (F) (occurrence probability). Frequency is estimated with experience feedback capitalised in tools such as SIMEO™ Consulting (software that takes into account the ageing mechanisms), but also by experts when mechanisms simulations are complex or in case of missing information;

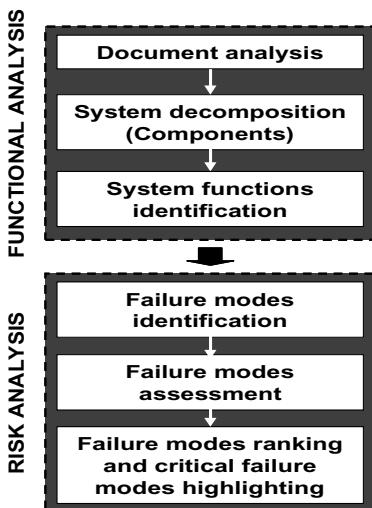


Figure 1. Risk analysis methodology applied to pile-supported wharves.

Component	Mode failure	Design stage			
		F	G	D	C
Platform	Lack of mechanical resistance	1	5	0	5
Platform	Loss of mechanical resistance	1	5	0	5
Piles	Lack of mechanical resistance	2	6	1	12
Piles	Loss of mechanical resistance	1	6	1	6
Embankment	Loss of the passive earth pressure and pile-soil adherence	1	6	1	6
Embankment	Leakage of particles from the backfill	1	4	1	4
Back-quay wall	Lack of mechanical resistance	2	6	0	12
Back-quay wall	Loss of mechanical resistance	1	6	0	6
Anchoring	Lack of mechanical resistance	3	6	2	30
Anchoring	Loss of mechanical resistance	1	6	2	12
Cut-off	Leakage of particles from the backfill	1	4	2	8

Figure 3. Results of pile-supported wharves risk analysis.

- the gravity of failure mode (**G**), which means the consequence level on the owner’s stakes (safety and availability of wharves’ operations);
- the detection means of signs that a failure mode is on the way (**D**). This parameter is defined according to conditions of access to components.

### 3.3 Results

The results of failure modes assessment are presented in Figure 3. Tie-rods are identified by risk analysis as fundamental components. Their behaviour is very sensitive to building conditions and their structural health can only be identified from the information acquired by monitoring. That’s why in a logic of risk management, this action must be anticipated from the design stage.

## 4 STRUCTURAL INSTRUMENTATION

Each wharf has been instrumented on twelve tie-rods (regularly distributed along the length of the structure) in order to measure the normal load in the tie-rods. These tie-rods are cylindrical steel bars. In the case of the TMDC-4 wharf, some sets of two vibrating wire strain gauges diametrically opposed and clamped by means of flanges screwed on each tie-rod have been used. In the case of Cheviré-4 wharf, resistive strain gauges have been used: two gauges bonded parallel to the axis of the rod and diametrically opposed, and two others bonded perpendicular to the rod, mounted in a full Wheatstone bridge acting as an elongation sensor and avoiding bending effects. For both instrumentations, the sensors were required not to affect the corrosion protection of the tie-rods. The two tie-rods at both ends of the TMDC-4 wharf have been monitored with 3 couples of vibrating wire sensors, instead of one, in order to study the evolution of the normal load and the bending moment along the tie-rod.

In addition, sensors measuring the water level in the embankment (piezometers) are implanted behind the

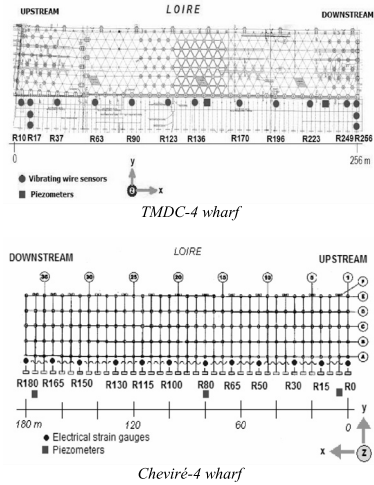


Figure 4. Instrumentation implanted in each wharf.

back-wharf wall and linked to a “Campbell Scientific CR10X” data logger; 3 piezometers on the Cheviré-4 at both ends and in the middle wharf and 2 on the TMDC-4 wharf at one end and in the middle. Finally, some tidal gauges (controlled by PANSN) measure the real tide level every 5 minutes. In the case of the TMDC-4, two tidal gauges are located in Donges (4 km upstream) and in Saint-Nazaire (2 km downstream), which allows to interpolate the water level in front of the wharf. For the Cheviré-4, a tidal gauge is located 1 km downstream the Cheviré bridge.

Figure 4 shows the distribution of the sensors along of each wharf. In a general way, the instrumented tie-rods are marked and named by an “R” letter and by their longitudinal abscissa position  $x$  in meters. By convention  $x = 0$  denotes the upstream extremity of the wharf.

## 5 MEASUREMENTS ANALYSIS

The analysis is performed at the tie-rods level. The main steps are: (i) data collection provided by the data logger; (ii) analysis of the untreated data and their physical meaning; (iii) data processing in order to highlight relevant correlations.

The acquisition period is 30 minutes, ensuring to observe the tide effects on the landing. The untreated signals saved by the acquisition system provide the local physical measurements; these are frequencies in the case of the TMDC-4 and electric voltages in the case of the Cheviré-4. A classical pre-processing of the measurements must be made in order to deduce the normal load in the tie-rods. Uncertainties of measurements are estimated: they are of less than 20 kN

for the TMDC-4 wharf and 10 kN for the Cheviré-4 wharf. All the measures taken into account for the present analysis are for service period without loading by ships (interval October 2002 to July 2003 for TMDC-4 wharf, interval January 2004 to October 2005 for Cheviré-4 wharf).

Two types of variations characterize the loads in the tie-rods:

- *temporal*: medium-term variations, where we question the levels of loads during a month (period of the moon rotation) and short-term variations where we are interested in the amplitude of the loads during a tide with a period of approximately 12 hours;
- *spatial*: variations of the load along the wharf, in each spatially distributed tie-rod.

We concentrate in this study in the medium-term evolutions.

### 5.1 Medium-term evolutions and statistical analysis

The medium-term load variations, for the non-operational phase, in the tie-rods studied for the two wharves, show a small evolution (Yáñez-Godoy et al., 2008a). They come on the one hand from the embankment loading and the conditions of service life and on the other hand from the seasonal cycles of the tide.

The analysis of the spatial load variation shows an important scatter from a tie-rod to another. This spatial variation of load shows a very distinct behaviour of the in-service structure compared to the design

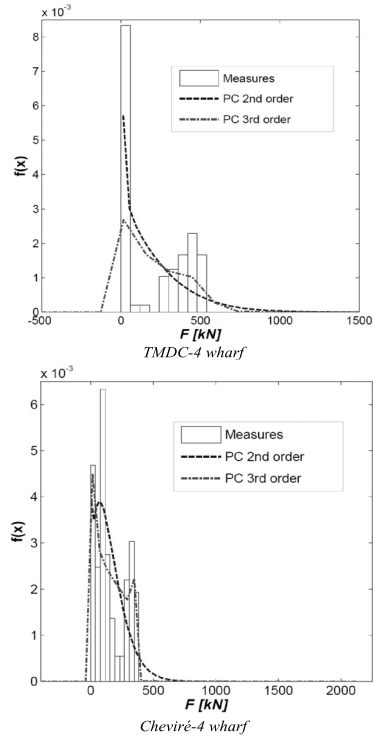


Figure 6. Statistical distribution and fitting with a polynomial chaos in each wharf.

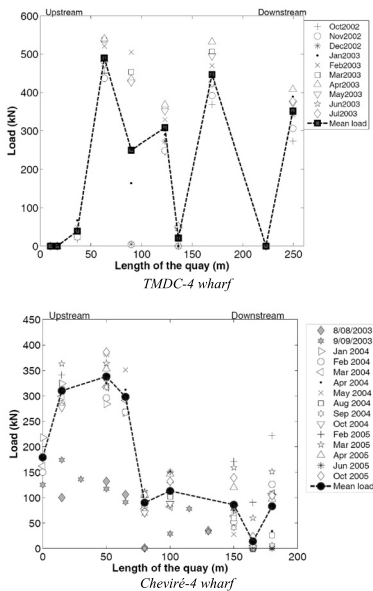


Figure 5. Medium-term loading evolutions in each wharf.

hypothesis. Research on the reasons of this variability taught us to have a prompt survey during the phase of construction (Yáñez-Godoy et al., 2008a). It underlines the need to define well the way of laying down tie-rods in order to keep an in-service behaviour as close as possible to the assumed and computed one.

Figure 5 represents the monthly average measured load in the tie-rods along the TMDC-4 wharf, during the period from October 2002 to July 2003, and the Cheviré-4 wharf, during the period from August 2003 to October 2005. The drawn mean profiles are obtained from monthly averages.

We can get statistics from monthly average measured load in the tie-rods along every wharf. To represent the considered measurements, we decided to use histograms (see Fig. 6).

### 5.2 Structural health assessment of wharves

We present now how to qualify the current structural state of the wharves from the information acquired by monitoring and its probabilistic analysis. We focus mainly on the tie-rods during service loading (non-operational phase). Two studies using in-service measurements are performed in the following sections:

- Verification of design load
- Verification of corrosion level

### 5.3 Verification of design load

This study lies on the loads obtained in design notes. They are considered implicitly as reasonable by the designer. The question is then to assess the probability to overrun this design value. This can be done by both methods, fitting predefined probability density function (pdf) to histograms or fitting with a polynomial chaos (PC) decomposition. In case of multimodal distribution (see Fig. 6), the first method implies identifying families of tie-rods by fitting several distributions. On the other hand, the second method systematizes the fitting from a data base and is selected in the following. This choice is also made to perform structural stochastic computations using spectral stochastic finite element method (Ghanem et al., 2003). We chose the estimate of maximum likelihood for the identification of PC decomposition (Desceliers et al., 2007). Then the problem is to identify the coefficients  $f_i$  of the one-dimensional polynomial chaos decomposition:

$$f(\theta) = f(\xi(\theta)) = \sum_{i=0}^p f_i H_i(\xi(\theta)) \quad (1)$$

where  $p$  is the order of the PC decomposition,  $\xi(\theta)$  the Gaussian germ, i.e. a standardized normal variable and  $H_i$  the Hermite polynomial of degree  $i$ . By using the maximum likelihood method, coefficients  $f_i$  are solution of the optimization problem:

$$L(F) = \arg \max_F L(F) \quad (2)$$

where  $F$  is the vector of components  $f_i$  ( $F = [f_0, \dots, f_p]$ ) with dimension  $(p + 1)$ , and  $L$  is the likelihood function:

$$L(F) = \prod_{j=1}^N p_f(f(\theta_j); F) \quad (3)$$

The likelihood function (3) takes values first very close to the numerical precision. Then the problem (2) is modified into:

$$-\log(L(F)) = \arg \min_F (-\log(L(F))) \quad (4)$$

The algorithm for solving the optimization problem (4) is detailed in (Schoefs, et al., 2007, Yáñez-Godoy, et al., 2008b). We make use of it to estimate coefficients  $f_i$  for every random variable. Distributions of every random variable are well represented by a first dimension 3rd degree PC (see Fig. 6).

This probability to overrun design value is called probability of failure from now on: the safety margin is then ' $M = F - F_d$ '. This service value is known

for Cheviré-4 wharf but unknown for TMDC-4 wharf. To progress in the analysis, we assume that the safety factor i.e. the ratio between the limit tensile strength  $F_e$  and the computed load in the design notes is the same for the two wharves. For Cheviré-4 wharf and for limit tensile strength  $F_e$  (1590 kN) and design value (691 kN) the safety factor is around 0.4.

We estimate from Figure 6:

- For TMDC-4 wharf:  $P(F > 0.4 F_e) = 8.2e-3$
- For Cheviré-4 wharf:  $P(F > 0.4 F_e) = 5.0e-4$

Moreover, we know that the service limit states correspond to a probability of occurrence on the life of the structure of about 0.5 (50%) to 0.01 (1%).

In both cases, the probability of failure for the non-operational phase is less than  $1e-2$ : it is convenient for service limit state. If the selected safety factor is 0.3 the probabilities of failure are respectively  $1.3e-2$  and  $1.2e-3$  for TMDC-4 and Cheviré-4 wharves.

### 5.4 Verification of corrosion level

This second study concerns the estimation of an acceptable corrosion level for tie-rods. In fact, assuming an acceptable level of failure probability allows addressing a new question: which acceptable corrosion level respects this safety target? We consider here for the service limit states, two levels of acceptable safety level: they refer to probabilities of failure of  $10^{-1}$  and  $10^{-2}$ . Cumulative density functions (*cdf*) can be obtained from Figure 6 and allow assessing the load in tie-rods corresponding to an acceptable safety level. These *cdf* and the corresponding experimental data are plotted for both wharves on Figure 7.

By knowing the load, the minimal residual steel area can be computed. The residual area for the three selected safety targets is summarized on Table 1:

This residual area divided by the initial area (56.7 and 44.2 [cm<sup>2</sup>] respectively for TMDC-4 and Cheviré-4 wharves) gives the percentage of loss of mater in terms of area (value between brackets in Table 1).

Higher is the target probability, less is the loss of steel area. The acceptable residual thickness is in the range [21%; 36%] depending on the target probability and the wharf. Note that Eurocode 3 (ENV 1993, Eurocode 3: Design of steel structures) allows the loss of 3 mm of thickness during 50 years of lifetime if no protection is provided. Here, it leads to residual

Table 1. Residual area allowed for tie-rods (cm<sup>2</sup>).

Probability of failure	TMDC-4 wharf	Cheviré-4 wharf
$10^{-1}$	13 (23%)	9 (21%)
$10^{-2}$	20 (36%)	10 (24%)



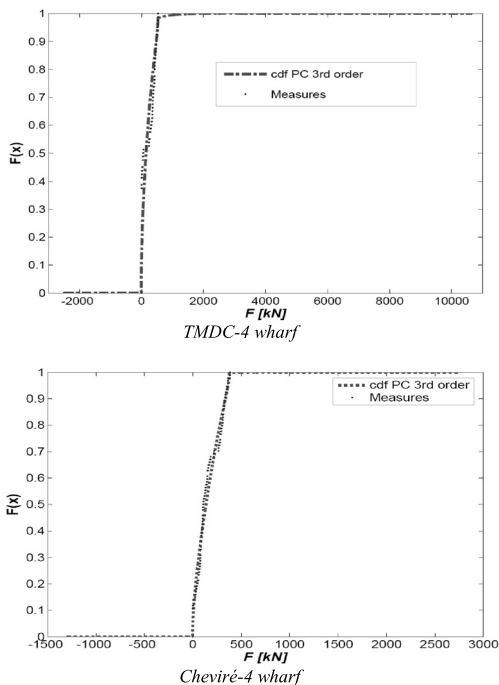


Figure 7. Cumulative density functions in each wharf.

area 49 cm<sup>2</sup> (86%) and 37.4 cm<sup>2</sup> (85%) respectively for TMDC-4 and Cheviré-4. Whatever the safety target, the acceptable residual area we obtain is lower than these values. It leads to conclude that the safety of tie-rods under service loading is satisfactory. This example is useful to reevaluate older structures since here tie-rods have an anticorrosion protection.

## 6 CONCLUSIONS

Risk analysis methodology led to a hierarchical scale of risks and highlighted tie-rods as fundamental components for two main reasons: the first being that their behaviour is very sensitive to building conditions and secondly they are hardly accessible after the building period. The profits of this analysis justified the important means of instrumentation to be foreseen since the design stage. Afterward, interpretation of the first measures has supplied to risk analysis the updating of the maintenance decision-making process.

Analysis of measured loads in tie-rods during service loading of the two pile-supported wharves showed a small evolution of medium-term load variation, though an important scatter of spatial load variation

has confirmed the sensibility to building conditions of tie-rods.

Structural health assessment (frequency of failure modes) of tie-rods has been performed to verify design load and corrosion level. The probabilistic analysis has been obtained from the information acquired by monitoring. A decomposition of measured loads in tie-rods on polynomial chaos is selected to represent more faithfully their probability distribution. Computed safety of tie-rods under service loading is satisfactory, risks are weak, and the analysis appears to be useful to reevaluate older structures. Future works will integrate loading of wind on container cranes and of ships and the use of mechanical models.

## REFERENCES

Billard Y., Bernard O., Lasne M., Capra B., Schoefs F., Boéro J., 2006. Risk analysis for survey optimization of harbour. In *Third International Colloquium of the Network for Integrating Structural Analysis, Risk and Reliability, ASRANet Colloquium, 10–12 July, 2006*, Glasgow, UK, paper 028–109 on CD-Rom.

Billard Y., Bernard O., Lasne M., Schoefs F., 2007. Risk analysis and reliability of repaired concrete quays. In *Proceeding of 10th International Conference on Applications of Statistics and Probability in Civil Engineering*, 2007, Tokyo, paper on CD-Rom, 8 p.

Crouigneau S., Bourdon L., Billard Y., Person J.L., Schoefs F. Risk analysis to support operation and maintenance of an ageing dock-gate for the Port of Marseille Authority. 1st International Conference on Construction Heritage in Coastal and Marine Environments (MEDACHS'08), 28–30 January 2008, Lisbon, Portugal.

Desceliers C., Soize C., Ghanem R., 2007. Identification of chaos representations of elastic properties of random media using experimental vibration tests. *Computational Mechanics* 39 (6): 831–838.

Ghanem R., Spanos P., 2003. *Stochastic finite elements: a spectral approach*, revised edition. New York: Dover.

Schoefs F., Yáñez-Godoy H., Nouy A., 2007. Identification of random material properties from monitoring of structures using stochastic chaos. In *Proceedings of the 10th International Conference on Applications of Statistics and Probability in Civil Engineering (ICASP10)*, 31 July–3 August, 2007, Tokyo, Japan, paper on CD-Rom, 8 p.

Verdure L., Schoefs F., Casari P., Yáñez-Godoy H., 2005. Uncertainty updating of an on-pile wharf after monitoring. In: *Proceedings of the 9th International Conference on Structural Safety and Reliability (ICOSSAR 2005)*, June, 2005, Rome, Italy, pp. 1347–1354.

Yáñez-Godoy H., Schoefs F., Casari P., 2008a. Statistical Analysis of the Effects of Building Conditions on the Initial Loadings of On-piles Quays. *Journal Structural Health Monitoring* (in press).

Yáñez-Godoy H., Schoefs F., Nouy A., 2008b. Overall “soil-sod-anchoring plate” stiffness identification of a monitored pile-supported wharf by a polynomial chaos representation. *Journal Structural Safety* (submitted to Journal in August 2007).

*Life-cycle cost of structures and infrastructures*

# Maintenance—LCC analysis based on real data

Carolin Bahr & Kunibert Lennerts

*Institute for Technology and Management in Construction (TMB),  
Department for Facility Management, University of Karlsruhe (TH), Germany*

**ABSTRACT:** While architects and planners can refer to various tools for the planning and calculation of construction costs, calculation methods for operational costs are scarce and not very accurate. Maintenance costs account for 25%–30% percent of the complete operational costs and are therefore an important factor. The BEWIS (Optimized upkeep strategies to maintain value of buildings) project uses real data to analyze the maintenance costs of 18 buildings over their complete life cycle. The analysis shows that existing calculation methods only deliver very inaccurate results for maintenance budgets and cannot satisfy real-life requirements.

## 1 INTRODUCTION

### 1.1 *Maintenance costs as part of LCC*

At the beginning of the 21th century, researchers as well as real estate companies center their attention on the holistic cost analysis for complete building life cycles. The forecasting and estimation of life cycle costs will be more and more important in the future (Riegel, 2004). International and European attempts to reach a common definition of terms like Life Cycle Costs (LCC) and Whole Life Costs (WLC) (ISO, 2000) demonstrate how important this topic is. Operational costs and therefore also maintenance costs are part of the life cycle costs of a building. While architects and planners can refer to various tools for the planning and calculation of construction costs, calculation methods for operational costs are scarce and not very accurate (Institut für Bauforschung e.V., 2001). A number of scientific publications (Pelzeter, 2006), (Riegel, 2004), (Naber, 2002) focus on this topic. Generally, these papers are, however, at a very early stage. Besides infrastructural services, maintenance costs build the biggest part of operational costs for industrial buildings, accounting for 25%–30% of the latter (Helbling, 2000). They are hence an important part of operational costs. To date, maintenance is unfortunately often not taken into account.

### 1.2 *Real estate—A special case*

Unlike short-lived consumer goods, buildings are used over decades. Exact cost forecasts are therefore difficult. Due to the complexity and interdependencies of the parameters involved, the calculation of maintenance costs for buildings deserves special attention.

Maintenance costs are defined by building-dependent parameters as well as kind of use and location. Other factors, e.g. political influences play an important part as well. To date, maintenance cost cannot be forecast reliably. Science urgently needs to develop reliable means to quantify maintenance costs and define the main cost-influencing parameters. To this end, the department of Facility Management of Karlsruhe University (FH) started the BEWIS (Optimized upkeep strategies to maintain value of buildings) project.

## 2 THE BEWIS PROJECT

### 2.1 *Project scope*

The BEWIS project analyzed the maintenance measures carried out to 18 buildings with typical histories and comprehensive data records. The portfolio comprises office and administrative buildings as well as school facilities. The analyzed buildings encompass over 160,000 m<sup>2</sup> gross floor area at a replacement value of 186.6 million Euros. Altogether, over 23,900 maintenance measures were carried out. For 2004, the year the study refers to, this corresponds to overall maintenance costs of 1.76 billion Euros.

### 2.2 *Methodology*

The analysis of the examples gives an insight into classical maintenance histories. For each building, all maintenance measures carried out over the complete building lifecycle were described and their cost quantified. Data collection alone took approximately 18 months.

Each single measure from the construction year to the year of documentation (2004) was registered.

The data stems mainly from archived single documents provided by cities and communities, partly also from community budgets, consisting of operating and financial investment budgets. Depending on the kind, age and size of a building, between 700 and 2,500 datasets per building were collected. Each dataset represents one maintenance or modernization measure. The database comprises over 29,000 datasets and gives detailed information on when which kind of measure was carried out to which building component and why. The costs of each measure as well as a detailed description are provided as well.

Additionally, the location and construction costs of all buildings were registered. A thorough evaluation of the building structure was done for each building in order to evaluate the effect of measures carried out in the past. Based on this information, the maintenance backlog in Euros was calculated. To enable cross-year comparisons, costs were consistently referred to the 2004 construction price index.

The registered data can be evaluated regarding the following factors:

- Cost development over the complete lifecycle
- Amount per single measure
- Most common measures
- Specific costs per different age periods
- Typical reasons for a measure
- Cost-intensive building parts
- Relation between age and price of a measure
- Relation of recurring and one-time measures
- Time and cost of costly one-time measures, e.g. roof reconstruction
- Current maintenance backlog of a building
- Construction costs of a building

### 3 EVALUATION

#### 3.1 Maintenance costs in relation to age

The expected useful life of a building varies between 20 and 80 years. The following figure shows the maintenance costs for the buildings analyzed for the BEWIS project over 55 years.

The analysis shows that the maintenance requirements of a building vary over its lifecycle. Age considerably influences the maintenance costs of a building.

Therefore, maintenance budgets need to take into account the differing maintenance requirements of buildings of different ages.

#### 3.2 Budgeting methods validation

Today, there are no well-founded and realistic methods for the calculation of maintenance budgets. This causes problems for maintenance experts, who—year

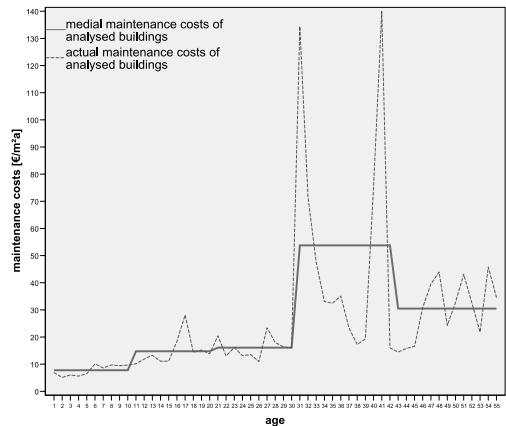


Figure 1. Maintenance costs of analyzed buildings.

after year—face the challenge of budgeting the maintenance expenditures for their building portfolio. As they lack real knowledge of the maintenance requirements as well as the cost-influencing factors, many experts refer to last year's values or other key figures. This leads to very imprecise calculations. The following graphic shows the key figures of several maintenance institutions.

The graphic shows that the key figures cover a wide range and show great deviations from the real costs. High cost differences are due partly to the fact that a number of cost-relevant parameters were weighted differently or neglected. The building age, e.g. was only taken into account by the second regulation on calculation (II. BV) as can be seen from the peaking costs in year 22 and 32 (figure 2).

Real data from the BEWIS project is used to contrast the maintenance costs calculated via key figures with the actual maintenance expenditures for the analyzed buildings.

The graphic shows that the average annual maintenance costs (red solid line) considerably deviate from the values calculated using key figures. While the key figure values show a static curve (apart from the second regulation on calculation), the actual costs vary with the building age. This means that the real costs were dynamic.

In order to compare the key figures with the real values from the examples, five age blocks of 10 years each were built:

The key figure values show differing deviations from the real costs for the different periods of life. For clarity, the deviations between the key figures and the real costs are displayed graphically in figure 4.

It can be seen that, except for the figures from the second regulation on calculation (II. BV), all key

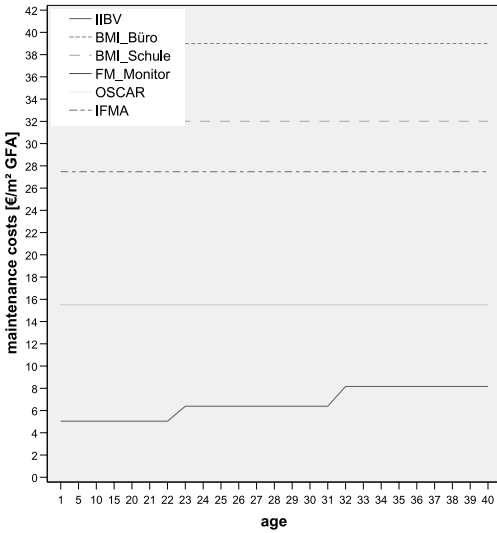


Figure 2. Maintenance key figures of different institutions.

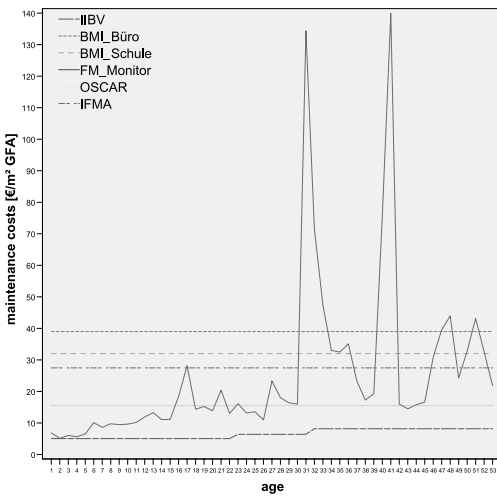


Figure 3. Comparison with actual maintenance costs.

figures are above the real costs for the first and second period of life. This changes during period three and especially four. Here, the calculated values are clearly below the real costs. As maintenance experts in general do not know when maintenance activities will be required, most of them do not reserve extra savings for future maintenance activities. The question then is if these requirements can be covered by the money saved. The following graphic shows the cumulated deviations between key figures and real maintenance expenditures. All values are indexed to

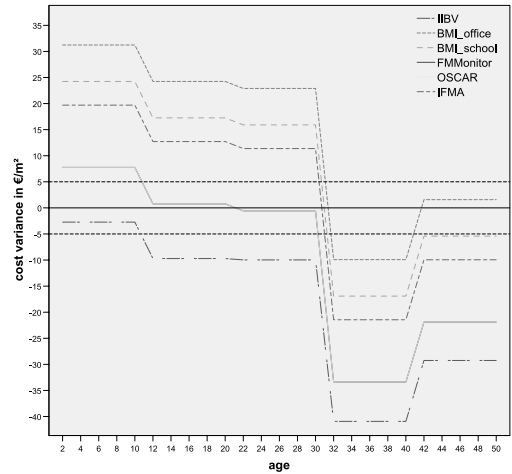


Figure 4. Cost deviations.

Table 1. Average maintenance costs.

	II. BV	BMI office	BMI school	FM Monitor	OSCAR	IFMA	Real costs
1. Period of life	5,0	39,0	32,0	15,5	15,5	27,5	7,8
2. Period of life	5,0	39,0	32,0	15,5	15,5	27,5	14,8
3. Period of life	6,1	39,0	32,0	15,5	15,5	27,5	16,1
4. Period of life	8,0	39,0	32,0	15,5	15,5	27,5	48,9
5. Period of life	8,2	39,0	32,0	15,5	15,5	27,5	37,4
Total	6,6	39,0	32,0	15,5	15,5	27,5	25,4

the year 2004 according to the construction price index from the German Federal Statistics Office.

The analysis shows that the figures from IFMA (IFMA, 2005) and BMI (BMI, 2005) were clearly too high for the first 30 years. Even though the financial resources were partly consumed by maintenance activities after that period, not all the money had been used after 50 years. The buildings' owners could have made better use of the excess money elsewhere. The figures from FM Monitor (FM Monitor, 2003) and the OSCAR Report (OSCAR, 2006) were only slightly too high for the first 30 years. The money saved during this period cannot cover the maintenance measures required during the following 20 years, causing a maintenance backlog. The figures from the second regulation on calculation (II. BV, 2003) are below the real costs as of year 1, causing an enormous maintenance backlog over the years.

Obviously these key figures are not suitable for the calculation of maintenance budgets.

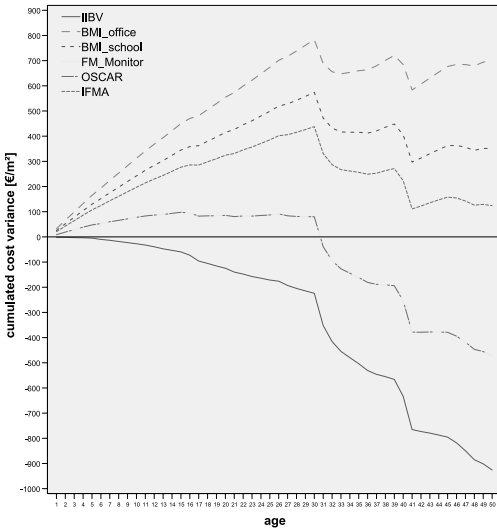


Figure 5. Cumulated cost deviations.

#### 4 CONCLUSIONS

Scientific and real-life scenarios lack well-suited calculation methods for maintenance costs. This causes severe problems especially for maintenance experts, as they do not know which means to refer to when calculating their maintenance budgets. Every year, they face the challenge of preparing the maintenance budget for their building portfolios. As they lack sound knowledge of the real maintenance requirements or the cost-relevant factors, most of them refer to last year's figures. The research presented in this paper shows, however, that a budget based on last year's figures is very imprecise and cannot satisfy real-life requirements.

Using the real data from the BEWIS project, cost-defining parameters can be identified and evaluated.

Based on these findings, a scientifically founded budgeting method shall be developed.

#### REFERENCES

- BMI, 2005: Building Maintenance Information: *Review of Maintenance Costs*. Serial 341 BMI Special Report—May 2005, RICS, London.
- FM Monitor, 2003: *Der Schweizer Facility Management-Markt im Überblick*, pom + Consulting AG, Zürich.
- Helbling Management Consulting, Studie, 2000: "*Facility Management in der Immobilienwirtschaft*", Zürich.
- IFMA, 2005: *IFMA Benchmarking Report*, Herausgegeben von der IFMA Deutschland e.V., Karlsfeld b. München.
- Institut für Bauforschung e.V. 2001: *Bauunterhaltungskosten beanspruchter Bauteile in Abhängigkeit von Baustoffen und Baukonstruktionen*; Forschungsbericht, Hannover, International Standard ISO 15686-1 2000: *Buildings and constructed assets- Service life planning—Part 1–9: General principles*, ISO copyright office, Genf, Schweiz.
- II. BV, 2003: *Verordnung über wohnungswirtschaftliche Berechnungen nach dem zweiten Wohnungsbaugesetz: II. Berechnungsverordnung*. Stand: Neugefasst durch Bek. Vom 12.10.1990, 2178; zuletzt geändert durch Art. 3V v. 25.11.2003.
- Naber, S. 2002: *Planung unter Berücksichtigung der Baunutzungskosten als Aufgabe des Architekten im Feld des Facility Management*, Peter Lang GmbH, Europäischer Verlag der Wissenschaften, Frankfurt.
- OSCAR, 2006: *Büroebenenkostenanalyse, Office Service Charge Analysis Report*, Jones Lang Lasalle GmbH, 2006.
- Pelzeter, A. 2006: *Lebenszykluskosten von Immobilien*. Herausgegeben von Prof. Dr. Karl-Werner Schulte und Prof. Dr. Stephan Bone-Winkel. In: *Schriften zur Immobilienökonomie*, Verlag Rudolf Müller, Köln.
- Riegel, G. 2004: *Ein softwaregestütztes Berechnungsverfahren zur Prognose und Beurteilung der Nutzungskosten von Bürogebäuden*. Dissertation des Fachbereich Bauingenieurwesen und Geodäsie der Technischen Universität Darmstadt.

# A new efficient methodology for large scale outsourcing of maintenance

J. Bakker, P. Boersma & J. Volwerk

*Civil Engineering Division, Ministry of Transport, Public Works & Water Management, Utrecht, The Netherlands*

**ABSTRACT:** This paper describes a new approach for large scale outsourcing of maintenance. The new approach delivers considerable efficiency gains for road operators. A reduction in costs of contract preparation and management in the order of 80% of the costs of a traditional approach can be achieved. Time needed to prepare a maintenance contract is considerably shortened. In addition the method minimizes traffic disruption. The new approach was developed in a project named “KOSMOS”. The aim of this project was to deal with a maintenance backlog on 1200 structures (mainly bridges) in a period of two and a half years, where in a traditional approach the time between the decision to repair a bridge and the start of the works would typically be two years.

The key elements of KOSMOS concept are:

- Early and intense involvement of possible contractors in contract intake;
- Functional demand specification as basis for contract;
- Competitive dialogue between individual contractors and the Client
- Tender award on the basis of the Economically Most Advantageous Tender (EMAT)
- System Based Contract Management (SBCM);
- Quality control carried out by the contractor;
- A Technical Inspection Service reports to both contractor and Client on the risk management and the quality of work execution.

The new KOSMOS-concept has so far enabled Rijkswaterstaat to outsource large scale maintenance on schedule. Traffic disruption has been considerably reduced compared to traditional approaches. Contractors are encouraged to develop innovative maintenance solutions with a low Life Cycle Cost and minimal traffic disruption.

## 1 INTRODUCTION

### 1.1 *General*

Rijkswaterstaat is responsible for the construction and management of the state infrastructure in The Netherlands. Since 2006 Rijkswaterstaat operates as a government agency. By means of a Service Level Agreement (SLA), Rijkswaterstaat and the ministry of Transport, Public Works and Water Management have agreed on a required quality level and availability for the state infrastructure against a fixed yearly budget for a period of four years.

However, in order to meet this fixed quality level an initial maintenance backlog had to be dealt with. Rijkswaterstaat was given a two-year period to do so, providing that traffic disruption would be minimized and that utilization of contractors was maximized. A maintenance backlog was defined for 1200 structures in total, varying from simple repair of guardrails to the strengthening or replacement of whole bridge decks.

The total budget for this backlog was roughly four hundred million Euros.

As the demand to deal with this backlog in such a short period emerged, it became obvious that a traditional approach would not suffice. The time to prepare for maintenance on a typical bridge varies between half a year to two years. Furthermore the resources needed to prepare and manage maintenance work are usually relatively high compared to building a new construction. The manpower needed to manage this extra workload on top of the normal work wasn't available by far. The problem was exacerbated by a recent restructuring within Rijkswaterstaat which reduced the number of personnel by approximately 20%.

### 1.2 *The approach*

A project team, by the name of “KOSMOS”, set out to tackle this complex task. “KOSMOS” is a Dutch alliteration for “Civil structure Maintenance

in Cooperation with Contracting parties by way of System Based Contract Management”. This name represents the ambition and intentions of Rijkswaterstaat: To realize the goals in full cooperation with contracting parties. These intentions were substantiated by inviting contracting parties to a series of “Public-Private Debates” on the conditions for cooperation. The earliest possible participation of contracting parties, and full transparency towards them, were important conditions indicated by the industry. The commission would need to be sufficiently flexible in terms of solutions and operations, leaving a more explicit responsibility for the end result with the contractor. Besides this, the opportunities for small and medium sized contractors to participate were to be ensured. It was clear at this stage KOSMOS would not only be challenging for the Client. In the years preceding KOSMOS the demand on contractors had sharply increased and order books were strained. Within six months a completely new concept for large scale commissioning of maintenance was developed by KOSMOS. This article describes this concept step by step.

## 2 THE “KOSMOS” CONCEPT

### 2.1 General

The following paragraphs incrementally describe the KOSMOS concept (Fig. 1). For each step the principle is addressed first, followed by a description of the way it was applied or executed in KOSMOS.

### 2.2 Pre-contractual preparation

The pre-contractual preparation focuses on determining the scope of the commission and the (pre-) selection of tenderers.

#### 2.2.1 Scope determination

*Principle:* Preceding the involvement of tenderers the general scope is determined by deciding the objects (civil structures) that will be subject of the commission. At this stage the scope gives no indication of the technical content.

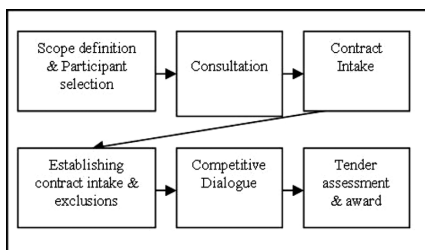


Figure 1. Steps in the procurement concept.

*Application in KOSMOS:* In KOSMOS the scope was determined by performing a “quick scan” on all objects (app. 5000 structures) managed by Rijkswaterstaat. This entailed a global visual inspection with the sole purpose of detecting a backlog in relation to described Basic Level of Maintenance. The emerging list of objects was completed with ‘known’ problem cases, caused by the fact that not all maintenance backlog is visually detectable. Subsequently the list of approximately 1200 objects was divided into 9 geographically and functionally consistent ‘work parcels’.

#### 2.2.2 (Pre-) selection of tenderers

*Principle:* The procurement of these ‘work parcels’ is publicly announced and tenderers are invited to contend. A selection of 4 contenders is determined on the basis of fulfilling tender requirements. From here on in contenders are referred to as ‘participants’.

*Application in KOSMOS:* In KOSMOS a low threshold to contend was deliberately set, in order to maximize the quantity of contractors available to contend. Also contractor combinations were admitted, in order to give small and medium sized contractors ample opportunity. This, however, induced that a lottery (for lack of a better procedure) had to be used, besides tender requirements, in order to determine 4 participants.

### 2.3 Consultation phase and contract intake

This phase focuses on the Client and participants jointly determining the ‘problems’ that are to be solved by maintenance.

#### 2.3.1 Consultation phase

*Principle:* The consultation phase is started up with all 4 participants combined. The purpose of this phase is to jointly determine which data needs to be gathered by way of contract survey, in order to realize a reasonable level of demand specification and suitability for pricing the commission. This phase requires the utmost sincerity of the Client.

*Application in KOSMOS:* The “quick scan” results and all additional object information known within KOSMOS were made available to the participants. In addition to this a (third) party is provided by the Client to perform the contract intake. Jointly the assignment for the contract intake (CI) party was defined. The assignment varied per object, ranging from desk-top analysis of maintenance history only, to a detailed site inspection.

#### 2.3.2 The contract intake

*Principle:* A contract intake entails the determination of “problems” with regard to the required functional



or technical state carried out by or on behalf of the participants. The description of problems should not introduce limitations in the contractor's responsibility to provide solutions. On the other hand the description of problems should enable a tenderer to assess the risks within reason in order to determine a competitive bid.

*Application in KOSMOS:* The required functional and technical state was defined by an "Analysis framework for inspection". This framework describes or refers to the requirements in terms of RAMS (RAMS = Reliability, Availability, Maintainability & Safety [CENELEC 1999]). The contract intake findings emerged not only from site inspections. Desk-top analysis also led to discoveries of functional shortcomings unrelated to physical defects. Also an unreliable mechanical installation, indicated by unacceptable failure rate, could be defined as a "problem". Due to the amount of maintenance it was, in many cases, unnecessary to assess detailed data such as the thickness of asphalt on a viaduct. A contractor can estimate on the basis of experience, knowing that he will lose and gain per location. As soon as a problem was sufficiently assessed it was labelled an "X-category problem", which meant that the problem description was, to the satisfaction of the Client and participants, fit for a 'fixed price' bid. If problems couldn't be defined on the basis of 'expert-judgement' and would require more research in order to determine the cause, resulting in unacceptable financial (bidding) risks, they were labelled a "Y-category problem". The results of additional research would change the status of a problem from 'Y' to 'X', however due to the given time schedule for procurement this wasn't realized in all cases. KOSMOS intended merely to resolve problems which constituted a maintenance backlog or would result in one within 2 years. Despite this, all foreseen problems for a 2–7 year period were inventoried along with a proposal to exclude the problem from the commission. The actual decision to in- or exclude a problem was made by Rijkswaterstaat. The contract intake was executed by a third party in command of the participants. They were given full opportunity to attend the complete intake. Some participants did just that, others limited themselves to the 'high risk' objects or problems.

## 2.4 Establishing the contract intake

*Principle:* In this phase the Client and participants establish whether the described problems are sufficiently clear and explicit for bidding. By way of formal statement by each participant the contract intake is established. Subsequently the Client determines the exclusion of problems from the commission.

*Application in KOSMOS:* After the joint intake each participant evaluated the contract intake. During

this phase ample discussion was conducted regarding X- or Y-category labelling of problems. The outcome of this discussion is significant because it determines the allocation of risks to the Client or participants. Some participants tried to evade risks altogether. For the Client it was paramount not to be drawn into details as every deviation will lead to additional work or contract alterations and the administrative burden that entails. It proved difficult for the 'contract intake parties' to actually describe the problem, instead of the 'visual symptoms' or 'defects' resulting from a problem. For Rijkswaterstaat it was of the utmost importance that the problem (the cause) should be addressed and not just 'the damage'. The determination of problems to be in- or excluded was based on:

- estimated costs for resolving the problem;
- the 'road unavailability' caused by addressing the problem;
- risks induced by not addressing the problem;
- efficiency: some maintenance works should always be combined for reasons of efficiency.

## 2.5 The tender period

The Tender period focuses on the realisation of bids. In this phase the opportunity is provided for participants to ask questions regarding the contract (terms, conditions and formulation) and for the Client to respond with an information notice. In addition, a procedure of 'competitive dialogue' enables the Client to come to specific terms with each individual participant regarding the spreading of (execution) risks between the Client and that tenderer. The tender period leads to the submission of an offer by each participant, in which a price is bid for solving each of the established problems included in the commission. In addition to the documents required for a valid bid, the submission contains information to evaluate quality aspects.

### 2.5.1 The competitive dialogue

*Principle:* A competitive dialogue [European Parliament, 2004] is intended to reach consensus over the allocation responsibility for risks (during realisation) between the Client and the tenderer. In addition a tenderer may propose innovative solutions in a private setting.

*Application in KOSMOS:* During the competitive dialogue tenders could submit proposals to take over risks regarding Y-category problems. For each Y-category problem several maintenance scenarios were given with an estimated chance of occurrence. This chance multiplied with the estimated costs for commissioning this scenario results in an 'estimated

value' of that individual scenario and subsequently in an 'estimated value' of the problem as a whole. Effectively the price Rijkswaterstaat is willing to pay to transfer the risks to a tenderer. If a tenderer is unwilling to take over such a problem the estimated value is added to his bid, but the risks remains with the Client. In many cases the tenderer opted to take over the risk once he determined that his calculation of the 'estimated value' was lower than the estimated value determined by Rijkswaterstaat. During the competitive dialogue a consensus was reached with each individual tender on the risk annexation of one or more maintenance scenarios or a Y-category problem as a whole for a fixed price. Alternatively a tender could propose the annexation of a problem in alliance with Rijkswaterstaat. In such a case a consensus was reached on a fixed price for a problem agreeing to share the deficit or surplus of actual execution costs, on the basis of a fixed risk bearing percentage, between the Client and the contractor.

### 2.5.2 The tender

*Principle:* In the tender a contractor bids to solve the X-category problems established during the contract intake and included in the commission with a minimum warranty for the solution and the option to offer an extended warranty. On top of this it must be guaranteed that the solution or execution doesn't invoke new or other problems. In addition an 'estimated value' for Y-category problems is offered according to the consensus reached in the competitive dialogue. The tender also includes an offer for the extent of interference in road availability. Besides the bid a separate submission is made containing his plan for Quality Control. The price offered, the length of warranty (LCC surplus value), the Y-category problems taken over, the interference in road availability (a budget for road unavailability) and plan for quality control together constitute the basis for assessment.

*Application in KOSMOS:* A database application was used during the contract intake to register and establish all problems to be commissioned. This database was converted into a bid registration tool for each tenderer. A bid was made for the solution of each problem with a 7 year warranty. If an extended warranty was registered by the tenderer, the database application would calculate and show the estimated result for future cost reductions for the Client [Bakker & Volwerk, 2007]. The same application would calculate and show the 'estimated value' of costs for the Client regarding the solution of Y-category problems. Finally the database application was used to calculate and show the capitalized interference of road availability. Constituting a fixed budget for 'traffic disruption'. This budget is computed on the basis of the hours of 'road unavailability' estimated by

the tenderer. 'Traffic disruption' is defined by the work hours resulting in 'road unavailability' outside timeslots of 'permissible road unavailability' predetermined by the Client. Maintenance executed in timeslots of 'permissible road unavailability' (generally night time and weekends) is presumed not to cause disruption of traffic. As such the risk during these timeslots is born by the Client. Maintenance, involving temporary lane closures or speed restrictions, executed outside these timeslots is presumed to cause major traffic congestion or disruption. Each estimated hour of lane closure outside the permitted timeslots was valued at €15.000,-. Similarly each hour of set speed restrictions was valued at €3.500,-. The total of capitalized interference of road availability constitutes the budget for 'traffic disruption'. In a separate envelope the tenderer submitted a plan for quality control and plan of execution for maintenance on an "example viaduct".

### 2.6 Tender assessment and award of contract

*Principle:* The assessment of submitted tenders consists of establishing whether the tender meets the formal tender requirements and the assessment of the quality and value aspects. The score given to the plan of quality control, the price and 'estimated values' bid for the solution of problems, the surplus value of extended warranties, the budget for 'traffic disruption' are all added up and a "nominal price" is computed. The tenderer submitting the lowest "nominal price" is awarded the contract.

*Application in KOSMOS:* After the Client received the tenders and established their validity, the assessment of the plan of quality control executed by two separate 'assessment teams'. Each team ranked the submitted plans by mutual comparison. The results of each team were merged and the final ranking was determined. The final ranking was processed by nominally in- or decreasing the bid price on the basis of a percentage of the median of the tenders. The resulting total was decreased by subtracting the LCC (Life Cycle Costs) surplus value due to extended warranties. This resulting total was increased by adding the 'estimated value' for all Y-category problems as taken over and determined by the tenderer or as left with and determined by the Client. Finally the calculated budget for 'traffic disruption' is added.

The grand total for the 'nominal price' is made up of: (Price) +/- (value of quality) - (LCC value) + (estimated value Y-problems) + (budget traffic disruption).

### 2.7 Engineering and execution

*Principle:* After the contract is awarded the contractor will start engineering the solutions in accordance

with the principles of Systems Engineering [ISO/IEC 2002]. As an integral part of the systems engineering process the contractor is obliged to verify whether the considered solution meets all the commissioned (functional) requirements and local interfacial derivative requirements. Subsequently the contractor validates that the considered solution will actually solve the problem indicated in the commission. The contractor bears sole responsibility for risk and quality management on all processes initiated in the execution of contract, including surveying, audits and tests. The Client keeps in touch with the quality delivered by the contractor by performing System Based Contract Management (SBCM) surveys. SBCM entails a combination of surveys on the contractor's quality control system, procedures and resulting products on the basis of risk analysis repeatedly performed. Both the contractor and the Client are informed of findings with regards to the quality of work execution as well as risks identified in the surveys performed by an independent third party. The limitation of 'traffic disruption' was further encouraged by a system premiums and penalties.

*Application in KOSMOS:* Immediately after a contract was awarded the contractor proceeded to derive the set of requirements regarding engineering. In some cases requirements were indicated for specific problems. More often requirements comprised standards and guidance notes generically applied to the project as a whole. The interfacial requirements often had to be developed or determined by the contractor. His responsibility exceeded working in accordance with prevailing standards and guidance notes. He was obliged to guarantee solving the problem as a whole. Part of the engineering involved producing a plan for traffic management. This plan had to be agreed with the principal traffic manager. This plan played a crucial part in contract management as heavy penalties (€100.000, -) were imposed if deadlines were exceeded. An incentive was incorporated in the contract to encourage the contractor to reduce traffic disruption pivoting round the agreed budget for 'traffic disruption'. If the contractor actually realized less 'road unavailability' then 80% of the remaining budget was awarded to him. If however the budget was exceeded a 120% penalty was imposed. The contractor conducted his own quality control and risk management. A third party, called the "Technical Inspection Service" (TIS) was hired by the Client to perform independent surveys and report the findings on the quality of work execution and emerging risks to both the Client and the contractor. The Client performed a limited amount of system orientated surveys on the execution of work by the TIS as well as the contractor (Fig. 2). Payments were made on the basis of a notice of execution by the contractor, a judgement on the delivered quality by the TIS and the results of our own SBCM surveys.

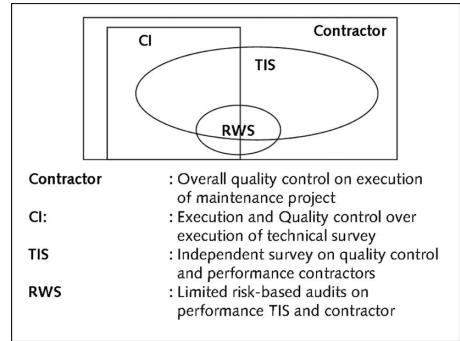


Figure 2. Scope of the quality control by all involved participants.

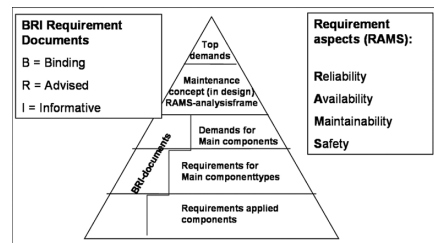


Figure 3. Structure of demand requirements.

### 3 THE CONTRACT STRUCTURE

For KOSMOS a particular and exceptional structure of documents was used to clarify the contract. All contracts consisted of the following elements:

- Descriptive documents for each phase in the tender;
- The main contract
- Demand specification 1: "Product Requirements"
- Demand specification 2: "Process Requirements"
- The "Tender registration tool" database application and guides;
- Object library (digital) including all available object data;
- Supporting documents for specific subjects (varying in content)

This set of contract documents was used as the standard for all 9 'work parcels'. This was applicable despite the broad variety in roughly 5000 problems for over 1200 objects varying in function, setting and local utilization. For a large part this was due to the structure of demand requirements implemented in specification 1 (Fig 3). A set of 'top demands' describe the general overall requirements for infrastructural assets managed by Rijkswaterstaat. These requirements are translated to 'aspect requirements' in terms of RAMS,

which were also used during the contract intake. In some cases these were specified more explicitly for specific elements in a civil structure or even potential solutions, depending on the risks involved. Adjacent to this structure of requirements a set of informative or binding standards and guides was incorporated in the contract.

#### 4 THE KOSMOS RESULT

The first couple of KOSMOS 'work pack contracts' are nearing completion as this article is written. The others are being executed. The KOSMOS concept has been fully applied resulting in the execution of a large amount of maintenance being finished reasonably within time, despite an extremely short run time and very limited Client staff capacity. Also the goals for minimal traffic disruption are amply met. It appears that most of the maintenance can be done in provided timeslots. The goals regarding cooperation and maximum utilization of contracting parties have been achieved to the satisfaction of both Client and contractors. Contractors were encouraged to come up with clever and innovative solutions for work execution and minimizing traffic disruption. Responsibilities have been transferred, taken over and born by contractors to a far greater extent, due to the fact he was involved in the definition of the commission and the engineering and execution of the work. He has been made responsible not only for execution of maintenance, but also the effect of it: solving the problem.

There are also many lessons to be learned from KOSMOS. The sheer amount of innovative elements (content, procedure and process) implemented for both parties has prevented the concept to live up to its full potential. A clear sign of maturing is detectable. Although the effectiveness of successive contracts is on the increase the potential of the KOSMOS concept has not been fully exploited. An evaluation has already been set up as a joint undertaking to clarify learning points.

#### 5 CONCLUSIONS

The KOSMOS concept constitutes a new and innovative approach for large scale outsourcing of maintenance. The described concept enables a Client to

carry out maintenance with a considerable reduction in the amount of personnel required compared to a traditional approach. By involving contractors earlier and more intensively before the tender period a significant reduction in preparation time is realized as a broader responsibility is taken by contractors. Awarding the contract on the basis of the Economically Most Advantageous Tender (EMAT) instead of lowest price encourages a tenderer to compete in quality as well as price. An Engineer and Construct commission, in which the demand is specified in terms of problems to be solved, leaves more room for innovative solutions while simultaneously transferring a broader responsibility towards the contractor. Incorporating incentives to reduce traffic disruption both in EMAT assessment as well as the adoption of a system of premium and penalty proved an effective to encourage the contractor to keep traffic disruption to a minimum.

#### REFERENCES

- CENELEC, Comité Européen de Normalisation Electro-technique. 1999. *EN 50126 Railway applications—The specification and demonstration of Reliability, Availability, Maintainability and Safety (RAMS)*. Brussels: CENELEC.
- European Parliament, Council Directive. 2004. EU directive 2004/18/EC of the European Parliament and of the Council of 31 March 2004 on the coordination of procedures for the award of public works contracts, public supply contracts and public service contracts, procedure COD (2000) 0275. Brussels.
- Bakker, J. & Volwerk, J. 2007. *Life Cycle Cost tenders for infrastructure projects* proceedings 5th International Workshop on Life Cycle Cost Analysis and Design of Civil Infrastructure Systems (LCC5), Seoul, Korea: Balkema.
- Mousset, P. & Vis, K. 2008. *Stimulation of innovations with the right procurement strategy*. Third International Conference of the CRC for Construction Innovation; Gold Coast, Queensland Australia.
- ISO/IEC 2002. *ISO/IEC 15288 Systems engineering—System Life cycle processes -first edition* Ref nr. ISO/IEC 15288:2002 Geneva Switzerland: ISO Copyright Office.

# Life cycle cost evaluation of the as-built cover layer in reinforced concrete bridge decks

C.L. Barnes & J.-F. Trottier

*Dalhousie University, Halifax, Nova Scotia, Canada*

**ABSTRACT:** The thickness and bulk chloride diffusivity of the protective cover layer provided in reinforced concrete bridge decks are the two most important design parameters affecting the corrosion induced maintenance requirements over the service life of the structure. Cover thickness requirements are usually dictated by environmental exposure conditions according to a particular design code, while the chloride diffusivity of the concrete material has tended to be indirectly specified through the rapid chloride permeability test. A more logical approach for deck design would instead consider local conditions including specified cover thickness, annual temperature variations, chloride application rates and typical surface chloride concentrations to determine an appropriate bulk diffusion coefficient to achieve the desired design life. The following paper presents an analytical approach to predicting maintenance requirements during the service life of a deck using ground penetrating radar measurements of the as-built cover thickness with bulk chloride diffusion testing of core samples from the deck. The analysis uses a finite difference model to evaluate the effects of time and temperature dependant changes in the chloride diffusivity over the as-built spatial distribution of cover on predicted optimal repair times. The present value of future repair costs are evaluated against a theoretically optimal repair schedule for an actual structure in order to suggest an appropriate bonus or penalty to the contractor for the construction quality.

## 1 INTRODUCTION

Durability considerations in the design of exposed reinforced concrete bridge decks have typically been addressed by specifying cover thickness and compressive strength from a structural viewpoint. Damage caused by chloride-induced corrosion of the reinforcement may be the most prevalent and costly of all the possible deterioration processes affecting reinforced concrete structures in northern climates where de-icing salts are used regularly. Designers tend to specify standard concrete mixtures that can provide a wide range of protection against chloride ion ingress, despite quality assurance testing on these materials employing such tests as the compressive strength and Rapid Chloride Permeability (RCP) as performance indices. RCP testing has been generally correlated to the capacity of the concrete to resist chloride ingress and tends to encompass a wide range of resistance within the range of acceptable indices. RCP does not provide sufficient information to model the rate of chloride ingress over time or to determine the expected corrosion initiation time.

The interaction between cover thickness and diffusive properties of the concrete dictate when sufficient chloride ion will reach the reinforcing bar to initiate active corrosion in the deck and should demand a

much greater focus on their measurement for improved quality assurance of new construction. Current quality control practice for cover thickness tends to consist of measuring the difference in a few locations across the deck between the top of the reinforcing bar and the top of the deck formwork prior to placing the concrete. Very few agencies require post-construction measurements of the as-built cover thickness to verify the cover layer thickness provided.

This paper presents a hybrid analysis of new deck construction using finite difference modeling of water soluble chloride ion diffusion in concrete with Ground Penetrating Radar (GPR) survey analyses of the decks to predict when reinforcement corrosion and cracking occur over the range of actual cover thickness provided across the entire surface of each deck. The present value cost difference between the predicted first repair and the design service life value can be used as the basis of a pay adjustment in an end-result performance specification construction contract.

## 2 CHLORIDE DIFFUSION IN CONCRETE

The ability of Portland cement concrete to resist chloride ion ingress generally results from the porosity of the cementitious matrix surrounding the relatively

less permeable aggregates. Chloride ions will migrate through moisture contained within interconnected pore spaces throughout the matrix as a change in concentration over time through a diffusive process governed by Fick's second law (Fick, 1855) as shown in Equation 1.

$$\frac{\partial \phi}{\partial t} = D \frac{\partial \phi^2}{\partial x^2} \quad (1)$$

The average rate of diffusive movement of chloride through the bulk of the concrete, including cementitious matrix, air-voids, and aggregates, can be described using the bulk diffusion coefficient,  $D$ . The resistance to chloride ion ingress, which depends largely on the porosity being affected by aggregate gradation, cementitious material and water content, and maturity, can be highly affected by mixture design, proportioning and construction modifications. The diffusivity coefficient has been shown to be variable over temperature and time (Thomas & Bamforth, 1999), according to Equation 2, implying that annually cyclic seasonal temperature variations will have an effect on the rate of chloride ingress.

$$D(t, T) = D_{ref} \left( \frac{t_{ref}}{t} \right)^m \cdot \exp \left[ \frac{U}{R} \cdot \left( \frac{1}{T_{ref}} - \frac{1}{T} \right) \right] \quad (2)$$

where  $D(t, T)$  = diffusion coefficient at time,  $t$ , and temperature,  $T$ ;  $D_{ref}$  = diffusion coefficient at some reference time,  $t_{ref}$ , and temperature,  $T_{ref}$ ;  $m$  = a constant which depends upon mixture proportions and cementitious materials;  $U$  = activation energy of the cement in the diffusion process;  $R$  = universal gas constant; and  $T$  = absolute temperature.

The inclusion of fly ash or blast furnace slags with silica fume in the cementitious materials used in the concrete will have a very significant impact on how the diffusivity will change with time by changing the  $m$ -value (0.5 to 1.2) shown in Equation 2. The diffusivity of these concrete mixtures will decrease at higher rates over extended periods of time as these materials react with hydration by-products from the Portland cement and decrease the available pore space in the matrix (Neville & Brooks, 1987). Ordinary Portland cement (PC) or binary blends of Portland cement and silica fume only (PC/SF) tend to lesser rates of diffusivity development, exhibiting  $m$ -values between 0.1 and 0.3 (Thomas & Bamforth, 1999) (Boddy et al., 1999).

The diffusion coefficient of concrete can be estimated using a bulk diffusion test (ASTM 1556-04) by matching the experimental variation in chloride content versus depth to a theoretical solution of Fick's second law, using a finite difference model or an

approximate solution based on the error function, shown in Equation 3.

$$C(x, t) = C_0 \left[ 1 - \operatorname{erf} \left( \frac{x}{2\sqrt{Dt}} \right) \right] \quad (3)$$

where  $C(x, t)$  = concentration of chloride ion at a depth,  $x$ , and time,  $t$ ;  $C_0$  = surface concentration of chloride at  $x = 0$ ; and  $\operatorname{erf}$  = error function.

The error function approximation only provides a reasonable solution for the case where the diffusion coefficient remains constant over time. Finite difference methods are preferable when considering the time and temperature dependant diffusivity of concrete materials and can also incorporate models for evaluating acid-soluble chloride binding in the concrete and the time required for cracking to occur once corrosion has initiated. Neglecting the effects of chloride binding will provide a more conservative estimate of the corrosion initiation time for a given cover depth.

Bazant (1979a, b) provided a theoretical basis for predicting corrosion induced cracking in concrete, shown in Equations 4–6. The rate of rust production depends on the availability of oxygen (mainly to the cathodic region), the size of the anodic and cathodic regions of the corrosion area, relative to the cover thickness, and bar diameter. For concrete exposed to dry air and having a 40% water saturation, Bazant (1979b) provides a rate of rust production,  $j_r = 2.08 \times (10^{-8})$  g/m<sup>2</sup>/s for large scale corrosion.

$$t_{cor} = \rho_{cor} \left( \frac{D}{s} \right) \left( \frac{\Delta D}{j_r} \right) \quad (4)$$

$$\Delta D = 2f_t \frac{L}{D} \delta_{pp} \quad \text{where } L \leq (s - D)/2 \quad (5)$$

$$\Delta D = f_t \left( \frac{s}{D} - 1 \right) \delta_{pp} \quad \text{where } L > (s - D)/2 \quad (6)$$

where  $t_{cor}$  = time required to cause cracking in the concrete after corrosion has initiated;  $\rho_{cor}$  = density of corrosion product;  $D$  = bar diameter;  $s$  = bar spacing;  $j_r$  = rate of rust production per unit area of plane surface;  $f_t$  = tensile strength of the concrete;  $L$  = cover depth; and  $\delta_{pp}$  = bar hole flexibility, as shown in Equation 7.

$$\delta_{pp} = \frac{1}{2} \left( \frac{D(1 + \nu)}{E} + \frac{4D^3}{s^2 E} + \frac{D(1 + \nu + D^2)}{2Eh(h + D)} \right) \quad (7)$$

where  $h$  = cover depth;  $E$  = elastic modulus of the concrete; and  $\nu$  = Poisson's ratio of the concrete.

Bazant (1979b) provides for either inclined cracking above a single bar in Equation 5 or a 'cover peeling' or delamination type cracking in Equation 6.

Liang et al. (2002) provide a correction to an error they detected in Bazant's equation for inclined cracking from a single bar, shown in Equation, and suggested that the equations presented by Amey et al. (1998) be used to determine the time to corrosion initiation and their modified Bazant equation for determining the time required to crack the concrete after corrosion has begun.

$$\Delta D^* = P_r \delta_{pp} = f_t' \left[ 2 \left( \frac{L}{D} \right) + 1 \right] \delta_{pp} \quad (8)$$

where  $\Delta D^*$  is substituted for  $\Delta D$  in (5) above.

The 90-day water soluble chloride diffusion coefficient can provide a relatively simple and inexpensive test result which can be used to determine the expected in-service corrosion life of a given deck using the chloride diffusion and cracking models. The drawback to this test is in the time required to conduct the test and obtain results, which may be onerous given typical need for quick results in substantiating construction contract payments. Future research should examine if accelerated bulk diffusion testing at elevated temperatures might provide a faster test result without affecting the measured diffusivity coefficient.

### 3 EFFECT OF SEASONAL TEMPERATURE VARIATIONS ON CHLORIDE INGRESS

A finite difference model was used to evaluate the effect of seasonal temperature variations on the corrosion initiation time for various cover depths and two different 90-day diffusivity values that might occur in practice. A threshold of 0.4% water soluble chloride ion by mass of cement in the concrete mixture was selected to evaluate the time corrosion initiation occurs at various cover depths. This threshold was determined through studies by the United States Federal Highways Administration (Thangavel, 2004) and is commonly used throughout North America. Two different concrete mixtures were modeled, differing by their cementitious material content and composition: 1) a 450 kg/m<sup>3</sup> high performance ternary blend of 72% Portland cement, 8% silica fume and 20% fly ash; and 2) 350 kg/m<sup>3</sup> of Portland cement only. Typical 90-day diffusivity coefficient and m-values were assumed to be  $1.5 \times (10^{-12})$  m<sup>2</sup>/s with  $m = 0.4$ , and  $5.0 \times (10^{-12})$  m<sup>2</sup>/s with  $m = 0.15$ , respectively. The surface chloride concentration was assumed to be 15 kg/m<sup>3</sup> of concrete. This surface concentration is typical of values determined from field core specimens by plotting the variation in water soluble chloride concentration versus cover depth and extrapolating the diffusion curvature to the surface. Two different temperature profiles were considered and are shown

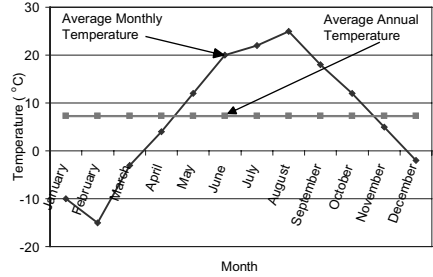


Figure 1. Temperature variation profiles.

in Figure 1. The first profile consisted of a typical monthly variation that might occur in Nova Scotia, Canada, while the second is a constant monthly temperature equal to the average annual temperature of the first profile.

The activation energy,  $U$  (J/mol), shown in Equation 9, used in adjusting the controlled temperature diffusion coefficient to an in-service temperature, if unknown, can be estimated for Portland cement (Schindler, 2004) based on the mass ratios, relative to the total Portland cement content, of the tricalcium aluminate,  $p_{C3A}$ , and tetracalcium aluminoferrite,  $p_{C4AF}$ , components of the cement, and on the Blaine specific surface of the cement. The modification factor  $f_E$  depends on the mass ratios of fly ash,  $p_{FA}$ , and slag,  $p_{SLAG}$ , present in the total cementitious blend, and on the mass ratio of lime in the fly ash to the total fly ash,  $p_{FACaO}$ , as shown in Equation 10.

$$U = f_E \cdot \left( 22,100 \cdot p_{C3A}^{0.30} \cdot p_{C4AF}^{0.25} \cdot Blaine^{0.35} \right) \quad (9)$$

$$f_E = 1 - 1.05 \cdot p_{FA} \cdot \left( 1 - \frac{p_{FACaO}}{0.40} \right) + 0.40 \cdot p_{SLAG} \quad (10)$$

It is observed in Figure 2 that ternary blend concrete far outperforms normal Portland cement concrete, providing longer times required for cracking to develop in the deck that increase with cover depth and illustrating the benefits of high performance concrete for increasing service life expectancy. The use of a monthly variation in service temperatures significantly reduced corrosion initiation times compared to the results using the constant average annual temperature because the diffusion rate is dramatically increased at higher temperatures.

Figure 3 shows the variation in the time required for cracking to occur in the deck, using the variable temperature model, over a range of cover thickness for a series of different diffusion coefficients corresponding to ternary (solid lines) and binary PC/SF or PC-only (dashed lines) based concrete mixtures.

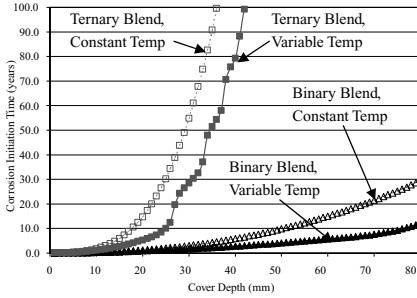


Figure 2. Difference between constant and variable temperature profiles on expected corrosion initiation time versus cover depth.

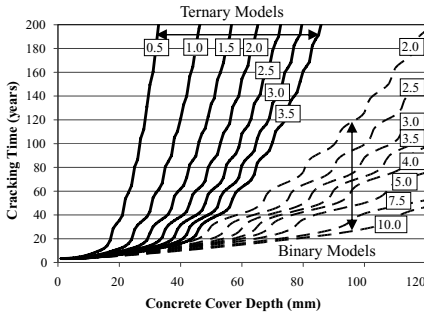


Figure 3. Service life required for concrete cover cracking using variable temperature profile over range of typical diffusion coefficient values ( $\times 10^{-12} \text{ m}^2/\text{s}$ ).

A wide variation in the expected service life exists, depending on the value of the 90-day diffusion coefficient and on the nature of the cementitious blend that was used in the concrete. Specified RCP test results of 1000 Coulombs for concrete at 90 days of age can be achieved using a wide range of diffusion coefficients ranging from  $0.4\text{--}5.0 \times (10^{-12}) \text{ m}^2/\text{s}$  using Portland cement only, binary, and ternary cementitious blends. Figure 3 indicates a range of 37 to >200 years of service life for ternary blends with diffusion coefficients between  $3.5\text{--}1.0 \times (10^{-12}) \text{ m}^2/\text{s}$  and 15–30 years for Portland cement or Portland cement/silica fume cements with diffusion coefficients between  $5.0\text{--}2.0 \times (10^{-12}) \text{ m}^2/\text{s}$  for a cover thickness of 50 mm. This striking difference clearly demonstrates the superiority of bulk diffusion testing over the RCP test as a means to define the expected service life of a reinforced concrete structure.

The finite difference model incorporating seasonal temperature variations effects on the diffusion of water soluble chloride ions in concrete can be used to determine the combination of diffusion coefficient and

minimum cover thickness required to achieve a design service life. Alternatively, the model can be used to evaluate the expected service life performance for quality assurance purposes of a newly constructed deck when coupled with extensive GPR-based cover thickness surveys.

#### 4 GROUND PENETRATING RADAR

GPR has become a common method for locating reinforcing bars and evaluating their depth in concrete. Bar depth is determined based on the velocity of the radar signal through the concrete and the travel time difference between signal reflections occurring between the concrete surface and the reinforcing bar, as shown in Equation 11.

$$h = [(r/2)^2 - (s/2)^2]^{1/2} = [(vt/22)^2 - (s/2)^2]^{1/2} \quad (11)$$

where  $h$  = depth to the reflecting boundary;  $s$  = transmitter/receiver spacing;  $v$  = signal velocity in the material; and  $r$  and  $t$  are the ray path length and signal travel time, respectively, from the transmitter to the reflecting boundary to the receiver.

The velocity of the signal in low loss materials is generally dictated by the relative dielectric constant,  $\epsilon_r$ , or permittivity, as shown in Equation 12. The permittivity of concrete generally ranges between 5 and 12, depending on the moisture content and abundance of ions in the pore water solution.

$$v = \frac{c}{\sqrt{\epsilon_r m_r}} \quad (12)$$

where  $c$  = speed of light in free space = 300 mm/ns; and  $m_r$  = relative magnetic permeability.

The permittivity of the surface layer can be determined using an air-launched radar antenna based on the relative difference in reflection coefficients between reflection amplitudes measured from the material surface and from a flat metal plate, which is assumed to totally reflect the transmitted signal. The resulting velocity is assumed to be representative over a depth of one half of the signal pulse width using the determined velocity. Alternatively, it is common to obtain drilled core specimens from known locations for calibrating the velocity in the overlying material using Equation 12. The total thickness to the subsurface reflecting boundary is used to calibrate the signal velocity, providing a more representative estimate of the material properties than the reflection coefficient technique. It is typical to obtain several drilled core specimens over a range of thickness values to obtain a representative velocity for the entire



structure. However, the reflection coefficient method permits velocity measurements at each data point, while the drilled core specimen requires an assumption of uniform velocity distribution throughout the structure and can result in larger errors between an estimated and actual thickness.

GPR provides a powerful tool for quickly measuring a representative sample of the cover thickness distribution across a reinforced concrete deck. This data can then be used to evaluate the location and extent of cover thickness variations over a deck surface relative to the specified value. These measurements can be used as inputs to the finite difference chloride diffusion model discussed above to estimate the time required for cracking to develop at each measured reinforcing bar location. Plan view contour maps can then be constructed detailing the location and extent of corrosion-induced cracking predicted in the deck at specific future times. Specific surface areas of damage can be predicted in order to forecast optimal maintenance scheduling. This maintenance forecast can then be used to evaluate the predicted corrosion life performance of the as-built deck structure versus the desired design performance in terms of a present value cost or benefit if a present value cost per unit surface area for repairs and long term trends in the interest rate and rate of return on investment are assumed.

## 5 CASE STUDIES

The cover thickness variations from three actual bridge decks were surveyed using GPR for this study and were found to vary normally, as listed in Table 1.

The cover thickness distributions from these real decks were used to demonstrate the effect of variations in the cementitious blend and diffusion coefficient on the predicted time for the repair of the first 20% of the deck surface versus the intended first repair time being equal to a zero-maintenance design life (70 years) of the decks. The time required after corrosion initiation to crack the concrete at each bar location was evaluated using a typical 35 MPa compressive strength Portland cement concrete mixture. The predicted first-repair times over a typical range of diffusivity is presented in Table 2 for Portland cement

only or binary PC/SF blend. The present value cost difference between the predicted repair time and the maintenance-free design service life corresponding to these diffusivity variations are listed in Table 3.

The difference in first-repair timing and present value cost difference appear to be more related to differences in the average cover thickness instead of the standard deviation of the each distribution. It was only possible to achieve the desired 70 year maintenance-free design period using  $D = 2.0 \times (10^{-12})\text{m}^2/\text{s}$  on the White Rock bridge for the cover thickness distributions that were measured. High performance ternary blend concrete mixtures would significantly prolong the predicted first-repair times by one to two orders of magnitude, and reduce the present value cost differences shown in Table 3, especially at the higher diffusion rates.

The interactive effect between the as-built cover system and the both temperature and time dependent diffusion coefficient require more sophisticated models than the traditional error function estimates of the diffusion equation can accommodate, but provide a reasonable physical model for predicting the expected service life of the structure based on the physical properties of the actual system.

Another important process which should be closely controlled to maximize the service life during reinforced concrete deck construction is curing. Improper curing by allowing the cover material to dry or by the late placement of curing compounds can lead to the development of shrinkage cracks in the concrete surface. Shrinkage cracks permit unimpeded access to the underlying cover material, effectively negating the protective capacity of the cover layer above the crack

Table 1. Cover thickness distribution statistics.

Structure	Minimum (mm)	Maximum (mm)	Average (mm)	Standard deviation (mm)
Hodgdon	39.8	95.2	61.8	6.3
White rock	54.3	110.5	84.9	8.6
Valleyfield	34.0	138.0	86.0	15.7

Table 2. First 20% deck repair timing (years).

Structure	Binary diffusion coefficient ( $\times 10^{-12}\text{m}^2/\text{s}$ )						
	2.0	2.5	3.0	4.0	5.0	7.5	10.0
Hodgdon	38.9	32.8	23.8	18.6	17.1	15.3	14.3
White rock	70.8	58.6	45.2	38.0	30.1	19.0	17.1
Valleyfield	68.6	54.8	46.0	36.5	29.4	21.1	19.3

Table 3. Present value cost difference (\$1000) between predicted and design repair time.

Structure	Binary diffusion coefficient ( $\times 10^{-12}\text{m}^2/\text{s}$ )						
	2.0	2.5	3.0	4.0	5.0	7.5	10.0
Hodgdon	9.3	11.8	16.2	19.1	20.0	21.1	21.7
White rock	0.0	0.6	1.4	2.0	2.7	4.0	4.2
Valleyfield	0.1	1.3	2.3	3.5	4.6	6.1	6.4

depth. An appropriate reduction in overall cover thickness can be applied to the measured cover distribution depending on the average crack depth and density of cracking on the concrete surface.

The ability of this model to evaluate the combined interactive effects of the water soluble chloride ion diffusivity in concrete and the as-built spatial cover thickness variations, along with adopting an average thickness reduction penalty in the cover layer to account for shrinkage crack effects, provides the capacity to assess the service life impact of the three most influential construction variables that a contractor can control for a given deck. As a result, the present value cost difference between the predicted and design first-repair times can be used as part of a performance specification contract system for deck construction, providing significant incentive for the contractor to place more emphasis on ensuring that these variables are adequately controlled in order to maximize the bonus which may be received for exceeding design requirements. Conversely, the model can also aid the deck owner in recuperating lost value that may result due to poor construction performance. If the present value cost difference were used as the basis of contract pay adjustments, the use of high performance concrete versus conventional concrete mixtures would result in a \$7,715 bonus to the contractor versus a penalty of \$9,250 for  $D = 2.0 \times (10^{-12}) \text{ m}^2/\text{s}$  on the Hodgdon Road Overpass. The net increase in cost resulting from the shrinkage crack cover thickness reduction for the Hodgdon Road Overpass with a ternary blend diffusion coefficient,  $D = 2.0 \times (10^{-12}) \text{ m}^2/\text{s}$ , is approximately \$14,000 resulting in a change from a bonus of \$7,715 to a penalty of \$6,300 for the contractor. Such effects are even more amplified when dealing with PC or PC/SF binary cementitious blends.

## 6 CONCLUSIONS

A finite difference model was presented incorporating time and temperature dependant diffusive transport of water soluble chloride ions in concrete; corrosion induced cracking models; and ground penetrating radar surveys of the as-built spatial variations in cover thickness to provide conservative, yet realistic, estimates of the location and extent of corrosion damage on actual reinforced concrete decks surface over time. It was observed from the model that the time required for sufficient water soluble chloride ions to diffuse to the various bar depths and initiate sufficient corrosion to crack the concrete cover layer may be significantly decreased by considering seasonal variations in temperature, compared an average constant annual temperature. Service life may be overestimated by using the error function approximate solution of the diffusion equation using a constant average annual

temperature. The sensitivity of the finite difference model in predicting the first 20% deck repair timing to variations in diffusion coefficient was evaluated with GPR cover surveys conducted on three newly constructed reinforced concrete decks. Repair time estimates, as a function of the diffusion coefficient, as-built cover system, and shrinkage crack cover thickness reductions, were also used to evaluate the present value cost difference between the expected repair time versus the design service life. Shrinkage crack effects on the service life were shown to have significant effect on the predicted service life of the deck. The present value cost difference evaluation of the as-built reinforced deck can be used for payment adjustments in performance specification contract systems, providing valuable incentive to contractors to produce more durable and long term maintenance free reinforced concrete structures.

## REFERENCES

- Amey, S.L., Johnson, D.A., Miltenberger, M.A. & Farzam, H. 1998. Temperature dependence of compressive strength of conversion inhibited high alumina cement concrete. *ACI Structural Journal* 95(1):27–36.
- ASTM Standard C1556. 2004. *Standard Test Method for Determining the Apparent Chloride Diffusion Coefficient of Cementitious Mixtures by Bulk Diffusion*. ASTM International, West Conshohocken, PA, [www.astm.org](http://www.astm.org).
- Bazant, Z.P. 1979a. Physical model for steel corrosion in concrete sea structures—theory. *ASCE Journal of the Structural Division* 105(6):1137–1153.
- Bazant, Z.P. 1979b. Physical model for steel corrosion in concrete sea structures—application. *ASCE Journal of the Structural Division* 105(6):1155–1166.
- Boddy, A., Bentz, E., Thomas, M.D.A. & Hooton, R.D. 1999. An overview and sensitivity study of a multimechanistic chloride transport model. *Cement and Concrete Research* 29:827–837.
- Fick, A. 1855. *Ann. Physik*, Leipzig, 170:59.
- Liang, M., Lin, L. & Liang, C. 2002. Service life prediction of existing reinforced concrete bridges exposed to chloride environment. *ASCE Journal of Infrastructure systems* 8(3):76–85.
- Neville, A.M. & Brooks, J.J. 1987. *Concrete Technology*. Essex, England: Longman Scientific and Technical.
- Schindler, A.K. 2004. Effect of temperature on the hydration of cementitious materials. *ACI Materials Journal* 101(1):72–81.
- Thangavel, K. 2004. The threshold limit for chloride corrosion of reinforced concrete. *Corrosion reviews* 22(1):55–70.
- Thomas, M.D. & Bamforth, P.B. 1999. *Cement and Concrete Research* 29:487–495.

# Recycling C&DW: a way for closing the concrete loop

V. Corinaldesi & G. Moriconi

*Dept. of Materials and Environment Engineering and Physics, Università Politecnica delle Marche, Ancona*

L. Dezi

*Dept. of Architecture, Constructions, Structures, Università Politecnica delle Marche, Ancona*

**ABSTRACT:** Within the European Union, the construction and demolition wastes (C&DW) amount to at least 180 million tons per year. Roughly 75% of the waste is disposed to landfill, despite its major recycling potential. However, the technical and economical feasibility of recycling has been proven, thus enabling some Member States (in particular Denmark, The Netherlands and Belgium) to achieve recycling rates of more than 80%. On the other hand the South European countries recycle very little of their C&DW. At present, recycled aggregates are mainly used untreated as obtained from demolition for excavation filling, roadbeds or floor foundation. However, several authors have studied the possibility of using recycled aggregates to manufacture structural concrete and in 2002, the CEN/TC 154 Technical Committee drew the EN 12620 "Aggregates for concrete" in which artificial or recycled aggregates are considered beside natural aggregates for use in concrete. The use of secondary raw materials in construction is highly essential from the viewpoint of Life Cycle Assessment (LCA) and effective recycling of construction wastes. In order to promote the reuse of C&DW in concrete, it is necessary to achieve three basic concepts: guarantee of safety and quality, decrease of environmental impact and increase of cost effectiveness of construction. Results of this study will show that recycled aggregate concrete can acquire satisfying quality as structural concrete and/or precast concrete elements through design by using materials conforming to all the related quality standards.

## 1 INTRODUCTION

### 1.1 *The European market of C&DW*

At more than 450 million tons per year the construction and demolition waste form the largest waste stream in quantitative terms within the European union, apart from mining and farm wastes (European Commission 2000). If one excludes earth and excavated road material the amount of construction and demolition waste generated is estimated to be 180 million tons per year.

About 72% of the waste is disposed to landfill, despite its major recycling potential. This represents very large quantities (more than one million tons per year) occupying existing landfills. However, the technical and economic feasibility of recycling has been proven, and certain member states (in particular Denmark, The Netherlands and Belgium) achieve recycling rates of more than 80%.

At present, the South European countries (Italy, Spain, Portugal, Greece) recycle very little of their C&DW. Their natural resources are of a sufficient quality and quantity to meet the demand for building materials at a moderate cost, thus implying a delay in the market for recycled materials to develop.

Nevertheless, mainly for environmental reasons, also in this part of Europe there is a growing interest in the possibility of recycling these materials. More recent data relative to the Italian market testified that almost 40% of C&DW were re-used or recycled in 1998 instead of 9% in 1996.

### 1.2 *Community policy on C&DW management*

Since 70's, the European Community started up a program directed to the waste management by means of the 75/442 CEE directive and the following 78/319 CEE, 84/631 CEE, 91/156 CEE and 90/639 CEE.

Within this general policy, which has among its main scopes the increase in production prevention, and the waste reduction trough the new clean technologies' development, the problem of C&DW assumes some relevance since 1992. In fact, in that year, the waste coming from the building process were included among the priority waste flows and, in order to study them, a specific workgroup was established, the "Construction and Demolition Waste Project Group".

Really, C&DW put management problems not so much for the presence of hazardous substances

(such as asbestos, chromium, cadmium, zinc, lead, mercury), that are little or nothing present, but for the huge amounts produced.

The "Construction and Demolition Waste Project Group" had as a main purpose the elaboration of a strategy for achieving a draft normative to be approved by the Council. The C&DW Project Group put its works (ended in June 1995) into practice by drafting two documents "Information" and "Recommendations". The "Information" document gave a picture of the current situation concerning construction and demolition waste. On the other hand, the "Recommendations" document suggested a series of measures and actions that, if undertaken by the various Member States, could widely develop the recycling of construction and demolition waste.

The European Community strategy (European Commission 1999), and the results of the researches carried out, sensitized the Member States which thought it right to acknowledge at national level the EU proposals. Therefore, each Member State adopted various political-economical tools that are giving encouraging results in terms of C&DW recycling.

In 1998 the Mandate M/125, concerning the execution of standardisation work for harmonized standards on aggregates, was issued by the Commission to CEN/CENELEC. This Mandate was subsequently correlated by several documents, dated 2002, in which artificial or recycled aggregates are considered together with natural aggregates: in particular, the CEN/TC 154 Technical Committee drew the EN 12620 "Aggregates for concrete".

## 2 LIFE CYCLE ASSESSMENT OF CONCRETE

As defined by EN ISO 14040 (CEN 2006), life cycle assessment (LCA) "addresses the environmental aspects and potential environmental impacts (e.g. use of resources and the environmental consequences of releases) throughout a product's life cycle from raw material acquisition through production, use, end-of-life treatment, recycling and final disposal (i.e. cradle-to-grave)".

In practice, in order to promote the application of recycled aggregate concrete, it is necessary to secure a suitable balance between 1) environmental impact, 2) safety and quality, and 3) cost-effectiveness.

### 2.1 *Environmental impact*

The building construction sector uses much energy and emits large quantities of carbon dioxide (CO<sub>2</sub>) to the atmosphere. Energy is used for extracting, transporting, processing and assembling materials, and CO<sub>2</sub> is emitted by fossil fuel combustion, land-use practices and industrial processes reactions, such as chemical reactions in the production and use of cement.

#### 2.1.1 *Environmental impact of cement*

During cement manufacture, mineral raw materials are heated in a kiln to produce clinker. Fuel combustion for kiln firing is the largest source of energy use and CO<sub>2</sub> emission during cement manufacture. The energy required for clinker production depends on the kiln design and the moisture content of the raw materials. The moisture content of kiln feed material can vary from about 0.5% when using the dry process to about 38% when using the wet process, with less energy being needed at lower moisture content (Worrell et al. 2001). Using exhaust gas to pre-heat feed material also reduces energy requirement. Gustavsson & Sathre (2006) compare the most efficient process using a short dry rotary kiln with pre-heater and precalciner to the least efficient, wet rotary kiln process that uses an average of 3.2 GJ more fuel (coal) per tonne of clinker. Electricity consumption for grinding and other uses is similar in both processes.

In normal Portland cement, clinker is ground and mixed with 5% gypsum to produce the finished product. Other materials whose reactivity has been increased through thermal processing, such as fly ash and ground granulated blast furnace slag (GGBS), can also be used as cement binders instead of clinker. Cement construction made of a blend of clinker and other additives is becoming more commonly used (Gartner 2004). When cement is made with a blend of clinker and by-products of other industrial processes, total energy use is reduced because less clinker must be produced. CO<sub>2</sub> emission is reduced in two ways: less fossil energy is needed for the production of the lower quantity of clinker, and lower clinker production means less CO<sub>2</sub> emission from the chemical reaction of limestone calcination.

If the whole life cycle of cement-based products is taken under consideration, there is a positive CO<sub>2</sub> emission from calcinations reaction during cement manufacture but also a negative emission due to carbonation reaction during the building lifecycle, which partially reduce cement environmental impact.

Pade & Guimaraes (2007) showed as the impact that concrete carbonation has in the assessment of CO<sub>2</sub> emissions from cement production has not been fully documented. Specifically, they showed a lack of knowledge about the carbonation of demolished and crushed concrete. In fact, the existing models for calculating carbonation do not take into account what takes place after the concrete has been demolished. Consequently, the contribution of the cement and concrete industry to net CO<sub>2</sub> emissions may be significantly overestimated.

Gustavsson & Sathre (2006) compare a clinker to cement ratio of 65% (used in the very common CEM II-B/L) to the 95% used in normal Portland cement. For the blended cement kiln fuel consumption is reduced by 1.4 GJ/tonne (Worrell & Galitsky 2004).

The electricity use increases by 0.06 GJ/tonne due to the need for grinding of the blending materials. The decrease in clinker manufacture reduces CO<sub>2</sub> emission from process chemical reactions by 32%.

### 2.1.2 *Environmental impact of aggregates*

Aggregate in the form of sand and gravel is an essential component of concrete, composing over 80% by weight of a typical concrete mixture. Aggregate of suitable size and quality occurs naturally in some places, requiring only extraction, washing, and transportation.

Where natural aggregate is not available or cannot be extracted, large stone is quarried, crushed and graded to the required sizes. Extraction of one tonne of natural aggregate requires 20 MJ oil and 9 MJ electricity, while one tonne of crushed gravel requires 120 MJ oil and 50 MJ electricity (Worrell et al. 1994). These evaluations do not include transport energy, which will depend on the locations of the resource and the batching site.

In practice, by using natural gravel instead of crushed gravel as concrete aggregate, there is a less fossil fuel consumption and a less CO<sub>2</sub> emission but the local availability of natural gravel is often a problem and the environmental impact of its extraction too.

A promising alternative is demolished concrete structures which can be crushed to produce aggregate. In this case the energy required for production at the recycling plant can be estimated to be about 40 MJ oil and 15 MJ electricity (Nicosia et al. 2000). In addition, by using demolished concrete as aggregate, non-renewable resources consumption can be limited and such waste materials can be recovered for a useful application instead of disposing of them at landfill.

## 2.2 *Safety and quality*

### 2.2.1 *How to improve C&DW quality: design for sustainable building*

One of the main problems of sustainable building is that the existing systems don't lead to clean and direct reusable secondary building materials after demolition.

Generally, when a building has reached its end of life, it is demolished and it becomes demolition waste. Unfortunately, a lot of different building materials are mixed together during the demolition process and much care is needed before construction and demolition waste (C&DW) can be reused.

In order to solve this problem, two steps need to be taken. Firstly, during the stage of design, a building should be designed for recycling, and secondly, during the demolition stage, all buildings should be dismantled into elements or reduce to in clean secondary materials.

In the stage of design a suitable dismantle building system should be chosen, enabling all the elements and components to be re-used easily and directly after dismantling. This stage of design is called design for dismantling (DFD). On the other hand, design for recycling (DFR) is another building system where, during the stage of design, consideration is given to what to do with the building materials after demolition (te Dorsthorst et al. 2001). In this way, separation of building materials would be rather simple during the demolition process and after further processing (for example crushing), and the separated materials could be used as raw materials for the production of new building materials. For example steel scraps can be employed for the production of new finished steel products instead of primary steel (obtained by mining and reducing iron ore).

The second alternative is the attempt to improve the recycling of materials and elements at the demolition site. This is the most effective solution nowadays, because the greater part of the buildings already built, where not designed for dismantling them. Firstly, buildings should be dismantled into elements and components if possible, for the reuse of elements. Secondly, if dismantling is not an option, buildings should be selectively demolished and the materials should be reused at the 'materials level'.

Obviously, the first options, before dismantling and/or demolishing, is upgrading existing buildings if possible (mainly from a safety and economical point of view) for giving them a second life, in agreement with the concept of minimizing waste production.

Concerning new buildings, they should be built and assembled with reusable elements and materials by means of DFD and DFR and by using secondary materials as much as possible.

Almost all current constructions were not built using DFD and DFR. The reuse of these constructions at all levels is difficult and demolition of these constructions results in mixed construction waste. Therefore, almost all of the C&DW ends up in road based layers, which however is a useful application.

### 2.2.2 *Fields of employ for C&DW*

Although concrete waste is presently used almost entirely for roadbeds, the demand for this application is not expected to increase, largely due to a decrease in new road construction. Meanwhile, toxic substances such as hexavalent-chromium and lead are present in the concrete waste since they are originally contained in cements (Dosho 2007). Taking soil contamination into consideration, it is necessary to develop other uses apart from roadbed for recycled concrete. At this purpose, a previous study (Sani et al. 2005) carried out on the leaching behaviour of concrete mixtures prepared with recycled aggregates showed as the ion

leaching rates expressed for unit of specific surface area are generally under the acceptable limits.

The most promising alternative uses for C&DW are recycled-aggregate concretes, recycled-aggregate mortars and, concerning the finest fraction, as filler for self-compacting concrete as well as for cement production.

Several authors (Kasai 1988, Hansen 1992, Dhir et al. 1998) studied the possibility of using recycled aggregates to prepare structural concretes and its feasibility was proved. In particular, these studies showed also that, in recycled-aggregate concrete, the fine recycled-aggregate fraction is particularly detrimental to both mechanical performances and durability of concrete.

For this reason the more recent approach is to recycle for concrete production only the coarse recycled fraction. In particular, the Italian Standards UNI EN 12620 and UNI 8520 allow the use of the only coarse recycled aggregate and it makes a difference between the aggregate coming from building demolition (which can be used only for low-strength concretes under 25 MPa strength class) and the aggregate coming from demolished concrete (which can be used for concretes up to 35 MPa strength class). In this way, a huge amount of fine recycled materials cannot be reused neither in concrete neither in roadbeds or floor foundation (where higher particle size is requested).

In order to find an alternative application for the fine recycled-aggregate fraction, the authors in previous works (Corinaldesi et al. 2002, Moriconi et al. 2003) studied mortars containing recycled instead of natural sand. Results obtained showed how, from a mechanical performance point of view, recycled-aggregate mortars are weaker than conventional mortars but the same isn't true when comparing the behavior of masonry walls made of these mortars. In fact, the mechanical performance of the overall mortar-brick system is strictly related to the mortar-brick adhesion, and recycled-aggregate mortars show excellent bond strength with bricks, due to their rheological properties. In fact, bond strength is related to the quality of the adhesion of fresh mortar to the brick (McGinley 1990, Robinson 1996, Brocken et al. 1998), and thus to the rheological properties of the mortar (Moriconi et al. 2003).

With the final target of a 100% recycling of C&DW, a further step is the attempt to reuse the fine fraction (less than 0.150 mm) of recycled concretes, produced during their processing, as mineral addition for preparing self-compacting concrete (Corinaldesi & Moriconi 2003, Corinaldesi & Moriconi 2004). The so-called 'rubble powder' proved to be effective when added to self-compacting concrete mixture in terms of improvement of its resistance to segregation. In this way even the reject of a reject could become useful. Moreover, this 'dust' proved to be particularly detrimental for the

mechanical performance of recycled-aggregate concrete, due to its high water absorption, and its removal from recycled aggregates allows improvement of their quality.

Concerning cement production, van Loo (1993) showed as the fine fraction (less than 0.150 mm) of recycled concrete, if suitably thermally treated, and used besides to clinker results in a compressive strength development of the same order of magnitude as coal fly ash.

Another field in which recycled concrete can be effectively recycled is that of precast concrete production. In fact, scraps coming from the manufacture of precast concrete elements, can be re-used as recycled aggregates to partially replace natural aggregates for manufacturing new reinforced concrete elements with unchanged mechanical performance. Since the waste material volume in prefabrication plants is relatively low, limited replacement of natural with recycled aggregate could be sufficient to dispose the entire production scraps by contemporarily gaining further environmental advantage, in terms of reduced extraction from quarries. In particular, the results obtained by the authors (Corinaldesi & Moriconi 2007) showed that the quality of the old concrete influences the maximum substitution percentage which can be tolerated, and in particular when the original strength class is 55 MPa the substitution can be carried out at a percentage of even 30%.

### 2.2.3 *Safety of recycled aggregate concretes*

The quality of recycled aggregate strongly depends on the kind of recycling plant (generally, fixed are better than mobile plants) and on the care of the quality checks at the input of recycling plant. In fact, hazardous materials such as asbestos must be rejected and also materials such as chalk wall waste should be previously removed in order to avoid future internal sulphate attack problems due to the presence of gypsum in the recycled aggregate.

In Italy, since 2006, quality controls concerning geometrical, physical and chemical properties of recycled aggregates must be carried out for their CE label according to EN 12620, before using them in concrete.

A comparison between a conventional scenario and a recycling scenario is carried out in the following part of the paper. At this purpose two concrete mixtures were compared, one made of virgin crushed aggregates (indicated as 'conventional mixture') and one made of 70% virgin crushed aggregates and 30% recycled concrete (indicated as 'recycling mixture'), coming from a fixed recycling plant based on the so-called R.O. S.E. technology (Italian acronym for 'homogenised recovery of building waste materials'). Concrete mixture proportions are reported in Table 1. In both cases a blended cement type CEM II-B/L 32.5 R according to

Table 1. Mixture proportions of one cubic meter of concrete.

Mixtures	Conventional mixture	Recycling mixture
W/C	0.55	0.53
Water, kg	185	185
Cement type CEM II-B/L, kg	335	350
Fine sand (0–4), kg (% by volume of total inert)	346 (20)	343 (20)
Coarse sand (0–5), kg (% by volume of total inert)	348 (20)	345 (20)
Fine crushed gravel (6–12), kg (% by volume of total inert)	526 (30)	–
Recycled concrete (6–12), kg (% by volume of total inert)	–	499 (30)
Crushed gravel (11–22), kg (% by volume of total inert)	527 (30)	524 (30)
Superplasticizer, kg (% by weight of cement)	3.3 (1.0)	3.5 (1.0)
Air-entraining admixture, kg (% by weight of cement)	0.2 (0.06)	0.2 (0.06)

Table 2. Mechanical and elastic performances of concretes.

Mixtures	Conventional mixture	Recycling mixture
28-day compressive strength (MPa)	30	30
28-day tensile strength (MPa)	1.92	1.96
28-day secant elastic modulus (GPa)	31.18	31.08
180-day drying shrinkage (mm/m)	–0.700	–0.650

EN-197/1 was used. The only difference in composition is a slight higher content of cement in the case of the ‘recycling mixture’ in order to achieve the same strength.

On the other hand, data relative to their mechanical and elastic performances are reported in Table 2. On the basis of the data reported in Table 2 the two concretes seem to achieve the same safety level.

Previous studies (Corinaldesi & Moriconi 2006, Corinaldesi & Moriconi 2008) about recycled-aggregate concretes made of 100% recycled aggregate (both coarse and fine fractions), coming from the C&DW treatment at the same fixed recycling plant above mentioned, showed satisfying results in terms of expected durability in comparison to conventional concrete. In particular, the use of recycled aggregates by compelling a lower water to cement ratio for achieving the same strength class (Tabs. 1–2) can be beneficial in increasing the service life of concrete structures because it extends the initiation period for reinforcement corrosion (Corinaldesi & Moriconi 2008).

Table 3. Traditional and eco-balanced costs referred to one cubic meter of concrete.

Type of concrete	Traditional cost (€)	Eco-balanced cost (€)
Conventional scenario	64.01	>64.01
Recycling scenario	63.15	38.20

Moreover, recycled-aggregate concrete submitted to low-cycle loading (characterized by a load history containing few cycles but having a large range of bond reversal stresses in order to simulate real structures subjected to earthquake or high winds) gave experimental evidence of the suitability of recycled-aggregate concrete for structural use (Corinaldesi & Moriconi 2006).

### 2.3 Cost effectiveness

Rough estimates of the prime costs of the two concrete mixtures are reported in Table 3.

The traditional cost evaluation was carried out bearing in mind that at present (year 2007), in Italy, cement costs about 89 €/tonne, superplasticizing admixture costs about 2.4 €/kg, air-entraining admixture about 1.7 €/kg, natural sand (0–4 mm) and (0–5 mm) cost 19.6 and 15.7 €/tonne respectively, crushed gravel (6–12 mm) and (11–22 mm) cost 13 €/tonne, and finally recycled aggregate cost 12 €/tonne.

Besides to the traditional cost of aggregates, it would be important to take into account their environmental costs. As suggested by Tazawa (1999), the eco-costs should be considered, the in this case are the expenses necessary to eliminate the environmental impact caused by the extraction of virgin aggregates (not well valuable) and also the negative eco-costs, that would be the expenses to eliminate the environmental load if rubble from building demolition are not used for preparing concrete. At the Italian current costs related to disposal of at landfill equal to 0.05 €/kg, the eco-balanced costs of concretes were calculated and reported in Table 3.

In addition, it could be predictable that the recycled-aggregate in the future could result cheaper than natural aggregate concrete because the former could have a decreasing market price while the latter will have an increasing one.

## 3 CONCLUSIONS

Results of this study show that recycled aggregate concrete can acquire satisfying quality as structural concrete through design by using materials conforming to all the related quality standards.

In addition, the use of recycled aggregates can improve both environmental impact and cost (in particular eco-balanced cost) of concrete.

Dosho (2007) also showed that if recycled coarse aggregate concrete having a 30–50% replacement ratio is assumed to be applied to new building construction, costs can be reduced by about 34–41% and CO<sub>2</sub> emissions by about 23–28% with the same quality and safety levels of conventional concretes.

## REFERENCES

Brocken, H.J.P., Spiekman, M.E., Pel, L., Kopinga, K. & Larbi, J.A. 1998. Water extraction out of mortar during brick laying: A NMR study. *Materials and Structures* 31 (205): 49–57.

CEN (European Committee for Standardization) 2006. EN ISO 14040:2006, Environmental management—Life cycle assessment—Principles and framework.

Corinaldesi, V., Giuggiolini, M. & Moriconi, G. 2002. Use of rubble from building demolition in mortars. *Waste Management*. 22(8): 893–899.

Corinaldesi, V. & Moriconi, G. 2003. The Use of Recycled Aggregates from Building Demolition in Self-Compacting Concrete. In O.Wallevik & I. Nielsson (eds.) *Self-Compacting Concrete, RILEM Proceedings PRO 33, Proc. 3rd Int. RILEM Symp., Reykjavik, Iceland, 17–20 August 2003*, Bagnex (France): RILEM Publications S.A. R.L.

Corinaldesi, V. & Moriconi, G. 2004. The Role of Recycled Aggregates in Self-Compacting Concrete. In V.M. Malhotra (ed.), *Fly Ash, Silica Fume, Slag and Natural Pozzolans in Concrete, ACI SP 221–57, Proc. Eighth CANMET/ACI Int. Conf., Las Vegas, USA, 23–29 May 2004*. Farmington Hills (USA): ACI Publishing.

Corinaldesi, V. & Moriconi, G. 2006. Behavior of Beam-Column Joints Made of Sustainable Concrete under Cyclic Loading. *Journal of Materials in Civil Engineering* 18(5): 650–658.

Corinaldesi, V. & Moriconi, G. 2007. Utilizzazione di aggregati in calcestruzzo riciclato in prefabbricazione (Recycling concrete aggregate in precast concrete production). *Calcestruzzo & Prefabbricazione International (Concrete Plant International)* 4: 86–94.

Corinaldesi, V. & Moriconi, G. 2008. The influence of mineral additions on performance of recycled-aggregate concrete. *ACI Materials Journal*, in press.

Dhir, R.K., Henderson, N.A. & Limbachiya M.C. (eds.) 1998. *Use of Recycled Concrete Aggregate*. London: Thomas Telford Publishing.

Dosho, Y. 2007. Development of a sustainable concrete waste recycling system. *Journal of Advanced Concrete Technology* 5(1): 27–42.

European Commission 1999. *Construction and Demolition Waste Management Practices, and their Economic Impacts, Final Report*: 1–208. Symonds Group Ltd, in association with ARGUS, COWI and PRC Bouwcentrum.

European Commission (Directorate-General Environment, DG ENVE.3) 2000. *Management of Construction and Demolition Waste. Working Document no 1*: 1–26.

Gartner, E. 2004. Industrially interesting approaches to low-CO<sub>2</sub> cements. *Cement and Concrete Research* 34(9): 1489–1498.

Gustavsson, L. & Sathre, R. 2006. Variability in energy and carbon dioxide balances of wood and concrete building materials. *Building and Environment* 41: 940–951.

Hansen, T.C. (ed.) 1992. *Recycling of Demolished Concrete and Masonry. RILEM TC 37-DRC-Demolition and Reuse of Concrete*. London: E & FN Spon.

Kasai, Y. (ed.) 1988. *Demolition and Reuse of Concrete and Masonry. Reuse of Demolition Waste*. London: Chapman and Hall.

McGinley, W.M. 1990. IRA and the flexural bond strength of clay brick masonry. *Masonry: Components to Assemblages. ASTM Special Technical Publication* 1063: 217–234.

Moriconi, G., Corinaldesi, V. & Antonucci, R. 2003. Environmentally-friendly mortars: a way to improve bond between mortar and brick. *Materials & Structures* 36 (264): 702–708.

Nicosia, S., Lucchese, A., Rizzo, G. & Ercoli, L. 2000. Riciclo di Rifiuti da Demolizione: un Contributo all'Ecobilancio. In: C.I.P.A. (ed.), *Innovation in Waste Management; Proc. IV Europ. Waste Forum, Milan, 30 November–01 December 2000*, Milan: C.I.P.A. Editore.

Pade, C. & Guimaraes, M. 2007. The CO<sub>2</sub> uptake of concrete in a 100 year perspective. *Cement and Concrete Research* 37: 1348–1356.

Robinson, G.C. 1996. Adhesion mechanisms in masonry. *American Ceramic Society Bulletin*, 75(2): 81–86.

Sani, D., Moriconi, G., Fava, G. & Corinaldesi, V. 2005. Leaching and mechanical behaviour of concrete manufactured with recycled aggregates. *Waste Management* 25(2): 177–182.

Tazawa, E. 1999. Engineering scheme to expedite effective use of resources. In P.K. Metha (ed.), *Concrete Technology for Sustainable Development in the Twenty-First Century, Proc. Int. Symp. Hyderabad, India, 9–11 February 1999*, New Delhi (India): Radha Press.

te Dorsthorst, B., Fraaij, A., Kowalczyk, T. & Sluimer, G. 2001. From grave to cradle: reincarnation of building materials. In V.M. Malhotra (ed.), *Recent advances in concrete technology, ACI SP 200–5, Proc. Fifth CANMET/ACI Int. Conf., Singapore, 30 July–01 August 2001*, Farmington Hills (USA): ACI Publishing.

van Loo, W. 1998. Closing the concrete loop—from reuse to recycling. In Dhir, R.K., Henderson, N.A. & Limbachiya, M.C. (eds.), *Use of recycled concrete aggregate*: 83–97. London: Thomas Telford Publishing.

Worrell, E., van Heijningen, R.J.J., de Castro, J.F.M., Hazewinkel, J.H.O., de Beer, J.G., Faau, A.P.C. & Vringer, K. 1994. New gross energy requirement figures for material production. *Energy* 19(6): 627–40.

Worrell, E., Price, L., Martin, N., Hendriks, C. & Meida, L.O. 2001. Carbon dioxide emissions from the global cement industry. *Annual Review of Energy and the Environment* 26: 303–29.

Worrell, E. & Galitsky, C. 2004. Energy efficiency improvement opportunities for cement making. *Report LBNL-54036*. Berkeley: Ernest Orlando Lawrence Berkeley National Laboratory.



# Life Cycle Cost Analysis in pavement type selection: state-of-the-practice

Zeynep Guven

*Skanska USA Civil Southeast Inc., Virginia Beach, Virginia, USA*

Prasad Rao Rangaraju & Serji N. Amirkhanian

*Clemson University, Clemson, South Carolina, USA*

**ABSTRACT:** Performing Life Cycle Cost Analysis (LCCA) in the design phase of a transportation project can result in economical strategies that might result in savings for highway agencies. Many state agencies have adopted the LCCA approach for aiding their decision process in pavement type (flexible or rigid) selection. Also, LCCA is increasingly being used to assess the relative costs of different rehabilitation options within each type of pavement. However, most of the input parameters that feed into the analysis are inherently uncertain. In order to implement the LCCA process in a reliable and trustworthy manner, this uncertainty must be addressed. This paper summarizes the findings of a research project that investigated the state of the-practice in LCCA across the United States and Canada. As part of this study, a preliminary survey and a final survey were conducted to gauge the level of LCCA activity in different states. The responses obtained from the web surveys were analyzed to observe the trends regarding the various input parameters that feed into the LCCA process. The survey results showed LCCA is used widely among transportation agencies. However, the extent of the analysis varies widely and is presented here. This paper also presents case studies that study the effects of the variation in discount rate and analysis period on Net Present Value (NPV). The case studies showed that by altering the analysis parameters, a break-even point is observed in the results and the lowest cost alternative is altered. Therefore, the importance of conducting a probabilistic analysis using statistical data was shown.

## 1 INTRODUCTION

### 1.1 Background

There is consensus in the highway industry that quality LCCA in the design phase of both new construction and rehabilitation projects can result in more appropriate strategies, considerable total savings (agency and road user) and better cash flow management (Jones et al. 2005 and Walls & Smith 1998). While the economic concepts that support this type of analysis are fairly straightforward, their application presents a number of challenges. Frequently there are uncertainties as to how LCCA should be employed and what assumptions should be made during the course of the analysis (FHWA 2002).

In 1998, the Federal Highway Administration (FHWA) issued an "Interim Technical Bulletin on LCCA" which provided guidelines on the computation of agency and user costs (2). In addition, the guidelines greatly improved the existing methodology (deterministic approach) by introducing a "probabilistic" approach in the treatment of uncertain LCCA inputs. In early 2005, the South Carolina

Department of Transportation (SCDOT) commissioned a research study to investigate the state-of-the-practice of LCCA across the nation and Canada and develop a comprehensive LCCA approach for SCDOT. In order to identify and quantify factors that need to be considered in developing realistic life cycle cost analysis, a comprehensive literature review of historical data was conducted. To complement the literature review, a preliminary web survey was developed and sent to the State Highway Agencies Departments of Transportations (DOTs) in all 50 States and Canada to capture their current level of LCCA endorsement and implementation. The second and final survey was sent out to State DOT officials that had responded to the first survey in order to gain a deeper understanding of their LCCA practices.

This paper documents the current state-of-the-practice of LCCA in many State Highway Agencies (SHA) in the US and Canada. This paper also presents case studies that study the effects of the variation in discount rate and analysis period on Net Present Value (NPV).

## 1.2 Work outline

The initial web survey was launched on September 2005. It contained questions about the general practice of LCCA, such as the use of any software; the analysis period used, and assigned initial performance life. Agency guidelines or policies regarding the pavement selection process were retrieved. The final survey was sent out in April 2006. The questions in the final survey were more in depth and aimed particularly at addressing the treatment of the uncertainty in LCCA parameters and finding out the inputs used in the analysis.

## 2 SURVEY RESULTS

### 2.1 LCCA practice

For the initial study, a total of 33 States and 2 Canadian Provinces participated in the preliminary survey. Out of these, 94% of the agencies indicated that they use LCCA as part of the decision process for selecting pavement type. A total of 23 States participated in the Final Survey. Among the 23 states, one state did not have concrete pavements and another state did not have an LCCA process in place. Their responses were discarded in questions related to the use of LCCA in the pavement type selection process, but were included where applicable.

### 2.2 Concerns with LCCA process

Of the 21 states that practiced LCCA and responded to the final survey, 14 states indicated that they were either satisfied or only had minor concerns with their existing LCCA process. However, 7 states indicated that they had significant concerns about the current practice of LCCA for pavement type selection process. The specific concerns raised by these states included:

- Unreliable quality of the input data into LCCA models;
- Lack of adequately trained individuals who understand the importance and implication of the input parameters into LCCA programs such as RealCost and DARwin;
- Difficulty in predicting cost of materials in a period of rapidly fluctuating prices;
- Lack of long-term field performance data for newer asphalt and concrete pavement designs and materials;
- Disagreements with asphalt and concrete pavement industry about the most appropriate inputs such as the determination of the timing of future rehabilitation, and determination of salvage value; and

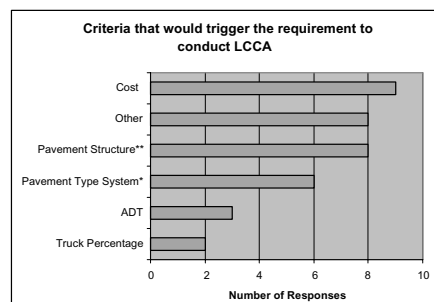
However, some states that presently do not use LCCA indicated that they would be willing to consider LCCA if initial construction costs of asphalt and concrete pavements become more comparable. Approximately 62% of the responding states indicated that they are considering revisions to the LCCA process to achieve a more realistic comparison between pavement alternatives. The nature of revisions being considered range from incorporating a probabilistic approach to LCCA to including user costs in the analysis.

Out of the 21 States that responded to the survey, 13 of them reported updating their LCCA process for pavement type selection within the last 3 years. Several DOTs modified their LCCA process to reflect a methodology that is based on FHWA's RealCost software program, while several other States are adjusting their processes constantly to reflect minor changes and clarifications.

### 2.3 Criteria that trigger the requirement to conduct LCCA

In the next question state officials were asked to select the criteria (more than one if necessary) that would trigger the requirement to conduct LCCA for pavement type selection. Figure 1 shows the results of the survey indicating that cost of the project was the most selected criteria, while some states base their need to perform an LCCA on the pavement structural consideration such as Structural Number, with a predetermined inclination towards one or the other pavement type.

In conducting LCCA, it is important to be aware of the fact that the LCCA has a life of its own and in some cases the data used in the analysis might lose its validity even before a decision is being made. The life of the cost of materials, life of the design, and change in



\*Pavement Type System (e.g., Interstate, Secondary Roads, etc.),

\*\*Pavement Structure (e.g., Structural Number, etc.)

Figure 1. Criteria that triggers the requirement to conduct LCCA.

traffic conditions must be considered for some additional criteria that should trigger the requirement to re-conduct LCCA.

## 2.4 *Methods to conduct LCCA*

In general, two approaches to LCCA may be employed—deterministic and probabilistic. In the deterministic approach, input variables are treated as discrete fixed values. However, the majority of input variables are uncertain. Uncertainty results from the assumptions, estimates, and projections that are made for the input parameters (Walls & Smith 2002). This uncertainty can be treated either by using risk analysis (the probabilistic approach) or by performing sensitivity analysis (Ozbay et al. 2004). A sensitivity analysis is often performed to assess the effects of various input parameters on the developed model. However, the sensitivity analysis does not necessarily reveal areas of uncertainty that may be a critical part of the decision-making process (Reagle et al. 2002). By including all possible inputs into the analysis and weighing the probability of occurrence of each, risk analysis alleviates the debate from the validity of LCCA results (Herbold 2000).

Ozbay et al. reported that in late 2002 none of the state DOTs followed the probabilistic approach. In 2006, 4 years after the introduction of the FHWA Probabilistic LCCA Software—RealCost—only 5% used a probabilistic approach. Majority of the states (80%) surveyed by the authors still used a deterministic approach, while 15% used a combination of probabilistic and deterministic approaches for different aspects of LCCA. In addition, 25% of the SHAs utilizing a deterministic approach perform sensitivity analysis on several parameters to address the uncertainty in LCCA, while another 25% expressed their intention of using the probabilistic approach in the future. Currently discount rate, analysis period, timing of rehabilitations, unit costs of materials in both initial construction and future rehabilitation projects are the parameters considered in sensitivity analysis by different states.

Use of software programs is necessary in a probabilistic approach or in conducting a sensitivity analysis in deterministic approach. The 2005 survey results showed that 50% of the responding agencies use RealCost—an LCCA program developed by FHWA, DARWin—a pavement design program—developed by AASHTO or some customized software to conduct LCCA. Among these states, 6 states use RealCost, 6 states use customized software, and only one state uses DARWin. Remaining states use a combination of the available software programs. In comparison, the results of a survey conducted in 2001 showed that 8 out of 16 responding State DOTs used software, predominantly DARWin and customized software, to compute

life cycle costs (Ozbay et al. 2003). Based on the results of this survey, it appears that after the release of RealCost program in 2002 by FHWA (FHWA 2003), most state agencies have adopted this program for conducting their LCCA calculations.

## 2.5 *LCCA parameters*

### 2.5.1 *Agency costs*

Agency costs play a key role in the life cycle cost determination for any given project. The survey results indicated that all the responding DOTs consider the initial construction costs and rehabilitation costs in the analysis. However, there is a lack of consensus on the inclusion of other agency costs elements such as traffic maintenance, engineering, etc. that are incurred by the agency over the analysis period. Out of the 21 states that responded only 12 included the maintenance of traffic costs, 10 included the routine and preventive maintenance costs, 9 included preliminary engineering costs, 8 included construction management costs, and only three states included associated administrative costs.

### 2.5.2 *User costs*

User costs typically are an aggregation of three separate components: Vehicle Operating Costs (VOC), Crash Costs, and User Delay Costs (Walls & Smith 2002). There has been a vast amount of research performed on the subject and VOC components are proven to be significant based on years of empirical and theoretical research results (Daniels et al. 2000) & (Ozbay et al. 2004). According to some researchers, not considering user costs during normal operations in the LCCA is a serious shortcoming (Ozbay et al. 2004). However, most of the states (approximately 58%) do not consider any type of user cost, let alone consider VOC or crash costs. Most of the State DOTs incorporating user costs into the analysis, calculate only user delay costs during major rehabilitation activities. However, there has been improvement in the recent years in this regard, as states are experimenting with probabilistic approach to include costs.

User costs are often similar to and can be larger than agency costs (Lindley et al. 2004). Considering that there is a large amount of uncertainty inherent in the user cost calculation process, it is particularly important to address the uncertainty through use of validated probabilistic data. Of the State DOTs that responded to the survey, Washington and Maryland DOTs use a probabilistic approach when dealing with user costs. Colorado DOT uses probabilistic values for annual traffic growth rate. Indiana DOT is implementing a probabilistic approach on a trial basis. Michigan DOT uses a deterministic approach in assessing the user costs.

### 2.5.3 Discount rate

When estimating future costs of transportation projects, discount rates play an important role, and can—like any other variable with some inherent uncertainty—alter the results as will be shown in Section 3 of this paper. The 2005 survey results showed that at the time this uncertainty was addressed only by 5 states as can be seen in Figure 2. Of those 5 states, 3 of them conduct a probabilistic LCCA which incorporates probabilistic values for the discount rate, while 2 other states run sensitivity analysis to determine the effect of the discount rate on their analysis results.

### 2.5.4 Analysis period

Figure 3 illustrates the analysis period used by state agencies. The State Highway Agency using the longest analysis period was New York State Department of Transportation (NYSDOT) which at the time reported using an analysis period of 65 years for pavement type selection process. Some states indicated that the analysis period they use depends on the proposed design life or on the network level of the pavement. The percentage of these states that determine the analysis period on a project-by-project basis was 22% in 2005.

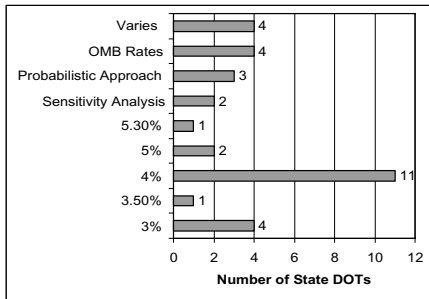


Figure 2. Discount rate as utilized by state DOTs in 2005.

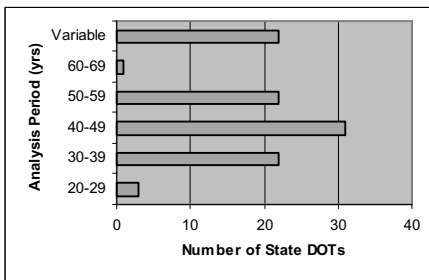


Figure 3. Analysis period as employed by state highway agencies.

### 2.5.5 Rehabilitation timings

Performance life for the initial pavement design and the life of subsequent rehabilitation activities have a major impact on LCCA results. Approximately 40% of the states surveyed indicated that they base their decisions on their pavement management system. However, other states indicated their decisions are based on available funding, maintenance treatment decision trees produced by their local districts and expert opinions. A summary of the responses from different DOTs on the performance life of initial pavement design, the life of subsequent rehabilitation activities for both flexible and rigid pavements can be found in the Master's Thesis by Guven; "Life Cycle Cost Analysis of Pavements: State-of-the-Practice".

### 2.5.6 Salvage value

Salvage value can have two fundamental components associated with it: residual value and serviceable life. Residual value refers to the net value from recycling of the pavement while serviceable life represents the remaining life in a pavement alternative at the end of the analysis period.

The survey results showed that 56% (18 out of 32) of the State DOTs included salvage value in their calculations. Majority of the respondents (8 out of 10) indicated that they calculate only serviceable life, and the rest calculate both residual value and serviceable life. One of the DOTs that calculate residual value, incorporate the benefit of reusing any in-place bituminous or concrete material, which can be recycled back into the new pavement structure into the initial cost estimate.

## 3 CASE STUDIES

As mentioned earlier, sensitivity analysis shows the independent effect of the variability of one of the inputs and is conducted by some of the DOTs surveyed. In the following case studies, the effects of the variation in discount rate and analysis period on Net Present Value (NPV) were investigated.

The LCCA consisted of comparing a hot mix alternative (HMA) versus Portland cement concrete (PCC) alternative. The data was provided by Colorado DOT. It evaluates the life cycle costs of keeping a one mile section of State Highway 119 in Boulder County of Colorado, over a certain serviceability index. The initial service life assigned for the HMA alternative had a mean value of 10 years with a standard deviation of 3.1 years. Each of the HMA rehabilitation activities also had a mean value of 10 years of assigned service life with a standard deviation of 3.1 years. The PCC alternative had an assigned initial service life with a mean value of 22 years and a standard deviation of

6.6 years. Each of the PCC rehabilitation activities had an assigned service life of 18 years with a standard deviation of 4 years. User costs were included in the analysis.

### 3.1 Finding the discount rate that changes the lowest cost alternative

In this sensitivity analysis, the effect of the change in discount rate on NPV was investigated. Discount rates were varied between 2% and 8% and incremented by 0.5%. A break-even point was observed in the results. Figure 4 shows that the change in the discount rate alters the ranking of the alternatives in terms of the agency costs around a value of approximately 6%. For this example, user costs do not seem to differentiate between the alternatives for different discount rates. As can be seen in Figure 5, above a discount rate of approximately 6%, the ranking of the alternatives change and alternative 1 becomes the lowest cost alternative.

### 3.2 Altering analysis period

Analysis period was altered between 10 and 70 years keeping all other parameters constant. In this analysis, the analysis period was limited with 70 years, because the input data for Alternative 1 covered a period of 70 years; an initial construction with a service life of 10 years, followed by 6 rehabilitation activities, each with a service life of 10 years. RealCost allows the user

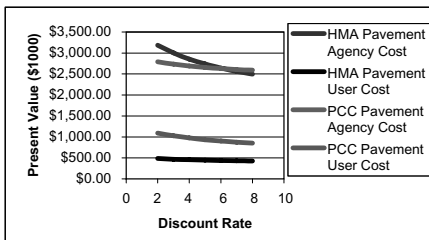


Figure 4. Effects of discount rate on agency and user cost.

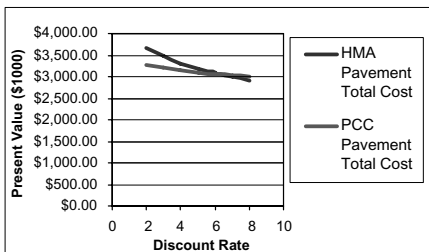


Figure 5. Effects of discount rate on total cost.

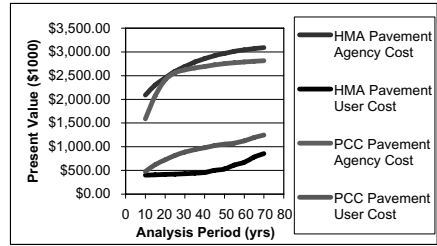


Figure 6. Effects of analysis on agency and user costs.

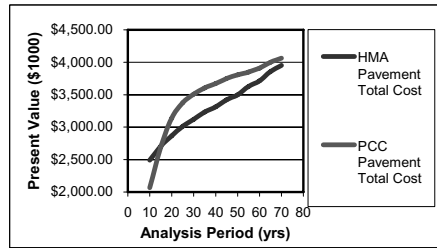


Figure 7. Effects of analysis period on total cost.

to enter data for 6 rehabilitation activities following initial construction. RealCost is currently being modified by FHWA to allow for an analysis containing more rehabilitation activities. As Figure 6 shows, alternative 2 agency costs always remain less than alternative 1 agency costs. However, around an analysis period of 20, the agency costs become very close. It is also worth noting that, in terms of agency costs, alternative 2 is the lower cost option, while in terms of user costs, alternative 1 is the lowest cost option. The change in analysis period, does not alter the ranking of the alternatives in terms of agency and user costs. However, the ranking is changed when total costs are considered. As Figure 7 displays, for analysis periods less than approximately 15 years, alternative 2 is the lowest cost option. For longer analysis periods, alternative 1 is the lowest cost alternative.

The case studies showed that by altering the analysis parameters, a break-even point is observed in the results and the lowest cost alternative might be altered.

## 4 CONCLUSIONS

This paper reported on the results of a nationwide survey that showed the variation in the extent of the LCCA conducted by SHAs.

- Cost, pavement structure (e.g., structural number), and pavement type system (e.g., Interstate, Secondary Roads, etc.) were reported, by many states,

to be the major criteria that would trigger the requirement to conduct LCCA.

- So far, 4 States have implemented the probabilistic approach and several others are conducting research to start implementing it.
- Over 50% of the responding agencies use Real-Cost, DARWin, or some customized software to conduct LCCA. Over one half of the responders indicated that they use RealCost software.
- In calculating the agency costs, maintenance of traffic costs, routine and preventive maintenance costs are considered by approximately 57% and 48% of the agencies, respectively.
- Approximately 58% of the SHAs do not consider any type of user cost. Most of the SHAs incorporating user costs into the analysis, consider only work zone user delay costs.
- Most of the states use a 4% discount rate. Approximately 15% of the respondents address the uncertainty in the discount rate by using a range of values, 3 to 5.3%, instead of using discrete input values. Some states use the OMB discount rate.
- State DOTs are moving towards using longer analysis periods. The majority of the respondents use a 40 year analysis period. However, 20% of the responding agencies use an analysis period of 50 years and one State DOT uses an analysis period of 65 years.
- Majority of state DOTs use historical data from pavement management systems to determine their rehabilitation timings.
- Approximately 56% of the respondents include salvage value in their analysis. Out of these, 80% calculate only serviceable life, and the rest calculate both residual value and serviceable life.
- The sensitivity analysis conducted by the authors showed that by altering the analysis parameters, a break-even point is observed in the results and the lowest cost alternative is altered. Therefore, the importance of conducting a probabilistic analysis using statistical data was shown.

#### ACKNOWLEDGEMENTS

This research was supported by the South Carolina Department of Transportation and Federal Highway

Administration. This support is both acknowledged and appreciated. The contents of this paper reflect the views of the authors who are solely responsible for the facts and the accuracy of data presented herein. The contents do not necessarily reflect the official views of SC DOT, FHWA, Clemson University, or Skanska USA Civil Southeast Inc.

#### REFERENCES

- Daniels, G., Stockton, W.R. & Hundley, R. 2000. Estimating Road User Costs Associated with Highway Construction Projects-Simplified Method. In Transportation Research Record: *Journal of the Transportation Research Board*, No. 1732, TRB, National Research Council: 70–79.
- FHWA (Federal Highway Administration), 2002. Life-Cycle Cost Analysis Primer. Office of Asset Management, Washington, DC.
- FHWA. 2003. *Economic Analysis Primer*. Washington, DC: Federal Highway Administration, Office of Asset Management.
- Guyen, Z. 2006. Life Cycle Cost Analysis of Pavements: State-of-the-Practice. Master's Thesis, Clemson University.
- Herbold, K. 2000. Using Monte Carlo Simulation for Pavement Cost Analysis. Public Roads.
- Jones, D., Lee, C. & Harvey, J. 2005. Economic Implications of Selection of Long-Life versus Conventional Caltrans Rehabilitation Strategies for High-Volume Highways. Draft report prepared for the California Department of Transportation.
- Lindly, J.K. & Clark, P.R. 2004. Characterizing Work Zone Configurations & Effects. Tuscaloosa, AL. University Transportation Center for Alabama, UTCA Report 04406.
- Ozbay, K., Parker, N., Jawad, D. & Hussain, S. 2003. Guidelines for Life Cycle Cost Analysis. Research Project Final Report. Report No: FHWA-NJ-2003-012 New Jersey Department of Transportation, Trenton.
- Ozbay, K., Parker, N., Jawad, D. & Hussain, S. 2004. Life Cycle Cost Analysis: State-of-the-Practice vs State-of-the-Art", *83rd Annual TRB Meeting*, Washington, DC.
- Reigle, J.A. & Zaniewski, J.P. 2002. Risk-Based Life-Cycle Cost Analysis for Project-Level Pavement Management. In Transportation Research Record: *Journal of the Transportation Research Board*, No. 1816, TRB, National Research Council, Washington DC. pp. 34–42.
- Walls, J., III, & Smith, M.R. 1998. Life-Cycle Cost Analysis in Pavement Design. Technical Bulletin FHWA-98-079. FHWA, U.S. Department of Transportation.

# Financial viability of TPSM applied continuous composite bridges

Jun-Hwan Kim, Jin-Hee Ahn, Chi-Young Jung & Sang-Hyo Kim

Yonsei University, Seoul, Korea

**ABSTRACT:** The negative bending moment near the intermediate supports of continuous composite girder bridges induces tensile stresses in the concrete deck and transverse cracks are repeatedly reported. The cracks rapidly deteriorate the concrete deck, giving rise to frequent need for maintenance work. Prestressing methods are usually utilized in this kind of situation for the concrete structures, but no effective and feasible method has yet been proposed for steel-concrete composite structures. A new type of prestressing method entitled TPSM (Thermal Prestressing Method) has been proposed for innovative construction of continuous composite girder bridges by Kim et al. (2007), for effective prestressing of the deck at the negative bending moment regions. This study describes the methodology for the economic analysis of TPSM applied bridges and introduces case studies for demonstration of the financial viability of the TPSM applied bridges compared to conventional continuous composite girder bridges.

## 1 INTRODUCTION

### 1.1 General description of TPSM

The negative bending moment near the intermediate supports of continuous composite girder bridges induces tensile stresses in the concrete deck. Although relatively high ratio of reinforcement is present in these regions, tensile cracks are repeatedly reported. The tensile cracks rapidly deteriorate the concrete deck, giving rise to frequent need for maintenance work. Also due to the tensile stresses, the concrete deck sections at the negative bending moment regions are ignored in the design process and this kind of design concept is a huge drawback regarding effective use of materials. Prestressing methods are usually utilized in this kind of situation for the concrete structures, but no effective and feasible method has yet been proposed for steel-concrete composite structures. A new type of prestressing method entitled TPSM (Thermal Prestressing Method) has been proposed for innovative construction of continuous composite girder bridges (Kim et al. 2007a,b).

In the application of TPSM to continuous composite bridges, downward deflection at the mid-span of the steel girders is induced by temporary heating, which is subsequently used as a prestressing force for developing initial stresses in the concrete deck. Tensile stresses can be eliminated or reduced by thermal prestressing, so that the stress level of the concrete deck due to design loads can be maintained under the allowable tensile stress. As a result, tensile cracks can be mitigated, significantly increasing the

service life of the structure and decreasing maintenance costs.

The additional construction procedure is also straight forward and can be synchronized with the general construction procedure so that no extra construction period is required. Table 1 shows the general construction sequence of the TPSM. First, the steel girders are erected, ready for casting of the deck concrete (Stage 1). Then the heating plates are attached to the lower flanges of the predetermined heating regions before the deck concrete is poured. As a result of heating, the lower part of the girder becomes hotter than the upper part, forming a temperature gradient in a heated section, which causes downward deflection at the mid-span of the steel girder (Stage 2). During the curing

Table 1. General sequence of construction using Thermal Prestressing Method.

Stage	Construction Process
1	
2	
3	
4	

: current phase  
 : previous phase

process of the deck concrete, the temperature gradient is maintained at a predetermined level, which can be achieved without difficulty by using an automatic controller (Stage 3). The heating plates are removed after the deck concrete is cured to a proper strength, which may require 3 to 7 days depending on the type of concrete and its long-term behavioral characteristics. After the girders are cooled down to the ambient temperature, the restoring force of the deformed steel girder induces initial stresses in the concrete deck (Stage 4). Simple equipment and construction procedure will allow considerable reduction in both initial construction cost and the lifetime cost.

For the developed TPSM to be put into practice, the financial viability or the economic feasibility must be guaranteed. In this study, an economic analysis of TPSM applied composite girder bridges versus conventional composite girder bridges is performed for this purpose. The basic theories for the economic analysis will be described within this chapter and some case studies will be shown to demonstrate the financial viability of the TPSM applied bridges.

## 2 FINANCIAL VIABILITY OF TPSM

The life-cycle cost of a TPSM applied composite girder bridge shall include initial construction costs, maintenance costs, and demolition costs. Since virtually no difference exists between the appearance of the conventional and TPSM applied bridges, only the initial construction costs and the maintenance cost will be considered herein. Since most of the factors contributing to the LCC are site and time specific, the cost analysis in this study will assume construction in the mid-US and all the costs will be normalized to the year 2006.

### 2.1 Initial construction cost

Construction costs include design cost and all initial material and labor costs for construction of a bridge. Assuming the design cost difference between conventional bridges and TPSM applied bridges is negligible, the material/labor cost and the thermal prestressing cost, are the factors in need for comparison of the initial construction costs of the two structures. In this study, unit material/labor cost were assumed according to the research by McEleney (2004) and the general contractors price list of the St. Marys Cement Inc. (2006).

The thermal prestressing cost consists of items such as depreciation cost of a heating system, depreciation and fuel cost of engine generators, and additional labor cost due to thermal prestressing. The unit costs of the items were assumed based on the experience learned

during the construction of TPSM applied prototype bridges (Kim et al. 2007b).

### 2.2 Maintenance costs

Of all the elements in a bridge superstructure, bridge decks require the maximum maintenance, for reasons ranging from the cracks, deterioration of the wearing surface, or degradation of the deck itself. For comparing the life-cycle cost of conventional versus TPSM applied composite girder bridges, only the deck maintenance is assumed to make difference in the maintenance cost since other elements of the bridges are scarcely different.

While cost analyses of rest of the categories are straight forward, the calculation of the maintenance cost can be rather difficult. The main reason for this difficulty is due to the cracking of the concrete deck. Observation data to assume the probability of early age cracking is very limited and experiment data is insufficient to presume the effect of thermal prestressing on increasing the durability of the deck. Moreover, the life time or the durability of the concrete deck on continuous composite girder bridges can differ depending on the construction method, weather of the location, concrete mix, design, and etc. In this study therefore, a number of assumptions are made to compute the approximate maintenance cost based on the references available.

It has been verified from the preceding analysis and experiments (Kim et al. 2007a,b) that the initial compressive stresses in the deck induced by TPSM can effectively prevent the transverse cracks. However, it is difficult to predict the effect of TPSM on extending the life time of the concrete deck since thermal prestressing is a newly developed method and more research and observation of bridges constructed using thermal prestressing method is required. As an alternative, analytical measures are utilized to predict the effect of the thermal prestressing method on increasing the durability of the deck.

The durability of the concrete structures, including concrete bridge deck, is mainly affected by the corrosion of reinforcing steel. Corrosion may significantly reduce the long-term performance of reinforced concrete structures, particularly in aggressive environments. Corrosion of reinforcement and/or spalling of the concrete cover may lead to loss of strength (reduction in area of steel or loss of bond) and unserviceability as shown in Figure 1.

Corrosion can be initiated either by direct penetration through flexural cracks or by chloride concentration due to de-icing salt (Fig. 2). Both modes of corrosion initiation are checked for estimation of the limit state. Since the concrete deck is not a critical member regarding the structural integrity, only the serviceability limit state, which refers to a state of the deck



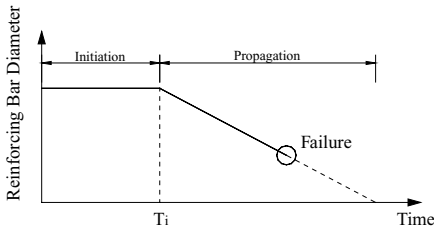


Figure 1. Deterioration process for loss of reinforcing steel.

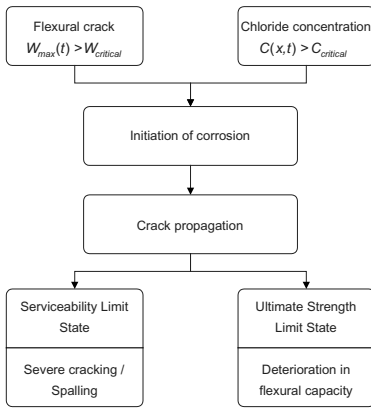


Figure 2. Deterioration process of concrete slabs.

where severe cracking or spalling occurs, is considered in this study.

Once the time to serviceability limit state is calculated, repair cycle can be determined from which the maintenance cost is estimated. For computation of the time to serviceability limit state, methodology for predicting the time to excessive cracking presented in many works (e.g., Liu & Weyers 1998, Stewart & Val 2003) is adopted. For computation of the chloride content, equation presented by Hoffman & Weyers (1994) was adopted. For estimation of the flexural crack width, various design equations are available in design codes, such as Gergely-Lutz equation, the equation in CEB-FIP (1993), and in Eurocode 2(2004). Among these equations, Gergely-Lutz equation is used in this study, which is recommended in ACI-318-99 (1999) and in AASHTO-LRFD specifications (1998).

### 2.3 User costs

User costs accrue to the direct users of the maintenance events. Maintenance and repair of an existing bridge, along with the rerouting of traffic, can impact drivers' personal time and the operating cost of vehicles sitting

in traffic. Accidents, involving harm to both vehicles and human life, tend to increase in road work areas.

The traffic delay costs, idle-capital costs, and accident costs can be computed using simple formulas and traffic statistics. Three types of user cost are considered in this study, which are; (i) driver delay costs-the personal cost to drivers delayed by roadwork, (ii) vehicle operating costs-the capital costs of vehicles delayed by roadwork, and (iii) accident costs-the cost of damage to vehicles and human due to roadwork. For example, the driver delay cost can be calculated based on the following equation:

$$\text{Driver Delay Costs} = \left( \frac{L}{S_a} - \frac{L}{S_n} \right) \times ADT \times N \times w \quad (1)$$

where  $L$  is the length of affected roadway or which cars drive,  $S_a$  is the traffic speed during bridge work activity,  $S_n$  is the normal traffic speed,  $ADT$  is the average daily traffic, measured in number of cars per day,  $N$  is the number of days of road work, and  $w$  is the hourly time value of drivers.

While the calculation is straight-forward, the parameters in the equations are site specific and can vary largely. Therefore, it is difficult to make generalizations about these costs. Instead, the following case study will be presented based on the data acquired from a bridge in a rural Virginia county (Ehlen 2003). The medium level of average daily traffic (ADT) is assumed, starting at 10,000 and linearly increasing to 20,000 by the end of the bridge's service life, assumed as 75 years.

## 3 CASE STUDY OF TWO-SPAN BRIDGE

For comparison of the LCC of conventional and TPSPM applied bridges, a typical 2-span continuous composite girder bridge is considered. Principal design factors of the bridges, such as the girder height and spacing, width and thickness of the concrete slab are assumed to be identical. Material properties of the bridges are also taken to be the same except that of the deck concrete. The deck concrete of the conventional bridges are assumed as 27 MPa grade, whereas 30 MPa concrete is assumed for the TPSPM applied bridges according to the clause regarding the strength of prestressed concrete decks in the *Korean Design Codes for Highway Bridges* (2005).

### 3.1 Description of considered bridge

Figure 3 shows the elevation of the designed conventional and TPSPM applied 2-span continuous bridges. The variation in the flange thickness is determined

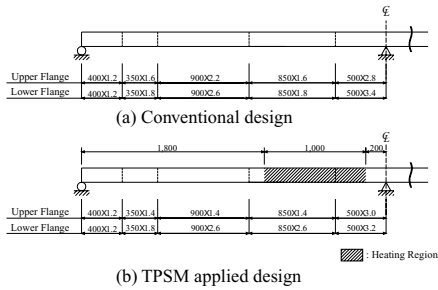


Figure 3. Elevation of conventional and TPSM applied bridges.

Table 2. Total initial cost of two-span continuous bridge.

Components		Conventional (US\$)	TPSM (US\$)
Initial construction costs	Material/fabrication	713,948	712,234
	TPSM	–	8,456
Total		713,948	720,690

based on the ratio of allowable stress to the working stress upon design loads. The flange thickness of the two bridges in Figure 3 share similar level of stress ratio within difference less than 10%. As can be observed from the figure, the upper flange thickness at the positive bending region of the TPSM applied bridge is relatively thinner compared to the conventional bridge. This is made possible due to the initial stresses resulting from thermal prestressing. Near the intermediate support, there is slight increase in the lower flange and a tradeoff decrease in the upper flange. Overall, the total amount of steel decrease when the TPSM is employed.

### 3.2 Initial cost

The total initial construction cost of the conventional and TPSM applied 2-span continuous composite bridges are summarized in Table 2. The cost for the deck concrete increase by a small margin of 1,100 US\$, whereas 2,800 US\$ is saved from the steel girder by application of the TPSM. Due to the thermal prestressing cost, however, the overall initial cost of the TPSM applied 2-span continuous girder bridge is more expensive compared to the conventional bridge by an amount of 6,742 US\$, which is less than 1% of the total initial construction cost. Nevertheless, this may be an insignificant figure considering the economical advantage in aspect of LCC.

### 3.3 Maintenance cost

The time until the serviceability limit state for the 2-span continuous bridge was analyzed. Using the chloride content equation and the flexural crack equation, the time to corrosion initiation must be calculated first. Since the chloride content equation is composed of multiple random variables, Monte Carlo simulation was used. Table 3 shows the input parameters for computation of the time to corrosion initiation due to chloride concentration.

Figure 4 shows the mean chloride concentration at 40 mm depth of the concrete deck with time in years obtained by Monte Carlo simulation using MATLAB with the sample size of 10,000. The probability of corrosion initiation obtained was obtained taking the mean value of 10,000 simulations for each year as shown in Figure 5. The jagged shape of the plotted probability is due to the critical chloride content, which is modeled as a uniformly distributed random variable. Despite of the jagged shape however, it can be judged that the time required for a 50 percentile value of corrosion initiation is approximately 25 years.

Corrosion initiation by flexural cracking can be computed using the previously mentioned equations. Since there are no probabilistic parameters in the equations, the time to corrosion initiation can be calculated deterministically. With the input parameters shown in

Table 3. Statistics of input parameters for computation of chloride concentration.

Parameter	Mean	C.O.V	Distribution
$x$	40 mm	–	–
$D$	$2.0 \times 10^{-8} \text{ cm}^2/\text{s}$	0.75	lognormal
$C_0$	$3.5 \text{ kg/m}^3$	0.5	lognormal
$C_{crit}$	$0.6\text{--}1.2 \text{ kg/m}^3$	–	uniform

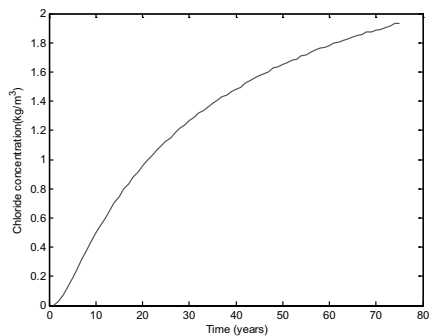


Figure 4. Chloride concentrations at 40 mm depth of the concrete deck.

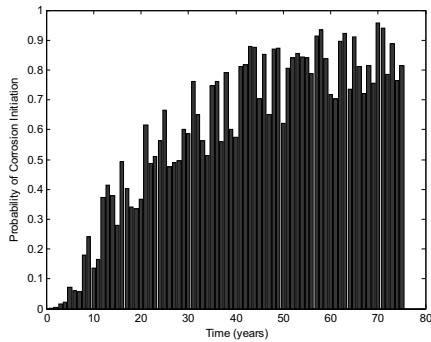


Figure 5. Probability of corrosion initiation.

Table 4. Input parameters for computation of flexural crack.

Parameters	Unit	Conventional method	TPSM
Distance to the neutral axis from the centroid of reinforcement ( $d_1$ )	mm	684.4	385.0
Distance to the neutral axis from the extreme tension fiber ( $d_2$ )	mm	735.4	436.0
Thickness of the concrete cover ( $d_c$ )	mm	40.0	40.0
Diameter of the reinforcing steel ( $D$ )	mm	22.0	22.0
Width of concrete deck ( $b$ )	mm	2260.0	2260.0
Stress calculated in the reinforcement at service loads ( $f_s$ )	MPa	62.63	4.08

Table 4, the time to corrosion initiation for the considered bridge is calculated as depicted in Figure 6. After the flexural crack width breaches the critical crack width threshold, shown in the figure as the hatched area, direct ingress of chlorides will initiate corrosion of the reinforcing steel.

From the analysis of chloride concentration and flexural cracking, the critical path for the corrosion initiation was determined as flexural cracking. Following the works by Stewart & Val (2003), the time to limit crack width, which is the sum of the time to corrosion initiation ( $T_i$ ), the time from corrosion initiation to first cracking ( $T_{1st}$ ), and the time from first cracking to the time when crack width reaches limit crack width ( $T_{ser}$ ), was obtained as summarized in Table 5. It was found that there is a significant difference between the calculated limit crack width between the two types of bridges due to the prestress induced in case of the TPSM applied bridge. Based on the results, repair interval of the deck is assumed as 9 and 16 years

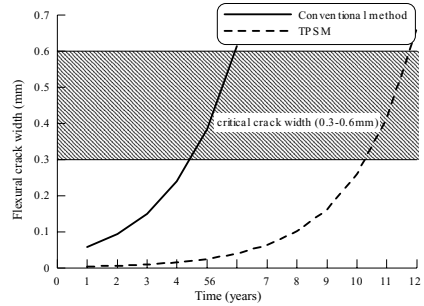


Figure 6. Flexural crack width.

Table 5. Calculated time to limit crack width of 1.0 mm.

Parameters	Conventional method	TPSM
Time to corrosion initiation ( $T_i$ )	6 years	12 years
Estimation of time to propagate to limit crack width ( $T_{sp}$ ) with $T_{1st}$ and $T_{ser}$ obtained using constant corrosion rate	3.10 years	4.20 years
Total time to reach limit crack width	9.10 years	16.20 years

for the conventional and TPSM applied bridge, respectively, while the service life of the deck was assumed as 40 years according to the report from the Korea Ministry of Construction and Transportation (2003). Finally, the maintenance cost can be estimated based on the calculated time to limit crack width as shown in Table 6.

### 3.4 User costs

From the repair/replacement cycle, the user cost can be calculated using the formulas for each costs as summarized in Table 7.

### 3.5 Life-cycle cost comparison of conventional and TPSM applied bridges

The total life-cycle cost of the conventional and TPSM applied 2-span bridges are summarized in Table 8. In spite of the 6,742 US\$ cost increase in the initial cost due to extra cost for thermal prestressing, the total LCC cost savings owing to the application of thermal prestressing was calculated as 43,219 US\$ in present value.

Table 6. Repair/replacement cost during the service life of considered bridges.

Conventional bridge			TPSM		
Year	Repair/replacement	Cost in PV (US\$)	Year	Repair/replacement	Cost in PV (US\$)
9	Repair	10,117	16	Repair	7,688
18	Repair	7,108	32	Repair	4,105
27	Repair	4,994	40	Replacement	75,184
36	Repair	3,509	56	Repair	1,601
40	Replacement	75,184	72	Repair	855
49	Repair	2,107	—	—	—
58	Repair	1,480	—	—	—
67	Repair	1,040	—	—	—
Total		105,541	Total		89,433

Table 7. Total calculated user costs.

User costs	Conventional		TPSM	
	Cost (US\$)	PV (US\$)	Cost (US\$)	PV (US\$)
Driver delay costs	133,703	32,552	101,056	21,387
Vehicle operating costs	213,926	52,083	161,690	34,219
Accident costs	57,760	14,062	43,656	9,239
Total user costs	405,389	98,697	306,402	64,844

Table 8. Life-cycle cost of conventional and TPSM applied 2-span bridges.

Components		Conventional (US\$)	TPSM (US\$)
Initial construction costs	Material/fabrication	713,948	712,234
Maintenance costs	TPSM	—	8,456
	Deck repair/replacement	105,541	89,433
	User costs	98,697	64,844
Total		918,186	874,967

#### 4 CONCLUSIONS

In this paper, the financial viability of the TPSM applied bridge has been examined on basis of the life-cycle cost. Initial costs as well as maintenance costs including the user costs have been estimated and compared with those of conventional continuous composite girder bridges. Through a case study of 2-span continuous bridge, it has been elucidated that the life-cycle efficiency of the TPSM applied bridges exceeds that of the conventional bridges as shown in Table 8.

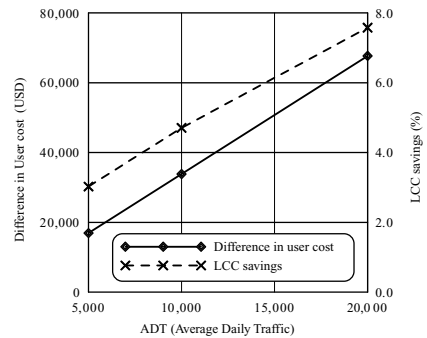


Figure 7. User cost and LCC savings.

By application of the TPSM, the LCC can be reduced as much as approximately 5% compared to that of conventional bridges. Although this is only a general figure and may differ depending on the location of the bridge and environment, it is deemed that the TPSM applied bridge possess significant economical competitiveness over the conventional bridges.

Maintenance cost being the major component of the LCC savings, the TPSM is expected to be more competitive for aggressive environment with relatively larger ADT. Figure 7 shows the changes in the user cost difference and LCC savings depending on the ADT of the considered 2-span bridge. The difference in the user cost, that is the difference between the user cost of the conventional bridge and the TPSM applied bridge, increases linearly with the ADT. In case of the subject 2-span continuous bridge, therefore, the plot shows that as much as 7.8% of the total LCC can be saved compared to the conventional bridges in case of a bridge with ADT of 20,000. Considering the preventing effect of early age cracking and extra cost savings as the technology gets more mature, the cost effectiveness may further increase.

#### ACKNOWLEDGMENTS

This study was supported by “the Korean Ministry of Construction and Transportation under Award Number A-02 (2001) through Korea Institute of Construction Technology”. The work was also supported in part by Yonsei University, Center for Future Infrastructure, a Brain Korea 21 program, Korea. The authors are grateful for their support and is a part of the “Improvement and Standardization of Construction Specifications and Design Criteria of Materials and Facilities Based on Performance” study from the “Standardization of Construction Specifications and Design Criteria based on Performance”, the “Construction & Transportation R&D Policy and Infrastructure Project (‘06~’11)”.

## REFERENCES

- AASHTO. 1998. *AASHTO LRFD Bridge Design Specification, SI units, 2nd edition*, American Association of State Highway and Transportation Officials, Washington, D.C.
- American Concrete Institute. 1999. *Building Code Requirements for Structural Concrete and Commentary and Notes*, ACI 318-99.
- British Standards. 2004. *Eurocode 2: Design of concrete Structures*, BS EN 1992-1-1.
- CEB. 1993. *CEB-FIP Model Code 1990*, CEB Bulletin d'Information, N° 213/214, Thomas Telford, London.
- Ehlen, M. 2003. *BridgeLCC 2.0 Users Manual: Life-Cycle Costing Software for the Preliminary Design of Bridges*. National Institute of Standards and Technology, Report #NIST GCR 03-853, Gaithersburg, MD.
- Hoffman, P.C. & Weyers, R.E. 1994. Predicting Critical Chloride Levels in Concrete Bridge Decks. In Schueller, G.I., Shinozuka, M., Yao, J.T.P., Balkema, A.A (eds), *Structural Safety and Reliability: Proceedings of ICOSSAR '93*: 957–959. Rotterdam.
- Kim, S.H., Kim, J.H., Ahn, J.H. & Song, H.W. 2007a. An Analytical Investigation of Thermal Prestressing Method for Continuous Composite Girder Bridges, *Magazine of Concrete Research* 59 (3): 165–178.
- Kim, S.H., Kim, J.H., Ahn, J.H. & Song, H.W. 2007b. An Experimental Investigation of Thermal Prestressing Method for Continuous Composite Steel Girder Bridges, *Magazine of Concrete Research* 59 (3): 179–188.
- Liu, Y. & Weyers, R.E. 1998. Modeling the Time-to-Corrosion Cracking in Chloride Contaminated Reinforced Concrete Structures, *ACI Materials Journal* 95 (6): 675–681.
- McEleney, W. 2004. Minimizing Steel Costs, GoBridges.com for the Business of Bridge Design and Rehabilitation, <http://www.gobridges.com/article.asp?id=358>. Date accessed: November. 2006.
- MOCT. 2005. *Korean Design Codes for Highway Bridges*, Ministry of Construction and Transportation (in Korean).
- MOCT. 2003. *LCC analysis of Highway Bridges Depending on Structural Type*, Ministry of Construction and Transportation (in Korean).
- Stewart, M.G. & Val, D.V. 2003. Multiple Limit States and Expected Failure Costs for Deteriorating Reinforced Concrete Bridges, *Journal of Bridge Engineering* 8 (6): 405–415.
- St. Marys Cement Co. 2006. General Contractor's Price List (2006), [http://www.stmaryscement.com/saintmaryscementinc/SMC\\_cementProd.asp](http://www.stmaryscement.com/saintmaryscementinc/SMC_cementProd.asp). Date accessed: November 2006.

# Effect of cumulative seismic damage on life-cycle cost of reinforced concrete bridges

R. Kumar, P. Gardoni & M. Sanchez-Silva

Zachry Department of Civil Engineering, Texas A&M University, TX, USA

**ABSTRACT:** This paper presents a probabilistic approach to compute the life-cycle cost of reinforced concrete (RC) bridges in earthquake prone regions. The approach is based on low-cycle fatigue theory of damage accumulation. The proposed methodology accounts for the uncertainties in the ground motion parameters, the distance from source and the seismic demand on the bridge. The statistics of the accumulated damage and the cost of repairs throughout the bridge life-cycle are obtained by Monte-Carlo simulation. As an illustration, the effect of design parameters on the life-cycle cost of an example RC bridge is studied. The results show to be valuable in better estimating the condition of existing bridges and, therefore, can help schedule inspection and maintenance programs. In addition, by taking into consideration the deterioration process over a bridge life-cycle, it is possible to make an estimate of the optimum design parameters by minimizing, for example, the expected cost throughout the life of the structure.

## 1 INTRODUCTION

Bridges experience various damages and deteriorations during their service life. Therefore, they need regular inspections, maintenance and repairs to ensure that they perform above a minimum performance level at all times. A large amount of funds are required today for the repairs and upgrade of deficient bridges. For example, according to USA TODAY (2006), the Federal Highway Administration puts the current cost of upgrading bridges at \$63 billion. This situation makes optimum fund allocation and life-cycle cost analysis a priority for bridge management systems and resource allocation.

The problem of the change in failure probability of a bridge over a period of time due to cumulative seismic damage has not been addressed in much detail in *LCC* analysis of bridges. The objective of this paper is to present a methodology to include the effect of cumulative seismic damage of reinforced concrete (RC) bridges in the life-cycle cost analysis. A variation of the low-cycle fatigue theory (Kunnath et al. 1997) that takes into consideration the deterioration in concrete and steel is used in this work.

The methodology is developed for a single-column bridge idealized as a single degree of freedom (SDOF) system. The formulation of the cumulative seismic damage for bridges with multiple columns can be built on the proposed approach but is beyond the scope of this paper. As a practical illustration, the proposed formulation is used to assess the life-cycle cost (*LCC*) of an example bridge.

## 2 SEISMICITY AND STRUCTURAL DEMAND

Structural *LCC* analysis requires first to estimate the seismic characteristics of a region (e.g., earthquake sources and rates of occurrence). This section presents the probabilistic model used in the proposed methodology to simulate the occurrence and the magnitude of earthquakes. In addition, this section describes the computation of structural demand parameters like drift, seismic energy, and number of inelastic cycles of the response of an equivalent SDOF system.

### 2.1 Seismicity modeling and prediction of ground motion parameters

In this study, the moment magnitude  $M_w$  is used to express the intensity at the source of an earthquake. Magnitudes are sampled independently of the time of occurrence of each earthquake using a cumulative distribution function from the frequency-magnitude relationship given by Gutenberg and Richter (1944) as

$$N_{eq}(M_w) = 10^{a-bM_w} \quad (1)$$

where,  $N_{eq}(M_w)$  is the cumulative annual rate of earthquakes having magnitudes greater than  $M_w$ ,  $a$  and  $b$  are dimensionless parameters that depend on the regional

seismicity. The derived sampling distribution is then written as

$$F(M_w) = 1 - \frac{10^{a-bM_w}}{10^{a-bM_{w,\min}}} \quad (2)$$

where,  $M_{w,\min}$  is the smallest possible magnitude of earthquakes for the given region.

The occurrence of earthquakes is modeled as a Poisson's process with a mean rate appropriate for the region. The Poisson distribution is written as

$$f(x) = \frac{(v)^x}{x!} \exp(-v) \quad (3)$$

where,  $x$  is the number of occurrences of an earthquake in the time window  $T_H$  which is the time span over which  $LCC$  is computed,  $v$  is the mean number of earthquake occurrences in  $T_H$  and  $f(x)$  is the probability density function (PDF) of  $x$ . In a Poisson's process the time intervals between two occurrences follow an exponential distribution. Therefore, the time of occurrences of the  $(M + 1)$ th earthquake is simulated as follows:

$$t_{M+1} = t_M + \Delta t \quad M = 1, 2, 3, \dots \quad (4)$$

where,  $t_M$  is the time of occurrence of the  $M$ th earthquake and  $\Delta t$  is the time interval between two earthquakes simulated using the following PDF

$$f(\Delta t) = \left(\frac{v}{T_H}\right) e^{-\left(\frac{v\Delta t}{T_H}\right)} \quad (5)$$

The peak ground acceleration  $A_H$  and peak ground velocity  $V_H$  at the bridge site are computed using the ground motion attenuation relationships given by Campbell (1997) from  $R_{SEIS}$ , which is the distance of the source from the site of the bridge,  $F$ , which is an index variable used to indicate the style of faulting and  $D$ , which is depth to the base rock from ground surface at the bridge site.

## 2.2 Spectral acceleration and seismic energy demand

The demand parameters needed in the proposed formulation are the spectral acceleration,  $S_a$ , and the seismic energy demand,  $E_I$ , for each simulated earthquake. The spectral acceleration  $S_a$  is computed by scaling  $A_H$  following Kunnath and Chai (2004) as follows:

$$S_a = \Omega_a A_H \quad (6)$$

where,  $\Omega_a$  is a scaling factor defined as

$$\Omega_a = \begin{cases} 1 + 2.5(C_a - 1) \frac{T}{T_c} & 0 < T \leq 0.4T_c \\ C_a & 0.4T_c < T \leq T_c \\ 2\pi C_v \frac{V_H}{A_H T} & T < 0.4T_c \end{cases} \quad (7)$$

where,  $T$  is the fundamental period of the bridge (or the equivalent SDOF system),  $T_c$  is the characteristic period of ground motion,  $C_a$  is the ratio of elastic spectral acceleration to peak ground acceleration in the short period range, and  $C_v$  is the ratio of spectral velocity to peak ground velocity in the velocity controlled region of the response spectrum. The values of  $C_a$  and  $C_v$  are 2.5 and 2.0, respectively. The value of  $T_c$  is given by Eq. (8).

$$T_c = 2\pi \frac{C_v V_H}{C_a A_H} \quad (8)$$

The seismic energy demand  $E_I$  is defined by Kunnath and Chai (2004) as

$$E_I = \frac{1}{2} m v_e^2 \quad (9)$$

where,  $v_e$  is the equivalent input energy velocity given by Eq. (10)

$$v_e = \Omega_v V_H \quad (10)$$

where,  $\Omega_v$  is a velocity amplification factor defined as

$$\Omega_v = \begin{cases} \Omega_v^* \left[ \frac{2T}{T_c} - \left( \frac{T}{T_c} \right)^2 \right] & T \leq T_c \\ \Omega_v^* \left[ \frac{T}{T_c} \right]^{-\lambda} & T > T_c \end{cases} \quad (11)$$

where,  $\Omega_v^*$  is an energy amplification factor given as

$$\Omega_v^* = \frac{0.25 A_H}{V_H} \sqrt{t_d T_c} \sqrt{\frac{\lambda + 0.5}{2\lambda + 2}} \quad (12)$$

where,  $\lambda$  is an input energy spectrum parameter equal to 0.5 as suggested by Kunnath and Chai (2004), and  $t_d$  is the strong ground motion duration. The value of  $t_d$  is given by Trifunac and Brady (1975) as follows:

$$t_d = -4.88s + 2.33M_w + 0.149R_{SEIS} \quad (13)$$

where  $s$  is a geologic site parameter and is equal to 0.0, 1.0 and 2.0 for alluvium, intermediate and rock, respectively. The type of soil used for the numerical example shown later in this paper is alluvium.

### 2.3 Peak displacement demand

The quantities  $S_d$  and  $T$  are used to compute the peak displacement demand  $U_{\max}$  based on the probabilistic demand model developed by Gardoni et al. (2003) as

$$\ln\left(\frac{U_{\max}}{H}\right) = 0.61 + 3.90\theta_{\delta 2} + (1 + \theta_{\delta 2})\hat{d}_{\delta} + \sigma_{\delta}\varepsilon_{\delta} \quad (14)$$

where,  $H$  is the clear height of the column,  $\theta_{\delta 2}$  is a model parameter equal to  $-0.153$  and  $\sigma_b = 0.216$ . The variable  $d_{\delta}$  is the natural logarithm of the deterministic drift demand computed using a deterministic procedure originally proposed by Chopra and Goel (1999) for the case of buildings and later modified by Gardoni et al. (2003) for the case of bridges, and  $\varepsilon_{\delta}$  is a random variable that has the standard normal distribution.

### 2.4 Number of inelastic cycles

For a given earthquake response, the equivalent number of constant amplitude inelastic cycles  $N$  corresponding to a certain amplitude is needed to compute the seismic damage. The value of  $N$  corresponding to  $U_{\max}$  is obtained from cyclic demand spectrum (Kunnath and Chai, 2004) as

$$N = \frac{\alpha E_I}{4\alpha_h V_y U_{\max}} \quad (15)$$

where  $V_y$  is the lateral force at yield and the parameter  $\alpha$  is the ratio between the hysteretic energy and the seismic energy demand,  $E_I$ , that can be written as

$$\alpha = 1.13 \frac{(\mu - 1)^{0.82}}{\mu} \quad (16)$$

where,  $\mu$  is the ductility demand given by

$$\mu = \frac{U_{\max}}{U_y} \quad (17)$$

where  $U_y$  is the displacement at yield of the column top. The parameter  $\alpha_h$  is a coefficient suggested by Kunnath and Chai (2004) to account for the deterioration of stiffness due to cyclic loading and is equal to 0.5.

## 3 CUMULATIVE SEISMIC DAMAGE

Under earthquake loading, bridge columns undergo several cycles of inelastic deflections. Therefore, low-cycle fatigue analysis is used in this paper to evaluate the seismic damage. In addition, an approximate strength degradation equation suggested by Das et al. (2006) is used to compute the structural properties of the damaged structure. This section first presents the background and the method adopted to model the low-cycle fatigue. Then, the computation of damage

index  $DI$  is discussed. Lastly, the methodology to compute structural properties of a damaged structure is presented.

### 3.1 Low-cycle fatigue

Based on Coffin (1954) and Manson (1953), the Coffin–Manson theory of fatigue formulates the behavior of longitudinal bars under reversed cyclic loading as

$$\varepsilon_p = \varepsilon_f' (2N_f)^c \quad (18)$$

where,  $\varepsilon_p$  is the plastic strain amplitude,  $\varepsilon_f$  and  $c$  are material constants determined experimentally,  $2N_f$  is the number of half cycles for the first fatigue crack on the longitudinal reinforcement bar. Mander et al. (1994) obtained the following expression for  $\varepsilon_p$  based on experiments on reinforcement bars:

$$\varepsilon_p = 0.08(2N_f)^{-0.5} \quad (19)$$

Similarly, Kunnath et al. (1997) obtained the following expression:

$$\varepsilon_p = 0.065(2N_f)^{-0.436} \quad (20)$$

In this study, instead of the relation between  $\varepsilon_p$  and  $N_f$  (i.e., Eqs. (18) through (20)) we use a modification of the relation suggested by Kunnath and Chai (2004) to model the low-cycle fatigue behavior for circular ductile RC columns as follows:

$$N_f = \left(\frac{c_1}{\mu}\right)^{c_2} \quad (21)$$

where,  $N_f$  is number of cycles to failure corresponding to the ductility demand  $\mu$ ,  $c_1$  is a constant equal to 8.25 and  $c_2$  is a constant equal to 4.0. The above expression can be used only for the first earthquake and has to be modified for the future earthquakes because the column deteriorates with every experienced earthquake. We propose a variation of Eq. (21) to make it suitable for damaged columns as follows

$$N_{fM} = \left(\frac{8.25}{\mu}\right)^4 - \sum_{i=1}^{M-1} N_i \quad M = 2, 3, 4, \dots \quad (22)$$

where,  $N_{fM}$  is the number of cycles to failure for the  $M$ th earthquake and  $N_i$  is the number of cycles in the  $i$ th earthquake that preceded. The expression in Eq. (22) can be explained using Figure 1. If  $N_i$  is the number of cycles used up in the  $i$ th event, then  $N_i$  has to be subtracted from the column capacity for the  $i$ th event to obtain the deteriorated capacity for the  $(i + 1)$ th event. Thus, the fatigue curve after the  $i$ th event is translated by the amount  $N_i$  towards the left.



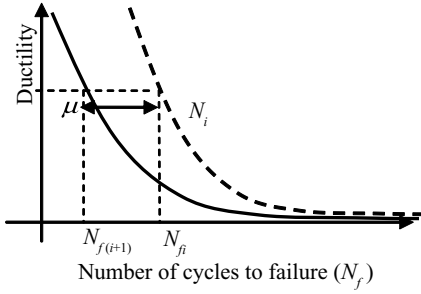


Figure 1. Updating fatigue curve.

### 3.2 Cumulative damage index

Using the well known Miner's rule explained in Miner (1945), the cumulative damage index can be written as follows:

$$DI = \sum_{j=1}^m \frac{1}{2N_{fj}} \quad (23)$$

where,  $DI$  is the cumulative damage index after  $m$  half-cycles,  $N_{fj}$  is the number of cycles to failure corresponding to the displacement in the  $j$ th half-cycle of loading. Eq. (23) can be modified to compute the cumulative seismic damage index after the  $M$ th earthquake as follows:

$$DI_M = \frac{N_M}{N_{fM}} + DI_{M-1} \quad M = 2, 3, 4, \dots \quad (24)$$

where,  $N_M$  is the equivalent number of constant amplitude inelastic cycles in the  $M$ th earthquake computed using Eq. (15) and  $N_{fM}$  is the number of cycles to failure for the peak displacement of  $M$ th earthquake computed using Eq. (22). Based on the Miner's rule, failure is assumed to occur when  $DI \geq 1.0$ .

### 3.3 Structural properties of damaged structure

The structural properties  $\mathbf{x}_p$  of the pristine bridge are defined as follows:

$$\mathbf{x}_p = (k, T, U_y, V_y) \quad (25)$$

where,  $k$  is the lateral column stiffness. The vector  $\mathbf{x}_p$  in Eq. (25) is represented by  $\mathbf{x}_{pM}^-$  right before the  $M$ th earthquake and by  $\mathbf{x}_{pM}^+$  right after the  $M$ th earthquake.

$$\mathbf{x}_{pM}^- = (k_M^-, T_M^-, U_{yM}^-, V_{yM}^-) \quad M = 1, 2, 3, \dots \quad (26)$$

$$\mathbf{x}_{pM}^+ = (k_M^+, T_M^+, U_{yM}^+, V_{yM}^+) \quad M = 1, 2, 3, \dots \quad (27)$$

Due to structural damage it is expected that column stiffness  $k$  decreases due to each experienced earthquake. The cyclic loading during each earthquake also results in the failure of the bond between steel and

Table 1. Statistical parameters for seismicity modeling.

Variable	Distribution	Parameters
$M_w$	See Eq. (3) $M_w \geq 5.5$	$a = 4.56 \quad b = 0.91$
$R_{SETS}$	Uniform $75 \text{ km} \leq R_{SETS} \leq 100 \text{ km}$	
$D$	Uniform $3 \text{ km} \leq D \leq 6 \text{ km}$	
$F$	Bernoulli $F = 0, 1$	$p = 0.5$
$x$	Poisson $x \geq 0$	$v = 150$
		$T_H = 75 \text{ yrs}$

Table 2. Structural properties of the example bridge.

Quantity	Symbol	Value
Axial load on column	$P$	$0.1A_g f_c$
Height of column	$H(\text{mm})$	4,000
Diameter of column	$D(\text{mm})$	1,500
Area of longitudinal bars	$\rho_l(\%)$	2.0
Diameter of transverse reinf.	$d_s(\text{mm})$	9.5
Spacing of transverse reinf.	$s_v(\text{mm})$	60
Nominal strength of concrete	$f'_c(\text{MPa})$	36
Nominal yield strength of steel	$f_y(\text{MPa})$	475

concrete, which results in a larger displacement at yield  $U_y$ . Das et al. (2006) suggested Eqs. (28) and (29) to account for any change in the stiffness and displacement at yield due to an earthquake.

$$k_M^+ = k_M^- \left[ 1 - \frac{U_{\max M} - U_{yM}^-}{U_u - U_{yM}^-} \right]^{0.1} \quad M = 1, 2, 3, \dots \quad (28)$$

where,  $k_M^-$  and  $k_M^+$  are column stiffness right before and after the  $M$ th earthquake. The quantity  $U_u$  is the maximum displacement under monotonic loading of the pristine column. The yield displacement  $U_{yM}^+$  after the  $M$ th earthquake is given by Eq. (29)

$$U_{yM}^+ = \left[ \frac{k + k_M^-}{k + k_M^+} \right] U_{yM}^- \quad M = 1, 2, 3, \dots \quad (29)$$

where,  $k$  is the pristine column stiffness. As expected, these equations show that the earthquake loading decreases the column stiffness and increases the displacement at yield. The values of  $T_M^+$  and  $V_{yM}^+$  can be found from following equations:

$$T_M^+ = 2\pi \sqrt{\frac{m}{k_M^+}} \quad M = 1, 2, 3, \dots \quad (30)$$

$$V_{yM}^+ = k_M^+ U_{yM}^+ \quad M = 1, 2, 3, \dots \quad (31)$$

A basic Monte-Carlo simulation using the random variables listed in Table 1 and the structural parameters listed in Table 2 is performed to compute the

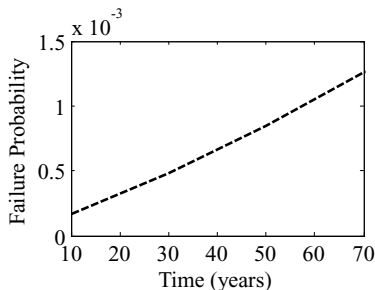


Figure 2. Effective of cumulative seismic damage on annual failure rate. Numerical error or simulation = 2%.

failure probabilities at various time instances during the service life of an example bridge typical of current California's practice. As expected it is found that the failure probability increases with the age of the bridge due to the damage accumulated during past earthquakes (Figure 2).

#### 4 LIFE-CYCLE COST ANALYSIS

The  $LCC$  of a bridge can be expressed mathematically as follows:

$$LCC = C_C + NPV(C_{IN}) + NPV(C_M) + NPV(C_F) \quad (32)$$

where,  $C_C$  = initial construction cost,  $C_{IN}$  = cost of inspections,  $C_M$  = routine maintenance costs,  $C_F$  = failure costs. Inspections, failures and maintenances occur at different instances in time, thus it is necessary to transform all the costs to the net present value (NPV). This paper focuses only on the computation of  $C_F$ , accounting for the effects of earthquakes. The bridge is allowed to deteriorate until collapse (i.e.,  $DI \geq 1.0$ ) without receiving any maintenance. The entire bridge deck and column is replaced at collapse and the bridge is assumed to regain full strength after replacement. Given the focus of this paper, the values of  $C_{IN}$  and  $C_M$  are taken equal to zero.

The cost of failure includes the indirect losses due to the disruption of the activities that relied on the use of the bridge, and direct costs like the loss of the existing structure and the cost of rebuilding it. This study focuses on the direct costs of failure only. Stewart and Val (2003) assumed the total cost of failure including all direct and indirect costs due to collapse to be ten times the construction cost (i.e.,  $C_F = 10C_C$ ). For this study we focus only on direct costs of failure and assume it to be equal to  $2C_C$ . Following the works of Kong and Frangopol (2003) and Stewart and Val (2003) the NPV of  $C_F$  is given by

$$NPV(C_F) = \frac{C_F}{(1+r)^{t_F}} \quad (33)$$

where,  $r$  is the discount rate and  $t_F$  is the time of failure. Substituting the values of NPV ( $C_F$ ) in Eq. (32) we obtain

$$LCC = C_C + \sum_{i=1}^{n_F} \frac{2C_C}{(1+r)^{t_F}} \quad (34)$$

where,  $n_F$  is the number of failures in the time window  $T_H$ .

The total cost of the bridge construction  $C_C$  can be partitioned into the construction cost of the piers  $C_{pier}$ , the deck slab  $C_{deck}$ , and the piles  $C_{pile}$ . Therefore,  $C_C$  can be written as

$$C_C = C_{pier} + C_{deck} + C_{pile} \quad (35)$$

The value of  $C_{pier}$  is computed as

$$C_{pier} = \frac{\pi d^2 H C_{uc}}{4} + \frac{\pi [\rho_t d^2 + \rho_s (D - 2d_c)^2] H \gamma_s C_{us}}{4} \quad (36)$$

where,  $C_{uc}$  is the cost per unit volume of the concrete work in column,  $C_{us}$  is the cost per unit weight of steel reinforcement work. It should be noted that the unit costs  $C_{uc}$  and  $C_{us}$  include the cost of material, labor and equipment used in the construction. The parameter  $\gamma_s$  is weight density of steel,  $\rho_t$  is area ratio of longitudinal steel to gross column area, and  $\rho_s$  is volumetric ratio of shear reinforcement to the column core. To illustrate of the relation between  $LCC$  and design parameters, the  $LCC$  analysis is carried out by varying the column diameter  $D$ . The column strength parameters can also be varied by changing the percentage of steel reinforcement, grades of steel and concrete. But for convenience and economy in construction and design process usually the choices in these parameters are limited.

The values of  $C_{deck}$  and  $C_{pile}$  are independent of  $\rho_t$  and  $D$  and are thus assumed to be constant in the  $LCC$  analysis. They are computed using the unit construction costs provided by CALTRANS Contract Cost Data (2006). The total deck area is assumed to be 40 m by 10 m and pile depth is assumed to be 15 m. Table 3 provides the values of all the parameters used in the computation of  $C_C$ .

A Monte-Carlo simulation technique is used to compute the expected  $LCC$ . Figure 3 shows the plots for failure probability for different values of column diameters at  $t = 0$  (dashed line) and  $t = 75$  years (solid line). As expected, the failure probability is found to increase with time due to accumulated seismic damage and to decrease with  $D$  increasing. Figure 4 shows the plot of the mean  $LCC$ , mean  $C_F$  and  $C_C$  for different values of  $D$ . As expected the value of  $C_F$  decreases and  $C_C$  increases by increasing  $D$ . The mean  $LCC$  is the

Table 3. Parameters used in computing life-cycle cost.

Item	Cost
Steel work	\$2.25/Kg
Concrete work	\$800/m <sup>3</sup>
$C_{deck}$	\$450/m <sup>2</sup>
$C_{pile}$	\$250/m
Length of bridge	#2,20 m spans
Width of bridge	10 m
Pile depth	15 m
$C_L$	2 $C_c$
$r$	2%

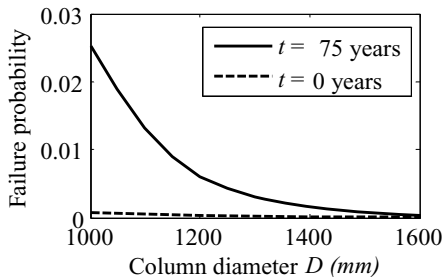


Figure 3. Failure probabilities at  $t = 0$  years and  $t = 75$  years.

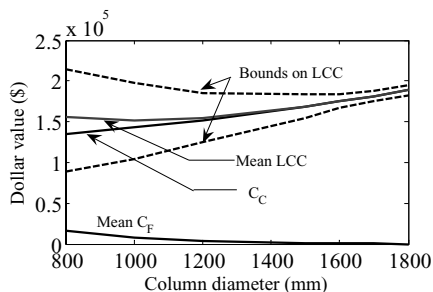


Figure 4. Relation of  $LCC$ ,  $C_F$  and  $C_C$  on column diameter. sum of  $C_C$  and mean  $C_F$ . It was found that the mean value of  $LCC$  is minimum for  $D$  close to 1,000 mm.

## 5 CONCLUSIONS

A methodology is presented to include the effect of cumulative seismic damage in the life-cycle cost analysis of bridges. The uncertainties in the ground motion parameters, seismic demand on the bridge are accounted for in the methodology. The same methodology can also be used to account for the uncertainties in distance to the source and the style of faulting.

Using an example bridge typical of current California's practice, it is shown that the failure probabilities increase significantly over a bridge service-life. This is because of the damage accumulated during

the repeated occurrence of small earthquakes that do not lead to a failure the bridge. The developed methodology can be used in a life-cycle cost analysis to assess the optimal design parameters for a bridge. As a practical illustration, the proposed formulation was used to assess the  $LCC$  of the example bridge and find the optimal column diameter.

## REFERENCES

- California Department of Transportation (Caltrans). (2006). Contract Cost Data Book—A summary of cost by items for highway construction projects, Caltrans, Sacramento, Calif.
- Campbell, K. (1997). "Empirical Near-source Attenuation Relationship for Horizontal and Vertical Components of Peak Ground Acceleration, Peak Ground Velocity, and Pseudo-absolute Acceleration Response Spectra." *Seismological Research Letters*, 68 (1), 154–197.
- Chopra, A.K. and Goel, R.K. (1999). "Capacity-demand-diagram methods for estimating seismic deformation of inelastic structures: SDF systems." *Pacific Earthquake Engineering Research Center, University of California, Berkeley, California, Report Number PEER-1999/02*.
- Das, S., Gupta, V.K. and Srimahavishnu, V. (2006). "Damage Based Design with No Repairs for Multiple Events and its Sensitivity to Seismicity Model". *Earthquake Engineering and Structural Dynamics*, 36 (3), 307–325.
- Gardoni, P., Mosalam, K.M. and Kiureghian, A.D. (2003). "Probabilistic Seismic Demand Models and Fragility Models for RC Bridges." *Journal of Earthquake Engineering*, 7 (1), 79–106.
- Gutenberg, B. and Richter, C.F. (1944). "Frequency of Earthquakes in California" *Bulletin of the Seismological Society of America*, 34 (4), 185–188.
- Jones, C. (2006). "Upkeep Costs Rises as USA's Bridges Age." <<http://www.usatoday.com>> (April 15, 2007).
- Kong, J.S. and Frangopol, D.M. (2003). "Life-Cycle Reliability-Based Maintenance Cost Optimization of Deteriorating Structures with Emphasis on Bridges". *Journal of Structural Engineering*, 129 (6) 818–828.
- Kunnath, S.K. and Chai, Y.H. (2004). "Cumulative Damage-based Inelastic Demand Spectrum." *Earthquake Engineering and Structural Dynamics*, 33 (4), 499–520.
- Kunnath, S.K., El-Bahy, A., Taylor, A.W. and Stone, W.C. (1997). "Cumulative Seismic Damage of Reinforced Concrete Bridge Piers." *National Institute of Standards and Technology Internal Report (NISTIR) 6075*.
- Mander, J.B., Panthaki, F.D. and Kasalanati, A. (1994). "Low-cycle Fatigue Behavior of Reinforcing Steel." *Journal of Materials in Civil Engineering*, 6 (4), 453–468.
- Stewart, M.G and Val, D.V. (2003). "Multiple Limit States and Expected Failure Costs for Deteriorating Reinforced Concrete Bridges." *Journal of Bridge Engineering*, 8 (6), 405–415.
- Trifunac, M.D. and Brady, A.G. (1975). "A study on the Duration of Strong Earthquake Ground Motion". *Bulletin of the Seismological Society of America*, 65 (3), 581–626.

# An information model for life-cycle cost management of cable-stayed bridge

S.H. Lee, M.G. Huang & B.G. Kim

*School of Civil and Environmental Engineering, Yonsei University, Seoul, Korea*

Y.H. Park

*Korea Highway Corporation, Dongtan-myeon, Hwasung-si, Gyeonggi-do, Korea*

**ABSTRACT:** In this paper, an information model is proposed for the life-cycle cost data management of cable-stayed bridges. Firstly, a unit cost model for all cost data throughout bridge lifetime is proposed in an attempt to detailedly represent various cost elements in a general expression. Each cost element has a dollar value which could be deterministic, probabilistic, or fuzzy. Then, an information model based on ISO/STEP standard is developed for the integrated cost data management of highway bridges. The cost information is categorized into initial cost, operation and maintenance cost, decommission cost, and others. Finally, the developed information model is applied to the Seohae Grand Bridge, which is currently the longest cable-stayed bridge in South Korea, to illustrate its applicability and efficiency. The model can be an integral part of an interoperable bridge project information system because it is international standard based. Future works for the study are given in the conclusion.

## 1 INTRODUCTION

Concepts of life cycle cost analysis, whose purpose is to specify and schedule an economically efficient set of actions (TRB 2003), and asset management, which is a systematic process of maintaining, updating, and operating physical assets cost-effectively (FHWA 2004), have been widely accepted as useful and powerful tools for the decision making of civil infrastructure. More recently, FHWA (Friedland et al. 2006) is initiating Long Term Bridge Performance (LTBP) program which will instrument, monitor, and evaluate a large number of bridges in USA in order to capture performance over 20-year period of time. Both concepts and the program require for comprehensively collections and integrated management of life cycle cost data and information.

Meanwhile, the life cycle cost management should be interoperable in order to reduce the cost of rework due to inadequate interoperability throughout bridge life cycle. Regarding the cost of inadequate interoperability, US National Institute of Standards and Technology (NIST) (Gallaher et al. 2004) reported that \$15.8 billion in annual interoperability costs were conservatively quantified for the capital facilities industry in 2002. Lee & Jeong (2006) also suggested to using standardized information model based on open standards for maximizing the reusability of data and information.

In this paper, a unit cost model and an information model based on ISO/STEP standard are proposed for the life-cycle cost data management of cable-stayed bridge in order to collect and provide high-quality and quantitative cost data and to bridge the data gaps for the interoperability. The proposed unit cost model gives each cost element a dollar value which could be deterministic, probabilistic, or fuzzy. The international standard based information model serves as the basic data type for the integrated management and interoperable operation. Finally, the applicability and efficiency of the proposed method is illustrated by applying to Seohae Grand Cable-Stayed Bridge.

## 2 BRIDGE LIFE CYCLE COST

The general life cycle of bridge structures, which are expected to achieve a 50- to 100-year service life, is shown in Figure 1.

Bridge life cycle cost models are various because of the diverse ways to categorize the cost data. The following equation is an example of a widely-used life cycle cost model,

$$LCC_{Total} = C_{INI} + C_{MAI} + C_{DIS} + C_{USER}$$

where,  $LCC_{Total}$  represents the total LCC,  $C_{INI}$  represents the initial cost which consists of the costs of

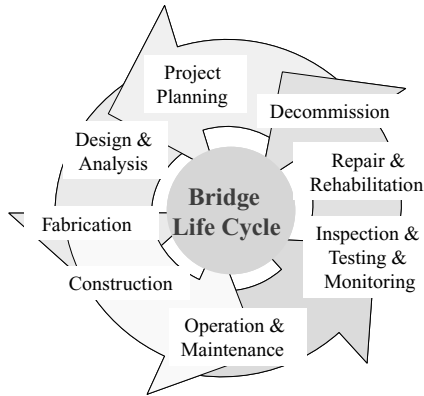


Figure 1. Bridge life cycle.

planning, design, construction, and supervision,  $C_{MAI}$  represents the maintenance cost which includes the costs of operation, maintenance, inspection, repair etc.,  $C_{DIS}$  represents the disposal cost which can be obtained by subtracting the recycle cost from the sum of break up cost and scrap cost, and  $C_{USER}$  is the user cost which includes vehicle operation cost and delay cost.

### 3 INFORMATION MODEL FOR COST MANAGEMENT

#### 3.1 Unit cost model

A unit cost model which is the building block of cost data management should be defined before developing any information model. Unit cost models can be based on materials, members, time, activities etc. In this study, the unit cost model (Fig. 2), which includes indirect\_cost and direct\_cost in general, is developed; the data types in Figure 2 are given in the Appendix. Cost\_data\_type is select from deterministic\_type and probabilistic\_type; entities of deterministic\_type and probabilistic\_type are also given in the Appendix. The unit cost model is based on bridge components and life cycle activities. As a result, the proposed information model for cost management in the following section is capable to be integrated with the 3D configuration based design information model. (Lee & Jeong 2006).

#### 3.2 Interoperable information model

In this section, an ISO/STEP based information model, which is subdivided into three sub-models, is developed for integrated and interoperable life cycle cost data management of highway bridge structures. The life\_cycle\_cost model (Fig. 3) encompasses bridge overview, life cycle cost description, and total cost data; the three sub-models are initial\_cost,

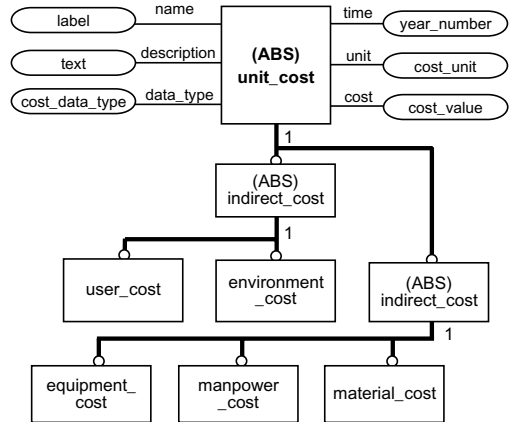


Figure 2. Partial EXPRESS-G diagram of unit cost model.

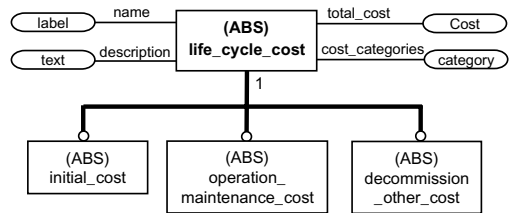


Figure 3. Partial EXPRESS-G diagram of life cycle cost model.

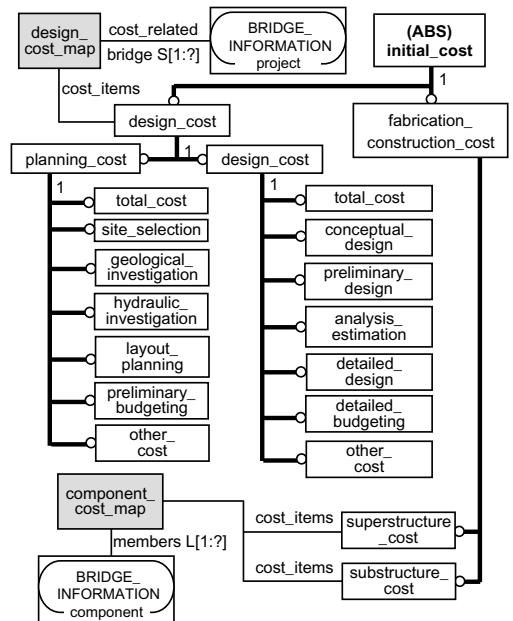


Figure 4. Partial EXPRESS-G diagram of initial cost model.

operation\_maintenance\_cost, decommission\_other\_cost models. Figure 4 gives the partial EXPRESS-G diagram of initial\_cost model, which consists of desing\_cost entity which is bridge life cycle activities based and fabrication\_construction\_cost entity which is bridge components based; both entities can be mapped to bridge 3D shape-based information model (Lee & Jeong 2006).

Figure 5 shows the partial EXPRESS-G diagram of operation\_maintenance\_cost model which is divided into regular\_maintenance, programed\_maintenance, and reactive\_maintenance entities according to the different types of maintenance actions. The operation\_maintenance\_cost model can be integrated with external schema such as bridge reliability and condition. Figure 6 is the partial EXPRESS-G diagram of decommission\_other\_cost model. End users can add entities in this model according to the needs of different projects. Using the proposed unit cost model and information model, the life cycle cost data of highway bridge structures can be integrated managed with interoperability.

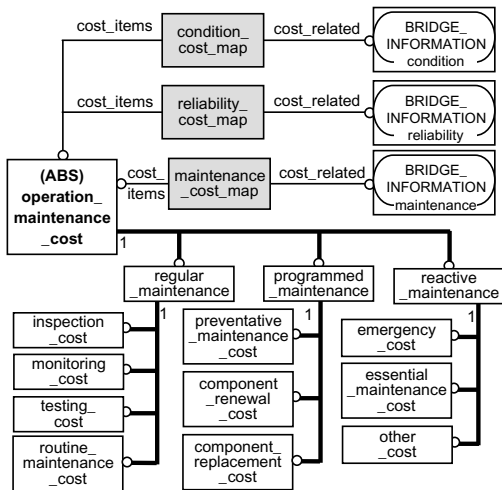


Figure 5. Partial EXPRESS-G diagram of operation & maintenance cost model.

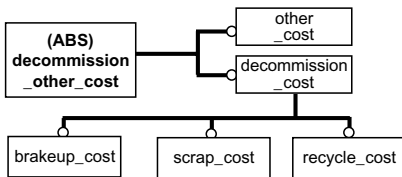


Figure 6. Partial EXPRESS-G diagram of decommission & other cost model.

## 4 IMPLEMENTATION TO CABLE-STAYED BRIDGE

### 4.1 Seohae Grand Bridge

Seohae Grand Bridge is currently the longest cable-stayed bridge in South Korea under service. It was constructed in December, 2000 and located on the Seohae Expressway, Chungcheongnam-do. It is 990 m long with a main span of 470 m. Both of its pylons are of 182 m high. Figure 7 shows the physical and digital profile of Seohae Grand Bridge; the digital profile is created using 3D configuration-based information modeling techniques for bridges (Lee et al. 2005).

### 4.2 Life cycle cost estimation

Life cycle cost of highway bridge structures is of increasing interests to transportation agencies. Usually, bridge life cycle cost prediction is based on structural element and system reliability analysis (Ang & Tang 2007) for determining the schedule of lifetime maintenance scenario. Bridge reliability analysis involves various assumptions and random variables on the performance of bridge members, which is out of the scope of this study. Consequently, the maintenance scenario for the life cycle cost estimation is based on KHC (KHC 2002). Existing cost data and information from KHC research report is stored in a database which



Figure 7. Physical and digital configuration of Seohae Grand Bridge.

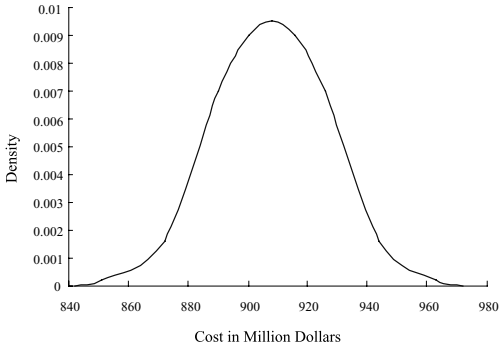


Figure 8. Life cycle cost estimation of Seohae Grand Bridge.

uses the proposed information model as its data structure. Then the bridge is assumed to be rehabilitated in year 38 and the bridge 80-year's life cycle cost can be calculated (Fig. 8); the cost is probabilistic as the cost element in the database are defined as probabilistic data.

## 5 CONCLUSION

A unit cost model and an information model for life cycle cost data management of highway bridges are proposed. The unit cost model is bridge components and life cycle activities based so as to be capable of integrating with 3D configuration model. The information model is ISO/STEP standard based so that the cost data can be shared and transferred among the shareholder. By using these two models, the life cycle cost data can be systematically collected, stored, and analysis for optimal funding and life cycle decision making. In this way, cost of reworks due to inadequate interoperability is reduced. The application to Seohae Grand Bridge illustrated the applicability of the proposed model. However, future studies are required on areas such as cost variant factors, sensitivity analysis, web-based service environment etc.

## ACKNOWLEDGEMENT

This work was supported by the Korea Research Foundation Grant funded by the Korean Government (MOEHRD) (KRF-2007-211-D00116) and Korea Bridge Design & Engineering Research Center sponsored by the Ministry of Construction and Transportation. We sincerely appreciate their help.

## REFERENCES

- Ang, H.-S. & Tang, W.H. 2007. *Probability Concepts in Engineering: Emphasis on Applications to Civil and Environmental Engineering*, 2nd Edition, John Wiley & Sons, Inc.
- FHWA. 2004. *FHWA Asset Management Position Paper*, Cambridge Systematics, Inc., USA.
- Friedland, I.M., Ghasemi, H. & Chase, S.B. 2006. *The FHWA long-term bridge performance program*, FHWA, USA.
- Gallaher, M.P., O'Connor, A.C. & Dettbarn, J.L. & Gilday, L.T. 2004. *Cost Analysis of Inadequate Interoperability in the U.S. Capital Facilities Industry*, NIST, USA.
- KHC. 2002. *Research on life cycle analysis of highway bridge members*, Korea Highway Corporation, Seoul, Korea.
- Lee, S.-H., Jeong, Y.-S. 2006. A system integration framework through development of ISO 10303-based product model for steel bridges, *Automation in Construction*, Vol.15, pp. 212–228.
- Lee, S.-H., Kim, B.-G. & Jeong, Y.-S. 2005. A new strategy for the information management of bridge maintenance, *Proceeding of 9th International Conference on Inspection, Appraisal, Repairs & Maintenance of Structures*, pp. 305–313, Changsha, China.
- TRB. 2003. *Bridge life-cycle cost analysis guidance manual*, NCHRP Report 483, part II, USA.

## APPENDIX. Data Types in Unit Cost Model

```

TYPE cost_data_type =SELECT
    (deterministic_type,
    probabilistic_type);
END_TYPE;

TYPE cost_unit = ENUMERATION OF
    (dollar,
    dollar_per_meter,
    dollar_per_centiare,
    dollar_per_stere);
END_TYPE;

TYPE cost_value = REAL;
END_TYPE;

TYPE year_number = INTEGER;
END_TYPE;--STEP Part 41

TYPE label =STRING;
END_TYPE;--STEP Part 41

TYPE text =STRING;
END_TYPE;--STEP Part 41

ENTITY deterministic_type;
    value :REAL;
END_ENTITY;

ENTITY probabilistic_type;
    mean_value :REAL;
    standard_deviation :REAL;
END_ENTITY;

```

# Guidelines for LCC analysis and evaluation of public construction projects in Korea

Tai Kyung Kang & Yoo Sub Lee

*Korea Institute of Construction Technology*

**ABSTRACT:** The report of the Korean Board of Audit and Inspection (BAI) on May 2007 indicates the problems of Life Cycle Cost (LCC) analysis and evaluation in the Design-Build (Turn-Key) and alternative bidding system. The point which the report indicates is that the cost estimation system for LCC analysis has nothing in common with each other and there's no consistency among the repair cycle and ratio per facilities parts. For solving these problems, BAI demands the establishment of the guidelines for LCC analysis and evaluation from the competent authority Korean Ministry of Construction and Transportation (MOCT). The objective of this study is to develop the improvement directions for LCC analysis and evaluation which are suitable to the public construction projects, especially for the Design-Build and alternative bidding system in Korea. For this study, the LCC related laws and regulations, LCC analysis guidelines of public cooperation, actual condition of LCC analysis and evaluation which includes, the elements of LCC, the estimation rules of the initial cost and the maintenance cost, the analysis standards of time value of money, etc. are investigated to provide the improvement directions for LCC analysis and evaluation

## 1 INTRODUCTION

### 1.1 *Background and purpose*

In order to forecast accurate Life Cycle Cost (LCC), various difficult problems should be solved. For example, since there are some areas such as geological conditions that can not be perfectly estimated in advance, while judging only from the initial construction cost, it is a general practice, in many cases, to increase/reduce the construction cost through design change after the contract conclusion. If accurate advance forecasting of even the construction cost only would be difficult while the construction period of building the facilities holds only a very short period of time among the total life cycle, it could be assumed without difficulties that LCC involving the whole life cycle would be affected by more complicated and diversified uncertain factors.

On the preposition that this type of uncertainties could be dealt with properly, notwithstanding the above background, anticipation is getting higher as a general tendency to the effect that selection of economic alternative design through LCC evaluation could be achieved and fundamental data for medium/long term budget utilization could be obtained and furthermore, reasonable decision-making and efficiency of budget investment covering the overall project could be enhanced.

Starting from 2000 domestically, as the design value engineering (hereinafter called 'VE') including

LCC evaluation is institutionalized in the public sector and LCC evaluation criteria for the specific facilities including expressway is suggested by a part of investment institutions including Korea Expressway Corporation, concern over LCC has started to increase. In particular, as LCC is reflected as an assessment factor for selecting qualified contractors of the public construction and private funding projects being implemented in the form of design-build system or alternative bidding system. An opportunity to take-off has been provided with a new business area that exclusively handles LCC evaluation business professionally being formed.

However, request for improvement for this system has also been cited along with the reality that the Board of Audit and Inspection has raised the question of LCC evaluation and its assessment system mainly for design-build project and alternative bidding project.

In this view, this study intends to suggest any improvement directions taking the status and problems of LCC evaluation and its assessment system into consideration mainly in terms of design-build bidding project and alternative bidding project.

### 1.2 *Research flow and method*

In order to suggest improvement directions for LCC evaluation and its assessment system, basic investigation for LCC relevant regulations and matters to be



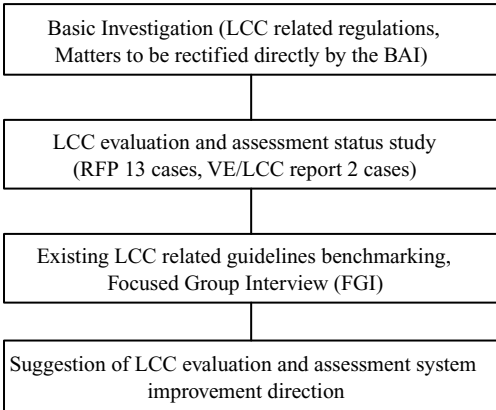


Figure 1. Research flow and method.

rectified directed by the Board of Audit and Inspection has been carried out in advance and LCC evaluation and its assessment reality has been examined by collecting 13 cases of Request for Proposal (hereinafter called ‘RFP’) for design-build bidding project and alternative bidding project and 2 cases of VE/LCC. Afterwards, through bench-marking existing LCC-related guideline and group interview (Focused Group Interview; FGI) with experts in charge of marketing design-build bidding or private funding project of the construction industry and experts in charge of VE/LCC business as proxy, improvement directions for LCC evaluation and its assessment system was suggested.

Research flow and method are shown in Figure 1:

Provided, however, that the objects of this study were limited to LCC evaluation and its assessment system for design-build bidding project or alternative bidding project and the private funding project, another category of the project, was excluded from this research scope. Since the main body of operation and maintenance is the governmental authorities in case of design-build bidding project or alternative bidding project while the main body of operation/maintenance of the private funding project is private contractor for a certain period of time, there are some delicate difference between LCC evaluation and its assessment system.

## 2 INVESTIGATION OF BASIC DATA

### 2.1 Status of relevant regulations

In accordance with Article 13, Clause 38, of the implementation regulations of Construction Technology Management Law (Ministry of Construction &

Table 1. Assessment items and marking criteria of design-build bidding project and alternative bidding project.

Assessment items	Assessment contents	Weight criteria
Planning Constructability	Design criteria	20~30
	Working method, ancillary/safety facilities plan, propriety of quality control plan	
Operation/ maintenance Safety	Propriety/easiness of operation/maintenance	10~20
	Structural/sectional design, prevention of disaster, safety control plan	
Economic efficiency	Operation/maintenance cost estimate, economic efficiency	10~20
	Environmentally friendly level, harmonizing with environment	
Environmental	Environmentally friendly level, harmonizing with environment	5~10
Others	Working period reduction, application of new technology/working method.	5~10

Transportation; MOCT) regulating construction work of its total construction cost exceeding 10 billion Won, VE including LCC evaluation is a mandatory obligation and in this connection, MOCT is suggesting a general guideline regulating the concept and procedure of VE by “Implementation guideline for reviewing design VE (the said Ministry gazette 58824-791 dated July 29, 2000)” and “Business manual for design VE (the said Ministry construction environment team No. 224, dated February 3, 2006)”, respectively.

Meanwhile, according to Article 1, Clause 3 of the provisional clause of the said Ministry guideline and the business manual, in case that LCC evaluation regarding VE is not easy or required an alternative is exceptionally allowed to be assessed. By the initial cost and any details regarding LCC evaluation and its assessment is not regulated giving emphasis only on VE.

On the other hand, in connection with the assessment for the LCC evaluation results, “Research on design VE (VE/LCC report)” of the design-build bidding project and alternative bidding project as per Item 3, Article 1, Clause 20 of “Operation regulation for the construction technology development and management (the said Ministry order No.686 dated October 30, 2007)” is regulated to be included in the bidding documents and according to Item 1, Article 3, Clause 26 of the same regulation, it is recommended to be reflected in the assessment for contractor selection.

Figure 1 shows assessment items and marking criteria for the design-build bidding project and alternative

Table 2. Example of assessment criteria for design-build bidding, etc.

Assessment items	Weight criteria	Weight per each case													Average weight
		A	B	C	D	E	F	G	H	I	J	K	L	M	
Planning	20–30	30	30	50	30	30	25	30	30	40	30	25	40	40	33.1
Constructability	20–30	25	26	10	20	20	25	20	31	15	25	15	20	20	20.9
Operation & maintenance	10–20	10	10	15	10	14	10	10	8	10	10	10	15	0	10.2
-LCC propriety		0	2	N/A*	N/A	N/A	2	N/A	2	N/A	0	N/A	N/A	N/A	
Safety	10–20	15	10	10	15	15	13	10	8	10	15	10	10	10	11.6
Economic efficiency	10–20	10	12	10	10	14	10	15	9	15	10	10	5	10	10.8
-LCC propriety		2	2	N/A	N/A	N/A	0	N/A	2	N/A	2	N/A	N/A	N/A	
Environmentalty	5–10	5	5	5	10	7	8	10	7	10	5	20	5	5	7.8
Others	5–10	5	7	0	5	0	9	5	7	0	5	10	5	15	5.6

\* N/A: Though classified as detailed items, marking was not detailed and it was suggested as total of the higher items including 'operation/maintenance' or 'economic efficiency'.

bidding project and “Facility plan through propriety and economic efficiency of operation/maintenance cost estimate” of “economic efficiency” item is considered to be directly associated with LCC evaluation and its assessment.

## 2.2 Questions raised by the board of audit & inspection

Summary of problems and recommendations suggested by the Board of Audit & Inspection in connection with LCC evaluation and its assessment on May, 2007 are as follows.

Regarding the initial cost, arbitrary application of actual working cost, estimation, private data without principle by the bidders.

Regarding operation/maintenance cost, its cost was improperly estimated to be reduced by way of intentional omission of main items of operation/maintenance, extension of replacement cycle of material/spare parts, underestimation of replacement unit price of material/spare parts, etc.

In case of alternative bidding for a bridge work, for example, suspension bridge which was excluded from the original design due to high LCC, was suggested as an alternative by the bidder with manipulating LCC it being rather lower.

Subsequently, design assessment members were forced to take the average value of ‘planning’ and ‘constructability’ items as a criterion for assessing ‘economic efficiency’ item and as a result, ‘economic efficiency’ item became unreasonably questioned.

When assessing ‘economic efficiency’ item, detailed LCC estimation criteria shall be provided so that LCC could be utilized as an objective indicator and by modifying the said Ministry order, proper action

has been taken so that LCC could be reasonably utilized for assessment in the process of the client’s LCC verification.

## 3 LCC EVALUATION AND ANALYSIS OF ITS ASSESSMENT STATUS

### 3.1 Status of RFP preparation

Contrary to the indication by the Board of Audit & Inspection, regarding the initial cost, in all 13 cases of RFP “preparation guideline of estimation description”, it was revealed that the basic principle was suggested that the construction cost should be estimated with applying objective criteria including standard estimation, actual working cost, etc., based on the regulation of the working rule for estimated price preparation.

On the other hand, regarding the detailed criteria (repair, replacement cycle, unit price, etc.) for estimating operation/maintenance cost, in all 13 cases, it was confirmed that even the minimum guideline had not been suggested therein as indicated by the Board of Audit & Inspection.

Meanwhile, as shown on Table 2, actual marking for ‘economic efficiency’ item was an average of 10.8 points for 13 cases and it could be noticed that mostly minimum marking was applied. Regarding ‘economic efficiency’ in particular, in case that the detailed item for the total proprieties of operation/maintenance and LCC that had nothing to do with the initial investment cost was established, which means the detailed marking for pure LCC was reflected, it was found that the detailed marking did not exceed 2 points. Sometimes LCC-related detailed item

could be established in 'operation/maintenance' parts, but detailed marking did not exceed 2 points as well.

### 3.2 Preparation status of VE/LCC report

Summary of LCC evaluation status was suggested based on LCC evaluation contents included in VE/LCC report presented by the bidder for actual design-build bidding project as shown on Table 3.

Table 3 above, it was revealed that the bidders had been submitting VE/LCC report including the detailed contents. Additionally, though there is an analysis that the new business market of preparing such report vicariously is on the decline, this market has enjoyed prosperity for the past couple of years being supported by the activation of private projects.

### 3.3 LCC Evaluation and study on assessment

Summary of LCC evaluation and assessment status of design-build or alternative bidding project is as in the following.

Since the bidder is not the main body of operation/maintenance in case of design-build or alternative

bidding project, contrary to the private financing project, it is a general practice to lower the operation/maintenance cost for immediate advantageous assessment.

Since the contents related to LCC evaluation suggested by the bidders are similar due to their outsourcing, the power of judgment is insignificant in reality and in actual assessment, minimum marking recommended by the government authorities are mostly applied.

Propriety assessment for the operation/maintenance of the suggested design proposal(or alternative) is solely relied on individual judgment of the assessment officer.

Since any detailed instruction manual for efficient operation/maintenance of the facilities by the government authorities is not presented after the completion of design-build bidding project or alternative bidding project, in-depth assessment of LCC evaluation is hard to be carried out in reality.

Though any government-level guideline for LCC evaluation is not available, but when judging from each facility elements, the contents of VE or LCC related guideline which is being utilized by some clients are mostly being applied.

Table 3. LCC evaluation cases of VE/LCC report.

Type of work		Road expansion/ pavement
LCC component item		Initial cost, operation/ maintenance cost, dismantling/disposal cost
LCC evaluation period		50 years for bridge, 20 years for road
Time value of money		Converting to current value
Discount rate	Estimate model	Actual discount rate utilizing producer price index, interest rate, of the Bank of Korea
		Applied figure
Background of cost estimate		3.3%
		Construction cost: standard estimate, actual working cost engineering fee: based on engineering consideration
		Application of basic conversion of the Korea Expressway Corp. guideline
		Demolition/ disposal cost
		Application of basic conversion of the Korea Expressway Corp. guideline

## 4 BENCH-MARKING FOR LCC-RELATED GUIDELINE

### 4.1 Type of LCC-related guidelines

When looking at LCC-related guideline at home and abroad, in terms of application and detailed drawing, it could be noticed that there are two main types as follows.

The first type of guideline is the LCC evaluation guideline for the pavement design suggested by Federal Highway Administration (hereinafter called 'FHWA') on 1998. This guideline with total pages of 100 is a detailed guideline including operation/maintenance cycle or unit price criteria for any specific facilities (road pavement) and in terms of its forms and detailed drawing, it could be considered as an original form of guideline of LCC evaluation guideline for pavement and bridge, etc., prepared by Korea Expressway Corporation.

### 4.2 Contents of existing domestic LCC-related guideline

In connection with the detailed guideline for estimating operation/maintenance cost which is a part of matters having been pointed out by the Board of Audit & Inspection on 2007, government-level guideline is not available but a case of operating guideline for any specific facilities by a certain part of clients could

Table 4. Characteristics of domestically existing LCC evaluation-related guideline and summary of its main contents.

Guideline	A	B	C	D
Application area	bridge, road pavement	bridge	dam	water treatment con'c structures
Main body of operation	Korea Expressway Corp.	Korea Expressway Corp.	Korea Water Resources Corp.	Korea Water Resources Corp.
Date of preparation	2001.12	2003.12	2004.11	2006.3
Characteristics	LCC evaluation guideline	research report(to be utilized for practical LCC guideline)	VE guideline(LCC evaluation inclusive)	VE guideline(LCC evaluation inclusive)
LCC evaluation period	bridge:100 years, pavement:35years	100 years	70 years	55 years
Cost integration	(Net Present Value, NPV)	same as left	same as left	same as left
Discount rate model	Actual discount rate utilizing producer price index, interest rate of Bank of Korea	same as left	same as left	same as left
Discount rate figure	4.54%	4.5%	6%	4.5%
LCC component item	initial cost, operation/maintenance cost, disposal cost, user cost	same as left	initial cost, operation/maintenance cost, disposal cost	initial cost, operation/maintenance cost
Probabilistic approach method	not applied	same as left	same as left	same as left
Basic data for cost estimate	const. cost per km/m <sup>2</sup> , linear regression method for estimating operation/maint cost	Repair maintenance cycle/rate	yearly operation/maintenance cost	repair/maintenance cycle

be noticed domestically. Summary of main contents of existing domestic LCC evaluation-related guideline is as shown on the Table 4.

As shown on Table 4, while the guidelines of Korea Expressway Corporation are intended for LCC evaluation, the guidelines of Korea Water Resources Corporation also contains LCC evaluation-related contents but these guidelines are fundamentally aiming at VE and therefore there is a little difference in terms of structure and contents.

### 4.3 Points of suggestion

Summary of points of suggestion obtained through bench-marking for LCC evaluation-related guideline at home and abroad are as follows.

Detailed guidelines are hard to be suggested in general since detailed guidelines including maintenance/replacement cycle or unit price for LCC evaluation differ depending on each type of facilities.

For this reason, detailed guidelines for LCC evaluation are being operated as per each facility both at home and abroad.

Among detailed contents of domestic LCC evaluation-related guideline, evaluation period or the contents of LCC component item, basic data for cost

estimate, etc., differ depending on applied facilities but time value of money or estimate model of discount rate which is in compliance with FHWA's pavement-related LCC guideline, is substantially identical in terms of broad framework.

## 5 IMPROVEMENT DIRECTIONS FOR LCC EVALUATION AND ASSESSMENT SYSTEM

The status of LCC evaluation and assessment system together with improvement directions as per each issues were suggested and its summary is as shown on Figure 2.

### 5.1 Improvement directions of LCC evaluation system

1) Arrangement of relevant guidelines:

It is judged that the arrangement of detailed guideline for all the facilities should be carried out as per each client on a medium to long term basis. Actually a certain part of the clients had already established detailed guidelines for LCC evaluation of their own.

But in a short term basis, it is judged to be meaningful to introduce the concept of the purpose of LCC evaluation, general procedures, time value of money

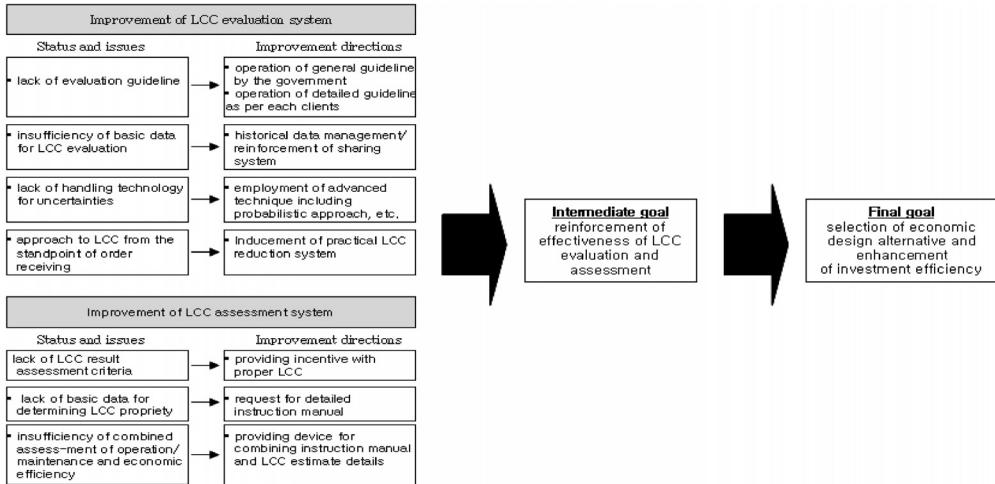


Figure 2. Improved directions for LCC evaluation and assessment system.

concept, and operate the general guidelines by the government. In this regard, the contents and forms of LCC Primer of FHWA could be referenced.

## 2) Establishment of LCC evaluation basic data:

For enhancing effectiveness of LCC evaluation, huge basic data that can estimate the relevant cost reasonably is required. For this objective, historical management system for repair/maintenance cycle or required cost of the facilities should be reinforced and a system of effectively sharing historical management information should be established.

## 3) Employment of advanced evaluation technique:

LCC evaluation is a process of forecasting future probabilities based on the past data, which inevitably entails uncertainties. In order to deal with these uncertainties effectively, it is necessary to employ advanced evaluation techniques led by the relevant industry.

### 5.2 Improvement directions of LCC assessment system

#### 1) Arrangement of assessment criteria for LCC estimate result:

It will be necessary to arrange the assessment system by giving advantages to the bidders who propose reasonable operation/maintenance price, instead of 'The lower, the better' policy having been applied previously.

#### 2) Request for instruction manual of facilities:

At the time of proposing design alternatives, instruction manual including operation/maintenance-related activities should be actually provided with the clients or assessment members and requesting this

material is the natural right of the clients. In addition, under the preposition of this material being provided, linked assessment of 'operation/maintenance' and economic efficiency' to be mentioned hereunder could be possible.

#### 3) System establishment for linked assessment of operation/maintenance and economic efficiency:

As a result of evaluation for 13 cases of RFP, it was understood that the detailed assessment item for applicability of operation/maintenance cost is classified as either detailed item of 'operation/maintenance' or detailed item of 'economic efficiency'. In view of this, it could be judged that these two higher assessment items of 'operation/maintenance' and 'economic efficiency' have something in common in terms of LCC concept.

Once the instruction manual for the facilities is made available, linked assessment of 'operation/maintenance' and 'economic efficiency' will be possible as a more objective assessment as to whether operation/maintenance-related activities presented clearly by documents, not by any objective judgment of the assessment members, is being reflected substantially without any mutual contradictions.

## 6 CONCLUSIONS

As mentioned previously, since LCC evaluation is preconditioned on the huge assumption for the future couple of decades, uncertainties are inevitably accompanied thereby and minimizing these uncertainties could be possible, but eliminating these uncertainties at all will be impossible with realistic

limitation. Therefore, in order to improve LCC evaluation and its assessment system practically, consistent and sustained common efforts of the government, the clients and the industry are required.

In the U.S.A. in 1995, the government had ruled LCC evaluation for the bridge, tunnel and pavement works with respective project amount exceeding \$0.25 million as an obligation but this regulation had been revoked on 1998 due to this fundamental limitation (FHWA, 2002) obviously implies significant messages to the domestic stakeholders who are looking for formulation of LCC guideline.

Notwithstanding this background, since it is the global trend to give more emphasis on decision-making from the standpoint of LCC rather than decision-making from the standpoint of the initial cost. Regarding the project cost, sustained subsequent research on itemized discussion for LCC evaluation and its assessment system is considered to be required.

#### ACKNOWLEDGEMENT

This research was supported by a grant (06 CIT A03) from Construction Infra Technology Program funded by Ministry of Construction & Transportation of Korean government.

#### REFERENCES

- Federal Highway Administration(FHWA). 2002. Life Cycle Cost Primer.
- Korean Ministry of Construction and Transportation(MOCT). 2000. Implementation guideline for reviewing design VE.
- Korea Expressway corp. 2001. Provisional guideline for LCC evaluation technique for expressway.
- Korea Expressway Corp. 2003. LCC evaluation research as per each type of bridges of expressway.
- Korea Water Resources Corporation. 2004. Design VE/LCC evaluation standard guideline for water pour dam facilities.
- Korea Water Resources Corporation. 2006. Practical technique for VE of water treatment con'c structure repair/reinforcing working method.
- Korea Land Corporation. 2006. Invitation to alternative bid for Inchun Chungra region development project.
- MOCT. 2006. 'Design VE business manual'.
- MOCT. 2007. Operation regulation for construction technology development.
- The Board of audit & Inspection. 2007. Report on audit result for the status of design build and alternative bidding system in Korea.

# Design of green engineered cementitious composites for pavement overlay applications

M.D. Lepech & G.A. Keoleian

*Center for Sustainable Systems, University of Michigan, Ann Arbor, Michigan, USA*

S. Qian\* & V.C. Li

*Department of Civil and Environmental Engineering, University of Michigan, Ann Arbor, Michigan, USA*

*\*Now at Microlab, Delft University of Technology, Delft, The Netherlands*

**ABSTRACT:** The construction, repair and rehabilitation of concrete pavements relies on the production and flow of large quantities of concrete and its constituents. Within the US, nearly 43 megatons of cement are used annually for the construction, repair and rehabilitation of concrete pavements, accounting for over 39 megatons of CO<sub>2</sub> emissions. To reduce environmental impact and improve the sustainability of pavement overlay systems, a class of materials called Engineered Cementitious Composites (ECC) has been designed for durable rigid pavement overlays.

ECC overlays are designed to enhance sustainability in two ways. First, “greener” ECC materials incorporate high volumes of industrial wastes including fly ash, ground granulated blast furnace slag (GGBFS), and waste foundry sands and carbon residue to reduce the environmental impacts of material production. Fundamental micromechanics carefully guide the green material design to maintain pseudo-strain hardening material behavior under tension. This ductile behavior is critical to the second mechanism for sustainability enhancement. Through a distinct fracture phenomenon, the ductility of ECC effectively eliminates reflective cracking, a major cause of premature overlay failure, thereby increasing durability and reducing life-cycle maintenance. Experimental and theoretical analyses verify the green material and durable overlay design approaches. Incorporating industrial wastes, over 70% of ECC virgin constituents have been replaced without reducing critical mechanical performance characteristics. The combination of green raw materials, a 50% reduction in overlay thickness, and a doubling of service life as compared to concrete overlays, leads to significant sustainability improvements have been achieved. This paper presents the methodology and results of incorporating green cementitious materials design into rigid pavement overlay systems.

## 1 INTRODUCTION

The construction and maintenance of streets and highways in the United States alone consumed an estimated 43 million metric tons of cement in 2006 (PCA 2007; vanOss 2007). The production of this cement resulted in the emission of nearly 39 million metric tons of CO<sub>2</sub>, over 111 thousand metric tons of NO<sub>x</sub>, and over 85 thousand metric tons of SO<sub>x</sub>. The greater impacts of this consumption, and its related emissions, are becoming increasingly apparent in the form of acid rain, public health, and global climate change.

In developed countries, much of this construction is targeted at maintenance, rehabilitation, and reconstruction of existing highway pavements. Currently, two systems are used for the rehabilitation of existing rigid pavements (i) an unbonded concrete overlay

and (ii) a hot mixed asphalt (HMA) overlay. For either of these overlay systems, reflective cracking is often the ultimate failure mode and limits the service life of the overlay (Tayabji et al 1985; NCHRP 1999; Huang 2004). Such reflective cracking is characterized by repeated traffic loads causing new cracks to “reflect” through the new overlay from pre-existing joints or cracks in the substrate. Current techniques to limit reflective cracking include the use of a bond-breaking layer (i.e. HMA) under concrete overlays which relieve stress concentration at the source of reflective cracking, complete rubblization (breaking concrete into aggregate-like particle *in situ*) of the substrate concrete, or extensive repair of existing pavement deterioration before overlaying. Currently, none of these approaches has been able to effectively eliminate reflective cracking in rigid pavement overlays.

### 1.1 Ductile rigid pavement overlays

To overcome the fracture-based phenomenon of reflective cracking, a ductile cement-based material is considered. Within the class of high performance fiber-reinforced cementitious composites (HPFRCC), Engineered Cementitious Composite (ECC) has been designed to exhibit ductility more commonly exhibited by ductile metals than brittle cement-based matrices. Developed through micromechanical tailoring of the components (i.e. cement, sand, and fibers), ECC exhibits an ultimate tensile strain capacity of 3%–5%, depending on the specific mixture (Li 2003). This tensile ductility, over 300 times that of normal concrete, is realized through the formation of a large number of closely spaced microcracks under load.

Previous laboratory research has investigated the use of ECC material as repair layer over an existing concrete substrate under both monotonic and fatigue loads (Lim & Li 1997; Kamada & Li 2000; Zhang & Li, 2002). Those researchers found that through a unique “kinking-and-trapping” mechanism, the material’s ductility effectively prevents substrate cracks from reflecting through an ECC overlay. Building from these results, Qian (2007) showed that ECC overlays are significantly more effective than unbonded concrete or HMA overlays in reducing reflective cracking, thereby extending the service life of an ECC rigid pavement overlay.

### 1.2 Sustainability of ECC overlays

Numerous researchers have studied the life cycle costs and impacts of pavement systems (i.e. asphalt versus concrete pavement systems) (Horvath & Hendrickson 1998; Zapata & Gambatese 2005; Chen et al 2007). Results from these studies have shown that Portland cement concrete pavements exhibit lower energy consumption and related impacts during the first three life cycle stages (extraction of raw material, manufacture, and placement) as compared to asphalt pavements. But energy consumption and emissions throughout service life is heavily dependent upon local parameters, such as traffic volume, truck loads, and climate.

Zhang et al (2007) has looked at the overall sustainability of unbonded concrete overlays, HMA overlays, and ECC overlays using economic, environmental, and social metrics. Zhang et al found that ECC overlays were able to improve the sustainability of rigid pavement overlays by using ECC materials to extend overlay service life and reduce surface roughness thereby improving vehicle fuel economy. Most important among these findings was the large impact that service life and the suppression of reflective cracking failure mechanisms have on overlay system sustainability.

The motivation behind this research is the development of new ECC composites that incorporate large

proportions of industrial waste streams for use in rigid pavement overlay applications. These new versions of ECC are controlled to incorporate waste while maintaining high ductility, high fatigue resistance, and the “kinking-and-trapping” mechanism for suppression of reflective overlay cracking.

## 2 GREEN ECC MIX DESIGNS

A total of 14 ECC mixes were designed incorporating a variety of industrial waste streams. These wastes include fly ash from coal-fired thermoelectric power generation, a variety of sands and wastes from metal casting processes, post consumer carpet fibers, wasted cement kiln dust from cement production, and expanded polystyrene (EPS) beads from lost foam foundry operations. The mix proportions and material properties are shown in Table 1. The incorporation of industrial wastes is governed by micromechanical models for the design of ECC materials as described in Lepech et al (2005; 2007).

A set of metrics capturing consumption and environmental impacts was computed for each of the 14 mix designs. These values result from a life cycle inventory assembled for cement-based materials and summarized by Kendall et al (2007). These values are shown in Table 2.

Mix 4 represents an early version of ECC which was not designed specifically for reduced environmental impact. Comparing Mix 4 with Mix 13, the ECC mixture with the lowest environmental impact, significant improvements are apparent. Total energy consumed in production (from raw material extraction through component manufacturing and transportation) is reduced by 58%. CO<sub>2</sub>, NO<sub>x</sub>, PM<sub>10</sub>, and SO<sub>x</sub> emissions are reduced by 76%, 53%, 83%, and 71% respectively. Virgin material consumption is also cut by 74% through the use of industrial waste streams. As seen in Table 1, only slight tradeoffs in mechanical performance were seen in these substitutions.

## 3 ESTIMATION OF SERVICE LIFE

As noted by Zapata & Gambatese (2005) and Zhang et al (2007), in order to assess the overall environmental impacts and sustainability metrics of a pavement overlay system, a model for service lifetime is needed. In the case of an ECC overlay, this model is based on the flexural fatigue life of the ECC material. Zhang & Li (2002), and later Qian (2007), showed experimentally that ECC, when laid over a cracked or damaged pavement substrate, is subjected to flexural fatigue loads until failure. This mechanism is shown schematically in Figure 1.

Based on this failure mechanism, the flexural fatigue behavior of the ECC materials listed in Table 1



Table 1. Material mix proportions and materials properties (kg/L unless noted otherwise).

Mix	Cement	Sand	Gravel	Water	Foundry Sand	Fly Ash	CKD	EPS	Carpet Fiber	PVA Fiber	PE Fiber	HRWR	HPMC	MOR (MPa)	$\epsilon_u$ (%)	$f'_c$ (MPa)
1	0.578	0.462		0.319		0.693				0.026		0.00751		13.43	2.5	55
2	0.414	0.456		0.319		0.829				0.026		0.0058		12.42	3.5	46
3	0.324	0.453		0.317		0.907				0.026		0.00518		10.83	3.7	38
4	1.266	0.633		0.321						0.02		0.0126	0.00063	12.15	3.8	65
5	0.845	0.845		0.361						0.026		0.0169	0.00127	7.83	4.9	57
6	0.59	0.472		0.288		0.708				0.026		0.01934		8.91	4.5	54
7	0.322	0.709		0.281		0.709				0.026		0.01934	0.00016	9.99	4	54
8	0.322	0.709		0.281		0.709				0.026		0.01934	0.00016	10.53	4.3	55
9	0.373	0.822		0.325		0.448				0.026		0.02241	0.00028	8.37	4.3	57
10	0.583		0.467	0.298		0.7				0.026		0.0175		6.75	3.5	46
11	0.578		0.462	0.319	0.462	0.693				0.026		0.00751		10.53	3.6	55
12	0.578	0.462		0.319		0.693		0.0026		0.023		0.013		8.64	3.7	55
13	0.231			0.319	0.462	0.693	0.347			0.026		0.00751		9.45	3.5	54
14	0.419	0.335		0.239		0.503		0.005		0.026		0.00125		8.37	3.8	45
Concrete	0.39	0.676	1.041	0.166										7.2	0.01	47

CKD—Cement Kiln Dust; EPS—Expanded Polystyrene; PVA—Polyvinylalcohol; PE—Polyethylene; HRWR—High Range Water Reducer; HPMC—Hydroxypropylmethyl Cellulose; MOR—Modulus of Rupture.

will govern the end of service life of overlays designed with these materials. The flexural fatigue behavior is characterized by S-N curves. To facilitate fatigue evaluation of the 15 material mixes shown above without completing millions of cycles of experimental fatigue loading, a fatigue model for ECC materials developed by Suthiwarapirak & Matsumoto (2004) is used. This model, based on previous work by Zhang (1998) and Suthiwarapirak & Matsumoto (2003), is shown as Equation 1.

$$\frac{\sigma_N}{\sigma_1} = 1 - (0.025 + 1.5 \times \epsilon_t) \text{Log}_{10}(N) \quad (1)$$

where,  $\sigma_N$  is the maximum allowable flexural stress (i.e. fiber bridging stress) at the N-th loading cycle,  $\sigma_1$  is the material MOR,  $\epsilon_t$  is a deformation parameter capturing the maximum tensile strain at a given load cycle, and N is the fatigue cycle count.

For Mixes 1, 2, and 3 of Table 1, flexural fatigue testing was carried out. Four point bending tests were

Table 2. Consumption and environmental impacts for individual mix designs.

Mix	Total E (MJ)	CO <sub>2</sub> (g)	NO <sub>x</sub> (g)	PM <sub>10</sub> (µg)	SO <sub>x</sub> (g)	BOD (g)
1	6.69	669.7	3.55	5.88	2.62	0.21
2	5.56	506.1	2.97	5.7	1.98	0.21
3	4.95	416.3	2.63	5.75	1.63	0.21
4	9.11	1228	4.46	9.5	2.82	0.16
5	7.60	876.1	3.73	6.82	2.08	0.21
6	6.03	634.6	3.04	4.63	1.56	0.21
7	4.74	400.8	2.37	3.03	1.04	0.21
8	4.74	400.8	2.37	3.03	1.04	0.21
9	5.07	450.3	2.51	3.51	1.15	0.21
10	5.49	572.9	2.873	3.74	1.42	0.21
11	5.7	608.9	2.97	4.01	1.5	0.21
12	5.7	614.7	2.86	4.53	1.5	0.21
13	3.85	296.4	2.08	1.6	0.82	0.21
14	5.04	476.3	2.59	3.29	1.21	0.21
Concrete	2.46	373.3	1.06	3.47	0.81	0

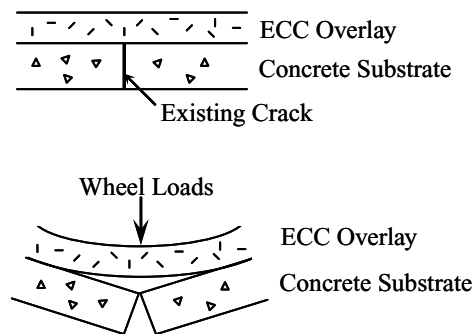


Figure 1. ECC overlay loading mechanism.

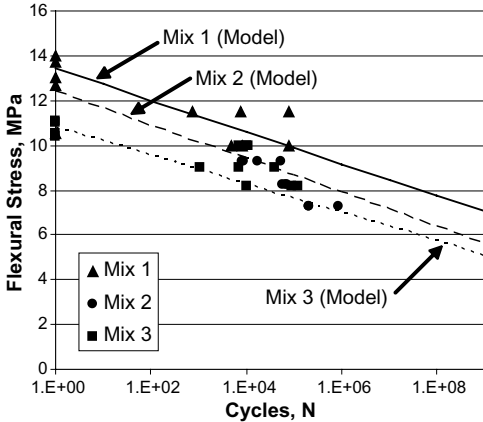


Figure 2. Comparison of experimental fatigue tests and predictive fatigue model.

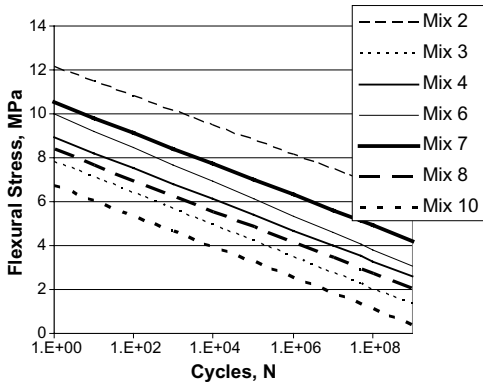


Figure 3. Fatigue degradation curves for a set of green ECC materials.

run as described in Qian (2007). The results of this fatigue testing and comparison with the above fatigue degradation model is shown in Figure 2. The fit with experimental data is sufficiently accurate among these three mix designs to apply to the larger population of ECC mixes shown in Table 1.

Using Equation 1, MOR values from Table 1, and measured tensile strain under bending load for each specimen, a family of S-N curves was developed for the green ECC mix designs. For clarity a small number of these curves are shown in Figure 3.

#### 4 DESIGN OF ECC OVERLAY

To assess the impact of green ECC mix designs on the larger rigid pavement overlay system, a series of structural design charts were developed by Qian (2007) for concrete and ECC overlays. These structural design charts are based on FEM modeling of ECC and

concrete overlaying a cracked concrete substrate. This is shown in Figure 4.

Using this model, a relationship between maximum stress developed during edge loading of a 1 ESAL (80kN) dual axle load and overlay thickness was determined. Existing slab and subgrade parameters were held constant ( $E_{existing} = 20.7 \text{ GPa}$ ,  $k_{subgrade} = 27.1 \text{ MN/m}^3$ ). The elastic modulus of the ECC overlay was also held constant at 20.7 GPa for all mix designs. For the design of a concrete overlay, the elastic modulus was increased to 34.5 GPa.

From the FEM model, the following overlay design chart was developed, relating overlay design thickness with the maximum stress level in the overlay. This relationship is shown in Figure 5.

For validation of FEM results, maximum stresses in an uncracked substrate scenario were compared to the classical Westergaard solution for maximum tensile stress within a semi-infinite pavement slab under edge loading (Westergaard 1926). As the size of the slab within the FEM model increases, the maximum tensile stress within the system approaches the Westergaard solution asymptotically as expected.

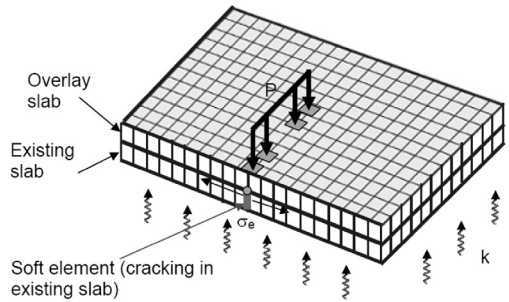


Figure 4. FEM model of overlay system with existing cracked concrete substrate.

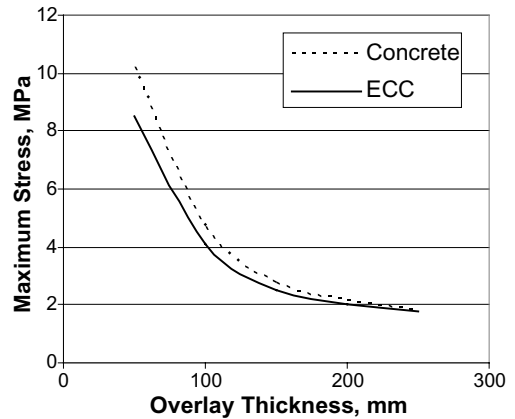


Figure 5. Design chart for overlay thickness.

## 5 OVERLAY APPLICATION ANALYSIS AND DESIGN

As noted by Zapata & Gambatese (2005), the overall environmental impacts of a specific overlay system are tied closely to the local application site, maintenance scheme, and traffic volume. For this research, an application site was chosen in southeast Michigan, near metropolitan Detroit. Interstate I-94 was selected. For pavement rehabilitation of site, the Michigan Department of Transportation typically would design a 175 mm–200 mm thick unbonded concrete overlay with a predicted service life of 20 years (MDOT 2005). Average daily truck traffic for the selected site is 12,000 with an assumed annual traffic growth rate of 5%. Over the 20 year service life, this results in approximately  $5 \times 10^7$  equivalent single axle loads. For this analysis, all overlay systems (concrete and ECC) are designed to last an equivalent lifetime of 20 years.

Using the fatigue degradation curves shown in Figure 3 (in addition to those for ECC mix designs not shown in Figure 3) the maximum flexural stress allowable with the ECC material can be determined. The maximum allowable flexural stress is shown for each ECC mix design in Table 3.

Using this maximum overlay stress, the minimum design overlay thickness can be calculated from Figure 5. The calculated minimum overlay design thicknesses for each of the 14 ECC mix designs and a concrete overlay are also shown in Table 3. As seen, as the fatigue performance of a specific ECC mix falls, the required overlay thickness increases to reduce the maximum tensile stress level within the overlay. This is most apparent with ECC Mix 10, which requires an overlay thickness of over 280 mm.

Table 3. Computed fatigue stress at  $5 \times 10^7$  loading cycles and required overlay thickness.

Mix	Stress at $5 \times 10^7$ Cycles (MPa)	Overlay Thickness (mm)
1	8.02	52
2	7.01	59
3	5.42	76
4	7.01	59
5	2.42	168
6	3.50	117
7	4.23	91
8	5.12	81
9	2.70	151
10	1.43	282
11	5.12	81
12	3.23	127
13	4.04	102
14	2.96	138
Concrete*	2.3	180

\* Concrete overlay stress level determined through fatigue testing results.

## 6 ENVIRONMENTAL METRICS

From this design, the overall environmental performance of the overlay design can be evaluated. Comparing trends within Tables 2 and 3, a trade-off between lower material environmental impact and greater overlay thickness is apparent in some cases. To best compare these design alternatives, comparisons between the 14 ECC and one concrete overlay material are made on an “installed” basis.

For this study, the width of the highway is assumed to be 7.32 m and the length of the project is 1000 m. Using the resource consumption and environmental impacts per volume of material shown in Table 2 and the minimum required overlay thicknesses from Table 3, the resource consumption and environmental impacts per kilometer of overlay installed are shown in Table 4 (for an overlay with 20 year service life).

As seen, the tradeoff between material performance and actual resource consumption or environmental impact can result in seemingly “greener” materials producing higher overall system impact. Once again, Mix 10 demonstrates this finding most clearly. Although Mix 10 exhibits significant environmental improvements over other ECC mix designs, its lower mechanical performance requires a much higher overlay thickness, resulting in an overall greater environmental impact per kilometer of overlay constructed. The best overlay material, considering primary energy, from the group developed is Mix 2. When considering CO<sub>2</sub> emissions, Mix 2 is also the best option. However, the significant non-linearity of these results with regard to other impact categories highlights the difficult decisions confronting transportation designers and government agencies.

Table 4. Resource consumption and environmental impact of overlay materials per kilometer installed.

Mix	(MJ) Total E	CO <sub>2</sub> (kg)	NO <sub>x</sub> (kg)	PM <sub>10</sub> (mg)	SO <sub>x</sub> (kg)	BOD (kg)
1	2,538	254,056	1,347	2,231	994	80
2	2,407	219,121	1,286	2,468	857	90
3	2,759	232,027	1,466	3,205	908	117
4	3,947	532,005	1,932	4,115	1,222	69
5	9,346	1,077,328	4,587	8,387	2,558	258
6	5,163	543,362	2,603	3,964	1,336	180
7	3,373	285,229	1,687	2,156	740	149
8	2,794	236,226	1,397	1,786	613	124
9	5,612	498,417	2,778	3,885	1,273	232
10	11,320	1,181,232	5,924	7,712	2,928	433
11	3,360	358,880	1,751	2,363	884	124
12	5,280	569,404	2,649	4,196	1,390	195
13	2,863	220,453	1,547	1,190	610	156
14	5,086	480,704	2,614	3,320	1,221	212
Concrete	3,241	491,834	1,397	4,572	1,067	–

This analysis does not include the impacts of required life cycle maintenance, changing surface roughness, and end-of-life scenarios of these overlay systems as addressed by Zhang et al (2007). While greatly complicating the analysis, this more complete analysis will be undertaken in the future.

## 7 CONCLUSION

The use of greener cementitious materials for repair and rehabilitation of rigid pavement systems represents significant potential for the reduction of material and energy resource consumption and pollutant emissions. Additionally, the incorporation of industrial waste streams into new overlay materials can successfully divert large waste flows from landfills. However, the incorporation of such industrial wastes must be carefully controlled to maintain overall system performance over the entire design life cycle.

Presented within this paper is a novel integrated approach to materials and structures design that leverages materials greening and structural design to rehabilitate existing rigid pavements. The results of this are a potential reduction of primary energy use and CO<sub>2</sub> emissions by 21% and 55% respectively. Findings from this study can be used by highway engineers and government agencies to systematically guide future rigid pavement rehabilitation projects toward lower resource consumption and pollution emissions.

## ACKNOWLEDGEMENTS

The authors would like to thank the US National Science Foundation MUSES Grant (CMS-0223971 and CMS-0329416) for funding this research.

## REFERENCES

- Chen, A., Keoleian, G.A., Gabler, E. 2007. Evaluation of Life-Cycle Cost Analysis Practices Used by the Michigan Department of Transportation. Submitted to *Journal of Transportation Engineering*.
- ERES Consultants, Inc. 1999. *NCHRP Report 415, Evaluation of Unbonded Portland Cement Concrete Overlays*, Transportation Research Board, Washington, D.C.
- Horvath, A., Hendrickson, C. 1998. Comparison of Environmental Implications of Asphalt and Steel-Reinforced Concrete Pavements. *Transportation Research Record*. 1626 (1) 105.
- Huang, Y.H. 2004. *Pavement Analysis and Design, 2nd edition*, Pearson Education, Upper Saddle River, NJ 07458.
- Kamada, T. & Li, V.C. 2000. The Effects of Surface Preparation on the Fracture Behavior of ECC/Concrete Repair System. *J. of Cement and Concrete Composites*, 22(6), 423–431.
- Lepech, M.D., Li, V.C. & Keoleian, G.A. 2005. Sustainable Infrastructure Material Design, In Nowak and Frongopol (eds) *Proceedings of The 4th International Workshop on Life-Cycle Cost Analysis and Design of Civil Infrastructures Systems, Cocoa Beach, Florida, May 8–11 2005*, 83–90.
- Lepech, M.D., Li, V.C., Roberston, R.E., Keoleian, G.A. 2007. Design of Green Cementitious Composites for Improved Sustainability. Submitted to *ACI Materials Journal*.
- Li, V.C. 2003. On Engineered Cementitious Composites (ECC)—A Review of the Material and its Applications, *J. Advanced Concrete Technology*, 1(3) 215–230.
- Lim, Y.M. & Li, V.C. 1997. Durable Repair of Aged Infrastructures Using Trapping Mechanism of ECC, *J. of Cement and Concrete Composites*, 19(4), 373–385.
- Michigan Department of Transportation. 2005. *Pavement Design and Selection Manual* Lansing, Michigan USA.
- Portland Cement Association. 2007. <http://www.cement.org/market/> (accessed on 12/6/07).
- Qian, S. 2007. *Influence of Concrete Material Ductility on the Behavior of High Stress Concentration Zones*. Ph. D. Thesis. University of Michigan, Ann Arbor.
- vanOss, H. 2007. *Mineral Commodity Summaries: Cement*. United States Geological Survey, Reston, VA USA.
- Suthiwarapirak, P., Matsumoto, T. 2003. Fiber Bridging Degradation Based Fatigue Analysis of ECC under Flexure *Journal of Applied Mechanics, JSCE*, 6, 1179–1188.
- Suthiwarapirak, P., Matsumoto, T. 2004. 3D Fatigue Analysis of RC Bridge Slabs and Slab Repairs by Fiber Cementitious Materials. In V.C. Li et al (eds) *Proceedings of Fracture Mechanics of Concrete Structures 5, Vail, Colorado USA April 12–16 2004*.
- Tayabji, S.D. & Okamoto, P.A., 1985. Thickness Design of Concrete Resurfacing, *Proc., 3rd Int'l Conf. on Concrete Pavement Design and Rehabilitation*, 367–379.
- Westergaard, H. 1926. Stresses in Concrete Pavements Computed by Theoretical Analysis. *Public Roads*. Vol. 7. pp. 25–35.
- Zapata, P. & Gambatese, J. 2005. Energy consumption of asphalt and reinforced concrete pavement materials and construction. *Journal of Infrastructure Systems*, 11(1) 9–20.
- Zhang, H., Lepech, M.D. & Keoleian, G.A. 2007. Dynamic Life Cycle Modeling of Pavement Overlay System: Capturing the Impacts of Users, Construction, and Roadway Deterioration. Submitted to *Journal of Transportation Engineering*.
- Zhang, J. 1998. *Fatigue Fracture of Fiber Reinforced Concrete—An Experimental and Theoretical Study*. Ph. D. Thesis, Department of Structural Engineering and Materials, Technical University of Denmark.
- Zhang J. & Li, V.C., 2002. Monotonic & Fatigue Performance in Bending of Fiber Reinforced ECC in Overlay System, *J. of Cement and Concrete Research*, 32(3), 415–423.

# Development of life-cycle cost based budget allocation system for bridge group

Ayaho Miyamoto

*Yamaguchi University, Ube, Japan*

Hidehiro Uchino

*Fuji P.S. Corporation, Tokyo, Japan*

**ABSTRACT:** The authors have been developing a Bridge Management System (J-BMS) for single bridge, which integrated with the Concrete Bridge Rating Expert System (BREX) that can be used to evaluate the serviceability of existing concrete bridges. The J-BMS will be able to predict the deterioration process of existing bridge members, construct a maintenance plan for repair and/or strengthening based on minimizing maintenance costs and maximizing quality, and estimate the maintenance costs in single bridge. In this system, the Genetic Algorithm (GA) technique was used to search for an approximation of the optimal maintenance plan. In the present study, a comprehensive decision support system is developed for maintenance strategies with/without annual budget limitations based on life cycle cost analysis of an entire bridge inventory, which form part of a highway network. Since formulation of an optimum bridge maintenance program for an entire stock of bridge structures is usually impeded by a lack of sufficient information on their existing conditions, the capability of the system was tried out, with a view to enhancing its capability, by applying it to a limited number of individual existing bridges, categorized as belonging to a typical bridge inventory. Genetic Algorithm is adapted, in order to obtain the semi-optimal solutions in this problem.

## 1 INTRODUCTION

In Japan, many highway bridges were constructed under the national highway network project launched in 1955. However, due to such factors as the increase in traffic volume and weight of vehicles, many bridges have seriously deteriorated over the years. Such bridges must be repaired or strengthened depending on the severity of their deterioration. However, due to the limited budget, funds must be split equally between maintaining the deteriorated bridges and constructing new ones.

In practice, however, since around 1990, bridge maintenance costs have increased more than the cost of constructing new ones in many developed countries. Thus, the increasing maintenance costs must be reduced by changing bridge maintenance methods, which once were limited to emergency measures against unpredicted events. The new concept of designing and constructing more durable bridges and thus reducing maintenance costs is becoming common in many countries. The highway networks in Japan are comparatively newer than those in other advanced nations. Thus, the financial situation regarding maintenance costs has not faced serious problems yet. However, one report estimates that by around 2010,

the ratio of bridges of 50 years of age will be about 35%. For this reason, comprehensive bridge management systems are essential. The systems should not only evaluate the serviceability of bridges, but also make an optimum maintenance plan considering the limited funds available.

In the present study, a comprehensive decision support system is developed for maintenance strategies with/without annual budget limitations based on life cycle cost analysis of an entire bridge inventory, which form part of a highway network. Since formulation of an optimum bridge maintenance program for an entire stock of bridge structures is usually impeded by a lack of sufficient information on their existing conditions, the capability of the system was tried out, with a view to enhancing its capability, by applying it to a limited number of individual existing bridges, categorized as belonging to a typical bridge inventory. Genetic Algorithm is adapted, in order to obtain the semi-optimal solutions in this problem.

The authors have been developing a Bridge Management System (J-BMS) for single bridge, which integrated with the Concrete Bridge Rating Expert System (BREX) that can be used to evaluate the serviceability of existing concrete bridges (Miyamoto A., et al. 1998.). The J-BMS will be able

to predict the deterioration process of existing bridge members, construct a maintenance plan for repair and/or strengthening based on minimizing maintenance costs and maximizing quality, and estimate the maintenance costs in single bridge. In this system, the Genetic Algorithm (GA) technique was used to search for an approximation of the optimal maintenance plan. In the present study, a comprehensive decision support system is developed for maintenance strategies with/without annual budget limitations based on life cycle cost analysis of an entire bridge inventory, which form part of a highway network. Since formulation of an optimum bridge maintenance program for an entire stock of bridge structures is usually impeded by a lack of sufficient information on their existing conditions, the capability of the system was tried out, with a view to enhancing its capability, by applying it to a limited number of individual existing bridges, categorized as belonging to a typical bridge inventory. Genetic Algorithm is adapted, in order to obtain the semi-optimal solutions in this problem.

## 2 MAINTENANCE STRATEGY FOR BRIDGES

This study proposes the maintenance management procedure considering the actual condition of a local government and develops the support system for each maintenance management business (see Figure 1),

because no any existing studies have explicitly specified the position of a general maintenance management procedure. In this maintenance management procedure, first of all, the bridge administrator performs initial inspection before it starts service life. For the existing bridge, a regular inspection assumed to be an initial inspection. The bridge administrator diagnoses using the result of this initial inspection, and sets the maintenance classification. Usually, the bridge administrator consigns the regular inspection to the enterprise based on the maintenance classification. In addition, the performance evaluation and the deterioration factor presumption are diagnosed by using the results of the regular inspection. The performance deterioration curve intended for two or more bridges is set by using this diagnosis result, and the budget allocation and the maintenance management plan are done. As a result of the budget allocation, it performs the detail inspection in the bridge judged that measures are necessary for current year. On the other hand, in the bridge where a detail inspection was judged it is unnecessary, the inspection cycle is reviewed and the maintenance classification is set newly. The above-mentioned content is macro management in the bridge maintenance strategy. Next, the factor of the deterioration that occurs in the object bridge is specified from the result of a detail inspection, and the performance deterioration curve that considers the factor and an external environment, etc. is set. The maintenance

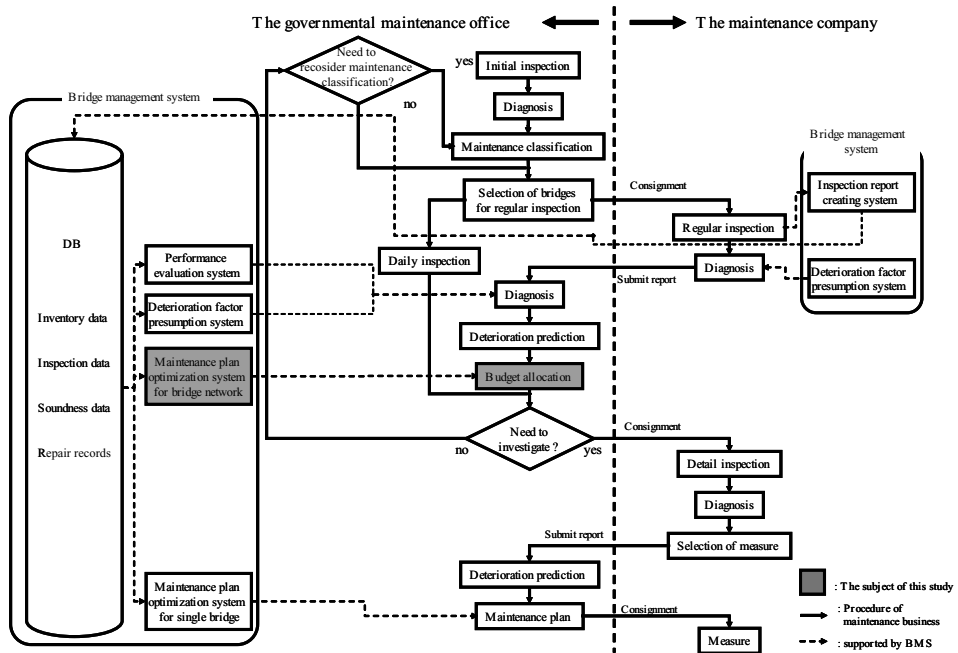


Figure 1. Position of maintenance plan optimization & budget allocation system.

plan of the object bridge at the life cycle is settled on by using the distribution budget calculated when this performance deterioration curve and the maintenance management plan are settled on. It is micro management in the bridge maintenance strategy.

### 3 BUDGET ALLOCATION METHOD

#### 3.1 Maintenance effects and deterioration curve

The existing maintenance plan optimization system applies relatively detailed maintenance strategies separately to main girders and slabs. The system's outputs include the approximate maintenance costs, an outline of maintenance plan and the bridges selected for detailed inspection. The system aims at the optimal allocation of roughly estimated budgets to respective bridges. New maintenance measures should be defined accordingly.

#### 3.2 Maintenance effects quantification

Concrete structures are maintained for four major purposes; blocking the factors of deterioration, controlling the deterioration speed, removing deterioration factors and controlling steel corrosion considerably, and enhancing load bearing capacity and deformability. In this study, repair of a small scale, repair of a large scale and reinforcement are discussed. The effects of repair and reinforcement are quantitatively assumed as described below based on the papers of Miyamoto et al. (Miyamoto A., et al. 1998.) and Japan Civil Engineering Contractors' Association.

##### Effects of repair

- (1) Soundness in terms of durability is enhanced to 100.

The soundness in terms of durability is assumed to be enhanced to 100 by repair because repair generally aims at restoring the durability to the level at the time of construction.

- (2) Rate of deterioration in load carrying capability is reduced.

Repair is expected not only to increase durability but also to reduce the rate of deterioration in load bearing capacity. Determining the ratio of improvement involves numerous uncertain factors.

##### Effects of reinforcement

- (1) Soundness in terms of load carrying capability is enhanced to 100.

Existing performance evaluation systems evaluate the load carrying capability of a bridge according to the specifications to which it is designed. Of the bridges with similar deformation, the load carrying capability of the one designed to older specifications is rated

lower. Reinforcing a bridge based on the present specifications therefore results in the soundness exceeding 100. In this study, it is considered appropriate to restore the soundness in terms of load carrying capability to 100, or achieve an effect of reinforcement of 100, at all times. To that end, the soundness is specified according to the current specifications at the start of service (e.g. the initial load carrying capability is set lower than 100) rather than setting the soundness at the start of service represented by the deterioration prediction curve at 100.

#### 3.3 Maintenance effects on deterioration curve

In this study, individual methods or combinations of repair and strengthening are discussed. The effects of the maintenance measures on the deterioration prediction curves for respective performance parameters are defined based on the equations for the deterioration prediction curves and the effects of the methods (see Table 1).

#### 3.4 Procedure of budget allocation

The bridge for the budget allotment is selected based on the deterioration model used in Miyamoto et al. research work (Miyamoto A., et al. 1998.). The selection procedure of the method of setting the deterioration curve and the budget allotment target bridge in a load carrying capability and durability is shown Figure 2 and as follows.

##### Step 1

The standard deterioration curve of load carrying capability is set based on load carrying capability soundness data and the parameter data in each material of each bridge. It groups from items such as the bridge type, the traffic volume and applied a Japanese standard for bridge, and each group sets the standard deterioration curve. From load carrying capability soundness data of each bridge, the standard deterioration curve of load carrying capability is set by

$$f(t) = b_L - a_L t^4 \quad (1)$$

where,  $b_L$ ,  $a_L$ : Parameter of deterioration curve for load carrying capability,  $t$ : Age of bridge.

##### Step 2

The load carrying capability deterioration curve of each bridge is set based on the standard deterioration curve set with Step 1. This method can be leveled considering the standard deterioration curve even if the precision of actual soundness data is low. And if the inspection is two times or more in addition, the setting of the curve becomes possible easily.

##### Step 3

The durability deterioration curve of each bridge is set from the load carrying capability deterioration

Table 1. Cost and benefit of repair and strengthening.

Maintenance measures	Construction cost (U/m <sup>2</sup> )		Deterioration curve expected after maintenance operation
	Slab	Main girder	
(i) Neither repair nor reinforcement is applied	0.0	0.0	Load bearing capacity: $f_{(i)}(t) = b_{L(i-1)} - a_{L(i-1)}t^4$ Durability: $g_{(i)}(t) = b_{D(i-1)} - a_{D(i-1)}t^c$
(ii) Repair			
A) a small scale	A) 23.8	23.8	Load bearing capacity: $f_{(i)}(t) = \{b_{L(i-1)} - a_{L(i-1)}t''^4\} - a_{L(i-1)}(t - t'')^4$
B) a large scale	B) 33.6	33.6	Durability: $g_{(i)}(t) = 100 - a_{D(i-1)}t^c$
(iii) Reinforcement			
A) a small scale	A) 94.6	132.1	Load bearing capacity: $f_{(i)}(t) = 100 - a_{L(i-1)}(t - t'')^4$
B) a large scale	B) 104.4	141.9	Durability: $g_{(i)}(t) = 100 - a_{D(i-1)}(t - t'')^c$

Note: Option A is adopted for soundness of 50 or higher in terms of durability, and option B is employed for soundness of less than 50.

$f_{(i)}(t)$ : Deterioration prediction curve for post-maintenance load bearing capacity.

$g_{(i)}(t)$ : Deterioration prediction curve for post-maintenance durability.

$b_{L(i-1)}, a_{L(i-1)}$ : Constant for deterioration prediction curve for pre-maintenance load bearing capacity.

$b_{D(i-1)}, a_{D(i-1)}$ : Constant for deterioration prediction curve for pre-maintenance durability.

$t$ : Number of years in service for the bridge,  $t''$ : Number of years at the time of the maintenance operation is carried out for the bridge.

$c$ : The degree of durability prediction curve ( $1 \leq c \leq 4$ ).

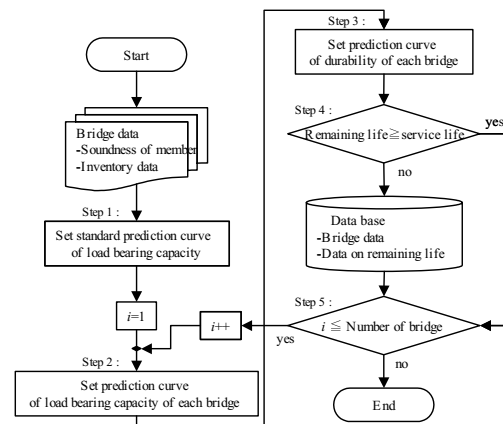


Figure 2. Procedure of selection of bridge requiring budget allocation.

curve set with Step 2. This curve is set in consideration of the correlation that a load carrying capability has decreased by durability's decreasing, too. Moreover, the age that durability and load carrying capability to be unable to serve that load carrying capability is 0 when durability is 0 is corresponding. In addition, the soundness when initial is constructed is also corresponding. Therefore, durability is deteriorated because of a degree that is lower than load carrying capability degree. From durability soundness data of each bridge, the durability deterioration curve is set by

$$g(t) = b_L - a_D t^c \tag{2}$$

where,

$$1 \leq c \leq 4 \tag{3}$$

$$a_D = \frac{b_L}{(b_L/a_L)^{\frac{c}{4}}} \tag{4}$$

where, it is necessary to show the standard deterioration curve of durability in the third curve.

**Step 4**

A remain life is calculated from the deterioration curve set by Step 2 and 3. The data of the bridge that A remain life is shorted is stored in DB.

**Step 5**

It does iterating the procedure of Step 2 to 4 for the number of the bridge.

The maintenance management plan is settled on so that three types of maintenance management measures shown to each age for the remaining life in Table 1 may be exclusively selected for the bridge where the budget allocation is necessary, and these bridges may satisfy the remaining life. The budget allocation problem is optimized by two stages that the long-term maintenance management plan problem of each bridge and the mid-term maintenance management plan problem of two or more bridges. In the long-term maintenance plan problem of each bridge, the LCC minimization at the remaining life is settled on and the maintenance management plan is settled on to the purpose.



Moreover, the maintenance management plan is settled on in the mid-term maintenance management plan problem of two or more bridges to assume the annual budget to be a restriction condition and to maximize the quality of the entire bridge group. It is because the solution space broadens hugely, and deriving the optimal solution becomes difficult when the budget allocation problem is only captured as enhancing the maintenance management plan problem at the singular bridge level, and two or more bridges are optimized at the same time. The procedure of the budget allocation is shown Figure 3 and as follows.

**Step 1**

The combination of the maintenance measures to which the life cycle cost is minimized is settled on from among the combination of the maintenance measures that satisfy condition that is not falling below soundness 0 at the remain period in the place where the maintenance measures  $m$  are executed in bridge  $i$  in the planned year  $t$ . The genetic algorithm is used for the decision of the maintenance plan assumed to be cost minimization of the life cycle, because there is innumerable the combination of the maintenance measures since  $t + 1$ . The formulation in this problem is shown below.

**Objective function:**

$$LCC_{i,\tau_i,t,m} = \sum_{\tau=\tau_{i,t}}^{L_i} C_{i,\tau} \rightarrow \min \tag{5}$$

where,

$$C_{i,\tau} = IM_{i,\tau} \cdot CM_{i,m} + IS_{i,\tau} \cdot CS_{i,m} \tag{6}$$

**Constraints:**

$$\begin{aligned} S_{SL_i}(\tau) > 0, S_{SD_i}(\tau) > 0, \\ S_{ML_i}(\tau) > 0, S_{MD_i}(\tau) > 0 \end{aligned} \tag{7}$$

where,  $LCC_{i,\tau_i,t,m}$ : Life cycle cost of maintenance measure  $m$  of age  $\tau_{i,t}$

- $i$ : Number of the bridge (1 through  $M$ )
- $M$ : Number of bridges
- $t$ : Year of maintenance (1 through  $T$ )
- $T$ : Planned period of maintenance (in years)
- $L_i$ : Expected service life of bridge  $i$  (in years)
- $C_t$ : Maintenance cost in  $t$ -th year (in U)
- $CM_{ijm}$ : Cost of maintenance of main girders in span  $j$  of bridge  $i$  carried out in  $t$ -th year
- $CS_{jim}$ : Cost of maintenance of slabs in span  $j$  of bridge  $i$  carried out in  $t$ -th year
- $IM_{i,t}$ : Measure or not in main girders of bridge  $i$  in  $t$ -th year
- $IS_{i,t}$ : Measure or not in slabs of bridge  $i$  in  $t$ -th year
- $S_{SL_i}(t)$ : Soundness of slabs of bridge  $i$  in terms of load carrying capability in  $t$ -th year
- $S_{SD_i}(t)$ : Soundness of slabs of bridge  $i$  in terms of durability in  $t$ -th year
- $S_{ML_i}(t)$ : Soundness of main girders of bridge  $i$  in terms of load carrying capability in  $t$ -th year
- $S_{MD_i}(t)$ : Soundness of main girders of bridge  $i$  in terms of durability in  $t$ -th year

**Step 2**

The process of Step 1 is iterated in the maintenance measure of 8 types, and the minimized maintenance plan is selected, because 3 types “NO measures”, “Repair”, and “Reinforcement” can be taken as both member, slab and main girder.

**Step 3**

It does iterating the procedure of Step 1 to 2 for the number of the bridge.

**Step 4**

The combination of the maintenance measures execution bridge where the quality is assumed to be the maximum under the budget constraint for the age of plan year  $t$  is calculated. GAs is used from the innumerable existence also of the combination of the measures execution bridge for the budget allocation problem to assume the quality to be the maximum. The formulation in this problem is shown below.

**Objective functions:**

$$Q_t = \sum_{i=1}^M Q_{t,i} \rightarrow \max \tag{8}$$

where,

$$Q_{t,i} = \left\{ 1 - \frac{\sqrt{(x_0 - q_{S,i}(t))^2 + (y_0 - q_{M,i}(t))^2}}{\sqrt{x_0^2 + y_0^2}} \right\} \times 100 \tag{9}$$

**Constraints:**

$$C_t \leq bud_{p,t} \tag{10}$$

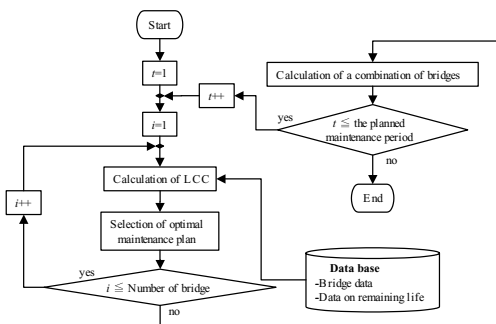


Figure 3. Procedure of maintenance plan problem.

$$bud_{p,1} = \frac{Bud_p}{\sum_{\tau=1}^T (1+r)^{\tau-1}} \quad (11)$$

$$bud_{p,t} = bud_{p,1} \times \prod_2^t (1+r) \quad (12)$$

$$Bud_p = BudT \times \left\{ 1 + \frac{1}{N_D} (N_D + 2 - 2p) \alpha \right\} \quad (13)$$

where,  $Q_t$ : Total quality in  $t$ -th year

- $Q_{t,i}$ : Quality of bridge  $i$  in  $t$ -th year
- $q_{S,i}(t)$ : Quality of slabs of bridge  $i$  in  $t$ -th year
- $q_{M,i}(t)$ : Quality of main girders of bridge  $i$  in  $t$ -th year
- $x_0$  and  $y_0$ : The reference values for load carrying capability and durability and are set at 100
- $bud_{p,t}$ : Budget for maintenance plan  $p$  for  $t$ -th year
- $Bud_p$ : Total budget for maintenance plan  $p$
- $BudT$ : Total budget (in U)
- $r$ : Rate of increase of annual budget
- $\alpha$ : Rate of change in budget amount
- $p$ : Number of the maintenance plan (1 through  $N_D + 1$ )
- $N_D$ : Number of budget plans (only even numbers are applicable)

Quality  $Q_{t,i}$  is calculated from the quality of the slabs and main girders in the span. Maintenance plans can be developed flexibly under a budget that allows for a margin of fluctuation rather than a fixed budget. In this study, therefore, multiple draft plans are developed while making the total budget flexible by introducing two variables,  $N_D$  and  $\alpha$ . The total budget for each draft plan  $Bud_p$  is obtained from the total budget  $BudT$ ,  $N_D$  and  $\alpha$  that the user determined, using Eq. (13). Optimizing the maintenance plan produces  $N_D + 1$  semi-optimal solutions with the total budget as constraints. Then, the budget for maintenance plan  $p$  for the  $t$ -th year under the total budget constraint is calculated by Eqs. (11) and (12). The semi-optimal solution here is defined as the one that is not optimal but not contradictory. The problem of maintenance plan optimization aims at providing the user with a wider choice of plans by presenting  $N_D + 1$  draft plans. This problem is free from the trade-off relationships of general multi-purpose optimization: trying to improve the value of an objective function worsens the value of another. Quality increases basically reduce the deterioration in soundness. The solution with the lower deterioration in soundness of the two of the same quality is regarded as an optimal solution.

*Step 5*

It does iterating the procedure of Step 1 to 4 for the planned period.

In this study, GAs (genetic algorithms) are applied to the optimization of the maintenance planning problem to accelerate solution search.

*Coding for maintenance measures*

Each of the three maintenance measures listed in Table 1 requires two bits for representation by a binary code. Assigning two-bit binary codes to the three measures leaves two-bit binary codes. The remaining codes with the code for “neither repair nor strengthening” are classified under the category of others in order to avoid the deterioration in calculation efficiency due to the generation of lethal genes. In the former J-BMS, genotypic coding is the sum of combinations of measures for the planned number of years of maintenance (Miyamoto A., et al. 2002.). The efficiency of calculation is not always high in the problem of maintenance planning for multiple bridges that involves numerous combinations. In this study, therefore, the period of maintenance is generally set at three to five years. The maximum period is assumed to be approximately 10 years. Not only the maintenance measures but also the time of maintenance is coded. The problem of maintenance planning is modeled by combining the codes based on the assumption that measures are taken less than three times during the planned period of maintenance. The model of the plan is represented by “maintenance measure  $k$  in the  $t$ -th year” for each span of main girders and slabs in a bridge.

*Optimization procedure*

The gene that models the maintenance plan is optimized by GAs. “Selection”, “Crossover” and “Mutation” that is the gene manipulation, use the following methods. The fitness value of each individual is calculated by linear scaling, and the individual selected by using together about the roulette selection and the tournament selection. The crossover rate is set so that crossover may assume the one to use one point crossover, and maintain the diversity of the individual as 1.0. The mutation is assumed to be the one to set the number of mutated gene from the viewpoint of the necessity of the calculation efficiency improvement. In that case, do not mutate in each individual but elect the mutated gene at random from among the number of individual times number of gene seats.

*Quality maximization of bridge group*

To calculate the combination of the bridge where the quality is maximized under the budget constraint of fiscal year, the genotype of the binary number code in which the presence of measures shown in Figure 5 is expressed is used and optimized. “1” expresses the measures none by “0” of the binary number code and

expresses. The quality of the bridge group is maximized using the maintenance measure optimized about each bridge when there are measures. Even if the number of bridges increases, it becomes easy to search for a semi-optimal solution because the gene is expressible only by the number of bits of numbers of bridges by modeled by the genotype that shows the maintenance plan decision problem of the bridge group in the budget allocation problem.

## 5 CONCLUDING REMARKS

In this study, an attempt was made to increase the applicability of the “maintenance plan optimization system”, a subsystem of the J-BMS that the authors have been developing, by solving the problems inherent in the system and made it applicable to multiple

bridges as well as single bridges. The GAs which are one of optimization methods, were adopted for solving the problem of maintenance plan optimization efficiently to derive semi-optimal solutions.

## REFERENCES

- Miyamoto A., Kawamura, K. & Nakamura, H. 1998. Development of Optimal Maintenance Plans for Existing Bridges using Bridge Management Systems (BMS), *Proceedings of the Japan Society of Civil Engineers (JSCE)*, No. 588/VI-38, pp. 191–208.
- Miyamoto A., Kawamura K. & Ong K.C.G. 2002. Bridge Management System for Existing Bridge Groups, *Reliability and Optimization of Structural Systems*, pp. 69–78.

# LCC case studies for bridges in different design phases

S. Noponen

*Ramboll Finland Ltd., Finland*

A. Jutila

*Laboratory of Bridge Engineering, Helsinki University of Technology, Finland*

**ABSTRACT:** The paper focuses on LCC case studies of two bridge projects. The objective is to incorporate all important issues of LCC studies on new bridges.

Two existing design projects of Ramboll Finland Ltd are discussed. The first one has reached the structural design phase already, but the second one is in the general design phase. In the LCC studies, the user costs are included in the analysis. Because the structural details of the bridges are valid in a common way, the deterioration of the components progresses at an average rate typical for the Finnish climate and maintenance policy. The deterioration and rehabilitation history is derived from the deterioration models developed in the Finnish Road Administration's (Finnra) previous research projects. If the components are designed with new details or by using new design codes, the deterioration rates can be estimated with mathematical deterioration equations. The maintenance and rehabilitation costs, the obsolescence factors (such as widening or strengthening needs) and the estimation of service life time are taken into account. The various possibilities of the bridge life are considered in different scenarios or risk analyses.

By analysing these bridge cases, it is possible to determine ways to minimize life cycle costs. In the general design phase a LCC study could be a tool in designing on the most economical bridge structures. In the same way, in the structural design phase such a study could provide a tool to determine the most economical bridge details and construction procedures.

## 1 INTRODUCTION

The research work carried out is based on the knowledge derived from the effective inspection and management systems developed in Finland. This development work was started already as early as the late 70's. The first Finnish approach to the life cycle cost (LCC) calculations and the Marcow chain deterioration models were done in the early 90's by VTT Technical Research Centre of Finland.

During the year 2007, there have been cases where the construction costs of large infrastructure construction projects in the contractor's tenders have been several tens of percents higher than the estimated initial construction costs. Therefore, it is important to improve the calculation methods for estimating initial costs as well as LCC for infrastructure projects.

## 2 PRINCIPLES FOR LCC

### 2.1 Calculating costs

Finnra provides some instruction books for calculating the costs of construction and rehabilitation of bridge

components or materials for designers. The costs taken from the Finnra's cost estimation guide are based on the 1995 costs and need to be increased by the bridge construction index.

The life cycle costs,  $C$ , are calculated by the well known net present value equation:

$$C = \sum_{t=0}^N \frac{C_t}{(1+r)^t}$$

where  $N$  = number of years in the calculation,  $C_t$  = cost over a specified period of time  $t$  (years), and  $r$  = discount rate. Some of the costs over a specified period of time are for example the initial cost, maintenance costs, user costs and demolition costs. For real discount rates Tupamäki has suggested the following values for different kinds of purposes: natural economy 0%, national economy 3%, state economy 6% and in business economy 9%. In Finnra's LCC calculations, the discount rate has normally been 4 or 5%. In this study the average discount rate is primarily estimated at 4%.

Design and supervision costs are included in the initial costs. They are normally estimated to be about 15% of the initial cost. In Finland bridge rehabilitation, e.g. rehabilitation of deteriorated bridge parts is normally included in the larger contracts. The quality of the work is assumed to be equal to that of a new product. This kind of rehabilitation is called basic rehabilitation. Average basic rehabilitation contract costs per bridge deck are estimated at 500...600 €/m<sup>2</sup>. An estimate of the basic rehabilitation intervals is presented in chapter 2.4. Finnra's budget for minor rehabilitation and general and special bridge inspections has been about 20% of the basic rehabilitation budget. Cleaning, yearly inspections and rehabilitations for bridge site structures are additional costs to be considered.

## 2.2 User costs

Bridge construction and rehabilitation cause disturbance to the road user. The effect of construction depends on the construction method and how traffic has been arranged. The various traffic arrangements can include the use of temporary bridges, detours and redirecting traffic to finished bridge sections. The user costs are divided into driver delay costs, vehicle operating costs and accident costs. Disturbances to users can be analysed by traffic simulations or by the use of simplified methods.

There are different simplified rules concerning calculation of, for example, driver delay costs. In this study, we make a comparison between two alternatives of calculating delay costs. The first method of estimating user costs caused by driver delay,  $C_{driver}$ , is given in equation:

$$C_{driver} = \left( \frac{L}{S_a} - \frac{L}{S_n} \right) \cdot T_{traffic} \cdot D_{ays} \cdot c_{ost}$$

where  $L$  = length of the road worksite,  $S_a$  = average velocity of the vehicle due to construction and  $S_n$  = velocity without construction,  $T_{traffic}$  = estimated daily traffic amount,  $D_{ays}$  = time needed for work and  $c_{ost}$  = driver delay cost for one vehicle. In Finland costs per hour have been set at 126.08 € for a bus, 19.57 € for a truck and 16.03 € for a car. The above driver delay costs are calculated based on assumed average wages and equivalent free time expense equal to 35% of the worker's wages. Vehicle operating and accident costs are not taken into account due to their minor influence on user costs.

Another way to estimate the user cost estimation in Finland has been to set the costs for the bridge construction site at 0.2 €/vehicle, when traffic is 500 vehicles per day. If the traffic amount is 25,000 vehicles per day, then the costs are 0.5 €/vehicle. For other traffic amounts, the costs are assumed to behave

linearly through these given points. This way of calculation has been developed from a couple of earlier construction projects.

In the first approach, the length of the road work site or the effective length where the construction site causes disturbance and lowers velocity of traffic should be known. This can only be accurately determined by doing traffic simulations.

A simple comparison of these two approaches calculating user costs is still done here. An assumption is made that normally the average speeds are reduced from 80 km/h normally to 40 km/h during construction. By substituting these values for  $S_n$  and  $S_a$ , respectively, and using the assumed daily cost to traffic discussed above, the length of road affected by construction can be solved. For a traffic level of 500 vehicles per day, the length equates to 800 m and for 25,000 vehicles per day, it equates to 2 km.

## 2.3 Maintenance costs

In the LCC calculations maintenance, inspection, cleaning and minor repair costs are taken into account as annual costs. For this kind of annual costs, the information is extrapolated from the data given in Finnra's publication "Life cycle costs of small bridges".

For basic rehabilitations the interval is estimated by the method given below. The system is based on the assumption that basic rehabilitation works are carried out when the bridge exceeds condition class 3. The estimated basic rehabilitation costs are based on the information given in Finnra's instructions.

## 2.4 Deterioration and interval of rehabilitations

Finnra's Bridge Management System is mainly based on general inspections. The average interval for general inspections is about five years. An inspector evaluates the damages and deterioration visually and records them into the register. The deterioration classification is given in Finnra's Bridge Inspection Guide. A bridge is divided into nine main structural components. In the evaluation these components are substructure, edge beam, superstructure, pavement, other surfaces, railings, expansion joint, other equipment and bridge site. The inspector's evaluation points  $C_{condition}$  (from 0 to 4) reflect the condition of the main components. The further deterioration process of the components can be estimated mathematically with the Markov chain method as shown by Finnra (Figure 1.).

In this analysis, the critical components of concrete bridges, that set of a need for basic rehabilitation, are assumed to be the edge beams that cause problems to railing connection, water isolation systems including drainage, expansion joints, bearings, surfaces of the superstructure and substructure. The basic rehabilitation interval can be estimated by calculating the

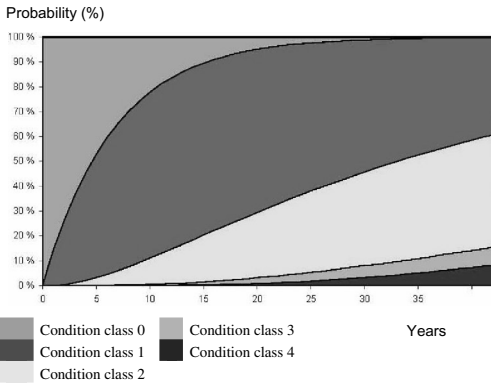


Figure 1. Condition class probability for corrosion protected steel culvert in waterway environment.

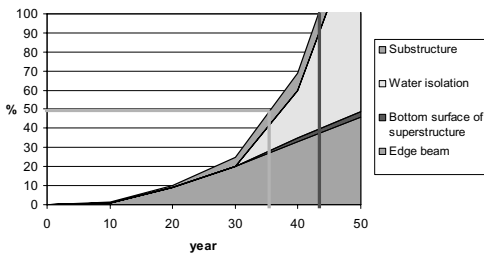


Figure 2. Example (Ampumarata flyover) of summing up the condition class 3 probabilities of the critical components together to get a prognosis for the time interval of basic rehabilitation.

combined deterioration likelihoods of these components and observing when the probability of reaching the condition class 3 exceeds 50%. That is the time when basic rehabilitation is needed.

In the example shown in Figure 2, 50% probability of basic rehabilitation, to the specific bridge, appears at the approximate age of 36 years. If we neglect some of the edge beam rehabilitation needs, the 50% probability is achieved later. Note that in this example the specific bridge does not have bearings and expansion joints. 100% probability of the bridge basic rehabilitation will occur at the approximate age of 43.

### 2.5 *Obsolescence and deconstruction costs*

In Finland bridges are designed to last at least 100 years for 95% probability, when good maintenance policy is used. This way of thinking does not take the obsolescence, i.e. changes in human based functionality or safety requirements into account. This kind of

phenomena are for example strengthening and widening of the bridge or changing the route of the road completely at the bridge site. Possible ways to consider these effects in the LCC calculations are by: increase the discount rate, decrease the lifetime of the bridge or assume the probabilities and costs caused by obsolescence.

Deconstruction includes many kinds of work, starting from designing and managing work. Even before the actual deconstruction work starts, traffic has to be directed away from the construction site and some of the carrying structures have to be supported. It is always important to do the deconstruction work in the right order following the instructions of the deconstruction plans and using the right machines for different face of work. After demolishing the bridge, the different structural materials, for example concrete and steel, must be separated from each other and transported to waste product treatment and rubbish dumps or reproducing factories. In this study, the deconstruction cost is taken from the construction cost information program Rapal, which estimates the demolishing cost for a bridge to be 176 €/m<sup>3</sup>. Rubbish dump payment of concrete (without reinforcement) is less than 30 €/m<sup>3</sup> in Finland.

### 2.6 *Sensibility study by considering different scenarios*

As the initial construction costs can vary tens of percents, it is more likely that there are still bigger risks for forecasting the whole LCC of a bridge. The bridge managing systems and maintenance strategies may change considerably in the long run. It is possible only to guess how politicians will prioritize the condition of the national traffic network in their future budgets. Also when calculating user costs, it should be remembered that the future traffic amounts are rough estimates. The functional or aesthetical needs may change and it may be decided that a bridge is useless before the structural life time has ended. These uncertainties should be studied by sensibility analysis or by considering different scenarios e.g. the worst and the best scenario of LCC. Carrying out these kinds of studies makes it possible to evaluate the reliability of the LCC calculation.

## 3 EXAMPLE OF LCC CALCULATION IN THE CONSTRUCTION DESIGN PHASE

### 3.1 *Aspects of LCC in the construction design phase*

Usually, when a bridge construction design project is started, the main functional goals of the bridge are

already known. Normally, there is a preliminary general drawing, in which also the main aesthetical forms are described. But of course there are many important details that the designing bridge engineer can influence to make the bridge LCC-effective. The most important things to be considered are usually the need of bearings and expansion joints as well as a choice of the most suitable substructure type. In addition, the user costs have to be minimized, especially on busy roads.

### 3.2 Introduction to the Ampumarata flyover project

The Ampumarata flyover will be constructed to improve the traffic connection between Helsinki city suburbs Viikkinmäki and Viikki. The suburb Viikkinmäki and its municipal technology are already under construction. There is a linking frame type bridge between the suburbs, but the width of the Hernepelto road going underneath the bridge and the pedestrian and bicycle lanes have to be improved. The over bridge passing highway Vt4 is one of the main roads to Helsinki and the daily traffic amount of the road is about 50,000 vehicles. Highway Vt4 is now a 3-lane road to both directions but it will likely be widened to a 4 + 4-lane road.

The Ampumarata flyover is designed to consist of two bridges, A and B, with effective width of 20.25 meters. So the extra lanes can be added without widening the bridge. The bridge type is three-span cast in situ reinforced concrete slab bridge with spans 8 + 16 + 8 m. These main measurements of the bridge have been decided in the general design phase.

The geotechnical conditions change quite dramatically at the bridge site. In the east corner, rock is less than two meters from the road level, whereas on to west side the distance to rock is almost 20 meters. The earth layers are the highway filling layers, clay and moraine. In sites where piles were needed, a rock socket pile was chosen, because there are more contractors for that pile type than e.g. for drilled piles. The estimated costs of these piles were quite equal.

In the structural design phase, the most important thing was to design the bridge so that it affects traffic on the highway Vt4 as little as possible during the construction period, and to design the foundation principals properly and cost effectively. In this kind of demanding bridge design task, the bridge engineer needs professional help from geotechnical, road, traffic, municipal and landscape designers.

One of the first tasks in the project was to find out what was the best way to build bridges A and B. The best solution was to start the construction from bridge A. The rock socket piles will be drilled and cut near the road level. The piles will directly carry the bridge after demolishing the falsework. For aesthetical reasons, column mantels are constructed later around the

pile. At this stage, when bridge A is being built, traffic is directed over the east side of the existing old frame type Ampumarata flyover. After bridge A is constructed, the traffic is directed on to it, and work can start on bridge site B. Excavation on the bridge site can start, because it does not affect traffic. In support lines 1, 2 and partly in support line 4, the bridge is supported on rock socket piles. Elsewhere, the concrete foundation slabs are constructed on rock. After finishing bridges A and B, the work will be continued by excavating the earth under the bridges, installing municipal pipes beneath the bridge and building the new Hernepelto road. Thereafter traffic on the Hernepelto road can be directed from the old route to the new one. Demolition of the old bridge can start next to bridge B, and after filling work and diverting the temporary road to bridge B, deconstruction of the remaining old bridge next to bridge A can be done.

For temporary roads, the speed limit is lowered from 80 km/h to 60 km/h. Every temporary road consists of 2 + 2 lanes, and in the edges and middle of the road, temporary concrete railings are used. The Hernepelto road can be used at every stage, so the trucks of Viikkinmäki suburb contractors and buses can use the road.

The construction of bridges is always quite demanding when the work is carried out close to busy roads. In this case, many good LCC decisions can be found. These include e.g. planning of temporary traffic arrangements, neglecting the use of bearings on support line 4, and including the construction of the bridge to its final width in the initial contract to avoid widening in the near future. In the next chapter the calculated portions of different effects in LCC are shown.

### 3.3 LCC calculations

In this chapter, the results of the Ampumarata flyover LCC calculations are presented. Three different scenarios for the life cycle of the bridge are taken into account. The average assumption scenario results are discussed in detail and the other results are shown from a sensibility aspect.

In the average calculation, the following assumptions have been made: the bridge is constructed in 6 months, life time of the bridge is 80 years, discount rate is 4%, annual maintenance costs without basic rehabilitation is 3 €/m<sup>2</sup>, one basic rehabilitation is needed at the age of 36 years, traffic cross-section will be changed at the age of 10 years and the changes take 1 month. The results of these calculations are shown in Figure 3. The whole LCC was about 9 M€, while the initial construction costs were about 2.4 M€.

It can be seen from Figure 3 that the biggest portions added to initial costs are user costs. User costs for this project are here 65% of the whole LCC. The large portion is natural due to the high traffic highway. In this

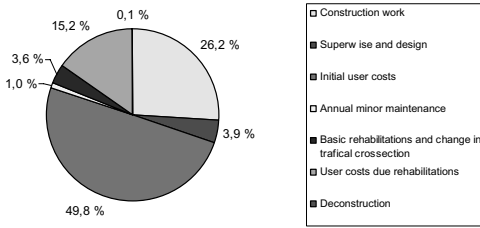


Figure 3. LCC portions of the Ampumarata flyover.

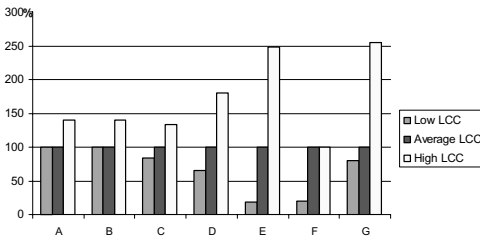


Figure 4. Sensibility study of the Ampumarata flyover LCC, in which A = Construction cost, B = Supervision and design cost, C = Initial user cost, D = Annual routine maintenance cost, E = Basic rehabilitations and change in traffic cross-section costs, F = User cost due to rehabilitation, G = Deconstruction cost.

case, the assumed rehabilitation costs are low, because bearings and expansion joints are avoided. The average results are not only interesting as such, but also the sensibility of the calculation is considered. Two other scenarios have been made for low and high LCC. The sensibility study is shown in Figure 4.

When calculating the LCC based on low cost scenario, the following assumptions different from those above have been made: the bridge is constructed in 5 months, life time of the bridge is 50 years, discount rate is 6%, basic rehabilitation is not needed (short life time) and traffic cross-section will be changed at the age of 20 years. In the scenario of high LCC: the initial costs are 40% higher compared to those of an average LCC case, the bridge is constructed in 8 months, life time of the bridge is 100 years, discount rate is 2%, two basic rehabilitations are needed (at the age of 30 and 60 years) and traffic cross-section will be changed at the age of 10 years.

So, by using different scenarios, the result is quite different. The sum of the low LCC is about 6.9 M€ and the high LCC is 12.2 M€. If the construction work of the Ampumarata flyover could be carried out in 5 rather than 8 months, 2.2 M€ of user costs would be spared. This is almost the same sum as the initial construction cost.

## 4 EXAMPLE OF LCC CALCULATION IN THE GENERAL DESIGN PHASE

### 4.1 Aspects of LCC in the general design phase

The most important aspects in the general design phase are: functionality, aesthetics and costs of the bridge. All these three things should be kept in mind when determining the best bridge solution for a specific bridge site. Functionality, e.g. the width and length of the bridge, is generally the thing where compromises are not wanted. Such compromises can cause increased user costs that could not be easily taken into account in the bridge engineers cost calculations. In general, the design phase LCC calculations can provide an appropriate tool for comparing the differences in LCC of e.g. steel and cast-in-situ concrete bridges. In these calculations, the effect of user costs can be taken into account. For example, the bridge scaffolding can restrict traffic so much that it is more cost effective to do the formwork carried by the main beams of superstructure. A simple comparison of this kind of user cost calculation is made in the next chapter.

### 4.2 Introduction to the project of the kivikko flyovers and a landscape bridge

These bridge sites are located in the city of Helsinki. The intention is to improve the traffic connection between the suburbs of Kivikko and Latokartano and to ease the pressure of traffic on the Ring Road I.

This general design phase project consists of six bridges. Two of the bridges, Kivikko flyovers, are very similar to the Ampumarata flyover discussed earlier. Traffic should be diverted to one bridge part or site at a time while the other is being constructed. The most interesting bridge in this project is a landscape bridge over the Ring Road I, which will continue from the side of the Latokartano suburb as a landscape park over a busy road. The length of the bridge is about 100 meters, and the effective width varies from some 10 m to 20 m. The daily traffic is about 60000 vehicles. The distance between the two bridge sites is about 250 m. The other three bridges do not much affect the LCC examination discussed next.

The interest in this project from a LCC point of view is to determine the user costs of the landscape bridge construction phase, and to examine, which bridge type is the most economical one. In this design phase, it is not sure that the Kivikko flyovers and the landscape bridge are awarded as one contract to be built at the same time. This fact has great effect on the user cost calculations. If they are constructed at the same time, bottle neck effect evaluation cannot be separated from the two bridge sites. This is because the sites are situated so close to each other.



#### 4.3 LCC comparison of the alternatives

Two alternatives, steel and prestressed concrete beam bridge for the landscape bridge are compared. The estimated initial cost for the steel and for the concrete bridge option are 3.2 M€ and 2.7 M€, respectively. For the steel bridge option, falsework is not needed, because the steel beams can carry the weight of the formwork and wet concrete. For the concrete bridge option, extra falsework with holes for the Ring I traffic is needed. This kind of a hole can be obtained by temporarily installed steel beams. The two temporary traffic holes below the landscape bridge should be at least 10 m wide.

In the following text, two ways of contracting the concrete bridge are evaluated by the aspect of user costs. In the first case, the flyovers and landscape bridge are constructed at the same time. The temporary road route length will increase 250 m, which is the distance between the bridges. By using the equation given in Chapter 2.2, the increased cost will be calculated with assumptions that 80 km/h average speed is lowered to 40 km/h in the temporary route, and the falsework of the landscape bridge restricts traffic for about 2.5 months. The increased user cost is then about 228,000 €.

The other option is to construct the bridges at different times. Then, the overall construction time increases and there will be two separate bottle necks in the work site. In this case, the effect caused by the narrow temporary road can be estimated with the second calculation method described in Chapter 2.2. The user costs for the 2.5-month period are estimated to be 2.25 M€. The difference in user costs in the first and second contract model is notable. By using a steel beam bridge type, the contract types do not affect the user costs, because the falsework is not needed in this bridge type.

When adding the extra user cost to the initial costs it is noticed that building a concrete bridge using the first contract case could be the cheapest one. But in this calculation, the extra costs of temporary steel beams are neglected, and the increased accident costs caused by vehicle collision to falsework columns or temporary beams are not added to LCC. For this reason, the steel beam is recommended for the bridge type, although the maintenance of a steel bridge could be higher.

## 5 CONCLUSIONS

The LCC calculation system, based on earlier research results and amended by some new findings, has been

described in this study. Some existing projects have been introduced and examples of structural and general design phases have been calculated.

In the study, the time interval of average basic rehabilitations is predicted by summing up the condition class 3 probabilities of critical components. After calculating the average results, a sensibility study is carried out by considering different scenarios.

The user costs have been calculated in two different ways. In the first method, accurate information of the length of the road work site and decreased velocity of the vehicles are needed. The second method is easier for the bridge LCC purposes. These two simplified approaches are not adequate enough in all cases, and it is recommended that traffic simulation is used as often as possible for difficult bridge construction projects. The user costs make up large portions of the whole LCC as noticed in the case studies, where the bridge site is on busy traffic routes.

## REFERENCES

- Bridge Life Cycle Optimisation—Jutila, A. & Sundqvist, H., Etsi Project (Stage 1), Helsinki University of Technology Publications in Bridge Engineering, TTK-SRT-37. 2007. Tampere: Domus-Offset Ltd, ISSN 1456-6273.
- Noponen, S. Rehabilitations of Finnish road Bridges. Life-Cycle and Performance of Civil Infrastructure Systems—Cho, Francopol & Ang. 2007. London: Taylor and Francis Group, ISBN 978-0-415-41356-5.
- Rautakorpi, H. Pienten siltojen elinkaarikustannukset (Life cycle costs of little bridges), Finnra, TIEH 4000405. 2004. Helsinki: Edita, ISSN 1457-991X.
- Sillan kustannusarvio (Cost estimation of bridge), Internal publications of the Finnish Road Administration (Finnra), TIEH 2100012-02. 2002. Helsinki: Edita, ISBN 951-726-865-3.
- Siltojen verkko- ja ohjelmointitason hallinnan kehittäminen (Development of bridges network and project level management), Finnra, TIEH 3201003. 2006. Helsinki: Edita, ISBN 951-803-731-0.
- Siltojen ylläpito (Maintenance of bridges), Finnra, TIEH 1000090-05. 2005. Helsinki: Edita, ISBN 951-803-461-3.
- Sillantarkastuskäsikirja (Bridge inspection manual, The directives for bridge inspection procedures.) 6th renewed edition in Finnish, Finnra, TIEH 2000003-04. 2006. Helsinki: Edita, ISBN 951-726-873-4.
- Tieliikenteen ajokustannusten yksikköarvot 2005 (Unit costs for road traffic 2005), Finnra, TIEH 2100039-05. 2005. Helsinki: Edita, ISBN 951-803-606-3.
- Tupamäki, O. 2003. Total LCC and Sustainable Construction. *Proceedings: RIL/RILEM/CIB Symposium ILCEDES 2003*. Kuopio.

# Life-cycle cost assessment and service life estimate of precast concrete culverts

D.K. Panesar

*University of Toronto, Toronto, Ontario, Canada*

C.J. Churchill & S.E. Chidiac

*McMaster University, Hamilton, Ontario, Canada*

E. Kling

*Hanson Pipe and Precast, Cambridge, Ontario, Canada*

**ABSTRACT:** This study evaluates the influence of ground granulated blast furnace slag (GGBFS) used as cement replacement on the service life and cost effectiveness of precast concrete culverts in Canada which are partially exposed to the outdoor environment including de-icing salts. The mix design variable considered in this study pertaining to dry-cast concrete is the percentage of GGBFS (0, 25 and 50%) added. Reinforcement corrosion service life estimates based on the concrete's air permeability measurements are made for two exposure conditions: carbonation and chloride penetration. A life-cycle cost assessment is conducted to evaluate the economic feasibility of alternative concrete mix designs. Agency costs for construction, and maintenance, as well as social costs over the culvert's service life are accounted for.

## 1 INTRODUCTION

Sustainable reinforced concrete structures which are durable and economical are being designed with service lives over 100 years. To achieve adequate long-term performance and the designed service life it is critical to understand the impact of materials selection and material design on economic and durability performance. The performance and durability of precast concrete pipe is of great concern to cities and municipalities that have new and existing infrastructure pipeline systems (OCPA 2003, NRC 1998). Box culvert structures are partially buried pipe and so are exposed to Canada's severe environmental conditions including freeze-thaw cycles and exposure to de-icing salts.

Although flow determination and structural analysis aspects of buried pipeline design are well established, investigation of concrete pipe durability and life-cycle costing is warranted to ensure that precast concrete pipe will fulfill the 100 year design life. Currently, the "design practice does not include an assessment of long term value through cost-benefit or life-cycle cost analysis" and there is a need to incorporate this into design and construction decisions (OCPA 2003). Partially exposed box culverts are vulnerable to deterioration on the interior and exterior of the pipe. The scope of this research is in context with external

exposure to de-icer salts and carbonation. This study pertains to the use of ground granulated blast furnace slag (GGBFS) as cement replacement on a typical dry-cast box culvert structure (2.4 m high  $\times$  3.0 m wide  $\times$  2.5 m long) and reveals its impact on service life estimations and life-cycle costs. To analyze life-cycle costs of three alternative mix designs this study adopts the present worth method as prescribed by ASTM C1131 (2006) which captures agency costs for various decision variables including construction, maintenance, and social costs such as CO<sub>2</sub> abatement.

## 2 SERVICE LIFE OF PRECAST CONCRETE CULVERTS

### 2.1 *Experimental program—concrete materials and curing*

Table 1 provides the mixture proportions of the concrete using type 10 ordinary Portland cement (OPC), GGBFS, crushed coarse aggregate with a maximum size of 13 mm, and fine aggregate consisting of natural rounded silica sand. After mixing and casting, the specimens were placed in lime-saturated water tanks at a temperature of  $23 \pm 2^\circ\text{C}$  for 14 days and then air-cured in a controlled environment with a

Table 1. Concrete mix design composition.

% GGBFS	Total binder (kg/m <sup>3</sup> )	Fine aggregate (kg/m <sup>3</sup> )	Coarse aggregate (kg/m <sup>3</sup> )	w/b
0	360	1275	847	0.38
25	360	1257	843	0.38
50	360	1257	843	0.38

Table 2. Air permeability measurements.

% GGBFS	Permeability 10 <sup>-16</sup> (mm <sup>2</sup> )
0	0.077
25	0.028
50	0.018

temperature of 23 ± 2°C and a relative humidity of 50 ± 5% for 14 days.

### 2.2 Air permeability as a durability indicator

The Torrent Permeability tester was used to measure the air permeability, assessing the quality of the near surface concrete. Results given in Table 2 are the average of two measurements.

Permeability has been used as a durability indicator of the covercrete’s air tightness (Torrent 2007, Dhir et al. 1989). In Torrent’s study, laboratory and site investigations have revealed that the logarithm of permeability at 28 days correlates linearly with carbonation depth and chloride diffusivity with age. Based on Torrent (2007), equations (1) and (2) shows that when the carbonation depth and the chloride penetration depth, respectively, are equal to the cover depth of the reinforcement (*c*), the service life (*SL*), of the structure is reached:

$$c = A \ln(kT/0.01)SL^{0.5} \tag{1}$$

And based on Fick’s 2nd law of chloride diffusion:

$$c = 2B(10^{-12}kT^{0.7}SL)^{0.5} \tag{2}$$

*A* and *B* = the parameters depending on exposure conditions, cement type etc., *t* = time (years), and *kT* = coefficient of air permeability (10<sup>-16</sup> m<sup>2</sup>).

### 2.3 Service life estimates

In accordance with OPSS 1821 (1993), the concrete cover to the welded wire fabric is 40 ± 5 mm and the cover to reinforcing bars is 50 ± 15 mm. This analysis assumes a reinforcing steel cover depth of

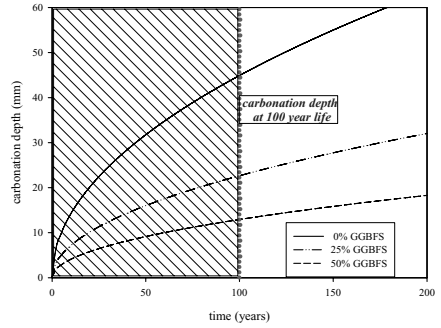


Figure 1. Influence of GGBFS on carbonation depth with age.

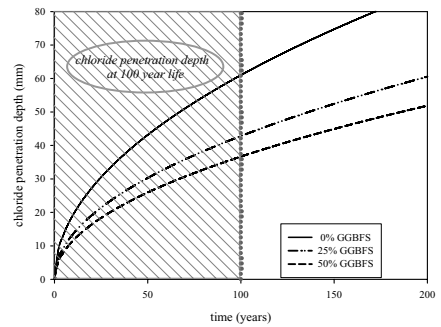


Figure 2. Influence of GGBFS on chloride penetration depth with age.

50 mm and based on equations (1) and (2), the service life is reached when the carbonation depth or chloride penetration, respectively, reaches 50 mm. In this study, to evaluate alternative mix designs, it is considered that the service life is reached at the onset of the corrosion propagation stage. Figure 1 shows that the depth of carbonation is lower with increasing percentages of GGBFS based on the 28 day air permeability measurements. When the carbonation depth is 50 mm, Figure 1 shows that the service life estimate of concrete containing 0% GGBFS is 124 years, and beyond 400 years for the 25% and 50% GGBFS mixtures. In comparison, when the chloride penetration depth equals 50 mm, Figure 2 shows the service life estimates, corresponding to the initiation stage of reinforcement corrosion, of concrete containing 0%, 25% and 50% GGBFS are 68 years, 138 years and 186 years, respectively. This analysis reveals that the service life of dry-cast concrete is limited by chloride penetration, and that concrete containing 0% GGBFS has a service life estimate approximately half that of concrete with 25% GGBFS addition.

### 3 LIFE-CYCLE COST ANALYSIS

Life-cycle costs of infrastructure elements consist of the sum of all expected costs and revenues to the end of the structures lifetime including operation, maintenance, repair and disposal costs (ACI 2002). Equation (3) represents the generic equation used for the present value of total life-cycle cost (*PVLCC*) (Ehlen & Marshall 1996). The costs are compared in real (inflation adjusted) prices and are discounted in order to derive their value.

$$PVLCC = IC + PVOMR + PVD \quad (3)$$

Initial construction (*IC*) costs are generated from design, surveying, material expenses, installation and final inspection. The present value of operation, maintenance and repair (*PVOMR*) costs include performance requirements such as inspection, repair and replacement of the structure. At the end of a culvert's service life, it may be ground and used as aggregate but its residual value is small and the present value of disposal, (*PVD*), is considered to be negligible since it is discounted over such a long period (70–100 years).

Equation (4) is used to convert future cashflows into an equivalent present worth and is influenced by the sum of all costs ( $C_t$ ), incurred at time ( $t$ ), using a real discount rate ( $d$ ), over the number of time periods in the study period ( $T$ ). Various approaches were studied to select a discount rate including the cost of borrowing, the cost of capital, the opportunity value, and the minimum attractive rate (Riggs et al. 1997; Wonsiewicz 1990). A range of discount rate values from 8% to 12% was suggested for public projects by the Treasury Board of Canada (1998) and a value of 10% was chosen in this analysis as a base.

$$PVLCC = \sum_{t=0}^T \frac{C_t}{(1+d)^t} \quad (4)$$

#### 3.1 Decision variables

##### 3.1.1 Real interest rate

A 'real interest rate' ( $d$ ) as expressed in equation (5) is a function of the actual interest rate ( $i$ ) and the inflation rate ( $f$ ) and reflects the purchasing power of the future cashflow by setting the discount rate to negate inflation and using constant dollars in the analysis.

$$d = \frac{1+i}{1+f} - 1 \quad (5)$$

##### 3.1.2 Annuities

Repair, replacement and user losses are structure and site specific. The box culverts analyzed in this study

are not part of the roadway infrastructure and therefore do not incur the large user costs that similar elements do when they are closed down for repair and rehabilitation (Purvis et al. 1994). The extent of the operation, maintenance and repair is therefore limited to annual inspections and localized restoration of deteriorating sections.

##### 3.1.3 Study period

To compare the three concrete mix designs the same study period must be used. Two of the mix designs (25% and 50% GGBFS) have service lives greater than 100 years. The design life of most infrastructure systems is 100 years and therefore this was the study period chosen for this study. Corresponding to the propagation period of active corrosion, the service life estimate of the concrete containing 0% GGBFS is 68 years (Fig. 2), at which time the costs necessary to remove, demolish and replace the culvert are accounted for in this analysis.

##### 3.1.4 Capital cost

The capital cost of the culvert includes cost of the design, material, quality assurance, labour and equipment. The capital cost for a 2.5 m span of culvert is between \$7000 and \$8000 and approximately \$3000 for installation yielding a total capital cost of approximately \$10 000 (OPSS 1821). This value is used in this analysis and is supported by various sources including R.S. Means (2006) and manufacturers' price listings.

#### 3.2 Pollution abatement

Third party costs such as pollution do not necessarily impact the agency in charge of the facility nor the direct users. It has been well documented that the concrete industry produces a significant amount of CO<sub>2</sub> in the creation of its products (Roskovic & Bjegovic 2005). Concrete production releases CO<sub>2</sub> but with age the occurrence of carbonation processes re-assimilates the CO<sub>2</sub> through the exposed surface area and this exchange could be interpreted as a positive cashflow. Owing to the CO<sub>2</sub> uptake process, other strategies for CO<sub>2</sub> abatement can be avoided and the corresponding cost would be incorporated as a benefit in the cashflow of the culvert's life-cycle. The methodology presented by Pade and Guimaraes (2007) for estimating the CO<sub>2</sub> uptake in concrete was adopted in this analysis. It is comprised of three calculations including determination of the carbonation depth, volume of carbonated concrete and the amount of CO<sub>2</sub> absorbed per volume of carbonated concrete. The amount of CO<sub>2</sub> released during the construction phase of the culvert was also calculated using the results reported in Prusinski et al. (2004) and the data was interpolated using a cubic spline for the mix design containing 25% GGBFS mixture.

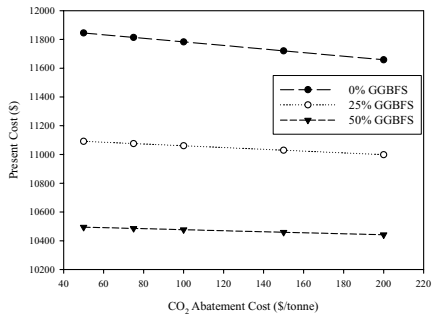


Figure 3. Influence of GGBFS on present cost of CO<sub>2</sub> abatement.

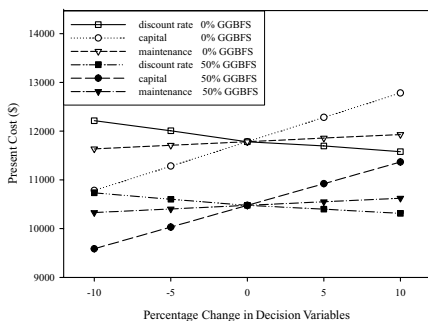


Figure 4. Sensitivity of discount rate, capital and maintenance costs for 0 and 50% GGBFS mixtures.

Abatement of CO<sub>2</sub> can be a costly endeavour and strategies range from switching to low emission fuels to sequestering the CO<sub>2</sub> in underground reservoirs. The costs of these abatement strategies has been estimated to range from \$25 to \$300 per tonne of CO<sub>2</sub> (Johnson & Keith 2004, Newell et al. 2006, Jaccard et al. 2003). Many of the strategies tend towards the lower end of this spectrum so a base case of \$100/tonne of CO<sub>2</sub> was chosen for the analysis. In addition \$50, \$75, \$150 and \$200/tonne of CO<sub>2</sub> were also evaluated to assess its sensitivity to the present worth analysis as shown in Figure 3.

### 3.3 Discussion of results and sensitivity of decision variables

In order to evaluate the influence of the discount rate, maintenance cost, and capital cost on the present value analysis, a sensitivity study was conducted using  $\pm 10\%$  of the base case as shown in Figure 4. All values are in Canadian dollars and all results were negative indicating a present cost. When comparing the base case for the three mix designs the present worth of 25%

and 50% GGBFS concrete is approximately 6% and 12%, respectively, less than concrete containing 0% GGBFS as shown in Figure 4.

The results indicate that capital cost is the most sensitive variable and this is expected because it is the largest single cost in the culvert's life-cycle and construction occurs during the initial time period and is not discounted. One of the primary differences between the present costs of the mix designs is attributed to the use of supplemental material which reduces the production costs of the culverts. In addition, the mix design that contains 0% GGBFS has a service life which is less than the design life of 100 years. At the end of its estimated service life of 68 years (Section 2.2), the existing culvert must be removed and a new one installed. This is a substantial expense and the analysis reveals that the 0% GGBFS mixture option is at a disadvantage compared to the mix designs with 25% and 50% GGBFS which do not need to be replaced during the design life.

The CO<sub>2</sub> abatement costs have a linear effect on the present worth of each mix design as seen in Figure 3. A relatively high abatement cost lowers the overall present cost of the mix designs. If the cost of abatement were to reach sufficiently high numbers such as several thousand dollars per tonne of CO<sub>2</sub> the present worth could become positive.

## 4 CONCLUDING REMARKS

The primary findings from this study revealed the following:

- The service life corresponding to the onset of active reinforcement corrosion of dry-cast concrete containing 0, 25 and 50% GGBFS as cement replacement is limited by chloride penetration and not carbonation. The reinforcement corrosion service life of concrete containing 0%, 25%, and 50% GGBFS is estimated to be 68 years, 138 years, and 186 years, respectively.
- Concrete containing 25%, and 50% GGBFS reduce the present cost of the mix designs containing 25% and 50% GGBFS by approximately 6% and 12%, respectively as compared to concrete containing 0% GGBFS.
- The environmental benefits evaluated in terms of CO<sub>2</sub> abatement are greater for concrete containing GGBFS as compared to OPC concrete based on estimates of CO<sub>2</sub> pollution emissions and CO<sub>2</sub> uptake.
- Application of the present worth method is an effective tool that can be used to evaluate the economic feasibility of alternative mix designs accounting for the durability and service life of precast pipe.

- Future studies will be conducted to further explore the effect of other mix design variables, and the effects of user costs and the influence of repair and rehabilitation.
- Further analysis will be conducted to assess the influence of variations in cover depth on the service life and life cycle costs. This is necessary to account for the range of specified cover depths and allowable tolerances for welded wire fabric and steel reinforcing bars.

## REFERENCES

- American Concrete Institute (ACI) 2002. Guide for Estimating Corrosion Service Life and Life Cycle Cost of Reinforced Concrete Structures. *ACI Committee 365*.
- American Society for Testing and Materials (ASTM), 2006. Standard Practice for Least Cost (Life Cycle) Analysis of Concrete Culvert, Storm Sewer and Sanitary Sewer Systems. ASTM Volume 04.05, C1131–95.
- Bai, J., Wild, S. & Sabir, B.B. 2002. Sorptivity and Strength of Air-Cured and Water Cured PC-PFA-MK Concrete and the Influence of Binder Composition on Carbonation Depth. *Cement and Concrete Research* 32: 1813–1821.
- Bentz, D.P., Clifton, J.R., Ferraris, C.F. & Garboczi, E.J. 1999. Transport Properties and Durability of Concrete: Literature Review and Research Plan. Building and Fire Research Laboratory, National Institute of Standards and Technology NISTIR 6395. pp. 41.
- Dhir, R.K., Hewlett, P.C. & Chan, Y.N. 1989. Near Surface Characteristics of Concrete: Intrinsic Permeability. *Magazine of Concrete Research* 41: 87–97.
- Ehlen, M.A. & Marshall, H.E. 1996. The economics of new-technology materials: a case study of FRP bridge decking [NISTIR 5864]. Gaithersburg (MD): National Institute of Standards and Technology.
- Jaccard, M., Loulou, R., Kanudia, A., Nyboer, J., Bailie, A. & Labriet, M. 2003. Methodological contrasts in costing greenhouse gas abatement policies: Optimization and simulation modeling of micro-economic effects in Canada. *European Journal of Operational Research* 145: 148–164.
- Johnson, T.L. & Keith, D.W. 2004. Fossil electricity and CO<sub>2</sub> sequestration: how natural gas prices, initial conditions and retrofits determine the cost of controlling CO<sub>2</sub> emissions. *Energy Policy* 32: 367–382.
- National Research Council Canada (NRC) 1998. Durability and Performance of Gravity Pipes: A State-of-the-Art Literature Review. pp. 60
- Newell, R.G. Jaffe, A.B. & Stavins, R.N. 2006. The effects of economic and policy incentives on carbon mitigation technologies. *Energy Economics* 28: 563–578.
- Ontario Concrete Pipe Association (OCPA) 2003. MTO-QA/QC of gravity drainage products. Presented by P. Smeltzer. *Infrastructure Symposium 2003– Sustainability for the Next 100 Years, Ontario Concrete Pipe Association*, Toronto, Ontario.
- Ontario Provincial Standard Specification (OPSS) 1993. Material Specification for Precast Reinforced Concrete Box Culverts and Box Sewers OPSS 1821. 9p.
- Pade, C. & Guimaraes, M. 2007. The CO<sub>2</sub> uptake of concrete in a 100 year perspective. *Cement and Concrete Research* 37: 1348–1356.
- Purvis, R.L., Khossrow, B., Clear, K.C. & Markow, M.J. 1994. Life-Cycle Cost Analysis for Protection and Rehabilitation of Concrete Bridges Relative to Reinforcement Corrosion. Strategic Highway Research Program, National Research Council, Washington D.C.
- Prusinski, J.R., Marceau, M.L. & VanGeem, M.G. 2004. Life Cycle Inventory of Slag Cement Concrete. *Eighth CANMET/ACI International Conference on Fly Ash, Silica Fume, Slag and Natural Pozzolans in Concrete*. 33p.
- R.S. Means 2006. Means Heavy Construction Cost Data 2007.
- Riggs, J.L., Bedworth, D.D., Randhawa, S.U. & Khan, A.M. 1997. Engineering Economics: Second Canadian Edition. McGraw-Hill Ryerson Limited.
- Roskovic, R. & Bjegovic, D. 2005. Role of mineral additions in reducing CO<sub>2</sub> emission. *Cement and Concrete Research* 35: 974–978.
- Torrent, R. 2007. Performance—Based Specification and Conformity Control of Durability. *International RILEM Workshop on Performance Based Evaluation and Indicators for Concrete Durability, Madrid, Spain*. 41–50.
- Treasury Board of Canada 1998. *Benefit-Cost Analysis Guide*. Government of Canada.
- Wonsiewicz, T. 1990. Life cycle cost analysis discount rates and inflation. Pipeline Design and Installation, Proc., ASCE Int. Conf., K. Kienow, Ed., ASCE, New York 639–648.

# A successive LCC model development of marine RC structures exposed to chloride attack using a Bayesian approach

Heungmin Park

*Korea University, IAM Corporation, Seoul, Korea*

Hyunjun Jung, Jungsik Kong & Goangseup Zi

*Korea University, Seoul, Korea*

**ABSTRACT:** A new life-cycle cost (LCC) evaluation scheme for marine reinforced concrete structures is proposed. In this method, unlike the conventional LCC evaluation performed during the design process, the LCC is updated successively whenever new information of the chloride penetration is available. This updating is performed based on the Bayesian approach. For important structures, information required for this new method can be obtained without any difficulties because it is a common element of various types of monitoring systems. Using this new method, the life-cycle maintenance cost of structures can be estimated with a good precision.

## 1 INTRODUCTION

The RC structures exposed to the marine environment are subjected to constant threat to the durability due to the chloride ions infiltrating from the surface. The chloride infiltrating to the inside of the RC structures neutralizes the alkalinity of the concrete to promote the corrosion of the concrete, resulting ultimately in the corrosion of the reinforcing steel bars inside the concrete structure. Therefore, the RC structures should be designed to improve the durability in consideration of degradation mechanism. In case of chloride attack particularly, the structure could be severely damaged. Therefore, the durability design considered LCC is performed without repair & maintenance during the life cycle. The maintenance design at a design stage, however, becomes somewhat different from the LCC design because of environmental and construction factors. In case of chloride attack, in general, it's estimated that the physical life of the RC structures is over when the critical chloride ion concentration is exceeded a design criteria at the level of steel bars. Even though the target life is not achieved, the lifetime for the degradation should be correctly estimated and the degraded structures should be properly repaired in order to keep the target life at a minimum cost. In order to improve the durability of the degraded structures, therefore, maintenance interventions should be timely done. Besides, it's very important to estimate the application time of maintenance interventions in terms of safety of the structure and cost efficiency.

The technique suggested in this paper seems very useful in structures whose monitoring data have been constantly accumulated. Furthermore, it's deemed that uncertainty could be reduced by using the statistical method. This paper used the Bayesian method to reduce the uncertainty of the model variables of RC structures subject to chloride attack by using regular monitoring results. The LCC of the RC structures exposed to the marine environment has been estimated also.

This paper is organized as follows: The first section describes degradation mechanism of marine RC structures, necessity of maintenance, and applicability of this study. Section 2 explains the durability of marine RC structures against chloride attack using the Bayesian approach. The third and fourth sections suggest a life-cycle cost model for marine RC structures based on the estimation of durability against chloride attack and show an example of calculation of the life-cycle cost. The Section 5 describes conclusions.

## 2 PREDICTION OF DURABILITY OF MARINE RC STRUCTURES USING BAYESIAN APPROACH

### 2.1 *One-dimensional analysis model of chloride damage*

The chloride inside of reinforced concrete structures, which has a direct impact on steel-bar corrosion can be classified into free chloride ion and fixed chloride ion. The two ions exist in equilibrium. The former has a

direct impact on corrosion of steel bars while the latter has no direct impact on the corrosion unless dissociation occurs. Under the ordinary environment, the fixed chloride ion does not dissociate. Under marine environment, however, it dissociates and converts into free chloride ion. Besides, under this marine environment, the surface humidity is high so that the impact of carbonation is minor. In this study, it's been assumed that there is no impact of carbonation in the concrete structure exposed to marine environment and the concrete is saturated (both inside and outside). Because the structure is exposed to the marine environment, the second law of Fick is used in order to analyze the chloride ions infiltrating from the surface.

Based on the law of conservation of mass of chloride ion, the equation can be stated as follows:

$$\frac{\partial C(X, t)}{\partial t} + \nabla \cdot J = I_{chloride} \quad (1)$$

Here,  $C(X, t)$  is the concentration of chloride ion ( $kg/m^3$ ) at the distance of  $X$  from the surface for the time period of  $t$  (seconds).  $t$  is then the time for the chloride to begin its diffusion,  $X$  is the distance measured from the surface (mm), and  $\nabla$  is the differential operator.  $J$  is the chloride ion flux and  $I_{chloride}$  is the second unit tensor of chloride ion. As Fick's first law, the flux  $J$  can be shown as follows:

$$J = -D \cdot \nabla C \quad (2)$$

Here,  $D$  is the chloride ion diffusion coefficient ( $\times 10^{-12} m^2/s$ ). If  $D$  is the homogeneous and isotropic one-dimensional model, the equations (1) and (2) can be combined as follows:

$$\frac{\partial C(X, t)}{\partial t} = D \frac{\partial^2 C(X, t)}{\partial X^2} \quad (3)$$

Here,  $I_{chloride}$  is ignored to make the equation simpler. A typical solution of the equation (3) under abnormal conditions can be described as

$$C(X, t) = C_S \left\{ 1 - erf \left( \frac{X}{2\sqrt{D_m t}} \right) \right\} \quad (4)$$

Here,  $erf$  is an error function, and  $C_S$  is the concentration ( $kg/m^3$ ) of chloride ion at the surface. Additionally, experimental equations (5) and (6) are used to reflect the change in the diffusion coefficient with the aging of the concrete. The equations (5) and (6) are generally used for correction in most field practice and research.

$$D_m = \frac{D_0}{1-n} \left( \frac{t_0}{t} \right)^n, \quad (t < t_c) \quad (5)$$

$$D_m = D_0 \left[ 1 + \frac{t_c}{t} \frac{n}{1-n} \right] \left( \frac{t_0}{t_c} \right)^n, \quad (t \geq t_c) \quad (6)$$

where,  $t_c$  is the point in time when there is no change in the diffusion coefficient of chloride ion, and, in this study, 30 years is used pursuant to the previous research by J.S. Kim et al  $t_0$  was set to 28 days of concrete age.  $D_0$  is a diffusion coefficient at time  $t_0$ , and the index  $n$  indicates the change in the coefficient of chloride ion diffusion. Additionally, equation (4) is an analytical solution obtained when the diffusion coefficient of the chloride ion  $D_m$  is a constant.

## 2.2 Updating durability based on the Bayesian approach

### 2.2.1 Bayesian updating

In order to correctly determine a probabilistic model, it's important to acquire sufficient data for random variables. The prior distribution for the point in time when the concentration of chloride ion reaches to a pre-specified value is calculated based on a statistical and deterministic method. This paper has used the Bayesian approach which has been applied to the problem of long-term deflection of prestressed segment bridge by Bazant et al. (1989) The chloride prediction model which is based on the Bayesian approach needs continuous monitoring results. The probability distribution of the initial model (prior) and the probability distribution updated (posterior) in consideration of measured data are expressed as  $P'(\vartheta)$  and  $P''(\vartheta)$ , respectively. The relationship between these two probabilities is then established by the Bayes' theorem.

$$P''(\vartheta) = c_1^* P(\underline{X} | \vartheta) P'(\vartheta) \quad (7)$$

where,  $\vartheta$  is the model variable. This study used model variables such as diffusion coefficient of chloride ion ( $D_0$ ), time-dependent index ( $n$ ), concentration of chloride ion at the surface of the concrete ( $C_S$ ).  $c_1^*$  is a constant determined by the condition of law of total probability.  $P(\underline{X} | \vartheta)$  is the conditional probability of the measured data  $\underline{X}$  given the model variable  $\vartheta$ .

$$P(\vartheta) = P(\underline{X}) \quad (8)$$

Here,  $P(\vartheta)$  becomes  $P(X)$  as shown in the equation (8) above for monotonically increasing problems such as creep without loading and irreversible chloride penetration. In other words, the uncertainty of the model constant for  $k$  th zone is the same as the uncertainty of the corrosion prediction.



### 2.2.2 Latin Hypercube sampling

The Latin Hypercube sampling divides the range of values for the input variables into  $K$  ranges and then selects  $K$  samples evenly one from  $K$  ranges randomly and non-repetitively when deriving the result data from the input variable space. It is a method to form  $K$  arrays and then to select the values for the input variables from one of arrays randomly and non-repetitively in order to select  $K$  values. The model variable  $\vartheta$  forms  $K \times N$  matrix. The Latin Hypercube Sampling is useful to analyze a problem associated with a lot of random variables.

Let  $X_m$  denote the concentration of the chloride measured at the time  $t_m (m = 1, 2, 3, \dots, M)$ . The mean ( $\bar{X}'_m$ ) and the standard deviation ( $\sigma_m^{X'}$ ) for the concentration of the measured chloride  $X'$  with the initially measured data before the revision, i.e. not considering the additional data obtained through monitoring, are given by the following equation.

$$\bar{X}'_m = \frac{1}{K} \sum_k X_m'^k, \quad \sigma_m^{X'} = \sqrt{\frac{1}{K} \sum_k (X_m'^k - \bar{X}'_m)^2} \quad (9)$$

And the probability of chloride damage is divided into  $k$  zones of equivalent probability.

Where,  $\bar{X}'_m, \sigma_m^{X'}$  are functions of time  $t_m$ . After the chloride concentration  $X_m$  is measured at time  $t_m$ , the likelihood function  $p_k$  is computed as follows:

$$p_k = \exp \left[ - \sum_m \frac{1}{2} \left( \frac{X_m - X_m'^k}{\sigma_m^{X'}} \right)^2 \right] \quad (10)$$

where, the standard deviation of the likelihood function  $\sigma_m^{X'}$  should be estimated from the existing laboratory data or field data. The average value for the model prediction,  $X_m''$ , is established as follows

$$\bar{X}_m'' = \sum_k P'' (X_m^k) X_m'^k = c_0 \sum_k p_k X_m'^k \quad (11)$$

The revised standard deviation,  $\sigma_m^{X''}$ , for the predicted chloride concentration,  $X_m''$ , becomes as follows:

$$\sigma_m^{X''} = \sqrt{c_0 \sum_k p_k (X_m'^k - \bar{X}_m'')^2} \quad (12)$$

### 2.3 Limit state function

If the chloride ion infiltrates into the concrete and spreads, it becomes imbedded in the concrete as aging. If the accumulated chloride ion infiltrates to the location of steel bars, the passive-state cover is formed on

the surface of the steel bars. The passive-state membrane brings corrosion on the steel bars and in turn deteriorates the durability of the structure. The point in time when the concentration of chloride ion reaches to a pre-specified value is defined as the service limit state, and the probability of corrosion at this point in time is computed. The limit state function to compute the probability of corrosion at the limit state can be defined as follows:

$$\underline{\vartheta} = \underline{\theta}(C_s, D_0, n), \quad R = r(\underline{\vartheta}), \quad S = s(\underline{\vartheta}) \quad (13)$$

$$G = R - S \quad (14)$$

where,  $C_{cr}$  is the critical chloride ion concentration, the load function represents the chloride ion concentration changing with time,  $D_0$  is initial diffusion coefficient,  $n$  is time dependant coefficient and  $\theta$  is a function. The critical state function can be expressed as a corrosion probability  $P_f$ . In real practice, a reliability index is more often used than the corrosion probability  $P_f$  to express the probability of corrosion. The corrosion probability and the reliability index  $\beta$  have the following relationship to each other:

$$P_f = \int_{-\infty}^0 f_G(g) dg \quad (15)$$

$$\beta = \frac{\mu_G}{\sigma_G}, \quad P_f = \Phi(-\beta) \quad (16)$$

where,  $\sigma_G$  denotes the standard deviation of  $G$ ,  $\mu_G$  indicates the mean of  $G$ .

### 2.4 Analysis for repair & reinforcement points in time through Bayesian update

In this paper, the design parameters were the diffusion coefficient of the initial chloride ion concentration  $D_0$ , a time-dependent index  $n$ , and the chloride ion concentration at the surface of the concrete  $C_s$ . The number of Latin Hypercube samples used in this study was fixed at 18 sets. In case of the prior probability, the values of design variables were decided based on the previous research by J.S Kim et al in general.

However, in this study, a significant difference has been detected between the predicted value and the monitoring data of the target structures. Therefore, the prior distribution was corrected with two data measured at the site, and then the posterior distribution was calculated. According to Costa (1999), the minimum cover thickness of ENV 1992-1-1 should be revised in case of RC structures. However, the minimum cover thickness of ENV 992-1-1 is set to 40 mm. Therefore, this paper has used Bayesian approach considering that the cover thickness is 40 mm based on an assumption that Dock 20 has followed the BSI Code.

Table 1 demonstrates the chloride attack into the concrete in Dock 20 over time. In this paper, the measured data are called, 'Dock 20.' In order to estimate prior distribution, the data in Table 4 are used as initial design variables:

In Fig. 1 below, the grey line represents prior distribution and the black line represents posterior distribution.

According to Fig. 1, the steel bars start to be corroded at the critical value of chloride ( $1.2 \text{ kg/m}^3$ ). Then, the difference between prior distribution and posterior distribution to reach up to  $1.2 \text{ kg/m}^3$  would be about 40 months. If a repair is done with a higher or lower critical value of chloride, a clear difference is observed in terms of mean and reliability index of limit-state function. Besides, a different prediction result is expected in terms of the remaining service life.

Table 1. Measured data in the field, Dock 20.

Cx		Time (months)	
Type	depth (mm)	36	48
Dock 20	40	0.300	0.384

Table 2. Variables for prior-estimation, Dock 20.

Design parameters		Prior-estimation (mean, standard deviation)
Dock 20	$D_0 (\times 10^{-12} \text{ m}^2/\text{s})$	$N(6, 1.2)$
	$n$	$N(0.4, 0.08)$
	$C_S (\text{kg/m}^3)$	$N(9, 1.8)$

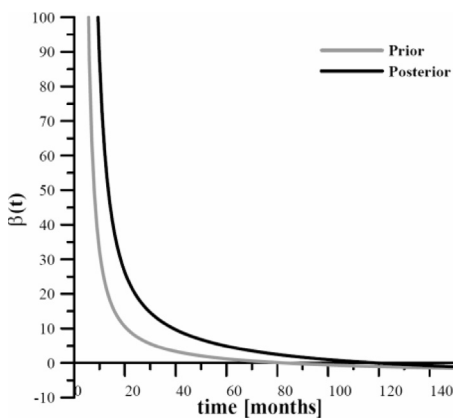


Figure 1. The change of samples compared with the change of chloride reliability index measured at 40 mm distance from the surface.

### 3 ANALYSIS ON DURABILITY AGAINST CHLORIDE ATTACK AND LIFE-CYCLE ANALYSIS SCENARIO

This table shows that applied analysis procedure of durability against chloride attack and life-cycle cost in this study.

Table 3. Analysis procedure of durability against chloride attack and life-cycle cost.

- 
- Stage 1. Application of chloride attack analysis model
1. Select design variables
  2. Create design variables and cumulated distribution functions using normal distribution
  3. Sample design variables using Latin Hypercube Sampling technique
  4. Arrange the samples randomly and group the design variables
  5. Calculate chloride ion concentration using the grouped design variables
  6. Calculate prior distribution based on the chloride ion concentration
- Stage 2. Application of Bayesian approach
1. Calculate initial likelihood function using the initial monitoring data
  2. Correct prior distribution using the calculated initial likelihood function
- Stage 3. Determination of application times of repair & maintenance
1. Determination of application times of repair & maintenance based on limit-state function
  2. Calculate reliability index
  3. Compare reliability indexes before and after updating
  4. Determine the time of repair & maintenance before and after updating
- Stage 4. Comparison results before and after updating and evaluation of LCC result
1. Develop a LCC model
  2. Apply probability variable (repair & maintenance cycle) of LCC model before and after updating
  3. Calculate lifecycle cost
  4. Compare LCC analysis results
- 

### 4 SUGGESTION OF LCC MODEL OF MARINE STRUCTURES

#### 4.1 Outline of LCC analysis of marine structures

LCC is a main tools to conduct economic assessment and analyzes cost through the life cycle of structures.

The general LCC analysis model is applying to select a cost-efficient alternative plan in basic plan or basic design stage.

Based on the alternative plan, the national budget could be efficiently distributed. In a maintenance stage, LCC optimum design or LCC optimum reinforcement could be applied through LCC analysis.

'Dock 20' is located at a port in Setenave estuary Portugal. According to 4-year monitoring on the 'Dock 20,' the marine structure has been flooded 22 times. In order to predict the maintenance costs, in particular, the repair and reinforcement cycle before and after Bayesian update have been calculated to obtain an efficient cost management scenario.

In terms of LCC analysis, there are deterministic and probabilistic models. In practice, the former has been widely used. For practical LCC analysis, however, it's important to decide how to handle the uncertainty efficiently. In this study, probabilistic approach has been applied because the uncertainty problem could be handled rationally.

The probabilistic LCC analysis based simulation technique using the data such as type of distribution, maximum expectation, and variation. Compared to deterministic approach, it's a more rational and more scientific method with no need of a wide range of sensitivity analysis because computer simulation tools can be used. The probabilistic approach is recommended by FHWA (Walls III & Smith, 1998).

#### 4.2 Life-cycle analysis model for marine structures

If a concrete structure is timely repaired, the durability can be recovered. This timing is lost, however, the degradation could be accelerated and structures might be remodeled or replaced as a result. The LCC model proposed in this study can predict the application times for repair based on the information updated by the Bayesian approach.

The probabilistic LCC analysis model applied in this study can be stated as follows:

$$E[C_{TOT}(X, n_k)] = C_{INI} + \sum_{k=1}^N \frac{1}{(1+q)^{n_k}} \times \{E[C_{MAI}(X, n_k)]\} + \frac{1}{(1+q)^N} C_{DIS} \quad (17)$$

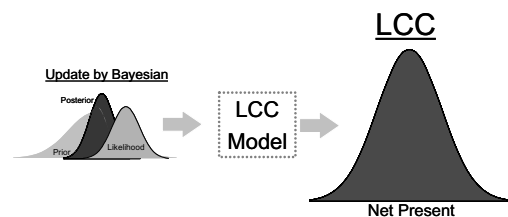


Figure 2. Outline of probabilistic LCC analysis in consideration of uncertainty of repair cycle.

where  $C_{TOT}$  is the life cycle cost.  $C_{INI}$  is initial cost, and  $C_{MAI}$  is maintenance cost obtained by Bayesian updating, and  $C_{DIS}$  is disposal cost.  $q$  is the discount rate and  $n$  is an year of expenditure, and  $N$  is the life cycle year.

Based on the Bayesian approach, The LCC is calculated by assuming that repair and reinforcement are done when the value of chloride reaches  $1.2 \text{ kg/m}^3$ .

If statistical data are sufficient, the probability distribution and variation are applied as they are. If they are insufficient, however, the evaluation would be—performed using subjective values obtained based on experts' opinion. The probabilistic approach considered the uncertainty of cost and risk factors is very useful method by using cost distribution and cumulative distribution. An economical maintenance planning can be done by efficient LCC calculation by comparing results before and after Bayesian updating. Besides, change of LCC can be accurately predicted.

## 5 EXAMPLE OF LCC CALCULATION BASED ON THE RECOMMENDED LCC ANALYSIS METHOD

### 5.1 Input variables and assumptions for LCC calculation

In the LCC calculation, the initial construction cost and disposal cost of the target facility were same. So they were not be considered. And the maintenance cost only has been analyzed. The variables include chloride density at the surface, chloride ion diffusion coefficient, concrete cover thickness, time-dependent index of diffusion coefficient.

The target service life of the concrete structure can be defined, 'a time period that no significant reduction of performance or corrosion of steel bars.' In many cases, the service life is calculated up to the time when steel bars start to corrode. In this study, a time for repair is defined as the time when corrosion on steel bars is detected even though no symptom of degradation is found on the surface.

Table 4. Durability by target service life of the domestic concrete structures (KCI, 2004).

Durability	Description	Target service life
1st level	Structure that requires an extremely high level of durability	100 years
2nd level	Structure that requires a high level of durability	65 years
3rd level	Structure that requires a low level of durability	30 years

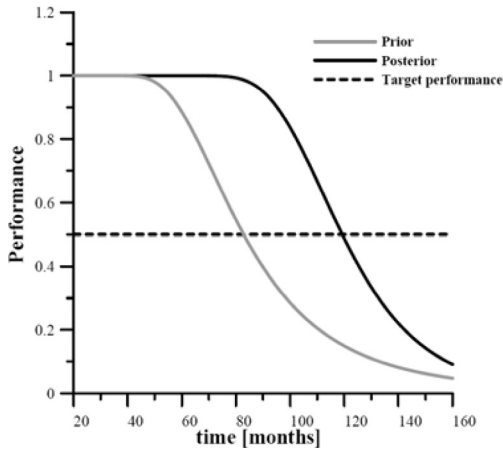


Figure 3. LCP model.

Table 5. Application value of repair cycle.

Repair cycle	Before update	After update
Mean value	82 months	120 months
Standard deviation	0.316	0.389

### 5.2 Application items of target structures and repair & reinforcement engineering method

There are lots of repair & reinforcement methods for concrete structure against chloride attack such as reinforcement plus surface cover thickness, continuous-fiber adhesion, electric method, realkalization plus surface cover thickness, desalination plus surface cover thickness, dismantlement, renewal, surface cover thickness (prevention), electric method. In this study, LCC has been calculated for the steelbar corrosion repair method.

The steel-bar corrosion repair method eliminates a cause of degradation with chemical treatment and reinforces the concrete surface after removing the part that has been rusted by chloride attack and applying a degradation treatment and surface recovery system (500 mm thick and 100 mm wide). The repair cost is KRW 248,673/m<sup>2</sup> (Standard of Estimate 2001 by Ministry of Construction and Transportation).

### 5.3 LCC calculation

In order to evaluate uncertainty, a probabilistic LCC method has been applied and Bayesian approach has been adopted in this study. The LCC cost that has been estimated on the RC structures exposed to the marine

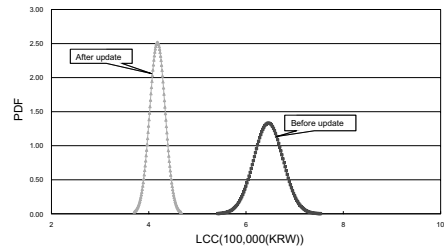


Figure 4. Existing and improved LCC probability graphs (PDF).

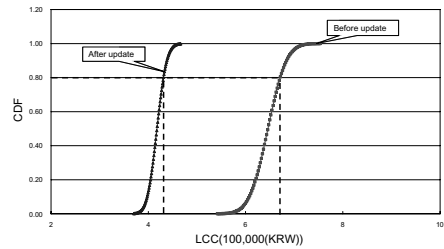


Figure 5. Existing and improved LCC probability graphs (CDF).

Table 6. Comparison of LCC results.

	Category	Cost
Before update	Initial cost	–
	Maintenance cost	KRW 645,10
After update	Initial cost	–
	Maintenance cost	KRW 430,61

environment and the LCC cost that has been estimated based on Bayesian approach in consideration of uncertainty have been comparatively analyzed. For probability analysis, MCS technique has been applied.

As shown in the Figs. 4, 5 above, an uncertainty of variables has considered in LCC. And LCC after update through Bayesian update is compared to LCC before update. More precise LCC cost has been obtained.

## 6 CONCLUSIONS

In existing LCC calculation models, design variables are mostly calculated by applying the mean value based on database and records. In this study, however, a more precise LCC calculation model has been developed in consideration of environmental and structural factors of main variables through a probabilistic analysis. In particular, an optimum repair & reinforcement

timing was calculated by predicting the performance degradation of concrete structure through Bayesian update. Then, the LCC cost before and after update has been compared. As a result, we could get more exact LCC after update. With a more exact prediction of a time for repair & reinforcement, besides, it's expected that the model could save time and money through a repair and reinforcement of the structure on time.

#### ACKNOWLEDGEMENTS

The work presented in this paper was funded by Center for Concrete Corea (05-CCT-D11), supported by Korea Institute of Construction and Transportation Technology Evaluation and Planning (KICTTEP) under the Ministry of Construction and Transportation (MOCT) & the Korea Science and Engineering Foundation (KOSEF) grant funded by the Korea government (MOST) (No. R11-2002-101-02005-0).

#### REFERENCES

Boulfiza, M., Sakai, K., and Banthia, N., et al. "Prediction of chloride ions ingress in uncracked and cracked concrete," *ACI materials journal*, Vol.100, No.1, 2003, pp.38-48.

Costa, A., and Appleton, J. "Chloride penetration into concrete in marine environment-Part I: Main parameters affecting chloride penetration," *Materials and Structures*, Vol.32, No.218, 1999, pp.252-259.

Costa, A., and Appleton, J. "Chloride penetration into concrete in marine environment-Part II: Prediction of long term chloride penetration," *Materials and Structures*, Vol.32, No.219, 1999, pp.354-359.

Bazant, Z.P., and Kim, J.K. "Segmental Box Girder - Deflection Probability and Bayesian Updating," *Journal of Structural Engineering*, Vol.115, No.10, 1989, pp.2528-2547.

Crank, J. "The Mathematics of Diffusion," *Oxford University Press*, 1975, pp.48-73, 114.

ENV 1992-1-1 (2004): Eurocode 2. Design of concrete structures. Part 1-1: General rules and rules for buildings, 2004, pp.49-52.

Ang, A.H.-S., and Tang, W.H. "Probability concepts in engineering planning and design," *Basic principles. John Wiley and Sons*, Vol.1, 1975, pp.329-359.

Mckay, M.D., Beckman, R.T., and Conover, W.J. "A comparison of three methods for selecting values of input variables in the analysis output from a computer code," *Technometrics*, Vol.21, 1979, pp.239-245.

Kim, J.S., Jung, S.H., Kim, J.H., Lee, G.M., and Bae, S.H., "Probability-Based Durability Analysis of Concrete Structures under Chloride Attack Environments" *Journal of Korea Concrete Institute* Vol.18, 2006, pp.239-248.

# Optimal floor plan design of high-rise apartment buildings based on life-cycle cost consideration

Keun Jun Park

*Department of Architectural Engineering, Hoseo University, Korea  
Visiting Professor, University of California, Irvine*

A.H-S. Ang

*Research Professor, University of California, Irvine*

**ABSTRACT:** An approach for determining the optimal floor plans of high-rise apartment buildings is proposed. The optimization process is based on minimizing the life-cycle cost (LCC) associated with a prescribed floor plan or plans for a building. The LCC of a floor design is based on specific criteria such as unit plan, building depth, building length, story of building and number of buildings. There are some methods to find the optimum design by cost modeling techniques, cost geometry, structured search system and expert system.

However, it is impossible to determine a model through traditional non-linear programming under the non-linear constraints in planning a design because they are applied to estimate the cost after the design is completed. Therefore, this study aims to propose an optimum floor plan design alternative for high-rise apartments based on LCC at the preliminary design stage.

## 1 INTRODUCTION

For a high-rise apartment building, the floor design by LCC is based on the criteria such as unit plan, building depth, building length, story of building and number of buildings. The optimum design alternative may be based on minimizing the life-cycle cost. There are methods for determining the optimum design such as cost modeling techniques, cost geometry, structured search system and expert system.

This study aims to propose an optimum floor design alternative of high-rise apartments from the stand point of life-cycle cost at the preliminary design stage.

Recently, increase of resource price, energy cost and labor cost by inflation is related to an inadequate use of limited resources such as construction material, energy, financing and time. Accordingly, it is important to propose a new approach for the design of optimal floor plans for high-rise apartments by integrating limited resources. The major objectives of this research are to study the principles and methods of floor plan design for high-rise apartments in order to minimize the life-cycle cost.

It needs to analyze the relationships between the life-cycle cost of high-rise apartment and the factors which affect the optimum floor plan design. The first step is to survey the basic principles and methods of architectural planning to minimize the life-cycle cost of high-rise apartments and to maintain its quality at

a reasonable level. The second step is to search the application method of life-cycle cost analysis technique for floor plans of high-rise apartments. The third step is to find factors that influence the life-cycle cost of floor plans as functions of the elements of building shape. Through this process, we can determine an optimum floor dimension of high-rise apartments.

## 2 THE OPTIMIZATION OF FLOOR PLAN DESIGN

Basically, the building cost is based on all stages of a project integrated from preliminary development to construction excluding the cost of maintenance and operation. But, to estimate the overall building life-cycle cost, the maintenance and operation costs must be included for a total economic building management. Accordingly, the integration of the overall building cost requires a methodology for the optimization of building project cost based on life-cycle cost. In this paper, we propose such a methodology for determining the optimal alternative floor plan of high-rise apartments.

The factors that affect the floor plan designs of high-rise apartments can be considered in terms of the building elements, building shapes and forms. The total life-cycle cost of high-rise apartments may be described as a linear-fractional equation and can

be increased or decreased as a function of the apartment unit plan. The optimum dimension of a high-rise apartment unit plan can then be calculated by taking the derivative of the equation.

### 3 THE ALTERNATIVE OF MINIMUM LIFE CYCLE COST

#### 3.1 *General stage of decision making for the selection of optimum design*

Although floor plan designs based on life-cycle cost has been considered, the minimum life-cycle cost floor plan has not been developed or applied.

The selection of a high-rise apartment floor plan design requires a preliminary architectural plan for estimating the construction cost and the building cost for a prescribed alternative high-rise apartment floor plan design. In order to consider life-cycle cost, the building elements such as building structures, walls, finishing and several types of openings must be included. In particular, these must include the initial cost, development cost, design cost, bidding cost, energy consumption cost and maintenance & operation cost. The energy cost can be estimated through a regression model which was developed by simulation of the simulated energy loads in residential units.

#### 3.2 *Total cost formulation*

Generally, the available statistics and data base of costs are useful. However, these must be supplemented by simulation of cost planning for a specific design of a high-rise apartment building to forecast the total budget cost. These require repeated simulations for several design alternatives and are possible to produce the costs and evaluate the alternatives but will not furnish the information needed for minimizing the life-cycle cost of high-rise apartment building.

We need the design that minimizes the total cost of the preliminary stage, planning stage, bidding stage, construction stage, and maintenance & operation stages. In this case, we need a methodology for high-rise apartments that integrates and optimizes the total life-cycle cost.

Generally, the basic approach is to decide the size and shape of a unit plan which is ordinarily selected through the preferences of the architectural designer.

#### 3.3 *Preliminary cost models*

The important building items that contribute to the project cost include the architectural design plan, the construction method, schedule of activities expressed as parameters of cost.

The building element quantity factor index (QFI) for cost planning is represented by the building shape, the size and the height of the building. The QFI influences overall cost according to the change of building composition of the main elements.

After the building element unit price is multiplied by the construction quantities, we obtain the total construction cost of the element. To simplify this process, we can replace this by the building QFI.

### 4 COST GEOMETRY METHOD

One of the most effective method for optimizing floor plan design is the *cost geometry* method. This is formulated as a function of the building shape (e.g. rectangular), ceiling and story heights, perimeter length, floor area, length of interior partitions, openings (doors and windows) and width of corridors. Moreover, the costs for each of the above elements are required to formulate the cost equation for a particular floor plan design.

#### 4.1 *LCC parameters of the cost geometry method*

The cost of a building element requires estimating the designated building element cost such as floor, wall, ceiling and column which comprise the building space. For example, the cost of the exterior wall would include the interior and exterior finish cost plus the cost of the wall structure. Accordingly, we obtain the total building cost by calculating the sum of the building element costs.

Observe that the QFI, defined as the ratio of wall length to floor area, decreases with increasing floor area. For example, consider floor plans with a given story height. In [Table-1](#) is shown the QFI according to the ratio of wall length to the square floor plan area.

#### 4.2 *LCC according to different building shape*

There are many decision factors for building shape like exterior wall, story height and building height. The exterior wall contributes a most important factor for the LCC of construction cost among these factors. The same system of exterior wall and exterior windows is usually used repeatedly in the high-rise apartment building which is related with the LCC. According to this viewpoint, the shape of the exterior wall is most significant in determining the LCC.

For the same floor area, the unit floor plan with the shortest exterior wall perimeter is, therefore, best for cost saving of LCC. From this stand point, the circle plan would be the best one, but there are many shortcomings such as uselessness of floor area for the building and inefficient interior space which is the main reason that most architects avoid this kind of

Table 1. QFI according to the ratio of wall length to floor plan area.

Floor plan	Floor area	Length of exterior wall	QFI
$a \times a$	$a^2$	$4a$	$4/a$
$2a \times 2a$	$4a^2$	$8a$	$2/a$
$4a \times 4a$	$16a^2$	$16a$	$1/a$

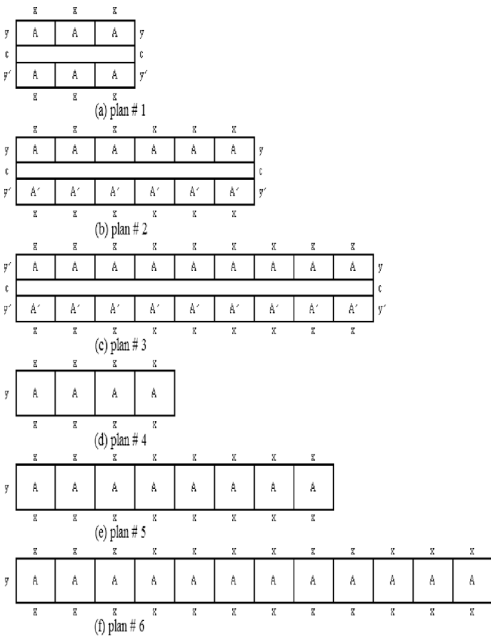


Figure 1. High-rise apartment floor plans.

floor plan in architectural planning. As a result the building shape has an effect on the LCC efficiency of a building. With these considerations, we can use the LCC geometry for evaluating the LCC efficiency of different building shapes.

### 4.3 Application of cost geometry for developing the high-rise apartment floor plan

It is not sufficient to minimize only the cost of wall if we are considering the overall LCC of high-rise apartment buildings because not only the exterior wall, but also the exterior entrance and windows have effects on the LCC.

From this viewpoint, we can use the cost geometry and apply it to the exterior wall system. With reference

to Fig.-1 and Table-2, we formulate the LCC model as follows:

Legend:

- $A'$ —unit area ( $m^2$ )
- $A$ —unit area ( $m^2$ )
- $H$ —story height (m)
- $W$ —LCC of wall ( $\$/m^2$ )
- $G$ —LCC of windows ( $\$/m^2$ )

Assume that the total area of windows occupies 15% of the total floor area.

- $P$ —LCC of partition ( $\$/m^2$ )
- $h$ —ceiling height (m)

For floor plan #1 of Fig. 1

$$\begin{aligned}
 LCC = & [(2 \cdot 3X + 2(Y + Y' + C)) \\
 & \times H - 3(A + A') \cdot 0.15] \\
 & \times W + (2 \cdot 3X + 2Y + 2Y') \\
 & \times hp + 3(A + A') \cdot 0.15G = 6(WH + hp) \\
 & \times X + 2(AWH + A'WH + Ahp + A'hp)/X \\
 & + 2CHW - 0.45(A + A') \\
 & \times W + 0.45(A + A')G \tag{1}
 \end{aligned}$$

For floor plan #2 of Fig. 1

$$\begin{aligned}
 LCC = & 12(WH + hp)X + (A + A') \\
 & \times (2WH + 5hp)/X + 2CHW \\
 & - 0.9(A + A')W + 0.9(A + A')G \tag{2}
 \end{aligned}$$

For floor plan #3 of Fig. 1

$$\begin{aligned}
 LCC = & 18(WH + hp)X + (A + A') \\
 & \times (2WH + 8hp)/X + 2CHW \\
 & - 1.35(A + A')W + 1.35(A + A')G \tag{3}
 \end{aligned}$$

For floor plan #4 of Fig. 1

$$\begin{aligned}
 LCC = & \{(2 \cdot 4X + 2Y)H - 4A \cdot 0.15\} \\
 & \times W + 3Y \cdot hp + 4A \cdot 0.15G \\
 & = 8WHX + A(2WH + 3hp)/X \\
 & - 0.6AW + 0.6AG \tag{4}
 \end{aligned}$$

For floor plan #5 of Fig. 1

$$\begin{aligned}
 LCC = & 16WHX + A(2WH + 7hp)/X \\
 & - 1.2AW + 1.2AG \tag{5}
 \end{aligned}$$



Table 2. The ranges of unit LCC for building elements (cost statistics from Korea).

No.	W: Exterior wall LCC (\$/m <sup>2</sup> )	P: Interior wall LCC (\$/m <sup>2</sup> )	G: Window LCC (\$/m <sup>2</sup> )	H: Story height (m)	h: Celing height (m)	C: Corridor width (m)
1	530	160	215	3.2	2.4	2.0
2	640	245	273	3.3	2.5	2.2
3	750	330	331	3.4	2.6	2.4
4	860	415	389	3.5	2.7	2.6
5	970	500	450	3.6	2.8	2.8

Table 3. x value for minimum LCC of each formula.

No.	Formula	x value (m)	Minimized LCC (\$)	A(m <sup>2</sup> )	A'(m <sup>2</sup> )	W(\$/m <sup>2</sup> )	P(\$/m <sup>2</sup> )	G(\$/m <sup>2</sup> )	H(m)	h(m)	C(m)
1	(7)	7.6	173015	83	93	530	160	215	3.2	2.4	2.0
2	(8)	6.1	262406	83	93	530	160	215	3.2	2.4	2.0
3	(9)	6.8	421333	126	139	530	160	273	3.2	2.4	2.0
5	(11)	5.3	127382	83	-	530	160	215	3.2	2.4	-
6	(12)	4.3	202668	83	-	530	160	215	3.2	2.4	-
7	(13)	4.0	273751	83	-	530	160	215	3.2	2.4	-

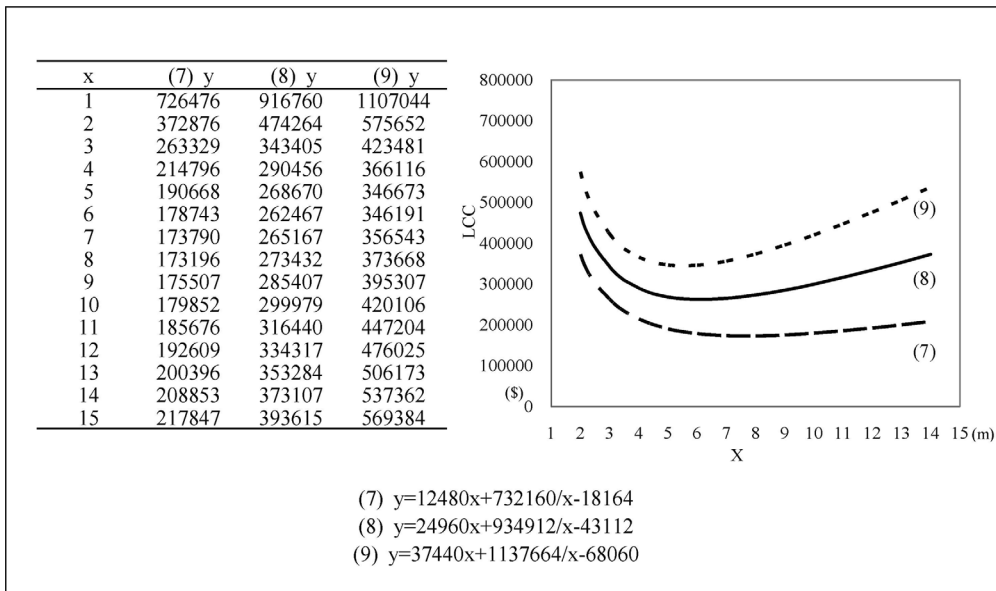


Figure 2. Graphics of eqs. (7)~(9).

For floor plan #6 of Fig. 1

$$LCC = 24WHX + A(2WH + 11hp)/X - 1.8AW + 1.8AG \tag{6}$$

In Table-2, we show the ranges of input data for LCC of each high-rise apartment building element, i.e.

element of exterior wall LCC, interior wall LCC and window LCC based on the cost statistics in Korea. For example, the ranges of unit LCC of exterior wall element, interior wall, window are 530~970 \$/m<sup>2</sup>, 160~500 \$/ m<sup>2</sup>, 215~450 \$/ m<sup>2</sup>, respectively, whereas the LCC ranges for the story height, the ceiling height and the corridor width are 3.2~3.6 m,

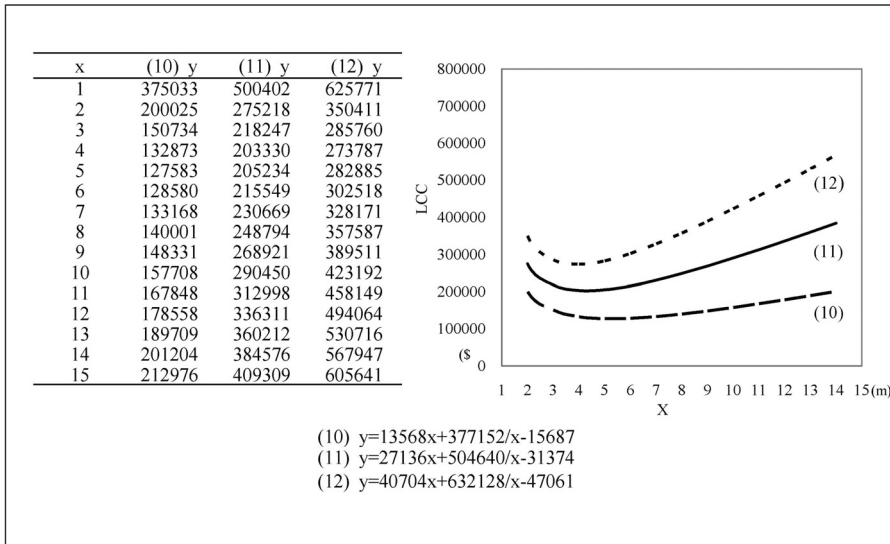


Figure 3. Graphics of eqs. (10)~(12).

2.4~2.8 m, 2.0~2.8 m, respectively. From Table-2 and Fig.-1, we can produce the formulas of Eqs. (1)~(6) which are derived from the variation of unit quantity and corridor type of high-rise building plans. If we input the variation of the story heights (3.2~3.6 m), the ceiling heights (2.4~2.8 m) and the corridor widths (2.0~2.8 m), we obtain the various LCC as indicated in Table 3 and shown graphically in Figs. 2 and 3, for each formulation. If we shift the area of unit plan from 83 m<sup>2</sup> to 150 m<sup>2</sup> for types A and A' in addition to the variation of LCC W, LCC P, LCC G, H, h, C, we obtain the LCC of Eqs. (1)~(6). If we input the data from Table-2 for A, A', W, P, G, H, h, C, we obtain the LCC formula for minimizing the LCC of high-rise apartment building, namely Eqs. (7) through (12) as follows:

For floor plan #1 of Fig. 1

$$LCC = 12480x + 732160/x - 18164 \quad (7)$$

For floor plan #2 of Fig. 1

$$LCC = 24960x + 934912/x - 43112 \quad (8)$$

For floor plan #3 of Fig. 1

$$LCC = 37440x + 1712960/x - 85158 \quad (9)$$

For floor plan #4 of Fig. 1

$$LCC = 13568x + 377152/x - 15687 \quad (10)$$

For floor plan #5 of Fig. 1

$$LCC = 27136x + 504640/x - 31374 \quad (11)$$

For floor plan #6 of Fig. 1

$$LCC = 40704x + 632128/x - 47061 \quad (12)$$

Taking the derivatives of the respective LCC equations (dLCC/dx) we obtain the minimum LCC of the high-rise apartment building for the specified values of A, A', W, P, G, H, h and C. The corresponding x value of each formulas (7)~(12) are shown in the 3rd column of Table-3.

According to Table-3, we find that the minimum LCC for the center-corridor-type floor plan is influenced mainly by the unit value of LCC W. With this value we obtain the optimal floor dimension x of floor plan design such as 7.6 m, 6.1 m and 5.1 m for the center corridor type of high-rise apartment building. For the case of a hall type high-rise apartment building, we obtain the corresponding optimal floor dimension x of floor plan design such as 5.3 m, 4.3 m and 4.1 m. It means that the value of x above or below this optimal x will increase the respective LCC.

#### 4.4 Optimal floor plan design

As illustrated above, we can develop an optimal floor plan design for high-rise apartments on basis of LCC at the preliminary design stage.

We reviewed several current methods for optimizing design of high-rise apartments and identified the planning variables that are pertinent and important for determining floor plans that are feasible. In this process, we selected the planning variables that are essential in the cost geometry method such as element of exterior wall, interior partition, story heights, floor area, corridor width and ceiling heights. With these parameters we developed the appropriate formulas to determine the optimal floor plan design of high-rise apartment buildings based on minimum LCC.

This methodology would be a useful tool for cost saving in planning floor plans of high-rise residential apartment building projects.

## 5 SUMMARY AND CONCLUSIONS

An approach for determining the optimal floor plans of high-rise apartment buildings at the preliminary design stage is proposed and developed. For this purpose, we reviewed several methods for floor plan designs and determined that the cost geometry method is the most effective for planning the optimal dimension of a residential architectural building based on LCC.

Using the available cost statistics and data base (e.g., from Korea), it is possible to forecast the optimal budget cost for a project. Through the simulation of cost planning of a high-rise-apartment building which was developed in this study we can determine the optimal floor plan design of the building during the preliminary design stage based on LCC.

The proposed cost geometry method requires the evaluation of the optimal value of  $x$ . This  $x$  value depends on the input data of the unit element LCC.

Therefore, in applying the proposed method, it is essential that the value of  $x$  must be evaluated in accordance with the condition of the regional environment or economy. With this consideration, this methodology should provide a useful tool for optimizing the unit floor plan design based on life-cycle cost consideration for high-rise apartment buildings.

The proposed floor design method may be used for planning and design of new high-rise apartments, for evaluating existing high-rise apartments, as well as for evaluating the cost efficiencies of new materials, standardization of architectural designs and building codes.

## REFERENCES

- Alphonse J. Dell'isola*: Value Engineering in the Construction Industry, Van Nostrand Reinhold Company, 1984.
- Douglas J. Ferry & Peter S. Brandon*: Cost Planning of Buildings, Granada Publishing LTD, 1984.
- Park, Keun Jun*: A Selection Method of Preferential Building Component for an Effective VE application, Journal of the Architectural Institute of Korea, Vol.19 No.12 (Serial No.182), December 2003.
- Park, Keun Jun*: Cost Model for Cost Saving on Each Building Phase by Integration of Factor, Journal of the Architectural Institute of Korea, Vol.18 No.7 (Serial No.165), July 2002.
- Radford, A.D.*: Design by Optimization in Architecture, Building and Construction, Van Nostrand Reinhold Company, New York, 1988.
- Riverso, M.E.*: A life-cycle Cost System for Value Engineering in Building Design and Construction, Purdue University, 1984.
- Sydney, Newton*: An agenda for Cost Modeling Research, Construction Management and Economics, Vol.18 No.7 (Serial No.165), July 2002.

# Life-cycle cost analysis for fire protection of buildings

L. Razdolsky

*LR Structural Engineering Inc., Lincolnshire, IL, USA  
Northwestern University, Evanston, Illinois, USA*

**ABSTRACT:** This research paper has focused on specifying cost-effective responses (CER) to natural disasters, and abnormal fires. The parametric estimating methodology has been used in this study. In this case, the process of estimating cost is defined by using mathematical equations that relate cost to one or more physical characteristics of the building. A simple example of a parametric estimate is the use of square footage to estimate building costs. The objective of this study is to construct such equation that will have the independent variables (fire-induced thermal load) on one side, and the dependent variable (the repair cost from abnormal fire) that is unknown. To make an estimate using CER, the theory of probability and statistics has been employed in this study. An example is provided to illustrate a parametric estimating process at the design development stage with possible fire damage during the life span of the building.

## 1 INTRODUCTION

In the case of designing and maintaining a building, the cost-effective building designs, construction processes, and repair strategies are those that minimize the costs to the owners and users of the building over its life or life cycle. Structural engineers designing a new building or repairing an existing building will typically—and are often required to—compare and choose from several alternative strategies, such as “steel structure vs. concrete structure” or “repair the structure vs. replace the structure.” In many cases the engineer has an existing, “base case” technique or strategy and “alternatives” that represent specific changes to this base case. Currently, for alternatives that provide the same technical performance, including code compliance and service life, construction costs are typically used to compare and ultimately decide on the design strategy. But an alternative with higher initial construction costs may have significantly lower operation, maintenance, and repair costs, and therefore life-cycle costs. Life-cycle cost analysis allows the engineer to determine which alternative is cost effective over its intended life. Beginning in the mid-1980s, the building regulatory systems of many countries are now partially or fully performance based. Under Performance Based Regulatory Systems (PBRs), end objectives representing society’s expectations for the built environment are specified in terms of quantifiable performance requirements in specific context of use. What PBRs demands is the ability to predict the performance of a specific

assembly to an arbitrary fire exposure during the life cycle of a building. These issues make the specification of appropriate design fires a significant problem in the context of performance-based designs under either performance codes or under the equivalency clause in prescriptive codes. The interrelationships between structural design and fire protection make it highly desirable to find a way to treat fire as yet another building design load. Additionally, in a performance system it is highly desirable to be able to describe a range of design fires for which a given building design is required to perform. This is clearly demonstrated by the Design Performance Levels concept incorporated into the International Code Council (ICC) Performance Code for Buildings and Facilities. This, in turn, constitutes the necessity to include the fire-induced damages/ repairs of a building in the cost-effective structural design. For the fire endurance, this means to design for the lifetime needed and the fire severity expected rather than for a fixed time and standard fire. Modern fuels and ventilation conditions would rarely be expected to produce the standard time-temperature curve in any space and extrapolating the fire endurance to another exposure condition is not possible. The fire load is defined as a thermal load resulting from the flame propagation within a building space. The energy needed to produce the required temperature is a function of the heat release and losses thru the vent areas; geometry of the building, and ventilation system (McCaffrey, 1981). Typically, the structural engineer would use a co-called T-squared heat release with a growth rate

(slow, moderate and fast) (Milke, 2002). The corresponding responses of different structural systems and possible structural damages to the building system have been discussed in (Razdolsky, 2007). In all cases, the maximum temperature of a fire has been used as a main global loading parameter and the structural system was substituted by the One Degree of Freedom (ODF) system.

## 2 PARAMETRIC ESTIMATING

Parametric estimating is the process of estimating cost by using mathematical equations that relate cost to one or more physical characteristics (maximum temperature due to fire load) of the item being estimated (the fire induced structural repair work of a building). A simple example of a parametric estimate is the use of square footage to estimate building costs. Square footage is a physical characteristic of a building that has been shown through statistical analyses of building trends to be one way of estimating building costs. Parametric estimates are often used in the early phases of a system's life cycle. At that stage of the life cycle, basic physical or performance characteristics may be available, but detailed designs may not be. Thus, parametric approaches may be the only option. Even later in a system's life cycle, however, a parametric approach might be used, for instance for certain elements of a detailed estimate. Parametric estimating equations are often called Cost Estimating Relationships or CERs. Even after the start of the development and construction phases, CERs can be used to estimate the costs of non-hardware elements. For example, they can be used to make estimates of O&S costs (fire-induced structural partial collapses or structural repair work). This may be especially important when trying to determine downstream costs of alternative design, performance, or support choices that must be made early in the development (design) process. For example, as it is shown below, by providing some additional reinforcement in structural elements at the design stage the fire endurance of the whole structural system can be substantially increased and therefore, the fire-induced structural damage and the O&S repair cost could be substantially decreased and the progressive collapse of the building can be prevented. In Building Life-Cycle Cost (LCC) analysis the user should using the probabilistic methods of lifecycle cost outcomes based on uncertainty about the value and timing of a fire-induced structural repair project cost, parameters such as the real discount rate, and area of a building affected by fire. The probabilistic methods produce distributions of life-cycle cost, allowing the user to see the range of life-cycle costs that can result from the uncertainty in costs and parameters.

## 3 DEVELOPING CERs

The construction cost of a square foot of a building, which can be estimated early in a building's design (development) stage, to predict fire-induced structural repair (rebuild) cost, which is not known until much later in the program's life. As more cost information becomes available, more detailed methods (e.g., engineering methods) of costing become feasible. CERs can play a valuable role in estimating the cost of a design approach, especially when conceptual studies and broad configuration trade-offs are being considered. To make an estimate using CERs, the cost estimator must use the statistical information available with respect to fire-induced structural repairs cost (Beitel, 2002). The purpose of this section is to describe the mathematical steps required to construct a CER method in our case, and introduce several related statistics used to evaluate the quality of the CER. Although the discussion in this article is limited to simple CERs (i.e., a single independent and a single dependent variable), the generalization to multiple, independent variables is briefly discussed. The classical CER in our case relates the maximum fire temperature to the construction cost of a fire-induced repair (rebuild) area of a building. This is an example of a simple relationship developed from a set of two-variable data. Suppose two measurements were taken on a building, where  $X_i$  denotes the maximum fire temperature  $T$  (the range of temperature for all practical purposes is:  $100^\circ\text{C} < T < 1200^\circ\text{C}$ ) and  $Y_i$  denotes the cost of construction repair work due to fire-induced damages to the building. Then one would obtain a set of "n" pairs of measurements:  $(X_1, Y_1)$ ;  $(X_2, Y_2)$ ;  $(X_n, Y_n)$ . The objective in developing a CER is to determine the relationship, if any, between  $X$  and  $Y$ . If such a relationship is found, it can be used to predict the costs of other fire-induced damage to the building if the cost estimator has some information on the new fire temperature (for example, ultra fast fire) that will be consistent with the nature of the combustible materials that would be found in the space. One way to proceed is to construct a functional relationship between  $X$  and  $Y$  based on so-called regression analysis. The first step in regression analysis is to hypothesize a relationship, usually involving one or more parameters, between the independent and dependent variables. There are essentially two approaches to hypothesizing a functional relationship between the independent and dependent variables in a regression analysis. The first approach is to hypothesize a relationship on the reasonable to hypothesize that the repair costs increase as a fire temperature increases (at least within a certain range). The cost estimator must review what factors might cause costs to increase and measure them directly or indirectly. The temperature relationship seems reasonable. Other

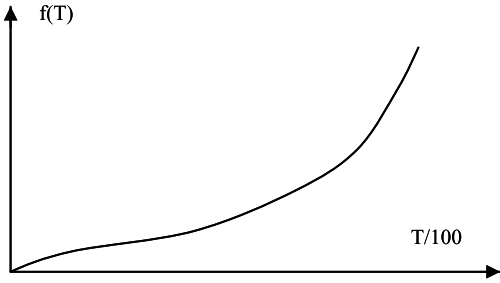


Figure 1. Scatter diagram.

relationships might be hypothesized for which there is no direct measure. For example, the construction's technology level could affect costs, but there is no direct measure of technology. Hence, the cost estimator may resort to an indirect measure such as time. Once the cost estimator has a list of hypothetical relationships, the cost estimator should determine what kind of relationship is expected. Is the relationship expected to be positive (as temperature increases repair cost increases) or negative? Determining this before collecting and analyzing the data enables the cost estimator to judge the reasonableness of the estimating relationship. The second approach is to construct and study (a scatter diagram) of the two variables. For example, the relationship between the X and Y variables could be linear or non-linear. In practice, it is best to employ both approaches. That is, after hypothesizing one or more functional relationships between the independent and dependent variables, the cost estimator should plot the data on a scatter diagram. If the scatter diagram does not confirm the hypothesized relationship, the cost estimator should rethink the prior notions and try to explain the discrepancy. There is no simple and direct way of determining a functional relationship; the process requires good judgment and experience that is gained only through repeated use of CERs. Once the relationship has been hypothesized and the data collected and normalized, the cost estimator should use curve-fitting techniques to specify the relationship in mathematical terms. Here are the steps to hypothesize a relationship in our case:

3.1. The simple One-Degree-Of-Freedom (ODOF) system can represent any element of a building structure: beam, truss, girder etc. or the whole structural system: frame system, tubular system, composite system etc. The mass motion (in terms of temperature as a design load) has two components: due to temperature itself, and dynamic effect created by the acceleration (second derivation) of temperature-time relationship and mass. The corresponding differential equation is:

$$\ddot{y}_d + \omega^2 y_d = -\ddot{\Delta}_t \quad (1)$$

Where:  $y_d$ —displacement due to inertial force action;  $\Delta_t$ —displacement due to temperature action;  $\omega$ —natural frequency of a given structural system (beam, girder, truss etc.);  $m$ —total mass.

To solve equation (1) let's assume that  $T(t) = -m\ddot{\Delta}_t$  basis of a prior assumption. For example, it is:

$$y_d = A \sin \omega t + B \cos \omega t + 1/(m\omega) \times \int_0^t T(u) \sin \omega(t-u) du \quad (2)$$

Where: arbitrary constants A and B could be obtained from the initial conditions:  $y_{t=0} = 0$  &  $\dot{y}_{t=0} = 0$ . If the explosion load is presented by the pressure function P (t) (Razdolsky, 2007), then the integral in Eq. (2) should be changed to:  $\int_0^t [T(u) + P(t)] \sin \omega(t-u) du$ . It is important to underline, that the total displacement of a given mass "m" is:

$$y_{tot.} = y_d + \Delta_t \quad (3)$$

Where:  $\Delta_t$ —is the displacement of a given structural system at a point, where the mass "m" is located, and the temperature load is applied statically. For fire resistance evaluation based on ASTM E119 Standard (ASTM, 2000) requirements any building assemblies, such as beam, column, wall etc., are exposed to heating in a furnace, following a specified temperature-time curve (ASTM, 2000), therefore the function T (t) in Eq. (2) is given. The curve T (t) is presenting in this study all three types of fire. The real temperature-time curve has some fluctuations of maximum temperature due to the hydrodynamic effect of fire propagation (Magnusson, 1970). Solving equation (1) one can obtain all interior forces: bending moments, shears etc., and therefore establish the areas of the building that are overstressed due to fire-induced loading conditions.

3.2. Estimate the structural repairs cost based on a given areas of concern.

3.3. For any given maximum fire temperature establish a functional relationship: "temperature-estimated cost"

$$ECR = (EC)f(T)(DF) \quad (4)$$

Where:

ECR—Effective cost of repair work

EC—Effective cost

f(T)—non-dimensional function obtained from (1) (Razdolsky, 2007)

$$f(T) = [(T_{mlt} - T)/(T - T_o)] \{ [(T_{mlt} - T_o) / \times ((T_{mlt} - T_o)^2 - T^2)^{1/2} - 1] \times (E_T/E)(M_n/M_u) \quad (5)$$

Where

- $T_{mli}$ —melting point of steel
- $T_o$ —room temperature
- $T$ —maximum fire-induced temperature
- $E_T$ —reduced modulus of elasticity at the fire temperature  $T$
- $E$ —non-reduced modulus of elasticity
- $M_n$ —nominal capacity of a structural element (moment, shear etc.)
- $M_u$ —ultimate exterior force (moment, shear etc.)

3.4. In order to account for the time of application of fire-induced design load, calculate DF using the following formula:

$$(DF) = ((1 + I)/(1 + i))^n \quad (6)$$

Where:

- $n$ —time of fire load application (years)
- $I$ —inflation rate
- $i$ —discounting rate

3.5. Draw non-dimensional scatter diagram, where  $X_n = T/100$  and corresponding  $Y_n = (ECR)/(EC)$  from (4) and (5).

3.6. Using regression analysis draws fitting curve (or straight line) and calculates mean value and standard deviation.

3.7. Use normal probability distribution to calculate the range of the effective cost of structural repair work due to fire-induced damage.

3.8. For alternate LCC design calculate the new nominal capacity of a structural element and repeat steps 2 thru 7.

#### 4 EXAMPLE #1

Data: Mid-rise reinforced concrete building (life span—100years; reoccurrence of fire—50 years) has a reinforced concrete beam (main structural typical element), restrained against longitudinal expansion. End span  $L_n = 30'$ , Data is taken from CRSI Handbook, 1984 (CRSI, 1984): Service load: D.L. = 87psf; 25% L.L. = 43psf. Spacing -14'-0". Total service load: 1.8klf; total ultimate load 6.4klf. Concrete: 4<sup>ksi</sup>. Steel  $f_y = 60^{ksi}$ . Section:  $w=16''$ ;  $h=30''$ . Reinforcement: top 4-#11; bottom 4-# 10 with #5 @13" o. c. ties. Modulus of elasticity  $E = 3600^{ksi}$ . Maximum temperature:  $T_m = 600^\circ C$ . Natural frequency  $\omega = 30.9$  rad./sec.  $t_o = .203$  sec.  $\epsilon = \lambda T_m = .0055L = 1.98''$ . Total moment and shear:  $M = 299.1^{ft-k}$

4.1. Solving equation (1) the interior forces are [ ]:  $M_n = 327^{ft-k}$  &  $V_n = 131.6k$ . Corresponding exterior forces are:  $M_u = 299^{ft-k}$  &  $V_u = 131.6k$ . Modulus of elasticity:  $E = 3600^{ksi}$  and the reduction coefficient due to fire-induced temperature  $n = 2.07$ .

Table 1. Non-dimensional function  $f(T)$ .

T/100	1	4	5	6	7	8
f(T)	.009	.0242	.0329	.0622	.0841	.1016
T/100	9	10	11	12		
F(T)	.1226	.1487	.1826	.229		

4.2. Floor area:  $100 \times 50 = 5000$  sq. ft.—area of concern.

4.3. Non-dimensional function  $f(T)$  from (5). The data arrange as follows:

4.4. Calculate the discount factor DF, if  $I = 5\%$  and  $i = 7\%$ :  $DF = .389$

4.5. Draw non-dimensional scatter diagram based on the data from Table 1.

4.6. The fitting curve in this case:  $f(T) = .1354(T/100)^2 + .2083(T/100) + 1$ . If the assumption is that for  $T/100 < 5$  there is no structural damage due to fire (slow fire), then the fitting curve is the straight line:  $f(T) = 2(T/100) - 6$ . The mean value and the standard deviation are as follows:  $f(T)_{aver.} = .0807$  and  $s = .0045$ . For normal distribution with 5% uncertainty the temperature interval expected:  $640^\circ C < T < 709^\circ C$ . The non-dimensional cost (ECR/EC) in this case:  $ECR/EC = .0807$ .

4.7. Alternate LCC design: additional 2-#10 bottom bars and 14-#5 ties were provided at the design stage in order to prevent structural damage from the fire-induced load, which results in 2% of the base cost of a square foot of a building. Using the same discount factor  $DF = .389$  the total increase is as follows:  $EC_1/EC = .064 < .0807$ . Therefore the alternate LCC design is acceptable.

#### 5 CONCLUSIONS

5.1. This article has dealt with the subject of parametric estimating (CER). Parametric estimating is the process of estimating cost by using mathematical equations that relate cost to one or more physical or performance characteristics of the item being estimated. Since physical or performance characteristics of a system are known early in a system's life cycle, parametric estimating methods are particularly needed for early life cycle estimates. The use of parametric methods has gained increasing acceptance because of the inherent advantages of the methods; they can generate complete estimates with little detail and relatively small time investment.

5.2. The fire-induced damages/repairs of a building should be included in the cost-effective structural design. For the fire endurance approximate formulas

are provided to account for the thermal load in the reinforced concrete design.

5.3. Simple non-dimensional formulas have been developed for the LCC analysis and design.

5.4. Regression analysis and the normal probability law have been used in order to estimate some unknown parameters.

## REFERENCES

- ASTM. 2000. *Standard Test Methods for Fire Tests of Building Construction and Materials*, ASTM E119. American Society for Testing and Materials, West Conshohocken, PA, USA.
- Beitel J., Ivankin N., Analysis of Needs and Existing Capabilities for Full-Scale Fire Resistance Testing, *National Institute of Standards and Technology, NIST GCR 02-843*, Baltimore, MD, 2002.
- CRSI. *Handbook, 1st Edition*, Concrete Reinforcing Steel Institute, 1984. USA.
- Magnusson S.E., and Thelandersson S. 1970. "Temperature-Time Curves of Complete Process of Fire Development in Enclosed Spaces," *Acts Polytechnica Scandinavia*.
- McCaffrey B.J., Quintiere J.D., and Harkleroad M.F., Estimating Room Temperature and Likelihood of Flashover Using Fire Data Correlations, *Fire Technology*, 17 (2), pp98-119, NFPA Quincy, MA, 1981.
- Milke J., Kohur V., Marrion C., Overview of Fire Protection in Buildings, *Federal Emergency Management Agency (FEMA), World Trade Center Building Performance Study*, USA, 2002.
- Razdolsky L., Extreme Thermal Load and Concrete Structures Design, *Fifth International Conference on Concrete under Severe Conditions Environment and Loading, Proceedings*, Tours, France, 2007.



# FRP bridge deck life cycle cost analyzer

Sidharta Sahirman, Robert C. Creese & Hota V.S. GangaRao

West Virginia University, Morgantown, WV, USA

**ABSTRACT:** Current Life Cycle Cost (LCC) analyses of Fiber Reinforced Polymer (FRP) bridge decks vs. concrete bridge decks consider only the manufacturing and erection costs in its cost calculation. They do not consider the most important advantage of FRP for construction, i.e. its light weight. The proposed model includes the cost savings in support structures when FRP is chosen as opposed to concrete as well as the user and third party costs occurring during the bridge installation process. It is believed this approach will provide a fair comparison between the two choices. A computer program, FRP Bridge Deck LCC Analyzer, was developed for conducting the comparison analysis. Beside the cost saving sub-module, the program incorporate service life estimation of the FRP deck based on the Factor Method. An LCC comparison between FRP Bridge Decks and SRC Bridge Decks for Sugar Run Bridge in West Virginia was done using the program.

## 1 LIFE CYCLE COST PROGRAM OVERVIEW

There are 17 input values for Life Cycle Cost Analyzer; the outputs of this program include: (1) total initial cost, (2) annual maintenance cost, (3) total disposal cost as well as the cost breakdowns. The program consists of five modules, i.e. Service Life Prediction, Initial Cost, Maintenance/Repair Cost, Disposal Cost and LCC modules.

Initial Cost modules consists 3 itemized costs (1) Agency Costs, (2) User Costs, and (3) Cost savings when FRP is used. It includes manufacturing costs, installation costs, and cost savings. The savings considered in this module was from the reduced weight of the steel girders used in FRP bridge deck construction as compared to the girders used for the concrete bridge deck construction.

Manufacturing cost is a function of total square footage of bridge deck area, which is the product of the length of the bridge deck times the width of the bridge deck. Manufacturing cost is calculated by multiplying the deck surface area by cost of bridge deck per square foot, which vary based on total square foot of bridge deck and year the bridge deck was built. The cost of bridge deck per square foot is estimated using learning curve method.

Bridge deck installation leads to lost time for the drivers of the vehicles, higher vehicle operation costs and increased accident rate. These costs can be sizable, depending on the total installation time as well as expected delay time. The expected delay time is a function of average daily traffic and length of the affected road work. These times were multiplied by the value of user's time to obtain lost time for drivers,

and were multiplied by vehicle operation cost per unit time to obtain increased vehicle operation cost. The equation used to obtain these costs was adapted from Ehlen and Marshall (1996):

$$\text{Costs} = \text{ADT} * N * ((\text{RL}/\text{CS} - \text{RL}/\text{NS}) * (\text{HC} + \text{VC}) + \text{RL} * (\text{CA} - \text{NA}) * \text{AC}) \quad (1)$$

Where

- ADT = Average Daily Traffic (vehicles per day)
- RL = length of affected roadway over which cars drive (miles)
- CS = traffic speed during bridge work activity (miles/hr)
- NS = normal traffic speed (miles/hr)
- N = number of days of road work (days)
- HC = hourly time value of drivers (\$/hr)
- VC = hourly vehicle operating cost (\$/hr)
- CA = during construction accident rate per vehicle-mile (#/vehicle-mile)
- NA = normal accident rates per vehicle-mile (#/vehicle-mile)
- AC = cost per accident (\$/accident)

The Life Cycle Cost Analyzer determines the annual average costs of the bridge deck alternatives during the service life. Since FRP bridge decks and concrete bridge decks have different life spans, the equivalent annual cost or annuity method was chosen as it can be applied for any combination of service life A and B. This approach was performed by determining a fixed study period based on the life of the girders and abutments. For the medium bridges, the study period can

range from 50–70 years while for large bridges the study period is 100 years. Based on the given study period, the average annual costs of the two bridge decks will be calculated and compared. In the program, the study period is determined based on the researcher judgment. For this case study, i.e. a medium size bridge, a study period of 70 years was assumed. The following assumptions were applied to enable this analysis:

1. Present values of maintenance cost are first obtained and then converted to average annual costs.
2. Replacement and Disposal Costs are applied since the life of concrete or FRP deck is less than the study period. For the LCC analysis the replacement and disposal costs are calculated using the present worth method for the time for the life of the deck and then annualized. These costs are assumed to continue over the life of the study period as the replacements of the decks are of the same type. The final decision to replace the entire structure or the deck will not be made until the structure enters the final stage of its life. At that time the decision must be made to replace the deck, repair the deck for the remaining life of the structure, or replace the structure and the deck. Since the life of the decks and structure are only approximate values, the use of annual average costs appears to be the best approach to the problem as other methods have additional problems.
3. End of life/Disposal costs are annualized by converting the future disposal cost to an average annual cost.

Figure 1 shows the implementation for the case study, i.e. structure life = 70 years, FRP service life = 70 years, and concrete service life = 35 years. This figure also illustrated the policies used, in which the black arrows represent biannual maintenance/inspection costs, as well as supplemental inspection costs which occur every 25 years for concrete and tri-annual maintenance/inspection costs as well as supplemental costs which occur every 25 years for FRP. The orange arrows represent the repair costs that in place every 3 years starting at year 20 for concrete and 5 yearly repair costs starting at year 25 till the overlay replacement for FRP. The yellow arrow represents overlay replacement that occur 35 years after deck installed. The purple arrows represent disposal costs which occur at the end of bridge deck service life, and the blue arrows represent initial/construction costs. The red arrows represent the NPV resulting from the maintenance, repair, replacement, and disposal costs. The average annual cost can be obtained by multiplying NPV with the capital recovery factor.

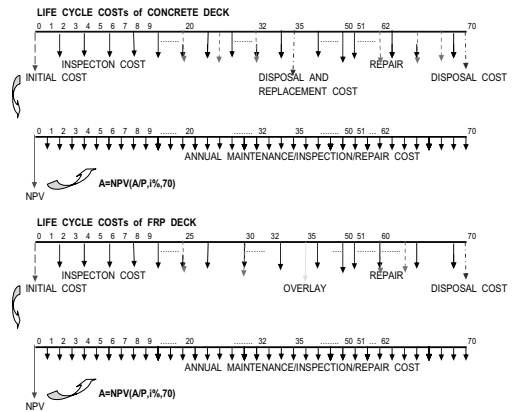


Figure 1. Life cycle cost analysis approach.

### 1.1 Inspection/maintenance/repair cost module

The inspection, maintenance and repair schedule for FRP bridge deck and concrete applied in this module is as presented in Figure 1. The following steps were applied to handle inspection/maintenance/ repair costs.

1. If the study period is N years and the concrete bridge deck service life is m, where  $2\text{ m} < N$  then the Total Present Value of these costs

$$(TPV) = MR + MR(A/P, i\%, m) \times (P/A, i\%, N - m) * (P/F, i\%, m) \quad (2)$$

where MR = present value of maintenance costs during m years of service life.

2. An approximate value for the annual costs

$$(AC) = TPV(A/P, i\%, N) \quad (3)$$

This assumes the costs will remain constant over the study period of N years even though m is not a multiple of N.

### 1.2 Service life prediction

The factor method was applied to estimate FRP bridge deck service life. The Delphi method was chosen to develop that application. The Delphi method comprises a series of questionnaires sent either by mail or via computerized systems to a pre-selected group of experts. The outcome of a Delphi application is an analysis of the opinions of the experts who respond to the questionnaires. There were two questionnaires sent to the experts for their opinions. The objective of the first questionnaire was to determine all important factors should be included in the estimations. Once

these factors were determined, the second set of questionnaire was distributed to gather expert opinions about (1) their estimates of RSLC = Reference Service Life of the Component and (2) estimates of service life given certain conditions, to determine the values of each modifying factors (A, B, C) in the following equation:

$$\text{Estimate Service Life} = \text{RSLC} * A * B * C \quad (4)$$

## 2 APPLICATION EXAMPLE

### 2.1 Inputs

In this case study an FRP deck and an SRC bridge deck with service life of 70 and 35 years were considered. The service life of the structure was assumed 70 years. The default value of FRP bridge deck cost/ square feet is \$47.42 (based on Bedford data) while concrete bridge deck is \$25/sq ft (average cost/sq ft for North Eastern States, Lopez-Anido, 2001). The Discount rate was 3%. The Sugar Run Bridge data of West Virginia was used with the following input data:

1. Deck Length = 39 ft
  2. Deck Width = 15 ft
  3. Deck Thickness = 8 inches
  4. N = 21 days (concrete), 2 days (FRP)
  6. RL = 0.1 mile
  8. NS = 55 miles/hour
  9. CS = 50 miles/hour
  10. Freeze thaw cycle is mild
  11. Light and UV exposure is mild
  12. Wearing surface is polymer concrete overlay
- The screen shot of the input data is given in Figure 2.

### 2.2 Model results

As discussed in the previous report, each cost component (initial, maintenance/repair and disposal) is breakdown into two cost classifications: agency costs and user costs. For that reason, in this analysis life cycle costs are classified into two main categories: agency costs and user costs.

The life cycle cost analysis performed for Sugar Run Bridge gave the following annual costs:

#### 2.2.1 User costs

The user costs for FRP bridge deck is less than the one for concrete bridge deck. For this case study, the user costs for FRP for both the installation and the disposal processes was 10% of the corresponding costs

Figure 2. Input's screen shot.

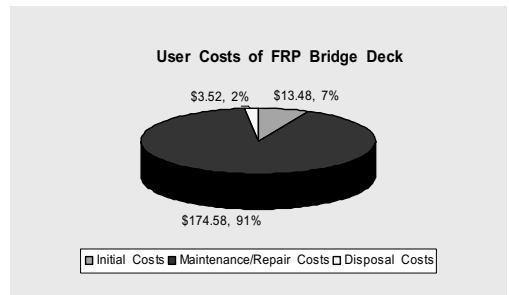


Figure 3. The user cost distribution for FRP bridge deck.

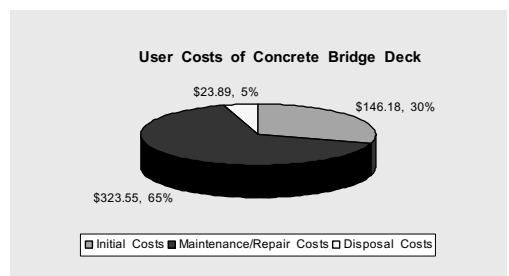


Figure 4. The user cost distribution for concrete bridge deck.

for concrete, mainly because of the big difference in time required to perform those activities.

Maintenance activities accounted for 91% of total user costs of FRP bridge deck and 65% of that of concrete bridge deck as illustrated in Figures 3 and 4.

Table 1. Cost/Sq ft for 70 years study period.

Agency costs	FRP	Concrete
Manufacturing and erection costs	\$47.6	\$33.9
Beam savings	\$2.7	
Maintenance/repair costs	\$3.8	\$5.2
Disposal costs	\$14.5	\$19.7
User costs		
Construction	\$0.7	\$7.3
Maintenance/repair	\$8.7	\$16.1
Disposal	\$0.2	\$1.2
	\$72.7	\$83.3

User costs for maintenance activities are \$8.7/sq ft and \$16.1/sq ft for FRP and concrete bridge respectively. These figures were obtained based on assumption that FRP bridge decks need less frequent maintenance and repair activities—as suggested by experts. As expected, the user cost of FRP bridge deck is lower than the one for concrete. On the contrary, initial construction activities only account for 7% of total user costs of FRP bridge deck but play significant role for concrete, i.e. it accounts for 30%. If we considered delays, i.e. opening a concrete bridge deck needs more than 21 days as estimated in this case study; the user costs during installation for concrete will increase tremendously. Under this situation, the user costs for FRP will be much less than the one for concrete.

The unit user costs (\$/sq ft) are summarized in Table 1.

### 2.2.2 Agency costs

The agency life cycle costs for the FRP deck is higher than the corresponding costs for the concrete deck. This emphasizes the importance role of FRP bridge deck cost as well as maintenance and repair cost in determining the economic viability of FRP bridge deck. The largest agency cost component of FRP deck is the initial costs (manufacturing and installation costs), which account for about 72% of the total agency cost (\$47.6/sq ft) as depicted in Figure 5. Hence, FRP bridge deck cost plays an important role in determining the economic viability of FRP bridge deck. In this case study, given that FRP bridge deck service life is 70 years, FRP is financially viable compared to concrete. However, the cost/sq ft applied is an optimistic value. As estimated by Sahrman and Creese (2003), if the improvement rate of FRP bridge deck cost remains at the same rate as the first FRP's produced, the average cost of \$40/sq ft would be reached by year 2013. However, with the changing world conditions it is unlikely that the improvement rate will remain constant. Based on one manufacturer estimates the manufacturing cost will be closer to \$45/sq ft for 4" bridge decks and most

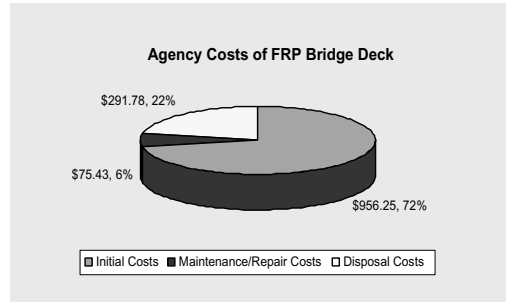


Figure 5. The agency cost distribution for FRP deck.

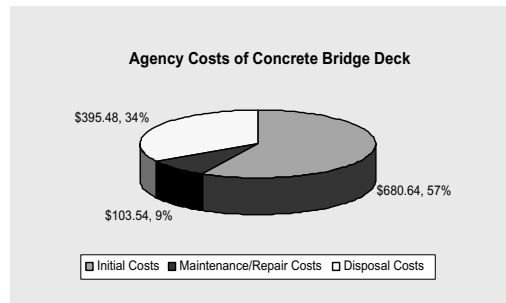


Figure 6. The agency cost distribution for concrete deck.

probably close to \$55/sq ft for 8" bridge decks. For that reason, the effects of this input is discussed in sensitivity analysis section.

### 2.2.3 Total costs

The Average Annual Value for FRP bridge deck for study period 70 years if cost saving considered was \$1,460 while that for the Concrete bridge deck was \$1,673 (Corresponding to \$72.7/sq ft and \$83.3/sq ft respectively). Based on the given scenario, the FRP bridge deck was more economical than the concrete deck.

This shows that FRP decks can compete with concrete deck if the FRP deck material and when the PC overlay meets the specific durability requirements, a certain amount of reduction in cost/sq ft of FRP bridge deck can be obtained.

Based on the above annual cost distribution, the main benefit of using FRP deck was in the user cost during construction and replacement. The high initial cost of FRP deck is the main concern for this application. Reduced maintenance costs and long service life are the two parameters that could balance this out to make FRP competitive.

### 3 BREAKEVEN ANALYSIS

Breakeven analysis indicates the maximum or minimum values of key parameters necessary for an alternative material to be cost effective. The breakeven analysis was done by re-computing the costs for FRP bridge deck by changing one parameter at a time to determine the level at which that the total life cycle cost of the FRP bridge becomes competitive or uncompetitive. The results are as follow:

1. Given the same values for all other parameters in the model, maximum FRP bridge deck to be cost competitive with concrete deck is \$59/sq ft. The relationship between FRP bridge deck and LCC cost/sq ft is depicted in Figure 7. The basic assumption of the results was the assumed schedules for the two bridge decks. If the FRP maintenance cost was not as low as expected, the conclusions would change. To illustrate the effect of maintenance cost, the same analysis was done using different assumption. If we assumed that an FRP maintenance cost is about 80% of the concrete, the maximum FRP bridge deck to be cost competitive with concrete deck is slightly below \$55/sq ft (\$54.8/sq ft).
2. The relationship between FRP service life and its LCC as given in Figure 8 showed that FRP with \$50/sq ft manufacturing cost will remain competitive with concrete if its service life at least 65 years.

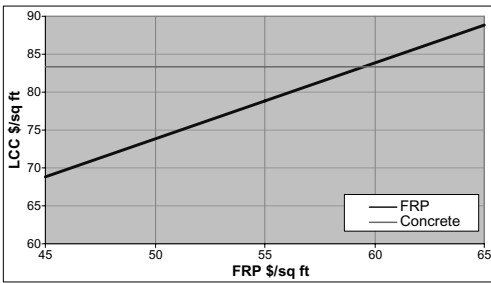


Figure 7. Effects of FRP cost/\$q ft on life cycle cost.

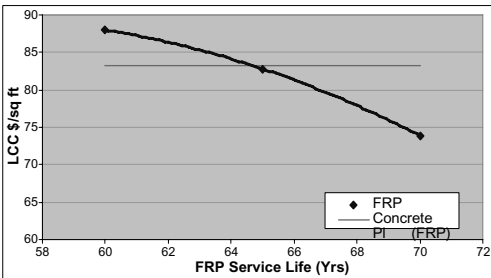


Figure 8. FRP deck service life and its life cycle cost.

In this study the study period assumed to be 70 years, the same as the structures (abutments and girders) service life and other parameters remain unchanged. Hence, if the service life reduced below 65 years, FRP deck cost/sq ft should be reduced to remain economically viable.

### 4 PRODUCTION COST MODEL

The above life cycle cost model, initial cost module particularly, assumed that manufacturing cost is a function of time. Hence, FRP bridge deck costs will decrease with time as the learning curve reaches the steady state. This model implicitly assumed that resin and fiber costs will be steady. An analysis on Effect of Resin and Fiber Costs to Manufacturing costs using Production Cost Model (Creese and Patrawala (2000)) was conducted. This model required twelve basic inputs as well as other inputs including raw material costs, and provides the manufacturing cost and its components.

The parameters used for this simulation analysis are raw material cost input, which include mat, roving, resin costs and the output studied is FRP manufacturing cost/ft. The values are expressed as percentage of the default values, i.e. ratio of material cost = material cost inputted/default cost and price ratio = FRP manufacturing output/default output.

FRP manufacturing cost simulation performed based on Creese and Patrawala's model showed that FRP bridge deck cost for a given year is a function of material costs. A ten percent increase of material costs will result in about six percent increase of bridge deck price.

Based on the above relationship, one should be caution when performing life cycle cost analysis of FRP bridge deck. Since FRP bridge deck cost is not a fixed number, this parameter value is part of important factors should always be considered in sensitivity analysis.

Utilizing the same model, estimation of FRP bridge deck costs were performed for different deck specifications. For FRP bridge deck with specifications similar to Prodeck 8 (Bedford Plastic Inc, weight 15.7 psf and 27 in sq of section area) was \$53.72/sq ft, while for Superdeck (Creative Pultrusion, weight 20 psf and 20 in sq of section area) was \$60.04/sq ft. The results which based on labor rate \$20/hr show that cost of \$50/sq ft is a reasonable estimate for 8" FRP bridge deck for the near future.

### 5 CONCLUSIONS

The costs of fiber reinforced polymer (FRP) bridge decks have higher initial costs than the traditional steel

reinforced concrete (SRC) bridge decks. The improved corrosion resistance of the FRP decks increases the deck life over that of the SRC bridges, but this by itself does not offset the effect of the higher initial costs. Additionally, the weight reduction would have an effect on the initial costs as the structure to support the deck would be reduced as the weight of an FRP deck approximately 20–25 percent that of a SRC deck. The major reductions would be in that for the steel bridge girders/beams/rollers required to support the bridge deck. Unfortunately, combination of both effects (higher service life and initial cost savings) do not always offset the effect of the higher initial costs.

However, if the savings from the concrete support foundations is considered from the loss in deck weight, the values will be more competitive.

Another key parameter for FRP competitiveness is the maintenance cost. When the required maintenance frequency for FRP deck is less than the one for concrete as predicted by experts and as assumed in the model, FRP bridge deck is competitive to concrete bridge deck.

The analysis has shown if the maintenance/repair costs of FRP bridge deck are at least 20% lower than ones of concrete bridge deck and the service life is as expected (70 years), FRP will be financially viable when deck cost is about \$55/sq ft. However, the deck cost need to be reduced to \$50/sq ft to remain competitive when the service life is only 65 years. The deck cost of \$50/sq ft can be reached in the near future as reflected from Bedford data as well as from Patrawala Model estimates.

## REFERENCES

- Creese, R.C. & T.B. Patrawala. 2000. A Cost Model for the Pultrusion Process. *Cost Engineering* 42 (6): 38–43.
- Ehlen, M.A. & H.E. Marshall. 1996. The Economics of New-Technology Materials: A Case study of FRP Bridge Decking. NISTIR 5864, U.S. Department of Commerce.
- Lopez-Anido, R. 1998. Life-Cycle Cost Evaluation of FRP Composite Bridge Decks. Technical Report, West Virginia University Research Corporation, Morgantown, WV, June 1998.
- Lopez-Anido, R. 2001. Life-Cycle Cost Survey of Concrete Bridge Decks—A Benchmark for FRP Bridge Deck Replacement. TRB ID Number:01-3166; Transportation Research Board 80th Annual Meeting; Washington, DC;
- Munley, E. 2000. FHWA's program in FRP Composites. ERC Bridge Technology Workshop, Boston.
- Nathan, T.R. & O.U. Onyemelukwe. 2000. Comparison of Bridge Deck Alternatives Using Life Cycle Costs. 8th ASCE Specialty Conference on Probabilistic Mechanics and Structural Reliability.
- Nystrom, H.E. et al. Financial Viability of Fiber-Reinforced Polymer (FRP) Bridges. *Journal of Management in Engineering*, January 2003, pp 1–8.
- O'Connor, J.S. 2002. New York's Experience with FRP Bridge Decks. *Polymer Composites II 2001: Applications of Composites in Infrastructure Renewal and Economic Development* CRC Press, New York.
- Sahirman, S. & R.C. Creese. 2007. Cost Analysis. Final Report. Unpubl. June 2007. Center of Excellence, Constructed Facilities Center, College of Engineering & Mineral Resources, West Virginia University, Morgantown, West Virginia.
- Field Inspection of In-Service FRP Bridge Decks. 2006. TRB Publication: NCHRP Report #564.

# Life cycle cost and function analysis in value based design decision

C. Utomo

*Sepuluh Nopember Institute of Technology, Indonesia*

A. Idrus

*Universiti Teknologi Petronas, Malaysia*

**ABSTRACT:** This paper presents an analysis of life cycle cost (LCC) and function in value based design decision. The object study is an affordable public housing and infrastructure in Indonesia. The objective of LCC analysis is to choose the most cost effective approach from a series of alternatives to achieve the lowest long-term cost of project and infrastructure. Decision analysis techniques applied to determine the relative value of the alternative solutions for performing the function. Criteria for evaluating value are initial cost, energy cost, return in profit, functional performance, reliability, and maintenance ability. Model formulates and its implementation based on application of Analytic Hierarchy Process (AHP) method for multi criteria decision-making. The implementation results demonstrate a process to select priorities each alternatives to each decision. It further emphasizes the importance of performance evaluation in the design process, and provides a focus for future research into performance evaluation techniques and their application.

## 1 INTRODUCTION

The need to provided energy-efficient design becomes more important. This is especially true in relationship to the design life of project. A means of accounting for the energy uses for the construction and operation of building is needed. New building display an increasing awareness of sustainability but invariability assumed a level of technical sustainability and concentrate on economic and social sustainability. At times it is difficult to quantify and qualify the importance of values other than those relating only cost. In a value analysis study, we do our primary investigations centered on the cost and the price of the project. Criteria for evaluating value are initial cost and energy cost as the LCC, return in profit, functional performance, reliability, and maintenance ability.

This paper focuses on a methodology of design decision that can more effectively align the design and performance evaluation with user expectations and economic imperatives. If reducing costs results in an inferior solution then it is possible that this solution will be of significantly less value. Therefore value should be the main consideration when choosing a solution.

Value Analysis (Woodhead and McCuish, 2002) seeks to determine the value of a particular solution, not only in terms of its associated costs but also by taking into account how well it meets the objectives of a

particular purpose. The basis of the methodology was founded on many years of practice in the field of value engineering (Wixson, 1999). Value engineering has been extensively applied in both construction management and systems engineering, however its application to the design and development of computer-based systems is a relatively recent development and still very much in the research stage. This application area presents some interesting challenges to current value analysis methods.

## 2 VALUE BASED DESIGN DECISION

Kirk, Turk and Hobbs (2007) describe traditional design versus value based approach. Value based as a new approach involves using a multidisciplinary team that includes representatives of the owner, user, facility manager, and constructor. Real-time decisions are reached using value-based methods in a team setting: function analysis, quality modeling, group creativity/innovation techniques, life-cycle costing, design/cost simulation modeling, and choosing by advantages.

The power of value-based team decision making is in the methodology. The meaning of value may be open to interpretation but generally the value of product will judged on some factor such as a high level of performance, capability, emotional appeal, style,

etc. relative to its cost (Crow, 2002). This can be expressed as:

$$\begin{aligned} \text{Value} &= (\text{Performance} + \text{Capability})/\text{Cost} \\ &= \text{Function}/\text{Cost} \end{aligned} \quad (1)$$

Value analysis is a powerful problem solving tool that can reduce cost while maintaining or improving performance requirements (Woodhead and McCuish, 2002; Kelly and Male, 2004). Hussain (2001) present research attempts to design called Value engineering expert system in suburban highway design (VESSHHD) that employ the power and abilities of expert system in solving complex problems to assist decision team in suburban highway design.

The problem solving process focuses on increasing value in the all-powerful triad of cost, quality, and performance. Value analysis is not concerned with simply minimizing cost. It is possible to increase the value of a product by increasing its function even when this results in greater cost, provided that the added function increases more than the additional cost. This leads to the concept of functional worth, which is defined as the lowest cost to provide a given function.

Value-based decision is a function-oriented methodology that allows a sound understanding of the relationship between the functions of the system and the purpose of their existence to be developed. It also identifies the criteria that can be used to determine whether or not a function is being performed correctly. Each criterion then needs to be weighted according to its importance to purpose. Decision analysis techniques can then applied to determine the relative value of the alternative solutions for performing the function (Clemen, 1996). This analysis will also take as parameters items such as the estimated costs, estimated complexity of the solution, and assessments of the risks involved in developing and producing the solution.

### 3 LIFE CYCLE COST

The term life cycle cost means [Kirk and Dell'Isola, 1995; Barringer, 2003] process for evaluating the total economic worth of a usable project segment by analyzing initial costs and discounted future costs, such as maintenance, user costs, reconstruction, rehabilitation, restoring, and resurfacing costs, over the life of the project segment. Life Cycle Cost is an essential design process for controlling the initial and the future cost of building ownership. LCC can be implemented at any level of the design process and can also be an effective tool for evaluation of existing building systems. LCC can be used to evaluate the cost of a full

range of projects, from an entire site complex to a specific building system component. As defined earlier, Life Cycle Cost is the total discounted cost of owning, operating, maintaining, and disposing of a building or a building system over a period of time. LCC equation can be breakdown into three variables: the pertinent costs of ownership, the period of time over which these costs are incurred, and the discount rate that is applied to future costs to equate them with present day costs [Landers, 1996; Fabrycky and Blanchard, 1991; Bull, 1993].

As the total cost of ownership of machinery and equipment, including its cost of acquisition, operation, maintenance, conversion, and/or decommission, LCC are summations of cost estimates from inception to disposal for both equipment and projects as determined by an analytical study and estimate of total costs experienced in annual time increments during the project life with consideration for the time value of money [Bull, 1993; Kirk and Dell'Isola, 1995; Woodward, 1997]. Figure 1 present key factors in LCC. The objective of LCC analysis [Barringer, 2003] is to choose the most cost effective approach from a series of alternatives to achieve the lowest long-term cost of ownership. LCC is an economic model over the project life span. Usually the cost of operation, maintenance, and disposal costs exceed all other first costs many times over.

For calculation of LCC, the following equation is used.

$$\begin{aligned} \text{PW of LCC} &= \text{Investment cost} \\ &+ \text{PW operation cost} \\ &+ \text{PW maintenance cost} \\ &+ \text{PW energy cost} \\ &+ \text{PW replacement cost} \\ &+ \text{PW salvage value} \end{aligned} \quad (2)$$

Present worth (PW) can be calculated using theory of time value of money

$$P = F \left[ \frac{1}{1+i} \right]^N = F(1+i)^{-N} \quad (3)$$

$$P = A \left[ \frac{(1+i)^N - 1}{i(1+i)^N} \right] \quad (4)$$

Where P = present value; F = future value; A = annual value; i = rate per period (year); N = number of time periods (years).

Based on the equation (2) four cost driver of building was calculated, here salvage value was not calculated because it was not practice in Indonesia. Table 1 and figure 2 present LCC and the proportion for each category; initial cost (including investment



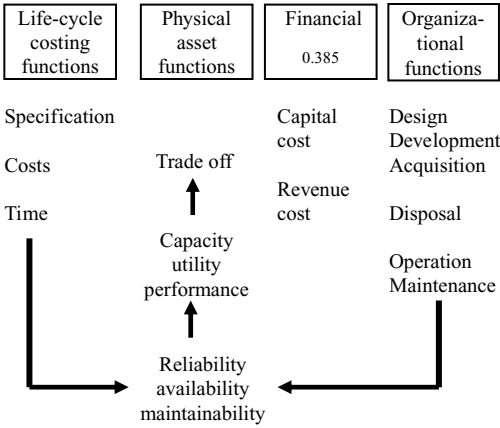


Figure 1. Key factors in life cycle costing (Woodward, 1997).

Table 1. Life cycle cost of a public housing and infrastructure (1000 USD).

Cost category	Present worth (1000USD)
Initial	2102
Energy	135
Operation & Maintenance	1115
Replacement	83
<b>Total cost</b>	<b>3437</b>

Source: Analysis.

cost), energy cost, operation and maintenance (O&M) cost and replacement cost. O&M cost and energy cost have annual basis, so they use equation (4) to calculate. Equation (3) was used for replacement cost that has variability in period.

In the calculation of LCC of the public housing and infrastructure, it is essential that the risk and associates with statistical parameters such as discount rate be properly considered. As an affordable building, two most important variables be considered for sensitivity analysis, that are discount rate and minimum attractive rate of return (MARR). Sensitivity analysis is a technique for evaluating how stability of the result or outcome depends on the variation in various input parameters.

Tables 2 and 3 shows the variation in total LCC of the example building at different discount rate and MARR. The table indicates that at lower MARR, the PW of LCC will decrease significantly. In this case of the project (an affordable public housing) better that shareholder give the lowest MARR or in minimum value for sustainability.

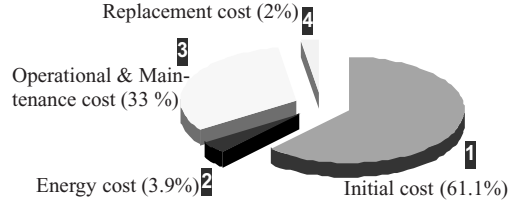


Figure 2. Life cycle cost of an affordable public housing.

Table 2. Sensitivity PW to discount rate.

i	PW (Thousand USD)	% Change PW	$\Delta$ %PW
7.5%	3054	-11%	1.8540%
7%	3117	-9%	2.0231%
6.5%	3187	-7%	2.2101%
6%	3263	-5%	2.4170%
5.5%	3346	-3%	2.6464%
5%	3437	0%	2.9007%
4.5%	3537	3%	3.1830%
4%	3646	6%	3.4967%
3.5%	3766	10%	3.8456%
3%	3898	13%	4.2340%
2.5%	4044	18%	

Source: Analysis.

Table 3. Sensitivity PW to MARR ( $r^2$ ).

$r^2$	PW (Thousand USD)	%Change PW	$\Delta$ %PW
13.332%	4,446	29%	7.6015%
12.443%	4,185	22%	6.6136%
11.554%	3,958	15%	7.5640%
10.666%	3,760	9%	5.0129%
9.777%	3,588	4%	4.3680%
8.888%	3,437	0%	3.8087%
8.00%	3,307	-4%	3.3236%
7.110%	3,192	-7%	2.9028%
6.222%	3,092	-10%	2.5738%
5.333%	3,005	-13%	2.2212%
4.444%	2,929	-15%	

Source: Analysis.

LCC Analysis can be performed on large and small buildings or on isolated building systems. Both owners and designer are taking into consideration the future maintenance and replacement costs in their selections. While initial cost is a factor in their decisions, it is not the only factor.

#### 4 DECISION MODEL FORMULATING

In many of the areas to which value analysis has previously been applied the evaluation of alternative solutions has been relatively straightforward. Therefore, in addition to each process that may offer an alternative solution, there are also several possible implementations for each of these modeling and evaluating.

By applying value analysis we can arrive at the solution that offers maximum benefit, and therefore avoid the possibility of wasting effort through implementing a less optimal solution. Because of the potential in the number of possible realizable solutions for each function, a hierarchical approach to evaluation is needed, and it is important to eliminate unsuitable solutions at the highest level of abstraction as possible. Figure 3 present the methodology that has been used in this research.

Some functions it may decided that a set of generic process are needed to perform the function, each of which will give rise to an associated set of possible specific processes. A number of processes may be identified as being probable candidates for performing the function. In many of the areas to which value analysis has previously been applied the evaluation of alternative solutions has been relatively straightforward. The solution to how a particular function will be performed will generally take the form of some process (or procedure). In this research there are three function of sustainability, that are technical, economic, and social (presented in level 3 figure 4) as the basis for alternative priority. By evaluating a number of alternative solutions and applying value analysis it can

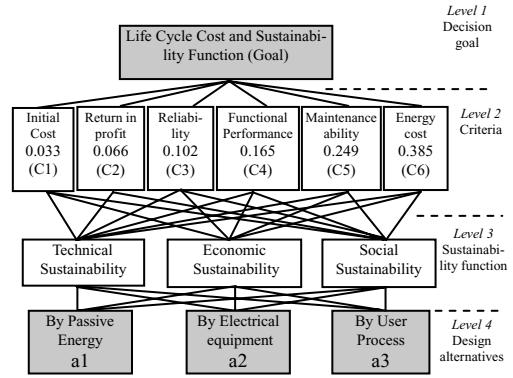


Figure 4. Decision hierarchy model.

arrive at the solution that offers maximum benefit, and therefore avoid the possibility of wasting effort through implementing a less optimal solution. Every sustainability decision has own alternative priority.

Figure 4 shows a model of decision hierarchy of LCC and sustainable function for an affordable public housing and infrastructure in Indonesia. Each of the objects in this model contains attribute representing their various properties and different preference. In this model, energy building system is used as object study. Firstly, attribute of decision was set based on previous study and standard function analysis ASTM E06.81 "Building Economics", 2004. Further, a set of questionnaire survey should be conduct to get data and knowledge of energy building system domain. The model has been test to the decision in a public housing project. Three stakeholders involved and give their own preference. Since every stakeholder has his own priority, and the project need a single alternative, main value has been used for this purpose.

Weighting and scoring technique are relevant in Value analysis exercise [Kelly, Male and Graham, 2004; Cariaga, El-Diraby and Osman, 2007, Nassar, Thabet and Beliveau, 2003] where a decision needs to be made in selecting an option from a number of competing options and the best option is not immediately identifiable. Many study in value-based design decision using the decision tools [Cariaga, El-Diraby and Osman, 2007; Sanchez, *et al.* 2005; Fan, Shen and Lin, 2007]. A paired comparison is held to determine the weighing to be given to each attribute.

#### 5 DESIGN DECISION AND ITS OPTIMIZATION

Based on decision hierarchy in figure 4, three stakeholders give their preferences using a set paired

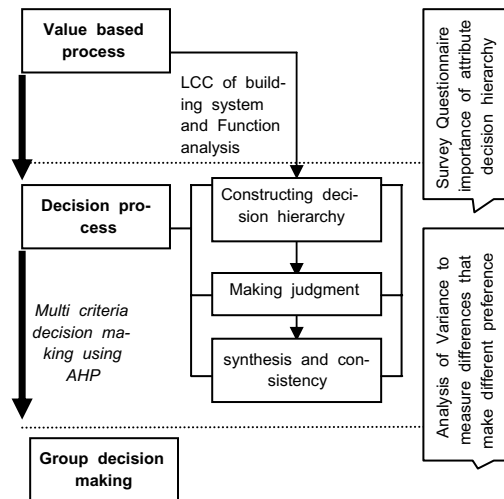


Figure 3. Process of value-based decision.

Table 4. Synthesis of analytic hierarchy process.

Weight of alternative	Weight of criteria					
	C1	C2	C3	C4	C5	C6
	.033	.066	.102	.165	.249	.385
<b>Technical sustainability</b>						
By passive energy 0.24646	.750	.723	.700	.059	.054	.206
By electrical equipment 0.37842	.060	.061	.088	.467	.512	.413
By user process 0.37511	.190	.216	.212	.474	.434	.381
<b>Economic sustainability</b>						
By passive energy 0.25430	.171	.198	.164	.254	.115	.386
By electrical equipment 0.35679	.570	.491	.539	.294	.459	.228
By user process 0.38891	.259	.312	.297	.452	.426	.386
<b>Social sustainability</b>						
By passive energy 0.28055	.180	.254	.354	.313	.277	.263
By electrical equipment 0.12502	.071	.098	.090	.198	.129	.110
By user process 0.594444	.748	.647	.556	.491	.595	.627

comparison questionnaire. Using mean value from their preferences, calculation matrix for each level of hierarchy that are: weighing factor of each criteria, 0.033 (initial cost), 0.066 (return in profit), 0.102 (reliability), 0.165 (functional performance), 0.249 (maintenance ability), 0.385 (energy cost). Tables 4 and 5 indicate that every sustainability function have their own preference priority. Using electrical equipment for energy system was chosen by three stakeholders as first priority for technical sustainability function. Different priority presents in both economic and social sustainability. These two functions put electrical equipment in lowest priority.

Since the decision priority is different for each sustainability function, further method can be used for optimization such as goal programming or advance method in artificial intelligent. In this case, design by user process was decide for an affordable public housing building and infrastructure. This decision based

Table 5. Each alternatives for each decision.

Priorities	Decision Alternatives to Function		
	Technical Sustainability	Economic Sustainability	Social Sustainability
	By electrical equipment	By user process	By user process
	By user process	By passive energy	By passive energy
	By passive energy	By electrical equipment	By electrical equipment

on qualitative synthesis of LCC analysis and the AHP result by the owner and designer.

## 6 CONCLUSION

The implementation results demonstrate a process to select priorities each alternatives to each decision. Value analysis can help to provide a better alignment between business objectives and the choice of design solutions. Life cycle cost and value analysis lead to effort in the initial design process and an increased active in the evaluation stage. However, given that implementation is the part of the development process that requires the greatest effort, and in many case accounts for the largest proportion of development costs, it believe that this additional effort represents a good investment when compared to the implications of an unsuitable implementation.

It further emphasizes the importance of performance evaluation in the design process, and provides a focus for future research into performance evaluation techniques and their application. Follow up research is particularly required, primarily a study of decision support system and expert systems, and artificial intelligent such as Multi Agent System.

## REFERENCES

- ASTM (2004). *Building Economics*.
- Barringer, P. 2003. A life cycle cost summary. *International Conference of Maintenance Societies*.
- Bull, John W. 1993. *Life cycle cost for construction*, 1st ed., London: Blackie Academic & Professional.
- Cariaga, I., El-Diraby, T. & Osman, H. 2007. Integrating value analysis and quality function deployment for evaluating design alternatives. *Journal of Construction Engineering and Management* 133(10):761–770.
- Clemen, R.T. 1996. *Making hard decision*, 2nd ed. Belmont CA: Duxbury Press.

- Crow, K. 2002. *Value analysis and function analysis system technique*, 31 June 2007. <http://www.npd.solution.com/va.html>.
- Fabrycky, W.J. & Blanchard, B.S. 1991. *Life-cycle cost and economic analysis*, New Jersey: Prentice-Hall.
- Fan, S., Shen, Q. & Lin, G. 2007. Comparative study of idea generation between traditional value management workshop and GDSS-supported workshop. *Journal of Construction Engineering and Management* 133 (10): 816–825.
- Hussain, M.A.D. 2001. *Value engineering expert system in suburban highway design (VESSHSD)*. PhD dissertation. University of Pittsburg.
- Kelly, J. & Male, S. 1993. *Value management in design and construction: the economic management of projects*, London: E & FN. Spon.
- Kelly, J., Male, S., Graham, D. 2004. *Value management of construction Project*. London: Blackwell Science.
- Kirk, S.J. & Dell'Isola. 1995. *Life cycle costing for design professionals*, 2nd edition. New York: McGraw-Hill, Inc.
- Kirk, S.J., Turk. R.G., & Hobbs, R.W. 2007. *Value based team design decision making*. The American Institute of Architects.
- Landers, R.R. 1996. *Product assurance dictionary*, New York: Marlton Publishers.
- Nassar, K., Thabet, W., & Beliveau, Y. 2003. A procedure for multicriteria selection of building assemblies. *Automation in Construction* 12:543–560.
- Sanchez, M. et al. 2005. Multiple criteria evaluation for value management incivil engineering. *Journal of Management in Engineering* 21 (3): 131–137.
- Wixson, R.J. 1999. *Function analysis and decomposition using function analysis system technique*, Proceedings of INCOSE.
- Woodhead, R & McCuish, J. 2002. *Achieving results: how to create value*. London: Thomas Telford.
- Woodward, D.G. 1997. Life cycle costing-theory, information acquisition and application. *International Journal of Project Management* 15 (6): 335–344.

# Equipment replacement decisions based on life-cycle cost analysis

José Weissmann

*The University of Texas at San Antonio*

Angela J. Weissmann

*TransAnalysis Engineers and Planners*

**ABSTRACT:** The Texas Department of Transportation (TxDOT) maintains an active fleet of approximately 17,000 units, annually replacing about ten percent. It also maintains a comprehensive data base that includes data relevant to life-cycle cost analysis. Ideally, equipment units whose life cycle costs have been increasing longer and/or at a faster rate should have higher replacement priority than those still amortizing. However, fleet managers could not routinely use life-cycle costs as replacement criteria because there was no reliable method to automatically prioritize thousands of life-cycle cost histories. This paper summarizes three innovative concepts in fleet management developed and implemented by the authors: (1) Bayesian analysis of life-cycle costs. This project used a SAS algorithm to adjust a trend component to each life-cycle cost time series; (2) Trendscore, a concept that enables a computer to mimic replacement decisions made by a person visually inspecting life-cycle cost Bayesian trends; and (3) Multi-attribute priority ranking, an algorithm that ranks replacement priorities based on the condition of the units relative to the rest of the fleet within its class or group, instead of the current practice of slating a unit for replacement when it reaches some threshold value. The replacement budget can be matched to the units with top replacement priority, making budget shortfalls clearly visible. These concepts were implemented through a menu-driven decision aid software that calculates life cycle cost profiles and trends, and generates replacement priority lists based on the concepts described above.

## 1 INTRODUCTION

According to Bibona (1996), in 1993 Loren Wiseman of Pacific Electric Co. surveyed the utility industry to find the “perfect” equipment replacement program. After analyzing over 100 responses, he found almost as many variations in programs and criteria as there were responses. Some, but not all, methods included mathematical models. This project’s literature review, which included a survey of approaches currently in use by state highway departments, indicated that replacement programs can be classified into the following six groups (Weissmann, A. & Weissmann, J., 2003):

1. Threshold criteria. Equipment units become candidates for replacement when they reach predetermined threshold values of indicators such as age, mileage, repair cost, and downtimes. This was the method in use by the Texas Department of Transportation (TxDOT) while this project was under development.
2. Historical costs as percent of new costs. Equipment units become candidates for replacement when their lifetime maintenance costs reach a predetermined percentage of the cost of a new unit.
3. Probability of failure. Probability models predict when a unit is approaching failure. This requires developing a subjective definition of “equipment failure”. Units are replaced when their estimated probability of failure reaches a predetermined threshold.
4. Unit cost (e.g., cost per mile). Equipment units become candidates for replacement when their cost per mile reach a predetermined percentage of the cost per mile for a given class of equipment.
5. Life-cycle cost analysis. Equipment units become candidates for replacement when their estimated total cost of ownership and operation reaches a minimum. A variation of this method uses incremental costs rather than costs over the entire life.
6. Weighted factor method. Relevant parameters (such as age, usage, downtimes, etc.) are divided by base figures, and the resulting ratios are weighted and added up. Equipment units become candidates for replacement when their sums exceed a predetermined threshold value.

The most important conclusion of this literature review is that, conceptually, all strategies above are the same. They compare the condition of a challenged unit to

some pre-determined threshold, defined for attributes such as mileage, cumulative downtime, either individually or combined (groups 1 and 6); cost variables (groups 2, 4 and 5), or probability of failure (group 3).

None of these strategies provides a way to verify where a challenged unit's condition stands with respect to all others. There is no fleet-level analysis. Fleet managers recognize that the ideal equipment replacement system should check the units' condition against the entire fleet and rank them on this basis, while at the same time finding units that automatically qualify for replacement based on one or more obsolescence criteria. However, none of the approaches in use can do this, because they all check the condition of each unit against predetermined values.

## 2 UTILIZATION OF THE LIFE-CYCLE COST CONCEPT

The total Life Cycle Cost (LCC) of an equipment unit is the sum of all costs incurred during the entire equipment life. It can be viewed as the sum of capital costs (purchase), periodic expenditures needed to operate and maintain the unit during its entire life, and resale. Ideally, it should also include the monetary value of intangibles such as downtimes, equipment depreciation and obsolescence (Brown et al., 1985; Dhilon, 1989; Grant, 1990; Weissmann and Euritt, 1991).

If the Equivalent Uniform Annual Life-Cycle Costs (EUALCC) are calculated for each year a unit is in operation, and plotted against time, one should obtain figure 1. In the beginning of the equipment life, the cost of acquiring the unit is spread into a small number of installments and weighs heavily on the annual cost, while the maintenance costs are low. As time passes, the initial investment offsets over the years, while repair costs increase. Adding these two costs results in

the equivalent uniform annualized LCC curve, which decreases as the initial investment offsets over the years, and increases as the operating costs become greater than the capital cost installments. Theoretically, the total EUALCC reaches a unique point of minimum (optimal region in figure 1). There is a region of low EUALCC before and after this minimum where the first derivative of the EUALCC with respect to age is very small, i.e., the EUALCC changes little with time. Then, the slope increases faster, until the EUALCC equals that of new equipment.

## 3 IMPLEMENTATION OF THE LIFE-CYCLE COST CONCEPT

Private and public agencies do not routinely include life-cycle costs in their replacement methodologies because, until now, the only way to automate the inspection of thousands of life-cycle cost histories was to define threshold values of EUALCC acceptability. Most fleet managers rightfully consider this practice inaccurate. What managers really needed was a way to compare and sort these histories.

For example, a fleet manager interested in using life-cycle costs to prioritize replacement of the three six-year old automobiles in figure 2 would replace the auto already in the upward region, and keep the one still amortizing. S/he might decide to replace the auto starting to leave the optimal region (dotted line) if there was an unexpected budget surplus—and s/he would consider additional criteria to make this decision.

In order to mimic this type of decision-making process in a computer, the authors first used a Bayesian time series adjustment to eliminate the random and seasonal components, leaving only the trend. This step is necessary because the variations in operational costs observed in figure 2 are the norm. Next, the authors defined an algorithm based on a variable they

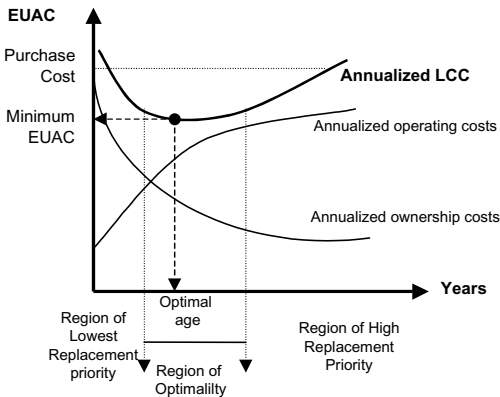


Figure 1. Theoretical EUACs of owning and operating an equipment unit.

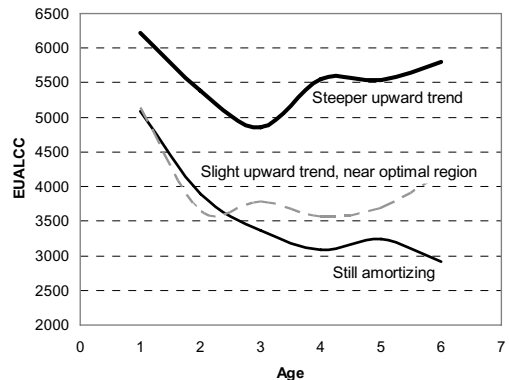


Figure 2. EUALCC trends.

called trendscore. Trendscore examines life-cycle cost trends in a way that accurately reflects fleet manager's decisions, allowing the computer to rank the fleet by life-cycle cost replacement priority.

#### 4 EUALCC SERIES ADJUSTMENT

The graph of EUALCC versus age meets the mathematical definition of a time series: a series of autocorrelated values with a general trend in time that is a function of external factors, with or without seasonal components, and disturbed by a random component. Among the many techniques for analyzing time series, the research team selected a Bayesian method developed by Akaike (1980), first programmed in FORTRAN by Akaike and Ishiguro (1987), and later included in the SAS Institute's package for matrix programming (SAS Institute Inc., 1993). Akaike's method decomposes a time series  $Y_t$  into a three components: random, seasonal, and trend, as shown in equation 1.

$$Y_t = T_t + S_t + \varepsilon_t \tag{1}$$

Where:

$Y_t$  = Variable under study (in this case, EUALCC in each year or age "t")

$T_t$  = Trend component.

$S_t$  = Seasonal component. This component either captures periodic maintenance costs. It can be absent for some equipment types.

$\varepsilon_t$  = Random component.

Akaike (1980) tested his method with artificial time series developed by disturbing a curve with a multiplicative seasonality and random irregularities. His procedure accurately separated the original curve, the multiplicative seasonal disturbance and the random component without any of the special considerations often necessary in other methods.

Figure 3 shows the actual EUALCC history and the fitted trend for the oldest unit still in use, a

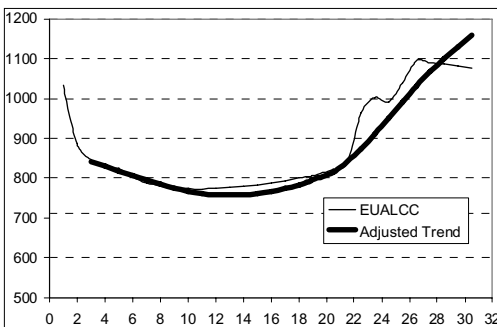


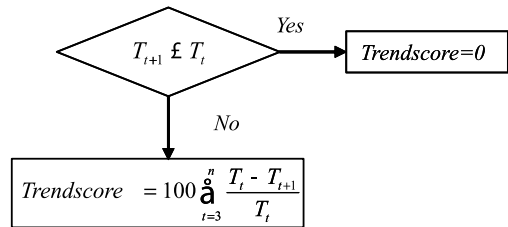
Figure 3. Adjusted EUALCC trend.

31-year old water tank. While testing Akaike's method, the authors found that the initial depreciation always caused a sharp downward slope in the first two years of the EUALCC curve. These years are not relevant for equipment replacement analysis, and the sharp negative slope often biased the trend estimate, especially for newer equipment units. They decided to start trend calculations in the third year of the equipment's life.

#### 5 THE EUALCC TRENDScore

Once the researchers were satisfied with the numerical method to isolate the EUALCC trend component, it was necessary to develop an algorithm to make a computer mimic a fleet manager looking at the graphs and making decisions based only on life-cycle costs. This person prioritizes the unit whose life-cycle cost has been increasing for the longest time and at the steepest rate. S/He eliminates from consideration all units that are still amortizing (negative trend) or in the optimal region (slope close to zero). Looking at figure 4, this manager would keep the unit that is still amortizing, replace the unit with the steep upward trend, and consider replace the one starting to leave the optimal region if there was a surplus. The trendscore, summarized in figure 3, captures this decision in a way that can be handled by computer logic.

As shown in figure 4, trendscore is a simple algorithm to successively "look" at each pair of consecutive time series points, eliminating the part of the curve that is not relevant for replacement decisions, and considering only the part with upward trend. The trendscore is greater than zero only for the part of the EUALCC history that has an upward trend. For these cases, the steeper the upward trend, the higher the trendscore; also, the longer the unit has presented an upward trend, the higher the trendscore. For example, the trendscores of the units shown in figure 2 are



Where:

T = EUALCC trend component

n = total number of years in service

t = time (in years of service).

Figure 4. The trendscore concept.

as follows: the unit with the upward slope has a trendscore of 11, followed by the one starting to leave the optimal region with a trendscore of 0.5. The unit that is still amortizing has a trendscore of zero. A computer sorting these trendscores in descending order would assign the correct replacement priorities to these units.

## 6 REPLACEMENT METHODOLOGY

The inclusion of life-cycle cost criteria was only one objective of this project. In order to be implementable, the new replacement methodology had to:

1. Make fleet-level replacement decisions based on a combination of factors that included, but were not restricted to, life-cycle costs.
2. Provide a gradual transition between the old threshold method and the new one.
3. Rely on available data, and therefore be immediately applicable to the entire fleet.
4. Use attributes that are easy to visualize, such as usage, downtime, and repair expenses.
5. Take advantage of the fleet managers' experience, allowing them to select the most relevant attributes for each specific equipment class,
6. Allow the manager to use the old threshold criteria if desired, combined with the new method.
7. Allow the fleet manager to assign units to the top of the replacement list due to obsolescence criteria defined by experience, such as expired warranties.

The objectives above were accomplished through the development of two additional concepts: multi-attribute priority ranking and automatic qualification.

### 6.1 Multi-attribute priority ranking

In order to address other factors relevant to equipment replacement and to add flexibility to the decision process, the authors developed and implemented a multi-attribute priority ranking method. This multi-attribute priority ranking process allows the manager to compare the challenged unit to all other active units within a desired class. The multi-attribute priority ranking is based on the conceptual approach developed by Weissmann, Burns and Hudson (1991) for TxDOT's Bridge Division. Weissmann's method for bridge rehabilitation and replacement ranking has been successfully used for over 10 years at TxDOT, giving the researchers confidence that a similar approach will also be useful for equipment management.

Numerically, the attributes are represented by their cumulative percentiles with respect to the rest of the fleet in that equipment class. The percentiles ("P") are calculated from the historical data set. Figure 5 shows an example of percentiles for the mileage attribute. This figure summarizes the cumulative mileages of

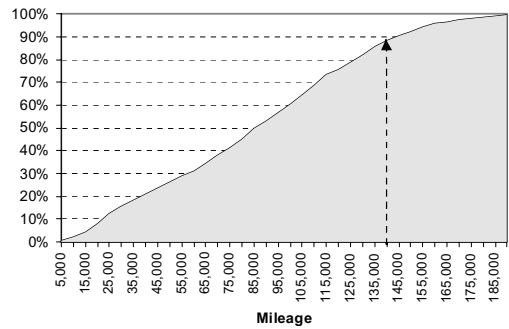


Figure 5. Example of attribute percentiles.

the single rear axle, six yd3 dump truck fleet. There are 1,308 dump trucks in this class. A dump truck with 140,000 miles of use is in the 89% percentile. This means that 89 percent of the dump trucks in this class have less mileage than this unit, and 11 percent have more.

The attributes selected for the multi-attribute decision-making process are the trendscore (life-cycle cost trends, as previously discussed), repair costs, cumulative usage, and cumulative downtime. Each unit's replacement priority rank is calculated for the combination of attributes and relative weights selected by the manager. A unit has replacement priority ("R") over other units based on the weighted average shown in equation 2.

$$R = \sum_{i=1}^n w_i P_i \quad (2)$$

Where:

R = Replacement priority (rank), a number between zero and 100.

i = Attribute (such as age, downtime, etc.)

n = Number of attributes

w = Weight of attribute "i", a number between zero and 1, assigned by the manager.

P = Cumulative percentile of attribute.

### 6.2 Automatic qualification

The system allows the user to input thresholds for automatic replacement qualification, if desired. When an automatic qualification threshold is selected for an attribute, the system uses a two-level ranking procedure. Units above that threshold go to the top of the list, ranked by the multi-attribute method. They are followed by units below the threshold, also ranked by the multi-attribute method. This is a very important practical feature. The old threshold method often led to budget overruns, flagging considerably more units



for replacement than the available budget. The manager can enforce TxDOT threshold policies while at the same time ranking units and using the priority list as a decision aid tool, and incorporating life-cycle cost concepts in the decision.

The manager can also take into account obsolescence issues such as warranties expiring at a certain usage level, or excessive repair costs. Finally, automatic qualification by threshold also helps the managers make a smooth transition between the old threshold method and the new fleet-level ranking method.

## 7 PRACTICAL EXAMPLE

An example clarifies the proposed method. Assume a manager wants to prepare a replacement priority list for a fleet of 1,308 six yd3 dump trucks with single rear axle. The manager knows from previous experience that mileage is a very important factor in replacement decisions, but wants to assign equal importance to life-cycle costs. The user also wanted to ignore the thresholds from the old method,

Figure 6 shows one of the screens for the developed computerized system. The manager enters weights of 0.5 for usage and 0.5 for trendscore, since s/he wanted to calculate the replacement priorities based on mileage and life-cycle costs, assigning equal importance to them, and ignoring the thresholds by leaving blank all the boxes labeled “automatic qualifier”.

The box labeled “generate replacement priority list” applies the methodology described above and displays the priority table. The leftmost column of list, partly covered by the graph, shows the priorities from first to last, followed by the unit unique identification tag, and values of the variables used in the calculations. The list scrolls vertically and horizontally, showing all 1,308 units and all cost variables.

Figure 6 shows two superimposed screens. The top box shows the values input by the user: the equipment class code, and the weights for the desired attributes. The superimposed graph screen shows the life-cycle cost and its trend, for the top priority according to the selected criteria, a truck with trendscore of 55 and 124,018 miles. This graph pops up when the user selects the desired unit and clicks on a button that is hidden behind the graph in figure 6.

According to the old threshold method, the top priority should be truck 05664C, with the highest usage (over 230,000 miles), but a low trendscore of 6. This truck would appear at the top of the replacement priority list if the user had entered 140,000 as the usage “automatic qualifier” in the appropriate box. However, the unit is barely starting an upward life-cycle cost trend. The proposed method correctly assigns this

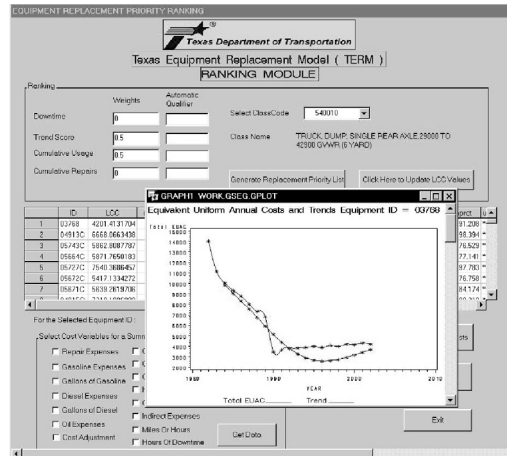


Figure 6. Computerized system results screen.

unit a lower priority, even when the manager wants mileage to weigh heavily on the replacement decision.

## 8 CONCLUSIONS

The old threshold method states that dump trucks in this class should be replaced when they reach either 140,000 miles or 10 years of age. Together, these criteria flag 701 dump trucks for replacement, or over half the fleet in this class. According to the historical database, the average cost of this class of dump truck is \$28,000. At this average cost, the replacement budget just for this equipment class should be almost 20 million dollars. Application of the threshold method to every equipment class in the database would require a replacement budget of about one billion dollars at the average costs stored in the historical data base. The threshold method does not solve the managers’ main problem: decide which units to keep and which ones to replace. While replacement thresholds can be useful, they are limited and can lead to decisions to replace an economically feasible unit and keep another that is not cost-effective.

The authors developed an automated, menu-driven system that prioritizes units for replacement according to a multi-attribute ranking method combined with an option for automatic replacement qualification based on thresholds. This method takes advantage of fleet managers’ experience with attributes such as mileage, downtimes, and repair expenses. Except for life-cycle cost calculations, it does not require assigning monetary values to factors before including them in the decision-making process. This is important especially

when or attributes known to be difficult to quantify, such as cost of downtime.

The multi-attribute method relies on the most recent available data, and allows the manager to input the relative importance of factors s/he considers important for replacement decisions. The user can easily compare two or more different replacement schedules based on different attribute priorities, and make informed decisions. The system generates data tables and graphs of every cost variable in the database. It calculates and, most importantly, automatically compares life-cycle cost histories and trends.

The life-cycle cost method theoretically combines all parameters that are relevant for replacement decisions into an annualized cost time-series that is quite straightforward to evaluate visually. The trendscore, developed to allow a computer to mimic replacement priorities assigned by a decision maker looking at life-cycle cost graphs, is a powerful tool to implement the information provided by annualized life-cycle cost graphs. However, it reflects all advantages and disadvantages of the life-cycle cost concept. The major disadvantage is the need to assign monetary values to all parameters. Vorster, C.M., and J.M. Garza (1992) found that downtime is especially difficult to quantify. The authors ran a sensitivity analysis and found that life-cycle costs are sensitive to downtime cost variations greater than \$20.00 an hour. Discount rates have less overall impact, and the slope of the life-cycle cost curve is not sensitive to discount rate variations within the range observed in the U.S. in the past 10 years. Life-cycle cost values also depend on the equipment residual (or resale) value, and this can be difficult to predict. All other costs are accurately recorded in a historical database.

Repair costs include both major equipment upgrade (which should make replacement a low priority) and major repair expenses (which should rise the priority). Unless the database discriminates between repair and upgrade expenses, a replacement list based on life-cycle costs may assign high replacement priorities to units that have been subject to upgrades. By the same token, a mileage threshold can assign high replacement priority to a reliable unit, often chosen over the others exactly because of its reliability.

In summary, the proposed method is especially useful for agencies with large fleets. The advantages over using only thresholds are numerous. The method allows thresholds (automatic qualification) while at the same time ranking units that met the threshold based on sound criteria and fleet-level decisions. It includes the most important attribute in equipment replacement, the unit's life-cycle costs. It considers the

manager experience with relevant replacement factors. Moreover, if the manager has reasons to believe that the cost data for a particular equipment class is not reliable, s/he can still rank units based on downtimes and usage, with no need to assign monetary values to these factors.

## REFERENCES

- Akaike, Hirotugu. Likelihood and the Bayes Procedure. *Bayesian Statistics: Proceedings of the First International Meeting Held in Valencia, Spain*, pp. 143–157, Valencia, Spain, University Press, 1980.
- Akaike, Hirotugu, and Ishiguro, Makio. *A New Time Series Analysis and Control Package*. American Statistical Association, Business and Economic Statistics Section, 1987 issue, pp. 33–42.
- Bibona, Salvatore. *Vehicle Replacement Strategies*. *Utility Fleet Manager*, October 1996, pp. 19–27.
- Brown, R.J. and Yanuck, R.R. *Introduction to Life Cycle Costing*. Prentice Hall, Englewood Cliffs, 1985.
- Dhilon, B.S. *Life Cycle Costing*. Gordon and Breach Science Publishers, New York, 1989.
- Grant, E.L., Ireson W.G. and Leavenworth. R.S. *Principles of Engineering Economy*. John Wiley and Sons, New York, 1990.
- SAS Institute, Inc. *SAS/IML Interactive Matrix Programming*. Cary, NC: SAS Institute Inc., 1999.
- SAS Institute, Inc. *SAS/ETS User Guide, Version 6*. Cary, NC: SAS Institute Inc., 1993.
- SAS Institute, Inc. *SAS/AF User Guide, Version 6*. Cary, NC: SAS Institute Inc., 1999.
- Vorster, C.M., and Garza. J.M. *Consequential Equipment Costs Associated with Lack of Availability and Downtime*. *ASCE, Journal of the Construction Engineering and Management*, Vol.116, No. 4, Dec. 1990.
- Weissmann, Angela J., and Weissmann. J. *Development of an Automated Fleet-Level Equipment Replacement Methodology*. Research Report 4941–2. The University of Texas at San Antonio, Department of Civil Engineering. July 2003.
- Weissmann, J., Weissmann, Angela J. and Gona, Srinivas. *Texas Equipment Replacement Model (TERM): Software Manual*. Research Report 4941–3. The University of Texas at San Antonio, Department of Civil Engineering. July 2003.
- Weissmann, J., Burns, N.H. and Hudson, W.R. *Operating the Texas Eligible Bridge Selection System (TEBSS)*, Research Report N° 1911–1F, Center for Transportation Research, The University of Texas at Austin, 1991.
- Weissmann, José, R. Harrison, and Euritt, M. *Conversion of the Texas Department of Transportation 6- and 10- yard Dump Truck Fleet from Standard to Automatic Transmissions*. Research Report 979–1F, Center for Transportation Research, Bureau of Engineering Research, The University of Texas at Austin, November, 1991.

# Life cycle analysis of waterfront structures (a qualitative process model)

John L. Wilson

*Department of Civil & Environmental Engineering, Lehigh University, Bethlehem, PA, USA*

Charles B. Kubic

*Civil Engineer Corps, U.S. Navy, Pearl Harbor, HI, USA*

**ABSTRACT:** This paper presents a life cycle evaluation strategy and its implementation to help ensure consistent, prudent life cycle decisions for naval waterfront structures. Planners and designers can use it to review both the impact that decisions have on life cycle cost and to determine alternatives that reduce life cycle cost of a waterfront facility. First, a relational database is used to identify the impact a specific scoping, planning or design decision has on costs across life cycle stages. Next, interrelationships among these decisions are used to identify inconsistent or incompatible choices. Then, summary reports are generated that contain specifics on life cycle costs that are affected by these decisions and potentially imprudent choices that might have been made. This tool provides communication of design alternatives and serves as a conceptual design framework for all parties involved in the life cycle process.

## 1 INTRODUCTION

The Real Property & Installation Lifecycle Management (RP&ILM) Support for the Department of Defense is, in part, designed to manage and access common data pertaining physical plants (buildings, utilities, real estate, and natural and cultural resources), Tinsley (2007). The research results presented in this paper are a natural extension to this effort. Waterfront structure operation standards were analyzed by the authors to identify and understand better the relationships among the critical life cycle decisions and their affected costs.

The authors have been involved in the study of life cycle engineering for several years. Their main objective in this field is to develop methods for the evaluation of life cycle cost and performance of large structural systems (Wilson et al, 1989), Shi & Wilson (1989). Research performed by the Construction Industry Institute (CII) Task Force on Life Cycle for Projects has shown that life cycle principles are relatively well established but decision makers often tend to make inconsistent life cycle choices because they do not share a common method and sound strategy that enables them to coordinate their decisions.

The method presented here considers all stages of a facility's life as an integrated process. The logical framework or backbone of the life cycle model is a driver-cost matrix that serves as a tool to help users

conceptualize the relationship between drivers of cost and the cost elements as they plan and execute projects. The decisions that affect the cost elements are called drivers. The cost elements, when totaled, give the entire cost of a facility over its planning horizon. The drivers and cost elements are organized in a sample driver-cost matrix as shown in Table 1, Driver-Cost Matrix. *The rows* are the design decisions (drivers) that are grouped into three phases: scoping, planning and design. Each driver will have a set of associated choices for that driver (explained in Section 3.1). *The columns* are the cost elements organized from: planning/design, construction, maintenance, operations, through to remediation and demolition. *Cells* contain the qualitative impact (high to negligible) a driver has on a cost element.

## 2 OVERVIEW

The life cycle system presented herein consists of three components as shown in Figure 1, System Components. First, the Input consists of driver choices made by a user. Second, the Toolbox contains three tools: a) the driver-cost matrix that contains the relative impact of a specific "design" decision (driver) on any given cost element; b) interrelationship matrices that represent relationships between related drivers and their choices; and c) the waterfront knowledge advisor that

Table 1. Driver-cost matrix framework.

Cost elements		Planning/ design	Construction	Maintenance	Operation	Remediation demolition
Phase	Driver					
Scoping phase	Types of ships					
	Facility capacity					
	Facility function					
	Date required					
	Site selection					
Planning phase	Facility flexibility					
	Facility layout					
	Security requirements					
	Facility design life					
	Utility supply/collection					
	Reliability requirements					
	Infrastructure req.					
Design phase	Environmental req.					
	Load carrying capacity					
	Construction materials					
	Manpower maint. req. Construction methods					

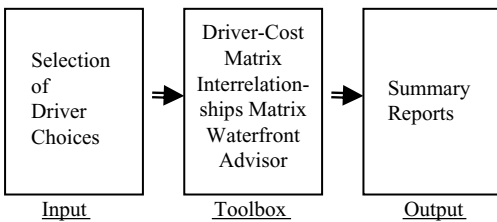


Figure 1. System components.

uses to analyze the cost and performance implications of the driver choices. Third, summary reports provide a user with information needed to make prudent life cycle decisions that are consistent with a sound life cycle plan.

### 3 SYSTEM COMPONENTS

#### 3.1 Driver-cost matrix

The driver-cost matrix framework as shown previously in Table 1 organizes information to help provide answers to the following types of questions. First, what decisions (drivers) have the most impact on life cycle cost? Second, what are the typical costs over the life of a structure? Third, what is the relative impact a specific decision has on a given cost element?

Table 2 on the next page shows the results of synthesized data for a subset of the driver-cost matrix for the highest cost elements for waterfront structures-Structural Maintenance, Utility Operation and Dredging. An H in the cells indicates where a driver has a

Table 2. Selected driver-cost impacts.

Cost elements	Str. maint.	Util. oper	Dredging
<b>Driver</b>			
Types of ships	H	H	H
Facility capacity			
Facility function		H	
Date required			
Site selection			H
Facility flexibility			
Facility layout			
Security requirements			
Facility design life	H		
Utility supply/collect		H	
Reliability req.			
Infrastructure req.			
Environmental req.		H	H
Load carrying capacity			
Construction materials	H	H	
Manpower maint. req.	H	H	
Construction methods	H		

significant affect on the corresponding cost element. For example, the driver Types of Ships has a significant affect on the cost element Structural Maintenance.

It is worthwhile to note that both the cost of failure and the cost of energy consumption for a facility are becoming increasingly important and, as more data become available, can be included in the driver-cost matrix.

Each driver has a set of associated choices. Table 3 shows the drivers and their associated driver choices for the scoping phase. (For brevity of presentation,

the planning and design phase drivers are omitted). Military handbooks related to the design of waterfront structures and interviews with naval personnel were used to select the driver choices and to determine their effects on each other and on the cost elements NAVFACENGCOM (1988). The full set of drivers and their choices is presented in Kubic (1999).

### 3.2 Driver interrelationships

Drivers which have an effect on each other, as well as on cost elements are interrelated. These relationships are known as driver interrelationships and were determined through interviews with a diverse cross section of naval personnel. Waterfront structures have several interrelated drivers that are analyzed to understand better the implications decisions have on cost(s) and performance. These interrelationships are used to help ensure prudent, consistent life cycle choices.

### 3.3 Interrelationship matrices

Interrelationship matrices are used to check consistency of driver choices across the three phases of scoping, planning, and design. Table 4, Interrelationship Matrices, gives an example for the drivers "Type of Ship" and "Load Capacity". For example, the upper left cell in the table shows the two drivers that are being evaluated. The leftmost column and top row show the choices associated with the two drivers. A positive sign (+) in a cell of the matrix indicates there is not a conflict between the choices. For example, this table

Table 3. Drivers and driver choices for the scoping phase.

Driver	Driver choices
Types of ships	Submarines, Surface combatants, Aircraft carriers, Small craft, Ammunition/supply, Tankers/others
Facility capacity	Heavy, Medium, Light
Facility function	General berthing, Repair, Supply, Ammunition, Fueling, Small craft
Date required	Early, Regular
Site selection	Geophysical issues, No geophysical issues
Facility flexibility	High, Low

Table 4. Interrelationship matrix: type of ship and load capacity driver choices.

Type of ship/ Load capacity	Submarine	Surface combatants	Aircraft carriers	Small craft	Ammunition/ supply	Tankers others
High	+	+	+	-	+	+
Medium	+	+	+	+	+	+
Low	+	+	-	+	-	-

shows that it would be acceptable (not inconsistent) to have a facility for an aircraft carrier to have a high load capacity. A negative sign (-) represents a combination that might present a problem and could have a significant detrimental effect on life cycle cost of a structure. The complete assemblage of matrices is presented in Kubic (1999).

### 3.4 Waterfront advisor

The Waterfront Advisor is a knowledge inference system that is used to review the impact that scoping, planning design decisions have on life cycle costs, and to assist the decision maker in finding alternatives to lower the life cycle cost of a waterfront facility. In the current work, it uses the knowledge and judgment of seasoned professionals to assist the decision maker to produce a more effective life cycle solution that will specifically lower operation and maintenance costs of a waterfront facility. The costs of maintenance, operations (and dredging) were determined by Kubic (1999) to be the most significant costs for waterfront facilities.

Specifically the Waterfront Advisor was implemented to do the following:

- Convey an understanding of scoping, planning and design decisions to a user.
- Communicate a project strategy and plan to individuals at each stage of the overall process.
- Help a user make prudent, consistent life cycle decisions.

During the scoping phase, it can provide an early alert to decision-makers to see the implication of their decisions on future decisions. During the planning phase, it can provide advice on the downstream effects of planning decisions and how these decisions affect the scope of the project. During the design phase, it can provide advice on how design alternatives can lower the life cycle costs of a facility.

The Waterfront Advisor is programmed in Visual Basic and is highly interactive allowing a user to interrogate terminology, knowledge and reasoning behind the advice provided by the system. (For brevity, actual screen captures during a session are omitted here).

The operation of the software is briefly described next. For each of the three phases, the decision-maker selects drivers and driver choices. After the

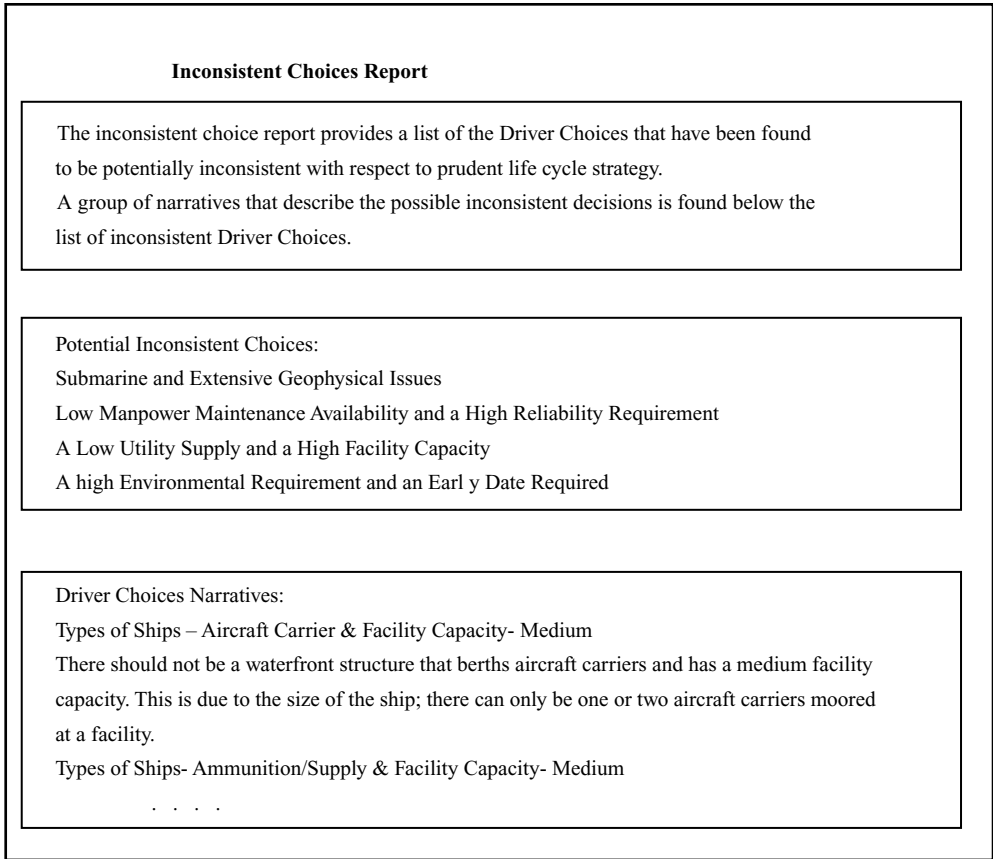


Figure 2. Inconsistent choices report.

driver choices are input, the user may further explore the alternatives for each driver choice or proceed to summary reports that present information on cost elements that have been increased or decreased, along with potential inconsistent choices. The user may then change any selections at his/her discretion and produce additional summaries.

Figure 2 shows a sample summary report where inconsistent choices have been made.

Summary reports showing how the cost elements are affected by the driver choices are automatically generated for examination by the user; but, for brevity, they are not included here.

#### 4 SUMMARY AND CONCLUSIONS

Life cycle decisions are often inconsistent because of poor communication among participants at different stages of the life cycle process and lack of utilization

of knowledge gathered from experience. The life cycle method presented herein was designed to assist decision makers in making consistent decisions to lower life cycle cost. Input is analyzed using three different tools: a driver-cost matrix; interrelationship matrices; and a knowledge inference system.

The driver-cost matrix provides a logical framework for the affect drivers have on life cycle cost elements. The interrelation matrices evaluate related driver choices in order to determine potentially inconsistent decisions. The knowledge inference system analyzes the driver choices affect on life cycle cost. The software produces summary reports that focus on the operation and maintenance costs and potential inconsistent choices that are affected by the user's input for waterfront structures.

This qualitative model can help create more effective waterfront facilities by improving communication and providing tools to encourage planners to explore the ramifications of their decisions for a facility

during its entire planning horizon. Current efforts are directed toward expanding the data for additional cost elements such as the cost of failure and the cost of energy consumption and providing a quantitative cost and performance model.

## REFERENCES

- Kubic, C.B. 1999, The Life Cycle Analysis of U.S. Naval Waterfront Structures, MS Thesis, Department of Civil Engineering, Lehigh University, Bethlehem, PA, May 1999, 1–34.
- NAVFACENGCOCOM, 1988, Military Handbook, General Criteria for Waterfront Construction, MIL-HDBK-1025/6, US Navy, May 15, 1988.
- Shi, C. & Wilson, J.L. 2000, Group Decision Support for Product Design- A Computational Design World, *Group Technology/Cellular Manufacturing World Symposium-2000*, University of Puerto Rico, San Juan, PR, March 27–29, 2000, 211–214.
- Tinsley, H. 2007, Enterprise Governance for Installation Geospatial Information and Services, *The Defense Installation Spatial Data Infrastructure Group*, May 22, 2007, 1–9.
- Wilson, J.L., Wagaman, S.J., Veshosky, D.A., Shi, C.G., Audry, P. & Beidleman, C.R. 1997. Life-cycle Engineering of Bridges, *Journal of Microcomputers in Civil Engineering, Special Issue*, pp. 445–452.

# An integrated life cycle assessment and life cycle analysis model for pavement overlay systems

H. Zhang, G.A. Keoleian & M.D. Lepech  
*University of Michigan*

**ABSTRACT:** Pavement systems have significant impacts on the environment and economy due to large material consumption, energy input, and capital investment. To evaluate the sustainability of rigid pavement overlay designs, an integrated life cycle assessment and life cycle cost analysis model was developed to calculate the environmental impacts and costs of overlay systems resulting from material production and distribution, overlay construction and maintenance, construction-related traffic congestion, overlay usage, and end of life management. An unbonded concrete overlay system, a hot mix asphalt overlay system, and an alternative engineered cementitious composite (ECC) overlay system are examined. Model results indicate that the ECC overlay system reduces total life cycle energy by 15% and 72%, greenhouse gas (GHG) emissions by 32% and 37%, and costs by 40% and 58% compared to the concrete overlay system and the HMA overlay system, respectively, over the entire 40 year life cycle. These advantages are derived from the enhanced material properties of ECC which prevent reflective cracking failures (discussed in a complementary paper). Material consumption, traffic congestion caused by construction activities, and roughness effects caused by overlay deterioration are identified as three dominant factors that influence the environmental impacts and costs of overlay systems.

## 1 INTRODUCTION

Pavement systems are fundamental components of our automobile transportation systems. While the transportation of people and goods is increasing rapidly, pavement systems have serious impacts on the environment and the economy. Yet, the American Society of Civil Engineers (ASCE) report card assigns US roads a grade of D (poor condition). This poor road condition costs US motorists an estimated \$54 billion annually in vehicle repair and operating costs (ASCE 2006). Sustainability is increasingly adopted as a framework for designing and constructing pavement systems. Life cycle assessment (LCA) and life cycle cost analysis (LCCA) methodologies provide the means for evaluating the sustainability of pavement systems.

An integrated LCA and LCCA model (LCA-LCCA) was developed to provide sustainability indicators for pavement systems, in this case a pavement overlay system. As pavements age and deteriorate, maintenance and rehabilitation are required to provide a high level of safety and service (Huang 2004). For pavements subjected to heavy traffic, one of the most prevalent rehabilitation strategies is placement of an overlay on top of the existing pavement (DOT 1989). An overlay provides protection to the pavement structure, reduces the rate of pavement deterioration,

corrects surface deficiencies, and adds some strength to the existing pavement structure. Depending on local conditions (i.e. traffic volume, truck loads, etc) and existing pavement, two possible designs are generally used: an unbonded concrete overlay or a hot mixed asphalt (HMA) overlay. The use of either concrete or asphalt poses significant environmental challenges. Additionally, concrete and asphalt have some physical limitations that contribute to durability concerns, which increase the likelihood of pavement overlay failure and maintenance frequency. Consequently, alternative materials are being developed to improve overlay performance. Part of the process to introduce new materials into application includes evaluation of the environmental impacts at each stage of the material life cycle from resource extraction through manufacturing, transportation, construction and final disposal.

LCA is an analytical technique for assessing potential environmental burdens and impacts. LCA provides metrics that can be used to measure progress toward environmental sustainability (Keoleian and Spitzley 2006). LCA studies the environmental aspects and potential impacts throughout a product's life from raw material acquisition through production, use and disposal (ISO 1997). An LCA model of a pavement overlay system was developed prior to this study's integration of an LCA and LCCA model. The LCA development is described in Zhang et al (2007).



LCCA model evaluates the monetary values of processes and flows associated with a product or system (Keoleian and Spitzley 2006). Like LCA models, LCCA models vary in scope and depth, accounting for different kinds of costs. For example, LCCA models may account only for internal costs (agency costs), such as construction costs and maintenance costs; it may also account for social costs, such as user costs which are incurred by motorists who are delayed or detoured by construction related traffic, or environmental costs including environmental damage costs associated with construction events.

The life cycle model in this study was applied to compare the environmental impacts for an overlay built using concrete, HMA, and a new material—Engineered Cementitious Composites (ECC), a high performance fiber-reinforced cementitious composite (HPFRCC).

ECC is a unique fiber-reinforced composite developed using a microstructural design technique driven by micromechanical principles. ECC is deliberately designed as a fiber reinforced cementitious material with a deformation behavior analogous to that of metals (Li 2003). Experimental testing of ECC overlays reveals significant improvements in load carrying capacity and system ductility over concrete or steel fiber reinforced concrete overlays (Qian 2007). Thereby, ECC can eliminate common overlay system failures such as reflective cracking (Li 2003). ECC is a promising candidate material for road repairs, pavement overlays, and bridge deck rehabilitation (Li 2003).

The objective of this research is to create a model that can analytically measure the sustainability indicators of pavement overlay systems. In addition, pavement construction and maintenance, roadway deterioration, and the impacts of traffic are dynamically captured. This integrated model is unique in its ability to capture pavement overlay life cycle energy consumption, environmental impacts, and costs including the upstream burdens of materials and fuel production. In the following section, the system boundary is defined and the integrated LCA-LCCA models are described. Subsequently, the life cycle model is applied to compare the environmental impacts and the costs of three pavement overlay systems. Finally, sensitivity analysis is performed for different traffic growth rates and fuel economy improvement scenarios.

## 2 METHODOLOGY

### 2.1 System definition

The overlay designs analyzed in this study are constructed upon an existing reinforced concrete pavement. The annual average daily traffic (AADT)

is approximately 70,000 vehicles with 8% heavy duty trucks (MDOT 1997). In the baseline scenario, the annual traffic growth rate is 0%. The three overlay systems are modeled as 10 km long freeway sections in two directions. Each direction has two 3.6 m wide lanes, a 1.2 m wide inside shoulder, and a 2.7 m wide outside shoulder. The thickness of the overlay depends on the material (concrete, HMA, or ECC) and construction methods. The concrete overlay is 175 mm thick and unbonded from the existing pavement by a 25 mm asphalt separating layer. The ECC overlay is 100 mm thick and constructed directly on the existing pavement. The HMA overlay is 190 mm thick. These pavement overlay designs are based on the results from experimental studies conducted at the University of Michigan and typical pavement overlay designs (Qian 2007 and Huang 2004). In the LCA model, the concrete and HMA overlays are designed for a 20 year service life by the Michigan Department of Transportation (MDOT 2005). The service life of ECC overlay is expected to be twice that of the concrete overlay by preventing commonly observed overlay failure modes, such as reflective cracking (Li 2003).

### 2.2 Integrated LCA-LCCA model

Figure 1 shows the integrated LCA-LCCA model framework. The LCA model is divided into six modules: material production, consisting of the acquisition and processing of raw materials; construction, including all construction processes, maintenance activities, and related construction machine usage; distribution, accounting for transport of materials and equipment to and from the construction site; traffic congestion, which models all construction and maintenance related traffic congestion; usage, including overlay roughness effects on vehicular travel and fuel consumption during normal traffic flow; and end of life, which models demolition of the overlay and processing of the materials. Details of each module are described in Zhang et al (2007). Input and output data from each module are evaluated to capture the material consumption, energy

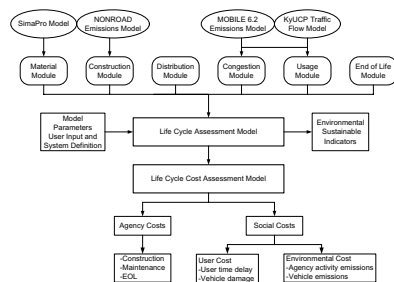


Figure 1. Integrated LCA-LCCA model framework.

consumption, and environmental impacts of the overlay system throughout its service life. Several datasets are required to provide the life cycle information for input materials or processes. For example, the dataset for ECC production provides the raw material consumption, total primary energy consumption, pollutant emissions, and wastes associated with producing a unit volume of ECC. Raw material consumption quantifies the non-fuel material inputs, such as the mass of cement required. Total primary energy consumption includes the energy required for extraction, refining, transportation, and processing the material. The air and water pollutant emissions and solid wastes are also modeled for each life cycle stage. These datasets and sources can be found in Keoleian et al and Zhang et al (Keoleian et al 2005; Zhang et al 2007).

The LCA model is linked to four external models: (1) a material environmental impact model, SimaPro 7.0 developed by PRe Consultants (Pre 2007); (2) a vehicle emissions model, MOBILE 6.2 developed by U.S. Environmental Protection Agency (EPA) (US EPA, 2002), and four localized MOBILE 6.2 data inputs for the winter and summer seasons which include annual temperature range, Reid vapor pressure, age distribution of the vehicle fleet, and average vehicle miles traveled data (SEMCOG 2006); (3) a construction equipment model, NONROAD, also developed by the EPA (US EPA, 2005); (4) and a traffic flow model developed at the University of Kentucky (KTC 2002).

The LCCA model incorporates the results of life cycle assessment modeling to calculate agency and social costs. The framework of the LCCA model was first developed by Kendall et al (2006).

Agency costs include all costs incurred directly by the Michigan Department of Transportation over the lifetime of the overlay system. These are typically construction and maintenance costs including material costs, equipment rental and operating costs, and labor costs. The actual agency costs were obtained directly from MDOT construction contracts.

Social costs are often not directly considered in the evaluation of DOT construction and maintenance activities. Generally, social costs include user costs and environmental costs. User costs are more likely to be considered in more densely populated states or urban areas, while environmental costs are not considered by any transportation agency in the US (Chan 2006). Even so, the literature is limited in examining how social costs are actually applied by state DOTs.

As mentioned in description of the LCA model, overlay construction and maintenance activities, and overlay deterioration will affect traffic flow. These traffic impacts result in user costs, since they are incurred by highway users traveling on the system. User costs are the differential costs incurred while driving between normal operations and work zone

operations or poor pavement conditions. User costs are an aggregation of user delay costs, vehicle operating costs (including fuel costs), and risk of traffic accidents (Wilde et al 2001).

User delay costs normally dominate user costs. The total cost of travelers sitting in traffic is determined by multiplying the value of driver time with the additional number of hours spent in work zone congestion or on detours as compared to the number of hours spent traveling the equivalent distance in normal traffic flow conditions. The value of time (delay costs rate) for passenger vehicles, single unit trucks, and combination trucks is \$11.58/veh-hr (vehicle hour), \$18.54/veh-hr, and \$22.31/veh-hr respectively, estimated by the Federal Highway Administration (Wall and Smith 1998). Costs are in 1996 dollars and updated to 2006 dollars in the LCCA model using the Consumer Price Index.

Vehicle operating costs account for higher fuel consumption and thus higher fuel costs when driving through a work zone or on a deteriorated overlay as compared to normal conditions. If drivers choose to detour to avoid congestion, they will travel a greater distance which also increases fuel consumption. Due to surface deterioration, the overlay surface roughness increases continuously over time. Roughness is often measured using the International Roughness Index (IRI), which was developed by the World Bank in 1986 (Sayers and Gillespie 1986). Increased road roughness is estimated to reduce onroad fuel economy. The effect of roughness on fuel consumption is shown in Equation 1 (WesTrack 1999), where FCF is the fuel consumption factor (greater than 1.0).

$$FCF = 0.0667IRI + 0.8667 \quad (1)$$

User costs are also based on increased risk of traffic accidents. Both traveling through construction work zones and traveling additional distances when detours are chosen contribute to increased costs of traffic accidents. In the state of Michigan, an additional \$0.13/VMT traveled in the construction zone and a \$0.09/VMT traveled in a detour are used to estimate the increased risk costs (MDOT 2003).

User costs should be considered when deciding the proper long term design of an overlay system, since user costs associated with overlay construction and maintenance usually exceed agency costs significantly (Zhang et al 2007 and Wilde et al 2001). Minimizing the interruption of traffic flow during construction and maintenance activities over the total life cycle of an overlay is important for highway designers.

Environmental costs include the pollution damage costs over the entire life cycle of an overlay system. These costs are related to both direct and indirect impacts to human health from air pollution; the inhaling of air pollutants detrimental to human health, and

Table 1. Air pollution damage costs by impacted region (Kendall et al 2006).

Pollutants	Average cost (2006 US \$/t)			
	Urban	Urban fringe	Rural	Global
SO <sub>x</sub>	\$6,732	\$3,013	\$877	
NO <sub>x</sub>	\$171	\$71	\$21	
CO	\$186	\$96	\$23	
PM <sub>2.5</sub>	\$2	\$1	\$0	
Pb	\$4,333	\$2,256	\$526	
VOC	\$2,147	\$2,147	\$2,147	
CO <sub>2</sub>				\$23
CH <sub>4</sub>				\$7,792
N <sub>2</sub> O				\$421

greenhouse gases that result in global warming. Six criteria pollutants specified by the US EPA which have direct impact to human health are considered, including sulfur dioxides (SO<sub>x</sub>), nitrogen oxides (NO<sub>x</sub>), carbon monoxide (CO), particular matter (PM<sub>2.5</sub>), lead (Pb), and volatile organic compounds (VOC). Three major greenhouse gases that are inventoried include carbon dioxide (CO<sub>2</sub>), methane (CH<sub>4</sub>), and nitrous oxide (N<sub>2</sub>O). The marginal costs of those pollutants are shown in Table 1 (Kendall et al 2006). Since the criteria pollutants are sensitive to geographic region, values for urban, urban fringe and rural areas are calculated separately. GHG emissions have global consequences, therefore global costs are used.

The discount rate is a central element to economic analysis which can significantly influence LCCA results. Historical trends over last several years indicate that the real time value of money ranges approximately between 3% to 5% (Wilde et al 2001). In the LCCA model, a real discount rate is used. Real discount rates reflect the true time value of money with no inflation premium. The real discount rate of 4% for agency and user costs was estimated based on values recommended by the U.S. Office of Management and Budget (OMB) (Office of Management and Budget 2005).

Environmental costs are not discounted traditionally, due to the significant uncertainty in environmental impacts and their associated costs. A series of sliding-scale discount rates was developed by Weitzman using a gamma discounting approach. The discount rate was divided into following scale: for the immediate future (years 1–5), a 4% discount rate is used; for the near future (years 6–25), a 3% discount rate is used; for the medium future (years 26–75), a 2% discount rate is used (Weitzman 2001).

### 2.3 Pavement overlay deterioration model

Pavement overlay deterioration modeling is important to connect pavement maintenance strategies to

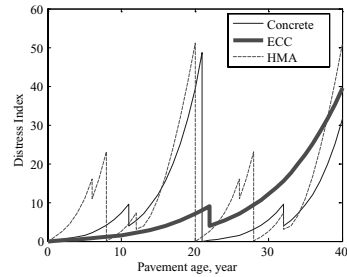


Figure 2. Distress index of each pavement.

impacts on users. In Michigan, a Distress Index (DI), which represents a holistic measure of pavement condition (including surface roughness and deterioration), is used rather than IRI to gauge pavement conditions (MDOT 2005). However, DI and IRI are correlated. No mechanics based theoretical model for DI exists as it depends on many factors such as temperature, traffic flow and load, types of pavements, and age of pavement. Currently, MDOT uses a threshold of DI of 50 to indicate the need for overlay reconstruction.

The construction and maintenance strategies for the concrete and HMA overlay systems are based on historical maintenance and pavement management records (MDOT 2005). The life cycles for each of the three systems begin with overlay construction. The concrete overlay is reconstructed in its 21st year, with major maintenance events at year 11 and year 31. The HMA overlay is reconstructed in its 20th year, with major maintenance events in year 8 and year 28, and minor maintenance events in year 6, 12, 26, and 32. The ECC overlay lasts for a 40 year service life with a single maintenance event and no reconstruction. Based on these construction and maintenance strategies, Figure 2 shows the DI increasing trends over time.

## 3 RESULTS

### 3.1 Life cycle assessment result

Total life cycle results represent the environmental impacts from the material module, construction module, distribution module, traffic congestion module, usage module (roughness effect on vehicle fuel economy) and end of life (EOL) module over a 40 year timeline. The environmental indicators in this study include energy consumption and greenhouse gas emissions.

The primary energy consumptions for 10 kilometers of the concrete, ECC and HMA overlays are  $6.8 \times 10^5$  GJ,  $5.8 \times 10^5$  GJ and  $2.1 \times 10^6$  GJ, respectively. As shown in Figure 3, the life cycle energy consumption for the three overlay systems is dominated by material

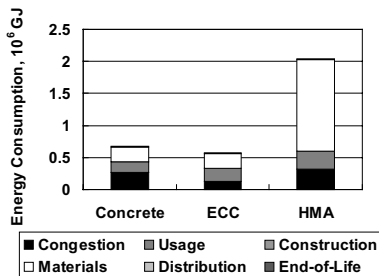


Figure 3. Primary energy consumption by life cycle phase.

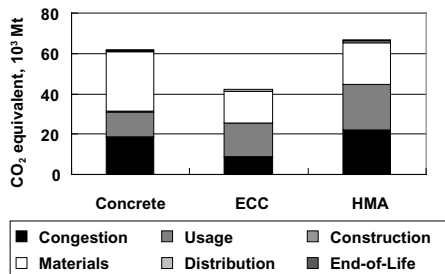


Figure 4. Greenhouse gas emissions by life cycle phase.

production energy, traffic congestion related energy, and roughness related energy. Roughness related fuel consumption has not been previously studied using LCA methods. Without considering surface roughness effects, the life cycle energy consumptions of three overlay systems decreases by 23%, 36%, and 14%, respectively.

Due to the superior material properties of ECC, which can double overlay service life compared to the other materials, the ECC overlay uses about 15% and 72% less energy than the concrete overlay and the HMA overlay, respectively. The high energy consumption for an HMA overlay is caused by the high feedstock energy contained in asphalt which accounts for 30% of the total life cycle primary energy consumption for HMA system.

Greenhouse gas (GHG) emissions inventoried in this study include CO<sub>2</sub>, methane, and nitrous oxide. The global warming impact is characterized by GHG emissions in metric tons of CO<sub>2</sub> equivalent. This is calculated by multiplying the mass of each GHG emission by its global warming potential (GWP), where GWP for CO<sub>2</sub> is 1, for methane is 23, and for nitrous oxide is 296. Figure 4 shows the global warming impact of each overlay system.

CO<sub>2</sub> emissions significantly dominate the contribution to global warming impact. In the concrete overlay system CO<sub>2</sub> represents 99.2% of total life cycle GWP,

Table 2. Life cycle costs for overlay systems.

	Concrete	ECC	HMA
Agency cost	\$10.1 m	\$6.2 m	\$14.8 m
User cost	\$61.9 m	\$37.4 m	\$84.2 m
Environmental cost	\$0.9 m	\$0.7 m	\$1.1 m
Total cost	\$72.9 m	\$44.3 m	\$100 m

in the ECC system CO<sub>2</sub> represents 99.4% of total life cycle GWP, and in the HMA system CO<sub>2</sub> represents 94.4% of total life cycle GWP. The ECC system reduces GHG emissions by 32% and 37% compared to the concrete overlay system and HMA overlay system, respectively. Generally, CO<sub>2</sub> emissions correlate with energy consumption; however, cement production releases CO<sub>2</sub> during calcination of limestone, which results in twice the CO<sub>2</sub> that would be produced from energy consumption alone (Keoleian et al 2005). Additionally, a large amount of primary energy consumption in the HMA overlay system is the feedstock energy. Carbon embodied in the material is fixed and does not generate CO<sub>2</sub> unless it is burned. This relationship is evident in the comparison of Figure 3 and Figure 4 wherein the CO<sub>2</sub> emission of the HMA overlay system is not significantly higher than the other two systems.

### 3.2 Life cycle cost analysis result

Table 2 shows the results for life cycle costs. The ECC overlay system demonstrates a cost advantage over the other two overlay systems in all cost categories assessed.

Despite higher initial construction costs for the ECC overlay system, the lower maintenance frequency due to improved ECC material properties results in an accumulated agency cost savings for ECC compared to the concrete and HMA overlay systems.

User costs account for more than 80% of total life cycle costs in each overlay system. Environmental costs are small compared to agency and user costs. Essentially, the cost distribution is driven by traffic parameters. Since this research deals with a high traffic volume freeway, congestion-related user time delays are significant. Thus, user costs overwhelmingly dominate total life cycle costs. If assumed traffic volume is lower, the likely impact of user costs in total life cycle costs will decrease and the impact of agency costs and environmental costs will rise.

## 4 CONCLUSION

The results of this study show that an ECC overlay system had lower environmental burdens and life cycle costs over a 40 year service life compared to concrete

and HMA overlay systems. By extending the service life and minimizing maintenance frequency, the ECC overlay system reduces total life cycle energy by 14%, GHG emissions by 32%, and costs by 40%, compared to the concrete overlay system. Material, traffic, and roughness effects were identified as the greatest contributors to environmental impacts throughout the overlay system life cycle. User costs significantly dominate total life cycle costs. Both the service life and maintenance schedule are key factors which determine the overlay system performance. Alternative overlay design strategies, such as varying overlay thickness and different maintenance schedules, can be implemented based on local traffic conditions and pavement requirements. Using this approach, the decision maker is able to design a more optimal overlay system among a number of alternative materials.

The integrated LCA-LCCA model outlined in this paper dynamically captures cumulative traffic flows, overlay deterioration over time, and maintenance activities to evaluate life cycle environmental burdens and costs. The incorporation of pavement overlay roughness effects on fuel consumption and related life cycle environmental burdens represents a significant extension of existing models. The resulting life cycle model enables decision makers to evaluate pavement infrastructure projects from a more holistic, long term perspective while providing criteria for more sustainable infrastructure material selection.

## ACKNOWLEDGEMENTS

The authors would like to graciously thank the US National Science Foundation MUSESE Grant (CMS-0223971 and CMS-0329416) for funding this research.

## REFERENCES

- American Society of Civil Engineering (ASCE). 2006. *Road to Infrastructure Renewal—A Voter's Guide*. Reston: ASCE.
- Chan, A., Keoleian, G., and Gabler, E. 2006. Evaluation of life-cycle cost analysis practices used by the Michigan Department of Transportation. *Journal of Transportation Engineering*. Submitted.
- Huang, Y.H. 2004. *Pavement analysis and design*. Upper saddle River: University of Kentucky.
- Kendall, A. 2004. *A Dynamic Life Cycle Assessment Tool for Comparing Bridge Deck Designs*. Ann Arbor: University of Michigan.
- Keoleian, G.A., and Kendall, A. 2005. Life cycle modeling of concrete bridge design: Comparison of engineered cementitious composite link slabs and conventional steel expansion joints. *Journal of infrastructure systems* 11(1): 51–60.
- Keoleian, G.A., and Spitzley, D.V. 2006. *Sustainability science and engineering*. The Netherlands: Elsevier.
- Kentucky Transportation Center (KTC). 2002. *The Costs of Construction Delays and Traffic Control for Life-cycle Cost Analysis of Pavements*. Lexington: University of Kentucky.
- Li, V.C. 2003. Durable overlay systems with engineered cementitious composites (ECC). *International Journal for Restoration of Buildings and Monuments* 9(2): 1–20.
- Michigan Department of Transportation (MDOT). 1997. *1997 Noninterstate Freeway Segments: Deficient Segments-URBAN*. MDOT: Ann Arbor.
- Michigan Department of Transportation (MDOT). 2003. *Standard Specifications for Construction*. MDOT: Ann Arbor.
- Michigan Department of Transportation (MDOT). 2005. *Pavement Design and Selection Manual*. MDOT: Ann Arbor.
- Office of Management and Budget. 2005. *Discount Rates for Cost-Effectiveness, Lease, Purchase and Related Analyses. Appendix C to Guidelines and Discount Rates for Benefit-Cost Analysis of Federal Programs*. Office of Management and Budget: Washington D.C.
- Portland Cement Association (PCA). 2002. *Environmental Life Cycle Inventory of Portland Cement Concrete*. PCA: Skokie.
- Product Ecology Consultant (Pre). 2004. *SimaPro 6.0*. Pre: Netherlands.
- Qian, S. 2007. *Influence of Concrete Material Ductility on the Behavior of High Stress Concentration Zones*. University of Michigan: Ann Arbor.
- Sayers, M.W., Gillespie, T.D., and Queiroz, C.A.V. 1986. *International Experiment to Establish Correlations and Standard Calibration Methods for Road Roughness Measurements*. World Bank: Washington, D.C.
- Southeast Michigan Council of Governments (SEMCOG). 2006. *Ozone and Carbon Monoxide Conformity Analysis for the Proposed Amendment of the 2030 Regional Transportation Plan for Southeast Michigan*. SEMCOG: Detroit.
- The Athena Sustainable Material Institute. 1999. *Life Cycle Embodied Energy and Global Warming Emissions for Concrete and Asphalt Roadways*. The Athena Sustainable Material Institute: Merrickville.
- The International Organization for Standardization (ISO). 1997. *Environmental Management: Life Cycle Assessment: Principles and Framework*. ISO: Geneva.
- United States Department of Transportation (DOT). 1989. *Rehabilitation of Concrete Pavements, Volume II*. DOT: Washington, D.C.
- United States Environmental Protection Agency (EPA). 2002. *MOBILE 6.2*. EPA: Ann Arbor.
- United States Environmental Protection Agency (EPA). 2005. *NONROAD2005 Model*. EPA: Ann Arbor.
- Weitzman, M.L. 2001. Gamma discounting. *American Economic Review* 91(1): 260–271.
- WesTrack. 1999. *The Road to Performance-related Specifications*. WesTrack Interim Reports: Carson City.
- Zhang, H., Lepech, M.D., and Keoleian, G.A. et al. 2007. "Dynamic Life Cycle Modeling of Pavement Overlay System: Capturing the Impacts of Users, Construction, and Roadway Deterioration." *Journal of Transportation Engineering*. Submitted.

*Life-cycle oriented computational tools*

# Advanced fragility curves of Interdependent Lifelines Using Decision Making Process

M.N. Alexoudi, K.G. Kakderi & K.D. Pitalakis

*Department of Civil Engineering, Aristotle University of Thessaloniki, Greece*

**ABSTRACT:** Lifeline systems' co and post seismic performance are controlled by the vulnerability and intra-connectedness of their components. The main objective of this research is the estimation of the expected seismic performance of infrastructure components through a probabilistic approach taking into account their interactions with other lifeline systems. The method proposed is based on the use of adequate interdependency indices between lifeline systems. They are evaluated using the Analytical Hierarchy Process which is enlisted in the most popular multicriteria decision making procedures. The notions of pair-wise comparisons, in terms of verbal or arithmetic preferences, of the production of reciprocal square matrix and the accepted consistency index and of the systemic vulnerability or "vulnerability of interdependent elements" are introduced. Fragility curves of the interdependent components are estimated based on vulnerability functions of independent elements and the reciprocal square matrix. The applicability of the proposed methodology is illustrated using an explanatory example.

## 1 INTRODUCTION

Lifelines are vital for the community, the quality of living, the degree of development and the growth of a society. Based on most recent data from strong earthquakes they are proved to be quite vulnerable during earthquakes. The mid and long-term effects of lifeline damages could be very important, as they can result in malfunction of urban activities and can have serious socioeconomic losses.

In complex city environment lifelines are highly intra-dependent and inter-dependent systems, showing a great degree of coupling between sub-components of the same system and with other infrastructures. The inherited complexity makes the assessment of interdependent lifeline systems' performance a difficult task and a very challenging issue for advanced seismic risk management solutions.

A major concern for the quantification of lifeline elements' interactions is the description of the typology and the functioning of systems involved, the nature of the reciprocal influence, when the specific synergy is evolved (normal, co-seismic or restoration/recovery period) and the importance of the link (slight/strong) between components and systems. Several types of interdependencies exist described by different researchers (Rinaldi et al. 2001, Tang et al. 2004, Yao et al. 2004): (1) function interaction/physical, cyber interaction, (2) collocation

interaction/geographic, space, physical damage propagation, (3) substitute interaction/back-up functions of substitute systems, (4) restoration/recovery interaction, (5) cascade interaction/functional damage propagation/system interaction, (6) general interaction, (7) logical interaction/financial markets.

Interdependencies in the seismic risk analysis of lifelines were studied by several researchers; although little research has been made so far for interactions between different critical infrastructures which may seriously affect the seismic risk management and mitigation. The research work presented in this paper accounts for the logical and the general interaction between different critical infrastructure elements, which derives from the compilation of the operational productivity offered from one lifeline element to another.

Several approaches can be used for the estimation of such interactions: economic, fuzzy logic, decision making or composite approaches (Wong & Isenberg 1995, Giannini and Vanzi 2000, Amin 2001, Little 2002, Brown et al. 2004, Bernhardt & McNeil 2004, Haines & Jiang 2001, Santos & Haines 2004, Dueñas-Osorio et al. 2006, Li & He 2002). The methodology presented herein (Fig. 1) is based on the use of multicriteria decision making procedure in order to estimate adequate interdependency indices between different elements of lifeline systems, that are used to evaluate "systemic fragility curves" of interdependent lifelines.

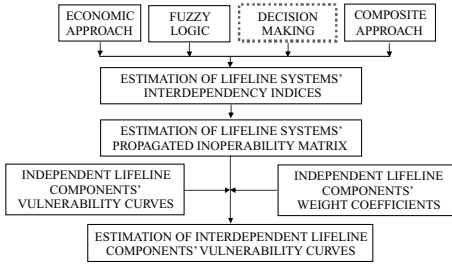


Figure 1. Flowchart of the proposed methodology.

## 2 INTERACTIONS BETWEEN LIFELINE SYSTEMS

As previously mentioned, lifelines are highly interconnected; thus the risk of failure or deviation from normal operating conditions in one lifeline system (or part of it) can affect the risk in another. In case of an earthquake, malfunction of a system's components can result in cascading effects within the same system and other connected systems. The nature of the identified interactions, as well as the degree of inter-connectedness (type and degree of coupling) is the determinant of the interdependent systems' seismic behavior. Equation 1 describes the seismic risk (S.R.) of interdependent lifeline systems:

$$\{S.R.\}_{interdependent} = \{S.R.\}_{independent} * \{\text{Interaction function}\} \quad (1)$$

Lets us consider three lifeline networks (systems 1, 2 and 3). Each node represents the lifeline elements that compose the system. If systems 1, 2 or 3 were independent, the failure of one system's component would influence the operability of the connected lifeline elements inside the system and the functionality of the system as a whole lifeline. In the case of systems' dependency, it could be considered that systems 1, 2 and 3 are dependent on the functionality of others through node N. Node N represents one lifeline system element that participates in system 1 but also influences systems 2 and 3. The functionality of node N is unsatisfactory (event  $E_N$ ) if system 1 fails between supply node 1 and node N (event  $E_1$ ) or system 2 fails somewhere between its supply node 2 and node N (event  $E_2$ ) or systems 3 fails between supply node 3 and node N (event  $E_3$ ).

The probability of the event  $E_N$  (interdependent event) for a three systems' interconnectivity can be written as:

$$P(E_N) = P(E_1) + (1 - P(E_1)) * P(E_2) * a_{12N} + (1 - P(E_1)) * P(E_3) * a_{23N} \quad (2)$$

where:  $P(E_1)$  denotes the probability of event 1 (event inside system 1—system 1 independency),

$P(E_2)$  denotes the probability of event 2 (event inside system 2—system 2 independency) and  $P(E_3)$  denotes the probability of event 3 (event inside system 3—system 3 independency),  $a_{12N}$  denotes a cross impact factor representing the degree of probabilistic contribution (functional dependence) of system 1 and 2 to the lifeline element of node N and  $a_{23N}$  denotes a cross impact factor representing the degree of probabilistic contribution of system 2 and 3 to the lifeline element of node N.

## 3 ESTIMATION OF COMPOSITE—“INTERDEPENDENT” FRAGILITY CURVES

The vulnerability of a system of interacting lifeline elements depends on the vulnerability of the individual components, the way in which the components are connected and the degree of their interdependency. The fragility of the system can differ significantly from the fragilities of its components. The concept of systemic vulnerability or “vulnerability of interdependent elements” is introduced to evaluate the system fragility in addition to the individual component fragilities. Fragility curves are described in terms of the probability of exceeding, in an independent lifeline component, a specific limit state as a function of ground motion intensity. Each system's element is examined as an individual component with no interaction between subcomponents of the same system or/and other external infrastructures. Thus, fragility curves of the interdependent components are estimated based on vulnerability functions of independent elements and the cross impact matrix. Fragility curves are usually described by (cumulative) lognormal distribution functions defined by a median value and a standard deviation  $\beta$  (e.g. NIBS, 2004). The conditional probability of being or exceeding, a particular damage state  $ds_i$ , given the peak ground acceleration (PGA) is defined by the relationship:

$$P(ds \geq ds_i / PGA) = \Phi \left[ \frac{1}{\beta_{dsi}} \ln \left( \frac{PGA}{PGA, ds_i} \right) \right] \quad (3)$$

where:  $\overline{PGA, ds_i}$  is the median value of peak ground acceleration at which the component reaches the threshold of the damage state  $ds_i$ ,  $\beta_{dsi}$  is the standard deviation of the natural logarithm of the peak ground acceleration for damage state,  $ds_i$  and  $\Phi$  is the standard normal cumulative distribution function.

For each PGA level  $a$ , and for each damage state, the final discrete probability of each infrastructure element  $j$  is estimated from the following function:

$$dPa_j^* = \sum dPa_{1j} * a_{1j} + dPa_{2j} + \dots + dP_{mj} * a_{mj} = \sum dpa_{ij}^* \leq 1, \text{ for } i = 1, \dots, m \quad (4)$$



where:  $dPa$  is the discrete probability at PGA level  $a$ ,  $i$  is the respective damage state and  $j$  is the examined infrastructure's component.

#### 4 CROSS IMPACT ANALYSIS

Cross impact analysis is a systemic method to evaluate probabilities of occurrences of various events in an interactive relationship. This method inevitably involves complex interactions among events and high uncertainty. It involves the following steps: (1) construct a structural model of interrelationship of all systems under consideration, (2) quantify expert opinions for the importance of each lifeline system or element compared to another (3) convert the opinions into the form of a cross impact matrix composed of elements representing degree of corresponding impact and (4) modify probability of an event occurrence using the cross impact matrix. In this study the principle of a cross impact analysis is employed for evaluation of system interactions, whereas the impacted probability is formulated on the rigorous basis of probability theory, decision making procedure and a systematic approach of seismic risk analysis.

#### 5 ANALYTICAL HIERARCHY PROCESS (AHP)

The Analytical Hierarchy Process (AHP) method is used to estimate the degree of probabilistic contribution of system 1 and 2 to the lifeline element of node  $N$  (see par. 2). AHP is listed in the most popular multicriteria decision making procedures as it employs simplicity, accuracy, it has theoretical robustness, it can handle both intangible and tangible criteria and most important it has the capability to directly measure the inconsistency of the respondent's judgments (Saaty 1980, Vargas 1990). The AHP combines subjective and objective alternatives into a single measure in a hierarchical or network framework. The assessment is based on a ratio scale and pair-wise comparisons for the estimation of lifelines interactions either verbally or numerically.

The AHP method requires the following steps: (1) structuring the hierarchy and collecting input data by pair-wise comparisons, (2) using the eigenvalue method to yield priorities, (3) calculating Consistency Ratio (CR) of individual expert to check the reliability of the experts, (4) estimating Consistency Index (CI) for the group of experts. The larger the CR the less consistent the expert is. In case of inconsistency, the procedure continues until consistency is accomplished.

##### 5.1 Structuring the hierarchy and collecting data by pair-wise comparisons

In order to structure the hierarchy a process of breaking down the levels continues until a bottom level

Table 1. Conversion table used in AHP to translate verbal preferences into numbers (Saaty, 1988).

Verbal judgment	Numerical judgment
Equally preferred	1
Equally to moderately	2
Moderately preferred	3
Moderately to strongly	4
Strongly preferred	5
Strongly to very strongly	6
Very strongly preferred	7
Very strongly to extremely	8
Extremely preferred	9

criterion is reached. Once the hierarchical structure is established, the relative importance (weights) of all decision elements is explicitly captured and revealed through ratio scale approach. Pair-wise comparison of these elements within the same hierarchical level, with respect to the parent elements in the next higher level, is established. Table 1 shows conversion used to translate verbal preferences into numbers judgments. The numerical scales range from 1 to 9 according to the preferences of experts.

The input data can be achieved from individual interviews of several experts. For each expert, the derived pair-wise comparisons of relative importance  $a_{ij} = w_i/w_j$  for all decision elements and their reciprocals  $a_{ji} = 1/a_{ij}$  are inserted into a "reciprocal square matrix"  $A = \{a_{ij}\}$  as shown in Equation 5.

$$A = \begin{bmatrix} w_1/w_1 & w_1/w_2 & \dots & w_1/w_n \\ w_2/w_1 & w_2/w_2 & \dots & w_2/w_n \\ \dots & \dots & \dots & \dots \\ w_n/w_1 & w_n/w_2 & \dots & w_n/w_n \end{bmatrix} \quad (5)$$

##### 5.2 Eigenvalue method

According to the eigenvalue method (Saaty 1980), the normalized right eigenvector  $W = \{w_1, w_2, \dots, w_n\}$  associated with the largest eigenvalue ( $\lambda_{\max}$ ) of the square matrix  $A$  provides the weighting values for all decision elements:

$$A * W = \lambda_{\max} * W \quad (6)$$

The analytical solution of Equation 6 then provides the relative weights for each decision elements.

##### 5.3 Consistency Ratio (CR) of individual expert

A Consistency Index (CI) is used to measure the degree of inconsistency in the square matrix  $A$ . The CI is defined as  $CI = (\lambda_{\max} - n)/(n - 1)$ , where  $n$  is the number of elements and  $\lambda_{\max}$  is the largest right eigenvalue estimated from each individual expert. Saaty (1980) compared the estimated CI with the same index derived from a randomly generated square matrix, called the Random Consistency Index (RCI) shown in Table 2. The ratio of CI to RCI for the same

Table 2. The Random Consistency Index (RCI)—Saaty, 1994.

n	1	2	3	4	5	6	7
RCI	0.00	0.00	0.52	0.89	1.11	1.25	1.35

order matrix is called the Consistency Ratio (CR). The judgmental consistency of each expert is determined. Generally, a CR of 0.10 or less is considered acceptable; otherwise matrix A will be revised to improve the judgmental consistency.

### 5.4 Group consistency index

The Geometric Mean Method (GMM) (Saaty, 1989), as shown is Equation 7 is being employed to aggregate different judgments from several experts. It should be noted that only consistent expert judgments are included in this step.

$$a_{ij}^{gp} = (a_{ij}^1 \times a_{ij}^2 \times \dots \times a_{ij}^h \times \dots \times a_{ij}^H)^{1/H} = \left( \prod_{h=1}^H a_{ij}^h \right)^{1/H} \quad (7)$$

where,  $a_{ij}^h = (w_i/w_j)$  is an element of the square matrix A of a decision maker h;  $(a_{ij}^{gp})$  is the geometric mean of the paired comparisons conducted by each expert; and H is the total number of experts. The Group Consistency Index (GCI) is defined as  $GCI = (\lambda_{max} - n)/n$ , where  $\lambda_{max}$  is the largest right eigenvalue estimated from the group pair-wise comparison matrix. The group consistency ration (GCR) is calculated in the identical way as the typical CR value ( $GCR = GCI/RCI$ ). The group judgment is considered consistent if the GCR is less than 0.10. In this study, it is assumed that the consensus among different individuals can be mathematically achieved by applying the GMM approach.

## 6 ILLUSTRATIVE EXAMPLE

A system of four interacting lifeline systems is assumed as illustrated in Figure 2. Table 3 presents the multiple connections between the four lifeline components in economical terms. The table inputs represent the cost which is provided by the  $i^{th}$  lifeline system's product (commodity) and consumed by the  $j^{th}$  lifeline system in order to operate. For example, EPS generate products that cost 15,000 euros. From these (15,000 euros), 7,000 euros are used by EPS itself, 2,000, 3,000 and 2,000 euros are supplied to PWW, NGMR and TC accordingly. Naturally, consumption between independent systems can be assumed as zero. The total supply for each component is calculated by the summation of intermediate consumptions.

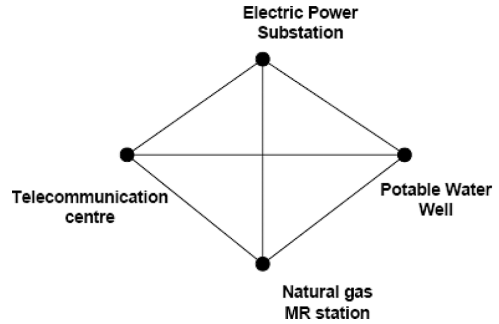


Figure 2. Indicative system of interacting lifeline components.

Table 3. Multiple connections between the four lifeline components in economical terms.

	EPS	PWW	NGMR	TC
EPS	7500			
PWW	2500	500		
NGMR	3000	700	1800	
TC	2000	1300	2200	500
TOTAL SUPPLY	15000	5000	8000	6000

### 6.1 Estimation of cross impact factors between lifeline components using AHP

The triggering issue of this research is to translate the relations between the elements of lifelines as given in Table 3 into words or number that present the importance of each lifeline element compared to the other. The method used for such purpose is the AHP. Six experts were selected according to their experience to lifelines and earthquake engineering.

Firstly, it was decided to structure a very simple hierarchy. Only one level approach was employed that direct links the four lifeline components of four different lifeline systems to each other without indirect links and second level elements. Table 3 illustrates the direct links between the components. Secondly, the six experts filled questionnaires using the conversion table provided in Table 1 and making pair-wise comparisons between the components. All experts used the number mode of the conversion table and not the verbal. Six “reciprocal square matrices” were produced for each one of the six experts. As an example two of them are given below:

$$A_{ale} = \begin{bmatrix} 1 & 0.20 & 0.14 & 0.25 \\ 5 & 1 & 0.17 & 0.33 \\ 7 & 6 & 1 & 2 \\ 4 & 3 & 0.5 & 1 \end{bmatrix},$$

$$A_{kak} = \begin{bmatrix} 1 & 0.20 & 0.25 & 0.17 \\ 5 & 1 & 1 & 1 \\ 4 & 1 & 1 & 0.50 \\ 6 & 1 & 2 & 1 \end{bmatrix}$$

Using the eigenvalue method  $w_i$  and  $\lambda_{max}$  were estimated for each one of the six experts (Table 4).

Performing the steps of the methodology described above the Consistency Index (CI) and Consistency Ratio (CR) of each individual expert were estimated (Table 5).

Afterwards Geometric Mean Method was employed to aggregate different judgments from the four consistent experts. Employing Equation 7, a new square matrix  $A_{group}$  was produced.

$$A_{group} = \begin{bmatrix} 1 & 0.20 & 0.18 & 0.17 \\ 4.95 & 1 & 0.36 & 0.44 \\ 5.60 & 2.78 & 1 & 0.51 \\ 6 & 2.28 & 1.97 & 1 \end{bmatrix}$$

The weight coefficients assigned to all four infrastructure elements as estimated from  $A_{group}$  are:

$$[w_i]^T = [w_{EPS} \ w_{PWW} \ w_{NGMR} \ w_{TC}]^T \\ = [0.500 \ 0.100 \ 0.300 \ 0.42]$$

Performing the steps of the methodology described above the Consistency Index (CI) and the Consistency Ratio (CR) of the group is 0.050 and 0.056 respectively. The relative importance of each element compared to another as derived from the normalized  $A_{group}$  matrix is then used in the “systemic vulnerability”.

$$A_{normalgroup} = \begin{bmatrix} 0.06 & 0.03 & 0.05 & 0.08 \\ 0.28 & 0.16 & 0.10 & 0.21 \\ 0.32 & 0.44 & 0.29 & 0.24 \\ 0.34 & 0.36 & 0.56 & 0.47 \end{bmatrix}$$

For an example the cross impact between EPS and PWW is  $a_{EPSPWW} = 0.28$ , the cross impact between

Table 4. Calculated weights and max eigenvalues.

A/A	Names	$w_{EPS}$	$w_{PWW}$	$w_{NGMR}$	$w_{TC}$	$\lambda_{max}$
1	ale	0.06	0.14	0.53	0.27	4.27
2	kak	0.06	0.31	0.25	0.38	4.04
3	arg	0.05	0.29	0.27	0.40	4.36
4	plia	0.04	0.08	0.24	0.63	4.31
5	pit	0.07	0.14	0.35	0.44	5.27
6	hatz	0.11	0.24	0.43	0.22	4.90

Table 5. Estimated Consistency Index (CI) and Consistency Ratio (CR).

A/A	Names	CI	RCI	CR	Acceptable
1	ale	0.088	0.89	0.10	YES
2	kak	0.014	0.89	0.02	YES
3	arg	0.120	0.89	0.13	YES
4	plia	0.103	0.89	0.11	YES
5	pit	0.422	0.89	0.47	NO
6	hatz	0.303	0.89	0.34	NO

EPS and NGMR is  $a_{EPSNGMR} = 0.32$  and between EPS and TC is  $a_{EPSTC} = 0.34$ .

## 6.2 Estimation of composite—“Interdependent” fragility curves

Fragility curves for the individual components (without taking into account the interdependency between them) are provided by (cumulative) lognormal distribution functions defined by a median value and a standard deviation  $\beta$ .

Figures 3–6 illustrate the comparison between the fragility curves of independent lifeline component (illustrated with “0” mode) and the ones of interdependent components as calculated from the procedure described above (illustrated with “1” mode).

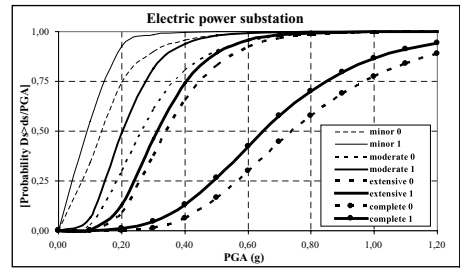


Figure 3. Fragility curves of electric power substation (EPS)—independent “0”/interdependent “1” component.

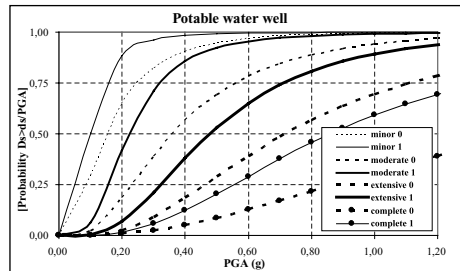


Figure 4. Fragility curves of potable water well (PWW)—independent “0”/interdependent “1” component.

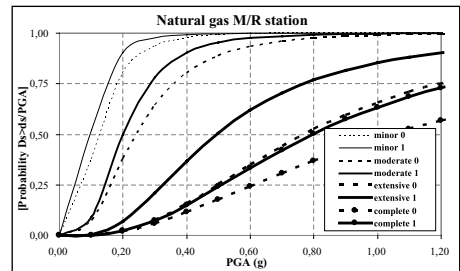


Figure 5. Fragility curves of Natural Gas M/R Station— independent “0”/interdependent “1” component.

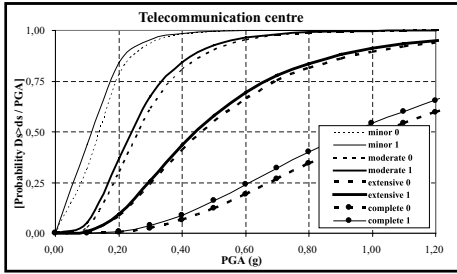


Figure 6. Fragility curves of Telecommunication Centre—dependent “0”/interdependent “1” component.

If infrastructure  $i$  depends on infrastructure  $j$ , and  $j$  has a high risk of failure, then the likelihood of  $i$  being disrupted or failing is correspondingly higher than if  $i$  was independent of  $j$ . In the case of the three interconnected elements (EPS, PWW and NGMR) of the example, the derived fragility curves are quite different from those referring to independent elements. Especially, in the case of NGMR the fragility curve of the extensive damage state of the independent component is similar with the fragility curve of complete damage state of the interdependent component. Moreover, for the EPS component, important differences exist in the case of minor and moderate damages especially in Peak Ground Acceleration (PGA) values in the range between 0.20 g to 0.30 g. For the case of the PWW, important differences between independent and interdependent fragility curves exist in the case of moderate and extensive damages in the range of 0.20 g and 0.40–0.80 g respectively. On the other hand, there are small differences between the fragility curves of the communication center estimated taking or not into account the existing interdependencies with other lifeline elements.

## 7 CONCLUSIONS

Infrastructure systems are highly intradependent and interdependent systems. Capturing and quantifying lifeline interactions are very important aspects within an advanced seismic risk management study of a complex city system. Within this framework, a method is proposed to simulate interdependent lifelines' vulnerability. Interdependency indices are estimated based on an Analytical Hierarchy Process. Furthermore, the notion of propagated inoperability and systemic vulnerability or “vulnerability of interdependent elements” is introduced. Fragility curves of the interdependent components are estimated based on vulnerability functions of independent elements and the “reciprocal square matrix”  $A$ . Using an illustrative example, it is demonstrated the efficiency of the proposed methodology to evaluate the expected seismic performance of complex interacting lifelines (electric power sub-stations, potable water wells, natural

gas M/R stations and telecommunication network) through a probabilistic approach. In general the interdependency of sub-components of different systems increases the seismic vulnerability. In certain cases (i.e. potable water wells), this increase may be very high in case of strong earthquakes (i.e. PGA = 0.4 g). Incorporation of systems' intra-dependencies and generalization of the proposed methodology to address the vulnerability assessment of multiple interacting infrastructure systems consisting of a number of different subcomponents, are the issues where future research will focus on.

## REFERENCES

- Amin, M. 2001. Toward Self-Healing Energy Infrastructure Systems. *IEEE Computer Applic. in Power* 14(1): 20–28.
- Bernhardt, K.L.S. & McNeil, S. 2004. An Agent Based Approach to Modeling the Behavior of Civil Infrastructure Systems. *Engin. Systems Symposium*. Tang Center, MIT.
- Brown, Th. et al. 2004. Assessing infrastructure interdependencies: the challenge of risk analysis for complex adaptive systems. *Int. Journal of Critical Infrastructures* 1(1).
- Dueñas-Osorio, L., et al. 2006. Seismic response of critical interdependent networks. In Press, *Journal of Earthq. Engin. and Structural Dynamics*.
- Giannini, R. & Vanzi, A. 2000. Seismic Reliability of Electric Networks and Interaction with other Damage Indicators. *Proc. 12th World Conference on Earthquake Engineering*.
- Haines, Y.Y. & Jiang, P. 2001. Leontief-based model of risk in complex interconnected infrastructures. *Journal of Infrastructure Systems* 7(1): 1–12.
- Li, J. & He, J. 2002. A recursive decomposition algorithm for network seismic reliability evaluation. *Journal of Earthquake Engin. and Structural Dynamics* 31: 1525–1539.
- Little, R.G. 2002. Controlling Cascading Failure: Understanding the Vulnerabilities of Interconnected Infrastructures. *Journal of Urban Technology* 9(1): 109–123.
- National Institute of Building Sciences (NIBS). 2004. Earthquake loss estimation methodology. HAZUS. Technical manuals, Federal Emerg. Manag. Ag., Washington, D.C.
- Rinaldi, S.M. et al. 2001. Identifying, Understanding, and Analyzing Critical infrastructure interdependencies. *IEEE Control Systems Magazine* 21(6).
- Saaty, T.L. 1980. *The analytical hierarchical process*. Wiley, New York.
- Saaty, T.L. 1988. *Decision Making For Leaders*. RWS Publications, Pittsburgh, Pennsylvania.
- Saaty, T.L. 1989. Decision making, scaling, and number crunching. *Decision sciences*, 20, 404–409.
- Saaty, T.L. 1994. *Fundamentals of decision making and priority theory with the AHP*. Pittsburgh, PA. RWS Public.
- Santos, J.R. & Haines, Y.Y. 2004. Modeling the Demand Reduction Input-Output (I-O) Inoperability Due to Terrorism of Interconnected Infrastructures. *Risk Analysis* 24(6).
- Tang, A.P. et al. 2004. Lifeline Systems Interaction and their Seismic Performance Assessment. *Proc. 13th World Conf. on Earthquake Engineering*, Vancouver, B.C., Canada.
- Vargas, L.G. 1990. An overview of the analytic hierarchy process and its applications. *European Journal of Operational Research*, 48, 2±8.
- Wong, F.S. & Isenberg, J. 1995. Effects of Lifeline Interaction on Seismic Performance of Communications Networks. *Proc. 4th U.S. Conf. on Lifeline Earthq. Engin.* TCLEE/ASCE, Monograph No.6, edited by J. O' Rourke.
- Yao, B. et al. 2004. Study Effect on Lifeline Interaction under Seismic Conditions. *Proc. 13th World Conf. on Earthq. Engin.*, Vancouver, B.C., Canada.

# Intelligent agents for life cycle management of structures and infrastructures in seismic areas

G.M. Atanasiu

*Department of Civil Engineering, Technical University of Iași, Romania*

F. Leon & M.H. Zaharia

*Department of Computer Science and Engineering, Technical University of Iași, Romania*

**ABSTRACT:** The performance monitoring and life-time management of structures can be increased by accumulating knowledge on their structural behaviour for several events during the life cycle. Each stage within the management of the structural life cycle can be assisted by an expert system that accumulates the experience of the system or organization involved. Intelligent agents are programs situated in their execution environment and capable of autonomous action in order to meet their design objectives. They can be reactive, pro-active and manifest social ability. Based on intelligent agents, the expert systems of different branches of an organization involved in structural monitoring during life time can communicate and exchange data that are useful for new challenges. In the design phase, the knowledge base of the expert systems can refer to the constraints imposed by different building standards. During the building phase, they can retain different cost-efficient solutions for the construction problems. In the operational phase, the intelligent agents can collect information from different sensors to monitor structural stress or vibrations response. Finally, in the maintenance phase, they can predict structural damage based on adaptive fragility curves.

## 1 INTRODUCTION

The management of seismic risk in urban areas involves not only practitioner engineers, but the whole community, and especially the administrative stakeholders at local, regional and national level. In order to provide practical, simple information for decision support as a prevention measure in case of high risk seismic events, new methods have to be developed. In this paper, we describe a methodology based on intelligent agents for the monitoring of structures during their life cycle, taking into account the design, construction, operation, and maintenance phases.

## 2 INTELLIGENT AGENTS

According to Wooldridge (2000), an agent is a computer system that is situated in its environment and is capable of autonomous action in order to meet its design objectives.

Agent Oriented Programming, AOP, is a fairly new programming paradigm that supports a societal view of computation. In AOP, objects known as agents interact to achieve individual goals. Agents can exist in a

structure as complex as a global internet or one as simple as a module of a common program. Agents can be autonomous entities, deciding their next step without the interference of a user, or they can be controllable, serving as an intermediary between the user and another agent (Wikipedia, 2007).

Intelligent agents retain the properties of autonomous agents, and in addition show a so-called “flexible” behaviour (Wooldridge & Jennings, 1995): reactivity, the ability to perceive their environment, and respond in a timely fashion to changes that occur in it, pro-activeness, the ability to exhibit goal-directed behaviour by taking the initiative, and social ability, to interact with other agents and possibly humans.

## 3 SEISMIC RISK ANALYSIS

Deterministic and probabilistic approaches to assessing seismic hazards and vulnerability of urban exposed infrastructure have differences, advantages, and disadvantages that often make the use of one advantageous over the other. Probabilistic methods can be viewed as inclusive of all deterministic events with a finite probability of occurrence. In this context, proper deterministic methods that focus on a single earthquake

ensure that that event is realistic, i.e. that it has a finite probability of occurrence. The complementary nature of deterministic and probabilistic analyses should be emphasized: deterministic events can be checked with a probabilistic analysis to ensure that the event is realistic (and reasonably probable), and probabilistic analyses can be checked with deterministic events to see that rational, realistic hypotheses of concern have been included in the analyses.

Determinism and probabilities are not a dichotomy, but a continuum in which both analyses are conducted, but more importance can be given to one over the other, i.e. the weight in the decision-making process, regarding whatever choices are available for risk reduction or loss mitigation (McGuire, 2007). This includes system layout, design, insurance, disaster planning, and recovery efforts. The best perspective is gained if both deterministic and probabilistic analyses are conducted. Factors that influence the choice include the decision to be made, i.e. the purpose of the hazard or risk assessment, the seismic environment, whether the location is in a high, moderate, or low seismic risk region, and the scope of the assessment, whether one is assessing a site risk, a multi-site risk, or risk to a region. On the other hand, the seismic vulnerability of the urban infrastructure can also be approached using deterministic or probabilistic methods, in strong connection with the characterization of the seismic event.

A straightforward equation defines the concept of seismic risk:

$$Risk = Hazard \times Vulnerability \quad (1)$$

The hazard is determined by the natural configuration of a specific location and cannot be changed. So far, the best analysis that can be made to evaluate the seismic hazard is by building a probabilistic map, containing the chances that an earthquake exceeding a certain magnitude will occur within a time interval.

On the other hand, seismic vulnerability is determined by human factors, and it can be reduced by a proper seismic design.

#### 4 DESIGN PHASE

Intelligent agents can be used to support the design phase of a structure. A civil engineering organization can have a wide variety of designs in its database, and ideally all designs should be made available when a new problem appears. The previous experience can be thus stored in different knowledge bases within the expert systems of the organization. The intelligent agents can visit all these distributed knowledge bases and provide help for the designers of new structures.

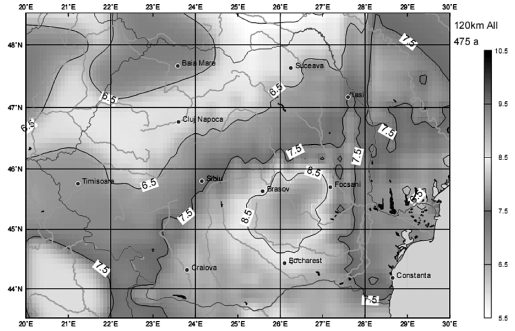


Figure 1. Seismic hazard for a recurrence period of 475 years in Romania region.

The first component of an organization knowledge base is comprised by hazard maps, which can mainly rely on public sources. An example of a seismic hazard map for Romania is given in Figure 1 (Ardeleanu, Leydecker, et al., 2005, Leon & Atanasiu, 2007), for a recurrence period of 475 years, i.e. probability of exceedance of 10% in 50 years,  $p_{50} = 0.1$ , as recommended by the Eurocode 8 (CEN, 2001).

Using these maps the designer can make informed decision about the seismic safety measures that should be taken for building the structure in a certain geographic location.

Second, such an agent can provide general advice regarding the design phase, such as (Rossetto, 2006):

- Choose an adequate lateral load resisting design;
- Maintain regularity in plan and elevation concerning both the stiffness and mass distribution;
- Ensure right connection between structural elements;
- Avoid designing in critical locations of stress concentration;
- Consider in dynamic response the needed spacing between buildings, in order to avoid pounding;
- Adopt concept capacity load for seismic design in order to control the failure modes;
- Estimating the real damage potential on non-structural elements.

Beside recommendations, the intelligent agents can provide actual help in this phase by ensuring that the design satisfies the constraints given by different standards, such as Eurocode 8 (CEN, 2001).

A third function of the agents relies on their data mining capabilities. They can analyze the knowledge bases of the organization and extract general models of “good” or “bad” designs. The design must be described by a set of attributes that take different values for each specific design. Based on the values of the attributes for each considered instance (design), a

classification model can be built, either in an explicit form such as a decision tree, or an implicit form such as an instance-based model.

#### 4.1 Decision trees

One of the most popular decision tree inducers is the C4.5 algorithm. It is an extension of the basic ID3 algorithm designed by Quinlan (1993) to address the following issues not dealt with by ID3: avoiding over-fitting the data, determining how deeply to grow a decision tree, reduced error pruning, rule post-pruning, handling continuous attributes, choosing an appropriate attribute selection measure, handling training data with missing attribute values, handling attributes with differing costs, improving computational efficiency (Hamilton, Gurak, et al., 2002).

The C4.5 algorithm generates a classification-decision tree for the given dataset by recursive partitioning of data. The algorithm considers all the possible tests that can split the dataset and selects a test that gives the best information gain. If by entropy one can understand the “impurity” of an exemplar set  $S$ , it is possible to estimate the efficiency of an attribute for the classification of these exemplars. The information gain measures the expected entropy reduction caused by the set partitioning after the values of an attribute  $A$ :

$$IG(S, A) = H(S) - \sum_{v \in Val(A)} \frac{card(S_v)}{card(S)} H(S_v), \quad (2)$$

where  $Val(A)$  is the set of the values of attribute  $A$ ,  $S_v$  is the subset of  $S$  for which attribute  $A$  has the value  $v$ , and  $H(S)$  is the entropy of set  $S$  with  $n$  classes, each with a probability of occurrence  $p_i$ :

$$H(S) = \sum_{i=1}^n -p_i \log_2 p_i. \quad (3)$$

For each discrete attribute, one test is considered with a number of outcomes equal to the number of distinct values of the attribute. For each continuous attribute, binary tests involving every distinct value of the attribute are considered. In order to compute the entropy gain of all these binary tests efficiently, the training data set belonging to the node in consideration is sorted for the values of the continuous attribute, and the information gains of the binary cut based on each distinct values are calculated in one scan of the sorted data. This process is repeated for each continuous attribute.

For the structure in Figure 2 (Atanasiu, Leon & Popa, 2007), a time-history analysis for a structural module was conducted using real data of some major earthquakes occurring in Romania, and particularly their effect on Iași city region. A decision tree that

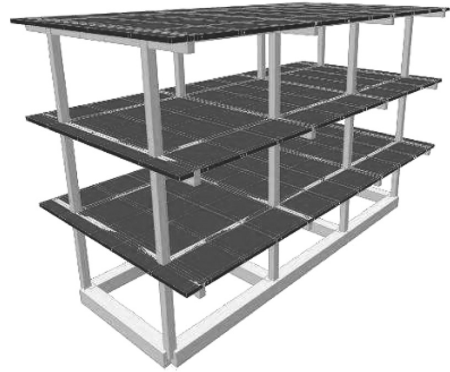


Figure 2. Structural model used for the finite element analysis.

```

pga = High
| h = High => displacement = Low
| h = Medium => displacement = High
| h = Low => displacement = High
pga = Low => displacement = VeryLow
pga = VeryHigh
| h = High => displacement = Medium
| h = Medium => displacement = VeryHigh
| h = Low => displacement = High
pga = Medium
| h = High => displacement = VeryLow
| h = Medium => displacement = Medium
| h = Low => displacement = Low
pga = VeryLow => displacement = VeryLow

```

Figure 3. Decision tree estimating the displacement of a structure.

specifies the displacement given the peak ground acceleration (PGA) of an earthquake, and the depth of its hypocenter, is displayed in Figure 3.

#### 4.2 Instance-based models with generalized exemplars

The generalized exemplar model is a form of inductive learning from examples, which extends the nearest neighbour classification method. It is a learning paradigm based on class exemplars, where an induced hypothesis has the graphical shape of a set of hyper-rectangles in an  $n$ -dimensional Euclidean space (Leon, 2006). Exemplars of classes are either hyper-rectangles or single training instances, i.e. points, known as “trivial hyper-rectangles”.

The input is a set of training examples, each described as a vector of numeric attribute/value pairs and an associated class. The  $n$  attributes used for describing

the examples define the  $n$ -dimensional Euclidean space in which the concept will be represented.

The method generalizes an initial user-defined set of points, or seeds, in the  $n$ -dimensional Euclidean space, expanding (or in some special situations shrinking) them along one or more dimensions, as new training examples are presented. The choice of which hyper-rectangle to generalize depends on the distance metric. In a universe where the attributes have crisp values, such a metric is a weighted Euclidean distance, either point-to-point or point-to-hyper-rectangle.

Attributes (dimensions) have different importance weights and a class distribution may be greater on a dimension than on another. Mean and standard deviation are computed independently for each dimension. Therefore, a formula is used for computing similarity, analogous to the axis-parallel elliptical (instead of radial) basis functions:

$$s(I, P) = e^{-\frac{\sum w_i \cdot (d_i(I, P))^2 / \sigma_i^2}{2D}}, \quad (4)$$

where  $w_i$  are the attribute weights,  $d_i()$  is the distance projected on dimension  $i$ ,  $\sigma_i$  is the standard deviation for dimension  $i$ , and  $D$  is the number of dimensions where attribute values are defined (known) for the considered instance  $I$ .

This optimized version of using generalized exemplars instead of normal instances decreases the memory need and increases the speed of the classification. It can thus classify a new design by means of similarity to old existing ones. A distinction between a “good” and a “bad” design is generic displayed considering the frame structure of Figure 4.

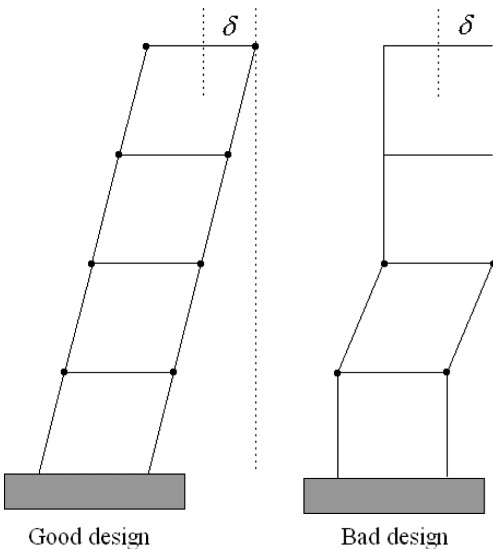


Figure 4. Design classification.

## 5 BUILDING PHASE

The capital cost for a construction project includes the expenses related to the initial establishment of the facility (Hendrickson, 2003):

- Land acquisition, including assembly, holding and improvement issues;
- Construction, including materials, equipment, and labour activities;
- Field supervision of construction;
- Construction financing;
- Insurance and taxes during construction;
- Owner’s general office overhead costs;
- Equipment and furnishings not included in construction;
- Inspection and testing costs.

During the building phase, the intelligent agents can help the organization to make a benefit-cost analysis. The main issues here are to decrease the construction costs, and at the same time to increase the seismic resistance. Based on previous experience, the agents can retrieve from the knowledge base an estimate of the optimal investment  $C$  that can decrease the sum of construction costs  $C_C$  and the expected maintenance costs  $C_M$ :

$$C = \arg \min_{C_c} \left( C_C + \sum_i C_M^{(i)} \cdot \gamma^{t_i - t_0} \right) \quad (5)$$

The maintenance costs at several moments are discounted by a factor  $\gamma < 1$ , revealing that a cost at a future time has less importance than the same cost at present, when  $\gamma$  would be equal to 1. The maintenance costs can be viewed as a function of the construction costs and previous maintenance investments.

Beside this analysis, the agents can assist the organization by organizing the information regarding previous contractors and suppliers. As the building phase develops, the agents will add new knowledge to the expert systems. The pieces of knowledge will not necessarily store concrete information about certain companies, although this can be useful as well sometimes in order to avoid deficient partners. The knowledge base will be mainly organized as records of generic conditions when a problem happened and the solutions found by the people involved.

It is relatively easy to use existent databases at different levels within the organisation. Also the use of artificial intelligence to create a wrapping layer, for federated databases between various queries and data sets is already functional. The technology chosen to implement different agent frameworks can also vary. Nowadays, the two dominant technologies, J2EE and .NET, have enough support to develop powerful agent applications.



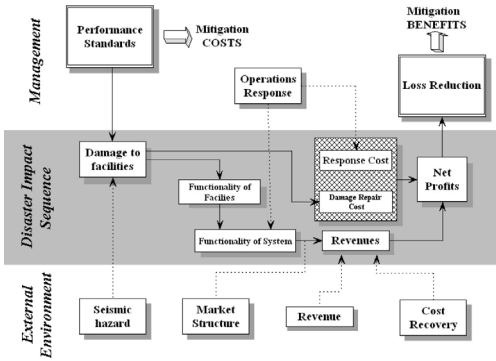


Figure 5. Flow chart on relationship between various costs for mitigation purposes.

The way of development will be probably driven from the powerful headquarters in the system, and slowly disseminate to all organizational branches. This process will be slow to minimise the organisation costs. Various types of agents will be used, from static agents to mobile intelligent agents. In fact, at the organisation level when this process starts, the only effort needed will be to establish a local standard related to agent communication language (such as KQML) and to the metadata structure. After that, the “seeds” can develop at their own growth rate depending especially on the admissible investments in the system.

In this way, the agents can help the risk management of the building phase and also increase the organizational intelligence by not allowing good solutions to encountered problems to be lost.

The main processes during the building, operation and maintenance phases are succinctly displayed in Figure 5 with respect to the seismic analysis, adapted after Zerbe & Falit-Baiamonte (2001).

## 6 OPERATION PHASE

In the operation phase, each building can be considered as monitored by an intelligent agent. The agent receives data from an array of sensors placed in key locations within the structure. Instead of transmitting all the input data to a centralized database, the agent first analyzes the sensors data, and tries to extract relevant knowledge in the form of operation rules, using data mining algorithm such as those presented in paragraph 4.

The intelligent agent sends only the defined rules, or alerts to the knowledge base of the expert system. By monitoring the sensor data over a user-defined period of time, the agent can correlate operation patterns.

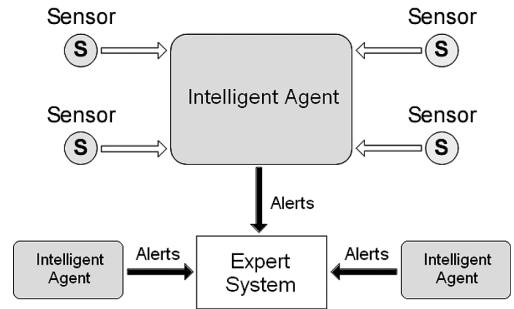
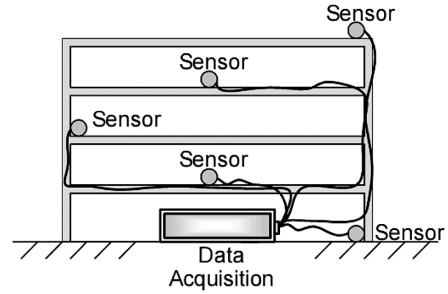


Figure 6. The network of local sensors and distributed intelligent agents.

For example, it can correlate the structural stress in key points of the structure with external events such as the speed of the wind, or ground vibrations, such as low intensity earthquakes.

The process is represented in Figure 6, adapted after (Lynch, 2002).

## 7 MAINTENANCE PHASE

The maintenance phase is correlated to the operation phase. Since each structure has an intelligent agent that monitors it, the agent can also use information about the vulnerability of the structure, and its variation during the cycle of operation and repair.

Fragility curves, also known as damage functions (Reinhorn, Barron-Corverra & Ayala, 2001) are used to approximate the structural damage from natural hazards data. The term of fragility means the probability of attaining a limit state, conditioned on a particular value of random demand (Ellingwood, 2001). More simply, fragility is a measure of vulnerability or an estimate of the overall risk. Fragility functions can be developed using different methods, heuristic, empirical, analytical or a combination of two methods.

Following the HAZUS methodology (FEMA, 1999), the damage states for a certain structure can include slight, moderate, extensive, and complete damage.

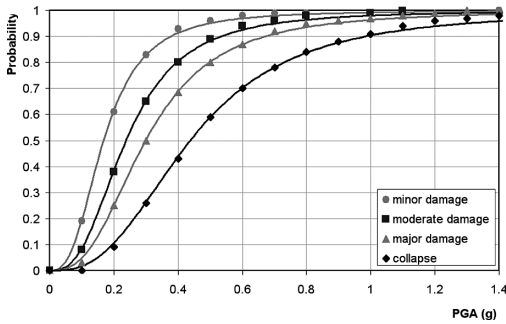


Figure 7. Set of fragility curves using the Simplified Multiple Multiplicative Factor Model.

In a previous article (Leon & Atanasiu, 2007), a simplified expression for fragility curves has been obtained using regression based on evolutionary algorithms. The best results were given by a Simplified Multiple Multiplicative Factor Model:

$$y(x) = \frac{x^e}{\varphi + x^e} \quad (6)$$

The corresponding graphical representation of the fragility curves is displayed in Figure 7.

This model is flexible enough to account for the continuous effects of the environment on a certain structure, including disasters such as earthquakes. The resulting fragility curves can be used to estimate the damage risk of a building given the estimated peak ground acceleration (PGA) of an earthquake. For example, as the structures undergo their lifecycle, the action of the environment causes the  $\varphi$  coefficient to increase, which in turn increases the damage risk when a seismic event occurs. By conducting repairs on a structure, its  $\varphi$  coefficient will decrease, and this will lower the seismic damage risk. Work remains to be done on the actual formulas relating these coefficients to the behaviour of a building during its lifecycle.

## 8 CONCLUSIONS

The use of distributed artificial intelligence in handling monitoring during lifecycle phases of structures located in seismic high potential areas is a new modern powerful tool, able to increase the reaction time and efficiency in the process of seismic vulnerability identification at various organisation levels. Our approach, applicable also for other various classes of extreme events to which the built infrastructure might be exposed during lifetime, can also increase the collaborative effort efficiency providing a quick response for structural safety problems that can appear at various levels in the structure and infrastructure lifecycle.

The gradual start is proposed due to the need of the system to accumulate new organisation knowledge because the changes that appear in human mentality, such as learning and acceptance, are rather slow. The cost problems can neither be neglected. Compared to the specific budget needed for design and execution for important investment, the related costs for starting and developing such a collaborative software platform would be negligible.

## REFERENCES

- Ardeleanu, L., Leydecker, G., Bonjer, K.P., Busche, H., Kaiser, D. & Schmitt, T. 2005. Probabilistic seismic hazard map for Romania as a basis for a new building code, *Natural Hazards and Earth System Sciences* vol. 5: pp. 679–684.
- Atanasiu, G.M., Leon, F. & Popa, B.F. 2007. A Scenario for Seismic Risk Mitigation in Urban Areas Using Data Mining Techniques, *The 3rd International Conference Lifetime Oriented Design Concepts, Sonderforschungsbereich 398*, Bochum, Germany.
- CEN, Comité Européen de Normalisation, EUROCODE 8. 2001. *Design Provisions for Earthquake Resistance of Structures*, Brussels, Belgium.
- Ellingwood, B.R. 2001. Earthquake risk assessment of building structures, *Reliability Engineering and System Safety* vol. 74: pp. 251–262.
- FEMA, 1999. HAZUS, Earthquake Loss Estimation Methodology, *Technical Manual, National Institute of Building Sciences for the Federal Emergency Management Agency*.
- Hamilton, H., Gurak, E., Findlater, L. & Olive, W. 2002. Knowledge Discovery in Databases, University of Regina, Canada, <http://www2.cs.uregina.ca/~hamilton/courses/831/notes/ml/dtrees/c4.5/tutorial.html>.
- Hendrickson, C. 2003. *Project Management for Construction: Fundamental Concepts for Owners, Engineers, Architects and Builders*, Department of Civil and Environmental Engineering, Carnegie Mellon University, Pittsburgh, <http://www.ce.cmu.edu/pmbbook>.
- Leon, F. & Atanasiu, G.M. (2007). Seismic Hazard Analysis of Iași City using Geographical Information Systems, *2nd Nordic Geographers Meeting, Meeting the Waves of Globalisation—Local, Regional and Environmental Response*, Bergen, Norway.
- Leon, F. & Atanasiu, G.M. 2007. Estimating Fragility Curves of Buildings using Genetic Algorithms, *Proceedings of the Ninth International Conference on the Application of Artificial Intelligence to Civil, Structural and Environmental Engineering*, Civil-Comp Press: Stirlingshire, Scotland, UK.
- Leon, F. 2006. *Intelligent agents with cognitive capabilities*, Tehnopress: Iași, Romania.
- Lynch, J.P. 2002. Decentralization of Wireless Monitoring and Control Technologies for Smart Civil Structures, John A. Blume Earthquake Engineering Center, *Technical Report #140*, Stanford University, Stanford CA., <http://www-personal.umich.edu/~jerlynch/papers/BlumeReport140Lynch.pdf>.

- McGuire, R.K. 2007. Deterministic vs. Probabilistic Earthquake Hazards and Risks, *Risk Engineering*, <http://www.riskeng.com/PDF/Deterministic.pdf>.
- Quinlan, R. 1993. *C4.5: Programs for Machine Learning*, Morgan Kaufmann Publishers: San Mateo, CA.
- Reinhorn, A.M., Barron-Corverra, R. & Ayala, A.G. 2001. Spectral Evaluation of Seismic Fragility of Structures, *Proceedings of ICOSSAR 2001*, Newport Beach CA.
- Rossetto, T. 2006. Earthquake Engineering, Civil & Environmental Engineering, University College London, [http://www.es.ucl.ac.uk/people/sammonds/17Earthquake engineering.pdf](http://www.es.ucl.ac.uk/people/sammonds/17Earthquake%20engineering.pdf).
- Wikipedia, The Free Encyclopedia, 2007. Agent Oriented Programming, [http://en.wikibooks.org/wiki/Computer\\_programming/Agent\\_Oriented\\_Programming](http://en.wikibooks.org/wiki/Computer_programming/Agent_Oriented_Programming).
- Wooldridge, M. & Jennings, N.R., 1995, Intelligent agents: Theory and practice, *The Knowledge Engineering Review* vol. 10 (1): pp. 115–152.
- Wooldridge, M., 2000. Intelligent Agents, in G. Weiß (ed.), *Multiagent Systems—A Modern Approach to Distributed Artificial Intelligence*. The MIT Press: Cambridge, Massachusetts.
- Zerbe, R.O., Falit-Baiamonte, A. 2001. The Use of Benefit-Cost Analysis for Evaluation of Performance-Based Earthquake Engineering Decisions, *Research Report, CMS-98121531*, Pacific Earthquake Engineering Research Center, College of Engineering, University of California, Berkeley, [http://peer.berkeley.edu/publications/peer\\_reports/reports\\_2002/0206.pdf](http://peer.berkeley.edu/publications/peer_reports/reports_2002/0206.pdf).

# Hierarchical ordering of extensometers readings from Itaipu dam

A.S. Dyminski & M.T.A. Steiner

*Federal University of Parana, Curitiba, Brazil*

R. Villwock

*University of Western Parana, Francisco Beltrão, Brazil*

**ABSTRACT:** A proper instrumentation system capable of monitoring dam structures lifetime behavior and their foundation is of vital importance. Commonly the instrumentation readings generate a large data set. It is crucial to select the correct array of information to understand dam behavior and to guarantee its safety. In this paper, data mining techniques were used to group and hierarchically organize a real instrumentation data set, comprised of 72 extensometers rods installed in Sector F of Itaipu dam. Each rod has had its displacement read periodically since 1980. In this work, the readings taken into consideration ranged from January/1995 to December/2004. A methodology composed of 8 stages was proposed to group the readings and to select the most important displacement measurements. The results showed that only 25 rods among the 72 installed could be considered relevant.

## 1 INTRODUCTION

Dams were conceived with the purpose of bringing great benefits to society. It is expected that their construction, operation and eventual decommissioning should occur safely. If a dam breaks down the destruction scale may be very high; it may put not only the environment in the surrounding areas at risk but also human lives. Therefore, adequate design, construction and operation of dams is a worldwide concern. International guidelines aiming at dams' safety and many productive discussions about this theme have been proposed by the ICOLD—*International Commission on Large Dams* (ICOLD, 2007).

The concept of "Dam Safety" should involve structural, hydraulic, geotechnical, environmental and operational aspects. All these features must be considered during a dam's lifespan. A proper instrumentation system capable of monitoring the dam's geotechnical and structural behavior is essential to assess its behaviour and integrity. A good overview about the relevance of instrumentation to evaluate dam safety can be found in Dibiagio (2000).

Generally, this monitoring generates a large data set composed of periodical readings taken during several years. It is important to select the correct array of information to better understand the dam's behaviour and solve occasional problems as soon as they occur. Decision making based on instrumentation data usually occurs throughout the lifespan of a dam. An interesting

discussion about risk assessment and decision making in dam safety is presented in Bowles et al. (2003).

Focusing on this aspect, the present paper proposes a methodology based on data mining techniques that selects the most important information in a dam's instrumentation data set, in order to contribute to the operation engineering team decision making process. This methodology was applied in a real data set, composed by displacement measurements of Itaipu Dam foundation.

## 2 ITAIPU DAM

Itaipu Dam is one of the biggest dams in the planet, located on the border of Brazil and Paraguay. It is 7,700 m long, built between the two margins of Parana river. Itaipu is the world's largest hydro electrical power producer (ITAIPU, 2007). There are more than 2200 instruments installed in the dam's structure and foundation (i.e. piezometers, extensometers, pendulums and flow gauges). These instruments have been periodically monitored since 1986 and eventually gathered a huge data set comprised of several instruments readings.

Itaipu company implanted an automatic data acquisition system in approximately 210 instruments in 2006. The company's team of engineers selected these instruments for automation considering their

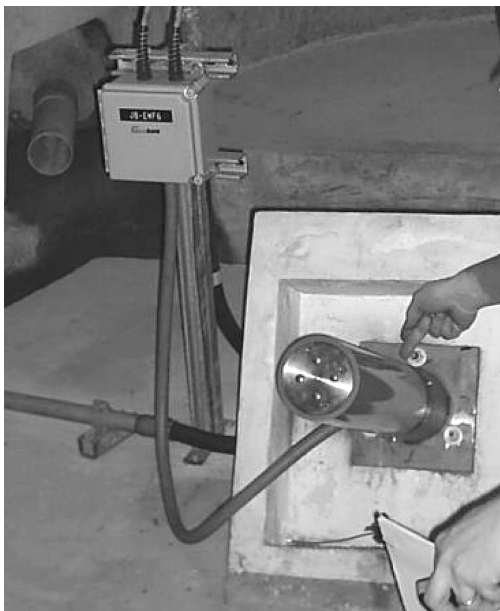


Figure 1. Automated extensometer installed in the Itaipu rock foundation.

importance for the diagnosis of the structures' safety, due to their location and past results, among other reasons.

Itaipu dam is divided into sectors. Sector F is the tallest and most central part of the main concrete dam—and it is considered the most important one. The structure of this sector is hollow gravity type and its maximum height is 196 m. In Sector F there are 30 instruments called extensometers. An automated extensometer picture is shown in figure 1.

Using the extensometers, it is possible to measure the vertical displacements of the basaltic rock mass where dam foundation is based on. A typical geological profile of Sector F rock mass foundation can be observed in figure 2. Settlement monitoring is very important and a special attention is given to the rock mass discontinuities like joints, faults and rock contacts. Each extensometer is installed in a specific location and can be composed by multiple rods of different lengths. Thus it is possible to monitor the vertical displacement of each geological discontinuity separately.

Each of the 30 extensometers has one, two or three rods, totaling 72 displacement measurements. Twenty four of these rods have automated acquisition data. In this work we use a data set composed by the readings of the Sector F extensometers that ranged from January/1995 to December/2004, totaling 72 time series of 120 readings each.

Due to the large amount of collected and stored data, as well as to the possibility of useful but hidden

information, it is necessary to use techniques that may allow us to transform data into knowledge, aiming at the decision making process related to dam's safety during its lifespan.

### 3 THE KDD PROCESS

The KDD—Knowledge Discovery in Databases—process is a set of continuous activities that shares the knowledge discovered in databases. This set is composed by 5 steps: data selection, pre-processing and data cleaning, data transformation (Data Warehouse), Data Mining, result interpretation and evaluation (Fayyad et al., 1996).

The KDD process starts with an organized clustering of the data mass. The data-cleaning step is performed by pre-processing those data in order to adapt them to the mathematical algorithms. Next, those data go through a transformation that will store them adequately in order to use the Data Mining techniques, which start by selecting the tools that shall be used. The main tasks in Data Mining are association, classification and clustering (Witten & Frank, 2005). In the end of the Data Mining process, a discovery report is produced. The interpretation of this report generates knowledge. The greatest advantage of Data Mining is that the information is discovered without being expected, because it was unnecessary to present a previous hypothesis.

In this work, the KDD process was used to select and point out the most important displacement reading series within the 72 attributes by applying mathematical models capable of performing this task.

### 4 METHODOLOGY

Time series is a set of observations sequentially generated in time which can show a serial dependency among them. Some purposes of analyzing time series are: to forecast future values in the series, describe the series' behavior and identify the mechanism that generates the series (Box et al., 1994).

Each one of the 72 rods displacement measures composed a time series and was called a "variable" identified with a code: for instance, equip4\_1, means extensometer 4 and rod 1. As the readings used were dated from January/1995 to December/2004, totaling 120 readings, we had a data matrix of order  $120 \times 72$ . For most instruments there was a monthly reading, but some of them presented more than a reading per month and in these cases we took the monthly average. Some of the instruments had missing readings and, in these situations, forecasts were made by Box & Jenkins methodology (Box et al., 1994). Using this procedure, all instruments had exactly 120 readings.

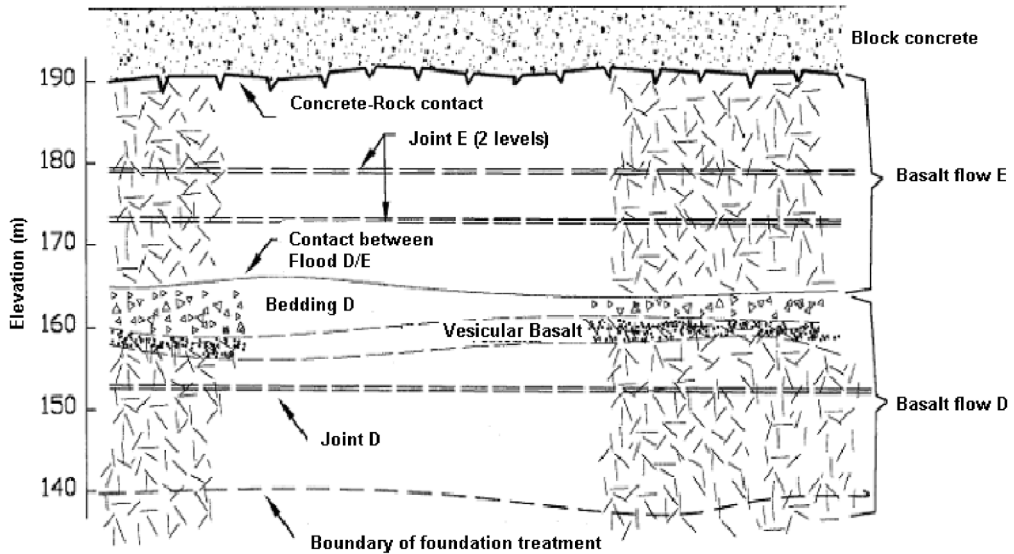


Figure 2. Basaltic geological profile of Itaipu Dam rock foundation—Sector F.

After time series pre-processing, we carried out the following analysis: Principal Component Analysis, Factor Analysis and Clustering Analysis (Johnson & Wichern, 1998). These tasks were done with the aid of the computational software Statgraphics Centurium XV.

The Principal Component Analysis was used to analyze the relationship among the variables of a set, transforming the original set into a new one composed by non-correlated variables called Principal Components, which have special properties in terms of variances. The Principal Components consisted in linear combinations of the original variables and they were obtained in a descendant priority order. The larger part of the data variability may be explained by a small number of principal components.

The main objectives of the Principal Component Analysis were: to reduce the number of variables and to indicate which variables or variable sets explain the larger part of the total variability, revealing which kind of relationship exists among them. In the Principal Components Analysis, it was possible to verify, for example, that some components represent a non-significant portion of the total variability (less than 1%) and that some variables are important (weights greater than 0,5 or less than -0,5) for these components. The most important variables corresponding to the less important components should not be selected.

Factor Analysis was a technique used to explain the correlations between a large set of variables in

terms of a set of few non-observable random variables, which were called factors. Within the same group, variables can be highly correlated between one another and correlations can be only a few from one group to another. Each group represents a factor that is responsible for the observed correlations. Communality is the variable variance part that is distributed throughout the factors.

Therefore, an additional criterion to select variables may be discarding those variables that had a lower communality. A low communality value indicated that the instrument and/or the corresponding rods did not work well or were not representative, in the case being analyzed.

Clustering Analysis is a technique in which clustering is made based on similarity or distance. Clustering may be hierarchic or non-hierarchic. In the hierarchic clustering there are as many groups as there are objects. Several different objects are clustered first. Then, these initial clusters are merged according to their similarities and eventually, by relaxing the similarity criterion, those subgroups merge until they form one single cluster. Clustering is carried out through connections. The most common connection types are: simple connection (closest neighbor), complete connection (most distant neighbor), average connection (distances average), Centroid Method and Ward's Method. The non-hierarchic clustering is used when the intention is to form  $k$  clusters. The most used non-hierarchic Clustering Method is the  $k$ -averages algorithm.

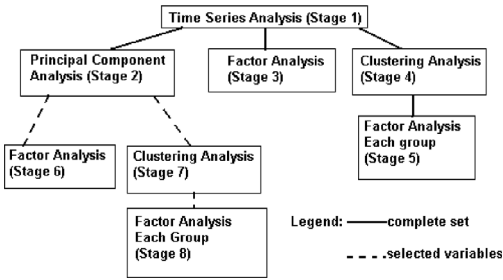


Figure 3. Flowchart of the proposed methodology.

The method used in this work was the Ward's one. The Ward's method does the fusion of two groups based on "loss of information" criterion (Johnson & Wichern, 1998). This criterion could be represented by the Square Quadratic Error (SQE). To each group  $i$ , the group mean (or centroid) and the square quadratic error ( $SQE_i$ ) were calculated. The  $SQE_i$  was obtained through the sum of square error of each variable of the group in relation to the group mean. To  $k$  groups we had  $SQE_1, SQE_2, \dots, SQE_k$  becoming possible the definition:

$$SQE = SQE_1 + SQE_2 + \dots + SQE_k \quad (1)$$

To each pair of groups  $m$  and  $n$ , the mean of the new formed group (group  $mn$ ) was calculated. Then the square quadratic error of group  $mn$  ( $SQE_{mn}$ ) was calculated. The square quadratic error (SQE) could be recalculated using:

$$SQE = SQE_1 + SQE_2 + \dots + SQE_k - SQE_m - SQE_n + SQE_{mn} \quad (2)$$

The groups  $m$  and  $n$  that resulted in the smallest increase in SQE (or the lowest "loss of information") could be merged. This method tends to create groups with the same size due to the minimization of the internal variation (Hair et al., 2005).

In Clustering Analysis, clusters were formed so that the variables within each cluster were highly correlated. Thus, the variables selection criterion in this work was aimed to select variables in order to keep at least one variable to represent the cluster. In this way, we applied Factor Analysis into each one of the formed clusters in order to select the variables that should remain in the cluster to represent it.

The methodology described above and adopted to reach the proposed goal is presented in a flowchart (Fig. 3).

As shown in flowchart, for the 1st stage composed by Temporal Series, the model was automatically chosen according to the Akaike criterion (AIC) and also

observing the root mean squared error (RMSE). We observed the residual integrated periodogram and in some cases, after analyzing the p-values in the parameters' "t" testing, the model was substituted by other considered more adequate or more economical.

Once performed the pre-processing of time series (Stage 1), Principal Component Analysis (PCA) was the next stage. It could select the variables based on their significance. After this stage (Stage 2), the next stages could be performed using the complete data set (solid line) or only variables selected during PCA. Then, factor and clustering analysis could be done. As a result of clustering analysis, the data were divided in groups and in each cluster was applied again factor analysis.

## 5 RESULTS

Firstly, the 120 time series were pre-processed leading to the uniformity of series size and periodicity of readings. Then in the principal component analysis (Stage 2), 63 components represent a non-significant portion of the total variability (less than 1%). Observing the important variables to these components, i.e. those which weights were greater than 0.5 or smaller than -0.5, only nine variables were discarded, remaining 63 variables. Among these ones, 17 variables were common with those automated by Itaipu. The single use of PCA was not a good selection criterion, because it could remain an excessive quantity of variables.

In the Factor Analysis, stage 3, it would be discarded the variables with low communalities, but no variable presented communality smaller than 0.71. Communality equal to 0.71 indicated that 71% of the variance of the variable was distributed to the factors and that only 29% was random. It meant that the corresponding instrument or rod works well. Therefore, 25 variables with higher communalities were selected. Among these ones, 14 variables were common with those automated by Itaipu.

In the Clustering Analysis (Stage 4), five clusters were observed. A common way to represent the hierarchical grouping is a dendrogram, which shows the similarity levels of grouping formation (Jain et al., 1999). The dendrogram can be "cut" in a specific level leading to a number of groups. The dendrogram with the clustering of stage 4 is shown in Figure 4. It was cut in the level of 5 clusters.

Observing the five clustering groups, the Factor Analysis were applied to each group in order to identify which instruments were the most important (Stage 5). The five variables with the highest communalities in each group were selected, totalizing 25 variables. Among these ones, 11 variables were also considered important by Itaipu's team.

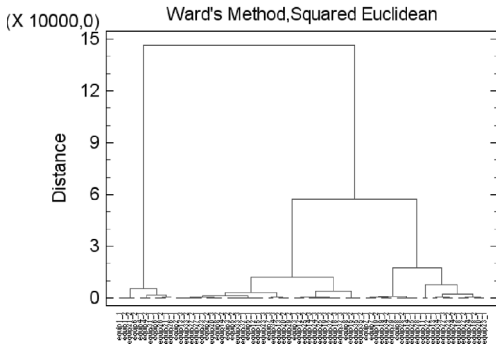


Figure 4. Dendrogram generated by Ward's Method (Squared Euclidean Distance) showing how the five clusters were formed—72 variables.

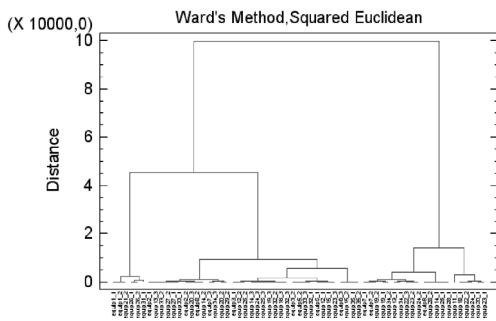


Figure 5. Dendrogram generated by Ward's Method (Squared Euclidean Distance) showing how the five clusters were formed—63 variables.

A different approach was also used to study the same problem. After PCA (Stage 2), only 63 selected variables were used to Factorial Analysis (Stage 6), where 25 variables were selected. The 63 variables were also used in Clustering Analysis (Stage 7) being divided in 5 groups, as shown in the dendrogram of figure 5. In each group was applied Factor Analysis (Stage 8) and the highest communality variables were selected. In both cases (stage 6 and stage 8 results), 25 variables were selected and 10 of them were common with those automated by Itaipu.

The results were organized in Table 1, where each line corresponds to an extensometer rod and the columns represent the selection criteria: Itaipu Engineering Team (IET); PCA/Stage 2 (ST2); Factor Analysis/Stage 3 (ST3); Clustering and Factor Analysis/Stage 5 (ST5); Factor Analysis of selected data/Stage 6 (ST6) and Clustering and Factor Analysis of selected data/Stage 8 (ST8). "X"s mark the variables selected for each criterion.

Table 1. Important variables selected using different criteria.

	IET	ST2	ST3	ST5	ST6	ST8
equip1_1	x	x	x		x	x
equip1_2	x	x	x		x	x
equip2_1		x				
equip2_2		x				
equip3_1		x	x		x	x
equip3_2		x		x		
equip4_1	x		x	x		
equip4_2	x		x	x		
equip5_1		x	x		x	x
equip5_2		x				
equip6_1	x		x	x		
equip6_2	x		x			
equip7_1		x				
equip7_2		x				
equip7_3		x				
equip8_1		x				
equip8_2		x				x
equip8_3		x				
equip11_1		x	x		x	x
equip12_1		x				
equip12_2		x				
equip13_1		x			x	
equip13_2					x	
equip13_3		x		x		x
equip14_1		x		x	x	x
equip14_2		x				
equip14_3		x	x	x	x	x
equip15_1		x				
equip15_2		x				
equip18_1		x				x
equip18_2						
equip18_3		x				
equip19_1		x				
equip19_2		x		x	x	
equip19_3		x		x		
equip20_1		x				
equip20_2		x				x
equip20_3		x				
equip21_1	x		x	x		
equip21_2	x	x	x	x	x	x
equip22_1	x		x	x		
equip22_2	x	x	x		x	x
equip22_3	x	x	x	x	x	x
equip23_1		x	x	x	x	x
equip23_2		x	x	x	x	x
equip23_3		x				
equip24_1		x	x	x	x	x
equip24_2		x	x		x	
equip24_3		x				
equip25_1			x			
equip25_2		x				
equip25_3		x		x	x	
equip26_1	x	x				
equip26_2	x	x			x	x
equip27_1	x	x				
equip27_2	x	x			x	
equip28_1		x	x		x	
equip28_2		x		x		x

(Continued)



Table 1. (Continued)

	IET	ST2	ST3	ST5	ST6	ST8
equip29_1	x		x	x		
equip29_2	x	x	x	x	x	x
equip31_1	x	x				x
equip32_1	x	x				
equip32_2	x	x				
equip32_3	x	x				
equip33_1		x				
equip33_2		x	x		x	
equip33_3		x		x	x	x
equip34_1	x	x			x	x
equip34_2	x	x		x		
equip34_3	x	x	x	x	x	x
equip35_1		x		x		
equip35_2		x		x		
Total	72	72	72	72	63	63
Selected	24	63	25	25	25	25
Common with IET	–	17	14	11	10	10

Columns: Criterion of Variable Selection:

IET= Itaipu Engineering Team

ST2=Principal Component Analysis/Stage 2

ST3= Factor Analysis/Stage 3

ST5= Clustering and Factor Analysis/Stage 5

ST6= Factor Analysis of selected data/Stage 6

ST8= Factor Analysis of selected data/Stage 8

## 6 CONCLUSION

This paper presented a methodology based on Data Mining techniques that can be useful to the decision making process related to a dam safety. Different criteria of variable selection were used to point out which instruments were the most relevant within a real data set of readings. From 72 extensometers rods installed in Sector F of Itaipu dam, 25 were selected as the most important to represent the behavior of dam foundation, for 4 of 5 adopted criteria. However, the selected rods were not exactly coincident among the diverse criteria.

There were also some differences between instruments chosen to automation and the selected for the proposed methodology. These differences have been discussed and some instruments indicated as relevant in the present analysis can be automated in a near future.

Other engineering and mathematical criteria are in development by the authors. The presented and the new criteria must be implemented in a user friendly software that will be available soon.

## ACKNOWLEDGMENTS

The authors would like to thank FINEP for its financial support to the research project AIEVC—“Uncertainty Analysis and Estimation of Control Values for the Geotechnical-structural Monitoring System at the Itaipu Dam”, to CAPES for the third author’s scholarship and to the Itaipu civil engineering team for instrumentation data and technical contributions.

## REFERENCES

- Box, G.E.P., Jenkins, G.M. & Reinsel, G. *Time Series Analysis: forecasting & control*. 3rd. Edition, Prentice Hall, 1994.
- Bowles, D.S., Anderson, L.R., Glover, T.F. & Chuhan, S.S. *Dam Safety Decision-Making: Combining Engineering Assessments With Risk Information, Proc. of 2003 US Society on Dams Annual Lecture*, 2003.
- Dibiagio, E. Question 78—Monitoring of Dams and Their Foundations—General Report: *Proc. Of Twentieth Congress on Large Dams, ICOLD*, 1459–1545, Beijing, 2000.
- Fayyad, U.M., Piatetsky-shapiro, G., Smyth, P., & Uthuramy, R. *Advances in knowledge Discovery & Data Mining*. MIT Press, 1996.
- Hair JR, J.F., Anderson, R.E., Tatham, R.L. & Black, W.C. *Análise Multivariada de Dados*. Bookman. São Paulo, 2005.
- Icold, *International Commission on Large Dams*. Available in: <http://www.icold-cigb.org/> Accessed in: Jan/02/2008.
- Itaipu. *Itaipu Binacional*. Available in <http://www.itaipu.gov.br>. Accessed in April/01/2007.
- Jain A.K., Murty M.N., & Flynn P.J. Data clustering: a review. *ACM Computing Surveys*. v. 31, n. 3, set. 1999.
- Johnson, R.A. & Wichern, D.W. *Applied Multivariate Statistical Analysis*. 4th Edition. Ed. Prentice Hall, 1998.
- Osako, C.I. *Drain Maintenance of Dam Foundation—Itaipu Hydrelectrical Power Plant Case Study*. M.Sc. Dissertation, Federal University of Paraná, Curitiba, 2002 (in portuguese).
- Witten, I.H. & Frank, E. *Data Mining—Practical Machine Learning Tools and Techniques*. 2nd. Edition. Ed. Elsevier, 2005.

# Algorithm for identification of damage on bridge piers

A.S. Kiremidjian, P. Sarabandi, A. Cheung, C. Cabrera & K.K. Nair

*Department of Civil and Environmental Engineering, Stanford University, Stanford, California, USA*

G. Kiremidjian

*Sensametrics, Inc., Palo Alto, California, USA*

**ABSTRACT:** Data from a quarter scale four-span three-pier bridge subjected to gradually increasing earthquake motion is collected using wireless sensing system as part of the experiment conducted at the University of Nevada, Reno under the NSF-NEES Research Program. The data are used to compute a damage measure based on the Mahalanobis distance between undamaged and various damage states of the bridge, where the data are modeled as a Gaussian mixture. Based on the results from the data analysis, the algorithm is to identify the onset of damage and an excellent agreement is found between the measured and observed damage states.

## 1 INTRODUCTION

Structural health monitoring methods that utilize statistical pattern recognition methods have become increasingly popular (see Chang 1999, 2001, 2003, 2005 and 2007). In all these methods, either an autoregressive, AR, (e.g., Sohn et al. 2005, Nair and Kiremidjian 2006, 2007, Lynch et al. 2006, Noh et al. 2007) or a wavelet (Nair 2007) is fitted to measurement data and the parameters of the model are used in formulating a damage sensitive feature. In addition, Nair and Kiremidjian (2006) showed that changes in the first three AR coefficients are related to changes in the stiffness of the structure. These methods have gained popularity because of their computational efficiency making them particularly suitable for embedding on a small form microprocessor such as those used in wireless structural monitoring systems. The initial testing and validation of these methods was limited to the ASCE Benchmark structure and the results were indeed very promising. Additional testing and validation is needed, however, for data collected on a variety of structures under different loading and environmental conditions.

In this paper, we present the results of the application of one of the damage models developed by Nair and Kiremidjian (2007) to data collected from a four-span three-pier one quarter scale bridge. The test was part of the National Science Foundation Network for Earthquake Engineering Simulation Program that was conducted on February 12–15, 2007 at the University of Nevada Reno in collaboration with the California Department of Transportation (CALTRANS). The data, which was collected with a wireless monitoring

system, was tested with several algorithms; however, in this paper we present the results from the application of the data to the AR model with a Gaussian Mixture model to describe the migration of AR coefficients as damage is induced to the structure. Excellent results are obtained both for identifying and quantifying the damage on the bridge piers which was the main damage mode observed from the experiment.

## 2 DESCRIPTION OF BRIDGE TEST

The University of Nevada, Reno performed a series of tests on a one quarter scale four-span bridge with three piers and two abutments mounted on three shaking tables and connected to additional actuators to enable two dimensional shaking at the piers and shaking at the abutments. The model for the bridge is shown in Figure 1.

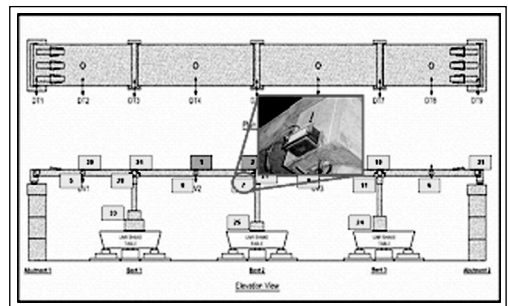


Figure 1. Test set-up of four-span three pier bridge with wireless sensor installation.

Seventeen wireless structural monitoring sensing units were installed on the bridge and their locations are shown with a sample photo of the sensing unit. Each sensing unit was equipped with two three-dimensional accelerometers, one for low noise vibration measurements with a noise floor of  $10^{-6}$ g and a dynamic range of 10 g but scaled to 5 g for increased accuracy and a three dimensional strong motion accelerometer with a noise floor of  $10^{-4}$ g and dynamic range of 6 g. In addition, three of the sensing units had built-in Whitstone bridges and six strain gages embedded in the piers were connected to the sensing units. The sensing units also had temperature and humidity gages. Each sensing unit was equipped with two microprocessors—one microprocessor for managing the unit and a computational microprocessor for analysis of the data with embedded algorithms. Data collected by the sensors in the unit was stored on an SD card. The sensing system was controlled wirelessly from a laptop which contained a decision support system and served as the system manager. Information from the units was also wirelessly transmitted to the decision support system. The wireless communication was achieved through a multi-hopping ZigBee compliant wireless communications network using 802.15.4 wireless radios.

The bridge was subjected to a series of unidirectional white noise motions in both the transverse and the longitudinal direction of the bridge and bidirectional strong ground motions scaled gradually to increasing amplitudes. Table 1 lists the characteristics of the various input motions for the test. Data were collected from all test runs.

### 3 DAMAGE MODEL OVERVIEW

Several damage detection models have been developed by Nair and Kiremidjian (2006, 2007) and Nair (2007) that use statistical pattern classification methods. In this paper we use the autoregressive moving average model, ARMA, to characterize the ambient response data at various test runs. The response to the white noise excitation is treated as ambient vibrations for that purpose. In this approach, the vertical response acceleration time history  $x(t)$  at a particular location on the structure is modeled with an ARMA function given by

$$x(t) = \sum_{k=1}^p \alpha_k x(t-k) + \sum_{k=1}^q \beta_k \varepsilon(t-k) + \varepsilon(t) \quad (1)$$

Where  $\alpha_k$  are the AR coefficients and  $\beta_k$  are the MA coefficients,  $\varepsilon(t)$  are the residuals of the function.

After testing and validation of variety of data, it was found that the AR coefficients are sufficient to the

Table 1. Test schedule of input motions

Test No.	Motion level	Test type	Motion PGA (g) Trans.	Motion PGA (g) Long.
WN01		White Noise (Trans.)		
WN02		White Noise (Long.)		
1A	1	W/Restrainer	–	0.09
1B	1	W/Restrainer	–	0.09
1C	1	Longitudinal	–	0.09
1D	1	Biaxial	0.075	0.09
WN11		White Noise (Trans.)		
WN12		White Noise (Long.)		
2	2	Biaxial	0.15	0.18
WN21		White Noise (Trans.)		
WN22		White Noise (Long.)		
3	3	Biaxial	0.25	0.3
WN31		White Noise (Trans.)		
WN32		White Noise (Long.)		
4A	4	W/Restrainer	–	0.60
4B	4	W/Restrainer	–	0.60
4C	4	Longitudinal	–	0.60
4D	4	Biaxial	0.50	0.60
WN41		White Noise (Trans.)		
WN42		White Noise (Long.)		
5	5	Biaxial	0.75	0.90
WN51		White Noise (Trans.)		
WN52		White Noise (Long.)		
6	6	Biaxial	1.00	1.20
WN61		White Noise (Trans.)		
WN62		White Noise (Long.)		
7	7	Biaxial	1.00	1.20

vibration signals. Furthermore, Nair and Kiremidjian (2006) showed that the first three AR coefficients are functionally related to the structural stiffness. Thus, the damage detection algorithm uses only  $\alpha_x, \alpha_y$  and  $\alpha_z$  to form its feature vector  $A = \{\alpha_x, \alpha_y, \alpha_z\}^T$ . To obtain statistics of these coefficients, a signal  $x(t)$  is divided into  $n$  segments and the AR model is fitted to each segment resulting in a set of data  $\{\alpha_{xi}, \alpha_{yi}, \alpha_{zi}\}$ . The input motion is white noise stationary Gaussian and the response measurements, thus will also be white noise stationary Gaussian. We use this property to develop a damage detection algorithm.

The premise for the damage detection algorithm is that the first three AR coefficients will change as damage is introduced to the structure. Since the process is white noise Gaussian, the first three AR coefficients are samples from a three dimensional Gaussian model. If the pre- and post- damage signals are different, then the properties of the AR coefficients are likely to be different thus resulting in different Gaussian models. For this purpose we use a Gaussian Mixture model which starts with the assumption that the pre- and post-damage AR coefficient data most likely come from different mixtures. The Gaussian mixture model, GMM, is given by

$$f(A_{1:N}) = \sum_{i=1}^M \pi_i \phi_i(A; \theta_i) \quad (2)$$

where  $\mathbf{A}$  is the collection of  $N$  feature vectors,  $\phi_i \sim N(\mu_i, \Sigma_i)$  is a Gaussian vector with mean vector  $\mu_i$  and covariance matrix  $\Sigma_i$  and  $\pi_i$  is the non-negative mixture weight for each class. The unknown parameters  $\Theta = \{\mu_i, \Sigma_i, \pi_i \mid i = 1, 2, \dots, M\}$  of the GMM can be estimated using the maximum likelihood principle. The direct maximization of the likelihood function is quite difficult and analytically intractable. For this purpose, the expectation maximization (EM) algorithm is used. The derivation of the EM algorithm and its working is given in Nair and Kiremidjian (2007).

### 3.1 Damage Identification

As damage is introduced to the structure, the vector of AR coefficients  $\mathbf{A}$  will migrate and the Gaussian distributions corresponding to each mixture will move away from each other. Thus, if we determine that  $M$ , the number of mixtures in the data of AR coefficients is 2 or greater, then there are more than two Gaussian vectors represented in that data and the data is coming from two distinct populations. Thus, we conclude that if  $M$  is 2 or greater, then damage has occurred. To determine how many mixtures are present, we use the Gap statistic as introduced by Tibshirani et al. (2001). (See Nair and Kiremidjian 2007 for detailed explanation of the gap statistic application to damage identification).

### 3.2 Damage Quantification

In general, as damage to the structure increases, the two Gaussian mixtures will migrate further apart from each other. The distance between the mixtures can then be used as a measure of the damage extent. The authors first considered the simple Euclidean distance which does not include any information on the dispersion of the data around the mean value of each Gaussian model. Then a damage measure based on

the Mahalanobis distance was defined which weighs the mixture separation distance with the covariance matrices of the two vectors of data. It was found that the damage measure using the Mahalanobis distance is a more robust measure of damage and thus it was used in the application presented in this paper.

The Mahalanobis distance between two vectors  $\mathbf{x}$  and  $\mathbf{y}$  with a covariance matrix  $\Sigma$  is defined as follows:

$$\Delta(\mathbf{x}, \mathbf{y}; \Sigma) = \sqrt{(\mathbf{x} - \mathbf{y})^T \Sigma^{-1} (\mathbf{x} - \mathbf{y})} \quad (3)$$

Thus the damage measure DM is defined in terms of the distance between the mean value vectors of the two Gaussian mixtures,  $\mu_u$  and  $\mu_d$ , corresponding to the undamaged and damaged states of the structure, respectively, weighted with respect to the cross-covariance matrix  $\Sigma_{ud}$ :

$$DM = \sqrt{(\mu_u - \mu_d)^T \Sigma_{ud}^{-1} (\mu_u - \mu_d)} \quad (4)$$

A normalized measure is proposed by Nair and Kiremidjian (2007) and by Noh et al, 2007; however, only the results from the application of equation 4 are presented in this paper.

## 4 MODEL APPLICATION TO BRIDGE TEST DATA

Three dimensional acceleration data from the various tests were sampled at a 200 Hz. Only the vertical response motions were used in the analyses presented in this paper. The data collected from the bridge test was used to test the ability of the model to detect and quantify damage. For that purpose the data were first de-noised and filtered. Figure 2 shows data collected at the mid-span of the deck between bents 1 and 2. The top figure shows the variation of the signal with time due to the warm-up period required by the sensor. Thus, we first remove the effect of temperature, and then filter the signal resulting in the record shown in the bottom of the figure. The signal is then tested for satisfying stationary and Gaussian properties. In all cases the data showed that we have a stationary and Gaussian time history (see Rice 1999).

The white noise data from runs WN01 and WN02 were used as the baseline cases corresponding to the undamaged case. A one minute time history was used for each analysis. Each time history was divided into segments each with a minimum of 400 points. Previous tests performed by the authors have shown that the AR coefficients become stable at samples of 400 or more. The Akaike Information Criteria was used to determine the order of the AR function and for all cases an order  $p = 5$  was found to be sufficient.

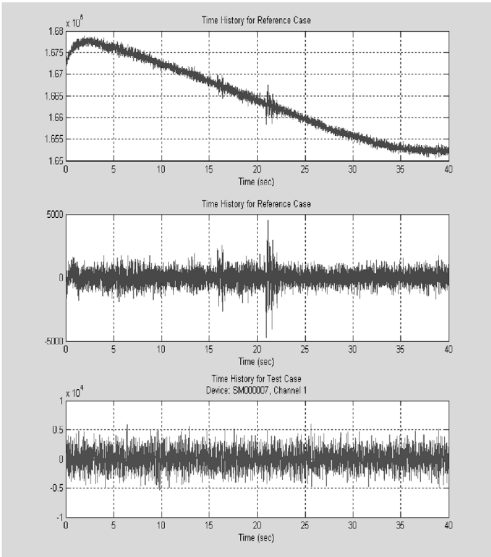


Figure 2. Detrending and denoising of recorded signal.

Table 2. Damage measure based on Mahalanobis distance.

Test	Damage Measure
Reno—Setup Day DC1 and DC2	baseline
Mild Shaking Day 1, White Noise 31	21
Mild Shaking Day 2, White Noise 41	36.8
Moderate Shaking Day 3, White Noise 51	57
Final Test Day, White Noise Run 61	60

The AR coefficients were then computed for each sample of the undamaged time history. Since there were two input white noise motions, two response acceleration time histories were used in the analysis.

The same analysis was also performed with the response motions to the white noise excitation obtained after each strong ground motion. Thus a set of AR parameters is obtained after ground motion levels 2, 3, 4 and 5 (see Brockwell and Davis, 2002 for methods of computing AR coefficients). The damage measure was computed in each case and is listed in Table 2.

As can be seen from Table 2, the damage measure, DM, increases gradually from the baseline case to 21, 36.8, 57 and 60. It is interesting to note that with the last test the damage measure does not increase significantly mostly because the structure is near the limit at which it is considered to be almost next to collapse.

The migration of the  $A$  coefficients from no damage to damage corresponding to white noise motions WN11 and WN41 are shown on the top of Figure 4

and those from the corresponding longitudinal input white noise WN12 and the response vertical acceleration WN42 are shown on the bottom of Figure 4. Two distinct and well separated clouds are shown in both cases as also confirmed by the gap statistics of these data; however, the dispersion in the alpha coefficients from the response motion to the longitudinal input appears to be much greater than that from the transverse input white noise. The damage measure is estimate to be 36.8.

The response acceleration records in the vertical direction obtained from the baseline white noise WN11 input motion and the response to the white following the shaking WN41 are shown on Figure 3.

At ground motion level 4 there was significant damage to the bridge piers with the largest damage observed to the piers in bent 1. The concrete cracked extensively and spalled exposing the rebar at the base of the pier. Figure 5 shows the damage to one of the pier at bent 1.

Figures 6 shows the recorded acceleration from the baseline white noise WN11 and the response motion from WN61 after the 0.50 g and 0.60 g biaxial strong motions were applied to the structure. Figure 7 shows the alpha coefficients for the respective undamaged and damaged states. The alpha clouds are further separated but the dispersion appears to be increasing as damage to the structure increases. The damage measure for this case is evaluated to be 60.

Figure 8 shows the damage to one of the piers corresponding to the biaxial motions of 1.0 g and 1.2 g. The damage to the pier is extensive, the concrete had already spalled at earlier strong motions and the rebar had buckled with this ground motion.

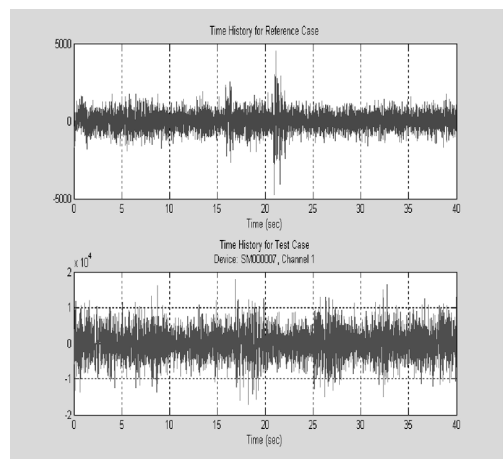


Figure 3. White noise data. The blue (on top) is obtained from WN11 and the red (bottom) is from WN41.

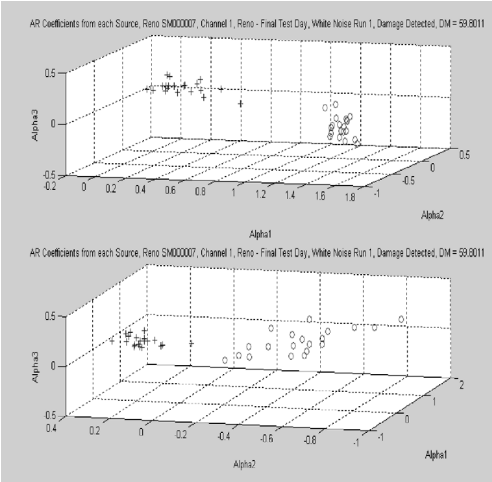


Figure 4. White noise data AR coefficients. The top graph combines WN11 and WN41. The bottom graph combines WN12 and WN42.

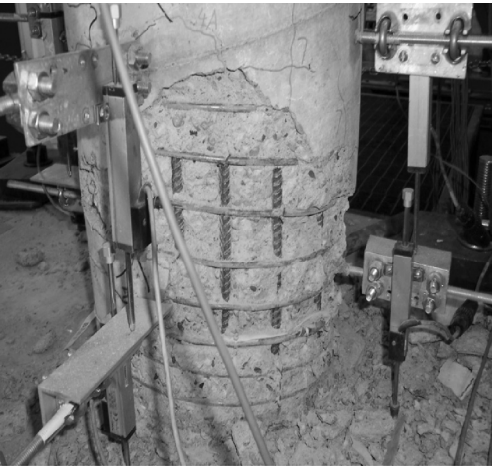


Figure 5. Damage to bridge pier after ground shaking level 4. Damage measure DM = 36.8.

Similar results were obtained from measurements at other locations on the bridge further confirming the robustness of the algorithm. In addition to this algorithm previously developed algorithms using statistical significance testing were also validated successfully with these data. Furthermore, a wake-up algorithm was tested with the system with three of the units that detected the strong biaxial shaking. This algorithm is intended to put the sensing units to sleep under normal operating conditions and to wake them up when an earthquake strong motion has occurred

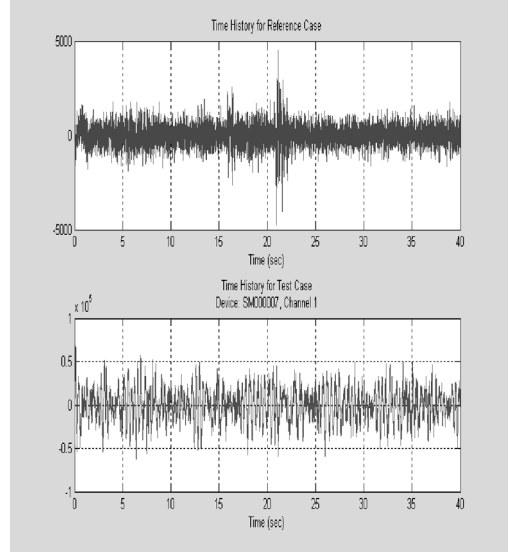


Figure 6. White noise data. The blue (on top) is obtained from WN11 and the red (bottom) is from WN61.

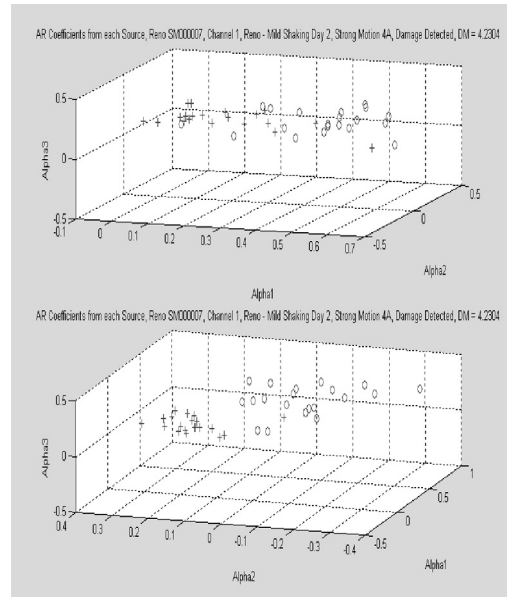


Figure 7. White noise data AR coefficients. The top graph combines WN11 and WN61. The bottom graph combines WN12 and WN62.

instructing them to start data collection of the response of the structure to the strong motion. Instructions are also given to the unit to collect ambient vibrations immediately after the strong motion has ceased.

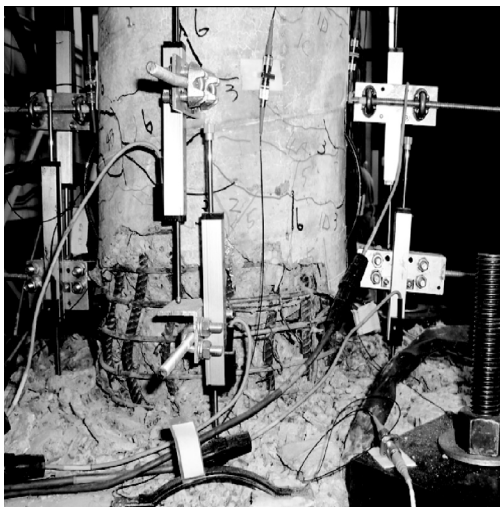


Figure 8. Damage to bridge pier at bent 1 after ground shaking level 5.

## 5 CONCLUSIONS

Analysis of the data from the strong earthquake motion test of a four-span three pier bridge at the University of Nevada, Reno demonstrated that the algorithm based on AR model fitting through the vibration signals with a Gaussian mixture modeling of the AR coefficients is able to detect damage at all the stages of damage that were induced to the structure. These included initial hairline cracking of the concrete at the base of the piers, extensive cracking at higher ground motions, spalling of the concrete and exposing of the rebar, buckling of the rebar and breaking of the rebar with increasing levels of biaxial ground shaking. The damage measure based on the Mahalanobis defined in this paper is found to correlate well to the degree of damage varying from 21 to 36.8 to 57 to 60 with each value corresponding to successively higher level of damage.

This test is another demonstration of the efficacy of the algorithm as illustrated with earlier applications with simulated and small scale laboratory test. Additional test, however, still need to be performed under varied environmental conditions to further validate the model. Furthermore, data from well controlled field experiments need to be generated and used in validating the algorithm under operating conditions. Similarly, additional tests need to be performed for calibration of the damage measure. It is not clear how the magnitude of the damage measure will behave with more complex structures where local damage may have different implications on the overall structural

performance. These issues still need to be investigated before the algorithm can be applied in practice.

## ACKNOWLEDGEMENTS

This research was partially supported by the NSF-NEESR Grant—15BBK16379 and by the NIST-ATP program. The authors gratefully acknowledge their support. We also thank Sensametrics, Inc. for providing all the data collected with their system.

## REFERENCES

- Brockwell, P.J. and Davis, R.A. (2002). *Introduction to Time Series and Forecasting*. Springer-Verlag, Second Edition, New York.
- Chang, F.-K. (ed.) (1999, 2001, 2003, 2005, 2007 and), *1st, 2nd, 3rd, 4th and 5th International Workshops on Structural Health Monitoring*, Stanford University, Stanford, CA 94305.
- Lynch, J.P., Wang, Y. Lu, K.-C., Hou, T.-C. and Loh, C.-H. (2006). "Post-Seismic Damage Assessment of Steel Structures Instrumented with Self-Interrogating Wireless Sensors," *Proceedings of the 8th National Conference on Earthquake Engineering* (8 NCEE), San Francisco, CA.
- Nair, K.K. (2007). "Signal Processing Based Damage Detection Algorithms for Structural Health Monitoring", Ph. D. Dissertation, Department of Civil and Environmental Engineering, Stanford University, Stanford, CA 94305.
- Nair, K.K., Kiremidjian, A.S. and Law, K.H. (2006). "Time Series-Based Damage Detection and Localization Algorithm with application to the ASCE Benchmark Structure," *Journal of Sound and Vibration*, 291 (2), 349–368.
- Nair, K.K. and Kiremidjian, A.S. (2007). "Time Series-Based Structural Damage Detection Algorithm Using Gaussian Mixtures Modeling," *Journal of Dynamic Systems, Measurement, and Control*, 129, 285–293.
- Noh, H., Nair, K.K., Kiremidjian, A.S. and Loh, C.-H. (2007). "Application of a Time Series-Based Damage Detection Algorithm to the Taiwanese Benchmark Experiment," *International Conference on Applications of Statistics and Probability in Civil Engineering*, CD Rom, Chiba, Japan. ISBN 978-0-415-45211-3.
- Rice, J.A. (1999) *Mathematical Statistics and Data Analysis, Second Edition*, Duxbury Press, Second Edition, New York.
- Sohn, H., Farrar, C.R., Hunter, H.F. and Worden, K. (2001). "Applying the LANL Statistical Pattern Recognition Paradigm for Structural Health Monitoring to Data from a Surface-Effect Fast Patrol Boat", *Los Alamos National Laboratory Report LA-13761-MS*, Los Alamos National Laboratory, Los Alamos, NM 87545.
- Tibshirani, R., Walther, G. and Hastie, T., (2001). "Estimating the Number of Clusters in a Dataset via the Gap Statistic," *Journal of the Royal Statistical Society: Series B*, 63 (2), pp. 411–423.

# Analysis, heuristics, and uncertainty of hybrid life cycle assessment: agriculture and construction case studies

A.E. Landis & M.M. Bilec

*University of Pittsburgh, Pittsburgh, Pennsylvania, USA*

**ABSTRACT:** The outcome of a life cycle assessment (LCA) is heavily reliant on the input data acquired during the life cycle inventory (LCI), the approach utilized to construct the LCI, and the methods used to develop the life cycle impact assessment (LCIA). LCI is generally developed using either a process or input-output (I-O) approach; both techniques have advantages and disadvantages. The main shortcoming of the process model is the subjectivity and inconsistencies of boundary selection, whereas the I-O method produces highly aggregated results. Additionally, neither typically incorporates uncertainty. By combining the two methods into a single framework the best aspects of each inventory approach are developed, while the weaknesses are minimized. Two case studies, corn production and on-site construction processes, are presented to demonstrate the advantages and disadvantages of LCA approaches. Although seemingly different, the case studies exemplify the use of hybrid LCA for disparate systems. The on-site construction case study explores the differences between process, I-O, and hybrid inventories. The corn production case study focuses on uncertainty in the inventory and impact assessment stages of LCA.

## 1 INTRODUCTION

### 1.1 *Background*

The outcome of an LCA is heavily reliant on the input data acquired during the life cycle inventory (LCI), the approach utilized to construct the LCI, and the methods used to develop the life cycle impact assessment (LCIA). The LCI phase of a LCA is often the most data and time intensive. Incorporating uncertainty and variability estimates for both input parameters and models is a daunting but essential step in the growth of more detailed and accurate LCAs. Typically one number will be used to represent a parameter within the LCI, when in many systems one number is insufficient for representing the range, variability and uncertainty in reality. If LCA is to continue as viable method to evaluate the environmental impacts of a product or process, then minimizing the time, improving the data quality, and providing practical options to develop an LCI and LCIA are critical.

### 1.2 *LCI modeling approaches*

Currently, three modeling options exist for the LCI: process, input-output, and hybrid. Process and input-output methods are widely used and have strengths and limitations. Hybrid modeling combines both approaches and attempts to address limitations in each approach.

The process LCI method systematically models the known environmental inputs and outputs by utilizing a process flow diagram. The scope of the process model continues to the point where the flow between process and emissions are negligible. The process approach was further developed with the framework established in the ISO 14040 series. This approach requires data collection from public sources, company or product specific information, and published research.

Another LCI method is input-output (I-O) analysis. Economic I-O analysis was developed by Wassily Leontief in the 1930s (Leontief 1936). Leontief developed an interdependency model that quantifies proportional interrelationships among economic sectors in an economy. I-O LCA combines national sector-by-sector economic interaction data, which quantifies the dependencies between sectors, with sector level environmental effects and resource use data. Using matrix operations, a change in economic demand from a sector can be quantified in environmental effects or resource use. While the US has the largest number of defined sectors and a broad range of publicly available environmental data, other countries, including Japan, Netherlands, and Australia, have developed I-O LCAs (Kondo et al. 1998; Lenzen 1998; Pesonen et al. 2000), using similar techniques to link economic and environmental data. Early work combining I-O data with energy analysis was completed by Bullard et al. (1978). Carnegie Mellon University has developed an I-O



based LCA tool, Economic Input-Output LCA (EIO-LCA) (Lave et al. 1995; Hendrickson et al. 1998).

### 1.3 Hybrid LCA

Because of advantages and disadvantages associated with both process and I-O, several researchers have proposed a hybrid approach that combines the strengths of both methods. One of the major limitations of the process model is the subjective determination of the boundary location; conversely, I-O LCA effectively eliminates the boundary issue by considering the interactions in an entire economy. The boundary for process LCAs is typically drawn around the direct impacts and to a point acceptable to the LCA practitioner; whereas, the boundary using I-O is able to capture all of the components, including indirect impacts. The exclusion of "indirect impacts" is important as results show that 132 first-order LCAs produced truncation errors of higher than 50% (Lenzen 2001). A major disadvantage of I-O LCA is that it typically does not include the use and end-of-life phases, necessitating the combination of process data. Because errors in process LCA models can be high and there is no scientific basis for determining an LCA's boundary, the credibility of pure process LCI as a technical tool is questionable (Lave et al. 1995; Suh et al. 2004).

Hybrid LCI models offer possible solutions to the process/I-O issues. Within the hybrid LCI realm, there are four general types of hybrid models: tiered, input-output based, integrated, and 'augmented process-based.' Although the models are classified into groups, they all combine process and I-O methods and differ primarily in the proportions of input-output and process data. As a whole the models represent a continuum of hybrid model development. Tiered hybrid analysis uses mainly input-output data and augmented process-based uses the largest proportion of process information.

### 1.4 Uncertainty in LCA

Incorporating uncertainty and variability estimates for both input parameters and models is a daunting but essential step in the growth of more detailed and accurate LCAs. The outcome of an LCA is heavily reliant on the input data acquired during the LCI as well as the methods used to develop the LCIA. Typically one number will be used to represent a parameter within the LCI, when in many systems one number is insufficient for representing the range, variability and uncertainty in reality. Monte Carlo simulation is a technique used to quantify uncertainty by propagating known uncertainties from probability distributions to the output variable. Monte Carlo analysis (MCA) within an LCI framework allows for the capture of parameter

variability and uncertainty. IA models contain both variability and uncertainty, as well as uncertainty associated with the model itself.

The IMPACT 2002 impact assessment model is one of the few IA tools that incorporates estimates of uncertainty into its factors. Parameter uncertainty is estimated for human toxicity (combined cancer and non-cancer) and ecotoxicity (combined aquatic and terrestrial ecotoxicity) for chemicals in the IMPACT 2002 database (Pennington et al. 2005). The uncertainty information is not incorporated into the overall impact assessment tool, IMPACT 2002+ (Jolliet et al. 2003). Nearly 1000 characterization factors for human toxicity, aquatic ecotoxicity and terrestrial ecotoxicity are derived from the IMPACT 2002 model. Using a risk-based approach, the model estimates toxicological impacts per unit emission based on chemical fate and transport as well as the risk and exposure of an effect for Western Europe. Parameter uncertainty associated with fate and human exposure as well as human health effects was developed by Hofstetter (1998) and were expressed as a set of fixed factors based on representative distributions for groups of chemicals with similar attributes. The factors are the square geometric standard deviation associated with lognormal distributions and are classified into three different certainty classes: high, medium, and low.

## 2 CASE STUDIES

### 2.1 On-site construction case study

The on-site construction processes case study used the 'augmented process-based' hybrid model, which was also employed by Guggemos and Horvath (2005) for modeling the life cycle of a commercial building. Since construction is a deregulated sector in the US, process data is limited. However, when available, process data was used in conjunction with typical project records and practices. Additionally, the construction industry has existing financial construction data in estimating software and scheduling tools. This monetary data can be used in I-O tools such as EIO-LCA without the need to collect additional data.

The scope of this case study focused on understanding the environmental impacts of primarily on-site construction processes for buildings, since building research has focused on other phases of a building's life cycle (materials, use, and end-of-life). The on-site construction phase is often overlooked when the entire life cycle is considered, leading to a gap in understanding the whole spectrum and possible sources of environmental impacts on the built environment. Since construction represents a significant portion of the U.S. economy, approximately 5 to 10% of the gross domestic product (GDP), opportunities exist to

examine the construction phase and identify areas where a reduction in environmental impacts could occur.

The hybrid LCA construction model was created in the software program, Analytica, a highly visual modeling tool that creates, analyzes, and communicates process decision models (Lumina Decision Systems 2006). Analytica has been used with other LCAs (Thabrew et al. 2007), (Lloyd et al. 2007). Attractive features of Analytica are its statistical capabilities and uncertainty analyses. The model's overall organization and process models are based on CSI format and R.S. Means (R.S. Means 2006). The model combines several data sources, including both process and EIO-LCA data, into one common LCA framework. Examples of the type of user input required are dollar value of construction, quantity of brick, and hours of generator. The model's scope is on-site construction activities, transportation from the manufacturer or supplier to the construction site, and construction service sectors. The model is able to produce both life cycle inventory and life cycle impact assessment results.

## 2.2 Comparison of LCI results—process, EIO-LCA, and hybrid

A comparison of the construction phase only was made between the steel framed case study from Guggemos and Horvath (2005), results from this research, and pure EIO-LCA results. The external demand was \$13 million representing the cost of construction in the Commercial and Institutional sector in EIO-LCA model. Since the EIO-LCA results contain both the material and construction phases, the results for the material phase were subtracted, using the averages from the material phases values from Junnila et al. (2006) and Guggemos and Horvath (2005). CO<sub>2</sub> emissions and energy were compared with the results showing that the hybrid model falls between EIO-LCA and Guggemos and Horvath results as shown in Figure 1 and Figure 2. Similar results were found for

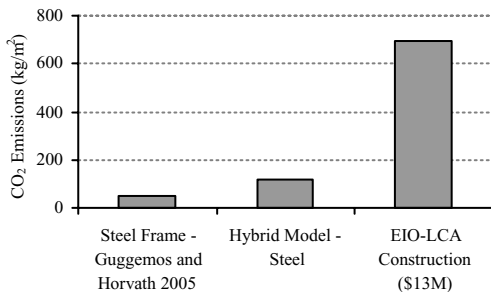


Figure 1. Construction CO<sub>2</sub> case study comparison.

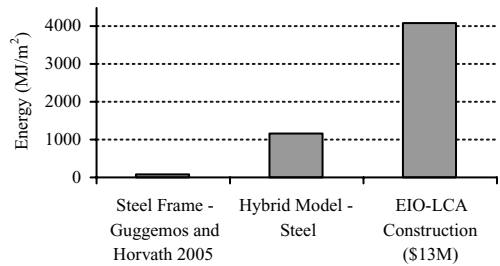


Figure 2. Construction phase-energy case study comparison

SO<sub>2</sub>, and NO<sub>x</sub>; the hybrid model is higher for PM<sub>10</sub> than both studies.

## 2.3 Agriculture case study

Incorporating agricultural air and aqueous emissions into LCAs has historically been problematic since data varies greatly by the scale of the system (within regions, states, and farms) and since nonpoint sources are customarily difficult to model. The corn case study inventory is of importance as it is a major agricultural feedstocks for both food and bioethanol production in the US. An increasing number of LCAs are being conducted to determine the energy balance and environmental impacts of corn-derived bioethanol fuels.

The process LCI data for the corn-soybean rotation in the US Corn Belt was developed previously to account for the variability in natural and extremely large systems (Miller et al. 2006; Landis et al. 2007). The major focus of the completed LCI was to evaluate the carbon and nitrogen material flows (including energy use, several other EPA criteria pollutants, pesticide and phosphorus flows). Each documented inventory flow has an associated probability distribution that was developed from a large input data set and Monte Carlo Analysis.

The uncertainty and variability from the LCI was combined with the uncertainty presented for IMPACT 2002 impact assessment tool. The probability distributions for the resultant LCIA were calculated utilizing MCA over 10,000 trials to ensure the reproducibility of the forecasts at the 95% confidence level. For comparative purposes, single-point estimates were calculated from the IMPACT 2002, TRACI, and CML impact assessment tools utilizing the mean LCI data for aqueous atrazine emissions, the mean IMPACT 2002 characterization factor for the corresponding point estimate, and the original units of the TRACI model- kg equivalents of 2,4-D.

TRACI and IMPACT 2002 model the combined aquatic and terrestrial ecotoxicity. For comparative

purposes, they are compared to the combined freshwater aquatic and terrestrial ecotoxicity calculated from CML.

## 2.4 Results and comparison of LCIA point estimates

Atrazine's probability distribution contribution to the IMPACT 2002 ecotoxicity midpoint is presented in Figure 3. Atrazine's contribution to the ecotoxicity midpoint is also compared to the corresponding values from the TRACI and CML tools. USEPA's TRACI (Tool for the Reduction and Assessment of Chemical and Other Environmental Impacts) model was developed specifically for the US, while Leiden University's CMLCA model was developed for the Netherlands and can be extrapolated to Western Europe and the World (Bare et al. 2002; Gorrée et al. 2002).

The disparate results amongst the three models result from the indicators used to represent the environmental impact to ecotoxicity. Ecotoxicity within IMPACT is derived from the mean hazardous concentration affecting 50% of present species (*HC50*). TRACI produces very similar results and is based on ecotoxicity potentials which are derived from predicted environmental concentrations (PEC) and a standard measure of harm such as the fraction of species adversely affected. CML ecotoxicity potentials are determined within the USES-LCA model from the ratio of weighted risk characterization ratios of the assessed substance and the reference substance (Huijbregts et al. 2000).

Life cycle uncertainty information displayed in probability format such as in Figure 3 has many benefits compared to single point LCA estimates. For example, probability distributions can illustrate areas of overlap when ranking the importance of relative emissions or when comparing different products or processes. LCAs utilizing single data points without uncertainty can not exhibit this depth of information. With the use of statistical approaches such as the Chi-squared test of homogeneity, life cycle

practitioners will also be able to determine whether compared environmental impacts are statistically significant. Finally, probability distributions allow for 'worst-case scenario' questions to be answered. For example, the 'worst case' of corn ecotoxicity due to atrazine would occur at the far right of the distribution in Figure 3.

## 3 CONCLUSIONS

Research opportunities exist for refining life cycle assessment modeling and results. Our work focused on hybrid LCI modeling and incorporating uncertainty in LCAs. For hybrid modeling, it cannot be definitively stated that hybrid modeling is the best option for *all* LCAs, or which approach to hybrid modeling would be preferred in a given application. The LCA practitioner will need to make the decision based on the best available data and information. Including both process and I-O data—especially service sector data—does provide a broader picture of the product or process under analysis. As countries shift away from manufacturing sectors towards service sectors, without reductions in emissions, including service sectors becomes significant because not including service sectors limits the LCA. Additionally, life cycle uncertainty in LCAs is becoming more available in terms of incorporation into LCI databases but is only in its infancy within IA tools. The presented analysis has only addressed parameter uncertainty and variability within the LCI and has not tackle the issue of model uncertainty, which can also provide a significant source of error to life cycle estimates. When extended to the LCIA, the majority of IA tools does not quantify and incorporate the uncertainty associated with the various parameters which make up the characterization factor. To represent the probability throughout the entire LCA, variability and uncertainty must be addressed within IA tools.

The modeling and uncertainty techniques were applied to two different case studies, demonstrating broad application in two disparate areas. Future work will combine both hybrid LCI modeling and uncertainty into one common framework. Future results will be compared with current results.

## REFERENCES

- Bare, J.C., G.A. Norris, D.W. Pennington and T. McKone (2002). TRACI: The Tool for the Reduction and Assessment of Other Environmental Impacts. *Journal of Industrial Ecology* 6(3–4): 49–78.
- Bullard, C.W., P.S. Penner and D.A. Pilati (1978). Net energy analysis, Handbook for combining process and input-output analysis. *Resources and Energy* 1(3): 267–313.

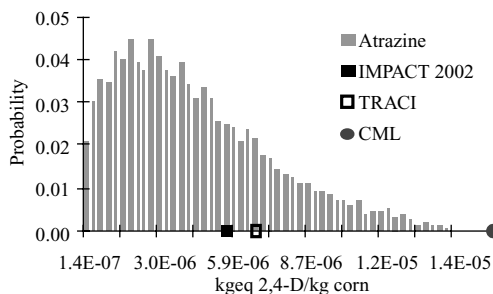


Figure 3. Ecotoxicity due to Atrazine.

- Guinée, J.B., M. Gorrée, R. Heijungs, G. Huppes, R. Kleijn, A. d. Koning, L. v. Oers, A.W. Sleswijk, S. Suh, H.A. U. d. Haes, J.A. d. Bruijn, R. v. Duin and M.A.J. Huijbregts, Eds. (2002). *Handbook on Life Cycle Assessment: Operational Guide to the ISO Standards (Eco-Efficiency in Industry and Science)*. Boston, Kluwer Academic Publishers.
- Guggemos, A. and A. Horvath (2005). Comparison of environmental effects of steel- and concrete-framed buildings. *Journal of Infrastructure Systems* 11(2): 93–101.
- Hendrickson, C., A. Horvath, S. Joshi and L. Lave (1998). Economic input-output models for environmental life-cycle assessment *Environmental Science and Technology* 32(7): 184A–191A.
- Hofstetter, P. (1998). *Perspectives in life cycle impact assessment: A structured approach to combine models of the technosphere, ecosphere and valuesphere.*, Kluwer Academic Publishers.
- Huijbregts, M.A.J., U. Thissen, J.B. Guinee, T. Jager, D. Kalf, D. Van de Meent, A.M.J. Ragas, A.W. Sleswijk and L. Reijnders (2000). Priority assessment of toxic substances in life cycle assessment. Part I: Calculation of toxicity potentials for 181 substances with the nested multi-media fate, exposure and effects model USES-LCA. *Chemosphere* 41(4): 541–573.
- Jolliet, O., M. Margni, R. Charles, S. Humbert, J. Payet, G. Rebitzer and R. Rosenbaum (2003). IMPACT 2002+: A New Life Cycle Impact Assessment Methodology. *The International Journal of Life Cycle Assessment* 8(6): 324–330.
- Junnilla, S., Horvath, A. and Guggemos, A.A. (2006). Life-Cycle Assessments of Office Building in Europe and the United States. *Journal of Infrastructure Systems* 12(1): 10–17.
- Kondo, Y., Y. Moriguchi and H. Shimizu (1998). CO<sub>2</sub> Emissions in Japan: Influences of Imports and Exports. *Applied Energy* 59(2–3): 163–174.
- Landis, A.E., S.A. Miller and T.L. Theis (2007). Life cycle of the corn-soybean agroecosystem for biobased production. *Environmental Science and Technology* 41(4): 1457–1464.
- Lave, L.B., E. Cobasflores, C.T. Hendrickson and F.C. McMichael (1995). Using Input-Output-Analysis to Estimate Economy-Wide Discharges. *Environmental Science & Technology* 29(9): A420–A426.
- Lenzen, M. (1998). Primary Energy and Greenhouse Gases Embodied in Australian Final Consumption: An Input-output Analysis. *Energy Policy* 26(6): 495–506.
- Lenzen, M. (2001). Errors in conventional and input-output based life-cycle inventories. *Journal of Industrial Ecology* 4(4): 127–148.
- Leontief, W. (1936). Quantitative input and output relations in the economic systems of the United States. *The Review of Economic Statistics* 18(3): 105–125.
- Lloyd, S. and R.J. Ries (2007). Incorporating Spatial and Temporal Resolution in the Life Cycle Inventory of Residential Buildings using Hierarchical Modules and Geographical Information. *Accepted In Dynamics of Industrial Ecosystems*.
- Lumina Decision Systems (2006). Analytica. Los Gatos, CA.
- Miller, S.A., A.E. Landis and T.L. Theis (2006). Use of Monte Carlo Analysis to Characterize Nitrogen Fluxes in Agroecosystems. *Environmental Science and Technology* 40(7): 2324–2332.
- Pennington, D.W., M. Margni, C. Ammann and O. Jolliet (2005). Multimedia Fate and Human Intake Modeling: Spatial versus Nonspatial Insights for Chemical Emissions in Western Europe. *Environmental Science and Technology* 39(4): 1119–1128.
- Pesonen, H.L., T. Ekvall, G. Fleischer, G. Huppes, C. Jahn, Z.S. Klos, G. Rebitzer, G.W. Sonnemann, A. Tintinelli, B.P. Weidema and H. Wenzel (2000). Framework for scenario development in LCA. *International Journal of Life Cycle Assessment* 5(1): 21–30.
- R.S. Means (2006). *Building Construction Cost Data*. Kingston, MA, R.S. Means Company, Inc.
- Suh, S., M. Lenzen, G. Treloar, H. Hondo, A. Horvath, G. Huppes, O. Jolliet, U. Klann, W. Krewitt, Y. Moriguchi, J. Munksgaard and G. Norris (2004). System boundary selection in life-cycle inventories *Environmental Science and Technology* 38(3): 657–664.
- Thabrew, L., S. Lloyd, J. Hamilton, C. Cypcar and R.J. Ries (2007). Life Cycle Assessment of Industrial and Institutional Water-based Acrylic Floor Finish Maintenance Programs. Submitted to the *International Journal of Life Cycle Assessment*.

# Advanced performance evaluation system for existing concrete bridges with machine learning

Ayaho Miyamoto

*Yamaguchi University, Ube, Japan*

Jun-ichi Ishida

*Yamaguchi Prefectural Government, Yamaguchi, Japan*

**ABSTRACT:** The management of existing concrete bridges has become a major social concern in many developed countries due to the large number of bridges exhibiting signs of significant deterioration. This problem has increased the demand for effective maintenance and renewal planning. In order to implement an appropriate management procedure for a structure, a wide array of corrective strategies must be evaluated with respect to not only the condition state of each defect but also safety, economy and sustainability. This paper describes a new performance evaluation system for existing concrete bridges. The system evaluates performance based on load carrying capability and durability from the results of a visual inspection and specification data, and outputs the necessity of maintenance. It categorizes both of the girder and slab as either unsafe, severe deterioration, moderate deterioration, mild deterioration, or safe. The technique employs an expert system with an appropriate knowledge base in the evaluation. A characteristic feature of the system is the use of neural networks to evaluate the performance and facilitate refinement of the knowledge base. Generally, although a neural network is a powerful machine-learning tool, the inference process becomes a “black box,” which renders the representation of knowledge in the form of rules impossible. However, the neural network proposed in the present study has the capability to prevent an inference process and knowledge base from becoming a black box. It is very important that the system is capable of detailing how the performance is calculated since the road network represents a huge investment. The effectiveness of the neural network and machine learning method is verified by comparison of diagnostic results by bridge experts.

## 1 INTRODUCTION

Information technologies such as cellular phones, car navigation systems, etc. have been advancing more rapidly than concrete technologies, and have been applied globally. There has been growing interest in the maintenance of civil infrastructure systems not only in Japan but worldwide (Miyamoto A. and Nakamura H. 2003.). Then, rational and economical diagnostic and remedial measures through the sharing of maintenance experience in Japan and other countries are required. One of the means of meeting the demand is rapidly advancing computer and information technologies. The authors have been developing a “Bridge Management System (J-BMS)” aimed mainly at increasing maintenance efficiency and assisting bridge administrators’ decision making for concrete bridges (Kawamura K., et al. 2000.). J-BMS is an integrated system composed of the “BMS database”, “Concrete Bridge Rating Expert System (BREX)” (Kawamura K., et al. 2000.), “maintenance planning optimization system” and “maintenance measure

selection system”. J-BMS was built using state-of-the-art information technologies including database systems based on information networks, and neural networks (Miyamoto A. 2004.). This paper describes the application of the concrete bridge rating expert system (BREX) to existing bridges. It specifically presents a method for efficiently building a Web-based database using the Internet, application of the durability diagnostic system to existing concrete bridges, and the effect of knowledge update (learning) in the system.

## 2 BRIDGE MAINTENANCE DATABASE SYSTEM USING THE WEB

This chapter first describes the composition of a Web-based bridge maintenance database system and outlines the system (Konno M., et al. 2003.). Then, specific methods for using the database system are discussed.

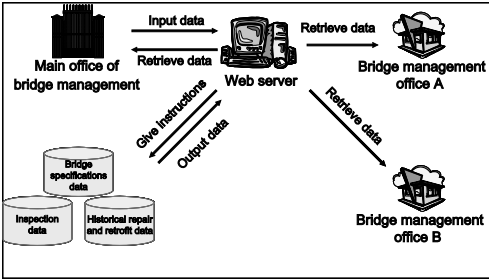


Figure 1. How the bridge maintenance database system works.

### 2.1 Composition and outline of Web-based database system

The database system stores the “bridge specifications data”, basic data on bridges, “historical inspection data”, the results of investigations and inspections conducted for bridge diagnosis, and “historical repair and retrofit data”, the history of repair and retrofit work performed for damaged or deteriorated bridges. A system is operated to centrally control these data (Figure 1). The database system is made accessible via an intranet to prevent the drainage of management data and enables the main and branch offices for bridge management to share bridge data.

For smooth bridge maintenance, not only inputting and retrieving data in the database system but also sharing the bridge data stored in the database with other systems is necessary. It has thus been made possible to output bridge data in the XML (eXtensible Markup Language) format which is widely used in the field of information processing. To store data smoothly, an inspection report preparation support system was developed as a subsystem of the database system to improve inspection procedures. To increase the efficiency of bridge maintenance, the database system has been equipped with bridge data output and inspection report preparation support features in addition to ordinary retrieval, input and update features.

### 2.2 Use of the database system

#### 2.2.1 Improvement of inspection procedure

At present, no bridge administrators inspect bridges or take remedial measures by themselves but administrators generally contract bridge inspection to private contractors, which have authorized inspection engineers inspect bridges. The private contractor submits an inspection report to the bridge administrator. No standard formats are available for inspection reports. The format often varies according to the private contractor. Inspection data may generally be voluminous.

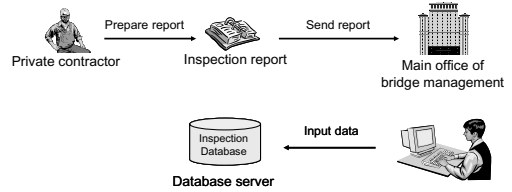


Figure 2. Input of inspection data in conventional procedure.

The bridge administrator may require much time in inputting inspection data based on the inspection report, and run the risk of making input errors. Conventional inspection procedures are inefficient because both the bridge administrator and the private contractor are separately involved in the digitization of data. An inspection report preparation support system was therefore built to help private contractors with their maintenance work. As a result, the procedure shown in Figure 2 was changed to the one in Figure 3.

First, the private contractor inspects bridges on a contractual basis, and inputs inspection results into the inspection report preparation support system. At the completion of inspection data input, the contractor outputs XML files containing inspection data and prepares an inspection report using features of the inspection report preparation support system. The contractor submits to the bridge administrator via CD or other electronic media XML files that is prepared using the inspection report preparation support system, and digital files of images of deterioration and damage obtained during inspection. The bridge administrator stores the digitized data in the database using CD received from the contractor.

Storing inspection data in XML files enables the bridge administrator to input inspection data to the database system by simply having the database read XML files containing inspection data. Thus, work efficiency is increased.

### 2.3 Inspection report preparation support system

The inspection report preparation support system is capable of preparing inspection reports referring to inspection data input into the system, and of outputting inspection data in the XML format to facilitate data input into the database system.

The inspection report preparation function automatically generates “an inventory of photographs” and “list of deformation cases” based on the inspection data from the inspection report preparation support system. An example of photograph inventory is given in Figures 4.

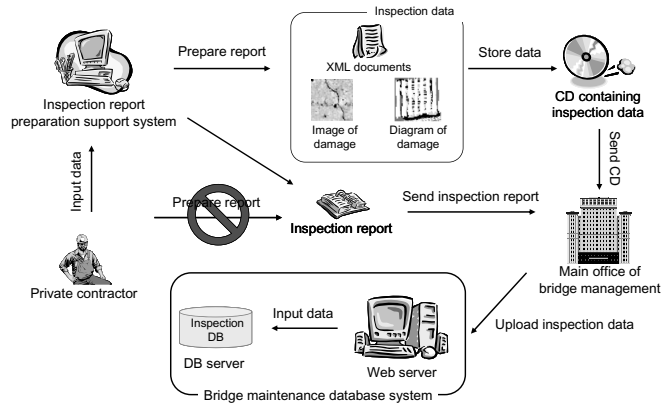


Figure 3. Improved procedure for inspection data input.

Photographs of dam age (xx bridge)						
Photograph No.	1	Span No.	3	Member No.	3	
Deformation No.	1	Type of deformation	Crack		Deformation No.	2
Deformation No.		Type of deformation			Deformation No.	2
Photograph No.	3	Span No.	2	Member No.	3	
Deformation No.	3	Type of deformation	Crack		Deformation No.	4
Deformation No.		Type of deformation			Deformation No.	4

Figure 4. An inventory of photographs.

## 2.4 Use of XML

To meet the input and output requirements described below, the database system is based on the assumption of using XML documents for bridge maintenance because XML can be used on the Internet and serve general purposes.

### 2.4.1 Data transfer to bridge maintenance support system

The diagnostic system, one of the bridge maintenance support systems described later, requires bridge specifications and inspection data. The system requires

much work for manually inputting a large volume of data, so it is not so practical. Using the XML format in the database system facilitates the transfer of bridge data to the bridge maintenance support system. Each piece of data is identified by a data tag where XML is used. Thus, necessary data can be read smoothly, and data can be input automatically. This makes the bridge maintenance support system more practical.

### 2.4.2 Data transfer from private contractor to bridge administrator

Authorized inspection engineers, at the request of the bridge administrator, generally inspect bridges and

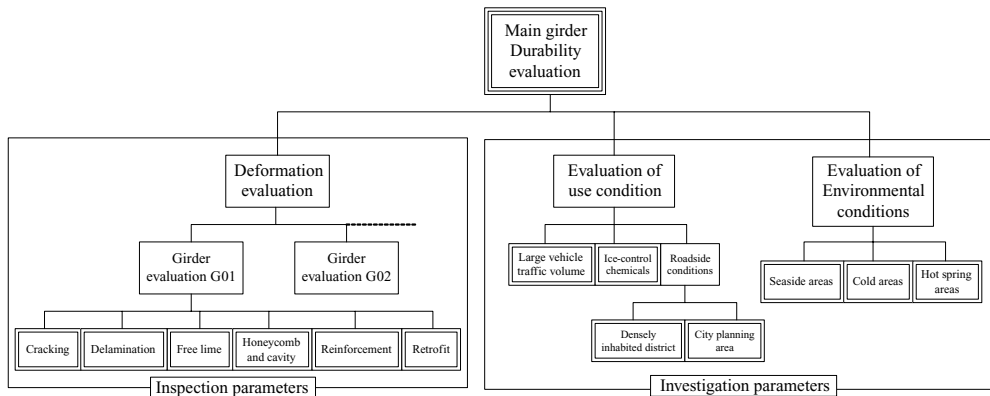


Figure 5. Diagnostic process for evaluating the durability of main girder.

submit a report on inspection results to the administrator. Then, errors in inspection data input and inefficiency of duplicate manual input of the same data into the inspection report and database system may be of concern. To solve such problems, a system was developed to use the benefits of XML. Keeping inspection date that are input to the inspection report preparation support system in the XML format enables smooth transfer of inspection data to the database and other application systems.

### 2.4.3 Data compatibility with systems of other organizations

Bridges have a service life of approximately 100 years, longer than other structures. Bridge-related data may vary in the service life. Existing systems are therefore expected to be enhanced. What is desirable in the future about bridge data are the digitization of the documents that are prepared in the life-cycle of bridges, or in the investigation through design and maintenance phases, and the centralized control of the documents for data sharing among those concerned. Migration to new systems or integration of existing systems is therefore expected for the purpose of sharing bridge data among those concerned. Defining a uniform XML format will enable smooth systems integration or migration to new systems without re-defining bridge data.

## 3 APPLICATION OF DIAGNOSTIC SYSTEM TO ACTUAL BRIDGES USING A DATABASE

### 3.1 Outline of diagnostic system

The diagnostic system evaluates the needs of repair and retrofit of the main member (main girder and slab) of the bridge in each span by grading durability and

load bearing capacity on a scale from 0.0 to 100.0 which is classified as the “soundness”. Appropriate measures are selected according to the soundness. Input data include visual inspection result, use condition and environmental condition. The diagnostic system is used for determining the need of remedial measures, a critical decision-making process. The system is therefore designed so that the diagnostic process can be accounted for. The system also enables knowledge update to effectively incorporate empirical and subjective knowledge of experts. Outlined below are the knowledge representation method and functional composition of the diagnostic system (Kawamura K., et al 2000.), (Izumoto M. 2004.) & (Miyamoto A. 2004.).

#### 3.1.1 How to represent knowledge

The diagnostic system hierarchically represents the process of experts’ diagnosis of existing performance parameters of bridges such as load bearing capacity and durability. For diagnosing individual parameters, If-Then rules are used to represent knowledge. The diagnostic system also employs fuzzy membership functions to handle subjective vagueness of engineers. The diagnostic process and knowledge representation rules are outlined below.

##### (i) Diagnostic process

The diagnostic process hierarchically represents the thought process of engineers when they diagnose bridges by integrating various inspection results. The diagnostic process is essential to the diagnostic system that the authors are trying to develop. Figure 5 shows a diagnostic process for the durability of a main girder.

##### (ii) Knowledge representation rules

Human knowledge is generally represented in natural language. For example, “if you have a slight fever



and a very sore throat, then you certainly have a cold.” In the diagnostic system, therefore, empirical or subjective knowledge of engineers is represented using If-Then rules.

### 3.1.2 Functional composition

The diagnostic system has five functions to enable accountability support and knowledge update (Figure 6). The functions are described below.

#### (i) Knowledge base

Knowledge base is a collection of experts’ knowledge, experience and learning patterns.

#### (ii) Inference engine

Inference engine efficiently processes the knowledge in the knowledge base to solve problems. The diagnostic system uses hierarchical neural networks with each level having a specific meaning, for accountability support and knowledge update. Figure 7 shows a hierarchical neural network for evaluating the durability of main girder.

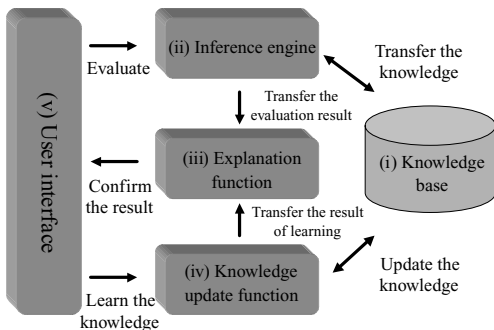


Figure 6. Functional composition of diagnostic system.

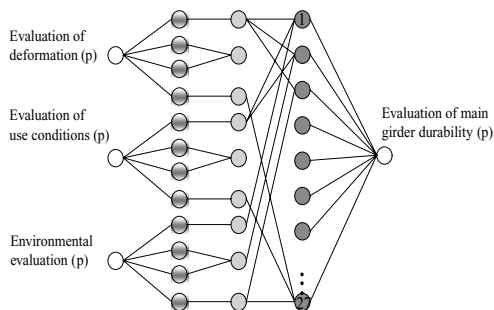


Figure 7. Application of hierarchical neural network.

#### (iii) Explanation function

The explanation function enhances the credibility of inspection and learning results. The diagnostic system has the following two explanation functions.

#### Explanation of diagnostic process

This function is aimed at explaining the path to inspection results. It supports accountability, one of the features of the diagnostic system. At the time of explanation of diagnostic process, it is possible to confirm the diagnostic process and knowledge representation rules that are used, and what emphasis is placed on which parameters (Figure 8).

#### Explanation of learning results

This function is performed to explain the basis on which knowledge is learned in the diagnostic system, and helps users determine whether knowledge should be updated or not. The diagnostic system enables the verification of changes in error and difference in inspection result before or after learning, to provide material for decision making (Figure 9).

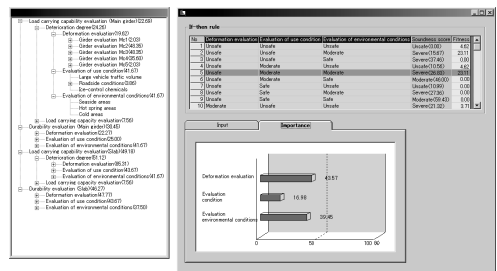


Figure 8. Output using the explanation function in the diagnostic process.

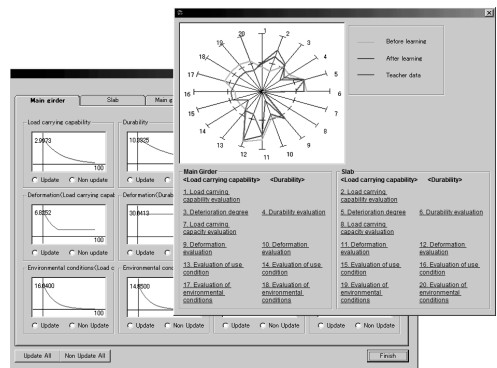


Figure 9. Explanation of learning results.

(iv) *Knowledge update function*

Knowledge in the knowledge base is updated to increase the accuracy of inspection results obtained by the diagnostic system. Engineers generally have subjective and empirical knowledge, which is very difficult to extract. In the diagnostic system, knowledge is updated through learning by error back-propagation based on the correlation between inspection and diagnostic results input into the neural network and training data (expert answers) collected through questionnaire surveys among engineers. More detailed explanations about the knowledge update function is provided in the Reference (Izumoto M. 2004.).

(v) *User interface*

User interface serves as a liaison between the system and the user to facilitate system use by the user. The user interface of the diagnostic system supports the input of inspection results, and enables the verification of diagnostic results and learning effects. Using the user interface in combination with the maintenance database system described in Chapter 2 enables an efficient use of the diagnostic system.

#### 4 CONCLUSIONS

This paper described the results of application to an existing reinforced concrete bridge a concrete structure durability diagnostic system using an XML-based database system and state-of-the-art information technology, and the knowledge update method in the

diagnostic system based on the diagnostic data using a neural network. Further system enhancement will be required for greater practicability. The authors are glad that a total system has been built for durability diagnosis.

#### REFERENCES

- Miyamoto, A. and Nakamura, H. (Eds.) 2003. Lifetime Management of Civil Infrastructure Systems, *Proceedings of 2003 High-tech Symposium*, Faculty of Engineering, Yamaguchi University, Vol. 1, pp. 1–79.
- Kawamura, K., Miyamoto, A., Nakamura, H. and Miyake, H. 2000. Practical Application of Concrete Bridge Rating Expert System using Hierarchical Neural Networks, *Journal of Construction Management and Engineering*, Japan Society of Civil Engineers (JSCE), Vol. 49, No. 665, pp. 45–64.
- Konno, M., Kawaraya, H., Miyamoto, A. and Nakamura, H. 2003. Practical Application of Database System for Bridge Maintenance Management, *Journal of Applied Computing in Civil Engineering, Committee on Civil Engineering Information Processing*, JSCE, Vol. 12, pp. 179–186.
- Izumoto, M. 2004. Development of Reinforced Concrete Bridge Performance Evaluation System with Accountability and Proposal of Knowledge Update Method, *Master's Thesis, Graduate School of Science and Engineering*, Yamaguchi University, pp. 1–64.
- Miyamoto, A. 2004. Advanced Structural Diagnostics, Cement and Concrete, *Japan Cement Association*, No. 684, pp. 1–9.

# Cost versus sustainability of reinforced concrete building frames by multiobjective optimization

I. Payá-Zaforteza, V. Yepes, F. González-Vidosa & A. Hospitaler  
*School of Civil Engineering, Technical University of Valencia, Valencia, Spain*

**ABSTRACT:** This paper describes a multiobjective simulated annealing (MOSA) algorithm applied to the design of reinforced concrete framed structures typically used in building construction. The economic cost of the frames and their sustainability are the two objective functions considered. The sustainability objective function is evaluated by the Ecoindicator 99's life cycle assessment of the materials of the structure. The evaluation of solutions follows the Spanish Code for structural concrete. Stress resultants and envelopes of framed structures are computed by an internal matrix method program. Design loads are in accordance to the national codes for building structures. The example studied is a symmetrical building frame of 2 bays and 6 floors. This example has 115 design variables including 6 material types of concrete, the type of steel, 36 cross-section dimensions and 72 passive reinforcement bars following a standard setup in columns and beams. Pareto results of the MOSA algorithm indicate that more sustainable solutions than the lower cost solution are available at a cost increment acceptable in practice. It is concluded that MOSA optimization algorithms are a forthcoming option for improving the environmental and economic design of real RC building framed structures.

## 1 INTRODUCTION

Since its appearance in the mid-fifties, artificial intelligence has dealt with a variety of fields that include the optimization of constrained problems. In spite of the potential capabilities of artificial intelligence, present design of economic concrete structures is very much conditioned by the experience of structural practitioners. Basically, the design of concrete structures is a problem of selection of design variables subject to structural constraints for which artificial intelligence is very much suited. Design variables include material grades, cross section dimensions and reinforcement. Most present design office procedures are still based on the adoption of cross-section dimensions and material grades based on sanctioned common practice. Once the structure is defined, it follows the analysis of stress resultants and the computation of passive and active reinforcement that satisfy the limit states prescribed by concrete codes. Should the dimensions or material grades be insufficient, the structure is redefined on a trial and error basis. Such process leads to safe designs, but the economy and sustainability of the concrete structures are, therefore, very much linked to the experience of the structural designer.

The methods of structural optimization may be classified into two broad groups: exact methods and heuristic methods. The exact methods are the traditional approach. They are based on the calculation of

optimal solutions following iterative techniques of linear programming (Hernandez & Fontan 2002). The second main group are the heuristic methods, whose recent development is linked to the evolution of artificial intelligence procedures. This group includes a broad number of search algorithms, such as Genetic Algorithms (Goldberg 1989), Simulated Annealing (Kirkpatrick et al. 1983), Tabu Search (Glover & Laguna 1997), etc. These methods consist of simple algorithms, but require a great computational effort, since they include a large number of iterations in which the objective function is evaluated and the structural constraints are checked. Among the first works of heuristic optimization applied to structures, the contributions of Jenkins (1991) and of Rajeev & Krishnamoorthy (1992) are to be mentioned. Both authors applied genetic algorithms to the optimization of the weight of steel structures. As regards reinforced concrete (RC) structures, early applications in 1997 include the work of Coello et al, who applied genetic algorithms to the economic optimization of a simply supported RC beam. Recently, there have been a number of RC applications (Camp et al. 2003, Lee et al. 2003, Leps & Sejnoha, 2003, Govindaraj & Ramasamy 2005), which optimize RC beams and building frames by genetic algorithms. More recently, our research group has used non evolutionary algorithms such as Simulated Annealing or Ant Colony to optimize earth retaining walls, portal and box road

frames, building framed structures, road vaults and bridge piers (Gonzalez-Vidosa et al. 2005, Paya et al. 2006, Perea et al. in press, Carbonell et al. 2007, Yepes et al. in press). On the other hand, studies on multi-objective optimization are less common and mainly focused on the application of evolutionary algorithms to steel structures (Hajela & Lin 1992, Greiner et al. 2004). A recent survey on heuristic structural optimization can be found in Paya-Zaforteza (2007).

The structures object of this work are building frames which are usually part of the structure of buildings. Building frames have typical horizontal beams of 5.00 to 10.00 m of horizontal span that sustain the vertical loads of the floors and transfer them to vertical columns of height between 3.00 to 6.00 m. Moderate horizontal loads are usually included in the design, but high levels of horizontal loading are usually transferred to adjacent shear walls. Building frames are calculated to sustain the loads prescribed by the codes and have to satisfy all the limit states required as an RC structure. The method followed in this work has consisted first in the development of an evaluation computer module where dimensions, materials and steel reinforcement have been taken as variables. This module computes the cost and a function that measures the sustainability of a solution and checks all the relevant limit states. Multiobjective simulated annealing, MOSA henceforth, is then used to search the solution space, so as to determine the Pareto set of combinations relating to the two objectives considered, which are the economic cost of the structure and its sustainability.

## 2 PROPOSED MULTIOBJECTIVE OPTIMIZATION PROCEDURE

### 2.1 Introduction

The problem of structural concrete multiobjective optimization that is put forward in the present work has two objective functions. First, it deals with the minimization of the cost function  $f_1$  of expression (1); and additionally, it deals with the minimization of function  $f_2$  in expression (2) that counts the environmental impact of the structure. Solutions are feasible when they satisfy the constraints of expressions (3).

$$f_1(x_1, x_2, \dots, x_n) = \sum_{i=1,r} p_i \times m_i(x_1, x_2, \dots, x_n) \quad (1)$$

$$f_2(x_1, x_2, \dots, x_n) = \sum_{i=1,s} d_i \times m_i(x_1, x_2, \dots, x_n) \quad (2)$$

$$g_j(x_1, x_2, \dots, x_n) \leq 0 \quad (3)$$

Note that the objective function in expression (1) is the sum of unit prices  $p_i$  (Table 1) multiplied by

Table 1. Unit prices considered for RC framed structures.

Unit	Description	Cost (€)
kg	Steel B-400	1.27
kg	Steel B-500	1.30
m <sup>3</sup>	Concrete HA-25	78.40
m <sup>3</sup>	Concrete HA-30	82.79
m <sup>3</sup>	Concrete HA-35	98.47
m <sup>3</sup>	Concrete HA-40	105.93
m <sup>3</sup>	Concrete HA-45	112.13
m <sup>3</sup>	Concrete HA-50	118.60
m <sup>2</sup>	Formwork in beams	25.05
m <sup>2</sup>	Formwork in columns	22.75
m <sup>2</sup>	Scaffolding for beams	38.89

Table 2. Environmental punctuations of the materials used in this study.

Unit	Description	Environmental punctuation
kg	Steel B-400	61
kg	Steel B-500	61
m <sup>3</sup>	Concrete HA-25	39100
m <sup>3</sup>	Concrete HA-30	41400
m <sup>3</sup>	Concrete HA-35	42000
m <sup>3</sup>	Concrete HA-40	50200
m <sup>3</sup>	Concrete HA-45	55600
m <sup>3</sup>	Concrete HA-50	61300

the measurements  $m_i$  of the construction units (concrete, steel, formwork, etc). In order to measure the sustainability of the structure (function  $f_2$ ) an environmental punctuation  $d_i$  has been given to each one of its materials by means of its life cycle assessment. This punctuation was obtained using Ecoindicator 99 (Goedkoop & Spriensma 2001) and the sustainability function (EC henceforth) is the sum of environmental punctuations  $d_i$  (Table 2) multiplied by the measurements  $m_i$  of the construction materials. Given a structure, the higher its EC value is, the lower its sustainability will be.

Finally, it is necessary to say that the restrictions in expression (3) are all the service and ultimate limit states that the structure has to satisfy.

### 2.2 Single objective simulated annealing

The basic search method used in the present MOSA algorithm is the single objective simulated annealing (SA henceforth), that was originally proposed by Kirkpatrick et al. (1983) for the design of electronic circuits. The SA algorithm is based on the analogy of crystal formation from masses melted at high temperature and let cool slowly. At high temperatures, configurations of greater energy than previous ones may randomly form, but, as the mass cools, the

probability of higher energy configurations forming decreases. The process is governed by the Boltzmann expression  $\exp(-\Delta E/T)$ , where  $\Delta E$  is the increment of energy of the new configuration and  $T$  is the temperature. The algorithm starts with a feasible solution randomly generated and a high initial temperature. The initial working solution is changed by a small random move of the values of the variables. The new current solution is evaluated in terms of cost. Greater cost solutions are accepted when a 0 to 1 random number is smaller than the expression  $\exp(-\Delta E/T)$ , where  $\Delta E$  is the cost increment and  $T$  is the current temperature. The current solution is then checked against structural constraints and if it is feasible, it is adopted as the new working solution. The initial temperature is decreased geometrically ( $T = kT$ ) by means of a coefficient of cooling  $k$ . A number of iterations called Markov chains is allowed at each step of temperature. The algorithm stops when the temperature is a small percentage of the initial temperature or when there are no improvements in a number of Markov chains (typically 1% and 1–2 Markov chains). The SA method is capable of surpassing local optima at high-medium temperatures and gradually converges as the temperature reduces to zero. The SA method requires calibration of the initial temperature, the length of the Markov chains and the cooling coefficient. The initial temperature is usually adjusted following different methods like the one proposed by Medina (2001), which consists in choosing an initial value and checking whether the percentage of acceptances of higher energy solutions is between 20–40 percent. If the percentage is greater than 40%, the initial temperature is halved; and if it is smaller than 20%, the initial temperature is doubled. Computer runs are performed a number of times so as to obtain minimum, mean and standard deviation of the results with respect to the optimum result.

### 2.3 Multiobjective simulated annealing

The flow-chart of the proposed multiobjective simulated annealing algorithm is summarized in Figure 1. The main features of the algorithm were proposed by Suppaitnarm et al. in 2000 and it is usually referenced in literature as the SMOSA algorithm. The present algorithm starts with a feasible solution generated randomly. Then, it follows the adoption of initial temperatures for the two objective functions, i.e. the cost of the structure and its sustainability. This is done following Medina's method as explained above for the single objective simulated annealing. Once the initial temperatures are adjusted, a random small move to the values of the variables is applied, so as to obtain the new working solution. This working solution is checked against the Pareto condition, which is met when the solution is not shadowed by any former element of the Pareto set of solutions. If it qualifies

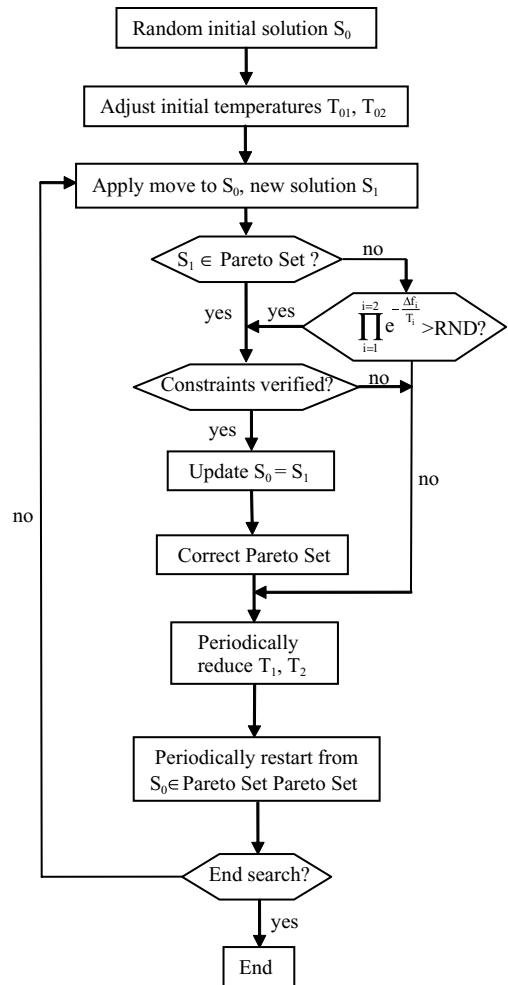


Figure 1. Flowchart of the proposed SMOSA algorithm.

for the Pareto list, then the structural constraints are checked, and if so, the current solution is updated and it is included in the Pareto list. Otherwise, when the solution does not qualify for Pareto, it is checked the SMOSA acceptance criterion. This criterion is met when the cost and the sustainability are smaller than for the previous solution, or when the expression (4) is greater than a random number between 0 and 1. In this latter case, the Pareto set is not improved, but the working solution is taken as a start for next iteration. The temperatures of the two objective functions are reduced after a number of iterations called Markov chains. Additionally, the algorithm restarts periodically from any of the extreme solutions in the Pareto set. The algorithm proposed in Figure 1 agrees with the original SMOSA algorithm in that it only accepts

feasible solutions, which the original recommended instead of alternative procedures, such as minimizing the constraint violations.

$$\prod_{i=1}^{i=2} e^{-\frac{\Delta f_i}{T_i}} \quad (4)$$

In order to obtain statistical valid results nine computer runs were performed.

### 3 SMOSA APPLICATION TO REINFORCED CONCRETE BUILDING FRAMES

The example studied relates to RC frames used in building construction (Paya-Zaforteza 2007). Figure 2 shows a typical symmetrical frame of 2 bays and 6 floors which will be used for the analyses below. This frame has a total of 115 design variables.

All the variables are discrete in this analysis. Variables include the type of reinforcing steel; the compressive characteristic strength of the concrete for the columns and beams of each floor, which can vary from a minimum of 25 MPa (HA-25) to a maximum of 50 MPa (HA-50) in steps of 5 MPa; the dimensions of the cross section of each column of the frame; the dimensions of the cross-sections of the beams; and the reinforcement steel variables which follow a

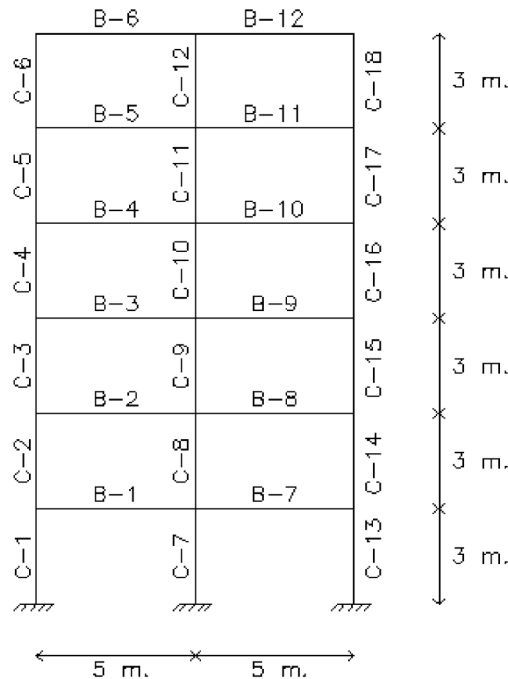


Figure 2. RC frame of 2 bays and 6 floors studied in this work.

standard reinforcement setup. Figure 3 shows a typical longitudinal reinforcement setup of the beams of the structure. It includes a basic top and bottom bars and positive and negative extra reinforcements of a standard length. Variables for beam stirrups include 3 zones of left, central and right positions of transverse reinforcement (Figure 4). Columns longitudinal and transverse reinforcement is shown in Figure 5. The longitudinal one can have 330 possible values varying from a minimum of  $4\phi 12$  to a maximum of  $34\phi 25$ . On the other side, transverse reinforcement of columns includes 21 possible values. It is worth noting the large number of variables required for the modelling of this type of structure in order to make a realistic RC frame design, i.e. 115 for the structure of Figure 2. This number is much larger than that of previous works (i.e. Lee & Ahn 2003, used 13 variables).

The most important parameters are the horizontal spans of the bays, the vertical height of the columns, the vertical and horizontal loads considered and the partial coefficients of safety. Structural constraints considered followed standard provisions for Spanish design of this type of structure (Dirección General para la Vivienda 1988, Comisión Permanente del Hormigón, 1999), that include checks of the service and ultimate limit states of flexure, shear and instability for the stress envelopes due to the vertical loads and the horizontal wind loads. Vertical loads amount to a total uniform distributed load of 35 kN/m (7.00 kN/m<sup>2</sup> of self weight plus live load and 5.00 m of spacing between parallel frames). As regards wind loads, they amount to a total uniform distributed load of 4.5 kN/m. Stress resultants and reactions were calculated by an

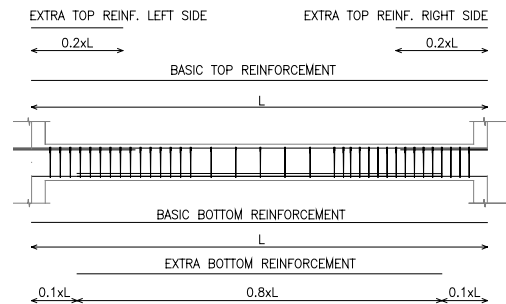


Figure 3. Typical longitudinal reinforcement bars of the beams.

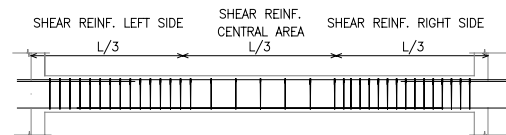


Figure 4. Typical shear reinforcement bars of the beams.

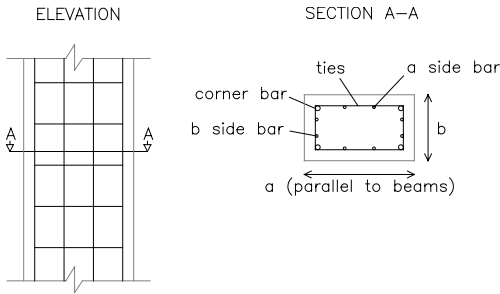


Figure 5. Typical reinforced concrete column reinforcement.

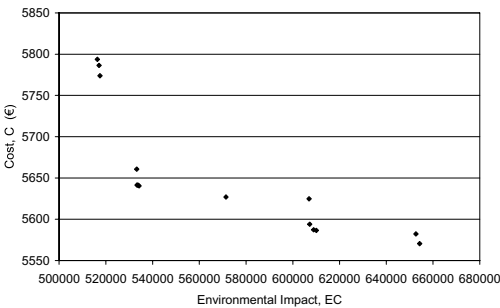


Figure 6. Final Pareto set of solutions.

internal matrix method program using a 2-D mesh. Deflections were limited to 1/250 of the horizontal span for the total load and to 1/400 for the active deflection; which is the part of the deflection measured after construction of the elements that can be damaged due to vertical displacements.

The SMOSA algorithm was programmed in Fortran 77. Typical runs for the RC frame of 2 bays and 6 floors of Figure 2 amounted up to 80 minutes in a Pentium IV of 3.20 GHz. The calibration recommended Markov chains or cycles of 135000 iterations and a cooling coefficient of 0.80 for the SMOSA algorithm. The most efficient move found was random variation of 3 or up to 3 variables of the 115 of the problem. Figure 6 shows the final Pareto set of solutions and tables 3, 4 and 5 detail the main results of the lower EC solution for this RC frame of 2 bays and 6 floors. Steel reinforcement is of 500 MPa of characteristic strength. Concrete in columns and beams is HA-35 (35 MPa of compressive strength) from the first to the fourth floors and HA-25 (25 MPa of compressive strength) in the rest of the structure. The cost of this SMOSA solution is 5793.75 €, whereas the cost of the best cost solution is 5561.81 € (4% more economic). As regards the sustainability, the lower EC solution has an environmental punctuation of 516,369.44 units and the most economic solution has 654,261.5 units (26.7% more EC). It is worth noting that the cost increment

Table 3. Beams results of the SMOSA solution with lower environmental impact.

Name	Dimensions		Top reinforcement		
	Depth (cm)	Width (cm)	Base	Extra Left	Extra Right
B-1	48	20	3φ10	3φ16	3φ20
B-2	50	20	3φ16	1φ16	2φ16
B-3	48	20	4φ16	–	2φ12
B-4	42	20	5φ16	1φ16	–
B-5	46	20	2φ25	–	–
B-6	47	20	2φ25	1φ10	1φ12

Table 4. Beams results of the SMOSA solution with lower environmental impact.

Name	Bottom reinforcement		Shear reinforcement		
	Base	Extra	Left	Central	Right
B-1	3φ10	2φ12	φ10/25	φ6/20	φ8/5
B-2	4φ12	1φ12	φ8/20	φ6/20	φ10/25
B-3	2φ12	2φ20	φ8/20	φ6/20	φ8/20
B-4	4φ16	2φ20	φ8/20	φ6/20	φ10/25
B-5	3φ20	2φ20	φ10/25	φ6/30	φ10/25
B-6	3φ20	3φ20	φ10/25	φ6/30	φ10/25

Table 5. Column results of the SMOSA solution with lower environmental impact.

Name	Dimensions		Long. Reinf.		
	a (cm)	b (cm)	Corner	b side	Ties
C-1	35	25	4φ12	–	φ6/15
C-2	35	25	4φ16	–	φ6/15
C-3	30	25	4φ16	–	φ6/15
C-4	30	25	4φ12	4φ12	φ6/15
C-5	30	25	4φ12	4φ12	φ6/15
C-6	30	25	4φ20	–	φ6/20
C-7	40	30	4φ12	2φ12	φ6/15
C-8	40	25	4φ12	–	φ6/15
C-9	40	25	4φ12	–	φ6/15
C-10	35	25	4φ12	–	φ6/15
C-11	30	25	4φ12	–	φ6/15
C-12	25	25	4φ12	–	φ6/15

is clearly justified as regards the improvement in the sustainability of the structure.

#### 4 CONCLUSIONS

From the above work the following conclusions may be derived:

- The study of this RC building framed structure shows the capability of the SMOSA algorithm for

the optimization of cost and sustainability of this kind of structures.

- Results give an example for which a cost increment of 4% results in a substantial reduction in the environmental impact of the structure of 26.7%, which leads to the tentative conclusion that more sustainable structures can be designed at a cost increment well acceptable in practice.

## REFERENCES

- Camp C.V., Pezeshk S. & Hansson H. 2003. Flexural Design of Reinforced Concrete Frames using a Genetic Algorithm. *ASCE Journal of Structural Engineering* 129 (1): 105–115.
- Carbonell A., Martinez F., Yepes V. & Gonzalez-Vidosa F. 2007. Threshold accepting optimization of road vaults and rectangular hollow bridge piers. *Proc. of the Tenth International Conference on Computer-Aided Optimum Design in Engineering*, Myrtle Beach (USA).
- Coello C.A., Chistiansen A.D. & Santos F. 1997. A Simple Genetic Algorithm for the Design of Reinforced Concrete Beams. *Engineering with Computers* 13 (4): 185–196.
- Comisión Permanente del Hormigón. 1999. *Instrucción de hormigón estructural*. EHE. Madrid: Ministerio de Fomento.
- Dirección General para la Vivienda y la Arquitectura. 1998. *NBE AE-88. Acciones en la edificación*. Madrid: Ministerio de Obras Públicas y Transportes.
- Glover F. & Laguna M. 1997. *Tabu Search*. Boston: Kluwer Academic Publishers.
- Goedkoop M. & Spriensma R. 2001. *The Ecoindicator 99. A damage oriented method for Life Cycle Impact Assessment*. Methodology Report. Amersfoort: Product Ecology Consultants.
- Goldberg D.E. 1989. *Genetic Algorithms in Search, Optimization and Machine Learning*. Boston: Addison-Wesley.
- Gonzalez-Vidosa F., Yepes V., Alcalá J., Carrera M. & Perea C. 2005. Simulated annealing optimization of walls, portal and box reinforced concrete road structures. *Proc. of the Ninth International Conference on Computer-Aided Optimum Design in Engineering, Skiathos (Greece)*.
- Govindaraj V. & Ramasamy J.V. 2005. Optimum detailed design of reinforced concrete continuous beams using genetic algorithms. *Computers and Structures* 84: 34–48.
- Greiner D., Emperor J.M. & Winter G. 2004. Single and multiobjective frame optimization by evolutionary algorithms and the auto-adaptive rebirth operator. *Computer Methods in Applied Mechanics and Engineering* 193: 3711–3743.
- Hajela P. & Lin, C.Y. 1992. Genetic search strategies in multicriterion optimal design. *Structural Optimization* 4: 99–107.
- Hernández S. & Fontan A. 2002. *Practical Applications of Design Optimization*. Southampton: WIT Press.
- Jenkins W.M. 1991. Structural Optimization with the Genetic Algorithm. *The Structural Engineer* 69 (24): 419–422.
- Kirkpatrick S., Gelatt C.D. & Vecchi M.P. 1983. Optimization by Simulated Annealing. *Science* 220 (4598): 671–680.
- Lee C. & Ahn J. 2003. Flexural Design of Reinforced Concrete Frames by Genetic Algorithm. *ASCE Journal of Structural Engineering* 129 (6): 762–774.
- Leps M. & Sejnoha M. 2003. New Approach to Optimization of Reinforced Concrete Beams. *Computers and Structures* 81: 1957–1966.
- Medina J.R. 2001. Estimation of Incident and Reflected Waves using Simulated Annealing. *ASCE Journal of Waterway, Port, Coastal and Ocean Engineering* 127 (4): 213–221.
- Paya I., Yepes V., Clemente J. & Gonzalez-Vidosa F. 2006. Heuristic optimization of reinforced concrete building frames (in Spanish). *Rev. Int. Met. Num. Calc. Dis. Ing.*, 22 (3): 241–259.
- Paya-Zaforteza I. 2007. *Optimización heurística de pórticos de hormigón armado de edificación*. Doctoral thesis. Valencia: Technical University of Valencia, Construction Engineering Dept.
- Perea C., Alcalá J., Yepes V., Gonzalez-Vidosa F. & Hospitaler A. Design of reinforced concrete bridge frames by heuristic optimization. In press *Advances in Engineering Software*, doi:10.1016/j.advengsoft.2007.07.007.
- Rajeev S. & Krishnamoorthy C.S. 1992. Discrete Optimization of Structures using Genetic Algorithms. *ASCE Journal of Structural Engineering* 118 (5): 1233–1250.
- Suppaitnarm A., Seffen K.A., Parks G.T. & Clarkson P.J. 2000. A Simulated Annealing Algorithm for Multiobjective Optimization. *Engineering Optimization* 33: 59–85.
- Yepes V., Alcalá J., Perea C. & Gonzalez-Vidosa F. A parametric study of optimum earth retaining walls by simulated annealing. In press *Engineering Structures*, doi: 10.1016/j.engstruct.2007.05.023.



# Model based reasoning for life-cycle structural engineering

Ian F.C. Smith & Prakash Kripakaran

*Ecole Polytechnique Fédérale de Lausanne (EPFL), Lausanne, Switzerland*

**ABSTRACT:** Good behavior models contribute to effective management of civil infrastructure. This paper describes recent work in the application of model-based reasoning to structural identification. Rather than selecting one model, iterative filtering of multiple models is proposed. This approach is shown to address several shortcomings associated with model updating methods that use a single model. Multiple models are generated through sampling, model composition and selection of models that provide measurement-prediction values below a threshold that is determined by statistical treatment of measurement and modeling errors. Finally it is shown how this approach can be used to select and position sensors so that measurements are more useful.

## 1 INTRODUCTION

System identification involves determining the state of a system and values of system parameters through comparisons of predictions with observed responses. (Ljung 1999). When applied to structural engineering, this is equivalent to finding the parameter values for models that may represent the behavior of a given structure. Conventional system identification strategies, such as model updating, use optimization methods with measured data to calibrate a mathematical model of a structure that is often based on the model used for design. Model updating in structural engineering may be performed using vibration measurements (Brownjohn 2003; Brownjohn et al. 2003; Friswell and Motterhead 1995; Koh et al. 2003) or using static responses (Banan et al. 1994; Sanayei et al. 1997; Sanayei and Onipede 1991; Sanayei and Saletnik 1996).

Although conservative design models result in safe and serviceable structures, they are usually not appropriate for interpreting measurements from structures in service (Smith 2005). Moreover, since system identification is an intrinsically abductive task, there may be many models that fit observed measurements (Robert-Nicoud et al. 2005a; Robert-Nicoud et al. 2005b). A multiple model approach to system identification in which each model represents different sets of assumptions is capable of incorporating large numbers of modeling possibilities.

Errors play a major role in the system identification process. Errors from different sources may compensate each other such that predictions of bad models match measurements (Robert-Nicoud et al. 2005a). Modeling and measurement errors have been

investigated in previous research. Banan et al. (1994) stated that the selection of an appropriate model is difficult; it is problem-dependent, and usually requires the intuition and judgment of an expert in modeling. For example, mathematical models may not be able to exactly capture variations in cross-sectional properties, existing deformations, residual stresses, stress concentrations and variations in connection stiffness. Sanayei et al. (1997) emphasized that errors in parameter estimates may arise from many sources, the most significant of which are measurement errors and modeling errors. A statistical evaluation of the performance of a system identification methodology must account for modeling and measurement errors.

Robert-Nicoud et al. (2005a) proposed a multiple-model identification methodology based on compositional modeling and stochastic global search. Stochastic search was used to generate a set of candidate models. The objective function for the search was defined to be the root-mean-square of the difference between measured values and model predictions (RMSE). When the RMSE value was less than a certain threshold value, the model was classified as a candidate model. The threshold was evaluated by assuming reasonable values for modeling and measurement errors through reference to previous studies in finite element analysis and sensor precision. A model involving the right set of assumptions and correct values of parameters has a cost function value that is less than or equal to this threshold when errors due to mathematical modeling and measurement are equal to estimated maximum values. A limitation of this study is that the threshold value is not qualitatively associated with the reliability of identification.

This paper describes new research done at EPFL in the area of system identification. Recent advances that incorporate errors in the system identification process and provide a statistical basis to reasoning with multiple models are described. Random variables are introduced for the errors in modeling and measurements. A new objective function is introduced for the stochastic search. The new form of the function uses threshold values at each measurement location. These threshold values are determined through reference to the required reliability of identification and probability distributions of errors. The paper then describes an entropy-based method that finds locations for subsequent measurement such that these are likely to eliminate the maximum number of models from the candidate model set.

## 2 SYSTEM IDENTIFICATION

### 2.1 Methodology

The framework of multiple-model system identification research at EPFL is shown in Figure 1. At the beginning, modeling hypotheses lead to a number of possible models using measurements from the structure. The model generation module compares measurements with predictions to identify a set of candidate models. A stochastic global search algorithm called PGSL (Raphael and Smith 2003) is used for optimization. A feature extraction module extracts characteristics of these models.

This paper examines the reliability of system identification. A reliability of 100% requires that the following three conditions are met: all possible models are considered in the set of models; there are sufficient measurement data to filter out wrong models and; all errors are zero. Fulfilling these three conditions completely is never feasible. However, for the purposes of this paper, it is assumed that the first two conditions are met. Many structures can be evaluated using the assumption that through use of good stochastic

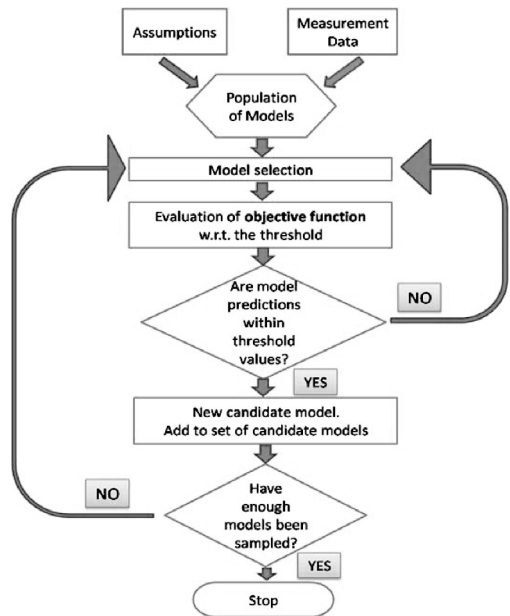


Figure 2. Algorithm for generating candidate models.

search algorithms and high tolerance limits all possible models are generated. The second condition requires the assumption that enough measurement data is available to filter out wrong models. Since a goal of this research is to determine systematically the best path to fulfillment of this condition, it is assumed that this goal is reached.

Estimating the reliability of structural identification, as discussed in this paper, involves calculation of a threshold range of errors given a statistical tolerance limit. When the assumptions discussed above are not possible, evaluations of reliability that are described in this paper provide upper-bound values. In the following section, errors that affect the reliability of identification are discussed.

## 3 ERRORS IN SYSTEM IDENTIFICATION

### 3.1 Modeling errors

Modeling error ( $x_{mod}$ ) is the difference between the predicted response of a given model and that of an ideal model that accurately represents behavior. Modeling error has been studied by many researchers (Banan et al. 1994; Frangopol and Liu 2007; Kong and Frangopol 2003; Liu and Frangopol 2004; Sanayei et al. 1997). Liu and Frangopol (2004) have studied the effect of modeling uncertainties in bridge maintenance planning. They consider two types of uncertainties—aleatory uncertainty and epistemic

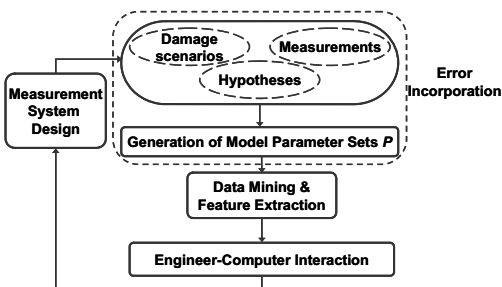


Figure 1. System identification methodology using multiple models.

uncertainty. Aleatory uncertainty is introduced by the inherent randomness in the model parameters. Epistemic uncertainties arise due to lack of knowledge or imperfect modeling.

We classify the modeling error in a more detailed manner. It has three components— $x_{mod,1}$ ,  $x_{mod,2}$ , and  $x_{mod,3}$ . The component  $x_{mod,1}$  is the error due to discrepancy between the behavior of the mathematical model and that of the real structure. Component  $x_{mod,2}$  is introduced during numerical computation of the solution of partial differential equations. Component  $x_{mod,3}$  is the error arising from inaccurate assumptions made during simulation.

Component  $x_{mod,3}$  is further separated into two parts— $x_{mod,3a}$  and  $x_{mod,3b}$ . The error part,  $x_{mod,3a}$ , arises from assumptions made when using the model (typically assumptions related to boundary conditions such as support characteristics and connection stiffness). The error part,  $x_{mod,3b}$ , arises from errors in values of model parameters such as moment of inertia and Young's modulus. While it might be impossible to separate the components in practice, it is still important to distinguish between these errors since the only error source that is usually recognized by traditional model calibration techniques is  $x_{mod,3b}$ .

To compare with the notation used by Liu and Frangopol (2004), aleatory uncertainties are represented by  $x_{mod,3b}$  and epistemic uncertainties by  $x_{mod,1}$ ,  $x_{mod,2}$  and  $x_{mod,3a}$ . Liu and Frangopol (2004) study the effect of aleatory uncertainties only and neglect epistemic uncertainties. Epistemic uncertainties are hard to quantify. They can be reduced by using appropriate element types, better meshing and sophisticated analysis techniques. However, such strategies cannot eliminate epistemic uncertainties completely for complex structures. Our approach provides an opportunity to explicitly account for  $x_{mod,3a}$  by allowing multiple modeling assumptions in the identification process. Thus it has the potential to enhance uncertainty studies by including epistemic uncertainties.

### 3.2 Measurement errors

Measurement error ( $x_{meas}$ ) is the difference between real and measured quantities in a single measurement. Measurement errors result from equipment as well as on-site installation faults (Sanayei et al. 1997). In addition to sensor precision values reported by manufacturers, the stability and robustness (for example, with respect to temperature), and the effects of location characteristics (for example, connection losses) also account for measurement error. While it is tempting to quantify measurement error as a sum of individual sources, it is more reasonable to quantify them probabilistically using sensor precision and on-site information obtained during sensor installation.

## 4 MODEL GENERATION

### 4.1 Methodology for bounded errors

The model generation task requires an objective function that accounts for the errors to generate a set of candidate models. Robert-Nicoud et al. (2005a) assumed that upper limits for modeling and measurement errors are known. The objective function is formulated as follows. If  $x_a$  is the real value of a behavior quantity such as deflection,  $x_{meas}$  is the measured value and  $x_{mod}$  is the value computed using a model, the following relationships have been obtained for a single measurement.

$$x_a = x_{meas} + e_{meas} \quad (1)$$

$$x_a = x_{mod} + e_1 + e_2 + e_3 \quad (2)$$

Model calibration procedures minimize the absolute value of the difference between  $x_{meas}$  and  $x_{mod}$ . The difference between  $x_{meas}$  and  $x_{mod}$  is known as the residue  $q$ . Rearranging the terms in Equations 1 and 2,

$$q = |x_{meas} - x_{mod}| = |e_1 + e_2 + e_3 - e_{meas}| \quad (3)$$

Thus, model calibration techniques minimize the quantity  $(|e_1 + e_2 + e_3 - e_{meas}|)$ . This is equivalent to inaccurately assuming that this quantity is always zero. The objective function that is minimized during the optimization routine is the root-mean-square composite error (*RMSE*) which was calculated as

$$RMSE = \sqrt{\frac{\sum q_i^2}{n}} \quad (4)$$

where  $q_i = |x_{i,meas} - x_{i,mod}|$  difference between the value measured at the  $i$ th measurement point and the predicted value computed using the model. Any model that gives an RMSE value less than a threshold value is considered to be a candidate model. The threshold is computed using an approximate estimate of modeling and measurement errors. From Equation 3, since errors could be positive or negative

$$q \leq |x_{mod}| + |x_{meas}| \leq |e_1| + |e_2| + |e_3| + |e_{meas}| \quad (5)$$

$$q \leq \text{Threshold} = e_{mod}^{est} + e_{meas}^{est} \quad (6)$$

$e_{mod}^{est}$  and  $e_{meas}^{est}$  are estimates of the upper bound for modeling errors and measurement errors respectively. For quantifying threshold,  $e_{mod}^{est}$  has been assumed to have a value of 4% (from finite element simulations) and  $e_{meas}^{est}$  was taken to be the precision of the sensor (Robert-Nicoud et al. 2005b).

#### 4.2 Model generation under statistical errors

The formulation described in the previous section for evaluating candidate models is improved by combining errors using statistical methods. Modeling error  $x_{mod}$  is difficult to quantify. It is problem dependent and can be minimized using modeling expertise (Banan et al. 1994). Assuming an ideal situation,  $e_1 = 0$ . The other errors can be modeled probabilistically.

Consider  $x_{meas}^i$  as the measured value at the  $i$ th measurement location and  $e_{meas}^i$  as the measurement error at that location. Similarly,  $x_{mod}^i$  is the predicted value at the  $i$ th measurement location and ( $e_{mod}^i = e_1 + e_2 + e_3$ ) is the total modeling error. In the absence of errors, predictions from a candidate model exactly match the measurements. Since errors are present, this is represented in mathematical terms as,

$$x_{meas}^i + e_{meas}^i = x_{mod}^i + e_{mod}^i \quad (7)$$

$$\Delta x^i = x_{meas}^i - x_{mod}^i = e_{mod}^i - e_{meas}^i \quad (8)$$

Modeling error is defined by a variable that follows a probability distribution with mean  $\mu_{mod}$  and standard deviation  $\sigma_{mod}$  and measurement error is defined by a variable  $e_{meas}$  that follows a probability distribution with mean  $\mu_{meas}$  and standard deviation  $\sigma_{meas}$ . Assume that the probability distribution for  $e_{mod}$  remains the same for one modeling problem. However, this may depend on element types and in reality, for a complex structure with different element types, the distribution for  $e_{meas}$  could be different at each location. Since values of measurement error depend on sensor and location characteristics, the distribution for  $e_{meas}$  changes for each measurement location. Assuming both probability distributions to be Gaussian distributions, the combined error is defined by a variable  $Z$  with mean  $\mu_Z$  and standard deviation  $\sigma_Z$ , such that

$$\mu_Z = \mu_{mod} - \mu_{meas} \quad (9)$$

$$\sigma_Z = \sqrt{\sigma_{mod}^2 + \sigma_{meas}^2} \quad (10)$$

Following from Equation (9), the threshold values for a certain reliability of identification are given by

$$r_1^i \leq (x_{meas}^i - x_{mod}^i) \leq r_2^i \quad (11)$$

such that

$$P(r_1^i \leq Z \leq r_2^i) = p_{reqd} \quad (12)$$

and

$$r_1 = \mu_Z - c, r_2 = \mu_Z + c \quad (13)$$

where  $c$  is the value that is determined from the required statistical tolerance limit,  $p_{reqd}$ .

The function,  $f_i$ , is defined as

$$f_i = \begin{cases} 0 & \text{if } r_1^i \leq \Delta x^i \leq r_2^i \\ (\Delta x^i - r_1^i)^2 & \text{if } \Delta x^i < r_1^i \\ (\Delta x^i - r_2^i)^2 & \text{if } \Delta x^i > r_2^i \end{cases} \quad (14)$$

where superscript  $i$  refers to the  $i$ th measurement location.

The significance of  $f_i$  is that the difference between measurement and prediction at each measurement location is compared with the corresponding threshold value. A model is a candidate model only if it satisfies condition at each measurement location, i.e., the difference is within the specified threshold for every single measurement location. This requirement is encapsulated in a new objective function as follows

$$E = \sqrt{\sum_{i=1}^n \frac{f_i}{n}} = 0 \quad (15)$$

The new objective function  $E$  in Equation (15) is employed for the case study in the next section. Equation (15) could be considered to be a form of the classical error function that is employed for curve fitting since it includes values of errors at each measurement location and provides a probabilistic basis for the reliability of candidate models.

## 5 OPTIMAL SENSOR PLACEMENT

A stochastic search such as PGSL (Raphael and Smith 2003) that uses the objective function defined in Equation (14) generates a set of candidate models. All the models in the set are considered to have same probability of being the correct model. The goal of system identification is to use measurements to identify the single model that truly represents the behavior of the structure. To eliminate models from this set of candidate models, more measurements are required. Given that there are many locations for placing sensors, computational approaches can assist in placing sensors at locations such that subsequent measurements eliminate the maximum number of models.

Let  $N$  be the number of sampled models generated by stochastic search.  $N$  depends upon the modeling assumptions and engineer preferences. Thus, there are  $N$  sets of predictions  $p$ . The goal is to place sensors at locations that offer maximum separability between these  $N$  model predictions.

To measure the separation between model predictions, the notion of entropy is used. Shannon's entropy

function (Shannon and Weaver 1949) is a mathematical representation for the uncertainty in a set. This expression comes from the field of information theory and it formulates the disorder within a set. In our case, a set is an ensemble of model predictions for a system identification task. For a random variable  $X$ , the entropy  $H(X)$  is given by the following equation.

$$H(X) = - \sum_{i=1}^N P_i \cdot \log(P_i) \quad (16)$$

$P_i$  are the probabilities of the  $N$  possible values of  $X$ . For practical purposes,  $0 \cdot \log(0)$  is taken to be 0. When a variable takes  $N$  discrete values, the entropy is a maximum when all values have the same probability  $1/N$ . For a binary variable, the maximum of the entropy function is  $H(X) = 1$  when  $P_1 = P_2 = 0.5$ . Thus entropy is a measure of uncertainty of the variable and is a maximum when the variable has equal probability of taking all possible values. The entropy for a given sensor location is calculated from the histogram of model predictions. The probability  $P_i$  of an interval is the ratio of the number of models in the interval to the total number of models. At the best measurement locations, model predictions should have maximum variation. The location with the highest entropy among model predictions is chosen for subsequent measurement.

## 6 ILLUSTRATION

### 6.1 Schwandbach bridge

The Schwandbach Bridge. (Billington 1979) (see Figure 3) designed by Maillart in 1933 is an early example of a deck stiffened open-spandrel arch. The elliptic horizontal ground-plan curve that is supported by a vertical curved thin-walled arch is also an example of daring structural engineering that has inspired engineers for over seventy years. The proposed methodology is demonstrated for identifying connection behavior of the Schwandbach bridge.

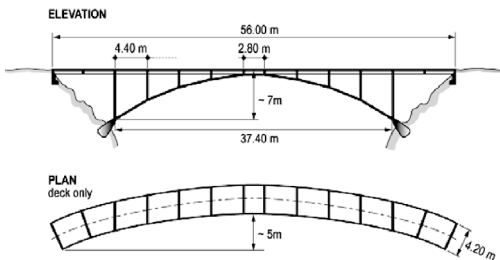


Figure 3. A schematic diagram of the Schwandbach bridge.

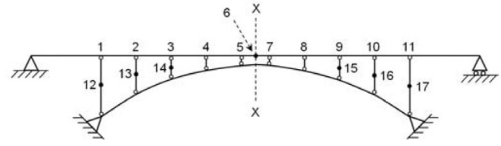


Figure 4. Modeling assumptions in Schwandbach bridge.

Connection behavior is difficult to understand in most structures. While they are modeled as fully hinged or fully rigid during design, it is well-known that connections exhibit semi-rigid behavior in practice. There are 20 connections in the Schwandbach bridge as shown by small circles in Figure 4. A finite element model of the bridge is created. Connections are modeled as rotational springs. To simulate sensor measurements, stiffness values are specified for all connections. This set of stiffness values is the correct model for the structure that should be found using system identification. A truck load test is simulated by modeling equivalent loads on the bridge model. Three load cases that represent two trucks at three different positions on the bridge are simulated. Each truck has a front axle and rear axle loads of 17 kN and 44 kN respectively.

The starting measurement system consists of inclinometers at 5 locations—1, 6, 11, 14 and 15, that are symmetric about mid-span. The inclinometers have a precision of  $1 \mu R$ . The rotations at the following locations for the three load cases are taken as the measurements from the inclinometers. These measurements are given as input to the model generation module. The spring stiffness values  $k_i$  of connection  $i$  are permitted to vary between 0 (hinged) and  $10^8$  (fully rigid). The model parameters are  $\log k_i$ —the logarithms of the spring stiffness  $k_i$ .

### 6.2 Results

For illustration purposes let us assume that the mean and standard deviations for modeling and measurement errors are the same at all sensor locations. Measurement errors can be estimated from laboratory experiments on sensors and also repeating measurements onsite. Let  $\mu_{meas}$  and  $\sigma_{meas}$  be 0 and  $4 \mu R$  respectively. Let  $\mu_{mod}$  and  $\sigma_{mod}$  be 0 and  $2 \mu R$  respectively. From Equations (9) and (10),  $\mu_z$  and  $\sigma_z$  are 0 and  $4.47 \mu R$  respectively. For an identification reliability of  $p_{reqd} = 95\%$  (see Equation (12)),  $c = 8.76 \mu R$  in Equation (13). Therefore  $r_1$  and  $r_2$  are  $-8.76 \mu R$  and  $8.76 \mu R$  respectively.

Using these values for  $r_1$  and  $r_2$ , candidate models that satisfy  $E = 0$  in Equation (15) are generated using PGS�. It generates 1083 candidate models and thus there are 1083 equivalent model predictions. Entropy

Table 1. Entropy of predictions at possible sensor locations.

Sensor location	2	3	4	5	7	8
Entropy	2.60	2.71	2.69	1.65	1.89	2.93
Sensor location	9	10	<b>12</b>	13	16	17
Entropy	2.64	2.62	<b>4.11</b>	3.56	4.00	3.74

of the model predictions are calculated at the remaining 12 possible sensor locations. These are tabulated in Table 1. It is seen that the entropy is maximum at location 12. This is the best location for subsequent measurement to eliminate the maximum number of models from the current candidate model set. It can also be observed that the sensor locations on the vertical slabs have higher entropy values than those on the bridge deck. Thus sensors on vertical slabs are likely to provide more useful information than those on the bridge deck.

## 7 CONCLUSIONS

Conclusions from this study are the following.

1. A multiple model approach has the potential to explicitly account for epistemic uncertainties in the system identification process.
2. An explicit statistical formulation of the objective function provides a useful basis for identifying candidate model sets.
3. Probabilistic characterizations of errors ensure an estimate of the reliability that the candidate model set includes the correct model.
3. A greedy strategy is useful when augmenting an existing measurement system with additional sensors.

Future work involves experimental error quantification using full scale studies. Experiments in controlled environments are required to estimate probability density functions for measurement and modeling errors. Subsequent tasks in multiple-model system identification include data mining in order to classify them into clusters and engineer-computer interaction for improved knowledge visualization. Finally there is much potential to combine this approach with methodologies that treat aleatory uncertainty.

## ACKNOWLEDGMENTS

This work is funded by the Swiss National Science Foundation under contract no. 200020-109257. The authors would like to thank B. Raphael, S. Ravindran and S. Saitta for participating in this project.

## REFERENCES

- Banan, M.R., Banan, M.R., and Hjelmstad, K.D. (1994). "Parameter Estimation of Structures from Static Response. II: Numerical Simulation Studies." *Journal of Structural Engineering*, 120 (11), 3259–3283.
- Billington, D. (1979). *Robert Maillart's Bridges*, Princeton University Press.
- Brownjohn, J.M.W. (2003). "Ambient vibration studies for system identification of tall buildings." *Earthquake Engineering & Structural Dynamics*, 32 (1), 71–95.
- Brownjohn, J.M.W., Moyo, P., Omenzetter, P., and Lu, Y. (2003). "Assessment of Highway Bridge Upgrading by Dynamic Testing and Finite-Element Model Updating." *Journal of Bridge Engineering*, 8 (3), 162–172.
- Frangopol, D.M., and Liu, M. (2007). "Maintenance and management of civil infrastructure based on condition, safety, optimization, and life-cycle cost." *Structure & Infrastructure Engineering: Maintenance, Management, Life-Cycle Design and Performance*, 3, 29–41.
- Friswell, M., and Motterhead, J. (1995). *Finite Element Model Updating in Structural Dynamics*, Kluwer Academic Publishers.
- Koh, C.G., Chen, Y.F., and Liaw, C.Y. (2003). "A hybrid computational strategy for identification of structural parameters." *Computers & Structures*, 81 (2), 107–117.
- Kong, J.S., and Frangopol, D.M. (2003). "Life-Cycle Reliability-Based Maintenance Cost Optimization of Deteriorating Structures with Emphasis on Bridges." *Journal of Structural Engineering*, 129 (6), 818–828.
- Liu, M., and Frangopol, D.M. (2004). "Optimal bridge maintenance planning based on probabilistic performance prediction." *Engineering Structures*, 26 (7), 991–1002.
- Ljung, L. (1999). *System Identification—Theory for the User*, Prentice Hall.
- Raphael, B., and Smith, I.F.C. (2003). "A direct stochastic algorithm for global search." *Applied Mathematics and Computation*, 146, 729–758.
- Robert-Nicoud, Y., Raphael, B., Burdet, O., and Smith, I.F.C. (2005a). "Model Identification of Bridges Using Measurement Data." *Computer-Aided Civil and Infrastructure Engineering*, 20 (2), 118–131.
- Robert-Nicoud, Y., Raphael, B., and Smith, I.F.C. (2005b). "System Identification through Model Composition and Stochastic Search." *Journal of Computing in Civil Engineering*, 19 (3), 239–247.
- Sanayei, M., Imbaro, G.R., McClain, J.A.S., and Brown, L.C. (1997). "Structural Model Updating Using Experimental Static Measurements." *Journal of Structural Engineering*, 123 (6), 792–798.
- Sanayei, M., and Onipede, O. (1991). "Damage Assessment of Structures Using Static Test Data." *Aiaa Journal*, 29 (7), 1174–1179.
- Sanayei, M., and Saletnik, M.J. (1996). "Parameter Estimation of Structures from Static Strain Measurements. I: Formulation." *Journal of Structural Engineering*, 122 (5), 555–562.
- Shannon, C., and Weaver, W. (1949). *The Mathematical Theory of Communication*, University of Illinois Press.
- Smith, I.F.C. "Sensors, Models and Videotape." *Computing in Civil Engineering 2005*, Cancun, Mexico, 1–1.

# Value analysis for decision making on highway cross-sections

N. Villegas, B. De los Ríos, A. Aguado & R. Núñez

*Department of Construction Engineering, Technical University of Catalonia (UPC), Barcelona, Spain*

**ABSTRACT:** This work presents a value-analysis based methodology for choosing among highway construction methods. It derives from a conceptual model centred on three axes: *requirements, components* and *life-cycle*. The methodology stipulates various stages for valuation: definition of a requirements tree (initial analysis); qualification of the response of an alternative relative to an indicator; creation of the value function; weighting of each hierarchical level; calculation of the value of each alternative for each requirement; and sensitivity analysis. The two alternatives analysed here comprise the traditional paving system used in Spanish highways and a new system featuring prefabricated reinforced concrete slabs. The different levels (requirements, criteria and indicators) are weighted using the Analytic Hierarchy Process (AHP) as a mathematical support tool.

## 1 INTRODUCTION

Highways are constantly being improved due to growing demand from society and from the highway sector itself. Advanced technology, such as new methods for design and construction, is being applied to equip roads with better features for travellers. Moreover, the highway construction sector, conscious of social, economic, environmental and, above all, safety issues, is making a marked effort to adapt to new situations and is incorporating these factors into its routines.

The aforementioned elements have been used to value highways in various studies. For example, Douglas (2002) adopted the theory that currently, the planning and design of highways is directly linked to their lifetime performance. Chao (2005) reported that correct functioning of roads entails proper assignment of criteria as well as the relationships among them. These conditions suggest that valuation of a highway is based on valuating economic, temporal or social components which are related.

This article aims to apply a methodology based on value analysis developed for use in cross-sections of highways over their lifespan. The objective of said methodology is to value highways according to their attributes (*e.g.* social, temporal, economic and aesthetic).

## 2 STATE OF THE ART

Highway evaluation systems are very broad. Researchers continue to improve their valuation methodologies on a daily basis, namely by incorporating attributes to make their projects more sustainable.

There are presently methodologies which emphasise economic aspects during highway construction (*e.g.* that of González [2000]). For example, some are based on the premise that the total cost of a road fundamentally depends on its volume and on its singular constituent elements. These clearly emphasise the incorporation of new attributes derived from ever increasingly important investment studies (*e.g.* those of Benzekri [2000] and Wibowo [2005]).

A second fundamental aspect of these methodologies is time. They are based on Herbsman's (2005) principle of 'time is money', in which the builder is paid in function of the duration of the project. However, these attributes are often associated with various factors. Odeh (2000) and Manoj (2003) included factors that directly influence projects, including deficiencies in decision making; construction methods; building errors; inadequate planning; and poor communication.

This article presents a methodology which represents a clear improvement for highway pavement analysis; however, it does not analyse different evaluation systems for highway segments.

## 3 VALUE ANALYSIS

Value analysis was developed by L.D. Miles in 1961. According to Miles, "*Value analysis is a system for use when better than normal results are needed.*"

In the context of highways in Europe, decision making on roads generally entails a traditional method of cost-benefit analysis. This is down to the facility with which this method can identify the respective

benefits of each alternative considered and determine the required values of yields and resource quantities.

The use of cost-benefit analysis has been systematically marginalised by administrations within the EU, which has firmly insisted on the development of new analysis methods for projects. These elements could be decisive in creating other evaluation methods in the sector (APAS, 1996).

In Spain value analysis is used in various sectors—typically the design and fabrication of products from small and medium-sized companies as well as corporate management; however, it is only scarcely applied to highways.

This work clearly confers added value to the development of a value analysis methodology for highways.

## 4 THE ANALYTIC HIERARCHY PROCESS

The Analytic Hierarchy Process (AHP) is a multicriteria evaluation and decision method invented by Saaty (1980). In the AHP, a complex situation is broken down according to a hierarchical model, and then solved by evaluating the model to obtain a ranking of the alternatives. Some of the components involved can be easily measured because they deal with quantitative aspects.

AHP is advantageous because it allows incorporation of qualitative objectives that are not usually included in analyses because they are difficult to measure, but that may nevertheless be relevant for certain parties involved in the decision making.

AHP generally has two applications in highway planning: decision making for entire routes, and decision making for cross-section.

The factors considered in making decisions on entire routes comprise choice of the best route according to orography, whereby engineering is combined with a decision model (Piantanakulchai, 2003); consideration of economic aspects in the improvement of road networks (Sanaei, 2003); and comparisons of maintenance, renovation and reconstruction (James, 2006).

Those considered in decisions on segments encompass selection of criteria (Ababutani, 2002; and Vannieuwenhuyse, 2003); quantification of the environmental and conservation costs of building a road.

The first step is to identify the decision that is to be made, the limits of the system (*i.e.* the project conditions), and the available alternatives.

The next step is to establish a multi-level tree to aid in decision making. These normally encompass three levels: requirements, criteria and indicators. The work reported here is based on the tree used in the MIVES project (Aguado et al., 2007).

Once the tree has been established, the relative importance of each indicator must be gauged against a

homogeneous scale (*e.g.* indicators associated with the same criterion). This is performed by weighting each indicator, criterion or requirement with a percentage value such that, in order for the calculations to be correct, all values within each group must sum to 100%.

Each alternative is assigned a score corresponding to each indicator. The final evaluation in the work presented here was performed according to the value functions established by Alarcón (2006), whereby the sum of the weights of each indicator is expressed as a number between zero and one.

## 5 TECHNICAL DESCRIPTION OF THE NEW CONSTRUCTION SYSTEM

### 5.1 Background conditions

Validation of the proposed methodology through value analysis requires a minimum of two alternatives. In this work, two different highway pavement construction systems are compared: a new one proposed by De los Ríos (2007) within the context of technology transfer, which is defined below; and flexible pavement, which is the system traditionally used in Spain.

The new system was designed for construction of new layers of highway. Technologically, it is based on the prefabrication of reinforced concrete elements, which offers a simple, high-quality system which is readily and more quickly constructed.

### 5.2 Cross-section geometry

The geometric cross-section considered here comprises the platform only; it does not include the berm. It thus includes the two traffic lanes as well as the exterior and interior verges, as shown in figure 1. The total width of the platform is 10.50 m (3.50 m per lane + 2.50 m for the exterior verge + 1.00 m for the interior verge).

### 5.3 Structure

The structure to be used is made up of robust, prefabricated modular slabs of reinforced concrete in dimensions optimised for fabrication, transport, storage and assembly. They are designed to maximise the laying process by covering the maximum area possible.

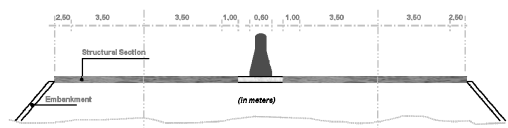


Figure 1. Cross-section of the highway segment studied.



Option	Cross Section
Traditional System (flexible pavement)	Road surface
	Middle layer
	Base layer
New System (Prefabricated concrete slabs)	Road surface
	Reinforced concrete

Figure 2. Cross-sections of the two systems considered.

Likewise, given that the joints between panels can affect ride comfort, especially in the direction perpendicular to traffic, the slabs are designed to imply the least number of joints possible.

Supporting the slabs on beams instead of directly on level ground is a way to reduce the risk of erosion and cantilever action in the slab, which in certain stripped areas could lead to local breakage.

The slabs are supported by reinforced concrete beams. Each slab of reinforced concrete used for the works is 3.20 m by 10.5 m (1 × w) at its shortest face.

Figure 2 illustrates the two types of cross-sections (*i.e.* the limits of the system) considered in this paper for validating the value analysis methodology.

A highway built with the new system would eventually require maintenance for problems such as damaged slabs (whose reinstallation would require interruption of traffic) and poorly sealed cross-joints (which can cause rider discomfort during vertical movements).

## 6 APPLICATION OF THE AHP TO HIGHWAY CONSTRUCTION

### 6.1 Alternatives

In the case at hand, the decision to be made is which of the two construction systems described above to use for paving a highway. Alternative 1 is the prefabricated slab system, and Alternative 2 is flexible paving, the system traditionally used in Spain (fig. 2). However, as Alternative 1 has not been evaluated experimentally, the validation ranges and indicator responses used for this work have been calculated based on research precedent and according to relevant literature (Häkinnen, 2000).

### 6.2 Defining the requirements tree

Table 1 shows the decision tree broken down into three hierarchical levels: requirements, criteria and indicators (Villegas, 2007).

Table 1. The decision tree used.

	Criterion	Indicator
Temporal	Project duration	Construction time (days/km)
		Maintenance frequency (days/km)
	Risk of project delays	Climatic conditions incidents (days/km)
Orographic conditions incidents (days/km)		
Labour conflict incidents (days/km)		
Economic	Costs	Initial construction cost (€ mil/km)
		Maintenance cost (€ /km)
	Risk of exceeding project budget	ISS <sup>1</sup> installations cost (€ mill/km)
Environmental	Capacity for use of recycled material	Exceeding budget due to external factors (%/km)
		Proportion of recycled material used in the structure (%/km)
	Consumption	Quantity of energy consumed (gigajoules/km)
Functional	Emissions	Starting material used (T/km)
		Water used (L/km)
	Integrated Services System (ISS)	CO <sub>2</sub> (T/km)
		Amenability of the structure to services (points)
		Adaptability of the structure to the use of prefabricated elements (points)

<sup>1</sup> ISS (Integrated Services System) refers to the amenability a structure to diverse services (*e.g.* telephone or electrical wiring, and fibre optics).

The qualitative valuation is performed in function of the requirements and criteria, whereas the quantitative valuation is done according to the indicators.

The first level of requirements comprises temporal, economic, environmental and functional aspects.

The requirements tree was thus established with 16 indicators, a number which was considered adequate for proceeding. Increasing the number of indicators does not always enable a more accurate evaluation; it implies more work, complicates the dependency relationships among attributes, and above all, leads to decreased reliability (by diluting weights).

### 6.3 Determination of the weights

The weights are assigned via AHP at each hierarchical level. The process entails pair-wise comparison of

Table 2. Comparison matrix.

Requirement	Temp.	Econ.	Env.	Func.	Weight
Temporal	1	0.666	2.5	1.5	0.30
Economic	1.5	1	2.5	1	0.33
Environmental	0.4	0.4	1	0.5	0.12
Functional	0.666	1	2	1	0.25

each element to be studied with all of the other elements in its branching level (*i.e.* the other indicators for the same criterion). The comparison is based on a scale developed by Saaty (1980), which features the following intermediate and inverse situations:

1. Equal importance
2. Slightly more important or preferred
3. More important or preferred
4. Much more important or preferred
5. Absolutely or extremely preferred

A comparison matrix is obtained for each comparison block. It is characterised by the following:

- It is a diagonal matrix with a value of 1 along its diagonal (because comparing an element with itself yields the same result for importance).
- An inverse element in the matrix takes on the inverse value. For example, if the temporal aspect has a relative importance of 2.5 compared to the environmental aspect, then the latter has a relative importance of 1/(2.50) compared to the former.

Table 2 shows the comparison matrix for the requirements. The matrix vector (shaded column) defines the weights of each requirement used: temporal (30%), economic (33%), environmental (12%) and functional (25%).

The consistency of the comparisons should also be calculated. For example, if A is twice as important as B, and B is twice as important as C, then logically, we expect that A will be four times as important as C.

### 6.4 Value functions

To quantify the alternatives using the indicators, a value function is applied to each attribute assigned. The indicators are valued on a scale of zero to one, which represents the state of satisfaction with the response of the indicator. This non-dimensional scale is needed in order to sum indicators that are measured in different units.

The value function has four parameters which, upon variation, can yield plots of all types of shapes: S-curve, concave, convex, or linear. This function is

provided by the following equation [1]:

$$V_{ind} = B * \left( 1 - e^{-K_i^* \left( \frac{|X - X_{min}|}{C_i} \right)^{P_i}} \right) \tag{1}$$

whereby  $X_{min}$  is the origin of the x-axis of the indicator, which is usually equal to zero;  $P_i$  is a factor which determines the plot shape (concave [ $P_i < 1$ ], linear [ $P_i = 1$ ], or S-shaped or convex [ $P_i > 1$ ]) as well as the plot slope at the inflexion point (coordinates  $C_i, K_i$ ; whereby  $C_i$  is the x-axis of the inflection point, and  $K_i$  is the y-intercept of the inflexion point);  $X_{max}$  is the x-axis of the indicator that generates a value of 1; and B is the factor (defined by equation [2]) that restricts the function to a value range of 0 to 1.

The aforementioned functions can be increasing or decreasing, depending on the maximum value at the x-axis,  $X_{max}$  or  $X_{min}$ , respectively. In the latter case, equation [1] lacks the 1 and takes the opposite sign, such that, for  $x = 0$ , the value is 1, whereas for the x-axis,  $X_{max}$ , the value is 0.

$$B = s \left( 1 - e^{-K_i^* \left( \frac{|X_{max} - X_{min}|}{C_i} \right)^{P_i}} \right)^{-1} \tag{2}$$

It should be pointed out that the range of the function ( $X_{min}$  to  $X_{max}$ ) must be well defined. Hence, if the range between  $X_{min}$  and  $X_{max}$  is much greater than the range of results, then nearly all of the alternatives will be evaluated similarly. If this occurs, it means that the indicator employed was useless, since it failed to discriminate among the alternatives.

Owing to the limitations of this article, each indicator is not described here in detail. To illustrate the concepts described above, one function corresponding to the studied case is presented in the following two subsections.

#### 6.4.1 Value function of the maintenance frequency indicator

Before showing the value function of the maintenance frequency indicator, we first describe here the indicator itself so that the reader can grasp how a function can both discriminate among and value the two alternatives being considered.

In Spain, the frequency of maintenance for road surfaces constructed with flexible paving is approximately two to three years, although the application of new technologies (*e.g.* better materials) to a road can influence maintenance demands.

To develop the value function for this indicator, we met with highway specialists. They suggested that for layers of micro-agglomerates, a maintenance frequency of two to three years should also be used.

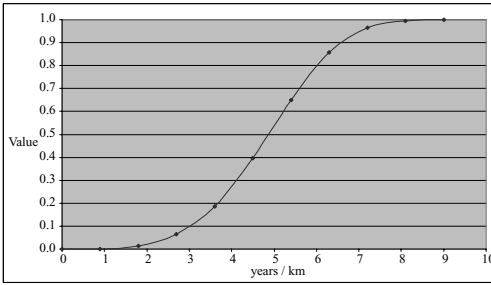


Figure 3. Value function for the *maintenance frequency* indicator.

Hence, we assigned a value of three years for the new system.

Values below this range are considered to imply a partially favourable situation for the alternative in question. As observed in figure 3, this value ( $C = 3$  years) was taken as x-axis of the inflexion point, with a y-intercept which represents 10% ( $k = 0.10$ ), whereby  $X_{max} = 9$  years,  $X_{min} = 0$  years and  $p = 4$ . The value of  $X_{max}$  could be exploited for use in advertising the long life of highways constructed by the new method.

Also as observed in figure 3, satisfaction begins to increase with the third year of maintenance frequency. This is due to the threshold (of three years) implied by the traditional alternative. A reduction in the frequency of maintenance therefore represents an added value for the alternative being evaluated.

## 7 RESULTS

### 7.1 The weight of each attribute

Table 3 shows the weight (shown in parenthesis as a percent value) obtained through AHP for each indicator, criterion and requirement of the two construction systems. Certain features of the table are worth mentioning: in the *temporal* area, the concern of the risk specialists over project duration is clearly evident, as is the specific importance given to maintenance frequency (83%) and to environmental protection, as reflected in the weight assigned to the consumption of raw materials (50%).

### 7.2 Value indices

Table 4 lists the valuations of the two alternatives in each of the four requirements, as well as the *value index* (i.e. the final score) for each alternative (far-right column), which incorporates the corresponding weights for each indicator, criterion and requirement.

The indicators were scored based on the recommendations of a committee of experts on highway

Table 3. The weight of each attribute in the requirements tree (expressed as %).

	Criterion	Indicator
Temporal (32)	Project duration (33)	Construction time (17)
	Risk of project delays (67)	Maintenance frequency (83)
		Climatic conditions incidents (17)
Economic (51)	Costs (75)	Orographic conditions incidents (83)
		Labour conflict incidents (83)
	Risk of exceeding project budget (25)	Initial construction cost (45)
		ISS installations cost (10)
Environmental	Capacity for use of recycled material (33)	Exceeding budget due to external factors (100)
	Consumption (33)	Proportion of recycled material used in the structure (100)
		Emissions (33)
Functional	Integrated Services System (100)	Starting material used (50)
		Water used (25)
		CO <sub>2</sub> (100)
		Amenability of the structure to services (33)
		Adaptability of the structure to the use of prefabricated elements (67)

Table 4. Valuations of the two alternatives in each requirement.

Alternative	Temp	Econ.	Envir.	Func.	Value index
1	0.20	0.22	0.04	0.02	0.52
2	0.26	0.25	0.06	0.06	0.59

construction and use. Of course, the points vary with the experience of the decision maker.

## 8 CONCLUSIONS

- Herein we have presented a method to improve evaluation of highway construction methods. It is based on value analysis and the integrated study of various factors implied in choosing a construction method. The tools used in the methodology were extracted from relevant literature.
- The use of weighted indicators provides accurate results (thereby partly avoiding biased results).
- The priorities of the attributes can be demonstrated through the use of sensitivity analysis.
- Comparison of the two construction systems revealed that the new one, based on pre-fabricated

concrete modules, is clearly the better alternative (0.59 vs. 0.52). Nonetheless, the valuations used for the new system could vary as experience with it is gradually acquired.

## ACKNOWLEDGMENTS

The authors thank the companies UNILAND and ICA for support provided through formal collaborations with UPC. Noé Villegas thanks the Mexican National Science and Technology Council (*CONACyT México*) for a doctoral grant at the UPC. This work is part of the MIVES II project (BIA 2005-09163-C03-01), which is financed by the Spanish Ministry of Education and Science (*MEC*), who is also thanked for their support. Lastly, the *Escuela Técnica Superior de Ingenieros de Caminos, Canales y Puertos* is thanked for funding support for this article.

## REFERENCES

- Ababutain, A. 2002. "A Multicriteria Decision-Making Model for Selection of both toll road proposals with the Public Sector". Pittsburgh University, Engineering School
- Aguado, A., Manga, R. Ormazabal, G. 2007. "La medida de la sostenibilidad en edificación industrial". Capítulo 6 del libro "Los aspectos conceptuales del proyecto MIVES". UPV-EHU.
- Alarcón, B. 2006. "Modelo integrado de valor para estructuras sostenibles". Tesis doctoral. ETS, Ingenieros de Caminos, Canales y Puertos. (UPC). 3 Marzo 2006. Directores de Tesis: Antonio Aguado y Alejandro García Josa.
- APAS 1996. Transport Research Report: "Action de Promotion D'Accompagnement et de Suivi et Autres Activités". Directorate General of Transport, European Commission.
- Benzrekri, J. 2000. "El presupuesto dedicado a las carreteras". Revista Carreteras. #109. Julio-Agosto. p. 17–20.
- De los Ríos, B. 2007. "Nuevo sistema constructivo para firmes en carreteras". Tesis doctoral en desarrollo. ETS, Ingenieros de Caminos, Canales y Puertos (UPC) Directores de Tesis: Antonio Aguado and Félix Pérez.
- Chan, A. 2002. "Framework of success criteria for build the design and building of projects" Journal of management in Engineering. July pp. 120–127.
- Chao-Hui, W. 2004. "Statistical Analysis of Causes for Design Change in Highway Construction on Taiwan". International Journal of Project Management #23. p. 554–563.
- Choocharukul, K. 2004. "User Perceptions and engineering Definitions of Highway Level of Service: an Exploratory Statistical Comparison". Transportation Research Part A. Vol. 38. #9–10. pp. 677–689.
- Douglas, W. 2002. "New Elements of Highway Geometry". TR News N. 223, November-December. pp. 3–7.
- El-Rayes, K. 2005. "Time-Cost-Quality Trade off Analysis for Highway Construction". Journal of Construction Engineering and Management, ASCE. April. pp. 477–486.
- González, B., Rodríguez, A., Fe, J. 2000. "Evaluación de los costes de construcción en la red de carreteras de Andalucía". Revista Carreteras. #107. Marzo-Abril. pp. 45–60.
- Häkkinen, T., Mroueh, U., Laine-Ylijoki, J., Wellman, K. 2000. "Life cycle assessment of road construction" TIELAITOS, Finnra Reports 17/2000. Finnish National Road Administration.
- Herbsman Z., Tong Chen W., Epstein W. 1995. "Time is money: Innovative Contracting Methods in Highways Construction". Journal of construction Engineering and management/ September. pp. 273–281.
- James, T., Tighe, S. 2006. "Analytic Hierarchy Process as a Tool for Infrastructure Management" Transportation Research Board of the National Academies. Volume 1974–2006. pp. 3–9. Department of Civil Engineering. Waterloo University. Ontario, Canadá.
- Kwangho, P. 2003. "Quantitative Assessment of Environmental Impacts on Life Cycle of Highways". Journal of Construction Engineering and Management. January–February. pp. 25–31.
- Manoj, K. 2003. "Criteria Based Decision Support System for Selecting Highway Alignments". Journal of Transportation Engineering. January–February. pp. 33–41.
- Odeh, A., Battaineh, H. 2002. "Causes of Construction Delay: Traditional Contracts" International Journal of Project Management. #20. pp. 67–73.
- Piantanakulchai, M. 2003. "Evaluation of Alternatives in Transportation Planning Using Multi-stakeholders Multi-objectives AHP Modelling". Proceedings of the Eastern Asia Society for transportation Studies. Vol. 4, October. pp. 1613–1627.
- Saaty, T. 1980. "AHP: The Analytic Hierarchy Process" McGraw-Hill.
- Villegas, N. 2007. "Análisis de valor para la toma de decisión aplicado a carreteras: secciones transversales". Tesis doctoral en desarrollo. ETS, Ingenieros de Caminos, Canales y Puertos. (UPC). Director: Antonio Aguado.